

Rajesh Singh
Sushabhan Choudhury
Anita Gehlot *Editors*

Intelligent Communication, Control and Devices

Proceedings of ICICCD 2017

Advances in Intelligent Systems and Computing

Volume 624

Series editor

Janusz Kacprzyk, Polish Academy of Sciences, Warsaw, Poland
e-mail: kacprzyk@ibspan.waw.pl

About this Series

The series “Advances in Intelligent Systems and Computing” contains publications on theory, applications, and design methods of Intelligent Systems and Intelligent Computing. Virtually all disciplines such as engineering, natural sciences, computer and information science, ICT, economics, business, e-commerce, environment, healthcare, life science are covered. The list of topics spans all the areas of modern intelligent systems and computing.

The publications within “Advances in Intelligent Systems and Computing” are primarily textbooks and proceedings of important conferences, symposia and congresses. They cover significant recent developments in the field, both of a foundational and applicable character. An important characteristic feature of the series is the short publication time and world-wide distribution. This permits a rapid and broad dissemination of research results.

Advisory Board

Chairman

Nikhil R. Pal, Indian Statistical Institute, Kolkata, India
e-mail: nikhil@isical.ac.in

Members

Rafael Bello Perez, Universidad Central “Marta Abreu” de Las Villas, Santa Clara, Cuba
e-mail: rbellop@uclv.edu.cu

Emilio S. Corchado, University of Salamanca, Salamanca, Spain
e-mail: escorchado@usal.es

Hani Hagrass, University of Essex, Colchester, UK
e-mail: hani@essex.ac.uk

László T. Kóczy, Széchenyi István University, Győr, Hungary
e-mail: koczy@sze.hu

Vladik Kreinovich, University of Texas at El Paso, El Paso, USA
e-mail: vladik@utep.edu

Chin-Teng Lin, National Chiao Tung University, Hsinchu, Taiwan
e-mail: ctlin@mail.nctu.edu.tw

Jie Lu, University of Technology, Sydney, Australia
e-mail: Jie.Lu@uts.edu.au

Patricia Melin, Tijuana Institute of Technology, Tijuana, Mexico
e-mail: epmelin@hafsamx.org

Nadia Nedjah, State University of Rio de Janeiro, Rio de Janeiro, Brazil
e-mail: nadia@eng.uerj.br

Ngoc Thanh Nguyen, Wroclaw University of Technology, Wroclaw, Poland
e-mail: Ngoc-Thanh.Nguyen@pwr.edu.pl

Jun Wang, The Chinese University of Hong Kong, Shatin, Hong Kong
e-mail: jwang@mae.cuhk.edu.hk

More information about this series at <http://www.springer.com/series/11156>

Rajesh Singh · Sushabhan Choudhury
Anita Gehlot
Editors

Intelligent Communication, Control and Devices

Proceedings of ICICCD 2017

 Springer

Editors

Rajesh Singh
Institute of Robotics Technology (R&D)
University of Petroleum and Energy Studies
Dehradun, Uttarakhand
India

Anita Gehlot
Department of Electronics &
Instrumentation Engineering
University of Petroleum and Energy Studies
Dehradun, Uttarakhand
India

Sushabhan Choudhury
Department of Electronics &
Instrumentation Engineering
University of Petroleum and Energy Studies
Dehradun, Uttarakhand
India

ISSN 2194-5357 ISSN 2194-5365 (electronic)
Advances in Intelligent Systems and Computing
ISBN 978-981-10-5902-5 ISBN 978-981-10-5903-2 (eBook)
<https://doi.org/10.1007/978-981-10-5903-2>

Library of Congress Control Number: 2017948236

© Springer Nature Singapore Pte Ltd. 2018

This work is subject to copyright. All rights are reserved by the Publisher, whether the whole or part of the material is concerned, specifically the rights of translation, reprinting, reuse of illustrations, recitation, broadcasting, reproduction on microfilms or in any other physical way, and transmission or information storage and retrieval, electronic adaptation, computer software, or by similar or dissimilar methodology now known or hereafter developed.

The use of general descriptive names, registered names, trademarks, service marks, etc. in this publication does not imply, even in the absence of a specific statement, that such names are exempt from the relevant protective laws and regulations and therefore free for general use.

The publisher, the authors and the editors are safe to assume that the advice and information in this book are believed to be true and accurate at the date of publication. Neither the publisher nor the authors or the editors give a warranty, express or implied, with respect to the material contained herein or for any errors or omissions that may have been made. The publisher remains neutral with regard to jurisdictional claims in published maps and institutional affiliations.

Printed on acid-free paper

This Springer imprint is published by Springer Nature
The registered company is Springer Nature Singapore Pte Ltd.
The registered company address is: 152 Beach Road, #21-01/04 Gateway East, Singapore 189721, Singapore

Preface

The Department of Electronics, Instrumentation & Control Engineering, University of Petroleum and Energy Studies, Dehradun, has organized Second International Conference on Intelligent Communication, Control and Devices (ICICCD 2017) during April 15 and 16, 2017. The conference focusses on the integration of intelligent communication systems, control systems, and devices related to all aspects of engineering and sciences. ICICCD 2017 aims to provide an opportune forum and vibrant platform for researchers, academicians, scientists, and industrial practitioners to share their original research work, findings, and practical development experiences. The proceedings are published in Advances In Intelligent Systems and Computing (AISC) book series of Springer.

The general aim of the conference is to promote international collaboration in education and research in all fields and disciplines of engineering. ICICCD 2017 is an international forum for those who wish to present their projects and innovations, having also the opportunity to discuss the main aspects and the latest results in the field of education and research.

The organizing committee is extremely grateful to the authors who had shown tremendous response to the call for papers. Over 300 papers were submitted from the researchers, academicians, and students on wide area of three parallel tracks on Intelligent Communication, Intelligent Control and Intelligent Devices, along with the poster presentation session and working model competition.

We are obliged to our Honorable Chancellor Dr. S.J. Chopra, Vice Chancellor Dr. Shrihari Honward, Vice President—Academic Affairs Dr. S.R. Das, Dean Dr. Kamal Bansal, and Director Dr. Suresh Kumar, for their confidence they have invested on us for organizing this international conference ICICCD 2017.

We extend our thanks to all faculty members and staff with different committees for organizing the conference and made it a grand success.

Dehradun, India

Dr. Rajesh Singh
Dr. Sushabhan Choudhury
Anita Gehlot

Steering Committee

Chief Patron

Dr. S.J. Chopra, Chancellor, UPES, Dehradun (India)

Patron(s)

Mr. Utpal Ghosh, President & CEO, UPES, Dehradun (India)

Dr. Shrihari Honwad, Vice Chancellor, UPES, Dehradun (India)

Dr. S.R. Das, Vice President, Academic Affairs, UPES, Dehradun (India)

General Chair

Dr. Kamal Bansal, Dean, College of Engineering Studies, UPES, Dehradun (India)

Program Chair

Dr. Durgesh Pant, Director, USAC, Dehradun

Organizing Chair

Dr. Suresh Kumar, Director (COES), UPES, Dehradun (India)

Dr. Manish Parteek, Director (CIT), UPES, Dehradun (India)

Dr. Piyush Kuchhal, Assoc. Dean (COES), UPES, Dehradun (India)

Dr. S.K. Banerjee, Assoc. Dean (COES), UPES, Dehradun (India)

Organizing Co-chair

Dr. Sushabhan Choudhury, HOD (EIC), UPES

Dr. Rajesh Singh, Assoc. Prof. & Head Institute of Robotics Tech. (R&D), UPES

Publicity Chair

Dr. R. Gowri, Prof., EIC, UPES

Dr. N. Siddiqui, HOD (HSE), UPES

Dr. Adesh Kumar, A.P (SG), EIC, UPES

Dr. Vikas Garg, HoD, Civil Engg., UPES

Public Relation Chair

Dr. Jitendra Kumar Pandey, Head (R&D), UPES

Dr. Paawan Sharma, A.P (SG), EIC, UPES

Dr. Mukul Gupta, A.P (SG), EIC, UPES

Session Management Chair

Dr. Ranjan Mishra, Assoc. Prof., EIC, UPES

Dr. N. Parsanthi, Assoc. Prof., EIC, UPES

Editors (AISC Book Series—Intelligent Communication, Control & Devices, 2017)

Dr. Rajesh Singh, Associate Prof. & Head Institute of Robotics Tech. (R&D), UPES

Dr. Sushabhan Choudhury, HOD (EIC), UPES

Anita Gehlot, Assistant Prof. (EIC), UPES

Organizing Committee

Convener

Dr. Sushabhan Choudhury, HOD (EIC), UPES

Dr. Rajesh Singh, Assoc. Prof. & Head Institute of Robotics Tech. (R&D), UPES

Conference Secretary

Ms. Anita Gehlot, A.P (SS), EIC, UPES
Dr. Adesh Kumar, A.P (SG), EIC, UPES

Finance Committee

Mr. Roushan Kumar, A.P (SS), EIC, UPES
Dr. Mukul Gupta, A.P (SG), EIC, UPES
Mr. Vinay Chowdhary, A.P, EIC, UPES
Mr. Raj Gaurav, A.P (SG), EIC, UPES

Technical Support

Dr. R. Gowri, Professor, EIC, UPES
Dr. Rajesh Singh, Associate Prof. & Head Institute of Robotics Tech.
(R&D), UPES
Dr. Adesh Kumar, A.P (SG), EIC, UPES
Dr. Ranjan Mishra, Assoc. Prof., EIC, UPES
Dr. Madhu Sharma, Assoc. Prof., UPES
Dr. Gagan Anand, Assoc. Prof., UPES
Ms. Anita Gehlot, A.P (SS), EIC, UPES
Mr. Vivek kaundal, A.P (SG), EIC, UPES
Dr. Rishi Dewan, A.P (SG),UPES
Dr. Amit Mondal, A.P (SS), EIC, UPES
Mr. Roushan Kumar, A.P (SS), EIC, UPES
Mr. Arpit Jain, A.P (SS), EIC, UPES
Mr. Tarun Kumar, A.P (SS), EIC, UPES
Mr. Raj Gaurav, A.P (SG), EIC, UPES
Dr. Paawan Sharma, A.P (SG), EIC, UPES
Mr. Ankur Dumka, A.P, CIT, UPES
Mr. Vishal Kaushik, A.P (SG), CIT, UPES
Dr. Inder Singh, A.P (SS), CIT, UPES
Dr. Om Parkash, HOD, Aerospace Engg., UPES
Mr. Sudhir Kumar Chaturvedi, A.P (SS), Aerospace Engg, UPES

Sponsorship Committee

Dr. R. Gowri, Professor, EIC, UPES
Mr. Arpit Jain, A.P (SS), EIC, UPES
Mr. Vivek kaundal, A.P (SG), EIC, UPES
Mr. Roushan Kumar, A.P (SS), EIC, UPES
Dr. Mukul Gupta, A.P (SG), EIC, UPES
Mr. Deepak Kumar, A.P (SS), EIC, UPES
Dr. Amit Mondal, A.P (SS), EIC, UPES
Mr. Raj Gaurav Mishra, A.P (SG), EIC, UPES
Dr. Rupendra Pachauri, A.P (SS), EIC, UPES
Dr. Abhinav Sharma, A.P (SS), EIC, UPES

Registration Committee

Dr. Adesh Kumar, A.P (SG), EIC, UPES
Dr. N. Parsanthi, Assc. Prof., EIC, UPES
Mr. Vinay Chowdhary, A.P, EIC, UPES
Mr. Khalelu R. Rehman, A.P, EIC, UPES
Dr. Abhinav Sharma, A.P (SS), EIC, UPES
Ms. Isha Kansal, A.P, EIC, UPES
Ms. Meera C.S., DRF, EIC, UPES
Ms. Varnita, DRF, EIC, UPES

Session Management

Dr. N. Parsanthi, Assc. Prof., EIC, UPES
Ms. Anita Gehlot, A.P (SS), EIC, UPES
Mr. Arpit Jain, A.P (SS), EIC, UPES
Mr. Khalelu R. Rehman, A.P, EIC, UPES
Dr. Madhu Sharma, Assc. Prof., EPG, UPES
Ms. Isha Kansal, A.P, EIC, UPES
Dr. Amit Mondal, A.P (SS), EIC, UPES

Hospitality Committee

Mr. Khalelu R. Rehman, A.P, EIC, UPES
Mr. Sallauddin, A.P, EIC, UPES
Mr. Vinay Chowdhary, A.P, EIC, UPES
Mr. Arpit Jain, A.P (SS), EIC, UPES
Mr. Vivek kaundal, A.P (SS), EIC, UPES
Mr. Deepak Kumar, A.P (SS), EIC, UPES
Ms. Meera C.S, DRF, EIC, UPES
Ms. Varnita, DRF, EIC, UPES

Venue Arrangement Committee

Mr. Vivek kaundal, A.P (SS), EIC, UPES
Mr. Arpit Jain, A.P (SS), EIC, UPES
Mr. Khalelu R. Rehman, A.P, EIC, UPES
Mr. Sallauddin, A.P, EIC, UPES
Mr. Vinay Chowdhary, A.P, EIC, UPES
Mr. Bhan Parkash, A.P (SS), EIC, UPES

Transport Committee

Mr. Sallauddin, A.P, EIC, UPES
Mr. Khalelu R. Rehman, A.P, EIC, UPES
Mr. Vinay Chowdhary, A.P, EIC, UPES
Mr. Arpit Jain, A.P (SS), EIC, UPES
Mr. Vivek kaundal, A.P (SS), EIC, UPES
Dr. Rupendra Pachauri, A.P (SS), EIC, UPES
Mr. Raja Roa, A.P (SS), EIC, UPES

International Committee

Dr. S.N. Singh, Fellow IEEE, IIT Kanpur
 Dr. M.V. Kartikeyan, IIT Roorkee
 Dr. Y.N. Singh, IIT Kanpur
 Dr. Giridhar K, IIT Madras
 Dr. Debashish Ghosh, IIT Roorkee
 Dr. K.J. Vinoy, IISc, Bangalore, India
 Dr. Arunkumar D. Mahindrakar, IIT Madras
 Dr. Nagendra Prasad Pathak, IIT Roorkee
 Dr. Nitin Khanna, IIT Gandhinagar, India
 Dr. Puneet Goyal, IIT Ropar, India
 Dr. S. Raghavan, NIT Trichy
 Dr. Prabhat Sharma, NIT, Nagpur, India
 Dr. L.M. Saini, Professor, NIT, Kurushetra, India
 Dr. Babita Saini, NIT, Kurushetra, India
 Dr. Vrijendra Singh, Associate Professor, IIIT, Allahabad, India
 Dr. Vijaynath, Birla Institute of Technology, Mesra, India
 Mr. Shailesh Mishra, NSIT, Delhi, India
 Dr. Lini Mathew, NITTTR, Chandigarh, India
 Dr. Ramesh Lalwani, Vice Chancellor, ICFAI University, India
 Dr. Nasimuddin, Scientist, A*STAR, Singapore
 Dr. Arjun Kumar, Scientist, Intel Corporation, USA
 Shri. Rajeev Jyoti, Deputy Director, MRSA
 Shri. V.K. Kaushik, Sci-‘G’, DEAL, Dehradun
 Shri. Ajay Malik, Sci-‘G’, DEAL, Dehradun
 Shri. Ashik Kalra, Sci-‘G’, DEAL, Dehradun
 Dr. R.P. Dixit, Sci-‘G’, DEAL, Dehradun
 Shri. Mehakar Singh, Sci-G, DEAL, Dehradun
 Dr. A.S. Shukla, Sci-‘F’, SAC, Ahmedabad
 Mr. Ankur Kumar, ST Microelectronics, Noida, India
 Mr. Purnendu Shekhar Pandey, THDC IHET, Tehri Garhwal, India
 Mr. Sushil Kumar, Bhushan Steel Limited, Engineer, Ghaziabad, India
 Ms. Sunita Chandel, Uttarakhand Technical University, Dehradun, India
 Dr. M.S. Yadav, Kurukshetra University, Kurukshetra, India
 Dr. Yogesh Chauhan, Gautam Budha University, G. Noida, India
 Dr. Dilip Kumar Sharma, GLA, Mathura
 Dr. Loviraj Gupta, Lovely Professional University, India
 Dr. S. Sri Gowri, Prof and Head ECE Department, SRK Institute of Technology,
 Enikepadu, Vijayawada, India
 Dr. Preeti Singh, Panjab University, Chandigarh, India
 Dr. M.R. Tripathy, Amity University, Noida, India
 Dr. Jaydeep Chakarvorty, Baddi University, Baddi, Solan (HP)
 Dr. Sandeep Chakarvorty, Baddi University, Baddi, Solan (HP)

Dr. Vinay Bhatia, Baddi University, Baddi, Solan (HP), India
Dr. Harbinder Singh, Chandigarh University, Chandigarh, India
Mr. Kuldeep Singh, Baddi University, Baddi, Solan (HP), India
Dr. Sonal Singhal, Shiv Nadar University, NCR, GB Nagar, India
Dr. M.D. Singh, Thapar University, Patiala, India
Dr. Mayank Srivastava, Amity University, Noida, India
Mr. Manish Sharma, Amity University, Noida, India
Dr. Y.K. Awasthi, M.R.University, Faridabad, India
Mr. Gaurav Verma, Jaypee University of Information Technology, Noida, India
Mr. Anuj Kumar Sharma, DIT University, Dehradun, India
Mr. Dileep Jaiswal, Maya Institute of Technology, Dehradun, India
Mr. Anand Nayyar, KCL Institute of Management and Technology,
Jalandhar, India
Dr. Namit Gupta, Shri Vaishnav Institue of Technology & Science, Indore, India
Dr. N.M. Singh, VJTI Mumbai, India
Dr. Faruk Kazi, VJTI Mumbai, India
Dr. Debdatta Kandar, NEHU, India
Dr. Chandra Mohan, Bapatla Engg College, India
Mr. Vinod Kumar Yadav, HRIT, Ghaziabad, India
Mr. Kulshrest Paraliya, JBIT, Dehradun, India
Dr. Mayank Singh, KEC, Ghaziabad, UP, India
Mr. Vishal Jain, BMIET, Sonapat, India
Dr. B.S. Jassal, Dean Projects, GEU, Dehradun
Dr. Vedprakash Dubey, GEHU, Dehradun, India
Dr. Rishi Prakash, GEU, Dehradun
Dr. Anurag Vidyarthi, GEU, Dehradun, India
Dr. M.R. Tripathy, Professor, Amity School of Engineering and Technology,
Noida(U.P.), India
Mr. Ravindra Sharma, Nimbus Academy of Management, Dehradun, India
Dr. I.A. Pasha, Dean (R&D), BVRIT, India
Dr. Himashu Monga, Director, SIET, Bilaspur, India
Dr. Ramesh Kumar Vobulapuram, Rajeev Gandhi Memorial College, India
Raj Kumar Chaurasia, ICFAI University, India
Dr. S. Sri Gowri, SRK Institute of Technology, India
Md. Yousuf, VBIT, Hyderabad, India
Mudassir Basha, BVRIT, India

Keynote Speakers

Chief Guest



Dr. A. Senthil Kumar
Director, IIRS, ISRO
Dehradun

Guest of Honor



Dr. R.P. Dixit Sc 'G'
DEAL, Dehradun

Program Chair



Dr. Durgesh Pant
Director, USAC
Dehradun

Keynote Speakers



Dr. Tan Cher Ming
Professor, Chang Gung University
Taiwan



Dr. Soumen Das
Professor, IIT Kharagpur
India



Dr. Loviraj Gupta
Executive Dean
LPU, Jalandhar, India



Prof. D.V. Gadre
Professor, NSIT
New Delhi, India

Contents

Impact of Sand Erosion on Hydroturbines: A Case Study of Hydropower Plant in Himachal Pradesh, India	1
Robin Thakur, Muneesh Sethi and Sourabh Khurana	
Design, Analysis, and Assessment of Efficiency of Three-Phase Squirrel-Cage Induction Motors Operating Under the Rated Voltage: A Design Consideration for Rural Areas	13
Raj Kumar Saini, Devender Kumar Saini, Rajeev Gupta, R.P. Dwivedi and Piush Verma	
Tunable Universal Filter in ± 0.5 V 32 nm CNFET for ISM 2.4 GHz Bluetooth/Zigbee Transceivers	23
Jyoti Sharma, Mohd. Samar Ansari and Sudip Kundu	
Morphology of Plants Using Spatial Domain Image Enhancement Technique for the Mildew Detection	33
Deepak Kumar, Prashanta Bhuyan, Manish Sharma and Amit Kumar	
A High-Throughput FPGA-Based Architecture for Advanced Encryption Standard: AES-512 Using Pre-ciphered Lookup Table	41
Vivek Kumar, Purnendu Shekhar Pandey and Praful Ranjan	
Design and Calculation of Power Aperture Parameters with Variable SNR	49
Prabhansh Varshney, Shagun Bishnoi, Sudhir Kumar Chaturvedi, Dipen Patel and D. Tejaswini	
Low Power Adder Circuit Based on Coupling Technique	55
Arpan Roy, Aashwin Sharma, Anu Mehra and Sachin Kumar Rajput	

Analysis of the Relationship Between Substrate Properties and Patch Dimensions in Rectangular-Shaped Microstrip Antennas	65
Raj Gaurav Mishra, Jeevani Jayasinghe, G. Chathuranga and Ranjan Mishra	
Dual-Band Square Patch Antenna for Bluetooth and WiMAX Applications	73
Praful Ranjan	
Estimation of Probability of Detection and False Alarm Alert for Swerling Targets	83
Prashant Singh, Shivam Kapri, Rajat Saklani, Prateek Mehta and Sudhir Kumar Chaturvedi	
Tsallis Entropy Segmentation and Weighted KNN Classifier-Based Automatic DR Detection from Retinal Fundus Images	95
Ravindra D. Badgujar and Pramod J. Deore	
Contact Resistance-Dependent OTFT Behaviour: Effect of Channel Length	107
Shruti Nautiyal, Pranjali Nautiyal, Shubham Negi and Poornima Mittal	
Enhancement in Efficiency of Hybrid Organic Photovoltaics by Variation in Anode Material	115
Pranjali Nautiyal, Arun Pratap Singh Rathod, Shruti Nautiyal and Poornima Mittal	
Performance Analysis of Double Block Layer OLED and Variation in Ratio of Double Block Layer	123
Shubham Negi, Poornima Mittal and Brijesh Kumar	
Design and Performance Evaluation of Frequency Compression Algorithm for Marathi Hearing Aid Users	129
Prashant G. Patil, Arun K. Mittra and Vijay S. Chourasia	
Emotion Recognition System for Patients with Behavioral Disorders	139
Aakash Verma, Astha Dogra, Ketan Malik and Meenkshi Talwar	
A Review on Computer-Aided Modelling and Quantification of PET-CT Images for Accurate Segmentation to Bring Imagination to Life	147
Ziaur Rahiman Shaik and Ch. Sumanth Kumar	
Genetic Algorithm-Based Optimized Gabor Filters for Content-Based Image Retrieval	157
D. Madhavi and M. Ramesh Patnaik	

Optimal ISA-PID-Based Drug Concentration Control in Cancer Chemotherapy	165
Pandey Vivek, Pachauri Nikhil, Rani Asha and Singh Vijander	
Implementation of Adder Circuit Using Quantum-Dot Cellular Automata-Based Logic Gates	173
Priyanka Kumari, Abhay Sharma and Arpita Singh	
FPGA Implementation of High Speed Multiplier with Optimized Reduction Phase	187
Arpita Singh, Abhay Sharma and Priyanka Kumari	
A Sustainable Approach to Home Automation System in Perspective of Ensuring Energy Efficiency and Security	197
Jaideep Saraswat, Nikhil Mall, Varima Agarwal, Sayali Rajale and Mainak Mukherjee	
Low-Offset High-Speed CMOS Dynamic Voltage Comparator	209
Priyesh P. Gandhi and Niranjana M. Devashrayee	
Vehicle Control Using Raspberry pi and Image Processing.	219
Rohit Tiwari and Dushyant Kumar Singh	
Self-organized Bacterial Evolutionary Dynamics: Fractal Characteristics	229
Saurabh Shanu, Sudepto Bhattacharya, Ajay Prasad and Apurva Gupta	
Diet Recommendation for Diabetic Patients Using MCDM Approach.	239
Kirti Sharawat and Sanjay Kumar Dubey	
Software Component Quality Models: A Survey	247
Munishwar Rai and Kiranpal Singh Virk	
Achievable Spectral Efficiency with SIT-Based Channel Estimation Method in Next Generation Cellular Networks	257
Rajarao Manda and Mohammad Salauddin	
Comparative Analysis of Workflow Scheduling Policies in Cloud Platforms	267
Kamal Kumar and Jyoti Thaman	
Effect of Ratio of Protrusion Height to Print Diameter on Thermal Behaviour of Al₂O₃-H₂O Nanofluid Flow in a Protrusion Obstacle Square Channel	277
Sunil Kumar, Alok Darshan Kothiyal, Mangal Singh Bisht and Anil Kumar	

PI-Based DSTATCOM Controller for Voltage Control in Weak Power Systems	289
Subhadip Bhattacharya and Benjamin A. Shimray	
Comparative Survey of Swarm Intelligence Optimization Approaches for ANN Optimization	305
Jaspreet Kaur, Ashima Kalra and Dolly Sharma	
Face Recognition Using Various Methods and Applications—Survey	315
Rajwant Kaur and Dolly Sharma	
A Review of Various Categories of Satellite Image Processing in Remote Sensing.	325
Rupinder Kaur and Dolly Sharma	
RNA: Structure, Prediction, and Visualization Tools	335
Dolly Sharma, Shailendra Singh, Trilok Chand and Pardeep Kumar	
Data Traffic Modeling of ML-MAC for Wireless Sensor Networks.	347
Aarti Kochhar, Pardeep Kaur and Preeti	
Supervised Learning Technique for Prediction of Diseases	357
Bharti Yadav, Shilpi Sharma and Ashima Kalra	
A Critical Review on the Application and Problems Caused by False Alarms	371
Vishal Sharma, Arun S. Varma, Atul Singh, Divyansh Singh and Bikarama Prasad Yadav	
Enhancement of Transient Stability of Multimachine System Using TCSC, SSSC and UPFC	381
Lokesh Garg, S.K. Agarwal and Vivek Kumar	
Linear Flight Control of Unmanned Aerial Vehicle	393
Alok Kumar Pandey, Anshuman Shukla, Ashutosh Gupta and Manjeet Singh Gangwar	
Hybrid Encryption Algorithm in Wireless Body Area Networks (WBAN).	401
Sameer Farooq, Deepak Prashar and Kiran Jyoti	
Integrated Sensors for Risk Assessment in Industries and Residential Sectors: A Review.	411
Vishal Kumar Singh, Ashish Maindolia, Abhishek Singh, Shubham Bhardwaj and Bikarama Prasad Yadav	
A Novel Approach for Node Localization in Wireless Sensor Networks	419
Abhishek Kumar and Deepak Prashar	

A Purely Active Circuit Simulator for Realizing Electronically Tunable Floating Resistance 429
 Mayank Srivastava, Ajay Roy and Dinesh Prasad

Comparative Study of OLSR, DSDV, AODV, DSR and ZRP Routing Protocols Under Blackhole Attack in Mobile Ad Hoc Network 443
 Ankit Singh, Gurpreet Singh and Mandeep Singh

Lead-Free Piezoelectric Energy Harvester Design for Lower Order Random Vibrations 455
 Oshin Garg, Sukesha Sharma and Preeti

Design and Development of IoT-Based Transmission Line Monitoring System 465
 Nikhil Kalra, Abhishek Sharma, Nitish Kumar, Rajesh Singh and Anita Gehlot

Critical Analysis and Review of Occupational, Environmental and Health Issues Related to Inadequate Disposal of E-Waste 473
 Shivam Kumar, Divyanshi Garg, Prashasti Sharma, Shubham Kumar and Sayed Mohammad Tauseef

Design and Development of Air and Water Pollution Quality Monitoring Using IoT and Quadcopter 485
 Aditya Agarwal, Vishakha Shukla, Rajesh Singh, Anita Gehlot and Vikas Garg

Network Forensic Process Model and Framework: An Alternative Scenario 493
 Prabhjot Kaur, Anchit Bijalwan, R.C. Joshi and Amit Awasthi

Modeling and Simulation of ECG Signal for Heartbeat Application 503
 B. Khaleelu Rehman, Adesh Kumar and Paawan Sharma

Fingerprint Acquisition Methodologies and Its Upgradation with IoT 513
 Rohit Samkaria, Rajesh Singh, Anita Gehlot, Rohit Sanket, Ateev Aggarwal, M.S. Yadav, Ashok Kumar, Rupendra Pachauri and Sushabhan Choudhury

Security Issues in Vehicular Ad Hoc Network: A Critical Survey 527
 Mohammad Arif and Shish Ahmad

Impact of Buried Oxide Layer Thickness on the Performance Parameters of SOI FinFET at 22 nm Node Technology 537
 Ravneet Kaur, Charu Madhu and Deepti Singh

Line-Based Successive Cancellation Decoder with Reduced Complexity	545
G.M.G. Madhuri, B. Praveen Kitti and N. Prasanthi Kumari	
Metal Artefact Reduction from Dental CBCT Image Using Morphology and Fuzzy Logic	553
Anita Thakur, Vishu Pargain, Pratul Singh, Shekhar Raj Chauhan, P.K. Khare and Prashant Mor	
Mitigation of Signal Interference by Positioning FFT Window for OFDMA System	561
Salauddin Mohammad, Madan Gopal, Rajarao Manda and Khaleel Rehman	
Effect of Skin Impedance on Delay and Crosstalk in Lossy and Non-uniform On-Chip Interconnects	569
Yenikepalli Ramesh and Vobulapuram Ramesh Kumar	
Modeling of Coupler Dynamics of Gatimaan Express	577
P.K. Jha and S.S. Gokhale	
Soil and Environment Conditions Based Smart Analysis System for Plant Growth Using IoT	587
Aakanksha Panwar, Avi Gaba, Rajesh Singh and Anita Gehlot	
Design of Novel Through Silicon via Structures for Reduced Crosstalk Effects in 3D IC Applications	599
Mounika Ganimidi and Vobulapuram Ramesh Kumar	
A Cost Effective and Performance Enhanced Deadlock Recovery Scheme for Wormhole Routed Networks	607
Jameel Ahmad, Akheela Khanum and A.A. Zilli	
Performance Enhancement of Point-to-Point FSO System under Rain Weather Conditions	623
Aditi Malik, Sanjeev Kumar, Preeti Singh and Pardeep Kaur	
Choice of Right Dimension and Position of Microstrip Feedline for the Bandwidth Improvement of Microstrip Antenna	633
Ranjan Mishra, Raj Gaurav Mishra, Piyush Kuchhal and Piyush Dua	
Recommendation and Interest of Users	639
Baljeet Kaur Nagra, Bharti Chhabra and Dolly Sharma	
A Life-Saving Approach: Traffic Control System to Prioritize Ambulance on Road	647
Sagar Majumdar, Rohan Sharma, Akshansh Jain, Rajesh Singh and Anita Gehlot	

Save the Real Nectar: Water Distribution System in Multi-storied Apartments 653
 Rohan Sharma, Sagar Majumdar, Tanushree Khattri, Rajesh Singh and Anita Gehlot

Domain Dictionary-Based Metadata Construction for Search Over Encrypted Cloud Data 661
 S.K. Mahreen, M.R. Warsi and S.K. Neelam

Reconstruction Using Sparse Approximation 671
 Rana Sameer Pratap Singh and Rosepreet Kaur Bhogal

A Corporate Network-Fed Quasi-lumped Resonator Antenna Array 679
 Seyi Stephen Olokede and Babu Sena Paul

Optimal Placement of Solar PV as Active Power Source in Primary Distribution System for Loss Reduction. 687
 Vani Bhargava, S.K. Sinha and M.P. Dave

Electrodynamic Study of a Novel Microstrip Ring Based on Finite Integral Technique Numerical Computational Code 699
 Seyi Stephen Olokede and Babu Sena Paul

Decaying Objects of Constant Demand Speed and Dependent of Time Within Permitted Delay in Imbursement of the Model of Inventory Level. 709
 Jasvinder Kaur and Arun Kumar

A Highly Secure Video Steganography Inside DWT Domain Hinged on BCD Codes 719
 Sonali Rana and Rosepreet Kaur Bhogal

Development of Multi-verse Optimizer (MVO) for LabVIEW 731
 Kumar Vivek, Mehta Deepak, Chetna, Jain Mohit, Rani Asha and Singh Vijander

Edge Detection Using Fuzzy Logic (Fuzzy Sobel, Fuzzy Template, and Fuzzy Inference System). 741
 Rachita Katoch and Rosepreet Kaur Bhogal

Performance Analysis of COADM-Based Transparent Optical Network 753
 Satnam Singh and Neeraj Sharma

ZigBee and GSM Based Fault Detection System for Low Tension Pillar 761
 Ram Nath and Ritula Thakur

Performance Evaluation of Wavelet-Based Image Compression Techniques	769
Nishat Bano, Monauwer Alam and Shish Ahmad	
Intelligent AVR Control of a Single Thermal Area Combined with LFC Loop	779
Devashish Sharma, Varsha Kushwaha, Kamlesh Pandey and Nibha Rani	
Object Size Determination Grasped by a Four-Finger Gripper Using Workspace Analysis	791
Nazma Ehtesham, S. Mukherjee and Mohd Suhaib	
Estimation of Parameters of Target Using RADAR Data Sets	799
M. Raja, Sudhir Kumar Chaturvedi, Hutanshu Kamal, Cris Thomas and Rahul Kummamuri	
Implementation of Smart Home Automation System on FPGA Board Using IoT	805
Rohit Chhabra, Manpreet Kaur Khurana and Anshuman Prakash	
Mobile App-Based Device Control for Robotic Movement	811
Navodit Sharma, Ishfaq Gaffar Dar and Manish Sharma	
Feature Recognition of Face with Real-Time Variations Using Eigen Face Approach Methodology with PCA Algorithm	819
Ishfaq Gaffar Dar, Azzan Khan and Manish Sharma	
Speed Regulation of a Non-linear Separately Excited DC Motor Using Optimized Fuzzy Logic Control	829
Arpit Jain, Piyush Kuchhal and Mukul Kumar Gupta	
Ranking of Educational Web Sites in Indian Perspective for Usability Evaluation	839
Heena Gupta and Sanjay Kumar Dubey	
Adaptability Evaluation of E-commerce Websites in Indian Perspective	847
Shivani Gupta and Sanjay Kumar Dubey	
Improvement and Approval of Impediment Recognition and Activity for Power Window	855
Roushan Kumar, Neelu J. Ahuja and Mukesh Saxena	
Design and Performance Analysis of Four-Port Discontinuous Patch Antenna	865
K. Shreekant, Parth Sharma and Shuchismita Pani	
A Compact, High-Radiation Efficient, and High-Gain Micro-Strip Patch Antenna Array for Millimeter Wave Applications	873
Beenish Kachroo and Malay Ranjan Tripathy	

Automatic Street Lighting System	879
Adesh Kumar, Roushan Kumar, Akansh Jain, Anand Pandey, Shubhankar Thapliyal and Akshay Sharma	
Efficient Method to Implement Arithmetic Operations Using Binary Logarithmic Algorithms for Reduced Circuit Complexity with Error Analysis	889
Sayyed Waize Ali, Manish Sharma and M.R. Tripathy	
Design of Efficient DC Power Supply for High-Voltage Low-Current Applications	895
Archana Singh, Sanjay Kumar Sinha, Kamlesh Pandey and Nibha Rani	
Design and Performance Analysis of High Gain Narrow Band Patch Antenna Array at X-Band	907
Madhukant Patel, Piyush Kuchhal, Kanhaiya Lal, Virendra Singh and Hemangi Patel	
Design of an Efficient Rectifier Circuit Based on Karthaus-Fischer Voltage Multiplier for Energy Harvesting	913
Asmita Rajawat, Karush Suri and Mohit Mohta	
Longitudinal Control of Small Unmanned Aerial Vehicle by PID Controller	923
Alok Kumar Pandey, Tanu Chaudhary, Shubham Mishra and Shrestha Verma	
Control Schemes for Permanent Magnet Synchronous Generator-Based Variable Speed Wind Turbine	933
Rupendra Pachauri, Pradeep Rana, Yogesh K. Chauhan and S. Choudhury	
Auto-Sensing Moisture Control for a Photo-Voltaic Based Irrigation System	943
Ginni Gupta, Kaushiki and Deepak Kumar	
Hardware Implementation of Solar Assisted Automatic Curtain Control System	951
Prateek Singh, Yogesh K. Chauhan, Rajesh Singh and Rupendra Pachauri	
Performance Analysis of Automatic Cleaning System for Solar PV Modules	963
Rupendra Pachauri, Himanshu Rai Anand, Anurag Koushal, Anurag Singh, Yogesh K. Chauhan and S. Choudhury	
Double Gate Tunnel Field Effect Transistor with Extended Source Structure and Impact Ionization Enhanced Current	973
Deepak Kumar and Prateek Jain	

Integration of Cognitive Radio with Heterogeneous Smart Grid Communication Architecture	981
Lipi Chhaya, Paawan Sharma, Adesh Kumar and Govind Bhagwatikar	
Comparison Between the Performance of Trigate Junctionless Transistor and Double-Gate Junctionless Transistor with Same Device Length	991
Deepti Singh, Renu Vig, Charu Madhu and Ravneet Kaur	
Analysis of Mahout Big Data Clustering Algorithms	999
Ishan Sharma, Rajeev Tiwari, Hukam Singh Rana and Abhineet Anand	
Bandwidth Enhancement of Micro-strip Patch Antenna Using Disconnected U-Shaped DGS	1009
Shraddha Kumari, Shubham Sachan and Asmita Rajawat	
Effect of the Dimension of Feedline for the Enhancement of Bandwidth of Square Microstrip Antenna	1019
R.K. Chaurasia, Vishal Mathur, Ranjan Mishra and Raj Gaurav Mishra	
Optimization of Data Centres for Heat Management	1025
Saurabh Singh, Abhineet Anand and Rajeev Tiwari	
Controlling of PMSG-Assisted Wind Energy Conversion System with Maximum Power Tracking Technique	1033
Diwaker Pathak, Rupendra Pachauri and Yogesh K. Chauhan	
Design of a Single-Axis Solar Tracker Using LDRs	1041
Utkarsh Jadli, Shailesh Uniyal and Ishita Uniyal	
2D Modelling and Simulation of Heat Transfer in Blast Furnace Hearth Using ANSYS	1051
Satish Kumar and Vijay Singh Bisht	
Offline Graphical Analysis of Signatures Using Geometric Features and Artificial Neural Network	1065
Parvesh Saini, Ishita Uniyal and Neeraj Singh	
Energy Efficient Image Compression Techniques in WSN	1079
Nishat Bano, Monauwer Alam and Shish Ahmad	
Real-Time System Monitoring and Control of Automation Industry Using IoT-Based Cloud Platform	1089
G.N.L. Ravi Teja, S. Sukumar, Surya Kompella, Raga Sudha and G. Pallavi	
Performance Estimation of Adaptive Beamforming Algorithms in Smart Antennas	1101
R. Gowri, Abhinav Sharma and Sanjay Mathur	

**Automatic Forest Fire Detection and Monitoring Techniques:
A Survey** 1111
 Vinay Chowdary and Mukul Kumar Gupta

**Design and Simulation of Implantable Blood Pressure Sensor
Using COMSOL Multiphysics** 1119
 K.S.N. Murthy, M. Siva Kumar, K. Suma Bindu, K. Satyanarayana,
 D. Sivateja and G. Sai Hemanth

**V-Band SIW Wideband Band-Pass Filters for
mm-Wave Applications.** 1127
 K. Bharath Kumar and T. Shanmuganatham

Alarming System for Railway Crossing. 1137
 Aishwarya Chauhan, Satish Kumar, Neha Gupta and Rajesh Singh

**Performance Investigation of Hill-Climbing MPPT Techniques
for PV Systems Under Rapidly Changing Environment** 1145
 Vibhu Jatelly and Sudha Arora

**Adaptive Beamforming for Linear Antenna Arrays Using
Gravitational Search Algorithm.** 1159
 Abhinav Sharma, Sanjay Mathur and R. Gowri

Design of a Low-Cost Potato Quality Monitoring System 1171
 Ayush Agrahari, Revant Pande, Paawan Sharma and Vivek Kaundal

Bionic Functionality of Prosthetic Hand 1177
 Shweta Gupta and Adesh Kumar

**Pollution Control by Installation of MQ-Smoke Sensors
in Car Exhausts with IOT-Based Monitoring** 1191
 Abinash Borah, Sandeep Jangid, Amisha Kumari, Anita Gehlot
 and Rajesh Singh

Bluetooth-Controlled Robot Using Windows Phone Application. 1199
 Abhay Kumar Gupta, Revanta Tikku, Sumit Kumar, Gaurav Verma
 and Adesh Kumar

**Threshold Sensitive Modified Leach Protocol for Energy
Saving in Wireless Sensor Network** 1207
 K. Shreekant, Parth Sharma, Sindhu Hak and Shuchismita Pani

Antenna Array Composed of Unit Cell Resonators 1215
 K. Shreekant, Sambhav Jain and Shalini Sah

**IOT-Based Hydroenergy Generation with the
Application of Sensors** 1225
 Pranjal Chaturvedi, Abinash Borah, Anamika Singh, Abhas
 and Rajesh Singh

Active Regeneration of Diesel Particulate Filter Using Microwave Energy for Exhaust Emission Control	1233
Caneon Kurien and Ajay Kumar Srivastava	
Approach to Find Shortest Path Using Ant Colony Algorithm	1243
Mudasar Basha, M. Siva Kumar, Vemulapalli Sai Pranav and B. Khaleelu Rehman	
Review of Expert System and Its Application in Robotics	1253
Ajay K.S. Singholi and Divya Agarwal	
Analysis of Multiple Shortest Path Finding Algorithm in Novel Gaming Scenario	1267
Aqsa Zafar, Krishna Kant Agrawal and Wg. Cdr Anil Kumar	
Design and Analysis of Beam-Steering Antenna Array	1275
S. Vijayadharshini, Apoorva Bhardwaj and Suchismita Pani	
Study of Various Ontologies	1283
Amit Verma, Iqbaldeep Kaur, Dolly Sharma and Dimple Nagpal	
Software Component Retrieval System	1289
Amit Verma, Dolly Sharma, Iqbaldeep Kaur and Monisha Kumari	
SRR-Loaded Clover Leaf-Shaped Minkowsky Fractal for Multiband Applications	1297
C. Elavarasi and T. Shanmuganantham	
Microstrip Transition to Substrate Integrated Waveguide Slot Antenna for Multiband Applications	1307
M. Nanda Kumar and T. Shanmuganantham	
A Comparative Analysis of PID Controller Design for AVR Based on Optimization Techniques	1315
Ishita Uniyal and Afzal Sikander	
Aadhaar Card-Based Android Application for Patient Monitoring System	1325
Parth Sharma, Jagriti Raizada, Faraz Siddiqui and Haneet Rana	
Analysis of Zernike Moment-Based Features for Sign Language Recognition	1335
Garima Joshi, Renu Vig and Sukhwinder Singh	
Accidents Avoidance Using Smart Traffic Regulation System	1345
Venkata Sai Gokul Gadamsetty, Kiran Kumar Vayalada and Arpit Jain	
Prioritization for Regression Testing Using Ant Colony Optimization Based on Test Factors	1353
Sheikh Fahad Ahmad, Deepak Kumar Singh and Preetam Suman	

Optimizing the Available Technology: Tunnel Safety and Energy Conservation System 1361
 Sagar Majumdar, Akshansh Jain, Harsh Lawaniya, Kartik Mudgal, Rajesh Singh and Anita Gehlot

A Navigation Device with Voice for Visually Impaired People 1369
 S.K. Nehal, Rajat Kumar Obheroi, Ajay Anand and Haneet Rana

Fuzzy Nutrition Recommendation System for Diabetic Patients 1381
 Aryaman Gupta and Sanjay Kumar Dubey

Physical and Chemical Properties of Mahua and Sal Seed Oils 1391
 Deepak Kumar, Vijay Kumar Chibber and Ajay Singh

Analysis of Sub-threshold Inverter and 6T SRAM Cell for Ultra-Low-Power Applications. 1401
 D. Sudha, Sreenivasa Rao Ijjada and Ch. Santhirani

Temperature- and Color-Based SDSS Stellar Spectral Classification Using Automated Scheme 1415
 Amit Goyal, Jayash Kumar Sharma, Darpan Anand and Manish Gupta

Experimental Investigation on SP and TCT PV Array Configurations to Reduce Power Losses During PSC. 1427
 Aditya Chaudhary and Mamta Chamoli Kala

A Multiband Circular Patch Microstrip Antenna for K and Ka Applications. 1437
 Ashna Kakkar, Nirdosh and Shalini Sah

RFID Device Based Home Security System to Detect Intruder Trespassing 1445
 Sanjana Minocha and Ankur Dumka

Review of Sockets for Transfer of Files Between Systems 1455
 Pranav Arora and Ankur Dumka

GSM-Based Prepaid Meter 1467
 Shruti Chaudhary, Adesh Kumar and Vivek Kaundal

Design of 2-Bit Vedic Multiplier Using PTL and CMOS Logic. 1481
 Gaurav Bajaj, Kabir Grover, Anu Mehra and Sachin Kumar Rajput

Computer Aided Diagnosis of Cervical Cancer Using HOG Features and Multi Classifiers. 1491
 Ashmita Bhargava, Pavni Gairola, Garima Vyas and Anupama Bhan

IC Engine-Powered Arial Vehicle for Medical Assistance 1503
 Priyal Kumar Sogani, Dushyant Dixit, Rajesh Singh and Anita Gehlot

A Critical Study on Role of Sensor-Based Electronic System for Toxic Gas Identification in the Mining (Coal) Industry	1511
Vishal Sharma, Taksh, Kritarth Srivastav, Priyam and Nihal Anwar Siddiqui	
Companding-Based Technique to Improve Signal to Noise Ratio and Power Dissipation in Analog to Digital Convertor Operating at CTDSP.	1523
Anustha, Mahima Gupta, Haneet Rana and Gagan Minocha	
Analysis of Parametric Effects on PEMFC Performance and Power Management Schemes	1529
Ekta Joshi and Sandeep Negi	
Comparative Analysis of MEMS Piezoelectric Materials for the Design of a Piezotube-Type Pressure Sensor.	1537
Sachin Kala, Varij Panwar, Lokesh Panwar and Sushant Sharma	
Design and Analysis of SEPIC-Based Single-Stage Three-Phase Inverter	1551
G. Mehta, V.K. Yadav and R. Verma	
Inductive Power as Wireless Energy in Electrical Applications.	1565
Shubham Kumar, Adesh Kumar, Vivek Kaundal and Mukul Kumar Gupta	
VGA Application in Text Display Using FPGA	1575
Akarsha Mishra, Adesh Kumar and Rakshita Parihar	
Survey on Implementation of Security in Cloud	1587
Deepak Garg and Jagpreet Sidhu	
Iterative Basic Block Pipelining Implementation as Fast Computation Technique.	1595
Parul Shikha, Manish Sharma and Sachin Rajput	
An Approach to Inter-vehicle and Vehicle-to-Roadside Communication for Safety Measures	1603
Rishita Prakash, Himanshu Malviya, Arushi Naudiyal, Rajesh Singh and Anita Gehlot	
Performance Evaluation of Big Data Frameworks: MapReduce and Spark	1611
Jaspreet Singh, S.N. Panda and Rajesh Kaushal	
Design and Analysis of PV Analyzer on LabVIEW	1621
Prateek Raj, Ankit Yadav, Farhan Nizam, Vinay Gupta and Peeyush Garg	
An Approach to Monitor Construction Site Based on Radio Frequency Identification and Internet of Things.	1629
Avi Gaba, Aakanksha Panwar, Rajesh Singh, Anita Gehlot and Vikas Garg	

The Real-Time Hardware of Smart Digital Alarm Clock Integrated with Microcontroller 1641
 Ginne Rani, Purnendu Shekhar Pandey, Praful Ranjan, Gaurav Negi and Saurabh Kavi

Design and Development of Oil Tank Monitoring System Using GSM MODEM in Distribution Transformer 1651
 Irfan Ansari, Shubham, Anurag Singh, Puneet Verma, Rajesh Singh and Anita Gehlot

Trends of Publications and Work Done in Different Areas in Energy Saving in Cloud Computing: A Survey 1661
 Nagma, Jagpreet Sidhu and Jaiteg Singh

Arduino- and IoT-Based Tools and Inventory Tracking System in Construction Sites 1677
 Aditya Agarwal, Aadrita Tanwar, Rajesh Singh, Vikas Garg and Anita Gehlot

Circumvention of Friction-Induced Stick-Slip Vibration by Modeling and Simulation 1687
 Jitendra Yadav and Geeta Agnihotri

Wireless Control System for Enhancing Passenger Safety in the Event of Driver Hostilities for Commercial Vehicles 1697
 Aviral Rawat, Gaurav Verma, Navneet Phadke, Yajur Pruthi and Deepak Kumar

Cybersecurity Issue and Online Information Source 1707
 Lalit Mohan Joshi and Rajendra Bharti

White Cane Navigation Using Arduino Uno 1719
 Mohd. Faizan Khan and Ankita Kumar

A Cheilosopic Approach for Unique Identification Among Indian Subpopulation 1729
 Shilpi Jain, V. Poojitha and Madhulika Bhatia

Weighted Transformation and Wavelet Transforms-Based Image Resolution and Contrast Enhancement 1739
 N. Prasanthi Kumari, T.V. Hyma Laksmi, D. Bhavani and G. Mohana Durga

Fat Tree NoC Design and Synthesis 1749
 Arpit Jain, Alok Kumar Gahlot, Rakesh Dwivedi, Adesh Kumar and Sanjeev Kumar Sharma

Big Data Issues in Medical Healthcare 1757
 Manish Madhava Tripathi and N.K. Joshi

Android-Based Home Automation Using Bluetooth and ESP8266 1767
Akhil Bhatt, Apurva Saxena, Shubhi Chauhan, Utkarsh Jaiswal and Yashaswi Verma

Embedded-Based Smart Solar Grid of 2 × 2 Monitoring System Using Smart Sensors 1777
Rohit Samkaria, Rajesh Singh, Anita Gehlot, M.S. Yadav, Ashok Kumar, Varchas Choudhary, Sushabhan Choudhury, Rupendra Pachauri and Anvesh Aggarwal

Author Index 1789

About the Editors



Dr. Rajesh Singh is currently associated with University of Petroleum and Energy Studies, Dehradun, as Associate Professor and with additional responsibility as Head Institute of Robotics Technology (R&D). He has been awarded a gold medal in M.Tech. and honors in his B.Tech. His area of expertise includes embedded systems, robotics, and wireless sensor networks. He has organized and conducted a number of workshops, summer internships, and expert lectures for students as well as faculty. He has twelve patents and published around hundred research papers in referred journals/conferences. Under his mentorship, students have participated in national/international competitions including Texas competition in Delhi and Laureate award of excellence in robotics engineering in Spain. Twice in last four years he has been awarded with certificate of appreciation from University of Petroleum and Energy Studies for exemplary work. He got certificate of appreciation for mentoring the projects submitted to Texas Instruments Innovation Challenge India Design Contest, from Texas Instruments, in 2015. He has been honored with young investigator award at the International Conference on Science and Information in 2012. He has published a book on “**Embedded System based on Atmega Microcontroller**” with NAROSA publishing house. He is editor to a special issue published by AISC book series, Springer, with title “Intelligent Communication, Control and Devices 2016”.



Dr. Sushabhan Choudhury is Head of the Department of Electronics, Instrumentation, and Control in the University of Petroleum and Energy Studies. He has teaching experience of 26 years, and he has completed his Ph.D. from the University of Petroleum and Energy Studies, M.Tech. (Gold Medalist) from Tezpur Central University, India, and received his B.E. degree from NIT, Silchar University, India. He has published more than 70 papers in various national/international conferences/journals. He has filed 10 patents. His area of interest is Zigbee-based wireless networks. He has been selected as the outstanding scientist of the twenty-first century by the Cambridge Biographical Centre, UK. He has also been selected in the who's who of the world in science by Marquis Who's Who, USA.



Ms. Anita Gehlot has more than 10 years of teaching experience in embedded systems and wireless sensor networks. She has **10 patents** in her account. She has published more than **fifty research papers** in refereed journals and conferences. She has organized a number of workshops, summer internships, and expert lectures for students. She has been awarded with certificate of appreciation from University of Petroleum and Energy Studies for exemplary work. She has published a book on “**Embedded System based on Atmega Microcontroller**” with NAROSA publication house.

Impact of Sand Erosion on Hydroturbines: A Case Study of Hydropower Plant in Himachal Pradesh, India

Robin Thakur, Muneesh Sethi and Sourabh Khurana

Abstract Sand erosion is the system of unfaltering avoidance of the solid from the surface of the hydroturbine hardware which relies on the concentration, size, hardness of sand particles, stream speed, and properties of material of different parts of turbine and working hours of the turbine. It is one of the major and complex issues in Himalayan area particularly amid storm season. Various investigations on erosion of turbine have demonstrated that the material of turbine apparatus dissolved because of sand particles. This paper depicts the exhaustive examination of silt, disintegration of runner cutting edges, and guide vanes of 300 MW Chamera-II hydrocontrol plant. It has been observed that hardness, size, and shape are vital parameters concerning their impacts on disintegration of water-driven turbines. Ultimately, weight lessening of turbine and subsequent fall in the productivity of force plant because of residue disintegration was likewise investigated.

Keywords Sand erosion · Efficiency · Guide vanes · Runner blades

List of Symbols

W	Loss of thickness per unit time
b	Turbine coefficient at eroded part
V	Relative flow velocity

R. Thakur (✉)

Department of Mechanical Engineering, Shoolini University, Solan
Himachal Pradesh 173212, India
e-mail: robinthakur@shooliniuniversity.com

M. Sethi

School of Engineering & Technology, AP Goyal Shimla University,
Shimla, Himachal Pradesh 171005, India
e-mail: sethi612@yahoo.com

S. Khurana

Department of Mechanical Engineering, OM Institute of Technology,
Juglan, Hisar 125001, India
e-mail: sourabhnth@gmail.com

© Springer Nature Singapore Pte Ltd. 2018

R. Singh et al. (eds.), *Intelligent Communication, Control and Devices*,
Advances in Intelligent Systems and Computing 624,
https://doi.org/10.1007/978-981-10-5903-2_1

a	Average grain size coefficient on the basis of unit value for grain size 0.05 mm
K_1 and K_2	Shape and hardness coefficient of sand particles
K_3	Abrasion resistant coefficient of material
SSC	Suspended sediment concentration
SSL	Suspended sediment load
ppm	Part per million
MWh	Megawatt hour
μm	Micrometer
x, y	Exponent values for concentration and size coefficients

1 Introduction

Hydroturbines are utilizing energy of water into mechanical energy and afterward encourage generators that are utilized to change over the mechanical energy into electrical energy. Turbines are effectively harmed by the effect of sediment particles. Hardness of sand relies on its mineral substance, size, shape, and the harshness of its surface. Numerous examiners have broken down regarding this matter, and, however, have not yet possessed the capacity to thoroughly portray what is best material for turbine to oppose corruption by sand since sand is exceptionally dissolving substance. Sediment supply and its vehicle in the Himalayan district are very huge and are thought to be most astounding on the planet. Topographically, the Himalayas are thought to be genuinely youthful mountains that are still in a dynamic stage [1].

Foremost parts of this sediment are having hard rough sand and sediment which thoroughly destruct the turbine hardware. Due to increment in grouping of sediment particles in water during rainstorm season causes damage to the submerged segments in hydro power plants, especially parts of turbine to disintegrate which definitely lessens productivity of turbine, changes in stream flow, vibrations and lastly failure of hydro turbines [2, 3]. Runner cutting edges, nozzle, guide vanes, ring liners, inlet valve seals, labyrinths, etc., are those parts of hydroapparatuses which are unfavorably influenced by residue [4]. Erosion due to sand results in rejection of material brought on by steady twisting and cutting activities and essentially unique parameters like concentration of sediment, size of residue, and hardness of residue material, normal speed of molecule, particles shape, point of impingement and properties of material are in charge of the consistent expulsion of material [5]. The precarious and rough geology of Himalaya prompts to many shake and slant dangers, which shape the essential wellspring of dregs for waterway frameworks. Three most vital waterways of Himalayas, in particular, the Ganges, the Brahmaputra, and the Indus, convey around 9.45% of aggregate yearly load from the landmass to the seas overall [6]. The issue of rough particles in hydro-electric plants is not new and in Norway, such instances of dregs disintegration had

been accounted for with fine silt coming into the stream from icy masses [7]. This sort of trouble is by all accounts more noticeable for the Himalayan district in India and the Andes Mountains in South America.

Suspended sediments transported from the high-altitude regions settle down in the reservoir and reduce their water storage capacity, which in turn reduces power generation. Among assortments of results, disintegration of pressure-driven structures harms to hydromechanical and electromechanical parts and constrained blackout of force plants every year may bring about gigantic loss of income to the exchequer. The present study deals with an investigation of severe erosion of turbine parts, including runner blade and guide vanes of a hydropower project located at Chamera, HP, India, through collection of field data, for example, discharge and sediment data, sediment sampling at relevant locations and measurement of parameters related to the efficiency of turbine.

1.1 Related Works

Pradhan [1] reported the study of Jhimruk River and found that the value of silt sediment concentration varying from 2000 to 6000 ppm during the peak monsoon and that value was reached up to 20,000 to as high as 60,000 ppm. It clearly indicates that the discharge during the monsoon is very high for generating same power under constant head as compared to the discharge before monsoon. The author also gives a relationship between the silt sediment load and the efficiency of turbine that is corresponding decreasing over a time period and concluded that 4–8% of efficiency was lost at 25% load.

Thapa et al. [2] led a review to distinguish a suitable erosion model for Francis turbine of Jhimruk hydroelectric focus (JHC) involved two standard disintegration model were chosen to evaluate the silt disintegration rates and back to back diminishment in effectiveness of the runner. An enhanced empirical erosion model to gauge disintegration rate and misfortune in runner productivity of Francis turbine was additionally created from the consequences of existing disintegration model to gauge disintegration rate and misfortune in runner proficiency and contrast them and the exploratory information. For JHC, the enhanced disintegration display gauges drop in proficiency of the runner alone to around 1% every year, and this is steady to the aftereffects of field estimations. The new disintegration model can be utilized as a powerful apparatus to detail proper plan and support system for the Francis runner at particular site.

Poudel et al. [8] detailed a contextual analysis of Modi waterway in Nepal in which a rotating disk was utilized to examine the way of residue impact on an example of turbine. This review revealed that shape, measure, streaming properties of water, and mineral substance of dregs are the central point which are basically in charge of the disintegration of material. The perceptions show that at downstream and upstream of water, the dissolving properties of dregs elements of Modi River were same. It is finished up finally from the outcomes that when the silt moving

down from upstream to downstream, its size and shape changes and discovered less disintegrating property.

Khurana et al. [9] has directed trial to decide the impact of residue disintegration of Turgo impulse turbine blades and reasoned that the erosive wear rate increments with an expansion in sediment fixation, residue size, and flow velocity. It was watched that disintegration was most extreme at the profundity of the cutting edge and at the scores. In light of the exploratory information, a relationship was produced for wear rate as an element of residue size, fixation, fly speed, and working hours of turbine. The connection created in this review can be utilized to foresee disintegration of the Turgo impulse turbine at the assembling phase of a turbine at specific site.

As per Frunzaverde et al. [10], constant vortex development and pressure fluctuation in the draft tube cone upgrading the likelihood of harm to hydromachineries specially turbine by working the plant at incomplete and over load condition. Alongside this pressure fluctuation, therefore of vortex arrangement, the draft tube stream causes overwhelming vibration and commotion in apparatuses and builds the odds of disappointment of hydroturbines.

Padhy and Saini [11] concentrated the impact of sediment disintegration on execution of a Pelton turbine tentatively and revealed that the silt concentration, silt size, velocity of jet, and the working hours of the turbine were solid parameters for proficiency misfortune in Pelton buckets. It was presumed that with an expansion in the silt concentration, sediment size, and stream speed the rate effectiveness loss of a Pelton turbine expanded. It was watched that with the loss of weight of Pelton basins the turbine control yield was diminishing. The rate of force misfortune was at first found at a higher rate; however, the rate of influence misfortune was observed to be at lower rates in the wake of working the turbine over a drawn out stretch of time. The expansion in freedom between guide vane and face plates, spillage through labyrinth seals, and friction loss misfortune in the disintegrated harsh surface prompts to misfortune in pressure-driven effectiveness.

Tsuguo [12] built up a relationship of fundamental parameters which are in charge of disintegration of turbines in light of 8 years of disintegration information of 18 hydropower plants. He proposed following relation to calculate erosion in turbines.

$$W = \beta \cdot C^x \cdot a^y \cdot k_1 \cdot k_2 \cdot k_3 \cdot V^m \text{ [mm/year]}$$

2 Location of Study

The Chamera Dam seizes the stream Ravi and backings the hydroelectricity extends in the locale. It is situated close to the town of Dalhousie, in Chamba locale in the condition of Himachal Pradesh in India. The repository of the dam is Chamera.

After finishing of the primary stage, the Chamera-I creates 540 MW (3×180 MW) of power though the second stage, Chamera-II Dam produces 300 MW (3×100 MW) of power.

The third stage, i.e., Chamera-III which was begun in 2012, creates 231 MW (3×77) of power. The one of a kind element of the area is the fluctuating day and night temperature. The temperature amid the day close to the dam ascends to 35 °C and drops to at least 18–20 °C during the evening.

The water level in the Chamera Lake ascends to a greatest of 763 m, while the base water level is 747 m. This plant consists of 3 units having 100 MW capacity of each and installed with Francis turbine, each having 15 runner blades.

The water conductor system consists of about 200-m long cut and cover section near the forebay followed by a 7.83-km long head race tunnel of 7 m equivalent dia leading to the surface power house. The general layout of the Chamera-II project is shown in Fig. 1.

For excluding particles coarser than 200 μm , a 375-m long, 16-m wide, and 21.75-m deep hopper-type sediment chamber was constructed as shown in Fig. 2.

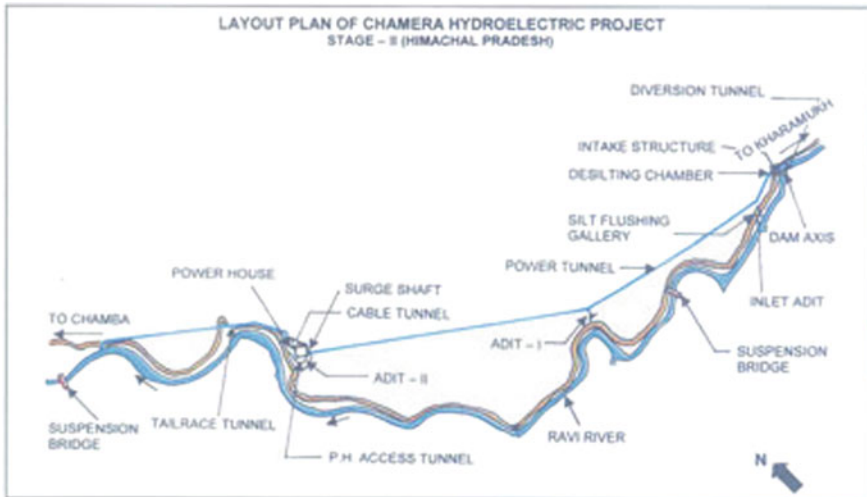


Fig. 1 General layout of Chamera-II

Fig. 2 Desilting chamber of Chamera-II



3 Data Collection

3.1 SSC and River Discharge

The variation of SSC in terms of eroded particles in a river discharge is extremely reliant on the hydraulic conditions, velocity gradient, and the flow capacity of river. From January 2013 to December 2014, the data was collected for 2 years regarding the SSC and discharge of river. By collecting the silted water sample at Chamera Lake, stage-II, the river discharge and SSC were measured with the help of a suspended sediment analyzer on an hourly basis. In a similar manner, water samples were also collected at the forebay of Chamera-II on an hourly basis and actual suspended sediment load (SSL) is also measured for each machine which passes through turbine. Similarly, the running hours of each machine during the running period was noted and the average suspended load (SSL) faced by each machine was also calculated at the plant.

The averaged electricity generated (MWh) by each machine was obtained by recording its total electricity generation (MWh) during operation. The variations of power generated and river discharge for years 2013 and 2014 at the said location are shown in Figs. 3 and 4.

3.2 Weight Loss of Hydromachinery

The annual maintenance period was from October 2013 to March 2014 in which all the mechanical components of the machines, i.e., runner, guide vanes, and upper and lower labyrinths were repaired consecutively. For further analysis, guide vanes,

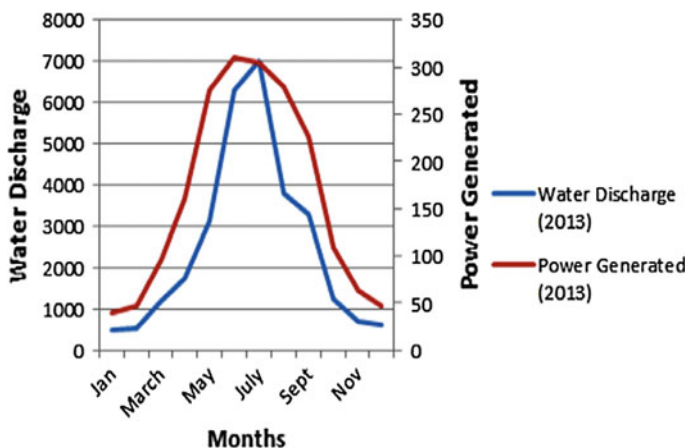


Fig. 3 Monthly variation of Water discharge and power generated for year 2014

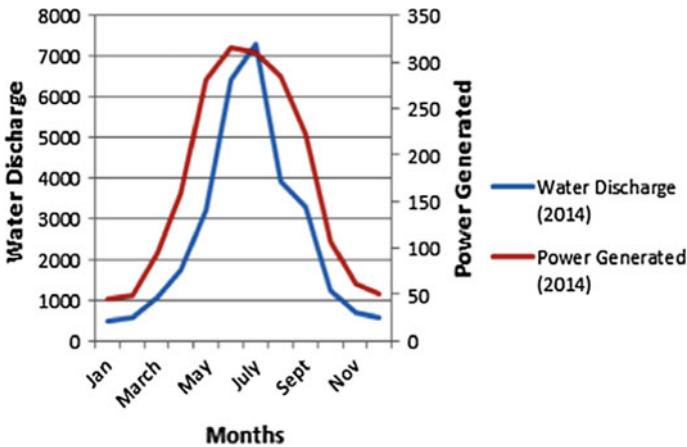


Fig. 4 Monthly variation of water discharge and power generated for year 2013

eroded runners, and upper and lower labyrinths of the turbine were taken out and the weights of the eroded runners were noted down for each machine.

4 Data Analysis

The sediment data collected in the Chamera Lake (intake), discharges, and corresponding power generated by the turbine have been analyzed, and their results are discussed in succeeding paragraphs. Various parts of hydroturbines eroded due to the presence of silt as shown in Fig. 5a–c. Eroded bucket of Pelton turbine of Aleo power plant, Manali (2×1.5 MW), is shown in Fig. 5d.

4.1 Suspended Sediment Concentration Pattern

Singh et al. [13] studied SSC and sediment load from the Gangotri Glacier from where Bhagirathi originates. Based on four years' observations (2000–2003), the author observed that the daily mean variation of SSC in the melt stream varied between 70 and 11,093 ppm. During the monsoon in year 2000–2003, the mean monthly SSCs were 1943, 2062, 3657, 2550, 735, and 135 ppm for May to October, respectively. The mean SSC was 1966 ppm, whereas the mean SSC (May–October) for 3 years (2008–2010) noted at MB-II was 1827 ppm for their entire sampling period (May–September).

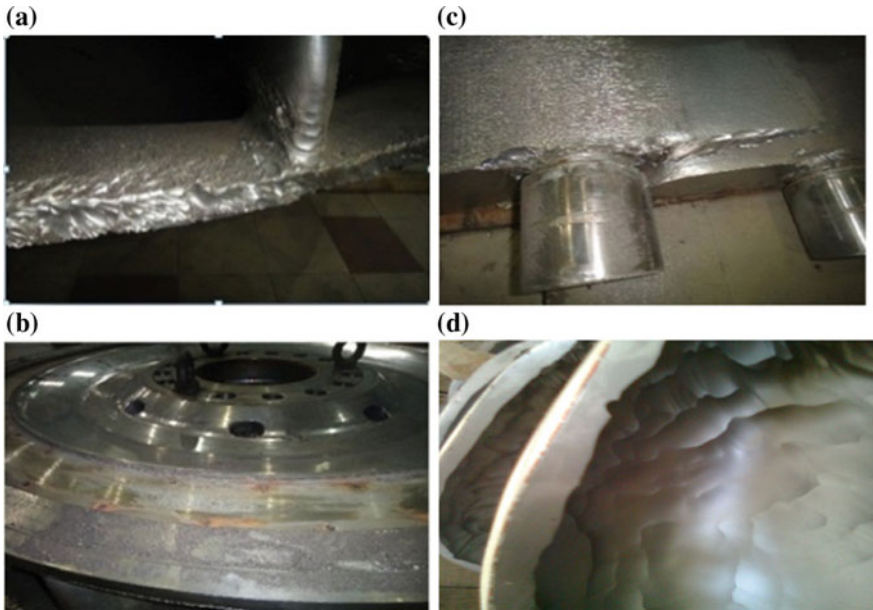


Fig. 5 a Eroded runner, b eroded lower face plate, c eroded guide vane, d eroded bucket of Pelton

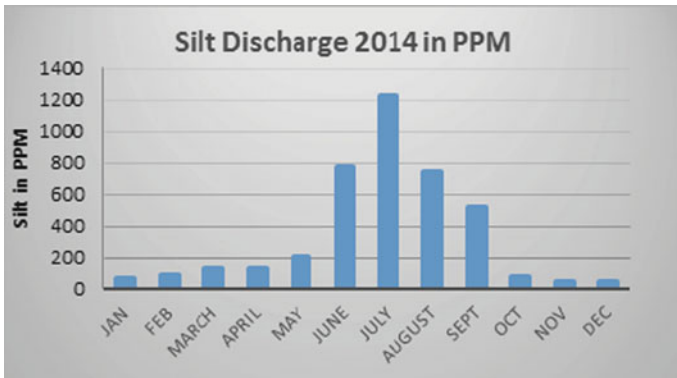


Fig. 6 Silt discharge of 2014 in PPM

At Chamera stage-II, the daily average concentration varied and the monthly SSCs for 2013 and 2014 from January to December are shown in Figs. 6 and 7.

In this study, the maximum sedimentation concentration was recorded in the month of July, i.e., 1221 ppm in 2014 and 1300 ppm in 2013.

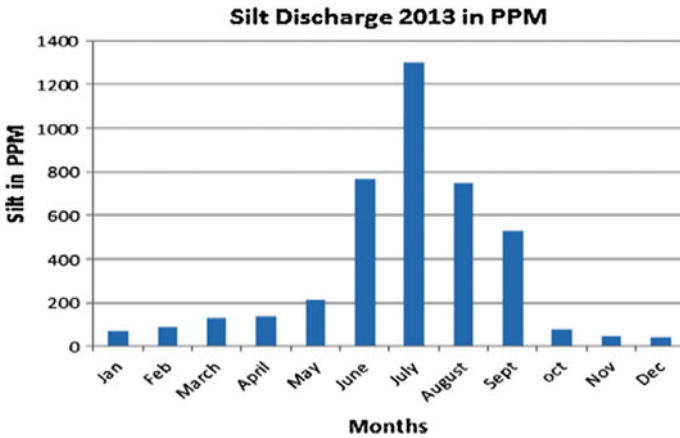


Fig. 7 Silt discharge of 2013 in PPM

4.2 Size Analysis of Sediment Particles

Dregs qualities are essential factors to be considered while determining its effect on hydroturbine material. Hard particles like quartz and feldspar are available in substantial sum in the majority of the waterways over the Himalayan bowls. The molecule size of suspended dregs in the frosty soften water is administered by the mineralogical five unique areas that was sieved to sort the elements into three distinct sizes. The strainer analyzer was shaken for 10 min to isolate every specimen size, in their individual sifter plate. Among these distinctive strainer classifications, molecule of sizes 62–250 μ is more inclined to bring about impact on turbine material. Other huge particles were separated to go into turbine area. The review was done on those four distinctive sifter classifications as it was. This lake dreg is used to discover the disintegration effect on turbine, and its disintegration rate is resolved to comprehend the sand disintegration of this waterway. The outcomes demonstrate that sand particles with more noteworthy size have high disintegration rate than littler particles streaming with water. The size assumes the significant part; however, it could be according to shape, mineral substance, and so on.

4.3 Mineralogy of Sediments and Shape Analysis

The analysis regarding mineralogy of the suspended sediment present in the water provides understanding in terms of geology of sediments and process of sediment yield. The mineralogical information of the suspended sediments present in the lake was analyzed with the help of X-ray diffractometer. This sand analysis provides a clear view of the geology of the suspended sediments and process of sediment yield.

Table 1 Mineralogical information from sand analysis

S. No.	Mineral	Samples (%)				Average (%)	Hardness (Mohr's scale)	Properties of minerals
		1	2	3	4			
1	Quartz	56	57	62	60	59	7	Hard mineral, resist weathering
2	Feldspar	6	7	5	8	7	6	Weathered white color
3	Carbonate	8	9	9	11	9	5	–
4	Magnetite	0.3	0.5	0.8	0.9	1	6	Shining dark gray, magnetic
5	Chlorite	0.8	0.3	0.4	0.6	1	2–2.5	Soft flaky mineral, green
6	Mica	20	16	18	19	18	2–3	–
7	Other minor	–	–	–	–			Very fine dust particles, clay, and other minerals

All four samples of suspended sediment collected from different location of Chamara-II were analyzed to have the following composition of different minerals as shown in Table 1.

The quartz and feldspar with high hardness index 7 and 6, respectively, are responsible for erosion of all turbine components. These sediments can be easily removed with the help of desilting chamber which is a sediment exclusion device, before the entering of these sediments into the power house.

4.4 Effect of Silt Erosion on Performance of Hydroturbines

Turbines are the critical portions of hydropower; it assumes key part in its execution which straightforwardly has effect on plant effectiveness and swing to power creation and life of force plant. It is qualified to study dregs of stream where control plant will manufacture; it gives clear depiction on choice of settling bowl, hydromechanical gear, and turbine material. The disintegrating way of sand relies on the size, shape, mineral substance of silt, and streaming properties of water.

The discharge and efficiency of Unit 2 corresponding to various machine loads (MW), measured between 21 and 30 September 2014, were compared with the discharge and efficiency data of April 2014, that is, before the monsoon period (Table 1).

The discharges and efficiencies of three units (3×100) were also compared graphically before and after the monsoon period (Fig. 8).

The normal values for suspended silt concentration amid the pinnacle rainstorm range from 1200 to 1400 ppm, which indicated that for generating same power under constant head, the discharge required for monsoon period is more as compared to discharge before monsoon.

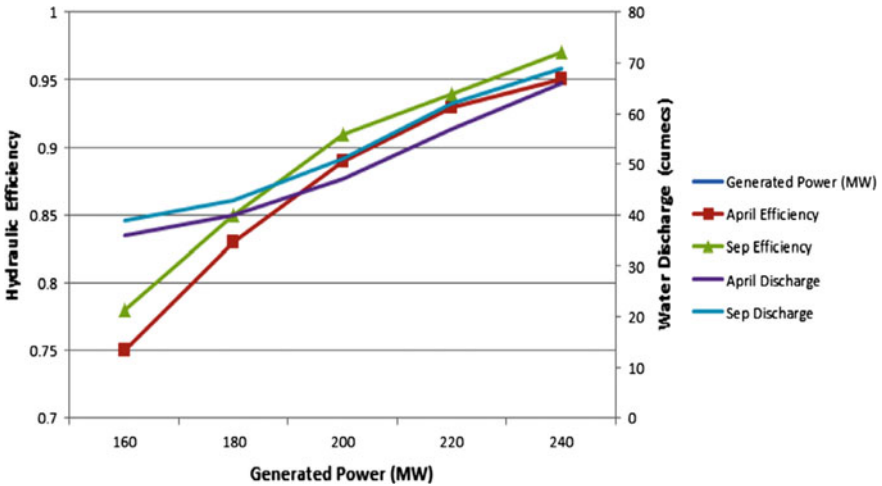


Fig. 8 Efficiency curve and discharge versus generator power of three units of Chamera-II (i.e., 3×100 MW)

It can be clearly observed from Fig. 8 that there is a significant increase in the requirement of discharge for generating the same power under the same head after the monsoon period and before the monsoon and reduction in the efficiency of turbine in corresponding periods.

5 Conclusion

1. The observation demonstrates sand as a standout among the most dissolving component and more noteworthy size sand particles have high disintegration rate than small particles streaming with water. The size assumes the key part, yet it could be according to shape, mineral substance, and so on.
2. Mainly Quartz and Feldspar are the main mineral substance found in dregs of Chamera-II and have high hardness effect on incentive than different minerals.
3. Maximum power was generated in the month of June in 2014, i.e., before monsoon and after that the downfall starts as the quantity of SSC starts increasing with the arrival of monsoon from July. It indicates the downfall of efficiency of the plant with the increase in the SSCs.
4. Due to drastic effect of silt sediments on the turbine machinery, a significant weight loss in the turbine components like runner, guide vanes, labyrinths, was found during the monsoon.
5. The performance in terms of efficiency of three units (3×100 MW) of Chamera-II due to silt erosion has been examined. The efficiency curve shows

the comparison of April 2015, i.e., before monsoon and September 2015, i.e., after monsoon. It indicates a downfall in the performance of hydroturbines in terms of power generation after monsoon.

References

1. Pradhan, P. M. S.: Improving sediment handling in the Himalayas, OSH Research, Nepal (2004).
2. Thapa, B.S., Thapa, B., Dahlhaug, O.G.: Empirical modelling of sediment erosion in Francis turbines, *Energy*, 41, 386–91 (2012).
3. Padhy, M.K., Saini, R.P.: Study of silt erosion on performance of a Pelton turbine, *Energy*, 36 (1), 141–147 (2011).
4. Goyal, D.K. et al.: Slurry erosion behaviour of HVOF sprayed WC-10Co-4Cr and $\text{Al}_2\text{O}_3 + 13\text{TiO}_2$ coatings on turbine steel, *Wear*, 289, 46–57 (2012).
5. Duan, C.G., Karelin, V.Y.: Abrasive erosion and corrosion of hydraulic machinery, London: Imperial College Press (2002).
6. Milliman, J.D., Meade, R.H.: Worldwide delivery of river sediments to the oceans, *J Geology*, 9, 11–19 (1983).
7. Brekke, H.: The influence from guide vane clearance gap on efficiency and scale effect for Francis turbine, XIV IAHR Symposium, Trondheim (1988).
8. Poudel, L. et al.: Sediment Impact on Turbine Material: Case Study of Modi River, Nepal, Kathmandu University journal of Science, Engineering and Technology, 8, 88–96 (2012).
9. Khurana, S., Varun; Kumar, A.: Effect of silt particles on erosion of Turgo impulse turbine blades, *Ambient Energy*, 35, 155–162 (2014).
10. Frunzaverde, D. et al.: Failure analysis of a Francis turbine runner. In: 25th IAHR Symposium on hydraulic machinery and system, IOP Publications, Romania, 2010.
11. Padhy, M.K., Saini, R.P.: Study of silt erosion on performance of a Pelton turbine, *Energy* 36, 141–147(2011).
12. Tsuguo, N.: Estimation of repair cycle of turbine due to abrasion caused by suspended sand and determination of desilting basin capacity. In: Proceedings of international seminar on sediment handling technique, NHA, Kathmandu, 1999.
13. Singh, P., Singh, R.D., Sharma, K.D.: Runoff forecasting and estimates of suspended sediment for sustainable development of hydropower scheme in Himalayan region, In Proceedings of International Workshop on Sediment Management for Hydro Projects, Supplementary Volume, India Hydro, New Delhi, 55–60 (2005).

Design, Analysis, and Assessment of Efficiency of Three-Phase Squirrel-Cage Induction Motors Operating Under the Rated Voltage: A Design Consideration for Rural Areas

Raj Kumar Saini, Devender Kumar Saini, Rajeev Gupta,
R.P. Dwivedi and Piush Verma

Abstract Three-phase induction motors are broadly utilized as a part of ventures and in residential purposes due its techno-financial points of interest. The issues involved in the design of three-phase induction motors are that the motors which are designed at rated voltage, however, working under the rated voltages specific in the provincial zones far from the utility Centers are highlighted. Such sorts of motors when work under the evaluated voltage cause more copper losses, derating, throbbing torque, and wastefulness. The aim of this paper is to break down the misfortunes and discover the optimized parameters to enhance the execution of the motors working on appraised to under evaluated voltages. The new designed parameters are compared with the standard one and salient features are talked about by utilizing MATLAB and JMAG Express.

Keywords Three-phase induction motor · Rated voltage · Below rated voltage Unbalanced voltages · JMAG express

R.K. Saini (✉) · D.K. Saini · R. Gupta
Department of Electrical Engineering, University of Petroleum and Energy Study,
Dehradun, Uttarakhand, India
e-mail: rajsaini.acet@gmail.com

D.K. Saini
e-mail: dksaini@ddn.upes.ac.in

R. Gupta
e-mail: rajeevgupta@ddn.upes.ac.in

R.K. Saini · R.P. Dwivedi
School of Electrical and Computer Science Engineering, Shoolini University,
Solan, Himachal Pradesh, India
e-mail: rpdwivedi@shooliniuniversity.com

P. Verma
Rayat–Bahra Group of Institutes, Patiala Campus, Patiala, India
e-mail: pverma19@yahoo.co.uk

1 Introduction

Energy conservation is an essential step toward overcoming the growing problems of the industries development. By reducing the wasteful energy, the performance of the electrical machines can be improved up to some extent. In Refs. [1, 2], the authors portrayed that the three-phase induction motors assume an essential part for the improvement of item in the industries. The horticulture nation like India a huge number of enlistment motors are quickening pump sets in the rustic zones are working under the rated voltages. The effectiveness of the enlistment motors can be expanded by lessening the losses, flux density, improving the cross section of the conductors, and modifying the design of the motor. Low voltage viewed as a power quality issue of noteworthy worry at the power dispersion level. Due to unbalance voltages, current leads to exclusive losses in the stator and rotor which relates to inefficiency of the induction motors. The motor unbalanced may also occur due to the problem of manufacturing process such as unequal number of turns in the rewinding process of the machines. The country conveyance system is far from the creating stations, because of this reality the utilities are finding exceptionally hard to keep up the managed control supply, which influences the motors execution, in spite of the fact that induction motors are intended to endure some level of unbalance power supply. In Refs. [3, 4], creators depicted that the unbalanced voltages likewise expands the temperature of the machine which prompts to decrease in productivity and shorter life time of the machine. At the end of the day, motors chipping away at lopsided voltage may have more proficiency than a motor taking a shot at adjusted or rated voltages. In Ref. [5], the creator discovers a few strategies to enhance the effectiveness of low voltage squirrel-cage induction motor. Out of 25 input components, 12 variable components are discovered which influence the productivity of the motor. In Ref. [6], P. Pillay analyzed the conduct of the induction motor working under lopsided voltages and clarified the impact of positive and negative arrangement voltages on the execution of the motor. In Ref. [7], authors clarified that the expanded scope of uneven voltage effectsly affects rotor misfortunes when contrasted with stator misfortunes in light of the fact that the rotor streams have an extensive deviation when contrasted with stator ebbs and flows. In Ref. [8], a complete investigation is done on the three-phase induction motor by considering a complex unbalanced voltage factor. The author of Ref. [9] investigated that by increasing the stack length, the efficiency, and power factor can be improved up to some extent. In Ref. [10], the author made a diagnostic review on three-phase induction motor affected by unbalanced voltages. The intricate voltage unequal component has been utilized as a record voltage lopsided for the investigation of the outcomes. The affectability of streams have been computed because of unequal voltages and its impacts on the productivity and slip of the motor are watched. The authors of the Ref. [11] presented a new technique on 1.5 kW induction motor to calculate the efficiency and other characteristic by using a

bacterial foraging algorithm (BFA) and also consider harmonic distortion conduction as one of a factor under distorted grid voltages. In Ref. [12], author presented a method to measure the prediction of temperature rise in the winding of the machine due to harmonics without having much knowledge of thermal properties of the machine under distorted voltage conditions.

1.1 Effects of Under Voltages

Because of unbalanced voltages, the sum of average voltages in the three phases is generally low, which expands the aggregate losses of the machine. These losses are partitioned in three sections, specifically the stator and rotor copper losses, core losses and mechanical losses. When the motor is working under the evaluated voltages, it will affect the variable losses as compared to constant losses. The grinding and windage losses (mechanical losses) as a rule happen in the scope of 1–2% of the total output of the machine. The constant losses rely on the constructional fates, and it fluctuates in the scope of 2–3%. In this research article for a 3.75 kW squirrel-cage induction motor, core and mechanical misfortunes are accounted for as 198 and 45 kW by the producer, while the stray misfortunes have been disregarded. Keeping in mind the end goal to dissect the execution of three-phase induction motor working as far as appraised to under evaluated voltage, a 3.75 kW three-phase squirrel-cage induction motor has been proposed with the accompanying information determinations as appeared in Table 1.

1.2 Results, Discussions and Recommendations

The calculation for unbalanced voltages due to which the motor is operating under the rated voltages have been investigated experimentally with the help of digital voltmeter at the motor terminal over a period of 8 days and 4 times in a day from 8 am to 10 pm. The percentage calculations for average voltages and percentage

Table 1 Input specifications

Particulars	Input values
Rating of machine (pi)	3.75 kW
Number of phases (<i>n</i>)	3
Voltage (Es)	400 V
Frequency (<i>f</i>)	50 Hz
Full load efficiency (<i>n</i>)	0.84
Synchronous speed (Ns)	1500 R.P.M.
Electric loading (ac)	21,000
Magnetic loading (Bav)	0.45
Winding factor (kW)	0.955

below the rated voltages of three phases have been calculated to calculate the variables losses of stator, rotor, and efficiency as shown in Table 2.

This is observed that the most effected parameter with the variation of voltages is the stator copper material. The number of turns of the stator winding will change with the variation of the voltage, which affects the variables losses and changes others parameters of the motor. By applying the rated voltage, the rated efficiency

Table 2 Calculations for average voltages, percentage below the rated voltage variables losses, and efficiency of a 3.75 kW three-phase induction motor

S. No.	Average voltage (V)	Stator copper losses without modified stator parameters	Rotor copper losses without modified stator parameters	% efficiency
1	361	314.83	186.69	83.75
2	371.33	306.08	181.57	84.01
3	371.67	305.8	181.41	84
4	370	307.18	182.22	83.98
5	371.67	305.8	181.41	84.02
6	371.33	306.08	181.57	84.01
7	365.33	311.11	184.51	83.61
8	365.33	311.11	184.51	83.61
9	373	304.72	180.78	84.04
10	375.67	302.55	179.51	84.11
11	375.67	302.55	179.51	84.11
12	366.33	310.26	184.01	83.88
13	375.33	302.83	179.67	84.1
14	360.67	315.14	186.86	83.75
15	372.67	304.99	180.93	84.04
16	358.67	316.89	187.88	83.69
17	360	315.72	187.2	83.54
18	370	307.19	182.22	83.98
19	364	312.25	185.18	83.83
20	365.67	310.83	184.34	83.87
21	365.67	315.43	187.03	83.74
22	360.33	312.54	184.51	83.82
23	363.67	312.83	184.51	83.81
24	363.33	311.17	182.22	83.86
25	370	307.18	186.35	83.98
26	361.67	314.26	181.58	83.77
27	371.33	306.08	180.79	84
28	373	304.72	180.94	84.05
29	372.67	304.99	185.18	84.03
30	364	312.25	186.35	83.83
31	361.67	314.27	185.34	83.77
32	363.67	312.54	184.37	83.82

Table 3 Parameters calculations for percentage change in parameters at appraised and under the evaluated voltage

Parameter calculations at rated voltage (400 V)	Parameter calculations under rated voltage (360 V)	Percentage change
Stator turns per phase = 310	Stator turns per phase = 279	(-)10
Total stator conductors = 1860	Total stator conductors = 1860	(-)10.53
Conductors per slot = 74	Conductors per slot = 69	(-)6.75
Current per phase = 1.88 A	Current per phase = 5.43 A	(+)10.13
Dia of stator conductor = 1.092 mm	Dia of stator conductors = 1.116 mm	(+)2.15
Stator resistance/phase = 3.970 Ω	Stator resistance/phase = 3.21 Ω	(-)18.56
Efficiency at rated voltage = 84.64%	Efficiency under rated voltage = 84.64%	Nil

of the motor is estimated 84.64%. This is also observed that by applying 10% less voltage of the rated voltage, i.e., at 360 V, the proficiency of the motor can likewise be accomplished up to its appraised productivity with the accompanying changes in the stator parameters of the motor as talked about in Table 3.

Nine perceptions are applied from Table 2 to watch the variety of productivity with adjusted and without changed stator turns. This is observed that with adjusted stator turns when the motor is working under the appraised voltage, the evaluated productivity of the motor can be accomplished as appeared in the figures underneath.

Figures 1 and 2 demonstrate that the stator and rotor copper misfortunes increase with the variety of voltages. These misfortunes can be kept up stable with upgraded stator turns and others parameters as appeared in Table 3, while by lessening the stator and rotor copper losses the effectiveness of the motor can be enhanced as appeared in Fig. 3.

1.3 Performance Optimization

This model of examining the execution of the motor depends on the numerical displaying of three-phase squirrel-cage induction motor under the variety of voltage, however to get the more helpful outcomes, the exhibited scientific model will be more valuable by the usage of improvement process. The geometrical parameters of stator and rotor are upgraded under the variety of voltages from evaluated to under the appraised voltages at greatest effectiveness as a protest work. The JMAG express (an electric motor design software) is utilized for this reason. The geometrical parameters of stator and rotor are ascertained as far as affectability examination at most extreme proficiency as a protest work as appeared in Table 4. For this reason, rim_001 with round bar rotor is utilized with So_013 parallel tooth opening, round base teeth width with space profundity is utilized to get the greatest productivity under the variety of voltages (Table 5).

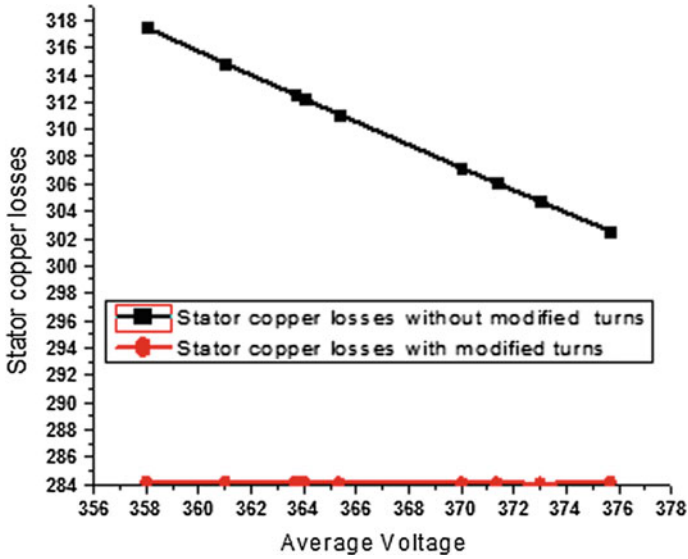


Fig. 1 Stator copper losses versus average voltage

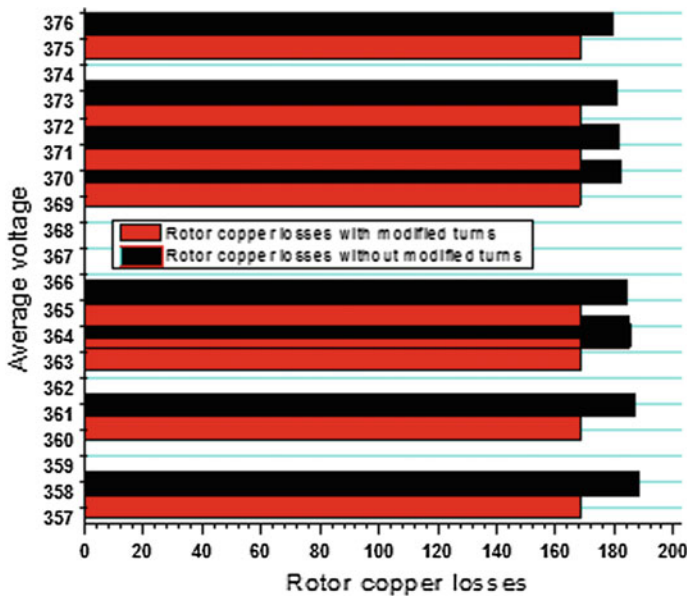


Fig. 2 Rotor copper losses versus average voltage

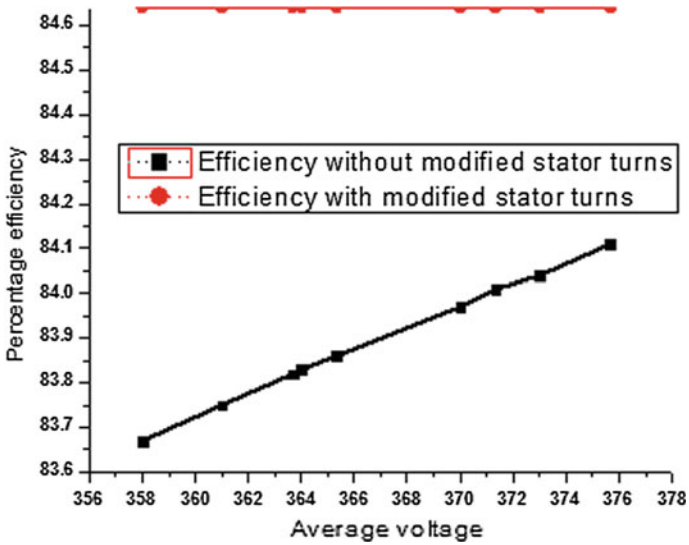


Fig. 3 Efficiency versus average voltage

Table 4 Figuring of stator and rotor measurements as far as affectability investigation under the variety of voltage

Variables	Values
Bore diameter of stator	43.3 mm
Outside diameter of rotor	42.44 mm
Stator tooth width	1.82 mm
Bar diameter of rotor	4.25 mm
Slot opening width	1.27 mm
Depth of stator slot	13.19 mm
Stator tooth height	1.54 mm
Width of stator slot	0.515 mm
Stator outside diameter	84.91 mm
Angle of stator tooth	22.9 Deg
Bar center depth	2.55 mm
Number of turns	365
Shaft diameter	12.7 mm

Table 5 Calculation for optimized efficiency versus speed of motor under the variation of voltage

Speed (R.P.M)	75	225	375	525	825	975	1125	1425
Optimized efficiency	4.97	13.14	21.48	30.04	47.84	56.72	65.96	85.16

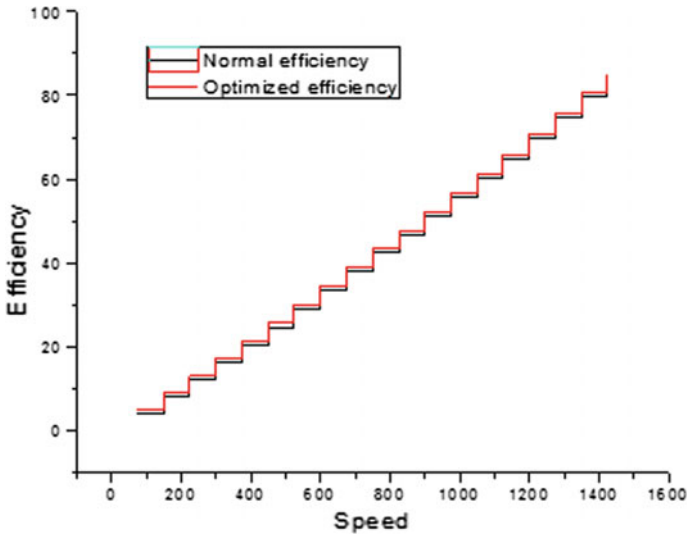


Fig. 4 Optimized efficiency versus speed

Figure 4 shows the relationship between normal and optimized efficiency on the bases of above said stator and rotor design.

2 Conclusion

This is broke down that the three-phase induction motors working under the rated voltage diminish the proficiency of the motors, which lead to decrease in overall performance of the motors. The present review in this exploration article demonstrates that the diminishment in effectiveness because of low voltage can be enhanced up to its appraised proficiency by advancement handle with the guide of appropriate determination of stator and rotor outline. This sort of study will be a gainful device for sparing vitality, specific in the villages where the appropriation of electrical supply is poor because of reactive power demand. With the aid of optimization process, the failure of motor can be avoided under the extreme conduction of power quality. The proposed design will not only save the operating cost of the motor, but it will also increase the operating life of the machine with more warranty period.

References

1. Sridhar, L, Jha, C.S, Singh, B.P, Murthy, S.S.: Design of energy efficient motor for irrigation pumps operating under realistic conduction IEE Roc.-Electr. Power Appl., Vol. 141, No. 6, pp. 269–274 (1994).
2. Von Jouanne, Annette, Banerjee, Basudeb (Ben): Assessment of Voltage unbalance. IEEE Trans on power delivery, VOL. 16, No. 4, pp. 782–790 (2001).
3. Williams.: Operation of three-phase induction motors on unbalanced voltages. AIEE Trans, Pt-III-A, and Power Apparatus Syst, pp. 125–133(1954).
4. Faiz, Jawad.: Influence of unbalanced voltage supply on efficiency of three Phase squirrel cage induction motor and economic analysis. Elsevier, Energy Conversion and Management VOL. 47, pp. 289–302(2006).
5. Hasuiké, K.: Efficiency improvement study of low voltage three phase squirrel cage induction motor for general purpose. IEEE Trans on power apparatus System, VOL. PAS-102, No. 12, (1993).
6. Pillay, P, Hofmann P, Manyage, PM.: Derating of induction motor operating with combination of unbalanced voltages and over-or-under voltages. IEEE Power engineering society winter meeting, VOL 3, pp. 1365–1371(2001).
7. Gilbert, AJ.: The influence of rotating machine design standards on the design of traction supplies. Conference on main line railway electric power, pp. 241–245(1989).
8. Wang, YJ.: Analysis of effects of three-phase voltage unbalance on induction motors with emphasis on the angle of the complex voltage unbalance factor. IEEE Trans on Energy Convers pp. 270–275(2001).
9. Emmanuel, B, Agamloh, Aldo, Togliatti, Cavagnino, Andrea.: The Incremental design Efficiency Improvement of Commercially Manufactured Induction Motors. IEEE Trans on industry applications, VOL. 49, no. 6, pp. 2496–2504(2013).
10. Wang, Yaw-Juen.: An Analytical Study on Steady-state Performance of an Induction Motor Connected to unbalanced three-phase voltage. IEEE Power engineering society, VOL 1, pp. 159–164 (2000).
11. Vladimir Sousa Santos, Percy, R, Viego Felipe, Julio, R, Gomez Sarduy, Enrique C. Quispe, Balbis, Milen.: Procedure for Determining Induction motor efficiency working under distorted grid voltages. IEEE Trans on Energy Conversion, VOL. 30, no. 1, pp. 331–339 (2015).
12. Gnacinski, P.: Prediction of windings temperature rise in induction motors supplied with distorted voltage. Elsevier, Energy Conversion and Management 49, pp. 707–717 (2008).

Tunable Universal Filter in ± 0.5 V 32 nm CNFET for ISM 2.4 GHz Bluetooth/Zigbee Transceivers

Jyoti Sharma, Mohd. Samar Ansari and Sudip Kundu

Abstract Carbon nanotube field-effect transistors (CNFETs) have emerged as practicable replacements to conventional MOSFETs for contemporary analog/digital design. This work highlights a current-mode tunable universal filter (CMUF), which can provide band-reject, low-, band-, and high-pass filtering functions, by making use of a new CNFET-based second-generation current-controlled conveyor (CCCII) and grounded capacitors only. The circuit operates on lower power supply and bias currents, and uses smaller capacitors as compared to CMOS counterparts. Corner frequencies (for LPF and HPF) and center frequency (for BPF) have been obtained in the GHz range. Tunability of filter outputs with respect to bias current has been demonstrated. This CMUF is suitable for operation in 868–915 MHz, and 2.4–5 GHz bands used by Zigbee and Bluetooth, respectively. Noise and Monte Carlo analyses have also been performed. The performance of both the CCCII and the CMUF is verified with extensive SPICE simulations.

Keywords Carbon nanotube FET · CNFET · Current-controlled conveyor
Universal filter · Bluetooth · Zigbee

J. Sharma (✉)

Department of Electronics and Communication Engineering, BIT Mesra,
Jaipur Campus, Jaipur, India
e-mail: jyotisharma@bitmesra.ac.in

Mohd. S. Ansari

Department of Electronics Engineering, AMU, Aligarh, India
e-mail: mdsamar@gmail.com

S. Kundu

Department of Electronics and Communication Engineering, BIT Mesra, Ranchi, India
e-mail: kundu.sudip@gmail.com

1 Introduction

Over the past three decades, CMOS technology has been the dominant force behind the exponential growth of the electronics industry. Well-controlled processes and high reproducibility from concept to silicon were the two most important factors which led to CMOS becoming ubiquitous in the integrated circuits industry. However, as feature sizes reduce to tens of nanometers, CMOS begins to introduce several challenges including, but not limited to, escalating transistor and IC power dissipation; swelling process and device variabilities, poorer scaled device performance; challenging lithography and process complexity and degraded interconnect performance. The reliability and performance of circuits implemented using such small channel length MOSFETs are degraded, thus limiting the possibilities of further scaling in conventional MOSFETs. In order to overcome these limitations, the novel materials and devices such as double- and multi-gate transistors, silicon-on-insulator FETs, and finFETs are explored for future electronic design applications. SOI FET is not been actively used presently due to its higher substrate costs, low thermal conductivity causing heating problem and floating body electrical effects. FinFETs also offer challenges such as formation of thin Si fins, limitations of lithography, S/D resistance, and simulators needed to model 3D quantum effects. Hence, the most promising of the various upcoming technologies appears to be the carbon nanotube field-effect transistors (CNFETs).

CNFETs exhibit better electron mobility, improved current density, more transconductance, stricter control over channel development, and improved threshold voltage [1–5]. CNFETs have atomically smooth surfaces, reduced electronic states at the dielectric interface, and higher drive currents than MOSFETs [6]. The main objective of this paper is to explore an analog signal processing building block design and its subsequent use in the current-mode universal filter design.

The ‘current-mode’ (CM) approach deals with currents as operating entities. Such an approach promises advantages like high speed, low power consumption at high frequency, high signal dynamic range, low cross-talk, schematic simplicity, and well suited for low voltage [7].

Bluetooth is a wireless technology used to transfer data between different electronic devices. It operates in the ISM 2.4 GHz/5 GHz band and is a typical protocol for near-range RF communication between several diverse types of gadgets, including cell phones, PCs, home entertainment systems, tablets. Zigbee is another similar, but less popular, technology operating in the ISM 2.4 GHz/5 GHz in most jurisdictions worldwide: 868 MHz in Europe and 915 MHz in the USA and Australia.

This manuscript is organized as per the following. The overview and performance assessment of the newly proposed CCCII has been presented in Sect. 2. Section 3 presents the proposed CNFET-based CMUF and its mathematical analysis. Section 4 contains results of extensive performance assessments (simulation as well as analytical) performed over the proposed CMUF. Lastly, Sect. 5 concludes the paper.

2 CNFET-Based Analog Building Block

The CCCII or the second-generation current-controlled conveyor is a current-mode device, which facilitates realization of electronic functions operational at higher frequency. The symbol of a CCCII and its related mathematical quantities are presented in Table 1 from where it can be observed that R_X is adjustable by a bias current I_B . This electronic control of the resistance at X-terminal imparts tunability to all circuits designed using a CCCII [8]. CCCII-based circuits are very suitable for high-frequency applications. It is widely used for implementing various analog signal processing functions, viz. amplifiers, integrators, rectifiers, differentiators, oscillators, filters [8–13]. Figure 1 shows a CNFET-based implementation of the CCCII. The circuit of Fig. 1 has been analyzed to yield the voltage transfer ratio (α), the current transfer ratio (β), and impedances at X, Y, and Z nodes as given by (3)–(7).

$$\alpha = \frac{V_X}{V_Y} = \frac{(g_{m4} + g_{m2})r_{o4} \| r_{o2}}{1 + (g_{m4} + g_{m2})r_{o4} \| r_{o2}} \quad (3)$$

$$\beta = \frac{I_Z}{I_X} = \frac{g_{m2}g_{m10}g_{m12} + g_{m4}g_{m11}g_{m13}}{g_{m11}g_{m10}(g_{m4} + g_{m2})} \quad (4)$$

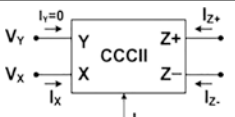
$$Z_X = \frac{1}{g_{m4} + g_{m2}} \quad (5)$$

$$Z_Y = \frac{1}{g_{ds6} + g_{ds9}} \quad (6)$$

$$Z_Z = \frac{1}{g_{ds13} + g_{ds12}} \quad (7)$$

The CNFET-based CCCII of Fig. 1 has been implemented in HSPICE, and DC, transient, and AC analyses were performed. Simulation results as shown in Fig. 2 depict that the proposed CCCII circuit correctly follows the mathematical formulations given in Table 1. Optimized design parameters of the CNFET-current-controlled conveyor used for simulation are summarized in Fig. 1b. Variation of performance parameters with frequency, pitch, and number of CNTs is presented in Fig. 3.

Table 1 Symbol and opposite expressions for CNFET-based CCCII parameters

Symbol of CCCIIs	Port relationships of CCCIIs	Port-X resistance
	$\begin{bmatrix} V_X \\ I_Y \\ I_{Z+} \\ I_{Z-} \end{bmatrix} = \begin{bmatrix} R_X & 1 & 0 \\ 0 & 0 & 0 \\ +1 & 0 & 0 \\ -1 & 0 & 0 \end{bmatrix} \begin{bmatrix} I_X \\ V_Y \\ V_Z \end{bmatrix} \quad (1)$	$R_X = \frac{1}{\sqrt{8\mu_n C_{ox} \frac{W}{L} I_B}} \quad (2)$

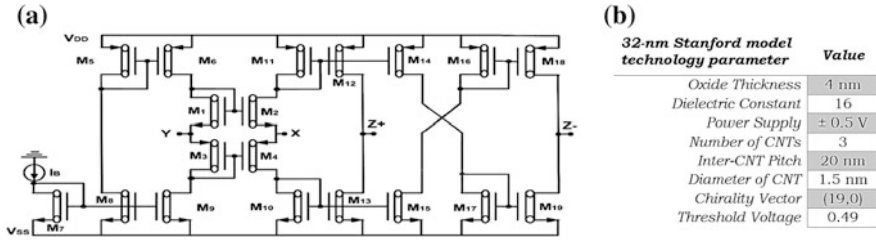


Fig. 1 a CNFET-based CCCII implementation. b 32 nm CNFET parameters

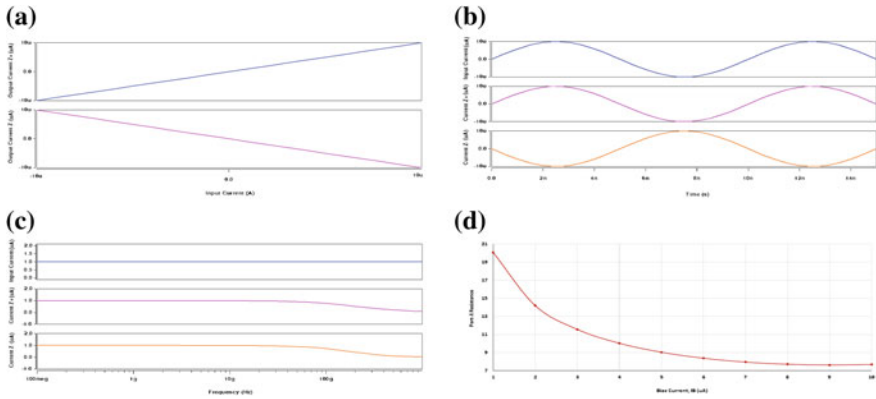


Fig. 2 Simulated results for positive and negative Z outputs of the current-controlled conveyor of Fig. 1: a DC, b transient, c AC analysis, and d port-X resistance variation with respect to bias current

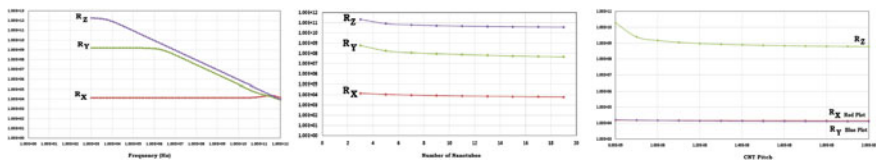


Fig. 3 Variation of performance parameters with respect to frequency, CNT count, and CNT pitch

3 Proposed CNFET-Based CM Universal Filter

The current-controlled conveyor (CCCII) finds use in the implementation of single-input and three-output CM filters with reduced number of passive components [14], [15]. In this section, the design and subsequent implementation of a CMUF using two CNFET CCCIIs has been discussed. The proposed CMUF has a

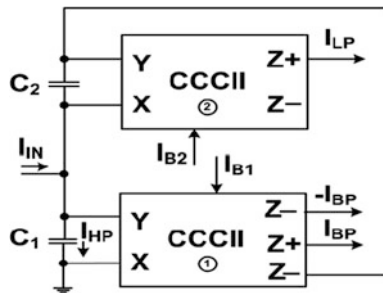


Fig. 4 Proposed CNFET-based CM universal filter

single-input and three-independent outputs for low-, high-, and band-pass filters. Figure 4 shows the proposed CMUF circuit using two CCCII and two capacitors. The transfer functions of various filtering functions available are given by (8)–(10).

$$\frac{I_{HP}}{I_{in}} = \frac{s^2}{s^2 + as + b} \quad (8)$$

$$\frac{I_{LP}}{I_{in}} = \frac{-b}{s^2 + as + b} \quad (9)$$

$$\frac{I_{BP}}{I_{in}} = \frac{as}{s^2 + as + b} \quad (10)$$

where

$$a = \frac{1}{R_{X1}C_1}$$

$$b = \frac{1}{R_{X1}R_{X2}C_1C_2}$$

Band-reject response may be obtained by connecting I_{HP} and I_{LP} together. The natural frequency ω_0 , the bandwidth ω_0/Q , and quality factor Q are given in (11). Values of ω_0/Q and ω_0 can be tuned by bias currents, I_{B1} and I_{B2} , of the two CCCII.

$$\omega_0 = \frac{1}{\sqrt{R_{X1}R_{X2}C_1C_2}}; \quad \frac{\omega_0}{Q} = \frac{1}{R_{X1}C_1}; \quad Q = \sqrt{\frac{R_{X1}C_1}{R_{X2}C_2}} \quad (11)$$

4 Performance Evaluation

4.1 Simulation Results

To verify the performance of the proposed circuit in Fig. 4, HSPICE simulations were undertaken. The DC supply voltages are taken as ± 0.5 V. For all the simulations, the capacitance values were chosen as follows: $C_1 = C_2 = 3$ fF, and bias currents were set as $I_{B1} = I_{B2} = 2$ μ A. Figure 5a, b shows the simulation results for LP, HP, BP, and BR filters. Electronic tuning of all filter responses with bias current is shown in Fig. 5c, d.

Electronic tuning by varying the bias current can be used to achieve the full frequency range of Bluetooth and Zigbee frequencies as shown in Fig. 6. Noise and Monte Carlo analyses have also been performed on the CMUF, and the results are shown in Fig. 7. Table 2 presents a comparative assessment of the proposed CMUF via-a-vis existing circuits on technology used, transistor count, supply voltage, active element count and type, number of resistors, capacitors, and frequency obtained.

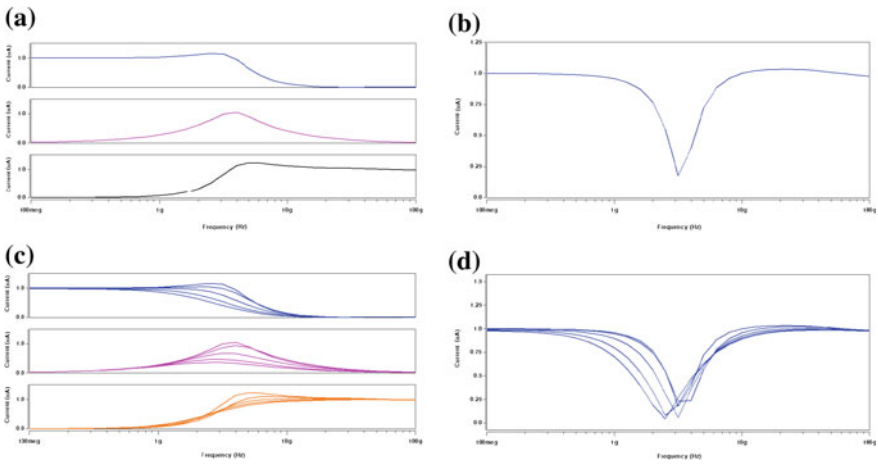


Fig. 5 Frequency responses of the proposed CMUF. **a** LP, HP, and BP responses, **b** band-reject response, **c** LP, HP, and BP tuning, **d** band-reject tuning (electronic tuning for variation in bias currents I_{B1} and I_{B2} from 2 to 10 μ A in steps of 2 μ A)

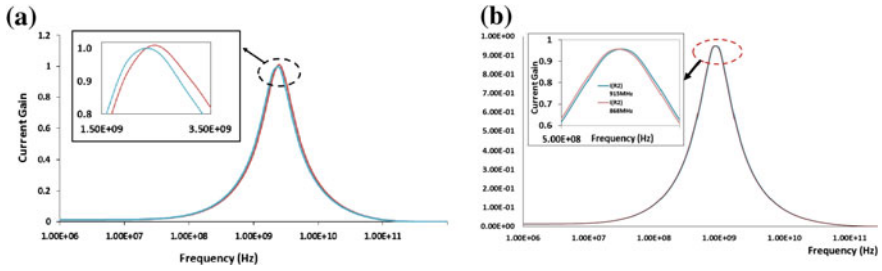


Fig. 6 Tuning of center frequency of BPF for **a** Bluetooth and **b** Zigbee

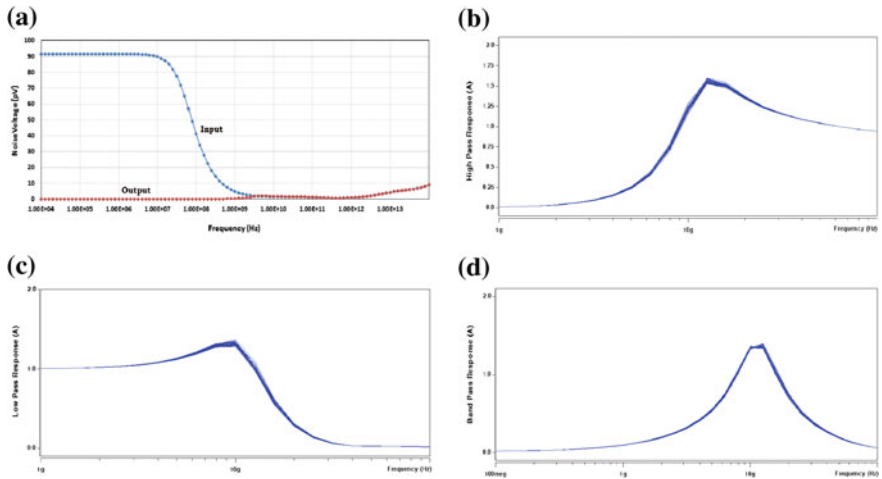


Fig. 7 Results of **a** noise analysis; **b** through **d** Monte Carlo analysis of low-pass, high-pass, and band-pass responses of the proposed CMUF

Table 2 Comparison of present work with previous works

Parameter	Reference			
	[10]	[11]	[7]	This work
Process	CMOS	CMOS	CMOS	CNFET
Technology node	0.35 μm	0.35 μm	65 nm	32 nm
Transistor count	17	19	19	17
Supply voltage	± 1.65 V	± 2.5 V	± 0.5 V	± 0.5 V
Bias current	–	200 μA	2 μA	2 μA
Capacitor	25 pF	0.5 nF	250 fF	3 fF
Active element	1 CCCII–	2 CCCII \pm	2 CCCII \pm	2 CCCII \pm
No. of resistors	1 floating	0	0	Resistor-less
No. of capacitors	2	2	2	2
Frequency range	MHz	MHz	MHz	GHz

Table 3 Non-ideal and parasitic analyses of the proposed CNFET-based CMUF

Non-ideal analysis	Parasitic analysis
$\frac{I_{HP}}{I_{in}} = \frac{s^2}{s^2 - \frac{\alpha_2 \beta s}{R_{X1} C_1} - \frac{\alpha_2 \beta}{R_{X1} R_{X2} C_1 C_2}}$	$\frac{I_{HP}}{I_{in}} = \frac{(sC_2 Z_3 Z_4 + Z_4) Z_2}{(Z_1 Z_3 + Z_1 Z_2)(1 + sC_2 Z_4) + Z_2 (sC_2 Z_3 Z_4 + Z_4)}$
$\frac{I_{BP}}{I_{in}} = \frac{\frac{\alpha_1 \beta s}{R_{X1} C_1}}{s^2 - \frac{\alpha_2 \beta s}{R_{X1} C_1} - \frac{\alpha_2 \beta}{R_{X1} R_{X2} C_1 C_2}}$	$\frac{I_{BP}}{I_{in}} = \frac{(sC_2 Z_3 Z_4 + Z_4) Z_1}{(Z_1 Z_3 + Z_1 Z_2)(1 + sC_2 Z_4) + Z_2 (sC_2 Z_3 Z_4 + Z_4)}$
$\frac{I_{LP}}{I_{in}} = \frac{-\frac{\alpha_2^2 \beta}{R_{X1} R_{X2} C_1 C_2}}{s^2 - \frac{\alpha_2 \beta s}{R_{X1} C_1} - \frac{\alpha_2 \beta}{R_{X1} R_{X2} C_1 C_2}}$	$\frac{I_{LP}}{I_{in}} = \frac{-(Z_1 Z_3 + Z_1 Z_2)}{(Z_1 Z_3 + Z_1 Z_2)(1 + sC_2 Z_4) + Z_2 (sC_2 Z_3 Z_4 + Z_4)}$
where	where
$\begin{bmatrix} V_X \\ I_Y \\ I_{Z+} \\ I_{Z-} \end{bmatrix} = \begin{bmatrix} R_X & \beta & 0 \\ 0 & 0 & 0 \\ \alpha_1 & 0 & 0 \\ \alpha_2 & 0 & 0 \end{bmatrix} \begin{bmatrix} I_X \\ V_Y \\ V_Z \end{bmatrix}$	$Z_1 = \frac{1}{sC_1} \parallel \frac{1}{sC_{Y1}} \parallel R_{Y1} \quad Z_2 = R_{X1} + \frac{1}{sC_{X1}}$ $Z_3 = R_{Z1} - \left\ \frac{1}{sC_{Z1-}} \right\ \parallel \frac{1}{sC_{Y2}} \parallel R_{Y2} \quad Z_4 = R_{X2} + \frac{1}{sC_{X2}}$

Table 4 Results of sensitivity analysis

Sensitivity	Value	Sensitivity	Value	Sensitivity	Value	Sensitivity	Value
$S_{R_{X1}}^{G0}$	-0.5	$S_{C_2}^{G0}$	-0.5	$S_{R_{X1}}^Q$	0.5	$S_{R_{X2}}^{BW}$	0
$S_{R_{X2}}^{G0}$	-0.5	$S_{C_1}^{BW}$	-1	$S_{R_{X2}}^Q$	-0.5	$S_{C_1}^Q$	0.5
$S_{C_1}^{G0}$	-0.5	$S_{C_2}^{BW}$	0	$S_{R_{X1}}^{BW}$	-1	$S_{C_2}^Q$	-0.5

4.2 Non-ideal and Parasitic Considerations

Non-idealities in the device operation as well as the parasitics associated with the analog building block cause deviations from the expected behavior of the circuit. It is therefore imperative to include such considerations in the actual design of any circuit. For the case of the proposed CMUF, Table 3 lists all the pertinent design relationships of the CMUF including the non-ideal and parasitic effects.

4.3 Sensitivity Analysis

Sensitivities of various circuit parameters such as ω_0 , bandwidth (BW) and quality factor (Q) with respect to passive components, reported in Table 4, are well below unity (one) in magnitude which illustrates that variations/tolerances in the values of the external resistor and capacitors are not expected to affect the circuit performance significantly.

5 Conclusion

In this paper, a second-generation current-controlled conveyor (CCCII) was implemented using 32 nm CNFET technology. Using a DC supply of ± 0.5 V, DC, transient, and AC analyses were performed using HSPICE. The simulation results indicated accurate operation of the CNFET-based CCCII up to few GHz. A current-mode universal filter was then designed that employed CNFET-based CCCII and grounded capacitors. All the four functions low-pass, high-pass, band-pass, and band-reject are obtained using this filter. Tunability of the filter outputs has also been analyzed with respect to bias currents. Non-idealities of the active elements were also considered along with the parasitics involved, to evaluate the actual performance of the proposed filter. HSPICE simulation results established the suitability of the CMUF for operation in the Zigbee and Bluetooth range. Such CNFET-based designs could be viable alternatives for replacing CMOS circuits in the next-generation low-power and high-frequency applications.

References

1. Baldonado, M., Chang, C.-C.K., Gravano, L., Paepcke, A.: The Stanford Digital Library Metadata Architecture. *Int. J. Digit. Libr.* 1 (1997) 108–121
2. Frank, D. J., Dennard, R. H., Nowak, E., Solomon, P. M., Taur, Y., Wong, H. S. P.: Device scaling limits of SiMOSFETS and their application dependencies, *IEEE*, Vol. 89, no. 3 (2001) 259–288
3. Dresselhaus, M. S., Dresselhaus, G., Avouris, P.: *Carbon nanotube*, Springer-Verlag
4. Sedra, A. S., Smith, K. C.: A second generation current conveyor and its applications, *IEEE Trans. Circuit Theory*, Vol. 17, no. 1 (1970) 132–134
5. Bielek, D., Biolkova, D., Viera: First-order voltage-mode all-pass filter employing one active element and one grounded capacitor, *Analog Integrated Circuits and Signal Processing*, Vol. 65, no. 1 (2010) 123–129
6. Stanford university CNFET model. <http://nano.stanford.edu/model.php?id=23>
7. Beg, P., Siddiqi, M. A., Ansari, M. S.: Multi output filter and four phase sinusoidal oscillator using CMOS DX-MOCCII, *International Journal of Electronics*, Vol. 98, no. 9 (2011) 1185–1198
8. Ranjan, A., Paul, S. K.: Voltage mode universal biquad using CCCII, *Journal of Active and Passive Electronic Components* (2011) pp. 1–5
9. Sharma, J., Ansari, M. S., Sharma, J.: Current-mode electronically tunable resistor-less universal filter in 0.5 V 32 nm CNFET, *Int. Conf. on Devices, Circuits and Communications (ICDCCom)*, (2014) 1–6
10. Sharma, J., Ansari, M. S., Sharma, J.: Electronically tunable resistor-less universal filter in 0.5 V 32 nm CNFET, *Fifth International Symposium on Electronic System Design (ISED)* (2014) 206–207
11. Singh, S. V., Maheshwari, S.: Current-processing current-controlled universal biquad filter, *Radioengineering*, Vol. 21, no. 1 (2012) 317–323
12. Chang, Chun-Ming, Huang, Tzu-Hao, Tu, Shu-Hui, Hou, Chun-Li, Horng, Jiun-Wei: Universal Active Current Filter Using Single Second-Generation Current Controlled Conveyor, *International Journal of Circuits, Systems and Signal Processing*, Vol. 1(2007) pp. 194–198

13. Abbas, Z., Scotti, G., Olivieri, M.: Current controlled current conveyor (CCCII) and application using 65 nm CMOS technology, World Academy of Science, Engineering and Technology Vol. 55
14. Parkash, J., Kumar, P.: Voltage mode second order biquadratic filters using single CCCII, International Journal of Electronics Engineering Vol. 3 (2011) pp. 257–260
15. Tripathi, S. K., Ansari, M. S.: Voltage-mode universal filter for ZigBee using ± 0.9 V 32 nm CNFET ICC-II. In: Confluence The Next Generation Information Technology Summit, 5th International Conference-IEEE (2014) 471–475

Morphology of Plants Using Spatial Domain Image Enhancement Technique for the Mildew Detection

Deepak Kumar, Prashanta Bhuyan, Manish Sharma
and Amit Kumar

Abstract Managing diseases (Arivazhagan et. al., CIGR, 15(1):211–217, 2013 [1]) in plant is a challenging task. Diseases are mostly seen on the leaves or stem or fruits of the plant. Systematic disease identification should be undertaken so that crop yield can be maximized. Some diseases can be handled by the farmer before the disease spreads. Farmers will find automatic disease identification with the system and easier in their occupation. A large of such diseases can be identified using the leaves of the plants. The proposed system automatically detects the patterns of diseases in their early stage.

Keywords Geometric correction · Powdery mildew diseases · Grayscale manipulation · Spatial domain

1 Introduction

In India, the agricultural [2] segment gets a vigorous place in the overall budget of the country. Agriculture segment offers livelihood to 65–70% of the total inhabitants. Numerous large and minor scale trades are to be subjected on agriculture area for their raw material which usually lie as some sugar factory, jute textile industries, food industries, pharmaceutical industries, etc. All trades need good fineness in raw material. So, study in agricultural sector is meant toward rise of efficiency and superiority. Herbal disease is one of the critical reasons that decreases amount and reduces quality of the agricultural production. Disease is a damage of well-being or a state of irregular working. Plant diseases are usually produced by microorganisms, worms, and molds [3]. The rate of plant illnesses also rests on environmental disorder. Sickness needs cautious analysis and treatment at right time to defend the

D. Kumar · P. Bhuyan (✉)
HRIT, Ghaziabad, India
e-mail: pramsu@gmail.com

M. Sharma · A. Kumar
Amity University, Noida, Uttar Pradesh, India
e-mail: manish.nsit07@gmail.com

shrub from dense damages. Disease can be originated in dissimilar portions of the plant like fruit, leaves, vegetable, and stem. Observing sickness in a plant plays a main role in the ground of agriculture. Observation of health and discovery of disease in plants and trees is serious for maintainable agriculture.

2 Background

Powdery mildew [2, 4] is a fungal illness which disturbs a large number of plants and fruits. These illnesses are caused by dissimilar species of fungi like Erysiphales [5], with *Podosphaera xanthii* [5], said to be the maximum cause of the illness.

Erysiphe cichoracearum [4, 6] was the most prominent cause in the world many years back. This illness is said to be most easily recognized as the white patches [6] that we see on the leaves are easily seen through our eyes. The lower leaves are usually said to be very exaggerated, but the white patches appear on the surface of the leaves. They can be easily spotted as they are visually very prominent. It grows well in the environment where rainfall is very frequent. The atmosphere undergoes wide change in the temperature, and thus, it leads to the vital variation in the prominent regions [4]. Severe and repetitive infections weaken the plant strength [2] and its ability to produce fruits or vegetables.

There are two techniques that can enhance a digital image.

1. Spatial domain.
2. Frequency domain.

Spatial domain [7] deals with the image pixels directly. The pixel values of the image are manipulated to achieve enhancement. Pixels in images i and g are denoted by r and s , respectively. The pixel values r and s are related by the expression,

$$s = F(r) \quad (1)$$

Here, F is a transformation that maps a pixel value r into a pixel value s .

A. Image Negative

Negatives of digital images are needed in many of the applications, like in various medical appliances the devices which use monochrome rays and characteristics. Transformation $T: G(x, y) = L - F(x, y)$, where L is said to be the maximum intensity level of an image.

B. Contrast Stretching

We obtained the images with very bad contrast which can be mainly due to poor brightness [7]; the dynamic range of the sensor is very inadequate; the aperture of the lens is very small, and thus, a proper corrective measure can be taken.

C. Logarithmic Operation

The expression of the logarithmic operation is given by

$$s = C \log(1 + r) \quad (2)$$

Here, C is the constant with the value of r greater than or equal to zero.

It shows that the input image with the low-intensity level is mapped with the output image of high-intensity level.

D. Power-Law Transformation

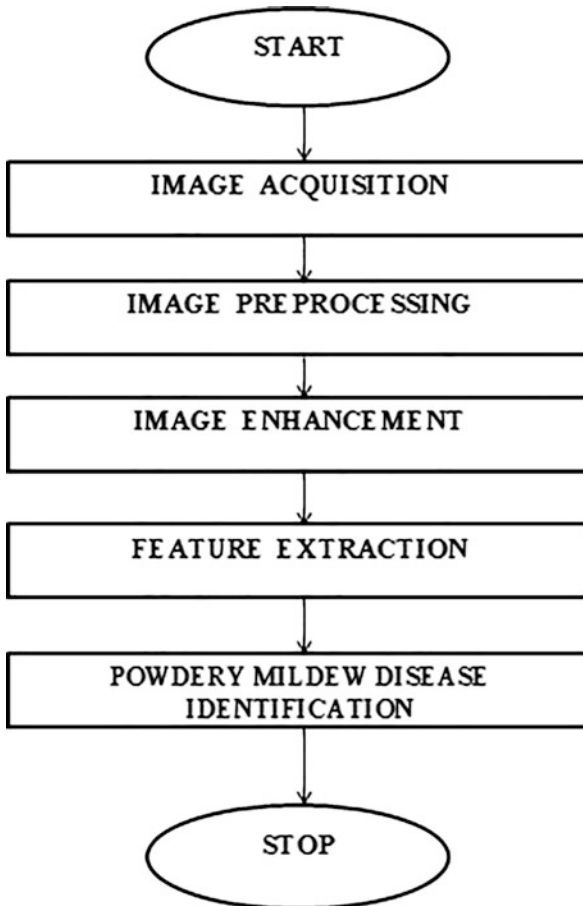
Here, different values of γ give different levels of enhancement, which is also known as gamma correction. It is not important or essential that the contrast of the image will always increase.

It can be simply defined by the relation.

$$s = Cr^\gamma \quad (3)$$

where C and r are positive constants.

3 Design and Implementation Flowchart



4 Results

See Figures 1, 2, 3, 4, 5, and 6.

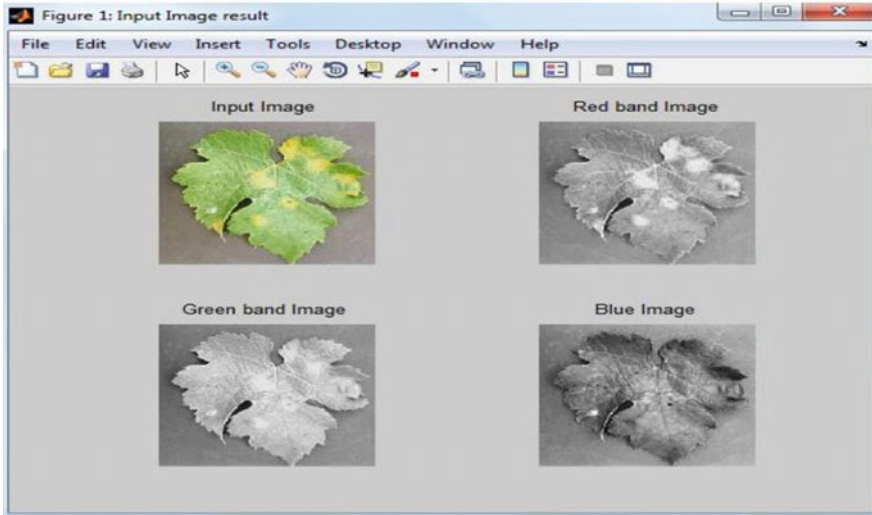


Fig. 1 Representation of RGB image of diseased grape leaf

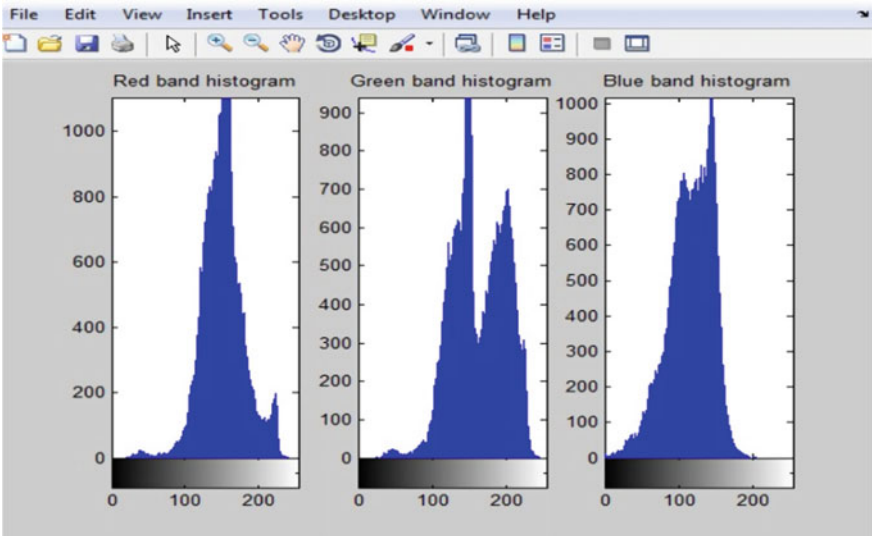


Fig. 2 Representation of histogram of diseased grape leaf

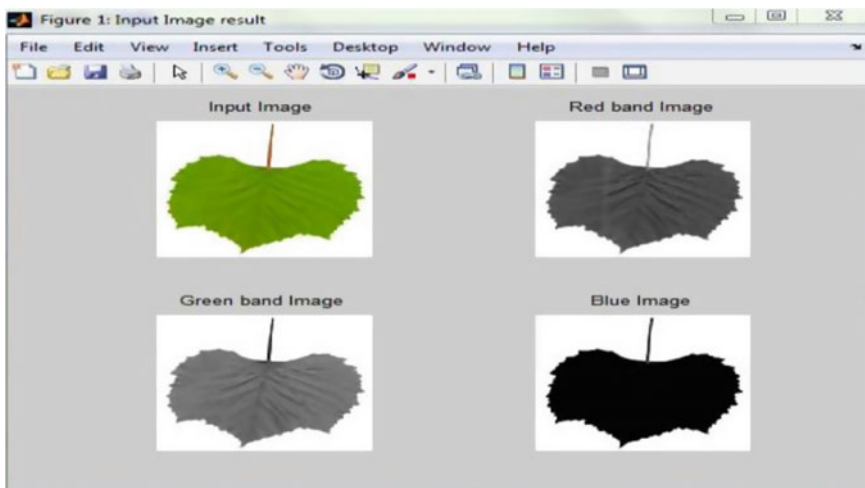


Fig. 3 Representation of RGB image of non-diseased grape leaf

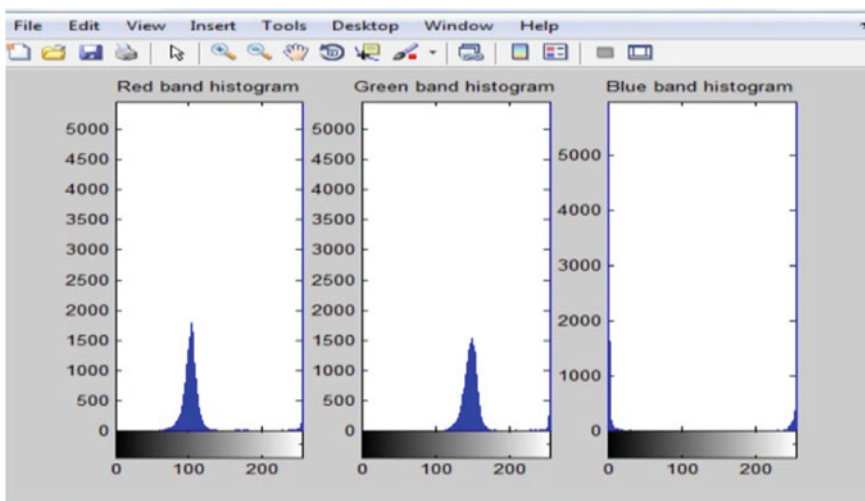


Fig. 4 Representation of histogram of non-diseased grape leaf

Fig. 5 Representation of diseased lemon leaf



Fig. 6 Representation of logarithmic operation on diseased lemon leaf



References

1. S. Arivazhagan, R. Newlin Shebiah, S. Ananthi, S. Vishnu Varthini, "Detection of unhealthy region of plant leaves and classification of plant leaf diseases using texture features", CIGR, vol. 15(1), pp. 211–217, March 2013.
2. Wilcox, W. 2003, Grape Disease Identification sheet, Cornell University Cooperative Extension.
3. C. Y. Lin, M. Wu, J. A. Bloom, I. J. Cox, and M. Miller, "Rotation, scale, and translation resilient public watermarking for images," IEEE Trans. Image Process., vol. 10, no. 5, pp. 767–782, May 2001.
4. Ellis, M. Doohan, D. Bordelon, B. Welty, C. Williams, R. Funt, R. Brown, M. 2004. Midwest Small Fruit Pest Management Handbook. The Ohio State University Extension. 125–129.
5. Mohit Agarwal, Manish Sharma, Shantanu Thakur "2D to 3D image transformation using Wavelet Technique" MEDCOM, 2014, IEEE Xplore, Nov. 2014.

6. Pscheidt, J. 2007, Grape-Powdery Mildew, Oregon State University Extension. Pearson, R. Goheen, A. 1998. Compendium of Grapes: How to Manage Pests, 2006, University of California Statewide Integrates Pest Management Program.
7. Rombough, L. 2002, The Grape Grower, A Guide to Organic Viticulture, Chelsea Green Publishing, pg. 97–101.

A High-Throughput FPGA-Based Architecture for Advanced Encryption Standard: AES-512 Using Pre-ciphered Lookup Table

Vivek Kumar, Purnendu Shekhar Pandey and Praful Ranjan

Abstract This paper proposes an FPGA architecture for a 512-bit AES implementation using a pre-ciphered lookup table approach. The hardware realization uses a 512-bit block message and a 512-bit key. The architecture is designed to give an increased throughput for applications where session keys are used for communication. The architecture exploits the fact that session key does not change for substantial duration for an entire session; therefore, a pre-ciphered lookup table can be used to enhance the encryption throughput. The design is suitable for applications where communication is performed in sessions and the key does not alter frequently, such as HTTP, Telnet remote login session in the application layer. An FPGA architecture is developed using Verilog HDL and synthesized using Virtex-7 device which shows a 290.71% increase in the throughput achieved in comparison with the previous implementation.

Keywords Session key · Advanced encryption standard · Crypto-accelerator
Symmetric key encryption

V. Kumar (✉)

Department of Computer Science and Engineering, THDC Institute of Hydropower Engineering and Technology, Bhagirathipuram, Tehri, Uttarakhand, India
e-mail: vivek9837@gmail.com

P.S. Pandey · P. Ranjan

Department of Electronics and Communication Engineering, THDC-IHET, Bhagirathipuram, Tehri, Uttarakhand, India
e-mail: purnendu12345@gmail.com

P. Ranjan

e-mail: prf98354@rediffmail.com

1 Introduction

Encryption of the digital information has been the most widely used technique of data security for communications over insecure channels. Data encryption falls under two main categories of symmetric and asymmetric key encryption where a shared key is used for symmetric key encryption, while separate pair of public and private keys are used for asymmetric key encryption. Asymmetric key encryption is extensively employed in digital signatures where data is of short size, but the mathematical complexity hinders its use for encryption of data of large size. To encrypt the data of larger bit size, symmetric key encryption is used; one of the most famous symmetric key algorithms is advanced encryption standard (AES). AES [1] was published by NIST in 2001 as a replacement of its predecessor, the DES algorithm [2]. So far AES has been the most commonly used algorithm for symmetric encryption because of its simplicity and has thus attracted the use of crypto-accelerator architectures for enhanced throughput.

AES-128, AES-256 [3, 4] are the commonly used variants of the AES algorithm, where key sizes are 128 and 256 bits, respectively. A more secure version of AES, AES-512 bits, is proposed here which uses a pre-ciphered lookup table (LUT), suitable for the digital communication where information is exchanged in sessions and validity of the symmetric key is of substantial duration. The use of LUT enhances the throughput with an endured area increase which is due to the size of the key and message block, both of which are of 512 bits. Mathematically for a particular key, any plain character will always map to a defined ciphertext. Therefore, if the known characters are encrypted beforehand and are stored in an LUT together with their ciphertexts, the message to be encrypted can then be replaced by the pre-ciphered characters by replacing the plain characters with their corresponding ciphertexts.

The proposed AES-512-bit architecture performs the encryption in two phases, where Phase 1 is where all the characters from standard ASCII character set are ciphered and stored in an LUT. Phase 2 is where the actual encryption of the input plaintext is performed by substituting the characters with their corresponding ciphertext. Phase 1 has 4 major byte-orientated transformations. First transformation is AddRoundKey where a XOR operation is performed between a 512-bit key and a 512-bit input matrix. Second is the SubBytes transformation where each byte is substituted with a pre-defined byte using a substitution box (S-BOX). Third transformation is the ShiftRows, where each row of the input matrix is shifted cyclically with different degrees. And fourth is the MixColumns transformation where the input matrix is columnwise multiplied with a constant matrix. The input plaintext goes through a number of rounds, each round contains the-above mentioned transformations. For a 512-bit variant of AES, there are a total of 16 rounds employed in the proposed architecture.

2 Related Work

Several hardware implementations have been proposed for AES, majority of which were of 128, 256-bit block size. Emphasize has always been on the throughput achieved with lesser area requirement. A parallel hardware implementation of 128-bit AES proposed [5] used four 32-bit data blocks in parallel and was able to outperform previous 128-bit architectures in terms of throughput and area usage. In [6], researchers have implemented and analyzed the performance and impact of the area of several cryptographic algorithms such as AES, Camelia, and SMS4 on two different LUT-size FPGA devices. As pipelining is lucrative method for attaining a decent throughput, researchers over the years have proposed many pipelined architectures for AES. A reconfigurable pipelined architecture [7] using parallel connections excelled in processing speed and throughput achieved. Another hardware architecture using pipelining for AES algorithm over $GF((2^4)^2)$ [8] was implemented by partitioning the ten rounds of AES-128 into repeated AES modules. A more secure hardware variant of AES, AES-512 architecture proposed by [9] showed a high-throughput achievement with tolerable area increase and as key search space was now 2^{512} , was also more resilient to cryptanalysis.

The proposed AES-512-bit architecture, which targets a high throughput of encryption, avails the advantage of using pre-ciphered LUTs and as anticipated gives a faster processing speed with an endured area increase.

3 Hardware Implementation of AES-512

The AES-512 module assumes that the communication between network entities is performed using the standard ASCII character set. In a secure communication whenever the information exchange starts, the communicating parties share a session key and for a limited period of time (it is recommended to change session key frequently) every data sent or received is encrypted using this key. For a given character if the encryption key does not change, it will always encrypt to the same ciphertext. The architecture exploits this fact, and all of the characters from the standard ASCII set are encrypted and stored in a pre-ciphered lookup table using the session key.

This task is carried out in Phase 1 (Fig. 1). Input plaintext message is encrypted in Phase 2. Plaintext message is an array of characters, and each character has already been ciphered (in Phase 1), now only a substitution operation is required where each character in the message is substituted with its corresponding ciphertext using the pre-ciphered lookup table. Substitution operation in Phase 2 is a low-cost operation; therefore, the encryption of the input message is quite fast and as anticipated, a significant throughput is achieved. However, the technique is viable till the validity of the key. A key change will mean that the pre-ciphered LUT is obsolete, because now the plain characters will encrypt to an altogether different

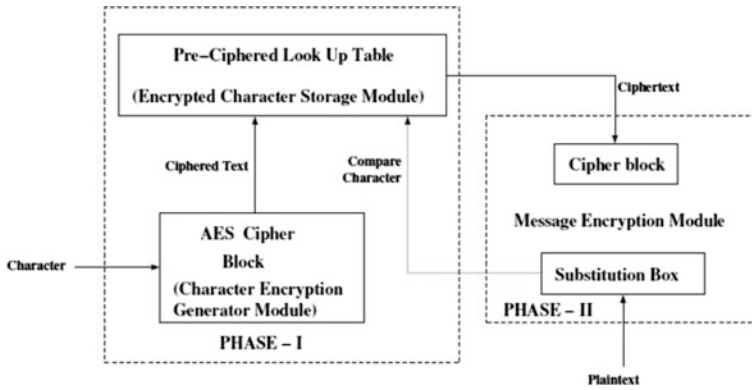


Fig. 1 Pre-ciphered lookup table encryption approach

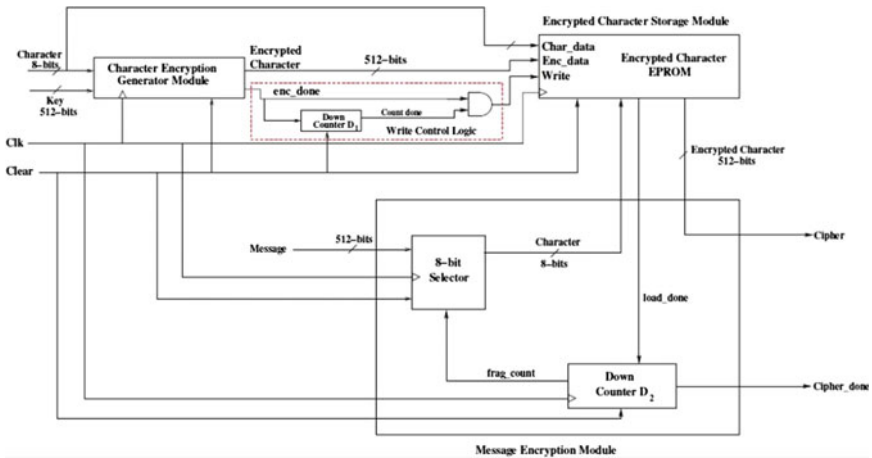


Fig. 2 Architecture layout of the AES-512-bit LUT-based encryption

ciphertext due to the introduction of the new key and using old LUT will produce incorrect results; therefore, production of a new LUT will be required. A switching may be performed between normal course of message encryption and the substitution-based encryption depending upon the validity of the session key. If the key validity is of shorter duration, a normal course of encryption must be adopted, but for key with significant validity, a LUT-based substitution encryption will propel the throughput achieved.

The architectural layout of the proposed encryption technique for AES-512 is depicted in Fig. 2. The architecture comprises of three major functional communicating blocks, the character encryption generator (CEG) module, the encrypted character storage (ECS) module, and message encryption (ME) module. A write

control logic (WCL) functioning between the CEG and ECS module ensures a synchronous write operation from CEG to ECS module. The detailed functionalities of modules are discussed in subsequent subsections.

3.1 Character Encryption Generator (CEG) Module

The CEG module is the functional block which performs the encryption of the ASCII character set using AES-512-bit algorithm. There are 128 characters in the standard ASCII character set; therefore, 8 bits suffice to represent them all. The first input to the module is an 8-bit ASCII character. The other input is a 512-bit key; this is the session key shared between the communicating entities. It is presumed that the key is shared using some standard key sharing protocol. Now, because the message block and key block must be of 512 bits in size, the 8-bit character is padded with 504 bits of bogus character to yield a 512-bit message block. Once padded, the message block and key are fed to the algorithm, and the obtained character cipher block, together with the original 8-bit character, is transmitted to the encrypted character storage (ECS) module. The procedure is repeated for all the 128 characters of the ASCII set.

3.2 Encrypted Character Storage (ECS) Module

The ECS module is an EPROM which is used for storing the ASCII characters together with their corresponding ciphertext. The ECS module takes the plain character together with the encrypted text and stores them in a form of a 2-D array, indexed using the 8-bit character representation. A write control logic works between CEG and ECS module to ensure a synchronous write operation. Whenever the CEG module generates a 512-bit encrypted character, it also generates an `enc_done` signal which is fed to a down counter D1. D1 counts the number of characters that have been encrypted and transmitted to the ECS module. Once all the characters have been encrypted, it transmits a low-count-done signal which disables further write operations on ECS module. Once filled with all the 128 encrypted ASCII characters, the ECS module will be operative for the message encryption (ME) module which encrypts the actual input message.

3.3 Message Encryption (ME) Module

The actual input message encryption is performed by the ME module. The module takes as input, a 512-bit message, and substitutes each character of the input message with its corresponding ciphertext using the pre-ciphered lookup table. The

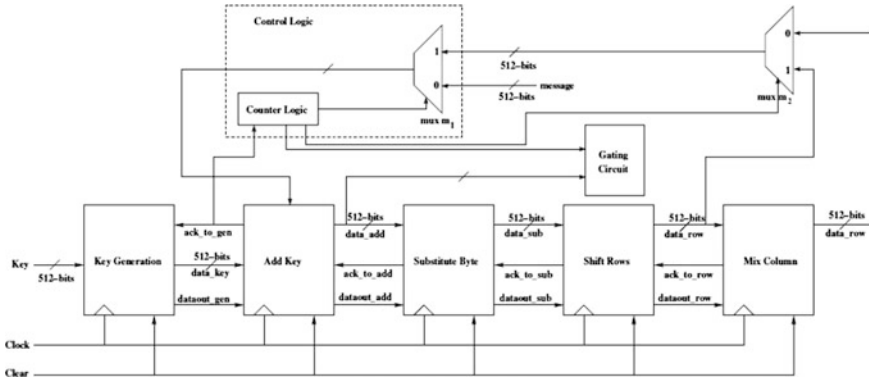


Fig. 3 Architectural design of character encryption generator

input message is fragmented into chunks of 8-bit character using the 8-bit-selector sub-module. The selected 8 bits are transmitted to the ECS module which looks for a matching character. Once the match is found, the corresponding ciphertext is transmitted back to the ME module together with a load-done signal. The received 512-bit cipher block is produced at the output port and the load-done signal is fed to the down counter D2 which counts the number of input message fragments that have been processed. It transmits a high_frag count signal to the bit-selector sub-module which selects the next 8 bits and the process is continued. The 512-bit message will have 64 chunks of 8-bit characters. The down counter D2 counts these 64 chunks and when all the bits are exhausted, it transmits a low_frag count signal to the bit-selector sub-module which in turn resets value to entertain a new 512-bit message.

Figure 3 depicts a detailed architecture of AES-512-bit character encryption generator (CEG) module. The architecture comprises of a KeyGeneration module with four integral transformation modules, namely AddKey, SubstituteByte, ShiftRows, and MixColumn. An external input of a 512-bit key is fed to the KeyGeneration module which expands it. The key together with the input message is given as input to the AddKey module, and after subsequent transformations, the output data is fed back to the AddKey module. A control logic is provided for the selection of the data that needs to be fed to the AddKey module; a counter logic initially set to 0 selects the input plaintext message from mux m1 for the first round of AES, and for subsequent rounds, transformed data from MixColumn is selected as input for AddKey.

Table 1 AES-512-bit implementation results

Device	Freq (MHz)	Area (CLBS)	Throughput (MBPS)
VIRTEX-7	926.6	5813	3381
VIRTEX-6	695.3	5813	2540

Table 2 AES-512-bit implementation results

Design	Area (CLBS)	Throughput (MBPS)
AES-512	5813	3381
[9]	6701	1163
[10]	3528	294
[11]	5673	353

The last round of AES does not have a MixColumn transformation, and a final AddRoundKey transformation is followed after ShiftRows. Mux m2 is used for the selection of data from MixColumn module except for the last round where data from ShiftRows transformation is selected. A 512-bit ciphertext is produced at gating circuit when counter logic is done with 16 rounds.

4 Results and Evaluation

The proposed AES-512-bit encryption technique was designed in Verilog for verification and simulation. Both families of Virtex-6 and Virtex-7 were used as target devices, while Xilinx ISE 14.1 was used to synthesize the Verilog codes. Virtex-7 family are new FPGA devices with higher performance and bandwidth. Table 1 shows the synthesis results. The result includes device family, area (in terms of configurable logic blocks (CLBs)), operating frequencies, and throughput obtained. The proposed encryption technique was able to achieve 290.71% higher throughput compared to previous 512-bit design. The area increase was, however, 64.76% (in terms of the increased CLB usage). Table 2 depicts the comparison of the implemented design with previous implementations, [9] is the 512-bit design. The area increase is evident from the bigger key size and block size. Also, increased key size makes the algorithm more resilient for the brute-force attack.

5 Conclusion

A high-throughput crypto-architecture is demanded in real-time applications like the multimedia and scientific research applications. The paper proposed and implemented a high-throughput LUT-based AES-512-bit algorithm which used a pre-ciphered lookup table which propelled the throughput. The architecture is more viable for the applications which carry out communication in session like the TELNET- and HTTP-based applications.

References

1. Daemon J, Rijmen V. The Rijndael Block Cipher AES Proposal. NIST, Version. 1999 Mar; 2.
2. Parikh C, Patel P. Performance evaluation of AES algorithm on various development platforms. In 2007 IEEE International Symposium on Consumer Electronics 2007 Jun 20 (pp. 1–6). IEEE.
3. Liberatori M, Otero F, Bonadero JC, Castieira J. Aes-128 cipher. High speed, low cost FPGA implementation. In 2007 3RD Southern Conference on Programmable Logic 2007 Feb (pp. 195–198). IEEE.
4. Orlic VD, Peric M, Banjac Z, Milicevic S. Some aspects of practical implementation of AES 256 crypto algorithm. In Telecommunications Forum (TELFOR), 2012 20th 2012 Nov 20 (pp. 584–587). IEEE.
5. Chang CJ, Huang CW, Chang KH, Chen YC, Hsieh CC. High throughput 32-bit AES implementation in FPGA. In Circuits and Systems, 2008. APCCAS 2008. IEEE Asia Pacific Conference on 2008 Nov 30 (pp. 1806–1809). IEEE.
6. Gao X, Lu E, Li L, Lang K. LUT-based FPGA Implementation of SMS4/AES/Camellia. In Embedded Computing, 2008. SEC'08. Fifth IEEE International Symposium on 2008 Oct 6 (pp. 73–76). IEEE.
7. Guo Z, Li G, Liu Y. Dynamic reconfigurable implementations of AES algorithm based on pipeline and parallel structure. In Computer and Automation Engineering (ICCAE), 2010 The 2nd International Conference on 2010 Feb 26 (Vol. 3, pp. 257–260). IEEE.
8. Abdel-hafeez S, Sawalmeh A, Bataineh S. High performance AES design using pipelining structure over GF((2⁴)/2). In Signal Processing and Communications, 2007. ICSPC 2007. IEEE International Conference on 2007 Nov 24 (pp. 716–719). IEEE.
9. Moh'd A, Jararweh Y, Tawalbeh LA. AES-512: 512-bit Advanced Encryption Standard algorithm design and evaluation. In Information Assurance and Security (IAS), 2011 7th International Conference on 2011 Dec 5 (pp. 292–297). IEEE.
10. Wolkerstorfer J, Oswald E, Lamberger M. An ASIC implementation of the AES SBoxes. In Cryptographers Track at the RSA Conference 2002 Feb 18 (pp. 67–78). Springer Berlin Heidelberg.
11. Elbirt AJ, Yip W, Chetwynd B, Paar C. An FPGA-based performance evaluation of the AES block cipher candidate algorithm finalists. IEEE Transactions on Very Large Scale Integration (VLSI) Systems. 2001 Aug; 9(4):545–57.

Design and Calculation of Power Aperture Parameters with Variable SNR

Prabhansh Varshney, Shagun Bishnoi, Sudhir Kumar Chaturvedi,
Dipen Patel and D. Tejaswini

Abstract The paper represents a process for designing search radar and power aperture calculation for variable signal-to-noise ratio (SNR) methods. Surveillance or search radars regularly search defined volume in space scanning for preys. These are usually used to excerpt prey data such as range, angular position, and probably prey velocity. Various search patterns are to be accepted, relying on the radar design and antenna. To accomplish this goal, we use the extension of radar range equation which is used to analyze and design the surveillance radar which is most frequent in large radar system, and the performance measurement is usually used to classify the radar kinds is power aperture product that is the product of the radar average power and the effective radar antenna area. Tracking radars use pencil beam patterns of antenna. It is because of this that a different search radar is desired to facilitate prey acquisition by the tracker. For making this, we are taking the assumption that we must have to search the angular region, and taking all azimuths and elevation area of the sector is small. The area may be in various shapes, in any coordinate system. The most opted surveillance regions are the area of the surface of a sphere surrounded by few elevation and azimuth stretch.

Keywords Search radar · Radar design and antenna · Prey acquisition
Azimuths and elevation area

1 Introduction

Radar is a system of substance exposure which operates on radio waves for calculating substance range, angle as well as velocity. They help in aircrafts, ships, space crafts, missiles (guided), vehicles detection, weather developments. It dwells for transmitter, generating electromagnetic waves within radio/micro-contour,

P. Varshney · S. Bishnoi · S.K. Chaturvedi (✉) · D. Patel · D. Tejaswini
Department of Aerospace Engineering, University of Petroleum and Energy Studies,
Dehradun 248007, Uttarakhand, India
e-mail: sudhir.chaturvedi@ddn.upes.ac.in

emitting antenna, receiving antenna for abducting few reconciles from articles in way of emitted signal, receiver along with processor for calculating the characteristics of the substances(s).

2 Search Radar Equation

2.1 Radar Range Equation

Minimum aperture prey radar range equation evaluates power at input to receiver of prey for provided radar cross area at a defined range. A signal exemplary, thereby, pretends as deterministic. Hence, equation of input power to receiver is:

$$P_r = \frac{P_t G_t G_r \lambda^2 \sigma}{(4\pi)^3 R_t^2 R_r^2 L} \quad (1)$$

here,

P_r is power received (watts).

P_t is peak power transmit (watts).

G_t is transmitter gain.

G_r is receiver gain.

λ is functioning frequency wavelength of radar (meters).

Σ is prey's non-fluctuating cross area of radar (square meters).

L is general loss factor (system as well as propagation loss).

R_t is range to prey from transmitter.

R_r is range to prey from receiver.

Identical transmitter as well as receiver ranges if monostatic radar.

Power equation at input to receiver shows signal style within signal-to-noise (SNR) ratio. For exemplifying noise style, consider receiver thermal noise in having white noise power spectral density (PSD) stated as: [1, 2]

$$P(f) = kT \quad (2)$$

here k —Boltzmann constant, T —effective noise temperature. Receiver behaves like winnow for architect white noise PSD. Consider magnitude squared receiver frequency response near rectangular refine alongside bandwidth same as reciprocal of pulse span, $1/\tau$. Total noise power at receiver output is:

$$N = \frac{kTF_n}{\tau} \quad (3)$$

here F_n —receiver noise figure.

Product of effective noise temperature with receiver noise factor can be assigned as *system temperature* as well as symbolized as T_s ; therefore, $T_s = TF_n$.

Employing equation for received signal power as well as output noise power, we get receiver output SNR:

$$\frac{P_r}{N} = \frac{P_t \tau G_t G_r \lambda^2 \sigma}{(4\pi)^3 k T_s R_t^2 R_r^2 L} \quad (4)$$

Hence,

$$P_t = \frac{P_r (4\pi)^3 k T_s R_t^2 R_r^2 L}{N \tau G_t G_r \lambda^2 \sigma} \quad (5)$$

2.2 Monostatic Radar Maximum Detectable Range

Consider minimum detectable SNR at receiver (monostatic) radar functioning at 1 GHz is 13 dB. The radar equation is applied for calculating the maximum detectable range for prey having non-fluctuating RCS as 0.5 m square, if radar contains peak transmit power as 1 MW. Considering transmitter gain as 40 dB with radar transmitting pulse of 0.5 μ s as span.

2.3 Bistatic Radar Receiver Output SNR

Assess output SNR for prey with RCS as 1 m square. Radar is being bistatic. Prey is placed 50 km from transmitter as well as 75 km from receiver. Radar functioning frequency is 10 GHz. Transmitter at peak transmit power is 1 MW having gain is 40 dB. Pulse width is 1 μ s. Receiver gain is 20 dB [1].

3 Kalman Filter

An algorithm which needs sets of measurements noted over a span, consisting statistical noise as well as various defects, along with producing projection of variables which are more accurate than ones built on just one measurement, by applying Bayesian inference as well as projecting a combined possibility circulation over variables for every time frame is Kalman filtering or linear quadratic estimation (LQE) [3].

Kalman filter contains various uses for the field of technology. An everyday use is for guidance, navigation, vehicles control, especially aircraft as well as spacecraft. Moreover, Kalman filter is an extensively used approach in time sets analysis applied in terrains like processing of signals or econometrics. Kalman filters central subjects in terrains in robotic motion planning, control, as well as admitted in trajectory optimization [4].

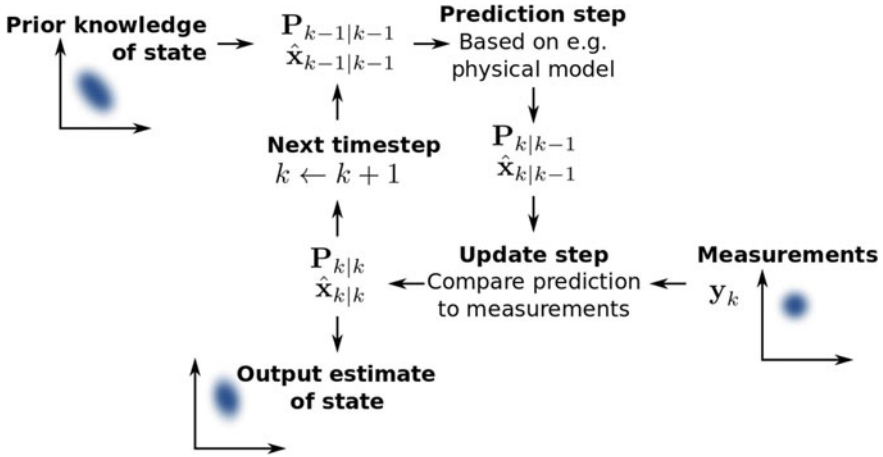


Fig. 1 Representation of Kalman filter process [5]

Algorithm operates on two-stride technique. For prognosis stride, Kalman filter yields evaluation of present state variables and their defects. Once outcomes of adjacent measurement (compulsorily corrupted with few, as random noise) are noted, these evaluates are updated applying weighted average and adding more weight to evaluates with greater certainty. Algorithm becomes recursive. It runs in real time, needing just current input measurements along with previously determined state and its defected matrix; no further past data is needed (Fig. 1).

3.1 Algorithm

Algorithm forecasts location of non-stationary article built on its past locations applying a Kalman filter estimator. It evaluates current location by updating Kalman state vector that consists of location (x, y) , velocity (V_x, V_y) as well as acceleration (A_x, A_y) for non-stationary article [6].

Kalman filter adopts laws of motion to evaluate new state:

$$X = X_0 + V_x \cdot dt, Y = Y_0 + V_y \cdot dt, V_x = V_{x0} + A_x \cdot dt, V_y = V_{y0} + A_y \cdot dt \quad (6)$$

The laws of motion secure the state transition matrix that is matrix which consists of coefficient codes of location, velocity, and acceleration.

3.2 Filtering Process

Filtering process contains two stages:

- Predicted state and covariance,
- Estimation.

Filter requires present dimensions, z , along with forecasted state, x_{prd} , for evaluating precise resemblance of present state.

4 Results and Conclusion

Using the various algorithms and MATLAB codes, for basic radar equations, we found that:

1. 5.6 kW is calculated as required peak power.
2. 345 km is calculated as maximum detectable range.
3. 9 dB is the estimated SNR.

As Simulink of Kalman filter runs the exemplary, it traces the path of body highlighted by blue as well as Kalman filter estimated location by green. Originally, it requires less time for evaluated location to assemble with real location of article. Slowly few abrupt shifts in location develop—every time Kalman filter adapts and records article after some iterations (Fig. 2) [7].

For variable power aperture from 2 to 50 msg, the output is shown below in bar graph as well as plot.

Variable aperture is plotted on the x -axis, whereas point index on the y -axis. Point index is nothing but the ratio of power available to change in time (Fig. 3).

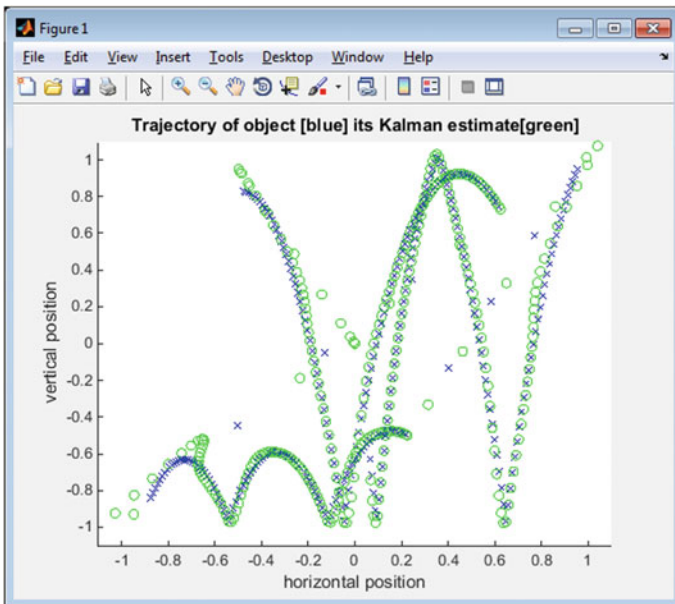


Fig. 2 Graph for Kalman trajectory

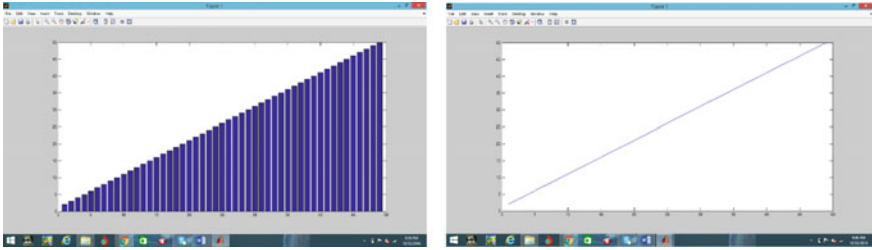


Fig. 3 Output for variable power aperture from 2 to 50 ms as bar graph as well as plot

References

1. Pang J, Lin Y, Xu X. 2013. Radar Signal Recognition Algorithm Based on Fractal Theory and Neutral Network. *Advanced Science and Technology Letters* Vol. 31 (MulGraB 2013), pp. 189–192 <http://dx.doi.org/10.14257/astl.2013.31.42>.
2. C. Windsor, L. Capineri and P. Falorni, “The Classification of buried pipes from radar scans”, *INSIGHT, Journal of the British Institute of Non Destructive Testing*, Vol. 45, N.12, December 2003, pp. 817–821.
3. David A, Puma LA, Jeffrey JB. March 2013. Radar Analysis of Bird Migration stopover sites in the Southeastern US. Final Report. Aeroecology Program, Department of Entomology and Wildlife Ecology, University of Delaware. SILVIS Lab, 1630 Linden Drive, Department of Forestry and Wildlife Ecology, University of Wisconsin, Madison.
4. Lengenfelder R. September 1998. The Design and Implementation of Radar Stimulator. Final Report. Department of Electrical Engineering, University of Cape Town.
5. Chanda, N., “Redundant Transmitting System in Aircraft (RTSA),” *SAE Technical Paper* 2015-01-2443, 2015, doi:[10.4271/2015-01-2443](https://doi.org/10.4271/2015-01-2443).
6. Sen S, Nehorai A. APRIL 2011. Sparsity-Based Multi-Prey Tracking Using OFDM Radar. *IEEE TRANSACTIONS ON SIGNAL PROCESSING*, VOL. 59, NO. 4.
7. G. Falorni, L. Capineri, L. Masotti and G. Pinelli, “3-D imaging of buried utilities by features estimation of hyperbolic diffraction patterns in radar scans”, *GPR 2004 conference proceedings*, Delft, June 2004. [2] D.J. Daniels, “*Ground Penetrating Radar*, 2nd Edition”, IEE London, 2004.
8. Huang, L., Chen, H., Yu, Z., and Bai, J., “Multi-Prey Tracking Algorithm in the Complicated Road Condition for Automotive Millimeter-wave Radar,” *SAE Technical Paper* 2016-01-0120, 2016, doi:[10.4271/2016-01-0120](https://doi.org/10.4271/2016-01-0120).

Low Power Adder Circuit Based on Coupling Technique

Arpan Roy, Aashwin Sharma, Anu Mehra and Sachin Kumar Rajput

Abstract Today's technology is continuously scaling itself, thereby resulting in increasing density of the transistors leading to high power dissipation on the chip. Therefore, we need to reduce this power consumption of these circuits and make them more efficient. In this paper, we have introduced two transistors in the Static Energy Recovery Full adder circuit by twisted coupled technique to achieve the power reduction of the circuit. The circuitry proposed in this paper is intended to be operated at 1 V supply with 0.12 mW on 90 nm CMOS technology.

Keywords Adders · MOS · SERF · Low power

1 Introduction

The most basic and fundamental arithmetic operation is addition used in ALU, Microprocessors, and DSP units. Expansion shapes a reason for different operations like subtraction, successive division, and so on. In this way, such adder circuits are the quintessence of processing units of most as of now utilized gadgets. Symmetric adder is a primary adder, which utilizes 28 transistors. In recent years, adders with less transistor count have been proposed [1–8]. With an increase transistors count on the chip, their control has turned into an issue and a few methods have been

A. Roy · A. Sharma · A. Mehra (✉) · S.K. Rajput (✉)
Department of Electronics and Communication Engineering,
ASET, Amity University, Noida, Uttar Pradesh, India
e-mail: amehra@amity.edu

S.K. Rajput
e-mail: skrajput@amity.edu

A. Roy
e-mail: royarpan09@gmail.com

A. Sharma
e-mail: aashwin.sharma@yahoo.in

brought forward to diminish power [6]. Various procedures are utilized to decrease the power by bringing down the swing of the signal [7].

Three major sources which account for dissipation of power in a digital circuit are given below as:

$$P = p_t f_c (C_L V_{DD} V_{sig}) + (I_{SC} V_{DD}) + (I_{leakage} V_{DD}), \quad (1)$$

where power,

$$\begin{aligned} p_t f_c (C_L V_{DD} V_{sig}) & \text{ due to switching,} \\ I_{SC} V_{DD} & \text{ due to short circuit,} \\ I_{leakage} V_{DD} & \text{ due to Leakage.} \end{aligned}$$

For the power component $p_t f_c (C_L V_{DD} V_{sig})$, every time, a input transition from 0 to 1 or 1 to 0, output node sense switching activity, which in turn is input combinations dependent. The dynamic power component reduces when swing level of output signal goes down [7]. In case the level of swing of signal V_{DD} , at output node is lowered, then the switching power is slashed by a factor of $\left(\frac{V_{sig}}{V_{DD}}\right) \times 100\%$. This paper proposes a modified 12 transistor adder, connected via twisted diode transistors which enabled us to achieve reduction in the consumption of power, along with low power-delay product (PDP). Our approach introduces two additional diodes in the overall circuit, thereby increasing the area for fabrication on a chip yet reducing the power and delay significantly as compared to the 10T adder circuit [4]. As a result, the power-delay product (PDP) is also considerably reduced.

Section 2 describes the proposed adder design along with the 10T adder circuit [4] and compares the mathematical output power of each individual circuit. Section 3 shows the power, delay, and PDP analysis of the proposed circuit at the operating voltages of 1 V supply. Section 4 gives the comparative analysis of the power, delay, and PDP of the proposed adder with the 10T adder circuit [4].

2 Adder Design

In Fig. 1a [4], *10TSERF* adder circuit is shown.

Figure 1b shows the present work with the proposed *12T* adder with alteration to the *10TSERF* adder. A twisted diode connected coupler is inserted at node 'O1.' By this method, the swing gets reduced which ultimately reduce the consumption of power in the circuit. By the arrangement of the twisted transistors, 'O1' node voltage should be lower than V_{DD} even though 'O1' was at a 'HIGH' logic level in the pre-charge mode. Compared with the full swing level, the small-swing level of output at first stage and then at second stage helps to reduce the dynamic power.

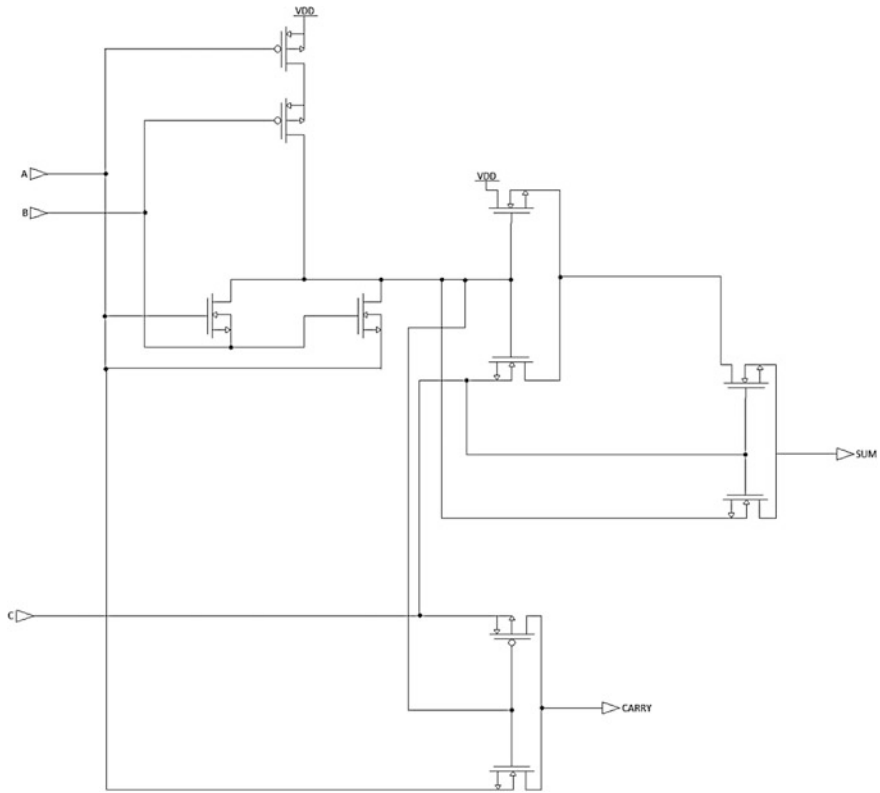


Fig. 1 SERF full adder

Output node voltage is given by Eqs. (2) and (3).

$$V_{\text{out_H}} = V_y \left(1 - e^{-t_{\text{chg}} / R_{\text{MP2}} \cdot C_{\text{load}}} \right), \quad (2)$$

$$V_{\text{out_L}} = V_x \left(e^{-t_{\text{dchg}} / R_{\text{MP2}} \cdot C_{\text{load}}} \right), \quad (3)$$

where

$$R_{\text{MP}} = \frac{1}{\mu_p C_{\text{OX}} \left(\frac{W_{\text{MP}}}{L} \right) (V_{\text{SG}} - |V_{\text{THP}}|)}, \quad (4)$$

$$R_{\text{MN}} = \frac{1}{\mu_n C_{\text{OX}} \left(\frac{W_{\text{MN}}}{L} \right) (V_{\text{GS}} - V_{\text{THN}})}. \quad (5)$$

A reduced output voltage level leads to lower the power as given by Eqs. (1) and (2).

3 Analysis and Simulation of 12T Adder Circuit

3.1 Power Analysis

Table 1 shows the simulation results of power analysis for 12T adder and is plotted in Fig. 2. From the plot, it can be observed that power and V_{dd} vary almost linearly and has a finer curve as compared to the one obtained in case of the 10T one (Fig. 3).

Table 1 Power analysis of 12T adder

V_{DD} (V)	Power (W) for 12T
1	0.00012133
1.1	0.00017203
1.2	0.000231
1.3	0.00029004
1.4	0.00036689
1.5	0.00044296

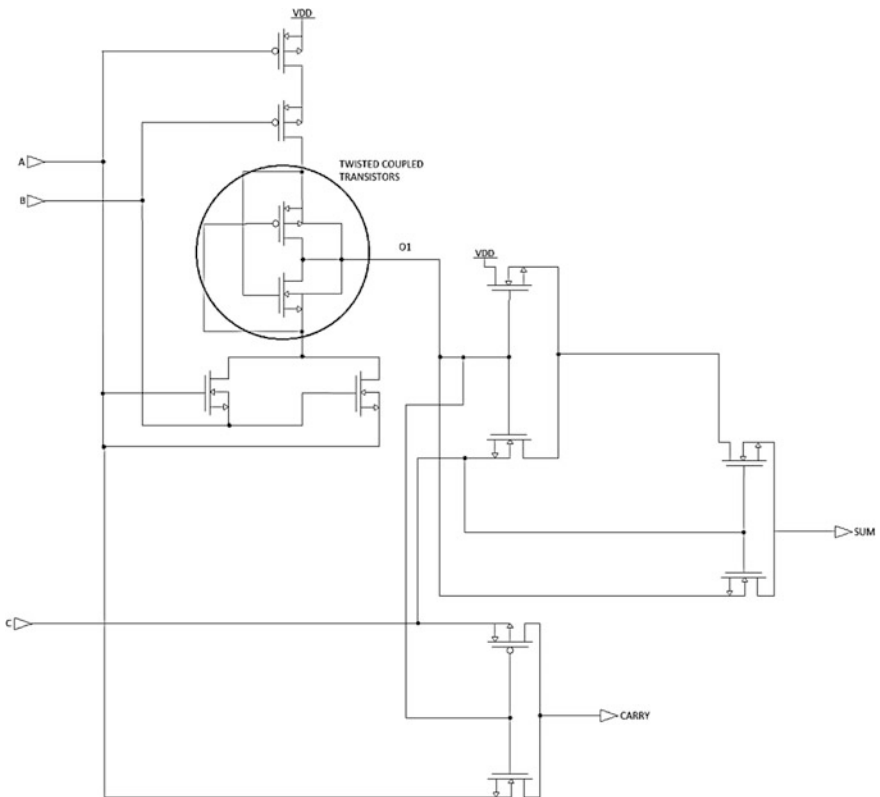


Fig. 2 Proposed 12T full adder

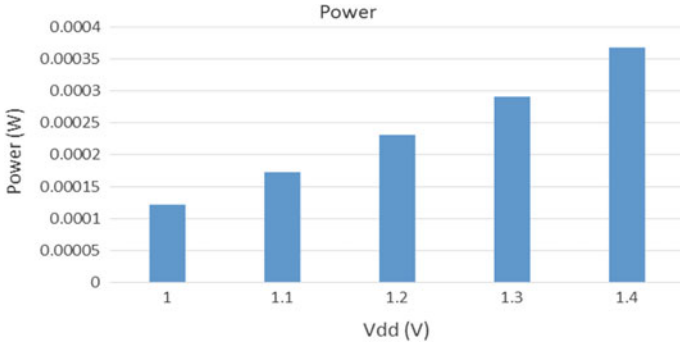


Fig. 3 Power characteristics of 12T adder

3.2 Delay Analysis

The low power mode is used to examine the design. The result of delay in seconds is listed below. An exponential decrease is observed in case of the 12T one, similar to that of the 10T one (Table 2; Fig. 4).

Table 2 Delay analysis of 12T adder circuit

V _{DD} (V)	Delay(s) for 12T
1	1.7089E-11
1.1	1.042E-11
1.2	7.4723E-12
1.3	5.7728E-12
1.4	4.9872E-12
1.5	4.4029E-12

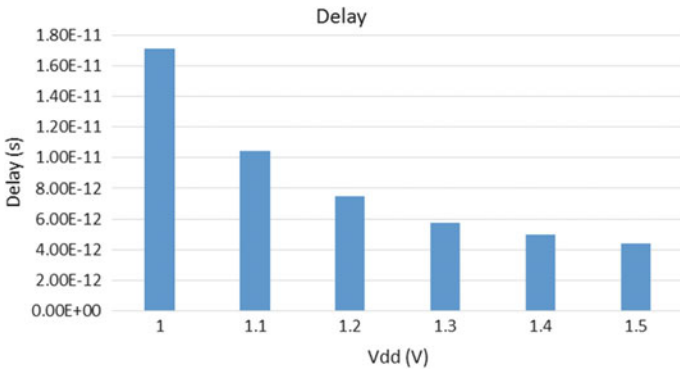
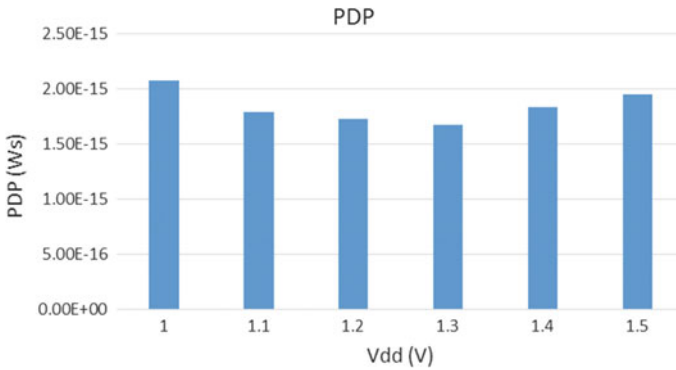


Fig. 4 Delay characteristics of 12T adder

Table 3 PDP characteristics of 12T adder circuit

V_{DD} (V)	PDP (Ws) for 12T
1	2.07347E-15
1.1	1.79252E-15
1.2	1.72608E-15
1.3	1.67431E-15
1.4	1.82976E-15
1.5	1.9503E-15

**Fig. 5** PDP characteristics of 12T adder

3.3 PDP Analysis

The result of delay in Watt-s is listed below. For a voltage range of 1–1.5 V, minimal change is obtained in the PDP, although there is a significant change in the value of the PDP at the operating value of 1 V when compared to the 10T adder circuit (Table 3; Fig. 5).

4 Comparative Analysis and Simulation of 10T and 12T Adders

4.1 Power Analysis

A comparison of power analysis for 10T and 12T adder is given Table 4 and the same is plotted in Fig. 6. The graphs show a significant drop in the 12T circuit's power, as compared to the 10T. The maximum percentage of power reduction of 16.58% is obtained at 1.5 V. This affirms the twisted diode-based connection of the transistors for power reduction technique.

Table 4 10T and 12T adder —power analysis comparison

V_{DD} (V)	Power (W) for 12T	Power (W) for 10T
1	1.2133E-04	1.42E-04
1.1	1.7203E-04	1.98E-04
1.2	2.31E-04	2.65E-04
1.3	2.9004E-04	3.43E-04
1.4	3.6689E-04	4.32E-04
1.5	4.4296E-04	5.31E-04

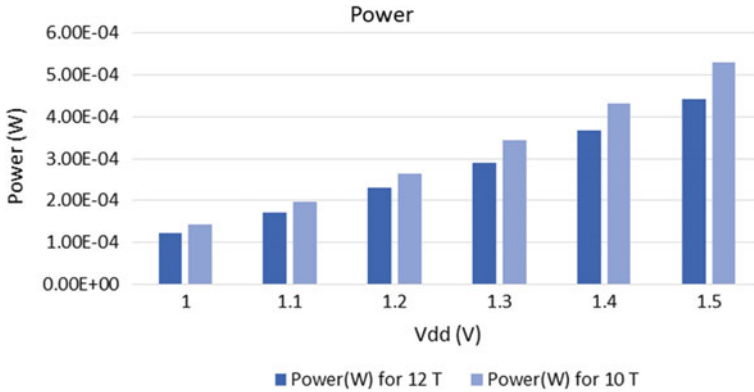


Fig. 6 Power comparison of 10T and 12T adder

4.2 Delay Analysis

Since the low power node is considered to examine the design, the simulation has been carried out for $V_{DD} = 1-1.5$ V. The result of delay in s is listed below. For a voltage range of 1–1.5 V, the reduction in the delay varies from 86.75 to 30.41% respectively (Table 5; Fig. 7).

Table 5 Delay comparison between 12T and 10T adder circuit

V_{DD} (V)	Delay (s) for 12T	Delay (s) for 10T
1	1.7089E-11	1.29E-10
1.1	1.042E-11	3.54E-11
1.2	7.4723E-12	1.66E-11
1.3	5.7728E-12	1.0557E-11
1.4	4.9872E-12	7.838E-12
1.5	4.4029E-12	6.3273E-12

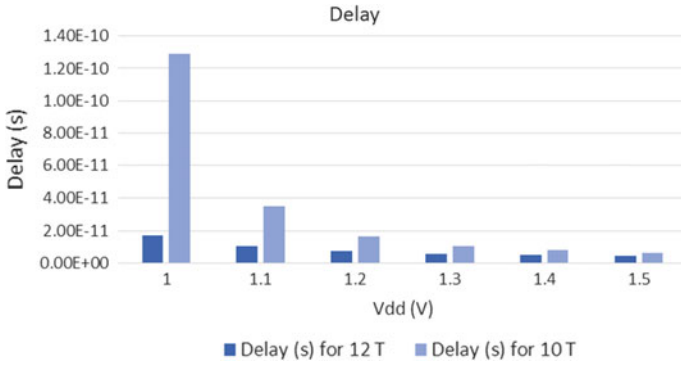


Fig. 7 Delay comparison of 10T and 12T adder

Table 6 Comparison of PDP between 12T and 10T adder circuit

V _{DD} (V)	PDP (Ws) for 12T	PDP (Ws) for 10T
1	2.07347E-15	1.83E-14
1.1	1.79252E-15	7.01E-15
1.2	1.72608E-15	4.4E-15
1.3	1.67431E-15	3.62E-15
1.4	1.82976E-15	3.38E-15
1.5	1.9503E-15	3.36E-15

4.3 PDP Analysis

The result of delay in s is listed below. For values ranging from 1 to 1.5 V, the drop in PDP varies from 88.66 to 41.95%, respectively (Table 6; Fig. 8).

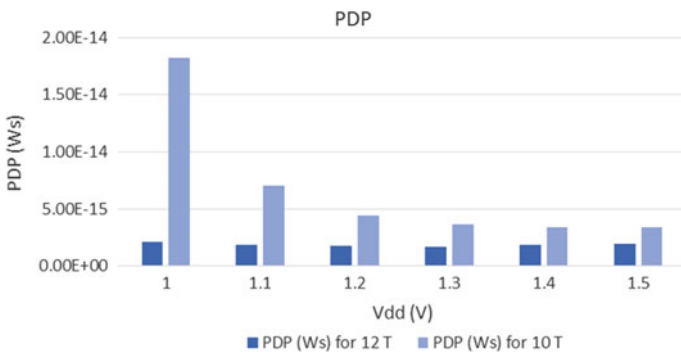


Fig. 8 PDP comparison of 10T and 12T adder

5 Conclusion

This paper therefore deals with an efficient method of reducing the power up to 16.58% in the adder circuit and also highly increasing the delay efficiency up to 86.75% as compared to the 10T SERF adder circuit. As a result, the power-delay product is also reduced up to 88.66% in this proposed adder circuit. This is achieved by using twisted diode connected coupler in the original circuit which assists in decrementing the voltage swing at the output node. This confirms the technique of power reduction, whose basis is formed on twisted diode connection transistors. The introduction of two transistors in the 10 T adder circuit [4] by twisted coupled technique does increase the area required for its fabrication on the chip but shows significant improvements in its power, delay, and PDP as a result.

References

1. Murmann, B. et al. "Impact of scaling on analog performance and associated modeling needs" IEEE Trans. Electronic Devices vol. 53 no. 9 pp. 2160–2167 Sep. 2006.
2. Uyemura, J. P. "Introduction to VLSI Circuits and Systems" Wiley John & Sons Inc. 2002.
3. Kumar, M., Arya, S. K. and Pandey, S., "Single bit full adder design using 8 transistors with novel 3 transistors XNOR gate," International Journal of VLSI design & Communication Systems, vol. 2, no. 4, pp. 47–59, December 2011.
4. Jin-Fa Lin, Yin-Tsung Hwang, Ming-Hwa Sheu, and Cheng-Che Ho, "A Novel High Speed And Energy Efficient 10 Transistor Full Adder Design," IEEE Transactions On Circuits And Systems—I: Regular Papers, vol. 54, no. 5, pp. 1053–54, May 2007.
5. Alluri, S., Dasharatha, M., Naik, B. R., "Design of low power high speed full adder cell with XOR/XNOR logic gates", 2016 International Conference on Communication and Signal Processing (ICCSP), pp. 0565–0570, DOI:10.1109/ICCSP.2016.7754203.
6. Singhal, S., Gaur, N., Mehra, A., Kumar, P., "Analysis and Comparison of Leakage Power Reduction Techniques In CMOS Circuits," IEEE Conference on SPIN, Feb. 2015, pp. 936–944, DOI: 10.1109/SPIN.2015.7095351.
7. Ahn, S. Y. and Cho, K., "Small-Swing Domino Logic Based on Twist-Connected Transistors," Elec. Letters, vol. 50, no. 15, pp. 1054–1056, July 2014.
8. Mehra, A., Bahukhandi, A., Kaur, A., Katyar, S., Khajuria, S., Rajput, S. K., Gaur, N., "A Novel Power Efficient 12T Full Adder", International Journal of Simulation Systems, Science & Technology, vol. 15, pp 44–48, 2014.

Analysis of the Relationship Between Substrate Properties and Patch Dimensions in Rectangular-Shaped Microstrip Antennas

Raj Gaurav Mishra, Jeevani Jayasinghe, G. Chathuranga and Ranjan Mishra

Abstract Microstrip antennas contain one dielectric substrate in its basic form. Properties of the substrate play a vital role in design of microstrip antennas. Therefore, understanding the impact of the substrate is important to the antenna research community. This paper analyzes the relationship between substrate properties and patch dimensions by designing numerous rectangular-shaped microstrip antennas working at different resonant frequencies.

Keywords Microstrip antennas · Permittivity · Resonant frequency
Substrate

1 Introduction

In the basic structure, a microstrip antenna is consisting of a substrate, a radiating patch on one side of the substrate along with the ground plane on the other side. When a microstrip antenna is designed to resonate at the fundamental mode, properties of the substrate are highly considered [1]. Primarily, patch dimensions depend on the thickness and the permittivity of the substrate. The resonant frequency of the microstrip antenna depends on all these properties. Narrow bandwidth, low gain, and low efficiency are inherent drawbacks of rectangular-shaped microstrip antennas. Therefore, understanding the impact of the substrate on the performance of the antenna is very important.

R.G. Mishra (✉) · R. Mishra

Department of Electronics, Instrumentation and Control, CoES, University of Petroleum and Energy Studies, Dehradun, India
e-mail: rgmishra@ddn.upes.ac.in

J. Jayasinghe · G. Chathuranga

Department of Electronics, Wayamba University of Sri Lanka, Kuliypitiya, Sri Lanka
e-mail: jeevani@wyb.ac.lk

© Springer Nature Singapore Pte Ltd. 2018

R. Singh et al. (eds.), *Intelligent Communication, Control and Devices*, Advances in Intelligent Systems and Computing 624, https://doi.org/10.1007/978-981-10-5903-2_8

To extend the efficiency as large as 90%, the height of the substrate has been increased [2]. Further, bandwidth has been increased up to about 35%. Thick substrates with low dielectric constant are preferable for good antenna performance as they provide features like better efficiency, loosely bound fields for radiation, and larger bandwidth [1]. However, as the height of substrate increases, surface waves are generated. They are not desirable because they extract power from the total available power for direct radiation. Another disadvantage of using substrates with low dielectric constant is they result in larger element size. On the other side, thin substrates having higher dielectric constants are desirable for microwave circuitry because substrates with higher dielectric constants result in smaller element size. However, they are less efficient due to their greater losses and have relatively smaller bandwidths [2].

Some researchers have done experiments on the properties of the substrates up to some extent. Reference [3] presented microstrip antennas on low dielectric-constant substrates, while [4] presented the impact of thick substrates on antennas' input impedance. Reference [5] analyzed the effect of substrate permittivity and thickness on printed circuit with dipole properties. Reference [6] illustrated the variation of resonant frequency for substrates with different thickness and permittivity. Effect of substrate thickness on the antenna performance for a circular disk microstrip antenna was presented in [7]. Moreover, in some research publications, effects of substrate properties have been explored in order to design an improved antenna by selecting the most suitable substrate. However, in those publications the major objective was to design a good antenna but not to analyze the impact of substrate properties in detail. For an example, impact of several substrates on efficiency, gain, directivity, and the antenna size of a microstrip antenna designed for LTE and Bluetooth technologies was discussed in [8]. The effect of curvature on the performance of conformal microstrip antenna on cylindrical bodies for TM₁₀ mode was studied in [9] for three dielectric substrates. Reference [10] investigated the effect of various dielectric constants on rectangular microstrip patch antenna performance by keeping the substrate thickness constant. It concludes that higher the value of the dielectric constant, the lower the gain and bandwidth. Five antennas with different heights were designed using same dielectric substrate material for the purpose of the application of wireless LAN in [11] and conclude that substrates with greater height can be used to achieve better directivity. In addition to the substrates, superstrates have also been studied. For example, considering the effect of the superstrate layer, a method for accurately determining the resonant frequency of such structures has been obtained by varying the patch dimension in [12]. A broadband microstrip antenna design with slot is presented in [13–15]. The significance of selection of size and position of the slot on the antenna design is also discussed.

As per the results, increasing the substrate thickness reduces the resonant frequency and increases the bandwidth. However, the relationships between the substrate properties, patch dimensions, and resonant frequencies have not been quantified so far.

This paper comprehensively analyzes the relationships between substrate properties and patch dimensions at different resonant frequencies. Section 2 presents the impact of substrate thickness, and Sect. 3 presents the impact of substrate permittivity. Finally, conclusions are given in Sect. 4.

2 Relationships Between Substrate Thickness and Patch Dimensions

This section analyzes the impact of substrate thickness on patch dimensions and antenna performance at different resonant frequencies in the range of 1–10 GHz. The substrate material is Rogers RO4003 (tm), which has a relative permittivity of 3.38 and a loss tangent of 0.0027. For the substrate height, 10 values in the range of 0.127–3.175 mm have been used. This range covers the commercially available substrate heights. Dimensions of a rectangular-shaped patch corresponding to each substrate thickness have been calculated in order to make the antenna resonate at the fundamental mode. The substrate thickness does not influence on the patch width W as per Eq. 1.

$$W = \frac{v_0}{2f_r \sqrt{\frac{\epsilon_r + 1}{2}}} \quad (1)$$

where v_0 is the speed of light in vacuum, f_r is the resonant frequency, and ϵ_r is the relative permittivity of the substrate. The substrate thickness impacts the effective substrate permittivity ϵ_{reff} and extension of the length ΔL and hence on the patch length L as per Eq. 2.

$$L = \frac{v_0}{2f_r \sqrt{\epsilon_{\text{reff}}}} - 2\Delta L \quad (2)$$

First, the variation of the patch length with respect to the substrate thickness is studied. At each resonant frequency, the plots show a similar pattern. The pattern at 4 GHz is shown in Fig. 1a. As per the results, when the substrate thickness increases, the required patch length reduces.

Figure 1b shows the variation of patch dimensions against the resonant frequencies for different substrate thickness values. At resonant frequency of 1 GHz, the patch lengths corresponding to the lowest and highest substrate thicknesses (0.127 and 3.175 mm) have a slight difference of 0.84 mm. It is only about 1% of the median patch length and therefore negligible. This difference increases with the resonant frequency. At 10 GHz, the difference between patch lengths is 1.84 mm which is about 29% of the corresponding median patch length. Comparison of patch width W and patch length shows that at any frequency of interest the patch width W is greater than the patch length L . However, this difference reduces with the frequency.

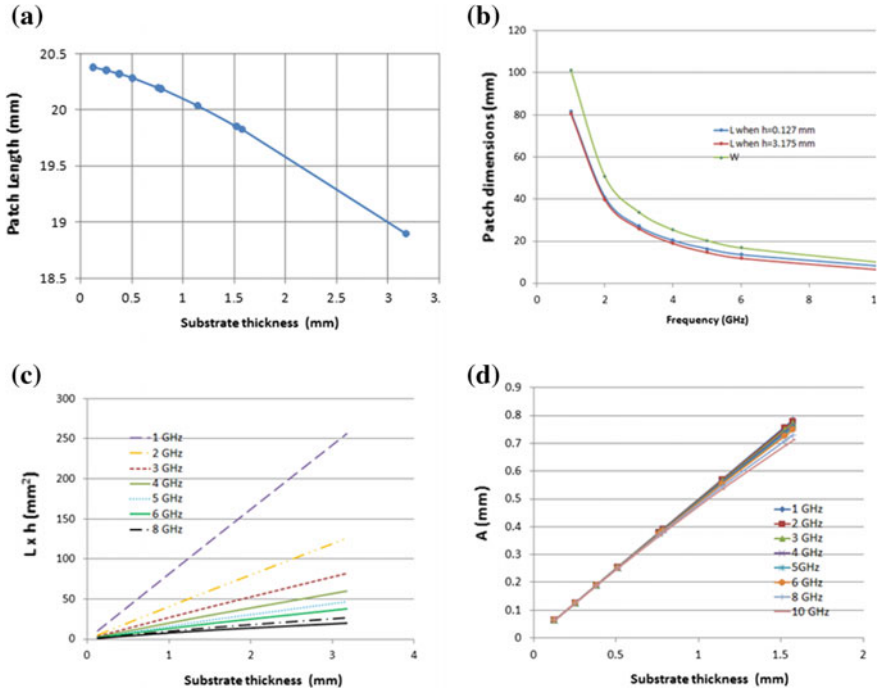


Fig. 1 Impact of substrate thickness **a** Variation of the patch length with the substrate thickness at 4 GHz. **b** Variation of patch dimensions with the resonant frequencies for different substrate thickness values. **c** Variation of patch length \times substrate thickness with the substrate thickness. **c** Variation of A with the substrate thickness

Figure 1c shows variation of patch length (L) \times substrate thickness (h) against the substrate thickness at several frequencies. At each resonant frequency, the variation is linear with different slopes. Lower resonant frequencies have a higher gradient. Further analysis of this graph shows A ,

$$A = \frac{L \times h}{\lambda} \tag{3}$$

where λ is the wavelength of the substrate, and the graphs at any frequency are approximately linear and coincide (Fig. 1d). The gradient of the graph is approximately 0.48.

3 Relationships Between Substrate Permittivity and Patch Dimensions

As per Eqs. 1 and 2, both patch width W and patch length L change according to the relative permittivity of the substrate. Variation of patch dimensions at 4 GHz is shown in Fig. 2a. At each resonant frequency in the range of 1 GHz to 10 GHz with interval size of 1 GHz, the graphs show the same pattern. As per the results, when using substrates with higher permittivity values, smaller patches can be used (Fig. 2b). The impact of substrate permittivity is similar at any frequency (Table 1). At resonant frequency of 1 GHz, the patch lengths corresponding to the lowest and highest substrate permittivity values (2.08 and 10.8) have a considerable difference of 58 mm which is about 77% of the median patch length. At resonant frequency of 10 GHz, the patch lengths corresponding to those substrate materials show a slight difference of only 5.3 mm. But this difference as a percentage of the median patch length is about 80%. The impact of substrate permittivity on the patch width is also similar at any frequency (Table 2). At resonant frequency of 1 GHz, the patch widths corresponding to substrate permittivity of 2.08 and 10.8 have a considerable difference of 59 mm which is about 64% of the median patch width. At resonant frequency of 10 GHz, the patch widths corresponding to those substrate materials show a slight difference of only 5.9 mm. But this difference as a percentage of the median patch length is again 64%. Therefore, the impact of substrate permittivity is higher than that of substrate thickness.

The impact of substrate material has been analyzed further and B ,

$$B = (L + W)^2 \times \epsilon_r^2, \tag{4}$$

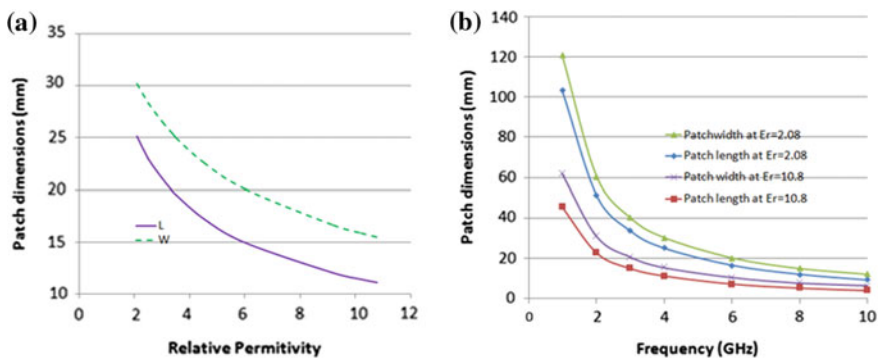


Fig. 2 Impact of substrate permittivity **a** Variation of patch dimensions with the substrate permittivity at 4 GHz. **b** Variation of patch dimensions with the resonant frequencies for different substrate materials

Table 1 Variation of patch length with resonant frequency

Resonant frequency (GHz)	Patch length			
	For $\epsilon_r = 2.08$ (mm)	For $\epsilon_r = 10.8$ (mm)	Difference (mm)	Difference (%)
1	103.30	45.65	57.65	77
2	51.23	22.68	28.54	77
3	33.84	14.97	18.87	77
4	25.12	11.09	14.04	77
6	24.51	10.76	13.76	78
8	18.39	8.07	10.32	78
10	9.36	4.00	5.36	80

Table 2 Variation of patch width with resonant frequency

Resonant frequency (GHz)	Patch width			
	For $\epsilon_r = 2.08$ (mm)	For $\epsilon_r = 10.8$ (mm)	Difference (mm)	Difference (%)
1	120.87	61.75	59.12	64
2	60.44	30.88	29.56	64
3	40.29	20.58	19.71	64
4	30.22	15.44	14.78	64
6	20.15	10.29	9.85	64
8	15.11	7.72	7.39	64
10	12.09	6.18	5.91	64

has been plotted against the relative permittivity (ϵ_r) for different resonant frequencies (Fig. 3a). The variation is linear and shows a higher gradient at lower resonant frequencies. When these results are divided by the square of the free space wavelength, the plots coincide (Fig. 3b). Variation of C ,

$$C = \frac{L \times f_r}{\epsilon_r}, \quad (5)$$

with the substrate permittivity is also analyzed (Fig. 3c). At any frequency, the plots overlap. The variation shows a similar pattern for patch width (Fig. 3d) where

$$D = \frac{W \times f_r}{\epsilon_r}. \quad (6)$$

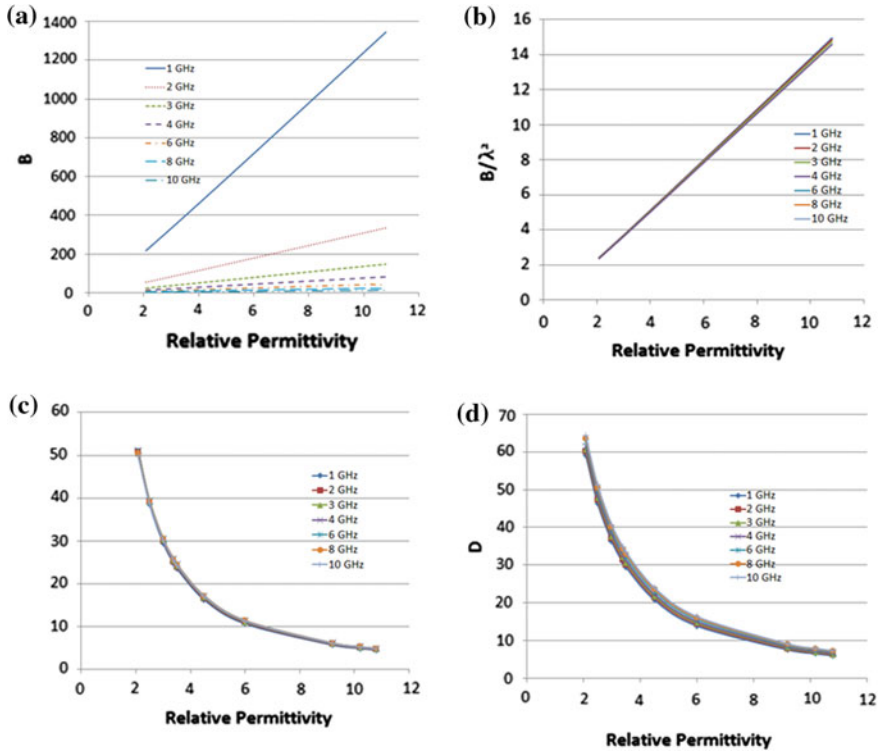


Fig. 3 Impact of substrate permittivity **a** Variation of B for different substrate materials (in thousands). **b** Variation of B/λ^2 for different substrate materials. **c** Variation of C with the substrate permittivity. **d** Variation of D with the substrate permittivity

4 Conclusions

When the substrate thickness increases, a slightly smaller patch length can be used and this is applicable to any resonant frequency. Impact of substrate thickness increases with frequency. Both patch length and patch width reduce with resonant frequency. However, the substrate thickness does not affect the patch width. Variations of patch length \times substrate thickness/wavelength against the substrate thickness are approximately linear and coincide at all resonant frequencies.

By using substrates with higher permittivity values, smaller patches with reduced length and width can be used. Impact of the substrate permittivity on both patch length and patch width is considerable at any frequency. Variation of $(\text{patch length} + \text{patch width})^2/\text{wavelength}^2$ for different substrate materials is linear and coincide at any resonant frequency. Moreover, plots of patch length or width \times resonant frequency/permittivity with the substrate permittivity for all frequencies coincide.

References

1. C.A. Balanis, *Antenna theory: analysis and design*. John Wiley & Sons, 2005.
2. D.M. Pozar, "Microstrip antennas." *Proceedings of the IEEE*, Vol. 80, no. 1, pp. 79–91, 1992.
3. G.P. Gauthier, A. Courtay & G.M. Rebeiz, "Microstrip antennas on synthesized low dielectric-constant substrates". *Antennas and Propagation IEEE Transactions on*, Vol. 45, No. 8, pp. 1310–1314, 1997.
4. M. Davidovitz & Y.T. Lo, "Input impedance of a probe-fed circular microstrip antenna with thick substrate". *Antennas and Propagation IEEE Transactions on*, Vol. 34, No. 7, pp. 905–911, 1986.
5. P. Katehi & N.G. Alexopoulos, "On the effect of substrate thickness and permittivity on printed circuit dipole properties". *Antennas and Propagation, IEEE Transactions on*, Vol. 31, No. 1, pp. 34–39, 1983.
6. D.H. Schaubert, D.M. Pozar & A. Adrian. "Effect of microstrip antenna substrate thickness and permittivity: comparison of theories with experiment". *Antennas and Propagation, IEEE Transactions on*, Vol. 37, No. 6, pp. 677–682, 1989.
7. J.S. Dahele & K.F. Lee "Effect of substrate thickness on the performance of a circular-disk microstrip antenna". *IEEE Transactions on Antennas and Propagation*, Vol. 31, pp. 358–360, 1983.
8. B. Ahmed, I.S. Zahra, H. Khurshid & S. Muzahir Abbas. "Analytical study on effects of substrate properties on the performance of microstrip patch antenna". *International Journal of Future Generation Communication and Networking*, Vol. 5, No. 4, pp. 113–122, 2012.
9. Elrashidi, K. Elleithy & H. Bajwa, "Resonance Frequency, Gain, Efficiency and Quality Factor of a Microstrip Printed Antenna as a Function of Curvature for TM01 mode Using Different Substrates". *Journal of Wireless Networking and Communications*, Vol.1, pp. 1–8, 2011.
10. K.V. Rop, D.B.O. Konditi, H.A. Ouma & S. Musyoki, "Application of adaptive neuro-fuzzy inference system technique in design of rectangular microstrip patch antennas". *Journal of Agriculture, Science and Technology*, Vol. 15, No. 1, pp. 147–160, 2014.
11. V. Hanumante, P. Bhattacharjee, S. Roy, P. Chakraborty & S. Mait, "Performance Analysis of Rectangular Patch Antenna for Different Substrate Heights". *International journal of Innovative Research in Electrical, Electronics, Instrumentation and Control Engineering*, Vol. 2, No. 1, pp. 515–518, 2014.
12. G.S. Dev & A. Singh, "Design and Analysis of Multidielectric Layer Microstrip Antenna with varying Superstrate Layer Characteristics". *International Journal of Advances in Engineering & Technology*, Vol.3, pp. 55–68, 2012.
13. Raj Gaurav Mishra, Ranjan Mishra, Piyush Kuchhal, Design of Broadband Monopole Microstrip Antenna Using Rectangular Slot, Volume 479, *Advances in Intelligent Systems and Computing*, pp. 683–688, ISBN: 978-981-10-1707-0. http://dx.doi.org/10.1007/978-981-10-1708-7_78.
14. Ranjan Mishra, Jeevani Jayasinghe, Raj Gaurav Mishra, Piyush Kuchhal, Design and Performance Analysis of a Rectangular Microstrip Line Feed Ultra-Wide Band Antenna, *International Journal of Signal Processing, Image Processing and Pattern Recognition*, SERSC Publications, vol. 9, No. 6, pp. 419–426, July, 2016. <http://dx.doi.org/10.14257/ijsp.2016.9.6.36>.
15. Ranjan Mishra, Raj Gaurav Mishra, Piyush Kuchhal, Analytical Study on the Effect of Dimension and Position of Slot for the Designing of Ultra Wide Band (UWB) Microstrip Antenna, 5th IEEE International Conference on Advances in Computing, Communications and Informatics (ICACCI), 978-1-5090-2028-7, Sept 2016.

Dual-Band Square Patch Antenna for Bluetooth and WiMAX Applications

Praful Ranjan

Abstract This paper offers a fruitful designing of dual -band square microstrip patch antenna, which resonates at the dual frequency of 2.52 and 4.33 GHz. This design offers proper impedance matching. This antenna has been designed for dual frequency using HFSS software and hardware implementation and tested. This antenna achieves -35 dB at 2.52 GHz and -15 dB at 4.33 GHz return loss. The proposed antenna design has good directional properties and radiation efficiency.

Keywords Microstrip square patch antenna · Dual band · Return loss
HFSS

1 Introduction

Microstrip patch antennas are playing a big role in communication devices [1–5]. A microstrip patch antenna is very simple planer structure type of antenna which is low profile. Microstrip patch antenna is very easy to manufacture, and very thin. Due to this, these antennas provide more advantages than other antennas. Microstrip patch antenna comes in various shapes like Rectangular, Circular Square, Triangular. Microstrip patch antenna can be designed in any shape like circular, triangular, square, and rectangular.

Microstrip antennas are very useful in today's scenario. These antennas are most widely used today. The advantages of these antennas are lightweight, compatibility with any shape and size, low cost, and easy to install on any kind of surface. These antennas can be designed to operate in circular polarization, dual-band, narrow-band and multi-band applications. This antenna is important in many microwave applications [6]. Microstrip antennas are compatible to all applications in planer structure. The size of antenna is being reduced by different techniques for cost saving and reduction of the size [7–10].

P. Ranjan (✉)

Department of Electronics and Communication Engineering, THDC Institute of Hydropower Engineering and Technology, Bhagirathipuram, Tehri, Uttarakhand, India
e-mail: prf98354@rediffmail.com

This paper presents a miniaturized square patch antenna with four slits cut which is suitable for dual band 2.52 and 4.33 GHz frequency. The purpose of this design is to obtain reduction in size, low cost, reduction in weight for miniaturizing antenna for achieving good antenna parameters and characteristics [11, 12].

Impedance matching is very important parameter in designing of antenna. This mismatch degrades antenna performances, and efficiency and is not suitable for maximum power transfer [13–16]. This is done by coaxial feed by proper 50 Ω matching. It has done by High Frequency Structure Simulation (HFSS).

2 Designing of Square Patch Antenna

The geometry of proposed microstrip square patch antenna has designed the basic formula [4], which has been given in Eqs. (1–5). The structure of microstrip patch antenna is square in shape. The square patch antenna which is feed with a 50 Ω microstrip strip line or 50 Ω coaxial feed. The square patch antenna is designed on first side of a substrate which is made of FR4 substrate with a thickness (h) and a dielectric constant ($\epsilon = 4.4$) of and second side is treat as ground of the substrate.

The 50 Ω microstrip feed line either edge feeding, side feeding, or coaxial feeding excites the microstrip patch antenna, which is revealed in Fig. 1, and it is along the X-direction in positive side. Top view and cross view of this antenna are shown in Figs. 2 and 3. The location of the feed position can also be calculated by

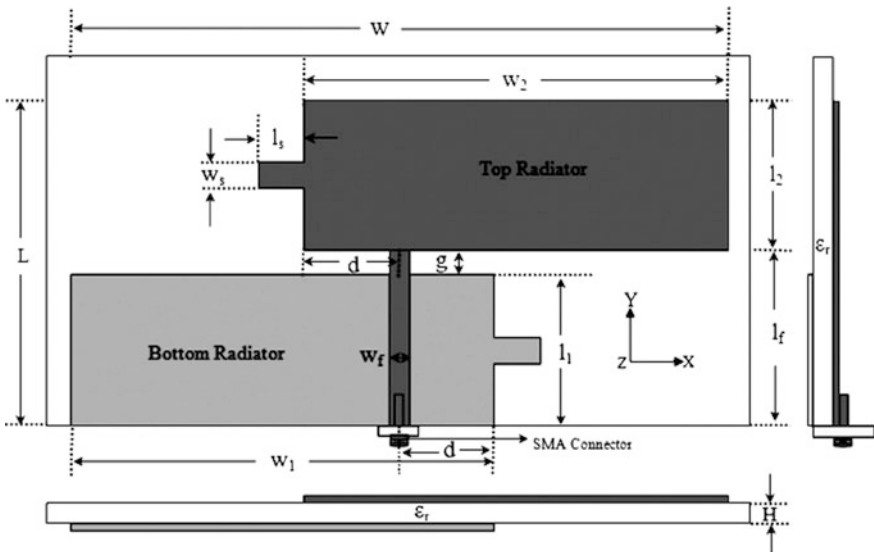


Fig. 1 General microstrip antenna structure

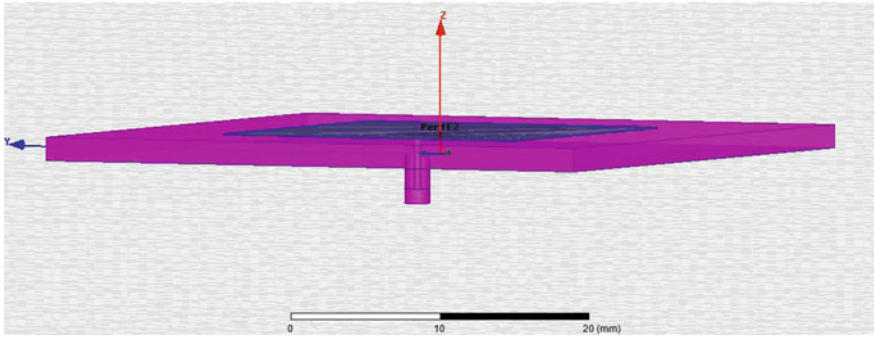


Fig. 2 Cross view of simulated square patch antenna

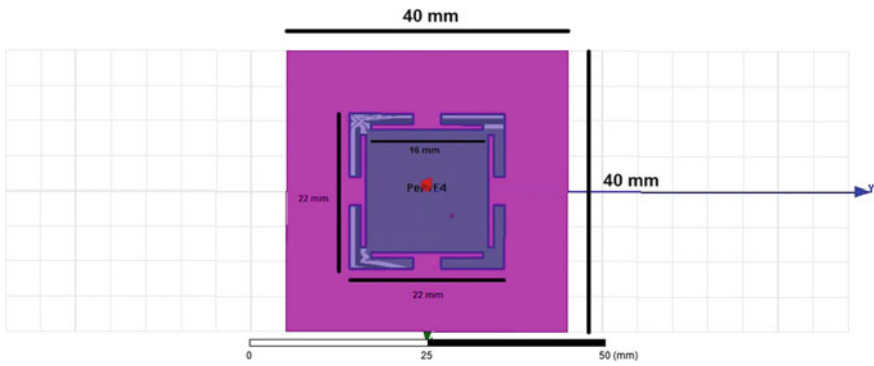


Fig. 3 Top view of simulated square patch antenna

the formula according to the condition of feed line. In this paper, feed position is at a distance “ d ” from one side of the edges of the square microstrip patch antenna. The top and bottom surface of square microstrip patch antenna can be distinguished with gap “ g ,” along the Z -axis, where $(W/h > 1)$

$$W = \frac{1}{2fr\sqrt{\mu_0\epsilon_0}} \sqrt{\frac{2}{\epsilon_r + 1}} \tag{1}$$

$$\epsilon_{\text{eff}} = \frac{\epsilon_r + 1}{2} + \frac{\epsilon_r - 1}{2} \left(\frac{1}{\sqrt{1 + \frac{12h}{w}}} \right) \tag{2}$$

$$L = L_{\text{eff}} - 2\Delta L \tag{3}$$

$$L_{\text{eff}} = \frac{C}{2f_r \sqrt{\epsilon_{\text{eff}}}} \quad (4)$$

$$\frac{\Delta L}{h} = 0.412 \frac{(\epsilon_{\text{eff}} + 0.3) \left(\frac{w}{h} + 0.264 \right)}{(\epsilon_{\text{eff}} - 0.258) \left(\frac{w}{h} + 0.8 \right)} \quad (5)$$

where

- ϵ_r Dielectric constant of substrate,
- ϵ_{reff} Effective dielectric constant,
- W Width of the patch,
- L Patch length,
- h Height of dielectric substrate,
- ΔL Effective length,
- f_r Resonating frequency.

Actual dimensions of antenna for dual-band frequency resonating at 2.52 and 4.33 GHz are as follows:

Parameters of the antenna	Unit (mm)
Patch antenna length (l)	22 mm
Patch antenna width (w)	22 mm
Height of substrate (h)	1.6 mm
Substrate length (L)	40 mm
Substrate width (W)	40 mm
Permittivity of substrate (ϵ)	4.4
Internal length and width	16 mm
Loss tangent of substrate	0.02

3 Results and Discussion

The square patch antenna has been simulated in above dimension in HFSS. Return loss of square microstrip antenna is shown in Fig. 4. Radiation pattern of square microstrip patch antenna of 2.52 GHz is shown in Fig. 5. Smith chart of impedance on both frequencies is shown in Fig. 6. The proposed antenna has been simulated first by ANSOFT HFSS software and analyzed; simulated microstrip square patch antenna has been designed using FR4. By using LKPF machine, connectors are used for feeding. The antenna has been fabricated and tested on network analyzer which is mentioned in Fig. 7.

Result of S_{11} (return loss) and impedance of tested and fabricated antenna are shown below in Figs. 8 and 9, respectively. The fabricated and simulated result of antenna is almost same. Hardware of the antenna is also shown in Fig. 10.

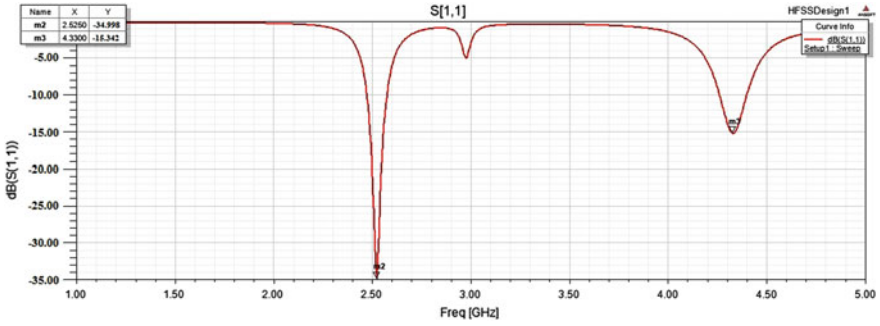


Fig. 4 Scattering parameter of square patch antenna

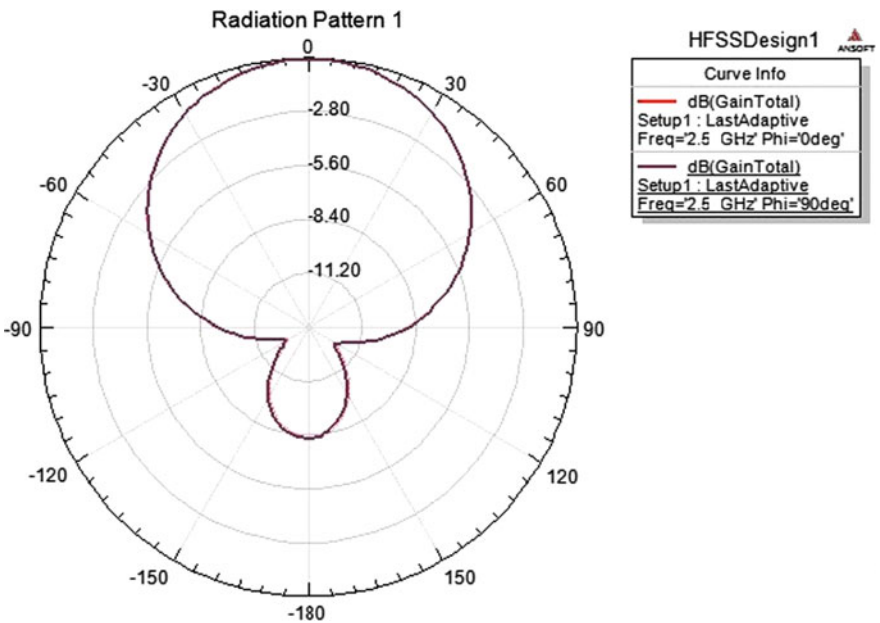


Fig. 5 Radiation pattern of square patch antenna

4 Conclusions

In this paper a microstrip square patch antenna with all corner slit has been simulated at 2.52 and 4.33 GHz for dual-band operation. This design achieved -35 and -15 dB return loss at 2.52 and 4.33 GHz, respectively. Proposed design is very compact and compatible with microwave devices and shows good agreement with

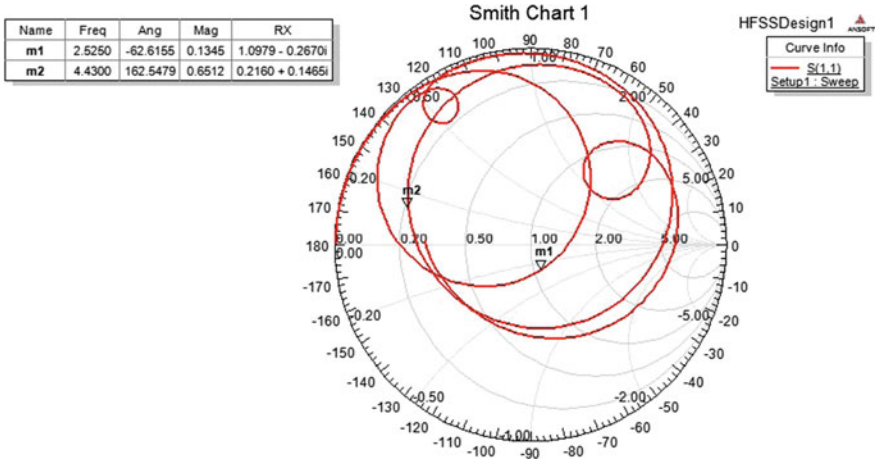


Fig. 6 Impedance matching of simulated antenna in Smith chart

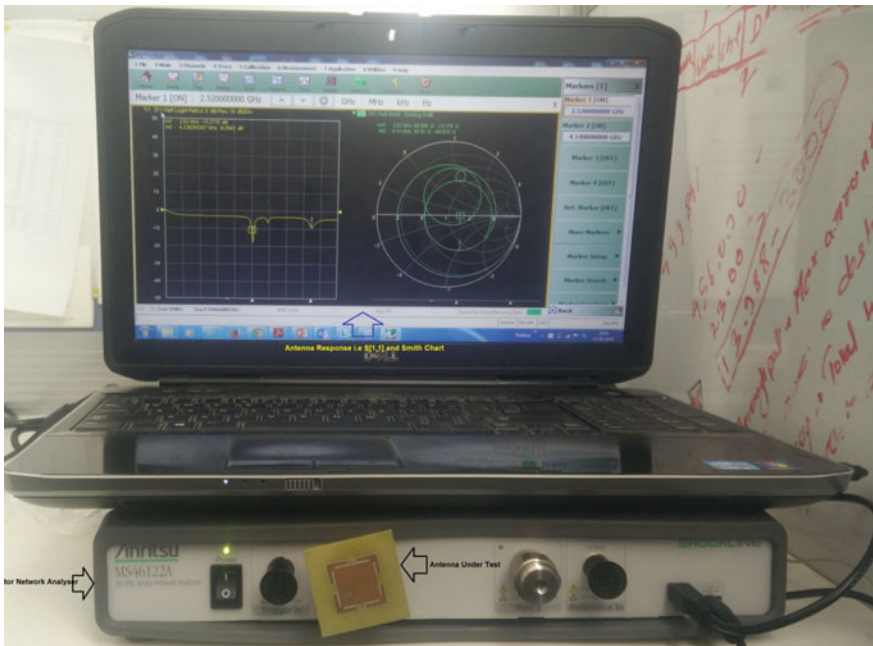


Fig. 7 Testing of fabricated antenna with VNA

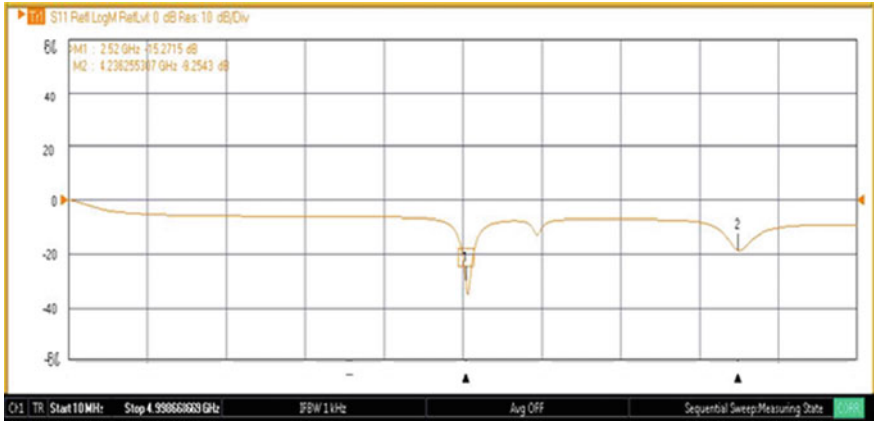


Fig. 8 Return loss of the antenna analyzed by VNA

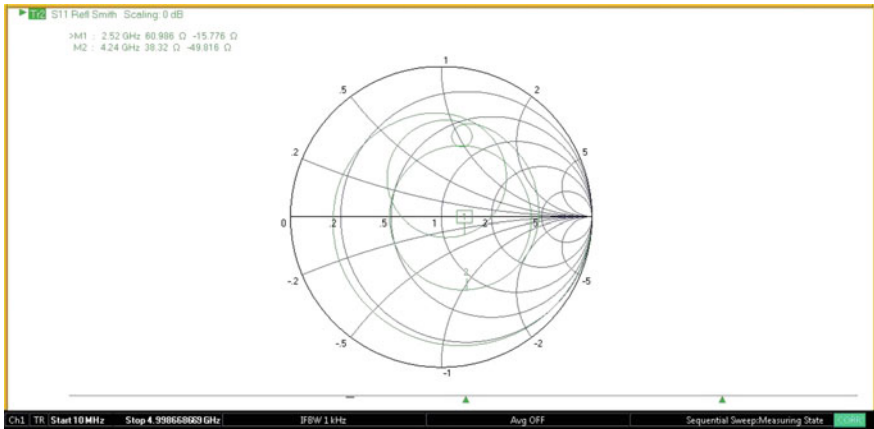


Fig. 9 Smith chart result of Impedance matching by VNA

antenna design parameters. The square patch antenna is applicable in Bluetooth, WIFI and Local area communication. Gain and efficiency of this antenna can be more improved in future.

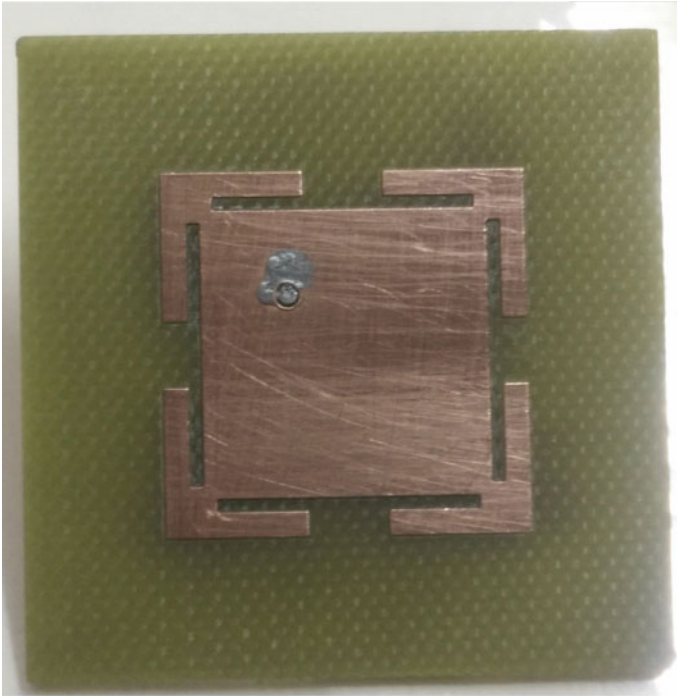


Fig. 10 Hardware of the square microstrip antenna

References

1. M. Ben Ahmed, M. Bouhorma, F. Elouaai, A. Mamouni, "Design of new multistandard patch antenna GSM/PCS/UMTS/HIPERLAN for mobile cellular phones", *European journal of scientific research* ISSN 1450-216X, vol. 32, No. 2(2009), pp. 151–157.
2. W. L. Stutzman, G. A. Thiele, "Antenna Theory and design", John Wiley & Sons, 2nd Ed., New York, 1998.
3. David M. Pozar, "Microwave Engineering", 3rd Edition, John Wiley & Sons, 2004.
4. C. A. Balanis, "Antenna Theory and Design", John Wiley & Sons, Inc., 1997.
5. Y. Rahmat-Samii and J. S. Colburn, "Patch antennas on externally perforated high dielectric constant substrates," *IEEE Trans. Antennas Propagation*, pp. 1785–1794, vol. 47, no. 12, December 1999.
6. A. D. Yaghjian and S. R. Best, "Impedance, Bandwidth, and Q of Antennas," *IEEE Trans. On Antennas and Wave Propagation*, vol. 53, No. 4, pp. 1298–1324, 2005.
7. D. M. Pozar, and D. H. Schaubert, "The Analysis and Design of Microstrip Antennas and Arrays", IEEE Press, New York, 1996.
8. Ramesh Garg, Prakash Bartia, Inder Bahl, Apisak Ittipiboon, "Microstrip Antenna Design Handbook", pp. 1–68, 253–316 Artech House Inc. Norwood, MA, 2001.
9. I. J. Bahl and P. Bhartia, *Microstrip Antennas*. Boston, Ma: Artech House, 1980.
10. A. K. Verma, D. Chakraverty and N. V. Tyagi, "Input impedance of probe fed multilayer rectangular microstrip patch antenna using the modified Wolff model," *Microwave Opt. Technology Lett.*, pp. 237–239, vol. 31, no. 3, 2001.

11. F. Abboud, A. Papiernik, and J. P. Damiano, "Simple model for the input impedance of the coax-feed rectangular microstrip patch antenna for CAD," *Proc. Inst. Electrical Eng.*, pp. 323–326, vol. 135, no. 5, 1988.
12. R. E. Collin, "Field theory of guided waves", Piscataway, NJ: IEEE Press, 1990.
13. Praful Ranjan," Design of Circularly Polarized Rectangular Patch Antenna with single cut," *CAC2S 2013*, Atlantis Press, pp. 174–177, 2013.
14. Praful Ranjan and N.prashanti, "Design of Double sided Metamaterial Antenna for Mobile Handset Applications," *SPIN 2014*, IEEE 978-1-4799-2866-8/14, pp. 675–678, 2014.
15. Praful Ranjan," Cylindrical Metallic pin structure microstrip patch antenna for wideband application," *ICICCD 2016 Springer SBIN 978-981-10-1708-7*, vol. 479, 2016.
16. Praful Ranjan, Prof. G.S. Tomar, Dr. R. Gowri, "Metamaterial Loaded Shorted Post Circular Patch Antenna" published in *International Journal of signal Processing and Patteren Recognition* Vol. 9, No. 10, (2016) pp. 217–226

Estimation of Probability of Detection and False Alarm Alert for Swerling Targets

Prashant Singh, Shivam Kapri, Rajat Saklani, Prateek Mehta
and Sudhir Kumar Chaturvedi

Abstract The objective of this research is to find the probability of detection of fluctuating targets. The plot between detection probability, false alarm probability, and signal-to-noise ratio (SNR) will be made for Swerling fluctuating target models. The variation of the scattered signal is based on radar cross section (RCS). We have taken two Swerling targets: SWI represents scan-to-scan fluctuating targets, where SWII represents fast pulse-to-pulse fluctuation. We have used the mathematical relation for respected targets. On the basis of mathematical formula, we have done MATLAB coding to find the graphs between probability of detection and false alarm probability, and graphs between other parameters define the correct target.

Keywords RADAR · Detection · False alarm · Probability · Swerling
SNR · RCS

1 Introduction

Swerling representation of fluctuating targets includes majority of the actual radar targets. There are four categories of such targets namely SWI, SWII, SWIII, and SWIV. Out of the four categories, only two have been discussed in this paper namely SWI and SWII. SWI represents scan-to-scan fluctuating targets, while SWII represents fast pulse-to-pulse fluctuation. Exact expressions are given for the probability of detection of these models. The formulas for detection probability will be used to plot curves between detection probability and range for Swerling I and II. Detection probability " P_d " is the ratio of detected target to the number of all possible hits on the radar screen.

P. Singh · S. Kapri · R. Saklani · P. Mehta · S.K. Chaturvedi (✉)
Department of Aerospace Engineering, University of Petroleum and Energy Studies,
Dehradun 248007, India
e-mail: sudhir.chaturvedi@ddn.upes.ac.in

© Springer Nature Singapore Pte Ltd. 2018
R. Singh et al. (eds.), *Intelligent Communication, Control and Devices*,
Advances in Intelligent Systems and Computing 624,
https://doi.org/10.1007/978-981-10-5903-2_10

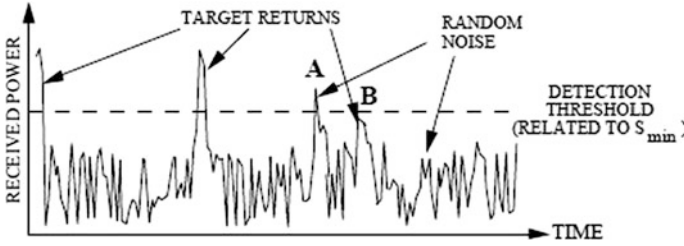


Fig. 1 Received power variation with time

$$P_d = \frac{\text{detected targets}}{\text{sum of all possible blibs}} \times 100$$

False Alarm: The false alarm is an important parameter in detection of target which is described by taking the threshold value as a reference (Fig. 1).

Here, A is false alarm and B is miss detection, thereby setting the threshold too low will result in greater number of target detection, although amount of false alarms will rise. Similarly, setting the threshold too high will result in lesser number of target detection, although amount of false alarms shall decline. Miss detection and false alarm are subject to trade-off. For achieving a desired probability of false alarm, the setting of threshold is done in most radar detectors [1].

Radar Cross Section (RCS): Radar cross section (RCS) tells us how detectable an object is with radio detection and ranging. A large RCS shows object being more easily detected than a target having small radar cross section. It is given by:

$$\sigma = \lim_{R \rightarrow \infty} 4\pi R^2 \frac{|E_s|^2}{|E_o|^2} \quad (1)$$

E_o = electric field strength of incident wave on target, E_s = that of scattered wave at the radar. Radar cross section varies with radar aspect angle. For illustration consider, isotropic point scatterers. Incident waves are scattered equally in all directions by these types of scatterers. In Fig. 2, two 1 m^2 aligned isotropic scatterers along with located radar boresight i.e., aspect angle is zero, and spacing between the two scatterers is taken as 1 m. RCS of both scatterers is calculated by varying aspect angle from 0° to 180° . This RCS contains superposition of both single radar cross sections. Composite RCS changes due to change in electrical spacing along both scatterers with variation in aspect angle.

$$\text{Electrical spacing} = [2 \times \text{scatter spacing} \times \cos(\text{aspect angle})]/(\text{wavelength})$$

RCS also depends on frequency of transmission, considering radar boresight aligned with two unity isotropic scatterers. Composite RCS is calculated as

Fig. 2 Variation of electrical size with aspect angle [2]

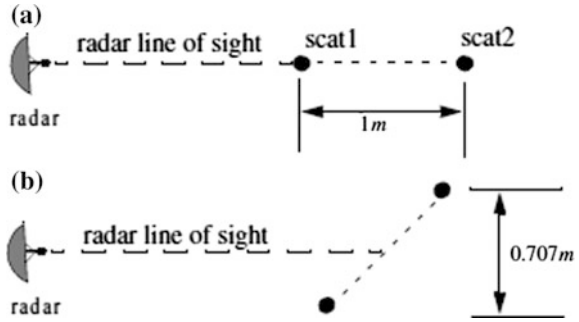
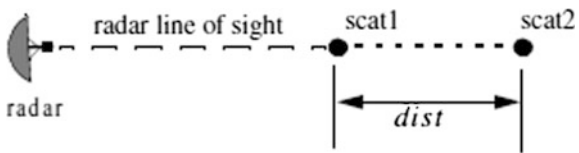


Fig. 3 Condition for variation of RCS with different frequencies



frequency is declined from 8 to 12.5 GHz. Figures 9 and 10 show the RCS variation with frequency of scatterer spacing 1.5–0.5 m (Fig. 3).

From those two figures, we come to know that a small frequency shift will lead to higher RCS fluctuation, when scatterer spacing increases tremendously as compared to closer centered scattering.

2 Methodology and Modeling

The research involves the analysis of Swerling targets I and II. The problem being discussed requires complex analysis. Two cases of Swerling have been described below which help in estimation of probability of detection of Swerling targets.

2.1 Swerling Case I

The returned signal power per pulse being assumed is the time constant upon target within the duration of one scan, but varies independently from scan to scan. The fluctuations of target RCS are picked up as fluctuations of signal-to-noise ratio in receiver. The probability density for input signal-to-noise power ratio is assumed to be

$$\omega(x, \bar{x}) = \frac{1}{\bar{x}} e^{-x/\bar{x}} \quad (x \geq 0), \quad (2)$$

where x is input signal-to-noise power ratio and \bar{x} is avg. of overall target fluctuations.

2.2 Swerling Case II

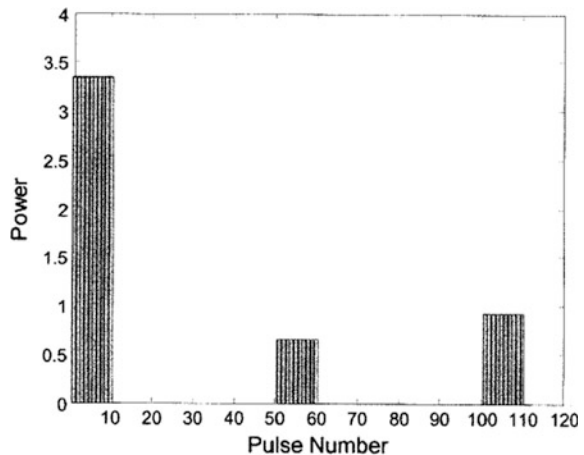
The fluctuations occur from pulse to pulse. The probability density function varies according to previous equation (as given in case 1). Swerling cases I and II functions on the target composed of many scatterers of roughly equal areas [3].

Figure 4 shows the power is constant for a scan and is varying for different scan. Each pulse received during a particular scan has same power. This is scan-to-scan fluctuation and represents the behavior of Swerling I target. Figure 5 shows that during a single scan, power is varying for each pulse sent during a scan. This is pulse-to-pulse fluctuation and represents the behavior of Swerling II target.

2.3 Pulse Integration

A pulse integrator improves the detection probability by using multiple transmit pulses. This gain is achieved by inserting a radar signal processor adding radar

Fig. 4 Fluctuations for Swerling I



returns from successive pulses. Depending on the location of the integrator the integration can be of two types.

1. coherent integration and
2. non-coherent integration.

Coherent Integration: Inside coherent integration, the integrator can be inserted between the matched filter and amplitude detector. Then the return is sampled and added by the signal processor, the amplitude detection and threshold check are done after this process. For this type of integration, it is assumed that the signal level at the input of the integrator does not vary with different pulses. This indicates Swerling I target type. Coherent integration is not useful for Swerling case II because the signal of these targets varies with each pulse.

Non-coherent Integration: The integrator is located after amplitude or square-law detector. The signal undergoes amplitude detection first, so the phase information is lost. The non-coherent integrator can be said to operate as the coherent integrator because it sums the returns from N pulses before the threshold check (Fig. 6) [4].

Fig. 5 Fluctuations for Swerling II

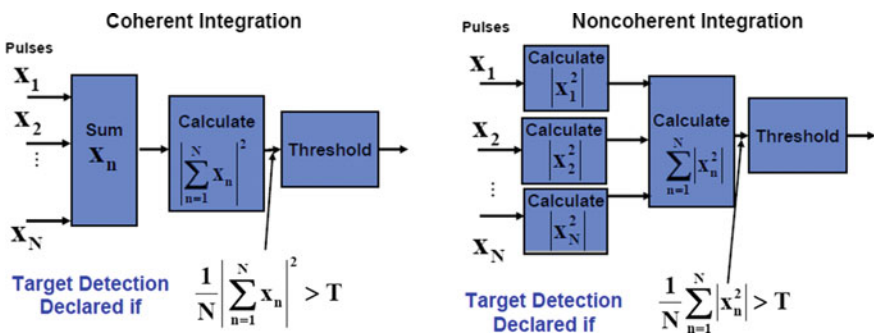
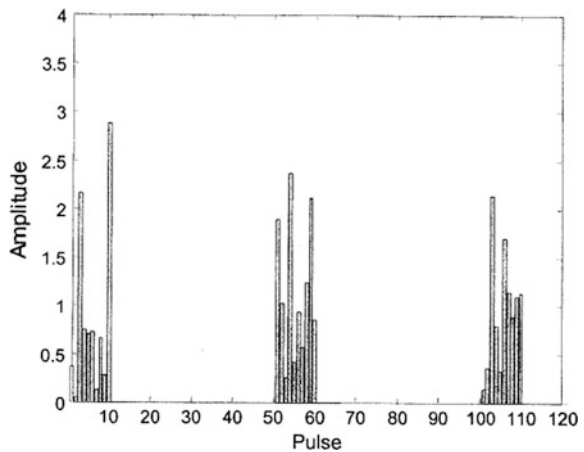


Fig. 6 Coherent and non-coherent integrations

The basic equation which needs to define the probability of detection is given below.

2.4 Swerling Target I

This methodology will be taken when probability of false alarm is very less ($P_{fa} \ll 1$) and $NX > 1$ and for exact $N = 1$

$$P_d = e^{[-Y_b/(1+X)]} \quad (3)$$

For $N > 1$

$$P_d = 1 - I\left[\frac{Y_b}{\sqrt{N-1}}, N-2\right] + \left[1 + \frac{1}{NX}\right]^{N-1} I\left[\frac{Y_b}{1 + \frac{1}{NX}\sqrt{N-1}}, N-2\right] e^{-\frac{Y_b}{1+NX}} \quad (4)$$

where I is the incomplete gamma function.

Generally, the incomplete gamma function for integer N is given by,

$$\Gamma_l(x, N) = \int_0^x \frac{e^{-v} v^{N-1}}{N-1!} dv \quad (5)$$

2.5 Swerling Target II

This methodology will be taken for a perfect case. The following values of P_d are valid only up to $N-1 \leq 50$ [5].

$$P_d = 1 - I\left[\frac{Y_b}{(1+X)\sqrt{N}}, N-1\right] \quad (6)$$

Beyond this point, an Edgeworth series can be used to calculate the probability of detection.

$$P_d = \frac{1}{2} [1 - \varphi^{-1}(T)] - c_3 \varphi^{(2)}(T) - c_4 \varphi^{(3)}(T) - c_6 \varphi^{(5)}(T) \quad (7)$$

where

$$\varphi(T) = \frac{1}{\sqrt{2\pi}} \exp\left[-\frac{T^2}{2}\right] \quad \varphi^{-1}(T) = \frac{1}{\sqrt{2\pi}} \int_{-T}^T \exp\left[-\frac{t^2}{2}\right] dt$$

$$T = \frac{Y_b - N(1+X)}{\sqrt{N(1+X)}} \quad c_3 = \frac{1}{3\sqrt{N}}, c_4 = \frac{1}{4N}, c_6 = \frac{1}{18N}$$

Here, $\varphi^{(2)}, \varphi^{(3)}, \varphi^{(5)}$ are derivatives of φ where

- Y_b is the normalized threshold.
- N is number of pulses integrated.
- X is input signal-to-noise power ratio for single pulse.
- \bar{X} is the average of X over all target fluctuation.
- P_d is the probability of detection.

3 Result and Discussion

Our aim in this research is the analysis of probability of detection of target having fluctuating cross section. The formulas for detection probability have been used to plot curves between detection probabilities and range for two different fluctuation models called Swerling targets.

Figure 7 shows the relation between probability density and radar cross section (RCS), this is the first graph which drawn in the MATLAB, this graph shows that when radar cross section increases, the probability density will decrease, so from this graph it is necessary to keep less radar cross section of any target in order to get

Fig. 7 Probability density versus RCS

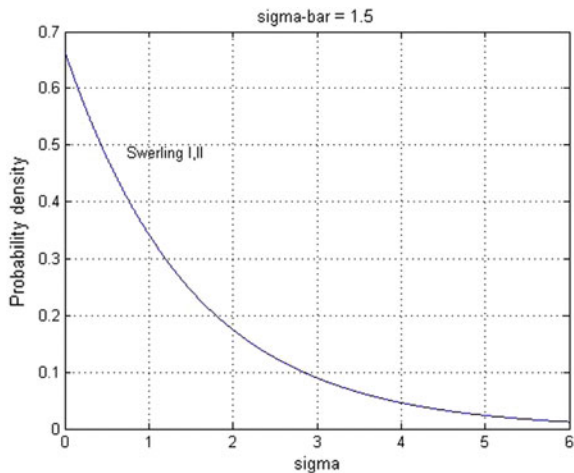


Fig. 8 RCS versus aspect angle

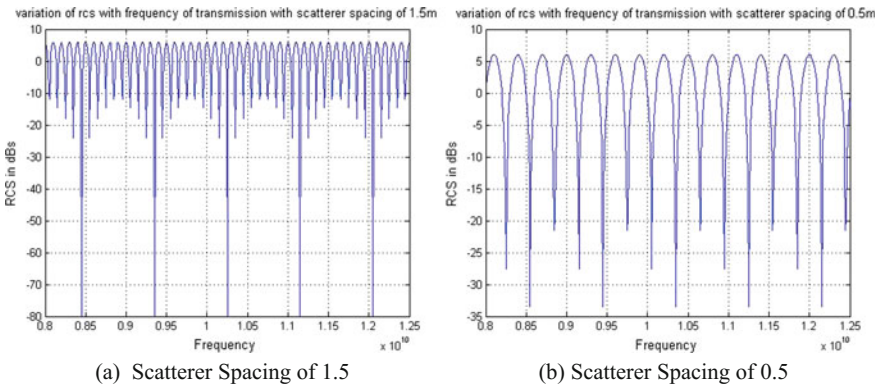
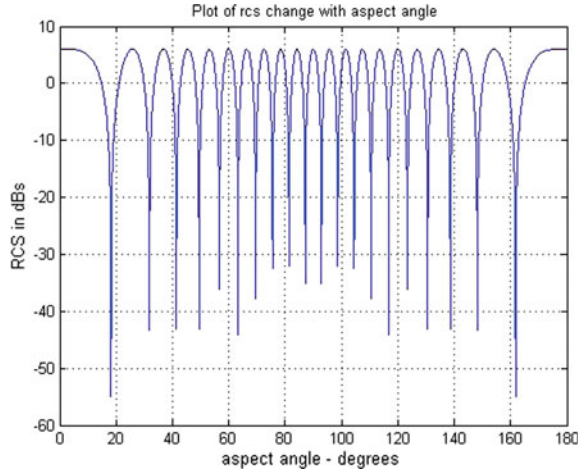


Fig. 9 Variation of RCS with frequency of transmission **a** scatterer spacing of 1.5, **b** scatterer spacing of 0.5

high probability density. Figure 8 shows the relation between aspect angle and radar cross section.

Figure 9a presents relationship among radar cross section and frequency when the scatterer spacing of 1.5, and Fig. 9b presents relationship among radar cross section along with frequency when the scatterer spacing of 0.5.

3.1 Final Observation and Comparison of Swerling I and Swerling II

The above graphs show the final observation and relation between detection probability and signal-to-noise ratio for different false alarm, where different false alarm has been shown by different colors, and the other graphs show the relation between detection probability (P_d) and false alarm (P_{fa}) for different SNR, where different SNR has been shown by different colors. In the above graphs, there is no pulse integration done, so the plots of Swerling I and II are identical because of same probability density function (Figs. 10, 11, 12, and 13).

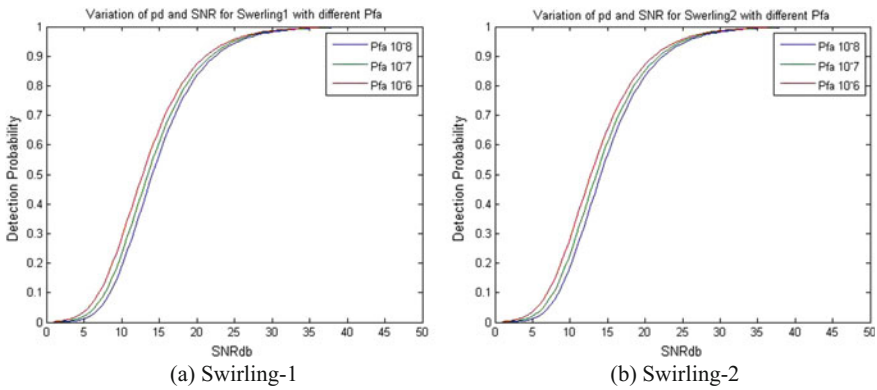


Fig. 10 Variation of detection probability with SNR for different P_{fa} . a Swerling I, b Swerling II

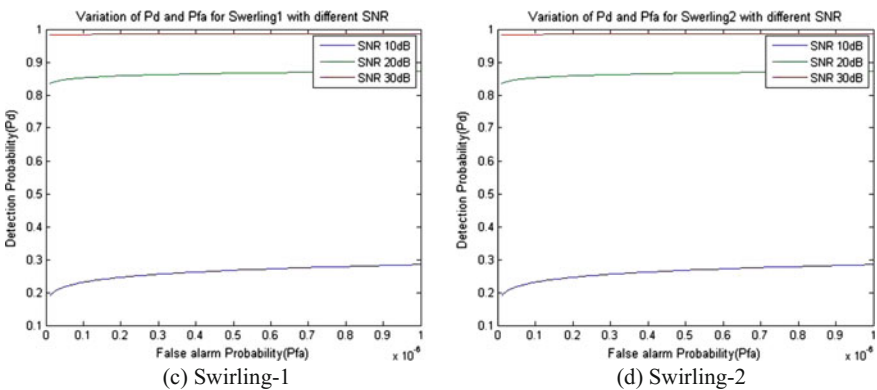


Fig. 11 Variation of detection probability with false alarm for different SNR. c Swerling I, d Swerling II

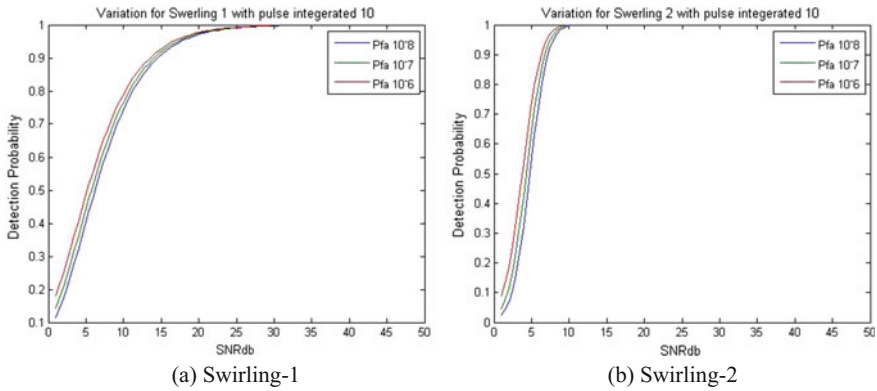


Fig. 12 Variation of detection probability with SNR for pulse integration. **a** Swerling I, **b** Swerling II

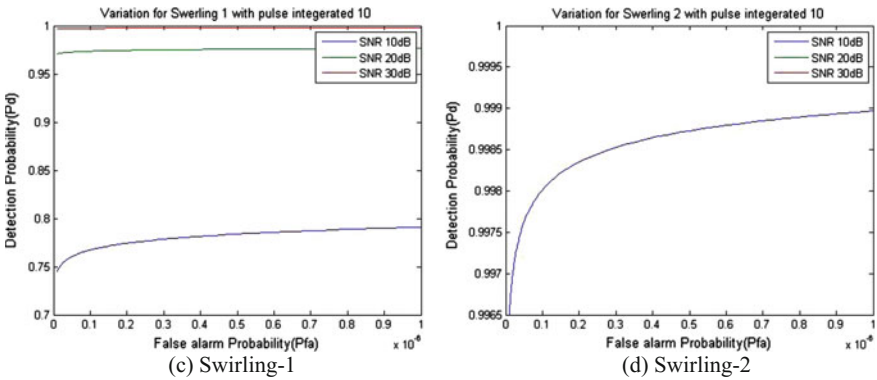


Fig. 13 Variation of detection probability with false alarm probability for pulse integration. **c** Swerling I, **d** Swerling II

In the above plots, pulse integration has been used to improve the detection probability, and it also helps in differentiation between Swerling target models I and II.

4 Conclusion

The main purpose of this research is to find the probability for detection and false alarm alert of fluctuation target. We have given detail analysis for probability for detection and false alarms of individual swerling targets. First, we have taken the parameter which requires for the analysis i.e., mathematical formula. We have taken

the mathematical relation which covers probability of detection and false alarm. On the basis of this mathematical relation, we have done the MATLAB analysis and then we have got the graphical relation between probability of detection and false alarm, and after the proper analysis the result has been taken. Along with this relation, we have also got the relation of signal-to-noise ratio and other parameter to more justify our result.

References

1. Marcum J. I., A Statistical Theory of Target Detection by Pulsed Radar, The Rand Corporation, Research Memorandum RM-754, December 1, 1947.
2. Swerling, P.: Probability of Detection for Fluctuating Targets, *IRE Trans.*, vol. IT-6, pp. 269–308, April 1960.
3. Skolnik, M. L: “Introduction to Radar Systems,” McGraw-Hill Book Company, New York, 1980.
4. Richards, M.A: “Fundamentals of Radar Signal Processing,” McGraw-Hill Book Company, New York, 2005.
5. Marcum J. I., A Statistical Theory of Target Detection by Pulsed Radar: Mathematical Appendix, The Rand Corporation, Research Memorandum RM-753, July 1, 1948.
6. Mahafza, B.R: “Radar Systems Analysis and Design using Matlab”, CRC Press LLC, 2000 N.W.

Tsallis Entropy Segmentation and Weighted KNN Classifier-Based Automatic DR Detection from Retinal Fundus Images

Ravindra D. Badgujar and Pramod J. Deore

Abstract Retina of individuals suffering from diabetes mellitus for several years signifies characteristic group of lesions of diabetic retinopathy (DR). DR is an asymptotic disease and emerging as one of the primary cause of vision loss in developing world. Ophthalmologist uses the retinal fundus image for manual screening of DR. To overcome the limitations of manual screening like highly subjective, time-consuming, prone to error, and requirement of expert availability, automated techniques are developed. We propose automated DR detection algorithm which uses retinal fundus images and detects exudates as sign of DR. Initially, the fundus image is preprocessed using Gaussian filter to remove the image noise. The preprocessing is followed by segmentation of fundus image. Optic disc is segmented using morphological operation and eliminated. The exudates which are prime sign of DR are segmented using Tsallis entropy segmentation and classified using weighted KNN. Various performance measures of the proposed technique are evaluated and compared with the existing exudate detection algorithms.

Keywords Diabetic retinopathy · Exudate · Tsallis entropy · w-KNN classifier

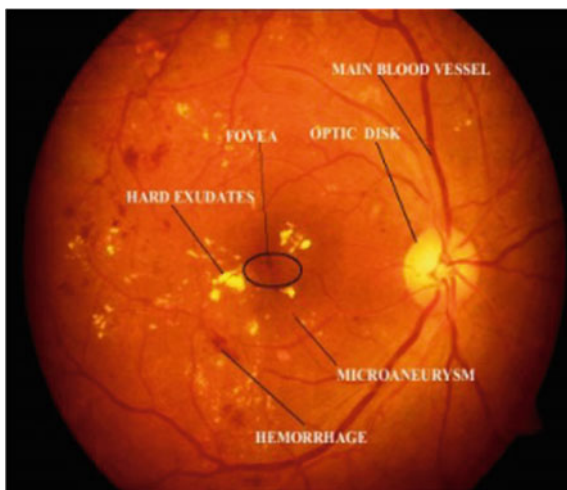
1 Introduction

More than 285 million citizens are visually impaired globally, as per factsheet of World Health Organization (WHO). Out of this, 246 million have low vision and 39 million are blind. The reason of visual impairment and blindness is uncontrolled diabetes [1]. In 2014, 422 million people were living with diabetes and global

R.D. Badgujar (✉) · P.J. Deore
Department of Electronics & Telecommunication Engineering,
RCBIT, Shirpur, Maharashtra, India
e-mail: ravindra_badgujar@yahoo.com

P.J. Deore
e-mail: pjdeore75@gmail.com

Fig. 1 Different signs of diabetic retinopathy captured in fundus image



prevalence of diabetes among adults has been doubled [2]. More than 75% of people with diabetes for more than 20 years will be prone to retinal diseases like diabetic retinopathy. The symptoms of DR are not detected until the disease is reached to a severe level. So its early detection and better treatment planning are vital. This opens a wide field of research to design and develop automatic screening systems to detect and diagnose the DR in early stages (Fig. 1).

Microaneurysms, hemorrhages, exudates, and inter-retinal microvascular abnormalities are different signs of diabetic retinopathy. Traditional retinal disease detection methods depend on human intervention; this is time-consuming, prone to error, and vastly subjective. Hence, it is necessary to develop an automated technique which is used to detect and diagnose the DR at a primary level. Early detection and diagnosis of diseases like diabetes related to the retina are of great importance. The exudate in a fundus image is one of the most prevalent earliest signs of diabetic retinopathy. These exudates must be detected from the original retinal image to classify the fundus images into normal and abnormal.

2 Literature Review

Automated detection of exudate is crucial for the early detection of the disease. The literature review summarizes various methods used for the detection of exudates in retinal fundus images. A three-stage model, comprising preprocessing, retinal image analysis, and classification, has been proposed by [3]. They used an extension of the m-Medoids-based modeling technique and combined it with a Gaussian mixture

model in an ensemble to form a hybrid classifier. G. Mahendran et al. developed a method for detection of exudates of a non-dilated, low contrast retinal fundus image. They performed segmentation using neighborhoods-based technique. For classification, PNN and SVN are used [4]. Machine learning techniques are proposed by [5] for exudates detection. To detect exudates, different statistical measures are used. Malay Kishore et al. proposed algorithm which removes false detection. They used threshold and edge detection approaches to eliminate different types of noises [6]. A deep convolutional neural network is proposed by [7]. Pre and post processing have not used hence results in lower segmentation efficiency. Anushikha S. et al. proposed a method for detection of exudates using intensity thresholding and morphological processing. They detected small exudates and removed the false positives and the noise sources from blood vessels and reflections during image capture making the detection of exudates accurate [8]. New preprocessing methods are proposed by Zhang et al. [9], which perform normalization, noise and motion artifact removal. Mathematical morphology-based techniques are used for segmentation, and random forest algorithm is used to detect the exudates.

3 Method

To detect, diagnose, or monitor retinal abnormality, fundus imaging is widely used. In this process, 2-D image of 3-D retinal semi-transparent tissues is projected onto the imaging plane. Ophthalmologists are using retinal fundus images for detection and diagnosis of eye-related diseases as a principal tool [10]. The proposed automated screening system is shown in Fig. 2, retinal fundus images are used as input images. Gaussian filtering is utilized for noise and background removal in preprocessing. Segmentation of different retinal anatomical structure like optic disc, and exudates is carried out. By considering important features of DR, only exudates are detected and classified using w-KNN classifier.

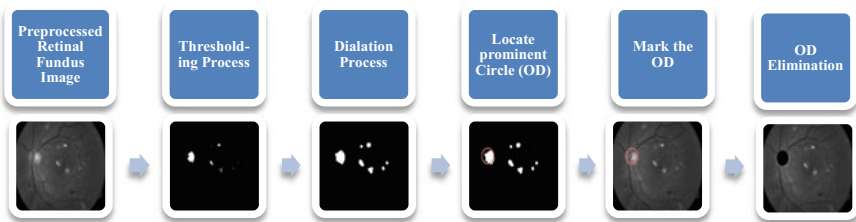


Fig. 2 Process of OD detection and elimination


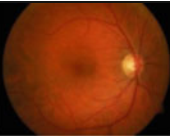

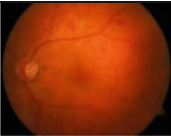
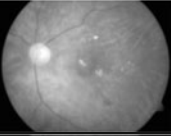
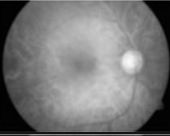
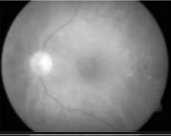
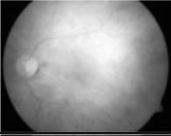
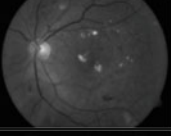
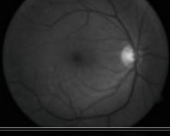
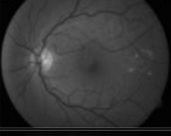
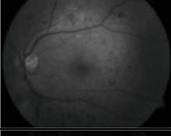
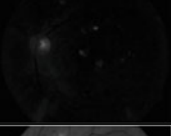
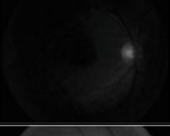
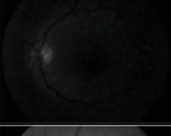

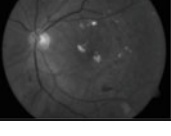
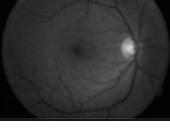

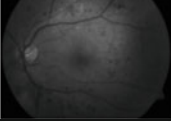
3.1 Preprocessing

Preprocessing consists of extraction of green channel and noise removal using Gaussian filter. Gaussian filter is an image-blurring filter in which transformation is calculated using Gaussian function for each pixel in input image [11], and it is given by

$$g(p, q) = \frac{1}{2\pi\sigma^2} e^{-\frac{p^2+q^2}{2\sigma^2}}. \tag{1}$$

The simulation results for the preprocessing of retinal fundus images are shown in Table 1. The results show green channel has most vital information. Hence, it is utilized for further processing. Gaussian filter is used for smoothing or averaging of fundus images, and it uses the mask of 9×9 with standard deviation of 1.75.

Table 1 Simulated results for different steps of preprocessing

DRIVE Dataset	Image1	Image 5	Image 11	Image 18
Original Image				
Red Channel				
Green Channel				
Blue Channel				
Gaussian Filtered Image				

3.2 Segmentation

For automatic detection of DR, exudate plays significant role. Intensity level of these retinal anatomical structures falls in the intensity range of exudates, and hence, it demands the elimination of OD to avoid false detection. In this paper, we focused on exudate for accurate detection of DR.

3.2.1 OD Detection and Elimination

Optic disc is located at the center of the retina. Optic disc (OD) is circular-to-oval white (bright) area measuring about 2×1.5 mm across. The exudates can be detected using their higher intensity trait from retinal images. In retinal images exudates and optic disc has same (higher) intensity range, and thus, it demands need to detect the optic disc and must be eliminated to avoid false detection. In this paper, OD detection and elimination are done using following morphological operation which includes following steps, and flow for OD detection and elimination is shown in Fig. 2.

3.2.2 Exudate Detection

After optic disc detection and elimination, the processed image is used to detect the exudates. Exudates are emerged with different properties, such as color, size, and shape. Exudates are of yellow and whitish colors and large in shape. Exudate detection process includes following image-processing steps. Contrast Stretching: OD-eliminated images are normalized using contrast stretching technique. Contrast stretching is a simple image enhancement technique utilized to improve the contrast in an image. For each pixel, the original value r and output value s are mapped using following function:

$$S = (r - c) \left(\frac{b - a}{d - c} \right) + a, \quad (2)$$

where a and b are lower and upper limits, respectively, and c and d are lowest and highest pixel values in image, respectively. The normalized image is segmented using threshold value. Image can be segmented in two parts as background and objects using thresholding methods based on histograms, clustering, or entropy. For image segmentation, non-extensive entropy thresholding may prove to be a powerful technique. Researchers [12] proposed and applied Tsallis entropy-based segmentation. We are using *the* Tsallis entropy-based exudate segmentation in this research work.

Tsallis Entropic segmentation

Let us consider an image having k gray levels. The set of all gray values $\{0, 1, 2, \dots, k\}$ usually has $k = 255$, and p_1, p_2, \dots, p_k are distribution of probabilities of each level. Here, we have defined two classes of probabilities based on this distribution, one is exudate (Class A) and another is background (Class B). Let us assume a bi-level threshold t for the gray levels, and two classes A and B are introduced with their probability distributions:

$$pA = \frac{p_1}{PA}; \frac{p_2}{PA} \dots \frac{p_t}{PA}, \quad (3)$$

$$pB = \frac{p_{t+1}}{PB}; \frac{p_{t+2}}{PB} \dots \frac{p_k}{PB}, \quad (4)$$

where $A = \sum_{i=0}^t p_i$, and $pA = \sum_{i=t+1}^k p_i$. The a priori Tsallis entropy for each distribution is defined as

$$S_q^A(t) = \frac{1 - \sum_{i=1}^t \left(\frac{p_i}{pA}\right)^q}{q - 1}, \quad (5)$$

$$S_q^B(t) = \frac{1 - \sum_{i=t+1}^k \left(\frac{p_i}{pB}\right)^q}{q - 1}. \quad (6)$$

Tsallis entropy $S_q(t)$ mainly depends on the threshold value t , for the exudate and background. It is devised as the sum of each entropy and defined in Eq. (7).

$$S_q(t) = \frac{1 - \sum_{i=1}^t (PA)^q}{q - 1} + \frac{1 - \sum_{i=t+1}^k (PB)^q}{q - 1} + (1 - q) \left(\frac{1 - \sum_{i=1}^t (PA)^q}{q - 1} \right) \left(\frac{1 - \sum_{i=t+1}^k (PB)^q}{q - 1} \right). \quad (7)$$

The Tsallis parameter q has great influence in the thresholding value and segmentation results. Proper value selection of Tsallis parameter q is important and is selected using numerous iterations and observing the segmentation results. The value of q can vary from 0.25 to 4. In this medical application, we selected the Tsallis parameter value in range of 0.5–1.5. After selection of Tsallis parameter the optimal threshold value is calculated. The optimum threshold value for luminance level t is obtained using $S_q(t) \Big|_{\max}$ and calculated using Eq. (8).

$$t_{\text{opt}} = \arg \max \left[S_q^A(t) + S_q^B(t) + (1 - q) \cdot S_q^A(t) S_q^B(t) \right]. \quad (8)$$

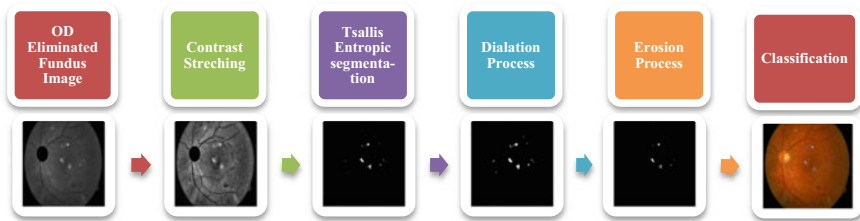


Fig. 3 Process of exudate detection and classification

The normalized retinal image is segmented using the Tsallis optimal threshold value calculated from Eq. (8). The output of thresholding gives us a binary image consisting white blob on black background. The white blob obtained after thresholding contributes to the exudates.

3.3 Post-Processing

The detected exudates are not precise hence the exudate detection is followed by post-processing operations. It includes the dilation of threshold image using disc structure followed by erosion process. The detected exudates are marked on original image. Various parameters are extracted and used for DR detection and grading purpose. Figure 3 represents the overall process of exudate detection and classification.

3.4 Classification and Optimization

Various exudates detected are classified using weighted KNN classifier. The attributes of the instances are used to perform an evaluation in w-KNN. Each attribute is evaluated to obtain a weight value. In w-KNN classifier, index of discernibility is used to evaluate every attributes of the training data set. The weights are applied to both the training and the testing data set.

4 Results

4.1 Simulated Results

In this proposed work, we are using the DRIVE database available online for evolution and testing of various retinal image-processing applications. In proposed

algorithm, the retinal images are preprocessed using prime morphological and filtering operations. Optic disc and exudates have similar characteristics like intensity, color, and shape. Hence for accurate detection of exudates and DR, OD should be detected and eliminated from retinal images. OD detection and elimination are done using morphological operation.

4.2 Performance Evaluation

Exudates detected using proposed algorithms are shown in Table 2. It shows that the exudates of the retinal image are detected accurately and shown on original

Table 2 Simulation results

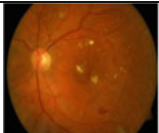

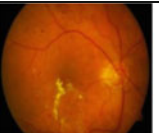
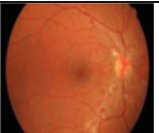
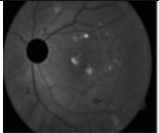
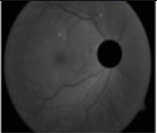
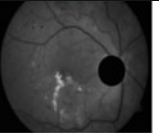
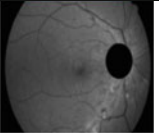
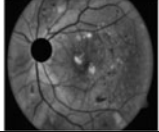
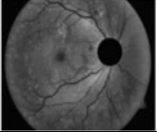
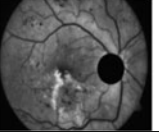
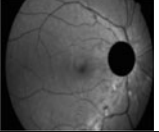





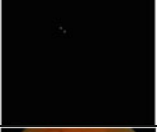


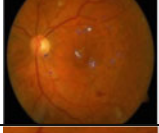
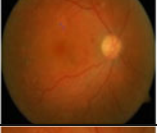

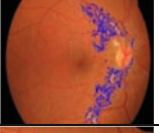
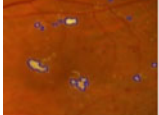

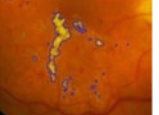
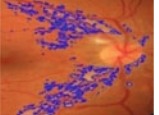
DRIVE Dataset	Image1	Image 6	Image 7	Image15
Original Image				
OD Eliminated fundus Image				
Contrast stretching				
Tsallis entropy Segmentation				
Post Processing				
Detected Exudates				
Closer View of detected Exudates				

Table 3 Statistical measures for proposed method

Measures	TP abnormal	TN normal	FP	FN
Data set (40)	26	11	1	2
Performance parameters	Sensitivity (%)	Accuracy (%)	Specificity (%)	Precision (%)
	96.29	92.5	91.67	96.29

Table 4 Comparisons with existing methods

Automated system	Sensitivity (%)	Specificity (%)
Proposed method	96.29	91.67
Bhalerao et al. [13]	82.6	80.2
Iqbal et al. [14]	98	61
Sopharak et al. [15]	81.61	99.9
Rumano et al. [16]	85.4	83.1

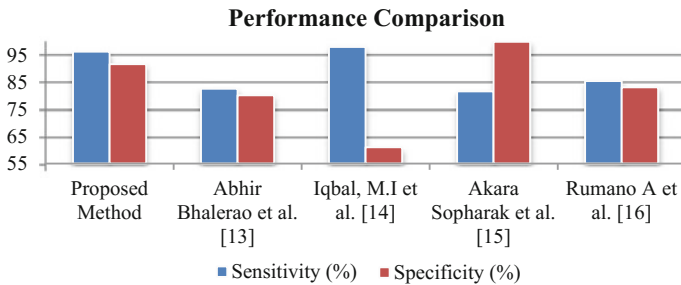
**Fig. 4** Graphical representation of performance evaluation

image. The exudates are represented by the boundary of blue color. For testing phase, the source fundus image data set contains 40 fundus retinal images, respectively. Tables 3 and 4 represent the statistical measure of the proposed system for DRIVE data set and compared with existing methods. Results illustrates that the proposed method provides better sensitivity and specificity as compared to existing algorithms (Fig. 4).

5 Conclusion

DR is prime eye-related disease which causes partial or entire vision loss. It demands the development of automatic system for detection of DR. The proposed DR detection algorithm uses morphological processing and Tsallis entropy segmentation for exudate detection in retinal fundus images. The retinal fundus images

are preprocessed using Gaussian filter for smoothing or averaging of fundus images, and it uses the mask of 9×9 with standard deviation of 1.75. Optic disc segmentation is performed using morphological operations. OD is eliminated from fundus image to avoid false detection of exudates. Exudates are segmented using Tsallis entropy optimization algorithm using the Tsallis parameter. Finally w-KNN classifier is used for accurate classification of the exudates and performance evaluation of proposed algorithm and comparison with existing algorithm is performed. Results illustrates that the proposed method provides better sensitivity and specificity as compared to existing algorithms.

References

1. World Health Organization Factsheet 2005: <http://www.who.int/mediacentre/factsheets/fs282/en> (Accessed on Dec 25, 2016).
2. International Diabetes Federation, Fifth Edition 2011: <http://www.idf.org/diabetesatlas/news/fifth-edition-release>.
3. M. Usman Akram, Shehzad Khalid, Anam Tariq, Shoab A. Khan, Farooque Azam, "Detection and classification of retinal lesions for grading of diabetic retinopathy" Elsevier Journal of Computers in Biology and Medicine 45 (2014) pp: 161–171.
4. Mahendran G, Dhanasekaran R. "Investigation of the severity level of diabetic retinopathy using supervised classifier algorithms." Comput Electr Eng (2015), <http://dx.doi.org/10.1016/j.compeleceng.2015.01.013>.
5. P. R. Asha and S. Karpagavalli, "Diabetic Retinal Exudates Detection using Machine Learning Techniques", International Conference on Advanced Computing and Communication Systems (ICACCS-2015), Jan. 05–07, 2015, Coimbatore, INDIA.
6. Malay Kishore Dutta, Kshitij Srivastava, Shaunak Ganguly, Shaumik Ganguly, M. Parthasarathi, Radim Burget, and Jiri Prinosil, "Exudates Detection in Digital Fundus Image Using Edge Based Method & Strategic Thresholding", 8th International Conference on Telecommunications and Signal Processing, TSP 2015, Prague, Czech Republic, July 9–11, 2015. IEEE 2015, ISBN 978-1-4799-8498-5.
7. Pavle Prentašić, and Sven Lončarić, "Detection of Exudates in Fundus Photographs using Convolutional Neural Networks", 9th International Symposium on Image and Signal Processing and Analysis (ISPA 2015), September 7–9, 2015, Zagreb, Croatia.
8. Anushikha Singh, Namita Sengar, Malay Kishore Dutta, Kamil Riha, and Jiri Minar, "Automatic Exudates Detection in Fundus Image using Intensity Thresholding and Morphology." 7th International Congress on Ultra Modern Telecommunications and Control Systems and Workshops (ICUMT).
9. Xiwei Zhang et al, "Exudate Detection in Color Retinal Images for Mass Screening of Diabetic Retinopathy", Accepted Manuscript (To appear in Medical Image Analysis).
10. P. Perona, J. Malik, 'Scale Space and Edge Detection Using Anisotropic Diffusion' IEEE Transaction on Pattern Analysis, Vol. 12, July 1990, pp 629–639.
11. Kazufumi Ito and Kaiqi Xiong, "Gaussian Filters for Nonlinear Filtering Problems", IEEE Transactions on Automatic Control, Vol. 45, No. 5, May 2000, pp 910–927.
12. Portes de Albuquerque, M.et al "Image thresholding using Tsallis entropy.", Pattern Recognition Letters, 25, 1059–1065. DOI:[10.1016/j.patrec.2004.03.003](https://doi.org/10.1016/j.patrec.2004.03.003).
13. Abhir Bhalerao et al. "Robust Detection of Microaneurysms for Sight Threatening Retinopathy Screening." IEEE Computer society, 2008, pp 520–527.

14. Iqbal, M.I et al. "Automatic Diagnosis of Diabetic Retinopathy using Fundus Images.", Blekinge Institute of Technology. 2006.
15. Akara Sopharak et al. "Automatic Microaneurysm Detection from Non-dilated Diabetic Retinopathy Retinal Images Using Mathematical Morphology Methods." IAENG International Journal of Computer Science, 2011.
16. Alan D. Fleming et al. "Automated Microaneurysm Detection Using Local Contrast Normalization and Local Vessel Detection.", IEEE Transactions on Medical Imaging, Vol. 25, No. 9., September 2006, pp 1223–1232.

Contact Resistance-Dependent OTFT Behaviour: Effect of Channel Length

Shruti Nautiyal, Pranjali Nautiyal, Shubham Negi
and Poornima Mittal

Abstract The charge injection occurs from contact metals into semiconductors can be inefficient process i.e., non-ohmic. This is due to significant difference amid work function of contact metal and lowest unoccupied molecular orbit (LUMO)/highest occupied molecular orbit (HOMO) level of n/p-organic semiconductor (OSC). Therefore, the contacts in OTFT drop a noteworthy sum of voltage due to occurrence of contact resistance. The effect of contact resistance can be observed at low channel length devices. The electrical characteristics and parameter extractions are done for SG-OTFT at various channel lengths, and the results are observed and analysed using organic module of Atlas 2-D simulator.

Keywords Thin film transistor (TFT) · Organic thin film field-effect transistor (OTFET) · SG-OTFT (single gate organic thin film transistor) OSC (organic semiconductor)

1 Introduction

The branch of electronics dealing with material science concerning the design, synthesis, chemical structures of conductive polymers and conductive small molecules is called organic electronics. Organic electronic devices are less expensive, more flexible and lighter in weight than inorganic counterpart electronics devices. This is the reason of attraction of intense research in this field in recent years. In current scenario, there has been noteworthy improvement in the overall performance of OTFTs. OSCs (organic semiconductors) have shown novel exciting potentials for applications entailing mechanical flexibility, low-temperature

S. Nautiyal (✉) · P. Nautiyal · S. Negi · P. Mittal
Department of Electronics and Communication Engineering,
Graphic Era University, Dehradun 248002, India
e-mail: shrutinautiyal91@gmail.com

P. Mittal
e-mail: poornima2228@gmail.com

processing, large area, lightweight and cost-effectiveness [1–4]. Although the performance of organic thin film transistors (OTFTs) is not comparable to the conventional MOS transistors, nevertheless it owns some worth mentioning advantages that include usage of bendable substrates like paper, plastic, fibre, cloth and foil, processing at low temperature and deposition of organic materials through solution processing techniques [2–5]. OTFTs have come in sight as a field of intense research field with emphasis on fundamental concepts and significance in numerous high-performances low-end applications [5–9]. Regardless of the extensive advancement made recently in enhancing the performance of OTFTs, several of design, material, and process constraints influencing OTFT performance are still poorly understood and poorly controlled. OTFTs can present deformation at the origin of the output characteristics, due to non-ohmic contacts at drain and source. One constraint like this is contact resistance [7–9]. In this paper, performance of OTFTs has been analysed at different channel lengths through simulation using organic module of Atlas 2-D simulator and analysed that there is 60% reduction in current from channel length 10 to 50 μm . This is due to presence of contact resistance in the transistors. Effect of contact resistance in transistors can be observed through carrying out simulations and channel length variation.

The paper consists of five sections, together with the present introduction Sect. 1. Next Sect. 2 describes the set-up required for simulation done for examining the characteristics then observing the outputs. Further, Sect. 3 is divided into two parts 3.1 and 3.2. In Sect. 3.1, electrical characteristics and output curves are depicted. In Sect. 3.2, parametric extraction is done for the device. Thereafter, in Sect. 4, analysis is done based on channel length (L) variation and observations are noted. Section 5 gives conclusion, and finally references are quoted.

2 Simulation Set-up

A BGTC (bottom gate top contact) single gate OTFT structure is employed. A BGTC structure is preferred as it contributes (a) low contact resistance, (b) high mobility, (c) high current and (d) large channel length compared to other OTFT structures.

The BG-OTFT structures simulated here begins from a bottom gate followed by depositing dielectric layer of Al_2O_3 . After that, comes the organic semiconducting layer of pentacene and lastly source and drain contacts of gold. The schematic drawing is represented in Fig. 1. The device structure of device simulated is depicted in Fig. 2.

The simulated device has L (channel length) of 10 μm and w (channel width) of 100 μm . Gate electrode was deposited by aluminium to a thickness of 20 nm. Then, dielectric layer of 5.7 nm was deposited. Next, the organic semiconductor of 30-nm thick film of pentacene was deposited. Finally, 30-nm thick gold source/drain contacts were deposited. The analysis of organic single gate transistor is done by making use of Atlas 2-D numerical device simulator [10].

Fig. 1 Schematic diagram of single gate OTFT

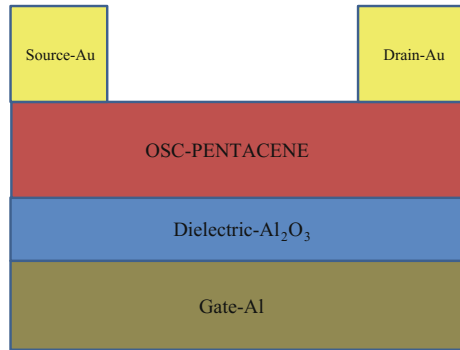
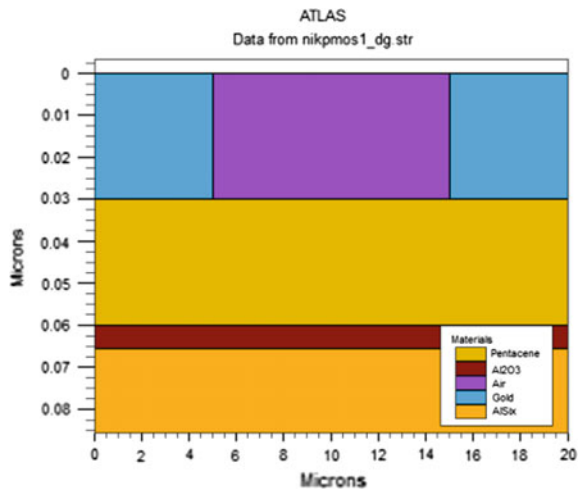


Fig. 2 Simulated device structure



3 SG-OTFT Electrical Characteristics and Parametric Extraction

3.1 Electrical Characteristics

The output curves of device simulated are depicted in Fig. 3. In Fig. 3a, Drain current versus Gate-Source Voltage curve through simulation is shown, in Fig. 3b, Drain Current versus Drain Source Voltage curve of device is plotted.

3.2 Parameter Extraction

The drain saturation current is defined by the formula (1–4)

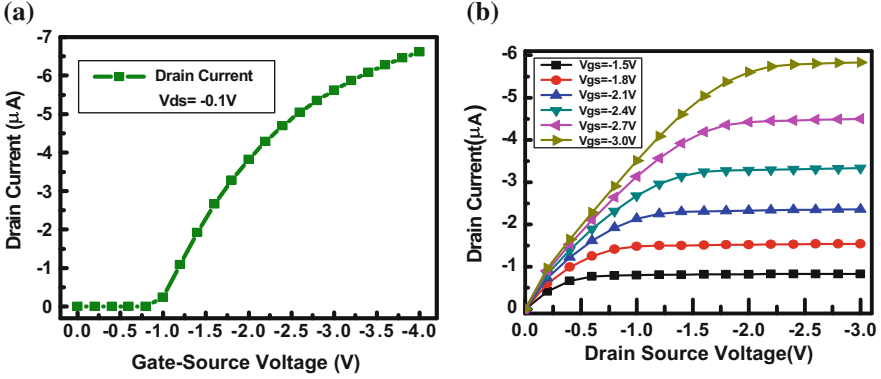


Fig. 3 Simulated results of SG-OTFT **a** SG-OTFT transfer characteristic, as simulated in Atlas 2-D device numerical simulator, **b** output characteristics of SG-OTFT. Output curve is plotted at different V_{GS} . It can be observed that from above graph, on increasing V_{GS} , I_D increases. The simulations are done for device of channel length = 10 μm and channel width 100 μm

$$I_D = \frac{\mu C_{ox} W}{2L} (V_{GS} - V_T)^2 \quad (1)$$

where I_D denotes drain saturation current, the field mobility is represented by μ , capacitance per cm^2 of gate oxide is denoted by C_{ox} , V_T represents the threshold voltage, gate-to-source voltage is denoted by V_{GS} , W is denoted for channel width, L is used for channel length.

The field-effect mobility or field mobility at saturation regime is determined by given formula

$$\mu = \frac{2L}{WC_{ox}} \left(\frac{\partial \sqrt{I_D}}{\partial V_{GS}} \right)^2 \quad (2)$$

Transconductance for SG-OTFT is calculated by the formula given below

$$g_m = \mu C_{ox} \frac{W}{L} (V_{GS} - V_T) \quad (3)$$

Threshold voltage is given by formula

$$V_T = \frac{QN_a t_{osc}}{C_{ox}} \quad (4)$$

Table 1 Experimental data versus simulated data

Name of parameters	Experimental [1]	Simulated
Drain Current (I_D)	5.0	4.84
Field-effect mobility μ (cm^2/Vs)	0.4	0.45
Transconductance (g_m)	5.0	4.8
Threshold Voltage V_T (V)	-1.0	-0.88

where Q , N_a , t_{osc} , C_{ox} are denoted by charge of electron/hole, doping concentration, thickness of OSC layer and oxide capacitance, respectively.

The simulated results are summarized in Table 1. The following results have been attained in the simulation applying the formulae discussed above.

4 Analysis Based on Channel Length Variation

For estimating simulated device contact resistance, variation in channel length of the device is done, ranging from 10 to 50 μm . The results are recapitulated in Fig. 4.

For estimating the simulated device contact resistance, the channel length (l) of device is varied ranging from 10 to 50 μm . The simulated results are recapitulated in Fig. 4. It is illustrated from Fig. 4a that on decreasing l from 50 to 10 μm , drain current (I_D) increases but the reduction in I_D is more prominently observed below channel length of 20 μm , as contact resistance effect on drain current becomes prominent at low channel lengths. According to Eq. (1), I_D is proportional to inverse of channel length. But it is observed through simulator in Fig. 4b that I_D is not varying appreciably as expected, this deviation is due to presence of contact resistance in the device. It can be observed from Fig. 4c that on decreasing l from 50 to 10 μm , I_D increases from 2.29 to 5.83 μA . On the other hand from Fig. 4d it can be observed that the threshold voltage is approximately equal for all channel lengths ranging from 10 to 50 μm i.e., V_T is observed approximately same for this range of channel lengths. In Fig. 4e, transconductance scales as predicted by Eq. (3).

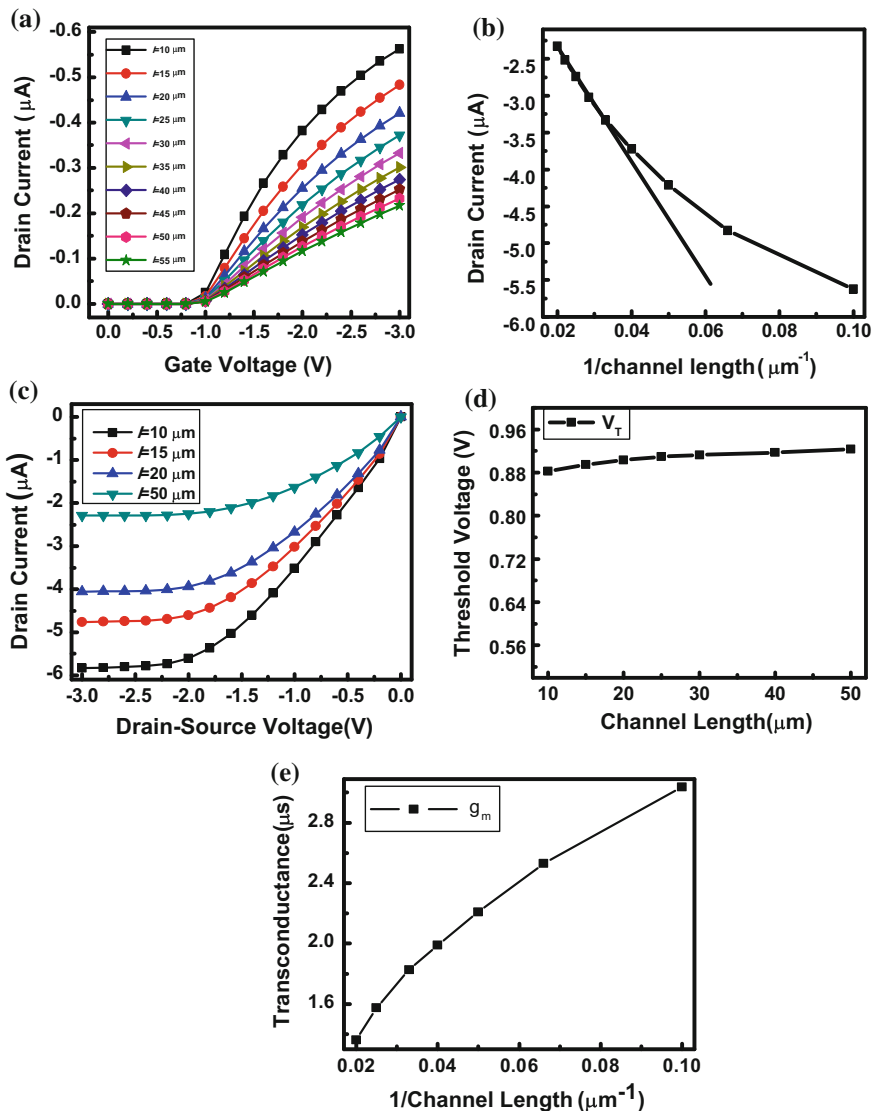


Fig. 4 a I_D versus V_{GS} curve at different channel lengths, b I_D versus $(1/\text{channel length})$ curve, c I_D versus V_{DS} curve, d threshold voltage versus channel length curve and e transconductance versus $1/\text{channel length}$ curve

5 Conclusion

In this paper, single gate OTFT with channel length 10 μm based on pentacene has been simulated. Subsequently, the paper has been compared characteristics of the SG-OTFT with experimentally reported paper [1]. Further, channel length of device has been varied ranging from 10 to 50 μm to observe the effect of contact resistance. The effect of contact resistance is observed at low channel length devices. Effect on drain current can be observed considerably. 60% reduction in current from channel length 10 to 50 μm is analysed, transconductance scales as predicted by Eq. (3), while threshold voltage is approximately the same for all channel lengths between 10 to 50 μm .

References

1. Klauk, H., Zschieschang, U., Halik, M.: Low-voltage organic thin-film transistors with large transconductance. *Journal of Applied Physics*, 102(7), 074514 (2007).
2. Kumar, B., Kaushik, B. K., Negi, Y. S.: Organic thin film transistors: Structures, Models, Materials, Fabrication, and Applications: A review, *Polymer Review*, Vol. 54:1, pp. 33–111 (2013, September).
3. Shim, C. H., Maruoka, F., Hattori, R.: Structural analysis on organic thin-film transistor with device simulation. *IEEE Transactions on Electron Devices*, 57(1), pp. 195–200 (2010).
4. Guo, W., Shen, L., Liu, C., Chen, W., Ma, D.: Analysis and extraction of contact resistance in pentacene thin film transistors. In *Nano/Micro Engineered and Molecular Systems, NEMS 2008*. 3rd IEEE International Conference, pp. 99–102 (2008, January).
5. Mittal, P., Negi, Y. S., Singh, R. K.: An analytical approach for parameter extraction in linear and saturation regions of top and bottom contact organic transistors. *Journal of Computational Electronics*, 14(3), pp. 828–843 (2015).
6. Khan, A. R., Yadav, S. C., Chauhan, S. S., Kumar, B., Kaushik, B. K., Negi, Y. S., Iyer, S. S. K. (2011, September). Vertical organic thin film transistor to achieve sub ten micron channel length devices. In *2011 2nd International Conference on Computer and Communication Technology (ICCCCT-2011)*.
7. Gundlach, D. J., Zhou, L., Nichols, J. A., Jackson, T. N., Necliudov, P. V., & Shur, M. S. (2006). An experimental study of contact effects in organic thin film transistors. *Journal of Applied Physics*, 100(2), 024509.
8. Jung, K. D., Kim, Y. C., Park, B. G., Shin, H., Lee, J. D.: Modeling and parameter extraction for the series resistance in thin-film transistors. *IEEE Trans. Electronic Devices* 56, 431–440 (2009).
9. Necliudov, P. V., Shur, M. S., Gundlach, D. J., & Jackson, T. N. (2003). Contact resistance extraction in pentacene thin film transistors. *Solid-State Electronics*, 47(2), 259–262.
10. ATLAS user's manual: Device simulation software. Silvaco International Santa Clara (2014).

Enhancement in Efficiency of Hybrid Organic Photovoltaics by Variation in Anode Material

Pranjali Nautiyal, Arun Pratap Singh Rathod, Shruti Nautiyal and Poornima Mittal

Abstract An efficient hybrid photovoltaic cell is demonstrated using different anode material. Graphene on PET substrate is being used as anode in the device and compared with performance of conventional device having ITO as anode. Because of outstanding transparency, conductivity, and flexibility, device with graphene anode shows higher performance in terms of current density. By using graphene as anode, current density is increased from 10.9 to 19.6 mA/cm² and shows an enhancement of 79.8%. This enhancement leads to the enhancement in the power conversion efficiency of the device.

Keywords Graphene · Hybrid photovoltaics · Transparent electrodes

1 Introduction

It is the statistics that in per 30 years energy consumption has increased by 56%. As demand for energy increases rapidly, solar energy comes out to be a perfect alternative to conventional fossil fuels. In recent years, solar energy capabilities by implementing organic solar cell have also been come out to be an emerging technology.

Organic materials are promising for low-cost solar cell devices, due to the inexpensive fabrication and room temperature processing. Organic solar cell devices have become a reason for attracting the attention, due to mild temperature

P. Nautiyal (✉) · A.P.S. Rathod · S. Nautiyal · P. Mittal
Department of Electronics and Communication Engineering, Graphic Era University,
Dehradun 248002, India
e-mail: nautiyalpranjali@gmail.com

P. Mittal
e-mail: poornima2822@ieee.org

processing, flexibility, potentially economic cost, and portable consumer advantage [1]. Unfortunately, the power conversion efficiency (PCE) of this class is not comparable with the PCE of inorganic solar cells. On the other side of coin, inorganic wafer-based photovoltaic cells have high PCE but their fabrication requires high deposition temperature and ultra-clean ambience, which increases its production cost and makes them unsuitable for the development of photovoltaics (PVs) in large-scale. In order to meet out solution for the above given issues, hybrid organic and inorganic semiconductor photovoltaic cells have been proposed as an emerging technology to attain high PCE with economic production cost [2, 3].

In this paper, we provide a basic overview of hybrid photovoltaic cells, different transparent electrode material for PV cells. Herein, we will also review the device structures, basic working mechanism of photovoltaics, and at last results are analyzed and discussed.

2 Hybrid Photovoltaic Cells

Hybrid solar cell combines organic and inorganic materials. In hybrid cells, organic material is used as donor which transports holes. Inorganic material is used as acceptor and electron transporter. Both organic and inorganic materials in hybrid photovoltaics are combined to form a photoactive layer. The organic material which acts as photon absorber and exciton donor and is assembled with inorganic material which facilitates exciton dissociation at junction. The whole combined assembly provides greater power conversion efficiency than single layer [4, 5]. Hybrid PV cells take the advantages of both inorganic semiconductor material and organic semiconductor material. To add to this, their low-cost production, processability, and high PCE make them interesting and attractive technology in the recent years.

3 Transparent Electrodes in PV Cells

For solar energy generation, a photovoltaics must have a transparent electrode. Transparent electrodes play a vital role in device by solving the issue low carrier collection. Furthermore, they act as protective layer and thus prevent the degradation of semiconductor material. Currently, ITO is the most commonly used electrodes in solar cell applications. Due to its electrical conductivity and optical transparency in visible range, it acts as a electron-collecting electrode in solar cell devices. However, there are some drawbacks, including limited supply of available indium, high production cost, brittleness, and lack of transparency in infrared region which restricts its ability to gather a wide range of solar energy [6].

Graphene has also gaining attention since last few years because of its outstanding electrical conductivity and optical properties. Another graphene's standout property is its inherent strength. It is the strongest material ever discovered [7]. In addition, it exhibits excellent flexibility and has inexpensive and abundant source material (carbon). Because of these properties, graphene possesses the innate potential to replace the convention electrode ITO in solar cell devices. Thin films of ITO are deposited by physical vapor deposition, whereas chemical vapor deposition (CVD) is being used for the production of large-scale graphene sheets [8].

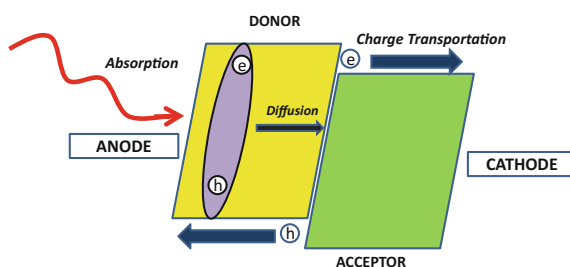
Several researchers have proposed photovoltaic cells and their potential applications, but increasing the performance of these cells is greatly required. Very few work has been done in terms of performance improvement with respect to material and moreover with architecture. In this paper, to improve the power conversion efficiency (PCE), we propose the hybrid photovoltaic cells having different anode material. We investigated the efficiency of photovoltaics with graphene as electrode is higher than that of device with conventional ITO.

4 Basic Working Principle of Heterojunction Photovoltaics

The basic working principle of organic photovoltaic device includes four fundamental steps: absorption, dissociation, separation, and transportation. Figure 1 illustrates the basic steps of the working principle of an organic solar cell.

When light (photon) gets incident on photoactive layer through transparent electrode (anode), electrons get excited; i.e., upon absorption of the light, material get energized, and excitons (coulomb bound electron-hole pair) are formed. After absorption and exciton formation, excitons undergo through diffusion followed by dissociation. Dissociation does occur due to different work function of acceptor and donor. Excitons dissociate at LUMO level of acceptor and HOMO level of the donor [9]. Dissociation is then followed by charge separation. It occurs at organic semiconductor/metal interfaces. Once they get separated, charge transportation does occur, and they get collected by respective electrodes.

Fig. 1 Fundamental mechanism to photon-to-electron conversion in heterojunction solar cells



5 Device Structure

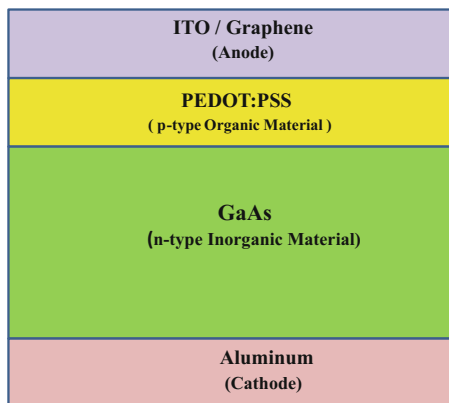
An OPV cell comprises a film of organic photovoltaic active layer, sandwiched between two electrodes (anode and cathode). The basic device structure of the proposed hybrid photovoltaic cell is shown in Fig. 2. The structure consists of transparent anode (ITO/graphene), poly(3,4-ethylenedioxythiophene)-poly(styrenesulfonate) PEDOT:PSS (acceptor), GaAs (donor), and a metal electrode (aluminum).

Thickness of ITO and aluminum is 40 and 100 nm, respectively. Graphene is transferred to polyethylene terephthalate (PET) substrate to act as anode for hybrid photovoltaics. Poly(3,4-ethylenedioxythiophene)-poly(styrenesulfonate) (PEDOT:PSS) of thickness of 40 nm is used as *p*-type organic material, and GaAs is used as *n*-type inorganic material. PEDOT:PSS is one of the doped materials which transports the holes rather than electrons. Its features like solution processability, high conductivity, and transparency in visible range make it popular to be used in PVs [10, 11]. GaAs has advantage of high carrier mobility and direct band-gap. Both PEDOT:PSS and GaAs constitute a heterojunction active layer for photovoltaic device.

6 Results and Analysis

The proposed device is simulated in Atlas simulator. It is 2D and 3D device simulator framework. It predicts the electrical behavior of specified semiconductor structures and provides insight into the internal physical with device operation. It can also solve the physical equations describing thermodynamics of carrier in device. Through simulation characteristics of two different hybrid photovoltaic device structures having different transparent electrodes are framed and studied. Figure 3a shows the simulated device structure with ITO as anode.

Fig. 2 Device structure of the proposed hybrid photovoltaics



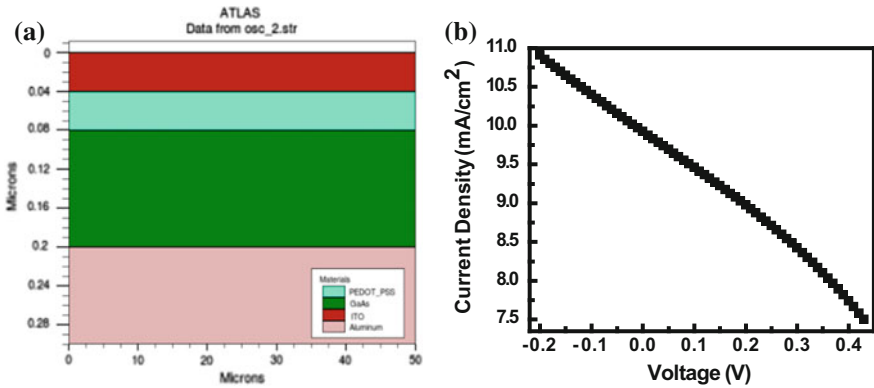


Fig. 3 a Simulated device structure of hybrid photovoltaics with ITO as anode and b current density–voltage characteristics

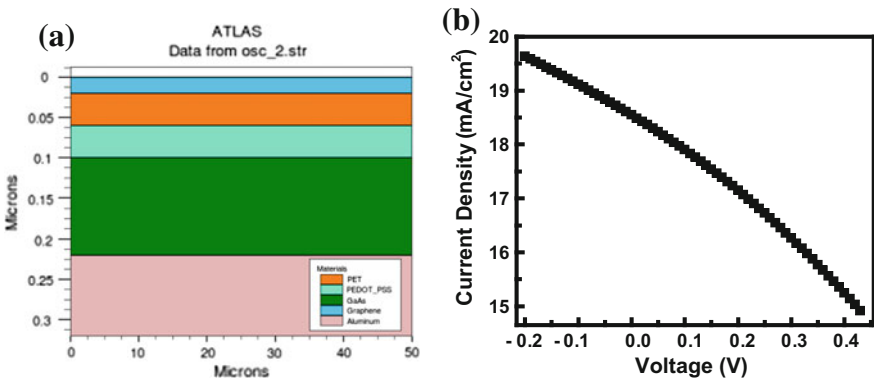


Fig. 4 a Simulated device structure of hybrid photovoltaics with graphene as anode and b current density–voltage characteristics

Figure 3b illustrates the simulated current density–voltage (J–V) characteristics curve of proposed device. The same device structure is simulated again but with different anode. In the second device, ITO is replaced by graphene. The simulator device structure with graphene as anode is shown in Fig. 4a.

Figure 4b illustrates the simulated current density–voltage (J–V) curve for hybrid PV cells with graphene anode. Power conversion efficiency (PCE, η) of a photovoltaic device is defined by the equation [9]

$$\eta = (J_{sc} * V_{oc} * FF) / (P_{in}) \tag{1}$$

where J_{sc} , V_{oc} , FF, and P_{in} are short circuit current density, open circuit voltage fill factor, and power of incident light, respectively. Enhancement in current density

Table 1 Comparison of hybrid PV cells with different anode

Device structure	Material			V (Volts)	J (mA/cm ²)
ITO/PEDOT: PSS/GaAs/Al	Anode	Active layer	Cathode	−0.2	10.9
	ITO	PEDOT: PSS/GaAs	Aluminum		
G/PET/PEDOT: PSS/GaAs/Al	Graphene	PEDOT: PSS/GaAs	Aluminum	−0.2	19.6

somehow gives rise to the value of PCE of device, and ultimately performance of device increases. The photovoltaic device structures, materials, and the parametric values of each device are summarized and compared in Table 1. By using graphene as transparent anode material for hybrid PV, the efficiency is greatly enhanced as compared to the conventional ITO.

It is observed that maximum attained value of current density in the device having ITO as anode is 10.9 mA/cm². The improved result of value 19.6 mA/cm² is obtained in other device which is having graphene as anode. The overall enhancement in the device performance in terms of current density has come out to be 79.8%. The increment in the value of current density of later device signifies the corresponding enhancement in the device efficiency.

7 Conclusion

We have demonstrated different structures for hybrid cell having different materials for anode. It is investigated and analyzed that by having graphene as anode in the device there is a sound improvement of 79.8% from 10.9 to 19.6 in the device performance in terms of current density.

Lightweight and flexible graphene electrode in PVs offers various possible route for applications that would not be possible with conventional silicon-based photovoltaics. Due to their flexibility, they could be applied to irregular walls and rooftop surfaces. Also they could be stacked on top or other solar cells, which results improved power generation from a given area. And thus hybrid solar cells having graphene as anode can be viewed as a stepping stone toward high-performance organic photovoltaics.

References

1. Bagher, A. M.: Comparison of organic solar cells and inorganic solar cells. *Int J Renew Sustain Energy*, 3, pp. 53–58 (2014).
2. Wright, M., Uddin, A.: Organic–inorganic hybrid solar cells: A comparative review. *Solar energy materials and solar cells*, 107, pp. 87–111 (2012).

3. Adikaari, A. D. T., Dissanayake, D. N. M., Silva, S. R. P.: Organic–inorganic solar cells: recent developments and outlook. *IEEE Journal of selected topics in quantum electronics*, 16 (6), pp. 1595–1606 (2010).
4. Liu, R.: Hybrid organic/inorganic nanocomposites for photovoltaic cells. *Materials*, 7(4), pp. 2747–2771 (2014).
5. Chi, D., Qi, B., Wang, J., Qu, S., Wang, Z.: High-performance hybrid organic-inorganic solar cell based on planar n-type silicon. *Applied Physics Letters*, 104(19), 193903 (2014).
6. Singh, V., Suman, C. K., Kumar, S.: Indium Tin Oxide (ITO) films on flexible substrates for organic light emitting diodes. In *Proc. of ASID*, vol. 6, no. 8, p. 388 (2006).
7. Park, H., Chang, S., Smith, M., Gradečak, S., Kong, J.: Interface engineering of graphene for universal applications as both anode and cathode in organic photovoltaics. *Scientific reports*, 3 (2013).
8. Huang, C. H., Yu, S. C., Lai, Y. C., Chi, G. C., Yu, P.: Efficiency enhancement of organic/GaAs hybrid photovoltaic cells using transparent graphene as front electrode. *IEEE Journal of Photovoltaics*, 6(2), pp. 480–485 (2016).
9. Su, Y. W., Lan, S. C., Wei, K. H.: Organic photovoltaics. *Materials Today*, 15(12), pp. 554–562 (2012).
10. Lai, T. H., Tsang, S. W., Manders, J. R., Chen, S., So, F.: Properties of interlayer for organic photovoltaics. *Materials Today*, 16(11), pp. 424–432 (2013).
11. Yi, C., Hu, X., Gong, X., Elzatahry, A.: Interfacial engineering for high performance organic photovoltaics. *Materials Today*, 19(3), pp. 169–177 (2016).

Performance Analysis of Double Block Layer OLED and Variation in Ratio of Double Block Layer

Shubham Negi, Poornima Mittal and Brijesh Kumar

Abstract OLED is the field of organic electronics that has improved tremendously in the past decade and so much that it can be a substitute to the conventional LED. Here in this paper, a simulation of the multilayered OLED with double block layer has been done. Thereafter, the change in ratio of thickness of the two layers comprising the double block layer is made, and its effect on the performance of the device is observed.

Keywords Organic semiconductor material (OSC) · Organic Thin Film Transistor (OTFT) · Organic light-emitting diode (OLED) · Double hole block layer (DBL)

1 Introduction

Organic light-emitting diodes (OLEDs) are one of the applications of the organic electronics which has improved itself by leaps and bounds in the recent decades. In fact, it is the only application which has surpassed the inorganic counterparts and is now being actively used by the industry [1–3].

OLEDs possess many advantages over the inorganic counterparts which have made it the device of choice to be used in the displays [4–6]. To sum up its advantages, it can be said that it has a very large variety of colors available for the display which has not even been provided by the inorganic counterparts [1]. The characteristics of color shown by the OLEDs are also highly appreciated for its quality and at the same time providing a good contrast between them, which enhances the picture quality.

S. Negi (✉) · P. Mittal
Department of Electronics and Communication Engineering,
Graphic Era University, Dehradun 248002, India
e-mail: Shubhamnegi0192@gmail.com

B. Kumar
Madan Mohan Malaviya University of Technology, Gorakhpur, India
e-mail: brijesh2228@gmail.com

Adding on to this, they have shown a good efficiency and the reason for this could be their power consumption which is low along with the low driving voltage [5]. They also have a high-speed electronic response time [4, 5]. The viewing angle, as wide as provided by the OLEDs, has never been achieved before. These all the advantages of the OLED are accompanied by the technological advantages of the organic electronics which includes the thin, flat, and light devices which are cheaper to manufacture, and at the same time, one can transform them for the flexible devices if all the organic materials are used for the device fabrication [2–6]. So in a nutshell, it can be said that OLED can provide a uniform source of light which has the property of self-emission and it can cover a large surface area.

In this paper, simulation of the multilayered OLED with double block layer has been done and further comparison of this device is made with the devices in which there is a variation of ratio of thickness of the two block layers which have been used. The simulations are done with the help of Silvaco Atlas tool [7].

This paper is divided into five sections, including the current introductory Sect. 1. This is followed by Sect. 2 where the basic knowledge about the multilayered OLED with double block layer has been explained. Thereafter in Sect. 3, the simulation setup is discussed for obtaining the results. This setup is employed for the analysis of the performance of multilayered OLED with double block layer. It is followed by the comparison of the properties of multilayered OLED when the ratio of thickness of the layers comprising the DBL is changed in Sect. 4. After this, concluding remarks have been given in Sect. 5.

2 OLED with Double Block Layer

Organic materials known are mostly the *p*-type materials, i.e., they favor the transportation of holes through them. The *n*-type organic materials are less known, and their performance is not too good. Also the speed of holes is more than the speed of electrons in the organic materials. When a multilayered OLED was made, the properties of material were taken for the injection of charge carriers, and this indeed helped in the recombination of holes and electrons. But as just mentioned above, the speed of holes is more than that of the electrons, so still some of the holes escape the EML layer and reach the cathode and get wasted. To prevent this, an additional layer is used and this layer is called the hole block layer (HBL). Sometimes, to further enhance the blocking properties, two HBLs are used, and that type of OLED is called double block layer. The structure of multilayered OLED with double block layer is shown in Fig. 1.

It can be seen in Fig. 1 that there are two new layers above the previously-defined layers of the multilayered OLED. These are the BA1q layer and the BPhen layer. The sole purpose of these layers is to block the flow of holes from the emission layer (EML) to the cathode. This is achieved by choosing the HOMO level of the block layer which is quite high, so that the holes can not easily jump the

Fig. 1 A multilayered OLED with double block layer



Table 1 Dimensions of the layers of device A used for simulation

S. No.	Layer name	Thickness of layer (in nm)
1	ITO (anode)	50
2	m-MTDATA (HIL)	45
3	NPB (HTL)	10
4	Alq ₃	5
5	QAD (EML)	0.1
6	Alq ₃	10
7	BAIq (HBL)	8
8	BPhen	8
8	Alq ₃ (ETL)	44
9	LiF (cathode)	1
10	Al (cathode)	50

energy barrier and thus they get trapped in the EML layer which improves the recombination.

The secondary task of these block layers is to enhance the electron injection, and if not, then not to interfere with the transportation of the electrons. This is achieved by having a LUMO level which is very close to the cathode layer.

3 Simulation Setup

The structure of multilayered OLED with double block layer is shown in Fig. 1. The different layers which have been used are clearly mentioned in the figure. The dimensions of the different layers are given in Table 1. The width of the device is 1 μm. The structure starts with the basic anode ITO over which the different OSC materials have been deposited. Firstly, a hole injection layer (HIL) is there of the

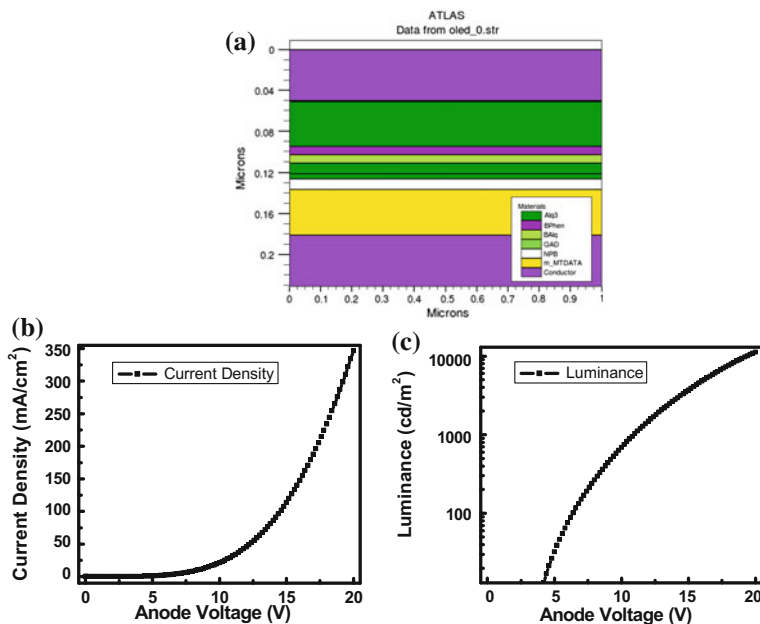


Fig. 2 The simulated results for the multilayered OLED with double block layer **a** simulated structure, **b** plot for current density and anode voltage and **c** plot for luminance and anode voltage

material m-MTDATA, followed by the hole transport layer (HTL) of NPB. Then the combination of Alq₃ and QAD layer is used for the EML layer. Above it, there are the two hole block layers of BAq and BPhen used. Their ratio in this device is 1:1, i.e., they both are in equal with respect to the thickness of the layers. Above it, there is again a layer of Alq₃ which functions here as an electron injection layer (EIL). Then at the top, there is a bilayer of Al/LiF which is the cathode. This device is the device A in the simulation.

The simulated structure of the device is shown along with the results for the current density and the luminance with respect to the anode voltage in Fig. 2.

It can be seen clearly from Fig. 2 that the performance of the OLED with double block layer is good, and the luminance characteristics and current density are of a good level.

4 Comparison of Variation in Ratio of Double Block Layer

In this section, a comparison of the change in ratio of the two block layers used has been made. The multilayered OLED which has been simulated in Sect. 3 has 1:1 ratio of the two block layers, i.e., 8 nm of BPhen and 8 nm of BAq. Now the effect

of change in the ratio is seen. For this, different ratios of BPhen–BAIq layer are taken and their impact on the current density and the luminance is noticed. The ratios that have been taken here are 1:1, 3:1, 7:1, 15: 1, 1:3, 1:7, and 1:15. These ratios are taken for BPhen–BAIq.

The plots for the current density versus the anode current are shown in Fig. 3. It appears from the plot in Fig. 3a that the effect of change in the thickness of layers is not prominent, but once the plots are zoomed near the end points the specific difference can be seen. The increment of ratio of thickness of BPhen layer decreases the performance of the device, whereas on the other hand, the increment in the ratio of BAIq increases the performance of the device. This increment is not very much for the current density.

Similarly, the plots for the luminance of the device are obtained and are shown in Fig. 4. Again like the previous case, it is seen from the graph that the effect of change in ratio is not there but once the graph is zoomed at the maximum operating voltage it shows the same results.

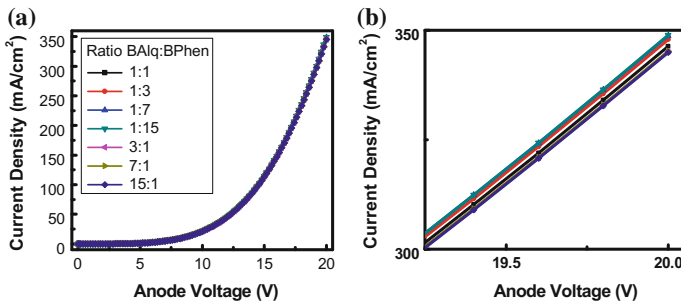


Fig. 3 a plot of current density versus the anode voltage at different ratios of block layer, b the zoomed view of the plot in (a) to show the effect of ratio variation

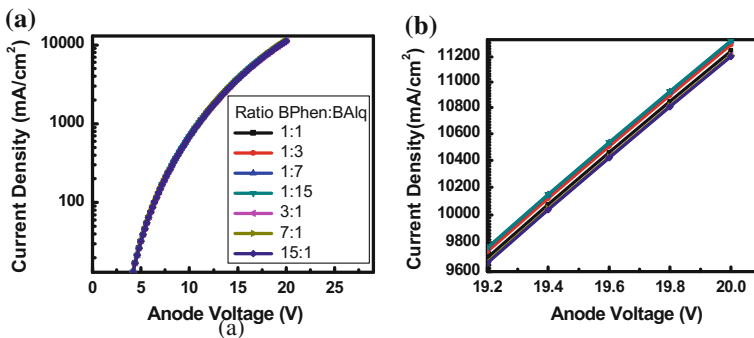


Fig. 4 a plot for the luminance versus the anode voltage for the different ratios of double block layers, b the zoomed version of the plot in (a) to show the effect of ratio change

The performance of the device is increased whenever the ratio is in favor of BAQ layer as compared to the BPhen layer. It can thus be perceived that the BAQ layer is a better layer for the blocking of holes when compared to the BPhen layer.

There is one more result from this which can be seen on closely observing the graphs in Figs. 3 and 4. Though the performance is increased on changing the ratio in favor of BAQ, it is also noted that when the ratio is increased too much that the other layer becomes almost insignificant, and the performance resembles the single block layer device and this performance is overall poorer when compared to the double block layer with ratio 1:1. Thus, increasing the ratio can lead to good performance, but only till the contribution of both the block layers in DBL are significant.

5 Conclusion

The conclusion that can be drawn from the simulations that have been shown in this paper are that the change in the ratio of thickness of the layers of double block layer has a small but significant effect on the performance of the device. The BAQ layer is considered as the better HBL than BPhen layer, and thus in the DBL, whenever the ratio of BPhen layer is increased, the performance is decreased; when the ratio of BAQ layer is increased the performance is improved. The second conclusion is that increasing the ratio of double block layer so as to get one layer in negligible thickness leads to the overall performance degradation of the performance compared to the DBL with ratio 1:1.

References

1. B. Kumar, B. K. Kaushik and Y. S. Negi, "Organic thin film transistors: Structure, models, materials, fabrication, and applications: A review", *Polymer Review*, vol. 54, no. 1, pp. 33–111, Sept. 2013.
2. B. Kumar, B. K. Kaushik and Y. S. Negi, "Static and dynamic characteristics of dual gate organic TFT based NAND and NOR circuits", *Journal of Computational Electronics*, vol. 13, no. 3, pp. 1–12, Sept. 2014.
3. B. Kumar, B. K. Kaushik, Y. S. Negi, and V. Goswami, "Single and dual gate OTFTs based robust organic digital design," *Microelectronics Reliability*, vol. 54, no. 1, pp. 100–109, Jan. 2014.
4. D. Ammermann, A. Bohler and W. Kowalsky, "Multilayered organic light emitting diodes for flat panel displays", pp. 48–58, Annual Report, Institute fur Hochfrequenztechnik, TU Braunschweig, 1995.
5. H. Yang, Y. Zhao, J. Hou and S. Liu, "Organic light emitting diodes with double block layer", *Microelectronics Journal*, vol. 37, no. 11, pp. 1271–1275, 2006.
6. S. Negi, A. Rana, A. K. Baliga, P. Mittal and B. Kumar, "Performance analysis of dual gate organic SR latch application," *ICCCA 2015*, pp. 1323–1328, 2015.
7. ATLAS User's Manual Device Simulation Software. Silvaco International Ltd., Santa Clara, USA, 2014.

Design and Performance Evaluation of Frequency Compression Algorithm for Marathi Hearing Aid Users

Prashant G. Patil, Arun K. Mitra and Vijay S. Chourasia

Abstract High frequency hearing loss for hearing aid user is hurdle for speech recognition in different background speaker–listener environment. In North Maharashtra region, patient suffered from moderate hearing loss at high frequency is unable to understand consonants and some vowels. In Marathi language, more confusing consonants are difficult to understand which will confuse HA user. Many Marathi words start with these confusing words. To design a hearing aid, we need to control and limit parameters like gain, compression time constants, processing attack time, compression ratios which clears that fast processing time will increase objectively speech intelligibility and slow processing time affect on sound quality. In this study, we designed MATLAB-based digital hearing aids according to the need of user. This digital hearing aid will fulfil all requirements of hearing aid users to limit the gain, frequency shaping of speech signal. In this method, speech signal is processed for different types of hearing impaired people which will make more audible for them. 1730 pre-processed Marathi sound recordings recorded in different background conditions are differing in parameters like compression ratio, compression speed and signal-to-noise ratio. Experimentation results show that all listeners are recognizing Marathi vowels and consonants very well in all background conditions.

Keywords Hearing aid · High frequency · Hearing loss
Marathi vowels · Frequency compression

P.G. Patil (✉) · A.K. Mitra · V.S. Chourasia
Department of Electronics Engineering, Manoharbai Patel Institute
of Engineering & Technology, Gondia 441601, Maharashtra, India
e-mail: patilpg232@gmail.com

A.K. Mitra
e-mail: akmitra@gmail.com

V.S. Chourasia
e-mail: chourasiav@gmail.com

1 Introduction

Nowadays hearing loss is affecting strongly on society, which occurs by diseases affecting middle ear or inner ear, age related or negligence at the initial level of detection. In India, 6.3% of total population suffered from hearing loss. According to national sample survey (NSS) taken in 2014 shows hearing disability in India is second major disability. In urban areas, high frequency hearing loss is about 9% of total disability, and in rural areas it is up to 10% of total disability. Depending upon the level of a person's inability to hear, the degree of hearing disability was ascertained. It is found that in Maharashtra, the number of persons with high frequency hearing disability was up to 2.291%. The percentage was higher in rural (2.310%) as compared with urban regions (2.236%). It is found that about 22% of the people suffered from profound loss (person could not hear at all or could hear only loud sounds) and 14% had severe hearing disability (not able to hear normal words). The survey shows that about 4% of people suffered from hearing loss from birth. In north Maharashtra region, 43 and 51% population reported the hearing disability in the 50–55 years of age in the rural and urban regions, respectively. Hearing loss is associated with age, and it is found clearly present in new birth children, teenagers and young adults. Normal person without any hearing loss can perceive a wide range of sounds in terms of pitch and loudness level in any background environment. Hearing is the primary sense of action by which we learn speech and mother language first. The ability to hear clearly after 6–8 months of birth is important to learn speech and language skills, auditory processing skills. A survey is done for four districts of north Maharashtra region (Table 1).

In this study, survey was taken at NGO-operated school shows that children's age between 12 and 20 years has difficulty to hear many Marathi words. These Marathi words always used in daily communication, many of them start from consonants so initial alphabet of word will wrongly recognized by HA user. All of these users wear low-cost hearing aid given by government or purchased by NGO's. Our prime goal is to improve recognition of Marathi alphabets in different listener's background condition. Here, we designed MATLAB-based DHA which will be useful to remove high frequency hearing loss and proper recognition of Marathi vowels and consonants. These will be useful for 6-year-old HA user as an assistive tool for learning Marathi alphabets.

Table 1 District wise patient suffered from high frequency hearing loss

District	No. of patients
District Hospital, Nandurbar	409
Govt. Medical College Dhule	1868
District Hospital, Jalgaon	2585
District Hospital, Nasik	1647
Maharashtra	168,559

<https://sadm.maharashtra.gov.in/sadm/en/getDetailedReport.gov>

2 Hearing Aid and Design Consideration

Hearing aids carry sounds from the outside environment into ear and make them audible nearer to patient requirement. The digital hearing aid has powerful battery, small microphones which collect sounds from the environment. An amplifier converts the all incoming sound (speech and speechless) then amplified signals are processed back to sound waves and delivered to ears through speakers of hearing aid.

According to World Health Organization, “Guidelines for Hearing Aids and Service for Developing Countries” in 2004 which states that total world production of HAs is less than 10% of the actual need and HAs and their regular services are expensive and often neglected by HA users. Main reason behind this awareness by HA user is inappropriate for developing countries. A survey shows that in deaf school, most of the students are coming from below poverty line (BPL holders). In India, most of the hearing disabled persons think that after wearing HA, we will hear well as normal person. WHO suggested that HA’s outcomes produced must meet the minimal requirements of user. Following parameters are playing key role in designing hearing aid in MATLAB

- Input speech signal is sampled at 16 kHz and hamming windowed 25 m s.
- Windows are overlapped ranging from 25 to 75%. Part of spectrum will compress the energy of 500 Hz bandwidth sliding windows are calculated with 100 Hz spacing from 1 to 8 kHz.
- Hick’s frequency compression Eq. (1) is considered for both low and high frequency ratio. Gain referred as amount of amplification applied to signal.
- If output has 120 dB SPL and input has 30 dB SPL then keep hearing in comfort zone.

$$\frac{F_{in}}{F_s} = \frac{1(1-a)}{\pi(1+a)} \tan\left(K \cdot \pi \frac{f_{out}}{f_s}\right) \quad (1)$$

Compression threshold (knee point) is defined as the input SPL is processed in the hearing aid will be reduced in the factor of K (± 0.5) dB. It is the point on the input/output function where the output level is 2 dB lower than it would be if no compression had occurred. If the input signal is louder then compression will be activated (input > threshold level); the compression ratio (CR) will decide amount of signal to be compressed.

$$CR = \Delta \text{Input} / \Delta \text{Output} \quad (2)$$

If input increases from 60 to 80 dB SPL, then output increases from 80 to 100 dB SPL then we need to set CR 2:1. Depending on the need of patient, system may have high or low CRs. A high Compression ratio 4.0 is used to limit the output of a hearing aid so that it does not exceed the user’s loudness discomfort levels. On

Fig. 1 Flowchart for signal processed in MATLAB simulation model

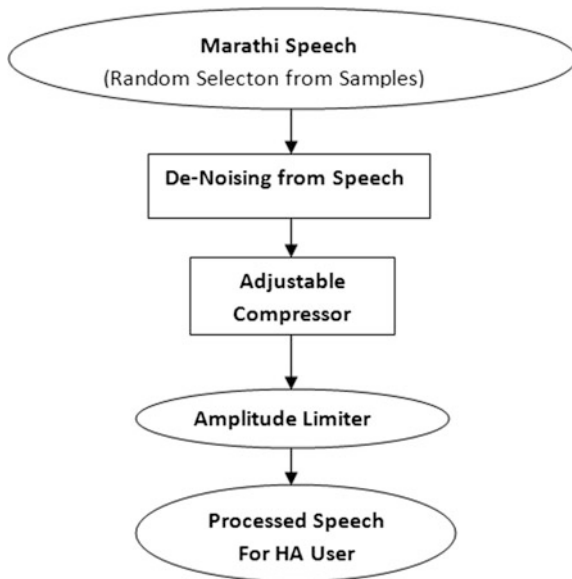
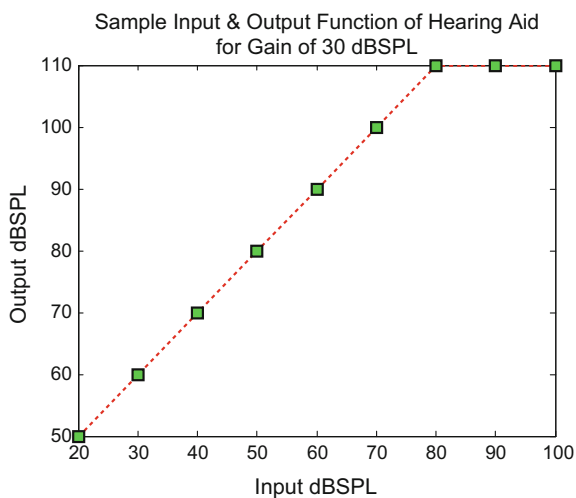


Fig. 2 Input and output function of signal with gain of 30 dB SPL in compressor



the other hand, a low CR typically set between 1.0 and 2.0 is used to improve audibility of the soft spoken speech and to restore loudness perception (Figs. 1 and 2).

- Maximum sampling frequency 44.1 kHz providing for excellent sound quality.
- A gain is added in between 30 and 45 dB.
- Low delay in processing (6.3–15.7 ms).
- Increasing audibility with low compression threshold (CT).

- Attack time and release time for compression (faster to avoid unwanted processing).
- Input versus output controlled compression.
- Multi Channels and Bands.

3 Processing Conditions of Compressor

Attack time (AT) is the time delay which occurs when the level of input signal loud enough to start compression process which is occurred if input signal is greater than threshold knee which will result reduction in gain to its target value (desired level or comfort zone of HA user. Release time (RT) is the time delay that occurs when offset of an input signal sufficiently loud to activate compression, which occurs when input signal is less than threshold knee. The details of proposed methodology are as follows:

- The objective is to develop hearing aid which will reduce moderate hearing loss for 4 HA users, who has difficulty in hearing high frequency, gain added in hearing 30–45 dB and threshold pain 90–110 dB

$$\text{Gain } G = \text{Output } Y(f) - \text{Input } x(f). \quad (3)$$

- Marathi speech signal has been inputted as wave file which contained noise, and then denoise function has been used to remove noise from speech signal.
- Wide range of compressor with different CR and threshold value.
- Time domain signal is converted to frequency domain ($N = 64$).
- Decide Minimum and maximum level of CR, T_{attack} , T_{Release} , compression threshold.
- Gain is set for first frequencies—signal is converted to samples where the total number of samples for signal is divided into number of frequency ranges. Entire frequency vector of signal has same sampling frequency.
- K = Pointer for number of samples has been modified.
- N = Total number of samples, T = sampling time.
- The pointer K would be modified in between 1000 and 2000 Hz.
- Amplitude level of individual sample is compared with $V_{t \text{ min}}$ and $V_{t \text{ max}}$ levels.
- If the signal level is more than knee threshold of user, then reduce the signal level to comfort zone of user.
- Processed Marathi speech samples are random play backed and listened to HA user by using PC and wireless headset in different environments.
- Multiple experiments were conducted to each listener for improvement and taken a decision to decide set of needed parameters for configurable compressor.

4 Simulated Results for Marathi Vowel

In this algorithm, we are processing pre-recorded Marathi vowels, consonants, syllables and rhyming words (confusing words for HA user) in different speech background environments. For simplicity, here we used only vowels to test and validate the algorithm, reason behind this is all Marathi vowels are distinctly separated by frequencies. In adjustable compressor, set of all parameters are varied from minimum value to maximum value to find suitable condition where HA user will find greater accuracy, comfort and higher recognition rate; M1 and M2 are corresponding set of parameters at minimum and maximum value, respectively. They are compared with own hearing aid performance then again tests are conducted to find moderate value parameters to achieve task (Fig. 3).

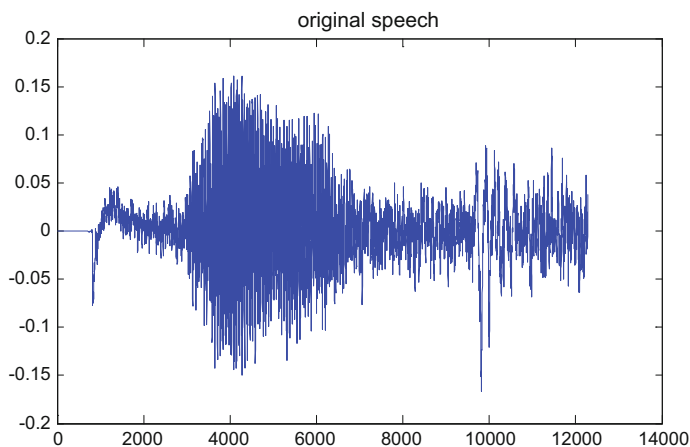


Fig. 3 Input Marathi vowel ऌ by female speaker in noisy room

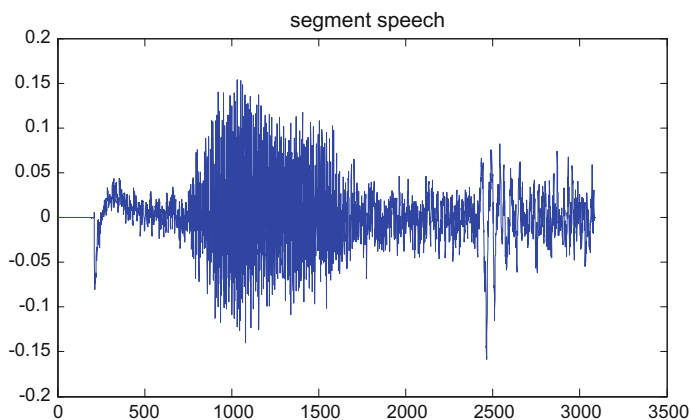


Fig. 4 Compressed Marathi vowel ऌ by factor of 4

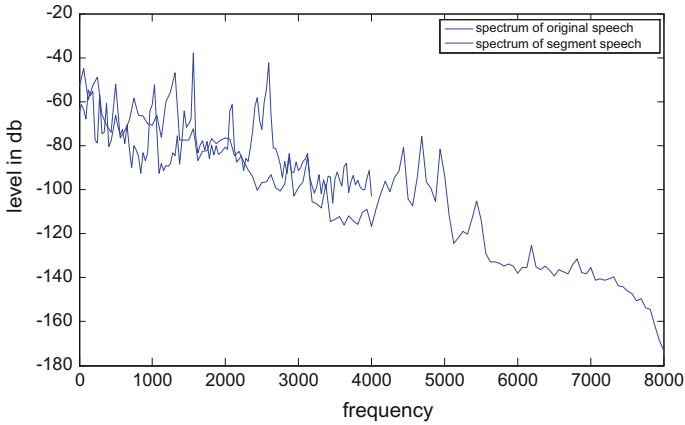


Fig. 5 Spectrum of original and segmented Marathi vowel ᳵ without overlapping

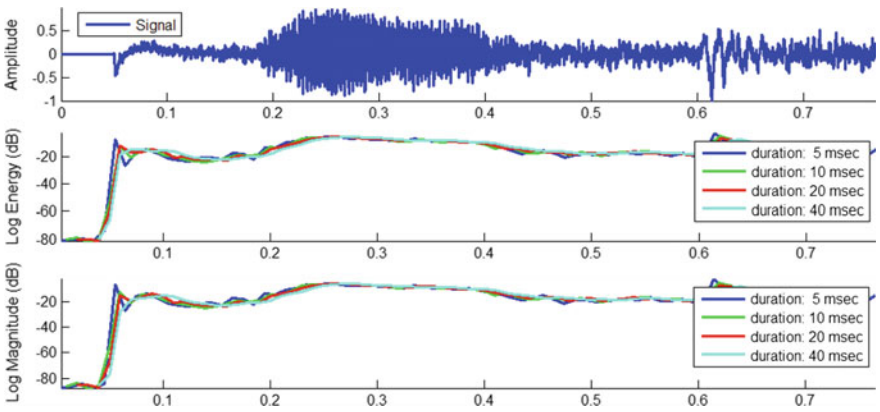
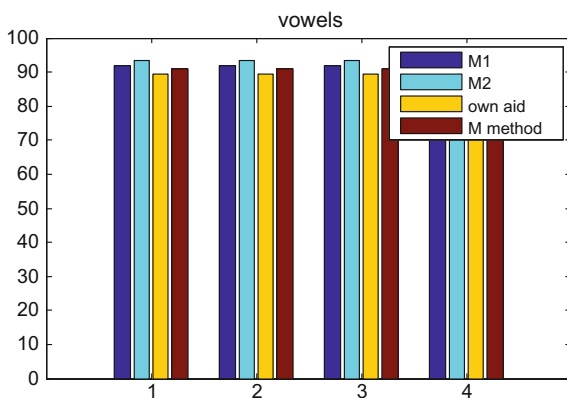


Fig. 6 Log energy levels of vowel ᳵ (noisy environment) in Marathi for different processing time

In Marathi language, individual vowels are not conveying important part of message sometimes with consonants, these are important. So here vowels are tested by group of 4 listeners in noisy environment. All participants were ready to adopt new algorithm with few changes (Figs. 4, 5, 6 and 7).

Fig. 7 Comparison of vowels recognition rate by 4 HA listener using min (M1), max (M2), owned HA and moderate set of parameter



5 Conclusion

This reconfigurable MATLAB-based frequency compressor tool is more capable for fine-tuning the speech with less distortion in the quality. Digital hearing aids system implementation using MATLAB is an approach towards satisfaction of hearing aid user; it is possible to refine the sound signal, for instance, by reducing noise and improving speech signals. In addition, by using this approach, the amplification will be done only at the range of frequencies which user needs to amplify. This will eliminate the problems with unwanted processing of vowels and consonants. All 4 HA users are satisfied with configurable approach but take it needs lots of experiment to find suitable set of parameters. Gender wise every listener need to set different parameters which is difficult and time-consuming process. To overcome this condition in future, we extend towards designing of intelligence-based compressor where manual adjustment will be done by decision-making device under some circumstances. Compressor plays a vital role to design and build intelligent compressor which is a big task in future.

Acknowledgements This research work was carried out at the Priyadarshini Deaf Residential School, Shirpur Dist-Dhule (India). We have obtained all ethical approvals from an appropriate ethical committee of institutional review board. If any issue arises hereafter then we will be solely responsible. The scientific responsibility is assumed by the authors. The institute had given the researcher permission to use our data as part of their experimental study. Institute have no objection to publish the experimental data in conference or journal paper.

References

1. James M. Kates, Senior Member, IEEE, and Kathryn H. Arehart, "The Hearing-Aid Audio Quality Index (HAAQI)" IEEE/ACM Transactions on Audio, Speech & language Processing, Vol. 24, No. 2, February 2016.

2. Francisco J Fraga, Leticia Pimenta C, S prates, Alan M Marotta, "Frequency lowering Algorithms for Hearing Impaired, A Text book of Speech technologies", Book Chapter 18, pp. 361 –388.
3. Danielle Glista, Susan Scollie, Marlene Bagatto, "Evaluation of nonlinear frequency compression: Clinical outcomes". *International Journal of Audiology* 2009; 48: pp 632644.
4. Harry Levitt, "A Historical Perspective on Digital Hearing Aids: How Digital Technology Has Changed Modern Hearing Aids", *Trends in Amplification* Volume-11, Number 1, March 2007. pp 7–24.
5. Joshua M. Alexander, "Individual Variability in Recognition of Frequency-Lowered Speech", *Seminars in Hearing*, Volume 34, No 2, Dec 2013.
6. Francis Kuk, "Considerations in Verifying Frequency Lowering", Published on January 19, 2013. *International Journal of Audiology* 2013.
7. Ying-Yee Kong, Ala Mullangi, "On the development of a frequency-lowering system that enhances place-of-articulation perception", *Speech Communication* 54 (2012) 147–160.
8. Pandurangarao N. Kulkarni, Prem C. Pandey, Dakshayani S. Jangamashetti "Multi-band frequency compression for improving speech perception by listeners with moderate sensorineural hearing loss" *Speech Communication* 54 (2012) 341–350 Elsevier 29 September 2011.
9. Shilpi Banerjee, Starkey Hearing Research & Technology. "An overview of the characteristics and applications of compression amplification". Process handbook Published in 2014.
10. Joshua M. Alexander, *Frequency Lowering in Hearing Aids*, March 29–31,2012 ISHA Convention.
11. Ruiyu Liang, Ji Xi, Jian Zhou, Cairong Zou, Li Zhao, An improved method to enhance high-frequency speech intelligibility in noise, *Applied Acoustics* 74 (2013) 71–78.
12. J. Fraga Francisco, C. S. Prates Leticia Pimenta, M. Marotta Alan, Martinelli Iorio Maria Cecilia, *Frequency Lowering Algorithms for the Hearing Impaired*, ISBN 978-953-307-996-7.
13. Veugen, Lidwien CE, Maartje ME Hendrikse, Marc M. van Wanrooij, Martijn JH Agterberg, Josef Chalupper, Lucas HM Mens, Ad FM Snik, and A. John van Opstal, "Horizontal sound localization in cochlear implant users with a contralateral hearing aid", *Hearing research*, Vol. 336, pp. 72–82, 2016.
14. Finke, Mareike, Andreas Büchner, Esther Ruigendijk, Martin Meyer, and Pascale Sandmann "On the relationship between auditory cognition and speech intelligibility in cochlear implant users: an ERP study", *Journal on Neuropsychologia*, Vol. 87, pp. 169–181, 2016.
15. Liang, Ruiyu, Ji Xi, Jian Zhou, Cairong Zou, and Li Zhao, "An improved method to enhance high-frequency speech intelligibility in noise," *Journal on Applied Acoustics*, Vol. 74, No. 1, pp. 71–78, 2013.
16. Sang, Jinqiu, Hongmei Hu, Chengshi Zheng, Guoping Li, Mark E. Lutman, and Stefan Bleeck, "Speech quality evaluation of a sparse coding shrinkage noise reduction algorithm with normal hearing and hearing impaired listeners", *Hearing research*, Vol. 327, pp. 175–185, 2015.

Emotion Recognition System for Patients with Behavioral Disorders

Aakash Verma, Astha Dogra, Ketan Malik and Meenkshi Talwar

Abstract According to a WHO survey in 2014, “One in four people in the world will be affected by mental or neurological disorders at some point in their lives.” This survey tells that a lot of population is affected with mental disorders, going through various struggles, which they did not opt for. They usually do not understand different emotions and are even unable to express them. So, this paper presents an Arduino-based wearable system for detecting emotions for patients with behavioral disorders. GSR sensor and pulse sensor record body parameters to assess the emotion of wearable and display it using different colors on the light indicator mounted on the wearable itself so that the patient can be taught about different emotions using color of indicator and other persons can be made aware of the mood of the patient. This data will also be saved using IoT enabling the doctor to do real-time monitoring.

Keywords Behavioral disorders · Emotions · Graph · GSR sensor · IoT
Pulse sensor · Wearable

1 Introduction

The processing as well as expressing emotions is elementary for normal socialization and social interaction [1]. Human intelligence is made up of mathematical, verbal, and emotional intelligence—the last one being the most important one. Potential to recognize emotions is essential for being emotionally intelligent but not everyone is capable and blessed enough to recognize as well as express themselves like others can do [2]. Perception of emotions by others also plays a vital role in deciding the quality of life a person with behavioral and emotional disorder will get. Such patients are neither able to communicate their emotions through facial expressions nor they have the right voice quality to express themselves through

A. Verma · A. Dogra · K. Malik (✉) · M. Talwar
University of Petroleum and Energy Studies, Dehradun, India
e-mail: ketanmalik@gmail.com

speech. Thus, this makes their existence even more difficult and challenging, making their lives vulnerable to an extent which cannot be imagined [3]. This problem has been acknowledged by various scientists, researchers, doctors, and empathetic individuals who have come up with different solutions in their respective fields of study.

Petrushin et al. implement a system which uses voice signals to assess the emotion associated with the voice and then stores it for future references [4]. Narayanan et al. describe an emotion recognition system which not only uses verbal communication but also non-verbal communication to estimate human emotional behavior. It receives the signals from speaker and then modifies it to draw the conclusion about emotional state [5]. Picard et al. explain an “affective wearable” which is nothing but a wearable system integrated with various sensors to recognize different emotions and behavioral patterns of the person wearing it [6]. Peter et al. discuss the need for introducing authentic and powerful technology in field of affective computing. A system was presented which used fusion of various body parameters and sensors to fabricate a multi-sensor variable system serving the purpose of emotion recognition and data-logging for references [7].

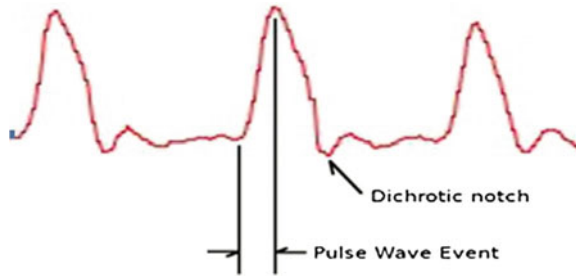
Walking on the same path, this paper introduces an Arduino-based emotion recognition wearable system with behavioral disorders. It uses GSR and pulse sensors to sense the body parameters, an OLED display as well as light indicator to display results, and an Arduino which processes the information and controls the display unit. The recorded data will also be stored using IoT for future references. The galvanic skin response (GSR) sensor measures the electrical conductance of skin. Human body starts microswearing due to excitement or stress which in turn changes the conductance of the skin, and this change is measured by GSR [8]. The pulse sensor measures the transparency of the skin and provides Arduino with live heart-rate data for measurements [9]. The data recorded using the two sensors was used to develop a graph in software which would reveal the state of emotion the person is in [10]. The recorded data can also be displayed and stored on cloud using IoT and hence, provides real-time monitoring for doctors and other concerned people.

Thus, a robust and efficient wearable system is presented which will not only display the mood of person wearing it but also provide the real-time data particularly to doctors for better treatment of people suffering from behavioral disorders [11].

2 Hardware Development

2.1 Components

- Pulse Sensor (SEN-11574): It is a non-invasive heart-rate monitoring sensor. The output of the sensor is voltage analogous to the pulse rate of the heart (Fig. 1). When the heart pumps blood, it generates a pulse throughout the body. This sudden change is recorded by using a LED and photodiode, and analogous

Fig. 1 Pulse rate of the heart

voltage is given as output. When the red LED is on all the time, the change in value of the photodiode due to pulse changes the voltage at the output.

- **GSR Sensor:** Various glands present on human body secrete body fluid such as sweat due to sympathetic activities. This change occurs in unconscious state. The change in sweat causes change in body conductance. Thus, by measuring the skin conductance, one can predict the emotion of the person. The GSR sensor measures the skin conductivity and gives analogous output. Thus, by measuring the GSR values, one can predict the emotional arousal such as happy state as well as sad state. The sensor is non-invasive and hence can be easily attached. The concentration of the sweat gland in human body varies from part to part. Thus, attaching GSR sensor to the part where more sweat glands are present, i.e., hands, will increase the level of accuracy.
- **Arduino LilyPad:** It is low-power Arduino board using ATmega168V microcontroller. On interfacing the device with various sensors, it will receive analog data in form of voltage from the sensor. It will then apply the algorithm to convert the analog data received to produce results which can be understood. The result will be then displayed on the OLED display, and accordingly, the result will be shown using LED. As it is a programmable device, the algorithm can be altered according to user's desire. Also the Arduino LilyPad is washable and will make the product more handy.
- **OLED display:** The OLED display is interfaced with the microcontroller to display the data. This provides better user interface and hence will help in better diagnostics.

2.2 Block Diagram

See Fig. 2.

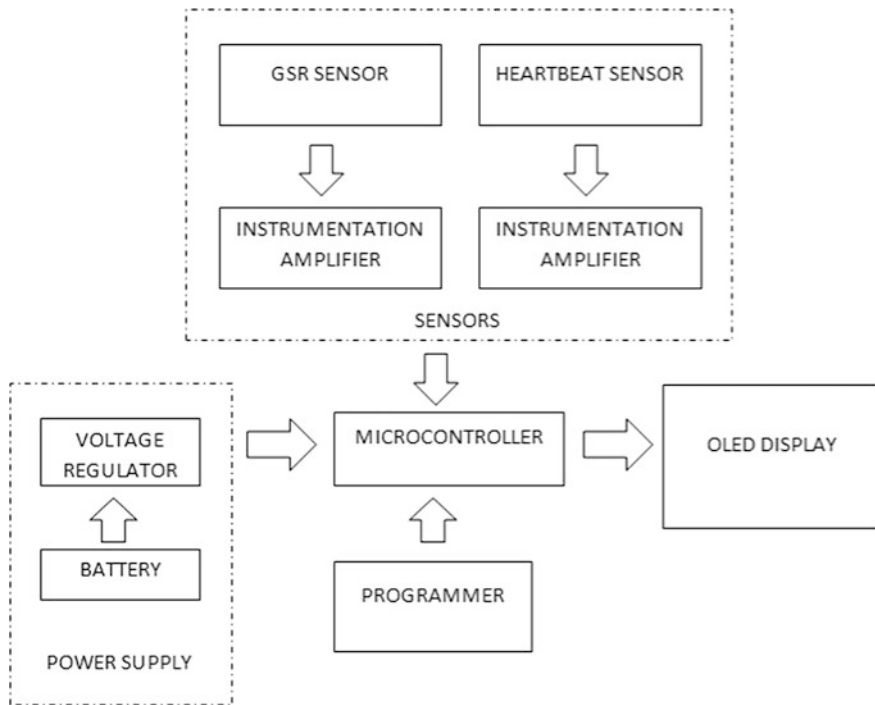


Fig. 2 Block diagram of the system

3 Working

This wearable device senses the state of emotion of the patient suffering from behavioral disorder by incorporating a pulse sensor and a GSR sensor. Corresponding to every emotion, the level of sweat produced in the skin differs. Since the GSR sensor measures the electrical conductance of the skin, for different values levels of sweat there would be different value provided by the GSR sensor. Hence, different values of GSR sensor can be used to indicate different emotions. Also, by using the pulse sensor, the pulse rate can be measured to infer the emotional state of the patient wearing the device. The data from both the sensors will be collected by the Arduino at its analog pin, and this data will further be used to plot a graph on MATLAB. This graph gets plotted in real time. On comparing this graph with the standard one (with emotions known), the emotional state of the patient is concluded. Same graph will be displayed for reference of doctor/psychologist. Also, an indication for the patient will be shown according to the emotion using a light indicator. The data collected in real time will be stored using IoT, so that it can be referred to whenever required.

4 Software Development

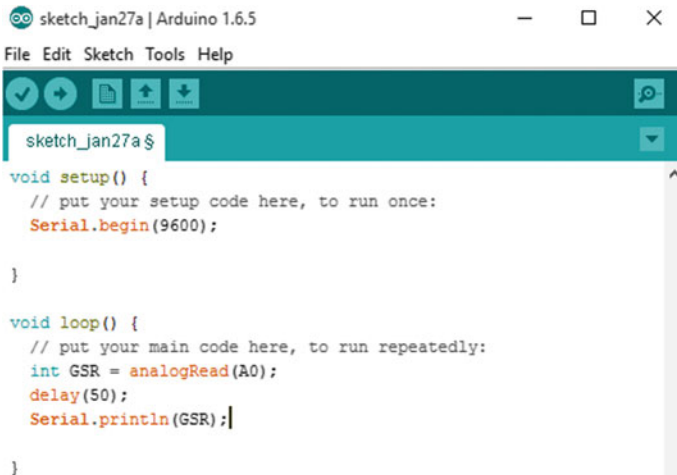
Arduino is the main processing unit of information. It collects data from sensors and controls the display unit. The sensors integrated with Arduino are GSR reader and pulse sensor.

The GSR sensor measures the electrical resistance through the body. The two leads are connected to two fingers of the person, and the analog output is fed to Arduino. This setup can be used to measure GSR at equal intervals, say 50 ms. Each reading is graphed, and changes in output according to mood can be seen in the graph and serial monitor by using the code as shown in Fig. 3.

The pulse sensor attached to digital input of Arduino will also send analog values at equal time interval according to the live pulse of the person. This information can also be recorded on a separate graph and can be verified on the serial monitor by using the code as shown in Fig. 4.

Taking into account the above two values, a graph can be plotted and compared to the reference graph as shown in Fig. 5.

This graph will be used to recognize the emotion and control the display unit accordingly. The same information can also be stored using IoT.



```
sketch_jan27a | Arduino 1.6.5
File Edit Sketch Tools Help
sketch_jan27a $
void setup() {
  // put your setup code here, to run once:
  Serial.begin(9600);
}

void loop() {
  // put your main code here, to run repeatedly:
  int GSR = analogRead(A0);
  delay(50);
  Serial.println(GSR);
}
```

Fig. 3 Program for serial monitoring of data

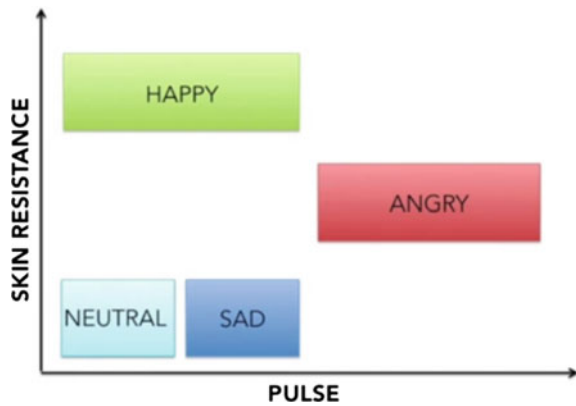
```

sketch_jan27a | Arduino 1.6.5
File Edit Sketch Tools Help
sketch_jan27a $
void setup() {
  // put your setup code here, to run once:
  Serial.begin(9600);
}

void loop() {
  // put your main code here, to run repeatedly:
  int HR = digitalRead(2);
  Serial.println(HR);
}
    
```

Fig. 4 Program for serial monitoring of data for heart beat

Fig. 5 Reference graph to recognize the emotion



5 Conclusion

This paper provides a technique to detect emotions of people with behavioral problems who are either unable to express emotions or have difficulty in understanding what they are feeling themselves. The wearable device discussed in this paper detects and displays the state of mind of the patient in the form of a color. This display of color allows the mood of the patient to be identified and understood by not only themselves but also by other people improving the quality of life of such patients. The data is saved on cloud and can be accessed by the doctors or other people concerned to monitor and note the variations enabling the doctors to give suitable treatment to patients with behavioral problems. In this way, the gap between the patient and other people which was formed due to lack of or improper

communication is reduced, and the treatment received by the patients is in accordance with their state of mind. This device offers an easy-to-read and reliable option to people with disabilities for displaying their emotion and be understood despite their ability to do so by themselves.

References

1. Blair, Robert James Richard, and Melanie Coles. "Expression recognition and behavioral problems in early adolescence." *Cognitive development* 15.4 (2000): 421–434.
2. Picard, Rosalind W., Elias Vyzas, and Jennifer Healey. "Toward machine emotional intelligence: Analysis of affective physiological state." *IEEE transactions on pattern analysis and machine intelligence* 23.10 (2001): 1175–1191.
3. Laukkanen, Anne-Maria, et al. "On the perception of emotions in speech: the role of voice quality." *Logopedics Phoniatrics Vocology* 22.4 (1997): 157–168.
4. Petrushin, Valery A. "System, method and article of manufacture for an emotion detection system improving emotion recognition." U.S. Patent No. 6,353,810. 5 Mar. 2002.
5. Narayanan, Shrikanth S. "Emotion recognition system." U.S. Patent No. 8,209,182. 26 Jun. 2012.
6. Picard, Rosalind W., and Jennifer Healey. "Affective wearables." *Personal Technologies* 1.4 (1997): 231–240.
7. Peter, Christian, Eric Ebert, and Helmut Beikirch. "A wearable multi-sensor system for mobile acquisition of emotion-related physiological data." *International Conference on Affective Computing and Intelligent Interaction*. Springer Berlin Heidelberg, 2005.
8. Bakker, Jorn, Mykola Pechenizkiy, and Natalia Sidorova. "What's your current stress level? Detection of stress patterns from GSR sensor data." *Data Mining Workshops (ICDMW), 2011 IEEE 11th International Conference on*. IEEE, 2011.
9. Kioumars, Amir Hoshang, and Liqiong Tang. "Wireless network for health monitoring: heart rate and temperature sensor." *Sensing Technology (ICST), 2011 Fifth International Conference on*. IEEE, 2011.
10. Orha, Ioan, and S. Oniga. "Wearable sensors network for health monitoring using e-Health platform." *Carpathian Journal of Electronic and Computer Engineering* 7.1 (2014): 25.
11. Villupuram, Tamil Nadu, and Tamil Nadu Villupuram. "IOT BASED HEALTH MONITORING SYSTEM."

A Review on Computer-Aided Modelling and Quantification of PET-CT Images for Accurate Segmentation to Bring Imagination to Life

Ziaur Rahiman Shaik and Ch. Sumanth Kumar

Abstract Image segmentation is a process of dividing image into smaller parts to identify the individual objects. Often, this process helps in the quantification of digital images related to disease complications for metabolic process. This work reports on the use of computer-aided modelling tools and rapid prototyping technology to document, preserve and reproduce in three dimensions, and historic machines and mechanisms are used for accurate medical diagnosis. Epidemiological and clinical trials have confirmed the greater incidence and prevalence of deaths due to the inability to acquire qualitative information from the acquisition of images in primary stage itself. Rapid prototyping gives a better understanding of clinical and physiologic mechanisms of various disorders and pain, lesion detection. In image segmentation process, thresholding method is suitable for defining optimal value for identification and detection of region of interest. The standard uptake value (SUV) is based on selecting threshold value to utilize a similarity metric between the grey level of image and data points obtained from the threshold values. This is based on the intensities or inhomogeneity of clustering framework. Affinity propagation is used for images as a matrix by measuring the square patches from similarity texture. A major challenge in computer vision is to extract this information directly from the images available to us, help users, and to see and feel as an actual part in order to bring a computer image to life. Actually, the framework is given by PET-CT images which is used to identify and detect malignant tissues in a human body with accurate measurements of SUVs. This process involves ROI identification, segmentation, rendering and SUV functional quantification for promising results. The results

Z.R. Shaik (✉)

Department of ECE, K.L.M College of Engineering, Kadapa 516003, Andhra Pradesh, India
e-mail: ziaur.rahiman786@gmail.com

Ch. Sumanth Kumar

Department of ECE, School of Technology, GITAM University, Bengaluru 562163,
Karnataka, India
e-mail: c_sumanth@yahoo.com

© Springer Nature Singapore Pte Ltd. 2018

R. Singh et al. (eds.), *Intelligent Communication, Control and Devices*,
Advances in Intelligent Systems and Computing 624,
https://doi.org/10.1007/978-981-10-5903-2_17

147

obtained from computer modelling are transformed into real substance by rapid prototyping technology to feel and provide accurate diagnosis to patient.

Keywords Quantification · SUV · Epidemiological · Rapid prototyping

1 Introduction

Computed tomography, magnetic resonance imaging tomography, and positron emission tomography are used for clinical practice as diagnostic devices in examining the abnormalities of the human body. These diagnostic devices are also used as a visual aid to support various diseases. These devices will make design iterations faster, produce early feedback, identify flaws, detect inflammations and define early problems to save money and future of patient by identifying the disease in early stages. It provides better surgical results with fewer procedures and also improves the functionalities to a considerable extent [1]. These include skin soft tissues, hard tissues and extra hard bones such as jaws and teeth. The significance of the imaging modalities is that they highlight the affected region and also represent the complete face after chopping the selected portion in three different dimensions such as coronal, sagittal and axial. The realistic models developed by computer modelling can also be made into real life by rapid prototyping technology. Diagnosing in 3D is not much costly affair when compared with other medical imaging modalities. This dynamic CAD model proposed makes the forecasting and treatment of a patient on priority [2]. Physicians could use the results of computer analysis as a second opinion to make the final decision. However, the pathology detection and anatomical structures are used for therapeutic and diagnostic purposes. The structural and functional description of molecular biology is easily represented by PET images with higher sensitivity and specificity. Assessing functional images is possible with uptake values and radiotracers accumulated with abnormalities [3]. Imaging modalities are combined together to accumulate brain, kidney, liver, heart with various diseases to identify and detect earlier diagnosis of diseases. The clinical studies prove that the imaging of PET-CT provides higher resolution and accurate diagnosis at different stages in different fields of medicine such as cardiology, oncology and neurology. The high dose of radiation and targeted volume area minimizes the damage to the tissues and ensures early measures by identifying and detecting the inflammation and infection in the various parts of the human body. In this work, boundary is detected and also it easily identifies the malignant tissues involved with better clinical practice involved by segmentation methods. F-FDG is the deoxyglucose fluorine which is used to identify and localize the cells of the human body affected, and information provided will be of high resolution and predictable [4].

1.1 Use of Quantification in Clinical Practice for Standardized Uptake Value

PET/CT imaging modality uses fludeoxyglucose (F-FDG) as an imaging biomarker in identifying or detecting pathology in oncology, cardiology and neurology. This modality is a view of metabolic information and anatomical structures of various organs of the human body [5]. Therefore, the SUV information provided to this modality is suitable in characterizing the lesions for better therapeutic procedures

$$\text{SUV} = \frac{\text{Activity concentration} \left(\frac{\text{KBq}}{\text{ml}} \right)}{\text{Injection dose} \frac{\text{MBq}}{\text{Bodyweight (kg)}}}$$

1.2 Problems in Medical Image Segmentation

One of the major problems with PET/MRI/CT images is recognition, and another is outline boundary detection. These two yield a difficulty in distinguishing the malignant and nonmalignant tissues in the human body. One more aspect is defining the region of interest and uptake value of the region based on the human parts of the body. Usually, any segmentation process involves better resolution, identifying and detecting pathologies, shape, texture, position and external noise. Any algorithm suffers from imaging artefacts, motion artefacts, streaking artefacts, scanning artefacts, etc. The above artifacts make pathology detection difficult to understand and analyse, so in order to overcome these problems, a suitable algorithm is required to carry out all these tasks successful [6]. Hence, SUV measurement and quantitative calculations will overcome this problem to provide a second opinion to the doctor. The resultant image can be used for rapid prototyping of cosmetic surgical applications. Hence, there is a need for accurate and robust technique that can perform all the multimodal images in a real time for better clinical facilities with use of upgraded technology.

1.3 Patient Preparation

Usually for any imaging modalities, patient is made to check his weight for SUV measurement. The system invariability is found out with respect to his fat percentage and body mass. For PET scanning, the acquisition time will be 60 min and an injection is given for a patient with ^{18}F -FDG and repeated twice depending on the requirement of malignancy. Glucose level and blood pressure are monitored

with accurate reconstruction parameters. Monitoring glucose level is used to reduce SUV variability. The dose level defines activity concentration of a patient. These factors define the activity recovery concentration and breathing motion artefacts as the major problems in CT scanning, where many elements such as instrumentation and detector system provide the artefacts from various sources defined above. Some of the methods used are attenuation and registration for real-time pathology detection. Some of the related organs and tissues depend on Hounsfield units (HU) for tissues such as heart, liver, lungs and abdomen. The quantitative results are defined by quantification, efficiency and superior resolution. This type of scanning results is used for diagnostic confidence, treatment monitoring and therapy planning which can be seen in real time for lesion detection and accurate quantification [7].

2 Methods

2.1 Segmentation Methods Based on Region of Interest

Homogeneity in the image is the major consideration for detecting the boundaries of the defined image. Usually, segmentation methods use intensities of each region for local distribution. There are two groups that define the region while considering PET images: Two groups are graph cut and region growing, where these methods define the intensities based on histogram. The seed value is given by the user according to the standard deviation and mean. The pixels of image are connected together to define homogeneity matrix. Every pixel is identified from the statistics, and entire region is dissected from the segmented portion to highlight the exact boundary. The ROI is used to work for low-resolution and motion artefact images. Region growing is used to avoid the false positives in segmentation based on user-defined seed value. This algorithm is able to determine the boundaries of lesion over sharp regions with number of iterations. The required target structure can be chopped for the segmented areas depending on the user selection area.

Graph cut methods are used to separate foreground and background seeds based on user-defined value. This automatically locates objects in an image based on pixel similarities for optimum value [8].

2.2 Affinity Propagation

Usually, the image is divided into clusters based on the similarities as data points. These clusters provide better efficiency and low error rate as k -means clustering is used for each data point over the spatial region provided by the affinity function of radio tracer of PET. Usually, the AP divides the spatial region of the image into two

data points: availability and responsibility. These points are of scalar values indicating an angle between each other as $a(i, k)$ where k is a responsible point and i is an exemplar point. These message points send the information indicating the angle useful for serving each other. Here, $r(i, k)$ defines the responsibility point and $a(i, k)$ defines the availability point with respect to voxels for easy classifications and similarities between two points.

$$r(i, k) < -s(i, k) < -\text{Max}\{a(i, k') + s(i, k')\}$$

$$a(i, k) < -\min\{0, r(k, k) + \sum_{i'(i' \neq i, k)} \max\{0, r(i', k)\}\}$$

2.3 *Boundary Detection*

Segmentation of image involves boundary detection for low resolution and noise in the images. The source statistics of the PET images define the homogeneities in locating and defining boundaries using either level set or active contours or gradient-based methods. Active contours are used to detect or identify the object of interest based on the energy functions [9]. These energies are usually classified into external and internal energies, where external energy defines the contour or shape based on the texture, edge and gradient values.

2.4 *Qualitative and Quantitative Parameters*

This work involves oncology, cardiology and neurology as their clinical studies which are to be very accurate for recovery and therapeutic treatment. This diagnosis is done by using PET which is very harmful to the body in extreme cases and results in cancer also. The objective is to find the lesion and malignant tissues in the human body and provide a better analytic procedure for a doctor in providing accurate second opinion. The results obtained are developed in a prototype for measurements and quantification so this step is very important to start the work. Initially, the quantification of three parts involves PET scanning in extreme case for better synthesis. Our method is used to quantify all the details of the patient such as radio tracer life of F18 injection, weight, scanning time and injection dosage [10].

2.5 *Rendering and 3D Modelling*

Medical imaging uses texture mapping to render the slices of a 3D volume in an aligned position with reasonable quality. This rendering is often known clearly when it is rotated with volume at every transition. Actually, the image is in the form

Table 1 CT values of abdominal tissues for Hounsfield units

Tissue	CT value (HU)		Organ	15-year-old patient	70-year adult
	Mean	SD			
Air	-1006	2	Heart wall	0.29	0.22
Fat	-90	18	Kidneys	0.089	0.074
Skin	+16	11	Brain	0.072	0.070
Spinal canal	+23	15	Bone surface	0.052	0.041
Kidney	+32	10	Liver	0.076	0.058
Blood (aorta)	+42	18	Lungs	0.092	0.064
Muscle	+44	14	Skin	0.037	0.030
			Other tissues	0.052	0.042

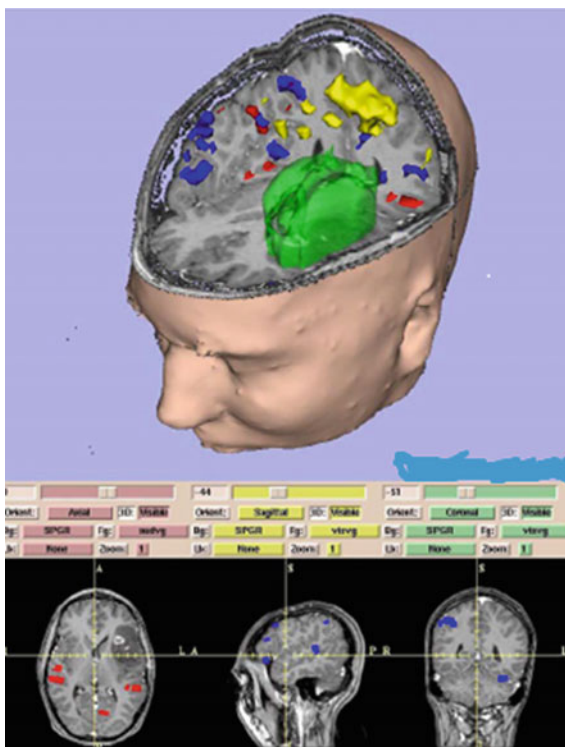
of slices which are aligned based on the viewing angle of the user. These are sliced through the volume at every angle defined and adjusted by the user. Classification determines the attenuation in each voxel, and from the attenuation, the represented tissue is determined. The main four tissues represented in CT are fat, soft tissue, bone and contrast medium-enhanced tissue [11]. 3D modelling is the process of developing a mathematical representation of any three-dimensional surface of object (either inanimate or living) via specialized software. The product is called a 3D model. It can be displayed as a two-dimensional image through a process called 3D rendering or used in a computer simulation of physical phenomena. The model can also be physically created using 3D printing devices (Table 1) [10].

3 Design Procedure

Usually, this work involves MATLAB software and rapid prototyping technology with 3D modelling software to bring imagination to life. It uses PET-CT imaging and performs all types of basic steps to identify the malignant tissues and lesion for performing better surgical procedures. In the first step, the image is preprocessed and its region of interest is detected for accurate segmentation. The segmented parts use boundary cut and graph cut segmentation to define the affinity propagation by similarities and level cut formulation. The second step involves the clinical procedures to avoid adverse reactions so the details of imaging are recorded and it is quantified to find out the level of segmentation. The third step shows rendering with volume and surface for the lesion detected based on user-defined viewing angle. Those surfaces are modelled based on the organs of the human body, and the dose injection is based on the Hounsfield units and basic values of PET-CT.

Finally, the obtained results are brought into real life through rapid prototyping technology, and the rendered model is built into a 3D model for better surface to have better and accurate opinion in surgical procedures. The general principle of 3D reconstruction is composed of the following steps.

Fig. 3 Rendered GUI with 3D using 3D slicer



5 Conclusion

Throughout the discussion, it is observed that the PET-CT imaging is the best and suitable tool for quantitative functional information on diseases. Image segmentation is basic step for image processing followed with 3D modelling for extracting the information defined by the user. In this work, different segmentation methods are used for defining boundaries and ROI for various organs of the human body. The recent advances applied in these techniques are suitable for PET, PET-CT and MRI-PET images. The investigated results of segmentation methods for smooth and sharp regions are evaluated through quantitative variations of SUV with peak and minimum values. The justified results obtained are given as input to 3D modelling software to render the identified lesions and malignant tissues involved in critical parts of the human body. We investigated different segmentation methods in detail; results were listed and compared throughout this review. These results of 3D modelled software are used to develop the imagination to life through rapid prototyping technology. Thus, this provides the clinicians and doctors a second opinion to perform therapeutic treatment. It is observed the PET image segmentation method is optimal for all applications and can compensate for all of the difficulties inherent to PET images. The changing techniques can also be easily incorporated

for anatomical information in metabolic activities for some hybrid frameworks (PET-CT, PET-CT and MRI-PET-CT) which is encouraging, and it is open to further investigations.

References

1. Brent foster, Ulas Bagci, Awais Mansoor, Ziyue Xu, Daniel J Mollura, "A Review on segmentation of Positron Emission Tomography Images", IEEE trans. Biomedical Engineering, Vol. 1 (3), 76–96, April, 2014.
2. Segmentation of PET images for Computer Aided Functional Quantification of Tuberculosis in Small Animal Models" IEEE trans. Biomedical Engineering, Vol. 61(3), 711–724, Nov, 2013.
3. Partha Ghosh, "Reproducible Quantification in PET-CT: clinical Relevance and Technological Approaches" White paper, SIEMENS, www.Siemens.com.
4. Brent Foster, Ulas Bagci, Ziyue Xu, Bappaditya Dey, Brian Luna, William Bishai, Sanjay Jain "Segmentation of PET Images for Computer—Aided Functional Quantification of Tuberculosis in Small animal models," IEEE Trans. Biomedical Engineering, vol. 61, No.3, March 2014.
5. W. Sun, B. Starly, J. Nam, and A. Darling "Bio-CAD modelling its applications in Computer-aided tissue engineering", pp. 29–47.
6. M. Viceconti, C. Zonnoni, and L. Pierotti. TRI2SOLID: "An application of reverse engineering methods to the creation of cad models of bone segments". pp. 211–220.
7. R.A. Armistead and J.H. Stanley "Computed Tomography: A Versatile Technology." Advanced materials & Processes 151 (2). pp. 33–36.
8. Sun W, Starly B, Darling A, Gomez C. "Computer-aided tissue engineering: application to biomimetic modelling and design of tissue scaffolds", J Biotechnol Appl Biochem 39(1). pp. 49–58., 2004;
9. Ziaur Rahiman Shaik, D. Madhavi, N. Jyothi and Ch. Sumanth Kumar: Development of 3D Model with Iso Surface Reconstruction Algorithm in Cosmetic Surgical Applications, Pak. J. Biotechnology. Vol. 13 (special issue on Innovations in information Embedded and Communication Systems) pp. 193–198 (2016).
10. Ziaur Rahaman Shaik, Ch. Sumanth Kumar "A Survey on Professional CAD software for Digital fabrication of Human Head Phantom using Rapid Prototyping system" Published by International Journal of Engineering Sciences Research-IJESR Vol. 5 Dec 2015.
11. Brent Foster, Ulas Bagci, Brian luna, Bappaditya Dey, William Bishai, Sanjay Jain, Ziyue Xu, Daniel J Mollura, "Robust Segmentation and Accurate Target definition for PET Images using Affinity Propagation, International Symposium on Biomedical imaging, San Fransco, USA, Pg.No:1461-1464, March 2013.

Genetic Algorithm-Based Optimized Gabor Filters for Content-Based Image Retrieval

D. Madhavi and M. Ramesh Patnaik

Abstract Fast and exact searching of digital image from the large database is the great demand. In this paper, a hybrid technique to improve the efficiency of content-based image retrieval (CBIR) is proposed. It uses combination of color, texture, and shape feature extraction methods. Color features are extracted using HSV histograms. For texture feature extraction, instead of traditional Gabor filter, four Gabor filters are simultaneously tuned in the desired direction using genetic algorithm and features are extracted in each direction simultaneously. The shape features are obtained using shape signature function with polygonal fitting algorithm. By the sequential process of these three stages, the retrieval performance is greatly improved. The simulation results prove that the proposed analysis gives significant improvement with respect to retrieval performance and computational complexity with the other proposed schemes.

Keywords Gabor filter · Genetic algorithm · Image retrieval · Precision Recall

1 Introduction

CBIR is the important technique in computer vision for image retrieval. Its applications are needed in various fields such as remote sensing and surveillance. CBIR system analyzes image content using color, texture, and shape features for indexing and performance measurement.

D. Madhavi (✉)

Department of ECE, GIT, GITAM University, Visakhapatnam 530045,
Andhra Pradesh, India
e-mail: dmadhavi336@gmail.com

M. Ramesh Patnaik

Department of Instrument Technology, College of Engineering, Andhra University,
Visakhapatnam 530003, Andhra Pradesh, India
e-mail: ramesh_patnaik@yahoo.com

A CBIR system proposed by Yang et al. [1] utilizes the color, texture, and shape features using color content of the image, filtering analysis, and pseudo-Zernike moment and by using different similarity measures. Kato [2] presented image retrieval from a huge set of images, using color analysis and boundary representation of images. Zhang et al. [3] proposed feature extraction using non-uniform quantization of color histogram. Huang et al. [4] presented an image retrieval system using wavelet filter banks and discrimination using fuzzy classification.

In this paper, a content-based image retrieval system using a sequential process of three feature sets is developed. It is having three stages. In the first stage, color features are obtained from the database of several images using HSV histograms [5, 6]. In second stage, genetic algorithm (GA)-based optimized Gabor filters are proposed for texture feature extraction [7, 8]. Instead of computing a large number of texture features using traditional Gabor filter [9], four Gabor filters are tuned simultaneously in the desired orientation and features are extracted in each direction [10]. In the third stage, shape features are extracted using Fourier descriptors of the signature functions [11].

The proposed method not only improves maximum average recall and average precision rate but also reduces computation complexity involved in the retrieval system.

This paper is structured as follows. Section 1 gives the suggested scheme of the image retrieval process. Section 2 provides the individual stage feature extraction of the proposed system. Experimental evaluation and simulation outputs are presented in Sect. 3. Some conclusions are discussed in Sect. 4.

2 Proposed Method

The block diagram of a three stage retrieval process of the proposed scheme is shown in Fig. 1. A database of N images is considered as input, and it is given as the input to stage 1. In this stage, N_C best possible images are retrieved by using color feature extraction with color histogram.

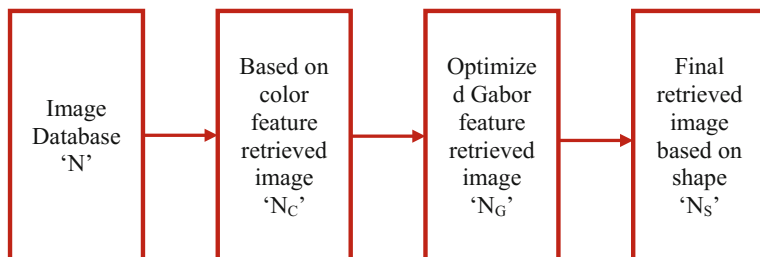
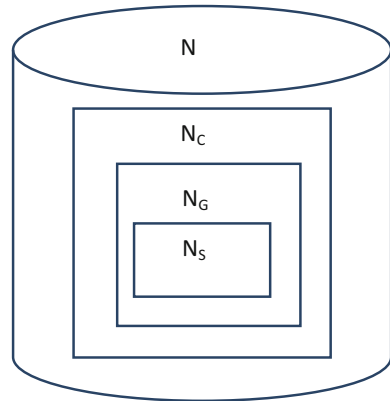


Fig. 1 Block diagram of different stages of CBIR

Fig. 2 Total number of retrieval images in each stage



These images are given as the input images for stage 2. In stage 2, texture features are extracted using a set of Gabor filters which are tuned in different orientations and scales. The filter parameters are optimized using genetic algorithm to reduce the number of computations and N_G best possible images are acquired. These sets of images are applied as input database for third stage. Here, feature extraction from images is carried out using shape descriptors using polygonal fitting algorithm with signature functions. From this last stage, N_S best possible relevant images to the query image are obtained. The sequential process of these three stages removed the irrelevant images, making the system efficient.

The relation between N database images and retrieval of images at different stages are related by the Eq. (1) and is shown in Fig. 2.

$$N > N_C > N_G > N_S \quad (1)$$

2.1 Feature Extraction Using HSV Color Histograms (Stage 1)

For retrieving N_C images from the database of N images, we used hue, saturation, and value (HSV) color model instead of RGB MODEL. The HSV model dissociates the gray scale and color information effectively. It separates the intensity component from the color carrying data in a color image which makes natural and intuitive to humans. The hue is not a variant for camera direction. The color histograms [12] of all images in the data set are computed. The color histogram finds the distribution of the pixels and the color content of an image. The similarity is measured using distance (D) measurement and is given by the Eq. (2).

If p and q denote two histograms with size ‘ k ,’ then the distance D between the histograms p and q can be given by Eq. (2)

$$D = \frac{\sum_{i=0}^{n-1} \min(p[i], q[i])}{\min(|p|, |q|)} \quad (2)$$

where $|p|$ and $|q|$ are magnitudes of histograms. This distance metric is arranged in ascending order, and first N_C images are selected which are having best similar images to query image.

2.2 Feature Extraction Using 2D Gabor Filters with Optimized Genetic Algorithm

Texture feature is the important feature in image retrieval systems. Gabor filters are widely used for this. The Gabor filter is modulation of Gaussian envelop with complex sinusoidal signal and is given by Eq. (3)

$$g(x, y) = \frac{1}{2\pi\sigma_x\sigma_y} \exp\left[-\frac{1}{2}\left(\frac{\tilde{x}^2}{\sigma_x^2} + \frac{\tilde{y}^2}{\sigma_y^2}\right)\right] \exp[2\pi jW\tilde{x}] \quad (3)$$

$\tilde{x} = x \cos \theta + y \sin \theta$, $\tilde{y} = -x \sin \theta + y \cos \theta$, where σ_x and σ_y denote scaling variables. W is the radial frequency of sinusoid. θ is orientation of the filter.

The Fourier transform of the Gabor function is given by

$$G(u, v) = \exp\left[-\frac{1}{2}\left(\frac{(u - W)^2}{\sigma_u^2} + \frac{v^2}{\sigma_v^2}\right)\right] \quad (4)$$

where $\sigma_u = \frac{1}{2}\pi\sigma_x$, $\sigma_v = \frac{1}{2}\pi\sigma_y$

The Gabor filters with different orientation and scales are selected, and features are extracted. To reduce the number of convolutions of these Gabor filters with the query image, a tunable Gabor filter is selected and the parameters are selected using a four-channel genetic algorithm and is shown in Fig. 3.

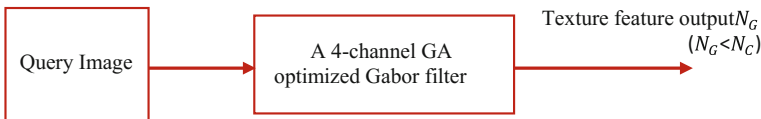


Fig. 3 Block diagram of tuned Gabor filter for texture feature extraction of stage 2

Here, the Gabor filters are tuned in four different directions and four different parameters are computed, and these are used to retrieve similar type of images corresponding to the query image. The fitness function is optimized by computing the energy responses using genetic algorithm. It provides best optimal search for obtaining characteristic vector. In image retrieval systems, fitness function determines the classification of individuals exactly.

The fitness function [5] can be evaluated by Eq. (5)

$$F = E_D D - E_C C \quad (5)$$

Here, D is the distance measure with weight E_D . C is the correlation measurement with weight E_C .

The best N_G images are obtained based on the minimum distance computation of texture feature vector of the required image and N_C input images in stage 2.

2.3 Feature Extraction Using Shape Signature Functions (Stage 3)

The N_G images that are obtained from stage 2 are given as input database for stage 3. In this, the most N_S similar images to the query image are obtained using shape signature functions and polygonal fitting algorithm. The shape signature function describes a unique shape and captures the perceptual feature of the shape. From the signature functions, Fourier descriptors are used to obtain frequency domain representation of the shape feature. These are invariant to scaling, translation, and rotation. The boundary coordinators of the images are obtained by applying polygon fitting algorithm.

The Fourier representation of the signature function $f(t)$ is given by Eq. (6)

$$a_k = \frac{1}{N} \sum_{t=0}^{N-1} f(t) e^{\frac{-j2\pi kt}{N}} \quad (6)$$

The magnitude of Fourier coefficients $\{a_k\}$ gives the shape descriptors. Shape features of required image and all input data set of this stage are evaluated, and the similarity is measured by calculating Euclidean distance which can be given by Eq. (7)

$$d = \sqrt{\sum_{i=0}^{N-1} |f_q^i - f_d^i|^2} \quad (7)$$

where f_q is the characteristic vector of required image, and f_d is the characteristic vector of all input data set of stage 3.

3 Experimental Results

The experimental analysis of the proposed system is evaluated using Wang database [13] by taking 500 images of five classes. A flower image in that data set is given as the query image. The values of N_C , N_G , N_S are taken as 12, 8, and 5, respectively. From stage 1, best 12 images are obtained and are given as input set for stage 2. From stage 2, eight best possible images are obtained and it is given as input database for stage 3. Finally, from stage 3 best five possible images are obtained. The efficiency of the proposed retrieval scheme is measured by using standard performance metrics Average precision (P) and average recall (R) are defined by Eq. (8)

$$P = \frac{N_{RI}}{T_I} \text{ and } R = \frac{N_{RI}}{N_{RD}} \tag{8}$$

where

- N_{RI} No. of relevant images retrieved,
- T_I No. of images retrieved,
- N_{RD} No. of relevant images in the data set.

The retrieval performance is evaluated for every image in each of the five classes. The performance comparison of proposed scheme with two different existing models is shown in Figs. 4 and 5. It is observed that the scheme considered

Fig. 4 Comparison of average precision of different models

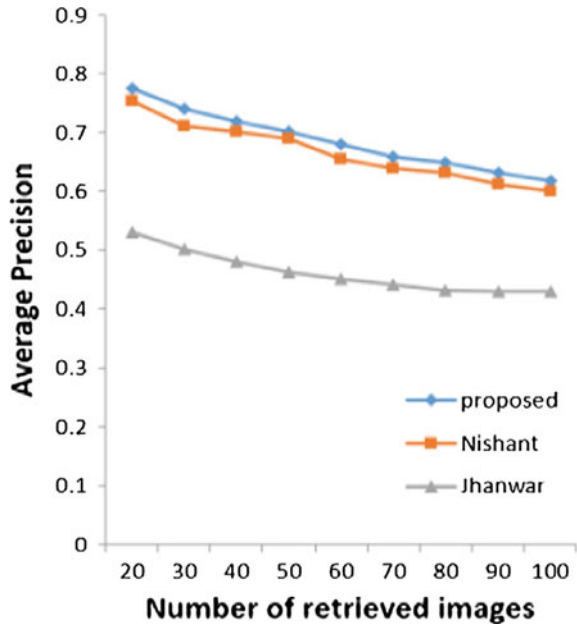
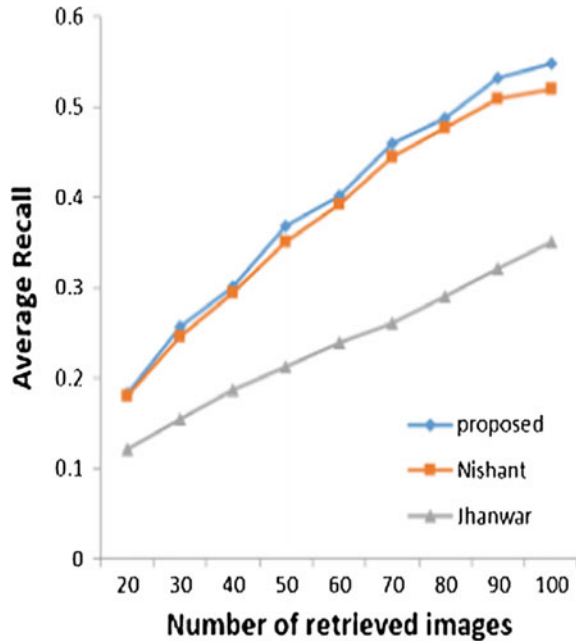


Fig. 5 Comparison of average recall of different models



shows high values of precision and recall in all five groups considered, which represents a good performance retrieval.

4 Conclusion

Content-based image retrieval is a challenging task for obtaining similar images from a large database. In this paper, a sequential process of color, texture, and shape feature analysis of a CBIR system has been proposed. The analysis of texture features using a tunable Gabor filter significantly improves the retrieval performance. The effectiveness of the proposed system is verified using performance metrics of average precision and average recall. Simulation results show that the proposed method provides better performance than traditional feature extraction techniques.

References

1. Yang, W.X: An Effective image retrieval scheme using color, texture & shape features, *computer Standards & Interfaces*, vol. 33, Issue 1, pp. 59–68. (2011)
2. T. Kato: Database architecture for content-based image retrieval. In: *Proceedings of the SPIE —The International Society for Optical Engineering*, vol. 1662, pp. 112–113. (1992)

3. Zhenhua Zhang: An Improving Technique of Color Histogram in Segmentation-based Image Retrieval. In: Fifth International Conference on Information Assurance and Security, pp. 381–384. IEEE Computer Society (2009)
4. Huang, P.W., Dai, S.K: Image retrieval by texture similarity. *Pattern Recognition*, Vol. 36, pp. 665–679. (2003)
5. Krishna, S., Balasubramanian, V., Black, J., Sethuraman, P: Person-Specific Characteristic Feature Selection for Face Recognition. *Biometrics: Theory, Methods, and Applications* Wiley publications. (2009)
6. Shrivastava N: An efficient technique for retrieval of color images in large databases. Dept. of Computer Science and Engineering, Jaypee University of Engineering and Technology, Raghuagarh, Guna 473226, India
7. Tsai, D. M., Lin, C. P., Huang, K.T: Defect Detection in Colored Texture Surfaces using Gabor Filters. *The Imaging Science Journal*. vol. 53, pp. 27–37. (2005)
8. Chisti, K. M., Srinivas, K. S., Prasad G: 2D Gabor filter for surface defect detection using GA and PSO optimization techniques. *AMSE Journals*. vol. 58, pp. 67–83. (2015)
9. Manjunath, B., Ma, W: Texture features for Browsing and retrieval of image data. *IEEE transactions on pattern analysis and machine intelligence*, vol. 18, No.8, pp. 837–842. (1996)
10. Madhavi, D., Patnaik, M.R: Image retrieval using GA optimized Gabor filter. *Indian Journal of Science and Technology*, vol. 9(44), pp. 1–11. (2016)
11. Hu, R.X: Angular Pattern and Binary Angular Pattern for Shape Retrieval., *IEEE Transactions on Image Processing*, vol. 23, No. 3, pp. 1118–1127. (2014)
12. Jhanwar, N: Content based Image Retrieval using Motif Cooccurrence matrix. *Image and Vision Computing*, vol. 22, pp. 1211–1220. (2004)
13. Wang Database: <http://wang.ist.psu.edu/>

Optimal ISA-PID-Based Drug Concentration Control in Cancer Chemotherapy

Pandey Vivek, Pachauri Nikhil, Rani Asha and Singh Vijander

Abstract The aim of this work is to design an efficient controller for optimum scheduling of drug during cancer treatment. The conceptual design of ISA-PID controller is applied for this purpose, and its parametric values are optimized by applying the cuckoo search algorithm (CSA) which results to the CSA-ISAPID controller. The simulated annealing (SA) and genetic algorithm (GA) are also used for comparative study. Simulation results reveal that CSA-ISAPID is able to control drug concentration more precisely in comparison with other designed controllers with minimum overshoot and settling time. Further results demonstrate that reduction in cancerous cells is high for CSA-ISAPID.

Keywords Cancer chemotherapy · ISA-PID · Genetic algorithm (GA) Simulated annealing (SA) · Cuckoo search algorithm (CSA)

1 Introduction

Chemotherapy is one of the important subjects that had gain interest over the past years for effective treatment method of cancer. Cancer chemotherapy aims at reducing maximum number of cancerous cells when chemotherapy drug injected in patient's body after a regular time period during treatment. However, the injected drug not only kills the cancer cells, but also damage normal cells due to its toxic

P. Vivek (✉) · P. Nikhil · R. Asha · S. Vijander
Instrumentation and Control Engineering Division, NSIT, Azad Hind Fauz, Marg,
Sec-3 Dwarka, 110078 New Delhi, India
e-mail: vivek.aei@gmail.com

P. Nikhil
e-mail: nikhilpchr@gmail.com

R. Asha
e-mail: ashansit@gmail.com

S. Vijander
e-mail: vijaydee@gmail.com

Table 1 Literature of various control schemes for cancer chemotherapy

Author	Controller	Performance characteristics
Algoul et al. in 2011 [1]	PID and IPD	No. of cancerous cells remain = 15
Martin and Teo in 1994 [2]	Optimal control	No. of cancerous cells remain = 4.878×10^4
Khadraoui et al. in 2016 [3]	Cascaded PID	No. of cancerous cells remain = 1.078
Algoul et al. in 2011 [4]	MOGA IPD	No. of cancerous cells remain = 99%
Algoul et al. in 2013 [5]	PSO PID	No. of cancerous cells remain = 98%

nature. Therefore, during treatment, it is necessary to assess desirable amounts of chemotherapeutic dose. So the concentration and toxicity remain within the threshold level during the course of treatment. Various approaches suggested by researchers for optimizing drug dose in cancer chemotherapy are concise in Table 1.

In this work, ISA-PID control scheme is proposed for optimum drug dose scheduling during chemotherapy. The enactment of suggested control strategy is compared with conventional PID. The optimal parametric values of ISA-PID controller are calculated using cuckoo search algorithm. This paper is structured as: in Sect. 2, mathematical modeling of cancer chemotherapy is described; in Sects. 3 and 4, structure of ISA-PID and cuckoo search algorithm are discussed, respectively. Sections 5 and 6 describe result and conclusion of the paper.

2 Mathematical Modeling of Chemotherapy

As already mentioned in previous section, the toxic nature of chemotherapy drugs affects cancerous as well as normal cells. Hence, a closed-loop control is needed to provide optimum drug concentration level and toxicity level below threshold value in patient body to kill maximum number of cancerous cells with minimum toxicity. The cancer chemotherapy model under contemplation and its parametric values have been considered from Martin [2]. The block diagram for closed-loop drug scheduling is shown in Fig. 1.

$$\frac{dX(t)}{dt} = -\alpha * X(t) + k(D(t) - \beta)H(D(t) - \beta) \quad (1)$$

$$\frac{dD(t)}{dt} = u(t) - \gamma * D(t) \quad (2)$$

$$\frac{dT(t)}{dt} = D(t) - \mu * T(t) \quad (3)$$

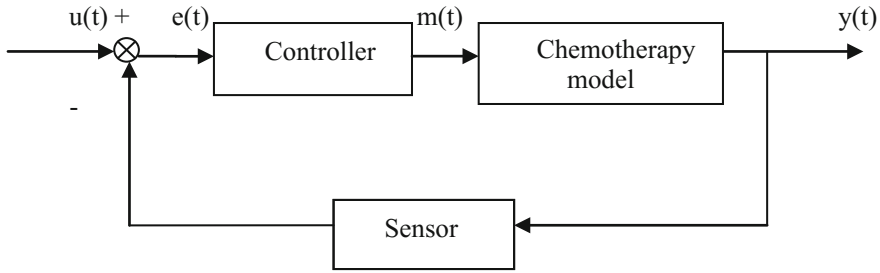


Fig. 1 Block diagram of closed-loop drug scheduling

$$H(D(t) - \beta) = \begin{cases} 1 & \text{if } D(t) \geq \beta \\ 0 & \text{if } D(t) \leq \beta \end{cases} \tag{4}$$

$$N(t) = 10^{12} \times e^{-X(t)} \tag{5}$$

3 ISA-PID Controller

The precise control of drug concentration is obtained by applying an efficient control scheme recognized as ISA-PID. The ISA-PID is described in the Laplace form as follows [6]:

$$M(s) = E(s) \left(K_p(\eta * U(s) - Y(s)) + \frac{(U(s) - Y(s))K_i}{s} + \frac{(K_d * s(v * U(s) - Y(s)))}{(1 + K_d * s / K_p * N)} \right) \tag{6}$$

Equation (6) can be rewritten as

$$M(s) = U(s) * F(s) - Y(s) * H(s) \tag{7}$$

$$H(s) = K_p + \frac{K_i}{s} + \frac{K_d * s}{(1 + K_d * s / K_p * N)} \tag{8}$$

$$F(s) = \eta * K_p + \frac{K_i}{s} + \frac{K_d * v * s}{(1 + K_d * s / K_p * N)} \tag{9}$$

where the description of above equation parameters is given in [6].

4 Cuckoo Search Algorithm (CSA)

The effectiveness of any controller is entirely relies on the tuning of designed parameters. Therefore, a newly proposed optimization algorithm, i.e., CSA, is utilized to estimate optimum parameters value of control structure. The preliminaries of CSA implementation are given below [7].

- (a) Firstly, a population of s host nests is generated having S_j —number of generations.
- (b) Randomly select a cuckoo (j) with the help of L'evy flights.
- (c) Randomly choose a nest i from s nests.
- (d) Compute the objective function J_j .
- (e) If $J_j < J_i$, then consider i as a new result or else substitute i by a new result.
- (f) Rejects shoddier nests and fresh nests are formed.
- (g) After that ranks are assigned to the solution and locate the current best.
- (h) Verify the termination state is fulfilled, if not return back to step b.

5 Simulation Results

The cancer chemotherapy model stated in aforementioned section is virtualized on Intel® Core™ i3 (1.8 GHZ) processor with 2 GB RAM in MATLAB 2011 version. ISA-PID and conventional PID are designed and implemented for drug concentration control in chemotherapy. The tuning of any controller is a tedious task, but due to progress in area of optimization, it is easy to find optimum parameters' value of a controller. The CSA is employed to assess the values of ISA-PID parameters. Selecting an appropriate objective function is the important task of optimization. Hence, weighted sum of number of remaining cancerous cells (N) and average toxicity (T) is selected.

$$J = w_1 * N(t_f) + w_2 * \frac{1}{t_f} \int_0^{t_f} T(t) dt \quad (10)$$

The values of w_1 and w_2 are determined after meticulous experimentation.

The parameters of ISA-PID controller (K_p , K_I , K_D , N , η , and v) are estimated using three algorithm, i.e., CSA, SA, GA. All these algorithms are run for 100 iterations on the similar objective function. Figure 2 shows the convergence graph for all the algorithms. It is deduced from Fig. 2 that GA is prematurely converged, SA reaches to its optimum values after 70 iteration, whereas CSA took only 15

Fig. 2 Convergence curve of SA, CSA, and GA

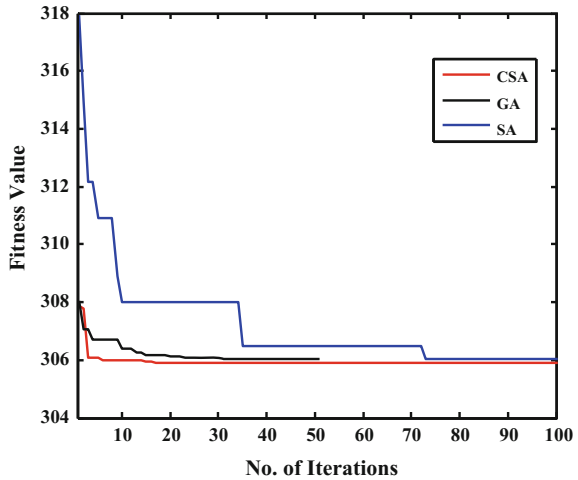


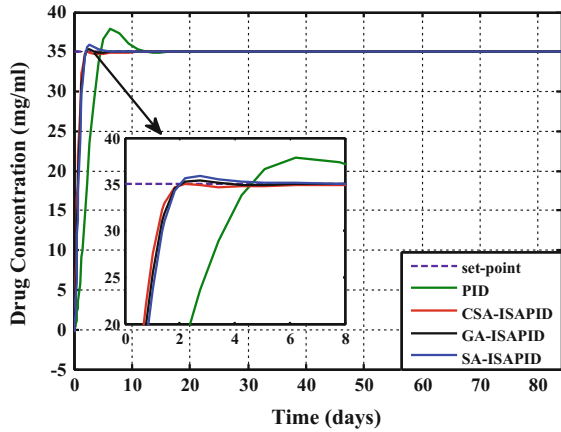
Table 2 ISA-PID and PID controller parameter values

Controllers	K_P	K_I	K_D	η	ν
PID	0.317	0.143	0.343	–	–
CSA-ISAPID	1.500	0.557	0.350	0.912	0.991
GA-ISAPID	1.245	0.402	0.356	0.970	1.013
SA-ISAPID	1.123	0.457	0.357	0.920	0.987

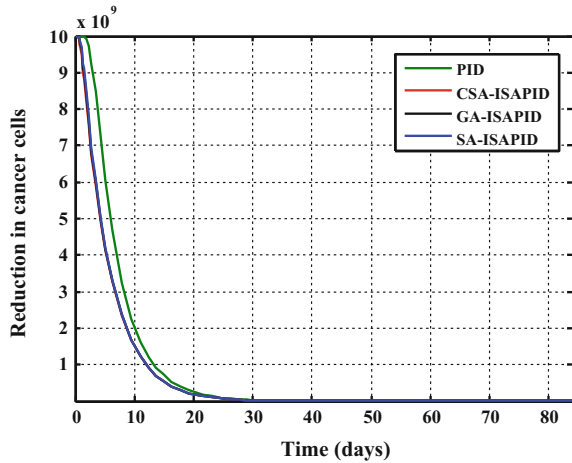
iterations to reach its optimum fitness values which show CSA is considerably quicker in comparison with SA and GA. The least values of objective function for SA, GA, and CSA are 306.10, 306, and 305.8, respectively. Table 2 shows the optimum values of designed controllers.

The performances of all the controllers are analyzed for drug concentration control. It is evident from Fig. 3 that proposed CSA-ISAPID controller is able to control the drug concentration more precisely w.r.t other implemented control techniques. The number of cancerous cells reduced is also highest in case of CSA-ISAPID (524) with minimum level of toxicity (87.490 mg. Day/ml). The quantitative analysis for all controllers is shown in Table 3. From Table 3, it is confirmed that CSA-ISAPID is more proficient as compared to other controllers, as it takes minimum time to settle with minimum overshoot.

Fig. 3 Drug concentration control by all the designed controllers



(a) Drug concentration



(b) Reduction in cancer cells

Table 3 Quantitative analysis of all designed controller

Controllers	% overshoot	Settling time (days)	Rise time (days)	No. of cancerous cell remaining
ZN-PID	8.12	37.50	8.650	691
CSA-ISAPID	0.1258	1.738	1.106	524
GA-ISAPID	1.0206	1.792	1.148	525
SA-ISAPID	2.5660	3.118	1.194	526

Bold values represents Proposed Controller

6 Conclusion

In this work, ISA-PID controller is proposed for drug concentration control during cancer treatment. The design parameters of ISA-PID are optimized using CSA, GA, and SA. The convergence graph demonstrates that CSA converges fast and reaches to minimum fitness value around 15th iteration, whereas GA and SA take 30 and 72 iterations, respectively, to reach their final value of objective function. All designed controllers are compared for drug concentration control at tumor site during chemotherapy. The quantitative analysis shows that CSA-ISAPID controller is proficient to other employed controller for drug concentration control.

References

1. S. Algoul, M. S. Alam, M. A. Hossain, M. A. A. Majumder “ Multi-objective optimal chemotherapy control model for cancer treatment”, *Med Biol Eng Comput* 49, 51–65 (2011).
2. Martin R, Teo KL “Optimal control of drug administration in chemotherapy tumour growth”. World Scientific, Singapore, 1–10 (1994).
3. S. Khadraoui, F. Harrou, H. N. Nounou, M. N. Nounou, A. Datta, S. P. Bhattacharyya “A measurement- based control design approach for efficient cancer chemotherapy”, *Information Science* 333, 108–125 (2016).
4. S. Algoul, M. S. Alam, M. A. Hossain, M. A. A. Majumder; “MOGA-Based Multi-drug Optimization for Cancer Chemotherapy” 5th International Conference on Practical Applications of Computational Biology & Bioinformatics of the series *Advances in Intelligent and Soft Computing* 133–140 (2011).
5. S. Algoul, M. S. Alam, M. A. Hossain, M. A. A. Majumder; “Chemotherapy Drug Scheduling: A Particle Swarm Optimization Approach” *Dhaka University Journal of Science*, 61, 35–40 (2013).
6. Ubaid Imtiaz, Sudhanshu S. Jamuar, J. N. Sahu, P. B. Ganesan, Bioreactor profile control by a nonlinear auto regressive moving average neuro and two degree of freedom PID controllers, *Journal of Process Control*, 24, 1761–1777 (2011).
7. Gandomi, A. H., Yang, X.-S., and Alavi, A. H., Cuckoo search algorithm: a metaheuristic approach to solve structural optimization problems. *Eng Comput.* 29, 17–35 (2013).

Implementation of Adder Circuit Using Quantum-Dot Cellular Automata-Based Logic Gates

Priyanka Kumari, Abhay Sharma and Arpita Singh

Abstract Quantum-dot Cellular automata (QCA) is nanotechnology that can be acquired to replace transistor-based design. The approach of transistor is based on charge transport; the primitive element in QCA is a cell; the communication between cells is solely Columbic hence there is no physical transport of charge. The major feature includes higher packaging density and lower power consumption. QCA cell-based structures can implement the logic gates, wires, memory units, combinational and sequential logic circuits. Digital logic design employing QCA cell is the main focus of this paper. In this paper, structure for Exclusive OR operation is proposed with primary goal of application in adder circuit to reduce the area. QCA designer is the EDA tool used for implementation and functional verification of the proposed structures.

Keywords Quantum-dot cellular automata (QCA) · EXOR gate
Half adder · Full adder

1 Introduction

As VLSI technology has made striking development which is continuously waning in future. The fundamental limit of MOSFET technology is its dimensional scaling which suffers from short channel and narrow channel effect which reduces

P. Kumari (✉) · A. Singh
Department of Electronics and Communication Engineering, Graphic Era University,
Dehradun 248002, India
e-mail: kumari.priyanka710@gmail.com

A. Singh
e-mail: assingharpita77@gmail.com

A. Sharma
Department of Electronics and Communication Engineering, Graphic Era Hill University,
Dehradun 248002, India
e-mail: abhay.ece.gehu@gmail.com

performance. Other limitation deals with it is interconnects problem and power dissipation of the devices. In the trend of minimization of device size, researchers are trying to find other alternatives supplement to conventional transistors [1]. And QCA technology is one of its representatives.

In this paper, a QCA EX-OR circuit is proposed which is further being used in a half adder circuit as reposing the severe clocking scheme. There are three majority gates, and one inverter is being used in the proposed circuit. In QCA, the device can be used as an interconnect [2].

The QCA approach is firstly introduced in [3] as an effective ultra dense devices with higher performance. Basically a QCA cell is quadratic in shape that exhibits 3D quantum confinement. There are four quantum dots in a single cell oriented at the corner sides of the square which are coupled capacitively and tunnel barrier [4]. A quantum dot is a region of low potential encompasses by higher potential region which is able to detain electron of lower energies known as potential well [5]. These quantum dots comprise by the constitute of group II-VI, III-V, and IV-V Ex-CdSe, PbSe, and InP [1, 6].

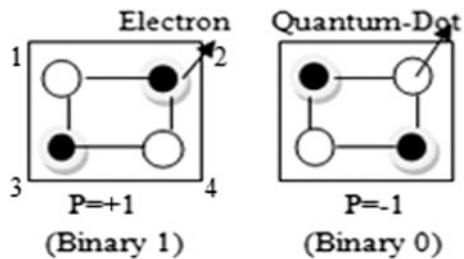
These QCA cell can contain two electrons, which are free to move between adjacent dots known as tunneling. In a QCA cell, transfer of information does not depend on the transport of electron as in conventional transistor, while on the location and adjustment of electron in a small area. And when feature size approaches to nanometer size, then quantum effect tunneling take place [3] by which electrons changes their position as depicted in Fig. 1.

There exist two charged electrons in a cell which always try to achieve the opposite corners due to repulsive electrostatic force. According to electron position in a cell, these two kinds of cell polarization or binary values take place and the values of these polarizations are defined by following equation:

$$P = \frac{(P_2 + P_4) - (P_1 + P_3)}{P_1 + P_2 + P_3 + P_4},$$

where P_j is the columbic charge at dot j . This equation shows that location of electrons at site 2 and 3 yield $P = +1$ polarization and location at site 1 and 4 will give $P = -1$ polarization. The fundamental idea of QCA cell is generic and can be

Fig. 1 QCA cells with electrons indicating logic level



implemented by various methods: molecular implementation, semiconductor implementation, and magnetic implementations [5, 7, 8]. Arrangement of these cells in an array is used to perform all logical functions like wires, memories, logic gates, all combinational and sequential circuits.

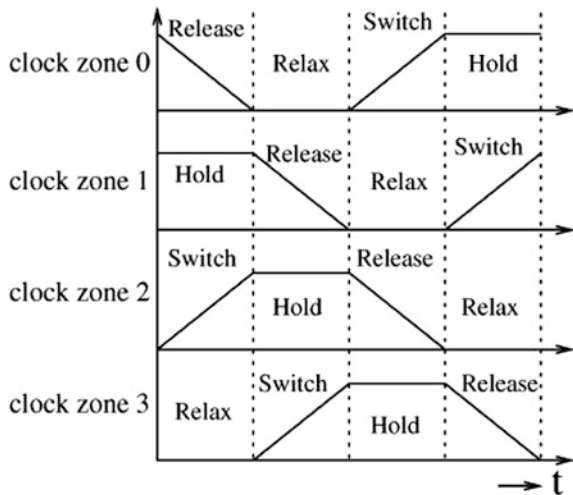
QCA designer tool is being used for an extant work of layout for quantum-dot cellular automata (QCA) by the Walus Group of B. Columbia University produces a fast and accurate simulation [9] by providing the powerful CAD features. QCA designer can simulate more complex computational circuits for general purpose.

2 Clock Zone

To attain the controllable data direction, cells are set into the four clock zones. For the synchronization of QCA circuit, clock plays a very crucial role [5]. A QCA array is categorized into four clock zones which are 90 degree in phase shift from one clock zone to another (Fig. 2).

These clock zones have four states: low-to-high, high, high-to-low, and low which are correspondingly referred as relax, switch, hold, and release [10]. These cells start computing during the high-to-low and hold the value during the low state [5]. Switch phase occurs when cells being unpolarized and having low potential barrier in increasing order. High potential barriers are achieved in the hold phase and lower potential barriers attained in release phase [11]. In relax phase, barriers cells are kept in unpolarized state at low level [12, 13].

Fig. 2 QCA clocks zones [2]



3 QCA Wire

A series of Quantum cell driven by the fixed polarization work as a wire and flow of signal is controlled with clock. The binary signals propagate from one end to another end by the electrostatic interaction between cells [14]. The state of the first polarized drive cell induces the same polarization in the complete series of the cells [15]. By this method, information propagated from first cell to last cell. There are two kinds of configuration of wire (Fig. 3).

4 Logic Gates Based on QCA Logic

4.1 Majority Gate

It is the fundamental logic function being used in QCA which uses odd number of input more than one. In Fig. 4, majority gate has been shown. It is denoted as $M(A, B, C) = AB + BC + CA$. By using these majority gates, two input AND gate and OR gate can be implemented by fixing one of its input at polarization-1 (binary 0) and polarization+1 (binary 1), respectively.

For AND operation: $-M(a, b, 0) = a \cdot b$,

For OR operation: $-M(a, b, 1) = a + b$.

4.2 Inverter

It is another basic logic gate used in QCA. On applying 1 at input, output 0 is attained and vice versa. It is denoted in (Fig. 5).

To implement the circuit of an inverter cell should be arranged at overlapping condition at input side and at other ends corner of the cells should be matched to invert the value at output.

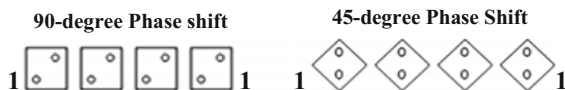


Fig. 3 QCA wires configurations

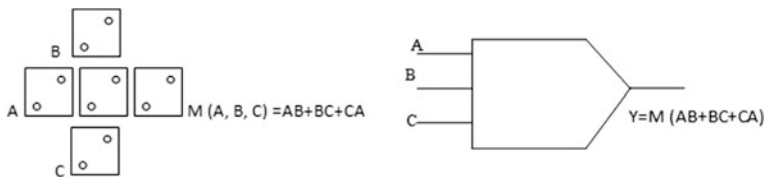


Fig. 4 QCA majority gate

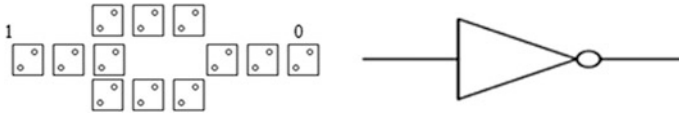


Fig. 5 QCA inverter circuit

5 QCA Cell Placement Technique: Crossover Technique

The printing area is 122 mm; crossover techniques introduce the concept of building QCA devices which are able to execute computation as a function of synchronization. QCA follows two kinds of crossover or can say interconnection technique known as coplanar and multilayer techniques. A coplanar technique is one layer technique either regular or rotated or simultaneous cell configuration technique. While multilayer technique uses bridge kind of structure, i.e., one layer deposited over another layer. It is complex in nature due to deposition of one layer over another and it is fiddle to implement [10, 11, 16, 17] (Fig. 6).

6 Conventional Circuit Using Multilayer Architecture

6.1 EX-OR Gate

It is a universal gate and used in various adder circuits and comparator and so many. EX-OR gate gives high at different level input and low at same level input.

$$Y_{out} = PQ' + P'Q.$$

This Boolean expression has been implemented in the circuit designing depicted in Fig. 7, using the multilayer crossover technique and can be realized more than one way. This technique uses the three majority gates and two inverters.



Fig. 6 Crossovers technique

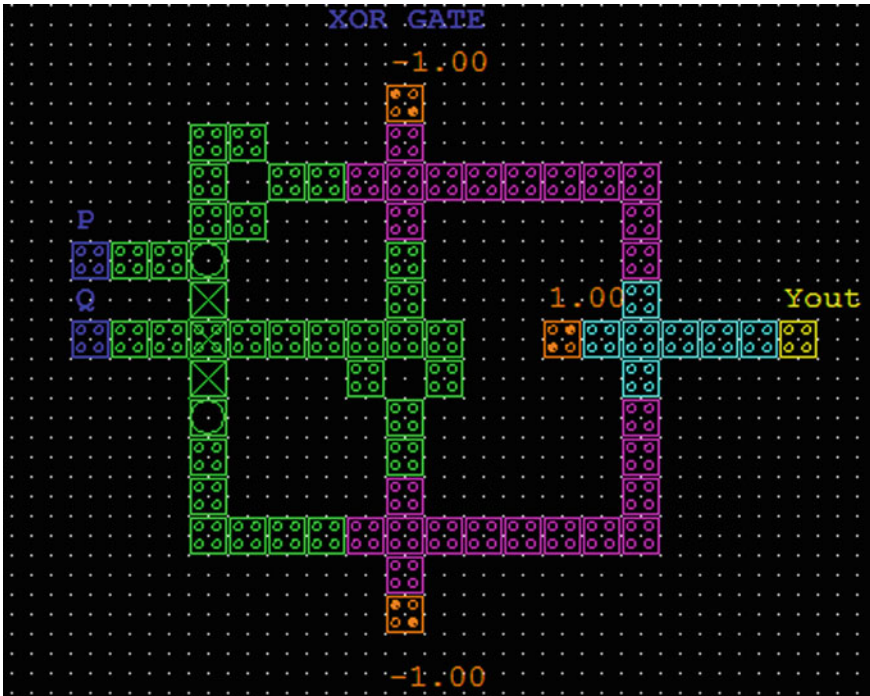


Fig. 7 Conventional EX-OR gate

6.2 Half Adder

Half adder is an arithmetic circuit which is used for addition of two numbers and produces a sum and carries as the output, e.g., if P and Q are the inputs then the sum will be the EX-OR of P and Q and the carry will be the AND of P and Q [6] (Figs. 8 and 9; Tables 1 and 2).

6.3 Full Adder

A one-bit full adder used to add three one-bit numbers and generate a carry. If P , Q , and R three input bits then the sum will be the EX-OR of P , Q , and R and the carry will be $PQ + QR + PR$. Layout and simulation of full adder have been shown in Figs. 14 and 15, respectively, (Table 3).

$$\text{SUM} = P \text{ XOR } Q \text{ XOR } R, \text{ CARRY} = PQ + QR + PR.$$

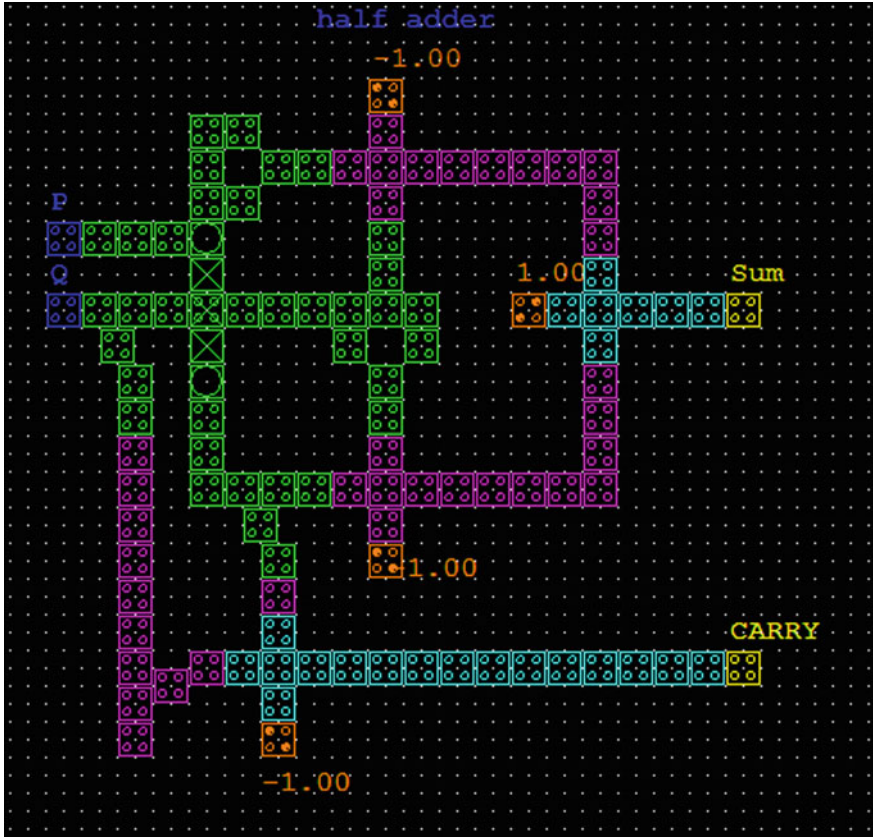


Fig. 8 Half adder circuit

Fig. 9 Logical implementation of EX-OR gate

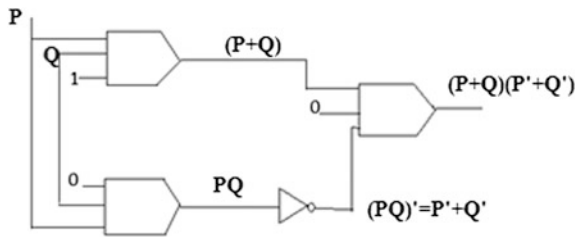


Table 1 EX-OR gates truth table

P	Q	Y_{out}
0	0	0
0	1	1
1	0	1
1	1	0

Table 2 Half-adder gates truth table

P	Q	Sum	Carry
0	0	0	0
0	1	1	0
1	0	1	0
1	1	0	1

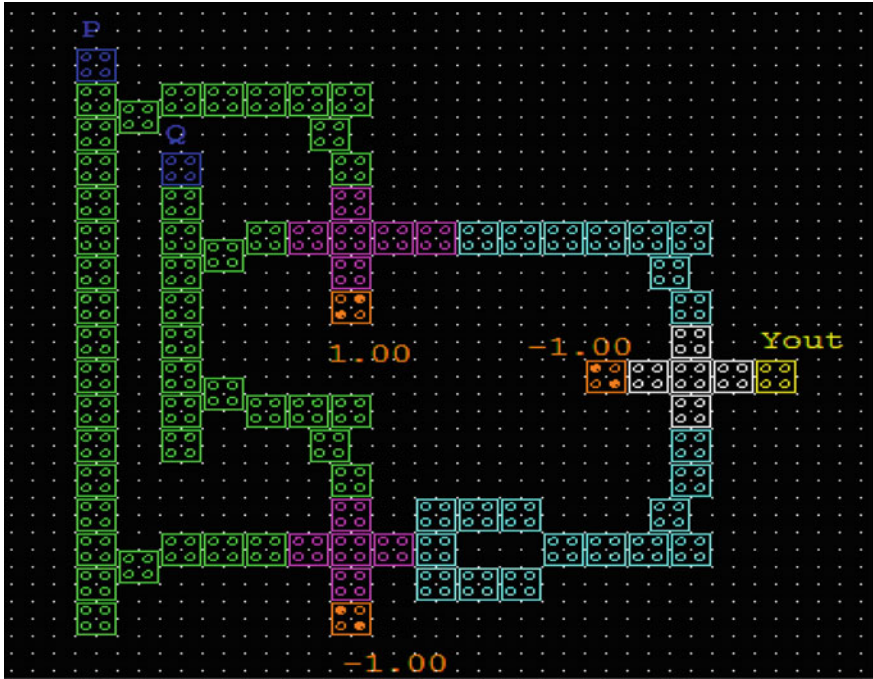


Fig. 10 Layout of EX-OR gate

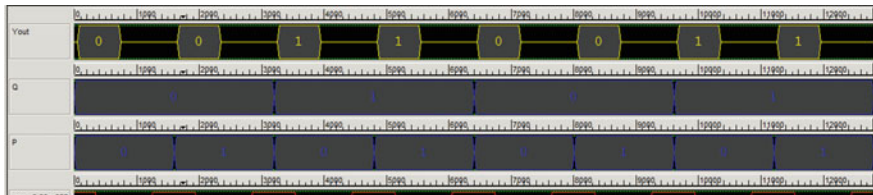


Fig. 11 Simulation of EX-OR gate

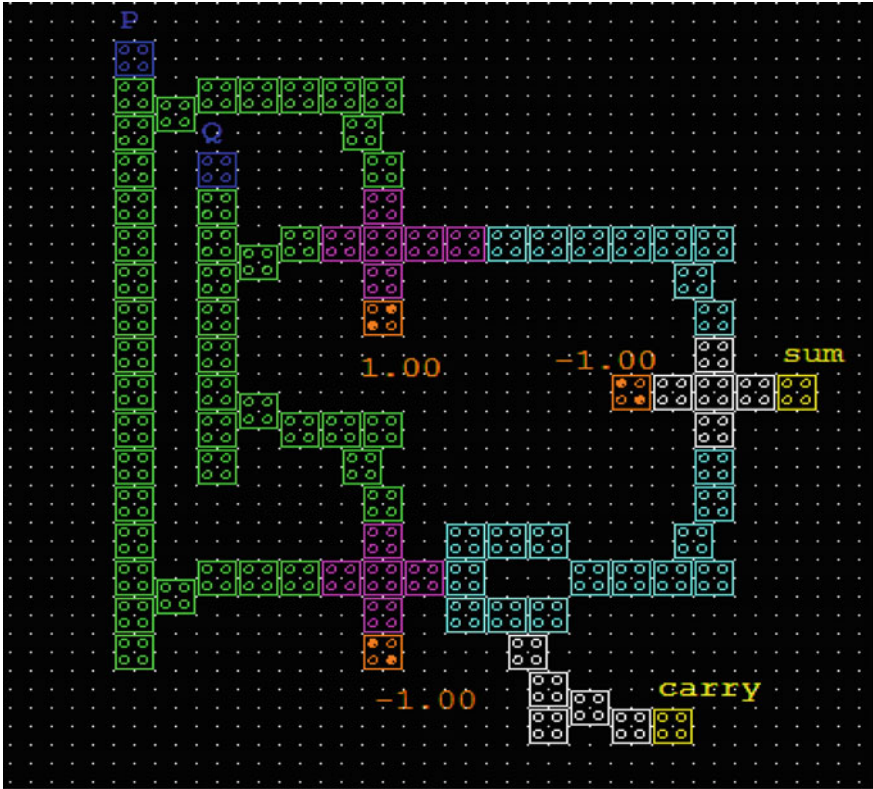


Fig. 12 Layout of half-adder using coplanar EX-OR gate

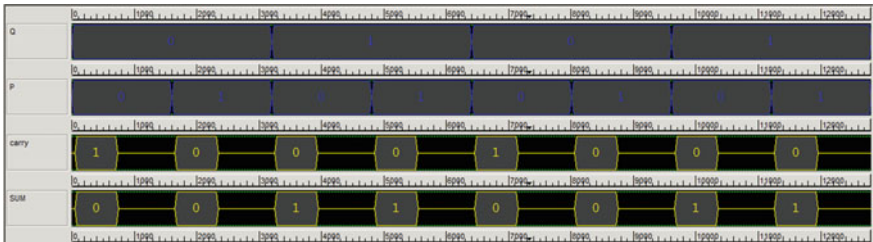


Fig. 13 Simulation of half adder

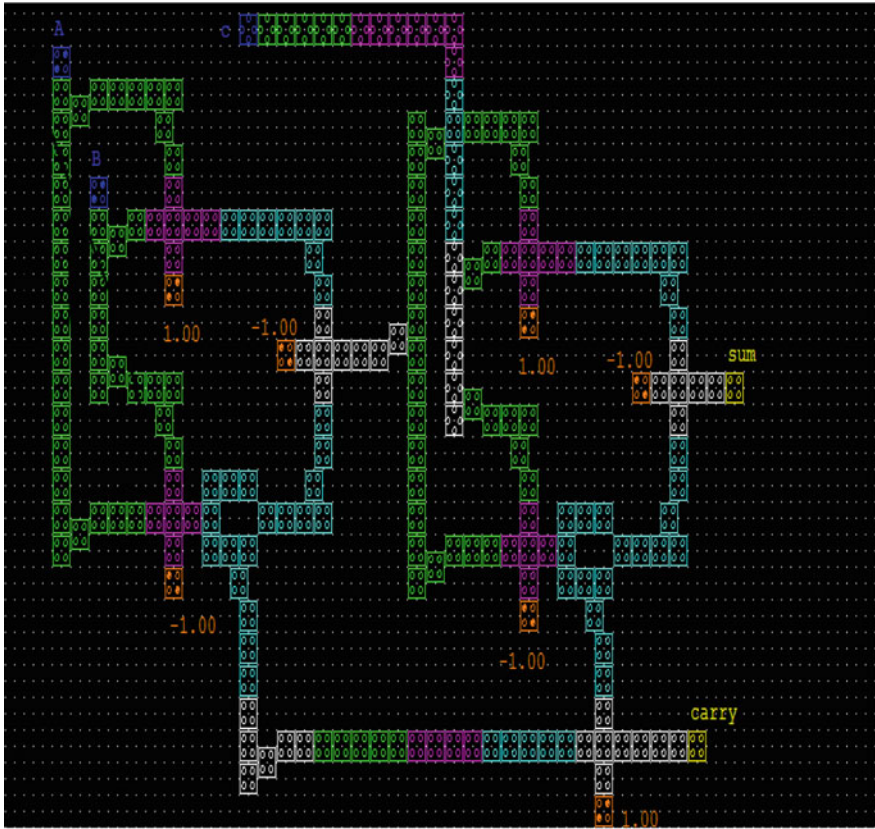


Fig. 14 Layout of full adder using coplanar half adder

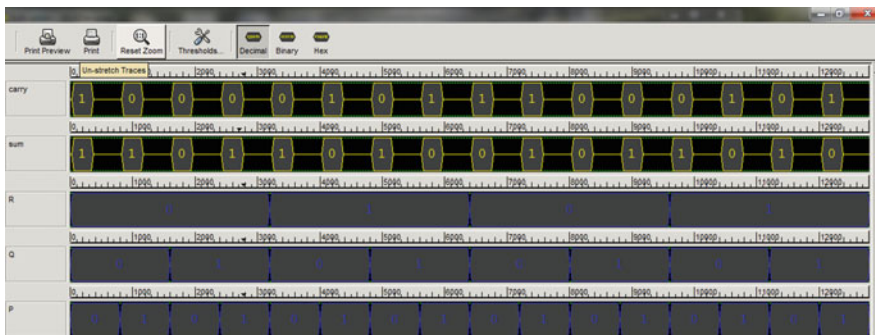


Fig. 15 Simulation of full adder using half adder

Table 3 Full adder truth table

P	Q	R	Sum	Carry
0	0	0	0	0
0	0	1	1	0
0	1	0	1	0
0	1	1	0	1
1	0	0	1	0
1	0	1	0	1
1	1	0	0	1
1	1	1	1	1

7 Proposed Circuit of EX-OR Gate, Half Adder, and Full Adder Using Coplanar Technique

In the proposed circuits, three majority gates and one inverter are being used [14].

$$\text{Sum} = (P + Q).(PQ)' = (P + Q).(P' + Q') = P'Q + PQ'$$

$$\text{Carry} = PQ.$$

The layout of the above Boolean expression has been shown in Figs. 10 and 12 along with the simulation result in Fig. 11 and in Figs. 13, 14 and 15.

8 Comparison

See Table 4.

Table 4 Area comparison between different structures

Crossover structure	Cell count	Area (nm ²)
Multilayer XOR	77	12,663
Multilayer half adder	114	185,318
Coplanar XOR	88	137,706
Coplanar half adder	94	141,954
Coplanar full adder	221	370,670

9 Conclusion

QCA is the answer for transistor-less design. In this paper, it is demonstrated how QCA cells can be arranged to obtain exclusive or operation. Further, it was proposed that half adder and full adder operation can be implemented employing the QCA cell-based structure. It was also observed that coplanar crossover architecture for EX-OR gate was less complex in terms of implementation when compared to multilayer crossover structure. Area was significantly reduced in half adder and full adder designs when the proposed architecture for EX-OR operation was used. This fact is illustrated in Table 4 where comparison of various adder structures has been provided. All the QCA cell-based structures were implemented on QCA designer tool with multi-phase clock propagation.

References

1. Kim, K., Wu, K., Karri, R.: The robust QCA adder designs using composable QCA building blocks. *IEEE transactions on computer-aided design of integrated circuits and systems*, 26(1), 176–183 (2007).
2. Pudi, V., Sridharan, K.: Efficient design of a hybrid adder in quantum-dot cellular automata. *IEEE transactions on very large scale integration (VLSI) systems*, 19(9), 1535–1548 (2011).
3. Lent, C.S., Tougaws, P.D., Porod, W., Bernestine, G.H.: Quantum cellular automata. *Nanotechnology*, Vol. 4, pp. 49–57 (1993).
4. Snider, G.L., Orlov, A.O., Amlani, I., Bernstein, G.H., Lent, C.S., Merz, J.L., Porod, W.: Quantum-dot cellular automata: Line and majority logic gate. *Japanese Journal of Applied Physics*, 38(12S), 7227 (1999).
5. Radhika, P., Tiwari, N., Pant, Y.: Design of adder and multiplier using quantum dot cellular automata based on nanotechnology. In Presented at the National Conference on Emerging Technologies (2011).
6. Cho, H., Swartzlander, Earl E.: Adder designs and analyses for quantum-dot cellular automata. *IEEE Transactions on Nanotechnology*, 6(3), 374–383(2007).
7. Wang, W., Walus, K., Jullien, G.A. (2003, August). Quantum-dot cellular automata adders. In *Nanotechnology, 2003. IEEE-NANO 2003. 2003 Third IEEE Conference on* Vol. 1, pp. 461–464 (2003).
8. Azghadi, M.R., Kavehie, O., Navi, K.: A novel design for quantum-dot cellular automata cells and full adders. *Journal of Applied Sciences*, Vol. 7, No. 22, pp. 3460–3468 (2007).
9. Lent, C.S., Tougaw, P.D., Porod, W.: Quantum cellular automata: the physics of computing with arrays of quantum dot molecules. In *Physics and Computation, 1994. PhysComp'94, Proceedings, Workshop on IEEE*, pp. 5–13 (2014).
10. Srivastava, S., Bhanja, S.: Hierarchical probabilistic macromodeling for QCA circuits. *IEEE Transactions on Computers*, 56(2), (2007).
11. Walus, K., Jullien, G.A.: Design tools for an emerging SoC technology: Quantum-dot cellular automata. *Proceedings of the IEEE*, 94(6), 1225–1244 (2006).
12. Blair, E.P., Yost, E., Lent, C.S. (2010). Power dissipation in clocking wires for clocked molecular quantum-dot cellular automata. *Journal of computational electronics*, 9(1), 49–55 (2010).
13. Graunke, C.R., Wheeler, D.I., Tougaw, D., Will, J.D. (2005). Implementation of a crossbar network using quantum-dot cellular automata. *IEEE Transactions on Nanotechnology*, 4(4), 435–440 (2005).

14. Walus, K., Dysart, T. J., Jullien, G. A., Budiman, R. A.: QCA Designer: A rapid design and simulation tool for quantum-dot cellular automata. *IEEE transactions on nanotechnology*, 3(1), 26–31(2004).
15. Perri, S., Corsonello, P.: New methodology for the design of efficient binary addition circuits in QCA. *IEEE Transactions on Nanotechnology*, 11(6), 1192–1200 (2012).
16. Walus, K., Dysart, T.J., Jullien, G.A., Budiman, R.A.: QCADesigner: A rapid design and simulation tool for quantum-dot cellular automata. *IEEE transactions on nanotechnology*, 3(1), 26–31(2004).
17. Galatsis, K., Khitun, A., Ostroumov, R., Wang, K.L., Dichtel, W.R., Plummer, E., Kim, K. W.: Alternate state variables for emerging nanoelectronic devices. *IEEE transactions on Nanotechnology*, 8(1), 66–75 (2009).
18. Sridharan, K., Pudi, V.: Design of arithmetic circuits in quantum dot cellular automata nanotechnology. Springer Vol. 599 (2015).
19. Reddy, D.T., Reddy, S.P., Reddy, K.S.K., Reddy, S.N., Khasid, S.K.: Area-Delay Efficient Binary Adders in QCA. Editorial Committees, 52.
20. BASU, S.: Realization of Xor and Xnor gates using qca basic gates (2014).

FPGA Implementation of High Speed Multiplier with Optimized Reduction Phase

Arpita Singh, Abhay Sharma and Priyanka Kumari

Abstract Multipliers play an important role in DSP applications hence, the delay executed by them is a dominating factor. Various multiplication algorithms are used to enhance the speed of the device. All these multipliers are then compared based on look up table (LUTs) and path delays. The simulated results show that the Wallace tree multiplier is the fastest multiplier, and by using carry look-ahead adder (CLA) for addition, delay is further reduced.

Keywords Wallace tree multiplier • Reduced partial products
Carry look-ahead adder • Delay • LUTs

1 Introduction

Multiplication is an integral function in arithmetic operations. A binary multiplier is an electronic circuit which multiplies two binary numbers using binary adders. Multipliers are used in a variety of applications such as digital signal processing (DSP), involving FFT (fast fourier transform), filtering, convolution, and in ALUs. Performance of these operations depends upon the performance of multipliers used i.e., the time executed by multipliers. The speed of any device has been its advertised feature. With advancement in technology, reduction in delay, area, and power consumption has become the rising requirement of user and a challenge for a

A. Singh (✉) · P. Kumari
Department of Electronics and Communication Engineering, Graphic Era University,
Dehradun 248002, India
e-mail: assingharpita77@gmail.com

P. Kumari
e-mail: kumari.priyanka710@gmail.com

A. Sharma
Department of Electronics and Communication Engineering, Graphic Era Hill University,
Dehradun 248002, India
e-mail: abhay.ece.gehu@gmail.com

designer. Various algorithms have been applied to increase the speed of multiplication, and hence, different multipliers have been used for this purpose, such as array multiplier, vedic multiplier, Wallace tree multiplier, booth multiplier, and dadda multiplier.

In this chapter, we have analyzed the performance of Array, Wallace tree, and Dadda multiplier in verilog language using Xilinx software and compared the performance of each multiplier. Multiplication process occurs in three phases: (1) Generation of PP (partial product), (2) Reducing Partial Products, and (3) Accumulation [1]. By multiplying the bits of multiplier and multiplicand, partial products are generated. These partial products are then accumulated using shift and addition operation to give the multiplied output. The speed of a multiplier depends upon the reduction stage of these partial products; greater the partial products are reduced, lesser the addition for them is required.

2 Array Multiplier

Array multiplier uses an array of Half and Full adders to perform the simultaneous addition of partial products. For an n -bit array, $n \times n$ number of AND gates, $n \times (n - 2)$ FA (full adders), and n HA (half adders) are used [2]. A composite figure of array multiplication for 4-bit is shown below. PP (partial products) are added using half and full adders, having carry of previous adder as third input. The length of multiplier and width of multiplicand are denoted by number of rows and width of each row in a multiplier, respectively. A total number of $(N - 1)$ adders are required to perform the multiplication of N -bit long multiplier.

In array multiplier, carry save adders (CSA) are used for addition to pass the sum and carry signal to the next stage. Although this process of multiplication is simple, it generates higher delay and occupies larger area (Fig. 1).

3 Wallace Tree Multiplier

Wallace tree multiplier is used to compensate the disadvantage of simple array multiplier which is higher delay and area occupied. In Fig. 2, a dot representation of wallace multiplier for 8-bit input is shown.

CSA (carry save adder) is used for the addition of PP (partial products) in this multiplier. In first step, three rows of partial products are formed and added using full adders and half adders until two rows are left [3]. The sum bit of the adder goes to the next stage at the same position, whereas the carry bit goes to the next stage at the next position which can be easily understood by the following dot diagram. Carry ripple adder is used for addition of last two rows (Fig. 2).

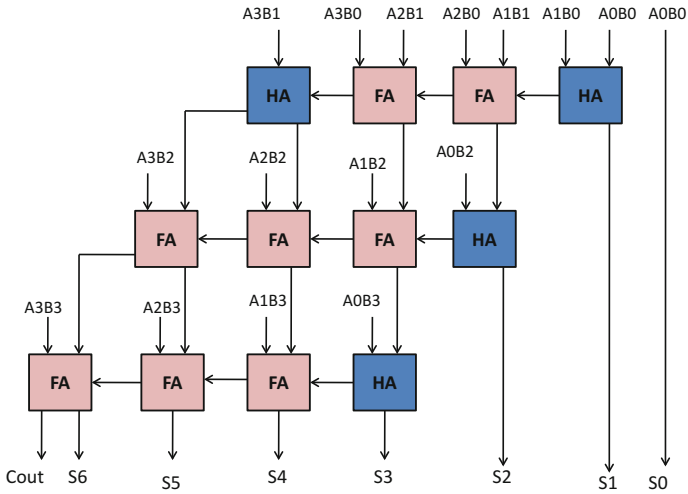


Fig. 1 A 4-bit array multiplier

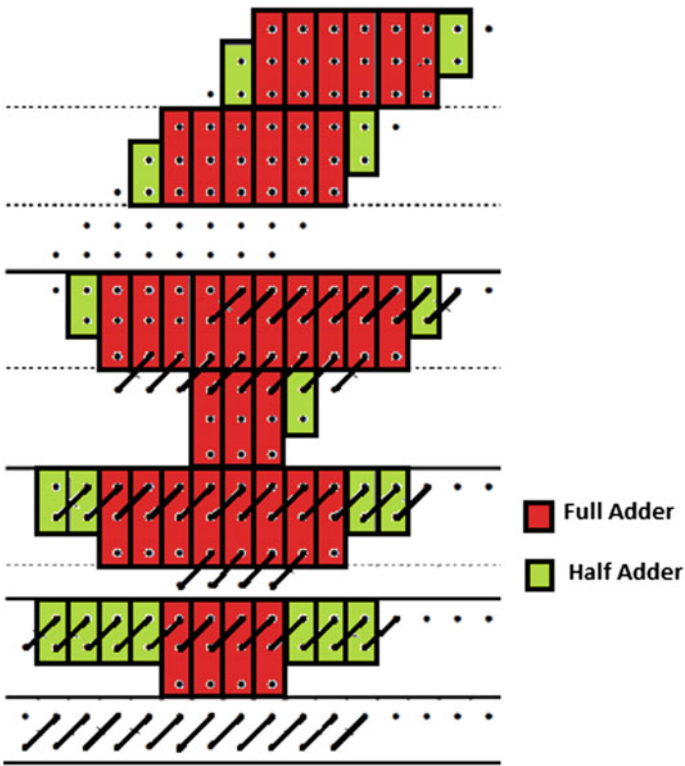


Fig. 2 A dot representation of Wallace tree multiplication

4 Dadda Multiplier

In Wallace tree multiplication, the partial products are reduced using (3:2) and (2:2) counters at column level. This reduction process is maximized in dadda multiplier. The steps for the algorithm are given below:

- Take $d_i = 2$ and $d_{i+1} = \lceil 1.5 \cdot i \rceil$, d_i represents the height of the matrix for the i th level. Find value of i such that d_i is less than the maximum number of bits in the highest bit column.
- In the i th stage from the end, (3:2) and (2:2) counters are used such that each column has maximum of d_i bits.
- For $i = i - 1$, second step is repeated until two rows are left which are added using carry ripple adder [4].

Dadda multiplier is found to give slightly faster response than Wallace multiplier and less hardware structure. A dot representation of dadda multiplication is shown in Fig. 3. The sum bit of adder goes to the next level at the same position of the bit, and to the next position of the next level, carry bit is placed.

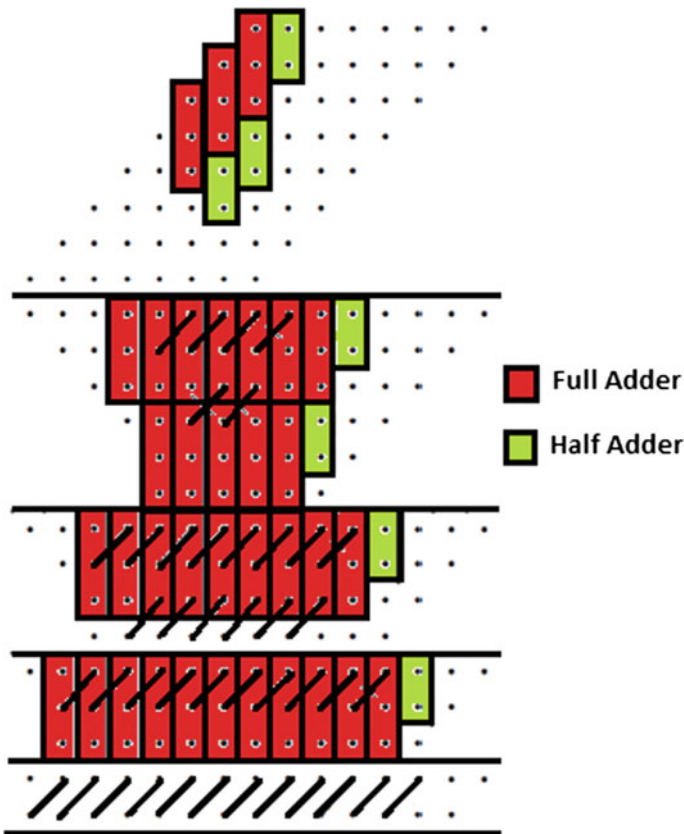


Fig. 3 A dot representation of Dadda multiplication

5 CLA (Carry Look-Ahead Adder)

Carry is forwarded to subsequent adder in carry ripple adder which results in computation of every carry, and hence, delay is caused by execution of each carry. The carry can be pre-computed ahead of time to improve this algorithm using carry look-ahead adder (CLA) [5] (Fig. 4).

In conventional 4-bit CLA (carry look-ahead adder), a CLA Logic and 4 full adders are used. In carry look-ahead logic, only one carry is propagated i.e., instead of executing each carry for each adder, the addition operation depends upon only one carry, and other carry values are represented in terms of that single carry. In this chapter, we have used MFA (modified full adder) instead of FA (full adder) in CLA.

6 Multiplier Using CLA

In this technique, CLA (carry look-ahead adder) with and without carry is used. CLA takes the 9-bit partial product terms and gives the output of 5-bit including carry out, which results in reducing the PP (partial products) [6]. Using CLA (carry look-ahead adder), PP (partial products) are reduced until final output is obtained. A dot representation is shown in Fig. 5.

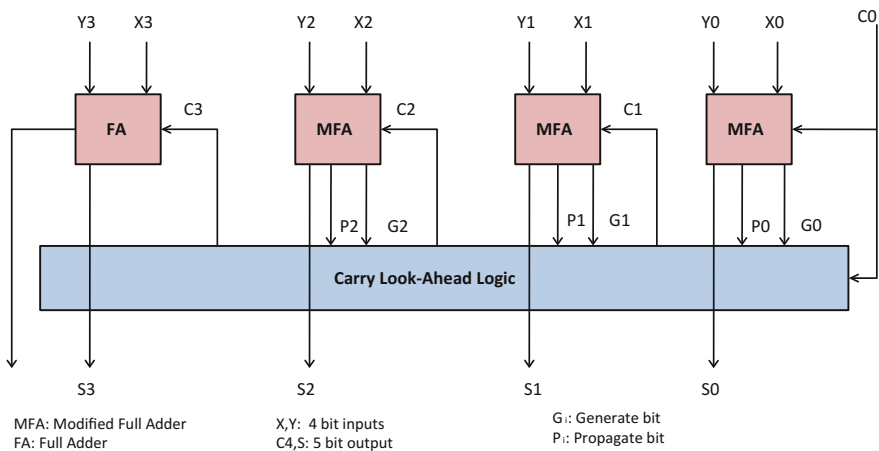


Fig. 4 A block diagram of 4-bit CLA

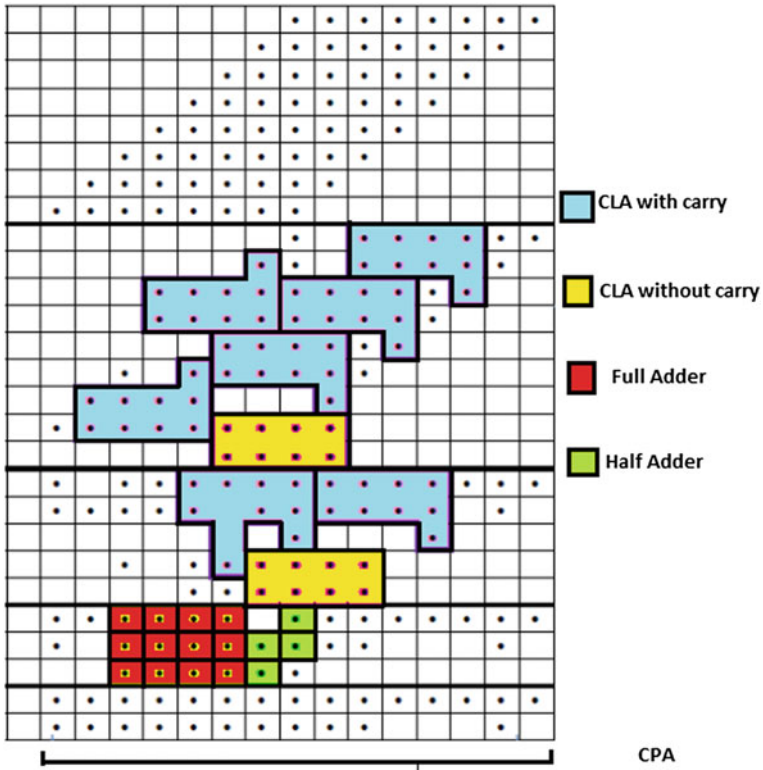


Fig. 5 A dot representation of multiplier using CLA in reduction phase

7 FPGA

A field programmable gate array (FPGA) consists of an array of generic logic cells and programmable switches which are two dimensional in nature. Hardware description languages VHDL and Verilog are used for modeling of a digital system [7]. Xilinx ISE 14.7 is used for design entry and implementation. Then, the design is implemented on Basys3 board. Basys3 is a digital circuit platform which is based on the latest Artix-7 FPGA.

8 FPGA Implementation

8.1 Simulation Result

Following figures show the stimulated output for array, wallace, dadda, and CLA multipliers respectively (Figs. 6, 7, 8 and 9).

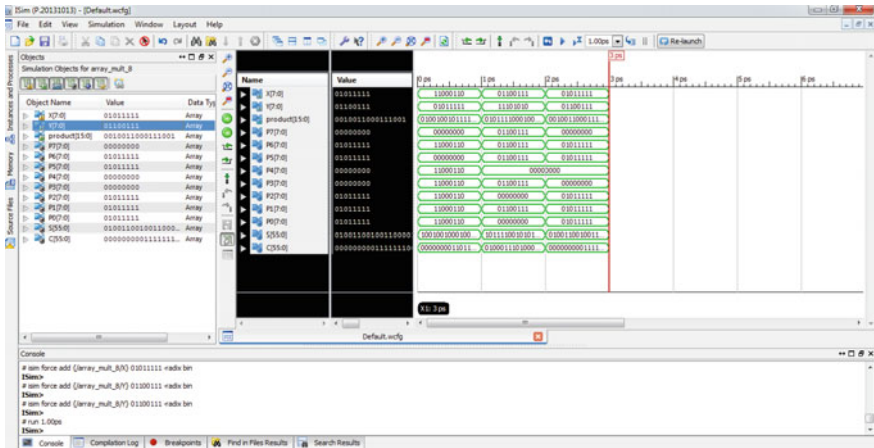


Fig. 6 A screenshot image of simulated output of 8-bit array multiplier

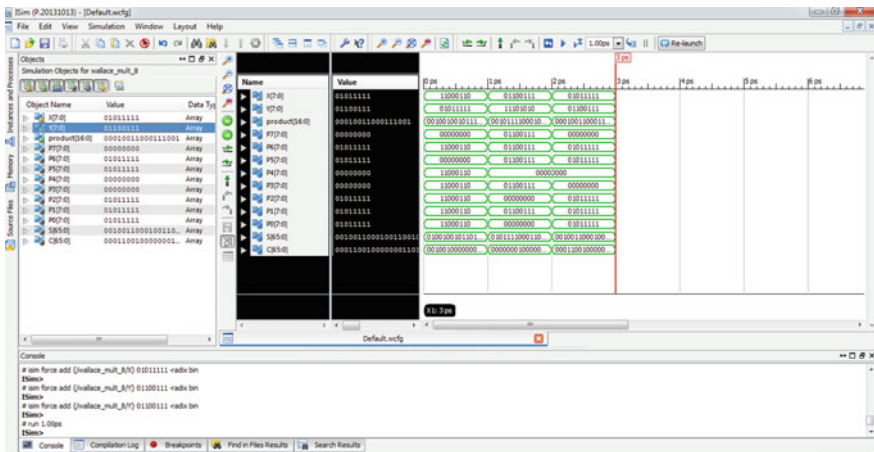


Fig. 7 A screenshot image of simulated output of 8-bit Wallace tree multiplier

Table 1 Estimated logic utilization

Multiplier type	Input size (bits)			
	4-bit	8-bit	12-bit	16-bit
	LUTs	LUTs	LUTs	LUTs
Array	28	132	296	520
Wallace	30	164	383	683
Dadda	36	207	511	610
CLA	33	191	462	541

Table 2 Maximum combination path delay

Multiplier type	Input size (bits)			
	4-bit (ns)	8-bit (ns)	12-bit (ns)	16-bit (ns)
Array	14.0224	30.105	45.743	61.429
Wallace	12.951	26.264	36.821	44.870
Dadda	14.112	25.471	36.188	45.363
CLA	11.716	24.350	32.007	40.131

9 Conclusion

In this chapter, we have implemented array, wallace, and dadda multiplier and compared their results in terms of delays and LUTs used in the execution. Further, we have used CLA in reduction phase which results in less delay after implementation. We used CLA of 4-bit because for higher input bits, the overall delay of multiplier is increased.

References

1. Krishna, K.G., Santhosh, B., & Sridhar, V.: Design of Wallace Tree Multiplier using Compressors. *International journal of engineering sciences & research Technology*, 2, 2249–2254 (2013)
2. Gaikwad, K.M., & Chavan, M.S.: Analysis of Array Multiplier and Vedic Multiplier using Xilinx. *Analysis*, 5(1) (2016)
3. Kunnathettu, M., Thomas, T., Manuel, A., Rachel, A., & Cheriyan, R.: FPGA Implementation of an Efficient High Speed Wallace Tree Multiplier
4. Sharma, A.: FPGA Implementation of a High Speed Multiplier Employing Carry Lookahead Adders in Reduction Phase. *International Journal of Computer Applications*, 116(17) (2015)
5. Mano, M. Morris, Ciletti: *Digital Design*, 4th ed. Pearson (2008) pp. 68–73
6. Chu, W., Unwala, A.I., Wu, P., & Swartzlander, E.E.: Implementation of a high speed multiplier using carry lookahead adders. In *Signals, Systems and Computers. Asilomar Conference on* (pp. 400–404). IEEE. (2013)
7. Palnitkar, Samir: *Verilog HDL: A Guide to Digital Design and Synthesis* 2nd ed. Pearson (2003)

A Sustainable Approach to Home Automation System in Perspective of Ensuring Energy Efficiency and Security

Jaideep Saraswat, Nikhil Mall, Varima Agarwal, Sayali Rajale and Mainak Mukherjee

Abstract In this paper, a sustainable approach to home automation system has been emphasized upon bearing in mind to optimize opportunities of energy saving and home security. Home automation systems serve as an addition to conventional construction, thereby ensuring consumption of energy in a synchronized method. It also leads to continuous monitoring of the home perimeter to ensure the highest level of safety of the residents. Apart from these, it ensures optimum indoor environment for maximum comfort. Home automation directly engages with the energy ingestion in installed lighting, HVAC system, perimeter security, etc. With technology proliferation, modern homes and buildings are progressively adopting technologies which would not only safeguard energy but would also sustain for a longer period.

Keywords Home automation · Energy efficiency · SVAGRIHA
Energy conservation · Renewable energy integration · Sustainability

1 Introduction

Home automation as the name suggests is using control systems and telecommunication network for automatic and efficient working and monitoring of home. Home automation should look into various aspects like reducing energy consumption, furnishing optimum indoor climate, providing the residents with a sense of security, distant monitoring and control to ensure safety even in one's absence, etc. One of the vital things is to record data for future use to know the amount of

J. Saraswat · N. Mall · V. Agarwal · S. Rajale
University of Petroleum & Energy Studies, Dehradun, India

M. Mukherjee (✉)
Department of Electrical Power & Energy, University of Petroleum & Energy Studies,
Dehradun, India
e-mail: mmukherjee@ddn.upes.ac.in

energy consumed to make better choices in the future. Home automation will rise as the most pragmatic approach soon.

The main intention for home automation is to redefine the living style of people with more ease and reliability with lesser energy consumption. Currently, there are many energy monitoring technologies available in the market, but a mere usage of energy monitoring technologies is like having a scale to check your weight. We know the weight is increasing but what are our efforts to reduce it? We need to implement energy efficient technologies for saving energy.

Home automation system which is linked to PLC in turn supported by the communication network is installed throughout the home. For this paper, it is divided into six major subsystems as shown in Fig. 1. They are perimeter intrusion detection system, HVAC, lighting system, CCTV system, fire and gas detection system, solar PV tracking automation. All of these are connected to PLC using communication bus.

The input to this multilayered subsystem is from various sensors, different terminals, signals from custom switches, mobiles, etc. These signals trigger the PLC which gives command to the appliances to give the desired output.

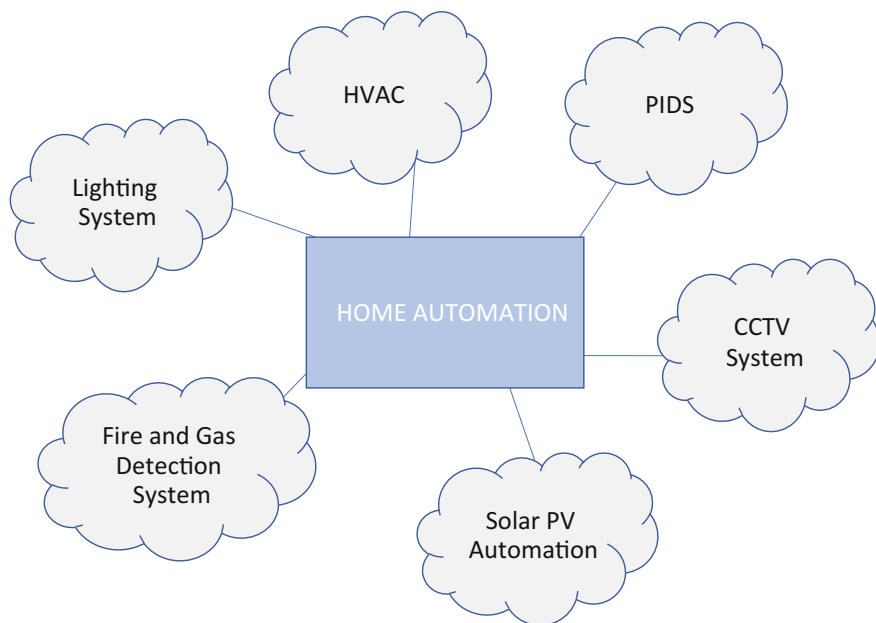


Fig. 1 Components of home automation

2 Paper Preparation

Home automation, apart from providing safe residential place, optimum indoor environment is more emphasized because of the energy efficiency measures it supports. In this paper, home automation is divided into six major subgroups for better understanding. Working of each of the subgroup is provided along with system architecture to furnish overall feel of the system. Also, each system was studied in detail to learn their role and significance in home automation. Comparison of scenarios in presence and absence of each system is underlined as well.

2.1 *Lighting System*

As per Centre for Climate and Energy Solutions, lighting accounts for 11% of electrical energy usage in residential buildings [1]. Optimizing the use of lighting will ultimately lead to significant reduction in consumption of electricity which in turn will lead to lower electricity bills.

Lighting system involves automation of the illumination lamps to make them work as needed. Lighting automation can work vastly from turning on/off the lights in the presence or in the absence of a person, to the amount of light that will be needed at the time of the day. It is also interlinked with security system like a provision of panic button near the bed to turn on the lights of the whole house at the time of an emergency. Lighting automation can be used for both indoor as well as outdoor lighting solutions.

This will lead to a significant reduction in energy consumption for lighting purposes and will help meeting the green building criteria. SVAGRIHA stands for Small Versatile Affordable Green Rating for Integrated Habitat Assessment is green building rating system popular in India. There are fourteen criteria in this rating system designed by GRIHA Council and TERI. These fourteen criteria's are divided into larger subgroups such as landscape, energy, water and waste, materials and lifestyle [2]. Lighting automation provides efficient artificial lighting technique for use (Fig. 2).

2.2 *PIDS—Perimeter Intrusion Detection System*

Perimeter intrusion detection system has become the need of the hour in today's world. There are majorly five factors that influence the selection of the type of perimeter intrusion detection system. They are risk, location, terrain, structure and standards. [3].

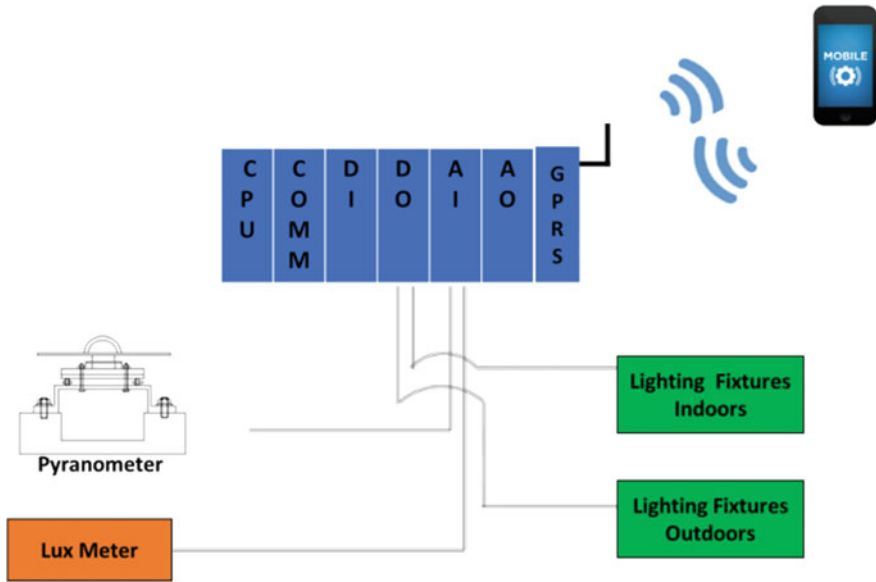


Fig. 2 System architecture of lighting system

Fibre-optic-based perimeter intrusion detection system for boundary of the perimeter is selected. Whenever there is an intrusion, it is being detected by the fibre-optic cable and sends the signal to the PIDS controller that an intrusion has occurred. The controller will then send a signal to the PLC controller which will then generate an alarm and will send a message to the resident to notify him.

Light is send into the optical fibre ring using a photodiode. The light is split by the optical coupler and is send through the ring in two different directions. When intrusion occurs, a vibration is applied to the fibre; the strength of the interference light fluctuates due to the change of refractive index in the region of the cable vibration. The emitted light arrives at a vibration point with some difference in time of flight. After passing the vibration point, the two counter directional light packets are combined to cause the interference. This interference is then detected by the photodiode at the receiving end which then sends signals to the controller [4] (Fig. 3).

2.3 HVAC and Indoor Air Quality Management

Heating, ventilation and air conditioning in single home dwellings can be carried out using VRV units and heat pump compressors. The indoor temperature and humidity levels are measured using temperature and humidity sensors. This ensures optimum temperature throughout the day. Using temperature sensors and humidity

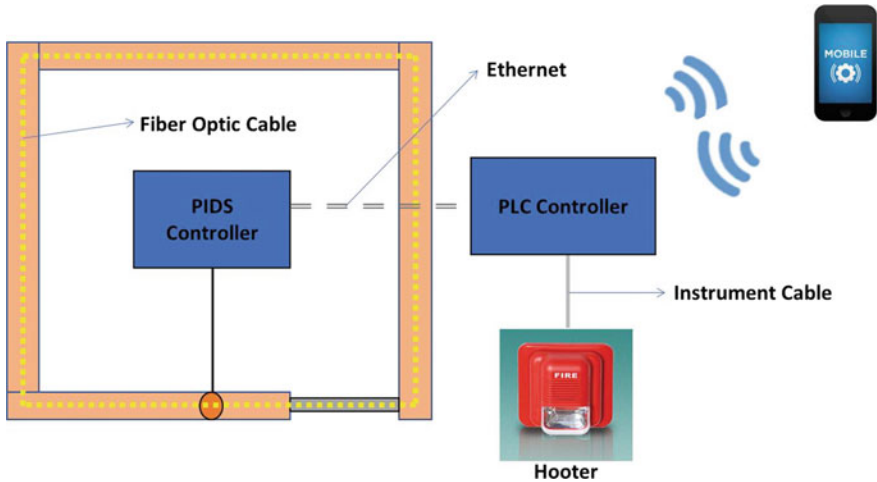


Fig. 3 System architecture of PIDS

sensors the ventilation and air conditioning plant will turn on as per the user requirement. Not only this, but flexibility in controlling the environment in each room is provided using the automation system. This can be well assisted by programmable thermostats. There can be a reduction of at least 30% in energy consumption through individual room control. With home automation there is an evident reduction in thermal energy demand by a factor of 30% [5].

In many areas, using evaporative cooling instead of VRV units can be beneficial in numerous ways. Evaporative coolers are cheaper to operate than refrigerative cooling. They can work best in areas where slight variation in temperature is not a problem. As compared to an air conditioner they use 75% less electricity, costs about half the price of an air conditioner, their installation is easy [6]. Also, the air supplied by evaporative coolers has high moisture content. Using cellulose filled pads in the rooms can dormant this issue (Fig. 4).

Indoor air quality is referred to the maintenance of optimum environment inside and around the house. It includes maintaining optimum temperature, humidity, carbon dioxide, volatile organic compounds, etc. Table 1 shows various issues related to IAQ of a house and how HVAC addresses to them.

2.4 Fire and Gas Detection System

Fire and gas detection system is one of the most important disciplines in home automation. In India, on an average, approximately 25,000 people die due to fires and related causes out of which females account for 66% of the total deaths. It is estimated that about 42 females and 21 males die everyday in India due to fire [8]. Leakage of gas

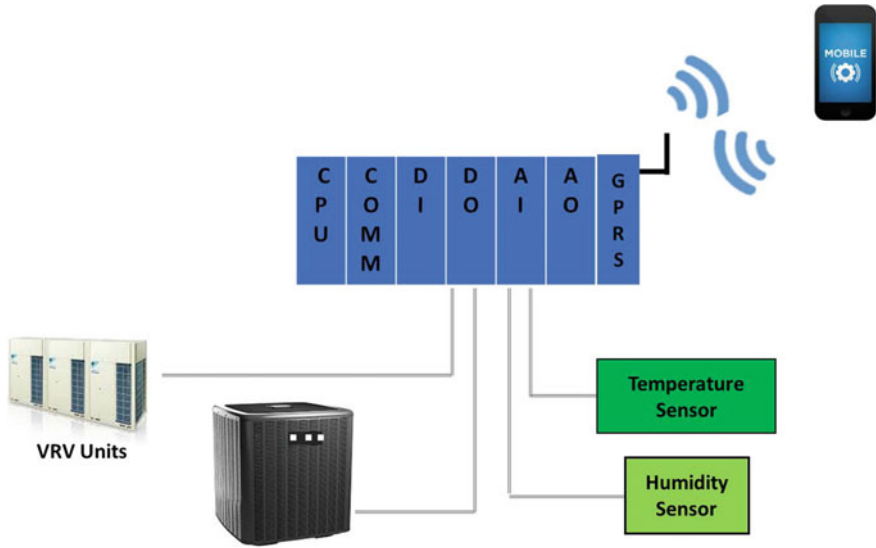


Fig. 4 System architecture of HVAC

Table 1 Comparison between air source heat pump and ground source heat pump [7]

S. No.	Parameter	Problem	Solution
1	Purification	Odours and chemical vapours	Constant intake and release of air containing these particles
2	Filtration	Small, respirable particles and bioaerosols	HVAC combats this problem by capturing even the smallest contaminants
3	Humidity control	Too much moisture	Dehumidifiers or humidifiers work with HVAC system or usage of cellulose filled pads

or outbreak of fire in a house can lead to massive destruction of life and property. Moreover, it can have adverse impacts on the environment. So, this system detects the presence of smoke and flame inside the house. The detectors then send a digital signal to the PLC controller. The controller then turns on the hooter to alert the residents as well as sends a text message to the mobile of the resident (Fig. 5).

2.5 CCTV System—Closed Circuit Television

Closed circuit television system is one of the oldest concepts for securing the parameter. It is not that businesses, industries, media houses require security but

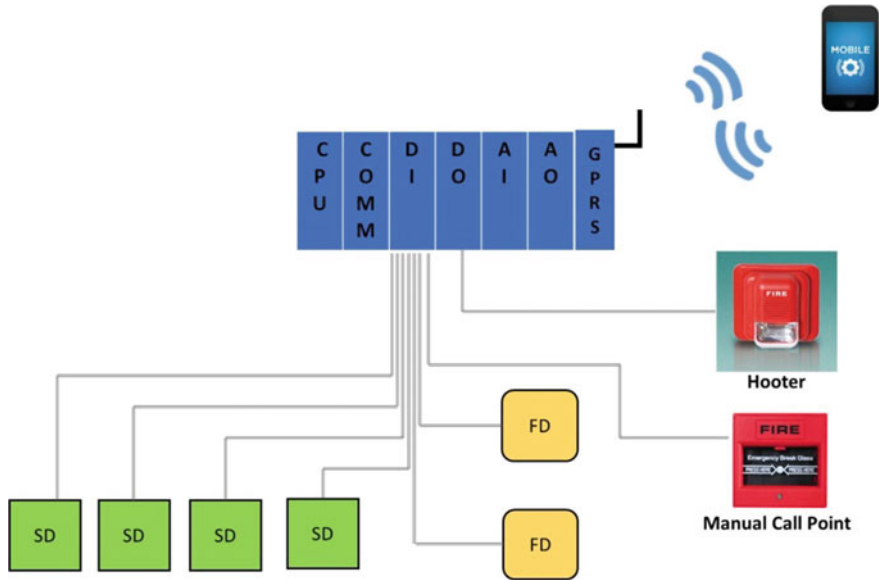


Fig. 5 System architecture of fire and gas detection system

homes do need it as well. With increasing crimes like burglaries, theft, etc. in current day and age, their importance is very much evident. CCTV system has proved to be one of the most trustworthy and cost effective options in recent times. The need of CCTV system lies in the fact that it can prevent crime, it can act as a useful piece of evidence, help law enforcement solve crime etc. [9]. The technology related to CCTV has constantly evolved with time. Recent development has eliminated the need for dedicated network cabling. Signal transmissions of IP address cameras can be carried out over power line for approximately 300 m (Fig. 6).

3 Integration of Renewable Energy Systems in Home Automation

3.1 Solar Tracking System

Solar energy is the energy which we get in the form of heat and light from the sun. We can harness this energy using various technologies such as:

1. solar thermal systems
 - (a) solar water heating system (flat plate collector or evacuated tube collector)

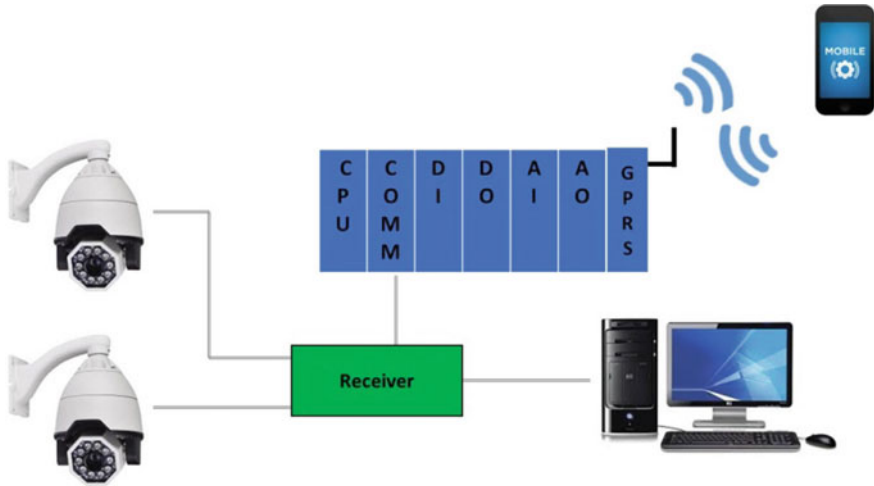


Fig. 6 System architecture of CCTV system

(b) solar thermal power system (power tower, parabolic trough collector).

2. solar photovoltaic systems (stand-alone SPV power plant, grid connected solar system, building integrated solar system).
3. other means such as artificial photosynthesis.

A solar photovoltaic panel is designed in such a way that it absorbs the sunrays as a source of energy and generates electricity. It produces a DC power which is converted into AC power using an inverter. The efficiency of panel depends on the material which it is made up of. The efficiency is usually between 10 and 20% [10]. In order to maximize the above-mentioned efficiency, solar tracking systems are installed. A solar tracker is used to orient the panel towards the sun. The incident sunlight consists of direct beam and diffused beam. Direct beam is approx. 90% and rest is diffused beam. More is the incident radiation on the solar photovoltaic panel; more will be the output power of the system.

There are two types of solar tracking system:

- Single-axis tracker—it has one degree of freedom which acts as the axis of rotation. It tracks from east to west. It is used to vary the solar azimuth angle.
- Dual-axis tracker—it has two degree of freedom that acts as the axes of rotation. These two axes are normal to each other. The panel can move from east to west direction and also rotates on its own axis. It is used to vary the solar azimuth angle as well as the tilt angle of the panels.

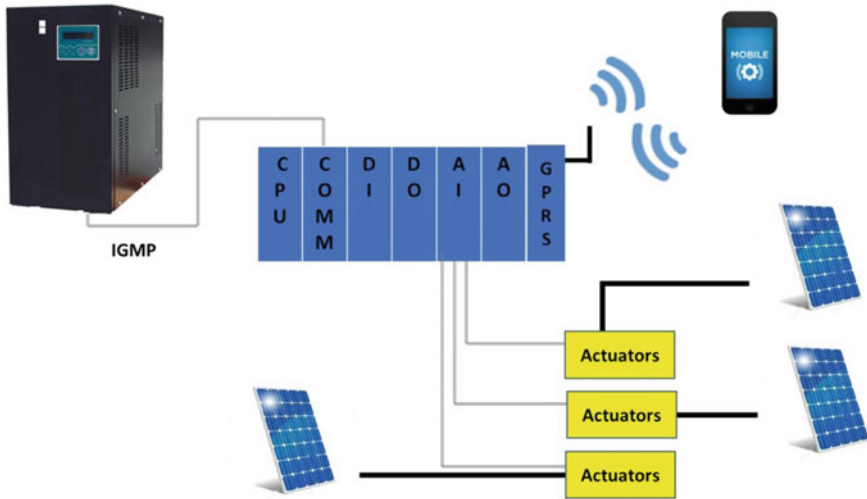


Fig. 7 System architecture of solar tracking and solar inverter

Single-axis tracking system involves using light detecting resistors (LDR) on the edges of the panel. When the light incidents on the resistors, their resistance changes. The panel will orient itself in the direction of minimum resistance with the help of stepper motor. Same is the case with dual-axis tracking system. It involves using four LDRs on each edge of the panel and two stepper motors. Apart from the tracking system, there is an important need of pooling the data from solar inverter to keep a track on the amount of energy generated everyday (Fig. 7).

3.2 *Scope for Geothermal in Fulfilment of Partial Energy Needs*

Geothermal Energy is used to reap the heat present in the earth. Unlike the change in the ambient temperature of the earth with changes in the seasons, the temperature below the earth is fairly constant. The temperature increases at a rate of 1 °F for every 70 feet depth below the earth [11]. It can meet both heating and cooling requirements of the building. It can extract heat from the building and transfer it to the ground or vice versa. Also, the heat pump can deliver about five times the energy for every 1 kWh of electricity consumed. It should be underlined that if the electricity used for heat pump is not coming from renewable energy source then it is not a green technology altogether. A comparison between air source heat pump and ground source heat pump is shown in Table 2.

Table 2 Comparison between air source heat pump and ground source heat pump [12]

S. No.	Parameter	ASHP	GSHP
1	Installation cost	Much less	High
2	Operation cost	High as efficiency is less	Significantly low as efficiency is very high
3	Maintenance cost	High as it is vulnerable to external environment	Low as it has stable geology environment
4	Life cycle cost	High	Low

4 The Future of Sustainable Homes

Mankind is constantly evolving with time. Earlier, focus was on acquiring energy to carry out day-to-day activities. But now the focus has shifted to acquiring sustainable form of energy to meet the needs. This evolution will bring a pleasant change in the coming years.

The two most popular terms related to homes are sustainable and zero carbon. A sustainable home is realized by constructing the house with greener practices; using the natural resources efficiently; protect the occupants health; minimum emission of GHG in the environment during its lifecycle and maintenance and demolition using greener practices. Zero carbon houses on the other hand can also be termed as negative carbon houses are the houses that generate more energy that what they consume along with their carbon dioxide emission being minimal. Realization of both requires implementation of renewable energy sources along with energy efficient technologies like solar PV systems, composting toilets, etc. With constant research in this field, economic realization of the same looks viable.

5 Conclusion

1. Implementation of automation in home leads to both thermal as well as electrical energy efficiency. It was also seen that implementation of individual room control was augmenting the efficiency.
2. It is clear from above that security is a crucial aspect for homes as well. An elevated level of security can be achieved using perimeter intrusion detection system as well as CCTV system.
3. Security of life and property from fire outbreak or smoke congestion can be achieved with optimum efficiency using fire and gas detection system.
4. Solar PV is a renewable source of energy. Utilizing solar tracking system will lead to an increase in the efficiency of the same. This will be an add-on advantage for solar PV. Though, solar tracking system is more beneficial for the regions that are near to the equator. It will furnish maximum efficiency of solar PV in the areas where the Sun is more or less overhead at the noon [13].

5. It is quite evident that dual-axis tracking system is more efficient as compared to a single axis.
6. A feasibility study should be carried out for geothermal source of energy. If the feasibility study is favourable then implementation of ground source heat pump is beneficial in comparison to air source heat pump. This is due to minimum operational, maintenance and life cycle cost for ground source heat pump.

References

1. Lighting Efficiency, Centre for Climate and Energy Solutions. Available at: <https://www.c2es.org/technology/factsheet/LightingEfficiency>
2. SVA GRIHA, SVA GRIHA Rating. Available at: http://www.grihaindia.org/index.php?option=com_content&view=article&id=86
3. Peter Houllis, Need Perimeter Intrusion Detection System? Here are your options and How to decide. Available at: <https://www.ifsecglobal.com/need-perimeter-intrusion-detection-here-are-your-options-and-how-to-decide/>, September 9, 2015
4. AFL, Fibre Security, Optical Fibre Perimeter Intrusion Detection System. Available at: http://www.astrec.com/uploads/5/9/7/1/5971541/afl_fibersecurity.pdf, Pg. No. 3 of 8
5. Heating, Ventilation and Air Conditioning. Available at: <http://www.buildingtechnologies.siemens.com/bt/global/en/buildingautomation-hvac/hvac-building-automation.aspx>
6. Evaporative Cooler versus Air Conditioning: A True Comparison. Available at: <http://www.air-n-water.com/evaporative-cooler-ac-comparison.htm>
7. Common Indoor Air Quality Problems and Solutions. Available at http://www.indoorairqualityhvac.com/problems_solutions.php
8. R.R. Nair. Fire Safety in India-An Overview. Available at <http://www.ind-safety.com/Articles/fire-safety-in-india-an-overview/242025/5254725/5250000>, October, 2013
9. Importance of CCTV. Available at <http://www.clvresources.com/Importance-Of-CCTV/>
10. Andrew Sedy. Efficiency of Solar Panels. Available at: <http://www.solarreviews.com/solar-panels/efficiency-of-solar-panels/>, April 8, 2018
11. Geothermal Heating and Cooling Technologies, United States Environmental Protection Agency. Available at: <https://www.epa.gov/rhc/geothermal-heating-and-cooling-technologies>
12. Ruqun Wu: Energy Efficiency Technologies—Air Source Heat Pump vs Ground Source Heat Pump, Pg. No. 6 of 10, Journal of Sustainable Development
13. Deepthi. S, Ponni. A, Ranjith. R, Dhanbal. R: Comparison of Efficiencies of Solar Tracker systems with static panel Single Axis Tracking System and Dual-Axis Tracking System with Fixed Mount, Pg. No. 3 of 9, International Journal of Engineering and Technology (IJET)

Low-Offset High-Speed CMOS Dynamic Voltage Comparator

Priyesh P. Gandhi and Niranjan M. Devashrayee

Abstract In this paper, authors have proposed low-offset high-speed voltage comparator which can be realized in A/D converters. It features low-offset and larger input swing at lower operating voltage. A comparison between typical comparator and the proposed comparator in 180 nm has been made. In the proposed comparator, the ICMR is considerably improved with reduction in offset voltage and power consumption. The power consumption of the proposed comparator is about 20% less as compared to conventional comparator, and its offset voltage is 28% less in comparison with other mentioned conventional comparators.

Keywords CMOS · Dynamic comparator · Offset · Speed · Analog-to-digital converters (ADCs)

1 Introduction

The growth in portable battery-operated communication devices increases the demand for low-power and high-speed ADC. A prime circuit required for conversion of the continuous signal to digital signal is the comparator. Generally, moving toward the smaller feature size allows for the reduction in the power consumption and higher speed. However, the process variation and mismatch increase at finer processes and limit the performance of the ADCs. One of the critical parts of an ADC greatly influenced by the process variation and mismatch is the comparator [1].

P.P. Gandhi (✉) · N.M. Devashrayee
Nirma University, Ahmedabad, India
e-mail: priyeshgandhi@gmail.com

N.M. Devashrayee
e-mail: nmd@nirmauni.ac.in

The comparator circuits should be immune to speed, power, and offset trade-off. Most of the high-speed ADCs required high-speed, low-power comparator with low offset for high-speed conversion from continuous signal to digital signal. Due to low propagation delay, less power utilization, high input impedance, and full-swing dynamic comparators are in demand. The design of comparator with low propagation delay suitable to operate at low supply voltages is more demanding from designer. In conventional comparators, the mismatch between the cross-coupled circuits determines the trade-off between the speed, offset, and the power utilization of the comparator.

The characteristics of a comparator are defined by its input-referred offset voltage for a given power dissipation, speed, and the area [2]. Scaling CMOS technology shrinks the headroom voltage and the full-scale range of input voltage. This effect gives a major thrust in recent comparator designs [3]. As the comparator is one of the main building blocks which confines the conversion speed of the A/D converters, its optimization is of major significance. Hence, the design of a high-performance comparator is one of the key challenges in an ADC design.

In comparators, a lower offset comes at the cost of bigger transistor dimension; therefore, it will lead to more power dissipation and increase in delay. In addition, the traditional comparators are difficult to design and there are not many design procedures to lower the offset voltage. To decrease the power utilization and the area of comparators, dynamic comparators are proposed [3–6]. However, such comparators generally experience comparatively large offset voltage in comparison with static comparators [6, 7]. Some designs have been proposed for dynamic comparators in the literature. The dynamic comparators are categorized into three groups: resistor divider [5], differential pair, and charge sharing dynamic comparator [2]. Other structures are mainly derived from these architectures [3–8].

As high speed is the great demand of today's portable devices, we present a performance comparison of existing dynamic comparators with proposed architecture in terms of delay, offset, ICMR, and power dissipation.

In order to break the deadlock between offset and power consumption, a new architecture is proposed. The single-tail architecture will make design more robust against any misalignment and non-idealities. More importantly, it involves a significantly smaller input offset voltage without a significant rise in power and delay. The organization of this paper is as follows: In Sect. 2, the existing architecture is presented along with the summation results. In Sect. 3, proposed architecture is presented along with the simulation results, while Sect. 4 concludes the paper.

2 Existing Architecture

The existing comparator architecture is illustrated in Fig. 2 [3]. When Φ_{clk} increases, comparator makes the decision. Rather using the same clock as top switches which swings from V_{ss} to V_{dd} , a phase-limited voltage swing clock ($\Phi_{\text{clk},B}$) has been used for the tail-clock signal. To make sure that tail current should not

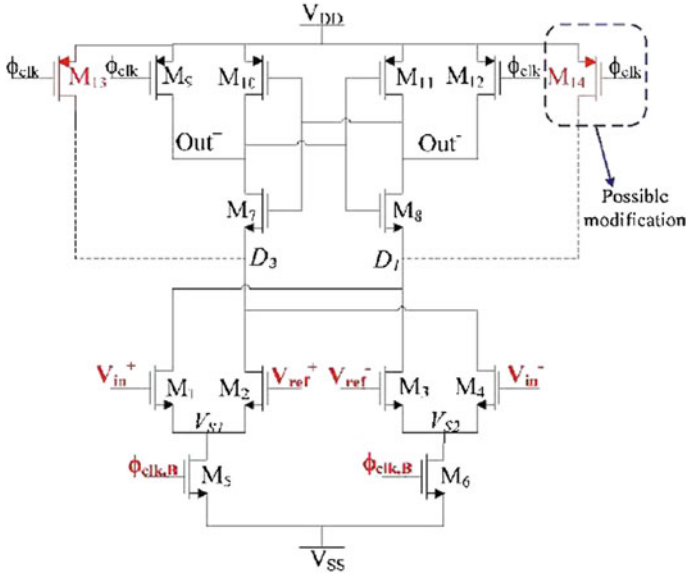


Fig. 1 Typical dynamic comparator by Katyal et al. [3]

enter into linear region, limited clock swing leads to tail current that remains in the saturation region. This is very crucial while the comparator is in evaluation phase.

To ensure all input transistors M_1 to M_4 have same currents, differential pair V_{in+} and V_{ref+} (and V_{in-} and V_{ref-}) is combined in single differential pair for a case where all the input transistors are of the equal dimension and no inequity is present [9, 10]. During the time of decision, all input transistors will contribute.

When comparator is in ideal mode, the nodes D_1 and D_2 can be reset to V_{DD} and help comparator to retune all the nodes prior to the comparator enters into evaluation mode (Fig. 1).

2.1 Simulation Results

Figures 2 and 3 show the simulation results for the typical dynamic comparator. From simulation, it has been observed that propagation delay is 0.162 ns, offset voltage is 1.021 mV, ICMR ranges from -0.29 V to 0.45 V.

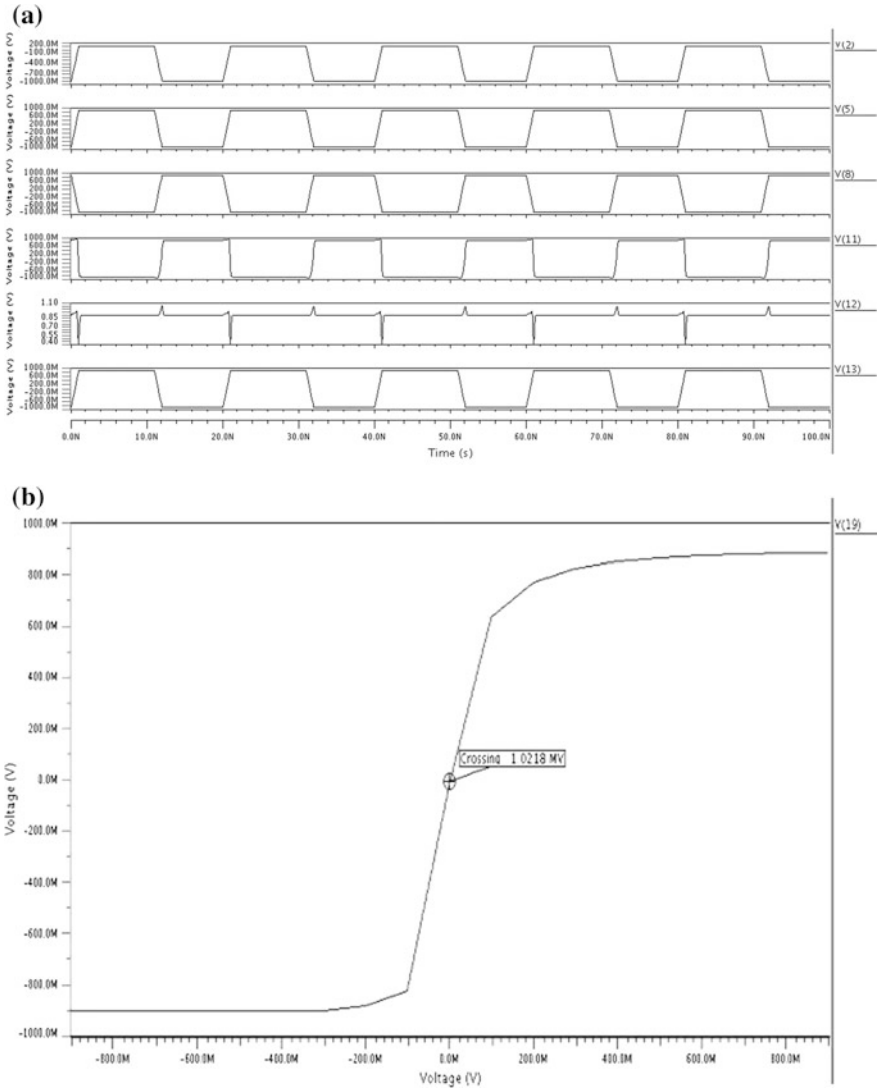


Fig. 2 a Transient analysis and b offset analysis of typical dynamic comparator

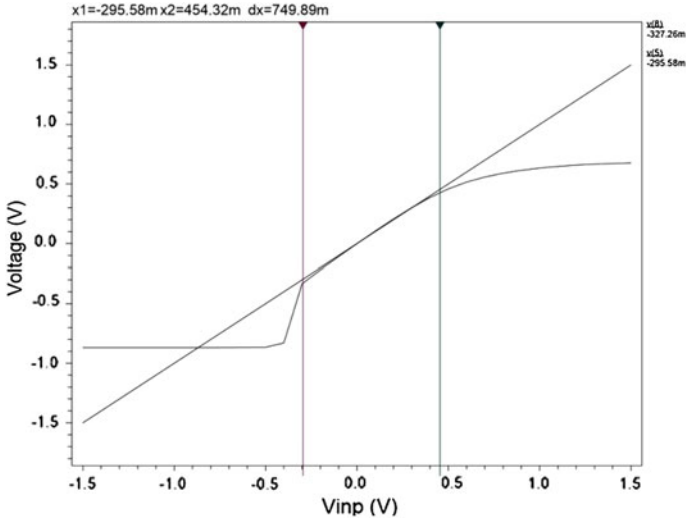


Fig. 3 ICMR for typical dynamic comparator

3 Proposed Comparator

The proposed comparator architecture is illustrated in Fig. 4. A small alteration has been made to the architecture in comparison with the architecture shown in Fig. 1. The modification is carried out for the tail transistor; a single tail transistor of higher area with phase-limited voltage swing clock ($\Phi_{clk,B}$) has been used. As an alternative; designing two identical transistors and to keep both in saturation at the same time, a single tail transistor will add the advantage and make design more robust against any misalignment and non-idealities. The single tail transistor ensures that limited current flows through both of the output branches, and it illustrates strong dependability on delay and offset voltage with common-mode input voltage.

3.1 Simulation Results

Figures 5 and 6 show the simulation results for the proposed comparator. From simulation, it has been observed that propagation delay is 0.87 ns, offset voltage is 0.73 mV, ICMR ranges from -0.40 to 0.57 V.

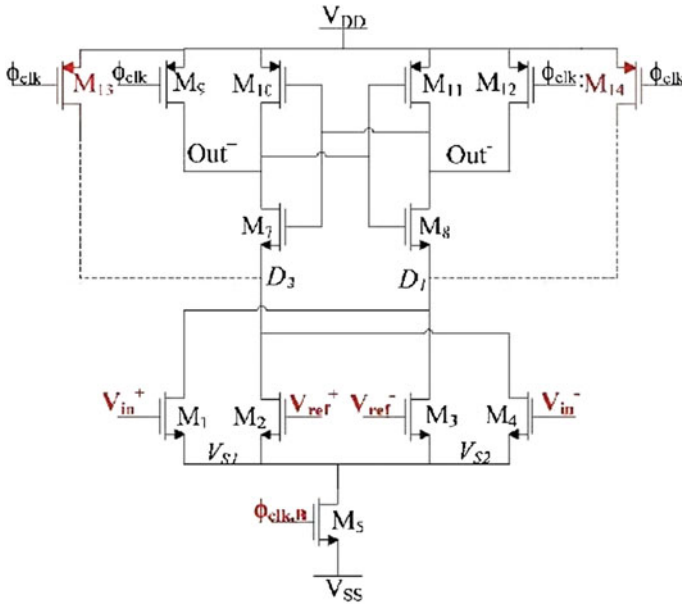


Fig. 4 Proposed comparator

Figure 7 illustrates the sensitivity of the offset voltage to common-mode voltage (V_{CM}). It shows that a variation in offset voltages is less in proposed comparator as compared to reference comparator against common-mode voltage.

The performance of proposed and reference comparators is verified and compared with each other in 180-nm CMOS technology. Table 1 compares the comparators' performance in terms of delay, offset, ICMR, and power consumption. The power dissipation and offset voltage of the proposed comparator are 20 and 28% less as compared to reference comparator, respectively.

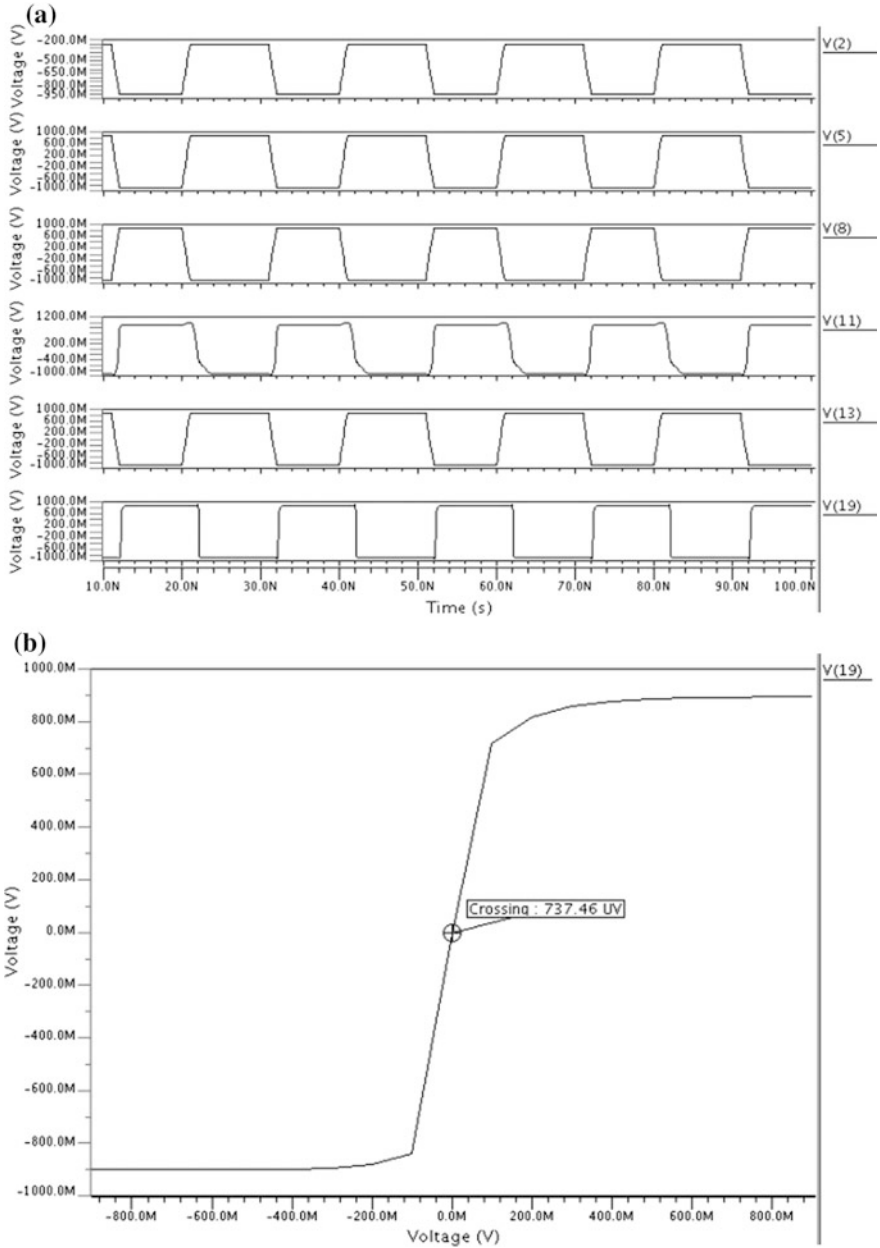


Fig. 5 a Transient analysis and b offset analysis of proposed comparator

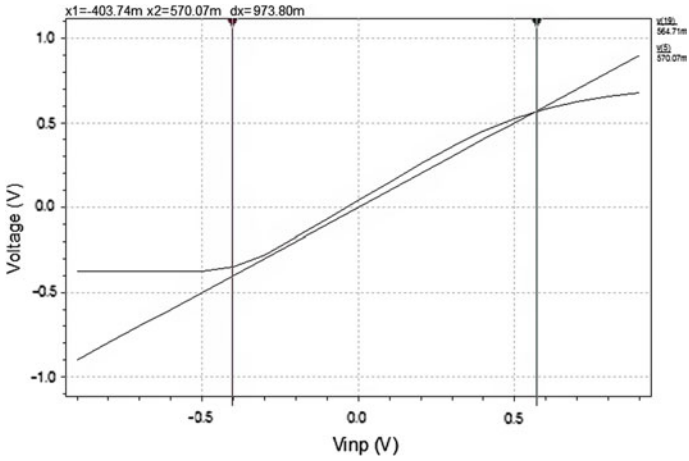


Fig. 6 ICMR of proposed comparator

Fig. 7 Offset voltage versus common-mode voltage

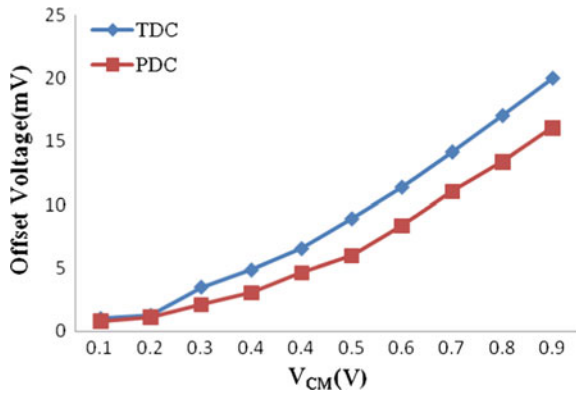


Table 1 Comparative result analysis

Parameter	Typical dynamic comparator	Proposed comparator
Technology (nm)	180	
Supply voltage (V)	± 0.9	
Delay (ns)	0.162	0.87
Offset (mV)	1.021	0.73
ICMR (V)	-0.29 to 0.45	-0.40 to 0.57
Power dissipation (μW)	379.90	300.23

4 Conclusion

In this paper, authors have projected a comparator which is mismatch insensitive dynamic comparator. The performance of the comparator has been verified by simulation featuring not only small offset voltage with low power dissipation. Offset and power dissipation of the proposed comparator are improved as compared to reference comparator with moderate increase in propagation delay. Thus, proposed comparator is a competitive choice for ADCs implemented in advanced process.

References

1. R. Jacob Baker, Harry W. Li, David E. Boyce, "CMOS Circuit Design, Layout and Simulation", IEEE Press Series on Microelectronic Systems, 1997, pp. 685–699.
2. Phillip E. Allen, Douglas R. Holberg, "CMOS Analog Circuit Design", Oxford University Press, Second Edition, 2002, pp. 439–488.
3. Vipul Kalyal, Randall L. Geiger and Degang J. Chen, "A New High Precision Low Offset Dynamic Comparator for High Resolution High Speed ADCs", IEEE Asia Pacific Conference on Circuits and Systems, 2006 (APCCAS 2006) pp. 5–8, Dec. 2006.
4. P. Uthaichana, E. Leelarasmeek, "Low Power CMOS Dynamic Latch Comparators", TENCON 2003, Conference on Convergent Technologies for the Asia-Pacific Region, pp 605–608 Vol. 2 Oct 2003.
5. HeungJun Jeon, Yong-Bin Kim, "A CMOS Low Power Low Offset and High-Speed Fully Dynamic Latched Comparator", SOC Conference (SOCC), 2010 IEEE International, pp. 285–288, 2012.
6. M. Hassanpourghadi, M. Zamani and M. Sharifkhani, "A Low-Power Low-Offset Dynamic Comparator for Analog to Digital Converters", Microelectronics Journal, 2013. pii/S0026269213002863 Elsevier, pp. 256–262. 2013.
7. Dhanisha N. Kapadia, Priyesh P. Gandhi "Design and Comparative Analysis of Differential Current Sensing Comparator in Deep Sub -Micron Region". Proceedings of 2013 IEEE Conference on Information and Communication Technologies (ICT 2013).
8. Dhanisha N. Kapadia, Priyesh P. of CMOS Charge Sharing Dynamic Latch Comparator in 130 nm and 90 nm Technologies". Proceedings of 2013 IEEE Conference on Information and Communication Technologies (ICT 2013).
9. L. Sumanen, M. Waltari, V. Hakkarainen, K. Halonen, "CMOS Dynamic Comparators for Pipeline A/D Converters," IEEE ISCAS, vol. 5, pp. 157–160, May 2002.
10. T. W. Matthews, P. L. Heedley, "A Simulation Method for Accurately Determining DC and Dynamic Offset in Comparators," IEEE MWSCAS, pp. 1815–1818, Aug. 2005.

Vehicle Control Using Raspberry pi and Image Processing

Rohit Tiwari and Dushyant Kumar Singh

Abstract The goal of the proposed work is to execute the accessible method to identify the stop board and red movement motion for a self-governing auto that makes a move as indicated by activity motion with the assistance of raspberry pi3 board. The framework likewise utilizes ultrasonic sensor for separation estimation with the end goal of speed control of vehicle to maintain a strategic distance from impact with ahead of vehicle. Rpi camera module is used for billboard recognition, and ultrasonic sensors are utilized to get the separation data from the genuine world. The proposed framework will get the picture of this present reality from the camera and after that covering and shape strategies are utilized to recognize the red signs of the activity and to decide the movement board signs like stop board framework will utilize haar course method to decide the stop words. So auto will have the capacity to make a move and diminishes the odds of human blunders like driver oversights that outcomes street mischances. The coding for this entire framework is in Python, and for picture handling, opencv is utilized that is much effective as contrast with the MATLAB. Ultrasonic sensor is utilized for the deterrent location set-up of camera since separation finding from the camera is more unpredictable and computational as contrast with the ultrasonic sensor. Ultrasonic sensor specifically gives the snag separate in front of it without more mind-boggling calculations.

Keywords Raspberry pi3 · Traffic flag detection · Obstacle recognition
Python

R. Tiwari (✉) · D.K. Singh
Lovely Professional University, Phagwara, Punjab, India
e-mail: rohitt202@gmail.com

D.K. Singh
e-mail: dushyantkumarsingh83@gmail.com

© Springer Nature Singapore Pte Ltd. 2018
R. Singh et al. (eds.), *Intelligent Communication, Control and Devices*,
Advances in Intelligent Systems and Computing 624,
https://doi.org/10.1007/978-981-10-5903-2_24

1 Introduction

As a result of a survey, more than 90% of road accidents happen due to the driver mistakes. These mistakes are red signal jumping, over speeding, not following road signs like stop board, etc. So to overcome this problem, designing of a system that itself takes the real-world data of the traffic and take action in the cause driver will not responding according to the traffic signals. So that we can reduce the human error as well as reduce the traffic problems caused by human due to phone calls and other facilities of entertainment or by the human avoidance of the traffic signals. So proposed system can assure that the people in the car and outside the car both are saves while travelling to their destinations. Designed system helps the car to get the distance of the next vehicles running ahead of designed vehicle and accordingly control the speed of the car. By the use of ultrasonic sensor designed car or vehicle will able to get distance of any obstacles come across while running car and it will help in avoiding the accident. People will also able to do their work while driving because car itself takes the responsibility and performs required action such as controlling brakes, speed, wheel control.

2 Methodology

Due to low budget, we used a two wheel chassis for the car and implemented all the techniques that give accurate results (Fig. 1).

2.1 *Traffic Signs and Signal Detection*

The main work of the proposed system is to detect the signboards like stop board and signals like red light signal. For red signal, system will always try to determine between the lower and upper range of the red colour and a rectangle be formed on the red signals. Whenever red signal occurs while running designed vehicle system will generate a rectangle around red signal and system will get high or 1 as input to the controller to stop the vehicle [1].

For the detection of the stop board sign system used cascade classifier in which it compares the xml file of different sizes of stop word with the input available from real world of traffic signboards using camera. After match found, it generates a signal so the pi sends a control signal to the l293d to control the motors of the chassis.

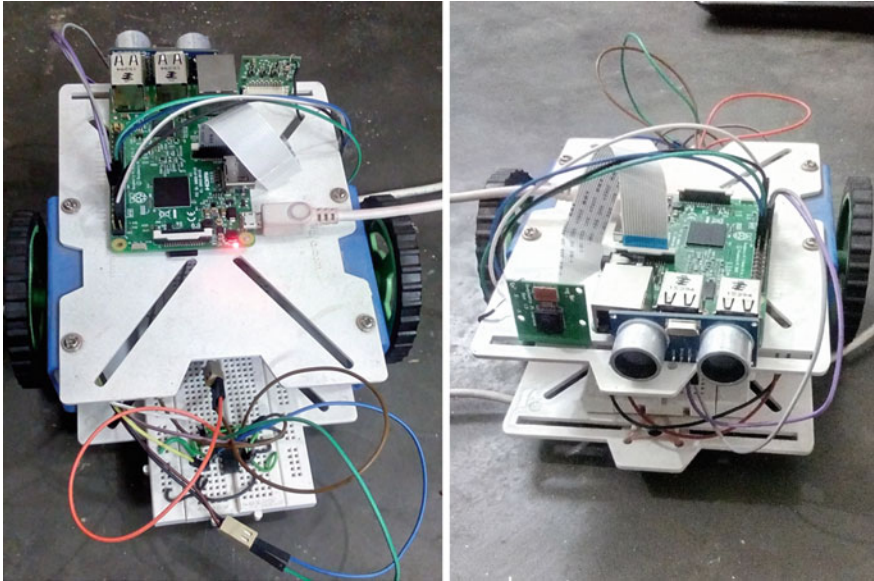


Fig. 1 Designed two wheel chassis car

2.2 Obstacle Detection

Using the ultrasonic sensor system, we get the distance of the objects ahead of the car [2]. Ultrasonic sensor gives distances of vehicle running ahead of designed vehicle and generate signal for stopping car when any objects will come near to the designed vehicle [3].

2.3 Security for Parking

While parking the car many times car backside parts get damaged due to any obstacles comes behind the car so by the use of ultrasonic sensor we can avoid all those damages. So by the use of an ultrasonic sensor, we can save our time and money as well and design a car more technically efficient in performance.

2.4 Speed to Overtake

In this project using ultrasonic sensor and image processing, we can get the exact speed to overtake a vehicle ahead of us. When any vehicle comes at the range of my car, ultrasonic sensor finds the distance of the next car at regular interval and backside ultrasonic sensor also finds the distance of the result, and so by getting distance of the next car at regular time, we can calculate the maximum speed of our car to overtake the next vehicle that is ahead of my car.

A. Raspberry pi3

Raspberry pi3 is a small chip that is like single-board computer. There are various models of raspberry pi available in the market, i.e. the Raspberry Pi1 Model B, Raspberry Pi1 Model B+, Raspberry pi2, Raspberry Pi3 Model B. These all differ in memory capacity and hardware features like Raspberry pi3 that has inbuilt Bluetooth and Wi-fi modules, whereas in previous versions, these modules were not available. It has 1.2 GHz 64-bit quadcore ARMv8 CPU with 1 GB of RAM [4].

B. Pi camera

Camera is used to take the continuous images to get the traffic signs and signals from the real world. According to the images available through the camera, we can send these images to the raspberry pi to perform the action to control the car [5] (Fig. 2).

C. Ultrasonic sensor

Ultrasonic sensor (hc-sr04) is used to detect the obstacles and avoid the accident [2]. It has 4 pin vcc, gnd, trig, and echo [6]. It gives up to 4 m information, and we need to stop our vehicle at the distance of 1 m before any vehicle is ahead of ours.

D. Motor driver IC

L293D is a motor driver IC that can control two DC motors at a time. Inputs 00 and 11 stop the motors, whereas logic 01 and logic 10 start the rotation of the motors in clockwise and anticlockwise directions, respectively (Fig. 3; Table 1).

Fig. 2 Pi camera

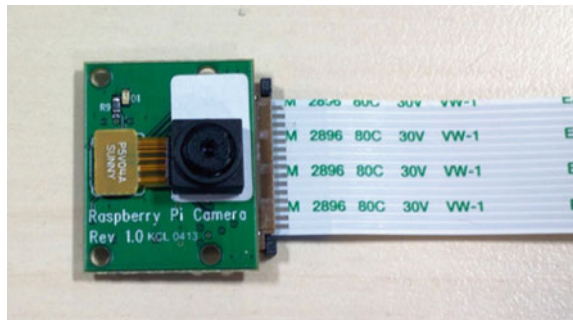


Fig. 3 Motor driver IC

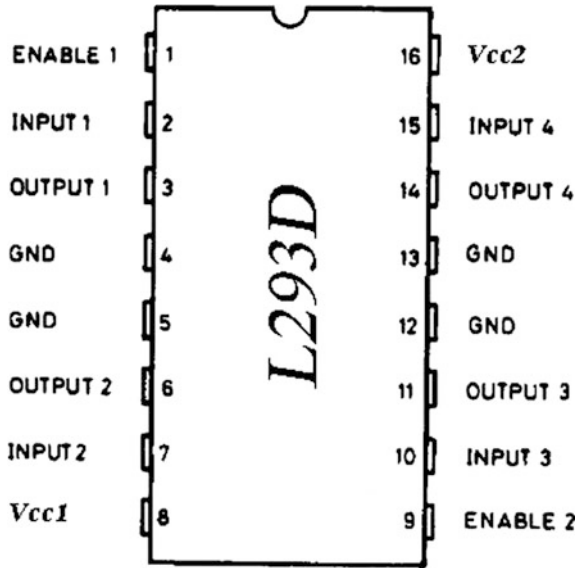


Table 1 Truth table to control the motors from l293d pins

Pin 2	Pin 7	Output
High	High	Stop
Low	Low	Stop
Low	High	Clockwise
High	Low	Anticlockwise

E. Python software

Python is a high-level, general-purpose programming language used widely in industries and research work and also used in making general-purpose projects [7]. Its software comes in various versions, i.e. IDLE Python 2, Python 3; also, in these two types, different versions of Python IDLE are available for programming the Python language.

F. Opencv

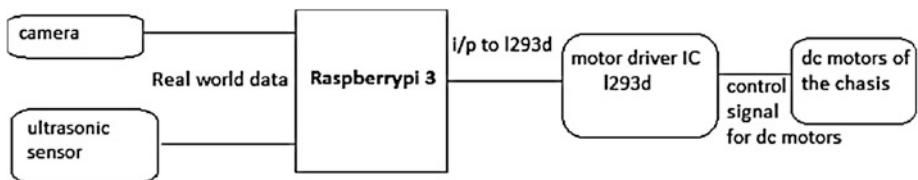
It stands for Open Source Computer Vision. It has a library of programming function mainly for real-time computer visions. It has more than 2500 optimized algorithms for the set of classical algorithm as well as for the state-of-the-art algorithms in the computer visions [8]. Opencv is basically used for image processing in which we used it for the face detection, object detections, image recognition, traces, and also other functions.

3 Hardware Connection

The 2 wheels of chassis are connected with two motors. Motor driver IC L293d is basically used to control the DC motors, and one motor driver IC can control only two motors. So the proposed system used one L293d that is enough to control the motors. So the input for motor driver IC is given by the Raspberry pi, and the output pins of the motor IC are connected to the motor of the chassis.

For movement of the car in forward and backward directions, system will rotate the wheels in equal speed, whereas to move left or right system will slow down the one wheel as compare to the other one according to the turning points, i.e. if system need to rotate the turn in left direction system has to slow down the left wheel and if there is need to turn in right direction system has to slow down the right wheel. In the proposed system, the input to the motor driver IC is given from the GPIO pins (2,3) for driving the left motor and GPIO pins (9,10) are used to drive the right motor from L293d.

Block diagram of connection:



4 Project Phases

4.1 Phase 1: Remote Control Car

A car can be designed that will control remotely for this we can use any wireless modules or we can designed website from where we can send signal to control vehicle. But on remote control car, car was not able to take any actions by itself, and to drive that car, every action accordingly real-world data has been taken by a person so that it was just like a person is driving a car not more than that. Also the problems of delay occurred because for each signal send by a person, it may be low or high data that take some amount of time and it generates the delay. There may be the chances of error since each low and high signal has individual operation, and while sending every time new data if signal exchanges, then it causes a problem due to human errors [8].

4.2 Phase 2: Autonomous Obstacle Avoidance

Cars comes up with the obstacle avoidances features using IR sensors in which distance measurement problem at low cost price sensor and it also not accurate with every colours so it was not good to use. Another method to measure the distance is camera but by the use of camera delay will increase time for that, whereas in this proposed system ultrasonic sensor is used that takes less computation time and gives accurate results in the form of the distances [8].

5 Results

See Figs. 4 and 5.

6 Conclusion

In this paper, the method used to make a self-responsible robot car is represented. Working of different hardware components is described. A way to find the stop signboard and red signals has been defined, and also way to detect the obstacles has been defined. All methods and algorithms given in this paper are successfully implemented in a robot car of chassis having two wheels.



Fig. 4 Stop sign and red light detection

Fig. 5 Distance measured by ultrasonic sensor

```

File Edit Shell Debug Option
Python 2.7.3 (default, Jan 13 2013,
[GCC 4.6.3] on linux2
Type "copyright", "credits" or "lic
>>> =====
>>>
Distance measurement in progress
Waiting For Sensor To Settle
Distance: 4.1 cm
Waiting For Sensor To Settle
Distance: 3.05 cm
Waiting For Sensor To Settle
Distance: 4.61 cm
Waiting For Sensor To Settle
Distance: 5.73 cm
Waiting For Sensor To Settle
Distance: 8.88 cm
Waiting For Sensor To Settle
Distance: 5.16 cm
Waiting For Sensor To Settle
Distance: 5.64 cm
Waiting For Sensor To Settle
Distance: 5.4 cm

```

7 Future Work

To enhance it more in the future, machine learning algorithms can be used so it can be able to determine each objects. The current performance is good but to make it more efficient it is necessary to implement it using machine learning and other algorithms so it will understand more things. So in future to make it more advance, it has to learn by own such things like—

- Distance of the obstacles between nodes.
- Remember the breakers and how to take action.
- Stores the data about every vehicles and different objects as well.
- Stores the dimensions of every object for the future action when they come in its way.

References

1. “Julian Balcerek, Adam Konieczka, Tomasz Marciniak, Adam Dabrowski, Krzysztof, Mackowiak, Karol Piniarski, “Automatic detection of traffic lights changes from red to green and car turn signals in order to improve urban traffic”, Signal Processing Algorithms, Architectures, Arrangements and Applications (SPA 2014), September 22–24th, 2014
2. Biqiang Du, Shizhao Liu, “A common Obstacle Avoidance Module Based on Fuzzy Algorithm for Unmanned Aerial Vehicle”, The 6th Annual IEEE International Conference on Cyber Technology in Automation, Control and Intelligent systems, June 19–22, 2016
3. Kiran Rafique Memon, Sugandh Memon, Batool Memon, Azam Rafique Memon, “Real time implementation of path planning algorithm with obstacle avoidance for autonomous car”, International Conference on Computing for Sustainable Global Development, 2016
4. G. Senthilkumar, K. Gopalkrishnan, V. Sathish Kumar, “Embedded image capturing system using raspberry pi system”, International Journal of Emerging Trends & Technology in Computer Science (IJETTCS), Volume 3, Issue 2, March–April 2014
5. S. Raju, K. Sanjay, T. Sathish Kumar, B. Madhini, “Semi Autonomous Vehicle To Prevent Accident”, International Journal of Technology Enhancements And Emerging Engineering Research, Vol. 2, Issue 5, 2014
6. Prof. D. S. Vodhya, Miss Delicia Perlin Rebelo, Miss Cecilia Jane D’Silva, Mr. Linford William Fernandes, Miss Clarissa Joella Costa, “Obstacle detection using Ultrasonic sensors”, International Journal for Innovative Research in Science & Technology, Vol. 2, Issue 11, April 2016
7. Rahul Singh, Someet Singh, Navjot Kaur, “A Review: Techniques of vehicle detection in Fog”, Indian Journal of Science and Technology, December 2016
8. Gurjashan Singh Pannu, Mohammad Dawud Ansari, Pritha Gupta, “Design and Implementation of Autonomous Car using Raspberrypi”, International Journal of Computer Applications (0975–8887) Volume 113 – No. 9, March 2015

Self-organized Bacterial Evolutionary Dynamics: Fractal Characteristics

Saurabh Shanu, Sudepto Bhattacharya, Ajay Prasad
and Apurva Gupta

Abstract In recent years, a new theory of the evolution of microbes under normal and stressed conditions has emerged, mainly in reference with the development of fractals and of self-organized mapping (SOM) concepts. This theory has much improved our understanding of the growth pattern of microbes like bacteria which determine their dynamics of evolution. In the first part of this paper, the main ideas in the theory of microbial self-organization are outlined, and some remarkable features of the resulting growth patterns are presented. In the second part, we apply conceptual tools developed in the context of fractal geometry to the study of the scaling properties of the bacterial growth in context with SOM patterns. We observe that such growth patterns appear to be more complex than simple fractals, although in some cases a simple fractal framework may be adequate for their description.

Keywords Fractals · Bacteria · Evolution · Self-organized maps
Evolution

S. Shanu (✉)

Department of Virtualization, School of Computer Science & Engineering,
University of Petroleum and Energy Studies, Bidholi, Dehradun 248007,
Uttarakhand, India
e-mail: sshanu@ddn.upes.ac.in; SaurabhShanu@ddn.upes.ac.in

S. Bhattacharya

Department of Mathematics, School of Natural Sciences, Shiv Nadar University,
Greater Noida, Gautam Buddha Nagar 201314, UP, India
e-mail: SudeptoBhattacharya@ddn.upes.ac.in

A. Prasad

Department of Cyber Platform, School of Computer Science & Engineering,
University of Petroleum and Energy Studies, Bidholi, Dehradun 248007,
Uttarakhand, India
e-mail: AjayPrasad@ddn.upes.ac.in

A. Gupta

Department of Informatics, School of Computer Science & Engineering,
University of Petroleum and Energy Studies, Bidholi, Dehradun 248007,
Uttarakhand, India

© Springer Nature Singapore Pte Ltd. 2018

R. Singh et al. (eds.), *Intelligent Communication, Control and Devices*,
Advances in Intelligent Systems and Computing 624,
https://doi.org/10.1007/978-981-10-5903-2_25

1 Introduction

Microbial organisms form interacting groups which show dense systems that offer a rich database for studying and learning about the interesting domains of complexity [1, 2]. These organisms may exhibit characteristic patterns of self-organized collective behavior, forming spatial aggregation [3–5].

In this paper, we study an evolving bacterial colony as a generation of information transfer and complexity. A single bacterium cell has been treated as a dense and complex molecule which interacts with its neighboring colonies, communicates with other individuals, replicates, and undergoes evolution and mutation [6]. When a huge number of bacteria act collectively as a colony, a large variety of different, fascinating spatial patterns can be seen emerging as a result of interaction of individual bacteria colony to be treated as agents with respect to its neighbors as well as with the environment. These patterns can be considered as the emergent result of local communication (communication within the surrounding of each individual colony) through exchange and processing of information over discrete time, and environmental conditions and can be usefully viewed as being encoded by the particular way the bacteria in question interacts as well as by the particular way these bacteria respond to environmental signals.

Evolving colonies or density of bacteria (and thus the bacterial colonies) carry and mediate information via communication by them locally and globally. Each colony is considered to receive a finite set of information or signal from its surrounding (as well as the environment) in the form of signals by the surrounding colony in the model. This input space decides the structural and functional shift of the bacterial colony to the next state in a definite discrete time step, producing a target set (the next generation). Bacterial colonies therefore could be thought of as a finite automaton [7–9].

Fibonacci series, which is a mathematical sequence of the positive integers, that appears as 1, 1, 2, 3, 5, 8, 13, 34, ... [10, 11, 12]. Observe that excepting the first two members of the sequence, each member is obtained by adding its two immediate predecessors in the sequence. And on taking the ratio of two successive numbers in a Fibonacci series such that the greater number is the numerator and the lesser is the denominator, we get values that converge to the golden ratio or golden number, i.e., 1.61803.

The principle of Fibonacci series also hold in case of fractal patterns. A fractal is a fragmented or rough geometric structure that can be further divided in leading sections, each of which is a miniature size copy of the complete structure. This means that they usually contain small copies of themselves deep inside the original (Fractal Structure). Fractals are enormously available in nature. An ordinary example is twigs on trees appear like the branches which they grow on, which appear like the tree itself. This satisfies the profile of fractals as the sections of the tree are copies of the larger unit, the entire tree. With this knowledge, it is easier to see how fractals exist in everything we see around us: leaves, cauliflowers, systems

of blood vessels and pulmonary vessels, rocks, mountains, coastlines, river networks, and in the bacteria.

We can explain fractals with a help of small example as follows.

Here, there are 4 copies of each line in every step. Thus, every time the observer descends, it is observed that the no. of lines get multiplied and all the daughter lines have a length of 1/3 of the parent line. So it can be deduced that the fractals have a particular dimension (d) and have linearity in their graph. The dimension can be explained for the above-mentioned example as (Fig. 1).

Since we get 4 copies of 1/3 times dimension

$$3^d = 4$$

$$d = 1.625$$

We intend to derive the growth of bacterial colonies under both stressed and normal conditions using the Fibonacci series and the iterative golden ratio with the irrelativeness of chaos and want to create an algorithm for pattern recognition scheme to identify the growth of microbes in the host bodies. Our main concentration would be to find a rule and thus a programmable machine code that will describe the spatial-temporal evolution of the modeled bacterial system. By using this, we also intend to diagnose the natural cooperation and defection carried out at all the levels by various communities in order to survive. The work to be carried out in this paper would be purely based on the logics of interactions, Fibonacci series, and the golden iterative ratio through the relatedness of chaos theory. We intend to generate a 2-D graph in order to derive a result for the evolution of the bacterial colonies and thus understand the lateral growth of the agents with time and space which has also be termed as cell growth dynamics in time and space [13].

To study the bacterial growth under both normal and stressed conditions, the following parameters have been used.

Materials and specifications used:

Bacterial strain: *Bacillus subtilis*.

Chemicals: Peptone, Agar, NaCl, K_2HPO_4 .

Antibiotic: Septran (cotrimoxazole).

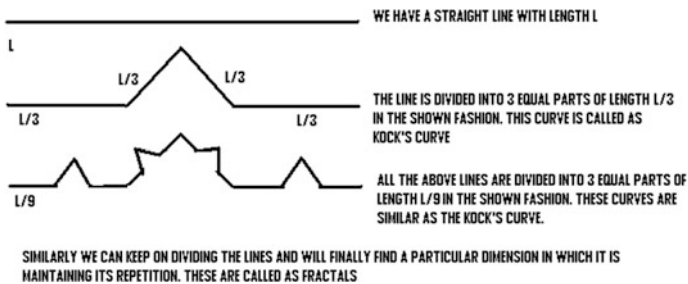
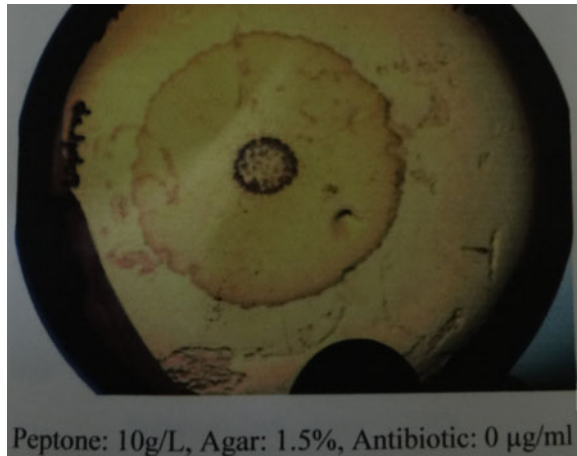


Fig. 1 Cock's curve

Fig. 2 Bacterial growth under normal conditions



Peptone concentrations: 1–5 g/L.

Agar concentrations (%): 1.25, 1.5, 1.75, 2.0.

Stresses used:

Nutrient Stress—here, less nutrients are to be supplied to the bacterial inoculums to observe the growth patterns and the fractals formed during this stress.

Agar (Substrate) Stress—here, the medium for the growth of the bacterial colonies is made stronger and stronger to observe the growth pattern of the colonies under the situation of drought.

Antibiotic Stress—here, at the time of growth of the microbial colonies, some antibiotics are introduced to the petri plates in order to see the cooperation of the colonies at time of foreign indulgence (Figs. 2 and 3).

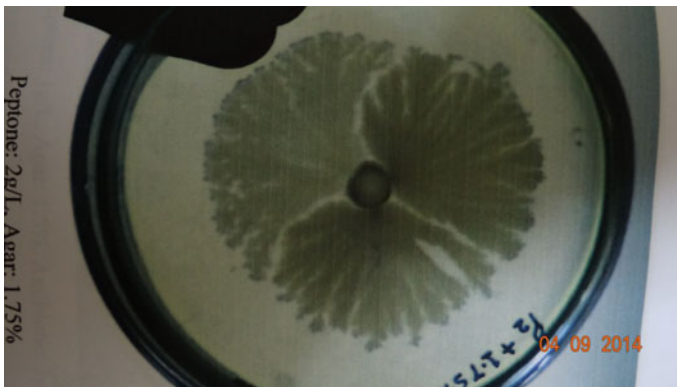


Fig. 3 Bacterial growth under stressed conditions

2 Bacterial Modeling Using Fibonacci Series

At different concentrations of peptone, agar and septrin (an antibiotic) for the growth of bacteria as follows.

It is observed from Table 1 that calculating the ratio of areas of any two successive days of a particular concentration gives an approximate iterative golden ratio.

For example: Concentration of peptone (%) is 0.4 than the ratio of areas of two successive days for each concentration of Agar (%) and Septrin (%) (Table 2).

Average of the above ratios: 1.454611047 (which shows the iterative golden ratio in growth of bacteria). And after more days, the ratio will tend to be much closer to golden ratio.

The area of bacteria is directly proportional to the time which is observed from the table (area of bacteria at equal intervals of time, i.e., 24 h). The graph of area versus parameters is illustrated in Plot 1.

It is good to see that the graph of each day showing similar fractal patterns and can be generated for any day without even knowing the area.

The simplest model used as of now was based on calculus [14–16]. If $P(t)$ is the area occupancy of the bacterial population at time t , then the Malthusian model of exponential growth is given by

$$\frac{dP}{dt} = rP$$

With some default conditions, $P(0) = P_0$. Parameter $r > 0$ is termed as growth rate and must be measured [17].

$$N(t) = N_0 e^{rt}$$

The solution has the rather unrealistic feature of getting larger without bound as t increases. Basically, the model ignores that bacteria require resources to grow and that these resources are finite which we have considered in our model.

For our model, we consider an iterated function of chaotic behavior

$$X_{n+1} = R x_n (1 - x_n), \quad n \in N \text{ and } n = \text{no. of iterations};$$

Using the previous two states of the area growth of the bacterial colonies, a value of 3.5 for the relatedness R is obtained, and further simulations for the predictive modeling are obtained based on this value of R . The simulations obtained were done through the tool of cellular automata, and a similar growth pattern is obtained which gives an insight to our devised logic.

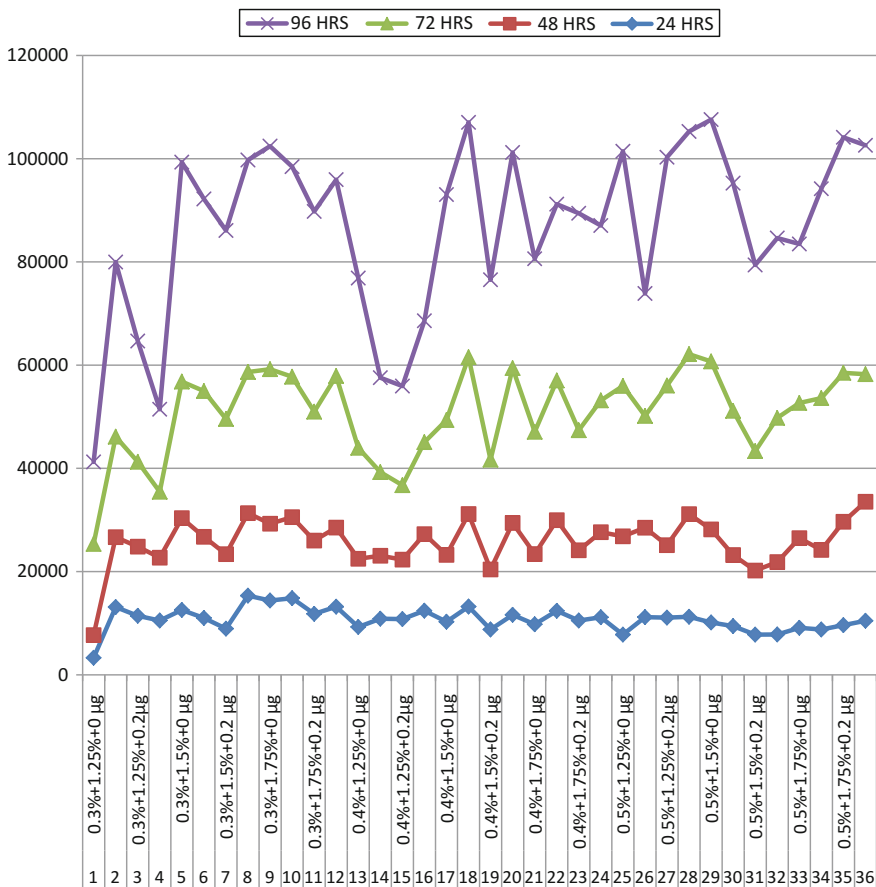
So computationally, we state that a bottom-up parsing [18, 19] had been conducted in with respect to the objective of obtaining the value of relatedness for predicting the spatial–temporal bacterial growth dynamics (Plot 2).

Table 1 Area occupancy of the bacterial colonies at different conditions at different time intervals

S. No.	Peptone % + Agar % + Seprtin µg	24 h	48 h	72 h	96 h
1	0.3% + 1.25% + 0 µg	3290	4390	17,660	15,904
2	0.3% + 1.25% + 0.1 µg	13,124	13,540	19,468	33,840
3	0.3% + 1.25% + 0.2 µg	11,432	13,388	16,438	23,416
4	0.3% + 1.25% + 0.3 µg	10,508	12,176	12,778	15,990
5	0.3% + 1.5% + 0 µg	12,562	17,786	26,452	42,528
6	0.3% + 1.5% + 0.1 µg	11,000	15,736	28,240	37,216
7	0.3% + 1.5% + 0.2 µg	8930	14,446	26,190	36,524
8	0.3% + 1.5% + 0.3 µg	15,320	15,990	27,362	41,068
9	0.3% + 1.75% + 0 µg	14,396	14,870	29,932	43,226
10	0.3% + 1.75% + 0.1 µg	14,842	15,710	27,192	40,696
11	0.3% + 1.75% + 0.2 µg	11,812	14,192	24,964	38,812
12	0.3% + 1.75% + 0.3 µg	13,202	15,320	29,372	38,040
13	0.4% + 1.25% + 0 µg	9264	13,204	21,500	32,896
14	0.4% + 1.25% + 0.1 µg	10,864	12,196	16,198	18,308
15	0.4% + 1.25% + 0.2 µg	10,798	11,514	14,424	19,204
16	0.4% + 1.25% + 0.3 µg	12,421	14,834	17,827	23,508
17	0.4% + 1.5% + 0 µg	10,283	12,946	26,128	43,695
18	0.4% + 1.5% + 0.1 µg	13,204	17,962	30,374	45,496
19	0.4% + 1.5% + 0.2 µg	8778	11,626	21,274	34,860
20	0.4% + 1.5% + 0.3 µg	11,606	17,800	30,024	41,772
21	0.4% + 1.75% + 0 µg	9778	13,618	23,688	33,528
22	0.4% + 1.75% + 0.1 µg	12,394	17,562	27,054	34,170
23	0.4% + 1.75% + 0.2 µg	10,518	13,618	23,252	42,028
24	0.4% + 1.75% + 0.3 µg	11,148	16,475	25,534	33,892
25	0.5% + 1.25% + 0 µg	7792	19,032	29,144	45,471
26	0.5% + 1.25% + 0.1 µg	11,170	17,324	21,672	23,713
27	0.5% + 1.25% + 0.2 µg	11,070	14,034	30,936	44,256
28	0.5% + 1.25% + 0.3 µg	11,238	19,886	30,996	43,160
29	0.5% + 1.5% + 0 µg	10,144	18,014	32,544	46,873
30	0.5% + 1.5% + 0.1 µg	9434	13,782	27,916	44,118
31	0.5% + 1.5% + 0.2 µg	7790	12,410	23,142	36,062
32	0.5% + 1.5% + 0.3 µg	7802	14,034	27,934	34,860
33	0.5% + 1.75% + 0 µg	9108	17,360	26,208	30,808
34	0.5% + 1.75% + 0.1 µg	8778	15,408	29,426	40,568
35	0.5% + 1.75% + 0.2 µg	9622	20,026	28,852	45,646

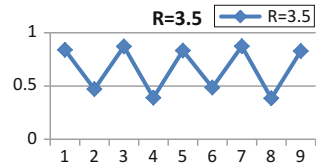
Table 2 Ratio of area occupancy of the bacterial colonies at different conditions at different time intervals

1	Peptone% + Agar% + Seprin%	48 h/24 h	72 h/48 h	96 h/72 h
2	0.4% + 1.25% + 0 µg	1.425302245	1.628294456	1.530046512
3	0.4% + 1.25% + 0.1 µg	1.122606775	1.328140374	1.130262995
4	0.4% + 1.25% + 0.2 µg	1.066308576	1.2527358	1.331392124
5	0.4% + 1.25% + 0.3 µg	1.194267772	1.201766213	1.318673922
6	0.4% + 1.5% + 0 µg	1.258971117	2.018229569	1.672343846
7	0.4% + 1.5% + 0.1 µg	1.36034535	1.691014364	1.497860012
8	0.4% + 1.5% + 0.2 µg	1.324447482	1.829864098	1.638619912
9	0.4% + 1.5% + 0.3 µg	1.533689471	1.686741573	1.39128697
10	0.4% + 1.75% + 0 µg	1.392718347	1.739462476	1.415400203
11	0.4% + 1.75% + 0.1 µg	1.416975956	1.540485138	1.263029497
12	0.4% + 1.75% + 0.2 µg	1.294732839	1.707446027	1.80750043
12	0.4% + 1.75% + 0.3 µg	1.477843559	1.549863429	1.327328268
	Average	1.322350791	1.59783696	1.443645391



Plot 1 Area occupancy of the bacterial colonies at different conditions at different time intervals

Plot 2 Relatedness of bacterial growth at discrete intervals



<i>n</i>	<i>R</i> = 3.5
1	0.84
2	0.4704
3	0.871933
4	0.390829
5	0.833286
6	0.486221
7	0.874336
8	0.384555
9	0.828354

$$R \in (3, 4)$$

We can observe that the graph of this iterative function is similar to the graph of area versus parameters.

3 Conclusion

Bacterial evolutionary dynamics can be understood as an iterative process with the appropriate computational logic, modeling the interactions and consequent evolution by cellular automata, and the chaotic behavior of evolution of the microbial colonies. This can be very useful to determine the pattern and then let the individuals and machines learn, how and when to deal with the microbial issues based on the gravity of the growth. So in our understanding from the observational work, the specificity of bacterial responses to stress stimulation is very well observed by the temporal and spatial dynamics of growth networks. Computational models provide insights into the interacting bacterial colonies with the available stresses. These temporal dynamics are interlinked to precipitous spatial gradients of growth and stress reactions, which not only guide nodal intracellular processes, but also necessitate mechanisms to facilitate communication across a cell.

References

1. Axelrod, R., Hamilton, W.D., (1981), The evolution of cooperation, *Science*, 211,4489, pp. 1390–1396.
2. Axelrod, R., (1984), *The Evolution Of Cooperation*, Basic Books, Inc., New York.
3. Binmore, K.G., Samuelson, L., (1992), Evolutionary stability in repeated games played by finite automata, *Journal of Economic Theory*, 57, 2, pp. 278–305.
4. Binmore, K., (2007), *Game Theory- A Very Short Introduction*, Oxford University Press.
5. Heylighen, F., (2005), Evolution, selfishness and cooperation, *Journal of Ideas*, 2, 4, pp 70–76.
6. Jacob, E.B., Cohen, I., Gutnick, D., Cooperative organization of bacterial colonies: from genotype to morphotype (1998), *Annu. Rev. Microbiol.*, 52, pp. 779–80, doi:[10.1146/annurev.micro.52.1.779](https://doi.org/10.1146/annurev.micro.52.1.779).
7. Bonanno, G., (1991), The logic of rational play in games of perfect information, *Journal of Economics and Philosophy*, 7, pp 37–65.
8. Osborne, M. J., (2002), *An Introduction to Game Theory*, Oxford University Press.
9. Page, R.D.M., 1996. TreeView: an application to display phylogenetic trees on personal computer. *Comput. Appl. Biosci.* 12, 357–358.
10. Kholodenko, B. N. (2006). CELL SIGNALLING DYNAMICS IN TIME AND SPACE. *Nature Reviews. Molecular Cell Biology*, 7(3), 165–176. <http://doi.org/10.1038/nrm1838>.
11. Bhattacharya, Sudepto and Shanu, Saurabh and Srivastava, Gaurav and Agarwal, Dushyant, Pattern Formation Through Cooperative Self-Organization in Stressed Bacterial Colonies: A Complexity Perspective (July 23, 2012). *The IUP Journal of Environmental Sciences*, Vol. V, No. 4, pp. 53–69, November 2011.
12. Paul, D., Pandey, G., Meier, C., van der Meer, J.R., Jain, R.K., 2006. Bacterial community structure of a pesticide-contaminated site and assessment of changes induced in community structure during bioremediation. *FEMS Microbiol. Ecol.* 57, 116–127.
13. Schloss, P.D., Handelsman, J., 2005. Introducing DOTUR, a computer program for defining operational taxonomic units and estimating species richness. *Appl. Environ. Microbiol.* 71, 1501–1506.
14. Wanger, M., Loy, A., 2002. Bacterial community composition and function in sewage treatment systems. *Curr. Opin. Biotechnol.* 13, 218–227.
15. Wexler, M., Bond, P.L., Richardson, D.J., Johnston, A.W., 2005. A wide host-range metagenomic library from a wastewater treatment plant yields a novel alcohol/aldehyde dehydrogenase. *Environ. Microbiol.* 7, 1917–1926.
16. Hopcraft, J., Ullman, J., (2004) *Introduction to Automata Theory, Languages and Computation*, Addison Wesley, Reading, MA.
17. Jacob, E.B., (2009), Learning from bacteria about natural information processing, *Natural Genetic Engineering and Natural Genome Engineering*, *Ann. N.Y. Acad. Science*, 1178, pp. 78–90, doi: [10.1111/j.1749-6632.2009.05022.x](https://doi.org/10.1111/j.1749-6632.2009.05022.x).
18. Park, H.Y., Kim, K.K., Jin, L., Lee, S.T., 2006. *Microbacterium paludicola* sp. nov., a novel xylanolytic bacterium isolated from swamp forest. *Int. J. Syst. Evol. Microbiol.* 56, 535–539.
19. Jacob, E.B., Cohen, I., Golding, I., Gutnik, D.L., Marianna T., Helbing, D., (2000), Bacterial Cooperative Organization under antibiotic stress, *Physica A: Statistical Mechanics and its Application*, 282, pp. 247–282.

Diet Recommendation for Diabetic Patients Using MCDM Approach

Kirti Sharawat and Sanjay Kumar Dubey

Abstract In today's fast and developing world, as everyone is growing at a very rapid speed, there are also various severe diseases that are growing around. We see in our surrounding that people are affected by various harmful diseases. There are various diseases whose vaccination is not even discovered by scientists. Diabetes is a disease which is found in a large number of people who can be child, youth, and male or female, anyone. This is a very harmful disease which just doubles the risk of early death of a person's life. So, its prevention and cure is very must. As it is caused due to high content of sugar in blood, therefore in this disease, it is recommended by doctors to give a proper diet to a diabetic patient. So, in this paper we aim to find out which type of food or diet is good for a diabetic patient. For this purpose, we use AHP method to find out the best diet for a diabetic patient. In this diet, quality is judged on the basis of various qualifying factors which must be considered for preparing the diet of a diabetic patient. The result is also validated by using fuzzy topsis method.

Keywords Diabetes · AHP · Fuzzy · Topsis · Health carbs

1 Introduction

Diabetes is commonly referred as diabetes mellitus. It is a group of metabolic diseases. The most common type of diabetes is type 1, type 2, and gestational diabetes. Approximately 90% cases of diabetes are of type 2 and only 10% is of type 1 while gestational diabetes affects the females during their pregnancy. Diabetes is caused by high blood glucose level, and it is a continued for a very

K. Sharawat (✉) · S.K. Dubey
Department of Computer Science and Engineering, Amity University
Uttar Pradesh, Sec-125, Noida, UP, India
e-mail: kirti.Sharawat21@gmail.com

S.K. Dubey
e-mail: sanjukundan@gmail.com

long-time sometimes for lifetimes. To prevent diabetes, doctor preferred some precautions that must be taken in an individual's diet. So, a proper diet is mandatory to control the blood glucose level of a human being. That proper diet must be prepared by considering various important factors that control the high sugar content and give proper nutrients to the patient [1].

As we know diabetes is a life threatening disease, it causes a lot of weakness in human body, so they must be compensated or fulfilled by giving a proper diet full of required nutrition's and less sugar content [2]. So, in the proposed paper we try to find out that which type of diet is best for a diabetic patient. Here, we divide the type of food on the basis of their nature which can be liquid, solid, or fluid. The best diet is one which gives all the proper nutrition to a diabetic patient and its sugar content must be less so it is not harmful for a diabetic patient.

1.1 Model Development

To find out the best quality diet, a model is proposed to develop an approach that helps to prepare a best quality diet. This diet is judged on the basis of various factors such as calories burned, body fat, health carbs, and dietary needs. To find out the best quality diet, decision is taken by using multicriteria decision-making (MCDM) approach. For this, AHP method is used to find out the rank of type of diet which is best for a diabetic patient, and validation is done by using Fuzzy topsis method. The following figure shows the hierarchical structure of the proposed model.

1.2 Defining Factors for Best Diet Selection

Firstly, we establish the factors which are used to evaluate the diet. In order to meet the factors and their importance for the selection process of diet, the data is collected by taking reviews from the people itself. Defining factors for diet selection contain the step-by-step procedural collection of factors such as body fat, calories burned, health carbs, and dietary needs and based order to select and decide which factor will be useful to the research model, each factor is given numbers rating (1–9), if a factor rates in between the numbers (1–7) then it may not be considered, but if a criteria lies between (7–9) then it is selected to be processed further [3, 4].

2 Decisions Parameters

2.1 *Body Fat*

In today's developing world, the eating pattern of people has drastically changed. People are quickly moving towards fast foods and junk food; they are unaware that food they are eating practice leads to diabetic disaster. Person suffering from type 1 diabetics starts losing weight while person suffering from type 2 diabetic starts gaining weight, these both conditions are not good for the health of a person. So, the amount of fats in diet is very important. It should be judged properly that whether diet of a diabetic patient should contain saturated fat or unsaturated fat. Therefore, this is considered as an important factor in preparing diet for a diabetic patient.

2.2 *Calories Burned*

The diet that a diabetic patient takes should be balanced according to the calories burned by them. It is not considerable that the diet contains a lot of nutrients, but we do not burn enough calories, then this can lead to increase the body weight of a person which is not good for a diabetic patient.

2.3 *Health Carbs*

There are different types of sugar for different people. For a diabetic patient, artificial sweeteners are included; while in diet of a healthy persons diet, normal sugar is there.

2.4 *Dietary Needs*

Sometimes it may be possible that a person suffering from diabetes may also suffer from some other disease. So, for such type of people there may be some special requirements in their diet so that they get proper nutrition in their diet.

3 Approach

In the proposed approach, a relationship is established between different types of food that is taken (F1, F2, and F3) and the selection factors (C1, C2, C3, and C4) as shown in Fig. 1. The variety in food is done on the basis of their type that is solid,

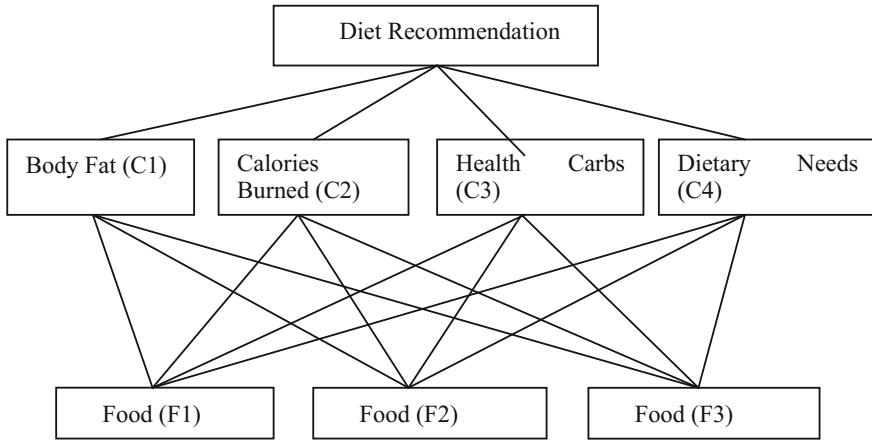


Fig. 1 Proposed hierarchical model

liquid, and fluid. By using multicriteria decision-making problem, we try to find out which type of food is the best for a diabetic patient. For this, firstly we create the decision hierarchy. After creating the decision hierarchy for the concerning problem, the weights of the criteria's are used for evaluation, and AHP method is used for the calculation in the second phase.

4 The AHP

AHP is due to Saaty (1980), and this method is very popular and concisely used especially in military for analysis. It is a highly outstanding management tool for complex multicriteria decision-making problems. Analytical hierarchy process has its own ability to make rank of the choices, in order to make an effective result out of conflicting objects. If the judgments between two or more object are relatively important and equal than one another, using AHP it can be resolved out [5].

5 Fuzzy Topsis

This is a procedure utilized for finding the request of inclination called FUZZY TOPSIS, which is a basic leadership strategy, created by Hwang and Yoon in 1981 [6, 7]. Later with couple of more improvements, it was given by Yoon in 1987. In this strategy, we picked the right option by finding the geometric mean from the positive perfect arrangement and the biggest geometric separation from the negative perfect arrangement [8, 9].

6 Experimental Work

We use AHP method to rank the types of food we consider in this paper on priority vector basis [10]. All the alternatives are taken from expert’s judgment. Firstly, all types of food are compared w.r.t each factor (C1 to C4). Then, all the taken factors are compared to show their relative importance. Below, we show all the matrices that we have taken. From these matrices, we calculate the nth root, eigenvector (EV), consistency index (CI), and consistency ratio (CR). These are as follows (Table 1).

We calculate the priorities of all the factors, and calculation is shown in the above matrices. These matrices are used to carry out the final priorities. For all the matrices, we have taken it is important that the value of CR (consistency ration) should be less than or equal to 0.1.

Now, the diet index is calculated by combining the respective vector and the weight of each factor. The factors proposed in the model, i.e. C1, C2, C3, and C4. W_i are the eigenvectors, calculated from the pairwise judgments taken for the factor only (Tables 2, 3, 4, and 5) F1, F2, and F3 are the three types of food and their eigenvectors taken from each of the matrix of factors (Table 6). To calculate the rank of the food, we calculate the diet index as follows.

Diet index = \sum weight of $C_i V_i^*$ * weight of $C_i W_i$ ($i = 1$ to 4) for the sample tables.

Table 1 Matrix for body fat (C1)

	F1	F2	F3	Nth	EV
F1	1	3	5	2.444	0.634
F2	1/3	1	3	1	0.259
F3	1/5	1/3	1	0.409	0.106
Total				3.853	0.999

$$\lambda_{\max} = 3.034, CI = 0.017, CR = 0.029$$

Table 2 Matrix for calories burned (C2)

	F1	F2	F3	Nth	EV
F1	1	5	9	3.512	0.748
F2	1/5	1	3	0.844	0.179
F3	1/9	1/3	1	0.337	0.071
Total				4.693	0.998

$$\lambda_{\max} = 3.024, CI = 0.012, CR = 0.020$$

Table 3 Matrix for health carbs (C3)

	F1	F2	F3	Nth	EV
F1	1	6	8	2.444	0.754
F2	1/6	1	4	0.606	0.181
F3	1/8	1/4	1	0.755	0.065
Total				3.805	1.0

$$\lambda_{\max} = 3.136, CI = 0.068, CR = 0.025$$

Table 4 Matrix for dietary needs (C3)

	F1	F2	F3	Nth	EV
F1	1	1/3	1/5	0.409	0.106
F2	3	1	1/3	1	0.259
F3	5	3	1	2.44	0.633
Total				3.849	0.998

$\lambda_{\max} = 3.035, CI = 0.017, CR = 0.029$

Table 5 Matrix for criteria

	C1	C2	C3	C4	Nth	EV
C1	1	5	3	7	3.2010	0.567
C2	1/5	1	1/7	5	0.6140	0.108
C3	1/3	3	1	6	1.5650	0.277
C4	1/7	1/5	1/6	1	0.2620	0.046
Total					5.642	0.998

$\lambda_{\max} = 4.14, CI = 0.046, CR = 0.051$

Table 6 Diet index

	C1	C2	C3	C4	Diet index
W_{C_i}	0.567	0.108	0.277	0.046	
W_{F1}	0.634	0.748	0.754	0.106	0.651
W_{F2}	0.259	0.179	0.181	0.259	0.226
W_{F3}	0.106	0.071	0.065	0.633	0.114

Food having the highest diet index will be ranked on the top, and others will be followed by it. From the above formula, we calculated the respective rank of food and it is shown in Table 6.

For all the taken samples, food type F1 has the highest diet index; therefore, vendor F1 is ranked I, F2 is ranked II, and F3 is ranked III.

7 Validation

After calculating the rank of food by using the AHP method, the result is validated by using fuzzy topsis method. Three decision makers defined as M1, M2, and M3 are used to determine the importance and weight of the criteria. Firstly, we calculate the decision matrix (X) and the weight vector (W), which are shown in Table 7.

$W = (0.468, 0.185, 0.302, 0.044)$, Then, we calculate the fuzzy performance matrix that represents the overall performance of all the alternatives with respect to each criterion (Table 8).

The positive ideal solutions are: (0.283, 0.134, 0.210, 0.026).

The negative ideal solutions are: (0.047, 0.012, 0.019, 0.004) (Tables 9 and 10).

On the basis of the closeness coefficient of three alternatives, the ranking order of three alternatives is determined as $F1 > F2 > F3$.

Table 7 Decision matrix (X)

0.605	0.726	0.696	0.102
0.291	0.203	0.239	0.291
0.102	0.069	0.062	0.605

Table 8 Normalized performance matrix (Z)

0.283	0.134	0.134	0.210	0.004
0.136	0.136	0.037	0.072	0.012
0.047	0.047	0.012	0.019	0.026

Table 9 Distance of each alternative from FPIS to FNIS

	d+	d-
D1	0.0115	0.1870
D2	0.1279	0.0560
D3	0.1870	0.0115

Table 10 Closeness coefficient

Diet	CCi
F1	0.9420
F2	0.3045
F3	0.0579

Therefore, $R^3I_1 = 0.9420$; this is the rank for first type of food.

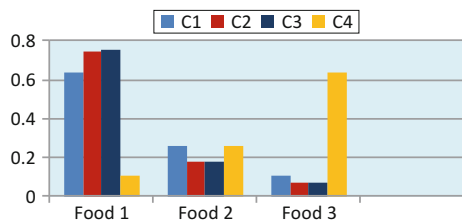
Similarly, for the second type of food, $R^3I_2 = 0.3045$.

And for the third type of food, $R^3I_3 = 0.0579$.

8 Results and Analysis

By using AHP, we get the result that the food type F1 has rank 1 among all the available alternatives. The result is also validated by using Fuzzy Topsis method which is as same as the rank found by AHP. So, it is validated that the food type F1 is the best among all the alternatives. The graph that shows the analysis between factors and weight is shown in Fig. 2.

Fig. 2 Ranking chart



9 Conclusion

As we know that lot of people are suffering from diabetics, it becomes necessary to find out a diet which is best for a diabetic patient. This type of diet helps to prevent diabetes and good for people who are suffering from diabetes. In this presented paper, best diet for diabetic patient was found out by using AHP (analytic hierarchy process), and the result shows the best optimum selection among the available list of different types of food on the basis of various criterion. The result is also validated by using fuzzy topsis method. The ranking is done on the basis of decision parameters so these are very important. This present approach helps to find the best quality diet for the diabetic patients. And we include this type of diet in our daily life, then it will help us to prevent diabetes, and this will lead to a healthy youth which is very important for a country and for a healthy surrounding.

References

1. Lukmantoa, R.B., Irwansyah, Ea.*.: The Early Detection of Diabetes Mellitus (DM) Using Fuzzy Hierarchical Model. In: Jl. KH. Syahdan No. 9, Kemanggisan, Jakarta 11480, Indonesia (2015).
2. Wang, M.H., Hagra, H., Lee, C.S.: A Type-2 Fuzzy Ontology and Its Application to Personal Diabetic-Diet Recommendation. In: IEEE Transactions on fuzzy systems, Vol. 18, NO. 2, APRIL (2010).
3. Rajeswari, K., Vaithyanathan, V.: Fuzzy based modeling for diabetic diagnostic decision support using Artificial Neural Network. In: IJCSNS International Journal of Computer Science and Network Security, VOL. 11 No. 4, April 20 (2011).
4. Sarhan, Z.A., Jordan, A.: Application of Analytic Hierarchy Process (AHP) In the Evaluation and Selection Of an Information System Reengineering Projects. VOL. 11 No. 1 (2011).
5. Omkarprasad, Vaidya, S., Kumar, S.: Analytic hierarchy process: An overview of applications. In: Department of Mechanical Engineering, Army Institute of Technology, Pune 411 015, (2004).
6. Panda1, B.N., Biswal, B.B., Deepak: 1 Integrated AHP and fuzzy TOPSIS Approach for the Selection of a Rapid Prototyping Process under Multi-Criteria Perspective. In: 5th International & 26th All India Manufacturing Technology, Design and Research Conference (AIMTDR 2014) December 12th–14th, (2014).
7. Ayhan, M.B.: a fuzzy AHP approach for supplier selection problem: a case study in a gearmotor company. In: International Journal of Managing Value and Supply Chains (IJMVSC) Vol. 4, No. 3, September (2013).
8. Sun, C.C.: A performance evaluation model by integrating fuzzy AHP and fuzzy TOPSIS methods: In: Expert Systems with Applications (2010).
9. Nagpal, R., Mehrotra, D., Bhatia, P.K., Sharma, A.: Rank University Websites Using Fuzzy AHP and Fuzzy TOPSIS Approach on Usability. In: I.J. Information Engineering and Electronic Business, (2015).
10. Elaalem, M., Comber, A., Fisher, P.: Land Evaluation Techniques Comparing Fuzzy AHP with TOPSIS methods. In: 13th AGILE International Conference on Geographic Information Science (2010).

Software Component Quality Models: A Survey

Munishwar Rai and Kiranpal Singh Virk

Abstract Design of reusable software component model is the essential research area of the software development. Component reusability has been the key driving factor behind the component model-based software engineering. There are other factors also that have contributed in the core development process of the software engineering models. Factors and related metrics are the basis for any software component quality model. Numerous software component quality models have been proposed, some general and some specific in nature. The aim of this paper is to conduct the literature survey for exploring the most popular software component quality models.

Keywords Quality models · Software components · Software development
Software engineering · Software quality

1 Introduction

Over the period of time, the world has seen tremendous growth using computing power. In this growth, software has played an important role to facilitate the diversity of the work that a computer could do. With diversified applications of computers, every aspect of human life became dependent upon it. As software has become a significant part of our daily life, a need arises for new application areas for which software are to be continuously evolved or re-invented.

M. Rai (✉)

M.M. Institute of Computer Technology & Business Management, Maharishi
Markandeshwar University, Mullana, Ambala, Haryana, India
e-mail: munishwar.rai@mmumullana.org

K.S. Virk

Department of Computer Science, Guru Nanak Khalsa College, Yamuna Nagar 135001,
Haryana, India
e-mail: kiranpal.virk@yahoo.com

Evolution of software systems requires moving to a new technology. Harnessing the new technology along with ever increasing domain complexity affects the software quality, productivity and development costs. Also, some systems include such complex components that developing them from scratch would be impossible, if profit is desired. Component development and its reusability are one of the solutions for sustainable profits. Component-based engineering practices are important. Software engineering being youngest to other well-established engineering practices, an analogy could be established between the complexity issues faced by software developers/engineers and the civil/mechanical engineers.

From its beginnings in the 1960s, software development meant writing few line of code and was not seen as a profession till 1980 when software engineering evolved as an established development paradigm. The first major breakthrough in software productivity came with the high-level languages [1]. Researchers have proposed numerous software models that intend to bring in the concept of quality in software engineering practices. Software component quality models and frameworks have been the part of the review papers and the concept papers. Every new model or framework takes previous knowledge as foundation for the proposed work. With a number of quality models available, it would be well justified to undertake systematic literature review to identify the relevant software component quality models.

The paper is organized as follows: The second section describes research method used to review papers on software component quality models. The third section discusses the application of research method and analysis of relevant research papers. The fourth section contains the review results and answers the research questions. The fifth section concludes the topic.

2 Research Method

Systematic literature review methodology of research work [2, 3] is followed in this paper.

2.1 Research Question

The paper intends to answer the following research question:

RQ1: Which are the top five most referred software component quality models in research papers published till 2016?

2.2 Search Strategy

Software component quality models have been searched on several scientific databases and social networking websites: Shodhganga (open source digital

repository of theses and dissertations from Indian universities), IEEE Xplore, ACM Digital Library, CiteSeerx, Google Scholar, ResearchGate and Semantic Scholar. To obtain the relevant papers, following search queries will be executed on title, abstract, keywords and other available metadata:

- SQ1: *Quality model*
- SQ2: *Software model*
- SQ3: *Software quality model*
- SQ4: *Quality of software*
- SQ5: *Evaluation of software quality*
- SQ6: *Software component*
- SQ7: *Component quality.*

2.3 Selection Criteria

The criteria for including and excluding the relevant research papers for our research are listed in Table 1.

2.4 Data Extraction Strategy

The papers shortlisted after the application of selection criteria will be thoroughly read and examined for relevant data extraction. The selected papers would constitute final set of papers and would be stored in Mendeley (bibliographic management software) to further ease the search and management of the bibliographic and citation data.

3 Overview of the Included Papers

3.1 Selection Process

Execution of search queries resulted in a set of 359 papers. After the removal of duplicate studies, application of inclusion and exclusion criteria and availability of

Table 1 Selection criteria

Inclusion criteria	Exclusion criteria
<ul style="list-style-type: none"> • Papers written in English language only • Papers appearing in conferences and journals related to software engineering • Papers focused on software component quality model • Papers published till 2016 	<ul style="list-style-type: none"> • Papers written in a language other than English • Papers appearing in conferences and journals not related to software engineering • Duplicated studies

Table 2 Year-wise distribution of papers

Year	No. of papers	Year	No. of papers	Year	No. of papers
1968	1	1995	2	2007	8
1969	1	1996	1	2008	5
1976	2	1998	2	2009	8
1977	2	1999	2	2010	3
1983	1	2001	10	2011	8
1984	1	2002	7	2012	10
1986	1	2003	8	2013	11
1987	1	2004	5	2014	16
1993	2	2005	10	2015	11
1994	2	2006	6	2016	27

full text, the revised set of papers contained 174 entries. The papers are categorized according to their year of publication. Table 2 shows the year-wise categorized count of published papers.

3.2 Year-Wise Trends of Paper Publishing

Figure 1 shows the line chart plotted for year-wise papers published using the data in Table 2. It clearly marks an overall upward trend in the publishing of papers dealing with software component quality models. The trend further affirms the interpretation that for pursuing research software component quality model is an important topic.

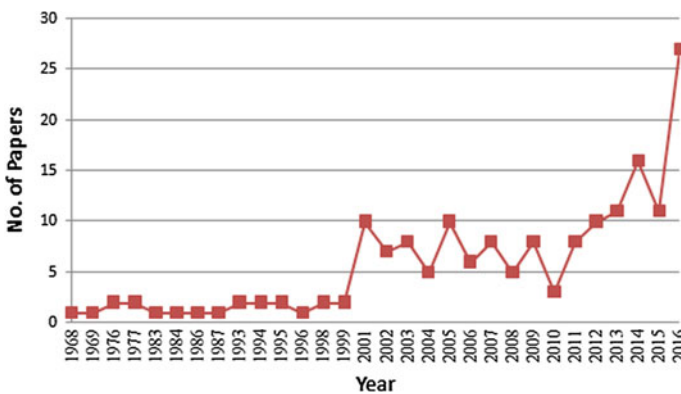


Fig. 1 No. of papers published per year

3.3 Most Referred Software Quality Models

All 174 papers were searched for the reference of various software component quality models. Quality model names were identified in each paper. The quality model-wise count is made and sorted information is stored in Table 3. Information is in descending order of paper frequency.

The top five quality models are ISO 9126, Boehm, McCall, Dromey and ISO 25010. There is a marginal difference between the ISO 25010 and FURPS. FURPS was devised by Hewlett-Packard in 1992. This model evolved as FURPS+ after it was embraced by IBM Rational Software [4].

ISO 25010 was devised in 2010 [5]. The time gap between ISO 25010 and FURPS is around 18 years. This clearly gives ISO 25010 an edge over FURPS. Hence, we take only first five models from Table 3 for further analysis.

3.4 Model-Wise–Year-Wise Trend of Paper Publishing

Quality models devised in 1970s by Barry Boehm, James McCall and others were assimilated into international standard ISO 9126 developed in 1990s [6]. It would be informative to know how our top five models have been cited in papers over the years. We further dig in for publishing year of all the papers that cited our top five quality models. Model-wise–year-wise line charts are plotted and shown in Figs. 2, 3, 4, 5 and 6. We have removed the year from the axis in which no research paper referring the respective quality model was published.

Table 3 Model-wise paper frequency

Quality model	No. of papers cited the model
ISO 9126	53
Boehm	50
McCall	31
Dromey	28
ISO 25010	18
FURPS	16
Alvaro	13
Bertoa	10
Rawashdeh	7
Cappemini	6
Georgiadou	6
Quamoco	5
Sqa-Oss	5
Al-Badreen	4
OpenBRR	4
QualOSS	4
MIDAS	1

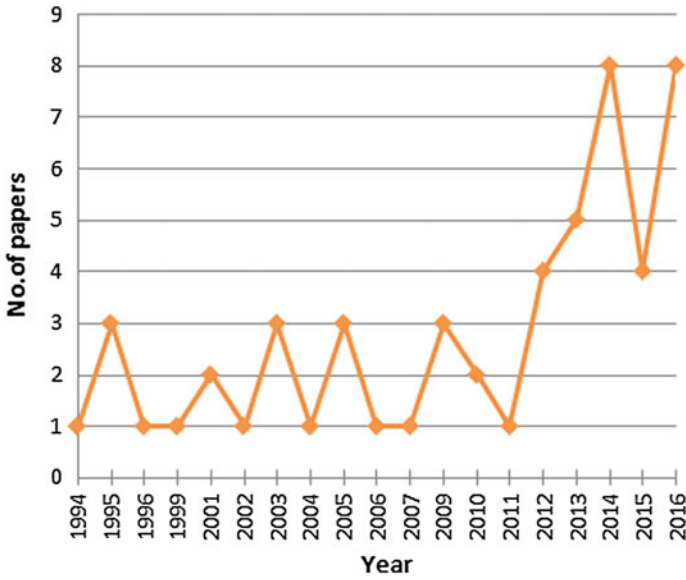


Fig. 2 Year-wise publication of papers citing ISO 9126 model

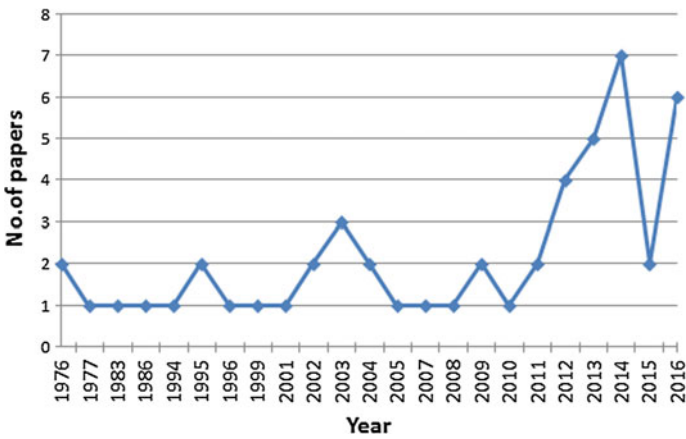


Fig. 3 Year-wise publication of papers citing Boehm model

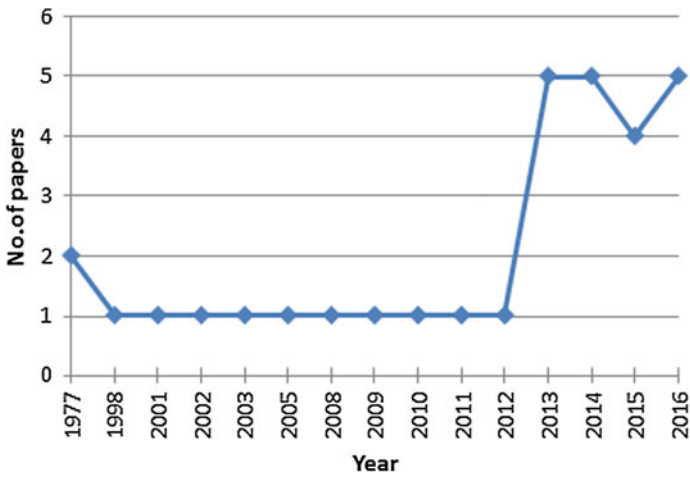


Fig. 4 Year-wise publication of papers citing McCall model

Fig. 5 Year-wise publication of papers citing Dromey model

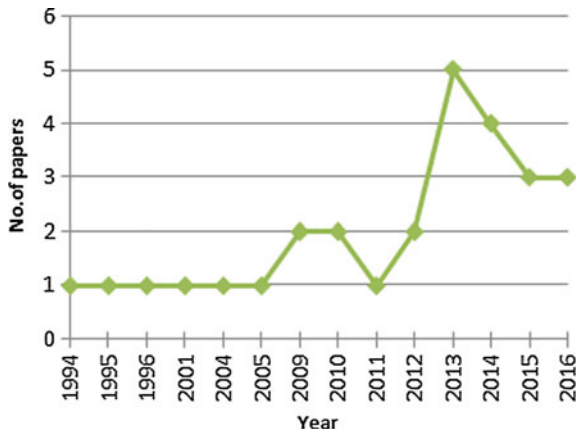
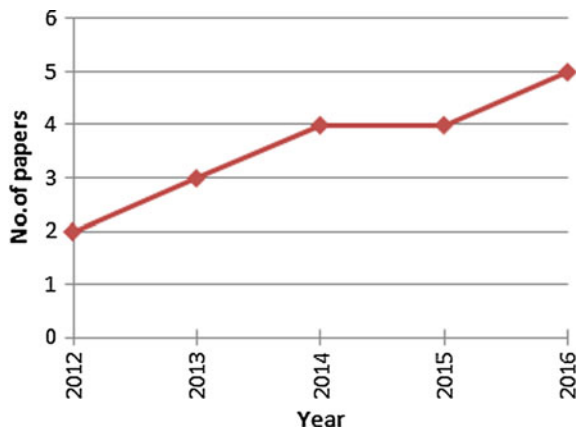


Fig. 6 Year-wise publication of papers citing ISO 25010 model



4 Review Results

4.1 *Relevance of Pursuing Review of Existing Quality Models*

Ascending trends in plotted graphs of Figs. 2, 3, 4, 5 and 6 clearly mark the relevance of pursuing the review of existing quality models in any research related to software component quality. The popularity of previous models like McCall, Boehm and Dromey comes from the citations. The McCall, Boehm and Dromey models among the top five models have stood the test of the times and still motivate the researchers. This strengthens the argument that ISO 9126 has taken under its fold the work of Barry Boehm and James McCall.

4.2 *Research Question*

RQ1: *Which are the top five most referred software component quality models in research papers till 2016?*

Table 3 gives us the top five software component quality models i.e. ISO 9126, Boehm, McCall, Dromey and ISO 25010.

5 Conclusion

There are few quality models that have stood the test of the times. Our results have concluded that the top five software component quality models are ISO 9126, Boehm, McCall, Dromey and ISO 25010. Detailed study of these models along with the quality metrics would be valuable for pursuing the further research in software component quality models. The other conclusion that could be derived is that twentieth century has seen the models as an outcome of individual researcher working in some organization. McCall work is with General Electric Company and US Rome Air Development Centre [7]. Boehm work is with TRS systems and Energy Group [8]. Dromey in 1995 presented his views as academic researcher [9]. The concrete steps for the quality of software as an engineering practice have been widely documented by ISO in 9126 standard [10]. ISO has since then amalgamated with the contemporary best practices in its standards of which ISO 25010 is a typical example. In twenty-first century, no model suggested by an individual researcher has been able to make its mark. There are few domain specific models or organization specific models or paradigm specific models that cater to tailored

requirements only. The popularity of ISO standards also points to the fact that researchers have accepted the lead of the ISO in devising the software component quality standards.

References

1. Brooks, F. P.: No Silver Bullet - Essence and Accident in Software Engineering. *IEEE Computer* 4, No. 2, 10–19 (1987).
2. Mijac M., Stajic Z.: Reusability Metrics of Software Components: Survey. In: 26th European Conference on Information and Intelligent Systems, pp 221–231. Varaždin, Croatia, Sep 23–25 (2015).
3. Miguel J.P., Mauricio D., Rodríguez G.: A Review of Software Quality Models for the Evaluation of Software Products. *International Journal of Software Engineering & Applications*, vol. 5, no. 6, pp. 31–54 (2014).
4. Al-Qutaish R. E.: Quality Models In Software Engineering Literature: An Analytical and Comparative Study. *Journal of American Science*, vol. 6, no. 3, pp. 166–175 (2010).
5. ISO/IEC 25010: Systems and Software Engineering—Systems and Software Product Quality Requirements and Evaluation (SQuaRE)—System and Software Quality Models. International Organization for Standardization, Geneva (2010).
6. Denning P.J.: Software quality.: *Commun. ACM*, vol. 59, no. 9, pp. 23–25, Sep (2016).
7. McCall J.A, Richards P.K., Walters G.F.: Factors in Software Quality: Concept and Definitions of Software Quality, RADC AFSC, Griffis Air Base, New York, RADC-TR-369, vol I. November (1977).
8. Boehm B.W., Brown J.R., Lipow M.: Quantitative evaluation of software quality. In: 2nd Int. Conf. Softw. Eng., pp. 592–605 (1976).
9. Dromey R.G.: A Model for Software Product Quality. In: *IEEE Trans. Softw. Eng.*, vol. 21, no. 2, pp. 142–162, (1995).
10. ISO/IEC IS 9126: Software Product Evaluation - Quality Characteristics and Guidelines for their Use, International Organization for Standardization, Geneva, Switzerland, 1991.

Achievable Spectral Efficiency with SIT-Based Channel Estimation Method in Next Generation Cellular Networks

Rajarao Manda and Mohammad Salauddin

Abstract Based on today's foreseen service requirements, such as live TV, video streaming, and file uploading and downloading; its needed to increase the data rates up to extreme level. This enhancement of data rates is highly depending on the usage of spectrum that how we are utilizing the available band to transmit data efficiently. In the present generation cellular networks, the channel estimation consumes some band of frequencies to determine the characteristics of wireless channel. Due to its (wireless channel) dynamic characteristics with respect to time and frequency, the conventional methods uses the more number of frequency bands hence the spectral efficiency decreases. This paper provides a technique to achieve higher spectral efficiency in next generation mobile networks with better system performance. In this method, a training sequence (reference pilot sequence) is superimposed along with the data sequence. At the receiver side, the same training sequence is used for estimating channel impulse response and then the data detection through the equalization. This estimated data are used recursively for channel re-estimation to increase the accuracy by minimizing the mean square error. From the simulation results and the numerical analysis, we show that the proposed method offers the better system performance with good spectral efficiency requirements.

Keywords LTE · OFDMA · SNR · Multiple-input multiple-output (MIMO) Superimposed training sequence · Reference symbols

R. Manda (✉) · M. Salauddin
Department of Electronics and Communication Engineering, University of Petroleum & Energy Studies, Dehradun, India
e-mail: rmanda@ddn.upes.ac.in

M. Salauddin
e-mail: msalauddin@ddn.upes.ac.in

1 Introduction

The future mobile devices are capable of performing the extreme advanced functionalities, such as voice telephony, Web browsing, multimedia steaming, and data transfer. Out of these functionalities, the last two require a high-speed data network. Recently, some systems have been proposed such as 4G-Long Term Evolution (LTE), 5G, and Worldwide Interoperability for Microwave Access (WiMAX) for high-speed data transfer. Due to high mobility, the achievable data rates cannot be achieved. This paper proposes a method to enhance the data rates in the above-mentioned systems. The two main resources for every communication system are power and bandwidth. These resources could affect the peak data rates of the communication networks defined by the Shannon's capacity theorem that the data rate can never exceed the channel capacity.

$$\text{i.e., } R_b \leq C = BW \log_2 \left(1 + \frac{S}{N} \right), \quad (1)$$

where BW = bandwidth and S/N = received signal power to noise power ratio. From Eq. (1), it is clear that the achievable data rates can be limited by mainly three factors: the available bandwidth (BW), the S/N ratio, and the spectral efficiency (R_b/BW). The most straightforward ways to enhance the data rates are increase or add more bandwidth (i.e., carrier aggregation) and increase received signal power using multiple antennas at the transmitting or receiving end (i.e., MIMO technology) [1–3]. But the wider transmission bandwidth impact on the complexity of the radio equipment and the information signal is more corrupted by the frequency-selective channel (i.e., due to multi-path fading). For remedy of this problem, orthogonal frequency division multiplexing (OFDM) has been selected as best transmission scheme for broadband wireless communication systems like WiMAX, LTE, and LTE-A, due to its robustness in multi-path fading channel and its spectral efficient. But OFDM is more sensitive to time dispersive property of multi-path propagation. In case of time dispersive channel, the estimation of channel impulse response is a challenging task.

The present and future generation cellular networks are designed with massive multiple-input multiple-output (MIMO) technology along with the combination of OFDM in both downlink and uplink, this further aggregate the channel estimation problem. In last few decades, some methods were proposed to estimate the channel. The pilot-based channel estimation method was used in conventional cellular networks. But these methods use separate spectrum for this purpose hence the spectral efficiency decreases. For better system performance especially in case massive MIMO-OFDM, these methods use large number of pilots and consume more bandwidth hence further degrade in the spectral efficiency [4–6]. Recently, a new method has been proposed in which a training sequence is superimposed on the data sequence for estimating of channel state information, which gives good performance with good spectral efficiency [7].

This paper follows as: the conventional method that is used in present generation cellular networks was discussed in Sect. 2, also mentioned their performance and comparison in terms of data rates and spectral efficiency. In Sect. 3, discussed the proposed method and its analysis. In Sect. 4, the simulation results and performance comparison are discussed between conventional and proposed method, and Sect. 5 concludes the paper.

2 Conventional Method

The main objective of channel estimation is to regulate the magnitude and phase shift caused by the wireless channel from the available information. For this module, a number of methods and algorithms can be hired. Most practical wireless communication networks such as WiMAX, 3G, and LTE systems adopt with pilot-based scheme that inserts the known pilots in both time and frequency domain.

2.1 System Modeling

As per the technical requirements, the best suited transmission scheme for the broadband wireless and cellular networks is MIMO-OFDM [1, 8]. Consider a basic block diagram of FFT-based OFDM transmitter and receiver system with pilot-assisted channel estimation as shown in Fig. 1. At the transmitter end, the modulated (PSK or QAM) data streams are mapped with subcarriers and given

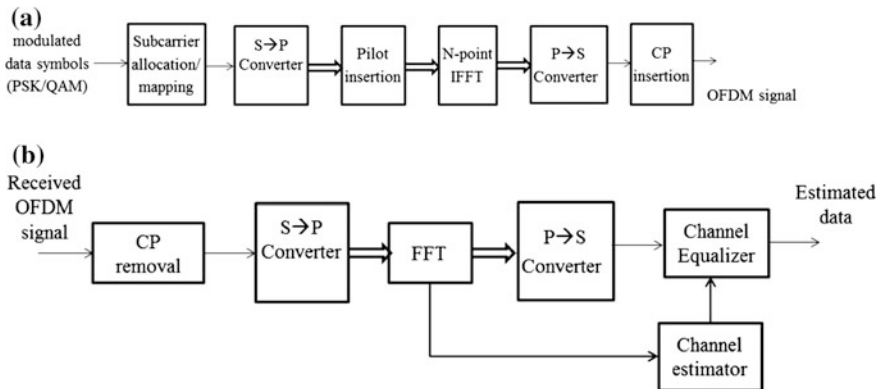


Fig. 1 a A simple schematic block diagram of OFDM transmitter with pilot-assisted channel estimation method b A simple block diagram of OFDM receiver

these data as input to the OFDM modulator. The OFDM signal is generated by passing through IFFT. It is defined in discrete time domain as

$$s_n = \sum_{k=0}^{N-1} d_k e^{\frac{j2\pi kn}{N}} \quad (2)$$

The known pilot symbols are inserted periodically at the transmitter end in both time and frequency before IFFT block in a predetermined manner through some subcarriers. The same pilot symbols are used at the receiver to determine the channel coefficients on the pilot subcarriers, and further these are used to determine the channel coefficients on others using interpolation methods.

2.2 Pilot Pattern

In 3GPP LTE network, assigned the user's data to a specific number of subcarriers for predetermined amount of time. This is named as physical resource block (PRB) which has both frequency and time dimensions (12 subcarriers and 6 or 7 OFDM symbols). So the reference/pilot symbols are inserted in two-dimensional manner, i.e., both time and frequency domain as shown in Fig. 2. Generally, the space between two pilot (reference) symbols depends on the time and frequency dispersion parameters of the wireless channel. The space required in time domain between two pilot symbols can be found from the maximum supported Doppler shift ($f_c v/c$), at the mobile speed (v) of range 350–500 km/h. Under the above assumptions, the maximum Doppler spread of from 972 to 1389 Hz. In order to reconstruct the channel, the minimum required sampling duration is given by approximately 0.5 ms. This indicates that the channel characteristics can be determined if there are at least two reference symbols inserted per slot in time domain. In case of frequency domain, the space between the two reference symbols can be obtained by calculating the coherence bandwidth. According to ITU channel model, this value is 20 kHz with 90% correlation and 200 kHz with 50% correlation. In LTE network, it is considered as 45 kHz; therefore, there is at least one reference symbol need to transmit for every 3 subcarriers.

The data rate of the system per one PRB is calculated as

$$\begin{aligned} & (\text{total number of subcarriers per PRB}) \times (\text{no. of bits per subcarrier}) / \\ & 0.5 \text{ ms} = 12 \times 7 \times 4 \text{ (for 16-QAM)} \times 2 \times 10^3 \text{ bps} = 672 \text{ kbps.} \end{aligned}$$

For 5 MHz channel bandwidth, the peak data rate is $25 \times 672 \text{ kbps} = 16.8 \text{ Mbps}$. But when we use some subcarriers for reference (pilot) signal transmission, the data rate reduces and hence the spectral efficiency. According to the given pilot pattern based on assumptions, there are 8 reference symbols per PRB. Therefore, the peak

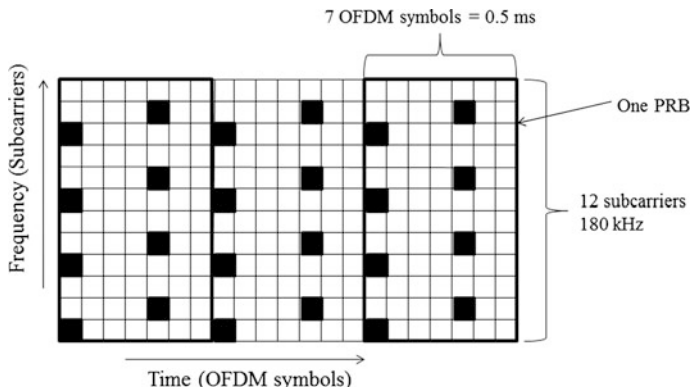


Fig. 2 Pilot pattern in LTE downlink

Table 1 Comparison of peak data rates

Channel bandwidth (MHz)	1.4	3	5	10	15	20
Number of occupied subcarriers	72	180	300	600	900	1200
Number of PRBs	6	15	25	50	75	100
Peak data rate in mbps without reference symbol transmission; QPSK modulation	2.016	5.04	8.4	16.8	25.2	33.6
16-QAM	4.032	10.08	16.8	33.6	50.4	67.2
64-QAM	6.048	15.12	25.2	50.4	75.6	100.8
Number of reference symbols per PRB	8					
Number of data subcarriers per PRB	76					
Peak data rate in mbps with reference symbol transmission using separate subcarrier; QPSK modulation	1.824	4.56	7.6	15.2	22.8	30.4
16-QAM	3.648	9.12	15.2	30.4	45.6	60.8
64-QAM	5.472	13.68	22.8	45.6	68.4	91.2

data rate = $25 (76 \times 4) \times 2 \times 10^3 \text{bps} = 15.2 \text{Mbps}$. The comparison is given in the Table 1.

3 Proposed Method

In pilot-assisted channel estimation, the spectral efficiency is reduced furtherly by transmitting more number of pilot symbols to get good system response in high-mobility scenarios. Instead of using the separate subcarriers for pilot symbols, if the pilot symbols are superimposed with data on same subcarrier we can improve

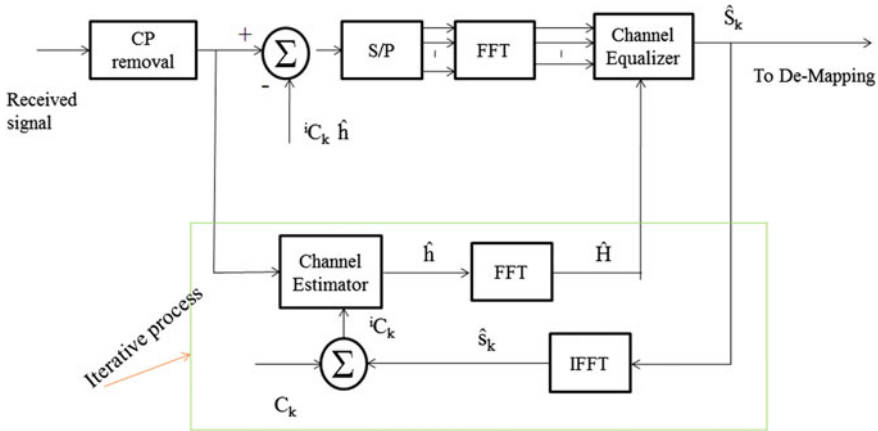


Fig. 3 OFDM receiver for proposed method

the spectral utilization as well as the system response by exploiting time and frequency characteristics of channel. In this proposed method, the pilot or reference symbols are arithmetically added to the data symbols on the same subcarrier with desired power allocation ratio. This pilot sequence is known as superimposed training sequence. The receiver model for the proposed method is shown in Fig. 3.

The superimposed training sequence is added on each subcarrier along with data sequence at OFDM transmitter after IFFT block and before CP insertion. At the receiver, the same training sequence is used to determine the channel response using least squares method. To increase the accuracy of the channel estimation, the estimated data is added to the training sequence then it is used to re-estimation of the channel response. This process is called interactive process.

The algorithm involves the following steps:

Let the received data sequence of k th OFDM symbol after removal of CP is

$$y_k(n) = (S_k + C_k)h_k + w_k,$$

where S_k and C_k are Toeplitz matrices of the data sequence and superimposed training sequence of the order $N \times L$; h_k = fading channel coefficients of order $L \times 1$; L = channel order, and w_k = AWGN noise sequence; k represents the k th OFDM symbol.

```

For i = 0 to 2 (number of iterations)
  If i = 0 Ck,i = Ck (Toeplitz matrix of the superimposed training
sequence)
  Else Ck,i = ŝk,i + Ck where ŝk,i = Toeplitz matrix (ŝk)
    For k = 1 to 7 (block length i.e. 7 OFDM symbols channel is
constant for this duration)

      ĥk =
      (Ck,iH Ck,i) Ck,iH yk          estimated channel coefficients

      End
      ĥ =  $\frac{1}{7} \sum_{k=1}^7 \hat{h}_k$ 
      ŝk =  $\text{ifft} \left( \frac{\text{fft}(y_k)}{\text{fft}(\hat{h})} \right)$ 
    end
  end
end

```

4 Simulation Results and Its Performance Analysis

The simulation results of the proposed method and conventional method are shown in Fig. 4. In first two iterations (0 and 1), the system performance is not good in terms of bit error rate (BER) compared to the conventional method. But with second iteration, the proposed method has given the improved system performance compared to the two-dimensional pilot-based method. It is clear that from the simulation results, for an acceptable BER of 1×10^{-3} , the proposed method could save up to 1 dB power, and approximately 10% spectral efficiency can be improved (from Table 1) compared to the conventional method. As per the 3GPP requirements, the maximum spectral efficiency is 30 bps/Hz with maximum 8 antennas [2]. We achieved the required spectral efficiency using the spectral efficiency by including overhead bits as shown in Fig. 5.

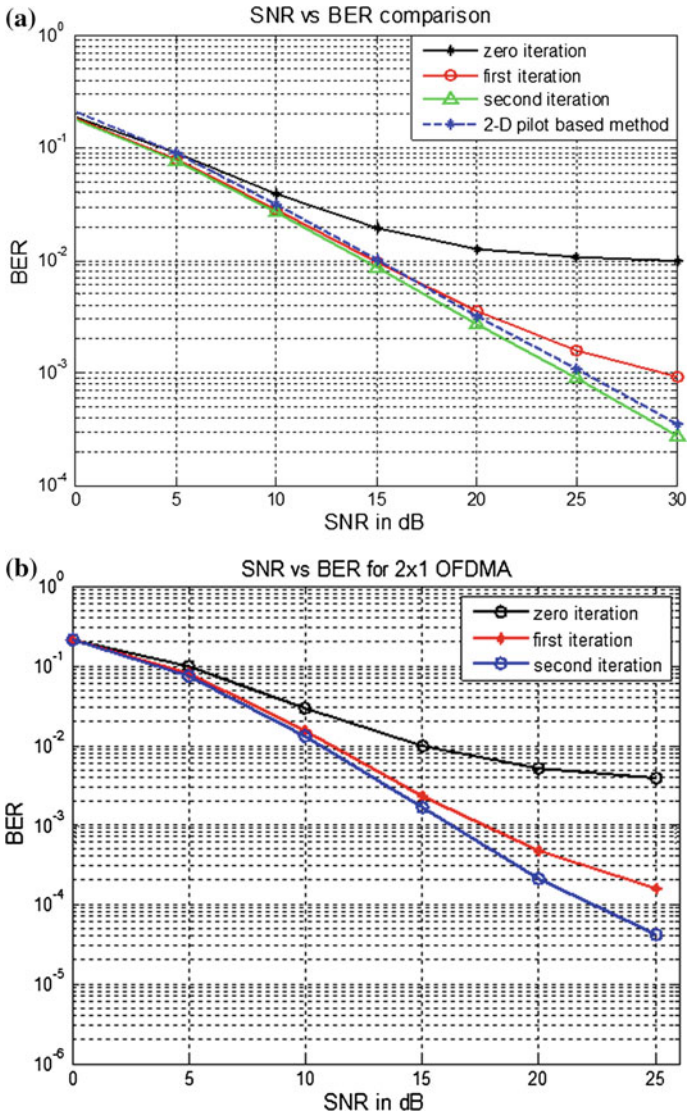
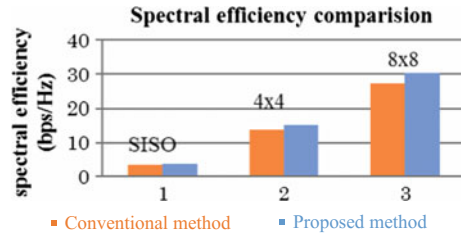


Fig. 4 BER versus SNR **a** performance comparison between proposed and conventional channel estimation method for 1×1 OFDMA systems; **b** for 2×1 OFDMA system

Fig. 5 Spectral efficiency comparison between conventional and proposed method for MIMO-OFDMA system supported by 64-QAM modulation scheme



5 Conclusion

In this paper, it was observed that the spectral efficiency degraded by transmitting the reference symbols on separate subcarriers and in case of high-mobility scenarios, the spectral efficiency could degrade furtherly to get better system performance. It provides a spectral efficient channel estimation method, and the simulation results were shown that the method gives a better system performance with achievable high data rates and spectral efficiency.

References

1. Uma Shanker Jha, Ramjee Prasad "OFDM towards fixed and mobile broadband wireless access" *Artech House Universal Personal Communications Series, 2007*, ISBN-13: 978-1-58053-641-7.
2. 3GPP, "Requirements for further advancements for Evolved Universal Terrestrial Radio Access (E-UTRA) (LTE-Advanced) (Release 9)", 3GPP, Technical Report TR 36.913 v9.0.0.
3. Shinsuke Hara, Ramjee Prasad "Multicarrier Techniques for 4G Mobile Communications". Artech House universal personal communications series, 2003, ISBN 1-58053-482-1.
4. J.W. Choi and Y.H. Lee, "Design of 2-D channel estimation filters for OFDM systems," *IEEE International Conference on Communications*, vol. 4, pp. 2568–2572, May 2005.
5. Won-Gyu Song and Jong-Tae Lim, "Pilot-symbol aided channel estimation for OFDM with fast fading channels," in *IEEE Transactions on Broadcasting*, vol. 49, no. 4, pp. 398–402, Dec. 2003. doi: 10.1109/TBC.2003.819049.
6. S. Park, B. Shim and J. W. Choi, "Iterative Channel Estimation Using Virtual Pilot Signals for MIMO-OFDM Systems," in *IEEE Transactions on Signal Processing*, vol. 63, no. 12, pp. 3032–3045, June 15, 2015.
7. Rajarao, M.; Kumar, R.V.R.; Madhuri, D.; Latha, M., "Efficient channel estimation technique for LTE air interface," in *Microelectronics and Electronics (PrimeAsia), 2012 Asia Pacific Conference on Postgraduate Research in*, vol., no., pp. 214–219, 5–7 Dec. 2012 doi: 10.1109/PrimeAsia.2012.6458657.
8. <http://www.3gpp.org/technologies/keywords-acronyms/97-lte-advanced>.

Comparative Analysis of Workflow Scheduling Policies in Cloud Platforms

Kamal Kumar and Jyoti Thaman

Abstract Cloud computing platforms are most suitable platforms for assessment of performance characteristics of any scheduling algorithm. Tasks in cloud platforms are represented as either set of independent tasks or workflows. Workflows technology imitates the industrial flows in digital forms. The optimal scheduling of tasks in a workflow may help in resequencing the activities in an industry. This paper utilized WorkflowSim simulator which extends CloudSim toolkit by incorporating workflow management through workflow engine, workflow planner, and workflow scheduler. Several modifications led to incorporation of overhead and failure layers into WorkflowSim. This paper presents a review of scheduling policies supported by WorkflowSim. An exhaustive review presents strength and weakness of various scheduling policies using varied task types.

Keywords Scheduling · Makespan · Performance analysis · CloudSim Workflows · HEFT

1 Introduction

The idea of cloud computing is based on the concept of reusability of IT capabilities. Cloud computing supports on-demand self-service dashboard through user login, where service user can subscribe or unsubscribe for services, without human intervention. Cloud platform gives different benefits to users like reduced cost, increased storage, flexibility. Different types of tasks are entered by user in cloud. Service providers must take all these tasks and ensure the desired processing as per user's demands. Workflows is special set of tasks which depicts the constraints, dependency and scheduling algorithms balance the load across all servers and

K. Kumar (✉)

School of Computer Science and Engineering, UPES, Dehradun, Uttarakhand, India
e-mail: kkumar@ddn.upes.ac.in

J. Thaman

M.M. University, Sadopur, Ambala, Haryana, India

© Springer Nature Singapore Pte Ltd. 2018

R. Singh et al. (eds.), *Intelligent Communication, Control and Devices*,
Advances in Intelligent Systems and Computing 624,
https://doi.org/10.1007/978-981-10-5903-2_29

267

improve the performance of cloud data center. The scheduling of workflows requires complex algorithms which not only respect the specified constraints but also improve the performance metrics of the computing platform. When scheduling of tasks uses common queue of tasks and does not consider device-level optimization, such scheduling is referred to as global scheduling, whereas when device-level queue of tasks and optimizations are undertaken, such scheduling is known as local scheduling.

This paper presents experimental analysis of these scheduling algorithms by using simulation environment. Simulations of workflows have been carried out in WorkflowSim. Different scheduling algorithms like FCFS, DAS, Max-min, Min-Min, HEFT, DHEFT for workflow scheduling are compared with makespan, utilization, speedup, and energy consumption parameters. A novel taxonomy for scheduling schemes is presented in this paper. This paper is organized into six sections. Section 2 presents a brief of related work. Section 3 presents new taxonomy proposed through this paper. Section 4 presents the algorithms of local scheduling schemes discussed in this paper. Section 5 presents the algorithms of global scheduling schemes discussed in this paper. Section 6 presents the simulation and discussion of simulation-based results. Finally, Sect. 7 presents the conclusion.

2 Related Work

In [1], authors proposed to compute the complexity and capacity of processing elements; authors presented two scheduling algorithms for scheduling tasks and carried out the experiments in CloudSim toolkit. The proposed algorithms gave good performance under heavy loads. In [2], authors reviewed workflow scheduling algorithms and produced a table on the basis of algorithm used, parameter considered like which method and factors are considered in algorithm, explanation, and development environment. In [3], authors presented a review of various energy-efficient task scheduling methods in a cloud environment. In [4], authors reviewed different scheduling algorithms in different environments with their respective parameters like what are their objective, which type of tool used, scheduling factors, and environment for implementation. In [5], authors performed comparative study of the different algorithms for their suitability, feasibility, adaptability in the context of cloud scenario after that author proposed the hybrid approach to enhance the existing platform that can help cloud providers to offer better quality of services. In [6], author presented a survey of workflow applications with respect to management and scheduling techniques and reviewed the existing scheduling algorithms in terms of their objective. Authors presented a load balancing approach based on GA in [7]. Authors [8] have proposed a greedy method based on task scheduling to decrease in the makespan and improved utilization. Authors in [9] targeted scheduling optimization and proposed heuristic algorithm-based approach and compared the performance with PSO embedded in

crossover and mutation. In [10], the authors reviewed several taxonomies for classification of challenges in workflow scheduling schemes. In [11], authors proposed a new taxonomy for classification of task scheduling algorithms based upon the goal-oriented or constraint-oriented approach. A large number of proposals were considered and classified in various categories as proposed by taxonomy.

3 Workflow Scheduling Taxonomy

Through this review paper, a new classification is proposed. In general, scheduling algorithms either try to optimize the execution times of the submitted jobs by using device-level optimization. Another way to achieve had been through global optimization, where common ready queue of jobs is considered instead of device-level ready queue. This difference in mechanism is novel classification proposed through this proposal. Scheduling approaches are classified through new taxonomy. Figure 1 presents the taxonomy in diagrammatic form.

4 Local Scheduling Policies

WorkflowSim supports many dynamic scheduling policies which respect parent-child relationships between tasks and jobs in the original or clustered workflows. Dynamic scheduling is the need of cloud environment. This section introduces dynamic scheduling schemes supported in WorkflowSim.

Data-Aware Scheduling (DAS): DAS algorithm is one of the favorite algorithms for scheduling. It uses the concept of time to transfer the data from input or output files corresponding to cloudlet. A cloudlet is scheduled on a virtual machine (VM) if data transfer time for pair of (cloudlet, VM) is minimum. Pseudo-code corresponding to DAS is as shown in Fig. 2. Figure only shows cloudlet VM mapping code.

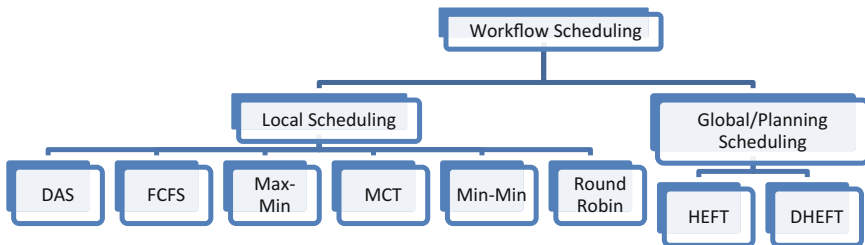


Fig. 1 New taxonomy for task scheduling algorithms in WorkflowSim

Algorithm: **DAS** (VMList, CloudletList)

```

For each vm in VMList
  If (vm.State ==Idle && DataTransferTime(cloudlet,vm)<
    DataTransferTime(cloudlet, FirstIdleVM))
    FirstIdleVM = vm
    vm.State =Busy
  End-If
End-For
Schedule cloudlet on FirstIdleVM

```

Fig. 2 Algorithm for data-aware scheduling

First-Come-First-Serve (FCFS): FCFS scheduling algorithm is simplest in terms of its implementation. FCFS schedules first unscheduled cloudlet on first available VM. The pseudo-code of FCFS is as shown in Fig. 3. The FCFS scheduling is fair in the formal sense or human sense of fairness, but it is unfair in the sense that long jobs make short jobs wait and unimportant jobs make important jobs wait (Fig. 3).

```

Algorithm: FCFS (VMList, CloudletList)

Step 1: For each cloudlet in CloudletList

Step 2: cloudlet_Status = False

Step 3: For each VM in VMList

  If (VM.State ==Idle)

    Schedule Cloudlet on VM

    Cloudlet_Status = True

    Break;

  End-If

End-For

Step 5: If (cloudlet_Status == False)

  Goto Step 7

End-If

Step 6: End-For

Step 7: End-FCFS

```

Fig. 3 Algorithm for FCFS

Max-min: Max-min scheduling algorithm has been most attractive scheduling algorithm. It uses the concept of scheduling cloudlets with maximum length to VM with minimum remaining capacity. It results in minimizing the execution time of smallest cloudlet by subjecting it to fastest VM (Fig. 4).

Minimum Completion Time (MCT): MCT scheduling algorithm schedules cloudlet in such a manner that next unscheduled cloudlet is completed in minimum possible time. Selection of VM is based on the remaining MIPS. VM with maximum remaining capacity is selected for execution of the cloudlet (Fig. 5).

Min-Min: Min-Min scheduling algorithm schedules the next cloudlet with minimum length on VM with remaining capacity. It results in scheduling smaller tasks on slower machines.

Round Robin (RR): RR scheduling algorithm schedules cloudlets in ascending order of their Id on idle VMs in order of their Id. This is the simplest form of scheduling, and performance depends upon the quantum of allocation. Large quantum size is equivalent of FCFS. RR is default preemptive algorithm. In WorkflowSim, RR is considered non-preemptive.

```

Algorithm: MaxMin (VMList, CloudletList)
For each cloudlet in CloudletList
  If Length.cloudlet >Length.MaxCloudLet
    MaxCloudLet = cloudlet
  End-if
End-For
For each vm in VMList
  If vm.State ==Idle
    FirstIdleVM = vm
  End-If
End-For
Schedule MaxCloudLet on FirstIdleVM

```

Fig. 4 Algorithm for Max-min scheduling

```

Algorithm: MCT (VMList, CloudletList)
FirstIdleVM = NULL
For each vm in VMList
  If vm.State ==Idle
    FirstIdleVM = vm
  End-If
End-For
For each vm in VMList
  If (vm.State==Idle&&vm.RemainingMips>FirstIdleVM.RemainingMips)
    FirstIdleVM = vm
  End-If
Schedule cloudlet on FirstIdleVM

```

Fig. 5 Algorithm for minimum completion time scheduling

5 Global/Planning Algorithm

Global planning algorithm uses a global ready queue instead of per device or VM ready queue. This prevents the usage of other machines and scheduling of independent tasks together. This section discusses HEFT and DHEFT algorithms.

Heterogeneous Earliest Finish Time Algorithm (HEFT): HEFT [12] works on the centralized approach and computes the ranks of all the tasks in the workflow by using bandwidth, task length, and parent–child relationships. Mean execution time for each task and average communication time between resources of two successive tasks on the basis of parent–child relationship between concerned tasks are computed in HEFT.

DHEFT Algorithm: DHEFT is distributed version of HEFT and utilizes the available resources in distributed manner such that a task is mapped to a machine only if it executes the given task in minimum possible time. The performance of DHEFT is much better than HEFT. No ranks are computed in HEFT though.

6 Simulation and Discussion

To complete the review of promising local and global scheduling algorithms, we considered WorkflowSim [13] as simulation tool.

6.1 Simulation Setup

The simulation of all the scheduling schemes was performed in WorkflowSim toolkit. WorkflowSim supports many facilities for simulation of cloud environment. Specific to this proposal, Xen VMs, four VMs types, $VM_MIPS = \{2500, 2000, 1000, 500\}$, $VM_RAM = \{870, 1740, 1740, 613\}$, $VM_BW = 100000$ have been considered with heterogeneous computational characteristics. Each VMs is considered to support only one processing elements. Sufficient repetitions of experiment have been performed to arrive at the results.

6.2 Discussion

From Table 1, it can be easily seen that the performance of local scheduling algorithms varies widely. Figure 6 discusses the makespan of local and global scheduling algorithms under different scheduling schemes. Under local scheduling algorithms, Max-min reduced the makespan by minimizing the execution time of smallest cloudlet by subjecting it to fastest VM. In Fig. 6, utilization of resources

Table 1 Simulation results in local scheduling algorithms and global scheduling algorithms

Schemes	Makespan	Utilization (%)	Energy consumption
DAS	1684.71	36.08	340415.397
CFS	795.61	42.92	164840.062
Max-min	371.13	67.84	83831.972
MCT	536.81	49.61	113915.113
Min-Min	617.42	45.87	129286.367
RR	926.54	40.99	190629.362
HEFT	866.52	37.69	173052.92
DHEFT	567.50	33.29	113405.76

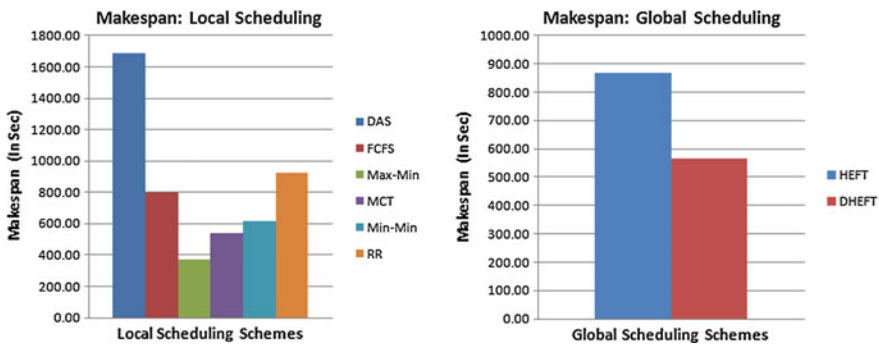


Fig. 6 Makespan characteristics of local and global scheduling algorithms

with local and global scheduling is discussed. Utilization of resources is higher in Max-min scheduling scheme than others. The reason for this is attributed to the fact that longer tasks continue to use slower machines, and at the same time smaller tasks continue to complete from faster machines. This keeps the utilization on higher sides (Fig. 6).

$$E = (P^{\max} \times 0.70 + P^{\max} \times 0.30 \times \text{util}) \times \text{makespan} \tag{1}$$

Using Eq. (1) [14], we compute the energy consumption due to specific local scheduling scheme. The energy consumption in Max-min is better than other scheduling schemes as higher utilization results in faster rate of energy consumption but for shorter duration. Graphs in Figs. 6, 7, and 8 complement the tabular results and clearly dictate that Max-min is promising scheduling approach for local scheduling for set of independent tasks. Formally, global scheduling algorithms are known as planning algorithms also. If system uses planning algorithm, local scheduling becomes ineffective. In global scheduling, DHEFT produced a reduced amount of makespan as compared to HEFT. The reason behind this is approximation of ready queue in DHEFT which is much better than that of HEFT and

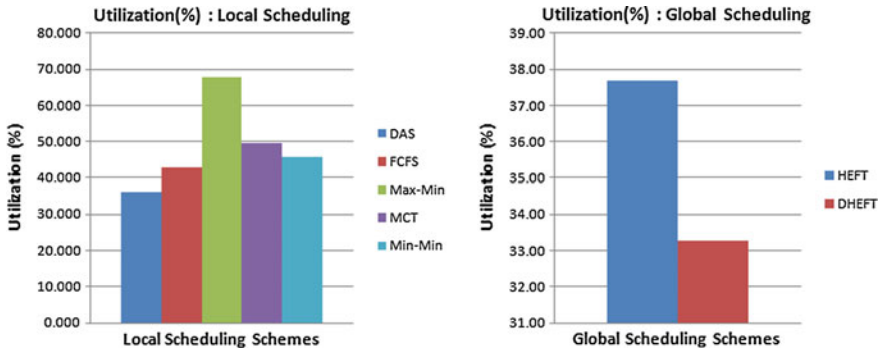


Fig. 7 Utilization characteristics of local and global scheduling algorithms

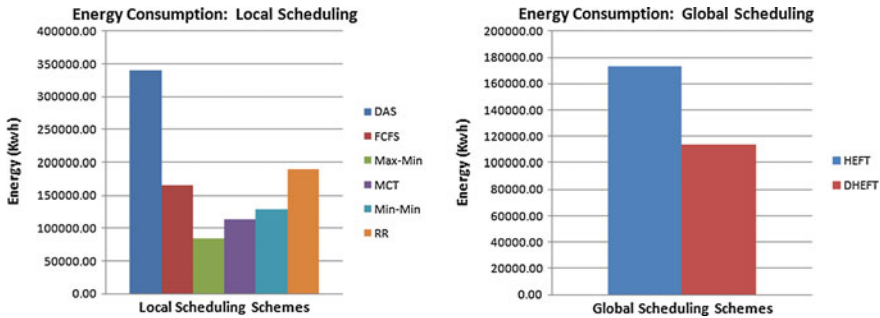


Fig. 8 Energy consumption characteristics of local and global scheduling algorithms

distributed decisions in DHEFT. DHEFT is able to exploit the resources at hand in better way than that of centralized approach used in HEFT. Results in Table 1 shows that DHEFT performs better than that of HEFT. The makespan characteristics, utilization characteristics, and energy efficiency of global scheduling algorithms in graphs of Figs. 6, 7 and 8 established that DHEFT outperforms HEFT. DHEFT is most promising global scheduling algorithm.

7 Conclusion

This paper presents a new taxonomy for classification of scheduling schemes in cloud computing paradigm. A large number of scheduling schemes were discussed and simulated for presenting a thorough review of available schemes. This review establishes that not all the scheduling algorithms are suitable. Local scheduling schemes were reviewed, and Max-min was declared as most promising local scheduling scheme. DHEFT was concluded as most promising global scheduling

scheme among global scheduling schemes. The conclusion here can be drawn that distributed decision is able to exploit the resources better than centralized approaches. Similarly, criteria-based task-machine mapping results in better resource utilization. Energy efficiency of the system is better if we choose better scheduling algorithm which has low makespan and better utilization. Hybrid of local and global scheduling approaches may improve the performance further.

References

1. Sindhu, S., & Mukherjee, S. (2011). Efficient task scheduling algorithms for cloud computing environment. In *High Performance Architecture and Grid Computing* (pp. 79–83). Springer Berlin Heidelberg.
2. Arya, L. K., & Verma, A. (2014, March). Workflow scheduling algorithms in cloud environment-A survey. In *Engineering and Computational Sciences (RAECS), 2014 Recent Advances in* (pp. 1–4). IEEE.
3. Atiewi, S., Yussof, S., Ezanee, M., & Almiani, M. (2016, April). A review energy-efficient task scheduling algorithms in cloud computing. In *Long Island Systems, Applications and Technology Conference (LISAT), 2016 IEEE* (pp. 1–6). IEEE.
4. Shimpy, E., & Sidhu, M. J. (2014). Different scheduling algorithms in different cloud environment. *International Journal of Advanced Research in Computer and Communication Engineering*, 3(9).
5. Singh, R. M., Paul, S., & Kumar, A. (2014). Task Scheduling in Cloud Computing: Review. *International Journal of Computer Science and Information Technologies*, 5(6), 7940–7944.
6. Liu, L., Zhang, M., Lin, Y., & Qin, L. (2014, May). A survey on workflow management and scheduling in cloud computing. In *Cluster, Cloud and Grid Computing (CCGrid), 2014 14th IEEE/ACM International Symposium on* (pp. 837–846). IEEE.
7. Kousik Dasgupta, Brotoji Mandal, Paramartha Dutta, Jyotsna Kumar Mondal, Santanu Dam, “A Genetic Algorithm (GA) based Load Balancing Strategy for Cloud Computing”, *Procedia Technology*, 10 (2013) 340–347.
8. Ji Lia, Longhua Fenga, Shenglong Fan” An Greedy-Based Job Scheduling Algorithm in Cloud Computing” *JOURNAL OF SOFTWARE*, VOL. 9, NO. 4, APRIL 2014.
9. Lizheng Guo1, Shuguang Zhao, Shigen Shen, Changyuan Jiang” Task Scheduling Optimization in Cloud Computing Based on Heuristic Algorithm” *JOURNAL OF NETWORKS*, VOL. 7, NO. 3, MARCH 2012.
10. Alkhanak, E. N., Lee, S. P., & Khan, S. U. R. (2015). Cost-aware challenges for workflow scheduling approaches in cloud computing environments: Taxonomy and opportunities. *Future Generation Computer Systems*.
11. Thaman, Jyoti, and Manpreet Singh. “Current perspective in task scheduling techniques in cloud computing: A review.” *International Journal in Foundations of Computer Science & Technology* 6 (2016): 65–85.
12. Topcuoglu, H., Hariri, S., Wu, M.Y. (2002). Performance-Effective and Low-Complexity Task Scheduling for Heterogeneous Computing. *IEEE Transactions on Parallel and Distributed Systems* 13(3), 260–274.
13. Chen, Weiwei, and Ewa Deelman. “Workflowsim: A toolkit for simulating scientific workflows in distributed environments.” In *E-Science (e-Science), 2012 IEEE 8th International Conference on*, pp. 1–8. IEEE, 2012.
14. Beloglazov, A., Abawajy, J., & Buyya, R. (2012). Energy-aware resource allocation heuristics for efficient management of data centers for cloud computing. *Future generation computer systems*, 28(5), 755–768.

Effect of Ratio of Protrusion Height to Print Diameter on Thermal Behaviour of $\text{Al}_2\text{O}_3\text{-H}_2\text{O}$ Nanofluid Flow in a Protrusion Obstacle Square Channel

Sunil Kumar, Alok Darshan Kothiyal, Mangal Singh Bisht and Anil Kumar

Abstract Thermal behaviour of turbulent alumina nanofluids flow in a protrusion obstacles square channel is numerically investigated. The ratio of protrusion height to print diameter varied from 0.83 to 1.67, streamwise spacing of 1.8, spanwise spacing of 1.8, size of nanoparticles of 30 nm, and concentration of 4.0%. The computations are performed under uniform heat flux over a range of Reynolds number varied from 4,000 to 18,000. The best improvement in thermal performance is observed to be 4.35 times higher over smooth surface square duct for the ratio of protrusion height to print diameter of 1.0.

Keywords Energy · Streamwise spacing · Spanwise spacing · Nanofluids
Nomenclature

d_p	Print diameter of protrusion obstacles, mm
D	Hydraulic diameter, mm
e_p	Height of protrusion, mm
f	Friction factor
f_{rsave}	Average flow friction of rough surface
E	Energy, J
f_{ssave}	Average flow friction of smooth surface
I	Heat flux, W/m^2

S. Kumar (✉) · A. Kumar
School of Mechanical and Civil Engineering, Shoolini University, Solan, India
e-mail: reachtome.sunil@gmail.com

S. Kumar
Uttarakhand Technical University, Dehradun, India

A.D. Kothiyal
Baba Farid Institute and Technology Dehradun, Dehradun, Uttarakhand, India

M.S. Bisht
Govind Ballabh Pant Engineering College Pauri Garhwal, Pauri, Uttarakhand, India

k	Turbulent Kinetic energy, m^2/s^2
Re_n	Reynolds number
M_t	Turbulent Mach number
P_r	Prandtl number
P_{rt}	Turbulent Prandtl number
v	Total velocity, m/s
u	Velocity in X-direction, m/s
X_s/d_p	Streamwise spacing
Y^+	Dimensionless distance from walls
Y_s/d_p	Spanwise spacing
ΔP_{ave}	Average pressure drop across
e_p/d_p	Protrusion height to print diameter
Nu_{rsave}	Average Nusselt number of rough wall
Nu_{ssave}	Average Nusselt number without protrusion wall

Greek Symbols

μ	Dynamic Viscosity, Ns/m^2
ρ	Density, kg/m^3
μ_t	Turbulent Viscosity, Ns/m^2
η_o, β_o	Model Constant
η_p	Hydraulic thermal parameter

1 Introduction

Rise in heat exchange is one of the major aims for any firm; so as of late, a few vital research works have been done to clarify and comprehend the reasons for the upgrade or control of heat exchange utilizing nanofluids [1]. Additionally, the lessening in the flow friction for frameworks that produce high liquid pressure drop is extremely clear. Subsequently, the objective for attaining the improvement of heat exchangers needs be dependably to upgrade the energy exchange and simultaneously limits the ascent in the flow friction [2, 3]. Lee and Choi [4] considered convective heat transfer of laminar flow of an inconclusive nanofluid in smaller scale channels and observed nanofluids can disseminate heat four times more than unadulterated water.

Xuan and Li [5] computed convective heat transfer coefficient of Cu–H₂O nanofluids and discovered generous heat exchange upgrade. Santra et al. [6] mathematically examined the after effect of Cu–H₂O over parallel wall conductor in transition constrained convection. They experimented that the rate of convective heat transfer augmented with a growth of Reynolds number and the volume fraction. Pak and Cho [7] have mathematical examined the turbulent friction and convective heat transfer behaviour of water-based nanofluids Al₂O₃ and TiO₂

having average diameters of 13.44 and 27.23 nm, respectively. Xuan and Li [8] have measured the convective heat transfer of Cu–H₂O nanofluid with little pressure-driven distance across level tube under laminar stream conditions. Nu of the nanofluid having concentration 2.21% rises to 38.5% that of unadulterated water.

Li and Xuan [9] have tentatively researched convective heat transfer and stream qualities of Cu–H₂O beneath laminar stream in a square metal duct. The exploratory outcomes demonstrate that the nanofluid has bigger heat exchange coefficient than immaculate water at equal Reynolds number. Kumar et al. [10] numerically studied the enhancement in heat transfer rate using Al₂O₃–H₂O nanofluid flowing through square mini channel with protrusion obstacle. Manay et al. [11] investigated the heat transmission and hydraulic appearances of Cu–H₂O inside a passage with square conduit utilizing the blend demonstrate. The forecasts demonstrated that the Cu–H₂O rises the heat transfer rate while the volume part and Reynolds number of Cu–H₂O are expanding.

2 CFD Simulation

In the present article, a numerical examination is led to dissect the 3D incompressible streams over protrusion obstacles on thermal behaviours in square channel. A commercial ANSYS 16.0 (Fluent), CFD software was utilized to re-enact fluid elements and heat transfer. Computational area, frame work era, representing conditions, limit conditions, determination/approval of appropriate turbulence model, and arrangement strategy are given in detail in the accompanying sub-segments.

2.1 Computational Geometry

The square channels with protrusion obstacles embedded in the heated wall are displayed in Fig. 1. The square channel had width $W_c = 10$ mm and height $H_c = 10$ mm. The total length of the channel is 340 mm. The length of the test section is $L_t = 108$ mm, with an upstream length of 200 mm to guarantee a completely created stream in the test segment. The downstream segment (leave segment) has the length of 32 mm which is connected to keep away from the event of adversative pressure impacts brought on by switched move through the computational space. The protrusion height = 1.0 mm.

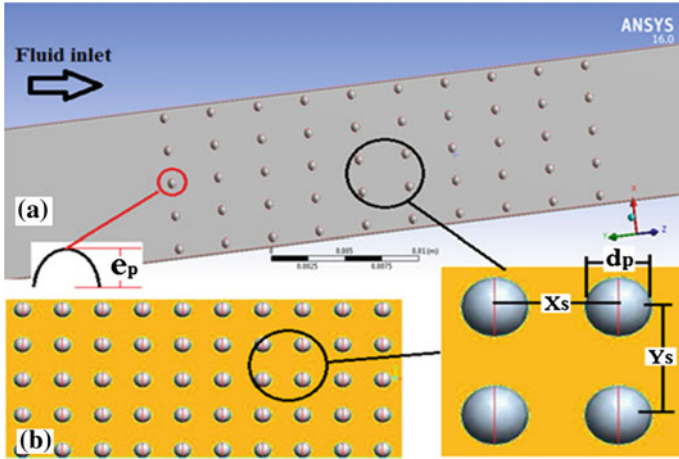


Fig. 1 Domain solutions for CFD analysis

2.2 Mathematical Equations

In present investigation, 3-D CFD simulation of Nu_{rs} and f_{rs} was shown by using software, namely ANSYS 16.0 (Fluent). Simulation elaborated the numerical results for equations of mass, momentum, and energy. These equations composed for incompressible fluid flow were as follow [12]:

Equation of continuity:

$$\nabla \cdot (\rho \cdot v) = 0 \tag{1}$$

Equation of momentum:

$$\nabla \cdot (\rho \cdot v \cdot v) = -\nabla p + \nabla \cdot (\mu [(\nabla v + \nabla v^T) - 2/3 \cdot \nabla \cdot v I]) + \rho g \tag{2}$$

Equation of energy:

$$\nabla \cdot (v(\rho E + p)) = \nabla \cdot (k_{eff} \nabla T - hJ + (\mu [(\nabla v + \nabla v^T) - 2/3 \cdot \nabla \cdot v I] \cdot v)) \tag{3}$$

Turbulent RNG $k-\epsilon$ model was used in the present investigation [12]. Turbulence kinetic energy (k) and (ϵ) its rate of dissipation, respectively, for RNG $k-\epsilon$ was found from the subsequent transport equations:

$$\partial/\partial X_i(\rho k u_i) = \partial/\partial X_i(\alpha_k \mu_{eff} \partial k/\partial x_j) + G_k + G_b - \rho \epsilon - Y_M + S_k \tag{4}$$

$$\begin{aligned} \partial/\partial X_i(\rho \epsilon u_i) = & \partial/\partial X_i(\alpha_\epsilon \mu_{eff} \partial \epsilon/\partial x_j) + C_{1\epsilon} \epsilon/k \cdot (G_k + G_{3\epsilon} G_b) - C_{2\epsilon} \rho \epsilon^2/k \\ & - R_\epsilon + S_\epsilon \end{aligned} \tag{5}$$

The model constants $C_{1\epsilon}$ and $C_{2\epsilon}$ in Eq. (5) are 1.42 and 1.62, respectively.

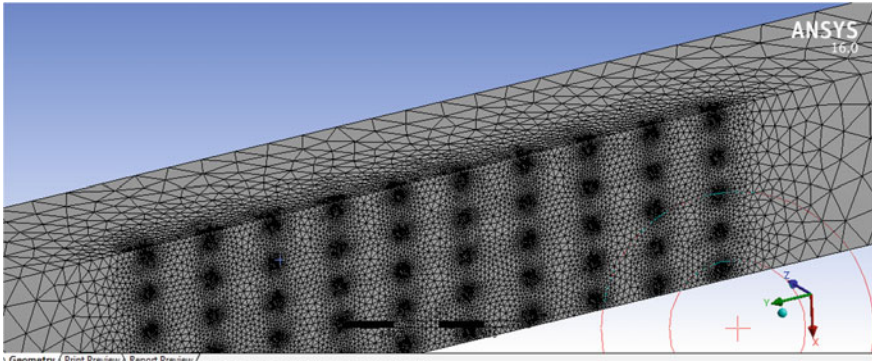


Fig. 2 Grid system

2.3 Grid Independence Test

The grid of the domain is through using ANSYS software. Figure 2 shows the graphic of grid systems. The different densities for grid (178219 cells, 187926 cells, 198338 cells, 201745 cells, 210984 cells) are applied to choose proper mesh size which acclimates with near-wall treatment. The wall distance Y^+ is taken for choosing correct near-wall treatment. To increase the grid density, the grid independence test has been done until additional increment displays a change of less than 2.0% in two successive groups of outcomes.

3 Properties of Nanofluid

$\text{Al}_2\text{O}_3\text{-H}_2\text{O}$ nanofluid is the mixture of H_2O base fluid and Al_2O_3 nanoparticle having diameter of 30 nm. The various properties of H_2O and Al_2O_3 are presented in Table 1, at 300 K reference temperature. The single-stage model [10] is considered to locate the physical properties of $\text{Al}_2\text{O}_3\text{-H}_2\text{O}$ nanofluid. The models applied to find specific heat, density, dynamic viscosity, and thermal conductivity, respectively, are as follow.

Density model:

$$\rho_{nf} = (1-\varphi)\rho_{bf} + \varphi\rho_{np} \quad (6)$$

Specific heat model [13]:

$$(\rho C_p)_{nf} = (1-\varphi)(\rho C_p)_{bf} + \varphi(\rho C_p)_{np} \quad (7)$$

Table 1 Thermophysical properties of water-based nanofluid Al_2O_3 with $d_{np} = 30$ nm and $\varphi = 0.04$ at $T = 300$ K

Nanoparticle and base fluid	ρ (kgm^{-3})	k ($\text{Wm}^{-1}\text{K}^{-1}$)	C_p ($\text{Jkg}^{-1}\text{K}^{-1}$)	μ (Nsm^{-2})
Al_2O_3	3773.07	36.00	765	0.001522
Base fluid	998.20	0.613	4182	0.001003

Dynamic viscosity model [13]:

$$\mu_{nf} = \mu_b(123\varphi^2 + 7.3\varphi + 1) \quad (8)$$

Thermal conductivity model (Bruggeman model) [14]:

$$k_{nf} = [(3\varphi - 1)k_p + (2 - 3\varphi)k_b + (\Delta)^{1/2}] \quad (9)$$

$$\Delta = [(3\varphi - 1)k_p + (2 - 3\varphi)k_b]^2 + 8k_pk_b \quad (10)$$

4 Validation of CFD Models

For validation of CFD turbulence models, the Nu_{rsave} results were compared to CFD turbulence model outcomes with Dittus–Boelter equation on smooth wall square channel. For Nu_{ssave} , the Dittus–Boelter equation (Eq. 11) was used.

$$Nu_{ssave} = 0.023 Re_r^{0.8} P_r^{0.4} \quad (11)$$

Figure 3 shows the observed Nu_{ssave} with Re_n for different models and comparison with Dittus–Boelter equation on smooth wall. It has been seen that the outcomes got RNG k - ε model are in very close with Dittus–Boelter equation results. It is therefore for present CFD investigation, RNG k - ε model was applied to simulating heat exchange and fluid flow of nanofluid flowing through square mini channel.

5 Results and Discussion

5.1 Heat and Fluid Flow

Numerical simulations are conducted to generate the Nu_{ave} and f_{ave} for Al_2O_3 – H_2O nanofluids flow through protrusion obstacle square channel of different e_p/d_p , while the flow Re_n is varied from 4000 to 18,000. To examine the effect of system and operating parameters on Nu_{ave} and f_{ave} , plots are discussed for different roughness configurations.

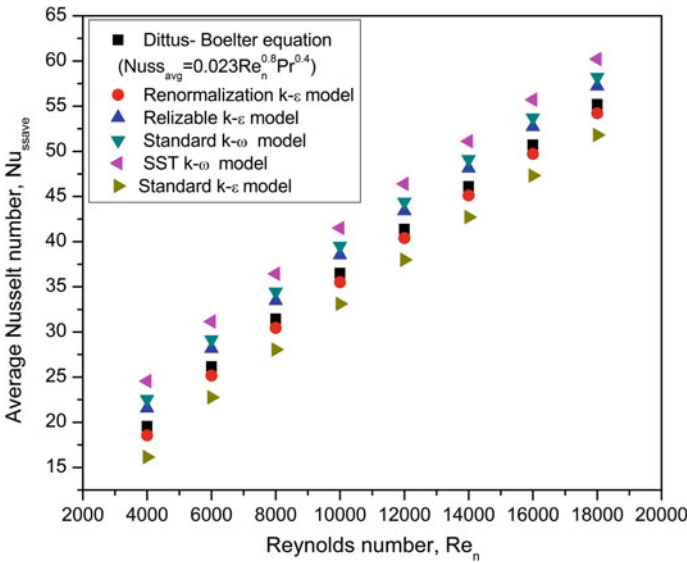


Fig. 3 Comparison between average Nusselt number for various CFD models and Dittus–Boelter equation

Figure 4a displays the variation of Nu_{ave} with Re_n for the various values of e_p/d_p for fixed parameters $X_s/d_p = 1.8$ and $Y_s/d_p = 1.8$. It is observed that Nu_{ave} rises with rise in e_p/d_p for all value of Re_n due to increased flow stream which causes more turbulence, thereby resulting in a rise in Nu_{ave} . The highest Nu_{ave} is received at e_p/d_p of 1.0. Figure 4b displays the variation of Nu_{ave} with respect to e_p/d_p for Al_2O_3 – H_2O nanofluids flow through protrusion obstacle square channel at distinct selected Re_n . It can be observed that highest Nu_{ave} is received at e_p/d_p of 1.0 for all value of Re_n .

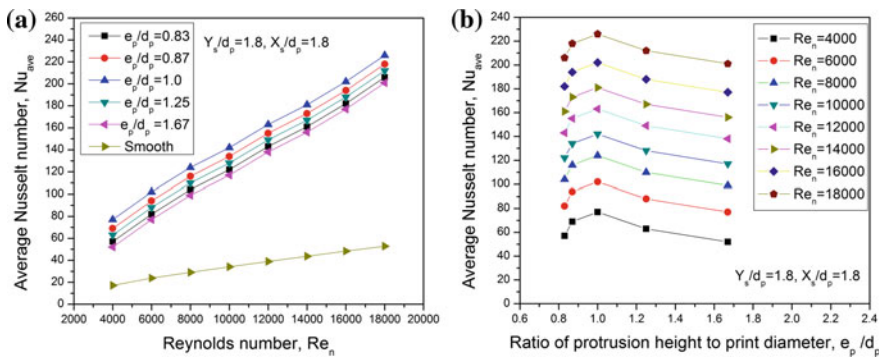


Fig. 4 a Variation of Nu_{ave} with Re_n at different e_p/d_p b Variation of Nu_{ave} with e_p/d_p at different Re_n

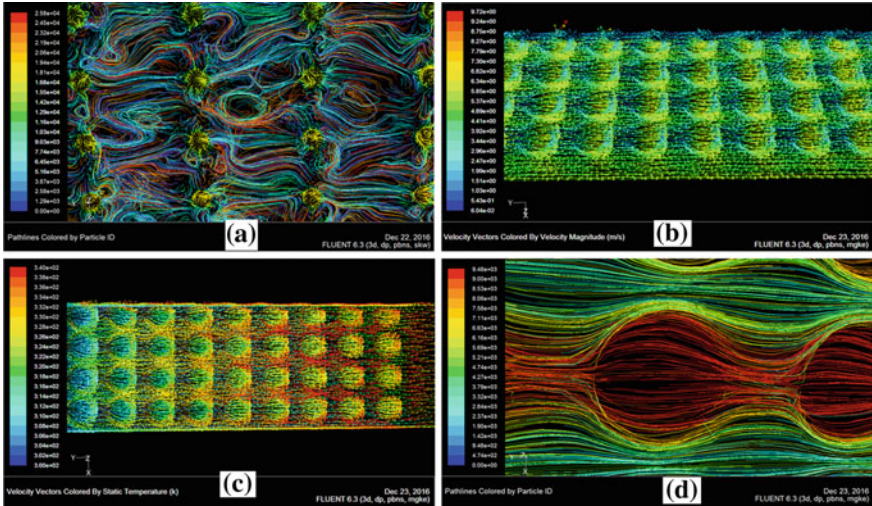


Fig. 5 Flow pattern in protrusion obstacles square channel **a** Velocity pathlines, **b** velocity magnitude, **c** velocity vector coloured by static temperature, **d** temperature pathlines

The outcomes of f_{ave} have been introduced as capacity of Re_n for various estimations e_p/d_p in Fig. 6a, for fixed values of blockage parameters, such as $X_s/d_p = 1.8$ and $Y_s/d_p = 1.8$. The values of f_{ave} for protrusion blockage are greater as compared to without protrusion blockage for the given Re_n , due to the presence of $Al_2O_3-H_2O$ nanofluids flow obstacles which is inattentive in case of without protrusion obstacles square channel. It has been observed from this plot that for a given e_p/d_p data f_{ave} reduces with rise in Re_n . The highest f_{ave} is received at e_p/d_p of 1.0. (Figure 5)

Figure 6b displays the deviation of f_{ave} with respect to e_p/d_p for $Al_2O_3-H_2O$ flow through protrusion obstacle square channel at distinct selected Re_n . It can be observed that highest f_{ave} is received at e_p/d_p of 1.0 for all value of Re_n . It is due to the fact that as e_p/d_p of 1.0 protrusion extends more and more into the core stream resulting in rise in turbulence level as well as the f_{ave} .

5.2 Thermal Hydraulic Performance

The numerical study of the protrusion obstacle square channel shows that e_p/d_p has a marked influence on Nu_{ave} and f_{ave} of the $Al_2O_3-H_2O$ nanofluids flow protrusion obstacles square channel. As implied from the above discussion, the protrusion roughness outcomes in rise in Nu_{ave} with corresponding increase in f_{ave} . A thermohydraulic performance parameter based on equal pumping power (η_p) define by various investigators consider both the heat transfer and pressure drop enhancement [15].

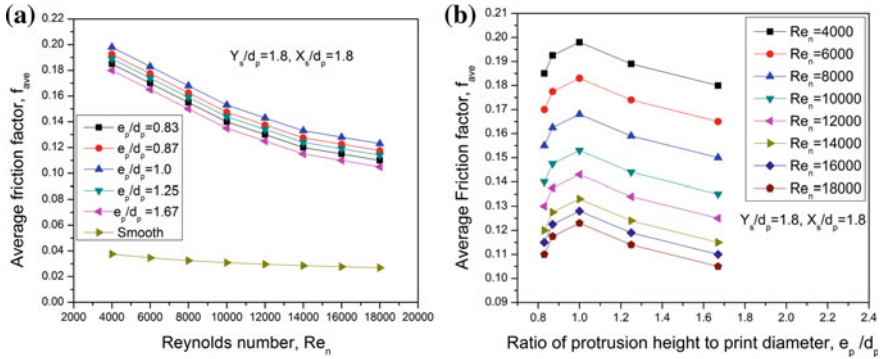


Fig. 6 a Variation of f_{ave} with Re_n at different e_p/d_p , b variation of f_{ave} with e_p/d_p at different Re_n

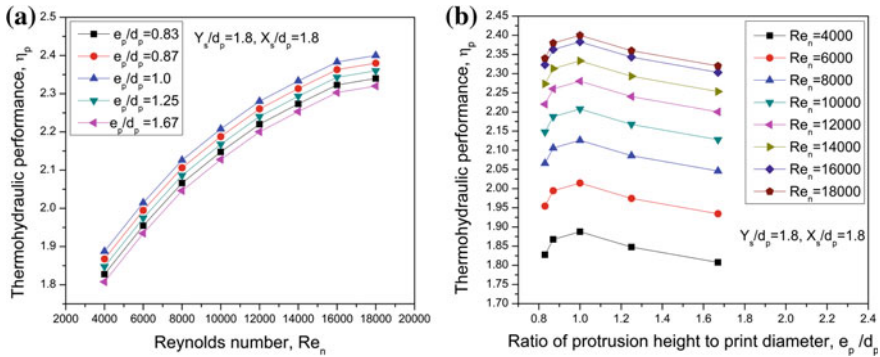


Fig. 7 a Variation of η_p with Re_n at different e_p/d_p , b variation of η_p with e_p/d_p at different Re_n

$$\eta_p = (Nu_{ave}/Nu_{ssave})/(f_{ave}/f_{ssave})^{0.33} \tag{12}$$

The effect of Re_n on this parameter η_p for various values of e_p/d_p is shown in Fig. 7a. It is highest for $e_p/d_p = 1.0$, thereby indicating that it is advantageous to use protrusion obstacles with $e_p/d_p = 1.0$, as compare to other value of e_p/d_p . The highest value of thermal hydraulic parameter obtained is 2.39 as clearly observed in Fig. 7b.

6 Conclusion

Numerical analysis of forced convection heat transfer through a protrusion obstacles mini square channel with $Al_2O_3-H_2O$ nanofluids having volume fraction of 4%, nanoparticle diameter 30 nm and the flow parameter in the range of

$4000 \leq Re_n \leq 18,000$ has been carried out. According to the obtained results, the conclusions can be drawn as follow:

- In case, protrusion obstacle results in considerable enhancement in Nu_{ave} of Al_2O_3 - H_2O nanofluids flowing in square channel, and this improvement depended on print diameter.
- The RNG $k-\varepsilon$ numerical model has been employed in the present examination as it exhibited decent agreement without protrusion blockage wall square channel. Model RNG $k-\varepsilon$ has been valid for smooth wall square channel, and grid independency test has also been employed to check the change with increase in number of grid cells.
- The best improvement in heat transfer is observed to be 4.35 times higher over smooth wall surface square channel.
- The thermal hydraulic performance parameter is higher for 1.0 ratio of protrusion height to print diameter.

References

1. Maiga, S.E.B., Nguyen, C.T., Galanis, N., Roy, G., Mare, T., Coqueux, M.: Heat transfer enhancement in turbulent tube flow using Al_2O_3 nanoparticle suspension. *Int J Numer Methods Heat Fluid Flow*. 16:275–292 (2006).
2. Veeranna, S., Lakshmi, N.S.: Al_2O_3 -based nanofluids a review. *Nanoscale Res Lett*. 6:456–471 (2011).
3. Saeed, Z.H., Seyyed, H.N., Elham, T., Javad, S.: Numerical investigation of Al_2O_3 -water nanofluid laminar convective heat transfer through triangular ducts. *Nanoscale Res Lett*. 6:179–188 (2011).
4. Lee, S., Choi, S.U.S.: Application of metallic nanoparticle suspensions in advanced cooling systems. *Proceeding of International Mechanical Engineering Congress and Exposition Atlanta, USA; 1996*.
5. Xuan, Y., Li, Q.: Investigation on convective heat transfer and flow features of nanofluids. *J Heat Transf*. 125:151–155 (2003).
6. Santra, A.K., Sen, S., Chakraborty N.: Study of heat transfer due to laminar flow of copper water nanofluid through two isothermally heated parallel plates. *Int J Therm Sci*. 48:391–400 (2009).
7. Pak. B.C., Cho, Y.: Hydrodynamic and heat transfer study of dispersed fluids with submicron metallic oxide particles. *Experimental Heat Transfer*. 11(2), 151–70 (1998).
8. Xuan, Y., Li, Q.: Flow and heat transfer performances of nanofluids inside small hydraulic diameter flat tube. *Journal of Engineering Thermophysics*. 25(2), 305–17 (2004).
9. Li, Q., Xuan, Y.: Convective heat transfer and flow characteristics of Cu-water nanofluids. *Technology Science*. 45(4), 408–16 (2002).
10. Kumar, S., Kothiyal, A. D., Bisht, M.S., Kumar, A. Numerical analysis of thermal hydraulic performance of Al_2O_3 - H_2O nanofluid flowing through a protrusion obstacles square mini channel. *Case Studies in Thermal Engineering* 9, 108–121 (2017).
11. Manay, E., Sahin, B., Yilmaz, M., Gelis, K.: Thermal performance analysis of nanofluids in microchannel heat sinks, *World Academy of Science, Eng. Technol*. 67 (2012).
12. Fluent Inc., *Fluent 6.3 user's guide*; 2006.
13. Kumar, A. Kim, M.: Solar air-heating system with packed-bed energy-storage systems, *Renewable and Sustainable Energy Reviews*. 72, 215–227 (2017).

14. Maiga S.E.B., Palm S.J., Nguyen C.T., Roy G. and Galanis N. Heat transfer enhancement by using nanofluids in forced convection flows. *International Journal of Heat and Fluid Flow*. 26: 530–546 (2005).
15. Kumar, R. Ranchan, C. Muneesh, S. Kumar. A.: Experimental investigation on overall thermal performance of fluid flow in a rectangular channel with discrete v-pattern baffle, *Thermal Science*. 17, 125–137 (2016).

PI-Based DSTATCOM Controller for Voltage Control in Weak Power Systems

Subhadip Bhattacharya and Benjamin A. Shimray

Abstract In this chapter, we present the problems associated with various types of loading and faults occurring in an interconnected power system. Reliability and quality are the two most important facets of any power delivery system. The basic objective of this chapter is two folds—first, to understand the various types of fault disturbances in a power system and ways to mitigate these problems using DSTATCOM. Power Electronic converters have played a pivotal role in the control of power quality mainly due to their fast action, reliability, and lower cost in comparison to conventional electro-mechanical controllers. To obtain the desired objective, IGBT-based voltage source converter (VSC) operating at high frequencies using sinusoidal pulse width modulation (SPWM) is used. For efficient reduction in harmonic contents, passive LCL filter is used at the point of common connection (PCC). Here, various kinds of faults commonly occurring in a power system are induced, and their impact on power quality is monitored. All the simulation is done using MATLAB Simulink using Sim Power Systems Blockset (PSB) Toolbox.

Keywords DSTATCOM • Voltage source converter (VSC) • Custom power devices (CPD) • DVR • UPQC • LCL filter • PI controller • Sinusoidal pulse width modulation (SPWM)

S. Bhattacharya (✉) · B.A. Shimray
Department of Electrical Engineering, National Institute of Technology Manipur,
Imphal, India
e-mail: subhadip.eee@gmail.com

B.A. Shimray
e-mail: benjaminshimray@gmail.com

1 Introduction

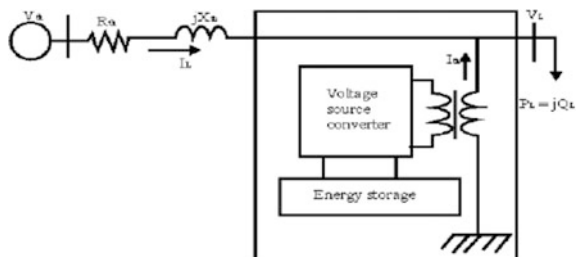
Power quality is absolutely a noteworthy worry in the present time. It has turned into a vital angle in power conveyance with the proliferation of complex power electronic devices whose execution is extremely touchy to the quality of power supply [1]. The electronic devices are prone to sensitivity issues owing mainly due to disturbances, and thus, majority of consumer appliances become less tolerant to power quality problems such as voltage dips due to external loading, voltage swells due to removal of external loads, and harmonic distortions due to switching operations of converters [2]. Power quality variations are classified as either disturbances which are transient or steady state variations. Basically, we have two types of interconnected grid systems—weak or compliant grid and stiff grid based on short circuit ratio (SCR). A compliant or weak grid has more losses and substantially poorer transient load response but has the potential to be more stable from massive disturbances that initiate rapid faults; however, generally we opt for a stronger grid to suppress disturbances effectively with a lower impedance distributed over the grid with online tap changers at source and predictive failure sensors. The quality of power reaching the ultimate customers is regulated by numerous international standards for e.g., IEEE 519 [3] standard which specifies a set of standard boundaries for harmonic elimination and reactive power compensation to be followed for nonlinear loads. To circumvent the challenges associated with poor power quality like poor power factor coupled with harmonic distortions and highly unbalanced supply systems, mechanisms utilizing custom power devices (CPD) have been devised, and since then, majority of the problems have been addressed [1]. Custom power devices are mainly of three types [4] :

- Distribution static compensator (DSTATCOM) [5–8]
- Dynamic voltage restorer (DVR) [9, 10]
- Unified power quality conditioner (UPQC) [9, 10]

All the devices have been explained in a greater detail in [10].

Distribution STATCOM is a shunt-connected device with identical structure as that of a STATCOM Fig. 1.

Fig. 1 Schematic diagram of DSTATCOM [10]



2 Principle of Operation

DSTATCOM as shown in Fig. 2 is inserted in transmission line to suppress voltage variation due to changing load conditions and control reactive power. As mentioned, it is connected in shunt to transmission line with point of common coupling (PCC) in phase with system voltage [5, 10].

The interesting feature of a DSTATCOM is its ability to compensate any load from inductive to capacitive. Figure 3 depicts the vector representation at nominal frequency for capacitive and inductive modes of operation. The bus voltage (V_{bus}) equals the summation of the voltage source converter terminal voltage (V_{VSC}) and voltage across the transformer used at the PCC (V_L) in both capacitive as well as inductive operating regions. Therefore, the DSTATCOM acts like a physical inductor drawing reactive power whenever there is a voltage swell and also as a physical capacitor bank injecting reactive voltage when there is sudden drop in terminal voltage during temporary load outages i.e., during voltage sags [11].

Fig. 2 Schematic diagram of DSTATCOM connected to the distribution network

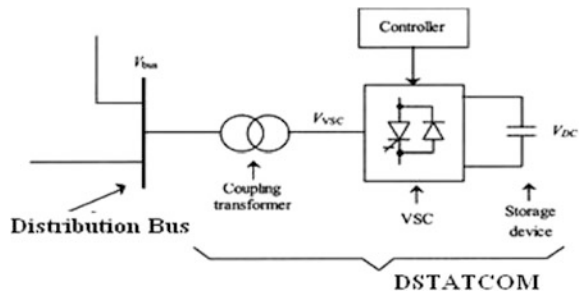
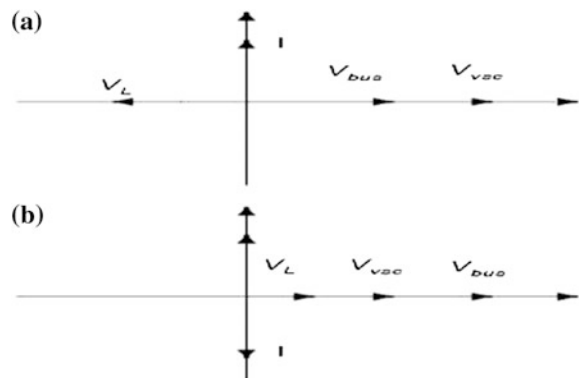


Fig. 3 Vector representation for the working modes of a DSTATCOM, a capacitive mode, b inductive mode



3 Objectives

- Modeling of a Transmission Line.
- Effect on Load Voltage on varying fault conditions like LLLG, LLG, LL, and LG.
- Effect on Load Voltage on Load outages.
- Designing of DSTATCOM for Load voltage compensation.
- Optimal design of the Control circuit for gate pulse firing of DSTATCOM.
- Design of the Filter Circuit (Fig. 4).

4 System Modeling

The system as shown in Fig. 6 consists of a 3-phase balanced source which may be an alternator or turbo generator with a line-line voltage of 220 kV, but in actual case, it is only about 1/10th of this value due to insulation reasons which is later stepped up to nearly 20 times to maximize the power transfer limit of the system. For the ease of schematics, this is obliterated. A 3-phase transformer is connected at the end of the 800-km-long line which is connected in delta/star/star which reduces the transmission level voltage to ordinary distribution level. There are 2 loads

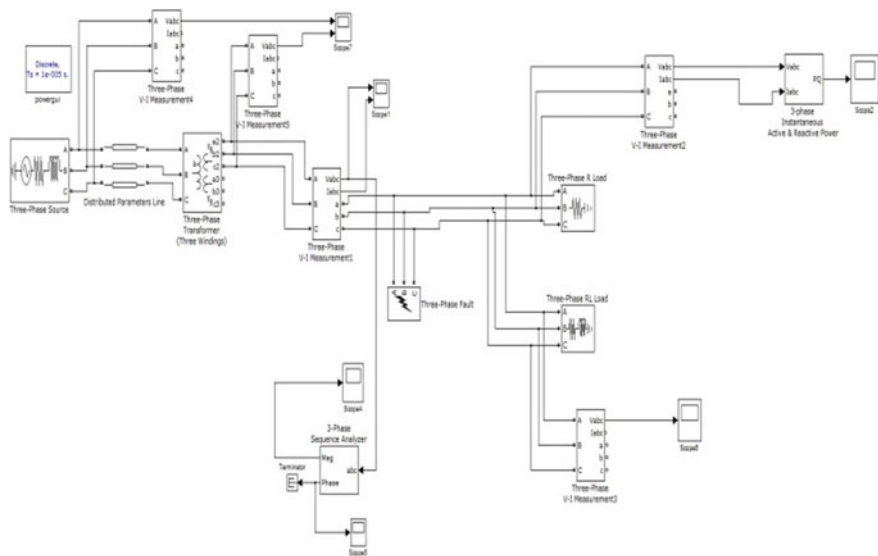


Fig. 4 Simulink model for fault analysis

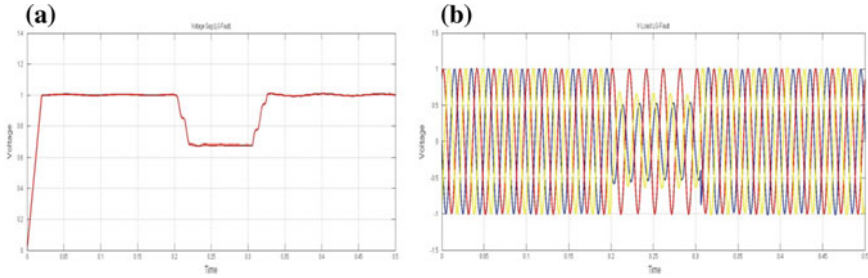


Fig. 5 a Load voltage (rms) pu sag at LG fault, b load voltage 3 Φ sag at LG fault

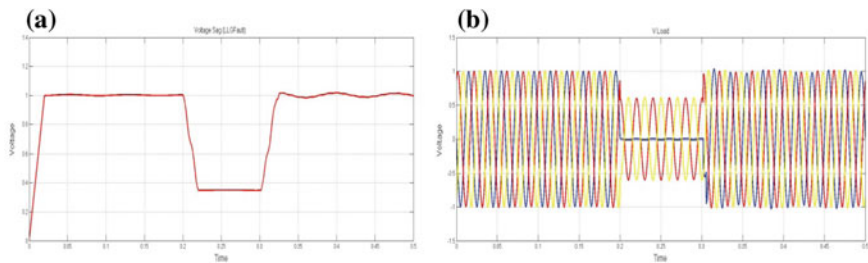


Fig. 6 a Load voltage (rms) pu sag at LLG fault, b load voltage 3 Φ sag at LLG fault

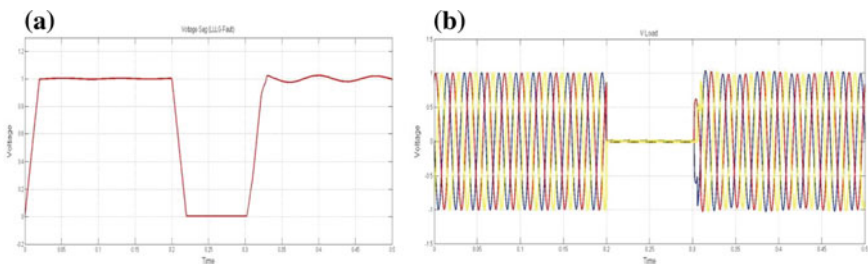


Fig. 7 a Load voltage (rms) pu sag at LLL fault, b load voltage 3 Φ sag at LLL fault

connected at the distribution side—one is a unity power factor load and the other a lagging power factor load. Various kinds of faults include single phase to ground fault, line-line fault, double line to ground fault, and line-line-line-ground fault. The fault severity is given as $LLL G > LLL > LLG > LL > LG$. Voltage sags at various levels of fault are monitored as given in Figs. 5, 6, and 7 [2].

5 Achievements

The following should be achieved after applying compensation due custom power devices (CPD):-

- Interruption of supply should be rare.
- Limitation imposed on the amplitude and time span of over-voltages and under-voltages.
- Harmonic distortion in the supply voltage kept minimum.
- Reduced phase unbalance mostly due to single-phase loads.
- Minimum voltage flicker.
- Frequency of the supply voltage should be within specified limits.

6 System Parameters

S. No	Elements	Values
1	3 Φ balanced source	220 kV, 50 Hz
2	3 Φ transmission line	800 km, 50 Hz
3	3 Φ 3 winding transformer ($\Delta/Y/Y$)	250 kVA, 220/11/11 kV
4	Load 1, load 2	50 kW, 60 kVA
5	Fault resistance	0.4 Ω
6	PI controller	$K_p = 0.5$ $K_i = 50$
7	PWM carrier frequency	450 kHz
8	Vdc, R, C	700 V, 600 Ω , 3 mF

As observed, with the increase in severity of fault, the sag of voltage increases. Now, at last, the most severe fault i.e., three-phase fault occurs when the voltage becomes 0 pu with no transfer of power. The fault resistance in all the cases is 0.4 Ω . The fault persists for 5 cycles from 0.2 to 0.3 s.

Lastly, when a load is removed from the system, the voltage in the line increases which is known as voltage swell. To demonstrate this fact, a circuit breaker (CB) is used Fig. 8 in place of the fault block, and the CB operates at 0.2 s (Fig. 9).

7 Effect After Inserting DSTATCOM

With the introduction of DSTATCOM in the network, the voltage unbalance is considerably reduced as shown in Fig. 11. The DSTATCOM is inserted as shown in Fig. 10 in shunt with the network.

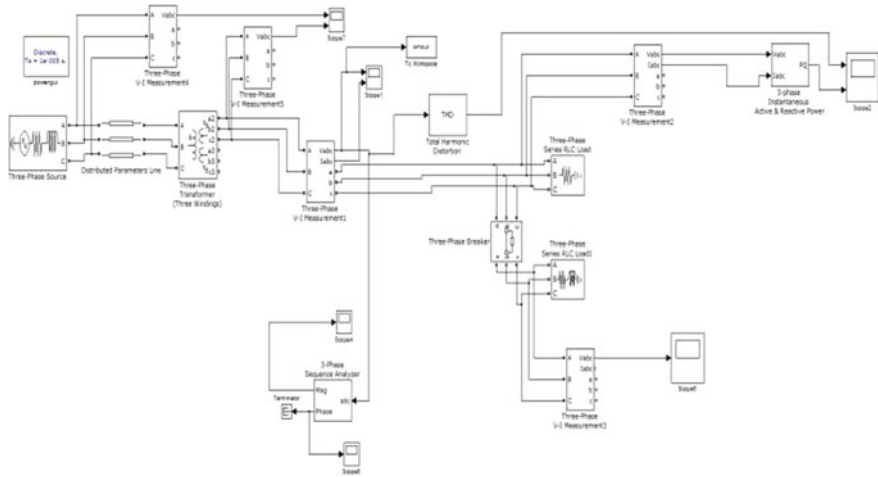


Fig. 8 Simulink model for voltage swell analysis

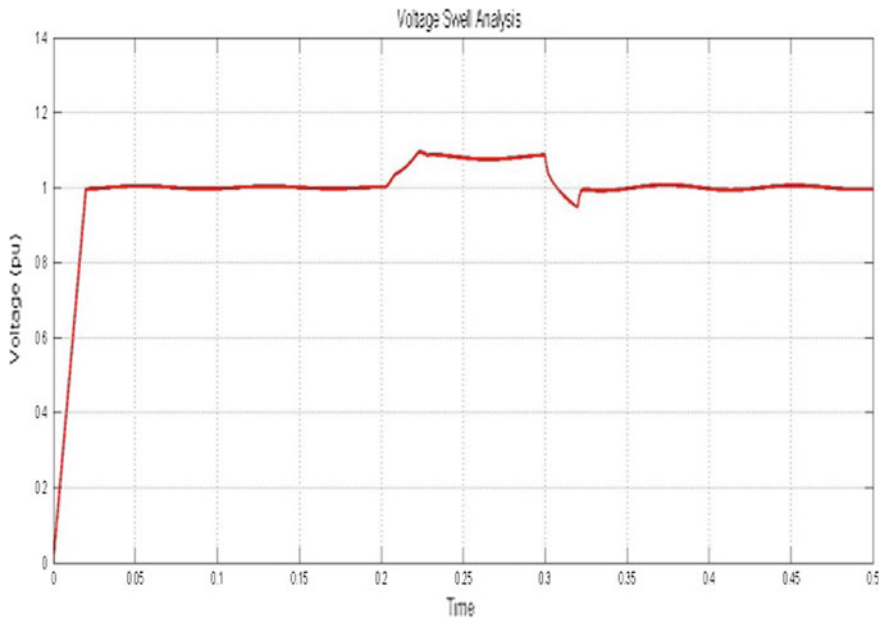


Fig. 9 Load voltage (rms) pu due to voltage swell analysis

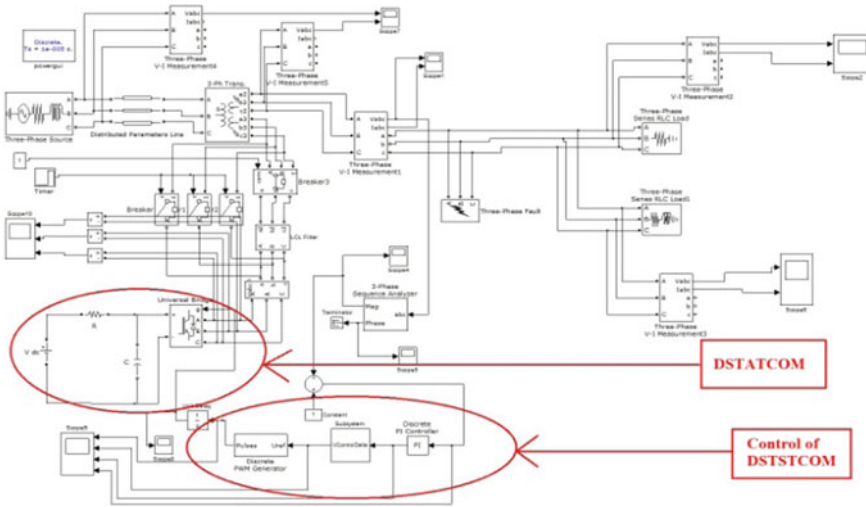


Fig. 10 Introduction of DSTATCOM in the network

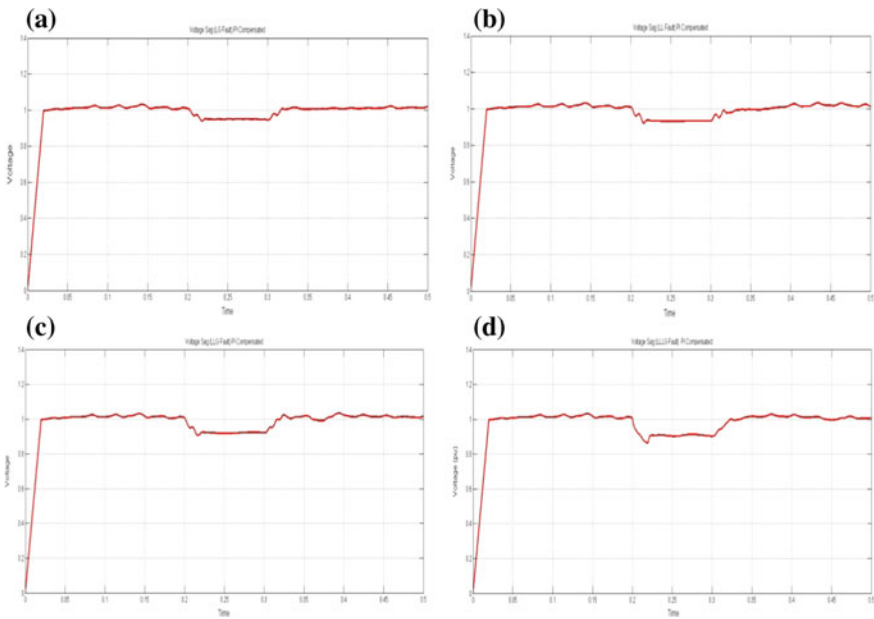


Fig. 11 a Compensation of LG fault, b compensation of LL fault, c compensation of LLG fault, and d compensation of LLLG fault

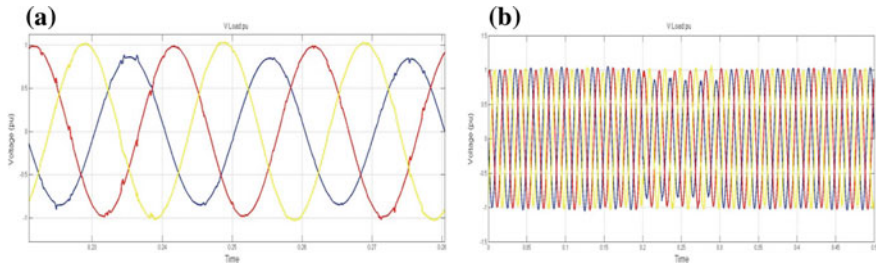


Fig. 12 **a** Spikes in load voltage waveform (zoomed) and **b** compensated load voltage waveform after inserting DSTATCOM

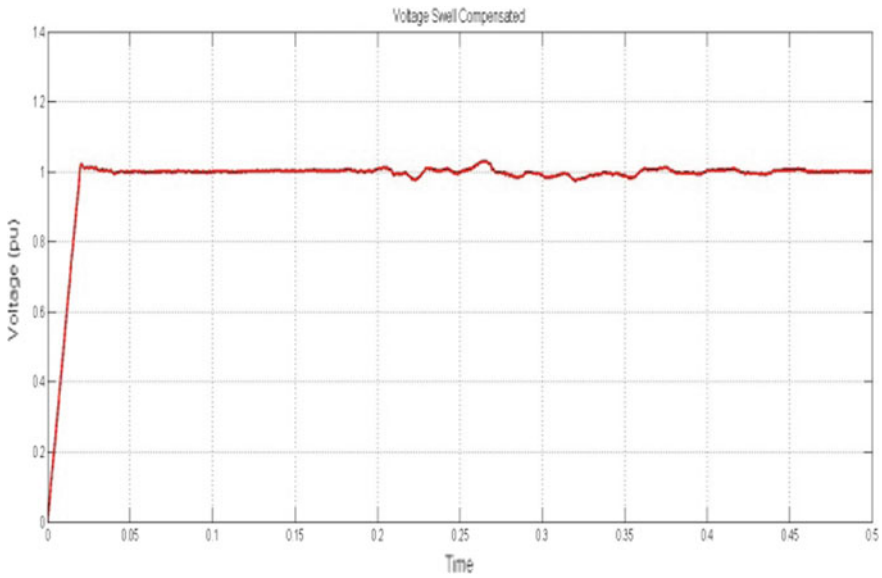


Fig. 13 Load voltage (rms) pu swell after compensation

The observed voltage spikes in the load voltage waveform are due to the switching action of the VSC bridge. It is easily visualized that the load voltage imbalance in the case of fault without DSTATCOM compensation Fig. 5b is eased out in Fig. 12b. Now, for all the other types of faults, the nullification of load voltage imbalance is shown in the following Figs. 11a–d.

The compensation similarly works for voltage swells as well reducing the voltage surge level thus maintaining a flat voltage profile as seen Fig. 13.

8 Control Strategy

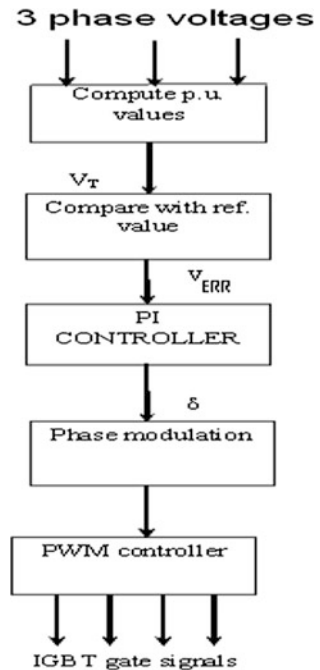
The primary purpose of any control system is that it should be responsive, accurate, higher dynamic range, easy to implement, cost friendly, and at the same time robust. We try to achieve these objectives in the following ways:

- Measuring the system voltage (pu).
- Comparing it with a known preset value.
- Modulating the error response.
- Feeding this error response as firing pulses to the VSC thyristors.

Phase Shift Control method is used in our control strategy. In this method, the required voltage regulation at the Point of Common Coupling is achieved by measuring the rms voltage (pu) at the load point and comparing it with a preset voltage value which is termed as the error response [12].

This error response, obtained by comparing the rms voltage with the fixed value of preset voltage of 1 pu (as all reference values of voltages are taken to be 1 pu), is fed to a PI controller which in turn generates the angle δ which decides firing instances of the valve of the VSC (Masand et al.) [1]. The angle is added to the phase angle of the three-phase balanced supply voltages which are symmetrically spaced by 120° as shown in Fig. 16.

Fig. 14 Control scheme for firing angle control of DSTATCOM



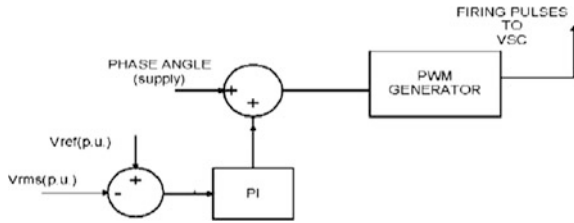


Fig. 15 Block diagram using phase shift control

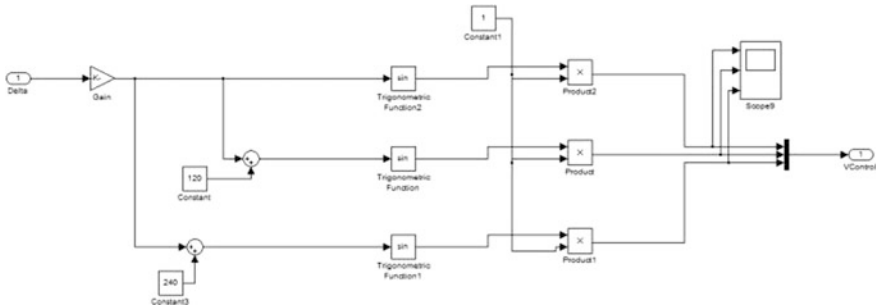


Fig. 16 Block diagram using phase modulation (Simulink® model)

This creates the necessary synchronizing signal to work the PWM Generator block. The DC source voltage of the VSC is held constant at the desired value with the help of capacitors as shown in Fig. 10 (Figs. 14 and 15).

Desired phase—modulation is achieved with the help of angle δ obtained as an output of the PI Controller Fig. 16.

i.e.,

$$\begin{aligned}
 V_A &= K * \sin(\omega t + \delta) \\
 V_B &= K * \sin(\omega t + \delta + 120^\circ) \\
 V_C &= K * \sin(\omega t + \delta - 120^\circ)
 \end{aligned}$$

where $K = \text{Gain} = 1$ in this case (Fig. 17).

9 Filter Design

A LCL filter is frequently used to interconnect an inverter to the utility framework keeping in mind the end goal to filter out the harmonics produced by the inverter thus mitigating the output ripple and smoothening the output load voltage waveform. The LCL filter gives a higher attenuation as well as being economic, given

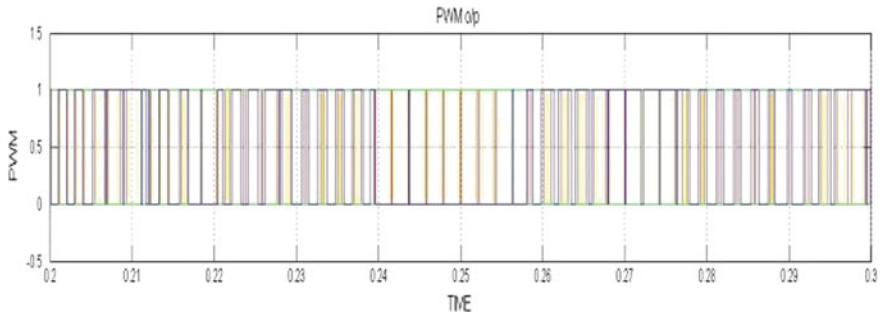


Fig. 17 PWM pulses feeding the thyristor valves of VSC

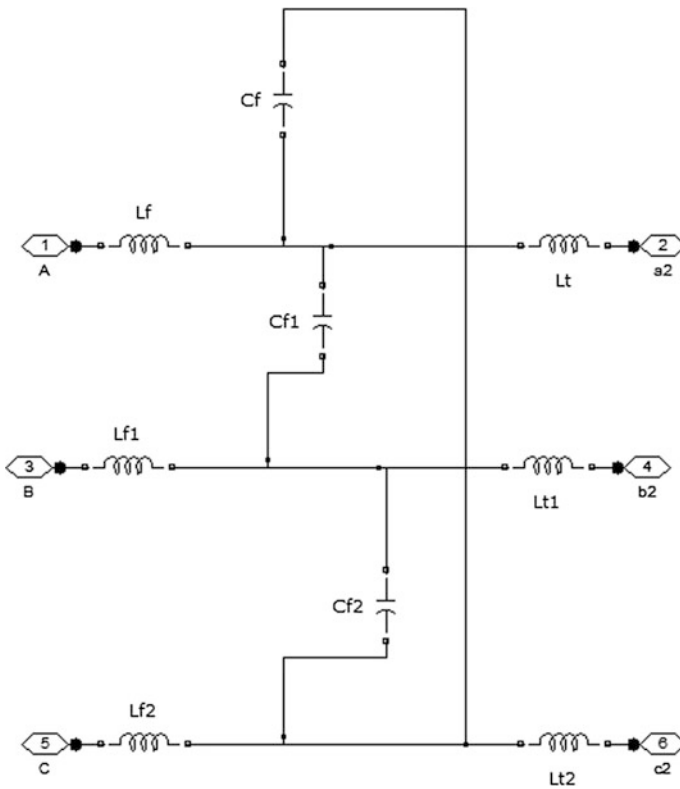


Fig. 18 LCL filter model Simulink® with delta connected capacitor bank

the general weight and size curtailment of the parts. It should be kept in mind while designing inductors that it causes voltage drop across them, and therefore, the grid side inductor should be kept small (Fig. 18).

Filter parameters per phase		
$L1$	Inverter side inductor	1.33 mH
$L2$	Grid side inductor	0.05 mH
C	Δ connected capacitor bank	3 mF

10 Harmonic Reduction

There is a considerable reduction in the load voltage waveform from the proper designing of the filter in the DSTATCOM compensation. Figures 19 and 20 show the improvement in total harmonic distortion (THD) in the load voltage waveform before and after compensation using DSTATCOM. The harmonic distortion can be further improved using other types of controller like fuzzy logic controllers (FLC).

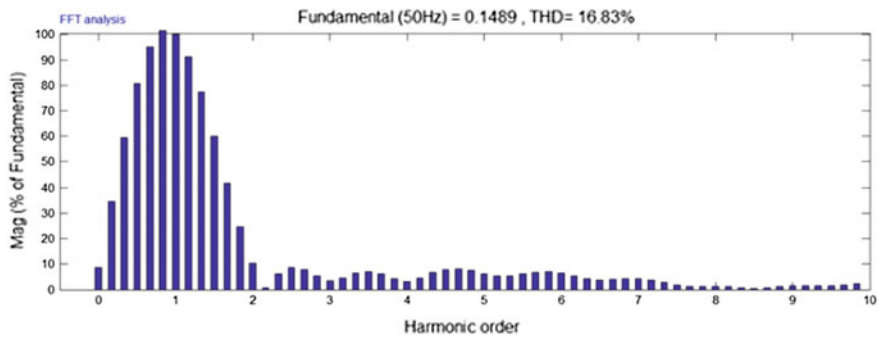


Fig. 19 THD before DSTATCOM = 16.83%

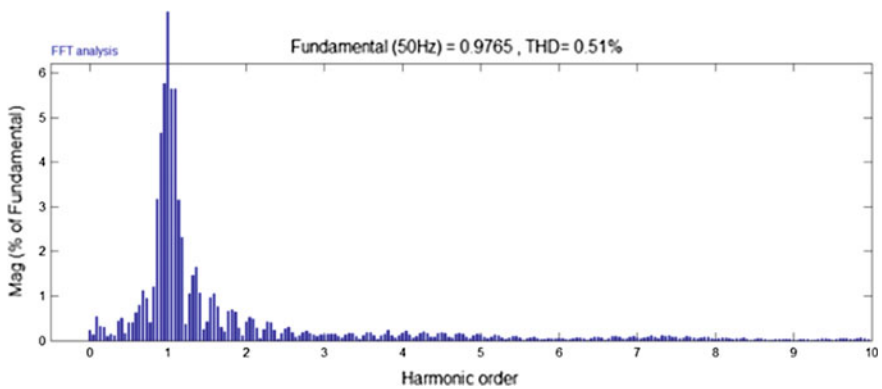


Fig. 20 THD after DSTATCOM compensation = 0.51%

11 Conclusion

In this chapter, a comprehensive analysis of distribution side voltage regulation using Distribution STATCOM is presented. It can be concluded that though DSTATCOM is conceptually similar to a STATCOM in the transmission side, their control is altogether different. The role of the voltage source inverter (VSI) is very important in this respect as the DSTATCOM may frequently need to infuse current in a specific phase free of the other two phases. The desired results of load voltage compensation have been achieved using this PI-based controller. It can be concluded thus that the use of DSTATCOM along with LCL filter effectively increases voltage compensation in the distribution network. There are also other control schemes through which the firing angle of the VSC can be controlled using advanced techniques of adaline-based neural fuzzy logic [13] and using genetic algorithm optimization and sliding mode control [14, 15] which will be done in my future works.

References

1. Gayatri Agnihotri, Deepika Masand. "Control Algorithms for Distribution Static Compensator", 2006 IEEE International Symposium on Industrial Electronics, 07/2006.
2. Parag Nijhawan, Ravinder Singh Bhatia, Dinesh Kumar Jain, "Role of DSTATCOM in a power system network with induction furnace load" IEEE 5th Power India Conference, Dec.19–22, 2012.
3. IEEE-519-1992 "IEEE Recommended Practices and Requirements for Harmonic Control in Electrical Power Systems", 1993.
4. B. Singh, P. Jayaprakash, D. P. Kothari, A. Chandra, and K. Al-Haddad, "Comprehensive study of DSTATCOM configurations", IEEE Trans. Ind. Informatics, vol. 10, no. 2, pp. 854–870, 2014.
5. B. Singh, J Solanki " A Comparison of Control Algorithms for DSTATCOM", IEEE Transactions On Industrial Electronics, vol. 56, no. 7, July 2009.
6. A. Ghosh and G. Ledwich, "Load compensating DSTATCOM in weak AC systems," IEEE Transactions on Power Delivery, Vol. 18, No. 4, ct. 2003 pp. 1302–1309.
7. P. Jayaprakash, B Singh, D.P. Kothari, "Three-Phase 4-Wire DSTATCOM Based on H-Bridge VSC with a Star/Hexagon Transformer for Power Quality Improvement", 2008 IEEE Region 10 Colloquium and the Third International Conference on Industrial and Information Systems, Kharagpur, 2008.
8. Bhim Singh. "Three-Leg Voltage Source Converter Integrated with T-connected Transformer as Three-phase Four-wire Distribution Static Compensator for Power Quality Improvement", Electric Power Components and Systems, 08/2009.
9. Afshin Lashkar Ara and Seyed Ali Nabavi Niaki, "Comparison of The Facts Equipment Operation In Transmission and Distribution Systems", 17th International Conference on Electricity Distribution Barcelona, Session No.2, Paper No.44, pp:12–15 May 2003.
10. Arindam Ghosh and Gerard Ledwich, "Power Quality Enhancement Using Custom Power Devices", Kluwer Academic Publishers, 2002.
11. D. Masand, "Control Algorithms for Distribution Static Compensator", 2009.

12. A. Joshi. "Inverter control using output feedback for power compensating devices", TENCON 2003 Conference on Convergent Technologies for Asia-Pacific Region TENCON-03, 2003.
13. B. Singh, J. Solanki, "Neural Network Based Control of DSTATCOM with Rating Reduction for Three-Phase Four-Wire System", IEEE PEDS 2005.
14. B. Singh, V.C. Sekhar, K.Kant, "Sliding mode control of static shunt compensator", IEEE Int. Conf. on Pow. Elec., Drives and Energy Systems, PEDES, 2014.
15. S. Srivastava, A. Manaktala, K. Sadhwani, M. GUpta, "On Comparing the Performance of Genetic Algorithm Optimized PI and Fractional Order PI Controller for Power Quality Enhancement", IEEE Int. Conf. on Power and Energy Sys. (ICPS), 2011.
16. M. G. Molina, "Control Design and Simulation of DSTATCOM with Energy Storage for Power Quality Improvements", 2006.

Comparative Survey of Swarm Intelligence Optimization Approaches for ANN Optimization

Jaspreet Kaur, Ashima Kalra and Dolly Sharma

Abstract Swarm intelligence (SI) approaches are a group of populace-dependent, nature influenced meta-heuristic approaches that are impressed via collective intelligence of homogeneous insects, birds, etc. These algorithms simulate the behaviour of the group of homogeneous biological entities to get a global ideal solution in optimization problems, where classical optimization algorithms may fail. Examples consist of a flock of birds, colonies of bees, colonies of ants, school of fish, etc. This paper presents a comparative study of different swarm intelligence approaches: particles swarm optimization (PSO) algorithm, intelligent water drop (IWD) approach, artificial bee colony (ABC) algorithm and ant colony optimization (ACO) algorithm for the optimization of single-layer neural networks.

Keywords Swarm intelligence · Particles swarm optimization algorithm
Intelligent water drop approach · Artificial bee colony algorithm
Ant colony optimization approach

1 Introduction

The complications about the use of classical optimization techniques on a wide-ranging engineering problems have contributed to evolution of alternative solutions. Traditional optimization techniques are often trapped in local optima minima in solving problems with many variables, wide explore area, etc. To vanquish these problems, researchers have been suggested SI algorithms for obtaining a global best solution. SI algorithms are population-based meta-heuristic algorithms

J. Kaur (✉) · A. Kalra · D. Sharma
Electronics & Communication Engineering, Chandigarh Engineering College, Landran, India
e-mail: jaspreet.bank@gmail.com

A. Kalra
e-mail: uppal.ashi@gmail.com

D. Sharma
e-mail: dolly.azure@gmail.com

that are inspired by collective intelligent nature of the group of homogenous insects, birds, etc. These algorithms simulate the behaviour of a group of biological entities. The behaviour of biological entities is guided by learning, adaptation and evolution. Artificial neural networks (ANN) are models which are inspired by biological neural networks. To improve the prediction accuracy of ANN, we need to find out optimal values of some ANN parameters like a number of neurons for input, output and hidden layers, weight values and activation function [1]. The literature has been suggested a number of SI algorithms that are best known for ANN optimization over traditional optimization algorithms. After going through the literature survey, we select four SI approaches for scrutiny: particle swarm optimization (PSO) approach, intelligent water drop (IWD) approach, artificial bee colony (ABC) and ant colony optimization (ACO) approach.

The manuscript presents a survey of above-mentioned four SI approaches along with their comparison. This paper is divided into seven sections. Section 2 of this paper presents a related work; Sect. 3 gives an overview of artificial neural network. Section 4 gives an overview and details of different SI optimization approaches. Section 5 describes the ANN training using SI approaches. Section 6 introduces comparison between different swarm optimization algorithms. Section 7 concludes the paper.

2 Related Work

Studies have confirmed that classical approaches have some drawbacks—trapping in local optimum, slow convergence rate [1], etc. SI algorithms have been applied to optimize feed-forward ANN models and proposed to overcome the shortcomings of traditional optimization algorithms. A rich survey of available classical and swarm approaches is found in the literature [2, 3]. A population-based heuristic particle swarm optimization algorithm was introduced in 1995 by Dr. Kennedy and Elbehart [4]. For load forecasting, Bashir and El-Hawary [6] have applied the PSO approach to optimize ANN. A probabilistic SI approach, ant colony optimization, was proposed by Dorigo and Di Caro in 1999. Kumar et al. [5] used ACO to optimize the ANN model for biometric fusion. Another SI algorithm artificial bee colony (ABC) was introduced in 2007 by Karaboga and Basturk for optimization of numerical problems. It was also used by Farshidpour and Keynia [7] for software defect prevention. An intelligent water drop is a nature excited SI optimization approach proposed by Shah-Hosseini in 2007. It may be used for minimizing and maximizing problems, and it was used by Hosseini for travelling salesman's problem [8]. There is a requirement to compare different SI algorithms in their ability to train single-layer feed-forward neural networks for some benchmark functions and also to accomplish the optimal set of parameters to achieve the better performance. Aforementioned inspired us to build an ANN model for minimizing the benchmark functions and optimize it using various SI algorithms.

3 Artificial Neural Network

The simplified model of human nervous system represents artificial neural network. ANN is comprised of many faux neurons to achieve the required functionality. It is a conjecture function that maps inputs onto outputs. Its learning capability and adaptability to data sets makes it pertinent in various fields. The output of ANN system is function of its inputs and weight values. Let X_i input, W_i is weight, thus output (Y) of ANN is given as:

$$Y = \sum_{i=1}^n X_i W_i. \quad (1)$$

ANN is made up of three kinds of layers: input, hidden and output layers. The number of hidden layers may vary.

4 Swarm Intelligence Algorithms

SI algorithms are meta-heuristic algorithms that are inspired by collective intelligent nature of the group of homogenous insects, birds, etc. A brief description of four SI algorithms that are used to obtain a best optimal solution of optimization problems is described in the next subsections.

4.1 Particle Swarm Optimization Algorithm

Overview, Initialization and Swarming Method: PSO was very first optimization algorithm originated by Eberhart and Kennedy. Initialization is first step of PSO algorithm. It is initialized with a random swarm, i.e. population of PSO. Each individual in the swarm has its own current position and velocity. Consider D-dimensional search space and S number of initial particles, i.e. S is swarm size. Let i th is any initial solution in D-dimensional arena. The location of i th solution is personified as a point in given search arena. Let X_i is position vector for initial population which provides current position of each individual and V_i is velocity vector which provides current flying velocity of each individual. The third parameter to be monitored by each i th particle is its P_{best} that represents best position achieved by i th particle in its previous cycle. The parameter to be monitored on the basis of P_{best} taken by all the particles is known as G_{best} , i.e. global best. In the previous position, P_{best} and G_{best} are considered to improve the location and velocity of each individual. The updated velocity of i th particle is provided using the following Eq. 2:

$$V_i^{(k+1)} = wV_i^k + \eta_1 r_1 (P_{\text{best}}^k - X_i^k) + \eta_2 r_2 (G_{\text{best}}^k - X_i^k). \quad (2)$$

The position/locality of i th particle is amended using Eq. 3:

$$X_i^{(k+1)} = X_i^k + V_i^{(k+1)} \quad (3)$$

where w is inertia weight that manages the effect of preceding particle velocity on the next updated velocity, η_1 and η_2 are learning rates, r_1 and r_2 are randomly and uniformly distributed variables within range of $(0,1)$. To avoid the roaming of particles outside the search space, a minimum (V_{\min}) and a maximum (V_{\max}) range of velocity is defined, i.e. $V_{\min} \leq V_i^{(k+1)} \leq V_{\max}$ [9]. The algorithm is repeated until a predefined stopping criterion is fulfilled.

4.2 Intelligent Water Drop Algorithm

Overview, Initialization and Swarming Method: The IWD is a nature excited optimization approach and introduced in 2007 by Shah-Hosseini [10] for travelling salesman problem. It is based on the concept of the functional performance of rivers, actions and replies that appear amid the water drops in rivers. Initialization phase of the IWD optimization algorithm includes problem formulation. First plot the given problem in terms of nodes and edges. Let N is a set of nodes and E is a set of edges. Graph (N, E) represents the problem. Each water drop travels from one node to another node of the graph along with the edges of graph. The solution of IWD completes when it reaches all other nodes and when all the IWDs completed their solution, then first iteration said to be completed. Similarly, that in PSO, after each iteration of the algorithm, the iteration best (I_{best}) result is found and utilized to modify the total iteration best T_{best} solution of the algorithm. The soil on the edges of I_{best} is reduced on the basis of the quality of the solution. During another iteration, the amount of soil on the lanes between nodes remains same as in the first iteration. The IWD algorithm ends when terminating condition is reached, i.e. may be maximum iterations I_{max} or expected T_{best} . IWD algorithm consists of two types of parameter such as constant or static parameters and dynamic parameters [10].

Static Parameters:

1. Number of water drops that represented as nodes ($N_{\text{IWD}} = N$).
2. Group of parameters utilized to manage the velocity improve function, i.e. $a_v = 1$, $b_v = 0.01$ and $c_v = 1$.
3. Group of parameters utilized to manage soil improve function, i.e. $a_s = 1$, $b_s = 0.01$ and $c_s = 1$.
4. Maximum number of iteration (I_{max}) is set by user and remains constant throughout the algorithm and used as terminating condition to atop algorithm.

5. $0 < \rho_n < 1$ and $0 < \rho_{iwd} < 1$ parameters are used to update local soil and global soil, respectively. These are set to $\rho_n = 0.9$ and $\rho_{iwd} = 0.9$.

Dynamic Parameters:

1. The number of visited nodes (N_{visit}) by k th IWD changes during the algorithm.
2. Initial velocity of k th IWD, i.e. V_{init}^k .
3. Initial soil that is loaded on k th IWD (S_{init}).

The values used in this paper are same as used by Hosseini [8]. The probability of choosing visited node j (not in visiting node list) for the k th IWD that is residing on the node i is given in Eq. 4 [11]:

$$P_i^k(j) = \frac{f(\text{soil}(i,j))}{\sum_{\forall l \notin N_{visit}} f(\text{soil}(i,l))}. \quad (4)$$

Velocity of k th IWD updated at every movement of IWD from i node to j node and is given in Eq. 5 [11]:

$$V^k(t+1) = V^k(t) + \frac{a_v}{b_v + c_v * \text{soil}(i,j)}. \quad (5)$$

$V^k(t+1)$ is updated velocity. Soil within the k th water drop (soil^k) and soil on path from node i to node j of k th water drop, i.e. $\text{soil}(i,j)$, are modified with following Eqs. 6 and 7:

$$\text{soil}^k = \text{soil}^k + \Delta\text{soil}(i,j) \quad (6)$$

$$\text{soil}(i,j) = (1 - \rho_n) * \text{soil}(i,j) - \rho_n * \Delta\text{soil}(i,j). \quad (7)$$

After updating the above parameters, find the I_{best} solution from the solutions of all IWD, i.e. T_{iwd} within an iteration using equation:

$$I_{best} = \arg \min / \max_{\forall T_{iwd}} y(T_{iwd}) \quad (8)$$

where $y(T_{iwd})$ quality of solution. Soil that provides the I_{best} solution needed to update, and updated soil is given as [11]:

$$\text{soil}(i,j) = (1 + \rho_{iwd}) * \text{soil}(i,j) - \rho_{iwd} * \text{soil}_{best}^k * 1/q(I_{best}). \quad (9)$$

Now, update the T_{best} , i.e. global best solution using I_{best} solution. And T_{best} is given as:

$$T_{best} = \begin{cases} T_{best} & \text{if } q(T_{best}) > q(I_{best}) \\ I_{best} & \text{otherwise} \end{cases} \quad (10)$$

4.3 Ant Colony Optimization Algorithm

Overview, Initialization and swarming method: ACO initially developed by Dorigo and Di Caro to optimize the discrete problems in 1997 [12]. The fundamental objective of ACO algorithm is to simulate the communal behaviour of ant armies in order to find the food source. With the help of pheromone, ants discover the shortest lane from their locality to the food resource, as they are blind insects. Initialization stage of ACO algorithm starts by generation of ants' population and assigning each ant (λ) as an initial solution. Then, set the initial pheromone train. The algorithm works in two modes such as forward manner and reverse manner. In forward manner, ants form a solution in probabilistic manner using initial pheromone train. While in reverse mode, ants estimate the constructed solution and its quality. These solutions are used to update the pheromone train. Let λ th ant is initially at city x and to go from city x , it chooses x' as a next city. The probability function used to select next shortest path from their current location to food source is given as [13]:

$$P_{xx'}^\lambda(t) = \begin{cases} \frac{[\tau_{xx'}(t)]^{r_1} [1/d_{xx'}]^{r_2}}{\sum_{x \in N_x^\lambda} [\tau_{xx}(t)]^{r_1} [1/d_{xx}]^{r_2}}, & \text{for } x' \in N_x^\lambda \\ 0, & \text{otherwise} \end{cases} \tag{11}$$

where t is time instant, $\tau_{xx'}$ is pheromone intensity, $d_{xx'}$ is distance between the two cities x and x' . r_1 and r_2 are two positive control parameters used to manage pheromone intensity and length of the path. N_x^λ is set of neighbours of city x , i.e. x' . The pheromone intensity is balanced on shortest path using $(1 - p)$, where p is pheromone decay factor and lies in middle of 0 and 1, i.e. $0 < p < 1$ after the completion of journey of each ant. After finding the shortest lane distance, the intensity of pheromone is to be improved using:

$$\tau_{xx'}(t + 1) = (1 - p)\tau_{xx'}(t) + \Delta\tau_{xx'}(t) \tag{12}$$

$\Delta\tau_{xx'}(t)$ is the quantity of pheromone added by ants to initial pheromone train to update it and is given as:

$$\Delta\tau_{xx'}(t) = \sum_{\lambda=1}^k \Delta\tau_{xx'}^\lambda(t) \tag{13}$$

where k is ant population, i.e. total number of ants. For global best journey with distance d_{gb} , the pheromone intensity is given as [14]:

$$\tau_{xx'}(t) = \begin{cases} \frac{1}{d_{gb}}, & \text{if } xx' \in \text{global best journey} \\ 0, & \text{otherwise} \end{cases} \tag{14}$$

4.4 Artificial Bee Colony Optimization Algorithm

Overview, Initialization and swarming method: ABC algorithm is introduced by Karaboga and Basturk in 2007 for numeric optimization problems [14, 15]. It imitates the seeking foraging nature of honeybees. The main job of these bees is to discover the food spot. The best food source location is corresponding to solution of optimization problem, and the quantity of nectar gives the fitness quality. Initialization phase creates a uniformly distributed solution, and each solution is of D dimensions. And D is equal to number of variables of optimization problem. Let F_i ($i = 1, 2, \dots, S_n$) represents location of food sources in D -dimensional search space and S_n is total number of available food source. The location of food source is given as:

$$F_{ij} = f_{\min}^j + \text{rand}(0, 1) * (f_{\max}^j - f_{\min}^j) \quad (15)$$

where f_{\max}^j and f_{\min}^j are upper and lower limits of location vector of j th dimension ($j = 1, 2, \dots, d$). The probability associated with selection of food source is given in Eq. 16:

$$P_s = \frac{\text{fit}(F_i)}{\sum_{i=1}^{S_n} \text{fit}(F_i)} \quad (16)$$

where fit is fitness function of food source, i.e. solution. If fitness function associated with new food source is higher than that of old one, then the position of old source is required to be updated with the new one and is done by using Eq. 17 [9]:

$$F_{ij}^n = F_{ij} + \Psi(F_{ij} - F_{kj}). \quad (17)$$

When non-improvement situation occurs, then scout bees start random search for new food sources.

5 ANN Using Swarm Intelligent Algorithms

Familiarizing with the SI algorithm to optimize the ANN includes some basic steps regardless of which SI Algorithm is taken into account. Since the hidden layer and output layer weights are require to be adjusted, they require to be traced as the vital entity contingent on the SI approach. The problem area holds the amalgamation of all feasible weight values for all layers. This hunt area is of n -dimensions where n is the set of weights that requires to be adjusted. The SI approach is implemented, and target function is depending on the projection accuracy of ANN. The weights are mapped onto the needed object of the approach, like a particle position in PSO. While calculating the fitness in SI, the weights are allocated to the ANN and its prophecy accuracy is obtained. If the fitness is the finest till now, then it will be

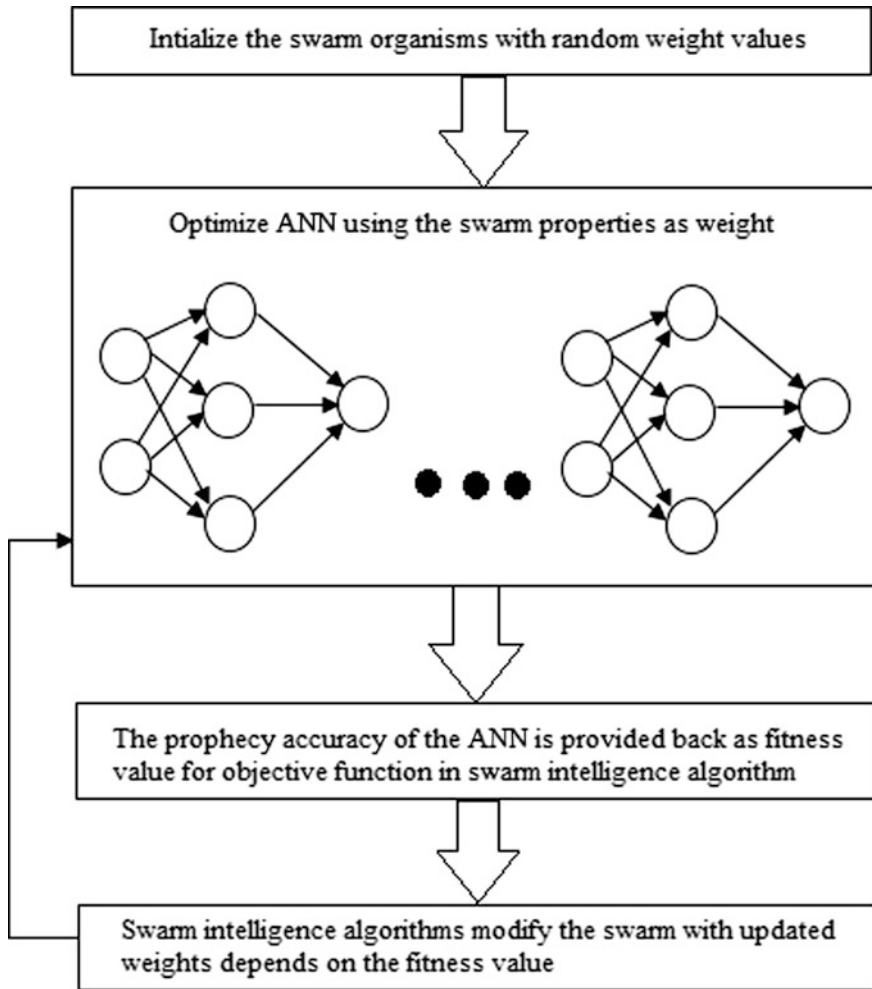


Fig. 1 ANN optimization using swarm intelligence algorithms

recorded as the finest set of weights and thus the finest result till now according to the SI Algorithm. The stages for an ANN optimization using SI algorithms are stated and summarized in Fig. 1.

6 Comparison

This section gives comparative study of different SI algorithms on the basis of their application, basic updating parameters, MSE, accuracy, convergence rate, etc. Each algorithm is suitable for different optimization problems. Table 1 gives the comparative study of different SI algorithms.

Table 1 Comparison of different swarm optimization algorithms

S. No.	Algorithm	Applications	Basic parameters to be updated	Mean square error	Convergence rate
1	Particle swarm optimization algorithm	Travelling salesman problem (TSP) and classification problem	Position and velocity of particles, i.e. birds	Low accurate	Convergence rate is quick, i.e. premature convergence not able to converge in local area
2	Intelligent water drop algorithm	Combinatorial and function optimization problems	Velocity of each IWD, soil within IWD, soil on path from one IWD to another	low	Better convergence
3	Ant colony optimization algorithm	Efficient for TSP	Intensity of pheromone train	low	Slow convergence rate
4	Artificial bee colony optimization algorithm	Classification Problems	Position of food source	Better performance	Slow convergence for local minimum

7 Conclusion

In this paper, four SI algorithms and ANN training with SI algorithms have been discussed. Each algorithm has different application areas, and different parameters are taken into account to reach the optimal solution by each algorithm. It is concluded that one algorithm is not suitable for all optimization problems. Each algorithm has some advantages and disadvantages. These SI algorithms overcome the problem such as slow convergence rate and trapping in local optimum. The comparative study of different optimization algorithms is always helpful to strengthen the performance of neural networks. We will also apply the hybrid of above-mentioned algorithms to deal with the optimization problems to get better results. Hybridization of two swarm algorithms has a fascinating research scope.

Acknowledgements The authors would like to convey special thanks to the Direction of Research and Innovation Centre in CEC-ECE Department of CGC Landran to give the special assistance that made preparation of this paper possible.

References

1. N. Kayarvizhy, S. Kanmani, R. V. Uthariaraj, "ANN Models Optimized using Swarm Intelligence Algorithms", WSEAS Transactions on Computers, vol. 13, pp. 501–519, 2014.
2. A. Kalra, S. Kumar, S.S Waliya. "ANN Training: A Survey of classical and Soft Computing Approaches", International Journal of Control Theory and Applications, Vol. 9, pp. 715–736, Dec-2016.
3. A. Kalra, S. Kumar, S.S Waliya. "ANN Training: A Review of Soft Computing Approaches", International Journal of Electrical & Electronics Engineering, Vol. 2, Spl. Issue 2, pp. 193–205, 2015.
4. J. Kennedy and R. Eberhart, "Particle swarm optimization," Neural Networks, 1995. Proceedings., IEEE International Conference on, Perth, WA, 1995, Vol.4, pp. 1942–1948.
5. A. Kumar, Amioy, M. Hanmandlu, H. Sanghvi, and HM Gupta, "Decision level biometric fusion using Ant Colony Optimization." 17th IEEE International Conference on Image Processing, pp. 3105–3108, Sept-2010.
6. Z. A. Bashir, M. E. El-Hawary, "Applying Wavelets to Short-Term Load Forecasting Using PSO-Based Neural Networks," IEEE Transactions on Power Systems, vol. 24, no. 1, pp. 20–27, Feb. 2009.
7. S. Farshidpour, F. Keynia, "Using Artificial Bee Colony Algorithm for MLP Training on Software Defect Prediction", Oriental journal of Computer Science & Technology, Vol. 5, No. 2, pp. 231–239, Dec-2012.
8. H.S Hosseini, "The intelligent water drops algorithm: a nature-inspired swarm-based optimization algorithm", International Journal of Bio-Inspired Computation, Vol. 1, pp. 71–79, 2009.
9. M. Mahi, O.K. Baykan, H. Kodaz, "A new hybrid method based on Particle Swarm Optimization, Ant Colony Optimization and 3-Opt algorithms for Traveling Salesman Problem", Elsevier Applied soft Computing, Vol. 30, pp. 484–490, Jan. 2015.
10. H.S. Hosseini, "An approach to continuous optimization by Intelligent Water Drop Algorithm", ELSEVIER Procedia-Social and Behavioural Sciences, pp. 224–229, 2011.
11. B.O. Alijla, "A modified Intelligent Water Drop Algorithm and its applications to optimization problems" International Journal of Expert Systems with Applications, Model 5G, pp. 1–15, May 2014.
12. M. Dorigo, G. Di Caro, "Ant colony optimization: a new meta-heuristic," Proceedings of the 1999 Congress on Evolutionary Computation-CEC99, Washington, DC, 1999, Vol. 2, pp. 1477.
13. R. Jovanovic, M. Tuba, "Ant Colony Optimization Algorithm with Pheromone Correction Strategy for the minimum connected dominating Set Problem" Journal of Computer Science and Information Systems, Vol. 10, pp 133–149, 2013.
14. D. Karaboga, B. AKay, "A Comparative study of Artificial Bee Colony Algorithm" ELSEVIER Applied Mathematics and Computation, Vol. 214, pp 108–132, 2009.
15. D.Karaboga, B.Basturk, "A powerful and efficient algorithm for numerical function optimization: artificial bee colony (ABC) algorithm", Journal of Global Optimization, Vol.39 Issue 3, pp.459–471,2007.

Face Recognition Using Various Methods and Applications—Survey

Rajwant Kaur and Dolly Sharma

Abstract Face recognition has many significant applied presentations, like observation and access control. Facial recognition is disturbed through the difficulties of accurate verification face images and conveying them to individuals in a data set. This system is gradually being arranged in an extensive variety of real requests. In this document summary, various methods in all of these classes are provided and several of the difficulties handled by the recognition system are declared. This study prior technique in recognition of face has been a quick fast increasing, stimulating and stimulating field applications in real time. The huge amount of facial recognition procedures has been advanced in the last periods. In face recognition is in holistic advance, a total face object is reserved into an explanation as contribution records into the facial infectious network. Individual of the major instances of general techniques is eigenfaces. Characteristics-based techniques in these approaches basic characteristics such as nose, eye and mouth are initialling of all extract, and their positions are served into a structural classifier.

Keywords Face recognition · Feature-based approach · Holistic methods and applications

1 Introduction

The digital image processing area refers to dispensation 3D pictures from resources of a computer ordinal. A 3D image is collected of a limited quantity of basics, every of which has a certain position and importance. The elements are called elemental imagery, image essentials, pals and pixels. The image pixel is the period used most

R. Kaur (✉) · D. Sharma

Department of Computer Science, Chandigarh Group of Colleges, Landran,
Mohali, Punjab, India
e-mail: rimmysaini13@gmail.com

D. Sharma

e-mail: dolly.azure@gmail.com

© Springer Nature Singapore Pte Ltd. 2018

R. Singh et al. (eds.), *Intelligent Communication, Control and Devices*,
Advances in Intelligent Systems and Computing 624,
https://doi.org/10.1007/978-981-10-5903-2_33

315

widely to denote the elements of a digital double [1]. An idea is the main progressive of our intellects, so it is not amazing that pictures production the individual most significant role in humanoid awareness. Although, the human different, who are inadequate to the visual band of the electromagnetic spectrum, imaging apparatus protection almost the complete electromagnetic area, extending from gamma to radio waves. They could function on pictures produced by source that commoners are not familiar to associate with imagery. This comprises ultrasound, electron microscopy, and computer-produced pictures. The digital image dispensation encompasses a worldwide and several areas of application.

Automated techniques biometrics of identifying a user depends upon physiological or behavioural features [2]. The authentication includes verification of person by characteristic build features, marks or a combination of additional physical standards, such as eye colour, height and face. The current characteristics are facial verification, handwriting, handgeometry, fingerprints, iris, finger vein, voice and retinal scan. The biometric authentication technique is nowadays attractive basis of worldwide set of huge enhanced empathy and confidential authentication. Level of confidential opening and operation trick rises; the requirement for better identification and personal authentication tools is an attractive apparent. Current actions had led to growth attention insecure that would make authenticate into popular use. The field of common use comprises Internet transactions, workstation and system access, receiver connections and in portable and sightseeing. Various kinds of biometrics: Particulars are long standing and others are newer technology. The most familiar biometric skills are fingerprinting, iris identification, hand geometry, sign identification, speech obligation, iris verification and face recognition.

Facial identification has developed a very dynamic exploration field in current years, primarily determined by the situation, extensive requests such as in community have, humanoid mainframe communication, and economic retreat [3]. The binary main face recognition jobs are identification and authentication. In the verification task, a duplicate of an unidentified feature is similar to the Galleria of recognized people. In identification, the job is to accept or repudiate the uniqueness requested by an individual. Consequently, assumed binary facial imageries, the area is choosing whether the binary imageries are of the similar distinct or never. The technique discussed in this paper discourses the documentation job. Facial recognition below well-known gaining situation is created established and offers high verification rates even once a huge number of focuses is in the Galleria. Though, once this job is achieved below uninhibited situations such as unrelated illumination and verified in facial impressions, accurate values significant reduction. Facial presences might verify when attainment situations are unrestrained, creation the recognition problematic though. For illustration, there could be some exciting radiances, terms and out of attention images. Outstanding for the high size of accurate porticoes, not only the correctness but also the scalability of a facial ID network requires to be measured. The central scalability problems are subsequent. First, the numeral of focus in the galleria can be relatively huge; hence, mutual

exploration methods such as instinctive force closest nearest working to contest investigation expressions do not rule well [4].

2 Related Work

Bhattacharya [5] described as, recommend a new method of captivating the strength of the SIFT process and removes the underlying weakness to develop SIFT equivalent in phase difference. This was completed by raising the size of the examine database to an assured degree of receipt. Our offer to pick up SIFT equivalent and rise up by a process to discover the position of a picture. Stress verified our procedure against several pictures and gets constantly good results for both flat and vertical differences in position.

Narang and Singh [6] features appreciation from picture and audio–visual was a prevalent topic in biometrics study. It was lots of significant useful applications, similar close watch and access control. It was troubled through the quandary of appropriately classify facial pictures and conveying them to individuals in a database. Suggest an effectual face expression technique based on SIFT technique for characteristics extraction and by Liebenberg–Marquardt BPNN for the cataloguing. The future technique, we allocate the extracted structures of the expression imageries as contribution routed to our NN in its place of by impartial the rare information as the contribution. The trial completed on the Yale face database, display that the makeover pictures can be familiar by the future expression verification technique capably. Likewise, the usual facial recognition procedures are associated with the planned process to express its efficacy.

Arun et al. [7] discussed the Internet-based safety soft robot was model; using soft is calculating examples for trouble solving and decision making in composite and ill prearranged condition. Soft robot displays the workplace through multimedia plans and instruments using the Internet request database. The prototype has sensual sub-systems such as invader recognition, which perceives attackers, capture picture and sends to the server, and a trouble escaping element to perceive the matters in the pathway of the movable electric automation. These various structures with mixture soft calculating methods proceed the established forgiving automation from the obtainable development, prove that the streaming skill established and move towards importantly improves the receptivity of robot teleportation.

3 Methods of Face Recognition

For the analytic methods, spaces and angles between feature opinions on the face, numbers of facial features or limited features, e.g. intensity standards extracted from facial features and components commonly applied to face recognition [8]. The main benefit of analytic methods is to permit a flexible distortion at the key feature points

so that pose variations can be compensate. In both templates and geometrical feature-based logical methods are implemented and compared. For pattern-based method, facial regions are matched through templates of eyes, nose and mouth individually, and the similarity scores of every facial feature are essentially added into an overall mark for face recognition. For geometrical feature-based techniques, eyes, mouth and nose facial features are initially detected (Fig. 1).

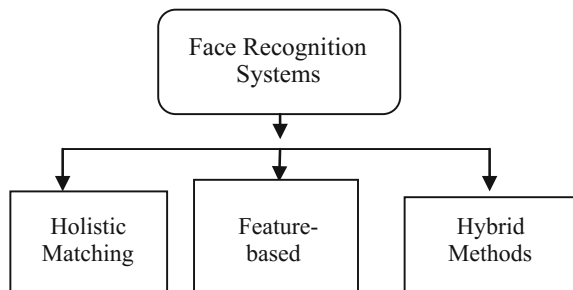
The spaces between significant points wherever charity to identified faces, e.g. size the detachment between the iris or additional significant opinions or calculating dissimilar viewpoints of facial machinery. Nevertheless, then again, it is essential that the face credit structures are completely routine. The face acknowledgement is such a stimulating yet inspiring unruly that it has involved researchers who need dissimilar conditions: sensibility, strategy gratitude, neural systems, computer vision and computer illustrations [9].

3.1 Complete Method

In complete advance, the total expression section is occupied into version as participation data into the appearance infectious structure. One of the finest occasions of all-inclusive approaches is eigenfaces, principal component analysis, line discriminated analysis and independent component examination, etc.

Formerly, the facial attendances are removed. The facial acknowledgement method is anew recognized into binary parts: face mask metrics and eigenfaces. Face mask metrics technology depends on the measurement of the detailed face mask structures. eigenfaces facial recognition process is grounded on classifying faces, allowing to the gradation of appropriate by a secure set of 150 master’s eigenfaces. These methods have alike forces and approaches that are cast-off in generating a representation; the only modification is that double treating is unconscious and grounded on an actual image. Each expression is allocated a grade of fit to every of the 150 principal eigenfaces; only the 40 pattern eigenfaces through the maximum degree of faith are essential to recreate the face through the throughput of 99 age %. Refining the processes for expression location, the existing software often does not discover the expression at all or discoveries “an expression”

Fig. 1 Types of techniques



at an improper place. These sign kinds the outcomes inferior. Improved outcomes can be completed if the worker is capable to express the structure precisely, wherever the irises are located [10] (Fig. 2).

3.2 Feature-Based Method

In these approaches, limited structures such as retina, nose and entrance are first of all extract and their positions and resident figures are fed into an essential classifier. A large face up to feature representation out approaches is featuring “installation”, after the structure tries to rescue structures that are imperceptible due to very big variation, e.g. head pose once we are relating a forward picture through a contour picture. Distinguish amongst the 3 different extraction techniques:

- generic techniques based on ends, lines and arcs [11],
- feature pattern-based techniques,
- structural similar techniques that take into inspection geometrical limitations on the features.

3.3 Mixture Methods

Mixture face appreciation structures are used as a group of together rounded and article extraction techniques. Commonly, 3D pictures are cast-off in mixture

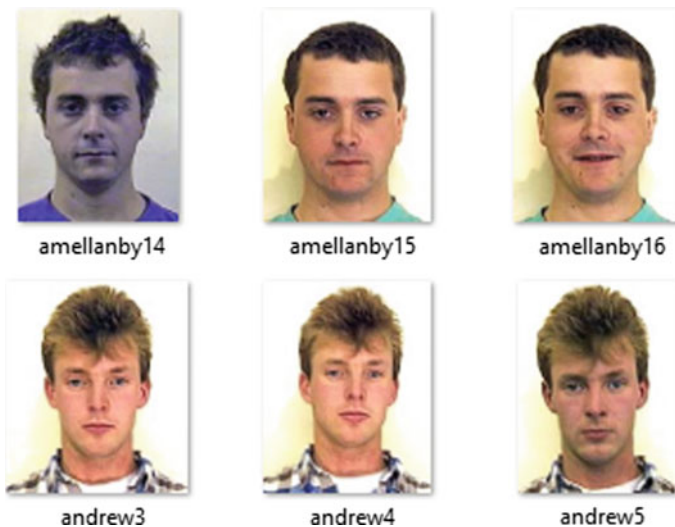


Fig. 2 Data set (face recognition) [http://pics.stir.ac.uk/2D_face_sets.htm]

techniques. The picture of a being's face is wedged in three-dimensional, permitting the structure to communicate the arcs of the appreciation openings, for illustration, or the shapes of the jawl or brow. Smooth a face in profile would serve, since the system uses complexity, and a partnership of extent, which gives it enough information to build a full face. The three-dimensional system frequently profits thus: uncovering, place, dimension, symbol and corresponding.

- **Discovery**—capture a face any a perusing a picture or picture a person's face in an actual interval.
- **Place**—formative the position, size and viewpoint of the bean.
- **Dimension**—transmission capacity to every arc of the expression to brand a pattern with detailed attention on the external of the retina, the confidential of the iris and the angle of the beak.
- **Symbol**—convert the pattern into a cipher, a geometric picture of the expression.
- **Corresponding**—compare the established data through expressions in the obtainable database.

4 Applications of Face Recognition

The presentations of biometrics could be separated into the subsequent three main classes:

4.1 *Commercial*

Commercial applications, i.e. computer system login, automated statistics security, e-commerce, Internet admittance, ATM, recognition card, corporeal access control, cellular phone, PDA, medical files management, detachment knowledge, etc.

4.2 *Government*

Government requests, i.e. general ID card, accurate facility, teamster's license, communal security, well-being payment, boundary control, permit control, etc.

4.3 Forensic

Forensic applications that are carcass ID, illegal investigation, extremist ID, paternity, determination, misplaced children, etc. [11].

This system is also beneficial in human computer communication, simulated authenticity, DB recovery, programming language, computer, entertaining, information safety example Windows, medical files, net banking, Biometric, e.g. Confidentiality ID—IDs, driver authorizations, Automatic identity authenticate—edge panels, Law implementation e.g. audio—visual surveillances, examination, Individual Security—driver observing system, home audio—visual surveillance network.

- **Face Verification:** Face identification networks recognize individual by their facial imageries. Face identification systems create the attendance of an official user relatively than impartial examining whether a legal document (ID) or an important is existence cast-off or whether the client distinguishes the underground individual verification statistics (Pins) or keywords. Subsequent is an illustration. To remove copies in a national constituent recording system since nearby are suitcases anywhere the similar individual was dispensed more than individual ID amount [12]. The face identification system non-stop associates the facial imageries of the constituencies and does not use the PIN number to discriminate single from the others. Once the highest binary matched facials are huge same the enquiry facial copy, physical evaluation is compulsory to the kind certainly they are certainly dissimilar clients so as to remove copies.
- **Entrée Controller:** In numerous of the admission control requests, such as official admittance or processor logs on, the shape/scope of the collection of user that required to be known is somewhat small. The expression images are also fixed underneath normal situations, such as forward faces and indoor lighting. The face authentication system of this presentation can accomplish high recognize rate deprived of much cooperation from the user. The considering is the sample. Face verification knowledge is second hand to display constantly who is in obverse of a computer incurable. It gives the user to authority the lethal deprived of selecting records and sorting out. Once the consumer plants for a predetermined interval time, a screen investor defences up the effort and restricts the hardware devices. When the consumer comes back and verified the display saver disperses and the existing meeting looks as it was left handed. An additional consumer who tries to logon deprived of agreement is deprived of.
- **Secure:** Now, additional than always, safety is a principal apprehension at airfields and for flag office and customers. Airport defines classifications that use face respect, knowledge have been executed at numerous airports around the creation. The succeeding are the two illustrations. In Oct 2001, Fresno Yosemite International (FYI) airport in California planned Visage's face ID field for airfield security determinations. The organization is considered to prepare fly's airport community protection captains when a single consistent the entrance of a known radical suspicious enters the airport protection barrier. Everyone

identified by the scenario would have additional exploratory procedures by communal safety captains. Processor protection has also realized the request of technology of facial recognition. To avert somebody else from modifying records are showing to others when the appropriate distinct greeneries the computer complete for a less time, consumers are always unaffected, checking that the distinct indistinguishable of the processor monitor or at a worker is the similar approved user who logged in [13].

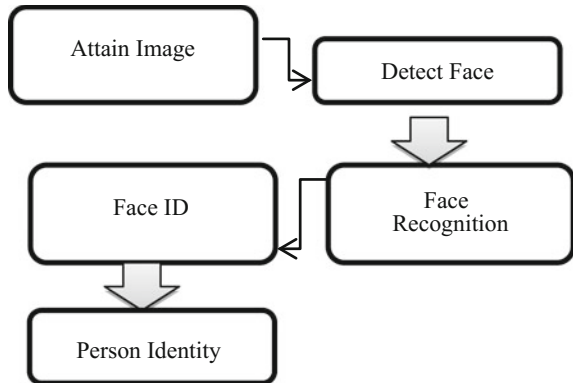
- **Searching Database Images:** It is licensed drivers, advantage recipients, disappeared children, migrants and forces bookings. General identity confirmation: electoral registration, funding, electronic commerce, recognizing newborn's, general IDs, permits, operative IDs.

4.4 Process of Face Recognition

This procedure of Processor-Vision that customer expressions to the purpose to verify a creature or authenticate a being's requested ID. It is included five processes to done their steps [14] (Fig. 3).

- Step 1 attaining the image of a person's face; binary ways to attain images:
1. numerically examination the previous representation;
 2. attain a sentient representation of a focus.
- Step 2 *Find appearance of an expression:* software is charity to determine the expressions in imagery that has been attained.
- Step 3 *Study of makeover copy:* software minor expression conferring to its opinions and valleys; efforts on the internal expanse of the appearance familiar as the "excellent threesome", values are used to generate a look reproduction with their feature points [15].

Fig. 3 Identification procedure



Step 4 *Assessment*: the expression pattern framed by the software is associated with all appearance designs the scheme has deposited in its data sets.

Step 5 *Same/no maintains*: software chooses whether or not some evaluations after step 4 are faster sufficient to announce a conceivable same.

Face appreciation exploits characteristic structures of the appearance adding the higher summaries of the appreciation openings; the expanses close the cheekbones, the edges of the opening and the position of the nose and eyes to achieve identification and confirmation. Maximum fields are impartially resilient to diffident modifies in haircut as they do not adventure extents of the appearance situated near the hairline. When second hand in documentation method, facial gratitude is normally yielding consumer inclines of adjacent contests as opposite to frequent an only conclusive competition.

5 Conclusion

In this appreciation is an interesting issue in the area of copy investigation and computer vision that established an excessive deal of reflection, over the preceding few eons since of its various submissions in numerous fields. Face recognition is a both interesting and significant recognition approach. Study has been showed dynamically in this extent for the prior four interval periods or so, and none the less large growth has been completed, inspiring outcomes have been gotten and existing expression identification systems have prolonged to a certain degree of adulthood when effective below uncomfortable situations; although, they are remote from attaining the model of actuality able to achieve passably in all the numerous conditions that are frequently faced by submissions searching these methods in real world existence.

References

1. Wilhelm, Burger and Mark J. Burge. *Digital image processing: an algorithmic introduction using Java*. (2016), Springer.
2. Fierrez-Aguilar, Julian, Javier Ortega-Garcia, Joaquin Gonzalez-Rodriguez, and Josef Bigun. “Discriminative multimodal biometric authentication based on quality measures.” (2005) *Pattern recognition* 38, no. 5: 777–779.
3. Ahmad, Faizan, Aaima Najam, and Zee Shan Ahmed. “Image-based face detection and recognition:” state of the art”, (2013), *arXiv preprint arXiv:1302.6379*.
4. Lin, Shang-Hung. “An introduction to face recognition technology.” *Informing Science* 3, no. 1, pp: 1–8, (2000).
5. Bhattacharya, Bhaskar, and Minhui Zhu. “Handling pose variation in face recognition using SIFTS.” In *IEEE Applied Imagery Pattern Recognition Workshop (AIPR)*, (2011), pp. 1–4. IEEE.

6. Narang, Gautam, Soumya Singh, and Arjun Narang. "Robust face recognition method based on SIFT features using Levenberg-Marquardt Back propagation neural networks." In *Image and Signal Processing (CISP)*, (2013) 6th International Congress on, IEEE, vol. 2, pp. 1000–1005.
7. Arun, S., G. Harish, K. Salomon, R. Saravanan, K. Kalpana, and J. Jaya. "Neural networks and genetic algorithm based intelligent robot for face recognition and obstacle avoidance." In *International Conference on Current Trends in Engineering and Technology*, (2013).
8. Verma, Seema, and Sonu Agrawal. "A Study on "A Soft Biometric Approach: Face Recognition"." *International Journal* 3, (2013), no. 3.
9. Schwartz, William Robson, Huimin Guo, Jonghyun Choi, and Larry S. Davis. "Face identification using large feature sets." *IEEE Transactions on Image Processing* 21, no. 4 (2012): 2245–2255.
10. Bhatia, Renu. "Biometrics and face recognition techniques." *International Journal of Advanced Research in Computer Science and Software Engineering* 3, (2013), no. 5.
11. Bhele, Sujata G., and Vijay H. Mankar. "A review paper on face recognition techniques." *International Journal of Advanced Research in Computer Engineering & Technology* 1, no. 8, pp: 339–346 (2012):.
12. Geng, Cong, and Xudong Jiang. "Face recognition using sift features." In *Image Processing, (2009) 16th IEEE International Conference on*, pp. 3313–3316. IEEE.
13. Srinivasan, A. "A Framework for Face Recognition Using Adaptive Binning and Adaboost Techniques." *The International Journal of Multimedia & Its Applications* 3, no. 1, (2011) pp.: 76–88.
14. Ahonen, Timo, Abdenour Hadid, and Matti Pietikäinen. "Face recognition with local binary patterns." In *European conference on computer vision*, (2004), pp. 469–481. Springer Berlin Heidelberg.
15. Shan, Caifeng, Shaogang Gong, and Peter W. McOwan. "Facial expression recognition based on local binary patterns: A comprehensive study." *Image and Vision Computing* 27, (2009), no. 6 pp.: 803–816.

A Review of Various Categories of Satellite Image Processing in Remote Sensing

Rupinder Kaur and Dolly Sharma

Abstract Satellite images may be unclear for many reasons. Consequently the important information in the images may not be easily seen. Image enhancement can improve a satellite image that has widespread information, but is not detectable. Image enhancement techniques are used to enhance the quality of the picture to get useful information, and many techniques have been developed to enhance the satellite images. Remote sensing technology has an important role for applications regarding the examination of the Earth. This chapter gives information and techniques useful for satellite image enhancement purposes. The general issues with satellite images are enhancement of gray scale image, noise, artifacts, distortion, resolution, less color information, and high frequency content, among others. Digital image processing is the basic concept distinctly preferred for satellite image processing. Essentially, satellite image processing information could be assembled into three types: (i) restoration, (ii) image rectification, and (iii) extracted data.

Keywords Satellite images · Image processing · Image enhancement
Information extraction · Restoration

1 Introduction

The process of remote sensing is the gathering of information nearby an entity or field and will be in direct relation to it. Satellite sensors are not in straight interaction. The required data are a physical medium to transport the data from the sensor fields. The high rays are cast off as an information importer in remote sensing. Generally remote sensing concerns the attainment of ground information.

R. Kaur (✉) · D. Sharma

Department of Computer Science, Chandigarh Group of Colleges, Landran, Mohali, Punjab,
India

e-mail: rupinder6704@gmail.com

D. Sharma

e-mail: dolly.azure@gmail.com

© Springer Nature Singapore Pte Ltd. 2018

R. Singh et al. (eds.), *Intelligent Communication, Control and Devices*,

Advances in Intelligent Systems and Computing 624,

https://doi.org/10.1007/978-981-10-5903-2_34

The remote sensing system is an imagery expressive procedure of the experimental division frequently called remote sensing imageries [1].

After allowing that the image might be either an image or limitations connected to the image, the process of image processing for which the contribution is a duplicate, such as a picture or film frame of the production, image processing is used in many fields such as remote sensing, medical applications, and the like. There are many types of images including panchromatic, multispectral, hyperspectral, synthetic aperture radar, and so on. Different parts of the electromagnetic spectrum are captured by different earth observation satellites. The satellite images have issues with their resolution, therefore the images may lose their high frequency content and appear blurred. Also, there are numerous problems connected to the satellite images. Therefore improvement of the image is needed to enhance the discernibility of the image to eliminate undesirable noise and artifacts, to improve contrast, and to uncover more details in order that some useful information may be extracted to get an enhanced image. This is an important reason behind image enhancement methods [2].

The main objective of this chapter is to understand the terms related to the enhancement of satellite images. Image enhancement techniques are utilized to make satellite images useful, so they may be readily interpreted by the human eye. The meaning of enhancement is the modification of the presence of an image in such a way that the information restricted in that image is more freely understood visually (Fig. 1).

Satellite images have been used mostly for land cover identification and classification of various features on the land surface taken from satellites. The land-cover and land-use mapping data that are remotely sensed are used in different applications such as environment, forestry hydrology, agriculture, geology, and many more. Therefore, in different kinds of fields images have a different role to perform. Image enhancement is used for making an image more interpretable for a particular kind of application, therefore this technique is very useful for satellite imagery that is generally suitable for all kinds of images [3].



Fig. 1 Image enhancement before and after enhancement

2 Related Work

Sharma et al. [4] introduced a new satellite image resolution that contrasts the method of enhancement which was constructed by the combination of two other methods, the discrete wavelet transform and particular value decomposition. As stated above, satellite images are used in numerous fields such as in meteorology, oceanography, fishing, agriculture, forestry, geology, education, intelligence, and warfare. The significant quality factors in images arise from their determination; here this method decays the image into four occurrence bands by using wavelet transform and the high-frequency subband descriptions from DWT have been interposed. By adding the alteration image of the input image along with this method, estimations of the changed remarkable matrix value from the LL subbands of the histogram secure the image and LL subband in the input image to obtain a brightness-enhanced image.

Kumar et al. [5] threw light on the accessible grouping systems and procedures, clustering being recycled to classes and satellite image in HVS and red-green-blue color difference. A basic satellite image originates with information and attacks. In order to extract regional information proficiently clustering is required and image and clustering-based pixel classification are significantly affected by the cool-space they designate, because image studies in scenarios of the blue, green, and red mechanisms are more demanding as calculated in some terms, capacity, and price in setting the difference of an entity.

Coumar et al. [6] discussed improvement of satellite images using a progressive block-based frequency domain approach. The difference enhancement technique uses the study of pre-eminent cover levels and appropriate stable radiant transformation which achieves frequency domain transformation in optimizing image rate, which is defined as input, by a collection of band-restricted parts by a sample factor, called Max–Min, maximum, minimum, and Min–Maxreplace bands. The intelligence data are controlled in the minimum subband where the contribution image with the pre-eminent glaze level is evaluated. According to the pre-eminent cover level the minimum subband is degenerated into a trilayer. The bendable radiant transformation is managed in the degenerated trilayer of the subband using the function of knee-shift, glaze level dominant, and gamma alteration function. The complete enhanced image is developed by resources on the use of the reverse frequency domain approach.

Santha et al. [7] defined computer vision as a larger and newest field of 3D-image processing with past, on-going, and planned research to complete the target of evaluating an optical intelligence for processors such as humanoid graphic scheme considerations, dispensation, categorizing, changing, and recalling descriptions based on their types. The main focus is on giving a clear route map describing the standing of sympathetic bio-medical, satellite images, and real-time accurate images for computer vision. The objective of the recent research proposes a complete training of methods and algorithms implemented by existing investigators and originating the best hybrid technique to cover all the various image

categories and create processor operations to appreciate the enhanced images as people do with the assistance of machine learning procedures by relating intelligence methods.

3 Several Categories in Satellite Imagery

In this section we have discussed various types of categories of satellite images.

3.1 Register Image [8]

The image register is the complete manner under numerical image processing that analyzes how to consider the same regions of the path image to relate copy taken at dissimilar intervals, angles, and sensors. Secure registered methods are important in the utilization of mosaic satellite images, uncovering the planet's area over interval change or divided image, and monitoring an environment and forecasting climate. There are various image registration techniques that fall into the subsequent eight kinds:

- (1) Imagery dimensionality
- (2) Register creation
- (3) Geometrical transformation
- (4) Interface gradation
- (5) Reduction procedure
- (6) Modalities
- (7) Subject and object.

3.2 Rectification

The geometric correction process is an image that can be denoted on a planar surface, in imitation of other images or maps. This is a process by which the geometry of an image completes the metric plan. It is required when secure fields, direction, and distance dimensions are needed to be made from the imagery. It is considered by converting information from the individual network system into the additional network system using symmetrical transformation [9].

The specific pixels are ground control points in the contribution image by which the production map coordinates are recognized. By using major opinions required to resolve the change equations, at least place solutions might be found that minimize the sum of squares of the exception. Maintenance should be trained when choosing ground-control points as their quantity, eminence, and delivery disturb the consequences of the modification.

3.3 *Enhanced Images*

Enhanced image methods recover the features of an image to make them apparent to a person. This technique is most beneficial because numerous satellite images when studied on a color presentation give insufficient information for image explanation. An extensive variety of methods exists for enhancing image features. Difference gives, concentration slicing, region enhancement, and longitude filtering are the more normally used methods [9]. Image enhancement is attempted after the image is modified for radiometric and geometric distortions. Improved image approaches are applied unconnected to every group in a multispectral image. Digital methods have been originated to be more acceptable than the photographic method for enhancing images for the positive true value and wide variety of digital procedures.

3.3.1 Contrast

This normally refers to the dissimilarity in gray-level values in an image and is a significant feature. It could be distinct as the ratio of the maximum concentration to the lowest concentration over an image. The difference ratio has a robust behavior on the solving influence and perceives the ability of an image. This ratio is superior the more relaxed it is in understanding the image. Satellite images need contrast development.

3.3.2 Enhanced Contrast

This technique expands the brightness values range in an image so that the image can be competently presented in a manner customarily anticipated by the expert. The thickness values in a division are accurately dragged farther separately, that is, protracted over a greater range. The consequence is to grow the graphic contrast between binary fields of different yet identical concentrations. This supports the expert in effortlessly differentiating between fields originally having an unimportant alteration in density.

3.3.3 Stretch Linear Contrast

This is the humblest dissimilarity given the technique. The gray principles in the real image and the adapted imagery survey a linear relative in this algorithm. The concentration amount in the lesser amount of the original histogram is allocated to extremely black and a cost at the high end is assigned to extremely white. The left pixel values are dispersed linearly between these dissipations. The structures or particulars that were unclear on the unique image would be clear on the difference stretched image.

3.3.4 Spatial Filter

Typical of distantly detected images is a limitation called spatial frequency, defined as various variations in the brightness value per unit detachment for any specific part of an image. If there are very few variations in the brightness value in a given field in an image, it is denoted as a low frequency area. Equally, if the brightness value changes intensely over short distances, this is an area of high frequency. Spatial filtering is the technique of separating the image into its important spatial frequencies and selectively changing confident spatial occurrences to highlight some image structures. This technique evolves according to the expert's ability to classify parts.

3.4 Classification [10]

The classification image spontaneously types both pixels in an image into land-area groups. Usually, multispectral data are recycled to perform the organizer and the spectral design present within the data for all pixels is used as a statistical beginning for classification. That is, different characteristic types give obvious different groupings of Digital Numbers (DNs) based on their essential spectral reflectance and productions. The classifier factors refer insecurely to a software program with greatly varying designs. Therefore, it is significant that the forecaster appreciates the substitute approaches for image classification.

4 Classification Techniques in Remote Sensing

There are three kinds of image classification techniques in remote sensing:

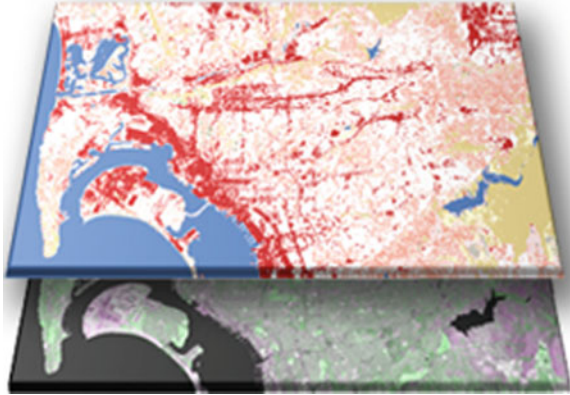
- Unmanaged/unsupervised image classification
- Managed/supervised image classification
- Entity-based image analysis

Pixels are the minimum unit characterized in an image. Image classification uses the reflectance figures for separate pixels. Unmanaged and managed image division methods are the binary major common techniques. However, entity-based organization has been seen as more powerful of late [11].

4.1 Unmanaged Classification

The grouped pixels are based on the reflectance belongings of image pixels. These are the so-called "groups." The user classifies the quantity of groups to

Fig. 2 Unsupervised classification



generate and which groups to use. With this information, the image division forms software product clusters. There are dissimilar image clustering techniques such as K-means clustering.

The manual user recognizes each cluster with programmed land-cover. It is repeatedly the case that numerous collections characterize a single land-cover class. The user combines clusters into a land-cover type. The unmanaged division image classification approach is normally used when no model sites occur (Fig. 2).

4.2 *Managed Classification Rate*

The user chooses preventative models for each land-cover group in the digital image. These model land-cover modules are known as “training sets.” An imagery grouping software uses the training locations to verify the land-cover classes in the complete image. The division of land-cover is based on the name in the exercise set. The 3D image division software determines each class on what it most resembles in the preparation set. The normal managed arrangement. The normal managed arrangement methods are supreme probability and less-distance grouping [12].

Classification Managed Steps:

- Choice training areas
- Produce signature file
- Categorize

4.3 *Entity-Based Image Classification Examination*

Traditional pixel-dependent processing produces square secret pixels. Entity- based image organization is very dissimilar in that it produces entities of diverse scale and shape. This is known as multidetermination subdivision (Fig. 3).

Fig. 3 Object-based classification



Multidetermination subdivision produces the same image of things by assemblage pixels. Entities are evaluated with dissimilar scales in an image similarity. These entities are more expressive than the rational pixel-based subdivision because they can be divided based on consistency, background, and geometry. An entity-based duplicate study allows the use of numerous groups for multiresolution subdivision and organization. Illustration, ultraviolet, promotion, or previous shape files can immediately be recycled to categorize image objects. Numerous layers can be connected to each other. This background comes with the method of neighborhood associations, immediacy, and distance between deposits.

5 Conclusion

In this chapter, we have given a survey of some papers related to satellite image enhancement and the approaches the authors used in their work. The 3D image processing of satellite data could be principally assembled into three types: image rectification and restoration, improvement, and feature extraction. Image refinement is the preprocessing of satellite statistics for geometric and radiometric connections. Improvement is applied to image data in order to display data successfully for succeeding graphic explanation. Feature abstraction is based on digital arrangement and is used for producing a digital thematic plan. These methods help improve the quality of satellite images so that they become more informative and useful in many

applications. This chapter outlines the study of new and better techniques for satellite image improvement. As stated there are a number of applications in which satellite images are used.

References

1. P. Suganya, N. Mohanapriya, B. Kalaavathi, "Satellite image resolution enhancement using multi wavelet transform and comparison of interpolation techniques", *International Journal of Research in Engineering and Technology*, (2014), eISSN: 2319-1163| pISSN: 2321-7308, Volume: 03 Special Issue: 07.
2. Rode, Gauri, and V. K. Shandilya. "A Literature Review of Satellite Image Enhancement Methods." *International Journal of Science and Research* 5 pp: 506–509 (2016).
3. Pandya, Arpita, and Priya R. Swaminarayan. "CLASSIFICATION OF VEGETATION AREA FROM SATELLITE IMAGES USING IMAGE PROCESSING TECHNIQUES." *International Journal of Research in IT, Management and Engineering*, (2015), ISSN 2249-1619, Impact Factor: 4.433, Volume 5, Issue 3 (2015).
4. Sharma, Aditi, and Ajay Khunteta. "Satellite image contrast and resolution enhancement using discrete wavelet transform and singular value decomposition." In *Emerging Trends in Electrical Electronics & Sustainable Energy Systems (IEEE)*, International Conference on, pp. 374–378., (2016).
5. Kumar, Gautam, P. Parth Sarthi, Prabhat Ranjan, and R. Rajesh. "Performance of k-means based satellite image clustering in RGB and HSV color space." In *Recent Trends in Information Technology* (2016), International Conference on, pp. 1–5, 2016.
6. Oudaya Coumar, S., R. Aravindraja, S. Arulambalam, R. Raam Naaraayan, and R. Senthil Prasad. "Contrast enhancement of satellite images using advanced block based DWT technique." In *Recent Trends in Information Technology*, (2016) International Conference on, pp. 1–6, IEEE.
7. Santha, T. "The significance of Real-time, biomedical and satellite Image Processing in understanding the objects & application to Computer Vision." In *Engineering and Technology*, 2016 International Conference on, (IEEE), pp. 661–670.
8. Chandrakala, M., and Mrs R. Amsaveni. "Classification of Remote Sensing Image Areas Using Surf Features and Latent Dirichlet Allocation." *ijarcse* 3, (2013), no. 9.
9. Eastman, J. R. "Introduction to remote sensing and image processing." *Idrisi for Windows User's Guide*. (2001), Cap 3.
10. Sreenivas, B., B. Narasimha Chary, and INDIA KARIMNAGAR. "Processing Of Satellite Image Using Digital Image Processing." In *A world forum on Geospatial*. (2011).
11. Radhadevi, P. V., V. Nagasubramanian, Archana Mahapatra, S. S. Solanki, Krishna Sumanth, and Geeta Varadan. "Potential of high-resolution Indian remote sensing satellite imagery for large scale mapping." In *ISPRS Hannover Workshop, 'High-Resolution Earth Imaging for Geospatial Information'*, June, (2009), pp. 2–5.
12. Dalmiya, C. P., and V. S. Dharun. "A survey of registration techniques in remote sensing images." *Indian Journal of Science and Technology* 8, (2015) Vol no. 26.

RNA: Structure, Prediction, and Visualization Tools

Dolly Sharma, Shailendra Singh, Trilok Chand and Pardeep Kumar

Abstract RNA has been found to be associated with many diseases, especially in humans. To understand the correlation of RNA with disease, an individual needs to understand its structure. As prediction of three-dimensional structure of RNA is complex and costly affair, researchers are focusing on the secondary structure of RNA. RNA secondary structure has been predicted by various algorithms, and various tools have been developed for its automatic prediction. Several components of RNA secondary structure have been acknowledged, namely hairpin loop, stacked pair, bulge loop, internal loop, and junction. The motive of this paper is to explore various RNA structures, techniques prediction of RNA secondary structure, and visualizations tools.

Keywords RNA · RNA secondary structure prediction · Visualization tools

1 Introduction

Bioinformatics is solving molecular biology problems using computer science techniques [1]. Biological problems have been proved to be solved efficiently by application of various algorithms and techniques of information technology. Techniques of information technology include science, statistics, mathematics, and engineering. Various databases are used to stock up, organize, and retrieve biological data. Further,

D. Sharma (✉) · S. Singh · T. Chand
Department of Computer Science, PEC University of Technology, Chandigarh, India
e-mail: dolly.azure@gmail.com

S. Singh
e-mail: shailendrasingh@pec.ac.in

T. Chand
e-mail: trilokchand@pec.ac.in

P. Kumar
School of Computer Science, Lingaya's University, Faridabad, Haryana, India
e-mail: erpardeepkaushik@gmail.com

the biological data is analyzed using various algorithms in techniques like artificial intelligence, soft computing, and simulation which includes neural networks, genetic algorithms, etc. The algorithms are being worked upon by various researchers. The algorithms have strong mathematical foundations supported by discrete mathematics. Some frequently used software technologies in bioinformatics are MATLAB, Java, BioJava, JavaPearl, C#, XML, Perl, C, C++, Python, SQL, CUDA, and spreadsheet applications [2]. This paper has been organized as follows. An overview of RNA and its functions is prearranged in Sect. 1.1. Section 1.2 discusses briefly all the types of RNA. Section 1.3 discusses RNA Secondary Structure and its components. Various methods, techniques, and tools for RNA secondary structure prediction are discussed in Sects. 2.1 and 2.2. Conclusion and Future scope is discussed in Sect. 3.

1.1 RNA

Biologically, living organisms must follow certain rules, regulations, and guidelines such that the living cell is functioning properly. This very information is out carried by RNA which stands for Ribonucleic acid. It is a universal fact that proteins are building blocks of life. Without the above-mentioned information being transferred properly from nucleus to ribosomes, production of accurate protein is impossible. This very fact conveys the importance of RNA. Underproduction, overproduction, or faulty production of protein leads to diseases [3]. The structure of RNA is as follows: RNA is single-stranded molecule that folds upon itself to imitate double helix structure of DNA (Deoxyribonucleic acid). The backbone of RNA contains ribose as sugar with four bases: Adenine, Cytocine, Guanine, and Uracil. Phosphate groups are also attached to ribose. The bases of RNA form pair called base pair in order to form secondary and further tertiary structure. RNA can be synthesized from DNA. DNA (unlike RNA) has double helix structure and stores the genetic code for long duration. As compared to DNA, RNA is more versatile. Apart from having significant role in protein synthesis, RNA carries out biochemical reactions, gene regulation, methylation, etc. Also, RNA does not have replicating capability like DNA. The life period of various types of RNA varies. Some of them have long life, and some get destroyed soon after their creation [3].

1.2 Types of RNA

RNA has been majorly categorized into three categories according to their nature, function, and structure, namely rRNA, tRNA, and mRNA. They play major role in protein assembly process. Apart from these, other types of RNA do exist having significant roles as discussed below.

- (A) Ribosomal RNA (rRNA): One of the RNA components of the ribosome which is necessary for the protein synthesis. Due to critical functions of rRNA, protein synthesis occurs. Ribosome exists in all organisms and helps translate the information in mRNA (messenger RNA) into protein. Ribosome has 60% rRNA approximately [4]. An rRNA structure is represented in Fig. 1.
- (B) Transfer RNA (tRNA): Transfer RNA acts as physical connection between the DNA and RNA sequence of nucleic acids and protein sequence of amino acid. It helps in decoding of mRNA (messenger RNA). tRNA is an important component of protein translation and contains 75–95 nucleotides [5]. A tRNA structure is represented in Fig. 2.
- (C) Messenger RNA (mRNA): mRNA transfers genetic information from DNA to the ribosome and is the biggest family of RNA molecules. mRNA was discovered by two scientist Elliot Volkin and Lazarus Astachan in 1956. DNA is copied into mRNA and then decoded into proteins. One molecule of mRNA is needed to encode the information of one protein, but for bacteria, more than one protein’s information can be encoded into one molecule of mRNA [6]. An mRNA structure is represented in Fig. 3.

Fig. 1 rRNA

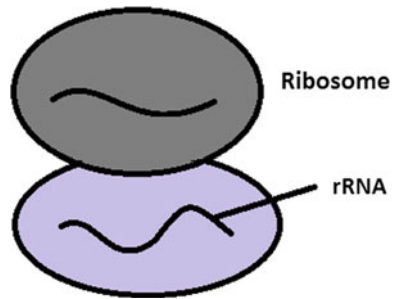


Fig. 2 tRNA

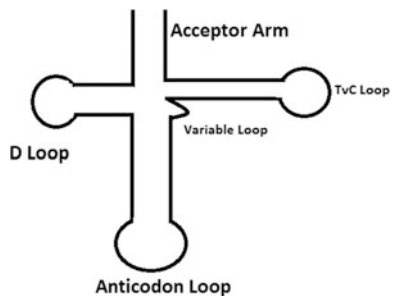
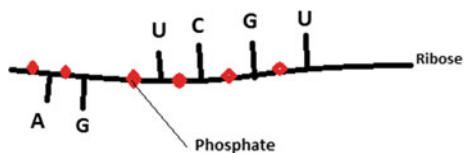


Fig. 3 m-RNA



- (D) Non-coding RNA (ncRNA): These are functional molecule of RNA that does not encode into protein. But still, non-coding RNA contains crucial information and has several functions. One of the functions of ncRNA is to regulate the gene expression at transcription level [7].
- (E) Transfer-messenger RNA (tmRNA): These are the RNA molecules that have similar properties like both tRNA and mRNA. Mostly, bacteria produce single one-piece tmRNA; however, a few permuted tmRNA encode two-piece tmRNA. It works like a quality control system which monitors the protein synthesis [8].
- (F) Small nuclear RNA (snRNA): These are small RNA molecules and are involved in splicing or other reactions of RNA. The approximate length of snRNA is 150 nucleotides. Complexes of snRNA are also known as snRNP which are conserved RNA-protein complexes (small nuclear ribonucleoproteins) generally called as “snurps” [9].
- (G) MicroRNA (miRNA): MicroRNA also comes from family of non-coding RNA. It plays an important role in regulation of gene expression and RNA silencing. These are single-stranded RNA molecules and are very short in length, only 22 nucleotides approximately. Both animals and plants have MicroRNA [10].
- (H) Small interfering RNA (siRNA): Small interfering RNA is also known as silencing RNA or short interfering RNA. siRNA leads to silencing of gene for a short span. siRNA is a synthetic RNA formed from double-stranded RNA molecular sequence of length 20–25 base pairs. siRNAs are used for knock-down of non-protein coding genes [11].
- (I) Small nucleolar RNA (snoRNA): These are a special category of small RNA molecules that signify the chemical changes of other RNAs mainly ribosomal RNA, Transfer RNA, and snoRNA (small nuclear RNA). It is also proposed that these came from evolution in gene duplication of transfer RNA (tRNA) [12].
- (J) Antisense RNA (asRNA): These are single-stranded RNA complementary to messenger RNA. asRNA is sometimes referred to mRNA-interfering complementary (micRNA), but micRNA is not so popular and not adopted widely. asRNA is used for down regulating a gene by inhibiting gene expression process [13].
- (K) Signal recognition particle RNA (SRP RNA): SRP is a RNP (ubiquitous) complex that results secretory proteins and membrane. These are required for co-translational protein targeting. The common family known as Alu came from a gene of 7SL RNA when the central sequence is deleted [14].

1.3 RNA Secondary Structure

RNA structures are of three types: primary, secondary, and tertiary structure. Primary structure is the linear sequence of the bases adenine (A), cytosine (C), guanine (G), and uracil (U). A primary RNA sequence is shown in Fig. 4. The single-stranded RNA primary structure folds upon itself to form helix structure specifically called secondary structure of RNA. The basic unit of structures thus formed is “Base pairs.” Two types of base pairs exist for RNA structures—Watson Crick base pairs and wobble base pairs. Watson Crick base pairs are C-G and A-U. Wobble base pairs are G-U. It is said that Wobble Base pairs are generally less stable than Watson crick base pairs because of the difference in hydrogen bonding. Various substructures of RNA secondary structure are loops, stacked base pairs, junction, knots, etc. [15].

In the real world, RNA molecules exist in tertiary structure inside organisms. Regrettably, it is quite costly and time consuming to predict tertiary structure as the structure is too complex. Moreover, it has been noticed that many of the structural elements present in secondary structure have also been found in secondary structure [15].

Thirdly, it is computationally costly to determine tertiary structure. Therefore, it is better to find out the secondary structure first and then use that information to predict the tertiary structure.

2 Components of RNA Secondary Structure

An RNA secondary structure consists of a number of smaller substructures. Figure 5 shows RNA secondary structure which contains substructures as discussed below.

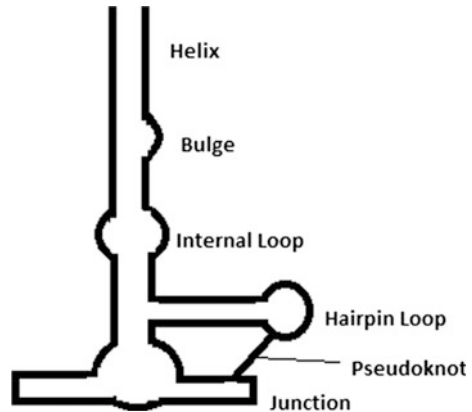
The different parts of RNA secondary structure are as follows:

1. Helix (or a stem): Consecutive base pairs form a stem or helix. If 1, 2, 3, and 4, respectively, are four bases in RNA sequence such that 2 appears somewhere after 1, and 4 appears somewhere after 3 in the sequence, then 1 pairing with 4 and 2 pairing with 3 forms a helix or stem [16, 17].
2. Internal loop: If there is an unpaired base on both sides of stem, it is termed as Internal loop [16, 17].
3. Bulge: If there is an unpaired base on any one side of stem, it is termed as bulge [16, 17].
4. Hairpin loop: A stem or helix containing at least 2 unpaired bases on one side is termed as a hairpin loop [16, 17].

Fig. 4 RNA primary structure

UCAAUGCCACCGCCUA

Fig. 5 Motifs of RNA secondary structure



5. Multi-branched loop: Multi-branched loop consists of structure having two or more interior base pairs existing in a loop [16, 17].
6. Pseudoknot: Pseudoknot is formed when four bases (1; 2; 3; 4) in sequence pair such that 1 is paired with 3, and 2 is paired with 4. The frequency of occurrence of pseudoknot is very less as compared to other RNA secondary structure as mentioned above [16, 17].

2.1 RNA Secondary Structure Prediction Techniques

In last 2–3 decades, many computer techniques and methods have developed in the area of RNA secondary structure prediction. Some of them are Grammars-based methods [18, 19], dynamic programming techniques, Matching Methods, EA (evolutionary algorithms), Genetic Algorithm, Artificial Neural Network, and fuzzy Logic techniques.

The First techniques developed for RNA secondary structure prediction was energy minimizing techniques, and concept of dynamic programming was used in these techniques. One of the simplest methods was developed by Nussinov in 1978 with complexity of $O(n^3)$ time (n represents the RNA sequence's length). Later on, Akutsu proposed a new dynamic programming algorithm which can deals with simple pseudoknots with the complexity of $O(n^4)$ [2] and with more advanced and complex structure of pseudoknots in time complexity of $O(n^5)$. Other software programs were also developed using the energy minimization techniques like Vienna RNA package [20] and mfold [21] for secondary structure prediction, but these software packages were not able to predict the pseudoknots in secondary structure. And, the accuracy of energy parameters in energy minimization techniques was not correct, and performance was also poor.

In 1995, maximum weighted matching (MWM) methods came into existence. In these techniques, the problem of discovering matching base pairs was described as finding out the maximum number of weighted matches between two sets (of the bases). Stormo et al. developed one of this kind of method known as the ILM (iterated loop matching) algorithm. ILM was capable of predicting pseudoknots with time complexity of $O(n^4)$ [22]. Evolutionary computation method is used for RNA structure prediction in another technique e.g., Evolutionary Algorithms (EA's). The logic of this method is to maintain a population (set of possible solutions) and search and evaluate from a series and finally select the best one. The algorithm tries to simulate the Darwinian evolution [21, 23] that's why called as evolutionary method. The disadvantage of EA's is slow speed.

Rivas and Eddy also suggested an algorithm based on the concept of dynamic programming for RNA structure predicting including pseudoknots [24, 25]. The worst case time complexity of the algorithm was $O(N^6)$, and worst case space complexity was $O(N^4)$. Also, the description of algorithm was complex. Knudsen and Hein introduced a new algorithm for RNA secondary structure prediction based on stochastic Context-Free Grammar [26]. The phylogenetic tree relating the sequence can be found by maximum likelihood estimation from the proposed model. This model uses stochastic context-free grammar for prediction.

2.2 RNA Visualization Tools

Various tools exist for visualization of molecular data. They are .NET Bio, BioJava, BioJS, Bioclipse, and UGENE. These tools facilitate molecular researchers to visualize their molecular sequence data in various formats.

.NET Bio is an open source tool developed by Microsoft initially named as Microsoft Biology Foundation (MBF). It is used for Genomics research and is developed by Microsoft .NET framework is a language neutral toolkit. Lots of parser techniques of RNA sequences, file formats, and set of connectors (NCBI BLAST) are implemented in it. Some of the supported alignment algorithms are Smith-Waterman, Needleman-Wunsch, Pairwise-Overlap, MUMmer, and NUCmer [27–29]. It supports RNA, DNA, and protein sequences. It can be extended easily by adding new functions, and the algorithms are themselves scalable. There is flexibility for programmers to choose any language like Visual Basic, C#, F#, or Python as per their expertise. It is very compatible with all type of technologies and applications like cloud, webs services, API, and REST web services. It is a cross platform i.e., it can run on windows, Mac, or Linux. .Net Bio comes in two variations, one for the command prompt and other .NET Excel. Help function is associated with each command so that novice user can learn commands. Commands like NucmerUtil, MumUtil, ComparativeUtil, etc., are used for sequence alignment. Specifically, NucmerUtil is for multiple sequence alignment. MumUtil is for maximum unique match between given sequence and multiple input sequences. ComparativeUtil is for sequence comparison. .NET Bio Excel comes as a plug-into

excel. It works well with NCBI, EBI, and Blast databases. .NET Bio is available at <http://bio.codeplex.com>.

BioJava is another open source tool developed on JAVA framework to deal with biological data. This tool is suitable for rapid application development. BioJava has parsers for RNA file formats, and it provides the ability of manipulation of sequence and 3D structures. It also provides different analytical and statistical methods and routines for sequence alignment, annotation, graphical interfaces, and utilities. It can also accommodate external scripts and snippets and can also run external programs so that code can be reused. It handles various sequence formats, like Embl, genbank, gff, blast, etc. It is also possible to input a sequence in one format and output it in a different format. It contains toolkit for Dynamic Programming and Hidden Markov Model. It also supports probability distribution over alphabets. Apart from RNA and DNA, it also supports Proteomics, clusters, ontologies [30], evolutionary trees, and expression data. BioJava can be downloaded from biojava.org/wiki/BioJava%3ADownload_4.1.0.

BioJS stands for Bio Java Script. BioJS tool [31] is a powerful tool which provides the ability to represent the biological data on web. It is an open source tool having java script components to visualize the biological data. Currently, more than 25 components are available. Interactivity and reusability are the best features of BioJS. BioJS have lot of small components and building block which can be reused in other application easily, and it is very easy to integrate it in other web application for programmers. It enables the full-featured biological workbench for Internet browser using the state-of-art web technologies [32]. One of the important features is Gene Expression summary which is providing information on under expression or over expression of a gene. Another component is for chromosome visualization. Another one is Protein Portfolio that shows protein description and its alignments. Apart from reusing the component, BioJS has feature to develop new components as well as ability to combine various components which may be published there and then so that they are further available to the community. This tool is available at <https://github.com/biojs/biojs> and inherited by others and provides additional functionality. It has capability to visualize the 2D and 3D data and different file format conversion. It allows editing 2D structures, manipulating 3D modeling, and predicting molecular behavior. Its components are JChemPaint, JMol, and various plugins. This tool is freely available on Internet for both open and commercial purposes. Bioclipse tool is available at <http://www.bioclipse.net/> [33].

UGENE [34] is another cross platform and open source software for bioinformatics. It supports Window, Linux, and Mac OS and is written in C++ using Qt framework. It provides the functionality to study, analysis, and visualize the genetics data. Database can be stored locally and shared environment. It has a common user interface in which lot of bioinformatics tools are integrated. Some excellent features of this tool are fast searching, shared database storage, RNA sequence data analysis with turbo pipeline, and ability to search online databases like PDB, NCBI, and DAS servers. It supports sequence alignment, phylogenetic tree generation, annotations, etc. UGENE is available at <http://ugene.net/>.

Some tools are specifically designed for RNA and are not open source. They are implemented keeping a specific goal in mind. One of those tools is QuickRNASeq Pipeline [35]. QuickRNASeq Pipeline is a GUI-based tool for large-scale primary RNA sequence data analysis. The tool is written in bash script and java script using HTML. It is an interactive tool that enables data sharing among end users in dynamic environment. Results are managed using a compression tool before sending to the web browser for display. For large-scale data, processing in parallel fashion and otherwise processing is done in serial fashion. QuickRNASeq pipeline is available at <http://quickrnaseq.sourceforge.net>.

RNAsoft [36] is an array of tools designed for visualization of DNA as well as RNA structures. Apart from visualization, this tool predicts the structure also, specifically RNA secondary structure. RNAsoft includes tools like Pairfold, Hotknots, and RNA Designer. Pairfold tool takes as input pair of RNA/DNA sequence and outputs its secondary structure. Hotknots also predict RNA secondary structure, but it includes prediction of pseudoknots also. The function of RNA Designer is just the reverse of any RNA secondary structure prediction algorithm. RNA Designer takes as input the structure of RNA and outputs sequence that will fold into the said structure.

3 Conclusion and Future Work

Prediction of RNA structure helps us recognize its function. Various types of RNA are used nowadays to fight with diseases. But this is possible only when RNA structure is predicted. Various Tools, Techniques, Algorithms have been used by researchers to predict and model RNA secondary structures. In this paper, we described various types of RNA and their importance. Also, we discussed different tools and techniques available to analyze and predict the RNA secondary structure. In existing research, there is restriction of type of structures to be predicted. Our future work will be to predict RNA secondary structure including all the sub-structures with lower time and space complexity.

References

1. T. Akutsu. Dynamic programming algorithms for RNA secondary structure prediction with pseudoknots. *Discrete Applied Mathematics*, 2000(104): 45–62.
2. Pardeep Kumar, Dolly Sharma, String Algorithms for Counting DNA Nucleotides, Transcribing DNA to RNA and Complementing a Strand of DNA, International Conference on Data Acquisition Transfer Processing and Management (ICDATPM-2014), Lingaya's University, Faridabad, 28–29 March, 2014, pg no. 244–247.
3. Jacques Cohen. *Bioinformatics—An Introduction for Computer Scientists*, ACM Computing Surveys, 2004(36):2, 122–158.

4. Michael T. Dixon and David M. Hillis. Ribosomal RNA Secondary Structure: Compensatory Mutations and Implications for Phylogenetic Analysis, University of Chicago. *Mol. Biol. Evol.* 1993(10):1, 256–267.
5. Alexander Rich and U. L. Rajbhandary. Transfer RNA: Molecular Structure, Sequence, and Properties. *Annual Review of Biochemistry.* 1976(45), 805–860.
6. Svetlana A. Shabalina, Aleksey Y. Ogurtsov and Nikolay A. Spiridonov, A periodic pattern of mRNA secondary structure created by the genetic code, *Nucleic Acids Research, National Center for Biotechnology Information*, 2006(34) :8.
7. Sean R. Eddy. Non-Coding RNA Genes and the Modern RNA World, Macmillan Magazines Ltd, 2001 (2).
8. Douglas R. Tanner, Jonathan D. Dewey, Mickey R. Miller, and Allen R. Buskirk. Genetic Analysis of the Structure and Function of Transfer Messenger RNA Pseudoknot, *The Journal Of Biological Chemistry*, 2006 (281):15, 10561–10566.
9. Douglass J. Forbes, Thomas B. Kornberg, and Marc W. Kirschner, Small Nuclear RNA Transcription and Ribonucleoprotein Assembly in Early Xenopus Development, *The Journal Of Cell Biology*, 1983(97).
10. Shi-Lung Lin, Joseph D. Miller, and Shao-Yao Ying, Intronic MicroRNA (miRNA), *Journal of Biomedicine and Biotechnology*, 2006(2006), 1–13.
11. Richard W. Carthew, Erik J. Sontheimer, Origins and Mechanisms of miRNAs and siRNAs, *Northwestern University, Cell*, 2009(136), 642–655.
12. Ting-Ting Liua, Danmeng Zhua, Wei Chena, Wei Dengb, Hang Hea, Guangming Hea, Baoyan Baib, Yijun Qic, Runsheng Chenb and Xing Wang Deng, A Global Identification and Analysis of Small Nucleolar RNAs and Possible Intermediate-Sized Non-Coding RNAs, *Molecular Plant Advance Access published September 17, 2012*.
13. Stuti Gupta, Ravindra Pal Singh, Nirav Rabadia, Gaurang Patel, Hiten Panchal, ANTISENSE TECHNOLOGY, *International Journal of Pharmaceutical Sciences Review and Research*, 2011 (9):2, Article-007.
14. Christian Zwieb, Rob W. Van Nues, Magnus Alm Rosenblad, Jeremy D. Brown, And Tore Samuelsson, A nomenclature for all signal recognition particle RNAs, *RNA Society, RNA Society, RNA*, 2005(11):1.
15. Anne Condon, Problems on RNA Secondary Structure Prediction and Design, Chapter, *Automata, Languages and Programming*, Volume 2719 of the series *Lecture Notes in Computer Science*, 2003(2719): 22–32.
16. Shubhra Sankar Ray and Sankar K. Pal, RNA Secondary Structure Prediction, Using Soft Computing, *IEEE/ACM Transactions On Computational Biology And Bioinformatics*, 2013 (10):1.
17. Donna K. Hendrix, Steven E. Brenner and Stephen R. Holbrook RNA structural motifs: building blocks of a modular biomolecule, *Quarterly Reviews of Biophysics.* 2006(38) :3, 221–243.
18. Dolly Sharma, Shailendra Singh, Trilok Chand, Formal Grammar Algorithms for Prediction of RNA Secondary Structure including Pseudoknot, *International Conference on Data Acquisition Transfer Processing and Management (ICDATPM-2014)*, Lingaya's University, Faridabad, 28–29 March, 2014, pg no. 206–208 Smith, T.F., Waterman, M.S.: Identification of Common Molecular Subsequences. *J. Mol. Biol.* 147, 195–197 (1981).
19. Dolly Sharma, Shailendra Singh, Trilok Chand, RNA Secondary Structure Prediction Algorithms Including Pseudoknots. 9 (3):268–283, 2013.
20. I. L. Hofacker, W. Fontana, P. F. Stadler, L. S. Bonhoeer, M. Tacker, and P. Schuster. Fast folding and comparison of RNA secondary structures (vienna rna package). *Monatshe. Chem.* 1994 (125), 167–188.
21. M. Z. et al. Algorithms and thermodynamics for rna secondary structure prediction: A practical guide in rna biochemistry and biotechnology. In *NATO ASI Series 1999*, Kluwer Academic Publishers, 1999.
22. J. Ruan, G. Stormo, and W. Zhang. An iterated loop matching approach to the prediction of rna secondary structures with pseudoknots. *Bioinformatics*, 2004 (20):1, 58–66.

23. K. C. Wiese, A. Deschenes, and E. Glen. Permutation based rna secondary structure prediction via a genetic algorithm. In R. Sarker, R. Reynolds, H. Abbass, K. C. Tan, B. McKay, D. Essam, and T. Gedeon, editors, Proceedings of the 2003 Congress on Evolutionary Computation CEC2003, pages 335–342, Canberra, 8–12 December 2003. IEEE Press.
24. E. Rivas and S. Eddy. A dynamic programming algorithm for rna structure prediction including pseudoknots. *Journal of Molecular Biology*, 285(5):2053–2068, 1999.
25. E. Rivas and S. R. Eddy. The language of RNA: a formal grammar that includes pseudoknots. *Bioinformatics*, 16(4):334–340, 2000.
26. B. Knudsen and J. Hein. RNA secondary structure prediction using stochastic context-free grammars and evolutionary history. *Bioinformatics*, 15:446–454, 1999.
27. Smith, Temple F. & Waterman, Michael S. Identification of Common Molecular Subsequences. *Journal of Molecular Biology*. 147: 195–197, 1981.
28. Needleman, Saul B. & Wunsch, Christian D. A general method applicable to the search for similarities in the amino acid sequence of two proteins. *Journal of Molecular Biology*. 48 (3): 443–53, 1970.
29. Arthur L. Delcher, Adam Phillippy, Jane Carlton, and Steven L. Salzberg. Fast algorithms for large-scale genome alignment and comparison. *Nucleic Acids Res.* Vol 30: 11, 2478–2483, 2002.
30. R. C. G. Holland, T. A. Down, M. Pocock, A. Prlić, D. Huen, K. James, S. Foisy, A. Dräger, A. Yates, M. Heuer and M. J. Schreiber. BioJava: an open-source framework for bioinformatics. *Bioinformatics*, 24:18, 2096–2097, 2008.
31. John Gómez, Leyla J. García, Gustavo A. Salazar, Jose Villaveces, Swanand Gore, Alexander García, Maria J. Martín, Guillaume Launay, Rafael Alcántara, Noemi del-Toro, Marine Dumousseau, Sandra Orchard, Sameer Velankar, Henning Hermjakob, Chenggong Zong, Peipei Ping, Manuel Corpas and Rafael C. Jiménez. BioJS: an open source JavaScript framework for biological data visualization. *Bioinformatics*, vol 29:8, 1103–1104, 2013.
32. <http://biojs.net/>.
33. Ola Spjuth Email author, Tobias Helmus, Egon L Willighagen, Stefan Kuhn, Martin Eklund, Johannes Wagener, Peter Murray-Rust, Christoph Steinbeck and Jarl ES Wikberg. Bioclipse: an open source workbench for chemo- and bioinformatics. *BMC Bioinformatics* vol 8:59, 1–10, 2007.
34. Konstantin Okonechnikov, Olga Golosova, Mikhail Fursov. Unipro UGENE: a unified bioinformatics toolkit. *Bioinformatics*, vol 28:8, 1166–1167, 2012.
35. Shanrong Zhao, Li Xi, Jie Quan, Hualin Xi, Ying Zhang, David von Schack, Michael Vincent and Baohong Zhang. QuickRNASeq lifts large-scale RNA-seq data analyses to the next level of automation and interactive, visualization. *BMC Genomics* vol 17:39, 1–15, 2016.
36. Mirela Andronescu, Rosalía Aguirre-Hernández, Anne Condon and Holger H. Hoos. RNA soft: a suite of RNA secondary structure prediction and design software tools. *Nucleic Acids Research*, vol 31: 13, 3416–3422, 2003.

Data Traffic Modeling of ML-MAC for Wireless Sensor Networks

Aarti Kochhar, Pardeep Kaur and Preeti

Abstract Wireless sensors collect the data and transmit it to the base station through a network of nodes. The flow of data through the network can also be termed as traffic flow. The nature of traffic flow in a network depends upon application for which network is designed. Modeling traffic flow for a wireless sensor network (WSN) is as important as designing the MAC or routing protocol. In fact, estimating the flow of expected traffic is a prerequisite of designing a protocol. Efficient estimation of traffic flow helps in determining resource requirements. Overestimation and underestimation of the traffic pattern and flow can lead to wastage or exhaustion of resources. Medium access control (MAC) protocol is responsible for shared access of media among nodes. Poisson distribution is used for shaping of traffic for multilayer MAC (ML-MAC). This paper proposes another traffic profiles such as Pareto and generalized Pareto distribution (GPD) for ML-MAC which are more realistic than Poisson. Further, it simulates ML-MAC for the proposed traffic models. Finally, this paper compares the results in terms of energy consumption and average delay. The results are further justified and concluded by providing supporting applications.

Keywords Wireless sensor networks (WSN) · Protocols · ML-MAC
Traffic modeling · Poisson · Pareto

1 Introduction

Wireless sensor network is a network of randomly deployed sensing nodes. Since WSN has no continuous power supply, nodes are highly energy constrained. These nodes sense the data, process the data, and transmit it to another node or base station. Maximum energy is consumed for communication by radio in WSN [1]. Activity of a radio is controlled by MAC protocol design. So to reduce energy

A. Kochhar (✉) · P. Kaur · Preeti
University Institute of Engineering and Technology, Panjab University, Chandigarh, India
e-mail: aarti.kochhar92@gmail.com

consumption, MAC protocols need to be efficiently designed. MAC protocols have various energy consumption factors such as idle listening, overemitting, over-hearing, and collisions [2].

Multilayer MAC (ML-MAC) is duty cycling-based MAC protocol in which nodes listen for the half of the duty cycle and sleep for the other half of the duty cycle to save energy. Owing to multiple layers, ML-MAC has less number of collisions, reduced energy consumption, and prolonged network lifetime. ML-MAC reduces the energy consumption due to idle listening and collisions.

Proper estimation of traffic helps in the design process of protocol stack. Analysis of traffic eases the process of pretransmission data processing. A good estimation of traffic flow in the network helps in efficient allocation of resources such as battery power, processor time, among nodes. It can provide a solution to energy constraints of WSN. It also aids the planning of congestion control mechanism. Communication traffic further consists of data traffic, control packet traffic, route discovery traffic, etc. This paper mainly focuses on data traffic modeling for multilayer-based MAC. WSN is an application-specific technology, and each application has different profiles of traffic. Demirkol et al. [3] investigated binary sensing traffic model and Elfes sensing traffic model for intrusion detection. Messier et al. [4] present traffic models for medical WSN.

This paper is divided into following sections. Section 2 provides related work. Section 3 presents the analysis of different traffic models. Section 4 deals with the simulation results. Finally, the paper is concluded in Sect. 5.

2 Related Work

Ye et al. [5] suggested reducing the energy consumption due to idle listening. Nodes listen for 50% of the duty cycle and sleep for rest of the 50% of the duty cycle. Authors simulated the designed protocol for different traffic loads. No particular traffic model is considered for simulations. So, the effectiveness of the protocol design may decrease under variable traffic flow.

Jha et al. [6] proposed ML-MAC which is a distributed contention-based MAC protocol. The listen period of nodes is further divided into layers to reduce energy consumption due to collisions and idle listening. Let number of layers be L , and listen period is divided into L non-overlapping layers as shown in Fig. 1. Nodes are uniformly distributed among these layers, and at particular instant, nodes from only one layer are active. Simulations show that ML-MAC outperforms S-MAC. ML-MAC saves 52% more energy than S-MAC for heavy traffic load and 64% energy for light traffic load. Authors considered Poisson distribution or shifted exponential distribution for modeling of traffic. Multiple layers reduce the duty cycle and hence the probability of collision. The concept of multilayer has great potential to solve energy constraints of WSN. Apart from WSN, the concept of multiple layering can benefit other wireless ad-hoc networks also [7].

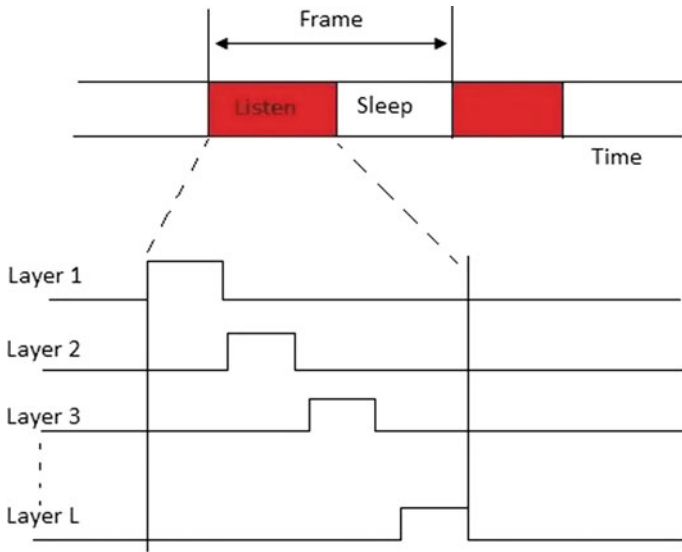


Fig. 1 Design of ML-MAC

Khurana et al. [8] suggested the deployment of relay nodes to reduce energy consumption caused by clock skew. Hardware clocks of nodes in WSN need to be synchronized for efficient operation. Quartz crystal in hardware clocks produces drift in the clock. Different drifts in each node lead to lack of synchronization among nodes. Unsynchronized network has more packet loss, delay, and energy consumption than synched network. Authors proposed a two-tier network with an additional tier of relay nodes to improve synchronization and reduce packet loss.

2.1 Traffic Modeling

Traffic modeling [9] is necessary to design MAC protocols efficiently. ML-MAC is a duty cycle-based MAC protocol. G. Romaniello et al. proposed traffic-aware duty cycle-based MAC protocol for WSN-HEAP (Ambient Energy Harvesting Protocol). For simulations, three parameters, energy harvesting rate, battery level, and traffic load, were chosen to manage and take decisions regarding duty cycle. Results show that traffic-aware protocol has better performance than traffic-unaware protocols in terms of delay and packet delivery ratio [10]. Traffic models are based upon concepts given below.

Sequence of Packets

Certain types of packets have to appear in a particular sequence. For example, acknowledgment packets can be sent only after receiving request messages. So

traffic for a network can be modeled on the basis of relation among these packets. Finite state machine (FSM) can be used to represent the sequence, or the sequence can be learned by the network.

Load Distribution

All the nodes in WSN may not have the same capabilities. So data traffic load cannot be distributed uniformly among nodes. Full Function Devices should be assigned with more traffic load, whereas Reduced Function Devices should handle fewer loads. For example, nodes near the base station tend to have more traffic than nodes away from the base station. So traffic profile can be modeled on the basis of load distribution. Nodes with more traffic need comparatively more resources.

Traffic Inter-arrival Time

Inter-arrival time is a time difference between arrivals of two packets. If T_n is time of arrival of n th packet and T_{n+1} is time of arrival of $(n + 1)$ th packet, then $I_n = T_{n+1} - T_n$ represents time interval between two arrivals. I_n is a random variable, and traffic profile can be modeled by using different distributions for I_n . For example, Poisson distribution is most widely used distribution for modeling traffic inter-arrival time. Modeling of packet inter-arrival time for traffic profiling has been discussed in more detail in Sect. 3.

3 Mathematical Analysis of Traffic Inter-arrival Time Models

Poisson distribution is most widely used distribution for profiling of traffic flow, but Wang et al. [11] stated the inappropriateness of Poisson process for modeling of bursty traffic. Poisson distribution can be used for traffic with variable bit rate but only if it is not bursty [12]. Paxson et al. [13] used traces of arrival processes to determine the error introduced by Poisson distribution modeling of inter-arrival time. The mathematical representation of few distributions (along with Poisson) for inter-arrival time pattern modeling has been discussed below.

3.1 Parameters of Distribution Function

A distribution can be characterized by its variables. These variables are also called as parameters. Various parameters that define probability density function (PDF) of a distribution can be location parameter, a ; shape parameter, b ; scale parameter, c . Change in location parameter changes the position of distribution graph on horizontal axis. Scale parameter either stretches or shrinks the distribution, whereas shape parameter varies the general shape of distribution. Some distributions use rate parameter, λ , instead of scale parameter. Rate parameter is reciprocal of scale

parameter. These parameters can be expressed as a function of various other variables such as explanatory variables and/or stochastic variables. These are called as generalized additive models for location, scale, and shape (GAMLSS) [14].

3.2 Poisson Distribution

The inter-arrival time in Poisson is exponentially distributed and independent. So it is appropriate for applications where main traffic flow consists of several independent traffic streams multiplexed together. PDF of Poisson is given as follows:

$$f(t) = \lambda e^{-\lambda t} \quad (1)$$

where λ is mean arrival rate of packets. Authors in [6] found the representation in Eq. (1) to be less realistic to characterize traffic. So they modified the equation as below:

$$f(t) = be^{-b(t-a)} \quad (2)$$

where a is location parameter, and b is shape parameter.

3.3 Pareto Distribution

Model in Eq. (2) was not realistic enough for modeling of traffic for ML-MAC. Pareto shapes inter-arrival time to be self-similar and independent, but it can model self-similar or identical traffic only over short duration of periods. In Pareto, larger portion of the data is represented by a smaller portion of the distribution. This is called as Pareto principle. PDF of Pareto distribution can be expressed as:

$$f(t) = \frac{bc^b}{t^{b+1}} \quad (3)$$

Infinite variance for $b \geq 2$ and infinite mean for $b \leq 1$ make Pareto more realistic for traffic characterization.

3.4 Generalized Pareto Distribution (GPD)

Generalized Pareto distribution models the tail of distributions. GPD is generalized as it consists of a number of special cases. So parameters of data traffic decide

which special case of distribution is appropriate. PDF of GPD is expressed below if $a < t$ when $b > 0$, or $a < t < a - \frac{c}{b}$ when $b < 0$

$$f(t) = \frac{1}{c} \left[1 + b \frac{(t-a)}{c} \right]^{-1-\frac{1}{b}} \quad (4)$$

If $a = c/b$ and $b > 0$, GPD is analogous to Pareto distribution with scale parameter c/b and shape parameter $1/b$.

For Eq. (4), b cannot be zero. For $b = 0$, PDF is as follows:

$$f(t) = \frac{1}{c} e^{-\frac{(t-a)}{c}} \quad (5)$$

For $a < t$, if $a = 0$ in Eq. (5), GPD is analogous to exponential distribution in Eqs. (1) and (2). Major advantage of GPD is that it allows the data traffic to choose the model, i.e., run-time adaptation depending upon application. GPD can also characterize traffic for bursty data applications like wireless multimedia sensor networks (WMSN).

4 Simulation Results

Here in this paper, ML-MAC, a well-known MAC protocol, is analyzed for different traffic generation models using MATLAB. Since the protocol assumed unlimited buffer size, no packets are dropped but ML-MAC does consider delay due to queuing of packets. The only reason for packet loss is collisions. Wireless channel is assumed to be without losses. Datasheet of TR1000 transceiver from RF monolithic is used for modeling of power consumption. Other simulation parameters are summarized in Table 1.

Inter-arrival time of traffic depends upon the distribution used. Source traffic can be characterized using three parameters: average data rate, λ ; maximum burst rate,

Table 1 Simulation parameters

Parameter	Value	Unit
Number of nodes	100	
Number of layers	1–10	
Frame duration	1	s
Layer duration	300/L	ms
Number of initial reservation slots	8	
Listening power of node	13.5	mW
Sleeping power of node	15	μ W
Transmitting power of node	24.75	mW
Data transmission rate	19.2	Kbps
Packet length	38	Bytes

β ; and average packet length, l . Distribution parameters (a , b , c) can be calculated from source traffic parameters (λ , β , l) using Eqs. (6)–(8).

$$a = \frac{l}{\beta} \quad (6)$$

$$b = \frac{\beta\lambda}{l(\beta - \lambda)} \quad (7)$$

$$c = \frac{1}{\lambda} \quad (8)$$

Simulations provide us good estimation value of various factors such as energy consumption, delay, and number of collisions. These values need to be considered while designing of WSN hardware and protocols. For example, energy consumption value helps in understanding the resource requirement of the WSN deployment. The values shown below are the result of an average of values taken over 10 rounds.

4.1 Energy Consumption

Energy consumption value when three distributions are used for traffic modeling is shown in Fig. 2. It shows that at packet inter-arrival time of 3 s, energy consumption is 347.7045 mJ for Poisson distribution and 398.5503 mJ for GPD. Thus, energy consumption increases by approximately 50–55 mJ for bursty traffic which is modeled using GPD. More bursty traffic has more number of collisions, and hence, the energy consumption increases. Poisson underestimates the energy requirement of WSN by 15% which may be misleading while deployment. Values produced are not worth relying upon as Poisson is not able to capture the bursty or heavy traffic. Deviation of 50 mJ is significant and considerable for WSN. Similarly, for Pareto distribution at same packet inter-arrival time of 3 s, energy consumption is 353.7444 mJ. Thus, a deviation of 6–10 mJ from Poisson is shown, which is only considerable in the applications with tight energy constraints. Pareto and GPD are also able to capture the variance in traffic. Hence, it produces a more reliable value for energy consumption.

4.2 Average Packet Delay

Delay calculated here is combined value of transmission delay, and the delay due to the time spent by messages in buffer until the next destination node is in sleep mode. Authors in [6] show that average delay for ML-MAC is more than average

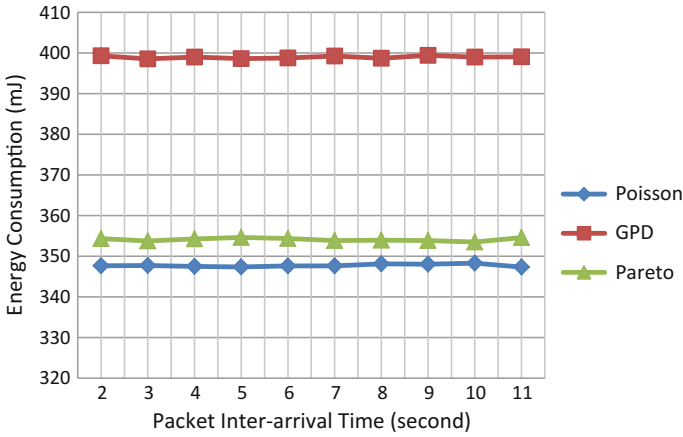


Fig. 2 Average energy consumption for $L = 3$ using various distribution models

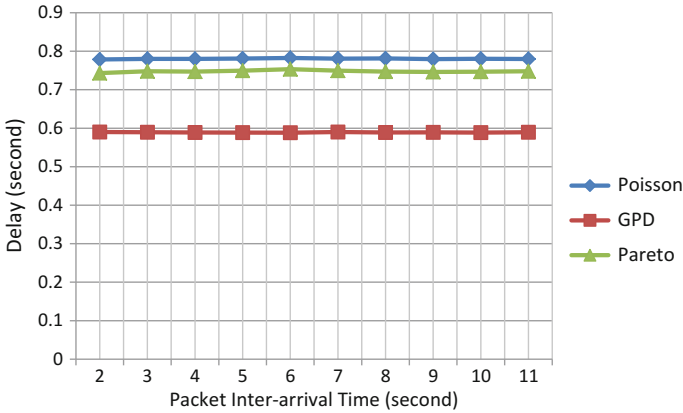


Fig. 3 Average packet delay for $L = 3$ using various distribution models

delay for S-MAC because nodes spend more time in sleep mode. Figure 3 shows average delay values for 10 rounds with varying packet inter-arrival time. Average delay at $L = 3$ and packet inter-arrival time of 3 s are 0.778291 s for Poisson, 0.58842 s for GPD, and 0.752952 s for Pareto. Result proves the efficiency of GPD over Poisson as the average delay decreases by approximately 0.18–0.22 s. This deviation can increase up to 0.45–0.50 s under various simulation parameters. This time difference is critical for security and medical applications.

Poisson distribution cannot capture the traffic for high-speed networks. Poisson modeling does not allow the nodes to be prepared for fast arriving packets and again underestimates the resource requirement. GPD can have traffic inter-arrival time as small as 0.23 s under various simulation parameters. For delay or

Table 2 Summary

Distribution	Traffic type	Targeted type of network for ML-MAC	Example of application for ML-MAC
Poisson	Light and independent	Networks capturing rare occurring events	Gas leakage alerts, fire alarms
Pareto	Self-similar and independent	Networks following Pareto principle	Target detection and tracking
GPD	Bursty data with run-time adaptation	Heavy traffic networks and high-speed networks	WMSN used in defense

time-constrained applications like defense application, for which sensed alarms need to travel to the base station or control center at the earliest, GPD distribution can be used. Processing speed of the nodes needs to be improved for traffic with such short traffic inter-arrival time. Pareto modeling produces deviation of 0.02 s from Poisson, which is not much significant.

Above simulations can be summarized and tabulated in the form of Table 2. Column two represents the type of traffic generated by corresponding distribution. Column three represents the type of application that the distribution model can support for ML-MAC. Column four shows the example of corresponding application. WMSN used in defense represents an application with heavy traffic and delay constrains (high speed).

5 Conclusion

As shown in the present paper, a proper understanding of traffic flow can provide new insights into network optimization techniques. ML-MAC is a protocol with high potential applications, but the potential can be exploited only if a reliable traffic model is used for the estimation of resources. The credibility of a traffic model depends upon how well it can represent actual traffic. Poisson underestimates heavy-tailed and bursty traffic. GPD and Pareto models can efficiently capture the correlating characteristics of the traffic. Hence suits best for bursty data. Owing to the density of traffic, number of collisions and energy consumption increases in the case of GPD and Pareto modeling.

GPD has less average packet delay, so it also fits for the profiling of traffic for high-speed WSN. So GPD proves out to be most realistic candidate for traffic modeling of ML-MAC. It can derive the full benefit of ML-MAC protocol. If GPD is used for traffic modeling while designing of ML-MAC, hardware and software requirements can be more closely approximated. Similarly, other recent protocols can be optimized using efficient traffic modeling. Other than the models discussed above, there are several other distributions that can be exploited for traffic modeling.

References

1. Didioui A (2015) Energy-Aware Transceiver for Energy Harvesting Wireless Sensor Networks. *Signal and Image Processing*.
2. Abozahhad M, Farrag M, and Ali A (2015) A Comparative Study of Energy Consumption Sources for Wireless Sensor Networks. *International Journal of Grid Distribution Computing*. vol. 8, no. 3, pp. 65–76.
3. Demirkol I, Alagoz F, Delic H and Ersoy C (2006) Wireless Sensor Networks for Intrusion Detection : Packet Traffic Modeling. *IEEE Communications Letters*. vol. 10, no. 1, pp. 22–24.
4. Messier GG and Finvers IG (2007) Traffic Models for Medical Wireless Sensor Networks. *IEEE Communications Letters*. vol. 11, no. 1, pp. 13–15.
5. Ye W, Heidemann J, and Estrin D (2002) An energy-efficient MAC protocol for wireless sensor networks. *Proceedings of IEEE Infocom 2002*. pp. 1567–1576.
6. Kumar M, Kumar A, Pal D, and Mohan A (2011) An energy-efficient multi-layer MAC (ML-MAC) protocol for wireless sensor networks. *International Journal of Electronics and Communications (AEÜ)*. vol. 65, no. 3, pp. 209–216.
7. Ngoc D, Dang M, Nguyen V, and Tra H, Hong C, Choe J (2016) An efficient multi-channel MAC protocol for wireless ad hoc networks. *Ad Hoc Networks*. vol. 44, pp. 46–57.
8. Khurana M, Thalore R, Raina V and Jha MK (2015) Improved time synchronization in ML-MAC for WSN using relay nodes. *International Journal of Electronics and Communications (AEÜ)*. vol. 69, no. 11, pp. 1622–1626.
9. Q. Wang (2010) Traffic Analysis & Modeling in Wireless Sensor Networks and Their Applications on Network. *Network Protocols and Algorithms*. vol. 2, no. 1, pp. 74–92.
10. Romaniello G, Alphand O, Guizzetti R and Duda A (2015) Sustainable Traffic Aware Duty-Cycle Adaptation in Harvested Multi-Hop Wireless Sensor Networks. *IEEE 81st Vehicular Technology Conference (VTC Spring)*.
11. Wang Q and Zhang T (2008) Source traffic modeling in wireless sensor networks for target tracking. In: *Proceedings of the 5th ACM International Symposium on Performance Evaluation of Wireless Ad-Hoc, Sensor, and Ubiquitous Networks (PE-WASUN'08)*. pages 96–100.
12. Ma Y and Aylor JH (2004) System Lifetime Optimization for Heterogeneous Sensor Networks with a Hub-Spoke Topology. *IEEE Transactions on Mobile Computing*. vol. 3, no. 3, pp. 286–294.
13. Paxson V and Floyd S (1995) Wide-Area Traffic : The Failure of Poisson Modeling. *IEEE/ACM Transactions on Networking*.
14. Jong RD, Buuren SV and Spiess M (2016) Computation Multiple Imputation of Predictor Variables Using Generalized Additive Models. *Communication in Statistics-Simulation and Computation* 45:3, 968–985.

Supervised Learning Technique for Prediction of Diseases

Bharti Yadav, Shilpi Sharma and Ashima Kalra

Abstract Lifestyle of a human being is changing day by day and leads human being to an unhealthy life. Apart from the routine exercise and healthy food, the health monitoring at a regular interval also becomes necessary to live long and healthy life. So, in this paper a system is proposed which will help in decreasing the progressive visits to the center moreover help in the early determination of risky sicknesses. This paper proposed a superior health monitoring framework utilizing neural network. In this, neural network (NN)-based health monitoring system is proposed as a solution to human health monitoring. In this, we are taking 276 instances and monitor their health by using 11 number of attributes. The dataset is got from UCI machine learning and from local specialist. All these attributes w.r.t patient are processed using NN in MATLAB and accordingly a result will be drafted. The previous techniques which were used to predict the heart, skin, liver disorder, diabetes, and cancer diseases are fuzzy logic, data mining, radial basis function network, recurrent network, etc. This paper presents our underlying attempt to grow such a framework with the assistance of NN by supervised learning method. In this proposed work, training part is 90% that means 248 instances used for training and rest 10% means 28 instances used for testing and validation. This system gives the more accurate result as compared to previous work, and it is the modified version of health monitoring system. This system shows an accuracy of 98.34% for training part which is the very good value for any data.

Keywords Artificial neural network · Health · Multilayer perceptron
Attributes

B. Yadav (✉) · S. Sharma · A. Kalra
Chandigarh Group of Colleges, Landran, Punjab, India
e-mail: bhariyadav60@gmail.com

S. Sharma
e-mail: shilpisharma.ece@cgce.edu.in

A. Kalra
e-mail: uppal.ashi@gmail.com

1 Introduction

Our health administrations are not that tremendously equipped with skills. The health monitoring framework is important to identify sicknesses effortlessly by just putting dataset of patients. This proposed framework can identify the diseases in patients with more accuracy when contrasted with past frameworks which took care of this issue. In this, health monitoring framework, for identifying the illness, has been led by particular indications related, for identifying the infections with more exactness. So, in this paper artificial neural networks (ANNs) used in health monitoring system. NN shows a seriously diverse way to deal with utilizing PCs as a part of the working environment. NN is utilized to study pattern and relationship in information.

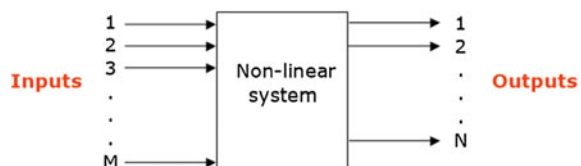
1.1 General Theory of Artificial Neural Networks

Artificial neural networks are no more than an interconnection of artificial neurons. ANNs learn the relations between selected inputs and outputs from the previous experiences. ANNs also perform their tasks simultaneously (i.e., parallel processing), which makes ANNs very fast. A typical ANN can identify and learn the relationships between the inputs and the outputs of a nonlinear multidimensional system (see Fig. 1).

The neural network is an imitation of the neurons in the human nervous system. The human brain consists of over 100 billion neurons and over thousand times more synapses (the interconnections between the neurons). A tree-like structure extends from neuron cell that accepts inputs from other neurons. They are called dendrites. The carrier of the outputs from neuron to the dendrites in another is called an axon.

In a very simple form, an artificial neural network may be considered as a directed graph with nodes and weighted connections between the nodes. The network has one or more input nodes to accept sensory inputs and one or more output nodes to get back the response. The output from the network is a function of the input variables and the corresponding connection weights between them. Compared to the biological neuron system, the nodes are identical to the cell body, the connections are identical to the synapses, and the connection weights are identical to the synaptic efficiency.

Fig. 1 Nonlinear multidimensional system



The general classification of networks is done on the basis of how these connections are established and how the connection weights are modified to minimize some error measure on the response of the network to a stimulate. In some networks like the Hamming net or Hopfield net, the weights are fixed. However, in most other networks, the connection weights are updated in the training process. The process of minimizing the error measure by weight update is known as learning. Some networks have the ability to learn their own and are thus known as unsupervised networks.

On the other hand, supervised networks require a training set that is a set of possible stimulants and the corresponding output expected from the network. The later is thus a form of interactive learning in which, as a student learns from the teacher, the network adjusts its internal connection weights so as to produce the exact answer expected in the training set for each stimulates. The training in supervised networks is evaluated by another set of data known as a test set that is identical to the training set but contains stimulants not seen in the training process. It is possible to picture the training process as some curve fitting or parameter estimation process for the series expansion of a function. If the training has resulted in a proper convergence of the network on the training data, one should also expect a minimum error in the testing process. If that in the case, the network has a good generalization ability and the learning is ideal. The second possibility is that the network produces very good results on the training set but fails considerably on the test set. This is typical of what we call over fitting of data.

1.2 Artificial Neural Networks Training Methods

The learning procedure is called training and is performed by principles, which are grouped into the two fundamental after sorts:

- Supervised learning: where both inputs and outputs are known, this implies the system can decide its prescient execution from given input.
- Unsupervised learning: where the outputs are not known and the neurons, however, need to figure out how to oversee them, this technique is not considered in this.

1.3 Characteristics

Artificial neural networks (ANNs) or connectionist systems are computing systems inspired by biological neurons, performing likewise as a human brain henceforth, the trademark incorporates the ability for storing information and making it available for utilizing at whatever point essential, liking to recognize designs, even in noise, bent for taking past experiences and make inference and judgments about new circumstances.

1.4 Applications

- Capacity to display straight and nondirect frameworks without the need to make presumptions certainly;
- Data preparing, including filtering and clustering;
- Computational neuroscience and neurohydrodynamics;
- Forecasting and expectation;
- Estimation and control.

2 Literature Review

Konstantina et al. in [1] proposed a prognosis and prediction of cancer using application of machine learning (ML). ML has a unique ability to detect the key feature from complicated datasets. Many techniques are preset to predict the disease like Bayesian networks, decision tree, and ANN. But according to this paper, ML method is more convenient to understand the cancer progression. ML also has a branch of artificial intelligence. Its aim is to design a model which can be used for prediction, estimation, and classification. For classification, author analyzed the model base on sensitivity, accuracy, and specificity. Validation method used is— fivefold cross-validation, cross-validation, and hold out. In this paper, author compares the work which all published recently for cancer prognosis by using ML methods. This comparative study will help us to opt for best method to design the system.

Giduthuri Sateesh et al. [2] presented metacognitive learning in a radial basis function network for classification problems. This system is inspired by metacognitive principles which have two components. One is metacognitive and second is cognitive component. To verify the result of a designed system, they choose low and high features small and large number of dataset. The dataset is from UCI machine learning. In this, author works on the dataset of liver disorder, breast cancer, and diabetes on low-dimensional feature which consist of around 200 samples this work shows and improvement of 7 and 14% as compared to previous result. The result from this sample is around 75%. In this, result used different–different method such as sequential multi-category RBF network, extreme learning machine (ELM), metacognitive RBF network (MCRBFN), self-adaptive resource allocation network (SRAN).

Amin et al. [3] in this paper evaluated that data mining is more appropriate technique for prediction of heart diseases. This technique is widely used for prediction and detection of many diseases, to get good accuracy. The important application of this diseases is to determine heart disease, based on the input attributes such as hypertension, age, obesity, tobacco, alcohol intake, and physical activity. This paper used two techniques for data mining, i.e., genetic algorithm and

neural networks. This technique is implemented for diagnosis of 50 patients using MATLAB software. A multilayer feed forward network used, which consists of input, hidden, and output layer, first to initialize the weights and train LM function used to update weight and bias values. Author used 70% data for training and 15% for testing. The result which author got from this software is 89% accurate.

Ankeeta et al. [4] presented a neural network system for diagnosis of heart disease; heart diseases are classified in four ways—normal person, stroke one, stroke two, and stroke three. The author used multilayer feed forward network, this can be done in two steps, training and testing, the 13 input parameters are used in this to get the best output, and it repeats the training so many times to get the accuracy. Dataset taken from the Cleveland Data uses 297 training pairs. To map the input attributes value to the output target value, two-layer feed forward back propagation network is used, hidden layers are 15 and input layer 13. Tansig is used in training function. In the end, the work is classified in four classes—Class 0, normal person, Class 1: first stroke, Class 2: second stroke, and Class 3: third stroke.

Sonawane et al. [5] presented a method in the medical field for the diagnosis of heart-related problems using neural network. There are 13 features that are used in this paper, and the system is trained by back propagation algorithm. A large number of patients are increasing everyday because of heart diseases; this is the reason that he worked for this diseases. Back propagation network first initialized the weight of each neuron. Then, receive output signal from the training data and send it to the hidden unit. This hidden unit computes the value of net input by using the below equation.

$$Z = V_{oj} + \sum (i = 1 \text{ to } N)X_i \cdot V_{ij}. \quad (1)$$

Then, the output i is calculated by using the activation function. The dataset contains 303 data values out of which 164 are related to healthy category and 139 are related to heart diseases. From 303, 212 values are related to training and other 91 are used for testing. The machine gives 98% accuracy when 20 neurons are used for 1000 iterations.

Jasdeep et al. [6] approached different methods: scaled conjugate gradient and Levenberg-Marquardt propagation. These different methods are used to diagnose the thyroid diseases. The thyroid dataset is first trained using LM propagation and output is noted. Then, the dataset is trained by conjugate gradient back propagation. The aim of this paper is to represent the general point for the use of ANNs in medical field. This method is also used for classification, forecasting, and problem solving. This also has three layers. Hidden layer consists of 20 neurons. This paper consists of 7200 patient dataset. This dataset is divided into three categories—normal, hyperfunction, and subnormal functioning. For training, 5040 samples are used, 1030 are used for validation, and 1030 are used for testing.

Gokul et al. [7] presented the application of a fully complex-valued radial basis function network (McFCRBF) and extreme learning machine (ELM) for the diagnosis of Parkinson's diseases. The two components of this are cognitive component and metacognitive component. It is a neurological degenerative effect. This disease slows down the movement, and it affects also speaking and writing. In this, result is based on the unified Parkinson's disease rating scale (UPORS), and its values range from 0 to 176, in which 0 represents the healthy and firm condition and 176 represents the unhealthy or disability condition. The scale is based on three factors—mood, behavior, and daily leaving activities. The dataset contains 804 samples out of 575 are used for training and 229 are used testing. This contains four inputs and one target. Model is trained for 1000 epoch. From this paper, they conclude that MC-FCRBF is more appropriate method as compared to FC-RBF and ELM.

Ayush et al. [8] illustrated that the diabetes is worse than all other diseases. Diabetes causes many diseases such as blindness, Alzheimer, and kidney failure. This paper illustrates that human lifestyle such as sleeping habit, physical activities, eating habit plays a major role for any disease. Diabetes is a chronic disease which occur either when pancreas does not produce enough insulin or when the body cannot use it properly the insulin produced. The questionnaires set made for interaction with doctor, and then these questionnaires asked localities to collect data. It depends on amount of sugar intake, physical activities performed, fried food intake, rice intake and sleeping time, etc. These are the important factors which cause diabetes. Other factors are BMI (body mass index), hereditary diabetes history of chronic disease. Two types of dataset were prepared—diabetic person and nondiabetic person. *K*-fold cross-validation method is used for result validation. In that, $k = 5$ (means data divide into five parts). By this method, the author got the accuracy of 75% correct from the collected dataset.

Agarwal et al. [9] discussed the most effective and friendly model for expert to help in medical field. The model was motivated by biological nervous system. ANN can be categorized in many types—single-layer feed forward network, multilayer feed forward network. ANN has the ability of learning. ANN has three types of learning process—supervised, unsupervised, and reinforcement learning. This study illustrates the usefulness of artificial neural network technique in the diagnosis of cancer. In ANN, two methods are used for best result—MLP gives 97% accuracy, PNN gives 96% accuracy, and ART shows 92% accuracy.

Panduranga et al. [10] observed that data mining is more powerful tool to diagnose the diseases. They collected dataset from north coastal regions. Dataset of 504 people used and this dataset consists of 56 input attributes. Main work of data mining is to extract the pattern from dataset and convert it to gainful data. For this, MATLAB software is used to analyze the information. This method increases the accuracy of data. In this, probability neural network method is used to analyze the

Table 1 Comparison of different techniques

Paper title	Author	Method used	Year
Machine learning application in cancer prognosis and prediction	Konstantina Kourou, Themis P. Exarchos, Konstantina P. Exarchos, Michalis V. Karamouzis, and Dimitrios I. Fotiadis	Fivefold cross-validation	2014
Sequential projection-based metacognitive learning in a radial basis function network for classification problem	Giduthuri Sateesh Babu and Sundaram Suresh	MCRBFN, ELM, SRAN	2013
Genetic neural network-based data mining prediction of heart disease using risk factors	Syed Umar Amin, Kavita Agarwal, and Dr. Rizwan	Data mining	2013
Heart disease diagnosis using neural network	Ankeeta R. Patel and Maulin M. Joshi	Multilayer feed forward network	2013
Prediction of heart disease using multilayer perceptron neural network	Jayshril S. Sonawane and D. R. Patil	Back propagation algorithm	2014
A novel method for medical disease diagnosis using artificial neural network	Jasdeep Singh Bhalla and Anmol Agarwal	Scaled conjugate gradient and Levenberg Marquardt back propagation	2012
Parkinson's disease prediction using machine learning approaches	S. Gokul, M. Shivachitra, and S. Vijaychitra	Fully complex-valued radial basis function network	2013
Prediction of diabetes based on personal lifestyle indicators	Ayush Anand and Divya Shakti	K-Fold cross-validation method	2015
Neural network technique for cancer prediction; a survey	Shikha Agarwal and Jitendra Agarwal	Multilayer perceptron	2015
A probabilistic neural network approach for classification of dataset collected from north coastal districts of AP, India using MATLAB	T. Pamduranga Vital, G.S.V. Prasada Raju, K. Sreemamurthy, and V. P. Venkata Charan	Probabilistic neural network	2015

dataset from which confusion matrix is computed and trains that network to get the appropriate result. Results are in the form of receiver operating characteristic (ROC) plot, a plot of sensitivity versus specificity. The R value from this method is 0.69%, and the means accuracy is 69% (Table 1).

3 Methodology

The information analysis might be performed by neural systems. There is one neural system display utilized as a part of this examination: back propagation systems. It gives a computationally proficient technique for changing weight in a feed forward network, with differentiable activation work units [11]. The preparing of a system by back propagation includes three stages: the feed forward of the input training design, the calculation and back propagation of the related error, and adjustment of the weight. There are three noteworthy strides in the neural system: preprocessing, architecture, and post-processing.

- In preprocessing, data are gathered that could be utilized as the input sources and output of neural systems [12–14]. This information is initially standardized or scaled for decreasing the variance and noise.
- In design, an assortment of neural system models is fabricated that could be utilized to catch the connections between the information of sources of input and output.
- In post-processing, distinctive systems are connected to the estimating results to boost the ability of the neural network prediction (Fig. 2).

The diagnosis of diseases is done by collecting data. Than data uploaded in MATLAB so it will pass from training and testing part. After its result if the result is more than a threshold value, then the practitioner assumed that person have chances of that diseases and recommends the patient to go for a laboratory test to assure about the result. By the test, it confirmed that which particular disease we have and what is the stage of that (Fig. 3).

3.1 Simulation Tool Used MATLAB

The name MATLAB remains for matrix laboratory. In MATLAB, neural network toolbox is one of the usually utilized, effective, industrially accessible programming instruments for the advancement and outline of neural systems. The product is easy to understand and grants adaptability and accommodation in interfacing with different tool kits in a similar situation to build up a full application [15]. It can simply open by command nntool in MATLAB command window.



Fig. 2 Design steps for ANN

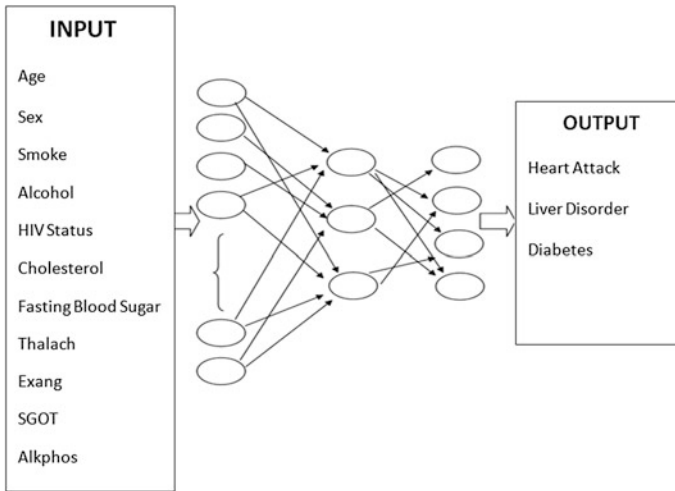


Fig. 3 Input and output attributes

4 Result

Parameters are as follows:

- Network Type = FeedforwardBackprop;
- Train Function = TRAINLM;
- Adaption Learning Function = LEARNGDM;
- Performance Function = MSE;
- Numbers of Layers = 2;
- Hidden neurons = 100.

After, assigning the value of these parameters. Next, divides the samples in training, validation, and testing. Here, we divide into the ratio of 90, 5, and 5%, respectively.

Figure 4 shows a simulink diagram of neural network in which x_1 shows its input and y_1 indicates a output for this network and Fig. 5 shows a neural network training model in this first layer is input layer [16], 11 inputs are given to this system then, its feedback is given to the middle layer which is hidden layer neurons taken in this layer are 100. After this step, it will preprocess the information and give its result at the output layer. So in this model, we already set its output to 3.

Then, training NN train tool plots the various state, i.e., performance, training state, error histogram, and regression [17–19].

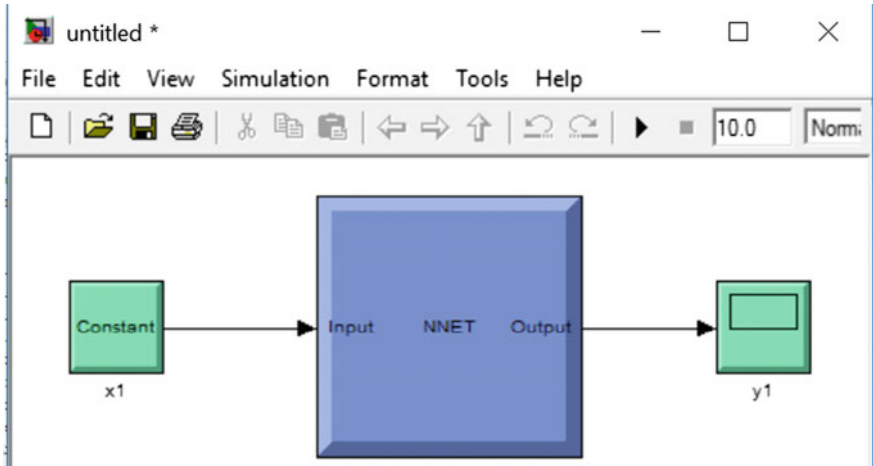


Fig. 4 Simulink diagram of NN

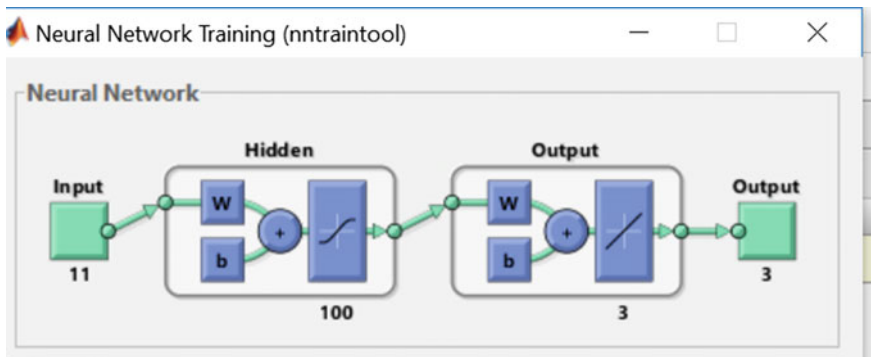


Fig. 5 Neural network model with different layers

Here, one plot is attached which is neural network training regression plot.

Figure 6 represents training, validations, and testing graphs of regression analysis. In this, training shows an accuracy of 98.34%, validation shows an accuracy of 19.41%, testing shows an accuracy of 15.61%, and overall result for this implementation is 88.67%.

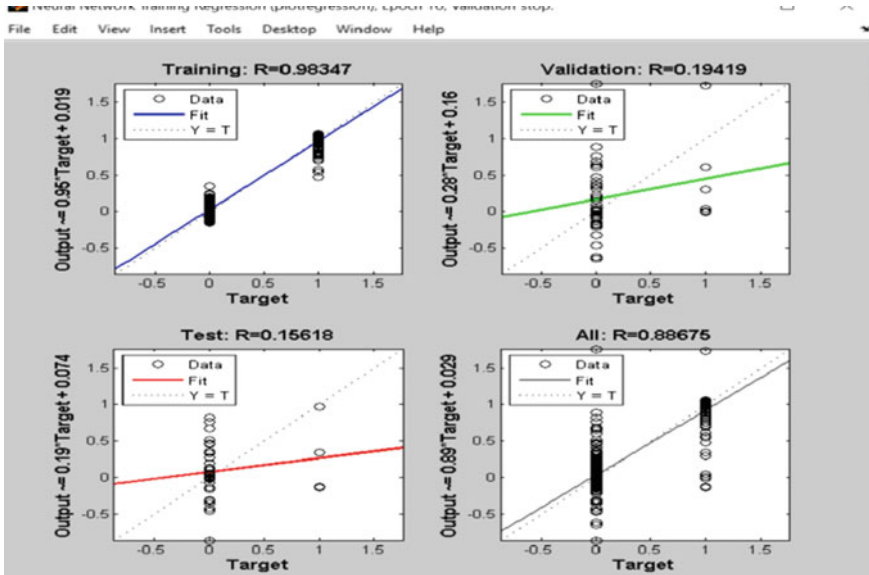


Fig. 6 Regression plot

5 Conclusion

This paper represents a tendency to access or utilization of ANN system for prediction of medical diseases. The idea of artificial neural systems in the field of medical is considered not extremely developed; the considerable measure of exploration is going on [20]. Thusly here, we designed simulated neural systems for diseases determination which prepared to utilize feed forward back propagation method. This model has been tried on a dataset that included patient data for determination of heart diseases, liver disorder, and diabetes datasets gathered from a UCI and nearby doctors. The parameters such as age, sex, blood pressure are important for prediction of disease in human health monitoring system. However, an addition of more feature such as HIV status, alkaline and phosphate added more carefulness to this system. From the results, it is observed that multilayer perceptron necessitated less number of neurons, less computation time as compared to other methods. ANN is adaptive, and this makes diagnose more reliable. In this system is trained first by using of datasets gathered form various sources, and then results are measured. Artificial neural systems illustrate noteworthy outcomes in managing and working with medical diseases dataset information. Results construed that this conclusion neural system-based model could be an important investigation of neural systems in the field of medical determination of diseases. In this architecture, the success rate of 88.67% was achieved.

6 Future Work

The proposed health monitoring system is based on MLP-NN that is more efficient. This system can be used in a wide range of medical field to help the professionals. But, the research is never ending process; a new beginning is always waiting. So, as a future work, more attributes can be used for training the system to increase the efficiency and accuracy of this system, which gives more appropriate results as compared to this. Also, new techniques can be applied for this.

Declaration I Bharti Yadav hereby declare that half of the data used to do the testing of my above work is collected from a hospital (ethical committee) of live patient and another half is from a central repository on Internet. If any issue arises hereafter, then I will solely be responsible for this.

References

1. Konstantin koura, Themis P. Exarchos, Konstantina P. Exarchos, Michalis V. Karamouzis and Dimitrios I Fotiadis, "Machine learning applications in cancer prognosis and prediction", computational and structural Biotechnology journal published Elsevier, vol 13, (2015), PP 8–17.
2. Giduthuri Sateesh Balri & Sundaram Suresh, "Sequential Projection Based Met cognitive Learning in a Radial Basis function Network for Classification Problems" IEEE transaction on neural networks and learning systems, vol 24 No 2 (2013).
3. Syed Umar Amin, Kavita Aggarwal and Dr. Rizwan Beg, "Genetic Neural Network Based Data Mining in Prediction of Heart Diseases using Risk factors", Proceeding of 2013 IEEE conference on Information and Communication Technologies (ICT 2013).
4. Anbeeta R. Patel & Maulin M. Joshi "Heart Diseases Diagnosis using Neural Network", 4th ICCCNT (IEEE), Tiruchengode, July 4–6 (2013).
5. Joyshril S. Sonawane & D.R Patil, "Prediction of Heart Diseases using multiplayer Perception Neural Network", ICICES 2014-SA Engineering College, Chennai, Tamil nadu (IEEE 2014).
6. Jasdeep Singh Bhalla and Anmol Agarwal, "A Novel method for Medical disease diagnosis using artificial neural network", The international conference on biomedical engineering and informatics 2008.
7. Gokul S, Shivachitra M and Vijayachitra S, "Parkinson's disease prediction using machine learning approaches", Proceeding IEEE 5th International Conference on advanced Computing 2013.
8. Ayush Anand and Divya Shakti, "Prediction of diabetes based on personal lifestyle indicators", First International Conference on next generation computing technologies (IEEE) 2015.
9. Shikha Agarwal and Jitendra Agarwal, "Neural Network Technique for Cancer prediction; A Survey", 19th International conference on knowledge based and intelligent information and engineering system, Published by Elsevier 2015.
10. T. Pamduranga Vital, G.S.V Prasada Raju, K. Sreemamurthy and V.P Venkata Charan, "A Probabilistic Neural Network Approach for classification of dataset collected from North Coastal Districts of AP, India using Matlab", International Conference on intelligent computing, communication and convergence, Elsevier, procedia computer science 48 (2015).
11. I.A Basheer and M. Hajmeer, "Artificial neural network : fundamentals computing diseases and application", Journal of micro biological methods 43, published by Elsevier 2000.

12. Dimitrios H. Mantzaris, George C. Anastassopoulos and Dimitriou K. Lymperopoulos, "Medical disease prediction using neural network", Published by research gate 2008.
13. Dr K. Usha Rani, "Analysis of Heart Disease dataset using Neural Network", International journal of data mining and knowledge management process, Volume 1, number 5, September 2011.
14. K. Balachandran and Dr R. Anitha, "Supervised Learning processing techniques for predignosis of lung Cancer diseases", International journal of computer application (0975-8887) Volume 1 number 4 2011.
15. Muhammad Akmal Sapon, Khadijah Ismail Suehazlyn Zainudin, "Prediction of Diabetes by using artificial neural network", International conference on circuits—systems and simulation Volume 7, 2011.
16. Dr R.R. Janghel, Dr Anupam Shukla and kshitiy Verma, "Soft computing based expert system for hepatitis and Liver disorder", 2nd IEEE International conference on engineering and technology (ICE Tech) 2016.
17. Xin Yao Senior Member, IEEE and Yong Liu, "A new evolutionary system for evolving Artificial Neural Networks", IEEE Transaction on Neural Network Vol. 8, No-1, May 1997 Transactions on information Technology in Biomedicine Vol 11, No. 3, (2012)
18. E. Sathish, M. Sivachitra, Ramasamy Savitha, and S. Vijayachitra, "Wind profile prediction using a metacognitive fully complex-valued neural network," IEEE Internation conference on Advanced computing (ICoAC), pp 1–6, (2012).
19. Kaur K. "Optical Multistage Interconnection Networks Using Neural Network Approach", Master of Engineering, Thapar University (2009).
20. "Artificial Neural Networks in Medicine World Map" published in 2011, It was published in USENET, in July 21, (2011).
21. Mohammad A.M Abushariah, Assal A.M. Alquadah, Omar Y. Adwan, "Automatic Heart Disease diagnosis system based on Artificial neural network and adaptive neuro fuzzy inference system approaches", Journal of software engineering and applications, 2014.

A Critical Review on the Application and Problems Caused by False Alarms

Vishal Sharma, Arun S. Varma, Atul Singh, Divyansh Singh and Bikarama Prasad Yadav

Abstract Emergency evacuation, mock drills, and response collected by detectors and sensors play an important role in averting the risks and disasters. Recent scenario gives the detailing of the false alarm predictions which do affect the general time line of the organization but also create the panic situation which somewhere results in loss of life and property. The use of fire alarms which are also connected with sensors plays an important role in emergency preparedness. Fire alarm work in coordination with detectors and sensors play an effective role as a best response. False Alarm is the result of poor installation, neglect in maintenance, environment, and anthropogenic factors. According to one of the data, Great Britain noticed somewhat 312,000 false alarms in the year 2011–12. The review paper analyzes the trends and latest developments in fire alarms both in industries and residential areas. The paper discusses and gives a critical view of the current problems of fire alarms/false alarms and its future implications in dealing with emergency response and evacuation.

Keywords False alarm · Emergency evacuation · Preparedness
Mock drills · Sensors

V. Sharma (✉) · A.S. Varma · A. Singh · D. Singh · B.P. Yadav
University of Petroleum and Energy Studies, Dehradun, Uttarakhand, India
e-mail: vishalsharma7r@gmail.com

A.S. Varma
e-mail: arunsvarmasandhu@gmail.com

A. Singh
e-mail: atul79346@gmail.com

D. Singh
e-mail: divssayush@gmail.com

B.P. Yadav
e-mail: bpyadav@ddn.upes.ac.in

1 Introduction

In the modern world, technology has conquered every problem up to a certain limit. Safety can be achieved only if the technology is being rightfully used. Accidents have consumed the lives of many people, not only lives but it has also caused problems to the properties. Residential and industrial fire has caused many problems socially, economically, and environmentally. According to studies about 86,400 nonresidential building fires were reported to United States fire department, each year it consumes the lives of approximately 85 people and causes injuries to about 1325 people. About \$2.6 billion property loss are being reported annually [1]. The situation is worse in developing and underdeveloped countries.

Many technique and fire preventions methods are used to prevent accidents. Proper handling of combustible and flammable materials, safe housekeeping, keeping proper fire extinguishing agents, proper investigation, etc., are used to minimize the fire [2]. Even for fire accident scenario fire drills, evacuations strategy, smoke and heat sensors for fire detection and fire alarms are used.

Automatic fire detection systems, when combined with various elements of emergency response and evacuation plan, can effectively reduce material damage, personal injuries, and loss of life from fire in the organization [3]. The alarm's and sensor's main function is to quickly identify a developing fire and alert building occupants and emergency response personnel before extensive damage occurs [4].

Evacuation strategy plays an important role during fire accidents, earthquake, and other natural calamities. A fire evacuation strategy must be there in light for risk assessment and other fire precautions which are intend to put in place. Two types of fire evacuation plans are considered, i.e., simultaneous evacuation and vertical phase evacuation. In simultaneous evacuation, in case of a fire alarm people are orderly moved to a safe premise [5]. Vertical phase evaluation is normally done by immediate evacuating of the floor where the fire is located and the floor above, after their evacuation people below are evacuated in an orderly manner.

According to the studies mostly fire in residential areas occur at night, i.e., when most people are asleep. People notice the fire only when it becomes out of control. In such situations, there arises a necessity for fire alarms in buildings for early detection of fire and help people to respond to the situation in time to save life and property. Early detection will allow them to escape or extinguish the fire [6]. Mainly the following detectors are used for fire detection such as heat detector, smoke detector, flame detector, and fire gas detector.

According to the studies by NFPA and the US fire administration, the usage of fire alarm has risen from 10% in 1975 to about 95% in 2000 and it might rise up to 135% in 2018 [7]. Also deaths due to fire accident in residential areas have decreased considerably since the last couple of years. It shows us the effectiveness of use of fire alarms. It has been observed that well installed and maintained fire alarms save lives of many people. It can be effectively used only when the main properties of the detector like good durability, authenticity, sensitivity are proper and it should not give any false alarms [8].

In case of a fire, according to the studies,

- Death due to fire is 51% less in homes when compared with homes without fire alarms, i.e., chance of deaths due to fire is minimized by half.
- 65% of deaths in 2004 happened in homes where the fire alarms were not used.
- When fire alarm and sprinklers are both used, the chances of survival increased up to 82% [9].

Technology can be tricky sometimes, nothing is perfect. Sometimes the sensors sense something other than fire which could activate the fire alarm it may be smoke, fog, and other things. The main cause will be unintentional like power surges during lightening and equipment failure. False alarm causes many problems, so it will be wise to understand the problems and make solutions for such problems [10].

2 Fire Alarm System

Fire detection and alarm combined help in notifying the presence of fire in its vicinity. Fire alarms are crucial with the help of sensors and detectors to detect harmful circumstances that involve fire and smoke [11]. A control panel is used to control both fire detectors and fire alarms which is controlled manually. Its main job is to coordinate the fire alarm system. We cannot underestimate the damages caused by fire, and it can be nullified by detection of fire in which fire alarms play an important role [12]. Warning is provided by fire alarm for taking the action during any fire accident.

3 Fire Detectors & Sensors

A fire detector or sensor works on the principle of optical processing. The main functions of fire detectors are identifying the situation of fire; it also helps in actuating both audial and visual signals, also helps in alerting the fire brigade and security on time. The mode of operation can be manual or automatic [13]. If we have installed or maintained the system then it will be able to work 24 h a day and 365 days a year. Mostly five types of fire detectors are used; they are smoke detector, heat detector, flame detector, smoke-heat detector-laser beam technique, and other combustion products detectors [14]. During any combustion process, it gives out smoke particles which may be solid or liquid. In smoke detector, these kinds of solid/liquid particles are identified by their ability to obstruct and reflect light. The particle size of smoke is between the range 0.5 mil microns to 10 microns. During some stages of fire, it produces particles which are lesser than 0.5 mm that cannot be identified, but it can be detected by their ability to attract ionized particles. Light attenuation detector, light scattering detector, and ionization

detector come under smoke detectors. Light attenuation detector works on light obscuration techniques. An electronic receiver and light emitter are present inside light attenuation detector [15]. Light scattering detector works on Tyndall effect. Ionization detector works on particles having low size, here two positive and negative electrodes and radioactive source are present. When the smoke particles enter the detector it gets attached to the alpha particles. The alpha particles are charged and heavy in nature, here positive and negative particles are formed. These particles get accumulated between the plates which will go to the circuit and it actuates the alarm. A heat detector is used to detect the temperature change using a heat sensitive element. Heat detectors are based on fixed temperature type and rate of rise of temperature [16]. The fixed temperature device works when the heat sensitive material reaches up to a certain point called eutectic point in which solid changes to liquid. The heat detector works when the surrounding temperature exceeds the operating temperature. Flame detectors are based on UV and IR rays [17].

3.1 Fire Alarm

The sensor will provide a signal to the alarm, and it will automatically produce a large siren followed by big flashing lights. It will help people identify that fire has occurred. Fire alarm can be automatic or manual [18].

3.2 Problems and Solutions for False Alarm Systems and Evacuation Strategies

A false alarm is caused when the similar conditions that are observed during a fire are detected by the sensors. It could be caused by mechanical, electrical, or unintended interference. Smoke that arises when cooking food could cause the tripping of fire alarm same goes for bonfires and smoking cigarettes. Lightening can be a cause of false alarms/malfunctioning. If we are using low-voltage fire alarm systems without any surge arrestors then the sudden surge of electricity could actuate the fire alarm or can cause malfunctioning [19]. Intentionally tripping the alarm is not big news, but it is the false alarm which consumes the time of fire brigades. False alarm could be caused from equipment failure and low battery. According to the report from the “fire statistics,” Great Britain, 2011–2012

- Local authorities and rescue services handled 584,500 fires or false alarm and less than 7% fewer than 2010–2011,
- False alarm is reduced from a rate of 339,000 during the year 2010–2011 to a rate of 312,000 during the Year 2011–2012.

During the year 2004–05 (see Table 1) total fire and false alarm were 845,000 in which 433,000 were false alarms which are approximately 51.2% of the total fire and false alarm. The fire and false alarm were reduced during the years, but the false alarm during the year 2011–12 (see Table 1) were 312,000 which is approximately about 53% of total fire and false alarm. This shows that even though the government has taken considerable steps to reduce the false alarm the rate of false alarm is not down (Fig. 1).

A false alarm went off at a Paris museum called Louvre museum on Wednesday July 20, 2016. The museum was evacuated by the officials immediately after the fire alarm. The official does not confirm the reason behind the tripping. The visitors say the guards were well trained as well as effective during the situation. Louvre museum is one of the largest museums in the world [20]. It may cause problems toward the reputation of the organization; it also causes business disruption and time loss.

False alarms can cause difficulties in day-to-day works by creating the time loss. Reducing the false alarm in residential places is a big challenge because of all the cooking activities. There are few ways to decrease the number of false activations of such alarms. First is installation and maintenance of fire alarm which will decrease the probability of false fire alarms and other is awareness among the residents about the use of detector is likely to lead a substantial reduction in false alarms [21].

Table 1 Fires by location and false alarm, Great Britain, 2004/05–2011/12 (figure are rounded thousands for understanding purpose)

Year	Fires and false alarms	Total fire	Building fires	Outdoor fires	Chimney fires	False alarms
2004–2005	845	412	93	311	8	433
2005–2006	832	409	90	310	9	423
2006–2007	838	411	86	318	8	426
2007–2008	770	364	80	276	9	406
2008–2009	694	309	74	225	11	385
2009–2010	654	299	74	216	10	354
2010–2011	627	288	74	204	10	339
2011–2012	585	272	71	193	8	312

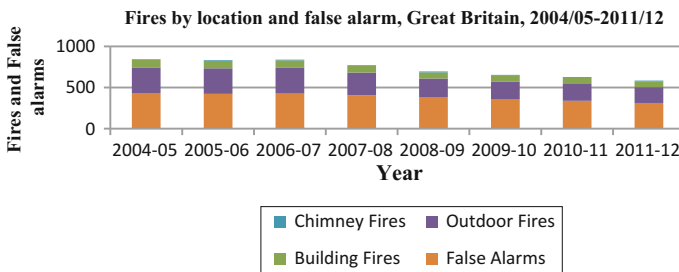


Fig. 1 Fires by location and false alarms

3.3 Comparison Between India and Japan Evacuation Strategies

Firecracker caught fire leaving a woman dead in Maradu Kottaram Bhagavathy Temple on April 11, 2016. The fire caused widespread damage to houses in surrounding areas. Fire tragedy in Kollam district was certainly a shock to people of Kerala. But the state seems to be living amidst such accidents. Since 1952 many such accidents have occurred across the state, for example, in 1990 at least 26 people were charred to death as the fireworks created havoc in Duryodhana Temple in Kollam. Also in 1984, during Kandashamkadavu Church festival a cracker blast disaster claimed the lives of least 20 lives [22]. If the Government had taken the proper actions against fire by learning from such events and proper evacuation procedure plans present there, then it would have reduced the loss to life and property.

On December 22, 2016 in Japan about 140 buildings were burnt due to massive fire spread in Japanese prefecture of Niigata. According to the report, there were two minor injuries due to fall and inhalation of harmful smoke. The authorities were able to evacuate 740 people from 360 homes at a high risk [23]. In Indian scenario such kind of accidents makes a widespread panic among the people which badly affect the evacuation procedures which can ultimately lead to deaths. In countries like Japan, evacuation becomes easy because they are prepared for such accidents. Everyone there knows how to deal with such hazards due to regular fire drills and strong evacuation plan.

3.4 Causes of False Alarms

Today in India we are facing problems related to false alarms which sometimes cause more loss than the actual accident due to the panic behavior of frightened citizens. As identified from the data collected, false alarms happen due to two main reasons, i.e., false alarms due to apparatus and malicious false alarms [24]. The false alarms are mainly caused due to damaged or broken apparatus. It is recorded that even smoke from cooking, smoking a cigarette, chemicals, and steam can set off the alarm causing havoc. Incorrect positioning, poor maintenance, and even sometimes power surge can result in false alarms. So the proper maintenance and cleaning of fire alarms are necessary on a regular basis.

The main reasons behind the false alarm and its rate are shown in Fig. 2. According to this detail, most of the false alarm is caused by fault in the system. This figure helps us to prioritize the things we must take to reduce the false alarms.

The number of malicious calls, also the reason for false alarm, to fire brigade is increasing consequently, public safety is being imperiled, and it is a complete wastage of money. Every year Shropshire Fire and Rescue Service receive around 600 malicious calls. Due to the availability of mobile phones people are able to call from anyplace which ultimately increases the malicious false alarm calls. The

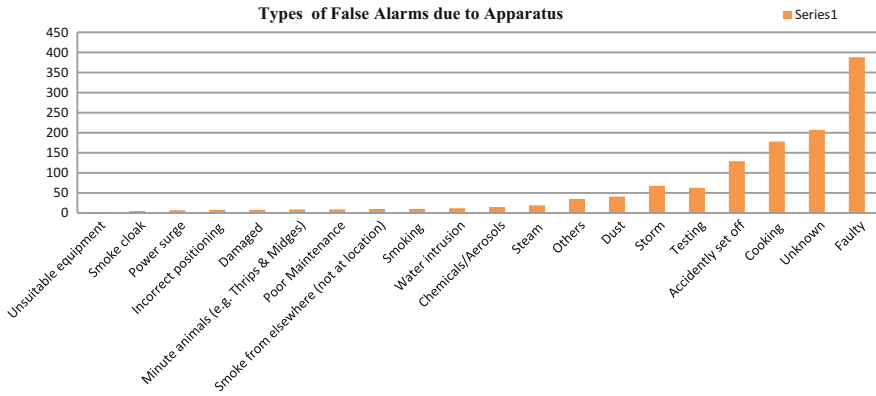


Fig. 2 Types of false alarms due to apparatus

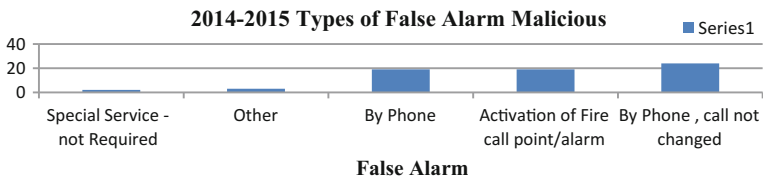


Fig. 3 Malicious false alarm

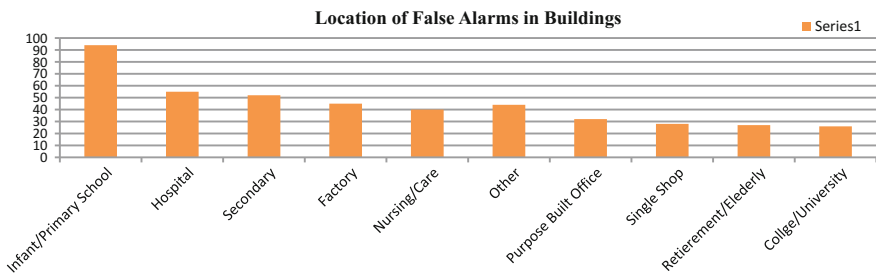


Fig. 4 Location of fire alarms in building

increase in the number of prepaid mobile phones used by young people has only increased frequency of the occurrence of such conditions and also it is hard to locate those mobile users [25]. The data regarding malicious false alarm is shown in Fig. 3.

Studies proved that the rate of false alarm (Fig. 4) is highest in infant/primary schools than college or universities. The main reason for this difference is the awareness of college students toward fire alarms. Awareness about basic things in life must be taught at an early stage of life [26].

4 Solutions

Overcoming the false alarms and the suppression problems present in the prior art fire detectors can be accomplished by the present inventions. This can be achieved using combined color spectrum discrimination and flame flicker frequency selection. Technically, speaking the rate of false alarms can be reduced by managing the low-level signals and only allowing the fire alarm to actuate only if the signals are coming continuously for a certain period of time. This method also provides a connection through radio between fire detecting systems and the alarm system. Video monitoring systems can be used to identify the false alarm. If there is a video surveillance in the false alarm area then we will be able to identify the alarm cause.

A surge arrester is a device used to control the voltage in the system, if any fault happens in the system then surge arrester which is connected in series to the fire detector will bypass the extra voltage in the system to earth which would ultimately protect the system [27]. Aspirating smoke detectors used in industrial areas uses pipes to intake air samples. The pollutants which come with air actuate the false alarm. If more fine air filters are used in these pipes the pollutants will be removed and the false alarm can be avoided.

There are few techniques which could minimize the rate of false alarm. Multisensors which would sense smoke and heat that are present inside the house. Until and unless both the sensors in the detector sense the problem the alarm won't actuate, it would help in reduction of the time loss and would avoid unwanted panic among the people. This will also increase the accuracy of the fire alarm.

5 Conclusion

Fire alarm system plays an important role in emergency preparedness, response, and mitigation. As fire alarm system works in the combined way with detectors and sensors, their effectiveness and efficiency purely depend on the usage and working of the sensors. Mainly five types of fire detectors based on the characteristics of fire and smoke are used. The problem of false alarm system has been the cause of many adverse situations which has led to loss of life and resources damage. The situation of false alarm can be regulated by the system of sensors and detectors. As discussed in the earlier part that the false alarm brings up the occurrence of panic, violence, psychological disorder, and mob behavior. There is a need to find the solution to prevent such scenario of false alarm by the use of best available technologies. In order to hinder such problems regular mock drills, inspections both in industrial and residential sectors are necessary. This will lead to proper communication to workers and inhabitants which will give them chance to understand the signals and respond accordingly. Industries, universities, hospitals, residential buildings are much prone to hazards and emergency conditions, these alarms (fire alarms) pave the way for safe protection. The basic concern therefore is to minimize the response and

condition of false alarms and to propagate its effectiveness in all the sectors so that the emergency preparedness and response may be implemented in a best possible way and saving people from risks and disasters.

References

1. Topical Fire Report Series Volume 14, Issue 5/June 2013 Nonresidential Building Fires (2009–2011).
2. Löwy, Michael, and Chris Turner. *Fire alarm: Reading Walter Benjamin's On the concept of history*. Verso, 2005.
3. Costa, Hilario. "Fire alarm system with method of building occupant evacuation." U.S. Patent No. 7,218,238. 15 May 2007.
4. Asatryan, D., & Hovsepyan, S. (2015, September). Method for fire and smoke detection in monitored forest areas. In *Computer Science and Information Technologies (CSIT)*, 2015 (pp. 77–81). IEEE.
5. Executive summary National Fire Protection Association (NFPA) and the U.S. Fire Administration, sited and retrieved on 24th January 2017.
6. Marbach, Giuseppe, Markus Loepfe, and Thomas Brupbacher. "An image processing technique for fire detection in video images." *Fire safety journal* 41.4 (2006): 285–289.
7. Drawings, C. Shop. "For fire-alarm system." Include plans, elevations, sections, details, and attachments to other work 1: 283111–2.
8. MacFarlane, R. K. (1999). U.S. Patent No. 5,896,082. Washington, DC: U.S. Patent and Trademark Office.
9. Kimura, T., Tanaka, S., & Suzuki, T. (1985). U.S. Patent No. 4,525,700. Washington, DC: U.S. Patent and Trademark Office.
10. Zhang, Lei, and Gaofeng Wang. "Design and implementation of automatic fire alarm system based on wireless sensor networks." *Proceedings of the International Symposium on Information Processing, Huangshan, China*. Vol. 2123. 2009.
11. Giglio, Louis, Wilfrid Schroeder, and Christopher O. Justice. "The collection 6 MODIS active fire detection algorithm and fire products." *Remote Sensing of Environment* 178 (2016): 31–41.
12. Asif, Omar, et al. "Fire-Detectors Review and Design of an Automated, Quick Responsive Fire-Alarm System Based on SMS." *Int'l J. of Communications, Network and System Sciences* 7.09 (2014): 386.
13. Ko, Byoung Chul, Kwang-Ho Cheong, and Jae-Yeal Nam. "Fire detection based on vision sensor and support vector machines." *Fire Safety Journal* 44.3 (2009): 322–329.
14. Qureshi, Waqar S., et al. "QuickBlaze: early fire detection using a combined video processing approach." *Fire Technology* 52.5 (2016): 1293–1317.
15. Nguyen-Ti T, Nguyen-Phuc, T, Do-Hong, T.: Fire detection based on video processing method. In: 2013 International Conference on Advanced Technologies for Communications (ATC), pp. 106–110 (2013) 16 Fire and disaster management agency, ministry of internal affairs and communications, firefighting white paper 2009; <http://www.fdma.go.jp/html/hakusho/h21/index.html>.
16. Chen, Thou-Ho, et al. "The smoke detection for early fire-alarming system base on video processing." *Intelligent Information Hiding and Multimedia Signal Processing*, 2006. IHH-MSP'06. International Conference on. IEEE, 2006.
17. Bellecci, C., et al. "Application of a CO2 dial system for infrared detection of forest fire and reduction of false alarm." *Applied Physics B: Lasers and Optics* 87.2 (2007): 373–378.
18. Ishii, Hiromitsu, and Takashi Ono. "Fire alarm system, sensor and method." U.S. Patent No. 4,871,999. 3 Oct. 1989.

19. Bahrepour, Majid, Nirvana Meratnia, and Paul JM Havinga. Automatic fire detection: A survey from wireless sensor network perspective. No. TR-CTIT-08-73. University of Twente, Centre for Telematics and Information Technology, 2008.
20. Chen, Shin-Juh, et al. "Fire detection using smoke and gas sensors." *Fire Safety Journal* 42.8 (2007): 507–515.
21. Albert, David E. "Enhanced fire, safety, security and health monitoring and alarm response method, system and device." U.S. Patent No. 7,173,525. 6 Feb. 2007.
22. Rinsurongkawong, Suchet, Mongkol Ekpanyapong, and Matthew N. Dailey. "Fire detection for early fire alarm based on optical flow video processing." *Electrical engineering/electronics, computer, telecommunications and information technology (ecti-con)*, 2012 9th international conference on. IEEE, 2012.
23. Ahrens, Marty. "Home smoke alarms: the data as context for decision." *Fire Technology* 44.4 (2008): 313–327.
24. Shehata, Mohamed S., et al. "Video-based automatic incident detection for smart roads: The outdoor environmental challenges regarding false alarms." *IEEE Transactions on Intelligent Transportation Systems* 9.2 (2008): 349–360.
25. Cannon Jr, Thomas Calvin. "Personal alarm and surveillance system." U.S. Patent Application No. 12/020,663.
26. Seeley, John E., and Mitchell Black. "Communication system for a fire alarm or security system." U.S. Patent No. 7,429,921. 30 Sep. 2008.
27. Izadi, Iman, et al. "An introduction to alarm analysis and design." *IFAC Proceedings Volumes* 42.8 (2009): 645–650.

Enhancement of Transient Stability of Multimachine System Using TCSC, SSSC and UPFC

Lokesh Garg, S.K. Agarwal and Vivek Kumar

Abstract This paper presents the transient stability enhancement of a multimachine system using series FACTS controllers. Series FACTS controller devices, i.e. TCSC, SSSC and UPFC, have been used in this paper for enhancing the transient stability of the system. Time-domain simulations are carried on PSAT (power system analysis tool box). The simulation results demonstrate that transient stability improves commendably of the multimachine system by using TCSC, SSSC and UPFC. Eigen value analysis also has been done during prefault condition, fault condition and with series FACTS controllers, i.e. TCSC, SSSC and UPFC. It also been observed that UPFC gives better transient stability enhancement as compared to TCSC and SSSC.

Keywords Power system • Power system analysis tool box • Unified power flow controller • Static synchronous series compensator • Transient stability Multimachine system

1 Introduction

Power system stability control is an important aspect. In the event of large disturbances, sudden faults, opening or closing of circuit breaker, load changes etc. or internal mechanical torques affects the power system stability of the system. Since power system is a large interconnected system, it is required that it must have secure

L. Garg (✉)
YMCAUST, Faridabad, India
e-mail: lokeshgarg123@gmail.com

S.K. Agarwal
Department of ECE, Faridabad, India
e-mail: sa_3264@yahoo.co.in

V. Kumar
Department of CSE, DCTM, Palwal, India
e-mail: principal@dctm.edu.in

and stable operation. In the last two decades, the flexible AC transmission system (FACTS) devices are becoming more popular. The main objectives of FACTS devices are to improve transient stability, voltage stability and line transfer capacity. Out of these three objectives, the improvement of transient stability is one of the most important aspects [1]. Using FACTS devices, the enhancement of transient stability can be done by controlling the real and reactive power during fault conditions. Blackout can occur if the system has low transient stability because of which the generators may go out of synchronism. Due to advancement of solid-state power electronic, FACTS devices have fast and reliable operation. Different types of FACTS devices are available like TCSC, SVC, SSSC, UPFC. [2]. In this paper, transient stability analysis has been done by using TCSC, SSSC and UPFC. The present paper is laid out as follows: Sect. 1—Introduction, Sect. 2—Study system, Sect. 3—Simulation results using PSAT model on IEEE 9 bus system pre-fault condition, faulty condition and post-fault condition with different types of FACTS controllers. Simulations results show that the transient stability of the system can be enhanced by different types of series FACTS controllers. UPFC has better transient stability enhancement characteristics as compared to other series FACTS controllers', i.e. TCSC and SSSC.

2 Study System

System under Study: In this model, there are nine buses, Bus no. 1 is taken as slack bus, voltage at this bus is 1 p.u. and buses 2 and 3 are generator buses (PV buses). Generator 1 rated with 100 MVA, 18 kV and 60 Hz, Generator 2 rated with 100 MVA, 16.5 kV and 60 Hz, and Generator 3 rated with 100 MVA, 13.8 kV and 60 Hz. Generator data, bus data, line data has been given in the Appendix 1. IEEE 9 bus system used here as a multimachine system. Study system is shown in Fig. 1 with pre-fault condition. All buses connected to each other by π section of transmission line. Assume that loads to be of constant impedance and all generators are operating with constant mechanical input power and with constant excitation. Power system analysis tool box (PSAT) software is used for the simulation. Transient stability is more in steady-state condition, i.e. pre-fault condition. The IEEE 9 bus system built using PSAT library. Rotor angle curve and voltage at all buses during pre-fault condition are shown in Fig. 6a, f, respectively.

2.1 Fault Condition

A three-phase fault is simulated at Bus no. 4 after start of simulation 0.8 s, and the fault clearing time is 1.05 s. As the fault occurs on the system, there may be loss of synchronism between the generators. It also affects the voltage at all buses during fault. Simulation result shows that the rotor angle positions of different generators

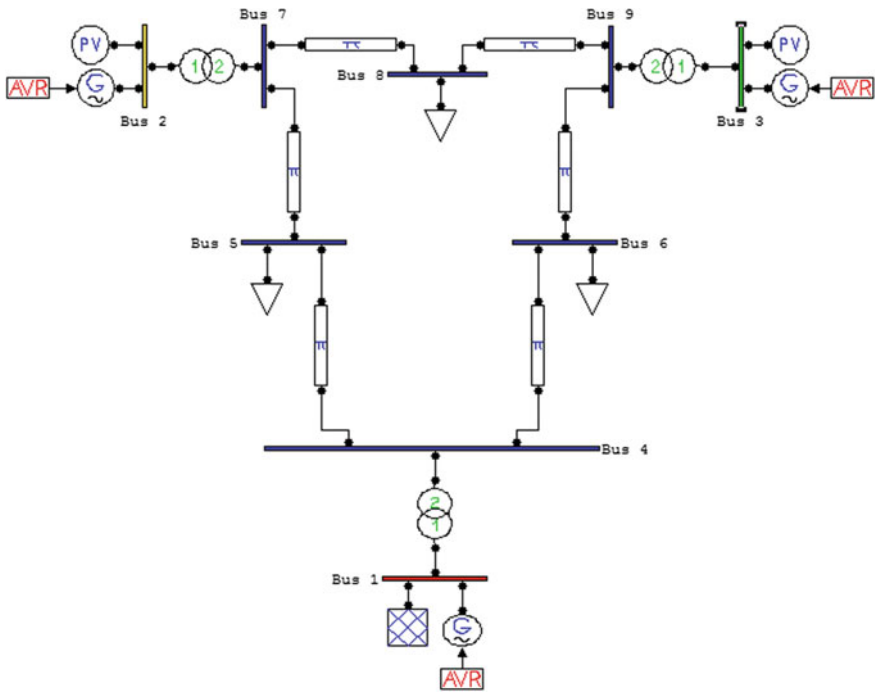


Fig. 1 IEEE 9 bus system pre-fault condition

change with reference to pre-fault condition and also the bus voltages at different buses have been changed with reference to pre-fault condition. Rotor angle curve and voltage at all buses during fault condition are shown in Fig. 6b, g, respectively (Fig. 2).

2.2 Post-fault Condition with TCSC

In order to maintain the synchronism and also enhanced transient stability of the system, different types of series FACTS devices, i.e. TCSC, SSSC and UPFC, are placed in the faulty system. TCSC has been placed in between buses 4 and 5. TCSC having 30% series compensation has been used for simulation. TCSC data has been given in the Appendix 2. Rotor angle curve and voltage at all buses in post-fault condition are shown in Fig. 6c, h, respectively (Fig. 3).

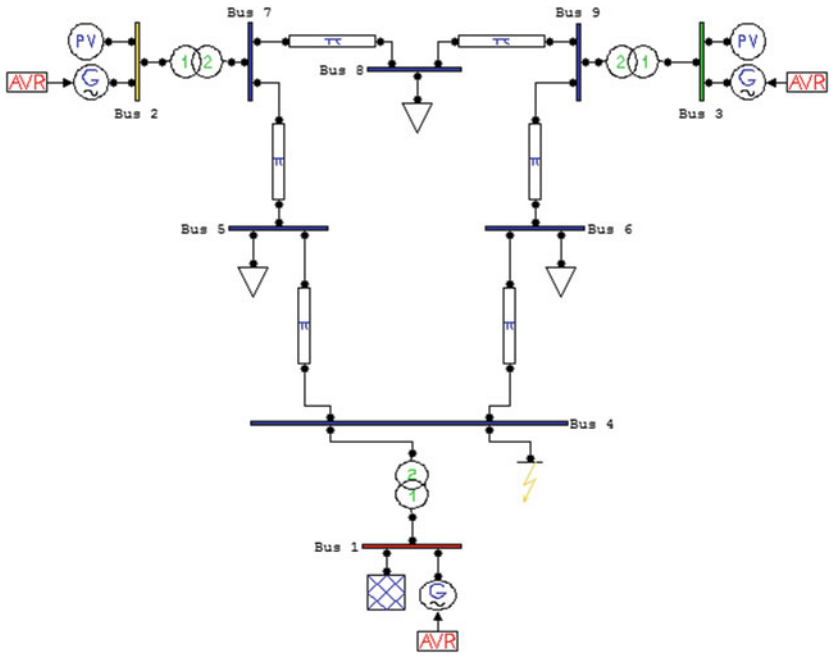


Fig. 2 IEEE 9 bus system fault condition

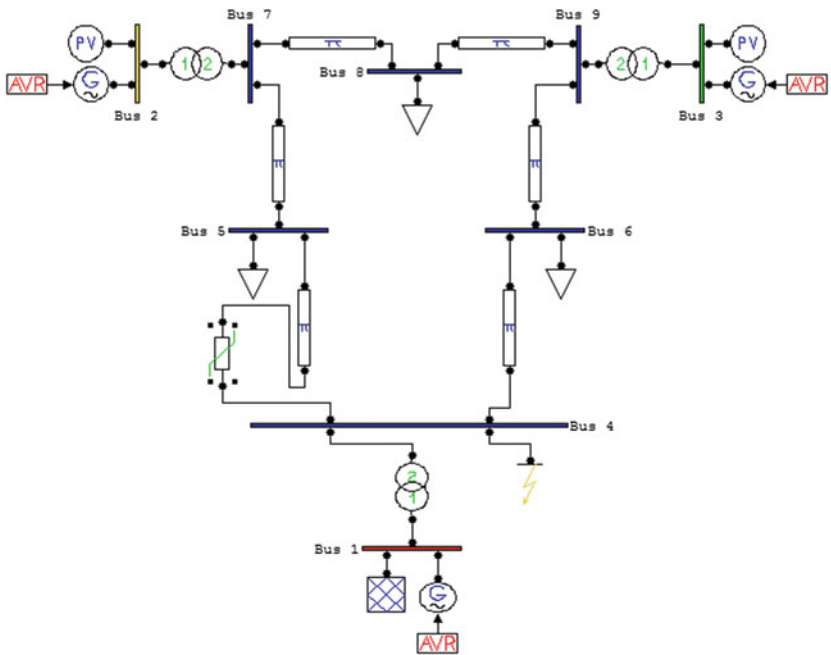


Fig. 3 IEEE 9 bus system with TCSC

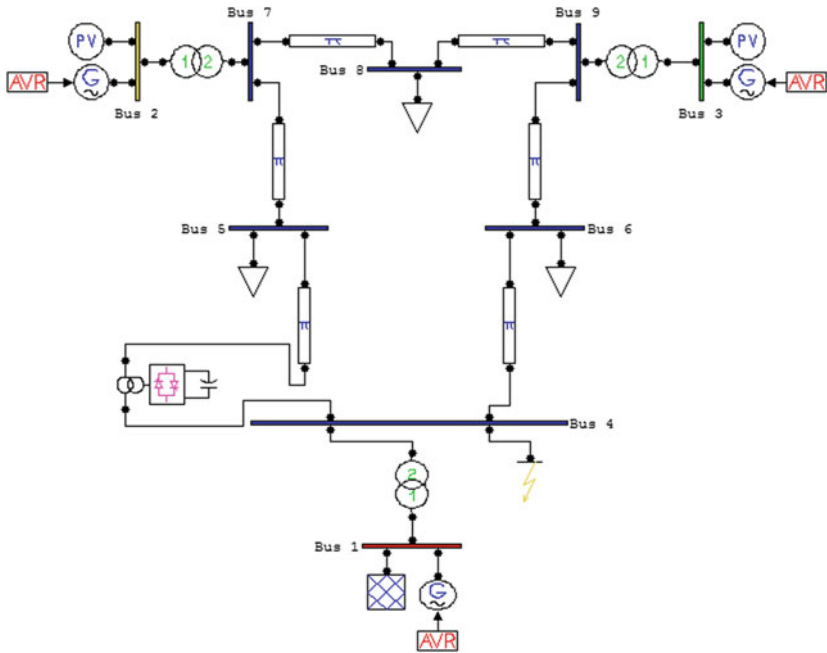


Fig. 4 IEEE 9 bus system with SSSC

2.3 Post-Fault Condition with SSSC

In order to maintain the synchronism and enhanced transient stability of the system, SSSC with 30% series compensation has been placed in the faulty system between buses 4 and 5. SSSC data has been given in the Appendix 2. Rotor angle curve and voltage at all buses in post-fault condition are shown in Fig. 6d, i, respectively (Fig. 4).

2.4 Post-fault Condition with UPFC

For enhancement of transient stability and to maintain the synchronism, UPFC has been installed between buses 4 and 5 with 30% series compensation. UPFC data also has been given in the Appendix 2. Rotor angle curve and voltage at all buses in post-fault condition are shown in Fig. 6e, j, respectively (Fig. 5).

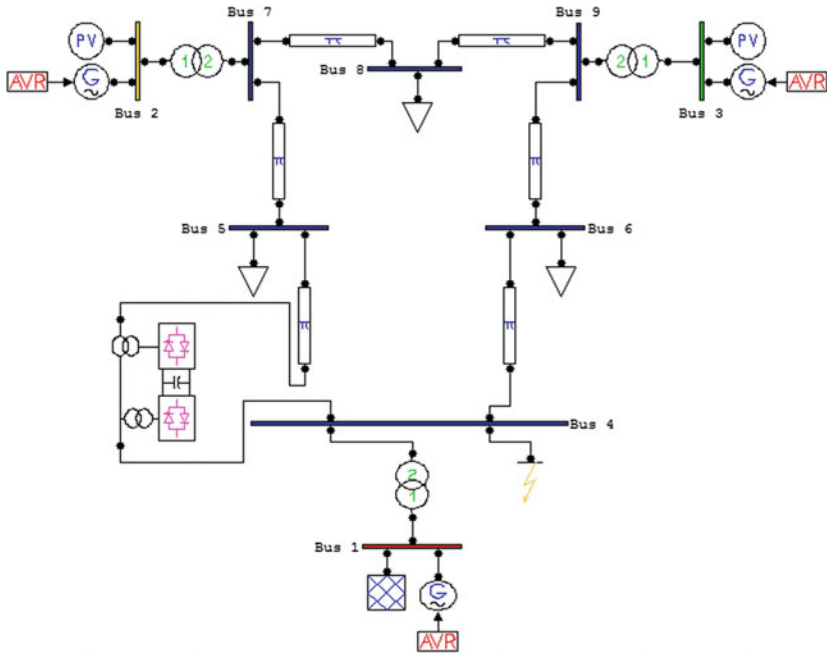


Fig. 5 IEEE 9 bus system with UPFC

3 Simulation Results

Simulation results from Fig. 6a–j show the rotor angle curve, voltage at all buses with pre-fault condition, fault condition and post-fault condition with TCSC, SSSC and UPFC.

4 Conclusion

In this paper, transient stability analysis has been studied on IEEE 9 bus system using PSAT software. Simulation results show the capability of TCSC, SSSC and UPFC on multimachine system for the improvement of transient stability. It has been concluded from eigen value analysis that UPFC is a better FACTS controller as compared to TCSC and SSSC for the improvement of transient stability of the system for the same level of series compensation.

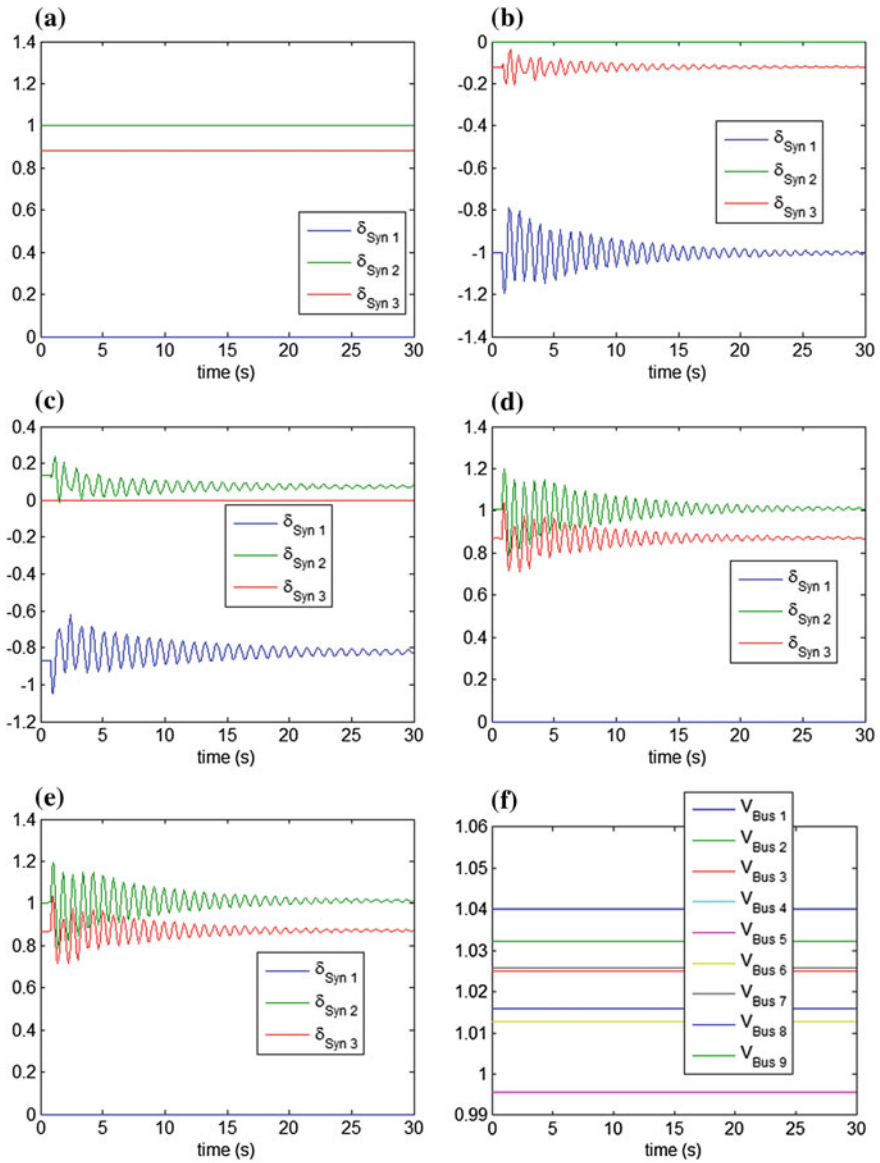


Fig. 6 **a** Rotor angle curve pre-fault condition. **b** Rotor angle curve fault condition. **c** Rotor angle curve with TCSC. **d** Rotor angle curve with SSSC. **e** Rotor angle curve with UPFC. **f** Voltage at all buses during pre-fault. **g** Voltage at all buses during fault condition. **h** Voltage at all buses with TCSC. **i** Voltage at all buses with SSSC. **j** Voltage at all buses with UPFC

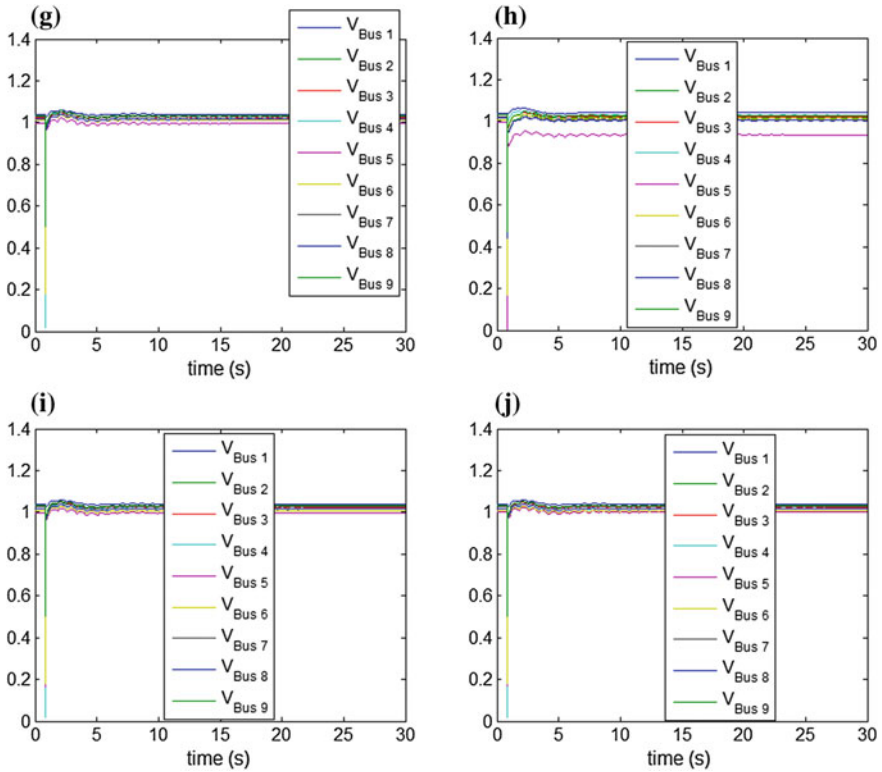


Fig. 6 (continued)

Appendix 1

<i>Generator data</i>					
	GEN 1	GEN 2	GEN 3		
MVA	100	100	100		
kV	18	16.5	13.8		
Hz	60	60	60		
R_a (p.u.)	0.00	0.00	0.00		
X_L (p.u.)	0.00	0.00	0.00		
X_d (p.u.)	0.8958	0.1460	1.3125		
X'_d (p.u.)	0.1198	0.0608	0.1813		
X''_d (p.u.)	0.0000	0.0000	0.0000		
<i>Transformer data</i>					
Bus no.	No. of i/p	No. of o/p	Voltage (kV)	Voltage (p.u.)	Angle (rad)
1	2	1	16.5	1.0	0.0

(continued)

(continued)

Transformer data

Bus no.	No. of i/p	No. of o/p	Voltage (kV)	Voltage (p.u.)	Angle (rad)
2	2	1	18	1.0	0.0
3	2	1	13.8	1.0	0.0
4	2	1	230	1.0	0.0
5	1	2	230	1.0	0.0
6	1	2	230	1.0	0.0
7	1	2	230	1.0	0.0
8	2	1	230	1.0	0.0
9	1	2	230	1.0	0.0

Line data

Line no.	From bus	To bus	Line impedance (p.u.)		Half line charging susceptance $B/2$ (p.u.)	MVA
			R (p.u.)	X (p.u.)		
1	4	5	0.01	0.085	0.0880	100
2	4	6	0.017	0.092	0.0790	100
3	5	7	0.032	0.161	0.1530	100
4	7	8	0.0085	0.072	0.7450	100
5	8	9	0.0119	0.1008	0.1045	100
6	6	9	0.039	0.170	0.1790	100

Appendix 2

Eigen value analysis

S. No.	Prefault condition	Fault condition	With TCSC	With SSSC	With UPFC
1	-1000 + j0	-1000 + j0	-1000 + j0	-1000 + j0	-1000 + j0
2	-1000 + j0	-1000 + j0	-1000 + j0	-1000 + j0	-1000 + j0
3	-1000 + j0	-1000 + j0	-1000 + j0	-1000 + j0	-1000 + j0
4	-0.720 + j12.745	-0.700 + j12.763	-0.740 + j1.267	-0.715 + j2.750	-0.711 + j12.758
5	-0.720 - j12.745	-0.700 - j12.763	-0.740 - j1.267	-0.715 - j2.750	-0.711 - j12.758
6	-0.190 + j8.365	-0.1534 + j8.290	-0.109 + j7.391	-0.1625 + j8.384	-0.1624 + j8.39
7	-0.190 - j 8.365	-0.1534 - j8.290	-0.109 - j7.391	-0.1625 - j8.384	-0.1624 - j8.39
8	-5.487 + j7.947	-5.4897 + j7.95	-5.552 + j7.982	-5.498 + j7.95	-5.4943 + j7.951
9	-5.487 - j7.947	-5.4897 - j7.95	-5.552 - j7.982	-5.498 - j7.95	-5.4943 - j7.951
10	-5.222 + j7.813	-5.2315 + j7.842	-5.225 + j7.844	-5.236 + j7.844	-5.2366 + j7.847
11	-5.222 - j7.813	-5.2315 - j7.842	-5.225 - j7.844	-5.236 - j7.844	-5.2366 - j7.847
12	-5.323 + j7.920	-5.330 + j7.927	-5.339 + j7.923	-5.33 + j7.927	-5.3345 + j7.927
13	-5.323 - j7.920	-5.330 - j7.927	-5.339 - j7.923	-5.33 - j7.927	-5.3345 - j7.927
14	-5.178 + j0	-5.1804 + j0	-5.006 + j0	-5.162 + j0	-5.1737 + j0

(continued)

(continued)

Eigen value analysis

S. No.	Prefault condition	Fault condition	With TCSC	With SSSC	With UPFC
15	-3.3996 + j0	-3.558 + j0	-3.431 + j0	-3.5762 + j0	-3.5744 + j0
16	-0.443 + j1.211	0.00125 + j1.083	-0.485 + j1.079	-4767 + j1.078	-0.4760 + j1.078
17	-0.443 - j1.211	0.00125 - j1.083	-0.485 - j1.079	-0.476 - j1.078	-0.4760 - j1.078
18	-0.439 + j0.7394	-0.445 + j0.732	-0.462 + j0.814	-0.445 + j0.7262	-0.4445 + j0.7264
19	-0.439 - j0.7394	-0.445 - j0.732	-0.462 - j0.814	-0.445 - j0.7262	-0.4445 - j0.7264
20	-0.425 + j0.496	-0.425 + j0.493	-0.442 + j0.515	-0.429 + j0.498	-0.4283 + j0.497
21	-0.425 - j0.496	-0.425 - j0.493	-0.4428 - j0.515	-0.429 - j0.498	-0.4283 - j0.497
22	0 + j0	0 + j0	0 + j0	0 + j0	0 + j0
23	0 + j0	0 + j0	0 + j0	0 + j0	-10 + j0
24	-3.225 + j0	-3.225 + j0	-3.2258 + j0	-3.2258 + j0	-3.2258 + j0
25	-	-	-2 + j0	-	-10 + j0
26	-	-	0 + j0	-	-10 + j0
27	-	-	-	-	-10 + j0

FACTS controller data

	TCSC	SSSC	UPFC
MVA	100	100	100
kV	230	230	230
HZ	60	60	60
Operating mode	Constant power	Constant reactance	Constant reactance
% Series compensation	30	30	30
Gain K_r (p.u.)	-	-	1.0
Time constant (s)	0.5	12	0.1
V_p Max	-	0.1	0.05
V_p Min	-	0.02	0.01
V_q Max	-	-	0.02
V_q Min	-	-	0.01
I_q Max	-	-	0.1
I_q Min	-	-	0.02
Xc (max.)	0.5	-	-
Xc (min.)	-0.5	-	-
K_p	5	-	-
K_i	1	-	-
Gain for stabilizing signal (K_r)	10	-	-

References

1. Poonam Singhal, S.K. Agarwal, Narender Kumar, "Transient Stability Enhancement of a Multimachine System using Particle Swarm Optimization based Unified Power Flow Controller" International Journal of Engineering Research and Applications, ISSN: 2248-9622, Vol.4, Issue 7, July 2014, Page 121-133.
2. N.G. Hingorani, "Understanding FACTS: Concepts and Technology of FACTS" IEEE Press 2000.

3. Sujith. S, T. Nanda Gopal, "Transient Stability Analysis of Multi machine System using Statcom" IOSR Journal of Engineering, ISSN: 2278-8719, Vol. 3, Issue 5, May 2013, Page No. 39–45.
4. K.R. Padiyar, Nagesh Babu, "Investigation of SSR Characteristics of UPFC" Electrical Power System Research 2015, Page 211–221.
5. Nagesh Prabhu, M. Janki, "Investigation of SSR Characteristics of SSSC with GA Based Voltage Regulator" World Academy of Science Engineering and Technology (75) 2011, page 1382–1389.
6. Anju Gupta, P.R. Sharma, "Static and Transient Voltage Stability Assessment of Power System by Proper Placement of UPFC with POD Controller" WSEAS Transactions on Power System, ISSN: 2224-350X, Vol. 8, Issue 4, October 2013, Page No. 197–206.
7. Prabha Kundur, "Power System Stability and Control" McGraw Hill 1993.
8. K.R. Padiyar, "Power System Dynamics Stability & Control" BS Pub Hyderabad Edition 2002.
9. Hadi Sadat, "Power System Analysis" TMH New Delhi Edition 2007.
10. K.R. Padiyar, "FACTS Controller in Power Transmission and Distribution" New Age Publishers.
11. L. Gyugyi, "A UPFC concept for FACTS" IEE proceedings- C, Vol. 139, No. 4, 1992, page 323–331.
12. Mukul Chankaya, "Transient Stability Analysis of power system with UPFC using PSAT" International Journal of Emerging Technology and Advanced Engineering, ISSN: 2250-2459, Vol. 2 Issue 12, December 2012, Page No. 708–713.
13. Ravi Kumar, Nagaraju, "Transient Stability Improvement using UPFC and SVC" APRN Journal of Engineering and Technology Vol. 2, No. 3, June 2007, Page 38–45.
14. Satish D. Patel, H.H. Raval, "Voltage Stability Analysis of Power System using Continuation Power flow method" ISSN: 2347-4718, Vol. 1 Issue 9, May 2014, Page No. 763–767.
15. Rajesh Ahuja, Mukul Chankaya, "Transient Stability Analysis of Power System with UPFC Using PSAT" international Journal of Emerging Technology and Advanced Engineering, ISSN: 2250- 2459, Vol. 2, Issue 12, December 2012, Page No. 708–713.
16. P.P. Panchbhavi, P.S. Vaidya, "Transient Stability Improvement of IEEE 9 Bus System with Shunt FACTS Device STATCOM" International Research Journal of Engineering and Technology (IRJET) ISSN: 2395-0056, Vol. 3, Issue 3, March 2016.
17. Vaibhav Desai, Vivik Pandya, "Enhancement of Transient Stability of Power System with Variable Series Compensation" International Journal of Engineering Research and Development" ISSN: 2278- 067X, April 2015.
18. Mohsen Darabian, Bahram, Mehdi, "Improvement of Power System Transient Stability Using an Intelligent Control Method" International Journal of Engineering and Advanced Technology (IJEAT), ISSN: 2249-8958, Vol.2, Issue 4, April 2013, Page 192–200.
19. Vinesh Agarwal, Diipeh M. Ptel, "Improving Power System Transient Stability by FACTS Controllers" International Journal of Engineering Research and Technology (IJERT), ISSN: 2278- 0181, Vol. 3, Issue 7, July 2014, Page 1–5.

Linear Flight Control of Unmanned Aerial Vehicle

Alok Kumar Pandey, Anshuman Shukla, Ashutosh Gupta
and Manjeet Singh Gangwar

Abstract In this chapter, state feedback controller with the help of full state feedback method or pole placement technique is designed to stabilize the lateral dynamics of unmanned aerial vehicle (UAV). Poles of the system are chosen such that system's performance meets the design specifications with the help of MATLAB. This chapter also analyzes the transient specifications.

Keywords UAV · Pole placement technique · State feedback controller

1 Introduction

An Unmanned Aerial Vehicle is basically a pilotless aircraft. They are mainly of three types: unmanned aerial vehicle (UAV), remotely piloted vehicles (RPV), and Drones [1]. The first ever UAV that was believed to be used on August 22, 1849, by Austrians in a war was an unmanned balloon-type structure. Since then, drones have been modified through various stages from past till now and are being used extensively. UAVs are being used in various applications and in various fields because of their versatility. This is arising interest in scientific communities for improving these UAVs more and more. The major advantage over manned aerial vehicles is of less involvement of human factor, lower cost, and high remote sensing capabilities. They have replaced manned aerial vehicles in various fields and are even capable to perform difficult tasks that cannot be performed by manned

A.K. Pandey (✉) · A. Shukla · A. Gupta · M.S. Gangwar
Electrical and Electronics Department, KIET, Ghaziabad, India
e-mail: pandeyalok507@gmail.com

A. Shukla
e-mail: anshuman2705@gmail.com

A. Gupta
e-mail: ashutosh02gupta@gmail.com

M.S. Gangwar
e-mail: manjeet5gangwar@gmail.com

vehicles. They are mostly used in military operations, but nowadays, they are being used in commercial, scientific, and other various applications [2]. Their other applications range from simple toys found for entertainment purpose to highly sophisticated commercial platforms performing unusual assignments like power station inspection and regulating and 3D modeling of buildings and structures [3]. Small size UAVs have been used by researchers in various disciplines, because of its operational simplicity and affordability [4]. The dynamics of majority fixed-wing aircraft exhibits nonlinearity and strong coupling among state variables that are subject to changes due to uncertainties because of external environment [5, 6]. Hence, UAV required well-specified control system. The goal of the chapter is to design and compare two types of systems so that we will be able to get the better one and provide more optimal control to the system at a lower cost.

2 Model Dynamics

This section explains the methodology of linear flight lateral control of unmanned aerial vehicle. The section consists of vehicle dynamics which explains the model equation for the vehicle and actuator dynamics which explains the controlling of the vehicle. Model of the vehicle used in this chapter is the linear version of small size flying wing vehicle. The flying vehicle which has nonlinear model is linearized using small disturbance theory around steady state conditions whose parameter values are given in Table 1 [7]. Assuming that derivations from the equilibrium condition are small, a linearized model is expected to provide useful and accurate information of the nonlinear model. Constants used to model the system are given below.

Table 1 Trim condition

Variable	Value
u_o	9.7 m/s
v_o	0 m/s
w_o	1.2 m/s
p_o	0 m/s
q_o	0 m/s
r_o	0 m/s
α_o	6.9°
β_o	0°
V_{air}	9.7739 m/s
h_o	150 m
δ_o	0°
θ_o	6.9°
φ_o	0°

Table 2 Aerodynamic coeff. and derivative

Lateral coefficients	Values
C_{Y_o}	0
C_{l_o}	0
C_{n_o}	0
$C_{Y_{\beta}}$	-0.06972
$C_{l_{\beta}}$	-0.093
$C_{n_{\beta}}$	0.001002
$C_{Y_{\delta_a}}$	0
$C_{l_{\delta_a}}$	0.1318
$C_{n_{\delta_a}}$	-0.0069
C_{Y_p}	0.0539
C_{l_p}	-0.256
C_{n_p}	0.0854

Calculation for stability derivatives for lateral condition by applying small disturbance theory on the nonlinear equations of the flying vehicle, we obtain the lateral liberalized model of the system vehicle having lateral steady derivatives mentioned in Table 4. From this lateral stability derivatives assuming value of constants, we have calculated these values respectively in Tables 2 and 3.

$Q = \frac{1}{2}\rho V_{air}^2$ is the dynamic pressure, m is the mass of the UAV in kg, S is the wing area, and b is the wing span.

Stability derivatives obtained are a function of static and dynamic stability coefficients.

From these tables, a generalized state space model is created. State space representation for the literalized lateral equation given is:

$$\begin{bmatrix} \Delta \dot{\beta} \\ \Delta \dot{\rho} \\ \Delta \dot{r} \\ \Delta \dot{\phi} \end{bmatrix} = \begin{bmatrix} \frac{Y_{\beta}}{\omega_o} & \frac{Y_p}{\omega_o} & -\left(1 - \frac{Y_r}{\omega_o}\right) & \frac{g \cos \theta}{\omega_o} \\ L_{\beta} & L_p & L_r & 0 \\ N_{\beta} & N_p & N_r & 0 \\ 0 & 1 & \tan \theta_o & 0 \end{bmatrix} \begin{bmatrix} \Delta \beta \\ \Delta \rho \\ \Delta r \\ \Delta \phi \end{bmatrix} + \begin{bmatrix} 0 \\ L_{\delta_a} \\ N_{\delta_a} \\ 0 \end{bmatrix} [\Delta \delta_a] \quad (1)$$

3 Controller Design Method

3.1 Pole Placement Method

Open loop poles of the system are $\{-2.33, -1.86, 0.0515 + 1.48i, 0.515 - 1.48i\}$. Two poles of the system are on left hand from origin, but two poles are conjugate as well as on right-hand side from origin, so system is unstable; therefore, the pole placement design is used to place all the poles in such a way that its $\zeta = 0.7$.

Table 3 Lateral stability derivatives

Lateral derivatives	Y_{β}	Y_p	Y_r	Y_{δ_a}	N_{β}	N_p	N_r	N_{δ_a}	L_{β}	L_p	L_r	L_{δ_a}
Formula	$\frac{QS}{m} C_{Y_{\beta}}$	$\frac{QSb}{2I_{yy}m} C_{Y_p}$	$\frac{QSb}{2I_{yy}m} C_{Y_r}$	$\frac{QS}{m} C_{Y_{\delta_a}}$	$\frac{QSb}{I_x} C_{N_{\beta}}$	$\frac{QSb^2}{2I_{yy}I_x} C_{N_p}$	$\frac{QSb^2}{2I_{yy}I_x} C_{N_r}$	$\frac{QSb}{I_x} C_{N_{\delta_a}}$	$\frac{QSb}{I_x} C_{L_{\beta}}$	$\frac{QSb^2}{2I_{yy}I_x} C_{L_p}$	$\frac{QSb^2}{2I_{yy}I_x} C_{L_r}$	$\frac{QSb}{I_x} C_{L_{\delta_a}}$

Table 4 Numeric value for lateral stability derivative

Variable	Y—force derivative	L—moment derivative	N—moment derivative
β	$Y_\beta = -2.6648$	$L_\beta = -11.1699$	$N_\beta = 0.0664$
p	$Y_p = 0.0730$	$L_p = -1.0893$	$N_p = 0.3634$
R	$Y_r = 0$	$L_r = 0.2319$	$N_r = -0.0655$
δ_a	$Y_{\delta_a} = 0$	$L_{\delta_a} = 15.830$	$N_{\delta_a} = -0.7353$

Desired locations of poles for the system are $\{-2.2, -0.7, -1.5 + i, -1.5 - i\}$ [8]. The necessary and sufficient condition for the placement of closed loop poles in the complex plane is that the system as

$$\dot{x}(t) = Ax(t) + Bu(t) \tag{2}$$

$$y(t) = Cx(t) \tag{3}$$

Is controllable, if all n state variables x_1, x_2, \dots, x_n can be accurately measured at all times, according to linear control law of the form

$$u(t) = k_1x_1(t) - k_2x_2(t) - \dots - k_nx_n(t) = -Kx(t) \tag{4}$$

where K is a constant state feedback gain matrix and for this model that is given below

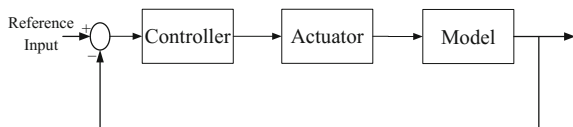
$$K = \begin{bmatrix} 3.0560 \\ 0.0837 \\ -0.6921 \\ -0.7381 \end{bmatrix} \tag{5}$$

The closed loop system is described by the state differential equation (Fig. 1)

$$\dot{x}(t) = (A - BK)x(t) \tag{6}$$

The feedback gain matrix K_1, K_2 should be such that the closed loop system is robust, in the sense that its poles are as insensitive to any changes in system as possible.

Fig. 1 Block diagram of model



4 Simulation Result

Without any controller, system is unstable and shown in Fig. 2. Results with PID controller are shown in Figs. 3, 4, 5, and 6. $G1$, $G2$, $G3$, and $G4$ are the transfer functions of different input and output sequentially.

$$G1 = \frac{6.381s^2 + 94s + 15.3}{s^4 + 1.388s^3 + 0.3939s^2 + 5.547s + 1.024}$$

$$G2 = \frac{15.83s^3 + 4.621s^2 - 3.839s + 0.4191}{s^4 + 1.388s^3 + 0.3939s^2 + 5.547s + 1.024}$$

$$G3 = \frac{-0.4571s^3 + 5.148s^2 + 1.199s - 3.464}{s^4 + 1.388s^3 + 0.3939s^2 + 5.547s + 1.024}$$

$$G4 = \frac{15.77s^2 + 5.244s - 3.694}{s^4 + 1.388s^3 + 0.3939s^2 + 5.547s + 1.024}$$

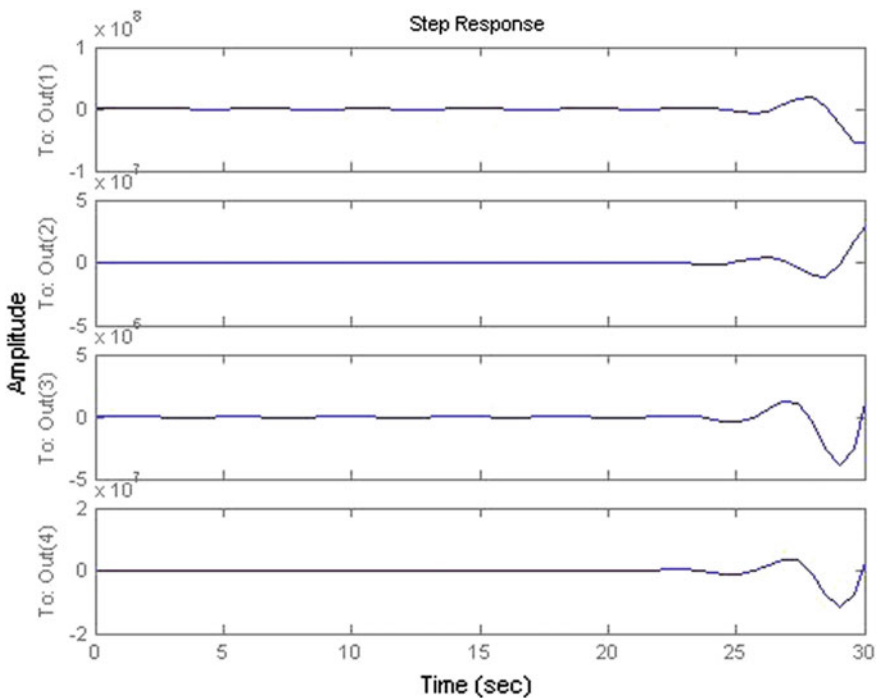


Fig. 2 Unstable system step response

Fig. 3 Response of $G1$

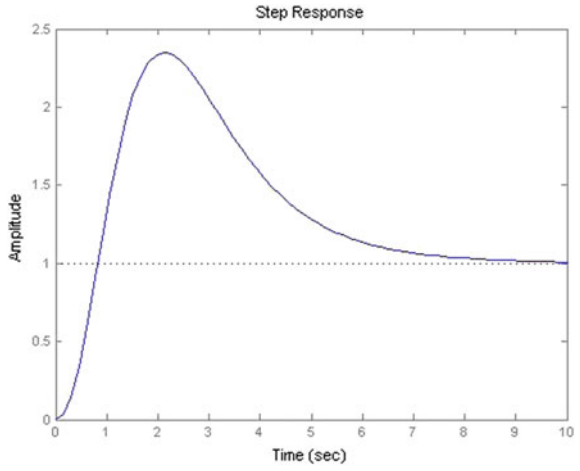


Fig. 4 Response of $G2$

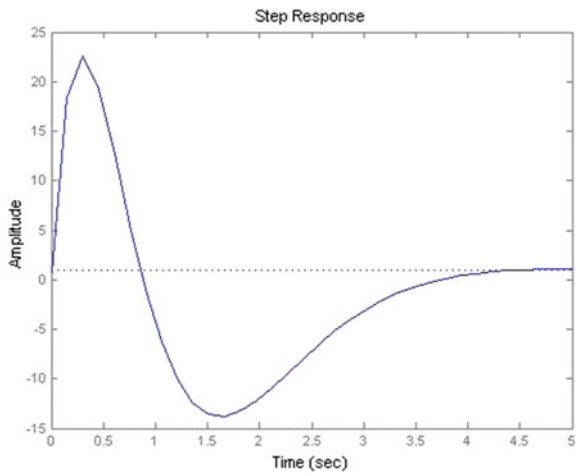


Fig. 5 Response of $G3$

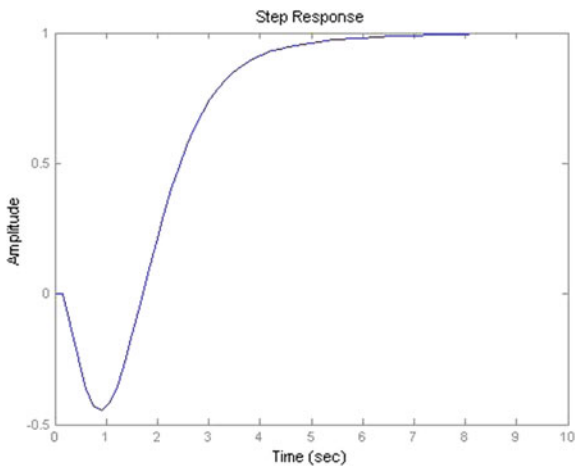
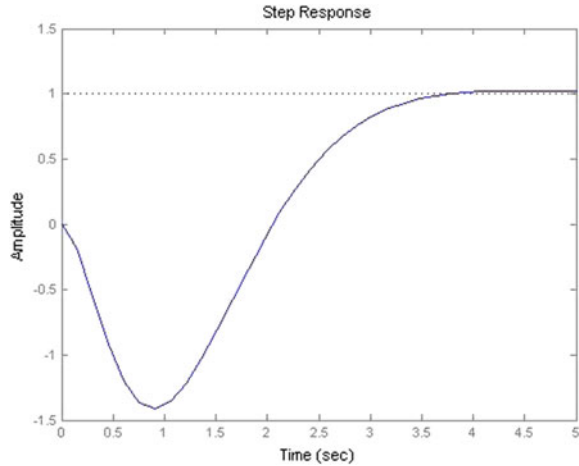


Fig. 6 Response of G_4 

References

1. Fahlstrom, P.G. and Gleason, T.J. (2012), *“Introduction to UAV Systems”*, JOHN WILEY.
2. Franke, Ulrike Esther (26 January 2015). “Civilian Drones: Fixing an Image Problem?” ISN Blog. International Relations and Security Network. Retrieved 5 March 2015.
3. Ali, N. Gageik, and S. Montenegro, “A review on distributed control of cooperating mini UAVs,” *Int. J. Artif. Intell. Appl.*, vol. 5, no. 4, pp. 1–13, Jul. 2014. [Online]. Available: <http://airccse.org/journal/ijaia/papers/5414ijaia01.pdf>.
4. Chao, H. Cao, Y. Chen, Y. Q. (2007), “Autopilots for Small Fixed-Wing Unmanned Air Vehicles: A Survey”, *Conference Proceedings, IEEE International Conference on Mechatronics and Automation, Harbin, China, August*, pp: 31443149.
5. B. Etkin, *Dynamics of Atmospheric Flight*. New York, NY, USA: Dover, 2005.
6. R. W. Pratt, *Flight Control Systems: Practical Issues in Design and Implementation*. Reston, VA, USA: AIAA, 2000.
7. “Modelling, Simulation and Control System Design for Civil Unmanned Aerial Vehicle (UAV)”, Shahriar Bagheri.
8. “Performance Analysis of Controllers for Linear Single Track Model of Sedan Car”, by Alok Kumar Pandey and B. A. Swarup.

Hybrid Encryption Algorithm in Wireless Body Area Networks (WBAN)

Sameer Farooq, Deepak Prashar and Kiran Jyoti

Abstract The wireless body area network is part of wireless sensor network in which both indoor and outdoor patients are monitored using sensors and wireless technology. The critical phase of monitoring is transmission of real time data from remote location to hospital community cloud, when patients outside the hospital at some remote location and is connected hospital cloud using Internet connection. So there is need to encrypt the data collected by sensor from patient before transmission. The paper is presenting the new concept, hybrid encryption algorithm (HEA) that is suitable for ad hoc as well as for wired networks also. The algorithm not only considers security of data but also the various constraints of sensor networks like battery power, bandwidth, limited processing capability, dynamic topology.

Keywords Hybrid encryption algorithm (HEA) · Wireless body area network (WBAN) · Elliptical curve cryptography (ECC) · Elliptical curve Diffie–Hellman (ECDH) · Advanced encryption standard (AES) · Cloud computing

1 Introduction

Wireless sensor network consists a group of autonomous sensing devices that are deployed over a particular geographic region or in some hostile environment for sensing physical and environmental conditions (such as temperature, humidity, pressure) or for monitoring and analysis purposes. It consists of an array of

S. Farooq (✉) · D. Prashar
Lovely Professional University, Phagwara, Punjab, India
e-mail: Sameerfarooq.lpu@gmail.com

D. Prashar
e-mail: Deepak.prashar@lpu.co.in

K. Jyoti
GNDEC, Ludhiana, Punjab, India
e-mail: kiranjyotibains@yahoo.com

autonomous sensors, and each sensor network node is capable to sense phenomena, perform computations on collected data and to communicate this data with rest of network nodes. A sensor node has typically several parts: a radio, transceiver, antenna, and microcontroller.

The broadcasting nature of the network and deployment of nodes in hostile areas or hazardous environments makes the networks prone to the various kinds of attacks and potential threats. Besides all this the dynamic network topology and limited resources availability, also makes these ad hoc networks, implementation difficult. So, the major challenge in ad hoc networks implementation is security of data and resource usage. The limited availability of power resource and memory space limitations makes implementation of high level security a daunting task. There are two main problems that arise in wireless ad hoc networks related to security algorithms. First, the complexity that security algorithms adds should be very low (in messages), because every bit (of message) that is processed by the sensor node needs power and thus decreases battery level of the sensor node for every second that computation needs. Second, the memory usage by processing activities in the node (encrypted text and cipher key) should be minimized to very less, because in sensor nodes we have limited memory spaces and limited bandwidth available. Due to the various constraints of wireless sensor networks such as limited battery power, limited bandwidth, limited processing capability of nodes and dynamic topology, the implementation of the complex and powerful algorithms is not possible. So we need to select the algorithm, which will provide better security, less computations, low power consumption, and small-sized output.

The main aim of designing the sensor networks is to collect and analyzes the real time data in hostile environments or hazardous locations, where human access is not possible. Because of this property of sensor networks, they are used in various applications of surveillance and monitoring like in battlefields, terrains, simulations, nuclear sites, space. The combination of sensing technology with the network technology makes it greater for wide variety of application and usages. Popular wireless sensor network applications include remote patients monitoring, wildlife monitoring, environmental monitoring, warzone surveillance, intelligent communications, industrial quality control, smart buildings, traffic monitoring, etc. Our topic is related to the application of the wireless sensor networks in healthcare system.

2 Wireless Body Area Networks (WBAN)

WSN has wide variety of application and usages everywhere particularly in healthcare system and defense industry. In healthcare system, they come under wireless body area networks (WBAN). The WBAN consists of a group of small

autonomous sensor node of different types that are wore by person or may be implanted on the patient's body in order to measure the various physiological activities (like ECG, EEG, EMG) and record them continuously for medical observation. The sensed data recorded by the sensors is sent to the hospital community cloud for diagnosis purpose where the clinicians (doctors) monitor the patients remotely. The physiological sensor is electrical equipment that is capable of sensing the various physiological conditions. The most commonly used physiological sensors are:

1. Electrocardiography (ECG): monitors heart functioning.
2. Electromyography (EMG): monitors muscle functioning.
3. Electroencephalography (EEG): monitors brain functioning.

There are also other types of sensors like blood pressure, tilt, movement, breathing, temperature. WBAN suffers from the same constraints as we discussed for wireless sensor networks like bandwidth, performance, dynamic topology, battery power, which makes them vulnerable to security attacks. However, WBAN has been successfully deployed in healthcare areas that includes monitoring of patients health remotely and e-health services. On connecting WBANs with the cloud, this increase its robustness, flexibility, availability; thus, overall throughput with sharing of data and computations among different devices located in the cloud. Thus, we can increase memory storage and computation power by connecting the WBAN network with the cloud to larger extent.

In this paper, we are going to implement the HEA algorithm on every sensor node which is collecting physiological data from patient's body and sending it to the sink (via PDA, mobile, laptop) that is hospital cloud, where doctors and other clinicians monitor patient's body activities. In this whole scenario we are dealing with WBAN, we have heterogeneous network clusters, so each node will act as its own cluster head, sending data to sink (hospital cloud) individually. The connection with sink is established through intermediate devices (viz. mobile, laptop, PDA, RBS, GPRS, WDCMA, LTE) using the HEA procedure step-by-step. We apply HEA at every sensor node interface, which encrypts the data collected, after fixed intervals of time. The encrypted data is then sent to sink via some nearest intermediate device (mobile, laptop, PDA, RBS, etc.). Figure 1 explains the whole scenario. Remember in case of WBAN, we have two types of patients, indoor patients and outdoor patients. Indoor patients are connected to hospital cloud through WLAN of hospital which is kept secure using firewalls, IDS, etc. The outdoor patients are connected through Internet to the hospital cloud. So the risk of attacks and intrusions is more, that is the reason we are using HEA.

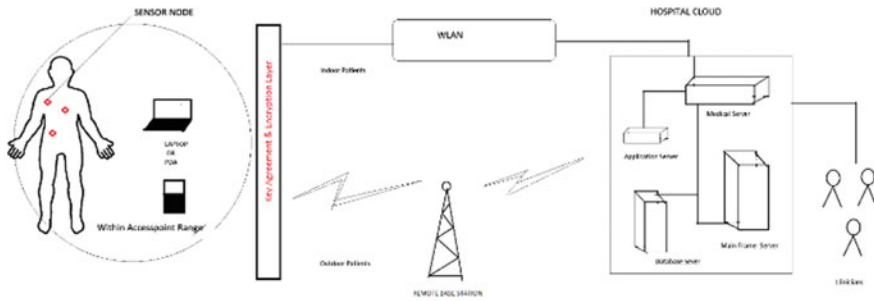


Fig. 1 Wireless sensor networks in healthcare systems

3 Literature Review

To date, many cryptographic algorithms have been proposed but most of them are not suitable for WSNs, due to the various constraints of ad hoc networks. Both asymmetric and symmetric cryptographic techniques offer both disadvantages and advantages. Symmetric encryption techniques are efficient and cost-effective for securing data; however, sharing the secret key is a problem. On the other hand, asymmetric techniques solve key distribution problem but they take more processing time in contrast to symmetric encryption and consume more resources. Therefore, the best solution is using of both techniques. This combining approach tries to get the advantages of both algorithms and also avoids the disadvantages of both techniques.

In 2012, Sadaqat and Bilal [1] proposed comparison on the basis of analysis that they did on different types of encryption techniques and cryptographic algorithms by using ad hoc networks. Their work resulted in providing the technique for selecting algorithms as per need by selecting different comparison matrices for communication device that includes details of processing time, energy consumption, memory expenses that satisfies both the needs as well as security for ad hoc environment. The security algorithm proposed by Subasree and Sakhivel [2] uses ECC algorithm for encryption. To generate the hash value, MD5 is used, which is then encrypted by using DUAL RSA algorithm, which is then sent to destination along with enciphered message. It has one disadvantage that it is slow due to ECC and DUAL RSA. Another problem is, if private key got compromised, the entire messages can be read. The third limitation is size of bits generated in the algorithm that is huge. In algorithm proposed by Dubal [3], it uses DUAL RSA as an encryption algorithm with key produced with ECDH. The calculated cipher text and the digital signature generated with ECDSA algorithm for more security is appended with the cipher text before sending it to destination through secured channel. In parallel, the hashing algorithm MD5 generates the hash value of the given cipher text. The algorithms used (DUAL RSA and ECDSA) are slow as compared to other algorithms. Also, the message can be decrypted by attacker if he knows private key. The requirement of secured channel is also a problem. Kumar

[4] proposed hybrid algorithm divided into two phases. In first phase, the plain message is enciphered with AES and in second phase with ECC algorithm. MD5 is used for hashing. Although algorithm uses both asymmetric as well as symmetric encryption algorithms and provides good quality of security, still is not used because it increases complexity in terms of time as well as in memory usage due to sequential encryption and decryption. In Farrukh Aslam Khan, Aftab Alia (2014) [5], proposed system uses multi-biometric-based scheme to get more secured and complex random key. Though there is no bound on sensor nodes like authentication of node, registered nodes of network, known node or friendly nodes, attacker can also send the malicious message in the network acting as a true node in the network. In the existing system, there is no bound on message freshness (time stamp checking) so the various attacks like DoS attack, DDoS attack, synchronization flooding attack are possible. The generation and usage of multi-biometric key in the system also increase complexity in terms of storage, computations, power consumption, and execution time. In Rizk and Alkady [6], the proposed architecture uses secret key for AES encryption. Although the key is encrypted with ECC algorithm, anyone who will know any of the parameter like trust center public key (TCPK) can easily decrypt the half block of cipher text (ci). The algorithm is using DUAL RSA, and so the algorithm is susceptible to prime factorization attack with which we can easily calculate the key. Thus, decrypt the remaining half block of cipher text (Ci). The algorithm uses XOR DUAL RSA the algorithm which is neither quantum computer resistant (QCR) nor next generation encryption (NGE) algorithm. Another problem of the algorithm is the computational complexity.

4 Proposed Framework

4.1 Introduction

The proposed framework consists of sensors that are implanted or attached on the patient's body. These sensors are of different types, viz. ECG, EGG, EMG, etc. They collect physiological data from the body of patient, the data collected is sent to nearer base station and then transmits it to the hospital cloud's servers securely via some intermediate devices (laptop/PDA) and base stations (RBS); here, the doctors and other medical staff take the readings of the data and then provide treatment to the patient accordingly. In the proposed system, we are dealing with the heterogeneous sensor network where all the nodes are of different types. Thus, there is no need of cluster formation or cluster head selection, as we have limited number of sensors attached to the patient's body, and all of them are of different types in their working sense and technology.

4.2 Details of Proposed System

The proposed framework is designed for secure communication between sink node and base station in cloud-based wireless body area networks (WBAN). The proposed framework is divided into five sections. Section 4.2.1 registration phase, section 4.2.2 authentication phase, section 4.2.3 ECDH key exchange phase, section 4.2.4 encryption phase, and section 4.2.5 decryption phase.

4.2.1 Registration Phase

In this phase, the patient who is going to use the wireless sensors for medical observation, the hospital community will provide him the unique registration number (RN), and the number is kept confidential. The different types of sensors are implanted or attached on the patient's body depending on types of illness. These sensors are given unique ID's (NID) under the given registration number. So each sensor on patient's body will be identified with unique registration number (RN) and node ID (NID).

4.2.2 Authentication Phase

Before any actual transmission of data between the base station (hospital cloud) and the sensor nodes both need to authenticate each other for prevention of any attack, viz. malicious node, man in the middle attack or worm hole, etc. In order to authenticate the sink nodes with the base station, few computation is done on both base station server side as well as the sink node side. Both sides use registration number (RN), node id (NID), and the time stamp (TM) for authentication and message freshness.

Sensor node	Base station
Compute $m1 = H(RN + NID) RN TM$ (send)	
	Extract $H(RN + NID)$, RN, TM from received $m1$. Fetch details of RN from databases and find corresponding NID value. Compute $H(RN + NID)$ and compare it with received one for integrity check and authentication.
	Compute $m2 = H(NID) RN TM$ (send)
Extract $H(NID)$, RN, TM from received $m2$. Compute $H(NID)$ and compare it with received one for integrity check and authentication.	

NID node ID, *TM* time-stamp value, *RN* registration number of patient, *H* MD5 hash function, *m1* message sent by sensor node to base station server, *m2* message sent by base station server to sensor node

After the successful integrity checks on the both side, the authentication will be achieved. Now, the sink and base station can communicate with each other and can send sensitive data to one another as both are authentic.

4.2.3 ECHD Key Exchange Phase

This phase includes exchange of key between sink node and base station that will be used for data encryption and decryption on sink node and base station side, respectively. The algorithm is used to exchange the key between sender and receiver is elliptic curve Diffie–Hellman. The steps to exchange key are:

$$\text{Elliptic curve equation: } y^2 = x^3 + ax + b$$

- P Field (modulo p)
- a, b Curve parameters
- G Generator (Base point)
- N Order (G)
- h Co-factor

The domain parameters (a, b, x, G) are known to everyone. The steps of key generation on both sides are given below:

1. First, the sink node will pick up a random key β , such that $1 < \beta < n - 1$. This will be his private key.
2. Similarly, the base station will also pick up a random key α , such that $1 < \alpha < n - 1$. This will be his private key.
3. Sink node will compute $S = \beta G$, and base node will compute $B = \alpha G$ ordinary.
4. Now, both will exchange the S and B though an ordinary channel. There is no need of secure channel.
5. Now, sink node will have $B = (x_B, y_B)$ and base station $S = (x_S, y_S)$. So, they both will multiply the received B, S with their private keys to get final keys:

$$\text{Key of sink node } P = \alpha.\beta.G.$$

$$\text{Key of sink node } Q = \alpha.\beta.G.$$

6. After computations, the final key K will be on both sink node side as well as base station side:

$$K = \alpha.\beta.G.$$

4.2.4 Encryption Phase

The proposed framework uses hybrid encryption algorithm (HEA). For encryption, this algorithm divides the plaintext message 'PT' into 'n' number of smaller units or blocks each of 128-bit in size. These units are then divided into two parts **Mi** (1 to n/2) blocks and **mi** (n/2 + 1 to n) blocks. In case, if the nth part is not equal to 128-bit size, the algorithm pads the block with null bits in order to make it equal to 128. In step 1, the first n/2 blocks '**Mi** (1 to n/2)' are encoded with ECC-128 bit algorithm. The algorithm uses key 'K' produced from ECDH algorithm. The first part is enciphered in the following way:

$$\mathbf{Mi} = \sum_{i=1}^{i=\frac{n}{2}} (\mathbf{PTi}) \quad 1 \leq i \leq \frac{n}{2}$$

Elliptic curve encryption function ECC_enc() enciphers the **Mi** (1 to n/2) with key **K** generated by ECDH algorithm. The cipher text produced will be

$$\mathbf{Ci} = \mathbf{ECC_enc}(\mathbf{Mi}, \mathbf{K})$$

In step 2 that will be performed in parallel with step 1, the remaining n/2 blocks **mi** (n/2 + 1 to n) are encrypted using AES-128 bit encryption algorithm. In this algorithm, the key **K** generated by ECDH algorithm is used for encryption. The cipher text produced will be:

$$\mathbf{mi} = \sum_{i=(\frac{n}{2}+1)}^{i=n} (\mathbf{PTi}) \quad \frac{n}{2} + 1 \leq i \leq n$$

$$\mathbf{ci} = \mathbf{AES_enc}(\mathbf{mi}, \mathbf{K})$$

MD5 hashing algorithm is used to generate hash values of the cipher texts **Ci** and **ci**.

$$\mathbf{Hi} = \mathbf{MD5}(\mathbf{Ci}).$$

$$\mathbf{hi} = \mathbf{MD5}(\mathbf{ci}).$$

And, finally, cipher text **CT** which is generated by padding **Ci** and **ci** is sent to the base station node. The hash values **Hi** and **hi** of the corresponding cipher texts **Ci** and **ci** are integrated (**HS** = **Hi** + **hi**) and are sent along with message to the destination.

$$\mathbf{CT} = \mathbf{Ci} + \mathbf{ci}$$

$$\mathbf{HS} = \mathbf{Hi} + \mathbf{hi}$$

4.2.5 Decryption Phase

In decryption, the received message **CT** which is in encrypted form is divided into '**n**' number of blocks each unit is of 128-bit size. The blocks are then grouped into two separate parts. The first half consists '**C_i**' (**1** to **n/2**) blocks and second half consists '**ci**' (**n/2 + 1** to **n**) blocks. For integrity check of received cipher text, either to accept or reject the hashing is done by using same hashing algorithm that is used by sender. In order to get the first half block of plaintext, the first half of received message '**C_i**' is decrypted by using ECC-128 bit algorithm decryption phase.

$$C_i = \sum_{i=1}^{i=(n/2)} (CT_i) \quad 1 \leq i \leq \frac{n}{2}$$

$$M_i = \text{ECC_dec}(C_i, K)$$

The remaining $n/2$ blocks (**ci**) are decrypted with AES-128 bit algorithms decryption phase as follows:

$$c_i = \sum_{i=(\frac{n}{2}+1)}^{i=n} (CT_i) \quad \frac{n}{2} + 1 \leq i \leq n$$

$$m_i = \text{D_AES}(c_i, K)$$

mi is the other part of the decrypted text. The process of decryption of '**C_i**' and '**ci**' is also in parallel like as in encryption. Finally, after the complete decryption of whole cipher message, the blocks are combined in same order as divided to get the complete message.

$$PT = M_i + m_i$$

5 Conclusion

The presented framework is sensor based on healthcare system using cloud, and main focuses are on outdoor patient's secure data transfer from sensor nodes (sink) to hospital cloud (base station). The proposed framework uses ECDH algorithm to generate a secured key for communication between the sink node and base station server. The framework uses hybrid algorithms: ECC-128 and AES-128 for data encryption. The work plan proposed is evaluated theoretically in sense of security of wireless ad hoc network in data communication. The proposed framework will be unique as it will provide a secure data movements in wireless body area networks (WBAN) with minimum costs and complexity without compromising the security.

References

1. Rehman, S. U., Bilal, M., Ahmad, B., Yahya, K. M., Ullah, A., & Rehman, O. U., "Comparison Based Analysis of Different Cryptographic and Encryption Techniques Using Message Authentication Code (MAC) in Wireless Sensor Networks (WSN)", *IJCSI International Journal of Computer Science Issues*, Vol. 9, Issue 1, No. 2, January 2012, ISSN (Online): 1694-0814.
2. Subasree, S., Sakthivel, N.K., 2010. Design of a new security protocol using hybrid cryptography algorithms. *IJRRAS* 2 (2), 95–103.
3. Dubal, M.J., Mahesh, T.R., Ghosh, P.A., 2011. Design of a new security protocol using hybrid cryptography architecture. In: *Proceedings of 3rd International Conference on Electronics Computer Technology (ICECT)*, vol. 5, India.
4. Kumar, N., 2012. A Secure Communication Wireless Sensor Networks Through Hybrid (AES + ECC) Algorithm, vol. 386. von LAP LAMBERT Academic Publishing.
5. F. Aslam, A. Ali, H. Abbas, N. Al, and H. Haldar, "A cloud-based healthcare framework for security and patients' data privacy using wireless body area networks," *Procedia-Procedia Comput. Sci.*, vol. 34, pp. 511–517, 2014.
6. R. Rizk and Y. Alkady, "Two-phase hybrid cryptography algorithm for wireless sensor networks," *J. Electr. Syst. Inf. Technol.*, vol. 2, no. 3, pp. 296–313, 2015.

Integrated Sensors for Risk Assessment in Industries and Residential Sectors: A Review

Vishal Kumar Singh, Ashish Maindolia, Abhishek Singh, Shubham Bhardwaj and Bikarama Prasad Yadav

Abstract Sensors and detectors technology has been very useful in recent years because of their widespread application in industries, residence, and in domestic application. From a giant process industry to a small iPhone gadget, sensors have marked their importance and need for the mankind by taking up automatic handling and precision data collection. As safety of vivid type of industries from fire and other hazards becomes the core obligation of government and private bodies, sensors use becomes nonnegotiable. Various types of sensors available in the market which can be used for protection, surveillances, and safety are now a days fashion and culture for the mega organizations which installs them in the significant places. The given review paper analyzes the latest trends in the field of sensor/detectors application with respect to safety. The review gives a significant collection of facts, data, and latest technological upgradation in sensor technology and its role in safety of processes to appliances.

Keywords Detectors · Industries · Process · Safety surveillance
Sensors

V.K. Singh (✉) · A. Maindolia · A. Singh · S. Bhardwaj · B.P. Yadav
University of Petroleum and Energy Studies, Bidholi via Premnagar,
Dehradun 248007, India
e-mail: Vishalksingh3011@gmail.com

A. Maindolia
e-mail: ashish.maindolia@gmail.com

A. Singh
e-mail: abhiss23595@gmail.com

S. Bhardwaj
e-mail: bhardwaj.shubham327@gmail.com

B.P. Yadav
e-mail: bpyadav@ddn.upes.ac.in

1 Introduction

Various technologies are employed for fire detection systems which are currently sensor-based systems which are categorized into infrared and optical-based sensors to detect the availability of heat, smoke, or radiation but no single technique is completely effective which can completely satisfy the users [1] in one of the survey. The characteristics of fire vary along with application and environment. As Indiaspend has reported, 6% of all unnatural deaths in India are caused due to accidental fires, which is third highest after car accidents (53%) and drowning (9%) [2]. Every month, there has been a case of fire due to leakage in LPG gas cylinder in the city. The loss of life and property has been escalating due to such tragedies. According to data provided by National Crime Records Bureau from 2010 to 2014, a total of 113,961 people had lost their lives in a fire accident with an average of 62 deaths a day. The death toll due to fire accidents in Maharashtra alone accounted to 21.3% of all deaths [3]. In one of the cases which took place on June 1, 1974, 28 people died and 36 were injured in an explosion caused by the leakage of cyclohexane in a chemical plant near Flixborough. The leakage of this chemical caused cloud formation of flammable hydrocarbons. On finding an ignition source, there was an explosion which caused fire that was burning for 10 days. The workers at the site and control room were unaware about the leakage as the detectors failed to give alarm. This gives the picture of a catastrophe and gives information that there are requirement of detector to warn people about any leakage of toxic or flammable gas or in case any fire broke out [4]. This results in increase in death toll due to unavailability or failure of fire detection system at the site [5]. However, sensors can be installed in a combination or individually which can affect the performance during its activity [6]. Their availability helps in evacuation of people on the site and can prevent any small incident from becoming a disaster. It also helps in prevention of fire at early stage. Detectors can help in mitigation of any type of accidents whether it is due to leakage of gas or fire caused due to various reasons.

There has been more than 50% increase in the usage of smoke detectors of total non residential market because of the fire broke out and massive fire explosion occurred in a restaurant in Petlawad town of Jhabua district, Madhya Pradesh which took the lives of 89 people. According to a Reuters report, gelatin sticks and other explosives accidental detonation which was illegally stored by a local businessman in his warehouse were the cause of the blast [7].

This paper discusses about the various accidents that occur due to absence of fire detectors system or failure of detection system which has proved be fatal for the people and organization and recent technologies which can be helpful to indicate firefighters so that they may respond to fire knowing whether a room is vacant or not, saving them the time of checking room for a potential rescue and reduce the impact of any fire so the fatalities can be prevented.

2 Problem Definition

Major accidents have happened due to the unsafe act of the people in the organization or due to negligence toward safety. Moreover, there were no active fire protection system available to reduce the impact of the accidents and the technologies used were not effective to counter large fires [8]. Two cases are explained below which show that the negligence of organization to implement the proactive system has led to disaster.

Bhopal Gas Tragedy (December 3, 1984)

Union Carbide factory, a pesticide plant in Bhopal at midnight of December 3 released 45 tonnes of methyl isocyanate (MIC) in the air causing the death of 10,000 people immediately. The gas caused irritation and breathing problem. Not only humans but animals also suffered. Those who left or survived the horror of night, suffered from genetic diseases [9]. The leaves were turned black, and the heavily populated city became a ghost town [10].

Cause—Due to cutoff in budget, the safety measure was compromised. Water carrying catalytic compound entered the tank 610 where MIC was stored. The tank was filled up to 85%, while only 50% of the tank was to be filled. The gas travelled from the water pipe connection and went through the scrubber into the atmosphere; and finally entered into the city.

The gauges failed to detect the increase in pressure in the tank, and there were no detectors to detect the leakage of the gas. The scrubber did not have any caustic soda, and the flare tower was under maintenance. It was a case of total absence and failure of safety system.

Missing Sensors—No sensors to detect the leakage and pressure gauge failure, and no sensor to inform that water is flowing back due to clog.

Chemical Runaway Reaction (June 11, 2003)

Industry—pharmaceutical plant

A runaway reaction occurred in a pharmaceutical plant due to extended heat output from a mixture consists of azoisobutyronitrile, N-bromosuccinimide, and cyclohexane. The safety disk of the reactor was ruptured, and almost 400 L of chemical was dispersed into the atmosphere.

Cause—The reactor was heated with a steam at a pressure of 0.5 bar by the technician and involved himself into another device. Within 10 min, the temperature of the mixture reached 56 °C, and then he stopped heating and stirring the reactor. When the pressure limit of 0.3 bar was exceeded, thereafter the safety disk ruptured at 0.5 bar. A temperature rise up to 84 °C of the reactor was seen by a workshop foreman, and then he immediately initiated the emergency shutdown routine [8].

Due to the absence of both temperature regulation and an alarm in the existing sensors, the operating protocols were mentioned inaccurately.

Missing Sensors—Temperature and pressure alarm triggers and temperature regulator.

3 Types of Sensors and Their Applications

3.1 *Smoke Detectors*

A smoke detection system continuously draws air from sampler using air pump/aspirator into a network of pipe to a centrally-located smoke detector through holes in the piping system. The smoke density is compared with a set of predefined smoke thresholds in the sampling; if smoke exceeds the thresholds in the sampled air, then an alarm is issued [11]. These detectors are divided into three main categories such as photoelectric, aspirating, and open-beam detectors. The photoelectric sensors are widely employed into residential sectors, and they are low cost. Comparatively, aspirating smoke detectors (ASDs) are more costly and have industrial application. While, projected beam of IR light is used in open beam detectors to detect smoke across residential, industrial and large commercial buildings.

3.2 *Heat Detectors*

A pneumatic heat detection system fitted on a sensing line accommodated with pressurized nitrogen using frangible bulb technology [12]. This results in activation of pressure switch which is triggered by the release of air trapped in the line, providing a fire signal and indicating the position of fire. To detect change in temperature along the length of the cable, linear sensors are used. Due to increase in temperature, declination in resistance occurs between the conductor and the metal screen [13]. Resistance changes can be monitored by a control module; if rate of temperature exceeds the fixed temperature, a fire warning signal can be provided. Their applications are in industrial facilities and can monitor section up to 3,200 m. It is also used as an alert fire detector for sections up to 2 by 250 m and also ensures safety in tunnels [14].

3.3 *Flame Detectors*

A flame emits IR and UV light which depends upon the chemical composition of burning material. The wavelength of light is monitored and detected by photodetectors which include photoconductive sensors which have wide band absorption [15]. A pyroelectric and thermopile sensor deals with narrow band interference filters. Some of the systems combine IR system with video imaging.

3.4 Gas Detectors

Various gases are studied extensively, but one of the reliable gas indicators for fire used is carbon monoxide (CO). Carbon monoxide is divided into two types for detection, i.e., nondispersive IR absorption (NDIR) and wet electrolyte [16]. The wet electrolyte is less expensive and widely used and can be used in composite with smoke and/heat sensors [11].

These detectors are classified according to the occupancy and have different advantages and drawbacks which are shown in Table 1.

Table 1 Different type of detectors with their occupancy, advantages, and disadvantages [17]

Sensors	Type	Occupancy	Advantages	Drawbacks
Smoke	Photoelectric	Residential	Least costly	Cannot be used in a room with high ceiling
	Aspirating	Industrial	More sensitivity, high smoke detection capability, used in area where smoke cannot reach the ceiling detectors	Costly. Pipes are used to draw air samples if contaminants are not removed might cause a false alarm
	Open beam	Assembly building	Detect smoke across large area, where point detection is uneconomical	
	Video-based	Electrical power generating station, aircraft hangar, historic buildings	The particle size that can be detected is limited by wavelength	Unable to operate in unlist situation
	Ionization	Residential	Small, inexpensive	Less responsive at smoldering stage (NFPA 72)
	Duct detectors		Early smoke detection system is moving in air through heating and ventilation system to prevent the recirculation of smoke from area of fire to unaffected region	

(continued)

Table 1 (continued)

Sensors	Type	Occupancy	Advantages	Drawbacks
Heat	Linear electrical fiber optic	Ducts, conveyors, tunnels, subway system	The length of sensing cable can be sensed	Can only be 1000 m long
	IR thermal imaging	Industrial coal	Can detect at smoldering stage of fire	Due to the high cost, it cannot be used in lower risk area [18]
		Storages coal stock pile		It cannot sense through glass and concrete
	Pneumatic	Aircraft	Highly sensitive	
Flame	UV detectors	Refineries	Works at full spectral region	False alarm might cause due to artificial sunlight, for example, artificial light, sunlight, etc.
	IR detectors	Chemical plants, drilling, gas processing, gas storage, gas turbine, aircraft hanger, printing paper, manufacturing		
Gas	Nondispersive IR absorption	Coal mines conveyors	Does not need early replacement	Costly
	Wet electrolyte		Smoldering phase detection	Early replacement
			Small, inexpensive	They do not fail safe High power consumption

4 Conclusion

The difference in technologies has been observed in detectors used in the past and in present. Earlier, we used to have smoke detectors followed by fire detectors and then heat detectors. The advancement in technology has enabled us to detect fire more accurately [19]. Now, we have smoke detectors which can detect how dense smoke rises alarm on the basis of smoke intensity. In some single process unit, a single detector is not enough to detect the leak or fire. So, we can use detectors in combination with place of lone detectors [20]. However, the advancement in technology has produced more chances of occurrence of accidents. The effectiveness of detectors varies with surrounding condition which can decrease their accuracy, life span, and sometimes raises false alarm [21]. Therefore, advancement in detectors technologies should be promoted to reduce these affects. To reduce the

nuisance of false alarms and reduce the time to detect actual fires, advancement in detectors, sensitivity adjustment, drift compensation, and indication for the maintenance of the detectors are necessary [22].

References

1. G. Brogi, L. Pietranera, Infrared sensor suitable for firefighting applications, US Patent 5422484, 1995.
2. Sethi, A.S. and India Spend Fire accidents kill 54 people daily in India, yet deaths have declined. (2015).
3. Dubbudu, R. Fire accidents caused an average of 62 deaths per day in the last 5 years. (2016).
4. Mahoney, D. G. Large property damage losses in the hydrocarbon- chemical industries: a thirty-year review (13th ed.). New York: M&M Protection Consultants. (1990).
5. Liu, Z.G., Crampton, G., Kashef, A., Lougheed, G., Gibbs, E., Su, J.Z. and Benichou, N. (no date) 'Fire Detectors, Fire Scenarios and Test Protocols'.
6. Systems, F. Thermal imaging cameras for fire prevention and detection - FLIR infrared.
7. Lees, F. P., Loss prevention in chemical process industries. London: Butterworth. (1996).
8. Lewis, D. J. Case histories of past accidents, the causes and consequences. In J. I. Petts, Major hazard installation: Planning and assessment. Lough borough University of Technology, UK. (1984).
9. Anderson Ayana R. "Division of Toxicology and Human Health Sciences, Agency for Toxic Substances and Disease Registry", CDC.
10. Pradyumna Mishra *et al.* Bhopal Gas Tragedy: review of clinical and experimental findings after 25 years; 22(3):193–202. (2009).
11. Palmer, K.N. Explosions in flammable smokes from smouldering fires. Loss Prevention and Safety Promotion, 4(3), D11 (1983).
12. Knisley, Joseph R. 'Technology trends in fire detection and alarm system', Contributing Editor| CEE News. (1 March, 1998).
13. Hemsley, R. Thermal imaging cameras – the future of firefighting (2015).
14. Fire Detectors, Fire Scenarios and Test Protocols Prepared by: Z. G. Liu, G. Crampton, A. Kashef, G. Lougheed, E. Gibbs, J.Z. Su and N. Benichou.
15. <http://electronicsdesign.com/article/digital/pir-based-motion-detection-sensor-to-solution-33099.aspx>.
16. D. S. Lee, D. D. Lee, S. W. Ban, M. Lee, and Y. T. Kim, "SnO₂ gas sensing array for combustible and explosive gas leakage recognition," IEEE Sensors J., Vol. 2, pp. 140–149, (2002).
17. Rob Bogue, "Sensors for fire detection", Sensor Review, Vol. 33 Iss 2 pp. 99–103. (2013).
18. Khan, F.I. and Abbasi, S.A. 'Major accidents in process industries and an analysis of causes and consequences', Journal of Loss Prevention in the Process Industries. (1999).
19. THE NEW GOLDEN AGE OF SENSOR MANUFACTURERS. www.usinenouvelle.com, March 27, (2008).
20. Shumard, "Implementation of wireless & intelligent sensor technologies in the propulsion test environment," Proc IEEE Conference on Sensor for Industry, pp. 135–138. Jan (2004).
21. J. Butler, "Robotics and Microelectronics: Mobile Robots as Gateways into Wireless Sensor Networks," Technology@Intel Magazine, Intel Corporation, May (2003).
22. INTELLIGENT SENSORS: NEW TECHNOLOGIES AND NEW PROBLEMS FOR OPERATIONAL SAFETY. F. Brissaud, D. Charpentier, A. Barros and C. Bérenguer - 16th Congress of Risk Management and Operational Safety – Avignon- Paper 3A-2. 6–10 October, (2008).
23. Taylor, J.R. Use of simulation for emergency planning and training. Health, Safety and Loss Prevention, 387, 114–119. W. M. Solano, J. Junell, J. L. Schmalzel and K. C. (1993).

A Novel Approach for Node Localization in Wireless Sensor Networks

Abhishek Kumar and Deepak Prashar

Abstract Numerous applications such as Internet of Things and robotics using sensors and wireless sensor networks (WSN) require localization and target tracking for their efficient implementation and functioning. Localization means determining the precise position of nodes within the network. Localization sometimes is also a precondition to other functionalities such as routing, self-organization capability. Various approaches and algorithms have been proposed to solve the localization problem. Most of these techniques involve use of some deployed nodes whose position coordinates are already known to us (using GPS or some other method) called landmarks or anchors. This paper presents a novel connectivity-based mobile localization approach for sensor networks and list of parameters on which a comparative study can be done.

Keywords WSN · Anchors · Range-based · Range-free · Mobility
Localization algorithms

1 Introduction

Wireless sensor networks are defined as a network of tiny sensor nodes. These sensor nodes are deployed in the field independently, and they operate coordinately through wireless links. There might be different kinds of sensor nodes in a network, some nodes with basic functionalities and some with expensive special functionalities. The network may be distributed over a small field, in a household, in an industry, or it can be operated over a large forest, deep oceans, or a traffic monitoring network in a city. Wireless sensor networks are not limited by the type of

A. Kumar (✉) · D. Prashar
School of Computer Science Engineering, Lovely Professional University,
Jalandhar, Punjab, India
e-mail: Abhisheikh.kmr@gmail.com

D. Prashar
e-mail: Deepak.prashar@lpu.co.in

data they monitor. The data can be seismographic readings or humidity levels or sounds in the forest or traffic camera recordings of a city.

Wireless sensor networks have become cost effective and small in size, thanks to the speed of evolution of technology. Flexibility, scalability, accuracy of sensor networks have made its manufacturing rapid, which in turn reduced the cost of development. Deployment of monitoring nodes has become simple with robust and reliable low-cost nodes. Design of wireless sensor networks has become application specific as the requirements are different in each application. A military application demands secure communication, a healthcare application demands accuracy, an environmental monitoring scheme demands for robustness, and a traffic monitoring scheme demands for longer lifetime. This might be the reason that the sensor networks are attracting attention of researchers to address these design constraints, improving existing protocols.

Wireless sensor networks just like ad hoc networks are subjected to the challenges such as limited power, limited coverage area of a node, no existing infrastructure, security issues, and interference to communication, channel restrictions, congestion etc. Several surveys in wireless sensor networks stated research domains such as routing techniques, MAC protocols, data congestion control, data aggregation, energy conserving mechanisms, localization, and security. And in addition, there were many application domains such as medical, and environment monitoring. WSN has umpteen number of applications in health, military, security, disaster prevention, and weather forecasting.

1.1 Overview of Localization

Localization is referred to the process of identifying the location of sensors with the help of anchor/beacon nodes. Wireless sensor networks as stated above have limited resources. All the sensor nodes cannot have location awareness independently as they are deployed in ad hoc manner in the network and some other factors such as cost, power constraints, size. In some cases, the GPS systems cannot be employed as the environmental conditions restrict the communication with satellites, e.g., monitoring applications in deep forests, ocean depths, household application in case of basements and dense concrete structures. Location of sensor node is very important in many applications. Without the location information, the data collected is of no use. Thus, the sensor localization is an important domain in WSN. Mobility is an important indicator of development. Mobile sensor nodes are required to have location awareness.

To determine the location of all the sensor nodes in the network, we deploy some nodes in the network that must be self-aware of their own position either by placing them in a fixed known location or by providing them with GPS like systems. These nodes are referred to as anchor/beacon nodes.

A sensor node to identify its own location communicates with the in-range anchor nodes. The beacon signals send the location of beacon nodes. The sensor

nodes find the distance and/or angle between anchor node and sensor node. From all the information of anchor nodes' locations and distances, sensor nodes calculate their own location.

1.2 Range-Based Schemes

Range-based techniques rely on node-to-node distance, angle measurement, and relative speed measurement for time computation. Once we have achieved the result of ranging, positions can be computed using either of triangulation, trilateration, or multilateration techniques. We will discuss three main ranging methods: RSSI [1–3], AoA [4], and ToA.

RSSI [5] is based on the fact that the energy of the transmitted signal decreases as the distance between the transmitter and receiver node increases. The attenuation is in polynomial terms, which is proportional to square of distance. To achieve localization using AoA data, two angle measurements are needed. A good demonstration is being presented in [6]. For ranging using Time of Arrival, time taken for the signal to propagate from transmitter to receiver is measured. It requires the sender and receiver to be synchronous and thus needing extra hardware support for maintaining synchrony.

1.3 Range-Free Schemes

Range-free localization algorithms avoid the above-mentioned techniques of ranging and intend to exploit the available connectivity and geometry among the sensor nodes and thus avoiding explicit use of ranging. The connectivity information is in the form of number of hops between any two sensing nodes. This hop count reflects how close or far the sensing nodes are. If two sensor nodes are directly within the communication range of each another, they will be called neighbors and the hop count will be one. Many such range-free estimation schemes use location-aware nodes called as anchors or landmarks. Typically, the anchors/landmarks are fixed and nodes may be fixed and mobile. But recently, several algorithms have been proposed which deal with mobile anchors too. More comprehensive study of range-free schemes has been done in Sect. 2 of the paper.

Another class of localization algorithms, anchor-based algorithms, requires anchors or landmarks for determination of the location coordinates of unknown sensor nodes. Most of the localization algorithms fall into this category. Conversely, anchor-free localization algorithms do not require any landmarks or other such nodes whose location is pre-known. But this class of algorithms requires more complex computation. Some of the anchor-free algorithms are the following: Spotlight Localization system which estimates the position by exploiting some space-time properties when an event is generated and time when this event is

perceived. Another such algorithm is Light House algorithm [7]. This technique uses a device known as lighthouse and finds out the distance between light house and sensor node. Range-free schemes have inherent advantages over the range-based schemes as they only exploit the connectivity information and hence do not need additional hardware.

2 Related Work

Nath and Niculescu [8] proposed that the underlying principle of DV-Hop is that the sensor nodes exchange the distance vector control packets; as a result every node maintains the minimum hop counts and the coordinates of every anchor node. Then, each landmark/anchor broadcasted their average computed distance of each hop contained along with data packets. When an unknown sensing node receives the average distance to each hop, it computes the distance to each anchor according to their recorded hop information. This approach does not require the distance to be calculated. In contrast to Centroid localization scheme, DV-Hop can solve the localization problem even in the sparse network. When the ratio of anchor increases, the localization mean square error of the algorithm decreases.

Liu et al. [9] developed a new concept called localizable collaborative body (LCB). It utilizes graph theory concepts to achieve localization. The unknown sensing node using this approach can localize itself with the help of multihop anchors or landmarks. Therefore, LCB can do away with indispensable requirement of having at least three landmarks to achieve localization. Under this scheme, the anchor nodes first broadcast their positions with the help of beacons. The sensing nodes receiving these beacons can model the network into a BN-tree. In this type of tree, only the parent node at first level that is the root node has at least three children, while rest of the parents may have two or more children nodes. LCB significantly reduces the computation overhead and cost of communication in the localization process. However, the major shortcoming of LCB is that individual localization errors result in cumulative error and the ongoing cooperative localization between sensing nodes results into localization error of one unknown sensing node having a significant repercussions on the position error of other sensing nodes.

Chen et al. [10] proposed a localization algorithm combining DV-Hop with assumption-based coordinates (ABC). In this, the algorithm first computes the distance between the anchor and unknown sensing nodes by employing the DV-Hop schemes and then computes the coordinates of position of unknown sensing node using ABC approach. It is a computationally simple approach with no overhead, but mean square error is high.

Liu [11] proposed a Distributed Mobile Location estimation algorithm. This algorithm epitomizes the idea of using the mobility to achieve localization. Under this, each unknown sensor node maintained a queue which is populated with information of three most recent locations, and based on that we can construct an

equation of the linear motion of an unknown node exploiting the history queue records. We can make an assumption that the sensing node whose position is to be determined is in linear motion in multiple short-time intervals and the acceleration is constant. Results showed that, the localization coverage of this algorithm can be achieved as high as 99% with correct choice of radio range.

Baggio and Langendoen [12] proposed two different schemes called Monte Carlo Localization and Monte Carlo Boxed Localization based on probability distribution. The algorithm comprises of two principal phases: prediction phase and filtration phase. In the prediction phase, an unknown sensor node envisages its assessed position using distributed switching equipment utilizing the mobility information of the mobile anchor. In the filtration phase, that unknown node removed any unreliable information from the computed position information. MCL can provide accurate position of nodes even with low anchor density and extremely irregular deployment conditions. In cases, when an unknown node cannot localize itself in first pass, the algorithm needs to be run in multiple passes. After the prediction stage, when we have collected samples and filtration of sampling fails, the MCL can create infinite loop filtering of the samples. The author runs simulations to show that the algorithm relies vastly on the posterior probability distribution utilizing discrete sampling. Hence, more the number of samples, better the localization accuracy, but this comes at the cost of more memory requirement and computational overhead.

Hu and Li [13] suggested an improvised DV-Hop localization algorithm. It is an improvisation of traditional DV-Hop localization algorithm. The traditional DV-Hop algorithm uses adjacent anchor node's metrics such as average hop distance which has perils of large computation errors. In this improvement, the authors used the mean hop distance from all the anchor nodes in n-hop range of a sensor node. After the position coordinates of sensor nodes are obtained, the location of anchor node is estimated again to compute the correction factor. This correction factor is broadcasted to all unknown nodes. All the correction factors from anchors are weighed, and average correction factor is used for location correction of unknown nodes. Similar to the conventional variant of DV-Hop algorithm, the improved version of algorithm also shows improved accuracy with improved node density.

Yang and Zhang [14] introduced an interhop distance correction approach in the DV-Hop localization. Four different communication radii were used, and based upon that the nodes were placed in four distant groups. Nodes regularly update the hop count based upon the packets they receive from adjacent nodes with different radii. Anchors compute mean error per hop and send that information to unknown nodes along with average hop distance. Unknown sensor node used that information to correct the hop distance and hence eliminate the incorrect calculations. Results showed that the proposed algorithm has better accuracy and stability over traditional DV-Hop.

Apart from that, several other range-free localization schemes have been implemented, such as improvised tetrahedron localization [15], HiRLoc [16], localization based on sphere intersections [17], localization based on voronoi regions [18], Dynamic Triangulation Localization [19], Target tracking Localization [20].

3 Scope of the Study

In this work, a problem statement for a novel range-free localization scheme has been presented. Most of the existing works in the area of localization have been subduing the mobility constraints and treated mobility as a burden. Through this study, an attempt has been made to analyze the various existing approaches first and find out the various parameters of interest in tracking the localization. This study will float out a network model for a new approach for connectivity-based localization schemes that scales well and efficiently with mobility. Further new insights and recurring challenges in achieving localization shall also be presented and described. Apart from this, this study also intends to propose a novel connectivity-based localization scheme.

4 Parameters of Consideration and Mobility

The various parameters of interest are the following:

- Area: $(100 \times 100) \text{ m}^2$
- Radio range: It is the communication radius of the node and will be taken as 20 m
- No. of nodes: 100
- Ratio of anchors: 10, 20, 30%
- No of times the simulations will be run: 1000.

Assumptions:

1. We assume that there is no interference among the signals send by anchors or received by them.
2. There is no attenuation in the signal strength while in transit.
3. There is no collision among two or more signals.
4. The mode of communication is line of sight.
5. The deployment region has no obstacles and is regular deployment.

The various factors for consideration and comparison are the following:

- A. **Localization Coverage:** It refers to the percentage or ratio of nodes correctly localized. We will run simulations with different percentage of anchors and find the change in localization coverage.
- B. **Localization Error:** The mean absolute error will be computed as: Suppose $(x_{\text{cen}}, y_{\text{cen}})$ is the computed position of a node and (x_i, y_i) is the actual position of the node, then the mean absolute error can be calculated as

$$\sum_{i=1}^n \frac{\sqrt{(x_{\text{cen}} - x_i)^2 + (y_{\text{cen}} - y_i)^2}}{n},$$

where n is the total number of nodes deployed.

- C. **Cost Trade-off:** We should look for a localization algorithm which uses less landmarks or anchors. The increase in quantum of anchors will lead to more cost burden. Furthermore increasing the number of anchors does not necessarily guarantee better localization coverage or accuracy. So we need to maintain an optimal anchor-to-nodes ratio. Cost will also depend on power equation.
- D. **Algorithmic Complexity:** The space and time complexity of centralized algorithm is less than distributed algorithm, but this comes at a cost of sustaining the fear of single point of failure in case of centralized algorithms. The intent is to reduce the memory requirement.
- E. **Anchor Placement:** The position where anchor is placed is also important. Some localization algorithms require anchor to be placed at corners of simulation area, whereas some require anchor to be placed at center and start moving.

Subroutine 1: Incorporating Mobility

Mobility in ad hoc and sensor networks can be modeled using techniques such as random waypoint (RWP) and Gauss Markov mobility model. Because of being lightweight and better fit for nondeterministic networks, this study uses Gauss Markov Model. We assume that movement occurs at fixed time intervals say ‘n.’ So the velocity and orientation or direction of mobile node at n th instant can be represented as:

$$S_n = \alpha * S_{n-1} + (1 - \alpha)\bar{S} + \sqrt{(1 - \alpha^2)} S_{X_{n-1}}, \tag{1}$$

$$d_n = \alpha * d_{n-1} + (1 - \alpha)\bar{d} + \sqrt{(1 - \alpha^2)} d_{X_{n-1}}, \tag{2}$$

where α is the turning parameter with value range $0 \leq \alpha \leq 1$.

If $\alpha = 0$, that means completely random movement.

And $\alpha = 1$ means linear movement.

\bar{S} and \bar{d} are the mean values of velocity and direction, respectively.

Location of the node at any instance ‘ t ’ can be represented as:

$$X_t = X_{t-1} + S_{t-1} \cos(d_{t-1}), \tag{3}$$

$$Y_t = Y_{t-1} + S_{t-1} \sin(d_{t-1}), \tag{4}$$

where $0 \leq d \leq 2\pi$.

We begin the movement at center of the area. Movement time is 1000 s. Time interval n is set to 1 s. Assume α is 0.75. $S_{X_{n-1}}$ and $d_{X_{n-1}}$ will be computed from Eq. (5) which represents a Gaussian distribution with value of μ as 0 and standard deviation σ as 1. \bar{c} is fixed to be 10 m/s, and \bar{d} is 90° .

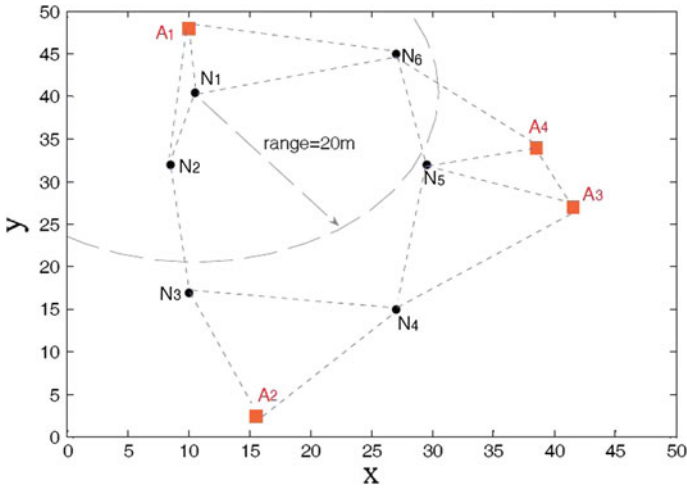


Fig. 1 Node deployment in the network using the mobility model of Subroutine 1

$$f(x|\mu, \sigma) = \frac{1}{\sigma\sqrt{2\pi}} e^{-\frac{(x-\mu)^2}{2\sigma^2}} \tag{5}$$

χ is the random variable with normal distribution or Gaussian function of distribution, σ is the standard deviation of input data, σ^2 is variance, and μ is the mean or median or mode as applied (Fig. 1).

5 Proposed Algorithm

- 1 Decide upon the parameters of interest and factors of comparison.
- 2 Call Subroutine 1. Implement with the above-mentioned values of direction and speed.
- 3 Assume there are n anchors: $A_1, A_2, A_3, \dots, A_n$.
- 4 For $k := 1$ to $n - 2$
 - a. Select A_k .
 - b. (X_k, Y_k) is the position of A_k .
- 5 For $l := (k + 1)$ to $n - 1$
 - a. Select A_l
 - b. (X_l, Y_l) is the position of A_l .
- 6 For $m := (l + 1)$ to n

Select A_m with its position as (X_m, Y_m) .

- 7 Call Subroutine 2 for the computation of location of unknown node N_x .
- 8 Exit.

For a sensor network with 100 nodes and 10% ratio of anchors, the Selective 3 DV-Hop gives C (10, 3) total number of combinations. Each of such combination will localize an unknown sensor using the trilateration. Average value of all such combinations and their corresponding locations will yield the estimated position. A typical combination of anchors (k, l, m) and its trilateration equation has been explained in Subroutine 2.

Subroutine 2: Position Matrix

Suppose that the location coordinates of unknown sensor N_x is (x', y') ,

$$\begin{cases} (x' - x_k)^2 + (y' - y_k)^2 = d_{k,N}^2 \\ (x' - x_l)^2 + (y' - y_l)^2 = d_{l,N}^2 \\ (x' - x_m)^2 + (y' - y_m)^2 = d_{m,N}^2. \end{cases}$$

Solving the above set of equations by trilateration method, we get the following

$$N_{\langle k,l,m \rangle} = \begin{bmatrix} X_{\langle k,l,m \rangle} \\ Y_{\langle k,l,m \rangle} \end{bmatrix} = C^{-1}B, \quad C^{-1} = -2 * \begin{bmatrix} x_k - x_m & y_k - y_m \\ x_l - x_m & y_l - y_m \end{bmatrix}.$$

$$B = \begin{bmatrix} d_{k,N}^2 - d_{m,N}^2 - x_k^2 - y_k^2 + x_m^2 + y_m^2 \\ d_{l,N}^2 - d_{m,N}^2 - x_l^2 - y_l^2 + x_m^2 + y_m^2 \end{bmatrix}$$

6 Conclusion

Sensor networks are full of inherent challenges to localization. The problem of fading, attenuation, incorrect computations prompted the researchers to move from range-based techniques to range-free techniques. Later, various algorithms to tackle the issue of mobility were also proposed. The intent was to use mobility as an advantage to solve the localization problem rather than considering it as a burden on the network. The proposed algorithm introduces mobility in the connectivity-based localization algorithm such as Selective 3 anchor DV-Hop algorithm. Incorporating mobility will lead to low cost, less processing time. The algorithm will be implemented using various tool boxes available in MATLAB, and the results obtained will be compared with the results of already existing range-free algorithms in terms of parameters such as accuracy (in terms of mean square error), coverage, cost (in terms of number of anchors), and complexity (in terms of processing time).

References

1. N. Patwari, A. O. Hero, M. Perkins, N. S. Correal, and R. J. ODea. Relative Location Estimation in Wireless Sensor Networks. *IEEE Transactions on Signal Processing*, Vol. 51, No. 8, August 2003.
2. J. Hightower, G. Boriello, and R. Want. SpotON: An Indoor 3D Location Sensing Technology Based on RF Signal Strength. Technical Report 2000-02-02, University of Washington, February 2000.
3. D. Niculescu and B. Nath. Ad Hoc Positioning Systems (APS). In *Proceedings of IEEE GLOBECOM '01*, November 2001.
4. B. H. Wellenhoff, H. Lichtenegger and J. Collins." *Global Positions System: Theory and Practice*". Fourth Edition. Springer Verlag, 1997.
5. Spread Spectrum Scene. "An introduction to indoor radio propagation". <http://sssmag.com/indoor.html>, June 2001.
6. Linqing GUI, "Improvement of Range free Localization Systems in Wireless Sensor Networks", Ph.D. thesis, University of Toulouse, 2013.
7. R  omer, K. "The lighthouse location system for smart dust". *ACM/USENIX International Conference on Mobile Systems, Applications, and Services (MobiSys)*", 2003.
8. Niculescu, D., & Nath, B. (2003). DV based positioning in ad hoc networks. *Journal of Telecommunication Systems*, 22(14), 267–280.
9. Liu, K., Wang, S., & Zhang, F. (2005). Efficient localized localization algorithm for wireless sensor networks. In *Proc. 5th international conference on computer and information technology* (pp. 21–23).
10. Shu, J., Liu, L., & Chen, Y. (2009). A novel three-dimensional localization algorithm in wireless sensor networks, wireless communications, networking and mobile computing. In *Proc. 5th international conference on wireless communications* (pp. 24–29).
11. Liu, Y. (2008). Distributed mobile localization algorithms of WSN. Master's thesis, Hunan Technology University, pp. 32–35.
12. Baggio, A., & Langendoen, K. (2008). Monte Carlo localization for mobile wireless sensor networks. *Ad Hoc Networks*, 6(5), 718–733.
13. Y. Hu and X. Li, "An improvement of DV-Hop localization algorithm for wireless sensor networks," *Telecommun. Syst.*, vol. 53, no. 1, pp. 13–18, 2013.
14. Xiaoying Yang, Wanli Zhang, "An Improved DV-Hop Localization Algorithm Based on Hop Distance and Hops Correction", *International Journal of Multimedia and Ubiquitous Engineering* Vol. 11, No. 6 (2016), pp. 319–328.
15. Chen, H. (2008). Novel centroid localization algorithm for three dimensional wireless sensor networks. In *Proc. of the 4th international conference on IEEE wireless communications* (pp. 1–4).
16. Lazos, L., & Poovendran, R. (2006). HiRLoc: high-resolution robust localization for wireless sensor networks. *IEEE Journal on Selected Areas in Communications*, 24(2), 233–246.
17. Lv, L., Cao, Y., Gao, X., & Luo, H. (2006). Three dimensional localization schemes based on sphere intersections in wireless sensor network (pp. 48–51). Beijing: Beijing Posts and Telecommunications University.
18. Wang, J., Huang, L., & Xu, H. (2008). A novel range free localization scheme based on Voronoi diagrams in wireless sensor networks. *Journal of Computer Research and Development* 45(1), 119–125.
19. Luo, R. C., Chen, O., & Pan, S. H. (2005). Mobile user localization in wireless network using grey prediction method. In *The 32nd annual conference of IEEE industrial electronics society* (pp. 2680–2685).
20. Hao, Y. (2006). Target localization and track based on the energy source. Master's thesis, Fudan University.

A Purely Active Circuit Simulator for Realizing Electronically Tunable Floating Resistance

Mayank Srivastava, Ajay Roy and Dinesh Prasad

Abstract This research article proposes a novel floating resistor simulation circuit with electronic control facility. Proposed simulator employs two voltage differencing transconductance amplifiers (VDTAs) only. The circuit structure of presented simulator is very simple and enjoys the following beneficial properties: (i) employment of only two active elements (VDTAs), (ii) no requirement of any external resistance so a purely active implementation, (iii) electronic control of realized resistance, (iv) no need to meet any active/passive element matching condition, (v) excellent behavior under non-ideal conditions, (vi) low values of sensitivity indexes, and (vii) full utilization of used active elements. The influence of VDTA terminal parasitics on high-frequency behavior of proposed circuit is also investigated. The working of presented circuit has been confirmed by designing a low-pass filter. To validate the behavior of realized circuits, simulations in PSPICE have been performed.

Keywords Active simulator · Resistance simulation · Floating resistance
VDTA

M. Srivastava (✉) · A. Roy
Department of Electronics and Communication Engineering,
KIET Group of Institutions, Ghaziabad, Uttar Pradesh, India
e-mail: mayank2780@gmail.com

A. Roy
e-mail: ajayroy@live.com

D. Prasad
Department of Electronics and Communication Engineering,
Jamia Millia Islamia, New Delhi, India
e-mail: dprasad@jmi.ac.in

1 Introduction

The active realization of passive components (inductors/capacitors/resistors) in floating form is a popular research domain for scientists and researchers. Numerous configurations for simulating floating passive elements using different ABBs have been presented in [1–18]. A resistor in floating state is an essential entity of many circuit configurations, but from the viewpoint of monolithic integration, it is not advisable to use a floating resistor as a resistor in floating state requires more area on chip as compared to a resistor connected to ground and also it is not easy to implement a floating resistor with precise value of resistance. Moreover, such resistor has fixed value which cannot be changed as per need. Therefore, tunable floating resistance simulation using active elements has become a fascinating research field of analog electronics domain. Many floating resistance simulation configurations using various active components like operational amplifier (OP-AMP) [6], operational transconductance amplifier (OTA) [7], modified current feedback operational amplifier (MCFOA) [8], current conveyors (CCII) [9–11, 14] differential difference current conveyor (DDCC) [12], current-controlled second-generation current conveyors (CCCII) [13], current backward transconductance amplifier (CBTA) [15, 16], current follower transconductance amplifiers (CFTA) [17], differential voltage second-generation current conveyor (DVCCII) [18], and voltage differencing transconductance amplifier (VDTA) [19] have been proposed in research work available in open literature, but unluckily these presented simulators undergo one or more of the following drawbacks: (i) excessive requirement of active components (more than two) [6, 9, 11, 13, 19], (ii) use of external resistor(s) [6–11, 14–16, 18], (iii) non-availability of electronic tenability feature [6, 8, 9–11, 18], (iv) need for active/passive component matching constraint (s) [16, 17], (v) degraded non-ideal performance [18], and (vi) partial utilization of ABB(s) [9, 12, 13, 15, 18, 19].

Therefore, the objective of this research paper is to propose a new solely active circuit configuration for simulating tunable floating resistor by using only two VDTAs. The presented simulator configuration offers the following profitable features: (i) use of only two VDTAs, (ii) no need of external resistor(s), (iii) electronic tuning in simulated resistance, (iv) no need of any active/passive element matching, (v) unaffected behavior under non-ideal environment, (vi) low active and passive sensitivities, and (vii) full utilization of VDTAs. As per the best awareness of authors, there is no simulator for floating resistor simulator available in the literature, which has all the above-mentioned features simultaneously.

2 Proposed Configuration

The voltage differencing transconductance amplifier (VDTA) is a new generation active element proposed in [20]. It finds numerous applications in analog signal processing [21–28]. The current–voltage relationships between different ports of VDTA are in terms of electronically controllable transconductance gains. Fig. 1 represents the block level representation of VDTA. Here, two input terminals are “N” and “P”, one auxiliary port is “Z”, and two output ports are “X+” and “X-”. All these terminals exhibit high impedances. The implementation of VDTA element by MOS technology has been shown in [20].

The current–voltage relations at the terminals of ideal VDTA can be described by the following current–voltage equation set:

Fig. 1 Electrical symbol of VDTA

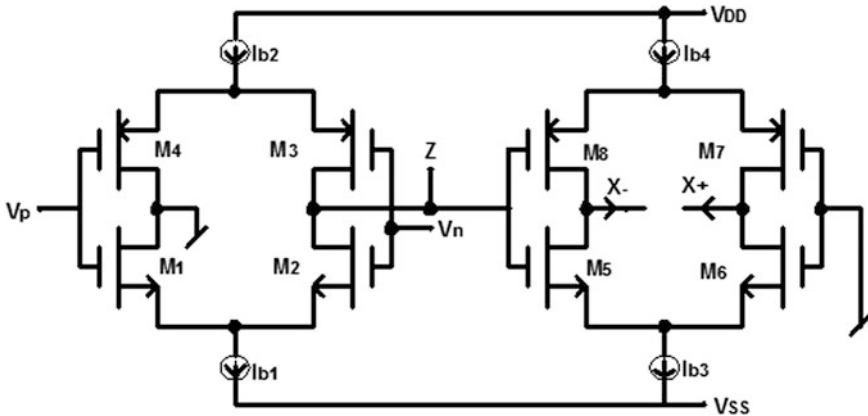
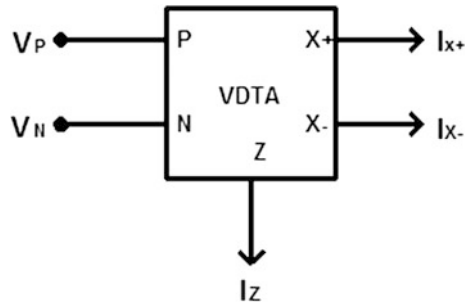


Fig. 2 CMOS implementation of VDTA [21]

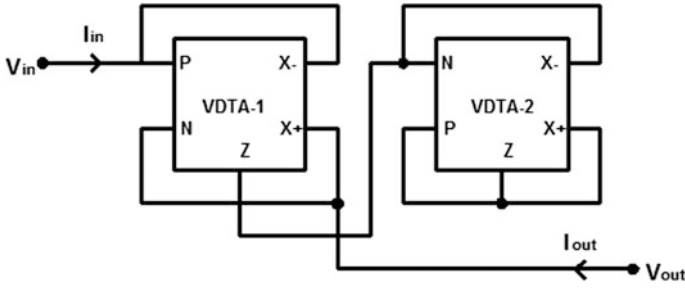
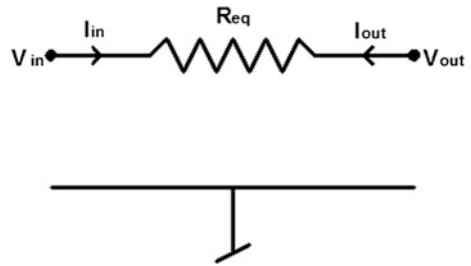


Fig. 3 Proposed purely active electronically tunable floating resistor simulator

Fig. 4 Equivalent circuit of VDTA circuit shown in Fig. 3



$$\begin{bmatrix} I_Z \\ I_{X^+} \\ I_{X^-} \end{bmatrix} = \begin{bmatrix} g_{m_1} & -g_{m_1} & 0 \\ 0 & 0 & g_{m_2} \\ 0 & 0 & -g_{m_2} \end{bmatrix} \begin{bmatrix} V_P \\ V_N \\ V_Z \end{bmatrix}. \tag{1}$$

In CMOS implementation shown in Fig. 2, the transconductance gains g_{m_1} and g_{m_2} are defined as follows:

$$g_{m_1} = \frac{g_3 + g_4}{2} \tag{2}$$

$$g_{m_2} = \frac{g_5 + g_8}{2} \quad \text{or} \quad g_{m_2} = \frac{g_6 + g_7}{2} \tag{3}$$

where k th MOS transistor’s transconductance “ g_k ” is defined as follows:

$$g_k = \sqrt{I_{B_k} \mu_k C_{OX} \left(\frac{W}{L} \right)_k}. \tag{4}$$

In Eq. (4), μ_k is charge carrier mobility, C_{OX} is layer (gate-oxide) capacitance per unit area, “ W ” is effective width of channel in MOS transistor, “ L ” is length of channel, and “ I_{B_k} ” is k th transistor’s biasing current.

The proposed purely active electronically tunable configuration for simulating floating resistance is shown in Fig. 3, and its equivalent circuit under ideal conditions is shown in Fig. 4.

The admittance matrix (short circuit) of circuit shown in Fig. 3 can be found as follows:

$$\begin{bmatrix} I_{in} \\ I_{out} \end{bmatrix} = \frac{g_{m_1}g_{m_2}(g_{m_3} + g_{m_4})}{g_{m_3}g_{m_4}} \begin{bmatrix} +1 & -1 \\ -1 & +1 \end{bmatrix} \begin{bmatrix} V_{in} \\ V_{out} \end{bmatrix}, \quad (5)$$

which replicates a “resistance in floating state” with equivalent resistance value defined as follows:

$$R_{eq} = \frac{g_{m_3}g_{m_4}}{g_{m_1}g_{m_2}(g_{m_3} + g_{m_4})}. \quad (6)$$

Here, (g_{m_1}, g_{m_2}) are the transconductances of VDTA-1 and (g_{m_3}, g_{m_4}) are of VDTA-2.

From Eq. (6), one can observe that the value of simulated resistance can be tuned by changing the transconductance gains g_{m_1} , g_{m_2} , g_{m_3} , and g_{m_4} . It is illustrated from Eqs. (2) and (4) that transconductances of VDTA can be controlled by bias current. Therefore, the resistance of simulated resistor can be changed by changing the bias currents and such control is known as electronic control which does not require any replacement of component(s) in circuit. By slight variation in connections of proposed configuration, a “negative resistor ($-R$) in floating form” can also be realized, which could be used for cancellation of parasitics in high parasitic circuits.

3 Non-ideal Analysis and Sensitivity Calculations

The current–voltage relationships of VDTA terminals under non-ideal condition are defined by equations given below:

$$I_Z = \beta_Z g_{m_1} (V_P - V_N) \quad (7)$$

$$I_{X+} = \beta_{X+} g_{m_2} V_Z \quad (8)$$

$$I_{X-} = \beta_{X-} g_{m_2} V_Z \quad (9)$$

where β_Z , β_{X+} , and β_{X-} are non-ideal transconductance gain errors.

To validate the performance of proposed circuit under non-ideal environment, it is reanalyzed using non-ideal Eqs. (7) and (9) of VDTA. The short-circuit admittance matrix under non-ideal environment can be obtained as follows:

$$\begin{bmatrix} I_{in} \\ I_{out} \end{bmatrix} = \frac{g_{m1}g_{m2}\beta_{z1}\beta_{x1-}(\beta_{z2}g_{m3} + \beta_{x2} + g_{m4})}{g_{m3}g_{m4}\beta_{z2}\beta_{x2-}} \begin{bmatrix} +1 & -1 \\ -1 & +1 \end{bmatrix} \begin{bmatrix} V_{in} \\ V_{out} \end{bmatrix}. \quad (10)$$

The simulated floating resistance “ R_{eq} ” in this case is as follows:

$$R_{eq} = \frac{g_{m3}g_{m4}\beta_{z2}\beta_{x2-}}{g_{m1}g_{m2}\beta_{z1}\beta_{x1-}(\beta_{z2}g_{m3} + \beta_{x2} + g_{m4})}, \quad (11)$$

where $\beta_{z1}, \beta_{x1+}, \beta_{x1-}, \beta_{z2}, \beta_{x2+}$, and β_{x2-} are the gain errors of VDTAs

So, it is important to note from Eq. (11) that even considering non-ideal conditions, the presented configuration simulates a resistor with no lossy term.

The sensitivity values of simulated resistance corresponding to $\beta_{z1}, \beta_{x1+}, \beta_{x1-}, \beta_{z2}, \beta_{x2+}, \beta_{x2-}, g_{m1}, g_{m2}, g_{m3}$, and g_{m4} are found as follows:

$$S_{g_{m1}}^{R_{eq}} = S_{g_{m2}}^{R_{eq}} = -1 \quad (12)$$

$$S_{\beta_{x2-}}^{R_{eq}} = 1 \quad (13)$$

$$S_{\beta_{x1-}}^{R_{eq}} = S_{\beta_{z1}}^{R_{eq}} = -1 \quad (14)$$

$$S_{\beta_{x2+}}^{R_{eq}} = -\frac{g_{m4}\beta_{x2+}}{(\beta_{z2}g_{m3} + \beta_{x2} + g_{m4})} \quad (15)$$

$$S_{\beta_{z2}}^{R_{eq}} = S_{g_{m3}}^{R_{eq}} = \frac{g_{m4}\beta_{x2+}}{(\beta_{z2}g_{m3} + \beta_{x2} + g_{m4})} \quad (16)$$

$$S_{g_{m4}}^{R_{eq}} = \frac{g_{m3}\beta_{z2}}{(\beta_{z2}g_{m3} + \beta_{x2} + g_{m4})}. \quad (17)$$

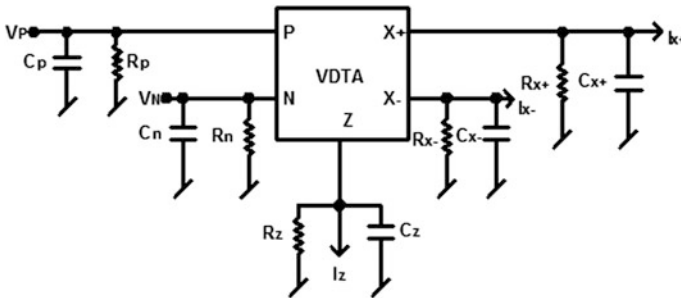


Fig. 5 Parasitic model of VDTA

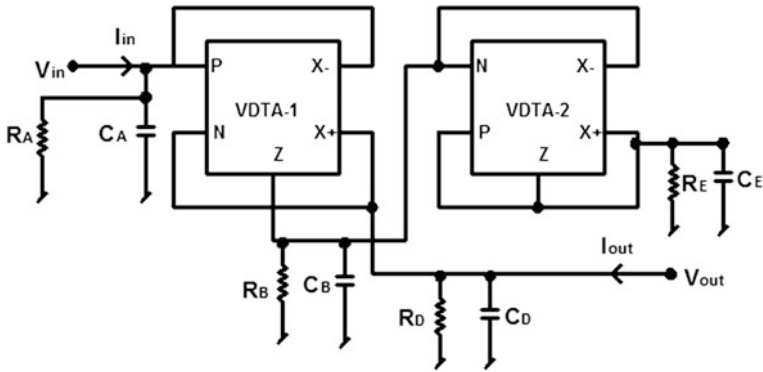


Fig. 6 Proposed floating resistor simulator with terminal parasitics of VDТАs

So, the values of all the sensitivity indexes are equal to or less than unity in magnitude.

4 Effects of Parasitics

In high-frequency condition, the parasitics at different ports of VDТА become significant and alter the behavior of VDТА-based circuits. A conventional VDТА along with its port parasitics is shown in Fig. 5.

To find the influence of parasitic impedances of VDТА on presented simulator, it was revisited taking parasitics under consideration. Proposed configuration with terminal parasitics of VDТА-1 and VDТА terminal-2 is shown in Fig. 6.

$$R_A = \frac{1}{\frac{1}{R_{p1}} + \frac{1}{R_{x1-}}} \tag{18}$$

$$R_B = \frac{1}{\frac{1}{R_{z1}} + \frac{1}{R_{n2}} + \frac{1}{R_{x2-}}} \tag{19}$$

$$R_D = \frac{1}{\frac{1}{R_{n1}} + \frac{1}{R_{x1+}}} \tag{20}$$

$$R_E = \frac{1}{\frac{1}{R_{p2}} + \frac{1}{R_{z2}} + \frac{1}{R_{x2+}}} \tag{21}$$

$$C_A = C_{p1} + C_{x1-} \tag{22}$$

$$C_B = C_{z_1} + C_{n_2} + C_{x_{2-}} \quad (23)$$

$$C_D = C_{n_1} + C_{x_{1+}} \quad (24)$$

$$C_E = C_{p_2} + C_{z_2} + C_{x_{2+}} \quad (25)$$

As the presented circuit is purely active realization, so there is no external passive element to alleviate the effect of parasitic impedances. Therefore, the behavior of circuit at high frequencies deviates from its intended behavior. The maximum operating frequency for proposed configuration can be evaluated as follows:

$$\omega_{0_{\max}} \left\langle \left\langle \min \left\{ \frac{\left(\frac{1}{R_{p_1}} + \frac{1}{R_{x_{1-}}} \right)}{\left(C_{p_1} + C_{x_{1-}} \right)}, \frac{\left(\frac{1}{R_{n_1}} + \frac{1}{R_{x_{1+}}} \right)}{\left(C_{n_1} + C_{x_{1+}} \right)}, \frac{\left(\frac{1}{R_{n_2}} + \frac{1}{R_{x_{2-}}} + \frac{1}{R_{z_1}} \right)}{\left(C_{n_2} + C_{x_{2-}} + C_{z_1} \right)}, \frac{\left(\frac{1}{R_{z_2}} + \frac{1}{R_{x_{2+}}} + \frac{1}{R_{p_2}} \right)}{\left(C_{z_2} + C_{x_{2+}} + C_{p_2} \right)} \right\} \right\rangle \quad (26)$$

The admittance matrix (short circuit) of circuit shown in Fig. 6 can be described as follows:

$$\begin{bmatrix} I_{\text{in}} \\ I_{\text{out}} \end{bmatrix} = Y \begin{bmatrix} 1 + \frac{(g_A + sC_A)}{Y} & -1 \\ -1 & 1 + \frac{(g_D + sC_D)}{Y} \end{bmatrix} \begin{bmatrix} V_{\text{in}} \\ V_{\text{out}} \end{bmatrix}. \quad (27)$$

From Eq. (27), it can be illustrated that circuit shown in Fig. 6 simulates a floating admittance configuration with admittance “Y”, where

$$Y = \frac{g_{m_1} g_{m_2} (g_E + sC_E - g_{m_3} - g_{m_4})}{[(g_B + sC_B)(g_E + sC_E - g_{m_3} - g_{m_4}) - g_{m_3} - g_{m_4}]} \quad (28)$$

$$R_F = \frac{g_B g_K - g_{m_3} g_{m_4}}{g_{m_1} g_{m_2} g_K} \quad (29)$$

$$C_F = \frac{g_B g_K - g_{m_3} g_{m_4}}{s g_{m_1} g_{m_2} C_E} \quad (30)$$

$$L_A = \frac{s g_B C_E}{g_{m_1} g_{m_2} g_K} \quad (31)$$

$$R_G = \frac{g_B}{g_{m_1} g_{m_2}} \quad (32)$$

$$L_B = \frac{s C_B}{g_{m_1} g_{m_2}} \quad (33)$$

$$R_H = \frac{g_K C_B}{g_{m_1} g_{m_2} C_E} \quad (34)$$

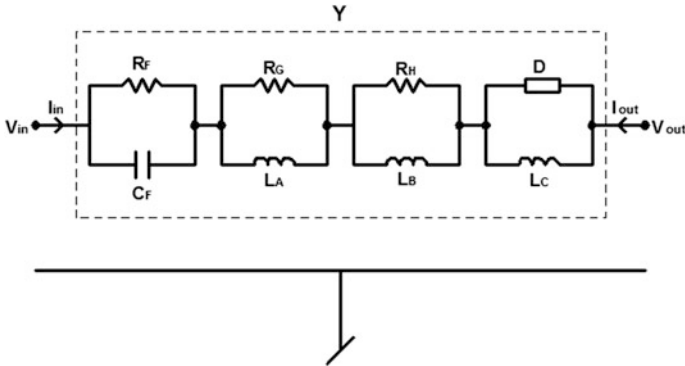
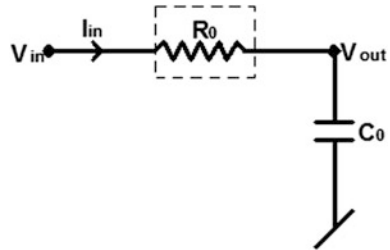


Fig. 7 Equivalent configuration of circuit shown in Fig. 6

Fig. 8 Application example

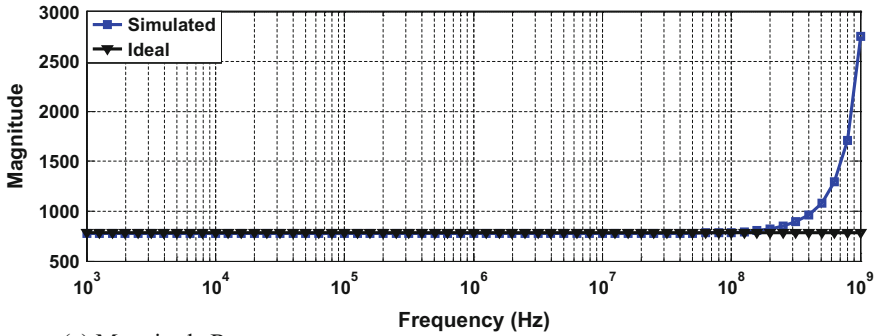


$$D = \frac{s^2 C_E C_B}{g_{m1} g_{m2} g_K} \tag{35}$$

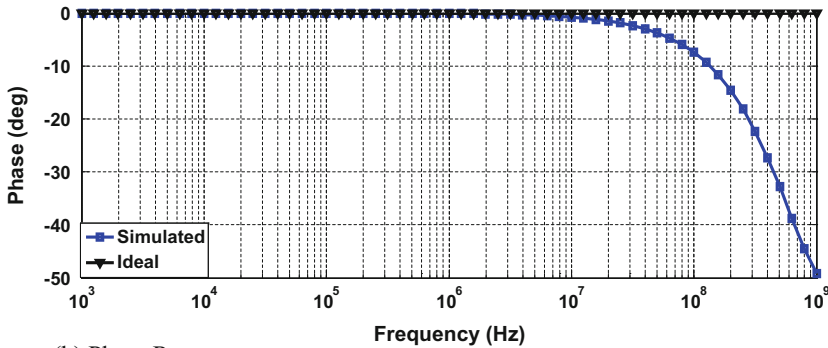
$$L_C = \frac{s C_B}{g_{m1} g_{m2}} \tag{36}$$

Equation (27) derives a circuit structure as shown in Fig. 7.

Now, it can be illustrated from Fig. 7 that considering the terminal parasitics of VDTAs, the designed pure floating resistor simulator becomes a lossy resistor simulator with lossy terms L_A , L_B , L_C , C_F , and D . These large number of lossy terms comes into the picture due to lack of parasitics balancing by external impedances. A carefully designed VDTA with low terminal parasitics is required to overcome this problem. The CMOS structure of VDTA implementation in this paper has very low values of parasitics capacitance values ranging from 0.05 to 0.15 pF and very high values of parasitic resistance of 10 MΩ order. So, parasitic effects are not very much significant on presented circuit.



(a) Magnitude Response



(b) Phase Response

Fig. 9 Frequency response of proposed circuit.

4.1 Application Example

To verify the workability of presented configuration, it has been used to design a low-pass filter (LPF). A conventional RC LPF and active implementation of this filter by replacing the floating passive resistor “ R_0 ” by proposed floating resistance simulator are shown in Fig. 8.

By mathematical analysis of simulated LPF illustrated in Fig. 8b, the voltage transfer function can be found as follows:

$$\frac{V_{out}(s)}{V_{in}(s)} = \frac{1}{1 + \frac{sC_0g_{m_3}g_{m_4}}{g_{m_1}g_{m_2}(g_{m_3} + g_{m_4})}}. \tag{37}$$

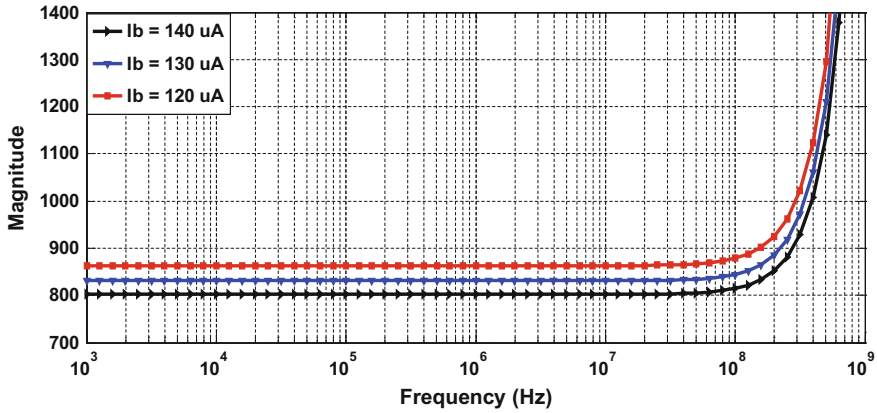


Fig. 10 Magnitude responses for different bias currents

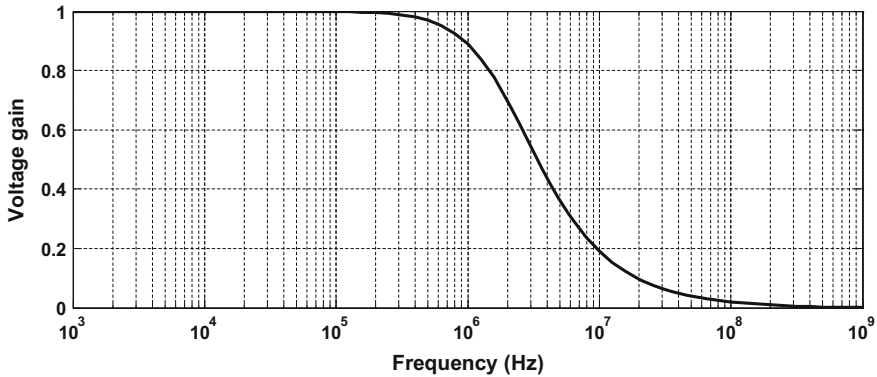


Fig. 11 Frequency response of synthetic floating resistor-based low-pass filter of Fig. 8b

5 Simulation Results and Discussion

To validate the behavior of realized circuit shown in Fig. 3, it is examined by PSPICE tool for circuit simulations. In simulation, the supply voltage for VDTAs is taken as ± 0.9 VDC. All the bias currents of VDTAs are chosen as $150 \mu A$. Fig. 9 shows the magnitude response and phase response of simulated impedance. It can be illustrated by Fig. 9a that the magnitude response of proposed simulator matches with ideal magnitude plot up to 292 MHz frequency. In the same manner it is clear from Fig. 9b that the simulated phase responses has strong agreement with ideal phase response up to 34 MHz frequency at high frequencies the simulated responses deviates from deal response due to effectiveness of parasitics.

To explain the electronic tuning capability of presented synthetic floating resistor, simulations have been done by varying bias current values. The magnitude responses for bias currents $I_b = 120, 130, \text{ and } 140 \mu\text{A}$ have been shown in Fig. 10. For $I_b = 120, 130, \text{ and } 140 \mu\text{A}$, simulated resistance values were found to be $0.864 \text{ k}\Omega, 0.830 \text{ k}\Omega, 0.802 \text{ k}\Omega$, respectively, while the ideal values were $0.878, 0.844, \text{ and } 0.813 \text{ k}\Omega$. So, simulated values have strong agreement with ideal values and deviation is not more than 1.5%.

The proposed simulator-based low-pass filter which is shown in Fig. 8b is also tested by SPICE simulations. For this purpose, CMOS VDTA with $\pm 0.9 \text{ VDC}$ supply has been used with $C_0 = 0.1 \text{ nF}$. The frequency responses of this filter obtained by SPICE simulation have been shown in Fig. 11.

6 Conclusions

A new solely active configuration for simulating electronically tunable floating resistor using only two VDTAs has been proposed. In open literature there is no electronically tunable floating resistor simulator using only two active component has been presented so far. The realized circuit configuration exhibits numerous advantageous properties such as electronic tunability of resistance, no element matching conditions, low values of sensitivity indexes, and no deviations under non-ideal conditions. The high-frequency limitations due to port parasitics of VDTA have been also studied out. A design example of low-pass filter employing proposed configuration has been given and validated. PSPICE simulations have been done with TSMC $0.18 \mu\text{m}$ CMOS technology to validate the theoretical analysis.

References

1. Minaei, S.; Yuce, E.; and Cicekoglu, O. (2006). A versatile active circuit for realizing floating inductance, capacitance, FDNR and admittance converter. *Analog Integrated Circuits and Signal Processing*, 47(2), 199–202.
2. Pal, K. (1971). New inductance and capacitor floatation schemes using current conveyors. *Electronics Letters*, 17(21), 807–808.
3. P. V. Ananda Mohan, (2008). Floating capacitance simulation using current conveyors,” *Journal of Circuits Systems and Computers*, 14(1), 123–128.
4. P. Mongkolwai, P.; Pukkalanun, T.; and Tangsirat, W. (2012). Electronically tunable floating capacitance simulator with only VDTAs and a grounded capacitor. 4th International Science, Social Science, Engineering and Energy Conference-2012.
5. Lahiri, (2010) DO-CCII based generalised impedance convertor simulates floating inductance, capacitance multiplier and FDNR. *Australian Journal of Electrical & Electronics Engineering*, 7(1), 55–59.
6. Senani, R. (1994). Realization of linear voltage controlled resistance in floating form. *Electronics letters*, 30(23), 1909–1910.
7. Riewruja, V.; and Petchmaneelumka, W. (2008). Floating current controlled resistance converters using OTAs. *International Journal of Electronics and Communications-AEU*, 62 (10), 725–731.

8. Yuce, E. (2007). On the implementation of the floating simulators employing a single active device. *International Journal of Electronics and Communications-AEU*, 61(7), 453–458.
9. Yuce, E.; Cicekoglu, O.; and Minaei, S. (2006). CCII-Based Grounded to Floating Imittance Converter and a Floating Inductance Simulator. *Analog Integrated Circuits and Signal Processing*, 46 (3), 287–291.
10. S. Minaei, E. Yuce and O. Cicekoglu, “A versatile active circuit for realizing floating inductance, capacitance, FDNR and admittance converter,” *Analog Integrated Circuits and Signal Processing*, vol. 47, no. 2, pp. 199–202, 2006.
11. Saad, R. A.; and Soliman, A. M. (2010). On the systematic synthesis of CCII-based floating simulators. *International Journal of Circuit Theory and Applications*, 38 (9), 935–967.
12. Kumngern, M.; Torteanchai, U.; and Dejhan, K. (2011). Voltage controlled floating resistor using DDCC. *Radioengineering*, 20 (1), 327–333.
13. Yuce, E.; Minaei, S.; and Cicekoglu, O. (2006). Resistorless floating imittance function simulators employing current controlled conveyors and a grounded capacitor. *Electrical Engineering*, 88 (6), 519–525.
14. Sagbas, M.; Ayten, U. E.; Sedef, H.; and Koksall, M. (2009). Floating imittance function simulator and its applications. *Circuits Systems and Signal Processing*, 28 (1), 55–63.
15. Ayten, U. E.; Sagbas, M.; Herencsar, N.; and Koton, J. (2012). Novel Floating General Element Simulators Using CBTA. *Radioengineering*, 21 (1), 11–19.
16. Sagbas, M. (2011). Component reduced floating $\pm L$, $\pm C$ and $\pm R$ simulators with grounded passive components. *International Journal of Electronics and Communications-AEU*, 65 (10), 794–798.
17. Li, Y. (2012). A series of new circuits based on CFTAs. *International Journal of Electronics and Communications-AEU*, 66 (7), 587–592.
18. Yuce, E. (2010). A novel floating simulation topology composed of only grounded passive components. *International Journal of Electronics*, 97 (3), 249–262.
19. Srivastava, M.; D. Prasad and Bhaskar, D. R. (2015). VDTA Based Electronically Tunable Purely Active Simulator Circuit for Realizing Floating Resistance. *Journal of Engineering Science and Technology Review*, 8 (3), 112–116.
20. Biolek, D.; Senani, R.; Biolkova, V.; and Kolka, Z. (2008). Active elements for analog signal processing: classification, review and new proposals. *Radioengineering*, 17 (4), 15–32.
21. Yesil, A.; Kacar, F.; and Kuntman, H. (2011) “New simple CMOS realization of voltage differencing transconductance amplifier and its RF filter application,” *Radioengineering*, 20 (3), 632–637.
22. Prasad, D.; Bhaskar, D. R.; and Srivastava, M. (2013) Universal Current-Mode Biquad Filter using a VDTA. *Circuits and Systems*, 4 (1), 32–36.
23. Prasad, D.; Bhaskar, D. R.; and Srivastava, M. (2013), “Universal voltage-mode biquad filter using voltage differencing transconductance amplifier. *Indian Journal of Pure and Applied Physics*, 51 (12), 864–868.
24. Prasad, D.; Srivastava, M.; and Bhaskar, D. R.; (2014). Transadmittance - type universal current-mode biquad filter using voltage differencing transconductance amplifiers. *International Scholarly Research Notices*, 4.
25. Prasad, D.; Srivastava, M.; and Bhaskar, D. R.; (2013). Electronically controllable fully uncoupled explicit current mode quadrature oscillator using VDTA and grounded capacitors. *Circuits and Systems*, 4 (2), 169–172.
26. Srivastava, M.; Prasad, D.; and Bhaskar, D. R. (2014). New Parallel R-L impedance using single VDTA & its high pass filter applications,” In *Proc. of International Conference on Signal Processing and Integrated Networks-2014 (SPIN-2014)*, Noida (India), 535–537.
27. Srivastava, M.; Prasad, D.; and Bhaskar, D. R. (2014). Voltage mode quadrature oscillator employing single VDTA and grounded capacitors. *Contemporary Engineering Sciences*, 27 (7). 1501–1507.
28. Srivastava, M.; Prasad, D.; Chitranshi, G.; Sengar, P.; and Mamta (2015). Novel Electronically tunable current-mode integrator employing VDTA. *IEEE-INDICON-2015*, 1–4, New Delhi (India).

Comparative Study of OLSR, DSDV, AODV, DSR and ZRP Routing Protocols Under Blackhole Attack in Mobile Ad Hoc Network

Ankit Singh, Gurpreet Singh and Mandeep Singh

Abstract Mobile ad hoc network consists of an independent set of moveable nodes who are exchanging information among one another within the network. Safety of ad hoc networks is the measure concern for transmitting the information among the wireless nodes. Wireless nodes are having friendly characteristics due to which they expose themselves to different kinds of malicious attacks which are very complicated to identify as each node contributes likewise in network process. Blackhole attack is a routing attack in which malicious node pretends to be the shortest route to reach target node then to all other routes. The purpose is to analyse the performance of various routing protocols of freely movable ad hoc network for instance OLSR, DSR, AODV, DSDV and ZRP under Blackhole attack. The performance factors which will be considered for analysis are packet drop rate, average throughput, average end-to-end delay of packet and packet delivery ratio.

Keywords MANET · OLSR · DSDV · AODV · DSR · ZRP and Blackhole attack

1 Introduction

From last few decades, it has been seen that people are more interested in using wireless technology, as the price tag of wireless-enabled devices has significantly decreased and at the same time functionality of wireless-enabled devices has enhanced effectively. Mobile ad hoc networks (MANET) are networks where each

A. Singh (✉) · G. Singh · M. Singh
Department of Computer Science & Engineering, Lovely Professional University,
Kapurthala, Punjab, India
e-mail: ankitsingh.lpu@gmail.com

G. Singh
e-mail: gurpreet.17671@lpu.co.in

M. Singh
e-mail: mandeep.13742@lpu.co.in

and every node participates for transmitting the information among themselves [1, 2]. This network works without any fixed infrastructure and centralized system. MANET can successfully operate in hostile environment where fixed infrastructure cannot be installed. In these types of networks, every node performs routing functionality as an intermediate node, contributing to successful transmission of information in the form of data packet transmitted by source node for valid destination node. Safety is a foremost concern in such ad hoc network which is operational in combat or rescue situation. As MANET is using multihop technique, the network is highly vulnerable to various attacks like Blackhole attack, Grayhole attack and Wormhole attack. This study illustrates performance of routing protocol in the presence of Blackhole node [3].

2 Related Works

Houda Moudni et al. [4] have performed an analysis to study the impact of different attacks over AODV routing protocol of fully active mobile ad hoc network. And attacks which were used to perform on AODV routing protocol are Blackhole attack, rushing attack and Flooding RREQ attack. The simulation of these attacks was performed using network simulator NS-2.35 over AODV routing protocol. The analysis was performed with certain parameters; they are as follow normalize route load, average end-to-end delay of packet and packet delivery ratio. From outcome, conclusion is that rushing attack has least substantial impact on effectiveness of AODV routing protocol and Blackhole attack is most substantial attack on performance parameter of AODV routing protocol. Deshmukh et al. [5] have proposed a methodology to detect Blackhole node over DSR routing protocol implemented in ad hoc network. This proposed methodology has used validity value along with RREP packet. This validity value is used by intermediate node to verify that the route is free from Blackhole node. It does not require extra processing. This paper illustrates the security issues of Blackhole attack over ad hoc network. Jain et al. [6] have analysed the quality of service for different sets of traffic pattern such as constant bit rate, pareto and exponential. This paper has performed a trust-based ad hoc network and concluded that exponential traffic pattern gives better result in the form of throughput and packet delivery ratio. Jaychandra et al. [7] have analysed the effect of Blackhole attack over AODV and MAODV routing protocols of ad hoc networks. The simulation of network has been performed in network simulator NS-2.35 with packet delivery ratio and average throughput as performance parameters. It concluded that MAODV has better performance than AODV as the number to node increases in ad hoc network. Kumari et al. [8] have performed an analysis of quality of service over routing protocols for freely movable ad hoc network as performance metric. The execution of these analyses was performed using network simulator NS-3. They have described the routing protocol like DSDV, OLSR and AODV; the performance metrics used in this analysis are routing overheads, average end-to-end delay of packet and packet delivery ratio.

These performances conclude that AODV gives better results than other protocols in the form of packet delivery ratio. Kaur et al. [9] have reviewed routing protocol of ad hoc network, for example, DSR, AODV, ZRP and prepared a comparative table on the basis of some quantitative parameter and described the advantage and disadvantage of these routing protocols on ad hoc network. Keerthika et al. [10] have proposed a methodology to eliminate the Blackhole attack effect from ad hoc networks using AODV trust model known as weighted trust ad hoc on-demand distance vector (WTAODV). Trust model works both directly and indirectly which uses factor such as link quality, neighbouring trust and normalized route reply misbehaviour. The sharing of this information results improvement in the malicious node detection in WTAODV model of mobile ad hoc network. This study has reflected that packet delivery ratio is improved by 15% in different situation.

3 Routing Protocol

There are numerous routing protocols which have been proposed by researchers for mobile ad hoc network. These functional routing protocols are categorized as proactive, reactive and hybrid. The proactive protocol is similarly named as table-driven routing protocol where table is need to be updated periodically, whereas reactive protocol is sometime also named as on-demand routing protocol where the path is searched when transmission needs to take place. And hybrid routing protocols is collaborating proactive routing protocol and reactive routing protocol [11, 12].

Following is description of functional routing protocols of network:-

3.1 *Destination Sequence Distance Vector (DSDV)*

The destination sequence distance vector (DSDV) is an effective routing protocol which is formulated using Bellman Ford algorithm to resolve the loop routing in MANET. This is one of the types of proactive routing protocol of freely movable network also called as table-driven routing protocols. Every node of mobile ad hoc network contains table of paths to neighbouring node with distance and sequence number in DSDV routing protocol. The sequence number in table is used for updating routes of the table with latest sequence number to prevent ad hoc network from loop routing. Since this routing protocol is table driven, therefore it is required to maintain the routes updated, each node broadcasts their routing table to the other nodes of network [13, 14].

3.2 *Optimized Link State Routing Protocol (OLSR)*

The Optimized Link State Routing Protocol is well-known protocol of Internet routing protocol which enhanced the working of freely moveable network. This protocol is a one type of proactive routing protocol of network which is also called as table-driven routing protocol. And this protocol operates with following control message to locate nodes and broadcast the link state information among the nodes for updating the routes with shortest possible routes of ad hoc network.

- (a) HELLO control message which is propagated to figure out the node present in one hop or two hop distance from their reply. Multipoint relay (MPR) is selected by the sender depending on one hop node offering shortest route to next hop nodes.
- (b) TOPOLOGY CONTROL (TC) is a control message of OLSR which is transmitted along with multipoint relay (MR) for broadcasting the neighbouring node information inside ad hoc network.

3.3 *Dynamic Source Routing (DSR)*

The Dynamic Source Routing Protocol is such a protocol that utilizes concept of source routing. This protocol is one of the types of reactive routing protocol which is also named as on-demand routing protocol. Source routing is also known as path addressing in which the route is discovered whenever node needs to propagate information for node of freely movable networks. When path is traced, then header is linked with data packet which contains the list of all nodes through which it will traverse for successful delivery of data packets to valid destination node. Each node in the route will process the header part of data packets and transmit it to the next listed node of route. And the same header is used for replying acknowledgement to sender in reverse order.

3.4 *Ad Hoc On-Demand Distance Vector (AODV)*

Ad hoc On-demand Distance Vector is fully functional routing protocol which uses principle of both Dynamic Source Routing Protocol for finding route and Destination Sequence Distance Vector routing protocol for latest information [15, 16]. Ad hoc on-demand distance vector (AODV) is functional routing protocol which belongs to reactive routing protocols also called as on-demand routing protocol. This protocol finds way for valid destination when a node requires to pass on the data packets to other node of present movable network [17, 18]. AODV routing protocol processes two measure function; they are route discovery for

destination and their maintenance [19, 20]. In AODV routing protocol, when a node of ad hoc network has to send some sort of information to other node of same network, then sender node broadcasts route request (RREQ) packet in freely movable network. And this RREQ packet will be retransmitted in same network by the intermediate node until the packet arrives at the target destination node. When route request (RREQ) packet via intermediate nodes arrives at correct destination node, node has to unicast a route reply (RREP) packet through same path to sender node and after that the transmission of actual data packets can start moving from source node of movable network to valid destination node. In between if the transmission of data packet link failure occurs, then route error (RERR) packet is generated from intermediate node and transmitted back to source node for restarting the route discovery process [21].

3.5 Zone Routing Protocol (ZRP)

Zone Routing Protocol is collectively using principle of proactive routing protocol and reactive routing protocol for transmission of information in the ad hoc network; hence, Zone Routing Protocol belongs to hybrid routing protocols. It was innovated for reducing the processing overhead and to increase the rate of delivery by proper implementation of most effective type of enhanced routing protocol over freely movable ad hoc network. Zone Routing Protocol creates zone for each node with some radius in the ad hoc network. Let the target destination node is present within the zone of source node, then it will use routing table for data packet delivery to destination node as proactive routing protocol delivers. If the destination node is present out of zone of source node, then source node uses the reactive routing protocol which checks every next zone in the ad hoc network whether the route of valid destination node. With this process, routing protocol is able to trim down overheads at the time of route discovery operation and packet delivery to the destination node. Zone Routing Protocol helps to deliver data packets immediately to valid destination node present within the zone using the routing table. It also helps to reduce the overheads for destination node outside the zone and the time to deliver of data packet [22].

4 Blackhole Attack

The mobile ad hoc network was innovated with an idea that the network will be working in risk-free environment. It was assumed the routing protocol will be effectively working in a trusted and cooperative atmosphere and hence there is no security mechanism for avoiding attack in mobile ad hoc network that can provide security against malicious nodes or attack to the ad hoc network [23, 24]. Thus, it cannot be ignored that the ad hoc network will work in threat-free environment or

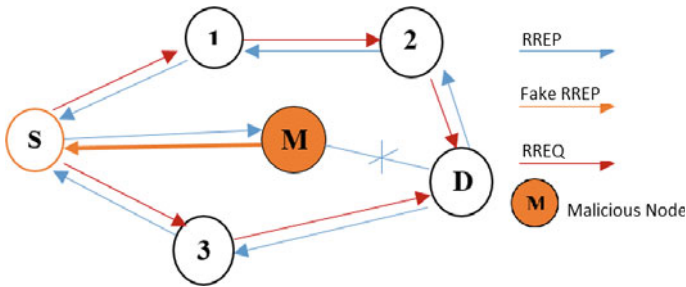


Fig. 1 Blackhole attack example

there is not any malicious node present in the ad hoc network, as its nature of open communication medium. This paper will examine the effect of Blackhole attack on different routing protocols. Blackhole attack is one of types of an active DoS-based attack [25, 26]. In Blackhole attack, a malicious node will broadcast its information to all the nodes of ad hoc network about its presence and wait till any other node is looking for route to other node through route request (RREQ) packet in same freely movable network, and at that point of time when RREQ packet reaches to malicious node, with immediate effect without looking into its routing table, it will generate a fake acknowledgement packet known as route reply (RREP) packet with latest sequence number and hop count as shortest route to valid destination node through itself [27, 28]. Therefore, the source node discards other RREP coming from other node and starts transmitting all its data packets towards the malicious node and consequently it drops all data packets, but not transmits it to valid destination node. In this kind of attack, the Blackhole node or malicious node is positioned at centre of the mobile ad hoc network by the attacker as shown in Fig. 1 [29, 30].

5 Experiment and Results

In the following segment of paper, we represent a controlled set of experiment for analysing the impact of Blackhole attack over routing protocols of functional ad hoc network. We have simulated these experiments over network simulator tool of version NS 2.35. These results are obtained on the basis of following listed parameter for analysing the influence of Blackhole attack on routing protocol of the ad hoc network. Following points are considered performance parameters:-

- (i) Average Delay: It is the amount of time taken by the informational data packets to move from application layer of source node of network towards the application layer of valid destination node. And it is also called as average end-to-end delay (as a parameter).
- (ii) Packet Delivery Ratio: It is the rate of coming data packets from source node to the rate of actual arrived data packets; it is the ratio of the amount of data

Table 1 Simulation parameters

Simulator	NS-2.35
Simulation time	400 (s)
Number of nodes	15, 25, 35...150
Simulation area	1500 × 1500 (m)
Routing protocols	OLSR, DSDV, AODV, DSR, ZRP
Pause time	10 (metre per second)
Maximum speed	20 (metre per second)
Traffic	Constant bit rate

packets delivered to valid destination node to the actual amount of transmitted data packet by initiating source node.

- (iii) Packet Drop Ratio: It is a proportion of the lost data packet to the data packets relayed from source node for delivery to valid destination node.
- (iv) Throughput: It is a number of successful delivery of data packet relay by source node of movable network to destination node over communication channel.

Table 1 represents the scenario of mobility which is performed over mobile ad hoc network on simulator. Following are the parameters on which simulation is performed using random waypoint model with nodes ranging from 15 to 150.

Figure 2 illustrates packet delivery ratio in the presence of Blackhole attack for routing protocols, for example, OLSR, DSDV, AODV, DSR and ZRP; it represents that AODV routing protocol gives better results than all other routing protocols.

Figure 3 illustrates average end-to-end delay in the presence of Blackhole attack for routing protocol, for example, OLSR, DSDV, AODV, DSR and ZRP; it represents that ZRP is higher than all other routing protocols.

Figure 4 illustrates packet drop ratio in the presence of Blackhole attack on routing protocol such as OLSR, DSDV, AODV, DSR and ZRP; it represents that ZRP is better than all other routing protocols.

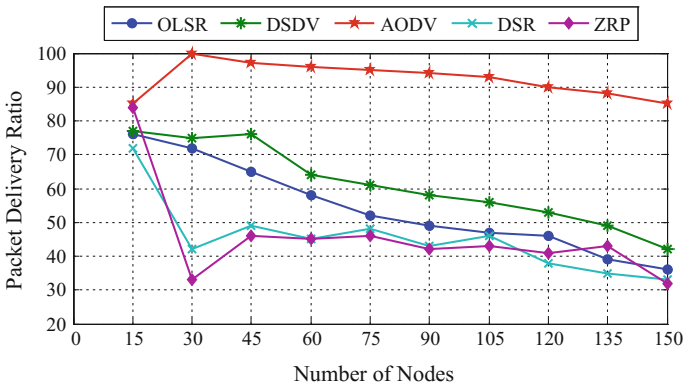


Fig. 2 Packet delivery ratio of routing protocol concealed by Blackhole attack

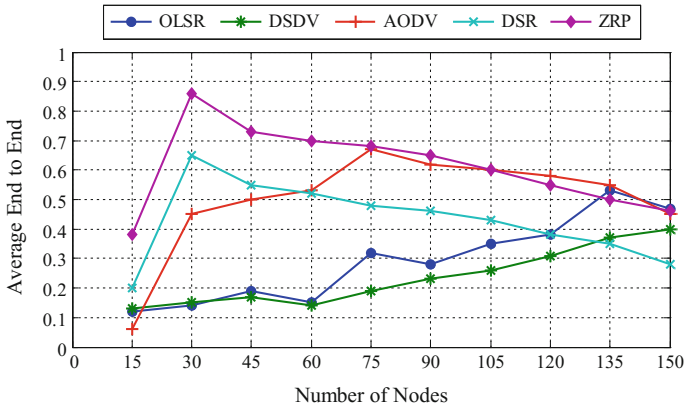


Fig. 3 Average end-to-end delay of routing protocols under Blackhole attack

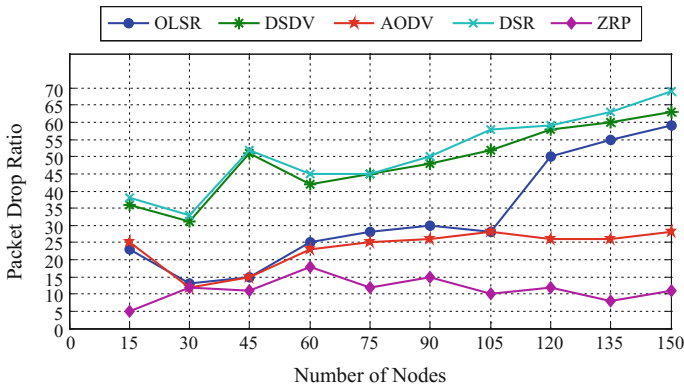


Fig. 4 Packet drop ratio for routing protocols under Blackhole attack

Figure 5 illustrates throughput of all scenarios in the presence of Blackhole attack on routing protocol such as OLSR, DSDV, AODV, DSR and ZRP; it represents that ZRP has greater throughput than all other routing protocols.

6 Conclusion and Future Work

At the starting where the strength of nodes is low, the ZRP values are at peak in the graph of average end-to-end delay, but as the strength of nodes in the network increases, it starts falling but DSDV has significantly maintained low end-to-end delay till the strength reaches to 90 node, further ZRP comes below it. ZRP has also performed better among all the routing protocols, and OLSR was worst among all

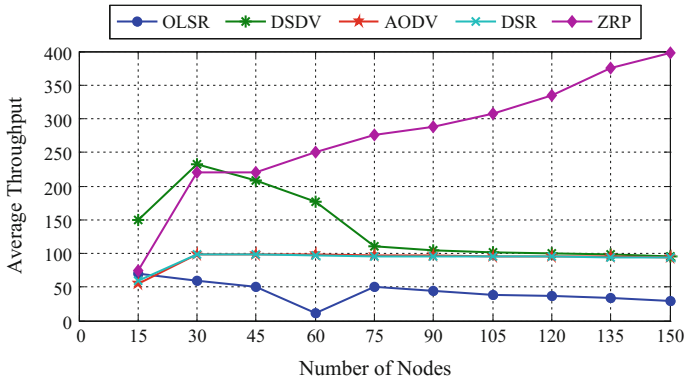


Fig. 5 Average throughput of routing protocol under Blackhole attack

in the presence of Blackhole attacking node. ZRP has also performed better in terms of packet drop ratio as well as in packet delivery ratio. All these results have represented that ZRP took over among all the routing protocols, and it has ability to function smoothly in mobile ad hoc network in the presence of Blackhole node. The Blackhole attacks are also harmful to technologies like IoT (Internet of Things) and VANET as for MANET.

For future, our aim is figure out the methodology that can eliminate the effects of Blackhole attack from performance parameter of mobile ad hoc networks so that ad hoc network can perform smoothly. We are going study to understand the impact of attack over all routing protocols performance parameter of Mobile Ad hoc Network.

References

1. Sushama Singh, Atish Mishra & Upendra Singh. Detection and Avoiding of Collaborative Blackhole attack on MANET using Trusted AODV Routing.. In Colossal Data Analysis and Networking (CDAN), Symposium. IEEE (2016).
2. Houda Moudni, Mohamed Er-rouidi, Hicham Mouncif, & Benachir El Hadadi. Modified AODV Routing Protocol to Improve Security and Performance against Blackhole attack. In Information Technology for Organizations Development (IT4OD), 2016 International Conference. IEEE (2016).
3. Kannan Govindan & Pransant Mohapatra. Trust Computations and Trust Dynamics in Mobile Ad-hoc Networks: A Survey. In IEEE Communication Surveys & Tutorials (Volume: 14, Issue: 2, Second Quarter 2016). IEEE (2016).
4. Houda Moudni, Mohamed Er-rouidi, Hicham Mouncif, & Benachir El Hadadi. Attacks against AODV Routing Protocol in Mobile Ad-Hoc Networks. In Computer Graphics, Imaging and visualization (CGIV), 2016 13th International Conference. IEEE (2016).
5. Sagar R. Deshmukh & Dr P.N. Chatur. Secure Routing to Avoid Blackhole Affected Routes in MANET. In Colossal Data Analysis and Networking (CDAN), Symposium. IEEE (2016).

6. Aporva Jain, Urmila Prajapati & Piyush Chouhan. Trust Based Mechanism with AODV Protocol for prevention of Blackhole attack in MANET. In Colossal Data Analysis and Networking (CDAN), Symposium. IEEE (2016).
7. S.H. Jaychandra, R Manjunatha, Nayab Hussain, B.U. Sujana, H.L. Gururaj & B.Ramesh. Analysis of Blackhole Attack in Ad-hoc Network using AODV and MAODV protocol. SPRINGER (2016).
8. Neelu Kumari, Sandeep Kumar Gupta, Rajini Choudhary & Shubh Laxshmi Agrwal. New performance analysis of AODV, DSDV and OLSR routing protocol for MANET. In Computing for Sustainable Global Development (INDIACom), 2016 3rd International Conference. IEEE (2016).
9. Parvinder Kaur, Dalveer Kaur & Rajiv Mahajan. A review and comparison of AODV, DSR and ZRP routing protocols on the basis of qualitative metrics. In Computing for Sustainable Global Development (INDIACom), 2016 3rd International Conference. IEEE (2016).
10. V.Keerthika & N. Malarvizhi. Mitigate black hole attack using trust with AODV in MANET. In Computing for Sustainable Global Development (INDIACom), 2016 3rd International Conference. IEEE (2016).
11. Ram Kishore Singh & Parma Nand. Literature review of routing attacks in MANET. In Computing, Communication and Automation (ICCCA), 2016 International Conference. IEEE (2016).
12. Sakshi Jain & Ajay Khuteta. Detecting and overcoming blackhole attack in mobile Adhoc Network. In Green Computing and Internet of Things (ICGCIoT), 2015 International Conference. IEEE (2015).
13. Mohamed A. Abdelshafy & Peter J. B. King. Dynamic source routing under attacks. In Reliable Networks Design and Modeling (RNDM), 2015 7th International Workshop. IEEE (2015).
14. Abhijeet Salunke & Dayan and Ambawade. Dynamic Sequence Number Thresholding protocol for detection of blackhole attack in Wireless Sensor Network. In Communication, Information & Computing Technology (ICCICT), 2015 International Conference. IEEE (2015).
15. Dhiraj Nitnaware & Anita Thakur. Blackhole Attack Detection and Prevention Strategy in DYMO for MANET. In Signal Processing and Integrated Networks (SPIN), 2016 3rd International Conference. IEEE (2016).
16. Sagar R.Deshmukh, P.N. Chatur & Nikhil B Bhople. AODV-based secure routing against blackhole attack in MANET. In Recent Trends in Electronics, Information & Communication Technology (RTEICT), International Conference. IEEE (2016).
17. Neeraj Arya, Upendra Singh & Sushma Singh. Detecting and avoiding of worm hole attack and collaborative blackhole attack on MANET using trusted AODV routing algorithm. In Computer, Communication and Control (IC4), 2015 International Conference. IEEE (2015).
18. Anurag Gupta & Kamlesh Rana. Assessment of various attacks on AODV in malicious environment. In Next Generation Computing Technologies (NGCT) 2015 1st International Conference. IEEE (2015).
19. Kriti Patidar & Vandana Dubey. Modification in routing mechanism of AODV for defending blackhole and wormhole attacks. In IT in Business, Industry and Government (CSIBIG), 2014 Conference. IEEE (2014).
20. Chaitali Biswas Dutta & Utpal Biswas. An energy aware blackhole attack for multipath AODV. In Business and Information Management (ICBIM), 2014 2nd International Conference. IEEE (2014).
21. Chaitali Biswas Dutta & Utpal Biswas. A novel blackhole attack for multipath AODV and its mitigation. In Recent Advances and Innovations in Engineering (ICRAIE-2014), International Conference. IEEE (2014).
22. Sivendra Prackash & Abhishek Swaroop. A brief survey of blackhole detection and avoidance for ZRP protocol in MANETs. In Computing, Communication and Automation (ICCCA), 2016 International Conference. IEEE (2016).

23. Sweta Dixit, Priya Pathak & Sandeep Gupta. A Novel Approach for Grayhole and Blackhole Detection and Prevention. In Colossal Data Analysis and Networking (CDAN), Symposium. IEEE (2016).
24. Siddhart Dhama, Sundeep Sharam & Mukul Saini. Blackhole Attack Detection and Prevention Mechanism for Mobile Ad-hoc Networks. In Computing for Sustainable Global Development (INDIACom), 2016 3rd International Conference. IEEE (2016).
25. Nirbhay Chaubey, Akshai Aggarwal, Savita Gandhi & Keyurbhai A Jani. Effect of pause time on AODV and TSDRP routing protocols under black hole attack and DoS attacks in MANETs. In Computing for Sustainable Global Development (INDIACom), 2015 2nd International Conference. IEEE (2015).
26. Pradeep R. Dumne & Arati Manjaramkar. Cooperative bait detection scheme to prevent collaborative blackhole or grayhole attacks by malicious nodes in MANETs. Reliability, Infocom Technologies and Optimization (Trends and Future Directions) (ICRITO), 2016 5th International Conference. IEEE (2016).
27. Vaishali Gaikwad Mohite & Lata Ragma. Security agents for detecting and avoiding cooperative blackhole attacks in MANET. Applied and Theoretical Computing and Communication Technology (iCATccT), 2015 International Conference. IEEE (2015).
28. Mohamed A. Abdelshafy & Peter J. B. King. Resisting blackhole attacks on MANETs. In Consumer Communications & Networking Conference (CCNC), 2016 13th IEEE Annual Conference. IEEE (2016).
29. Ankit D. Patel & Kartik Chawda. Blackhole and grayhole attacks in MANET. In Information Communication and Embedded Systems (ICICES2014), 2014 International Conference. IEEE (2014).
30. Hemant Sharma, Koushik Banerjee & Brijesh Kumar Chaurasia. Blackhole Tolerant Protocol for ZigBee Wireless Networks. In Computational Intelligence and Communication Networks, 2014 International Conference. IEEE (2014).

Lead-Free Piezoelectric Energy Harvester Design for Lower Order Random Vibrations

Oshin Garg, Sukesha Sharma and Preeti

Abstract The paper describes the design and experimental evaluation of piezoelectric energy harvester that can generate power from random vibrations of low frequency. The design consists of two aluminium cantilevers on which PVDF-based piezoelectric patches were bonded on both the sides and were serially connected. Two full wave schottky diode bridge rectifiers were used to rectify the output of each cantilever. The output of rectifiers was added using serial connections. The prototype generated a net DC output of 1.04 V and 16.85 μ W power under lower order vibrations.

Keywords Piezoelectricity · PVDF · Cantilever · Energy harvesting
Serial connection

1 Introduction

With the advancement in wireless technology, wireless sensors can be used in almost every field. Some of the applications are wireless sensor networks and military applications. Wireless sensors require their own power supply which in most of the cases is conventional battery. Batteries have limited lifetime, and they need to be replaced with time. The task to replace batteries is very tedious and expensive because most of the wireless sensors are placed in remote areas and work in harsh environment. Researchers are focusing on alternative ways to power these wireless sensors. Energy harvesting from vibrations is one of the most promising choice for powering wireless sensors or other low power devices [1–4]. The vibrational energy can be converted into electrical energy by using three principles, namely piezoelectric, electromagnetic and electrostatic. Out of these three techniques, energy harvesting using piezoelectric principle has been widely investigated because it requires no external voltage source and it has simple structure [5–7]. A piezoelectric energy harvester consists of three main components: transducer,

O. Garg (✉) · S. Sharma · Preeti
University Institute of Engineering and Technology, Panjab University, Chandigarh, India
e-mail: osh.scorpion@gmail.com

rectifier and storage unit. The transducer converts mechanical force or vibrations into electrical energy. It consists of a patch of piezoelectric material bonded to a cantilever with or without tip mass [8, 9]. There are several piezoelectric materials such as piezo ceramics PZT (lead zirconate titanite), PVDF (polyvinylidene fluoride), single crystals PMN-PT, PZN-PT. Different piezoelectric materials have different behaviours. Some are brittle but give larger voltage output; some are flexible but give higher voltage output [10]. Usually single crystals give higher voltage output but they have been hardly used for energy harvesting purposes because they are difficult to fabricate and are very expensive [11, 12]. Various materials have been investigated, and PZT has been most commonly used for energy harvesting purposes [13]. But it has been experimentally shown that despite its low piezoelectric coefficient, PVDF gives better results than PZT when subjected to low vibrations because of its high flexibility [14]. Also, PVDF is a lead-free material which is environment friendly [15]. The output of the transducer gives AC output, i.e., alternating current. The rectifier circuit converts the AC signal to DC, i.e., direct current. The DC output is then stored in capacitors or batteries [16].

There are various design parameters for the design of transducer such as loading mode, structure and choice of material. In this paper, series connection of two cantilevers with 3-1 loading mode [17] using PVDF-based material has been investigated under lower order random vibrations. For lower order vibrations, sometimes output voltage is very less and it could not even overcome the voltage drops of rectifier circuit. The motive of this paper is to enhance the voltage output by bonding piezoelectric patches to both the sides of cantilever and connecting them directly by using serial connections.

2 Simulations and Discussion

Simulations were done in LT SPICE simulator, and the two cases were compared. Case 1: piezoelectric patches were applied on different cantilever on single side. Case 2: piezoelectric patches were attached to both sides of cantilever. Since the AC output of different cantilevers is out of phase, so they cannot be directly added as it will result in net decrease in voltage output. To solve this problem, output of each cantilever is first rectified and then serially added. Figure 1a, b shows the simulation results of Case 1: piezoelectric patches are bonded on single side of cantilever, and Fig. 2a, b shows the simulation results of Case 2: piezoelectric patches are bonded on both sides of cantilever, respectively.

Table 1 summarizes the simulation results. The voltage and current obtained in Case 1 are 1.13 V and 11 μ A, whereas the voltage and current obtained in Case 2 are around 1.35 V and 22 μ A, respectively.

From the simulation results, it has been found that there is a voltage improvement of around 220 mV and current improvement of 11 μ A. Hence, a net power increase of 17.27 μ W has been achieved. Moreover in Case 2, we require only two rectifiers which results in reduction of external circuitry. Also, here we have

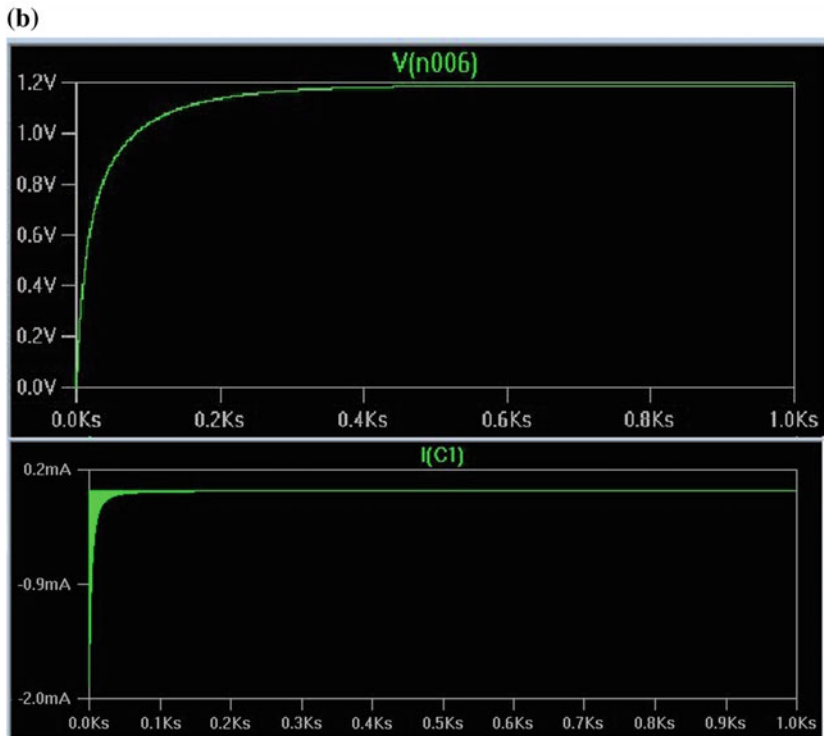
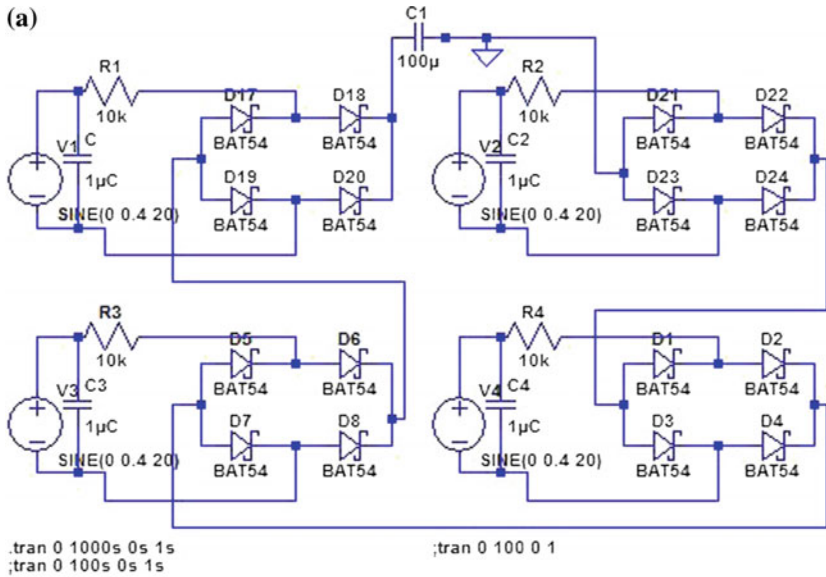


Fig. 1 a LT spice block diagram of Case 1: piezoelectric patches bonded on single side of cantilever. **b** Voltage and current response of Case 1

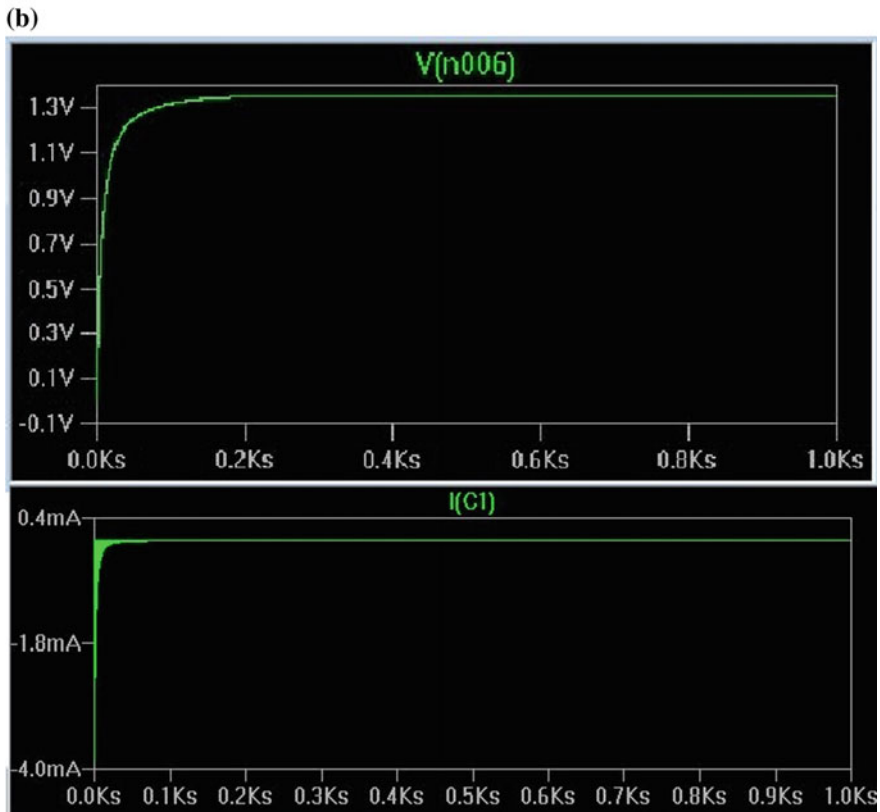
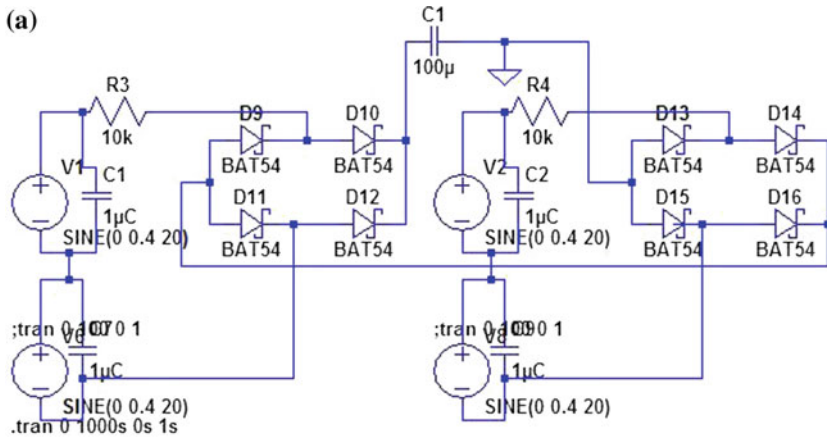


Fig. 2 a LT spice block diagram of Case 2: piezoelectric patches bonded on both sides of cantilever. b Voltage and current response of case 2

assumed that voltage output of each piezoelectric element is 400 mV which is greater than voltage drop of one rectifier. If the voltage generated from one piezoelectric element is less than the voltage drop of the rectifier then in Case 1, we will get only noise at the output, whereas in Case 2, we will be able to get the output due to direct serial addition of two piezoelectric patches.

3 Experimental Set-up and Results

The experimental set-up of a piezoelectric energy harvester consists of two cantilevers on which piezoelectric patches were bonded on both the sides and electrically connected in series. A cantilever beam type of structure with 3-1 loading mode has been chosen because of its simple structure. The set-up consists Fig. 3 shows the cantilever beam arrangement and Fig. 4 shows the experimental set-up of piezoelectric energy harvester. Table 2 shows the dimensions of cantilever beam and piezoelectric patches.

The aluminium cantilever beams were clamped on a clamper and were subjected to lower order random vibrations due to air flow of fan. The outputs of the cantilevers were rectified by means of two schottky bridge rectifiers. The rectified output of each cantilever was serially added which is stored in a capacitor. The responses were recorded by means of digital signal oscilloscope (DSO). It has been practically proved that cantilever with piezoelectric patches attached to both the sides and serially connected gives better output as compared to cantilever with

Table 1 Simulation results of Case 1 and Case 2

Case	Voltage (V)	Current (μ A)	Power (μ W)
Case 1: piezoelectric patches bonded on single side of cantilever	1.13	11	12.43
Case 2: piezoelectric patches bonded on both sides of cantilever	1.35	22	29.7

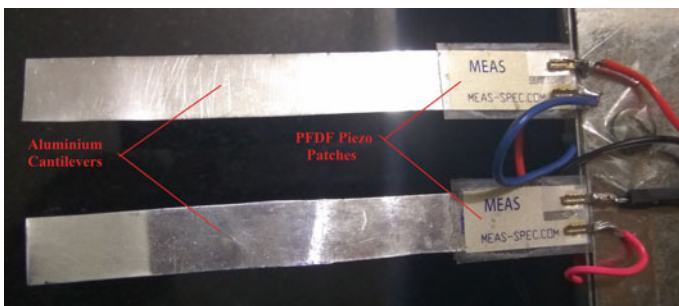


Fig. 3 Cantilever beam arrangement

Fig. 4 Experimental set-up of piezoelectric energy harvester

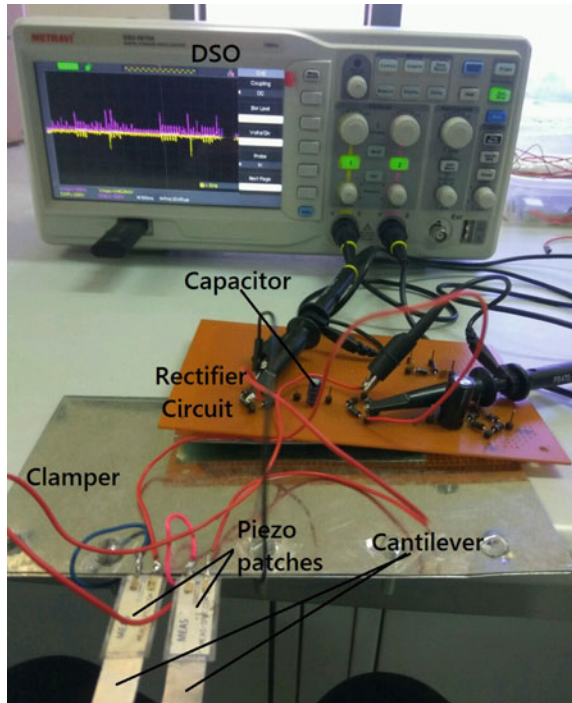


Table 2 Dimensions of cantilever beams and piezoelectric patches

Dimensions	Cantilever 1	Cantilever 2	Piezoelectric patch 1 (mm)	Piezoelectric patch 2 (mm)
Length	11 cm	11 cm	22	22
Width	10 mm	10 mm	10	10
Thickness	0.23 mm	0.23 mm	0.2	0.2

piezoelectric patch attached to single side. Figure 5 shows the time response of Case 1 and Case 2, i.e., piezoelectric patch attached to one side of the cantilever beam and piezoelectric patch attached to both sides of cantilever beam, respectively.

It has been observed that there is significant increase in the output voltage in Case 2. The RMS value of voltage obtained in Case 1 was about 0.5 V which is less than the voltage drop of a single rectifier which is around 0.74 V voltage drop of two schottky diodes whereas the RMS value obtained in Case 2 was about 1.2 V. Hence, there is a significant increase in the performance of piezoelectric cantilever when the piezoelectric patches were bonded on both sides of the cantilever as its sensitivity towards vibrations also increases. Hence, in the prototype, we have attached piezoelectric patches on both the sides of cantilevers. Two aluminium

cantilevers were used. Figure 6 shows the time response of cantilever 1 and Fig. 7 shows the time response of cantilever 2.

Since the responses of both the cantilevers are not in phase, they cannot be directly added. The outputs of both the cantilevers were rectified and then serially added. Figure 8 shows the phase delay between the responses of two cantilevers, and Fig. 9 shows the resultant DC voltage after serial addition of rectified voltages of both the cantilevers.

The performance of both the cantilevers and the voltage drop of both the rectifiers have been tabulated in Table 3.

The obtained RMS value of the output of cantilever 1 was 1.2 V, and the RMS value of the output of cantilever 2 was 1.4 V. The voltage drop of schottky diode

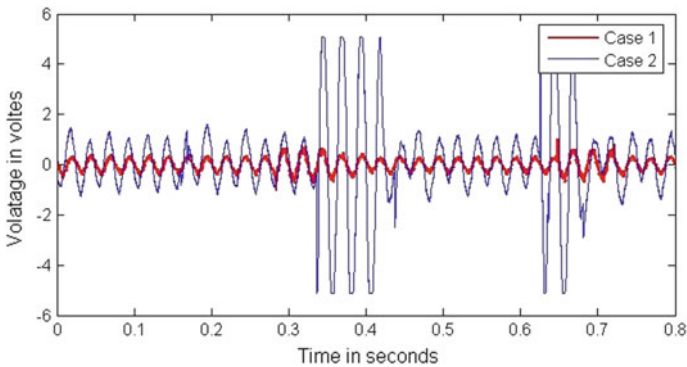


Fig. 5 Time response of Case 1: piezoelectric patch on one side of cantilever and Case 2: piezoelectric patch bonded on both sides and serially connected

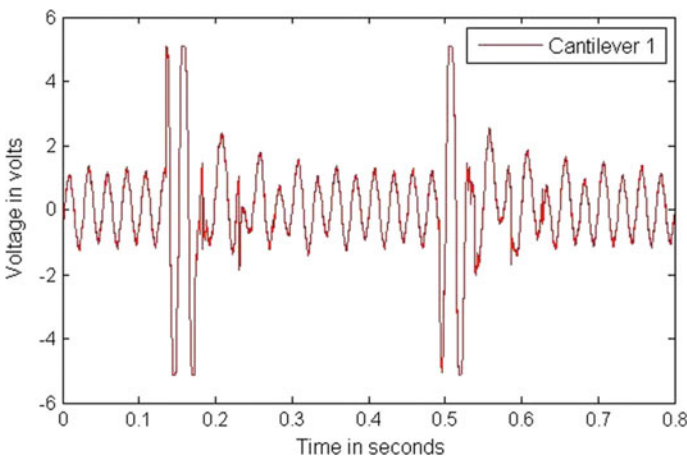


Fig. 6 Time response of cantilever 1

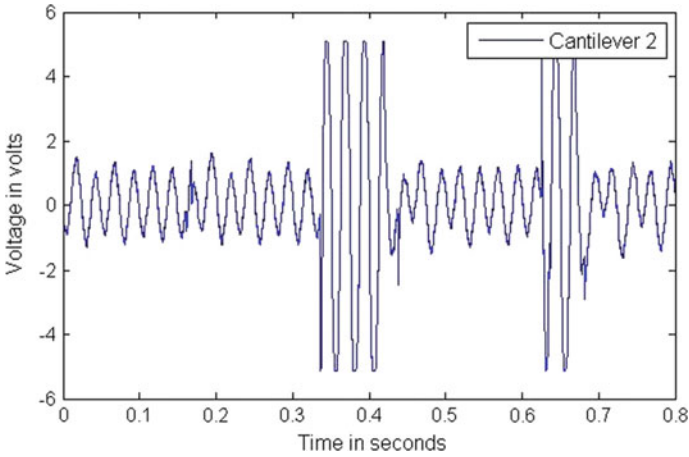


Fig. 7 Time response of cantilever 2

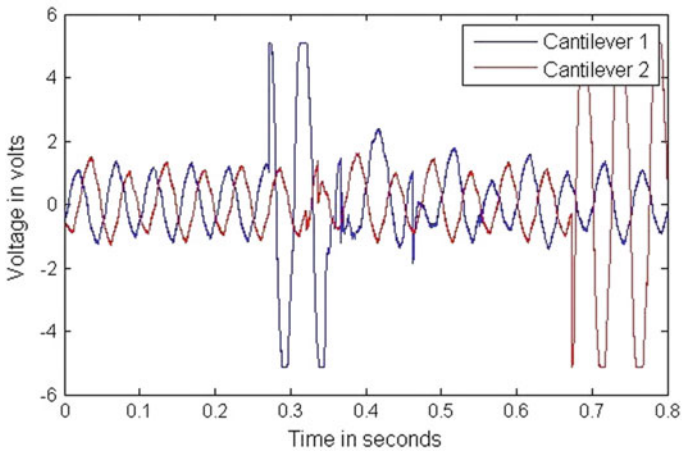


Fig. 8 Phase delay between the time responses of two cantilevers

bridge rectifier 1 was 0.74 V, and the voltage drop of rectifier 2 was 0.82 V. Final experimental results have been tabulated in Table 4.

The resultant DC voltage across the capacitor under lower order random vibrations was 1.04 V. For current measurement, voltage drop across a 1 K resistor has been measured, which was 0.016 V. Hence, net current was calculated as 16.47 μ A and net power of 17.13 μ W has been achieved which can be used for low-power applications.

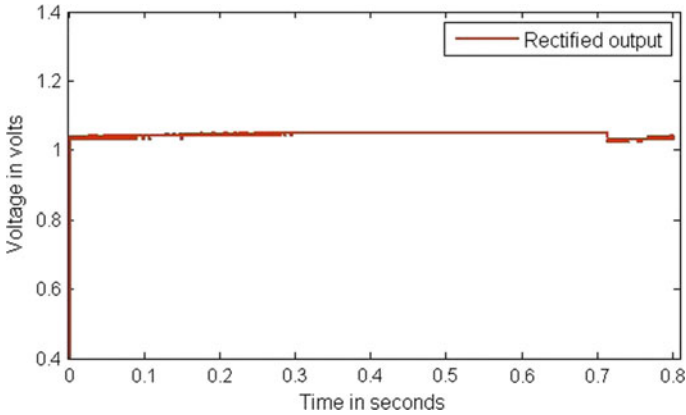


Fig. 9 Resultant DC output voltage response

Table 3 Performance of two cantilevers

Cantilever	Voltage in V		
	Before rectification (AC)	After rectification (DC)	Voltage drop of corresponding rectifier
1	1.2	0.46	0.74
2	1.4	0.58	0.82

Table 4 Final experimental results

Resultant DC values		
Voltage (V)	Current (μ A)	Power (μ W)
1.04	16.47	17.13

4 Conclusion

The output generated from normal cantilever arrangement for piezoelectric energy harvesting under lower order random vibration is very less. Sometimes, it cannot overcome the voltage drop of the rectifier. The designed prototype uses two cantilever arrangement with piezoelectric patches attached to both the sides and connected in series which results in the output voltage which is greater than the rectifier drop. For the transducer design, PVDF-based piezoelectric patches were used due to its high flexibility. The output of two cantilevers were individually rectified and then serially added. The net DC voltage of 1.04 V and power of 16.85 μ W have been obtained using this arrangement under lower order random vibrations.

References

1. Siddique ARM, Mahmud S, Van Heyst B., "A comprehensive review on vibration based micro power generators using electromagnetic and piezoelectric transducer mechanisms," *Energy Convers Manage* 2015;106:728–47.
2. Yang Z, Zu J., "High-efficiency compressive-mode energy harvester enhanced by a multi-stage force amplification mechanism," *Energy Convers Manage* 2014;88:829–33.
3. Guan M, Liao W-H, "Design and analysis of a piezoelectric energy harvester for rotational motion system," *Energy Convers Manage* 2016;111:239–44.
4. Zhou W, Zuo L., "A self-powered piezoelectric vibration control system with switch precharged inductor (spci) method," *IEEE/ASME Trans Mechatron* 2015;20(2):773–81.
5. Kim, H.S.; Kim, J.H.; Kim, "A review of piezoelectric energy harvesting based on vibration," *Int. J. Precis. Eng. Man.* 2011, 12, 1129–1141.
6. Chalasani, Sravanthi, and James M. Conrad. "A survey of energy harvesting sources for embedded systems." *Southeastcon*, 2008. IEEE. IEEE, 2008.
7. Y.C. Shu, I.C. Lien, "Efficiency of energy conversion for a piezoelectric power harvesting systems," *J. Micromech. Microeng.* 16 (2006) 2429–2438.
8. Andosca, Robert, et al. "Experimental and theoretical studies on MEMS piezoelectric vibrational energy harvesters with mass loading." *Sensors and Actuators A: Physical* 178 (2012): 76–87.
9. Chen, Shih-Nung, Gou-Jen Wang, and Ming-Chun Chien. "Analytical modeling of piezoelectric vibration-induced micro power generator." *Mechatronics* 16.7 (2006): 379–387.
10. S. M. Taware and S. P. Deshmukh, "A Review of Energy Harvesting From Piezoelectric Materials," *IOSR J. Mech. Civ. Eng.*, pp. 43–50, 2013.
11. Yang, Zhengbao, and Jean Zu. "Comparison of PZN-PT, PMN-PT single crystals and PZT ceramic for vibration energy harvesting." *Energy Conversion and Management* 122 (2016): 321–329.
12. Zibo Jiang, "PMN-PT crystal of less defects and more uniformity", *Applications of Ferroelectric International Symposium on Integrated Functionalities and Piezoelectric Force Microscopy Workshop 2015 Joint IEEE International Symposium on the*, pp. 56–59, 2015.
13. Karami MA, Bilgen O, Inman DJ, Friswell M, et al., "Experimental and analytical parametric study of single-crystal unimorph beams for vibration energy harvesting," *IEEE Trans Ultrason Ferroelectr Freq Control* 2011;58(7):1508–20.
14. Farinholt, K. M., Pedrazas, N. A., Schluneker, D. M., Burt, D. W. and Farrar, C. R., "An energy harvesting comparison of piezoelectric and ionically conductive polymers," *Journal of Intelligent Material Systems and Structures*, Vol. 20, No. 5, pp. 633–642, 2009.
15. Ji, Sang Hyun, et al. "Flexible lead-free piezoelectric nanofiber composites based on BNT-ST and PVDF for frequency sensor applications." *Sensors and Actuators A: Physical* 247 (2016): 316–322.
16. D. Kumar, P. Chaturvedi, and N. Jejurikar, "Piezoelectric Energy Harvester Design and Power Conditioning," *IEEE Students' Conf. Electr. Electron. Comput. Sci. Piezoelectric*, pp. 1–6, 2014.
17. Kim, Seon-Bae, et al. "Comparison of MEMS PZT cantilevers based on d_{31} and d_{33} modes for vibration energy harvesting." *Journal of Microelectromechanical Systems* 22.1 (2013): 26–33.

Design and Development of IoT-Based Transmission Line Monitoring System

Nikhil Kalra, Abhishek Sharma, Nitish Kumar, Rajesh Singh and Anita Gehlot

Abstract Transmission of electricity in India is now of far greater importance than ever thought of, it depends on high-voltage lines which at times has to cross kilometers of forests or mountains to reach a certain area, and a preventive check has to be done since even a single fault can stop power supply. In order to check for faults, shocks or corrosive element in the wire, the power supply has to be first cut down and interruption of energy flow is not always admissible. The author presents an octocopter, a new concept to translate on the power lines without any interruption of power supply. The paper presents the concept, implementation, and demand of the copter in present scenario.

Keywords IoT · Octocopter · Corrosion · Fiber optic

1 Introduction

High-voltage power lines link power generation sites in India to urban and rural areas. Since it is hazardous to run a power plant near residential areas, power lines have to cross thousands of kilometers, at times, to deliver power supply [1]. These transmission have to go through desert, mountains, and other areas where if any malfunction in power supply or power line happens then it takes a lot of time and manpower to get power lines back in working condition and deliver power supply to the specified area [2].

Any malfunction like light cuts, heavy power supply, or corrosive diametric extension in these lines severely affects thousands of lives since people have become dependent on power supply, and mere loss of supply for even a minute disturbs lives, at times [3]. Therefore, preventive measures should be used so that wire doesn't reach the condition where it cannot supply power at all [4]. Preventive maintenance of supply lines is a hectic task and specialized task, and highly trained

N. Kalra (✉) · A. Sharma · N. Kumar · R. Singh · A. Gehlot
University of Petroleum and Energy Studies, Dehradun, Uttarakhand, India
e-mail: nikhilkalra09@yahoo.com

people are required to move cables for preventive inspection and rectify accordingly [5]. And, as they inspect the cables, they usually inspected the cables for external cuts such as ruptured stands or melting wires that are caused mainly by lightning or excessive flow of power [6]. Since the check is manual, power supply has to be cut down and this is possible only at certain time in a year and that too shut down thousands of lives [7]. These limited numbers of checks prevent trained people to keep regular checks, and harm is not avoided, eventually.

With the use of robot for preventive checks, not only number of inspections can increase but highly trained people aren't even required to not down the data provided by the robot [8]. The foremost advantage of using a robot is that power supply interruption is not required at all [9].

In India, helicopters are used instead of cutting down the power supply but even remotely controlled helicopter can only note down external readings; it can't adhere to inner faults which usually occur in the power lines which stop power supply; therefore use of helicopters is a better way, but it doesn't give us sufficient data to avoid any major breakdown of power in future [10].

In order to overcome these limitations, a robot can be used which can check for both external and internal faults and give live readings; the major limitation in using a robot is when some obstacle come in the way then robot can malfunction, and this limitation has been rectified by the author's solution [11].

2 Server Section

The octocopter is primarily developed to inspect wires for any fault that can hamper power supply; the copter can inspect four wires at a time and has enough mobility to overcome any obstacle. ATMEGA microcontroller is used for functioning of various sensors and cameras. In this robot, XBEE mode of wireless communication is used which sends signals to the copter as well as base station. The copter has two IR sensors for detection of wire underneath it and two ultrasonic sensors for measuring the distance and a hook sensor (Fig. 1).

3 Robot Section

The copter employs two pulleys and a hook to move on the power lines and has a carbon fiber structure with a T-shaped base and a 2-DOF manipulator. The readings from ultrasonic and IR sensor are going to send signal to the hook to open up and get fitted on the transmission lines accordingly. When the copter senses any obstacle and needs to move from one tower to another, then the person using controller places copter on another tower in the same way (Fig. 2).

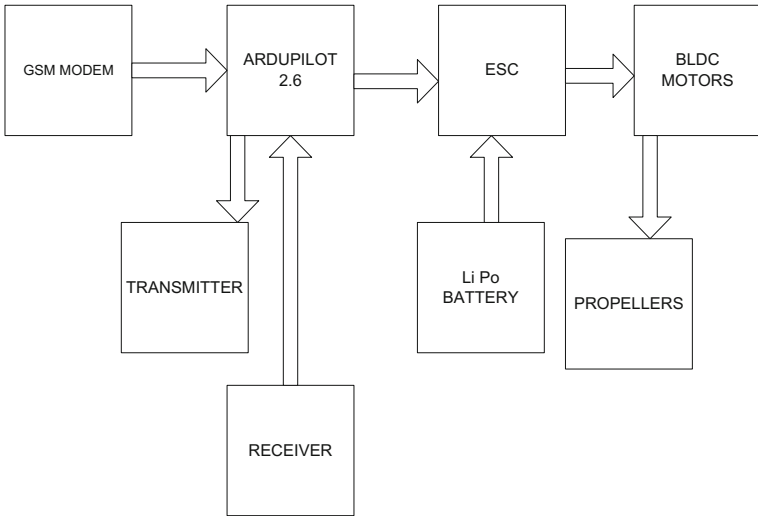


Fig. 1 Server section

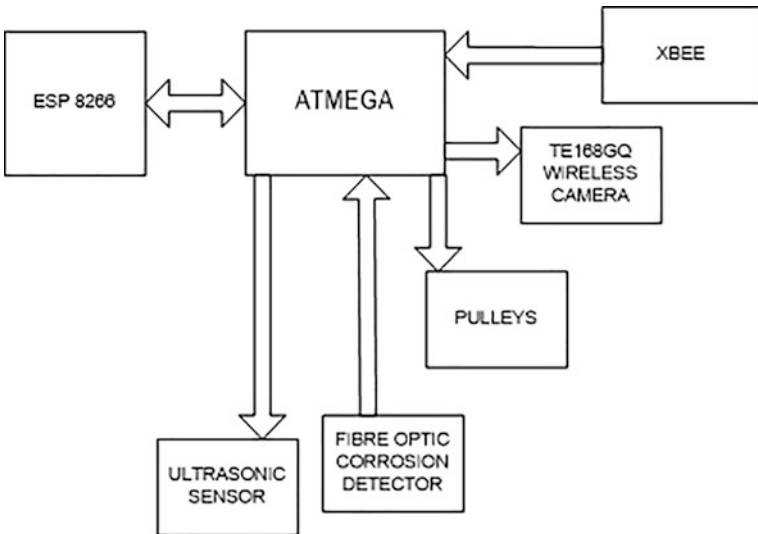


Fig. 2 Robot Section

4 Software Development

The most common types of failure in power wires are melted wires or some external cuts which are easily detectable with naked eyes or a camera, but internal corrosion is one of the areas which can't be detected using sensors, and corrosion is one of the reasons why undetectable faults lead to failure at very high level and lead to loss of power. For external damages, it is required to get images of cuts and damages and with octocopter this can be easily accomplished using a mini-camera. Corrosion often occurs in the core of aluminum conductor steel-reinforced cables which in turn leads to loss of power transmission and loss of wire too, and wire is needed to be replaced when corrosion extends to advanced stages in transmission wires. The problem with corrosion of transmission wires internally is that condition of wires keep deteriorating without an external change, so detecting any change in wire through naked eyes isn't possible. However, there is a slight change in diameter of the wire since wire starts expanding cylindrically with rate of corrosion. By employing laser sensors in octocopter to measure any change in diameter, it is possible to notice the change and replace wires accordingly. Both sensing technologies were assembled in a compact sensing unit and consist of a laser emitter and a receiver, with the cable between them. The optical fiber corrosion detector gives the reading of the diameter of transmission line; the corrosion at its third stage varies the diameter of wire up to 0.5–3.0 mm, so through this the attendant gets to know about the corrosion condition of the wire and attendant can get to know as to which part to attend first. If in case, there is any severe cut in the wire due to some external damage then the readings are going to be very abrupt; when there is reading as abrupt as beyond 3.0 mm then camera is taken to the spot where there is abrupt reading and live feed is taken and the cut is confirmed (Fig. 3).

5 Result

The designed system is tested on Proteus simulation software with the interfacing with MATLAB. Figure 4 shows the Proteus simulation model for the system.

6 Future Scope and Conclusions

With exacerbating demand of power in India, where power loss for a few hours is loss of cores worth of money, we can't afford to lose power because of corrosive fault in transmission wires on which a regular check isn't being kept on, and a mere manual check from helicopters only tells the operator about the external defects which isn't always sufficient to prevent the disaster.

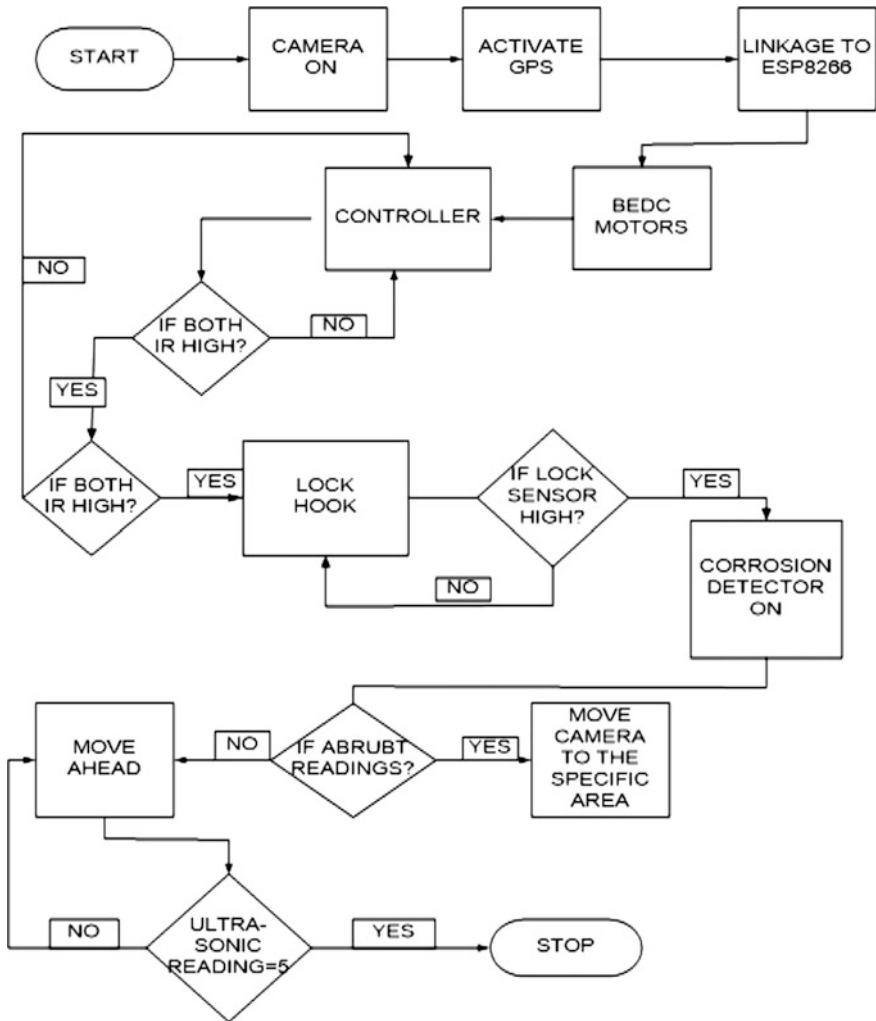


Fig. 3 System working algorithm

This project eyes on saving India from transmission loss using octocopter which is going to save a lot of time, since regular yearly checks are fruitless and time-consuming; save a lot of manpower, since keeping a manual check through operators demands a lot of people, and save a lot of money, since manual checks using helicopters are costly. Thus, this project, if implemented, is going to help India in lot of ways and transmission of power is not going to be lost to corrosion.

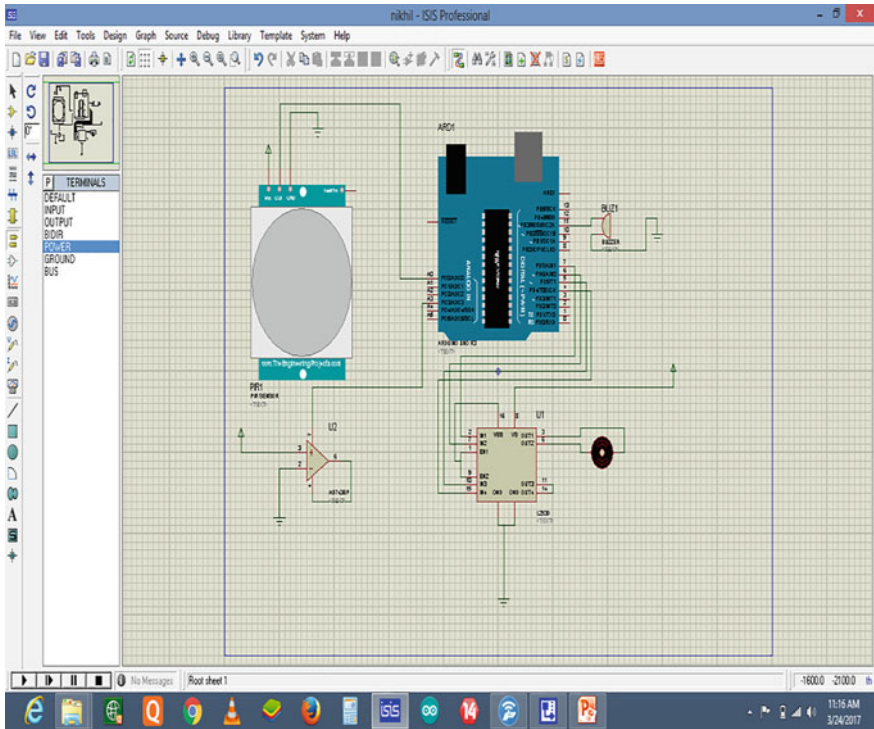


Fig. 4 Proteus simulation model for system

References

1. Trincavelli, Marco, et al. "Towards environmental monitoring with mobile robots." Intelligent Robots and Systems, 2008. IROS 2008. IEEE/RSJ International Conference on. IEEE, 2008.
2. Dunbabin, Matthew, and Lino Marques. "Robots for environmental monitoring: Significant advancements and applications." IEEE Robotics & Automation Magazine 19.1 (2012): 24–39.
3. Cooper, K. R., et al. "Optical fiber-based corrosion sensor systems for health monitoring of aging aircraft." AUTOTESTCON Proceedings, 2001. IEEE Systems Readiness Technology Conference. IEEE, 2001.
4. Fuhr, Peter L., and Dryver R. Huston. "Corrosion detection in reinforced concrete roadways and bridges via embedded fiber optic sensors." Smart Materials and Structures 7.2 (1998): 217.
5. Ishino, R., and F. Tsutsumi. "Detection system of damaged cables using video obtained from an aerial inspection of transmission lines." Power Engineering Society General Meeting, 2004. IEEE. 2004 [1].
6. Montambault, Serge, and Nicolas Pouliot. "The HQ LineROver: contributing to innovation in transmission line maintenance." Transmission and Distribution Construction, Operation and Live-Line Maintenance, 2003. 2003 IEEE ESMO. 2003 IEEE 10th International Conference on. IEEE, 2003.

7. Debenest, Paulo, and Michele Guarnieri. "Expliner—From prototype towards a practical robot for inspection of high-voltage lines." *Applied Robotics for the Power Industry (CARPI), 2010 1st International Conference on*. IEEE, 2010.
8. Er, Meng Joo, Shenghai Yuan, and Ning Wang. "Development control and navigation of Octocopter." *Control and Automation (ICCA), 2013 10th IEEE International Conference on*. IEEE, 2013.
9. Pouliot, Nicolas, and Serge Montambault. "Geometric design of the LineScout, a teleoperated robot for power line inspection and maintenance." *Robotics and Automation, 2008. ICRA 2008. IEEE International Conference on*. IEEE, 2008.
10. Intwala, Aditya, and Yash Parikh. "A Review on Vertical Take Off and Landing (VTOL) Vehicles." *International Journal of Innovative Research in Advanced Engineering (IJIRAE) 2* (2015).
11. Vera, Rosa, Diana Delgado, and Blanca M. Rosales. "Effect of atmospheric pollutants on the corrosion of high power electrical conductors: Part 1. Aluminium and AA6201 alloy." *Corrosion science* 48.10 (2006): 2882–2900. 4. Czajkowski, K., Fitzgerald, S., Foster, I., Kesselman, C.: *Grid Information Services for Distributed Resource Sharing*. In: *10th IEEE International Symposium on High Performance Distributed Computing*, pp. 181–184. IEEE Press, New York (2001).

Critical Analysis and Review of Occupational, Environmental and Health Issues Related to Inadequate Disposal of E-Waste

Shivam Kumar, Divyanshi Garg, Prashasti Sharma, Shubham Kumar
and Sayed Mohammad Tauseef

Abstract Even as we were struggling to find a solution to the ever increasing problem of municipal waste, we now have the problem of E-waste staring in our faces. Increasing electrical and electronic waste is a matter of grave concern as it leads to a number of health and safety problems. The E-waste disposal, especially in India, is done in a highly unorganized manner. The workers in this sector are not trained and have to work under hazardous conditions without access to proper gear, thereby exposing themselves and the environment to hazardous substances. It is estimated that more than one million workers are engaged in unorganized E-waste disposal sector in India. This paper analyses the current E-waste scenario globally and Indian context, its effects and management.

Keywords Occupational disease · E-waste · Toxic substances
Transplacental

1 Introduction

Globally, E-waste (WEEE) is a word used for Electronics waste. E-waste definition has been created and interpreted by many countries; WEEE is the term used to describe old, end-of-life or discarded appliances, using electricity, stated by WEEE directive. At the time of discarding, Electrical and Electronics waste, it comprises of

S. Kumar (✉) · D. Garg · P. Sharma · S. Kumar · S.M. Tauseef
University of Petroleum and Energy Studies, Dehradun 248007, Uttarakhand, India
e-mail: shivam.kasauli@gmail.com

D. Garg
e-mail: divyanshigargmicky80@gmail.com

P. Sharma
e-mail: prashasti.sharma99@gmail.com

S. Kumar
e-mail: shubhamkumar6075@gmail.com

sub-assemblies and parts of a product which are key issues and concerns for health and safety for workers and common beings [1].

A report by United Nations Environment Program has shown that 40 million tons electric waste is generated around the world [2]. E-waste easily finds its illegal entry in developing countries like India, Pakistan and China. Health and diseases have been noticed by the disposition of E-waste in the developing nation like China and Ghana where rapid increase of abnormalities has been noticed and informed [3]. These countries have been encouraged, intentionally or unintentionally for dismantling and recycling of E-waste [4]. Nowadays, it is a challenge for government and public to manage E-waste safely as it contains both lethal and expensive metals. Recycling of E-waste has been a global issue as the caducity of electrical and electronics waste has become shorter in last decades [5] (Fig. 1).

After China, India is considered to be the most populated country and in several years India has experienced rapid industrialization that has resulted adverse effects on ecosystem and human health where E-waste management directly as well as indirectly paves the way [6]. In India, suitable strategies for dealing E-waste is lacking or the available strategies are failed in implementing because of financial resources and lack of technology [7]. The Associated Chambers of Commerce of India is growing at a compound annual growth rate of around 25% and its likely to about 12.5 lakh MT per annum. The surveyed data of E-waste produced in Mumbai (96,000), Delhi NCR (67,000), Bangalore (57,000), Chennai (47,000), Pune (19,000) [8]. This waste cannot be controlled easily as number of electrical appliances will continue to increase on a large scale and usage of microprocessor is also increasing in daily routine. Market of electronics is one of the speedily expanding markets [9]. While selecting the treatment methods for E-waste, few points need to be considered such as characteristics of waste and its quantity, efficiency of treatment, space available for equipment, availability of local treatment technologies and options. For operating the technology, skill is also required (Fig. 2).

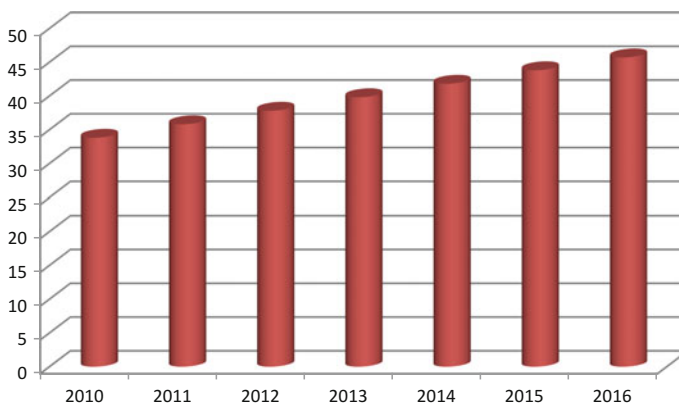
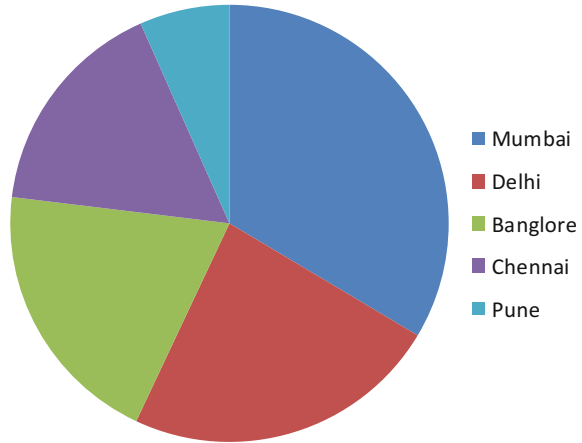


Fig. 1 Global E-waste generation (Mt)

Fig. 2 Producer of E-waste in India



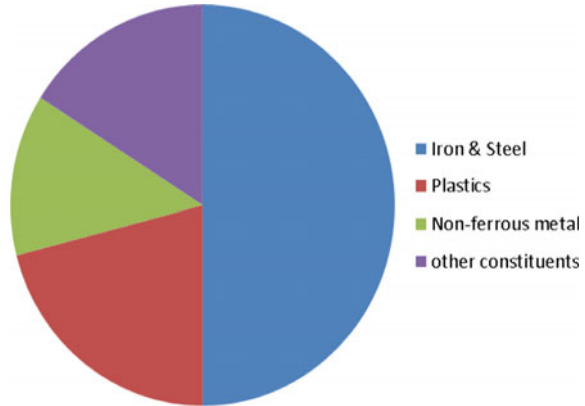
2 Classification and Effects of E-Waste

Hazardous and non-hazardous categories have been broadly formed to describe the composition of E-waste. E-waste comprises of ferrous and non-ferrous plastics, metal, printed circuit and other items. 50% of waste is comprised of iron and steel and 21% is contributed by plastics, whereas 13% followed by non-ferrous metals and other constituents [10]. The electronic waste is comprised of toxic substances such as lithium in mobile phones, batteries and photographic equipment nickel in alloys, relays semiconductors and pigments, lead and cadmium in computer batteries, highly toxic dioxins and furans are released while burning PVC cables. The materials are complex and hence it is difficult to recycle them in sustainable manner without hampering the health of workers even in developed countries [11].

There are many other toxic substances found in materials like americium, chromium VI, cadmium and zinc. Lead in high quantity can be fatal. It is a neurotoxin that affects kidney and the reproductive system, whereas beryllium is carcinogenic and lung diseases can be caused [12].

Due to unsafe recycling of E-waste, children residing in that area have higher lead level in blood. Study has been done that shows that immune system responding to vaccination for Hepatitis B is decreased [13]. E-waste is comprised of chemical products such as brominated flame retardant (BFRs), polychlorinated diphenyl ethers (PCBDs) and hexabromocyclododecane (HBCDs) [14]. If these materials are not treated properly, then they release hazardous substances such as furans, dioxins, PCBs and heavy metals like copper, lead and HG are also released into the environment that causes negative impacts [15]. And these pollutants that are released in environment effect human, if they are exposed [16] (Fig. 3).

Fig. 3 Constituents of E-waste generated



3 Global E-Waste Scenario

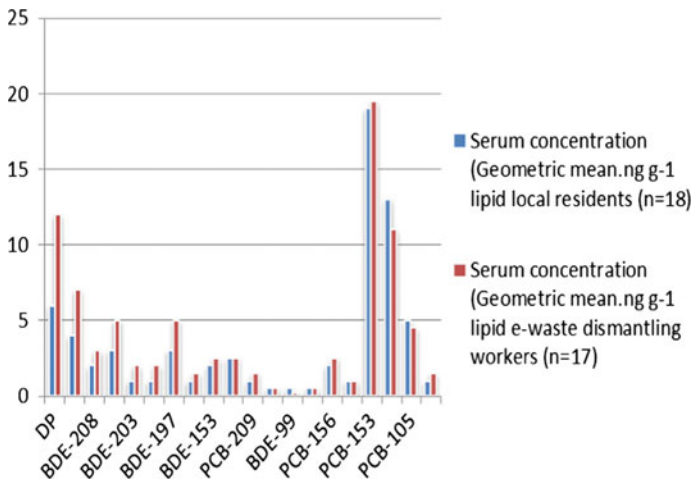
3.1 Africa, Ghana

The worst problem faced in the world right now is with Ghana as it is the centre of E-waste recycling site in West Africa and also imports E-waste from other developed nations. 85% of the E-waste dumped in Ghana is produced in Ghana and West Africa only. A significant part of Ghana's E-waste is bought to Agbogbloshie, a suburb of Accra. Out of the total waste, 30% of the imported goods are completely new and out of the other 70, 30% needs repairing and the rest, i.e. 22,500 million is of no use and treated as dump. Here, men extract copper, aluminium and other materials using methods that are dangerous to health and are harmful for environment which are shipped back to the factories and refineries in developed countries. The over accumulated quantity of E-waste in Agbogbloshie has started to become a threat for the workers and people living there. Because the method used for decomposition is not environment friendly as it involves burning of the electronics which results in the emission of many toxic gases like carbon monoxide, sulphur and carbon dioxide. This condition resulted in formation of a toxic gases cloud over the area which poisons air and also toxicates soil. Many health disorders occur due to this severe problem that includes abnormalities in newly born child, cancer and respiratory diseases. Condition of landfill is again a serious issue faced as a result of this scenario because a major amount of plastic and other scrap material stays at the dumpsite or end up in the river or the sea [17].

3.2 China

The south-eastern city in China named Guiyu is a major hub of the recollection and decomposition of E-waste. According to the survey conducted by US, 70% of the

electronics manufactured ended up in China and it is estimated that 450,000 people are involved in this business [18]. China has become the biggest industry in the world for the decomposition of industrial waste. The most toxic compounds emitted during the decomposition of E-waste comes from burning of circuit boards, plastic and copper wires, and copper and steel are recovered from them by washing with hydrochloric acid. These kinds of conditions have created massive health disorders in the country affecting every age group of people living there [19]. Over 60% children in Guiyu has been tested with more than average level of lead, arsenic and other harmful components which is affecting the development and growth of their brain and central nervous system. This condition created in many parts of world has affected the people, their vegetation and promoted unhealthy lifestyle causing threat to the development of new generation from an initial age [20].



3.3 India

Looking at the present scenario, India produces 1,200,000 MT of E-waste per year and is also an active market of waste import, but there is no large scale organized E-waste processing and recycling facility currently practised and therefore it exists in a highly unorganized sector. It is estimated that Maharashtra state produces up to 20,270 tons per year and an estimated 30,000 number of computers become obsolete every year. And the 70% of the E-waste handled in India is from other countries. The maximum amount of work is done in an unregulated environment where there is no control on emission of toxic gases [21]. These kinds of practices mainly take place in the urban slum areas of the country where over 10 lakh untrained workers perform the task risking their life without any personal protective

equipment. These procedures emit dioxins and harmful compounds. Most of the dismantling work is done in Delhi and outer areas. This harmful process emits toxic gases which are polluting the atmospheric air of Delhi and making it difficult for people to survive. There have been over 500 reported cases of diseases of cancer and mental disabilities found in affected areas. Newly born child are also affected severely as they are getting birth defects due to continues exposure towards toxins. India is ranking second in the world after china, in producing E-waste as well as importing it. The present scenario experienced here tells a story of great destruction and harmful circumstances in coming future [22].

4 Impacts of E-Waste on Health

Safety measures are important so that these toxic substances cannot affect the workers and others in the vicinity by entering in the body through inhalation, ingestion, transplacental and dermal effect.

There are many cases like Guiyu in China in which Hepatits B is reduced but it has uplifted the Pb levels in preschool children residing in recycling area [13]. This is the evidence that proves the health effect caused by the improper E-waste handling is fatal. These recycling activities of E-waste have retrograde local drinking water. A river water sample near a Chinese recycling village from Lianjiang River was assessed where lead levels were found 2400 times higher than the drinking water guidelines of World Health Organization, thereby involving a serious health hazard [23].

This impact has been worse in developing countries like India where people involved in recycling waste are mostly from unorganized sector and stay in close proximity to landfills of untreated waste. Moreover, they work without any protection and safeguards. Workers involved in the recycling process are uneducated or illiterate so they are unaware of the hazards associated with them [24].

A survey has been done with respect to E-waste handling which is affecting the health of the people. Below given data show the type of pollutants, its occurrence, sources and diseases which are the result of E-waste handling.

Pollutants in E-waste

S. No.	Pollutants	Occurrence	Sources	Disease
1	Arsenic	Semiconductor, diode, microwave, LED, solar cells	Dust and soluble materials	Lung cancer, fatality
2	Barium	Electron tubes, lubricant and additives	Inhalation, ingestion and dermal contact	Brain swelling damage to heart, liver and spleen

(continued)

(continued)

S. No.	Pollutants	Occurrence	Sources	Disease
3	Brominated flame proofing agent	Casing, circuit boards, cables and PVC cables	Inhalation, ingestion and transplacental	Delay mental and physical development
4	Cadmium	Batteries, pigment, solder, alloys, computer batteries, monitor, cathode ray tubes	Ingestion and inhalation	Weakness, fever, headache, sweating and muscular pain Chronic lung, cancer and kidney damage
5	Perfluoroalkyls	Fluoro polymers in electronics	Ingestion, dermal contact, inhalation, and transplacental	Chronic kidney disease
6	Cobalt	Insulators	Inhalation	Hard metal lung disease, decrease pulmonary function and asthma
7	Lead	Lead rechargeable batteries, solar transistors, lithium batteries, PVC	Ingestion, inhalation and dermal contact	Vomiting, diarrhoea Appetite loss, abdominal pain, constipation, fatigue, and headache
8	Copper	Conducted in cables, copper ribbons, coils, circuitry, pigments	Inhalation, Ingestion and dermal contact	Chronic respiratory disease, liver, kidney and skin disease, Wilson's disease
9	Polychlorinated biphenyl	Capacitors, transformer	Inhalation and ingestion	Cancer, effects immune system, reproductive system, nervous system, and endocrine system
10	Polyvinyl chloride	Plastic used in electronic appliances	Inhalation	Effect nervous and immune system, lung damage

(continued)

(continued)

S. No.	Pollutants	Occurrence	Sources	Disease
11	Selenium	Older photocopying machines	Inhalation	Hair loss, neurological abnormalities, Selenosis
12	Mercury	Fluorescent lamp, alkaline batteries and mercury wetted switches	Ingestion/inhalation	Brain and liver damage
13	Dioxins	Unwanted by-products release while manufacturing pesticide	Inhalation, Ingestion, transplacental and dermal contact	Malformation of foetus
14	Chlorofluorocarbon	Cooling units	Inhalation	Cardiac Arrhythmia, asphyxiation, effect central nervous system
15	Chromium VI	Data types, floppy disk	Inhalation and dermal contact	Damage of DNA, irritation to eyes, skin and mucous membrane
16	Americium	Medical equipment, fire detectors, active sensing element in fire detectors	Inhalation	Damage lungs, liver and thyroid, bone cancers
17	Toner dust	Toner cartridge for laser printer	Inhalation	Chronic inflammation and lung fibrosis
18	Zinc	Cathode ray tubes, metal coatings	Ingestion and inhalation	Blurred vision, nausea and vomiting
19	Nickel	Batteries	Inhalation, ingestion, dermal contact and transplacental	Pneumonitis, cancer of lung and sinuses
20	Beryllium	Computers, X-ray Machines, ceramic component of electronics	Inhalation, ingestion and transplacental	Berylliosis

5 Hazards and Risk Associated with E-Waste Recycling

Different kind of hazards can be caused to workers depending on their individual operations. During disassembling of electrical and electronics equipment various hazards can occur such as accident release and spillage of hazardous substances. For example, Mercury is found in fluorescent tubes can be released into atmosphere on breaking of a shell that can be absorbed in body or can be inhaled [25].

The primary hazards associated with mechanical process like shredding or other size reduction process results into generation of dust. The exposure of dust can be through inhalation and dermal contact. Air quality monitoring has been done in the shredding zone of E-waste where cadmium and lead exposure levels were high as 0.27 and 1.4 μg [26]. This shows that worker working in that kind of environments are not safe.

In motorized treatment of E-waste in a Swiss recycling plant, fine dust fraction of BFRs was detected [27]. This emphasizes that emissions of BFRs are high in the vicinity of mechanical treatment of E-waste.

A Norway Research-based group has investigated about the BFRs which is found in some of waste handling plants. The research team took the plasma sample of three occupational groups who were engaged in electronic dismantling facility production of PCBs and laboratory assistants. The result showed higher plasma level TBBPA and BDE-153, hepta-brominated congener BDE-183 was also detected in group.

6 Harmful Practices Related to Treatment of E-Waste

Smelting, a pyro-metallurgical process is practised in order to recover metal from E-waste. Hazards associated with this process are emission of copper cadmium and lead fumes. The emission of fumes of metals from smelting is hazardous [28]. Metal scrap was processed from E-waste as one of the feedstock [29]. These 35 different metals were found existing during smelting (Sr, Li, S, La, Ce, U, Al, Y, Ti, V, Cr, Fe, Ba, Na, Ni, Be, Co, Cd, Zn, Mo, Tl, As, Pb, Sb, In, Ag, Cu). The Zn, Pb and Cu concentrations were 149, 353, 525 $\mu\text{g/l}$. These values were compared from regional background where concentration of Zn, Pb and Cu were 1.6, 1.7 and 1.1 $\mu\text{g/l}$, respectively, the concentration found was very high to handle.

So, overall the available data show that there is no monitoring in the near areas of E-waste recycling plants. It will be helpful in designing of E-waste reprocessing plant to avoid work-related health risk. Thus, monitoring of the vicinity area near the recycling plant is must in order to reduce risks for the environment.

7 Hazards and Risk Associated with Burning of E-Waste

On the basis of their investigation Stewart and Lemieux mentioned that burning of a mixture of keyboards, motherboards and cases using pilot-scale rotary kiln incinerator. Emissions of metal consist of lead, copper, antimony while emission of PCD Ds/Fs was below regulatory limit. Thus, disposal of E-waste incineration is a good practice, if suitable particulate matter device is used to control emissions of metal [30].

Watanabe et al. [28] conducted experiment where PCBs waste in a pilot-scale incineration undergoes combustion where formation of PBD Ds/Fs, PCD Ds/Fs and PXD Ds/Fs occur. But brominated and chlorinated compound were removed during flue gas treatment. At the final exit, they were not observed [31].

So incineration is a good practice. Studies have shown that brominated and chlorinated compounds undergo combustion with effluents flue gas treatment system.

8 Conclusion

The E-waste has become one of the major issues in the present era for the developing nations like India and Africa. The developing nations are becoming the dump yard of E-waste for developed nations. The workers engaged in the treatment of WEEE are also exposed to the heavy metals and toxic fumes which have led to occupancy of various diseases. In India the E-waste management is one of the most unorganized sector which leads to detrimental environmental and occupational health impacts. Presently, we are lacking efficient technologies for the treatment of E-waste. **Even the advancement in technology is enhancing the cost of treatment and the production of WEEE.** Some of the recommendations that could be put to practice to improve the conditions of workers and to cope up with the problem of E-waste:

- Government should impose stringent laws on import of E-waste.
- Strict regulation for treatment and disposal of E-waste.
- Regulations for handling, disposal and safe practices for E-waste.
- Latest technologies to be adopted for treatment of E-waste in order to reduce negative impact on environment and health of workers.
- Collaboration with developed nations for technological advancements.

References

1. http://www.unep.or.jp/ietc/Publications/spc/EWasteManual_Vol1.pdf.
2. <http://www.thehindu.com/sci-tech/energy-and-environment/india-a-victim-of-ewaste-crime/article7202265.ece>.
3. China Nonferrous Metals Industry Association, The renewable non-ferrous metal industry development report in China (2013).

4. China Nonferrous Metals Industry Association, The renewable non-ferrous metal industry development report in China (2013).
5. J. Fu, A. Zhang, T. Wang, G. Qu, J. Shao, B. Yuan, Y. Wang, G.B. Jiang, Influence of e-waste dismantling and its regulations: temporal trend, spatial distribution of heavy metals in rice grains, and its potential health risk, *Environ. Sci. Technol.* 47 (2013) 7437–7445.
6. Awasthi AK, Zeng X, Li J (2016) Environmental pollution of electronic waste recycling in India: a critical review. *Environ Pollut* 211:259–270.
7. Electronic waste – time to take stock. *Lancet* 2013; 381(9885):2223.
8. Balabanicupnik M, Klemencic AK. Negative impact of endocrine disrupting compound on human reproductive health. *Reprod Fertil Dev* 2011; 23(3):403.
9. Association of Plastics Manufacturers in Europe (APME). Plastics – a material of choice for the electrical and electronic industry-plastics consumption and recovery in western Europe 1995. APME: Brussels:1; 2004.
10. UNEP, Ozone Secretariat. n.d. The Montreal Protocol on Substances that Deplete the Ozone Layer. Available: http://ozone.unep.org/new_site/en/montreal_protocol.php [5 May 2012].
11. X. Xu, X. Chen, J. Zhang, P. Guo, T. Fu, Y. Dai, S.L. Lin, X. Huo, Decreased blood hepatitis B surface antibody levels linked to e-waste lead exposure in preschool children, *J. Hazard. Mater.* 298 (2015) 122–128.
12. Eguchi A, Nomiyama K, Devanathan G, Subramanian A, Bulbule KA, Parthasarath P, Takahashi S, Tanabe S (2012) Different profiles of anthropogenic and naturally produced organohalogen compounds in serum from residents living near a coastal area and e-waste recycling workers in India. *Environ Int* 47:8–16.
13. Song Q, Li J (2014a) Environmental effects of heavy metals derived from the e-waste recycling activities in China: a systematic review. *Waste Manage* 34(12):2587–2594.
14. Song Q, Li J (2014b) A systematic review of the human body burden of e-waste exposure in China. *Environ Int* 68:82–93.
15. <http://www.prb.org/Publications/Articles/2013/e-waste.aspx>.
16. <http://interactive.aljazeera.com/aje/2015/ewaste/index.html>.
17. ourworld.unu.edu/en/assessing-and-improving-the-e-waste-problem-in-china.
18. Qu, W.Y., Bi, X.H., Sheng, G.Y., Lu, S.Y., Fu, J.M., Yuan, J., Li, L.P., 2007. Exposure to polybrominated diphenyl ethers among workers at an electronic waste dismantling region in Guangdong, China. *Environ. Int.* 33, 1029–1034.
19. <http://edition.cnn.com/2013/05/30/world/asia/china-electronic-waste-e-waste/>.
20. <https://www.ncbi.nlm.nih.gov/pmc/articles/PMC4446940/>.
21. http://www.unep.or.jp/ietc/Publications/spc/EWasteManual_Vol1.pdf.
22. Peters-Michaud, N., Katers, J., Barry, J., 2003. Occupational risks associated with electronics demanufacturing and CRT glass processing operations and the impact of mitigation activities on employee health and safety. In: *Proceedings of the Electronics and the Environment. IEEE International Symposium 2003*, pp. 323–328.
23. Morf, L.S., Tremp, J., Gloor, R., Huber, Y., Stengele, M., Zennegg, M., 2005. Brominated flame retardants in waste electric and electronic equipment: substance flows in a recycling plant. *Environmental Science and Technology* 39, 8691–8699.
24. Zdanowicz, C.M., Banic, C.M., Paktunc, D.A., Kliza-Petelle, D.A., 2006. Metal emissions from a Cu smelter, Rouyn-Noranda, Québec: characterization of particles sampled in air and snow. *Geochemistry: Exploration, Environment, Analysis* 6 (2–3), 147–162.
25. <https://www.ncbi.nlm.nih.gov/pmc/articles/PMC2796756/>.
26. Telme, K., Bonham-Carter, G.F., Kliza, D.A., Hall, G.E.M., 2004. The atmospheric transport and deposition of smelter emissions: evidence from multi element geochemistry of snow, Quebec, Canada. *Geochimica et Cosmochimica Acta* 68(14), 2961–2980.
27. Stewart, E.S., Lemieux, P.M., 2003. Emissions from the incineration of Electronics industry waste . In: *Proceedings of Electronics and the Environment, 2003. IEEE International Symposium*, 19–22 May, pp. 271–275.

28. Watanabe, M., Kajiwara, N., Takigami, H. Noma, Y., Kida, A., 2008. Fomation and degradation behaviours of bominated organic compounds and PCD/Fs duing thermat treatment of waste pinted circuit boards. *Organohalogen Compounds* 70, 78–81.
29. Townsend, T.G., Musson, S., Jang, Y.-C., Chung, I.-H., 1999. Characterization of lead leachability from cathode ray tubes using the toxicity characteristic leaching procedure. Report #99-5. State University System of Florida, Florida Center for Solid and Hazardous Waste Management.
30. Townsend, T., Vann, K., Mutha, S., Pearson, B., Jang, Y.-C., Musson, S., Jordan, A., 2004. RCRA Toxicity Characterization of Computer CPUs and Other Discarded Electronic Devices. State University System of Florida, Florida Center for Solid and Hazardous Waste Management.
31. Lindberg, S.E., Wallschlaeger, D., Prestbo, E., Bloom, N., Price, J., Reinhart, D., 2001. Methylated mercury species in municipal waste landfill gas sampled in Florida. *Atmospheric Environment* 35, 4011–4015.

Design and Development of Air and Water Pollution Quality Monitoring Using IoT and Quadcopter

Aditya Agarwal, Vishakha Shukla, Rajesh Singh, Anita Gehlot
and Vikas Garg

Abstract The earth is a resource for drinking water and fresh air, which comprises of many untapped elements that lies beneath. In India, one of the major problems in developing countries is that the water bodies are highly polluted and air is contaminated. Industrial facilities use a lot of chemical as raw materials. Some of them are very harmful and contribute to pollution. This results in the increasing in the emission of hazardous materials in air, water, as well as soil. Future prosperity and stability are determined by important natural resources that is air and water. So we have designed the Water and Air Monitoring System that will help the authorities in crisis management centers to discover and anticipate contamination of water and air. The system comprises of one master drone and four slave robots where the two of the slaves serve the purpose for detection of air pollution and the next two are used for water pollution.

Keywords Water · Air · Pollution · Master drone · Slave robots

A. Agarwal (✉) · V. Shukla · R. Singh · A. Gehlot · V. Garg
College of Engineering Studies, University of Petroleum and Energy Studies,
Dehradun 248007, Uttarakhand, India
e-mail: adityaa235@gmail.com

V. Shukla
e-mail: shuklavishakha52@gmail.com

R. Singh
e-mail: rsingh@ddn.upes.ac.in

A. Gehlot
e-mail: anita@ddn.upes.ac.in

V. Garg
e-mail: vgarg@ddn.upes.ac.in

1 Introduction

Clean water and fresh air are one of the most essential elements for the existence of humans and other living creatures, but with the alarming rate of pollution it is necessary to reduce the pollutants caused by mankind in order to protect the environment. Between November 1 and November 9, 2016 the nature showed that how bad air quality has become and so air pollution struck the capital of India (New Delhi) causing a great destruction for all the living organisms. On November 7, 2016 the particulate matter 2.5 levels had risen up to 999, even though only 60 microorganism is recommended [1]. On December 2002, it's been estimated that around 4000 deaths were caused due to great smog occurred in London [2]. The most vital element among natural resource is water which is essential for the existence of living being, production of food, and economic development. According to the National Sample Survey Organization (NSSO), 91.3% of rural households in Punjab use SBF to meet their energy needs for cooking [3]. Control of air and water pollution is no longer just a matter of conventional combustion products [4]. Recently, ambient air pollution with particulate matter (PM) has been classified as carcinogenic to humans (IARC, 2015) [5]. In India quiet a number of cities are facing the acute shortage of water; even though a wide variety of work depends on the water. Pure water has virtually zero conductivity [6]. Due to industrial waste say chemicals and other hazardous material not only degrades the quality of water but also serves as a poison for all the living organisms using it in a direct or indirect manner. There are several projects running for the removal of water pollution from various rivers but none of them has given the result up to the mark. Narmada project was started years ago and yet haven't been finished in cleaning up the river. According to the World Health Organization (WHO, 2011), the greatest risk to public health comes from microbes contaminated drinking water [7]. The US Environmental Protection Agency (EPA) has imposed stringent regulations on the concentrations of many environmental pollutants in air and water [8]. In the Narmada River, turbidity, BOD, and hardness are found in higher concentration when compared to the standard permissible limit. This study also revealed that the local residents were suffering from respiratory and skin diseases adversely [9]. Yellow fever and dengue were the most frequent diseases available in the nearby region. Due to increase in frequency, magnitude, and potential effects water problems have turned around to be a subject of global issue and are not confined to a particular places and areas [10]. Therefore, it is a high time for all the citizens to work upon this disastrous area for the betterment of the living being. The proposed system deals in the detection of the contamination of water as well as that of air to a greater extent without harming the nature's cycle and doesn't lead to destruction of the environment. One master drone and four slave robots will be present in the system and communication amongst them will be done through RF modem, thereby monitoring as well as revealing the information regarding the health of air and water.

2 Theory

2.1 Causes of Water Pollution

- 2.1.1. Humans usually dump and litter the solid wastes in rivers, lakes, and oceans. The cardboard, Styrofoam, aluminum, plastic, and glass are few littering items.
- 2.1.2. Oil is insoluble in water and thereby forms a thick sludge. During ship travel, accidentally if the oil gets spilled then it pollutes the water and hence leads to water pollution.
- 2.1.3. Sewage can lead to a major problem if chemicals and pharmaceutical substances are flushed in the toilet by people.

Air pollution equally contributes to the contamination of water bodies and effect the food chain adversely. In air pollution, algal blooms are caused by nitrogen compounds and also contribute to acidic nature of the water bodies thus causing in misbalance in health and environment as well. It may cause diseases, allergies, or cause death of any species. Due to air pollution an individual's medical conditions are aggravated and person suffers from asthma and emphysema, lung cancer, chronic respiratory disease, heart disease, and even damaging to the brain may occur.

2.2 Causes of Air Pollution

- 2.2.1. Emissions from industries and manufacturing activities.
- 2.2.2. Burning of fossil fuels. Carbon oxide (CO_x) is highly emitted from motor vehicles and hydrocarbons (HC) and nitrogen oxides (N_xO_y).
- 2.2.3. Household and farming chemicals (crop dusting, fertilizers dust emit harmful chemicals into the air).
- 2.2.4. Deforestation is also a main cause that contributes to air pollution and green-house effect.

2.3 Key Facts

- 2.3.1. Out of every 100 individuals almost more than 40 are affected due to water borne diseases and 30 are going through air borne diseases such as asthma.
- 2.3.2. Dead marine life on the coast and many other wind up on the beaches, killed by the contaminants in their habitat.
- 2.3.3. Likewise plants too are affected via different ways say acidification, eutrophication, and ground-level ozone.
- 2.3.4. People working in the outward region mostly suffers from the burning sensation in eyes and throat. Their lungs are also damaged and lead to several diseases.

3 Proposed System

See Fig. 1.

3.1 Master Drone

The proposed system consists of one master drone and four slave robots. The two slaves are flying robots and they will serve the purpose for detection of air pollution, and the next two slaves will be land robots and are used to monitor water pollution. The four slaves will always be accommodated inside the master drone which will have a payload of 1 kg. Each slave robot will weigh 200–250 gm. In that area where the pollution needs to be monitored, master drone will be sent and the four slaves residing inside it will come out. The four slaves will send real-time data to master drone through RF modem. In this way the exact location of all the slaves could be determined. The drone will help in recording and maintaining the data received from the four slaves (Fig. 2).

3.2 Flying Robot

It consists of Microcontroller (Arduino UNO), Dust Sampler, Air monitoring sensors like MiCS-2714 Gas Sensor (NO₂), MQ-9 Gas Sensor, MiSC-2614 Gas Sensor (Ozone), Humidity sensor, MQ-2 Gas Sensor and temperature sensors, RF modem, and DC power supply. The different kinds of sensor will serve the assigned

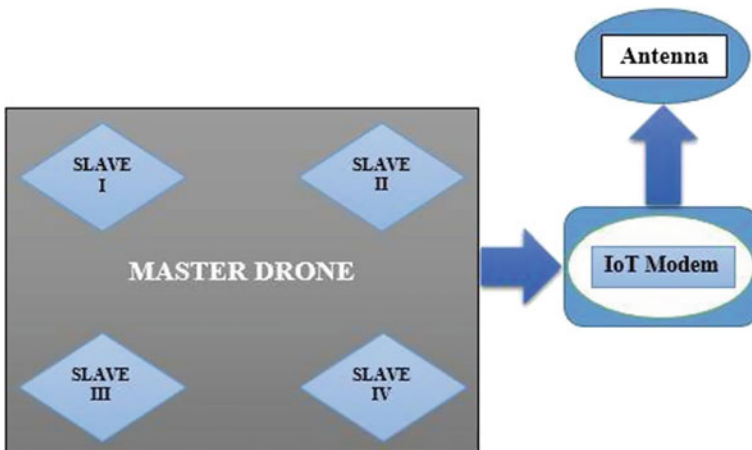


Fig. 1 Block diagram of main system

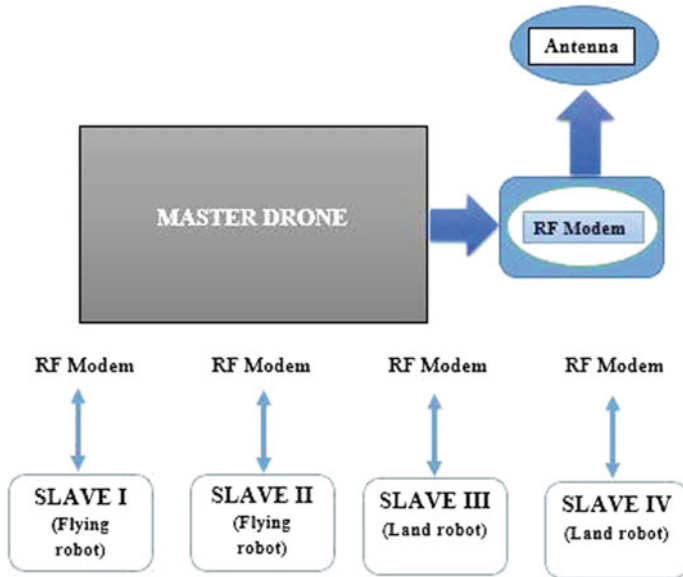


Fig. 2 Block diagram of master drone

purposes and send the real-time data to the master drone through RF modem. The data will be uploaded from master drone to the server via IoT modem and this will help in analyzing the different levels of air pollution present in that particular area, so that the necessary steps can be taken by the governing authority (Fig. 3).

3.3 Land Robot

It consists of Microcontroller (Arduino UNO), Water sensors which include oxidation–reduction potential (ORP), pH, conductivity (salinity), dissolved oxygen (DO), turbidity, temperature, various dissolved ions, RF modem, and DC power supply. Here also the different kinds of sensor will serve the assigned purposes and send the real-time data to the master drone through RF modem. The data will be uploaded from master drone to the server via IoT modem and this will help in analyzing the different levels of water pollution present in that particular area, so that the necessary steps can be taken by the governing authority (Fig. 4).

4 Component Description

See Table 1.

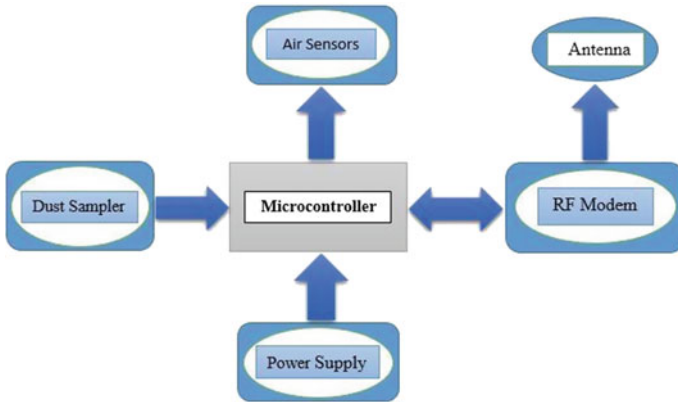


Fig. 3 Block diagram of air robot

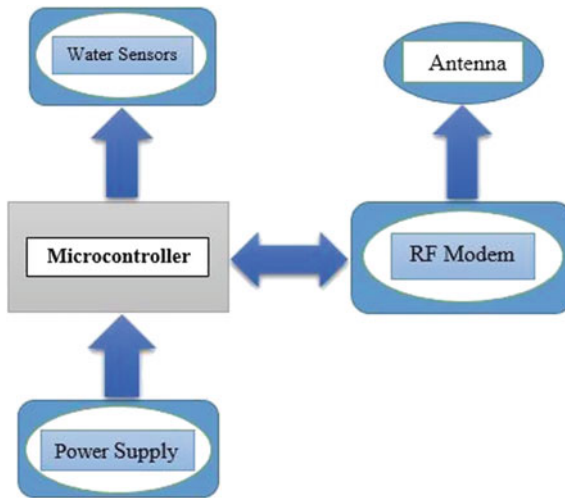


Fig. 4 Block diagram of land robot

Table 1 Equipments used

S. No.	Device	Specifications
1	Arduino UNO	Microcontroller board based upon the ATmega328P
2	RF modem	It works at a frequency of 2.4 GHz. Used to receive and transmit data
3	IoT modem	It's used to transmit data to the cloud
4	Water sensors	It's used to measure different levels of pollution in water bodies
5	Air sensor	Air sensor is designed to analyzed different levels of air pollution
6	Power supply	12 V/1A lithium ion battery, AC power supply

5 Result and Discussion

The air and water monitoring system is nowadays very important and essential. This technology minimizes the level of pollution which is present in the air as well as in water. In this way, the contamination would be highly reduced. The air–water borne diseases can not only be prevented but also the animals, humans, and plants can live in the healthy environment. The proposed system is efficient, cost effective, approachable, and environment friendly.

6 Future Scope of the Work

Access to clean water and air is indispensable to human life. Yet managing this access in an efficient and effective manner is an immensely complex challenge. Due to air pollution, people are highly prone to respiratory diseases, for example, bronchitis and heart problems which have increased the number of hospital beds. The air pollution has led to major health effects when compared to other environment factors. Contaminated water too leads to bad health and effect living creatures residing in the water bodies. Due to limited and lack of human efforts and modern technology, it isn't feasible to control pollution in each and every area. If this project is installed then organizations would get a better chance to control the pollution efficiently, thereby maintaining the fragile ecosystem, thus, making our environment a better place for each and every individual.

References

1. Sweta Goswami (7 November 2016). "Delhi's worst smog yet wakes up govt, emergency measures announced". *Hindustan Times*.
2. Brunekreef, Bert, and Stephen T. Holgate. "Air pollution and health." *The lancet* 360.9341 (2002): 1233–1242.
3. Sidhu, Maninder Kaur, et al. "Household air pollution from various types of rural kitchens and its exposure assessment." *Science of The Total Environment* (2017).
4. Thomas, Moyer D., and R. H. Hendricks. "Effects of air pollution on plants." *Air pollution* 239 (1961).
5. Pedersen, Marie, et al. "Ambient air pollution and primary liver cancer incidence in four European cohorts within the ESCAPE project." *Environmental Research* 154 (2017): 226–233.
6. Gehlot, Anita, et al. "WPAN and PSO based Water Quality Monitoring with LabVIEW as data logger".
7. Dixit, Rakhi Bajpai, et al. "Emergence of toxic cyanobacterial species in the Ganga River, India, due to excessive nutrient loading." *Ecological Indicators* 72 (2017): 420–427.
8. Ho, Clifford K., et al. "Overview of sensors and needs for environmental monitoring." *Sensors* 5.1 (2005): 4–37.

9. Katakwar, Mukesh. "Narmada river water: Pollution and its impact on the human health." *IJCS* 4.2 (2016): 66–70.
10. Markovic, Natasa, Aleksandar Stanimirovic, and Leonid Stoimenov. "Sensor web for river water pollution monitoring and alert system." 12th AGILE International Conference on Geographic Information Science "Advances in GIScience", Hannover, Germany, ISSN. 2009.

Network Forensic Process Model and Framework: An Alternative Scenario

Prabhjot Kaur, Anchit Bijalwan, R.C. Joshi and Amit Awasthi

Abstract Network forensic provides a way to trail the cyber criminals through analysis and trace back of collected network evidence. The prerequisite is the deployment of various network traffic collection tools such as Iris, NetIntercept, NetWitness, SoleraDS5150, Xplico. Network forensic analysis involves examination of network traffic to detect invasion and exploring how the crime took place, i.e., setting up crime scene for investigation and replays. In this paper, we have proposed the process model and compared with the existing network forensic process models and frameworks. Along with highlighting the research challenges at various stages, authors propose a high-level description of standard process model and framework.

Keywords Framework · Network forensic · Process model

1 Introduction

Internet is the medium for distribution of cyber-attacks. But it is something which is much needed in almost every aspect of a country's economy, i.e., in banking, education, transportation (railways, airways, buses, and taxis), healthcare, business, and many more. With the growth of Internet there is a need to protect the data.

P. Kaur · A. Bijalwan

Department of Computer Science & Engineering, Uttaranchal University, Dehradun, India

e-mail: info.prabh@gmail.com

A. Bijalwan

e-mail: anchit.bijalwan@gmail.com

R.C. Joshi

Graphic Era University, Dehradun, India

e-mail: chancellor.geu@gmail.com

A. Awasthi (✉)

University of Petroleum and Energy Studies, Dehradun, India

e-mail: aawasthi@ddn.upes.ac.in

© Springer Nature Singapore Pte Ltd. 2018

R. Singh et al. (eds.), *Intelligent Communication, Control and Devices*,

Advances in Intelligent Systems and Computing 624,

https://doi.org/10.1007/978-981-10-5903-2_50

Though traditional protection techniques such as firewalls, antivirus software are not sufficient enough, so it requires enhanced security measures. Protecting alone the system is not sufficient rather; it is necessary to trace back to the criminals in case of cybercrime. Network forensic provides a mechanism to track the criminals. It also provides a mechanism to trace the malicious traffic, and its analysis thus helps in investigation process.

Consider the cyber-attack at giant company LinkedIn in 2012 where password of nearly 6.5 million user accounts were stolen, and again in 2016 about 100 million hashed passwords and email addresses were leaked both from the same source, i.e., Russian cyber criminals. There has also been breach in the security of Apple's iCloud leading to the stealing of 500 private pictures of celebrities in year 2014. Various scenarios and frameworks have been developed so far to prevent the attacks and identify its origin in case of attack. In spite of many existing virtuous frameworks and techniques for network forensics, there is need for continuous development in this area and to overcome challenges in existing models. This paper reviews existing process models, frameworks and presents a high-level description of the design of process model and framework. Also research challenges at various stages of framework implementations are highlighted. Further sections of this paper include: related work in Sect. 2, proposed standard process model and suggested framework in Sect. 3, various research challenges at different stages of implementation in Sect. 4, and concluding remarks are given in Sect. 5.

2 Related Work

The existing process models are based on the steps involved during digital forensic investigation process. Pilli et al. designed the generic network forensic process model by extracting the key features from the existing digital forensic process models and tried to incorporate in their proposed model [1]. Likewise, the incident response phase provided by Mandia and Procise is included in their model with two-way link between detection and presentation phases [2]. Their model involves phases in the order of preparation phase [3], detection phase (newly introduced phase), incident response phase [2], collection phase, preservation phase, examination phase, analysis phase, investigation phase [4, 5], and presentation phase [6].

Kohn et al. defined a generic digital forensic process model to support the investigation process by following the standardized steps [7]. Liu et al. employed a logic-based network forensic process model using PROLOG in order to analyze the collected data evidence and remove other unrelated data [8]. This technique could be used to reconstruct the attack scenario and can be presented as a proof in the court of law. Lutui focused attention on design science, which involved the extensive study of multidisciplinary digital forensic investigation process model to give more emphasis on efficacy and coherence of the design phase [9].

There are numerous frameworks given by authors such as: ForNet stands for forensic network is a distributed system-based framework given by Shanmugasundaram et al.

that can identify extreme network events [10]. Similarly, another category is based on fuzzy decision tree-based network which is a soft computing-based framework [11]. Bijalwan and Pilli engrossed the psychology of criminals while breaching the network security framework and requirements associated with network forensic [12].

3 Process Model and Framework

3.1 Proposed Network Forensic Standard Process Model

After Ren and Jin [6] proposed the standard network forensic process model, then Pilli et al. [1] also proposed a generic process model for network forensics incorporating the new phase of detection where fast evaluation is done to check the alleged outbreak of crime. The proposed process model aims to first authorize the investigator to perform the investigation process. It is important to preserve the evidence while making an initial assessment. Here, there is an option to abort the investigation if in case certain prerequisites are not fulfilled such as pre-installed sensor and network traffic collector tools such as NetIntercept, Xplico, etc. In case of further investigation is to be carried out, then a strategy is planned to reduce the network traffic collected and document them. Further analysis is done, and review is made through to check for further improvement. The proposed standard network forensic process model is shown in Fig. 1. A brief detail of work performed at each phase is highlighted in this section.

Authorization: This phase involves obtaining legal permissions from the concerned authority to initiate the investigation process as shown in Fig. 1. Ciardhuain proposed the authorization phase to take consent from the internal and external organizations [13].

Preservation: Preservation phase implicates the avoidance of tempering of network evidence [1]. For example in case a mobile device is involved in the crime, then it must be switched off to avoid mitigating of call and network logs. This is the second phase as shown in Fig. 1.

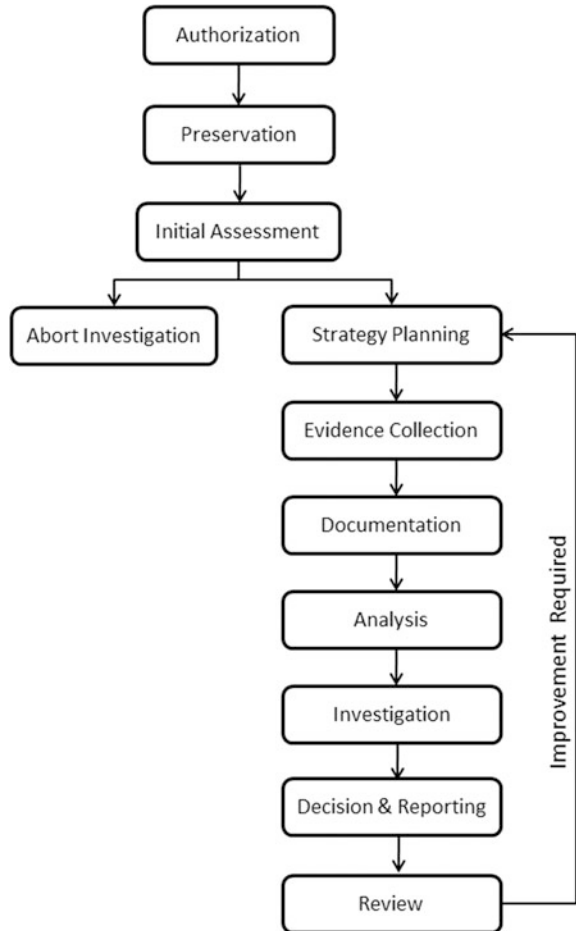
Initial Assessment: In this stage, an initial judgment is made whether to continue or abort investigation. If there are not pre-installed tools for network traffic collection, then the investigation is terminated [4]. This phase has two outward links, out of which only one is selected as displayed in Fig. 1.

Strategy Planning: This phase comprises to jot down the strategy to carry out further investigation, i.e., team members, duration of investigation, cost involved, and software use. This phase involves to construct a design strategy using design science given by Lutui [9], giving more stress on efficacy and coherence.

Evidence Collection: Evidence is collected at this stage which may either involve automatic or manual network traffic collection. Further, the huge data collected from the network can be reduced by eliminating superfluous data [14].

Documentation: Documentation is the process of writing all the relevant information required during the investigation process [4].

Fig. 1 Standard network forensic process model



Analysis: Analysis phase involves determination of attack patterns by employing various machine learning techniques. This phase involves the techniques such as PROLOG logic techniques to analyze the data as given by Liu et al. [8].

Investigation: Further investigation is done to reconstruct the attack scenario, and replay it at the investigator’s end [15].

Decision and Reporting: A decision is made at this stage about the type of attack and concerned authorities are informed to take appropriate actions.

Review: A review is done to check it for further improvement. In case of any improvement is required then strategy is rescheduled by taking the novel parameters.

3.2 Proposed Network Forensic Framework

The amalgamations of standard network forensic framework phases with the phases of network forensic process model are explained in this section. In this framework Fig. 2, the network traffic is collected automatically and reduced to an extent by eliminating the superfluous data and useful features are extracted which are transferred to the next phase. The analysis of the derived features is carried through to obtain a pattern. The newly derived pattern can be matched with the patterns stored in the knowledge base. If a match is found, then an initial quick response is made to the criminals stating warning to abort the attack. Further analysis is done to constantly derive new patterns in case no match is found. The reconstruction phase involves design of attack scenario which is then replayed by the investigator in the next phase.

Network Traffic Collector: The vast amount of traffic flows from the Internet. The network traffic can be collected in one of the following three manners: (1) automatic network traffic collection [16]; (2) collecting traffic on change in frequency at different intervals; and (3) manual network traffic collection Casey [4]. This phase involves taking permissions from the concerned authority to perform forensics in the concerned intruded network and thus collect network traffic. After obtaining the authorization, the network traffic is collected and the preservation phase involves keeping the data unaltered while examining the crime scenario. The three phases of process model acting at the network traffic collector phase is shown in Fig. 3. Nagesh proposed automatic network data collection using distributed mobile agents [16]. Initial assessment is done in order to check the feasibility of the

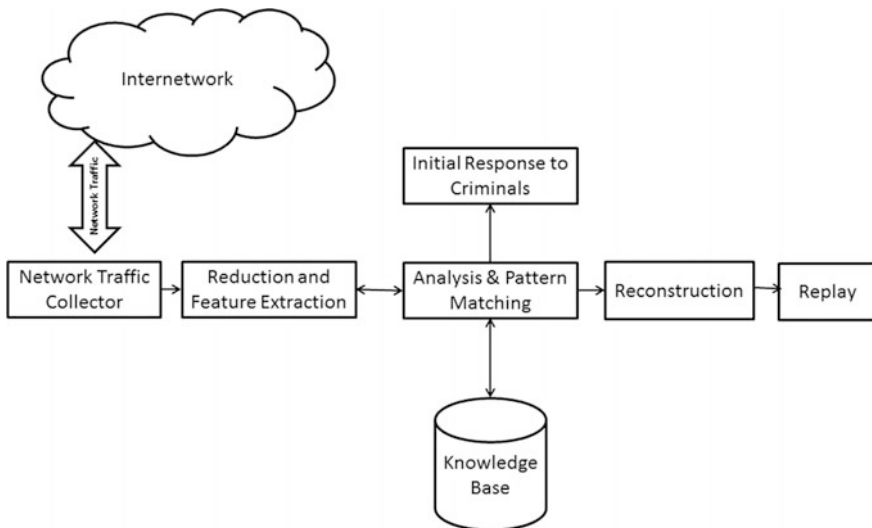
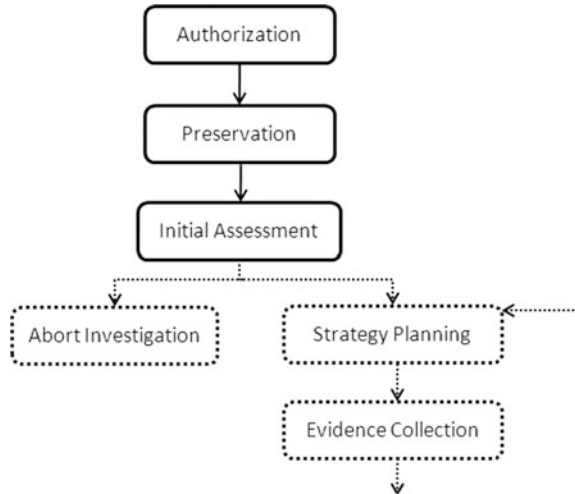


Fig. 2 Standard network forensic framework

Fig. 3 Three phases of process model acting at network traffic collector phase of framework



assessment. If the initial judgment seems to be infeasible, then investigation process is aborted.

Reduction and Feature Extraction: There are enormous data available on the network. Storing each and every bit of network traffic involves huge secondary storage media. This phase involves strategy planning to make the steps to reduce the data by eliminating the extraneous attributes. Similar kind of data can be represented using encoding techniques, for example, all http packets using run-length encoding scheme, i.e., 100 http packets can be represented as 100 http. After reducing the data wherever possible, the important features can be extracted using various machine learning techniques. Relevant points are documented such as what kind of features to extract, who is responsible for this, and what algorithms to employ. Chen et al. used a scalable network forensic method to reduce 97% of attack irrelevant traffic of network resulting in reduced overhead and better accuracy for self-propagating stealth attacks [17]. The strategy planning phase of standard network forensic process model acts at reduction and feature extraction phase of network forensic framework and is shown in Fig. 4.

Analysis and Pattern Matching: In analysis and pattern matching phase, the reduced network traffic is further examined to determine the attack pattern [1, 3, 4, 6, 9, 13, 17, 18]. Dependency graphs can be used to show the order of occurrence of events. Attack patterns are obtained which can then be matched with the existing patterns if any stored in the database. If the current attack pattern matches with the prevailing pattern stored in the knowledge base, then the investigator can move to the next phase. Thus, this helps in saving the investigator’s time and fastens the examination process. If new attack pattern is obtained during analysis phase, then it is stored in the knowledge base for future reference and further analysis is done to obtain additional attack patterns. The analysis phase of process model as shown in

Fig. 4 Three phases of process model acting at reduction and feature extraction phase of framework

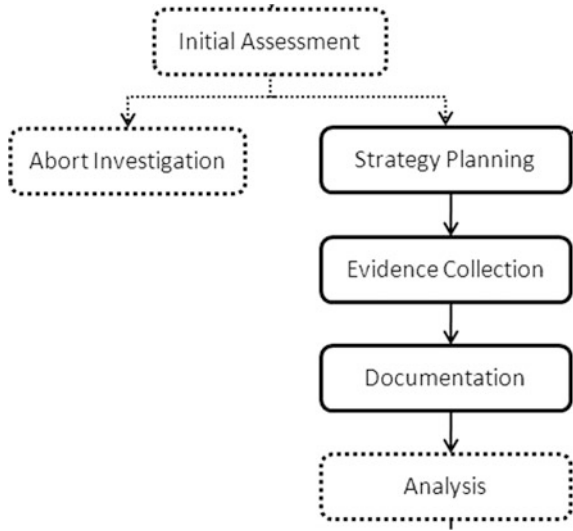


Fig. 5 Analysis phase of process model acting at analysis and pattern matching phase of framework

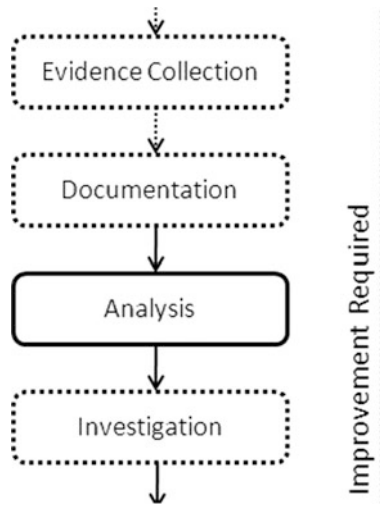


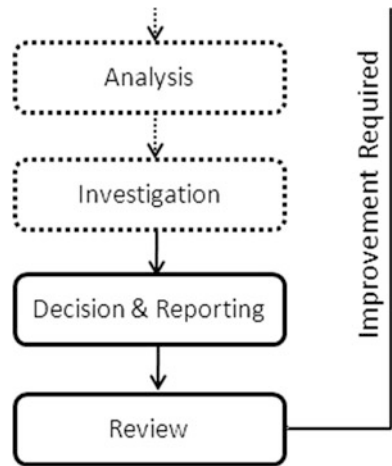
Fig. 1 acts at the analysis phase of framework Fig. 2, and the amalgamation is shown in Fig. 5.

Reconstruction: The pattern obtained from the analysis phase is reconstructed to generate the sequence of events [4]. The patterns are scrutinized according to the flow of packet stream. A proper investigation is done of TCP connection in order to obtain knowledge about the inflow and outflow of packets via which ports. The investigation phase of process model acts at the reconstruction phase of framework to obtain the attack patterns as shown in Fig. 6.

Fig. 6 Investigation phase of process model acting at reconstruction phase of framework



Fig. 7 Two phases of process model acting at replay phase of framework



Replay: In this phase, the pattern created in the previous phase is replayed in order to obtain the crime scenario. The replay of the attack scenario is done on the investigator end without harming the actual network. This is done using simulators to replay the constructed attack situation. The outcome of the simulation is compared with the actual attack scene, and reporting is done. Based on reporting, a decision is made whether to include more parameters and after exhaustive review of the replay process, the control goes back to the strategy planning phase if further improvements are required which is shown in Fig. 7.

4 Challenges

The authorization phase may sometimes face challenge of taking permission from external bodies located overseas, who may not permit due to their country's legal perspectives. The challenge arises in analysis of enormous network traffic; it is therefore suggested in this paper to reduce the network traffic by eliminating the irrelevant traffic based on some criteria. Before actually initiating the preservation phase, the intruder may clear its attack traces which could act as a base for investigation. While collecting evidence, it is necessary to reduce the network traffic data by using substantial data reduction techniques leading to the availability of only relevant data. Sometimes, it is difficult to understand the methodology and intension of the attacker while analyzing large volume of data. If the evidence collected cannot be presented in court of law, then that investigation is not considered fruitful. Liu et al. proposed techniques using which network evidence could be shown in the court of law whenever required [8].

5 Conclusion

In spite of much research is made on network forensic process models and frameworks, it still seems to be a young field. Many challenges faced at various stages are in the process of continuous improvement. The proposed model and framework have been constructed by taking the best features from the existing models and frameworks. This work aims to eliminate the above challenges faced at various stages of the process model to a fair extent. The future work aims at practical implementation of the proposed standard network forensic process model and standard network forensic framework design.

References

1. Pilli, E. S., Joshi, R.C., Niyogi, R.: Network forensic frameworks: Survey and research challenges. *Digital Investigation* 7, 14–27, (2010).
2. Mandia, K., Procise, C.: *Incident Response and Computer Forensics*. Osborne McGraw-Hill, New York, (2003).
3. Reith, M., Carr, C., Gunsch, G.: An Examination of Digital Forensic Models. *International Journal of Digital Evidence* 1(3), (2002).
4. Casey, E.: Network traffic as a source of evidence: tool strengths, weakness, and future needs," *Digital Investigation* 1, 28–43 (2004).
5. Palmer, G. L.: Forensic analysis in digital world. *International Journal of Digital Evidence*, 1 (1), 1–6 (2002).
6. Ren, W., Jin, H.: Distributed Agent-based Real Time Network Intrusion Forensics System Architecture Design. *Proceedings of the International Conference on Advanced Information Networking and Applications*, pp. 177–182, IEEE Press, New York (2005).

7. Kohn, M. D., Eloff, M. M., Eloff, J. H. P.: Integrated digital forensic process model. *Computer & Security* 38, 103–115 (2013).
8. Liu, C., Singhal, A., Wijesekera, D.: A logic-based network forensic model for evidence analysis. *IFIP Advances in Information and Communication Technology* 462, 129–145 (2015).
9. Lutui, R.: A multidisciplinary digital forensic investigation process model. *Business Horizons* 59, 593–604 (2016).
10. Shanmugasundaram, K., Memon, N., Savant, A., Bronnimann, H.: ForNet: A Distributed Forensics Network. *Digital Investigation* 7, 14–27 (2010).
11. Liu, Z., Feng, D.: Incremental fuzzy decision tree-based network forensic system. *Conference on Computational and Information Science* 3802, 995–1002 (2005).
12. Bijalwan, A., Pilli, E. S.: Crime psychology using network forensics. *Journal of Computer Engineering & Information Technology*, 3, (2014). doi: [10.4172/2324-9307.1000120](https://doi.org/10.4172/2324-9307.1000120).
13. Ciardhuain, S. O.: An extended model of cybercrime investigations. *International Journal of Digital Evidence*, 3(2), 1–22 (2004).
14. Tang, Y., Daniels, T. E.: A Simple Framework for Distributed Forensics. *Proceedings of the 25th IEEE International Conference on Distributed Computing Systems Workshops*, February 2005.
15. Selamat, S. R., Yusof, R., Sahib, S.: Mapping Process of Digital Forensic Investigation Framework. *International Journal of Computer Science and Network Security* 8, 163–169, (2008).
16. Nagesh, A.: Distributed network forensics using JADE mobile agent framework. Master's thesis, Arizona State University (2007).
17. Chen, L. M., Chen, M. C., Liao, W., Sun, Y. S.: A Scalable network forensics mechanism for stealthy self-propagating attacks. *Computer Communications*, 36, 1471–1484, (2013).
18. Ndatinya, V., Xiao, Z., Manepalli, V. R., Meng, K., Xiao, Y.: Network forensic analysis using Wireshark. *International Journal of Sensor Networks*, 10, 91–106, (2015).

Modeling and Simulation of ECG Signal for Heartbeat Application

B. Khaleelu Rehman, Adesh Kumar and Paawan Sharma

Abstract The heart disease is dangerous and threat to human life. Most number of heart diseases are observed in the recent years. The diseases are diagnosed and cured completely if predicted in advance. The ECG signal, which contains the data, can be processed by different methods; there is a huge movement for the healthcare applications, which consists portable, less-cost monitoring applications like wearable watches, T-shirts. Electrocardiogram signal processing module is implemented in VHDL and simulation on mentor graphics Modelsim simulator. The digital filtering with low pass FIR architecture (FIR is better than IIR). Filters shall remove the 50 Hz coupled noise and other high frequency noises; the filtered signal is fed to STFT (short-time Fourier transform) through which a lot of interference can be observed by the medical experts. An ECG signal which is a function of MATLAB is used as test input for Modelsim tool for simulation and functional verification.

Keywords Electrocardiogram (ECG) · VHDL · Modelsim · STFT

1 Introduction

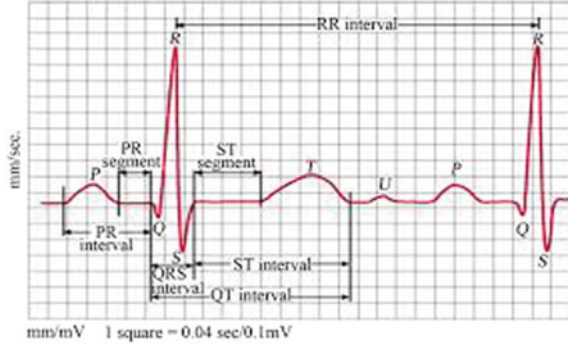
The ECG is the record of heart electrical activity. The abnormalities in the amplitude levels of voltage cause various cardiac arrhythmias [1]. The normal heart rate is called as electrically polarized. The previous ECG signal processing was depending on time domain analysis [2] but the time domain is not always useful to study all the characteristics of ECG signals; for this purpose, the frequency domain

B. Khaleelu Rehman (✉) · A. Kumar · P. Sharma
Department of Electronics, Instrumentation and Control Engineering,
University of Petroleum and Energy Studies, Dehradun 248007, India
e-mail: krehman@ddn.upes.ac.in

A. Kumar
e-mail: adeshkumar@ddn.upes.ac.in

P. Sharma
e-mail: paawan.sharma@ddn.upes.ac.in

Fig. 1 ECG signal characteristics



method is used to achieve fast Fourier transform (FFT) method [3] but the limitation in the FFT is it is unable to provide the exact location of frequency components of time domain. To overcome the limitation of FFT, the next tool available for the ECG signal processing is STFT. ECG is the electrical activity of heart where each cycle is represented with the combination of electrical waves with peaks and valleys. Any electrocardiogram signal gives the data regarding the heart abnormality condition. The ECG signal characteristics are shown in Fig. 1. Many researchers have found the validation of QRS complex detection using the real-time ECG signal processing [4–7].

2 Proposed Architecture of the Overall System

This article proposes the Modelsim simulation results of ECG signal processing.

The block diagram is showing the entire ECG signal processing in Fig. 2 including the FPGA. From the MIT-BIH [8] database and from the MATLAB, the voltage levels of P, Q, R, S, and T can be obtained and these values are incorporated in the sound card of the system as shown in Fig. 2; the values are sent to the 12-bit ADC. 50 Hz noise removal filter is used to discard power supply interference noise. After the removal of power supply noise, the filter coefficients are given to the notch filter to remove the high frequency noise. This filter is used for attenuating the signals which are not in the range of 0.05–100 Hz.

2.1 Coefficient Generation for Notch and High Pass Noise Removal Filter

The coefficients of Notch filter and high pass noise removal filter is generated with the help of MATLAB 2012 and the process is suggested below.

Start → MATLAB → toolboxes → filter design HDL coder → Filter Design and Analysis Tool (FDA tool) (Fig. 3).

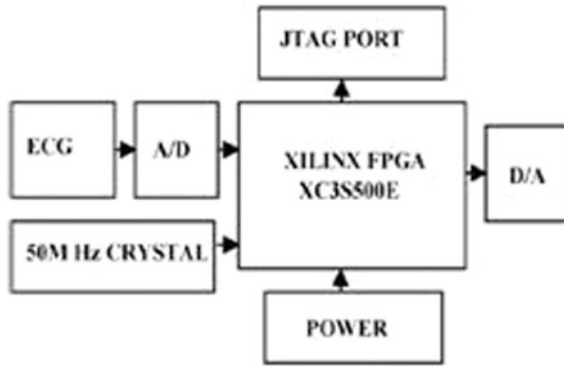


Fig. 2 Block diagram of ECG

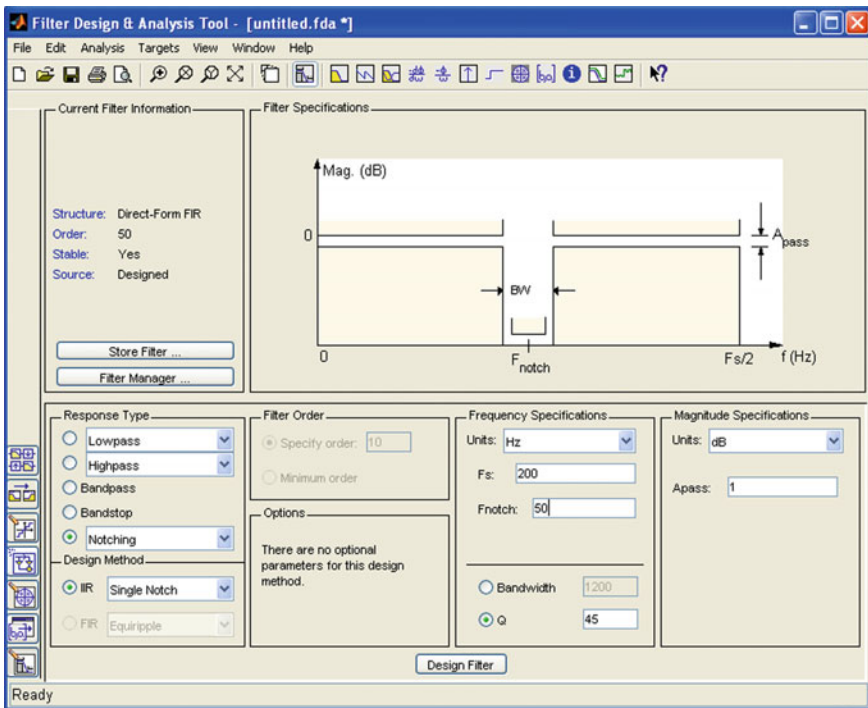


Fig. 3 Filter design and analysis test

Click design filter. Then, the coefficients will be generated (Fig. 4).

The window shown in Fig. 5 will open after “Open file select export” option and it will be remain opened using “click on export”, corresponding data is exported to workspace.

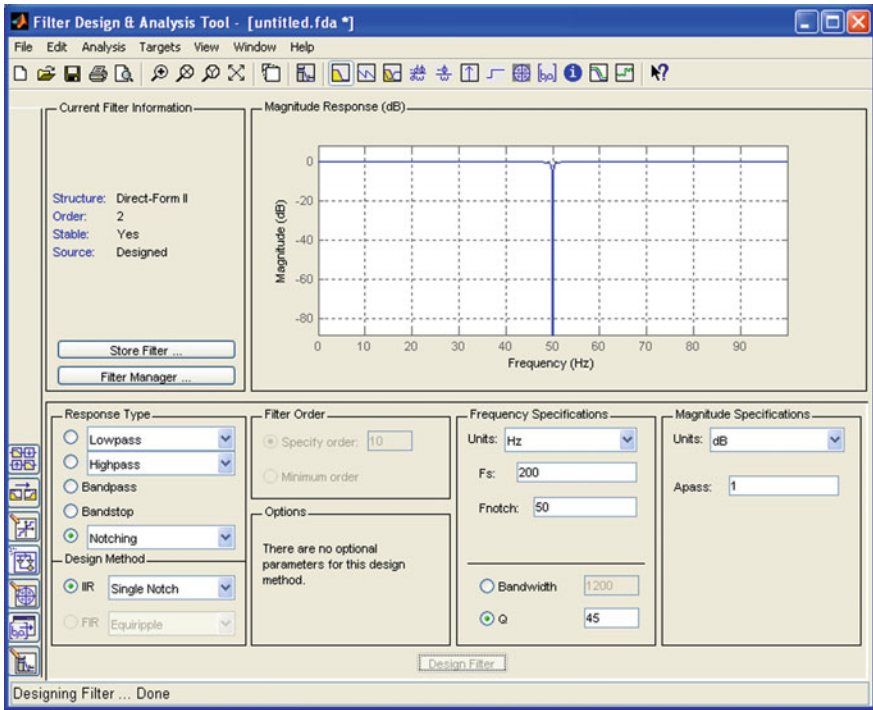


Fig. 4 MATLAB window for filter design

Fig. 5 Filter coefficients



A MATLAB code which converts the decimal numbers to binary values, taking the inputs from MATLAB workspace (i.e. coefficients) and in the program total length of binary values and no of fractional parts in it.

High Pass Noise Removal Filter.

Select specifications as shown below for high frequency noise removal filter, and then follow all the steps given for the notch filter to generate the coefficients (Fig. 6).

As the binary coefficients are generated, copy coefficients to the PFIR package and save them in the PFIR package by different naming as filter_notch for notch operation and filter_bpf for high frequency noise removal filter.

PFIR module: The package created which consists of the filter coefficients will be utilized by calling the package into program; PFIR structure is shown in Fig. 7. Input is taken as PFIR_in and is given to a multiplier in a loop; another input to multiplier is the filter coefficient (i) stored in the PFIR package. Result generated by the multiplier will be added with another multiplier in the loop ($i + 1$). Loop will be running till last coefficient is multiplied, and result is reflected on to output signal PFIR_out.

ECG ROM block: An ECG signal is generated from MATLAB by using the command ECG for a sampling rate of 160 as shown below because normal

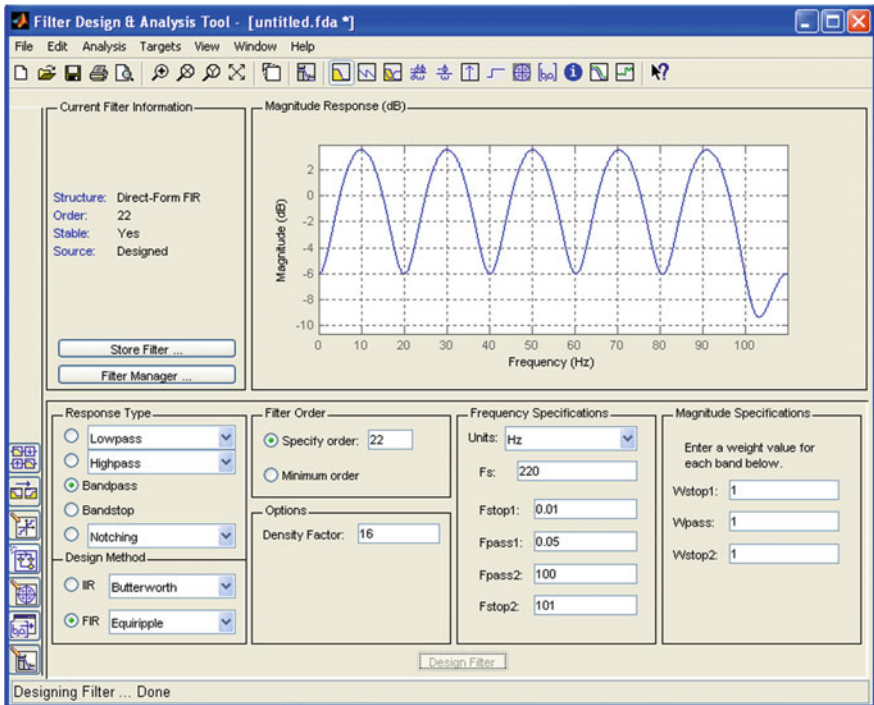


Fig. 6 High pass noise removal filter

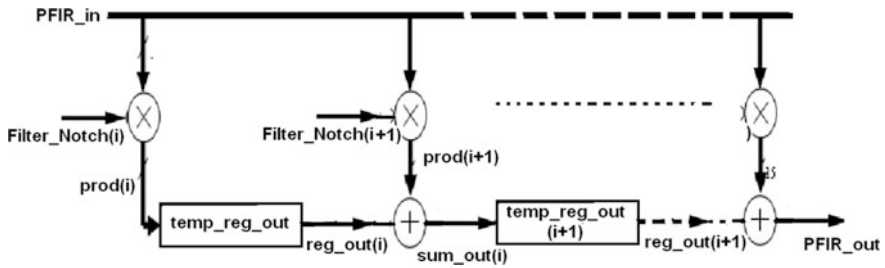


Fig. 7 PFIR filter design perspective

heartbeat rate is 72 beats per/min, i.e., 0.83 s for the beat so no. of samples taken for the beat is 160 samples as shown in the figure. A MATLAB code has been developed to convert data in the workspace to binary format according to specified length. The generated values in binary format are copied and saved in the ECG ROM. The output of the ECG signal is obtained based on clock signal.

3 Results and Discussion

As shown in Fig. 8, ECG_data_1 is the input from the MATLAB and the values are stored in the ROM memory of the FPGA. The DC value is set to zero because the ADC is unsigned and it will not predict negative values. The positive and negative peaks of the ECG signals are found by forcing DC_values as reference. The maximum value and maximum index are the peaks of P, R, T, and the minimum value and minimum index are Q and T values.

4 Waveform Description

It can be observed from Fig. 9 that the filtered ECG signal is given to FFT. The FFT output is real and imaginary part and plotted the FFT signal shows real and imaginary part so that magnitude signal is combined with the output signals. The paper implements only one notch filter at 50 Hz to remove the power supply noise and another filter with 0.05–100 Hz band pass characteristics.

Figure 10 shows the Modelsim output in which the second signal is the noisy signal when the noisy signal is passed through the filtering technique (high pass filter, notch filter); the output shown in the third graph is the smooth graph after filtering.

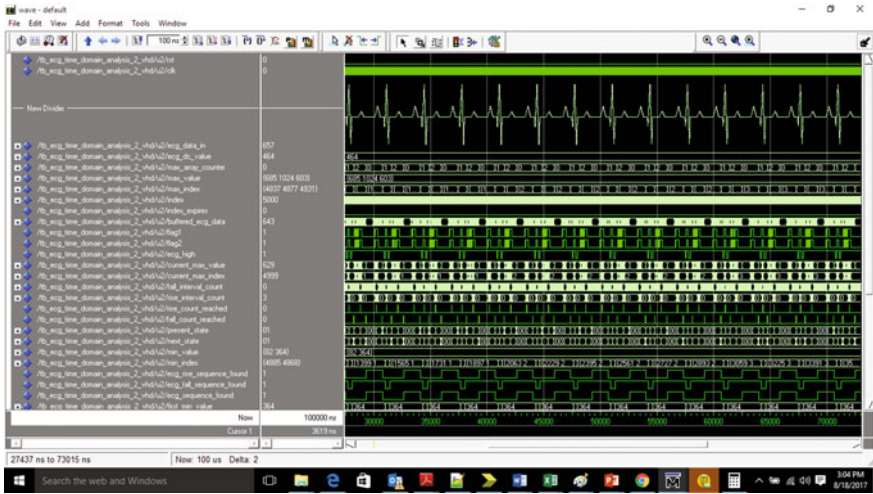


Fig. 8 ECG signal in Modelsim

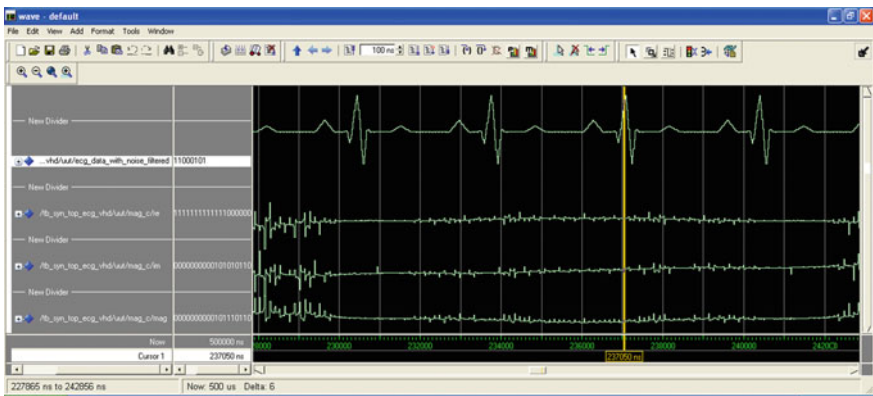


Fig. 9 Filtered ECG signal



Fig. 10 Modelsim overall simulated ECG signal

5 Conclusion

In the medicine area observing of unhealthy arrhythmia is linked with the rhythm of heart. Hence, it is utmost significant to implement a system which routinely finds the cardiac arrhythmia (i.e., heartbeat abnormalities). The persistence of this system is to simulate the ECG signal processing on the Modelsim simulator using VHDL programming language. The MATLAB code is verified successfully for the generated ECG signal and P, Q, R, S, T values are estimated with the help of sound card. This architecture provides the plurality of blocks through which it provides for the diagnosis of electrocardiogram signal and QRS complex detection. The functional simulation of the proposed architecture is done in Modelsim 10.0b student edition and it shows the succesful pattern of ECG signal.

References

1. E. El Mimouni, M. Karim, “Novel Simple Decision Stage of Pan & Tompkins QRS Detector and its FPGA-Based Implementation”, ISBN 978-1-4673-2679-7(set), pp. 331–336, 2015.
2. L. Cuiwei, Z. Chongxu, and T. Changfeng, “Detection of ECG Characteristic Points Using time domain Transforms”, IEEE Trans.Biomed. Eng, VOL. 42, NO. 1, pp. 21-28, 2015.
3. L. Nianqiang, W. Yongbing, Z. Guoyi, “A Preferable Method on Digital Filter in ECG Signal’s Processing Based on FPGA”, IEEE Computer society, 978-0-7695-4020-7, pp. 184–186,2016.
4. N. Debbabi, S. El Asmi, H. Arfa, “Real-time Correction of ECG baseline wander Application to the Pan & Tompkins QRS detection algorithm”, IEEE,2014.
5. C. Pavlatos, A. Dimopoulos, G. Manis and G. Papakonstantinou, “Hardware implementation of pan & tompkins QRS detection algorithm”, European Social Fund, Pned 2013.

6. S. Gradl, P.Kugler, C. Lohmuller, B. Eskofier, "Real-time ECG monitoring and arrhythmia detection using Android-based mobile devices", IEEE EMBS, pp. 2452–2455,2012.
7. J. Pan and W. J. Tompkins, "A Real-Time QRS Detection Algorithm", IEEE TRANSACTIONS ON BIOMEDICAL ENGINEERING, VOL. BME-32, NO. 3, pp. 230–236, MARCH 2015.
8. Massachusetts Institute of Technology. M-BIH ECG database Available: www.phisionet.com.
9. XILINX, Internet site address: <http://www.xilinx.com>.
10. www.irr-nancy.fr.

Fingerprint Acquisition Methodologies and Its Upgradation with IoT

Rohit Samkaria, Rajesh Singh, Anita Gehlot, Rohit Sanket, Ateev Aggarwal, M. S. Yadav, Ashok Kumar, Rupendra Pachauri and Sushabhan Choudhury

Abstract Fingerprint reader is an emerging technology, increasing at a tremendous rate due to its function that allows the fast identification and secure verification capabilities. This technology enables to recognize individual users without need of any password and the card swipes and works in a different ways rather than the swipe cards and other identification technologies. By using this technology, we can recognize and authenticate individuals based on the who they are, instead of the what they know, like their password and pins and what they possess, like keys and swipe cards. Fingerprint technology having important role with security application and e-commerce due to their ability of identifying and providing access to user through finger. This technology can be implemented in the various areas like Voters Identification, Passport verification, Population Census, Driver's license, and Professional ID and there data can be placed on cloud by using Internet of Things (IoT). If cloud-based technology incorporated with fingerprint identification and is properly used, then it has potential to create a highly secured verification environment. In this research, we have done extensive literature survey for future research areas in this field.

Keywords Fingerprint recognition · IoT · Quick response

R. Samkaria (✉) · R. Singh · A. Gehlot · R. Sanket · A. Aggarwal · M.S. Yadav · A. Kumar · R. Pachauri · S. Choudhury
Electronics Instrumentation and Control Engineering Department,
College of Engineering Studies, University of Petroleum and Energy Studies,
Dehradun 248007, Uttarakhand, India
e-mail: rohit.samkaria93@gmial.com

R. Singh
e-mail: rsingh@ddn.upes.ac.in

1 Introduction

Biometric-based system for identification is capable of identifying a person on the behalf of either physical characteristics or the behavior [1]. Nowadays, there are number of technologies available to identify a person through biometrics. Mostly these technologies include the signature dynamics, voice recognition, retina recognition, face recognition, recognition of hand, fingerprint recognition, iris recognition [2–4].

Fingerprint identification has great promise for diversified use in many applications which include numerous practical applications [5]. Now it is time to review this technology in depth with its implementation over cloud by using IoT and to consider its academic research and the future use of this technology [6]. In this review paper, we would focus on the management issue and technical issue with the fingerprint-based identification issue and implementation of fingerprint identification over cloud through IoT and its application [7]. The goal is to provide the detailed view of the fingerprint-based technology incorporated with IoT, so that researcher would be able to develop their own better idea with further research [8–10].

Whenever system verifies biometrics of a person, system should be capable of verifying some specific features of biometric of person and for this task it requires something with which it can compare [11]. Therefore, a template or profile required which stores the biometric properties of the person. The process of recording the biometric properties of a person in the system is called enrollment [12, 13]. During the process of enrollment to get the profile of a biometric of person, the biometrics characteristics are required to scan several time, mostly three or four times so that the profile we get should be independent of real-time variations that occurred in practice, like angle of placement of finger over the scanner [14–16]. Another thing required is the data we get after scanning should be compressed because the memory or storage capacities of these systems are small and some security technique requires to protect this data, therefore gives a high level of security [17, 18].

When enrollment process is completed and a biometric verification too occurred, a scan of finger of person is made and we get data corresponds to the finger [19]. This data from the finger is compared with the biometric profile in the system [20–22]. Now here two terms take place False Reject Rate (FRR) and False Accept Rate (FAR) and come from the margin error that we allowed in the person biometric characteristics [23]. And in case the required margin is very small then system rejects the right person and in case the margin is too large then malicious person treated as acceptance [24, 25]. Now the person identification data is loaded over the cloud and this can be monitored using Internet throughout the globe [26].

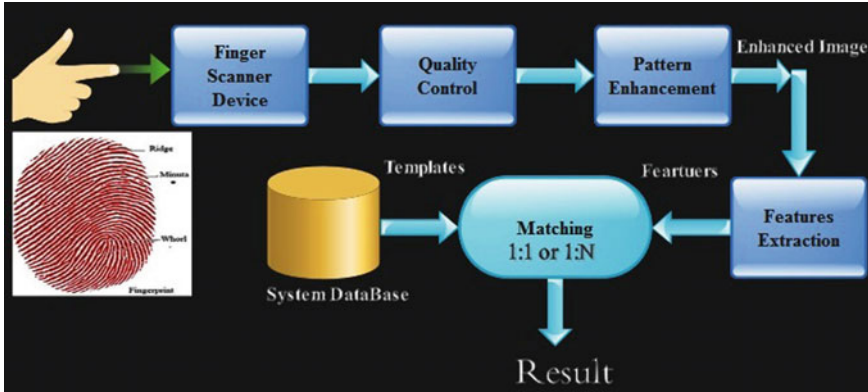


Fig. 1 Block diagram of the system

2 Fingerprint Verification Theory

Inside skin of the finger covers a pattern which consists of hills or valleys which varies from person to person. This is helpful for fingerprint identity verification of their owners. Although some of the fingerprint pattern recognition system based on the recognition does not compare to the original, most systems use certain features into the ridge pattern [27]. These features are the fact that the fingerprint pattern from the papillary ridges is not continuous line bit it ends, splits, or islands. Minutiae are the special points on the fingers, hundreds of minutiae are present in a fingerprint, the scanner scans around 30–40 minutiae (Fig. 1).

Minutiae are being used since hundreds of years by law enforcement agencies for accurate identification. In Europe, the 12 minutiae should be identified for positive identification. The 12 point rule is not based on stats; it is assumed that in the population of tens of millions no two persons will have same 12 point minutiae in fingerprints [28].

2.1 Terminology

The terminology that is used in the fingerprint is identification versus verification. There are five stages which are involved in the finger scan identification and verification: fingerprint image acquisition, image processing, and location of distinctive characteristics, template creations, and template matching (Fig. 2).

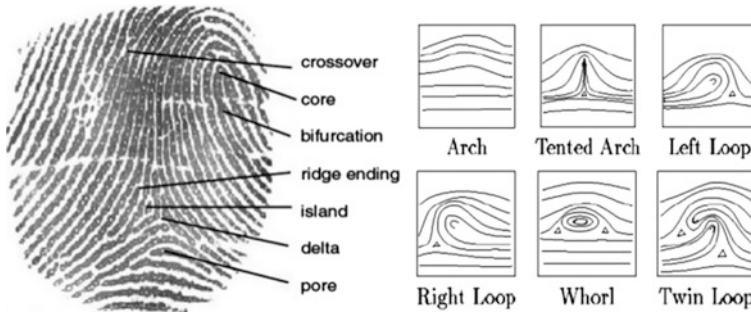


Fig. 2 Fingerprint structure

2.2 FAR and FRR

The biometric identification technology can be fine-tuned in either high security level or low level security. For the high security level, the biometric systems make more finicky and in this case the false rejection rate increases and rejects an authorized user and causes inconvenience to users. If the security is the system is set to very low than it causes FAR to increase.

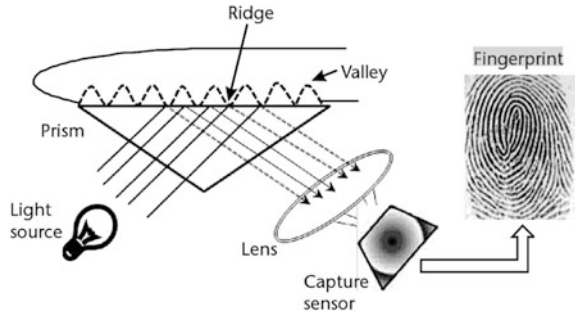
3 Fingerprint Scanning Technologies

Copies of the fingerprint found at crime scene are examined to match minutiae for over hundred years. This method is used when the person whose fingerprints are to be matched is not cooperating but for those who cooperate, proper systems are available so that they can access after verification. In mid-eighties, the first generation finger-print scanners were introduced, after that the technology evolved a lot for commercial purposes [29]. Optical techniques were used for the scanning of finger, currently a variety of techniques is used for the scanning of the fingerprints. The techniques are:

3.1 Inked Capture

The oldest form of the fingerprint acquisition is the inked method in which an ink is applied over the finger and impression of the finger is taken over a real physical substrate, then a highly trained operator oversees the capture. The capture over the physical substrate depends upon the amount of the ink applied to the finger and force applied over the finger [22]. The captured print might be too dark or too be very light pose to difficulty to extract the pattern.

Fig. 3 Working of optical sensor



3.2 Latent Fingerprint

Latent fingerprint applies the advantage of oily nature of the skin which leaves the ridgeline structure of the finger. These ridgeline trace is captured by various different chemicals. Latent fingerprint technology is mostly utilized in the forensic, criminalistics, or crime scene analysis and this technology requires a high degree of specialization to maintain the integrity of fingerprint.

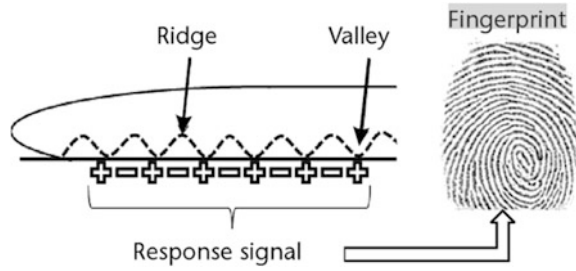
3.3 Optical Sensors

A LED light source illuminates the finger placed on the plate. The image is projected on the camera using a prism. The image is stored for analysis using frame grabber technique [18]. This advancement in this technology was frustrated total internal reflection. The refractive index of ridges and valleys is different, so when finger touches an optical mirror and corresponds to that a light is fall over the mirror, light falls on the valleys it is reflected back and light falls over the ridges do not reflect back and appears to be dark, and this image is captured in the system (Fig. 3).

3.4 Solids State Capacitive Sensor

The variations in capacitance between valleys and ridges of the finger-print are measured by an array of pixels. This is possible because of the difference between skin sensor and air sensor's capacitive values (Fig. 4).

Fig. 4 Working of solid state capacitive sensor



3.5 Ultrasonic Sensor

When some difference in acoustic impedance of the skin and air is there then ultrasonic sensor was discovered. The sensors used in the system are already in use in medical world. The frequency range is from 20 kHz to many gigahertz [30]. The resolution of 500 dots per inch is required for minutiae recognition for this high frequency is required.

3.6 Temperature Sensor

The size of the sensor is small even smaller than the finger due to the reason that the scan can be done just by swiping finger over the finger. The distinction between the temperature of the finger and air between the valleys helps the sensor to detect the finger.

4 Major Application Field of Fingerprint Reorganization Technology

For data protection, the password is not reliable method. It is human tendency that they might forget the password but biometrics methods do not require any password. Finger-print technology has been used for centuries and is unique and can verify very accurately. A review from International Biometric Group reveals the market share of the biometric technology is provided below in the figure [23] and the latest area of fingerprint technology that can be utilized are as (Fig. 5).

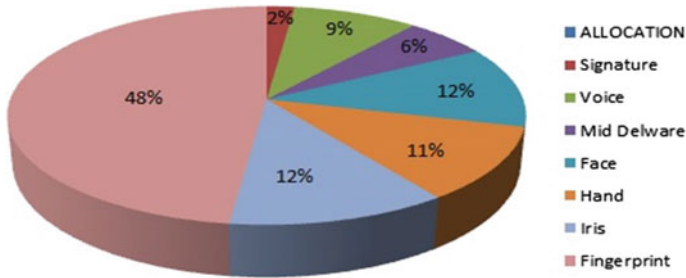


Fig. 5 Statistics of finger print technology

4.1 Voter Registration and Identification

Some democracies around the world are slowly embracing the appropriate technologies in the election process. Registration is the one process that is done through this process what we called (Biometric Voter Registration). For this task, some skilled operator is required who are having good computer knowledge.

4.2 Border Control via Passport Verification by Using Biological Parameter

This application is utilized in the airports where the identity of the passengers is verified through the biometric reorganization.

4.3 Population Census by Using Biometrics

Fingerprint reorganization is utilized for population census in various countries where the data is collected by the skilled operator along the area and is put over the data base. This provides the census report and another way increases the security of the particular area.

5 Management Issue in Fingerprint Acquisition Technologies

In the management applications, fingerprint pattern reorganization efforts were initially limited to case as all the sensors technology having their own advantages and disadvantages that make them suitable for particular application than others.

5.1 Research in Management Issue

The biometric data of person are unique and permanent characteristics of the individuals so in this case the privacy protection of the biometric pattern authentication scheme has become a common concern for various industries [31]. The fingerprint pattern is taken from the tip of the finger which is a small area from which the measurement is taken and the ridges patterns vary or can be affected by various factors like cuts, dirt, or even wear and tear and acquiring the high quality of the fingerprint pattern became a complicated task when people with no few minutia points often wash their hand with detergents (specially surgeons which wash their hands with strong detergents) face difficulties to enroll.

Although the fingerprints are very convenient in many industries but it is not suitable for the people who works in chemical industries because their fingerprints are affected by various chemicals. In manual labor industry, the worker is used to work with the hands, their fingers get rough and scratched and this situations lead to the miss-reading.

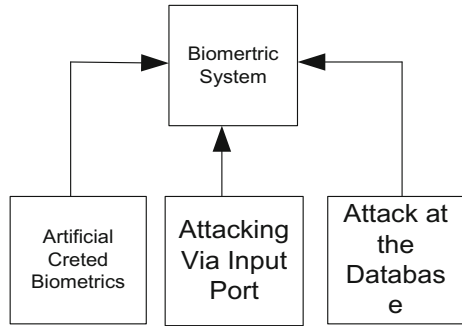
5.2 False Positive Rejects and False Negative Acceptance

The accuracy of the fingerprint reorganization must be determined or monitored constantly. The problem which arises are due to false positive reject in which a fingerprint could accidentally accept the person pattern and allow him/her in allocation who does not belong there [32]. On the one hand, a person who should be allowed to a location is kept outside due to the false rejection of biometrics.

5.3 Hardware and Software Problem

The fingerprint reorganization technologies face difficulties to implement in large public and private organizations where number of people to be enrolled is very large, this requires a large hardware to implement the system and a large storage is required to hold the finger pattern data of all the people of the organizations. The hardware involved in the system must be reliable and must be from reputable company, i.e., 'Re-furbished' hardware is not acceptable. Many biometric devices operated with the software that compares the pattern data with the stored data in the device. The extracted data is compared with the stored data and if software fails to compare this data then the whole system will fail.

Fig. 6 Block diagram of security attacks



5.4 Security Attacks

In the management side, there are several security threats which may harm the protect information of the management. Figure below shows the security attack over fingerprint-based biometric system (Fig. 6).

6 Limitation Within Fingerprint Technology

The biggest problem associated with the fingerprint scanning is that the scanner cannot differentiate the finger and the dummy. There are two methods creates the dummy of the fingerprint easily that can be scanned as a true fingerprint by the scanner. One of the methods is.

A plastic cast can be created for the finger, then silicone is filled in the cast to make a silicone dummy. The dummy can be used by any other person easily to fool the system [33]. This method is very useful in the case when the person is cooperating but if there is no cooperation then the fingerprint is required on the glass or on any other surface.

This making of dummy makes the system weaker; this may lead to many types of attacks like:

- A wrong person wants to get access can use this method to prepare the dummy, and then he can use it to get access of wherever he wants.
- If a cooperating person can prepare the dummies willingly then he can give access to anyone he wants to give.

Sensor	Limitations
Optical	Condition of finger skin such as moisture content, oiliness, and elasticity of the finger has a significant impact over the captured pattern. Sometimes affected by the residue of previous fingerprints and ambient light focused on the mirror plate
Ultrasonic	Ultrasonic sensors are comprised of various/several mechanical parts and which results in a large size and relatively having very high cost
Capacitive	In the capacitive sensors, the production cost is increased due to their large size. They are mostly affected by the electrostatic discharge (ESD) wet fingers
RF Sensor	Captured details at the epidermal dermal levels of skin provide high quality images from dirty and poor skin qualities. Production cost is high
Thermal	Ambient temperature has an impact over the fingerprint sensor

7 Fingerprint Sensor and IoT Application Gateway

Transformation of data between the fingerprint module and the IPv6 is executed by the program inside application gateway of IoT because the finger recognition nodes are not capable with Internet protocol to communicate [34] (Fig. 7).

Figure 8 shows the circuit diagram for fingerprint sensor interfacing with Arduino Nano to extract the code of individual fingerprint before its actual implementation. Connect Txout, search pins of fingerprint module to Rx and search pins of Arduino Nano, respectively.

To extract the code, follow the steps

1. Press the Empty switch to clear the previous data.
2. Place the finger on fingerprint and press 'Add' switch to add the fingerprint information to the memory of module.
3. The extracted code can be checked on the terminal V1.9b through MAX232.
4. Repeat the process to 'Add' more fingerprint information.

Once all these steps are performed, the identifications pattern is stored in the memory and this pattern is coded in digital format. So when users placed finger over the fingerprint module, system generate a digital code and Arduino Nano compare the code generated by the module with the stored code and it the generated

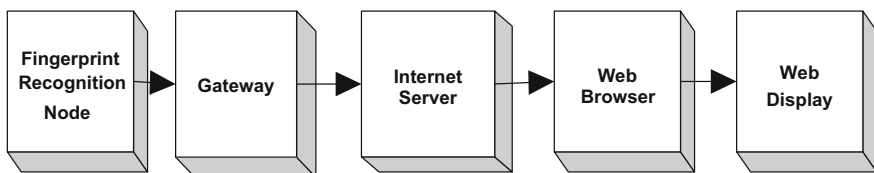
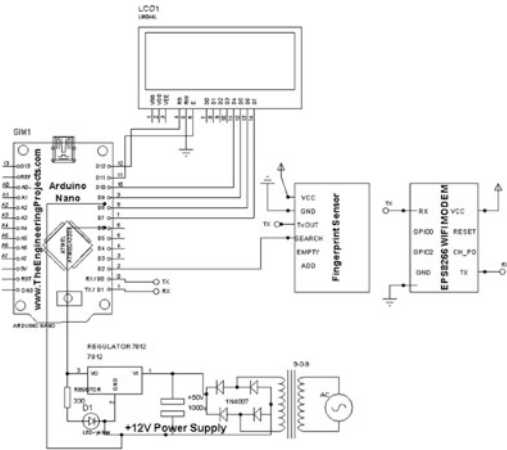


Fig. 7 Block diagram of the complete system

Fig. 8 Circuit diagram



code matched with the stored code then is provide the access to user and send the details of person behind the code to cloud through ESP8266 module which is the gateway to the Web server.

8 Conclusion and Result

We have surveyed the key features of the fingerprint pattern reorganization technology and described its management application, advantages, and limitation of the current fingerprint recognition technology and its incorporation with cloud-based monitoring system by using IoT. In future, research may include the high security level of the pattern by addition of fingerprint identification algorithm (correlation and features-based approaches), and cloud monitoring is an emerging technology to this field which can bring a drastic change in this technology. I hope this paper might help the researchers the general user’s in understanding of biometrics and fingerprint technology, particularly with its familiarity, utility, acceptability and moreover to lead the heightened of the awareness of the fingerprint technology with IoT to enhance the security of the system.

References

1. Jain, Anil K, Arun Ross, and Salil Prabhakar. "An introduction to biometric recognition." IEEE Transactions on circuits and systems for video technology 14.1 (2004): 4–20.
2. Poon, Carmen CY, Yuan-Ting Zhang, and Shu-Di Bao. "A novel biometrics method to secure wireless body area sensor networks for telemedicine and m-health." IEEE Communications Magazine 44.4 (2006): 73–81.

3. A. K. Jain, A. Ross, and S. Pankanti, "Biometrics: a tool for information security," *IEEE Transactions on Information Forensics and Security*, vol. 1, no. 2, pp. 125–143, 2006.
4. C. Roberts, "Biometric attack vectors and defences," *Computers and Security*, vol. 26, no. 1, pp. 14–25, 2007.
5. M1.4 Ad Hoc Group on Biometric in E-Authentication, "Study report on biometrics in E-authentication," Tech. Rep. INCITS M1/07-0185rev, International Committee for Information Technology Standards (INCITS), Washington, DC, USA, August 2007.
6. Tao, Fei, et al. "IoT-based intelligent perception and access of manufacturing resource toward cloud manufacturing." *IEEE Transactions on Industrial Informatics* 10.2 (2014): 1547–1557.
7. I. Buhan and P. Hartel, "The state of the art in abuse of biometrics," Tech. Rep. TR-CTIT-05-41, Centre for Telematics and Information Technology, University of Twente, Twente, The Netherlands, December 2005.
8. Tao, Fei, et al. "IoT-based intelligent perception and access of manufacturing resource toward cloud manufacturing." *IEEE Transactions on Industrial Informatics* 10.2 (2014): 1547–1557.
9. K. Ishikawa, *Guide to Quality Control*, Nordica International, Tokyo, Japan.
10. A. Ross, K. Nandakumar, and A. K. Jain, *Handbook of Multibiometrics*, Springer, Berlin, Germany, 2006.
11. Francioso, L., et al. "Flexible thermoelectric generator for ambient assisted living wearable biometric sensors." *Journal of Power Sources* 196.6 (2011): 3239–3243.
12. Jain, Anil K., Karthik, Nandakumar., and Abhishek, Nagar. "Biometric template security." *EURASIP Journal on Advances in Signal Processing* 2008 (2008): 113.
13. Chen, Shih-Lun, et al. "Wireless body sensor network with adaptive low-power design for biometrics and healthcare applications." *IEEE Systems Journal* 3.4 (2009): 398–409.
14. Roberts, Chris. "Biometric attack vectors and defences." *Computers & Security* 26.1 (2007): 14–25.
15. Alonso-Fernandez, Fernando, et al. "Quality-based conditional processing in multi-biometrics: application to sensor interoperability." *IEEE Transactions on Systems, Man, and Cybernetics-Part A: Systems and Humans* 40.6 (2010): 1168–1179.
16. Silva, Hugo, et al. "Study and evaluation of a single differential sensor design based on electro-textile electrodes for ECG biometrics applications." *Sensors*, 2011 IEEE. IEEE, 2011.
17. Christin, Delphine, et al. "A survey on privacy in mobile participatory sensing applications." *Journal of Systems and Software* 84.11 (2011): 1928–1946.
18. Piuri, Vincenzo, and Fabio Scotti. "Fingerprint biometrics via low-cost sensors and webcams." *Biometrics: Theory, Applications and Systems*, 2008. *BTAS 2008*. 2nd IEEE International Conference on. IEEE, 2008.
19. Text of Final Committee Draft 19795-1, *Biometric Performance Testing and Reporting—Part 1: Principles and Framework*, ISO/IEC JTC1/SC37 N908, 2005.
20. K. Asai, Y. Hoshino and K. Kiji, "Automatic fingerprint identification by minutia-network feature – Matching process," *Transactions of IEICE D-II, J72-D-II*, 5, pp. 733–740, May 1989 (in Japanese).
21. K. Uchida, et al, "Fingerprint card classification with statistical feature integration," *Proceedings of the 14th International Conference on Pattern Recognition*, Brisbane, Australia, pp. 1833–1839, Aug. 1998.
22. Text of Final Committee Draft 19795-1, *Biometric Performance Testing and Reporting—Part 1: Principles and Framework*, ISO/IEC JTC1/SC37 N908, 2005.
23. A. Monden, L. Huang and S. Yoshimoto, "A Performance Evaluation Assuring the Security Strength of Individual Fingerprints," *Proc. of the 2005 Symposium on Cryptography and Information Security*, pp. 541–546, 2005 (in Japanese).
24. A. Monden and S. Yoshimoto, "Fingerprint Identification for Security Applications," *NEC Res. & Develop.*, 44, 4, pp. 328–332, Oct. 2003.
25. L. Huang, A. Monden and S. Yoshimoto, "Fingerprint Identification Based on False Acceptance Probability," *Proc. of the 2004 Symposium on Cryptography and Information Security*, pp. 579–584, 2004 (in Japanese).

26. Amendola, Sara, et al. "RFID technology for IoT-based personal healthcare in smart spaces." *IEEE Internet of Things Journal* 1.2 (2014): 144–152.
27. S. Hiratsuka and Y. Hoshino, "The Intelligent Fingerprint Authentication System 'Secure Finger'," *NEC Res. & Develop.*, 43, 1, pp. 11–14, Jan. 2002.
28. Biometric System Laboratory - University of Bologna, "FVC 2006: the 4th international fingerprint verification competition," 2006, <http://bias.csr.unibo.it/fvc2006/default.asp>.
29. C. Wilson, A. R. Hicklin, M. Bone, et al., "Fingerprint vendor technology evaluation 2003: summary of results and analysis report," Tech. Rep. NISTIR 7123, National Institute of Standards and Technology, Gaithersburg, Md, USA, June 2004.
30. P. J. Phillips, W. T. Scruggs, A. J. O Toole, et al., "FRVT 2006 ' and ICE 2006 large-scale results," Tech. Rep. NISTIR 7408, National Institute of Standards and Technology, 2007.
31. M. Przybocki and A. Martin, "NIST speaker recognition evaluation chronicles," in *Proceedings of Odyssey: The Speaker and Language Recognition Workshop*, pp. 12–22, Toledo, Spain, May 2004.
32. T. Matsumoto, H. Matsumoto, K. Yamada, and S. Hoshino, "Impact of artificial "gummy" fingers on fingerprint systems," in *Optical Security and Counterfeit Deterrence Techniques IV*, vol. 4677 of *Proceedings of SPIE*, pp. 275–289, San Jose, Calif, USA, January 2002.
33. T. Matsumoto, M. Hirabayashi, and K. Sato, "A vulnerability evaluation of iris matching (part 3)," in *Proceedings of the Symposium on Cryptography and Information Security (SCIS'04)*, pp. 701–706, Iwate, Japan, January 2004.
34. Kelly, Sean Dieter Tebje, Nagender Kumar Suryadevara, and Subhas Chandra Mukhopadhyay. "Towards the implementation of IoT for environmental condition monitoring in homes." *IEEE Sensors Journal* 13.10 (2013): 3846–3853.

Security Issues in Vehicular Ad Hoc Network: A Critical Survey

Mohammad Arif and Shish Ahmad

Abstract A vehicular ad hoc network or VANET is a new and advanced approach for communication between vehicles while running on the roads. This has drawn the attention of many researchers. VANET is very helpful in enhancing the safety of the vehicles, passengers and drivers, and the management of traffic using real-time traffic information. VANET is the advancement of MANET. The key distinction between VANET as well as MANET is that in VANET the topology is extremely vibrant due to fast movement of the motor vehicles. VANET network is also susceptible to attacks. One of the very important goals of design of VANET is to prevent the communication from malicious intentions and the security attacks and setting up trustworthy end-to-end connection and having proficient data transfer. In this paper, we firstly focused on security features, confrontations, and different types of possible assaults on VANET and then we threw light on different types of security techniques.

Keywords MANET · VANET · Attacks · Security · Trust · Threats

1 Introduction

VANETs are particular case of mobile ad hoc networks. In such scenarios, two types of communications are performed. One is infrastructure-based wireless communication and the other is ad hoc communication. Infrastructure-based communication is performed between on-board units (OBUs) of vehicles and road-side units (RSUs) as revealed in Fig. 1. The ad hoc communication performed among the vehicles, which is also called vehicle-to-vehicle (V2V) communication or “Inter-Vehicle Communication (IVC).” VANETs have many applications like

M. Arif (✉) · S. Ahmad

Department of Computer Science, Integral University, Lucknow, UP, India
e-mail: arif_mohd2k@yahoo.com

S. Ahmad

e-mail: shish_parv@rediffmail.com

© Springer Nature Singapore Pte Ltd. 2018

R. Singh et al. (eds.), *Intelligent Communication, Control and Devices*,
Advances in Intelligent Systems and Computing 624,
https://doi.org/10.1007/978-981-10-5903-2_53

527

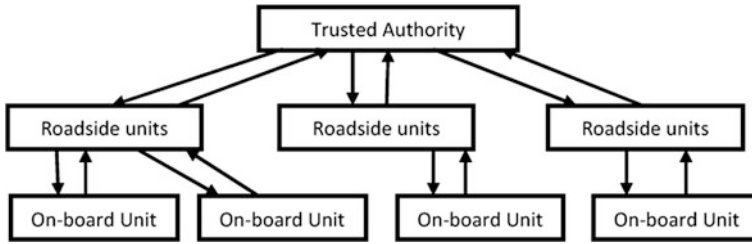


Fig. 1 VANET communication

traffic supervising, crash averting, advertisement, securing the roads from accidents, and safety of people on road. Unlike MANETs, VANETs have highly dynamic topology due to fast moving nodes on the road. VANETs have high possibility of network partitioning due to highly dynamic topology. One positive thing with VANET is that the nodes or vehicles have no constraint of battery power. VANETs show different characteristics on highways and inside city, as rate of change of topology is different on highways. “Wireless Access in Vehicular Environments (WAVEs)” are used at physical layer.

2 Security Requirements for VANETs

As VANET is comprised of wireless ad hoc network, there are some security requirements as follows [2, 3]:

- a. **Authentication and Integrity:** Authentication of data as well as sender is necessary. Data should be verified by all the vehicles. Sender authentication is also necessary to know about the genuineness of user. Integrity of data means that the receiver should receive the original data that was sent.
- b. **Confidentiality:** Confidentiality means that data should be kept confidential by the means of encryption. No data could be accessed by anyone from the channel.
- c. **Privacy and Anonymity:** Privacy means that sender’s identity should be kept private.
- d. **Access Control:** Data could only be accessed by authorized users.
- e. **Non-Repudiation:** If some one performs any action, he should not be able to deny that action.
- f. **Vehicle Traceability:** The capability to get the real identification of sending vehicles.
- g. **Scalability:** The capability of a VANET to acknowledge the varying size of network without any interruption or failure in data transportation or traffic management so that the performance is not degraded.
- h. **Availability:** The network should be available even in challenging conditions.

3 Challenges and Impact

The VANET has many challenges that can influence the security approaches to create secure network. Some of the challenges are as follows [15, 16]:

- a. **Network Volatility:** The transportation of data between nodes is momentary so the connection may be set up for a definite time period, and then it is finished due to the movement of vehicles.
- b. **Privacy:** The privacy of user is to be kept private. Also, privacy has to be set up for being definite of embracing that specific information by certified individual.
- c. **Time-Sensitive Applications:** Some time-sensitive applications which are very urgent should have small delay in reaching the destination. So, the routing technique should be opted in such a way that transmission delay is minimum.
- d. **Infrastructure:** In VANET, all the RSUs are connected to each other by a backbone, whereas the vehicles are connected to each other by ad hoc mode. So a trust rapport should be created among vehicles.

4 Types of Attacks

There are many attacks that can influence the performance of VANETs. Some of the attacks are due to insiders, and some are due to outsiders. Attacks are grouped as active attacks as well as passive attacks. Some of attacks are as follows:

- a. **Message Spoofing:** The masquerader sends false communication to other vehicles to misinform them and circulate wrong information.
- b. **Message Replay Attack:** The malevolent vehicle repeats sending earlier messages in order to choke the traffic.
- c. **Integrity Attack:** The malevolent vehicle can change in content of messages sent by genuine vehicles to misinform the other vehicles.
- d. **Impersonation Attack:** The malevolent vehicle states that it is a genuine vehicle to send false messages to some other vehicles.
- e. **Denial-of-Service (DoS) Attack:** The malevolent vehicle throws unrelated or petty messages to hold back large bandwidth of the channel and put away more resources of other nodes.

4.1 Nature of Attack

Some malevolent attacks cannot be sensed due to their environment. A malevolent node in VANET can satire itself like a lawful vehicle that other speaking vehicles cannot monitor, although these vehicles have accurate data about themselves. As a

result, some assault such as Sybil attacks cannot be sensed easily, and concerns should be recognized to construct a sturdy trust compromise depending on vibrant nature of VANETs.

4.2 Attack Target

The malevolent vehicles are powerfully proposed to attack a node when they can converse over long space. These nodes have more suppleness to send false messages and data for other vehicles at elongated distances. Hence, sensing such feature is tough than a local malevolent like man in the middle attacks.

4.3 Attack Impact

Impacts on vehicles also classify the attacks.

- a. If any vehicle is isolated and any malicious node is there near it, the attack can be undetected.
- b. If attack is detected but the information of vehicle is not sufficient, the attack will not be corrected. So the involved nodes will receive incorrect data.
- c. If vehicles are linked to some genuine node, the attack will be detected as well as corrected.

4.4 Classification of Attacks on Different Layers

- a. Threats in application layer: At application layer, the data of vehicle are dealt with. So vehicle information like position can be captured and misused. The malevolent code attacks and refutation attacks are the main attacks in the application layer [17].
- b. Threats in transport layer: The transport layer deals with authentication, securing process-to-process communication by encryption, delay handling, and packets loss. Some of the attacks at transport layer are denial-of-service attack, hijacking of session, acknowledge storm.
- c. Threats at network layer: Route maintenance is very tedious task in VANET due high speed vehicles and highly dynamic topology. The main objective is to set up a best possible and competent route such that broadcasting information can be widening effortlessly and swiftly to other vehicles [18].
- d. Threats at data link layer: The VANET is a point-to-point network. MAC layer is responsible to manage the medium access. The medium access is done either by distributed coordination function or by point coordination function. Data link layer is susceptible to DoS attack.

- e. Threats at physical layer: This layer is more susceptible to attacks. Some attacks on this layer are snooping. Some other attacks are interference and DoS. In VANET, radio signals can effortlessly be intercepted. Eavesdropping is the sensing and intercepting of communication. To overcome these threats, either “Direct Sequence Spread Spectrum (DSSS)” or “Frequency Hopping Spread Spectrum (FHSS)” is used.

5 Various Security Techniques

In past few years, a huge amount of research has been contributed to achieve a secure VANET. We have analyzed some of the techniques.

5.1 Identification Mechanism

In identification method a unique id number named “Vehicle Identification Number (VIN)” is assigned to each vehicle by the manufacturer. The concerned government department requires the registration number of the vehicle. In this system, vehicles will be visible and traceable [19].

5.2 Electronic Identification

Hubaux and Capkun in 2004 had proposed the electronic number plate. In this method, the identification included both the manufacturer id and the registration number. It helped in authenticating, maintaining the privacy, and tracing the vehicle more easily [20].

5.3 Pseudonymous Certificates

Trusted authority was responsible to issue such certificates. Raya, Papadimitratos, and Hubaux in 2006 have proposed to have a vehicular public key infrastructure (VPKI). There is a central certificate authority (CA) in each country and a delegate CA in each state. The delegate CA will assign the id to the vehicle and convey to central CA. If a vehicle crosses its state, it will also be traceable because central CA will broadcast the information of vehicle to all delegate CAs as shown in Fig. 2.

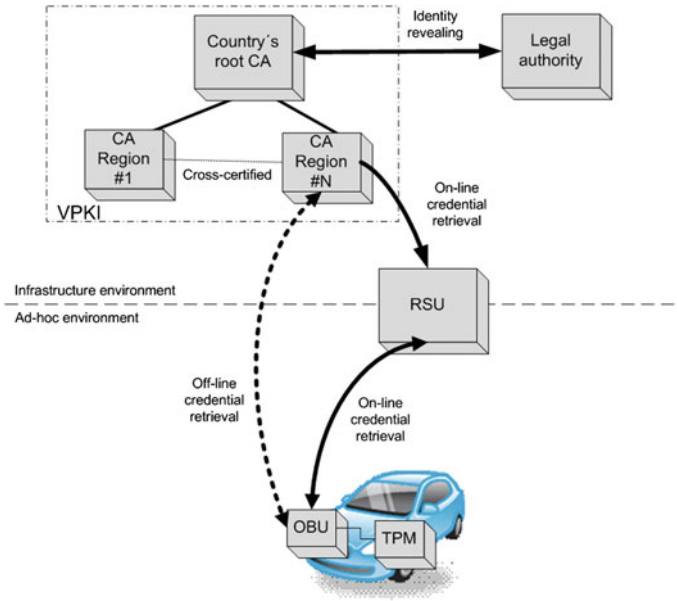


Fig. 2 Alternatives to retrieve vehicular credentials

5.4 Non-repudiation

Non-repudiation means to prevent any user to deny its action. “Non-Repudiation of Origin (NRO)” has vital role in VANETs. NROs are generally implemented by using digital signatures. The sender will have to sign before sending. The receiver will verify its signature using its public key. Signature verification is done in two steps. First is to check the signature. To check the signature, the received value and calculated hash value are compared. If both values are same, the entity is verified. Second is certification verification. It is necessary to know that certificate of sender is not obsolete [6].

5.5 Confidentiality

Confidentiality has very important role in V2V communication. Verma and Huang in 2009 had proposed that any vehicle entering within the range of any RSU will have to get itself registered with that RSU. After successful registration, the RSU will send the vehicle a short-lived public key. Hong, Huang, Gerla, and Cao in 2008 proposed to authenticate the vehicles using “Attribute-Based Encryption (ABE)” scheme. In this scheme, the private key is assigned to each vehicle and the public key will comprise of some attributes like type of vehicle and manufacturer’s name [12].

Table 1 Summary of different techniques for VANET security

S. No.	Authors	Title of Paper	Technique-Implemented	Attacks-covered in	Security-Dimensions
1	B. Dahill et al [20] (2002)	“A Secure Routing Protocol for Ad Hoc Networks”	Public and Private key distribution and certificate verification	DoS, and Replay Attack, False warning	Authentication, Message Integrity, non-repudiation
2	Priya Karunanithi, et al. [9] (2011)	“Efficient Distributed Group Authentication Protocol for VANET”	Signatures are assigned in groups. Also verified in groups	Spoofing and DoS	Authentication and privacy
3	Horng et al. [1] (2015)	“Enhancing Security and Privacy for Identity-based Batch Verification Scheme in VANET”	Signed messages are sent, Each vehicle is assigned unique Id.	Forgery and confidentiality attack	Message authentication, integrity, non-repudiation
4	Manish K Soni et al. [4] (2014)	“HAP: Hybrid Authentication for VANET”	Unique certificate is assigned along with group id	Sink hole attack	Authentication and reliability
5	Yiliang han, et al. [2] (2014)	“Aggregate syncryption based hybrid authentication for VANET”	Signatures are assigned in groups. Also verified in groups	Spoofing and DoS	Privacy, Authentication
6	Ghaleb, Fuad A., et al. [6] (2013)	“Security and privacy enhancement in vanets using mobility pattern”	Misconduct is detected using movement pattern	Disclosure, Masquerade attack	Privacy
7	Pouyan, et al. [3] (2014)	“Sybil Attack Detection In Vehicular Networks”	Traffic management and tracing the vehicles	Sybil attack	Privacy and authentication
8	Tong Zhou et. al. [8] (2011)	“P2DAP—Sybil Attacks Detection in VANET”	Eavesdropping by outsider node	Sybil attack	Privacy
9	X. Lin, et al. [11] (2007)	“GSIS: A secure and privacy-preserving protocol for vehicular communications”	Signatures are assigned in groups. Also verified in groups	Spoofing and DoS	Authentication and privacy
10	Adigun, et al. [5] (2013)	“Protocol of Change Pseudonyms for VANETs”	Public and Private key distribution	Authentication	Confidentiality and Non-repudiation

(continued)

Table 1 (continued)

S. No.	Authors	Title of Paper	Technique-Implemented	Attacks-covered in	Security-Dimensions
11	Y. C.Hu et al [14] (2002)	“Ariadne: A Secure On-Demand Routing Protocol for MANET”	Public and Private key distribution	DoS, and Replay Attack	Authentication
12	Catalin G et al. [10] (2010)	“Security protocol for vehicular distributed systems”	Digital Signature Algorithm is used	Spoofing and DoS	Integrity and non-repudiation
13	Alam, Nima, et al. [7] (2013)	“Relative positioning enhancement in VANETs”	Practical Vehicular progress in VANET	DoS	Privacy
14	Y. C. Hu et al [13] (2003)	“SEAD: Secure efficient DV routing for MANET”	Hash function is used one way	DoS	Availability
15	P. Papadimitra [12] (2003)	“Secure Data Transmission in MANET”	Authentication is done using MAC addresses.	Disclosure, Masquerade attack	Privacy and Authentication

5.6 Denial-of-Service and Availability

Suppose some nodes do not join in the routing and it burdens the medium with counterfeit requests, the network will not be able to arrive at the required performance. After verifying any sender by cryptographic values, the vehicle will do the plausibility checks. In his scheme, if a node A gets some message from a node B, then node A will act according to the previous information. Suppose node B is telling about jam but sensor of node A is not detecting any vehicle, then node A will not take B’s information seriously and trust of B will be reduced [10] (Table 1).

6 Conclusion

A lot of explorations in VANETs are enduring for a lot of years even then more are required. The present researches anticipated to face some explicit attacks. VANET is an ad hoc network with highly changing topology. It is susceptible to security threats as well. More research is required for securing the routing, management of keys and management of data inspection at various levels. In this review paper, we threw light on the requirements of security, its implications, different attacks at different layers, and various techniques to cope up the attacks.

References

1. Horng, S.; Tzeng, S.; Li, T.; Wang, X.; Huang, P.; Khan, M., 2015. Enhancing Security and Privacy for Identity-based Batch Verification Scheme in VANET, *IEEE Transactions on Vehicular Technology*, (2015).
2. Yiliang Han; Dingyi Fang; Zelun Yue; Jian Zhang, 2014. SCHAP: Aggregate syncryption based hybrid authentication protocol for VANET in *Springer international publishing Switzerland*, (2014).218–226.
3. Pouyan, Ali Akbar, and Mahdiyeh Alimohammadi. 2014. Sybil Attack Detection in Vehicular Networks In *Computer Science and Information Technology journal*, (2014). vol.2, no.4, pp. 197 –202.
4. Manish Kumar Soni and Ashish Vashistha. 2014. HAP: Hybrid Authentication Protocol for VANET in *IJCA Proceedings on NWNC (3):10–14*, (April 2014).
5. Adigun; Bensaber.;Biskri. 2013. Protocol of Change Pseudonyms for VANETs in *IEEE 38th Conference on LCN Workshops*, 2013.
6. Ghaleb, Fuad A., M. A. Razzaque, and Ismail Fauzi Isnin. 2013. Security and privacy enhancement in vanets using mobility pattern. In *IEEE Fifth International Conference on Ubiquitous and Future Networks (ICUFN)*, (2013).
7. Alam, Nima, A. T. Balaei, and A. G. Dempster. (2013). Relative positioning enhancement in VANETs: A tight integration approach. *IEEE Transactions on Intelligent Transportation Systems*, vol.14, no.1, (March 2013) 47, 55.
8. Tong Zhou; R.R Choudhury; Peng Ning; K Chakrabarty. 2011. P2DAP—Sybil Attacks Detection in VANET in *IEEE Journal on Selected Areas in Communications Volume:29*, Issue: 3 (2011).
9. Priya Karunanithi, Komathy Karuppanan. 2011. Efficient Distributed Group Authentication Protocol for Vehicular Ad Hoc Network In *Proceedings of International Conference, ACC 2011*, vol 192, (2011) 624–633.
10. Catalin Gosman, Ciprian Dobre, Valentin Cristea, 2010. A Security Protocol for Vehicular Distributed Systems, in 12th international conference on symbolic and numeric algorithms for scientific computing, *IEEE digital library* (2010).
11. X. Lin, X. Sun, P. H. Ho, and X. Shen, 2007. GSIS: A secure and privacy-preserving protocol for vehicular communications, *IEEE Transactions on Vehicular Technology*, vol. 56, no. 6, pp. 3442–3456, (2007).
12. P. Papadimitratos and Z. J. Haas, 2013. Secure Data Transmission in MANET, in *ACM Workshop on Wireless Security*, San Diego, CA, (Sept. 2003).
13. Y. C. Hu, D. B. Johnson and A. Perrig, 2003. SEAD: Secure efficient distance vector routing for MANETs, in *Elsevier B. V.* (2003) 175–192.
14. Y. C. Hu, A. Perrig and D. B. Johnson, 2002. Ariadne: A Secure On-Demand Routing Protocol for Ad Hoc Networks, *MobiCom’02*, (2002) 23–26.
15. Mohammad Arif, Tara Rani. “Enhanced Ant Colony based Routing in MANETs”. Published in the *Proceedings of 5th IEEE International Conference on Advanced Computing & Communication Technologies [ICACCT-2011]*. Pages: 48–54, Panipat, November 5, 2011. ISBN 81-87885-03-3.
16. Mohammad Arif, Tara Rani. ACO based Routing for MANETs. Published in *International Journal of Wireless & Mobile Networks*. April 2012, Volume 4. Number 2. ISSN: 0975-3834 [Online]; 0975-4679[Print]. Pages: 163–174.
17. Mohammad Arif and Khalid Imam Rahmani. Adaptive ARA (AARA) for MANETs. Published in *IEEE Xplore in the Proceedings of 3rd Nirma University International Conference on Engineering [NUICONE 2012]*, Ahmedabad, Gujarat, India, November 5, 2012. ISBN 978-1-4673-1720-7.
18. Mohammad Arif, Kavita Satija, Sachin Chaudhary, “ERBR: Enhanced and Improved Delay for Requirement Based Routing in Delay Tolerant Networks”. Published in the *Proceedings of*

NetCoM—2010, by SPRINGER, pages: 223–232, Chennai, December 27–29, 2010. ISSN: 978-3-642-17878-8_23.

19. Mohammad Arif, Abu Daud, “Adaptive Routing Techniques in Disruption Tolerant Networks”. Published in the Proceedings of the Second International Conference on Wireless & Mobile Networks (WiMoN—2010), by SPRINGER pages: 336–348, Chennai, July 23–25, 2010. ISSN: 978-3-642-14493-6_35.
20. Dahill, B.N. Levine, E. Royer and Clay Shields, A Secure Routing Protocol for Ad Hoc Networks, in Proceeding of IEEE ICNP (Nov. 2002), 78–87.

Impact of Buried Oxide Layer Thickness on the Performance Parameters of SOI FinFET at 22 nm Node Technology

Ravneet Kaur, Charu Madhu and Deepti Singh

Abstract In CMOS technology, as we decrease the gate length of MOSFET from μm to nm , its performance is effected due to increased short-channel effect (SCE) and leakage current (Xie et al. in *IEEE Trans Electron Devices* 59, 2012 [1]; Loan, Quresh, and Sundar Kumar Iyer in *IEEE Trans Electron Devices* 5, 2010 [2]). Multigate transistors like double gate, tri-gate transistors, FinFETs are proposed to reduce SCEs which finally result in improvement of current flowing through device (Agostinelli et al. in *IEEE Trans Very Large Scale Integr (VLSI) Syst* 5, 2010 [3]; Singha et al. in *Optimization of Underlap Length for DGMOSFET and FinFET*, 2015 [4]; Sahu et al. in *J Microelectron, Electr Compon Mater* 44(2), 2015 [5]). Buried oxide layer is introduced in the substrate of FinFET to decrease parasitic capacitance which is formed between source/drain region and substrate of FinFET (Sun et al. in *IEEE Trans Electron Devices* 58, 2011 [6]; Ponton in *IEEE Trans Circuits Syst* 56(5), 2009 [7]). Thus, the paper highlights the effect of variation in buried oxide layer thickness of SOI FinFET on electrical parameters like threshold voltage, drain-induced barrier lowering (DIBL), on current, off current, on/off current ratio. Various simulation results are shown in the research paper using TCAD software.

Keywords Silicon-on-insulator (SOI) · Short-channel effects (SCE) · Drain-induced barrier lowering (DIBL) · Fin-shaped field-effect transistor (FinFET)

1 Introduction

Downscaling in planar FETs is used to improve the performance, power, and current density with 22 nm process node [5]. As we decrease channel length of MOSFET, SCE like saturation velocity, hot carriers, surface scattering, etc., occurs in device [1]. Multigate transistors like double gate, tri-gate transistors, FinFET are

R. Kaur · C. Madhu (✉) · D. Singh
University Institute of Engineering and Technology, Panjab University, Chandigarh, India
e-mail: charu_uet@pu.ac.in

designed to reduce SCEs [3, 4]. FinFET has better control of channel as compared to MOSFET due to the presence of tri-gate in FinFET. There are two types of FinFET: SOI FinFET and bulk FinFET. FinFET built on bulk wafers is known as bulk FinFET, and FinFET built on silicon-on-insulator (SOI) wafers is known as SOI FinFET. Bulk FinFET has better heat transfer rate as compared to SOI FinFET [8]. Parasitic capacitance of FinFET has significant impact on circuit performance. The parasitic capacitance is defined as capacitance between the source/drain regions and substrate of the fin body, speed of the device also depends upon capacitances induced in the device [9]. However, bulk FinFET has more parasitic capacitance as compared to SOI FinFET [7, 9]. SOI FinFET has more drain current which flows from drain to source by applying specific threshold voltage as compared to bulk FinFET [10]. Short-channel effects are reduced in SOI FinFET as compared to bulk FinFET [11]. Off leakage current in SOI FinFET is also reduced as compared to bulk MOSFET [12]. Thus, research paper highlights the effect of variation in buried oxide layer thickness of SOI FinFET on various electrical parameters like threshold voltage, DIBL, on current (I_{on}), off current (I_{off}), I_{on}/I_{off} current ratio. Various simulations are shown in this research paper using TCAD software.

1.1 FinFET Device Structure

The bulk FinFET and SOI FinFET structures are designed by using visual technology computer-aided design (TCAD) software at 22 nm node technology. Due to the presence of parasitic capacitances in bulk FinFET which reduces the speed of device, SOI FinFET is frequently used [7, 9], and this research paper describes the variations in various electrical parameters by changing the buried oxide layer thickness (10, 50 nm) in SOI FinFET. The design parameters for SOI FinFET are described in the Table 1. The operating temperature of SOI FinFET is 300 K, and gate length of SOI FinFET is 22 nm [13, 14]. The physical model used in SOI FinFET is drift diffusion model to simulate the electrical characteristics [12]. SiO_2 acts as dielectric material in Gate oxide and buried oxide [14].

Table 1 Design parameters used in drawing SOI FinFET

S. No.	Parameters	SOI FinFET
1	Gate length	22 nm
2	Oxide thickness	1 nm
3	Buried oxide thickness	10 nm, 50 nm
4	S/D doping concentration	$1.0\text{e}+20$ (atoms cm^{-3})
5	Channel doping concentration	$1.0\text{e}+16$ (atoms cm^{-3})
6	Fin height (H_{fin})	20 nm
7	Fin width (W_{fin})	17 nm
8	Gate work function	4.45 eV

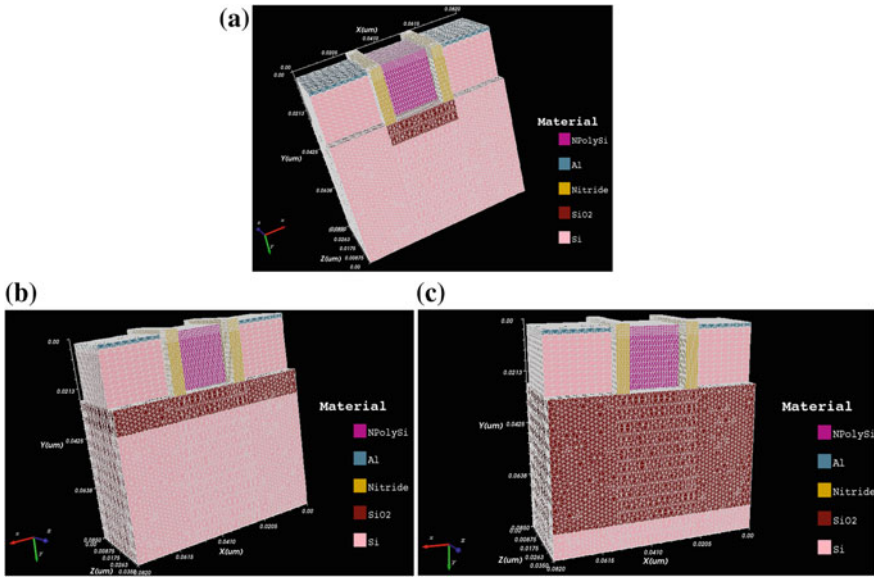


Fig. 1 a 3D view of bulk FinFET, b SOI FinFET having buried oxide thickness of 10 nm, c SOI FinFET having buried oxide thickness of 50 nm

Nitride (Si_3N_4) material is used as isolation material, S/D contact material used in SOI FinFET is aluminium, and gate material is poly silicon [15]. Donor doping concentration (N_d) of S/D in SOI FinFET and bulk FinFET is 1.0×10^{20} atoms cm^{-3} , and acceptor doping concentration (N_a) in channel of SOI FinFET is 1.0×10^{16} atoms cm^{-3} [8, 16] (Fig. 1).

2 Simulation Result and Discussion

Simulations are carried out for SOI FinFET by varying buried oxide layer thickness at 10 and 50 nm. Performance parameters such as threshold voltage, on current, off current, on/off current ratio, and SCE like DIBL are also discussed in this paper. Figure 2a demonstrates the effect of applied gate voltage on the drain current for SOI and bulk FinFET and Fig. 2b demonstrates the V-I curve for different buried oxide layer thickness 10, 50 nm.

Figure 2a demonstrates the drain current of SOI FinFET is more than drain current of bulk FinFET [10]. Comparing with SOI FinFET, off leakage current is higher in bulk FinFET [12].

Heat produced in SOI FinFETs is not transferred to the substrate due to the presence of buried oxide layer in the substrate of device [8]. Since the heat transfer rate from channel to substrate varies by varying buried oxide layer thickness;

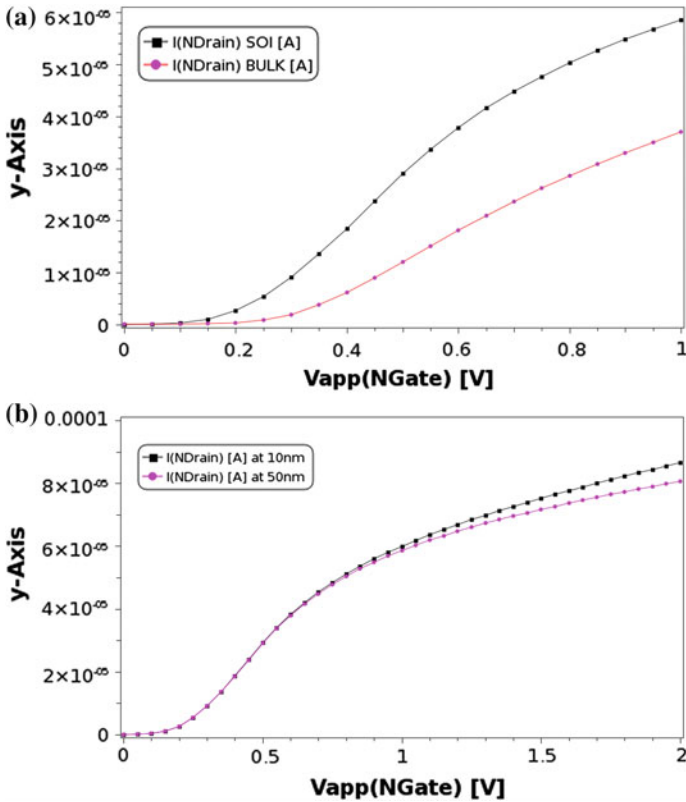


Fig. 2 a $I(\text{NDrain})$ as function of $V_{\text{app}}(\text{NGate})$ in SOI and bulk FinFET at drain voltage of 0.1 V showing that drain current in SOI FinFET is larger than bulk FinFET at work function = 4.45 eV, **b** $I(\text{NDrain})$ as function of $V_{\text{app}}(\text{NGate})$ for buried oxide layer thickness at 10, 50 nm of SOI FinFET and work function = 4.45 eV

Fig. 2b demonstrates SOI FinFET having buried oxide layer thickness 10 nm transfers the heat from channel to substrate which causes unwanted increase in the parasitic capacitance and device temperature also decreases which result in reduction of reverse saturation current and increase in drain current of SOI FinFET. SOI FinFET having buried oxide layer thickness 50 nm results in poor heat transfer rate from channel to substrate. The device temperature becomes larger and carrier mobility decreases with increase in device temperature, and the off current leakages increases with increase in device temperature and drain current decreases [8, 17].

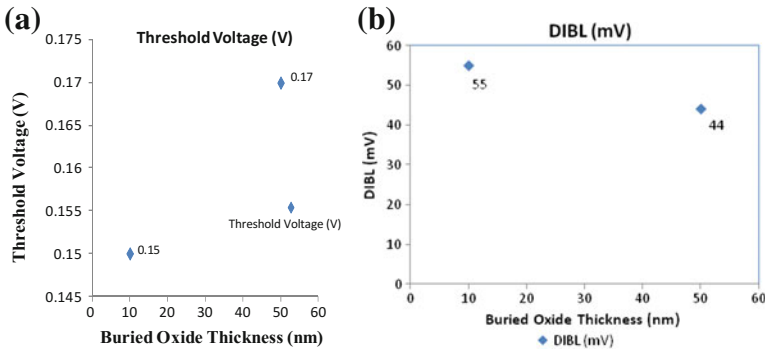


Fig. 3 **a** threshold voltage as function of buried oxide layer thickness of SOI FinFET at work function 4.45 eV, **b** DIBL as function of buried oxide layer thickness and results are taken at $V_{dd} = 0.1$ and 1 V, work function 4.45 eV

2.1 Threshold Voltage and DIBL as a Function of Buried Oxide Layer Thickness

Figure 3a, b demonstrates the variation in threshold voltage and DIBL of SOI FinFET with increase in buried oxide layer thickness. Threshold voltage defined as minimum gate to source voltage when transistor starts conducting from source to drain and minimum current starts flowing from drain to source through channel [18].

We observe that threshold voltage goes on increasing with increase in buried oxide layer thickness of SOI FinFET, and these results were taken at work function = 4.45 eV. DIBL is short-channel effect of MOSFET in which threshold voltage depends upon drain voltage, and threshold voltage reduces with increase in drain voltages and calculation of DIBL is done by using threshold voltage in linear and saturation region [19, 20]. The variation of DIBL decreases with increases buried oxide layer thickness from 10 to 50 nm.

2.2 Effect of Buried Oxide Layer Thickness on I_{on}/I_{off} Current Ratio of the Device

On current and off current of SOI FinFET as a function of buried oxide layer thickness are illustrated in Fig. 4a, b, respectively. On current is drain current which flows through channel when gate to source voltage goes from weak to strong inversion. Off current is the current which flows through channel when device is in off state [18]. It is observed that, on current decreases with increase in buried oxide layer thickness of SOI FinFET due to reduction in heat transfer rate at buried oxide thickness 50 nm as compared to buried oxide thickness 10 nm [8].

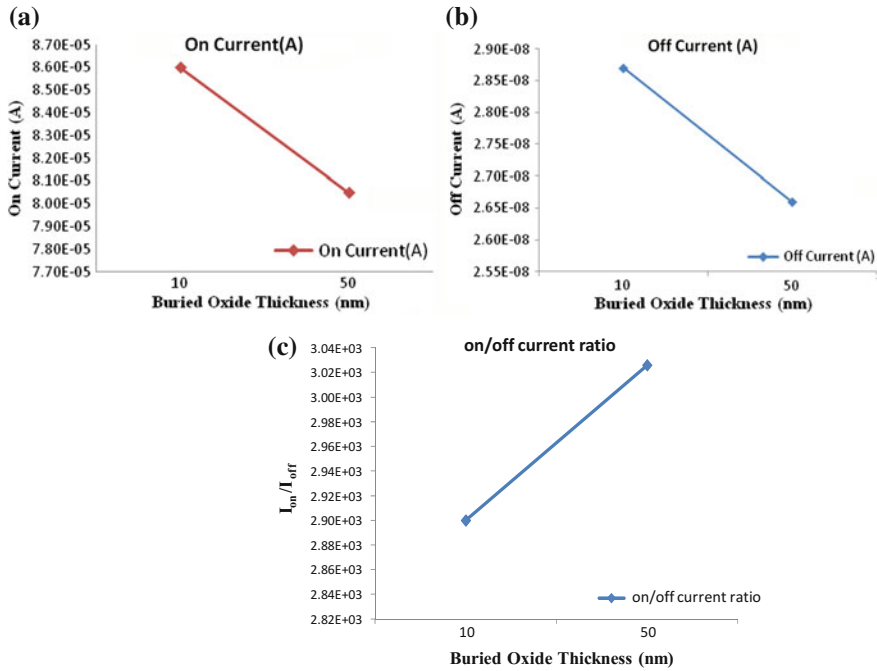


Fig. 4 **a** On current as function of buried oxide layer thickness of SOI FinFET and results are taken at $V_{dd} = 0.1$ V and work function = 4.45 eV, **b** off current as function of buried oxide layer thickness of SOI FinFET and results are taken at $V_{dd} = 0.1$ V and work function = 4.45 eV, **c** I_{on}/I_{off} current ratio as function of buried oxide layer thickness of SOI FinFET and results are taken at $V_{dd} = 0.1$ V and work function = 4.45 eV

The off current is also observed to decrease with increase in buried oxide layer thickness of SOI FinFET. These I_{off} and I_{on} current simulations are performed for $V_{dd} = 0.1$ V and work function 4.45 eV. It is also observed that as the buried oxide layer thickness of SOI FinFET is increased, I_{on}/I_{off} ratio also gets increased.

3 Conclusion

The effect on parameters like threshold voltage, on current, off current and DIBL was studied for buried oxide layer thickness 10, 50 nm of SOI FinFET. Threshold voltage which has to be low is achieved at buried oxide layer thickness 10 nm of SOI FinFET. Simulation was carried out using TCAD software. DIBL which has to be low for good performance is achieved at buried oxide layer thickness 50 nm of SOI FinFET. I_{on}/I_{off} ratio must be high for good performance which is achieved at buried oxide layer thickness 50 nm. In this research paper, channel length of device is 22 nm and it can also be changed according to the requirements.

References

1. Qian Xie, Jun Xu, and Yuan Taur "Review and Critique of Analytic Models of MOSFET Short-Channel Effects in Subthreshold" IEEE TRANSACTIONS ON ELECTRON DEVICES, VOL. 59, JUNE 2012.
2. Sajad A. Loan, S. Quresh, and S. Sundar Kumar Iyer, "A Novel Partial-Ground-Plane-Based MOSFET on Selective Buried Oxide: 2-D Simulation Study" IEEE TRANSACTIONS ON ELECTRON DEVICES, VOL. 5, MARCH 2010.
3. Matteo Agostinelli, Massimo Alioto, David Esseni and Luca Selmi, "Leakage-Delay Tradeoff in FinFET Logic Circuits: A Comparative Analysis With Bulk Technology" IEEE TRANSACTIONS ON VERY LARGE SCALE INTEGRATION (VLSI) SYSTEMS, VOL. 18, FEBRUARY 2010.
4. D. Singha, K. P Pradhana, S. K. Mohapatra, P. K. Saha "Optimization of Underlap Length for DG MOSFET and FinFET" 3rd International Conference on Recent Trends in Computing 2015 (ICRTC-2015).
5. P. K. Sahu, S. K. Mohapatra, K. P. Pradhan "Impact of Downscaling on Analog/RF Performance of sub-100 nm GS-DG MOSFET" Journal of Microelectronics, Electronic Components and Materials, Vol. 44, No. 2, 2014.
6. Xin Sun, Victor Moroz, Nattapol Damrongplisit, Changhwan Shin and Tsu-Jae King Liu "Variation Study of the Planar Ground-Plane Bulk MOSFET, SOI FinFET, and Trigate Bulk MOSFET Designs" IEEE TRANSACTIONS ON ELECTRON DEVICES, VOL. 58, NO. 10, OCTOBER 2011.
7. Davide Ponton, Pierpaolo Palestri, David Esseni, Luca Selmi, Marc Tiebout, Bertrand Parvais, Domagoj Šiprak, and Gerhard Knoblinger, "Design of Ultra-Wideband Low-Noise Amplifiers in 45 nm CMOS Technology: Comparison Between Planar Bulk and SOI FinFET Devices" IEEE Transaction on Circuits and System, Vol. no. 56, No. 5, May 2009.
8. Jong-Ho Lee "Bulk FinFETs: Design at 14 nm Node and Key Characteristics" Springer Science, Nano Devices and Circuit Techniques for Low-Energy Applications and Energy Harvesting, Springer science + business media 2016.
9. T. Chiarella, L. Witters, A. Mercha, C. Kemer, R. Ditttrich], M. Rakowski, C. Ortolland, L.-A. Ragnarsson, B. Parvais, A. De Keersgieter, S. Kubicek, A. Redolfi, R. Rooyackers, C. Vrancken, S. Brus, A. Lauwers, P. Absil, S. Biesemans and T. Hoffmann "Migrating from Planar to FinFET for Further CMOS Scaling: SOI or Bulk?", Proceedings of the European Solid State Device Research Conference, 2009.
10. Mirko Poljak, Vladimir Jovanović, Tomislav Suligoj "SOI vs. Bulk FinFET: Body Doping and Corner Effects Influence on Device Characteristics" Electrotechnical conference, IEEE Transaction of Electronic Devices, 2008.
11. S. Krivec, H. Prgić, M. Poljak and T. Suligoj "Comparison of RF performance between 20 nm-gate bulk and SOI FinFET" 37th International Convention on Information and Communication Technology, Electronics and Microelectronics (MIPRO), 2014.
12. Anterpreet Gill, Charu Madhu, Pardeep Kaur "Investigation of short channel effects in Bulk MOSFET and SOI FinFET at 20 nm node technology" IEEE INDICON 2015.
13. Takashi Matsukawa, Yongxun Liu, Shin-Ichi O'uchi, Kazuhiko Endo, Junichi Tsukada, Hiromi Yamauchi, Yuki Ishikawa, Hiroyuki Ota, Shinji Migita, Yukinori Morita, Wataru Mizubayashi, Kunihiko Sakamoto, and Meishoku Masahara, "Decomposition of On-Current Variability of nMOS FinFETs for Prediction Beyond 20 nm" IEEE TRANSACTIONS ON ELECTRON DEVICES, VOL. 59, NO. 8, AUGUST 2012.
14. Ulayil Sajesh Kumar and Valipe Ramgopal Rao, "A Thermal-Aware Device Design Considerations for Nanoscale SOI and Bulk FinFETs" IEEE TRANSACTIONS ON ELECTRON DEVICES, VOL. 63, NO. 1, JANUARY 2016.
15. Raghvendra Sahai Saxena and M. Jagadesh Kumar "Polysilicon Spacer Gate Technique to Reduce Gate Charge of a Trench Power MOSFET" IEEE TRANSACTIONS ON ELECTRON DEVICES, VOL. 59, NO. 3, MARCH 2012.

16. Farshad Moradi, Sumeet Kumar Gupta, Georgios Panagopoulos, Dag T. Wisland, Hamid Mahmoodi, and Kaushik Roy, "Asymmetrically Doped FinFETs for Low-Power Robust SRAMs" IEEE TRANSACTIONS ON ELECTRON DEVICES, VOL. 58, NO. 12, DECEMBER 2011.
17. Zhe Xu, Jinyan Wang, Yong Cai, Jingqian Liu, Zhen Yang, Xiaoping Li, Maojun Wang, Zhenchuang Yang, Bin Xie, Min Yu, Wengang Wu, Xiaohua Ma, Jincheng Zhang and "300 °C operation of normally-off AlGaIn/GaN MOSFET with low leakage current and high on/off current ratio" Electronics Letters, Volume: 50, IEEE, February 2014.
18. Vishal Narula, Charu Narula, Jatinder singh "Investigating Short Channel Effects and Performance Parameters of Double Gate Junctionless Transistor at Various Technology Nodes" International Conferences on Recent Advances in Engineering & Computational sciences (RAECS), December 2015.
19. Mahender Veshala, Ramchander Jatooth, Kota Rajesh Reddy, "Reduction of Short-Channel Effects in FinFET" International Journal of Engineering and Innovative Technology (IJEIT), Volume 2, Issue 9, March 2013.
20. Anurag Chaudhry and M. Jagadesh Kumar, "Controlling Short-channel Effects in Deep Submicron SOI MOSFETs for Improved Reliability: A Review", IEEE Trans. on Device and Materials Reliability, Vol.4, pp. 99–109, March 2004.

Line-Based Successive Cancellation Decoder with Reduced Complexity

G.M.G. Madhuri, B. Praveen Kittu and N. Prasanthi Kumari

Abstract The error-correcting codes which achieve Shannon's channel capacity are polar codes for infinite length. In this, we propose an efficient implementation for SC polar decoders with $O(\log_2 N)$ processing elements, where N is code block length. Here, SC decoding processing unit is implemented in logarithmic domain, thereby reducing the multiplication and division operations and low-complex partial sum logic. This decoder architecture has a low dispensation density that allows large polar codes to put into practice. Simulation is done using Xilinx, and simulation results are presented.

Keywords Successive cancellation decoder · VLSI · Polar codes
Partial sum logic

1 Introduction

Polar codes achieve Shannon's Channel capacity as the length leads to infinity and also have good error-correcting capability. The complexity of polar codes is $O(N \log_2 N)$ where N is the code length. Polar codes [1] have a particular and proficient encoding and decoding techniques. There are various decoding algorithm, successive cancellation (SC) decoding algorithm is of reduced complexity than other decoding algorithms.

In simplified successive cancellation (SSC) decoder [2], groups of frozen bits do not need to be explicitly decoded, since their values are already known (usually

G.M.G. Madhuri (✉) · B. Praveen Kittu
PSCMR College of Engineering and Technology, Vijayawada, India
e-mail: gmgmadhuri@gmail.com

B. Praveen Kittu
e-mail: praveenkittu17@gmail.com

N.P. Kumari
College of Engineering Studies, University of Petroleum and Energy Studies,
Dehradun, India

zero), and groups of information bits can be estimated by serial successive cancellation. SC algorithm in natural logarithm of likelihood proportion can be observed as sum-product algorithm which requires less number of calculations. In this paper, an improvement is made in the partial sum logic by using the DFFs and matrix generation block.

Section 2 explains about polar code encoding and decoding process in short. Section 3 explains the proposed SC decoder architecture. Finally, the simulation results and conclusion are presented in Sect. 4.

2 Polar Code Construction

Consider $W : X \rightarrow \hat{X}$ as a binary discrete memory-less channel (B-DMC). Let X be input where $X \in \{0, 1\}$, \hat{X} be the output, and conversion probabilities are $W\left(\frac{\hat{x}}{x}\right), \hat{x} \in \hat{X}, x \in X[1]$. The measure of capacity and rate of the channel W is represented by symmetric channel capacity $I(W)$ and Bhattacharya parameter $Z(w)$, where

$$I(W) = \sum_{\hat{x} \in \hat{X}} \sum_{x \in X} \frac{1}{2} W\left(\frac{\hat{x}}{x}\right) \log \frac{W\left(\frac{\hat{x}}{x}\right)}{\frac{1}{2W\left(\frac{\hat{x}}{0}\right)} + \frac{1}{2W\left(\frac{\hat{x}}{1}\right)}}$$

$$Z(W) \triangleq \sum_{x \in X} \sqrt{W\left(\frac{\hat{x}}{0}\right) W\left(\frac{\hat{x}}{1}\right)}$$

Some channels reach capacity $I(W)$ to 1, and some channel’s capacity reaches to 0. This type of polarization is used for polar codes.

Encoding of polar codes uses simple linear mapping for length- N -polar encoder; the generator matrix $G_N^{\otimes N}$ is defined as

$$G_N^{\otimes N} = B_N F^N$$

When $N = 2^n, 0 < n < \log_2 N$, as $N \geq 1, B_N F^{\otimes N}$ is a bit-reversal matrix and F^N is N th Kronecker power of the matrix.

$$F^{\otimes 1} = \begin{bmatrix} 1 & 0 \\ 1 & 1 \end{bmatrix}$$

$$F^{\otimes 2} = \begin{bmatrix} F^{\otimes 1} & 0 \\ F^{\otimes 1} & F^{\otimes 1} \end{bmatrix} = \begin{bmatrix} 1 & 0 & 0 & 0 \\ 1 & 1 & 0 & 0 \\ 1 & 0 & 1 & 0 \\ 1 & 1 & 1 & 1 \end{bmatrix}$$

A polar encoder has input u_1^N which is linear mapping to an output vector x_1^N , where $x_1^N = u_1^N G_N^{\otimes N}$ is sent over the channel.

2.1 SC Decoding

Polar SC decoder decodes the received code word \hat{x}_1^N at B-DMC, $W^N : X^N \rightarrow \hat{X}^N$, as \hat{u}_1^N . The decoder performs decoding by calculating intermediate values using information from channel likelihood. Received code word is denoted as llr . In [3] SC decoder computes \hat{u}_1^N hard decisions in a successive order from \hat{u}_1^1 to \hat{u}_1^N . The likelihood ratio of \hat{x} can be used to estimate \hat{u} with recursive procedure, and each decoded bit \hat{u}_1^N is obtained from decision function D as

$$\hat{u}_1^N = D(\text{LR}(\hat{x}, \hat{u}_1^{i-1}))$$

where $D(\text{LR}(\hat{x}, \hat{u}_1^{i-1})) = 1$, if $\text{LR}(\hat{x}, \hat{u}_1^{i-1}) < 1$ and i is not frozen bit, otherwise $\text{LR}(\hat{x}, \hat{u}_1^{i-1}) = 0$.

Depending on LR values of \hat{x} , processing element f and g are used to compute $\text{LR}(\hat{x}, \hat{u}_1^{i-1})$.

$$f = \frac{1 + ab}{a + b}, g = a^{1-2\hat{u}}b,$$

where a and b are LR values.

SC polar decoder carries complex divisions and multiplications which is not apt for hardware execution. In order to trim down the complexity, elements f and g are defined in log likelihood ratio (llr) domain in simplified SC decoding [4] as

$$\begin{aligned} f(l_a, l_b) &= 2 \tan h^{-1}(\tan h(\frac{l_a}{2}) \tan h(\frac{l_b}{2})) \\ g(l_a, l_b) &= l_a(-1)^{\hat{u}} + l_b \end{aligned}$$

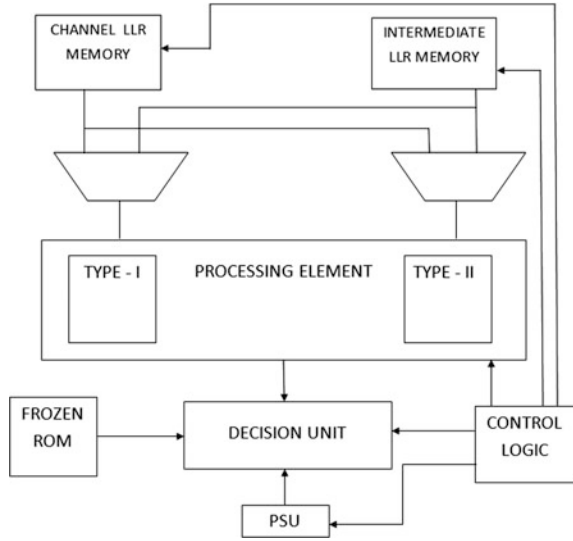
where l_a and l_b are llr values. This has hyperbolic functions. So we modified the f and g nodes using min-sum algorithm in our implementation [2].

3 Implementation

In this section, implementation of SC decoding algorithm is explained. The block diagram of the algorithm is shown in Fig. 1.

The main components of SC decoder are processing unit (PU), decision unit, partial sum logic, control unit and memory elements. PU calculates the intermediate llr values using the functions f and g .

Fig. 1 Block diagram of SC decoding algorithm



Processing unit: It consists of two types of processing elements (PE). Type I PE pre-computes two possible outputs for both adding and subtracting the operands together. Type I PE has an adder–subtractor architecture with q -bit quantization. Type II PE makes use of the min-sum algorithm. Figure 2 shows the architecture of PU.

Decision unit: The decision unit function is based on intermediate llr representation. The decision scheme depends on whether they are frozen or not. The frozen indices are pre-determined prior the transmission. Two bits frozen 1 and frozen 2 are defined such that frozen 1 is 1 when \hat{u}_{2i-1} is frozen, otherwise zero and frozen 2 is 1 when \hat{u}_{2i} is frozen, otherwise zero (Fig. 3).

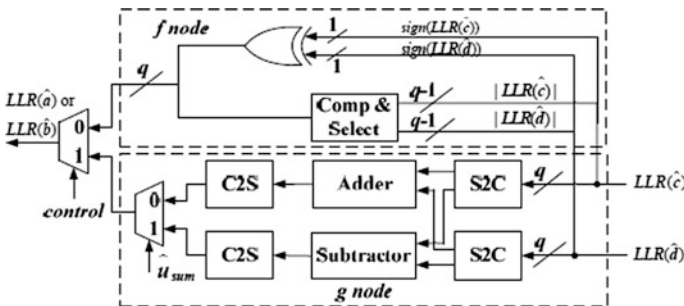


Fig. 2 Architecture of processing unit

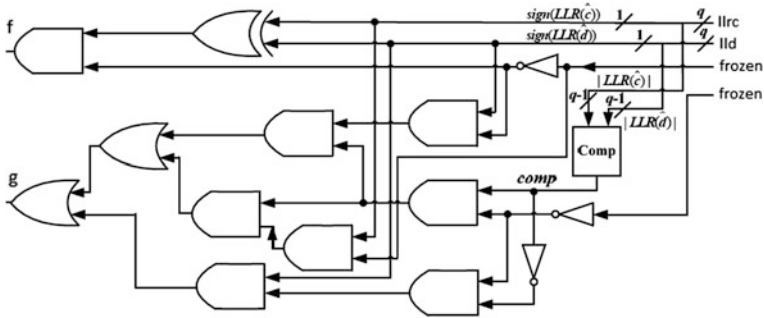


Fig. 3 Architecture of the decision unit

Boolean expression of \hat{u}_{2i-1} and \hat{u}_{2i} is derived as

$$\hat{u}_{2i-1} = \overline{\text{frozen}} 1 (\text{sign}(\text{llr}(\hat{c})) \oplus \text{sign}(\text{llr}(\hat{d})))$$

$$\hat{u}_{2i} = (\overline{\text{comp}} \overline{\text{forzen}} 2 \text{sign}(\text{llr}(\hat{d})) + \overline{\text{comp}} \overline{\text{forzen}} 1 \overline{\text{forzen}} 2 \text{sign}(\text{llr}(\hat{d})))$$

$$+ \text{comp} \overline{\text{forzen}} 1 \overline{\text{comp}} \overline{\text{forzen}} 2 \text{sign}(\text{llr}(\hat{c}))$$

where comp is the comparison result of $\text{llr}(\hat{c})$ and $\text{llr}(\hat{d})$. $\text{comp} = 1$ if $|\text{llr}(\hat{c})| > |\text{llr}(\hat{d})|$, otherwise 0 (Fig. 4).

Partial Sum Logic: Partial sum logic evaluates the partial sums which are required by PEs to calculate the function implemented by type I PEs. After decoding the bit \hat{u}_i , $0 \leq i < N/2$, PSL updates partial sum by “XOR” ing their values with \hat{u}_i . All the remaining partial sums maintain their present values. The partial sum does not have a regular structure to be stored as words in RAM. So $N/2$ -bit register is used to store the partial sum.

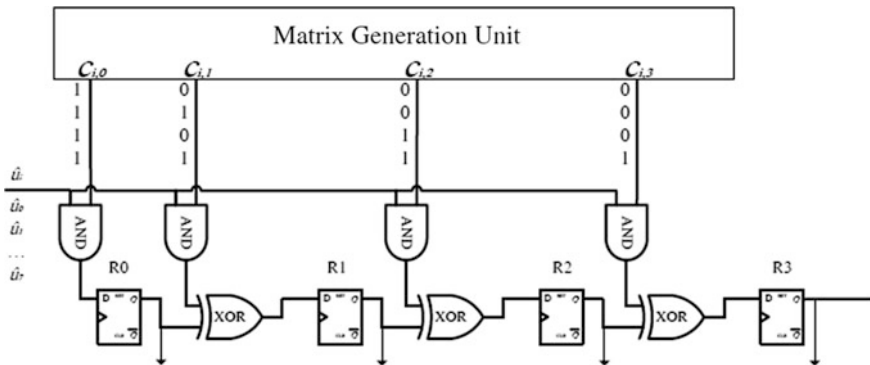


Fig. 4 Architecture of PSL

In this PSL architecture, if the control bit $C_{i,j} = 1$, the input to each DFF R_j is the value of R_{j-1} , which is EX-XORed with the current decoded bit \hat{u}_i . The partial sum is calculated for code length N as:

$$R_0 = \hat{u}_i \text{ and } C_{i,0}$$

$$R_j = R_{j-1} \text{ xor } (\hat{u}_i \text{ and } C_{i,j}) \quad \text{if } j > 0$$

All the partial sums for the PE are generated by the same DFF in this structure. The PSL can be a part of line SC decoder by connecting $N/2$ PEs to same DFF without the need for extra routing of partial sums to PEs.

The control matrix is represented as $C = \begin{matrix} j^{\otimes n-1} \\ j^{\otimes n-1} \end{matrix}$ whose element $C_{i,j}$ is the j th control bit generated at step i . The matrix $j^{\otimes n-1}$ is generated using linear feedback shift register (LFSR). The matrix generation unit produces the rows of C sequentially. LFSR of size $N/2$ is used to produce this sequence; i th row of C is given by

$$C_{i,0} = 1 \quad 0 \leq i \leq N - 1$$

$$C_{i+1,j} = C_{i,j-1} \text{ xor } C_{i,j} \quad 0 \leq i \leq N - 1, 0 \leq j \leq \frac{N}{2} - 1$$

Controller: The controller module facilitates the different stages in the decoding process. It generates distinctive control signals like the current decoded bit \hat{u}_i , the present stage j . It controls a multiplexer which chooses the channel llr memory as the input during the input stage, and during the decoding, the outputs of the PEs are stored in intermediate llr memory. Controller generates the select lines for the multiplexer to choose channel llr memory or intermediate llr memory.

4 Simulation Results



Fig. 5 Simulation results of PE

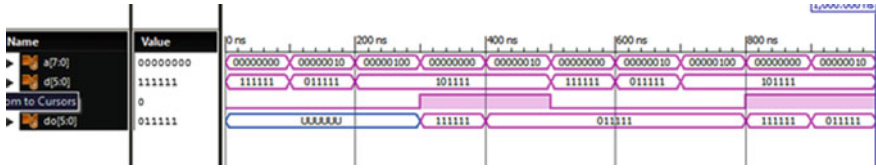


Fig. 6 Simulation results of *llr* memory



Fig. 7 Simulation results of decision unit

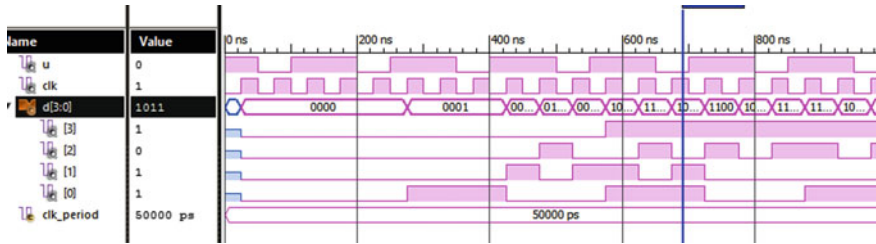


Fig. 8 Simulation results of partial sum logic

5 Conclusion

In this paper, architecture for SC is proposed for decoding of polar codes. Simulation results of PE, memory, decision unit, partial sum logic are presented. The performance of decoder is improved by reducing number of PEs with which the complexity is reduced. Future work will focus on reducing the critical path delay due to control logic and decision unit.

References

1. C. Leroux, A. J. Raymond, G. Sarkis, and W. J. Gross, "A semi-parallel successive-cancellation decoder for polar codes," *IEEE Trans. Signal Process.*, vol. 61, no. 2, pp. 289–299, January 2013.
2. A-Y Amin, and R.K. Frank, "A simplified successive cancellation decoder for polar codes," *IEEE Commun. Lett.*, vol.15, no.12, pp. 1378–1380, December 2011.
3. Boyaun, "Polar Codes", Ph.D. dissertation, University of Minnesota.
4. E. Arıkan, "Channel polarization: A method for constructing capacity achieving codes for symmetric binary-input memoryless channels," *IEEE Trans. Inform. Theory*, vol. 55, no. 7, pp. 3051–3073, July 2009.
5. C. Zhang, B. Yuan, and K. K. Parhi, "Reduced-latency SC polar decoder architectures," in *Proc. Int. Conf. Commun.*, pp. 3471–3475, June 2012.

Metal Artefact Reduction from Dental CBCT Image Using Morphology and Fuzzy Logic

Anita Thakur, Vishu Pargain, Pratul Singh, Shekhar Raj Chauhan, P.K. Khare and Prashant Mor

Abstract Cone beam computed tomography (CBCT) is a new-generation 3D image modality which is highly used in dentistry. As CBCT is a low-radiation imaging technique, reconstruction of image is prone to artefacts. Artefacts are the discrepancies between the original physical image and the mathematical modelling image process. In dental treatment, mostly metallic filling is done which produces metal artefact in imaging, in which it produces the reflection effect on imaging that misleads the diagnosis of treatment. In this paper, the proposed method reduces the reflection effect of metal artefacts and enhances the contrast of CBCT image. Here the proposed technique used morphological approach for reflection reduction, and fuzzy enhancement is used for contrast improvement. The output image has been analysed and evaluated using structure of similarity index matrix (SSIM) and peak value ratio in terms of signal versus noise (PSNR). Visual perception also shows the performance of the proposed work.

Keywords Metal artefact · Beam hardening · Morphology · Fuzzy contrast enhancement

A. Thakur (✉) · V. Pargain · P. Singh · S.R. Chauhan
Department of Electronics and Communication Engineering, Amity University, Noida,
Uttar Pradesh 201303, India
e-mail: athakur@amity.edu

V. Pargain
e-mail: vishupargain@gmail.com

P. Singh
e-mail: pratul.ujjain@gmail.co

S.R. Chauhan
e-mail: shekhar9dec@gmail.com

P.K. Khare · P. Mor
Electronic Department, RDVV, Jabalpur, India

1 Introduction

New-generation imaging technology in health monitoring system requires precision in terms of visual with low-radiation dose. These requirements are essential for head and neck span imaging diagnosis. So cone beam CT (CBCT) scanning has appeared to be a promising technique [1, 2]. Despite all, it is prone to be affected by artefact and low contrast in image which degraded the overall image quality. The main reason of this default is low radiation dose of X-ray. Artefact is the unwanted structure change in the original image due to external factor or imaging system default. The artefact can be classified into different types including metal artefact, streak artefact, ring artefact, cupping artefact, scatter artefact, and motion artefact. [3, 4].

Mostly in dental implantation, implant filling materials are of high density like amalgam, gold alloy, co-chrome, and silver alloy which produces reflection effect at imaging system. So, in craniofacial region imaging faces the challenge in terms of artefact-free CBCT/CT image. Because it is not like that every time patient may remove the metal filling and go for CT imaging. Metal artefact is originated in different forms like beam hardening, exponential edge gradient effect (EEGE), nonlinear partial volume effect and scattering [5]. In beam hardening, at the time of acquisition of the projection data, the attenuation of the photon energies occurred which produces the artefact around the metals. Exponential edge gradient effect occurred due to high contrast difference in neighbourhood structure. At the time of beam penetration, many photons are deviated from original path which are scattered that causes the scatter artefact.

Many research papers listed the metal artefact solution in terms of qualitative and quantitative methods. One of the common iterative reconstruction methods is used for reduction of metal artefact [6, 7], in which it requires accurate generation and attenuation of X-ray. Reconstruction is in repeated manner, so it is slow method. Other method is energy decomposition, in which they consider the different material energy attenuation for that required two or more X-ray energy sources [8, 9]. Most practical approach is sinogram in-painting method in which metal traces are detected in projection [10, 11], where threshold and interpolation approaches are used. This method is fast but accurate data estimation is still a challenge. So there is still a possibility to find the best solution for metal artefact reduction and contrast enhancement of CBCT dental images.

The proposed method is based on morphology approach for metal artefact reduction, and for contrast enhancement fuzzy approach is used. Most of this paper used the threshold segmentation-based and inpainting sinogram for metal artefact reduction. Here the proposed method uses the dilation method to abstract out the region of interested and with roll filling method unwanted reflection is filled as background.

The organization of paper is as follows: Sect. 2 described the proposed algorithm for metal artefact reduction with contrast enhancement. Section 3 shows the results with discussion and Sect. 4 comprises the conclusion.

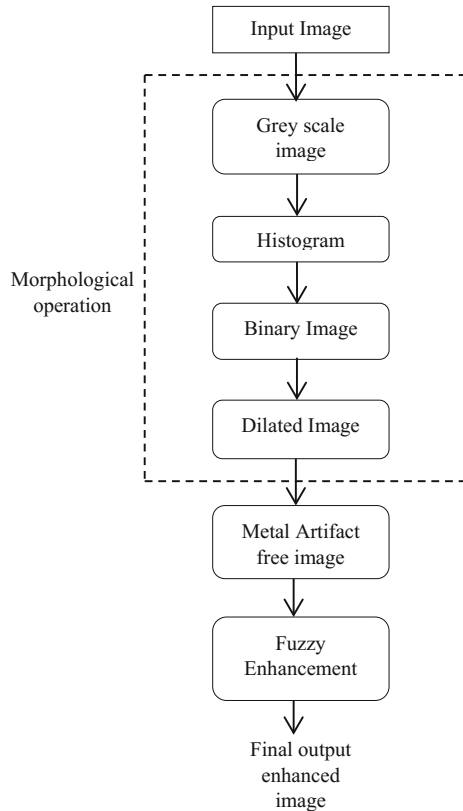
2 Proposed Method

In dental implantation, metal filling is the common method for treatment. Due to this, X-ray photons are scattered and attenuated from the path which produces metal artefact and low contrast in reconstructed images. The proposed method uses two approaches for solving these issues: first is morphological approach to reduce the reflection effect of metal in CBCT image, and other is the fuzzy-based contrast enhancement approach to get best visual image. Figure 1 shows the proposed method’s block diagram for metal reflection artefact reduction with contrast enhancement.

2.1 Morphology Approach to Metal Artefact Reduction

Morphology is nonlinear local operator-based efficient tool in image processing. Most of the researcher used morphology operation for filtering and segmentation application [12]. Feature extraction work is not so common with morphology. In the proposed

Fig. 1 Block diagram for metal reflection artefact reduction with contrast enhancement



method, we used the morphology dilation operation to extract the main feature of dental anatomy. Reflection of the metal filling in background image is filled with corresponding gray level without hiding the important information from the CBCT image. In morphology, dilation is a dynamic operator which is nonlinear supreme filter that considers the centre point and near neighbourhood pixel grid in image extraction.

In the proposed work, the original metal artefact image is first converted into grayscale image. Using histogram method, the histogram of the image is found. After that, specific region is extracted with the help of binary image thresholding method. Then with dilation of structuring element, the brightness of the extracted image will be generated. Small, dark, and reflected region is ‘fill in’ with surrounding similar intensity pixel. That will reduce the reflection of metal in image.

2.2 Fuzzy Approach for Contrast Enhancement

Fuzzy approach is used to handle the uncertainty in various applications. Researchers are developing many algorithms which work as fuzzy image processing [13, 14]. In the proposed method, fuzzy approach is used for contrast enhancement of CBCT images. In fuzzy enhancement method, images are first normalized, which means the dynamic range of gray level is decreased. Contrast mapping of pixel intensities measure is defined by Eq. 1.

$$I_{\text{FuzzyCon}} = \frac{I_{\text{Fuzzy}} - I_{\text{meanFuzzy}}}{I_{\text{Fuzzy}} + I_{\text{meanFuzzy}}} \quad (1)$$

Here, ρ is a fuzzy parameter which depends on the type of image. Fuzzy mapping rules are implemented to map the intensities of the image to change the low contrast to high level, and for that Eq. 2 is used.

$$I_{\text{FuzzyCon}} = \frac{1 - e^{-k \times I_{\text{FuzzyCon}}}}{1 - e^{-k}} \quad (2)$$

where K is a contrast-mapping function which is problem specific. After correcting, contrast-mapping fuzzification is implemented on image and an enhanced image is achieved using integration of fuzziness parameter.

3 Results and Discussion

The proposed algorithm is tested on different metal artefact CBCT dental images. Here morphology-based approach is used to reduce the reflection of metal filling in dental implantation. For improving the brightness of low-radiation CBCT image,

fuzzy enhancement is implemented. Figure 2 shows the experiment results of morphological operation on metal artefact CBCT image to reduce reflection effect.

Quality of images assessed is done using two parameters: peak signal-to-noise ratio (PSNR) and matrix structure of similarity index (SSIM) of the image. Table 1 shows the PSNR value of the morphology operation and fuzzy enhancement of metal artefact dental images.

From Table 1, the PSNR value of input images is higher at fuzzy enhancement, as our aim is to reduce the effect of metal artefact from the CBCT dental image.

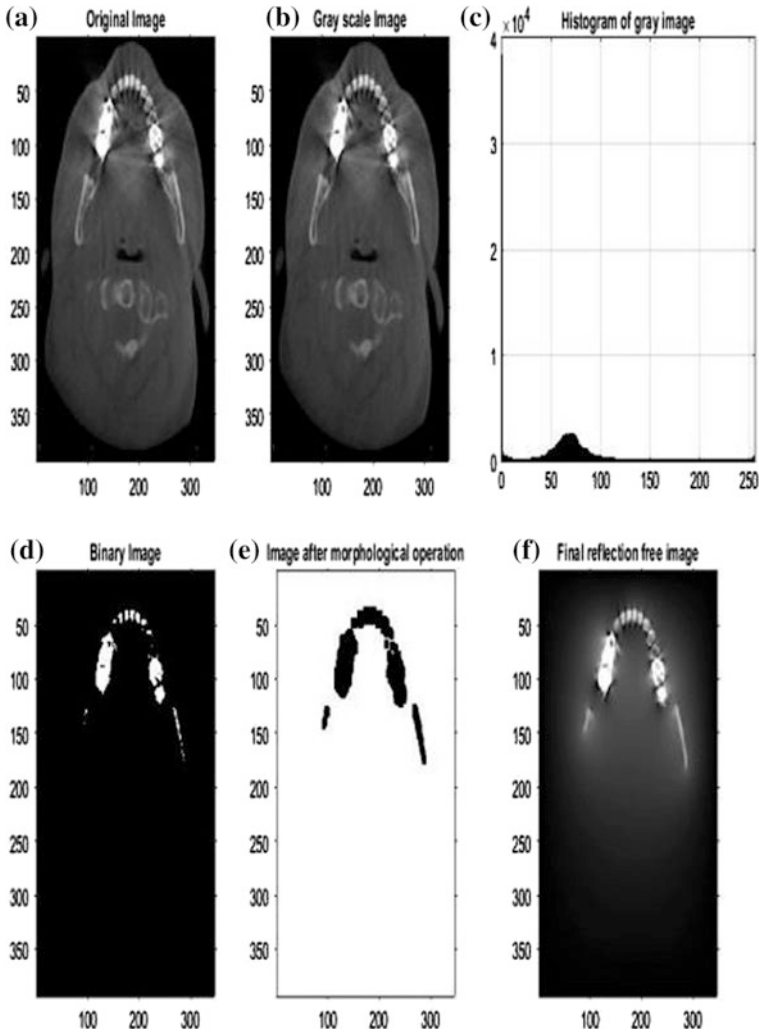


Fig. 2 a Artefact CBCT dental image. b Gray CBCT dental image. c Histogram of input dental image. d Binary image. e Dilated CBCT image. f Final reflection free CBCT image

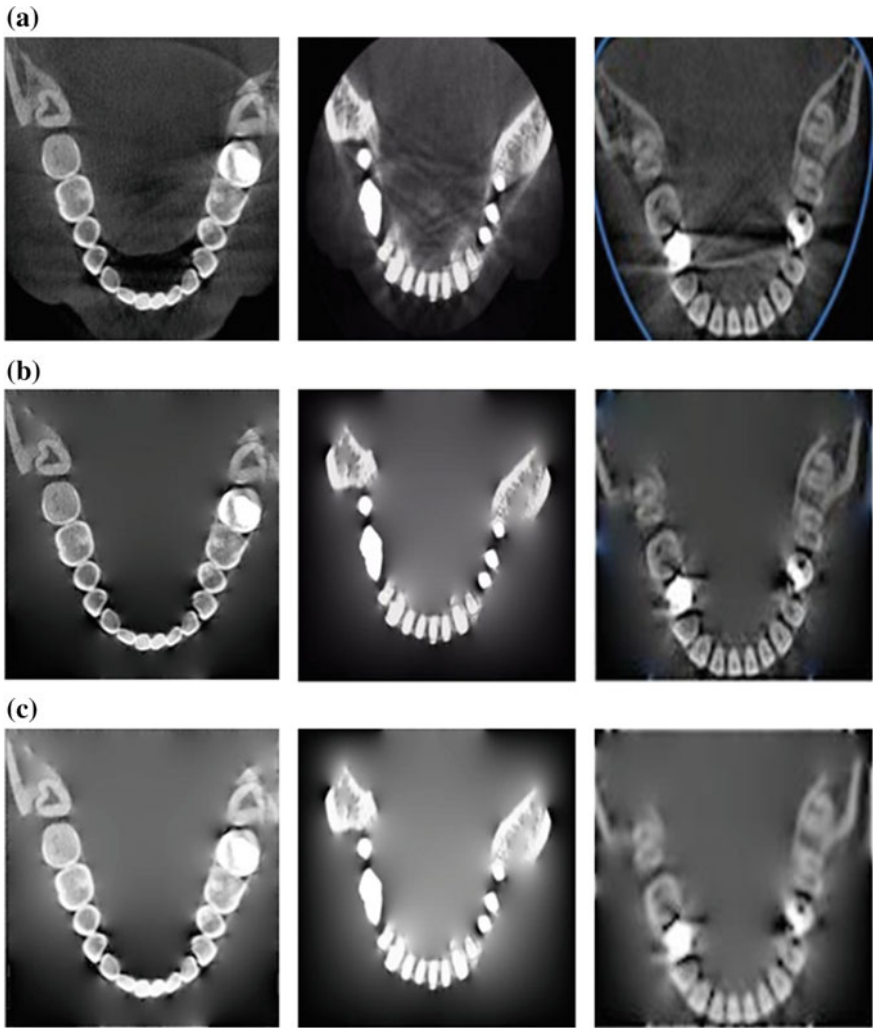


Fig. 3 a CBCT dental metal artefact image. b Output after morphological operation. c Output after fuzzy enhancement for dental image 1, 2 and 3 respectively

From Table 1, it found that morphological operation still needs to improve the contrast of images. So, fuzzy enhancement gives promising change in terms of PSNR and visual perception. Other parameter used to check the quality of image is SSIM which compares the image quality with reference to original image. Table 2 shows the SSIM of CBCT dental image with morphology and fuzzy enhancement operation.

Table 1 PSNR values after morphological operation and fuzzy enhancement

Dental image	Morphological operation	Fuzzy enhancement
Dental image 1	26.1388	89.8734
Dental image 2	20.8294	104.2938
Dental image 3	24.6505	92.5354

Table 2 SSIM values after morphological operation and fuzzy enhancement

Dental image	Morphological operation	Fuzzy enhancement
Dental image 1	0.7285	0.8572
Dental image 2	0.4905	0.5934
Dental image 3	0.6504	0.8472

From Table 2, it is shows that the value of SSIM is improved in fuzzy enhancement. SSIM value varies between -1 to 1 . If it reaches to near the unity, that means perception quality is improved.

4 Conclusion

Metal artefacts are present in CBCT images due to external and internal factors, which destroy the visual and important information of the images. As CBCT images are low radiation dose imaging technique which is easily affected by the artefacts. In this paper, morphology and fuzzy approaches are used to reduce the metal artefact effects on CBCT images and to improve the contrast of image. PSNR and SSIM values show the reduction of artefact in CBCT image. In future work, another algorithm is explored to reduce the different types of artefact in image modality.

Acknowledgements We would like to thank Department of Electronics and Communication, Amity School of Engineering & Technology, Amity University, Uttar Pradesh, for providing us resources and facilities for implementing this research.

References

1. Miracle AC, Mukherji SK. Conebeam CT of the head and neck, part 1: physical principles. *Am J Neuroradiol* 2009; 30: 1088–1095.
2. Miracle AC, Mukherji SK. Conebeam CT of the head and neck, part 2: clinical applications. *Am J Neuroradiol* 2009; 30: 1285–1292.
3. Yu L, Li H, Mueller J, Kofler JM, Liu X, Primak AN, et al. Metal artifact reduction from reformatted projections for hip prostheses in multislice helical computed tomography: techniques and initial clinical results. *Invest Radiol* 2009; 44: 691–696.

4. Nahmias C, Lemmens C, Faul D, Carlson E, Long M, Blodgett T, et al. Does reducing CT artifacts from dental implants influence the PET interpretation in PET/CT studies of oral cancer and head and neck cancer? *J Nucl Med* 2008; 49: 1047–1052.
5. Zhang Y, Zhang L, Zhu XR, Lee AK, Chambers M, Dong L. Reducing metal artefacts in cone-beam CT images by preprocessing projection data. *Int J Radiat Oncol Biol Phys* 2007; 67: 924–932.
6. X. Zhang and J. Wang, “Metal artifact reduction in X-ray computed tomography by constrained optimization,” *Med. Phys.* 38 (2) Feb. 2011.
7. G. Wang, T. Frei and M. Vannier, “Fast Iterative Algorithm for Metal artifact reduction in Xray CT,” *Acad Radiol.* 7 (8), August 2000.
8. Bamberg et al., “Metal artifact reduction by dual energy CT using monoenergetic extrapolation,” *Eur Radiol.*,10, 2010.
9. Alvarez and Macovski, “Energy-selective reconstructions in X-ray computerised tomography,” *Phys. Med. Biol.*, 21 (5), 1976.
10. M. Bal and L. Spies, “Metal artifact reduction in CT using tissue-class modeling and adaptive filtering,” *Med. Phys.*, vol. 33 (8), 2006.
11. W. Veldkamp et al., “Development and Validation of segmentation and interpolation for metal artifact suppression,” *Med Phys.*, vol 37 (2), 2010.
12. M. Iwanowski, S. Skoneczny, J.Szostakowski, “Image segmentation by advanced morphological filtering and clustering”, in:Proceedings of International Conference of The Quantitive Description of Materials Microstructure, Warsaw 16–19 April 1997 pp. 307–314.
13. BalasubramaniamJayaram, Kakarla V.V.D.L. Narayana, V. Vetrivel, “Fuzzy Inference System based Contrast Enhancement”, *EUSFLAT-LFA* July,2011 Aix-les-Bains, France.
14. Li Jiuxian, Sun Wei, Xia Liangzheng, “Novel fuzzy contrast enhancement algorithm”, *Journal of south east university (Natural Science Edition)*, Vol. 34 No 15, 2004.

Mitigation of Signal Interference by Positioning FFT Window for OFDMA System

**Salauddin Mohammad, Madan Gopal, Rajarao Manda
and Khaleel Rehman**

Abstract In today's generation, there is a need for achieving high-data rate to compete with the standard applications like OFDMA. The high speed depends on how efficiently the spectrum is being used to transmit the data from transmitter to the receiver. Due to the time-dispersive nature of the fast fading channels, the signal may get faded when reaching the receiver. The signal formed by group of symbols travels via multiple paths to reach the receiver. The fading caused by multipath propagation is called the multipath fading. To reduce the signal interference, many equalization technique algorithms have been proposed [1]. Apart from equalization algorithms, FFT operation window can be positioned at the downlink module of OFDMA system ensuring all the symbols have been received at the receiver to reduce the interference and increase the SNR. ModelSim 10.2 and MATLAB have been used to simulate and compare the results. The simulation results of the proposed method show 4.8% significant improvement of SNR.

Keywords OFDMA · FFT · Equalization algorithms · Signal interference

S. Mohammad (✉) · R. Manda · K. Rehman
Department of Electronics and Communication Engineering,
University of Petroleum and Energy Studies, Dehradun, India
e-mail: msalauddin@ddn.upes.ac.in

R. Manda
e-mail: rmanda@ddn.upes.ac.in

K. Rehman
e-mail: krehman@ddn.upes.ac.in

M. Gopal
JNTU, Hyderabad, India
e-mail: mekala.madan@gmail.com

1 Introduction

In the mid-1960s, frequency-division multiplexing (FDM) has evolved in which all the subcarriers are separated by a guard band in the frequency domain to overcome the signal interference. Later, it has been overcome by orthogonal frequency-division multiplexing (OFDM) technology in which all the subcarriers are placed orthogonally for the efficient use of available spectrum. Orthogonal frequency-division multiple access (OFDMA) [2] is the modified advanced version of OFDM in which all the subcarriers are formed as group of subchannels and transmitted to the receiver. Initially, 2048-pt FFT was proposed, but there is also scalable OFDMA Sc-OFDMA which can perform 128-pt FFT, 512-pt FFT, 1024-pt FFT and 2048-pt FFT depending on the channel and bandwidth [3]. The signal which is a group of symbols travels in multiple paths to reach the receiver called multipath propagation. There is a chance that the processing of FFT can start before all the symbols arrived at the input of the FFT processor causing intersymbol interference (ISI) [4]. Such type of interference can be combatted by using equalization technique algorithms like least mean squares algorithm (LMS), recursive least squares (RLS) algorithm, constant modulus algorithm (CMA) and 2D-MMSE algorithm [5]. However, in the most practical wireless systems it is not so easy to design the 2D-MMSE equalizer [6]. Hence, we propose a new technique for the mitigation of ISI in which the delay spread will be calculated and the FFT window will be positioned according to the delay. The delay can be produced by using the farrow filters which provide the fractional delay.

The rest of the paper is organized as follows: in Sect. 2, we introduce the system model of the OFDMA system along with the delay calculations. Section 3 gives the proposed positioning of the FFT window system followed by Sect. 4 to show the simulation results and the comparisons of simulated results, and the last section concludes the chapter.

2 Modelling of OFDMA System

At the downlink point of view, both OFDM and OFDMA technology remain same except the processing size of the FFT at the receiver and the block diagram of the same is shown in Fig. 1. The serial data is converted to parallel, and then, an appropriate digital modulation scheme is applied before performing the inverse fast Fourier transform (IFFT) operation. Usually, QAM-64 is used for high-data-rate applications like DVB-T and DVB-H systems.

Each symbol is prefixed by a cyclic prefix (CP) [7] in order to overcome the interference caused the symbols during the transmission in the channel. For an optimum case, the cyclic prefix must be kept at least four times larger than the expected delay spread. The output of the IFFT in the time domain can be given as in Eq. 1.

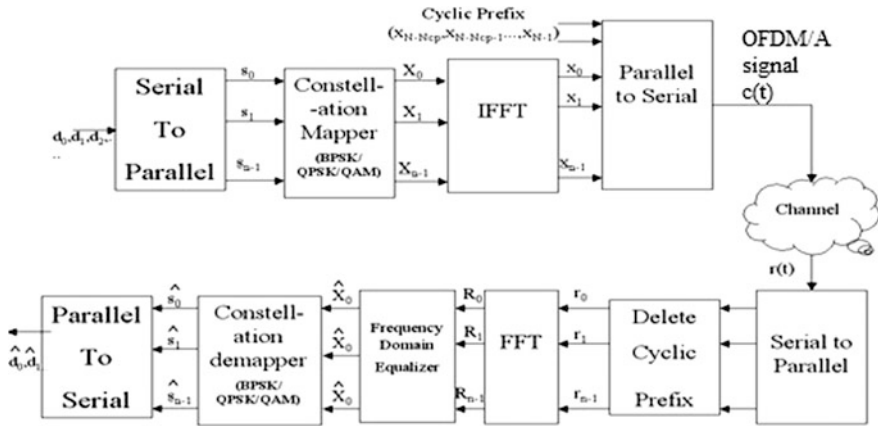


Fig. 1 OFDMA system block diagram

Table 1 BER of LMS, RLS and CMA equalizer for OFDM/A system

Equalization	BER of OFDM/A-based BPSK system	BER of OFDM/A-based QPSK system	BER of OFDM/A-based QAM system
LMS	0.845	0.909	0.874
RLS	0.848	0.878	0.938
CMA	0.818	0.939	0.874

$$X_k(n) = \frac{1}{\sqrt{N}} \sum_{i=0}^{N-1} X_m(i) e^{j2\pi \frac{ni}{N}} \tag{1}$$

$$0 \leq i \leq N - 1; 0 \leq n \leq N - 1,$$

where $X_k(n)$ and $X_m(i)$ represent the sequence in time and frequency domains, respectively. Similarly, the output of the fast Fourier transform in the frequency domain can be given in Eq. 2.

$$R_m(i) = \sum_{n=0}^{N-1} r_{k(n)} e^{-j2\pi \frac{ni}{N}} \tag{2}$$

The output of the FFT is fed into appropriate equalizer whose impulse response is the inverse of the channel response for the reduction of ISI. The BER of various equalizer algorithms [8] with different modulation schemes is shown in Table 1 (Fig. 2).

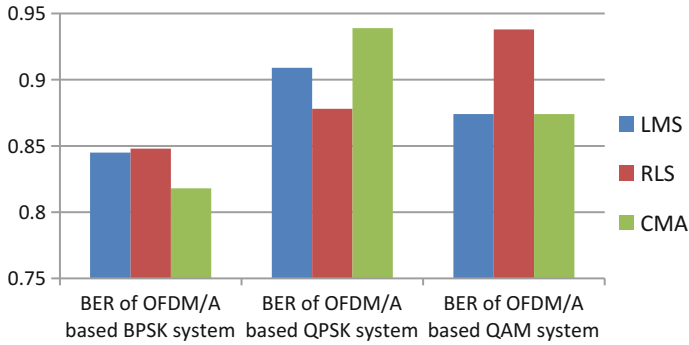


Fig. 2 BER of LMS, RLS and CMA equalizer for OFDM/A System

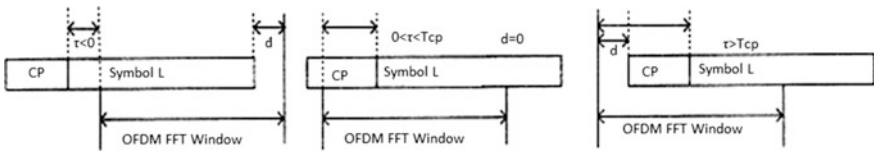


Fig. 3 Delays of FFT window

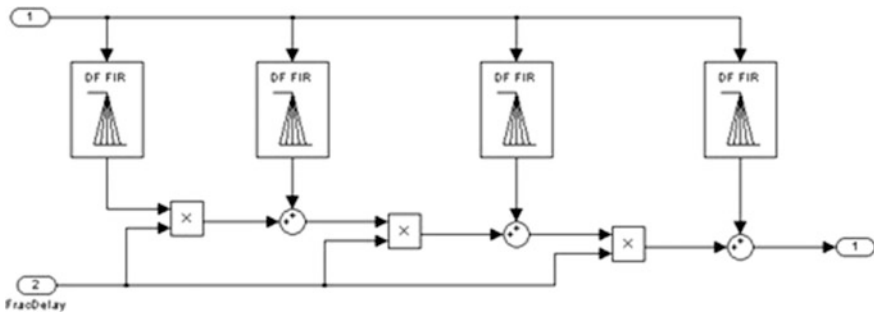


Fig. 4 Farrow structure for variable fractional delay

3 Proposed System

Various possibilities of delays at the receiver are shown in Fig. 3. Different symbols receive at different times at the receiver causing ISI. So, to combat the ISI the FFT window is adjusted to an optimum position ensuring all the symbols have been received prior to performing FFT operation.

The mean excess delay and the RMS delay spread are used to calculate the delay time of the symbols. The mean excess delay is given as

$$\bar{\tau} = \frac{\sum_k P(\tau_k)\tau_k}{\sum_k P(\tau_k)}, \tag{3}$$

where $\bar{\tau}$ is the RMS delay spread, $P(\tau_k)$ is the absolute power of the received signal, and delay of the k th detectable signal arriving at the receiver is denoted by $P(\tau_k)$.

The RMS delay spread can be derived from the mean excess delay as shown in Eq. 4.

$$\sigma_\tau = \sqrt{\tau^2 - \bar{\tau}^2}. \tag{4}$$

The RMS delay is also useful to estimate the type of the interference based on the coherence bandwidth. Coherence bandwidth is less than the signal bandwidth in the frequency-selective fading.

The relation between the RMS delay spread and coherence bandwidth is given as

$$B_C \approx \frac{1}{5\sigma_\tau}. \tag{5}$$

Based on the delay, the FFT window is shifted by passing the signal through a Farrow filter which is also known as fractional delay filters.

4 Simulation Results

The simulations have been carried out for the implementation of the window-positioned OFDMA in the presence of interference. For this to implement, inputs were taken from International Telecommunication Union (ITU). The power delay profiles given by ITU for a given specified time are shown in Table 2. Hence, both the conventional OFDMA and window-positioned OFDMA were simulated and the interference has been mitigated by delaying the FFT process by 1.6 μ s.

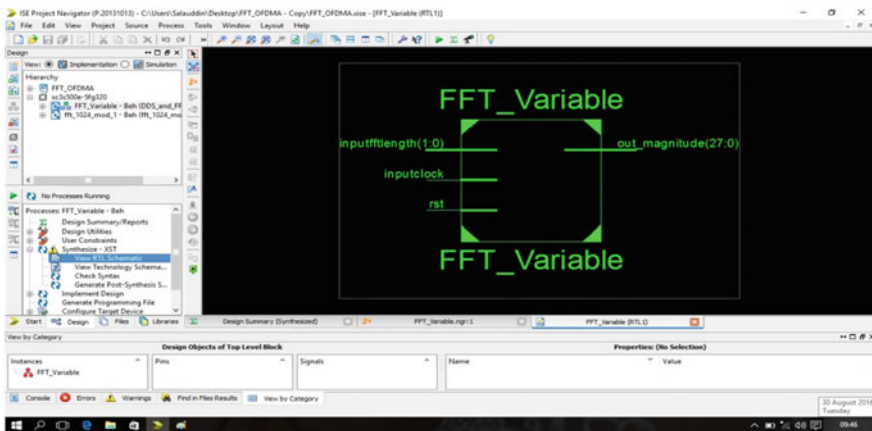


Table 2 ITU channel parameter values at a specific time

ITU-R	Delays (τ) in μ s	Power (P) in dB
Ped-A	[0 0.11 0.19 0.41]	[0 -9.7 -19.2 -22.8]
Ped-B	[0 0.2 0.8 1.2 2.3 3.7]	[0 -0.9 -4.9 -8 -7.8 -23.9]
Veh-A	[0 0.31 0.71 1.09 1.73 2.51]	[0 -1.0 -9.0 -10.0 -15.0 -20.0]
Veh-B	[0 0.3 8.9 12.9 17.1 20]	[-2.5 0 -12.8 -10.0 -25.2 -16.0]

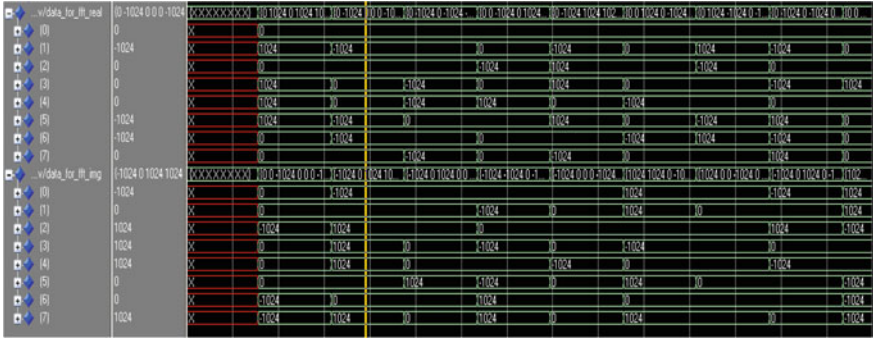


Fig. 5 Symbols going to the input of IFFT

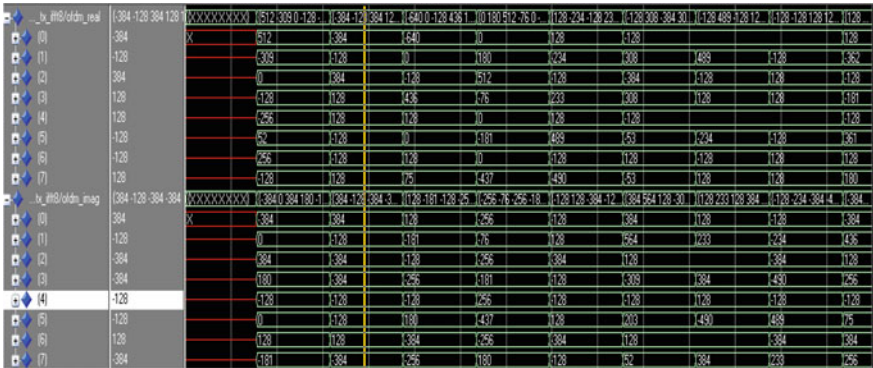


Fig. 6 Symbols going to the input of IFFT

The RTL view of the OFDMA system is shown in Fig. 4. For the implementation on the hardware, 16-bit input with 10-bit fractional part was considered. The 64-bit input which has been converted to parallel 8×8 data which is going as the input to the IFFT processing has been shown in Fig. 4.

The values obtained from Figs. 5 and 6 need to be divided by 1024 to get the obtained MATLAB results. And the initial set of data shown can be neglected which is due to the initial zeros. Similarly, the output of the IFFT processing is shown in Fig. 6.

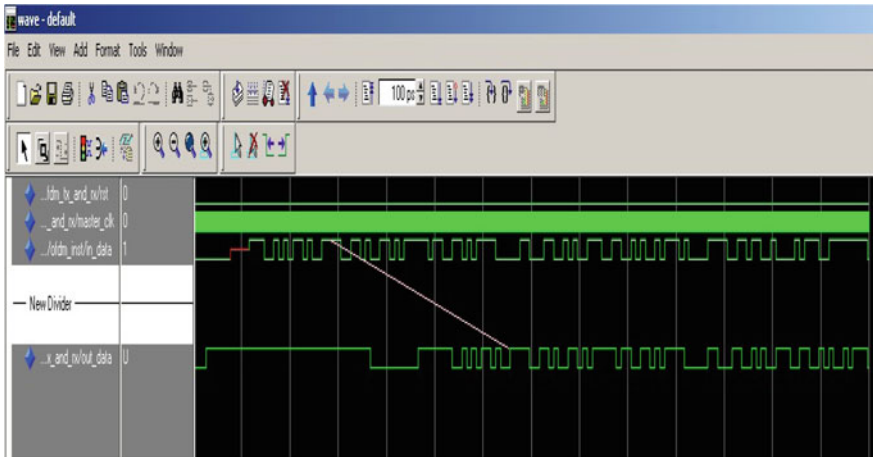


Fig. 7 Simulation of window-positioned OFDMA

And at last, Fig. 7 shows the comparison between the conventional OFDMA and the FFT window-positioned OFDMA. The results show that the delay given by the ITU has been considered and the FFT processing was delayed at the receiver. Hence, the proposed system ensures that all the symbols have been received at the receiver, and then, only the FFT processing is started to mitigate the signal interference.

5 Conclusion

The paper gives the following conclusions: In the high-data-rate applications like DVB-H and DVB-T, the ISI is an important parameter to consider and the signal interference is mitigated by positioning the FFT window in the case of interference. The results show the improvement of SNR by 4.8% for the proposed system over conventional OFDMA system. Hence, the same system can be used for the real-time applications and superimposed training sequence of symbols can be done to the same system to avoid cyclic prefix and utilize the bandwidth more efficiently.

References

1. Markus Rupp, "Convergence Properties of Adaptive Equalizer Algorithms" in IEEE Transactions on signal processing, VOL. 59, No. 6, June 2011.
2. E. Hari Krishna, K. Sivani, K. Ashoka Reddy, "Hardware implementation of OFDM transceiver using FPGA" in International Conference on Computer and Computational Sciences (ICCCS), 2015.

3. Chung-Ping Hung, Sau-Gee Chen and Kun-Lung Chen, "Design Of an Efficient Variable Length FFT Processor "in IEEE International Symposium on Circuits and Systems.2004.
4. Van Duc Nguyen, H.P. Kuchenbecker, "Inter carrier and inter symbol interference analysis of OFDM systems on time-varying channels" 4th IEEE Workshop on signal processing Advances in Wireless Communications, 2003.
5. Yang yang Fan, Xue Chen, Weiqin Zhou, Xian Zhou, Hai Zhu, "The Comparison of CMA and LMS Equalization Algorithms in Optical Coherent Receivers" in 6th International Conference on Wireless Communications Networking and Mobile Computing (WiCOM)- Electronic ISBN: 978-1-4244-3707-8.
6. Yao Liang, Weiou Zhou, Mingyu Zhou, Li He, "Research and implementation for 2D MMSE channel estimation" 12th International Conference on Signal Processing (ICSP)-[10.1109/ICOSP.2014.7015267](#).
7. Wei-Chang Chen, Char-Dir Chung, "Spectral Precoding for Cyclic-Prefixed OFDMA with Interleaved Subcarrier Allocation" in IEEE transactions on communications, vol. 61, No 11, Nov. 2013.
8. Jeffrey G. Andrews, Arunabha Ghosh, Rias Muhamed, Fundamentals of WiMAX: Understanding Broadband wireless Networking, Prentice Hall, 2007.

Effect of Skin Impedance on Delay and Crosstalk in Lossy and Non-uniform On-Chip Interconnects

Yenikepalli Ramesh and Vobulapuram Ramesh Kumar

Abstract An efficient finite-difference time-domain (FDTD) model is presented to analyse time delay and the crosstalk noise in lossy non-uniform interconnects. The complementary metal oxide semiconductor (CMOS) is used as driver for non-uniform interconnects and terminated with capacitive loads. Further, the resistive losses at high frequency due to skin effect and shrinking of interconnects are inculcated in the proposed model and analysed the high frequency effects. The improved alpha power law model represents the nonlinear behaviour of CMOS drivers, and the non-uniform interconnect is modelled including skin effect by FDTD technique. Hence, the proposed algorithm accurately estimates the crosstalk noise and delay in non-uniform interconnects at high frequencies and the results of FDTD are validated using HSPICE simulations.

Keywords Skin effect • FDTD • VLSI interconnects • CMOS

1 Introduction

In recent trends, faster and compact devices need smaller interconnect length and result in performance degradation in terms of delay, noise, and crosstalk. High-speed interconnects are normally modelled with an equivalent circuit having distributed RLGC parameters. Transmission lines with frequency-dependent variables are the best suit to describe electrical characteristics of on-chip interconnect. At earlier stages of VLSI design, it is necessary that CMOS technology needs keen

Y. Ramesh (✉)

Department of Electronics and Communication Engineering,
Koneru Lakshmaiah University, Guntur, India
e-mail: ramesh.yenikepalli@gmail.com

V.R. Kumar

Department of Electronics and Communication Engineering, Rajeev Gandhi Memorial
College of Engineering and Technology, Nandyal, India

modelling of CMOS gate-driven interconnect structures [1]. Driving of interconnects with the CMOS driver rises frequency/time conversion problem.

Recently, the authors in [2] proposed a model to analyse crosstalk accurately but it depends on even mode and odd mode and is suitable for loss less uniform interconnects. In [3], the authors proposed FDTD algorithm for analysing transients in CMOS gate-driven lossy uniform interconnects with frequency-dependent parameters. However, it is restricted to uniform interconnects, whereas for non-uniform interconnects it is unreported. In this work, the extension of frequency-dependent parameters is incorporated for non-uniform on-chip VLSI interconnects. In high-speed interconnects, due to skin effect, the current flows near the surface of the conductors and leads to increase in effective resistance [3]. In [4, 5], the authors proposed a method to explain propagation delay for non-uniform lossy transmission lines in time (t) domain using FDTD. In this work, parameters depending on frequency are also included. However, in this model a resistive driver is connected to transmission lines and terminates using resistive loads, so this analysis is not a practical one for on-chip interconnects which are having nonlinear drivers.

In this work, an efficient method is proposed for analyzing the crosstalk of CMOS gate driven loss non uniform interconnect system. Signal integrity issues are reported due to coupling in between the interconnect lines and nonlinear behaviour of CMOS driver. Further, CMOS driver's nonlinear behaviour is best described using improved alpha power law model and interconnects are modelled based on finite-difference time-domain (FDTD) model including frequency-dependence parameters.

2 Modelling of FDTD Algorithm for Non-uniform Lossy Interconnect System

In this section, the expressions for copper (Cu) interconnect line are developed using frequency-based skin impedance in (1) and the same is incorporated in FDTD model to find delay time and crosstalk at far end of the interconnect. The modelling part is represented below.

$$Z(z) = A_1(z) + B_1(z)\sqrt{s}. \quad (1)$$

2.1 Modelling of Non-uniform Lossy Interconnects with Frequency Dependency

Generally, transmission line model is best suit to analyse coupled interconnect lines because both have similar RLCG distributed elements [1]. The transmission line

(TL) expression with space and time dependency is modelled [7, 8] as in (2a) and (2b), and the equivalent two-coupled non-uniform lossy line is shown in Fig. 1.

$$\frac{\partial}{\partial z} v(z, t) + Z(t)i(z, t) = -l(z) \frac{\partial}{\partial z} i(z, t) \tag{2a}$$

$$\frac{\partial}{\partial z} i(z, t) + g(z)v(z, t) = -c(y) \frac{\partial}{\partial z} v(z, t) \tag{2b}$$

The internal impedance and current of the transmission line Eq. (2a) and (2b) are transformed to Laplacian domain as

$$Z(z, s) * i(z, s) = Z(z, t)i(z, t). \tag{3}$$

From Eq. (1) in Eq. (3),

$$L^{-1}\{Z(z, s)i(z, s)\} = A_1(z)i(z, t) + L^{-1}\left\{\frac{B_1(z)}{\sqrt{s}}\right\} * \frac{\partial}{\partial t} i(z, t). \tag{4}$$

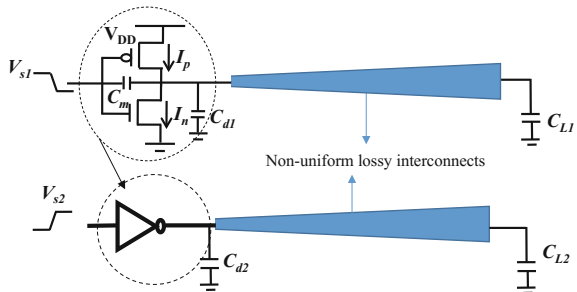
The term $(1/\sqrt{s})$ in (4) having inverse transform as from [6] is

$$\frac{1}{\sqrt{\pi t}} = \frac{1}{\sqrt{s}}. \tag{5}$$

By substituting Eq. (5) in (4) gives

$$Z(z, t) * i(z, t) = \left\{ A_1(z)i(z, t) + \left(\frac{1}{\sqrt{\pi}}\right) B_1(z) \int_0^t \frac{1}{\sqrt{p}} \frac{\partial}{\partial t} i(z, t-p) dp \right\}. \tag{6}$$

Fig. 1 Non-uniform lossy interconnect line existed by CMOS nonlinear gate



To solve lossy transmission line equations, FDTD is the most appropriate and widely used technique. By using this technique, the space position axis z is divided into equal subsections. Every adjacent V and I points are $\Delta z/2$ apart. Similarly, adjacent voltage and current time points are $\Delta t/2$ apart.

On applying finite-difference algorithm to Eq. (6) gives:

$$\int_0^t \frac{1}{\sqrt{p}} \frac{\partial}{\partial(t-p)} i(z, t-p) dp = \int_0^t \frac{L(z, t-p)}{\sqrt{p}} dp \tag{7}$$

where the function $L(z, t)$ is treated as constant over the time segment Δt . Thus, Eq. (7) becomes

$$\sum_{x=0}^n \int_{\Delta t(x)}^{\Delta t(x+1)} \frac{L(z, (n+1)(\Delta t - p))}{\sqrt{p}} dp = \sqrt{\Delta t} \sum_{x=0}^n L(z, (x+1)\Delta t - p) P_0(x). \tag{8}$$

On applying finite-difference approximation to TL equations in (2a), (2b) and substituting (8) in (2a), results in (9a) and (9b) [9–11]

$$l(k) \frac{-i_k^{n+1/2} + i_k^{n+3/2}}{\Delta t} + \frac{v_{k+1}^{n+1}}{\Delta z} + A_1(k) \frac{i_k^{n+1/2} + i_k^{n+3/2}}{2} + \frac{B_1(k)}{\sqrt{\pi\Delta t}} \sum_{x=0}^n P_0(x) \left\{ i_k^{n+3/2-x} - i_k^{n+1/2-x} \right\} = 0 \tag{9a}$$

$$c(k) \frac{v_k^{n+1} - v_k^n}{\Delta t} + g(k) \frac{v_k^n + v_{k-1}^{n+1}}{\Delta t} = - \frac{i_k^{n+1/2} - i_{k-1}^{n+1/2}}{\Delta z} \tag{9b}$$

where $k = 1, 2, \dots, N_z$. $v_k^n = v(\Delta z(k-1), \Delta t n)$; $i_k^n = (\Delta z(k-\frac{1}{2}), \Delta t n)$.

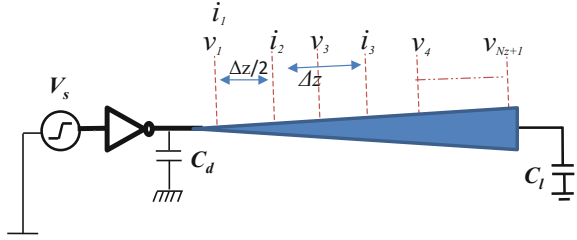
By solving (9a) and (9b)

$$\left[\frac{l(k)}{\Delta t} + \frac{A_1(k)}{2} + \frac{B_1(k)P_0(0)}{\Delta t} \right] i_k^{n+3/2} = \left[\frac{l(k)}{\Delta t} - \frac{A_1(k)}{2} + \frac{B_1(k)P_0(0)}{\Delta t} \right] i_k^{n+1/2} - \frac{v_k^{n+1} - v_k^{n+1}}{\Delta z} - \frac{B_1(k)P_0(0)}{\Delta t} \sum_{x=1}^n P_0(x) \left(i_k^{n-x+3/2} - i_k^{n-x+1/2} \right) \tag{10}$$

$$\left[\frac{C(k)}{\Delta t} + \frac{G(k)}{2} \right] V_k^{n+1} = \left[\frac{C(k)}{\Delta t} - \frac{G(k)}{2} \right] V_k^n - \frac{I_k^{n+1/2} - I_{k-1}^{n+1/2}}{\Delta z}. \tag{11}$$

A bootstrapping method is used to solve the Eqs. (10) and (11). The interconnect line voltage and current values are assigned as zero. After applying input to the line, from Eq. (11) the voltages are evaluated based on previous voltage and current

Fig. 2 Interconnect line with space discretization along its length for implementing FDTD model



solutions; later using Eq (10), currents are evaluated in terms of present current and past voltages. The space discretization for performing the bootstrapping mechanism along the line is shown in Fig. 2.

Putting $k = 1$ and $N_z + 1$ in Eq. (11) results (12) and (13) for near- and far-end equations, respectively.

$$\left[\frac{c(1)}{\Delta t} + \frac{g(1)}{2} \right] v_1^{n+1} = \left[\frac{c(1)}{\Delta t} - \frac{g(1)}{2} \right] v_1^n - \frac{i_1^{n+1/2} - i_0^{n+1/2}}{\Delta z/2} \tag{12}$$

$$\left[\frac{c(N_z + 1)}{\Delta t} + \frac{g(N_z + 1)}{2} \right] v_{N_z}^{n+1} = \left[\frac{c(N_z + 1)}{\Delta t} - \frac{g(N_z + 1)}{2} \right] v_{N_z}^n - \frac{i_{N_z+1}^{n+1/2} - i_{N_z}^{n+1/2}}{\Delta z/2}. \tag{13}$$

The line current at near end $z = 0$ is i_0 and at far end $z = 1$ as $i_{N_z + 1}$. Then, KCL expression is represented in (14) and (15), respectively.

$$i_0 = i_p - i_n + c_m \left(\frac{d(v_s^n - v_1^{n+1})}{dt} \right) - C_d \frac{dv_1}{dt} \tag{14}$$

$$i_{N_z + 1} = C_l \frac{\partial v_{N_z + 1}}{\partial t}. \tag{15}$$

By substituting Eq. (14) and Eq. (15) in (12) and (13) yields (16) and (17), respectively. These are the expressions for line voltage and currents at any point along the interconnect lines and for $k = N_a + 1$.

$$v_1^{n+1} = \left[\frac{c(N_a + 1)}{\Delta t} + \frac{g(N_a + 1)}{2} \right]^{-1} \left\{ \begin{aligned} & \left[\frac{c(N_a + 1)}{\Delta t} - \frac{g(N_a + 1)}{2} \right] v_1^n - \frac{2}{\Delta z} i_1^{n+1/2} \\ & + \frac{2}{\Delta z} \left(i_p^{n+1/2} - i_n^{n+1/2} - c_m \left(\frac{d(v_s^n - v_1^n)}{dt} \right) + C_d \left(\frac{dv_1^{n+1/2}}{dt} \right) \right) \end{aligned} \right\} \tag{16}$$

$$i_k^{n+3/2} = \left[\frac{l(k)}{\Delta t} + \frac{A_1(k)}{2} + \frac{B_1(k)P_0(0)}{\Delta t} \right]^{-1} \left\{ \left[\frac{l(k)}{\Delta t} - \frac{A_1(k)}{2} + \frac{B_1(k)P_0(0)}{\Delta t} \right] i_k^{n+1/2} - \frac{v_k^{n+1} - v_k^{n+1}}{\Delta z} \right. \\ \left. - \frac{B_1(k)P_0(0)}{\Delta t} \sum_{x=1}^n P_0(x) \left(I_k^{n-x+3/2} - I_k^{n-x+1/2} \right) \right\}. \tag{17}$$

3 Results and Discussions

In this section, the proposed FDTD model for interconnect lines is validated using HSPICE simulations for different input conditions. Consider a two-coupled non-uniform interconnects shown Fig. 1. The input excitation given as 0.9 V pulse with duty cycle of 50% and rise/fall times is 50 ps and pulse width of 300 ps.

The load capacitance (C_L) is 1fF. The interconnect line length is 1 mm, the spatial discretization of the non-uniform lines chosen to be 10 segments, and the time discretization is $\Delta t = 100\Delta t_{max}$.

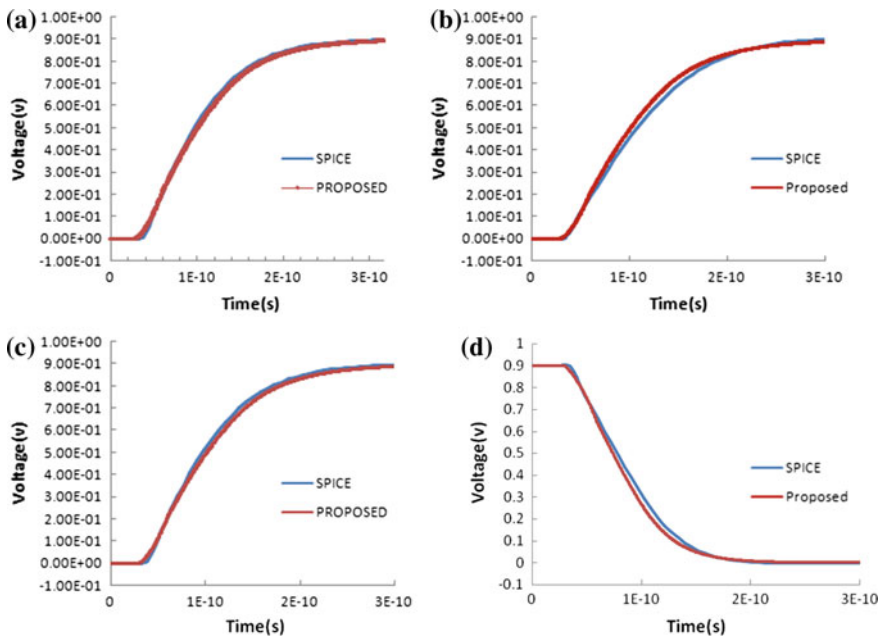


Fig. 3 Time-domain response at **a** port 3 in-phase, **b** port 4 in-phase, **c** port 3 out-phase, and **d** port 4 out-phase

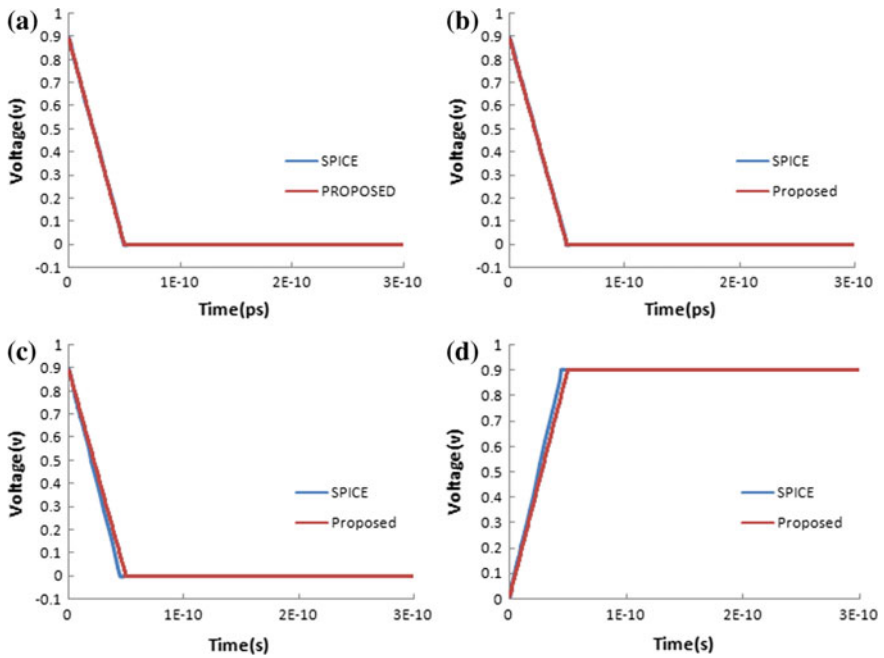


Fig. 4 Time-domain response at **a** port 1 in-phase, **b** port 2 in-phase, **c** port 1 out-phase, and **d** port 2 out-phase

The p.u.l parameters are represented as follows:

$$l = \begin{bmatrix} L_1 & L_{12} \\ L_{12} & L_2 \end{bmatrix} \text{ nH/m} \quad c = \begin{bmatrix} C_1 & C_{12} \\ C_{12} & C_2 \end{bmatrix} \text{ pF/m}$$

$$g = \begin{bmatrix} G_1 & 0 \\ 0 & G_2 \end{bmatrix} \text{ S/m} \quad R = \begin{bmatrix} R_1 & 0 \\ 0 & R_2 \end{bmatrix} \Omega/\text{m}$$

where $L_1 = L_2 = L(y) = 387/(1 + \lambda(y))$; $L_{m12}(y) = \lambda(y)L(y)$; $C(y) = 104.3/(1 + \lambda(y))$; $C_{12}(y) = -\lambda(y)C(y)$ $R_1 = R_2 = 60 \Omega/\text{m}$

$$G_1 = G_2 = G(y) = 0.001/[1 - \lambda(y)]$$

$$\lambda(y) = 0.25 \left[1 + \sin\left(6.25\pi y + \frac{\pi}{4}\right) \right]$$

At far end of interconnect, the transient response is observed and shown in Fig. 3a–d. At near end, the transient response is shown in Fig. 4a–d. The results are validated with HSPICE simulations.

4 Conclusion

An efficient frequency-dependent FDTD model is developed for non-uniform lossy interconnect lines to analyse near- and far-end transient analyses for interconnects. Further, the proposed algorithm is validated using HSPICE simulation results in very good accuracy in predicting the response. The time delay analysis is done by comparing the near- and far-end interconnect time delays using FDTD, and the same is validated using HSPICE. Hence, the model is verified accurately both in predicting the timing response and delay of the on-chip interconnect lines.

References

1. Rabaey J., Chandrakasan A., and Nikolic B.: Digital Integrated Circuits: A Design Perspective, 2nd ed. Englewood Cliffs, NJ: Prentice-Hall (2003)
2. Agarwal, K., Sylvester, D., and Blaauw, D.: Modeling and analysis of crosstalk noise in coupled RLC interconnects. In: *IEEE Trans. Comput.-Aided Des.*, vol. 25, no. 5, pp. 892–901 (2006)
3. Nahman, N.S., and HOLT, D.R.: Transient analysis of coaxial cables using the skin effect approximation $A + B\sqrt{s}$. In: *IEEE Trans. Circuit Theory*, vol. 19, No. 5, pp. 443–451 (1972)
4. Paul C.R.: Analysis of Multiconductor Transmission Lines. NY: Wiley Interscience (1994)
5. Orlandi and Paul C.R.: FDTD analysis of lossy, multiconductor transmission lines terminated in arbitrary loads. In: *IEEE Trans. Electromagn. Compat.*, vol. 38, no. 3, pp. 388–399 (1996)
6. Roden J.A., Paul C.R., Smith W.T., and Gednery D.: Finite-Difference, Time-Domain analysis of lossy transmission lines. In: *IEEE Trans. Electromag. Compat.*, vol. 38, No. 1, pp. 15–24 (1996)
7. Kumar, V.R., Kaushik B.K., and Patnaik A.: An unconditionally stable FDTD model for crosstalk analysis of VLSI Interconnects. In: *IEEE Trans. Compon Packag. Manuf. Technol.*, vol. 5 no. 12, pp. 1810–1817 (2015)
8. Li, X., Mao J., and Swaminathan M.: Transient analysis of CMOS-gate driven RLGC interconnects based on FDTD. In: *IEEE Trans. CAD Integr. and Circuits Syst.*, vol. 30, no. 4, pp. 574–583 (2011)
9. Kumar, V.R., Kaushik, B.K., and Patnaik, A.: An accurate FDTD model for crosstalk analysis of CMOS-gate-driven coupled RLC interconnects. In: *IEEE Trans. Electromag. Compat.*, vol. 56, no. 5, pp. 1185–1193 (2014)
10. Kumar, V.R., Kaushik, B.K., and Patnaik, A.: An accurate model for dynamic crosstalk analysis of CMOS gate driven on-chip interconnects using FDTD method, In: *Microelectronics Journal*, vol. 45, no. 4, pp. 441–448 (2014)
11. Kumar, V.R., Kaushik, B.K., Patnaik, A.: Improved Crosstalk Noise Modeling of MWCNT Interconnects Using FDTD Technique, *Microelectronics Journal* vol. 46, no. 12, pp. 1263–1268 (2015)

Modeling of Coupler Dynamics of Gatimaan Express

P.K. Jha and S.S. Gokhale

Abstract This chapter presents a mathematical model of coupler dynamics of Gatimaan Express. It has one locomotive class WAP5, one generator van, one second-class chair car, and one executive chair car, respectively. Overall, 180 (4×45) Degree of Freedom model is developed in Matlab/Simulink[®]. Lateral and longitudinal suspension forces of front bogie, rear bogie, and car body are considered in the model. The study is done with three different train's velocities such as 40, 60, and 160 kmph, respectively. The actual track geometry provided by Research Designs Standards Organization (RDSO), Lucknow, is simulated for this study. The result of coupler forces and its rotations on these velocities are discussed.

Keywords Coupler · Coupler rotation · Longitudinal suspension force
Lateral suspension force · Yaw motion · Matlab/simulink[®]

1 Introduction

Wagons of train are connected by couplers and draft gears which are elastic and damping in nature. Coupling system is one of major part of train, and it affects longitudinal and lateral dynamics of train. During the braking, coupler reduces the chance of collision between wagons. Large coupler rotation in curve track can produce additional lateral force to the wheelsets which results derailment. Hence, study of coupling dynamics is important for locomotive's safety and its dynamic stability. Rotational behavior of couplers causes derailment as its yaw becomes

P.K. Jha (✉) · S.S. Gokhale
Department of Mechanical-Mechatronics Engineering, The LNM Institute of Information
Technology, Rupa Ki Nangal, Post-Sumel, via Jamdoli, Jaipur 302031, India
e-mail: pkjha@lnmiit.ac.in

S.S. Gokhale
e-mail: ssg1@lnmiit.ac.in

unstable during emergency braking and generates large amount of longitudinal compressive force. Therefore, many researchers have developed models to study the dynamic performance of coupler force and its rotation.

Cole et al. [1] modeled a train of 103 wagons and 3 locomotives connected through couplers and studied three different cases: autocouplers with standard draft gears, autocouplers with draft gears and wedge with unlocking features, and the traditional drawhook buffer system, respectively. They found that autocoupler draft gear units have minimum fatigue damage.

Jeong et al. [2] performed the sensitivity analysis on their model and noticed that coupler dynamics has high potential for derailment on curve track.

Seid [3] proposed a 3D coupler model with draft gear in Ansys to determine the structural analysis of its critical parts during impact load.

Xu et al. [4] designed a model to analyze the coupler rotation behavior on the train dynamics. It was rubber draft gear model which had hysteresis characteristics, friction characteristics, and alignment-control characteristics of the coupler knuckles and the coupler shoulder, respectively. They noted that the rotational behavior of coupler on the different types of track affects railway vehicle dynamics performance, especially during braking. The impact of middle coach couplers is a main cause for the same.

Tianwei et al. [5] studied a model of couplers with different rotation angles and found that large coupler's rotation angle produced more longitudinal coupler compressive force than the coupler with small rotation angle.

Camil et al. [6] developed three case studies: vehicle equipped with buffers, vehicle with a traction device, and modified buffer characteristic with a stroke limiter for high speeds. They found that relative displacements and velocities of adjacent coaches correspond to the end of buffers, and maximum stroke of coupler are zero.

Wei et al. [7] made a train with coupler system model to study its coupler jackknifing behavior, and further, it was evaluated with the experiment data. Results indicated that a braking-induced impact due to coupler behavior has negative effects on the train dynamics.

Based on these prior researches, this chapter presents the study of inclusion of longitudinal dynamics, vehicle side slip, and yaw angle of car body in model. Model is developed with one Locomotive class WAP5, Generator van, Second-Class Chair car and Executive Chair. Track geometry provided by Track Machines of RDSO, Lucknow is incorporated in the model. Couple dynamics study is an extension of my previous work which had a model of 152 Degree of Freedom for the longitudinal, lateral, and vertical, roll, pitch, and yaw motions studies [8].

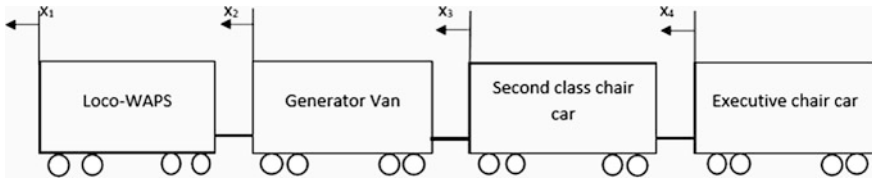


Fig. 1 Schematic diagram of Gatimaan express model

2 Equations for Coupling Dynamics of Gatimaan Express

Gatimaan Express has LHB bogie with Center Buffer Coupler (CBC). The coupler is opened manually but is closed automatically when they are mated adjacently. It has ant climbing features due to vertical interlocking [9].

A 180 DoF Gatimaan Express model is connected by three couplers. Couples CL_1, CL_2, and CL_3 between WAP5 and Generator Van, Generator Van and Second-Class chair, and Second-Class chair and Executive-Class chair. A schematic diagram of model is shown in Fig. 1. Longitudinal and lateral dynamic connections are made in mathematical modeling of the train. Tangent and curve tracks of 3500 m radius with cant angle 0.0238 rad with three different velocities 40, 60, and 160 kmph are taken in simulation. Forces acting on the coach is shown in Fig. 2. The equations for coupling dynamics are derived by modifying equations given by Xu et al. [4] below. Suppose a car body is in static equilibrium, and F_{fcbx} is the longitudinal force of car body, F_{bog1y} and F_{bog2y} are the lateral forces provided by the front and rear bogies, respectively. F_{fcy} , F_{rcy} , and F_{c1} are the lateral front coupler force, rear coupler force, and coupler pin force. Ψ , β and α are the yaw angle, vehicle side slip, and coupler angle. Assuming l_{c1} , l_c , and l_b are the length of coupler, length between front and rear couplers and length between front and rear bogies.

Assume force acting in upward direction and clockwise moment at the center of car body as positive.

$$F_{rcy} - F_{fcy} + F_{fcbx} \sin(\psi + \beta) = F_{bog2y} - F_{bog1y}. \quad (1)$$

$$0.5l_c^* (F_{rcy} + F_{fcy}) - 0.5l_b^* (F_{bog2y} + F_{bog1y}) - 0.5l_c^* F_{fcbx} \sin(\psi + \beta) = 0. \quad (2)$$

Equations of coupler force can be obtained as

$$F_{c1} = F_{rcy} \sin(\psi + \beta) - F_{rcy} \sin(\psi + \beta) \cos(\alpha). \quad (3)$$

$$\alpha = \arcsin(0.5l_c^* \sin(l_{c1})) + \beta. \quad (4)$$

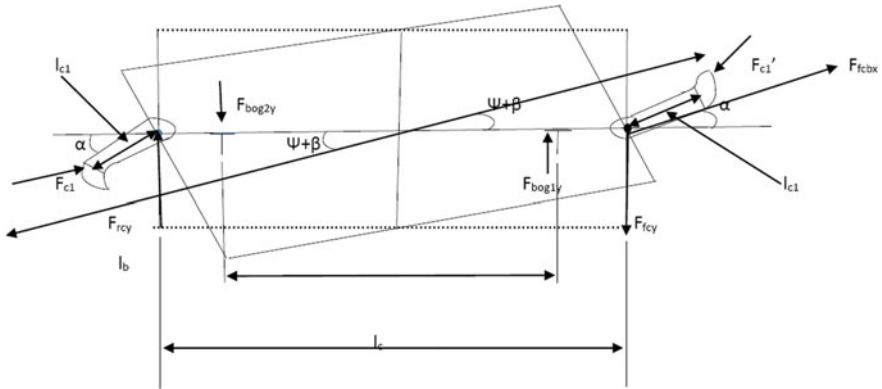


Fig. 2 Coupler force with other forces acting on the car body

Equations of coupler friction model:

Assume coupler surface generates friction force and the relative motion between two couplers. Apply Coulomb friction principles in the proposed model by adding the following equation. Suppose F_{f1} , x , v_f , and μ are friction force acting on the coupling surface, relative displacement, and velocity of couplers and friction coefficient, respectively.

$$F_{f1} = 0.5 * (1 + \text{sign}(x)) * (\mu F_{c1} \text{sign}(v_f)). \tag{5}$$

3 Development of Coupling Dynamics Model in Matlab/Simulink[®]

Different masses for locomotive WAP5, Generator van, Second-Class Chair and Executive chair, 56610, 33590, 29940, and 27115 kg, are considered in simulation.

The derived equations of coupler dynamics are presented in Matlab/Simulink[®] R2015b version, and Runge Kutta ode45 order solver with time step of 0.001 s is implemented. The simulation is performed at different speeds 40, 60, and 160 kmph on straight and right directional curve track of 3500 m with cant angle of 0.0238 rad. Simulation is performed for 20 s to study dynamic behavior of the model.

The simulated results of coupler rotational angle and couple forces are shown in Figs. 3, 4, 5, 6, 7, 8, and 9, respectively. The trains run up to 4 s on straight track and after that on curve track up to 16 s and finally on straight track.

The first coupler (Loco-WAP5) has large rotational angle than second coupler (Generator van) and third coupler (Second-Class Chair) as shown in Figs. 3, 4, and 5. It is indicated that behavior of couplers remains same on straight and curve

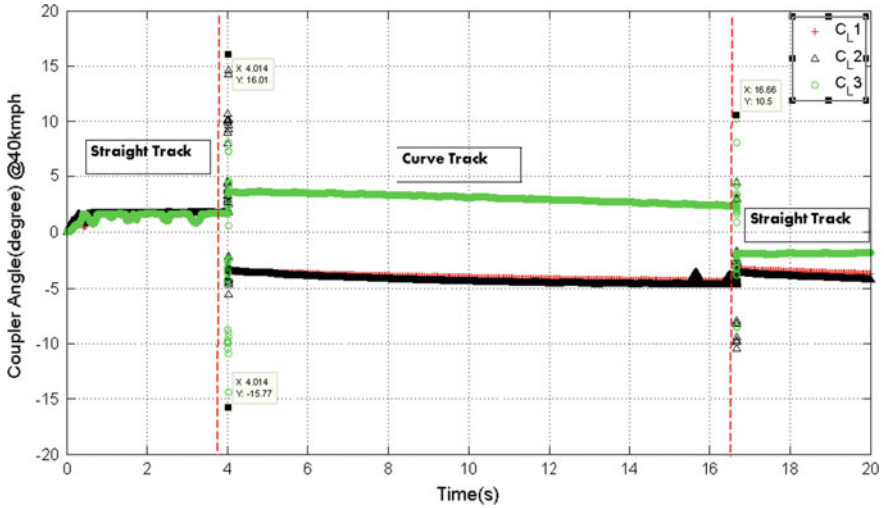


Fig. 3 Coupler angle (degree) at 40 kmph

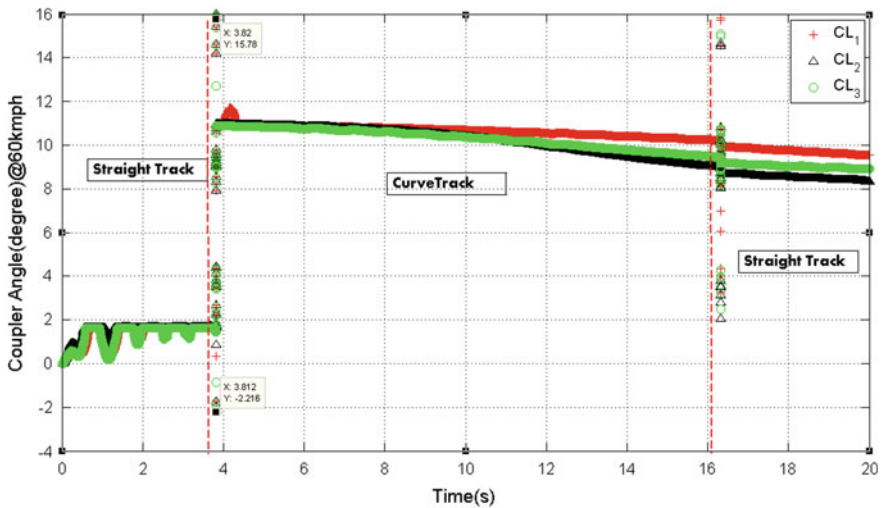


Fig. 4 Coupler angle (degree) at 60 kmph

tracks, but at the time of track switching, its behavior is changed significantly. The temporal nature of couplers can affect the railway vehicle stability.

The coupler rotational angles during track switching from straight to curve and curve to straight at speeds 40 and 60 kmph are about 16° and 10°. But its values at 160 kmph at the same switching conditions are about 4.3° and 9.3°.

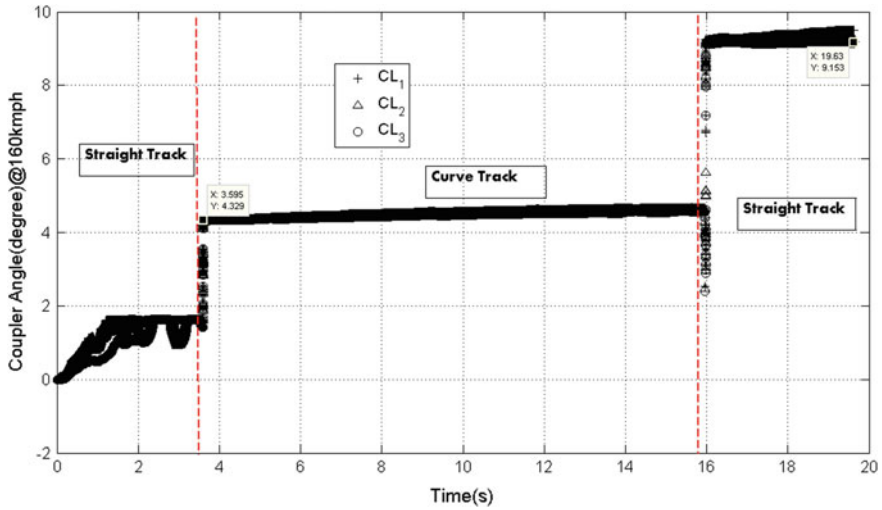


Fig. 5 Coupler angle (degree) at 160 kmph

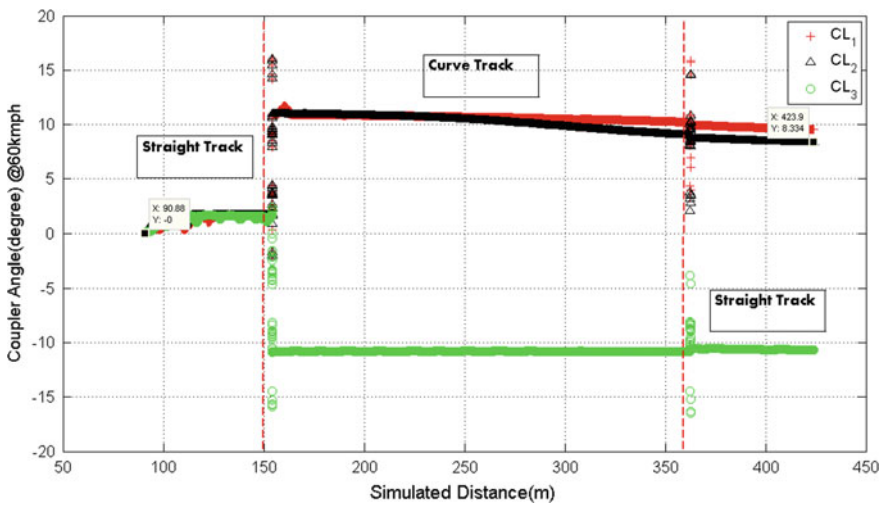


Fig. 6 Coupler angle (degree) at 60 kmph versus distance (m)

Coupler angle during the train travel for 20 s simulation is shown in Fig. 6. It is shown that the simulation starts from 99.88 m as it the length of train and covers the distance 339.02 m at the speed of 60 kmph.

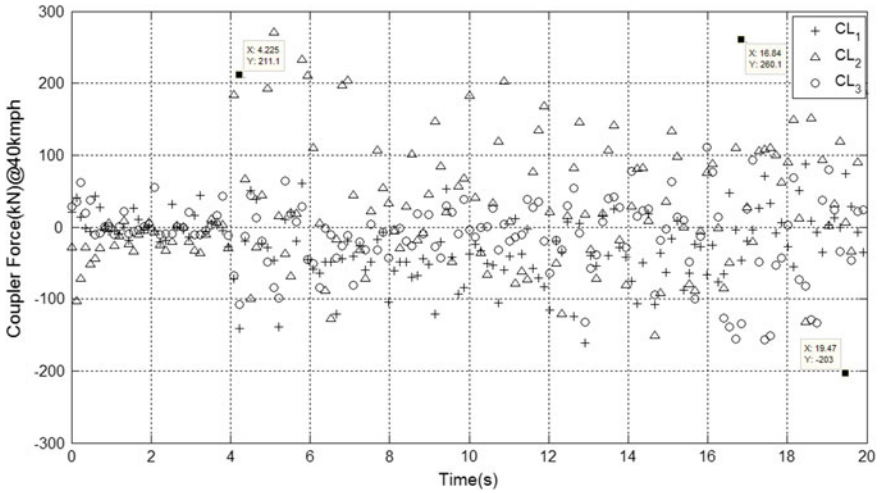


Fig. 7 Coupler Force (kN) at 40 kmph

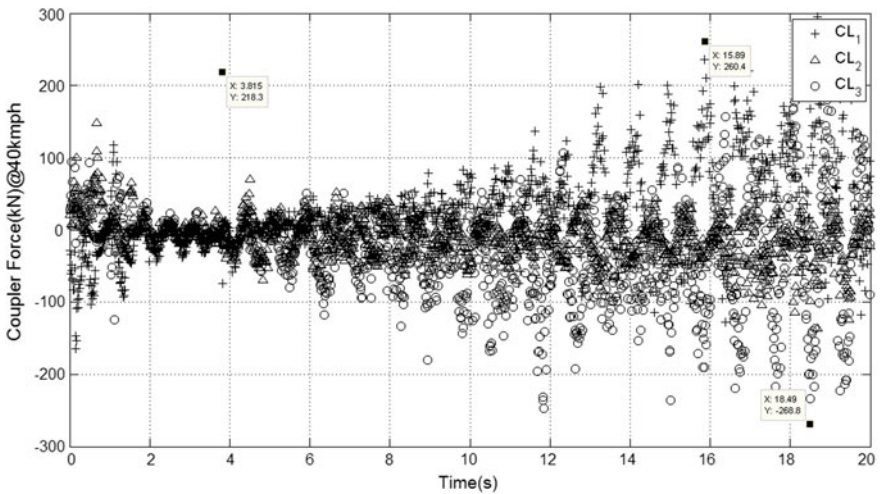


Fig. 8 Coupler Force (kN) at 60 kmph

From the Figs. 7 and 8, coupler maximum forces at 40 and 60 kmph are almost same i.e., 211 and 218 kN, respectively at the time of straight track switching to curve track. Whereas, switching from curve track to straight track, coupler maximum force is about 260 kN. Maximum forces at 160 kmph at about 4 and 16 s are 120 and 298 kN as shown in Fig. 9.

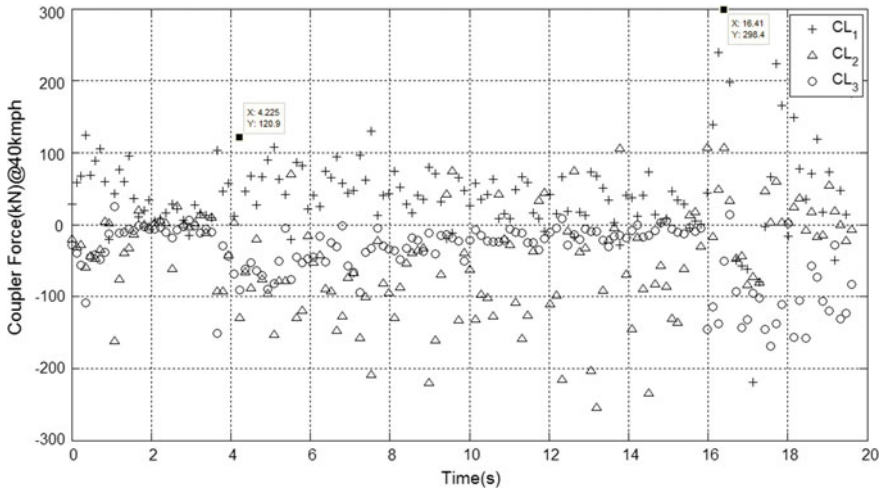


Fig. 9 Coupler Force (kN) at 160 kmph

4 Conclusion and Remarks

The dynamic coupler model of Gatimaan Express is studied. Third coupler has more rotational angle than others. It remains nearly constant on straight and curve tracks but changes significantly at the time of track switching. The coupler rotational angle plays one of the major roles in vehicle stability. It has less impact on longitudinal train dynamics.

Coupler forces at 40 and 60 kmph at track switching position are almost same.

5 Future Works

Buffer model will be appended to the current model to make robust. Large and free rotations of coupler behaviors are the major parts of coupler dynamics. Longitudinal dynamics also affected by braking, so its characteristics will also be reckoned in the extensive model. The derailment dynamics will be studied due to impact of coupler and barking performances.

References

1. Cole, C., Y Q Sun: Simulated comparisons of wagon coupler systems in heavy haul trains. *J. Rail Rapid Transit.* 220, 247–256 (2006)
2. Jeong., D., Lyons, M.L., Orringer, O, Perlman, A.B.: Equations of Motion for Train Derailment Dynamics. Proceedings of the 2007 ASME Rail Transportation Division Fall Technical Conference. Illinois, Chicago, USA (2007)

3. Seid, A. Mohammed: Structural Analysis and Dynamic Simulation of Heavy Haul Train coupler with gear for Rotational Effect. Master Thesis, Department of Mechanical and Industrial, Addis Ababa Institute of Technology, Ethiopia (2015)
4. Xu, Z.Q., W.H. Ma., Q. Wa., S.H. Luo.: Coupler rotation behavior and its effect on heavy haul trains. *Int. J. Vehicle Mechanics and Mobility*.vol. 51, pp. 1818–1838, Taylor & Francis (2013)
5. Tianwei, Q., Ma. Weihua, Wu. Dong, Luo Shihui: Influence of Coupler and Buffer on Dynamics Performance of Heavy Haul Locomotive. *J. The Open Mechanical Engineering* pp. 1033–1038, (2015)
6. Camil C., Ana-Maria., Tudor: Modeling the Buffers Hysteretic Behavior for Evaluation of Longitudinal Dynamics in Train Forces. Session of the Commission of Acoustics, (2012)
7. Wei, L., J. Zeng, Wang: Investigation of in-train stability and safety assessment for rail vehicles during braking. *J. Mechanical Science and Technology*. Vol. 30. pp. 1505—1525 (2016)
8. Jha, P. K., S.S. Gokhale: Modeling and Validation of Gatimaan Express with Matlab/Simulink. *Int. Journal of Transport Development and Integration*. WIT Transactions on the Built Environment. ISSN No.:1743-3509, Vol. 162. pp. 441–457, (2016)
9. Research Designs Standards Organization: Maintenance Manual for BG Coaches of LHB Design. pp. 26–27

Author Biographies

Mr. Jha is pursuing Ph.D. and working as an Assistant Professor in the LNMIIT since 2013. Mr. Jha has 13 years of experience in Research and Development in Automotive.

Dr. Gokhale is a Professor of Aerospace Department in IIT Madras and is Director of the LNMIIT since 2012. Professor Gokhale has published more than dozen papers in international journals. He worked on several research projects, especially on Aerospace Propulsion, Computational Fluid Dynamics, Simulation, and Optimization. Professor Gokhale has handled numerous research consultancies and institutions (Visvesvaraya National Institute of Technology-Nagpur, National Institute of Technology-Calicut, and IIT-Madras and many more).

Soil and Environment Conditions Based Smart Analysis System for Plant Growth Using IoT

Aakanksha Panwar, Avi Gaba, Rajesh Singh and Anita Gehlot

Abstract In today's world, we want plants to grow under healthy conditions with appropriate nutrients, required for their growth. This aim is achievable through smart electronic devices, which provide us very precise and accurate analysis of each and every factor needed for the growth of the plants. The device used in our research is pretty beneficial for plants in various plant's nurseries where different plants are grown for studying and testing purposes. This system has two micro-controller units in it, wirelessly connected with each other using RF module. Various sensors are used to measure factors related to soil and environment leading to an efficient and precise plant growth study. All the data recorded by the device is stored in a cloud server using local area network (LAN). The analysis will always be available to the user and is easily accessible using IoT.

Keywords IoT · Cloud server · Soil sensors · Plant growth · Water supply

1 Introduction

Innovation and advancement in technology could be seen anywhere around us. We humans have so much developed ourselves that now everything is becoming automated and self-driven. With modern machines and tools, accuracy of measurements

A. Panwar (✉) · A. Gaba · R. Singh · A. Gehlot
Electronics Instrumentation & Control Engineering Department,
College of Engineering Studies, University of Petroleum and Energy Studies,
Dehradun 248007, Uttarakhand, India
e-mail: aakankshapanwar@gmail.com

A. Gaba
e-mail: aaavigaba13@gmail.com

R. Singh
e-mail: rsingh@ddn.upes.ac.in

A. Gehlot
e-mail: anita@ddn.upes.ac.in

also gets increases. The area, which is yet to be introduced to modern machines and ideas, is agriculture and gardening area. The idea of bringing together modern technology and cultivation methods is inevitable. However, the projects which have been done until now, are very much expensive and large scale like ‘cropin’ [1]. So there is still need of a simple, user-friendly and cost-efficient device or a system, which can be used for smart gardening and agriculture techniques. There have been studies related to smart gardening as depicted in [2]. A device should be made, which is easily understandable and can be controlled without much efforts. Beside its simplicity, the device should be precise in its applications and measurements. This research is entirely developed on an Arduino-based smart device that will focus on precise agriculture and will measure the growth of a plant under variable soil conditions and forms. Whole project is based on various sensors attached to an Arduino board. A sensitive ultrasonic sensor is used in our study to measure the growth of the plant very precisely up to milli meters of length. Sensor will continuously sense and record the height of the plant very accurately and forward the data to Arduino UNO from which it is uploaded to cloud server using LAN [3]. With the help of it, we would get to know about growth of the plant (up to mm) at any instant and the rate of growth under certain soil conditions. Many time situations occur when we grow a plant and it does not go so well. It can be due to the type of soil. So with the help of this device, we can compare the growth of two plants in certain soil conditions and can come up to a result that which of the two plants is suitable for the growth in that certain type of soil. An ultrasonic anemometer is also attached with the system to measure the speed of the airflow in the atmosphere. Measured data would be transferred to the Arduino simply by connecting wires. We have used two Arduino boards in this project, which are connected with each other via RF module [4].

Major constituents of the soil that are responsible for appropriate plant growth are measured using sensors, with an additional automatic water supply to the plant.

This device will help us in measuring plants growth in different soil and environmental conditions. This device is designed in such a way that it can compare the growth of two plants whenever needed under certain soil, wind, and temperature conditions. This will help us to reach the conclusion, which will prevent us to grow plants under unfavorable conditions. This device helps in the optimization of time, cost, travel, and accuracy of information.

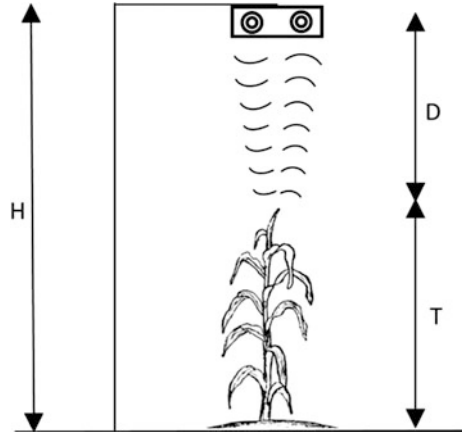
2 Experimental Discussion

2.1 *Variety of Sensors Used*

Ultrasonic sensor for measuring height of the plant:

Statistics of growth and height of the plant will be recorded with the help of an ultrasonic sensor HC-SR04. This sensor is easily available in the market. It can measure distance from 2 to 4 m and with a ranging accuracy up to 3 mm. It emits

Fig. 1 Plant height and growth measurement using ultrasonic sensor. Where H Height of sensor from ground. D Distance measured by sensor. T Height of the plant



sound waves of 40,000 Hz, which return after striking any obstacle in its way. The sensor is placed horizontally downward facing the ground just over the tip of the plant at some particular height (see Fig. 1). Here, the obstacle for sound waves emitted by the sensor is plant's tip. To measure the growth rate of the plant, sensor should emit and receive the sound wave again and again after a particular period of time, say 1 h. So in order to generate the continuous stream of ultrasound wave, trigger pin of the sensor is given high input for 10 μ s. It will transmit out an 8 cycle sonic burst, which will propagate at the speed of sound and is received at the echo pin of the sensor. According to [5], speed of sound wave is $v = 0.034$ cm/ μ s and it propagates easily through the air. To calculate distance from sensor to the obstacle, we have used Eq. (1). Height of the plant is calculated using Eq. 2, which is written in the formulas section. Proteus simulation of the ultrasonic sensor is shown in the Fig. 2, in which all the connections are done with an Arduino1 board. The data received by the sensor is then transferred to another Arduino2 board connected to local server using RF module. From there, all the information is uploaded to cloud server using IoT [6].

Anemometer for measuring speed of the wind flow:

Wind may affect the process which involves measuring height of the plant. It may lead to false values or in other words inaccurate results to some extent. So to prevent the data received by ultrasonic sensor from going toward inaccuracy, anemometer will be used in this research [7]. This will help to detect the speed of the wind and will give directions to the Arduino if the wind speed is beyond a value defined by us. If the speed of the wind gets increases from the predefined value, a signal from the microcontroller will be generated which will cut out the working of ultrasonic sensor until the flow of wind becomes normal. This will lead us to prevent the false reading of height and growth of the plant sensed by ultrasonic sensor. Recorded wind speed is also sent to another Arduino board using RF module. Arduino2, which will receive this data, is connected to LAN, and further all the data is uploaded to the cloud server using IoT.

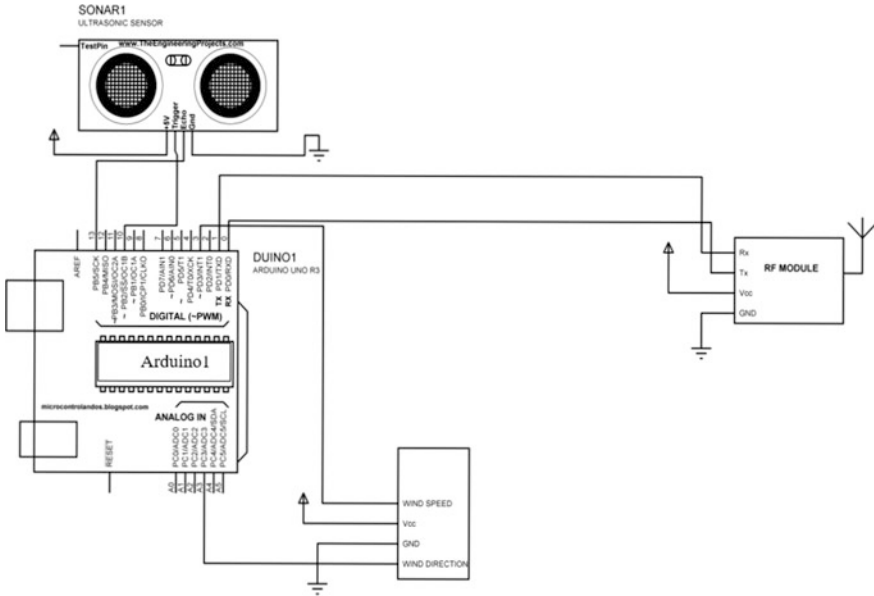


Fig. 2 Arduino unit for height and wind speed measurement

Temperature and Humidity sensor:

We have considered temperature and humidity sensor as a crucial part of this research. This part contributes in measuring the surrounding temperature and humidity. All the information regarding the temperature and humidity of the surrounding is received using a sensor named DHT11 [8], easily available in the market and online stores.

DHT11 sensor needs power supply of 3-6v DC voltage. A 100nF capacitor is connected between the Vcc and ground of the sensor for filtering purpose. All the data received by the sensor is then forwarded to the Arduino2, which will then upload the data on cloud server using IoT.

Soil Moisture sensor to measure moisture content in soil:

Water holding capacity of the soil is very important when it comes to plant growth. Right amount of water is necessary that is why it is necessary to take care of the water content of the soil for the fertility of soil as well as health of the plant.

In our research, soil moisture sensor, SEN-13322, is taken in use, which is easily available at some online stores [9]. This sensor is then connected to the analog pin of the Arduino2 say 'A1.' The Arduino2 board to which this sensor is connected is settled at the base of the plant that is further connected to a local area network. In order to measure the moisture content in soil, the sensor uses the capacitance value to find the dielectric permittivity of the soil. In soil, value of electric permittivity is directly proportional to the water content in it. Sensor will generate different

voltages with respect to the permittivity value of soil, and hence the water content will be measured by this. The readings sensed by the sensors will be sent to the cloud from time to time using IoT technology. These details will then be easily available to the user with the help of an application.

Automatic water supply to the plant using the readings of moisture sensor:

A motor is connected to the digital pin of Arduino2 board settled at the base of the plant. This motor is used here to control the water supply to the plant. A threshold value is predefined to the microcontroller, below which the soil is considered dry and above that value soil is considered as wet or water sufficient. As soon as the value of moisture content in the soil reaches just below the threshold value. A high signal is generated to the digital pin of the Arduino2, at which a motor is connected and the motor gets turn on therefore the water supply [10]. When the water content of soil gets sufficient enough, the water supply will automatically get turn off.

pH sensor for measuring pH value of the soil:

pH value of the soil is also the most important quantity for testing the fertility of soil. In our research, we are using Tris's Compatible Flat pH Sensor to measure the pH value of soil. The range of the sensor is pH 0–14. Electrode of this sensor is double-junction, gel filled, and sealed. Working temperature range of the sensor is 0–100 °C. To communicate with Arduino microcontroller, this sensor will need an interfacing shield [11]. We had made the Arduino program in a way that it will read the pH value of the soil after every 8 h or we can say three times a day. All the analog data received by the sensor is then converted to binary form using the Arduino program whose flowchart is drawn in 'Algorithm and Flow charts' section of this paper. All the data received is transferred to another microcontroller connected to local area network. Further all the data is uploaded to the cloud server using IoT.

2.2 RF Module for Sending Data from Arduino1 to Arduino2

As we are using two Arduino boards in our experiment, Arduino1 at some height and Arduino2 at the base of the plant, we need some connectivity between these two Arduino boards for experimental purpose. The data is from Arduino1 is to be transferred to Arduino2 which is connected to LAN. We are not connecting both the Arduino boards with separate LAN, as our objective is to build a cheap and simple device, which would not be possible if we will use two separate LAN connections. Hence, we need some connectivity between our two Arduino boards to communicate with each other. Therefore, a simple data transmitting and receiving device called RF module. As the name itself tells that it uses radio frequencies to

communicate. Frequency at which it works varies from 30 to 300 GHz. Tx/Rx pair of RF module works at a frequency of 434 MHz. Transmitter RF receives serial data from microcontroller and transmits the same through the antenna connected to it [12]. Ground and supply are provided either from the controller or from any pre-designed power supply. Similarly, receiver RF receives the data in radio frequency and converts it into serial data. A flowchart of the Arduino program used for transmission and reception of data using RF is shown in Sect. 2.4.

3 Figures and Explanations

Proteus simulation for the circuits used in the research.

Figure 2. Is the proteus simulation of the Arduino unit for health and wind speed measurement, which is then transferred to the other Arduino with the help of RF module, connected at the Tx pin of Arduino1.

Ultrasonic sensor is connected with pin no. 13 and pin no. 10 of the Arduino1. Power supply 5 V and ground are supplied to the sensor separately using a power supply.

Various types of application-based researches based on Arduino interfacing with sensors have been carried out alike [13, 14].

Anemometer is connected with both the analog and digital pins of Arduino1. For the measurement of wind speed, it is connected to the digital pin PD3 of Arduino1, and for measuring the direction of the wind, the anemometer is connected to the analog pin A3 of the Arduino1 board. 5v Vcc and ground are given by using the same power supply used for ultrasonic sensor.

All the data regarding the height of the plant and wind speed is continuously sensed by the sensors and forwarded to the Arduino1 board. Recorded data is transferred to another Arduino2 board connected to LAN. Data transmission is done with the help of RF module. Rx and Tx pin of RF is connected with Tx and Rx pin of Arduino1, respectively. Data transmitted from this side will be then received by another RF connected to the Arduino2 settled at the base of the plant (see Fig. 3).

Figure 3. is the Proteus simulation of the second Arduino board named as Arduino2 settled at the base of the plant and further connected to a LAN. Some sensors are connected to the Arduino board for the measurement of various constituents of soil, which affects the growth of plant.

A pH sensor is connected to the 'A0' pin of Arduino2, and Vcc and ground are supplied to the sensor using a power supply. All the data received by the sensor will be then forwarded to the Arduino2. Further data will be uploaded to a cloud server using LAN.

A temperature and humidity sensor is also connected to the Arduino2. Data pin of the sensor is connected to the analog pin 'A1' of the Arduino. Power is supplied to the sensor using a power supply. All the data about temperature and humidity will be sensed by the sensor and then forwarded to Arduino2 from where all the data is uploaded to a cloud server using IoT technology.

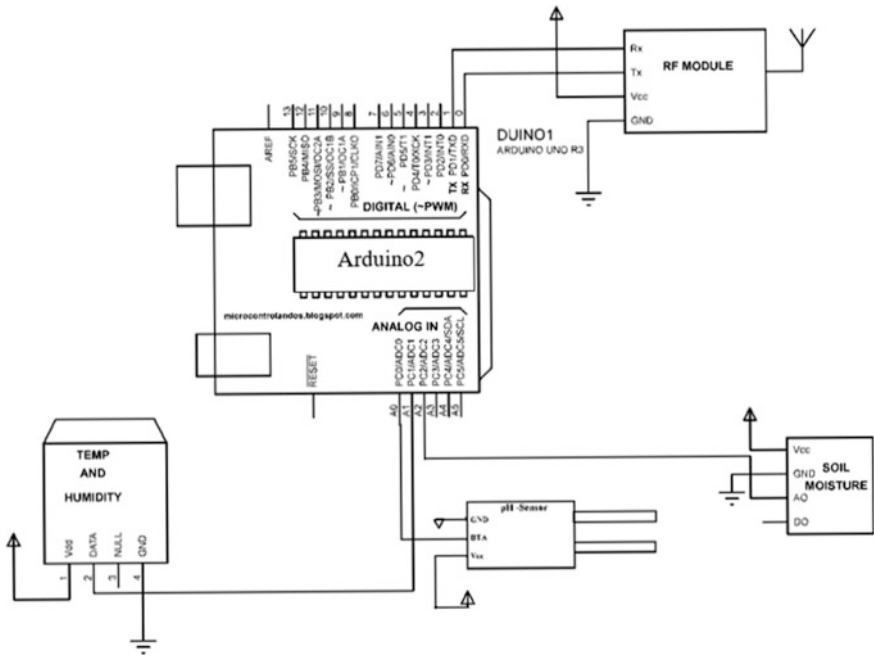


Fig. 3 Arduino unit consisting of some soil sensors and temperature/humidity sensor

A soil moisture sensor is also connected to the Arduino2 for measuring the moisture content in the soil. Analog pin ‘A0’ of the sensor is connected to ‘A2’ pin of Arduino2. Input power Vcc and ground are given to the sensor using a power supply shown in Fig. 4.

As the threshold value of moisture content is predefined to the Arduino, as soon as the value of moisture content in soil falls and reaches just below the threshold. A high signal is generated at the digital pin of Arduino2 at which a motor is connected which will get turn on and a water supply connected to it will get started, and when the moisture content in the soil becomes well enough, a low signal is generated at the same pin to turn off the water supply.

An RF module is connected to Rx and Tx pin of the Arduino2 which will receive all the data transmitted by the RF connected to the Arduino1.

All the data recorded by the sensors is forwarded to the Arduino board connected to LAN, which will be then uploaded to a cloud server using IoT technology.

The above Fig. 4 is the Proteus simulation of 5 and 12 Volts power supply. This power supply is used for the entire project to provide Vcc and ground to the sensors. This is simple power supply circuit which is converting 220–240 V into 5 and 12 V output. Here, we are using a step down transformer ‘TR1’, for transforming high voltage AC input into a low voltage. To convert the stepped down AC voltage into DC, a bridge rectifier is made using diodes. Further, the output of the rectifier is passed through capacitor for filtering purpose. Capacitor eliminates the

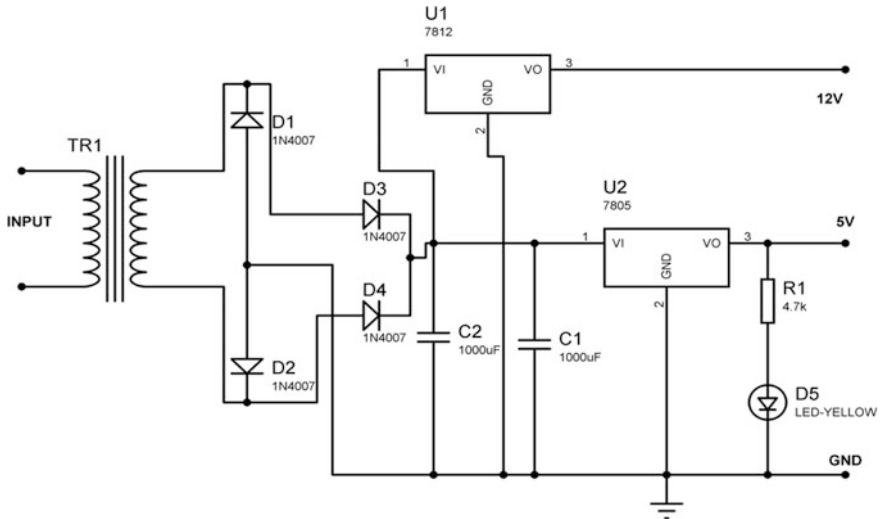


Fig. 4 Proteus simulation of the power supply used in our research

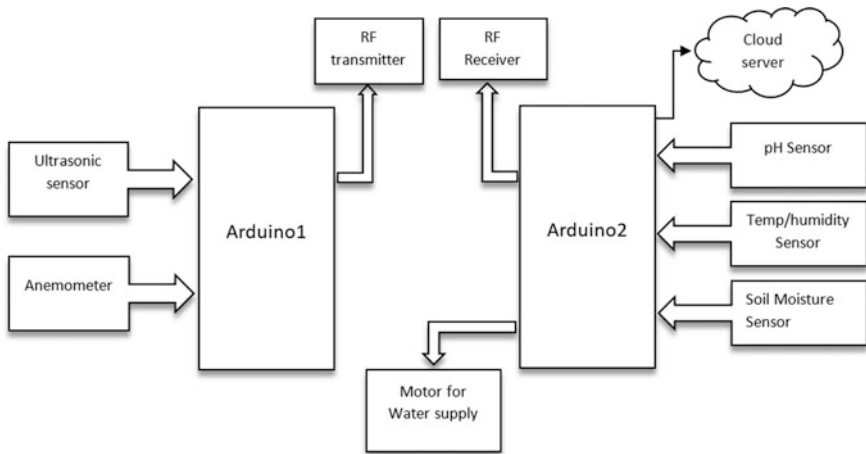


Fig. 5 Block diagram of the system

fluctuations in the voltage and provides a stable DC voltage, which is then fed to IC 7805 and IC 7812 for getting the desired 5 and 12 V power at the output.

Figure 5 is the block diagram for the whole experiment. In the block diagram, two Arduino boards are used, named as Arduino1 and Arduino2. Ultrasonic sensor and anemometer are connected to Arduino1, and data is transmitted through RF.

pH sensor, temperature/humidity sensor, and soil moisture sensor are connected to Arduino2. All the data transmitted from Arduino1 is received from Arduino2

using receiver RF. All the collected data is then uploaded to a cloud server using IoT technology. A water supply controlled by motor is also connected to Arduino 2.

4 Formulas

Equation (1) is used to calculate the distance from sensor to the tip of the plant. When we take the product of time 't' taken by the sound wave to travel to and back from the obstacle and the speed of sound wave which is 0.034, the result we get from that is double of the desired distance. That is why only we have divided the distance by 2 in the Eq. (1).

$$D = t \times 0.034/2 \quad (1)$$

Here,

D distance calculated by Ultrasonic sensor

t time taken by the sound wave

Similar work has been shown in [15]. To calculate the height and growth of the plant, the values of 'D' and 'H' are implemented repeatedly after a certain time period. 'H' is the height of the sensor fixed by us manually, and 'D' is the distance measured by sensor using Eq. (1). We will get the height of the plant by subtracting *D* from *H* as shown in Fig. 1. Ultrasonic sensor will continuously collect the value of 'D,' and microcontroller will do the mathematics to obtain the height of the plant.

$$T = H - D \quad (2)$$

Here,

H Height of sensor from ground.

D Distance measured by sensor.

T Height of the plant.

To measure the growth rate of the plant, we have constructed an equation labeled as Eq. (3) written below. As the ultrasonic sensor will record the value of *D* after each and every hour, the microcontroller will find the height of the plant after every hour simultaneously. All the obtained data of height of the plant is saved as T_1 for the first hour and T_2 for the second hour of the day. Then the growth of the plant is calculated by subtracting the previous recorded height (T_1) from the new height (T_2) that will be $T_2 - T_1$ shown in Eq. (4). Moreover, to obtain the growth rate of the plant in that 1-hour microcontroller will divide the obtained value with 60 to obtain growth rate in mm per min. Likewise height of the plant will be calculated after every hour from $T_1 - T_{24}$. In the end of the day, average of all the calculated heights is measured and then it is divided by 24 for getting the growth of plant in mm per

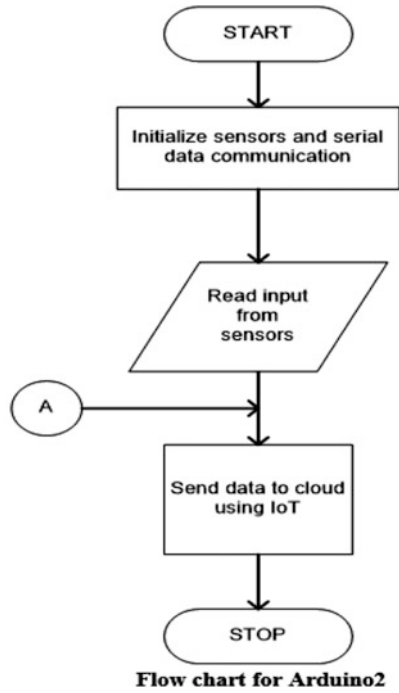
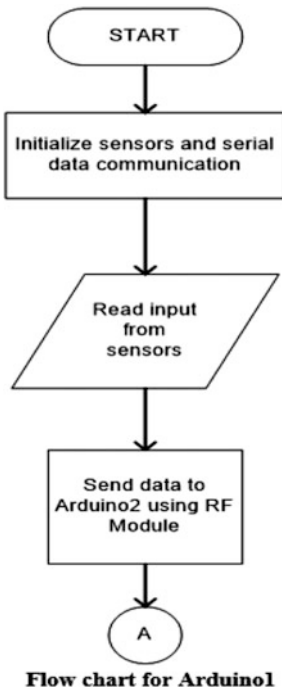
day. In the same way, we can set the unit for our calculations according to our requirement.

$$(T'_1 + T'_2 + T'_3 + \dots T'_{24})/24 = T_{\text{avg}} \text{ mm/day} \tag{3}$$

Where,

$$T'_1 = (T_2 - T_1)/60 \text{ mm/min} \tag{4}$$

5 Flowcharts



6 Conclusion

Plants growth measurement is very important factor in determining the healthy conditions of the vegetation. The design used in our study can be used to ensure the health of any plant. This device can be further used to implement on a large scale. The use of microcontrollers along with sensors is a very good combination that is very cost effective. Comparison between two plants can be carried out with the help of this device, thereby getting an idea of which plants require what soil and environmental conditions for its growth. Further actions can be taken to resolve the issue if out of two plants one plant is not showing good results. Moreover, the device is working on IoT technology such that all the data will get uploaded to the cloud and the user can access all the information just by having access to the Internet. Thus, the device is very user-friendly and easy to set up. After the setup of the device, its functioning is automatic and does not require any need of labor work.

References

1. <http://www.cropin.co.in.>, Cropin Technology Solutions PVT LTD, Bangalore, Karnataka.
2. Xiaojuan Duan, "Research on IoT based Smart Garden Project", *Applied Mechanics and Materials*, Vol. 608–609, pp. 321–325, 2014.
3. Raj Kumar Singh, A. K. Jain, "Research Issues in Wireless Network", *International Journal of Advanced Research in Computer Science and Software Engineering*, Volume 2, Issue for, April 2012.
4. N. K. Kaphungqi, "RF Based Remote Control for Home Electrical Appliances", *International Journal of Innovative Research in Electrical, Electronics, Instrumentation and Control Engineering*, Vol. 3, Issue 7, July 2015.
5. Dennis A Bohn, "Environmental Effects on the Speed of Sound", *J. Audio Eng. Soc.*, Vol. 36, No. 4, 1988 April.
6. S. R. Vijay Lakshmi, S. Muruganand, "Challenges in Integrating Wireless Sensor Network and Internet of Things for Environmental Monitoring", *World Scientific New* 41 (2016) 1–315.
7. Demurtas, Giorgio, et. al, "Calibration of a Spinner Anemometer for Wind Speed Measurements", *Wind Energy*, Volume 19, Issue 11, November 2016.
8. Vijay S. Kale, Rohit D. Kulkarni, "Real Time Remote Temperature and Humidity Monitoring using Arduino and Xbee S2", *International Journal of Innovative Research in Electrical, Electronics, Instrumentation and Control Engineering*, Vol. 4, Issue 6, June 2016.
9. <https://www.sparkfun.com/products/13322>. SparkFun Electronics® Niwot, Colorado.
10. Khole, Sagar, et. al, "Automated Drinking Water Supply System and Theft Identification using Embedded Technology", *International Journal of Innovative Research in Computer and Communication Engineering*, Vol. 3, Issue 3, March 2015.
11. <http://www.vernier.com/products/sensors/ph-sensors/ph-bta/>... ©2017 Vernier Software & Technology, Beaverton, OR 97005 United States of America.
12. Shende, Prashant, et. al, "RF based Automatic Energy Meter Reading System", *International Journal of Advanced Research in Computer Science and Software Engineering*, Volume 4, Issue 9, September 2016.

13. Katyal, Amber et. al, "Wireless Arduino based Weather Station", International Journal of Advanced Research in Computer and Communication Engineering, Vol. 5, Issue 4, April 2016.
14. Subhankar Chattoraj, "Smart Home Automation based on different sensors and Arduino as the master controller", International Journal of Scientific and Research Publications, Volume 5, Issue 10, October 2015.
15. Shrivastava, A. K. et. al, "Distance Measurement of an Object or Obstacle by Ultrasound Sensors using P89C51RD2", International Journal of Computer Theory and Engineering, Vol. 2, No. 1, February 2010.

Design of Novel Through Silicon via Structures for Reduced Crosstalk Effects in 3D IC Applications

Mounika Ganimidi and Vobulapuram Ramesh Kumar

Abstract In recent days, through silicon via (TSV) become a promising technology for integrated circuit packaging. The structure of the TSV composed of copper, insulating liner, and silicon substrate. The TSV is enclosed using insulating liner to troubleshoot the leakage in signal from copper (Cu) to silicon (Si) substrate. In the existing TSV structures, silicon dioxide (SiO_2) dielectric is used as insulation liner because of its material compatibility with the silicon substrate. On the other hand, several researchers were reported the problems of SiO_2 . Due to the high dielectric constant of SiO_2 , the insulating capacitance increases that result in increasing of delay. Therefore, SiO_2 is not suitable for high-performance applications. To alleviate the insulating capacitance, polymer liner is used rather than SiO_2 . A proposed novel TSV structure consists of the signal TSV is encompassed by utilizing the poly-propylene liner. For comparison purpose, we perform the simulations for both conventional and proposed TSV structures by varying different design parameters of TSV. It has been observed that the proposed TSV structure shows 25% decrease in crosstalk compared to conventional TSV structures.

Keywords Through Silicon Via (TSV) · Poly-propylene liner
Polymer capacitance · Crosstalk

1 Introduction

In present days, through silicon via (TSV) interconnects are playing vital role in 3-D IC integration. The TSV interconnects are short in length and consume less power. The TSVs support all blocks in integrated circuits are stacked vertically.

M. Ganimidi (✉)

Department of Electronics and Communication Engineering,
Koneru Lakshmaiah University, Guntur, India
e-mail: aaavigaba13@gmail.com; ganimidimounika@gmail.com

V. Ramesh Kumar

Department of Electronics and Communication Engineering, Rajeev Gandhi Memorial
College of Engineering and Technology, Nandyal, India

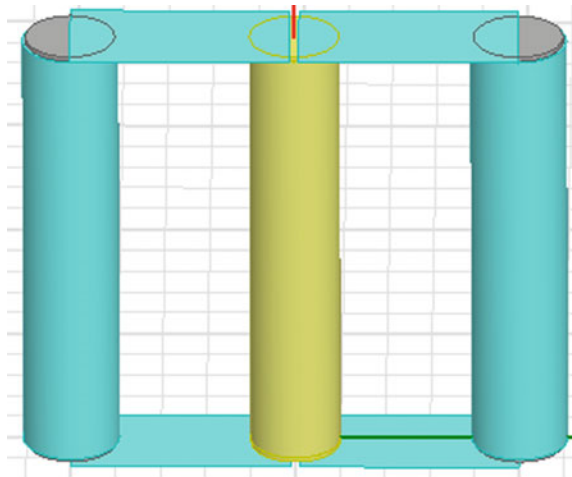
The structure of the TSV composed of Cu, insulating liner, and silicon substrate [1–4]. The usage of insulating liner is to troubleshoot the signal spillage from the copper (Cu) metal to silicon (Si) substrate. In the traditional TSV structures, silicon dioxide (SiO_2) is used as a liner for insulation because of its material compatibility with the silicon substrate. The oxide liner has small thickness which is roughly equivalent to $0.01 \mu\text{m}$, and it has large dielectric constant normally the value is 3.9. Because of high dielectric constant, SiO_2 liner develops a large insulating capacitance which impacts on degradation of TSV performance. Hence, SiO_2 liner is not appropriate for high-performance applications. To enhance the TSV performance and mitigate the insulating capacitance, low-dielectric constant liners are used instead of SiO_2 liners.

Normally, polymer liner has low dielectric constant, elastic modulus, and large thickness. Due to the low dielectric constant of polymer, it prompts a less insulating capacitance between metal and silicon substrate that results in decreasing of delay. Hence, polymer liners are well suitable for high-performance applications. In the proposed model, we considered a novel TSV structure with polypropylene polymer liner as insulating liner.

2 Electrical Modelling of TSV with Analytic Equations

The proposed TSV structure comprises of three cylindrical signal-ground-signal pattern with height $100 \mu\text{m}$ and radius $10 \mu\text{m}$ as shown in Fig. 1. The first and third cylinder is designed with copper surrounded by polypropylene liner thickness $0.1 \mu\text{m}$ and heavily doped silicon MOS depletion layer width $0.68 \mu\text{m}$. The middle cylinder is designed with copper and surrounded by doping layer thickness $0.1 \mu\text{m}$.

Fig. 1 Proposed TSV structure with Signal-Ground-Signal pattern



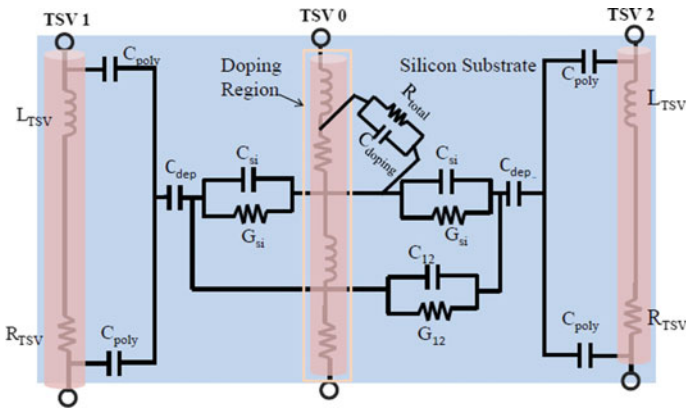


Fig. 2 Electrical equivalent model for the proposed TSV

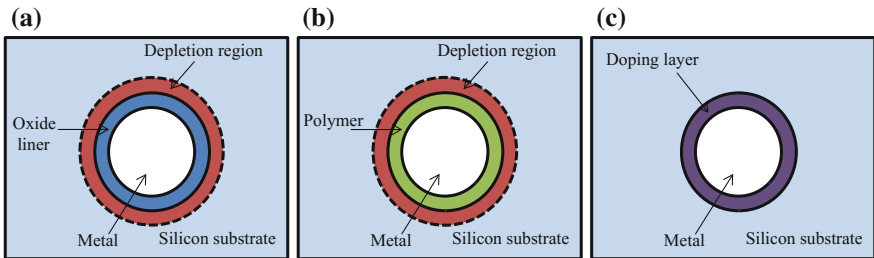


Fig. 3 **a** The top-view of conventional signal and ground TSV, **b** proposed signal TSV, **c** Top view of proposed ground TSV structure

The dielectric constant $\epsilon_{si}(\epsilon_r)$ of poly-propylene liner, SiO_2 , silicon, and copper are 2.3, 3.9, 11.9, and 1, respectively.

In this section, an equivalent circuit model for TSVs is reported with distributed RLGC components. The electrical equivalent model is framed using the analytic equations, which are formulated based on the material properties, frequency structural parameters, etc. Figure 2 shows the electrical equivalent circuit of the proposed TSV structures. The presented model is framed based on TSV's physical structure (Fig. 3).

The RLCG parameters based on the structure of TSV are reported below. The resistance and inductance of the TSV are analytically modeled as

$$R_{\text{TSV}} = \rho_{\text{TSV}} \times \frac{h_{\text{TSV}}}{\pi \left(\frac{d_{\text{TSV}}}{2}\right)^2} \tag{1}$$

$$L_{\text{TSV}} = \frac{1}{2} \left\{ \frac{\mu_0 \mu_r \text{TSV}}{2\pi} \times h_{\text{TSV}} \times \ln \left(\frac{\rho_{\text{TSV}}}{r_{\text{TSV}}} \right) \right\} \quad (2)$$

where h_{TSV} , d_{TSV} , r_{TSV} are the length, diameter, and radius of the TSV.

It is necessary to surround an insulating layer around the TSV, to isolate it from conductive silicon substrate. An insulation capacitance C_{polymer} will come into the picture because of this insulation layer [5]. A depletion capacitance C_{dep} which is in series with C_{polymer} is appeared owing to ground connection of substrate. The polymer capacitance and depletion capacitance can be calculated as

$$C_{\text{polymer}} = \frac{1}{2} \left\{ 2\pi \times \varepsilon_0 \varepsilon_{r,\text{polymer}} \times \frac{h_{\text{TSV}}}{\ln \left(\frac{r_{\text{TSV}} + t_{\text{poly}}}{r_{\text{TSV}}} \right)} \right\} \quad (3)$$

$$C_{\text{dep}} = \frac{\varepsilon_{\text{Si}} h_{\text{TSV}}}{\ln \left(1 + \frac{w_{\text{dep}}}{r_0} \right)} \quad (4)$$

The metal–semiconductor contact formed between the silicon substrate and the TSV conductor depends on doping concentration of substrate and type of metal, respectively. The metal and semiconducting silicon results in two types of contacts: an ohmic contact or a rectifying Schottky contact [1]. An ohmic contact is formed with highly doped silicon, when the concentration is around 10^{20} cm^{-3} or higher. The ohmic contact is a less resistance junction, and it provides less contact resistance between metal and silicon substrate. This contact resistance depends on the doping concentration. Further, the lower doping concentrations result increase in the metal–silicon contact resistance. Metal and semiconductor formation is an important parameter in dealing with TSVs. The total resistance comprises of contact resistance and the resistance of the doping region is expressed in (5)

$$R_{\text{Total}} = \frac{1}{2\pi h_{\text{TSV}}} \ln \frac{r_0 + t}{r_0} \cdot \frac{1}{\sigma_{\text{eq}}} \quad (5)$$

The doping capacitance in (6) comes in the model, and it is based on the dielectric material used in doping region.

$$C_{\text{doping}} = \frac{\varepsilon_{\text{Si}} h_{\text{TSV}}}{\ln \left(1 + \frac{t}{r_0} \right)} \quad (6)$$

The unit-length inductance and mutual-inductances of signal TSV are reported in (7) by treating ground TSV as the reference ground [6, 7]

$$L_{ij} = \frac{\mu_0}{2\pi} \ln \left(\frac{l_{i0}^2}{R_i R_0} \right), \quad (i = j)$$

$$L_{ij} = \frac{\mu_0}{2\pi} \ln \left(\frac{l_{i0} l_{j0}}{R_0 l_{ij}} \right), \quad (i \neq j)$$
(7)

The coupled capacitance C_{12} and inductance G_{12} between the TSVs are extracted from the following matrices [8]

$$C = \mu_0 \varepsilon_{\text{Si}} h_{\text{TSV}} L^{-1}, \quad G = \mu_0 \sigma_{\text{Si}} h_{\text{TSV}} L^{-1}$$
(8)

Where σ_{Si} is silicon conductivity and ε_{Si} is dielectric constant, height of the TSV is represented by h_{TSV} .

3 Proposed TSV Results and Its Analysis

The performance of conventional TSV structures and proposed TSVs structures is analyzed in this section. The radius of TSV is 15 μm , length is considered as 150 μm , and the polymer liner thickness is chosen as 0.15 μm . The pitch between TSVs is chosen as 25 μm . The conductivity of silicon (σ_{Si}) is 10 s/m, and ground doping conductivity is 0.1 s/m. The signal TSV with excitation of 0 V at low level and 1 V at high level, the depletion region of metal oxide semiconductor region is 680 nm. In conventional structure, the depletion region around the TSV for ground is 280 nm. The performance of a novel TSV structure is simulated using HSPICE software. The conventional TSV structure is also simulated for performance comparison with the proposed TSV. The proposed TSV structure simulation shows the reduction in crosstalk dramatically compared to the conventional TSV structure.

Considered the thickness of liner (t_{ox} , t_{poly}) is 0.15 μm , $r_{\text{TSV}} = 15 \mu\text{m}$, $h_{\text{TSV}} = 150 \mu\text{m}$, pitch between TSVs is 25 μm for both proposed and conventional TSV structure. The higher dielectric constant of oxide results in oxide capacitance is more compared to polymer capacitance. Due to the reduction in polymer capacitance, it leads to decrease in the crosstalk effect. In addition to that, depletion capacitance and doping capacitance of signal and ground TSV are also considered into account. In conventional TSV structure, there is depletion capacitance for ground TSV similar to the signal TSVs. In place of depletion capacitance, doping capacitance for the ground TSV is considered in proposed TSV structure. Compared to depletion capacitance, doping capacitance for ground TSV is negligibly small. Therefore, the crosstalk in proposed TSV structure is decreased nearly 25% compared to conventional TSV structure as shown in Fig. 4.

In addition to that, the proposed TSV structure is validated by 3-D field solver simulation results, HFSS. Many design parameters such as r_{TSV} , h_{TSV} , and ρ_{TSV} are swept to validate the proposed TSV structure until to reach the frequency by 20 GHz. Figure 5 shows the crosstalk in the proposed TSV structure. The

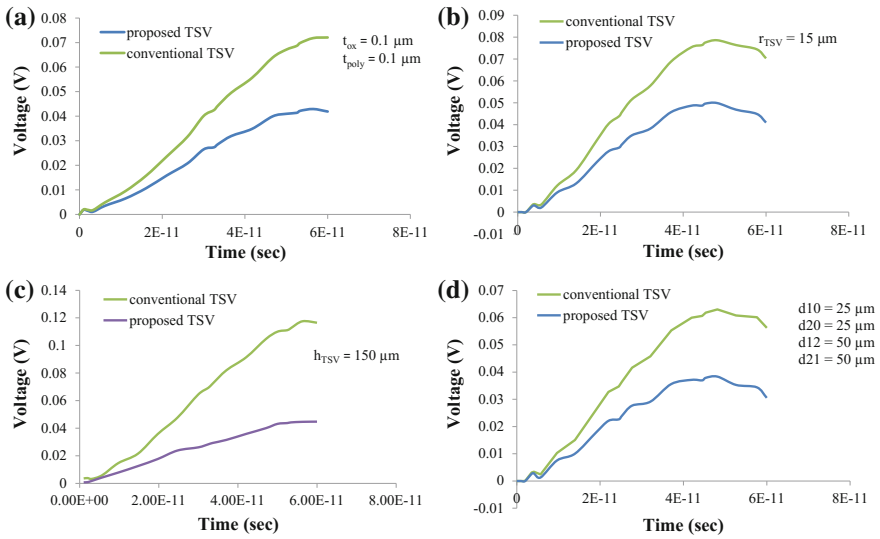
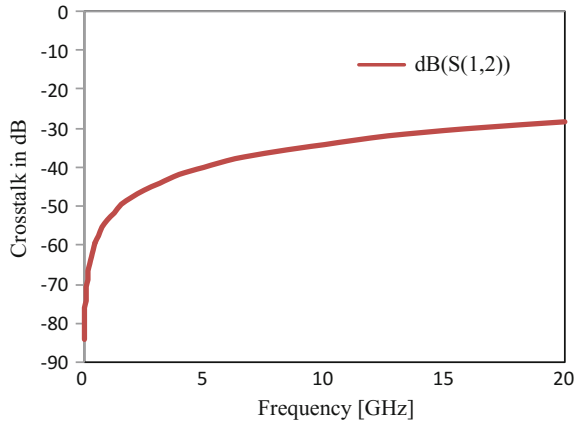


Fig. 4 Comparison of proposed TSV structure simulation with the conventional TSV structure. **a** t_{ox} , $t_{poly} = 0.15 \mu\text{m}$, **b** $r_{TSV} = 15 \mu\text{m}$, **c** $h_{TSV} = 150 \mu\text{m}$, **d** $d_{10} = 25 \mu\text{m}$, $d_{20} = 25 \mu\text{m}$

Fig. 5 Simulation results of proposed TSV structure with 3-D field solver



simulation results show crosstalk in proposed TSV structure which is approximately equal to 80 dB at lower frequencies.

4 Conclusion

A novel TSV structure is proposed for reducing the crosstalk effects. The proposed TSV structure uses poly-propylene polymer liner as insulating liner because of its low dielectric constant. The main contribution of this work is analyzing the impact

of insulating capacitance on crosstalk noise. For same value of parameters like TSV radius, we observe that the crosstalk decreases over conventional TSV structures. The proposed TSV structure shows 25% decrease in crosstalk compared to conventional TSV structures. The proposed TSV structure is also simulated using 3-D field solver.

Acknowledgements The authors would like to thank Science and Engineering Research Board (SERB), DST, Government of India for the financial support of the project file number ECR/2016/001070.

References

1. DC Yang, J. Xie, and M. Swaminathan, "A Rigorous Model for Through-Silicon Vias With Ohmic Contact in Silicon Interposer," *IEEE microwave and wireless components letters.*, vol. 23, no. 8, pp. 385–387, July 2013.
2. B. K. Kaushik, M. K. Majumder, and V. Ramesh Kumar, "Carbon nanotube based 3-D interconnects - A reality or a distant dream," *IEEE Circuits and Systems Magazine*, vol. 14, no. 4, pp. 16–35, Nov. 2014.
3. V. Ramesh Kumar, M. K. Majumder, and B. K. Kaushik, "Graphene based on-chip interconnects and TSVs – Prospects and challenges," *IEEE Nanotechnology Magazine*, vol. 8, no. 4, pp. 14–20, Nov. 2014.
4. M. K. Majumder, A. Kumari, A. Alam, V. Ramesh Kumar, and B. K. Kaushik, "Signal integrity improvement with peripherally placed MWCNTs in mixed CNT bundle based TSVs," in *Proc. IEEE Conference on Electron Devices and Solid-State Circuits*, Singapore, pp. 649–652, June, 2015.
5. G. Katti, M. Stucchi, K. De Meyer, and W. Dehaene, "Electrical modeling and characterization of through silicon via for three-dimensional ICs," *IEEE Trans. Electron Devices*, vol. 57, pp. 256–262, 2010.
6. T. Bandyopadhyay, K. J. Han, and D. Chung, "Rigorous electrical modeling of Through Silicon Vias (TSVs) with MOS capacitance effects," *IEEE Trans. Comp. Packag. Manufact. Technol.*, vol. 1, pp. 893–903, 2011.
7. E. Engin and N. S. Raghavan, "Metal semiconductor (MES) TSVs in 3D ICs: Electrical modeling and design," in *Proc. IEEE Int. 3D Syst. Integr. Conf.*, 2012, pp. 1–4.
8. B. K. Kaushik, V. Ramesh Kumar, M. K. Majumder, and A. Alam "Through Silicon Vias – Materials, Models, Design and Performance," *CRC Press, Taylor & Francis*, 2016.

A Cost Effective and Performance Enhanced Deadlock Recovery Scheme for Wormhole Routed Networks

Jameel Ahmad, Akheela Khanum and A.A. Zilli

Abstract Directly connected multicomputer systems provide massively high computational capacity when connected with an interconnection network, having their own components as local memory, processor and other peripheral devices and connected with some topology as mesh, hypercube, and tree [1]. These nodes communicate with each other by exchanging messages. Each node equipped with a router which deals with communication-related implications [2]. Various switching techniques are used to route the messages from source to destination node. The wormhole routing technique has been proved as most suitable switching technique in these systems [3], but faces challenges like flow control and deadlocks (Mohapatra in Wormhole routing techniques for directly connected multicomputer systems [4]). There are two common approaches to deadlock handling: deadlock detection and deadlock recovery. The proposed work is based on deadlock recovery. This is based on the existing scheme ‘Disha’ (Anjan and Pinkston in An efficient fully adaptive deadlock recovery scheme: DISHA, pp. 201–210 (1995) [5]). Full adaptive routing is allowed without any restriction, and a deadlock detection mechanism is applied to monitor the deadlocks, and if deadlock is detected, then a deadlock recovery mechanism is in place to resolve the deadlock cycles. To optimize the cost the proposed scheme suggests, not equipping every node with additional buffer but alternate nodes in the columns of a mesh can be equipped with additional flit buffer, and blocked packets can switch to the recovery path, and eventually reach to the destination. So enhanced performance is achieved on reduced complexity and optimized cost.

Keywords Wormhole switching · Adaptive routing · Recovery path
Deadlock buffer

J. Ahmad (✉) · A. Khanum · A.A. Zilli
Department of Computer Science and Engineering, Integral University Lucknow,
Lucknow, UP, India
e-mail: jameel@iul.ac.in

A. Khanum
e-mail: akheela@iul.ac.in

A.A. Zilli
e-mail: aazilli@yahoo.com

1 Introduction

The parallel computers provide high computational performance. These systems are assembly of nodes, each having its own processor, local memory, and other peripheral devices. These nodes are interconnected through some topologies categorized as direct and indirect. In direct networks, nodes are connected with direct connection or point to point, through some topology like mesh, hypercube, or tree. Each node is equipped with a router to deal with communication-related tasks [6]. The latency of communication is one of the important metrics in these networks. The wormhole routing has been found most suitable switching technique in these networks [4]. The wormhole switching faces the challenges like flow control and deadlocks. Deadlocks are crucial issue in the wormhole-routed networks. Deadlock avoidance and deadlock recovery are the two common approaches to deadlock handling[7, 8]. The proposed work is based on the deadlock recovery. The performance of the base scheme ‘Disha’ [5] has been enhanced by reducing the complexity of the routers [9]. The cost also has been reduced by reducing the number of resources and increasing their utilization [10]. So the proposed work is an attempt to provide enhanced performance on optimized cost.

2 Wormhole Switching

In the wormhole switching technique, a packet is further divided into small-sized transmittable units known as flits, and all the transmission between nodes is performed in the form of flits. One of the flit is designated as header flit that contains all the information related to routing, and rest all the flits of a message contain data. All the flits of a message flow in a sequence where all the data flits follow the header flit (Fig. 1).

Prevention of deadlock is one of the main issues in wormhole switching and usually accomplished by a suitable choice of routing function that selectively prohibits messages from taking all available paths, thus preventing cycles in the network. Selection of a routing algorithm is thus a major issue in wormhole-switched network [11].

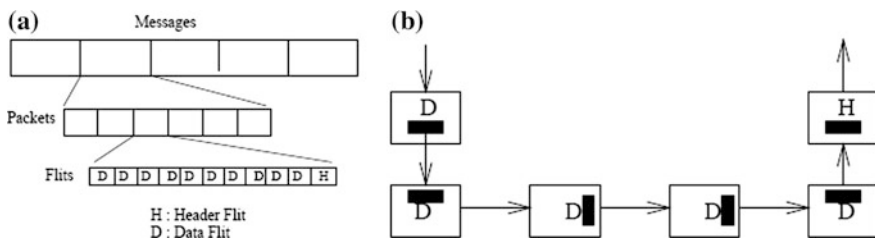


Fig. 1 Routing in wormhole switching [4]

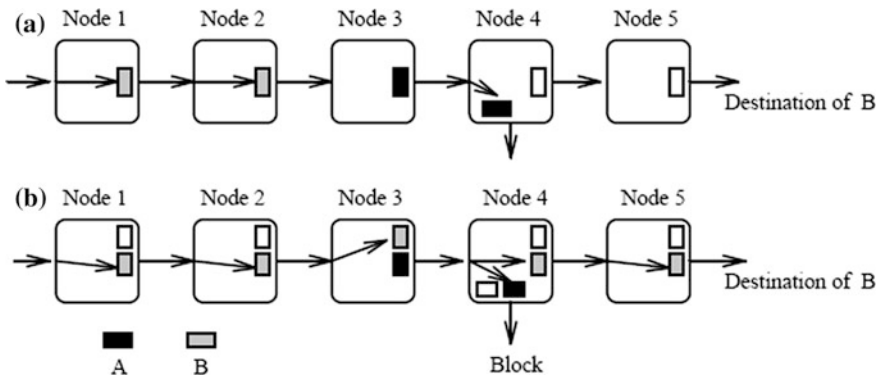


Fig. 2 Blocking of message and solution by virtual channel [4]

Virtual Channels: A virtual channel is logical abstraction of its physical channel [4]. Virtual channels provide alternative path and reduce the blocking effect [12]. These are used in multicomputer systems to improve performance and to design deadlock-free routing techniques (Fig. 2).

3 Deadlock Recovery Scheme ‘Disha’

The work is based on the deadlock recovery scheme ‘Disha’ [5] proposed by Anjan and Pinkston. In this scheme, routing is carried out without any restriction or use of virtual channels. In the case of formation of cycles resulting deadlocks, an additional flit buffer is provided with every node. The deadlock buffers provide alternative path to the blocked messages, and any one of the packets is shifted to the deadlock buffer lane and eventually reaches its destination and consumed. Once, one packet advances, the cycle breaks, and other packets resume their way.

4 Deadlock Recovery Scheme ‘Disha Enhanced’

The proposed work aims at optimizing the performance of routing of an interconnection network on reduced cost. This has been achieved by reducing 40% deadlock buffers from alternate columns of a mesh interconnection network against the base scheme ‘Disha’ and eventually reducing the cost of crossbar ports to reduce the cost and complexity of the routers and thereby speeding up the routers to enhance the performance of the deadlock recovery scheme. The cost and complexity of routers has been further reduced by reducing a number of virtual channels from alternate columns.

The base scheme ‘Disha’ has used additional deadlock buffer at every router [13], but the proposed scheme suggests to use deadlock buffers at alternate columns only to reduce the cost and complexity of the routers. A deadlock recovery path has been provided to support the recovery scheme. Some additional deadlock buffers have been equipped to complete the recovery path. If some packets are blocked due to formation of the deadlock cycle, any one packet is shifted to the deadlock buffer path and eventually reaching its destination, thereby breaking the cycle and resuming the network to precede other packets along their way. Only one packet is allowed to switch to recovery path to make sure that recovery path is deadlock free. So the proposed scheme is using lesser resources to recover from deadlocks and enhancing the performance of the scheme, suggesting a cost effective framework with enhanced performance.

4.1 Interconnection Network in the Proposed Scheme ‘Disha Enhanced’

The interconnection network given below has used deadlock buffers at alternate columns only, against the base scheme, which has used deadlock buffers at every router [14]. The shaded squares are indicating nodes equipped with deadlock buffers (Fig. 3).

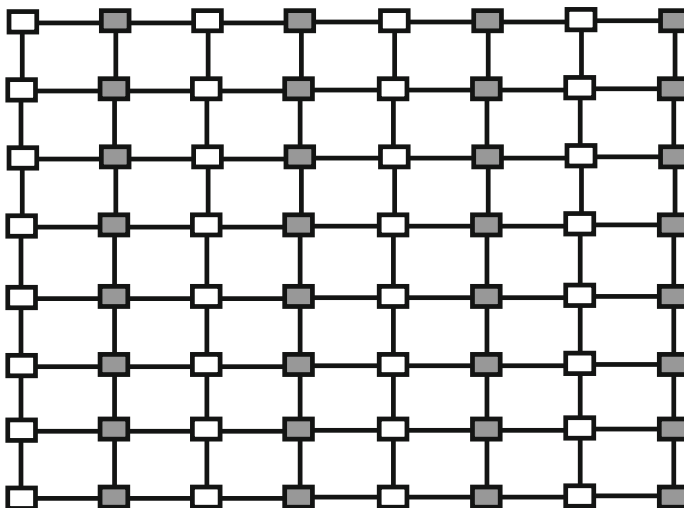


Fig. 3 Interconnection network ‘Disha Enhanced’

4.2 Recovery Path

In the case of deadlock situations, a recovery path has been provided to shift a packet on recovery path to ensure deadlock-free recovery scheme. Seven additional flit buffers have been taken to complete the recovery path. The recovery path is acyclic to guarantee that the packet on recovery path cannot further stick in cycle. The figure below shows the recovery path. As shown in the above figure, every node on the recovery path is equipped with deadlock buffer to facilitate deadlock-free routing on the recovery path (Fig. 4).

4.3 Deadlock Situations

Deadlock occurs when some packets endlessly wait for each other and no packet is able to proceed in the network due to formation of deadlock cycle.

Figure 5 shows a deadlock situation where four packets P1, P2, P3, and P4 are waiting for each other in a deadlock cycle. Here, $P1 \rightarrow P2 \rightarrow P3 \rightarrow P4 \rightarrow P1$.

In the cycle formed in above figure, two segments of the deadlock cycle are on the deadlock buffer equipped columns. Figure 6 shows the deadlock recovery scheme. The path equipped with deadlock buffers provides an alternative path for packet P1; hence, packet P1 shifts to recovery path and breaks the cycle. After P1, P4 can proceed on its path, and then, the packets P3 and P2 can resume their path and reach their destination, so the network is resumed by achieving recovery.

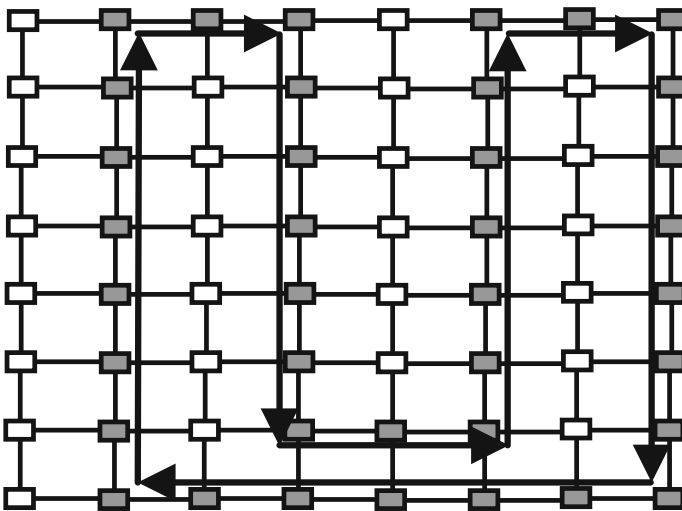


Fig. 4 Recovery path

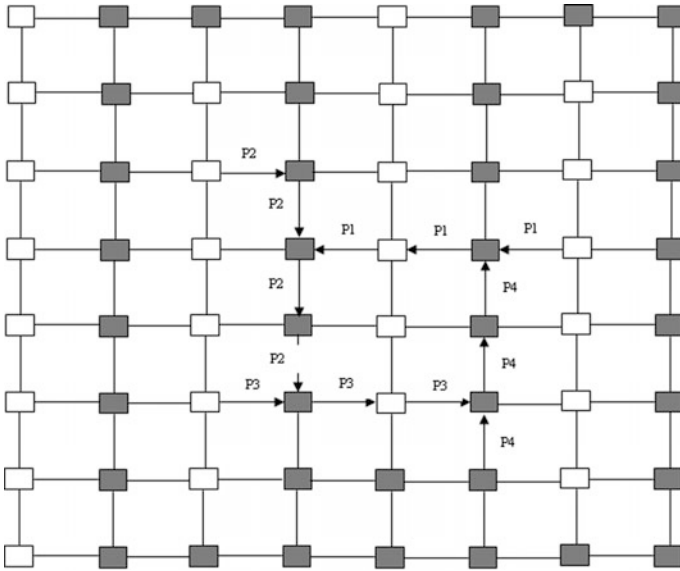


Fig. 5 Deadlock scenario

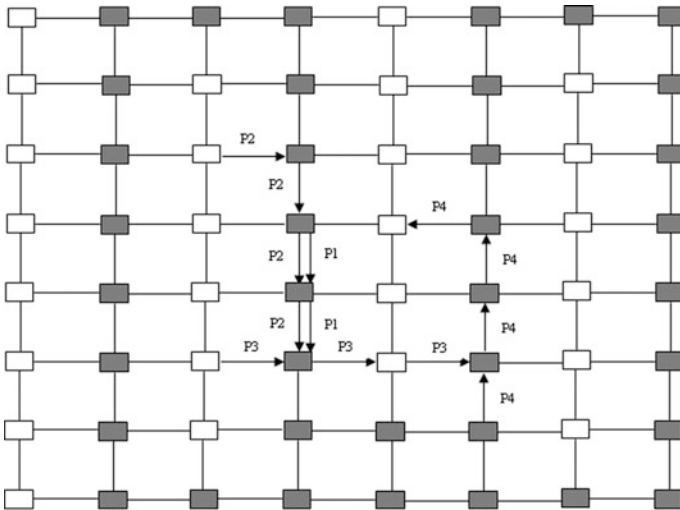


Fig. 6 Recovery scheme

4.4 Architecture of Routers

Two types of routers have been used in the proposed scheme:

Routers equipped with deadlock buffer: The routers with deadlock buffer are same as the base scheme. S_0, S_1, \dots, S_3 are showing the status line that makes tri-state deadlock buffers enable in presence of deadlock and keeps disable in absence of deadlock. The crossbar has been taken 6×5 , i.e., six inputs and five outputs (Figs. 7 and 8).

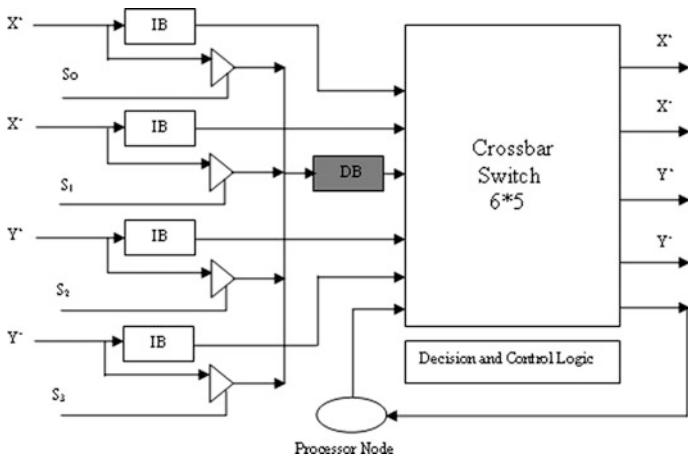


Fig. 7 Router in Disha

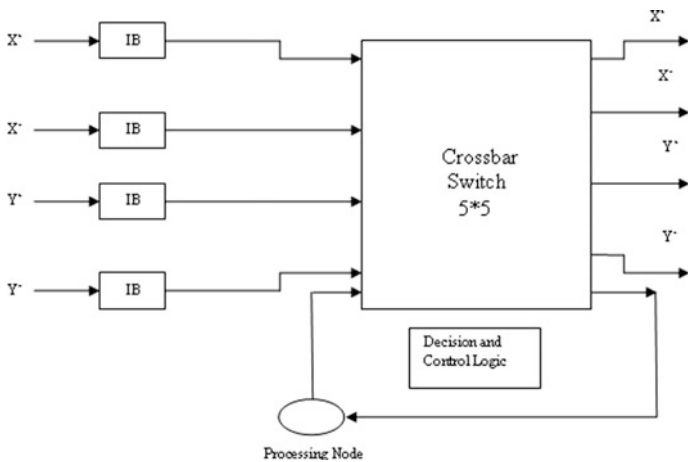


Fig. 8 Router without deadlock buffer

5 Performance of the Proposed Scheme

'Disha Enhanced': Cost Model

The cost of the proposed scheme 'Disha Enhanced' has been compared with 'Disha' scheme as per following'.

'Disha' and 'Disha Enhanced' both without virtual channels. 'Disha' with one virtual channel and 'Disha Enhanced' with one virtual channel at alternate columns only. 'Disha' with two virtual channels per physical channel and 'Disha Enhanced' with one virtual channel per physical channel.

Setup Latency

$$T_{Setup} = T_{Ad} + T_{Arb} + T_{Cb} + T_{Hsel} + T_{Vc}$$

T_{Setup} setup latency

T_{Ad} address-decoding latency

T_{Arb} arbitration delay

T_{Cb} delay through crossbar

T_{Hsel} header updation latency

T_{Vc} Virtual channel controller delay

Data Through Latency

$$T_{data-through} = T_{Fc} + T_{Cb} + T_{Vc}$$

T_{Fc} Flow controller delay

Values of Individual Latencies

$$T_{Ad} = C_3$$

$$T_{Arb} = C_4 + C_5 * \log F \quad (F : \text{Routing freedom} = \text{no. of o/p choices})$$

$$T_{Cb} = C_0 + C_1 * \log P \quad (P : \text{no. of ports input/output})$$

$$T_{Hsel} = C_6 + C_7 * \log F$$

$$T_{Vc} = C_8 + C_9 * \log V$$

$$T_{Fc} = C_2$$

Delay Constants

$C_0 = 0.4$, $C_1 = 0.6$, $C_2 = 2.2$, $C_3 = 2.7$, $C_4 = 0.6$, $C_5 = 0.6$, $C_6 = 1.4$, $C_7 = 0.6$, $C_8 = 1.24$, $C_9 = 0.6$ [9].

6 Cost Model

Disha (Without Virtual Channel)

At Setup

$$\begin{aligned}
 T_{disha} &= T_{Ad} + T_{Arb} + T_{Cb} + T_{Hsel} + T_{Vc} \\
 &= C3 + (C4 + C5 * \log F) + (C0 + C1 + * \log P) \\
 &\quad + (C6 + C7 * \log F) + 0 \quad (T_{Vc} = 0) \\
 &= 6.50
 \end{aligned}$$

At Data Through

$$\begin{aligned}
 T_{disha} &= T_{Fc} + T_{Cb} + T_{Vc} \\
 &= C2 + (C1 * \log P) + 0 \quad (T_{Vc} = 0) \\
 &= 2.2 + 0.6 * (\log 6 + \log 5) + 0 \\
 &= 3.088
 \end{aligned}$$

Cost Model: Proposed 'Disha Enhanced' (Without Virtual Channel)

At Setup

Let latency at router with deadlock buffer = T_{db}

Latency at router without deadlock buffer = T_s , then

$$\begin{aligned}
 TDE &= (T_{db} + T_s) / 2 \\
 T_{db} &= 6.5 \quad (\text{Same as disha}) \\
 T_s &= T_{Ad} + T_{Arb} + T_{Cb} + T_{Hsel} + T_{Vc} \\
 &= C3 + (C4 + C5 * \log F) + (C0 + C1 + * \log P) \\
 &\quad + (C6 + C7 * \log F) + 0 \quad (T_{Vc} = 0) \\
 &= 6.36 \quad 2.15\% \text{ faster} \\
 TDE &= (6.50 + 6.36) / 2 \\
 &= 6.43
 \end{aligned}$$

At Data Through

$$\begin{aligned}
 TDE &= (Tdb + Ts)/2 \\
 Tdb &= 3.10 \quad (\text{Same as disha}) \\
 Ts &= TFc + TCb + TVc \\
 &= C2 + (C1 * \log P) + 0 \quad (TVc = 0) \\
 &= 3.04 \quad 2\% \text{ faster} \\
 TDE &= (3.10 + 3.04)/2 \\
 &= 3.07
 \end{aligned}$$

Cost Model: 'Disha' (With One Virtual Channel)

At Setup

$$\begin{aligned}
 TDisha &= TAd + TArb + TCb + THsel + TVc \\
 &= 6.50 + (C8 + C9 * \log V) \\
 &= 7.74
 \end{aligned}$$

At Data Through

$$\begin{aligned}
 TDisha &= TFc + TCb + TVc \\
 &= 4.34
 \end{aligned}$$

Cost Model: Proposed 'Disha Enhanced' (One Virtual Channel at Alternate Columns Only)

At Setup

$$\begin{aligned}
 Tdb &= TAd + TArb + TCb + THsel + TVc \\
 &= 6.50 + TVc \quad (TVc = 0) \\
 &= 6.50 \quad 16\% \text{ faster} \\
 Ts &= TAd + TArb + TCb + THsel + TVc \\
 &= 6.36 + TVc \\
 &= 6.36 + (C8 + C9 * \log V) \\
 &= 7.60 \\
 TDE &= (6.50 + 7.60)/2 \\
 &= 7.05 \quad 9\% \text{ faster}
 \end{aligned}$$

At Data Through

$$\begin{aligned}
 T_{db} &= T_{Fc} + T_{Cb} + T_{Vc} \\
 &= 3.1 + 0 \quad (T_{Vc} = 0) \\
 &= 3.1 \quad 28.6\% \text{ faster} \\
 T_s &= T_{Fc} + T_{Cb} + T_{Vc} \\
 &= 3.04 + T_{Vc} \\
 &= 4.28 \\
 TDE &= (3.1 + 4.28)/2 \\
 &= 3.69 \quad 15\% \text{ faster}
 \end{aligned}$$

7 Analysis

Without virtual channel

As shown in the above graph, $TDE < TDisha$, both at Setup and Data Through (Figs. 9 and 10).

Proposed scheme is 4.15% faster than ‘Disha’ by reduced complexity at simple At Setup (without virtual channels)

Let latency at router with deadlock buffer = T_{db}

Latency at router without deadlock buffer = T_s , then

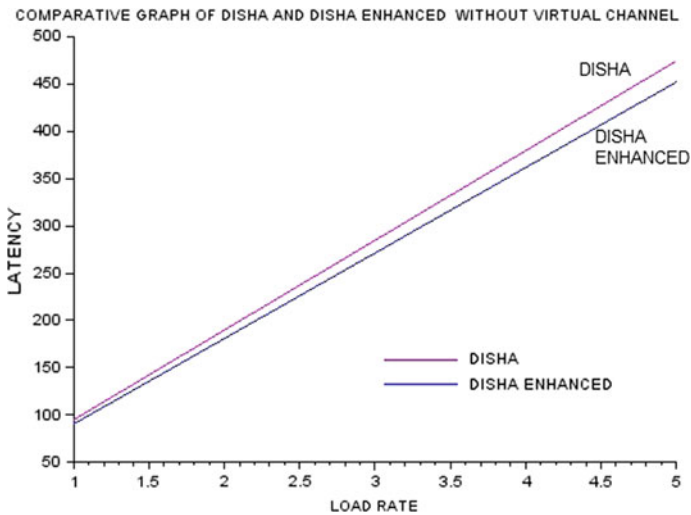


Fig. 9 Comparative graph Disha and Disha enhanced without virtual channel

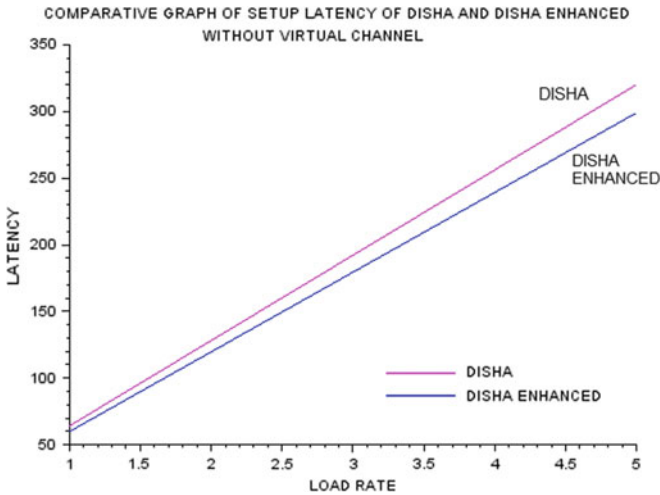


Fig. 10 Comparative graph of setup latency of Disha and Disha enhanced without virtual channel

$$\begin{aligned}
 TDE &= (Tdb + Ts)/2 \\
 Tdb &= 6.5 \quad (\text{Same as disha}) \\
 Ts &= TAd + TArb + TCb + THsel + TVc \\
 &= C3 + (C4 + C5 * \log F) + (Co + C1 + * \log P) \\
 &\quad + (C6 + C7 * \log F) + 0 \quad (TVc = 0) \\
 &= 6.36 \quad 2.15\% \text{ faster}
 \end{aligned}$$

At Data Through (without virtual channel) (Figs. 11 and 12)

$$\begin{aligned}
 TDE &= (Tdb + Ts)/2 \\
 Tdb &= 3.10 \quad (\text{Same as disha}) \\
 Ts &= TFc + TCb + TVc \\
 &= C2 + (C1 * \log P) + 0 \quad (TVc = 0) \\
 &= 2.2 + (0.6 * (\log 5 + \log 5)) + 0 \\
 &= 3.04 \quad 2\% \text{ faster}
 \end{aligned}$$

A minor difference is being shown due to the fact that a number of ports both in input and output have been reduced from 6 to 5.

Analysis

TDE < TDisha,
 Proposed scheme is 25% faster than ‘Disha.’

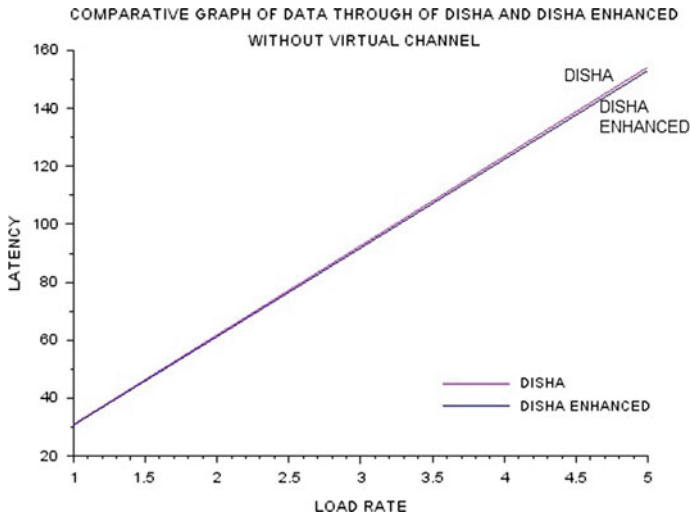


Fig. 11 Comparative graph of data through of Disha and Disha enhanced without virtual channel

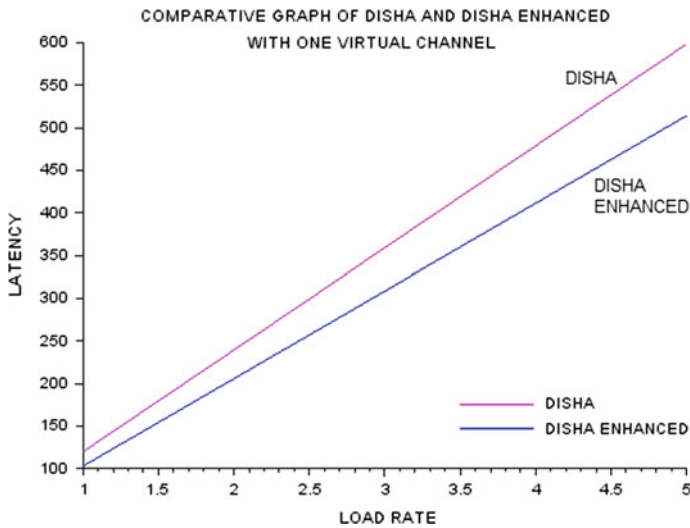


Fig. 12 Comparative graph Disha and Disha enhanced with one virtual channel

Cost saving: Cost of deadlock buffers has been reduced 40%. Cost of crossbar switches has been reduced from $6 * 5$ to $5 * 5$, thereby crossbar complexity has been reduced by 16.6%. Cost of virtual channels has been reduced by 50% (Figs. 13 and 14).

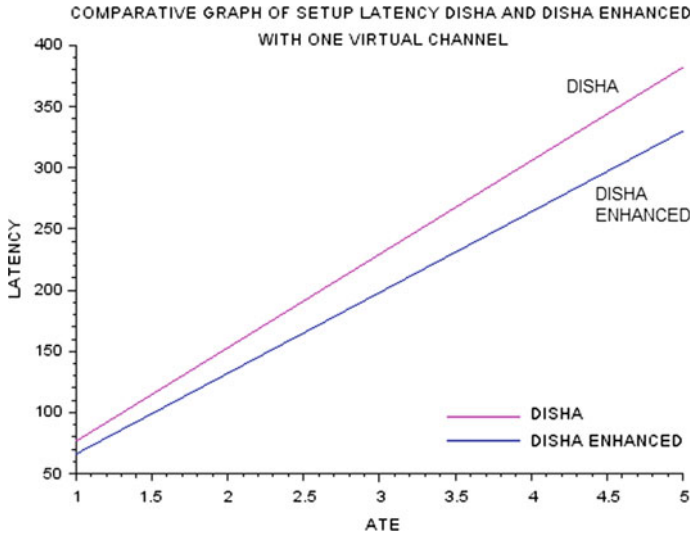


Fig. 13 Comparative graph of setup latency of Disha and Disha enhanced with one virtual channel

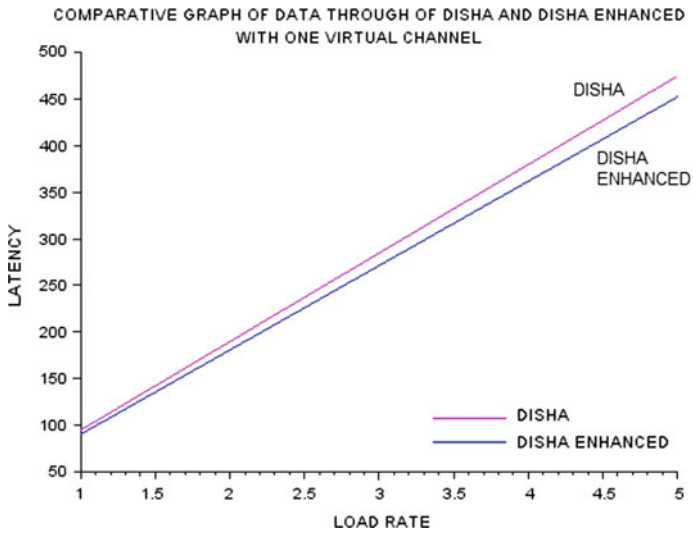


Fig. 14 Comparative graph of data through of Disha and Disha enhanced without virtual channel

At Setup

$$\begin{aligned}
T_{db} &= T_{Ad} + T_{Arb} + T_{Cb} + T_{Hsel} + T_{Vc} \\
&= 6.50 + T_{Vc} \\
&= 6.50 + 0 \quad (T_{Vc} = 0) \\
&= 6.50 \quad 16\% \text{ faster}
\end{aligned}$$

$$\begin{aligned}
T_s &= T_{Ad} + T_{Arb} + T_{Cb} + T_{Hsel} + T_{Vc} \\
&= 6.36 + T_{Vc} \\
&= 6.36 + (C_8 + C_9 * \log V) \\
&= 6.36 + 1.24 \\
&= 7.60
\end{aligned}$$

$$\begin{aligned}
TDE &= (6.50 + 7.60)/2 \\
&= 7.05 \quad 9\% \text{ faster}
\end{aligned}$$

At Data Through

$$\begin{aligned}
T_{db} &= T_{Fc} + T_{Cb} + T_{Vc} \\
&= 3.1 + 0 \quad (T_{Vc} = 0) \\
&= 3.1 \quad 28.6\% \text{ faster}
\end{aligned}$$

$$\begin{aligned}
T_s &= T_{Fc} + T_{Cb} + T_{Vc} \\
&= 3.04 + T_{Vc} \\
&= 3.04 + 1.24 \\
&= 4.28
\end{aligned}$$

$$\begin{aligned}
TDE &= (3.1 + 4.28)/2 \\
&= 3.69 \quad 15\% \text{ faster}
\end{aligned}$$

The proposed scheme outperforms and showing high improvement due to the increased utilization of virtual channels.

8 Conclusion

The proposed scheme suggests means for safely incorporating fully adaptive wormhole routing to support efficient communications in a parallel processing environment. The scheme is applicable to any network topology. It employs deadlock recovery as opposed to prevention with the objective of making the scheme faster. Consequently, it does not require virtual channels for deadlock freedom.

References

1. C. J. Glass and L. M. Ni, Adaptive Routing in mesh-connected networks, Intl. Conference on Distributed Computing Systems, pp. 12–19, 1992.
2. J.-H. Seo, (2013) “Three-dimensional Petersen-torus network: a fixed-degree network for massively parallel computers”, *Journal of Supercomputing*, Vol. 64, No. 3, pp 987–1007.
3. L. M. Ni and P. K. McKinley, “A survey of Wormhole Routing Technique in Direct networks”, *IEEE Computers*, vol. 26, no. 2, pp. 62–76, Feb. 1993.
4. Prasant Mohapatra, “Wormhole Routing Techniques for Directly Connected Multicomputer Systems” 201 Cover Hall, Iowa State University Ames, IA 50011.
5. K. V. Anjan and T. M. Pinkston, “An efficient fully adaptive deadlock recovery Scheme: DISHA, Int. Symp. On Computer Architecture, PP. 201–210, June 1995.
6. Amnah EL-Obaid, (2015), Three Dimension Hamiltonian Broadcast Wormhole- Routing, Vol 7, No. 3, May 2015, *International Journal of Computer Networks and Communication (ICNC)*, Department of Computer Science and Information, Technology, Al-Zaytoonah University of Jordan, Amman Jordan.
7. J. Duato. On the design of deadlock-free adaptive routing algorithms for multicomputers: design methodologies. In *Proceedings of Parallel Architecture and Languages Europe*, pages 390–405, June, 1991.
8. J. Duato. A Necessary and Sufficient Condition for Deadlock-Free Adaptive Routing in Wormhole Networks. In *Proceedings of the International Conference on Parallel Processing*, pages I142–I149, August, 1994.
9. Andrew A. Chien. A Cost and performance model for k-ary n-cube wormhole routers. In *Proceedings of Hot Interconnects Workshop*, August 1993.
10. Andrew A. Chien. and J. H. Kim. Planner-Adaptive Routing: Low-cost adaptive networks for multiprocessors. In *Proceedings of the 19th International Symposium on Computer Architecture*, IEEE Computer Society, pages 268–77, May, 1992.
11. J. Kim, Z. Liu and A. Chien. Compressionless Routing: A framework for adaptive and fault-tolerant routing. In *Proceedings of the 21st International Symposium on Computer Architecture*, IEEE Computer Society, pages 289–300, April, 1994.
12. Faizal Arya Samman, (2011) “New Theory for Deadlock-Free Multicast Routing in Wormhole-Switched Virtual Channel less Networks on-chip”, *IEEE Transactions on Parallel & Distributed System*, Vol. 22, pp 544–557.
13. K. V. Anjan and T. M. Pinkston, “An efficient fully adaptive deadlock recovery Scheme: DISHA, Int. Symp. On Computer Architecture, pp. 201–210, June, 1995.
14. J. Duato, C. Yalamanchili, L. Ni, (2003) “Interconnection Networks: An Engineering Approach”, Elsevier Science.
15. C. J. Glass and L. M. Ni, “The Turn model for adaptive routing,” *Jou. of the ACM*, pp. 874–902, vol. 41, Sept. 1994.

Performance Enhancement of Point-to-Point FSO System under Rain Weather Conditions

Aditi Malik, Sanjeev Kumar, Preeti Singh and Pardeep Kaur

Abstract FSO (free-space optics) is a new technology used to solve last mile problem in point-to-point communication. As name indicated, FSO link is a seamless communication link using air as a medium for transmission of optical information. For successful transmission, medium should be free of attenuation caused by different weather conditions like rain, haze, fog. In this paper, analysis of FSO systems has been done using two 32-channel WDM systems and then compared at a constant data rate of 2.5 Gbps. The system with single laser outperforms the system employing an array of 32 CW lasers in terms of link distance under different rain conditions.

Keywords FSO · WDM · Rain · BER · Laser power · Link length

1 Introduction

Free-space optics is used for communication between two points considering free space as the transmission medium [1]. It is also called as wireless optical communication. For the successful transmission of signal, a clear line of sight is required [2]. FSO is optical communication link where light is transmitted between transceivers and thus system is called having speed of light for transmission. FSO offers distinct advantages over microwave and optical fiber communication system [3]. Microwave installation is difficult, speed is less, and license is required as

A. Malik · S. Kumar (✉) · P. Singh · P. Kaur
University Institute of Engineering and Technology, Panjab University, Chandigarh, India
e-mail: sanjeev_esd@yahoo.in

A. Malik
e-mail: Aditi2202@gmail.com

P. Singh
e-mail: preeti_singh@pu.ac.in

P. Kaur
e-mail: Pardeep.tur@gmail.com

compared to FSO. FSO is mainly used where feasibility of optical fiber is difficult or rapid deployment is required [4]. High security and license do not required in case of FSO [5]. FSO system offers advantage of high-speed, broader bandwidth and does not suffer interference [6]. Electromagnetic and radio-magnetic interference cannot affect the transmission in FSO link. FSO poses characteristics like low-power usage per transmitted bit and dense spatial reuse [7]. FSO systems are used for implementation of different applications. It is used to increase the broadcasting area of an existing MAN, to interconnect two local area networks (LANs), to form a storage area network (SAN), to backup fiber links acting as a redundant links and deploy a new networks in lesser time [8]. Last mile problem is reduced by FSO where transmission rate is reduced significantly when cable network is employed [9].

FSO communication system has many advantages but there are some drawbacks also which reduce the link performance [10]. There are many factors in free-space medium which leads to the attenuation, distortion, diversion, or interference of an optical beam in FSO transmission [10]. If attenuated signal will exceed the dynamic range of optical receiver in FSO communication system, then losses occur will be undesirable [9]. As the transmission is done in the air, the atmospheric conditions are to be studied. System is vulnerable to atmospheric disturbance, imbibing, physical hindrances, scattering, building swing/seismic activity, and scintillation [7]. Atmospheric attenuation is attenuation in atmosphere which is the main factor which can affect FSO link. Absorption, scattering, and turbulence combine and form total atmospheric attenuation. Molecular and aerosol imbibing comprise the atmospheric absorption. Scattering is divided into three types: Rayleigh, Mie, and non-selective. Rayleigh scattering is caused due to molecules, Mie scattering is caused by aerosol of air, and non-selective is caused by geometric consideration of system [10]. Absorption is caused by merging of the optical beam's photons and air molecules existent in the medium of FSO link [11]. The rearrangement or deflection of optical beam can create a significant degradation of intensity of received light on the propagation pathway, and it is defined as scattering [10]. The warm air rising from the land can lead to the arbitrary changes in refractive index. This leads to fluctuation of signal amplitude which is called as scintillation [8]. Aerosols are the foreign elements present in the medium and cause absorption and scattering. Fogs, clouds, rain, snow, haze, etc. are responsible for the presence of aerosols [9, 11]. The performance analysis of transmission can be made in terms of certain parameters like bit error rate (BER), eye opening, and maximum quality factor. Analysis has also been carried out for clear and hazy weather conditions for different component configurations [12].

In this chapter, a system is designed using WDM technique to overcome the system degradation and enhance FSO link performance. Link distance is improved using different power transmission and data rate. Three different types of rain weather conditions are considered and studied using two different systems. A basic WDM-based FSO system is shown in Fig. 1.

There are totally 4 sections in this chapter. Section 1 introduces the concept. System design and considerations are discussed in Sect. 2 where 32-channel-based

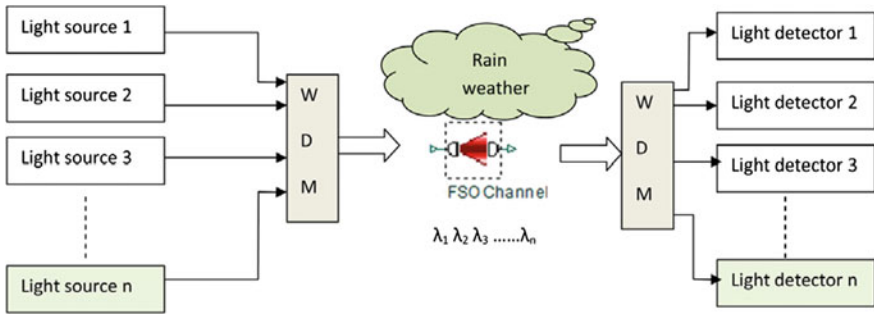


Fig. 1 WDM-based FSO system [13]

two-WDM FSO systems are designed. Section 3 reports the simulation results and its discussion. The paper is concluded in Sect. 4.

2 System Consideration

2.1 System Design

A FSO system has three basic systems, i.e., transmitter, FSO channel, and receiver. The transmitter system consists of pseudo-random bit (PRB) generator, non-return-to-zero pulse generator, continuous wave laser, and Mach-Zehnder modulator (MZM), while avalanche photodetector (APD) and LP Gaussian filter are used at receiving end [13]. BER analyzer and optical power meter is used to visualize the simulation value. There is a limit on incrementing the power of transmission for eye safety including many other factors [14].

2.2 Link Analysis

The received power at receiver end guarantees the reliability of transmission because minimum sensitivity of receiver depends upon it for given bit rate. It is needed that the level of the power should remains above the minimum sensitivity for successful transmission.

2.2.1 Rain

Attenuation present in a system can affect its performance. Atmospheric attenuation and geometric losses constitute all over the attenuation. In the present work, it is

considered that there is no beam spread, and hence, there will be no geometric losses [13]. Rain attenuation exists due to rain fall and is a non-selective scattering. This type of attenuation is wavelength independent [10]. Rain has the ability to produce the fluctuation effect in delivery laser. The visibility of FSO system depends upon the quantity of the rain. In case of heavy rain, water droplets have solid composed and it can either modify the optical beam characteristics or hinder the passage of beam by introducing absorption, scattering, and reflection [7]. There are different proposed models in the literature to calculate the loss due to the atmospheric turbulence [13]. Beer's law- and Stroke's law-based numerical model is derived. According to Beer's law, the laser power's weakening in the environment is [13]:

$$\tau(r) = \frac{P(r)}{P(0)} = e^{-\beta r}, \quad (1)$$

where r is the link range in meters, $P(r)$ is the laser power at range r , $\tau(r)$ is the transmittance at a range r (km), β is the coefficient of scattering (km^{-1}), and $P(0)$ is source's laser power (W). The scattering coefficient which is derived using Stroke's law [13]:

$$\beta_{\text{rainscat}} = \pi a^2 N_a Q_{\text{scat}} (a/\lambda), \quad (2)$$

where a is the radius of raindrop ($1 \times 10^{-3} - 0.1$ cm), λ is wavelength, N_a is the raindrop distribution, and Q_{scat} is the efficiency of scattering. The raindrop distribution N_a is measured using the following equation [13]:

$$N_a = \frac{Z_a}{\frac{4}{3}(\pi a^3)V_a}, \quad (3)$$

where V_a is the limit speed precipitation, Z_a is the rainfall rate (cm/s) as shown in Table 1. The limiting speed of raindrop can be calculated as [13]:

$$V_a = \frac{2a^2 \rho g}{9\eta}, \quad (4)$$

where η is viscosity of air, ρ is density of water (g/cm^2), and g is the gravitational constant.

Table 1 Different rainfall rates, Z_a , for different rainfall levels [13]

S. No.	Rainfall levels	Z_a in cm/s
1	Light rainfall	7.22×10^{-4}
2	Medium rainfall	1.11×10^{-3}
3	Heavy rainfall	2.22×10^{-3}

2.3 WDM-Based System Design

The WDM systems are designed in OptiSystem v 11.0. The working wavelengths are 850 and 1550 nm because FSO equipments are commercially available in these ranges. Other wavelength windows also exist, but their usages are limited because of the availability of devices, components, and practical implementation [10]. The power level of 1550 nm is more than 850 nm, and system performance is found much better with 1550 nm wavelength [13]. The aperture is kept 15 cm. Laser power is kept at constant value of 30 dBm for different attenuation values of rain. The system has been optimized at 2.5 Gbps data rate for all weather conditions. At light, medium, and heavy rain types of weather condition, attenuation is 6.27, 9.64, and 19.28 dB/km, respectively [13].

There are two systems designed in this paper: System I and System II.

System I:

System I uses CW laser of 32 arrays. Mux used at transmitter side and DeMux used at receiver end, respectively, consist of 32-channel WDM. Visualization of the output is done using BER analyzer with the use of selector [13].

System II:

In this system instead of using array of laser, single CW laser is used and fork is used to divide the output. Fork is a device where every output end has the same value as the input end [2, 14]. Before the signal in FSO channel is transmitted, the multiplexer (WDM) and modulation are used. At the output of WDM, DeMux power combiner is used and its output connected to BER analyzer is used to analyze it. Power combiner combined all the power of demultiplexed signals [15]. The layout of system is shown in Fig. 2.

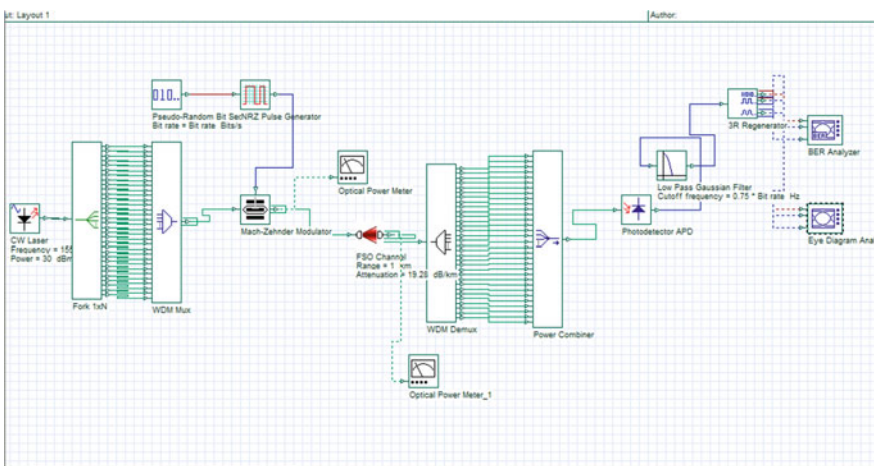


Fig. 2 OptiSystem layout for System II

3 Results and Discussion

Different parameters need to be optimized so that the performance of the system in the presence of different weather conditions does not degrade too low. The parameters are link distance, aperture size, data rate of transceiver, laser power. Simulations are carried out for the three weather conditions which are light, medium, and heavy rain conditions.

3.1 System I

System I is designed using an array of 32 CW lasers. The analysis of System I performance under light, medium, and heavy rain weather conditions is shown in Table 2. The analysis of BER has been done from the eye diagrams shown in Fig. 3. This can be easily derived from Table 2 that using the data rate of 2.5 Gbps and 30 dBm power laser, when the amount of attenuation is increased (according to respective weather condition), then a downfall in the maximum acceptable transmission distance with acceptable quality factor values. Analysis of Table 2 shows that when condition of weather (light rain) is used, then the distance up to which acceptable transmission distance can be done is 10 km while for heavy rain condition, the distance is reduced to 3 km.

3.2 System II

In this section, only one CW laser is used to design the system; thus, the system complexity is reduced as compared to System I. The conditions for the optimizations needed to be same only then the difference in the output is logical. For this, 2.5 Gbps data rate and 30 dBm laser powers are used. Analysis of output is done using weather conditions (light rain, medium rain, and heavy rain) for varying link

Table 2 Performance analysis of System I and System II under various rain conditions

S. No.	Weather condition	Attenuation (dB/km)	Acceptable transmission distance (in km)		Max Q factor		Min BER	
			System I	System II	System I	System II	System I	System II
1	Light rain	6.27	10	16	8.05145	6.74596	3.9979 e^{-16}	7.60062 e^{-12}
2	Medium rain	9.64	6	10	15.3104	16.9435	3.16075 e^{-53}	9.32409 e^{-60}
3	Heavy rain	19.28	3	5	15.6991	16.4522	7.42261 e^{-56}	4.04325 e^{-61}

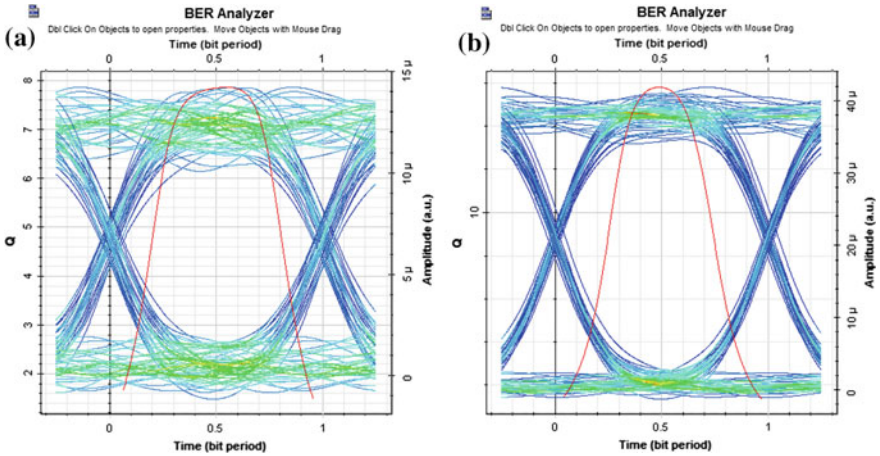


Fig. 3 Eye diagram of System I a BER analyzer at light rain and b BER analyzer at heavy rain

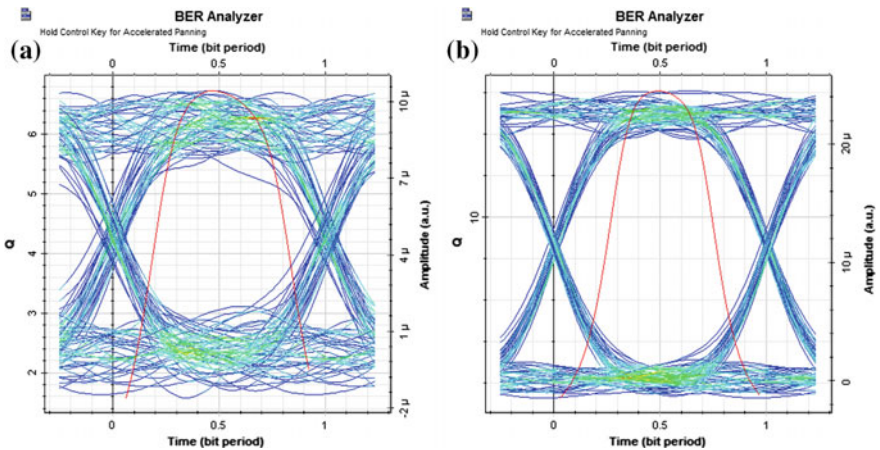


Fig. 4 Eye diagram of System II a BER analyzer at light rain and b BER analyzer at heavy rain

distances. The analysis of performance in terms of weather condition, distance, and BER is shown in Table 2. The performance in terms of eye opening can be observed from Fig. 4.

Analysis from Table 2 shows that when the weather condition (light rain) is used, then the acceptable distance of transmission is increased to 16 km, while a downfall in the acceptable transmission distance can be seen under heavy rain condition and its value is only 5 km. Similarly, the eye opening is more for light rain condition than for heavy rain condition and hence the Q factor.

3.3 *System I Versus System II*

Analysis of Table 2 shows that, when the maximum acceptable distance is increased, then a decrease in the value of quality factor is observed and performance of the whole system also degraded. Another observation from Table 2 shows that when the amount of attenuation is increased according to weather condition, a downfall has been observed in the value of quality factor. For heavy rainfall, the amount of attenuation is also high, at this condition the value of Q factor approaches to zero at a distance of 15 km, but when the attenuation is not high, it shows a downfall in its value after 15 km. It can be analyzed from Table 2 that under weather conditions (light, medium, and heavy rain), the maximum acceptable transmission distance of System II is higher than System I, which shows that System II support longer distance than System I (under assumed conditions of weather). Also, when the weather condition (light rain) is used, the System II link distance is nearly double of the link distance of System I.

4 Conclusions and Future Scope

FSO system is the new technology to solve the problem faced by previous systems in communication field. Researchers have shown a great interest on different mitigation techniques in FSO system to enhance its performance in extreme weather conditions and areas where FSO performance is degraded. Lots of technologies are used to derive the different weather conditions. Based upon these values, systems are being designed and analyzed. In this paper, simulation is done for two-WDM FSO communication systems under rain conditions, i.e., one with single CW laser (System II) and array of 32 CW laser (System I). Their performance is investigated keeping the optimized parameters alike. The data rate is kept constant at 2.5 Gbps. Observations has shown that when the weather condition (light rain) is used, the acceptable transmission distance that the System I can support upto 10 km while it shows an increase in distance when System II is used and its value is 16 km. When weather condition (heavy rain) is used, the System II shows increase in acceptable distance up to 5 km while the System I shows only 3 km acceptable transmission distance. Thus, it can be concluded that performance of FSO system under different weather conditions (light, medium and heavy rain) is improved for System II in terms of maximum acceptable transmission distance (link distance) while using WDM system. The present FSO-WDM system is analyzed for single beam. Further, it is proposed to extend system analysis for multibeam concept and in addition to weather conditions the performance can also be analyzed for scintillation effects.

References

1. Jitendra Singh, Naresh Kumar, "Performance analysis of different modulation format on free space optical communication system", Elsevier, *Optik* 124 (2013) 4651–4654.
2. S. Vigneshwaran, I. Muthumani, A. Sivananatha Raja, "Investigations on Free space optics communication system", Information Communication & Embedded Systems (ICICES), IEEE Conference Publication, 2013.
3. Naresh Kumar, Ashwani Kumar Rana, "Impact of various parameters on the performance of free space optics communication system", Elsevier, *Optik* 124 (2013) 5774–5776.
4. Samir A. Al-Gailani, Abu Bakar Mohammad, Redhwan Q. Shaddad, "Evaluation of a 1 Gb/s Free Space Optic System in Typical Malaysian Weather", 3rd International Conference on Photonics 2012, IEEE.
5. S.A. Al-Gailani, A.B. Mohammad, R.Q. Shaddad, "Enhancement of free space optical link in heavy rain attenuation using multiple beam concept", Elsevier, *Optik* 124 (2013) 4798–4801.
6. A.Z. Suriza, Islam Md. Rafiqul, A.K. Wajdi, A.W. Naji, "Effects of Rain Intensity Variation on Rain Attenuation Prediction for Free Space Optics (FSO) Links", International Conference on Computer and Communication Engineering (ICCCE 2012), IEEE.
7. A.K. Rahman, M.S. Anuar, S.A. Aljunid, M.N. Junita, "Study of rain attenuation consequence in free space optic transmission", Proceedings of IEEE 2008 6th National Conference on Telecommunication Technologies and IEEE 2008 2nd Malaysia Conference on Photonics.
8. Aditi Malik, Preeti Singh, "Free Space Optics: Current Applications and Future Challenges", International Journal of Optics, Hindawi, 2015 (2015) 1–7.
9. Vladimir Brazda, Onrej Fiser, Lubos Rejcek, Michal Mandlik, "Attenuation of Optical Signal in Free Space-Event Analysis", 13th Conference on Microwave Techniques COMITE, IEEE 2013.
10. Suriza Ahmad Zabidi, Wajdi Al Khateeb, Md. Rafiqul Islam, Ahmed Wathik Naji, "Investigation of Rain Attenuation Impact on Free Space Optics Propagation in Tropical Region", 4th International Conference on Mechatronics (ICOM), IEEE 2011.
11. Adnan R. Raja, Quaid J. Kagalwala, Taha Landolsi, and Mohamed El-Tarhuni, "Free-Space optics channel characterization under UAE weather conditions", International Conference on Signal Processing and Communications (ICSPEC), IEEE 2007.
12. Aditi Malik, Preeti Singh, "Comparative Analysis of Point to Point FSO System Under Clear and Haze Weather Conditions" Springer, *Wireless Personal Communications*, 80 (2015) 483–492.
13. Hilal A. Fadhil, Angela Amphawan, Harsul A.B. Shamsuddin, Thanaa Hussein Abdm Hamza M.R. Al-Khafaji, S.A. Aljunid, Nasim Ahmed, "Optimisation of free space optics parametes: An optimum solution for bad wheather conditions", Elsevier, *Optik* 124 (2012) 3969–3973.
14. Vishal Sharma, Gurimandeep Kaur, "High speed, long reach OFDM-FSO transmission link incorporating OSSB and OTSB schemes", Elsevier, *Optik* 124 (2013) 6111–6114.
15. Nur Haedzerin Md Noor, Ahmed Wathik Naji And Wajdi Al-Khateeb, "Performance Analysis Of A Free Space Optics Link With Multiple Transmitters/Receivers", *IJUM Engineering Journal*, 13 (2012).

Choice of Right Dimension and Position of Microstrip Feedline for the Bandwidth Improvement of Microstrip Antenna

Ranjan Mishra, Raj Gaurav Mishra, Piyush Kuchhal and Piyush Dua

Abstract Microstrip antenna has huge potential to meet the ongoing demand for wireless communication. Low conventional bandwidth of it hinders its use. Out of many ways of increasing the bandwidth, one of the simplest ways is the proper dimension and position of the feedline. A proper value has insightful effect in bandwidth enhancement by proper impedance matching. This chapter put some insight into it for a particular rectangular antenna at X band. The simulations are conducted using HFSS. A considerable improvement by this simple way has been noticed.

Keywords Bandwidth · Microstrip feedline · Impedance

1 Introduction

An increasing demand for the high-bandwidth microstrip antenna attracted significant attention of researchers recently. It is so owing to its huge demand in different wireless applications in radar, aircraft, missiles, and satellite. Microstrip antenna possesses certain potential, as described by Garg et al. [1], to meet this requirement. It has many such noticeable features as cited by Mishra [2]. The work by Pozar and Schaubert [3] put the microstrip antenna among the new trend in its research. A simple microstrip antenna suffers from low bandwidth of around 3–5%. This evokes the researcher for its bandwidth improvement.

R. Mishra (✉) · R.G. Mishra · P. Kuchhal · P. Dua
CoES, University of Petroleum and Energy Studies, Dehradun 248007, India
e-mail: rmishra@ddn.upes.ac.in

R.G. Mishra
e-mail: rgmishra@ddn.upes.ac.in

P. Kuchhal
e-mail: pkuchhal@ddn.upes.ac.in

P. Dua
e-mail: pdua@ddn.upes.ac.in

Bandwidth is an important parameter, and it determines the range of operating frequencies of it. Many researchers such as Deshmukh and Ray [4] and Mishra et al. [5] have shown by using slot on the patch. Sadat et al. [6] used square-ring slot, Islam et al. [7] introduced E-H shaped slot, Jolani et al. used M-shape slot [8], and Ansari and Ram [9] with M slot to maximize the impedance bandwidth. Mishra et al. [10] showed the use of proper size and position of rectangular slot to get UWB range, whereas its performance analysis is described [11].

Out of various feeding techniques in [2], microstrip feedline is simple in design and easily integrated in integrated circuits. It is easy in analyzing, and also, the fabrication is on the same feedline with the fabrication of patch itself. The feedline delivers the energy to the patch, hence its dimension and position have profound effect on the impedance matching. Subsequently, a proper matching yields an improvement in bandwidth.

2 Antenna Dimensions

The geometry of the rectangular and regular microstrip antenna has been manually selected. The dielectric constant (ϵ_r) and height (h), of substrate, are mainly responsible for determining the geometrical dimension of the antenna. The central resonant frequency (f) is chosen to be 6 GHz in our discussion. Substrate used is FR4-epoxy having dielectric constant of 4.4 and loss tangent of 0.027.

The initial dimensions including length (L) and width (W) of the microstrip antenna are calculated using equations formulated by Garg et al. [1] and Balanis [12].

$$\text{Length } (L) = \frac{c}{2f} \left(\frac{\epsilon_r + 1}{2} + \frac{\epsilon_r - 1}{2} \sqrt{\left[1 + 12 \frac{h}{W} \right]} \right)^{\frac{1}{2}} - 2\Delta L$$

ΔL is the correction factor and its value is 0.07.

$$\text{Width } (W) = \frac{c}{2f} \times \sqrt{\frac{2}{(\epsilon_r + 1)}}$$

The length of the antenna is found to be 12 mm. The height of the substrate is taken to be 1.6 mm. It neither marks the antenna bulky, and the antenna exhibits a better response in terms of bandwidth [13]. The width of the antenna is at the higher side and is taken to be 18 mm. The equations reveal that the length of the patch and height of the substrate depend on resonant frequency and dielectric constant. The width of the patch is varied from 14 to 20 mm. It has been observed in the simulation [5] that beyond 18 mm of width of the patch, the performance inclines below the required value of -10 dB of return loss. The simulation is performed in HFSS.

3 Observation and Discussion

The electromagnetic waves travel from source to feedline to the antenna, and then radiates to the free spaces. Whenever there is mismatch impedance at any of the interface, it causes some of the electromagnetic waves to reflect back. In the transmission line, it forms a standing wave. The standing waves can be reduced when impedance of the antenna is matched with characteristic impedance of the feedline. This eventually minimized the energy storage capacity of the feedline. Hence, the dimension of the microstrip feedline plays a significant role in the performance of the antenna. A good impedance matching enhances the performance, thereby increasing the bandwidth. On the other hand, a mismatch in the impedance hampers the performance of the antenna, and this results a decrease in the bandwidth.

In next discussion, the observation with different dimension of the microstrip feedline is done. The dimensions of the microstrip feedline are taken from the set of equations as reported [1]. The length of the feedline is approximately three times its width. For the given dimension of the patch and the substrate, the initial width and length of the microstrip feedline come out to be 4 and 9 mm. Observation is done with the variation of the bandwidth and the return loss with different dimension of the feedline. The variation in the absolute value of the return loss with respect to different length of the feedline is plotted in Fig. 1. Here, the length of the feedline is varied from 6 to 15 mm. 6 mm of the length is the initial theoretical length, and 15 mm is the length at which the bandwidth becomes zero. It is observed that the width of the feedline has more dominant effect than the length. The observation is carried with 4, 4.25, 4.5, and 4.75 mm width of feedline, and the best result is obtained with 4.5 mm.

Further simulations are carried in HFSS. HFSS has more real-time result since it also considers the substrate.

Fig. 1 The Bandwidth with varying dimension of feedline

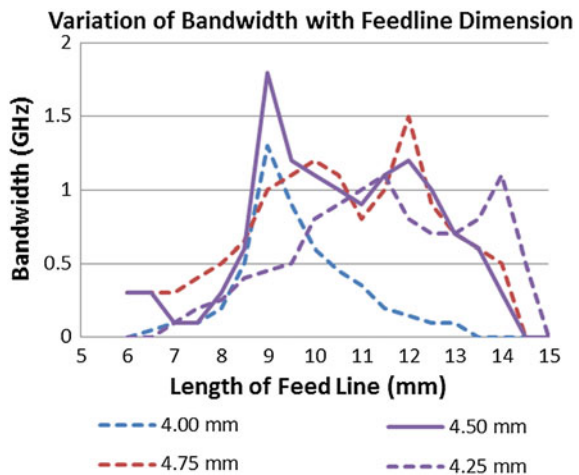


Fig. 2 Effect on return loss by varying length of feed line

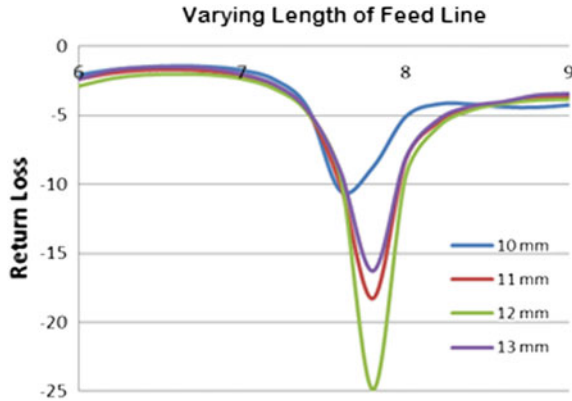


Fig. 3 Effect on return loss by varying width of feedline

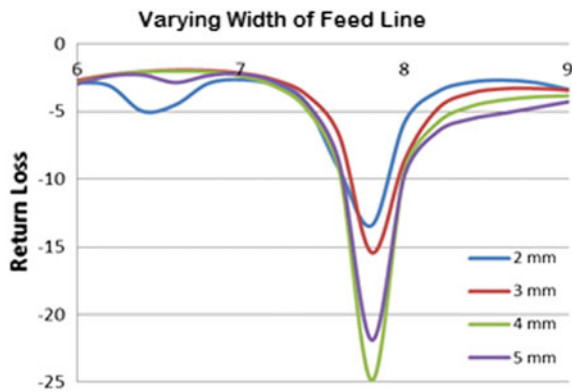


Figure 2 is the observation on the return loss and the corresponding bandwidth by varying the length of the microstrip feedline. The feedline length is varied from 9 to 13 mm. It depicts that the best result is with 12 mm length.

Figure 3 is the observation of the same aforesaid parameters by varying the width of the feedline. The width of the feedline is taken from 2 to 5 mm. The best result is observed with 4 mm of width.

Figure 4 is result obtained by observing how the position of the line affects the parameter. Here, the reading is noted from taking the feedline at the lower edge (0 mm) to upper edge (12 mm). Significant result is getting out when the feedline is away from the lower and upper edge. The best result is obtained when it is just at the center of the patch i.e., 6 mm above the lower edge.

The image of the simulated antenna is shown in Fig. 5.

The return loss (S1 parameter/reflection coefficient) with simulation from HFSS is shown in Fig. 6, which clears the fact that the antenna is yielding a wide band.

Fig. 4 Effect on return loss by varying the position of feedline

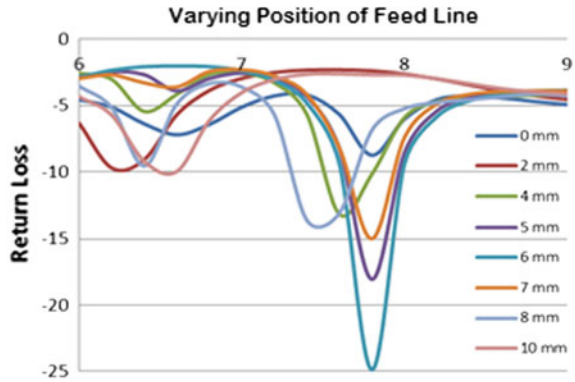


Fig. 5 Simulated diagram of antenna on HFSS

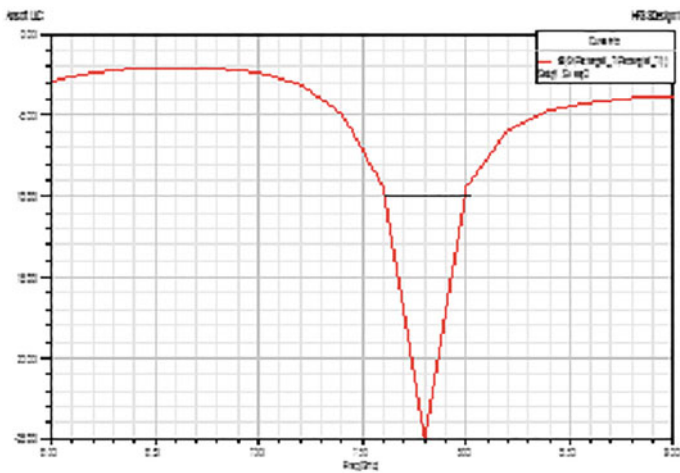
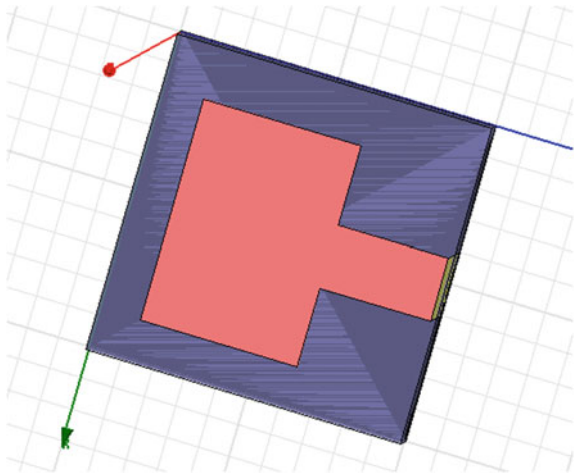


Fig. 6 S1 parameter of the observed antenna on HFSS

4 Conclusions

The best radiating result of the microstrip antenna is observed by proper matching between its impedance and the characteristic impedance of the feedline. A proper dimension of the slot inserting at the proper position contributes a perfect matching. This intensifies the electric field, and performance of the antenna gets enhanced. The perfect matching yields a high bandwidth with good return loss. Therefore, it is concluded that a proper selecting the dimension of the feedline on a suitable patch results in the broadening of the antenna conveniently.

References

1. R. Garg, P. Bhartia, and I. Bahl, Ittipiboon, *Microstrip Antenna Design Handbook*, Artech House, Norwood, Mass, USA, 2001.
2. R. Mishra, An Overview of Microstrip Antenna, *HCTL Open International Journal of Technology Innovations and Research (IJTIR)*, Volume 21, Issue 2, August 2016.
3. Pozar, D. M. and D. H. Schaubert, *Microstrip Antennas: The Analysis and Design of Microstrip Antennas and Arrays*, IEEE Press, New York, 1995.
4. A. A. Deshmukh and K. P. Ray, "Compact broadband slotted rectangular microstrip antenna," *IEEE Antennas and Wireless Propagation Letters*, vol. 8, pp. 1410–1413, 2009.
5. R.G. Mishra, R. Mishra, P. Kuchhal, "Design of Broadband Monopole Microstrip Antenna Using Rectangular Slot", *Advances in Intelligent Systems and Computing*, vol. 479, pp. 683–688, 2016.
6. S. Sadat, M. Fardis, F. Geran, and G. Dadashzadeh, "A compact microstrip square-ring slot antenna for UWB applications," *Progress in Electromagnetics Research*, Vol. 67, 173–179, 2007.
7. M. T. Islam, M. N. Shakib, and N. Misran, "Broadband E-H shaped microstrip patch antenna for wireless systems," *Progress in Electromagnetics Research*, vol. 98, pp. 163–173, 2009.
8. F. Jolani, A. M. Dadgarpour, and H. R. Hassani, Compact M – slot folded patch antenna for WLAN, *Progress in Electromagnetics Research Letters*, vol. 3, pp. 35–42, 2008.
9. Ansari J.A. and Ram B.R. Broadband stacked U-slot microstrip patch antenna. *Progress in Electromagnetics Research Letters* 2008, 4, 17–24.
10. R. Mishra, R. G. Mishra, P. Kuchhal, "Analytical Study on the Effect of Dimension and Position of Slot for the Designing of Ultra Wide Band (UWB) Microstrip Antenna", 5th IEEE International Conference on Advances in Computing, Communications and Informatics (ICACCI), 978-1-5090-2028-7, Sept 2016.
11. R. Mishra, J. Jayasinghe, R. G. Mishra, P. Kuchhal, "Design and Performance Analysis of a Rectangular Microstrip Line Feed Ultra-Wide Band Antenna", *International Journal of Signal Processing, Image Processing and Pattern Recognition* Vol. 9, No. 6, pp. 419–426, 2016.
12. Constantine A., Balanis; *Antenna Theory, Analysis and Design*, John Wiley & Sons, Inc., Hoboken, New Jersey, 2005.
13. R. Mishra, P. Kuchhal, A. Kumar, "Effect of Height of the Substrate & Width of the Patch on the Performance Characteristics of Microstrip Antenna", *International Journal of Electrical and Computer Engineering*, vol 5, no 6, pp 1441–45, 2015.

Recommendation and Interest of Users

Baljeet Kaur Nagra, Bharti Chhabra and Dolly Sharma

Abstract This paper tells the overall exploration of social recommender systems. All the people who are in participation of his work will become familiar with new featured recommendation system methods, classification of recommender system according to different purpose criteria, common estimated methodologies and possible apps that can employ the different social recommender systems. A recommender system's main purpose is to provide users with customize online service recommendations to deal the fast growing online information an excessive load of issues and to betterment the users' connection and its management. Various techniques of different types of recommender system have been produced and various software has been generated since 1995 and various kinds of recommender system software has generated lately for a different sort of apps. Researchers and management trainees recognized that recommender systems give a wide opportunities and challenges for limited sized tweets in the Twitter post, with more lately successful evolution of the recommender systems for real-world applications. The largeness of post on different subjects is enormous to social sites users who can be interested in a few subjects.

Keywords Social site · Customized recommendation · Social recommendation Users' interests

B.K. Nagra (✉) · B. Chhabra · D. Sharma
Department of Computer Science, Chandigarh Group of Colleges,
Landran, Mohali, Punjab, India
e-mail: baljeetkaur.nagra126@gmail.com

B. Chhabra
e-mail: cecm.cse.bharti@gmail.com

D. Sharma
e-mail: dolly.azure@gmail.com

1 Introduction

Twitter has come out as a most robust Web services. Twitter has more than 500 million users and the largeness of tweets one receives is continuously growing. In simple words, 80% of crowd is the omnipresent cell phone users [3]. Large amount of tweets is spreading lowering users' efficiency to the point out that 60% American companies have a policy for their employees about using the sites like Facebook, Twitter, Instagram while doing job [17]. A large volume of social sites like Twitter users' interest of posting tiny messages which throwing back the clarity of subject. Users' interests change by time, that is basically witness by the liberal mania twitter's characteristics of Twitter that gives suggestions like hash tags, raw data tags symbolized as #.

In this paper, we have reviewed a social recommendation which basically depends on users' behaviour like users' liking and disliking. This paper tells about researchers' work which mainly focus at the presentations of no tweets orderly in such a way that all post and tweets looks more attractive in appearance in look [7].

To attain this, it is very mandatory to figure out users' transforming behaviour by the passage of time. An algorithm named TRUPI was proposed by Mansour et al. [8]; it first figures out the behaviour then ranks the tweets according to the behaviour. It hires different types of classifiers that tell the behaviour of user on his timeline. Then all tweets go to ranking model and this model ranks to all according to their liking, disliking.

2 Basic Concepts

This section describes the basic concepts of Twitter recommender system-based machine learning.

2.1 Recommender System (RS)

RS is very popular information filtering technology which plays a very important role in aiding the users' internet systems to discover the appropriate data by providing the hints of relevant information of potential interest and search behaviour to the users'. Because of the possible outcomes of social correlation in SRS, social SRSs have gathered a lot of attention lately [14].

Presenting the analysis of existing recommender system and conversation of some of the research analysis direction, Researchers started by giving some authorized explanations of social recommendation and discussion of their distinctive attributes and its conclusions by comparing with old version recommender systems [15]. Then, the researchers lay out and then explained the existing and

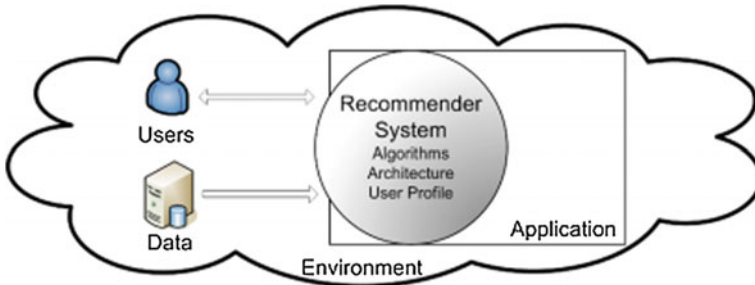


Fig. 1 Recommender system

verify social-based recommender system into memory-based and model-based social recommendations (Fig. 1).

As depending upon this, the rooted models took on to make and analyse system for every category. Some key finding given by the author from +ve and -ve experiences in making social recommender system for betterment of capabilities of social recommendations.

2.2 Content-Based Recommender Systems (CBRS)

If we take a look on information filtering research and information retrieval, content-based recommender system is main instance of it and has their maintained deep root in it [13]. On the users’ personal interest, behaviour or past search history which he/she preferred, recommender system recommends the similar items. Most of the existing CBRS keeps a keen eye on the verified [2]. Content-based recommender systems keep eye on recommended and verified goods with information related to text such as news, books and documents. Contents present in those sorts of systems are explained by some of keywords [5], and the keyword’s formative-ness to a document is evaluated by TF/IDF. A keyword’s TERM FREQUENCY weight in document indicates the number of that word present in the document, while INVERSE DOCUMENT FREQUENCY weight of a keyword is the inverse frequency of document of that word (Fig. 2).

Suppose, x_{jk} = TF/IDF weight of the k -th keyword in v_j and the v_j content can be expressed as

$$x_j = (x_{j1}, x_{j2}, \dots, x_{j\ell}).$$

With these representations of terms, the CBRS recommend the items to the customers which quite same as users’ liking in the past history maximum time and on the basis of their search like personal interest or search behaviour. Particularly, various persons’ goods are compared to the items which previously rated by the customers.

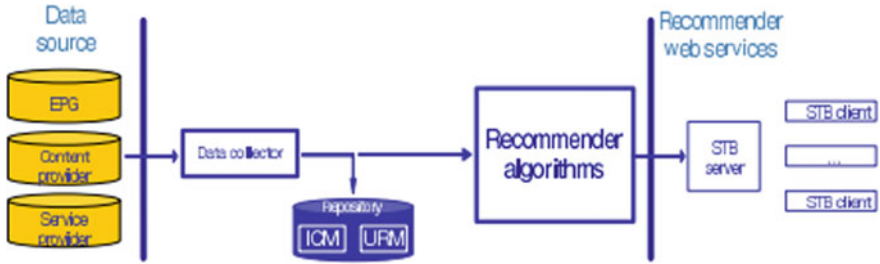


Fig. 2 Architecture of the recommender system

2.3 Collaborative Filtering (COF)-Based Recommender System (CFRS)

CF is powerful and important method which plays a vital role in the constructing a proposed recommender [13]. It can predict and make an estimate of the users' personal interest and behaviour directly by detecting a complex and unexpectedly complicated pattern from a customer's past or users' historical behaviours such as the rating of product without having knowledge of domain [9, 13]. The expected estimation and prediction of CFRS that if users have been concurred to each other in the past time then there are more likely chances to be concurred to each other in upcoming times than to be agreed with disorganize chosen users. Present CF methods may be classified into memory-based (MEB) and model-based (MOB) methods [4].

2.3.1 Memory-Based Collaborative Filtering (MBCF)

MBCF mainly uses few predictions. There is possibility of happening two types of predictions either the entire user-item matrix or a trial to create assumption, which can be further classified into two methods. First one named user-oriented methods [4, 13] and other one is item-oriented methods [12]. User-oriented methods assume an unreleased rating from the users' perspective on the basis of an item experience as all the ratings weighted average from his alike customers on the purchase, while item-oriented methods assume users' average rating of similar items of the identical users [18]. Main issues of a MBCF method are decoding, computing and combining some of the users' rating. User-oriented methods and item-oriented methods can hold same kind of techniques to deal with the two issues:

- User-oriented methods are used by us to explain the representative methods for computation and aggregation of users' ratings,
- Computing resemblance for user-oriented methods: It is a very difficult step for user-oriented methods.

2.3.2 Model-Based Collaborative Filtering (MOBCF)

MOB methods first predict a prototype for generation of users given ratings and then put in directly to the data mining and machine-based learning techniques to figure out the following patterns after training and testing the data [6] that might be used to figure out the assumption for anonymous users’ ratings. If we compared this to MBCF MOBCF keeps more number of aims to detect latent factors which describe estimated ratings [1, 16].

2.4 Hybrid Recommender Systems (HRS)

To overcome drawback of CBF and collaborative COF, hybrid was proposed. Hybrid is mixture of CB and COF techniques [5]. The main task of hybrid recommender system is to integrate recommendation techniques and to get the better result in the term of performance with limitations. To overcome ramp up problem, combination of CF filtering with other techniques takes place [5]. Hybrid recommendation system techniques flowchart are shown in Fig. 3.

2.5 Social Recommendation System (SRS)

First social system was appeared in 1998 [15]. Its main goal is to reduce the overloaded volume of data over the social sites like Facebook, Twitter, and Instagram. Social recommender system also focuses to increase the number of participation of beginner and old users of these sites [11]. Contents like Wikipedia, written blogs, number of tags, persons, groups use customize method to find out the users’ behaviour like users ‘liking and disliking’.

2.5.1 Memory-Based Social Recommender Systems (MBSORS)

MBSORS mainly uses MBCF models named user-oriented method. A union is done with the users’ missing rating to its related user who has some common

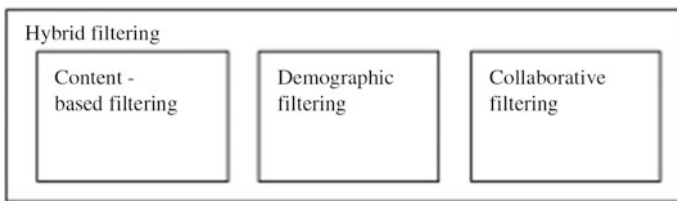


Fig. 3 Recommender system techniques

relation. It is called as an N positive [15]. For existing users, old user-oriented methods employ same types of N users. MBSORS employs N+ users who are correlated to each other that is obtained from both types of information rating as well social recommendation. SRS of this classification has two steps which are following as:

- Firstly, for specified users, it acquired N+ users.
- Secondly, MBCF combine users ‘rating who are related to each other that is acquired by first step which has missing rating’.

2.5.2 Model-Based Social Recommender Systems (MOBSOS)

MOBSRSs select the MOBCF techniques as fundamental modelling. Matrix factorization methods are the methods which utilize MOBCF Techniques [11, 15]. Some characteristics of it are given below:

- (1) To find the optimal solution, different types of optimization techniques are used and gradient-based method is one of them.
- (2) Matrix factorization has probabilistic interpretation with Gaussian noise.
- (3) This is reliable and granted to users to add prior knowledge.

3 Discussion

Social recommendation can potentially find out the solution, some drawback of traditional recommender systems like information sparsity problem and new item—new user [10].

It has gathered a lot of attention towards the area like both academia and industry. Social recommendation has become an area of study in the research literature. Many systems and method have been developed and improved performance of production of recommendation is obtained [14].

On the other hand, many victorious systems in industry area are hard to find and there is still need of a lot jobs to attain the victorious events by putting in the social recommender systems in research area. [19] Researchers give main key findings from both +ve and -ve experiences in putting the SRS to find out compatibility and then evolution of social recommendation occurs.

3.1 Positive Experiences in Social Recommendation

Some of key findings from victorious events given below:

- (1) For social recommendation, information of social media includes mandatory data and yield from analysis give the mandatory technical support.

- (2) Users' point of view, interests might generate through social networks that may overcome new users' size.
- (3) Social recommendation may be improved in the protection of recommendation.

3.2 *Negative Experiences in Social Recommendation*

In brief, key findings from –ve experiences in putting SRS are given below:

- (1) Social relations are very noisy. They create a –ve influence on recommender systems.
- (2) It is very tough for SRS to betterment of the performance of new users when they have very less number of co-relations.
- (3) Various social correlations have differ sort of impact on SRS and there is very difficult job to figure out the trust relations that might or might not be appropriate to other sort of relations.

4 Conclusion

Social recommendation has drawn the attention towards two fields' academics as well as industrial area, it's been a decade, there is much progress in the field of social media and many victorious social recommender systems have generated. In this paper, a brief knowledge of RS and social recommendation is given and we discussed the characteristics, its involvement in different things and developed techniques. Social recommender systems are categorized into memory-based social recommender systems (MBSORS) and model-based social recommender systems (MOBSORS). A review of SRS is represented model wise. Few key findings from +ve and –ve experiences are put at the social recommender systems. There is still need of improvement in the social recommendation so that the main goals can be attained easily.

References

1. Baeza-Yates, Ricardo, and Berthier Ribeiro-Neto. *Modern information retrieval*. Vol. 463. New York: ACM press, 1999.
2. Balabanović, Marko, and Yoav Shoham. "Fab: content-based, collaborative recommendation." *Communications of the ACM* 40, no. 3 (1997): 66–72.
3. Belkin, Nicholas J., and W. Bruce Croft. "Information filtering and information retrieval: Two sides of the same coin?." *Communications of the ACM* 35, no. 12 (1992): 29–38.
4. Breese, John S., David Heckerman, and Carl Kadie. "Empirical analysis of predictive algorithms for collaborative filtering." In *Proceedings of the Fourteenth conference on Uncertainty in artificial intelligence*, pp. 43–52. Morgan Kaufmann Publishers Inc., 1998.

5. Burke, Robin. "Hybrid recommender systems: Survey and experiments." *User modeling and user-adapted interaction* 12, no. 4 (2002): 331–370.
6. Chee, Sonny Han Seng, Jiawei Han, and Ke Wang. "Rectree: An efficient collaborative filtering method." In *International Conference on Data Warehousing and Knowledge Discovery*, pp. 141–151. Springer Berlin Heidelberg, 2001.
7. Chen, Bee-Chung, Jian Guo, Belle Tseng, and Jie Yang. "User reputation in a comment rating environment." In *Proceedings of the 17th ACM SIGKDD international conference on Knowledge discovery and data mining*, pp. 159–167. ACM, 2011.
8. Elmongui, Hicham G., Riham Mansour, Hader Morsy, Shaymaa Khater, Ahmed El-Sharkasy, and Rania Ibrahim. "TRUPI: Twitter recommendation based on users' personal Interests." In *International Conference on Intelligent Text Processing and Computational Linguistics*, pp. 272–284. Springer International Publishing, 2015.
9. Goldberg, Ken, Theresa Roeder, Dhruv Gupta, and Chris Perkins. "Eigentaste: A constant time collaborative filtering algorithm." *Information Retrieval* 4, no. 2 (2001): 133–151.
10. Guy, Ido. "Social recommender systems." In *Recommender Systems Handbook*, pp. 511–543. Springer US, 2015.
11. Herlocker, Jonathan L., Joseph A. Konstan, Al Borchers, and John Riedl. "An algorithmic framework for performing collaborative filtering." In *Proceedings of the 22nd annual international ACM SIGIR conference on Research and development in information retrieval*, pp. 230–237. ACM, 1999. 4.
12. Karypis, George. "Evaluation of item-based top-n recommendation algorithms." In *Proceedings of the tenth international conference on Information and knowledge management*, pp. 247–254. ACM, 2001.
13. Koren, Yehuda. "Factorization meets the neighborhood: a multifaceted collaborative filtering model." In *Proceedings of the 14th ACM SIGKDD international conference on Knowledge discovery and data mining*, pp. 426–434. ACM, 2008.
14. Lops, Pasquale, Marco De Gemmis, and Giovanni Semeraro. "Content-based recommender systems: State of the art and trends." In *Recommender systems handbook*, pp. 73–105. Springer US, 2011.
15. Ricci, Francesco, Lior Rokach, and Bracha Shapira. *Introduction to recommender systems handbook*. springer US, 2011.
16. Sopchoke, Sirawit, and Boonserm Kijsirikul. "A step towards high quality one-class collaborative filtering using online social relationships." In *Advanced Computer Science and Information System (ICACISIS), 2011 International Conference on*, pp. 243–248. IEEE, 2011.
17. Twitter (2006). <http://www.twitter.com/> (last accessed January 06, 2014).
18. Twitter Usage. <http://about.twitter.com/company> (last accessed January 06, 2014).
19. Yildirim, Hilmi, and Mukkai S. Krishnamoorthy. "A random walk method for alleviating the sparsity problem in collaborative filtering." In *Proceedings of the 2008 ACM conference on Recommender systems*, pp. 131–138. ACM, 2008.

A Life-Saving Approach: Traffic Control System to Prioritize Ambulance on Road

Sagar Majumdar, Rohan Sharma, Akshansh Jain, Rajesh Singh and Anita Gehlot

Abstract In order to have a long-term approach toward future endeavors, security of life is of utmost importance. The ambulance communicates with the traffic light controller at the nearest crossway through radio frequency technology using RF module, navigation system, and switch array. The command of traffic light guides the ambulance the way forward to reach the destination at the proper time. This paper illustrates the complete use of available techniques in an optimized manner and to utilize it for maximum benefit for the public of the nation. The proposed system has free space path loss equal to 99.16 dB approximately which is good for a wireless system configuration to work efficiently.

Keywords RF module · Navigation system (GPS) · Switch array

S. Majumdar (✉)

B. Tech (Electronics Engineering), University of Petroleum and Energy Studies,
Energy Acres, Dehradun, India
e-mail: sagarnandim@gmail.com

R. Sharma

B. Tech (Power System Engineering), University of Petroleum and Energy Studies,
Energy Acres, Dehradun, India
e-mail: rohansharma0394@gmail.com

A. Jain

B. Tech (Computer Science Engineering), University of Petroleum and Energy Studies,
Energy Acres, Dehradun, India
e-mail: sherjain98@gmail.com

R. Singh · A. Gehlot

Department of Electronics Engineering, University of Petroleum and Energy Studies,
Energy Acres, Dehradun, India
e-mail: rsingh@ddn.upes.ac.in

A. Gehlot

e-mail: anita@ddn.upes.ac.in

© Springer Nature Singapore Pte Ltd. 2018

R. Singh et al. (eds.), *Intelligent Communication, Control and Devices*,
Advances in Intelligent Systems and Computing 624,
https://doi.org/10.1007/978-981-10-5903-2_66

1 Introduction

India accounts to 1.34 billion population and is the second most populous country in the world. With the population growth rate of 1.2% annually, the predictions are reaching 1.53 billion in the coming years [1]. This new era of industrialization and urbanization has made people to shift to the cities leaving their ancestral homes for having a better standard of living, and this goes the same with all the families of the society [2]. Only the metropolitans of the nation itself account to population in the range between 65 lakhs and 2 crores [3]. The trend gives rise to increase in population within the city leading to more traffic. This adversely effects one of the important necessity of humans called ambulance facility. According to CIA (Central Intelligence Agency) world fact book, about 10.1% of deaths in India are caused due to late arrival of ambulance [4]. The term, we call as '*First Aid*,' is one of the prime requirements in a city which, in many cases, can only be provided by ambulances. As the health of the patient deteriorates, he/they require an immediate addressal toward a hospital, which is being fueled up through an early arrival of an ambulance. Though the services are available but are not being utilized at their potential.

According to some present instances like a man bled to death after a two-and-a-half-hour ambulance delay [5], a 15-min travel to hospital took about 45 min, sacrificing the life of an old-aged person [6], a six year old being rushed to hospital due to chronic problem, collapsed on the way due to extension in time of travel [7], pregnant woman died due to the same issue of reaching late [8]. So, it is correct to say that the delay in ambulance costs over to life of many people. The statistics of the increasing problem is, however, very alarming and needs a direct attention. The instant provision to the facility can be achieved if we open up our trafficking roads thus allowing the patient to be treated according to his/her ailment.

Here, we are proposing a system which will eliminate vehicles from the path of ambulance, so that it can reach its destination on time, with the help of proper signaling of traffic lights. The mode of communication between the ambulance and traffic light controller at a crossway is through RF (radio frequency) module where ambulance driver instructs the traffic light controller about its approaching and leaving path across the crossway with the help of navigation system and switch array.

2 Theory and Principle Involved

An idea is put forward only after taking into account all the main principles of the model and keeping in mind about the long-term benefits to mankind and environment from it. The operating principle of the proposed system includes that of RF module, navigation system, switch array. The RF modules use its transeceiving antennas in order to communicate between the ambulance and the traffic lights over

long distances, at the particular frequency of 433 MHz, operating at voltage range of 3–12 V [9] and at the rate of 1–10 kbps without any consideration of line of sight (LOS) communication issue [10].

The switch array with four buttons pointing left, right, up, and down allows the ambulance driver to communicate with traffic light controller, acknowledging about its leaving path from crossway by pressing the corresponding button. The navigation system or the GPS helps the driver to track the traffic light position and the status of traffic on the upcoming path on its way.

3 Fabrication and Methodology

The system works in the radius of 5 km, with traffic light at the center. This consists of two main units, that is, ambulance and traffic light control unit. The ambulance is equipped with a RF transceiver module, switch array, and a navigation system. On the other hand, the traffic light controller, which is controlling the lights with the help of relays and transistors [11], contains a RF module. Both the units are illustrated in the following Fig. 1.

The RF module inside the traffic light controller receives radio signals as soon as an ambulance enters the area within 5-km radius. This now manages the traffic in such a way that the path taken by the ambulance should possess less vehicles. The lights are controlled accordingly with the help of relays and transistors by the controller. From inside the ambulance, the RF module sends signal to the traffic light controller, acknowledging its presence. The navigation system is used to detect a nearby traffic light for the ambulance driver [12], so that the driver can send the direction of leaving the crossway to the traffic light controller, with the help of switch array [13]. The traffic light then makes the path, going to be used by the ambulance to leave the crossway, empty.

In Fig. 2, two ambulances are approaching the traffic light, which is at the center of the crossway. Ambulance from path 3 is at 3 km from traffic light, and it has to

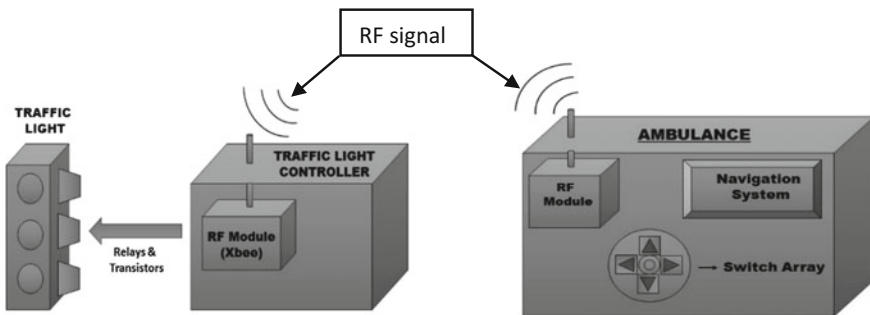


Fig. 1 a Traffic light control unit. b Ambulance unit

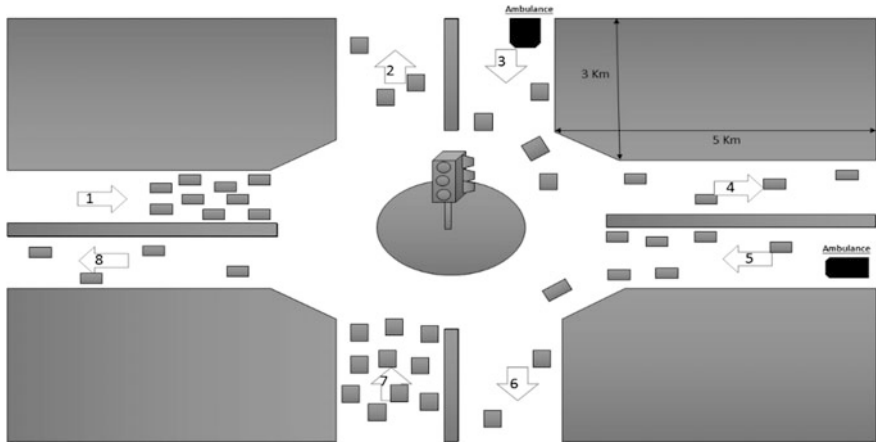


Fig. 2 Path cleared by the traffic light for the two ambulances in the crossway

go toward path 8. Similarly, another ambulance, at 5 km from traffic light, is approaching it from the path 5 and it has to go toward path 6. The traffic light now tends to clear the paths 3, 8, 5, and 6 for smooth run of the ambulances. The priority of the ambulance is decided by the traffic light on the basis of its distance from the ambulance, when more than one ambulance is approaching it simultaneously. In the case of Fig. 2, ambulance from side 3 is nearer than that of ambulance from side 5. Hence, there are less vehicles in path 3 as compared to path 5. More vehicles will be reduced from the path 5 when the ambulance on this path comes more close to the traffic light. Hence, the ambulance finds its way out of the traffic very easily.

4 Mathematical Calculation

We know free space path loss (FSPL) formula for a wireless communication system is given by [14],

$$FSPL(dB) = 20 \log_{10}(d) + 20 \log_{10}(f) + 32.45 \tag{1}$$

where

‘*d*’ is the distance from the transmitter (in kilometers) and

‘*f*’ is the signal frequency (in megahertz)

Taking the values as *d* = 5 km, *f* = 433 MHz, and substituting in Eq. (1),

we get,

$$\begin{aligned}\text{FSPL(dB)} &= 20 \log_{10}(5) + 20\log_{10}(433) + 32.45 \\ &= 13.97 + 52.73 + 32.45 \\ &= 99.159 \text{ dB.}\end{aligned}$$

Thus, FSPL is calculated out to be **99.159 dB**.

5 Conclusion

Precisely, this system holds good for the fact that WHEN THE CITY TRAFFIC HALTS, AN AMBULANCE LIVES and this can be achieved by the above-developed system and of course, through guided effort and cooperation of all individuals of the nation.

The good response from the system's free space path loss for the used dimensions will certainly help us to adopt this method of minimizing death rate due to late arrival of ambulance. The installation cost is also minimal as it only requires very common components for this system to work. Thus, if appreciated, it can act very beneficial in increasing life expectancy ratio for a patient availing the ambulance services.

References

1. Visaria, Pravin, and Leela Visaria. "Indian population scene after 1981 census: A perspective." *Economic and Political Weekly* (1981): 1727–1780.
2. Adelman, Irma. "An econometric analysis of population growth." *The American Economic Review* 53.3 (1963): 314–339.
3. Shaw, Annapurna, and M. K. Satish. "Metropolitan restructuring in post-liberalized India: separating the global and the local." *Cities* 24.2 (2007):148163.
4. Roy, Nobhojit, et al. "Where there are no emergency medical services—prehospital care for the injured in Mumbai, India." *Prehospital and disaster medicine* 25.02 (2010):145–151.
5. <http://www.itv.com/news/2017-01-25/man-bleed-to-death-after-2-5-hour-ambulance-delay/>.
6. <http://www.thehindu.com/news/cities/Hyderabad/Ambulances-delayed-patients-Suffer/article14985899.ece>.
7. <http://timesofindia.indiatimes.com/city/bengaluru/When-city-traffic-halts-ambulanceslives/articleshow/37055671.cms>.
8. <http://timesofindia.indiatimes.com/city/bhubaneswar/Ambulance-delay-leads-to-patient-death/articleshow/54455881.cms>.
9. Kazanchian, Armen E. "Antenna with integrated RF module." U.S. Patent No. 8,866,696. 21 Oct. 2014.
10. Hee-Joon, P. A. R. K., et al. "Design of miniaturized telemetry module for bi-directional wireless endoscopes." *IEICE Transactions on Fundamentals of Electronics, Communications and Computer Sciences* 86.6 (2003): 1487–1491.

11. Eckel, David P., et al. "Network based electrical control system with distributed sensing and control." U.S. Patent No. 6,388,399. 14 May 2002.
12. Howard, Damian, et al. "Integrating Navigation Systems." U.S. Patent Application No. 11/750,822.
13. Tannas Jr, Lawrence E. "Transparent keyboard switch and array." U.S. Patent No. 4,017,848. 12 Apr. 1977.
14. Alam, Didarul, and Rezaul Huque Khan. "Comparative study of path loss models of WiMAX at 2.5 GHz frequency band." *International Journal of Future Generation Communication and Networking* 6.2 (2013): 11–23.

Save the Real Nectar: Water Distribution System in Multi-storied Apartments

Rohan Sharma, Sagar Majumdar, Tanushree Khattri, Rajesh Singh and Anita Gehlot

Abstract In order to have sustainable development, the resources need to be judiciously utilized. This paper illustrates on how we can limit our water requirements according to our needs as well as its distribution among the multi-storied buildings which are being constructed within premises or outskirts of each and every city. The overhead tank being placed on the top of the building will furnish equal amount of water to each and every floor with the use of flow sensors, servomotor, and control valves that are operated by a microcontroller, helping the system to run efficiently yielding better output.

Keywords Flow sensor · Servo motor · Android application · Microcontroller controlling valves

R. Sharma (✉) · T. Khattri
B. Tech (Power System Engineering), University of Petroleum and Energy Studies,
Energy Acres, Dehradun, India
e-mail: rohansharma0394@gmail.com

T. Khattri
e-mail: tanuamazingworld@gmail.com

S. Majumdar
B. Tech (Electronics Engineering), University of Petroleum and Energy Studies,
Energy Acres, Dehradun, India
e-mail: sagarnandim@gmail.com

R. Singh · A. Gehlot
Department of Electronics Engineering, University of Petroleum and Energy Studies,
Energy Acres, Dehradun, India
e-mail: rsingh@ddn.upes.ac.in

A. Gehlot
e-mail: anita@ddn.upes.ac.in

1 Introduction

Rapid increase in population has led to scarcity of water. United Nations Environmental Programme 2002 states that, by 2025, the number of people who will be living in regions with absolute water scarcity will reach 1.8 billion [1]. Especially in developing countries, about two-thirds of the world population will be facing moderate to high water stress and remaining half will be facing problems due to water scarcity. Overexploitation of water resources, particularly underground water, is the result of wasteful attitude and mismanagement of resources in India. In urban settlements, the concentration of water-related problems will be more, where quantity of water resource is degrading day by day [2]. The pressure at the upper floors is very low and that at lower floors is high enough due to non-uniform distribution of water on the floors of buildings and a large population faces mismanagement. Around 800 L of water is required for five people in a flat in a day [3].

Indian cities face intermittent water supply. Except some public–private partnership systems, none provides 24×7 water supplies. Indian houses with fresh-water supply are only 64%. Between 1 and 6 h is the likeable duration of water supply [4]. With piped water distribution system, many areas inside India have poor water quality. Cracks and high leakages are present in many systems. Percentage of water supplied as per an international survey of water loss, in 1991, reports that water loss is from 8 to 24% in industrialized countries, water loss ranged from 15 to 24% in middle-income or industrialized countries, and water loss was estimated at between 25 and 45% in developing countries like India [5]. Contaminated water inside pipe through cracks is also a consequence of negative pressure in the pipes due to power outage [6].

Water can also be conserved by reducing water losses in pipes. Required water pressure can reach each floor efficiently with the help of efficient pressure booster pumps, flow meters, and pressure regulating valves. By the year 2050, it was estimated that half of India's population will be living in urban areas and will face acute water problems [7]. Water stress condition in these countries in addition to source limitation is due to factors such as poor distribution through pipe networks and inequalities in service provision between the rich and the poor [8]. The majority of the respondents are not connected to the water supply pipelines, and respondents, who do not have pipe connection in their houses, correspond to 71%. As stated earlier that the current supply caters for just about 30% of the daily water demand of the study area is reflected by these facts [9]. The paper, thus, suggests a way for uniform distribution of water in all the floors of an apartment.

2 Theory and Principle Involved

When the governing principle is approved for its long-term benefits to the population of a nation, the designing process is initiated full-fledged. The operating principle for the system revolves around flow sensors, microcontroller controlling valves, motor, pump, etc. As observed, an overhead tank placed on the top of an apartment distributes water in a fashion so that the ground floor receives maximum water compared to upper floors, since pressure goes directly in proportion to height of apartment floor [10].

The prime operation of the flow sensors will acknowledge the microcontroller about the level of water pressure at each floor, which will produce motion in valves that are to be motor controlled. An android app lets the user to manually control the flow of water, using the technique of wireless communication with the microcontroller, controlling the servomotors [11].

3 Fabrication and Methodology

The system works when the overhead tank supplies water to the residents of an apartment. The flow sensor senses the flow of water and sends information about the same to the microcontroller. The microcontroller then sends the command to the servomotor, which in turn controls the valve movement. At the same time, people of the apartment can manually regulate the valve movement through a mobile application, communicating wirelessly with the microcontroller. The process is illustrated in Fig. 1a, b.

Whenever the flow is more, the stepper motor minimizes the valve opening, and when the flow reduces, motor makes the valve wide open. One can manually alter the valve opening by giving manual command by using an android app, where the display shows the actual flow of water, user fed flow of water as well as buttons for

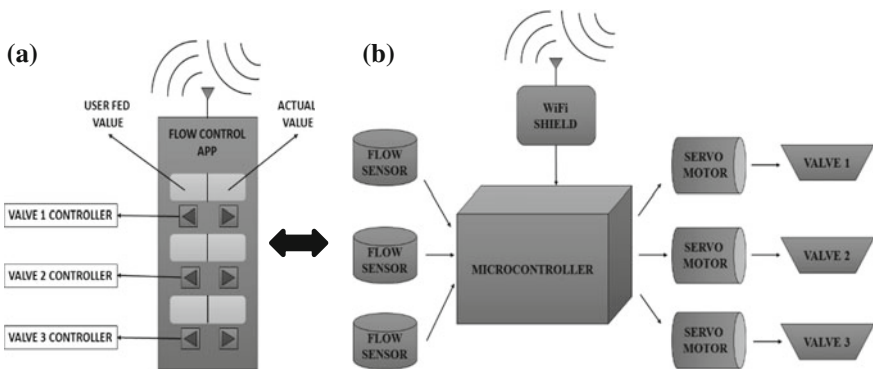


Fig. 1 a Mobile app display. b Flow control unit

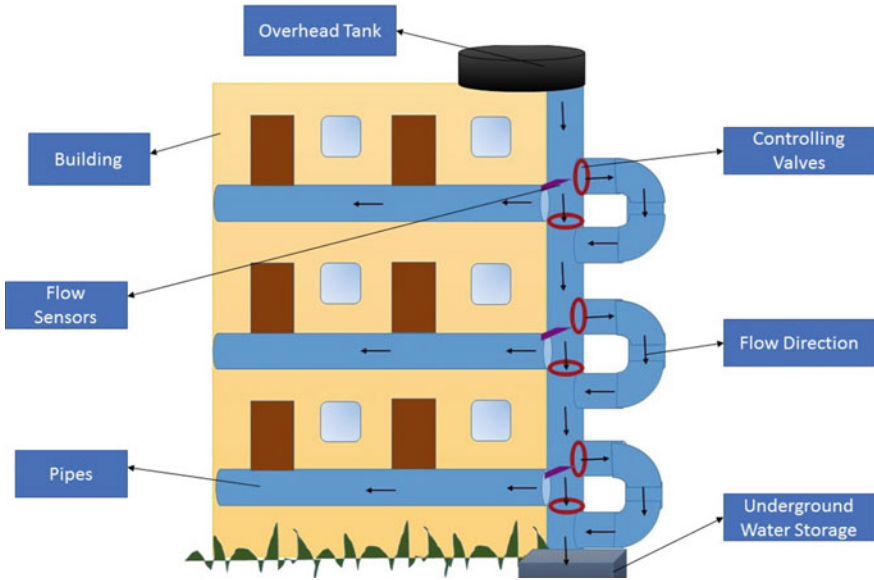


Fig. 2 Flow control system working

changing the openings of all the valves of the apartment floors so that amount of inlet water can be controlled. This app is communicating with the microcontroller, which closes the valve with the help of servomotor. When no one is there in the apartment floor, valve can be completely closed, blocking the water flow in that floor. Then, water is then supplied to the lower floors by a diverted pipeline as shown in Fig. 2. In this way, water wastage is minimized and each floor is supplied with equal amount of water.

Consider Fig. 1b, where the overhead tank is furnishing water to all the floors of the apartments. The water is flowing down, and the flow sensor's output is fed into the microcontroller. If no one is staying in the first floor (say), microcontroller makes the valve closed or it can be closed manually by android app. Now, the lower floors are fed with water, flowing through diverted pipelines. Finally, the extra water is stored in the underground water storage in order to eliminate water wastage [12].

4 Mathematical Calculation

Generally, the requirement of water by 1 person per day = **150 L** (including peak hours) and **10 L** (drinking water)

- **Total amount of water required = $150 + 10 \text{ L} = \underline{160 \text{ L}}$**
- So, for five people living in a floor,
Total amount of water required = $160 \times 5 = \underline{800 \text{ L}}$

- Thus, for a three-floor building,
Total amount of water required = 800 L × 3 = 2400 L
- Volume of water required (in cubic meters) = 2400/1000 = **2.4 m³**

Let capacity of the tank = **3600 L**

The equivalent dimensions are 1.5 × 2 × 1.2 m = **3.6 m³**

We know,

$$P = \rho gh,$$

where

P = pressure drop [in Pascal (Pa)]

$\rho = 1000 \text{ kg/m}^3$

$g = 9.81 \text{ m/s}^2$

h = height from the top of the tank to the base of each floor.

On substituting the values, we get

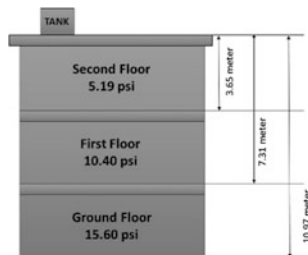
$$P = \{ (1000 \text{ kg/m}^3) * (9.81 \text{ m/s}^2) * h \}.$$

The illustration for a three-floor building can be represented as, for example,

- **2nd floor-** h = 12 ft. = 3.65 m; **P₂ = 5.19 psi**
- **1st floor-** h = 24 ft. = 7.31 m; **P₁ = 10.40 psi**
- **Ground floor-** h = 36 ft. = 10.97 m; **P_g = 15.60 psi**

This is the approximate existing situation without considering the losses (due to bending, sudden enlargement, contraction, friction, etc.)

Further, these pressures are being regulated for each and every floor of a building.



- The type of pipe to be used = 1/4 in.
- The pump to be used = Water booster pump of centrifugal type (Fig. 3).

These values state that water pressure rises as it moves downward, and thus, water is not equally distributed in all the floors. Hence, this proposed system can rectify this issue.

	Type K		Type L	
	Outside Diameter (inches)	Wall Thickness (inches)	Outside Diameter (inches)	Wall Thickness (inches)
	0.375	0.035	0.375	0.03
Flow (gpm)	Pressure Loss (psi/ft)	Velocity (ft/sec)	Pressure Loss (psi/ft)	Velocity (ft/sec)
1	0.146	4.4	0.125	4.1
2	0.528	8.8	0.451	8.2
3	1.118	13.2	0.956	12.4

Fig. 3 Pipe of nominal size 1/4 (in.) [13]

5 Conclusion

In brief, it can be said that PLANNING AND MANAGEMENT OF TODAY WILL BENEFIT US FOR TOMORROW. Since, water is the prime unit of life on Earth and the ground water table is significantly decreasing, hence it should be preserved as much as possible.

Further, the huge population needs habitation leading to construction of tall buildings which brings out the problem of water distribution, so it is the sole responsibility of each one of us to limit ourselves to its use according to the requirements. The minimal investment and good results can give better outputs with long-term goals with this proposed system.

References

1. Panwar, Ar Manoj, and Mr Sunil Antil. "Issues, Challenges and Prospects of Water Supply in Urban India".
2. Rosegrant, Mark W., Ximing Cai, and Sarah A. Cline. *World water and food to 2025: dealing with scarcity*. Intl Food Policy Res Inst, 2002.
3. Alperovits, Elyahu, and Uri Shamir. "Design of optimal water distribution systems." *Water resources research* 13.6 (1977): 885–900.
4. McKenzie, David, and Isha Ray. "Urban water supply in India: status, reform options and possible lessons." *Water Policy* 11.4 (2009): 442–460.
5. Suryakumari, D., S. V. Deshpande, and V. S. Deshpande. "The Relevance of Appreciative Inquiry In the context of Social Change, Social Research, Social Work and Social Entrepreneurship." *Imperial Journal of Interdisciplinary Research* 2.6 (2016).
6. McInnis, Duncan. "A relative-risk framework for evaluating transient pathogen intrusion in distribution systems." *Urban Water Journal* 1.2 (2004): 113–127.

7. Totsuka, N., Trifunovic, N., & Vairavamoorthy, K. (2004). Intermittent urban water supply under water starving situations, 505–512.
8. Singh, S. K., Chandel, V., Kumar, H. & Gupta, H. (2014). Remote Sensing and GIS Based Urban Land Use Change and Site Suitability Analysis For Future Urban Expansion of Parwanoo, Planning Area, Solan, Himachal Pradesh (India). *International Journal of Development Research*, Vol. 4.
9. Mohammed, Abdullahi B., and Abdulrahman A. Sahabo. “Water Supply and Distribution Problems in Developing Countries: A Case Study of Jimeta-Yola, Nigeria”.
10. Zacheus, Outi M., and Pertti J. Martikainen. “Occurrence of legionellae in hot water distribution systems of Finnish apartment buildings.” *Canadian Journal of Microbiology* 40.12 (1994): 993–999.
11. Brunette, Waylon, et al. “Open data kit sensors: a sensor integration framework for android at the application-level.” *Proceedings of the 10th international conference on Mobile systems, applications, and services*. ACM, 2012.
12. DeStefano, Gerard. “Water management system.” U.S. Patent No. 4,934,404.19 Jun. 1990.
13. <http://docs.engineeringtoolbox.com/documents/930/pressure-loss-copper-pipe-1.png>.

Domain Dictionary-Based Metadata Construction for Search Over Encrypted Cloud Data

S.K. Mahreen, M.R. Warsi and S.K. Neelam

Abstract With the massive increase in the amount of data generated every day and with the advent of the modern technology, cloud storage has become a need of the hour. Advancements in cloud computing led the data owners to outsource their intensive data to cloud servers like Amazon, Microsoft Azure, Google Drive, and so on. Cloud storage services permit users to store and/or accession of data in a cloud; irrespective of the time and geographical locations, in an on-demand basis using any device. However, entrusting the cloud service provider with the sensitive data raises the underlying security and privacy issues. In order to provide confidentiality, data are encrypted before safekeeping it on the cloud service provider (CSP). Although the encryption approach does strengthen the data security, it consequently effects the various operations to be performed on the data, most significant being data searching and retrieval. Various searchable encryption schemes are developed for search over outsourced encrypted data. Mostly these schemes perform index-based ranked search and employ frequency of search keyword in the document; hence, challenging the security and reducing efficiency. In this paper, we present a domain dictionary-based index generation scheme for search over encrypted data. We have proposed a novel concept of domain dictionary wherefrom a metadata-based index file is to be generated that is to be queried while performing searching operations.

Keywords Cloud · Domain dictionary · Index · Metadata

S.K. Mahreen (✉) · M.R. Warsi
Department of Computer Engineering, Aligarh Muslim University, Aligarh, UP, India
e-mail: mehkhani27@gmail.com

S.K. Neelam
Department of IT, NIT Srinagar, Srinagar, J&K, India

1 Introduction

In this era of speedy advancements in the technology, newer computing models are replacing the traditional ones. Also with enormous amounts of data being generated everyday at an enormous speed, the traditional and local storage systems do not cope up with the rising storage demands. Data owners are inclined toward moving their data to the cloud storage servers. Migrating data and computing services to the cloud infrastructures do provide benefits like rapid elasticity of resources, flexibility in services, reduced maintenance overhead, and over and above in a pay-as-per-demand fashion. Despite of all the ubiquitous benefits of cloud storage, there arise underlying security and privacy concerns when it come to outsourcing sensitive data to the cloud server. In certain scenarios, customers do settle for the flexibility of services at the cost of privacy. However, when it comes to enterprises and organizations with sensitive data to be stored on a server privacy and data security cannot be compromised. Therefore, in order to motivate data owners to migrate their sensitive data to cloud, the security and privacy issue need to be addressed. The straight forward approach is to apply cryptographic techniques to secure the sensitive data before being outsourced to the cloud server for storage. When the information is encrypted various operations to be performed on the data are limited as the data are in the unintelligible form. Efficient search over encrypted data still remains a challenge for the researchers.

Many search-enabled encryption schemes have been developed so far to perform search over encrypted data [1]. Most significant search techniques include keyword-based search schemes. Various indexing techniques have been suggested for keyword-based search schemes. Most of the index based techniques are based on frequency of the query keyword in the document; which in effect does causes leakage of data as the cloud might get insight of the document contents, hence challenging the security.

The goal is to perform search and retrieve the outsourced data in an effective and secure manner. In this paper, we present a novel index generation scheme based on domain dictionary for providing search capability over encrypted data.

2 System Model and Implementation

The system model can be viewed as an aggregation of three entities: the data owner, the data user, and the cloud server (C). The data owner owns a wide set of documents that are to be outsourced for safekeeping to the remote server. Prior to outsourcing information to the cloud in order to achieve confidentiality, the information needs to be encrypted. Also, a domain dictionary D has to be constructed. This domain dictionary D is an assemblage of all the keywords, contained in the files that are to be stored on a remote server, and their extended sets to include synonyms and related terms. Later, at the time of searching the required files are retrieved with the assistance of these extended keyword sets in the D .

After applying cryptographic techniques on the data, the encrypted data retrieval becomes a challenging task. So, in order to perform search operations over the outsourced encrypted data for retrieving data effectively, the construction of a searchable index becomes inevitable. Therefore, before outsourcing we construct a searchable index I from D for querying encrypted data and then along with the encrypted document collection, index I is outsourced to the cloud server. In the search phase, a trapdoor is to be generated against the query keywords submitted by the data user. The cloud server will look into the index I against the generated query trapdoor and then return the relevant search results to the end user.

2.1 Initialization Phase

Initialize (): The data owner selects the documents containing sensitive data, recognizes the keywords of interest representing those documents that are to be added to the domain dictionary. At the time of searching, these keywords are passed for querying while fetching the relevant files from the remote cloud server.

2.2 Metadata Construction

In order to build a searchable index for providing search capabilities, the metadata needs to be extracted from the data files to be outsourced. Metadata construction begins with the creation of the domain dictionary which can be viewed as a collection of data buckets. Each data bucket or domain in the domain dictionary contains id of the domain and all the keywords and their extended synonym set corresponding to the similar files out of whole set of documents.

Build-Domain-Dictionary (D): The set of keywords that represent the set of sensitive files F are identified by the data owner. Our proposed scheme allows the data owner to specify the file with more powerful keywords even if they don't occur in the file but are much relevant to its content. The selected keywords are expanded to include synonyms and related terms by the keyword set extension (KSE) process. The keyword synonym set is generated using the WordNet[®], which is a large lexical database of English, provided by Princeton University.

Using the expanded keyword set search quality is improved as not just the exact matching keywords but also the synonyms and related terms are also taken into consideration. For every new file that is to be uploaded, the domain dictionary is dynamically updated with a new set of keywords and their extended synonym sets. Before inserting a new entry, i.e., a keyword synonym set into D , a similarity score between the new keywords and the existing domains is calculated. If some existing domain(s) have similarity value greater than a threshold (≥ 0.4) the new entry is appended to the domain having maximum similarity with the new keyword entries. In this way, each domain is populated with the related keywords which in effect

represent the files that are conceptually related. The overall process of building the domain dictionary is described in the algorithm depicted in Fig. 1.

2.3 Index Construction

To build a searchable index out of the constructed metadata for every document F_i in the set F , we need to scan the entire metadata set and compute the appropriate relevance score with each domain D in the domain dictionary. Each index maps to a data bucket or the domain in the domain dictionary. At the time of searching, the user enters the search query and the relevance score for the extended query terms is calculated across the domains in domain dictionary which is then matched against the index entries for the retrieval of relevant files. Every index entry of the index I for each sensitive file will be stored in the format shown below:

$$D_i \rightarrow \langle F_j, S_j \rangle \langle F_x, S_x \rangle \dots \langle F_z, S_z \rangle$$

D_i is the domain id and F is a file having similarity S with D_i . Every time a new file is to be uploaded, the index file is updated by appending the new similarity value against the relevant domain id. The complete framework for search over

Algo 1:Build-domain(k_s, D)

K : Set of file keywords, *F*: sensitive files, *D* : Domain Dictionary
Output *D*.

1. Preprocessing:
 - I. Choose the keywords $K_w = (K_{w1}, K_{w2}, K_{w3} \dots K_{wn})$ from every file in the collection of sensitive files $F = (F_1, F_2, F_3 \dots F_m)$.
 - II. Expand selected keywords using the Keyword Set Extension (KSE) process to generate keyword synonym set.
2. Populating the domain dictionary
 - I. Calculate the similarity between the new keyword set and the domains that exist in the domain dictionary.
 - II. Identify the domains that have similarity value greater than a threshold (≥ 0.4)
 - III. Select the most similar domain having maximum similarity value and append the new extended keyword values to it.
3. Building the final domain dictionary
 - I. If no similar domain exists that satisfies condition at 2.II, add a new domain to domain dictionary $D = (D_1, D_2, D_3, \dots D_n)$.
 - II. This $D = (D_1, D_2, D_3, \dots D_n)$ is the final Domain Dictionary *D*.

Fig. 1 Details of build domain

cryptographic cloud data utilizing the proposed scheme of “Domain Dictionary based Metadata Construction” is described in detail in [2].

3 Analysis

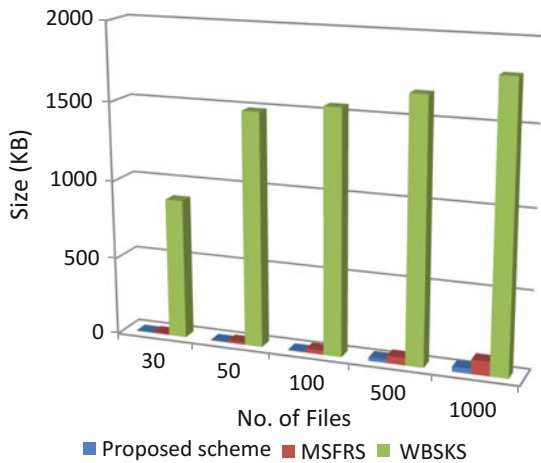
3.1 Space Analysis of the Proposed Scheme

For the purpose of analyzing the proposed scheme, we uploaded varying number of files to populate the data set and monitored the variations in the size of the generated index when the file upload frequency was increased. With the increase in number of uploaded files, index entries increased, hence resulting in increase in index file size. We also compared the size of index files generated in previous schemes like WBSKS [3] and keyword-based scheme MSFRS [4]. Figure 2 draws a contrast of the varying index file sizes. According to the statistics in Fig. 2, the index file generated by our developed scheme has significantly smaller storage requirements than those created by WBKS and MSFRS. This huge reduction in the index file size generated in our scheme is due to non-involvement of keywords in the index file. Hence, efficiency in terms of space requirements for the index file is improved.

3.2 Efficient and Secure Index Generation and Domain Building

An efficient feature of our scheme is that the index file entries are free from keywords; hence, there is no threat of data leakage to the remote CSP.

Fig. 2 Comparison of the index file sizes



Also, minimum overhead occurs while revising the index file entries and refurbishing the contents of domain dictionary. Figure 3 shows the average time taken to construct index and domain dictionary. It is evident from the results that time taken to construct index and domain dictionary in our scheme is almost the same. Also, the building time in both the cases increases with increase in number of keywords representing the file.

A comparison of the cost of index construction in the existing scheme MSFRS [4] and our proposed scheme was drawn. Figure 4 shows a contrast of average time used to build the index file with 100 files on cloud server; using the proposed scheme and MSFRS. The results in Fig. 4 clearly show that in both the schemes the time taken to construct the index file is almost same, but some hike in construction time was observed in case of MSFRS when the size of file to be uploaded increased. No such effect was observed in our scheme testifying that in the proposed scheme index construction time is independent of file size.

4 Related Work

In order to incorporate the search-enabled encryption schemes to cloud computing environments, researchers have been developing schemes to perform search over cryptographic cloud data efficiently [5]. Traditional way of searching included single keyword searchable encryption schemes [6, 7] wherein usually a searchable index is build and encrypted prior to remote storage. In these techniques, only single keyword search is possible. Also, some researchers have developed attribute-based encryption schemes that retrieve data on the basis of attributes of the data user. In attribute-based encryption schemes [8, 9], reverse encryption of cipher

Fig. 3 Time to build index file and domain dictionary with 100 files on C

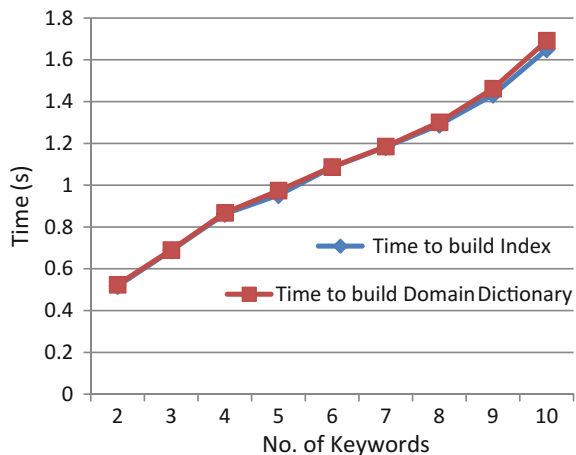
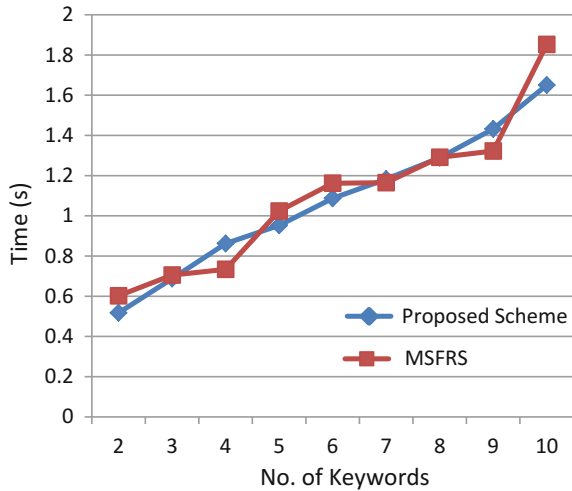


Fig. 4 Comparison of average index construction time with 100 files on C



text is possible only if there is a match between the attributes of the cipher text and the set of attributes of the user key.

To improve search functionalities over encrypted data, conjunctive keyword search [10, 11] has been proposed. In these schemes, huge complexity is incurred as conjunctive keyword-based search retrieves “all-or-nothing,” i.e., only those files are returned that contain each and every keyword included in the search query. The predicate encryption-based schemes [12, 13] are the recent proposed search approaches that support both conjunctive and disjunctive search. The disjunctive keyword-based search approach returns all those files that possess at least a subset of the query keywords, be it only a single keyword of significance. The lack of ranking mechanism owed to the wastage of processing time. In order to reduce this wastage of crucial processing time, order-preserving techniques were introduced [14, 15].

Wang et al. [16] proposed an encrypted inverted index for providing search capabilities over encrypted data. In this scheme, ranking of the retrieved documents was done according to the computed relevance score between documents and query.

Cao et al. [17, 18] were among the first few in the field to define ranked search problem with multi-keyword query. They proposed a latest architecture for multi-keyword-based ranked search while preserving privacy over encrypted cloud data (MRSE). They incorporated “inner product similarity” for evaluating document relevance. However, they employed static dictionary which needed to be regenerated every time a new keyword was inserted. Zhu et al. went on to propose an enhanced scheme “Efficient Multi-Keyword Rank Query on Encrypted Cloud Data” (MKQE) [19]. In MKQE, the count of computations required to expand keyword dictionary was reduced and also access frequencies of keywords were taken into consideration.

Moh and Ho [3] developed three different schemes “Synonym-Based Keyword Search (SBKS),” “Wikipedia-Based Keyword Search (WBKS),” and “Wikipedia-Based Synonym Keyword Search (WBSKS)”; among which WBSKS is an amalgam of SBKS and WBKS and incorporates the advantage of both the schemes to enhance the search to accommodate synonyms of the query keyword while managing a short index. In these schemes, index construction time was very high. Saini et al. [4, 20] proposed multi-keyword synonym-based fuzzy search supporting ranking over outsourced cryptographic cloud data (MSFRS) which supports multi-keyword, suggests synonyms; also, it returns ranked results by evaluating relevance scores on the basis of the frequency of the keywords in the files.

In order to support ranked multi-keyword search while accommodating synonym-based search as well, Fu et al. [21] put forth a flexible searchable scheme which utilized vector space model (VSM) to construct document index, and incorporated text information retrieval technique TFIDF. Also, they proposed a semantic feature extraction method known as E-TFIDF to improve the accuracy of search results.

5 Conclusion

In this paper, the goal was to address the issues of data security and data discovery of the outsourced encrypted data. Many disadvantages have been found in traditional techniques since they rely on evaluation of the encrypted files to find the relevance. Cloud server has to parse every relevant file that contains the keyword to find its relevance to the search query. This increases the computational complexity, and hence the searching time. To increase the efficiency of retrieval, we have been able to achieve a significant reduction in the index file size, which is credited to the fact that each index maps to a data bucket or the domain in the domain dictionary instead of listing up mappings from encrypted keywords to the comparable set of sensitive files that contain them. We introduced a novel concept of domain dictionary-based index construction wherein index file entries are free of keywords. By querying metadata file for searching and avoiding parsing of the encrypted files, search time can be reduced.

References

1. Neelam S. Khan and C. Rama Krishna. A Survey on Secure Ranked Keyword Search over Outsourced Encrypted Cloud Data. International Conference on Computer Networks and Information Technology (ICCNIT), March 20–21, 2014, NITTTR Chandigarh, pp. 347–357.
2. Mahreen S., Warsi M.R, Neelam S.: Secure Metadata based Search over Encrypted Cloud Data supporting Similarity Ranking: Unpublished.
3. Moh, T.S., Ho, K.H.: Efficient semantic search over encrypted data in cloud computing. In: International Conference on High Performance Computing and Simulation, pp. 382–390. Bologna (2014). <http://ieeexplore.ieee.org/abstract/document/6903711/>

4. Saini V., Challa R.K., Khan N.S.: An Efficient Multi-keyword Synonym-Based Fuzzy Ranked Search Over Outsourced Encrypted Cloud Data. In: *Advanced Computing and Communication Technologies. Advances in Intelligent Systems and Computing*, vol. 452. Springer, Singapore (2016). http://doi.org/10.1007/978-981-10-1023-1_43
5. Sharon. E, N. Saravanan.: A Survey on Keyword Based Search over Outsourced Encrypted Data. In: *International Journal of Engineering and Technology (IJET)*, vol. 5, pp. 905–909, (2013).
6. D. Song, D. Wagner, and A. Perrig.: Practical Techniques for Searches on Encrypted Data. In: *Proceedings IEEE Symposium. Security and Privacy*, (2000).
7. E.-J. Goh, “Secure Indexes,” *Cryptology ePrint Archive*, <http://eprint.iacr.org/2003/216>. 2003.
8. Sahai, A., Waters, B.: Fuzzy identity-based encryption. In: *Proceedings of EUROCRYPT*, pp. 457–473, (2005).
9. J. Bethencourt, A. Sahai, and B. Waters.: Ciphertext-policy Attribute based encryption. In: *Proceedings of IEEE Symposium. on Security and Privacy*, pp. 321–334, (2007).
10. L. Ballard, S. Kamara, and F. Monrose.: Achieving Efficient Conjunctive Keyword Searches over Encrypted Data. In: *Proceedings of Seventh Int’l Conference Information and Communication Security (ICICS ’05)*, (2005).
11. D. Boneh and B. Waters.: Conjunctive, Subset, and Range Queries on Encrypted Data. In: *Proc. Fourth Conf. Theory Cryptography (TCC)*, pp. 535–554, (2007).
12. J. Katz, A. Sahai, and B. Waters.: Predicate Encryption Supporting Disjunctions, Polynomial Equations, and Inner Products. In: *Proc. 27th Ann. Int’l Conf. Theory and Applications of Cryptographic Techniques (EUROCRYPT)*, (2008).
13. A. Lewko, T. Okamoto, A. Sahai, K. Takashima, and B. Waters.: Fully Secure Functional Encryption: Attribute-Based Encryption and (Hierarchical) Inner Product Encryption. In: *Proc. 29th Ann. Int’l Conf. Theory and Applications of Cryptographic Techniques (EUROCRYPT ’10)*, (2010).
14. A. Swaminathan, Y. Mao, G. M. Su, H. Gou, A. Varna, S. He, M. Wu, and D. Oard.: Confidentiality-Preserving Rank-Ordered Search. In: *ACM Storage SS*, pp. 7–12, (2007).
15. K. Li; W. Zhang; C. Yang; N. Yu.: Security Analysis on One to-Many Order Preserving Encryption-Based Cloud Data Search. In: *IEEE Transactions on Information Forensics and Security*, vol. 10, no. 9, pp. 1918–1926, (2015).
16. C. Wang, N. Cao, K. Ren, and W. J. Lou.: Enabling Secure and Efficient Ranked Keyword Search over Outsourced Cloud Data. In: *IEEE Transaction on Parallel Distributed System*, vol. 23, no. 8, pp. 1467–1479, (2012).
17. N. Cao, C. Wang, M. Li, K. Ren, and W. J. Lou.: Privacy-Preserving Multi-keyword Ranked Search over Encrypted Cloud Data. In: *IEEE INFOCOM*, pp. 829–837, (2011).
18. Cao, N., Wang, C., Li, M., Ren, K., Lou, W.: Privacy preserving multi-keyword search over encrypted cloud data. In: *IEEE Trans. Parallel Distrib. Syst.* 25, 222–233, (2014).
19. Z. Xu, W. Kang, R. Li, K. Yow and C. Xu.: Efficient multi keyword rank query on encrypted cloud data. In: *18th IEEE International Conference on Parallel and Distributed Systems*, pp. 244–251, (2012).
20. Khan Neelam, S., Challa, R.K.: Secure ranked fuzzy multi-keyword search over outsourced en-encrypted cloud data. In: *5th IEEE International Conference on Computer and Communication Technology (ICCT)*, Allahabad (2014).
21. Z. Fu, X. Sun, N. Linge, and L. Zhou.: Achieving Effective Cloud Search Services: Multi-keyword Ranked Search over Encrypted Cloud Data Supporting Synonym Query. In: *IEEE Transaction Consumer Electronics*, vol. 60, no. 1, pp. 164–172, (2014).

Reconstruction Using Sparse Approximation

Rana Sameer Pratap Singh and Rosepreet Kaur Bhogal

Abstract Interest in sparse approximations is prevalent in the recent years. The reason for this undivided engrossment is due to the large amount of applications. The process to find a sparse approximation can be very cumbersome since there is no specific method that can guarantee a solution in every situation. In this paper, we find sparse approximations and then analyze two algorithms: orthogonal matching pursuit (OMP) and least square orthogonal matching pursuit (LS-OMP).

Keywords Algorithms · Approximation methods · Least square Orthogonal matching pursuit (OMP) · Sparse

1 Introduction

Sparse is defined as the measurable quantity of a vector that means the vector employed is small in length. The main concern is not the length of the vector but the count of cardinal entries in the vector. The l_0 -norm is used to measure the sparseness of a vector, i.e., the count of cardinal terms. A number of advantages are associated with the use of sparse vectors such as calculations related to the multiplication of a vector by a matrix are tedious, while with the use of sparse vector the computations are reduced considerably. Another merit is that the sparse vectors require less storage space since only the location and the values of the entries are to be recorded.

Sparse approximation can be calculated in the more general form of an epitome mathematical problem. A wide range of applications make sparse approximation an important tool. Since vectors are required to represent a large amount of data, thus a large storage space will be required to hold or transmit it. By the use of sparse

R.S.P. Singh (✉) · R.K. Bhogal
Lovely Professional University, Phagwara, India
e-mail: sameer.rana1987@gmail.com

R.K. Bhogal
e-mail: rosepreetkaur12@gmail.com

approximation, the space required to store the vector would be reduced significantly. Sparse approximations are also employed to examine data by showing how the column vectors in a given basis join to produce the required data.

In order to produce approximations, one needs to gauge a signal onto a vacuous m -dimensional subspace. This is the most basic linear form of approximation. Furthermore, the use of interpolation by means of fixed polynomial makes it even simpler. Later, a series of nonlinear methods were developed to produce these approximations. One common and easy method is to impose a signal onto the superior linear subspace traversed by m entries of a fixed orthonormal basis. The reason for this simplicity is the rigid structure of an orthonormal system, thus yielding an improved approximation error [1, 2] as compared to the linear methods. But the main drawback of using the nonlinear methods is that sometimes the signal under supervision just does not fit into the orthonormal basis. Thus, researchers designed the best methods for approximating the linear combination of m elements from a random dictionary. This technique is known as the sparse approximation or nonlinear approximation.

How does one design a fast algorithm that can possibly calculate a nearly optimal sparse representation of a random input signal? This can be answered with the help of the two approaches, orthogonal matching pursuit (OMP) and the least square orthogonal matching pursuit (LS-OMP). OMP is the frequent voracious algorithm that chooses a segment prime associated with the unconsumed part of the signal under observation. After this, it produces a pristine approximation by imposing the signal onto the previous segments that were been preferred. Further, this technique is expanded to a minor voracious algorithm that helps in an orthonormal system. The LS-OMP has an advantage over OMP that it exactly recovers the signal within less number of iterations. In contrast to this, OMP has its own merit of giving simple and fast implementations [3, 4]. In this paper, experimental results show that the LS-OMP gives guaranteed signal recovery or reduced error in comparison with the OMP method.

2 Related Work

In 2011, Charles Soussen and Remi Gribonval [5] extended the research of Tropp for the scrutiny of OMP using the exact recovery condition (ERC). The orthogonal least squares (OLS) gives the first exact recovery analysis for a random signal within k iterations. The results also prove that while using OMP some subsets are never recovered for a particular set of dictionary.

Gagan Rath and Christine Guillemot in 2009 ventured a paper [6] related to the orthogonal augmentation of the foremost instigate complementary matching pursuit (CMP) algorithm used for sparse approximation of a vector. The basic procedure employed in CMP is homologous to the matching pursuit (MP) but carried out in the row space of the dictionary matrix. This algorithm tries to remove the problem

of MP that is sub-optimality by upgrading the elements of all stipulated entries at every step.

Tropp presented an article [7] in 2004 to resolve the sparse approximation muddle regarding random dictionaries using the voracious algorithm, namely OMP. It is been observed here that OMP and the Donoho's basis pursuit (BP) can recuperate the favorable solution of an exactly sparse signal, subjected to any condition. Thus, it dominates this theory by giving facts that OMP and BP give guaranteed results for every sparse input signal from a random dictionary.

Candes and Tao ventured in their paper [8] that if the signal under observation is sparse in affixed basis or compressible, then there is a prospect to reassemble it back from a small number of random measurements by solving a simple linear equation, within a predefined set of accuracy. It carries on this approach to a number of other random measurement entities, thus proving the point with a set of examples.

In 2002, Elad and Bruckstein [9] presented an evidence of an elementary uncertainty principle. The main work subsists the representations of vectors for different set of orthonormal basis. Thus, there is a candid impact on the lone attribute of the sparse representation of any vectors employed, by formulating a set of orthonormal bases as over-complete dictionaries.

3 Algorithms

A number of methods are been used for solving the sparse approximation problems in the recent years. The two algorithms used in this paper to solve sparse approximation issue are the OMP and the LS-OMP. OMP is a greedy algorithm for formulating the sparse approximation problem. This approach fosters an approximation through a series of iteration. For each iteration been carried out, the column vectors that precisely imitate the entailed vectors are selected, and then these vectors are worn to construct the panacea. In the least square OMP algorithm, an additional least square step is added in the solution update step.

A. OMP

Input:

- Signal y and matrix D .
- Terminate criterion which symbolizes the level of accuracy.

Output:

- Approximation vector c .

Algorithm:

1. Undertake the residual $R_0 = y$, the time $t = 0$ and the index set $V_0 = \emptyset$
2. Set $s_t = i$, a_i gives the panacea of $\max \langle R_t, a_k \rangle$, here a_k are the row vectors of D

3. Upgrade the set V_t with $s_t : V_t = V_{t-1} \cup \{s_t\}$
4. Enumerate the recent residual employing c

$$R_t = R_{t-1} - \sum_{j=1}^t c(s_j) a_{v_j}$$

5. Set $t \leftarrow t + 1$
6. Check the stopping criterion and if it is not satisfied return to step 2.

B. LS-OMP

Input:

- Signal y and matrix D .
- Terminate criterion which symbolizes the level of accuracy.

Output:

- Approximation vector c .

Algorithm:

1. Begin by setting the residual $R_0 = y$, the time $t = 0$ and the index set $V_0 = \emptyset$
2. Assume $s_t = i$, a_i gives the solution of $\max \langle R_t, a_k \rangle$ here a_k are the row vectors of D
3. Upgrade the set V_t with $s_t : V_t = V_{t-1} \cup \{s_t\}$
4. Resolve the least squares issue

$$\min_{c \in C^{V_t}} \left\| y - \sum_{j=1}^t c(s_j) a_{v_j} \right\|_2$$

5. Enumerate the recent residual using c

$$R_t = R_{t-1} - \sum_{j=1}^t c(s_j) a_{v_j}$$

6. Set $t \leftarrow t + 1$
7. Check the stopping criterion and if it is not satisfied return to step 2.

4 Experimental Results

The two algorithms, OMP and LS-OMP, are been tested for different set of random matrix, thus depicting the foremost contrast of the algorithms on the basis of the number of iterations and the average time they took while formulating the result.

The average time an OMP took to calculate solutions using different set of iterations is shown in Fig. 1. For the above calculations, a randomly generated 80×240 matrix is been used. As it is known that the OMP algorithm has to go through a set of n iterations to calculate a solution with $\|x\|_0 = n$, therefore it can be observed from the figure that OMP took an average 0.32 s to go through 80 iterations.

Further for OMP, the average error of the solutions that are been calculated for Fig. 1 is been demonstrated by Fig. 2. The OMP shows equitably precise approximations in calculations where the matrix used is an over-complete randomly generated one. The figure below shows that a small increase in the number of iterations yields a small increase in accuracy. It can be further understood in a simple way that an increase in the number of iterations will result in less error, thus giving an exact sparse approximation.

Fig. 1 Average time of solutions using OMP

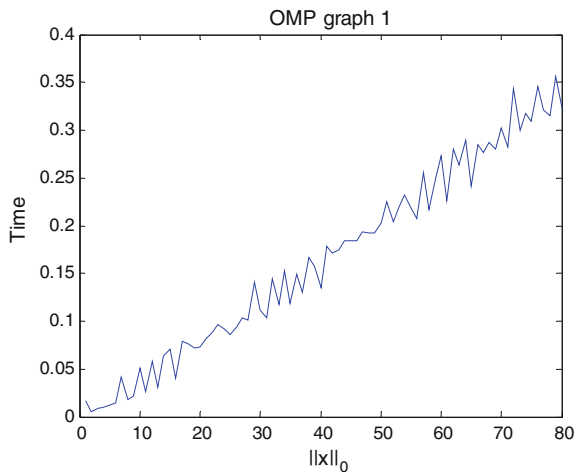
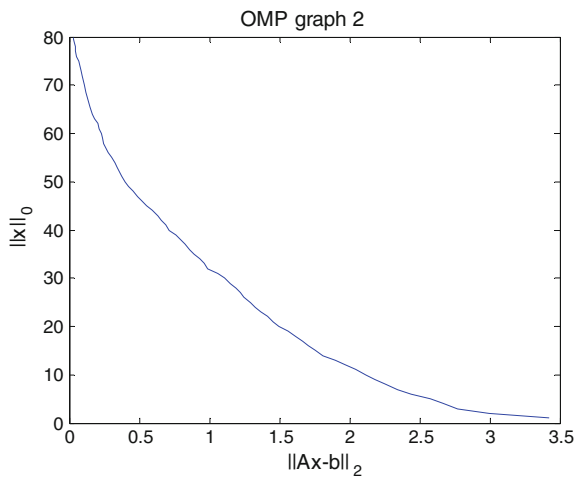


Fig. 2 Average error of solutions using OMP



For the LS-OMP algorithm, Fig. 3 shows the average time the algorithm took to calculate solution for a given set of iterations. For the above calculations, a randomly generated 80×240 matrix is been used. The LS-OMP algorithm has to go through a set of n iterations to calculate a solution with $\|x\|_0 = n$; therefore it can be observed from the figure that LS-OMP took an average 0.2 s to go through 80 iterations. Thus, the time taken by LS-OMP is fairly less than that of OMP algorithm, thus making it more efficient to calculate the sparse approximation results.

Similarly for LS-OMP, Fig. 4 depicts the average error of the solutions that are been calculated for Fig. 3. The LS-OMP algorithm shows equitable exact approximations in calculations where the matrix used is an over-complete randomly generated. The figure depicts that a slight increase in the number of iterations gives a small increase in the accuracy rate. It is simply said that as the number of iterations are incremented, the resulting error in sparse approximation is reduced significantly.

Fig. 3 Average time of solutions using LS-OMP

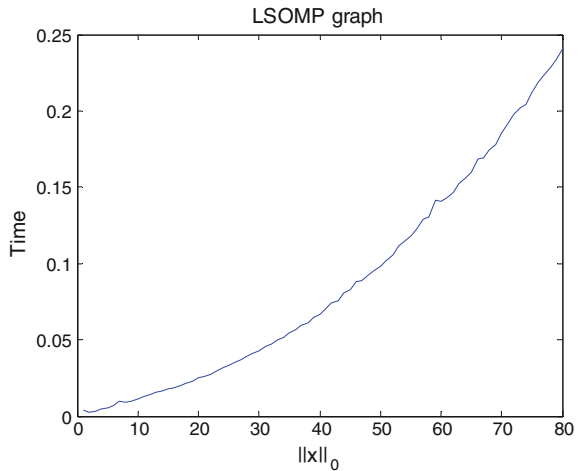


Fig. 4 Average error of solutions using LS-OMP

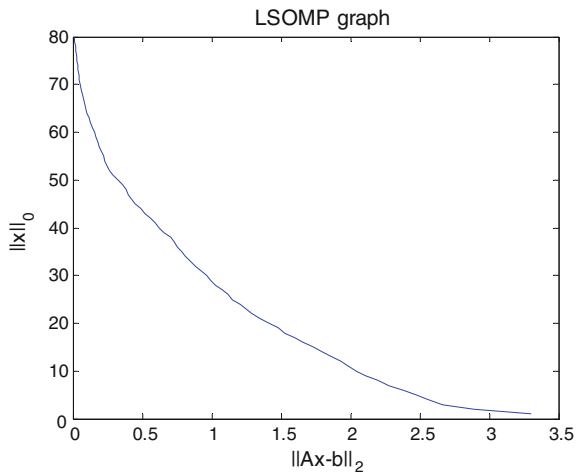


Table 1 Average time and average error values for OMP and LS-OMP

Algorithm	No. of iterations	Average time	Average error
OMP	40	0.1374	0.716
	60	0.2735	0.2278
	80	0.3224	0.0284
LS-OMP	40	0.0667	0.629
	60	0.1406	0.154
	80	0.2412	0.0001

In order to understand the average time and average error concept, different iteration values are taken for which these values are calculated related to both the algorithms. Finally, these values are been summarized in Table 1. It is clear from the table that for OMP the average time it took to give the solution is 0.1374 s, while LS-OMP took only 0.0667 s for an iteration value of 40. Further if the iteration values are increased, then LS-OMP gives us better result in calculating the solution within a small average time. Also the average error value for 40 iterations is 0.716 for OMP, while that for LS-OMP is 0.629. Thus, this signifies that LS-OMP gives us less average error within the same number of iterations performed for OMP. Furthermore, if we increase the number of iterations then LS-OMP settles to an insignificant error value while OMP still has a value of 0.0284. Therefore, OMP needs further iterations to be carried out in order to make average error near to zero.

5 Conclusion

In this paper two algorithms, OMP and LS-OMP, are been studied for different set of randomly generated matrix. The results obtained for the algorithms using a randomly generated 80×240 matrix show that OMP takes more time to calculate solution for a given set of iterations as compared to the LS-OMP. Also from the figures, it is observed that the average error in LS-OMP is reduced to zero within these 80 iterations while the OMP still need more iteration to do so.

References

1. R. A. DeVore, "Nonlinear approximation," *Acta Num.*, pp. 51–150, (1998).
2. V. Temlyakov, "Nonlinear methods of approximation," *Foundations of Comp. Math.*, vol. 3, no. 1, pp. 33–107, July (2003).
3. G. Davis, S. Mallat, and M. Avellaneda, "Greedy adaptive approximation," *J. Constr. Approx.*, vol. 13, pp. 57–98, (1997).

4. A. C. Gilbert, M. Muthukrishnan, and M. J. Strauss, "Approximation of functions over redundant dictionaries using coherence," in Proc. 14th Annu. ACM-SIAM Symp. Discrete Algorithms, Baltimore, MD, pp. 243–252, Jan. (2003).
5. Charles Soussen, Remi Gribonval, Jerome Idier, and Cedric Herzet, "Joint k-step analysis of orthogonal matching pursuit and orthogonal least squares," IEEE Trans. Inform. Theory, vol. 59, no. 5, pp. 3158–3174, May (2013).
6. Gagan rath and Christine guillemot, "Sparse approximation with an orthogonal complementary matching pursuit algorithm," IEEE trans., pp. 3325–3328, (2009).
7. Joel A. Tropp, "Greed is Good: Algorithmic results for sparse approximation," IEEE Trans Inform. Theory, vol. 50, no. 10, pp. 2231–2242, Oct (2004).
8. Emmanuel J. Candes and Terence Tao, "Near-Optimal signal recovery from random projections: universal encoding strategies," IEEE Trans. Inform. Theory, vol. 52, no. 12, pp. 5406–5425, Dec (2006).
9. Michael Elad and Alfred M. Bruckstein, "A generalized uncertainty principle and sparse representation in pairs of bases," IEEE Trans. Inform. Theory, vol. 48, no. 9, pp. 2558–2567, Sept (2002).

A Corporate Network-Fed Quasi-lumped Resonator Antenna Array

Seyi Stephen Olokede and Babu Sena Paul

Abstract A new class of antenna is presented. It consists of an interdigital capacitor in parallel with a straight strip inductor. The proposed antenna is fed through a new corporate feed network. The configurations designed, fabricated, and measured include 8×1 and 8×2 . Each resonator is fed at the non-radiating end with a view to achieving higher gain and better performance. The performance profile of the array antenna, including the reflection coefficient and radiation patterns, is investigated and presented. Reasonable measured gains of 12.8 and 16.9 dBi are obtained for 8×1 and 8×2 configurations, respectively. The size of each element of the array is $5.8 \times 5.6 \text{ mm}^2$, which makes it a potential candidate for wireless communication applications.

Keywords Compact antenna · Corporate feed array · Gain · Quasi-lumped antenna

1 Introduction

No doubt microstrip antennas possess many attractive features, but it is also true that they suffer major operational disadvantages, namely relatively large size, low power, spurious feed radiation, poor scan performance, narrow frequency pattern, and poor polarization purity [1]. Nonetheless, they do have valuable features such as a simple structure, conformability, the capability of wide application to various devices, ease of integration with active circuits, etc. Besides, no other available alternative antenna solution (aside from patch antennas) would neither disturb the aerodynamic flow nor protrude inward to disrupt the mechanical structure, save planar antenna and in particular Vivaldi antennas, which are usually too large in terms of both the footprint and estate, and thus unlikely to be readily used as

S.S. Olokede (✉) · B.S. Paul

Department of Electrical and Electronic Engineering Technology,
University of Johannesburg, Johannesburg, South Africa
e-mail: solokede@gmail.com

compact antennas. The premium of corporate feed networks as an efficient mode of excitation technique for patch arrays include better frequency pattern, no requirement for protrusion, great design flexibility, reduced mismatch losses [2], 2D array vertical integration with relative ease [3] and equal excitations of radiating elements with a large degree of versatility. Moreover, few of the practical array designs reported in the literature are excited by a coplanar corporate feedline. The advantages as reported by these authors centered on total construction simplicity with reduced size occupancy [4].

However, the corporate feeds are much less compact than the series feed. More losses are typically associated with them owing to longer line lengths. The purpose of this paper is firstly to examine other patch antenna alternatives that can deliver conformability attribute, yet with compactness capability; and secondly to propose a new compact corporate feed network. It is anticipated that this proposed alternative antenna will demonstrate compact premium in terms of estate occupation, especially when fed by compact feed network. This in turn will defray any excess estate area incurred by the corporate feed network. To this end, the design of a quasi-lumped element resonator antenna (QLERA) is presented. The simplest lumped element or QLERAs is formed by lumped or quasi-lumped inductors and capacitors resonating at $\omega_o = (LC)^{-0.5}$. Thus, the aperture dimension of the QLERAs is theoretically and numerically determined to be $5.8 \times 5.6 \text{ mm}^2$, translating to $0.21 \times 0.179\lambda$.

2 Proposed Antenna Array Design

2.1 Single Element Design

Generally, QLERAs exhibit substantial form factor reduction capability and are attractive candidates for compact antennas at microwave spectrum band. On the flip side, the unloaded Q-factor of a QLERAs is considerably lower with respect to the distributed resonator, as both the dielectric and conduction losses to a large extent influence the design performance. A realized design hence needs a compromise between compact premium and tolerable losses [5]. The center inductor is the finger shorted across the capacitor [6]. The pads capacitance connected at both ends of the QLERAs serves as capacitance to ground. These two capacitance can be varied to attain the frequency under consideration. The capture of the proposed QLERAs is shown in Fig. 1a of [7]. Equations to determine the radiation resonance of the QLERAs are concisely reported by Ain et al. in the same publication.

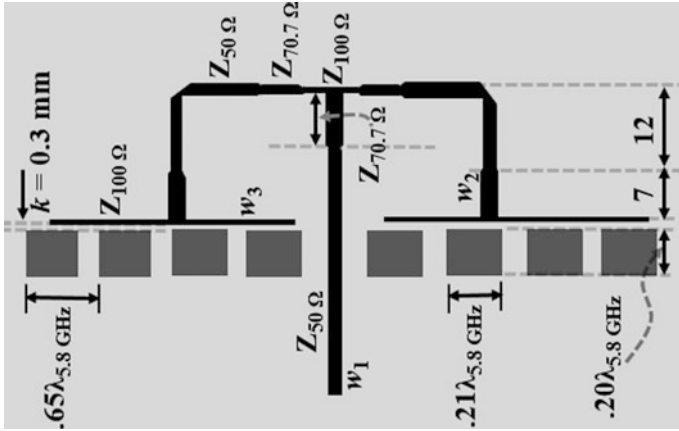


Fig. 1 8×1 array

2.2 8×1 Corporate-Fed Array

Figure 1 shows a prototype of an 8×1 array with a parallel (corporate) feed network where power splits into two sub-arrays, of four elements each. The equal length splits power in equal proportion in terms of magnitude and phase to the feed points. The power divisions can be 2^n such as 2, 4, 8, 16, etc., where $n = 1, 2, 3, 4$, etc. Thus, the required power division together with the number of the feeds are determined by the number of the patch radiators, as demonstrated in [8]. Each resonator is fed at the non-radiating edge. It is expected that the non-radiating edge-fed corporate network will naturally deliver higher gain, higher efficiency, wider bandwidth, etc. [9]. Doing this usually results in lower insertion loss. The inter-element spacing is 0.62λ , which is equal to 18.2 mm as against 0.5λ . The inter-element spacing is reasonably large to prevent the internal parasitics as a result of mutual coupling that may occur around the adjacent elements and junctions. It is so chosen in order to house the parallel feed network [10], which would otherwise has been impossible using inter-element spacing of 0.5λ even though it will be expedient in order to mitigate the sidelobe level. The entire structure is fed by a Wilkinson power divider by the T-junction in order to split the 50Ω line into two ($2 \times 100 \Omega$). The transformation from 50 to 100Ω and vice versa is implemented using a quarter-wavelength transformer. The transformation is determined by the equation $\sqrt{2}Z_0$ and estimated as 70.7Ω . The transmission line widths labeled w_1 , w_2 , and w_3 are determined based on the characteristic impedance at each location using equation (9) for $w/h \geq 1$. Using the said equation, $w_1 = 1.898$ mm, $w_2 = 1.05$ mm, and $w_3 = 0.46$ mm with the corresponding impedances of 50, 70.7, and 100Ω , respectively, based on Eq. (1) below.



Fig. 2 Geometry of the proposed array (8×1)

$$Z_0 = \frac{120\pi}{\sqrt{\epsilon_{\text{eff}}} \left[\frac{w}{h} + 1.393 + \frac{2}{3} \ln \left[\frac{w}{h} + 1.444 \right] \right]}, \quad (1)$$

where

$$\epsilon_0 = \frac{\epsilon_r + 1}{2} + \frac{\epsilon_r - 1}{2} \left[1 + 12 \left(\frac{h}{w} \right)^{-0.5} \right]. \quad (2)$$

2.3 8×2 Corporate-Fed Array

In Fig. 2, the proposed antenna configuration is presented. It is a direct reflection of the 8×1 elements, with two of them combined to form the 8×2 parallel array network with a common corporate feed. In order to understand the performance characteristics and the radiation pattern of the proposed antenna better, an analytical CST microwave studio using the finite integration technique is used for full-wave analysis.

3 Experimental Results and Discussions

3.1 8×1 Corporate-Fed Array

Both antenna structures are fabricated on Roger RO4003C duroid laminate board with substrate permittivity (ϵ_s) of 3.38 and a metallization of 0.813 mm. The measurements of the proposed antennas were done using HP 8720B network analyzer to observe the reflection and radiation characteristics (this time along with

the spectrum analyzer). Figure 3 shows the simulation and measured $|S_{11}|$ of the proposed QLERA.

For the 8×1 -element configurations, the simulated $|S_{11}|$ is -40 dB with a frequency pattern of $5.62\text{--}5.98$ GHz at about 5.8 GHz. The measured reflection coefficient is -35 dB, and an impedance frequency pattern of $5.65\text{--}5.98$ GHz occurs at about the same frequency as the simulated result. The input impedance in the form of a Smith chart is shown in Fig. 4a, and the impedance is $49.29 - j05.37 \Omega$.

Fig. 3 Reflection coefficient of the array. **a** 8×1 , **b** 8×2

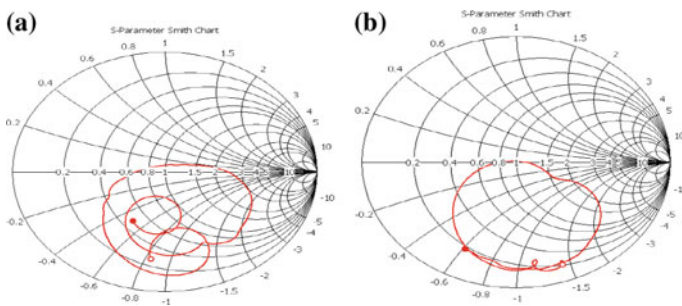
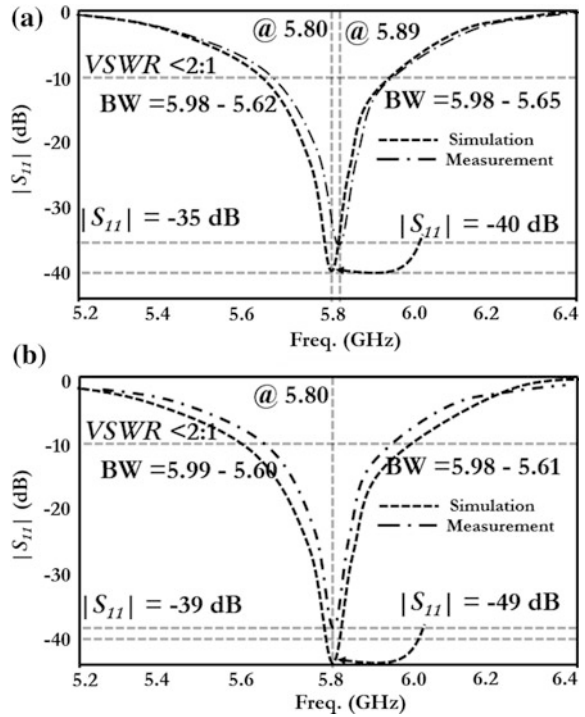


Fig. 4 Antenna impedance determination using the Smith chart

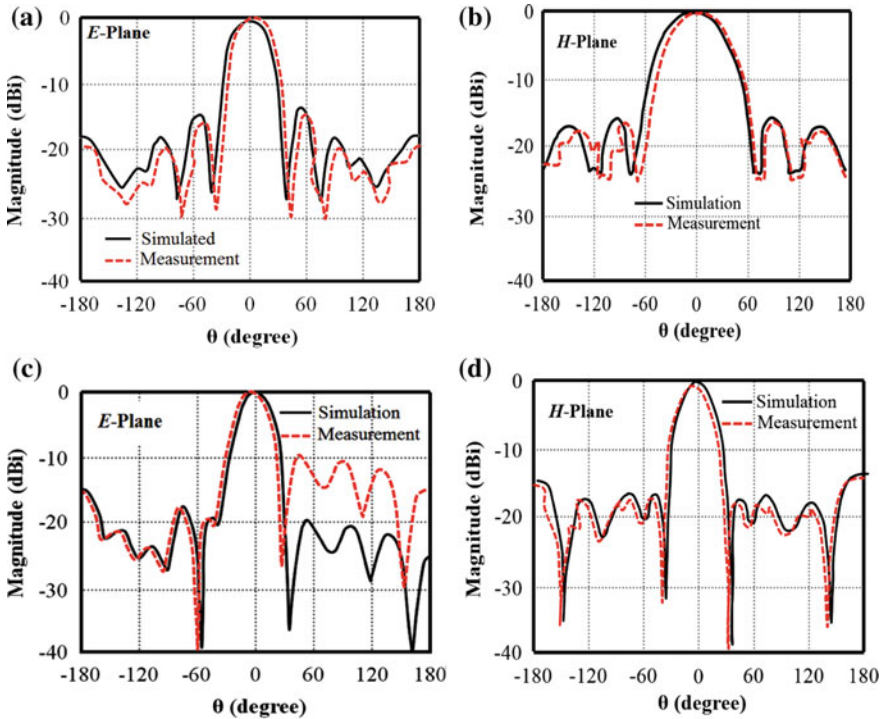


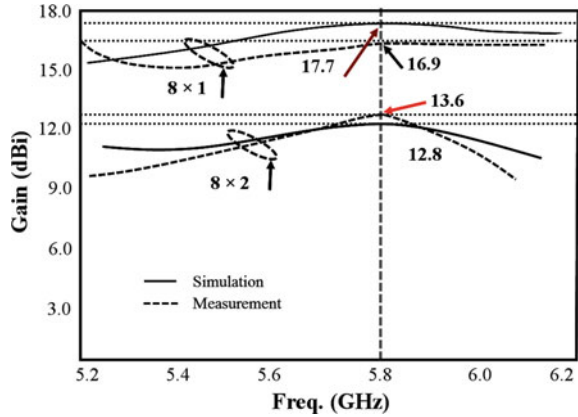
Fig. 5 Interconnect length versus lithographic resolution

Both reflection coefficients indicate a significant matching level and good agreement. Figure 5a, b show the simulated and measured radiation patterns of the 8×1 QLER sub-array in the *E*- and *H*-planes, respectively. Two reasonable side-lobe levels of about -15 dB (associated with the finite ground plane) are seen. The level of the side lobes is more visible in the *H*-plane polar plot shown in Fig. 5b. The measured *E*-plane agrees substantially with the simulated result.

3.2 8×2 Corporate-Fed Array

The simulated and measured $|S_{11}|$ of the 8×2 configuration of the proposed antenna are given in Fig. 5c, d. The simulated input $|S_{11}|$ is substantial and concisely put at -49 dB, indicating a very good impedance match. This assertion is supported by the Smith chart shown in Fig. 4b. The bandwidth pattern is $5.69 - 5.69$ GHz at about 5.79 GHz, and the input impedance is as shown in Fig. 4b. The measured $|S_{11}|$ at about 5.81 GHz is $5.61 - 5.98$ GHz with an impedance of $51.49 - j1.05 \Omega$. The simulated and measured radiation patterns of the 8×1 array antenna are depicted in Figs. 3a and 5c, and d gives the simulated and measured radiation pattern of the

Fig. 6 Gain versus frequency response



8 × 2 QLERA array configuration of both the *E*- and *H*-planes. The patterns are taken at the target resonant for which the maximum power is highest. The simulated and measured patterns of both planes agree significantly. The radiations are inclined upward at the principal axis ($\theta = 0$) with a measured gain advantage of 16.1 dBi, as shown in Fig. 6. A slight sidelobe level due to surrounding spurious radiations is noticed at the right hemisphere of the *E*-plane plot.

3.3 Comparison Between 8 × 1 and 8 × 2 Corporate-Fed Array

For the purpose of comparison, it is noted that a measured excess bandwidth difference of 40 MHz constituting about 12.1% impedance bandwidth differential is obtained in the case of the 8 × 2-element array compared to the 8 × 1-element array configuration. A similarly larger gain by an amount of about 27.61% is achieved in the 8 × 2-element array. Another observation is the reduced sidelobe level difference of about -4 dB for the *E*-plane, and -1 for the *H*-plane over the 8 × 2-element array. It is therefore obvious that 8 × 2-element array exhibited better bandwidth (in excess of 130 MHz), an enhanced directional characteristic, and a lower sidelobe level with a reasonable gain in excess of 4.1 dBi.

4 Conclusion

Experimental study on the design of a QLERA array with corporate feed has been carried out, both for 8 × 1- and 8 × 2-element arrays. All the designs demonstrated brilliant impedance match. The simulated and measured results are in good agreement. It was found that a QLER is not only suitable for antenna design but has

a compact size advantage. The 8×1 configuration demonstrated real estate of $1.94 \times 2.73\lambda \text{ mm}^2$ while the 8×2 indicated a size of twice the 8×2 array. Comparative analysis carried out between the 8×1 - and 8×2 -element sub-array showed that the 8×2 -element array had a better performance profile with a reasonable gain advantage of 4.1 dBi.

References

1. C. A. Balanis, *Antenna theory, analysis and design*, 2nd Edition, John Wiley & Sons, 722–783, 1997.
2. A. Petosa, *Dielectric resonator antenna handbook*, 209–245, Artech House Inc, 2007.
3. J. R. James, P. S. Hall, and C. Wood, *Microstrip antenna theory and design*, London: Peter Peregrinus, 1981.
4. P. S. Hall and C. M. Hall, “Coplanar corporate feed effects in microstrip patch array design,” *Proc. Inst. Elect. Eng.*, pt. H, Vol. 135, pp. 180–186, Jun. 1988.
5. M. Reppel, “Novel HTS microstrip resonator configurations for microwave bandpass filters,” Ph.D. Thesis, Bergish University, Wuppertal, Germany, 2000.
6. M. I. Lancaster, “Passive microwave device applications of high temperature superconductors,” Great Britain: Cambridge University Press, 1996.
7. M. F. Ain, S. S. Olokede, Y. M. Qasaymeh, A. Marzuki, J. J. Mohammed, S. Sreekantan, S. D. Hutagalung, Z. A. Ahmad, Z. Abdulla, A novel 5.8 GHz quasi-lumped element resonator antenna, *AEU—Int. J. of Electrons & Coms*, 2013.
8. R. E. Muson, “Conformal microstrip antenna and microstrip phased arrays,” *IEEE Trans. on Antennas and Propagation*, Vol. 22, No. 1, 74–78, 1974.
9. D. P. Gray; Ravipati, C. B.; Shafai, L., “Corporate-fed microstrip arrays with non radiating edge fed microstrip patches,” *IEEE Ant. & Propag. Society Int. Symposium*, pp. 1130–1133, 21–26 Jun 1998.
10. G. M. Pushpanjali, Konda, R. B., Mulgi, S. N., Satnoor, S. K., Hunagund, P. V. ‘Equilateral triangular microstrip array antenna for broadband operation,’ *Microwave and Optical Technology Letters*, *Microw. Opt. Tech. Lett.* 2008.

Optimal Placement of Solar PV as Active Power Source in Primary Distribution System for Loss Reduction

Vani Bhargava, S.K. Sinha and M.P. Dave

Abstract The general problem of DG placement deals with the size of DG and its location, but at the same time this placement must be economically justifiable. To gain benefits of DG placement, the DG must be optimally sized and placed. The paper uses analytical expressions for determination of optimal size and a methodology for optimal location of DG placement. The solar PV system is used as the distributed generator to be placed in primary distribution system for active power supply. The solar photovoltaic system is employed here as a type 1 distributed generator (DG) to supply active power to the distribution system. The methodology uses analytical expressions and is based upon the exact loss formula. Along with the optimal size and location, this paper also presents the economics of this placement considering loss reduction and capacity relieving of the distribution substation.

Keywords Optimal size · Optimum location · Exact loss formula
Distribution system · SPV

1 Introduction

In power system, when power flow takes place it results in continuous power or energy loss as well. In distribution system, the power loss is more as compared to the transmission system. The high R/X ratio of distribution system and the significant amount of the voltage drop cause a considerable amount of power and energy loss in distribution system. The loss reduction in distribution system hence became a matter of great concern. Over last few years, the distribution system reconfiguration and the capacitor placement were the ways of reducing those losses.

V. Bhargava (✉) · S.K. Sinha
Department of Electrical and Electronics Engineering, Amity University Uttar Pradesh,
Noida, India
e-mail: vanigarg03@gmail.com

M.P. Dave
Department of Electrical Engineering, Shiv Nadar University, Greater Noida, India

Recently, the electricity market liberalization and increased concern for saving environment supported DG penetration in distribution system. The DG so placed is capable of improving the voltage profile and reducing the power loss in distribution system.

The general problem of DG placement deals with the optimal size and location of DG, and at the same time the DG placement must be justified economically. So the economy of DG placement is a prime constraint while considering DG placement in distribution system.

The paper is written keeping in mind the single main objective function of energy loss cost minimization with the help of optimal DG placement in primary distribution system.

A number of methods are presented by a number of authors for optimization of DG placement for loss reduction in distribution system [1]. They are:

1. analytical methods, 2. numerical methods, and 3. heuristic methods.

The analytical methods are simplest in implementation but they are only an indicative as they are based upon certain assumptions.

The paper uses analytical expressions for optimal DG size determination followed by a methodology that provides the best site or optimal location for optimally sized DG placement.

2 Distributed Generation

The distributed generation is the electricity generation with the help of facilities/resources that are having sufficiently smaller capacities as compared to the generation by central conventional generating power plants.

As per CIGRE (International Council on Large Electricity Systems), the distributed generation is generation with generators having maximum power capacity of 50–100 MW and the generating units directly connected to the distributed network. These generations are neither centrally planned nor they are centrally dispatched.

Another definition comes from Chambers [2], as per Chambers, the distributed generators are relatively small-sized generators, typically 30 MW or less. These units are placed near to the consumer site to fulfill their specific requirements. In addition with fulfilling the consumer requirements, they can also support in economy of distribution system [3].

Dondi et al. [4] also defines the same as a small power generation source which lies in the range of few kilowatts to tens of megawatts, located in vicinity of the load and not connected to the central power system. They also included the provision of energy storage in their definition of the distributed power generation.

3 Sizing and Location Using Analytical Method

3.1 Optimal Size

The exact loss formula [2] mentioned here gives the total real power loss in the system. The same is given by the following equation

$$P_l = \sum_{i=1}^N \sum_{j=1}^N [\alpha_{ij}(P_i P_j + Q_i Q_j) + \beta_{ij}(Q_i P_j - P_i Q_j)], \quad (1)$$

where [2]

$$\alpha_{ij} = \frac{r_{ij}}{V_i V_j} \cos(\delta_i - \delta_j),$$

$$\beta_{ij} = \frac{r_{ij}}{V_i V_j} \sin(\delta_i - \delta_j),$$

and

$r_{ij} + jx_{ij} = Z_{ij}$ being ij th element of Z-bus matrix [Z-bus] and [Z-bus] = [Y-bus]⁻¹.

For the loss minimization, the total real power loss rate of change with respect to the injected power becomes zero.

$$\frac{\partial P_l}{\partial P_i} = 2 \sum_{j=1}^N (\alpha_{ij} P_j - \beta_{ij} Q_j) = 0.$$

With this, what follows is

$$\alpha_{ii} P_i - \beta_{ii} Q_i + \sum_{j=1, j \neq i}^N (\alpha_{ij} P_j - \beta_{ij} Q_j) = 0, \quad (2)$$

$$P_i = \frac{1}{\alpha_{ii}} [\beta_{ii} Q_i + \sum_{j=1, j \neq i}^N (\alpha_{ij} P_j - \beta_{ij} Q_j)].$$

In these equations, P_i is injected real power at i th node. The total real power injected at i th node is the difference of real power generated at and withdrawn from the i th node. The same can be written as

$$P_i = P_{DG_i} - P_{Di}. \quad (3)$$

P_{DG_i} being the injected real power from DG and P_{Di} is the load demand at the same i th node. Following previous two equations, the optimal size of DG e for each bus 'i' that would minimize the losses at each bus can be obtained [5].

The above equations can be arranged to obtain the following equation

$$P_{DG_i} = P_i - \frac{1}{\alpha_{ii}} \left[\beta_{ii} Q_i + \sum_{j=1, j \neq i}^N (\alpha_{ij} P_j - \beta_{ij} Q_j) \right]. \quad (4)$$

Equation obtained above is the equation of optimum value for DG capacity at each bus in an nth bus system. If DG of any other size, than this, is placed at a particular bus 'i' in nth bus system, it will give rise to higher losses as compared to the losses without DG unit placed in system [6].

After installing DG in system, the loss coefficients α and β get changed as they are dependent upon voltage magnitudes and their angles. Numerically, it is found that with updation of α and β values, the variation obtained in DG size is small and can be neglected. So assuming this to be the optimum size of DG in what follows.

3.2 Site for Optimal DG

After optimal sizing of DG, the other step is determination of optimal location for its placement. The site is so chosen that the total system losses are at the minimum. The procedure followed for obtaining optimal placement location for DG is as follows.

Using Eq. (4), optimal DG size is determined. The next step is determination of the total system losses using the exact loss formula with optimally sized DG placed at individual buses one at a time. After determining the total loss, the next step is the identification of the bus with minimum total loss [7, 8]. This is the optimal location for DG placement. The final step is running the load flow with updated value of power injection at selected location to obtain the final result.

4 The System Under Consideration and Test Results

To apply the analytical method, a program is developed in MATLAB environment. It is tested with 33-bus IEEE radial distribution system, and the validation of results is done with references [9] and [1]. It is concluded that the analysis can be extended to any practical system considering DG placement for loss reduction. The following figure shows the 33-bus IEEE-33 test distribution system line diagram (Fig. 1).

It is a 33-bus radial distribution system with 32 branches. Load on the given system is 3.72 MW and 2.3 MVAR. For implementation of methodology, a program is written in MATLAB. The results obtained are shown in Figs. 2, 3, 4 and 5. They include the voltage profile obtained with base case load flow analysis in Fig. 2. The optimum DG sizes as obtained with analytical method are shown in Fig. 3.

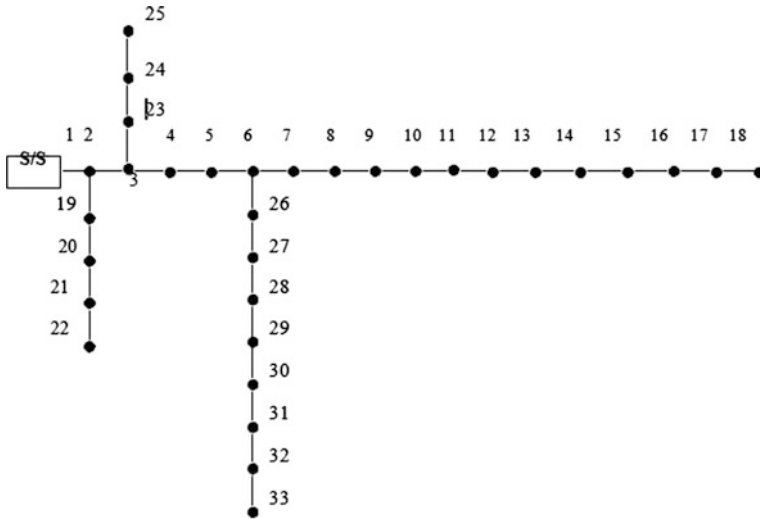


Fig. 1 IEEE-33 bus test distribution system

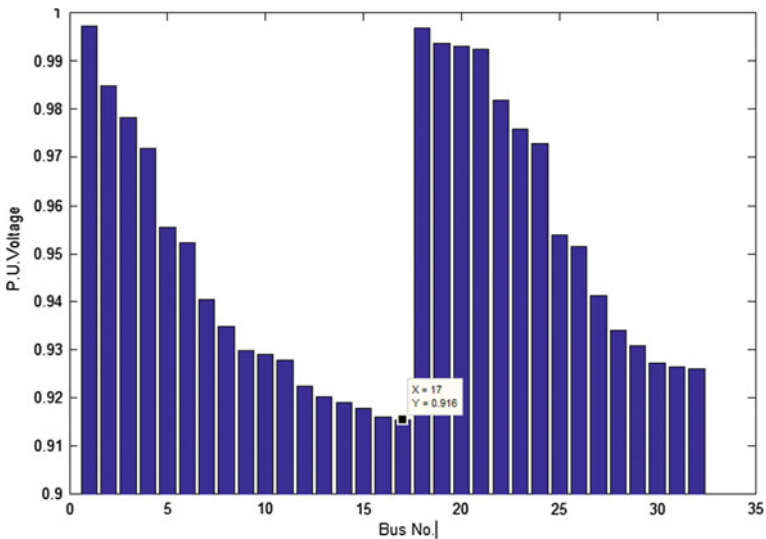


Fig. 2 Voltage profile at different buses without DG

Once the optimal DG size is obtained, the next step is the determination of losses with each DG unit placed one at a time. From Fig. 4, it can be seen that after DG placement of optimal capacity at respective busses, the minimum loss is obtained at bus no. 6. It implies that with DG placed at bus no. 6 the losses obtained are minimum hence bus no. 6 comes out to be the best location for a single type 1 DG

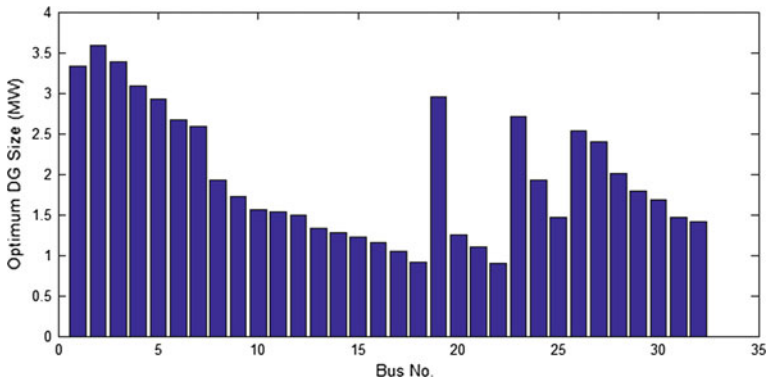


Fig. 3 Optimum DG size at various buses for 33-bus test distribution system

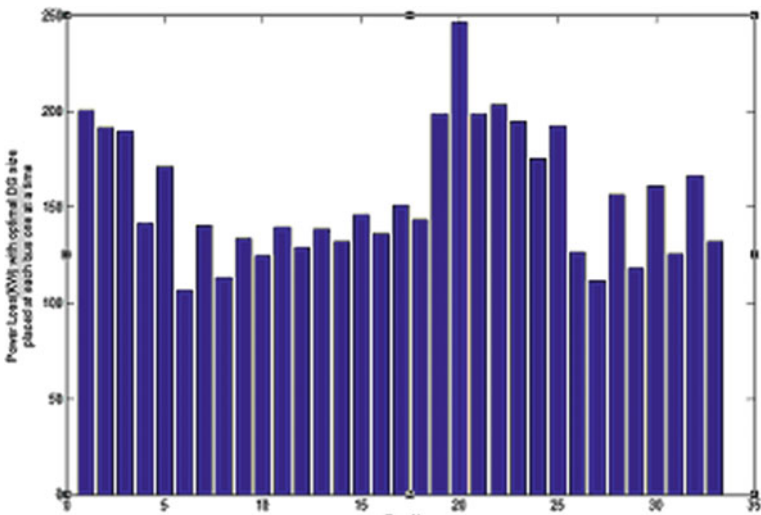


Fig. 4 Losses at various nodes with optimal DG placement

placement, in this case, a solar photovoltaic system. The optimal size of DG at bus number 6 is 2.6646 MW. The total system loss reduces to 108.037 KW against 200.1512 KW without DG placement. Figure 5 shows the profile of voltage obtained at various buses after DG placement. It can be seen that this voltage profile is also improved and the minimum p.u. voltage obtained is 0.952 at bus no. 17, which is in the permissible range.

If instead of placing one DG unit of 2.6646 MW at bus no 6, if three 3 DG units of 1 MW each are placed at bus no. 6,11, and 27, where the losses are minimum, the total system losses get reduced to 88.0583 KW, and voltage profile gets improved as [8, 10] shown in Fig. 6 with the minimum per unit voltage of 0.973 obtained at bus no. 32.

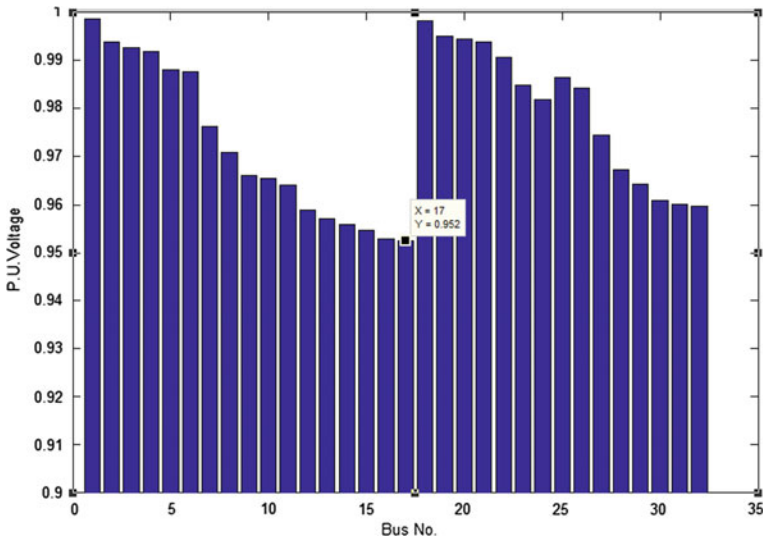


Fig. 5 Voltage profile at various buses after single DG placement at bus no. 6

Further, if the DG size placed at each bus, i.e., at bus numbers 6, 11, and 27, is 0.7 MW, the total losses are further reduced to 84.6148 KW and the minimum value of per unit voltage obtained is 0.96 at bus no. 32. The voltage profile is shown in the Fig. 7.

The summary of the result is shown in table given below: (Table 1)

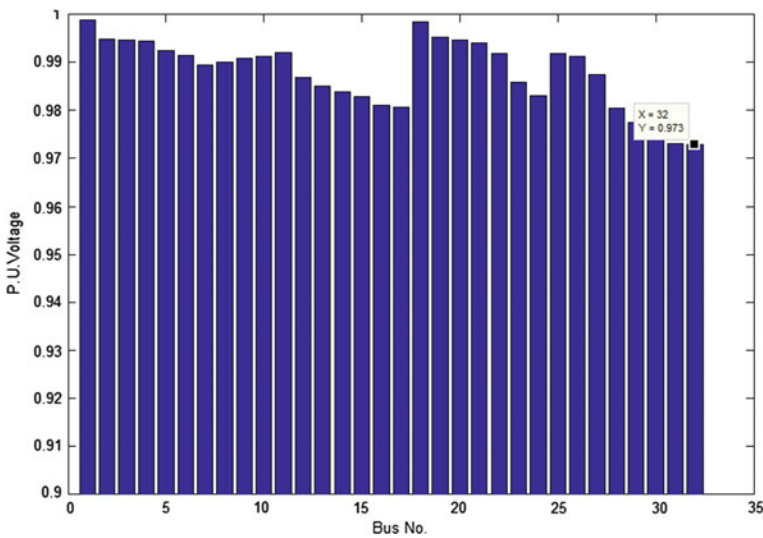


Fig. 6 Voltage profile after three DG placement of 1 MW each at bus no. 6, 11, and 27

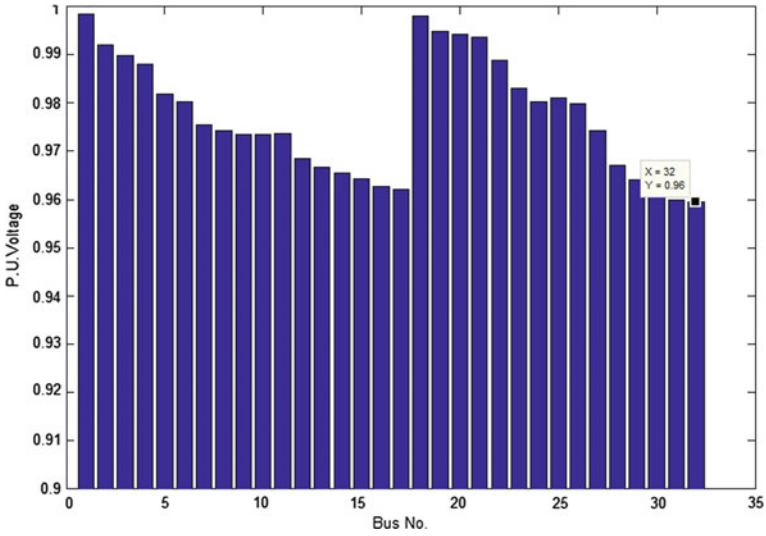


Fig. 7 Voltage profile after three DG placement of 0.7 MW each at bus no. 6, 11, and 27

5 Economics of SPV Placement

Cost of Energy Loss: The energy lost in a certain time can be determined as:

$$L_e = \sum_{i=1}^n L_{ei},$$

where

$$L_{ei} = I_i \times I_i \times R \times T.$$

Knowing L_{ei} , the cost of lost energy can be determined as

$$CEL = R_e \times L_e.$$

R_e is rate of energy, and L_e is the lost energy.

The economical benefit of SPV placement can be determined by comparing the benefit due to reduced energy loss cost, reduced cost of energy withdrawal from substation, and cost of SPV installation.

SPV Cost: The total SPV cost can be divided into two parts: the fixed installation cost and the variable cost.

$$CDG = C_{cv} * Q_{ck}. \tag{5}$$

C_{cv} and Q_{ck} are rate of SPV per MW and rating of SPV at kth bus.

Table 1 Summary of DG Placement

Base case	After single DG (SPV) placement at bus 6 (2.6646 MW)		After 3 DG (SPV) placement at buses 6,11 and 27 (1 MW each)		After 3 DG (SPV) placement at buses 6,11 and 27 (0.7 MW each)		
	Total loss (kW)	Per unit voltage (minimum)	Total loss (kW)	Per unit voltage (minimum)	Total loss (kW)	Per unit voltage (minimum)	
200.1512	0.916pu at bus no. 17	108.0375 KW	0.952 pu at bus no. 17	88.0583	0.973 pu at bus no. 32	84.6148 MW	0.96 pu at bus no. 32

The objective function for cost minimization can now be framed as:

$F = CEL + C_{cv} * Q_{ck}$; where F is the cost function for minimization.

Minimizing this, the net saving so obtained is

= SEL - CDG

where SEL is the saving due to energy loss reduction, and CDG is the cost of DG obtained from Eq. (5).

With the values obtained in the foregoing analysis of the given system, the following is the cost calculation table. The system is studied with the peak power demand. For the purpose of economics of loss calculations, the average loading per day is considered, which approximately 60% of the peak load demand is. The loss of power is dependent upon the current squared, so the reduction of power level from peak value to average value causes the loss to get reduced to 36%. Further it is assumed that the distributed generator (SPV) is supplying power for eight hours in a day. For rest of the time, i.e., for 16 h, the power is withdrawn from substation (Table 2).

Table 2 Cost Comparison among Various DG Placements and Base Case

S.No.	Base case	With one SPV (2.6646 MW)	With three SPV (1 MW each)
Total power lost (kW)	200.15 kW	108.0375 kW	88.0583 kW
Total average power lost (kW)	72.054 kW	38.89 kW	31.70 kW
Energy lost per day	1729.296 kWH	311.12 kWH	253.6 kWH
Cost of energy lost per day	Rs. 10,375.74	Rs. 1866.72	Rs. 1521.60
Cost of energy lost per year	Rs. 3,787,145.1	Rs. 681,352.80	Rs. 555,384.00
Without DG for 16 h	Rs. 2,524,763.4		
Total loss cost with 8 h SPV and 16 h. without SPV	–	Rs. 3,206,116.2	Rs. 3,080,147.4
Saving in loss cost	–	Rs. 581,028.9	Rs. 706,997.7
SPV size	–	2.6646 MW	3 MW (three units of 1 MW)
Substation supply required	3.72 MW 2.3 MVAR	1.0554 MW 2.3 MVAR	0.72 MW 2.3 MVAR
Cost of DG (SPV) ground mounted @ 5 crore per MW	–	Rs. 13.323 Crores	Rs. 15 Crores
Capital cost (10% interest and depreciation benchmark cost)	–	Rs. 1.3323 Crores Rs. 13,323,000.00	Rs. 1.5 Crores Rs. 15,000,000.00
Saving in energy units drawn from substation	–	Rs. 46,683,792.00	Rs. 52,560,000.00
Total savings per year	–	Rs. 47,264,820.9	Rs. 53,266,997.7

6 Conclusion

The work is carried out for the purpose of determination of the optimal sizes and locations of distributed generation units for their placement in radial distribution system. This is done for overall economy of the distribution system by DG placement. The problem formulated is solved in two steps. The first one is determination of optimal size and next is finding the location for optimal placement of DG units. The sizing issue, for a single DG placement, is solved using analytical expressions based upon exact loss formula. For multiple DG placements, best of candidate buses are selected on the basis of minimum power loss and with the use of repeated load flow runs, best combination of buses has been evaluated. To carry out the study, 33-bus radial distribution system is considered with solar PV as an active power DG source. The savings are obtained by reducing the loss cost and the substation withdrawal and the same is given in tabulated form for the purpose of comparison. In this paper, only active power injection is considered for loss cost reduction by optimally placing the solar photovoltaic systems as a distributed generator. The optimal values of reactive power to be injected can also be determined at the same time for further reduction in the loss cost.

References

1. W. Caisheng and M. H. Nehrir: Analytical approaches for optimal placement of distributed generation sources in power systems. In: *IEEE Transactions on Power Systems*, vol. 19, pp. 2068–2076 (2004)
2. Mukul Dixit, Prasanta Kundu, Hitesh R Jariwala: Optimal Placement and Sizing of DG in Distribution system using artificial Bee Colony Algorithm. In: *2016 IEEE 6th International Conference on Power Systems (ICPS) (2016)*
3. P. Dondi, D. Bayoumi, C. Haederli, D. Julian, and M. Suter: Network integration of distributed power generation. In: *Journal of Power Sources Volume 106, Issues 1–2, Pages 1–412 (2002)*
4. Lucian Ioan Dulau, Mihail Abrudean, Dorin Bica: Effects of distributed generation on electric power systems. In: *INTER-ENG, Elsevier Ltd (2013)*
5. H. Hedayati, S. A. Nabaviniaki, and A. Akbarimajd: A Method for Placement of DG Units in Distribution Networks. In: *IEEE Transactions on Power Delivery*, vol. 23, pp. 1620–1628 (2008)
6. Anastasia S. Safigianni, George N. Koutroumpetis, Vassilis C. Poullos: Mixed distributed generation technologies in a medium voltage network. In: *Electric Power Systems Research, 2012 Elsevier Ltd*
7. A. Changers: Distributed Generation- A Nontechnical Guide. In: *Penn Well, Tulsa, Oklahoma*, p. 283 (2001)
8. Duong Quoc Hung and Nadarajah Mithulananthan: Multiple Distributed Generator Placement in Primary Distribution Networks for Loss Reduction. In: *IEEE Transactions on Industrial Electronics*, vol. 60, no. 3 (2013)

9. Hung D.Q., Mithulananthan N. and Bansal R.C.: Analytical Expressions for DG Allocation in Primary Distribution Networks. In: *IEEE Transactions on Energy Conversion*, vol. 25, no. 3, pp 814–820 (2010)
10. N. Acharya, P. Mahat, and N. Mithulananthan: An analytical approach for DG allocation in primary distribution network. In: *International Journal of Electrical Power & Energy Systems*, vol. 28, pp. 669–678 (2006)

Electrodynamic Study of a Novel Microstrip Ring Based on Finite Integral Technique Numerical Computational Code

Seyi Stephen Olokede and Babu Sena Paul

Abstract We present a novel microstrip ring resonator (MRR) excited by a transmission line. The MRR is capable of controlling signal propagation along the peripheral of the resonator such that it is able to prohibit signal propagation within the vicinity of the narrow band closed to the target resonant, so long the magnetic component of the electromagnetic (EM) field is polarized with respect to the ring axis. The magnetic fields invariably induced current at the MRR loops via the distributed capacitance between the rings at target frequency, to ensure the frequency-selective characteristics. The selectivity behaviour is dependent on the degree of the induced current in the ring loop at the frequency under consideration can be explained by the induced current loops in the rings at resonance. We therefore investigate the electrodynamic propagation mechanism of this novel MRR to leverage on its frequency-selective behaviour to evolve miniaturized passive resonators.

Keywords Electrodynamic · 3D · Finite integration code · Numerical code
Ring resonator

1 Introduction

The need for portability necessitates the present pressing demands for miniaturization, in particular for radio frequency communications using many available wireless handheld devices such as personal and wireless communication devices, Tablet PCs, PDAs, GPRS, mobile phones, portable media gaming, barcode scanners, field data collection automation (FADA), point of sale (POS), portable media players. To meet the portability requirement in today's ever-changing mobile world, engineers are constantly confronted with stringent design constraints. The performance penalty

S.S. Olokede (✉) · B.S. Paul
Department of Electrical and Electronic Engineering Technology,
University of Johannesburg, Johannesburg, South Africa
e-mail: solokede@gmail.com

incurred by this unending demand for smaller form factor is severe. Alternative solutions to ameliorate these performance penalties are opening up new vistas of research endeavours while consolidating on the existing ones. Wireless sensors' aperture size requirement is often limited by their electrical length. The radiative resistance of these sensors depreciates with decreasing form factor. The Q factor also increases with decrease of form factor, which inadvertently worsen the resonance. The excitation mechanism of such compact sensors is problematic as most times. The excitation network is often bigger than the sensor itself, thus worsening the input impedance match, with severe degradation of the scattering parameters.

The introduction of this novel MRR structure has been very useful in the reduction of resonance with respect to its dimensions without any performance penalty, and yet with a size reduction premium. The split inserted along the MRR creates substantial capacitance values sufficient enough to lower the resonance, whereas the MRR dimensions are small compared to their electrical resonance. By implication, the radiative losses become negligible, but the Q factor becomes considerable [1–3]. In this paper, we examine the dynamics of the frequency reduction potential of the proposed MRR based on its frequency-selective behaviour. We demonstrate using a 3D finite integration numerical code that the magnetic fields are confined at the slit and perpendicular to the axis of the ring, whereas the electric field components of the EM waves propagate around the peripherals of the MRR conductors.

2 The Operational Principle

Figure 1 depicts the geometry of the proposed MRR, with the dimensional parameters as stated. The centre-inserted transmission line is the excitation mechanism connecting ports 1 and 2. When excited at these two ports, both magnetic fields and magnetic fields propagate along the transmission lines as demonstrated in Fig. 2a where both the magnetic field (H) and electric field (E) intensities are similarly as depicted in the Figure, forming H_y and E_x , respectively. As such, the power flow level is moderate such that the power flow—the poynting vector ($E \times H$)—directly demonstrates the rate of energy transfer per unit area of an electromagnetic field due to the two ports. The two electromagnetic fields (E and H) are orthogonal to each other and propagate along the z -direction (the direction of the flow). Ironically at the first resonance, the MRR demonstrates optimal electric charge densities within the gaps with unlike polarities, such that maximum current is observed around the resonator arm the rib with the gap labelled L as shown in Fig. 2b. This effect is further demonstrated from the FIT models shown in Fig. 3. At the TE_{01} resonance mode, the electric charge densities are optimum when there exist opposite signs (+, -) at the gap edges as also demonstrated in [4–10].

Consequently, the charge density is optimum at a location on the ring at the positions labelled L as demonstrated in Fig. 2b, whereas the current density is maxima elsewhere on the ring particularly at gap edges as demonstrated in Fig. 3a.

Fig. 1 The proposed microstrip ring resonator

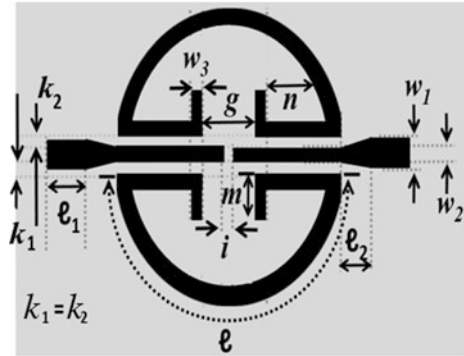
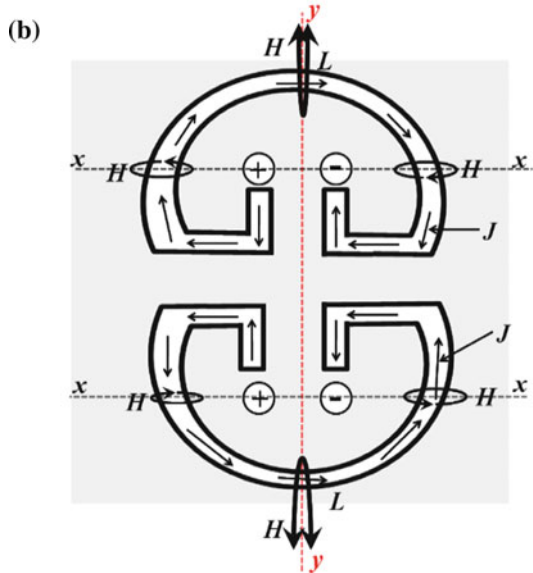
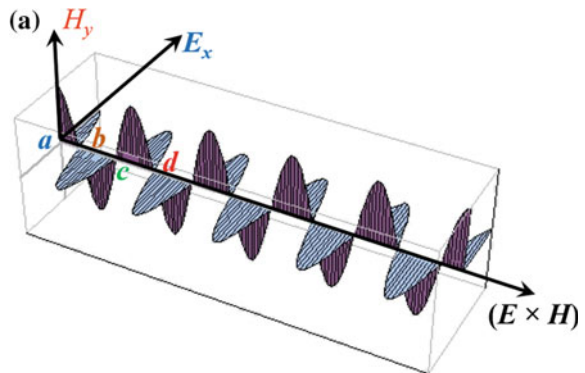


Fig. 2 Operation dynamics. **a** sinusoidal variation of E and H fields, **b** current density flow



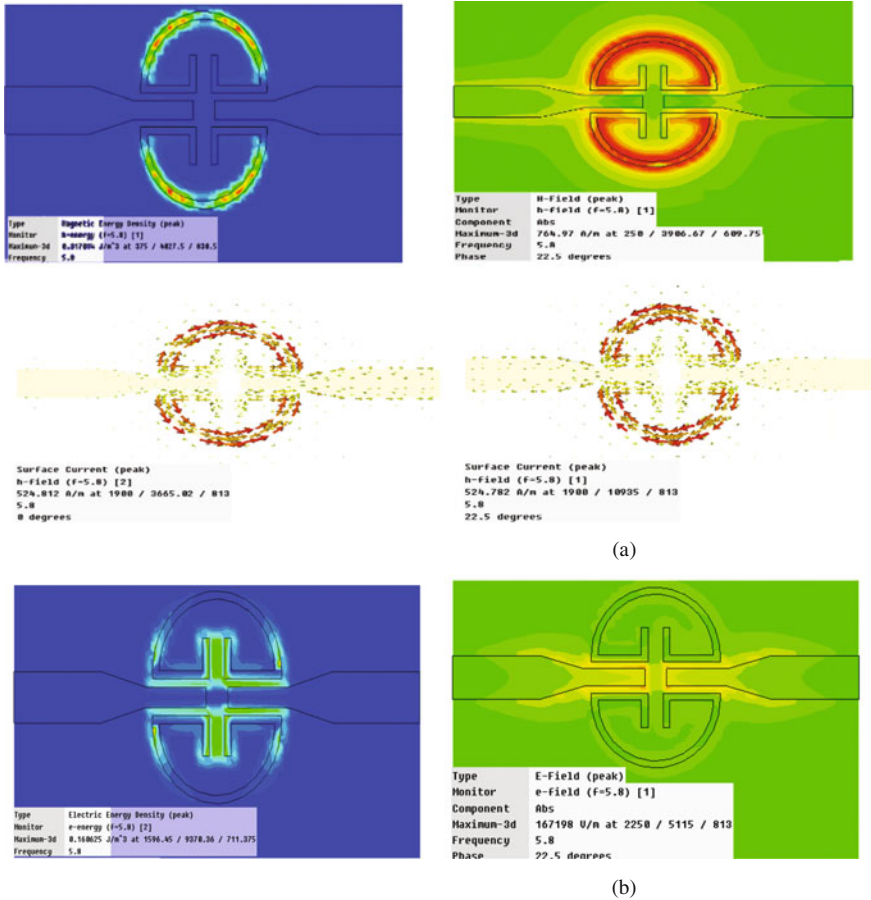


Fig. 3 The electrodynamic models of the proposed MRR. **a** Magnetic energy, **b** Electric energy

As a result, the vibrations of the electric component of the EM field in the two resonant halves of the ring—the right-hand sides (RHS) and the left-hand sides (LHS)—are opposite in phase in the two halves of the ring divided by vertical axis ($y-y$) with a red thread as shown Fig. 2b. The maxima of the electric component of the standing wave in addition with the minima of magnetic component of the standing wave were both observed at the gap edges’ vicinity. Thus, the minima of the electric component of the standing waves in addition with the maxima of the magnetic field standing waves are significantly close to the slit directly opposite to the MRR arm. In the second quadrant of Fig. 4c representing $(|E_x|, |H_y|)$ at the first crest between $(a$ and $b)$ of Fig. 2a, the electric field $(|E_x|, |H_y|)$ is optimum. The same $(|E_x|, |H_y|)$ is zero at the first quadrant representing the negative half-cycle of the sinusoid at a location between $(b$ and $c)$. The same scenario in the second quadrant repeats itself at the fourth quadrant representing the position between

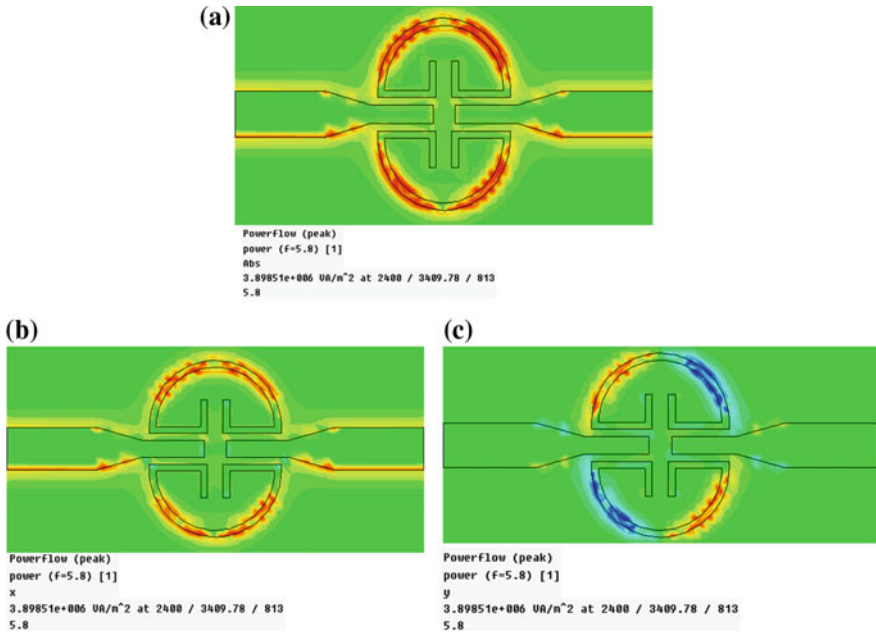


Fig. 4 Power flow of the MRR. a Absolute, b x-axis, c y-axis

(c and d), whereas the occurrence of the third quadrant representing positions between (d and a) is similar to that of the first quadrant. At position distances of (b and c) and (d and a) where H_y and E_x are both zero on the xy -plane of Fig. 2a were responsible for the power flow dissimilarity observed between Fig. 4a, b. Consequently, the maxima of the electric component of the standing wave along with the nodes of magnetic component of the standing wave are evident at the vicinity of the gap edges close to the gap directly opposite the ring circumference. Figure 3a (ii and iii) demonstrates the superposition theorem of the excitation from the two ports. The arrow shows the current density flow due to excitation from either of the ports. It is evident in Fig. 3a (ii) that the excitation is as a result of port 2, whereas Fig. 3a (iii) is the excitation through port 1.

Therefore, the possibility of controlling the electric response of an MRR is feasible by adjusting the orientation of its gap with respect to the applied electric field E . If the gap is parallel to the electric field E , an electric coupling is established. Simultaneously, there is also a magnetic resonance due to H -field though less strong compared to the electric resonance. Thus, the proposed resonator prevents the propagation of the signal within the narrow band close to the resonance under consideration; so long the magnetic field component of the EM is polarized along the ring axis. While Fig. 3a (i, ii, and iii) confirms that the magnetic field is polarized along the axis of ring, Fig. 4 shows the time-varying power flow along the proposed MRR particularly the absolute power flow shown in Fig. 4a when excited by the ports. In Fig. 4b, the power flow in x -direction is depicted, whereas

in y -direction is shown in Fig. 4c. The superposition of powers from the two ports is significant in Fig. 4a indicating the absolute power flow due to constructive combination of the power from both ports. It is the combination of Figs. 4b, c. As such, the power flow level is moderate in Fig. 4b compared to what was obtainable in Fig. 4a. In Fig. 4c, the power flow—the Poynting vector ($E \times H$)—directly demonstrates the rate of energy transfer per unit area of an electromagnetic field due to the two ports. Consequently, the maxima of the electric component of the standing wave in addition with the minima of magnetic component of the standing wave are evident at the vicinity of the gap edges directly opposite the ring axis near the gap edges and near the middle of the opposite side of the ring.

3 Experimental Results and Discussions

Figure 5 depicts the effect of magnetic field coupling on the proposed MRR over a coupling space of k . The resonance shifts (increase) to higher regime as the coupling space k increases. At this time, the electric field intensities with this coupling space are less dense. Therefore, the coupling between the two halves of the proposed MRR becomes relaxed and the coupling strength becomes inferior. It is expected that the reflection coefficients $|S_{11}|$ shown in Fig. 5a at this time should depreciate.

Unfortunately, the coefficient does not differ substantially to be able to confirm the extent of the relaxed coupling. We envisaged that there is likely possibility that this can be confirmed if the coupling space is further increased. The same observation is recorded as regards Fig. 5b where the insertion loss (S_{12}) also shifts upward side away from the target resonance of 5.8 GHz due to increase of the coupling space k . Interestingly, opposite of the above deductions holds. As the coupling space decreases, the resonance frequency shifts downward much below the target resonance. It is assumed that this shift is as a result of tight coupling. When this coupling space is reduced, the MRR structure becomes smaller. This makes the realization of miniaturized passives possible using the proposed structure based on the resonance split due to magnetic and electric field interactions as stated above.

Fundamentally, the proposed MRR is capable of exhibiting three resonance, namely (1) resonance as a result of the upper half-MRR, (2) resonance as a result of the lower half-MRR, and (3) resonance as the two halves MRR behaves as circular passive which is achievable as the separation gaps between the halves are joined together due to fringing effects. When the coupling space increases, the impedance bandwidth increases. Further increase of the coupling space will exert the capacity of the proposed MRR for increase impedance bandwidth that it eventually leads to dual band. Table 1 describes the dual band possibility of the MRR, the coupling space at which the dual band results, the insertion loss implications, and importantly, their respective reflection coefficients as demonstrated in Fig. 6.

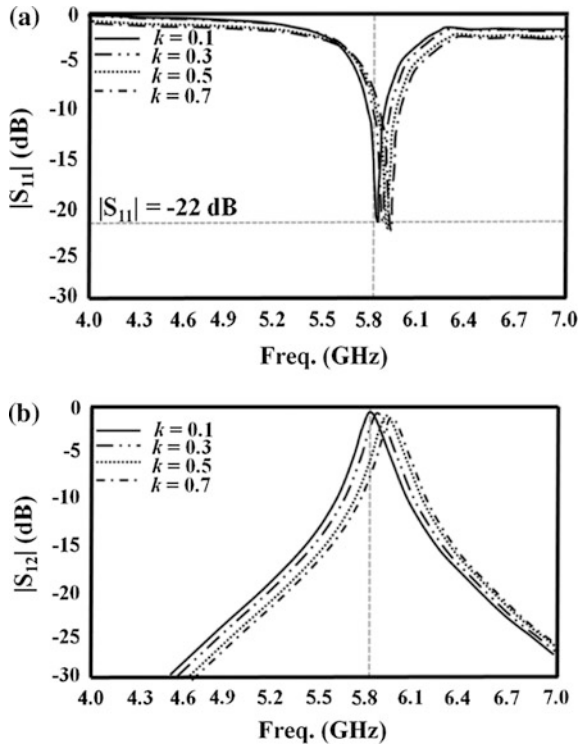


Fig. 5 Effect of magnetic coupling with respect to k coupling space. **a** $|S_{11}|$, **b** $|S_{21}|$

Table 1 Performance profile vs. coupling space

Coupling gap k (mm)	Resonant Freq. GHz		$ S_{11} $ (dB)		$ S_{12} $ (dB)		Bandwidth (MHz)	
			f_1	f_2	f_1	f_2	f_1	f_2
0.1		5.80	–	–21.5	–	–0.9	780	–
0.3		5.81	–	–22.0	–	–2.67	360	–
0.5		5.88	–	–22.4	–	–2.69	203	–
0.7		5.91	–	–22.6	–	–2.72	140	–
0.9	5.30	6.10	–22.3	–22.8	–2.75	–2.77	600	700

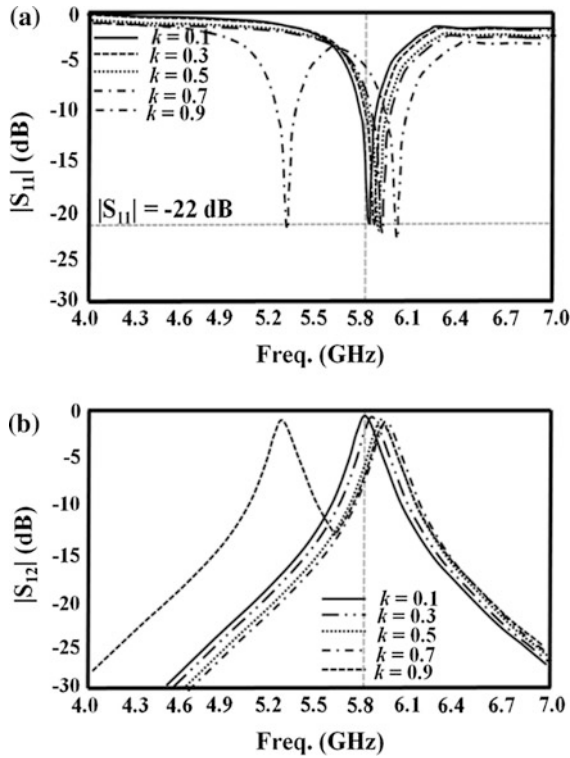


Fig. 6 Effect of magnetic coupling with respect to k coupling space. **a** $|S_{11}|$, **b** $|S_{21}|$

4 Conclusion

In this paper, an electrodynamic investigation of novel compact MRR based on finite integration technique numerical code is presented. The resonance response variance is observed when compared to the effect of electric field densities within the coupling space. The decrease of coupling space decreases the resonance, and also, the size occupancy. The proposed design presents apparent size reduction, as compared to conventional parallel-coupled or end-coupled microstrip bandpass filter, with reasonable performance enhancement.

References

1. C. M. Soukoulis, M. Kafesaki, and E. N. Economou, "Negative index materials: New frontiers in optics," *Adv. Mater.* 18, pp. 1941–1952, 2006.
2. R. Penciu, M. Kafesaki, T. F. Gundogdu, E. N. Economou, and C. M. Soukoulis, "Theoretical study of left-handed behavior of composite metamaterials," *Photon. Nanostruct.* 4, pp. 12–16, 2006.
3. J. B. Pendry, "Focus Issue: Negative Refraction and Metamaterials," *Opt. Express* 11, pp. 639–755, 2003.
4. H. Zhan, Li, Y.-Q., Chen, X., Fu, Y.-Q., Yuan, N.-C., "Design of circular polarisation microstrip patch antennas with complementary split ring resonator," *Microwaves, Antennas & Propagation, IET*, vol. 3, no. 8, pp. 1186–1190, December 2009.
5. Philippe Gay-Balmaz, Olivier J. F. Martin, (2002) Electromagnetic resonances in individual and coupled split-ring resonators. *Journal of Applied Physics* 92 (5):2929–2936
6. R. Marqués, J. Martel, F. Mesa, F. Medina, (2002) Left-Handed-Media Simulation and Transmission of EM Waves in Subwavelength Split-Ring-Resonator-Loaded Metallic Waveguides. *Physical Review Letters* 89 (18)
7. J.D. Baena, J. Bonache, F. Martin, R.M. Sillero, F. Falcone, T. Lopetegui, M.A.G. Laso, J. Garcia-Garcia, I. Gil, M.F. Portillo, M. Sorolla, *IEEE Transactions on Microwave Theory and Techniques* 53 (4):1451–1461
8. R. A. Shelby, Experimental Verification of a Negative Index of Refraction. *Science* 292 (5514):77–79
9. D. R. Smith, (2004) Metamaterials and Negative Refractive Index. *Science* 305 (5685): 788–792
10. T.F. Gundogdu, Mutlu Gökkavas, Kaan Güven, M. Kafesaki, C.M. Soukoulis, Ekmel Ozbay, (2007) Simulation and micro-fabrication of optically switchable split ring resonators. *Photonics and Nanostructures - Fundamentals and Applications* 5 (2–3):106–112

Decaying Objects of Constant Demand Speed and Dependent of Time Within Permitted Delay in Imbursement of the Model of Inventory Level

Jasvinder Kaur and Arun Kumar

Abstract This paper has an economic order quantity (EOQ) replica which is generated used for a decaying products having time dependent on demand. If late payment is allowable decaying value is considered to be fixed and time dependent on demand value is assumed to be a constant function of time. Models of mathematics is also taken from the two dissimilar cases, that is, for case (1): The financial standing time period is equal to or less than to the sequence time period used for an account settlement and for case (2): The financial standing time period is greater than the sequence time period used for an account settlement. And the outcomes are explained with mathematical examples. Explanation for analyzing a time constant demand and allowable late payment are tacked about.

Keywords Decaying product · Deterioration · Constant demand
Permissible delay in payment · Inventory

1 Introduction

In this economic order quantity (EOQ) classical model in light 1915, the production rate is real of a product was considered as many ways like as linear, exponential, quadratic etc. and in this real gross national product, the production rate of any item is every time in a coming on strong. And some inventory modelers had rewarded their concentration as dependent of time demand speed. Goyal et al. [1] used the deteriorating inventory in recent trends, and Sarkar [2] developed the model time dependent deteriorating rate with permissible delay in payment. Khanra et al. [3]

J. Kaur (✉)

Department of Mathematics, BFIT, Dehradun, Uttarakhand, India

e-mail: jasvinddn@gmail.com

A. Kumar

Department of Management, Sanjivani Parenteral Ltd., Dehradun, Uttarakhand, India

e-mail: suryaarun2007@gmail.com

© Springer Nature Singapore Pte Ltd. 2018

R. Singh et al. (eds.), *Intelligent Communication, Control and Devices*,

Advances in Intelligent Systems and Computing 624,

https://doi.org/10.1007/978-981-10-5903-2_73

developed the model for quadratic demand with deteriorating item under permissible delay in payment. Sarkar et al. [4] was grownup inflation and time value of money with time varying demand. Bhunia et al. [5] advanced for two warehouses inventory model for deteriorating products with backlogging under delay in payment. Ruxian Li, Hongjie Lan, John R. Mawhinney developed deteriorating product inventory model. Sana and Chaudhum [6] extended Huang [7] was developed inventory model for limited storage space. Pahi and VoB [8] and Lin et al. [9] and others. Jalan et al. [10] and Hariga [11] developed inventory model for shortages and deteriorating items with time dependent demand. Now in recent paper, we take that demand is constant and shortages are not allowed and unlimited price replenishment which is time dependent. In this paper, we have two cases. First is when $T > t_2$ and second is when $T < t_2$ then we get the value of economic order quantity, i.e., $A_0(T_1)$ and $A_0(T_2)$ and after that we write the examples for finding the value of $A_0(T_1)$ and $A_0(T_2)$ and write the sensitivity analysis of table.

2 Assumptions and Notations of This Paper

We are using the following assumptions in this paper

- (i) R Price of replenishment.
- (ii) T Sequence time period among two orders in the year.
- (iii) t_2 Allowable sequence time in year of delay in resolving the accounts by the dealer.
- (iv) δ Stable rate of decaying things within the period $0 < \delta < 1$.
- (v) h Cost of carrying inventory not including interest accuses/rupee of unit buying price/unit time.
- (vi) b Unit buying price of things.
- (vii) A_b Interest accuses/rupee asset in stock of inventory/year.
- (viii) A_e Interest earned/rupee in one year.
- (ix) $D(t_1)$ Consider the demand speed $D(t_1) = x$; $x > 0$. Where x is the initial value of the demand and which is time dependent.

We are using the following notation in this paper

- (i) Shortages are not permitted.
- (ii) The decaying value is stable/unit time period, and it is not substitution of the decaying things surrounded by the sequence.
- (iii) The demand value of the things is considered with a constant.
- (iv) Price of replenishment is unlimited.
- (v) Possibility of time is countless.

3 Mathematical Solution and Formulation of This Paper

The list of inventory rank $A(t_1)$ in any sequence time period t_1 is created by under the differential equation.

$$\frac{dA(t_1)}{dt_1} + \delta A(t_1) = -x; \quad 0 \leq t_1 \leq T. \quad (1)$$

Since demand speed $D(t_1) = x$, When $A(T) = 0$ at $t_1 = T$ Then we have

$$y = \frac{e^{\delta T}}{\delta} \cdot x \text{ Therefore } A(t_1) = \frac{x}{\delta} [e^{\delta(T-t_1)} - 1]; \quad 0 \leq t_1 \leq T. \quad (2)$$

When $A(0) = A_0$ at $t_1 = 0$ and $A(T_1) = A_0$.

Hence, the quantity of initial order is given by as of the Eq. (2) is

$$A_0 = A(0) = \frac{x}{\delta} [e^{\delta T} - 1]. \quad (3)$$

The entirety demand surrounded by the sequence time period $[0-T]$ is

$$\int_0^T D(t_1) dt_1 = \int_0^T x dt_1 = xT.$$

Entirety cost of inventory holding (CIH) surrounded by the sequence time period $[0-T]$ is

$$\text{CIH} = h \int_0^T A(t_1) dt_1 = \frac{hx}{\delta^2} [e^{\delta T} - 1 - \delta T]. \quad (4)$$

Entire cost of inventory decaying (CID) surrounded by the sequence time period $[0-T]$ is

$$\text{CID} = b \left[A_0 - \int_0^T D(t_1) dt_1 \right] = \frac{bx}{\delta} [e^{\delta T} - 1 - \delta T]. \quad (5)$$

Now from the case (1): when $T > t_2$ then

When the interest of inventory is payable surrounded by the sequence time period $[T-t_2]$ then the interest of inventory payable surrounded by the sequence time period $[0-T]$ is

$$Ab_1 = bA_b \int_{t_2}^T A(t_1)dt_1 = \frac{xbA_b}{\delta^2} \left[e^{\delta(T-t_2)} - 1 - \delta T + \delta t_2 \right]. \tag{6}$$

Hence the interest earned of inventory surrounded by the sequence time period $[0-T]$ is

$$AE_1 = bA_e \int_0^T t_1.D(t_1)dt_1 = \frac{bA_e T^2 x}{2}. \tag{7}$$

∴ The sum of changeable price (cp) using per sequence = price of replenishment inventory + price of holding inventory + price of decaying inventory + payable of interest surrounded by the permitted delay with period of time—interest earned of inventory surrounded by the sequence.

∴ Sum of changeable price (cp) using per sequence is

$$S_1(T) = \frac{R}{T} + \frac{CIH}{T} + \frac{CID}{T} + \frac{Ab_1}{T} - \frac{AE_1}{T} = \frac{R}{T} + \frac{hx}{T\delta^2} [e^{\delta T} - 1 - \delta T] + \frac{bx}{T\delta} [e^{\delta T} - 1 - \delta T]. \tag{8}$$

At present, we shall obtain the price of minimum changeable per unit time period.

$$\therefore \frac{dS_1(T)}{dT} = 0 \text{ and, } \frac{d^2S_1(T)}{dT^2} > 0.$$

At this time, putting the value of $\frac{dS_1(T)}{dT} = 0$, then we will be getting the value of T_1 Therefore

$$xT \left[\left(b + \frac{h}{\delta} \right) (e^{\delta T} - 1) + (e^{\delta(T-t_2)} - 1) \frac{bA_b}{\delta} - bA_e T \right] + \frac{xb}{\delta} [e^{\delta T} - 1 - \delta T] + \frac{bA_b x}{\delta^2} [e^{\delta(T-t_2)} - 1 - \delta(T - t_2)] - \left[R + \frac{hx}{\delta^2} (e^{\delta T} - 1 - T) \right] - \frac{bA_b T x}{2} = 0. \tag{9}$$

Therefore at this moment, we will be solving the Eq. (9) and we will get the value of T

$$T_1 = \sqrt{\frac{2R}{x[2\delta b + 2h + bA_b(1 - 2t_2) - 2bA_e]}}$$

In favor of the length of optimal sequence $T = T_1$, Hence $T = \sqrt{\frac{2R}{x[2\delta b + 2h + bA_b(1 - 2t_2) - 2bA_e]}}$.

And from this case (1), the economic order quantity (EOQ) is in the form of

$$A_0(T_1) = \frac{x}{\delta} [e^{\delta T_1} - 1]. \tag{10}$$

At the present from the case (2): when $T < t_2$ then

In this case (2), the purchaser obtain the interest at the deals income permitted delay in imbursement time period and find not interest is payable surrounded by the time period used for the manufactured goods in the warehouse.

Interest obtain used for the time sequence $[0-T]$ is

$$bA_e \int_0^T t_1 D(t_1) dt_1 = bA_e \int_0^T t_1 x dt_1 = \frac{bA_e x T^2}{2}. \tag{11}$$

Getting the interest with the allowable delay time $[T-t_2]$, it means

$$bA_e(t_2 - T) \int_0^T D(t_1) dt_1 = bA_e(t_2 - T) \int_0^T x dt_1 = bA_e(t_2 - T)xT. \tag{12}$$

Hance, the addition of getting the interest surrounded by the sequence is

$$AE_2 = bA_e \int_0^T t_1 D(t_1) dt_1 + bA_e(t_2 - T) \int_0^T D(t_1) dt_1 = \frac{bA_e}{2} x T^2 + bA_e(t_2 - T)xT. \tag{13}$$

At the present from the case (2).

The addition of cost of changeable per sequence (cc) = price of replenishment inventory + price of holding inventory + price of decaying inventory - interest earned of inventory surrounded by the sequence.

Hence, the addition of cost of changeable per sequence is

$$S_2(T) = \frac{R}{T} + \frac{CIH}{T} + \frac{CID}{T} - \frac{AE_2}{T} \\ = \frac{1}{T} \left[R + \frac{hx}{\delta^2} (e^{\delta T} - 1 - \delta T) + \frac{bx}{\delta} (e^{\delta T} - 1 - \delta T) - \frac{bA_e x T^2}{2} - bA_e(t_2 - T)xT \right]. \tag{14}$$

At this time, we will be finding the price o minimum changeable per unit time.

Hence, $\frac{dS_2(T)}{dT} = 0$ and, $\frac{d^2S_2(T)}{dT^2} > 0$.

At the moment, putting the value of $\frac{dS_2(T)}{dT} = 0$ and we will gett the value of T_2 .

Hence $\frac{dS_2(T)}{dT} = 0$,

$$Tx \left(b + \frac{h}{\delta} \right) (e^{\delta T} - 1) - bA_eTx(t_2 - T) + \frac{bx}{\delta} (e^{\delta T} - 1 - \delta T) - R - \frac{hx}{\delta^2} (e^{\delta T} - 1 - T) - \frac{bA_eTx}{2} (2t_2 - T) = 0. \tag{15}$$

Hence we will be solving the Eq. (15) and getting the solution of T .

$$\therefore T = \sqrt{\frac{2R}{x[2(\delta b + h) - bA_e(1 + t_2)]}} \text{ In favor of the length of optimal sequence } T = T_2, \\ \therefore T_2 = \sqrt{\frac{2R}{x[2(\delta b + h) - bA_e(1 + t_2)]}}. \tag{16}$$

And from this case (2), the economic order quantity (EOQ) is

$$A_0(T_2) = \frac{x}{\delta} (e^{\delta T_2} - 1) \tag{17}$$

At the present from the case (3): when $T = t_2$ then

the changeable price $S_1(T)$ and $S_2(T)$ both are the equal for the value of $T = t_2$ and the price of function is getting on putting $T = t_2$ in Eq. (14) or on putting $T = t_2$ in Eq. (8) and we will be setting the value of $S_3(T)$

$$\therefore S_3(T) = \frac{R}{t_2} + \frac{hx}{t_2\delta^2} [e^{\delta t_2} - 1 - \delta t_2] + \frac{bx}{t_2\delta} [e^{\delta t_2} - 1 - \delta t_2] - \frac{bA_e t_2 x}{2}. \tag{18}$$

\therefore From this case (3), the economic order quantity (EOQ) is in the form of

$$A_0(t_2) = \frac{x}{\delta} (e^{\delta t_2} - 1). \tag{19}$$

4 Mathematical Examples of Paper

We are solving the mathematical example as follows for all the cases (1), (2), and (3) of this inventory model.

Example-(i): Mathematical examples for the case (1)

When,

$x = 1200$ Units/Year,	$R = \text{Rs. } 250/\text{Order},$	$A_b = 0.17/\text{Year},$
$A_e = 0.15/\text{Year},$	$h = \text{Rs. } 0.14/\text{Year},$	$b = \text{Rs. } 15/\text{Unit},$
$\delta = 0.25,$ and	$t_2 = 0.20$ Year	

At this time, we are solving the Eq. (9) and we get $T_1 = 0.296$ year.

And the price of minimum average is $S_1(T_1) = \text{Rs. } 441.64.$

Again we will be solving the Eq. (16), and we have $T_2 = 0.287$ year.

And the price of minimum average is $S_2(T_2) = \text{Rs. } 718.55$ and we have $T_2 > t_2.$

Where the case (2) is contradicting and which is hold, only case (1).

Like as $T_1 > t_2$ hence in this case, the price of minimum average is $S_1(T_1) = \text{Rs. } 441.64.$

Which the length of optimum sequence is $T_1 = 0.296$ year.

And we are getting the result of economic order quantity (EOQ) is $A_0(T_1) = 355.20.$

Example-(ii): Mathematical example for the case (2)

When,

$x = 1200$ Units/Year,	$R = \text{Rs. } 250/\text{Order},$	$A_b = 0.17/\text{Year},$
$A_e = 0.15/\text{Year},$	$h = \text{Rs. } 0.14/\text{Year},$	$b = \text{Rs. } 15/\text{Unit},$
$\delta = 0.25,$ and	$t_2 = 1.20$ Year	

At this time, we are solving the Eq. (9) and we get $T_1 = 1.141$ year.

And the price of minimum average is $S_1(T_1) = \text{Rs. } 296.18.$

Again we will be solving the Eq. (16), and we have $T_2 = 0.286$ year.

And the price of minimum average is $S_2(T_2) = \text{Rs. } 177.94.$

And we have $T_1 < t_2$ where the case (1) is contradiction and which is hold, only case (2).

Like as $T_2 < t_2$ hence in this case, the price of minimum average is $S_1(T_1) = \text{Rs. } 296.18.$

Which the length of optimum sequence is $T_2 = 0.286$ year.

And we are getting the result of economic order quantity (EOQ) is $A_0(T_2) = 343.20.$

5 Sensitivity Analysis of Tables of This Paper

Outcome of sensitive analysis

Now we will be studying the changes results of the worth of the variable $x, A_b, A_c, R, \delta, h, b, t_2$ on most favorable sum of price and reordering number.

Now the outcomes of sensitive analysis is presented with changing every variable with 45%, 15% and -45%, -15% we assume the one variable with 45%, 15% and -45%, -15% variable are not changed and the outcomes of sensitive analysis are hold of example (i) and the outcomes are represented in above tables. In which we examine.

- (i) In the above-mentioned Table 1, we observed that the $S_1(T_1)$ and $S_2(T_2)$ are increased and the value of T_1 and T_2 are decreased by way of increasing in the value of variable x and the value of T_1 and T_2 are fairly sensitive of change with x and the value of $S_1(T_1)$ and $S_2(T_2)$ both are low sensitive of changes with x .
- (ii) In Table 2, we get that the value of T_1 is decreasing and the value of $S_1(T_1)$ is increasing by way of increasing in the value of the variable A_b and T_1 is fairly sensitive of changes with A_b and the value of $S_1(T_1)$ is few changes in the variable A_b and the value of $S_2(T_2)$ and T_2 are not affected by the way of the changing in the values of the variable A_b .

Table 1 Sensitivity analysis based on variable x

Variable	Percentage change in variable	T_1	T_2	$S_1(T_1)$	$S_2(T_2)$	Note $t_2 = 0.20$ year	Final result	Percentage change in optimum % price
x	-45	0.422	0.318	432.301	659.102	$T_1 > t_2$	$S_1(T_1)$	-11.87
	-15	0.397	0.289	499.589	684.574	$T_1 > t_2$	$S_1(T_1)$	-2.39
	15	0.292	0.199	586.521	879.312	$T_1 > t_2 > T_2$	$S_1(T_1)$	1.73
	45	0.265	0.185	621.311	923.137	$T_1 > t_2 > T_2$	$S_1(T_1)$	6.82

Table 2 Sensitivity analysis based on variable A_b

Variable	Percentage change in variable	T_1	T_2	$S_1(T_1)$	$S_2(T_2)$	Note $t_2 = 0.20$ year	Final result	Percentage change in optimum % price
A_b	-45	0.489	0.213	481.826	782.202	$T_1 > t_2$	$S_1(T_1)$	-11.06
	-15	0.426	0.213	525.732	782.202	$T_1 > t_2$	$S_1(T_1)$	-2.15
	15	0.375	0.212	576.956	782.202	$T_1 > t_2$	$S_1(T_1)$	2.25
	45	0.327	0.212	615.819	782.202	$T_1 > t_2$	$S_1(T_1)$	5.36

6 Conclusion

In this paper, we conclude that infeasible outcomes in this model used for the values -45 and -15% negative inaccuracies in R but the results may be because of the choice of the exacting variable values in these mathematical results. In the above table, we observed that the most possible rate is decreasing firstly by way of the increasing of the variable A_e which substantiated the genuine bazaar location. This benefit of the constant demand has inspired the creators for accepting it in the current replica for the genuine bazaar. We analyze that the providers propose their clients a convinced credit stage period not including interest for the duration of allowable late time stage period. Because a solution, it inspire client of order added amount since disbursing afterword not directly decreases the price of purchases.

References

1. S. K. Goyal, B.C. Gin, Recent trends in modeling of deteriorating inventory, *European journal of operational research*, 134(2001) 1–16.
2. Biswajit Sarkar, An EOQ Model with delay in payments and time varying deterioration rate, *mathematical and computer modeling*, 56 (2012) 367–377.
3. S. Khanra, S. K. Ghosh, K. S. Chaudhun, An EOQ model for a deteriorating item with time dependent quadratic demand under permissible delay in payment, *Applied mathematics and computation*, 218 (2011) 1–9.
4. Biswajit Sarkar, Shib Sankar Sana, Kripasindhu Chaudhun, An imperfect production process for time varying demand with inflation and time value of money- An EMQ Model, *Expert systems with applications*, 38 (2011) 13543–13548.
5. A. K. Bhunia, Chandra K. Jaggi, Anuj Sharma, Ritu Sharma, A two warehouse inventory model for deteriorating items under permissible delay in payment with partial backlogging, *Applied mathematics and computation*, 232 (2014) 1125–1137.
6. Ruxian Li, Hongjie Lan, John R. Mawhinney, A review on deteriorating inventory study, *service science & management*, 3 (2010) 117–129.
7. Yung-Fu Huang, An inventory model under two levels of trade credit and limited storage space derived without derivatives, *Applied mathematical modeling*, 30 (2006) 418–436.
8. Julia Pahi, Stefan VoB, Integrating deteriorating and lifetime constraints in production and supply chain planning: A survey, *European journal of operational research*, 238 (2014) 654–674.
9. C. Lin, B. Tan, W. C. Lee, An EOQ Model for deteriorating items with time- varying demand and shortages, *International journal of systems science*, 31(3) (2000) 391–400.
10. A. K. Jalan, R. R. Giri, K. S. Chaudhuri, EOQ model for items with weibull distribution deterioration, shortages and trended demand, *International journal of systems science*, 27(9) (1996) 851–855.
11. M. Hariga, An EOQ Model for deteriorating items with shortages and time- varying demand, *Journal of operational research society*, 46 (1995) 398–404.
12. Shib Sankar Sana, K. S. Chaudhun, A deterministic EOQ model with delays in payments and price-discount offers, *European journal of operational research*, 184 (2008) 509–533.

A Highly Secure Video Steganography Inside DWT Domain Hinged on BCD Codes

Sonali Rana and Rosepreet Kaur Bhogal

Abstract Prime need of hiding data from eavesdroppers is accomplished by the use of steganography, which is an area of research from years. Steganography is an artifice and science of hiding information inside a medium. Modern mediums are text, image, audio tracks and video streams. After the evolution of Internet, wide researches have been carried out on video steganography due to high capacity of information been stored in a video file. Hiding of information in a video file can be achieved in a variety of ways. Each and every technique used has its own merits and demerits. In this paper, a highly secure video steganography has been propounded rooted on BCD coding. To ameliorate the collateral of the algorithm, the covert message is first encoded by BCD coding. Then, it is implanted in the DWT coefficients of video frames. The middle and high frequencies zones of DWT are regarded as less sensitive to HVS, so the covert message is implanted only into mesial and high frequency DWT coefficients. The results of propounded algorithm are correlated with the LSB insertion method. The results manifest superior performance for propounded algorithm as compared to LSB insertion method, hence shows minimal trade-off of visual quality.

Keywords BCD (Binary coded decimal) codes • DWT (Discrete wavelet transform) • Eavesdroppers • HVS (Human visual system) • LSB (Least significant bit) • Video steganography

S. Rana (✉) · R.K. Bhogal
Lovely Professional University, Phagwara, India
e-mail: sonalirana85@gmail.com

R.K. Bhogal
e-mail: rosepreetkaur12@gmail.com

1 Introduction

Steganography is gleaned from Greek language for secret communication. It is a mixture of two words Steganos means ‘covered’ and graphy means ‘writing’. It is an art of embedding data inside a cover medium such as text, images and videos [1]. In simple words, steganography just substitutes the least significant bits of the covert data to the carrier media. Popular description for steganography is ‘hidden in plain sight’ means intruder can’t detect the very existence of the secret data. There is no particular law associated with the steganography, but one should be aware while choosing and reusing the video or audio file for data hiding. Steganography uses one drawback of ‘Human Visual System’ (HVS) as advantage, i.e. human eyes can’t detect small changes in the cover media. Figure 1 explains the traditional block diagram of the steganography. The robustness of the steganography system is determined by three factors: (1) Amount of data hidden (2) Detection of data (3) Difficulty of removal. Other parameters for Steganography are embedding payload and embedding efficiency. Steganography in video is similar to image steganography, except the fact that information is hidden in each frame of the video. There are two domain used to implement video steganography, i.e. spatial domain and transform domain techniques [2]. LSB insertion is a spatial domain technique and is a substitution-based technique. It replaces the superfluous data of the cover media with the LSBs of the concealed data. This scheme is advantageous because of easy implementation and simplicity. DCT, DWT are the examples of frequency domain techniques, in which cover media is converted into frequency components before embedding the secret data in it. Frequency domain techniques are resistant for any kind of attacks, and it is difficult to retrieve information for eavesdropper.

The steganography algorithm that embodies high implanting efficiency will be less prone to attacks and will be very strenuous to detect through stegoanalysis tools. To increase the embedding payload with nether alteration of the cover media, innumerable steganography methods have been propounded using different techniques. In this paper, the steganographic methods used for securing hidden text are BCD codes and sequential coding. Sequential encoding increases the randomness

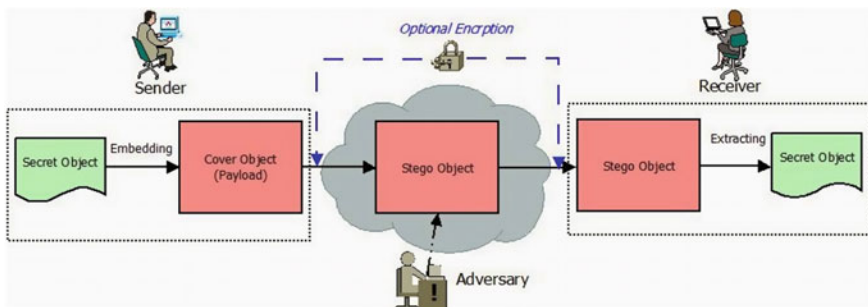


Fig. 1 Block diagram of Steganography

of the secret text and makes it more strenuous to detect by hackers. DWT [3] used in the embedding process enhances the visual feature after embedding the data inside it. DWT exploits two types of the functions, wavelet functions and scaling functions, which are chronicle including the low pass and high-pass filters. The propounded algorithm has used a key which is predefined by the sender in the embedding process. A key is used in order to enhance the security of the algorithm. The propounded algorithm provides satisfactory trade-off visual feature, embedding payload and robustness. The residue part of this paper formulated as: segment two bestows relevant work, segment three elucidates DWT (discrete wavelet transform), segment four unfolds BCD codes and segment five represents embedding process. Segment six exhibits and explains experimental results.

2 Relevant Work

In 2012, Zhang et al. propounded a coherent embedder using BCH code for steganography. In this paper [4], embedder obfuscates the secret data into cover media. The embedding process is accomplished by reforming the assorted coefficient values in the input line in harmony to fabricate pattern merits vacuous. Both storage capacity and computational cost are reduced by using this coherent embedder and is more robust in comparison with other methods. It improves system complexity from exponential to linear.

In 2015, Ramadhan J. Mstafa et al. ventured an algorithm [5] based on DWT domain based on BCH codes for video steganography. In this paper, DWT is used to enhance the textural features of the cover media after embedding data in it. This transform is more robust than DCT, FFT, etc. frequency domain techniques. BCH codes are cyclic error detecting and correcting codes which enhance the security of secret data and enhance the overall efficiency of the steganographic system.

In 2014, Ramadhan J. Mstafa et al. introduced an algorithm [6] based on Hamming codes for video steganography. In this paper, principle of linear block codes is used for implementing video steganography. Hamming codes are linear error correcting and detecting codes, which enhance the secrecy and security of the secret data. In hamming codes, the original data are encoded by adding some extra data with nadir amount of redundancy and known as codeword. By using Hamming codes, the security and the efficiency of the steganographic scheme were enhanced.

In 2015, Ramadhan J. Mstafa et al. proposed an algorithm [7], wavelet based on the KLT tracking algorithm and BCH code for video steganography. The proposed algorithm is divided into four different phases. In first part, secret data are encrypted with a secret key and BCH codes are tendered to it in order to produce an encoded message. In second part, face detecting and tracking algorithms are applied in order to extract facial features and regions from the cover video frames. In third part, the secret data are embedded in the middle and high frequency coefficients of the wavelet transform of the facial regions. In fourth part, data extraction is done by extracting secret memo from the mesial and high frequency coefficients of the

wavelet transform of the facial regions. The propounded algorithm bestows the high implanting efficiency and high implanting payload.

In 2009, R.O. El Sfy et al. propounded an algorithm [8] based on integer wavelet transforms (IWT) for video steganography. In this paper, IWT for cover media hides information in it, using optimum pixel adjustment (OPA) algorithm. The coefficients used are chosen using pseudorandom generator to enhance the security and secrecy of the secret data. The OPA is used to reduce the embedding error occurred during embedding process. The proposed algorithm increases and boosts the security of the steganographic system. Wavelet transform enhances the textural features of the cover media.

3 Discrete Wavelet Transform

A wavelet is a short wave with oscillatory nature, whose amplitude originates at zero, elevates and afterwards decreases back at zero again. Wavelets are functions defined over finite time duration. Wavelets are having two functions- wavelet function and scaling function. Wavelets are generated from mother wavelet function ψ . DWT [9] is a frequency domain technique used to transform signal from time domain to frequency domain. DWT sunders low, mesial and high frequencies and its borderlines from each other. Haar wavelet is the simplest form of DWT. DWT can be applicable for both 1D and 2D signals. For 1D signals, DWT provides the average and the difference of the pixel values.

For 2D signals, i.e. images, DWT will result in four different frequency sub-bands that are LL, LH, HL, HH. LL is the lower resolution approximation of the image. HL is horizontal attribute coefficient (CH), LH is vertical attribute coefficient (CV) and HH is diagonal detail coefficients (CD) as shown in the below diagram. High frequency sub-bands (HH, HL and LH) consist of texture and edge details of an image. High frequency components are worn in order to embed the secret data, as it is not detectable by HVS (Fig. 2).

4 BCD Codes

BCD stands for binary coded decimal which is an encoding scheme for decimal numbers where every digit has its own binary equivalent excerpt. These codes are widely used in electronic systems and computing systems. Its main douth is to permit facile transfiguration to decimal digits for printing or display and faster decimal metamorphosis. In BCD encoding, each decimal digit is victual in a four-bit nibble.

Let's take an example to demonstrate BCD conversion:-

Decimal : 0 1 2 3

BCD: 0000 0001 0010 0011

Therefore, BCD encoding for number 123 is:

0001 0010 0011

BCD encoded numbers can easily be unveiled by delineating each of the nibbles to a different character. They are very useful for manipulation of numerical data.

5 The Propounded Steganography Algorithm

The propounded algorithm utilizes a video stream for analyzing. In the starting phase, the video is dispersed into frames. Then few frames are selected for embedding data in it. But before implanting the secret data, 2D-DWT is applied on selected frames. Then secret data are encrypted by the secret key, and after that BCD codes are worn for encoding the secret data. Then triple secured secret data are fed to the DWT transformed frames.

5.1 Data Embedding Process

Here, the embedding process of video steganography using BCD codes is explained in the form of steps. The embedding process consists of two parts: First, encoding the secret data with secret key and BCD codes (steps 1–4) and second part is to apply 2D-DWT on selected video frames from a video and then encode the secret data in those frames (steps 6–11).

1. Input the secret message with .txt extension.
2. Apply secret key1 for changing the bit places of the covert message.

Fig. 2 Components of different level DWT decomposition

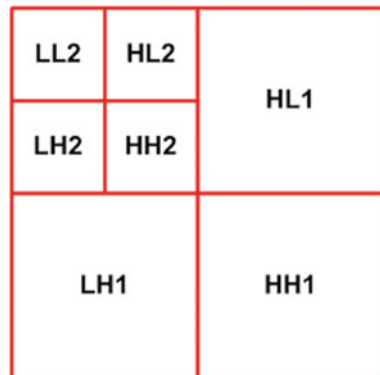
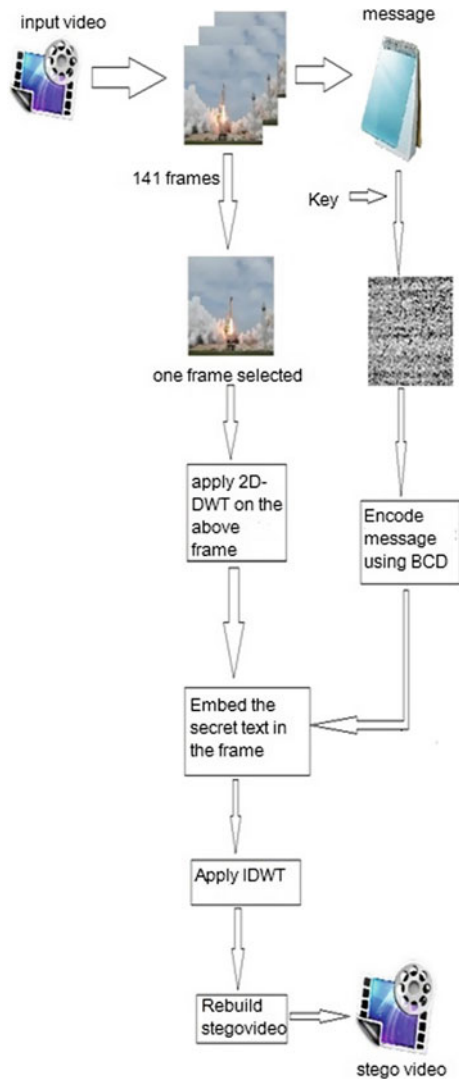


Fig. 3 Embedding process flowchart



3. Transfigure the covert message in a one-dimensional array (1-D).
4. Encode the encrypted secret message with BCD codes.
5. Input the cover video streams.
6. Disperse the video into number of frames.
7. Apply 2D-DWT on the selected video frames.
8. Implant the secret memo into mesial and high frequency coefficients (LH, HL, HH) of the frames.
9. Apply inverse two-dimensional DWT on the video frames.

10. Rebuild the stego frames after inverse DWT.
11. Combine the stego frames to rebuild the stego video for transmission.

The secret key worn in the propounded algorithm is predefined by the sender in the implanting phase. Secret key (key1) is used to change the bit positions of the secret data in order to make it more random and untraceable for eavesdroppers. Then BCD codes are used for encoding the encrypted secret data. BCD encoding provides the triple security to the secret data from the attacks. This improves the collateral and robustness of the propounded algorithm. Thus, the role of BCD codes been used in steganography is clear from the security it provides to the user data from any intruders. The embedding process gives three times more security to the secret data as compared to other techniques. Finally, the embedding process for video steganography is visualized with the help of a block diagram in Fig. 3.

6 Experimental Results and Explanations

In this section, three different videos are used with the file extension of audio video interleave (AVI) and .mp4. The videos have vehicular objects and musical instruments been displayed for a small duration of time. Thus, it was less time consuming in extracting the frames from the particular video and helped in reducing the time complexity.

In order to obtain the experimental results, R2013a version of MATLAB software is used. The pixel resolution of all videos is different with an extraction of 20 frames per second. The shuttle.avi video had a total of 121 frames, viplanedeparture.mp4 video had 337 frames and the xylophone.avi had 141 frames in total. The secret message used is an immense text file. After following the steps of the proposed algorithm, the frames that are extracted from the shuttle.avi video file is shown in the Fig. 4.



Fig. 4 Extracted video frames of shuttle.avi

6.1 Visual Calibre Factor

The foremost hurdle in video steganography is to handle the visual transparency that is the distortion should be fairly small in the stego video. Visual calibre is also known as the impalpability factor that depends on the similarity between the stego carrier image and the original carrier image. A video file is also signified using the authenticity factor also which lies between the resemblance of the extracted secret text and the original secret text. The above parameters can be computed with the help of the quantitative index like mean square error (MSE) and peak signal to noise ratio (PSNR). For the three video files that used the MSE and PSNR values are calculated using the below formulas.

$$MSE = \frac{1}{MN} \sum_{n=1}^M \sum_{m=1}^N [\bar{g}(n, m) - g(n, m)]^2$$

$$PSNR = -10 \log_{10} \frac{MSE}{S^2},$$

where $\bar{g}(n, m)$ is the stego carrier image and $g(n, m)$ is the original carrier image. M and N represent the width and height of the image, S is the maximum pixel value. The comparison between the carrier and stego image frame by frame is shown in Table 1. From the table, it is inferred that there is no possible distortion, thereby reducing the chance of recognizing the presence of secret data.

The propounded algorithm is been applied on four frames of the different video files used. After formulating the steps, the PSNR and MSE value of the red, green and blue planes of the frames are shown in the three tables. Table 2 gives detailed information of PSNR and MSE of shuttle.avi video file. Further, Table 3 shows the PSNR and MSE value of viplanedeparture.mp4 video file and Table 4 depicts the PSNR and MSE value of xylophone.avi video. A plot of the PSNR value for all videos is shown in the Fig. 5.

From the above Table 2, it is inferred that if the PSNR value is high and MSE value is small then the visual quality of the image is compact. The MSE value may be high according to the video file chosen, but it does not strike the visual calibre of the image. Since the MSE value also depends upon length of the text that is embedded in the video file.

Table 1 Comparison between carrier image and stego image







Cover video stream		Stego video stream
		
		

Table 2 PSNR and MSE value of Shuttle.avi

Cover image	Stego image	PSNR (dB)	MSE
Frame6.jpg	Stego.jpg	Red-35.22	Red-19.50
		Green-35.45	Green-18.53
		Blue-35.29	Blue-19.19
Frame9.jpg	Stego1.jpg	Red-42.60	Red-3.56
		Green-42.85	Green-3.37
		Blue-42.56	Blue-3.60
Frame11.jpg	Stego2.jpg	Red-40.45	Red-5.85
		Green-40.56	Green-5.70
		Blue-40.35	Blue-5.99
Frame13.jpg	Stego3.jpg	Red-35.74	Red-17.30
		Green-35.82	Green-16.99
		Blue-35.77	Blue-17.20

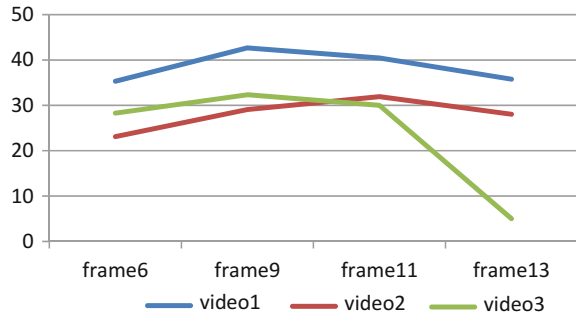
Table 3 PSNR and MSE value of viplanedeparture.mp4

Cover image	Stego image	PSNR (dB)	MSE
Frame6.jpg	Stego.jpg	Red-23.49	Red-290.76
		Green-22.96	Green-328.2
		Blue-22.83	Blue-338.89
Frame9.jpg	Stego1.jpg	Red-29.19	Red-78.19
		Green-29.09	Green-80.13
		Blue-28.96	Blue-82.48
Frame11.jpg	Stego2.jpg	Red-31.76	Red-43.35
		Green-32.04	Green-40.58
		Blue-31.99	Blue-41.09
Frame13.jpg	Stego3.jpg	Red-28.02	Red-102.53
		Green-28.11	Green-100.3
		Blue-28.01	Blue-102.77

Table 4 PSNR and MSE value of xylophone.avi

Cover image	Stego image	PSNR (dB)	MSE
Frame6.jpg	Stego.jpg	Red-29.05	Red-80.83
		Green-28.10	Green-100.5
		Blue-27.65	Blue-111.60
Frame9.jpg	Stego1.jpg	Red-32.82	Red-33.95
		Green-32.41	Green-37.27
		Blue-31.73	Blue-43.61
Frame11.jpg	Stego2.jpg	Red-31.02	Red-51.38
		Green-29.70	Green-69.52
		Blue-29.27	Blue-76.92
Frame13.jpg	Stego3.jpg	Red-28.42	Red-93.44
		Green-27.79	Green-108.2
		Blue-27.32	Blue-120.40

Fig. 5 PSNR values of the three videos



From the above Table 3, it is inferred that the MSE values also depend on the extension of video file and length of the secret message. MSE values are high for the frames of extension .mp4, doesn't mean that stego frames are distorted after embedding secret data in the frames.

In the above Table 4, the MSE value obtained is a bit high which is due to the length of the text that is been embedded in the video file. Rather this increase in the MSE value does not have any effect on the visual quality of the video frame thus making it secure from the unwanted intruders. The PSNR values of the three videos for different frames are shown in the Fig. 5. Video one denoted by blue is shuttle.avi file, and video two in red is for viplanedeparture.mp4. Similarly, the video three file in green is for xylophone.avi. From the below Fig. 5, the PSNR values calculated for the first video shuttle.avi are high and between the range of 35–45 dB. For the other two videos, the PSNR value is been quite small with a range value of 25–35 dB. This shows that PSNR values also depend upon the type of the video file extension chosen that are .avi and .mp4 in this case.

7 Conclusion

In this paper, a highly secure video steganography in the DWT domain rooted on BCD codes has been propounded. The propounded algorithm fragmented the cover video file into frames. Before the embedding process, the secret data are encrypted by the secret key (key1) and then encoded by using BCD codes, in order to enlarge the efficiency and accuracy of the proposed algorithm. The 2D-DWT is applied on the fragmented video frames in the mesial and high frequencies (LL, LH and HH) for implanting data. The main aim of using DWT is to enhance the texture and edges of the carrier video frames after implanting the data in it. This reduces the distortion and noise in the stego frames. The secret key is used to enhance the security of the system. In future work, we would enhance the other factors like implanting payload of the propounded algorithm with respect to the visual calibre factor. Also, we would apply other frequency domain techniques and error detecting and correcting code methods to enhance the security and robustness of the algorithm.

References

1. Eric Cole, *Hiding in Plain Sight: Steganography and the Art of Covert Communication*, Canada: Wiley, 2003.
2. Mennatallah M. Sadek, Amal S. Khalifa & Mostafa G.M. Mostafa, "Video steganography: a comprehensive review," Springer, pp. 1–32, Mar 2014.
3. Prabakaran. G & Bhavani. R, "A modified secure digital image steganography based on discrete wavelet transform," IEEE, pp. 1096–1100, 2012.
4. R. Zhang, et al., "Fast BCH Syndrome Coding for Steganography," in *Information Hiding*. vol. 5806, S. Katzenbeisser and A.-R. Sadeghi, Eds., ed: Springer Berlin Heidelberg, pp. 48–58, 2009.
5. Ramadhan J. Mstafa and Khaled M. Elleithy, "A high payload video steganography algorithm in DWT domain based on BCH codes (15, 11)," IEEE, pp. 1–9, Apr 2015.
6. Ramadhan J. Mstafa and Khaled M. Elleithy, "A highly secure video steganography using hamming codes (7, 4)," IEEE, pp. 1–6, 2015.
7. Ramadhan J. Mstafa and Khaled M. Elleithy, "A video steganography algorithm based on kanade-lucas-tomasi tracking algorithm and error correcting codes," Springer, vol. 75, issue 17, pp. 10311–10333, Sept 2016.
8. R. O. El Safy, H. H. Zayed & A. El Dessouki, "An adaptive steganographic technique based on integer wavelet transform," IEEE, pp. 111–117, 2009.
9. S. Faragallah, "Efficient video watermarking based on singular value decomposition in the discrete wavelet transform domain," *AEU - International Journal of Electronics and Communications*, vol. 67, pp. 189–196, 2013.

Development of Multi-verse Optimizer (MVO) for LabVIEW

Kumar Vivek, Mehta Deepak, Chetna, Jain Mohit, Rani Asha and Singh Vijander

Abstract LabVIEW is a versatile tool with various inbuilt toolkits to perform various measurement and control tasks. Hence, it is used in almost every field of engineering. However, it does not provide enough contribution in the field of optimization which is the major concern. It has only one optimizer based on differential evolution (DE) algorithm. Even though DE is a very effective global optimization technique, but its performance highly depends on parametric settings. DE contains high number of user-defined parameters; therefore, it becomes cumbersome for user to obtain best parametric settings for a given optimization problem. Recently, several nature-inspired algorithms are developed with reduced number of parametric settings to obtain the optimum solutions while solving complex black box optimization problems. Hence, to update the LabVIEW in the field of optimization, there exists a need of continuous development of other efficient global optimizers. Multi-verse optimizer (MVO) is considered as one of the latest but effective nature-inspired optimization algorithm with only two user-defined parameters. In this paper, MVO toolkit is developed for LabVIEW

K. Vivek (✉) · M. Deepak · Chetna · J. Mohit · R. Asha · S. Vijander
Instrumentation and Control Engineering Division, NSIT, Azad Hind Fauz Marg, Sec-3,
110078 Dwarka, New Delhi, India
e-mail: viv2011pratibha@gmail.com

M. Deepak
e-mail: dmehta9911@gmail.com

Chetna
e-mail: chetnasingh9395@gmail.com

J. Mohit
e-mail: nsit.mohit@gmail.com

R. Asha
e-mail: ashansit@gmail.com

S. Vijander
e-mail: vijaydee@gmail.com

platform and the efficiency of the proposed toolkit is validated on a test bed of five standard benchmark functions. The statistical analysis of results shows that the MVO is far better in solving optimization problems as compared to DE.

Keywords Multi-verse optimizer · LabVIEW · Optimization

1 Introduction

LabVIEW (Laboratory Virtual Instrument Engineering Workbench) is a well-known software platform used for measurement and automation. It supports visual or graphical programming environment called as G programming. Scientists and researchers use G programming environment as their primary tool in a wide range of applications from design to deployment of machines, remote monitoring, embedded systems, and other complex systems. Although LabVIEW offers several inbuilt toolkits which make the task of programming easy, but there is a scarcity of optimizers. It consists of only one global optimization toolkit which is differential evolution (DE) [1]. Over the past few years, a continuous development has been observed in this field and many solutions have been proposed in the form of LabVIEW toolkits like Grey Wolf Optimizer [2], Cuckoo Search algorithm [3], Bat algorithm [4], and Ant Lion Optimizer [5].

Due to the successful application of nature-inspired optimization algorithms in solving complex optimization problems, recently various optimization algorithms have been proposed such as ideal gas molecular movement algorithm [6], natural forest regeneration algorithm [7], efficient chaotic water cycle algorithm [8], improved monarch butterfly optimization algorithm [9] and multistage Krill Herd algorithm [10]. Multi-verse optimizer (MVO) is another innovative but effective nature-inspired optimization algorithm developed by Mirjalili et al. [11] with only two user-defined parameters. The main inspiration behind this algorithm is based on cosmological concepts. Universal phenomenon is always a good topic of research for cosmologists. MVO involves three main cosmological phenomena (a) white hole (b) black hole, and (c) wormhole. The structure of MVO is very easy to implement and user-friendly (less number of parametric settings). This algorithm is successfully applied in multilevel thresholding selection [12] and parameter extraction of photovoltaic generating units [13]. The present work is focused on development of an efficient as well as accurate optimization toolkit in LabVIEW based on multi-verse optimization algorithm. The brief introduction of MVO and its implementation in LabVIEW platform are discussed in the subsequent sections.

2 MVO Description

MVO takes inspiration from multi-verse theory of physics according to which multi-verse symbolizes the opposite of universe. According to this theory, existence of other universes is assumed apart from our own universe in which we all are living. The theory suggests that multiple universes not only interact with each other but also collide sometimes [11]. Apart from this, every universe is having its own inflation rate which defines its rate of expansion through space. Similar to other nature-inspired population-based algorithms, MVO also performs the search process in two ways, i.e., exploration versus exploitation. The cosmological concepts of black hole and white hole explore the search space while wormhole assists in exploiting the search space.

MVO performs the optimization based on the following rules [11]:

1. High inflation rate refers that there is high probability of white hole's existence and less probability of black hole's existence.
2. Objects are sent through white holes by the universes having high inflation rate while objects are received through black holes to the universes with less inflation rate.
3. Random movement of objects may be considered in all universes through wormholes towards the best universe irrespective of their inflation speed.

3 Development of MVO Toolkit

Development of MVO toolkit consists of various virtual instruments (VIs) which perform the following operations:

- I. Positions of universes are randomly initialized.
- II. Calculating inflation rate of each universe.
- III. Calculation of wormhole existence probability (WEP) as well as travelling distance rate (TDR) constants.
- IV. Calculation of best universe and best inflation rate.
- V. Updating the position of new universe.

The above operations are repeated from Step (II) till the desired result obtained. Each implemented virtual instrument (VI) with its corresponding function is discussed in the following sections.

3.1 *Generate Initial Universes.VI*

The function of this VI (Fig. 1) is to generate random initial universes (i.e., random initial population) on the basis of user-defined parameters like upper bound (UB),

Fig. 1 Generate initial universes.VI



lower bound (LB), dimensions (dim), and number of universes (Ns) using Eq. (1) defined as follows:

$$X = \text{Rand} \times ((\text{UB} - \text{LB}) + \text{LB}) \tag{1}$$

3.2 Inflation Rate.VI

This VI calculates the inflation rate (or fitness) of each universe with respect to the objective function to be optimized. Hence, it needs two inputs, first one is a two-dimensional array of search agents and other is objective function needed to be optimized. On the basis of these two inputs, VI gives one-dimensional array which contains the inflation rate corresponding to each position of the search agent. The implemented inflation rate VI is illustrated in Fig. 2.

3.3 Calculation of WEP and TDR.VI

This VI (Fig. 3) calculates wormhole existence probability (WEP) and travelling distance rate (TDR). WEP is increased linearly over the course of iterations for emphasizing exploitation. For calculating WEP, following equation is used:

$$\text{WEP} = \text{WEP}_{\text{Min}} + i \times \left(\frac{\text{WEP}_{\text{Max}} - \text{WEP}_{\text{Min}}}{i_{\text{max}}} \right) \tag{2}$$

where WEP_{Min} and WEP_{Max} are constants having values 0.2 and 1, respectively, for the present work, i denotes current iteration and i_{max} is the maximum number of iterations defined by the user. The travelling distance rate (TDR) is decreased over the iterations to have more precise local search around the best universe (exploitation). For calculating TDR, following equation is used:

$$\text{TDR} = 1 - \frac{i^{1/6}}{i_{\text{max}}^{1/6}} \tag{3}$$

Fig. 2 Inflation Rate.VI



Fig. 3 WEP_TDR.VI



3.4 Elitism.VI

This VI (Fig. 4) keeps the record of best inflation rate and best universe. Best universe is obtained by transferring the object from the universe with high inflation rate towards the universe of low inflation rate through white hole. The objects are transferred till the inflation rate reaches the best then only the best universe with the best inflation rate is obtained.

3.5 Position Updating.VI

This VI (Fig. 5) updates the position of the universes. For this purpose, the position of the sorted universe is compared with the position of random universe and then this VI updates the best solution found by providing an array of updated universe. It takes few more input parameters to perform the task such as WEP, TDR, and sorted inflation rate.

Fig. 4 Elitism.VI

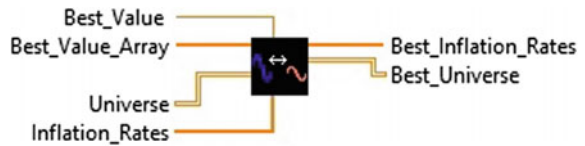


Fig. 5 Position updating.VI



4 Results and Discussion

The proposed MVO toolkit is developed in LabVIEW™ version 14.0 on PC having 64-bit operating system and Intel® Core™ i3-4005U processor operated on 1.70 GHz frequency with 4 GB RAM. The front panel of the designed toolkit is shown in Fig. 6 while its corresponding block diagram with valid connections of all Sub-VIs is shown in Fig. 7.

To test the effectiveness of the proposed toolkit, a comparative analysis of DE and MVO is performed on a test bed of five standard test functions. These functions have different characteristics such as unimodal (U), multimodal (M), separable (S) and non-separable (N). To have a fair comparison, both the algorithms are tested

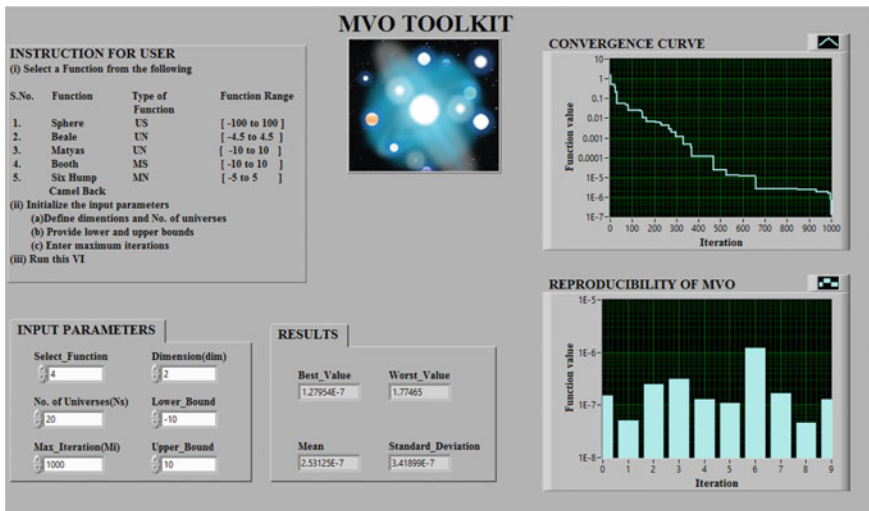


Fig. 6 Front panel of MVO toolkit

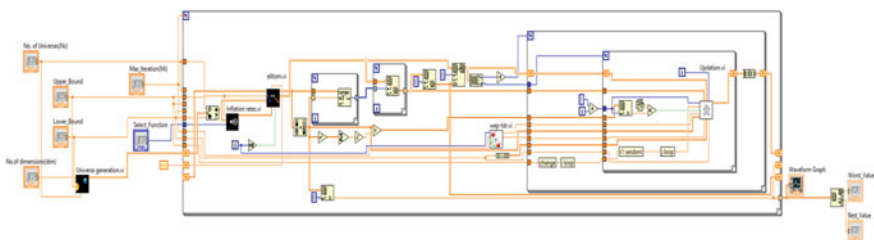


Fig. 7 Block diagram of MVO toolkit

on each considered benchmark function for ten independent trials with maximum 1000 iterations and fixed number of search agents =20. The best, worst, mean and standard deviation obtained during this statistical experimentation are recorded in Tables 1 and 2. It is observed from the results that overall performance of MVO is much better than DE while solving numerical optimization problems. Figure 8 represents the perspective view of multimodal booth function. Figure 9 shows the convergence plot of MVO and DE while solving this complex multimodal function. It is clear from Fig. 9 that DE got trapped in local minima for Booth function while MVO attained global minima. Therefore, MVO is found better for optimization in the LabVIEW environment in comparison with DE.

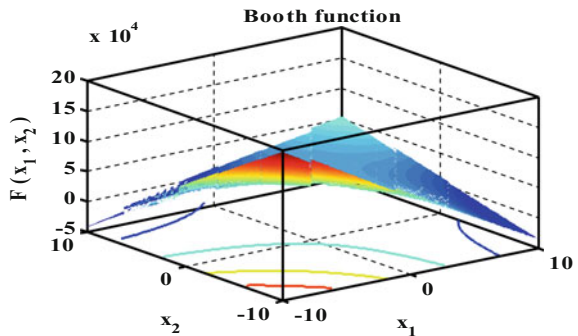
Table 1 Comparison of best and worst of MVO and DE for benchmark functions

Function	Type	Dim	Global min	Best		Worst	
				DE	MVO	DE	MVO
Sphere	US	2	0	0.034852	1.2027E-5	18.964	28.83
Beale	UN	2	0	0.000450	1.7342E-8	3.8274	7.1900
Matyas	UN	2	0	4.0908E-5	3.3624E-8	0.7706	0.1986
Booth	MS	2	0	0.000113	7.7043E-7	11.7287	19.9976
Six Hump Camel	MN	2	-1.03163	-1.0314	-1.03163	-0.08544	0.81226

Table 2 Comparison of mean and standard deviation of MVO and DE for 10 runs

Function	Mean		Standard deviation	
	DE	MVO	DE	MVO
Sphere	0.0365	9.1369E-6	0.03626	9.5502E-6
Beale	0.00033	0.2286	0.00038	0.3681
Matyas	0.00011	1.2650E-8	8.5887E-5	1.1411E-8
Booth	0.00198	3.6926E-7	0.00231	2.7917E-7
Six Hump Camel	-1.03059	-1.03163	0.00137	2.4749E-8

Fig. 8 Perspective view of multimodal booth function



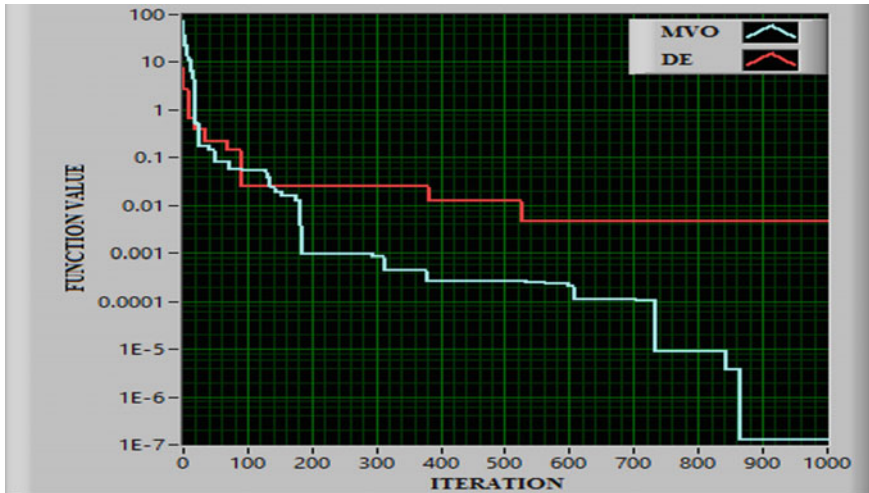


Fig. 9 Optimization of DE and MVO

5 Conclusion

The motive of this research work is to develop a toolkit in LabVIEW which can efficiently solve black box optimization problems. For this purpose, a recently proposed optimization algorithm named as MVO is successfully implemented in LabVIEW. The performance of MVO toolkit is validated on five standard benchmark functions, and achieved results are compared to DE. It is concluded from comparative analysis that MVO is much faster in convergence with sufficient level of accuracy as compared to the existing DE.

References

1. Storn, R. and Price, K., 1997. Differential evolution—a simple and efficient heuristic for global optimization over continuous spaces. *Journal of global optimization*, 11(4), pp. 341–359 (1997).
2. Gupta, P., Rana, K. P.S., Kumar, V., Mishra, P., Kumar, J. and Nair, S.S., Development of a Grey Wolf Optimizer Toolkit in LabVIEW™. In *IEEE International Conference on Futuristic Trends on Computational Analysis and Knowledge Management (ABLAZE)*, pp. 107–113 (2015).
3. Mishra, P., Kumar, V., Rana, K.P.S., Nair, S.S. and Kumar, J., Cuckoo search implementation in LabVIEW. In *IEEE International Conference on Computational Techniques in Information and Communication Technologies (ICCTICT)*, pp. 331–336 (2016).
4. Thakur, K.S., Kumar, V., Rana, K.P.S., Mishra, P., Kumar, J. and Nair, S.S., Development of Bat Algorithm Toolkit in LabVIEW™. In *IEEE International Conference on Computing, Communication & Automation (ICCCA)*, pp. 5–10 (2015).

5. Gupta, S., Kumar, V., Rana, K.P.S., Mishra, P. and Kumar, J., Development of Ant Lion Optimizer toolkit in LabVIEW™. In IEEE International Conference on Innovation and Challenges in Cyber Security (ICICCS-INBUSH), pp. 251–256 (2016).
6. Varae, H. and Ghasemi, M.R., Engineering optimization based on ideal gas molecular movement algorithm. *Engineering with Computers*, 33 (1), pp. 71–93 (2017).
7. Moez, H., Kaveh, A. and Taghizadieh, N., Natural Forest Regeneration Algorithm: A New Meta-Heuristic. *Iranian Journal of Science and Technology, Transactions of Civil Engineering*, 40(4), pp. 311–326 (2016).
8. Heidari, A.A., Abbaspour, R.A. and Jordehi, A.R., An efficient chaotic water cycle algorithm for optimization tasks. *Neural Computing and Applications*, 28 (1), pp. 57–85 (2017).
9. Wang, G.G., Deb, S., Zhao, X. and Cui, Z., A new monarch butterfly optimization with an improved crossover operator. *Operational Research*, pp. 1–25 (2016).
10. Wang, G.G., Gandomi, A.H., Alavi, A.H. and Deb, S., A multi-stage krill herd algorithm for global numerical optimization. *International Journal on Artificial Intelligence Tools*, 25 (02), p. 1550030 (2016).
11. Mirjalili, S., Mirjalili, S.M. and Hatamlou, A., Multi-verse optimizer: a nature-inspired algorithm for global optimization. *Neural Computing and Applications*, 27 (2), pp. 495–513 (2016).
12. Wangchamhan, T., Chiewchanwattana, S. and Sunat, K., Multilevel thresholding selection based on chaotic multi-verse optimization for image segmentation. In 13th IEEE International Joint Conference on Computer Science and Software Engineering (JCSSE), pp. 1–6 (2016).
13. Ali, E.E., El-Hameed, M.A., El-Fergany, A.A. and El-Arini, M.M., Parameter extraction of photovoltaic generating units using multi-verse optimizer. *Sustainable Energy Technologies and Assessments*, 17, pp. 68–76 (2016).

Edge Detection Using Fuzzy Logic (Fuzzy Sobel, Fuzzy Template, and Fuzzy Inference System)

Rachita Katoch and Rosepreet Kaur Bhogal

Abstract Prime edges in a digital image contain useful information that can be utilized in the processing of digital images. Edges of an image can be applied in disjointing of images, finding objects in images, for image registration, etc. Edge detectors are the tools that find out all the edge pixels that are present in a digital image. Edges are the points in an image where the intensity level changes very sharply from one pixel to other pixel. In this research paper, edge detection using three different methods of fuzzy logic has been done. The three different methods of fuzzy logic for edge detection are Sobel fuzzy edge detector, template fuzzy edge detector and fuzzy inference system. A comparison has been made among these three methods at different values of threshold. The result shows that the fuzzy inference method gives more good results than other two methods under all outlines.

Keywords Edge detection · Sobel · Template · Fuzzy inference system
Threshold

1 Introduction

Edges provide a backbone in image processing and in many applications of image processing. Edges provide an outline of the object in an image. In a digitized image, edges are present on those pixels where disruption exists for intensity value. These disruptions have their advantageous to calculate content, orientation, deepness, and characteristics of surface in a digital image [1]. The pixels on an edge are called edge points. Most edges are unique in space, i.e., their position and orientation

R. Katoch (✉) · R.K. Bhogal
School of Electronics and Electrical Engineering, Lovely Professional University,
Jalandhar, India
e-mail: rachitakatoch123@gmail.com

R.K. Bhogal
e-mail: rosepreetkaur12@gmail.com

remain the same in space when viewed from different points. When an edge is detected, the unnecessary details are removed, and keep only the important structural information.

Edge detectors are engaged to an image in order to cut down the data that is less concerning with processing, while secure the necessary information of an image. In today's world, edges detector plays important role in many areas, for example in medicine geography, military, robotics, meteorology, and pattern recognition systems [2–5].

The edge detectors tools are grouped into two categories: one is lean on gradient and second category is lean on Laplacian. In the first category, first of all, the gradient magnitude is calculated along x - and y -direction using smoothing filter. Then, the calculated gradient magnitude is used to figure out the location of edge pixels of edges in an image. Thus, first category works on first derivative. Examples are Sobel, Prewitt, and Robert, etc. In the second category, first of all, the second-order derivative is calculated of the image and then finds the zero crossing in the second derivative. Then, on the basis of zero-crossing edges are detected.

2 Literature Survey

In 1993, fuzzy logic provides linguistic statements in natural language that can be used to represent important data of the image that can further utilized in image rectification, image intensification, and for finds out edge pixels in an image. The proposed method can be utilized by any operator to accomplish the task without any strong background knowledge [6].

In 2011, a paper given a simple method of fuzzy based on thresholding that gives better result than the conventional algorithm such as Sobel, Canny, Robert, Prewitt. Result of simulation shows that the fuzzy logic that leans on thresholding for figure out edge pixels gives preferable results than traditional schemes. Although the result is better, computational complexity has increased [7]. In 2011, a simple edge detection and fast calculation method can be achieved using fuzzy rules. The maximum entropy principle is used for the adjustment of parameters [8]. The proposed method does not require any filtering process because the given method can detect edge pixels from any digitized image that is affected by noise.

In 2008, a new type of edge detector tool that lean on fuzzy has implemented that made use of thirty-two rules for figure out edge pixels in scanned image of head. A comparison is executed of the proposed technique and regular techniques, and result shows that the suggested technique has less computational complexity as analogy to other existing techniques [9].

In 1998, a new type of edge detection method is used that can detect edges in any type of digital image that is corrupted by noise. The proposed method used fuzzy logic approach in order to figure out edge pixels from any image without experience any affect from the noise that is present in an image. The outcome displays that the proposed technique shows more preferred outcome from

traditional methods on the basis of more good edge pixels and affectability of noise. In this the proposed method which is leaning on fuzzy, when a noise pulse is detected it reconstruct back to original data with the help of fuzzy reasoning [10].

In 2008, a new type of edge detection method has been proposed that combines fuzzy logic [11, 12] with cellular learning automata (CLA) [13–16]. In the proposed method, first of all, edges are detected by fuzzy logic, and then CLA is used to enhance the detected edges because CLA possess repeatable and neighborhood considering nature. In this paper, MATLAB is used to prepare the algorithms and their results.

3 Various Techniques for Edge Detection

Edge detection algorithm plays very important role in today's world, and it becomes an important part of image processing. Edge detection algorithm preserves important information of an image and removes unwanted information, thus deflate the chunk of material to be progress. Multitudinous edge detectors algorithms are maturate in order to find the perfect edge detector. The edge detection techniques can be segregate into two forms such as first technique gamble on gradient and second technique gamble on Laplacian in order to figure out edge pixels.

3.1 Edge Detection Lean on Gradient

In the gradient-based edge detection, first of all, the gradient magnitude is calculated along x - and y -direction using smoothing filter. Then, the calculated gradient magnitude is used to resolve the of edge pixels in an image. Thus, the first technique utilized first-order derivative of an image. Example of gradient-based method is Sobel, Prewitt, Robert, etc.

3.2 Edge Detection Lean on Laplacian (Zero Crossing)

In the second technique that lean on Laplacian-based methods, first of all, the second-order differentiation is enumerate of the image, and after that zero junction is enumerate from the second-order differentiation. Then, on the basis of zero-crossing edges are detected. The example of Laplacian-based method is Laplacian of Gaussian (LOG).

The gradient-based method is more societal than Laplacian-based method. In present, a large count of edge detector techniques is reachable, but there is no solitary technique is reachable for figure out edge pixels that realize robustly in whole feasible image ambience. Diversified edge detector techniques are passed

down to get down edge pixels like Sobel, Krisch operators which are exercised on peculiar images. But, the collection of edge detector that should exploit is gamble in on the properties of images like delicacy of noise, speed, delicacy of assimilation, and potency.

4 Applied Algorithms

4.1 Sobel Fuzzy Edge Detector

In fuzzy Sobel method, first of all, gradient in two directions using Sobel operator has been calculated and after that conjoins the gradients in deuce directions, i.e., x- and y-direction to get the finishing gradient. In this approach, edge pixels are reckoned by using different values of threshold that gamble on the user.

In Sobel fuzzy technique, the image is split into two different sectors. If the gray level value of the pixels having more diversity than their neighborhood pixels, then those pixels of the image are considered as edge pixels, and if gray level value of the pixels having less diversity with their neighborhood pixels, then those pixels of the image are considered non-edge pixels. The outline of the complete edge of the image is calculated by using threshold scruples, i.e., lesser level (LL), higher level (HL), lesser limit (LL), and higher level (HL) [22].

With the help of the considered threshold values, edge pixels and non-edge pixels are calculated. The gradient of the processing image which is denoted by $g(i, j)$ is calculated with the help of Sobel operator. The fuzzy logic (FL) method has been used to derive the outcomes of the suggested technique that is leaning on fuzzy in order to figure out edge pixels. Equation (1) defines the fuzzy rules

$$\begin{aligned}
 p(i, j) &= 255, \text{ if } g(i, j) \geq \text{HL} \\
 &= 0, \text{ if } g(i, j) \leq \text{LL} \\
 &= g(i, j) \cdot \max((\mu_{\text{SFR}}(i, j), \mu_{\text{EFR}}(i, j)))
 \end{aligned} \tag{1}$$

where μ_{SFR} is membership function (MF), μ_{EFR} is the MF of the image edge region, $g(i, j)$ is calculated gradient, and $p(i, j)$ is the calculated edge pixel.

4.2 Template Fuzzy Edge Detector

In template fuzzy edge detection, first of all, a set of templates edge images (TEI) is made, and after that convolution has been done of all these TEI with the original image. The size of the TEI is less than that of the image. In initial step, in order to get the pixels value between zero and one, normalized the values of intensity of every pixels. The total TEI that has been designed is designated as “ n ,” and all TEI

help to determine all the position of edge pixels that are present in the image. Every TEI is taken on the image at a particular position and on the other image that is denoted by "S." The size of the image window should be similar to the size of the template [21]. In order to check the presence of an edge pixel at a particular position in an image, comparison is performed between the pixels of image and templates edge images.

The templates for fuzzy method are as follow

$$\begin{bmatrix} a & a & a \\ b & b & b \\ c & c & c \end{bmatrix} \begin{bmatrix} a & b & c \\ a & b & c \\ a & b & c \end{bmatrix} \begin{bmatrix} a & c & b \\ b & a & c \\ c & b & a \end{bmatrix}$$

Thus, one can make more templates just by shifting the elements of matrix.

Place the templates of edge image on the complete image, i.e., at each point on the normalized image place the center of each template. Compute the divergence value of fuzzy between the template and every elements of the original image and choose the minimum value.

Consider the position of pixel at location (x, y) in the TEI be (x_T, y_T) , and the relative position in the original image be (x_I, y_I) . After that the measurement of homogeneity between the original image and all the pixels of template is computed by using Eq. 2.

$$H_T(x, y) = 1 - |\text{pixel}_I(x_I, y_I) - \text{pixel}_T(x_T, y_T)| \tag{2}$$

where $\text{pixel}_I(x_I, y_I)$ is the location of pixel for the original image, and $\text{pixel}_T(x_T, y_T)$ is the location of pixel for the template.

Similarly, for all the templates, the same method has been used. With the guidance of a normal max operation, the similarity measures of all the templates are combined together for finding the existence of edges for the image and the template.

$$H(x, y) = \max(H_T(x, y)), T = 0, 1, 2, \dots, n \tag{3}$$

where n = number of templates.

In order to show the best position of the presence of edge pixels, the resultant image has been operated using threshold method. Thus, all the values that deceit down the threshold is considered as zero, and other values that lie above the threshold value are considered as 1.

4.3 Detection of Edge Using Fuzzy Inference System (FZYIFSM)

FZYIFSM is a technique that takes input value and gives output count on the rules interpret by the user. With the help of editors and viewers of GUI present in the

toolbox of FZYIFSM, one can make the rules, denominate MF, and study the performance of a FZYIFSM. One can form the FZYIFSM with the help of GUI tool or command line function. The implemented algorithm is

Step 1 Import the image into MATLAB.

Step 2 Convert the image into gray scale image, so we can deal with a two-dimensional instead of a three-dimensional array.

Step 3 Convert image into double-precision data.

Step 4 Scale the image, so that its elements are in the $[0, 1]$ range.

Step 5 Obtain image gradients in the x-axis and y-axis. Take the image gradients as an input to FIS and take a Gaussian membership function with zero mean for each input. If the gradient value for a pixel is 0, then it comes under zero membership function having a degree of 1.

5 Comparison of Edge Detection

To apply these three algorithms, MATLAB tool has been used.

5.1 The Result of Sobel Fuzzy Edge Detector

See Figs. 1 and 2.

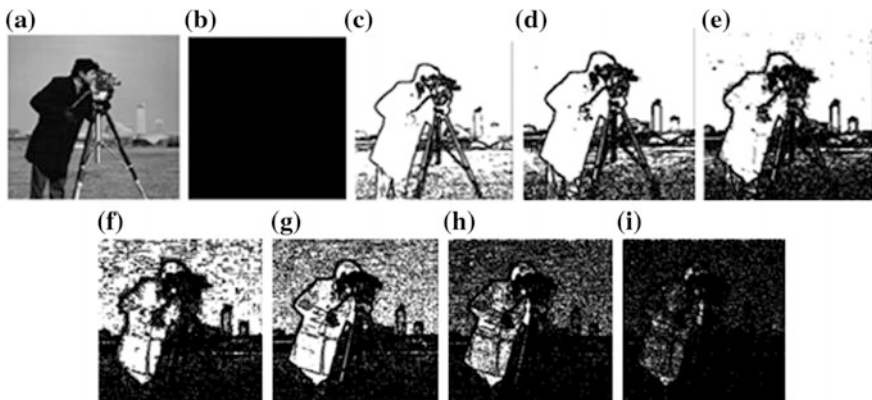


Fig. 1 a Original image, b threshold = 0.00, c $T = 0.01$, d $T = 0.02$, e $T = 0.04$, f $T = 0.09$, g $T = 0.10$, h $T = 0.20$, i $T = 0.50$



Fig. 2 a Original image, b threshold = 0.00, c T = 0.01, d T = 0.02, e T = 0.04, f T = 0.09, g T = 0.10, h T = 0.20, i T = 0.50

5.2 The Result of Fuzzy Template-Based Edge Detector

See Figs. 3 and 4.

5.3 The Result of Fuzzy Inference System

See Figs. 5 and 6.

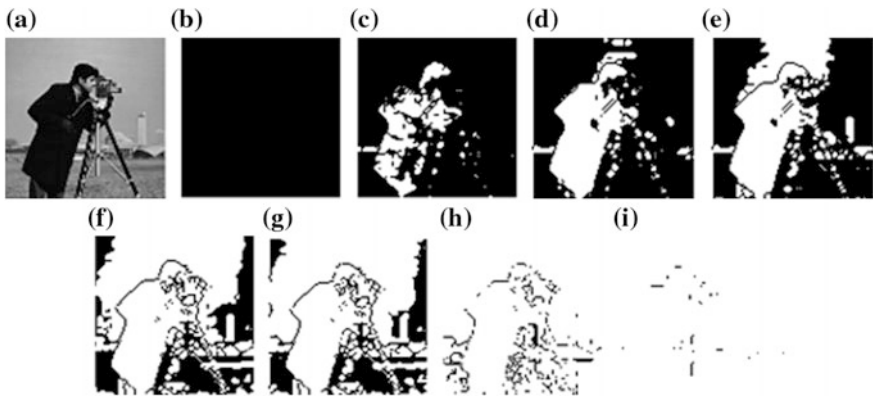


Fig. 3 a Original image, b threshold = 0.00, c T = 0.01, d T = 0.02, e T = 0.04, f T = 0.09, g T = 0.10 h T = 0.20, i T = 0.50

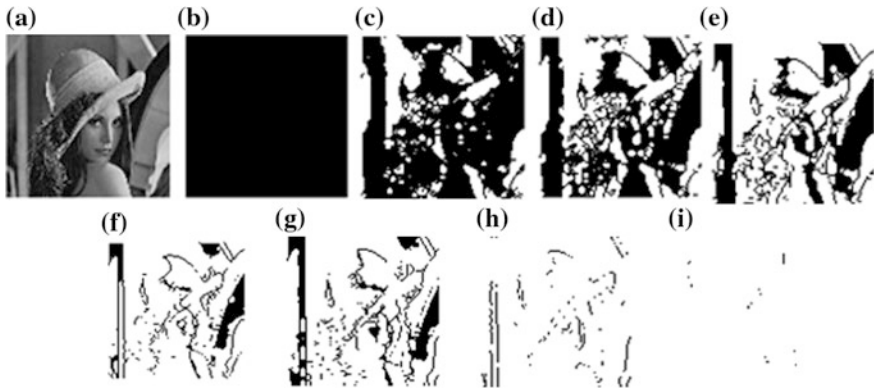


Fig. 4 a Original image, b threshold = 0.00, c T = 0.01, d T = 0.02, e T = 0.04, f T = 0.09, g T = 0.10, h T = 0.20, i T = 0.50

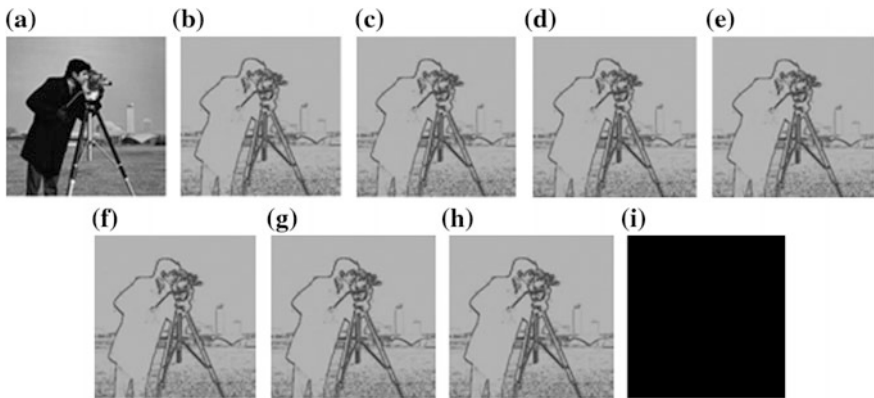


Fig. 5 a Original image, b threshold = 0.00, c T = 0.01, d T = 0.02, e T = 0.04, f T = 0.09, g T = 0.10, h T = 0.20, i T = 0.50

6 Results and Discussions

The experiment has been done by applying three different methods of fuzzy logic on two images, i.e., Lenna and Cameraman images, and edges are detected. The results obtained by Sobel fuzzy edge detector are given in Figs. 1 and 2. In Figs. 3 and 4, the edges detected by fuzzy template-based edge detector are given. Figures 5 and 6 show, the result obtained by fuzzy inference system. Sobel fuzzy edge detector gives best result at 0.01, and above 0.01 the result is getting poor. Fuzzy template-based edge detector gives best result at 0.09 values of threshold, and below 0.09 the result is not good. But, fuzzy inference system gives best result at all the values of threshold. Table 1 shows total number of edges at different values of

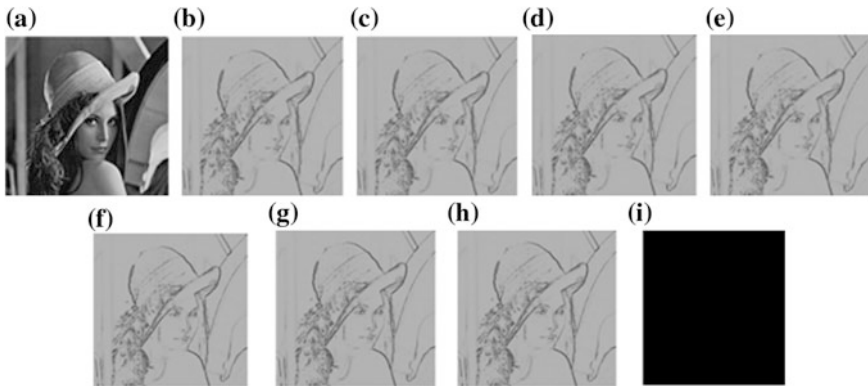


Fig. 6 a Original image, b threshold = 0.00, c T = 0.01, d T = 0.02, e T = 0.04, f T = 0.09, g T = 0.10, h T = 0.20, i T = 0.50

Table 1 Total edges at different values of threshold

Threshold	Algorithm		
	Sobel fuzzy	Template fuzzy	Fuzzy Inference System
0.00	0	0	64,700
0.01	64,674	12,321	64,721
0.02	64,000	13,231	64,724
0.04	60,000	14,000	64,731
0.09	30,000	64,000	64,727
0.10	28,384	64,531	64,783
0.20	20,321	44,689	64,798
0.50	11,573	135	0

The *bold* values show the maximum number of edges detected using particular algorithm at a different threshold

threshold for three algorithms. In table, fuzzy inference system gives maximum value of edges for all threshold values.

Thus, fuzzy inference technique is supreme beyond all techniques, because fuzzy inference algorithm can preserve the purity of proven information. Fuzzy inference system also certifies exactness of locality of the image.

Figure 7 shows graph for Sobel fuzzy edge detector. Graph shows that for threshold 0.01 the total number of edges is maximum, but as threshold value increases number of edges get reduced. From 0.05 to 0.10, the graph reduced sharply. Figure 8 shows graph for fuzzy template-based edge detector, and graph shows at 0.09 threshold total number of edges is maximum, but after 0.09 graph reduced sharply which shows that with increase in threshold the total number of edges get reduced, and at 0.5 there is minimum number of edges. Figure 9 shows graph for fuzzy inference system, and graph shows that from threshold value 0.00

Fig. 7 Graph of Sobel fuzzy

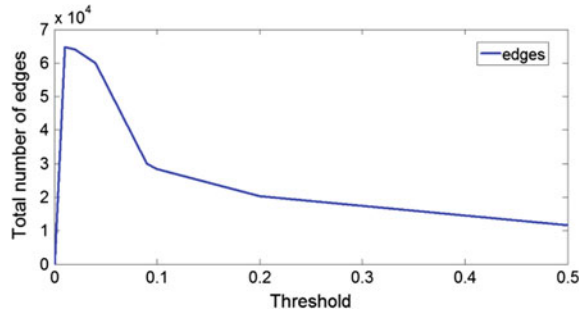


Fig. 8 Graph of fuzzy template

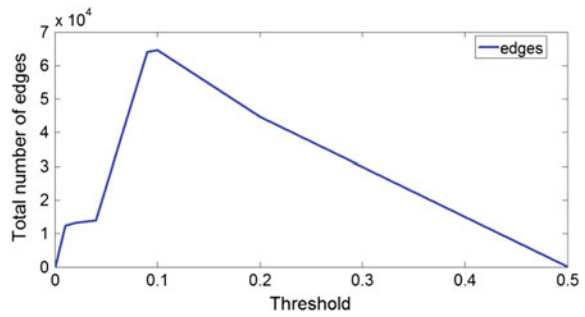
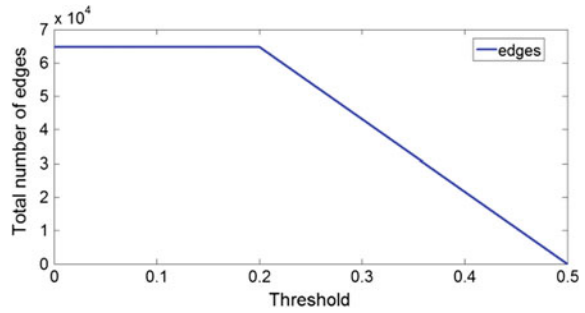


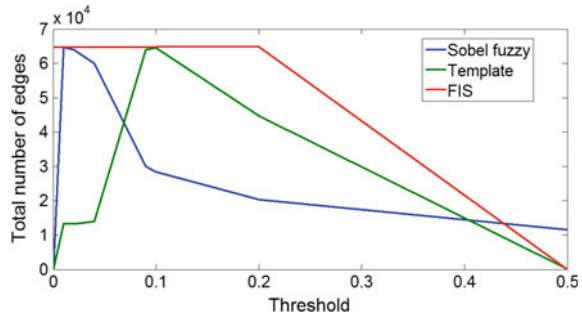
Fig. 9 Graph of fuzzy inference system



to 0.20 the total number of edges is maximum, but above 0.20 value of threshold edges get reduced.

Figure 10 shows comparison of all the three methods. In this graph, the FZYIFSM system gives plentiful edges for all threshold values. Sobel fuzzy edge detector gives best result at 0.01, and above 0.01 the result is getting poor. Fuzzy template-based edge detector gives best result at 0.09 values of threshold, and below 0.09 the result is not good.

Fig. 10 Comparison of three methods



7 Conclusions and Future Scope

In this paper, three different edge detection methods have been applied using fuzzy logic. These three methods are very effortless and short but capable to shorten the theory of artificial intelligence and in transformation of images. The algorithms have been developed in MATLAB environment. The three fuzzy rule-based algorithms recover all edges from the image. The three algorithms applied in this paper can be utilized in numerous areas. At the end, comparisons are elevated for all the three techniques.

FZYIFSM is supreme beyond all techniques, as FZYIFSM can preserve the purity of proven information. Fuzzy inference can certify exactness of locality of images. Further, the FIS method has less computational complexity than the fuzzy template and fuzzy Sobel methods and thus takes less time for edge detection. In future work, the techniques applied in this paper can be utilized by other intelligent methods like artificial neural network, genetic algorithm, etc. Also within the fuzzy logic technique, a modified version of fuzzy system, i.e., a type-2 fuzzy system can be used to get better results.

References

1. S.N. Sivanandam, S. Sumathi and S.N. Deepa, "Introduction to Fuzzy Logic using MATLAB," *Springer*, Berlin, 2007, pp. 2.
2. T. Shimada, F. Sakaida, H. Kawamura, and T. Okumura, "Application of an edge detection method to satellite images for distinguishing sea surface temperature fronts near the Japanese coast," *Remote Sensing of Environment*, vol. 98, no. 1, pp. 21–34, 2005.
3. A. A. Goshtasby, 2-D and 3-D Image Registration: for Medical, Remote Sensing, and Industrial Applications. 2005, pp. 21–34, 2005.
4. A. Kazerooni, A. Ahmadian, N. D. Serej, H. Saberi, H. Yousefi, and P. FarniaSerej, H. Saberi, H. Yousefi, and P. Farnia, "Segmentation of brain tumors in MRI images using multi-scale gradient vector flow," 2011, pp. 7973–7976.
5. B. Siliciano, L. Sciacicco, L. Villani, and G. Oriolo, *Robotics: Modelling, Planning and Control*. 2010, pp. 415–418.

6. Ching-Yu Tyan and Paul P. Wang, "Image Processing—Enhancement, Filtering and Edge Detection Using the Fuzzy Logic Approach," IEEE, pp. 600–605, 1993.
7. Mehul Thakkar, Prof. Hitesh Shah, "Edge Detection Techniques Using Fuzzy Thresholding," IEEE, pp. 307–312, 2011.
8. TALAI Zoubir "A Fast Edge Detection Using Fuzzy Rules," IEEE, pp. 1–5, 2011.
9. Fabrizio Russo "Edge Detection in Noisy Images Using Fuzzy Reasoning," IEEE, pp. 369–372, 1998.
10. S. K. Pal, R. A. King, "Image Enhancement Using Fuzzy Sets," Electronics Letters, Vol. 16, pp. 376–378, 1980.
11. Abdallah A. Alshennawy, and Ayman A. Aly, "Edge Detection in Digital Images Using Fuzzy Logic Technique" World Academy of Science, Engineering and Technology 51, pp. 178–186, 2009.
12. Saman Sinaie, Afshin Ghanizadeh, Siti Mariyam Shamsuddin, "A Hybrid Edge Detection Method Based on Fuzzy Set theory and Cellular Learning Automata." International Conference on Computational Science and Its Applications, ICCSA. IEEE Computer Society, pp. 208–214, 2009.
13. Dhiraj kumar Patel and Prof. S. A. More, "An Enhanced Approach for EDGE Image Enhancement using Fuzzy Set Theory and Cellular Learning Automata(CLA)", World Journal of Science and Technology, pp. 158–162, 2012.
14. P. Jebaraj Selvapeter, Wim Hordijk, "Cellular Automata for Image Noise Filtering" 978–1-4244-5612-3/09 IEEE 2009.
15. Yan Ha, "Method of edge detection based on Non-linear cellular Automata", Proceedings of the 7th World Congress on Intelligent Control and Automation, June 25–27, 2008.
16. Suryakant, Neetu Kushwaha "Edge Detection using Fuzzy Logic in Matlab," vol. 2, pp. 38–40, 2012.

Performance Analysis of COADM-Based Transparent Optical Network

Satnam Singh and Neeraj Sharma

Abstract The performance of conventional add drop multiplexer (ADM) was limited due to greater cost involved in optical to electrical and electrical to optical conversions during addition and removal of wavelengths (information) along the line. Configurable optical add-drop multiplexer (COADMs) give the flexibility of adding or removing the wavelengths without the optical to electrical and electrical to optical conversions. Secondly, COADMs are very cost effective. This paper studies the performance of a 4×4 wavelength COADM. The performance at various wavelengths is compared on the basis of gain, noise figure and optical signal to noise ratio (OSNR).

Keywords Add Drop Multiplexer (ADM) · Configurable optical add-drop multiplexer (COADM) · Optical To Electrical To Optical (OEO)

1 Introduction

Optical fibre is one the fastest growing technology and is in great demand. The emerging technologies use optical fibre in Internet, cable television, telephone and computer networking [1]. The enormous bandwidth, low BER and low error, makes the optical fibre even future proof.

There is no electronic equipment available which can directly deal with the enormous 50 THz bandwidth provided by optical fibre so as to take the advantage of such a high bandwidth. Optical fibre's bandwidth is further divided into smaller wavelengths. These wavelengths are multiplexed and are transmitted through optical fibre. Such systems are also termed as WDM systems. In WDM systems, the wavelengths supporting the communication between different end users are multiplexed and then carried by same optical fibre.

S. Singh (✉) · N. Sharma

Department of ECE, University Institute of Engineering and Technology,
Panjab University, Chandigarh, India
e-mail: er.satnamsingh1992@gmail.com

The WDM system needs add drop multiplexers for adding/dropping of wavelengths at any node. The add drop multiplexers convert the optical signal in the fibre to electrical and then extract the required information. In second step, it converts that electrical signal to optical and sends it through fibre. These optical to electrical and electrical to optical conversions require extra circuitry that increases the overall cost.

In order to remove that extra circuitry required for OEO, COADMs were introduced. COADMs consist of combination of optical multiplexers and demultiplexers along with optical switches [2]. This combination separates out the required wavelength without the need of any OEO. Also, it reduces the circuitry and overall cost.

The objective of this paper is to analyze the performance of a COADM using a simulator and compare different parameters like gain, noise figure and OSNR at different frequencies. The reason for the degradation in output is also discussed and future work for improvement in performance is purposed.

This paper is divided into four sections. In Sect. 2, system description is provided along with the explanation of working. In Sect. 3, a basic COADM is simulated using Optisystem simulator, and its performance is analyzed using different parameters. In Sect. 4, the paper is concluded with the discussion of future scope.

2 System Description

COADM consists of three main parts—optical switch, optical multiplexer and optical demultiplexer. This combination selects out the wavelength that is required without any OEO. In the following system, a laser array is used to transmit four frequencies at 193.1, 193.3, 193.5, 193.7 THz. These four frequencies are multiplexed to an optical fibre of 50 km. After 50 km, four more frequencies are added using COADM with line width = 10 nm. The effects of adding frequencies are discussed in Sect. III. Similarly, the frequencies are dropped using COADM. After dropping frequencies, the signal is passed through an optical fibre for 50 kms and then received at output.

Now three situations are taken into consideration. First is input to output insertion loss, it compares the overall loss in output with respect to input. Second is input to drop insertion loss, it compares the loss in input signal due to dropping of wavelengths. Third is adding to output insertion loss, it compares the loss in output due to the adding of wavelengths, simulation and results (Fig. 1).

3 Simulation and Results

The system defined above is simulated using Optisystem simulator [3]. A configurable optical add-drop multiplexer is used as a subsystem and is used for checking the losses in the optical signal during addition and dropping of the wavelengths as shown in Fig. 2.

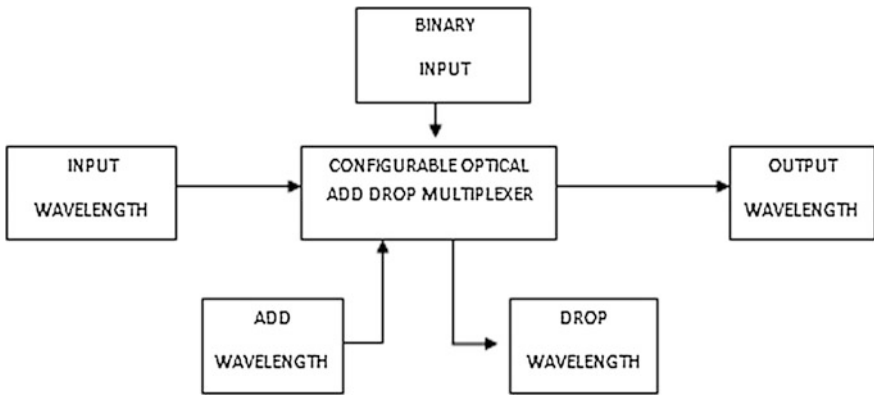


Fig. 1 Block diagram of simulated system

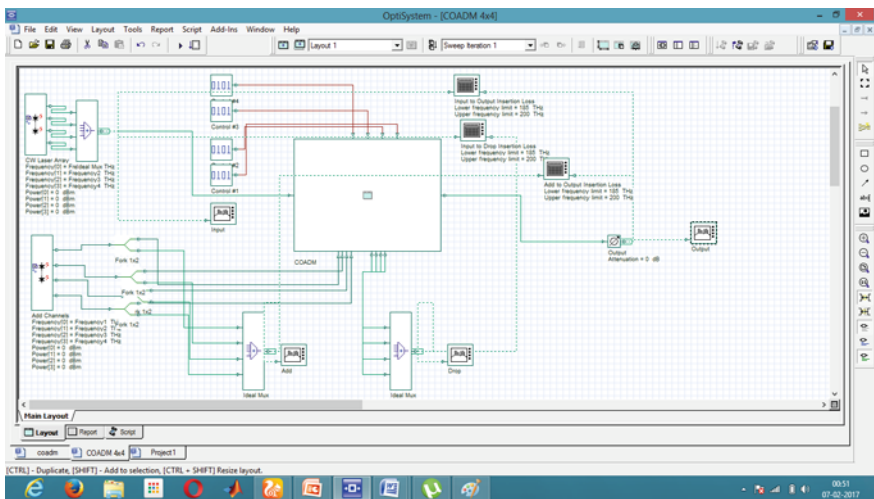


Fig. 2 Optisystem representation of proposed system

The laser array is used for four different frequencies 193.1, 193.3, 193.5, 193.7 THz. These four frequencies are multiplexed on to optical fibre. The line width between frequencies is taken as zero; hence, there is no distortion as shown in Fig. 3.

Four frequencies are added later on. Another laser array is used to generate optical signal at the same frequencies as the input, but the line width is varied to 10 MHz. Due to this line width, distortion can be noticed in the optical spectrum analyzer output as shown in Fig. 4.

The internal structure of the used subsystem consists of four optical switches, four optical multiplexers and four optical demultiplexers. Optical multiplexers add

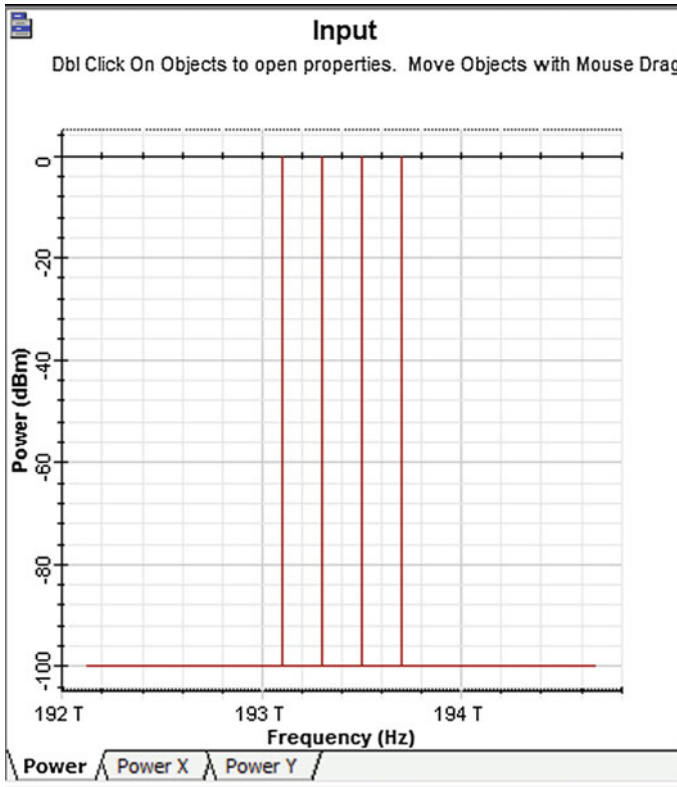


Fig. 3 Optisystem representation of input wavelengths

the wavelengths and optical demultiplexers drop the wavelengths. Binary input shown in the system description acts as a control to drive the optical switches as shown in Fig. 5.

The optical demultiplexers are used to drop the wavelengths, therefore four wavelengths that were added with 10 MHz line widths are dropped, and the optical spectrum analyzer output is shown in Fig. 6.

The dropped wavelengths contained distorted waveform because of the line width provided during adding so giving the proof that only those wavelengths are dropped those were added using optical multiplexers. The following figure shows the output waveform that contains the original frequencies that were transmitted in the start (Fig. 7).

At every frequency, the value of gain, noise figure, output signal and output SNR is taken out that compares the following losses.

From the Tables 1, 2, 3 and 4, it is quite evident that the gain is decreasing while adding and dropping wavelengths.

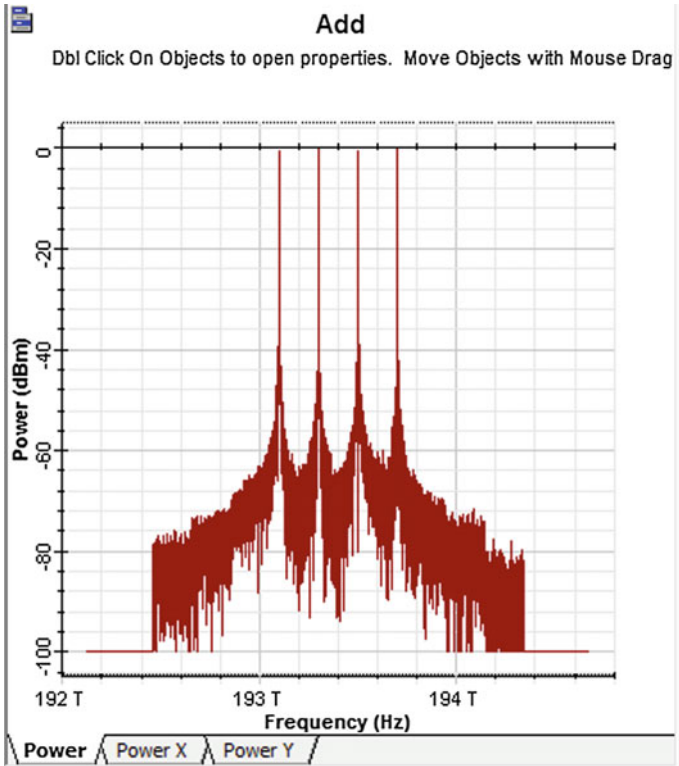


Fig. 4 Optisystem representation of added wavelengths

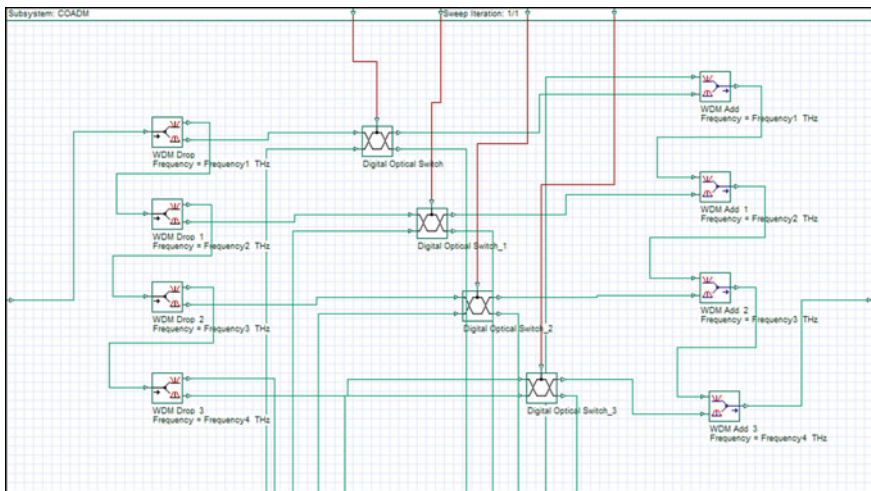


Fig. 5 Internal structure of the COADM

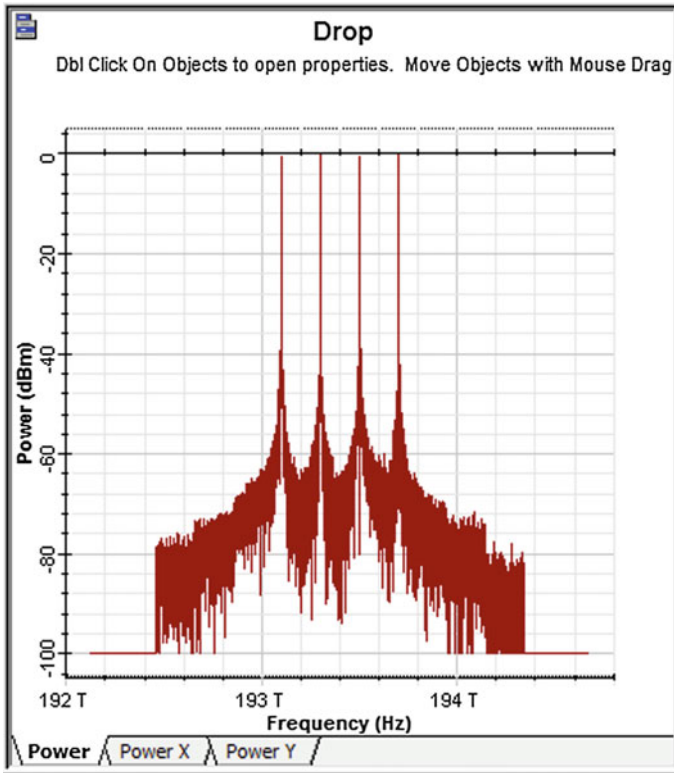


Fig. 6 Optisystem representation of the dropped frequencies

Similarly, noise figure is increasing during adding and dropping wavelengths, i.e. noise in the system is increasing.

Output signal and OSNR are showing slight modifications but are decreasing.

The reason for the decrease in the above parameters is regarded as crosstalk [4, 5], power excursions at high frequencies [6] and insertion losses.

4 Conclusion

The performance of configurable optical add-drop multiplexer (COADM) is analyzed using Optiwave simulator and degradation in gain, output signal, OSNR and subsequently noise figure is increased. The reasons behind this degradation are crosstalk, power excursions and insertion losses.

As the system is very cost effective and easily deployable. It can be used in CWDM systems easily. So there is a trade-off between cost and degraded gain and OSNR.

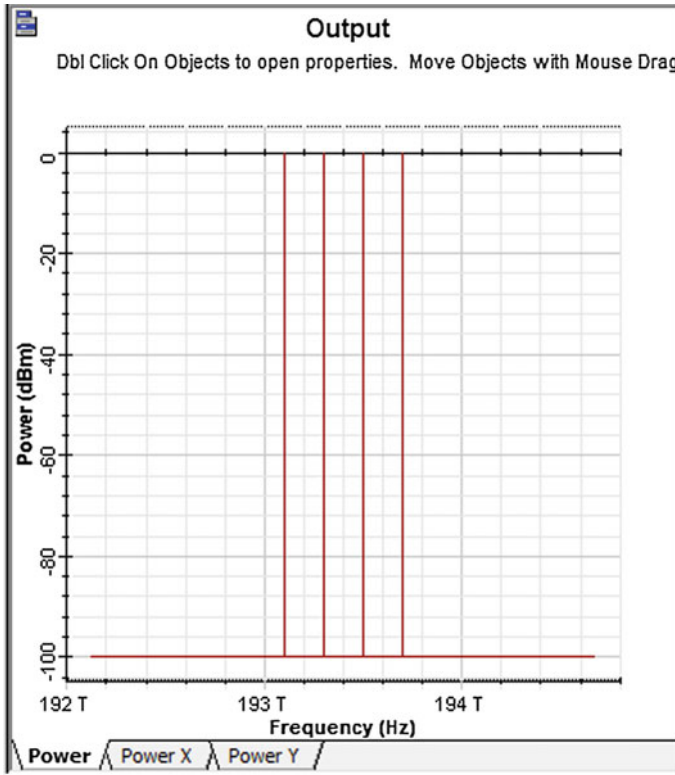


Fig. 7 Optisystem representation of the output frequencies

Table 1 Loss information at frequency 193.1 THz

Parameters	Input to output insertion loss	Input to drop insertion loss	Add to output loss insertion loss
Gain (db)	-0.00091865379	-0.00083182104	-8.6832743e-005
NF (db)	0.000918654	0.000831821	8.68327e-005
O/P Signal	-0.000918654	-0.000831821	-0.000918654
O/P OSNR	99.9991	99.9992	99.9991

Table 2 Loss information at frequency 193.3 THz

Parameters	Input to output insertion loss	Input to drop insertion loss	Add to output loss insertion loss
Gain (db)	-0.00098854529	-0.0008002439	0.0078116986
NF (db)	0.000988545	0.00080024	-0.0078117
O/P Signal	-0.000988545	-0.00080024	-0.000988545
O/P OSNR	99.999	99.9912	99.999

Table 3 Loss information at frequency 193.5 THz

Parameters	Input to output insertion loss	Input to drop insertion loss	Add to output loss insertion loss
Gain (db)	-0.00098854529	-0.0076586532	0.0066701079
NF (db)	0.000988545	0.00765865	-0.00667011
O/P signal	-0.000988545	-0.00765865	-0.000988545
O/P OSNR	99.999	99.9923	99.999

Table 4 Loss information at frequency 193.7 THz

Parameters	Input to output insertion loss	Input to drop insertion loss	Add to output loss insertion loss
Gain (db)	-0.00091865379	-0.012597847	0.011679194
NF (db)	0.000918654	0.0125978	-0.0116792
O/P Signal	-0.000918654	-0.0125978	-0.000918654
O/P OSNR	99.9991	99.9874	99.991

Future work is to reduce this degradation by eliminating the crosstalk and power excursions using different strategies.

References

1. Idachaba, F., Ike D.U., HOEO O.: Future Trends in Fiber Optics Communication. Proceedings of the World Congress on Engineering 2014 Vol I, WCE 2014, July 2–4, 2014, London, U.K
2. Configurable Optical Add-drop Multiplexer in Optisystem tutorials-Volume 2
3. www.optiwave.com
4. Cancela L.G., Srqueira D.G, Pinheiro B.R., Rebola J.L., Pires J.J.: Analytical Tools for Evaluating the impact of in-band Crosstalk in DP-QPSK Signals. 2016 21st European Conference on Networks and Optical Communications—(NOC)
5. Sharma N.: Effects of Crosstalk Propagation on the Performance of All-Optical Networks. 1st Int'l Conf. on Recent Advances in Information Technology RAIT-2012
6. Wang Z., Tsai J., Pan Y., Kilper D., Pavel L: Control for Suppression of Channel Power Excursions in ROADM-Based WDM Chain Networks. 2013 Conference on Control and Fault-Tolerant Systems (SysTol) October 9–11, 2013. Nice, France
7. Agrawal G.P, "Fibre Optic Communication Systems. John Wiley, 2002

ZigBee and GSM Based Fault Detection System for Low Tension Pillar

Ram Nath and Ritula Thakur

Abstract This paper represents the automation in distribution network on low-voltage side of distribution transformer. This project will help to automate the distribution network on LT side. The fuse of any phase blows off in low tension (LT) pillar due to any fault or overloading; it is difficult to find the fault location. Hence, restoration of power supply takes more time which affects the services to consumer. To maintain high standards of availability and reliability, it is required to reduce the restoration time and find the faulty location as soon as possible. In LT pillar, there are so many numbers of incoming and outgoing lines. In case of fault or over loading, any fuse blows off instantly, the proposed system will send the real time data to main control room automatically. Then operator will get information about which fuse has been blown off and then he will send fuse man to repair the fuse. This will save restoration time and improve reliability.

Keywords Distribution network · LT pillar · Distribution transformer Restoration

1 Introduction

Power distribution automation system means automation in distribution side for the better and safe operation of distribution network. The distribution network comprises of different type of sensors and actuators, communication network for the advancement of distribution grid which easily finds the fault location in low-voltage

R. Nath (✉)

Department of Electrical and Electronics Engineering,
Roorkee Engineering & Management Technology Institute, Shamli, India
e-mail: ramani.pr21@gmail.com

R. Thakur

Department of Electrical Engineering, National Institute of Technical Teachers'
Training & Research, Chandigarh, India
e-mail: ritula.thakur@gmail.com

© Springer Nature Singapore Pte Ltd. 2018

R. Singh et al. (eds.), *Intelligent Communication, Control and Devices*,
Advances in Intelligent Systems and Computing 624,
https://doi.org/10.1007/978-981-10-5903-2_78

761

distribution system [1]. For the improved reliability, and security and future extension power system network, each and every electric utility has to be accurately inventory the condition of the physical assets of grid. Geographical information system (GIS) is a very good information technology to reduce the complexity of electrical distribution system. It helps in locating the fault location, network optimization, load forecasting within a specific time of period; it also provides better scenario for monitoring distribution facility and helps in better management to provide the electricity to the consumer. For controlling and monitoring of electricity, distribution network GIS is a very effective tool [2]. Remote-controlled sectionalizers are good option to automate the distribution system; it is simple in operation and cost-effective. The main function of these sectionalizers is to isolate the faulty section very fast and provide the alternate routes for restoration of unfaulted section. If in distribution system extended outages are present, it will also be useful for step-by-step restoration of the network [3]. The aim of the distribution automation system (DAS) is to monitor and control the operation of the equipment connected at the distribution line and substation or poles remotely. Implementation of DAS, supports the low-voltage substations which distribute power to the end users. Supervisory control and data acquisition (SCADA) system helps in monitoring and controlling the distribution network. DAS operates remotely for fault detection, fault location and isolation, clearance, and supply restoration [4]. DAS is integrated with automated fault isolation system (AFIS) based on hardware and software system. For the implementation of AFIS, end user substation has been automated [5]. To automatically monitor the quality of service in the low-voltage grid, LV grid has needed to update to become the 'smart grid' [6]. Security, reliability, and economy of the power system are directly dependent on quality of planning, and play a vital role in electrical power system [7]. We know that distribution network is continuously developing, systems are becoming more reliable. To reduce the fault and its impact on distribution network for the improvement of reliability, relay protection is paid more attention. For high-voltage power network, existing relay allocation and setting a systems are more suitable as compared to low-voltage network because of different network topology, properties, and operation mode [8].

2 Hardware Development

Assume that in a city, there are n numbers of LT pillars present and the main utility center is far away from the LT pillar. So the information of each pillar is first received by a junction called coordinator. Every coordinator will to have capacity to store the information of no. of LT pillar. Then each Coordinator will communicate with the main control center room. Communication between the LT pillar and coordinator, we can ZigBee; for the long-range communication, GSM be used for communication between Coordinator and main control center. The generalized block diagram is shown in Fig. 1.

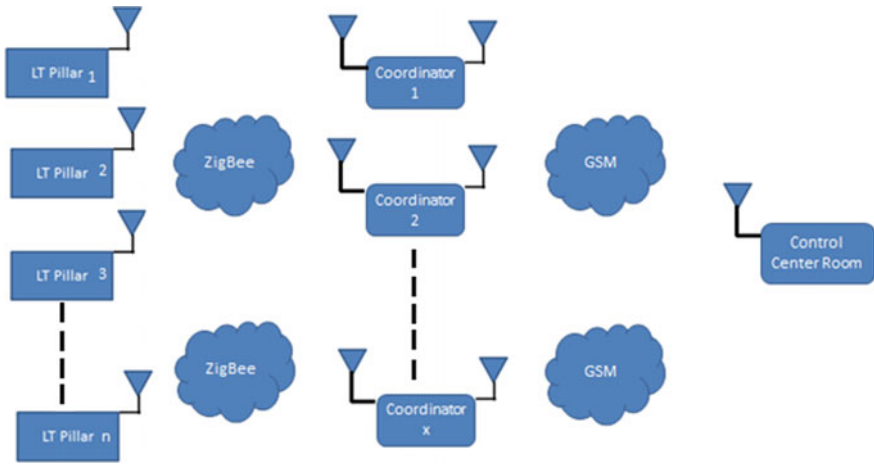


Fig. 1 Generalized block diagram of system

This paper will help in advancement of distribution grid by automating the low-voltage side of distribution transformer. To know about the healthy condition of LT Pillar, AND logic plays an important role and that information is sent to the coordinator through ZigBee module and from coordinator it will be transmitted to the main control room using GSM technique.

Every coordinator has one ZigBee modem and one GSM modem for the communication between the LT pillar and utility center, respectively. Power supply is needed to run the coordinator, and LCD is also present to show the condition of fuses in LT Pillar. Block diagram of Coordinator is shown in Fig. 2.

In main control center room, one GSM receiver will be present to receive the information which is send by the coordinator. Then GSM modem is connected with Arduino. The result will be shown in PC with the use of LabVIEW Graphic User Interface (GUI). Block diagram of control room is shown in Fig. 3.

Fig. 2 Block diagram of coordinator

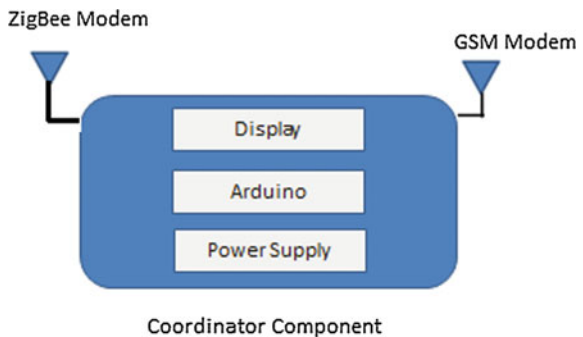
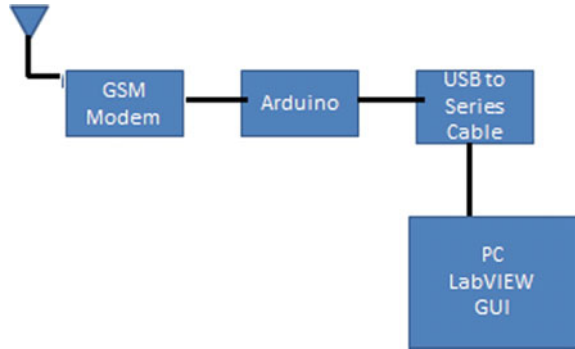


Fig. 3 Block diagram of control room



3 Software Development's

3.1 Proteus Simulation Model

Proteus simulation is used to make the easy calculation and it driven the execution of programs. Proteus simulation is used to get the accurate information about the time and the operational behavior of applications. With the use of Proteus simulator, we can get fast and accurate result and we can easily reproduce our results from real multiprocessor. Proteus has ability, by which it provides the user to control the accuracy level of simulation. For parallel software, it is an excellent platform which supports the troubleshooting, testing, tuning and evaluation of performance and graphical output. The Proteus model of proposed system is shown in Fig. 4.

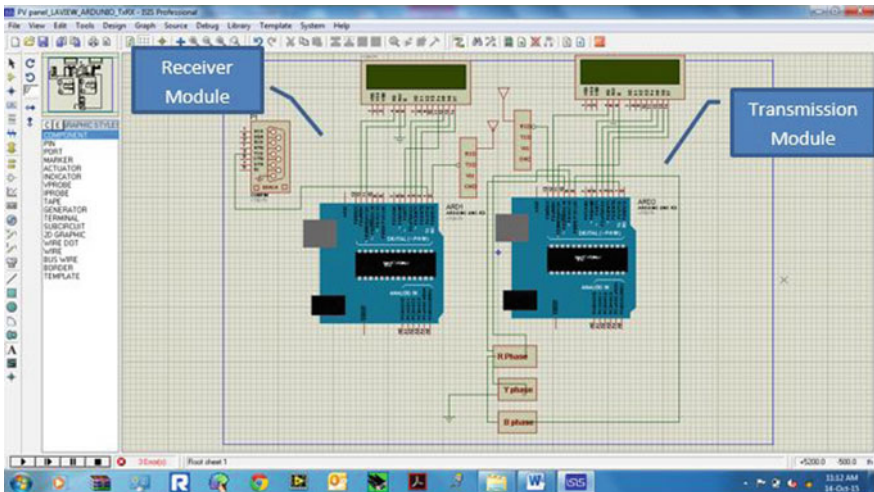


Fig. 4 Proteus model

3.2 LabVIEW Model

To get the result on PC in main control center, LabVIEW software is used in the present work. LabVIEW is a graphical programming language. It is a development tool that makes automation delight. LabVIEW gives graphical representation which has more spontaneous design notations than text-based code. LabVIEW model present system is shown in Fig. 5.

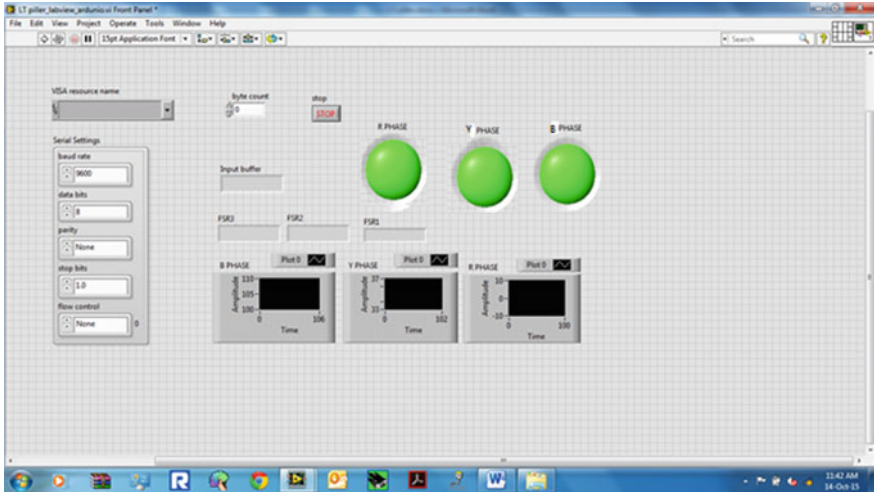


Fig. 5 LabVIEW model

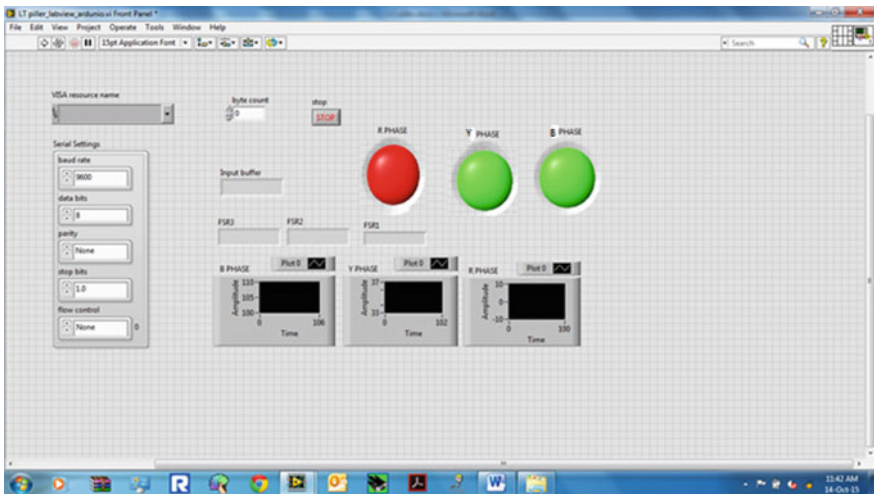


Fig. 6 Result when 'R' phase blow 'Off'

4 Results

By using Proteus model and LabVIEW GUI in PC, we can monitor the health of fuses in LT pillar of Distribution network with the use of AND logic gate and Arduino. It automates the LT side of distribution network. In case of any fault or if fuse blown off, this information is instantly sent to the main control center and it will be shown on personal computer. Suppose that due to fault, fuse of R phase blown off, this information is sent to the main control room by using ZigBee and GSM communication media. By using Lab VIEW model, red light will be shown on PC in main control center as shown below in Fig. 6.

When due to fault or overloading Y phase’s fuse blown off, it will shown on LabVIEW model in main control center room by glowing red light on Y phase as shown in Fig. 7.

If faults occur on B phase, then its fuse will be burnt and this result will be shown on PC by using LabVIEW model in main utility center by red light as shown in Fig. 8.

The above diagrams show the front panel of LabVIEW model and the main function run in back panel of LabVIEW is shown in Fig. 9.

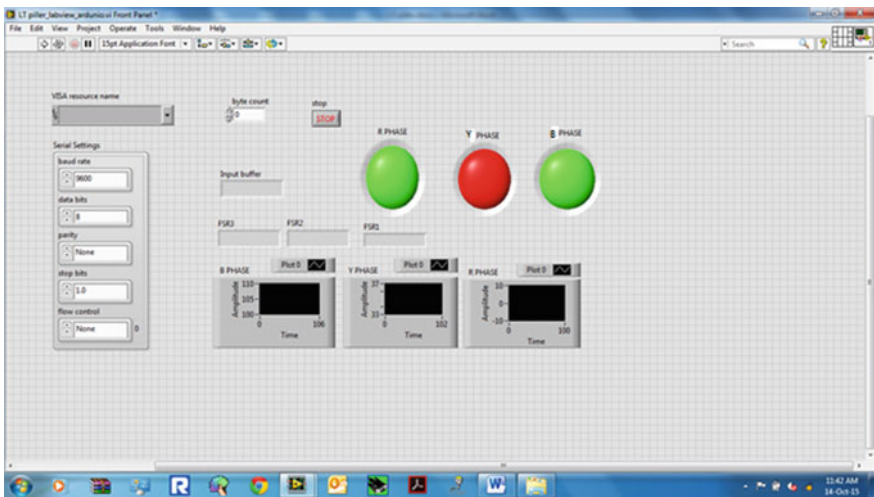


Fig. 7 Result when ‘Y’ phase blow ‘Off’

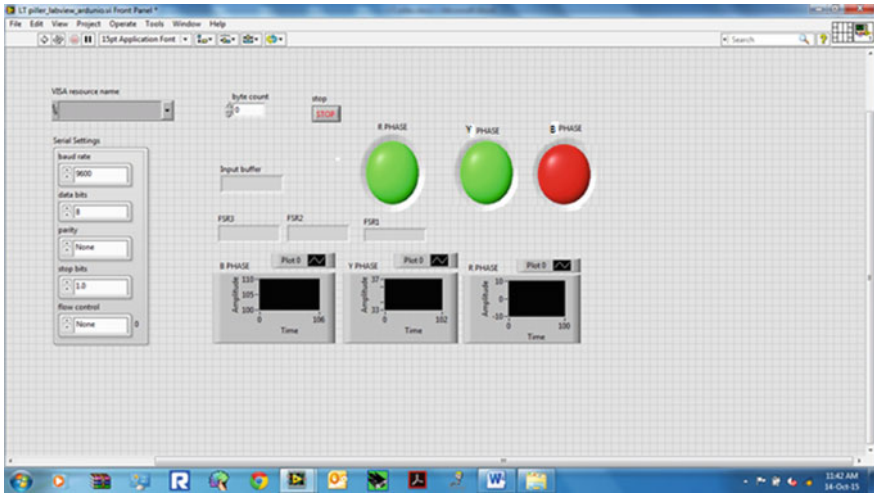


Fig. 8 Result when ‘B’ phase blow ‘Off’

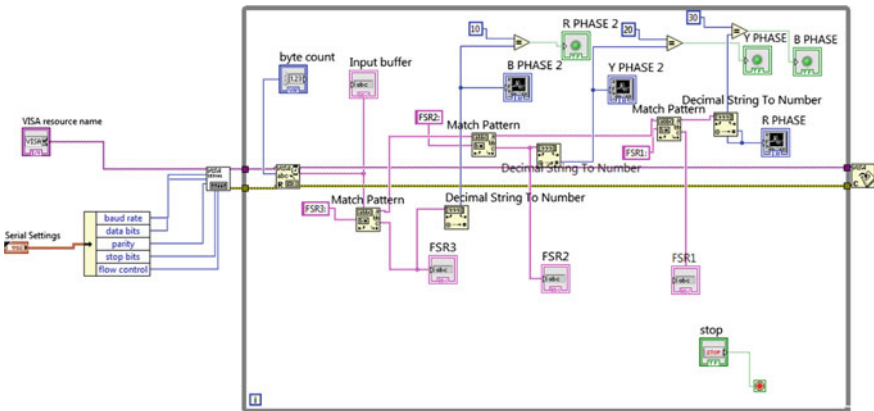


Fig. 9 Back panel view of model

5 Conclusion

This paper will help in advancement of distribution grid on LT side of distribution transformer. This is the first step to make the LT side ‘Smart, and this will help to improve the reliability of grid and also operation of self-healing grid that will make traditional grid to smart grid. This paper would basically be useful for distribution company to improve the reliability and availability of power supply by reducing the time period of restoration of power supply and easily find the location of fault in LT pillar.

The proposed system in the paper can be the part of smart grid in India. There are so many pilot projects going on, but in the field of power distribution only few efforts are seen. Initially, only up to 33 and 11 kV would be automated to make the LT side of distribution transformer automated. In future, it could be very much helpful to improve the power reliability and to maintain the standard of companies.

References

1. Zhihong L., Zhiyong, L.: Exploration and practice of the smart distribution network by the Yangjiaping Power Supply Bureau. In: Shanghai, China., Electricity Distribution, China International Conference on Electricity Distribution (CICED), Proceedings of IEEE, pp. 1–6, September, 2010.
2. Stephen O.E. and Damilola D.A.: Geospatial Modeling of Electricity Distribution Network in Ife Central Local Government Area, Osun State, Nigeria. In: Warri, Delta State, Nigeria, Science Journal of Environmental Engineering Research (SJEER), Vol. 2014, sjeer. 213, pp.1-7, February, 2014.
3. Pahwa, Anil: Role of distribution automation in restoration of distribution systems after emergencies. In: Manhattan, KS, USA, Transmission and Distribution Conference and Exposition, IEEE/PES, Vol. 2, pp.1204-05, November, 2001.
4. Ahmed, M. M. and Sulaiman, M.: New Low Voltage (LV) Distribution Automation System. In: Clearwater, Florida, USA , Proceedings of International Conference on Power and Energy System (IASTED), IASTED, Vol.539, No.813, pp.289-93, January, 2007.
5. Ahmed, M. M.: Development of automated fault isolation system on distribution systems in Malaysia. In: Malaysia, IEEE Conference, International Conference on Computer and Communication Engineering (ICCCE), ICCCE, pp. 587-593, July, 2012.
6. Snoeck, W.: Quality of Service Monitoring in the Low Voltage Grid by using Automated Service Level Agreements. In: Sweden, School of Electrical Engineering (EES), Industrial Information and Control System, KTH, Master Thesis/Dissertation, pp.1-169, 2013.
7. Wang, S.: An effective and applied method on evaluation of distribution network planning. In: Nanjing, China, Electricity Distribution, China International Conference on Electricity Distribution (CICED), Proceedings of CICED/IEEE, pp. 1–6, September, 2010.
8. He, C. and Zhang, B.: Relay protection setting calculation system in distribution networks. In: China, Electricity Distribution, China International Conference on Electricity Distribution (CICED), Proceedings of CICED/IEEE, pp. 1–4, September, 2010.
9. <http://www.ni.com/newsletter/51141/en/>.

Performance Evaluation of Wavelet-Based Image Compression Techniques

Nishat Bano, Monauwer Alam and Shish Ahmad

Abstract Wavelet transform provides excellent energy compaction and exploits redundancy for better image compression. This paper analyses the performance of wavelet-based image compression techniques, namely set partitioning in hierarchical trees (SPIHT), set partitioned embedded block (SPECK) and JPEG2000. Image quality measured as peak signal-to-noise ratio and computational complexity, i.e. encoding and decoding times, is calculated for these techniques. Simulation results show that JPEG2000 outperforms other state-of-the-art wavelet image codecs (SPIHT and SPECK) in coding efficiency and computational complexity. Simulation is carried out on various images of different dimensions at different bit rates using MATLAB software.

Keywords JPEG2000 · Set partitioning in hierarchical trees (SPIHT) · Set partitioned embedded block coder (SPECK) · Wavelet transform

1 Introduction

For computer applications before transmission, the redundant data needs to be compressed in order to reduce storage. In image compression, the highly correlated neighbouring pixels are discarded by reducing the redundant information in an image. Image compression techniques are becoming more complex with the improvement in efficiency. Image can be transformed using discrete cosine transform (DCT) [1] and discrete wavelet transform (DWT) [2, 3]. Joint Photographic

N. Bano (✉) · M. Alam

Department of Electronics Engineering, Integral University, Lucknow, UP, India
e-mail: nishatrizvi9@gmail.com

M. Alam

e-mail: malam@iul.ac.in

S. Ahmad

Department of Computer Science, Integral University, Lucknow, UP, India
e-mail: shish_parv@rediffmail.com

© Springer Nature Singapore Pte Ltd. 2018

R. Singh et al. (eds.), *Intelligent Communication, Control and Devices*,
Advances in Intelligent Systems and Computing 624,
https://doi.org/10.1007/978-981-10-5903-2_79

769

Experts Group developed (JPEG) coder [4, 5, 6] uses DCT and generates energy-compacted spectral components. Wavelet transform offers excellent energy compaction and eliminates redundant information present in an image. Shapiro [7] introduced EZW which is extremely fast, very effective and produces embedded bit stream. The performance of EZW is further enhanced by presenting a more efficient and faster technique known as set partitioning in hierarchical trees (SPIHT) developed by Said and Pearlman which is simple technique and offers excellent rate–distortion performance [8]. A. Islam and W. Pearlman proposed block-based wavelet transform coding technique with low complexity known as set partitioning embedded block (SPECK) [9]. JPEG2000 [10] provides higher compression efficiency which is faster than zerotree coders but it needs extra memory allocation. However, for high resolution images, SPIHT and SPECK need large memory bank which in turn increases the cost of hardware. The paper is organized as follows: Sect. 2 contains overview of the wavelet-based compression techniques, namely SPIHT, SPECK and JPEG2000. In Sect. 3, results are given. We conclude the paper in Sect. 4.

2 Overview of Wavelet-Based Compression Techniques

2.1 SPIHT

Set partition coding (SPC) has high energy compaction and zerotree properties of wavelet decomposition. This gives bitstream which is embedded in nature. This means that coding algorithm can be stopped at any time. SPIHT transmits decision by assigning bits. The pixel values are compared with the threshold using the following function:

$$\Gamma_n(X) = \begin{cases} 1, & \max_{(i,j) \in X} \{|c_{ij}|\} \geq 2^n, \\ 0, & \text{otherwise} \end{cases} \quad (1)$$

where 1 and 0 indicates the significance and insignificance of sets with respect to threshold.

The set partitioning rules are defined as:

$\hat{Q}(i, j)$ = A set of the co-ordinates of offsprings of node (i, j) ; $\hat{D}(i, j)$ = A set of the co-ordinates of descendants of node (i, j) ; $\hat{L}_r(i, j)$ = A set of co-ordinates of descendants excluding $\hat{Q}(i, j)$; $\hat{L}_r(i, j) = \hat{D}(i, j) - \hat{Q}(i, j)$.

SPIHT comprises two passes: sorting and refinement and consists of three lists to keep track of pixel values [8]. LIP is the list of insignificant pixels which has all the pixels of LL band (highest energy band). LIS is the list of insignificant sets that consist of sets with descendants only excluding tree root. LSP is the list of significant pixels that contains significant coefficients of all passes. During sorting pass or significance map testing, all the pixels in LIP are tested for significance. If they are significant, an output bit is generated and a sign bit is given. The significant

pixels are now sent to LSP. Now, tree sets with descendants are checked for significance. If they are found significant, they are detached from the list and then partitioned into four offsprings. These offsprings are tested and if found significant, they are sent to LSP otherwise they are sent to LIP. During refinement pass, those pixels which were significant in the previous sorting pass are refined and output the most significant bit of the pixel value [11, 12, 13].

2.2 *SPECK*

Set partitioned embedded block coding (SPECK) [9] is the block-based efficient state-of-the-art algorithm which has only two lists, namely LIS and LSP. There are three coding steps in SPECK algorithm: initialization, sorting and refinement. Initially, a threshold is set. The image is transformed using DWT and partitioned into a set \hat{S} which consists of root node of the pyramid and a set \hat{I} which consists of remaining coefficients. Initially, \hat{S} block coefficients are kept in LIS and LSP is empty. During the sorting pass, significance of \hat{S} and \hat{I} sets is checked. If \hat{S} is found to be significant, it is partitioned into four equal sized subsets added to LIS. All subsets of 1×1 are checked for significance and if found significant, the sign bit is coded. These subsets are then added to LSP. If the set \hat{I} becomes significant, it is divided into octave band partitioning. A total of four sets are generated: three \hat{S} sets and one \hat{I} set. When all sets are partitioned and made significant, the refinements pass starts which refines the quantized pixel values of LSP that are found significant in the earlier passes. Now, threshold is reduced in a step of two and the process is repeated until the desired bit rate is attained. Because of the linked lists of SPECK, huge memory is required that increases its complexity [14, 15].

2.3 *JPEG2000*

JPEG2000 [10] was developed by Joint Photographic Experts Group (JPEG) committee. It exploits the features of discrete wavelet transform (DWT), a benchmark in image compression and introduced several new features. These new features such as better low bit rate performance, grey and colour image compression, lossless and lossy compression, large images and image components, large dynamic range of pixels, progressive transmission, error resiliency, image security are effective for vast applications. The block diagram of JPEG2000 encoder is given in Fig. 1.

JPEG2000 encoder performs three steps in compression: discrete wavelet transform (DWT), quantization and entropy encoding. Each component after multi-component transformation is decomposed by DWT in different subbands which are then independently quantized. These quantized subbands are broken into equal sized small code blocks, generally 32×32 , 64×64 . These code blocks produce compressed bitstreams after independently entropy encoded by Tier-1 and Tier-2 coding

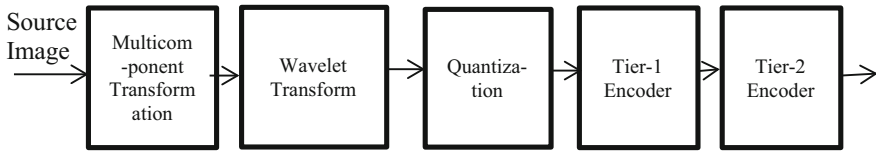


Fig. 1 JPEG2000 encoding process

engines. In Tier-1 coding process, each code block is divided into n bit planes, where n is the precision of number of elements in code blocks. They are encoded from n th bit plane to first bit plane by fractional bit plane coding using embedded block truncation optimization technique (EBCOT) [16] algorithm in three coding passes such that if a part of one bit plane is being encoded, other bit planes do not overlap. The three coding passes of EBCOT are significance propagation, magnitude refinement and clean-up pass. EBCOT generates context data and binary decision values which are coded by binary arithmetic coding (known as MQ-coder) and produce compressed bits for all code blocks. In Tier-2 coding, for each code block, a layer has all the coding passes from all consecutive bit planes and block summary information has length of compressed bitstreams, zero bit plane data and the number of coding passes data. Tag trees (quadtrees) are used to represent the layer and block summary data for all code blocks as compressed file header.

3 Simulation Results

The wavelet-based image compression techniques SPIHT, SPECK and JPEG2000 are simulated on MATLAB software. The results are tabulated as follows, and PSNR, encoding and decoding times are plotted against different bit rates for Lena and Barbara images (Tables 1 and 2).

Table 1 Image quality in terms of PSNR (dB) for image Lena

Image Size	Bit rate	SPIHT	SPECK	JPEG2000
256 × 256	0.03125	18.9583	18.9076	18.8
	0.0625	20.8117	20.8093	21.9
	0.125	22.837	22.7617	24.4
	0.25	24.9053	24.8546	26.8
	0.5	28.229	28.2168	30.4
512 × 512	0.01	19.9878	20.316	21.3
	0.03125	23.4453	23.5408	25.3
	0.0625	25.2964	25.3614	27.9
	0.125	28.0685	28.0842	30.9
	0.25	31.2954	31.2811	34.0
	0.5	34.8531	34.821	37.2

Table 2 Image quality in terms of PSNR (dB) for image Barbara

Image Size	Bit rate	SPIHT	SPECK	JPEG2000
256 × 256	0.03125	19.5478	19.558	20.2
	0.0625	21.1388	21.2202	22.2
	0.125	22.6964	22.7187	24.1
	0.25	24.4466	24.6391	27.1
	0.5	28.1264	28.4063	31.4
512 × 512	0.03125	21.4355	21.6194	22.4
	0.0625	22.4363	22.4943	23.8
	0.125	22.8963	24.1632	25.7
	0.25	26.4289	26.8417	28.8
	0.5	29.9908	30.2937	32.2

Figures 2 and 3 compare the coding performance (PSNR) (in dB) of SPIHT, SPECK and JPEG2000 algorithms for Lena image of dimension 256 × 256 and 512 × 512 against different bit rates. Figures 4 and 5 compare the PSNR (in dB) values of SPIHT, SPECK and JPEG2000 for Barbara image of 256 × 256 and 512 × 512 size, respectively. PSNR values (in dB) for JPEG2000 are best at all bit rates for these dimensions (Tables 3, 4, 5 and 6).

The encoding time is defined as the total time elapsed in wavelet transforming an image and then encoding the transformed coefficients. The decoding time is defined as the time elapsed in decoding the bitstream to reconstruct the image at a given bit rate. From Figs. 6, 7, 8 and 9, it is seen that at low bit rate, SPIHT and SPECK have

Fig. 2 PSNR (in dB) versus bit rate

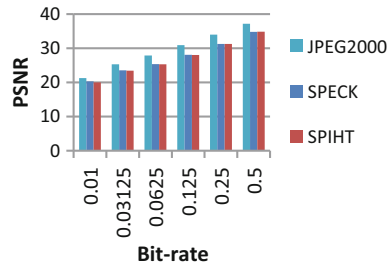


Fig. 3 PSNR (in dB) versus bit rate

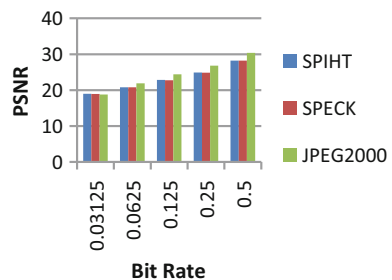


Fig. 4 PSNR (in dB) versus bit rate

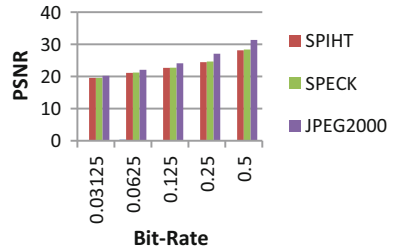


Fig. 5 PSNR (in dB) versus bit rate

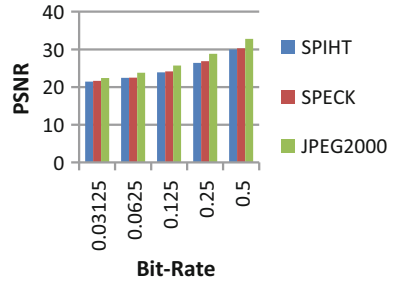


Table 3 Encoding and decoding times (in sec) for Lena image (256 × 256)

Bit rate	Encoding times			Decoding times		
	SPIHT	SPECK	JPEG2000	SPIHT	SPECK	JPEG2000
0.03125	0.371826	0.237291	0.545	0.041339	0.284069	0.265
0.0625	0.501402	0.452506	0.467	0.117489	0.388409	0.203
0.125	0.67561	0.891356	0.546	0.104909	0.631575	0.234
0.25	1.117004	1.778107	0.469	0.204936	0.896541	0.313
0.5	1.746806	3.577435	0.484	0.417989	2.010663	0.28

Table 4 Encoding and decoding times (in sec) for Lena image (512 × 512)

Bit rate	Encoding times			Decoding times		
	SPIHT	SPECK	JPEG2000	SPIHT	SPECK	JPEG2000
0.03125	0.986418	0.854543	0.67	0.11139	1.298324	0.546
0.0625	1.502201	1.717778	0.671	0.21293	2.567204	0.39
0.125	2.393825	3.384598	1.015	0.45045	5.192314	0.609
0.25	4.286269	6.804369	0.689	1.14808	10.47092	0.531
0.5	8.209132	13.54116	0.668	3.24535	20.70019	0.388

Table 5 Encoding and decoding times (in sec) for Barbara image (256 × 256)

Bit rate	Encoding times			Decoding times		
	SPIHT	SPECK	JPEG2000	SPIHT	SPECK	JPEG2000
0.03125	0.378639	0.215362	0.373	0.084359	0.44197	0.234
0.0625	0.513724	0.439732	0.514	0.06422	0.35901	0.202
0.125	0.655711	0.854807	0.404	0.110582	0.64911	0.264
0.25	1.18267	1.896267	0.545	0.211162	0.85683	0.234
0.5	2.932433	3.802933	0.594	0.447299	2.54111	0.329

Table 6 Encoding and decoding times (in sec) for Barbara image (512 × 512)

Bit rate	Encoding times			Decoding times		
	SPIHT	SPECK	JPEG2000	SPIHT	SPECK	JPEG2000
0.03125	1.03194	0.819432	0.716	0.099328	0.763043	0.404
0.0625	1.599716	1.651234	0.689	0.200636	1.003149	0.344
0.125	2.246898	3.326122	0.716	0.445806	2.163501	0.312
0.25	3.821626	7.586121	0.656	1.193864	5.805479	0.593
0.25	7.682409	13.91948	0.685	3.0199	15.50009	0.406

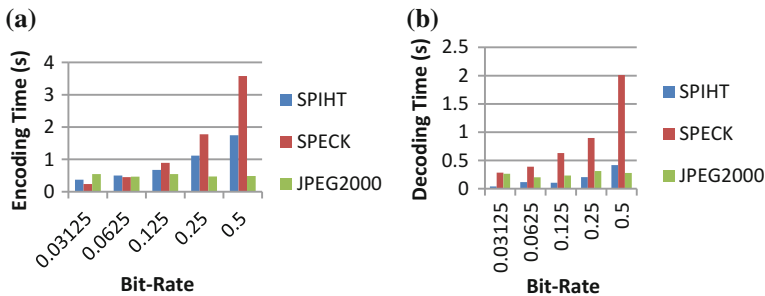


Fig. 6 Coding complexity: **a** encoding time (sec) and **b** decoding time (sec) for SPIHT, SPECK and JPEG2000 for Lena image of dimension 256 × 256

small values of the encoding and decoding times for Lena and Barbara image of 256 × 256 and 512 × 512 but at high bit rate, JPEG2000 outperforms them.

Figures 6 and 7 show the encoding and decoding times (in sec) for SPIHT, SPECK, JPEG2000 for Lena image of size 256 × 256 and 512 × 512 against different bit rates, and Figs. 8 and 9 show the encoding and decoding times (in sec) for Barbara image of size 256 × 256 and 512 × 512, respectively.

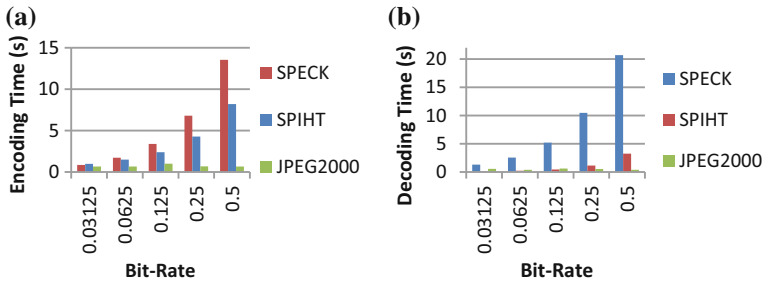


Fig. 7 Coding complexity: **a** encoding time (sec) and **b** decoding time (sec) for SPIHT, SPECK and JPEG2000 for Lena image of dimension 512 × 512

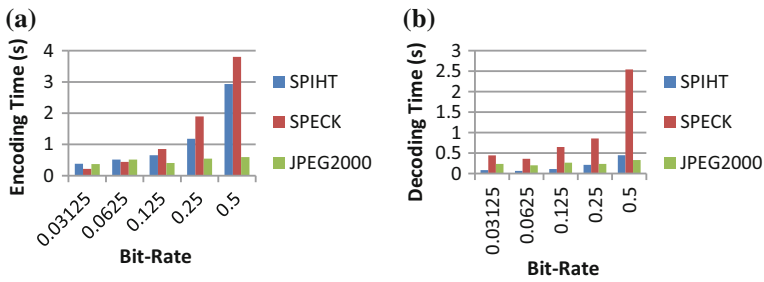


Fig. 8 Coding complexity: **a** encoding time (sec) and **b** decoding time (sec) for SPIHT, SPECK and JPEG2000 for Barbara image of dimension 256 × 256

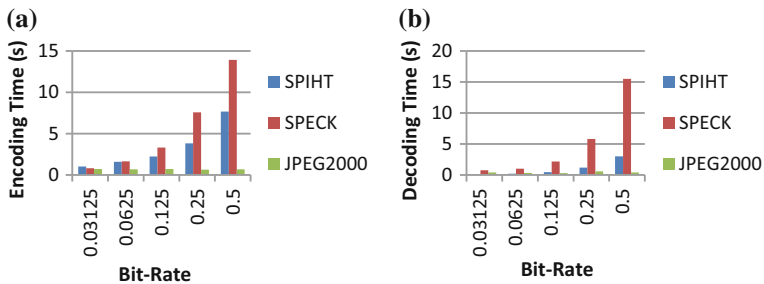


Fig. 9 Coding complexity: **a** encoding time (sec) and **b** decoding time (sec) for SPIHT, SPECK and JPEG2000 for Barbara image of dimension 512 × 512

4 Conclusion

This paper compares the set partition coding algorithms (viz. SPIHT and SPECK) and JPEG2000. The simulation results indicate that JPEG2000 technique is fast compared to set partition coding algorithms. The encoding and decoding times for

JPEG2000 are small compared to other algorithms. The PSNR values of JPEG2000 are better for a given bit rate for Lena and Barbara images of 256×256 and 512×512 .

References

1. Ahmed N., Natarajan T. and Rao K. R.: Discrete cosine transform: IEEE Transactions on Computers, vol. 23 no. 1, pp. 90–93 (1974)
2. Calderbank A. R., Daubechies I., Sweldens W., and Yeo B.L.: Lossless Image Compression Using Integer to Integer Wavelet Transforms, in Proc.: IEEE Int. Conf. Image Processing, vol. 1, Santa Barbara, CA, opp. 596–599. (1997)
3. Antonini M., Barlaud, M., Mathieu, P., and Daubechies, I.: Image coding using the wavelet transform, IEEE Trans. on Image Processing, 1, 205–220, (1992)
4. Wallace G.K., The JPEG still picture compression standard: IEEE Transaction Consumer Electronics, vol. 38, no. 1, Feb (1992)
5. ISO/IEC 1091 8 (JPEG), Information Technology-Digital Compression and Coding of Continuous-Tone Still Images.”
6. Pennebaker W. B. and Mitchell J. L.: JPEG: Still Image Compression Standard.: Van Nostrand Reinhold, New York (1993)
7. Shapiro J. M.: Embedded image coding using zerotrees of wavelet coefficients: IEEE Trans. Signal Process., vol. 41, pp. 3445–3462 (1993)
8. Said A. and Pearlman W. A.: A new, fast, and efficient image codec based on set partitioning in hierarchical trees: IEEE Trans. Circuits Syst. Video Technol., vol. 6, no. 3, pp. 243–250 (1996)
9. A. Islam and W. A. Pearlman: Embedded and efficient low-complexity hierarchical image coder: IEEE Transactions on circuits and systems for video technology, vol. 14, no. 11 (2004)
10. Taubman D.: High performance scalable image compression with EBCOT: IEEE Trans. Image Processing, vol. 9, pp. 1158–1170 (2000)
11. J.Z. Gang, G.X. Dong, L.L. Sheng: a fast image compression algorithm based on SPIHT: IEEE international conference (2009)
12. Akter M., Reaz M. B. I., Mohd-Yasin F., Choong F.: A modified set partitioning in hierarchical trees algorithm for real-time image compression: J. Commun. Technol. Electron., vol. 53, no. 6, pp. 642–650 (2008)
13. Pan H., Siu W.-C., and Law N.-F., A fast and low memory image coding algorithm based on lifting wavelet transform and modified SPIHT: Signal Process., Image Commun., vol. 23, no. 3, pp. 146–161 (2008)
14. Baojun H and Yan L.: An Improved SPECK Image Coding Algorithm.: IEEE Fifth International Conference on Information Assurance and Security, pp 227–229 (2009)
15. Senapati R. K., Pati U. C., Mahapatra K. K.: Listless block tree set partitioning algorithm for very low bit rate embedded image compression, Int. J. Electron. Commun., vol. 66, no. 12, pp. 985–995 (2012)
16. Taubman D., Ordentlich E., Weinberger M. and Seroussi G.: Embedded Block Coding in JPEG2000 (2001)

Intelligent AVR Control of a Single Thermal Area Combined with LFC Loop

Devashish Sharma, Varsha Kushwaha, Kamlesh Pandey
and Nibha Rani

Abstract This paper presents an intelligent control technique for voltage and frequency control of a single area power system. The two loops of AGC, i.e., LFC and AVR, are incorporated in the system to improve the system dynamics. The effect of cross-coupling of LFC loop with the AVR loop has also been taken into consideration. To prove the supremacy of intelligent control techniques, the conventional PID controller responses are compared with Fuzzy logic controller responses. It has been found that that the dynamic response of the system in terms of damping of oscillations, settling time, and peak overshoots is improved.

Keywords Automatic generation control · AVR · LFC

1 Introduction

A power system requires load and generation balance at all times for economic and reliable operation. Any imbalance between generation and load can cause voltage and frequency instability and blackouts. This makes automatic generation control (AGC) as the one of the most influential problem in the power system. The ultimate goal of the AGC is to reduce the transient oscillations and to make steady-state errors zero for frequency and voltage responses in a very small time. AGC consists of two main control loops—(1) Automatic voltage regulation (AVR), (2) Automatic load frequency control (ALFC). AVR accounts for the voltage fluctuations due to load variations. The voltage at the system terminals and its magnitude is regulated by the system's reactive power and is kept within the nominal ranges by incor-

D. Sharma (✉) · V. Kushwaha · K. Pandey · N. Rani
Department of Electrical and Electronics Engineering, ASET, Amity University
Uttar Pradesh, Noida, India
e-mail: debu909@gmail.com

K. Pandey
e-mail: pandey.1411@gmail.com

porating an AVR loop; a ALFC loop is used for maintaining frequency under restricted limits.

The main target of the LFC in an isolated area is to maintain frequency under the scheduled range. For a rise in active power demand, the steam to turbine must be increased by increasing the governor points to compensate for that increased load. Also for a rise in the reactive power at the load, there is a drop in voltage at the terminals. To compensate for this drop, the excitation field current must be raised to a value such that emf generated is increased, thereby increasing the reactive power supplied. So there is a need of controller in both loops to keep the voltage (V) and frequency (f) inside the permissible range. Various methods have been adopted by the researchers to control the deviations in voltage and frequency within the allowable range such as PI, PID, Fuzzy logic, neural networks, hybrid techniques, and evolutionary algorithms. It has been found that the intelligent controllers provide better dynamic response than the conventional controllers. Also the optimum values of gains of P, I, and D found using evolutionary algorithms give more optimum results.

Most researchers have considered these two loops as decoupled as the time constants of excitation field are much lower than those of LFC loop. Hence, the transients occurring in the AVR loop vanish at much faster rate, and its effect on the dynamics of LFC loop is neglected. However, there is some cross-coupling present between the LFC and AVR loops in practical systems. The cross-coupling accounts for the interaction between the two loops.

In this paper, an attempt to study the effect of cross-coupling existing in between LFC and AVR loops has been done using Fuzzy logic controller. A simulink model has been designed in the MATLAB, and the comparison between the results of FLC and PID controller has been made to show the superiority of the intelligent technique.

2 Modeling of FLC Loop

The purpose of the LFC loop is to retain the frequency within a nominal range. The LFC loop contains four main parts: governor model, turbine model, generator-load, and a controller. It contains two loops: primary and secondary. Governor, turbine, generator-load, and regulation constitute primary loop. This primary loop is not enough to get zero steady-state error. So, a controller is necessary and an integral-type controller is generally preferred due to its zero steady-state response and reset type characteristics. The load frequency is sensed by frequency and is fed back to the comparator whose output decides whether to increase or decrease the steam intake depending upon the change in frequency. Figure 1 shows a LFC loop for an isolated area.

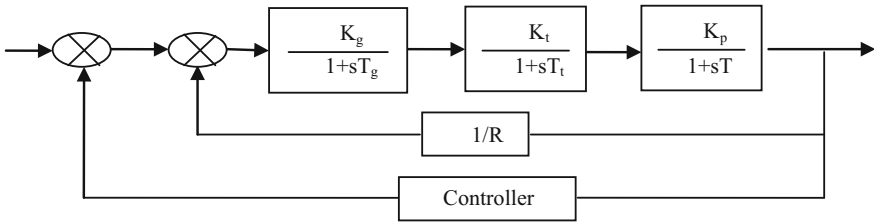


Fig. 1 LFC loop with controller

3 Modeling of AVR Loop

The ultimate task of an AVR loop is to keep terminal voltage constant. A typical AVR consists of an amplifier, an exciter, a field circuit, a transducer, and a controller. A potential transformer is used to sense the voltage magnitude in a phase. The sensed voltage is now used for generating error by comparing it to a DC reference signal. The error signal is amplified, and after amplification this error can be used to regulate the exciter field and restores its terminal voltage to nominal value. If the generator field current is increased, it results in an increase in the generated EMF and reverse happens if field current is decreased. Following are the components that constitute a AVR loop.

a. *Amplifier*

It amplifies the voltage error between the DC reference (V_r) and effective voltage (V_t), which is fed by the comparator. The output of the amplifier becomes exciter’s input. Due to delay in the response of amplifier, its transfer function model is:

$$\frac{\Delta V_{er}}{\Delta V_r} = \frac{K_a}{1 + sT_a} \tag{1}$$

where ΔV_r is the reference DC signal and ΔV_{er} is the error signal.

b. *Exciter*

The exciter has its input as the amplified error and excites the field windings to control the magnitude of the terminal voltage. The output of exciter is a function of field current, and due to saturation in the magnetic circuit it is not linear. But transfer function is linearly approximated to Eq. (2).

$$\frac{\Delta V_f}{\Delta V_{er}} = \frac{K_e}{1 + sT_e} \tag{2}$$

Here, ΔV_f is the voltage across field winding of the alternator.

c. *Generator Field*

The field voltage is applied to the field winding of the generator. Its transfer function is:

$$\frac{\Delta E}{\Delta V_f} = \frac{K_f}{1 + sT_f} \tag{3}$$

Here, ΔE is the variation in generated emf.

d. *Sensors*

A potential transformer is used to sense the actual output voltage magnitude continuously and feeds it to the comparator where it is compared with a reference dc voltage, to generate an error signal. It can be as its transfer function by:

$$\frac{V}{V_t} = \frac{K_s}{1 + sT_s} \tag{4}$$

E. *Controller*

The transient response considering peakshoots oscillations and settling time (t_s) can be enhanced through a controller. If a conventional PI controller is used, then the transfer function is given by Eq. (5) (Fig. 2)

$$\frac{K_{pS} + K_i}{1 + sT_f} \tag{5}$$

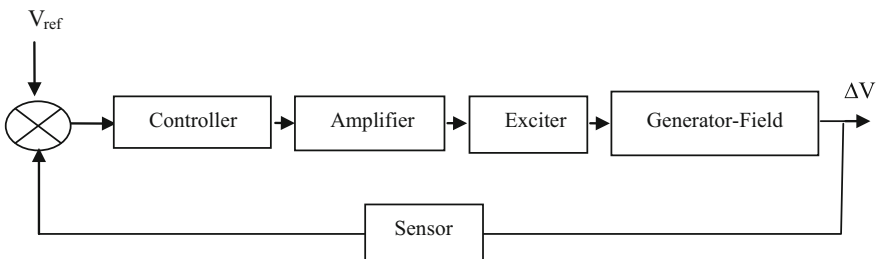


Fig. 2 AVR loop of a single power system

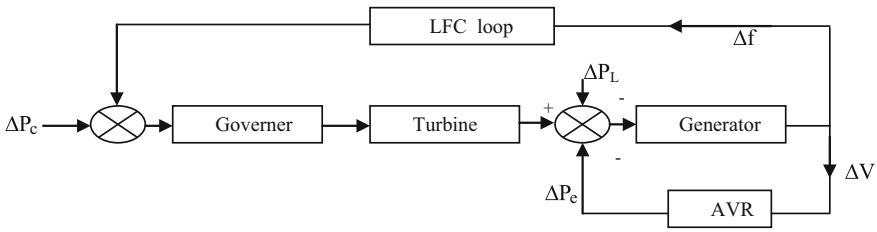


Fig. 3 LFC loop combined with AVR loop

4 Automatic Generation Control

The combination of both load frequency control and voltage control constitutes AGC. Both active and reactive power can be controlled through AGC. In steady-state conditions, the two loops behave as non-interacting, but during transient conditions become interacting and show that cross-coupling does exist between the two loops. Figure 3 below shows the schematic block diagram of LFC loop combined with AVR loop.

The magnitude of the active power is controlled by the generated emf E which is controlled by the AVR loop. Frequency depends on this active power; therefore, any alteration in AVR loop will cause subsequent changes in the LFC loop.

5 Control Methodology

There are various conventional and intelligent techniques that can be used for controlling the voltage and frequency in power network, e.g., PI, PID, Fuzzy logic, neural networks, hybrid techniques, and evolutionary algorithms. Here, conventional PID control and intelligent Fuzzy logic controller responses are compared.

5.1 Conventional Control: PID

PID controller in AVR is incorporated to control the voltage deviations by tuning the gains K_p , K_i , and K_d . The optimum of these gains can be found out using Ziegler–Nichls method. In LFC loop, the PID controller is used to control the frequency deviations. The simulink diagram of AVR with PID controller is shown Fig. 4.

Where e is the error, and u is the controlled output.

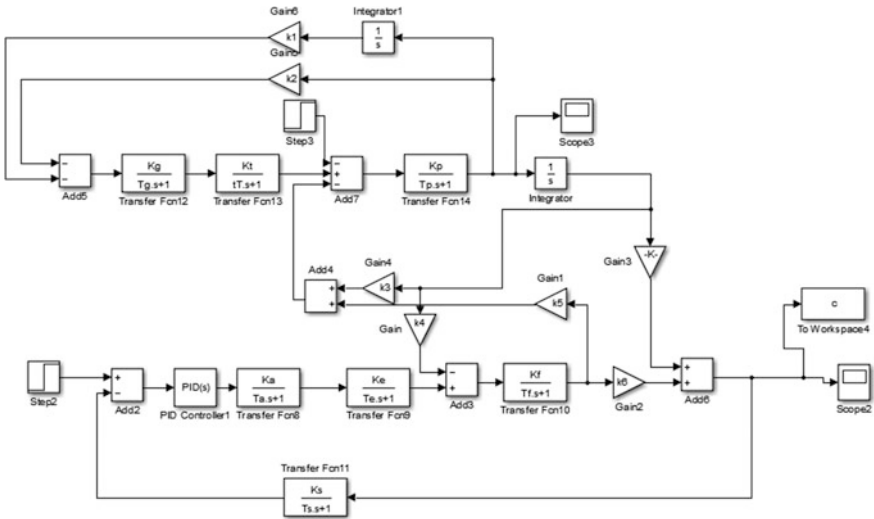


Fig. 4 Simulink diagram: AVR loop with PID controller

5.2 Intelligent Control: Fuzzy Logic

To map input vectors into output vector space with a knowledge base known as rule base, we use Fuzzy logic. It includes three parts, viz. Fuzzification (crisp to fuzzified), knowledge base formation, and defuzzification (fuzzified to crisp). Fuzzification involves the measurement of input variables and converting crisp measurement to fuzzified values and expressing them as input membership functions. A rule base is a set of rules that define a specific output to a particular input. The output membership functions are then defuzzified into real values.

A fuzzy inference system formed can be of two types: Mamdani-type or Sugeno-type. While Sugeno-type FIS is suitable with linear models only, Mamdani-type FIS is suitable with both linear and nonlinear systems. Here, we have used Mamdani-type models. Inputs to the Fuzzy logic controller are two, viz. error signal and derivative of the error, and has only one output (Fig. 5).

The seven input membership functions of both inputs and outputs are formed using triangular membership functions (mfs) with a range of -0.1 to 0.1 . A total of 49 rules have been formed using simple “if-then” statements. These rules and mfs are shown in Table 1 and Figs. 6, 7, and 8, respectively.

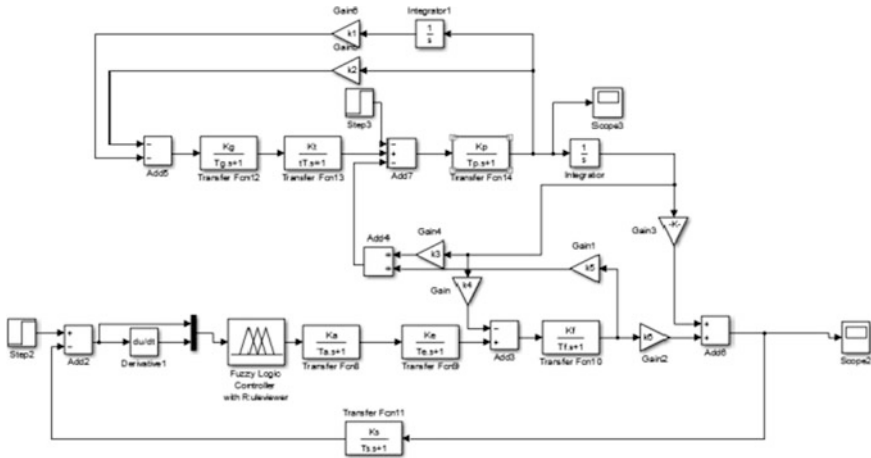


Fig. 5 Input error membership functions

Table 1 Rules for Fuzzy Inference System

error	de							
	UL	VL	L	ZE	H	VH	UH	
UL	UL	UL	UL	UL	VL	L	ZE	
VL	UL	UL	UL	VL	L	ZE	H	
L	UL	UL	VL	L	ZE	H	VH	
ZE	UL	VL	L	ZE	H	VH	UH	
H	VL	L	ZE	H	VH	UH	UH	
VH	L	ZE	H	VH	UH	UH	UH	
UH	ZE	H	VH	UH	UH	UH	UH	

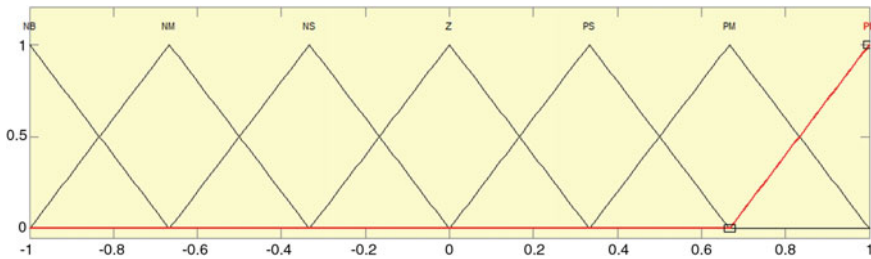


Fig. 6 Simulink diagram: AVR loop with Fuzzy controller

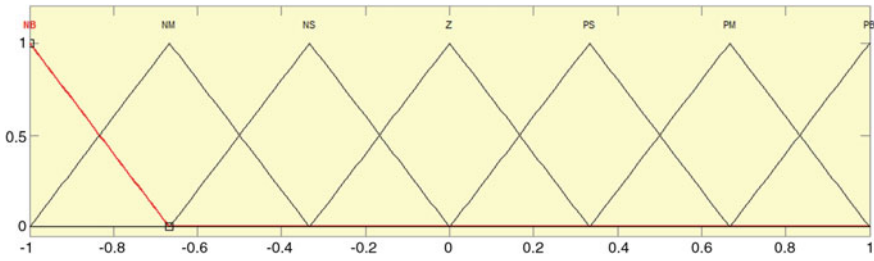


Fig. 7 Derivative of input error membership functions

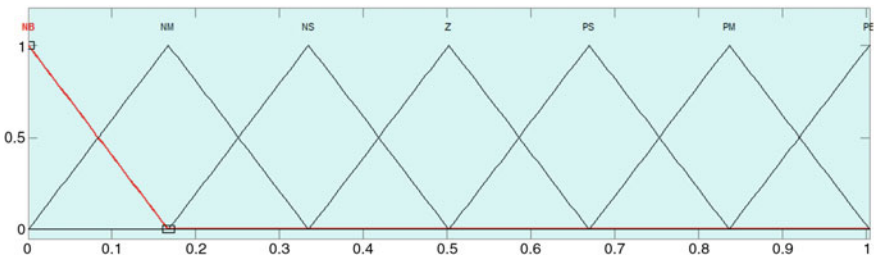


Fig. 8 Output membership functions

6 Results and Discussions

The system under investigation is simulated under following three cases, and the results are obtained:

CASE 1: Combined LFC and AVR loops without PID Control in AVR loop.

In this case, the system is incorporated with both LFC and AVR loops, but there is no controller present in the AVR loop. The voltage and frequency responses are obtained after simulation and shown in Fig. 9.

Case 2: Combined LFC and AVR loops with PID control in AVR loop.

In this case, the AVR loop is incorporated with a PID controller to reduce the steady-state error to zero. The simulation results show that the peakshoots and settling time have reduced, and the oscillations in the voltage response have been damped out (Fig. 10).

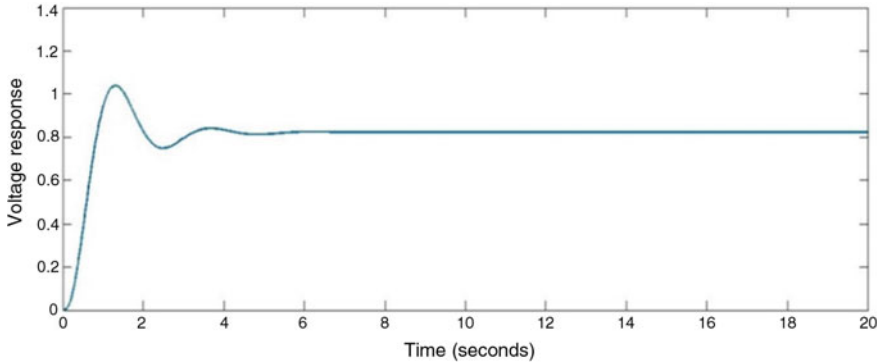


Fig. 9 Voltage response without any controller

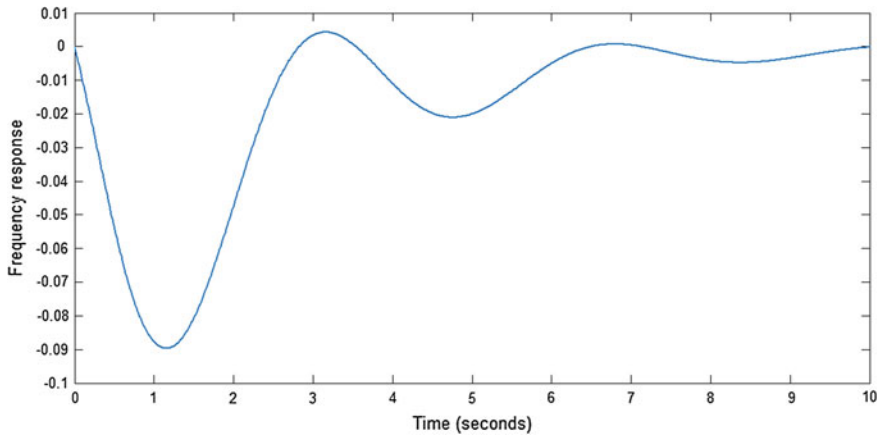


Fig. 10 Frequency response of LFC loop with AVR loop

CASE 3: Combined LFC and AVR loops with Fuzzy logic control in AVR loop.

In this case, the conventional controller is replaced by an intelligent controller, i.e., Fuzzy logic controller. The results show that the settling time is further reduced, and dynamic response is much improved (Figs. 11 and 12).

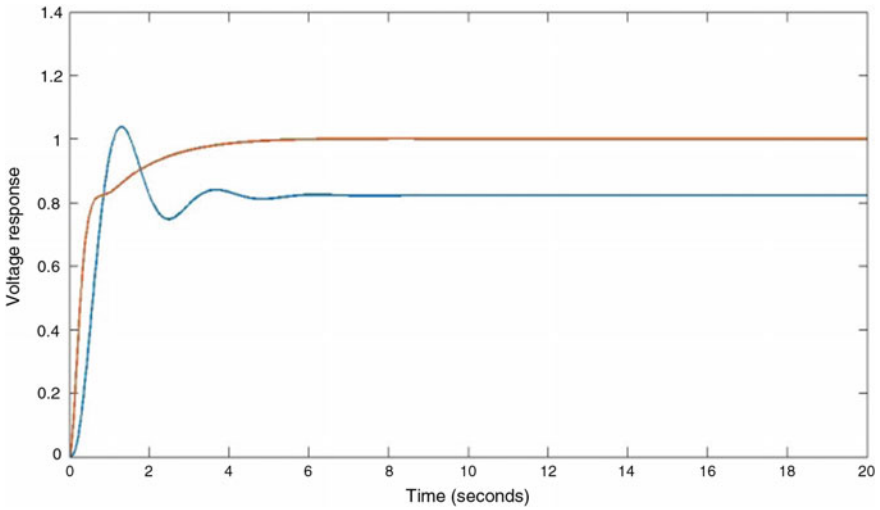


Fig. 11 Voltage response of with PID in AVR loop

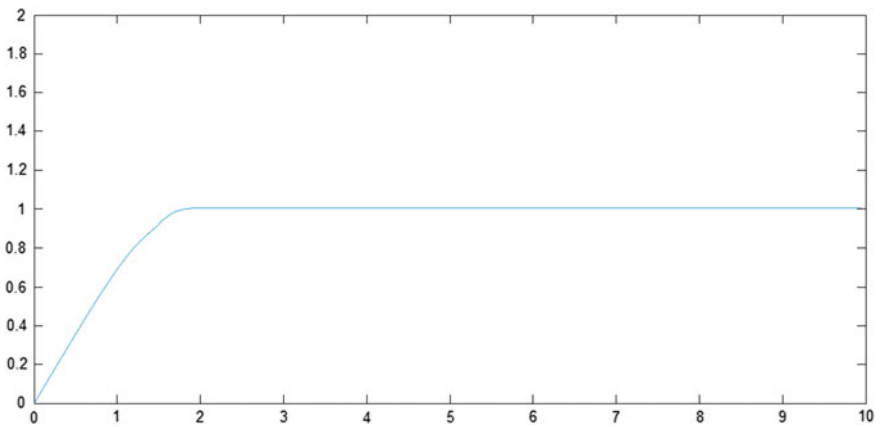


Fig. 12 Voltage response of with Fuzzy control in AVR loop

7 Conclusion

The frequency and voltage responses with different controllers were studied for the two loops. Also, the existence of cross-coupling in two loops and its effects (i.e., AVR and LFC) were analyzed. The oscillations present in the voltage response were successfully damped out using PID controller and FLC, and the outputs of the controllers were compared. It has been found that the intelligent Fuzzy control is

superior in controlling the voltage response than the conventional PID controller. The Fuzzy controller provides better dynamic responses considering the parameters such as damping oscillations, settling time, and maximum overshoots.

References

1. A. Gupta, A. Chauhan and R. Khanna, "Design of AVR and ALFC for single area power system including damping control," *2014 Recent Advances in Engineering and Computational Sciences (RAECS)*, Chandigarh, 2014.
2. Parveen Dabur, Naresh Kumar Yadav and Vijay Kumar Tayal *International Journal of Computer and Electrical Engineering*, Vol. 3, No. 2, April, 2011.
3. D.P. Kothari, I.J. Nagrath- "Modern power system Analysis"-TATA macgrawhill.
4. S. Satyanarayana, R. K. Sharma, Mukta and A. K. Sappa, "Automatic generation control in power plant using PID, PSS and Fuzzy-PID controller," 2014 International Conference on Smart Electric Grid(ISEG), Guntur, 2014.
5. A.M. Hamza, M.S. Saad, H.M. Rashad and A. Bahgat, "Design of LFC and AVR for single area power system with PID controller tuning by BFO and Ziegler methods," *IJCST*, vol. 4, issue 5, pp. 12–17, May 2013.

Object Size Determination Grasped by a Four-Finger Gripper Using Workspace Analysis

Nazma Ehtesham, S. Mukherjee and Mohd Suhaib

Abstract The performance of a multi-finger robotic gripper is measured in terms of its capability to grasp and manipulate objects successfully. Manipulation of an object is possible only if it is stable within its grasp. Moreover, most of the manipulation task is done only when the object is grasped by precision grasping rather than power grasping. Also, the manipulability of the object by a gripper depends upon size and shape of the object. It is, therefore, important to evaluate the shape and size range that a robotic gripper can grasp to understand its area of application. The work presented here proposes a method to identify the maximum size of an object which a gripper can grasp by precision grasping. The workspace of the hand is utilized for this purpose. The methodology is demonstrated on a new four-finger tendon-driven robotic gripper developed in the laboratory.

Keywords Workspace • Object size • Position vectors

1 Introduction

The object to be handled by a robotic gripper can be of various morphology, weight, and dimensions depending upon the task and environment. Custom-made grippers are required to handle particular set of objects and can execute defined set of manipulation. No universal gripper is suitable for all work pieces. However, advancement in technology has led to more developed universal gripping devices. These are called dexterous robot hands. Dexterous hands are capable to handle different size and shape objects more efficiently, but their design is generally very

N. Ehtesham (✉)
Amity University, Noida 201301, Uttar Pradesh, India
e-mail: nazma.e@gmail.com

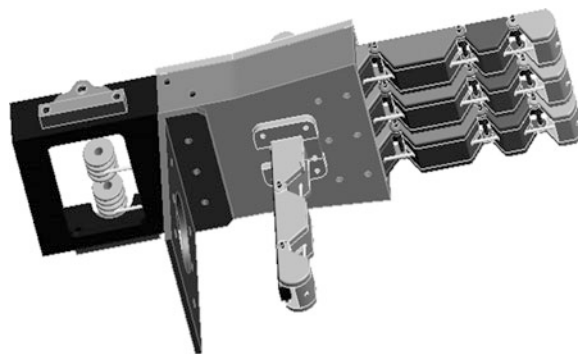
S. Mukherjee
Indian Institute of Technology, New Delhi 110016, India

M. Suhaib
Jamia Millia Islamia, New Delhi 110025, India

complex, cost is high, and the handling capacity is very low compared to task specific grippers. The underlying work evaluates the performance of a new four-finger gripper. The hand is developed to have better grasping capabilities with simple mechanism as the main objective (Fig. 1). The hand has total eleven joints (each finger having three revolute pairs and thumb having two revolute pairs). The actuation mechanism restricts total degree of freedom of hand to four, one for each finger and one for thumb. The actuation is provided through independent rope and pulley mechanism for all fingers and thumb. The actuator motion is transmitted from distal to middle and middle to proximal phalange through the rope. This causes the finger wrap partially. The workspace of the gripper is calculated and is used as an important parameter for evaluating its grasping capabilities. Workspace is the region in space which is within reach of the gripper [1]. The region within which each point is traceable by the gripper in at least one orientation is called reachable workspace. If the gripper can trace all the points within a region in all of its orientation, then the region is termed as denims workspace. Thus, the dexterous workspace can be considered as the subset of reachable workspace. The workspace of the hand if resembles to that of human hand indicates the degree of anthropomorphism and is discussed as a function of hand kinematics in [2, 3]. The thumb–finger precision workspace defines all positions which are possible for contact between tips of thumb and fingers in all configurations [4].

A number of approaches have been reported in the literature to investigate the workspace of robots, namely geometric analysis [5], random search method by Monte Carlo technique [6], and polynomial discriminant [7]. The workspace of human hand is analyzed analytically in [8]. Shin et al. [9] compared a robot hand and human hand by comparing their workspace which was calculated using forward kinematics. The appropriate locations of human–robot interaction—were determined in advance by computing the workspace of human and robot in their working area [10]. However, these methodologies never proved to be applicable for multi-fingered robotic grippers. In fact, limited analysis is available in this area. This is because of the complex mechanisms associated with these hands. Therefore, a simple and efficient method is an obvious need for investigating the workspace of multi-finger robotic hand.

Fig. 1 Four-finger tendon-driven gripper



2 Methodology

The thumb, middle and index finger are considered to play the most prominent role for grasping various objects. However, ring and pinky fingers are considered auxiliary [11, 12]. Moreover, for the hand under consideration, all three fingers other than thumb are identical in all aspects; therefore, the workspace created here involves thumb and only one of the three fingers. The work volume of the four-fingered gripper is generated by defining the position vectors of tip of middle finger and thumb in terms of joint rotations of individual phalanges. The range of joint rotations is taken in accordance with range of fingers and thumb of human hand as reported by ‘American Academy of Orthopaedic Surgeons’ [13]. The reference coordinate axes are defined along unloaded configuration of thumb and middle finger (Fig. 2), and their point of intersection is taken as the origin of coordinate axes. The position vectors of thumb and fingertip are plotted on the coordinate frame (Fig. 3), and their plots are generated using 3D surface plotter. (Figs. 4, 5, 6, and 7). The plots give entire range of tip movement within the workspace. The finger and thumb tip positions can directly be obtained from these plots for any rotation of joints. To calculate the maximum opening of hand for precision grasping, the joint rotations are defined in a logical way based on the physiology of human hand [14], and distance formula [15] from coordinate

Fig. 2 Finger–thumb arrangement on palm and definition of coordinate axes for the four-finger gripper

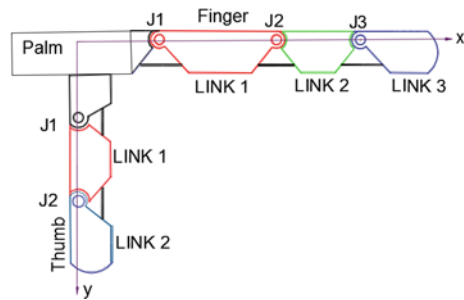
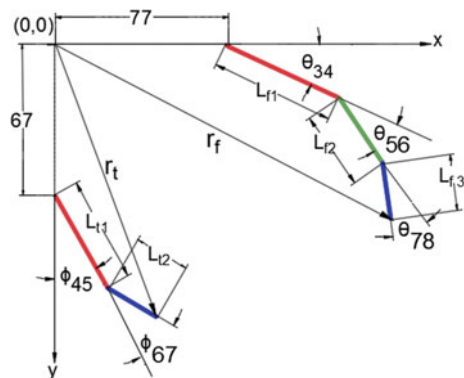


Fig. 3 Kinematic model representation of middle finger and thumb for the four-finger gripper



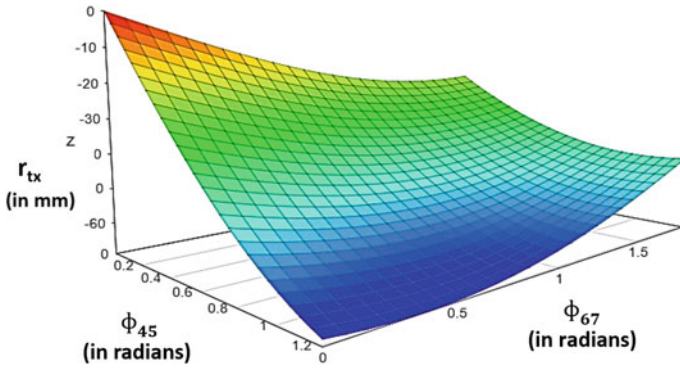


Fig. 4 Thumb tip vector along coordinate x-axis versus proximal and distal joint rotation

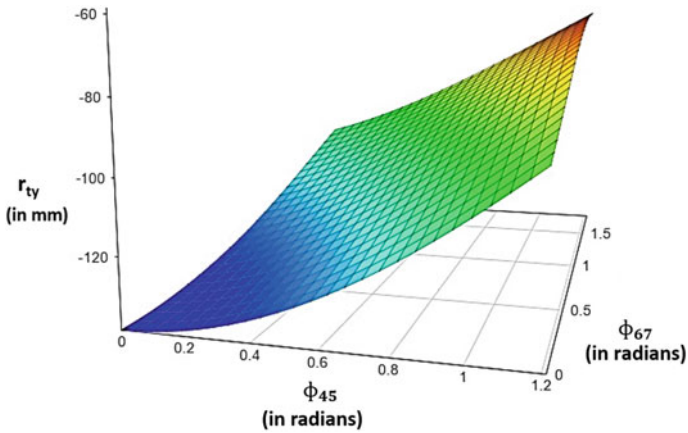


Fig. 5 Thumb tip vector along coordinate y-axis versus proximal and distal joint rotation

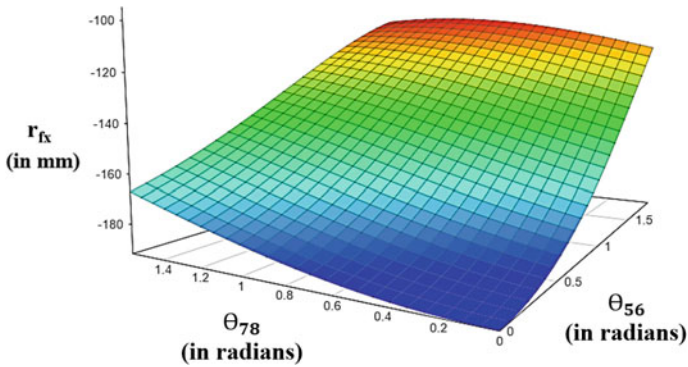


Fig. 6 Fingertip vector along coordinate x-axis versus middle and distal joint rotation

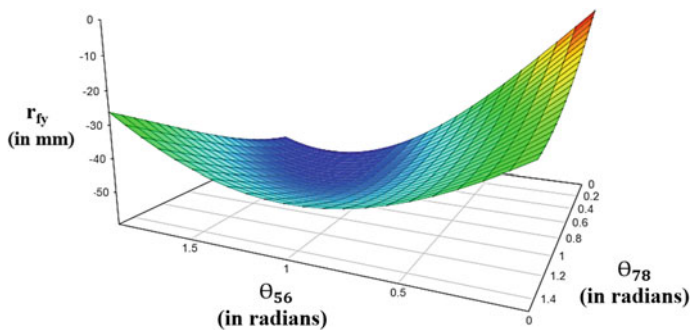


Fig. 7 Fingertip vector along coordinate y -axis versus middle and distal joint rotation

geometry is used for calculating distance between finger and thumb tip. The maximum distance between the tips gives a direct value of maximum size of the object that can be grasped by the hand.

3 Position Vectors

For deriving position vectors [16], coordinate frame and its origin is defined. The fingers and thumb are attached to the common base which can be considered as its palm. The point of intersection of the axes of finger joints and thumb joints defines coordinate frame and origin of the system as shown in Figs. 2 and 3. In this configuration, phalange rotations are only possible about z -axis.

3.1 Position Vector for Finger

From Fig. 3, the position vector r_f of the tip point of the finger is derived as:

$$\begin{aligned} \vec{r}_f = & -[L_{f1} \cos \theta_{34} + L_{f2} \cos(\theta_{34} + \theta_{56}) + L_{f3} \cos(\theta_{34} + \theta_{56} + \theta_{78}) + 77] \vec{i} \\ & - [L_{f1} \sin \theta_{34} + L_{f2} \sin(\theta_{34} + \theta_{56}) + L_{f3} \sin(\theta_{34} + \theta_{56} + \theta_{78})] \vec{j}. \end{aligned} \quad (1)$$

3.2 Position Vector for Thumb

Thumb is different than fingers as having only two phalanges. Also, the dimensions of the phalanges are different from fingers. The position vector of tip point for thumb is written as:

$$\begin{aligned} \vec{r}_i = & -[L_{i1} \sin \varphi_{45} + L_{i2} \sin(\varphi_{45} + \varphi_{67})] \vec{i} \\ & - [L_{i1} \cos \varphi_{45} + L_{i2} \cos(\varphi_{45} + \varphi_{67}) + 67] \vec{j}. \end{aligned} \quad (2)$$

4 Workspace

Workspace of finger and thumb can be analyzed by plotting graph of different parameters of tip of the finger and thumb. As the gripper is developed by taking human hand as model, therefore, the range for joint rotations is taken in conformity with human hand. Here, the plots are generated by taking the following values [7].

For finger: Proximal joint rotation = 0° – 90° , middle joint rotation = 0° – 90° , distal joint rotation = 0° – 90° . For thumb: Proximal joint rotation = 0° – 50° , distal joint rotation = 0° – 80° .

The phalange lengths are taken from gripper geometry $L_{f1} = 55$ mm, $L_{f2} = 35$ mm, $L_{f3} = 25$ for the finger and $L_{t1} = 47$ mm, $L_{t2} = 25$ mm for the thumb. The workspace of thumb and middle finger is generated using 3D surface plotter. Fingertip and thumb tip position can be obtained using these plots for any combination of joint rotation angle.

5 Maximum Size of the Object that the Hand Can Grasp for Precision Grasping

The hand can grasp an object of maximum size with precision only when the tips of finger and thumb have maximum opening or the distance between the two tips is maximum. This can be achieved if CMC and MCP joint of thumb are kept at minimum opening, while for finger, the MCP and PIP joint are at minimum opening (i.e., for thumb $\varphi_{45} = 0^\circ$ and for finger, $\theta_{34} = 0^\circ$ and $\theta_{56} = 0^\circ$) At the same time, the extension/flexion angle of IP joint of thumb and DIP joint of finger is set at maximum value (i.e., for thumb $\varphi_{67} = 80^\circ$ and for finger, $\theta_{78} = 90^\circ$) [8].

From Figs. 6 and 7 in Chap. 4, the fingertip coordinates corresponding to above-stated values ($\theta_{34} = 0^\circ$ and $\theta_{56} = 0^\circ$ and $\theta_{78} = 90^\circ$) are: $P_1(x_2, y_2) = (r_{fx}, r_{fy}) = (-167, -25)$. Also, from Figs. 3 and 4 in Chap. 4, the thumb tip coordinates corresponding to above-stated values ($\varphi_{45} = 0^\circ$, $\varphi_{67} = 80^\circ$) are: $P_2(x_2, y_2) = (r_{tx}, r_{ty}) = (-24.62, -118.34)$. The distance between these points using distance formula [15] from coordinate geometry is:

$$\begin{aligned} d &= \sqrt{(r_{fx} - r_{tx})^2 + (r_{fy} - r_{ty})^2} \\ d &= \sqrt{(-167 + 24.62)^2 + (-25 + 118.34)^2} \\ d &= 170.24 \text{ mm.} \end{aligned} \quad (3)$$

This is the maximum gap between the tip of the finger and thumb which is also the maximum size of the object that can be grasped by the hand. Thus, any object having dimension up to 170 mm in any direction can be grasped by the hand.

6 Conclusions

A simple approach is developed for creating workspace of a new four-finger robotic gripper. The methodology can be applied to any multi-finger gripper irrespective of the mechanism used to actuate the gripper. For the four-finger gripper, the workspace is generated using position vectors of thumb and finger. The plots are then utilized to calculate the largest object size that the hand can grasp. The maximum distance of fingertip from thumb tip is calculated as 170 mm. Thus, the hand can grasp any object of size up to 170 mm. This confirms the applicability of this gripper for all anthropomorphic purpose as far as the object size is concerned, as for an adult hand, the range for maximum object size varies from 160 to 190 mm [7]. The approach can further be utilized for plotting position vectors of all the fingers on the same plot, and the analysis can be extended to estimate the maximum size of object for power grasping. Further, the power grasp analysis for position vector can be extended for calculating minimum size of object.

References

1. Zhang Wenzeng, Zhao Deyang, Chen Qiang, Du Dong.: Linkage under-actuated humanoid robotic hand with of grasping force. In IEEE 2nd International Conference on Informatics in Control, Automation and Robotics (CAR). (Vol-2), (29 April 2010) doi: [10.1109/CAR.2010.5456585](https://doi.org/10.1109/CAR.2010.5456585).
2. Biagiotti L., Lotti F., Melchiorri C., Vassura G.: How Far is the Human Hand? A Review on Anthropomorphic End Effectors. DIES Internal Report, University of Bologna, Tech. Rep. (2004).
3. Biagiotti L.: Advanced robotic hands: Design and control aspects. Ph.D. dissertation, Università Degli Studi di Bologna, (2002).
4. L.C. Kuo, H.Y. Chiu, C.W. Chang, H.Y. Hsu, and Y.N. Sun: Functional workspace for precision manipulation between thumb and fingers in normal hands. *Journal of electromyography and kinesiology*, vol. 19, no. 5, pp. 829–839, (Oct 2009).
5. Gupta. K.: On the nature of robot workspace. *International Journal of Robotics Research* 5 (2):112–121 (1986). (Pubitemid 16592727).
6. Rastegar J., Perel D.: Generation of manipulator workspace boundary geometry using the monte carlo method and interactive computer graphics. In *ASME Trends and Developments in Mechanisms Machines and Robotics Vol.3* pages 299–305. (1988).
7. Hong Zhang: Efficient evaluation of the feasibility of robot displacement trajectories. In *IEEE Transactions on Systems Man and Cybernetics* 23(1):324–330. (1993).
8. J. Yang K., Malek Abdel, Nebel K.: Reach envelope of a 9-degree-of-freedom model of the upper extremity. *International Journal of Robotics and Automation* 20(4):240–259. (2005). (Pubitemid 41499038).

9. Shin Seunghoon, Han Sangchul, Lee Kunwook, Moon Hyungpil, Choi Hyouk Ryeol, Koo Ja Choon: A design framework for dexterous robotic hand. IEEE 8th International Conference on Ubiquitous Robots and Ambient Intelligence (URAI). (23–26 Nov. 2011).
10. Vahrenkamp Nikolaus, Arnst Harry, Wächter Mirko, Schiebener David, Sotiropoulos Panagiotis, Kowalik Michal, Asfour Tamim.: Workspace analysis for planning human-robot interaction tasks. IEEE-RAS 16th International Conference on Humanoid Robots (Humanoids), (15–17 Nov. 2016).
11. T. Feix, R. Pawlik, H. Schmiedmayer, J. Romero, D. Kragic: A comprehensive grasp taxonomy: In Robotics, Science and Systems: Workshop on Understanding the Human Hand for Advancing Robotic Manipulation. (June 2009). <http://grasp.xief.net>.
12. M. Cutkosky: On grasp choice, grasp models, and the design of hands for manufacturing tasks. Robotics and Automation, IEEE Transactions on, vol. 5, no. 3, pp. 269–279, (Jun 1989).
13. <https://www.fgc.edu/wp-content/uploads/2011/12/averages-of-rom.pdf>.
14. Marieb, Elaine N: Human Anatomy & Physiology (Sixth ed.). Pearson PLC. ISBN 0-321-20413-1. (2004).
15. William H. McCrea: Analytic Geometry of Three Dimensions. Courier Dover Publications, (Jan 27, 2012).
16. Spiegel M.R., Lipschutz S., Spellman D. Vector Analysis (Schaum's Outlines) (2nd ed.). McGraw Hill. ISBN 978-0-07-161545-7 (2009).

Estimation of Parameters of Target Using RADAR Data Sets

M. Raja, Sudhir Kumar Chaturvedi, Hutanshu Kamal, Cris Thomas and Rahul Kummamuri

Abstract Radar (radio detection and ranging) has large number of application ranging from remote sensing to missile guidance, but it is widely employed to estimate the velocity and position of a moving or presence of stationary targets. Different types of radars which are used for this purpose are pulse Doppler radar, MTI (moving target indicator) radar with different types of configuration like monostatic or bistatic. This work primarily focuses on the velocity and position estimation of a moving target using different radar data sets. Initially, Doppler effect and time delay of the received signal for a simple monostatic radar configuration are examined. Then, the graphical user interface (GUI) is developed in MATLAB to model the ambiguity function in order to derive the target parameters from the received signal.

Keywords Doppler effect · Doppler radar · MTI RADAR · Ambiguity function

1 Introduction

Radar is an electromagnetic system which is used to determine the velocity and position of an object [1]. All weather operability of radar systems helps it to find diverse form of application; application of radar system ranges from general parameters like position and velocity of the target to the weather monitoring and missile guidance [1]. A typical radar system consists of antenna, duplexer, transmitter, receiver, and a display unit (Fig. 1).

M. Raja (✉) · S.K. Chaturvedi · H. Kamal · C. Thomas · R. Kummamuri
Department of Aerospace Engineering, University of Petroleum and Energy Studies,
Dehradun, Uttarakhand, India
e-mail: mraja@ddn.upes.ac.in

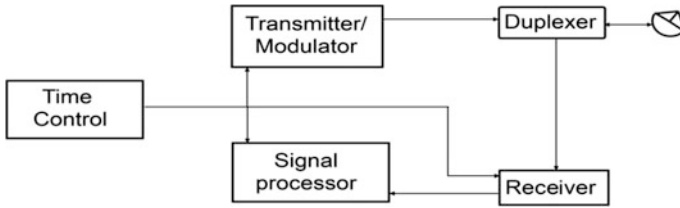


Fig. 1 Simplified block diagram of the pulse Doppler radar

1.1 Working of Typical Radar

RADAR emits electromagnetic waves through antenna into a specified volume in order to search for the objects, i.e., targets. These targets reflect a part of the incident waves to the RADAR; these reflected waves are termed as echoes. Echoes are further processed by the RADAR receiver in order to derive the desired information about the target like velocity, range, size, and direction of its movement.

1.2 Classification of RADAR

RADAR can be classified on the basis of the different modes of its operation which directly depends on the task it has to carry out. Configuration of any RADAR

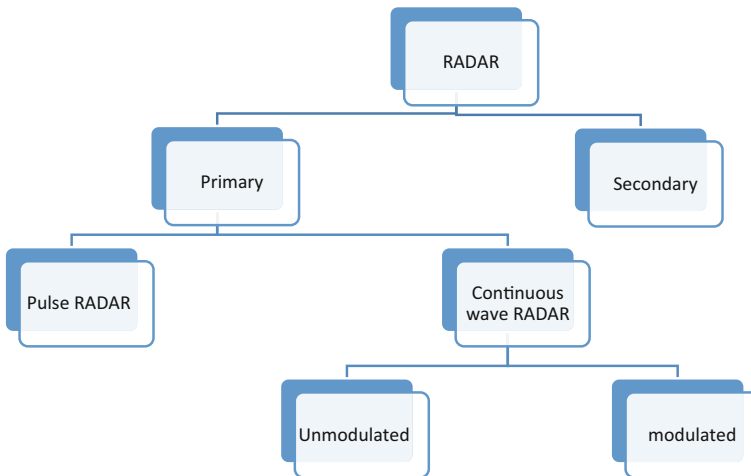


Fig. 2 Classification of RADAR [3]

depends upon the tasks to be performed, physical environment, and the interferers it is expected to encounter [2]. The work presented primarily focuses on the mono-static pulse Doppler radar (Fig. 2).

2 Methodology

Doppler effect holds good for the parameter estimation of moving target with the help of RADAR data sets. Doppler effect states that the frequency of the returned signal depends on the velocity and direction of the target (Fig. 3).

Ambiguity function is employed to determine the position and velocity of the moving target. The correlation function is defined as:

$$\theta(\tau, \gamma) = \int_{-\infty}^{\infty} s(t)s^*(\gamma t + \tau)dt. \tag{1}$$

Hence, ambiguity function can be defined as [4]:

$$(\tau, \gamma) = |(\tau, \gamma)|^2. \tag{2}$$

Considering $x(t)$ as sent signal and $y(t) = (\gamma t - \tau)$ as received signal, then γ and τ can be determined, which subsequently assist in determination of position and velocity of the target.

According to [5], the ambiguity function can be written as:

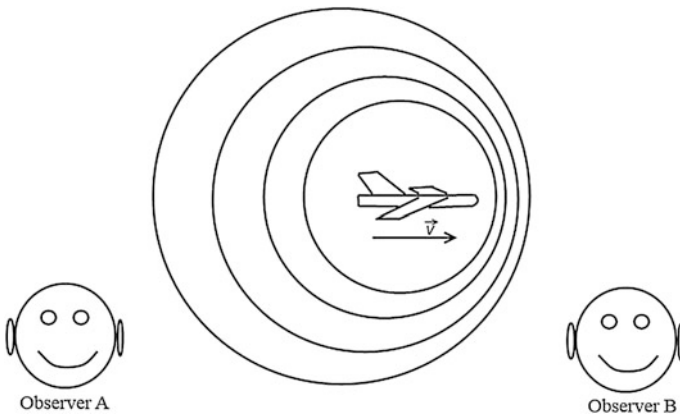


Fig. 3 Schematic depicting the Doppler effect

$$\psi(\tau, f_D) = \left| \int_{-\infty}^{\infty} s(t)s^*(t - \tau)e^{-jf_D t} dt \right|^2 \quad (3)$$

where f_D is Doppler frequency.

3 Implementation in MATLAB

A function `rcvdsig` is defined in MATLAB to simulate the received signal. This function is based on the following equation [4].

$$y(\alpha t + T_0) = x(t) \quad (4)$$

where

$y(t)$ is received signal,

$x(t)$ is original signal, and

α is Doppler factor.

In the above equation, the signal sent is delayed due to the finite propagation velocity of the signal.

Input parameters of the above-mentioned function are:

x the vector of emitted signal samples,

f_s the sampling frequency,

c the velocity of signal propagation,

v the speed of the target,

d the distance from the target at the time of the beginning of emitting,

ap the boolean operator, which is equal to 1 for the approaching target and 0 for the receding target.

Objective of the `rcvdsig` function is to simulate signal reflected from the target. Received signal is sampled at the same frequency as the input one. Resampling function in MATLAB can be used to generate the Doppler frequency shift, but the results of the resampling function go out of scope when target moves non-radial to the RADAR. Hence, interpolation function can be employed to overcome the short comings of the resampling function.

In order to estimate the velocity and position of a target, a function `ambf` is defined in MATLAB. `ambf` function is based on the following equation [4].

$$\psi(\tau, \alpha) = \left| \int_{-\infty}^{\infty} s(t)s(\alpha t + \tau) dt \right|^2. \quad (5)$$

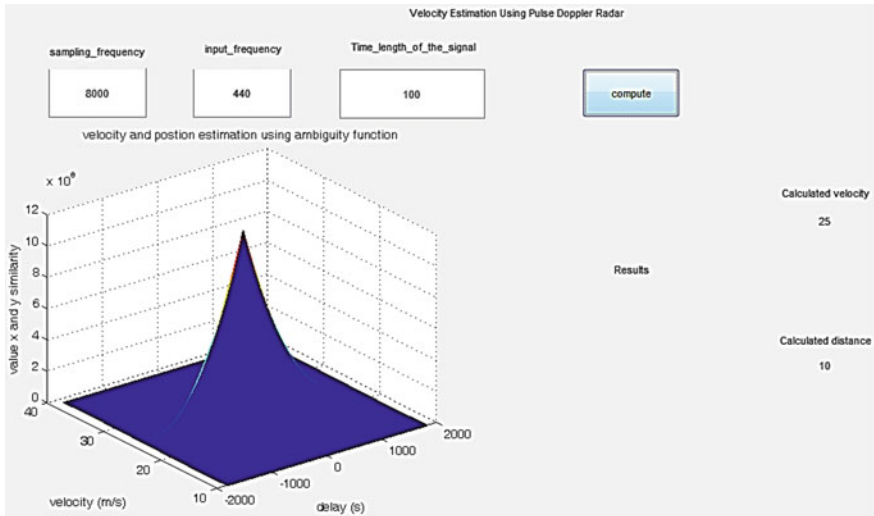


Fig. 4 Schematic of GUI

4 Results and Discussions

Received signal is sampled at the same frequency as the input one. Resampling function in MATLAB can be used to generate the Doppler frequency shift, but the results of the resampling function go out of scope when target moves non-radial to the RADAR. Hence, interpolation function can be employed to overcome the short comings of the resampling function.

Ambiguity function is the tool which can be used to estimate the target parameters by comparing the received and sent signal. Implementation of ambiguity function in MATLAB proves its utility for the determination of position and velocity. A GUI is developed in the MATLAB environment as shown in Fig. 4 to compute the velocity and range of the target using monostatic pulse Doppler radar. It also helps us to analyze the effect of variation in input parameter on the computation of the target parameters.

References

1. Skolnik I. Merrill: Introduction to RADAR Systems. Mcgraw-Hill, Singapore (1980) 1–5.
2. Edde Byron.: RADAR Principles, Technology, Applications. Pearson Education, Delhi (2004) 44–49.
3. Sharma K.K.: Fundamentals of RADAR, SONAR and Navigation Engineering. S.K.Kataria and sons, Delhi (2011) 18–19.

4. Swick, D. A.: An Ambiguity Function Independent of Assumptions about Bandwidth and Carrier Frequency. NRL Report 6471, Naval Research Laboratory, Washington, D. C. 1966.
5. Tsao, T.: Ambiguity Function for a Bistatic Radar. IEEE Transactions on Aerospace and Electronic Systems, 1997, ISSN 0018-9251.

Implementation of Smart Home Automation System on FPGA Board Using IoT

Rohit Chhabra, Manpreet Kaur Khurana and Anshuman Prakash

Abstract There has been a rapid introduction of network-enabled digital technologies in home automation. These technologies provide a lot of opportunities to improvise the connectivity of devices within the home. Internet helps to bring in with immediate solution for many problems and also able to connect from any of the remote places which contributes to overall cost reduction and energy consumption. Intelligence based on microprocessors is used by home automation to incorporate electronic structures in the household. The inducement in arrears' home mechanization is economical application of electrical energy. Thus, a spread of analysis and lots of resolutions on home automation has been planned. These structures use laptop, mobile web, GSM Bluetooth, and Zigbee network, etc. (Di Carlo and Cove, Smart Homes (Home Automation)" [1]; Krishna and Nagendram, Int J Comput Technol Appl 3(1):163–168, 2012 [2]). The proposed system is made with the help of FPGA and Wi-Fi. The appliances are controlled wirelessly through mobile phone connected with Wi-Fi.

Keywords IoT · FPGA · Home automation

1 Introduction

Verilog will be used to code the design being implemented using field-programmable gate array (FPGA) hardware. This system uses World Wide Web network to set up the communication between mobile/computer and controller. To improve the

R. Chhabra (✉)

Synopsys India Pvt. Ltd., Bangalore, India
e-mail: rohit.rohit.chhabra@gmail.com

M.K. Khurana

University of Petroleum and Energy Studies, Dehradun, India
e-mail: manpreetkhurana26@gmail.com

A. Prakash

THDC-IHET, Tehri, Uttarakhand, India

© Springer Nature Singapore Pte Ltd. 2018

R. Singh et al. (eds.), *Intelligent Communication, Control and Devices*,
Advances in Intelligent Systems and Computing 624,
https://doi.org/10.1007/978-981-10-5903-2_83

805

standards of living, the system uses wireless technology. GUI has been developed via Microsoft Visual Basic .NET. The speaking acknowledgment system was created with the assistance of Microsoft Speech [3]. Client system that has been accustomed captures the command and transfers the information to server via Wi-Fi-based wireless network. Server system is supplied to GUI administrator for executing the speaking acknowledgment system. Mobile-built vocal sound grasp management and observation system was planned wherever authors develop a rule that translates the vocalized feedback into writing note once haul out the options [4]. In the epitome style of Zigbee, primarily constructed assimilated device is mentioned. Such design theme has knack to regulate all piece of equipment while not extra hardware [5]. In mandate to attach by means of the house grid, a cellular mobile phone primarily centered on a piece of equipment scheme is conferred [6]. In the predicted system, design authors programmed the consumer cellular phone using the J2ME language. When the commands from the purchasers are once received by the mobile phone, it performs the actions accordingly to the request by PIC microcontroller. Opto-coupler and immobile control button (TRAIC) is employed to incorporate the expedients flanked by the PIC and also the home-based machines. Two dominant procedure strategies are mentioned, i.e., time and speech controlled through computer-developed exploitation VB 6.0 language, and they used Microsoft voice engine tools for voice recognition [7]. The papers show that earlier systems were wired and quality measurement was done manually which was time-consuming and laborious. Then automated wired systems were implemented in industries and institution. Later, warning systems were developed to warn the users in institution using sensors. The wired systems were changed to wireless systems. A system with GSM facility was introduced so that user can monitor the industry or household from anywhere. Then system with wireless technologies like Zigbee and RF came with different sensor nodes [8]. The research implemented is a home automation system which wirelessly monitors the appliances via Wi-Fi and sensor system used for the warning system [9–11].

2 Proposed Algorithm

2.1 Block Diagram

The interfacing unit and the Wi-Fi module are connected to FPGA-programmed central board through serial port. The data will be sent serially from the mobile/computer to the Wi-Fi module using the World Wide Web gateway.

The focal utility of the control unit is to receive the data from the Wi-Fi module. The UART has two constituents that are UART transmitter and UART receiver. The architecture of the system is shown in Fig. 1.

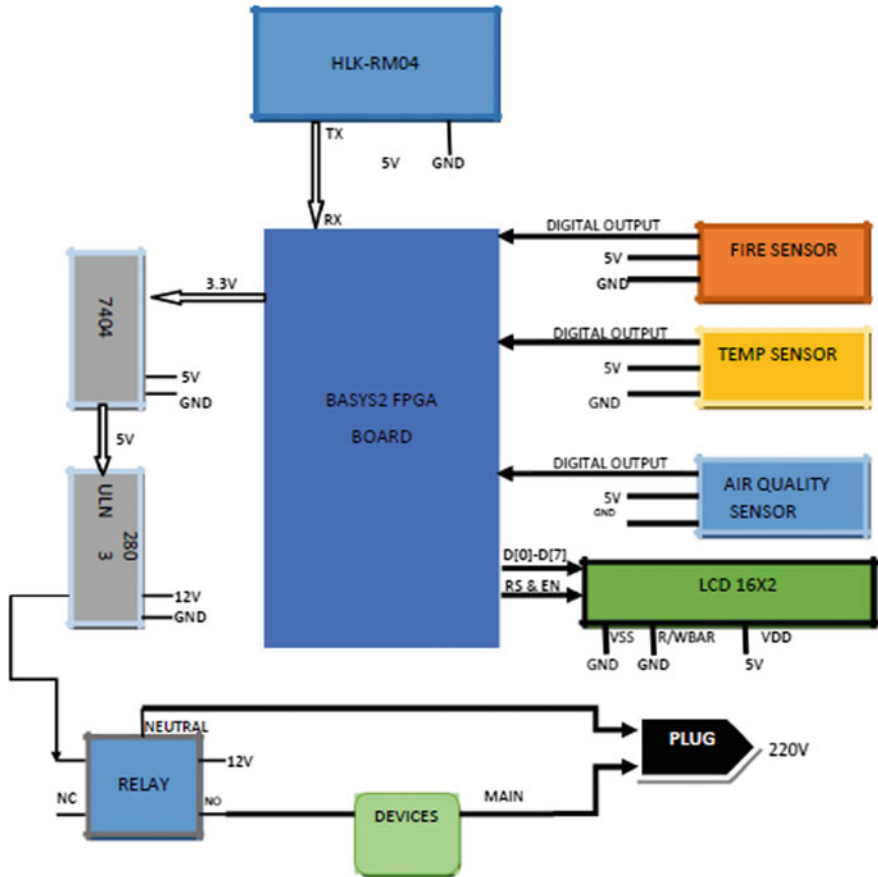


Fig. 1 Architecture of the system

2.2 Description

As shown in Fig. 1, from FPGA to HLK-RM04, there is only one connection, i.e., transmitter of the Wi-Fi module with the receiver of the FPGA. As we know that FPGA is not been provided with the UART pins, we had built a UART receiver set at 9600 baud rate. In the above figure, there is flow from the FPGA → 7404 → ULN2803; it is done because the output of the FPGA board is 3.3 V which is not supportive for ULN2803 to work out. It requires the voltage of 5 V to work. After that there is Relay which is electromechanical device used to connect between 12 and 220 V. The other important interface which plays very crucial role for the feedback of the system is LCD interface which works as a broadcaster as well as warning systems whenever sensor system crosses its threshold value. On basis of the values of the sensor, value on the LCD changes. LCD has been interfaced through FPGA in 8-bit mode, i.e., it has 8 data pins from which ASCII values of the characters have been sent,

one at a time by following the particular timing constraints as explained in LCD section of the previous section. The other two pins of the LCD that are connected with the FPGA are enabled and data/instruction registers. Whenever we have to write a data over the LCD, it is going to only happen with $1 \rightarrow 0$ transaction of the enable pin. In writing data over the LCD, we have to continuously swap between data and instruction mode. It happens as after every character printing, we have to move the cursor to the next point next to it and also to mention that to where to start from. The other connections are done as shown in the diagrams which are connected to the ground and Vcc pins. The sensor circuits shown in the above sections had only one digital output except from there supply and ground pins. These digital outputs come from the op-amp output after comparing their values with the threshold values adjusted by us through potentiometer. Depending upon their values, controller decides which warning has to be print to the LCD and for warning lights on FPGA is also switched on which on the other hand in any real application can be connected to the warning alarm.

3 Results

The data is being transmitted to the receiver of FPGA board via Wi-Fi module transmitter section, and data is being received on the FPGA, thus the proposed prototype is the handheld device through which a user can control the devices from

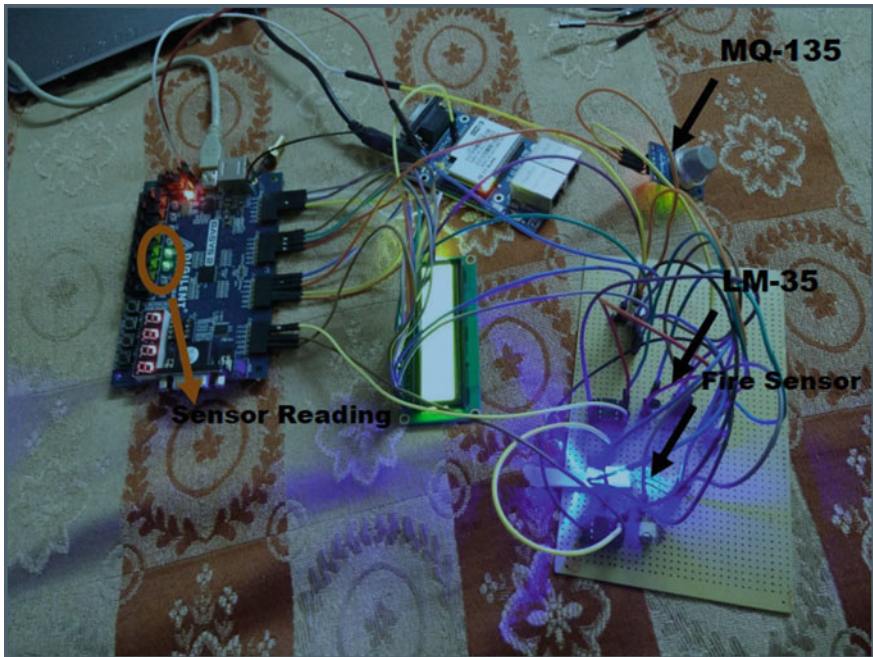


Fig. 2 Sensors attached with FPGA controller

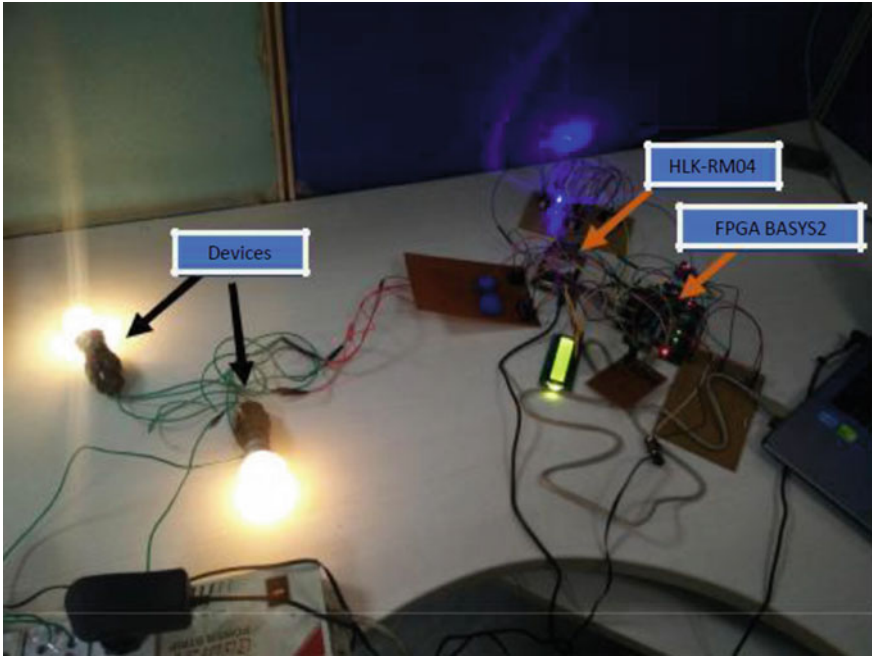


Fig. 3 Design controlling devices

the different areas, and also the sensors will check the institution from fire, temp, and air quality as shown in Fig. 2.

The complete working of devices controlled via Internet performed successfully as shown in Fig. 3.

4 Conclusion

The conclusion of the research is that an integrated smart home automation through FPGA has been developed which needs to be implemented. The system designed is a prototype of the concept proposed. This prototype can be implemented to independent houses, societies, cities, urban areas, etc.

5 Future Scope

The future scope of proposed research is wide in nature. This system can future be linked with the government authorities so that they can map the areas or households consuming more resources or wasting resources. Also the whole system can be automated through IoT. Other quality monitoring sensors can be incorporated with the system to improve the effort.

References

1. A. S. Di Carlo and G. Cove, "Smart Homes (Home Automation)", (2012) August 30, <http://www.aging.ny.gov/livably/resourcemanual/design/iv1c.pdf>.
2. Y. B. Krishna and S. Nagendram, "Zigbee Based Voice Control System for Smart Home", *International Journal Computer Technology & Applications*, vol. 3, no. 1, (2012), pp. 163–168.
3. B. Mardiana, H. Hazura, S. Fauziyah, M. Zahariah, A. R. Hanim and M. K. Noor Shahida, "Homes Appliances Controlled Using Speech Recognition in Wireless Network Environment", *International Conference on Computer Technology and Development (ICCTD)*, (2009), pp. 285–288.
4. N. P. Jawarkar, V. Ahmed and R. D. Thakare, "Remote Control using Mobile through Spoken Commands", *IEEE - International Consortium of Stem Cell Networks (ICSCN) 2007*, (2007), pp. 622–625.
5. I. -K. Hwang, D. -S. Lee and J. -W. Baek, "Home Network Configuring Scheme for All Electric Appliances Using Zigbee-based Integrated Remote Controller", *IEEE Transactions on Consumer Electronics*, vol. 55, no. 3, (2009) August, pp. 1300–1307.
6. M. S. Nasr, F. H. A. S. Azwai, "Friendly home automation system using cell phone and J2ME with feedback instant voice messages", *2009 IEEE/ACS International Conference on Computer Systems and Applications*, (2009), pp. 531–538.
7. S. M. A. Haque, S. M. Kamruzzaman and Md. A. Islam, "A System for Smart-Home Control of Appliances Based on Timer and Speech Interaction", *Proceedings of the 4th International Conference on Electrical Engineering & 2nd Annual Paper Meet*, (2006) January 26-28, pp. 128–131.
8. Pavithra.D, RanjithBalakrishnan "IoT based Monitoring and Control System for Home Automation", *Global Conference on Communication Technologies (GCCT 2015)*, 2015 IEEE.
9. Ming Wang, Guiqing Zhang, Chenghui Zhang, Jianbin Zhang, Chengdong Li, An IoT-based Appliance Control System for Smart Homes, *2013 Fourth International Conference on Intelligent Control and Information Processing (ICICIP) June 9 – 11, 2013, Beijing, China*, 2013 IEEE.
10. Anish NK, Kowshick B, S.Moorthi, Ethernet based Industry Automation using FPGA, 2013 IEEE.
11. N. Kaimal, P. Jadhav, S.Rizvi, MamtaKhatu, "Implementation OfIoT For Home Automation," *IJEERT*, vol. 3, no. 2, pp. 7–11, Feb 2015.

Mobile App-Based Device Control for Robotic Movement

Navodit Sharma, Ishfaq Gaffar Dar and Manish Sharma

Abstract As of late, there has been a gigantic development of mobile phones with over several billions of users all across the globe. Cell phone has made a great impact with our society. It is hard to imagine lives without cell phones. In this project, we have designed an android application to control a robot. The accelerometer sensor which is inbuilt in phone is used for controlling the motion of robot depending on the gesture made by phone. Bluetooth technology is used to interface the device with android application. The technology can be widely used in future for controlling any machine which can work on x and y coordinates (e.g. robot, vehicles, drones) by simple use of mobile and Bluetooth module (GSM for long ranges).

Keywords Robotic car · ATMEGA microcontroller · Accelerometer Embedded systems · Bluetooth module · Motor driver · Smartphone

1 Introduction

A mechanical device called robot [1], it can be called an artificial model or agent, and it also consists of programmable device that gives calmness to the humans and movements are controlled by same. So it is the system, which by virtue of its behavior and appearance, shows that it has capability to work by itself. Along these lines by its profound quality of sense, it gives genuineness in each field of science. Humans communicate in the physical world by the means of five senses. However, gestures play an important role in communicating with the physical world from age-old times; even before, there were no inventions of any language. Robots are portioned into two classes, i.e., remote-controlled robots (gesture-controlled robots)

N. Sharma (✉) · I.G. Dar · M. Sharma
Amity University, Noida, Uttar Pradesh, India
e-mail: navoditd@gmail.com

I.G. Dar
e-mail: ishfaqgaffar6@gmail.com

© Springer Nature Singapore Pte Ltd. 2018
R. Singh et al. (eds.), *Intelligent Communication, Control and Devices*,
Advances in Intelligent Systems and Computing 624,
https://doi.org/10.1007/978-981-10-5903-2_84

and autonomous robots (line- or edge-sensing robots); since this paper deals with controlling robot with gestures, the immediate focus will be on the remote-controlled robots only. The necessity of such devices dependably needs additional cost and complex microcontroller programming keeping in mind the end goal to create rationales for proper working of the device. So for the sake of reduction of price along with complexity, a tilt-dependent robotic car is made by using Atmega16 microcontroller, HC-05 Bluetooth module, and accelerometer (Smartphone) is proposed. The reception part of system which is present at robotic section gets control signals sent by transmitting section according to the orientation of the Smartphone (inbuilt accelerometer) [2] which controls the movements of robotic car, which follows the IEEE 802.15.4, and which is a standard protocol very well.

2 Approach Used

Two separate modules have been used to produce controlled motion of our wireless device. It comprises of a transmitter module and a receiver module. The transmitter here is a Smartphone using its accelerometer, and the receiver is seated on the body of robot consisting of four DC motors. Each motor is connected with low-weight wheel which helps it to have a decent adjust and a controllable movement. The transmitting section which is having an accelerometer tilt sensor [3], which captures the slant angle of the Smartphone operated by the user and sends the values remotely with the assistance of HC-05 Bluetooth module alongside the utilization of microcontroller AVR ATmega16 [1, 4]. The receiver station placed at the top surface of robotic car gets controlling signals sent by transmitting station.

2.1 Transmitter Diagram

The transmitter (Fig. 1) we are having in this project is simply an Android-based Smartphone which has an inbuilt accelerometer; here, we developed an Android app which continuously measures the X , Y , and Z coordinates and displays on Smartphone's screen. Whatever will be the position of Smartphone, it shall be captured by the Smartphone's accelerometer sensor and separate x , y , and z coordinate data will be sent accordingly from the transmitter station (Smartphone via Android app) to the receiver station (the robotic car). The transmitting and receiving station communicates with each other via HC-05 Bluetooth module which is mounted on the receiving end. The HC-05 Bluetooth has a range of 10 m approx.

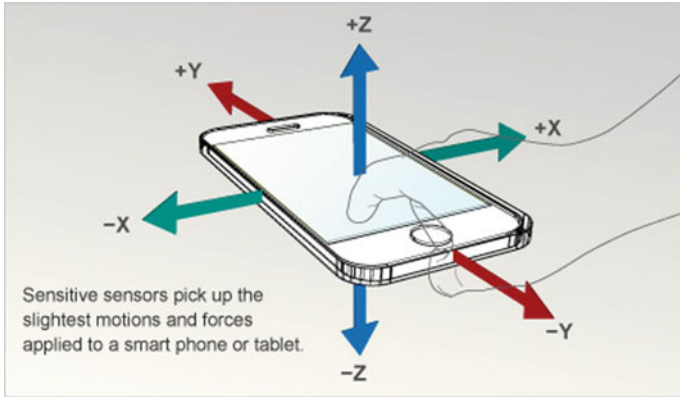


Fig. 1 Axes of a smartphone

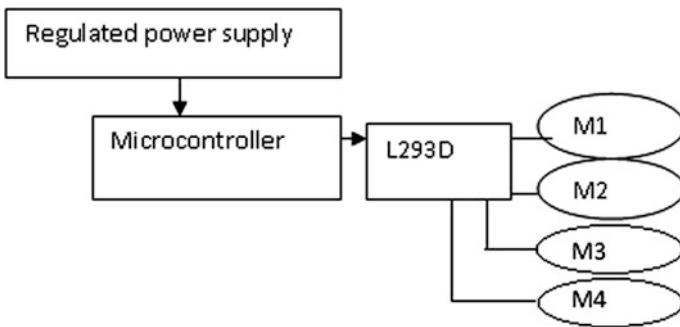


Fig. 2 Block diagram of receiver

2.2 Receiver Block Diagram

The receiving station (Fig. 2) has a fixed supply of +9 V, ATmega Microcontroller, HC-05 Bluetooth module, L293D motor driving IC, and four DC motors. The receiver station is placed on the top surface of body of robotic car which will behave in accordance with the instructions which will be sent with the help of the transmitter end for the movement of robot in balanced, stable, left, forward, right, and backward direction.

3 Working

The behavior of the remote-operated robotic car is isolated into mainly three sections:

3.1 Robot Body

Body of robot consists of four wheels each of which are connected to four DC motors attached to a plastic chassis. The wheels are free to pivot in two-directional level of flexibility, i.e., it is free to move about any direction which relies upon the course of constrain in a single plane.

3.2 Transmitter

The Android-based Smartphone is acting as a transmitter; in this part, the Android app developed continuously measure the X , Y , and Z coordinates by the virtue of inbuilt accelerometer which in turn transmits the instruction to the collector end. The slant position values [5] are captured by the movement of Smartphone in stable, right, left, backward, and forward directions, respectively.

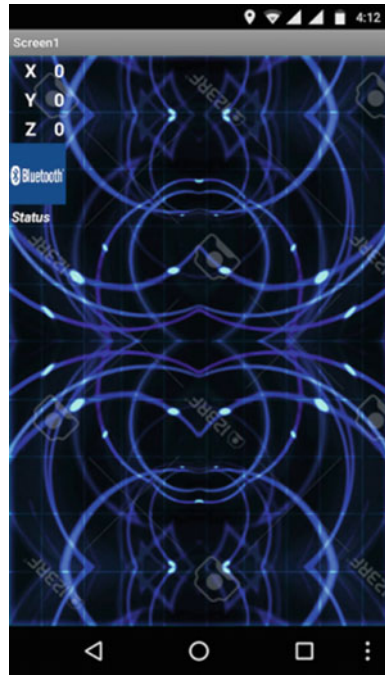
3.3 Receiver

The receiving part consists of ATmega16 microcontroller, L293D motor driving IC, and HC-05 Bluetooth module. Here, the microcontroller stores the values sent from the transmitting end (Smartphone) via HC-05 Bluetooth module, and these incoming characters are being compared with previously saved values of X , Y , and Z coordinates [6] in the microcontroller present in the receiver section. This forces the DC motors present on the robotic car by the assistance of L293D motor driving IC to actuate in balanced, stable, right, left, backward, and forward directions in a speedy reaction time.

Table 1 Comparative study

S. No.	Previous system	Proposed system
1	Wired systems	Wireless system
2	More efforts	Very less efforts
3	Very slow process	Very fast process

Fig. 3 Android-based app

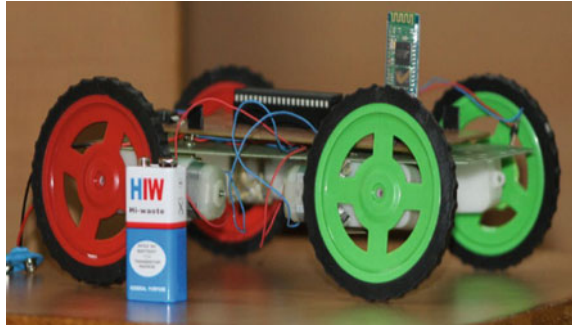


4 Experimental Results

It has been deduced that the system we proposed is very fast, very much precise, and secure. Table 1 shows the comparative analysis of the previously existing systems with our wireless system. It can be seen from the results below that our proposed system is fully functional.

5 Developed System

Figure 3 is the Android-based app which is installed in Smartphone in order to control the robotic car shown in Fig. 4.

Fig. 4 Robotic car

6 Conclusion

Wireless framework for the controlling of any object (here robotic car) which will respond in right, left, forward, and backward direction by the motion of Smartphone held in user's hand is made successfully. The system is made intelligent by programming of the ATmega32 microcontroller and by the sensing ability of accelerometer sensor. So by designing such type of wireless module, the need for wired system is overcome. The range (in meters) of smooth operation of the system is dependent on the Bluetooth module used (here HC-05), whose range is approximately 10 m.

7 Future Work

As far as the future scope of this technology is concerned, by improving accuracy and precision and by increasing the Bluetooth range of the system, more precise framework can be planned. This will be very much fruitful in the medical fields like the patients suffering from different kind of physical disabilities (e.g., spinal cord problem).

References

1. Mike Horton and John Suh, "A Vision for Wireless Sensor Networks", IEEE transactions on Industrial Electronics 0-7803-8846-1/05, 2005.).
2. Wei Y, Liu L, Zhong J, Lu Y, Sun L (2015) Unsupervised race walking recognition using smartphone accelerometers. In: Knowledge Science, Engineering and Management. Springer, pp 691–702.
3. Weiyun Jiao, Xiaojing Wang, Li Zhao, "Monitoring system of car-guardrail accident based on wireless sensor networks", ITST – 2008 ISBN: 978-1-4244-2858-8.

4. H. Sahin and L. Guvnec, "Household Robotics: Autonomous Devices for Vacuuming and Lawn Mowing", *IEEE Control Systems Magazine*, vol. 27, no. 2, pp. 20–96, Apr. 2007.
5. D. Mizell, "Using gravity to estimate accelerometer orientation", *Proc. 7th IEEE Int. Symp. Wearable Computers (ISWC 2003)*, pp. 252–253, Oct. 2003.
6. Ravi N, Dandekar N, Mysore P, Littman ML (2005) Activity recognition from accelerometer data. In: *AAAI*. vol. 5, pp. 1541–1546.

Feature Recognition of Face with Real-Time Variations Using Eigen Face Approach Methodology with PCA Algorithm

Ishfaq Gaffar Dar, Azzan Khan and Manish Sharma

Abstract Face is a composite multidimensional structure, and it needs great assessing methods for acknowledgment. Our approach regards confront acknowledgment as a two-dimensional acknowledgment issue. In this plan, confront acknowledgment is finished by foremost Component Analysis (PCA) (Biometric Technology Application Manual Volume One: Biometric Basics, National Biometric Security Project, 2008 [1, Turk and Pentland, “Face Recognition using Eigen-faces”, IEEE Conference on Computer Vision and Pattern Recognition, 1991 2]). The primary point is to execute the model (framework) for a chosen confront and separate it from a substantial number of as of now put away faces with some ongoing varieties also. The Eigen-confront approach utilizes Principal Component Analysis (PCA) calculation for the acknowledgment of pictures. It gives us efficient approach to discover the lower dimensional space. The face is characterized by Eigen-confronts which are Eigenvectors of the arrangement of confronts, which may not relate to general facial component, for example, lips, nose, and eyes. The framework (Velikiy Novgorod, “Pattern Recognition”, the 6th international Conference on Image Analysis, October 21–26, 2002 [3]) performs by anticipating pre-removed face picture onto an arrangement of face space that speaks to noteworthy varieties among known face pictures. Face will be labeled as perceived or not perceived face in the wake of coordinating with the present database. In the event that the client is new to the face acknowledgment framework, then his/her information (format) will be put away in the database else coordinated against the information (layouts) (Turk and Pentland, Face Recognition using Eigen-faces, IEEE Conference on Computer Vision and Pattern Recognition, 1991 [4]) which is as of now put away in the database. The dimensionality lessening through PCA represents the littler face space than the preparation set of appearances and henceforth more prominent computational adaptability (Debnath Bhattacharyya, Rahul Ranjan, Farkhod Alisherow, and Minkyu Choi, Biometric Authentication: A Review, Int J u- e- Service Sci Technol 2(3), 2009 [5]).

I. G. Dar (✉) · A. Khan · M. Sharma

Amity School of Engineering and Technology, Amity University, Noida 201303, UP, India
e-mail: ishfaqgaffar6@gmail.com

© Springer Nature Singapore Pte Ltd. 2018

R. Singh et al. (eds.), *Intelligent Communication, Control and Devices*,
Advances in Intelligent Systems and Computing 624,
https://doi.org/10.1007/978-981-10-5903-2_85

819

Keywords Feature recognition • Real-time variation • Principal component analysis algorithm • Face • Sociology • Vectors • Databases • Covariance matrix

1 Introduction

Confront acknowledgment from pictures is a subdue of the general protest acknowledgment issue. Finding a man from her or his face is the most nonintrusive modalities in biometrics [6]. Recognition or facial imaging identifies people by comparing sample images with stored images or templates using mathematical analysis of the acquired pixels. The systems that use technology of facial recognition take images using cameras and, like their technology of biometric counterparts, develop templates for comparing live images (faces) to an already saved template. The use of facial recognition is mostly found in criminal identification, security systems, verification mode, etc.

The primary methods used for facial recognition or identifications are as follows:

1. Local correlation method;
2. Support vector machines;
3. Elastic bunch graphing.

And in this report, we are using **Principle Component Analysis (PCA)**.

2 Approach Used

PCA (Principle Component Analysis) [4] is an advantageous technique that has application in fields like image compression and face recognition and for discovering designs [3] in information of high measurement. It is an approach to distinguish designs in information, and it is communicating the information in an approach to highly recognize their disparities and likenesses. The examples might be elusive in information of high measurements where solace of graphical portrayal is not accessible. Rule segment is a capable instrument for information breaking down. There are other principle elements of PCA that once the examples are found, the information can be packed, i.e., the quantity of measurements is diminished without that much loss of data.

2.1 Figuring the Principle Components

Eigenvalues and eigenvectors [7] of the information covariance [1] network are to be calculated in order to find the principle components. This is like the way toward

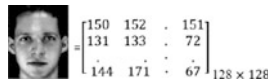
finding the hub framework in which the covariance lattice is corner to corner. The eigenvector having the biggest eigenvalue is the heading of most prominent variety; the one with the second biggest eigenvalue is the orthogonal course with the following most elevated variety et cetera.

3 Implementation

3.1 Face Viewed as a Vector

Confront acknowledgment is a case where standard segment investigation has been generally utilized; essentially, the quantity of factors is diminished. How about we take a case of 2D situation where we have an info picture and we need to contrast and an arrangement of information base pictures to locate the best match. Accepting the pictures is of a similar determination and is all similarly encircled (i.e., the countenances show up at a similar scale and same place in the pictures). Every pixel can be viewed as a variable consequently having a high dimensional issue which can be rearranged by rule segment investigation [8].

In a picture acknowledgment, a picture with “*n*” pixels is dealt with as a point in an “*n*” dimensional space for the most part called picture space. The individual coordinate of this speaks to the force estimations of every pixel of the picture and frames a column vector; $\mathbf{px} = (\mathbf{i1}, \mathbf{i2}, \mathbf{i3}::: \mathbf{in})$. This vector is framed by connecting each line of picture pixels, so for an unassuming estimated picture, say 128/128 determination it will measurement **16384**. For e.g.



Face viewed as a 2D matrix

Becomes as a vector;

[150; 152; _ _ _ 151; 131; 133; _ _ _ 72; _ _ _ 144; 171; _ _ _ 67]16K

Thus, we can express each image (face) in the matrix form and will use the same knowledge in our next section.

4 Steps to Be Followed for Face Recognition Using PCA

Step 1: Creating Training Set

2D images of size $\mathbf{m} \times \mathbf{n}$ can be spoken to as **1D** vector by linking lines [1, 8], i.e., picture is changed over into a vector of length $\mathbf{N} = \mathbf{m} \times \mathbf{n}$.

For example, the image of size $(\mathbf{64} \times \mathbf{64}) \times \mathbf{1}$ is shown below, and it can be represented by a single column by concatenation as



$$I = \begin{bmatrix} x_{11} & x_{12} & \dots & x_{1n} \\ x_{21} & x_{22} & \dots & x_{2n} \\ \dots & \dots & \dots & \dots \\ x_{m1} & x_{m2} & \dots & x_{mn} \end{bmatrix} \xrightarrow{\text{CONCATENATION}} \begin{bmatrix} x_{11} \\ \vdots \\ x_{1n} \\ \vdots \\ x_{2n} \\ \vdots \\ x_{mn} \end{bmatrix} = x.$$

Now by the same process, we will have m number of images in our training set.

Step 2: Moving Origin to the Mean of Data

To make sure that principle component the bearing of max fluctuation, it is compulsory to focus the framework. To begin with the vector of mean qualities, Ψ is resolved and afterward that vector is subtracted from each picture vector.

$$\Psi = \frac{1}{M} \sum_{i=1}^M x_i.$$

$$\phi_i = x_i - \Psi$$

Arrived at the midpoint of vectors are organized to frame another preparation network (measure $N \times M$);

$$A = \phi_1, \phi_2, \dots, \phi_M$$

For example, we have three faces in training set shown below, and hence we will get the mean of these three faces.



Step 3: Obtaining the Covariance Matrix

Now, we are going to compute the covariance lattice \mathbf{C} and assess its eigenvectors (\mathbf{ei}) and eigenvalues ($\lambda\mathbf{i}$) [5]. The mean-balanced framework “ \mathbf{A} ” calculated above the corresponding covariance matrix can be calculated simply by multiplying it with its transpose, i.e., \mathbf{A}^t .

$$\mathbf{C} = \mathbf{A} \times \mathbf{A}^t.$$

Step 4: Eigenvalues and Eigenvectors of Covariance Matrix

On the off chance that \mathbf{Vi} and $\mu\mathbf{i}$ are eigenvectors and eigenvalues of framework $\mathbf{A}^t\mathbf{A}$ separately, then:

$$\mathbf{A}^t \mathbf{A} \mathbf{Vi} = \mu\mathbf{i} \mathbf{Vi}.$$

Multiplying both sides of above equation with \mathbf{A} from the left, we get:

$$\mathbf{A}^t \mathbf{A} \mathbf{Vi} = \mathbf{A} \mu\mathbf{i} \mathbf{Vi},$$

$$\mathbf{A}^t \mathbf{A} (\mathbf{A} \mathbf{Vi}) = \mu\mathbf{i} (\mathbf{A} \mathbf{Vi}),$$

$$\mathbf{C} (\mathbf{A} \mathbf{Vi}) = \mu\mathbf{i} (\mathbf{A} \mathbf{Vi}).$$

Comparing conditions, we can reason that the principal $\mathbf{M} - 1$ eigenvectors \mathbf{ei} and eigenvalues $\lambda\mathbf{i}$ of the covariance framework \mathbf{C} are given by $\mathbf{A} \mathbf{Vi}$ and $\mu\mathbf{i}$, respectively.

Step 5: Sorting the Eigenvalues and Associated Eigenvectors

Eigenvectors connected with the most elevated eigenvalue mirror [9] the most astounding fluctuation, and the one connected with the least eigenvalue, consequently the littlest difference. Around 90% of the aggregate change is contained in the initial 5–10% eigenvector as eigenvalues decline exponentially. Along these lines, the vectors ought to be put away by eigenvalues so that the primary vector relates to the most astounding eigenvalue. These vectors are then standardized. Another network \mathbf{E} is framed so that each vector \mathbf{ei} is a segment vector. This network has measurements $\mathbf{N} \times \mathbf{D}$ where \mathbf{D} is the wanted number of eigenvectors. It is utilized for projection of information grid \mathbf{A} .

Step 6: Recognition

The last step is the acknowledgment of faces. Picture of the individual we need to discover in the test set is changed into a vector \mathbf{P} , lessened by the mean esteem Ψ and anticipated with a grid of eigenvectors (Eigen faces):

$$\omega = \mathbf{E}^t (\mathbf{P} - \Psi) \text{ [8].}$$

Arrangement is finished by deciding the separation, \mathbf{i} , among $\boldsymbol{\omega}$ and \mathbf{y}_i of grid \mathbf{Y} . The most widely recognized is the Euclidean separation; however, different measures might be utilized. On the off chance that \mathbf{A} & \mathbf{B} are two vectors of length \mathbf{D} [9], the separation between them is resolved as taken after:

Euclidean Distance:

$$d(\mathbf{A}, \mathbf{B}) = \sqrt{\sum_{i=1}^D (a_i - b_i)^2} = |\mathbf{A} - \mathbf{B}|.$$

On the off chance that the greatest separation between test face and training faces is higher than a limit θ [8, 5], the test face is thought to be obscure (Recognized), else it is known (Not Recognized).

5 Coding in MATLAB

Steps to be followed for face recognition utilizing PCA and eigen face [2] approach as examined in area 4.2 can be implemented in MATLAB as follows:

1. Read the images from the training set and reshape each face image (2D matrix) into a column vector. And generate a new matrix of size $n \times M$ (where n = no. of pixels in each image and M = no. of images in the training set) from these vectors, such that each vectors form a column of matrix. Following MATLAB functions were used for this purpose:

Imread: $\mathbf{A} = \text{imread}(\text{filename}, \text{fmt})$ puruses a grayscale or shading picture from the record determined by the string filename. On the off chance that the record is not in the present organizer, or in an envelope in a MATLAB way, determine the full pathname.

Reshape: $\mathbf{B} = \text{reshape}(\mathbf{A}, m, n)$ gives back the m -by- n grid \mathbf{B} whose components are taken section insightful from \mathbf{A} . A blunder comes about if \mathbf{A} does not have $m * n$ components.

2. Calculate the mean of these input face images (row-wise).
In MATLAB mean value of the elements of any row vector a computed using function mean.
3. Subtract the mean from each input image to obtain the matrix of mean-shifted images [3, 8].
4. Obtain the covariance matrix of this matrix of mean-shifted images.
For any given matrix, say \mathbf{A} , covariance matrix is obtained by simple multiplication of the transpose of matrix \mathbf{A} by \mathbf{A} , that is, $\mathbf{A}\mathbf{A}^t$.
5. Calculate the eigenvectors and eigenvalues of this covariance matrix.
In MATLAB, these are obtained by using the function **eig()**.

$[\mathbf{V}, \mathbf{D}] = \text{eig}(\mathbf{A})$ produces matrix of eigenvalues (\mathbf{D}) and eigenvectors (\mathbf{V}) of matrix \mathbf{A} , so that $\mathbf{A} * \mathbf{V} = \mathbf{V} * \mathbf{D}$. Matrix \mathbf{D} is the *conical form of A*—a

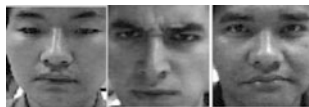
diagonal matrix with **A**'s eigenvalue on the main diagonal. Matrix **V** is the *modal matrix*, its columns are the eigenvectors of **A**.

6. Order the eigenvectors by their corresponding eigenvalues, in decreasing order.
7. Project the mean-shifted images on to the Eigen space using the retained eigenvectors. This is done by simple dot product of two vectors. **C = dot (A, B)** returns the scalar product of the vectors **A** and **B**. **A&B** must be the vectors of the same length. When **A&B** are both column vectors, **dot (A, B)** is the same as **A * B**.
8. Obtain the test image for recognition and reshape it as above.
9. Mean-shift it in the same way as was done in step 2.
10. Project the mean-shifted test image onto the Eigen space obtained above [1, 8].
11. Find the difference between the projection of test image and projections of all the images from training set (known as Euclidean distance) [7, 2].
12. Set the threshold value in order to distinguish between known and unknown faces.

6 Results

6.1 Test 1

Number of variable facial expressions recognized with three faces in training set.



Training set faces for test 1



Eigen faces for test 1

S. No.	No. of faces in training set	No. of Eigen faces used	No. of test faces	Success percentage			False hit rate
				Face 1 (%)	Face 2 (%)	Face 3 (%)	
1	3	3	3	100	100	100	0
2	3	3	5	100	100	100	0
3	3	3	22	100	81.81	86.37	0

6.2 Test 2

Number of variable facial expressions recognized with five faces in training set.



Training set faces for test 2



Eigen faces for test 2

S. No.	No. of faces in training set	No. of Eigen faces used	No of test faces	Success percentage					False hits
				Face 1 (%)	Face 2 (%)	Face 3 (%)	face 4 (%)	Face 5 (%)	
1	5	5	5	100	100	100	100	100	0
2	5	5	10	100	80	90	80	10	0
3	5	5	22	100	81.8	86.4	54.5	4.5	0

6.3 Test 3

In this test, we kept different number of images of the below person in the database [2, 6]. Fifteen images of the same person were tested for recognition, i.e., we kept fifteen images in test set. Each image (that in database and that in test set) was captured with the Web cam. We extracted the face portion from each image and converted each colored image into grayscale image using MATLAB functions.



Results of test 3

S. No.	No. of images in database	No. of test images	Success rate (%)	False accept rate (%)
01	6	15	61	9
02	9	15	67	5

6.4 *Following Conclusions Can Be Drawn from the Above Tests*

- (1) Training set may contain face images corresponding to one person only or a number of different persons.
- (2) Faces in the training set were exactly recognized in every test.
- (3) Different facial expressions corresponding to each face in training set were also recognized.
- (4) The successful recognition rate for greater variations in expressions or intensities can be increased by using more than one face image corresponding for a given person in the training set.
- (5) More quantity of face pictures in the training set, more will be the number of Eigen faces (Eigenvectors of covariance matrix). But the Eigenvectors corresponding very small Eigen values do not contribute much to the variance in data and hence can be neglected.

7 Conclusion and Future Scope

In this venture, the issue of dimensionality [10] is totally understood for face acknowledgment. The approach we utilized, i.e., Eigen countenances and PCA, is very fiery in the treatment of face pictures with differed outward appearances and also the headings. Additionally, it is very productive and basic in the preparation and acknowledgment stages, apportioning low-level handling [8] to confirm the geometry of face or separation between facial organs and their measurements. This approach is touchy to pictures with uncontrolled brightening conditions [9]. The confinement of Eigen face approach is the treatment of face pictures with abnormal state if variety in outward appearances and with glasses.

The eventual fate of this calculation can be stretched out to interfere with the outward appearance of a man or to perceive the sexual orientation of individual. Acknowledgment could be done under generally changing conditions; for example, scaled frontal view, subjects with scenes, frontal view, a 45° view [6], and so forth are attempted, while the preparation informational collection covers restricted perspectives. The calculation models are the ongoing differing lighting conditions also.

References

1. National Biometric Security Project, "Biometric Technology Application Manual Volume One: Biometric Basics" National Biometric Security Project 2008.
2. M. A. Turk and A.P. Pentland, "Face Recognition using Eigen-faces", IEEE Conference on Computer Vision and Pattern Recognition, 1991.

3. Velikiy Novgorod, "Pattern Recognition", the 6th international Conference on Image Analysis, October 21-26-2002, Russia.
4. M. A. Turk and A.P. Pentland, "Face Recognition using Eigen-faces", IEEE Conference on Computer Vision and Pattern Recognition, 1991.
5. Debnath Bhattacharyya, Rahul Ranjan, Farkhod Alisherow, and Minkyu Choi, "Biometric Authentication: A Review", International journal of u- and e- Service, science and Technology Vol. 2, No. 3, September, 2009.
6. Velikiy Novgorod, "Pattern Recognition", The 6th international Conference on Image Analysis, October 21-26-2002, Russia.
7. Salina Abdul Samad, Dzati Athiar Ramli, and Aini Hussain, "Person Identification using Lip-Motion Sequence", Apolloni et al. (Eds.): KES 2007/WIRN 2007, part 1,LNAI 4692, Springer-Verlag Berlin Heidelberg 2007.
8. A. k. Jain, A. Ross, and S. Pankanti, "Biometric: A Tool for Information Security", IEEE Trans. Information Forensics and Security, Volume 1, No. 2, jun. 2006.
9. H.E. Cetingul, Y. Yemez, E. Erzin, A.M. Tekalp "Discriminative Lip-motion Features for Biometric Speaker Identification," IEEE int. Conf. on Image Processing, Singapore, 2004.
10. Matthew Turk and Alex Pentland, "Eigenfaces for REcognition", Vision and Modelling Group, The Media Laboratory, Massachusetts Institute Technology in Journal of cognitive neuro science 1991,Vol. 3.

Speed Regulation of a Non-linear Separately Excited DC Motor Using Optimized Fuzzy Logic Control

Arpit Jain, Piyush Kuchhal and Mukul Kumar Gupta

Abstract This paper demonstrates the speed tracking for a separately excited non-linear DC motor using optimized fuzzy logic controller. Rotor speed is varied by changing the armature voltage of the motor while keeping the voltage in the constant torque region. Genetic algorithms optimization-based fuzzy logic control is used to track the speed change, and the results obtained from fuzzy logic control are compared with PID controller. Comparison indicate an improvement in performance for optimized fuzzy logic control exhibiting a reduction in overshoot, transient, and steady-state parameters as compared with PID controller.

Keywords Separately excited DC motor · Optimized fuzzy logic control
Genetic algorithms

1 Introduction

A separately excited DC motor (SEDM) is a device which translates electrical input energy into rotational mechanical energy [1]. Operating principle for SEDM employs placing a current carrying coil in a fixed magnetic field, this coil is subjected to a torque as a result the coil rotates continuously and therefore the shaft attached to it also rotates, and thus electrical input energy is translated into mechanical work. In SEDM, the motor field coils are provided from an outward source, for example motor generator set and the field current in the motor are

A. Jain (✉) · M.K. Gupta
Department of Electronics, Instrumentation and Control Engineering,
University of Petroleum and Energy Studies, Dehradun, India
e-mail: arpit.eic@gmail.com

M.K. Gupta
e-mail: mkgupta@ddn.upes.ac.in

P. Kuchhal
CoES, University of Petroleum and Energy Studies, Dehradun 248007, India
e-mail: pkuchhal@upes.ac.in

independent of any variations in the armature current [2]. To deal with uncertain/ambiguous systems L. Zadeh proposed fuzzy set theory [3]. Fuzzy set theory finds applications in various fields of engineering: control [4], image processing [5], data mining to name a few. Successful application of a fuzzy logic system (FLS) on a given system is governed by a various factors which generally include: choosing right membership function (MF), constructing proper rule base, selecting right inference engine to name a few [6]. MF selection replicates an important role in performance of a fuzzy system as an incorrect chosen MF may result in degradation of system performance even when other system parameters are chosen wisely [7].

1.1 Speed Control of a Separately Excited DC Motor

The objective of this investigation is to design an optimized FLC for SEDM speed tracking controller. Speed regulation is achieved through manipulating armature voltage [8]. Here the armature voltage (V_a) is adjusted while keeping field voltage (V_f) fixed at the rated voltage value. As the armature voltage is increased, firstly the armature current (I_a) rises and thus the torque increases, therefore speed of rotor also increases. As the drop across the armature resistance (R_a) varies, the speed of the motor changes in proportion to V_a . The speed corresponding to the rated V_a and rated V_f are acknowledged as the rated speed of the motor. The motor speed is always kept below the rated speed. The motor is expected to develop a high torque, and hence the V_f is kept at its rated value. The expression for the rotor speed in SEDM is given by the following equation:

$$\omega = (V_a - I_a R_a) / K \phi, \quad (1)$$

where

- ω rotor speed
- V_a armature voltage
- I_a armature current
- R_a armature resistance
- K constant
- ϕ flux per pole

From the above relation, it is clear that the speed (ω) of SEDM can be regulated by varying either of the following parameters:

- (i) V_a —Armature Voltage
- (ii) R_a —Armature Resistance
- (iii) ϕ —Flux

First two methods implicate a change in armature circuit, while the flux change can be achieved by a variation in magnetic circuit of the motor. Consequently, methods of speed tracking technique for SEDM can be categorized as either armature control technique or field control technique.

2 Fuzzy Logic Control and Optimization Algorithm

FLC is a controller which is established on a linguistic control strategy and originates from knowledge of a field expert. The basic principle of operation of a fuzzy logic controller (FLC) relies on system’s qualitative knowledge which is being controlled. Fuzzy logic deals with uncertain or imprecise situations as opposed to precise situations in crisp logic. The internal structure of a FLC consists of fuzzification, inference system, and defuzzification. Generally, triangular membership function (MF) is used in the analysis and center of gravity method is carried out for the purpose of defuzzification. The number of rule sets for the operation of a FLC depends upon the number of I/O variables and the number membership functions [9]. The optimization technique employs predefined MFs in which support function is optimized using maximum entropy algorithm [10]. The entropy of a fuzzy set is given by [11]:

$$H(A) = - \int_{-\infty}^{\infty} \{ \mu_i \log \mu_i + (1 - \mu_i) \log (1 - \mu_i) \} \tag{2}$$

where μ = membership value of a fuzzy set.

The support base of the pre-existing fuzzy sets is displaced by standard deviation obtained from initial experimental run of the system. Now, the objective function is obtained as:

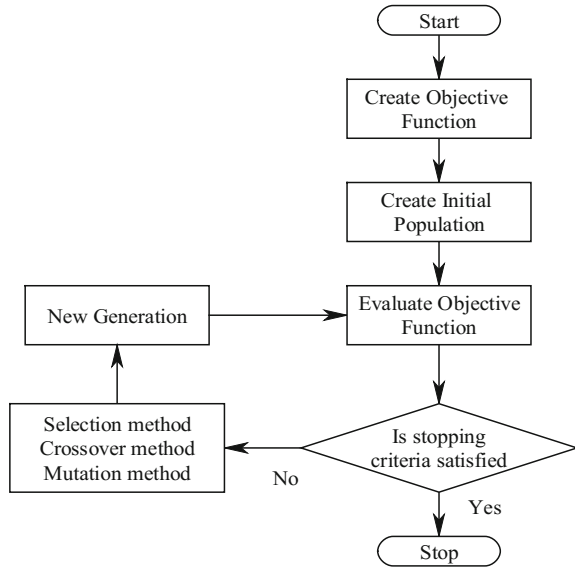
Maximize

$$H(\mu_{z^*}) = - \left[\int_{-\varepsilon \mp \sigma}^0 \left(\frac{x + \varepsilon \mp \sigma}{\varepsilon \mp \sigma} \right) \ln \left(\frac{x + \varepsilon \mp \sigma}{\varepsilon \mp \sigma} \right) dx + \int_{-\varepsilon \mp \sigma}^0 \left(- \frac{x}{\varepsilon \mp \sigma} \right) \ln \left(- \frac{x}{\varepsilon \mp \sigma} \right) dx \right] \\ - \left[\int_0^{\varepsilon \pm \sigma} \left(\frac{\varepsilon \pm \sigma - x}{\varepsilon \pm \sigma} \right) \ln \left(\frac{\varepsilon \pm \sigma - x}{\varepsilon \pm \sigma} \right) dx + \int_0^{\varepsilon \pm \sigma} \left(\frac{x}{\varepsilon \pm \sigma} \right) \ln \left(\frac{x}{\varepsilon \pm \sigma} \right) dx \right] \tag{3}$$

Subject to maximum $H(\mu) = \sum_{i=1}^n H(\mu_i)$

Genetic algorithms are used to optimize the value of objective function described above. Figure 1 depicts the optimization algorithm [12].

Fig. 1 Flowchart for genetic algorithm-based optimization



3 Speed Control of SEDM

In armature voltage control method for speed control of SEDM, the I_f is kept constant and therefore flux density (B) is remained fixed, and V_a is varied. A fixed I_f is achieved by exciting the field separately from a static DC source and since B is directly proportional to the I_f , B is also constant. Therefore, the torque is proportional only to the I_a .

A. PID-based control of SEDM

To benchmark results obtained from FLC, the control objective is initially achieved with help of PID controller. Initial PID gains are obtained using Zeigler–Nichols tuning method and these are then optimized for least mean square error:

$$K_p = 10.32 \quad K_I = 4.21 \quad K_D = 0.57$$

3.1 Architecture for Fuzzy Logic-Based Control of SEDM

We use a two input, one output FLC to design controller for SEDM. The inputs for FLC are error in angular speed of rotor [$\varepsilon(t)$] and rate of change of error [$\Delta\varepsilon(t)$]. The output variable is V_a .

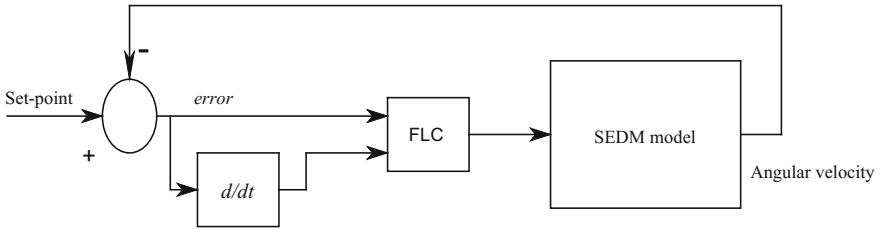


Fig. 2 FLC architecture

Mamdani-type FLC having triangular membership functions is chosen as they are faster than other membership functions. A set of seven membership functions with forty-nine rules is used to get a more precise and accurate result (Figs. 2 and 3).

The control surface obtained for the designed controller is depicted in Figs. 4 and 5 illustrates the MATLAB-Simulink™ program.

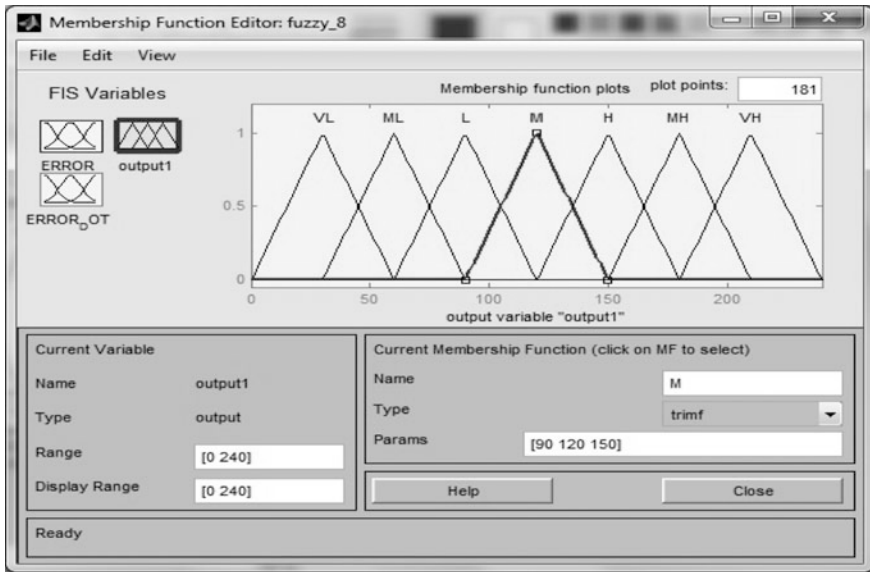


Fig. 3 Membership functions for FLC

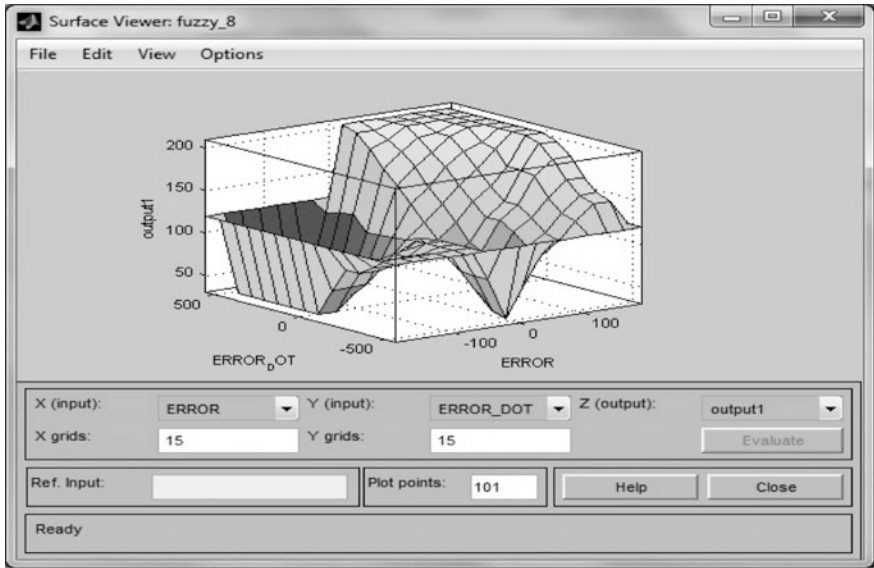


Fig. 4 Surface view of membership functions of FLC

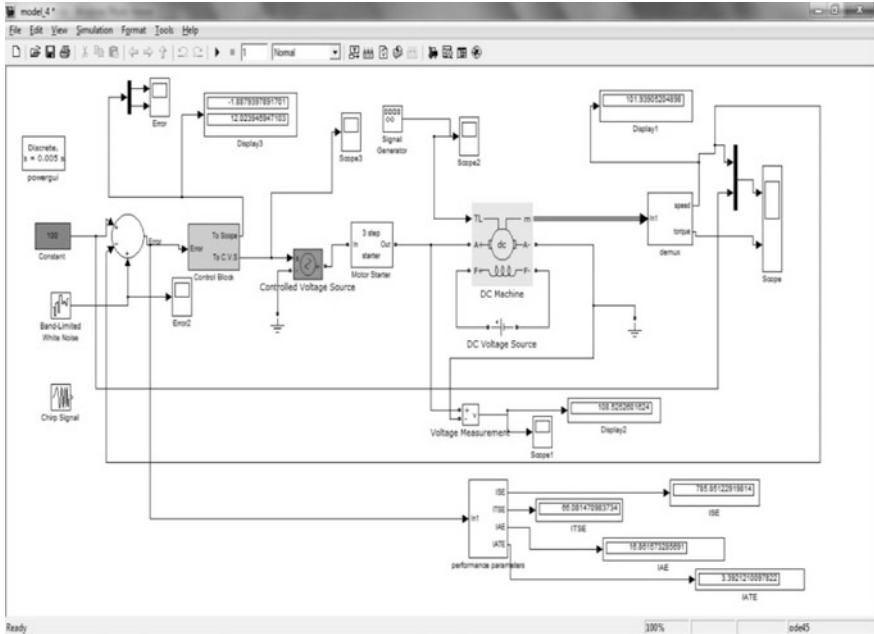


Fig. 5 MATLAB-Simulink™ program for SEDM

4 Results and Discussion

Results are obtained by simulating speed tracking of SEDM model using PID controller as well as optimized FLC. Parameters chosen for SEDM simulation model [2] (Table 1):

Parameters	Value	Parameters	Value
Rated motor power	5 HP	R_a	2.581 Ω
L_a	0.0281 H	V_a	240 V
R_f	281.3 Ω	L_f	156 H
V_f	300 V	J_m	0.0221 kg m ²
B_m	0.002953 N ms	K_v	1.25 V/rad/s
K_m	0.516 N m/A		

Simulation results for PID controller and optimized FLC are depicted in Figs. 6, 7, and 8, respectively. From the figures below, it is evident that the fuzzy logic controllers are better controllers than the PID controllers. Table 2 summarizes the transient response parameters for the two controllers.

Table 1 Rule base

$e/\Delta e \rightarrow$	BN	MN	NS	ZE	SP	MP	BP
BN	M	L	L	VL	VL	VL	VL
MN	M	M	L	ML	L	L	L
NS	M	M	M	L	ML	VL	VL
ZE	VL	ML	L	M	H	MH	VH
SP	L	M	H	H	MH	VH	VH
MP	M	H	H	MH	VH	VH	VH
BP	H	MH	VH	VH	VH	VH	VH

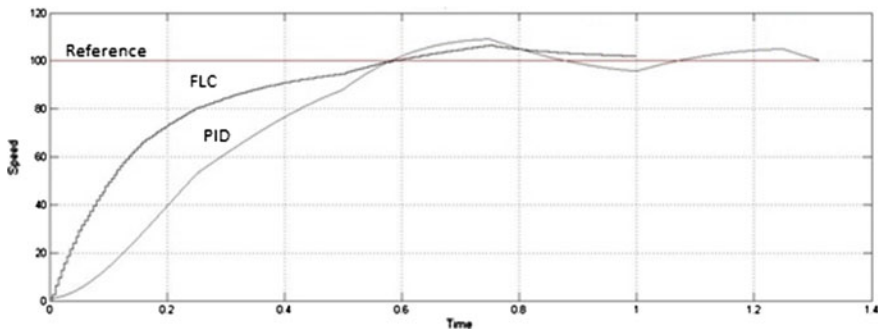


Fig. 6 SEDM response for PID and optimized FLC

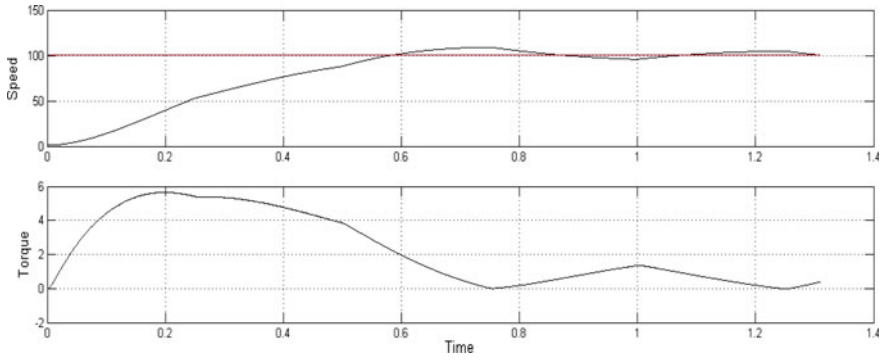


Fig. 7 SEDM response for PID

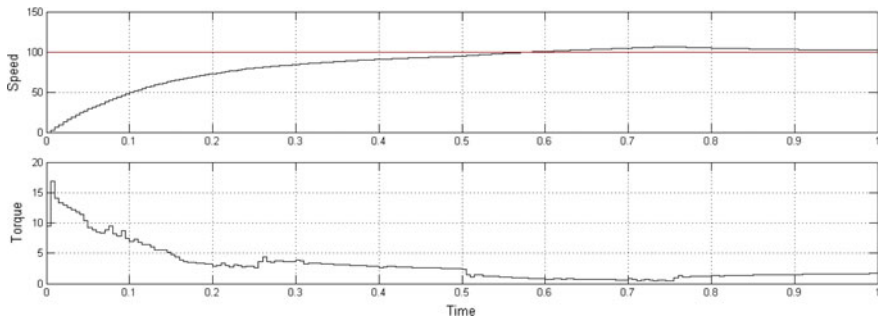


Fig. 8 SEDM response for optimized FLC

Table 2 Transient analysis between PID and optimized FLC

Parameters (units)	PID	Optimized FLC
Rise time (s)	0.52	0.4
Settling time (s)	1.3	1
Overshoot (%)	10	6.45
Linearization of SEDM model	Required	Not required

5 Conclusion

Simulated results indicate an improvement in transient response and torque characteristics for optimized FLC as compared with PID controller. FLC exhibits faster response along with a lower overshoot value. Also, the FLC response achieves an early steady-state value. The most important aspect of FLC is its ability to control

non-linear SEDM model. The gains for PID controller are calculated for linear model of SEDM. While the FLC is designed treating the motor model as a black box system, thereby eliminating the requirement of linearization.

References

1. A. Hughes, *Electric motors and drives*, Burlington: Elsevier Ltd., 2006.
2. M. George, "Speed Control of Separately Excited DC Motor," *American Journal of Applied Sciences*, vol. 5, no. 3, pp. 227–233, 2008.
3. L. A. Zadeh, "Fuzzy sets," *Information and Control*, vol. 8, no. 3, pp. 338–353, 1965.
4. C. C. Lee, "Fuzzy logic in control systems: Fuzzy Logic Controller - Part 1," *IEEE Transactions on systems, man and cybernetics*, vol. 20, no. 2, pp. 404–418, 1990.
5. T. J. Ross, *Fuzzy logic with engineering applications*, New Delhi: Wiley, 2015.
6. Cazarez-Castro, N. R., L. T. Aguilar and O. Castillo, "Fuzzy logic control with genetic membership function parameters optimization for the output regulation of a servomechanism with nonlinear backlash," *Expert Systems with Applications*, vol. 37, p. 4368–4378, 2010.
7. J. M. Mendel, "Designing Fuzzy Logic Systems," *IEEE Transactions on Circuits and Systems*, vol. 44, no. 11, pp. 885–895, 1997.
8. A. Jain, D. Tayal and N. Sehgal, "Control of Non-Linear Inverted Pendulum using Fuzzy Logic Controller," *International Journal of Computer Applications*, vol. 69, no. 27, pp. 7–11, 2013.
9. G. Rajeshkanna, "Modern Speed Control of Separately Excited DC Motor by Boost Converter Fed Field Control Method," in *International Conference on Computer Communication and Informatics (ICCCI -2013)*, Coimbatore, INDIA, 2013.
10. T. Hasuike, H. Katagiri, H. Tsubaki and H. Tsuda, "Constructing Membership Function Based on Fuzzy Shannon Entropy and Human's Interval Estimation," in *IEEE world congress on computational intelligence*, Brisbane, Australia, 2012.
11. A. Jain, S. Sheel and K. Bansal, "Constructing Fuzzy Membership Function Subjected to GA based Constrained Optimization of Fuzzy Entropy Function," *Indian Journal of Science and Technology*, vol. 9, no. 43, 2016.
12. A. D. Termini and S. Luca, "A definition of non probabilistic entropy in the setting of fuzzy set theory," *Information and control*, vol. 20, pp. 301–312, 1972.

Ranking of Educational Web Sites in Indian Perspective for Usability Evaluation

Heena Gupta and Sanjay Kumar Dubey

Abstract Educational Web sites are very popular among students these days for various educational needs. The success of such Web sites depends on the effective user interface, and the user interface is related to the usability. But users, especially students, find several difficulties in exploring these sites, e.g., some sites do not give what exactly the student wants, the lack of questions bank, no search boxes, and many more. The selection of best site is very difficult when several alternatives are available. To overcome these issues, the present paper proposed a hierarchical model to evaluate the rank of usability of educational sites in Indian context. The ranking is based on the various attributes of usability and is evaluated by using the AHP technique and later validated with the help of entropy method. With this technique, we can judge the mostly used Indian educational site among the given alternatives. This would become easy for the general people to find the most popular Web site in the future by using the presented approach.

Keywords Usability · AHP · Entropy · Education · Model

1 Introduction

In this era, the development is increasing so fast that sitting anywhere anyone can communicate with each other with the help of Internet connectivity. Many organizations, institutes, and coaching centers can communicate with general public with the help of their sites. In this paper, research is done about the usability of various popular Web sites on which attributes they are been used by the users. With this research, one can come to know about the Web sites why they are used and

H. Gupta (✉) · S.K. Dubey
Department of Computer Science and Engineering, Amity University
Uttar Pradesh, Sec.-125, Noida, UP, India
e-mail: heenaguptaa25@gmail.com

S.K. Dubey
e-mail: skdubey1@amity.edu

more popular. Basically, this is the comparison between the usability of Web sites on the basis of factors with the help of AHP tool and validated by entropy method. Usability is basically the interaction of the users with any kind of system, products, or any other user-friendly operated devices. Another definition is “Usability is one of the most important characteristics of any user interface; it measures how easy the interface is to use” [1]. Usability is “a measure of the quality of a user’s experience when interacting with a product or system—whether a Web site, a software application, mobile technology, or any user operated device” [2]. “A variety of usability evaluation methods have been developed to evaluate human interaction with an interface; these aim to identify areas for improvements in the interactions in order to increase usability” [3]. Here, the tool used is AHP. Analytic hierarchy process (AHP) is a method developed by Thomas L. Saaty [4]. This is the technique used to analyze complex decisions with the help of mathematical and psychological approach. And at last, the conclusion is extracted.

2 Research Methodology

In this research paper, we are going to present an analytic approach toward complex decisions, viz. AHP method. This method is useful for making the decision when there is some hierarchy is present [5, 6]. For this purpose, we proposed a hierarchal model in which top level of usability. The middle layer contains the important attributes which affect the usability of Web sites; for research purpose, we have chosen three Web sites, viz S1, S2, and S3. Due to some privacy matters, we are not enclosing the name of the sites. The selection of most usable site is decided by AHP, and it is validated by entropy method [7]. But we want to check which has the highest usability. Figure 1 shows the proposed hierarchical model.

The deciding attributes are ease of use, transparency, attractiveness, and usefulness.

Describing briefly the above attributes:

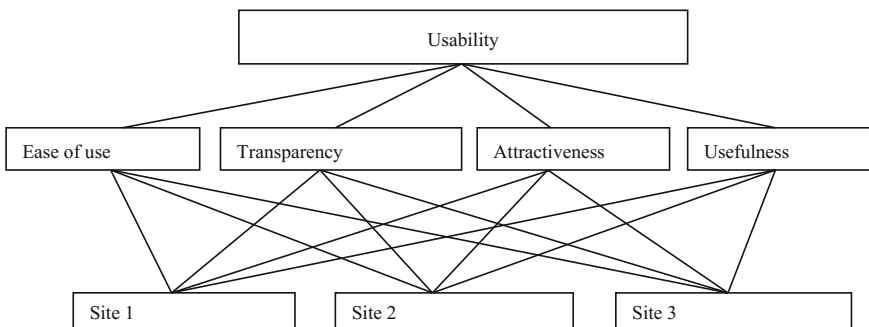


Fig. 1 Proposed usability model

Table 1 Matrix for ease of use (C1)

	S1	S2	S3	Nth	EV
S1	1	5	4	2.687	0.67
S2	0.2	1	0.33	0.409	0.10
S3	0.25	3	1	0.909	0.23
Total				4.005	1.00
$\lambda_{\max} = 3.09$				CI = 0.04	CR = 0.07

1. Ease of use (C1)—Ease of use is basically how much user-friendly the Web sites is to the user. It is the attribute that helps user to find the quick information the user actually wants. Having internal links and a search box will make the user get what they exactly want.
2. Transparency (C2)—This is the attribute that makes each and every people understand the content, the page, and everything related to the Web sites. Everything the user wants is clearly mentioned with the help of internal and external links in the Webpage.
3. Attractiveness (C3)—This attribute makes the page attractive, as general pupils want the Web site for studying in which they do not get bored. Everything they need to study should be precisely written, and if requires deep study, then external links should be there for their ease.
4. Usefulness (C4)—Usefulness of sites is important. As the data required related to any competitive examinations should be there, many mock tests, sample questions and answers, methodology to solve those questions, tricks, etc., should be present in the Web site.

3 Experimental Work

Here, we are going to provide the detailed AHP methodology for the selection of three educational Web sites in Indian scenario based on the above-mentioned method. Data are collected for survey, after that, we check the consistency. Saaty described that obtained tabular data are consistent if consistency ratio is less than 0.1 [8] (Tables 1, 2, 3, 4, 5, and 6).

Table 2 Matrix for transparency (C2)

	S1	S2	S3	Nth	EV
S1	1	0.25	0.2	0.368	0.097
S2	4	1	0.5	1.259	0.332
S3	5	2	1	2.154	0.569
Total				3.781	0.998
$\lambda_{\max} = 3.021$				CI = 0.0105	CR = 0.018

Table 3 Matrix for attractiveness (C3)

	S1	S2	S3	Nth	EV
S1	1	3	7	2.758	0.650
S2	0.33	1	5	1.181	0.278
S3	0.14	0.2	1	0.303	0.071
Total				4.242	0.999
$\lambda_{max} = 3.04$				CI = 0.02	CR = 0.0344

Table 4 Matrix for usefulness (C4)

	S1	S2	S3	Nth	EV
V1	1	3	1/3	1	0.259
V2	1/3	1	1/5	0.409	0.106
V3	3	5	1	2.444	0.634
Total				3.853	0.999
$\lambda_{max} = 3.034$				CI = 0.017	CR = 0.029

Table 5 Matrix for criteria

	C1	C2	C3	C4	Nth	EV
C1	1	5	3	7	3.201	0.553
C2	0.2	1	0.33	5	0.757	0.130
C3	0.33	3	1	6	1.561	0.270
C4	0.14	0.2	0.166	1	0.261	0.045
Total					5.780	0.998
$\lambda_{max} = 4.217$					CI = 0.072	CR = 0.08

Table 6 Usability index

	C1	C2	C3	C4	Usability index	Rank
S1	0.67	0.097	0.650	0.259	0.57	I
S2	0.10	0.332	0.278	0.106	0.178	III
S3	0.23	0.569	0.071	0.634	0.248	II
W (Ci)	0.553	0.130	0.270	0.045		

4 Validation by Entropy Method

The following entropy method is used for the validation purpose of the obtained results from above AHP technique [9]. The whole procedure is as follows (Table 7):

Results From Entropy Method:

STEP 1: $\alpha = \text{constant} = 1/\ln(n)$; whereas n is the number of options
 $\alpha = 1/\ln(3) = 0.91023$

Table 7 Weight table

$p = 1 \text{ to } k \downarrow$	$q = 1 \text{ to } n \rightarrow$		
	S1	S2	S3
C1	0.670	0.10	0.23
C2	0.097	0.332	0.569
C3	0.650	0.278	0.071
C4	0.259	0.106	0.634

Table 8 R^3I_i ranking table

	A	B	C
R^3I_i	0.453	0.1985	0.3426
Rank	I	III	II

STEP 2: $V_j = \alpha \sum (l_{pq} * \ln (l_{pq})$ for all q ($q = 1 \text{ to } k$) & ($p = 1 \text{ to } n$)

$$V_1 = 0.91023 [l_{11} * \ln (l_{11}) + l_{21} * \ln (l_{21}) + l_{31} * \ln (l_{31})]$$

$$V_1 = 0.91023 [0.67 * \ln (0.67) + 0.10 * \ln (0.10) + 0.23 * \ln (0.23)]$$

$$V_1 = 0.7615$$

Similarly,

$$V_2 = 0.8312$$

$$V_3 = 0.7497$$

$$V_4 = 0.7980$$

STEP 3: $E_p = (1 - V_p)$

$$E_1 = (1 - V_1)$$

$$E_1 = 1 - 0.7615 = 0.2385$$

Similarly,

$$E_2 = 1 - 0.8312 = 0.1688$$

$$E_3 = 1 - 0.7497 = 0.2503$$

$$E_4 = 1 - 0.798 = 0.2020$$

STEP 4: $W_q = E_q / \sum E_q (q = 1)$

$$W_1 = [E_1 / (E_1 + E_2 + E_3 + E_4)]$$

$$W_1 = [0.2385 / (0.2385 + 0.1688 + 0.2503 + 0.2020)]$$

$$W_1 = 0.2774$$

Similarly,

$$W_2 = 0.1963$$

$$W_3 = 0.2911$$

$$W_4 = 0.2349$$

STEP 5: $\sum W_q = W_1 + W_2 + W_3 + W_4 + W_5$

$$W_q = 0.2774 + 0.1963 + 0.2911 + 0.2349$$

$$W_q = 0.9997$$

STEP 6: $R^3I_p = \sum (l_{pq} * W_q)$ for all $p, q = 1 \text{ to } k$

$$R^3I_1 = (0.67 * 0.2774) +$$

$$(0.097 * 0.1963) + (0.650 * 0.2911) + (0.259 * 0.2349)$$

$$R^3I_1 = 0.453$$

Similarly

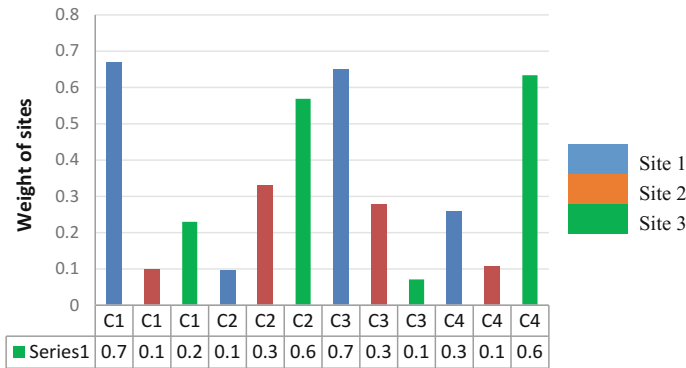


Fig. 2 Analysis and ranking chart

$$R^3I_2 = 0.1985$$

$$R^3I_3 = 0.3426$$

So the rank table is provided in Table 8.

5 Results and Analysis

Using entropy method, we have observed that the Web site S1 has the rank I among all other available educational Web sites. The ranking found by entropy method is same as the ranking found by AHP. So, result is validated, and thus, educational Web site S1 is the best alternate site among all the educational Web sites. The analysis graph between educational sites’ attributes and weight is shown in Fig. 2.

6 Conclusion

Usability of educational sites has an important role in the educational functionality of any organization or institution. This paper presents Web sites’ selection attributes using AHP technique, and the results showed the best selection among the available list of educational sites based on some important attributes. Approvals of the results are done using entropy method. Guidelines of the decisions to define the ranking among the substitutes were initiated on the basis of subjective data. The selection of the best educational sites will occur on the basis of the specified attributes by the help of the recent proposal. More number of decision criteria will be used for the research purpose and with different methods to get more perfect and effectual results in the coming time.

References

1. Nielsen, J.,: "Heuristic Evaluation". In J. Nielsen and R. L. Mack (Eds.); Usability Inspection Methods, John Wiley & Sons, New York, pp. 2564, 1994.
2. Anonymous, Step-by-Step Usability Guide, 2006 <<http://www.usability.gov>> [accessed 20.09.2011].
3. Gray, W., and Salzman, C.,: "Damaged Merchandise? A review of experiments that compare usability evaluation methods", Human-Computer Interaction, vol. 13, pp. 203261, 1998.
4. Saaty, T.L.,: How to make a decision: The analytic hierarchy process. European Journal of Operational research, pp. 9–26, 1980
5. Hasan, L.,: "Evaluating the Usability of Educational Websites Based on Students' Preferences of Design Characteristics". International Arab Journal of e-Technology, Vol. 3, No. 3, 2014.
6. Ahmet Menten, S.,: "Assessing the usability of university websites: An Empirical study on Namik Kemal University", TOJET: The Turkish Online Journal of Educational Technology, volume 11 Issue 3, 2012
7. Jabar, M., Abbas Usman, U., Awal, A.,: "Assessing The Usability Of University Websites From Users' Perspective". Australian Journal of Basic and Applied Sciences, 7(10), pp. 98–111, 2013
8. Saaty, T.L.,: The Analytic Hierarchy Process, New York: McGraw Hill. International, 1980.
9. Divyaa S K, Yadav N. and Dubey S. K.,: "Usability Evaluation of Mobile Phones By using Ahp-Entropy Approach", Proceedings of the 10th INDIACom; INDIACom-2016; 3rd International Conference on "Computing for Sustainable Global Development, pp. 5296–5300, 2016

Adaptability Evaluation of E-commerce Websites in Indian Perspective

Shivani Gupta and Sanjay Kumar Dubey

Abstract E-commerce websites are in much demand these days. Customers are moving towards these sites for buying the products because the trend of shopping from offline purchasing to online purchasing is increasing. Another reason is that there is no third party in between of customers and buyers. The online products are much cheaper in comparison with offline products. The customer lacks in the adaptation of these sites that which one is the best for one's purpose and which one is not. To solve this problem, a hierarchical model is proposed. With the help of proposed model and the Analytical Hierarchy Process approach, ranking of Indian e-commerce site is done. The model is then validated by using entropy method. Methodology in the present paper will help the online buyers to select the best e-commerce site according to their requirements.

Keywords Adaptability · AHP · Entropy

1 Introduction

In the recent years, there is a rapid growth in the consumers to make their purchases online. With the revolution of digitalization, more and more people are attracting towards online marketing and that has developed a need for the e-commerce websites to give all the information regarding their products over the Internet [1]. Websites that deliver everything to the consumers from clothes to groceries took advantage of this new information age. Since there is a lot of e-commerce websites

S. Gupta (✉) · S.K. Dubey
Department of Computer Science and Engineering, Amity University
Uttar Pradesh, Sec.-125, Noida, UP, India
e-mail: shivani95gupta@gmail.com

S.K. Dubey
e-mail: skdubey1@amity.edu

that are selling their products and too few consumers to make them all gainful. It is obvious from the fact that the websites which are the toughest will survive in the competition. And so with this, there is a need to develop the website keeping in mind about consumers that includes “who are the consumers”, “what is the searched information” and “how can this information can be regained easily” [2]. Adaptability is the degree to which the website is being easily used by the consumers. Basically, adaptability is the ease to which a consumer can easily interact with the website and make online purchase. So there must be a set of factors that must be kept in mind by the Web developers to make the website more adaptable and to increase the website users. In this research paper, we are some of the key factors that are helpful in making the website more adaptable. And according to these factors, we will rank the websites and find out which is the most adaptable website from the user’s perspective. The main objective of this paper is to decide the rank of sites on the basis of some important factors. This rank will help the online buyers to select the best e-commerce site for their purpose.

2 Literature Review

In the past few years, several work over the adaptability of e-commerce websites in different countries has been done. In this section, we review some of these work done in different countries and the also review about the adaptability factors proposed by different authors.

Authors	Adaptability factors
Austen [1]	Quality of information, ease of reading and appearance of website
Fangyu Lia [3]	Easy to use, search efficient and navigate easily
Natalija Guseva [4]	Navigation, internal search, architecture and content design
A.K. Abd El Aleem [5]	Performance, security, design and maintenance and user interaction
Oscar de Bruijn [6]	Attractiveness (in content and presentation) and usability
Nasrin Dehbozorgi [7]	Learnability, operability and understandability
Mohammad Alshehri [8]	Ease of use, ease of navigation and user satisfaction
QUIM model [9]	Efficiency, effectiveness, productivity, satisfaction, learnability, safety, trustfulness, accessibility, universality and usefulness
Renuka Nagpal [10]	Response time, ease of use, ease of navigation and informative

3 Methodology

In this paper, we are going to present the AHP method. This method is useful when making the decision when there is some hierarchy is present. For this purpose, we purposed a hierarchical model in which top level is adaptability. The middle layer contains the important factors that affect the adaptability of e-commerce websites. The factors are chosen on the basis of adaptability of Indian e-commerce websites. For research purpose, we have chosen three websites and the sites are chosen on the basis of their popularity. The sites chosen are having nearly equal popularity. Due to some confidentiality matter, we are not enclosing the name of the websites. The factors on which the adaptability of the e-commerce websites will be ruled on include:

- A. **Scalability:** “It is the ability of the website to work efficiently under heavy traffic”.
- B. **Search efficiency:** It is defined as how easily a customer can find what he/she wants. It is important that the customer experiences the e-commerce website as his own personal online store where whatever he wants is a click away.
- C. **Security:** It is defined as the protection of e-commerce assets from unauthorized access, use, alteration or destruction.
- D. **Ease of use:** It is defined as how easily the customer is able to access a particular website. It is a very important factor to define adaptability of a website since it is important that the customer can easily use the website (Fig. 1).

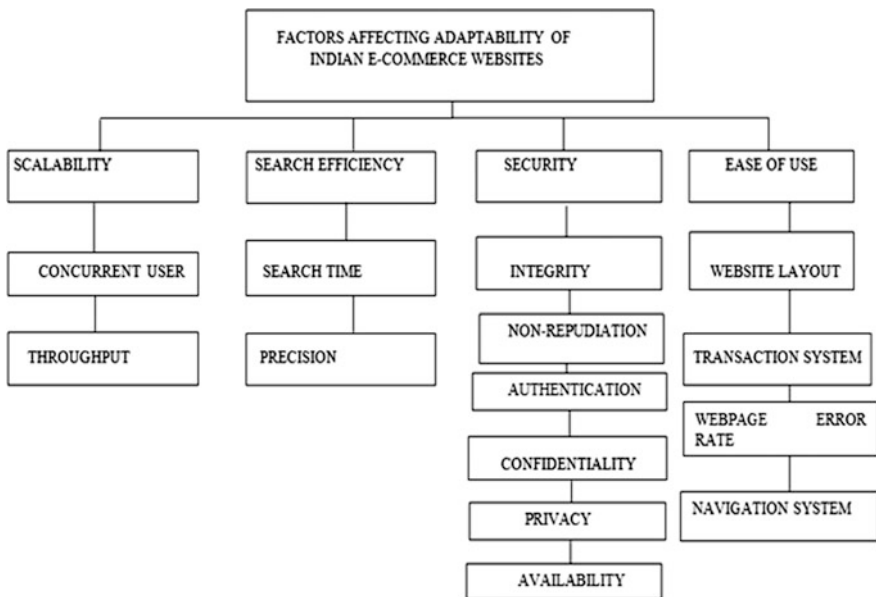


Fig. 1 Sub-factors of adaptability

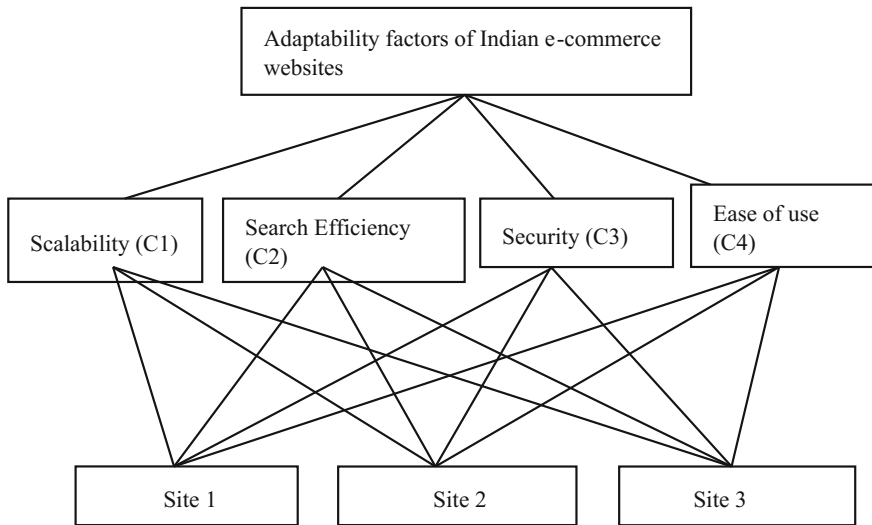


Fig. 2 Proposed hierarchical model

4 Approach

A relationship has been set up between the three e-commerce websites. The names of these sites are not giving due to privacy issue. The adaptability factors Scalability (C1), Search efficiency (C2), Security (C3) and Ease of use (C4). And by using the AHP approach which is discussed later in the section, the adaptability index has been calculated (Fig. 2).

5 Experimental Set-up

In this section, we will provide with detail of AHP methodology for choosing the three Indian e-commerce websites on the basis of proposed model. For the purpose of data collection which will be considered while checking the data consistency, we performed a survey of a group of people. And after the collection of data, we checked the consistency of the e-commercial websites. Saaty [11] described that obtained matrix data are consistent if the ratio is <0.1 (Tables 1, 2, 3, 4 and 5).

The consistency ratio for all the matrices is calculated. The consistency ratio must be <= 0.1. In above all the matrices, the CR is coming out to be <0.1, therefore the weights and the finding about the factors is satisfactory.

After this, the weight of each factor and the respective vector is combined to get the adaptability index. C1, C2, C3 and C4 are the factors Scalability, Search efficiency, Security and Ease of use, respectively, whereas vectors V1, V2 and V3 are

Table 1 Matrix for Scalability

	V1	V2	V3	Nth	EV
V1	1	1/3	5	1.18	0.8462
V2	3	1	7	2.73	0.1977
V3	1/5	1/7	1	0.30	0.2184
Total				4.21	0.991
$\lambda_{max} = 3.05$				CI = 0.0293	CR = 0.05

Table 2 Matrix for Search efficiency

	V1	V2	V3	Nth	EV
V1	1	4	7	3.00	0.70
V2	¼	1	3	0.909	0.212
V3	1/7	1/3	1	0.366	0.085
Total				4.275	0.997
$\lambda_{max} = 3.026$				CI = 0.01	CR = 0.017

Table 3 Matrix for Security

	V1	V2	V3	Nth	EV
V1	1	9	5	3.55	0.75
V2	1/9	1	1/3	0.33	0.07
V3	1/5	3	1	0.84	0.17
Total				4.72	0.99
$\lambda_{max} = 3.01$				CI = 0.009	CR = 0.015

Table 4 Matrix for Ease of use

	V1	V2	V3	Nth	EV
V1	1	1	7	1.90	0.514
V2	1	1	3	1.43	0.386
V3	1/7	1/3	1	0.366	0.099
Total				3.696	0.999
$\lambda_{max} = 3.07$				CI = 0.038	CR = 0.06

Table 5 Matrix for factors

	C1	C2	C3	C4	Nth	EV
C1	1	1/5	1/3	½	0.325	0.055
C2	5	1	2	4	3.378	0.572
C3	3	1/2	1	3	1.642	0.2783
C4	2	1/4	1/3	1	0.553	0.093
Total					5.898	0.999
$\lambda_{max} = 4.625$					CI = 0.0875	CR = 0.972

the e-commerce websites. To calculate the rank of the website, we will find the adaptability index of the websites. Adaptability index of e-commerce websites = $\sum \text{weight of } C_i V_i^* \text{ weight of } C_i W_i$ ($i = 1-5$) for the sample Table 6.

Table 6 Matrix for adaptability index

	C1	C2	C3	C4	Adaptability index	Rank
W_{V1}	0.8462	0.70	0.75	0.514	1.1481	I
W_{V2}	0.1977	0.212	0.07	0.386	0.2738	II
W_{V3}	0.2184	0.085	0.17	0.099	0.2454	III
WCi	0.58	0.381	0.436	0.124		

Therefore, according to the adaptability index of the three e-commerce websites, Site 1 is the most adaptable website from the user’s perspective.

6 Validation by Entropy Method

We have calculated the ranking of the e-commerce website by using AHP method. Now, we will validate our results by using the entropy method (Table 7).

A. Procedure to find the rank:

Step 1: $\beta = \text{constant} = 1/\ln(n)$: where n is the total number of websites.

$$\beta = 1/\ln(3) = 0.91023$$

Step 2: $V_j = -\beta \sum (l_{ij} * \ln(l_{ij}))$ for all j ($j = 1$ to k) and ($i = 1$ to n)

$$V_1 = -0.91023 [l_{11} * \ln(l_{11}) + l_{21} * \ln(l_{21}) + l_{31} * \ln(l_{31})]$$

$$V_1 = -0.91023 [0.8462 * \ln(0.8462) + 0.1977 * \ln(0.1977) + 0.2184 * \ln(0.2184)]$$

$$V_1 = 0.72$$

Step 3: $E_i = (1 - V_i)$

$$E_1 = (1 - V_1)$$

$$E_1 = 1 - 0.72$$

$$E_1 = 0.28$$

Similarly $E_2 = 0.28$, $E_3 = 0.36$ and $E_4 = 0.15$.

Table 7 Matrix for factors and websites

j = 1 to n ↓	i = 1 to n →		
	V1	V2	V3
C1	0.8462	0.1977	0.2184
C2	0.70	0.212	0.085
C3	0.75	0.07	0.17
C4	0.514	0.386	0.099

Table 8 Matrix for rank of websites

Website	Site 1	Site 2	Site 3
R^3I_i	0.73	0.19	0.15
Rank	I	II	III

Step 4: $W_j = E_j / \sum E_j$ ($j = 1$)

$$W_1 = [E_1 / (E_1 + E_2 + E_3 + E_4)]$$

$$W_1 = [0.28 / (0.28 + 0.28 + 0.36 + 0.15)] \Rightarrow W_1 = 0.26$$

Similarly $W_2 = 0.26, W_3 = 0.34, W_4 = 0.14$

Step 5: $\sum W_j = W_1 + W_2 + W_3 + W_4 + W_5$

$$W_j = 0.26 + 0.26 + 0.34 + 0.15 \Rightarrow W_j = 1.01$$

Step 6: $R^3I_i = \sum (I_{ij} * W_j)$ for all $i, j = 1$ to k

$$R^3I_1 = (0.8462 * 0.26) + (0.70 * 0.26) + (0.75 * 0.34) + (0.514 * 0.15)$$

$$R^3I_1 = 0.73$$

This is the rank for first website.

Similarly for the second website $R^3I_2 = 0.19$.

And for the third website $R^3I_3 = 0.15$ (Table 8).

7 Rank and Analysis

From the above analysis of websites corresponding to the factors, it is observed that the adaptability index of the first website is the highest. Since the website with the highest adaptability index is the most adaptable site, therefore Site 1 is the most adaptable site among the three with Rank I. And the result is also validated by using entropy. The analysis graph between e-commerce websites and the adaptability factors has been shown in Fig. 3.

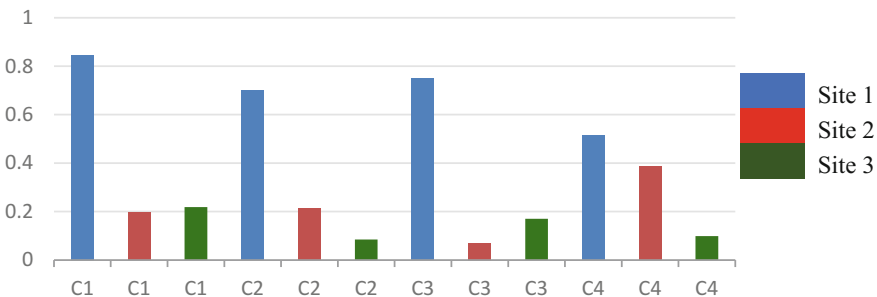


Fig. 3 Analysis and ranking chart of websites

8 Conclusion

In the recent years, the number of users for online marketing has seen a significant increase. With digitalization, a large population in India has access to the Internet and hence the e-commerce websites have seen a major growth in the number of customers. More people are accessing the Internet and doing their purchases online. The e-commerce website is much benefited from this age of digitalization. Since the a lot of people are using the e-commerce websites, there is a need for Web designers to keep certain factors in mind while designing the website to make it more adaptable to the users. It will be beneficial for the e-commerce website to make the website customer friendly so that they don't face any difficulty while using the website and they come to the same website again when they want to purchase anything online. This research paper proposed some factors that are useful for making website more adaptable, and according to those factors we calculated the rank of three popular e-commerce websites using the AHP technique and also validated the result using entropy method. Through this research, we find out that Site 1 is the most adaptable website among the three chosen websites.

References

1. Moore, A.R.: Usability Study on e-Commerce Web Sites, Instructional Technology, Dr. Liu's Design Strategies for New Media, April 17, 2005
2. Nagpal, R., Mehrotra, D., Bhatia, P.K.: Analytical Modelling Approach To Measure The Usability of Website, International Journal of Software Engineering and Its Applications Vol. 10, No. 5 (2016), pp. 125–142
3. Lia, F., Lib,a *, Y.: Usability evaluation of e-commerce on B2C websites in China, Procedia Engineering 15 (2011) 5299–5304
4. Guseva, N.: Looking for the e-commerce quality criteria: Different perspectives, ISSN 1392-1258. ekonomika 2011 Vol. 90(1)
5. Abd El-Aleem, A.K., Abd El-wahed, W.F., Ismail, N.A.: Efficiency Evaluation of E-Commerce Websites, International Journal of Computer, Electrical, Automation, Control and Information Engineering Vol. 1, No. 4, 2007
6. Bruijn*, O.D., Angeli, A.D., and Sutcliffe, A.: Customer experience requirements for e-commerce websites, Int. J. Web Engineering and Technology, Vol. 3, No. 4, 2007
7. Dehbozorgi, N., Jafari, S.: Proposing a Methodology to Evaluate Usability of E-Commerce Websites: QUEM Model, International Journal of Computer Applications (0975—8887) Volume 52—No. 6, August 2012
8. Alshehri, M., Aldabbas, H., Sawle, J., and Baqar, M.A.: ADOPTING E-COMMERCE TO USER'S NEEDS, De Montfort University, Faculty of Technology, Leicester, United Kingdom
9. Donyae, M., and Seffah, A.: QUIM: An Integrated Model for Specifying and Measuring Quality in Use, Eighth IFIP Conference on Human Computer Interaction, Tokyo, Japan, 2001
10. Nagpal, R., Mehrotra, D., Bhatia, P.K., and Sharma, A.: Rank University Websites Using Fuzzy AHP and Fuzzy TOPSIS Approach on Usability, I.J. Information Engineering and Electronic Business, 2015, 1, 29–36, DOI:10.5815/ijieeb.2015.01.04
11. Saaty, T.L.: How to make a decision: The analytic hierarchy process. European Journal of Operational research, (1980), 9–26

Improvement and Approval of Impediment Recognition and Activity for Power Window

Roushan Kumar, Neelu J. Ahuja and Mukesh Saxena

Abstract The paper focuses to bring high-quality innovative products based on automotive power window control system. Currently, market is moving very rapidly and technology drives the use of simulation models and different validation techniques for model design and rapid realization process. A model-based design technique provides higher efficiencies in product development cycle that boost the technocrats to deliver outcome on time and satisfies initial design requirements and their validation. This paper applies the model-based design model and also develops prototype and appropriate code from a model-based development tool code generation automatically. The research paper emphasis on the modeling and validation of obstacle detection and appropriate action on automotive power window and implementation on electronic control unit based automotive power window. The main objective of ECU-based power window system is to make automatic or circuit-based approach to raise up glass door and to lower down the glass door with help of an appropriate driver and passenger switches or the use of appropriate sensors like carbon dioxide sensor, thermocouple, current sensor, and proximity sensor to replace the conventional hand-turned crank handle manual automotive window, and whenever obstacle is detected, power window should lower down by 10 cm. Automatic power window control system consists of power electronic circuit, DC motor, and control algorithm. The control algorithm senses soft obstructions and hard obstructions and accordingly controls speed of DC motor as well as orientation control of DC motor that moves the window glass frame downward of 10 cm when any obstruction is detected. In other way the power window ECU faculties hindrances and with help of calculations it is keeping up information

R. Kumar (✉)

Department of Electronics Instrumentation and Control Engineering,
University of Petroleum and Energy Studies, Dehradun, India
e-mail: rkumar@ddn.upes.ac.in

N.J. Ahuja

Centre of Information Technology, University of Petroleum
and Energy Studies, Dehradun, India

M. Saxena

University of Technology and Management, Shillong, Meghalaya, India

© Springer Nature Singapore Pte Ltd. 2018

R. Singh et al. (eds.), *Intelligent Communication, Control and Devices*,
Advances in Intelligent Systems and Computing 624,
https://doi.org/10.1007/978-981-10-5903-2_89

which additionally control the engine development operation in three distinctive memory cushions that are routinely refreshed by the information beats that are identified with DC engine speed control. The whole framework is outlined as a clever control framework by applying number of conditions which results to the development of the power window.

Keywords Power window algorithm • BLDC motor • Intelligent power window control circuit

1 Introduction

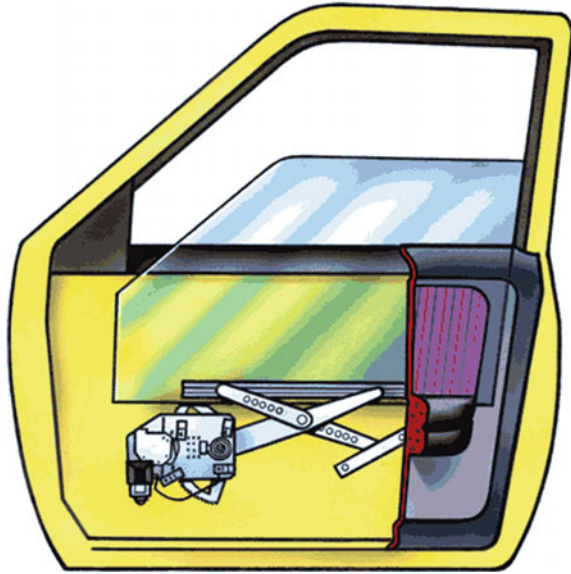
The ECU board comprises of numerous switches few are driver controlled and few are traveler's controlled, when specific switch is squeezed the DC engine circuit will control development of DC engine and further it will move the window outline upwards and comparatively when the opposite side of same switch is squeezed the window will additionally move toward downwards. With help of transfers, H connect circuits are utilized to alter the course of DC engine from anticlockwise to clockwise heading and clockwise to anticlockwise bearing. In both of the cases, we have utilized two closeness sensors on top side and base side of the car control window board. As far as possible and as far as possible is distinguished by the nearness sensor. In this investigations, LPG and temperature sensor are utilized. LPG sensor a particular esteem is characterized above which it is expected that there is gas spillage in the vehicle and window will move downwards until as far as possible is come to. For temperature sensor, when lodge temperature is above edge go, the power window glass edge will move consequently toward descending until as far as possible is detected.

In automobile, power window is a vital electrical DC motor-based system. This is located in every door of the particular vehicle. The main objective of this system is to raise up and lower down the power window-based glass door by applying a proper electrical-based two-way manual switch to replace the use of hand-turned crank mechanism-based automotive window. Automotive power window-based system includes DC motor, power electronics circuit, control algorithms, and multiple electromechanical switch as inputs [1].

A portion of the cutting-edge autos have a component of time deferral; this kind of frameworks permits the usefulness in the windows and other supporting assistants to be operational for quite a while even after the motor is halted [2]. Another components in some vehicle is the express-down window, which permits the window to be totally lower with one tap on the manual switch, as halted by holding the switch descending until the window achieves the level.

On mechanical structure-based criteria, any car control window framework is of two sorts. One is called as link sort control window framework and other sort is named scissors sort control window framework. The primary usefulness of both the frameworks is for raising and bringing down the vehicle windows outline utilizing a

Fig. 1 Power window system



DC engine which is further controlled through power window control calculations. The link sort of car power window framework has four noteworthy segments, for the most part of DC electric engine, railing, control hardware circuit, and driver and traveler switch [3]. The power window glass is mounted at the bearer plate, and the link is situated on the railing surface. DC motor is utilized to turn the link in order to move the window all over utilizing a rack and pinion outfit system which is further joined to the DC engine and the link-based circuit is represented in Fig. 1.

Power window systems are used in every vehicle, and it should meet the functional safety, standard, and ease of operation to prevent fatal accident like trapping pet neck in window frame and human body being trapped, leading to blockage because of malfunction or error in the power window system [4, 5].

Power window electrical control circuit and components are further divided into four types. One is relay-driven DC motor, second category is H bridge-driven DC motor, third category is brushless DC motor (BLDC), and last one is permanent magnet synchronous motor (PMSM) [6].

The association of paper is as per the following: Sect. 1 presents presentation, area 2 piece chart, segment 3 controller configuration, segment 4 exploratory setup, segment 5 result and discourse. Conclusion and Future work is spoken to in area 6.

1.1 Block Diagram

A block diagram of a system is represented in Fig. 1 in which the principal functions are represented by blocks connected by lines representing relation between the

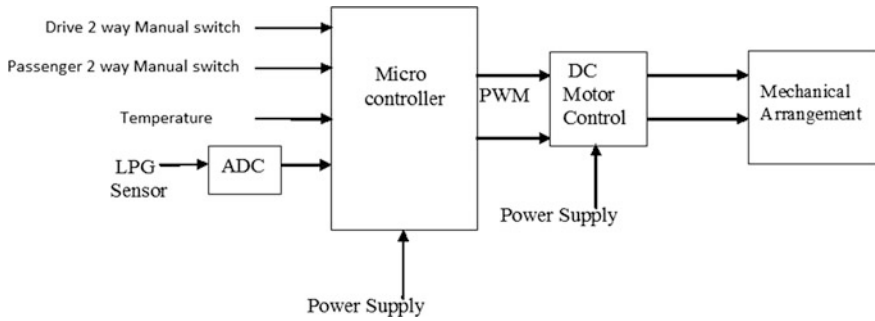


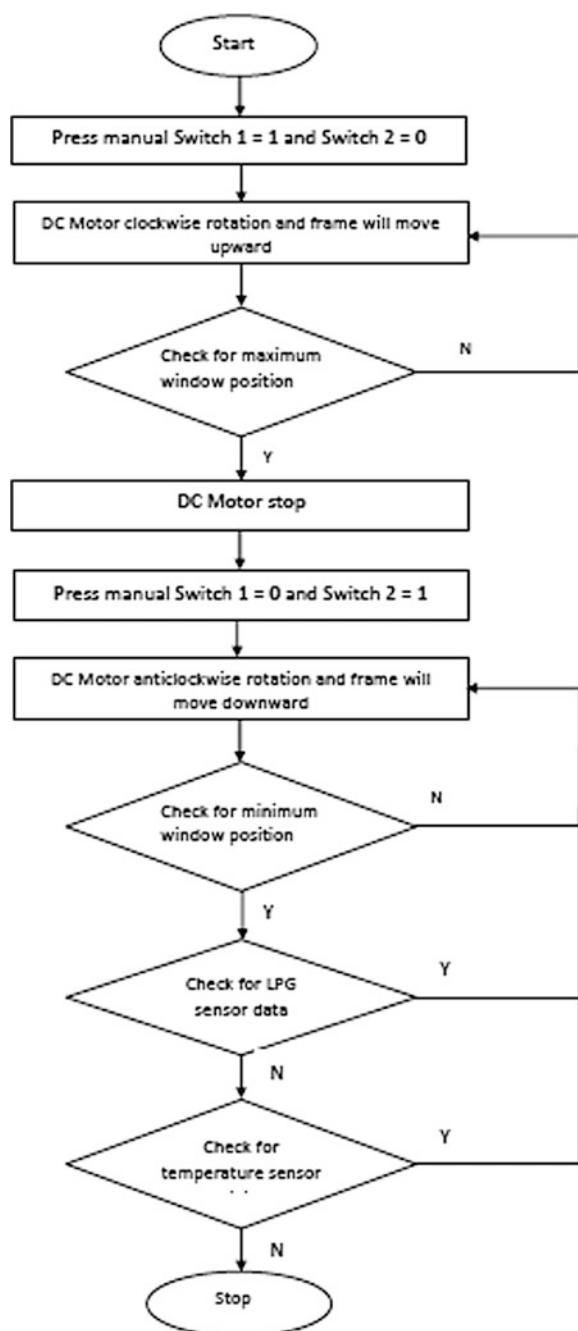
Fig. 2 Basic structure of power window system

blocks. The power window control system is further divided into hardware design, software design, electronic circuit design, and control process flow algorithms. In Fig. 2, multiple inputs like driver manual switch, passenger switch, different sensors are used as input to the system. Microcontroller-based system called ECU is used to control power window system. Two-way mechanical switch is pressed to move motor forward and backward and accordingly window frame will move in upward and downward direction. MOSFET-based H bridge circuit is used to control the motor, which further controls the direction of power window from anticlockwise to clockwise direction and clockwise to anticlockwise.

To effectively design the automotive power window system, it can be further classified as four subsystems:

- (a) ECU development
- (b) Hardware interfacing and signal conditioning circuit
- (c) DC motor and power electronics circuit
- (d) Lifting mechanism.

Power window frame consists of two sensors, one on top of the frame and other on bottom of the frame. Using sensor with appropriate electrical signal, the upper-level limit and lower-level limit are identified and accordingly DC motor stops until the next instruction from control algorithm is given. The two sensors LPG and temperature define input to controller if there is LPG gas leakage if its LPG based engine and internal cabin temperature is rises to threshold value then the power window glass move toward downwards side until the lower limit is sensed. The control algorithm flowchart related to software development procedure is demonstrated in Fig. 3.

Fig. 3 Control algorithm flowchart

2 Controller Design

Various challenges arise during the design of a vehicle ECU. Any vehicle in current market scenario consists of multiple larger subsystems like power train, engine, body electronics, automatic transmission, battery management system; every subsystem is of nonlinear nature and closed-loop time-varying system and because of that it is very complex. In this research the automotive power window controller i.e. microcontroller based ECU design is categorized into hardware design and development of software [1, 2].

This section offers information on switch-based controller implemented in integrated development environment. The ECU-based control algorithm structure is measured based on the block diagram inputs as shown in Fig. 1. For the development of ECU, the following inputs are taken for motor forward and reverse movement (Table 1).

From the above input to the controller, DC motor decides whether the power window will move in upward and downward direction.

2.1 Hardware Model

For prototype development, power window system is categorized into following five segments:

- Power supply unit
- ECU, i.e., microcontroller board
- Power electronics circuitry
- Sensors interfacing circuit
- Switch interfacing circuit.

Power supply is further classified into ON and Off board power supply unit. ON and Off board power supply unit contains of center-tap step down transformer and input applied to center-tap step down transformer is 220 V and 1 A and output is 12 V-0 V-12 V and 1 A. An electromechanical Switch, i.e., passenger and driver manual switch for ON and OFF the system. Indication of working system using LED is used in the system, Resistor of 1 k Ω , Full wave rectifier circuit is used which consists of four 1 N 4007 diodes, voltage regulator IC LM 7812 and LM 7805 are used for OFF voltage power supply, i.e., generation of constant 12 V

Table 1 Input characteristic

Input No.	Description
1	Driver two-way manual switch
2	Passenger two-way manual switch
3	Temperature input
4	LPG input

supply and LM 7805 is used for generation of 5 V as ON voltage DC power supply unit. For filtering circuit a the rating of a capacitor is 1000 μ F and 50 V.

ECU development board contains ON board power supply unit which requires input as 5 V and 600 mA, which is established by voltage regulator IC LM 7805. Motor circuitry is power electronics cum discrete electronics-based circuit used to run the motor in appropriate direction. In the protection circuit, freewheeling diode is used to limit the back EMF, i.e., electromotive force generated from relay and motor which comes under inductive load. A DPDT relay of 12 V, 5 A, with appropriate rated coil current and coil resistance is used with power transistor 2N3055 which is used for switching [7]. MOSFET-based H bridge circuit is another alternate over relay-based switching circuit. Q1 and Q3 are N-channel MOSFETs and IC used for IRF510 that supports 10 A current whereas Q2 and Q5 are P-channel and IC used for that is IRF9530 based IC is used which in turn control the position of the automotive power window glass shown in Fig. 4. According to DC motor characteristics and object detection system working model, some analysis was conducted for best threshold value and calculation for lower down value, i.e., 10 cm from maximum position. The best threshold calculation to identify obstacle is 92% of maximum current of rated DC motor during starting. This current value is identified with current sensor installed in series with DC motor circuit. According to data sheet of hall effect based current sensor ACS712 maximum current is 5 A and 185 mV/A output sensitivity. ATmega development board is used as ECU consists of Microcontroller IC, 16 \times 2 LCD for presenting upward and downward movement of power window system.

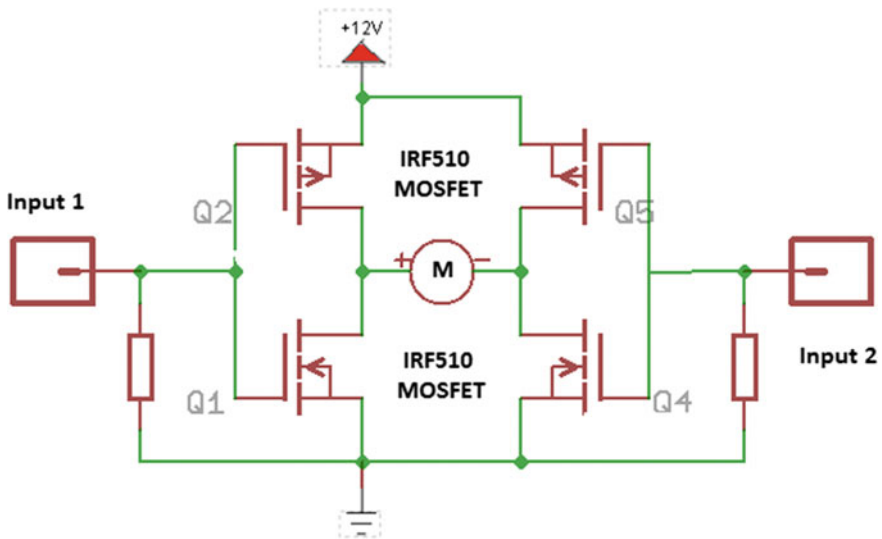


Fig. 4 MOSFET-based H bridge circuit

3 Results and Discussions

The experimental result on power window system is classified as obstacle measurement and action performed by the automotive power window. The experimental analysis was conducted for the prototype design using measurement and instrumentation system. The modeling and its prototype development are done successfully using MATLAB/Simulink software and tested on microcontroller called ECU. Simulink is used for altered investigation purposes. Implementation on hardware is done using microcontroller and desecrates electronics components cum modules like driver circuit, bridge circuit, power supply unit. The prototype developed is cost-effective and simple with respect to implementation on hardware device [8]. This type of retrofitted system can be implemented in types of vehicles for power window system, and further, it will safeguard occupant and passengers during accidents as shown in Fig. 5.

This is an example of an automated system that reduces human effort for operation and ease of interface with power window system. The obtainable experimental outcomes describe applicability of the innovative, robust, and modest

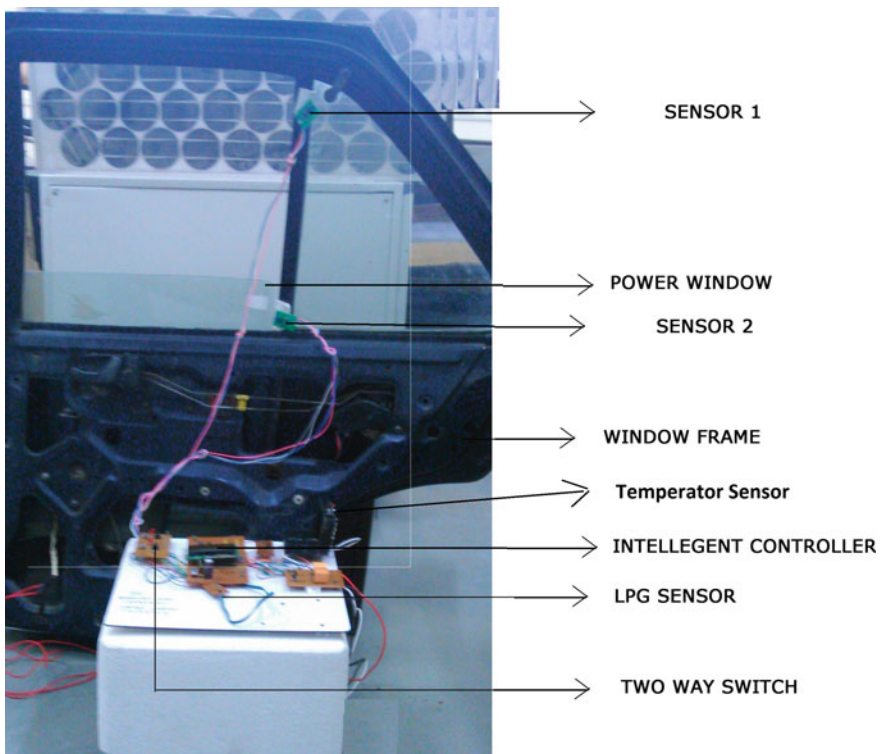


Fig. 5 Experimental setup

Table 2 Result comparison analysis

Parameters	Obstacle detection	Action performed	Experimental result	Ref. [9]	Ref. [10]
Movement time (upward)	Yes	10 cm below to maximum	1.3 S	3.27 S	4.00 S
Movement time (downward)	No	Not required	Not required	3.20 S	4.00 S

approach for power window control system in the traditional vehicle. The approach is all-purpose and can be implemented to other types of vehicles, i.e., commercial light vehicle light and heavy load vehicle.

Prototype illustrates the overall structure of our proposed automotive power window system. The automotive power window system uses a personal computer with MATLAB/Simulink and sensor for obstacle. An obstacle detection method aims to define the presence of obstacles and takes appropriate action by control algorithm to lower down the window frame exactly 10 cm below from maximum position.

The prototype of automotive power window experiment shows below optimal result in comparison with other obtainable work. Once obstacle is identified, then power window will move 10 cm toward downward side and time taken to travel 10 cm is 1.3 s. Similarly, overall time taken to move power window downside is 2.62 s. The evaluation table with reference to the existing work is represented in Table 2.

4 Conclusions

In this article, the modeling, design analysis, and development are carried out for the implementation of power window prototype, whereas safety of power window system is increased. Since because low cost and ease of availability of CNG and LPG Vehicles is increasing exponentially as its cost, effectiveness and efficiency is higher compare to conventional IC engine. To increase safety of the system, LPG sensors are incorporated and implemented in the automotive systems. In coming

Table 3 Abbreviations details

Abbreviation	Abbreviations details
IOT	Internet of things
CNG	Compressed natural gas
ECU	Electronic control unit
LDR	Light dependent resistor
BLDC	Brushless DC motor
LPG	Liquid petroleum gas
ADC	Analog to digital conversion

days, this technology can be recommended for high-end ECU and stretched for accidental information through Internet of things to control room. The above investigation is equated with similar work carried out with other scholars with existing technology and modern technology with respect to power window control, and it is assessed an prime result in terms of obstacle detection technique and action taken by control algorithm. Moving ahead, this research work can be extended to vehicle networking, fault lenience and electromagnetic interference and compatibility. The abridgements used for paper are listed in Table 3.

References

1. R. Kumar and A. Kumar, "Design and hardware development of power window control mechanism using microcontroller," in *International conference on Signal Processing and Communication*, IEEE Xplorer, pp. 361–365.
2. R. Kumar, N.J. Ahuja, M. Saxena and A. Kumar "Modelling and Simulation of Object Detection in Automotive Power Window" Volume 9, Issue 43, November 2016, ISSN (Print): 0974-6846 ISSN (Online): 0974-5645, Indian Journal of Science and Technology(IJST).
3. Wang Yi, Qiu Yunfeng, Yin Jie, "Application of automobile power window controller for peripheral interface controller", International Conference on Electronic Measurement & Instruments (ICEMI), IEEE Aug 2011, vol. 2, page 363–367.
4. J. H. Park, G. H. Choi, T. S. Yoon And J. B. Park, "A Sensorless Safety PowerWindow Control System in Automotive Application", International Conference on Control, Automation and Systems 2008, COEX, Seoul, Korea, pp 1457–1461.
5. Yi Wang, Yun-feng Qiu "A Low Cost Anti-Pinch Control System for Electrical Window", Proceedings of the Fourth IEEE International Conference on Information and Computing, April 2011, Page 385–387.
6. Liu Xiaoming, Shao Yahui, Wu Haowei, Zhong Yuanhong. Design of Car Window Anti-trapping Without Sensor. *Micromotors Servo Technique* 2007(4):48–49.
7. Zhang Yaming, Sun Fengchun, Zhang Xiaowei., "Development of Vehicle Control Unit for HEVs", *JOURNAL OF NORTH UNIVERSITY OF CHINA*, 2009, 30(6):530–535.
8. Kitae Yeom, Jinyoung Jang, Choongsik Bae, "Homogeneous charge compression ignition of LPG and gasoline using variable valve timing in an engine", *Science direct paper*, 2007.
9. Liu Xiaoming, Shao Yahui, Wu Haowei, Zhong Yuanhong. Design of Car Window Anti-trapping Without Sensor. *Micromotors Servo Technique* 2007(4):48–49.
10. Jung Hoon Park, Ga Hyung Choi, Tae Sung Yoon And Jin Bae Park, "A Sensorless Safety PowerWindow Control System in Automotive Application", International Conference on Control, Automation and Systems 2008, COEX, Seoul, Korea, pp 1457–1461.
11. Wang Yi, Qiu Yunfeng, Yin Jie, "Application of automobile power window controller for peripheral interface controller", International Conference on Electronic Measurement & Instruments (ICEMI), IEEE Aug 2011, vol. 2, page 363–367.
12. Daiqiang Wang, Shiyu Gao, Yuqing Chen, Yi Wang, Qiao Liu. Intelligent Control System Based on CAN-bus For Car Doors and Windows. Proceedings of the 3rd international conference on Anti-Counterfeiting, security, and identification in communication, IEEE Press Piscataway, 2009: 242–245.
13. Zhang, C.W., "Simulation Study of H8 Control for Regenerative Braking of Electric Vehicle", In Proceedings of the 2010 International Conference on Computing, Control and Industrial Engineering, Wuhan, China, 5–6 June 2010; Volume 1, pp. 439–441.
14. M. Ehsani, M. Rahman and H. Toliyat, "Propulsion System Design of Electric and Hybrid Vehicles", *IEEE Transactions on Industrial Electronics*, Vol. 44, No. 1, Feb. 1997.

Design and Performance Analysis of Four-Port Discontinuous Patch Antenna

K. Shreekant, Parth Sharma and Shuchismita Pani

Abstract A compact discontinuous microstrip slot patch antenna, which is operating at a frequency of 2.4 GHz, has been proposed for Bluetooth applications. It has one port, which is excited with the help of microstrip feed line mechanism. The proposed antenna is a 3-layer structure consisting of ground, substrate, and discontinuous patch. A patch antenna can be defined as narrowband, wide-beam antenna that is fabricated by etching the antenna element pattern into the metal trace, which is then bonded to a dielectric substrate, which is insulating in nature. Printed circuit board can be an insulating dielectric substrate, along with a continuous metal layer, which is bonded to the opposite side of substrate layer and which acts as a ground plane for the patch antenna. Common microstrip antennas consist of shapes such as square, rectangle, circle, but the shape is usually circular. But in the case of the discontinuous patch, it consists of a circular ring inscribed in a square ring. Both circular ring and square ring are connected through rectangular strips. A thorough study of various parameters has been carried out with performance optimization to reduce the size of area of an antenna. This antenna can achieve return loss of -23.01 dB and $VSWR \leq 1.5$ at frequency of 2.4 GHz. Antenna proposed in this paper can be used in various modern communication applications.

Keywords Discontinuous · Microstrip antenna · Square and circular rings
Four port

K. Shreekant (✉) · P. Sharma · S. Pani
Amity University, Noida, India
e-mail: shrikant.k.95@gmail.com

P. Sharma
e-mail: parthsharma2708@gmail.com

S. Pani
e-mail: spani@amity.edu

1 Introduction

In wireless communication, there is an increase in demand for antennas, which are capable of operating in various frequency bands without changing physical equipment [1]. Researchers are made to work hard to enhance the performance of microstrip patch antenna (MSA) to provide improved technology like MIMO [2]. In wireless systems, antenna propagates through free space, which leads to signal degradation. Signal degradation can be because of path loss; the power density of the electromagnetic wave is reduced as it propagates through space. This is tackled using various techniques like multiple-input multiple-output (MIMO), which increases quantities like the signal-to-noise ratio. The signal-to-noise ratio of a channel may be affected by fading, which will in turn start to affect the bit error rate, if the data being transmitted is digital. The main principal behind the MIMO is to provide multiple versions of the signal. Probability that the different signals will be affected at the same time will be reduced, if they can be affected in different ways to the signal path. One of the major advantages of multiple-input multiple-output is that it increases performance of wireless system without affecting or increasing the transmitting power or system bandwidth [3–6]. To reduce the area and size of an antenna, discontinuous patch antenna is the best alternative to achieve the above-mentioned merits. The other advantages of discontinuous patch antennas are as follows: (1) improved radiation pattern, i.e., the strength of the radio waves, which depend on the direction and which propagate from the antenna and (2) high input impedance, i.e., it allows the antenna to draw little power on the signal that means the circuit provides more power on the signal. The reconfigurable radiation patterns can be used to obtain broadside radiations in the omnidirectional direction and two end-fire radiations whose main beams are directed exactly in opposite directions [7]. Now, a planar structure consisting of four-element array based on a shape like L-shape can be used for a directional radiation pattern [8].

The radiation pattern can be configured using a new topology as well, with two diodes and two metal structures, where diodes are used for short circuit in the circuit [9]. Tunable antennas can also be created using different frequencies for different applications [10]. Now, the microstrip patch antenna can also be designed using asymmetrical p-i-n diodes for radiating purposes [11]. Discontinuous patches provide better solution when it is used for MIMO application, since the band gap difference arising due to the structure might be effectively used for radiating different frequency of antenna within the given range. Thus, in this paper, we have integrated the above-mentioned merits to design an antenna with four ports. But such design techniques have some drawbacks like increase in complexities of baseband processing. From the observations, we can propose and validate the design of a four-port discontinuous patch antenna. In Sect. 2, we have presented the designing details of discontinuous patch antenna constituting square and circular rings. In Sect. 3, the parametric results of the proposed antenna with simulated results have been carried out. The results have been studied and analyzed.

2 Antenna Design

For any antenna to work optimally, it should be receiving and transmitting signals in resonance frequencies; vibrating system or any other external source drives another system to oscillate with amplitude, which is greater than what it is currently oscillating at. The resonance frequency of the discontinuous antenna is 2.4 GHz. The substrate is made of FR-4 (lossy) material with thickness 1.2 mm. Dielectric constant of substrate is 4.3. The use of lossy medium is justified because of its characteristic to absorb a significant amount of energy of the propagating electromagnetic wave. The ground with 1.2 mm thickness is made of perfect electric conductor (PEC); a perfect electrical conductor is an idealized material, which exhibits infinite electrical conductivity or in other words equivalent to zero resistivity. The impedance of antenna is around 50 Ω. The dimensional parameters are given in Table 1. The parameters are optimized to obtain more accurate results.

The dimensions of discontinuous patch antenna are as follows:

- Outer square patch width (W) = 0.4λ
- Outer square patch length (L) = 0.4λ
- Where $\lambda = 125$ mm
- Optimized outer square patch width = 0.32λ
- Outer square patch length = 0.32λ
- Inner square patch width (w) = 0.3λ
- Inner square length (l) = 0.3λ
- Optimized inner square patch width = 0.28λ
- Inner square length = 0.28λ
- Outer circular radii = 0.14λ
- Optimized outer circular radii = 0.128λ
- Inner circular radii = 0.12λ
- Optimized inner circular radii = 0.112λ .

2.1 Figures

The simulation for discontinuous patch antenna is carried out with the help of commercial simulation software, CST Microwave Studio Simulator. The

Table 1 Computerized dimensions and optimized dimensions

Parameters	Computed dimensions	Optimized dimensions
Outer patch width = length	50	40
Inner patch length = width	37.5	35
Outer radii	17.5	16
Inner radii	15	14

optimization of the design is also conducted. The simulated result of various parameters likes of return loss; when a signal is returned or reflected by a discontinuity, the power may get reduced, VSWR; ratio of the maximum and minimum voltage in the standing wave. Large impedance mismatch will result in large amplitude of the standing wave and no voltage will be present in the standing wave if there will be perfect impedance matching, so the ratio of the maximum voltage to minimum voltage would be 1:1, Directive Gain; at a particular coordinate combination, the radiation intensity of an antenna which is divided by the radiation intensity from an isotropic antenna of same power radiated into the space, for four-port discontinuous patch antenna are tabulated in Table 2.

A discontinuous patch antenna with resonant frequency of 2.4 GHz gives a return loss of -23.01 dB. VSWR value lies in the range 1–2, and directive gain of 3.9 dB is obtained as shown in Table 2.

The S11 for the proposed discontinuous patch antenna is -23.01 , -15 , -32.89 , and -24.98 dB at 2.4, 3.9, 5.3, and 7.8 GHz, respectively, which has been observed as shown in Fig. 1.

The impedance value for the proposed patch antenna has been calculated as 50Ω at 2.4 GHz, as shown in smith chart in Fig. 2.

The maximum directivity for the proposed patch antenna has been calculated as 3.9 dB at 2.4 GHz, as shown in 3D in Fig. 3, of radiation pattern.

Table 2 Parameters and values of the proposed structure

Parameters	Values
Resonance frequency	2.4 GHz
Return loss	-23.01
VSWR	1.45
Directive gain	3.9

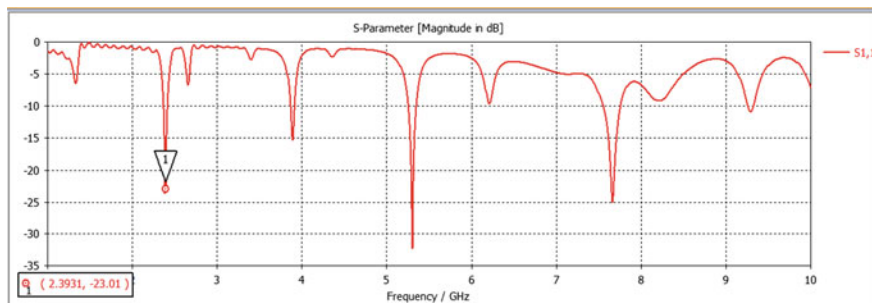


Fig. 1 Return loss of the proposed antenna

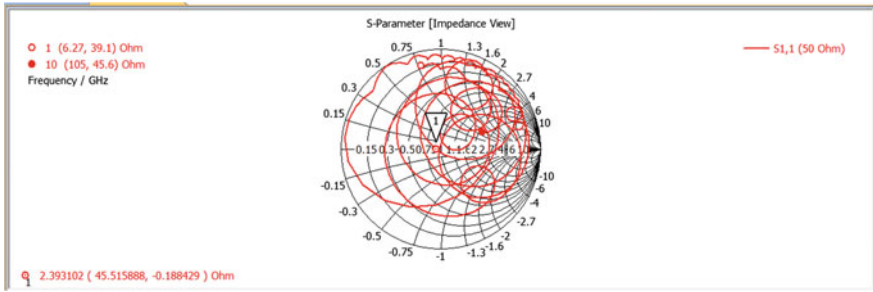


Fig. 2 S-parameter

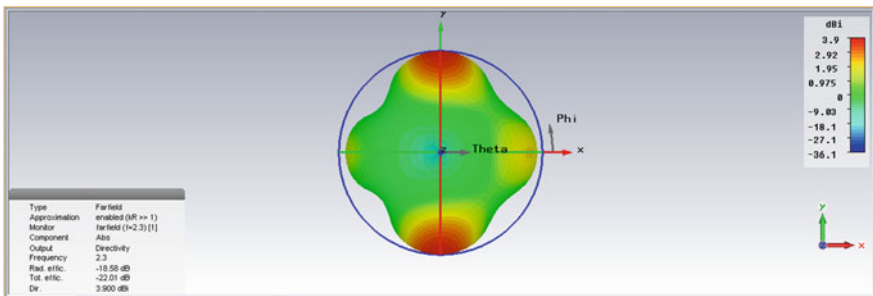


Fig. 3 3D radiation pattern

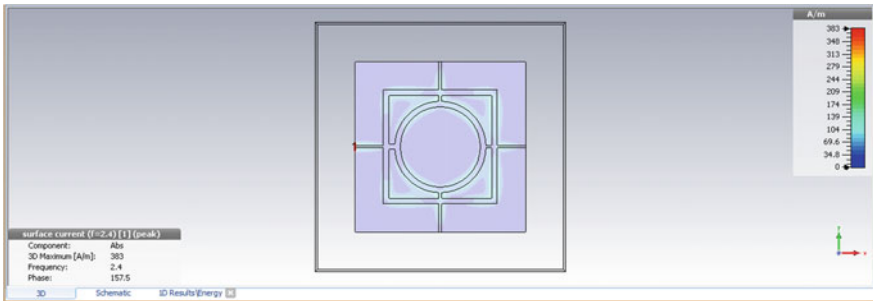


Fig. 4 Current distribution of the antenna

The 3D maximum for the proposed patch antenna current value is 383 at 2.4 GHz, as shown in Fig. 4.

The VSWR for the proposed patch antenna has been calculated as 1.45 at 2.4 GHz, as shown in Fig. 5.

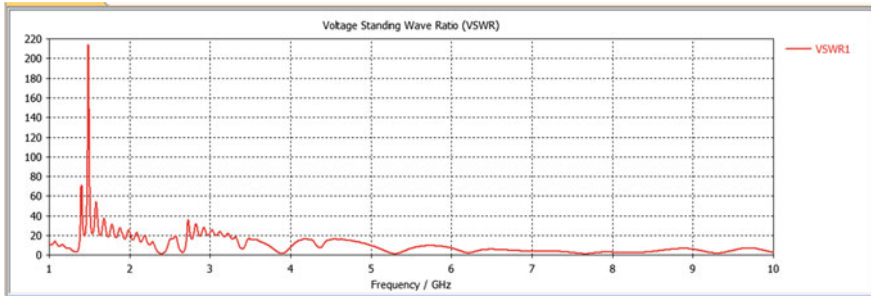


Fig. 5 VSWR of the four-port discontinuous patch antenna

3 Conclusion

A new four-port discontinuous patch antenna has been designed and simulated for the operating frequency of 2.4 GHz. This antenna is useful for Bluetooth applications. The simulation has been carried out using CST Microwave Studio. Optimization has been done to improve the efficiency of patch antenna. A comprehensive parametric study has been done by varying various dimensional parameters (width of square and circular ring) of the discontinuous patch antenna having three layers. A patch antenna is used because of the increased radiation intensity and high impedance because of the MIMO technology.

References

1. Jiajie, Z., Anguo, W., Peng, W., "A Survey on reconfigurable antennas", International Conference on Microwave and Millimeter Wave technology ICMWT, vol. 3, pp. 1156–1159, 2008.
2. Cheng, W.H., Feng, Z.H., "Planar reconfigurable pattern antenna by reactive-load switching", *Microw. Opt. Technol. Lett.*, 47, (5), pp. 506–507, 2005.
3. Piazza, D., Kirsch, N.J., Forenza, A., Heath, R.W., 2008, Dandekar, K.R., "Design and evaluation of a reconfigurable antenna array for MIMO systems" *Antennas Propag.*, 56, pp. 869–881.
4. Lai, M.-I., Jeng, S.-K., "Compact pattern reconfigurable antenna array based on L-shaped slots and PIN diodes for adaptive MIMO systems", *IEEE Antenna Propag. Soc. Int. Sym.*, 2008, 8, (1), pp. 6–9, 2008.
5. Mark, A.C.K., Corbett, R.R., Ross, D.M., "Low cost reconfigurable landstorfer planar antenna array", *IEEE Trans. Antennas Propag.*, 57, (10), p. 3051, 2009.
6. Piazza, D., Mookiah, P., D'Amico, M., Dandekar, K.R., "Experimental analysis of pattern and polarization reconfigurable circular patch antennas for MIMO systems", *IEEE Trans. Veh. Technol.*, 59, pp. 2352–2362, 2010.
7. Wu, S.-J., Ma, T.-G.: 'A wideband slotted bow tie antenna with reconfigurable CPW-to-slotline transition for pattern diversity', *IEEE Trans Antennas Propag.*, 2008, 56, pp. 327–334.

8. Lai, M.-I., Wu, T.-Y., Hsieh, J.-C., Wang, C.-H., Jeng, S.-K., "Compact switched-beam antenna employing a four element slot antenna array for digital home applications", *Antennas Propag.*, 56, pp. 2929–2936, 2008.
9. Lai, M.-I., Wu, T.-Y., Hsieh, J.-C., Wang, C.-H., Jeng, S.-K., "A compact pattern reconfigurable antenna design for handheld wireless devices", *IEEE Antennas Propag. Soc. Int. Symp.*, 1, pp. 5223–5226, 2007.
10. Peroulis, D., Sarabandi, K., Katehi, L.P.B., "Design of reconfigurable slot antennas", *IEEE Trans. Antennas Propag.*, 53, pp. 645–654, 2005.
11. Nair, S.V.S., Max, J.A., "Reconfigurable antenna with elevation and azimuth beam switching", *IEEE Antennas Wirel. Propag. Lett.*, 9, pp. 367–370, 2010.

A Compact, High-Radiation Efficient, and High-Gain Micro-Strip Patch Antenna Array for Millimeter Wave Applications

Beenish Kachroo and Malay Ranjan Tripathy

Abstract In this article, a design of a compact, high-radiation efficient, high-gain 4×4 micro-strip patch antenna array is proposed. The proposed micro-strip patch antenna array configuration is optimized to operate at millimeter wave frequency of 42 GHz. The design combines both the series- and the parallel-fed structures to form an array. The combined structure exhibits high performance in terms of gain (8.04 dB), reflection coefficient (-24.2 dB), and radiation efficiency (87.7%) and is ideal to use for the applications at millimeter wave. The excitation to the array structure is provided by a single co-axial feed placed at the center of the 2D planar arrangement.

Keywords Millimeter wave · Series fed · Parallel fed · 2D planar arrangement
Co-axial feed

1 Introduction

Millimeter wave (10–300 GHz) band frequencies, nowadays, are considered to be the potential carriers for a wide range of emerging applications such as wireless telecommunication, wireless high-definition video streaming, satellite communication, imaging, sensing, automotive radar, and standards like WiGig/802.11 [1, 2]. Due to the paucity of operational frequencies below 6 GHz, the millimeter wave frequencies found their way to the real-world applications and lured the attention of the researchers worldwide. On the basis of the Friis transmission in Eq. (1), it can be comprehended that the free space path loss is much higher in millimeter wave band than the current operating bands due to the shorter wavelength. Consequently,

B. Kachroo (✉) · M.R. Tripathy
Department of Electronics and Communication Engineering,
Amity University Uttar Pradesh, Sector-125, Noida, Uttar Pradesh, India
e-mail: beenishali99@gmail.com

M.R. Tripathy
e-mail: malay.amity@gmail.com

the gain of the base station and receiver antennas is to be increased without engrossing more power [3].

$$P_R = P_T + G_T + G_R - 20 \log(4\pi d/\lambda) \quad (1)$$

Given to the small electrical length of millimeter wave antennas, implementation of such antennas as an array at the terminals can be exploited to obtain a high gain. In literature, micro-strip patch antenna arrays have been extensively used because of their low profile, low cost, high gain, lightweight, flexibility to design and fabricate. Apart from aforementioned advantages, micro-strip antenna arrays are taken into the consideration because their integration with the millimeter wave and microwave circuits is relatively convenient. To compensate for the loss that occurs at the higher frequencies, simplify the design and prune the feeding network, a series-fed method is often chosen [4].

Two types of the array-feeding structures recurrently used are the parallel-fed and the series-fed. The parallel-fed structures use proportionately long transmission lines, the presence of which causes spurious radiation and notable dielectric loss to prevail. In contrast, the series-fed structure makes use of small transmission lines and elevates the antenna efficiency. However, if placed at the center, the parallel-fed structures corroborate that the combined beam of each half array is directed toward the broadside [5].

In this article, the design of a millimeter wave antenna array is proposed—keeping in mind the above illustrations. The proposed micro-strip patch antenna array is a series-fed array structure with parallel-fed network at the center. The array achieves high gain and high radiation efficiency, and the maximum power absorbed by the antenna is considerably low.

2 Antenna Array Structure

Figure 1 depicts the geometry of the proposed micro-strip patch antenna array. The antenna array spreads across the substrate in a 2D planar arrangement and employs total of 16 identical micro-strip antenna patches operating at the frequency of 42 GHz. The design in effect is the incorporation of both the series-fed and the parallel-fed structures. The antenna array is assembled of four rows of micro-strip patch antennas fed serially. The implementation is carried out by placing the patches in a manner similar to the one followed by elements of a 4×4 matrix. High-impedance micro-strip lines are used to connect a patch to its adjacent in the rows 1 and 2 and rows 3 and 4, both vertically and horizontally. The upper half of the array (amalgamation of rows 1 and two) and the lower half of the array (amalgamation of rows 3 and 4) are separated by a feed line of 26.58 mm, which along with a co-axial feed at the center and three other feed lines of length 6.6 mm form the feeding network for the proposed array structure. The co-axial feed has a port impedance of 50Ω and is preferred over the other feeding methods for two

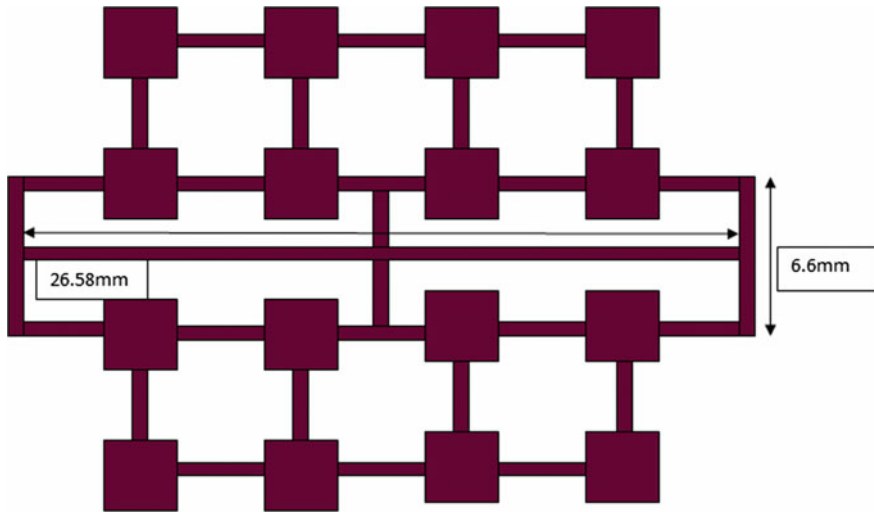


Fig. 1 Antenna array structure

reasons: one to eliminate the spurious radiations and two to reduce the overall system cost. A parallel interconnection is established between the upper half and the lower half of the antenna array through this feeding network.

The antenna array structure is developed on the substrate Rogers RT/Duroid 5880 of thickness $h = 2.2$ mm, dielectric constant $E_r = 2.2$, and a loss tangent of $\delta = 0.0001$. The simulation of the design is carried out on 3D EM simulation software high-frequency structure simulator (HFSS), based on the finite-element method (FEM).

3 Results and Discussion

The simulated performances exhibited by the proposed antenna array structure are presented. In this section, Fig. 2 represents the reflection coefficient, Fig. 3 represents gain versus frequency graph, representing the variation of gain with the values of theta and phi at the operating millimeter wave frequency of 42 GHz, and Fig. 4 represents the radiation pattern of antenna in the E-plane. The measured reflection coefficient of the proposed array structure is -24.2 dB (< -10 dB) which affirms that the antenna possesses a good matching capability. At theta equal to 300° and phi equal to 0° , the array attains a maximum gain of 8.04 dB. As we move away from value of theta equal to 300° , it is observed that there is difference of 1 dB between the consecutive values of gain, as shown in Table 1. The radiation pattern of the array is nearly omnidirectional with smaller side-level lobes and no squint in the main lobe. The antenna array is a narrowband antenna offering the total

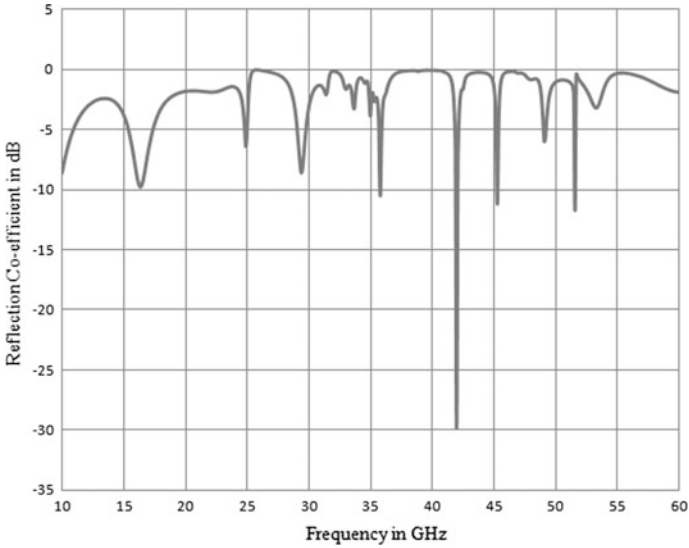


Fig. 2 Graph showing the reflection coefficient of the antenna array structure

Table 1 Variation of gain with the values of theta and phi

Gain (dB)	Theta (°)	Phi (°)
8.04	300	0
7.21	310	0
6.23	340	70
6.05	360	90
5.5	350	90

Table 2 Computed antenna parameters

Antenna parameters	Calculated values
Max U	0.46033 W/S _r
Peak directivity	6.2
Incident power	1 W
Accepted power	0.86 W
Power radiated	7.56 W

bandwidth of 338.1 MHz and radiation efficiency of 87.7%. Other computed antenna parameters such as maximum power radiated, peak directivity, power accepted and power radiated, and incident power are given in Table 2. And it is inferred from the calculations that the total power absorbed by the antenna array is relatively low which substantiates the use of series-fed antenna method in the proposed array structure.

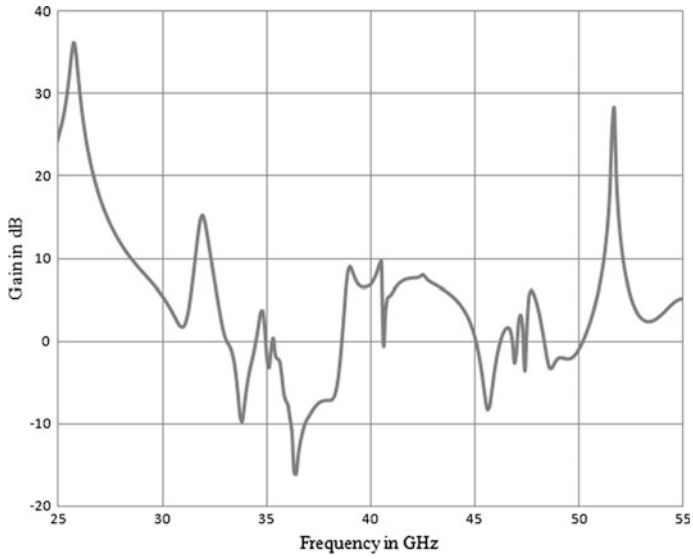


Fig. 3 Gain versus frequency graph

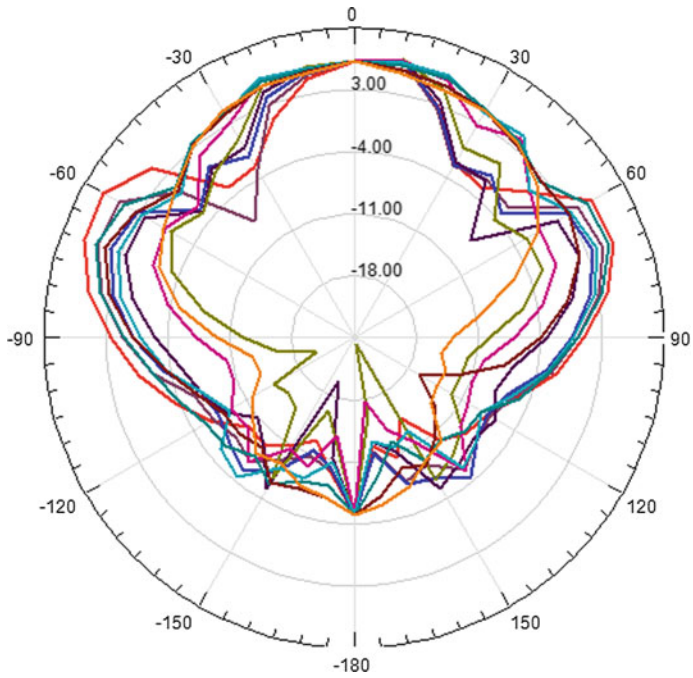


Fig. 4 E-plane radiation pattern of the proposed antenna array

4 Conclusion

In this article, the design of a hybrid series-fed and parallel-fed antenna array for the millimeter wave applications was proposed. The proposed design was aimed at achieving a high gain and high radiation efficiency to indemnify the losses that occur at the millimeter wave frequencies. The use of the hybrid structure along with the co-axial feed was made to decrease the spurious radiations, dielectric losses, cost and enhance the overall antenna efficiency. The concept, theory, design, and results showed a good agreement upon simulation—thereby making this article viable.

References

1. Abdellatif, A., Naeini, S.S, and Mohajer, M.: Novel Low Cost Compact Phased Array Antenna for millimeter wave 3D beam scanning applications. In: Proc. IEEE APSURSI, pp. 1145–1146. July (2016).
2. Bisognin et al, A.: Differential Feeding Technique for millimeter wave Series-fed Antenna Array: Electron Letters, vol. 49, no. 15, and pp. 918–919. July (2013).
3. Zhao et al. K.: mm-wave Phased Array in mobile terminal for 5G Mobile system with consideration of Hand Effect. In: Proc. 81st IEEE VTC Spring, pp. 1–4. (2015).
4. Chong, Y., Wenbig, D.: Micro-strip Series-fed Antenna Array for millimeter wave Automotive Radar Applications. In: Proc. IEEE MITIMW, pp. 1–3. (2012).
5. Kuo, F.Y., Hwang, R.B.: High Isolation X-band Marine Radar Antenna design: In IEEE Trans. Antennas Propagation, vol. 62, no. 5, pp. 2331–2337, May (2014).

Automatic Street Lighting System

Adesh Kumar, Roushan Kumar, Akansh Jain, Anand Pandey,
Shubhankar Thapliyal and Akshay Sharma

Abstract The considerable amount of electrical power is consumed in lighting up the streets in India. However, streets remain deserted for most of the time after night fall, and a minimum frequency of vehicles pass through the street in that duration of time. The conventional lighting system on road and highways is not automatic in India. The volume of traffic and passerby is very through the streets in nighttime, and light is on for the whole night. The larger amount of light is wasted on roads meaninglessly. The same issue can be addressed with the use of automatic or flexible-lighting system technology and LED lamps which can be as solution for power saving, fast, reliable, and efficient in operation to control the amount of light utilization in a street and city. In the paper, the prototype hardware for automatic street light system is being proposed, which will use an Arduino Uno microcontroller and estimates the saving of energy in nighttime.

Keywords Street lighting systems · Flexible-lighting technology
Light-emitting diode · Power-conserving · Automatic street lighting system
Arduino Uno microcontroller

A. Kumar · R. Kumar · A. Jain (✉) · A. Pandey · S. Thapliyal · A. Sharma
Department of Electronics, Instrumentation and Control Engineering,
University of Petroleum and Energy Studies (UPES), Dehradun 248007, Uttarakhand, India
e-mail: akansh.jain99@gmail.com

A. Pandey
e-mail: anandpandey725@gmail.com

S. Thapliyal
e-mail: shubhankar_thapliyal@stu.upes.ac.in

A. Sharma
e-mail: sharmaakshay890@gmail.com

1 Introduction

Automation, cost efficiency, and power consumption are the most important factors in the present field of electrical and electronics related technologies, and have been a backbone for rapid growth and development of new technologies in this field. The industry of street lighting systems has grown rapidly and is going to a much complex level with the rapid industrialization and the growth of cities. For controlling and maintaining this complex street lighting system more economically, various systems have been developed in many different countries. The development of such systems is done to reduce the energy consumption and control the particulate city's lighting system using different technologies, like cloud computing, vehicular emissions.

The lighting systems are still following the old standards and not having the latest control and advanced techniques. The manufacturing companies develop new methods but they are costly due to environmental issues and increasing cost of raw material. The use of the new technology in light sources may be an important and intuitive solution in terms of energy consumption. Light-emitting diode (LED) offers better efficiency, cost, and avoids greenhouse gas emissions effect. It can be very good enhancement in electricity utilization in streets and environment safety. The average life span of LED is 50,000 h, using a power source of 6–8 W, with total kWh used as 329 kWh/year with a total cost occurred being \$32.95/year. Due to these facts, a smart and automatic street light control system, which saves power, electricity, money, and environment, is the goal of this project, where we will be using an ultrasonic sensor, to find out the velocity of a particular vehicle. With the knowledge of the distance between the two lamp poles, and the velocity taken, we can calculate the time of the car appearing in the other pole.

2 Related Works

In our daily life, we can see a huge shortage of power in many areas across the country, due to which there have been power cuts still occurring in many places. Seeing street lights being open for the whole night, consumption of useless power is still rampant. Due to this, a need for an automatic street lighting system arises out of this situation, which drives us to proceed with the aim of curbing the situations mentioned above. Rajput et al. [1] described the Intelligent Street Lighting (ISL) system. This project consists the use of automatic, self-controlled devices embedded along with sensors which, in turn, monitors the environmental parameters like sound, fog, temperature, and carbon monoxide emission. Karthikeyan et al. [2] described one of the street light control systems, in which day and night detection is done to turn lamps on, and the lamp is working in nighttime only. They have used the infrared detectors and turn on lights automatically when pedestrians or vehicles pass by. Vipasha et al. [3] presented a cloud-based

automatic street light and monitoring system using infrared sensor. The movement of the human being is controlled with the help of dimming control circuit that is controlling the movement of the human being in specified range. The circuit turns on, brightens, and dims the street light system accordingly hence capable to save the larger amount of power. Srikanth et al. [4] described a ZigBee-based remote control automatic street light system. It also discusses an artificially intelligent system that can take automatic decisions only for ON/OFF/DIMMING, considering all movements of vehicles or pedestrians and also the surrounding light intensity. Natu et al. [5] proposed an intelligent street lighting system based on wireless GSM module. It is applied for the municipal street lighting and a cost-effective solution for the infrastructure point of view. In this, the completed street lighting lamps are connected to relay driving mechanism. The Java application is running in the base server that maintains the complete light information in the entire city. In case of the particular street light information in ON/OFF condition, the server is capable to send the SMS to street controller and further take any action with the help of GSM.

3 System Design and Methodology

The street lighting system will be divided into sections, each consisting of three street lamps. The street lamps of the section will be connected to a microcontroller, which will then perform the methodology mentioned as follows:

Sensing: In this project, the sensor is one of the most important components used. What we look at is the use of a sensor in measuring the speed of the vehicle, and to identify the presence of the vehicle. The project would adopt the use of an ultrasonic sensor which will calculate the speed of the moving vehicle.

Calculation: For calculations, a program will be installed in the microcontroller, which will look into calculating the time taken for the car to reach the next section (contain three lamp posts). This will be done by using the values of speed from the sensor and the distance between the two sensors.

Communication: In this part, each section, consisting of three lampposts, is connected to a microcontroller, which will provide the lampposts a medium of communication. If one section of lampposts gets the value of the speed of the car using sensor, it will also calculate the time for the car to reach the next lamppost.

Output: After all calculations, the microcontroller would blink an LED lamp, suggesting the opening of the street lamps in the section. After three minutes, if there is no vehicular traffic, the street lamp will automatically shut down.

3.1 Block Diagram

The system block diagram for the automatic street lighting system is shown in Fig. 1.

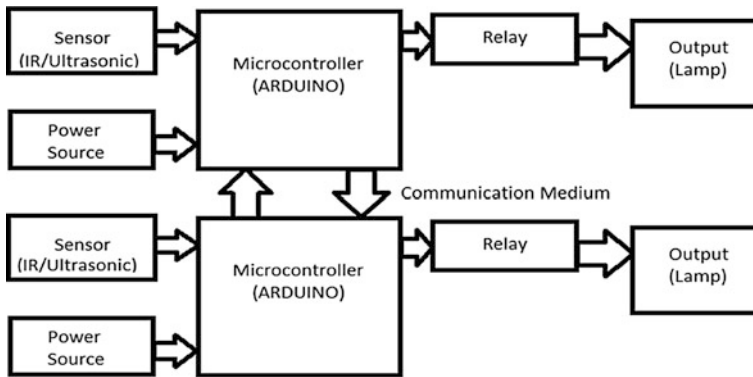


Fig. 1 System block decryption of automatic street lighting

The working is as follows:

- Step I The sensor will sense the vehicle and note the velocity.
- Step II The microcontroller will be used for calculating the time taken for the car to move to the next pole.
- Step III The power source will be used to power the microcontroller, which will be around 5 V.
- Step IV There will then be communication, undertaken by the microcontrollers of the first section, and the succeeding sections.
- Step V To operate like a mechanical switch, the relay is an electrically operated switch, used in electromagnet. The relay will work to produce the desired output in the circuit.
- Step VI The output will consist of the LED lamp. The opening of the lamp will also switch the streetlights in the section to on state. The lamps in the section will automatically shut down if no vehicle passes through the section.

3.2 Circuit Diagram

The circuit diagram of the system is shown in Fig. 2. The working is as follows:

- Step I In the ultrasonic sensor used in the above circuit, input is at echo pin, while the output is at the trigger pin. When input is given through the echo pin, the output pulse is sent by the trigger to the microcontroller.
- Step II From there, the microcontroller then directs the signal to the relay, via the resistor and transistor. The transistor acts as a switch, i.e., when the required signal is sent, only then will the transistor forward the signal to the relay, otherwise it will be grounded, i.e., OFF mode.

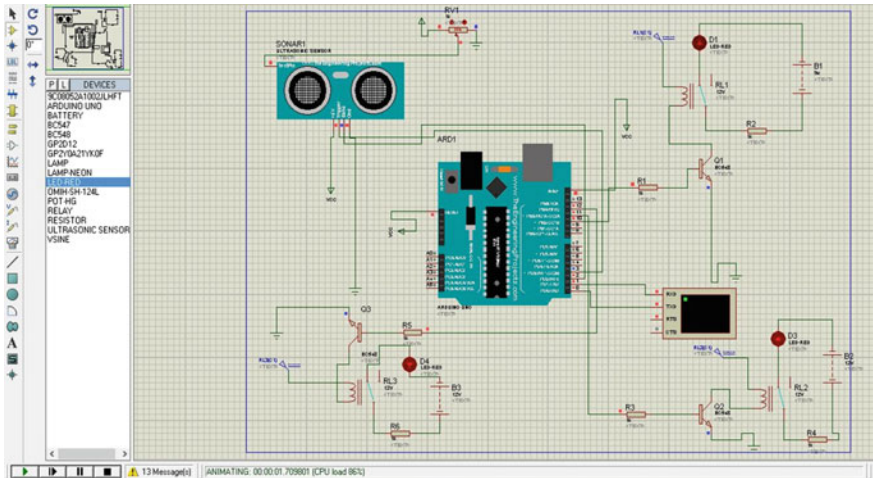


Fig. 2 Circuit simulation in Proteus

- Step III As soon as the relay will get the signal from the transistor, it will switch from normally open (NO) to the normally closed (NC) mode. When the relay switches from NO to NC mode, the output can be observed in the form of opening of the streetlights in a particular section simultaneously.
- Step IV While the relay is in NC mode, the lamps will continue to glow as long as the street is not vacant for a specified duration. If the street is vacant for more than the specified duration, then the lamps will go OFF and as a result, the relay will switch from NC to NO mode.

3.3 Component Description

The components used are as follows:

Step-down Transformer: The step-down transformer is used to reduce the voltage from primary winding to the secondary winding. The basic unit of the microcontroller is the power supply. To design the power supply, a step-down transformer is used which is stepping the 220–12 V supply.

Rectifier: The rectifier is the part of the power supply unit which has step-down transformer followed by PN junction diode which converts the AC input to uni-directional DC. This process is called rectification. The PN junction works in forward direction and conducts during positive half cycle. Hence, the rectifier converts AC voltage to pulsating DC voltage.

Filter: The rectified output is not pure DC in nature; it is pulsating DC output and having ripples. The filter circuit is used to remove the ripples presented in the rectified output. For this purpose, we use capacitor filter. The rating of capacitor is 1000 $\mu\text{F}/50\text{ V}$.

Ultrasonic Sensor: The ultrasonic sensor follows the sound waves instead of light. This feature makes it suitable for object present, clear objects in directly or dark places also. The sensor works very well for the measurement between moving and stationary objects. The ultrasonic sensor module HC—SR04 that provides 2–400 cm noncontact measurement and accuracy is of 3 mm. The internal circuit has ultrasonic transmitters, receiver, and control circuit. This module sends 40 kHz signal and detects the presence pulse signal back. The I/O triggering is occurring at least 10 μs with high signal. The high-level signal is backed, and the time of high output IO is considered as the period from sending ultrasonic to returning. Moreover, test distance = (high level time \times velocity of sound (340 M/S))/2. It has power supply: 5 V DC, ranging distance: 2–500 cm, quiescent current: <2 mA, 5 V TTL, or 3.3 V CMOS microcontrollers. Modulation at 40 kHz, positive TTL pulse, and require minimum 87 μs to maximum 30 ms (PWM).

Transistor: Generally, a transistor = transfer + resistor, used to amplify the current in the circuit. An npn BJT transistor is used in this circuit. It has a small amount of current at its base and controls the larger amount of current at emitter and collector terminals.

Resistor [2(10 K and 1 K)]: Resistors are the passive components and resist an electric current by a voltage drop between the two terminals. In the circuit design, we have used two 10 K and one 1 K resistors. The resistors follow the Ohm's law:

$$V = IR.$$

SPDT Relay: It is an electromagnetic device which is used to connect/interface two circuits mechanically, by separating them electrically. For example, a relay will make a 5 V DC battery circuit to switch into a 230 V AC mains circuit.

LED [3(RGB)]: It is a semiconductor device. Like transistors, and other diodes, LEDs are made up of silicon. Small amounts of chemical impurities that are added to silicon, such as gallium, arsenide, indium, and nitride, help in making the LED give off light. Photon emits when a current is passing through led.

Microcontroller: Microcontroller is the System on Chip (SoC) IC which has the processing unit, memory, and programmable input/output peripherals. In the project, an Arduino Uno microcontroller board, ATmega328 microcontroller, is used, available in removable, dual-inline-package (DIP). The controller has 14 digital input/output pins (of which six can be used as PWM outputs), reset button, one 16 MHz quartz crystal, six analog inputs, a power jack, a USB connection, and an ICSP header.

3.4 Flowchart

The flowchart to describe the complete operation is depicted in Fig. 3.

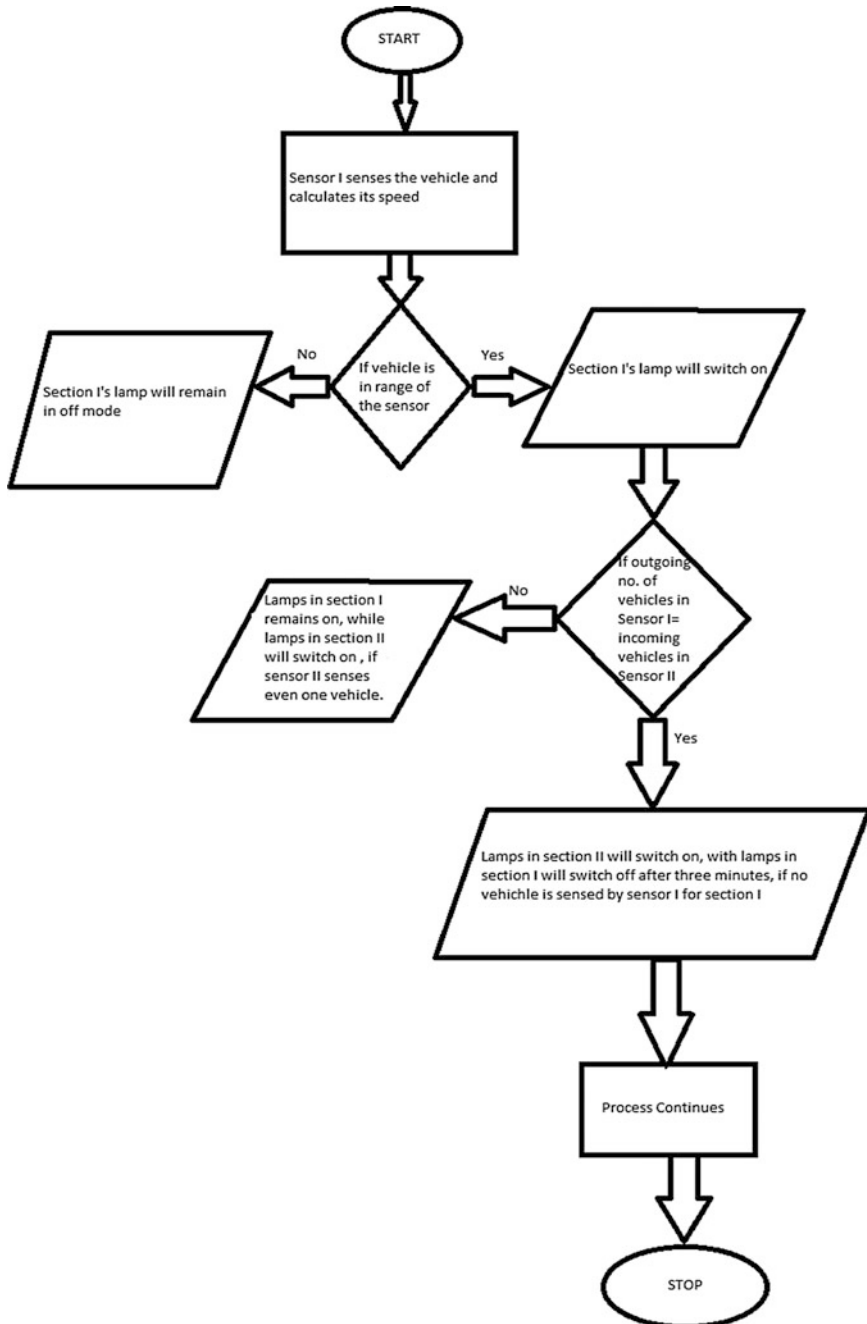


Fig. 3 Flowchart

4 Result

The expectations from this project indicate a reduction in power and electricity usage in street lighting system. As a result of this system, the net usage to street lighting can be reduced by a very large margin. This was tested at Nanda ki Chowki, near Premnagar, Dehradun, where the device functioned significantly well. Also the LED blinked, which signified the success of the module. The prototype of the developed system is shown in Fig. 4.

The values of distance of the obstacle from the ultrasonic sensor can be observed when the safe zone (range of sensor) is set to 50 cm on the virtual terminal screen shown below. Figure 5a shows the virtual terminal and corresponding values, when the obstacle has entered the safe zone, and Fig. 5b shows the virtual terminal and corresponding values, when the obstacle has not entered or is outside the safe zone.

The developed system can be one of the good systems which are helpful in the reduction of the street crime and preventing injury accidents in nighttime. The emergency services in the street are enabled with the effective use of CCTV in nighttime and assist the emergency operations to identify different locations and carry several duties. The development of such system helps promoting public transport, sustainable transport, walking, cycling, and 24 h support at leisure economy, facilitates the society for inclusion, and provides the full utilization of time and freedom to use the city in the dark time.

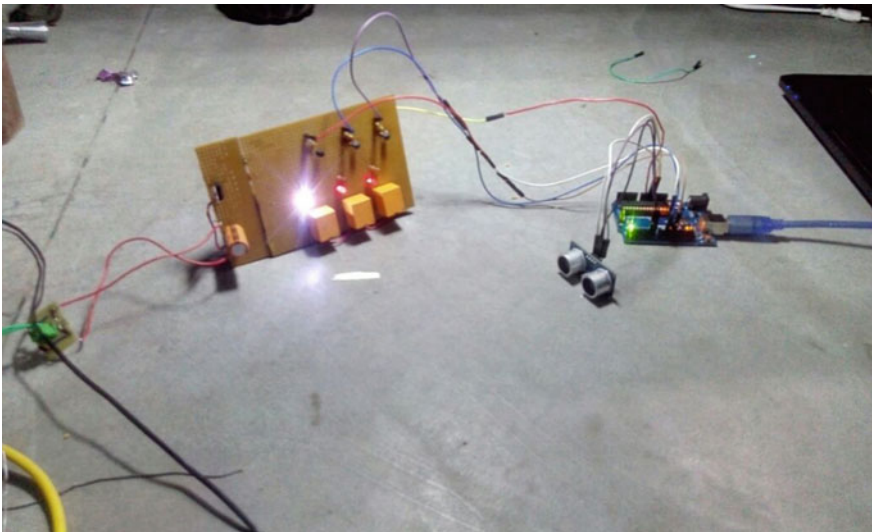


Fig. 4 Developed prototype

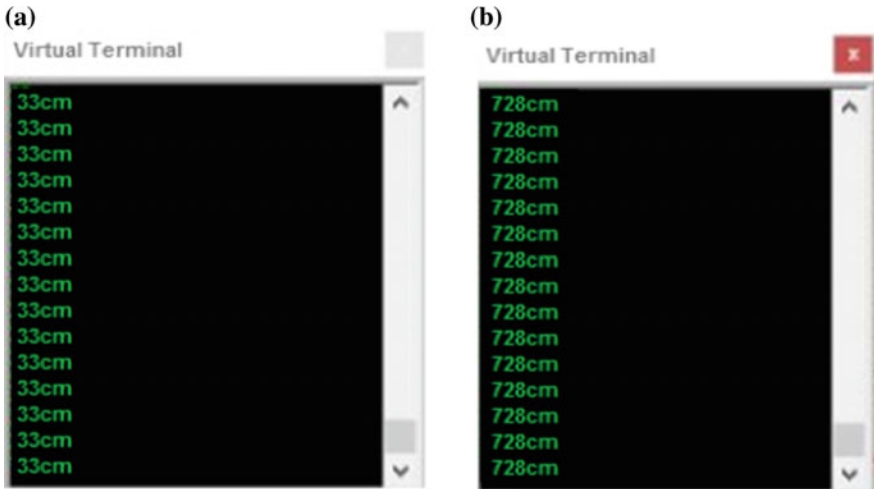


Fig. 5 a Safe zone. b Outside the safe zone

5 Conclusion

The power usage is estimated to reduce by a significant amount in street lighting. Excess usage of power in street lighting can now be checked, and also be supplied to households that still do not have electricity. With this, we can not only save electricity, but empower a new generation of technologies that can surface from this invention.

References

1. K.Y. Rajput, G. Khatav, M. Pujari, P. Yadav “*Intelligent Street Lighting System Using GSM*” International Journal of Engineering Science Invention, Vol. 2, 2013, pp 60–69.
2. Karthikeyan. M, Saravanan. V, Vijayakumar. S “*Cloud Based Automatic Street Light Monitoring System*”, International Conference on Green Computing. Communication and Electrical Engineering (ICGCCEE), IEEE Xplorer, 2014, pp 1–5.
3. Vipasha and Preeti Abrol, “*Design of Traffic Flow based Street Light Control System*”, International Journal of Computer Applications Vol. 72, No. 18, 2013, pp 0975–8887.
4. Srikanth M, Sudhakar K N, “*ZigBee Based Remote Control Automatic Street Light System*”, International Journal of Engineering Science and Computing, (IJESC), 2014, pp 639–643.
5. Natu, Omkar and Chavan, S. A. “*GSM Based Smart Street Light Monitoring and Control System*”, International Journal on Computer Science & Engineering, Vol. 5, No. 3, 2013, pp 187–189.

Efficient Method to Implement Arithmetic Operations Using Binary Logarithmic Algorithms for Reduced Circuit Complexity with Error Analysis

Sayed Waize Ali, Manish Sharma and M.R. Tripathy

Abstract An algorithm is developed for arithmetic operation with reduced circuit complexity and memory by using binary logarithm operations, and along with this comparative error analysis of logarithmic multiplier is discussed. Since logarithm of a binary number is approximated by shifting and counting the bits itself, thus no look-up table (LUT) or logic cell is required but errors are introduced which can be reduced based on parallel computation.

Keywords Logarithmic number system (LNS) · Logarithmic multiplier Mitchell's algorithm · Parallel processing

1 Introduction

Binary multiplication and division are mostly used operations in computation, and it consumes more time for calculation since a multiplication or a division is obtained by a series addition or subtraction with shift operations, especially in applications such as DSP and image processing because of generation of large numbers of partial products. By using LNS, a multiplication and division can be converted into simple addition and subtraction of two numbers. John N. Mitchell [1] introduces a method of converting a binary number into its logarithmic equivalence through straight-line approximation by using only shift and counting operation and in which no LUT is required. This reduces area of circuit and execution time but introduces error because of the single straight-line approximation of mantissa in numbers between power of two.

S.W. Ali (✉) · M. Sharma · M.R. Tripathy
Amity School of Engineering and Technology, Amity University, Noida 201303,
Uttar Pradesh, India
e-mail: sayyedwaizeali@gmail.com

© Springer Nature Singapore Pte Ltd. 2018
R. Singh et al. (eds.), *Intelligent Communication, Control and Devices*,
Advances in Intelligent Systems and Computing 624,
https://doi.org/10.1007/978-981-10-5903-2_93

1.1 Mitchell's Algorithm

By a piecewise linear approximation of a logarithmic curve, Mitchell successfully developed a method to get the log and antilog value by shifting and counting.

Following are the steps to calculate the log by Mitchell's algorithm [2];

Step 1: Calculate the leftmost "1" bit position, and the binary value of the position will be the characteristic.

Step 2: Bits right to the leftmost "1" bit will become mantissa.

$$\text{Example}(57)_{10} = (00111001)_2$$

Leftmost "1" bit position is 5 = 101; characteristic.

Bits right to the leftmost "1" bit are 11001; mantissa.

$$\text{So } \text{Log}(00111001) = (101.11001)_2$$

$$\text{Log}(57)_{10} = (5.78125)_{10}; 0.5376\% \text{ error}(5.8125 \text{ actual value})$$

Steps to calculate antilog value

Step 1: Convert the characteristic to decimal value.

Step 2: Replace the characteristic with 1.

Step 3: Shift the decimal point right with the amount of decimal equivalence of characteristic.

Step 4: Convert the number into decimal.

$$\text{Log}(57)_{10} = \text{Log}(00111001)_2 = (101.11001)_2$$

$$\text{Decimal equivalence of characteristic } 101 = 5$$

$$\text{Replacing characteristic by 1: } 1.11001$$

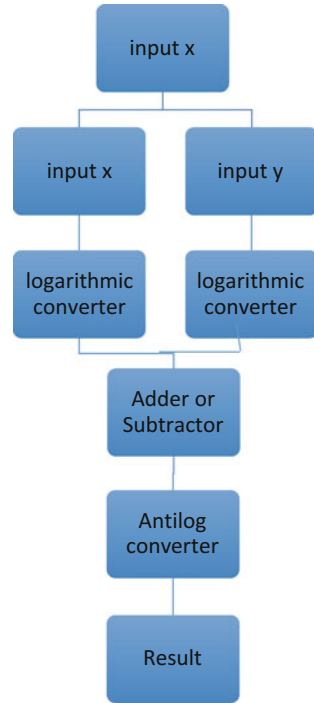
$$\text{Shifting decimal point by 5: } (111001)_2 = (57)_{10}$$

In Mitchell's algorithm for multiplication and division, log of input terms is calculated separately, then their sum for multiplication or subtraction for division is calculated, and further the antilog of the resultant is derived out which is the approximate result [1, 2]. The error in the result depends on the mantissa value of the inputs logarithm equivalence [1, 3] (Fig. 1).

$$\text{If we represent } \log(x) = m_1.x_1 \text{ and } \log(y) = m_2.x_2$$

Then, the error factor in multiplication E_m and division E_d is given by [1]

Fig. 1 Logarithmic-based arithmetic operation block diagram



$$E_M = \frac{1 + x_1 + x_2}{(1 + x_1)(1 + x_2)}; \quad x_1 + x_2 < 1$$

$$E_M = \frac{2(x_1 + x_2)}{(1 + x_1)(1 + x_2)}; \quad x_1 + x_2 \geq 1$$

$$E_D = \frac{(1 + x_1 - x_2)(1 + x_2)}{(1 + x_1)}; \quad x_1 - x_2 \geq 0$$

$$E_D = \frac{(2 + x_1 - x_2)(1 + x_2)}{2(1 + x_1)}; \quad x_1 - x_2 < 0$$

-11.1 and 12.5% are the maximum error in the multiplication and division operation, respectively. Note that the error in the multiplication is always negative and that in division is positive [1].

2 Approach Used

Since the error in the resultant term depends only on the mantissa value, thus this mantissa can be used separately for calculating the error factor from the main logarithmic multiplication or division operation, and the error factor can be used to

manipulate the resultant product or quotient term so that the error can be reduced to less than 1%.

2.1 Error Calculation

The error factors E_D and E_M for multiplication and division operations are calculated in parallel with the antilog generation of the product or quotient [4]. The result is fed to the ALU with the error factor specifically adder for multiplication process and subtractor for division process, and the error will be reduced. The log of error function is calculated as

$$\begin{aligned} \log(E_M) &= \log(P) + \log(n) - \log(Q) - \log(R) & P' < 1 \\ \log(E_M) &= 1 + \log(P') + \log(n) - \log(Q) - \log(R) & P' \geq 1 \\ \log(E_D) &= \log(S) + \log(R) - \log(Q) - \log(n) & S' \geq 0 \\ \log(E_D) &= \log(S'') + \log(R) - \log(n) - \log(Q) - 1 & S' < 0 \end{aligned}$$

If either x_1 or x_2 is 0, then $n = 0$
where

- P' ($x_1 + x_2$); with decimal
- Q' ($1 + x_1$); with decimal
- R' ($1 + x_2$); with decimal
- S' ($x_1 - x_2$); with decimal
- n $(10)^D$; D is the minimum decimal position from x_1 or x_2
- P ($1 + P'$); ignoring decimal
- Q Q' ; ignoring decimal
- R R' ; ignoring decimal
- S ($S' + 1$); ignoring decimal
- S'' ($S + 1$); ignoring decimal

3 Working

For generation of the logarithm of a given binary number, priority encoder [1] is required which detects the leftmost "1" bit position and a decimal to binary converter to convert the bit position and mantissa value into binary then registers to store the log value (characteristic and mantissa). Generation of log value and mantissa is done in parallel.

After this, for the selection of multiplication or division a multiplexer is used whose output select line decides among addition and subtraction operation by setting the value of select input of XOR-gated parallel adder/subtractor [5,6]. The value of select line is taken as 0 or 1 which decides addition or subtraction,

respectively. In parallel, with the addition or subtraction operation, the two conditions for $(x_1 + x_2)$ and $(x_1 - x_2)$ are checked for respective operations.

3.1 Example for Multiplication

$$\begin{aligned} \text{Let } z &= 14(x) \times 11(y) \\ (14)_{10} &= (1110)_2 \quad (11)_{10} = (1011)_2 \\ \text{Log}(x) &= 11.110 \quad \text{log}(y) = 11.011 \quad x_1 = (0.110)_2 \quad x_2 = (0.011)_2 \\ \text{Log}(z) &= \text{log}(x) + \text{log}(y) = 111.001 \quad = (0.75)_{10} \quad = (0.375)_{10} \\ \text{Antilog}[\text{log}(z)] &= z = (10010000)_2 \quad x_1 + x_2 \\ z &= (144)_{10}; -6.493\% \text{ error} \quad E_D = 0.935064 \\ Z_{\text{finl}} &= 153.99; 0.00064\% \text{ error} \end{aligned}$$

3.2 Example for Division

$$\begin{aligned} \text{Let } z &= 8(x) \times 5(y) \\ (8)_{10} &= (1000)_2 \quad (5)_{10} = (0101)_2 \\ \text{Log}(x) &= 11.00 \quad \text{log}(y) = 10.01 \quad x_1 = (0.00)_2 \quad x_2 = (0.01)_2 \\ \text{Log}(z) &= \text{log}(x) - \text{log}(y) = 00.11 \quad = (0.00)_{10} \quad = (0.25)_{10} \\ \text{Antilog}[\text{log}(z)] &= z = (1.11)_B \quad x_1 - x_2 < 0 \\ z &= (1.75)_D; 9.375\% \text{ error} \quad E_D = 1.09375 \\ Z_{\text{finl}} &= 1.60.0\% \text{ error} \end{aligned}$$

4 Experimental Results

We have calculated that the proposed method is generating more accurate results; even zero error result can also be obtained and executed with same time period, nearly comparable with execution time of traditional Mitchell’s algorithm [1]. Table below shows comparison of error.

Operation	Traditional Mitchell method error (%)	Proposed method error
11 ÷ 14	8.035	0.000006%
99 × 17	2.079	0.00000387%
54 × 122	0.90625	0.75

5 Conclusion

In the proposed design, the error generated due to approximation of mantissa is reduced as compared to traditional Mitchell's algorithm but power consumption is increased due to parallel processing. Since parallel processing is used, the condition of synchronization has to be kept in mind while designing the circuitry. As no LUTs are used, circuit complexity is reduced than LUT-based logarithmic multiplier [2]. This architecture can be used when precision is the main concern over power consumption.

6 Future Works

Talking about future scope, power consumption of circuit will be the area of work which will be worked upon by using less numbers of parallel processors and power-efficient processors.

References

1. Demetrious K. Kostopoulos "An Algorithm for Computation of Binary Logarithm", IEEE transaction on electronic computer, vol 40, No. 11, November 1991.
2. John N. Mitchell, "Computer Multiplication and Division using Binary Logarithm", IEEE transaction on electronic computer August 1962.
3. Mahalingum and N. Rangantathan "Improving accuracy in Binary logarithm using operand Decomposition." IEEE Transaction on Computers, Vol. 55 No. 2, pp 1523–1535, December 2016.
4. Tso-Bing Juang, Han-Lung-Kuo and Kai-Shaing, Jan " Lower error and area efficient antilogarithmic converters with bit correction Schemes." Journal of the Chinese Institute of Engineers, 2015.
5. P. Saha, A. Banerjee, A. Dandapat and P. Bhattacharya "High speed multiplier using high accuracy floating point logarithmic number system". Scientia Iranica Transaction D: Computer Science and Engineering and Electrical Engineering, Vol 21 No.3, pp. 826–841, 2014
6. R. K. Agrawal, and H. M. Kittur," ASIC Based Logarithmic Multiplier using iterative pipelined architecture," IEEE Conference on information & Communication Technologies (ICT) pp. 362–366 2013.

Design of Efficient DC Power Supply for High-Voltage Low-Current Applications

Archana Singh, Sanjay Kumar Sinha, Kamlesh Pandey
and Nibha Rani

Abstract High voltage generally means electrical energy of higher magnitude sufficient to inflict human beings. So, safety requirements and particulars are to be followed while designing the model. The objective of this paper is generation of high DC output voltage from two methods, namely flyback converter and Cockcroft–Walton voltage multiplier with input DC supply. Mathematical modeling, control strategy, circuit operation, and design considerations are discussed. High-voltage power supply for a particular application has become cheaper due to latest advance in power supply technology. Many applications are of high DC supply in industry, research work, dielectric testing of high-voltage equipment.

Keywords Flyback converter · DC voltage · Cockcroft–Walton voltage multiplier
Power supply · Transformer

1 Introduction

A high-voltage, compact power supply modules or products are in great demand in various fields like commercial, defense, research laboratories, especially in high-voltage testing, and in various instruments such as electro spray, lasers. Usually, power supplies having high power density and efficiency with low cost are preferred. Newly made modules operate at high frequencies (20–100 kHz). With

A. Singh (✉) · S.K. Sinha · K. Pandey · N. Rani
Department of Electrical and Electronics Engineering, ASET, Amity University Uttar Pradesh, Noida, India
e-mail: archanaeee21@gmail.com

S.K. Sinha
e-mail: sksinha6@amity.edu

K. Pandey
e-mail: kpandey@amity.edu

N. Rani
e-mail: nibharani279@gmail.com

the help of recent advances in power supply technology, it has become possible to make the design of module smaller, more efficient, and lighter due to higher levels of monitoring and process control.

Since high voltage is used in the module, it is important for the person operating with it, to keep in mind the danger associated with it. A specific guideline for safety practices can be followed which is found in IEEE standard 510-1983. According to the application, various power ranges of power supply are needed.

This paper aims at the generation of high DC voltage and low currents at output terminals of circuit of two different methods:

1. Flyback converter
2. Cockcroft–Walton voltage multiplier

A comparison is made to decide which method is more suitable and versatile.

Different parameters such as ripple, stability, accuracy, and consistency of the power supply are considered. It should perform consistently. The key components which have low losses and operate at higher frequency together with advanced power conversion techniques have led to the development in power supply field.

2 Literature Survey

2.1 *Flyback Converter*

Flyback converter is a type of switched mode power supply (SMPS) and is useful in both AC/DC or DC/DC conversion with inductor split so that to form a transformer. The principle behind these converters is based on energy storage in inductor during ON period and discharge of energy to load during OFF period.

Basically, there are two working modes—ON state and OFF state. In ON state, energy is transferred to the transformer by input supply, and in same time, output capacitor supplies energy to the load. In OFF state, energy stored in the transformer is supplied to the output load and capacitor [1].

These are popular because of the absence of inductor, single semiconductor switch, and coupled inductor. These are mostly preferred where the output voltage needs to be isolated from the main input supply. The input is unregulated DC voltage which is rectified by a capacitor filter.

Figure 1 shows a flyback converter circuit topology. It includes a single-controllable switch (MOSFET) with common switching frequency of 100 kHz which is used for controlling the duty ratio for desired output voltage. Both the windings of the transformer have good coupling and do not conduct simultaneously. The output section consists of filtration and rectification processes by using a diode and capacitor [2].

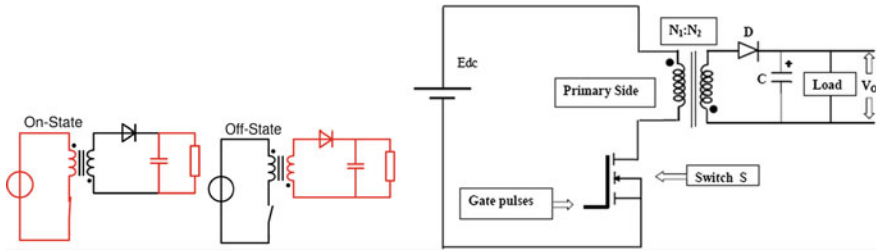


Fig. 1 Two different modes of flyback converter and its circuit diagram

Design strategy can be followed by using following steps:

1. Defining circuit parameters such as inductance L , full-load DC inductor current I_{FL} , ripple ΔI_{pp} , maximum peak instantaneous short-circuit current limit I_{scpk} , absolute loss limit, and max temperature rise.
2. Select material of core.
3. Find maximum flux density and maximum flux swing.
4. Selection of core shape and size.
5. Loss limit is determined.
6. Number of turns is calculated.
7. Calculation of gap length.
8. Winding resistance and conductor size are calculated.
9. Calculate winding loss, total loss, and temperature rise.

2.2 Cockcroft–Walton Voltage Multiplier

As we know, there are many methods to step up AC voltage, but when DC is considered, transformer is not applicable. Here, the use of voltage multiplier comes for generation of voltage or stepping up voltage by number of stages. In this case, the output voltage is several times greater than input supply. On the basis of the ratio of output voltage to input voltage, voltage multipliers are categorized as doubler, tripler, or quadrupler. Figure 2 shows a Voltage doubler [3].

Fig. 2 A voltage doubler

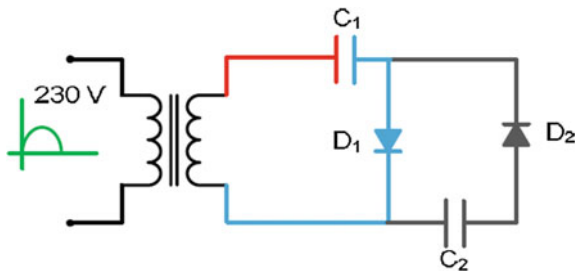
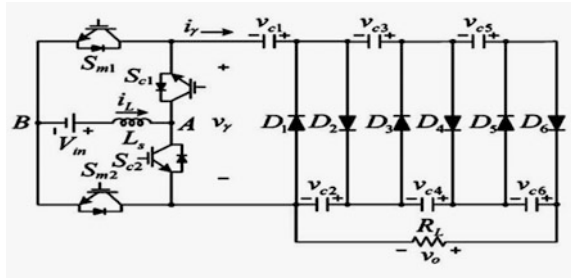


Fig. 3 Three stage CW voltage multiplier



CW voltage multiplier is made of voltage multiplier circuits cascaded to form a ladder-type network consisting of diodes and capacitors to generate high-voltage DC. Advantage of this method is that unlike transformers, it does not require heavy core and insulation in bulk. Due to this, these are lighter and cheaper. In this, peak-to-peak voltage would get doubled at each stage [4].

Figure 3 shows three-stage Cockcroft–Walton voltage multiplier. It converts relatively low DC input voltage to high DC output voltage. As seen, it is made up of ladder of capacitors and diodes. Two capacitors and two diodes form a single stage. Generally, an n -stage CW voltage multiplier has output voltage of $2n$ times the supply voltage magnitude. This circuit diagram shows four bidirectional switches ($Sc1$, $Sc2$, $Sm1$, and $Sm2$). L_s is boost inductor connected in series with the supply voltage. The control strategy which is applied includes two independent frequencies, one of high frequency and the other of low frequency [5, 6].

In case AC voltage is used as an input supply, then also high output DC voltage can be obtained by CW voltage multiplier. The diagram of such a model is shown in Fig. 4 [7].

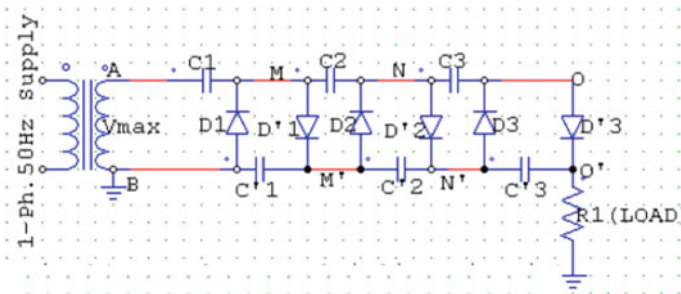


Fig. 4 AC supply fed to CW voltage multiplier

3 Model and Design

3.1 Flyback Converter

The model has been made in MATLAB with the help of Simulink feature. Simulink model of flyback converter consisting of all main parts and details is shown in Fig. 5.

Here, input DC source and a switching device (here MOSFET) are connected across primary winding of the transformer which acts as two magnetically coupled inductors and provides voltage isolation. On the secondary side, a diode and capacitor are connected across secondary winding which provides rectification and filtering of voltage.

The numerical value of various parameters is as follows:

- I/P voltage—100 V DC
- O/P voltage—1100 V DC (apprx.)
- Frequency—10 kHz
- Load resistor—10 K-Ω
- Primary v/g of Linear Transformer—100 V
- Secondary v/g of Linear Transformer—1100 V
- Number of nodes—8
- Number of branches—8
- Number of transformers—1
- Number of v/g sources—2
- Number of current sources—3
- Number of switches—3
- Total number of inductances and capacitors—3

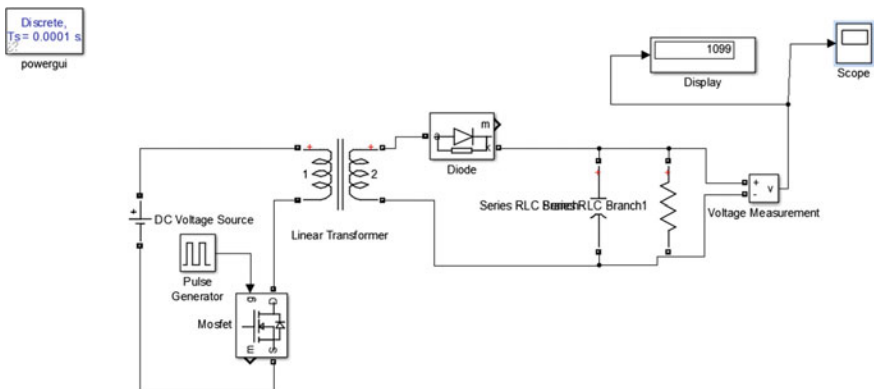


Fig. 5 Simulink model of flyback converter

In performing simulation, some assumptions are made such as the coupling is ideal, voltage drops in ON state of diodes and switches are ignored, linear magnetic circuit is assumed, core and capacitor are lossless.

Various other parameters in designing of the model are considered such as value of inductance L , maximum and minimum duty ratio, maximum ON and OFF time, inductor peak current, input and output power, flyback turn ratio. All these values are calculated with the help of their respective formula.

In the designing of transformer, selection of core (material, size, and shape), calculation of primary and secondary turns, etc., are considered. Value of primary inductance should be high for higher efficiency and reducing magnetizing current and losses.

3.2 Cockcroft–Walton Voltage Multiplier

The simulation and designing was done in MATLAB 2014a/Simulink. In this, the generation of high DC voltage is done with the help of multiplier circuit that consists of capacitors and diodes. The simulation circuit is shown in Fig. 6.

In this model, the input source is low-level DC source like a battery. It consists of three stages of multiplier with each stage containing a pair of diodes and capacitors. Multiplier multiplies the peak-to-peak voltage with number of stages to get the high voltage. It consists of one inductor used for boosting up the voltage level, four switches, and finally CW voltage multiplier. There are two operating frequencies, namely f_c (alternating frequency) and f_m (modulating frequency), which are kept high so that smaller capacitor and inductors can be used.

The output voltage depends on the number of stages of CW multiplier and the voltage across the capacitors.

$$V_o = n * V_c = n * V_{max}$$

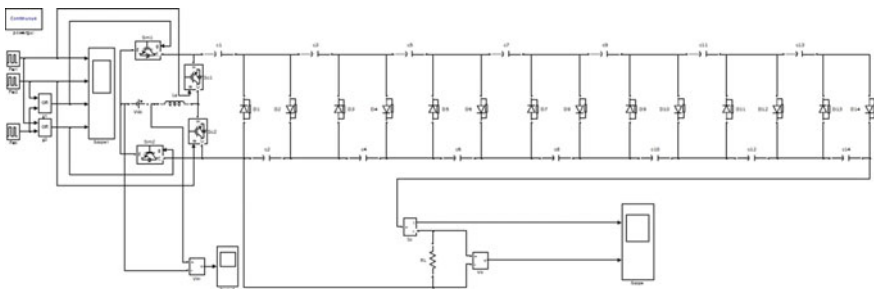


Fig. 6 Simulink model of a 7-stage CW voltage multiplier

Some assumptions were made while modeling the Simulink model:

1. Ideal circuit elements free from losses were considered.
2. Large value of capacitors was taken.
3. Ripple and drop in voltage are neglected.
4. The converter operates in conduction mode under steady-state condition.

Further, we need to carefully consider parameters of different components so as to make it reliable and predict circuit performance, keeping in mind the designing, ripple, and regulation. Capacitor and diode are selected very carefully. The capacitor is chosen on the basis of withstanding the maximum voltage according to the number of stages used. It may be a plus point to choose capacitors which have voltage rating double that of applied peak voltage.

For the selection of diodes, its various parameters such as repetitive peak reverse voltage, frequency of input signal, peak forward surge current, forward current and voltage are to be considered carefully.

4 Results and Output Waveforms

All the output waveforms are an outcome of the Simulink model made in previous section in MATLAB.

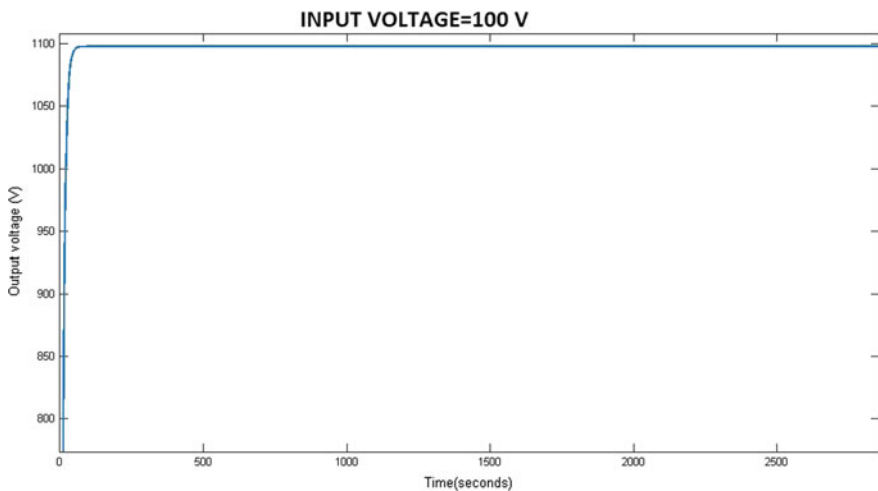


Fig. 7 Output voltage waveform

4.1 Flyback Converter

The output waveform shown in Fig. 7 shows a perfect DC voltage with some ripples of approximately 1100 V while applying 100 V DC at input section. Y-axis shows the voltage rating, and X-axis shows the time period. It is seen that by varying the input DC supply and secondary voltage of the transformer, the value of output voltage changes. We can therefore plot a graph showing the dependency of output on these two parameters (Figs. 8 and 9).

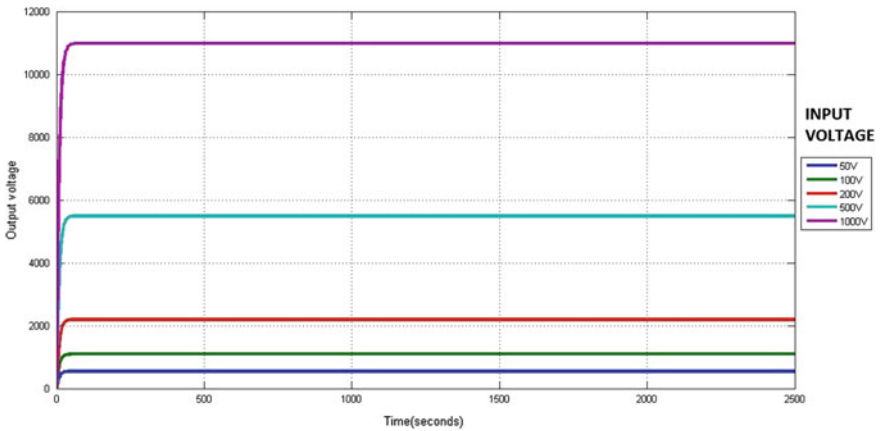


Fig. 8 Input voltage versus output voltage graph

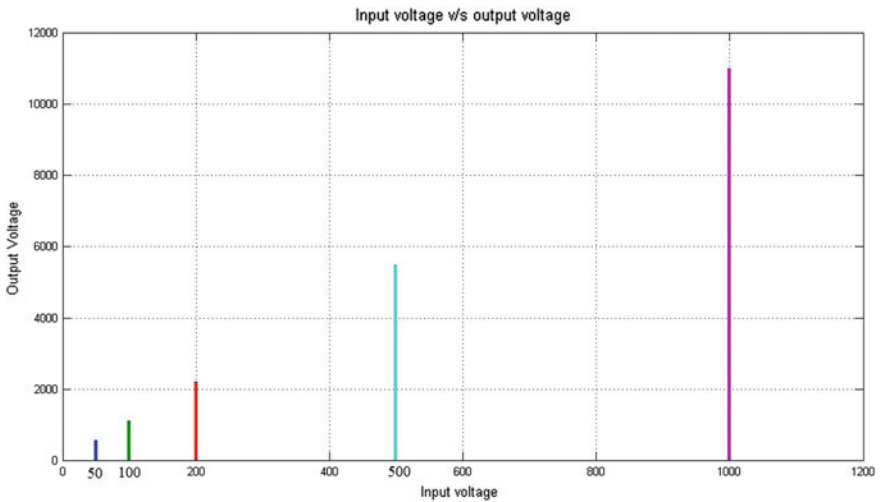


Fig. 9 Various output voltages from different input voltages

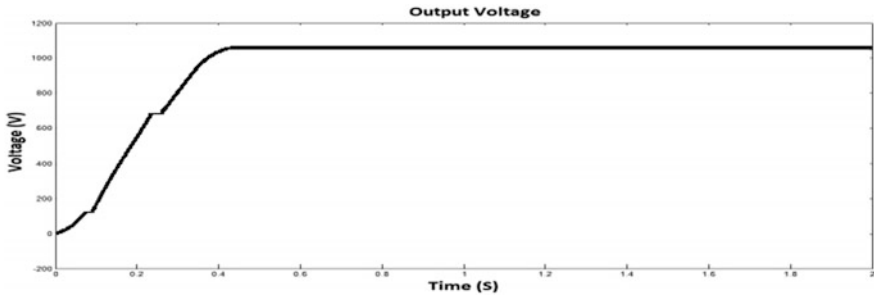


Fig. 10 Output voltage waveform of CW voltage multiplier

4.2 Cockcroft–Walton Voltage Multiplier

Waveforms of the converter at $V_{in} = 48 \text{ V}$, $\eta = 93.5\%$, and $V_o = 1.05 \text{ kV}$ are taken for simulation. The upper part of the s/g has four switches, in which $Sc1$ and $Sc2$ are operated at f_c , and $Sm1$ and $Sm2$ are operated at f_m .

Above given the output voltage waveform of the CW voltage multiplier (Fig. 10) which is a constant DC voltage.

Table 1 represents the value of different components used in designing of the Simulink model. Output voltage therefore is around 1.05 kV.

The waveforms of gate switching pulses which are given to the four switches in the model are shown in Fig. 11. During high load situation, the efficiency is decreased due to the conducting and resistance losses of diodes and capacitors.

Table 1 Values of different parameters

Parameters	Values
Input voltage DC	42–54 V
Output DC voltage	1.05 kV
Modulation frequency	60 kHz
Alternating frequency	1 kHz
Resistive load	1 K Ω
Number of stages	7
Boost inductor	1.5 mH
Capacitors	470 μF

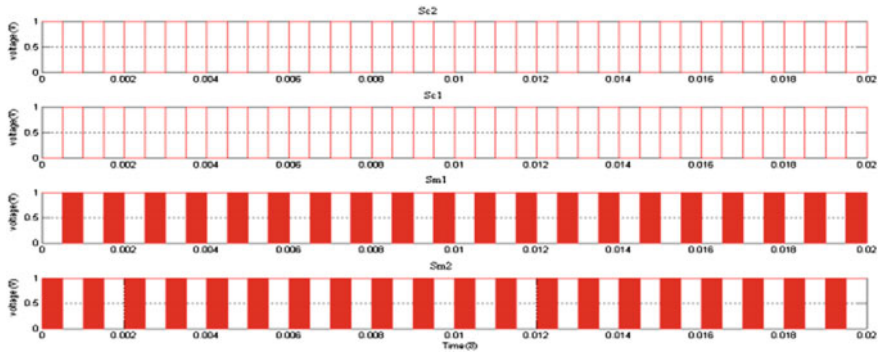


Fig. 11 Waveforms of gate switching pulses

5 Conclusions

Both the techniques are discussed in detail and the comparison is made between both of them. To generate a high-voltage DC output, some factors are considered on the basis of which both the above-mentioned techniques are compared. The best module accepted by the market would be the one which has low cost, maintenance free, less bulky, less variance in desired output value, more stability, less operating time, etc.

In flyback converter, because of its simple circuit, isolation transformer, small size, higher efficiency, and cost-effectiveness, it becomes a common and cheap mode of power supply. Knowing the application and the desired output voltage value, we can design the converter accordingly. These are popular in low-power applications where output voltage and input supply are isolated from each other. There is no output inductor present in the circuit due to which transient response is faster. Output voltage can be varied by varying the duty ratio of the pulse given to the switch which is connected to the primary of flyback transformer.

The output voltage of CW voltage multiplier is dependent on various factors such as value of input supply (AC/DC), value of boost inductor, and capacitors in filtering circuit, load resistance. This method of high generation of DC voltage can be adopted where no AC supply is present. It is highly reliable and has less cost. Since no AC supply is given, therefore, cost of rectifier for conversion of AC to DC voltage is omitted which further makes it cheaper. The circuit is small as it requires only cascading of diodes and capacitors which makes it portable and easy to handle. Different magnitudes of output DC voltage can be taken from different stages without varying input voltage level. Controllability of this circuit is easy.

Further, to increase output voltage to a higher level, design of flyback converter is added to voltage multiplier at the output terminals of transformer. This step minimizes the level of insulation for the transformer [8].

References

1. Karthika V L, Nimmy Sara George, "Design of a Power Supply Using Fly-Back Converter" International Journal of Advanced Research in Electrical, Electronics and Instrumentation Engineering.
2. Lesson 22 "Fly-Back Type Switched Mode Power Supply" Version 2 ee IIT, Kharagpur.
3. Nikhil M. Waghmare, Rahul P. Argelwar, Amol Thakare, Sneha Urkude, "Battery Operated Multistage High Voltage Generation By Cockcroft-Walton Multiplier", International Journal of Engineering Sciences & Research Technology, Vol.4, 2015.
4. Nikhil M. Waghmare, Rahul P. Argelwar, "High Voltage Generation by using Cockcroft-Walton Multiplier", International Journal of Science, Engineering and Technology Research, Vol. 4, 2015.
5. Amol R. Thakare, Senha B. Urkude, Rahul P. Argelwar, "Analysis of Cockcroft-Walton voltage multiplier", International Journal of Scientific and Research Publication., vol. 5, no. 3, 2015.
6. R. Prince, R. Kalaivani "DC-DC Converter Based On Cascade Cockcroft-Walton Voltage Multiplier for High Voltage Gain without Using Transformer", International Journal of Engineering Science and Innovative Technology, Volume 2, Issue 2, March 2013.
7. C. K. Dwivedi, M. B. Daigavane," Multi-purpose low cost DC high voltage generator (60 kV output), using Cockcroft-Walton voltage multiplier circuit||, International Journal of Science and Technology Education Research Vol. 2(7), pp. 109-119, July 2011.
8. Nader Barsoum, Glenn Isaiah Stanley, "Design of High Voltage Low Power Supply Device", Universal Journal of Electrical and Electronic Engineering, pp. 6-12, 2015.

Design and Performance Analysis of High Gain Narrow Band Patch Antenna Array at X-Band

Madhukant Patel, Piyush Kuchhal, Kanhaiya Lal, Virendra Singh and Hemangi Patel

Abstract The paper proposes a high gain narrow band array of rectangular microstrip patch antennas. Each element of the array is rectangular in shape. A high dielectric and low lossy material Rogers-3006 with dielectric constant 6.51, loss tangent of 0.002 and thickness 1 mm have been used as a substrate. 50 Ω microstrip line feed is used to exit the microstrip antenna. We cannot achieve high gain and directivity with single element so 8×1 patch antenna array designed to achieve high gain and directivity for intrusion detection application at precise operating frequency of X-Band. The patch array has been targeted for the application of "Intrusion Detection", where high gain, narrow bandwidth and higher directivity are needed.

Keywords Microstrip antenna · Corporate feed network · Antenna array X-Band

M. Patel (✉)

Reve Automation, Gandhinagar, Gujarat, India
e-mail: madhukant.patel@reveautomation.com

M. Patel

UPES, Dehradun, Uttarakhand, India

P. Kuchhal

CoES, University of Petroleum and Energy Studies, Dehradun 248007, India
e-mail: pkuchhal@ddn.upes.ac.in

K. Lal · V. Singh

Sahajanand Laser Technology Ltd., Gandhinagar, India
e-mail: kanhiyalal@sahajanandlaser.com

V. Singh

e-mail: vsingh@sahajanandlaser.com

H. Patel

IMP Consultancy, Gandhinagar, Gujarat, India
e-mail: hemangipatel79@gmail.com

© Springer Nature Singapore Pte Ltd. 2018

R. Singh et al. (eds.), *Intelligent Communication, Control and Devices*,
Advances in Intelligent Systems and Computing 624,
https://doi.org/10.1007/978-981-10-5903-2_95

1 Introduction

Antennas are a kind of transducers for converting input electrical energy into output electromagnetic energy as radiation [1]. Antennas are energy receiver to collect the electromagnetic energy from the free space and converting into electrical energy. Microstrip antenna has been used as pivotal in many microwave applications [2]. The microstrip antenna has substrate in between two radiating patches and ground plane. High dielectric constants of the substrate are helpful in miniaturizing the dimension of antenna.

Required gain and directivity cannot be achieved with a single patch antenna so 8×1 patch antenna array is designed to achieve high gain and directivity for intrusion detection application at X-Band. The corporate-fed network with quarter wave transformer is used to match patch element impedance to 50Ω input impedance [3].

At X-Band of high-frequency range (8–12 GHz), the microstrip antenna has acted as an effective response. A rectangular shaped array [3–5] of microstrip patch antenna, fed with suitable line [3], using RO3006 material provides high gain as compared with Teflon and FR4.

2 Dimension of Array Antenna

The first case in the design of the array is the right choice of the patch [6]. The suitable dimensions are critical for the performance of the array antenna.

For an efficient radiation from the antenna, the dimensions (length and width) of the rectangular microstrip antenna is given by the following equations [7].

The width, W , is:

$$W = \frac{c}{2f} \times \sqrt{\frac{2}{(\epsilon_r + 1)}} \quad (1)$$

Here, f is the resonant frequency and ϵ_r is the dielectric constant of the substrate. In our design, the substrate is chosen as Rogers-3006 with and ϵ_r of 6.51.

The length, L , is:

$$L = \frac{c}{2f} \left(\frac{\epsilon_r + 1}{2} + \frac{\epsilon_r - 1}{2} \sqrt{\left[1 + 12 \frac{h}{W} \right]} \right)^{-\frac{1}{2}} - 2\Delta L \tag{2}$$

The overall dimension is tabulated in Table 1.

The element can feed by single line or by multiple lines in a feed network arrangement so we refer to multiple lines in a feed network; it is a combination of corporate-fed network with quarter wave transformer as shown in Fig. 1 (8×1 array antennas),

8×1 array is shown in Fig. 1.

Table 1 Design parameter of single microstrip patch antenna for 9.65 GHz

Width of patch	7.93 mm
Length of the patch (L)	5.72 mm
Input resistance of patch	50 Ω
Width of microstrip line (w_0)	0.1 mm
Length of microstrip line	2 mm
Dielectric constant of the substrate	6.51 (RO3006)

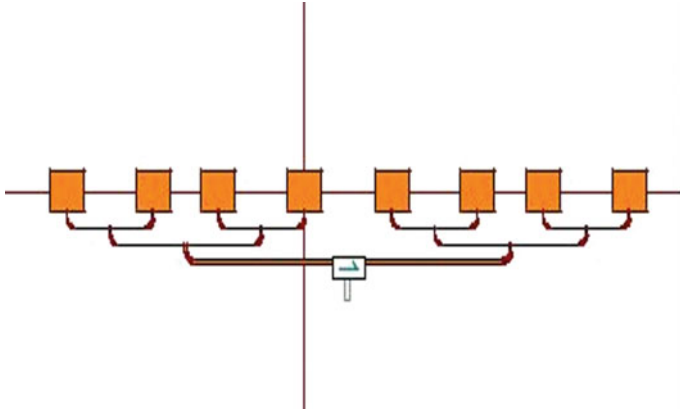


Fig. 1 Array of 8×1 microstrip square antenna

3 Results

A. Return Loss

This antenna has shown -17.76 dB return loss at 9.65 GHz resonant frequency which is shown in Fig. 2. At this frequency, antenna radiates maximum power and reflects minimum power.

B. VSWR

VSWR is a measure of how much the mismatch in impedance happens. Figure 3 is the VSWR plot of our observation, and it reveals that VSWR obtained is $1.30:1$. This is a good value because this ratio $1.30:1$ is well within the $2:1$ ratio of prescribed value of VSWR.

C. Total Gain Versus Frequency

Total gain of the antenna is 12.30 dBi for 9.65 GHz frequency as shown in Fig. 4.

Fig. 2 Return loss of 8×1 array antennas

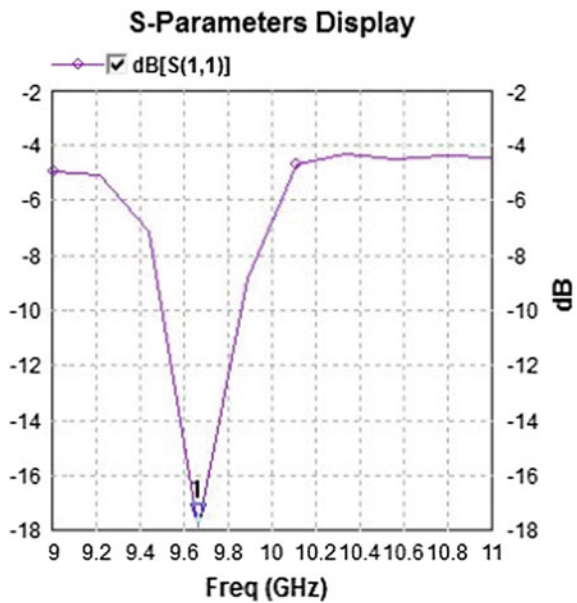


Fig. 3 Voltage standing wave ratio (VSWR) of array antennas

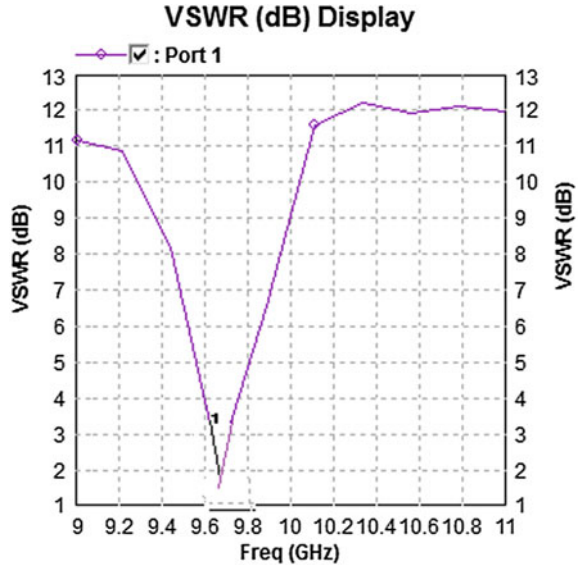
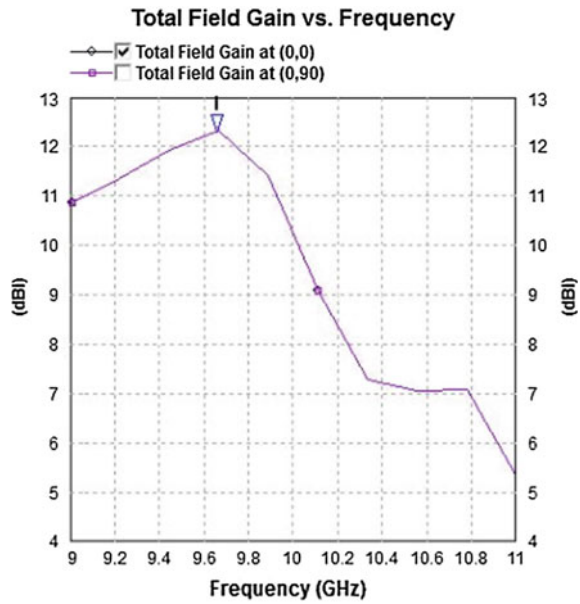


Fig. 4 Gain of 8×1 array antennas



4 Conclusion

Many applications in the areas basically of microwave sensors, the antenna should have very high directive characteristics, and the proposed array antenna is the one that fulfils this. An array antenna having multiple numbers of patches increases the gain (of 12.30 dBi), as obtained with our configuration. Hence, the given 8×1 patch antenna array gives enough confidence to use as intrusion detection sensor. The immediate further work is to build a prototype for lab testing and evaluation as intrusion detection sensor.

Acknowledgements This research was supported by Sahajanand Laser Technology Ltd, Gandhinagar. We are thankful to our colleagues Dr. Ranjan Mishra, UPES Dehradun who provided expertise that greatly assisted the research.

References

1. R. Garg, P. Bhartia, and I. Bahl, Ittipiboon, *Microstrip Antenna Design Handbook*, Artech House, Norwood, Mass, USA. (2001).
2. R. Mishra, *An Overview of Microstrip Antenna*, HCTL Open International Journal of Technology Innovations and Research (IJTIR), Volume 21, Issue 2. (2016).
3. R. Mishra, R. G. Mishra, P. Kuchhal, "Analytical Study on the Effect of Dimension and Position of Slot for the Designing of Ultra Wide Band (UWB) Microstrip Antenna", 5th IEEE International Conference on Advances in Computing, Communications and Informatics (ICACCI), 978-1-5090-2028-7. (2016).
4. Pozar, D. M. and D. H. Schaubert, *Microstrip Antennas: The Analysis and Design of Microstrip Antennas and Arrays*, IEEE Press, New York, (1995).
5. H. Errifi, A. Baghdad, A. Badri, and A. Sahel, "Design and Analysis of Directive Microstrip Patch Array Antennas with Series, Corporate and Series-Corporate Feed Network" *International Journal of Electronics and Electrical Engineering*. December. Vol 32. (2015).
6. R. Mishra, J. Jayasinghe, R. G. Mishra, P. Kuchhal, "Design and Performance Analysis of a Rectangular Microstrip Line Feed Ultra-Wide Band Antenna", *International Journal of Signal Processing, Image Processing and Pattern Recognition* Vol. 9, No. 6, pp. 419–426, (2016).
7. Constantine A., Balanis; *Antenna Theory, Analysis and Design*, John Wiley & Sons, Inc., Hoboken, New Jersey, (2005).

Design of an Efficient Rectifier Circuit Based on Karthaus-Fischer Voltage Multiplier for Energy Harvesting

Asmita Rajawat, Karush Suri and Mohit Mohta

Abstract Reduction in the usage of wires has been of significant importance to the power delivering process. Such transmission is obtained by using a rectenna which consists of a rectifier and an antenna. Antenna is used for receiving the signal, whereas the rectifier merely transforms the received RF signal into a DC signal. In this work, a rectifier circuit is designed for a 2.45 GHz GSM signal using Advanced Design System Software. Impedance matching of the antenna has been carried as per the matching circuit. Simulation of the circuit is carried out in order to analyze the power delivered. The Agilent HSMS 2862 Schottky diode is used for rectifying the signal in the voltage doubler circuit. DC voltage, current, and output power are plotted against input power. The rectifier designed can be used for ample number of applications in wireless transmissions.

Keywords RF power · DC output · Impedance matching · Voltage multiplier

1 Introduction

1.1 Related Work

In today's fast progressing world, wireless power transmission has a vital part of contributing power from the source to output of the device without the use of any wires or any contact. In recent past, the wireless transfer of data has profoundly increased and its market has widely expanded.

A. Rajawat (✉) · K. Suri · M. Mohta
Amity University Uttar Pradesh, Noida, Uttar Pradesh, India
e-mail: arajawat@amity.edu

K. Suri
e-mail: karushsuri@gmail.com

M. Mohta
e-mail: mohitmohitmohta@gmail.com

Rectennas have wide number of applications over other devices of its kind. Unlike batteries, rectennas have a higher lifetime and do not emit any pollutants. Further research in this area includes rectification of high frequency signals, use of super diodes in the rectification process, and the introduction of polymeric rectifiers.

The rectifying antenna (commonly known as rectenna) is a combination of the antenna and a nonlinear rectification unit. Integration of these two constituents into one circuit is carried so that the conversion of RF power to DC power can take place. Figure 1 depicts the block diagram of a simple Rectenna.

It is a combination of rectifier and antenna. Antenna receives the microwave power, and rectifier converts it into DC which can be used further. A low-pass filter is also connected between the antenna and rectifier to suppress the radiation of higher harmonics from the diodes. The microwave power that is converted into DC by rectenna is defined by its conversion efficiency [1].

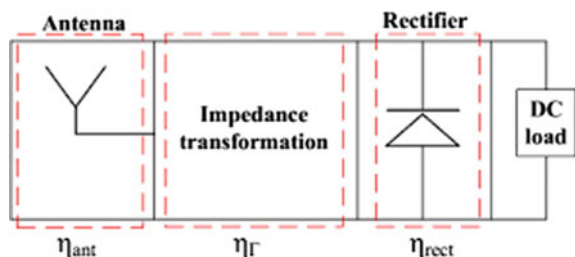
To increase the efficiency, two approaches can be opted. The first approach is to increase the antenna aperture, and the second approach is to design a new rectifying circuit.

Figure 1 shows the block diagram of a basic rectenna.

The receiving antenna captures the EM waves coming from the ambient radio waves. The rectifying circuit converts it into DC power. The impedance matching circuit connects and matches the receiving antenna with the rectifying circuit. The rectifying circuit consists of a voltage multiplier, which is finally connected to the load. Much research has been done on voltage multiplier circuits. In [2], resonance circuit transformation method was used which gave an output of 0.3 V for an input power level of -26 dBm. A Cockcroft Walton multiplier circuit was presented in [3] which produced an output of 1 V DC for an input of $1 \mu\text{W}$. In [4], the design proposed produced an output of 1.04 V which was based on the Villard voltage doubler circuit. In [5], Villard voltage multiplier comprises of CMOS technology; efficiency of the circuit was found to be 22.97% at $66 \mu\text{W}$ input, and the output voltage was 1.5 V. A seven-stage Schottky diode voltage doubler circuit was designed and simulated for an incident signal of 40 dBm which resulted in 3 mV across a $100 \text{ k}\Omega$ load [6].

For the wireless sensor network, a rectenna of 2.45 GHz has been realized using a modified Vivaldi antenna [7]. An energy harvester circuit [8] is designed by using a flexible one-directional antenna with a rectifier circuit and an impedance matching circuit. In [9, 10] energy efficient rectifier circuit at 900 and 2.45 MHz has been

Fig. 1 Block diagram of a rectenna



designed. A rectifier circuit is realized to elevate the power alteration efficiency from RF signal to DC signal. Many different forms of rectennas are used for WPTs and different energy harvesting applications.

In this suggested operation, the rectifier using Karthaus-Fischer voltage multiplier circuit is fabricated for a 2.45 GHz signal, and hence it is further connected with an impedance matching circuit and output load to complete the overall energy harvesting system.

1.2 Contribution

The research contribution of the paper is dedicated toward the study and simulation of Karthaus-Fischer voltage multiplier designs to obtain a good conversion efficiency and higher DC output voltage. The design concept of the paper is based on the concerned multiplier circuit with and without matching circuit and the respective output graphs.

1.3 Organization of Paper

The paper is organized as follows. Proposed multiplier design with and without matching circuit and its simulation results are presented in Sects. II and III which validates the accuracy of the analysis. Section IV concludes the paper.

2 Rectifier Design Based on Karthaus-Fischer Voltage Multiplier

The software used for designing is ADS, and the chosen value of the frequency in the task for simulation is 2.45 GHz. Schottky diode HSMS-2862 from Agilent Technologies is used for the voltage multiplier circuit. The diode can be used at high frequencies because of high switching speed and low forward voltage drop. The diode can also respond to noise spikes with rise times comparable to 1 ns because of picosecond switching. Signal degradation caused by waveshape loss is minimized by using low capacitance. Diode is not subjected to optimization. The values of the capacitances are chosen same as the analysis of the results after prior research exhibited that the rise time and output voltage were found to be better with equal values of capacitances.

An equivalent load resistance of 1000 Ω is connected to obtain the output across it. Capacitor would hold the value of voltage indefinitely if load resistor is not connected.

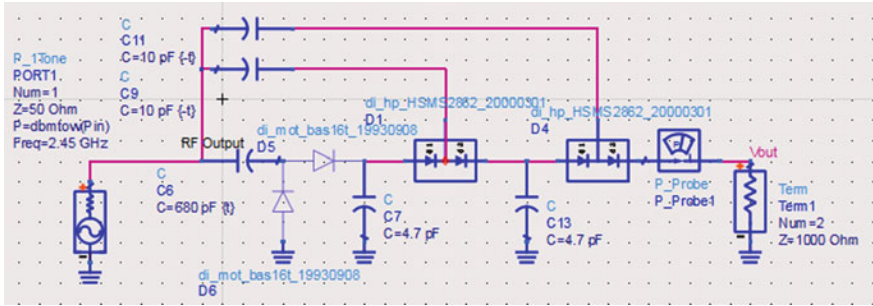


Fig. 2 Rectifier circuit of the unmatched circuit

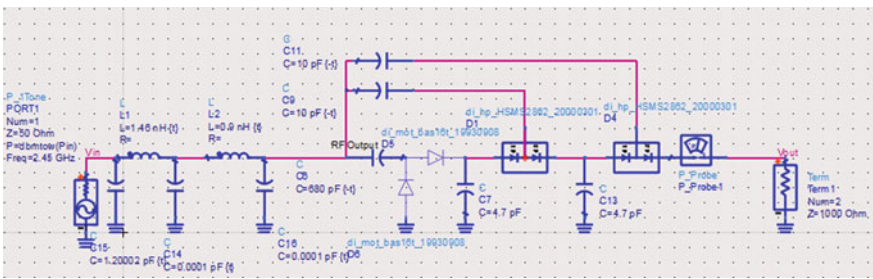


Fig. 3 Rectifier circuit with matching circuit

2.1 Unmatched Circuit

The unmatched circuit is obtained by removing all the lumped components of the matching circuit, i.e., by simply excluding the matching circuit. Figure 2 provides the circuit diagram for the unmatched circuit.

2.2 Matching Circuit

The matching circuit consisting of the lumped components is chosen in such a way so that the DC output obtained across the load by a significant extent. The technique of impedance matching is highly effective in fabricating complex high frequency designs. A self-generated source of 0–24 dBm power is used with impedance of 50 Ω. The filter section is used to remove the harmonics, and the final section consists of the rectifying circuit with impedance of 1000 Ω.

A proper matching circuit is designed by using the lumped components so that maximum transfer of signal takes place from the source to the diode. Figure 3 shows the rectifier circuit with matching circuit. The matching circuit enhances the output as a result of impedance matching.

3 Results and Discussion

3.1 Results of Unmatched Circuit

Design of the rectifier circuit consisting of the Karthaus-Fisher voltage doubler circuit is analyzed by distinguishing the results of the unmatched circuit from the matching circuit.

For the unmatched circuit, maximum output voltage of 3.351 V is observed with the maximum value of current as 3.351 mA. Figure 4 and 5 display the plots for output voltage and output current against the RF input power.

Output power delivered to the load is also observed with a peak value of -29 dBm in the range of 0–24 dBm input power. Figure 6 highlights the plot for output power against input power. Output power is described by the following equation:

$$P_{out} = (V_{out})^2/R_L.$$

Here, V_{out} is the output voltage measured across the load and R_L is the constant load resistance (1000 Ω).

DC conversion efficiency (η) is an essential measure to check the validity of the designed rectenna. Figure 7 gives the variation of conversion efficiency with the input power. Peak value of efficiency observed is 40.69%. DC conversion efficiency can be calculated with the help of the following equation:

$$\eta = P_{out}/P_{in}.$$

Here, P_{out} is the output power obtained after rectification and P_{in} is the input RF power.

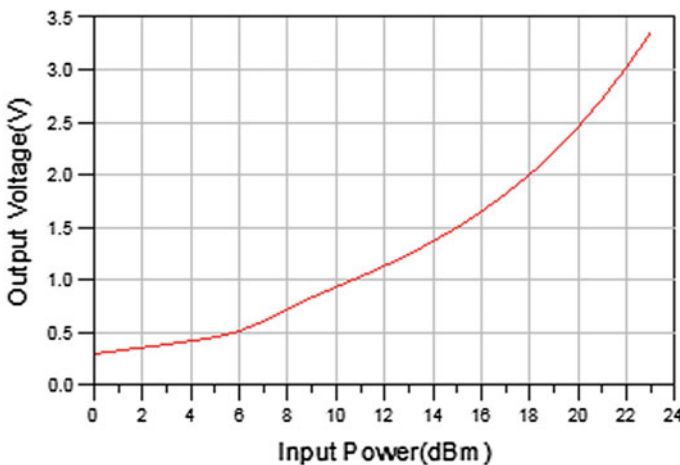


Fig. 4 Output voltage versus input power

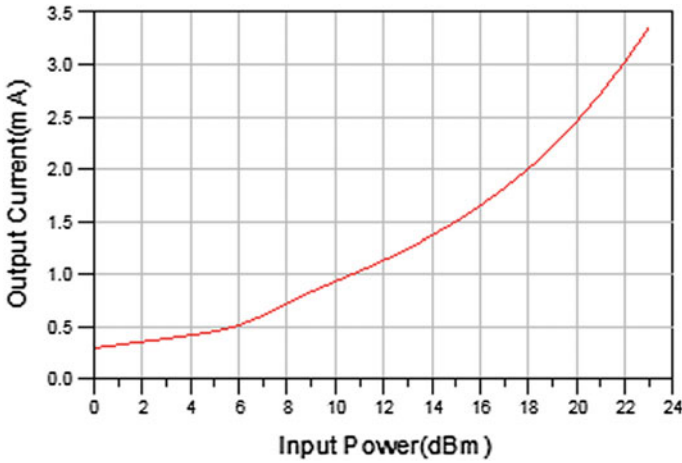


Fig. 5 Output current versus RF input power

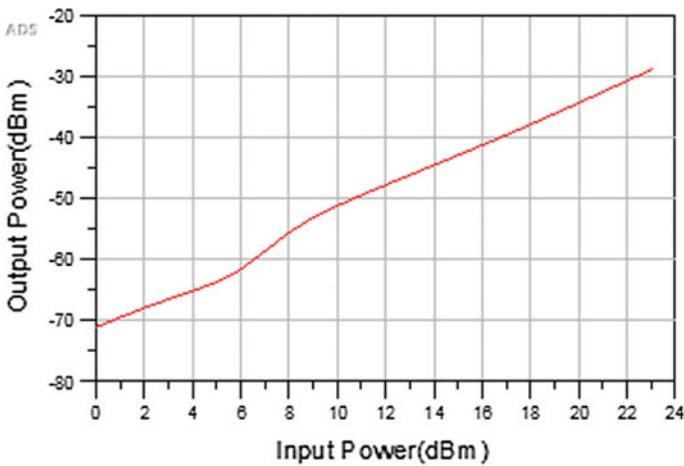


Fig. 6 Output power versus RF input power

3.2 Results of Matched Circuit

For the matching circuit, plots for output voltage and output current have been obtained against the RF input power. All the results have been obtained for a load of 1000Ω . Figure 8 and 9 show the results for output voltage and current against the input power of 0–24 dBm. A maximum DC voltage of 3.518 V has been obtained with the output current as 3.518 mA.

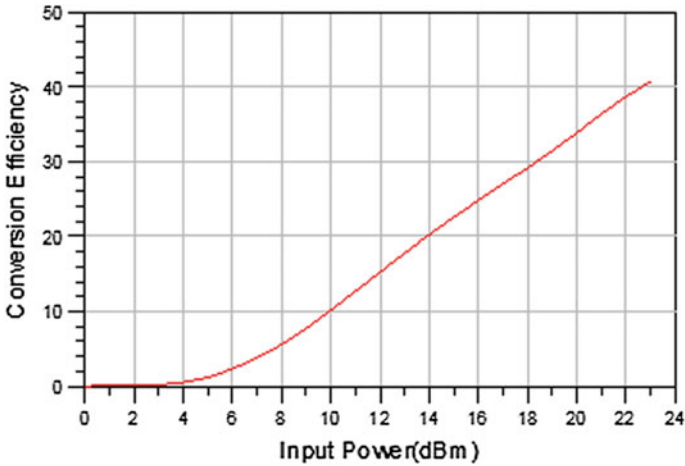


Fig. 7 Conversion efficiency for the unmatched circuit

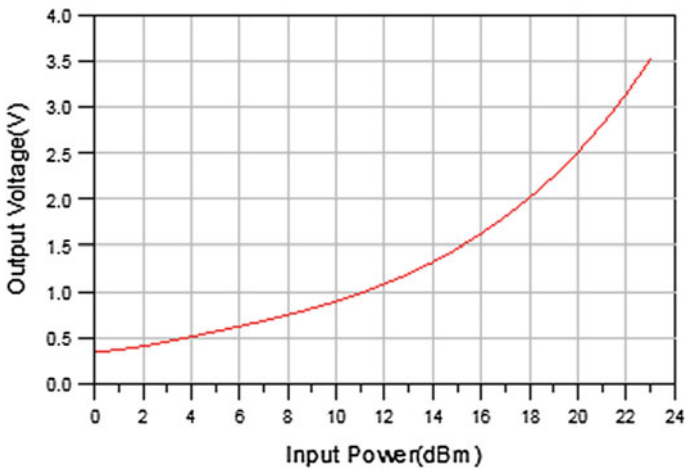


Fig. 8 Output voltage versus RF input power

Figure 10 shows the plot of output power against input power. A maximum value of -28.15 dBm is observed. Output power is described by the following equation:

$$P_{out} = (V_{out})^2 / R_L$$

where V_{out} is the DC voltage occurring across the output and R_L is the load impedance (1000Ω). Conversion efficiency for the matching circuit is observed at a peak value of 70.11%. Figure 11 displays the plot for conversion efficiency against input power.

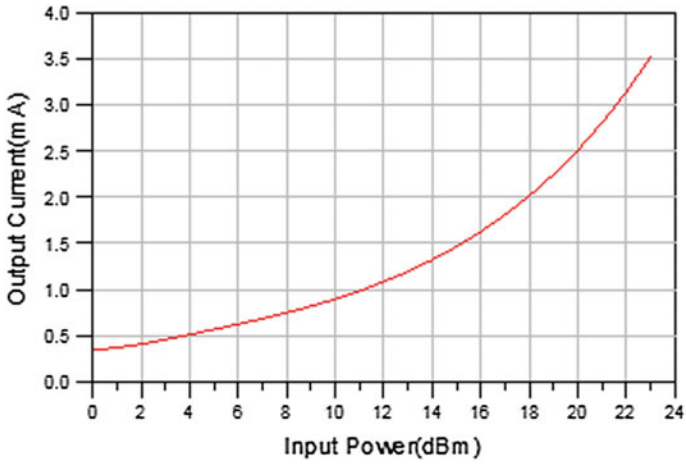


Fig. 9 Output current versus RF input power

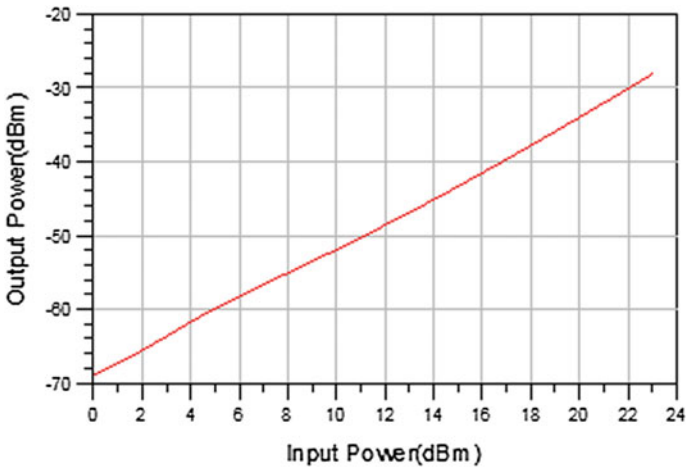


Fig. 10 Output power versus input power

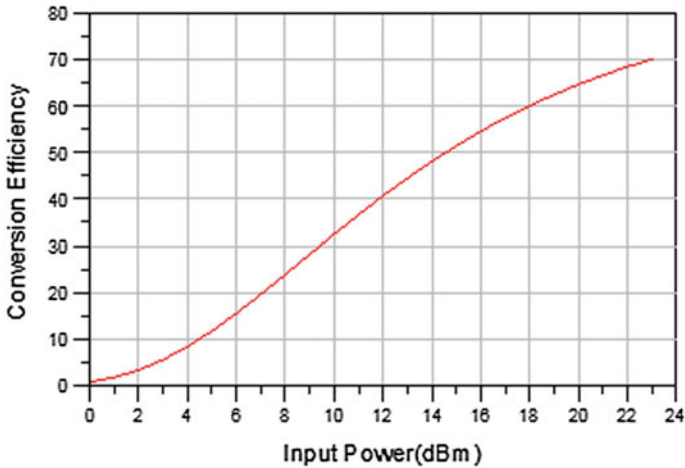


Fig. 11 Conversion efficiency for the matched circuit

4 Conclusion

Wireless power transmission has a sustainable future for accomplishing small-scale electrical power circuits which find their use in communication systems. In this suggested work, a rectifier has been fabricated for 2.45 GHz ISM band. This design of the matching circuit and rectifier circuit has been done using Advanced Design System (ADS). The result from its simulation gives the maximum output voltage of 3.518 V at an RF power of 23 dBm. Furthermore, the voltage doubler circuit produces an efficiency of 70.11% for rectification. Impedance matching has been utilized to match the source and rectifier impedances. This makes the rectifier convenient for applications related to rectenna.

References

1. W. C. Brown, "The receiving antenna and microwave power rectification", *Journal of Microwave Power*, vol. 5, pp. 279–92, (1970).
2. Ugan, T., Reindl, L. M.: "Concept for Harvesting Low Ambient RF-SourceforMicrosystems", http://www.imtek.de/content/pdf/public/2007/powermems_2007_paper_ungan.pdf, accessed 20th March (2010).
3. JiangWang, Liang Dong and Yuzhuo, Fu.: "Modeling of UHF voltage multiplier for radio-triggered wake-up circuit", *International Journal of Circuit Theory and Application*, DOI:10.1002,(2010).
4. M. Arrawatia, M. S. Baghini and G. Kumar, "RF energy harvesting system at 2.67 and 5.8 GHz", *Proceedings of Asia Pacific Microwave Conference*, 900–903, (2010).

5. H. Jabbar, S. S. Young and T. J. Taikyeong, "RF energy harvesting system and circuits for charging of mobile devices", *IEEE Transactions on Consumer Electronics*, 56(1): 247–253, (2010).
6. E. M. Ali, N. Z. Yahaya, N. Perumal and M. A. Zakariya "Design of RF to DC rectifier at GSM band for energy harvesting applications", *A Journal of Engineering, Science and Society*, 10(2): 15–22, (2014).
7. Fabrizio Congedo, "A 2.45 GHz Vivaldi Rectenna for the Remote Activation of an End Device Radio Node", *IEEE Sensor Journal*, Vol. No. 10, pp. 1536–1225, (2015).
8. Haruichi Kanaya, "Energy Harvesting circuit on a One-Sided Directional Flexible Antenna", *IEEE Microwave and Wireless Component Letters*, Vol.23, No.3, pp. 1351–1309, (2013).
9. K. Kaviarasu, V. Ganesh, "Design and Simulation of a 900 MHz Rectifier for Rectenna Applications", *IEEE ICCSP*, (2015).
10. Asmita Rajawat, P.K. Singhal, "Design of Energy Efficient Voltage Multiplier Circuit for RF Energy Harvesting", *ETAERE* (2016).

Longitudinal Control of Small Unmanned Aerial Vehicle by PID Controller

Alok Kumar Pandey, Tanu Chaudhary, Shubham Mishra
and Shrestha Verma

Abstract The paper presents the design of PID controller for longitudinal dynamics of small UAV. It also provides the state matrices by using physical parameters: aerodynamic coefficients and stability derivatives. PID controller provides the stability to UAV and transient specifications. The focus of this paper is on modelling and control design for a UAV system. The novel approach suggested in this paper is to use PID controller. PID controller is only used to provide the required transient response (Stevens and Lewis in Aircraft control and simulation. Wiley, Hoboken, [1]).

Keywords UAV · PID controller · Ziegler Nicholas tuning

1 Introduction

Number of organisations such as military and civilian have rapidly increased due to incremented interest in UAVs exploring to develop plenary autonomous UAVs. As the level of autonomy of the UAV increases, the complexity of its guidance and control system also goes beyond the level. Development of algorithm for that advanced guidance is necessary and obligatory for fulfilling the incipient requisites as the application area of the UAV is increasing and also for modelling UAVs in future and important technology related to it.

A.K. Pandey (✉) · T. Chaudhary · S. Mishra · S. Verma
Electrical and Electronics Department, KIET, Ghaziabad, India
e-mail: Pandeyalok507@gmail.com

T. Chaudhary
e-mail: tanu1995.kiet@gmail.com

S. Mishra
e-mail: parthsarthishubham@gmail.com

S. Verma
e-mail: Shresthaverma94@gmail.com

Control and stabilisation of larger UAV, however, is simpler than SUAV. This is because of several constraints associated with SUAV, like the low mass of the conveyance, lesser Reynolds numbers and light wing loading. For a system like UAV, for its control and development, dynamic modelling is a very crucial step. Indeed, for analysing various system possibilities and behaviour under different flight conditions, this dynamic model is used by the designer. This dynamic model plays a vital role for those UAVs as well whose event of failure is very high, i.e. risk of damage. Therefore, before realisation of a controller into a system, it is recommended to first check its simulation and tuning possibility [2].

Three simple steps are followed in designing and tuning of controller for both self-regulating and integrating processes: collect closed-loop dynamic process data, incorporate the data in simple linear model and, with the help of model parameters, obtain PID tuning parameter values. This method is discussed and shown in the remainder of this paper.

2 Model Dynamics

The yaw (ψ), pitch (θ) and roll (ϕ) are the concerning angles that transfer to the body frame from the vehicle frame. The behaviour of the aircraft is described by these Euler angles. The angle associated with the rotation between the stability frame and body frame and vice versa is called angle of attack (α) and from stability frame to the wind frame is sideslip angle (β). These are concisely discussed as follows [2].

The angle between the inertial north (x^1) and the inertial velocity vector projected on the horizontal plane is called course angle (χ). The difference between the course angle and the heading is called crab angle (χ_c). The two important angles to transform from body frame into flight frame are (χ , γ) [3]. When the wind is not present,

- $\chi_c = 0$.
- $\gamma = 0$.
- $V_a = V_g$.

The physical parameters of aircraft are presented in Tables 1 and 2 [4, 5].

During modelling, several posits have been taken. Albeit aircraft is genuinely elastic in nature, as concerning the elasticity of the UAV will not be fruitful as far as research is concerned. Two, the earth is considered to be an inertial reference frame. Three, throughout the simulation, mass properties of the aircraft are constant. Conclusively, there exists a plane of symmetry in the aircraft. The one and three postulations sanction for the point-mass treatment of the aircraft.

The condition in which all of the motion variables are constant or zero is called steady state for an aircraft. Following assumptions are also made for linearisation [1]

Table 1 Some physical properties of aircraft

Parameter	Symbol	Value
Wing span	B	1.27 m
Wing surface area	S	0.3097 m ²
Maincord	C	0.25 m
Mass	M	1.959 kg
	J_x	0.07151 kg m ²
Inertia	J_y	0.08636 kg m ²
	J_z	0.15364 kg m ²
	J_{xz}	0.014 kg m ²

- (a) All velocities are zero.
- (b) The acceleration is zero.
- (c) Earth is assumed to be totally flat.
- (d) Aircraft has a constant mass.
- (e) The variations in atmosphere density due to altitude are neglected.

For steady-state flight, the states and control action for UAV are

$$\dot{p}, \dot{q}, \dot{r}, \dot{u}, \dot{v}, \dot{w} \left(\text{or } \dot{V}a, \dot{\beta}, \dot{\alpha}, \right) = 0 \tag{1}$$

$$U = \text{constant} \tag{2}$$

The following are the derived aerodynamic coefficients and derivatives for the longitudinal dynamics.

$$\begin{bmatrix} \Delta \dot{u} \\ \Delta \dot{w} \\ \Delta \dot{q} \\ \Delta \dot{\theta} \end{bmatrix} = \begin{bmatrix} X_u & X_w & X_q + w_0 & -g \cos \theta_0 \\ Z_u & Z_w & Z_q - w_0 & -g \sin \theta_0 \\ M_u & M_w & M_q & 0 \\ 0 & 0 & 1 & 0 \end{bmatrix} \begin{bmatrix} \Delta u \\ \Delta w \\ \Delta q \\ \Delta \theta \end{bmatrix} + \begin{bmatrix} X_{\delta_e} & X_{\delta_r} \\ Z_{\delta_e} & 0 \\ M_{\delta_e} & 0 \\ 0 & 0 \end{bmatrix} \begin{bmatrix} \Delta \delta_e \\ \Delta \delta_r \end{bmatrix} \tag{3}$$

Table 2 Aerodynamic coefficients

Longitudinal coefficients	Value
C_{L_0}	0.2615
C_{D_0}	0.029
C_{M_0}	0
C_{L_z}	3.4424
C_{D_z}	0.8477
C_{M_z}	-0.4438
$C_{L_{\delta_e}}$	0.7450
$C_{D_{\delta_e}}$	0
$C_{M_{\delta_e}}$	-0.3438

2.1 State Space Model

The state space equations of longitudinal motion are stated as:

$$\dot{x}_{lon} \triangleq (u, w, q, \theta, h)^T, \tag{4}$$

and the input vector (control) is stated as:

$$U_{lon} \triangleq (\delta_e, \delta_\tau)^T \tag{5}$$

Let us consider that the wind speed and also the lateral states are zero (i.e. $\varphi = p = r = \beta = v = 0$) (Table 3).

Putting above values in state equation, state input and output matrix are given below

Table 3 Longitudinal stability derivatives

Longitudinal derivatives	Formula
X_u	$\frac{u\rho S}{m} [C_{x0} + C_{x_\alpha} \alpha + C_{x_{\delta_e}} \delta_e] - \frac{\rho S w C_{x_z}}{2m} - \frac{\rho S_{prop} C_{prop} u}{m}$
X_w	$\frac{w\rho S}{m} [C_{x0} + C_{x_\alpha} \alpha + C_{x_{\delta_e}} \delta_e] - \frac{\rho S u C_{x_z}}{2m} - \frac{\rho S_{prop} C_{prop} w}{m}$
X_q	$-w + \frac{\rho V_a S C_{x_q} C}{2m}$
X_{δ_e}	$\frac{\rho V_a^2 S C_{x_{\delta_e}}}{2m}$
X_{δ_τ}	$\frac{\rho S_{prop} C_{prop} K \delta_e}{m}$
Z_u	$\frac{u\rho S}{m} [C_{Z0} + C_{Z_\alpha} \alpha + C_{Z_{\delta_e}} \delta_e] - \frac{\rho S w C_{Z_x}}{2m}$
Z_w	$\frac{w\rho S}{m} [C_{Z0} + C_{Z_\alpha} \alpha + C_{Z_{\delta_e}} \delta_e] - \frac{\rho S u C_{Z_x}}{2m}$
Z_q	$u + \frac{\rho V_a S C_{z_q} C}{2m}$
Z_{δ_e}	$\frac{\rho V_a^2 S C_{Z_{\delta_e}}}{2m}$
M_u	$\frac{u\rho S c}{J_y} [C_{M0} + C_{M_\alpha} \alpha + C_{M_{\delta_e}} \delta_e] - \frac{\rho S w C_{M_x}}{2J_y}$
M_w	$\frac{w\rho S c}{J_y} [C_{M0} + C_{M_\alpha} \alpha + C_{M_{\delta_e}} \delta_e] - \frac{\rho S u C_{M_x}}{2J_y}$
M_q	$\frac{\rho V_a S c^2 C_{M_q}}{2J_y}$
M_{δ_e}	$\frac{\rho V_a^2 S c C_{M_{\delta_e}}}{2J_y}$

$$\begin{aligned}
 A_{\text{lon}} &= \begin{bmatrix} -0.0543 & -0.5332 & 0 & -9.7295 \\ -2.7791 & -10.3435 & 8.51 & -1.1732 \\ -0.3403 & -2.0302 & 0 & 0 \\ 0 & 0 & 1 & 0 \end{bmatrix} \\
 B_{\text{lon}} &= \begin{bmatrix} 2.4224 & 0.224 \\ -20.2054 & 0 \\ -18.4384 & 0 \\ 0 & 0 \end{bmatrix} \\
 C_{\text{lon}} &= \begin{bmatrix} 1 & 0 & 0 & 0 \\ 0 & 1 & 0 & 0 \\ 0 & 0 & 1 & 0 \\ 0 & 0 & 0 & 1 \end{bmatrix} \\
 D_{\text{lon}} &= [0]
 \end{aligned}$$

Initially, the step response of system is unstable that is shown in Fig. 2, so there is a need of controller to stabilise it.

3 Design of PID Controller

Integrating processes are obstinate. It is required to tune controllers for such type of processes in closed loop as they can reach dangerous levels if not regulated. Earlier, in PID controller, the reference input, the error and the linear combination of differential coefficient and integral were used to develop control signals, that is

$$u = K_p e + K_i \int e dt + K_d \frac{de}{dt} \tag{6}$$

where $e(t) = r(t) - y(t)$. Controller configuration block diagram is given in Fig. 1. Auto-tuning method has been used for obtaining PID controller parameters as $K_p = 2.49$, $K_i = 7.33$, $K_d = 0.187$. These values are used for obtaining system's step response that is shown in Figs. 2, 3, 4, 5, 6. The step response in figures shown, gives a peak overshoot of as high as 25% with relatively short rise time of 0.1 s. Settling time for the system is 1.3 s.

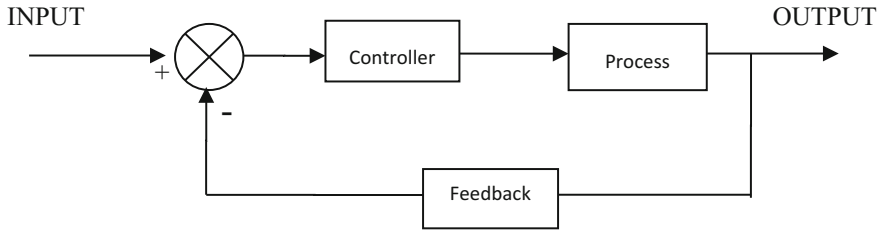


Fig. 1 Block diagram of a control system

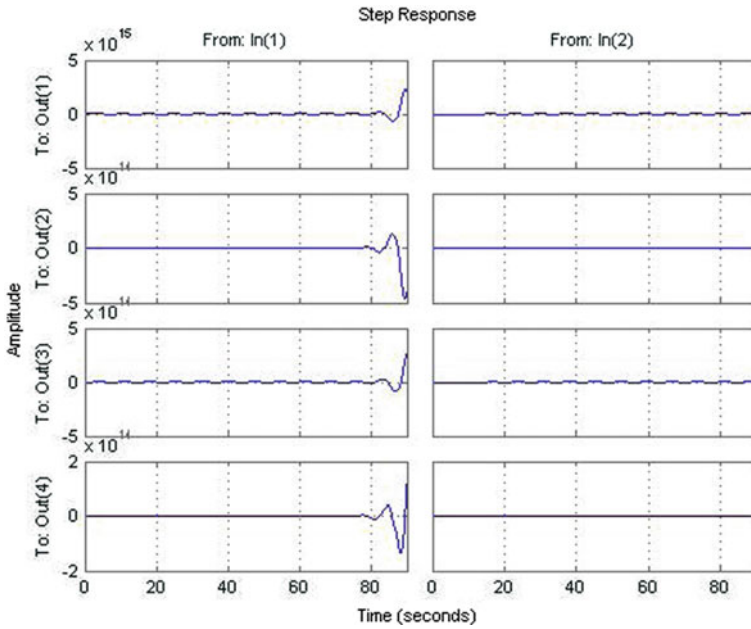


Fig. 2 Unstable system

4 Simulation Results

Without any controller system is unstable and shown in Fig. 2. Results of PID controller are shown in Figs. 3, 4, 5 and 6. G1, G2, G3 and G4 are the transfer functions of different input and output sequentially.

Time-domain specifications of system are given in Table 4.

Fig. 3 Response of G1

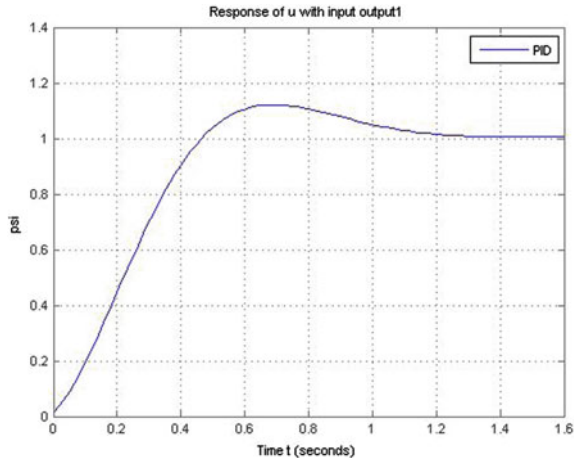


Fig. 4 Response of G2

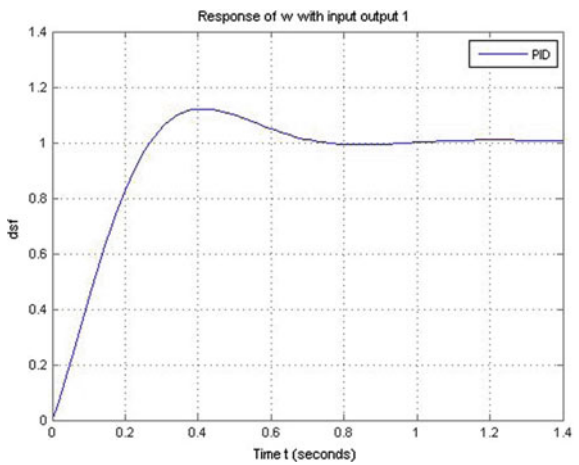


Fig. 5 Response of G3

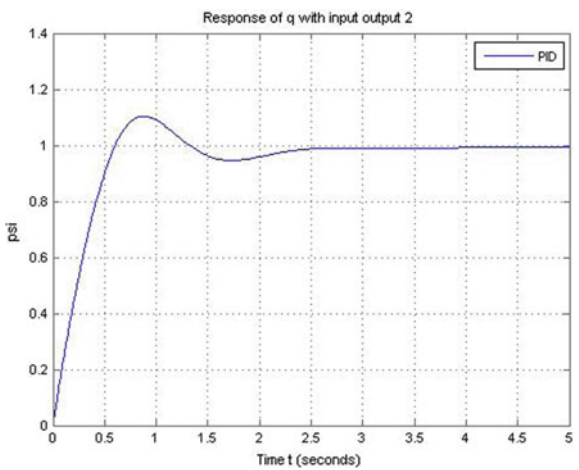


Fig. 6 Response of G4

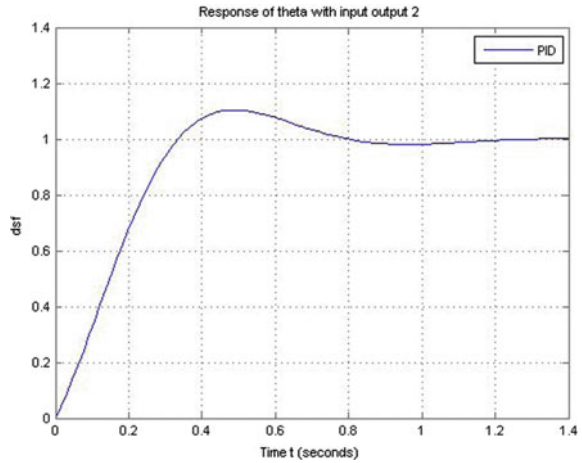


Table 4 Results

Parameters	G1	G2	G3	G4
Rise time (s)	0.2467	0.1991	0.4583	0.2467
Settling time (s)	0.7321	0.6666	2.3095	0.7321
Overshoot (%)	10.3971	12.1736	10.3218	10.3791
Peak time (s)	0.4873	0.4104	0.8806	0.4873

5 Conclusion

A PID controller has been developed to stabilise the longitudinal dynamics of mini-UAV, and time-domain specifications of system are analysed. Peak overshoot and settling time of the system are in under limit, but for smoother controller, we can propose advance controllers.

References

1. B. L. Stevens and F. L. Lewis, “*Aircraft Control and Simulation*”, Hoboken, NJ: John Wiley& Sons, Inc., 2nd ed., 2003.
2. A. Elsayed, A. Hafez, A.N., H. Eldin, H. Mohammad “Modelling of small UAV”, International Journal of Mechanical/Aerospace, Industrial, Mechatronic and Manufacturing Engineering, Vol. 9, No. 3, 2015.
3. D. T. Greenwood, “*Principles of Dynamics*. Englewood Cliffs”, NJ: Prentice Hall, 2nd ed., 1988.
4. Murch, A., Dorobantu, A., and Balas, G., “*University of Minnesota UAVFlight Control Research Group*,” <http://www.uav.aem.umn.edu>, 4 March 2013.

5. Murch, A., Paw, Y. C., Pandita, R., Li, Z., and Balas, G., “*A Low Cost Small UAV Flight Research Facility*,” CEAS Conference on Guidance, Navigation, and Control, Munich, Germany, 2011.
6. Edward AFB CA, “*Flying Qualities Phase. Vol. 2*”, USAF TEST Pilot School, 1988.
7. “*USAF Stability and Control DATCOM*”, Flight Control Division, Air Force Flight Dynamics Laboratory, Wright- Patterson Air Force Base, Oh, 1980.
8. Xinzhong Chen, Ahsan Kareem, “*Advances in Modeling of Aerodynamic Forces on Bridge Decks*”, Journal of Engineering Mechanics, November 2002.
9. Andrei Dorobantu, Austin M. Murchy, Bernie Mettlerz, and Gary J. Balasx, “Frequency Domain System Identification for a Small, Low-Cost, Fixed-Wing UAV” Department of Aerospace Engineering & Mechanics University of Minnesota, Minneapolis, MN, 55455, USA, pp. 1–13.
10. Randal W. Beard, Timothy W. McLain, “*Small Unmanned Aircraft: Theory and Practice*”, Princeton University Press, 2012.

Control Schemes for Permanent Magnet Synchronous Generator-Based Variable Speed Wind Turbine

Rupendra Pachauri, Pradeep Rana, Yogesh K. Chauhan
and S. Choudhury

Abstract In this paper, two control schemes such as direct control scheme (DCS) and vector control scheme (VCS) are presented for permanent magnet synchronous generator (PMSG) based adjustable speed wind turbine (WT) system. In DCS, all parameters are obtained in the stator reference frame to invalidate the need of continuous position of rotor. Furthermore, it is analyzed that the DCS acquires numerous advantages over traditional indirect VCS such as torque, flux control lacking any rotor location. It is lesser parameters dependence and sensor less operation. In both the techniques, the DCS can operate underneath fixed and dynamic wind velocity conditions. Both of these control schemes are implemented in MATLAB/Simulink software, and the obtained characteristics are shown which results effective and satisfactory performance.

Keywords Direct control scheme · Vector control scheme · Synchronous generator · Adaptable speed wind turbine

R. Pachauri (✉) · S. Choudhury
Electronics Instrumentation and Control Engineering Department,
College of Engineering Studies, University of Petroleum and Energy Studies,
Dehradun 248007, Uttarakhand, India
e-mail: rpachauri@ddn.upes.ac.in

S. Choudhury
e-mail: schoudhury@ddn.upes.ac.in

P. Rana · Y.K. Chauhan
Electrical Engineering Department, School of Engineering, Gautam Buddha University,
Greater Noida 201312, Uttar Pradesh, India
e-mail: rana.pradeep327@gmail.com

Y.K. Chauhan
e-mail: chauhanyk@yahoo.com

1 Introduction

The wind energy is highly desired refilled source of power generation to complete the renewable energy (RE) target all over the world to decrease the depletion of fossil fuels [1]. In present, dynamic wind turbine (WT) control techniques influence power production in the country because of their benefits on stable speed generation like maximum power point (MPP) operation, higher efficiency, and power quality [2].

Mostly variable speed WTs with gearbox are used, which is based on DF induction generator [3, 4]. The variable speed WT technology has an advantage of higher energy yield and lower power fluctuation as compare to fixed speed WT [5]. However, in these types of turbines, a gearbox is coupled to the generator system and which creates problems in turbine. Also gearbox has some drawbacks in these turbines, it requires regular maintenance as it suffers from fault and malfunction [6].

The operation can also be performed in extensive speed range (near cut-out speed) due to flux weakening to make constant power between rated and cut-out wind speed [7, 8]. The pulse width modulation (PWM) rectifier for three switches and vector-controlled PWM rectifier for six switches are required [8]. The previous work has been done on various control methods described in literature with PMSG-based dynamic speed WT like switched mode DC–DC boost rectifier [9]. The drawback of this types WT system is to control power factor of generator having great harmonic distortion, results in poor efficiency of generator [10]. In present, PMSG-based dynamic speed WECS used traditional vector control method [10, 11]. In this technique, generator torque through current control can control indirectly. The speed controller generates the output in the form of d - q axis on the rotor reference frame to involve coordinate transformation and the position sensor for torque curve [11, 12].

This research article presents the direct control scheme (DCS) and vector control scheme (VCS). It is concluded that during DCS performance, there is no need for coordinate transformations since all parameters are performed in stator reference frame to validate the control action. Therefore, it does not require the continuous rotor position (ω_r). Moreover, this technique found fundamentally sensor less and has so many benefits over the traditional indirect VCS. So, the need of a sensorless speed estimator is to calculate the rotor speed without an automated mechanical sensor which is proposed and implemented in this paper.

2 System Interpretation

The overall system is comprised mainly three important parts (a) wind turbine, (b) PMSG, and (c) control schemes (i) vector control scheme (VCS) (ii) direct control scheme (DCS). The layout of entire system is presented in Fig. 1.

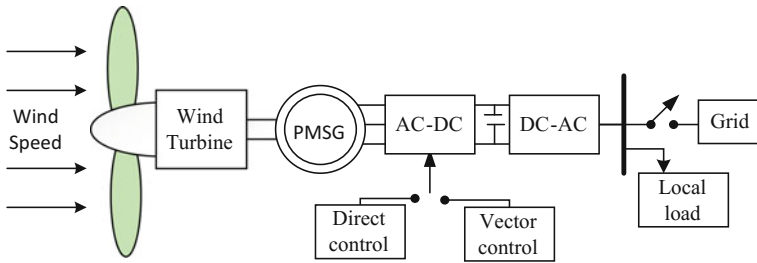


Fig. 1 Layout of control scheme of PMSG-based WT system

This research paper is categorized in seven basic sections—in Sects. 1 and 2, introduction of WT system with system layout description is described. In Sects. 3 and 4, WT and PMSG modeling are discussed in detail. Furthermore, control schemes (i) vector control scheme (VCS) and (ii) direct control scheme (DCS) are discussed in detail in Sect. 5. The results and discussion part of this paper is presented in Sect. 6. Section 7 concludes the paper.

3 Modeling of WT System

WT is used to transform the kinetic energy (KE) of the wind velocity into the mechanical power. Mechanical power (P_m) and torque (τ_{WT}) of the WT are calculated by Eq. (1) as,

$$P_m = \frac{1}{2} \rho A C_p V_\omega^3, \tau_{WT} = \frac{1}{2} \rho A C_p V_\omega^2 \frac{R}{G \lambda} \tag{1}$$

where C_p is the performance constant, R is the rotor radius, G is the gear ratio [7]. Tip speed ratio (λ) and C_p is given as,

$$\lambda = \frac{\omega_r R}{V_\omega}, C_p(\lambda, \beta) = \varepsilon_1 \left(\frac{\varepsilon_2}{\lambda_i} - \varepsilon_3 - \varepsilon_4 \right) e^{\frac{-\varepsilon_5}{\lambda_i}} + \varepsilon_6 \lambda \tag{2}$$

where ω_r is rotor speed (rad/sec), $\varepsilon_1, \varepsilon_2, \dots, \varepsilon_6$ are constants, β is pitch angle of blade and λ_i is initial tip speed ratio given by Eq. (2) [9, 13, 14].

4 Modeling of PM Synchronous Generator

PMSGs are utilized in WECS to bring out various advantages. These are self-excited synchronous generators, resulting elimination of the rotor copper losses used to transform the mechanical output of the turbines into the electrical power. An

external power supply is also not required and maintenance is eliminated since brushes and slip rings as well as rotor windings are also uninvolved. In this context, variable wind speed is used. The PMSG rotor and WT shaft rotate in synchronism with the same shaft [7]. The equations of d - q transformation of PMSG is given as in Eq. (3) as,

$$\frac{di_q}{dt} = \frac{(-R_s i_q + \omega_e (L_{qs} + L_{ls}) i_d + u_q)}{L_{qs} + L_{ls}}, \frac{di_d}{dt} = \frac{(-R_s i_d + \omega_e (L_{qs} + L_{ls}) i_q + u_d)}{L_{ds} + L_{ls}} \quad (3)$$

where i_d and i_q represent the phase currents of stator on d - q axis, respectively, R_s is resistance of stator, L_{qs} and L_{ls} are inductances of stator on the d - q axis, respectively, ω_e and τ_{em} are the electrical rotating speed (rad/sec) of the PMSG and electromagnetic torque, respectively, defined by Eq. (4) as,

$$\omega_e = p\omega_g, \tau_{em} = 1.5p\{(L_{ds} - L_{ls})i_d i_q + i_q \psi_f\} \quad (4)$$

where, p is number of pole pairs and ψ_f is magnetic flux of PMSG system.

5 Control Schemes for PMSG

5.1 Direct Control Scheme

The DCS for PMSG is presented in Fig. 2. This method does not require to control the stator currents. The generator torque and stator flux both can be adjusted freely and straight through two independent hysteresis controller bands for flux and torque [4, 8]. The selection rule is made in the way that errors available in torque and flux will be inside the hysteresis bands to get the desired flux and torque feedback. In

Fig. 2 DCS for PMSG system

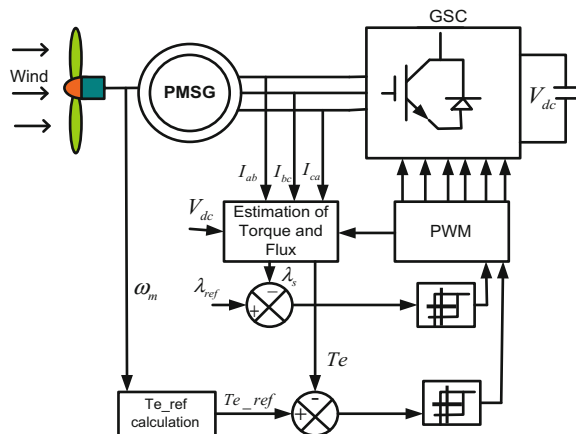
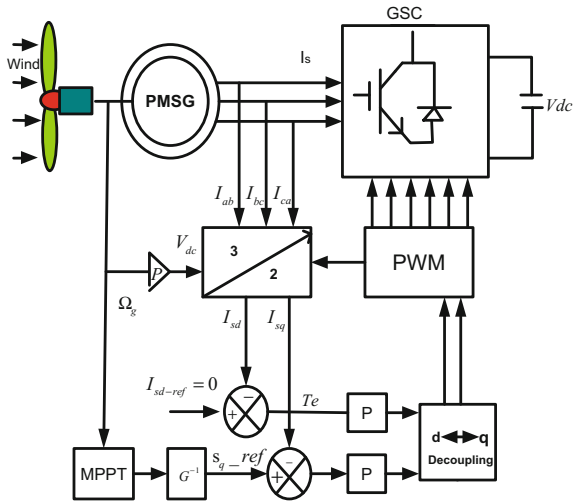


Fig. 3 VCS for PMSG system



direct control method, switching voltage vector which can be taken through switching voltage set. Various advantages of direct control technique are as follows,

- No need of coordinate transformation since every calculation has been done in stator reference frame.
- It doesn't need any rotor position sensor.
- Requires minimum parameters.
- Numbers of controller are minimizing as comparison of indirect vector control techniques.

5.2 Vector Control Scheme for PMSG

Indirect VCS is technique for determining the rotor flux position indirectly. For the calculation of the rotor flux position, stator current measurements and the angular quantity of rotor speed are necessary. To the measurements of rotor speed, this is summed with negative slip velocity. The VCS for PMSG is shown in Fig. 3.

6 Results with Discussion

The proposed schemes are modeled and simulated in MATLAB/Simulink software. The system constrained is specified in Appendix. The performance of system is investigated for both the traditional vector control and direct control under dynamic

wind speed in terms of WT torque and stator currents of PMSG, electromagnetic torque, and rotor speed.

The outcomes are deliberated for two situations as follows,

- Performance of system with traditional indirect vector control method.
- Performance of system with direct control.

6.1 Performance of System with Traditional Indirect Vector Control Method

Figure 4 reflects the system performance of dynamic speed WT and MATLAB/Simulink model of indirect VCS. The obtained results from traditional

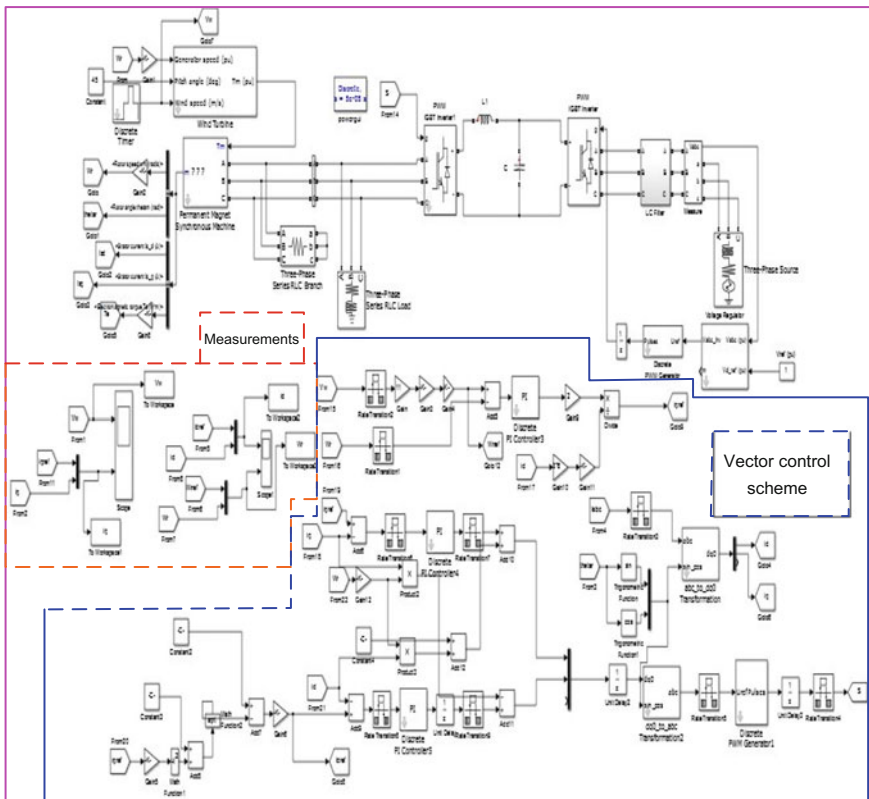


Fig. 4 MATLAB/Simulink model of traditional indirect VCS

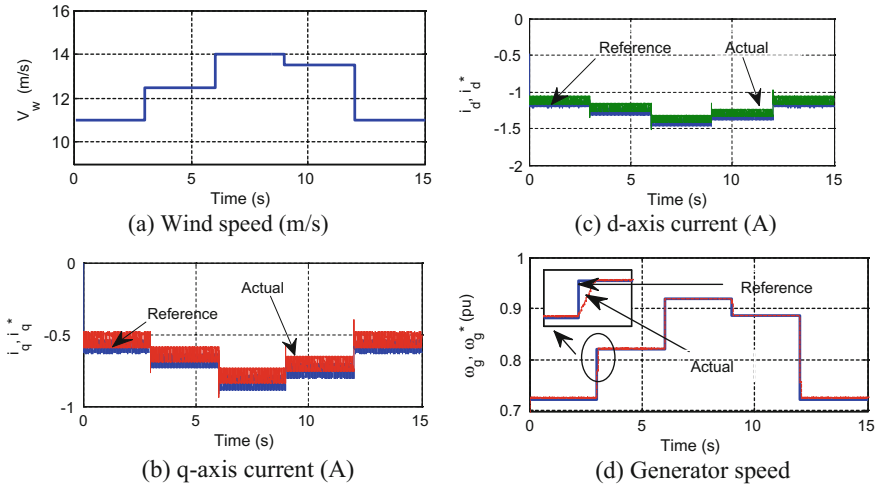


Fig. 5 Performance of the traditional indirect VCS for PMSG

indirect VCS are depicted in Fig. 5a–d. It is found that the transient analysis of WT-assisted PMSG system has been done in terms of varying wind speed, torque, flux, turbine rotor speed. The considered wind speed range of 11.5–14 m/s, depicted in Fig. 5a. The d - q axis currents and generator speed are tracked efficiently with the reference value. The overall performance of the considered system agreed with the obtained results and shown in Figs. 4 and 5.

6.2 System Performance with Direct Control Scheme

In Fig. 6, the results depicted and shows the behaviour of PMSG-based wind turbine and MATLAB/Simulink model of DCS in Fig. 6.

The obtained results from DCS are depicted in Fig. 7a–d, and it is found that the transient analysis of WT-assisted PMSG system has been done in terms of varying wind speed, torque, flux, turbine rotor speed. The considered wind speed range of 11.5–14 m/s, depicted in Fig. 5a. The d - q axis currents and generator speed are tracked efficiently with the reference value. The overall performance of the considered system agreed with the obtained results and shown in Fig. 7.

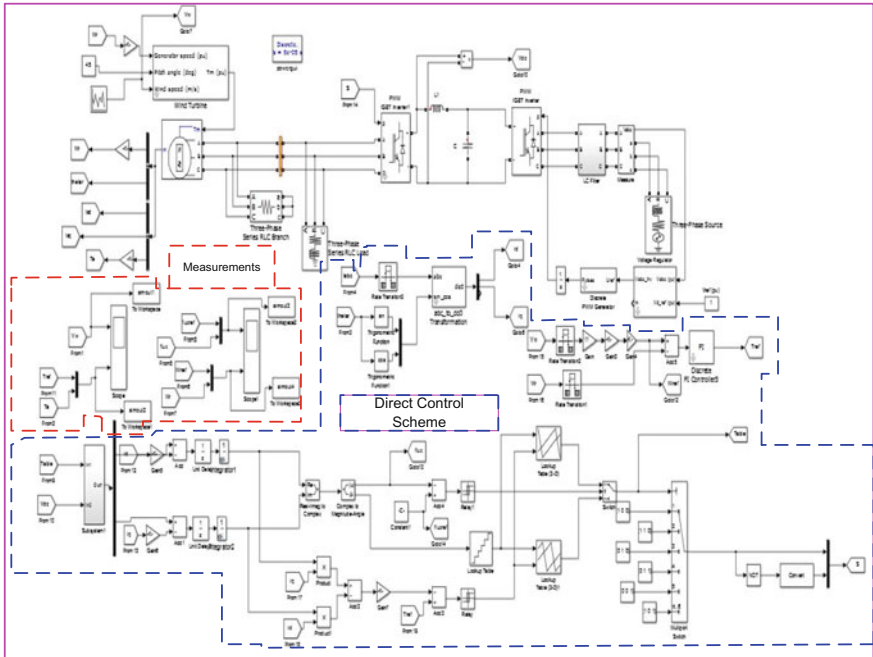


Fig. 6 Simulation diagram of DCS for PMSG

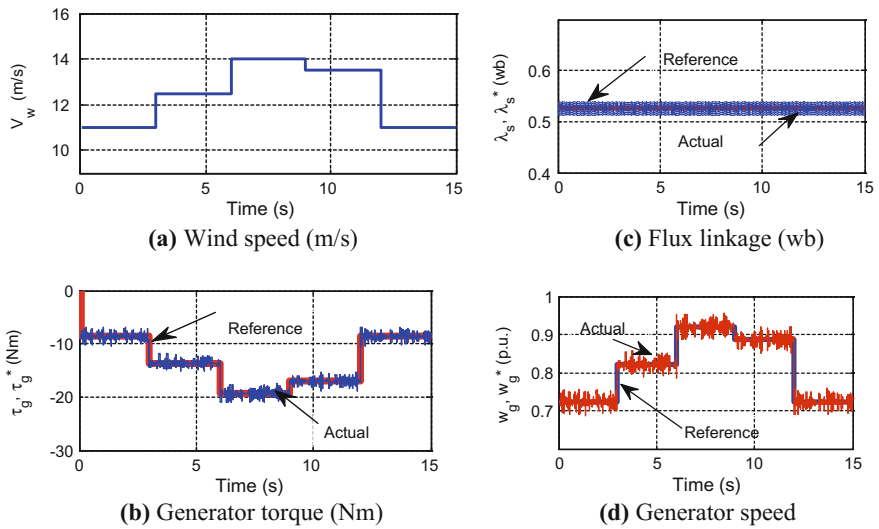


Fig. 7 a–d Performance of the DCS for PMSG

7 Conclusion

In this paper, two methods of control techniques such as direct control scheme (DCS) and vector control scheme (VCS) for PMSG-based dynamic speed WT system are implemented for performance analysis. A variable wind speed pattern is considered for WT-assisted PMSG system for transient analysis. In direct control technique, rotor location is validated as all the parameters obtained in the stator reference frame. In this both control schemes techniques, the DCS can work under fixed and variable wind speed conditions also. Both of these control schemes are implemented in MATLAB/Simulink, and the obtained results are closed agreed to reduce the torque and with ripples in speed. The simulation results for the DCS show that the estimator has calculated effectively the generator rotor speed with minimum error.

Appendix

See Table 1.

Table 1 Operating parameters of WECS

<i>PMSG parameters</i>		Gear ratio (G)	40
Rated power	4.7 kW	Air density	1.2 kg/m ³
Rated torque	34.8 Nm	Number of blades	3
Rated speed	1280/1600 rpm	Blade radius (R)	4.5
Magnetic flux linkage	0.525723 Wb	Air density (ρ)	1.2 kg/m ³
d -axis inductance (L_d) per phase	18.237 mH	Wind speed (V_w)	10–18 m/s
q -axis inductance (L_q) per phase	49.239 mH	Power coefficient (C_p)	0–0.59
Stator resistance	1.56 Ω	Tip speed ratio (λ)	7–9
No. of poles	6	Blade pitch angle (β)	0°–18°
Rotor inertia	0.0049 kg m ²	$\varepsilon_1, \varepsilon_2$	0.5176, 116
<i>WT parameters</i>		$\varepsilon_3, \varepsilon_4$	0.4, 5
Number of blades	3	ε_5	21
Blade radius	4.5	ε_6	0.0068

References

1. Pachauri, R. K., Chauhan, Y. K.: Assessment of Wind Energy Technology Potential in Indian Context. *International Journal of Renewable Energy and Research*, 2(2012) 773–780.
2. Muller, S., Deicke, M., Doncker, R. W. D. D.: Doubly Fed Induction Generator System for Wind Turbines. *IEEE Transaction on Industrial Applications*, 8(2002) 26–33.
3. Mohseni, M., Islam, M. S. M., Masoum, M. A.: Enhanced Hysteresis Based Current Regulators in Vector Control of DFIG Wind Turbine. *IEEE Transaction on Power Electronics*, 26(2011) 223–234.
4. Haque, M. E., Saw, Y. C., Chowdhury, M. M.: Advanced Control Scheme for an IPM Synchronous Generator Based Gearless Variable Speed Wind Turbine. *IEEE Transaction on Sustainable Energy*, 5(2014) 354–362.
5. Goodfellow, D., Smith, G. A.: Control Strategy for Variable Speed Wind Energy Recovery. *Proc. 8th BWEA Conference Cambridge, 1986*, 219–228.
6. Polinder, H., Van der Pijl, F. F. A., Vilder, G. J. D., Tavner, P. J., Comparison of Direct driven and Geared Generator Concepts for Wind Turbines. *IEEE Transaction on Energy Conversion*, 3(2006) 725–733.
7. Kumar, H., Gupta, A., Pachauri, R. K., Chauhan, Y. K.: PI/FL Based Blade Pitch Angle Control for Wind Turbine Used in Wind Energy Conversion System. in *Proc. IEEE Conference on Recent Developments in Control, Automation and Power Engineering*, (2015) 1–6.
8. Rao, Y. M., Rao, B. S.: Performance Evaluation of PWM Converter Control Strategy for PMSG Based Variable Speed Wind Turbine. *Journal of Engineering Research and Applications*, 3(2013) 1000–1006.
9. Pachauri, R. K., Chauhan, Y. K.: Mechanical Control Methods in Wind Turbine Operations for Power Generation. *Journal of Automation and Control Engineering*, 2(2013) 214–220.
10. Deghan, S. M., Mohamadin, M., Varjani, A. Y.: A New Variable Speed Wind Energy Conversion System Using Permanent Magnet Synchronous Generator and Z-Source Inverter. *IEEE Transactions on Energy Conversion*, 24(2009) 714–724.
11. Uehara, A., Pratap, A., Goya, T., Senjyu, T., Yona, A., Urasaki, N., Fnbashi, T.: A Coordinate Control Method to Smooth Wind Power Fluctuation of a PMSG Based WECS. *IEEE Transaction on Energy Conversion*, 26(2011) 550–558.
12. Pachauri, R. K., Kumar, H., Gupta, A., Chauhan, Y. K.: Pitch Angle Controlling of Wind Turbine System Using Proportional-Integral/Fuzzy Logic Controller. In: *International Conference on Advanced Computing, Networking and Informatics*, 43 (2015) 55–63.
13. Qiao, W., Qu, L., Harley, R. G.: Control of IPM Synchronous Generator for Maximum Wind Power Generation Consideration Magnetic Saturation. *IEEE Transaction on Industrial Application*, 45(2009) 1095–1105.
14. Pathak, D., Gupta, A., Pachari, R. K., Chauhan, Y. K.: Autonomous Operation of Wind-Battery Hybrid Power System with Intelligent Power Management Capability, *International Conference on Intelligent Communication, Control and Devices, Advances in Intelligent. Systems and Computing* 479(2016) 317–324.

Auto-Sensing Moisture Control for a Photo-Voltaic Based Irrigation System

Ginni Gupta, Kaushiki and Deepak Kumar

Abstract The principal objective of the proposed paper is to introduce an irrigation pump for rural areas, with the use of solar power, which can be automatically switched ON/OFF by sensing the soil moisture condition, and the same is to display on the LCD whether pump is in ON/OFF condition. Sensor-monitoring is made possible with the help of μ -controllers, enabled the dry soil observation, where the μ -controller would send the adequate command to the relay driver (IC) that could further be used to switch the motor, to the designed state, as per the soil condition.

Keywords PV array · Auto-irrigation · Moisture sensor · μ -controller 8051

1 Introduction

Adoption of an adequate method of irrigation plays an extremely vital role in agriculture. Exponentially augmenting population has continuously extracted the groundwater, reducing its level (normal) and leading to the gradual increase in proportion of non-irrigated land.

Water wastage is a ubiquitous problem to be encountered, and for the very same purpose, the author(s) proposes the system that effectively uses the water integrated with renewable source of energy [1]. The proposed system extracts electrical power from sunlight through photovoltaic array, and hence, the system under consideration is independent of the electricity. The mentioned circuit comprises of soil

G. Gupta · Kaushiki · D. Kumar (✉)
University of Petroleum and Energy Studies, Dehradun, India
e-mail: Deepak.kumar@ddn.upes.ac.in

moisture sensor which infers whether the soil is in wet or dry condition. Under the circumstance when the moisture level of the soil is measured to be lesser than the preset level, the sensor flags the soil as dry or moist and procures command for relay unit [2] which is associated with the switching element, shouldering the liability to put the motor either in “ON” or “OFF” condition. As far as the relay is concerned, it would act upon the input provided by the sensor, i.e. motor is turned “OFF,” if the soil is moist and vice versa. The content of moisture in the soil is percept by the mentioned sensing element inserted into the soil that facilitates the desired command to the μ -controller [3], depending on whether the land is required to be moist. The μ -controller stores the instructions obtained via comparator and assists to control the relay operation for the situational soil observation.

Photovoltaic array is represented as a DC current source, where a group of cells are combined to form a string and several strings (as per the required current and voltage level) are assembled together to form an array [4]. To obtain higher value of voltage at the array terminals, one uses more number of cells in series, whereas the higher magnitude of current can be achieved via implementing more number of strings in parallel.

The proposed system uses the electrical energy procured by PV panels to operate the irrigation pump. System (under consideration) is bound to perish gradually owing to the inadequate water supply, and hence, auto-sensing moisture control is proposed to get rid of the foresaid situation.

1.1 Characteristics of PVA

The fundamental equations of the photovoltaic array are mentioned in Eqs. (1–3) as taken from [5]:

$$I_{pv} = N_p I_{ph} - N_p I_{rs} \left[\exp \left\{ \frac{q(V_{pv} + I_{pv} R_s N_s / N_p)}{k T_{ac} N_s A} \right\} - 1 \right] \tag{1}$$

$$I_{ph} = G [I_{scr} + K_i (T_{ac} - T_r)] 0.001 \tag{2}$$

$$I_{rs} = I_0 \exp \left[\frac{q E_g}{k A} \left(\frac{1}{T_r} - \frac{1}{T_{ac}} \right) \right] \left[\frac{T_{ac}}{T_r} \right]^3 \tag{3}$$

Here are the values of constants and variables used in various equations (Table 1).

Table 1 Values of the KC200GT datasheet for the PVA (100 kW) at 298 K and 1 kW/m²

Parameters	Magnitude
V_{mp}	499.7 V
I_{mp}	206.55 A
V_{oc}	625.1 V
I_{sc}	221.67 A
K_v	-0.123 V/°C
K_i	0.0032 A/°C
P_{max}	100 kW

1.2 Microcontroller (8051)

The author studied about the microcontroller and its architecture and pin diagram [6] and applied the basics for programming for using soil moisture sensor.

Block Diagram

See Fig. 1.

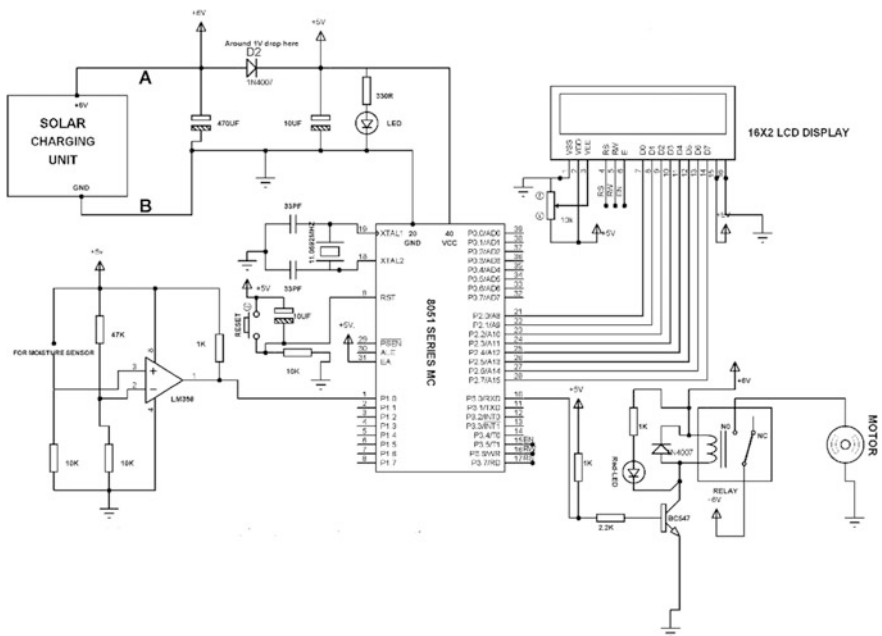


Fig. 1 Architecture of μ -controller-based PV-operated irrigation pump

```

#include<reg52.h>

sbit sense=P1^0;

sbit motor=P3^0;

sbit RS=P3^7;
sbit RW=P3^6;
sbit EN=P3^5;

#define lcd_port P2

void lcd_init();
void lcd_cmd(unsigned char);
void lcd_data(unsigned char);
void lcd_string(unsigned char *);
void delay(unsigned int);

void main()
{

sense=1; //make sense pin high
motor=0; //make motor pin clear
lcd_init(); // INITIALISE THE LCD

while(1)
{
if(sense==1) // if input is high
{
lcd_cmd(0x80); // lcd 1st line starting position
lcd_string(" WET CONDITION"); // display string on lcd
lcd_cmd(0xc0); // lcd 2nd line starting position
lcd_string(" MOTOR OFF"); // display string on lcd
motor=1; // relay OFF
}
else if(sense==0) //if input is low
{
lcd_cmd(0x80); // lcd 1st line starting position
lcd_string(" DRY CONDITION "); // display string on lcd
lcd_cmd(0xc0); // lcd 2nd line starting position
}
}
}

```



```

lcd_string(" MOTOR ON ");           // display string on lcd
motor=0;                             // relay ON
}
}
}

void lcd_init()
{
lcd_cmd(0x38);           // SET THE LCD IN 2 LINE 5X7 MATRIX MODE
lcd_cmd(0x0c);          // DISPLAY ON & CURSER OFF
lcd_cmd(0x01);          // CLEAR THE LCD
lcd_cmd(0x80);          // CURSER IS AT LCD 1ST LINE STARTING POSITION
}

void lcd_cmd(unsigned char cmd)
{
lcd_port=cmd;
RS=1;                   // RS = 1 FOR DATA
RW=0;                   // RW = 0 FOR WRITING
EN=0;                   // ENABLE IS LOW
EN=1;                   // ENABLE IS HIGH
}

void lcd_data(unsigned char data1)
{
lcd_port=data1;
RS=1;                   // RS = 1 FOR DATA
RW=1;                   // RW = 1 FOR READING
EN=0;                   // ENABLE IS LOW
EN=1;                   // ENABLE IS HIGH
}

void lcd_string(unsigned char *t) // for display string on LCD
{
while(*t)
{
lcd_data(*t);

t++;
}
}
}

```

1.3 Results

See Figs. 2, 3 and 4.

2 Calculation

Assuming rice crops, water required = 1.5 l/s/ha. Now, power of the pump to be used = $LPS * 10^{-3} * g * \text{density}/\text{efficiency}$.

where

$$g = 9.8 \text{ m/s}^2$$

$$\text{Water Density} = 1000 \text{ kg/m}^3$$

Let efficiency of pump to be 60% after considering all possible losses.
So,

$$P = 1.5 * 10^{-3} * 9.8/0.6$$
$$= 24.5 \text{ W} = 25 \text{ W (approx)}$$

Let it be a 12 V DC pump.
As

$$P = 25 \text{ W}$$
$$I = P/V = 25/12 = 2.08 \text{ A}$$

Suppose we require power for 10 h per day, so

$$= 25 * 10/12 = 20.8 \text{ AH}$$

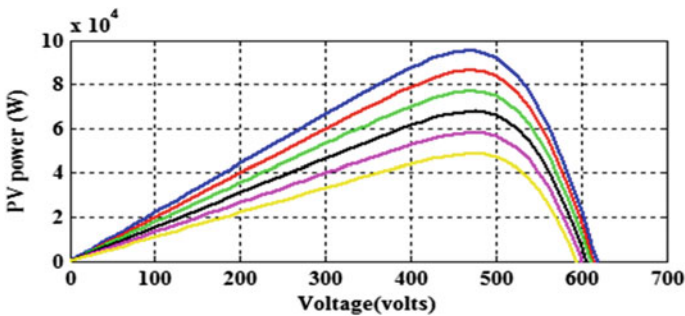


Fig. 2 P-V characteristics of the 100 kW photovoltaic array

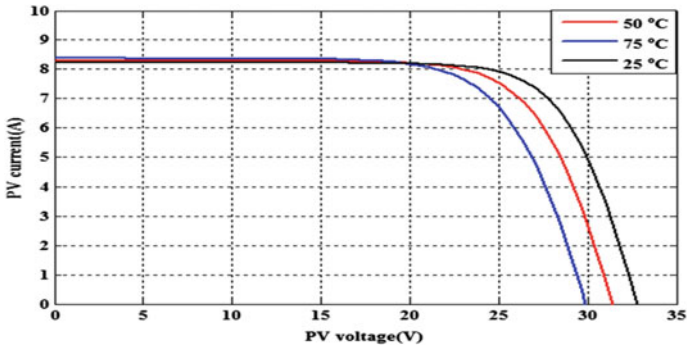


Fig. 3 I-V characteristics of a 100 kW PV array for different temperature profile

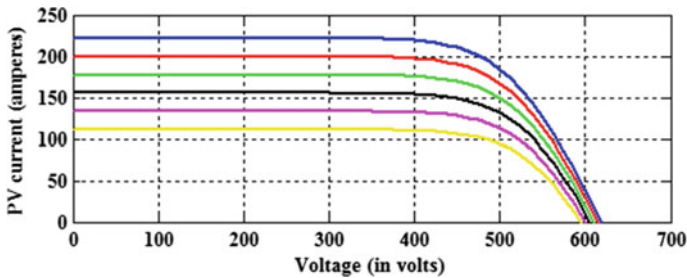


Fig. 4 I-V characteristics of a 100 kW PV array for varying Irradiation

For some extra backup of battery, <say> 24 AH battery:

$$\text{Charging current of battery} = 1/10\text{th of its Ampere Hours} = 24/10 = 2.4 \text{ A}$$

$$\text{Power required to be produced by solar panel} = 12 \text{ V} * 2.4 \text{ A} = 28.8 \text{ W}$$

So, solar panel required for working of pump should produce power of 30 W.

3 Conclusion

This irrigation system is beneficial to the farmers when this system is implemented. When the soil needs water, it is indicated by the sensor by this automatic irrigation system. Automatic irrigation system [7] is used to optimize the usage of water by reducing wastage and reduces the human efforts. The electrical energy needed to the water pump, and controlling system is given by solar panel. Using solar energy alleviates the energy crisis problem. The system requires minimal maintenance and attention because they are self-regulating.

References

1. H. J. Moller, *Semiconductors for Solar Cells*. Norwood, MA: Artech House, 1993.
2. M. Lincy Luciana, B. Ramya, and A. Srimathi, "Automatic Drip Irrigation Unit Using PIC Controller", *Proceedings of the International Journal of Latest Trends in Engineering and Technology*, Vol. 2, Issue 3, May 2013.
3. A. S. Sedra and K. C. Smith, *Microelectronic Circuits*. London, U.K.: Oxford Univ. Press.
4. A. L. Fahrenbruch and R. H. Bube, *Fundamentals of Solar Cells*. San Francisco, CA: Academic, 1983.
5. Kumar Deepak, "Modeling, simulation and performance analysis of a grid-tied voltage source inverter based photovoltaic system under balanced and non-linear load conditions", 2015 IEEE International Conference on Electrical Computer and Communication Technologies (ICECCT), 2015.
6. <http://www.edgefxkits.com/automatic-irrigation-system-on-sensing-soil-moisture-content>.
7. V. R. Balaji, M. Sudha, Solar Powered Auto Irrigation System, *IJETCSE*, Volume 20 Issue 2.

Hardware Implementation of Solar Assisted Automatic Curtain Control System

Prateek Singh, Yogesh K. Chauhan, Rajesh Singh and Rupendra Pachauri

Abstract An innovative effort on hardware design of an automatic curtain control system powered by solar PV array. To achieve the objective, a constant voltage controller (CVC) type maximum power point tracking (MPPT) method for PV system is implemented with a DC to DC boost converter circuit to find maximum power. Also, a motor controller unit is implemented to control the motor run time used in this system. The proposed system circuits which include CVC-MPPT circuit boost converter and motor control unit have been designed using Proteus environment. The closing and opening of curtain has been tested under different light intensity level. The performance analysis of entire system is observed acceptable.

Keywords Curtain control · CVC MPPT · DC–DC boost converter
Solar PV array

P. Singh (✉) · Y.K. Chauhan
Electrical Engineering Department, School of Engineering, Gautam Buddha University,
Greater Noida 201312, Uttar Pradesh, India
e-mail: prateek010@gmail.com

Y.K. Chauhan
e-mail: chauhanyk@yahoo.com

R. Singh · R. Pachauri
Electronics Instrumentation and Control Engineering Department, College of Engineering
Studies, University of Petroleum and Energy Studies, Dehradun 248007, Uttarakhand, India
e-mail: rsingh@ddn.upes.ac.in

R. Pachauri
e-mail: rupendrapachauri@gmail.com

1 Introduction

The grid power is one of the most demanding sources of energy for various applications. Still, a large amount of electrical energy is produced from the conventional sources of energy i.e. fossil fuels which include coal, oil and gas etc. Conventional energy sources are decaying very fast due to their excessive use in commercial and domestic applications [1].

The major renewable based energy source is the PV system. The sun irradiation can be converted into 30–40% electricity using a solar PV system only [2]. The electrical output of the PV system depends on the solar insolation and module temperature. This solar energy is treated as clean energy source and also easily available. Due to government initiatives and more focused on research in different aspects of PV field such as cost, size and efficiency etc.

The MPPT methods are utilized to achieve the maximum power from PV system. Various types of MPPT techniques i.e. Perturb and observe (P&O), Incremental and conductance (IC), constant voltage controller (CVC) techniques are commonly discussed in literature [3]. In paper [4], the author has proposed and hardware design of the feedback loop DC to DC boost converter for PV assisted HBLLED based system. System comprises of a PV system, a boost converter and a LED lighting load. To obtain the maximum power from PV system, a CVC based MPPT technique is designed as well as the boost converter using the PWM and a differential amplifier ($\mu A741$). The authors of [5] have proposed a P&O based MPPT system designed using DC–DC, Buck-Boost converter and controlled by PIC16F73 microcontroller. In [6], presents a CVC based MPPT method which tracks the reference location voltage according to varying climatic conditions automatically. A simple and economic based Analog feed forward PWM controller is designed to track regularly to search MPP of a PV system in accordance with varying climatic conditions. In [7], focuses on the bench work study, done on Brushless DC motor, which is integrated with a PV power assistance for water pumping application. An economic prototype controller is designed without the incorporation of current and position sensing unit, which reduces the cost of system dramatically. The dynamic behavior of the BLDC motor is investigated. The authors in [8], focused on development and construction of a DC to DC converter, which ensured the output voltage will rise from 12 to 24 V.

Above literature review motivates for this paper, in which the IRF840 sensor is used instead of IRF540, due to high ratings, does not heat up and switching characteristics are fast. Furthermore, the hardware implementation of CVC based MPPT is fabricated to achieve MPP through solar PV panel.

2 System Description

The experimental setup consists four parts as, (a) PV system (b) CVC type MPPT assisted DC to DC boost converter (c) motor controller unit (d) DC motor coupled load i.e. window curtain is attached with DC motor. The schematic diagram of the model is shown in Fig. 1.

2.1 Solar PV Technology

The Si solar cells are conventional and are normally wired in series. They are encapsulated in a solar module, protecting the cells from adverse weather conditions. It also has a tempered glass acting as a cover, a rear back sheet which is made from fire-resistant material and on the outer edge an aluminum frame [9–11].

The output of Photovoltaic cell is very much shading sensitive and these shading effects are very well known. The electrical output falls gradually when portion of a cell, module, or an array is shaded while the larger portion is sunlit. This is due to the phenomenon of internal ‘short-circuiting’. If the drawn current from the series string is not greater than that produced by the shaded cell, the current (and also power) are produced in limited amount [12, 13].

2.2 CVC Based MPPT Assisted DC–DC Boost Converter

This converter changes the uncontrolled input DC to controlled output DC voltage at a reference voltage level, by adjusting the duty ratio, the output voltage is regulated in this circuit. These types of circuits are also called switched-mode

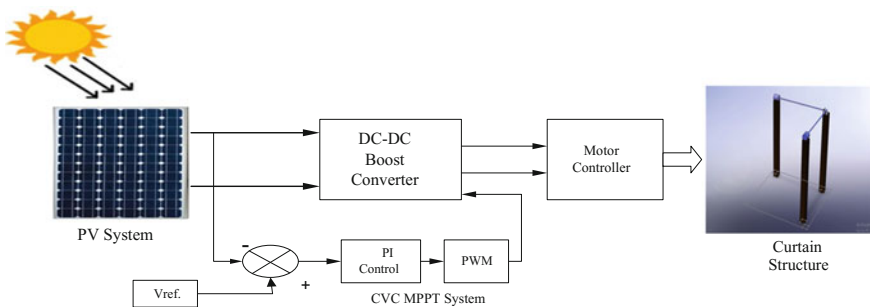


Fig. 1 Schematic diagram of solar assisted automatic curtain control system

circuits. The duty-cycle or the PWM signal can be calculated and expressed in Eq. (1) as,

$$\%D = 1 - \frac{V_i}{V_o} \times 100 \quad (1)$$

The various components used in this model are summarized as,

(i) **Differential amplifier** ($\mu A741$)

It is used to design the differential amplifier with gain 100. In this circuit, 9% of the desired output is given as the reference signal to compare it with the 9% of the boost converter output.

(ii) **PWM generator** ($LM555$)

This integrated circuit is used to design the PWM generator. In this circuit, the output signal of the differential amplifier is fed to LM555 timer circuit. To get the desired duty cycle of 50%, this is shown in Eq. (2) as,

$$D = \frac{R_1}{(R_1 + R_2)} \quad (2)$$

The timing capacitor is charged up through R_1 and discharged through R_2 .

(iii) **Voltage regulators (7812 and 7912)**

This voltage regulator is used to give a constant +12 V output to trigger the pin no. 7 of the differential amplifier, and second voltage regulator 7912 is used to give a constant -12 V output to trigger the pin number 4 of the differential amplifier.

(iv) **Variable resistor**

This variable resistor is used to drop the voltage level to +2.1 V to feed the input pin no. 3 of the differential amplifier.

(v) **Switching MOSFET (IRF840)**

A switching MOSFET is used for switching purpose of the circuit.

(vi) **Coils/inductor and capacitor**

The value of inductor used in this circuit is calculated and expressed in Eq. (3) as,

$$L = \frac{D(1 - D)^2 \times R}{2 \times F_s} \quad (3)$$

The output capacitance used in the circuit is calculated and expressed in Eq. (4) as,

$$C = \frac{D}{F_s \times R \times V_r} \quad (4)$$

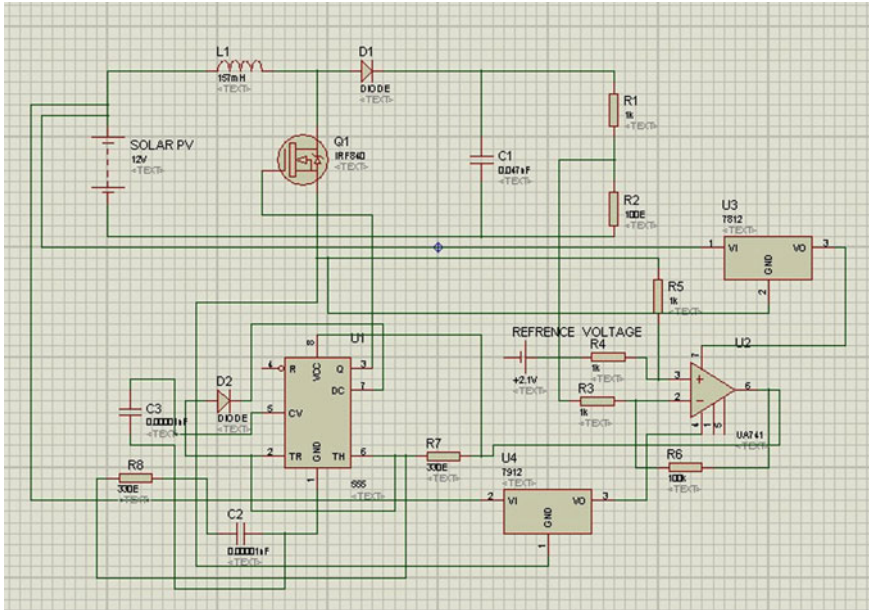


Fig. 2 CVC based type MPPT

where, V_r = output voltage ripple factor, R = output resistance, F_s = switching frequency. The circuit designed for the CVC based MPPT assisted DC–DC boost converter is shown in Fig. 2.

2.3 Motor Controller Circuit

In the circuit of motor controller, two integrated circuits i.e. Atmega 8 and L293D have been used where, Atmega 8 is the programming IC and L293 is the motor driving IC. The circuit designed for the motor controller circuit is shown in Fig. 3.

(i) **ATmega microcontroller**

An ATmega is an 8-bit microcontroller, high performance, low power consumption based architecture. It executes complex instructions in a single clock cycle. Its processing speed is high. It also has in-system programmable flash memory.

(ii) **Motor driver circuit**

L293D is a quadruple high current half bridge-H driver IC. It provides bidirectional drive currents of maximum value of 600 mA at voltages of 4.5–36 V. In it, the external high speed output clamp diodes are present internally. The drivers are permitted in pair with 1 and 2 drivers on the left side and the drivers 3 and 4 on the right side of the IC.

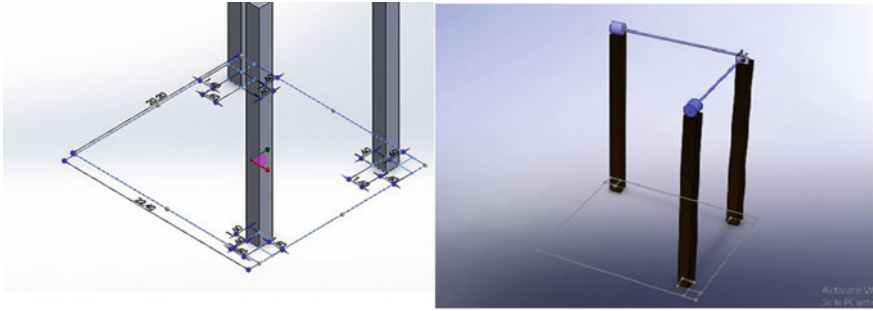


Fig. 4 Dimensions and design of curtain structure

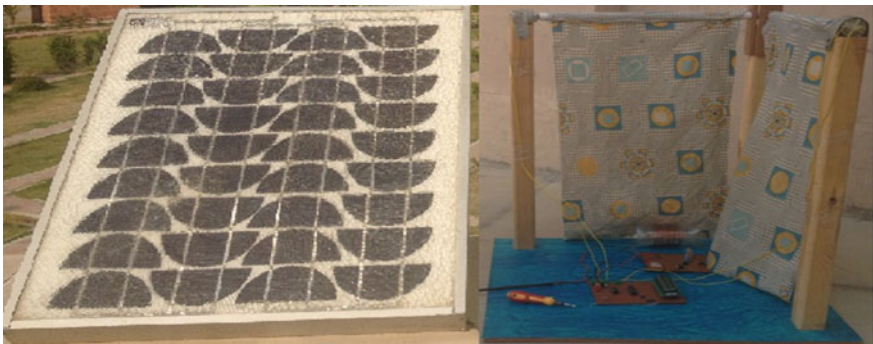


Fig. 5 Solar PV panel and window curtain structure

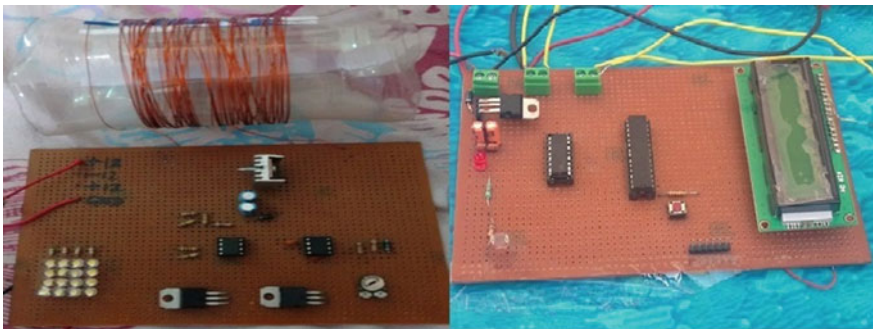


Fig. 6 Hardware implementation of proposed system

maximum of 0.5 V and thus, the solar array can produce maximum of 18 V. The output voltage of the array ranges from 12 to 18 V.

The circuits implemented in the hardware design of the CVC type MPPT DC to DC boost converter and the motor controller are shown in Fig. 6. The inductor used is an air-filled inductor with copper coils wound over a plastic base.

4 Results and Discussion

The solar PV (model PM 62 series) panel I-V and P-V curves are shown in Fig. 7a, b as,

The performance analysis or testing of the designed system has been done and the obtained results are summarized in Table 1.

The experimental setup of proposed system is shown in Fig. 8 and the output voltage of the solar PV system with and without MPPT technique is shown in Fig. 9.

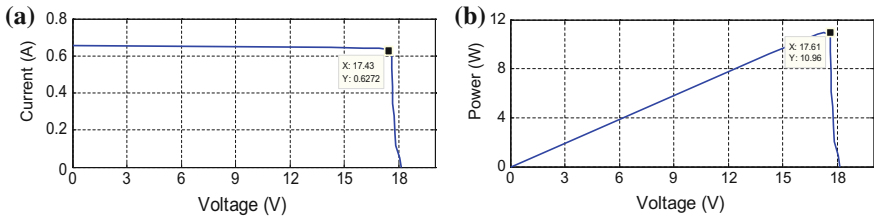


Fig. 7 a, b Panel I-V and P-V characteristics

Table 1 Input–output voltage of the implemented system

S. No.	V_{in} (V)	V_{out} (V)	V_{in} (V)	V_{out} (V)
1	10	21.20	14	22.79
2	11	21.54	15	22.80
3	12	22.40	16	22.80
4	13	22.63	17	22.81
5	13.92	22.68	18	23.00

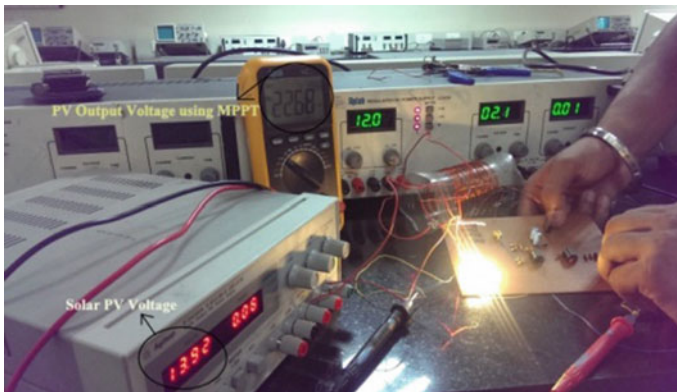


Fig. 8 Experimental setup under testing

Fig. 9 Output response of solar PV system with and without MPPT technique

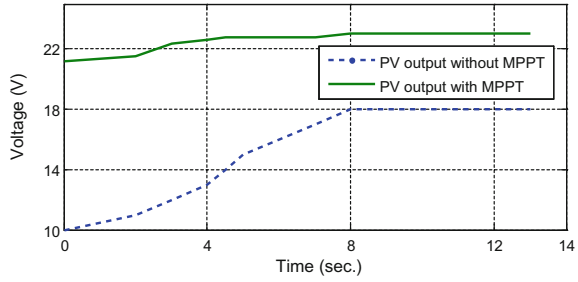


Table 2 Motion of curtain

S. No.	LDR voltage ADC values	Structure height for upward motion (in.)	LDR voltage ADC values	Structure height for downward motion (in.)
1	790	06.15	780	06.15
2	850	12.30	650	12.30
3	950	18.45	550	18.45
4	1020	24.60	450	24.60

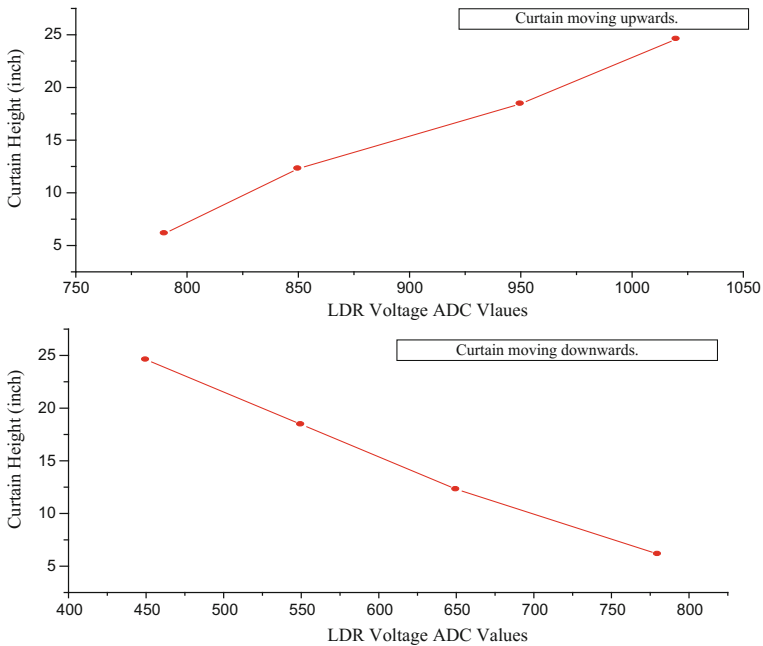


Fig. 10 Dynamic characteristics of curtain controller

The results of performance of the motor controller are given in Table 2.

In Fig. 10, the dynamic characteristics of window curtain moving upward and downward is shown clearly.

5 Conclusion

In this paper, hardware implementation of the CVC type MPPT for PV system using DC to DC boost converter has been carried out for motor driven automatic curtain control unit. The designing of MPPT, DC to DC boost converter and motor control of curtain has been done in Proteus software. The system performance has been tested under different light intensity level and found satisfactory as far as opening and closing of curtain is concerned.

Appendix

1. Solar PV panel

Maximum Voltage (V_{\max}) = 18 V, Maximum Current (I_{\max}) = 0.5 A, Maximum Power (P_{\max}) = 10 W.

2. MPPT assisted DC–DC boost converter parameters

Duty Cycle = 0.5, Inductor (L) = 157 μ H, Capacitor (C) = 47 μ F, Resistor (R) = 1100 Ω , P-I controller = μ A741, PWM Generator = LM555

3. Motor controller unit

Atmega 8 = 4.5–5.5 V, 3.6 mA, L293 D = 4.5–36 V, 1.2 A (peak output current)

References

1. Pachauri, R. K., Chauhan, Y. K., Assessment of Wind Energy Technology Potential in Indian Context. *International Journal of Renewable Energy and Research*, 2(2012) 773–780.
2. Gupta, A. Kumar, P. Pachauri, R. K., Chauhan, Y. K. Effect of Environmental Conditions on Single and Double Diode PV System: A Comparative Study. *International Journal of Renewable Energy and Research*, 4(2014), 849–858.
3. Noman, A. M., Addoweesh, K. E., Mashaly, H. M., Simulation and dSPACE Hardware Implementation of the MPPT Techniques using Buck Boost Converter. in *Proc. IEEE Conference on AFRICON*, (2013), 1–9.
4. Satya, P., Natarajan, R. Design and Implementation of 12 V/24 V Closed Loop Boost Converter for Solar Powered LED Lightning System. *International Journal of Electrical and Technology*, 5(2013), 254–264.
5. Ahmed, K. T., Datta, M., Mohammad, N. A Novel Two Switch Non-Inverting Buck-Boost Converter Based Maximum Power Point Tracking System. *International Journal of Electrical and Computer Engineering* 3(2013), 467–477.
6. Leedy, A.W., Liping, G, Aganah, K. A. A Constant Voltage MPPT Method for a Solar Powered Boost Converter with DC Motor Load. in *Proc. IEEE Conference on Southeastcon at Orlando* (2012), 1– 6.
7. Swamy, C.L.P. Experimental Investigations on a Permanent Magnet Brushless DC Motor Fed by PV Array for Water Pumping System. in *Proc. IEEE Conference on Energy Conversion Engineering* (1996), 1663–1668.

8. Ponniran, A., Said, A.F.M. DC-DC Boost Converter Design for Solar Electric System. in *Proc. International Conference on Instrumentation, Control & Automation at Bandung* (2009), 210–214.
9. Xiaoqing, L., Xiaoyan, L., Lijun, L. Study on the Application of Solar Technology in Oilfield Multi-Purpose Station. in *Proc. IEEE Conference on Energy and Environment Technology* (2009) 369–372.
10. Zanesco, *et al.*. Development of a PV System as a Way to Promote the Technology. in *Proc. IEEE Conference on Photovoltaic Specialists*, (2012), 526–530.
11. Dutter, M., *et al.* Low-cost Thin-Film Deposition Apparatus for Solar Applications. in *Proc. IEEE Conference on Systems and Information Engineering Design Symposium* (2014), 135–140.
12. Harvey, E. C., Gower, M. C. Laser Cutting Thin Films for Solar Panels. in *Proc. IEEE Conference on Compact Power Sources* (1996), 1–5.
13. Lanier, W. R., Fuschillo, N., Eggleston, F.K., Flat Plate Thermoelectric Solar Cells: Manufacturing Process and Life Testing. *IEEE Transactions on Aerospace and Electronic Systems*, (2008), 16–25.

Performance Analysis of Automatic Cleaning System for Solar PV Modules

Rupendra Pachauri, Himanshu Rai Anand, Anurag Koushal,
Anurag Singh, Yogesh K. Chauhan and S. Choudhury

Abstract An experimental setup for automatic cleaning of dust fouling on photovoltaic (PV) system is designed. Comprehensive observations are carried out for numerous types of tracking and cleaning conditions for the extensive comparative study. In this context, the performance of the designed system is compared with stationary, sun tracking, and tracking with cleaning conditions in terms of open-circuit voltage, current, and power. The obtained results are carried out to evaluate the designed system performance for solar PV modules and/or array in tracking and cleaning conditions simultaneously, which are found satisfactorily and superior. So, the present study is very helpful for the enhancement of the PV module efficiency and can be recommended to extract the maximum electrical energy from PV module in domestic as well as commercial applications.

Keywords Photovoltaic system · Solar tracker
Automatic solar cleaning system · Renewable energy

R. Pachauri (✉) · S. Choudhury
Electronics Instrumentation and Control Engineering Department, College of Engineering Studies, University of Petroleum and Energy Studies, Dehradun 248007, Uttar Pradesh, India
e-mail: rpachauri@ddn.upes.ac.in

S. Choudhury
e-mail: schoudhury@ddn.upes.ac.in

H.R. Anand · A. Koushal · A. Singh · Y.K. Chauhan
Electrical Engineering Department, School of Engineering,
Gautam Buddha University, Greater Noida 201312, Uttar Pradesh, India
e-mail: himanshu.anand23@gmail.com

A. Koushal
e-mail: anuragkoushal1993@gmail.com

A. Singh
e-mail: anuragsingh1890@yahoo.com

Y.K. Chauhan
e-mail: chauhanyk@yahoo.com

1 Introduction

With the present energy, the need to suffice the demand of population density and energy resources is shifted to renewable energy (RE) resource such as solar energy, wind energy, fuel cells. Solar energy is clean and abundantly available. But it lacks in efficiency, and only 30–40% conversion of sun irradiation energy into electrical energy is possible.

The authors in [1] show the enhancement of efficiency of PV model using different arrangement configurations. The performance of PV module is compared with or without reflectors in the presence of plane mirror, aluminum foil, etc. The obtained results are shown by the performance improvement of PV module with respect to conventional operating conditions. In [2], authors employed dual-axis solar tracking system using Arduino. The obtained results are compared for the performance evaluation of solar tracking with static solar PV module, which shows the enhancement of efficiency. In [3], the authors improved the efficiency of solar PV system using fuzzy logic controlled DC motor and LDR based solar PV tracking system. In [4], the authors designed a weather-based automatic solar tracking method. In this system, the solar positioning sensors, e.g., LDR, and solar trajectory algorithm is used to determine solar position to extract maximum power. The measured data for different weather conditions such as sunny, cloudy, and rainy days are compared for the performance evaluation. The authors in [5] developed single-axis automated solar tracking system, in which DC-gearred motors are employed to rotate the position of PV panel. The designed system consisted of two electromechanical relays and a microcontroller for its efficient operation. The obtained results of the developed system have shown the improvement in the efficiency of PV module. In [6], an automated sun tracking system using 8051 microcontroller with the assistance of stepper motor is developed. Without the use of synchronization for sun tracking, the PV module is cleaned using sliding brushes, while the solar panels are made to rotate 360° throughout the day. The results obtained from the system show improved efficiency of the developed system. The authors of [7] developed two types of systems: (i) single-axis tracker of angle ranging from 0–180° and (ii) double-axis tracker with horizontal axis and vertical axis limits between 180° and 90°, respectively.

The present literature review motivates to develop a presented system. So, the uniqueness of this system is to improve the performance of the PV module with the integration of cleaning and tracking approaches simultaneously for the performance enhancement of the PV modules and/or array. A hardware implementation is designed to claim and approval this approach.

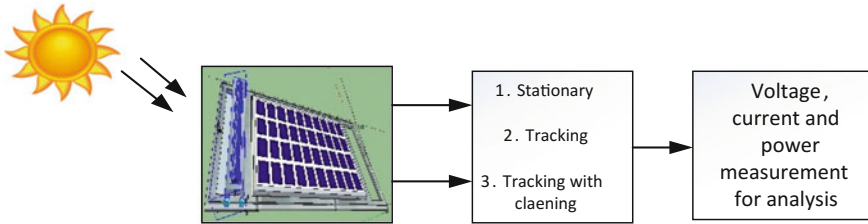


Fig. 1 Schematic diagram of complete system



(a) Outdoor working of the Solar PV system (b) Close view of automatic cleaning PV system

Fig. 2 a, b Hardware implementation of solar tracker assistance for PV module

2 System Description

In this paper, two 12 W PV modules (each of 6 W) are used for the performance analysis under the different scenarios such as (i) PV system in a stationary condition, (ii) PV system with solar irradiation tracking, (iii) PV system with solar irradiation tracking along with cleaning. Moreover, the stationary position of solar PV module is installed at tilt angle of 23.5° , and the PV modules are statically placed to face in the east direction as sun travels from east to west. Furthermore, a comparative study of PV module assistance with tracking and tracking and cleaning system in terms of current, voltage, and power is carried out for the performance evaluation (Fig. 1).

3 Experimental Setup

The bench work analysis of PV modules for different types of conditions such as solar tracking system statically and dynamically and solar tracking with cleaning system is shown in Fig. 2.

4 Results and Discussion

The performance evaluation of PV with the following experimental systems is carried out as,

- Performance evaluation of PV modules under stationary conditions,
- Performance evaluation of PV modules under sun tracking conditions,
- Performance evaluation of PV modules under sun tracking along with automatic dust cleaning conditions,
- Comparison of voltage, current, and power under the considered experimental setup conditions

4.1 Performance Evaluation of PV Modules Under Stationary Conditions

The hardware arrangement of PV system with supportive components is done for the measurement and performance evaluation at still position. The measurement of peak values of current, voltage, and power of solar PV system is considered for one month throughout the day from 08:00 AM to 05:00 PM (March 15–April 14, 2016) and summarized and shown in Table 1. The graphical representation of the measured data is exposed in Fig. 3a–c.

Table 1 Performance of PV modules at stationary position

Day	V (Volt)	I (A)	P (W)	Day	V (Volt)	I (A)	P (W)
1	9.71	0.91	8.8361	16	10.20	1.15	11.730
2	9.78	0.90	8.8020	17	10.18	1.13	11.5034
3	9.83	0.91	8.9453	18	10.10	1.07	10.807
4	9.89	0.92	9.0988	19	10.12	1.09	11.0308
5	9.95	0.96	9.552	20	9.97	0.97	9.6709
6	9.90	0.93	9.207	21	10.23	1.18	12.0714
7	9.92	0.95	9.424	22	10.22	1.17	11.9574
8	9.95	0.98	9.751	23	10.26	1.12	11.4912
9	10.05	1.00	10.05	24	10.27	1.11	11.3997
10	9.98	0.99	9.8802	25	10.22	1.08	11.0376
11	10.03	0.98	9.8294	26	10.26	1.10	11.286
12	10.09	1.10	11.099	27	10.27	1.14	11.7078
13	10.29	1.15	11.8335	28	10.24	1.12	11.4688
14	10.11	1.10	11.121	29	10.28	1.14	11.7192
15	10.08	1.00	10.08	30	10.05	0.96	9.648

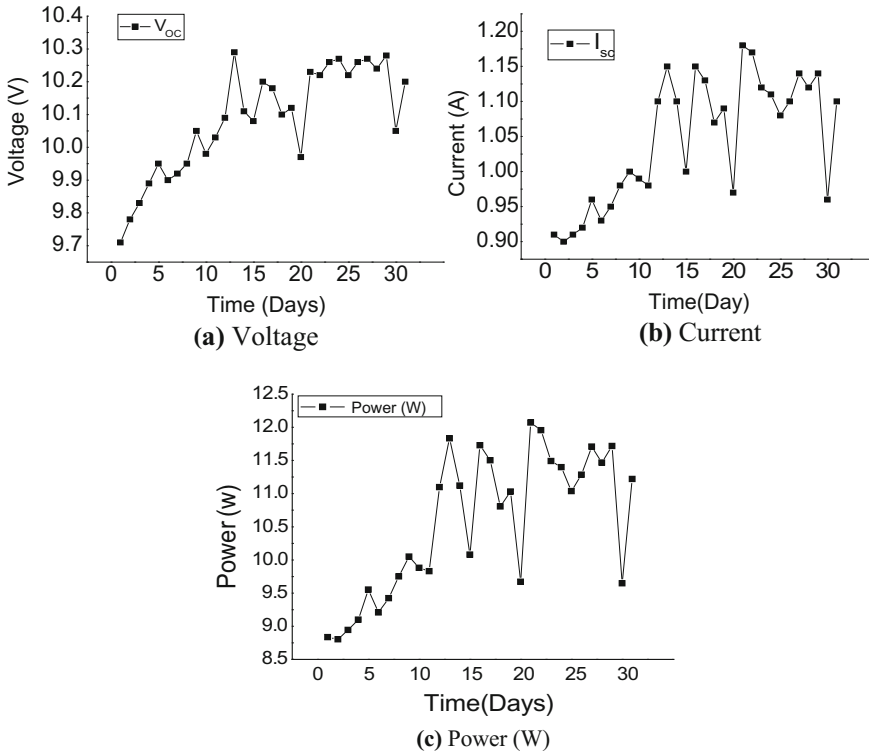


Fig. 3 a–c Performance of PV module in stationary condition

4.2 Performance Evaluation of PV Modules Under Sun Tracking Conditions

The experimental setup of solar PV modules and its supportive components is arranged with a single-axis solar tracker in order to attain the high amount of sun irradiation to improve the performance of system. The measurement of peak values of voltage, current, and power of solar PV module is taken over a period of one month (March 15–April 14, 2016) for 9 h daily with an interval of 30 min between every measurement, which is summarized in Table 2. The behavior of electrical parameters of solar PV modules is shown in Fig. 4a–c.

Table 2 Performance of solar PV module under tracking condition

Day	V (Volt)	I (A)	P (W)	Day	V (Volt)	I (A)	P (W)
1	9.96	1.01	10.0596	16	10.23	1.22	12.4806
2	9.97	1.03	10.2691	17	10.22	1.18	12.0596
3	9.98	1.06	10.5788	18	10.19	1.15	11.7185
4	10.03	1.08	10.8324	19	10.20	1.17	11.9340
5	10.07	1.17	11.7819	20	10.13	1.1	11.1430
6	10.01	1.13	11.3113	21	10.26	1.27	13.0302
7	10.04	1.14	11.4456	22	10.25	1.26	12.9150
8	10.06	1.16	11.6696	23	10.27	1.32	13.5564
9	10.17	1.18	12.0006	24	10.29	1.31	13.4799
10	10.07	1.19	11.9833	25	10.24	1.27	13.0048
11	10.11	1.17	11.8287	26	10.26	1.29	13.2354
12	10.14	1.21	12.2694	27	10.3	1.34	13.8020
13	10.25	1.22	12.5050	28	10.28	1.30	13.3640
14	10.15	1.15	11.6725	29	10.31	1.36	14.0216
15	10.12	1.09	11.0308	30	10.12	1.20	12.1440

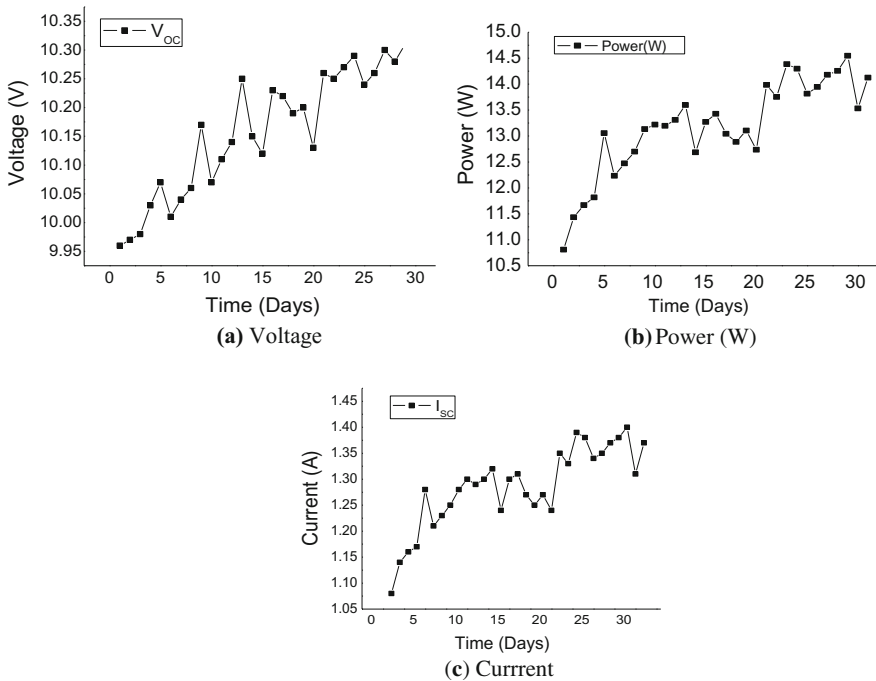


Fig. 4 a–c Performance of PV system with solar irradiation tracking

4.3 Performance Evaluation of PV Modules Under Sun Tracking Along with Automatic Dust Cleaning Conditions

The solar PV system is integrated with a dust cleaning system to attain the high amount of solar insolation for performance improvement. The measurement of peak values of voltage, current, and power of solar PV module is taken over a period of one month (15 March–14 April) for 9 h daily with an interval of 30 min between every measurement, which is given in Table 3. The behavior of electrical parameters of solar PV module is shown in Fig. 5a–c.

Table 3 Solar PV system with solar tracking along with cleaning system

Day	V (Volt)	I (A)	P (W)	Day	V (Volt)	I (A)	P (W)
1	10.01	1.08	10.8108	16	10.25	1.31	13.4275
2	10.03	1.14	11.4342	17	10.27	1.27	13.0429
3	10.06	1.16	11.6696	18	10.31	1.25	12.8875
4	10.10	1.17	11.817	19	10.32	1.27	13.1064
5	10.20	1.28	13.056	20	10.27	1.24	12.7348
6	10.11	1.21	12.2331	21	10.36	1.35	13.986
7	10.14	1.23	12.4722	22	10.34	1.33	13.7522
8	10.16	1.25	12.7	23	10.35	1.39	14.3865
9	10.26	1.28	13.1328	24	10.36	1.38	14.2968
10	10.17	1.30	13.221	25	10.31	1.34	13.8154
11	10.23	1.29	13.1967	26	10.33	1.35	13.9455
12	10.24	1.30	13.312	27	10.35	1.37	14.1795
13	10.3	1.32	13.596	28	10.33	1.38	14.2554
14	10.23	1.24	12.6852	29	10.39	1.40	14.546
15	10.21	1.30	13.273	30	10.33	1.31	13.5323

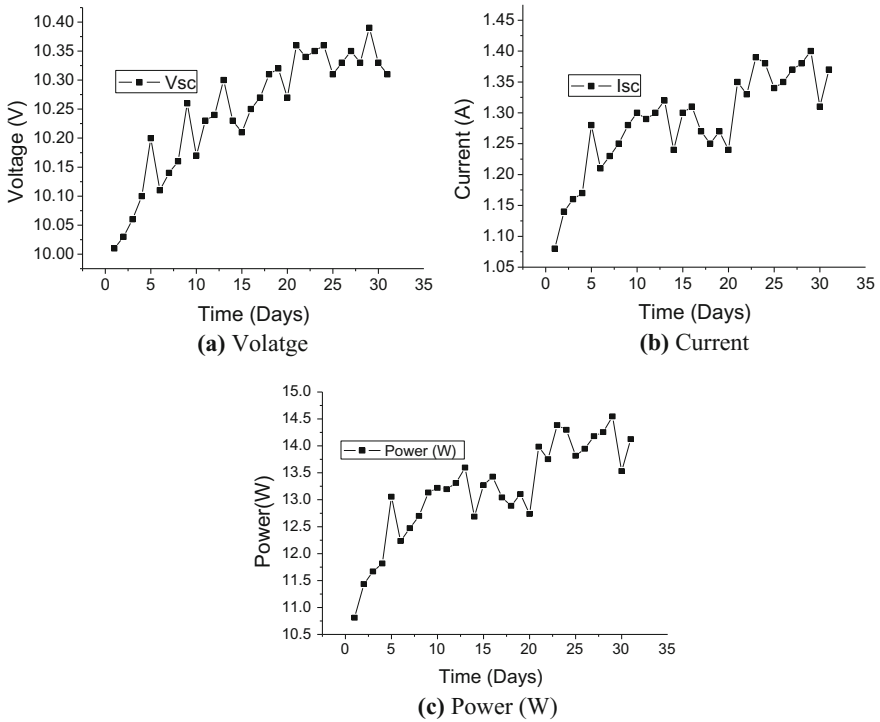


Fig. 5 a–c Performance of system under solar tracking along with cleaning system

4.4 Comparison of Electrical Parameters Under the Considered Experimental Setup Conditions

The measurement of electrical parameters has been carried out over a period of month, and the comparative studies are shown in Fig. 6a–c, which can be considered to study the performance of solar PV modules for various experimental conditions.

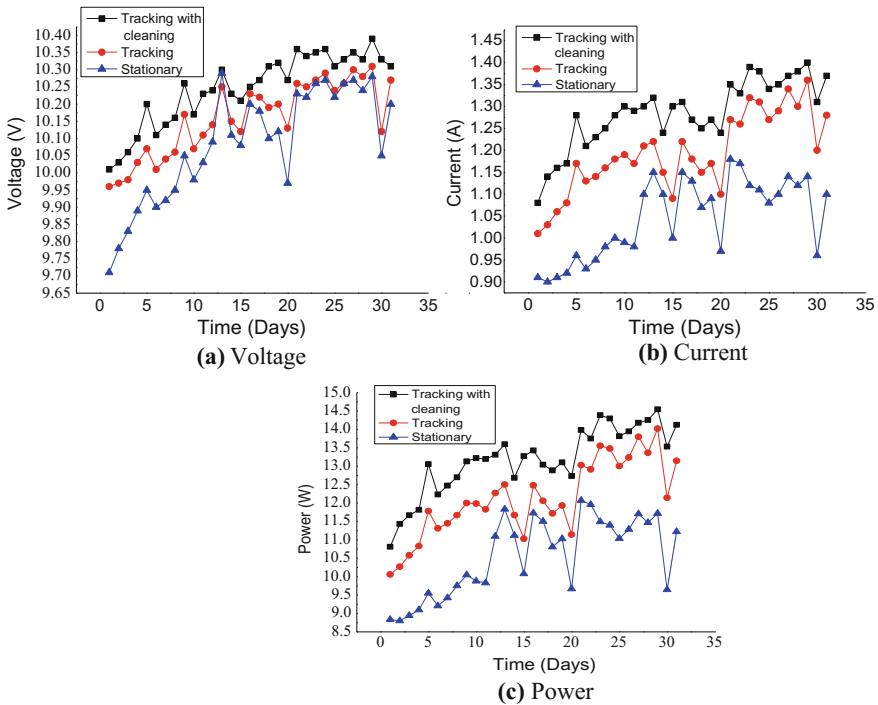


Fig. 6 a–c Performance comparison of solar PV system for different experimental arrangements

5 Conclusion

A holistic comparative study of solar PV arrangements is carried out in different scenarios. The performance parameters of PV modules are monitored continuously in electrical terms such as voltage, current, and power. On behalf of the obtained results, a comparison under different arrangements is made and it is observed that the PV system with cleaning and sun tracking system shows best results as compared to the stationary arrangement and sun tracking conditions of solar PV system. Overall study is useful in domestic-based stand-alone PV system.

References

1. Kumar, A., Pachauri, R. K., Chauhan, Y. K.: Analysis and Performance Improvement of Solar PV System by Solar Irradiation Tracking. in *Proc. IEEE Conference on Energy Economic and Environment*, (2015) 1–6.
2. Othman, N., Manan, M. I. A., Othman, Z., Al Junid, S.A.M.: Performance Analysis of Dual Axis Solar Tracking System. in *Proc. IEEE Conference on Control System, Computing and Engineering*, (2013) 370–375.

3. Abadi, I., Soeprijanta, A., Musyafa, A.: Design of Single Axis Solar Tracking System at Photovoltaic Panel using Fuzzy Logic Controller. in *Proc. IEEE Conference on Engineering and Technology*, (2014) 1–6.
4. Xu, J., Wu, K., Ma, L.: All Weather Automatic Solar Tracking Method Applied in Forest Fire Prevention. in *Proc. IEEE Conference on Electronic Measurement and Instruments*, (2009) 1805–1809.
5. Ponniran, A., Hashim, A., Munir, H. A.: A Design of Single Axis Sun Tracking System. in *Proc. IEEE Conference on Power Engineering and Optimization*, (2011) 107–110.
6. Tejwani, R., Solanki, C.S.: 360° Sun Tracking with Automated Cleaning System for Solar PV Modules. in *Proc. IEEE Conference on Photovoltaic Specialists Conference*, (2010) 2895–2898.
7. Tania, M. H., Alam, M. S.: Sun Tracking Schemes for Photovoltaic Panels. in *Proc. IEEE Conference on Developments in Renewable Energy Technology*, (2014) 1–5.

Double Gate Tunnel Field Effect Transistor with Extended Source Structure and Impact Ionization Enhanced Current

Deepak Kumar and Prateek Jain

Abstract The double gate tunnel field effect transistor with sandwiched SiGe/Si source extension is discussed. Here in addition to band-to-band tunneling for lower gate voltages, impact ionization sets in for higher gate voltages, boosting the ON state current by a factor of X. A sandwiched layer of Si between SiGe in the source is proposed to enable higher Ge mole fraction on the surface. SiGe is primarily used to exploit higher tunneling rate from the SiGe region and to utilize the large built-in electric field at the junction of SiGe with Si. Different encroachment of SiGe under the gates was explored to find that optimum performance is observed in the range of 2–4 nm extension. We also show that, impact ionization is confined to a very small region in the device and thus ON current increases without raising the reliability concern.

Keywords Gate controlled impact ionization
Band-to-Band tunneling (BTBT) • Impact ionization

1 Introduction

The design low-power circuits using MOSFETs is increasingly becoming difficult, since the limit of 60 mV/decade subthreshold does not allow the subthreshold region of operation to scale with area and power supply scaling [1, 2]. Tunnel field effect transistor (TFETs) [3–5] and impact ionization MOSFETs (IMOS) [6, 7] are some of the device ideas that circumvent this subthreshold problem. TFETs have been widely researched recently for low-power VLSI devices [1], because of its exceptional leakage power performance and low OFF current [8–10]. One of the

D. Kumar (✉)

University of Petroleum and Energy Studies (UPES), Dehradun 248007, India
e-mail: deepakkumar18207@gmail.com

P. Jain

Department of Electrical Engineering, Indian Institute of Technology Kanpur,
Kanpur 208016, India

main drawbacks of the TFETs is its low ON state current (I_{ON}) as compared to ITRS requirements [11] and stringent fabrications steps required for extracting performance (citation on doping requirements, etc.). Reported methods to increase I_{ON} in TFETs include structural modifications (hetero junction source [12, 13], tapered source (citation), etc.), doping optimization (retrograde doping, pocket implant source [14, 15], etc.), gate metal work function engineering (double gate, dual metal gate [16, 17]) improving electrostatics (gate all around structures [18, 19]), dielectric optimization (with one [20] or multiple [21] dielectrics). On the other hand, IMOS suffers from high operating voltage requirement, high I_{OFF} , threshold voltage shift due to hot carrier injection and associated concerns about reliability.

In this paper, we have performed 2-D device simulation to explore the effect of overlapping the lower band gap highly doped SiGe source with the gate. While current flows mostly due to BTBT, impact ionization sets in for higher gate voltages, thereby increases I_{ON} . The increment in I_{on} with increasing encroachment comes at the cost of degraded subthreshold slope and increases V_T . ON state current (I_{ON}) increases due to the controlled impact ionization with the SiGe encroachment under the gate.

2 Schematic of Double Gate TFETs

The proposed device structure is shown in Fig. 1. The device is conventional double gate tunnel field effect transistor (DGTFET) with a sandwiched SiGe/Si source structure that will be extended into the gate side of the channel. We consider a device of channel length 25 nm, silicon body thickness 8 nm, n-type doping in drain region of 10^{18} cm^{-3} , p-type doping in source of 10^{20} cm^{-3} , and body is low n-type doped (10^{16} cm^{-3}), hafnium oxide gate dielectric with 2 nm thickness [22] and Ge mole fraction in SiGe is 0.5 [23], work function of metal 4.2 eV. SiGe is primarily used to exploit higher tunneling rate from the SiGe region and to utilize the large built-in electric field at the junction of SiGe with Si, which is caused by the lower band gap of SiGe and the resulting discontinuity in the valence band.

Fig. 1 Schematic view of DGTFET with extended SiGe/Si source structure. X is the encroachment of SiGe (p +) under the gate



3 Device Simulation and Results

The simulation was done using Sentaurus 2D device simulator from Synopsys TCAD [24], where we have included all relevant physical effects. BTBT current was calculated using nonlocal tunneling model, which is the most versatile and dynamic model available in the software [25]. Gate leakage mechanism has been included via the direct tunneling model. For the devices that we have considered here, the gate current is limited to $\sim 10^{-13}$ A/ μm . High field mobility degradation has been accounted for by the Enormal model [26] and impact ionization was included via Van Overstraeten model [27]. To account for the very high doping in source, we have included band gap narrowing effects and used Fermi-Dirac statistics. Default model parameter values for Si and SiGe were used as we are primarily interested in showing the effect of the structural modification on the device operation, and have refrained from calibration to experimental data for SiGe, which at this time, have non-idealities that we did not want to delve into.

The simulated transfer characteristics for the device structure are shown below in Fig. 2. The gate voltage (V_G) axis is divided in two different regions which are indicated in the figure: low V_G (region 1) and higher V_G region (region 2). For low V_G operation, SiGe aligned to gate edge gives best BTBT generation rate. This is expected, since extending the p++ doping underneath the gate results in depletion in the extended part of source for $V_G > 0$ leading to a widening source-channel barrier, and concomitant lower BTBT rate, and increasing SS with increasing source extension. The average subthreshold slope which is computed as [28]:

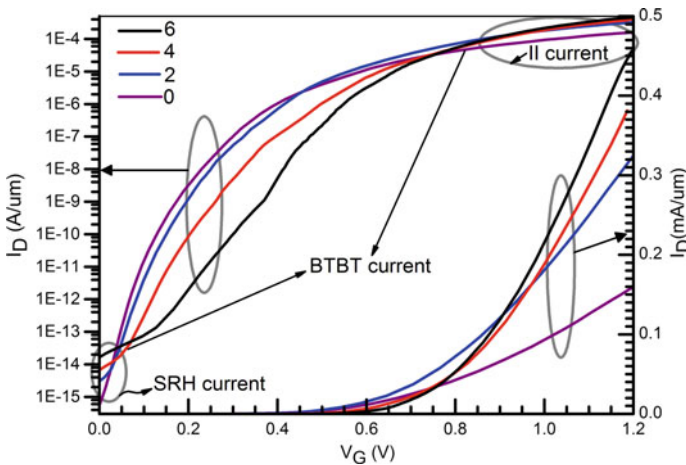


Fig. 2 Transfer characteristics of DGTfET with extended SiGe/Si source and 0.5 Ge mole fraction for different encroachment length (nm) inside the gate. I_{ON} is enhanced with different encroachment length of SiGe inside the gate, but the subthreshold slope is degraded

$$SS_{AVG} = \frac{(V_T - V_{OFF})}{(\log I_{VT} - \log I_{VOFF})}. \tag{1}$$

The threshold voltage termed as V_T , the gate voltage termed as V_{OFF} from which the drain current starts to take off, I_{VT} is the drain current at $V_{GS} = V_T$, and I_{VOFF} is the drain current of the device at $V_{GS} = V_{OFF}$.

For different extension comes out to be 35, 42, 47 and 52 mV/decades for 0, 2, 4 and 6 nm extension respectively. The threshold voltage (V_T) calculated using constant current of 100 nA/ μm also increases with increasing the source extension, with values being 0.295, 0.322, 0.394, and 0.447 V for 0, 2, 4 and 6 nm extension, respectively.

However, the area of the source-channel junction that experiences high electric field increases with increasing source extension, and at $V_G > 0.45$ V, the impact ionization current aids the I_{ON} for the devices with higher source extensions. The ON current (defined as I_{DS} at $V_{GS} = 1.2$ V for $V_{DS} = 1.0$ V) for 0,2,4, and 6 nm extensions comes out to be 159, 324, 391, and 456 A/ μm , respectively, which are a factor of 1.25,1.76, 2.41, and 2.81 higher if we do not include impact ionization.

In the OFF state, the BTBT current in the TFET is comparable or less than the reverse leakage diode current, which is dependent on the generation current inside the depletion region.

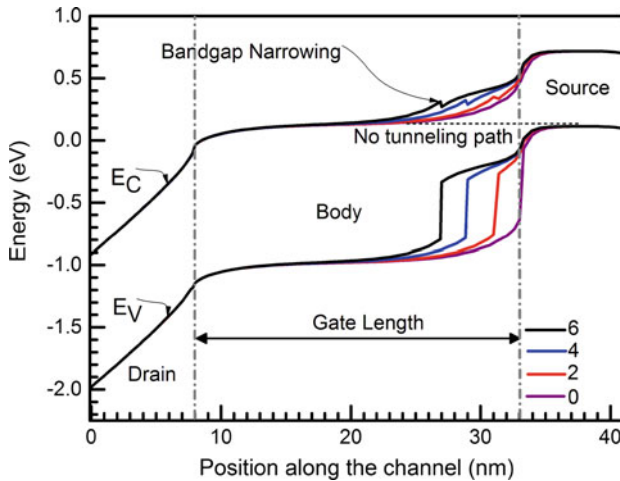


Fig. 3 Energy band diagram 1\AA below the gate in the OFF state ($V_{GS} = 0$ V and $V_{DS} = 1$ V). Dotted vertical line indicates the gate edges. No tunneling path is formed for any of the structures in the OFF state as shown by dotted lines

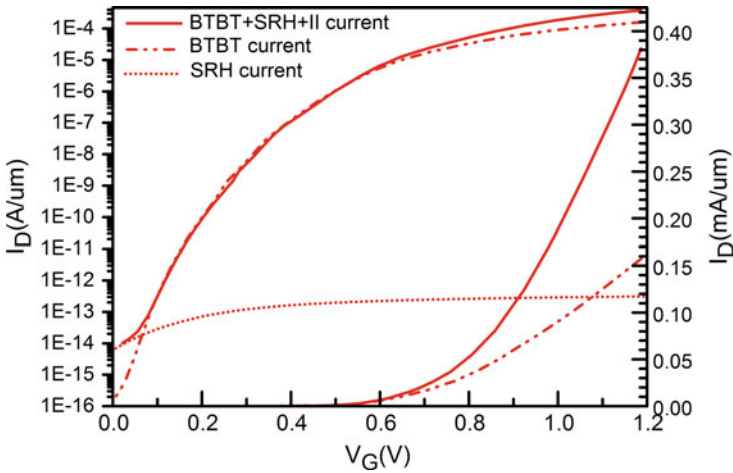


Fig. 4 Transfer characteristics broken into the various current components of DGTJET with extended SiGe/Si source and 0.5 Ge mole fractions for 4 nm encroachment length inside the gate

As can be seen from Fig. 3, in the OFF state, the source valence band and the channel band does not overlap and there is no tunneling path at the junctions. Hence I_{OFF} is limited by the SRH recombination leakage current. This generation rate is higher in SiGe than in Si due to its lower band gap and higher intrinsic carrier concentration. Extending the SiGe under the gate also results in depletion in the overlap region, resulting in higher SRH leakage currents, which gives the saddle points in the I_D-V_G at low V_G . This is apparent from Fig. 4, where we have broken the total current for 4 nm extension inside the gate into the constitutive components arising from SRH generation, BTBT generation, and impact ionization separately.

The ON current is maximum for the 2 nm extension in the higher V_G (region2) region for $V_G \leq 0.86$ V. The reason for this behavior can be explained as follows: Tunneling path is always shorter for the 0 nm extension as shown in Fig. 5a, however, the tunneling, which is from SiGe valence band to Si conduction band, mostly occurs in the Si region. On the other hand, for the 2 nm extension, at larger V_G , the whole tunneling path lies completely inside SiGe, which results in higher BTBT rate (due to lower reduced mass). This is evident from Fig. 5b where the generation rate from BTBT and impact ionization is plotted for $V_{GS} = 0.8$ V near the source-channel junction 1 Å below the top gate consistent with the other cut lines. For $V_G > 0.86$ V, as electric field in the source-channel junction increases, impact ionization sets in, this rate being higher for the devices which have higher extension into the source. We verify this from Fig. 5c, and also note that impact ionization is confined to a small region.

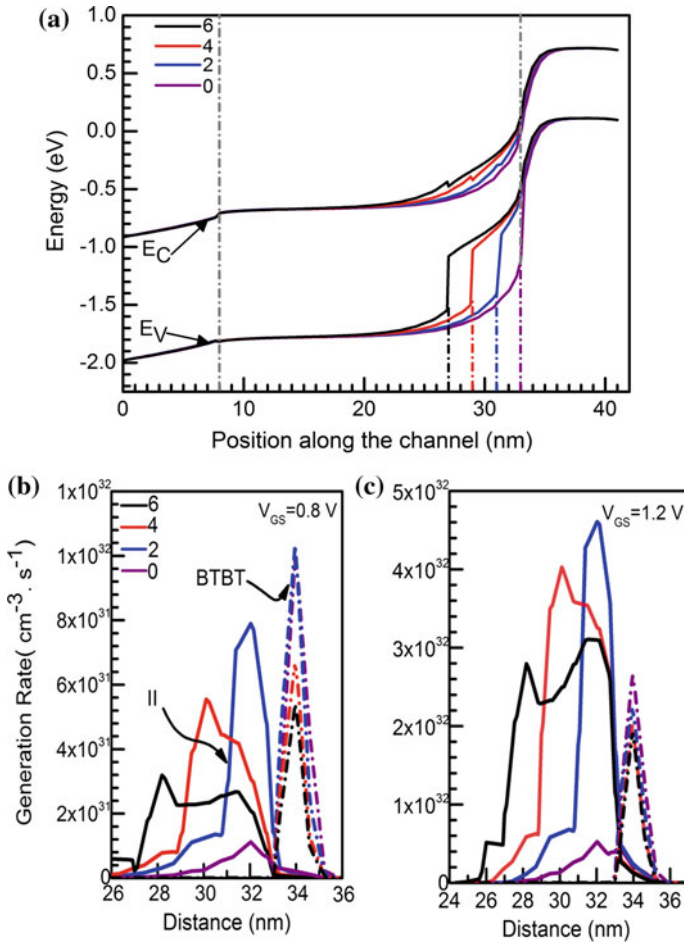


Fig. 5 .

In Fig. 5a Energy band diagram along a horizontal cut near to the surface calculated at ($V_{GS} = 0.8 \text{ V}$ and $V_{DS} = 1 \text{ V}$). The tunnel barrier width increases with the extension length which decreases the BTBT rate as evident from **b** BTBT and impact ionization rate near the source along the same horizontal cutline under the conditions of Fig. 5a ($V_{GS} = 0.8 \text{ V}$ and $V_{DS} = 1 \text{ V}$) 2 nm extension gives the best BTBT rate. Impact ionization current (proportional to area under curve) increases with the overlap length inside the gate. **c** BTBT and Impact ionization rate in the device for $V_{GS} = 1.2 \text{ V}$, other conditions being identical to Fig. 5b 0 nm gives best BTBT rate in this region; however, impact ionization current now dominates over BTBT

4 Conclusion

The use of Ge alone at the source will not give us the flexibility that we can get with SiGe. With SiGe using different mole fraction of Ge and modulating its band gap, we can control energy band diagram and can optimize the performance in various ways like the one we did in this paper. Higher Ge mole fraction can be grown on the surface using this device structure. Using this structure, we can get an intermediate performance between a TFET and IMOS. Different extensions length inside the gate degrades the subthreshold slope, but the increase in ON state current is large. Thus, we can have a compromise performance TFET with different extensions gate length. The concerning thing about the device is its reliability issue about this structure.

References

1. Robert H. Dennard, Fritz H. Gaensslen, et al., Solid State circuits, IEEE Journals., vol. 9, May 1974.
2. Mark Bohr IEEE SSCS Newsletter 12(1), 11–13, 2007.
3. Evan O kane, J. Appl. Phys. 32, 83 1961.
4. Adrian M. Ionescu, and heikiriell, Nature November 2011 doi:[10.1038/nature10679](https://doi.org/10.1038/nature10679).
5. W.M. Reddick, G.A. Amaratunga Applied Physics Letters, vol. 67, no. 4, pp. 494–496, Jul 1995.
6. KailashGopalakrishnan, Peter B. Griffin, and James D. Plummer, et al IEEE Transaction on electron devices, vol. 52, no. 1, Jan 2005.
7. K.E. Moselund, D. Bouvet, et al SSE, doi: sse.2008.04.021.
8. C.Hu, et al, IEDM Tech. Dig., pp. 387–390, 2010.
9. Q. Zhang, W. Zhao, and A. Seabaugh, IEEE Electron Device Lett., vol. 27, no. 4, pp. 297–300, Apr. 2006.
10. W. Y. Choi, B.-G. Park, J. D. Lee, and T.-J. K. Liu, IEEE, vol. 28, pp. 743–745, Aug. 2007.
11. Semiconductor Industry Association (SIA), International Technology Roadmap for Semiconductors, 2012 Edition.
12. Eng-HuatToh et al., App. Phys. Lett, 91, 243505 (2007).
13. Yue Yang, Pengfei Guo, et al, Journal of applied physics 111, 114514 (2012).
14. Dheeraj Mohata, et al 2011 Appl. Phys. Express 024105 doi:[10.1143/APEX.4.024105](https://doi.org/10.1143/APEX.4.024105).
15. Genquan Han, Ye Sheng Yee et al, Silicon Nanoelectronics Workshop (SNW), 2010.
16. W. Long, H. Ou, J. M. Kuo, and K. K. Chin, IEEE Trans. Electron Devices, vol. 46, no. 5, pp. 865–870, 1999.
17. M. Jagadesh Kumar and Sneha Saurabh, IEEE Trans. Electron Devices, vol 58, no. 2, Feb. 2011.
18. Jae Sung Lee et al 2012 Jpn. J. Appl. Phys. 51 doi:[10.1143/JJAP.51.06FE03](https://doi.org/10.1143/JJAP.51.06FE03).
19. Anne S. Verhulst, Bart Sorée, et al. J. Appl. Phys. 107, 024518 (2010).
20. K. Boucart and A. M. Ionescu, IEEE Trans. Electron Devices, vol. 54, no. 7, pp. 1725–1733, Jul. 2007.
21. Gibong Lee, Jung-Shik Jang Semicond. Sci. Technol. 28 (2013) 052001 (5 pp).
22. X. Garros, C. Leroux, D. Blin, J.F. Damlencourt1, A.M. Papon ESSDERC 2002.
23. Nayan Patel, A. Ramesha, Santanu Mahapatra Microelectronics Journal 39 (2008) 1671–1677.
24. Synopsys, TCAD Sentaurus device, ver. D2010-03, 2010.

25. Jiao Yipeng, Wei Kangliang, et al. *Journal of Semiconductors* Vol. 34, No. 9, sept. 2013.
26. M. N. Darwish et al. *IEEE Transactions on Electron Devices*, vol. 44, no. 9, pp. 1529–1538, 1997.
27. R. van Overstraeten and H. de Man, *Solid-State Electronics*, vol. 13, no. 1, pp. 583–608, 1970.
28. W. Y. Choi and W. Lee, *IEEE Trans. Electron Devices*, vol. 57, no. 9, pp. 2317–2319, Sep. 2010.

Integration of Cognitive Radio with Heterogeneous Smart Grid Communication Architecture

Lipi Chhaya, Paawan Sharma, Adesh Kumar
and Govind Bhagwatikar

Abstract The existing power grid is going through a massive transformation with an integration of electrical and communication architectures. Smart grid is a radical approach to overcome the limitations of existing electricity grid. Smart grid is characterized by full duplex communication, distribution automation, renewable energy integration, advanced metering infrastructure, active participation of consumers, fault diagnosis and isolation with self-healing capability, and complete monitoring and control of entire power grid. Integration of information and communication technologies for realization of intelligent grid requires huge amount of spectrum space. Bandwidth is a restricted resource. Cognitive radio technology can facilitate an effective use of available spectrum. This paper is expected to serve as a comprehensive review of application of cognitive radio technology for smart grid communication infrastructure and various spectrum sensing techniques for energy efficiency.

Keywords Cognitive radio · Communication · Energy efficiency
Gateway · Smart grid · Spectrum sensing

L. Chhaya (✉) · P. Sharma · A. Kumar
Department of Electronics, Instrumentation and Control Engineering,
University of Petroleum and Energy Studies (UPES), Dehradun 248007,
Uttarakhand, India
e-mail: lipi.chhaya@gmail.com

P. Sharma
e-mail: paawan.sharma@ddn.upes.ac.in

A. Kumar
e-mail: adeshkumar@ddn.upes.ac.in

G. Bhagwatikar
SANY Group, Pune, India
e-mail: gowind.india@gmail.com

1 Introduction

A power grid is a network which carries electricity from central power plant to customer premises. A grid is called smart or intelligent if it is integrated with information and communication technologies [1]. Smart grid is described by full duplex flow of electrical energy and information. It is a closed-loop system to monitor and control the entire system. The smart grid is a future generation power grid with self-healing capability. Smart grid technology ensures efficient, reliable, robust, and automated distribution system with enormous features. Integration of renewable energy resources will lead to reduced carbon footprint and emissions. It can be defined in various ways as per its functional, technological, or beneficial aspects. As per the definition given by US department of energy, “A smart power grid uses digital technology to improve security, reliability, and efficiency of the electric power system from large generation, through the delivery systems to electricity customers and an increasing number of distributed generation and storage resources.” Smart grid is beneficial in terms of efficacy, economy, safety, security, consistency, and environmental aspects of energy generation, transmission, and distribution system. Sensing, measurement, transmission, and control are the prime functionalities of smart grid communication architecture [2].

2 Heterogeneous Communication Architecture of Smart Grid

The communication architecture of smart power grid can be envisioned as a diverse and hierarchical network. As shown in Fig. 1, the smart grid communication architecture can be distributed into three basic hierarchical network layers.

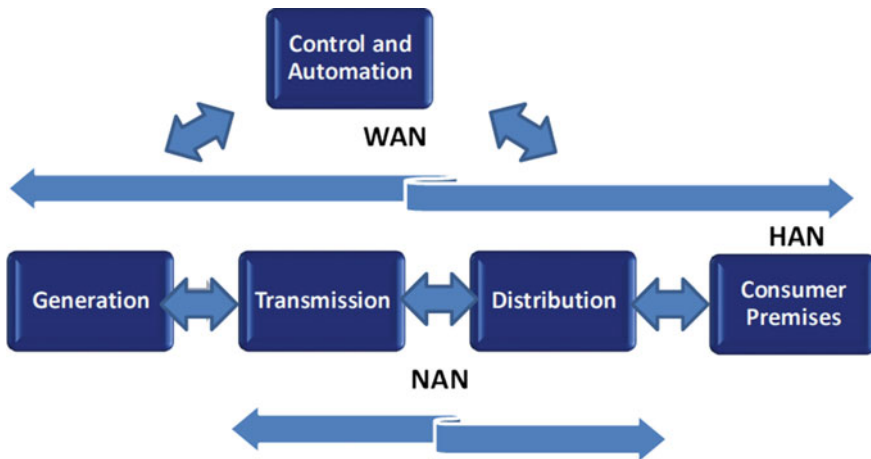


Fig. 1 Smart grid hierarchical communication network layers

Smart grid hierarchical and heterogeneous communication network can be designed on the basis of following layers [3, 4].

2.1 Home Area Network (HAN)

HAN is applicable for home automation. It is used for the consumer domain and consists of electronics appliances and wireless sensor networks. These consumer electronics appliances communicate their energy consumption statistics to central or main home monitor and regulator or smart meter. Central regulator or smart meter sends it to the central electricity grid for monitoring, control, fault detection, and billing purposes.

Smart meters receive the commands from central power grid, and they control the home appliances based on the received commands. The HAN ranges for the coverage area of few meters. IEEE 802.15.1, IEEE 802.15.4, IEEE 802.11, Narrowband PLC, etc. standards can be used for HAN [5].

2.2 Neighborhood Area Network (NAN)

The function of NAN is to communicate the information collected by smart meters to central controller. The NAN may contain few hundreds of smart meters deployed in HANs. Smart meters are linked with different gateways through NANs. The area covered by NANs is around 10 square miles. The requirement of data rates for NAN is around 10–1000 Kbps. WLAN, cellular, and PLC can be used for neighborhood area networks [5].

2.3 Wide Area Network (WAN)

The WAN connects various NANs. Data collection points are located, and the collected data is forwarded to central controller. The coverage area for WAN is around thousands of square miles. The requirements of data rates are around 10–100 Mbps.

Wide area requires very high bandwidth for its operation and management. WAN is suitable for supervisory control and data acquisition systems for monitoring, data acquisition, management, and control of power grid. IEEE 802.16 (Wimax) and cellular technologies such as LTE, 3G, 4G, 5G, EDGE, and GPRS are the suitable adoptions for wide area network applications [5].

This type of heterogeneous architecture will lead to efficient operation of various smart grid communication applications. Hierarchical architecture ensures reliable communication of information at generation, transmission, distribution, and control

of smart grid, but still there are enormous challenges to be overcome for the realization of full-fledged smart grid communication infrastructure. The home area networks generally use industrial, scientific, and medical (ISM) band of 2.4 GHz which is already preoccupied with many applications. The coexistence of Bluetooth, Wi-fi, and Zigbee technologies is the biggest hurdle for reliable communication. Moreover, the limited spectrum availability of ISM band with enormous applications to be served will result into congested and noisy communications. Cognitive radio has the capability to adapt the parameters, and it also provides resourceful use of spectrum. With the use of spectrum sensing technology in cognitive radio, a scheduled and coordinated communication system can be developed for various smart grid applications. The smart grid communication system requires large amount of information to be communicated for process, transmission, storage, control, and self-healing purposes. Cognitive radio can facilitate an efficient use of limited spectrum for reliable and hassle-free communications. The communication process in smart grid architecture comprises of data transmission and reception among various homogeneous and heterogeneous networks in HAN, NAN, and WAN. Cognitive radio technology is inevitable for this type of applications as smart grid devices require adaptability as well as reconfigurable hardware. The usage of IEEE 802.22 standard for proposed heterogeneous smart power grid communication architecture ensures the efficient utilization of available spectrum. Dynamic spectrum utilization can be used to exploit underutilized parts of spectrum in effective manner [6].

3 Standard for Cognitive Radio Applications

IEEE 802.22 is developed for wireless regional area network, and it is used for cognitive radio technology. Cognitive radio technology facilitates the use of unoccupied and available portions of television spectrum (television white space). A governing guideline for IEEE 802.22 is provided by FCC that permits consumers to use television white spectrum. As per the FCC guidelines, cognitive radio devices function within VHF and the UHF bands. The bandwidth of cognitive radio channels is 6 MHz, and the bands are 54–72 MHz, 76–88 MHz, 174–216 MHz, and 470–806 MHz. The television frequencies have greater transmission characteristics which can increase the coverage area and the capacity to enter the structures at lesser signal strength which provides improved broadband services for end consumers. An IEEE 802.22 standard lay emphasis on the access of wireless communication in distant and rural areas as the range of this standard is better than the contemporary broadband communication technologies like WiMAX. Smart grid communication infrastructure is a heterogeneous network which uses diverse set of communication standards. In the framework of smart grid technology, cognitive radio concept can be a prominent solution for energy efficiency and effective utilization of available bandwidth [7]. Spectrum sensing and management are the most

essential concepts to address the issue of spectrum scarcity in smart grid communications.

4 Integration of Cognitive Radio with Smart Grid Heterogeneous Communication Architecture

Bandwidth is a scarce resource in communication systems. The increasing demand for radio spectrum for various applications requires effective spectrum utilization. Effective use of limited bandwidth is a critical technical challenge. Experimental readings of occupied spectrum have confirmed that wide range of an existing licensed radio spectrum is sporadically used. The most efficient and promising solution to increase the usage of frequency spectrum is cognitive radio (CR) technology as it facilitates the resourceful occupation of spectrum spaces which are not used by primary users. In IEEE 802.22, primary users mean licensed consumers with greater legacy or priority privileges for the use of a particular fragment of the frequency spectrum. Secondary consumers are the users with the least priority, but they can use the spectrum such that they do not result into destructive interference to primary users with greater priorities. More apparently, on the basis of definition given by FCC, IEEE 802.22 has the capability to distinguish the portions of licensed band which are unoccupied at a specific period in a certain geographical region [6–8]. This is called the technique of spectrum sensing. It can be used to enhance the data throughput of secondary users by considering radio frequency emissions and by managing the distribution of available parts of spectrum equitably among SUs [7].

On the basis of access of spectrum and transmission methods of primary and secondary users, cognitive radio networks can be classified into three categories [7–10].

4.1 Interweave Cognitive Radio Networks

In interweave approach, secondary user senses an unoccupied portion of spectrum used by each primary user and opportunistically uses these unused portions for sending its data.

4.2 Overlay Cognitive Radio Networks

In overlay method, the channel occupation strategy of primary user is known to secondary user. This information is used by secondary user for communication provided that the shared slice of spectrum is not used by primary end user.

4.3 Underlay Cognitive Radio Networks

In this approach, secondary consumers can use the band in parallel with primary consumers by amending transmission parameters to avoid interference.

In this section, the various approaches for integration of cognitive radio in home, neighborhood, and wide area networks are discussed as displayed in Fig. 2.

4.4 Home Area Cognitive Networks

A home area network (HAN) manages the home energy system. The function of HANs is to identify new devices and ensure reliable and efficient communication between all the consumer devices. Interweave as well as underlay cognitive network approaches are suitable options for HANs. The real-time communication of energy consumption and billing information is inevitable for HAN. Metering and dynamic pricing information is collected by smart meter and sent to consumers for their active participation in energy usage. The wireless sensor networks built for facilitating an efficient home automation system may use different topologies such as mesh and star and various communication protocols such as Zigbee, Bluetooth, or Wi-fi. The cognitive home gateway must be capable of managing this heterogeneous topologies and technologies. The cognitive gateway operating in home area network must have the cognition capacity to sense the unused frequency spectrum and adapt the transmission features to use the unoccupied spectrum in efficient manner [10]. The cognitive gateway has to use the unoccupied spectrum by considering interference avoidance [10–12]. Cognitive home gateway also communicates with neighborhood area networks. HAN consists of sensors, actuators, consumer appliances, meters, control devices, etc. Cognitive home gateway manages the communication between different devices and assigns channels dynamically to all the devices.



Fig. 2 Cognitive radio network gateways for smart grid communications

4.5 Neighborhood Area Cognitive Networks

The functionalities of neighborhood area network (NAN) include meter reading, distribution automation, fault detection and isolation, multimedia applications, and data communication with HANs. The area covered by NANs is over thousand meters. So, the channel between smart meters and data accumulation points must be efficient and free of interference. Both underlay and overlay methods of spectrum access are suitable for NAN. An overlay approach is preferred for high speed communication requirement, and the underlay approach is preferred for low speed traffic requirement. The licensed spectrum should be used for NANs. The NANs collect data from customers through HANs and forward it to WANs [13].

Neighborhood area network consists of neighborhood area network cognitive gateway as well as home area network cognitive gateway. NAN cognitive gateways connect various HAN cognitive gateways. HAN cognitive gateways behave as data aggregators. Home gateways communicate with neighborhood gateways using licensed spectrum by means of cognitive radio technology. The use of both licensed as well as unlicensed spectrum is proposed for NAN gateways. This approach is called hybrid dynamic spectrum access. The NAN cognitive gateways allocate licensed bands to HAN gateways which are considered as primary users. Unlicensed bands can be occupied for greater data communication demand and HAN as well as NAN gateways can occupy these bands opportunistically as secondary users.

4.6 Wide Area Cognitive Networks

In wide area networks, NAN cognitive gateway behaves as a cognitive network node and communicates using unlicensed and unoccupied spectrum. The base stations of cognitive radio technology are located over extensive geographical region and connected to control center. They manage the communication between various NAN cognitive gateways. Overlay cognitive radio approach can be used for wide area networks. The wide area network uses core as well as backhaul network [14]. Cellular communication technology can be used for core network for communication with control center. Backhaul networks are used for NAN gateways connectivity and monitoring purposes and may use various heterogeneous wireless technologies [15]. The cognitive radio approach enhances efficiency, capacity, and coverage of smart grid communication networks.

5 Conclusion

The prime motive of this paper is to describe a comprehensive review of application of cognitive radio technology and spectrum sensing in smart grid communications. Smart power grid is a revolutionary technology of present era. The communication infrastructure of smart grid technology is a complex heterogeneous network with huge bandwidth requirement. Bandwidth is a scarce resource. The realization of complete communication infrastructure of smart power grid is only possible with effective use of limited spectrum. Cognitive radio is a prominent solution to use licensed as well as unlicensed bands efficiently. Heterogeneous and hierarchical communication network of smart grid can be designed and integrated with cognitive radio technology. Privacy and data security of these networks can be explored as a future work.

References

1. V. C. Gungor, B. Lu, G. P. Hancke: Opportunities and challenges of wireless sensor networks in smart grid. *IEEE Transactions on Industrial Electronics*, 57, 10, 3557–3564 (2010).
2. N. Binti Mat Isa, Tan Chee Wei, A. H. M. Yatim.: Smart grid technology: Communications, power electronics and control system. *International Conference on Sustainable Energy Engineering and Application (ICSEEA)*, Bandung, 10–14.
3. R. Yu, Y. Zhang, S. Gjessing, C. Yuen, S. Xie, M. Guizani: Cognitive radio based hierarchical communications infrastructure for smart grid. *IEEE Network*, 25, 5, 6–14 (2011).
4. H. Farooq, Low Tang Jung.: Choices available for implementing smart grid communication network. *Computer and Information Sciences (ICCOINS)*, 2014 International Conference on, Kuala Lumpur, 1–5 (2014).
5. Anzar Mahmood, Nadeem Javaid, Sohail Razzaq (2015) A Review of Wireless Communications for Smart Grid, *Renewable and sustainable reviews* 41, pp-248–260,
6. S. Haykin.: Cognitive Radio: Brain-Empowered Wireless Communications. *IEEE JSAC*, 23, 2, 201–20 (2005).
7. V. Kouhdaragh, D. Tarchi, A. V. Coralli, and G. E. Corazza.: Cognitive radio based smart grid networks. *Proc. TIWDC—Green ICT*, Sep. 23–25, 1–6 (2013).
8. W. Meng, R. Ma, H.-H. Chen: Smart grid neighborhood area networks: A survey, *IEEE Networks.*, 28, 1, 24–32 (2014).
9. Vineeta, J. K. Thathagar.: Cognitive radio communication architecture in smart grid reconfigurability. *Proc. Int. Conf. ET2ECN*, 1–6 (2012).
10. F. Liu, J. Wang, Y. Han, P. Han.: Cognitive radio networks for smart grid communications. *Proc. ASCC*, 1–5 (2013).
11. D. P. Shea, J. E. Mitchell.: Architecture to integrate multiple PONs with long reach DWDM backhaul. *IEEE Journal of selected areas of Communication*, 27, 2, 126–133 (2009).
12. A. Boustani, M. Jadhwal, H. M. Kwon and N. Alamatsaz.: Optimal resource allocation in Cognitive Smart Grid Networks. *12th Annual IEEE Consumer Communications and Networking Conference (CCNC)*, NV, 499–506 (2015).
13. A. Khan, M. H. Rehmani and M. Reisslein.: Cognitive Radio for Smart Grids: Survey of Architectures, Spectrum Sensing Mechanisms, and Networking Protocols. *IEEE Communications Surveys & Tutorials*, 18, 1, 860–898 (2016).

14. A. Ghassemi, S. Bavarian, L. Lampe.: Cognitive Radio for Smart Grid Communications. First IEEE International Conference on, Smart Grid Communications (SmartGridComm), Gaithersburg, MD, 297–302 (2010).
15. J. Wang, M. Ghosh and K. Challapali.: Emerging cognitive radio applications: A survey. IEEE Communications Magazine, 49, 3, 74–81 (2011).

Comparison Between the Performance of Trigate Junctionless Transistor and Double-Gate Junctionless Transistor with Same Device Length

Deepti Singh, Renu Vig, Charu Madhu and Ravneet Kaur

Abstract In this paper, we have compared double-gate junctionless transistor and trigate junctionless transistor for electrical parameters like I_{on} , I_{off} , I_{on}/I_{off} ratio, threshold voltage, drain-induced barrier lowering (DIBL). In CMOS technology, as we reduce the device dimensions, its performance gets affected due to short channel effects as well as leakage current. To minimize these short channel effects, different types of devices are introduced by the researchers. Junctionless transistor is a new CMOS technology and is easier to fabricate too. Junctionless transistor is a heavily doped semiconductor device which has gate electrode which is the controlling terminal [1]. Operation of junctionless transistor relies on the fully depletion of the semiconductor using the work function of the gate material to turn the device off [1]. If the number of gates is increased in a transistor device, it will provide the better control of the flow of current in the channel of the device. For the comparison of devices, various simulations were carried out using TCAD software.

Keywords Junctionless transistor (JLT)
Double-gate junctionless transistor (DGJLT)
Trigate junctionless transistor (TGJLT) · Work function
Channel length · Drain-induced barrier lowering (DIBL)

1 Introduction

Due to downsizing, the length of the channel of a device is reduced; because of this, the formation of junction is becoming very hard as formation of junction requires doping with different types of materials [1, 2]. Due to the short channel effects, leakage current in the device is increasing, which in turn degrades the performance of the device [3–5]. So to avoid these issues i.e., short channel effects as well as the

D. Singh (✉) · R. Vig · C. Madhu · R. Kaur
University Institute of Engineering and Technology, Panjab University,
Chandigarh 160014, India
e-mail: charu_uiet@pu.ac.in

© Springer Nature Singapore Pte Ltd. 2018
R. Singh et al. (eds.), *Intelligent Communication, Control and Devices*,
Advances in Intelligent Systems and Computing 624,
https://doi.org/10.1007/978-981-10-5903-2_104

formation of junction in the transistor device, some advanced research have discovered a notable technology in which no formation of junction is required between the source and drain which is called junctionless transistor technology (JLT) [4–6]. Junctionless transistor is a new introduction to the semiconductor industry with many advantages over conventional transistor [5–8]. In comparison with the conventional MOSFET fabrication process, the fabrication process of junctionless MOSFET is considerably simple since the device has no doping concentration gradient due to which no formation of junction takes place [4, 9]. Junctionless device consists of a narrow body with the channel heavily doped same carrier type as to the source and drain regions, and the device is turned off by body depletion using an appropriate work function of the gate [10]. Junctionless transistors require heavy doping to allow proper amount of current to flow when the device is turned on [9]. The switching of the transistor depends upon the work function difference of gate material used in the device and the material which is used to form the channel of the device [5, 11]. Work function is defined as the lowest energy required for removal of an electron from the solid surface of the device [11, 12]. In this paper, simulation is carried out using TCAD software [17].

1.1 Device Structure of Trigate Junctionless Transistor and Double-Gate Junctionless Transistor

The trigate junctionless transistor and double-gate junctionless transistor structures are designed by using technology computer-aided design software (TCAD) at 40 nm node technology. Due to the presence of short channel effects in transistor with junction which demerits the performance of the device, junctionless transistor can be used in its place [18]. The design parameters for trigate junctionless transistor and double gate junctionless transistor are mentioned in Table 1. The operating temperature for both the devices is 300 K, and gate length of both the devices

Table 1 Design parameters used in drawing both devices

S. No.	Parameter	Double-gate junctionless transistor	Trigate junctionless transistor
1	Thickness of oxide (nm)	1	1
2	Polysilicon thickness (nm)	1	1
3	Work function of gate (eV)	5.17	5.17
4	Doping (cm^{-3})	ND = 1.5e+19	ND = 1.5e+19
5	Gate length (nm)	12	12
6	Gate material	p+poly-Si	p+poly-Si

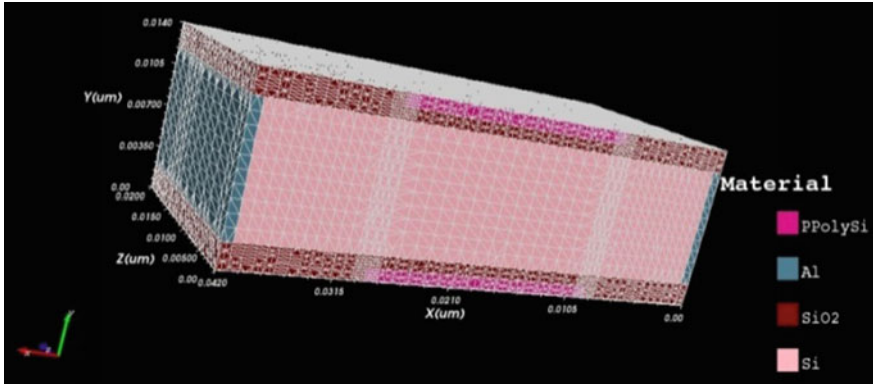


Fig. 1 3D structure of double-gate junctionless transistor

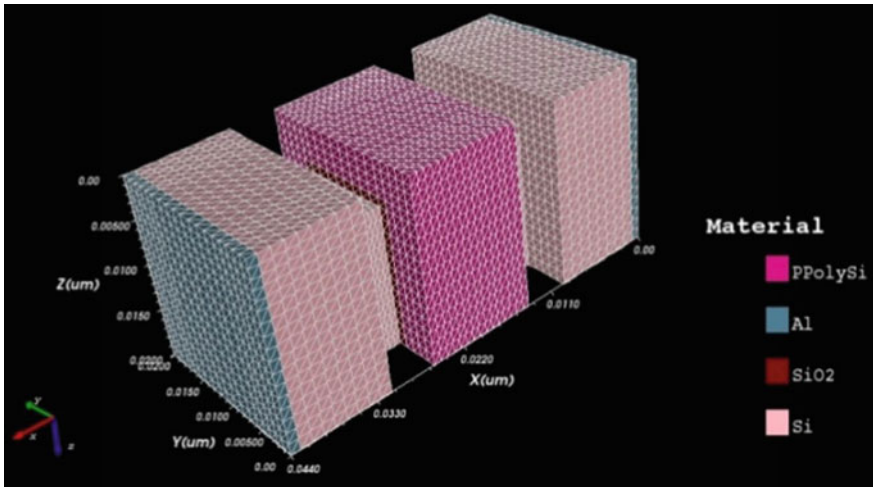


Fig. 2 3D structure of trigate junctionless transistor

is 12 nm. The physical model used in both the devices is drift-diffusion model to simulate the electrical characteristics [7, 11] (Figs. 1 and 2).

Gate material is polysilicon. Donor doping concentration (N_d) of S/D in trigate junctionless transistor and double-gate junctionless transistor is $1.5e+19$ atoms/cm⁻³ [19]. Work function used for both the device is 5.17 eV. Gate material used is p-type polysilicon [7].

2 Simulation Result and Discussion

In this paper, simulations were carried out for the devices for comparison of different electrical parameters for trigate junctionless transistor as well as double-gate junctionless transistor. Performance of different electrical parameters like ON current, OFF current, threshold voltage, ON/OFF ratio, and DIBL was discussed for both the devices.

A. Drain current versus applied gate voltage

Figure 3 shows the effect of applied gate voltage on the drain current for trigate junctionless transistor (TGT) and double-gate junctionless transistor (DGT) with drain voltage 0.1 V. Figure 4 shows the effect of applied gate voltage on the drain current at drain voltage 1 V. The work function for both the devices is kept constant at 5.17 eV.

B. Threshold Voltage

Threshold voltage of a device is that gate voltage at which the current starts flowing through the device having minimum current value [5]. If gate voltage is less than threshold voltage, current will not flow ideally in the device; but due to short channel effect, there is a very small amount of current that flows through the device called leakage current which degrades the performance of device [13, 16]. Figure 5 shows the change in threshold voltage as the drain voltage is changed. It is observed that trigate junctionless transistor has less threshold voltage as compared to the double-gate junctionless transistor.

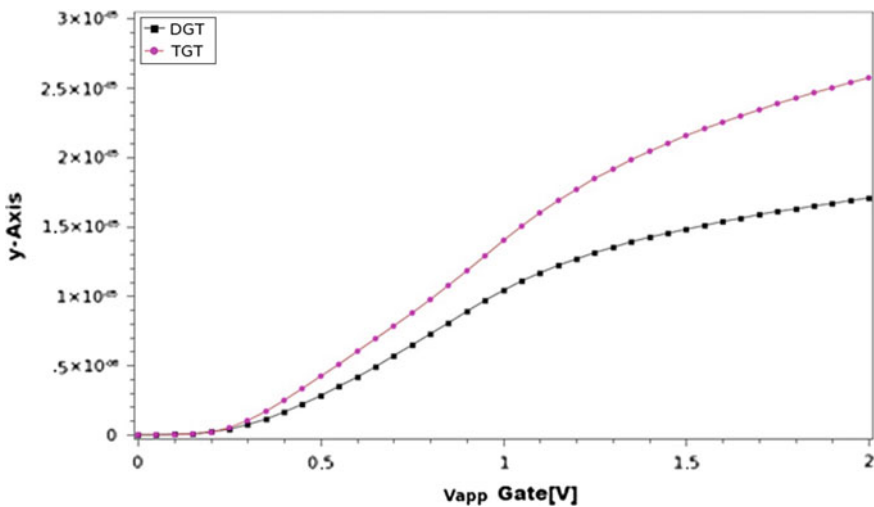


Fig. 3 I_d (drain) as function of V_{app} (gate) in trigate and double-gate junctionless transistor at drain voltage of 0.1 V keeping work function = 5.17 eV

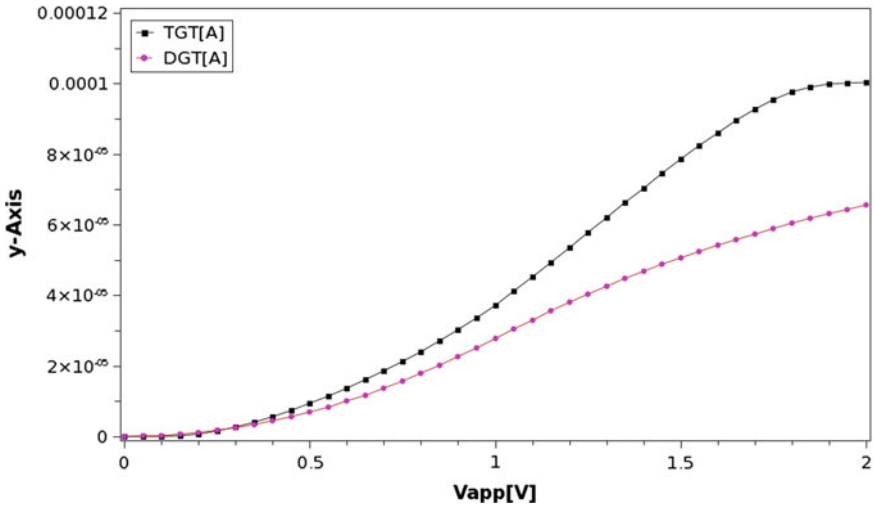
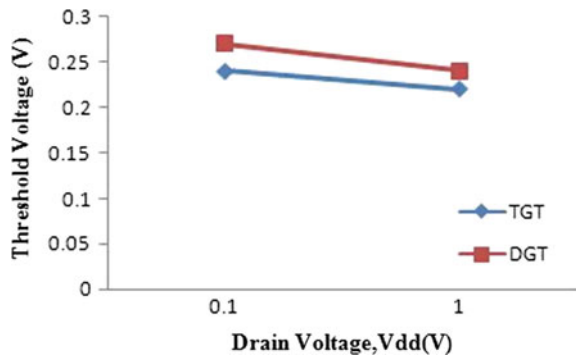


Fig. 4 I (drain) as function of V_{app} (gate) in trigate and double-gate junctionless transistor at drain voltage of 1 V keeping work function = 5.17 eV

Fig. 5 Graph between threshold voltage (V_{th}) and drain current (V_{dd})



C. ON current and OFF current

ON current is known as the current that flows through the channel of a device formed between the source and drain when the gate voltage is greater than the threshold voltage [2, 15]. OFF current is known as the current which flows in a channel of the device when the gate voltage is smaller than threshold voltage which also degrades the performance of the device [2, 3, 14, 15]. Due to OFF current, large power dissipation takes place in the device as there is current flowing through the device when the device should not be conducting [7, 11, 13]. The probable reason for change in ON current is that ON current is directly proportional to change in gate to source voltage and threshold voltage, i.e., as the threshold voltage increases, the change is decreasing and vice versa.

Table 2 Simulation result

S. No.	Parameter	Double-gate junctionless transistor	Trigate junctionless transistor
1	Threshold voltage at 0.1 V drain voltage (V_{th}) (V)	0.27	0.24
2	ON current (I_{on}) (A)	1.7e-05	2.57e-05
3	OFF current (I_{off}) (A)	2.59e-09	7.91e-10
4	I_{on}/I_{off} ratio	0.65e+04	3.2e+04
5	Threshold voltage at 1 V drain voltage (V_{th}) (V)	0.24	0.22
6	DIBL	3.3e-02	2.2e-02

D. I_{on}/I_{off} current ratio

It is observed that as ON current increases and OFF current decreases, so I_{on}/I_{off} current ratio also increases. It is observed that trigate junctionless has more ON current as and less OFF current as compared to the double-gate junctionless transistor, so trigate junctionless transistor has more I_{on}/I_{off} current ratio.

E. Drain-Induced Barrier Lowering (DIBL)

DIBL is a type of short channel effect in which reduction in the threshold voltage of the device takes place as the drain voltage is increased [11]. DIBL is directly proportional to the threshold voltage and inversely proportional to the change in drain voltage [7, 16]. It is observed that trigate junctionless transistor has less threshold voltage as compared to the double-gate junctionless transistor, which implies that trigate junctionless transistor has less DIBL.

Different simulation results for different parameters which are performed on double-gate junctionless transistor and trigate junctionless transistor are shown in Table 2.

3 Conclusion

Different parameters like threshold voltage, ON current, OFF current, and DIBL were studied for the comparison between trigate junctionless transistor and double-gate junctionless transistor. Simulations were carried out by using TCAD software. We have concluded that ON current which is required to be high is achieved by trigate junctionless transistor and OFF current which is required to be low is achieved by trigate junctionless transistor. DIBL must be low for good performance of the device is also achieved by trigate junctionless transistor. For further comparison between the devices, researches can change different parameters in their devices according to their requirements.

References

1. J.P. Colinge: "Silicon-On-Insulator (SOI) Technology", Manufacture and Applications.
2. Donald A. Neamen, "Semiconductor physics and devices", third edition, McGraw-hill.
3. International technology roadmap for semiconductors (ITRS) [online] available: <http://www.itrs.net>.
4. J., Colinge, C., Lee, A., Afzalian, N., Akhavan, R., Yan, I., Ferain, P., Razavi, O'Neill, A., Blake, M., White, A.M., Kelleher, B., McCarthy, R., Murphy "Nanowire transistors without junctions" Nat. Nanotechnology, Vol. 5. pp. 225–229, 2010.
5. J.P., Colinge, C.W., Lee, N., Dehdashti Akhavan, R., Yan, I., Ferain, P., Razavi, A., Kranti and R., Yu "Junctionless Transistor physics and properties" Solid-state electron, December 2010.
6. C. Lee, I. Ferain, A. Afzalian, R. Yan, N. Akhavan, P. Razavi, and J. Colinge, "Performance estimation of junctionless multigate transistors," Solid State Electron., vol. 54, no. 2, pp. 97–103, Feb. 2010.
7. Vishal Narula, Charu Narula, Jatinder Singh "Investigating Short Channel Effects and Performance Parameters of Double Gate Junctionless Transistor at Various Technology Nodes" RA ECS 2015 IEEE 2015.
8. R. Rios, A. Cappellani, M. Armstrong, A. Budrevich, H. Gomez, R. Pai, N. Rahhal-orabi, and K. Kuhn, "Comparison of Junctionless and Conventional Trigate Transistors With L_g Down to 26 nm", IEEE Electron Device Letters, Vol. 32, No. 9, September 2011.
9. A. Kranti, R. Yan, C.-W. Lee, I. Ferain, R. Yu, N.D. Akhavan, P. Razavi, J.P. Colinge, Junctionless nanowire transistor (JNT): properties and design guidelines, in: Proc. Euro. Solid-State Device Res. Conf. (ESSDERC), 2010, pp. 357e360.
10. R. Rios, A. Cappellani, M. Armstrong, A. Budrevich, H. Gomez, R. Pai, N. Rahhal-orabi, and K. Kuhn, "Comparison of Junctionless and Conventional Trigate Transistors With L_g Down to 26 nm", IEEE Electron Device Letters, Vol. 32, No. 9, September 2011.
11. Vishal Narula, Charu Narula, Jatinder Singh "Analysis and comparison of various performance parameters and short channel effects of n channel and p channel dual gate junctionless transistors at different technology nodes", I J C T A, 9(11) 2016, pp. 5301–5306.
12. Porag jyoti ligira, Gargi Khanna, "review on different types of junctionless transistor", International journal of emerging technologies in computational and applied sciences. Pp.404–408, Feb.2014.
13. Sohn, Chang Ki Baek, Sooyoung Park, M.j.Deen, Yoon-H Jeong, Jeong- Soo Lee "Electrical Characteristics of 20 nm Junctionless Si Nanowire Transistor" Solid State Electronics pp-7–10 2012.
14. Juan Pablo Duarte, Sung-Jin Choi, Yang-Kyu Choi "A full range Drain Current Model for double gate junctionless transistors" IEEE transactions on Electron devices, Vol 58, December 2011.
15. Ming-Hung Han, Chun-Yen Chang, Life Fellow, IEEE Hung-Bin, Chen, Ya-chi Cheng, Yung Chun "Device and circuit performance estimation of junctionless Bulk FinFet's" IEEE Trans Electron Devices pp. 1807–1813 2013.
16. Renan Doria Trevisoli¹, Rodrigo Trevisoli Doria², Michelly de Souza² and Marcelo Antonio Pavanello "Threshold voltage in Junctionless nanowire transistors", semiconductor science and technology, Semicond. Sci. Technol. 26, 2011.
17. TCAD Simulation Software Cogenda user Manual.
18. T. Poiroux, M. Vinet, O. Faynot, J. Widiez¹, J. Lolivier, T. Ernst, B. Previtali, S. Deleonibus, "Multiple gate devices: advantages and challenges", Microelectronic Engineering pp-378–385, 2005.
19. Nima Dehdashti Akhavan, Isabelle Ferain, Pedram Razavi, Ran Yu and Jean-Pierre Colinge, "Random Dopant Variation in Junctionless nanowire Transistors", IEEE 2011 International SOI Conference pp- 1–2, 2011.

Analysis of Mahout Big Data Clustering Algorithms

Ishan Sharma, Rajeev Tiwari, Hukam Singh Rana
and Abhineet Anand

Abstract Log data generated from any of the source or communicating devices is huge; to analyze such data we need to categorize them in some clusters. Depending upon clusters, data analytics can be done. Enabling the analytics in data helps in identification of business patterns and behavior of customers. Analyzing such big data is a major task, so distributed computing is used in Hadoop platform and machine learning library Mahout is used. Weighting technique TF-IDF is used for vectorization of data, and clusters are formed using clustering algorithms for doing analysis. Clustering algorithms K-mean, fuzzy K-Mean, LDA, and spectral clustering in Mahout are used and analyzed on basis of execution time, number of clusters, static or dynamic cluster creation.

Keywords Big data · Clustering · Mahout · Vectorization

1 Introduction

In the past couple of years, the data industry has seen a boom in the amount of data generated and used by all the digital users across the globe. Internet has been a huge contributor to that, whether its a video content, social networking content, or even simple text-related content, the amount of data we consume and create is increasing day by day. An IDC [1] study suggests that the amount of world's information is doubling day by day and is expected to reach 40ZB by 2020. This data burst is generally termed as big data and is one of the most interesting fields of research today. Big data has commonly three dimensions that are volume, velocity, and variety. But, the main problem with big data is that it is unable to be processed by traditional computing techniques, distributed systems, and databases.

I. Sharma · R. Tiwari (✉) · H.S. Rana · A. Anand
Department of Computer Science, UPES, Dehradun, India
e-mail: rajeev.tiwari@ddn.upes.ac.in

I. Sharma
e-mail: its.ishansharma@gmail.com

As a result, big data analytics and analysis are one of the growing sectors in today's industry. However, due to its variety the data poses a big problem during its analysis and a lot of times most of the data gets wasted due to the lack of analysis techniques. Big data also helps in the area of machine learning and artificial intelligence as machines can learn the pattern from the data and apply that learning to suggest valuable suggestions. Hadoop MapReduce [2] is a software framework which is used to process vast amount of data in parallel or large clusters of commodity hardware. It uses divide and conquer technique to process that huge sum of data, that is, it divides the large chunk of data into small pieces and then processes it. It has two phases, namely map phase and reduce phase. Generally, computing and storage nodes are basically the same which increase its efficiency. Apache Mahout [3] is one of the open-source machine learning frameworks which works alongside Hadoop to provide distributed analytics techniques. It basically focuses on three [4] main areas of machine learning techniques, namely recommendation, classification, and clustering.

Various big data analytics techniques are being deployed in various sectors in the industry such as health, finance, retailers, banking, insurance [5], and even in the energy sector [6]. In the current market place, big data analytics plays a critical role in driving business-related decisions. It is also suggested by an IBM study [7] that business intelligence is one of the key areas in the industry after virtualization and cloud computing.

This paper mainly focuses on the clustering part of machine learning framework in conjunction with big data processing. The technique uses Apache Mahout for clustering and categorizing text data for analysis. The technique uses Hadoop and HDFS for storage and processing of textual data. Section 2 defines the literature review and in Sect. 3 the technique is proposed. The results will then be evaluated followed by the conclusion.

2 Literature Review

Previously, a lot of work has been proposed in the field of analysis of the big data. First of all, the problem of processing and storage of big data led to the development of google file system (GFS) [8] and the MapReduce paradigm [9]. This allowed the processing of the big data to be easy and efficient without wasting money and other resources on the hardware itself. It allows computation on data on commodity servers by distributing and computing it on the same resource at the same time. It eliminates the need for sending data on the network and makes maintenance and load balancing of the system much more convenient. MapReduce framework takes care of scheduling, monitoring, and execution of tasks by itself and does not require any intervention. Since the storage and compute nodes are same, the bandwidth of the system is also very high across the cluster. The Framework comprises of master resource manager and slave node manager.

The application provides the map and reduces functions along with input and output locations with the help of suitable interfaces and/or abstract classes.

Apache also provides other solutions that work in conjunction with Hadoop that extend Hadoop capabilities. Mahout is one of them. It is an open-source machine learning platform that is used to provide distributed and scalable data analytics capabilities. Mahout supports three fundamental key areas of machine learning which are clustering, classification, and recommendation. The paper focuses on the clustering area in which Mahout provides various clustering algorithms, namely K-means [10], canopy [11], fuzzy K-means [12], streaming K-means [13], and spectral clustering [14]. Additionally, Apache also provides HBase for storage of data, and Hive which is a NoSQL database query platform, all supported by Mahout and Hadoop.

There are also various proprietary techniques [15] present in the market which can be used as per the need and convenience like Jaspersoft, Tableau Desktop, Pentaho big data, business analytics and BI, FICO big data analyzer, and Skytree, etc., for big data analytics.

Researches related to machine learning algorithms are well established and proved, and big data analytics and large scale distributed machine learning are still under development, like Mahout. There is some initial work that has been done and experimented upon.

Esteves et al. [16] proposed the use of Mahout K-means clustering on a 1.1 GB dataset which examines clustering and scalability of TCP dataset from an airforce LAN. Afterward, they applied fuzzy c-means and K-means on 11 GB of Wikipedia data that analyzes system performance and clustering algorithm.

Barrachina et al. [17] proposed another methodology for categorizing technical support requests. They used Mahout to categorize the support requests from VMware technical support data. They have proposed a proof of concept (POC) end-to-end solution that utilizes the Hadoop programming model, extended ecosystem, and the Mahout big data analytics library for categorizing similar support calls for large technical support data sets.

In contrast, the technique presented in the paper provides an integrated solution of Mahout along with Hadoop to solve the problem of text clustering and categorization for machine learning purposes.

3 Proposed Work and Its Implementation

In this paper, we present a collection of tools which can be used to categorize and classify any textual data. This can be used on the large scale as it supports Hadoop platform along with Mahout which is a machine learning library and all of the tools are open-source and can be used as per the requirements. The dataset which we will be using is Reuters-21578 which is the dataset of nearly 21578 news articles collected over a period of time. This result will come in the form of the clusters in which the input textual data will be classified and categorized.

3.1 Tools Used

The main components used in this technique are: (1) Hadoop [18] which is an open-source framework that is used for processing big data by using distributed computing over commodity hardware (2) Mahout [19] which is an open-source machine learning library that is used to provide distributed analytics capabilities and built on top of Hadoop.

4 Implementation Outline

Considering that Hadoop and Mahout are already installed, as installation process will be beyond the scope of this paper, we begin by downloading the Reuters-21578 data. Our work can be explained in following steps (Fig. 1).

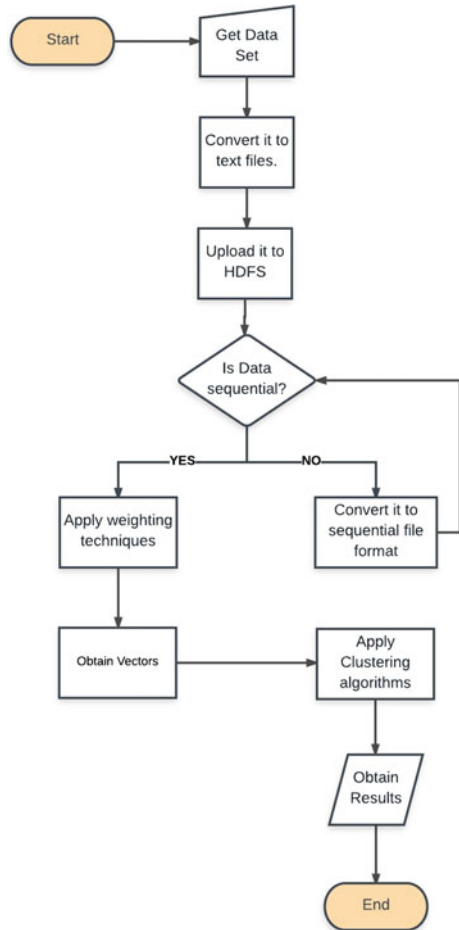
4.1 Extracting and Converting Data

First extract the data from its respective archive, the data are in the form of .sgm file format which is equivalent to .XML file format. It helps to compress the large textual data in proper organized way so that it can be extracted and used later. The extracted .sgm files cannot be used directly as Mahout cannot understand the data, those files first have to be converted into the text files.

4.2 Loading to Hadoop and Sequential File Creation

After converting all the files to text format, they have to be uploaded to the Hadoop distributed file system for processing and storage. The HDFS provides smooth and rapid access to the files and is much preferred storage technique for storing large chunks of data while using MapReduce queries. After uploading the data to HDFS all the text files need to be converted into the sequential file format. Sequential file format provides easy and fast access to file read and decreases all the I/O latency. The conversion of the files to sequential format is an important step, and if the files are not sequential then first they need to be converted to that format.

Fig. 1 Flow chart for creating clusters and their analysis



4.3 *Generating Weights and Vectors*

After the format conversion, weighting techniques can be applied so that the respective text vectors can be obtained. Mahout uses TF-IDF weighting technique to create text vectors. TF-IDF (text frequency inverse document frequency) is one of the most common text weighting techniques used to describe documents in vector space model. In this technique, initially the frequency of each word is calculated. This means, the more a word appears in the document the more is its word frequency or term frequency. Inverse document frequency (IDF) measures how infrequent a term is in the document. If a word has higher term frequency, then it is not considered important. Hence, the word which appears least is considered important according to the algorithm. Along with the vectors, a dictionary file will also be generated. The main aim of the dictionary file is to map the words along with their vectors.

4.4 *Applying Clustering Algorithms with Tested Scenarios*

After creating the vectors, the main aim is to apply the clustering algorithms on them. Mahout provides various clustering algorithms to test results depending upon execution time, no of clusters, etc.

- K-means
- Fuzzy K-means
- Latent Dirichlet Allocation (LDA)
- Spectral Clustering

K-means [20] clustering is one of the simplest clustering algorithms which classifies a given data set based on certain number of clusters which are provided. The basic technique is, first define k number of centroid for each cluster and place them far away from each other. Then take each point from the dataset and assign it to the nearest centroid until no point is left. Then again calculate the new k number of centroids as new centers of the clusters and again take each point and reassign them. Finally, do this process again and again till no points in the cluster moves. This results in groups instead of individual points after which further calculations can be done.

In fuzzy K-means [21] the data points are being partitioned into k clusters just like the K-means algorithm and the clusters are associated with their respective centroids. But here the relationship between a data point and the cluster is fuzzy. This means that a data point has a certain level of membership with a cluster which reflects its belongingness to that cluster.

In latent Dirichlet allocation (LDA) [22], the algorithm represents documents corpus based on mixture of latent topics. These topics are discovered from the sentences that are present in the corpus. LDA measures documents on the basis of mixture of topics. First, number of words in the document is decided (say by Poisson distribution). Then topic mixture for the document is selected using Dirichlet distribution over a set of k topics. Finally, each word in the document is generated by first picking up the topic and then using that topic to generate the word itself.

Spectral clustering first constructs a KNN graph or similarity graph for all the data points. Then it embeds those data points in a low-dimensional space (spectral embedding), in which clusters are more obvious, with the use of the eigenvectors of the laplacian graph. Finally, a classical clustering algorithm like K-means is applied to partition the embedding. Spectral clustering has better performance because it makes no assumptions on the shapes of clusters and also does not require iterative starts like other classical algorithms do. After applying the clustering algorithms, the output is taken out from the Mahout using cluster dumper tool. Since the output is still in the sequential format, it first has to be converted into text format with the help of the tool.

5 Results

After applying the clustering algorithms, the results are as in Figs. 2, 3, 4, 5 and Table 1.

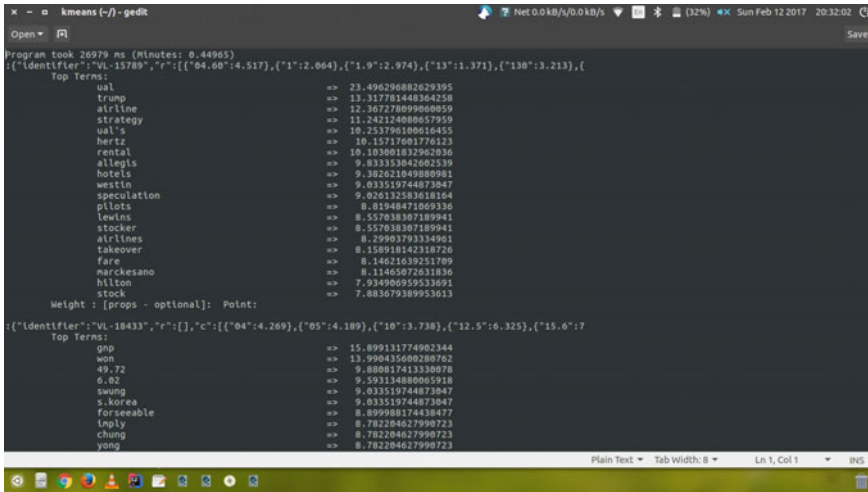


Fig. 2 K-means, execution time: 26,979 ms, and clusters: 20

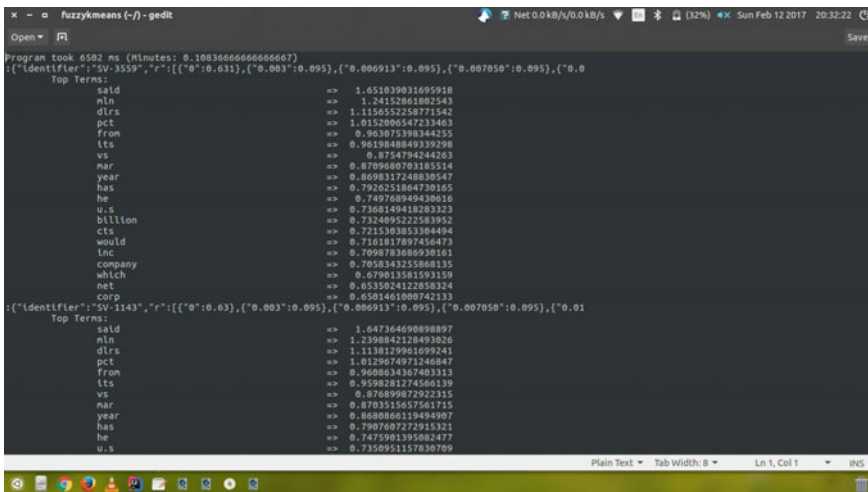
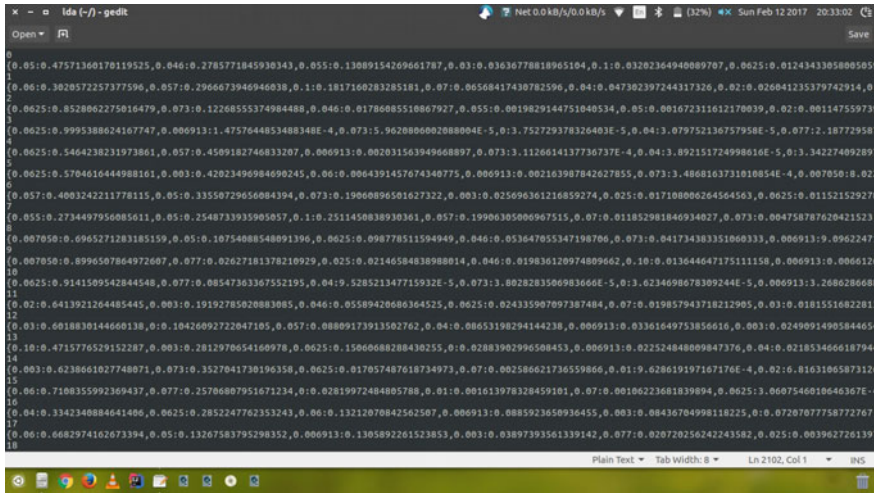
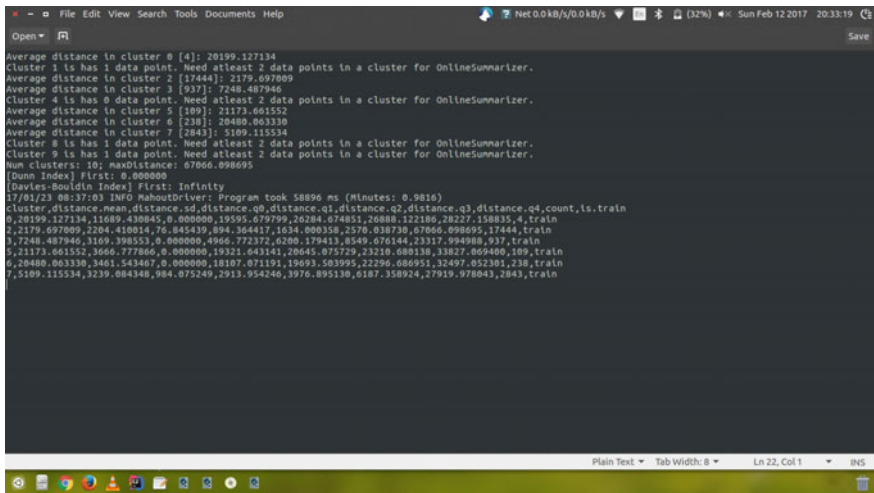


Fig. 3 Fuzzy K-means, execution time: 6502 ms, and clusters: 20



```
x - o lida (-) - gedit
0
0.05:0.47571360170119525,0.046:0.2785771845930343,0.055:0.13089154269661787,0.03:0.0363778818965104,0.1:0.03202364940089707,0.0625:0.0124343305809505
1
0.06:0.3026572257377596,0.057:0.2966673946946030,0.110.1817160283205181,0.07:0.06568417430782596,0.04:0.047302397244317320,0.02:0.026041235379742914,0
2
0.0625:0.8528062275016479,0.073:0.1226855374984488,0.046:0.01786085510807927,0.055:0.0019829144751040534,0.05:0.001672311612170039,0.02:0.00114755973
3
0.0625:0.9995388624107747,0.006913:1.4757644853488348E-4,0.073:1.52729378326403E-5,0.1:3.752729378326403E-5,0.04:3.079752136757958E-5,0.077:2.18772958
4
0.0625:0.5464238231973861,0.057:0.4589182746833207,0.006913:0.002031563949668897,0.073:1.1226614137730737E-4,0.04:3.892151724998616E-5,0.3:34227409289
5
0.0625:0.5704616444988161,0.003:0.42023498984690245,0.06:0.0064391457674340775,0.006913:0.002163987842627855,0.073:3.48681637310108054E-4,0.007050:0.02
6
0.057:0.004324221178115,0.05:0.33559729656084394,0.073:0.1966809651027322,0.003:0.025696361216859274,0.025:0.017108066264564563,0.0625:0.0115212927
7
0.055:0.2734497956085611,0.05:0.2548733935090507,0.1:0.2511450838930361,0.057:0.19966305006967515,0.07:0.011852981846934027,0.073:0.004758787620421523
8
0.007050:0.096521283185159,0.05:0.10754088548091396,0.0625:0.098778511504949,0.046:0.053647855347198706,0.073:0.041734303351060333,0.006913:9.0962247
9
0.007050:0.899507864972607,0.077:0.02627181378210929,0.025:0.02146584838988014,0.046:0.019836120974809662,0.10:0.013644647175111158,0.006913:0.006612
10
0.0625:0.9141509542844548,0.077:0.08547363367552195,0.04:9.528521347715932E-5,0.073:3.8028283506983666E-5,0.1:0.0234696878309244E-5,0.006913:3.268628668
11
0.02:0.6413921264485445,0.003:0.19192785020883085,0.046:0.05589426086364525,0.0625:0.024335907097307484,0.07:0.019857943718212905,0.03:0.0185156102281
12
0.03:0.601830144660138,0.0:0.10426092722047105,0.057:0.08809173913502762,0.04:0.08653198294144238,0.006913:0.03361649753856616,0.003:0.0249091490584465
13
0.10:0.471577629152287,0.003:0.2812970654160978,0.0625:0.15066088288430255,0.0:0.02803902996508453,0.006913:0.02254840809847376,0.04:0.02153466618794
14
0.003:0.623866102774801,0.073:0.3527041730196358,0.0625:0.017057487618734973,0.07:0.00258621736559866,0.01:9.62861919167176E-4,0.02:0.0163106587312
15
0.06:0.7108555992369437,0.077:0.25706087951671234,0.0:0.02819972484805788,0.01:0.001613978328459101,0.07:0.00106223681839894,0.0625:3.0607546016646367E-
16
0.04:0.334240884641406,0.0625:0.285247762353243,0.06:0.13212070842502507,0.006913:0.0885923650936455,0.003:0.0843674998118225,0.0:0.0720707758772767
17
0.06:0.6682974162673394,0.05:0.13267583795298352,0.006913:0.1305892261523853,0.003:0.03897393561339142,0.077:0.020720256242243582,0.025:0.0039627261339
18
```

Fig. 4 LDA, execution time: 84,662 ms, and indexes: 21578



```
x - o File Edit View Search Tools Documents Help
Average distance in cluster 0 [4]: 20199.127134
Cluster 1 is has 1 data point. Need atleast 2 data points in a cluster for OnlineSummarizer.
Average distance in cluster 2 [17444]: 2179.697809
Average distance in cluster 3 [937]: 7248.487946
Cluster 4 is has 0 data point. Need atleast 2 data points in a cluster for OnlineSummarizer.
Average distance in cluster 5 [109]: 21173.601552
Average distance in cluster 6 [238]: 20489.063330
Average distance in cluster 7 [2843]: 5109.115534
Cluster 8 is has 1 data point. Need atleast 2 data points in a cluster for OnlineSummarizer.
Cluster 9 is has 1 data point. Need atleast 2 data points in a cluster for OnlineSummarizer.
Num clusters: 10; maxDistance: 0766.09805
[Dunn Index] First: 0.000000
[Davies-Bouldin Index] First: Infinity
[7/61/23 05:37:03 INFO HuboutDriver: Program took 58896 ms (minutes: 0.9816)
cluster_distance,mean_distance,id,distance,q0,distance,q1,distance,q2,distance,q3,distance,q4,count,is_train
0,20199.127134,11689.438045,0.00000,19595.079799,20204.074051,26889.122189,28227.158835,4,train
1,2179.697809,2204.410915,76.845439,894.364451,1634.000338,2576.930730,0766.098050,17444,train
3,7248.487946,3169.398553,0.800000,4966.772372,6200.179413,8549.676144,23317.994988,937,train
5,21173.601552,3660.777866,0.000000,19321.643161,20645.075759,23210.688138,13827.869480,109,train
6,20489.063330,3461.643407,0.000000,18187.071191,19093.503995,22296.086951,32497.652393,238,train
7,5109.115534,3239.084348,984.075249,2913.954246,3976.895130,6187.358924,27919.978043,2843,train
```

Fig. 5 Spectral clustering, execution time: 58,896 ms, and clusters: 10

Table 1 Comparison of algorithms

Algorithm	Mahout command	Number of clusters	Execution time (ms)	Type of data clustering	Type (fixed/dynamic)
K-means	K-means	20	26,979	Text files	Fixed
Fuzzy K-means	Fuzzy K-means	20	6502	Text files	Fixed
LDA	lda	N/A	84,662	Text files	Dynamic
Spectral	spectral K-means	10	58,896	Text files	Dynamic

6 Conclusions

In today’s world, big data analytics is one of the key factors which gives useful insights to organizations for their business-related purposes. Machine learning is also one of the major areas which help in analyzing the data to give valuable suggestions. The technique presented in this paper presents a complete open-source solution for analytics of textual data for its categorization and clustering. Future work can examine more text weighting techniques to generate text vectors to improve the quality of results. Further, new machine learning models can also be used for creation and generation of better and improved results. Moreover, various automation techniques can also be used which can reduce the overall time consumed by the process.

References

1. Digital Universe Study (on behalf of EMC Corporation): Big Data, Bigger Digital Shadows, and BiggestGrowth in the Far East. 2012. <http://idcdocserv.com/I414>.
2. MapReduce Tutorial, <https://hadoop.apache.org/docs/stable/hadoop-mapreduce-client/hadoop-pmapreduce-client-core/MapReduceTutorial.html>.
3. Mahout, <http://mahout.apache.org/>.
4. Robin Anil, Sean Owen, and Ted Dunning. *Mahout in Action*. Manning, 2012.
5. Data Science Association, <http://www.datascienceassn.org/content/how-top-10-industries-use-big-dataapplications>.
6. Ibrahim, Shadi, et al. “Governing energy consumption in hadoop through cpu frequency scaling: An analysis.” *Future Generation Computer Systems* 54 (2016): 219-232.
7. IBM: The Essential CIO. 2011. <http://www-935.ibm.com/services/uk/cio/pdf/CIE03073-GBEN-01.pdf>.
8. Ghemawat, Sanjay, Howard Gobioff, and Shun-Tak Leung. “The Google file system.” *ACM SIGOPS operating systems review*. Vol. 37. No. 5. ACM, 2003.
9. Dean, Jeffrey, and Sanjay Ghemawat. “MapReduce: simplified data processing on large clusters.” *Communications of the ACM* 51.1 (2008): 107–113.
10. K-Means clustering, <http://mahout.apache.org/users/clustering/k-means-clustering.html>.
11. Canopy Clustering, <http://mahout.apache.org/users/clustering/canopy-clustering.html>.
12. Fuzzy K-Means, <http://mahout.apache.org/users/clustering/fuzzy-k-means.html>.

13. StreamingKMeans algorithm, <http://mahout.apache.org/users/clustering/streaming-k-means.html>.
14. Spectral Clustering Overview, <http://mahout.apache.org/users/clustering/spectral-clustering.html>.
15. Sharma, Ishan, Rajeev Tiwari, and Abhineet Anand. "Open Source Big Data Analytics Technique." Proceedings of the International Conference on Data Engineering and Communication Technology. Springer Singapore, 2017.
16. Esteves, Rui Maximo, Rui Pais, and Chunming Rong. "K-means clustering in the cloud—a Mahout test." Advanced Information Networking and Applications (WAINA), 2011 IEEE Workshops of International Conference on. IEEE, 2011.
17. Barrachina, Arantxa Duque, and Aisling ODriscoll. "A big data methodology for categorising technical support requests using Hadoop and Mahout." Journal of Big Data 1.1 (2014): 1.
18. Apache Hadoop, <http://hadoop.apache.org/>.
19. Apache Mahout, <http://mahout.apache.org/>.
20. K-Means Clustering, https://home.deib.polimi.it/matteucc/Clustering/tutorial_html/kmeans.html.
21. Chang, Chih-Tang, Jim ZC Lai, and Mu-Der Jeng. "A fuzzy k-means clustering algorithm using clustercenter displacement." J. Inf. Sci. Eng. 27.3 (2011): 995–1009.
22. Introduction to Latent Dirichlet Allocation, <http://blog.echen.me/2011/08/22/introduction-to-latentdirichlet-allocation/>.

Bandwidth Enhancement of Micro-strip Patch Antenna Using Disconnected U-Shaped DGS

Shraddha Kumari, Shubham Sachan and Asmita Rajawat

Abstract The paper presents the design to increase the bandwidth of an inset feed micro-strip patch antenna using disconnected U-shaped defected ground structure (DGS). Since defects in the ground of the antenna change the current distribution, the bandwidth changes. A critical and comparative analysis of the three different antenna designs has been done. The first design is of a simple micro-strip patch antenna with inset feed. The second design consists of three defects in the ground of the antenna. The third consists of the DGS as well as a slot in the patch of the antenna. Simulation results show that the bandwidth increases with each design especially when DGS is applied. The proposed design is applicable for the frequency of IEEE S band—3.6 GHz.

Keywords Inset feed · Micro-strip patch
Disconnected U-shaped defected ground structure

1 Introduction

1.1 Related Work

Due to the ever-growing developments in wireless communications, the need for affordable and efficient micro-strip patch antenna [1] continues to grow.

S. Kumari (✉) · S. Sachan · A. Rajawat
Amity University, Noida, Uttar Pradesh, India
e-mail: shraddha.kumari@gmail.com

S. Sachan
e-mail: kabirhappy94@gmail.com

A. Rajawat
e-mail: arajawat@amity.edu

An antenna is basically a transducer designed in such a way that it receives and transmits electromagnetic waves. Because of the various advantages a micro-strip patch antenna has over conventional antennas like manufacturing ease, low fabrication cost, light weight, they are widely used in various practical applications like wireless communication, RADAR, Wi-Max. The proposed antenna design works in the S band of IEEE standards and is further modified to enhance bandwidth.

In this paper, DGS is introduced for bandwidth enhancement [2] of a micro-strip slot antenna. Defected ground structure (DGS) [3–5] refers to a configuration that is etched periodic or cascaded non-periodic configuration. It creates a defect in the ground of transmission line. This changes the shield current distribution which changes the characteristics of the transmission line such as line capacitance or inductance. This further changes the gain or the bandwidth of antenna. A lot of research has been done in this field to modify the antennas as per the requirements.

There can be various slot geometries that can be etched in the ground plane like arrowhead-slot, spiral head, dumb-bell shape, H-shape [6, 7]. Due to these defects in the ground of the antenna, the capacitance/inductance changes. In this paper, DGS has been used to improve bandwidth of the antenna. Further inset feed has been used upon careful analysis [8, 9].

1.2 Contribution

The paper is dedicated toward the study and simulation of three different antenna designs. The design is modified by using disconnected U-shaped defected ground structure. The design of the antenna consists of an inset feeding technique because of its fabrication ease, and simple matching technique. It is shown that the first design without DGS has a lower bandwidth and bandwidth increases as we introduce defects in ground.

1.3 Organization of Paper

The paper is organized as follows: Sects. 2 and 3 consist of the proposed antenna designs with their simulation results with and without DGS, respectively. We can conclude our analysis from the simulation results. Section 4 concludes the paper.

2 Antenna Design

The paper presents three new micro-strip patch antenna designs. The simulation has been done on Computer Simulation Technology (CST). The working frequency has been chosen as 3.5 GHz. The first antenna is crafted on a 1.6-mm thick FR-4(lossy)

dielectric substrate having dielectric constant of 4.3. This material is used as it reduces the antenna size and makes it compact. The second antenna consists of the disconnected U-shaped defected ground structure. The third design consists of one slot in the patch of the antenna along with the previously etched DGS. The antenna designs are obtained for various parameters, and based on the results obtained, a comparison is made among them.

2.1 Antenna Design A

Figure 1 shows a design of a basic micro-strip patch antenna named as Design A which does not contain DGS. This model design is provided with an inset feed [4, 9] in the patch, and bandwidth and return loss are measured at 3.5 GHz frequency.

Measurements of patch are determined using the antenna equations [3]. These are further optimized for better results. The calculated parameters of Design A are shown in Table 1.

2.2 Antenna Design B

For enhancing the bandwidth of the antenna, the design has been modified and etched with a disconnected U-shaped defected ground structure as shown in Fig. 2.

The dimensions of the patch antenna are same as the previous design. A disconnected U-shaped slot is further cut in the ground of the antenna whose measurements have been mentioned in Table 2.

Fig. 1 Micro-strip patch antenna without DGS

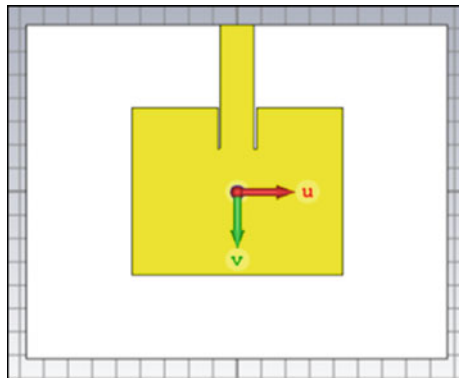


Table 1 Antenna A optimized parameters

Variable	Value (mm)
Length of patch	71.6
Width of patch	87.2
Height of substrate	1.6
Length of feed line	53.7
Width of feed line	14

Fig. 2 Ground plane with disconnected U-shaped DGS

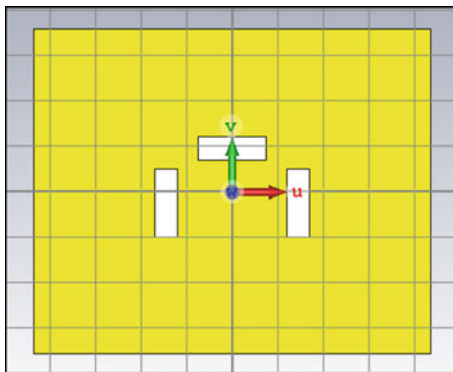


Table 2 Antenna B optimized parameters

Variable	Value (mm)
Length of patch	71.6
Width of patch	87.2
Height of substrate	1.6
Length of feed line	53.7
Width of feed line	14
Dimensions of slot	30 * 10

2.3 Antenna Design C

For enhancing the bandwidth, one additional slot in the patch of the antenna is done as shown in Fig. 3.

The dimensions of the patch as well as the slots in the ground remain same. The slot in the patch of antenna is the same as the slot in the ground whose dimensions are mentioned in Table 3.

Fig. 3 Patch of antenna with one slot

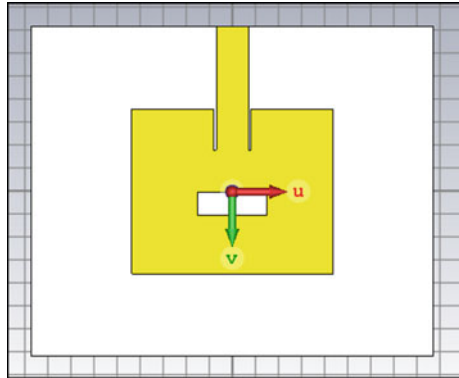


Table 3 Antenna C optimized parameters

Variable	Value (mm)
Length of patch	71.6
Width of patch	87.2
Height of substrate	1.6
Length of feed line	53.7
Width of feed line	14
Dimensions of slots in the ground	30 * 10
Dimensions of slot in the patch	30 * 10

3 Results and Discussion

Three micro-strip patch antennas with an inset feed have been designed. The first antenna Design A has a good gain but with limited bandwidth. The return loss is below -10 dB which is good. The Design B was proposed with a disconnected U-shaped defected ground structure in the antenna. The results show that with DGS, resonant frequency shifts to the lower side due to change in the current distribution of the radiating patch. The bandwidth increases with DGS, and the antenna behaves as a dual-band antenna with increased bandwidth. Another antenna Design C which is proposed consists of another slot in the patch of the antenna which increased the bandwidth even more. Table 4 shows the comparison between the three antenna designs.

3.1 Results of Design A

(a) Return Loss

For the antenna without defect ground structure, return loss is shown in Fig. 4. A resonant peak (RL = -34.195) for the resonant frequency 3.5 is obtained which is below -10 dB. The bandwidth for the same is 66 MHz.

(b) Radiation Pattern

The radiation pattern for frequency 3.5 GHz is shown in Fig. 5.

Table 4 Comparison between the three antenna designs

Design	Frequency (GHz)	Return loss	Bandwidth (MHz)
A	3.5	-34.195	66
B	3.22	-23.584	115
	3.65	-28.015	70
C	3.87	-24.371	80

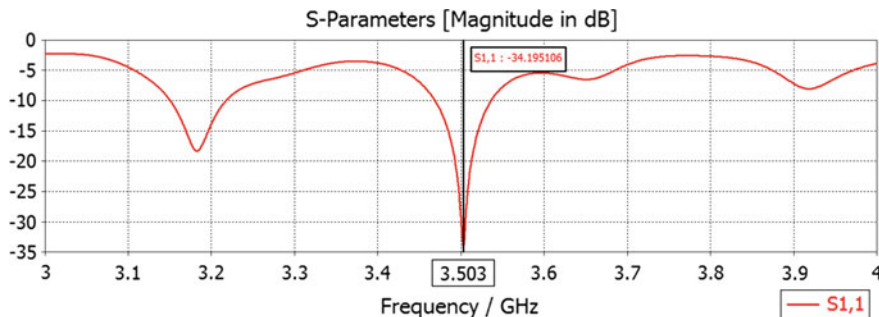


Fig. 4 S₁₁ of the antenna A

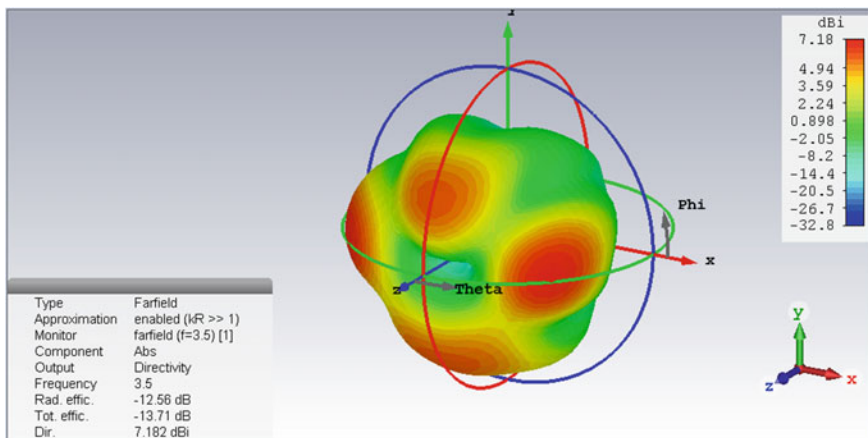


Fig. 5 Radiation pattern at 3.5 GHz

3.2 Results of Design B

(a) Return Loss

For the antenna with a disconnected U-shaped defected ground structure, return loss is shown in Fig. 6. For the resonant frequency 3.65 GHz, a resonant peak (RL = -27.916 dB) is obtained and at 3.22 GHz a resonant peak (RL = -23.584) is obtained which is below -10 dB. The bandwidth increases to 70 MHz for frequency 3.65 GHz and to 115 MHz for frequency 3.22 GHz.

(b) Radiation Pattern

The radiation pattern for frequency 3.65 GHz is shown in Fig. 7 and for frequency 3.22 in Fig. 8.

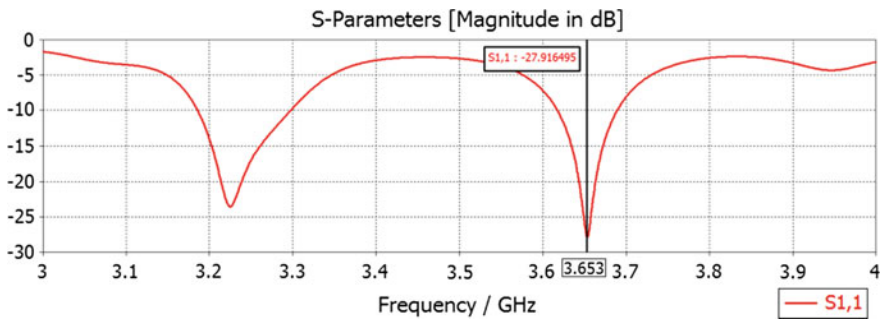


Fig. 6 S_{11} of the antenna B

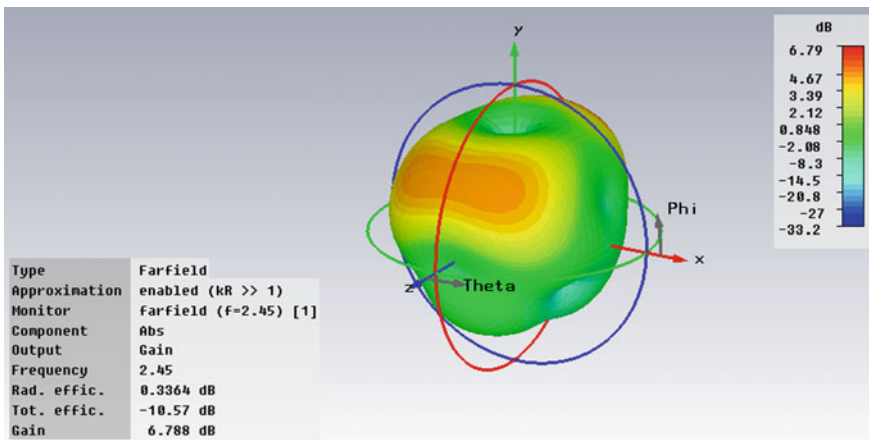


Fig. 7 Radiation pattern at 3.65 GHz

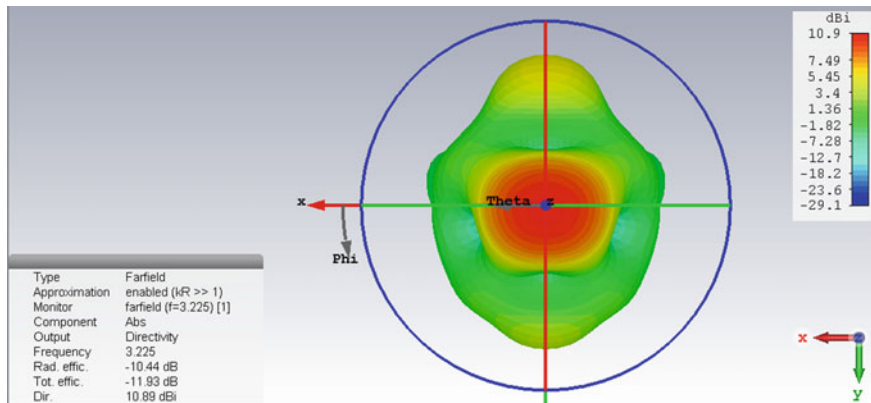


Fig. 8 Radiation pattern at 3.22 GHz

3.3 Results of Design C

(a) Return Loss

For the antenna with a U-shaped defected ground structure and one slot in the patch of the antenna, return loss is shown in Fig. 9. For the resonant frequency 3.87 GHz, a resonant peak (RL = -24.371 dB) for the patch antenna is obtained which is below -10 dB. The bandwidth further increases to 80 MHz.

(b) Radiation Pattern

The radiation pattern for frequency 3.87 GHz is shown in Fig. 10.

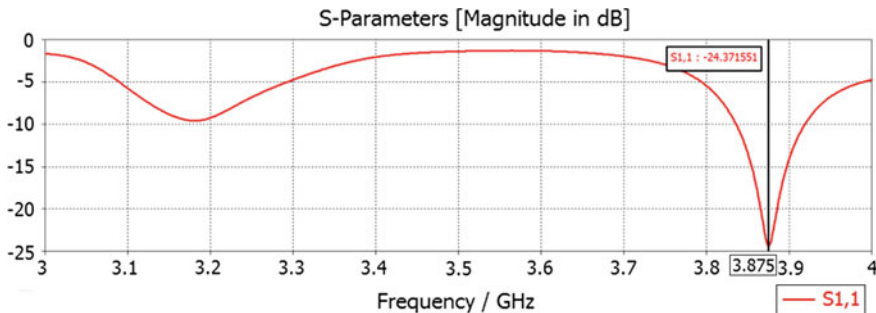


Fig. 9 S₁₁ of the antenna C

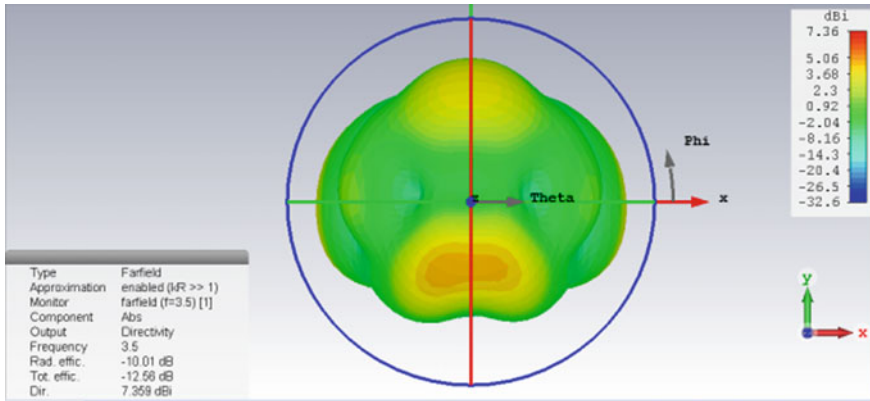


Fig. 10 Radiation pattern at 3.67 GHz

4 Conclusion

After analyzing the simulation, we can say that the bandwidth has increased to 80 MHz in Design C as compared to 66 MHz in Design A. Results also suggest that when we introduced defected ground structure in Design B, the antenna behaved as a dual-band with enhanced bandwidth at both the resonant frequencies. The bandwidth at frequency 3.22 GHz increased to 115 MHz which is an improvement of 74%. The change in bandwidth can be attributed to the relation between current distribution and bandwidth. The dual-band antennas can be used in long-distance communication like satellite communication, radars.

References

1. Constantine A Balanis, *Antenna Theory Analysis and Design*, 2nd Edition, Singapore, John Wiley and Sons (2002).
2. Varun Vaid, Sunil Agrawal, "Bandwidth Optimization using Fractal Geometry on Rectangular Micro-strip Patch Antenna with DGS for Wireless Applications", 2014 International Conference on Medical Imaging, UIET Punjab University, India.
3. A.K. Arya, M.V. Kartikeyan, A. Patnaik, "Efficiency Enhancement of Microstrip Patch Antenna with Defected Ground Structure", *MICROWAVE*, (2008) 729–731.
4. R. L. Dua, H. Singh, N. Gambhir, "2.45 GHz Micro strip Patch Antenna with Defected Ground Structure for Bluetooth", *International Journal of Soft Computing and Engineering (USCE)*, vol. 1, no. 6, pp. 2231–2307, January 2012.
5. Ashwini K. Arya, M.V. Kartikeyan, A. Patnaik, "Defected Ground Structure in the perspective of Microstrip antenna", *Frequenz*, Vol.64, Issues 5–6, Oct (2010) 79-84.
6. A. K. Arya, A. Patnaik, M.V. Kartikeyan, "Gain Enhancement of Micro-strip patch antenna using Dumbbell shaped Defected Ground Structure", *IJSRET*, Vol.2, Issue 4, July (2013) 184–188.

7. Asmita Rajawat, P.K Singhal, Sindhu Hak Gupta, Chavi Jain, Praneet Tomar, Kartik Kapur, "Gain Enhancement of Microstrip Patch Antenna Using H-Shaped Defected Ground Structure", 4th International Conference on Advanced Computing, Networking and Informatics (ICACNI 2016).
8. S. Sathamsakul, N. Anantrasirichai, C. Benjangkaprasert and T. Wakabayashi, "Rectangular patch antenna with inset feed and modified ground plane for wideband antenna", SICE Annual Conference 2008, The University Electro-Communications, Japan, August (2008) 20–22.
9. S. Bhunia, M.-K. Pain, S. Biswas, D. Sarkar, P. P. Sarkar, and B. Gupta, "Investigations on Micro strip Patch Antennas with Different slots and Feeding Points", Microwave and Optical Technology Letters, No. 11, Vol. 50, November (2008) 2754–2758.

Effect of the Dimension of Feedline for the Enhancement of Bandwidth of Square Microstrip Antenna

R.K. Chaurasia, Vishal Mathur, Ranjan Mishra
and Raj Gaurav Mishra

Abstract The need for the development of wideband microstrip antenna has been very well recognized. The present-day researchers are focused on developing novel design of microstrip antenna which would provide a good wideband. In this paper, the geometry of a microstrip antenna has taken to be square and feeding method also changed which is responsible for broadband. The antenna is fed with microstrip line by keeping a stub at source junction. It is done to improve the impedance bandwidth by the width of the structure of feedline adjustment is performed. This paper presents the study of a compact square antenna to operate in the frequency range of X-band from 8 to 12 GHz. The prototype planer antenna exhibits an overall wideband of bandwidth 560 MHz with a good reflection coefficient of -25 dB. This type of antenna is very useful in many broadband applications in X-band.

Keywords Antenna array · Return loss · X-band · Microstrip antenna

1 Introduction

Microstrip antennas are very popular in recent year because of economical efficiency, very small size, support to horizontal and vertical polarization, and many more. However, one of the major issues of the microstrip patch antenna is the small operating bandwidth. It is the most significant factor limiting the widespread use of the

R.K. Chaurasia (✉) · V. Mathur
ICFAI Tech School (ITS), The ICFAI University, Jaipur, India
e-mail: chaurasia.rajkg@gmail.com

V. Mathur
e-mail: wishalmathur@gmail.com

R. Mishra · R.G. Mishra
University of Petroleum and Energy Studies, Dehradun 248007, India
e-mail: rmishra@ddn.upes.ac.in

R.G. Mishra
e-mail: rgmishra@ddn.upes.ac.in

microstrip antenna in broadband application. Since microstrip antenna is very compact, low-cost, multitasking, and reliable wireless communication devices have become an essential part of our daily communication life, and the need for low-profile miniaturized multi- and wideband antennas has escalated [1]. Most of the wireless device operated in X-band communication needs separate antenna for different bands, but microstrip antenna can resonant more than once. The size of electronics needed for wireless applications is shrinking drastically, whereas their functionality has increased. The demand for the antennas for these various applications is of small size, lightweight, low cost, and integrality with electronic integrated circuits. Microstrip antennas with planer patch configuration meet the demands of these. The planer microstrip antenna suffers from narrow bandwidth (3–5%) and poor efficiency [2]. Its low bandwidth is not sufficient for most of the wireless applications nowadays. Various methods have been studied [3, 4] and reported to increase the patch antenna impedance bandwidth. The effects of notches are also reported in various literatures [5–7]. The effect of slot in broadening is also reported [8–10]. In very fundamental structure, a microstrip antenna is formed by two conductor: an upper conductor and lower conductor which are separated by dielectric substrate; an upper conductor is radiating patch, and lower conductor is ground plane for antenna.

2 Antenna Design

The design of the antenna depends on three parameters, namely resonant frequency (f), substrate material related to *dielectric constant* (ϵ_r), and *substrate height* (h). The resonant frequency selected for design of microstrip antenna is 11.0 GHz. The substrate whose dielectric constant must be lower volume and low tangent loss is chosen to achieve a broadband of microstrip antenna. Also, it is mandatory that the antenna should not be bulky, so the height of the dielectric substrate is selected as 1.57 mm. The feeding is required to transfer power from sources to antenna, a very simple microstrip feedline method has been used for feeding purpose, and the length and width of the antenna are calculated using the following equations [11]:

$$\text{The width, } W, \text{ is given as: } W = \frac{c}{2f} \times \sqrt{\frac{2}{(\epsilon_r + 1)}}$$

where f is the resonant frequency and ϵ_r is the dielectric constant of the substrate. In our design, the substrate is chosen as Duroid with and ϵ_r of 2.2.

$$\text{The length, } L, \text{ is given as: } L = \frac{c}{2f} \left(\frac{\epsilon_r + 1}{2} + \frac{\epsilon_r - 1}{2} \sqrt{\left[1 + 12 \frac{h}{W} \right]} \right)^{-1} - 2\Delta L$$

$$\text{where } \Delta L = 0.412h \left(\frac{(\epsilon_{\text{eff}} + 0.3) \left(\frac{W}{h} + 0.264 \right)}{(\epsilon_{\text{eff}} - 0.258) \left(\frac{W}{h} + 0.8 \right)} \right)$$

$$\epsilon_{\text{reff}} = \frac{\epsilon_r + 1}{2} + \frac{\epsilon_r - 1}{2} \sqrt{\left[1 + 12 \frac{h}{W} \right]}$$

where ϵ_{reff} = effective dielectric constant and ϵ_r = dielectric constant of substrate.

The effective length is the length owing to the fringing effect. The correction factor and the corresponding effective dielectric constant are calculated from the set of equations [12]. With these values, the length and width of the antenna, as calculated from the above sets of equations, are come out to be 8.15 and 10.77 mm; the structure of the antenna has been shown in Fig. 1; and the resultant bandwidth that come out to be 340 MHz of impedance bandwidth is shown in Fig. 2. The length and width of the square-shaped antenna are to be taken as 8.00 mm. The simulation was done using HFSS.

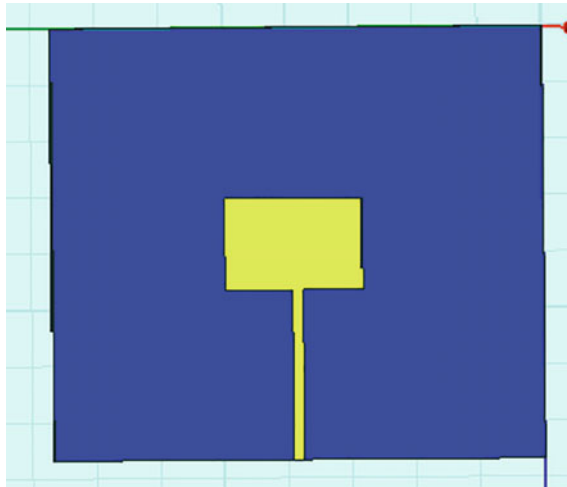


Fig. 1 Structure of design antenna

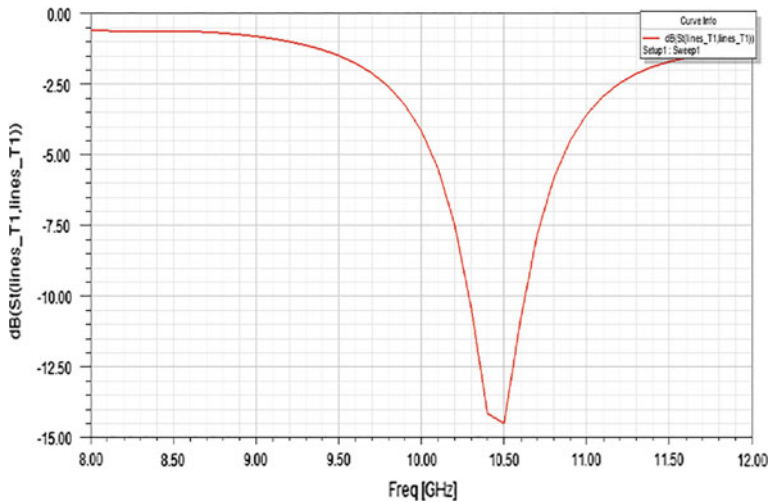


Fig. 2 Bandwidth of design antenna

3 Result and Discussion

The proposed antenna design structure is shown in Fig. 3. The dimension of the square microstrip antenna is provided in Table 1. In this design, we have modified the dimension of feedline structure at source side and in fact widen the feedline structure from 1.79 to 5.79 mm, and the maximum bandwidth obtained is 490 MHz.

It is reported that the higher width accounts for more bandwidth [13]. Our observation also validates this. The prototype antenna exhibits a good broad bandwidth when the width of the stub is kept at 4.79 mm. The impact of the variation of the stub width in the better reflection coefficient of -25.5 dB and higher broadband is shown in Fig. 4. The maximum bandwidth is obtained at 4.79 mm. When further increasing the width of the stub, its bandwidth remains constant, and above 5.79 mm width, the band of frequencies exceeds beyond 12 GHz of range.

Fig. 3 Structure of proposed antenna

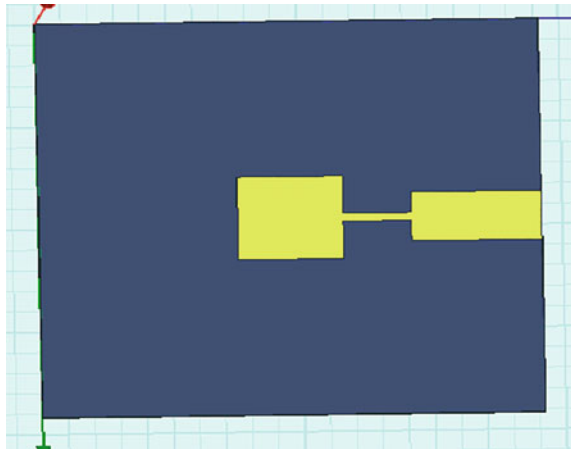


Table 1 Dimension of the square antenna

Width of the antenna	8.00 mm
Length of the antenna	8.00 mm
Length of stub line	9.90 mm
Width of stub line	4.79 mm
Length of substrate	38 mm
Width of substrate	38 mm
Height of substrate	1.5 mm

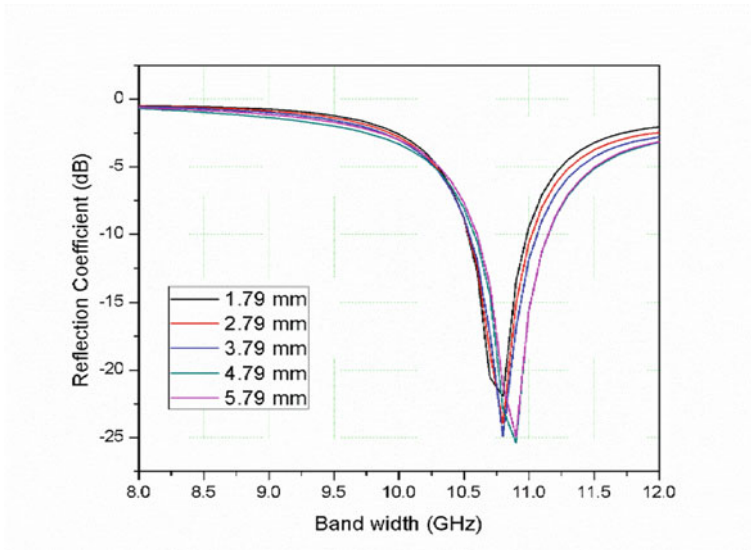


Fig. 4 Different stub widths of feedline with bandwidth

4 Conclusion

A novel design of the square microstrip antenna is presented. The effect of the dimension of the feedline for the enhancement of the bandwidth has been observed by placing a stub at source junction, and a broadband is obtained by the increment in the width of the stub of the feedline. The antenna has shown a good bandwidth of 560 MHz which is considerable for good broadband applications in the X-band.

References

1. R. Mishra, P. Kuchhal, A. Kumar, "Effect of Height of the Substrate & Width of the Patch on the Performance Characteristics of Microstrip Antenna", *International Journal of Electrical and Computer Engineering*, vol 5, no 6, pp 1441–45, (2015).
2. Amandeep Bath, Abhishek Thakur, Jitender Sharma, Prof. Basudeo Prasad, "Design of a rectangular Patch Antenna", *International Journal of Electrical and Electronics Engineering (IJEEE)*, Vol. 1, No. 1, pp. 1–6, February (2011).
3. Kushwaha, R.S.; Srivastava, D.K.; Saini, J.P.; Dhupkariya, S., "Bandwidth Enhancement for Microstrip Patch Antenna with Microstrip Line Feed," *Computer and Communication Technology (ICCCT)*, vol., no., pp. 183,185, 23–25 Nov. (2012).
4. R. Mishra, J. Jayasinghe, R. G. Mishra, P. Kuchhal, "Design and Performance Analysis of a Rectangular Microstrip Line Feed Ultra-Wide Band Antenna", *International Journal of Signal Processing, Image Processing and Pattern Recognition* Vol. 9, No. 6, pp. 419–426, (2016).

5. Dong-Zo Kim, Wang-Ik Son, Won-Gyu Lim, Han-Lim Lee, and Jong- Won Yu, "Integrated planar monopole antenna with microstrip resonators having band-notched characteristics", *IEEE Trans. Antennas Propag.*, vol. 58, pp. 2837–2842 (2010).
6. S. W. Su, K. L. Wong and C. L. Tang, "Band-notched ultra-wideband planar monopole antenna", *Microwave Optical Technology, Letter*, vol. 44, pp. 217–219 (2005).
7. Jia-Yi Sze and Wie-Shan Chang, "Dual-band square slot antenna with embedded crossed strips for wireless local area network applications," *IEEE Letter on Microwave and Optical Technology*, Vol. 51, pp. 435–439, (2009).
8. K. F. Lee, K. M. Luk, K. F. Tong, S. M. Shum, T. Huyn and R. Q. Lee, "Experimental and Simulation Studies of the Coaxially Fed U-slot Rectangular Patch", *IEEE Proceedings of Microwave Antenna propagation*, Vol. 144, No. 5, pp. 354–358 (1997).
9. Srilakshmi, A.; Koteswararao, N.V.; Srinivasarao, D., "X band printed Microstrip compact antenna with slots in ground plane and patch," *Recent Advances in Intelligent Computational Systems (RAICS)*, 2011 IEEE, vol., no., pp. 851,855, 22–24 Sept. 2011.
10. Kumar G and Ray K.P., "Broadband Microstrip Antennas", *Artech House*(2003).
11. C. A. Balanis., "Antenna Theory - Analysis and Design", *Wiley-Interscience*, (2012).
12. R. Mishra, An Overview of Microstrip Antenna, *HCTL Open International Journal of Technology Innovations and Research (IJTIR)*, Vol. 21, No. 2, (2016).
13. P. Kumari, P. Ranjan, R. Gowri and P. Kuchhal, "Design of double sided metamaterial antenna for mobile handset applications," *2014 International Conference on Signal Processing and Integrated Networks (SPIN)*, Noida, pp. 675–678. (2014).

Optimization of Data Centres for Heat Management

Saurabh Singh, Abhineet Anand and Rajeev Tiwari

Abstract Servers are backbone of our digital age. In recent times, operation and managing operation system has become a lot easier. But still server management comes with its own set of challenges like cost constraints, network latency, environment. The biggest obstacle in managing the server is heat management, because it indirectly affects other factors like operation cost, environmental impact and many more. There could be many ways to manage heat on the server, but one of the most effective ways could be to optimize the infrastructure of data centre. In this literature, we try to explore various fractural arrangement and practices to optimize data centre for heat management.

Keywords Data centre · Heat management · Cooling · Green computing

1 Introduction

With the advent of World Wide Web in 1990s, IT revolution started and big MNC, universities, researchers and ever individuals came online. Since then the number of user is accelerating. All this enormous user base is managed by hundreds of data centre located all around the world [1]. To address this huge user base, the solution was simple: “keep on putting more and more server to address the demand”. But soon the organizations felt the problem with this approach, because the servers come with its own set of challenges like cost, power, environmental effects. But the

S. Singh (✉) · A. Anand
SCSE, Galgotias University, Noida, India
e-mail: saurabhfly121@gmail.com

A. Anand
e-mail: abhineet.mnnit@gmail.com

R. Tiwari
Department of Computer Science, UPES, Dehradun, India
e-mail: rajeev.tiwari@ddn.upes.ac.in

most fundamental concern is heat and energy optimization. In this paper, our focus is on heat. Heat management is directly related to many other factors like

- Durability of hardware.
- Cost: as with increasing load on data centre increases heat dissipated which hence costs a lot to manage.
- Impacts of data centre on environment: managing heat would help data centre to manage constraints put up by environmental regulatory, many other green computing concerned authorities.

When it comes to manage heat [2], there can be three aspects in which it could be managed:

- Optimizing the data center infrastructure.
- Optimizing the hardware for server racks to manage heat flow.
- Optimizing through software and algorithms.

In general, circumstances all of the three aspects/approach are used to reach to the best optimized state. But in this literature, our work is confined to optimizing the data centre infrastructure [3]. Then Timothy M. work on reducing energy consumption by means of resource allocation methods has also motivated us for progressing in this work [4].

2 Proposed Ideas Through Which Problem Has Been Addressed

Every electronic machine in the data centre produces heat as a waste. As the data centre is an enclosed facility, if the heat is not given proper outlet, it could easily damage the server, thus the need for cooling is must. The American society of heating and air conditioning engineer (ASHRAE) [5] states parameter for data centre. These days, ASHRAE allowable temperature extends up to 104 °F for certain kind of devices.

The problem with heat management is that it requires a lot of energy, specific infrastructure, a considerable operation expense, etc. But still all such expense never ensures that one would get the desired result.

Data centre cooling is all about design, and it governs the efficiency and control of the data centre. It also helps to determine the expectation, energy inputs and capital requirements. Hence, it is very vital for planning.

There are many approaches/technique to optimize the data centre. But all these approaches generally tend to control airflow, humidity and other factor related to it, in order to manage the heat. The designs we would like to discuss in this literature are as follows.

2.1 Simple Raised Floor Cooling

This method has been there for decades, and it was one of the oldest approaches which was used for few of earliest data centre. It works on the principal of mixing the conditioned air with comparatively hot air in the chamber of servers; that is, little amount of cold air is mixed with the hot air. So, larger volume of air temperature comes down at the required level of temperature. This approach works well when information technology equipment (ITE) densities used to be low. This approach of mixing cold air into the hot air provides an uneven temperature, low density and poor efficiency for data centre. But, it has been seen at most of the data centre in the Asian region because of easy architectural requirement and maintenance majors (Fig. 1).

2.2 Cold Aisle Containment

Cold aisle environments are generally used along with the raised floor. It allows in the cooling system to keep different delivery systems like overhead duct facility with raised floor cooling system. It can be easily observed and has been observed that it becomes very hard to make any adjustment/change once the platform for server is arranged. In the raised floor, many cold air pods are included where amount of cold air to be pumped is regulated. Volume of cold air to be delivered to different pods depends on the area is being covered by that cold pod (Fig. 2).

With this approach of data centre, it is required to assume the flow of cold air will not be required to send on continuous basis. It will not be a very wise to take out tiles of the floor or adjust tiles. In few cases of data centre, computational fluid dynamics (CFD) is used to determine airflows which could be on real time data

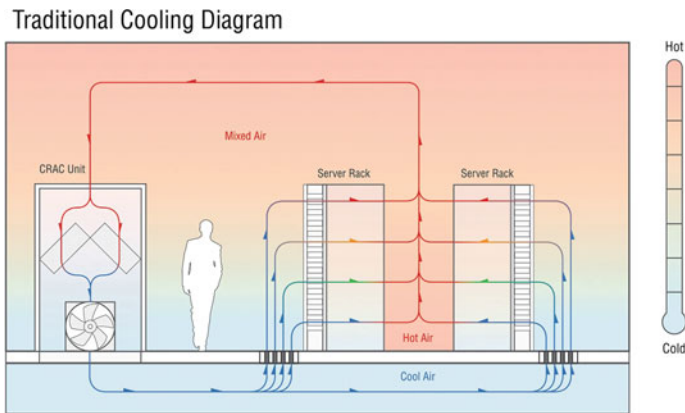


Fig. 1 Traditional cooling system

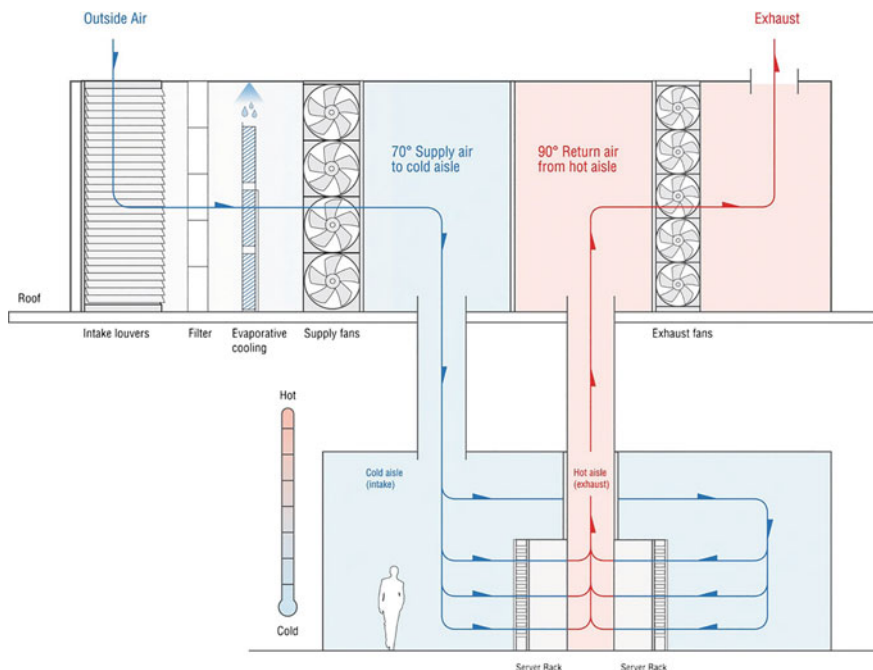


Fig. 2 Hot air is kept separately produced by the servers

depended, which can regulate cold air fan speed to get the correct amount of air to be pumped to correct pod. But, practically there is a limitation of volume of air to be delivered to particular pod with amount of tiles it is covering. Still the approach is being observed to be with great result where the loading of ITE remains stable.

2.3 Hot Aisle Containment

In the previous approach, methodology suggested to push the cold air into the system, whereas the next discussed approach is trying to pump out the hot air from the plenum. Hot aisle approach increases the flexibility for deploying containment. For users, it will be easy to deploy many pods easily with the different cabinet layout. The pod can be deployed like the chimney structure used in our household in the ceiling plenum, which can be easily detached like ceiling tile and allow the hot air to get out of chamber as the hot air will naturally go up. It allows for the flexibility to remove raised floor from design which allows to reduce cost and management.

2.4 *Liquid Cooling*

A liquid-based cooling design needs chillers that remove heat from the outside environment to provide cool water. The cool water transported is moved to the data centre, and also the pulse of liquid cooling includes the flexibility to deploy it in specified area by row or rack. It is reliable with few moving parts. But the challenge is that poses bigger technical and budget challenges in comparison to air cooling technologies.

2.5 *Economizer Cooling*

It is one of the most efficient cooling designs at present. Due to effectiveness and its approach, it is also called “free calling”. In this approach, the refrigerant cycle is turned off either part or all of the time. It limits the expense of chillers and compressors which are associated with traditional model. Economizer can be briefly classified into three types based on the sources where they get inputs into data centre, i.e. air side, waterside, evaporized.

Airside economizers bring air from outside to data centre, which is then allowed to mix with air returning to get the desirable conditions, before it is pumped into the data centre. There is an other technique which restrict outside air to enter the data centre and take heat from inside. Mainly this is applicable for the location where temperature used to be at very low level.

Evaporative cooling is one different approach where systems use evaporated water (direct or may be indirect) to replace the available cooling. It has been used for refrigerant-based cooling more efficiently. When the state of water change, it absorbs energy, lowering the dry bulb temperature to a point where it approaches the wet bulb (saturated) temperature of the air.

One other approach is waterside economizer systems, where lowering the temperature is not required, because outside environment is very cold and to maintain the temperature of plenum it only required to guide the cold and hot air at the required chambers. Heat exchanger is used to pump water and pass air through hot and cold water atmosphere to maintain the temperature required. The chilled water passes through a heat exchanger and rejects the heat directly to the condenser water loop.

This optimization technique is every efficient in optimizing both heat and energy. These days giants like Facebook are investing a lot on this approach. But still there is lot of scope of improvement as it has potential to be optimized more (Fig. 3).

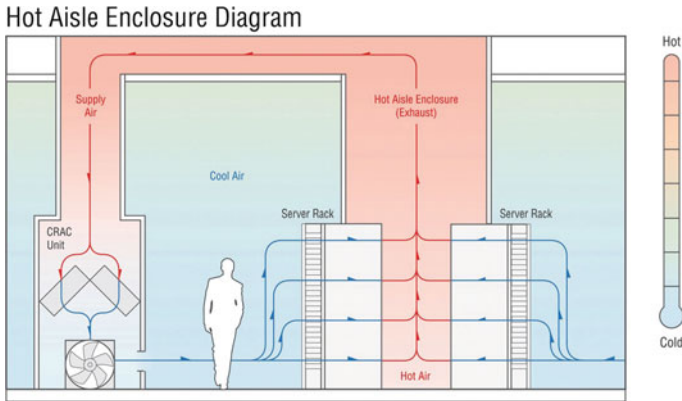


Fig. 3 Hot containment is used to separate the hot and cold air

3 Analytical Study

A simple raised floor cooling system is good for very primary system, but for larger set-up, it becomes futile and inefficient. Also it is not very static in nature and the cooling is uneven. It provides more flexibility than the simple raised floor cooler set-up.

Many articles and literature by different researchers and developers have been citing and discussing that the size of cloud computing environment and size of server and applicability have been growing with tremendous speed both at economical and consumer level and requirement level. One of the well solution for that is Project Natick [6] used by Microsoft where the data centre has been kept under water which has been suggested by **When Sean James**. The project is mainly focusing on those consumers where polluted lives near water. Idea behind the putting offshore data centre is growth of data in those populated area. Underwater installation of data centre will provide more cooling, renewable energy sources and easily controlled environment. By putting the server offshore, it will provide the benefits of **Rapid Provisioning** and **Reduced Latency Time**. Natick uses recycled material for its data centre, uses very less energy from outside as it recycle its energy generated by itself, consumes no water for cooling.

Closed isle system has better efficiency. The cooling is more concentrated and is more flexible in nature. IT is good for the normal data centre with average size, but it is not proved so much efficient for big data centre. Also it consumes lot of energy.

The economizer cooling system proves very efficient. IT draws air and moisture from outside which makes it environment friendly. It also reduces the cost of chillers and compressor which reduces its operation cost. Use of economizer cooling is prevalent these days. One big drawback is that it is dependent to some extent on the outside, which can be troublesome for some geographic location.

4 Conclusion

A simple raised floor cooling system is good for very primary system, but for larger set-up, it becomes futile and inefficient. Also it is not very static in nature and the cooling is uneven. It provides more flexibility than the simple raised floor cooling set-up.

Closed isle system has better efficiency. The cooling is more concentrated and is more flexible in nature. IT is good for the normal data centre with average size, but it is not proved so much efficient for big data centre. Also it consumes lot of energy.

The economizer cooling system proves very efficient. IT draws air and moisture from outside which makes it environment friendly. It also reduces the cost of chillers and compressor which reduces its operation cost. Use of economizer cooling is prevalent these days. One big drawback is that it is dependent to some extent on the outside, which can be troublesome for some geographic location.

From raised floor cooling technology to economizer cooling technology and then to the auspicious concept of underwater data centre. We have come a long way. Rigorous research and innovation is required to build more efficient technology. Unique design and auspicious do lay the foundation for future innovation but choice of data centre design for a typical organization is not depended upon latest design but on factors like constraints capital, floor space, need so such design which are more efficient and could be easily implemented by typical data centre should be promoted and improved.

5 Future Scope

Data centre cooling technology is one of the most important areas of research these days. More and more innovation is being put these days. One such considerable innovation is project Natick by Microsoft. Project Natick promises to end all the problems posed by open environment design. The idea here is to go underwater. It completely eliminated the need of water for data centre cooling. Some cooling also could be made more efficient by make use of the hot air/water that is put out as a water. It could be done through using hot air/water for energy generation.

References

1. John Peter Valiulis “Intelligent Controls: a Simple Way to Optimize Your Data Center Thermal Management System” BY INDUSTRY PERSPECTIVES ON AUGUST 19, 2015
2. A Beloglazov, J Abawajy, R Buyya “Energy-aware resource allocation heuristics for efficient management of data centers for cloud computing”- Future generation computer systems, 2012 - Elsevier

3. Kien Le, Ricardo Bianchini, Thu D. Nguyen, Ozlem Bilgir, Margaret Martonosi, "Capping the brown energy consumption of Internet services at low cost", Green Computing Conference 2010 International, pp. 3–14, 2010.
4. Timothy M. Lynar, Ric D. Herbert, Simon, William J. Chivers, "Reducing grid energy consumption through choice of resource allocation method", Parallel & Distributed Processing Workshops and Phd Forum (IPDPSW) 2010 IEEE International Symposium on, pp. 1–7, 2010.
5. http://www.apc.com/salestools/VAVR-5UDTU5/VAVR-5UDTU5_R2_EN.pdf
6. <http://natick.research.microsoft.com/>.

Controlling of PMSG-Assisted Wind Energy Conversion System with Maximum Power Tracking Technique

Diwaker Pathak, Rupendra Pachauri and Yogesh K. Chauhan

Abstract This paper develops a dynamic model of small-scale wind energy conversion system (WECS) based on diode bridge rectifier and permanent magnet synchronous generator (PMSG). The simple and effective perturb and observe (P&O) algorithm has been proposed for extracting maximum power point tracking (MPPT) of wind turbine (WT) in the moderate-to-cutout wind speed region by sensing input parameters of DC–DC buck–boost converter. The MPPT algorithm in addition to the DC–DC converter is being simulated in MATLAB/Simulink software. The obtained characteristics show the effectiveness of P&O MPPT technique for extracting maximum power from the wind and delivering it appropriately to the resistive load.

Keywords DC–DC buck–boost converter • Wind turbine • P&O controller
Permanent magnet synchronous generator (PMSG) • Renewable energy

1 Introduction

The energy composed from the sources which are replenished by nature such as sunlight, wind is defined as renewable energy (RE) [1]. RE sources exist on large geographical areas on earth in the form of various energies such as wind, solar, biofuel. The depletion of energy resources like fossil fuels is due to rapid and high

D. Pathak (✉) · Y.K. Chauhan

Electrical Engineering Department, School of Engineering, Gautam Buddha University,
201312 Greater Noida, India
e-mail: diwakernit29@gmail.com

Y.K. Chauhan

e-mail: chauhanyk@yahoo.com

R. Pachauri

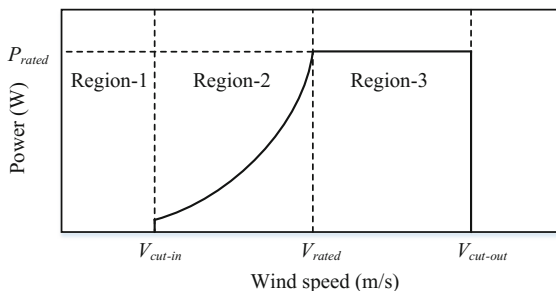
Electronics Instrumentation and Control, Engineering Department, College of Engineering
Studies, University of Petroleum and Energy Studies, Dehradun 248007, Uttarakhand, India
e-mail: rupendrapachauri@gmail.com

© Springer Nature Singapore Pte Ltd. 2018

R. Singh et al. (eds.), *Intelligent Communication, Control and Devices*,
Advances in Intelligent Systems and Computing 624,
https://doi.org/10.1007/978-981-10-5903-2_109

1033

Fig. 1 Ideal power characteristics of wind turbine



utilization. So exploring more energy sources is must. Therefore, a concept of power feedback based on the WECS is proposed in this paper.

The wind potential and direction can be used to generate electricity. But the characteristics of wind speed are highly variable in nature [2]. In this work, a WECS is integrated with P&O algorithm as maximum power extraction technique to investigate the connected resistive load under variable state of wind speed [3, 4].

Control techniques are implied to a wind turbines (WTs) to operate them in a specific range of wind velocity within cut-in (V_{cut-in}) and cutout ($V_{cut-out}$) velocities. Figure 1 shows the generalized power characteristics of a WT having three different operating regions, namely low-speed region (speed less than or equal to V_{cut-in}), moderate-speed region (speed between V_{cut-in} and V_{rated}), and high-speed region (speed between V_{rated} and $V_{cut-out}$). The center of attention of this paper is to analyze the WECS in moderate- and high-wind speed [5].

In [5], authors have concluded that P&O method is flexible and simple in implementation. However, they found P&O method as inefficient having some problems during the determination of optimal value of variable wind speed conditions. In [6], authors have proposed a control scheme for output power extraction from grid-integrated dynamic WECS. They analyzed the proposed MPPT algorithm in MATLAB/Simulink and found an effective technique. In [7], the authors have compared two MPPT algorithms and their implementation in small WECS, namely incremental conductance method (INC) and P&O to prove the effectiveness and reliability of the designed algorithms. In [8], the authors used the P&O algorithm to initialize the command for searching online a maximum power point (MPP) to operate an ideal relation-based technique. The authors in [9] derived a relation for the optimal current in terms of voltage to reach MPP.

This research work presents an effective algorithm, namely P&O for extracting the maximum power in the moderate and above wind speed regions. The WT has been modeled with the dynamic equations in MATLAB/Simulink comprising of PMSG, diode bridge rectifier, and a DC–DC buck–boost converter. The method used in this paper is focused on the concept of identifying the peak value and calculating the voltage and current at that value for the approximation of the duty cycle of buck–boost converter. Once the duty cycle is estimated, then this method can be implemented to determine the optimum output voltage and current for MPPT.

2 Wind Energy Conversion System Layout

The proposed WECS comprises a fixed blade pitch and fixed tip-speed ratio (TSR) WT, a PMSG, a diode bridge rectifier, a DC–DC buck–boost converter, and a resistive load as shown in Fig. 2.

2.1 Wind Turbine System Architecture

The wind power (P_{wind}), power (P_m), and torque (τ_{WT}) equation of a WT are expressed [2] as

$$P_{wind} = \frac{1}{2}A\rho V_w^3, \quad P_m = 0.5\rho AC_p V_w^3, \quad \tau_{WT} = 0.5\rho AC_p V_w^2 \frac{R}{G\lambda} \quad (1)$$

where A is the probe area of WT blades. ρ , V_w , and C_p are air density, wind velocity, and performance coefficient, respectively. R , G , and λ are rotor radius, gear ratio, and tip-speed ratio (TSR), respectively. C_p is expressed [1] as

$$C_p(\lambda, \beta) = C_1 \left(\frac{C_2}{\lambda_i} - C_3\beta - C_4 \right) e^{-\frac{C_5}{\lambda_i}} + C_6\lambda, \quad \frac{1}{\lambda_i} = \frac{1}{\lambda + 0.08\beta} - \frac{0.035}{\beta^3 + 1} \quad (2)$$

where C_1, C_2, \dots, C_6 are coefficients. β and λ_i are pitch angle and initial TSR, respectively. λ is the ratio of the speed of blade tips of a WT and wind velocity [3].

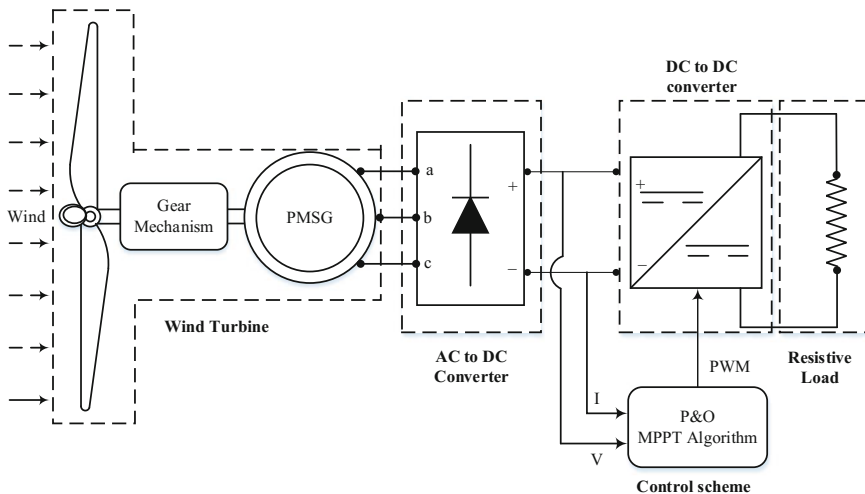
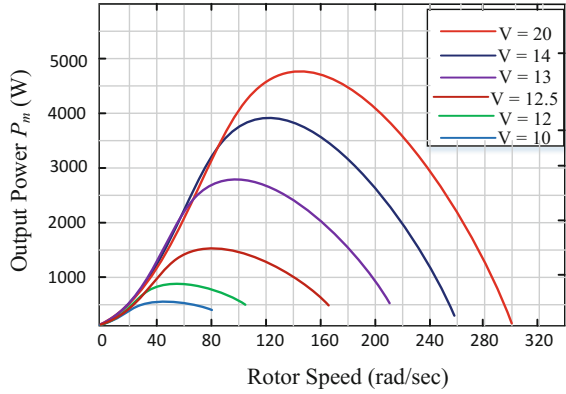


Fig. 2 Proposed system layout

Fig. 3 Power characteristics



$$\lambda = \frac{V_{TIP}}{V_w} = \omega_r \cdot R / V_w \tag{3}$$

where V_{TIP} is speed of tips of blades, and ω_r is rotor angular velocity. Figure 3 shows the power characteristic curves in various wind speed conditions.

2.2 DC–DC Buck–Boost Converter Architecture

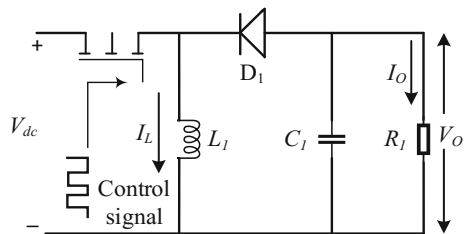
The buck–boost converter is one of the DC to DC PWM converters having output voltage level that must be larger or less than the input voltage level. Relation of the voltage and current is given by Eq. (4) as

$$V_{in} = L \frac{I_2 - I_1}{T_1} = L \frac{\Delta I}{T_1}, V_o = -L \frac{\Delta I}{T_2} \tag{4}$$

where V_{in} is input voltage, I_1 and I_2 are the minimum and maximum inductor currents, respectively. T_1 and T_2 are switching periods.

The equivalent circuit diagram of buck–boost converter is presented by Fig. 4.

Fig. 4 Equivalent circuit of buck–boost converter



The relation between the on time and off time of the switch and the total time duration is given in terms of duty ratio (D) [10] as

$$T_1 = DT, T_2 = (1 - D)T \tag{5}$$

where T is total switching period ($t_{on} + t_{off}$).

Combining both relations of Eqs. (5, 6) is derived as

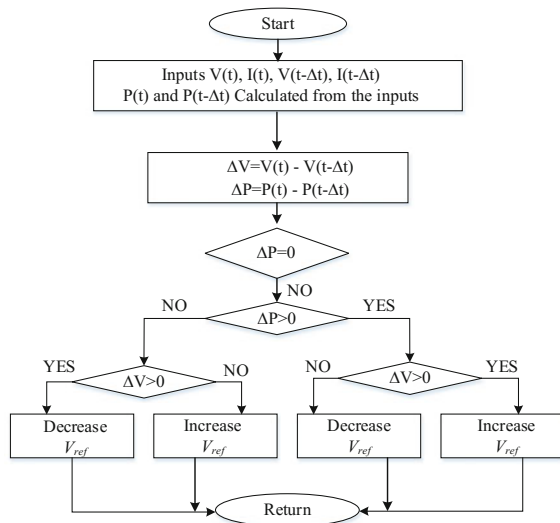
$$V_o = -\left(\frac{D}{1 - D}\right)V_{in} \tag{6}$$

3 Maximum Power Point Tracking System

In this paper, analysis of P&O method is presented. The P&O is one of the most extensively used methods in recent years. The output voltage and power of WT are changed by varying the D , and whether the new output power increases constantly or not is being observed. The operating power point on the left or right of the curve is perceived allowing the input voltage. Finally, whether the duty cycle D keeps changing in the same direction or not is determined. The MPP can be achieved by such repeated perturbation, observation, and comparison. The algorithm is presented by flowchart in Fig. 5.

The actual output DC voltage and current developed by MPPT method is applied as a source signal for comparison with the input parameters of buck–boost converter. Finally, the variation between outputs has been fed to duty cycle [8].

Fig. 5 Flowchart of P&O algorithm



4 Simulation Analysis Results

The proposed MPPT technique is analyzed and investigated under the dynamic wind speed as shown in Fig. 6. The WECS response is analyzed under the proposed strategy.

Figure 7a–b shows the WT generator performance. Figure 7a shows the response of electromagnetic torque of the WT, and Fig. 7b shows rotor speed of the PMSG. Initially, the wind speed is 20 m/s. At this moment, electromagnetic torque starts increasing and gets stable on 18 Nm. Negative sign shows the generating mode. At the same time, rotor speed also starts increasing from its standstill position and gets settled at 152 rad/s. After 0.5 s, wind velocity is step-decreased as shown in Fig. 3.

At $t = 1.5$ s, wind velocity is step-increased to 14 m/s. Both parameters of the WT generator start increasing. At this time, electromagnetic torque is again 16 Nm and rotor speed is 130 rad/s.

Figure 8a–c presents the performance characteristics of DC–DC buck–boost converter under the P&O technique when wind speed is varied stepwise. Initially, when wind speed is taken 20 m/s, output voltage of the DC–DC buck–boost

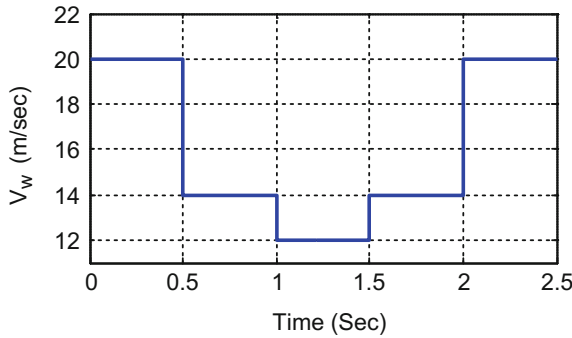


Fig. 6 Considered wind speed pattern

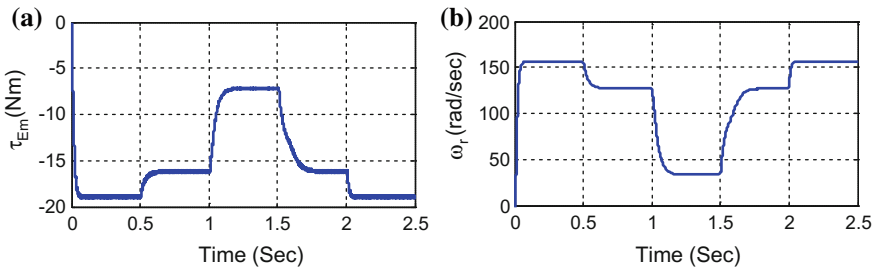


Fig. 7 a, b WT generator performance

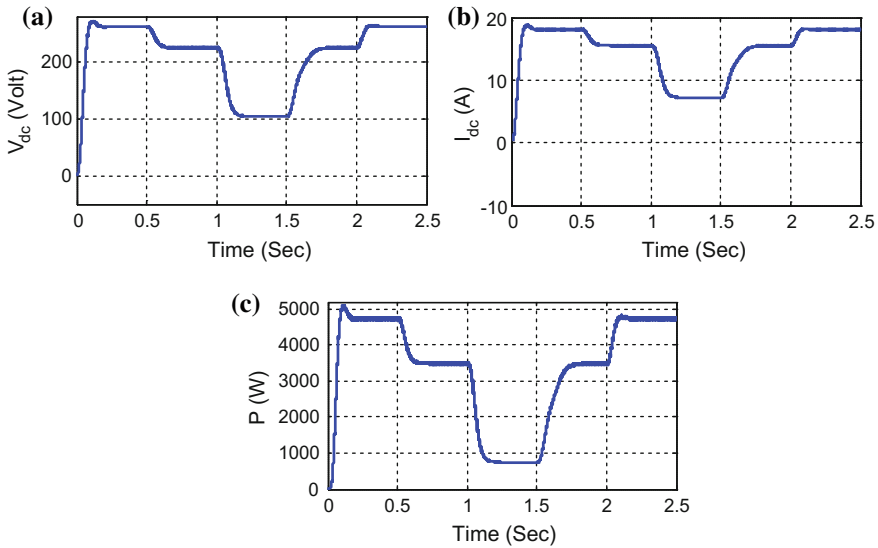


Fig. 8 a–c Output parameters at resistive load

converter is 263.88 V and current is 18 A. Therefore, power obtained by the MPPT technique is 4750 W.

Hence, it is investigated that maximum power tracked by the MPPT is 4750 W at rotor speed of the 152 rad/s when wind speed is 20 m/s. Above or below this wind speed and rotor speed, power gets reduced and efficiency of the WECS experienced very poor.

5 Conclusion

Investigations of WECS have been carried out by developing the Simulink model of complete system under consideration. The results have been discussed in detail to assess the performance of P&O MPPT-assisted WECS. The P&O controller operated in this paper used voltage and current generated by the WECS to generate the duty cycle by adjusting the parameter for different systems. The obtained results show a significant performance for WECS system with P&O algorithm. The study can be used to increase the system's stability by constant power generation in dynamic wind speed condition. Due to fewer controller parameters, the considered system is less complex, which is having good speed and stability. When this control is employed with small wind power system, it can be a cost-effective solution.

References

1. Pathak D., Gupta A., Pachauri R.K., Chauhan Y.K.: Autonomous Operation of Wind-Battery Hybrid Power System with Intelligent Power Management Capability. In proc. of Advances in Intelligent Systems and Computing, 479(2016) 317–324.
2. Kumar H., Gupta A., Pachauri R.K., Chauhan Y.K.: PI/FL Based Blade Pitch Angle Control for Wind Turbine used in Wind Energy Conversion System. In proc. of Recent Developments in Control, Automation and Power Engineering, (2015) 15–20.
3. Pachauri R. K., Chauhan Y. K.: Mechanical Control Methods in Wind Turbine Operations for Power Generation. Journal of Automation and Control Engineering, 2(2014) 215–220.
4. Pachauri R. K., Kumar H., Gupta A., Chauhan Y. K.: Pitch Angle Controlling of Wind Turbine System Using Proportional Integral/Fuzzy Logic Controller. Smart Innovation, Systems and Technologies, 43(2015), 55–63.
5. Abdullah M.A., Yatim A.H.M., Tan C.W., Saidur, R.: A Review of Maximum Power Point Tracking Algorithms for Wind Energy Systems. Renewable and Sustainable Energy Reviews, 16(2012), 3220–3227.
6. Kesraoui M., Korichi N., Belkadi A.: Maximum Power Point Tracker of Wind Energy Conversion System. Renewable Energy, 36(2011) 2655–2662.
7. Kuo N.Y., Chih K. L.: Applying Novel Fractional Order Incremental Conductance Algorithm to Design and Study the Maximum Power Tracking of Small Wind Power Systems. Journal of Applied Research and Technology, 13(2015) 238–242.
8. Abdullah M.A., Yatim A.H.M., Tan C.W.: An online Optimum Relation Based Maximum Power Point Tracking Algorithm for Wind Energy Conversion System. In proc. of IEEE Conference of Power Engineering, (2014), 1–6.
9. Zhang H. B., Fletcher J., Greeves N., Finney S. J., Williams B. W.: One power point operation for variable speed wind/tidal stream turbines with synchronous generators. IET Renewable Power Generation, 5(2011) 99–108.
10. Samavatian V., Radan A.: A High Efficiency Input/output Magnetically Coupled Interleaved Buck–Boost Converter with Low Internal Oscillation for Fuel Cell Applications: Small Signal Modeling and Dynamic Analysis. International Journal of Electrical Power and Energy Systems, 67(2015) 261–271.

Design of a Single-Axis Solar Tracker Using LDRs

Utkarsh Jadli, Shailesh Uniyal and Ishita Uniyal

Abstract Trackers are equipment which are used to get direct sunlight through a uniform orientation according to the position of sun in sky. They are intended to get maximum power through sunlight tracking. Solar technology has been playing a major role in generating electricity. Tremendous research is going in for designing the efficient solar trackers. The initial cost of solar trackers is no doubt high but their running cost and maintenance cost is quite low. Nowadays, solar trackers are becoming beneficial for the grids which are difficult to connect and setup. The smooth operation of solar trackers making them widely used for electricity generation. This paper presents a design of an Op-Amp and relay-based solar tracking system that uses the servo motor and light dependent resistors (LDRs) for the systematic and effective operation.

Keywords Single axis · Solar tracker · PV cell · LDRs · Servo motor

1 Introduction

A solar photovoltaic (PV) cell is similar to a basic p-n junction device that directly transforms solar irradiance into electrical energy. When, an n-type material is combined with a p-type material their Fermi level becomes equal and as a result the band bends as depicted in Fig. 1.

Due to this change in the band of p-n junction, electrons and holes find it difficult to move across the junction [1]. Unlike a normal p-n diode, on application of solar irradiance in a PV cell, an electron-hole pair is generated near the region of band bending. Hence, a larger area of solar PV cell should be exposed to solar irradiance and whole p-n junction should be over that area. A basic structure of PV cell is shown in Fig. 2. In this n-layer is kept very small as compared to p-layer, so that

U. Jadli (✉) · S. Uniyal · I. Uniyal
Department of Electrical Engineering, Graphic Era University,
566/6, Bell Road, Clement Town, Dehradun 248002, Uttarakhand, India
e-mail: utkarshjadli@gmail.com

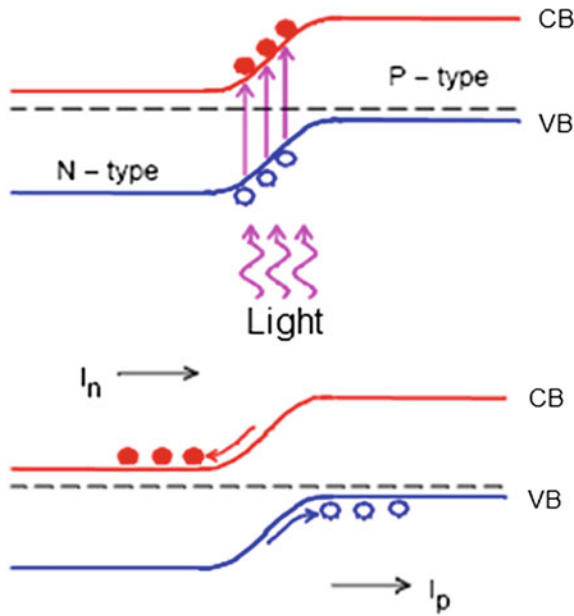


Fig. 1 Band diagram of p-n junction

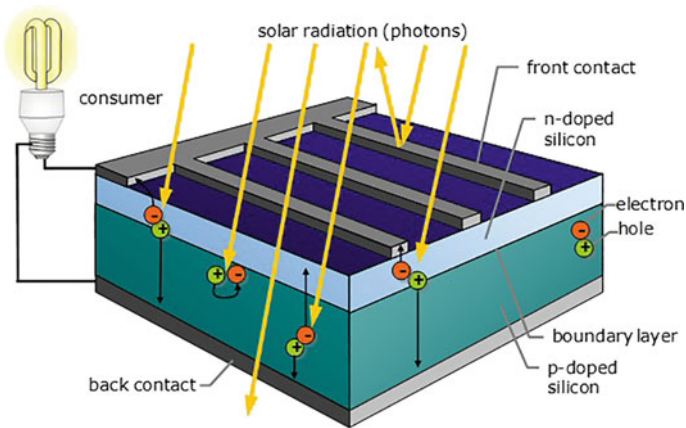


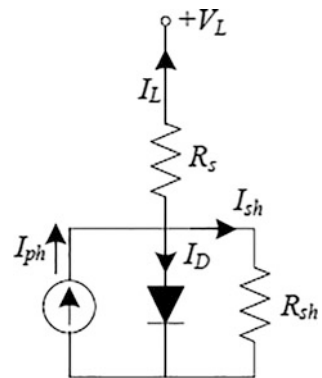
Fig. 2 Basic structure of PV cell

sun light can penetrate up to p-n junction as shown in Fig. 2 [1, 2]. Metal substrate is used to collect the charge carriers from the p-layer. However, charges are also collected from the n-layer as well. A metallic grid is laid over the n-type layer so that minimum sunlight is blocked and maximum exposure is provided [3–8].

2 Problem Statement and Modeling of PV Cell

Solar irradiance from the sun consists of two components, the “direct beam” and the “diffused sunlight.” The “direct beam” shares around 90% of the solar incident energy on Earth and the rest is shared by the “diffused sunlight.” As “direct beam” shares maximum energy, it is required to collect maximum power from the solar PV by maximizing solar irradiance to it. Greater the solar irradiance, greater is the solar cell or solar panel output. Many researches [9–22] have found out that tracking photovoltaic panels are more efficient and are able to capture more solar irradiance than a fixed photovoltaic panel. Going through such researches, it can be seen that by converting our fixed photovoltaic panel into a single-axis tracking panel, solar irradiance experienced by the photovoltaic panel increases up to 50%. And if the solar irradiance increases, output power of the photovoltaic panel also increases. MPPT greatly depends on the solar irradiance and if a tracking panel is used with MPPT, the efficiency of the overall system increases. Regardless of any techniques we have discussed in the MPPT section, all of them require a solar tracker which can track the sun for maximum solar irradiance. Each individual PV cell in an array produces a voltage of order of 0.7–0.8 V. So, in order to generate voltage and current of significant magnitude, these cells are used in series and parallel. For high voltage applications, cells are used in series, whereas for high current applications cells are used in parallel. However, by default, a PV cell is a current source because the radiation produces pairs of charges (electron-hole). These charges move across the junction and hence result in generation of current. Hence, the modeling of a solar PV cell is based on the current source and a diode connected inverted across the current source. A single diode model of a solar PV cell is depicted in Fig. 3. Here, R_s is the series resistance and R_{sh} is the shunt resistance of the solar PV cell, respectively [5, 7]. Series resistance (R_s) is the resistance of material which exists between bulk and the metal contact. Shunt resistance (R_{sh}) represents the recombination of electron-hole pairs.

Fig. 3 Single diode model of a PV cell



The mathematical model [23–27] of a PV cell can be obtained by applying various electrical laws on the model given in Fig. 3. Applying Kirchhoff's Current law (KCL), we get

$$I_{\text{ph}} = I_{\text{D}} + I_{\text{sh}} + I_{\text{L}}, \quad (1)$$

where I_{ph} is the photon current and is highly dependent on solar irradiance and I_{D} is the diode saturation current and is given by,

$$I_{\text{D}} = I_{\text{o}} \left[\exp\left(\frac{qV_{\text{d}}}{K\eta T_{\text{n}}}\right) - 1 \right], \quad (2)$$

From (1), we get

$$I_{\text{L}} = I_{\text{ph}} - I_{\text{sh}} - I_{\text{D}}. \quad (3)$$

Using (2) in (1), we get

$$I_{\text{L}} = I_{\text{ph}} - I_{\text{o}} \left[\exp\left(\frac{qV_{\text{d}}}{K\eta T_{\text{n}}}\right) - 1 \right] - \frac{V_{\text{d}}}{R_{\text{sh}}}. \quad (4)$$

Since, $V_{\text{d}} = V_{\text{L}} + I_{\text{L}}R_{\text{s}}$, we get

$$I_{\text{L}} = I_{\text{ph}} - I_{\text{o}} \left[\exp\left(\frac{q(V_{\text{L}} + I_{\text{L}}R_{\text{s}})}{K\eta T_{\text{n}}}\right) - 1 \right] - \frac{(V_{\text{L}} + I_{\text{L}}R_{\text{s}})}{R_{\text{sh}}}. \quad (5)$$

Solving Eq. (5) by Newton-Raphson Method, we get the famous I - V and P - V curve as shown in Fig. 4. As shown in Fig. 4, MPP describes the point where output panel power is at its peak. There are many factors such as temperature, dirt, shadow, spectral characteristics, insolation. which affect the efficiency of the solar cells. The PV cell output power is reduced due to the climatic conditions and variations in the ambient temperature [7]. The variation in the output of solar cell (as depicted by the characteristics) is proportional to the variations in the intensity of light. In general, the energy produced by each solar PV cell depends upon its operational and environmental conditions [7, 8].

If solar PV cells are connected to the load or battery directly, it results in the reduction of the output power. The reason for this is the mismatching in load or mismatching in load voltage. Since, the output characteristics of a solar PV cell are greatly affected by the various environmental and technical conditions such as temperature, solar irradiance, and load impedance, so in order to collect the maximum power from solar PV cell and to force the solar PV cell to operate on the maximum power point, a capable device is required. Solar PV panel generally converts 20–40% of the solar irradiation to electrical output. To enhance the efficiency of the solar panel, maximum power point tracking (MPPT) techniques are used. These techniques are generally based on the maximum power transfer

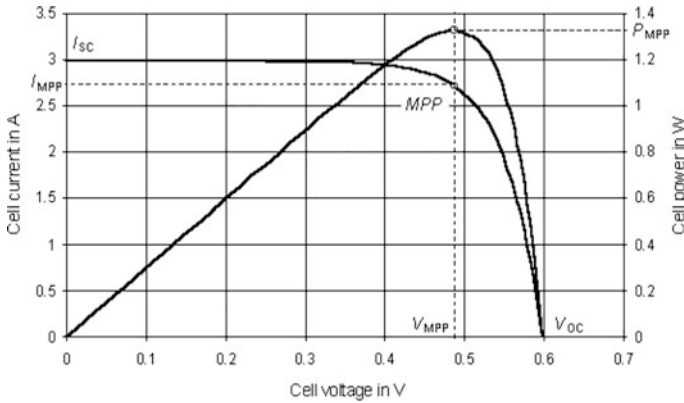


Fig. 4 Typical *I-V* and *P-V* characteristics of a PV cell [7, 8]

theorem. Hence the tracking of maximum power point depends on the impedance matching. There has been a lot of research on the MPPT [5, 9, 23–29].

3 Design Analysis

The proposed single-axis solar tracker as shown in Fig. 5 consists of two LDRs mounted with the solar panel. Both LDRs are connected to a supply of 5 V at one end and the other end of the two LDRs are connected to the input pins of the Op-Amp (IC AS358A), i.e., pin 3 and pin 5, respectively. The other inputs of the Op-Amp, i.e., pin 2 and pin 6, respectively, are connected with the 5 V supply with the help of variable resistors. Pin 8 and pin 4 of the Op-Amp are supply (5 V) and ground, respectively. Pin 1 and pin 7 of the Op-Amp are the outputs. Both the outputs of the Op-Amp are connected to the base of the transistors and later on connected to the relay. Transistors act as a switch for the relay. Variable resistors are used to change the light intensity of both the LDRs. When both LDRs are facing sunlight, both the input voltage to the Op-Amp remains same, which results in same output voltage. The output voltages will trigger both the relays which in turn will give equal voltages to the servo motor. Hence, the motor remains still. When one of the LDR is in dark side, it is open circuited. The output of the LDR is compared with the output coming from the variable resistor, by the Op-Amp, which in turn generates a low output. Similarly, the bright side LDR will produce less voltage as output which when compared with the variable resistor voltage produces high output voltage.

The high output will turn on the respective transistor, which will turn on the relay while the low output voltage will not be able to turn ON the transistor as well as the relay. When the one of the relay switches ON it will give signal to the servo motor. The servo motor will rotate till both the LDR produce the same output.

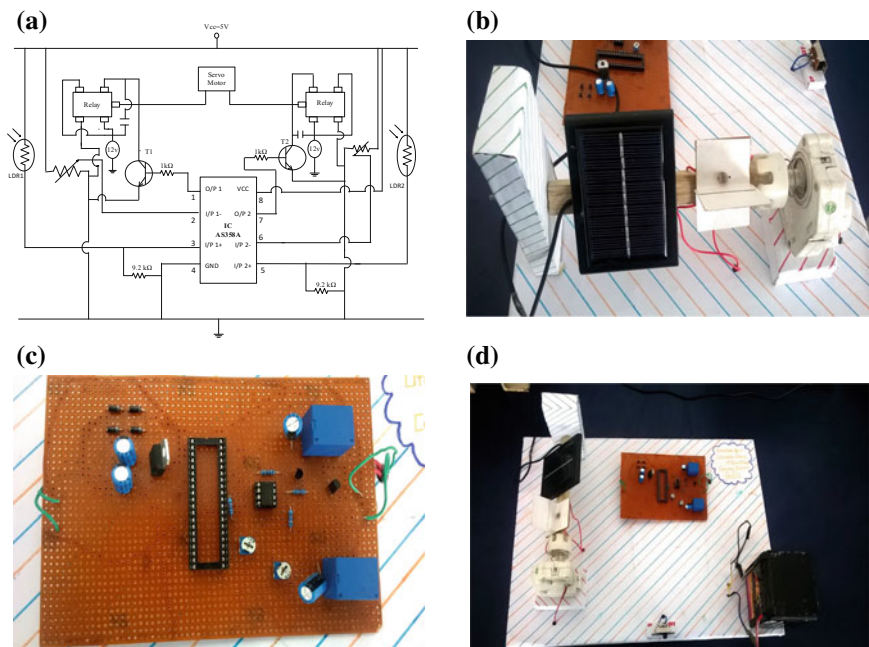


Fig. 5 a Circuit diagram of the proposed solar tracker using LDRs; b solar charger mounted on a servo motor with LDR arrangement; c circuitry of the proposed solar tracker; d the complete hardware of the proposed solar tracker

Table 1 Data showing specifications of solar charger being used for the experiment

V_{oc}	I_{sc}	V_m	I_m	P_{max}	Dimension
7 V	1.5 A	6.42 V	1.2 A	7.7 W	95 mm × 70 mm × 6 mm

4 Results

This section describes the results obtained from the solar tracker designed. The specifications of the solar charger are given by Table 1.

Table 2 shows the comparison of power produced from the PV panel without solar tracking device and with solar tracking device and the percentage change in output power.

The above data (power) of the solar charger can be plotted against time using MATLAB and is shown as:

Table 2 Data showing power of the solar charger, with and without tracker

Time	Without tracker			With single-axis tracker			Percentage change in power $\% = \frac{P_2 - P_1}{P_1} \times 100$
	V (V)	I (A)	Power (W) (P_1)	V (V)	I (A)	Power (W) (P_2)	
7 am	5.88	0.3	1.764	6.36	0.8	5.088	+188.43%
8 am	6.08	0.5	3.04	6.32	0.9	5.688	+87.11%
9 am	6.02	0.8	4.816	6.12	1.1	6.732	+39.78%
10 am	6.20	1.0	6.2	6.13	1.1	6.743	+8.76%
11 am	6.40	1.1	7.04	6.41	1.1	7.051	+0.16%
12 pm	6.41	1.2	7.692	6.41	1.2	7.692	0%
1 pm	6.40	1.2	7.68	6.40	1.2	7.68	0%
2 pm	6.36	1.1	6.996	6.39	1.1	7.029	+0.47%
3 pm	6.20	0.9	5.58	6.31	1.0	6.31	+13.08%
4 pm	6.00	0.6	3.6	6.12	0.8	4.896	+36.00%
5 pm	5.94	0.4	2.356	6.13	0.7	4.291	+82.13%
6 pm	5.83	0.2	1.166	6.05	0.4	2.42	+107.55%

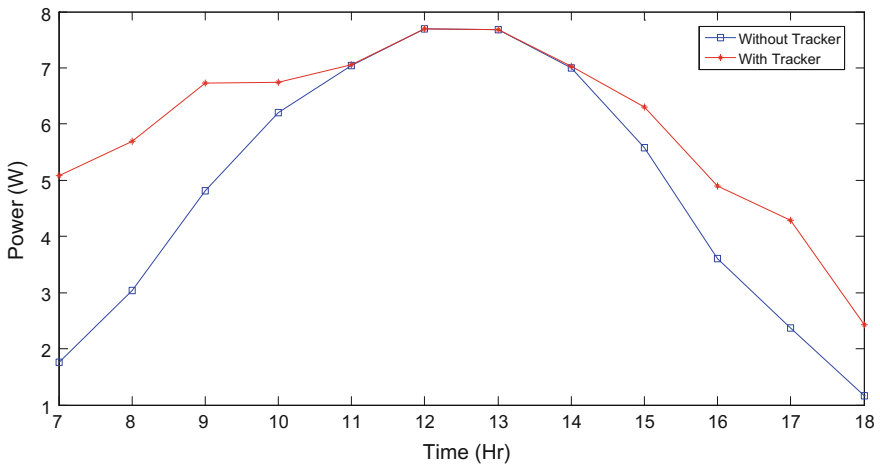


Fig. 6 Power versus time plot (with and without solar tracker)

5 Conclusion

The power produced by the single-axis tracking and fixed solar panel was investigated. Few exceptional conclusions can be drawn in this study as follow:

- (i) As single-axis tracking panel produces more power, hence, it is more efficient than the fixed one.

- (ii) At noontime or midday, both setups produce nearly equal amount of power.
- (iii) Single-axis tracking produces higher output power than the fixed panel during the entire day. It is seen that the single-axis tracker is utilizing most of available solar irradiation, efficiently.

The present work presented a simple single-axis solar tracker which is based on Op-Amp and a relay. The solar tracker has been designed practically and tested in real. The results have been simulated in MATLAB. However, more effective operation can be obtained by using microcontroller and can be compared with the other types of solar tracking systems. For more efficiency, the solar tracker can be modified for MPPT and can be used in a lot of solar applications efficiently.

References

1. YU, Peter, Cardona, Manuel, "Fundamentals of Semiconductors - Physics and Materials Properties", Springer-Verlag Berlin Heidelberg, 2010.
2. Volker Quaschnig, "Renewable Energy and Climate Change", 1st edition, John Wiley & Sons Ltd Chichester, 2010.
3. Kimiyoshi Kobayashi, Hirofumi Matsuo, and Yutaka Sekine, "An excellent operating point tracker of the solar-cell power supply system," in IEEE Trans on IE, vol. 53, no. 2, pp. 495–499, 2006.
4. F. Liu, S. Duan, B. Liu, and Y. Kang, "A variable step size INC MPPT method for PV systems," in IEEE Trans. Ind. Electron., vol. 55, no. 7, pp. 2622–2628, Jul. 2008.
5. T. Esrarn and P.L. Chapman, "Comparison of photovoltaic array maximum power point tracking techniques," in IEEE Trans. Energy Convers., vol. 22, no. 2, pp. 439–449, Jun. 2007.
6. G. Petrone, G. Spagnuolo, R. Teodorescu, M. Veerachary, and M. Vitelli, "Reliability issues in photovoltaic power processing systems," in IEEE Trans. Ind. Electron., vol. 55, no. 7, pp. 2569–2580, Jul. 2008.
7. Azadeh Safari and Saad Mekhilef, "Simulation and Hardware Implementation of Incremental Conductance MPPT With Direct Control Method Using Cuk Converter," in IEEE Transactions on Industrial Electronics, vol. 58, no. 4, April. 2011.
8. Huang BJ, Sun FS, "Feasibility study of one axis three positions tracking solar PV with low concentration ratio reflector," in Energy Convers Manage, vol. 48, pp. 1273–1280, 2007.
9. M. Veerachary, T. Senjyu, and K. Uezato, "Neural-network-based maximum-power-point tracking of coupled-inductor interleaved-boost-converter-supplied PV system using fuzzy controller," in IEEE Trans. Ind. Electron, vol. 50, no. 4, pp. 749–758, Aug. 2003.
10. Huld T, Cebecauer T, Šuri M, Dunlop E, "An analysis of one-axis tracking strategies for PV systems in Europe", in Progress in Photovoltaics Research and Applications, vol. 18, no. 3, pp. 183–194, 2010.
11. Neville RC, "Solar energy collector orientation and tracking mode," in Solar Energy, vol. 20, pp. 7–11, 1978.
12. Kalogirou S., "Parabolic trough collector system for low temperature steam generation: design and performance characteristics," in Applied Energy, vol. 55, no. 1, pp. 1–19, 1996.
13. Chang TP, "The gain of single-axis tracked panel according to extra-terrestrial radiation," in Applied Energy, vol. 86, pp. 1074–1079, 2009.
14. Chang TP, "Output energy of a photovoltaic module mounted on a single-axis tracking system," in Applied Energy, vol. 86, pp. 2071–2078, 2009.
15. Nann S., "Potentials for tracking photovoltaic systems and V-troughs in moderate climates," in Solar Energy, vol. 45, no. 6, pp. 385–393, 1990.

16. Helwa N, Bahgat A, El Shafee A, "Maximum collectable solar energy by different tracking systems," in *Energy Sources*, vol. 22, pp. 23–34, 2000.
17. Al-Mohamad A, "Efficiency improvements of photo-voltaic panels using a suntracking system," in *Applied Energy*, vol. 79, pp. 345–354, 2004.
18. Edenburn MW, "Performance analysis of a cylindrical parabolic focusing collector and comparison with experimental results," in *Solar Energy*, vol. 18, pp. 437–444, 1976.
19. Braun JE, Mitchell JC, "Solar geometry for fixed and tracking surfaces," in *Solar Energy*, vol. 31, no. 5, pp. 439–444, 1983.
20. Cucumo M, Kaliakatsos D, Marinelli V, "General calculation methods for solar trajectories," in *Renewable Energy*, vol. 11, no. 2, pp. 223–234, 1997.
21. Morcos VH, "Optimum tilt angle and orientation for solar collectors in Assiut, Egypt," in *Renewable Energy*, vol. 4, no. 3, pp. 291–298, 1994.
22. Kacira M, Simsek M, Babur Y, Demirkol S, "Determining optimum tilt angles and orientations of photovoltaic panels in Sanliurfa, Turkey" in *Renewable Energy*, vol. 29, pp. 1265–1275, 2004.
23. E. Koutroulis, K. Kalaitzakis, and N. C. Voulgaris, "Development of a microcontroller-based, photovoltaic maximum power point tracking control system," in *IEEE Trans. Power Electron.*, vol. 16, no. 1, pp. 46–54, Jan. 2001.
24. S. Jain and V. Agarwal, "A new algorithm for rapid tracking of approximate maximum power point in photovoltaic systems," in *IEEE Power Electron*, vol. 2, no. 1, pp. 16–19, Mar. 2004.
25. Pandey, N. Dasgupta, and A. K. Mukerjee, "Design issues in implementing MPPT for improved tracking and dynamic performance," in *Proc. 32nd IECON*, pp. 4387–4391, Nov. 2006.
26. K. H. Hussein, I. Muta, T. Hoshino, and M. Osakada, "Maximum photovoltaic power tracking: An algorithm for rapidly changing atmospheric conditions," in *Proc. Inst. Elect. Eng.—Gener., Transmiss. Distrib.*, vol. 142, no. 1, pp. 59–64, Jan. 1995.
27. T.-F. Wu, C.-H. Chang, and Y.-H. Chen, "A fuzzy-logic-controlled single stage converter for PV-powered lighting system applications," in *IEEE Trans. Ind. Electron.*, vol. 47, no. 2, pp. 287–296, Apr. 2000.
28. N. Femia, G. Petrone, G. Spagnuolo, and M. Vitelli, "Optimization of perturb and observe maximum power point tracking method," in *IEEE Trans. Power Electron.*, vol. 20, no. 4, pp. 963–973, Jul. 2005.
29. N. Femia, D. Granozio, G. Petrone, G. Spagnuolo, and M. Vitelli, "Predictive & adaptive MPPT perturb and observe method," in *IEEE Trans. Aerosp. Electron. Syst.*, vol. 43, no. 3, pp. 934–950, Jul. 2007.

2D Modelling and Simulation of Heat Transfer in Blast Furnace Hearth Using ANSYS

Satish Kumar and Vijay Singh Bisht

Abstract Iron blast furnace is used in the metallurgical field to extract molten pig iron from its ore through a reduction mechanism. Hearth is the most important part to find life of furnace. Campaign life of furnace is reduced due to erosion of refractory line. Temperature inside the blast furnace is very high and practically observe these process inside the hearth is very difficult. In order to overcome this problem, the hearth is modelled by using various computational fluid dynamics (CFD) softwares such as ANSYS Fluent, ANSYS-CFX, FLUENT. The numerical model is then supplied with data which are already known from practical situations as boundary conditions. Materials' proper physical properties are also used as input. The software runs several simulations and provides us with the result that can validate the experimental observations up to the most accurate level. In this study, temperature distribution profile inside a blast furnace hearth has been shown by modelling a simple hearth with the help of ANSYS 15.0 Workbench.

Keywords Blast furnace hearth · 2D modelling · ANSYS · Simulations

1 Introduction

Blast furnace:

Blast furnace is a large furnace which is used in metallurgical field to produce metals, especially pig iron. In the blast furnace, lead and copper are also produced.

S. Kumar (✉) · V.S. Bisht
Department of Thermal Engineering, Faculty of Technology,
UTU, Dehradun 248007, Uttarakhand, India
e-mail: satish10071992@gmail.com

V.S. Bisht
e-mail: vsinghbisht5@gmail.com

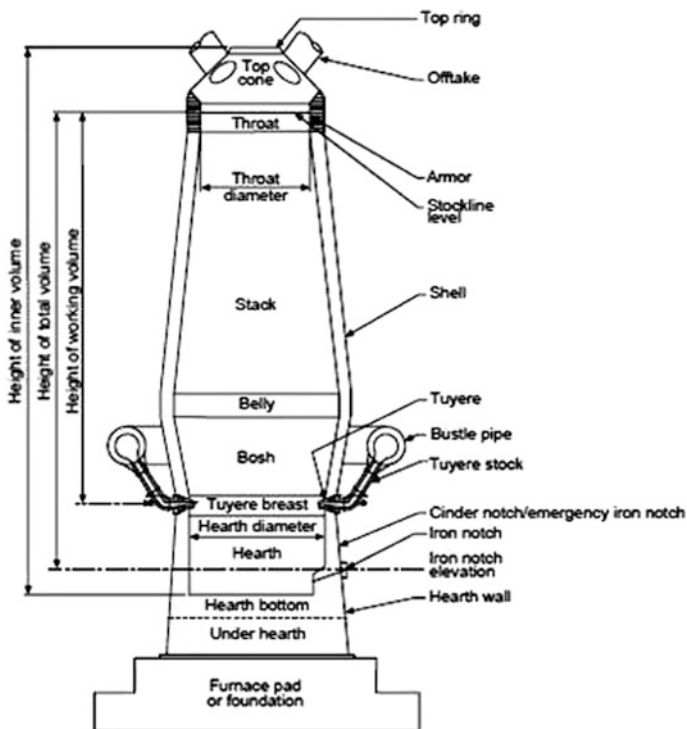


Fig. 1 Schematic diagram of an iron blast furnace

Various regions within an iron blast furnace:

It is composed of five main parts. They are:

- (i) **Hearth**—a crucible-shaped portion which is present at the bottom of the furnace;
- (ii) **Stack**—a vertical shaft that extends from stock line to mantle level;
- (iii) **Belly**—the cylindrical portion below the stack;
- (iv) **Bosh**—an intermediate zone between the hearth and the belly;
- (v) **Tuyeres**—series of pipes located around the circumference through which blast of the hot air is given or blown to the furnace (Fig. 1).

2 Modelling and Simulation

Modelling and simulation are the study or information without testing in reality or real life how something is behaving. So it represents the real system by mathematical models that represent the dynamics of the system through simulation.

3 Literature Review

Shinroku et al. [1] used mathematical model of blast furnace that was developed by Japan Nippon Corporation. He used mathematical model to analyse the operation and policies related to blast furnace. Their future task is the development of 3D models and non-steady-state models of solid particle behaviour.

Iwamasa et al. [2] used a commercial fluid dynamic package called TASC flow to simulate the heat transfer and thereby to estimate the refractory erosion of the blast furnace in hearth region. The Flat Products Division Port Kembla Steelworks Blast Furnace 6 was studied in this case. A parametric survey of various operating conditions for PK6 was done and the production rates, coke bed porosity, dead-man shape, iron level and inlet temperatures were predetermined. Then, several simulations were run by changing one parameter and keeping others constant. The results suggested that the shape and the location of the dead-man coke influence the wear of hearth refractory the most. The refractory wear is most rapid at the time when the coke is floating in the bottom of the hearth. Due to the vigorous recirculation zone driven by natural convection, the greatest erosion of refractory lining occurs at the walls and at the bottom of the hearth near the walls.

PanjkoVIC et al. [3] have studied the temperature distribution profile and the wear of refractories in the hearth portion of blast furnace. In their study, CFX 4.2 commercial package is used and successfully developed a computational fluid dynamics model of iron flow and heat transfer in the hearth.

Bryan et al. [4] refined the BlueScope Steel's No. 5 hearth which was earlier used by Panjkovic et al. [3]. This model developed by BlueScope Steel is known as Coupled Flow-Refractory Model (CFRM) which has been continuously improved over the years.

Maldonado et al. [5] separately investigated the reason behind the erosion of hearth by doing numerous simulations with the help of CFX 4.4 fluid flow package. In their case study considering the time period of January 2002 to January 2006. The temperature of centre pad was 510 °C during March 2002. It was simulated by using a uniform 400 mm coke-free layer. There was a gradual reduction of refractory temperature during March 2002 to October 2003. It was proposed that low-conducting build-up or deposit layers were gradually formed during this period of time. Then, there was a rapid increase in the temperature peaking late December 2003 (increasing to March 2002 level) which was attributed to the formation of a floating coke bed with a raised hemispherical-shaped coke-free layer. This was followed by another gradual decrease in the temperature to March 2004. Since then, the temperature fluctuated between 400 and 500 °C.

4 Modelling of Hearth

Two-dimensional models of a simple blast furnace hearth have been developed using the ANSYS 15.0 Workbench (Fig. 2).

4.1 Using Fluid Flow (Fluent) Two-Dimensional Modelling of Only Hearth Part

See Figs. 3, 4, 5 and 6.

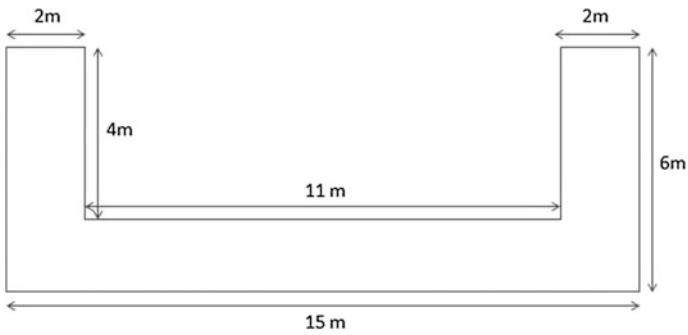


Fig. 2 Schematic diagram of the hearth model [6]

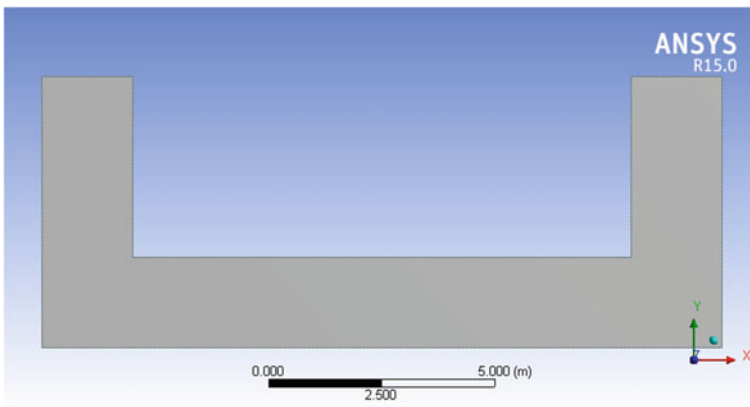


Fig. 3 Model of hearth

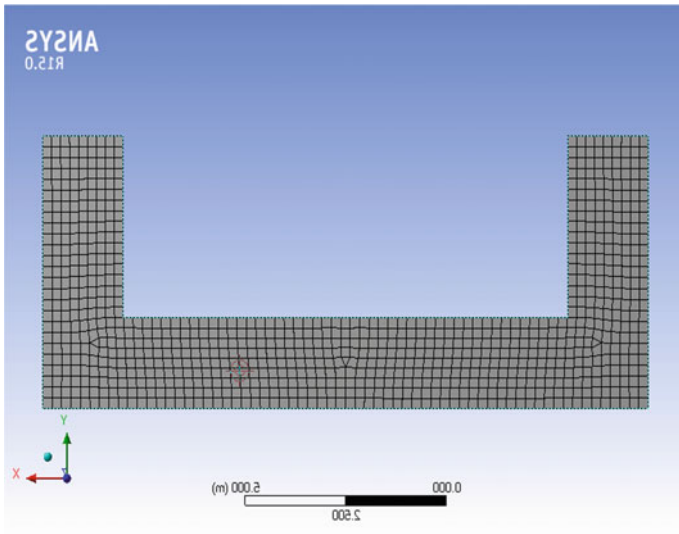


Fig. 4 Meshed structure of model

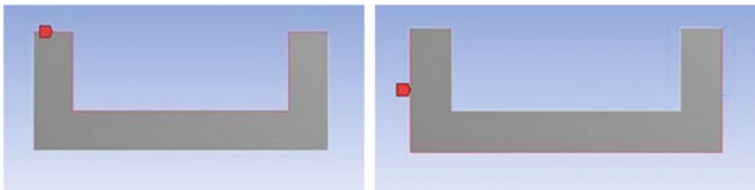


Fig. 5 Inner wall and outer wall

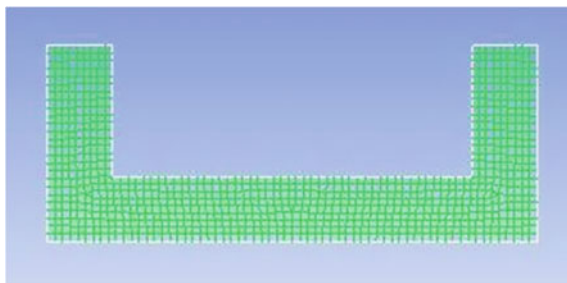


Fig. 6 Initial set-up diagram

4.2 Using Fluid Flow (Fluent) Two-Dimensional Modelling of Hearth Containing Hot Metal

See Figs. 7, 8, 9 and 10.

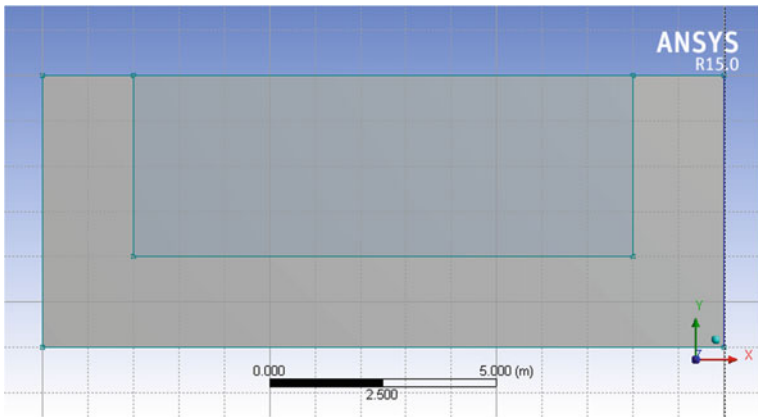


Fig. 7 Model of hearth

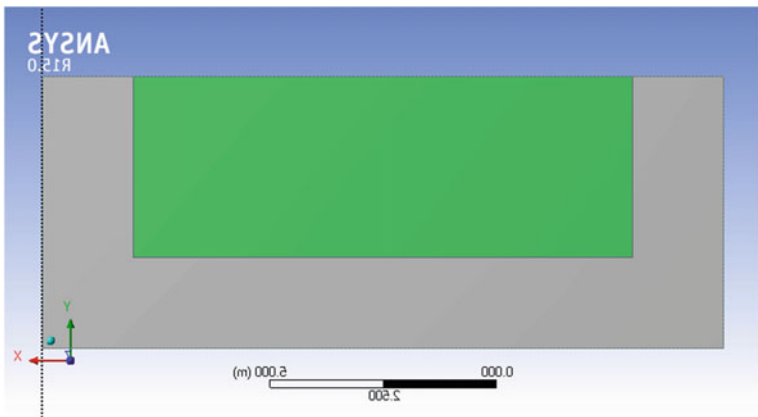


Fig. 8 Model of hearth containing hot metal

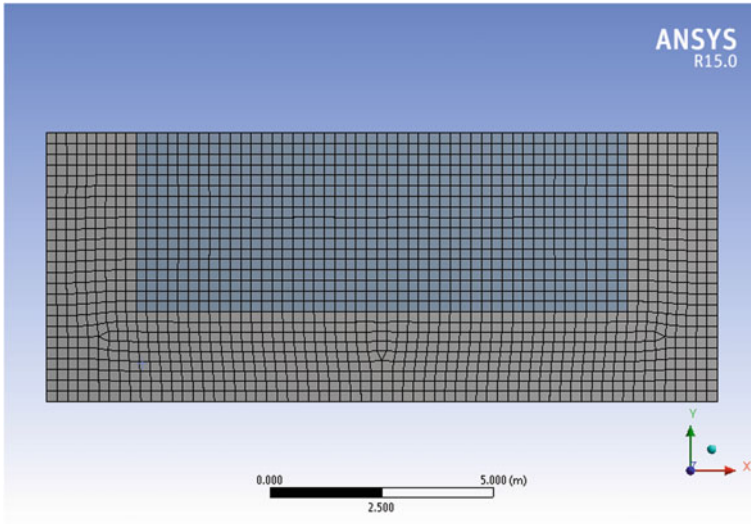


Fig. 9 Meshed structure of hearth containing hot metal

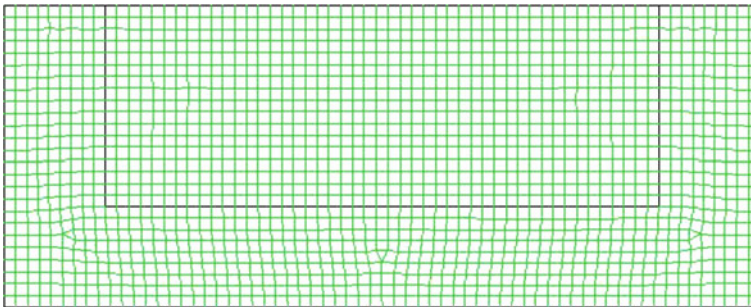


Fig. 10 Initial set-up diagram

5 Material Properties

Table shows the model parameters [3].

	Density (kg/m ³)	Specific heat (J/kg K)	Thermal conductivity (W/m K)
Carbon	2267	7000	2705
Hot metal (iron)	1260	850	–

6 Governing Equations

We have used only the conduction equation in our simulation. Conduction refers to the heat transfer between two bodies through molecules which are, more or less, static. According to Fourier's law of heat conduction, heat transfer rate is linearly proportional to the temperature gradient. Mathematically represents as,

$$q \propto dT/dx \quad (1)$$

$$q = -k(dT/dx) \quad (2)$$

where, q is the rate of heat flux in W/m^2 , dT/dx is the temperature gradient in the direction of heat flow x and k is the proportionality constant. It is a property of the material through which heat propagates property is called thermal conductivity ($W/m K$). dT/dx is negative because negative sign in the temperature gradient indicates that the heat flows from a high temperature to a low temperature. So, since we consider temperature difference in the temperature gradient term, we can take the temperature either in $^{\circ}C$ or in Kelvin ($1^{\circ}C = 1 K$).

7 Results and Discussions of Simulation

7.1 Only Hearth Part Simulation

Assumptions:

- (i) Steady-state process;
- (ii) Hot metal and slag presence is neglected;

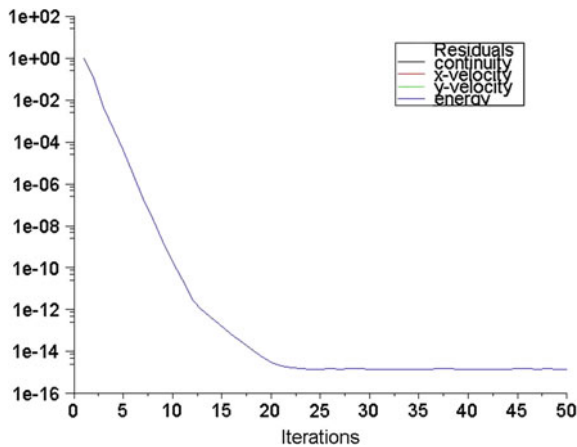


Fig. 11 Convergence of the simulation

- (iii) Refractory fireclay brick presence is neglected;
- (iv) Slag and hot metal chemical reaction are neglected.

Boundary conditions:

- (i) The inner side temperature of the hearth is taken to be 1400 °C.
- (ii) The outer walls temperature of the hearth is taken to be 27 °C (300 K).
- (iii) Two-dimensional heat transfer process is considered.
- (iv) Cross-sectional area is taken as unity.

Figure shows the number of iterations taken to complete the simulation process or convergence (Figs. 11, 12 and 13).

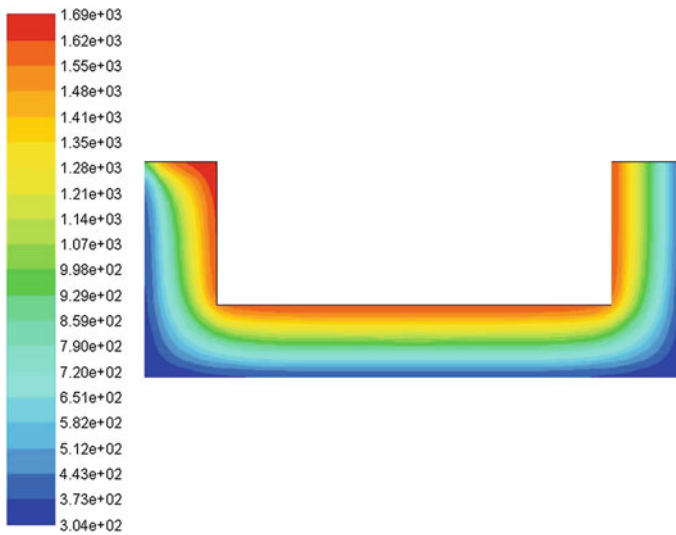


Fig. 12 Temperature distribution profile of hearth

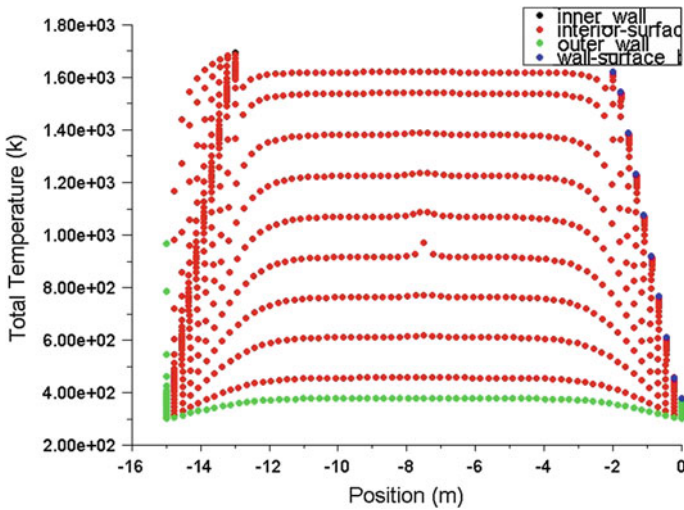


Fig. 13 Total temperature versus position(m)

7.2 *Hearth Containing Hot Metal Simulation*

Assumptions:

- (i) Steady-state process is considered.
- (ii) Slag presence is neglected.
- (iii) Refractory fireclay brick presence is not considered.
- (iv) Hearth and hot metal's chemical reaction are neglected.
- (v) Heat transfer mode is conduction.

Boundary conditions:

- (i) Constant liquid iron level;
- (ii) Outer surface temperature of the molten hot metal: 1500 °C;
- (iii) Hearth outer wall is at room temperatures, i.e. at 27 °C;
- (iv) Two-dimensional heat transfer process is considered;
- (v) Cross-sectional area—unity (Figs. 14, 15 and 16).

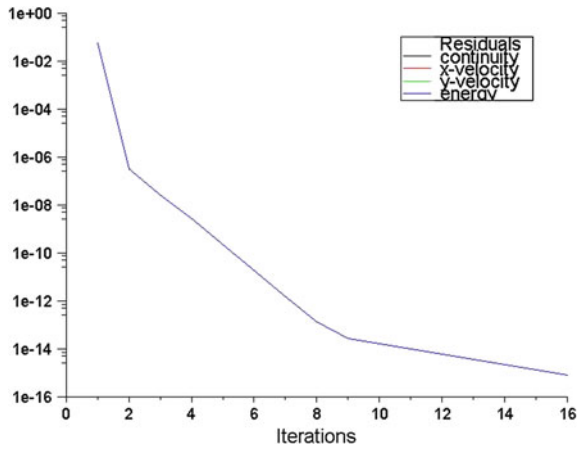


Fig. 14 Convergence of simulation

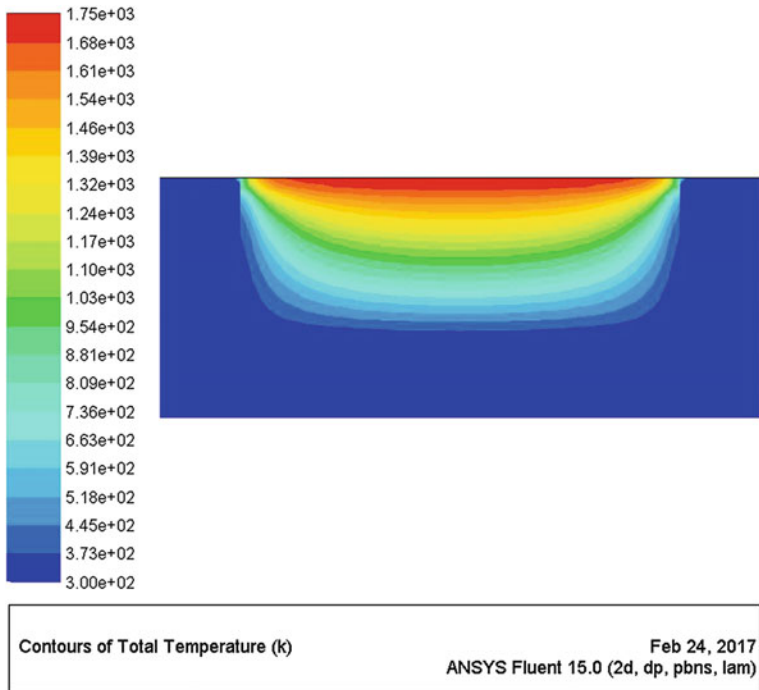


Fig. 15 Temperature distribution profile of hearth containing hot metal

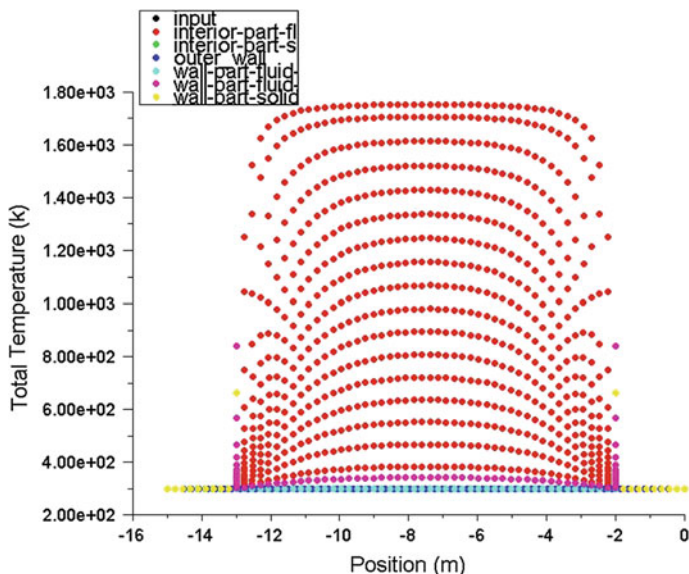


Fig. 16 Total temperature versus position

8 Conclusion

A simple blast furnace hearth is modelled by using ANSYS 15.0 Workbench. Several simulations are run with the help of fluid flow (FLUENT). Only hearth and hearth with hot metal are the two cases which are considered for simulation program. Their temperature distribution profiles are studied and displayed.

References

1. Shinroku matsuzaki, Akihiko shinotake, Masaaki naito, tsunehisa nishimura, Kazuya kunitomo, Takashi sugiyama, "Development of Mathematical Model of Blast Furnace", Nippon steel technical report No. 94, JULY 2006.
2. P K Iwamasa, G A Caffery, W D Warnica, S R Alias, "Modelling of Iron Flow, Heat Transfer and Refractory Wear in the Hearth of an Iron Blast Furnace", Inter Conf on CFD in Mineral & Metal Processing and Power Generation, CSIRO 1997.
3. Vladimir panjkovic, "Computational Fluid Dynamics Modelling of Iron Flow and Heat Transfer in the Iron Blast Furnace Hearth", Second International Conference on CFD in the Minerals and Process Industries, CSIRO, Melbourne, Australia, 6–8 December 1999.
4. Bryan wright, Paul zulli, Frank bierbrauer and Vladimir Panjkovic, "Condition Blast Furnace Hearth using Computational Fluid Dynamics Assessment of Refractory", Third International Conference on CFD in the Minerals and Process Industries, CSIRO, Melbourne, Australia, 10–12 December 2003.

5. D. maldonado, P. Zulli, B. Y. guo and A. B. yu, "Mathematical Modelling of Flows and Temperature Distributions in the Blast Furnace Hearth", Fifth International Conference on CFD in the Process Industries, CSIRO, Melbourne, Australia, 13–15 December 2006.
6. Biswajit dalai "cfD modelling of heat transfer in blast furnace", Bachelor thesis 2015, <http://www.thesis.nitrkl.ac.in>.

Offline Graphical Analysis of Signatures Using Geometric Features and Artificial Neural Network

Parvesh Saini, Ishita Uniyal and Neeraj Singh

Abstract Signature verification is an important research area in the field of personal validation because signatures have become an important and crucial tool for the human identification. The verification of human signature is substantial when dealing with the financial and non-financial transactions. Nowadays, it has become necessary to have a computer-based signature verification system. This helps in verifying the signatures in more convenient way. This paper presents graphical analysis of signatures (original and forged) of human on the basis of simple geometrical features. Artificial neural network has been used as a classifier to distinguish between original and forged signature. Algorithm has been developed, and results have been obtained through MATLAB.

Keywords Biometrics · Signature verification · Offline mode
Artificial neural network · Geometric features

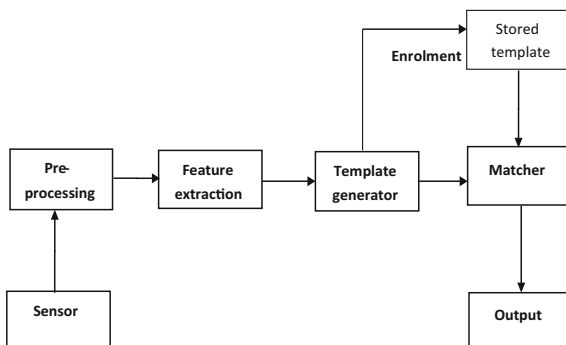
1 Introduction

There are two words in Greek, bios and metron. Bios means life and metron means measurement. These two words are combined to make biometrics. Biometrics deal with the identification and measurement of various human traits such as their physical and behavioral features [1]. Biometric has become advanced technique to bring security for personal authentication. A general biometric system has been shown in Fig. 1.

Human beings are recognized by their features or characteristics such as face, way of talking, walking, etc. These features of human have become a very crucial tool to be used for developing security system. It has become necessary to identify and to verify the human beings due to many reasons which include the singular

P. Saini (✉) · I. Uniyal · N. Singh
Department of Electrical Engineering, Graphic Era University, 566/6, Bell Road,
Clement Town, Dehradun 248002, Uttarakhand, India
e-mail: parv1606@gmail.com

Fig. 1 Basic block diagram of a biometric system [1]



activities across the international borders, increased use of financial documentation, and access to some crucial documentation leakage to which is a threat on the security of the country [2]. Conventional authentication techniques like identity documents and passwords are not enough to avoid identity theft and confirm security. These techniques generally fail because of the possibility that they can be forgotten, stolen, or lost [3]. Handwriting signature is one of the various biometric techniques which are used for the verification and/or identification of an individual [4, 5]. Signature is an important biometric trait of human being because most of the financial transactions involve signatures. For the authorization and authentication in the lawful transactions, signature is accepted as the prime tool [6]. Also signature gives a security and an authentication to a number of assets of signer [6]. Today, signature verification has been researched in all parts of the world because as the advancements are going on, forgeries are also taking up in all financial and legal transactions. To avoid and reduce the risk of forgeries, identification of authentic signature is of prime concern. A number of systems have been developed for signature verification and identification. Signature recognition or verification can be categorized as:

- Static (or offline) method
- Dynamic (or online) method

The challenge in signature recognition and verification is that the data are in the form of two-dimensional image. Generally, the identification or verification is done by comparing the signature image with the stored template. This is manual way of recognizing and verifying signatures. However, forgers have developed skills to imitate the original signatures which are difficult to be identified and verified manually. This requires the need of an intelligent and highly efficient system which can distinguish between an original and forged signature. This can be ensured by identifying the unique features of the signature image and designing an algorithm to extract those features from the signature image. This is a challenging task. Another challenge in signature identification and verification is the variation in the signatures by an original person. Due to various reasons (such as: health, ageing, etc.), there are possibilities that the signature by an original may vary. Generally there are

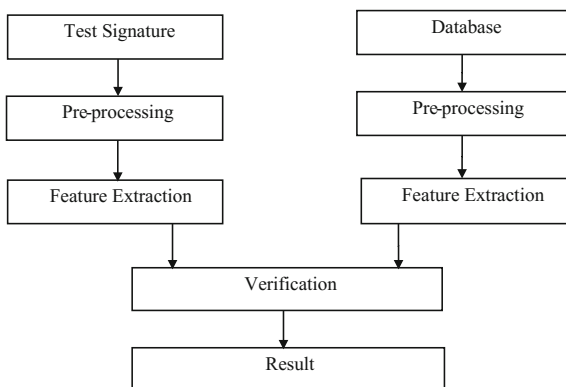
two types of discrepancies in the signature. These are inter-variations and intra-variations [5]. Forgery of a signature is done by copying the original signature by a forger. The forgers may develop random, skilled, or simple types of forgeries [5]. Apart from the above-mentioned forgeries, [7] describes a few more types of forgeries such as: simulation, tracing, cut and paste, electronic, and free-hand forgery. There are generally two types of approaches which are used for the signature identification and verification. These are: template matching and feature extraction. Most of the research done in this topic describe about the feature extraction. [8] describes a review on the signature verification system in offline mode which uses artificial techniques, while [9] explains about the state-of-the-art way of signature verification. Pixel matching technique for signature verification has been described in [10], a comparison of various offline signature verification techniques is given in [11], signature verification based on improved features in [12], shape dissimilarities in [13], support vector machine in [14], deep convolutional generative adversarial networks in [4], geometric feature extraction using artificial neural network in [5], neural networks in [6]. Some other approaches are: hidden markov model (HMM), contour method, ROC analysis, enhanced modified direction feature, etc. Most of the techniques presented in the research are based on feature extraction. For verifying or recognizing signature through feature extraction, it is important to identify some unique features of signature. A lot of such unique features have been identified till date and have been used through various algorithms. However, no system till date gives a 100 percent results. Like any biometric system, the efficiency of signature identification and verification is also justified through two important factors viz: false acceptance rate (FAR) and false rejection rate (FRR). This paper presents a design and analysis of signature verification system which makes use of artificial neural network as a classifier. The neural network is trained through an algorithm developed. A database of original signature of 6 persons has been created. And similarly, a database of forged signature in the category of simple, random, and skilled forgery has also been created. The methodology followed for signature verification in this paper has been explained in Sect. 2.

2 Methodology

The methodology and algorithms selected for image capture, processing of image, feature selection, and verification of signatures have been covered in this article. (Refer Fig. 2.)

For the present work, back-propagation technique of neural network is used for the verification of the signatures. Back-propagation technique is a systematic method of training multilayer artificial neural networks. Since signature verification is the behavioral parameter of biometrics and is used to authenticate a person [15], hence it needs a rigorous analysis of the data for verification purpose. A typical signature verification process includes: *data acquisition, pre-processing, feature*

Fig. 2 Proposed system for signature verification [1]



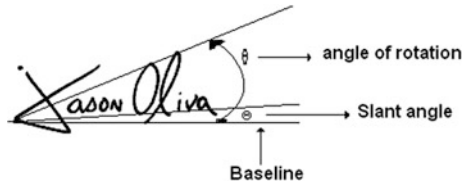
extraction, and verification [16, 17]. Data is in the form of images of the signatures which have been collected by scanning the signature images through scanner at the desired resolution. Thereafter, the signature images are pre-processed to enhance the quality of the images and to make them appropriate for feature extraction. The pre-processing involves the following processes done on signature images: image conversion, image segmentation, image smoothening, filtration. The image is converted from RGB to gray image and then gray to binary. Automatic global thresholding technique is used to convert the gray image into binary. After pre-processing of the images, the images are ready for feature extraction. The process of collecting the unique data of an image in statistical form is known as feature extraction. The current project work is based on simple geometrical features of signature to distinguish between original and forged signature. The unique features of signature image have been identified and extracted through MATLAB program. The geometric features which have been identified for this work are briefly described below:

- Angle of signature with baseline
- Length to breadth ratio of signature image (bounding box)
- Signature pixels to the bounding box ratio
- Center of mass of the pixels in signature image
- Line gradient fitting between the centers of gravity into two equal halves of the image.

2.1 Angle of Signature with Baseline

Signatures are assumed to be rested on an imaginary line which is known as baseline of the box bounding the signature. However, often signatures are inclined more or less with the baseline and this angle of inclination is known as slant angle (Θ) (shown in Fig. 3).

Fig. 3 Base angle of signature



2.2 Length to Breadth Ratio of Signature Bounding Box

A mathematical relation of length to breadth ratio is given by Eq. 1:

$$L - to - B = \frac{A_x}{A_y} \tag{1}$$

2.3 Signature Pixels to the Bounding Box Ratio

This is also known as normalized area (NA) and is given by:

$$N_A = \frac{A_{sp}}{A_x A_y} \tag{2}$$

where N_A is the signature pixels to bounding box ratio (or normalized area), and A_{sp} is the area occupied by the pixels of signature image.

2.4 Center of Mass of the Pixels in Signature Image

It is a unique geometric feature of an image. It can be termed as center of gravity and is given by:

$$X = \sum_{k=0}^{M-1} \frac{P_v(j) * J}{A_{sp}} \tag{3}$$

$$Y = \sum_{l=0}^{N-1} \frac{P_H(l) * l}{A_{sp}} \tag{4}$$

where P_v and P_H are the projection in vertical and horizontal direction, respectively.

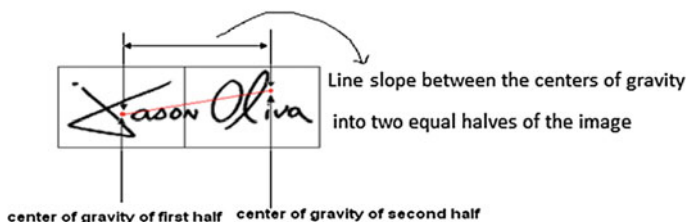


Fig. 4 Line slope between the centers of gravity into two halves of the image

2.5 Line Gradient Fitting Between the Centers of Gravity into Two Equal Halves of the Image

This feature is supposed to be one of the unique features of the signatures and is used to distinguish between the original and forged signatures (as shown in Fig. 4).

After feature extraction, the database is created, based on the geometrical features discussed above. This database is used for verification purpose. In verification, the signatures are finally tested to detect that either the signature is original or forged. During the verification process, the input signature of an individual is compared with the available database of that individual. The classification between original or forged signature is done with the help of artificial neural network.

3 Result Analysis

The results of the designed system for offline signature verification have been discussed in this section. As per the methodology, the system has been run and results have been checked for original and forged signatures. The performance measures of the biometric system are evaluated through two major criterions: (i) false rejection rate (FRR); and (ii) false acceptance rate (FAR). A graphical analysis of original and forged signature has been presented in this section along with the statistical results depicted in tables provided (Figs. 5, 6, 7, 8, and 9; Tables 1, 2, 3, 4, 5, 6 and 7).

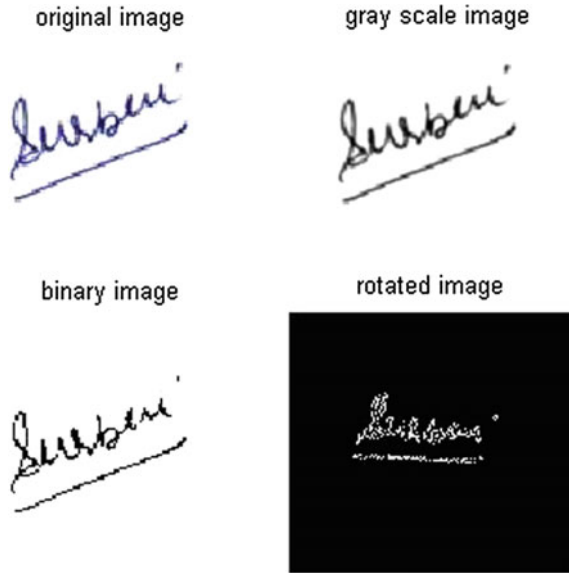


Fig. 5 Different processed images of original signatures from database—1

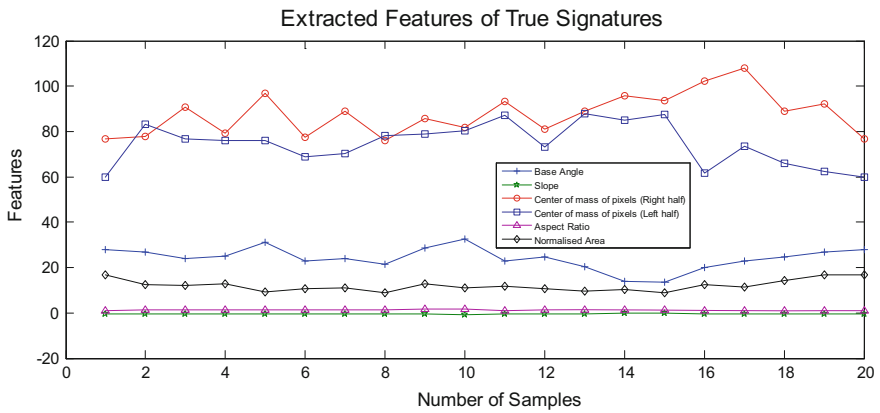


Fig. 6 All features of original signatures in one diagram

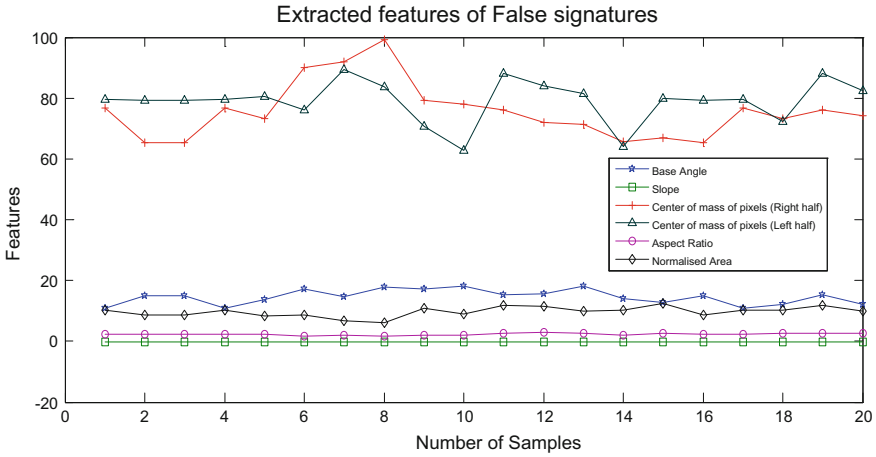


Fig. 7 All features of random forged signatures in one diagram

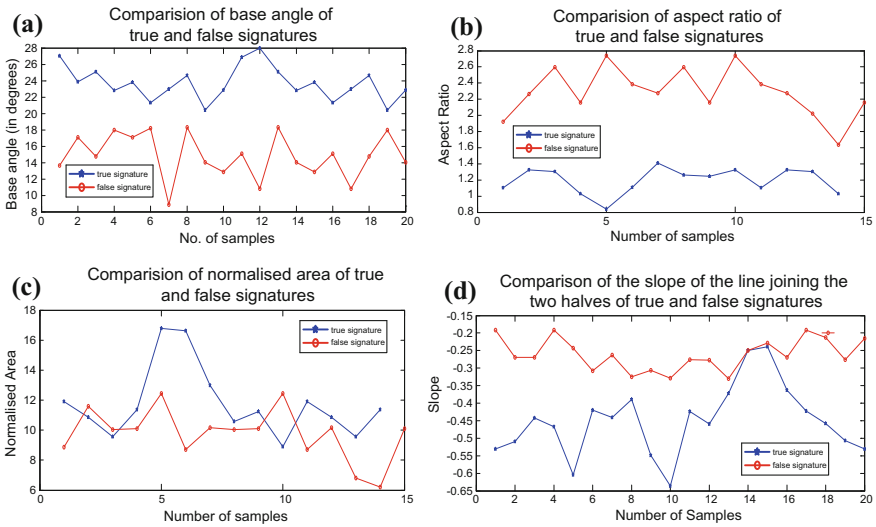


Fig. 8 Comparison of various features of a simple forged signature with original signature; **a** Comparison of baseline angle; **b** Comparison of aspect ratio; **c** Comparison of normalized area; **d** Comparison of the slope of the line joining the two halves signatures

4 Conclusion and Future Scope

The system proposed in this paper is a simple signature verification system which uses ANN to verify between original and forged signature. The verification is based on simple geometrical features of signature which makes this system a convenient

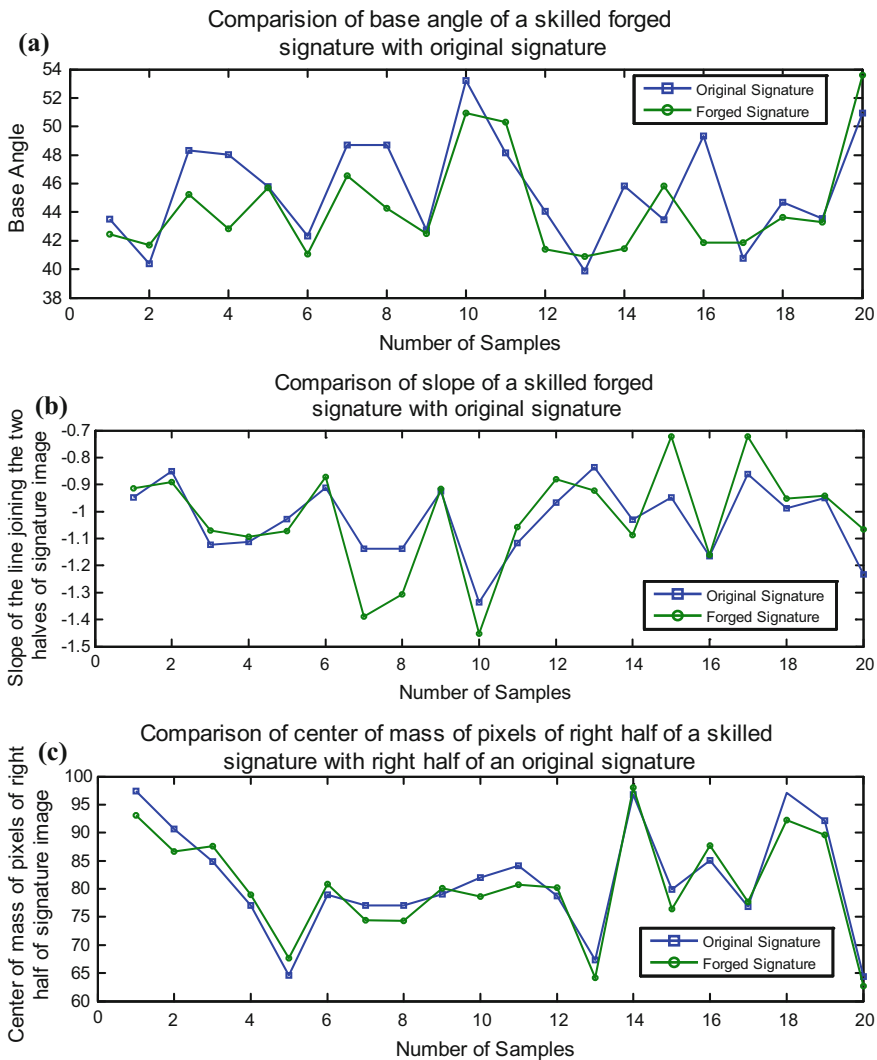


Fig. 9 Comparison of various features of a skilled forged signature with original signature; **a** Comparison of base angle; **b** Comparison of slope of signatures; **c** Comparison of center of mass of pixels of right half of a signatures; **d** Comparison of center of mass of pixels of left half of a signatures; **e** Comparison of aspect ratio; **f** Comparison of normalized area

method to deal with random and simple forgeries. However, the system does not give ample results when dealing with skilled forgeries. The results have been shown in Tables 1, 2, 3, 4, 5, and 6. The method can easily be utilized on computers in

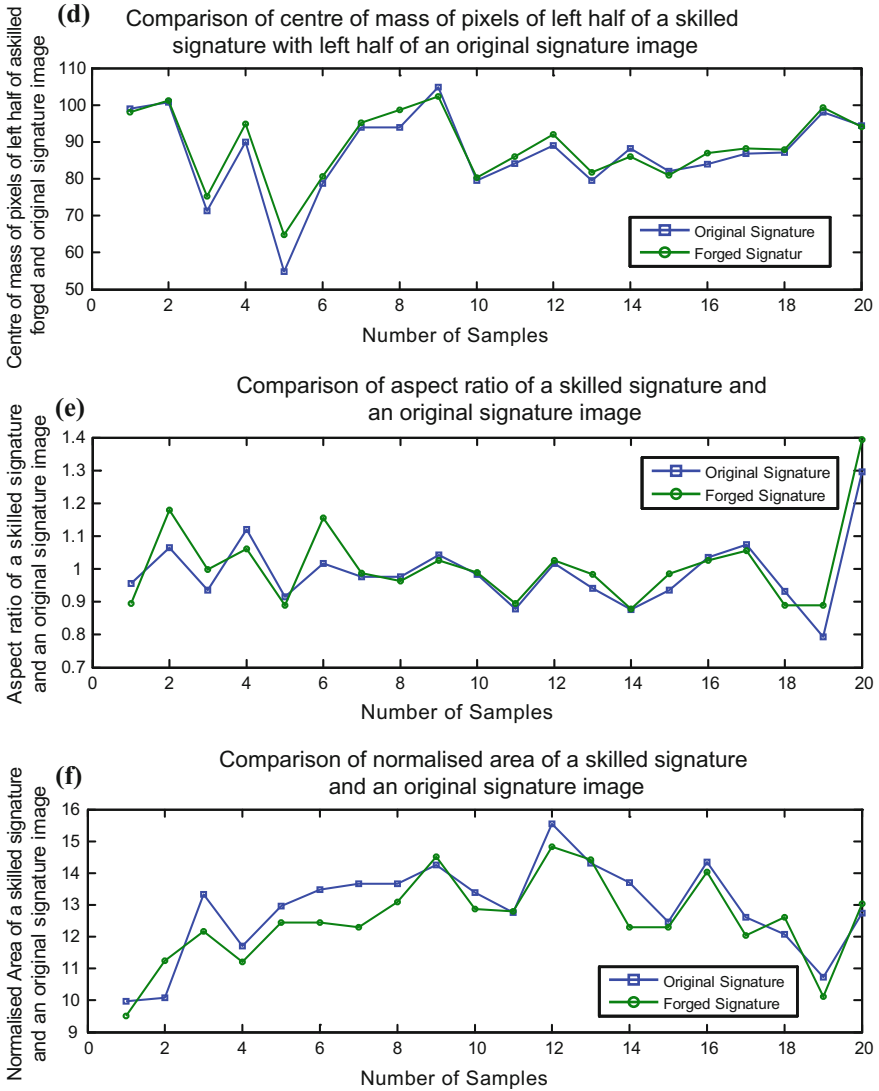


Fig. 9 (continued)

banks and other financial transaction for signature verification by developing a simple graphical user interface. To make the system efficient for skilled forgeries, some more new unique features can be found and extracted (Table 7).

Table 1 Results of database—1

Type of forgery	No. of samples for training	No. of samples for testing		FRR (%)	FAR (%)
		Original	Forged		
Random	20	20	20	10	3.33
Simple	20	20	20	10	16.66
Skilled	20	20	20	10	50

Table 2 Results of database—2

Type of forgery	No. of samples for training	No. of samples for testing		FRR (%)	FAR (%)
		Original	Forged		
Random	20	20	20	3.33	3.33
Simple	20	20	20	6.66	20
Skilled	20	20	20	3.33	60

Table 3 Results of database—3

Type of forgery	No. of samples for training	No. of samples for testing		FRR (%)	FAR (%)
		Original	Forged		
Random	20	20	20	00	6.66
Simple	20	20	20	3.33	10
Skilled	20	20	20	00	50

Table 4 Results of database—4

Type of forgery	No. of samples for training	No. of samples for testing		FRR (%)	FAR (%)
		Original	Forged		
Random	20	20	20	00	00
Simple	20	20	20	3.33	16.667
Skilled	20	20	20	3.33	60

Table 5 Results of database—5

Type of forgery	No. of samples for training	No. of samples for testing		FRR (%)	FAR (%)
		Original	Forged		
Random	20	20	20	00	3.33
Simple	20	20	20	6.66	10
Skilled	20	20	20	6.66	50

Table 6 Results of database—6

Type of forgery	No. of samples for training	No. of samples for testing		FRR (%)	FAR (%)
		Original	Forged		
Random	20	20	20	3.33	00
Simple	20	20	20	10	10
Skilled	20	20	20	6.66	50

Table 7 Details of ANN architecture used for signature verification

Type of ANN used	Feed forward
Algorithm	Back propagation
Activation function	Radial basis function
Number of epochs	5000
Learning rate	0.08
Input neurons	06
Output neurons	01
Number of hidden layer	01

References

1. James L. Wayman, 2008 “Biometrics in Identity Management Systems”, IEEE Computer Society, pp no. 30–37.
2. Robert W. Ives, Yingzi Du, Delores M. Etter, and Thad B. Welch, August 2005, “A Multidisciplinary Approach to Biometrics” IEEE Transactions on Education, Vol. 48, No. 3, pp no. 462–471.
3. Shantanu Rane, Ye Wang, Stark C. Draper, and Prakash Ishwar, September 2013 “Secure Biometrics”, IEEE signal processing magazine, pp no. 51–64.
4. S. Chandra and S. Maheskar, “Offline signature verification based on geometric feature extraction using artificial neural network,” 2016 3rd International Conference on Recent Advances in Information Technology (RAIT), Dhanbad, 2016, pp. 410–414.
5. Jyoti Singh and Manisha Sharma. Offline signature verification using neural networks. *i-Manager’s Journal on Information Technology*, 1(4):35, 2012.
6. Shashi kumar, D. R., K. B. Raja, R. K. Chhotaray, and Sabyasachi Pattanaik., “Biometric security system based on signature verification using neural networks”, 2010 IEEE International Conference on Computational Intelligence and Computing Research, 2010. Technology, Volume 10, 2013, Pages 970–977.
7. S. N. Robert and B. Thilagavathi, “Offline signature verification using support vectore machine,” 2015 International Conference on Innovations in Information, Embedded and Communication Systems (ICIECS), Coimbatore, 2015, pp. 1–6.
8. Vivek kr. Shrivastava, Imran Hussain, Vikash Shrivastava, “Review on offline signature verification methos based on AI technique”, *International Journal of Advancements in Research and Technology*, Vol 2, Issue 5, May 2013.
9. Donato Impedovo, Giuseppe Pirlo, September 2008, “Automatic Signature verification: The State of the Art”, IEEE Transactions on System, man and cybernetics, pp no. 609–635.
10. Indrajit Bhattacharya, Prabir Ghosh, Swarup Biswas, Offline Signature Verification Using Pixel Matching Technique, *Procedia* [10] U. A. Jain and N. N. Patil, “A comparative study of

- various methods for offline signature verification,” 2014 International Conference on Issues and Challenges in Intelligent Computing Techniques (ICICT), Ghaziabad, 2014, pp. 760–764.
11. K. V. Arya and R. Kumar, “Improved feature based offline signature enhancement and verification,” 2014 9th International Conference on Industrial and Information Systems (ICIIS), Gwalior, 2014, pp. 1–6.
 12. P. N. Narwade, S. V. Bonde and D. D. Doye, “Offline signature verification using shape dissimilarities,” 2015 International Conference on Communication, Information & Computing Technology (ICCICT), Mumbai, 2015, pp. 1–6.
 13. M. R. Deore and S. M. Handore, “A survey on offline signature recognition and verification schemes,” 2015 International Conference on Industrial Instrumentation and Control (ICIC), Pune, 2015, pp. 165–169.
 14. Z. Zhang, X. Liu and Y. Cui, “Multi-phase Offline Signature Verification System Using Deep Convolutional Generative Adversarial Networks,” 2016 9th International Symposium on Computational Intelligence and Design (ISCID), Hangzhou, 2016, pp. 103–107.
 15. Tee Wilkin and Ooi Shih Yin, 2011, “State of The Art: Signature Verification System”, 7th International Conference on Information Assurance and Security (IAS), pp no. 110–115.
 16. Anil K. Jain, Arun Ross and Salil Prabhakar, 2004 “An Introduction to Biometric Recognition”, IEEE Transactions on Circuits and Systems for Video Technology, pp no. 1–29.
 17. Daniel A. Reid, Mark S. Nixon, and Sarah V. Stevenage, June 2014 “Soft Biometrics; Human Identification Using Comparative Descriptions”, IEEE Transactions on pattern analysis and machine intelligence, vol. 36, pp no. 1216–1228.

Energy Efficient Image Compression Techniques in WSN

Nishat Bano, Monauwer Alam and Shish Ahmad

Abstract The increasing curiosity in the wireless sensor network (WSN) research measures physical phenomena, like pressure, temperature, which are transported through low bandwidth and low complexity data streams. The introduction of inexpensive CMOS cameras and microphones has promoted wireless multimedia sensor networks (WMSNs). WSN applications such as military, environmental, multimedia surveillance, health care are tailored to provide high energy efficiency. Energy efficiency is the most important parameter in WSN due to resource constraints. The aim of image compression is to reduce redundant information present in an image, thus providing energy efficiency. In this paper, we analyze image compression techniques, namely Set Partition in Hierarchical Trees (SPIHT), Set Partitioned Embedded BloCK Coder (SPECK), and JPEG2000 for energy constrained WSNs. We also compute energy consumption for transmitting a 512×512 Lena image from source to destination and compressed using SPIHT algorithm.

Keywords Energy efficiency · Image compression
Set partitioning in hierarchical trees (SPIHT)
Set partitioned embedded BloCK (SPECK) · JPEG2000

N. Bano (✉) · M. Alam

Department of Electronics Engineering, Integral University, Lucknow, India
e-mail: nishatriv9@gmail.com

M. Alam

e-mail: malam@iul.ac.in

S. Ahmad

Department of Computer Science, Integral University, Lucknow, UP, India
e-mail: shish_parv@rediffmail.com

© Springer Nature Singapore Pte Ltd. 2018

R. Singh et al. (eds.), *Intelligent Communication, Control and Devices*,
Advances in Intelligent Systems and Computing 624,
https://doi.org/10.1007/978-981-10-5903-2_113

1079

1 Introduction

Sensor systems arise due to the development of technologies such as micro-electromechanical systems (MEMS), VLSI, and wireless communications. WSN has grown interest in a swell of civil and military applications [1]. WSN comprises low-power sensor devices, embedded processor which are used to collect and process the data from sensor, communication channel, and power unit. Wireless sensor networks measure pressure, temperature, humidity, or object's location. These applications require low bandwidth and are delay tolerant. WMSNs are self-organizing systems, installed to retrieve, store, correlate, and fuse multimedia contents in real time. The availability of cost-effective CMOS cameras that capture audio streams, still images, and video has grown interest in wireless multimedia sensor network (WMSN) [2]. The design of image sensor nodes is influenced by hardware constraints, transmission media, and energy consumption [3, 4].

The efficient use of battery, available memory, processing competency, and attainable data rate of sensor devices is required. Sensors are battery controlled devices but multimedia applications yield large amount of data which require high transmission rates and widespread processing. Therefore, to maximize network lifetime, protocols, algorithms, and architectures are challenging while providing the quality of service (QoS) required by the application. The capability of each wireless link depends on the interaction of several functions, like energy consumption, routing, and rate policies, handled by all network devices. Hence, the capacity and the delay achieved by each link depend on location and vary continuously, building QoS provisioning a challenging task. Multimedia data, including snapshot data (e.g., still image) contain event triggered observation obtained in a small time-period and streaming data (video) obtained over a long time-period. State-of-art image and video encoders use compression algorithms that reduce the amount of information to be transmitted. WMSNs enable design of simple encoder due to data processing and energy constraint.

The organization of this paper is as follows: Related work is given in Sect. 2. In Sect. 3, we discuss energy efficient image compression techniques. System model is given in Sect. 4. Simulation results and analysis are given in Sect. 5. In Sect. 6, we conclude this paper.

2 Related Work

Over the past years, significant efforts are done which reduces the energy consumption of the wavelet-based image coders. D. Pham and S.M. Aziz [5] presented architecture and protocol that use low complexity JPEG2000 image compression technique in energy constrained WSN that consumes less energy and is fast. Sensor nodes are power constrained. H. Wu and A. Abouzeid [6] proposed a distributed JPEG2000 that distributes the amount of work of wavelet transform to several

nodes from source to the sink, thus eliminates computation power restriction of single nodes and increasing the lifetime of network up to fourfold. M. Nasri et al. [7] attempted to conserve energy using Skipped high pass subbands. Here multiple packets are combined, processed, and multiple copies are transmitted over network to reduce lifetime. The computational energy saving for SHPS technique is high for different compression levels, hence energy is conserved. D.M. Pham and S.M. Aziz [8] presented a reliable image transmission protocol to remove packet errors, and an efficient object extraction algorithm is also given that reduces the energy consumption of transmitted image. M. Nasri et al. [9] proposed a priority image compression technique based on wavelet transformation. A. Chefi and G. Sicard [10] proposed a low-power SPIHT-based image compression technique with hardware and software implementation in terms of energy conservation. Y. Rahman et al. [11] presented a novel object extraction technique that transmits image segments minimizing in-node energy consumption. W. Wang et al. [12] proposed a novel image component technique for efficient energy image transmission with improvement in peak signal-to-noise ratio.

3 Energy Efficient Image Compression Techniques

3.1 Image Compression

In image compression, the highly correlated neighboring pixels are discarded by reducing the redundant information in an image. An image compression system contains three steps:

- (1) Elimination or reduction in pixel redundancy,
- (2) Reducing entropy, and
- (3) Entropy coding.

Image compression is based on the two basic principles, namely spatial redundancy reduction and statistical redundancy reduction. Spatial redundancy is due to correlation between adjacent pixels that can be reduced using decorrelation techniques such as predictive coding, transform coding, subband coding. The statistical redundancy (or entropy coding) reduces the data by variable length coding (VLC) technique by allocating the techniques in a way that the symbols which appeared more are represented with less appearing pixels, thereby achieving compressed image (Fig. 1).

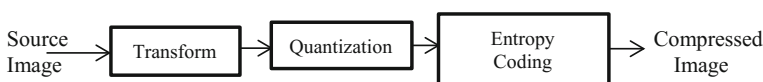


Fig. 1 Image compression process

Image can be transformed using DCT and DWT. JPEG coder uses DCT and generates energy-compacted spectral components. Discrete wavelet transform provides excellent energy compaction and exploits redundancy for better image compression. DWT offers higher compression efficiency than DCT, but it is complex. In order to remove complexity and memory requirement, lifting wavelet transform [13, 14] and fractional wavelet transform are used in an energy efficient way [15].

3.2 *Wavelet-Based Image Compression Techniques*

In digital images, redundant information is present. For energy conservation, we compress images and transmit them with small amount of data utilizing basic principle of image compression. Shapiro [16] introduced embedded zerotree wavelet (EZW) which is extremely fast, very effective, and produce embedded bit stream. The performance of EZW is further enhanced by presenting a simple, more efficient, and faster technique called set partitioning in hierarchical trees (SPIHT) developed by A. Said and W. Pearlman which has outstanding rate-distortion performance [17]. A. Islam and W. Pearlman proposed block-based wavelet transform coding technique with low complexity known as Set Partitioning Embedded bloCK (SPECK) [18]. Embedded block coding with optimized truncation (EBCOT) algorithm [8] adopted in JPEG2000 provides higher compression efficiency than SPIHT, but it is very complex and computationally intensive as it needs extra memory allocation. For hardware constraints, SPIHT is preferred over EBCOT [19]. However, for high resolution images, SPIHT needs large memory bank which in turn increases cost of hardware.

SPIHT comprises two coding passes: sorting and refinement pass and uses three lists (LIP, LIS and LSP) to store the transformed coefficients of the image. LIP contains the insignificant pixels of the high energy LL band. LIS contains list of insignificant sets that have descendants only. LSP is the list of significant pixels which is initially kept empty. Initially, a threshold is set and significance of coefficients is tested in a progressive way. The coefficients that are found to be significant are added to LSP. The significant coefficients of previous pass are refined and n th bit is output. The process is repeated by reducing the threshold to half until all coefficients are tested for significance. SPIHT is simple, fast and gives best rate-distortion performance, but the presence of three lists requires more memory and consumes more energy, thus increasing its complexity.

SPECK is a block-based image compression that consists of two linked lists, namely LIS and LSP and three coding stages: initialization, sorting, and refinement pass. The image is divided in two sets: set \hat{S} and set \hat{I} . Set \hat{S} is the root set of pyramid and set \hat{I} contains remaining pixels. During the sorting pass, significance of \hat{S} and \hat{I} sets are checked. If \hat{S} is found to be significant, it is partitioned into four equal sized subsets added to LIS. All subsets of 1×1 are checked for significance and if found significant, the sign bit is coded. These subsets are then added to

LSP. If the set \hat{I} found significant, it is divided into octave band partitioning. A total of four sets are generated: three \hat{S} sets and one \hat{I} set. When all sets are partitioned and made significant, the refinements pass starts which refine the quantized pixel values of LSP that are found significant in the earlier passes. Now threshold is reduced in a step of two. Repeat this process until the desired bit rate is attained. Reduction of linked lists in SPECK reduces memory requirement, but still there is need to reduce its complexity.

JPEG2000 is the wavelet-based version developed by Joint Photographic Experts Group committee. JPEG2000 introduces many new features that are effective for vast applications. JPEG2000 performs preprocessing that includes tiling, dc level shifting, and multicomponent transformation operations. JPEG2000 encoder performs three steps in compression: discrete wavelet transform (DWT) processing step, quantization step, and entropy encoding step. Each component after multicomponent transformation is decomposed by DWT in different subbands which are then independently quantized. These quantized subbands are broken into equal sized small code-blocks, generally 32×32 , 64×64 . These code-blocks produce compressed bit streams after independently entropy encoded by Tier-1 and Tier-2 coding engines. In Tier-1 coding process, each code-block is divided into n bit-planes, where n is the precision of number of elements in code-blocks. They are encoded from n th bit-plane to first bit-plane by fractional bit-plane coding using Embedded Block Truncation Optimization Technique (EBCOT) [19] algorithm in three coding passes such that if a part of one bit-plane is being encoded, other bit-planes do not overlap. These three coding passes of EBCOT are significance propagation, magnitude refinement, and clean up. EBCOT generates context data and binary decision values which are coded by binary arithmetic coding (known as MQ-coder) and produce compressed bits for all code-blocks. In Tier-2 coding, for each code-block, a layer has all the coding passes from all consecutive bit-planes and block summary information has length of compressed bit streams, zero bit-plane data, and the number of coding passes data. Tag trees (quad trees) are used to represent the layer and block summary data for all code-blocks as compressed file header (Table 1).

A comparative analysis is done among these image coders:

JPEG2000 has high coding efficiency, but requires high memory. So it is not energy efficient. SPECK algorithm also has high computation cost and requires huge memory compared to SPIHT. From this analysis, we can say that SPIHT is highly energy efficient although it has low compression quality than JPEG2000.

Table 1 Comparison of image compression techniques in terms of computation cost

	SPIHT	SPECK	JPEG2000
Transform	DWT	DWT	DWT
Memory needed	low	low	high
PSNR (image quality)	low	low	high
Encoding time	low	high	high

4 System Model

4.1 Energy Consumption Analysis

Following features are assumed while sending an image from source to destination upon receiving a request from destination:

- The characteristics of all sensors are same.
- The energy of a node remains same for the transmission of full image.
- The network path from source to destination remains the same during the entire process with n intermediate nodes numbered from 1 to n .

Consider a wireless sensor network which has n intermediate nodes equipped with camera. An image is transmitted from source to destination through a sensor. The energy consumption in transmitting a bit is

$$E_{tx} = \dot{\epsilon}_e + \dot{\epsilon}_a d^\alpha \tag{1}$$

The energy consumption in receiving a bit is

$$E_{rx} = \dot{\epsilon}_e \tag{2}$$

where $\dot{\epsilon}_e$ is the energy dissipation (per bit per meter²), $\dot{\epsilon}_a$ is the energy consumption per bit in the circuit, d is the distance between source and destination, and α is the path loss parameter.

4.2 Energy Model of Radio Transceiver

Energy is consumed by intermediate nodes when it is transmitted from source to destination. Consider a radio transceiver model [20].

- If E_{SW} Energy consumed in switching the mode;
- $E_{TX}(k, P_{out})$ Energy consumed in transmitting k byte of image;
- $E_{RX}(k)$ Energy consumed in reception of k byte image;

Then the energy consumed in transmitting k bytes of image from node i to node j is

$$E_{ij}(k) = 2E_{SW} + E_{TX}(k, P_{out}) + E_{RX}(k). \tag{3}$$

$$E_{ij}(k) = 2C_{SW} \cdot V \cdot T_{SW} + k \cdot C_{TX}(P_{out}) \cdot V \cdot T_{TX} + C_{RX} \cdot V \cdot T_{RX}. \tag{4}$$

where C_{SW} , $C_{TX}(P_{out})$, C_{RX} , T_{SW} , T_{TX} , T_{RX} , V are the currents drawn, operation time and battery voltage to switch the mode, to transmit the image, and to receive the image by the radio, respectively.

4.3 Energy Model of 2D-DWT Processing

Assume an input image of $M \times N$ pixels. If 2D-DWT is applied T times on image, then the energy consumption is given by

$$E_{DWT} = M \times N \cdot (10\epsilon_{shift} + 12\epsilon_{add} + 2\epsilon_{rmem} + 2\epsilon_{wmem}) \cdot \sum_{i=1}^T \frac{1}{4^{(i-1)}}. \tag{5}$$

where ϵ_{shift} , ϵ_{add} , ϵ_{rmem} , and ϵ_{wmem} signify energy consumption in shift, add, read, and write 1 byte, respectively.

4.4 Energy Model of Quantization and Entropy Coding

Energy consumption in quantization and entropy coding k bytes of image is given by

$$E_{ENT}(k) = \epsilon_{ENT} \cdot k. \tag{6}$$

5 Simulation Results and Analysis

5.1 Input Parameters

From technical documentation, we adopted the characteristics of crossbow Mica2 motes sensor [21, 20] given: (Table 2).

Table 2 Input parameters for Mica2 motes

Variable	Value	Variable	Value
$C_{TX}(0)$	20 mA	T_{SW}	0.25 ms
C_{RX}	15 mA	ϵ_{shift}	3.3 nJ
C_{SW}	15 mA	ϵ_{add}	3.3 nJ
T_{TX}	0.416 ms	ϵ_{rmem}	0.26 μ J
T_{RX}	0.416 ms	ϵ_{wmem}	4.3 μ J

Using these parameters and $V = 3 \text{ V}$, we can compute energy consumed in transmitting, receiving, and in DWT process for one byte is $E_{TX} = 24.96 \text{ }\mu\text{J}$, $E_{RX} = 18.72 \text{ }\mu\text{J}$, and $E_{DWT} = 9.19 \text{ }\mu\text{J}$ (from Eq. 5), respectively.

5.2 Effect of Image Compression

The energy consumed in entropy coding is 160 nJ per byte [6]. Initially, there are 32,768 bytes available in a 512×512 pixel image. The energy dissipated during entropy coding in an uncompressed image is 5.24 mJ from (6) and the total energy consumption in transmitting uncompressed 512×512 pixel image from node i to node j is 1430 mJ. The energy consumed in mode switching from Table 2 is

Table 3 Energy consumption in compression

Compressed bytes achieved (k)	Energy consumption in transmission (E_{TX}) (in mJ)	Energy consumption in reception (E_{RX}) (in mJ)	Energy consumption in entropy coding (E_{ENT}) (in mJ)	Total energy consumption ($E_{ij}(k)$) (in mJ)
16,381	409	307	2.62	716
8168	205	153	1.31	358
4091	102	76.6	0.655	179
2010	50	37.6	0.322	88
961	24	18	0.154	42
504	12.6	9.43	0.08	22

Fig. 2 Energy consumption (E_{ENT}) in quantization and entropy coding for SPIHT

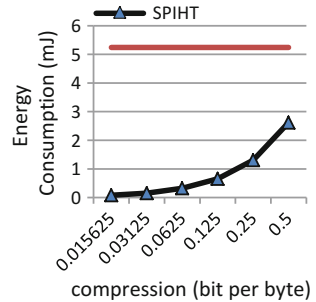
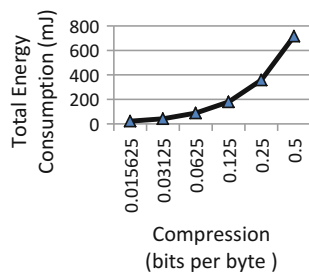


Fig. 3 Total energy consumption ($E_{ij}(k)$) for SPIHT



11.25 μ J. The energy dissipation at different compression rates using Eqs. (4), (6), and Table 1 is calculated and provided: (Table 3).

Figures 2 and 3 show the energy consumption during quantization and entropy coding and the total energy consumed in transmitting a 512×512 pixel Lena image from node i to node j at different compression ratio for SPIHT.

6 Conclusions

We review the existing energy efficient techniques in resource constrained wireless sensor network. The wavelet transformed image compression techniques (SPIHT, SPECK, JPEG2000) are analyzed. A comparative analysis of these techniques is shown in terms of computational cost and energy efficiency. From this, we conclude that SPIHT is highly energy efficient compared to other techniques. Using system model, the energy consumption for transmitting a 512×512 Lena image from source to destination which is compressed using JPEG2000 algorithm is reduced compared to uncompressed image.

References

1. Akyildiz I.F., Su W., Sankarasubramaniam Y., Cayirci E.: Wireless sensor networks: a survey, *Computer Networks* (Elsevier) 38 (4) pp. 393–422 (2002)
2. Akyildiz I. F., Melodia T., and Chowdhury K. R.: A Survey on Wireless Multimedia Sensor Networks. *Computer Networks* (Elsevier), vol. 51, no. 4, pp. 921–960, March (2007)
3. Melodia T., Akyildiz I. F.: Research challenges for wireless multimedia sensor networks: in *Distributed Video Sensor Networks*, London, U.K.: Springer-Verlag, 2011. pp. 233–246 (2011)
4. Downes I., Rad L. B., and Aghajan H.: Development of a Mote for Wireless Image Sensor Networks: in *Proc. Cognitive systems with Interactive Sensors (COGIS)*, Paris, France, (2006)
5. Pham D. M., Aziz S.M.: An Energy Efficient Image Compression Scheme for Wireless Sensor Networks: *IEEE, ISSNIP* (2013)
6. Huaming Wu and Abouzeid A.A.: Energy efficient distributed JPEG2000 image compression in multihop wireless networks: 4th Workshop on Applications and Services in Wireless Networks (ASWN-2004), pages 152–160. (2004)
7. Nasri M., Helali A., Sghaier H., Maaref H.: Energy conservation for image transmission over wireless sensor networks: *IEEE* (2011)
8. Pham D. M. and Aziz S. M.: Object extraction scheme and protocol for energy efficient image communication over wireless sensor networks: *Computer Networks*, vol. 57, pp. 2949–2960. (2013)
9. Nasri M., Helali A., Sghaier H., Maaref H.: Priority Image Transmission in Wireless Sensor Networks, 8th International multi-conference on systems, signals & devices, (2011)
10. Chefi A. and Sicard G: SPIHT-based image compression scheme for energy conservation over Wireless Vision Sensor Networks. *IEEE conference* (2014)

11. Rehman Y., Tariq M., Sato T.: A Novel Energy Efficient Object Detection and Image Transmission Approach for Wireless Multimedia Sensor Networks: *IEEE sensors journal* (2016)
12. Wang W., Peng D., Wang H., Sharif H.: A Novel Image Component Transmission Approach to Improve Image Quality and Energy Efficiency in Wireless Sensor Networks: *Journal of Computer Science*. 3 (5) pp. 353–360 (2007)
13. Sweldens W.: “The lifting scheme: A custom-design construction of biorthogonal wavelets,” *Appl. Comput. Harmon. Anal.*, vol. 3, pp. 186–200, (1996)
14. Sweldens W.: The lifting scheme: a construction of second generation wavelets: *SIAM J. Math. Anal.*, pp. 511–546, (1997)
15. Rein S., Lehmann S., and Gühmann C.: Fractional wavelet filter for camera sensor node with external Flash and extremely little RAM: in *Proc. ACM Mobile Multimedia Commun. Conf. (MobiMedia)*. pp. 1–7. (2008)
16. Shapiro J. M.: Embedded image coding using zerotrees of wavelet coefficients: *IEEE Trans. Signal Process.*, vol. 41, pp. 3445–3462 (1993)
17. Said A. and Pearlman W. A.: A new, fast, and efficient image codec based on set partitioning in hierarchical trees: *IEEE Trans. Circuits Syst. Video Technol.* vol. 6, no. 3, pp. 243–250 (1996)
18. Islam A., Pearlman W. A: Embedded and efficient low-complexity hierarchical image coder. *IEEE Transactions on circuits and systems for video technology*, vol. 14, no. 11, (2004)
19. Taubman D.: High performance scalable image compression with EBCOT: *IEEE Trans. Image Processing*, vol. 9, pp. 1158–1170, (2000)
20. Heintzelman W., R., Chandrakasan, A., and Balakrishnan, H.: Energy-efficient communication protocol for wireless microsensor networks: In *Hawaii International Conference on System Sciences HICSS*, volume 2. (2000)
21. Crossbow Technology Inc. (2007). Crossbow. <http://www.xbow.com>. Consulted in

Real-Time System Monitoring and Control of Automation Industry Using IoT-Based Cloud Platform

G.N.L. Ravi Teja, S. Sukumar, Surya Kompella, Raga Sudha
and G. Pallavi

Abstract Industrial manufacturing involves large calibrations of data and process. Security, optimal response time, and control are major constraints while describing a process in industry. Various technologies were in research to enhance the functional capabilities for better responses. IoRT is one such promising technology to provide a better solution in most advanced way. The architectural design of communication through IoT is one of the open challenges facing, and there is a futuristic viability in achieving a solution for such issues. This paper depicts an approach, implementation of a conveyor model of a simple assembly line to separate metal from nonmetal using a Python-controlled 2-axis robotic arm. The entire process can be monitored using a Web server, designed for real-time process application.

Keywords IoRT/IoT · Optimal response · Assembly line
Web server · Assembly line · Control

G.N.L.R. Teja (✉) · S. Sukumar · S. Kompella · R. Sudha · G. Pallavi
Kriyative Edge Technology Services (P) Ltd., Hyderabad, India
e-mail: raviteja@kriyative-edge.com

S. Sukumar
e-mail: sukumar@kriyative-edge.com

S. Kompella
e-mail: surya@kriyative-edge.com

R. Sudha
e-mail: ragasudha@kriyative-edge.com

G. Pallavi
e-mail: pallavi@kriyative-edge.com

1 Introduction

Everything around us is getting smarter and changing. The change is taking step toward a better and smart future. The major role of engineering focus to play a pivotal role in bringing those changes to make a point-breaking understanding of the technologies around us in a better way. A smart home can make a smart city, likewise a smart industry can revolutionize the process for a smarter maintenance. It is a small step in making smart industries by reducing the complexity of wired communication with replaceable—connecting devices and cloud platform for analysis and control [1]. This also solves the problem of complex hardware architecture by replacing structural complexity with logical devices and advanced communication devices.

This paper aims to deploy computing techniques in creating a barrier to integration, complexity, to provide more financial gains and energy savings. Sustainability of resources in many small- and medium-scale industries is a current dominant issue. Automated process is a very efficient and effective process on installing very-high-configured equipment, which is a possible constraint in small and medium industries. Consistent growth in market defines targets, but lack of resources has become a possible challenge in many ways.

A simple consideration of a mushroom harvesting plant, where the production process takes minimum of 14 weeks for the yield and most of the approach, is manual. A conveyor system would possibly reduce time of transporting yield; maintain the same environment and easy handling [2, 3]. But yet most of the process is manual and all the information is recorded by a person. This has a possible disadvantage of failure in certain conditions.

The problem persists in many other companies, where the process is dependent on manpower. To avoid problems of human error and to utilize all the manpower for a better production, this paper provides a brief insight of possible advantages of IoT in automation industry.

Initiating the process, identifying metal from nonmetal, handling the part as per requirement are the general insights briefed in this paper with real-time deployment. Usage of IoT concepts helps to monitor the process from any part of the world. One needs not to possibly be live at the moment to see the process. All the processes can be recorded, sorted, and are ready for analytics at an instance.

2 Internet of Things: A Case Study

The way of communication, life style, work culture, and ease of data extraction has changed with Internet. Connecting people bought revolution in once livelihood and next era of modernization is connecting various devices through Internet and cloud, by which smart and intelligent devices revolutionize once working methodology. A survey report stating the number of estimated connecting devices will be

50 billion at least by 2020 which are connected to cloud platform [4, 5]. A better and sophisticated way to connect with other devices is by machine-to-machine (M2M) applications. With IoT, the maximum allowance of physical devices connected to cloud platform would lead to mobile revolution. Comfort, safety, and efficiency are the driving factors for IoT, connecting physical objects to cloud Internet platform. The abbreviation IoT is not yet well defined; Cisco calls it Internet of Everything. Generally, it is Industrial Internet and IBM calls this as the same Internet. But all agree that IoT will make our physical systems much smarter.

2.1 Different Layers of IoT Protocols

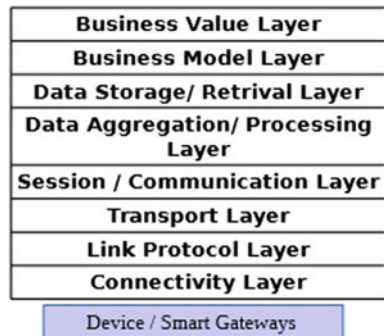
The layer of hierarchy is given below. It is not possible to discuss all the available protocols so the protocol stack below will be confined to most common and useful protocols in the current trends [5] (Fig. 1).

2.2 Networking Protocols and Standards for IoT

IoT got a lot of importance from recent past from both academic researches an industrial approach. Due its vast application, support a lot of funding for research is encouraged. Lot of financial aid is being supported and spent to IoT-related technologies and on research, yet a lot of research is being expected in the following years [5–7].

Considering the protocols related to IoT which are operating at various layers in the networking stack, which includes: MAC—medium access control layer, network and session layer. Representing IoT, the standards and protocols were supported by Internet Engineering Task Force (IETF), IEEE—Institute of Electrical and Electronics Engineers, ITU—International Telecommunication Union (ITU),

Fig. 1 Different layers to understand the protocol stack



and other standard organizations. A consistent research of half decade proposed a lot of standards for current and future necessity.

2.3 IoT Ecosystem

The IoT ecosystem defined the layer-level application support. The bottom layer defines the market domain and application domain, which is a smart grid-connected home, or smart health monitoring system, etc.; preceding second layer is sensors to enable the application. Sensors like temperature, humidity, gas, electrical utility meters, cameras [8] were considered as few examples supporting the second layer. The ecosystem is supported with third layer that will interconnect different other layers which allows the generated data or values from the sensors to the communication interference like cloud/Internet or data process center or a computational facility [9]. The entire data is summarized with other previously collected values or data sets representing geographical data or population growth or economic expansion and so on. Machine learning, data mining, artificial intelligence, and other advanced adaptive techniques were used to combine the data and analyze the results. Huge distributed data banks were to be enabled, so that the collaboration approach at application level with communication software like SDN—software-defined networking, SOA—service-oriented architecture. The top or prior layer is all about services that enable the market including health, education, logistics, energy (Fig. 2).



Fig. 2 IoT ecosystem with hierarchy

Developing a successful IoT application is still not an easy task due to multiple challenges [10, 11]. These challenges include mobility, reliability, scalability, management, availability, interoperability, and security and privacy.

3 Basic Concept

Industrial conveyor monitoring and handling control system involve parts which are aggregated into our proposed system. The system designed is represented into our proposed block diagram (Figs. 3 and 4).

3.1 Working Principle

Arduino Uno: Intelligent devices play a very crucial role in embedded systems. Most common MCU device by ATMEL is being used in Arduino Uno [12]. Being an open-source platform, it is preferably used in various projects on electronics and embedded systems. A physical circuit with MCU will be driven by the software program through IDE that runs from computer to the board (Fig. 5).

ESP8266. Esp8266 is an open-source IoT platform. It includes firmware which runs on Wi-Fi (Fig. 6).

A command from user will initiate the process; the part on the conveyor system is identified by a metal sensor integrated over the system. An ultrasonic sensor will identify the exact position of the part over conveyor and stop the sequence; every piece of working can be monitored by a custom-designed Webpage 1tuch.in.

Fig. 3 Basic concept of cloud integration of a conveyor system

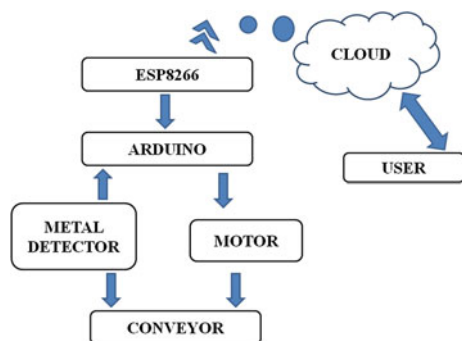


Fig. 4 Process describing the handling unit

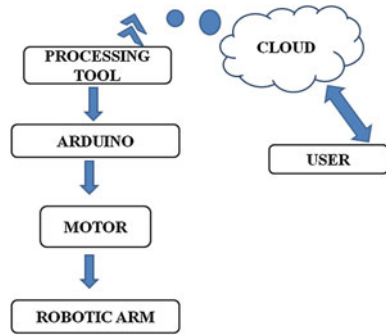
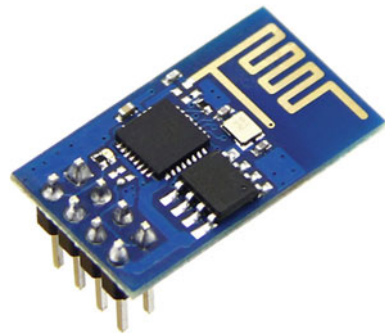


Fig. 5 Physical model of Arduino Uno



Fig. 6 Physical model of ESP8266 Wi-Fi module



Once the conveyor sequence is performed based on the results depicted by metal sensor and ultrasonic sensors, the robotic arm is given command to collect the part and place it in respective locations as per guidelines. To perform this action, the command center is designed using processing tool (Fig. 7).

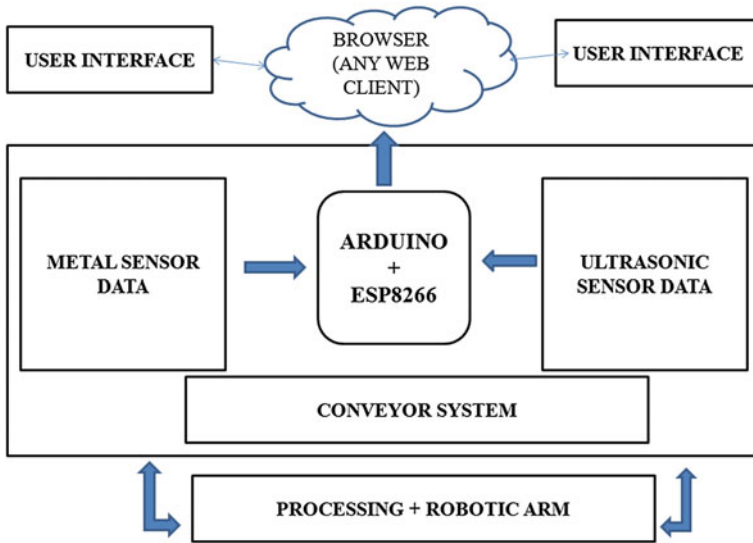


Fig. 7 Working principle of the defined hardware algorithm

4 Design and Implementation

Initial setup for the design is as follows: a metal sensor is interfaced to sense the metal objects or parts with better accuracy. MCU (Arduino Uno) is being used for automatic control of entire system which reduces the complexity of design and control. Entire input from sensor unit is provided to MCU for processing, the input from the sensor unit which senses the metal, the data is transmitted to user through Wi-Fi which is connected to cloud/Internet. Acceptance information is being monitored and maintained the server, which will send a message to the user, and the response from the user will decide the action to be performed by the robotic arm with respect to the status of metal sensor.

Later stages implementing the ultrasonic sensor for measuring exact location of part on conveyor reduced the complexity for robotic arm to take necessary action.

4.1 Programming Steps for Programming Arduino Uno Board

- (i) Connect Arduino Uno to USB port of computer.
- (ii) Initialize the board by selecting type of board being used and also with virtual port assigned to the board in the tools menu.

- (iii) An Arduino Uno sketch usually has five parts: declaring the variables; enabling the setup routine, which will initialize the variables and conditions to run the preliminary code; looping, is the place you add the main algorithm which will be executed repeatedly till an external reset is actively pressed or the sequence is terminated by the user; final section will be for other important functions to activate during the setup enablement and for loop routines.
- (iv) To test the device, upload a preloaded program. This will ensure the device functioning.
- (v) Once after testing, the board is ready for any purpose deployment. Once disconnecting from computer and integrating it with proposed projects directly.

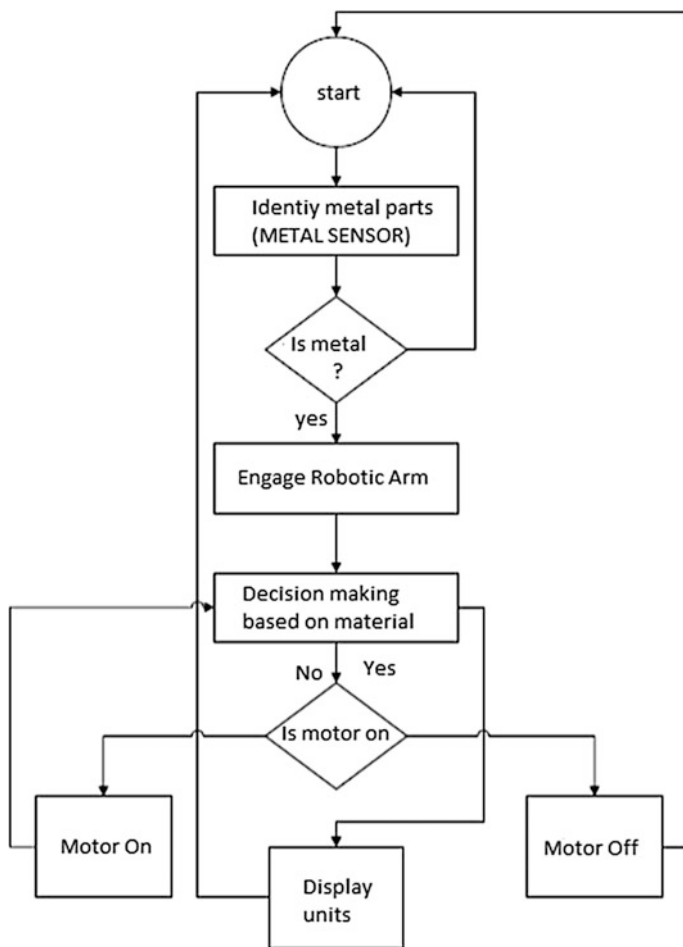


Fig. 8 Algorithm for the proposed system

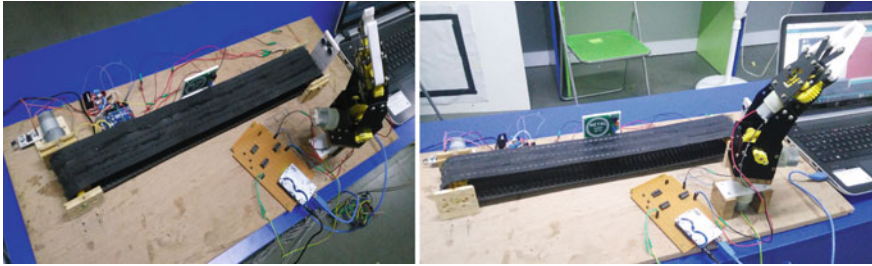


Fig. 9 Real-time system deploying conveyor model, robotic arm, circuitry interface

- (vi) Once the program is executed and compiled the project is converted into hex format and can be downloaded into device.
- (vii) Thus, the project life cycle is accustomed with the project implementation (Fig. 8).

4.2 Processing Programming Environment

This is a tool to learn how to program using flexible software sketchbook and within the context of visual arts. This open-source tool is more compatible for integrating with external devices like Arduino Uno.

4.3 Real-Time Model

See Fig. 9.

5 Results, Conclusion, and Future Scope

Through this approach, a lot of calibrations were recorded with few IoT protocols. Considering only one parameter like metal to provide results, being a repetitive process it needs better algorithms and advanced communication protocols to integrate more sensoric data into the cloud platform.

Among 15 iteration cycles, 2 cycles were out of the algorithm. This is a constraint to focus on. A general loop governing the system yields such a result. Further progress is achieved with control algorithms creating a feedback loop using PID tuning filter.

TCP protocol is being implemented for regular communication, with this algorithm, and by using open-source hardware equipment, the designed node could not resist the high-flow buffer rate and the timing function plays a vital role. Little iteration was satisfactory with a time lag of 3–4 s, while few took a time gap of above 10 s. This has a severe effect at the process and outcome. A server-to-server communication way is being implemented for further understanding. Considering packet ratio, durability, timing functions, the approach has given some satisfactory results. Despite this, a lot of research, implementation, and understanding is necessary.

Advanced protocols like MQTT have a benefit compared to TCP and UDP. Few other protocols should also be revised in this case.

This research review paper portrays the importance of IoT in manufacturing and assembly units, its current growth, protocols defining the rules, and further expansion in large scale.

References

1. Condie, S. J. T.: Distributed computing, tomorrow's panacea-an introduction to current technology, *BT Technol. J.* 17(2) (1999), pp. 13–23.
2. <http://www.hortidaily.com/article/19747/Canada-Automated-mushroom-harvester-can-change-the-industry>.
3. Saucy, P., and Mondada, F.: Open access to a mobile robot on the Internet, *IEEE Robotics and Automation Magazine* 7(1) (2000), pp. 41–47.
4. Goldberg, K., Gentner, S., Sutter, C. et al.: The Mercury project: A feasibility study for Internet robotics, *IEEE Robotics and Automation Magazine* 7(1) (2000), pp. 35–40.
5. Jia, S., and Takase, K.: Network-based human assist robotic system using CORBA, in: *The Sixth International Symposium on Artificial Life and Robotics*, Tokyo, Japan, 2001, pp. 105–109.
6. Siegwart, R., Wannaz, C., Garcia, P. et al.: Guiding mobile robots through the Web, in: *Proc. of 1998 IEEE/RSJ Conference on Intelligent Robots and Systems; Workshop on Web Robots*, Victoria, B.C. Canada, October 12–17, 1998, pp. 1–7.
7. Stein, M.: Painting on the Web, The PumaPaint Project, in: *Proc. of 1998 IEEE/RSJ Conference on Intelligent Robots and Systems; Workshop on Web Robots*, Victoria, B.C. Canada, October 12–17, 1998, pp. 37–43.
8. Jesus M. Corres, Carlos Ruiz, “Competition oriented learning experience in electronics: Robot fabrication from scratch”, *Global Engineering Education Conference (EDUCON) 2016 IEEE*, pp. 62–65, 2016, ISSN 2165-9567.
9. Ashraf Suyyagh, Benjamin Nahill, Alexandre Courtemanche, Evgeny Kirshin, Zeljko Zilic, Boris Karajica, “Managing the microprocessor course scope expansion”, *Microelectronic Systems Education (MSE) 2013 IEEE International Conference on*, pp. 36–39, 2013.

10. Peter Ferschin, Monika Di Angelo, Gerhard Brunner, "Rapid prototyping for kinetic architecture", Cybernetics and Intelligent Systems (CIS) and IEEE Conference on Robotics Automation and Mechatronics (RAM) 2015 IEEE 7th International Conference on, pp. 118–123, 2015, ISSN 2326-8239.
11. Dalton, B., and Taylor, K.: A framework for Internet robotics, in: Proc. of 1998 IEEE/RSJ, Conference on Intelligent Robots and Systems; Workshop on Web Robots, Victoria, B.C. Canada, October, 1998, pp. 15–23.
12. Arduino Uno official source: www.arduino.cc.

Performance Estimation of Adaptive Beamforming Algorithms in Smart Antennas

R. Gowri, Abhinav Sharma and Sanjay Mathur

Abstract Adaptive antenna also known as smart antenna is a combination of antenna array with digital signal processor. It optimizes the beam pattern of antenna array according to the changing electromagnetic environment. The two key signal processing approaches of adaptive antenna are identification of spatial signature of incoming signals and adaptive beamforming (ABF). The behavior of three different beamforming algorithms, i.e., conjugate gradient algorithm (CGA), affine projection algorithm (APA), and quasi-Newton algorithm (QNA), are analyzed in terms of their beam pattern characteristics and their convergence rate. The results obtained in the simulations show that CGA has greater null depth and has fastest convergence rate among all the three algorithms.

Keywords Smart antenna · ABF · CGA · APA · QNA

1 Introduction

In the area of wireless communication, there has been a substantial development in the wireless services. Third and fourth generation cellular services and personal communication services have attracted many users worldwide, which lead to increased traffic in the present wireless scenario. Smart antenna plays the leading role and is a novel development in the area of telecommunication as it satisfies the requirement of present wireless services such as higher channel capacity and data rates. The term smart signifies the signal processing aspect of the antenna. Smart antenna identifies the direction of incoming signals and optimizes the weights of antenna array in order to direct the antenna's major lobe in the direction of signal of interest (desired user) and nulls in the direction of interfering signals. Thus, the

R. Gowri (✉) · A. Sharma
Department of EIC, UPES, Dehradun, Uttarakhand, India
e-mail: ravigowri07@gmail.com

S. Mathur
Department of ECE, College of Technology, GBPUA&T, Pantnagar, India

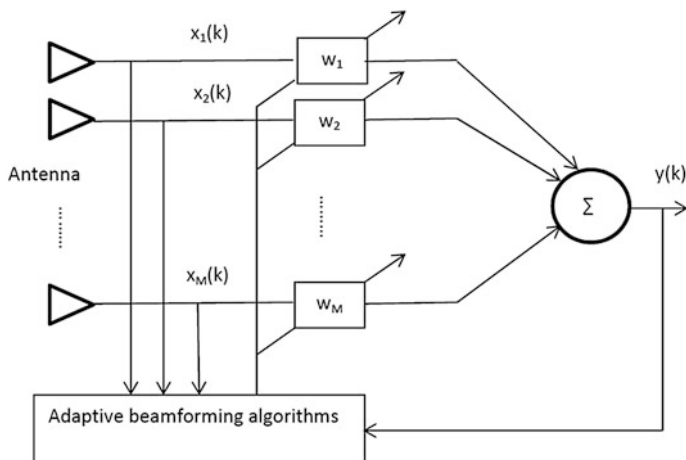


Fig. 1 Adaptive beamforming network

operation of smart antenna is governed by direction of arrival (DOA) estimation algorithm and ABF algorithms. Multiple signal classification (MUSIC), matrix pencil, capon, Root-MUSIC, ESPRIT are some of the efficient DOA estimation techniques already reported in literature [1–3]. As the DOA changes with time, ABF has to be employed by recalculating the optimum array weights. ABF technique is an improvement over the fixed beamforming technique as it continuously updates the array weights. Figure 1 shows the general ABF network.

The paper is organized in the following manner. Section 2 briefly discusses conjugate gradient, affine projection, and quasi-Newton ABF algorithms. In Sect. 3, results obtained from simulations are analyzed and compared. Section 4 provides a conclusive remark and the scope of future work.

2 Algorithms in ABF Techniques

In the field of array signal processing, adaptive beamforming often known as optimum combining was initially developed in 1960 for radar and sonar applications. The adaptation process keeps on recalculating the optimum array weights in changing electromagnetic environment based on certain optimization criteria. In this section, adaptive beamforming based on different optimization criteria, viz. conjugate gradient algorithm, affine projection algorithm, and quasi-Newton algorithm are briefly discussed.

2.1 Conjugate Gradient Algorithm

Conjugate gradient algorithm also called as accelerated gradient approach by Monzingo and Miller is an iterative technique which solves the unconstrained optimization problems by choosing the orthogonal paths in each new iteration [4]. CGA overcomes the limitation, i.e., slow convergence speed of steepest descent algorithm [3, 9, 10]. The weight update equation is given by:

$$\bar{w}(n+1) = \bar{w}(n) - \mu(n)\bar{D}(n), \quad (1)$$

where $\mu(n)$ and $\bar{D}(n)$ are the step size and the direction vector and are given by:

$$\mu(n) = \frac{\bar{r}^H(n)\bar{A}\bar{A}^H\bar{r}(n)}{\bar{D}^H(n)\bar{A}^H\bar{A}\bar{D}(n)}, \quad (2)$$

$$\bar{D}(n+1) = \bar{A}^H\bar{r}(n+1) - \alpha(n)\bar{D}(n), \quad (3)$$

where \bar{r} is the residual and is given by:

$$\bar{r}(n+1) = \bar{r}(n) + \mu(n)\bar{A}\bar{D}(n), \quad (4)$$

$$\alpha(n) = \frac{\bar{r}^H(n+1)\bar{A}\bar{A}^H\bar{r}(n+1)}{\bar{r}^H(n)\bar{A}\bar{A}^H\bar{r}(n)}. \quad (5)$$

The conjugate gradient algorithm finds wide applications in mobile communication as it reduces the BER and eliminates the multipath channel fading effect.

2.2 Affine Projection Algorithm

Affine projection algorithm is an efficient and less complex adaptive filtering algorithm. The algorithm is a generalization of normalized least mean square (NLMS) algorithm, as in the weight update equation, the algorithm utilizes all N projections vector of input signal instead of single vector of NLMS algorithm [7, 8]. The algorithm utilizes an arbitrary number of data pairs such that the new solution depends on the present and past data pairs. The weight update equation is defined as:

$$\bar{w}(k+1) = \bar{w}(k) + \mu X(k)t(k), \quad (6)$$

where $t(k) = [X^H(k)X(k) + \delta I]^{-1}e^*(k)$,

$$e(k) = d(k) - X^T(k)w^*(k).$$

The step size μ which lies between 0 and 2 controls the stability and speed of convergence of the algorithm [5].

2.3 Quasi-Newton Algorithm

A quasi-Newton algorithm based on Newton's method is a robust optimization technique which finds applications in ABF. The algorithm shows stable performance in high signal correlation and has good rate of convergence. The weights of the algorithm are updated as:

$$\bar{w}(k+1) = \bar{w}(k) + \mu(k)h(k), \quad (7)$$

where $\mu(k)$ is the step size and $h(k)$ is the direction of the update and is given by:

$$h(k) = -R^{-1}(k-1) \frac{\partial J_{w,w^*}}{\partial w^*}. \quad (8)$$

The cost function and the step size is given by,

$$J_{w,w^*} = |e(k)|^2, \quad (9)$$

$$\mu(k) = \frac{1}{2x^H(k)R^{-1}(k-1)x(k)}, \quad (10)$$

where $x(k)$, $R^{-1}(k-1)$, and $e(k)$ are the input vector, inverse of the correlation matrix, and the error vector, respectively [5, 6].

3 Results and Discussion

This section analyzes the performance of ABF algorithms discussed in previous section on the basis of radiation pattern and their convergence rate. An uniform linear array (ULA) having omnidirectional antenna elements with $\lambda/2$ distance between the array elements are considered. The cosine signal is considered as the signal of interest, and the random signals are signals not of interest. The directions of desired and interfering signals are $\{0^\circ, -30^\circ, 30^\circ\}$. The noise variance is 0.01, and the number of snapshots is 100. The beam pattern of APA, QNA, and CGA are analyzed with the variation of array elements. The number of array elements considered in the simulation is $\{10, 14, 18\}$.

Figures 2, 3, and 4 show the variation of beamwidth, SLL, and maximum null depth of APA, QNA, and CGA with the alteration of array elements. The simulation results present in Tables 1, 2, and 3 show that beamwidth decreases with the increase of array elements and hence increase in directivity. All the three algorithms show almost similar variation in beamwidth with the increase of array elements [4]. Since the number of antenna elements is greater than 10, thus the SLL varies randomly around -14 dB which is fulfilling the standards. The results show that null depth at two interferences is maximum for CGA as compared to other two algorithms.

Figures 5, 6, and 7 show the convergence of all the three beamforming algorithms. Since all the three algorithms are iterative algorithms, thus their rate of convergence is an important parameter to examine their performance. The mean square error of QNA and APA converges almost after 50 iterations while residual drops to almost zero after 5 iterations for the conjugate gradient algorithm. Thus, CGA has the fastest rate of convergence among QNA and APA.

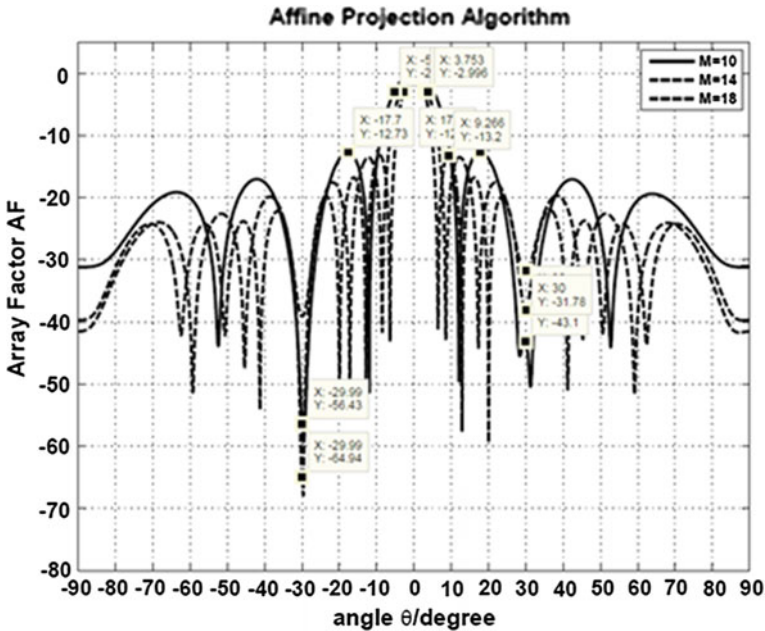


Fig. 2 Radiation pattern for affine projection algorithm

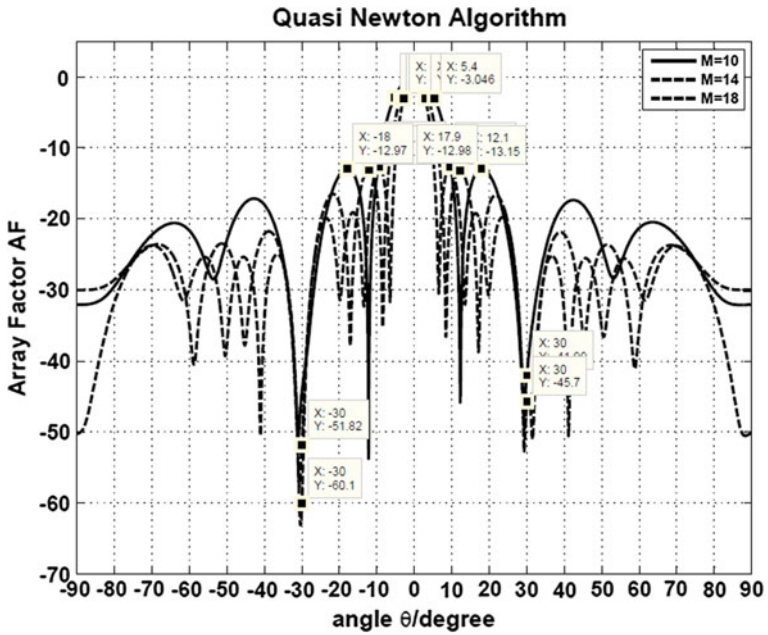


Fig. 3 Radiation pattern for quasi-Newton algorithm

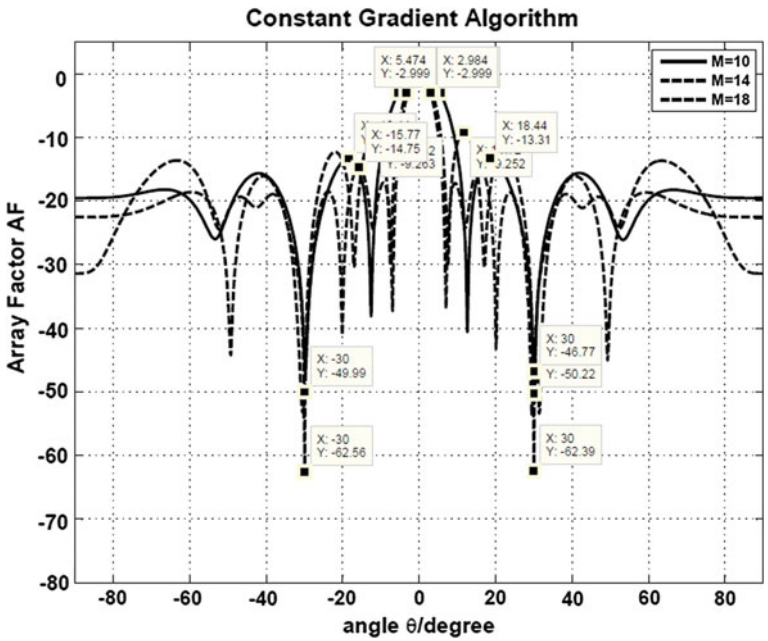


Fig. 4 Radiation pattern for conjugate gradient algorithm

Table 1 Characterization of affine projection algorithm

S. No.	Number of antenna elements	Beamwidth (°)	Maximum SLL (dB)	Null depth at 30° (dB)	Null depth at -30° (dB)
1	10	10.53	-12.73	-43.1	-56.43
2	14	7.492	-13.51	-31.78	-39.08
3	18	5.69	-13.2	-38.12	-64.94

Table 2 Characterization of quasi-Newton algorithm

S. No.	Number of antenna elements	Beamwidth (°)	Maximum SLL (dB)	Null depth at 30° (dB)	Null depth at -30° (dB)
1	10	10.6	-12.98	-41.99	-44.24
2	14	7.4	-13.14	-46.11	-51.82
3	18	5.8	-12.68	-45.70	-60.10

Table 3 Characterization of conjugate gradient algorithm

S. No.	Number of antenna elements	Beamwidth (°)	Maximum SLL (dB)	Null depth at 30° (dB)	Null depth at -30° (dB)
1	10	10.95	-13.36	-50.22	-44.84
2	14	6.926	-9.252	-62.39	-62.82
3	18	5.784	-14.76	-46.77	-49.99

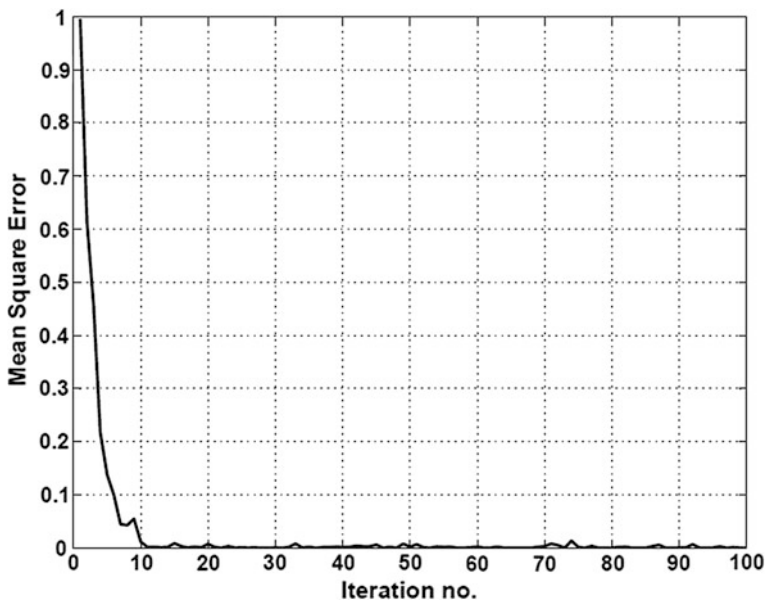


Fig. 5 MSE convergence of affine projection algorithm

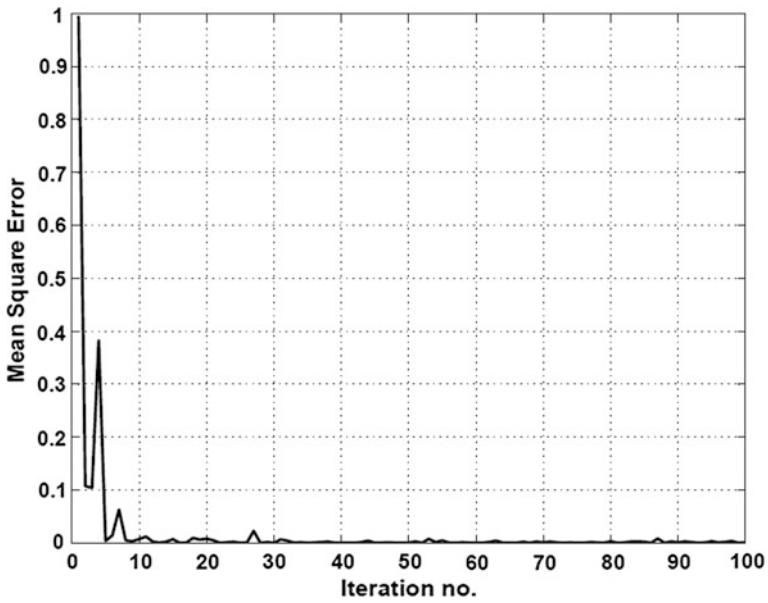


Fig. 6 MSE convergence of quasi-Newton algorithm

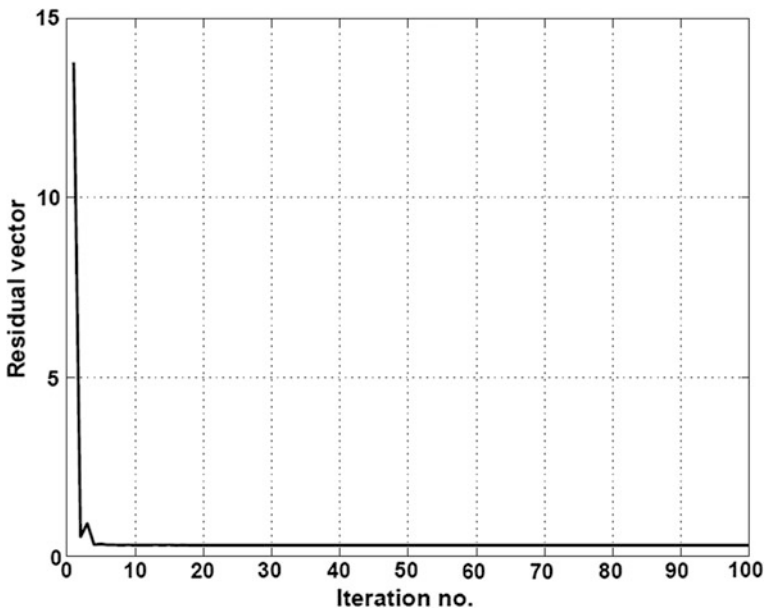


Fig. 7 Residual convergence of conjugate gradient algorithm

4 Conclusion

In this paper, three ABF algorithms, viz. QNA, APA, and CGA are studied in terms of their beam pattern characteristics and rate at which these algorithms converge. The results show that with the increase of array elements the beamwidth decreases and hence the directivity increases. All the three algorithms have almost similar variation of beamwidth with the increase of antenna elements. The CGA has the greatest null depth and fastest rate of convergence compared to other two algorithms in alignment with the results shown in [4]. As a proposal of future work, the beam pattern characteristics and rate of convergence of all the algorithms can be analyzed for planar and circular arrays. The behavior of other ABF algorithms, i.e., LMS, SMI, RLS, and CM algorithm can be compared with the discussed algorithms for linear and planar arrays.

References

1. Sharma, A., Mathur, S.: Performance Analysis of Adaptive Array Signal Processing Algorithms. *IETE Technical Review*, vol. 33, no. 5, pp. 472–491 (2016).
2. Sharma, A., Mathur, S.: Deterministic maximum likelihood direction of arrival estimation using GSA. *International Conference on Electrical, Electronics, and Optimization Techniques*, pp. 415–419 (2016).
3. Gross, F. B.: *Smart Antennas for Wireless Communications*, McGraw-Hill (2005).
4. Saxena, P., Kothari, A. G.: Performance analysis of adaptive beamforming algorithms for smart antennas. *IERI Procedia*, 10, pp. 131–137 (2014).
5. Balanis, C. A., Ioannides, P. I.: Introduction to smart antennas. *Synthesis Lectures on Antennas*, vol. 2, no. 1, pp. 1–175 (2007).
6. De Campos, M. L., Antoniou, A.: A new quasi-Newton adaptive filtering algorithm. *IEEE Transactions on Circuits and Systems II: Analog and Digital Signal Processing*, vol. 44, no. 11, pp. 924–934 (1997).
7. Gay, S. L.: The fast affine projection algorithm. In *Acoustic signal processing for telecommunication*, pp. 23–45. Springer US (2007).
8. Sankaran, S. G., Beex, A. L.: Convergence behavior of affine projection algorithms. *IEEE Transactions on Signal Processing*, vol. 48, no. 4, pp. 1086–1096 (2000).
9. Choi, S.: Application of conjugate gradient method for optimum array processing. *Progress In Electromagnetics Research*, 5, pp. 589–624 (1991).
10. Choi, S., Sarkar, T. K.: Adaptive antenna array utilizing the conjugate gradient method for multipath mobile communication. *Signal processing*, vol. 29, no. 3, pp. 319–333 (1992).

Automatic Forest Fire Detection and Monitoring Techniques: A Survey

Vinay Chowdary and Mukul Kumar Gupta

Abstract Natural disasters have always been mankind's constant companion since time immemorial. Forest fire is one such disaster which when occurs at large scale not only destroys the flora, fauna, vegetation of the forest but also puts the life of human being and animals at a very high risk. In the recent past years, managing this type of crisis, viz., a large scale fire has become a very difficult and challenging task. Things that are common in most of the forest fire that occur at large scale are loss of life (human or animal), loss of vegetation, loss of flora and fauna, and communication failure. Therefore, a comprehensive survey on the existing forest fire detection and monitoring mechanisms is highly desired. This article is aimed at providing a birds eye view of these existing detection and monitoring mechanisms for forest fires.

Keywords Forest fire detection • Monitoring • Wireless sensor networks

1 Introduction

As stated by National Institute of Disaster Management, Ministry of Home Affairs in their latest report on Forest Fire Disaster Management, forest fire is the major cause of injury and loss to forest. This loss due to fire has a major impact on forest ecosystem their by indirectly affecting the nature's ecosystem. As per one estimate of United Nations Development Program the loss due to such a fire in forest, economically will be around ₹9000/- per ha per annum (*Reference: <http://nidm.gov.in/pdf/pubs/forest%20fire.pdf>). This means a single event of forest fire at a

V. Chowdary (✉)
UPES, Dehradun, India
e-mail: vchowdary@ddn.upes.ac.in

M.K. Gupta
Department of Electronics, Instrumentation and Control Engineering,
University of Petroleum and Energy Studies, Dehradun, India
e-mail: mkgupta@ddn.upes.ac.in

large scale will always cause a loss of worth crores which will turn the net asset of forest into ashes. Therefore, greater emphasis is laid on the survey that can be used for the purpose of design and development of detection and monitoring system.

It is because of some activities such as an uncontrolled anthropogenic which makes a fire in the forest to occur at regular intervals. Incidents which lead to regular forest fires include man-made incidents, climate changes, and other factors; there has been a constant increase in the frequency of forest fires. Out of the incidents mentioned above, man-made incidents, i.e., deliberate cause is the most common one. In general fires that occur in the forest can be classified into three types which are:

1. Ground fires,
2. Surface fires, and
3. Crown fires.

Ground fires as given in Fig. 1 occur basically on the floor of forest which will produce much heat but without flames. This type of fire is a result of peaty leaves which will be always found on the floor of forest. One more cause can be the organic component of soil which will be formed by the process of decomposition of leaves and other plant materials by soil microorganisms. Ground type of fires is rarest of the three and has been rarely recorded because they normally occur at forests which are situated at very high altitudes such as Himalayan forests. To detect this type of fires, which is a very difficult task, sensors which can record and measure even a temperature difference of as small as 1°C also should be used.

Therefore, one can go for the implementation of thermal sensors and radiation sensors for this purpose. Authors of article [1] propose the use of animals to be used as biological sensors. The animal which is suited for detection of ground fire are

Fig. 1 Ground fire



Fig. 2 Surface fire



Fig. 3 Crown fire



reptiles like tortoise. But problem with this type of reptiles is their slow nature because of which their tracking will be very difficult (Figs. 2 and 3).

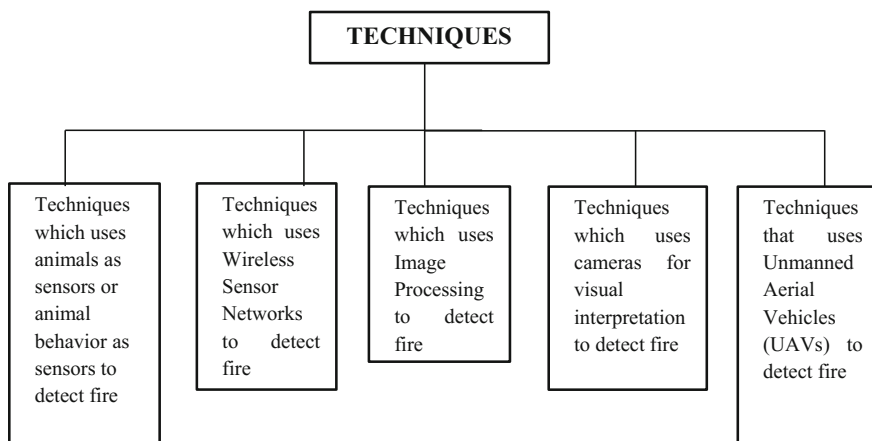
Surface fires occur on the ground and the spread of this type will always take a regular shape and will usually depend on the speed of wind. To detect this type of fire which will not only produce flames but will also generate smoke one can go for smoke sensor. One such use of smoke to detect fire in home environment is discussed in [2]. In this article, authors have given importance to the optimization of power in terms of both the hardware and software. Lastly, the crown type of fires

will burn the complete tree right from the root to the top most leaf through the stem. This type of fires will give much more flame than smoke. To detect these fires one needs a very robust sensor that can withstand a very high temperature.

2 Forest Fire Detection Techniques

With reference to the work carried out, development shown in the field of fire detection and monitoring, the techniques used can be under categories which use

1. Techniques which use animals as sensors or animal behavior as sensors to detect fire.
2. Techniques which use Wireless Sensor Networks to detect fire.
3. Techniques which use image processing to detect and monitor fire.
4. Techniques which use cameras for visual interpretation to detect fire.
5. Techniques that use Unmanned Aerial Vehicles (UAVs) to detect fire.



Under the first technique which uses animals as biological sensors is given in [1]. As described in previous section authors of [1] divide forest fires into three categories and give the possibilities of animals that can be used as biological sensor to detect each of this type of fire. In the article [3], authors mention the use of fire beetles. Fire beetles which are a creature with a specialty that it runs toward the light generated and not the other way as others do, whenever there is a fire. This phenomenon is used in this article for fire detection. Authors of this paper describe the use of infrared emission zone in order to detect fire from distance as large as 100 km, since beetles are capable of detecting fire from such a large distance. A very good comparison of beetles sensing capability with that of infrared

(IR) sensors sensing capability is presented because of which IR sensors are replaced by beetles in this article.

In the techniques which use Wireless Sensor Networks which is quite familiar technique and comparatively the scale of research in this field is more than other fields. Authors of article [4] discuss on crisis management using multi-agent system-based wireless sensor networks. An example of crisis mentioned by the authors is a large-scale city fire. Main objective of this article is described in its five features which are data aggregation, tracking, orientation of rescue people, multi-application management, and cooperation decision mechanism. Here the use of multi-agent system is restricted to software layer which aims to improve WSN performance by allowing cooperation between sensor nodes. A tool based on WSN is proposed in [5] which is for urban and industrial firefighting. Monitoring of fire and firefighter plus escape path guidance are the functionalities achieved by authors of this articles assuming that there is no pre-existing WSN. In [6], authors use temperature and humidity sensor to detect fire. Sensors in a cluster communicate to cluster head using Zigbee and cluster head sends data to control room using Wi-Fi. An early fire detection method is proposed in [7] which uses hierarchical Wireless Sensor Network. Results show that accurate fire detection with very rare false alarm has been achieved. FireWxNet of [8] which is a layered application based on Wireless Sensor Network for monitoring fire situation in a very rugged environment. It uses combination of sensors and cameras to detect and monitor events of forest fire. Also authors have addressed the deployment issue of nodes in this article. A low power and low-cost wireless smoke alarm system is proposed in [2] which is for home environments. Main features of interest from this article are low cost and low power requirements. The optimization technique adopted by authors gives autonomy of almost five years. In [9], an identification of smoldering approach and phases of flaming is proposed. Authors have also shown correlation analysis between combinations of different sensors which helps in identifying the perfect combination of sensors to implement in order to achieve high accuracy. Artificial neural network is combined with wireless multi-sensor in the result analysis part.

Techniques based on image processing for fire detection are comparatively less in number. In [10], authors have proposed an image processing model based on YCbCr rather than a normalized RGB model. The proposed method is adopted due its less complexity. In [11], authors present a technique based on data mining and image processing. Fire detection is carried through three phase's, viz., preprocessing, training, and detection phase. Adaptive Neuro Fuzzy Interface System is used for result validation. Using Sobel edge detection [12] and RGB color model, authors here proposed a fire detection model which is mainly comprised of Red R component.

The use of cameras for fire detection is proposed in articles [13, 14, 15]. Design & development of multi sensor wireless network, which uses IP cameras are used to detect fire. IP cameras need line-of-sight communication with sensors. Moreover these cameras should be placed at a high altitude to get good view. In [14], smoke is used as parameter for fire detection. Smoke is captured using IP camera and detection is done using discrete cosine transform (DCT). An early fire detection

method is proposed using IP camera and DCT. A fully wireless system based on optical imaging named SITHON is proposed which focuses on early detection and monitoring of forest fire [15]. The demonstration of this system was performed with small controlled fire and then the results were evaluated.

A comprehensive survey for the use of Unmanned Aerial Vehicles for forest fire detection monitoring and carrying out firefighting activities is given in [16]. First a brief review of development and next review of technologies related to UAVs are given. Challenges and their potential solution are also provided. Authors of [17] describe a fire index that can be applied to Unmanned Aerial System (UAS) in order to detect fire. Authors were able to achieve a detection precision of more than 96% with processing time of 4 min.

There are certainly other techniques also available in the literature other than those mentioned above to detect and monitor fire and also provide aid to firefighting. In [18] directional antennas are used as sensors for providing assistance to firefighters in case of large fire. A leader follower approach is applied in firefighter scenario. Authors of [19] present a radio acoustic sounding system which is used to develop an automated early fire detection system. Remote thermal mapping is the proposed solution for fire detection. This method can be used for crown and surface fire detection and not for ground fire. Sound signals may undergo attenuation thereby reducing the efficiency of this system.

3 Conclusion

A comprehensive survey covering the articles of last decade has been presented in this article. The potential benefits, feature of interest for forest fire detection monitoring and providing assistance to firefighting have been highlighted in the review of the literature. As forest fire is one of the most active disaster events in all most all the countries around the world, availability of information from multiple sources is always critical. The aim of this article was to provide a comprehensive view existing technologies with respect to different fields, viz., use of wireless sensor networks, use of image processing, use of cameras, use of animals as biological sensors, and use of UAVs to detect and monitor fire incidents. We as authors of this article hope to see a further improvement in the area of the literature review in the above-mentioned fields in the future.

References

1. Sahin, Y.G., *Animals as mobile biological sensors for forest fire detection*. Sensors, 2007. 7 (12): p. 3084–3099.
2. Luis, J.A., J.A.G. Galán, and J.A. Espigado, *Low power wireless smoke alarm system in home fires*. Sensors, 2015. 15(8): p. 20717–20729.

3. Bousack, H., et al., *Towards Improved Airborne Fire Detection Systems Using Beetle Inspired Infrared Detection and Fire Searching Strategies*. *Micromachines*, 2015. **6**(6): p. 718–746.
4. Sardouk, A., et al., *Crisis management using MAS-based wireless sensor networks*. *Computer Networks*, 2013. **57**(1): p. 29–45.
5. Clemente, A.D.S.B., J.R. Martínez-de Dios, and A.O. Baturone, *A wsn-based tool for urban and industrial fire-fighting*. *Sensors*, 2012. **12**(11): p. 15009–15035.
6. Ulucinar, A.R., I. Korpeoglu, and A.E. Cetin, *A Wi-Fi cluster based wireless sensor network application and deployment for wildfire detection*. *International Journal of Distributed Sensor Networks*, 2014.
7. Molina-Pico, A., et al., *Forest Monitoring and Wildland Early Fire Detection by a Hierarchical Wireless Sensor Network*. *Journal of Sensors*, 2016. **2016**.
8. Hartung, C., et al. *FireWxNet: A multi-tiered portable wireless system for monitoring weather conditions in wildland fire environments*. in *Proceedings of the 4th international conference on Mobile systems, applications and services*. 2006. ACM.
9. Yan, X., et al., *Real-Time Identification of Smoldering and Flaming Combustion Phases in Forest Using a Wireless Sensor Network-Based Multi-Sensor System and Artificial Neural Network*. *Sensors*, 2016. **16**(8): p. 1228.
10. Premal, C.E. and S. Vinsley. *Image processing based forest fire detection using YCbCr colour model. in Circuit, Power and Computing Technologies (ICCPCT), 2014 International Conference on*. 2014. IEEE.
11. Angayarkkani, K. and N. Radhakrishnan. *An effective technique to detect forest fire region through ANFIS with spatial data*. in *Electronics Computer Technology (ICECT), 2011 3rd International Conference on*. 2011. IEEE.
12. Poobalan, K. and S.-C. Liew. *Fire detection algorithm using image processing techniques. in Proceedings of the 3rd International Conference on Artificial Intelligence and Computer Science (AICS2015)*. 2015.
13. Lloret, J., et al., *A wireless sensor network deployment for rural and forest fire detection and verification*. *Sensors*, 2009. **9**(11): p. 8722–8747.
14. Millan-Garcia, L., et al., *An early fire detection algorithm using IP cameras*. *Sensors*, 2012. **12**(5): p. 5670–5686.
15. Tsiourlis, G., S. Andreadakis, and P. Konstantinidis, *SITHON: a wireless network of in situ optical cameras applied to the early detection-notification-monitoring of forest fires*. *Sensors*, 2009. **9**(6): p. 4465–4482.
16. Yuan, C., Y. Zhang, and Z. Liu, *A survey on technologies for automatic forest fire monitoring, detection, and fighting using unmanned aerial vehicles and remote sensing techniques*. *Canadian journal of forest research*, 2015. **45**(7): p. 783–792.
17. Cruz, H., et al., *Efficient forest fire detection index for application in unmanned aerial systems (UASs)*. *Sensors*, 2016. **16**(6): p. 893.
18. Min, B.-C., et al. *Using directional antennas as sensors to assist fire-fighting robots in large scale fires*. in *Sensors Applications Symposium (SAS), 2014 IEEE*. 2014. IEEE.
19. Sahin, Y.G. and T. Ince, *Early forest fire detection using radio-acoustic sounding system*. *Sensors*, 2009. **9**(3): p. 1485–1498.

Design and Simulation of Implantable Blood Pressure Sensor Using COMSOL Multiphysics

K.S.N. Murthy, M. Siva Kumar, K. Suma Bindu, K. Satyanarayana, D. Sivateja and G. Sai Hemanth

Abstract This paper presents the design and simulation of blood pressure sensor for healthcare and biomedical applications. Generally blood pressure can be measured by using sensors externally, but here is an implantable sensor which is used for continuous monitoring of blood pressure. The software used is COMSOL Multiphysics, a general purpose software platform for modelling and simulating the advanced applications. This work describes the design of nanotube-based sensor with a basic known technology of MEMS. The main physics used in this design is solid mechanics and time-dependent analysis which is performed to certain values of pressure that is applied on the model. The pressure versus displacement analysis is performed, and it is observed that the pressure is directly proportional to displacement. The device performance is compared by using materials like Si and Au. The result shows that Au has good sensitivity than Si which is verified by calibration method.

Keywords Blood pressure · Displacement · Biomedical applications · COMSOL

K.S.N. Murthy (✉) · M. Siva Kumar · K. Suma Bindu · K. Satyanarayana · D. Sivateja · G. Sai Hemanth

Department of Electronics and Communication Engineering, K L University,
Vaddeswaram, Andhra Pradesh, India
e-mail: ksnmurty@kluniversity.in

M. Siva Kumar
e-mail: siva4580@kluniversity.in

K. Suma Bindu
e-mail: kamavaram.suma@gmail.com

K. Satyanarayana
e-mail: kaminenisatyam574@gmail.com

D. Sivateja
e-mail: sivateja1034@gmail.com

G. Sai Hemanth
e-mail: saihemanthgalla@gmail.com

1 Introduction

An innovative technology, which has many attractions like miniaturization, low power consumption, performing multiple operations with single equipment, is MEMS. The technology of MEMS indicates that it produces the devices with the combination of both electrical and mechanical components [1]. The main advantage of MEMS is its size which ranges between few micrometres to millimetres. MEMS devices have greater ability in many domains like sensing, actuating and controlling [1]. The MEMS-based sensors can be used for biomedical applications also [5]. Bio-MEMS devices can be manufactured based on the operation of various parameters like temperature, pressure, capacitance, voltage and current. This paper provides a brief idea about blood pressure detection using pressure as a sensing element [2]. Pressure is an important parameter in real-life applications. It is defined as force per unit area [3]. The mathematical expression of pressure is

$$\text{Pressure } (p) = \text{Force/Area} \quad (1)$$

Blood pressure measurement which is the most important routine check-up in order to have well-being health. The normal blood pressure can be expressed in terms of systolic over diastolic pressure as 120/80 (mmHg) [6]. Systolic is the highest level of our blood pressure when the heart beats and diastolic is lowest level of our BP as heart relaxes between beats.

This raise and fall of blood pressure leads to many diseases.

1. High BP leads to hypertension which causes heart attacks or strokes, trouble with memory.
2. Low BP causes hypotension which results in dizziness, fainting, diarrhoea, etc.

In general, blood pressure can be measured by using some instruments like sphygmomanometer and some auscultatory methods. But these instruments have a limitation that they cannot detect blood pressure when the body has mobility. So, a design of MEMS-based sensor is proposed to implant in a human body, which is used for continuous monitoring of blood pressure [4, 6]. This helps the doctor to provide an early detection and an efficient treatment to the patients suffering with blood pressure. The implantable pressure sensor is interfaced to an external circuit for the wireless monitoring and digital display of blood pressure. The sensor is connected to RF microcontroller, a balun network and a chip antenna [4, 7] (Figs. 1 and 2).

The total work is performed with the help of software named COMSOL Multiphysics. COMSOL Multiphysics is finite element analyser, solver and simulation software for various physics and engineering applications [6]. The virtual blood pressure sensor model is designed using this tool followed by simulations. This paper describes a model for continuous monitoring of blood pressure using a nanotube-based design and also its analysis by using various parameters [9].

Fig. 1 An auscultatory method to measure blood pressure



Fig. 2 Measurement of blood pressure using manometer



2 Design Procedure

A virtual view of the model is designed in COMSOL [8], which has various physics and engineering applications. A 3D structure is developed by considering solid mechanics as the main physics which is a part of structural mechanics [6]. There are many different analysers present in the tool among which the time-dependent analysis is selected as the variations in blood pressure are observed with respect to time.

When the model is taken into consideration, the design is a nanotube-based sensor which is almost identical to cantilever sensor [10]. A component needs to be created which has many designing facilities like geometry, definitions, materials, physics used and meshing. In geometry, a cylindrical structure is designed with some dimensions like height and radius. Similarly, another cylindrical structure is designed and placed inside the first cylinder by using Booleans and partitions in

geometry. The structure has fixed base at one end and free suspension at other end. Since it is an implantable sensor, the size is an important parameter [6]. The structure is designed in micrometres (μm), as the diameter of the blood vessels where the sensor is placed is in micrometre range. A height of $8\ \mu\text{m}$ and radius of $2\ \mu\text{m}$ are used for design. After the structural design is performed, the sensing ability should be developed. As pressure is the main sensing parameter, some load like boundary or point load is applied to the design with the help of definitions in the tool. The materials like silicon (Si) and gold (Au) are opted by selecting the required domains in the model. In material analysis, the Young's modulus and Poisson ratio of Si and Au are considered.

For silicon,

1. Poisson ratio = 0.17
2. Young's modulus = 150 GPa

For gold,

1. Poisson ratio = 0.42
2. Young's modulus = 79 GPa

Meshing is performed which is a finite element analyser. Some parameters like pressure and displacement are created by entering certain values of pressure in Pa/kPa. The ranges of values between 5 and 11 kPa are provided. The model is simulated for a required amount of selected time. After computation, the displacement is recorded with the variation of pressure.

3 Simulation and Analysis Using COMSOL

The designed model is simulated with the help of COMSOL, and analysis is performed by varying dimensions of the sensor, material and pressure.

Some values of pressure that is higher and lower to normal blood pressure 120/80 are given to the model. Different boundary loads are applied at the free end, and their displacements are recorded simultaneously. The graphical analysis is also performed along with the simulation result.

3.1 Analysis

3.1.1 Material Analysis Using Si and Au

The working performance of the sensor changes with change in material. The model is simulated by using silicon and gold materials. The operating conditions change when different values of pressure are applied. The simulations and values of displacement for different values of pressure are recorded (Figs. 3 and 4; Table 1).

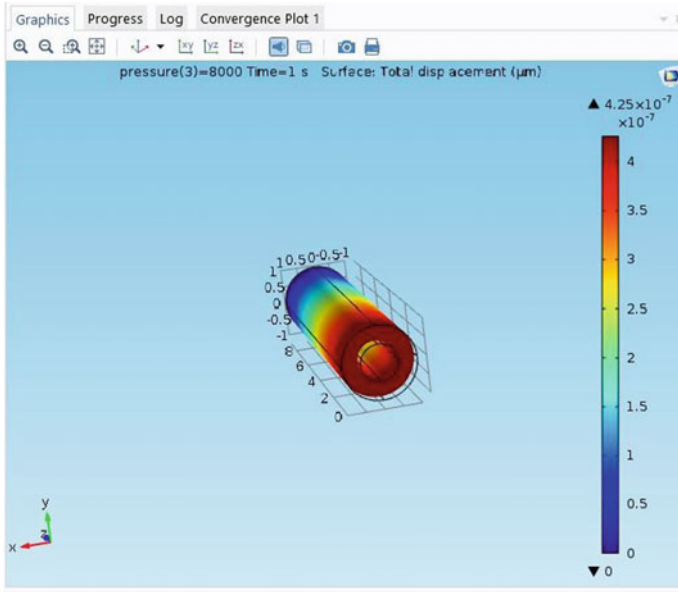


Fig. 3 Simulation of nano tube sensor for blood pressure sensor using silicon

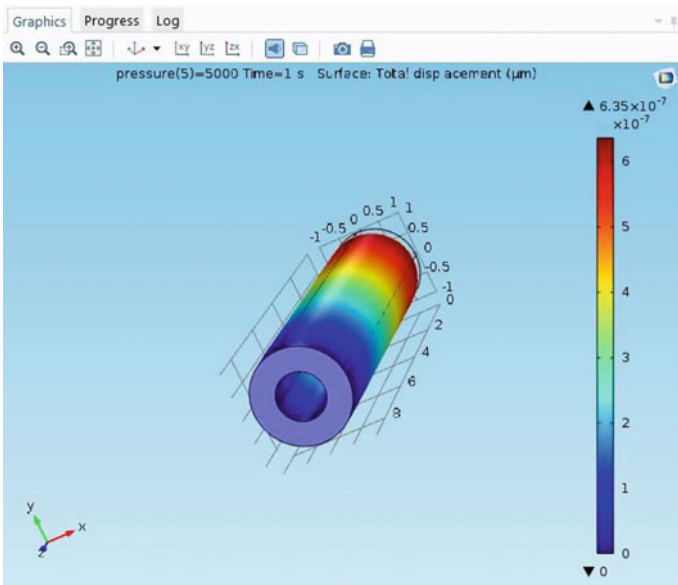


Fig. 4 Simulation of blood pressure sensor using gold

Table 1 Variation of displacement with pressure for Si and Au

Pressure (Pa)	Materials used	
	Silicon displacement (μm)	Gold displacement (μm)
11,000	0.58	1.4
9500	0.505	1.21
8000	0.425	1.02
6500	0.346	0.826
5000	0.266	0.635

3.1.2 Pressure versus Displacement Analysis

The boundary loads and point loads are applied to the model for the variation in pressure. The ranges of values are in between 5 and 11 kPa. After computation of the model, it is observed that there is an increase of displacement with increase of pressure. This shows that displacement is directly proportional to blood pressure. Thus, the blood pressure can be calibrated in terms of displacement of the sensor.

The graphical representation of pressure versus displacement is shown in Fig. 5.

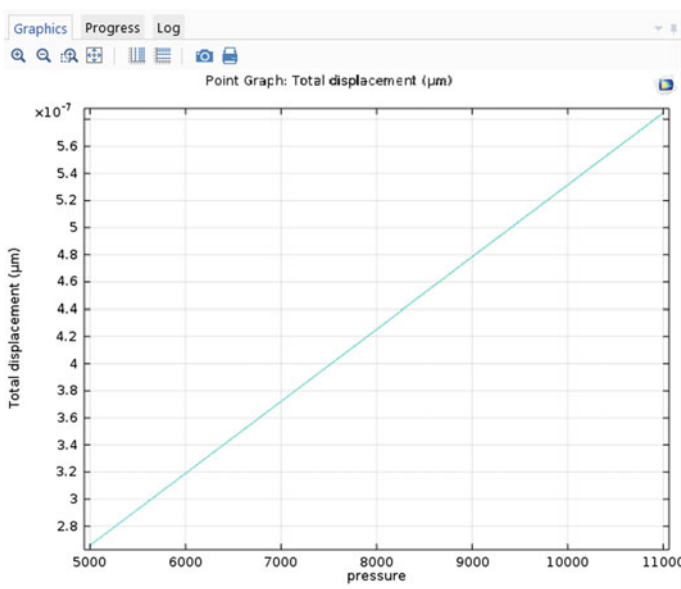


Fig. 5 Graph showing the variation of displacement with pressure

3.1.3 Calibration of the Sensor

The difference in displacement for 1500 Pa when Si material is used:

Between the pressure 11000–9500 Pa = 0.575 μm

Between the pressure 9500–8000 Pa = 0.080 μm

Between the pressure 8000–6500 Pa = 0.079 μm

Between the pressure 6500–5000 Pa = 0.080 μm

The difference in displacement for 1500 Pa when Au material is used:

Between the pressure 11000–9500 Pa = 0.190 μm

Between the pressure 9500–8000 Pa = 0.190 μm

Between the pressure 8000–6500 Pa = 0.794 μm

Between the pressure 6500–5000 Pa = 0.191 μm

The calibrated value of pressure sensor for 1 Pa with respect to silicon and gold materials is $1.566\text{e-}4$ and $2.2733\text{e-}4$ μm , respectively.

4 Conclusion

The analysis shows that there is an increase in displacement as pressure increases. So displacement is directly proportional to pressure. When materials are considered, the calibrated value of pressure sensor for 1 Pa to the silicon is **$1.566\text{e-}4$ and to the gold is $2.2733\text{e-}4$** . This shows that **gold has good accuracy and sensitivity** when compared to other materials. So it is concluded that gold is the preferred material for the implantation of blood pressure sensor.

5 Future Scope

Similar to blood pressure detection, protein concentration can also be detected since the displacement of nanotube is based on number of substances which is directly proportional to the protein concentration. So protein concentration can be detected by addition of some materials.

References

1. R. U. Sonje, S. V. Borde, "Micro-Electromechanical Systems (Mems)", IJMER, Vol. 4 Iss. 3 (Mar. 2014), 2249–6645, Page no: 1, 2.
2. Dr. Prasanna Kumar S.C., Jyothsna D., "Biomedical Applications Of Mems & Nems Pressure Transducers/ Sensors", IJIRD, Vol 2 Issue (5 May, 2013), 2278–0211, Page no: 6.
3. Nurul Amziah Md. Yunus, Izhal Abdul Halin, Nasri Sulaiman, Noor Faezah Ismail, Ongs Kai Sheng, "Valuation on MEMS Pressure Sensors and Device Applications", International

- Journal of Electrical, Computer, Energetic, Electronic and Communication Engineering, Vol: 9, No: 8 (2015), Page no: 2.
4. M. Theodor, J. Fiala, D. Ruh, K. Förster, C. Heilmann, F. Beyersdorf, Y. Manoli, H. Zappe, "Implantable accelerometer system for the determination of blood pressure using reflected wave transit time", ELSEVIER, Sensors and Actuators A 206 (2014) 151–158, Page no: 2.
 5. Shivam Kohli, Anish Sain, "MEMS BASED PRESSURE SENSOR SIMULATION FOR HEALTHCARE AND BIOMEDICAL APPLICATIONS", IJESSET, Volume 6, Issue 3, pp: 308–315 (Dec. 2013) 2231–6604, Page no: 1.
 6. Raghavendra Nagaralli, Kiran kumar B. Balavalad, B. G. Sheeparamatti, "Modeling Of Implantable Blood Pressure And Protein Sensor Using COMSOL/Multiphysics", IJIRS, Vol. 2 Issue 9 (September 2013) 2319–9725, Page no: 2, 3, 4.
 7. Peng Cong, Wen H. Ko and Darrin J. Young, "Wireless implantable Blood Pressure sensing Microsystem Design for monitoring of small Laboratory Animals", Sensors and materials, Vol. 20, No. 7(2008) 327–340, Page no: 3.
 8. P. Patnaik, S.K. Kamilla, Debi Prasad Das, "Alternate glucometer bio-Sensor based on Ultrasonic MEMS transceivers", Expert from the proceedings of the 2013 COMSOL Conference in Bangalore, page no: 3.
 9. Debashid Maji, Ravi Shankar Vunnam, C.P. Ravikumar and Soumen Das, "Simulation of MEMS Based flexible flow sensor for Biomedical Application", COMSOL Conference 2011, November 4–5, Page no: 3.
 10. S. Anand Selvin, S. Aravind Lovelin, N. Boovaraga Moorthy, Anju Gupta, M. Alagappan, Venkateswaran Ramalingam, "Design and Simulation of Carbon Nanotube based Piezo resistive Pressure Sensor", Expert from the proceedings of the 2011 COMSOL Conference in Bangalore, Page no: 3.

V-Band SIW Wideband Band-Pass Filters for mm-Wave Applications

K. Bharath Kumar and T. Shanmuganantham

Abstract This paper presents V-band band-pass filter, which is designed with high bandwidth and compact size by using planar structure technology, i.e., substrate integrated waveguide technology (SIW). Grounded coplanar waveguide (GCPW) is used as a transmission connecting path. This V-band filter design by using RT duriod 5880 substrate material with a height of 0.508 mm and ϵ_r as 2.2. Filter dimensions are $6.8 * 3.5 * 0.508 \text{ mm}^3$. Due to its dimensions and bandwidth, this filter is more suitable to develop 59–64 GHz RADAR applications. At 60 GHz, this V-band band-pass filter gives reflection coefficient of -54.156 dB , insertion loss of -0.25 dB and Voltage Standing Ratio of 1.004. At 60 GHz, this band-pass filter gives a quality factor of 1124 with surface currents of 43.1 dB (1 A/m). This structure is more suitable to design RADAR and %G components at millimeter wave frequency range.

Keywords SIW · RT duriod 5880 · RADAR · 5G · SIP · SOS
GCPW · SIC · BPF · Chebyshev

1 Introduction

With the increasing of high-density wireless communication resources, high bandwidth is required. Nowadays does not only require high bandwidth but also require less delay, low loss with compact size. To full fill all above requirements, high free spectrum is required. At millimeter wave frequency range (i.e., 30–300 GHz) [5], high free spectrum is available. In this frequency range, federal

K. Bharath Kumar · T. Shanmuganantham (✉)
Department of Electronics Engineering, Pondicherry University, Puducherry, India
e-mail: shanmugananthamster@gmail.com

communication commission (FCC) announced 57–64 GHz is unlicensed frequency. FCC announces 59–64 and 66–71 GHz frequency ranges for RADAR applications [6]. In 57–64 GHz, any unauthorized device can access any wireless communication systems. Especially, 59–64 GHz range of the spectrum is used for short distance RADAR applications freely any wear. In 57–64 GHz spectrum, 60 GHz frequency plays a key role in designing short distance RADAR applications. Nowadays, number of applications and technology increases which not only require high bandwidth but also consider design parameters such as high selectivity, compact size, low cost, and low insertion loss. Planar and non-planar technologies are incapable of providing these characteristics at the time of design. Non-planar circuits provide good quality factor but not in size and cost. Planar circuits provide compact size but not in quality factor. So the combination of planar and non-planar advantages developed new technology which is substrate integrated waveguide (SIW). This is a most suitable method for high-frequency application especially for millimeter and submillimeter applications [5–8]. SIW is made up of sandwiching two metal layers by a substrate and the side faced by rows of the array of metallic holes. These holes have a diameter and spacing small to appear as electric walls [5–10], which implies that certain modes cannot resonate. In the development of 60 GHz frequency modulated continuous wave (FM-CW), RADAR system millimeter wave unit design is very challenging one. The FM-CW millimeter wave unit block diagram is shown in Fig. 1.

Millimeter wave unit requires high bandwidth with good quality factor. But bandwidth and quality factors are inversely proportional. So it is impossible to get good bandwidth as well as a quality factor, but millimeter wave requires both to be in a good manner. Millimeter wave applications, such as RADAR, 5G, require above 1 GHz of bandwidth. To fabricate these components by using SIW fabrication technology, size is reduced. Due to this reduction of size, all the components

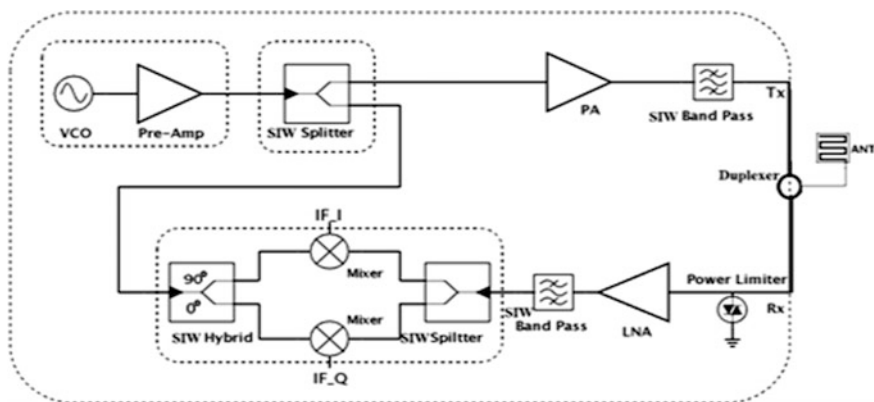


Fig. 1 Blocks diagram of millimeter wave unit in FM-CW

of this millimeter wave unit fabricate on the single package which is nothing but System In Package (SIP) [5] and also fabricated entire System on Substrate (SOS). Due to SIW technology, fabrication quality factor is also improved with less cost.

In this paper, the next section explains the design of SIW, CPW, and filter. The third section explains the result of proposed band-pass filter. Fourth sections explain comparisons between the results of proposed work with literature surveys. Final section explains the conclusion of proposed filter.

2 Design of SIW, CPW, and Filter Structure

2.1 SIW Design

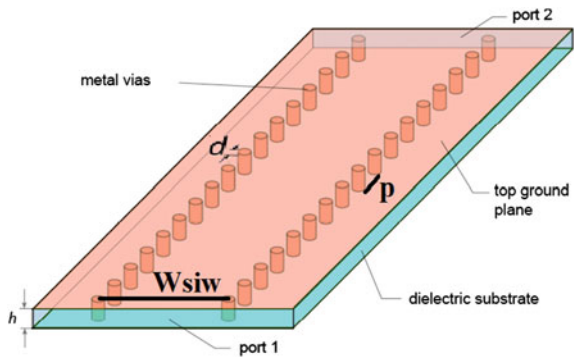
SIW structure is just like rectangular waveguide structure but in the place of sir in rectangular waveguide substrate is placed and two periodic arrays of metallic vias are used to connect the top and bottom conductor which shown in Fig. 2. SIW design parameter is via diameter (d) and spacing between two vias (P) and width between two conductor vias (W_{siw}) are decided the losses in the structure which are calculated by using below formulas [5–10].

$$W_{\text{eff}} = W_{\text{siw}} - d^2 / (0.95p) \tag{1}$$

$$W_{\text{eff}} = a / (\sqrt{\epsilon_r} \sqrt{\epsilon_r}) \tag{2}$$

$$P \leq 4d \tag{3}$$

Fig. 2 SIW structure and its parameters



Here, “ a ” is the standard dimension of normal width rectangular waveguide. ϵ_r is relative permittivity of the substrate. RT duriod 5880 substrates are used, which having $\epsilon_r = 2.2$ with dissipation factor $\tan\delta = 0.0009$. The height of the RT duriod 5880 substrates is $h = 0.508$ mm. The top and bottom of the substrate are coated with a copper layer with a thickness of 0.035 mm.

2.2 CPW Design

To connect the components in SIP or SOS, more accurate impedance matching is required, which is provided by GCPW. To avoid cross talk in between components, CPW to SIW transmission is good one. In CPW design, space width (S) between ground and signal carrying conductor and signal carrying conductor path width (W) parameters are important, which are calculated by using below formulas. Here, grounded CPW method is used because it gives good results compared with normal CPW connection

The design of CPW is shown in Fig. 3. The GCPW must respect the form factor [6, 7]. Here Imdg is nothing but guided wavelength (λ_g). By changing S , bandwidth also changes.

$$0.2 \leq \frac{w}{w + 2s} \leq 0.8 \quad (4)$$

Here, Fig. 3 shows the CPW structure. This figure gives all the parameters of CPW. Here, tapering section is used for good impedance matching. The length of this tapering section is calculated using below formula.

$$\lambda_g = \lambda_o / \sqrt{\epsilon_r} \quad (5)$$

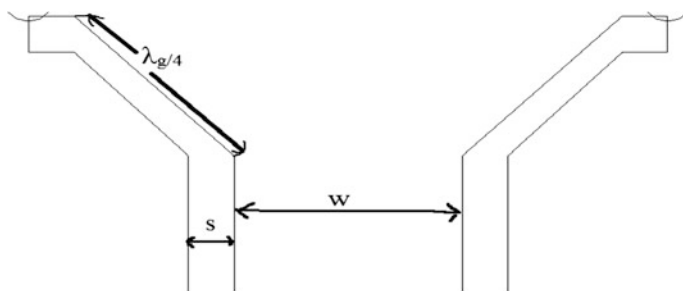
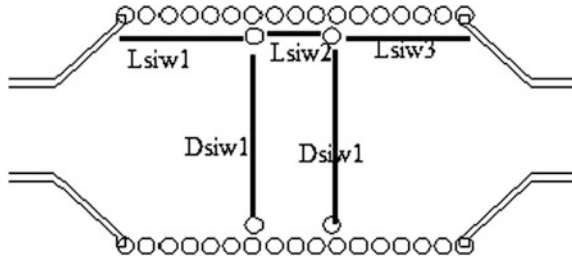


Fig. 3 GCPW structure

Fig. 4 Proposed BPF design structure and its parameters



2.3 Band-Pass Filter Design

Here, filter is designed by using inductive post topology. Band-pass filter consists of parallel resonance circuit [1–4]. First, we calculate the order or number of resonance present in the filter, which is calculated by using below formula in the case of Chebyshev synthesis.

$$N \geq \frac{\cosh^{-1} \sqrt{\frac{10^{(0.1LAs)} - 1}{10^{0.1LAr} - 1}}}{\cosh^{-1}(\Omega_s)} \tag{6}$$

N is the order of the filter, LAs is the level of out of band reject at pulsation $\Omega_s = 1$ rad/s, and LAr is maxed amplitude of ripple. Theoretical calculations of series and shunt capacitance and inductance values are calculated in [1–4]. The distance between the inductance posts and diameter of inductance post are calculated using [1–4] (Fig. 4).

To design BPF, consider LAs as -20 dB and LAr as 0.3 dB. Central operating frequencies are considered for the proposed of the filter is 60 GHz. This is fourth-order v-band filter, and those calculated values are present in Table 1 by using [1, 2].

Table 1 Proposed SIW filter design structure parameters

Parameter	Value (mm)
$L_{siw1} = L_{siw3}$	2
L_{siw2}	0.92
$D_{siw1} = D_{siw2}$	2.25
L	6.8
W	3.5
d	0.2
P	0.25
W_{siw}	2.72
λ_g	3.371
W_c	1.008
S	0.1
L_c	0.552

3 Results and Discussion

The simulation results of proposed BPF structure is shown in Fig. 5. In this, red line indicates reflection coefficient (S_{11}), and the green line indicates transmission coefficient (S_{12}). To calculate the bandwidth of proposed structure, -20 dB is taken as reference in simulation result. This -20 dB line touches S_{11} at $f_1 = 51.37$ GHz and $f_2 = 63$ GHz which is shown in Fig. 5. The bandwidth of proposed structure is $f_2 - f_1 = 11.631$ GHz, which covers almost 86% of an unlicensed band of frequency. At 60 GHz, reflection coefficient gives the maximum value of -54.16 dB and transmission coefficient of -0.25 dB which is shown in Fig. 6.

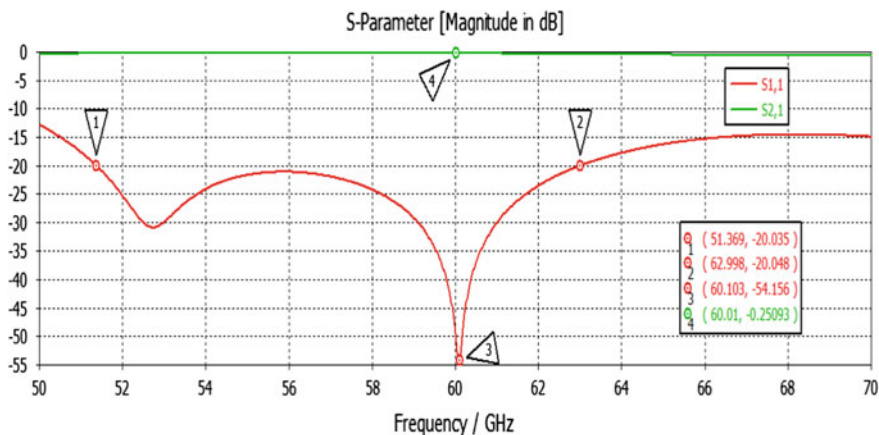


Fig. 5 Simulation results of proposed BPF

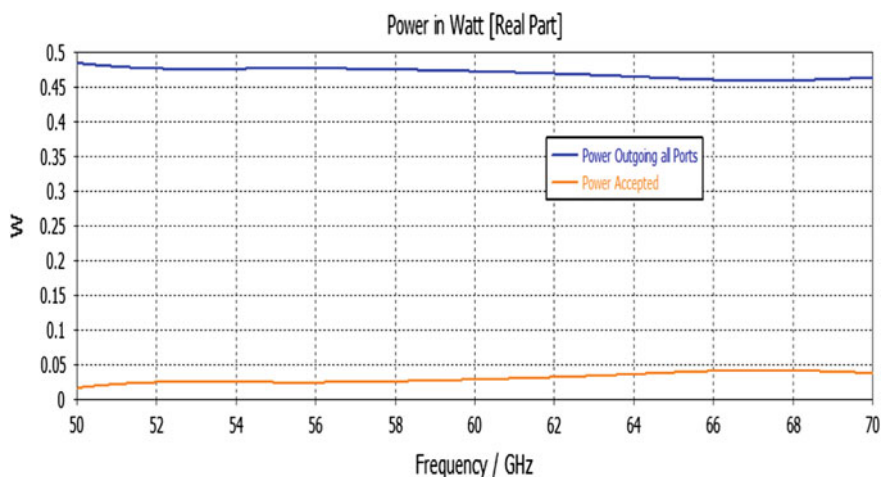


Fig. 6 Outgoing and acceptance power flow of proposed filter

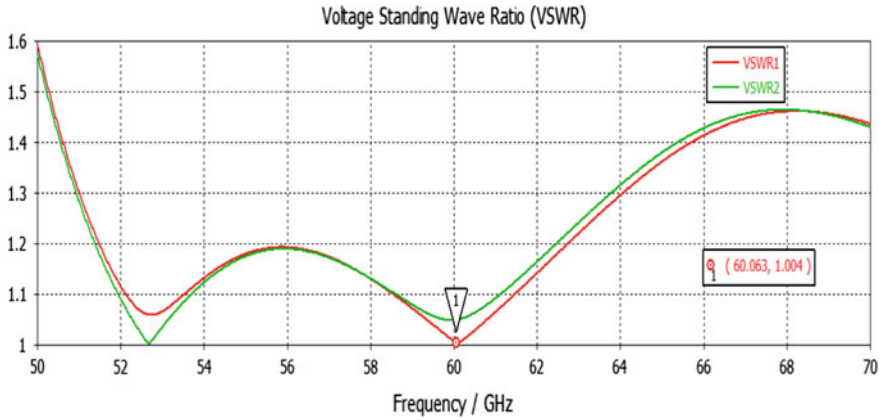


Fig. 7 VSWR curve of proposed BPF

Not only concentrated on bandwidth but also concentrated on power acceptance at both sides of the device. Figure 7 shows how the power accepted and passed on both sides of devices. In both ports, passing power is 0.5 W at bandwidth calculated places. Side1 and side2 are shown in Fig. 7.

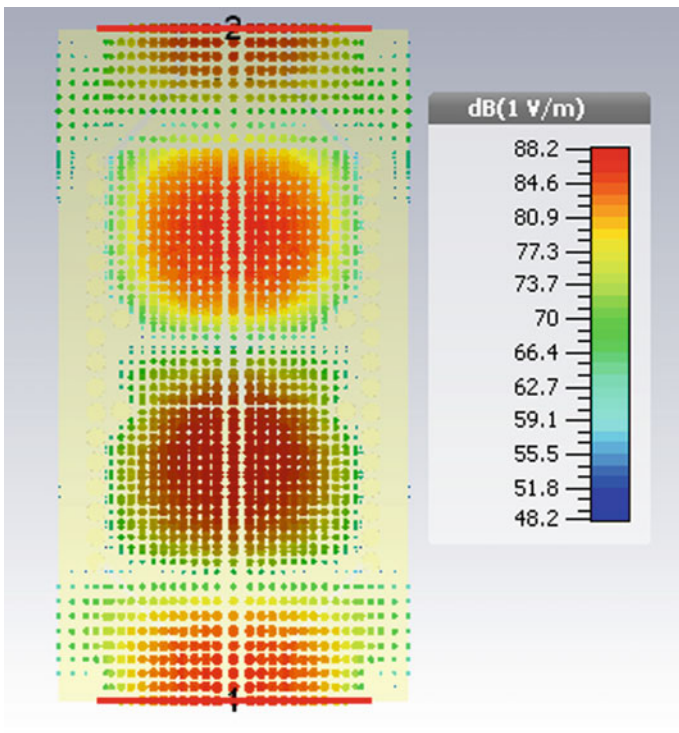


Fig. 8 Electric field distribution of proposed BPF

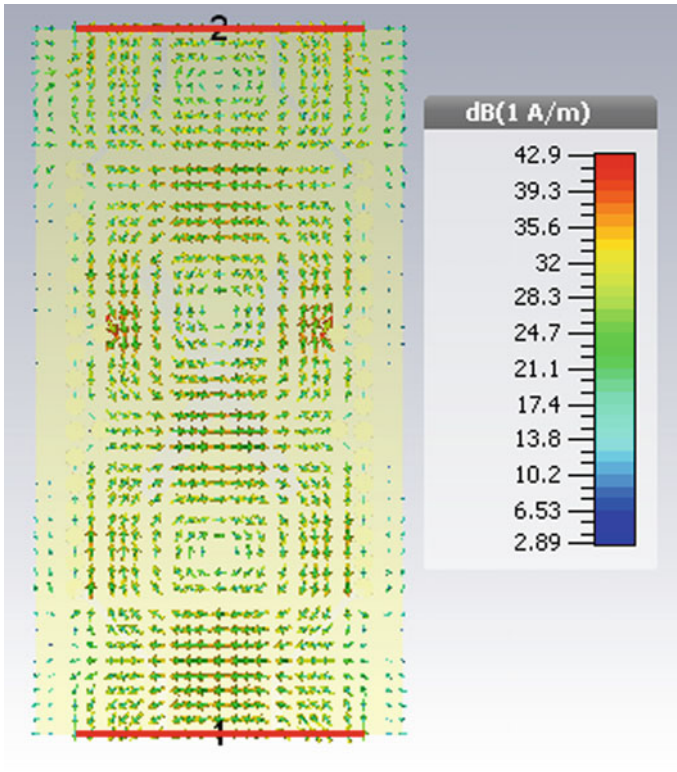


Fig. 9 Electric field distribution of proposed BPF

Voltage standing wave ration (VSWR) of BPF is shown in Fig. 7. Throughout the band, VSWR is maintained in between 1 and 2.

Electric field distributions of the BPF are shown in Fig. 8. At 60 GHz, BPF gives electric field strength of 88.2 dB (1 v/m) which also shown in Fig. 8.

Magnetic field distributions of the BPF are shown in Fig. 9. At 60 GHz, BPF gives magnetic field strength of 42.9 dB (1 A/m) which also shown in Fig. 9.

4 Comparisons

Here, Table 2 represent the comparisons between exit structures with the proposed structure.

Table 2 Comparisons between existing structures to proposed BPF

Parameters	Ref. [4]	Ref. [9]	Ref. [10]	Proposed design
Frequency (GHz)	60	60.2	60.4	60.1
ϵ_r	7.38	4.3	2.2	2.2
$\tan\delta$	0.01	0.025	0.0009	0.0009
Bandwidth (GHz)	1.35	41.11	1.5	11.63
Reflection coefficient (S11) (dB)	-21	-63.9	-52	-54.2
Transmission coefficient (S12) (dB)	-4.9	-0.9	-0.9	-0.25
Size (all in mm ³)	2.36 * 2.36 * 1.1	4.63 * 2.3 * 0.508	10.11 * 3.5 * 0.25	6.8 * 3.5 * 0.508

5 Conclusion

In this paper, V-band BPF is designed by using inductive post wall irises in the band of 50–70 GHz. This BPF provides a quality factor of 1125. At 60 GHz, V-band BPF provides good reflection coefficient, insertion loss, and VSWR. Due to its compact size and bandwidth, this device is more suitable to develop the RADAR system at millimeter wave frequency range. This filter covers 86% of unlicensed band frequency of 57–64 GHz. This is more suitable to RADAR application in the band of 59–64 GHz. In future, bandwidth will be increased, and these devices are also suitable for the machine-to-machine communication because of its compact size. If extend these software results into a prototype and measure the results which are suitable to millimeter wave application.

References

1. Dominic Deslandes, Student Member, IEEE, Ke Wu: Analysis and Design of Current Probe Transition from Grounded Coplanar to Substrate Integrated Rectangular Waveguides. In: IEEE transactions on microwave theory and techniques, VOL. 53, NO. 8, AUGUST 2005.
2. Ahmed Rhbanou, Seddik Bri: Design of Substrate Integrated Waveguide Pass Filter at [33–75] GHz Band. In: International Journal of Engineering and Technology, ISSN: 0975-4024, Vol 6 No 6 Dec 2014–Jan 2015.
3. Jia-She ng Hong, M. J. Lancaster: Microstrip filters for RF/Microwave applications. In: John Wiley and Sons, 2001.
4. Desong wang, Kuo-sheng chin, Wenquan Che, Yafen Wu, chin-chun chang: Compact 60 GHz low-temperature confined ceramic filter with quasi- elliptic band pass response. In: IET microwave, Antenna and Propagation research article, January 2016, Vol. 10 iss. 6, pp 664–669.

5. K. Bharath Kumar, T. Shanmuganatham: A Survey of Recent Technologies and Research Challenges of Substrate Integrated waveguide. In: IEEE 6th International Advanced Computing Conference, Bhimavaram, 2016.
6. K. Bharath Kumar, T. Shanmuganatham: Design of SIW Patch Fed U slot Antenna for Millimeter-Wave Applications. In: International Conference on Smart Engineering Materials, Bangalore, 2016.
7. K. Bharath Kumar and Dr. T. Shanmuganatham “Multiband E-shape SIW Antenna for mm-Wave Applications”, IEEE International Conference on Computer, Communication and Signal Processing, Chennai, 2017.
8. K. Bharath Kumar, T. Shanmuganatham: Four dielectric substrate analyses for millimeter wave application. In: Second International Conference on Large Area and Flexible Microelectronics, Bangalore, 2016.
9. K. Bharath Kumar, T. Shanmuganatham: Wideband SIW filter for mm-wave application. In: IEEE International Conference on Computer, Communication and Signal Processing, Chennai, 2017.
10. K. Bharath Kumar, T. Shanmuganatham: A Design of SIW filters for RADAR and 5G Applications. In: IEEE International Conference on Emerging Technological Trends 2016, Kolam, Kerala.

Alarming System for Railway Crossing

Aishwarya Chauhan, Satish Kumar, Neha Gupta and Rajesh Singh

Abstract The paper given below is the introduction of a new system on railway crossings. The following alarming system is to make people aware of the presence of the locomotive nearby and would warn them to clear the crossings before the locomotive to cross the track so as to reduce the number of accidents. The use of traffic lights as well as sensors help in the functioning of alarming system introduced. The traffic lights would in turn use conventional source of power that is solar power which will increase the efficiency of the system.

Keywords ASRC · Arduino uno · Vibration sensor · Solar panel
Power supply · Electrical bell · Traffic lights

A. Chauhan (✉) · S. Kumar · N. Gupta · R. Singh
Electronics Instrumentation and Control, Engineering Department, College of Engineering
Studies, University of Petroleum and Energy Studies, Dehradun 248007, Uttarakhand, India
e-mail: chauhanaishwarya15@stu.upes.ac.in

S. Kumar
e-mail: satishindian163@gmail.com

N. Gupta
e-mail: nkashyap2206@gmail.com

R. Singh
e-mail: rsingh@ddn.upes.ac.in

1 Introduction

The introduction of the concept is a distributed railway control system, and also the confirmation of principle algorithm is utilized for safe distributed control. The process includes the transformation of highly abstract algebraic specifications to directly implement distributed control processes using verification steps. The system model is separated to a domain model and also a controller mode, hence reducing the complexity. The domain model demonstrates physical framework in the absence of control. Controller model introduces the safety-related control mechanisms by monitoring whether it is safe for a train to move or a perspective to be switched [1].

New real-time methods are required to increase the efficiency and flexibility of railway systems. Along with the periodic trains, new charter trains are being introduced to increase safety. The trains already have timelines to meet irrespective of the conditions faced. Trains have pre-established routes with stations and tracks predefined along with the arrival timings. Distributed method is presented so as to fulfill the constraints. Block sections starting with station are dynamically allocated, and hence paths are already provided without leading to deadlocks [2].

This paper is a complete structural engineering survey of railway system model including the equipment and programming along with a case study included. Distributed constant control of crossings in a railway system is demonstrated. The present techniques are not efficient enough to ensure safety on the crossings. Real-time application interface is introduced for the detailed agent-based control scheme. The existing system shows un-deterministic behavior which is not acceptable in terms of safety [3].

In this paper, simulations are utilized for the distributed controllers to deal with the control problems, and these are further used for substantial scale purposes. Here, an algorithm is used to figure all possible ways so as to evade further mishaps. Trains are tasks with temporal behavior that must satisfy sure deadlines. Further, "IF conditions THEN actions" play an important role to seek an automatism for verification using temporal rules so as to implement control signals [4].

The paper works on the utility of radio technology that will successfully caution an individual that there is a train approaching the current region. This is basically a railroad impact collision framework. It incorporates transmitting pulse radio unit coupled to vehicle when locomotive has predetermined separation from a railroad crossing. The accepted impulse radio signal makes sure that an individual operating the vehicle is informed about the possibility of danger. Therefore, there will be a prior warning of the coming threat [5].

Various models using certain statistics examined the relationship between crossing accidents and features of crossings. With the increase in traffic volumes and number of train, crashes increased. Application of the paper is to provide a model to deal accident caused between vehicles and train at crossing [6].

In this, normal theory of accident and high-reliability theory are compared and evaluated. According to normal accident theory, no matter what the organizations do, accidents take place, whereas high-reliability theory state that organizations can contribute to prevent accidents. Further, these theories are applied in the case of railroad accidents [7].

The paper introduces a system for providing an alarm when at least two bodies are near the same collision point. This includes common loop verification between the car and collision point. The loop is explained as follows: first transmitter for transmitting first radio frequency signal, first receiver at a collision point; a second transmitter for transmitting second radio frequency from common collision point to first vehicle, and a second receiver in vehicle that is approaching the common collision point. Therefore, an indication is provided forming a closed loop between the vehicle and collision point [8].

Computer and communication technologies can be used to benefit large scale and network centric systems. With the use of given technologies, control solution optimal solutions can be computed within a short interval of time. In this paper, the process is demonstrated using a case study of scheduling vehicles traveling on a grid of intersecting roads. An optimization model for this problem is introduced that uses linear programming. Here, two heuristic algorithms are introduced to evaluate against the optimal approach. To ensure this heuristic technique to meet the requirements, it is compared with optimal methods [9].

The invention is related to railroad signaling systems and an automatic alarm control system which are adapted to for the prevention of collision of two trains. This comprises of beam lasers at the end of the train and a pair of separate photocell detectors for each laser. The beams of following are modulated and projected ahead. The circuit of following becomes conducting only when it receives two identical signals from the both detectors to operate alarm in time to prevent a collision [10].

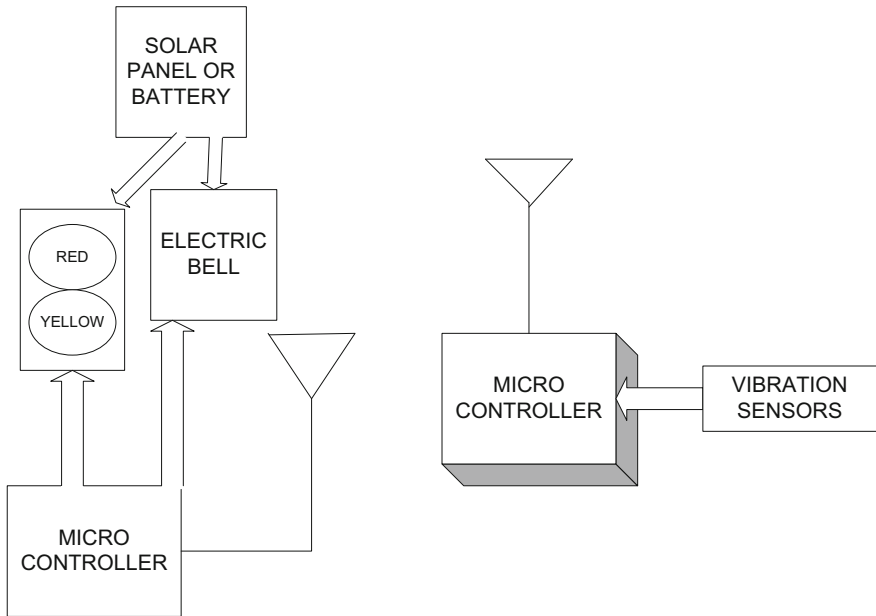
Vibration level of the ground will increase with the increase in speed of the train. For multi-story buildings, vibration is higher at top floor as compared to lower ones. Heavier train produces much more vibration than lighter train [11].

The frequency induced by vibration of a train is usually lower than 80 Hz. The ballasted track or the ballastless track can produce much larger train-induced ground vibration at frequencies above 40 Hz. Lateral vibration and longitudinal vibration are very small compared to vertical vibration [12].

2 Background of the Research

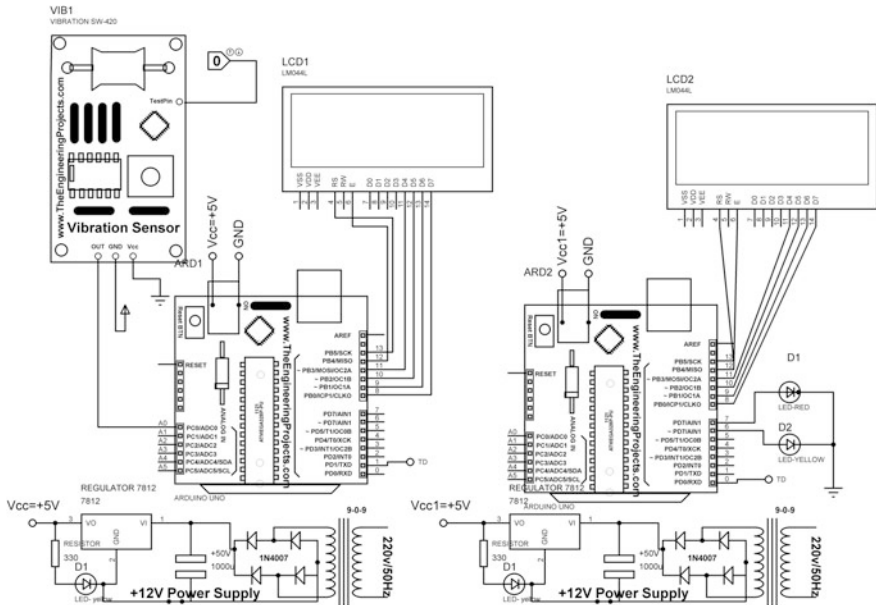
A number of lives are put to risk on the railway crossing. There are times when people unaware of the fact that the train would come at anytime, and they move on tracks, resulting in the loss of their lives. Many a time, people unknowingly fall prey to accidents on the tracks due to improper system designed for the crossing. Other situations are when vehicles get struck on the track and the fast-moving trains collide with it. This situation leads to loss of lives and happiness. Hence to avoid such situations, an alarming system for the railway track crossing is designed and is explained further.

3 Flow Diagram



Our idea is to create an alarming system that consists of vibration sensors, microcontroller and a traffic light as well as an electric bell to indicate persons on the crossing regarding the approaching locomotive.

4 System Description



5 Working

The system focuses on a communication channel between the train traversing a track and the people crossing the track. The tracks designed would have vibration sensors associated with them. Near the railway crossing, there will be a system called ASRC installed. This system consists of microcontroller, vibration sensors, SOP, TL and electrical bell. The vibration sensors would confirm the presence of the train on the track. The amount of vibration received from the sensors estimates the distance of the train from the railway crossing. As the train approaches the crossing, the vibration would increase. The crossing itself would have TL and electric bell which will use the solar energy for their working installed. In the absence of solar power, there is a battery backup. As soon as the train would approach the crossing, the light would glow. If the train is far from crossing, then yellow light would glow. As the train approaches near to the crossing above 40 Hz, red light would glow. Whenever there is red light, the bell would trigger and people traveling would have an idea that train is approaching and they must leave the track meanwhile.

6 Result and Discussion

The result of the above-mentioned alarming system for railway crossing is the prevention of number of accidents that take place regularly on the crossing due to negligent attitude of the people carelessly crossing it. How about an idea of informing people before falling prone to accidents. Yes, when the information of the coming tragedy is obtained beforehand there will be a considerable decrease in the number of accidents. The sole purpose of the alarming system produced in this paper is the improvement of systems at crossings to avoid tragedies and same will be the result of ASRC. Now, further discussing the importance and relevance of ASRC to improve the quality of railway system. The importance of the alarming system is the prevention of collisions on the crossings due to an improper communication channel between the train driver and the people walking on the tracks. The newly designed channel will focus on the methods to enhance the information from the trains traversing to the system designed for alarming people on the crossing. The entire proposed system is of utmost importance as we apply it to present scenario as the number of accidents because of improper management is increasing day by day, and therefore it is now time to create new ways to reduce the destruction and the accidents on railway tracks. Moreover, if there will be lesser number of accidents, it will not only give assurance of the safety to lives on the tracks but also assure lesser destruction to the economy. The amount spent by the railways to mend the tracks and trains can now be used for further development and hence would give the railway network a new shape.

7 Future Scope

Having a look at the present scenario, Indian railways are in dire need for improvement. There is a considerable increase in the number of accidents. To minimize this harm to lives and humanity, steps are to be taken. Therefore, this alarming system for railway crossings will act as a boon for the emerging and developing railway network. The alarming system is capable of informing the people about the approaching mobile on the track and would make it convenient for the people to leave the track before time so as to minimize the destruction to lives. The proposed system would be beneficial as well as conventional and hence can act as an advantage for the present system. The energy used is solar power and is therefore conventional. The use of such conventional energy resource brightens the future of this alarming system. A try to save a maximum number of lives using conventional methods brightens the scope of this project, and the economic feasibility also allows the railways to accept this model for the development of network at the crossings. If we sit and think, we will realize that there is nothing better in the entire world than saving lives and spreading happiness. Hence, this model of such an alarming system is a try by us to spread the smile and we consider that we have a good scope.

8 Conclusion

The conclusion of the paper produced is the introduction of ASRC that is an alarming system that works for the reduction in the number of accidents that take place when people cross the railway tracks without knowledge of the presence of the train traversing the same track. The system described below will throw light on an entirely new method of indicating people regarding the approaching mobile. The system also emphasizes on the technique of use of the solar power for the signaling lights and alarming the people regarding the coming threat. The introduction of an entirely new communication channel between the sensors on the track and the system designed on the crossing is explained above.

References

1. A.E. Haxthausen and J. Peleska, "Formal development and verification of a distributed railway control system", Software Engineering IEEE.
2. TiberiuLetia, MihaiHulea and RaduMiron, "Distributed scheduling for real-time railway traffic control", Computer Science and Information Technology 2008. IMCSIT 2008. International.
3. D.A. El-Kebbe and M. Gotz, "Distributed Real-Time Control of Railway Crossings Using Multi-Agent Technology", Computational Intelligence for Modelling Control and Automation 2005 and International Conference on Intelligent Agents Web Technologies and Internet Commerce International Conference.
4. Argo Rosin, Taavi Moller and JuhanLaugis, "Maintenance Analyses Control and Supervision System Design of Light Rail - An Application in Estonia", IEEE Industrial Electronics IECON 2006 - 32nd Annual.
5. Grisham, William T., and Mark D. Roberts. "Railroad collision avoidance system and method for preventing train accidents." U.S. Patent No. 6,759,948. 6 Jul. 2004.
6. Oh, Jutaek, Simon P. Washington, and Doohee Nam. "Accident prediction model for railway-highway interfaces." *Accident Analysis & Prevention* 38.2 (2006): 346–356.
7. Rijpma, Jos A. "Complexity, tight-coupling and reliability: Connecting normal accidents theory and high reliability theory." *Journal of Contingencies and Crisis Management* 5.1 (1997): 15–23.
8. Fuhrmann, Norbert, and Nick Friedman. "System for providing a warning when vehicles approach a common collision point." U.S. Patent No. 4,931,793. 5 Jun. 1990.
9. Argo Rosin, Taavi Moller and JuhanLaugis, "Maintenance Analyses Control and Supervision System Design of Light Rail - An Application in Estonia", IEEE Industrial Electronics IECON 2006 - 32nd Annual.
10. Henry, Frank Strauss. "Automatic collision prevention, alarm and control system." U.S. Patent No. 3,365,572. 23 Jan. 1968.
11. Xia, He, Nan Zhang, and Y. M. Cao. "Experimental study of train-induced vibrations of environments and buildings." *Journal of Sound and Vibration* 280.3 (2005): 1017–1029.
12. Zhai, Wanming, Zhenxing He, and Xiaolin Song. "Prediction of high-speed train induced ground vibration based on train-track-ground system model." *Earthquake Engineering and Engineering Vibration* 9.4 (2010): 545–554.

Performance Investigation of Hill-Climbing MPPT Techniques for PV Systems Under Rapidly Changing Environment

Vibhu Jatily and Sudha Arora

Abstract There has been a great push for harnessing of solar energy using photovoltaic (PV) systems. For improving the overall efficiency, maximum power point tracking (MPPT) is inevitable in most photovoltaic (PV) systems. The MPPT technique draws out maximum power from a PV module for different meteorological and load conditions. As the environmental conditions fluctuate throughout the day, maximum power point tracker along with the power converter forces the PV panel to deliver maximum power to the load. Performance indices like speed of convergence, accuracy, steady-state losses, implementation complexity, cost determine the overall suitability of a MPPT technique for a particular application. Researchers have proposed different techniques to achieve excellent dynamic response while maintaining low steady-state power loss. Among these techniques, hill-climbing-based algorithms are widely used for commercial and industrial applications. In this paper, a comparative performance analysis of the conventional and modified hill-climbing MPPT algorithms has been done. The simulation model of these techniques have been developed in MATLAB/Simulink environment, and results are presented.

Keywords Hill-climbing · MPPT · Perturb and observe
Incremental conductance · Incremental resistance

1 Introduction

The demand for electric energy is expected to grow continuously with the development of society. Bulk of this energy hitherto is met from coal-fired power plants. The adverse environmental effects associated with carbon emissions emanating from fossil fuel-based plants are likely to incur severe penalties from national and international regulating bodies [1]. For meeting the energy demands, the alternative

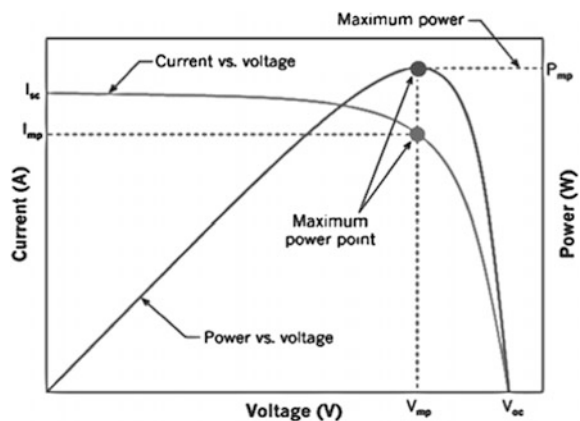
V. Jatily (✉) · S. Arora

Department of EE, College of Technology, GBPUA&T, Pantnagar, India
e-mail: vibhujatily@gmail.com

resources, preferably renewable ones will be harnessed to the extent possible. Solar, apart from wind, is the major option available for harnessing its unlimited source of energy to electricity, due to its abundance across the globe [2]. Conversion of solar energy into electrical energy using the photovoltaic cells has numerous advantages: clean and free energy, low maintenance, long life, location benefits, etc. The PV panel efficiency is generally about 20%, and the converter efficiency can be at above 90%. Therefore, to build an efficient PV system, use of a highly efficient MPPT algorithm is essential [3]. For a given atmospheric condition, the $I-V$ and $P-V$ characteristics of a solar cell are shown in Fig. 1. By observing the characteristic, one can easily understand that the MPP lies in the nonlinear region (knee) of the characteristic. Due to the variation in meteorological conditions, the $I-V$ and $P-V$ characteristics vary throughout the day and so does the MPP on these curves. Tracking this maximum power point (MPP) is a challenge for PV system designer engineers. The MPPT technique tries to track this point, so that maximum power can be extracted from solar array even under harsh environmental conditions [4].

A number of research and review articles have been published on tracking the MPP of photovoltaic panels. The commonly used MPPT techniques include perturb and observe (P&O), incremental conductance (INC), sliding mode control, ripple correlation control, soft computing, etc. P&O and INC are the most common hill-climbing techniques that are widely implemented for various applications. These are moderately efficient; however, these hill-climbing techniques fail to converge to the MPP for rapidly changing atmospheric conditions [5]. Sliding mode control was suggested by [6] for fast tracking of MPP under change in irradiance and load conditions. Although this technique is highly efficient, it involves complex computations and hence requires complex control circuitry. Ripple correlation control [7] uses inherent ripple present in the converter for MPPT and uses digital signal processors for complex computations, thereby increasing the complexity of the controller. Soft computing techniques like: fuzzy logic, neural network, particle swarm optimization, gravitational search algorithm [8] are highly efficient but

Fig. 1 Characteristic curve of a solar cell. *Source* ijaeie.com



require high computational processors, which increases the overall cost of the system.

Among all these algorithms, P&O is widely used technique because of its advantages of good efficiency and inexpensive implementation. Various improvements have been suggested to hill-climbing techniques [5, 9–12] to overcome its major drawbacks, as mentioned earlier. Zaheeruddin et al. suggested the use of two perturbation step sizes to improve the performance of the [11] P&O algorithm. Killi and Samanta [5] suggested the use of two sensors to determine the change in voltage and current between two perturbations in order to alleviate the drift-problem in P&O algorithm under rapidly increasing irradiance condition. Kollimalla et al. [10] proposed a current perturbation algorithm to efficiently track the MPP for varying irradiance. Comparative studies of some maximum power point tracking techniques were given in [13] and [14]. In spite of the fact that many highly efficient MPPT techniques have been introduced, perturb and observe is still the commercially accepted technique due to its low complexity and cost. In this paper, a comprehensive review of the classical and modified hill-climbing techniques is done on the basis of simulations runs under rapid changes in irradiance and temperature, and conclusions are drawn from the results obtained and evaluation of some important performance indices.

2 Commonly Used MPPT Algorithms

The solar energy conversion efficiency of a photovoltaic cell is around 16–20%. For maximum utilization of the energy under varying atmospheric conditions, MPP trackers are employed in most PV applications. Some commonly used MPPT techniques are discussed below.

2.1 *MPPT Based on Conventional Hill-Climbing Techniques*

2.1.1 Perturb and Observe (P&O) Algorithm

In this method, the panel voltage is purposefully perturbed (increased or decreased), and then the corresponding change in power is observed. If the observed power has increased, the next perturbation will be of the same sign, and if the power has decreased, the next perturbation will be of the opposite sign. The process-chart of this method is shown in Fig. 2. The amplitude of the perturbation step should be greater than the voltage ripple of the array voltage for accurate power calculations

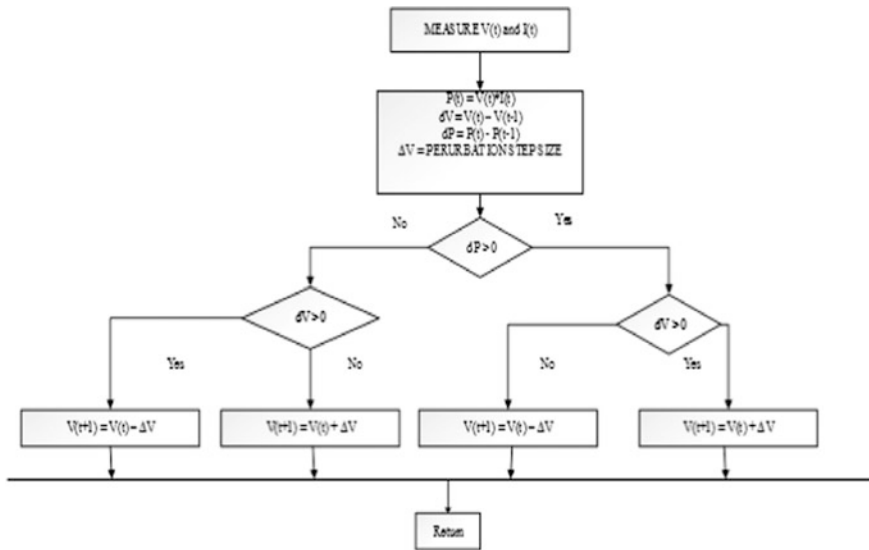


Fig. 2 Process-chart of perturb and observe (P&O) algorithm

and thus for true MPP tracking. Care must be taken to select a time interval between two perturbations that is larger than the settling time of the chosen converter; otherwise, the algorithm may give inaccurate results.

2.1.2 Incremental Conductance (INC) Algorithm

This method is derived by using the PV power curve ($P-V$). From Fig. 1, it can be easily seen that the slope is positive to the left of the peak point, negative to its right, and zero at the peak. The INC algorithm uses this relationship to track the MPP

$$\frac{dP}{dV} = \frac{d(I \cdot V)}{dV} = I + V \frac{dI}{dV} \tag{1}$$

To achieve maximum power, the power derivative must be zero.

$$\frac{dP}{dV} = 0 \quad \text{or} \quad \frac{dI}{dV} = -\frac{I}{V} \tag{2}$$

where $\frac{I}{V}$ represents the conductance and $\frac{dI}{dV}$ represents the incremental conductance. The process-chart of this technique is shown in Fig. 3.

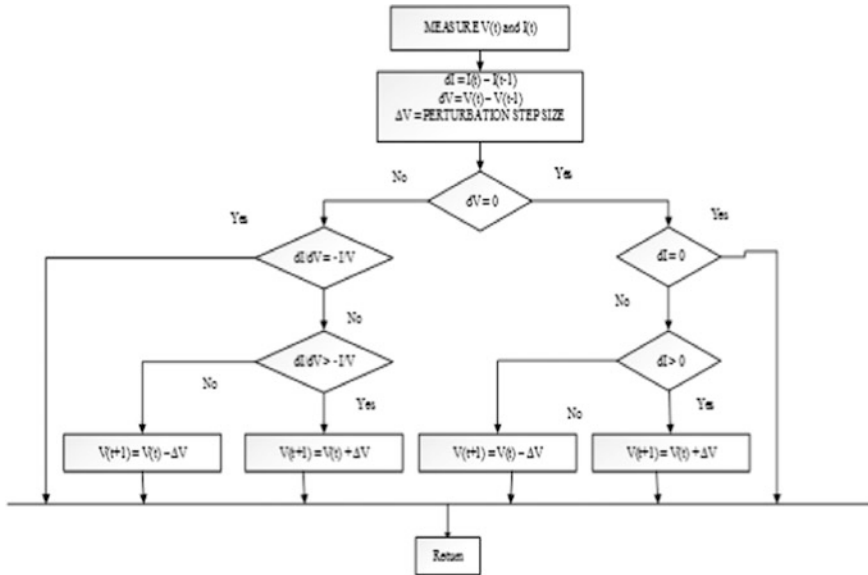


Fig. 3 Process-chart of incremental conductance

2.1.3 Incremental Resistance (INR) Algorithm

The incremental resistance method is analogous to the incremental conductance method. The INR differs from INC from the fact that it uses the knowledge of another power curve ($P-I$). By examining the $P-I$ curve in Fig. 4, we can easily see that the $P-I$ curve’s slope is positive to the left of the peak, negative to its right, and zero at the peak.

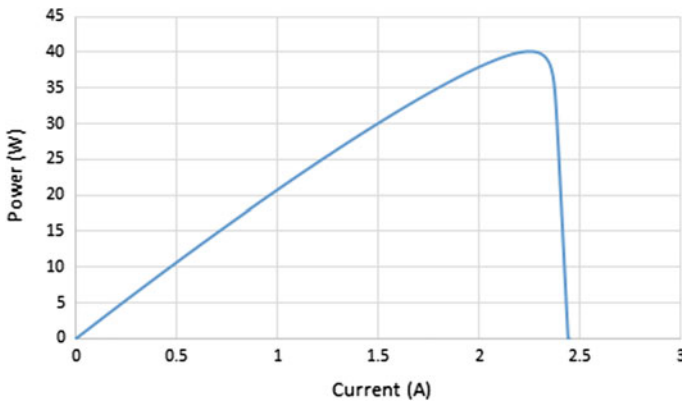


Fig. 4 $P-I$ power curve of a solar panel

Thus, the algorithm is developed as under:

$$\frac{dP}{dI} = \frac{d(V.I)}{dI} = V + I \frac{dV}{dI} \tag{3}$$

The condition for maximum power can be calculated by equating the power derivative to zero.

$$\frac{dP}{dI} = 0 \quad \text{or} \quad \frac{dV}{dI} = -\frac{V}{I} \tag{4}$$

where $\frac{V}{I}$ represents the resistance and $\frac{dV}{dI}$ represents the incremental resistance. The process-chart of this method is shown in Fig. 5.

2.2 MPPT Based on Modified Hill-Climbing Techniques

2.2.1 Variable Step Size (VSS) P&O Algorithm

This technique is a modification of the conventional P&O algorithm discussed above. Pandey [15] suggested this VSS algorithm by formulating an appropriate

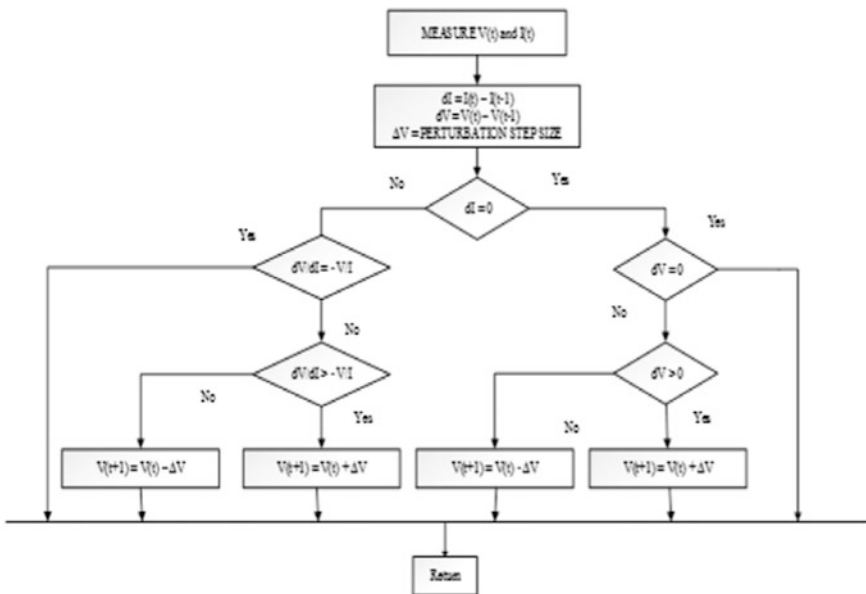


Fig. 5 Process-chart of incremental resistance algorithm

scaling parameter to determine the step size. The step size of VSS P&O is given in Eq. (5).

$$V(t + 1) = V(t) \pm M * \text{abs}\left(\frac{dP}{dV}\right) * \Delta V \tag{5}$$

The scaling factor M governs the convergence speed and MPP oscillations. The authors proposed determination of the value of scaling factor on the basis of Eq. (6):

$$M = \frac{|dV(\text{max})| * D(\text{max})}{|dP(\text{max})|} \tag{6}$$

where $D(\text{max})$ is the maximum permissible change in step size, $|dP(\text{max})|$ is the corresponding change in power, and $|dV(\text{max})|$ is the corresponding change in voltage. Hence, the scaling parameter step can be calculated from Eq. (6).

The process-chart of this algorithm is shown in Fig. 6.

2.2.2 Variable Step Size (VSS) INC Algorithm

In the conventional INC algorithm, the use of fixed step size creates a bargain between the dynamic and steady-state response. Liu et al. [16] used $P-V$ curve due to the smooth variation of $\frac{dP}{dV}$. A scaling factor N has been proposed by them for

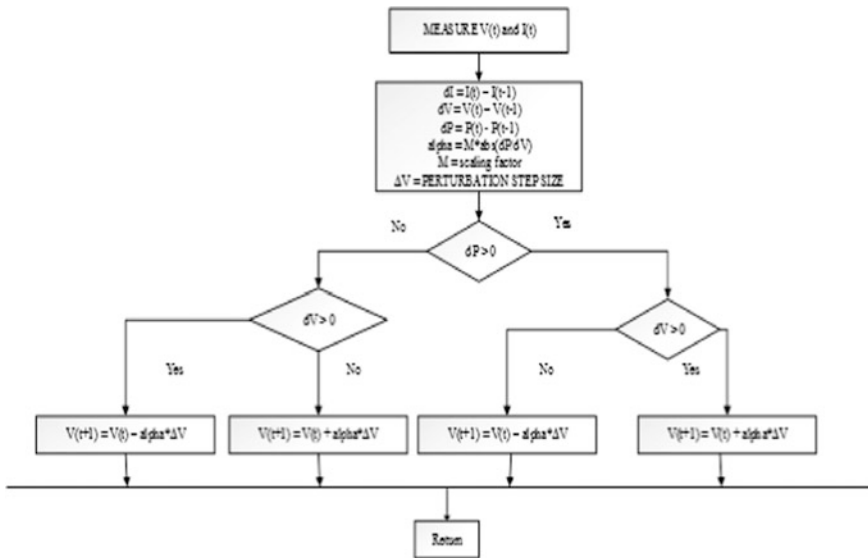


Fig. 6 Process-chart of VSS P&O algorithm

improving the performance of the MPPT algorithm. This scaling factor N can be determined from Eq. (7).

$$N = \frac{|dV(\max)| * D(\max)}{|dP(\max)|} \tag{7}$$

The process-chart of this algorithm is shown in Fig. 7.

2.2.3 Variable Step Size (VSS) INR Algorithm

Mei [17] proposed a VSS INR algorithm by using a scaling parameter to calculate the slope of $P-I$ power curve. The scaling factor N may be calculated as given in Eq. (8).

$$N = \frac{|dV(\max)| * D(\max)}{|dP(\max)|} \tag{8}$$

The VSS INR uses the knowledge of $P-I$ instead of $P-V$ power curves. The process-chart of this algorithm is shown in Fig. 8.

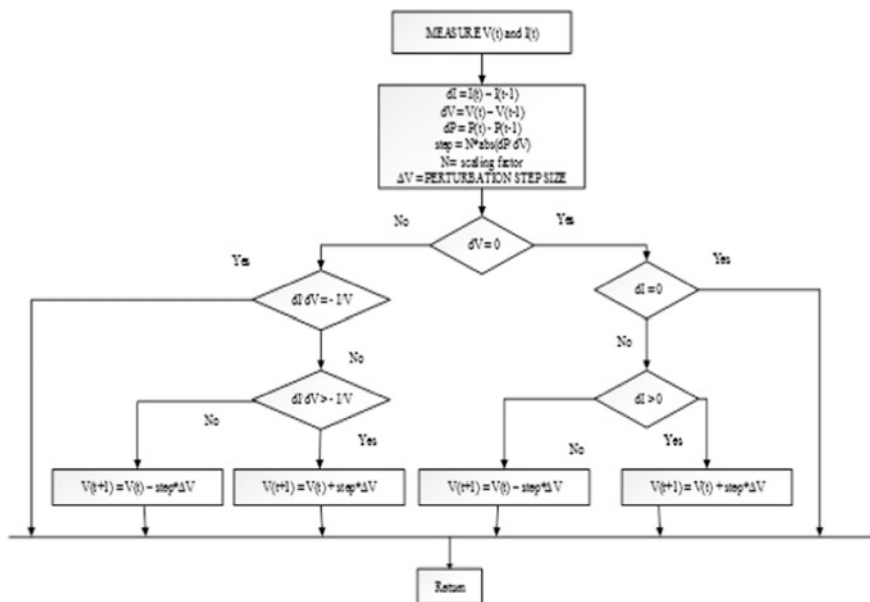


Fig. 7 Process-chart of VSS INC algorithm

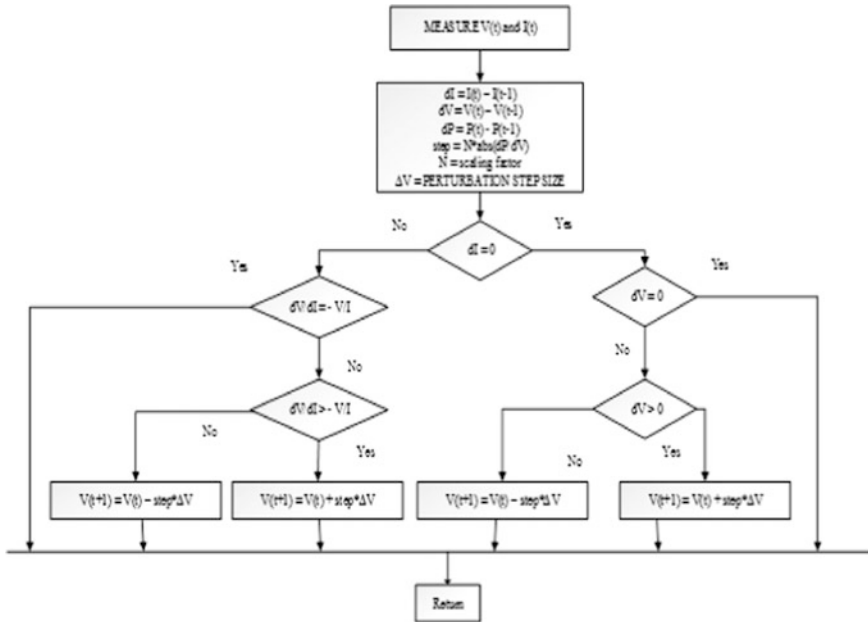


Fig. 8 Process-chart of VSS INR algorithm

3 Results and Discussion

The PV module considered here for simulation is a 49W SAMSUNG PV panel made of multi-crystalline cells. The specifications for the same are given in Table 1. The conventional algorithms were simulated and tested for various environmental conditions. A performance evaluation of six MPPT on the basis of output power observed in these simulations run and on their duty-cycle variations has been conducted.

Two case studies were performed by the authors, by varying both irradiance and temperature. By observing the behavior of output power, different comparative tables are developed on the basis of some qualitative and quantitative performance parameters. For the first case, the PV module was operated under constant temperature at STC (25 °C), but irradiance was rapidly increased from 600 to 1000 W/m² and then suddenly decreased to 500 W/m². The output power observed in case of six MPPT techniques in response to these step changes in irradiance is depicted in Fig. 9.

Table 1 Specifications of PV panel at STC

V_{OC}	I_{SC}	V_{MPP}	I_{MPP}	β_{oc}	α_{sc}
24.9	2.43	21.3	2.3	-0.27269	0.061745

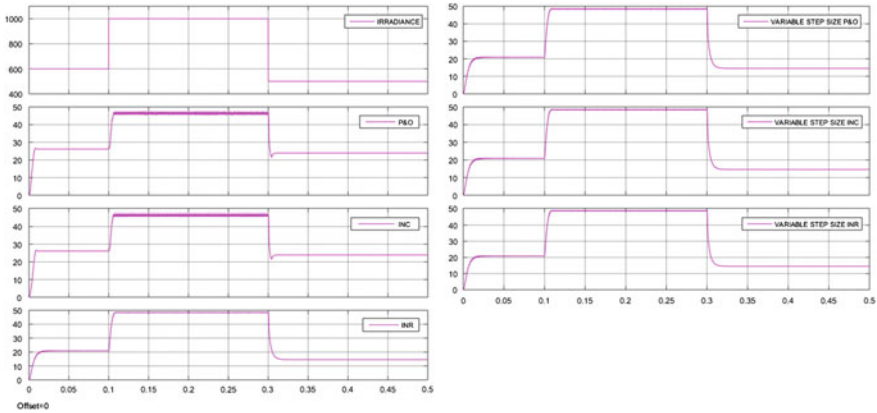


Fig. 9 $P-t$ curve showing comparison between P&O, INC, INR, VSS P&O, VSS INC, and VSS INR for a step change in irradiance

A qualitative comparison of these six techniques on the basis of three performance indices is shown in Table 2. These three indices are the static response, the dynamic response, and the ability to track peak power.

In order to compare the different algorithms, a similar step size of 0.0001 was chosen. It is observed that for low irradiance levels, P&O and INC algorithms are able to extract more power as compared to all other algorithms. INR and the modified approaches exhibit excellent steady-state response as compared to the conventional hill-climbing algorithms.

For the second case, the PV module was operated under constant irradiance at STC, but the temperature was rapidly increased from 30 to 50 °C and then suddenly decreased to 25 °C. The output power from these six techniques in response to these step changes in temperature is shown in Fig. 10.

Among all the classical algorithms, the modified INR algorithm displays an excellent response due to its use of $P-I$ curve. The steady-state response of the P&O and INC algorithm is inferior to that of their modified counterparts.

A qualitative comparison of these six techniques on the basis of three performance indices is shown in Table 3. As in the previous case, the three indices are the static response, the dynamic response, and the ability to track peak power.

Table 2 Qualitative comparison under conditions of a step change in irradiance

Technique	Static response	Dynamic response	Peak power tracking
P&O	Average	Good	Satisfactory
INC	Average	Good	Satisfactory
INR	Poor	Good	Doubtful
Variable step size P&O	Excellent	Excellent	Doubtful
Variable step size INC	Excellent	Excellent	Doubtful
Variable step size INR	Excellent	Excellent	Doubtful

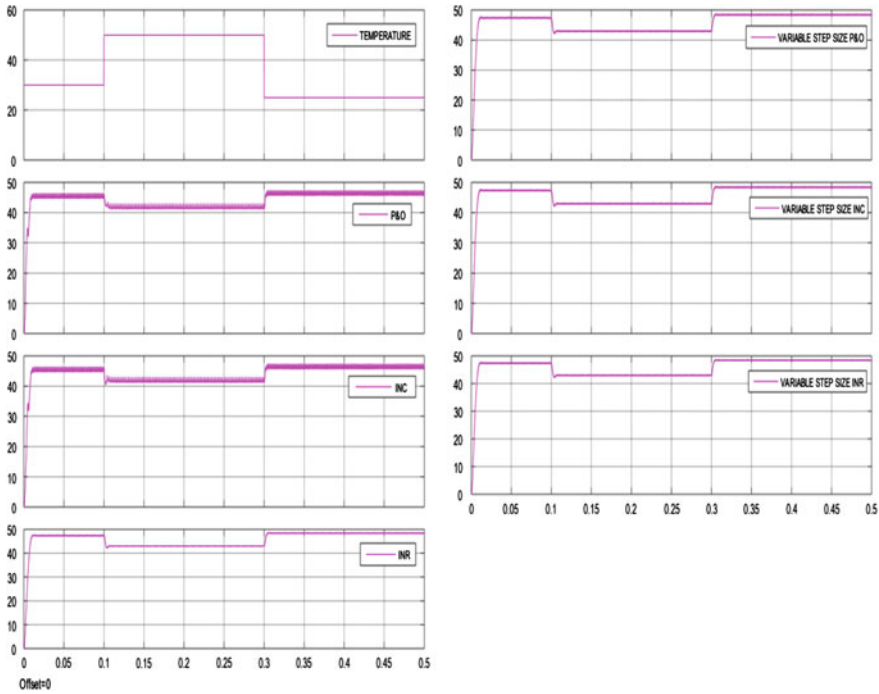


Fig. 10 *P-t* curve showing comparison between P&O, INC, INR, VSS P&O, VSS INC, and VSS INR for a step change in temperature

Table 3 Qualitative comparison under conditions of a step change in temperature

Technique	Static response	Dynamic response	Peak power tracking
P&O	Poor	Poor	Doubtful
INC	Poor	Poor	Doubtful
INR	Average	Good	Satisfactory
Variable step size P&O	Excellent	Excellent	Satisfactory
Variable step size INC	Excellent	Excellent	Satisfactory
Variable step size INR	Excellent	Excellent	Satisfactory

The irradiance in practical conditions keeps on changing during the day. These changes occur rather frequently during the rainy season. The technique chosen for tracking the MPP is required to perform efficiently under different levels of irradiance. The efficiency of all six MPPT techniques, therefore, has been computed at irradiance levels of 1, 0.8, 0.6, and 0.4 p.u., taking irradiance at STC (1000 W/m²) as the base value. A comparison of the efficiency obtained in case of these six techniques under these different levels of irradiance is shown in Table 4.

Table 4 Quantitative comparison of six MPPT techniques indicating efficiency for different irradiance

Algorithm	1 p.u. (%)	0.8 p.u. (%)	0.6 p.u. (%)	0.4 p.u. (%)
P&O	93.89	91.32	88.82	91.99
INC	93.69	91.32	88.82	91.99
INR	96.34	90.30	85.73	93.55
Variable step size P&O	97.97	92.60	70.64	47.97
Variable step size INC	97.97	92.60	70.64	47.97
Variable step size INR	97.97	92.60	70.64	47.97

These results show that as the irradiance decreases the modified approaches fail to track the true MPP. The conventional algorithms show satisfactory results, but then these suffer from steady-state power losses.

4 Conclusion

Sudden and rapid changes in irradiance levels in practical conditions are encountered by roof-top, terrace mounted PV panels or by panels mounted on building façades, as well as in case of terrestrial PV plants during cloudy weather. Such sudden changes in irradiance are likely to occur frequently on panels mounted on transport vehicles. Sudden changes of temperature also do occur in case of transport vehicles, when these happen to pass under shades of trees in the country side or under shades of nearby buildings in urban areas. The step changes in irradiance levels and temperature levels were, therefore, chosen carefully in this study, keeping these practical considerations in mind.

The performance investigation of the commonly used hill-climbing techniques under rapidly changing environmental conditions has been conducted. On the basis of the results obtained, it can be concluded that:

- For a rapid increase in temperature, P&O and INC algorithms exhibit poor performance as compared to their modified counterparts.
- For a rapid increase in irradiance, P&O and INC algorithms exhibit poor steady-state response but give satisfactory dynamic response even under low irradiance levels.

For both test cases, the variable step size P&O, INC, and INR algorithms display excellent steady-state response resulting in low steady-state losses.

References

1. David J. C. MacKay, *Sustainable Energy - Without the Hot Air*, first ed., UIT, 2008.
2. Mukund R. Patel, *Wind and Solar Power Systems: Design, Analysis, and Operation*, second ed., CRC, 2005.
3. C. S. Solanki, *Solar Photovoltaics*, second ed., PHI, 2012.
4. M. A. S. Masoum, H. Dehbonei, and E. F. Fuchs, "Theoretical and Experimental Analyses of Photovoltaic Systems With Voltage- and Current-Based Maximum Power-Point Tracking," vol. 17, no. 4, pp. 514–522, 2002.
5. M. Killi and S. Samanta, "Modified Perturb and Observe MPPT Algorithm for Drift Avoidance in Photovoltaic Systems," vol. 0046, no. c, pp. 1–10, 2015.
6. Y. Levron and D. Shmilovitz, "Maximum Power Point Tracking Employing Sliding Mode Control," vol. 60, no. 3, pp. 724–732, 2013.
7. T. Eswam, S. Member, J. W. Kimball, S. Member, P. T. Krein, P. L. Chapman, S. Member, P. Midya, and S. Member, "Dynamic Maximum Power Point Tracking of Photovoltaic Arrays Using Ripple Correlation Control," vol. 21, no. 5, pp. 1282–1291, 2006.
8. T. Logeswaran and A. Senthilkumar, "A Review of Maximum Power Point Tracking Algorithms for Photovoltaic Systems under Uniform and Non-Uniform irradiances," *Energy Procedia*, vol. 54, pp. 228–235, 2014.
9. A. K. Abdelsalam, A. M. Massoud, S. Ahmed, and P. N. Enjeti, "High-Performance Adaptive Perturb and Observe MPPT Technique for Photovoltaic-Based Microgrids," vol. 26, no. 4, pp. 1010–1021, 2011.
10. S. K. Kollimalla, S. Member, M. K. Mishra, and S. Member, "Variable Perturbation Size Adaptive P & O MPPT Algorithm for Sudden Changes in Irradiance," pp. 1–11, 2014.
11. Z. Sukumar and M. Ahteshamul, "Performance evaluation of modified perturb & observe maximum power point tracker for solar PV system," *Int. J. Syst. Assur. Eng. Manag.*, 2015.
12. S. Rajasekar, S. Member, R. Gupta, S. Member, A. Upadhyay, P. Agarwal, S. Kumar, Y. S. Kumar, and S. Member, "Modified Hill-top Algorithm Based Maximum Power Point Tracking for Solar PV Module," no. 3, pp. 1801–1806, 2012.
13. D. P. Hohm, "Comparative Study of Maximum Power Point Tracking Algorithms Using an Experimental, Programmable, Maximum Power Point Tracking Test Bed," 2000.
14. T. Eswam, S. Member, and P. L. Chapman, "Comparison of Photovoltaic Array Maximum Power Point Tracking Techniques." *IEEE Trans. Energy Conv.* 2007, 22, pp. 439–449.
15. A. Pandey, "High-Performance Algorithms for Drift Avoidance and Fast Tracking in Solar MPPT System," *IEEE Trans. Energy Conv.* Vol. 23, No. 2, pp. 681–689, 2008.
16. F. Liu, S. Duan, "A Variable Step Size INC MPPT Method for PV Systems," pp. 2622–2628, 2008.
17. Q. Mei, "A Novel Improved Variable Step-Size Incremental-Resistance MPPT Method for PV Systems," pp. 2427–2434, 2011.

Adaptive Beamforming for Linear Antenna Arrays Using Gravitational Search Algorithm

Abhinav Sharma, Sanjay Mathur and R. Gowri

Abstract Smart antenna is one of the leading innovations in the area of mobile communication which has drawn the attention of researchers as it fulfills the requirement of wireless services such as higher data rates and channel capacities. Adaptive beamforming (ABF) is one of the primary signal processing aspects of smart antenna. The problem of ABF is formulated as an optimization problem for linear antenna arrays. A novel gravitational search algorithm (GSA) is explored for optimizing the function which will effectively fit to the condition such as to direct the main lobe toward the desired direction of signal of concern (DS) and zero output (null) in the undesired direction of signals (UDS). The optimization algorithm shows good steering ability, and the simulation result verifies that the algorithm presents radiation pattern with reduced side lobe level (SLL) as compared to well-known minimum variance distortionless response (MVDR) technique. The simulations are carried out at different power levels of the incoming signals for analyzing overall performance of algorithms.

Keywords Smart antenna · ABF · GSA · SLL · MVDR

A. Sharma (✉) · R. Gowri
Department of EIC, UPES, Dehradun, Uttarakhand, India
e-mail: abhinav.sharma@ddn.upes.ac.in

S. Mathur
Department of ECE, College of Technology, GBPUA&T, Pantnagar, India

© Springer Nature Singapore Pte Ltd. 2018
R. Singh et al. (eds.), *Intelligent Communication, Control and Devices*,
Advances in Intelligent Systems and Computing 624,
https://doi.org/10.1007/978-981-10-5903-2_121

1159

1 Introduction

The modern wireless communication has become the backbone of the communication industry. There has been a tremendous growth in the users of the wireless services worldwide in last decade and it is expected to rise exponentially with the introduction of new research ideas to a concrete system. The demand of third- and fourth-generation modern cellular services and other personal communication services have motivated the researchers to explore new ways to maximize the spectral efficiency of the network. There exist numerous techniques such as advanced coding and compression techniques, higher order modulation technique, adaptive interference and dynamic spectrum management technique, smart antennas which enable the efficient utilization of the spectrum. Dynamic spectrum management is the basic outline of cognitive radios proposed by Joseph Mitola in 1998 which dynamically manage the spectrum based on the spectrum observation.

Smart antenna [1] also known as adaptive antenna has emerged as a promising technology in the field of wireless communication which proves economical for large range of potential users. Smart antenna is a combination of antenna array and digital signal processor which basically transmit and receive the signal in an adaptive manner. The antenna is governed by signal processing algorithms which identify the spatial signature of the incoming signals and calculate the weights of the beamforming network for exactly identifying the antenna beam toward the desired user by tracking it. The algorithms which dynamically calculate the array weights in real time so as to place the major lobe toward the signal of concern and null intensity in the undesired direction of signal are called ABF algorithms. The beamforming algorithm takes into account the direction of incoming signals. Multiple signal classification (MUSIC), Matrix Pencil, ESPRIT, and Maximum Likelihood are some of the well-known algorithms which estimate the direction of incoming signals. In [2, 3], authors had reviewed and compared different DOA estimation, blind and non-blind ABF algorithms. MVDR is an efficient ABF technique which maximizes the carrier to interference and noise ratio so as to steer the major lobe toward DS and nulls in the direction of UDS.

Computational intelligence has gained momentum in the field of science and technology to solve hard nondeterministic polynomial (NP) problems in an efficient manner. The principle constituents of soft computing approaches like neural network, heuristic approaches, and fuzzy logic are being efficiently used in the field of array signal processing. Heuristic approaches like genetic algorithm (GA), simulated annealing (SA), differential evolution algorithm, particle swarm optimization (PSO), ant colony optimization (ACO), and honey bee algorithm find an application in antenna arrays design and pattern synthesis problems. The pattern synthesis problems find the weights of antenna array by reducing the pattern mismatch. The problem of ABF is a real-time problem, thus the optimization algorithm used for beamforming should have a good rate of convergence. In [4], authors have used the variant of PSO algorithm, i.e., Adaptive Mutated Boolean Particle Swarm Optimization (AMBPSO) for ABF in linear antenna arrays. In [5], author combines

the soft computing capabilities of Mutated Boolean Particle Swarm Optimization (MBPSO) and neural network for ABF. In [6], authors used adaptive dispersion invasive weed optimization (ADIWO) for ABF and compare the results with PSO-based beamformer and MVDR technique.

In this article, GSA [7, 8] is utilized for optimizing fitness function so as to obtain complex weights of linear arrays for ABF. The amplitude of the interfering signals are uncertain thus the exact element values of the interfering correlation matrix are not taken into account. Therefore, the interference correlation matrix is taken as the identity matrix.

This paper is organized in the following manner. The data model for beamforming is briefly introduced in Sect. 2. The standard MVDR technique and GSA are discussed in Sects. 3 and 4. Section 5 presents the simulation results for ABF for different power levels. Section 6 provides a conclusive remarks.

2 Data Model for ABF

A uniform linear array of R sensor elements is considered which are symmetrically placed about the origin as shown in Fig. 1. Suppose ULA receives monochromatic signals and having distance of separation between the elements as ' d_0 ', respectively. The incoming signals consists of desired signal $s(l)$ coming from the angle θ_0 and N interference signals $i_n(l)$ coming from angle $\theta_n (n = 1, \dots, N)$. The received signals also include gaussian noise $n(l)$ having a variance of σ^2 .

The signal at the input of the m th array element can be modeled as:

$$\bar{y}(l) = \bar{b}(\theta_0) * s(l) + [\bar{b}(\theta_1) \quad \bar{b}(\theta_2) \quad \dots \quad \bar{b}(\theta_N)] * \bar{i}(l) + \bar{n}(l)$$

$$\bar{y}(l) = \bar{b}(\theta_0) * s(l) + \bar{B} * \bar{i}(l) + \bar{n}(l), \tag{1}$$

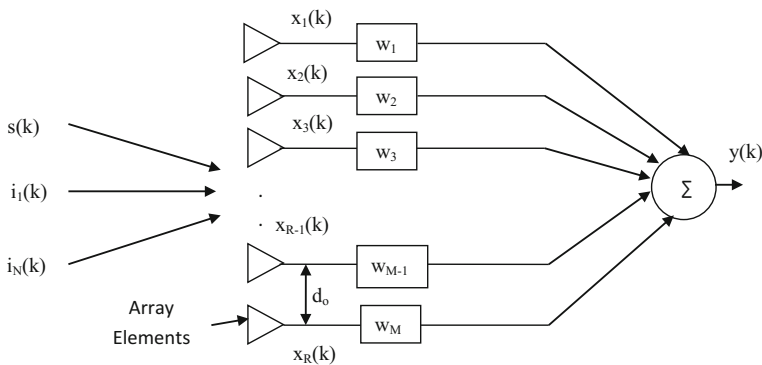


Fig. 1 Uniform linear antenna array

$$\bar{y}(l) = \bar{d}(l) + \bar{u}(l), \quad (2)$$

where $\bar{b}(\theta_n)$ represents the array steering vector which contains information of incoming signals and is given by:

$$\bar{b}(\theta_n) = \left[e^{j(r-1)\beta d \sin \theta_n} \right]^T, r = 1, \dots, R, \quad (3)$$

where θ_n is the angle from the array broadside, β is the phase constant related to operating frequency.

$\bar{d}(l) = \bar{b}(\theta_0) * s(l)$ represents the desired input signal vector,

$\bar{u}(l) = \bar{B} * \bar{i}(l) + \bar{n}(l)$ represents the interference plus noise signal vector.

The antenna array output is expressed by:

$$\begin{aligned} z(l) &= \bar{w}^H * \bar{y}(l) \\ z(l) &= \bar{w}^H * \bar{d}(l) + \bar{w}^H * \bar{u}(l), \end{aligned} \quad (4)$$

The mean value of the power radiated by an array in the desired direction is expressed by:

$$\sigma_d^2 = E \left[|\bar{w}^H \bar{d}(l)|^2 \right] = E \left[|\bar{w}^H \bar{b}(\theta_0) s(l)|^2 \right] = S \bar{w}^H \bar{b}(\theta_0) \bar{b}(\theta_0)^H \bar{w}, \quad (5)$$

where $S = E \left[|s(l)|^2 \right]$ is the mean signal power of desired signal is considered as unity and hence the output power of desired signal is given by:

$$\sigma_d^2 = \bar{w}^H \bar{b}(\theta_0) \bar{b}(\theta_0)^H \bar{w}. \quad (6)$$

The mean array output of the undesired signal is expressed by:

$$\begin{aligned} \sigma_u^2 &= E \left[|\bar{w}^H \bar{u}(l)|^2 \right] = E \left[|\bar{w}^H [\bar{B} * \bar{i}(l) + \bar{n}(l)]|^2 \right] \\ &= \bar{w}^H \bar{B} \bar{R}_{ii} \bar{B}^H \bar{w} + \bar{w}^H \bar{R}_{nn} \bar{w}, \end{aligned} \quad (7)$$

where $\bar{R}_{ii} = E \left[\bar{i}(l) \bar{i}^H(l) \right]$ is the interference correlation matrix,

$\bar{R}_{nn} = E [\bar{n}(l) \bar{n}^H(l) = \sigma^2 * I]$ is the noise correlation matrix.

Thus, using the above expressions of noise correlation matrix in Eq. (7) we obtain the expression:

$$\sigma_u^2 = \bar{w}^H \overline{BR}_{ii} \bar{B}^H \bar{w} + \sigma^2 \bar{w}^H \bar{w}. \tag{8}$$

In this article, we maximize the SINR so as to direct the major lobe toward the DS and form pattern nulls toward UDS. Using Eqs. (6, 8), we obtain the following expression for SINR:

$$\text{SINR} = \sigma_d^2 / \sigma_u^2 = \bar{w}^H \bar{b}(\theta_0) \bar{b}(\theta_0)^H \bar{w} / \left(\bar{w}^H \overline{BR}_{ii} \bar{B}^H \bar{w} + \sigma^2 \bar{w}^H \bar{w} \right). \tag{9}$$

The fitness function used in the optimization algorithm is the inverse of the SINR.

$$F = \left(\bar{w}^H \overline{BR}_{ii} \bar{B}^H \bar{w} + \sigma^2 \bar{w}^H \bar{w} \right) / \bar{w}^H \bar{b}(\theta_0) \bar{b}(\theta_0)^H \bar{w}. \tag{10}$$

As the function is minimized by the optimization algorithm, the major lobe of the array output is directed toward DS and zero output is formed toward interference signals.

3 Minimum Variance Distortionless Response

MVDR is a robust beamforming technique and its solution is similar to maximum likelihood (ML) solution. The goal of this technique is to minimize the mean array output of the undesired signal and thus maintaining the array output corresponding to the desired signal. Thus, the optimum weights of individual elements are derived by using:

$$\min \{ \bar{w}^H \overline{R}_{uu} \bar{w} \} \text{ while } \bar{w}^H \bar{b}(\theta_0) = 1. \tag{11}$$

The optimum array weights based on this criteria is expressed as:

$$\bar{w}_{mvd} = \overline{R}_{uu}^{-1} \bar{b}(\theta_0) / \bar{b}(\theta_0)^H \overline{R}_{uu}^{-1} \bar{b}(\theta_0), \tag{12}$$

where $\overline{R}_{uu} = E[\bar{u}(l)\bar{u}^H(l)]$ is the correlation matrix of $\bar{u}(l)$.

4 Gravitational Search Algorithm

GSA was developed by Rashedi et al. in [7] for getting a solution of complex and high-dimensional problems. Researchers have developed various optimization techniques inspired from social behavior, biological, or physical processes in the recent years. GSA is a stochastic optimization technique which is motivated from

Newton’s physical phenomena, which states that there exist an attracting force among the particles which is proportional to their masses and inversely proportional to their distance square. The algorithm considers agents as objects having masses and positions. There exists a gravitational force among all the agents which causes the agents to move in the direction of best solution.

Algorithm
<p>Step 1. Randomly initialize the position and velocity of the agents in the search space</p> $Y_i = (y_i^1, \dots, y_i^d, \dots, y_i^m) \text{ for } i = 1, 2, \dots, M.$ $vt_i = (vt_i^1, \dots, vt_i^d, \dots, vt_i^m) \text{ for } i = 1, 2, \dots, M.$
<p>Step 2. Assess the fitness of all the agents in the search space and determine the best and the worst fitness as:</p> $\text{best} = \min_{j \in \{1, \dots, K\}} \text{fitness}_j(t)$ $\text{worst} = \max_{j \in \{1, \dots, K\}} \text{fitness}_j(t)$ <p>where, $\text{fitness}_j(t)$ represents the fitness value of the j^{th} agent at time t.</p>
<p>Step 3. The gravitational constant G at iteration t is evaluated as:</p> $G(t) = G_0 \exp(-\text{beta} * \text{iter}/\text{maxit})$ <p>where, beta and G_0 are the gradient constant and initial value of gravitational constant while iter is the current iteration and maxit is the maximum number of iterations.</p>
<p>Step 4. Update the mass of the agents in each iteration by the following equations:</p> $\text{mass}_i(t) = \frac{\text{fitness}_i(t) - \text{worst}(t)}{\text{best}(t) - \text{worst}(t)}$ $\text{Mass}_i(t) = \frac{\text{mass}_i(t)}{\sum_{j=1}^N \text{mass}_j(t)}$
<p>Step 5. Determine the force acting on agent 'k' from agent 'r' at d^{th} dimension and t^{th} iteration as:</p> $\text{Force}_{kr}^d(t) = G(t) \frac{\text{Mass}_{pk}(t) * \text{Mass}_{ar}(t)}{R_{kr}(t) + \epsilon} (y_k^d(t) - y_r^d(t)).$ <p>where, $R_{kr}(t)$ is the Euclidean distance between the two agents 'k' and 'r' at each iteration t and ϵ is a zero offset constant.</p>
<p>Step 6. The total force that acts on agent 'k' in a dimension d is calculated as:</p> $\text{Force}_k^d(t) = \sum_{r=1, r \neq k}^N \text{rand}_r \text{Force}_{kr}^d(t),$ <p>where, rand_r is a random number in the interval $[0,1]$.</p>
<p>Step 7. Determine the acceleration of the k^{th} agents at iteration t as:</p> $\text{acceleration}_k^d(t) = \frac{\text{Force}_k^d(t)}{\text{Mass}_{kk}(t)}$
<p>Step 8. Determine the velocity and position of the agents at next iteration $(t+1)$ as:</p> $vt_i^d(t+1) = \text{rand}_j vt_i^d(t) + \text{acceleration}_i^d(t),$ $y_i^d(t+1) = y_i^d(t) + vt_i^d(t+1).$ <p>The algorithm is repeated from step 2 until the termination criteria is met.</p>

5 Adaptive Beamforming Methodology

The methodology of ABF using GSA optimization technique is briefly discussed. The algorithm iteratively tries to refine the magnitude and phase of ULA so as to direct major lobe and nulls in the defined directions with reduced SLL.

The methodology of ABF is as follows:

1. Initialize the population of agents with complex random position and velocities in the search space. The agents having the complex position represent the amplitude and phase of weight vectors. The dimension of the weight vector represents the number of sensor elements.
2. Determine the fitness of all the particles in GSA using Eq. (10).
3. The position and velocity of the particles are updated in each successive iteration. Since the problem of beamforming using GSA is modeled as a minimization problem thus the weights based on minimum fitness represent the required solution.

6 Results and Discussion

The results obtained through simulation are presented in order to validate the capabilities of GSA for ABF. We have considered 10 elements ULA with $\lambda/2$ spacing between the array elements. Three different scenarios are studied in order to analyze the effectiveness of the GSA over robust MVDR ABF technique. The parameters for GSA algorithm are as follows: population size is 30, maximum iterations are 1000, Gravitational constant (G_0) is 100, Gradient constant (alpha) is 20, and zero offset constant is $2.22e-16$. In the first scenario, ULA receives one desired signal arriving at 30° and eight interference signals arriving at $\{-70^\circ, -40^\circ, -30^\circ, -10^\circ, 0^\circ, 10^\circ, 50^\circ, 70^\circ\}$ with an SNR of 30 dB.

Figure 2 and Table 1 display and present the radiation pattern and the weights for MVDR and GSA algorithm for the first scenario.

In the second scenario, ULA receives one desired signal from 30° and eight interfering signals arriving from $\{-70^\circ, -40^\circ, -30^\circ, -10^\circ, 0^\circ, 10^\circ, 50^\circ, 70^\circ\}$ with an SNR of 15 dB.

Figure 3 and Table 2 display and present the radiation pattern and the weights for MVDR and GSA algorithm for the second scenario.

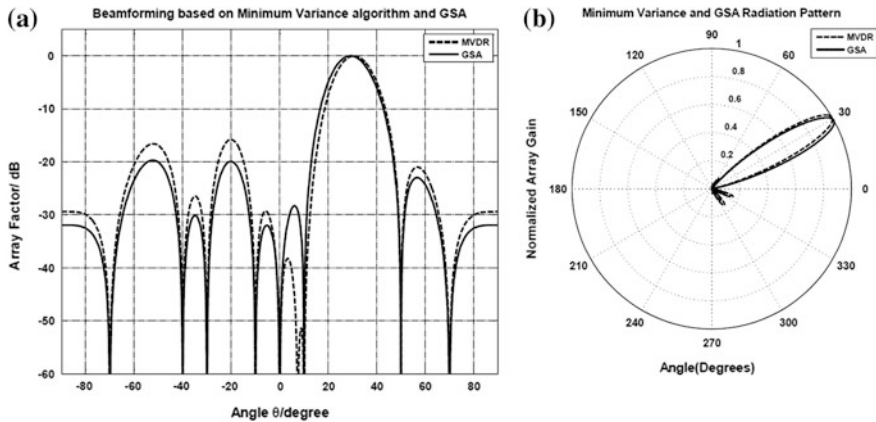


Fig. 2 a Linear plot b Polar plot for first scenario of beamforming using GSA and MVDR algorithm

Table 1 Estimated weights of first scenario of beamforming using GSA and MVDR algorithm

m	W_{MVDR}	W_{GSA}
1	$0.35245 - 0.22679j$	$0.41076 + 0.015865j$
2	$0.017253 + 0.40491j$	$-0.05278 + 0.50937j$
3	$-0.75025 + 0.15175j$	$-0.83341 - 0.026849j$
4	$-0.22043 - 0.89979j$	$-0.070759 - 1.0572j$
5	1.0	1.0
6	$0.34232 + 0.93958j$	$0.24772 + 1.0665j$
7	$-0.92089 + 0.10091j$	$-0.87421 + 0.15384j$
8	$-0.11425 - 0.75687j$	$-0.11762 - 0.66439j$
9	$0.38635 - 0.1224j$	$0.37239 - 0.19029j$
10	$-0.092439 + 0.4088j$	$-0.081946 + 0.19331j$

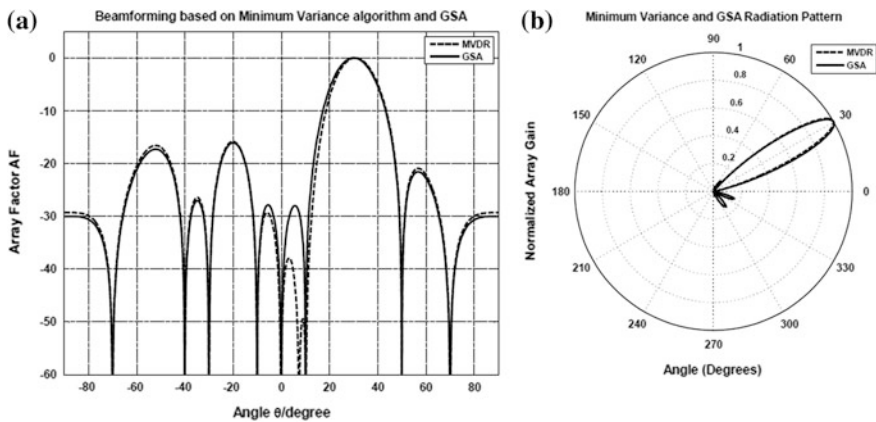


Fig. 3 a Linear plot b Polar plot for second scenario of beamforming using GSA and MVDR algorithm

Table 2 Estimated weights of second scenario of beamforming using GSA and MVDR algorithm

m	W_{MVDR}	W_{GSA}
1	$0.35407 - 0.22629j$	$0.52486 - 0.041515j$
2	$0.018068 + 0.407j$	$0.0073994 + 0.5335j$
3	$-0.75082 + 0.15166j$	$-0.91186 + 0.035403j$
4	$-0.21946 - 0.90085j$	$-0.16494 - 1.113j$
5	1.0	1.0
6	$0.34045 + 0.94026j$	$0.32004 + 1.0984j$
7	$-0.92175 + 0.10035j$	$-0.8547 + 0.12385j$
8	$-0.11301 - 0.7576j$	$-0.071041 - 0.67482j$
9	$0.38884 - 0.12158j$	$0.34309 - 0.17439j$
10	$-0.092227 + 0.40996j$	$-0.18896 + 0.21582j$

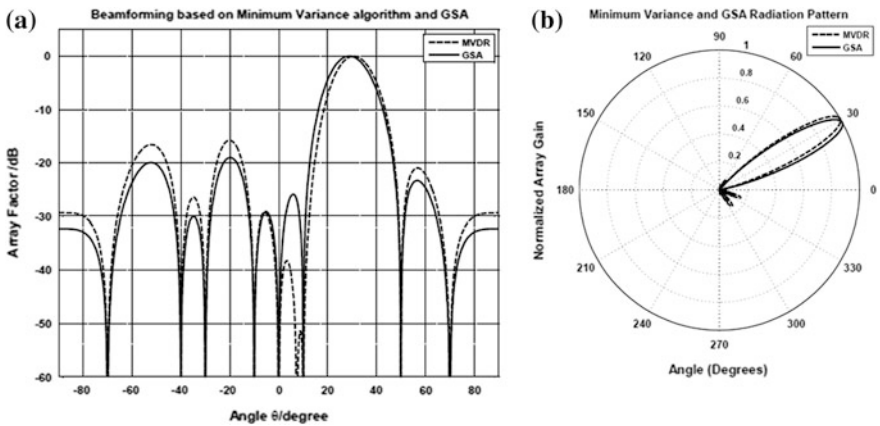


Fig. 4 a Linear plot b Polar plot for third scenario of beamforming using GSA and MVDR algorithm

Table 3 Estimated weights of third scenario of beamforming using GSA and MVDR algorithm

m	W_{MVDR}	W_{GSA}
1	$0.3524 - 0.22681j$	$0.43822 + 0.085019j$
2	$0.017227 + 0.40484j$	$-0.069042 + 0.54307j$
3	$-0.75023 + 0.15175j$	$-0.86553 - 0.076036j$
4	$-0.22046 - 0.89976j$	$-0.033305 - 1.11j$
5	1.0	1.0
6	$0.34238 + 0.93956j$	$0.22525 + 1.108j$
7	$-0.92086 + 0.10093j$	$-0.85816 + 0.1675j$
8	$-0.11429 - 0.75684j$	$-0.11475 - 0.63695j$
9	$0.38627 - 0.12243j$	$0.36534 - 0.2098j$
10	$-0.092446 + 0.40876j$	$-0.088023 + 0.1292j$

In the third scenario, one desired signal arrives at the 10 element array from 30° and eight interfering signals arrives from $\{-70^\circ, -40^\circ, -30^\circ, -10^\circ, 0^\circ, 10^\circ, 50^\circ, 70^\circ\}$ with an SNR of 50 dB.

Figure 4 and Table 3 display and present the radiation pattern and weights for MVDR and GSA algorithm for the third scenario.

The simulation results show that GSA-based ABF and MVDR algorithms direct the antenna's main lobe and nulls in the direction of SOI and SNOI. However, the GSA algorithm presents better SLL as compared to MVDR algorithm in all the three scenarios. But, in order to achieve specific value of SLL at certain angular region, a specific function of SLL must be added to the fitness function.

7 Conclusion and Future Work

The paper proposes GSA for ABF in linear antenna arrays. The capability of the algorithm is judged in three scenarios of distinct power levels. The GSA-based ABF algorithm applied on linear antenna arrays requires the knowledge of the direction of the incoming signals. The GSA-based beamformer succeeds not only to steer the main lobe toward direction of DS but also achieves radiation pattern with reduced SLL. Simulation results verify that GSA-based beamformer shows good rate of convergence and provides adequate steering ability of the major lobe and nulls with reduced SLL compared to popular MVDR-based beamforming technique. Thus, GSA-based ABF technique seems to be quite promising for array signal processing. As a proposal of future work the GSA could be applied on more complex fitness function so as to obtain reduced SLL at certain angular regions.

References

1. Gross, F. B.: *Smart Antennas for Wireless Communications with MATLAB*, Mc Graw-Hill, (2005).
2. Godara, L. C.: Application of antenna arrays to mobile communications. II. Beam-forming and direction-of-arrival considerations, *IEEE Proceedings of the*, vol. 85, no. 8, pp: 1195–1245, (1997).
3. Sharma, A., Mathur, S.: Performance Analysis of Adaptive Array Signal Processing Algorithms, *IETE*, Taylor & Francis, vol. 33, no. 5, pp: 472–491, (2016).
4. Zaharis, Z. D., Yiouitsis, T. V.: A novel adaptive beamforming technique applied on linear antenna arrays using adaptive mutated boolean PSO, *Progress In Electromagnetic Research*, vol. 117, pp: 165–179, (2011).
5. Zaharis, Z. D., Gotsis, K. A., Sahalos, J. N.: Adaptive beamforming with low side lobe level using neural networks trained by mutated boolean PSO, *Progress In Electromagnetic Research*, vol. 127, pp: 139–154, (2012).
6. Zaharis, Z. D., Skeberis, C., Xenos, T. D.: Improved antenna array adaptive beamforming with low side lobe level using a novel adaptive invasive weed optimization method, *Progress In Electromagnetic Research*, vol. 124, pp: 137–150, (2012).

7. Rashedi, E., Nezamabadi, S., Saryazdi, S.: A Gravitational Search Algorithm, *Information Sciences*, vol. 179, no. 13, pp. 2232–2248, (2009).
8. Sharma, A., Mathur, S.: Deterministic maximum likelihood direction of arrival estimation using GSA. *International Conference on Electrical, Electronics, and Optimization Techniques*, pp: 415–419, (2016).

Design of a Low-Cost Potato Quality Monitoring System

Ayush Agrahari, Revant Pande, Paawan Sharma and Vivek Kaundal

Abstract The paper reports design and fabrication of a low-cost solution for monitoring food quality. Owing to its widespread popularity worldwide for regular food item, potato has been chosen as an object to be classified according to quality features such as size, shape, surface texture, and color. The system design includes classifier design for potato detection, ROI segregation, and analysis of certain statistical parameter. For the present study, potatoes have been classified as *grade-1* and *grade-2*. Grade-1 potatoes are those which have to be retained while grade-2 potatoes have to be discarded. ARM-based embedded platform has been chosen for implementation. The system performance meets the required specifications.

Keywords Quality monitoring · Classifier design · OpenCV
Raspberry pi · Potato segregation

1 Introduction

In India the system of collection, distribution, storage, and retail of agricultural produce is evolving at a good pace. However, rotten and spoiled agricultural produce can cause various kinds of diseases, making a person vulnerable to food poisoning. There are shopping malls, complexes, grocery chains, and stores, etc., in every nook and corner selling fresh fruits and vegetables. Segregating good quality

A. Agrahari · R. Pande · P. Sharma (✉) · V. Kaundal
Department of Electronics, Instrumentation and Control Engineering, University of Petroleum and Energy Studies (UPES), Dehradun 248007, Uttarakhand, India
e-mail: paawan.sharma@ddn.upes.ac.in

A. Agrahari
e-mail: ayush.agrahari@gmail.com

R. Pande
e-mail: revantpande.v8@gmail.com

V. Kaundal
e-mail: vkaundal@ddn.upes.ac.in

vegetables and fruits are a very labor intensive and time-consuming effort. Various techniques have been discussed for this purpose in [1, 2].

Rotten and spoiled agricultural produce like fruits, vegetables, etc., can cause various kinds of diseases and health problems [3, 4], thereby making a person sick and more vulnerable to food poisoning, etc. A major device or system is most sought after presently which can segregate rotten agricultural produce from the good ones. The present study reports design of a system which can segregate rotten fruits and vegetables using color-based image processing. The importance of this prototype is that it will enable efficient segregation for large-scale facilities for large volumes of rotten fruits and vegetables through image processing. The proposed system can be utilized by fresh food chains across the country, together with the different states and central government too, also in e-mandis, for removal of rotten food produce. The target beneficiaries can be categorized as direct beneficiaries like fresh food chains, government mandis, distribution chains, middlemen involved in the agriculture sector, etc., and indirect beneficiaries could be the end consumers of the outlets or distributary bodies.

2 System Design

Several systems based on ARM-based Raspberry pi-embedded platform have been reported using image processing and analysis [5, 6]. The hardware in present study consists of a flash camera which takes images of the selected fruit or vegetable and sends it to a processing unit (Raspberry pi). This central processing unit performs image processing and searches for any cuts, bruises, black spots, unusual small size, unusual large size, unusual shape, unusual color, etc., of the fruit or vegetable and triggers accordingly to segregate it. A DC-gear motor runs the conveyor on which all this is done. This motor is controlled by the Raspberry pi module via an Arduino unit. The removal of the rotten product is done by triggering a servo motor which has an arm through which it turns to remove the rotten product. Figure 1 shows the training phase of classifier design. Figure 2 shows the implementation of classifier for potato classification.

As shown in Fig. 1, a large number of samples are collected, marked as positive and negative, and then used for performing HAAR training using OpenCV [7, 8]. The output of HAAR training is the classifier, which is an XML file corresponding to object to be detected.

Figure 2 represents the implementation of the system, where the samples taken at appropriate time are subjected to a classifier. The object is highlighted if present in the frame. Then, the object pattern is segregated from rest of the image to perform certain statistical analysis. These techniques prominently include histogram analysis. The potato is graded according to the numeric calculation performed on the cropped portion.

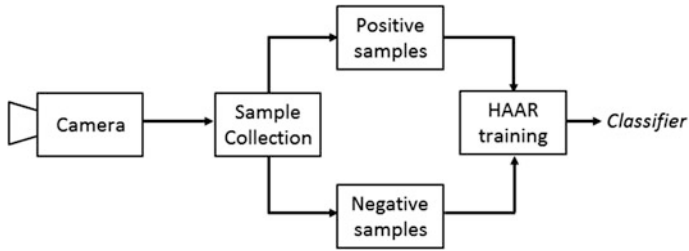


Fig. 1 Training phase

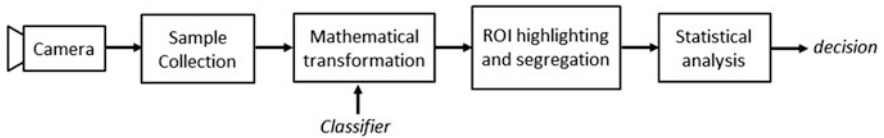


Fig. 2 Design and implementation phase

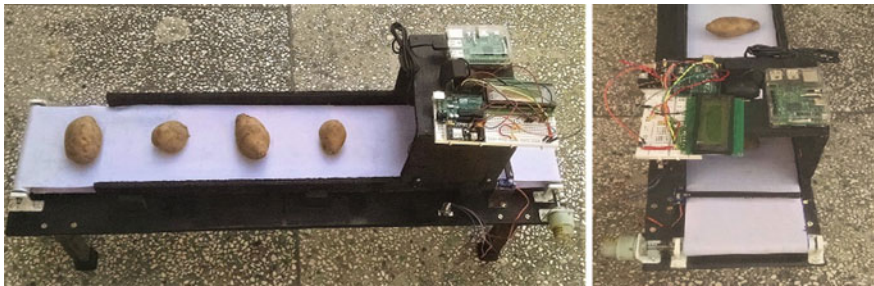


Fig. 3 Prototype design

3 Results and Discussion

Figure 3 shows the prototype design. The setup includes a conveyor belt mechanism fitted with Raspberry pi-based embedded platform. Raspberry pi is provisioned with several GPIO pins, camera input, and wireless connectivity.

Potatoes are fed to the system by placing them on the conveyor belt. This belt moves at a constant slow speed of 1 cm/s. As soon as the potato is detected via specifically designed classifier, belt is temporarily stopped. Figure 4 shows the detection and highlighting of the potatoes. It is to be noted that for better detection rate of potatoes, a black background is used. Then, the object segregation takes place followed by numerical calculations. The analysis is summarized in Table 1.

For testing and performance evaluation, several good and bad quality potatoes are used as shown in Fig. 5. It is to be noted that the size of object is a very important

Fig. 4 Object detection

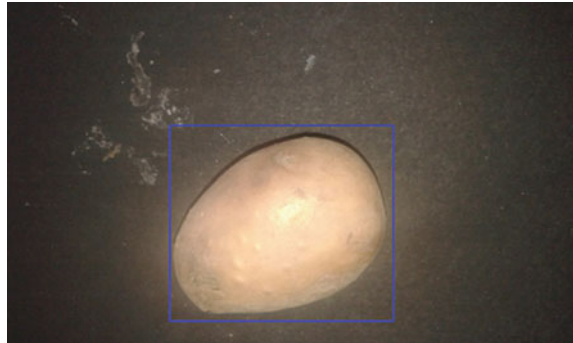


Table 1 Summary of numerical analysis

Sample no.	Grayscale level	Pixel count [A,B]	A/B	Grade
1	[0–55, 56–255]	[511,002, 47,590]	10.73	1
2	[0–55, 56–255]	[507,316, 46,359]	10.94	1
3	[0–55, 56–255]	[533,215, 55,066]	9.68	1
4	[0–55, 56–255]	[520,706, 55,354]	9.40	1
5	[0–55, 56–255]	[525,676, 62,493]	8.41	1
6	[0–55, 56–255]	[521,853, 73,721]	7.07	1
7	[0–55, 56–255]	[504,727, 43,392]	11.63	2
8	[0–55, 56–255]	[432,354, 32,405]	13.34	2

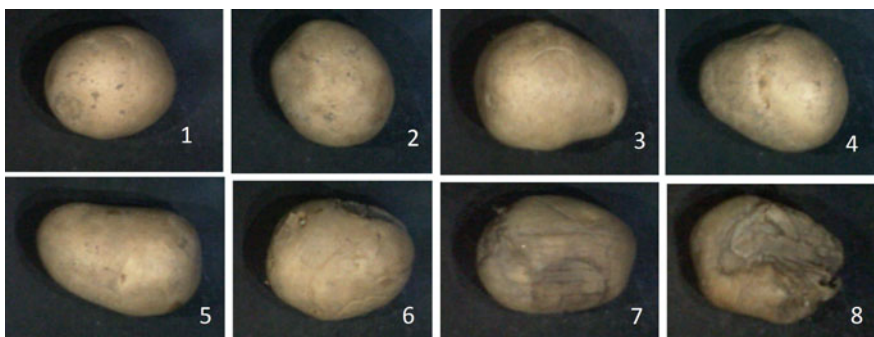


Fig. 5 Potato samples

parameter while designing the classifier itself. Efforts are required to maintain the size of potato almost same. This ensures smooth detection of potatoes.

It is clear from Table. 1 statistics that sample no. 7–8 are bad quality potatoes and possess relatively higher values for ratio A and B. The corresponding images for potatoes are shown in Fig. 5. The higher value can be justified by the increment

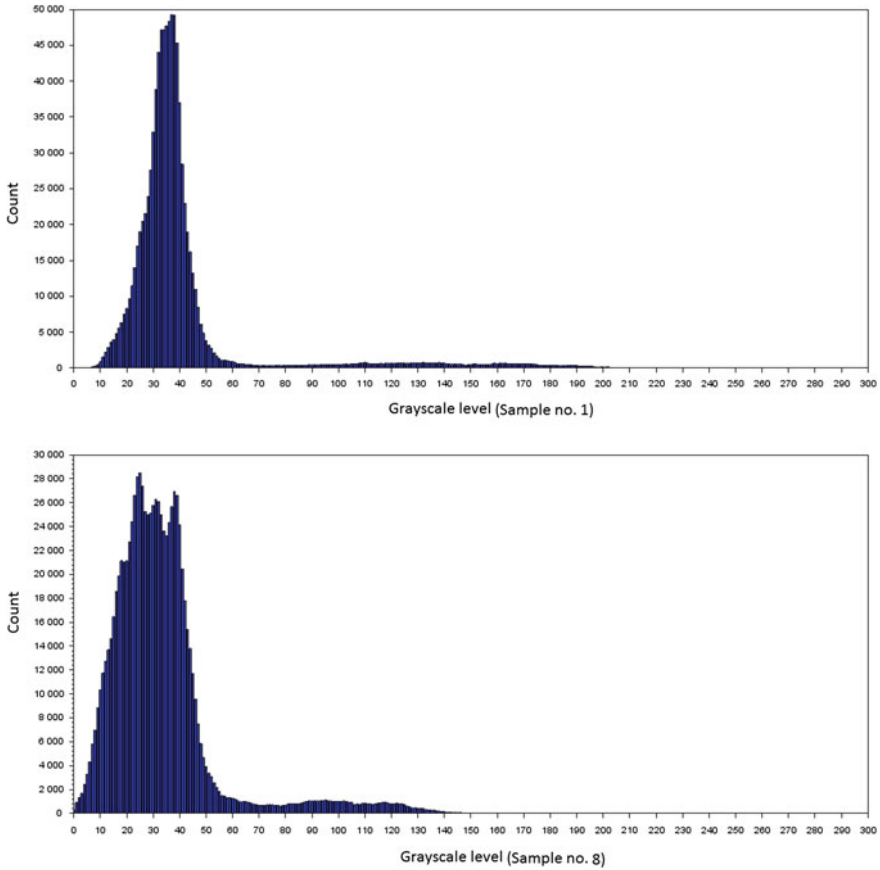


Fig. 6 Histogram comparison for sample no. 1 and 8

in number of pixels toward lower side (darker side). In common view, dark color potatoes are viewed as bad.

Figure 6 shows two histograms corresponding to sample no. 1–8, respectively. These figures explain the differences in numerical figures.

3.1 Program Code

```
import numpy as np
import cv2
pot_cascade = cv2.CascadeClassifier('potato2.xml')
dcap = cv2.VideoCapture(0)
while(True):
```

```

    get, wr = dcap.read()
    pot_im1 = wr
    pot_gr1 = cv2.cvtColor(img1, cv2.COLOR_BGR2GRAY)
    pot_s = pot_cascade.detectMultiScale(gray1, 1.9, 1)
    for (x,y,w,h) in pot_s:
        cv2.rectangle(img1, (x,y), (x+w, y+h), (255,0,0), 2)
        cv2.imshow('img1',img1)
        if cv2.waitKey(1) & 0xFF == ord('q'):
            break
    dcap.release()
    cv2.destroyAllWindows()

```

4 Conclusion

The design and implementation of a potato quality monitoring system was presented. The prototype is a low-cost solution based on ARM-based embedded platform. The software code was written in Python using OpenCV libraries. The system worked efficiently for various samples of potatoes of both grade-1 and grade-2. However, the system requires constant ambient light and object size for better performance.

References

1. Miertuš, Stanislav, Jaroslav Katrlík, Andrea Pizzariello, Miroslav Stred'anský, Juraj Švitel, and Jozef Švorc. "Amperometric biosensors based on solid binding matrices applied in food quality monitoring." *Biosensors and Bioelectronics* 13, no. 7 (1998): 911–923.
2. Rodríguez-Lázaro, D., Lombard, B., Smith, H., Rzezutka, A., D'Agostino, M., Helmuth, R., Schroeter, A., Malorny, B., Miko, A., Guerra, B. and Davison, J., 2007. Trends in analytical methodology in food safety and quality: monitoring microorganisms and genetically modified organisms. *Trends in food science & technology*, 18(6), pp. 306–319.
3. Tewari, G. and Juneja, V. eds., 2008. *Advances in thermal and non-thermal food preservation*. John Wiley & Sons.
4. Fellows, P.J., 2009. *Food processing technology: principles and practice*. Elsevier.
5. Sharma, P., Gupta, M.K., Mondal, A.K. and Kaundal, V., 2017. HAAR like Feature-Based Car Key Detection Using Cascade Classifier. In *Proceeding of International Conference on Intelligent Communication, Control and Devices* (pp. 689–694). Springer Singapore.
6. Wen, X., Shao, L., Xue, Y. and Fang, W., 2015. A rapid learning algorithm for vehicle classification. *Information Sciences*, 295, pp. 395–406.
7. Seo, N., 2008. Tutorial: OpenCV haartraining (rapid object detection with a cascade of boosted classifiers based on haar-like features). available on.
8. Elmer, P., Lupp, A., Sprenger, S., Thaler, R. and Uhl, A., 2015, June. Exploring compression impact on face detection using haar-like features. In *Scandinavian Conference on Image Analysis* (pp. 53–64). Springer International Publishing.

Bionic Functionality of Prosthetic Hand

Shweta Gupta and Adesh Kumar

Abstract This research paper emphasizes on unbelievable functionality of prosthetic hand. Till now, we have studied about prosthetic limbs for the amputees or the war soldiers or the people who have met with an accident, undergone the surgery and got the prosthetic hand. But what about the functionality of prosthetic hand. Can it open and pack your luggage or has an auto-grasp feature that nothing gets tumbled from the prosthetic hand. Is it the sensor technology it is using and if yes, then how it is implemented by the electronic component microprocessor and Bluetooth capabilities using bionics based wearable technology, controlled from smartphone, are the main components of this research paper.

Keywords Prosthetic hand • Bionics • Wearable technology • Bluetooth Smartphone

1 Introduction

Bionics is the development of engineering designs by mimicking nature biological methods. In past, scientists studied the bird flying and developed aeroplanes with the help of various methods available in engineering. In the biomedical field, we come up with the term Prosthesis (plural prostheses) is the replacement of the missing body part by the artificial device which may be lost due to accidental injury, illness or due to any other reason loss of body part takes place. It is basically the rehabilitation process, in which the arm, leg or any other body part is lost, it could be replaced by prosthetic device.

S. Gupta (✉)

Department of Electronics and Communication Engineering, Dr. K.N. Modi Institute of Engineering and Technology, Modinagar, Ghaziabad, Uttar Pradesh, India
e-mail: shwetagupta832000@gmail.com

A. Kumar

Department of Electronics, Instrumentation and Control Engineering, University of Petroleum and Energy Studies (UPES), Dehradun 248007, Uttarakhand, India

The replacement with such artificial limbs not only, helps to improve mobility and usual chores in the daily life. There are wide variety of prosthetic hand, leg and foot available in market. The basic design of the existing prosthetic hand involves:

1. Design of the socket adjusting the amputated limb into it.
2. A suspension wire or holding to hold the amputated limb into it.
3. Shaft to hold the limb.
4. A hand, foot etc. with cosmetic appearance.

The stump is protected with lining of foam or silicone. Special covering of socks are worn on the stump to ensure proper fitting of the stump and improved comfort [1].

Now, if we come down to the explanation of wearable technology, wearables, and fashion technology are a sort of smart electronic devices with embedded microcontrollers that are either implanted or worn on the body. Another most important component of wearable technology is graphene, a thin layer of tightly packed pure carbon atoms in the shape of hexagonal honeycomb lattice. Carbon is not only the thinnest compound known but lightest material and strongest compound discovered and best conductor of heat and electricity and excellent property of light absorption.

2 Working

2.1 Gesture Control

The gesture control feature provides the functionality of moving the prosthetic hand in one of the four directions with the help of preprogrammed grips normally prevalent in practical life with the help of an app as shown in Fig. 1.

App control may provide variety of grips throughout the day. By opening the app on the smartphone, user can select 24 different grips and 12 customized grips to perform different functions of daily routine in your day today life as shown in Fig. 2.

Fig. 1 Gesture control

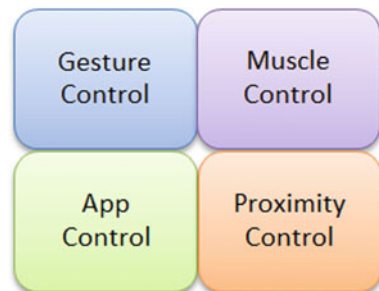


Fig. 2 App control to provide 24 different grips [8]



Index Point



Lateral Grip



Tripod Closed

Fig. 3 Different triggering positions of muscle with smartphone app



2.2 *Muscle Control*

The prosthetic limb uses myoelectric signals, which implies the muscles of the remaining part of the body give directions to move the artificial limb. Above two predetermined muscle sites, electrodes are placed on user's bare exposed skin. Whenever, there is contraction in these muscles, the immediate change in electrical pattern is registered and these signals are sent to microprocessor, resulting in opening and closing of prosthetic limb.

2.3 *Triggers*

The prosthetic limb can opened and closed into several different grips like lateral grip or precision punch as shown in Fig. 3.

Fig. 4 Demonstration of muscle triggers to pack the suitcase



Different triggering positions of the muscle are:

1. Hold open (opening of hand for certain particular time).
2. 'double impulse' (open hand is followed by two quickly open gestures).
3. 'triple impulse' (open hand is followed by three quickly open gestures).
4. 'Co-contraction' (opening and closing both hand muscles simultaneously).

Thus, with the help of above defined gestures [2], person can make any type of grip and perform the desired function as in Fig. 4.

2.4 Nearness Control

Proximity Control is made possible by chip technology in which small Bluetooth enabled devices are there.

2.5 Internal Design

This kind of prosthetic hand is ideal for an individual and each finger has its own motor. This allows fingers to run until the object is firmly grasped. Figure shows artificial limb holding the ball with a grip.

The energy for movement of hand comes from the battery, which is embedded in prosthetic limb. Each prosthetic limb has a unique identifying number depicted around the wrist, near the base of hand as shown in Fig. 5. But, this kind of prosthetic limb is not able to feel things like sweat, shock or heat. In case, lot of force is applied on the prosthetic limb, then it might get destroyed.

And the prosthetic hand is not water resistant, and might get damaged if water is poured on it. To protect the prosthetic hand from carrying load, weight should be evenly distributed at the tips of the hand in Fig. 6.

Fig. 5 Unique identification number on prosthetic hand [8]



Fig. 6 Weight evenly distributed across the hand tips to prevent damage [8]



3 Internal Specifications of the Prosthetic Hand

3.1 Socket Interface and Control

The socket or interface is required fit the prosthetic hand in the remaining hand and electrodes are required sense the brain command to open or close the artificial hand as shown in Fig. 7. The electrical activity given by the brain is picked by the electrode, but this process should not cause pain as shown in Fig. 8.

3.2 Battery Charging

Since this prosthetic limb is run by the battery, so we have to continuously charge it with battery. The amount of charging depends on the use, with no worry about the overcharging of the artificial limb.

The method to charge the arm, is to remove socket and turn the off button. To charge, the time approximately needed for 1300 mAh battery is 90 min and



Fig. 7 Internal specification of prosthetic hand [8]

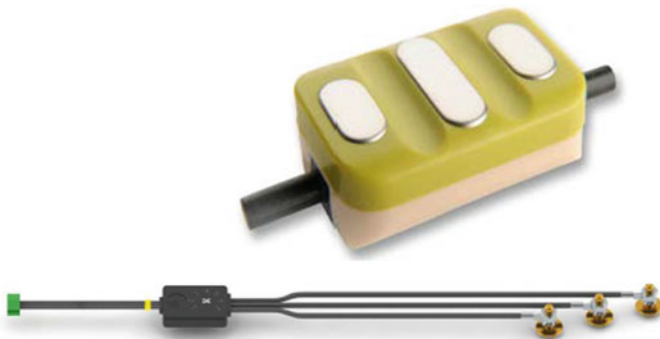


Fig. 8 Socket interface and control [8]

2000 mAh battery is 180 min. The different lights during the display are as follows: Red is for rapid charge, green for fully charge, Solid Amber is for Standby, Rapid flashing amber for error, Slow flashing green is for maintenance, Solid Green for

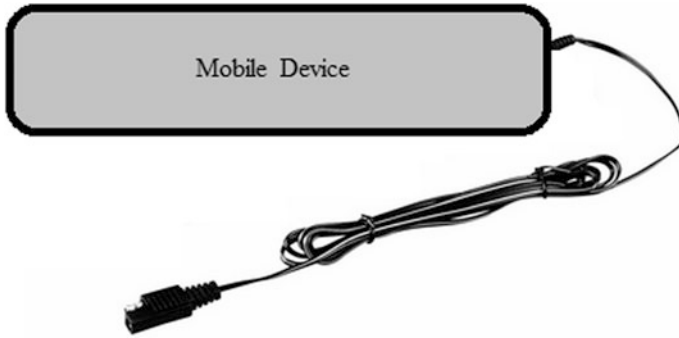


Fig. 9 Battery charger [8]

fully charged. Full discharge charging time is approximately 1300 mAh battery for 180 min and 2000 mAh for 180 min as shown in Fig. 9.

A click should be heard on connection.

3.3 *Bluetooth Capabilities of Prosthetic Hand*

A software program called Bluetooth is needed to wirelessly connect to prosthetic hand from the smartphone. Bluetooth could be used to select various grip patterns and various gestures. The software is loaded in smartphone and handshake signals are sent.

Within 10 meters range, handshake Bluetooth signals will be picked up. On your smartphone, welcome message would pop up after installation. In the app, then the request for inserting handshake request would pop-up. Then the Bluetooth has to be turned on and the indication of turning-on of the prosthetic hand would occur. Then, “connecting to device” would flash and finally, would go to “connect”. If more than one prosthetic device is in the vicinity then all the devices would be in the listed in the app, and correct would be connected.

4 Navigating the App

Once the app is connected, homepage as shown in Fig. 10 appears with four options illustrated. Four options are features, training, hand health and exit (Fig. 11).

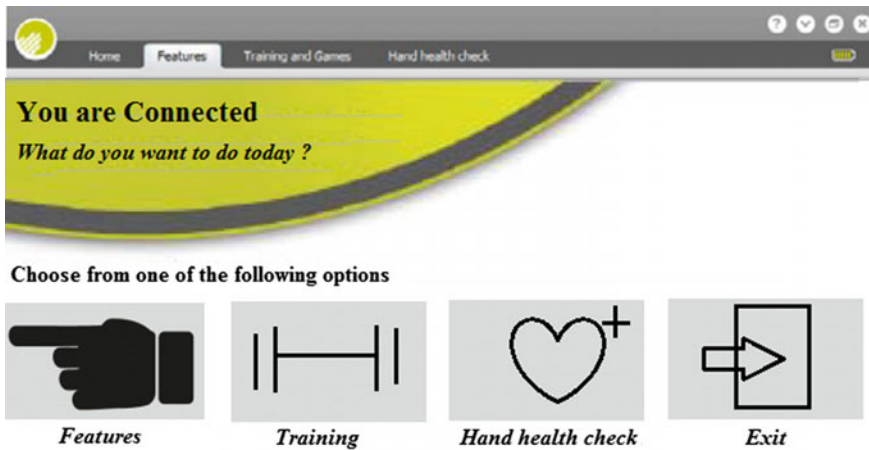
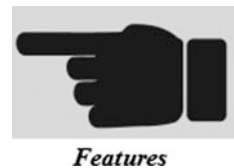


Fig. 10 Homepage of app [8]

Fig. 11 'Features' first icon on the home page [8]



4.1 Features

After selecting the features icon, different icons of hand are displayed, indicating the direction in which hand should move as shown in Fig. 12.

4.2 Training

It helps in the selection of the various grips and custom gestures and training or sending the required signals to the prosthetic hand as shown in Fig. 13.

4.3 Activity Checking

Diagnostic checking of hand for a particular selected gesture is handled by this icon to ensure its proper working as shown in Fig. 14.

Fig. 12 Actual movements of the hand [8]



Fig. 13 This provide various grips features to the prosthetic hand



Training

Fig. 14 Icon for diagnostic checking of prosthetic hand [8]



Hand health check

Fig. 15 Icon for exit from the application [8]

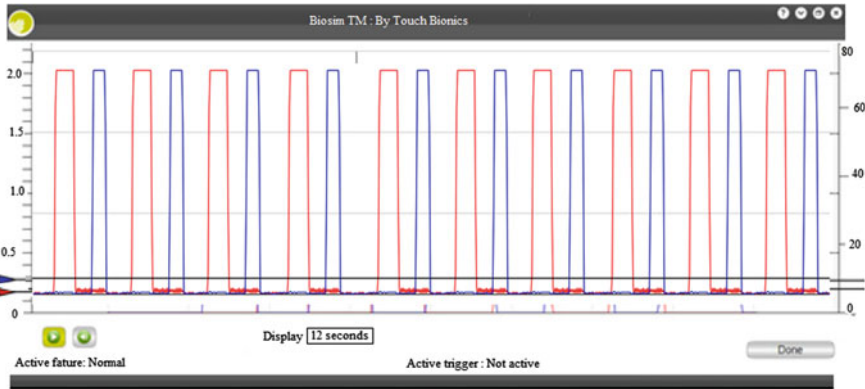
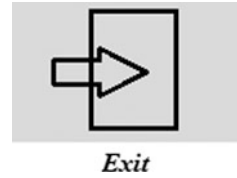


Fig. 16 Real time signals [8]

4.4 Exit

This helps in exiting from the application and from the particular gesture control as shown in Fig. 15.

5 Training

Training involves the variety of exercises for opening and closing of the hand.

5.1 Real Time Signals

Once you have selected the training, the real time signals as shown in Fig. 16 in blue and red help to monitor the movement of hand. Opening of hand is indicated by red signals and closing of hand by blue signals [3]. The strength of the signal is indicated by peak which should be at least half way through.

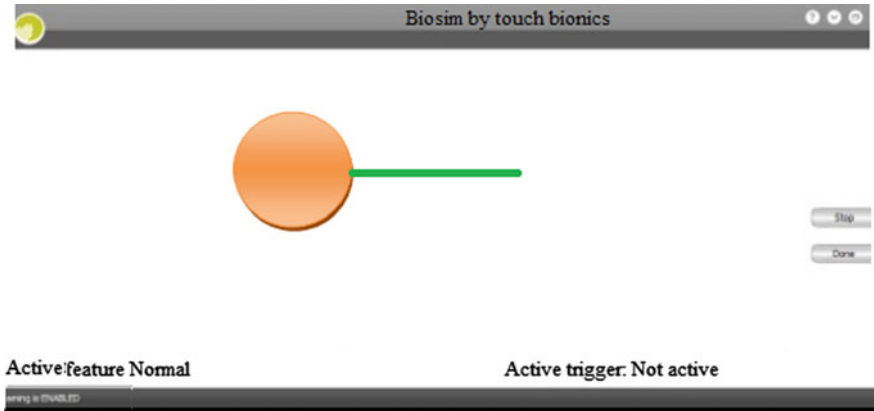


Fig. 17 Strength of signal [8]

5.1.1 Strength and Speed

To indicate strength of signal as shown in Fig. 17, ball is moved above the line and to increase the speed of motion of hand ball is moved on the steep hill again and again [4] (Fig. 18).

5.1.2 Co-contraction Signals

For quick stimulation of muscles, the following exercise of co-contraction involves movement of hand to top of hill [5] at the same time as shown in Fig. 19.

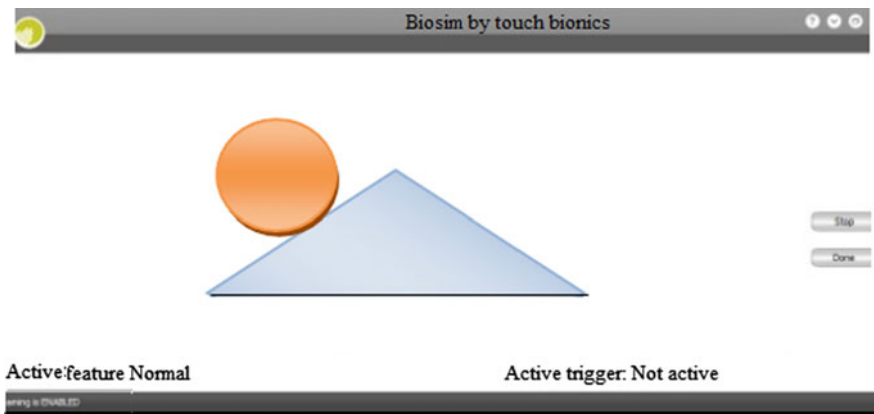


Fig. 18 Speed of signal [8]

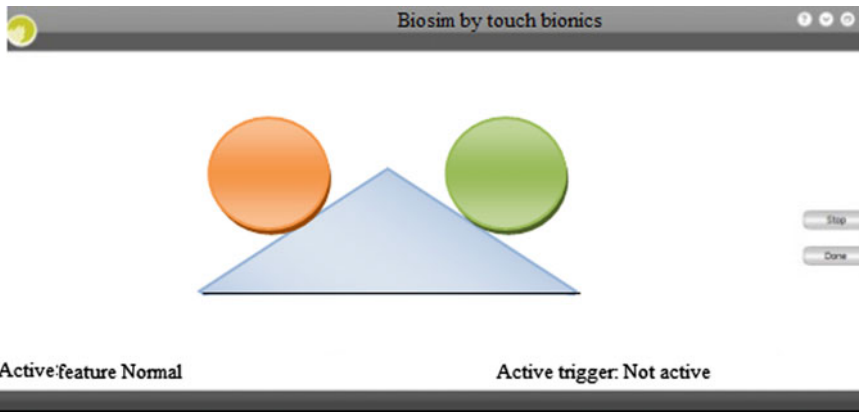


Fig. 19 Co-contraction of hand [8]

Fig. 20 Different coverings for the prosthetic hand [8]



6 Coverings

Different color covering for the prosthetic hand should be there matching the color of the skin [6] and should be protected against wear and tear as shown in Fig. 20.

6.1 Procedure to Put on the Covering

1. The position of the thumb should be 15 mm or 0.6 inches away from thumb as shown in Fig. 21.
2. Pull the plastic cover over the digits as shown in Fig. 22.

Place the covering over the hand and gently adjust it over the fingers [7]. While removing special care should be taken not to put extra pressure on thumb or index fingers as shown in Fig. 23.

Fig. 21 Thumb 0.6 inches away from thumb



Fig. 22 Placing the covering over the hand



Fig. 23 Adjusting the covering over the fingers [8]



7 Conclusion

Thus, prosthetic hand can be made with help of above listed methods and can be trained as the brain trains the human hand and is also given the artificial covering like the real hand.

References

1. M.C. Carrozza, P. Dario, F. Vecchi, S. Roccella, M. Zecca, F. Sebastiani, "The Cyberhand: on the design of a cybernetic prosthetic hand intended to be interfaced to the peripheral nervous system", *Intelligent Robots and Systems*, 2003. (IROS 2003). Proceedings. 2003 IEEE/RSJ International Conference on 27–31 Oct. 2003, ISBN -0-7803-7860-1.
2. Skyler A. Dalley, Tuomas A. Wiste, Thomas J. Withrow, Michael Goldfarb, "Design of a Multifunctional Anthropomorphic Prosthetic Hand With Extrinsic Actuation", *IEEE/ASME Transactions on Mechatronics*, Volume 14, Issue: 6, Dec. 2009.
3. Robert Bouge (2009), "Exoskeletons and robotic prosthetics: a review of recent developments", *Industrial Robot—An International Journal*, Volume 36, Issue 5, pp. 421–427. <http://dx.doi.org/10.1108/01439910910980141>.
4. D.P. Romilly, C. Anglin, R.G. Gosine, C. Hershier, S. U. Rascheke "A functional task analysis and motion simulation for the development of a powered upper-limb orthosis", *IEEE Transactions on Neural Systems and Rehabilitation Engineering*, Volume 8, Issue 4, Sep 1994.
5. M.C. Carozza, B. Massa, S. Micera, R. Lazzarini, M. Zecca, P. Dario, "The development of a novel prosthetic hand—ongoing research and preliminary results", *IEEE/ASME Transactions on Mechatronics*, Volume 7, Issue 2, Jun 2002.
6. A. B. Ajiboye, R. Fff Weir, "A heuristic fuzzy logic approach to EMG pattern recognition for multifunctional prosthesis control", *IEEE Transactions on Neural Systems and Rehabilitation Engineering*, Volume 13, Issue 3, Sept. 2005.
7. Elaine Biddiss, Dorcas Beaton & Tom Chau, "Consumer design priorities for upper limb prosthetics", pp. 346–357, Accepted 01 Oct 2007, Published online: 09 Jul 2009, <http://dx.doi.org/10.1080/17483100701714733>.
8. i-limbTM ultra User Manual on touch Bionics Part number: MA01069: Issue No. 2, March 2013.

Pollution Control by Installation of MQ-Smoke Sensors in Car Exhausts with IOT-Based Monitoring

Abinash Borah, Sandeep Jangid, Amisha Kumari,
Anita Gehlot and Rajesh Singh

Abstract Installation of the smoke sensors in the car exhausts of the personal vehicles can be major step in the pollution control system through which the concentration of the smoke can be calculated with the help of a simple circuit comprising of few electronic components like LEDs, buzzers. Various methods came into action to calculate the release of the CO₂, SO₂ gases with the help of individual sensors. But here, we are using only a single sensor for this, a few electronic components, and GSM module for transmission and IOT. This will keep a regular check of pollution level in individual automobile on a daily basis and set a limit of smoke emission for a particular vehicle and will play a major role in pollution control. The installation of this device will be made compulsory in the near future when the manufacturing of the automobile takes place, thus reducing the risk of pollution. Our system will also increase the use of public vehicles which is again a beneficiary factor for the pollution levels to reduce.

Keywords IOT-based pollution monitoring
MQ2 sensors in car exhausts • Pollution control using sensors

1 Introduction

In the last decade, many systems have been designed for the pollution level monitoring system in the automobiles and factories, since pollution has been a major cause of illness in cities and global warming. Our system is based on the IOT,

A. Borah (✉) · S. Jangid · A. Kumari · A. Gehlot · R. Singh
Electronics Instrumentation and Control, Engineering Department, College of Engineering Studies, University of Petroleum and Energy Studies, Dehradun 248007, Uttarakhand, India
e-mail: abinash.ab1996@gmail.com

A. Gehlot
e-mail: anita@ddn.upes.ac.in

R. Singh
e-mail: rsingh@ddn.upes.ac.in

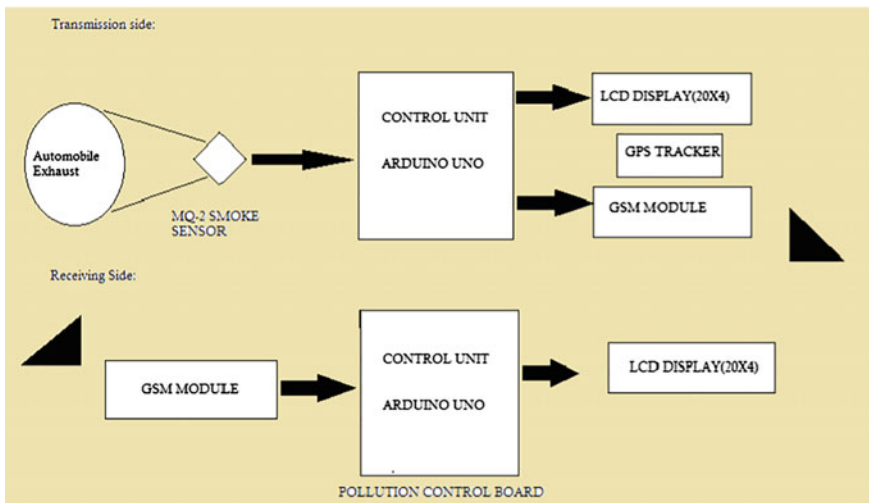
which can monitor the concentration of smoke (in PPM) with the help of MQ Smoke Sensor, a small circuit, GPS tracker, and a GSM module for data transmission which will be installed in the exhausts of the automobiles. This system will be sealed in every personal vehicle which a customer buys, and it shall be implemented newly in the cars at the time of purchase. Depending on the usage of the vehicles like long-distance goods carrier, daily usage for office employees, there will be a limit of PPM level set for each and every personally owned vehicle. As soon as the vehicle reaches the limit of PPM concentration released, it shall receive a note from the Pollution Control Board stating the data limit and his usage shall be reduced accordingly for the day. The pollution control will receive the data through the GSM module installed in the system. For further issues, there will be a GPS tracker installed in the vehicle which will definitely help to locate the vehicle and consult the owner. Thus in this way, if the concentration level of smoke released of each personal vehicle is known and the usage is limited by the help of this system, then the smoke density in the air reduces and the city will be a better place to be in.

2 Related Work

Various other methods are also in existence such as the pollution and emission control system by Neu, Steven W, and Bruce A Bergamn in which there is a catalytic converter which has an inbuilt oxygen sensor which is mounted in the exhaust of the vehicles and a control valve for the connection to the main engine which controls the amount of air supplied [1]. Then, there is wireless sensor network air pollution monitoring system (WAPMS) by Khedo, Kavi K, Rajiv Persedoss, and Avinash Mungur which shows the implementation of the wireless sensor for air pollution monitoring in Mauritius by deploying huge number of sensors in many parts of the island. It uses an Air Quality Index and Recursive Converging Quartiles which is a new algorithm used to merge data to eliminate duplicates and give accurate readings [2]. A wireless sensor network system used to monitor the conditions inside and outside of the building which is programmed to process the signals and give an output in suitable format. Then, the processing of signals takes place by the sensor nodes and the structure of the data is discussed to help to identify the key pieces of information and the data is made to be used. Basically, the research will show the use of wireless sensor networks for the monitoring of buildings [3]. Online GPRS Sensor for monitoring the pollution which has been implemented and tested. The system proposed by Tuan-Duc Nguyen consists of mobile data acquisition and pollution monitoring server, and the MDAQ comprises of a single chip microcontroller with pollution sensors, a GPRS modem, and GPS module. The database server which is created is attached to the server of the pollution to store the pollutants. It reports the real-time pollutants level on a daily basis [4]. An air pollution monitoring system with the help of sensor network to detect air pollution and wireless sensor network system which was based on ZigBee. The performance of the system was estimated in the actual real fields. TOSSIM Simulator was used by Zhou Yushan, Zhang Yiwei,

Chu Linlin, Liu Congning, and Shi Yunbo simulation of Nesc for efficient routing. The paper also makes a move in the digital convergence age by the research and development [5]. A pollution information transmitter with the integration of wireless network by Petite and Thomas which transmits the information on pollution, the nature of the pollution is detected by the use of Trans receivers coupled to the monitoring devices [6]. A participatory system for the monitoring of pollution and controlling it by Mendez and Diego which represents a P Sense system for air pollution monitoring and control by accessing the pollution data of the organizations and address their problems and needs. The Air Quality Index also is known by the help of this system [7].

3 System Description



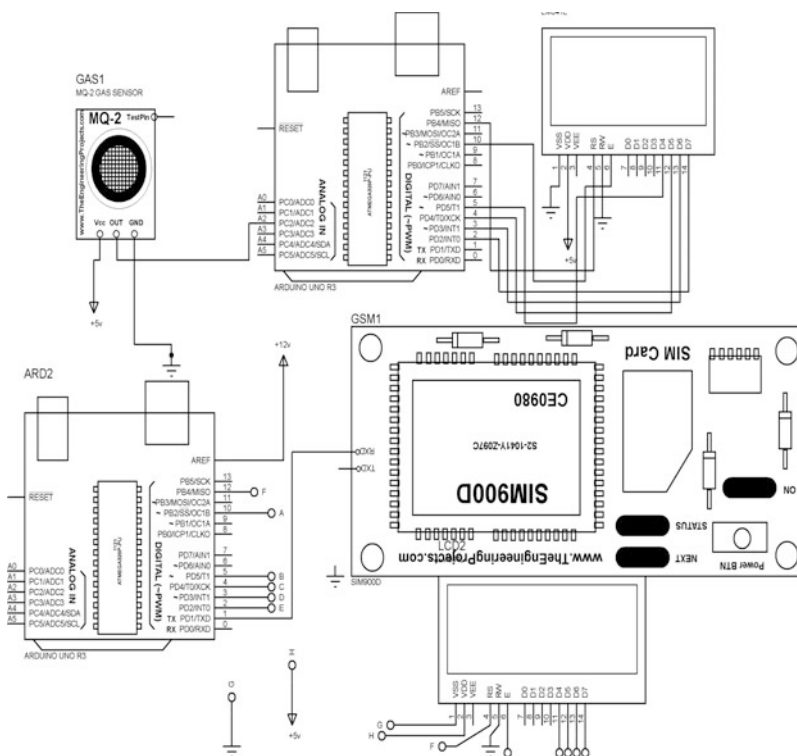
BLOCK DIAGRAM OF THE SYSTEM

As per the Block Diagram shown above, we have the transmission side and the receiving side as per follows.

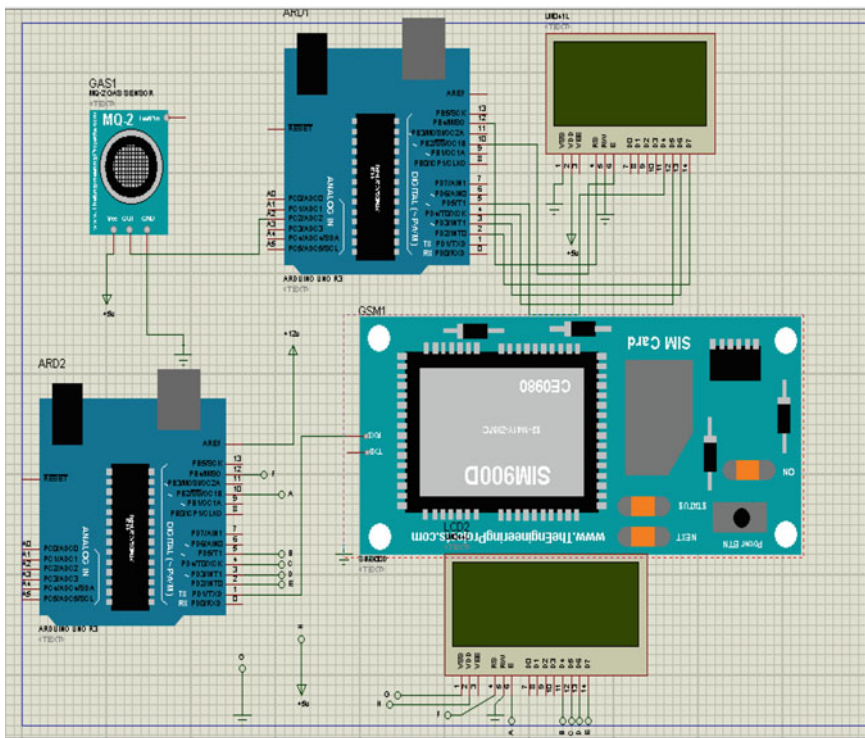
On the transmission side, we have a smoke sensor (MQ-2 Sensor) which is mounted in the exhaust of the personal automobiles which not only detects the smoke coming out of the exhaust but also the concentration of the smoke emitted with the help of a small circuit illustrated below. The circuit comprises of LEDs, a buzzard, and jumpers. The concentration level known to us is in the level of PPM. The data of the concentration is manipulated by the Arduino board and is displayed in a 20 × 4 LED as shown in the figure. The system also comprises of a GSM module which transmits the data from the automobile to the Pollution Control

Board which is on the receiving side. Here in the receiving side also, we have a GSM module which will receive the data and it will be displayed on the LCD. Thus on the basis of the permit of each and every vehicle, there will be a limit given to the vehicles as per daily basis and its concentration level will be monitored accordingly by the board. If a person exceeds the limit of the pollution given to his/her vehicle, he will be getting a warning from the Pollution control database and further actions will be taken based on the activity and the location of the car which will be traced by the GPS tracker attached in default. For further investigation, the local police authorities can be informed about the vehicle. This information of particular vehicles can be obtained on the cloud with the use of IOT, and the owner of the vehicle can easily access the information with his/her credentials.

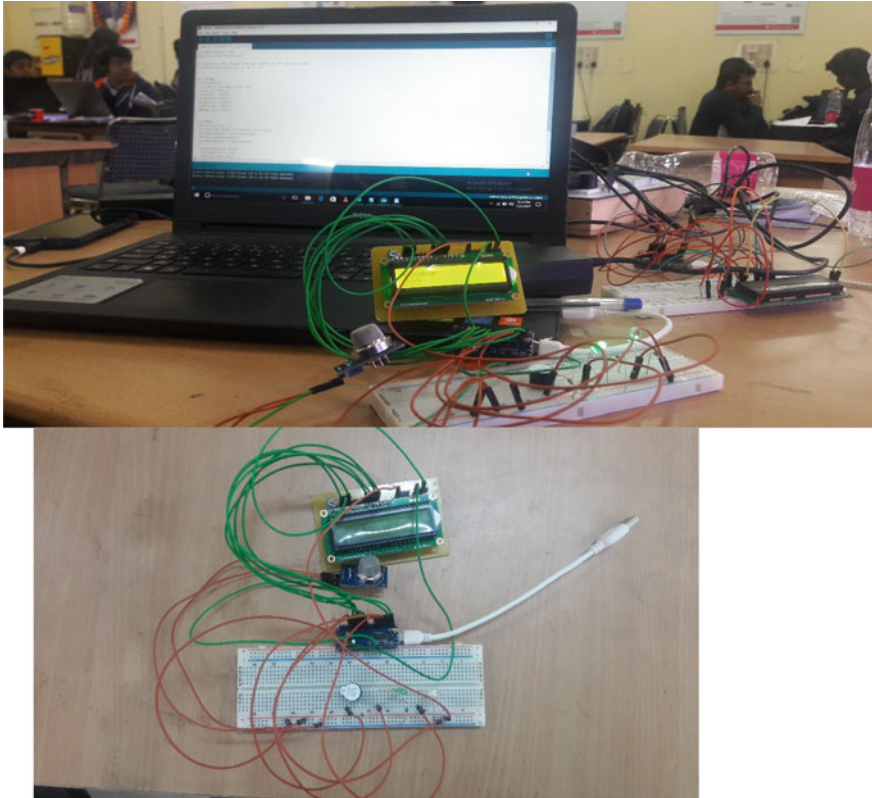
4 Circuit Model



4.1 Proteus Model



4.2 Actual View of the System



The programming part and the actual circuit

5 Result and Conclusion

Though many researchers have come with many systems which have been used to control and monitor the pollution level, our paper shows how the use of few sensors and electronics components can make us note the concentration level of individual personal vehicles and restrict the level of smoke released by them on a daily basis which would not only decrease the harmful gases in the atmosphere. This system in good hands can serve as a benchmark for future pollution control systems and provide drastic changes in the air we breathe. This system will also increase the use of public vehicles. The system can also be implemented in the chimneys of the factories and can help in the pollution control and monitoring.

References

1. Neu, Steven W., and Bruce A. Bergman. "Pollution control system for older vehicles." U.S. Patent No. 5,163,412. 17 Nov. 1992.
2. Khedo, Kavi K., Rajiv Perseedoss, and Avinash Mungur. "A wireless sensor network air pollution monitoring system." *arXiv preprint arXiv: 1005.1737* (2010).
3. Jang, Won-Suk, William M. Healy, and Mirosław J. Skibniewski. "Wireless sensor networks as part of a web-based building environmental monitoring system." *Automation in Construction* 17.6 (2008): 729–736.
4. Tuan-Duc Nguyen, "Energy efficient wireless sensor network and low power consumption station design for an urban water level monitoring system", *Information and Computer Science (NICS) 2016 3rd National Foundation for Science and Technology Development Conference on*, pp. 252–256.
5. Zhou Yushan, Zhang Yiwei, Chu Linlin, Liu Congning, Shi Yunbo, "Research in Automobile Exhaust Gas of Sulfur Dioxide and Nitrogen Dioxide Monitoring WSN and Optimization Coverage Algorithm", *Instrumentation and Measurement Computer Communication and Control (IMCCC) 2015 Fifth International Conference on*, pp. 1202–1205, 2015.
6. Petite, Thomas D. "System and method for transmitting pollution information over an integrated wireless network." U.S. Patent No. 7,424,527. 9 Sep. 2008.
7. Mendez, Diego, et al. "P-sense: A participatory sensing system for air pollution monitoring and control." *Pervasive Computing and Communications Workshops (PERCOM Workshops), 2011 IEEE International Conference on*. IEEE, 2011.
8. Imran, S., and Veeramuthu Venkatesh. "Cost Effective Air Quality Monitoring System Based on Xbee Wireless Sensor Networks." *Indian Journal of Science and Technology* 9.48 (2016).

Bluetooth-Controlled Robot Using Windows Phone Application

Abhay Kumar Gupta, Revanta Tikku, Sumit Kumar, Gaurav Verma and Adesh Kumar

Abstract A robot is basically an amalgamation of both mechanical and electronics working in synchronization which in turn are guided by electronics and computer programming. In this era of globalization and industrialization, robots are being developed and used tremendously in various domains of human life in order to ease their work and provide precision. There are many people who have worked on Android platform along with Arduino, but a combination of Windows app along with AVR Microcontroller is not a common sight. This paper presents the implementation of a robot which is capable of being controlled by a Windows phone application (smartphone) that acts as a wireless remote controller. This remote controller can be interfaced to the Bluetooth module using UART protocol. According to the commands received from the remote controller, robot performs the specified function.

Keywords Windows phone application · Robot · Bluetooth module

A.K. Gupta (✉) · R. Tikku · S. Kumar · G. Verma
Electronics and Communication Engineering, Jaypee Institute of Information Technology,
Sector-62, Noida, India
e-mail: abhay.k.gupta01@gmail.com

R. Tikku
e-mail: revanta.tikku@gmail.com

S. Kumar
e-mail: sumitkr.abit@gmail.com

G. Verma
e-mail: gaurav.iitkg@gmail.com

A. Kumar
Department of Electronics, Instrumentation and Control Engineering, University
of Petroleum and Energy Studies (UPES), Dehradun 248007, Uttarakhand, India
e-mail: adeshmanav@gmail.com

1 Introduction

According to Google, *smartphone is a mobile phone that performs most of the functions similar to a computer, usually has a touchscreen user interface, an access to the Internet, and capable of downloading and running apps* [1]. In the present world, smartphones have become an integral part of human life. A smartphone is capable of doing each and every task similar to a computer. Over the years, there has been a growth in wireless domain and a paradigm of wireless technology is **Bluetooth**. Bluetooth wireless technology was initially created in order to provide a wireless substitute to RS-232 data cables. Bluetooth technology can be used to switch data over slight distances by means of radio transmission [2]. Bluetooth is being used in millions of products from mobile phones, cars to medical devices, and computers. Bluetooth technology allows you to share data such as videos, photos, voices notes, and other information wirelessly between paired devices. Thanks to the ever increase in wireless technologies, that can be easily incorporated in smartphones, there has been an increase in the number of smartphone users. As the app market is mainly dominated by big players like Android and iOS. In recent years, there has been a significant growth in Windows app store as well. Microsoft supports Windows which provide an open-source platform for developers across the globe. In this paper, we put forth a view on how modern day robots can be controlled using our regular smartphones [3]. We are able to move the robot forward, backward, right, and left by using the Windows phone app. The objective of this work is to contribute in the growth of wireless communication with the robots, so that they can be used for welfare and enlightenment of humans. These kinds of robots can prove to be effective in diverse fields like surveillance, household, schools, etc. This can also be used as for educational purposes. It has a simple architecture, so students will be able to build their own robots with custom features and further use them for analyzes and experimentation [3]. There are many people who have worked on Android platform along with Arduino, but a combination of Windows app along with AVR Microcontroller is not a common sight. The following shows the control architecture of the project:

2 Hardware

2.1 ATmega32

Atmel has introduced a high-performance 8-bit microcontroller to the world, the ATmega32. It has RISC-based Harvard architecture. It is a low-power microcontroller which combines 32 KB of programmable flash memory and 2 KB of Static RAM along with 1 KB of EEPROM. It consists of an 8 channel 10-bit Analog to Digital converter. Customized with a JTAG interface for on-chip debugging, the device operates between 4.5 to 5.5 volts and a throughput of

16 MIPS at 16 MHz [4]. The Atmel ATmega32 has a higher performance compared to other microcontrollers which makes it a highly flexible and pocket-friendly solution to many microcontroller-based applications [3]. A better combination of power efficiency along with computing advantage is provided by no other microcontroller in its class. All megaAVR devices offer self-programmability for fast, secure, cost-effective in-circuit upgrades. You can even upgrade the flash memory while running your application. The ATmega32 provides the following standard features: The ATmega32 is a single-chip microcontroller with Harvard architecture that comes with standard features such as on-chip program (code) ROM, timers, and I/O ports [5].

2.2 *HC-05*

HC-05 Bluetooth device consists of a Bluetooth interface module along with an adapter. Bluetooth serial module functions by converting serial port to Bluetooth [3]. The device named after odd numbers can be used to perform both functions: master and slave. Hence, we have used HC-05 Bluetooth module. The default password of an HC-05 is 1234 (in our case). HC-05 is a very user-friendly device. It follows the serial port protocol (SPP) which is used for the wireless connection setup. HC-05 is a version 2.0 product with enhanced data rate (EDR) 3 Mbps Modulation with a 2.4 GHz transmitter and receiver. Developed along the lines of CMOS technology, it has a CSR BlueCore 04 single-chip Bluetooth system [6].

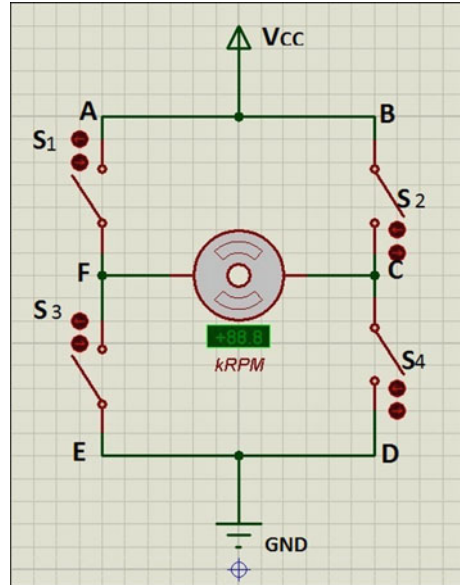
2.3 *L293D*

L293 and L293D are high current drivers. They are based on the principle of quadruple half-H bridge. The L293D is designed for bidirectional movement and have a current rating of up to 600-mA at a voltage range from 4.5 to 36 V [7]. The L293D is a motor driving IC. It allows the DC motors to rotate in either direction, i.e., clockwise or anticlockwise. It is a 16-pin IC that works on the concept of an H bridge which helps it control two DC motors simultaneously in either directions [8].

2.4 *Working of a DC Motor*

Figure 1 shows the controlling of DC motor. It contains four switches S_1 , S_2 , S_3 , and S_4 . There is a V_{cc} and ground connection to it. The motor is constructed in the following manner; if switch S_1 is closed, S_4 also closes automatically. Hence, the circuit AFCD is closed. Thus, making the motor rotate in a specific direction (say clockwise). If S_2 is closed, S_3 also closes, making the motor rotate in the opposite

Fig. 1 Schematic of a DC motor



direction (i.e., in this case anticlockwise). In the project, we have used two motors (i.e., two-wheel drive) in which we have programmed it to work in the following manner:

- For forward movement, all motors rotate clockwise,
- For backward, all motors work anticlockwise,
- To turn right, only the left sided motors rotate, and
- To turn left, only the right sided motors rotate.

2.5 Establishing Serial Communication Between Robot and App

According to Wikipedia, *Serial communication* in telecommunication and computer science is the process of sending data over a communication channel or computer bus sequentially, one bit at a time [9]. Universal asynchronous receiver/transmitter (*UART*) is usually an integrated circuit—most of the times it helps accomplish serial communication over a computer or peripheral devices. It is now commonly included in microcontrollers. ATmega32 has a special register allocated for data handling, called UDR. *Sending Data*—when using the USART for transmission, just writing a byte of data to the UDR register will ensure that your data are sent serially. *Receiving Data*—when using the UART for reception of data, the same register UDR is used to store the incoming data. On detection of a valid start

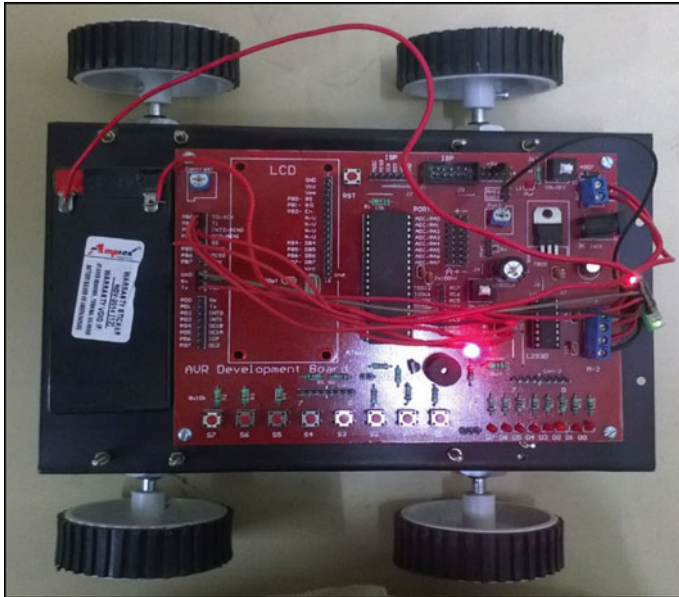


Fig. 2 Robot car top view

bit/start bit pattern, data start entering the UDR register and with the detection of a valid stop bit after the specified number of data bits (during initialization), the UDR register is ready to be read. Since, the UART can behave as either a receiver or a transmitter at a given time, there can be no confusion as to what UDR should contain, at a given instant (Fig. 2).

3 Software

3.1 Windows Phone Application Design

Talking about the software part, the Windows phone application is designed on Visual Studio 2013. The user interface is designed using XAML while the backend is programmed using Visual C#. The algorithm of the app is discussed as follows:

- First of all find all Bluetooth paired devices using *PeerFinder()* method [10].
- List all the Bluetooth paired devices in the *ListBox*, we displayed only three paired devices using *for loop* [10].
- Used *System.Windows.Input* [10] to take touch/gesture input from the user.

- If no item is selected, i.e., *Selected Item*==*null* then display message “No Device Selected! Try Again”.
- Else connect to the selected item.
- Send the command to the selected item using *DataWriter()* [10] as:
 - Forward (*W*) → Hex Code: 57,
 - Backward(*S*) → Hex Code: 53,
 - Left (*A*) → Hex Code: 41,
 - Right (*D*) → Hex Code: 44,
 - Stop(*X*) → Hex Code: 58.

These commands are sent to the microcontroller via Bluetooth module and accordingly the robot performs the specified functions as depicted in Fig. 2.

3.2 Application Instructions

Initially, pair HC-05 Bluetooth module with your smartphone using default password “1234”. Open the App, and select “HC-05” from the list of paired devices. The app interface consists of five button arrows which are “up,” “down,” “left,” “right,” and “stop” which when clicked sends hex codes 57(*W*), 53(*S*), 41(*A*), 44 (*D*), and 58(*X*) to the microcontroller via Bluetooth and the robot moves forward, backward, left, right, and stop, respectively as depicted in Fig. 3).

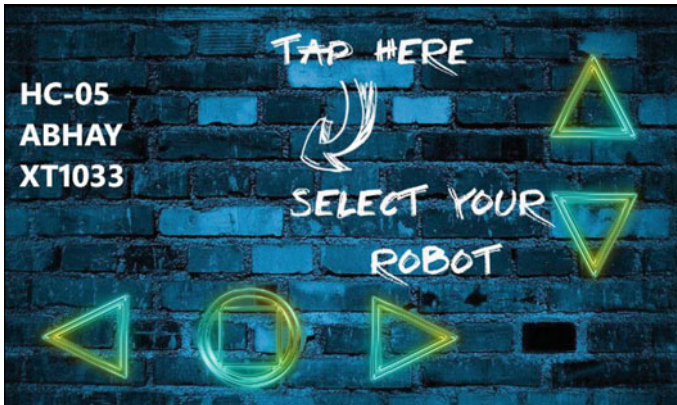


Fig. 3 Bluetooth app to control the robot

4 Conclusion

This research paper will serve as a means for comprehending the intricacies of using smartphone to control physical devices using Bluetooth technology. The system has been successfully designed to monitor and control the robot using Windows Bluetooth-enabled phone and Bluetooth module HC-05 [11]. The microcontroller is used to aid the robot to move in specified directions [12]. The Bluetooth module receives commands from the Windows phone and following the principle of UART protocol, communication among Bluetooth devices takes place. Visual Studio with Windows phone SDK is the platform on which the system was developed, which proved to be immensely efficient and easy to use [13].

References

1. Submitted to Istanbul Bilgi University—Student Paper
2. Bluetooth Fast Facts URL: <http://www.bluetooth.com/Pages/Fast-Facts.aspx>
3. <http://www.ijser.in>
4. Submitted to Universiti of Teknologi Malaysia—Student Paper
5. <http://www.popularmicrocontrollers.com>
6. Bluetooth HC-05 module URL: http://arduino-ua.com/docs/DS_BluetoothHC05.pdf
7. <http://www.electronicengineeringprojects.com>
8. L293D Motor Driver URL: <http://www.rakeshmondal.info/L293D-Motor-Driver>
9. <http://www.cclab13.noadol.com>
10. Bluetooth for Windows Phone 8 URL: <http://msdn.microsoft.com>
11. Sumit Jambhulkar, Aditya Vikram, Sukhbani Kaur Viridi, Priyank Sharma, Khushhali Goel, Gaurav Verma, “Android Application Based Mishap Identification and Warning System” International Journal of Control and Application, vol 9, No.8, pp. 41–48, September 2016.
12. Gaurav Verma et al, “Wireless Position Tracking of a DTMF based Mobile Robot using GSM and GPS” Indian Journal of Science and Technology”, vol 8, issue 17, IPL0161, August 2015.
13. Submitted to Victoria University—Student Paper.

Threshold Sensitive Modified Leach Protocol for Energy Saving in Wireless Sensor Network

K. Shreekant, Parth Sharma, Sindhu Hak and Shuchismita Pani

Abstract In wireless sensor networks (WSN), energy efficiency has been the main concern. Analysis of threshold sensitive modified LEACH protocol has been done in this paper. For the identical amount of initial energy and election probability the number of rounds, which a node lives in threshold, sensitive modified LEACH protocol is to a great extent higher than the traditional LEACH protocol suggested by critical comparative analysis and simulation results. Modified LEACH protocol mainly involves the modified cluster head scheme as well as the dual transmitting power level. The threshold sensitive modified LEACH protocol outruns the traditional LEACH protocol in terms of energy efficiency as shown by the results obtained.

Keywords Wireless sensor · Network · LEACH · Modified LEACH
Election probability · Initial energy

1 Introduction

Wireless networks are the most vital and useful technology, and the history of the WSN, which includes two most important programs namely distributed sensor networks (DSN) and sensor information technology (SensIT), which impact the development of sensor networks [1]. Nowadays, wireless sensor network is becoming popular in the field of research. WSN consists of a several mobile

K. Shreekant (✉) · P. Sharma · S. Hak · S. Pani
Amity University, Noida, India
e-mail: shrikant.k.95@gmail.com

P. Sharma
e-mail: parthsharma2708@gmail.com

S. Hak
e-mail: shak@amity.edu

S. Pani
e-mail: spani@amity.edu

terminals (MOTEs), which spread out them arbitrarily in harsh environment. Sensor nodes that are MOTEs have the capability to sense, process, compute, and also transmitting the information gathered by a specific event and location to the base station [2]. Every MOTEs have one thing in common that is, it comprises of a power source, a microprocessor, and also a low energy radio. Nodes are generally initiated by battery. The battery depletes at a quicker speed generally because of the process such as computing and communication. Due to this consumption of battery at a rapid rate recharging, repairing, and replacing battery becomes a tedious and almost an impracticable job to attain. Considering this case, low energy consumption becomes a key factor in WSN. Energy consumption is a key constraint while developing a wireless sensor system, and heterogeneous models where the difference between the sensors is not only in their available energy but also in their processing capabilities [3]. Another constraint which we need to address before designing a wireless sensor network which will increase the lifetime of WSN and offer the system with better and efficient functioning, is possible through clustering. By assuming the roles in the cluster hierarchy, the nodes in the WSN can be used to operate the actions, which are done before [4].

MIMO or multiple input multiple output has several advantages over single input single output, and one of them is the energy efficiency which it provides. Performance of MIMO's is much superior as compared with SISO, since it offers much higher data rate due to transmission of multiple symbols which use the multiple antennas present in the system. SISO is used in applications like radio, satellite, GSM, whereas MIMO is used for next generation technologies like WLAN-11n, 11ac, 3GPP LTE, etc., Pragmatic implantation of MIMO in a wireless sensor network is not possible because of the size constraint. There are physical limitations in MOTEs due to which it allows WSN to accommodate a single antenna in the transmission process. This specification makes it hard for a definite-sized sensor node to apply MIMO [5]. In order to make such system, there is a virtual MIMO in the WSN, and we require a supportive communication. Because of this, we can implement a single antenna wireless node in a many user environments or an environment where there are more than one users present. The sensor node contributes toward their antenna to attain transmission diversity. The basic idea behind the supportive communication between the various antennas sensor nodes is in the awakening of data theoretic property of the relay channels. We can acquire many advantages of MIMO from cooperative communication and that too without sensor nodes possessing multiple transmitters and multiple receivers, and hence it is known as virtual MIMO (V-MIMO).

To build wireless sensor network energy efficient network, modified LEACH has been projected and is applied. LEACH is the basic clustering protocol and was proposed by W.B. Heinzelman [6]. Some modifications were made in the LEACH protocol and were termed as modified LEACH [7].

Modified LEACH protocol was introduced in order to build cluster and cluster heads. As usage of energy is smaller while transmitting the data over a large area network, this is verified that huge area cooperative is much very flourishing as compared to SISO.

So, we can conclude cooperative communication is essential in order to improve sensor mode battery life, which in return improves the lifetime of wireless sensor networks

2 Modified Leach Proposed Scheme

To understand the scheme, here the study of LEACH protocol is done [1]. At each round, one cluster head is selected by the LEACH protocol. Once a node is being selected from the cluster, it is then not selected for the next ($1/P$) round in where the cluster head is getting formed, where ' p ' refers to the probability of a node which is going to get selected. So in every round, the cluster head is changing. Once selected cluster head is chosen, the next cluster head checks the energy before the new cluster head is getting formed. So a threshold value is set and if the present cluster head node has greater energy than the desired value left then it will stay as the cluster head. But if the energy is less than the energy of the threshold value, a new cluster head is chosen in the following round with LEACH protocol. With this, we can save energy in the proposed threshold sensitive modified LEACH protocol. We are saving this energy because the cluster head is not changing at every round. The LEACH protocol offers same amplification energy for all nodes, but here we are using dual transmitting power levels and with its help, we are able to use different types of modes of transmission like inter cluster transmission, intra cluster transmission, and cluster head to base station transmission method. The different types of modes, which are being used for transmission solely, depend upon the nature of transmission. If we tend to use different levels of power, it ends up saving more energy.

This flow graph shows threshold sensitive modified LEACH protocol is given in Fig. 1.

Figure 1 shows the flow graph of a modified LEACH protocol. In accord with the protocol, every round cluster head will not change. New cluster head is created among remaining nodes only when it spent much energy amid its residency. Again, we apply here hard and soft thresholding (HT & ST). For HT sensed value (sen.v) is more than threshold value (TH), and new sensed value is higher than sensed value of the HT for ST.

3 Results and Observations

Reproductions are directed utilizing MATLAB and to get exact plots, certainty interim is taken. Reproductions show that modified LEACH performs better considering measurements of system lifetime. The comparisons have been made between modified LEACH and the traditional LEACH, on the basis of election probability and initial energy variation.

Fig. 1 Flow graph

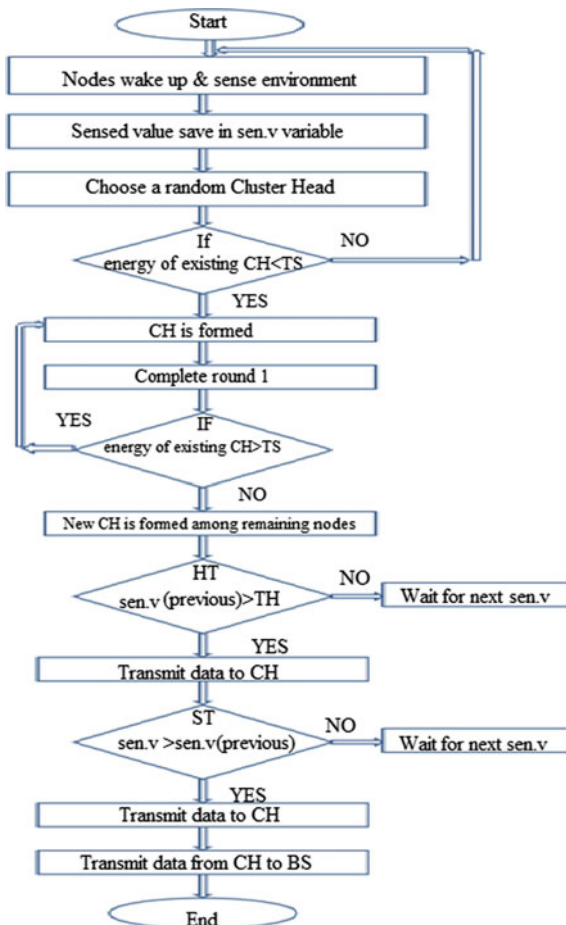


Figure 2 shows that the election probability of a sensor node increases and becomes a cluster head, and number of rounds also increases in the modified LEACH protocol. So modified LEACH protocol gives enhanced performance than LEACH protocol.

The detailed comparison of the performance of modified LEACH in comparison to traditional is given in Table 1, which shows the number of rounds with respect to the election probability. It clearly indicates that the performance of modified LEACH protocol is much better than the traditional LEACH protocol.

In Fig. 3, it analyzes initial energy utilization with expanding number of nodes in the system and depicts modified LEACH expands the framework lifetime, since the number of increase in nodes corresponds to the starting energy of the sensor node for the MODLEACH and is significantly more than the traditional LEACH technique (Table 2).

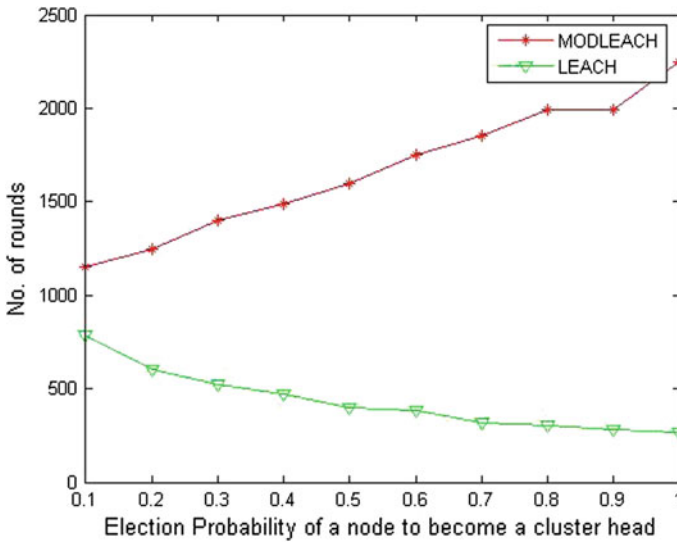


Fig. 2 Election probability variation with number of rounds

Table 1 Number of rounds with respect to probability

Probability	No. of rounds	
	LEACH	MODLEACH
0.1	785	1150
0.2	606	1250
0.3	525	1400
0.4	471	1490
0.5	398	1600
0.6	382	1750
0.7	318	1850
0.8	304	1990
0.9	282	1990
1.0	264	2250

4 Conclusion

Wireless sensor network is in exploration phase. In this paper, critical comparative analysis of proposed modified threshold sensitive modified LEACH is done in comparison to traditional LEACH. It is shown that for the same election probability, the number of the rounds performed by the node is proposed threshold sensitive modified LEACH is approximately 65.4% more, than the traditional LEACH (at election probability is 0.5).

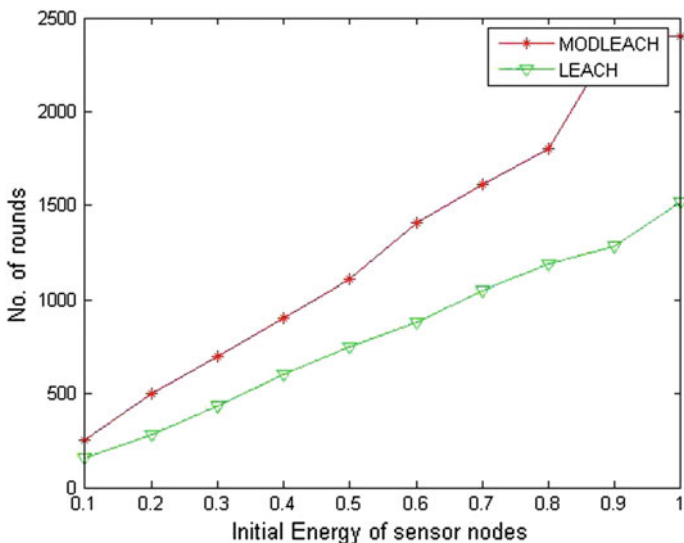


Fig. 3 Initial energy variation with number of rounds

Table 2 Number of rounds with respect to initial energy

Initial energy	No. of rounds	
	LEACH	MODLEACH
0.1	154	250
0.2	285	500
0.3	432	700
0.4	602	900
0.5	747	1110
0.6	878	1410
0.7	1047	1610
0.8	1188	1800
0.9	1286	2390
1.0	1520	2400

When the initial energy of sensor nodes is varied, it is observed that for the same amount of initial energy the life of nodes in proposed threshold sensitive modified LEACH is more. As the number of rounds conducted by a node in proposed traditional LEACH (at initial energy is 0.5). Hence, the proposed threshold sensitive modified LEACH protocol outperforms the traditional LEACH. It is clearly indicated that it will result in energy saving.

References

1. C. Y. Chongand, S. P. Kumar, "Sensor Networks Evolution, Opportunities and Challenges", Proceedings of the IEEE, pp. 1787–1792, 2003.
2. Mahmood, D., et al, "MODLEACH: A Variant of LEACH for WSNs," Broadband and Wireless Computing, Communication and Applications (BWCCA), IEEE, pp. 158–163, 2013.
3. Duarte-Melo Enrique J, Mingyan Liu, "Analysis of Energy Consumption and Lifetime of Heterogeneous Wireless Sensor Networks", Procof IEEE Globecom, Taipei, Taiwan, pp. 21–25,2002.
4. L. M. C. Arboreta and N. Nasser, "Comparison of Clustering Algorithms and Protocols for Wireless Sensor Networks", Canadian Conference on Electrical and Computer engineering, pp. 1787–1792, 2006.
5. M. Younis, P. Munshi, G. Guptaand, S. M. Elsharkawy, "On Efficient Clustering of Wireless Sensor Networks", Second IEEE Workshop on Dependability and Security in Sensor Networks and Systems, pp. 78–91, 2006.
6. Zhang Rui-Hua, Jia Zhi-Ping, Yuan Dong-Feng, "Lifetime analysis in heterogeneous wireless sensor networks", Jilin Daxue Xuebao, vol. 38, no. 5, pp. 1136–1140, 2008.
7. W. R. Heinzelman, A. Chandrakasan and H. Balakrishnan, "Energy Efficient Communication Protocols for Wireless Microsensor Networks", In Proceedings of Hawaiian International Conference on Systems Science, 2000.

Antenna Array Composed of Unit Cell Resonators

K. Shreekant, Sambhav Jain and Shalini Sah

Abstract The proposed design of an antenna is a novel microstrip antenna array composed of metamaterial structures, in the form of closed ring, and unit cell resonators developed on FR4 epoxy (Dielectric constant = 4.2) substrate, which will operate in the Ku band useful for satellite communication purposes. The use of unit cell resonators allows us to operate at wavelengths of 2 cm or 20 mm, which is much larger than the diameter of the outer circle, which is 7 mm of the unit cell structure. The feed is directly connected to the four of the left-handed metamaterial structures' circular ring resonators. The solution frequency has been set at 15 GHz for optimum performance. The proposed antenna has a gain of 5.67 dB and the return loss of -26.33 dBi with a bandwidth of 1.2 GHz from 15 to 16.2 GHz. The design and the properties of this particular antenna have been studied and performed using the HFSS software, and the results have been compared with vertical array antennas placed at the center and the right side of the substrate.

Keywords Microstrip antenna · Metamaterial · Unit cell resonator
Left-handed material

K. Shreekant (✉) · S. Jain · S. Sah
Amity University, Noida, India
e-mail: shrikant.k.95@gmail.com

S. Jain
e-mail: sambhavjai94@gmail.com

S. Sah
e-mail: sshah@amity.edu

1 Introduction

The growth of wireless communication and the number of applications based on it have been explosive over the past decade. This rapid rate, which includes everything from Web browsing to live video, is now at our fingertips, and we cannot imagine even a day without the wireless communication of any form. One of the most important parameters for wireless communication is an antenna. An antenna is basically a device that is used for transmitting and receiving radio frequency (RF) signals. Some of its salient features of an antenna include impedance matching. There should be impedance matching in the antenna. Another feature is that the antenna should be capable of transmitting and receiving only the desired signals and should be able to block all other signals. The gain of an antenna should be as high as possible. The radiation pattern is basically a graphical representation of the electric and magnetic fields radiated by the antenna in theta and phi coordinates. Radiation pattern may be unidirectional, bidirectional, or omnidirectional. Another important property of an antenna is its return loss, which is the magnitude of S_{11} versus the frequency [1]. Metamaterials are those materials, which are structured artificially and provide electromagnetic properties not usually encountered in nature [2]. Some of the applications of metamaterials allow for the use in imaging apparatus, planar light wave circuits, etc. They can also be used to improve the antenna's directivities [3]. Radio frequency identification (RFID) can also be used to establish a communication between a reader and an electronic tag. Left-handed metamaterials are used to improve the permeability and permittivity since their values are simultaneously negative [4, 5], where the E, H, and k form a left-handed system and the gain of the antenna is significantly improved [6]. Next-generation wireless devices will not meet the requirements of the ever-increasing demand for wireless communications, so instead of using one antenna, an array of antennas can be used, which will usually exist side by side in small space while on the other hand also preserving their low coupling support. Now, the array of antennas can be metamaterial phased arrays [7] and impedance matching is necessary for any wireless communication. Now, the array of metamaterial structures can be of any size and shape, and to increase the gain of circular waveguide structure, metamaterial antenna array is used [8].

We have come up with a metamaterial array antenna consisting of four unit cell resonators, on the left-hand side [9, 10]. Wireless communications have a need for low-cost, miniature size, and simple structure antennas, and coplanar waveguide fed antennas meet this requirement, since they provide large bandwidth, which is the most important parameter, but on top of that they have a singular metallic layer and are simple enough to fabricate [11]. The design of the unit cell resonator is based upon the structure resulted from three discontinuous resonant bands.

In this paper, this single-cell resonator is used to create the mentioned antenna in this paper, which consists of an array consisting of four such unit cells connected

vertically, which improves the parameters of the antenna greatly. Comparison of the proposed structure has been done with other experimental structures, but the vertical array antenna yields the best results.

2 Antenna Design and Geometry

2.1 A. Proposed Antenna and Unit Cell Design

The design of the antenna has been divided into two parts.

The first part involved the design and the simulation of a single circular antenna or a unit cell resonator. It has been developed on FR4 epoxy substrate with relative permittivity of 4.2. It consists of 6 different circles, with different radii, which are decreasing in descending order. The outer most circle with radius 3.5 mm is connected to the feed of the antenna (Figs. 1 and 2).

The equations for the design of the unit cell resonator are given as follows:

$$f_{\text{circular_nm}} = \alpha_{\text{nm}} / 2\pi r (\epsilon\mu)^{1/2} = \alpha_{\text{nm}} c / 2\pi r (\epsilon_r \mu_r)^{1/2} \tag{1}$$

$$f_{\text{gcircular_nm}} = 2\pi r / \alpha_{\text{nm}} \tag{2}$$

here in the two equations,

- $f_{\text{circular_nm}}$ —resonant frequency (of the disk resonator);
- $f_{\text{gcircular_nm}}$ —guided wavelength;
- α_{nm} —Bessel function (derivative m th zero having n order);
- r —circular disk radius;
- c —speed of light which is equal to 3×10^8 [11].

Fig. 1 Unit cell resonator

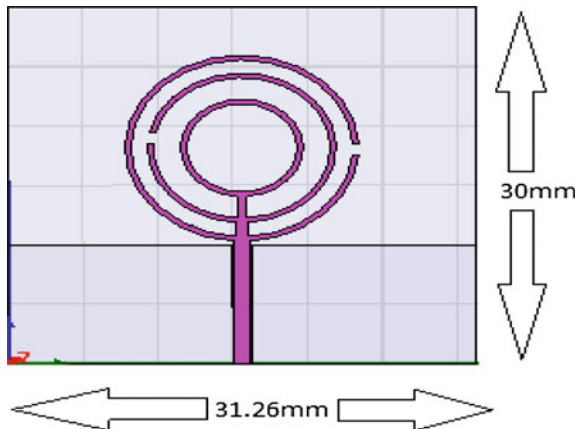
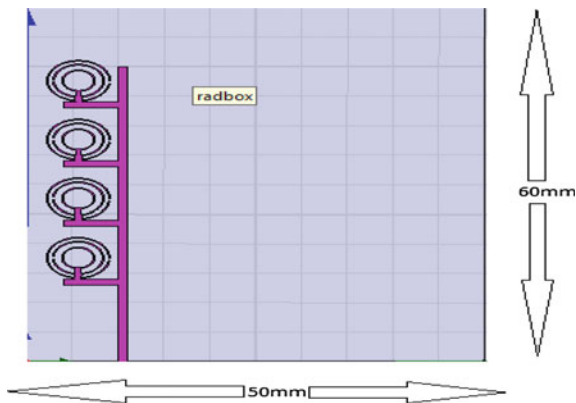


Fig. 2 Geometry of proposed antenna array using unit cell resonators



The dimensions of the unit cell are given in Table 1, consisting of 3 ring structures. Now in the paper, we have proposed the ideas of connecting four such circular ring resonators vertically, which are all connected using a single microstrip field. The ground size has been taken as 50×60 mm, for the design of the proposed antenna in this paper, and for the design of the unit cell or the circular unit cell structure, the ground has been taken as 30×31.26 . The substrate material used for the design of unit cell resonator is nonmagnetic FR4 epoxy, which has a corresponding permittivity of 4.2 and loss tangent of 0.02. The property of the FR4, which affects the frequency-dispersive properties, has not been taken into account. While designing the unit cell resonator, the geometrical parameters are kept equivalent for the front and backside.

2.2 B. Different Configurations

Figure 3 shows three different configurations of the array antenna with unit cells arranged vertically. The antenna (i) depicts the proposed structure of the vertical array antenna in the paper; antenna (ii) is the vertical array antenna placed in the center of the substrate; and antenna (iii) is the vertical array antenna placed at the right side of the substrate. The antenna (i), which is the proposed structure, yielded

Table 1 Dimensions of circular ring resonator

Parameters	Computed dimensions (mm)
Radius of outer most circle	3.5
Width of outermost circle	0.17
Radius of middle circle	2.83
Width of middle circle	0.18
Radius of inner circle	1.84
Width of inner circle	0.18

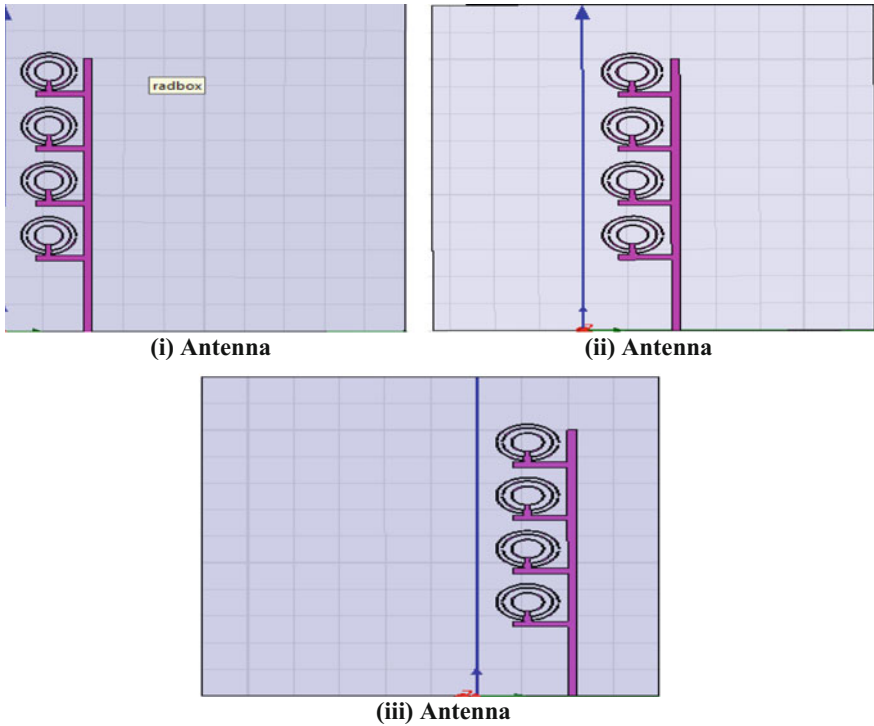


Fig. 3 Different configurations of the array antenna

-10 dB bandwidth of 8% along with a gain of 5.67, whereas the antenna (ii) yielded -10 dB bandwidth of 10% with a gain of 5.0047' and antenna (iii) with 8% with gain of 3.85. The unit cell or the unit cell resonator yielded -10 dB bandwidth of 8.5% which is a bit more than the antenna (i), but the gain is 1.88, which is much less than the proposed structure. For a fair comparison, all the configurations of the antennas were designed on the same conditions. Table 2 contains all the different configurations of the antennas, along with their parameters.

Table 2 Comparison of different metamaterial structures with the proposed structure

	Gain (dB)	Directivity	-10 dB bandwidth (%)
Antenna (i) (proposed)	5.67	10.738	8
Antenna (ii)	5.0047	9.56	10
Antenna (iii)	3.85	7.22	8
Circular unit cell resonator)	1.88	2.22	8.5

Table 3 Comparability of different array structures with proposed antenna

	Directivity	Gain (dB)	-10 dB bandwidth (%)
Antenna (i) (proposed structure)	10.738	5.67 dB at 15 GHz and 1.4 dB at 5.5 GHz	8%
Broadband microstrip antenna with LHM [1]	3	1 dB	63%
Dual-band circularly polarized antenna [3]	Not Specified	6.6 dBic at 920 MHz and 7.9 dBic at 2.4 GHz	3.4% at 908–939 MHz and 7.0% at 2.37–2.54 GHz
Patch antenna with metamaterial cover [2]	16.84	Not specified	Not specified
Circular waveguide antenna with metamaterial structure [8]	Not specified	7 dB	Not specified
Directive patch antenna with metamaterial cover [5]	Not specified	10 dB	Not specified

In Table 3, the likeness of the mentioned antenna has been done with referred papers on the basis of the parameters such as directivity, gain, and -10 dB bandwidth. As we can see, the proposed antenna has a higher bandwidth than the dual-band circularly polarized RFID reader [3] and higher gain than the broadband microstrip antenna with LHM [1].

3 Results and Observation

The parameters, which define the performance of an antenna, are usually the return loss, radiation pattern, gain, VSWR, and directivity. Return loss is characterized as the loss in signal power, when it is being transmitted due to a discontinuity or a disturbance. The directional dependence on the strength of an antenna depends on the radiation pattern.

In Fig. 4, the return loss of proposed design of the circular unit cell resonator is -26 dB. The more the return loss is, the less will be the power, which will get reduced due to discontinuities.

Here, red color represents E field and purple color represents H field. The radiation pattern of the circular unit cell used as a single unit cell for the array has been shown in the first image of Fig. 5. The second image of Fig. 5 shows the radiation pattern of the proposed antenna.

This vertical array was compared with other iterations of the vertical array located in different positions in the substrate. The gain in each of the other two cases was less than the proposed structure when operated at the same frequency of 15 GHz. In Fig. 6, return loss of proposed structure of antenna is being shown as -26.3 dBi. When a signal is returned or reflected by a discontinuity, the power may get reduced. So the more the return loss is, the less will be the power, which will get

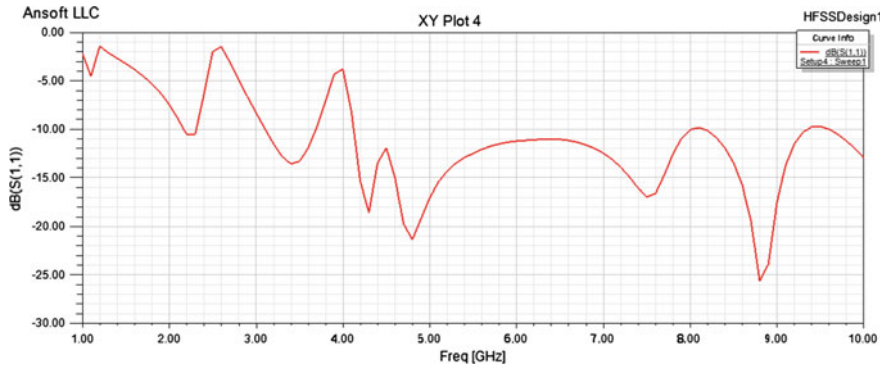


Fig. 4 Return loss of unit cell resonator

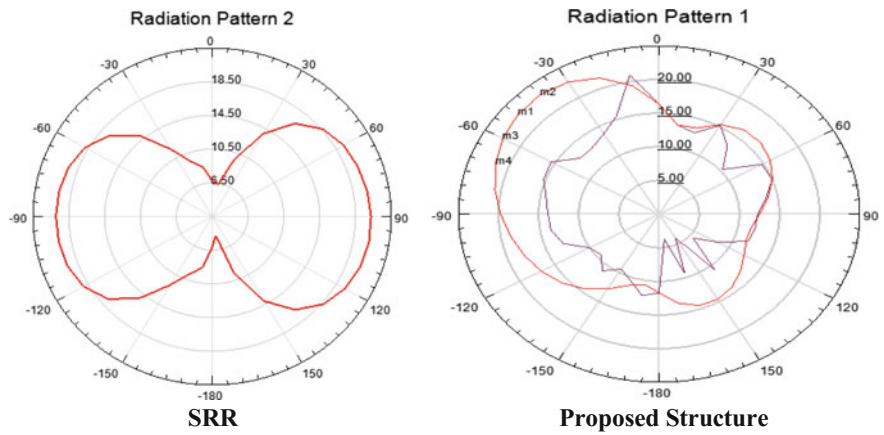


Fig. 5 Radiation pattern of SRR (unit cell resonator) and the proposed antenna

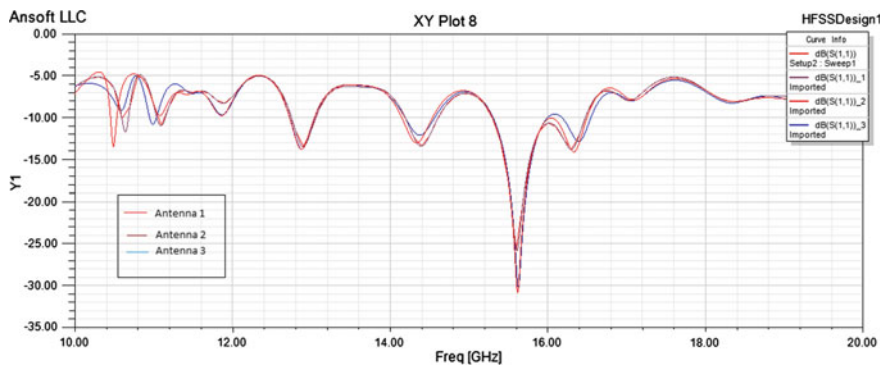


Fig. 6 Return loss of the proposed antenna structure compared with other configurations

reduced. As we can see, the return loss, of the second configuration, i.e., antenna (ii), was obtained as -27.6610 dBi, which is a bit higher than that obtained in the vertical array, at the left side of the substrate, but the gain here obtained is less than the proposed structure. In the third structure of the antenna (iii), the return loss of the right-sided vertical antenna is -31 dBi, but the gain of 3.85 is much less than the proposed vertical antenna on the left side of the substrate.

Figure 7 depicts all the different configurations of the vertical antenna array with their radiation patterns: antenna (i), which is the proposed structure, antenna (ii), and antenna (iii).

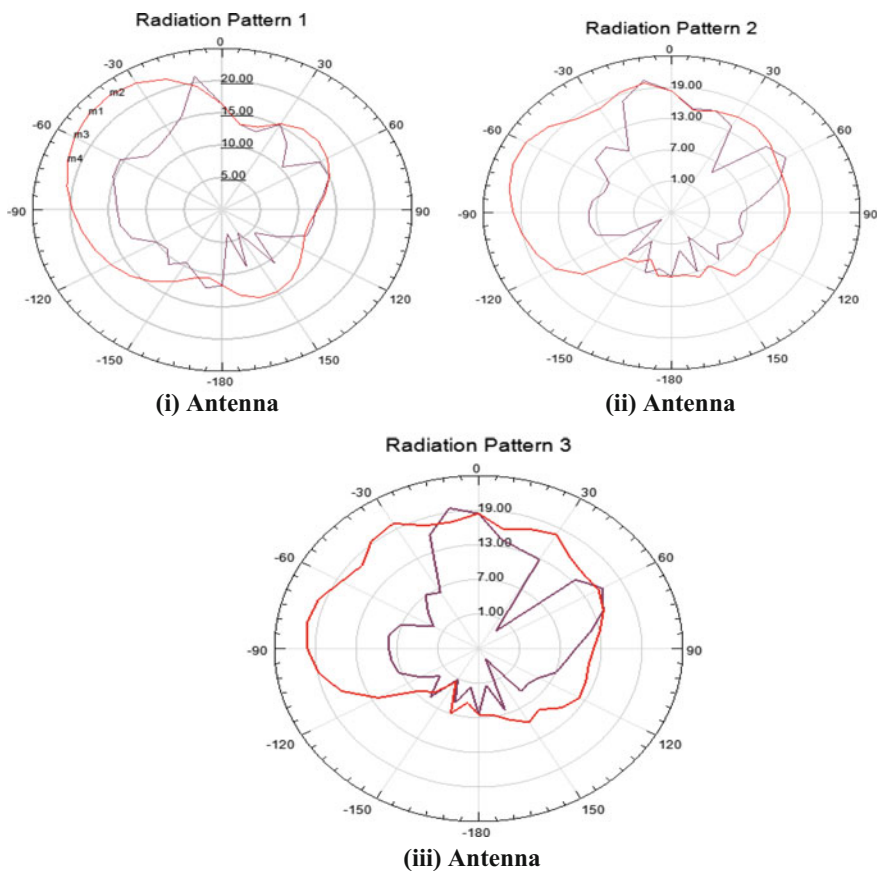


Fig. 7 Comparison of radiation patterns of disparate configurations of vertical antenna

4 Conclusion

A new microstrip vertical antenna array composed of four circular unit cell resonators has been proposed. The simulated results show that the gain of the vertical metamaterial array proposed in this paper is obtained to be 5.67 dB which is very large when compared to the other configurations of the vertical array antenna in which the gain was obtained to be 5.0047 dB in the case of antenna (ii), where the array was in the center of the substrate, and 3.85 dB for antenna (iii), where the array was on the right side of the substrate. The unit cell resonator can further be used for different configurations like horizontal array and various other shapes.

References

1. Merih palandoken, Andre Grede, and Heino Henke, "Broadband Microstrip Antenna With Left-Handed Materials", *IEEE Transactions on Antennas and Propagation*, Vol. 57, No. 2, February 2009.
2. HU Jun, YAN Chun-sheng, LIN Qing-Chun, "A new patch antenna with metamaterial cover", *Hu et al/ J Zhejiang Univ SCIENCE A*, 2006-7(1)-89-94.
3. Youn-Kwon Jung, Bomson Lee, "Dual band Circularly Polarized Microstrip RFID Reader Antenna using Metamaterial Branch-Line Coupler", *IEEE Transactions on Antennas and Propagation*, Vol. 60, No. 2, February 2012.
4. H.A. Majid, M.K.A. Rahim, T. Masri, "Microstrip Antenna's Gain enhancement using left-handed metamaterial structure" *Progress in Electromagnetics research*, Vol. 8, 235-247, 2009.
5. Zi-bin Weng, Nai-biao Wang, Yong-chang Jiao, Fu-shun Zhang, "A Directive Patch Antenna with Metamaterial Structure", *Microwave and optical technology letters*, Vol. 49, No. 2, February 2007.
6. Norberto Lopez, Cheng-Jung Lee, Ajay Gummalla, Macha Achour, "Compact Meta material Antenna array for Long term Evolution(LTE) handset Application", *IEEE Transactions on Antennas and Propagation* 2009.
7. S. Sajuyigbe, M. Ross, P.Geren, S.A. Cummer, M.H. Tanielian, D.R. Smith, "Wide Angle impedance matching metamaterials for waveguide-fed phased-array antennas", *IET Microw Antennas Propogation*, vol. 49, iss. 8, 1063-1072, 2010.
8. Li B., Wu B., Liang C.-H., "Study on High Gain circular waveguide array Antenna with Metamaterial Structure" *Progress in Electromagnetics Research*, *PIER* 60, 207-219,2006.
9. Maria Elena de Cos, Mohamed Mantash, Anne-Claude Tarot, Fernando Las-Heras, "Dual-band Coplanar waveguide-fed smiling monopole antenna for wiFi and 4G long-term evolution applications" *IET Microwaves, Antenna and Propogation*, Vol. 7, iss 9, pp. 777-782, 2013.
10. Chih-Yu Huang, En-Zo Yu, "A slot-monopole antenna for dual-band WLAN Applications", *IEEE Antennas and Wireless Propogations Letters*, Vol. 10, 2011.
11. L.-M. Si, X. Lv, "CPW-fed multi-band Omni-directional planar microstrip antenna using composite metamaterial resonators for wireless communications", *Progress in Electromagnetics Research*, *PIER* 83, 133-146, 2008.

IOT-Based Hydroenergy Generation with the Application of Sensors

Pranjal Chaturvedi, Abinash Borah, Anamika Singh, Abhas and Rajesh Singh

Abstract As we know, hydropower generation in almost every country has been proven as a durable and efficient method of production of electricity, the hydro-power type of power generation is cost efficient and can produce a good amount of electricity in need. Due to its renewability, hydropower serves almost 40% of the total energy production. Our paper is based on how few tanks, pumps, and turbines in an underground system can be used to produce energy with the rapid flow of water from the collector tank above. Basically, for the efficient working of the system, there are few sensors used for the water level check mounted in the tanks and in the pipes, respectively, for the water flow check. The whole system generation is put on the IOT which helps in the monitoring of the power generation. There are voltage and current sensors attached at the end of the system for the current and voltage sensing and marking. Thus, this system with the help of IOT and few sensors attached can give us the adequate data of the power generation

Keywords Hydropower energy production · IOT-based power generation
Efficient power generation · Sensor calibration

1 Introduction

Our system is basically a hydropower generation system with IOT-based data monitoring system which can produce adequate amount of energy by the rapid flow of water from a collector tank which collects water from the rain and many sources.

P. Chaturvedi (✉) · A. Borah · A. Singh · Abhas · R. Singh
Electronics Instrumentation and Control, Engineering Department, College of Engineering Studies, University of Petroleum and Energy Studies, Dehradun 248007, Uttarakhand, India
e-mail: pranjalnc@outlook.com

A. Borah
e-mail: abinash.ab1996@gmail.com

R. Singh
e-mail: rsingh@dd.upes.ac.in

Also, this way the rainwater can also be put to a good use and energy can produce from the rainwater source which is renewable. The main tank which is above the ground level provides a rapid flow down to the underground mechanism of turbine engine which is connected through pipes. Now, here the pipes are responsible for the water flow through the tanks located underground. Each pipe is mounted with sensors which will have the calibration and help provide the information of water flow in the pipes through the Arduino. The concept of the sensors attached in the tanks is basically for the water level indication which will restrict and allow the flowage of water into the tank accordingly when required. Here, the water used for power generation is never wasted but been used again and again to make it more efficient. The whole underground system is separately connected to an Arduino-based system which will comprise of the display and the WIFI modem for the data transmission to the IOT server. The Arduino takes care of the mechanism going on through the sensor calibration in the pipes and the tanks. All the data received is displayed on the LCD. Apart from the sensors in the pipes and tanks, there are voltage and current sensors attached which will sense the power generation accurately in required terms as per the parameter there. Thus, this way the whole information can be transmitted to the server through IOT, and the energy produced is noted.

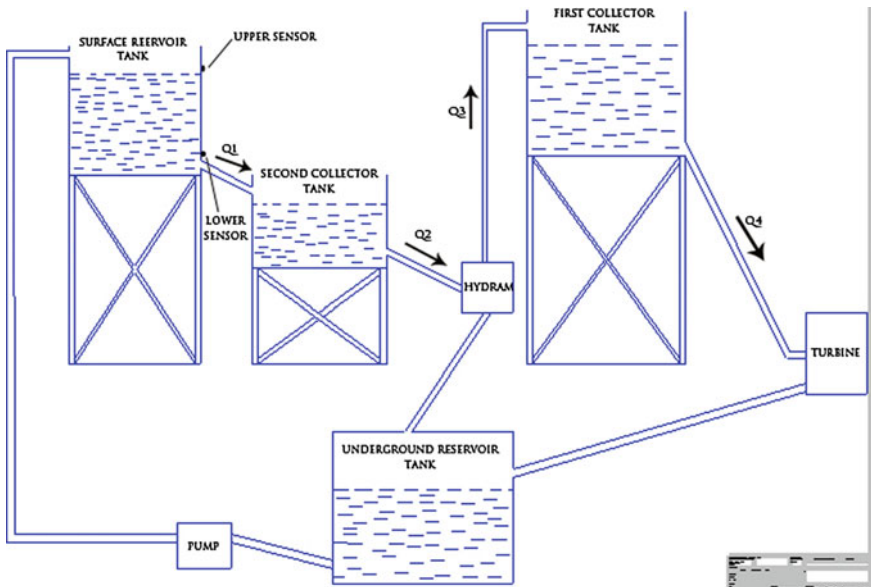
2 Related Works

As we know, the hydroelectric power generation has been used in many cases to overcome the needs of electricity; there are certain methods which also have good power generation through hydroelectric source. Thus, A.A. William set up a system in which centrifugal pumps play a vital role in power generation, which are used as hydraulic turbines due to its production in bulk in many countries. William stated that if the centrifugal pumps can play a role of the combined generator and turbine unit. Hence, this will be a low-cost method to generate electricity in developing countries [1]. A system introduced by M. Mohibullah, A.M. Radzi, and Hakim on the basis of hydropower plants converting potential energy of water into electricity. This hydroelectric power generated water can be used for irrigation facility and many other. Mohibullah and Radzi use MATLAB software for the calculation of the total head, the discharge rate once the capacity of the water is known [2]. Hydropower, however, plays the most important renewable system for electric power generation worldwide. According to statistics, it produces 19% of the electricity of the planet. Oliver Paish believes that small hydropower generation will be a major source for power generation in the country of Europe for the next decade. His paper summarizes the small hydrotechnologies and the new innovations which are being developed and the barrier for the development further [3]. S. Hemann here designs a hydroelectric source of power generation for the villagers to recharge the batteries, which are used by them in their houses for lights and other purposes. His paper throws a light on how the hydroelectric source can be a lifeline

for the villager and plays a major source of power [4]. C.A. Nwosu and Madueme’s paper shows the efficiency of a hydroelectric power generator by using several tanks, few sensors, and pumps to generate the electricity. Basically, there are few tanks which play a major role on producing electricity and collecting rainwater and which has a capability of meeting the requirements of power in the off-rain season. The system can be adapted in the remote locations [5]. S.N. Mohammed shows the efficiency of a hydraulic pump which has the capability of raising, transferring, and also compressing fluid. The hydraulic pump has a good durability which can deliver the water among different sources. Electricity required is zero [6].

3 System Description

Below is a systematic diagram explaining the hydroelectric power generation which is placed below the ground level except for the collector tank which is responsible for the water collection from the sources nearby and mostly rain water. Also, the locations of all the sensors are shown accordingly for correct calibration.

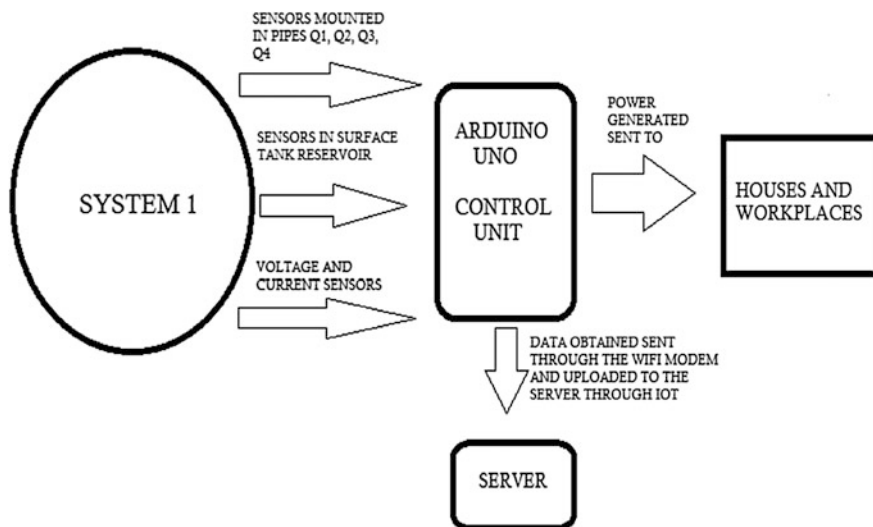


Schematic diagram for Micro-hydropower plant using hydam

As the figure above, the water collected above in the collector tank flow down through the pipe to the turbine below with rapid force due to the long pipe attached there, this rapid flows make the turbine to run and thus through this energy is produced in adequate amounts and is supplied for use. The voltage and current

sensors attached to the RHS of the turbine system gives the amount of power generation in different parameters. The water from the turbine is not being wasted here and is being sent to an underground reservoir tank which is stored and connected to the turbine again to the LHS. As the reservoir tank is filled to a certain level and the sensor mounted in the surface reservoir tank is triggered, the water pump attached to it is used to send the water collected to the surface reservoir tank. The surface reservoir tank as shown above in the figure has two sensors for the water level denotation. Now, when the water is full in the tank the upper sensor triggers, and the pump stops to ensure there is no overflow. The water collected here is again sent to the second collector tank. At the end of the second collector tank, there is a hydram or a hydraulic ram connected which is again connected to the surface collector tank. Thus, the hydram helps to pump the water up to the surface tank and thus the cycle continues.

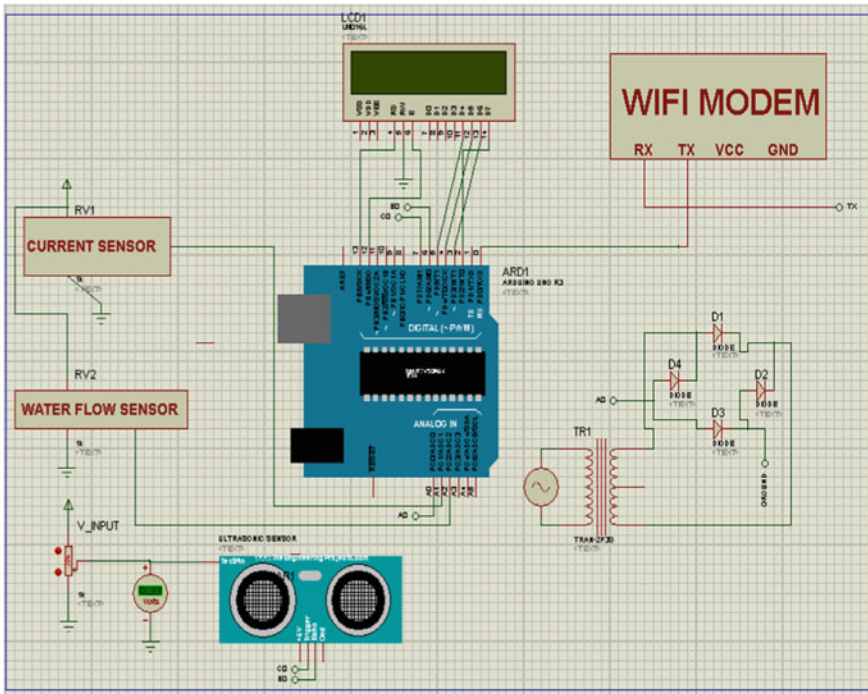
As we can see, there is no point of wastage of water in this system as all the water which makes the turbine run is used again and again and with the help of few sensors mounted on the pipes and the tanks everything is well organized and automated with no issues. The right side of the system comprises of the Arduino, LCD, and voltage and the current sensors which will notify the data of the power generation in parameters, and this data is uploaded on the server with the help of the IOT and transmitted through the WIFI modem. The IOT plays a major role in our system as it displays all the data regarding the power generation as per the work and which is easily feasible.



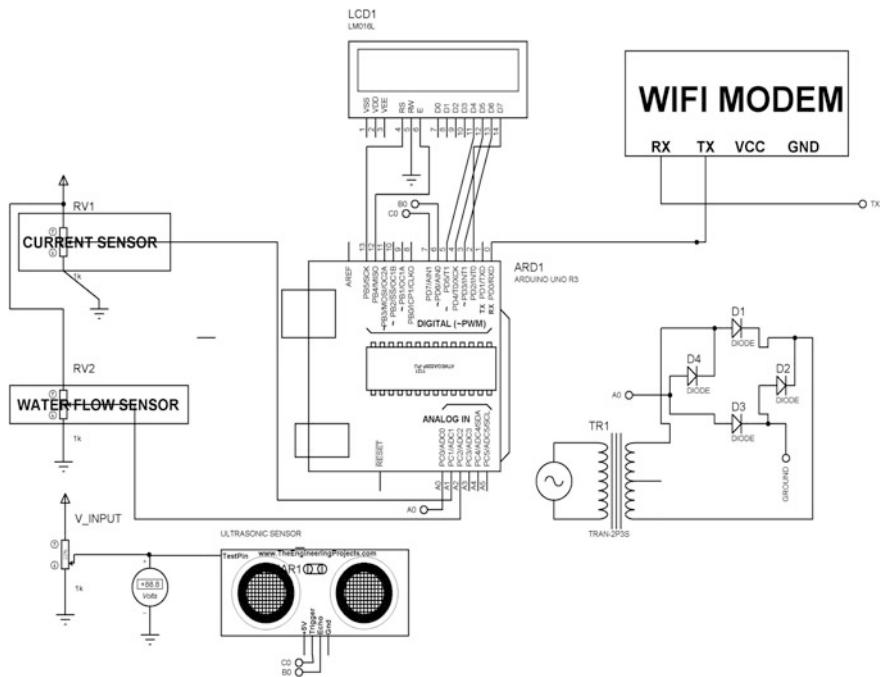
Block diagram of the system

In the block diagram above, the system 1 explains all the reservoir tanks and the control system of the hydropower generation, and the sensor calibration is done through the Arduino and then the data which is obtained is uploaded on the server through IOT and is transmitted by the WIFI modem.

4 Proteus Model



5 Circuit Diagram



6 Result and Conclusion

In the coming future, all the energy production will be done through the renewable sources, and this paper adds as an initiative to that. The system proposed plays an efficient role in the energy production in many factors. It is among the most convenient way of producing energy due to its durability and good work function. The source of energy which is the water used in the production can be used again and again. This way there is nothing to be lost in the system and everything used is well versed with the environment as it is located underground. The energy produced in this system also in adequate level and can be provided to the households easily. The power drawn is detected by the sensors there, and then it is worked out in the Arduino and transmitted to the server through the WIFI modem and also with the help of IOT.

References

1. Williams, A. A. (1996). Pumps as turbines for low cost micro hydro power. *Renewable Energy*, 9(1–4), 1227–1234.
2. Mohibullah, M., Radzi, A. M., & Hakim, M. I. A. (2004, November). Basic design aspects of micro hydro power plant and its potential development in Malaysia. In *Power and Energy Conference, 2004. PECon 2004. Proceedings. National* (pp. 220–223). IEEE.
3. Paish, O. (2002). Small hydro power: technology and current status. *Renewable and Sustainable Energy Reviews*, 6(6), 537–556.
4. Hemann, S. [2006]. Design of a micro-hydro powered battery charging system for rural village electrification (Master Thesis, Carl von Ossietzky University, Oldenburg, Germany). Retrieved from <https://www.researchgate.net/file.PostFileLoader.html?id=56c840c360614b99768b45ac&assetKey=AS%3A331152654127106%401455964353782>.
5. Nwosu, C. A. & Madueme, T. C. (2013). Recycled Micro Hydropower Generation using Hydraulic Ram Pump. *IMPACT: International Journal of Research in Engineering & Technology*, 1(3), 1–10.
6. Mohammed, S. N. [2007]. Design and Construction of a Hydraulic Ram Pump. *Leonardo Electronic Journal of Practices and Technologies*, 6(11), 59.

Active Regeneration of Diesel Particulate Filter Using Microwave Energy for Exhaust Emission Control

Caneon Kurien and Ajay Kumar Srivastava

Abstract The toxic nature of the exhaust gases emitted from diesel engines has led to the development of emission control systems like diesel oxidation catalysis, diesel particulate filtration and selective catalytic reduction. The particulate matter emitted by these engines is found to be carcinogenic in nature. Diesel particulate filter (DPF) is used for trapping the particulate matter which consists of soluble organic fraction and soot particles. The regeneration of these accumulated soot particles is one of the major problems faced in these systems. Active regeneration takes place in the traditional DPF by injecting the fuel to the filter and then initiating combustion by introducing spark. It will lead to uncontrolled combustion causing serious damage to the filter. Electromagnetic waves in microwave region can be used for regeneration of the accumulated soot. Detailed literature survey has been carried out on the application of microwave energy for the regeneration purpose, and an emission control system has been proposed in this paper.

Keywords Catalyst · Emission · Microwaves · Soot · Regeneration

1 Introduction

Environmental pollution caused due to the exhaust gases from the diesel engines has increased to a higher extent. The emission regulations have become more stringent, and the researches are going on to reduce the emissions to the acceptable levels. Pre-treatment techniques like engine modifications and blending of fuel cannot bring down the emissions to required levels. Post-treatment systems like diesel particulate filtration, diesel oxidation catalysis and selective catalytic

C. Kurien (✉) · A.K. Srivastava
Mechanical Engineering Department, University of Petroleum and Energy Studies,
Dehradun, India
e-mail: ckurien@ddn.upes.ac.in

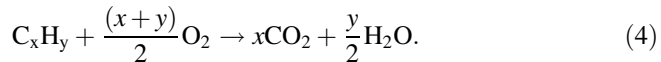
A.K. Srivastava
e-mail: akumar@ddn.upes.ac.in

reduction have to be employed. Oxidation of carbon monoxide, nitrides and hydrocarbons takes place in the diesel oxidation catalyst (DOC) filter. The particulate matter is trapped with the help of diesel particulate filter (DPF). The particulate matter consists of soluble organic fraction and soot particles. These are ultra-fine particles with its aerodynamic diameter in the size range of less than 2.5 μm , and it is also carcinogenic in nature [1]. Diesel particulate filters consist of square channels which are alternately plugged and porous in nature. Exhaust gas passes through these channels, and the particulate matter in the exhaust gases gets trapped in these walls. The soot particles will get accumulated in these channels leading to clogging of filters, and the backpressure will rise reducing the efficiency of the engine. Regeneration of the accumulated soot particles has to be carried out either by using active or passive regeneration techniques. Passive regeneration takes place continuously by the temperature of the exhaust gases and can also be carried out by using some catalysts. But passive regeneration alone cannot remove the trapped soot particles to required extent. Active regeneration technique has to be adopted to remove the accumulated soot. In commercial diesel particulate filters, active regeneration is carried out by injecting the fuel to the filter substrate and then burning it by producing spark. This will result in uncontrolled combustion inside the filter substrate and will also damage the filter reducing the service life of the filter. Microwave energy has been found to be a possible method for active regeneration since it has the ability to penetrate through the filter and also without heating the exhaust gases. The material of the filter has to be selected in such a way that it must have high dielectric properties which will help in absorbing microwave energy. Soot particles are a good absorber of microwave radiations. Combined use of microwave energy and catalysts will help in oxidation of soot at higher reaction rate and lower temperature. An exhaust emission control system has been proposed in this paper, and a model of the system has been designed using SOLIDWORKS $\times 64$. This system will serve as an effective after treatment system for meeting the stringent emission regulations.

1.1 Diesel Oxidation Catalyst Filter (DOC)

The exhaust gases released by the diesel engines consist of carbon monoxide, nitrogen oxides and hydrocarbons. Diesel oxidation catalyst filter consists of a monolith substrate with alumina wash coat in which catalysts are impeded, inlet/outlet lofts and a container housing the entire filter. Platinum is mostly used as a catalyst to promote the oxidation of carbon monoxide, nitrogen oxide and hydrocarbons. A slight portion of soot is also oxidized by these catalysts. It is suitably placed before diesel particulate filter since the oxidation of nitrates can be utilized for passive regeneration of the soot in the particulate filter. Reference [2] carried out catalysis in two stages, where the initial stage includes reduction of NO_x emissions using rhodium catalyst. The final stage is of the oxidation catalyst,

where it reduces the unburned hydrocarbons and carbon monoxide by oxidizing them over platinum and palladium catalyst. Various reactions taking place inside the DOC filter are as follows.



Most widely used oxidation catalysts in DOCs are platinum-based, but it is expensive and also will be poisoned easily by sulphates in diesel exhaust. This has led to the researches for alternative catalysts which can be used for meeting this application, and the results showed that only possible alternative is to dope non-noble metals into platinum-based catalysts. In reference [3], Impregnation method was used for preparing a series of Pt–V/Ce–Zr–O diesel oxidation catalysts with different Pt/V ratios and the effect of vanadium on catalytic activity and sulphur resistance was investigated in detail. The results of the tests showed that Pt–V/Ce–Zr–O with only 1 wt% Pt catalyst showed the highest catalyst performance with vanadium loading of 1 wt%.

At low temperatures especially during cold start, the performance of DOC was found to be low but most of CO and hydrocarbons are produced at this stage. In reference [4], the influence of hydrogen on the oxidation kinetics of exhaust gases was investigated and the results showed that smaller H₂ concentrations are more effective in improving the catalyst light-off temperature as well as promoting NO oxidation. CFD analysis is very much useful in analysis of the designed model and also for conducting simulation along with chemical analysis so that the effectiveness of the proposed model can be determined. Different combinations of chemicals suggested in above literatures can be subjected for chemical analysis and simulation as an initial step before manufacturing the prototype. The equations required for modelling the flow include conservation of mass, momentum and energy. A series of simulations on continuum model was performed in reference [5]. The results of these simulations showed that flow distribution is a strong function of properties like monolith cell density, diffuser angle and aspect ratio. In our previous works, we have conducted analysis of the designed DOC models in ANSYS by considering the flow as k-epsilon turbulence model. The results showed that circular DOC has better flow properties as compared to rectangular-shaped ones due to the reversed flow at the edges. The contours showing variation in pressure drop along the length of the filter for rectangular- and circular-shaped filters are showed in Figs. 1 and 2.

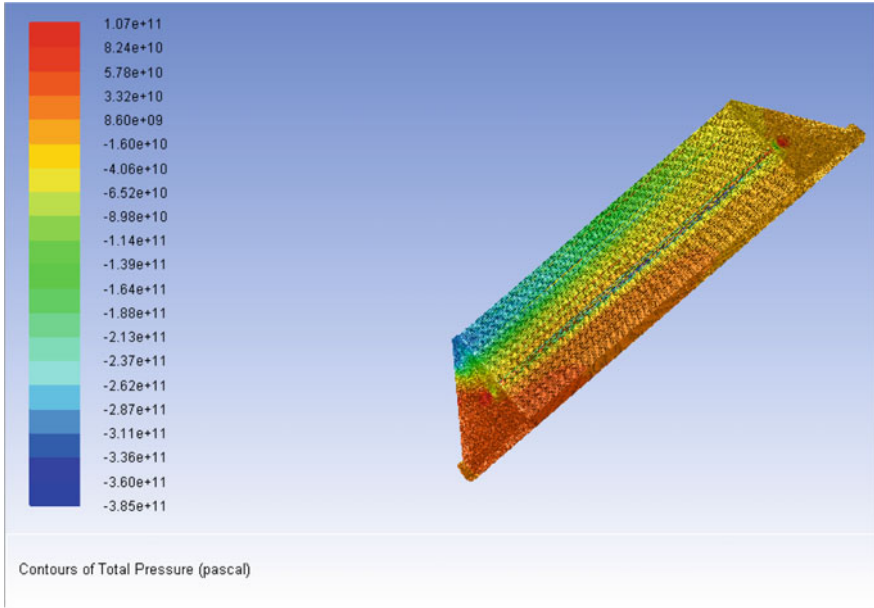


Fig. 1 Contours of pressure coefficient in rectangular-shaped DOC

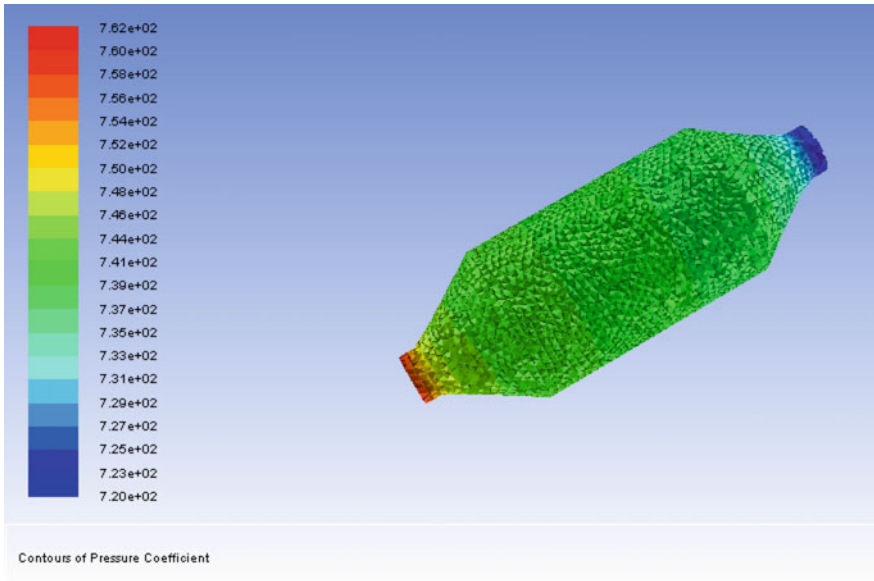


Fig. 2 Contours of pressure coefficient in circular-shaped DOC

1.2 Diesel Particulate Filter (DPF)

Diesel particulate filter has been the most promising technology for removing the particulate matter from the exhaust emissions. Particulate filter has monolith filter substrate with rectangular channels which are alternately plugged, and it is made up of porous material. In this, the particulate matter will be trapped initially and it has to be cleared periodically by regeneration. In traditional DPFs, the regeneration is carried out by injecting fuel into the filter and allowing it to burn the trapped soot particles. But it will result in reduction of efficiency, excessive use of fuel and also may damage the filter due to uncontrolled combustion [6]. This has raised the need for alternative methods for regeneration of soot particles trapped in the DPF.

Microwave-assisted catalytic regeneration has been carried out for biomass boilers in reference [7], where the results showed that the temperature, energy and time required for regeneration can be reduced by simultaneous use of microwave applicator and specially catalyzed DPF. Higher price of noble metals has raised the requirement for an alternative option for catalysts in place of Pt. The results of this study suggested that CePr active phase is a promising candidate for replacing Pt in real applications. Fuel injection strategies also have an effect on emission of particulate matter. In reference [8], the effects of fuel injection strategies on exhaust emissions were studied in detail. The results of the study showed that pre-mixed combustion can be enhanced by increased fuel injection pressure and advanced start of injection which could increase the NO_x emissions. Combined application of fuel injection strategies and DPF will also remove the trade-off correlation between the nucleation mode particles and accumulation mode particles for particulate matter emissions. Regeneration of the soot particles by combined application of microwave energy and fuel additives is called as composite regeneration. Multidisciplinary design optimization of the filter for composite was carried out in reference [9], where the energy consumption and utilization efficiency of the microwave energy were examined.

2 Proposed Emission Control System

An emission control system which is a combination of diesel oxidation catalyst filter and diesel particulate filter has been proposed in this paper. Microwave energy has been suitably considered to be used for regeneration purpose. The material of the particulate filter must have good permeability like ceramic, silicon carbide, etc. which will allow the microwaves to pass through it without heating the exhaust gases (Fig. 3).

The dielectric properties of a material determine its ability to get heated by microwaves. The dielectric constraints consist of real and imaginary components as shown in equation number 5.

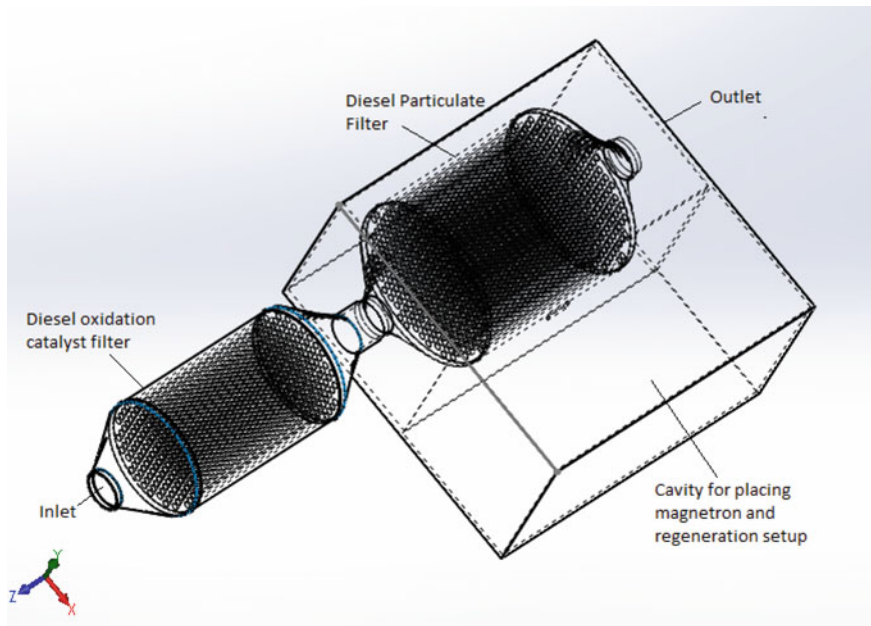


Fig. 3 Model of the designed system with DOC and DPF filter

$$\varepsilon' + j\varepsilon'' = \varepsilon. \quad (5)$$

When the trapped soot particles are subjected to microwave radiations, it gets heated up directly by the microwaves while the cordierite material will get heated up only by conduction or by convection of heat from soot. In the proposed set-up, microwaves are generated by the magnetron and its line diagram is shown in Fig. 4. The values of dielectric constant for different materials are given in Table 1.

The exhaust gas from the diesel engine is directed to the DOC filter, where the oxidation of carbon monoxide, nitrogen oxide and hydrocarbons take place. The nitrogen oxide is oxidized to nitrogen dioxide which promotes the passive regeneration of the trapped soot particles in the diesel particulate filter. It is one of the major reasons for placing the diesel oxidation catalyst before the diesel particulate filter. The diesel particulate filter is encased in a container which has two compartments. Regeneration set-up consisting of magnetron for producing microwaves is placed in one compartment and filter substrate is placed in the other. When the backpressure value goes beyond a certain limit, active regeneration is carried out by directing the microwaves to the filter substrate. The energy consumed by the regeneration set-up and time required for regeneration have to be determined by experiments.

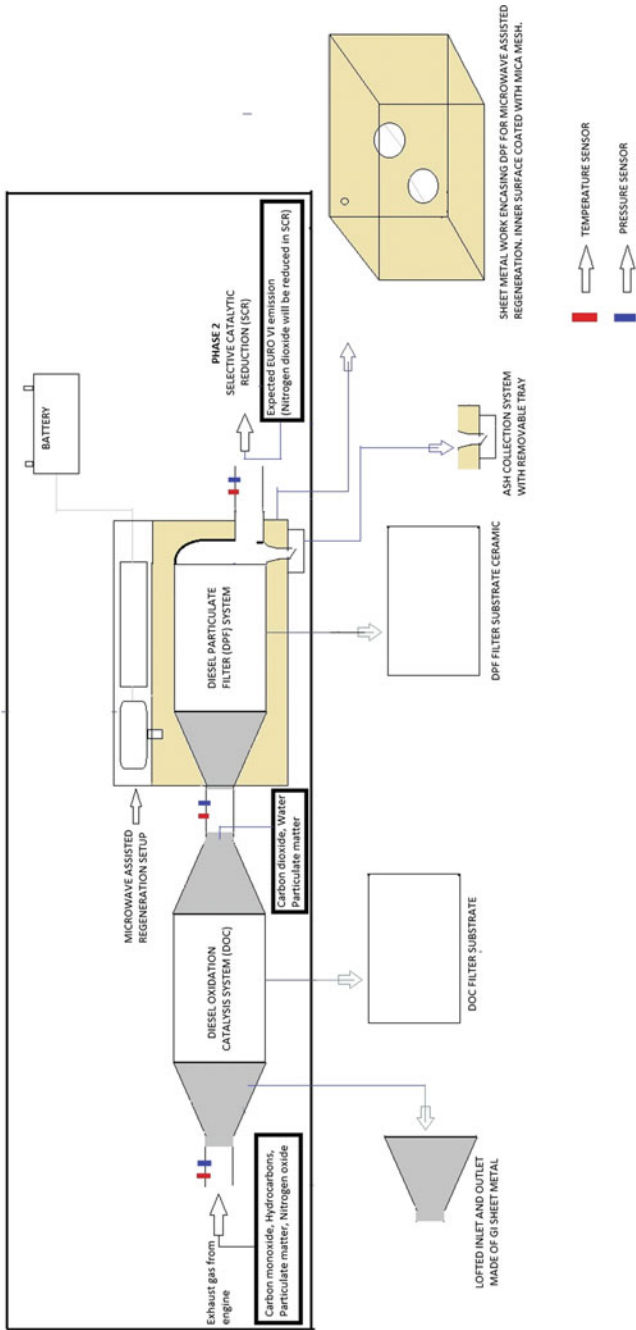


Fig. 4 Line diagram of the proposed emission control system

Table 1 Dielectric properties of materials

Material	Dielectric constant (ϵ')	Dielectric loss factor (ϵ'')
Diesel soot	10.70	3.60
Cordierite	2.90	0.140
Alumina ceramic	8.90	0.009
Quartz	3.80	0.0001

3 Conclusion

Higher efficiency and longer life of diesel engines have made it an integral part of automotive and other industry. Growing rate of air pollution has made the environmental regulations to be stringent, and also the EURO VI emission norms have to be adopted by all countries. The main challenges for implementing this are faced by the automobile companies and the oil marketing companies. Automobile companies have to design changes in vehicles, and oil marketing companies have to upgrade the fuel quality. Vehicles have to be fitted with exhaust control devices (DOC, DPF and SCR), and also the new designs must cope with the driving roads and ambient conditions. Researches are going on to meet these challenges. This project aims to develop a functional prototype which can be fitted to automobiles so that its emission can be controlled to meet EURO VI emission norms. One of the other challenges involved with this proposed system is sulphur poisoning of the catalyst used. CFD simulations have been very useful for analysing the designed models and also for optimizing various design parameters. CFD analysis involves analysing the flow and other parameters in a virtual environment as per the initial and boundary conditions fed to the system. Fabrication of the designed system has been initiated, and CFD simulations have been carried out to validate the geometric design.

References

1. Lee, Chanmin, et al. "Ag supported on electrospun macro-structure CeO₂ fibrous mats for diesel soot oxidation." *Applied Catalysis B: Environmental* 174 (2015): 185–192.
2. Taibani, Arif Zakaria, and Vilas Kalamkar. "Experimental and computational analysis of behavior of three-way catalytic converter under axial and radial flow conditions." *International Journal of Fluid Machinery and Systems* 5.3 (2012): 134–142.
3. Huang, Haifeng, et al. "Promoting effect of vanadium on catalytic activity of Pt/Ce–Zr–O diesel oxidation catalysts." *Journal of Environmental Sciences* 33 (2015): 135–142.
4. Herreros, J. M., et al. "Enhancing the low temperature oxidation performance over a Pt and a Pt–Pd diesel oxidation catalyst." *Applied Catalysis B: Environmental* 147 (2014): 835–841.
5. Hayes, R. E., et al. "CFD modelling of the automotive catalytic converter." *Catalysis today* 188.1 (2012): 94–105.
6. Corro, Grisel, et al. "Hydrogen-reduced Cu/ZnO composite as efficient reusable catalyst for diesel particulate matter oxidation." *Applied Catalysis B: Environmental* 165 (2015): 555–565.

7. Palma, Vincenzo, et al. "Catalytic DPF microwave assisted active regeneration." *Fuel* 140 (2015): 50–61.
8. Guan, Chun, et al. "Effects of fuel injection strategies on emissions characteristics of a diesel engine equipped with a particle oxidation catalyst (POC)." *Journal of Environmental Chemical Engineering* 4.4 (2016): 4822–4829.
9. Bin Zhang, Jiaqiang E, Jinke Gong, Wenhua Yuan, Wei Zuo, Yu Li, Jun Fu, (2016) Multidisciplinary design optimization of the diesel particulate filter in the composite regeneration process. *Applied Energy* 181:14–28.

Approach to Find Shortest Path Using Ant Colony Algorithm

Mudasar Basha, M. Siva Kumar, Vemulapalli Sai Pranav
and B. Khaleelu Rehman

Abstract This paper deals with Ant Colony Optimization (ACO). Our approach is to compare the run-time and accuracy of existing techniques using Ant Colony Optimization to find the shortest path. Here, we are going to study how to locate the shortest path using Dijkstra's, Bellman–Ford and Kruskal's algorithms, and comparisons will be done among all the algorithms. Ant lays pheromone on the path it travelled to identify the shortest path from its nest to the food source. We will also be studying what are the uses of implementing ACO algorithm on a XILINX ZYNQ-7000 PSoC (Programmable System on Chip) instead of implementing it on Arduino or Raspberry Pi.

Keywords Ant Colony Optimization (ACO) · Dijkstra's algorithm
Bellman–Ford algorithm · Kruskal's algorithm · Pheromone
Xilinx ZYNQ-7000 PSoC

1 Introduction

Ant Colony Optimization (ACO) was first introduced by Marco Dorigo in the early 1990s. The evolution of this algorithm was inspired by observing the ant colonies. ACO algorithm has been applied to many of the combinatorial optimization

M. Basha (✉) · V.S. Pranav
Department of ECE, BVRIT-N, Hyderabad, Telangana, India
e-mail: mudasar4u@gmail.com

V.S. Pranav
e-mail: pranav3993@gmail.com

M. Siva Kumar
Department of ECE, K L University, Vijayawada, AP, India
e-mail: siva4580@kluniversity.in

B.K. Rehman
Department of Electronics, Instrumentation & Control Engineering,
University of Petroleum & Energy Studies, Dehradun, Uttarakhand, India
e-mail: krehman@ddn.upes.ac.in

problems, and some of them are travelling salesman, quadratic assignment, etc. [1]. So, to find the shortest path, ant uses probabilistic function which will be complicate to calculate in the graphs. Although there is a technique to find the shortest path using probabilistic functions, we will be using Dijkstra's algorithm which is easy to understand and can be calculated easily in case of the graphs. Dijkstra's algorithm was visualized by Edsger W. Dijkstra in 1956 and was published after three years. All three algorithms with respective examples are discussed. Bellman–Ford algorithm was designed by Alfonso Shimbel in the year 1955, but this algorithm was titled after Richard Bellman and Lester Ford Jr., who publicized it in the years 1958 and 1956, respectively. Kruskal's algorithm was designed by Joseph Kruskal in the year 1956, which is a greedy algorithm in graph theory. Bellman–Ford, Kruskal's and Dijkstra's algorithms are compared with each other to decide which is better to find the shortest path. We can implement Ant Colony Optimization algorithm on the XILINX ZYNQ-7000 PSoC. This ZYNQ-7000 PSoC contains FPGA and two 1 GHz ARM Cortex-A9 processors. This PSoC is the faster and smarter way of creating a smarter system. FPGA is a semiconductor chip which consists programmable logic elements called 'logic blocks'. Here, we will also discuss that XILINX ZYNQ-7000 PSoC is better compared to Arduino and Raspberry Pi.

2 Ant Colony Optimization (ACO)

It is a meta-heuristic technique. Ants find the shortest path while they travel from their nest towards the food source using pheromone trails. Pheromone is a chemical substance that is produced by ants to lay on the ground, so that other ants could follow them till the food source. If the quantity of the pheromone deposited on ground is more, the probability of the path being followed by other ants will be more. Strength of the pheromone decreases as the time passes, and to increase the strength of the pheromone, other ants following the path will deposit pheromone. Ants decide to go from one node to another based on the probabilities calculated. It will also have the tour memory of the path that it travelled; that is, consider there are two nodes node-A and node-B, so if the ant travels from node-A to node-B then tour memory will be = {A, B}. This memory can be stated as Tabu list. Artificial Ant Systems have some memory called data structures, and they are also able to sense 'environment' if necessary (not just pheromone). If the object appears in the path, then ants decide whether to turn left or towards the right with uniform probability, but extra pheromones are deposited on the shortest path [2]. Some techniques to find the shortest path in ACO are discussed below. The flow chart represented below describes a general approach for all algorithms.

2.1 Flow Chart for the Process in ACO

The flow chart for the process in ACO is shown in Fig. 1.

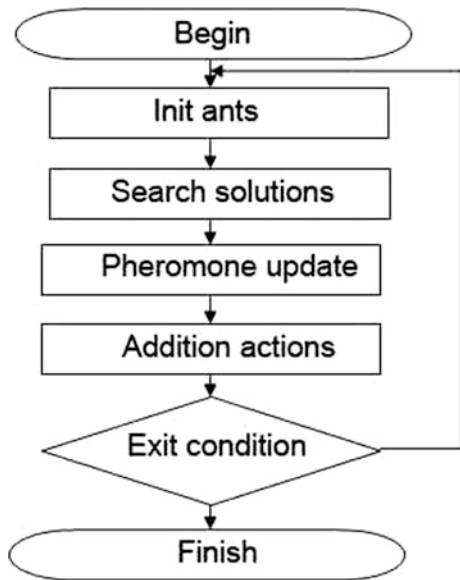
2.2 Applications of ACO

- Routing in telecommunication networks, travelling salesman.
- Bus routes, delivery routes, graph colouring.

The three techniques used to find out the shortest path and the theoretical analysis of these algorithms are discussed as follows:

- (1) Dijkstra’s algorithm,
- (2) Bellman–Ford algorithm and
- (3) Kruskal’s algorithm.

Fig. 1 Flow chart representation of all algorithms



2.3 Dijkstra's Algorithm

This is the shortest path channelling algorithm which is clear and uncomplicated to understand. Here, each node is labelled from source node to current node along its best-known path, so all nodes are labelled with infinity initially. While proceeding the algorithm, the shortest paths are known and infinity is replaced with concerned values [3]. Consider the following example whose starting point is node-A and ending point is node-F for the demonstration of algorithm (Fig. 2).

In the above example, the values are labelled with infinity; also, node-A is defined as working node initially. Node-A is made permanent; in the example, node-B has the smallest path than the node-C, i.e. ($1 < 2$), so node-B is made permanent. The path should always be in forward direction, and reverse direction is not considered in Dijkstra's algorithm (Fig. 3).

Now in the next step from node-B, the smallest path is towards node-E as it has the smallest value than node-D, i.e. ($3 < 4$); here, node-E is made permanent (Fig. 4).

In the last step, the shortest path is highlighted with the thick black line and the nodes are circled which reside in the shortest path. The result obtained after solving whole algorithm is shown in Fig. 5.

2.4 Bellman-Ford Algorithm

This method is somewhat similar to Dijkstra's algorithm, let us consider the same example that we demonstrated above. For solving the example in Bellman-Ford algorithm, some of the rules of Dijkstra's algorithm are followed [4]. In the first step of this algorithm, the shortest path from node-A is towards node-B when compared to node-C, i.e. ($1 < 2$), and the diagram for this is shown below. In Bellman-Ford algorithm, also the path should be in forward direction only. Here, the starting point is node-A and ending point is node-B (Fig. 6).

In the second step, from node-B, the shortest path is towards node-E when compared to node-D, i.e. ($3 < 4$). So, the names of the nodes are written inside the nodes. The path from node-A to node-C is not considered because it has the greatest value (Fig. 7).

Fig. 2 First step of Dijkstra's algorithm

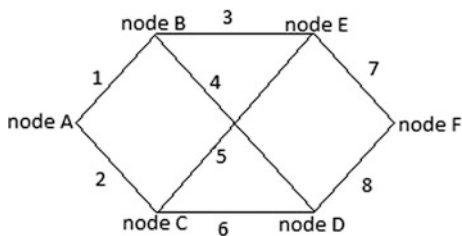


Fig. 3 Second step of Dijkstra's algorithm

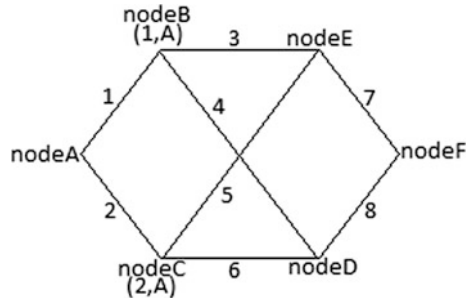


Fig. 4 Third step of Dijkstra's algorithm

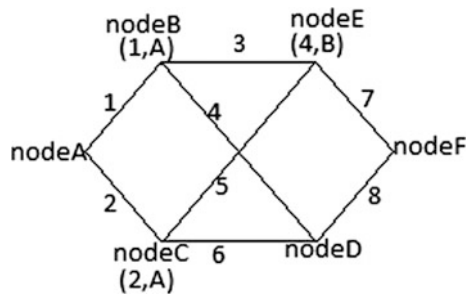


Fig. 5 Result of Dijkstra's algorithm

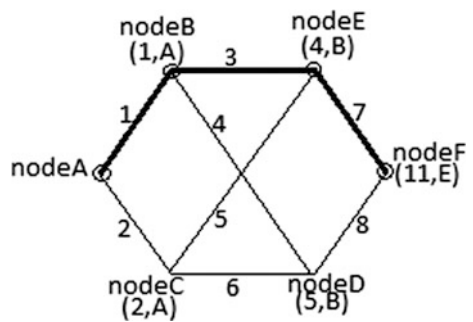


Fig. 6 First step of Bellman-Ford algorithm

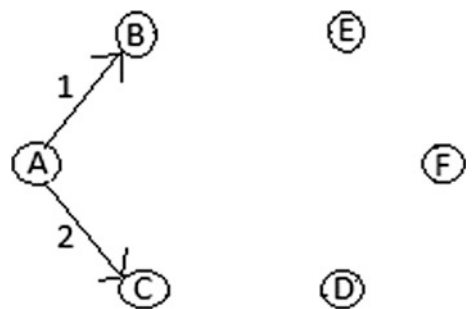
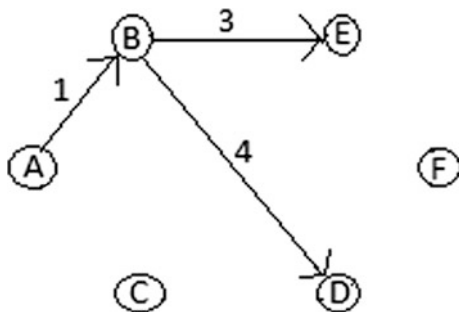


Fig. 7 Second step of Bellman–Ford algorithm

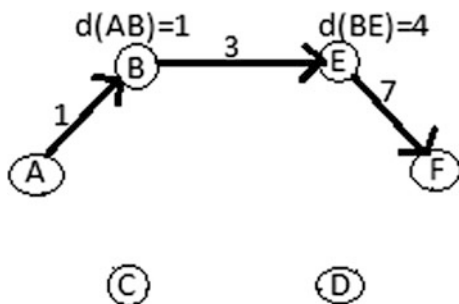


In the last step, as there no other nodes left the path will end at node-F which will give us the shortest path. The path obtained is highlighted with black line. Result for Bellman–Ford algorithm is shown in Fig. 8.

2.5 Kruskal’s Algorithm

This is also called as minimum-spanning tree algorithm. In Kruskal’s algorithm, given values are arranged in ascending order; after arranging these values, all possible paths are checked for path to be the shortest. Here, no loops should be formed while processing, because it may lead to more number of iterations; due to more number of iterations, run-time increases and load on CPU also increases [5]. Here, we consider the same example that we demonstrated in Dijkstra’s algorithm. In the first step of Kruskal’s algorithm, the shortest path from node-A is observed and we get the shortest path towards node-B. Now, the diagram for this step is shown in Fig. 9.

Fig. 8 Result of Bellman–Ford algorithm



In the second step from node-B, the shortest path observed is towards node-E, but the path to node-D is also included in diagram as no loop is formed. Now, if we consider node-C and draw the path towards node-D, the loop will be formed. So, it is neglected (Fig. 10).

In this step, from node-E, there is only one path left to go towards node-F and the path coming from node-D will be neglected as joining the path with node-F will result in the formation of loop. Hence, we get the shortest path. Result for Kruskal’s algorithm is shown in Fig. 11.

Fig. 9 First step of Kruskal’s algorithm

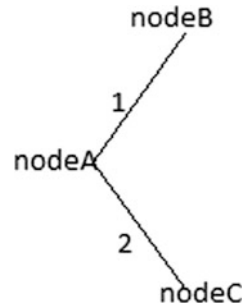


Fig. 10 Second step of Kruskal’s algorithm

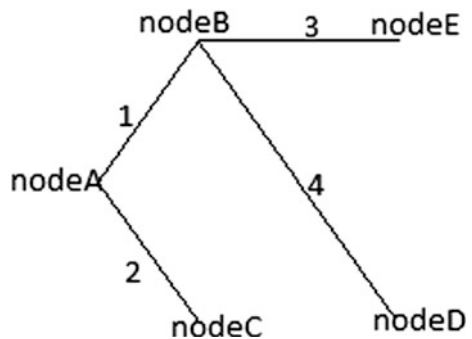


Fig. 11 Result of Kruskal’s algorithm

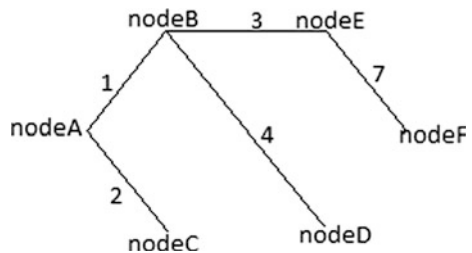


Table 1 Comparisons between three algorithms

S. No	Performance	Dijkstra's algorithm	Bellman–Ford algorithm	Kruskal's algorithm
1	Number of iterations	More	More	Less compared to Dijkstra's algorithm
2	Complexity	More compared to both algorithms	Less compared to Dijkstra's algorithm	Less compared to both algorithms
3	Accuracy	More compared to both	Less compared to Dijkstra's algorithm	Less compared to both
4	Speed	Less compared to both	Less compared to Kruskal's	More compared to both

2.6 Comparisons Between Dijkstra's, Bellman–Ford and Kruskal's Algorithms

The comparisons between Dijkstra's, Bellman–Ford and Kruskal's algorithms are shown in Table 1.

3 ZYNQ-7000 PSoC

ZYNQ-7000 PSoC is the product of Xilinx, where Xilinx is the American-based company. ZYNQ-7000 is a processor which offers the programmability of software, hardware and input/output in a single chip, and it incorporates 2 ARM Cortex A9 processors and FPGA [6].

The major functional blocks of ZYNQ-7000 are as follows:

- (1) Processing System (PS)
 - (a) Application processor unit (APU),
 - (b) Memory interfaces,
 - (c) Input/output peripherals and
 - (d) Interconnect;
- (2) Programmable Logic.

4 Simulation Results

The simulation results of the Dijkstra's algorithm for path 'A-B-E-F' will be obtained as shown below, and testing is done using Vivado (Xilinx) tool (Figs. 12 and 13).



Fig. 12 Simulation result for Dijkstra's algorithm

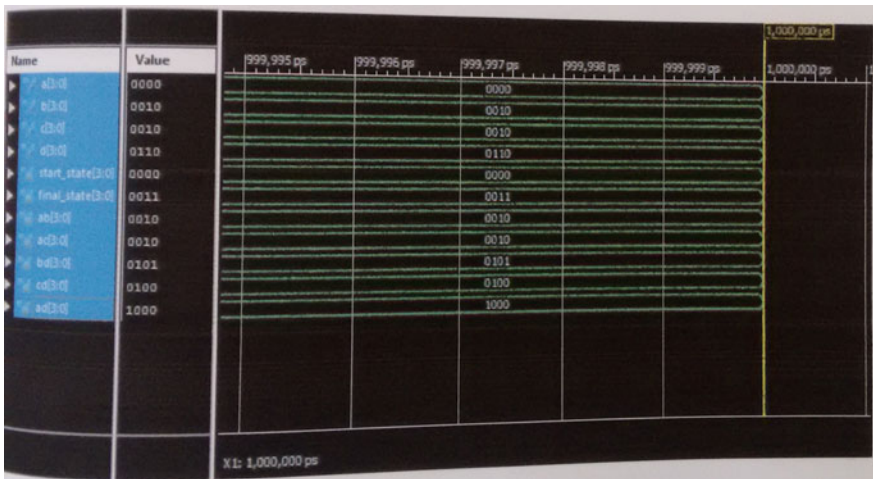


Fig. 13 Simulation result for Dijkstra's algorithm

5 Conclusion

We would like to conclude that according to our study, the shortest path can be found with Ant Colony Optimization using Dijkstra's algorithm accurately, and by implementing the ACO algorithm on XILINX ZYNQ-7000 PSoC, the run-time will be reduced and load on CPU will also be reduced as the logical or mathematical

calculations can be performed by ZYNQ-7000 PSoC that contains two 1 GHz ARM Cortex-A9 processors and FPGA. We can also conclude that ZYNQ-7000PSoC is better compared to Arduino and Raspberry Pi, because while executing a large number of instructions in ZYNQ-7000, the load on CPU will be reduced and execution time will be less.

References

1. Marco Dorigo, Thomas Stutzle, *Ant Colony Optimization*, ISBN 0-262- 04219-3, 2004
2. Michael Herrmann, *Natural Computing, Lecture 10: Ant Colony Optimisation*, 2010
3. V. S. Bagad, I. A. Dhotre, *Topic-Shortest Path Algorithm, Dijkstra's Algorithm*, Page No.-4-13, 1-14, June 2012
4. V. S. Bagad, I. A. Dhotre, *Topic-Shortest Path Algorithm, Bellman-Ford's Algorithm*, Page No.-4-16, 1-17, June 2012
5. An approach to parallelize Kruskal's algorithm using Helper Threads, Anastasios Katsigiannis, Nikos Anastopoulos, Konstantinos Nikas, and Nectarios Koziris
6. SoPC-Based Parallel ACO Algorithm and its application to Optimal Motion Controller Design for Intelligent Omnidirectional Mobile Robots, Hsu-Chih Huang Member, IEEE

Review of Expert System and Its Application in Robotics

Ajay K.S. Singholi and Divya Agarwal

Abstract A mechanical device or system, which can think and contemplate, observe, listen, walk, speak, and sense like a human, can be developed using a knowledge-based technique known as expert system. Expert system can be integrated with robotics to merge human intelligence with machines, so as to achieve smart work like that of humans by embedding features such as reasoning, knowledge/intelligence, and problem-solving capabilities. Methodologies implemented in expert systems have been surveyed in this paper along with the literature review related to the various applications of expert system in the field of robotics. This paper gives the literature reviews of articles with a keyword index and articles from different journals in order to explore the various applications of expert system. This paper also presents various types of expert system such as knowledge-based expert system rule and fuzzy-based expert system, characteristics and features of expert system and its advantages.

Keywords Expert system (ES) · Robotics · ES applications
ES methodologies · Inference engine

1 Introduction

Expert system (ES) is basically intelligence-based technique, comprising of knowledge database for all the application domains and an inference or reasoning system which solves problem with expertise and competence as that of the human beings [1–3]. Its strength is its ability to store and maintain a strong knowledge-based, comprising of all know-how of applications domains within industries [4, 5]. Expert system should not be considered as an alternative for

A.K.S. Singholi
G.B. Pant Government Engineering College, Okhla, Delhi, India
e-mail: ajay.igit@gmail.com

D. Agarwal (✉)
USICT, Guru Gobind Singh Indraprastha University, Delhi, India
e-mail: er.divya@gmail.com

decision maker, as they can take decisions only for the situations whose information is stored or predicted in its knowledge base; hence, they can be considered as mechanical substitutes of humans [6, 7].

The increasing capability of artificial intelligence (AI) in the field of robotics allows the developers to implement system that attempts to understand and imitate human behavior [8]. Expert system is an AI technique based on a computer system for emulating human-expert's decision-making capabilities to solve problems whose elucidation is already stored in their database [9]. Edward Feigenbaum while doing research in Heuristic Programming Project introduced the concept of expert systems, hence, regarded as father of expert system [10]. In the project, they created a knowledge base of complex infectious diseases (Mycin) to diagnose complex and unknown organic molecules (Dendral). The primary aim of ES is to create a strong database comprising of all the possible problems, their solution, prompt actions, how to handle emergency situations, etc., to a computer as an alternative to a human expert [10]. They are important for solving intricate problems such as in robotics applications for fault detection and fault tolerance, path and trajectory planning, obstacle detection in industrial robot. Decision migration in distributed robot, mobile robots controls, designing of robots, range and vision control of robot, control of welding gun in welding robots and performance optimization in planar robot etc. ES has the capability to learn from environment and experience by capturing it using coding and reuses the information already stored in it [5, 11]. Fundamentally, ES has the capability and expertise as that of the humans for the problems known to it, and it solves the problems with that expertise based on certain rules [12].

ES-based robot will produce robotic machines with intelligence and control as that of computers along with physical capabilities like that of humans [13]. It will be able to work in complex hazardous situations where it is difficult for humans to traverse and navigate such as mining, space exploration, sea/ocean exploration, etc., by imparting vision to a robot to interpret the information obtained from pictures [7, 14, 15]. This article surveys application of ES-based robots through a literature review of articles from 1990 to 2017. Further paper is organized as: Sect. 2 describes the expert system methodologies, architecture, characteristics, and advantages. Section 3 presents the literature review related to the applications of expert system in different research areas in robotics. Conclusion and future scope are discussed in Sects. 4 and 5.

2 Background of Expert System Methodology

Expert system is a computer system that mimics the knowledge processing capability of human beings [16]. The expert system consists of following three basic components:

- **User Interface** [14]: It is a computer program that is responsible for interaction and information exchange in between user/expert and system. The user inputs are facts, and the system answers these facts [17].

- **Knowledge Base [7]:** It contains knowledge and all related information on a particular subject to be stored for autonomous processing.
- **Inference Engine [18]:** It is a computer program that does interpretations from the knowledge and understanding it has been taught by an expert, to perform reasoning tasks.

2.1 Different Kinds of Expert System

There are three kinds of experts system:

2.1.1 Knowledge-Based ES

The knowledge-based system is human-centered and consists of certain evidences and facts to understand and imitate human expertise [19]. Components of knowledge-based system include: knowledge base, inference engine, engineering tool, and user interface [20] (Fig. 1).

2.1.2 Rule-Based ES

It contains and interprets information obtained from experts, in the form of if-then-else rules which can be used as an inference to perform operations on data to reach suitable conclusion based on a situation of one rule as a time. Inferences are

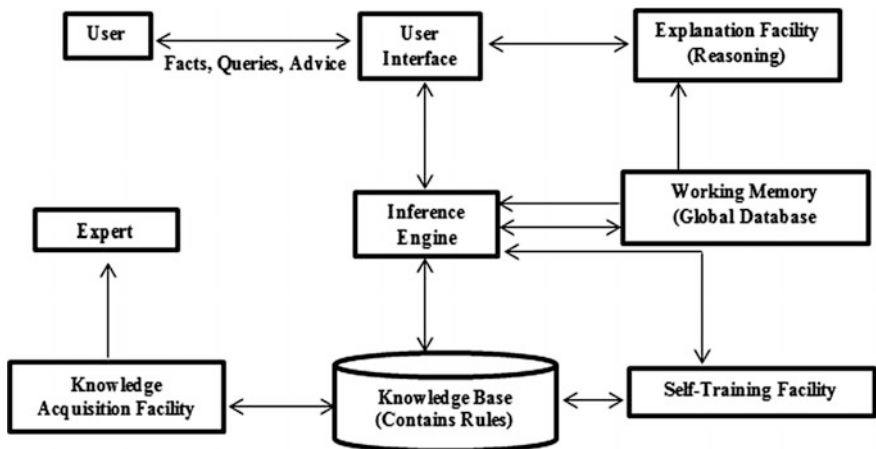


Fig. 1 Architecture of expert system

computer programs required for providing reasoning methodology relating to the information available in rule-based ES, for framing conclusion [14, 21].

2.1.3 Fuzzy-Based ES

Such systems are developed using fuzzy logic to deal with uncertainty and vagueness in the decision making for real-time situations [21, 22]. Using fuzzy sets and fuzzy logics simulates the normal reasoning process of humans by letting computer systems to perform more logically than the conventional systems. Fuzzy-based ES takes into consideration every possible option available rather than choosing in between two options such as black or white, true or false because in real-time situations there is certain vagueness in taking total precise values for practical applications [23, 24].

2.2 Characteristics of Expert System

The basic characteristics required for an expert system is given below [25]:

- High performance: The quality of advice given by expert system should be very high [3].
- Expertise: ES should produce good solutions both effectively and efficiently to eliminate wasteful or unnecessary calculations [26].
- Adequate response time: The system should be designed in such a way that it takes reasonable amount of time to produce solutions which are as that of the humans or are improved to it, for getting a conclusion or decision.
- Good reliability: Reliability is important because ES acts as a substitute for humans, so as to ensure safety of an enterprise or organization reliability must be high [14].
- Self-knowledge: ES must have the capabilities to examine reasoning process and explain operations.
- Understandable: ES should be understandable, i.e., it should be capable of explaining all the operations or processes it has to execute.
- Flexibility: The expert system should be flexible, i.e. it has the ability to add, change, and delete the knowledge from the knowledge base [5].

2.3 Advantages of Expert System

ES finds various applications in research as well as commercial field based on certain advantages discussed below [27]:

- **Accessibility:** There are situations where it is not possible for humans to be present all the time such as during emergency situation like natural disasters or fire breakouts, etc. For such situations, ES is a very good option because in it an elaborate knowledge base can be prepared by combining all the information after analyzing all the problems, circumstances, casualties, situations, adversities, conditions, etc., by many experts to make it more accessible all the time and ensure safety of both labor and equipments. Moreover in an ES, knowledge can be stored by many experts as it reads/captures and interprets information from all the data known to it in comparison with an individual human being [28].
- **Consistency:** ES-based robotic applications will be more consistent compared to the human counterparts as a robot will maintain its consistency over a period of time by being more accurate and providing good representation of knowledge with less errors [29].
- **Efficiency:** ES is more efficient compared to its human counterpart because it doesn't suffer from fatigue and can work the same or different tasks simultaneously without getting bored. Hence, ES-based industrial machines would be able to efficiently analyze all the operations concurrently.
- **Stability:** There are situations that a human expert working on a problem is absent or is replaced than in that case ES brings about stability by assisting the human expert in problem solving based on the previous learning [30].
- **Time constraints:** Training a new human expert is costly as well as time-consuming while copies of an expert system can be made very easily in a short interval of time. ES can perform much faster than its human counterpart with slight error rate [31].

3 Application Areas of Expert Systems in Robotics

Strength of an ES is to derive understanding and information from facts and figures gained from human experts or several other sources such as Internet. The hallmark of an ES is to draw conclusion or take decisions based on this knowledge [4, 28]. ES has online as well as offline memory capabilities which allow it to learn from the current scenarios in the industries or application areas as well based on certain facts and evidences for which ES acts as blank storage media to accumulate information and knowledge about circumstances [19]. ES finds applications in robotics as it provides both tangible and intangible benefits to enterprises by dramatically reducing the time and effort for solving a problem in comparison with a human individual [7]. ES works as a substitute for human experts if all the circumstances and its action are stored in its database so as not to hamper the overall performance of the organization.

ES plays a very important role in robotics. ES has been used by various researchers in robotics applications such as fault detection and fault tolerance, path and trajectory planning, obstacle detection in industrial robot, decision migration in

distributed robot, mobile robot controls, designing of robots, range and vision control of robot, control of welding robots, and performing optimization in planar robot. [1, 7]. Table 1 shows a summary of applications of ES in robotics. Following section includes ES-based robotics applications and their related literature survey.

3.1 *Fault Detection and Tolerance*

It is the competency of a robotic system to be capable of detecting failures within the enterprise or organization and to be able to tolerate failures so as to cope with the internal as well as external failures and continue performing all the assignment jobs without any human intervention [32]. Hubner and Hormann [32] presented and developed a prototype based on an ES for faults and failures diagnosis in a robotic system. Visinsky et al. [33] introduced a new approach for integrating this application area with robotics. Using ES would be helpful for strategizing failure mode analysis, to detect and repair errors, to tolerate and reconfigure failures within one

Table 1 Applications of expert systems

Author	Year	Subject
Hubner and Hormann	1991	Fault detection and fault tolerance
Visinsky et al.	1994	
Petterson	2005	
Morales and Savage	1994	Path and trajectory planning
Christensen and Piranians	1997	
Sanders et al.	2010	
Tudar and Moise	2013	
Sen et al.	2004	Performance optimization
Gardone and Ragade	1990	Mobile robot control
Mutambara and Litt	1998	
Meijer et al.	1991	
Djeda and Borenstein	2001	
Savege et al.	2008	
Ming et al.	1997	
Zhou, et al.	2005	Decision migration in distributed robot
Rai and Hong	2013	
Ludan et al.	2006	
Kaldested, et al.	2012	Obstacle detection
Chew et al.	1991	Robot designing and kinematics
Bhatia et al.	1998	
Tian and Gao	2013	Welding robot control
Popescu and Zhang	2001	Vision control
Correal et al.	2014	

scaffold. Petterson [34] proposed a Sapphire architecture-based monitoring and surveillance system, where expert system was integrated with linear temporal logic (LTL) comprising rules based on fuzzy logic, for fault detection and isolation.

3.2 Path and Trajectory Planning

Path planning is the method to predetermine and follow the path to reach goal position from its initial position without hitting any obstacle. Morales and Savage [8] proposed an approach to control motion of a mobile robot using integrated ES and ANN. This approach consists of two modules: high level and low level. In high level, there is a planner which is used to generate an action plan and a navigator that generates a path and the movement follow based on a map. In low level, there is a pilot who exhibits two behaviors: One is to reach the configuration and other is to avoid obstacles. The expert system is used to design the planner and navigator, whereas the ANN is used to implement pilot module. Tudar et al. [24] designed an efficient fuzzy ES to control robot's trajectory traversal by teaching it rules through an adaptive neuro-fuzzy system. Christensen and Pirjanian [35] proposed a model for planning and control in mobile robot which describes that how a behavioral system is controlled by a rule-based expert system. To design expert system, CLIP (c language interface production system developed by NASA) is used. Sanders et al. [36] developed an expert system-based teleoperated mobile robots using ultrasonic sensors to increase performance of robots in teleoperation applications. Initially, ES interprets data using joystick and sensors to identify dangerous conditions and then recommend safe course of action to perform tasks quickly.

3.3 Vision Control

Range estimation is to determine range information for omnidirectional vision system in robots. Popescu and Zhang [23] present a fuzzy ES for range estimation. This ES is built to accurately estimate range and position in an autonomous mobile robot. In this paper, new algorithm SFP (symmetry feature point extraction) is developed which detects symmetry points from a digital image. An omnidirectional system is used in order to capture the environment of the robot. Correal et al. [29] proposed an advanced expert systems approach which was able to capture images, correct it, and also reconfigure it to perform applications in the field of stereo vision. Here, ES is able to adjust image intensity with other images by automatically matching their histograms. ES also finds application for autonomous navigation of robots in industrial enterprises.

3.4 Performance Optimization

Sen et al. [37] designed and presented an ES-based adaptive control system to enhance the transient performance of planar robot. The structure proposed by them comprised of a supervisor-based ES to improve and optimize the performance of robot.

3.5 Mobile Robot Control

Meijer et al. [1] present a procedural ES to control robot in unstructured setup or environment autonomously centered across exception handling model. Gardone and Ragade [9] proposed taxonomy-based robot control ES based on fuzzy reasoning for selection of appropriate control algorithm. Mutambara and Litt [16] demonstrated a solution for joint position and joint rate limits problems of a manipulator using forward and inverse kinematics along with supervisory ES. Forward kinematics is used to quantify the weights obtained through conventional windup feedback scheme and supervised ES to get hold of closest desired goal. To test and validate the achievable manipulator task, inverse kinematics was used to evaluate subspace, available and constrained workspace. Djeda and Borenstein, [21] presented a fuzzy logic-based ES method for navigation (FLEXnav). The method was used to combine data from position and angular sensors to precisely approximate the heading and tilt of robot. Savage et al. [38] introduced ViRbot, a robotics architecture based on ES. It could control service operation of mobile robots. In this type of ES, commands are spoken to mobile robots in the form of rule-based system that takes conceptual dependency representation to accomplish the commands and makes path tracking problem of a robot easier to implement. One such service robot was also introduced by Schiffer et al. [39] and was named CAESER.

3.6 Decision Migration in Distributed Robot

Zhou et al. [2] introduced a new ES designed control strategy to be employed in real-time inspection for electric transmission line. Rai et al. [11] presented a conceptual framework within different physical components for dynamically migrating the decisions of multicomponent robots. They proposed a framework (using JAVA ES shell as a knowledge development tool), where the decision could be transferred to a robot handling multiple components or products so as to effectively maintain and manage faults, failures and emergency situations by providing non-hierarchical and organized control features. Ming et al. [40] proposed an intelligent planning strategy using distributed model network to deal with path

planning problem for several mobile robots working concurrently in an industrial setup. This approach guaranteed optimal time and energy considering kinematic and dynamic constraints of robots.

3.7 Obstacle Detection

Obstacle detection and obstacle avoidance, navigation control strategy for mobile robots was demonstrated [41]. The technique employed considered a robotic system centered across hybrid architecture ES taking into consideration environment state data as well as fuzzified obstacle data to process optimal navigation through obstacle. Kaldested et al. [42] proposed a CAD-based expert system for the online obstacle detection using a laser sensor. Here, ES is taught about the environment and information related to allowed objects and positions.

3.8 Robot Designing and Kinematic

Bhatia et al. [30] introduced an expert system for designing SCARA arm (selective compliance assembly robotic arm). In this proposed model, they developed an if-then-else rule-based ES in which they defined different rules to obtain different observations to reach achievable goals. Here, knowledge base is created to calculate static and complex mathematical equations for joint torques and load which helps in designing or choosing motor and bearing used. Chew et al. [43] describe an expert system developed to aid the designer in evaluating the most appropriate robot-hand kinematic structural concept from a large number of possible alternatives. The system uses representation method using graphs to demonstrate robot's kinematic structure. Such a representation scheme uses two sets of rules: fundamental knowledge and heuristic knowledge rule sets.

3.9 Welding Robot Control

Tian and Gao [25] proposed a model to control the position of welding gun for a robot used for welding application. In this model, welding gun position is obtained using the radial basis functional neural network, whereas the step angle is obtained using the expert system.

4 Conclusion

ES is an intelligent and smart computer program which is able to evaluate complex problems easily based on the knowledge stored in its database to style it as a substitute for its human counterpart by using task-specific information and inference techniques. This review article comprises of literature review from the previous last three decades of work in the area of expert systems and its applications in the area of robotics. It also summarizes the applications areas and the methodologies used for integration of ES in robotics. It is to be concluded that ES methodologies and its integration would set a trend in the near future because of its effectiveness, accessibilities, and expertise-oriented domain. Also it is very easy and faster to train and create replicas of ES compared to the training of human experts. From the literature, it can be concluded that ES has the capability to change, adapt, modify and to understand new concepts on its own from the experiences it goes through daily. This will not only create a boom in the industrial sector but will also increase productivity in lesser time. Integration of ES with robotics is a step toward factory automation which is the need of the hour. ES offers easy and total solution of the problem by taking into consideration all the aspects of the problem and takes necessary action as that of the human expert. Implementation of ES is also important because previously implemented tools and techniques were expensive and needed more time to develop and more computer resources for data storage and handing while it is easy to program ES both offline and online. ESs also suffer from certain limitations and gaps which are to be taken into consideration before implementing them for any application area. ESs suffer from the problem of limitation of technology because the initial setup is costly and complex, there are some problems with knowledge acquisition while feeding data into its database as all the data has to be entered and any loss or corrupt file will give erroneous result. Although ES serves to be a substitute of a human expert but it can't replace humans because human expertise is necessary for it to run smoothly and for a longer duration with consistency.

5 Future Scope

In real-life situation, there are certain ambiguous and biased values/data, for those ES with fuzzy-logic capabilities will result in handling of problem with more flexibility, thus controlled and organized manufacturing processes. Also if an expert system is given capabilities of human experts using neural network methodology then ES would be the best solution for working in hazardous environment where human involvement is risky. So work must be done in the area of expert system with neuro-fuzzy logic capabilities.

References

1. Meijer, G.R., Mai, T.L., Gaussens, E., Hertzberger, L.O., and Arlabosse F.: Robot Control with Procedural Expert System” In: Jordanides T., Torby B. (eds) Expert Systems and Robotics, 71, 217–232 (1991)
2. Zhuo, F.U., Wang, J.D., Li, Y.I.N.G. and Wang, J.: Control of an inspection robot for 110 KV power transmission lines based on expert system design models. Control Applications (2005)
3. Salunkhe, S., Hussein, S.K. and Hussein, M.A.: An Expert system for automation design of compound dies. AI Applications in Sheet Metal Forming: Part of the series topics in mining, metallurgy and materials engineering, 183–216. (2016)
4. Dunstan, N.: Generating domain-specific web-based expert systems” Expert Systems with Applications, 35, 686–690 (2008)
5. Amin, S.M., Ibrahim, K.H., Naggar, A.S., Rashwan, A.N., Sadek, A.E., AbdelGalil, M.A. and Badawi, A.H.: Parameterized Experience Exchange in Expert – Fellow Swarm Robotic System, Controller Performance Context. AIAA Information Systems, Texas, 1066, 1–7 (2017)
6. Giarratano, J.C. and Riley, G.D.: Expert system: principles and programming. 4th edition, Thomas learning, UK (2004)
7. Kishan, B., Chadha, V. and Maini, C.: A review of development and applications of expert system. International journal of advanced research in computer science and software engineering, 2(10), 319–325 (2012)
8. Morales, M. and Savage, J.: Motion control of a mobile robot using an expert system and artificial neural network. Parasol lab, technical report (1994)
9. Gardone, B.A. and Ragade, R.K.: IREX: an expert system for the selection of industrial robots and its implementation in two environments. IEA/AIE ‘90 Proceedings of the 3rd international conference on Industrial and engineering applications of artificial intelligence and expert systems, 2, 1086–1095 (1990)
10. Edward, F.A. Pamela, M.C.: The fifth generation: Artificial Intelligence and Japan’s Computer Challenge to the world. Addison-Wesley Publication Computer, 1st Edition (1983)
11. Rai, L. and Hong, J.: Conceptual framework for knowledge based decision migration in multi-component robot. International Journal Of Advanced Robotics System, 10(5), 237–249 (2013)
12. Omran M.G.H., Salman A., Engelbrecht, A.P.: Self-adaptive Differential Evolution. Computational Intelligence and Security CIS 2005, Lecture Notes in Computer Science, vol 3801, Springer edition, 192–199 (2005)
13. Kishore, R. and Thomas, A.: Effectiveness index of expert system applications in agriculture. International Journal of Agriculture, Environment and Biotechnology, 9(1), 117–121 (2016)
14. Liao, S.H.: Expert system methodologies and applications- a decade review from 1995–2004. Expert system with applications, 28(1), 91–103 (2004)
15. Khattak, S.B., Akhtar, R., Hussain, I., Ullah, M., Maqsood, S., and Haq, I.U.: Expert System for Lean Manufacturing at Tobacco Industry. Technical Journal of University of Engineering and technology, 21(1), 104–109 (2016)
16. Mutambara, A.G.O. and Litt, J.: A framework for a supervisory Expert system for robotic manipulators with joint position Limits and joint rate limits. NASA centre for aerospace information, Technical Report (1998)
17. Grafflin, C.P., Alumni, N., Suay, H.B., Mainprice, J., Lofaro, D., Berenson, D., Chernova, S., Lindeman, R.W. and Oh, P.: Toward a user-guided manipulation framework for high-DOF robots with limited communication. Intelligent Service Robotics, 7(3), 121–131 (2014)
18. Alma, Z., Torgyn, M., Marzhan, M. and Kanat, N.: The Methodology of Expert Systems Kantureeva Mansiya. IJCSNS International Journal of Computer Science and Network Security, 14(2), 62–66 (2014)
19. Wiig, K.M.: Knowledge management the central management focuses for intelligent-acting organization. Arlington Schema press, 1, (1994)

20. Dhaliwal, J.S. and Benbasat, I.: The use and effects of knowledge based system explanations: theoretical foundations and a framework for empirical evaluation. *Information Systems Research*, 7, 342–362 (1996)
21. Djeda, L. and Borenstein, J.: FLEXnav: Fuzzy logic expert rule based position estimation for mobile robots on rugged terrain. *International Conference on Robotics and Automation*, 10, 317–324 (2001)
22. Jamshidi, M.A., Titli, A., Zadeh, L. and Boverie, S.: *Applications of Fuzzy logic: towards high machine intelligence quotient systems*. Upper Saddle River. N.J. Prentice Hall (1997)
23. Popescu, D. and Zhang, J.: A fuzzy expert system for range estimation. *Studies in information and control*, 10, 1–11(2001)
24. Tudar, L. and Moise, A.: Automatic expert system for Fuzzy control of robot trajectory in joint space. *International Conference on Mechatronics and Automation*, 1057–1062 (2013)
25. Tian, J., Gao, M. and He, Y.: Intelligent control of welding gun pose for pipeline welding robot based on improved radial basis function network and expert system. *International Journal Of Advanced Robotics Systems*, 10, 1–8 (2013)
26. Waterman, D. A.: *A Guide to Expert Systems*. Addison-Wesley Publishing Company, Inc. (1986)
27. Kumar, Y. and Jain, Y.: Research aspects of expert system. *International Journal of Computing and Business Research*, 23–29 (2013)
28. Ali, S.A., Ghaffari, M., Liao, L. and Hall, E.: Mobile robotics moving intelligence. In book, *Mobile Robots Moving Intelligence*, Germany (2006)
29. Correal, R., Pajares, G. and Ruz, J.J.: Automatic expert system for 3D terrain reconstruction based on stereo vision and histogram matching. *Expert Systems with Applications*, 14, 2043–2051 (2014)
30. Bhatia, P., Thirunarayanan, J. and Dave, N.: An expert system based design of SCARA robot. *Expert systems with applications*, 15(1), 99–109 (1998)
31. Berenson, D., Abbeel, P. and Goldberg, K.: A Robot Path Planning Framework that Learns from Experience. *2012 IEEE International Conference on Robotics and Automation* (2012)
32. Hübner T. and Hörmann K.: A Model-Based Expert System for the Diagnosis of Faults in a Robot System for Cleaning Castings. In: Jordanides T., Torby B. (eds) *Expert Systems and Robotics*, 71, 655–661 (1991)
33. Visinsky, M.L., Cavallaro, J.R. and Walker, I.O.: Expert system framework for fault tolerance in robotics. *Computers and Electronics Engineering*, 20(5), 421–435, (1994)
34. Petterson, O.: Execution monitoring in robotics- A survey. *Robotics and automation system*, 53(2), 73–88 (2005)
35. Christensen, H.I., Pirjanian, P.: Theoretical methods for planning and control in mobile robotics. *1st International Conference On Knowledge Based Intelligent Electronic Systems*, 81–86 (1997)
36. Sanders, D.A., Jones, L.G. and Gegov, A.: Improving ability of tele-operators to complete progressively more difficult mobile robot paths using simple expert systems and ultrasonic sensors. *An International Journal of Industrial Robot*, 37(5), 431–440 (2010)
37. Sen, M.D.L., Minambres, J.J., Gaeride, A.J., Almanía, A. and Soto, J.C.: Basic theoretical results for expert systems: Application to the supervision of adaptation transients in planar robots. *Artificial Intelligence*, 152(2), 173–211, (2004)
38. Savege, J., Lareva, A.L., Carrera, G., Cuellar, S., Esparza, D., Minami, Y. and Penuelas, U.: Virbot: A system for the operation of mobile robots. *Robocup 2007: robot soccer, world cup XI*, 5001, 512–519 (2008)
39. Schiffer, S., Ferrein, A. and Lakemeyer, G.: CAESAR: an intelligent domestic service robot. *Intelligent Service Robotics*, 5(4), 259–273 (2012)
40. Ming, Z., Maoxiang, S.S., Yanhong, W. and Chaowan, Y.: Decentralized self-decision planning system for multiple intelligent mobile robots. *IEEE International Conference on Intelligent Processing System*, 2, 1385–1389 (1997)

41. Ludan, W., Hongguang, W., Lijin, F. and Mingyang, Z.: Research on obstacle-navigation control of a mobile robot for inspection of the power transmission lines based on expert system. *Climbing and Walking Robots* springer edition, 173–180 (2006)
42. Kaldested, K.B., Hovland, G. and Anisi, D.A.: CAD based training of an expert system and a hidden markov model for obstacle detection in an industrial robot environment. *International Federation of automatic control*, 45(8), 53–58 (2012)
43. Chew M., Issa G.F., and Shen S.N.T.: Expert System for Robot Hand Design Using Graph Representation. In: Dwivedi S.N., Verma A.K., Sneckenberger J.E. (eds) *CAD/CAM Robotics and Factories of the Future'90*, 466–471 (1991)

Analysis of Multiple Shortest Path Finding Algorithm in Novel Gaming Scenario

Aqsa Zafar, Krishna Kant Agrawal and Wg. Cdr Anil Kumar

Abstract The most important research area in gaming is shortest path finding. Many video games are facing the problem of path finding and there are many algorithms present to resolve the problem of shortest path finding such as breadth-first search, depth-first search, Dijkstra's algorithm and best-first search. A* algorithm has been proved the best algorithm for resolving the problem of shortest path finding in games. It provides the optimal solution for path finding as compared to other search algorithm. In the starting section, brief introduction about the path finding is given. Then the reviews of different search algorithm are presented on the basis of path finding. After that information of A* algorithm is described. In the last, application and examples of how the path finding techniques are used in the game are addressed and future work and conclusion are drawn. In this paper, comparison is drawn on search algorithm on the basis of path finding in games. A* algorithm gives the optimal solution in a faster way as compare to other algorithm. A* uses a heuristic function and movement amount from start node to any other node n, so A* select the most promising node for expanding due to this property A* gives optimal solution.

Keywords Path finding · Optimal path · A* algorithm · Shortest path Gaming scenario

1 Introduction

Path finding usually means to find the minimum distance node. There are many problems of path findings like transit planning, routing of telephone traffic, navigation of maze, and path finding of robot. Nowadays, importance of game industry

A. Zafar · K.K. Agrawal (✉)

Department of Computer Science, Amity University, Lucknow, India
e-mail: kkagrwal@outlook.com

Wg.C. Anil Kumar

Amity School of Engineering and Technology, Amity University, Lucknow, India

© Springer Nature Singapore Pte Ltd. 2018

R. Singh et al. (eds.), *Intelligent Communication, Control and Devices*,

Advances in Intelligent Systems and Computing 624,

https://doi.org/10.1007/978-981-10-5903-2_132

increases very fast and the problem of path finding in game industry is a popular and frustrating problem. In role playing and real-time strategy games, there are characters who move from their location to another place or player decided place. The most usual problem of path finding in video games is how to ignore barriers intelligently and find out the best efficient way over unique terrain [1].

A* algorithm is best for path finding and gives the optimal solution so many people are trying to improve the speed of A* algorithm. Many attempt and effort have been done for optimizing this algorithm over the last ten years and lot of reviewed algorithm has been found. This type of optimizations covers improvement of heuristic functions, optimize the map, introduce new data structure, and reduce the memory need. The next segment of this paper reviews on various path finding algorithms.

2 Literature Survey

Literature survey of this paper is basically the comparison of various search algorithms in terms of path finding. In this research survey, breadth-first search (BFS), depth-first search (DFS), Dijkstra's algorithm, best-first search, and A* algorithm are described in brief [2].

2.1 *Breadth-First Search (BFS)*

It is an algorithm which starts from root node, firstly the root node is expanded, and after expanding the root node next level nodes are expanded. In BFS, queue is used for storing the record of each node. BFS start with level 0, and it searches level-by-level until the goal is find. If there exist a solution more than one, BFS chooses the shortest solution in which less number of steps are required.

BFS start searching from node 1 then it expands its successor node 2 and node 3, then node 2 expands its successor node 4 and node 5 this process goes until all nodes are visited and goal is find.

The main drawback of breadth-first search is memory requirement because each level record must be saved for expanding the next level, so BFS requires a lot of memory for storing these records. If the goal is far away so BFS takes lot of time for finding the solution. Space complexity of BFS is $O(b^d)$ [3].

2.2 *Depth-First Search (DFS)*

This algorithm starts from goal node and generates all successor of start node and tests those nodes, unlike BFS which expands the siblings of nodes DFS expands

firstly the children nodes in deepest level and finds the solution [3]. If solution is found it don't expand other nodes, it stops searching, means if solution exist it explores one branch only.

DFS requires less memory because only one branch is expanded. DFS uses stack to keep record of visited nodes. DFS start from node 1 and expands its child node 1 then node 1 expands its child node 2 and goes inside deepest until the solution is found.

Drawback of DFS is that there is no assurance to discover the solution, and there is also no assurance to discover minimal solution, if there exists more than one result in the problem. Another drawback of DFS is that there is a chance that path finding may go under the left most path permanently. The complexity depends on the number of paths exist in the graph.

2.3 *Best-First Search*

Best-first search finds the evaluation function to know how far the goal node is from the particular node. Best-first search uses heuristic function $h(n)$ to expand the next node, the node that has less $h(n)$ value must be selected as a next node. BFS always find good paths to the goal. Formula for best-first search is-

$$f(n) = h(n) \tag{1}$$

The difference between best-first search and A* algorithm is that best-first search uses only heuristic value and A* algorithm uses heuristic value as well as movement value for each node, so A* algorithm gives more optimal path for path finding.

2.4 *Dijkstra's Algorithm*

Dijkstra's algorithm chooses the minimum distance from start node to any other node. Dijkstra's algorithm starts form the beginning node and choose the unvisited minimum distance node, and from that node it again selects its minimum distance neighbor node. Dijkstra's algorithm works only with non-negative weighted edges. Dijkstra's algorithm uses a priority queue to keep track the unvisited nodes [4].

Dijkstra's algorithm discover minimum distance path $O(E + V \log(V))$ if it uses min priority queue with Fibonacci heap. Otherwise if any other implementation of priority queue is taken so it takes $E \log(E) + V$ [3].

Uninformed searching is a major drawback of Dijkstra's algorithm, which results in quite a waste of time, the algorithm does not work on negative edges which come up to be an another shortcoming of Dijkstra's algorithm.

2.5 A* Algorithm

A* Algorithm is a type of search algorithm which discovers the shortest path between the start node and goal node. A* selects the most promising unvisited node for expanding [5]. A* finds the cost function of each node for expanding the next node, based on the cost function it select a node to expand next, node whose cost function is minimum is selected for further expanding. Cost function of each node is calculated by the formula given below

$$f(x) = g(x) + h(x) \quad (2)$$

where,

$g(x)$ = movement cost from the start node to any node x ,

$h(x)$ = movement cost from any node x to the goal node.

$h(x)$ is known as heuristic function. Cost function $f(x)$ is the addition of $g(x)$ and $h(x)$. A* Algorithm selects the next node whose $f(x)$ value is minimum. A* algorithm gives the assurance to discover a minimal path from initial node to the end node, if there exists a path. And it gives the optimal solution if $h(x)$ is permissible heuristic means value of $h(x)$ is always minimum or equivalent to the real minimal path cost from any node n to the goal node.

A* is the more useful and most well liked selection for path finding in computer games. According to the nature of game, it is applied on the game. A* algorithm finds the optimal solution of the problem in an efficient way (Fig. 1).

3 Analyzing—A* Is Better than Dijkstra's Algorithm

See Table 1.

4 Appropriate Utilization of A* in Computer Games

A* is very well liked path finding algorithm in game industry, it is easy to understand and easy to implement. A* algorithm is used in many computer games for finding the shortest path in game world [6]. In this section, discussion of many popular online games in terms of path finding and the use of these games as an example to show the effect of path finding in every unique game map representation.

```

A*//
1. Begin the O list.
2. Begin the C list.
3. Keep the initial vertex to the O list.
4. Iterate the following stages:
  a. See the node who has minimal f value in the
     open list, consider this vertex as a
     current vertex.
  b. Put this vertex into C list.
  c. For every accessible vertex from the
     present vertex-
     i.      If present on the C list, avoid
            this vertex.
     ii.   If this vertex is not in the O list
            keep it into the O list. Assign the
            present vertex the parent of this
            vertex. Find the heuristic value,
            movement value and the cost value of
            this vertex.
     iii.  If this vertex is present in the O
            list already, examine is this path is
            better. If yes, modify its parent to
            the present vertex, and again find the
            cost value and movement value.
  d. End when
     i.    Put the goal vertex to the C list.
     ii.   Unable to discover the goal vertex,
            the O list is now blank.
5. Sketch in opposite direction from the goal
   vertex to the initial vertex. This is the
   shortest path.

```

Fig. 1 Pseudocode of A* [5]

4.1 Path Finding Queries in Game Industry

Real-time strategy game, Age of Empires is an excellent game. In this game, grids are used to represent the map. A 256×256 grid produces 65,536 feasible positions. The motion of military unit is clarified as if going an object by a maze. A* star algorithm is used in Age of Empires. Lot of Age of Empires [7] players are irritated by the abominable path finding [8]. The problem occurs in this game is when a group of objects moved simultaneously at a same time half of them get

Table 1 Comparative table amongst A* algorithm and Dijkstra’s algorithm

Parameters	A*algorithm	Dijkstra’s algorithm
Searching algorithm	Best-first search	Greedy best-first search
Time-based complexity	For A* its $O(n \log n)$, where n —total number of nodes	For Dijkstra’s its $O(n^2)$
Heuristic function	A* algorithm— $f(x) = g(x) + h(x)$, where, $g(x)$ = traveling cost from start node to any other node x . $h(x)$ = traveling cost between any node x to the goal node	Heuristic function of Dijkstra’s algorithm is— $f(x) = g(x)$, $g(x)$ = traveling cost between starting node to any node x . Dijkstra’s algorithm is worst case scenario of A* algorithm

jammed in the tree, this problem occurs when the number of trees are increased [5]. Representation of Age of Empires is shown in Fig. 2.

One more real-time strategy game is Civilization V, in which representation of maps is shown by hexagonal tiles as shown in Fig. 3. A path finding algorithm is applied here for supervising the group of military going to the wanted place by a collection of “movable” hexagonal tiles. Civilization V also faces the problem of poor path finding. This game was published in November 2010 [5].



Fig. 2 A snapshot of Age of Empire [9]



Fig. 3 A snapshot of Civilization V [10]

In strategy game, hundreds and thousands of units move simultaneously, so they face problem in moving from one point to another point. A* algorithm performs well in first person shooter games because in this type of games few objects moved simultaneously at a same time, so objects are not jammed in the tress and don't take too much time for calculating the cost value [11].

5 Conclusion

This paper reviews the several algorithm for path finding, in which A* algorithm is better option for path finding in games, this A* algorithm is pleasing for path finding and gives the optimal solution of the problem. It is difficult to discover another algorithm until now A* is proved as optimal. A great amount of work has been done for improving the speed of A* and optimizes this algorithm in different ways. There are lot of ways to improve the performance of A* algorithm to introduce the new data structure, reduce the search space, and improve the heuristic function.

6 Future Work

A future work is to optimize the A* algorithm and improve the performance in terms of search space, memory usage, heuristic function, and data structure. Memory usage can be reduced, heuristic function can be improved, and new data structure can be introduced for improving the performance of existing path finding algorithm.

References

1. Xiang Xu and Kun Zou, “ An Improved Path finding Algorithm in RTS Games”, *Communications in Computer and Information Science—Springer* 153, pp. 1–7, 2011
2. Mehta Parth, Shah Hetasha, Shukla Soumya, Verma Saurav,” A Review on Algorithm for Path finding in Computer Games”, available at www.researchgate.net/publication/303369993
3. Amit S. Wale, Taranpreet Singh Saini, Ahmed Mohammad Ali, Vandana S. Jagtap, “Survey Heuristic Search for Shortest Path finding in Games,” *ISSN-Print 2393–8374, Online-ISSN 2394-0697, Vol 2, I 12, 2015*
4. Geethu Elizebeth Mathew, “Direction Based Heuristic for Path finding in Video Games”, *Procedia of Computer Science* 47, 262–271, 2015
5. Xiao Cui and Hao Shi, “A*- based Path finding in Modern Computer Games,” *IJCSNS, School of Engineering and Science, Victoria University, Melbourne, Australia, International Journal of Computer Science and Network Security*, p 125, Vol 11, No 1, Jan 2011
6. Rubén Tous, “Real Time Planning for Path-finding in Computer Games”
7. Age of Empire Game by Microsoft [www.microsoft.com/ games/ empires](http://www.microsoft.com/games/empires), read on January 10, 2017
8. Rubén Tous, “Real Time Planning for Path-finding in Computer Games”, *Universitat Pompeu Fabra (UPF), Department de Tecnologia, Spain*
9. Firaxis Games, “Sid Meier’s Civilization V”, www.civilization5.com, read on January 10, 2017
10. N. H. Barnouti, Al-Dabbagh S S M and Naser M A S “Path finding in Strategy Games & Maze Solving Using A* Search Algorithm” (2016) *Journal of Computer and Communication*, 4, 15–25. <http://dx.doi.org/10.4236/jcc.2016.411002>
11. Guni Sharon, “Thesis Summary Optimal Multi-Agent Path finding Algorithm”, Published at Twenty Ninth AAI-Conference on Artificial Intelligence Proceedings

Design and Analysis of Beam-Steering Antenna Array

S. Vijayadharshini, Apoorva Bhardwaj and Suchismita Pani

Abstract This research paper presents a novel microstrip antenna array composed of four rectangular patches, developed on FR4 epoxy substrate with dielectric constant 4.4. This proposed antenna gives good results at 17.5 GHz. At this solution frequency, the reflected power (S11) of 36.5 dBi is obtained. The design and the properties of this antenna have been studied and performed using the HFSS software, and its application beam steering is studied on MATLAB software.

Keywords Microstrip patch · Antenna array · Beam steering

1 Introduction

For any wireless communication, antenna has been playing the intermediate role between the transmitter or receiver and the propagation media. With the development of communication systems recently, the need for minimal cost, light weight, and easy to be fabricated antennas working over a wide range of frequencies has come up. Microstrip patch antennas have become very necessary nowadays. Their different geometries make them more varied in nature and hence can be used in diverse situations. Their structure which is extremely lightweight and their integratability with microwave circuits are some of their many advantages [1].

S. Vijayadharshini (✉) · A. Bhardwaj · S. Pani
Amity University, Noida, India
e-mail: vijayadharshini96@gmail.com

A. Bhardwaj
e-mail: apsi.apoorva@gmail.com

S. Pani
e-mail: spani@amity.edu

Microstrip patch antenna has a very simple construction having a one-layer structure which has the following four parts—ground, patch, substrate, and feeding line [2]. Wireless communications present a new challenge for antenna designing due to ample growth in terms of lesser cost, minimum profile antennas, lesser weight along with more reliability [3].

To make these antennas more compatible with the current need of communication, designing of many single patches in array configuration is done. The setup is very basic, comprising of proximity coupling between a substrate having microstrip feed line and rectangle shape microstrip fixed on a corresponding superstrate which is a little open-circuited tuning stub shunted with a feed line [4].

Antenna arrays are pretty dynamic and can produce a desired pattern which is difficult to be attained with single antenna element. Adding to this, scanning of antenna system beam, directivity improvement, and other functions tough to be performed with a single antenna element can be done effectively [5]. Likewise, assortment of antenna array design issues can be communicated as convex optimization issues, which can be (numerically) explained with great efficiency by as of late created interior point methods [6].

Not only radar and wireless communications but military and commercial applications also have been seen to be working on phased arrays whose key issue is electronic beam steering. Due to such high importance, electronic beam steering is being studied in detail [7]. M. Rammal for smart antenna synthesis has suggested to synthesis multi-beam patterns in the directions of different users and steered beams with zero in desired direction. This process is done by controlling the phases during synthesis [8]. Wireless networks in their most efficient form need to have considerable impact on proper use of the spectrum, minimum cost of setting up new wireless systems, and realization of transparent operations. Smart antennas are best to achieve the mentioned parameters, and hence their adoption in future wireless systems is expected [9].

Section two of this paper is antenna design which focuses on designing an antenna array of 4×1 configuration with the dielectric constant of 4.4 (FR4 epoxy) and the operating frequency of 17.5 GHz lying in Ku band for various applications like satellite communication and broadcasting services. Third section comprises of results and observations which contains the graph of radiation pattern, return loss, E - and H -fields, and the beam-steering radiation patterns at different angles.

2 Antenna Design and Geometry

The proposed 1×4 antenna array using microstrip rectangular patches is operating at a frequency of 17.5 GHz. It has been developed on FR4 epoxy substrate with relative permittivity of 4.4 and has been fed by the microstrip feed line (Fig. 1).

Now in the paper, we have proposed the idea of connecting four such rectangular microstrip patches to form a matrix of 1×4 resulting in an antenna array. All the

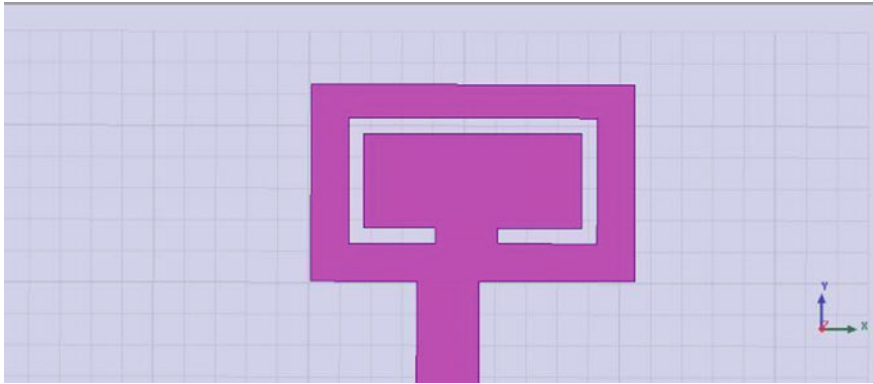


Fig. 1 Single antenna element

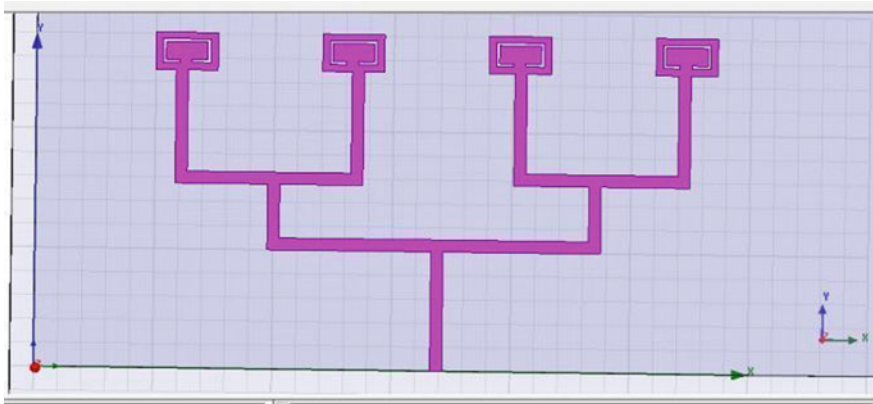


Fig. 2 Antenna array design

Table 1 Dimensions of rectangular microstrip patch

Parameters	Computed dimensions (mm)
Length of rectangular patch	5.21
Width of rectangular patch	3.13
Height of substrate	1.8
Width of feed lines	1

elements are connected using a single microstrip feed line. The ground size has been taken as 200×100 mm (Fig. 2; Table 1).

In the next part of our paper, we have shown the phenomenon of beam steering. For this, we have developed a code on MATLAB to observe the change in the main lobe direction of the radiation pattern. This is obtained by changing the phases relatively of the signals driving the antenna array.

3 Result and Discussion

Now, after arranging four such rectangular elements into an array, the following radiation pattern as in Fig. 3 has been obtained.

From Fig. 4, two dips can be clearly observed in the return loss curve. More significant S11 is observed at 19.2 GHz of 36.5 dB and the other S11 of 20 dB at 10.7 GHz. When a signal is returned or reflected by a discontinuity, the power may get reduced. So the more the return loss, the less will be the power, which will get reduced.

The polarization of radio wave is determined by the “E”-plane also known as electric field shown by red color in Fig. 5. For any antenna where the electric field

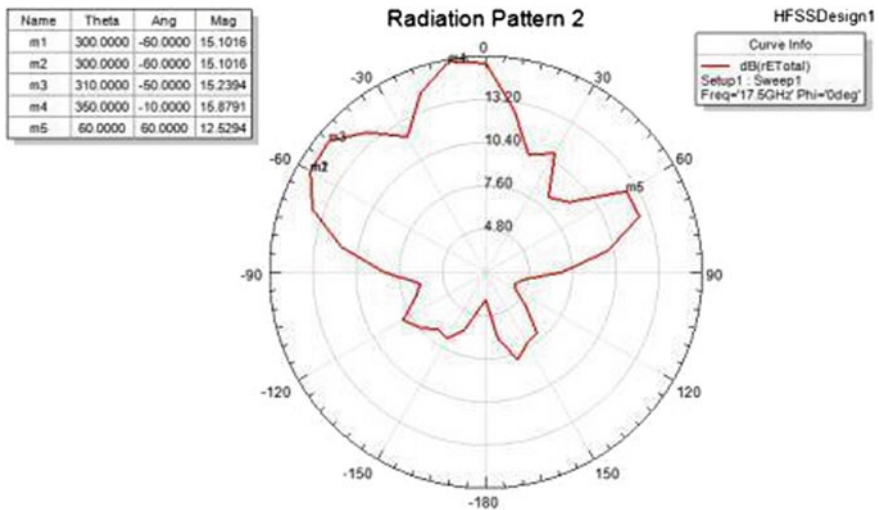


Fig. 3 Radiation pattern of microstrip patch antenna array

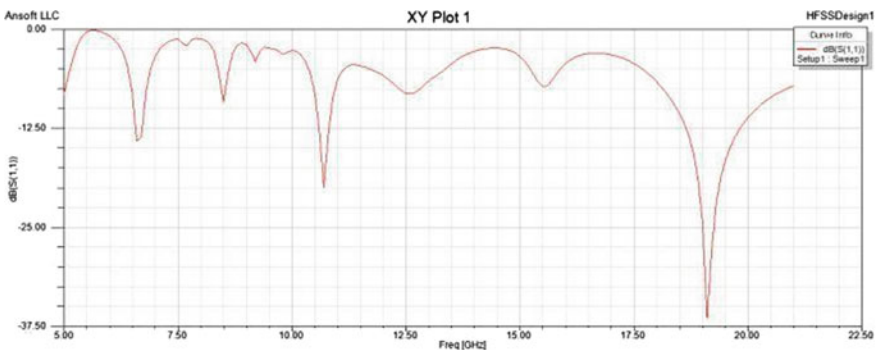


Fig. 4 Return loss of designed array

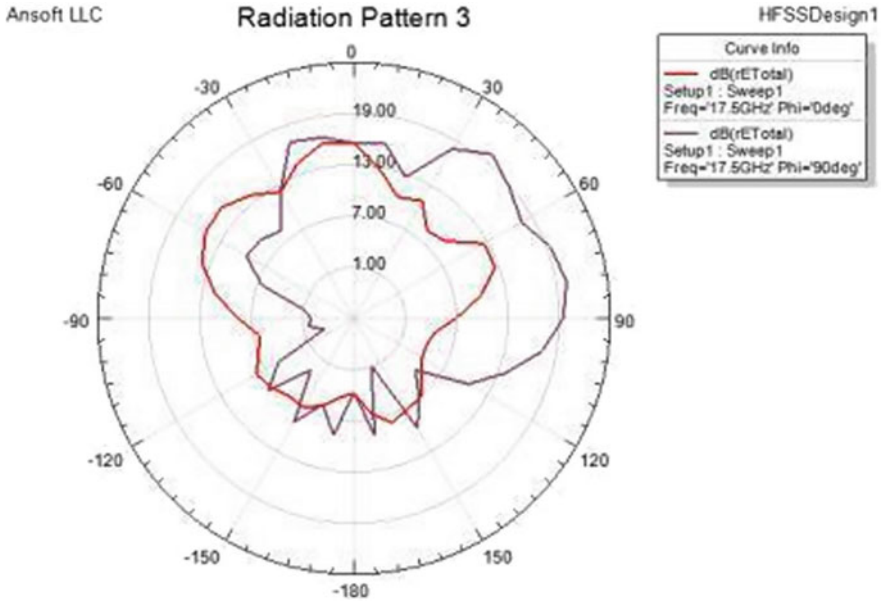


Fig. 5 Radiation pattern *E*- and *H*-field

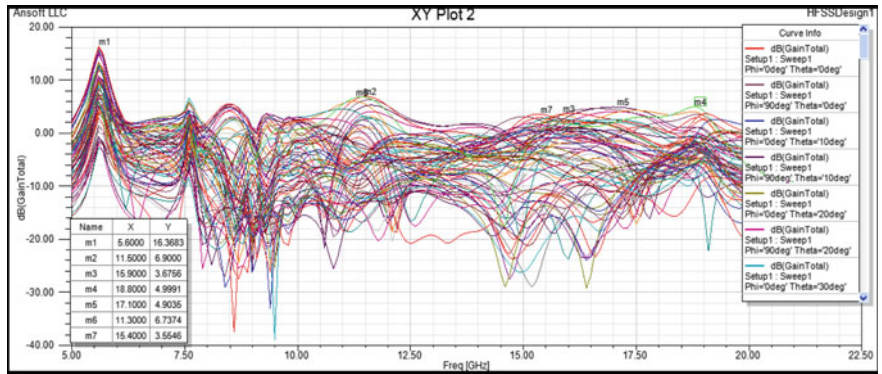


Fig. 6 Gain versus frequency plot

coincides with vertical plane constitutes to a vertically polarized antenna. Similarly, horizontal coincidence of azimuth plane with electric field happens for horizontally polarized antenna. Phase difference between *E*- and *H*-planes is 90°. The plane containing *H*-field and the direction of maximum radiation is called *H*-plane indicated by the purple color.

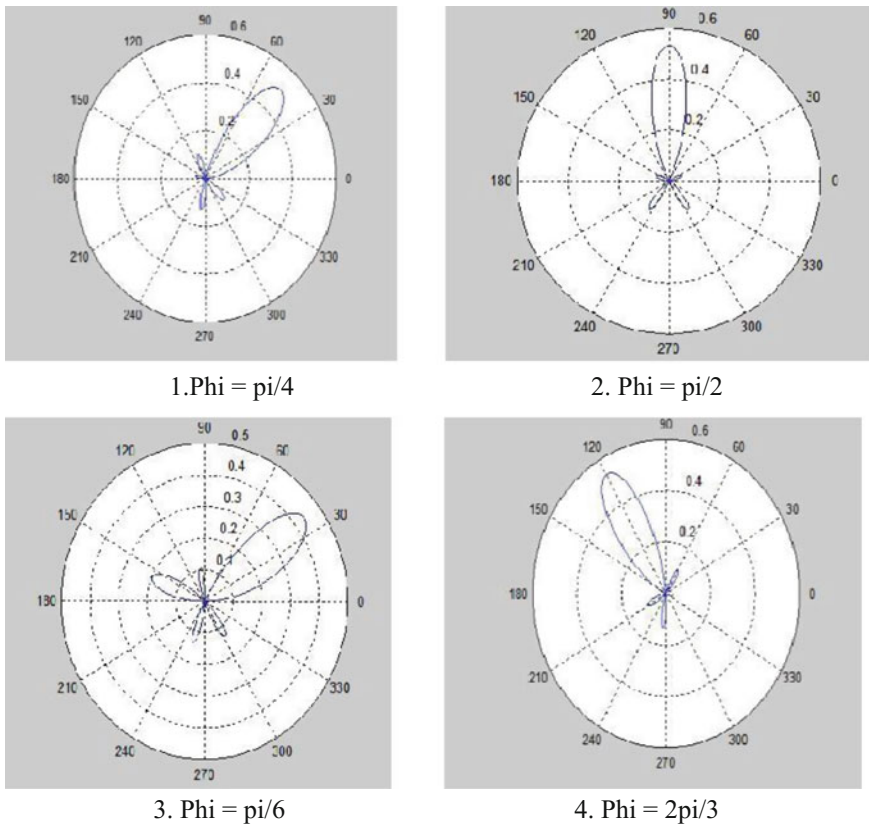


Fig. 7 Beam steering results on MATLAB for various values of phi

The gain versus frequency plot as shown in Fig. 6 shows different values of gain for different frequencies. For the Ku band application, maximum of 6.9 dB gain achieved with an operating frequency of 11.5 GHz (Fig. 7).

4 Conclusion

A novel antenna array composed of rectangular microstrip patches in the matrix form of arrangement 1×4 has been proposed. The gain obtained for the setup is 6.9 dB with a return loss of 36.5 dB. Beam steering, i.e., change in direction of major lobe of radiation pattern for different phi values, is also observed.

References

1. Md. Rabiul Hasan, Abdulla Al Suman, “**Substrate Height and Dielectric Constant Dependent Performance of Circular Micro Strip Patch Array Antennas for Broadband Wireless Access**”, Journal of emerging trends in computing and information sciences, Vol 3, No. 10 Oct 2012
2. A. De, C.K. Chosh and A.K. Bhattacharjee, “**Design and performance analysis of microstrip patch array antennas with different configurations**” International Journal of Future Generation Communication and Networking Vol. 9, No. 3(2016), pp. 97–110
3. N. Mohamed, Sabidha Banu, Dr. M. Ramkumar Prabhu & U.T. Sasikala “**Design A Square Micro strip Patch Antenna for S-Band Application**” , IOSR Journal of Electronics and Communication Engineering (IOSR-JECE)e-ISSN:2278–2834, p-ISSN: 2278-8735. Volume 10, Issue 2, Ver. IV(Mar–Apr. 2015), PP 24–30
4. D.M. Pozar, B. Kaufman, “**Increasing the bandwidth of a micro strip antenna by proximity coupling**”, Electronics Letters, Volume: 23, Issue: 8, April 9,1987
5. Ei Thae Aye, Chaw Myat New, “**Rectangular Micro Strip Patch Antenna Array for RFID applications using 2.45 GHz frequency range**”, International Journal of scientific and research publications, Volume: 4, Issue: 6, June 2014
6. H. Lebret, S. Boyd, “**Antenna array pattern synthesis via convex optimization**”, IEEE Transactions on Signal Processing, Volume: 45, Issue: 3, March 1997
7. G. Li, S. Yang, Y. Chen, and Z. Nie, “**Novel Electronic beam steering technique in time modulated antenna arrays**”, Progress in Electromagnetic Research, PIER97, 391–405, 2009
8. M. Rammal, M. Mouhamadou and P. Vaudon, “**Smart antenna array patterns synthesis: null steering and multi-user beamforming by phase control**”, Progress in Electromagnetic Research, PIER 60, 95–106, 2006
9. Angeliki Alixou, Martin Haardt, “**Smart antenna technologies for future wireless systems: trends and challenges**”, IEEE communications magazine, September 2004

Study of Various Ontologies

Amit Vermal, Iqbaldeep Kaur, Dolly Sharma and Dimple Nagpal

Abstract There is a tremendous growth of component retrieval in the field of component-based software engineering, but the lack of interrelations between concepts and interfaces is still an issue. The gap is fulfilled by the ontology so that the best component can be retrieved by providing interrelationships between components. The objectives of this paper are to study various ontologies that are built by human and to find out the process of ontology retrieval. This paper reviews the current tools and techniques for retrieving the component from repository. To attain good results for retrieving the component from repository, the components in the repository should not only be interlinked but also provide interrelationships of the component that can only be done by using ontology.

Keywords Component-based software engineering · Retrieval · Ontologies

1 Introduction

The analysis of the previous work related to component-based development is focused on the retrieval of component from repositories. Various classification and retrieval techniques are there for storing and retrieving the component from repository. In this, we study about the previous work on component-based retrieval.

A survey of component retrieval and numerous software repositories is given in [1]. Software repositories are designed in such a way so that component can easily

A. Vermal (✉) · I. Kaur · D. Sharma · D. Nagpal
Department of Computer Science, Chandigarh Group of Colleges, Landran, Punjab, India
e-mail: dramitverma.cu@gmail.com

I. Kaur
e-mail: iqbaldeepkaur.cu@gmail.com

D. Sharma
e-mail: dolly.azure@gmail.com

D. Nagpal
e-mail: dimplenagpal009@gmail.com

be retrieved from repository. Software repositories are required to facilitate storing and maintaining reusable software components efficiently. This paper provides a base for user-friendly interface which retrieves the component from a well-defined repository. Moreover, future work of this paper leads to the semantic search to increase the precision and recall ratio. The retrieval of component from semantic search technique not only gives precise output, but also the results that match the query syntactically and semantically.

In [2], concept of keyword-based retrieval using automated implementation is discussed. A newly developed tool named Automated Repository Exploration (ARE) version. 1.0.0 has been implemented. This technique retrieves the component relevant to the keyword based on user query. Then the ranked results were presented to users according to the reliance of the searched components. In this paper, working of the tool with keyword-based search is performed for retrieving relevant components from repository.

To improve search prospects and to rank the components, weights are assigned to individual components, so that the most relevant components rank higher than the non-relevant one.

In [3], an approach to software reuse was presented which is architecture based. Architecture-based approach presents an integrated approach to software reuse. The various reuse issues are addressed in this approach in semi-automatic fashion. These approaches encourage the component-based development automation along with supporting the design maintenance. A prototyping system ABRIE was described for supporting this approach.

As illustrated in [4], this paper presents the keyword-based retrieval. The implementation of this retrieval algorithm is done by a tool named Automated Repository Exploration. In this paper, ranking and retrieval of component is also done by assigning weights to each component. While there are several advantages of keyword-based retrieval, one should not avoid the limitation of it. The limitation of keyword-based retrieval is that the keyword queries are ambiguous and create many ambiguity like structural and keyword ambiguity. Moreover, the evaluation of results is difficult to find in keyword-based retrieval.

As illustrated in [5], this paper presents the retrieval by firstly classifying the component. The classification of component is the combination of attribute value and faceted classification. The retrieval of component is done by both keyword and query based, but the output of query based is more precise as compared to keyword. The comparison of query-based retrieval and keyword-based retrieval is shown in Table 1. But the problem with the query-based retrieval scheme is that it gives effective output on small number of components in repository. If the component repository is large enough, it does not give us precise output.

A technique that is required to retrieve the component semantically and syntactically is named as ontology. An ontology-based component retrieval is much more effective retrieval than any other technique. Basically, ontology provides the

Table 1 Query-based retrieval and keyword-based retrieval

The method of retrieval	Component in repository	Components retrieved	Relevant component retrieved	Relevant components in the index	Precision (%)	Recall (%)
$T_F R_L$	400	380	320	350	84	91
$M_{Fb} R_L$	400	372	323	348	86	92
$M_{Rb} R_L$	400	375	340	344	90	97
$M_{ROC} R_L$ (proposed method)	400	392	375	380	96	98

R_L retrieval; T_F traditional faceted; M_{Fb} MDL file based; M_{Rb} metadata repository based; M_{ROC} metadata repository and ontology-based component

relationship between concepts, classes, and individuals so that the component which is retrieved from the repository not only matches the query syntactically but also matches semantically. In [6], a component retrieval system that retrieves the component based on faceted and metadata repository is described.

In [7], the various component retrieval techniques that are based on facet description, signature matching, tree-based structure, hierarchical structure, and specification matching are described. These retrieval techniques not only help in effective retrieval but also the efficiency of the component can also be ensured by this. Moreover, it suggest an idea for further improving the precision and recall rates by extending the dictionary terms, or by expanding the query, or by designing a user-friendly interface, etc.

In [8], an ontology-based description of component is provided with the OWL (web ontology language). In this, the software is developed which retrieves the component semantically. For retrieving the component, a user query inputs the query in natural language that is being translated to OWL, so that the same semantic representation is deployed for matching the component on both sides, i.e., user query and the component sides. Moreover, the future work of this paper is to build a numerical control component repository under network management environment that is based on component description with the help of ontology.

In [9], for storage and retrieval of components, a metadata and faceted classification is presented that considers domain semantic information based on ontologies and taxonomies.

As compared to other repositories that extract the limited number of components, the proposed metamodel provides the recommendation of components, as ontology and taxonomies were involved in this. In this, the design of the model of software component retrieval and its architecture were made, and the matching algorithm was presented. The metadata repository was created from domain knowledge, according to the facet and term space relation, and was applied to the

component retrieval process. Then, the retrieval of component is done by matching the terms in the metadata repository to the software component which is described with the facet classification.

In [10], an ontological approach is presented to address the semantic gap. The proposed framework has the two main components, namely a reference architecture ontology and an architecture knowledge base. These components are important because through this, three frameworks processes are integrated. This paper presents an approach to remove the semantic gap by explaining model elements and then developing the refinement and representation processes. The distinguished feature of the proposed framework besides giving importance on the semantic aspect of model element is to achieve integration of framework by dependability relationships. The proposed work can be extended in many directions like establishing its effectiveness through complex case studies, and formalization of the framework activities can be developed as a future direction.

In [11], for developing a job knowledge ontology, a semantic framework is introduced that focuses on domains, i.e., task and knowledge domain. Exploiting the job knowledge (Job-know) ontology, yields knowledge elements obtained from different sources, bridging gaps, identification of knowledge shortages and from a comprehensive perspective the bridging requirement of education system was facilitated.

In [12], an ontology-based representation model and retrieval algorithm for component in order to solve the problem of uniform formulism for component storage and retrieval. For representing the knowledge of ontology, component ontology is employed, and the proposed algorithm for component retrieval is implemented by ontology query and reasoning.

2 General Ontologies

Besides the user-developed ontologies, there exist general ontologies by which human ontologies can be enhanced or developed. Some of the general ontologies are shown in Table 2.

Ontology plays a vital role in retrieving the component form repository, as it provides interrelationships between concepts, interfaces, axioms, provides rules, etc.

Table 2 General ontologies

Ontologies	Description	Contains
U.O	Defines the basic concepts that are similar across knowledge domains	Bunge–Wand–Weber (BWW), common semantic model (COSMO), unified foundational ontology (UFO), yet another more advanced top ontology (YAMATO), etc.
S.P.O	Software life cycles and the phases of software life cycles are defined	Waterfall model, prototype model, incremental model, rapid application development (RAD) model
A.D.O	The relationship between concepts are provided along with the knowledge representation of particular domain	–
V.O	All the different versions which are defined in this, which are produced till date	It contains all the concepts, i.e., revision, release, file, etc.
S.B.O	The behavior of software system is modeled, i.e., the various actions that can be performed under a particular scenario are determined	–
O.O.O	The vocabulary is defined to describe the object-oriented design	It contains concepts such as class, inheritance, polymorphism, member functions, interface, objects, subclass, method. The relationships, i.e., inheritance, realization are also included in this
P.O	A library of patterns is provided that is used for creating the software system	It contains the design patterns of content ontology
S.A.O	The various artifact that are produced during the evolution of software systems are defined	Dublin core metadata, IEEE learning object metadata
D.O	All the documents associated with software system are defined	Contains the documents that are evolved during different phases, i.e., formal specification, source code listing, DFD generated during various phases
Q.O	Varied quality attributes that are associated to software system, i.e., traceability, modularity, correctness are defined	Various tools that are used for measuring the software quality, i.e., run chart, scatter diagram
M.O	The maintenance-related concepts and their relationships are defined	Contains concepts like activity, person, i.e., maintenance engineer, procedure, i.e., method
T.O	A collection of different software development tools that can be used for developing a particular software	The information about the tool is provided with the help of semantic web techniques

3 Conclusion and Future Scope

This paper explains the various classification and retrieval techniques. Moreover, the concept of ontology with various tools to build the ontologies is explained. The findings of this paper are various ontologies that are built by human, study of various general ontologies and understanding the concept of ontology-based retrieval.

References

1. Bakshi, Amandeep, and S Bawa. "A Survey For Effective Search And Retrieval Of Components From Software Repositories." In *International Journal of Engineering Research and Technology*, vol. 2, no. 4 (April-2013). ESRSA Publications, Year 2013.
2. C. Ram, and H. Rathi. "To ameliorate component searching by automating keyword search technique." In *Computing for Sustainable Global Development (INDIACom), 2015 2nd International Conference on*, pp. 560–565. IEEE, Year 2015.
3. Chen, Yonghao, and B HC Cheng. "Facilitating an automated approach to architecture-based software reuse." In *Automated Software Engineering, 1997. Proceedings., 12th IEEE International Conference*, pp. 238–245. IEEE, 1997.
4. Chatterjee, Ram, and Himani Rathi. "To ameliorate component searching by automating keyword search technique." In *Computing for Sustainable Global Development (INDIACom), 2015 2nd International Conference on*, pp. 560–565. IEEE, 2015.
5. Bhatia, Vaneet Kaur. "Implementing Improved Classification and Multiple Search Criteria in Software Repository." PhD diss., THAPAR UNIVERSITY PATIALA, 2011.
6. Gupta, S., and Ashok Kumar. "Reusable Software Component Retrieval System." *International Journal of Application or Innovation in Engineering and Management* 2, no. 1 (2013): 187–194.
7. JATAIN, NIDHI AMAN. "Component Retrieval Techniques-A Systematic".
8. Quan, Liu, Jin Xinjuan, and Long Yihong. "Research on ontology-based representation and retrieval of components." In *Software Engineering, Artificial Intelligence, Networking, and Parallel/Distributed Computing, 2007. SNPD 2007. Eighth ACIS International Conference on*, vol. 1, pp. 494–499. IEEE, 2007.
9. Gupta, S., and Ashok Kumar. "Reusable Software Component Retrieval System." *International Journal of Application or Innovation in Engineering and Management* 2, no. 1 (2013): 187–194.
10. Kiwelekar, Arvind W., and Rushikesh K. Joshi. "An ontological framework for architecture model integration." In *Proceedings of the 4th International Workshop on Twin Peaks of Requirements and Architecture*, pp. 24–27. ACM, 2014.
11. Khobreh, Marjan, Fazel Ansari, Madjid Fathi, Reka Vas, Stefan T. Mol, Hannah A. Berkers, and Krisztián Varga. "An ontology-based approach for the semantic representation of job knowledge." *IEEE Transactions on Emerging Topics in Computing* 4, no. 3 (2016): 462–473.
12. Peng, Yong, Chunguang Peng, Jian Huang, and Kedi Huang. "An ontology-driven paradigm for component representation and retrieval." In *Computer and Information Technology, 2009. CIT'09. Ninth IEEE International Conference on*, vol. 2, pp. 187–192. IEEE, 2009.

Software Component Retrieval System

Amit Verma, Dolly Sharma, Iqbaldeep Kaur and Monisha Kumari

Abstract This paper describes the prerequisites of software component retrieval which further explore the information about the algorithms and tools of software component retrieval. These techniques and procedures are mainly used for analyzing the enormous software components and their parameters. There is a need to find enhanced and optimized result using advance technologies of software component analysis. The objectives of the paper are to understand the component retrieval concepts, to get acquainted with software component extraction, to analyze the enormous amount of component and its parameter and to understand the need of software component analysis.

Keywords Software component retrieval · Software component model
Software component retrieval approach

1 Introduction

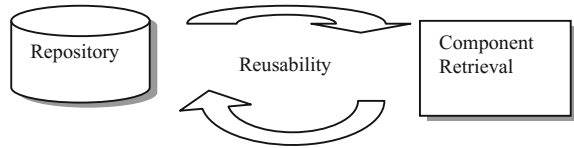
The part of Software Engineering named as component-based development which focuses on concept reusability of the components. The term software component refers to a unit of the software that has set of functional properties and can be integrated into the system independently. These set of properties are called interfaces and accepted by the provider of interface and software or another component that interacts with component (provider). Component-based development involves

A. Verma (✉) · D. Sharma · I. Kaur · M. Kumari
Department of Computer Science, Chandigarh Group of Colleges, Landran, Punjab, India
e-mail: dramitverma.cu@gmail.com

D. Sharma
e-mail: dolly.azure@gmail.com

I. Kaur
e-mail: iqbaldeepkaur.cu@gmail.com

M. Kumari
e-mail: monisha_nk@yahoo.in

Fig. 1 0-Level DFD

the steps to design and develop the system with reusable integrated parts (components). The component can be addressed as a software component, business component, distributed component and much more. There are requirements for the components to be fulfilled as the component should be fully documented, thoroughly tested, designed with awareness, return codes and robust. The software component is stored in the repository and relevant component can be retrieved from the repository for reuse (shown in Fig. 1).

The first time the consideration of software component is given by Doug McIlroy. In 1968, he introduced the concept differently in terms of mathematical routines library or utility libraries. The component retrieval is an important factor for improving the productivity and product quality in software development.

In component-based development, there exist some functional set of properties that are known by component (provider) and the software or component that interacts with the component (provider). There are two types of interface distinguish by component model. The provided interface is the action that is provided to the environment by the component. The required interface is the action the component required and provided by the environment.

Component deployment is a technique that empowers component integration into the system and the deployed component accessible to provide services. Binding is the process that provides the interaction between the components entrenched through interfaces. The component composition is the composition of component functions and component's functional properties. The component-based development system is based on the three principles: reusability, substitutability, and extensibility.

Reusability: Reusability is the extent to which a device can be reused that reduces the buildup from basics. There are three main reuse tasks in the retrieval process: (1) Based on partial specification, the component is searched and retrieved, (2) the reuse worth of retrieved component is accessed, (3) fitting the reusable parts to the specifics of the current issue.

Substitutability: The component should accommodate with the system and meet the requirements of the system. When one component replaces with another component, the system should maintain accuracy, this is called substitutability.

Extensibility: The components can be extended with the components which are part of the system or addition from the outer environment. The component extensibility is supported by providing multiple interfaces as shown in Table 1

Table 1 Three principles

Principles	Explanation	Feature
Reusability	Same component can be used again for different or same purpose	Reduce buildup from basics
Substitutability	Component accommodates with the system and meets requirements	Maintain accuracy of the system
Extensibility	Component can be extended with the component which is part of the system or addition from outer environment	Supported by providing multiple interfaces

1.1 Taxonomies of Component

The component can be business, or technology type. These are explained in Table 2.

1.2 Concept of Component Retrieval

The concept of the retrieval of the component from the repository is that to search the most relevant component from a large number of components present in the repository so that retrieved component can be reused. The aim of component retrieval is based on the concept of “one component from one repository”. The components can be extracted from the repository by using the component retrieval technique as shown in Fig. 2.

1.3 Evolutionary Stages of Component

The reuse of the component is not latest. In ancient times, the components like their tools and weapons were reused for different purpose of tasks.

1.3.1 Early Years of Component

In early Stone Age, the tools and weapons made up of organic material such as leather, wood, fiber, bone, and antler, and in early Iron Age the tools and weapons

Table 2 Taxonomies of component

Component Type	Instances
Bc	Au, Iv, Cr, Cc
Tc	Wss, Jc, Hc.

Bc Business component, *Tc* Technology component, *Au* Authentication, *Iv* Inventory, *Cr* component repository, *Cc* Credit card, *Wss* Web server services, *Jc* JSF components, *Hc* HSQLDB components

were made up of iron and metal. These tools and weapons are used for paintings, cultivation of wild cereals, pottery production, irrigation, domestication of goats, sheep and pigs. The reusability of tools and weapons as component has been used. The same tool or weapon has been used for different works. The communication between people had been based upon the symbols which make their communication keyword based, and the symbols were taught by their families and friends which was genetic algorithm based. The interaction between the people was cluster association based.

1.3.2 Modern Years of Component

Reuse of software component idea has been taken from producing industry and structural designing field. Producing of vehicles from parts and development of structures from blocks are the cases. Spare parts of an item ought to be accessible in business sectors to make it fruitful. The best case for this situation is:

- The producers of different autos would have not been so in profit and successful if these organizations have not make the spare parts available of their autos.

Programming organizations have utilized a similar idea to create programming in parts. These organizations have given parts with their virtual products to market themselves effectively. Programming parts are transported with the libraries accessible with software. These software segments are called components. Component development system has two sub-processes: application engineering and component engineering. In the application engineering, the application is built using the components and in the component engineering, the components are developed and identified that is highly useful.

1.4 Software Repository

The libraries of reusable components keep on growing; the issue of extracting components from the repository has observed the consideration of the software reuse group. The capacity and recovery of reusable assets in a repository has been the subject of dynamic research before reusable resources incorporate program particulars, source code, protest codes, documentations, and the UML particulars that are delivered in the project and can be reused later. But, finding components and reusing the suitable component are difficult, especially when confronted with a huge collection of software components and little documentation is there about how they can be reused. Numerous software repositories have been produced, extending the different searching approaches. Henceforth, it is getting difficult to search the component according to the client requirement. This work gives effective direction for finding and identifying relevant software components that fulfill client queries.

1.5 Software Component Retrieval Process

The process of software component retrieval has been discussed in the Table 3 below. This explains the concept of the software component retrieval process from the repository. The process starts with the selection of the software component after query matching. In the repository, assume that there are components in the repository $CR_{\text{repository}}$. There are n number of software components in the repository. C_1 is the first software component in the repository, and C_n is the nth software component in the repository. C_{ret} is the retrieved software component from the repository according to the user requirement UR_{eq} . The user will give some query for the search of the software component.

If the user’s requirement matches the software component present in the repository, then the software component is selected from the repository and can be retrieved. If the user requirement does not matches with the software components present in the repository, then the user needs to do the new search with the modification in the search. The search can be done till the software component does not match the user requirements.

Table 3 Algorithm for selection of component

Algorithm 1: Component selection	
Begin	
Initialize $CR_{\text{repository}}$	// Components in repository
Input: UR_{eq}	// UR_{eq} = User Requirement
Output: C_{ret}	// C_{ret} = Component Retrieved
C_1	// C_1 =First component in repository
C_n	// C_n = Last component in repository
$C_{\text{ret}} \in CR_{\text{repository}}$	
if ($C_{\text{ret}} = UR_{\text{eq}}$)	// C_{ret} =Component retrieved
{	
Select C_{ret}	
Break	
}	
else	
{	
Requirement modification ($UR_{\text{eq}}, C_{\text{ret}}, R_{\text{result}}$)	
return (UN_{req})	// UN_{req} = New user requirement
}	
End if	
{	
$C_{\text{ret}} = UN_{\text{req}}$	
}	

1.6 Conclusion

In this paper, the software component retrieval process has been explained. Different types of software component and the evolution of the software component have been discussed in this paper. The process of retrieval is done by using the different retrieval techniques. The component retrieval techniques and algorithms are integrated with the soft computing approaches like machine learning, neural network-based approach to enhance the better result. There are many software component models that can be used for the designing and development of the software component.

References

1. Zhongjie W, Xu X, Zhan D. A survey of business component identification methods and related techniques, *International Journal of Information Technology*. 2006 Oct, 2(4), pp. 229.
2. Andreas A S, Vogiatzis DG, Papadopoulos GA. Intelligent classification and retrieval of software components. In 30th Annual International Computer Software and Applications Conference (COMPSAC'06), IEEE. 2006, pp. 37–40.
3. Tania B, Gadou M, Ranka S. A genetic algorithm based approach for multi-objective hardware/software co-optimization. *Sustainable Computing: Informatics and Systems*. 2016 Jun, (10), pp. 36–47.
4. Kumar B R, Dave M, Joshi R C. Retrieval of Most Relevant Reusable Component Using Genetic Algorithms. In *SERP, Software Engineering Research and Practice*. 2006 Jan, pp. 151–55.
5. Anurag D, Saxena P C. Software component retrieval using genetic algorithms. In *Computer and Automation Engineering, 2009. ICCAE'09. International Conference on IEEE*. 2009 Mar, pp. 151–155.
6. Uğuz, Harun. A two-stage feature selection method for text categorization by using information gain, principal component analysis and genetic algorithm. In *Knowledge-Based Systems*. 2011 Oct, 7(24), pp. 1024–1032.
7. Vodithala S, Pabboju S. A dynamic approach for retrieval of software components using genetic algorithm. In 6th IEEE International Conference on Software Engineering and Services. 2015 Sept, pp. 406–10.
8. Wang L Z, Kung-Kiu. A taxonomy of software component models. On *Software Engineering and Advanced Applications in 31st EUROMICRO Conference*. 2005 Sept, pp. 88–95.
9. Amandeep B, Bawa S. A Survey For Effective Search And Retrieval Of Components From Software Repositories. In *IJERT International Journal of Engineering Research and Technology*. 2013 April, 2(4).
10. Rao CV, Niranjan G P. An integrated classification scheme for efficient retrieval of components. In *JCS Journal of Computer Science*. 2008, 4(10), pp. 821–25.
11. Lucredio D. A survey on Software Components Search and Retrieval. In 30th EUROMICRO conference. 2004, pp. 152–59.
12. Maarek Y S, Kaiser GE, Berry DM. An Information Retrieval approach for automatically constructing software libraries. *Software engineering based IEEE transactions*. 1991 Aug, 17(8), pp. 800–13.
13. William T, George T. Heineman C. *Component-based software engineering. Putting the pieces together*, addison-westley, 2001.

14. Hall P, Leonor B, Hall J. An introduction and history of software architectures, components, and reuse. In *Software Architectures*, Springer, London, 2000.
15. Mcheick H, Ah-Ki E, Godin R, Hamed M. An experiment in software component retrieval. In *IST Information and Software Technology*. 2003 Jul, 45(10), pp. 633–49.
16. Kung-Kiu, Wang Z. Software component models. *Software engineering based IEEE Transactions*. 2010, 10(33), pp. 709–24.
17. Frakes, Pole T P, William B. An empirical study of representation methods for reusable software components. *Software Engineering based IEEE Transactions*. 1994 Aug, 20(8), pp. 617–30.
18. Ibrahim B, Girardi MR. An approach to improve the effectiveness of software retrieval. In the 3rd Irvine Software Symposium Proceedings, Irvine, California, 1993.
19. Mitsuo G, Cheng R. Genetic algorithms and engineering optimization. 2000, 7.
20. Szyperski C, Ivica C, Stafford J. Software components beyond programming: From routines to services. In *IEEEsoftware*, 2011 May/Jun, 28(03), pp. 22–26.
21. Kaur J, Tomar P. Validation of Software Component Selection Algorithms based on Clustering. *Indian Journal of Science and Technology*. 2016 Dec, 9(45), pp. 1–4.
22. Verma A, Gupta S, Kaur I. Inconsistency Detection in Software Component Source Code using Ant Colony Optimization and Neural Network Algorithm. *Indian Journal of Science and Technology*. 2016 Oct, 9(40), pp. 1–11.
23. Kaghed H N, Al-Shamery S E, Al-Khuzai F E K. Multiple Sequence Alignment based on Developed Genetic Algorithm. *Indian Journal of Science and Technology*. 2016 Jan, 9(2), pp. 1–7.

SRR-Loaded Clover Leaf-Shaped Minkowsky Fractal for Multiband Applications

C. Elavarasi and T. Shanmuganatham

Abstract The split ring resonator [SRR] loaded clover leaf-shaped minkowsky fractal antenna for multiband applications is presented. This model fairs that the multiband presence of the antenna is a fall out of its fractal metamaterial nature with leaf patch. The antenna consists of iterations of minkowsky fractal with a complementary split ring resonator. In order to produce multifrequency band features, the SRR is positioned at the back of the substrate. The computer-generated results obtained monopole antenna which offers a multiple operating bands, 8.82 GHz by X band/12.76, 15.56, 15.56, and 17 GHz by Ku band. The size of the SRR-loaded clover leaf-shaped fractal antenna is 16 mm × 14 mm × 1.6 mm printed on FR4 substrate. The parametric studies plus simulated emission characteristics are existing. The proposed antenna effectively achieved return loss, VSWR, and fine radiation pattern with equitable gain across the operating bands.

Keywords Clover leaf · Fractal antenna · SRR · Minkowsky curve
Monopole antennas · Coplanar waveguide fed · Multiband

1 Introduction

Antennas are a predictable part of any wireless communication system, which is stand-in as a transducer among transmitter and free space. They are the well-organized radiators of electromagnetic energy into free space [1]. Owing to the gorgeous features of multiple bands, monopole antenna is the most regularly used antenna for microwave frequency band applications. To accomplish compact and multiband functions in a single device, symmetric coplanar waveguide method is used. Contrasting category

C. Elavarasi (✉) · T. Shanmuganatham
Department of Electronics Engineering, Pondicherry University,
Kalapet, Puducherry, India
e-mail: celavarasi19@gmail.com

T. Shanmuganatham
e-mail: Shanmuga.dee@pondiuni.edu.in

of the design part to a variety of client needs to be evidenced in literatures. These invent contains versatile formation which modify their difficulty on the way to mix with WLAN scheme [2–4]. With the growth in the number of amenities delivered and growing trend of miniaturization needs the design of compact multiband antennas. Several CPW feed antenna techniques have been projected to succeed the multiple band functional frequency [5]. The development of planar strategies like coplanar waveguide has more attention in recent days, which subsequently replace the wire antennas conservatively used for the wireless applications. Fractal metamaterial antennas have resolved this problematic to some extent, but the field of antennas needs more inventive study of the advanced ultra-compact designs [6, 7]. A fractal antenna is fashioned using fractal geometry, a self-similar outline erected from the reiteration of an artless shape. Almost fractals are certainly form in nature. These objects display self-similar structure over a span, but limited scale range [8]. Trees/ferns are fractal in essence and can be fashioned on a computer by applying a recursive algorithm. This recursive nature is accessible in these illustrations—a division from a tree or a leaf from a fern is a small replica of the total—not exact, but akin in nature. This connection helps to regulate and solve the eco-friendly issue of carbon emission plus control. Flowers are one of the splendid creations of nature, and artists have shaped several incredible insights as well [9–12]. Flowers are irregular in nature could be fractals, and they add an additional dimension to the whole landscape [13]. Fractals are only a muse- too rough pro-Euclidean geometry, iterative plus recursive in addition to ostensibly countless [14, 15]. They twist up within food with germs, plants along with animals, mountains along with water plus sky. From the macro-view of a flower, fractals turn up frequently. Here is one stunning example of flower fractals that found in nature is clover leaf. Metamaterials are non-natural materials engineered to have properties that are not institute in nature [16]. The negative refractive index is a utility of electric permittivity plus magnetic permeability which are properties relating to the presence of an electric and magnetic field, correspondingly [17, 18]. Considering Snell’s Law, when a wave lights a negative index material [NIM], the angle that the refracted wave marks with the common plane is much countless than that of materials with positive refractive index.

$$\eta = \sqrt{\epsilon\mu}$$

where, η = Refractive index; ϵ = Electric permittivity; μ = Magnetic permeability

In this paper, CPW fed SRR-loaded clover leaf-shaped patch with Minkowsky curve fractal antenna produce an X band—8.82 GHz and Ku band—12.76 GHz/15.56 GHz/17 GHz resonances. The CPW fed has the assistance of uniplanar feed along with denseness. A few CPW fed designs enlist large area, so it is tough in the analysis part. In order to progress the impedance bandwidth with compacted size, coplanar waveguide [CPW] feed has been originated because of their striking eventual [19]. One of the most basic properties of fractal is self-similarity which is nothing but each tiny petal of the bigger one has the equivalent shape in the complete flower. The clover leaf is one of the types found in

fractal [8] shapes. The acceptable conduct of the antenna such as reflection coefficient, gain, emission pattern, and impedance matching are enforced at almost all the functional bands. Parameters of the antenna were designed, and stimulated results are presented and conferred.

2 Antenna Design

The design going ahead with basic CPW fed circular patch configuration [1] gives a single fundamental mode of resonance at 11.54 GHz [−40.79 dB]. The matching of fundamental resonant mode was reduced, and it is improved when feed is changed to clover leaf shape and also with symmetric CPW ground (2) gives a single fundamental mode of resonance at 8.64 GHz [−24.29 dB] and 10.82 GHz [−18.45 dB].

The clover leaf-shaped patch with modified minkowsky curve fractal configuration provides a triple mode resonance (3) with better matching compared to its before stage which gives a triple resonance at 8.6 GHz [−18.54 dB], 12.35 GHz [−28.21 dB], and 15.3 GHz [−30.28 dB]. The matching and gain properties of multiple band of resonance improved by etching a complimentary split ring resonator loaded on reverse side of the substrate on stage (4) as shown in the Fig. 1. Figure 2a, b shows the configuration of the CPW fed circular patch and clover leaf-shaped patch. The proposed antenna is engraved on a flame retardant 4 substrate with dielectric constant $\epsilon_r = 4.4$ and loss tangent ($\tan \delta$) = 0.02. The SRR loaded with minkowsky curve fractal antenna dimensions is $16 \times 14 \times 1.6 \text{ mm}^3$ as shown in the Fig. 2c, d. The proportions of the designed SRR-loaded clover leaf-shaped fractal antenna are fixed in Table 1. The gap ‘g’ among the center strip plus ground is 0.3 mm. The clover leaf-shaped patch with minkowsky curve fractal and SRR is exotic to strengthen the coupling among the SRR-loaded leaf minkowsky patch which act as a superior contender for multiple functional band applications.

3 Simulation Results

Figure 3 shows the reflection characteristics of compact multiband CPW fed clover leaf-shaped fractal SRR antenna. The antenna projected shows the resonance at 8.8 GHz at X band and 12.76 GHz/15.56 GHz/17 GHz at Ku band. Consequently,



Fig. 1 Design evolution of the antenna proposed

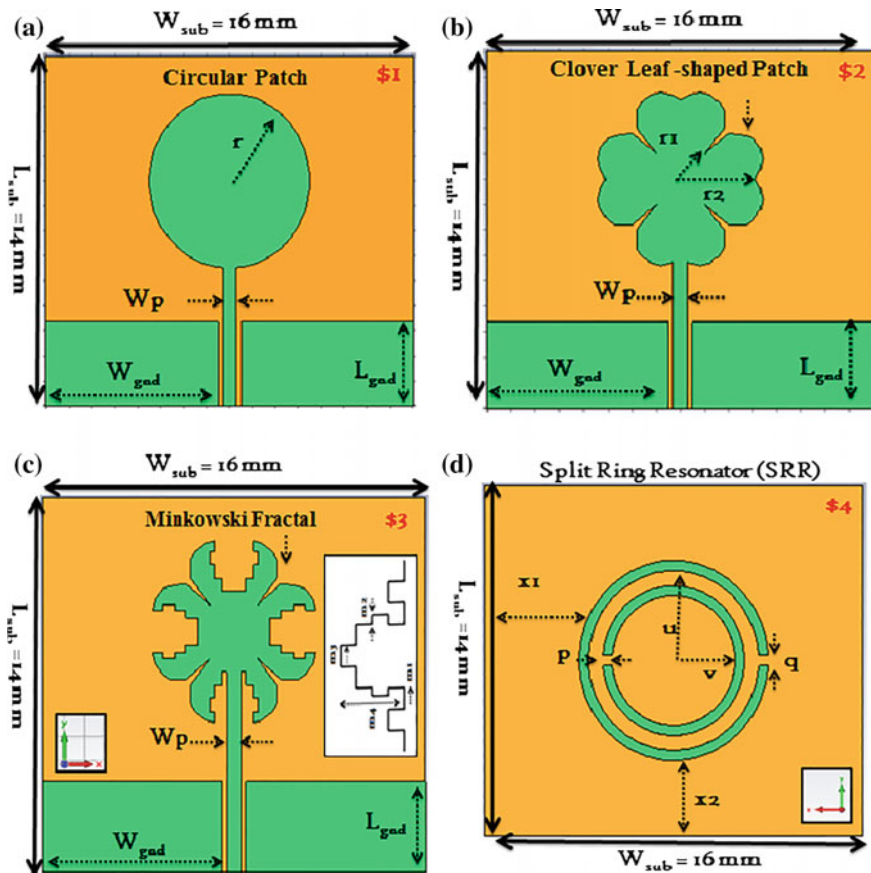


Fig. 2 Geometry of the CPW-fed circular patch antenna [1] (a), clover leaf patch [2] (b), Minkowski fractal [3] (c), split ring resonator fractal antenna [4] (d)

Table 1 Design parameters of the antenna

Parameter	Dimension	Parameter	Dimension
Wsub	16.0	m2	0.2
Lsub	14.0	m3	1.0
Wgnd	7.5	m4	2.0
Lgnd	3.4	r	3.5
Wp	0.6	r1	3.0
Lp	5.5	r2	1.5
u	3.0	t	1.6
v	2.0	gap	0.3
p	0.3	x1	3.0
q	0.3	x2	3.0
m1	0.5		

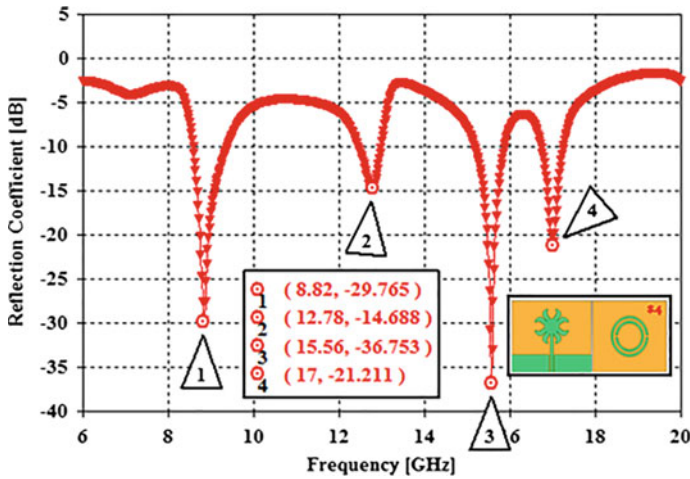


Fig. 3 Shows S11 versus frequency for SRR-loaded fractal metamaterial antenna

we can realize more multiple bands with fine magnifications of clover leaf with minkowsky fractal and split ring resonator. The parametric studies of the planned design for the comparison of reflection coefficient [dB] versus frequency [GHz] for CPW fed circular patch antenna [Ant 1]/clover leaf-shaped patch [Ant 2]/Minkowsky Fractal [Ant 3]/split ring resonator fractal antenna [Ant 4] are carried and shown in Fig. 4. Figure 5 demonstrate the simulated electric current distribution at the frequency of 8.8, 12.7, 15.5, and 17 GHz. Due to the pairing, the electric plus magnetic fields of the monopole cooperate with the SRR by electrifying both the inner along with outer slit rings. This excitation makes the SRR to reveal its metamaterial-like negative functions, thus provide a radiating mode that correlate to the smallest reverberating frequency of the SRR antenna.

The computer-generated radiation patterns of the clover leaf-shaped patch with minkowsky fractal metamaterial antenna exemplify in Fig. 6. It can be seen that the emission patterns found in the H plane are roughly omnidirectional, and radiation pattern in the E plane is bidirectional, which designate superior monopole like emission characteristics over the operating functional bands. The SRR is placed in the reverse side of the proposed antenna and is magnetically united to it. To validate the occurrence of negative permeability characteristics in the proposed SRR structure, waveguide method are used to describe. The real parts of permeability are extracted as shown in Fig. 7. Thus, effective material constraints extract the best manner to prove the realism of metamaterial property. The replicated crest gains against frequency are schemed in Fig. 8. It confirms that the anticipated antenna provides an elevated level of exclusion to signal frequencies inside the multiple functioning bands.

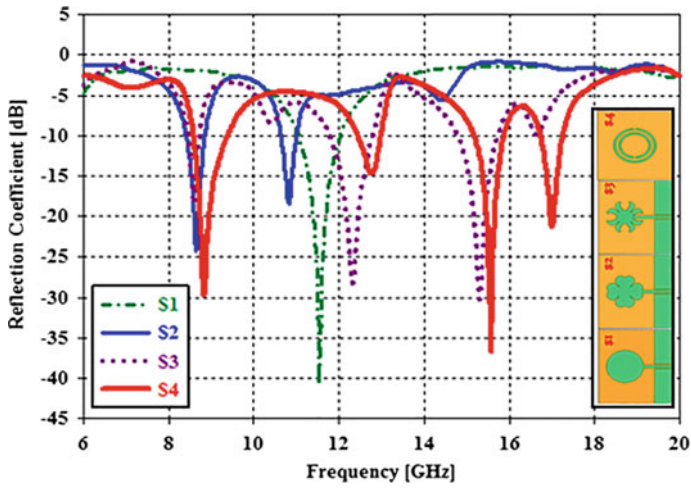


Fig. 4 shows comparison of S11 versus freq for CPW-fed circular patch antenna [S1]/clover leaf patch [S2]/Minkowsky fractal [S3]/split ring resonator fractal antenna [S3]

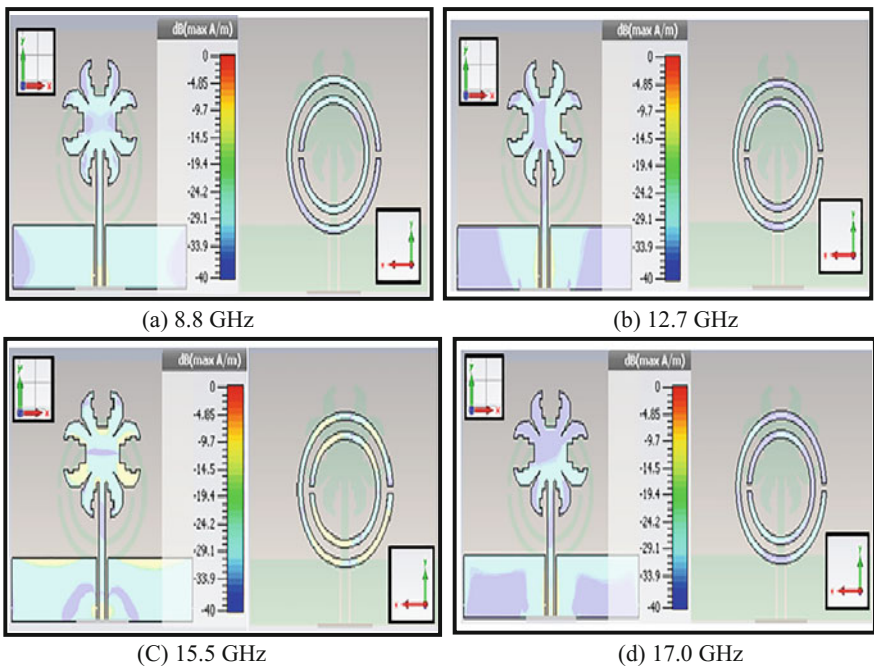


Fig. 5 Simulated current distributions for proposed antenna

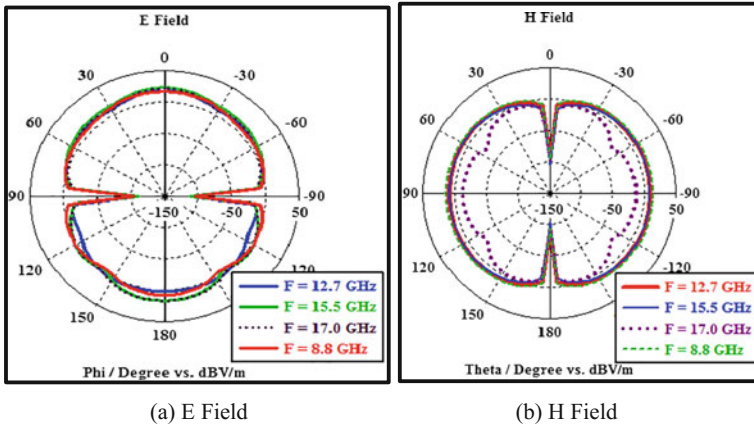
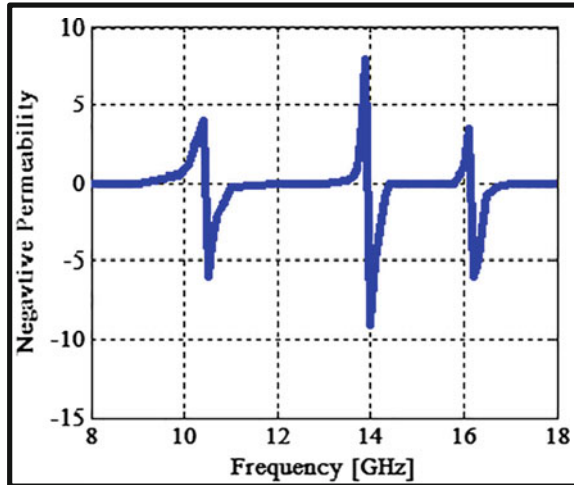


Fig. 6 Far-field pattern for proposed antenna

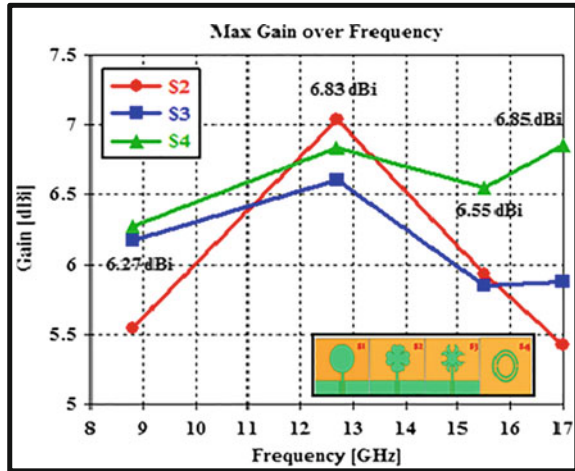
Fig. 7 Negative permeability



4 Conclusion

SRR-loaded clover leaf-shaped minkowsky fractal antenna with CPW feeding technique has existed in this paper. The computer-generated results indicate that the proposed antenna yields X and Ku bands. Fractal metamaterial antenna consists of compacted size ($16 \times 14 \text{ mm}^2$) which is for multiple operating frequencies. The result shows that antenna have good reflection coefficient and with compact size reduction and this minkowsky fractal SRR antenna is best suited for 8.82, 12.76, 15.56 and 17 GHz multiband applications.

Fig. 8 Peak gain



References

1. Yang Cai, Zuping Qian, Wenquan, Yingsong Zhang, Liu Yang, "Electrically large resonant cavity loaded with ϵ -ve and μ -ve Metamaterials", IEEE Ant. and Wirele. Propaga. Lette., Vol. 15, pp. 294–297, (2016).
2. Jayaram Kizhekke, Malathi Kanagasabai, "Circularly polarized broad band ant deploying fractal slot geometry", IEEE Ant. and Wirele. Propaga. Lette., Vol. 14, pp. 1286–1289, (2015).
3. S.C. Basaran, U. Olguun, and K. Sertel, Multi-band monopole ant with complement-ary split ring resonators for WLAN/Wi-MAX applications, IET Electro. Lette., 49, 636–638, (2013).
4. V. V. Reddy and N. V. S. N. Sharma, "Compact circularly polarized asymmetrical fractal boundary micro-strip ant for wireless applications", IEEE Ant. and Wirele. Propaga. Lette., Vol. 13, pp. 118–120, (2014).
5. Seyed Amir Hossein., Zahra Atlasbaf, "Miniaturized dual band CPW fed ant's loaded with U shaped Meta-materials", IEEE Ant. and Wirele. Propaga. Lette., Vol. 14, pp. 658–660, (2015).
6. Bashar B. Qas Elias, "Design of Broadband Circular Patch Microstrip Antenna for KU-Band Satellite Communication Applications", Int. Jo. of Microw. and optic Techn., Vol. 11, pp. 362–368, No. 5, (2016).
7. Xuxiang Chen, Yuehe Ge, T revor S. Bir d, "Reduction of sidelobe radiations of the standard pyramidal horn using a thin metamaterial lens", IET Electronics Lett., Volume 52, Issue 24, p. 1973–1974, (2016).
8. Maria C. Gonzalez, Bala subramaniam Preetham Kumar, George R. Branner, "Generalised design method of broadband array antennas usin g curved geometry", IET Microwaves, Antennas & Propagation, Volume 10, Issue 14, p. 1553–1562, (2016).
9. Hongyan T ang, Ke Wang, Runmiao Wu, Chao Yu, "Compact broadband CP monopole antenna with tilted branch", IET Electronics Lett., Volume 52, Issue 21, p. 1739–1740, (2016).
10. Nawel Seladji-Hassaine, Fethi Tariq Bendimerad, "Miniaturized Dual Band Triangular Microstrip Antenna with Sierpinski Fractal Ground", Int. Jo. of Microw. and optic Techn., Vol. 11, pp. 347–355, No.5, (2016).

11. C.Elavarasi, T.shanmuganantham, "Parametric analysis of water lily shaped SRR loaded fractal monopole antenna for multiband applications" WASET, Int. Jo. of Electrical, Comp., Energetic, Electronic and Communi. Engg. Vol: 10, No: 9, (2016).
12. Rajan Mishra, Ashish Pandey, "Asymmetric Crescent shaped Dual Band Monopole antenna for UWB and GSM 1800/1900 applications", Int. Jo. of Microw. and optic Techn., Vol. 11, pp. 356–361, No. 5, (2016).
13. Parul Dawar, N.S. Raghava and Asok De, "Ultra Wide Band, Multi-resonance Antenna Using Swastika Metamaterial", Int. Jo. of Microw. and optic Techn., Vol. 11, pp. 413–420, No. 6, (2016).
14. C. Elavarasi, T. Shanmuganantham, "CPW Fed CRR Coconut Tree Shaped Fractal Antenna for C/X Band Apps", Int. J. of Engg. Res. (IJER), vol. 1, Iss. 2, (2016).
15. Mohammed Alibakhshii Kenarri, Mohammad Naseer Moghadasii, Ramazaan Ali-Sadeghzadeh, Bal Singh Virdee, "Hexa band planar ant with ACS fork shaped radiator for the multi band and broad band comm. apps", IET Microwaves, Ant. and Prop., vol. 10, Iss. 5, pp. 471–478, (2016).
16. Debdeep Sarkaar, Kush manda Saurav, Kumar Vai. Srivastavva, "Dual band CSRR loaded printed di-pole ant arrays for pattern diversity MI/MO application", IET Microwaves, Ant. and Prop., vol. 10, Iss. 10, pp. 1113–1123, (2016).
17. Hao Jiang, Zheng hui Xue, Weimiing Li, Wu Ren, "Multi-band polarization insensitive meta-material absorber based on circular Fractal structure", IET Microwaves, Ant. and Prop., vol. 10, Iss. 11, pp. 1141–1145, (2016).
18. N. Mishra and R. K. Chaudhary, "A Miniaturized ZOR Antenna with Enhanced Bandwidth for WiMAX Applications," Microw. and Opt. Tech. Lett., vol. 58, Iss. 1, pp. 71–75, (2016).
19. Maryam Rahimi, Mahshid Maleki, Marjan Soltani, Afsaneh Saeed Arezomand, Ferdows B. Zarrabi, "Wide band SRR inspired slot antenna with circular polarisation for wireless application", AEUE Inte. J.of Electro. and Comm., vol.16, pp. 30212–6, (2016).

Microstrip Transition to Substrate Integrated Waveguide Slot Antenna for Multiband Applications

M. Nanda Kumar and T. Shanmuganatham

Abstract Substrate integrated waveguide is a good candidate for implementing millimeter wave applications. In this paper, we represented microstrip transition to substrate integrated waveguide slot antenna for multiband applications, which is developed by Rogers RT/duriod 5880 with a dielectric constant of 2.2, the substrate thickness of 0.381 mm and metallization thickness is 0.035 mm. The simulation results show reflection coefficient, VSWR, gain and radiation pattern. This antenna produces two resonant frequencies, one band is 2.2 GHz with a resonant frequency of 60 GHz (Suitable for wireless communication networks) and 3.05 GHz band with a resonant frequency 79 GHz (suitable for automotive radar systems).

Keywords Substrate integrated waveguide (SIW)
Substrate integrated circuits (SICs) • Wireless LAN (WLAN)
Printed circuit board (PCB)

1 Introduction

The frequency of millimeter wave technology is 30–300 GHz and plays a very important role in communications, attracted due to increasing growth of academia and industry applications. Some of the fixed unlicensed frequencies of millimeter wave technologies are 60 GHz (wireless communication networks) [1, 2], 79 GHz (automotive radar systems) [3, 4], and 94 GHz (millimeter wave imaging). For this application, investigation on broad band and high gain antenna is very important and growing attention in last decades.

M. Nanda Kumar (✉) · T. Shanmuganatham
Department of Electronics Engineering, Pondicherry University,
Kalapet, Puducherry, India
e-mail: nanda.mkumar12@gmail.com

T. Shanmuganatham
e-mail: Shanmuga.dee@pondiuni.edu.in

57–64 GHz band (7 GHz) is an unlicensed band which is assigned by federal communication commission (FCC) to access unlicensed devices, and resonant frequency is 60 GHz. This frequency band is used for high data rates [5], short-range applications such as wireless local area network (WLAN), automotive applications, and GIFL.

79–81 GHz band (4 GHz) is used for automotive radar applications with resonant frequency 79 GHz [6], which is assigned by federal communication commission, and it is an unlicensed band used to access an unlicensed devices.

For high frequency applications, microstrip lines are not used due to a small wavelength and high losses, and next suitable transmission line is a waveguide but a manufacturing process is tough due to very low value of wavelength.

To overcome the drawbacks of microstrip and waveguides, Introduces new transmission line that is substrate integrated waveguide (SIW) [7, 8]. It is mainly introduced to implement for high frequency applications like millimeter and centimeter applications and one type of substrate integrated circuits (SICs) [9–11]. The shape of SIW is a waveguide, integrated with the help of two rows (periodic) of holes or vias interlinked with the bottom and top ground planes of a substrate. Figure 1 describes the simple structure of a SIW.

Compared to microstrip lines, fabrication process of SIW is very simple, low weight, moderate size, and cost effective; compared to a rectangular waveguide, it has high quality factor, more power handling, low interference. The main advantage of SIW is integrated into a planar form and includes passive components, active components and antennas.

Wireless communications and slot antenna are attracted due to easy integration, low profile, conformability to planar, and better isolation from fed network.

The structure of paper is as follows. Section 2 describes about a design of antenna; Sect. 3 describes the structure; Sect. 4 describes the discussion of result. Finally, Sect. 5 describes about the conclusion.

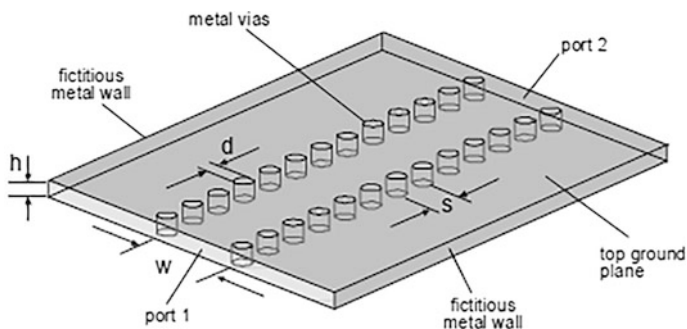


Fig. 1 Substrate integrated waveguide

2 SIW Design

SIW is one type of transmission line, designed mainly for millimeter and centimeter wavelength applications. TE_{10} is a dominant mode of rectangular waveguide and the width of a dielectric-filled rectangular waveguide is

$$a_R = \frac{C}{2 * f_c * \sqrt{\epsilon_r}} \quad (1)$$

where

a_R width of dielectric-filled rectangular waveguide,
 C speed of light.

The SIW width is also depended on d as well as s , as given in Eq. 2 [12–14].

$$a_R = a_S - \frac{d^2}{0.95s}. \quad (2)$$

To maintain loss free radiation between metallic vias, it must satisfy the below equation [12–14].

$$d \leq \frac{\lambda_g}{5} \quad (3)$$

and

$$s \leq 2d. \quad (4)$$

3 Proposed Antenna Structure

Figure 2 shows that the structure of proposed antenna is used for operation of 60 GHz frequency band, Rogers RT/duriod 5880 with a $\epsilon_r = 2.2$ material is used to design, height is 0.381 mm, and copper thickness of 35 μm . Where white colour represents for a dielectric substrate, yellow colour represents for copper and circles also filled by a nickel to create holes between top and bottom planes through dielectric substrate. Figure 2a–c are the bottoms, top planes and side view proposed antenna. In Fig. 2a, we used microstrip feeding with an input impedance of 50 Ω . The dimensions of proposed antenna is 4 * 9.034 * 0.381 mm and the top of substrate we introduce the slot. The parameters considered for designing of an antenna were mentioned in Table 1.

A quarter wavelength is chosen for microstrip and tapered microstrip length. The size of slot width is chosen in between half-guided wavelength to guided wavelength, and length will be less than a width of the slot.

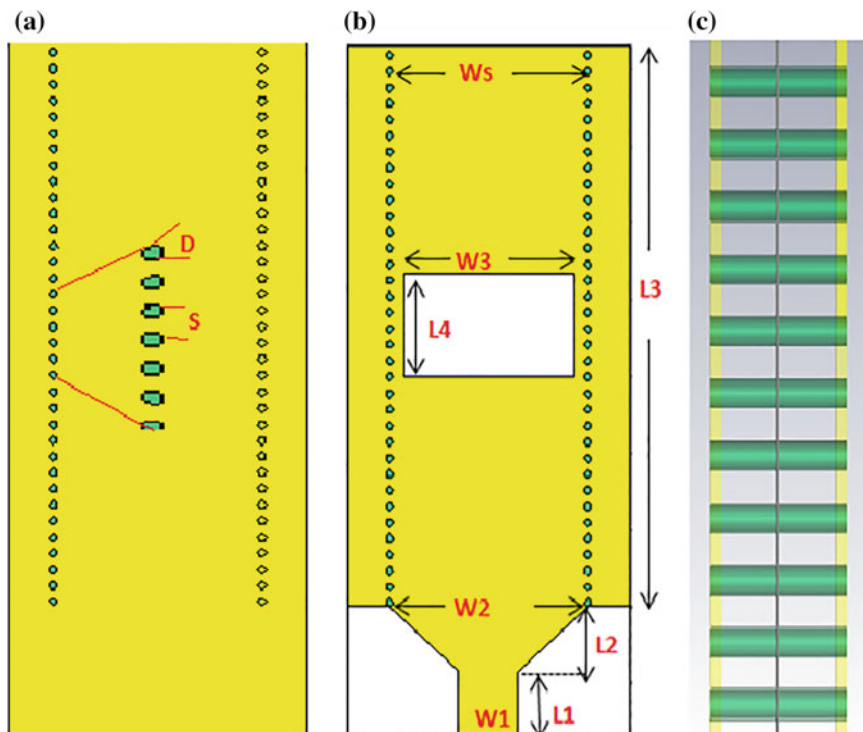


Fig. 2 Proposed antenna **a** bottom plane, **b** top plane, **c** side view

Table 1 Parameters used for design

Parameter	Value (mm)	Parameter	Value (mm)
S	0.21	L_4	1.35
D	0.1	W_1	0.842
L_1	0.842	W_2	2.8
L_2	0.842	W_3	2.4
L_3	7.32	W_s	2.8

4 Results and Discussion

Figure 3 shows the frequency (GHz) versus reflection coefficient (dB) in between frequency range 50–90 GHz and observed that two resonant bands 60 and 79 GHz and their return losses are -34.153 and -20.874 dB and also observed different bands with respect to -10 dB reference line, one is between 58.833 and 61.035 GHz (2.2 GHz bandwidth) and another one is 77.326–80.384 GHz (3.05 GHz bandwidth). The resonant frequency of 60 GHz is suitable for wireless communication networks, and second resonant frequency 79 GHz is suitable for automotive radar applications.

Fig. 3 Reflection coefficient versus frequency

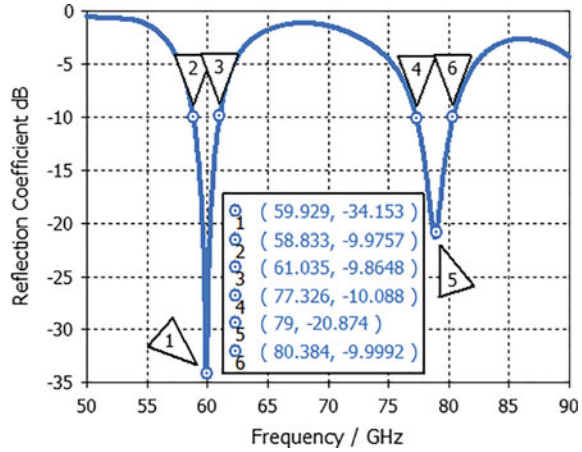


Fig. 4 Voltage standing wave ratio (VSWR)

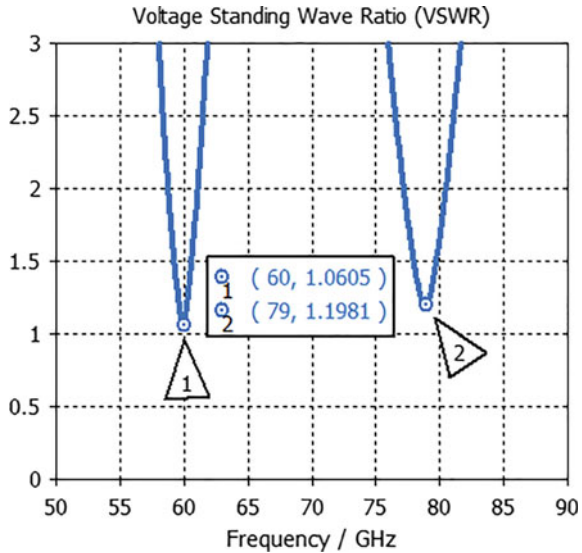


Figure 4 shows the VSWR for above-simulated antenna and observed the two resonant frequencies 60 and 79 GHz. The VSWR values are 1.0605 and 1.1981. This antenna can be suitable for two applications, one is wireless communication networks (60 GHz) and another one is automotive radars (79 GHz).

Figure 5 describes the 3D gain pattern for different frequencies (60 and 79 GHz), observed that the direction of propagation is along z-direction and gains are 5.432, 5.987 dBi at 60 and 79 GHz frequencies, and also observed that the radiation and transmission efficiencies are -0.026 dB (0.0994), -0.8318 dB

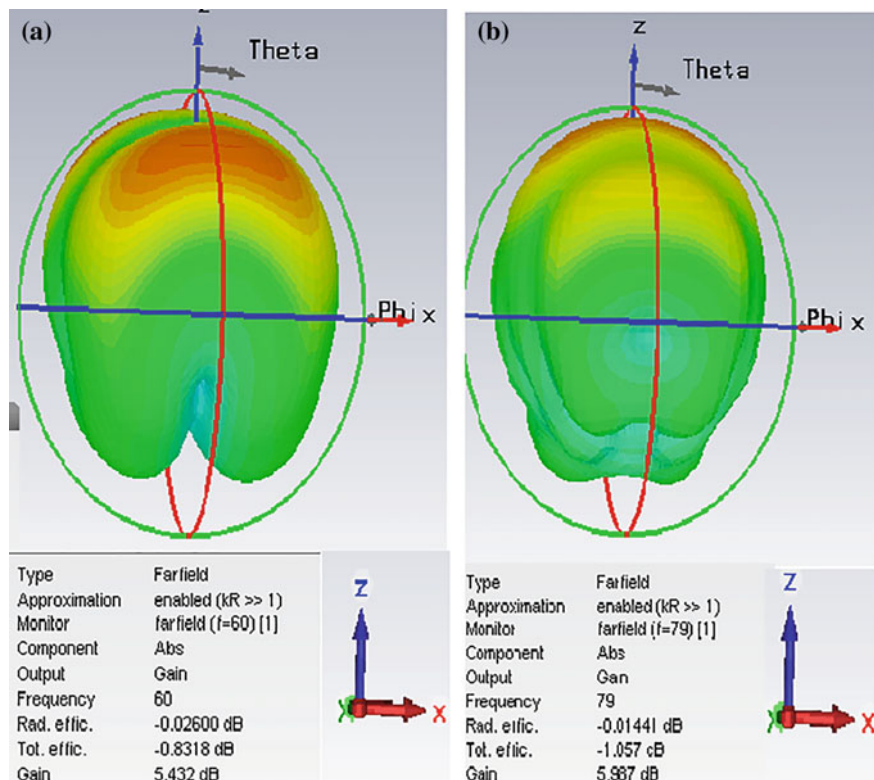


Fig. 5 3D gain patterns **a** 60 GHz, **b** 79 GHz

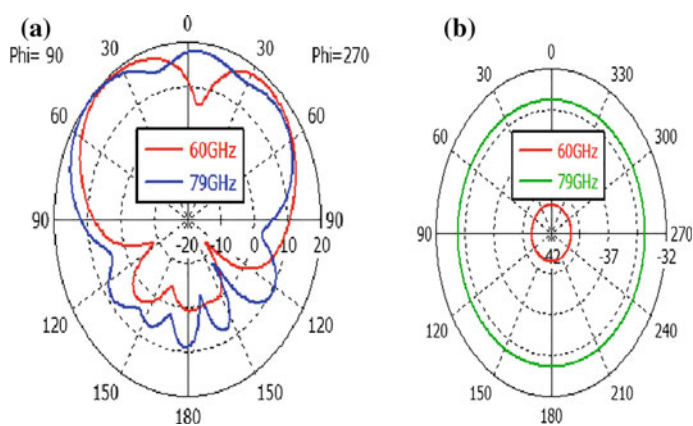


Fig. 6 Two-dimensional radiation pattern **a** E-field, **b** H-field

(0.0825) at 60 GHz and -0.01441 dB (0.09966), -1.057 dB (0.078397) at 79 GHz. Figure 6 shows the E-plane and H-plane patterns for different frequencies, i.e., 60 and 79 GHz.

5 Conclusion

This paper presents design of microstrip transition to SIW slot antenna for dual band applications and achieved two bands, one is around 2.2 GHz (58.833–61.035 GHz) with resonant frequency of 60 GHz and another is 3.05 GHz (77.326–80.384 GHz) with resonant frequency of 79 GHz with respect to -10 dB line and VSWR (2:1). The gain, radiation efficiency, transmission efficiency, VSWR, and reflection coefficient values are 5.432 dB, 99.4%, 82.5%, 1.0605, -34.153 dB at 60 GHz and 5.987 dB, 99.66%, 78.397%, 1.1981, -20.874 dB at 79 GHz. The 60 GHz frequency is suitable for wireless communication networks, and 79 GHz frequency is suitable for automotive radar applications.

References

1. Purva Shrivastava and T. Rama Rao "Performance Investigations with ATLSA on 60 GHz Radio Link in a Narrow Hallway Environment" *Progress in Electromagnetics Research*, vol. 58, pp. 69–77 (2015).
2. S. Ramesh and T. Rama Rao "Planar High Gain Dielectric Loaded Exponentially TSA for Millimeter Wave Wireless Communications" *Wireless Press Communication (Springer)*, pp. 3179–3192 (June 2015).
3. Junfeng Xu, Zhi Ning Chen, and Xianming Qing "CPW Center-Fed Single-Layer SIW Slot Antenna Array for Automotive Radars" *IEEE Transactions on Antennas and Propagation*, vol. 62, no. 9, pp. 4528–4536 (2014).
4. Yujian Li and Kwai-Man Luk "Low Cost High Gain and Broadband Substrate-Integrated-Waveguide-Fed Patch Antenna Array for 60-GHz Band" *IEEE Transactions on Antennas and Propagation*, vol. 62, no. 11, pp. 5531–5538 (2014).
5. D. Lockie and D. Peck, "High data rate Millimeter wave Radios," *IEEE Microwave Mag.*, Vol. 10, No. 5, pp. 75–83 (2009).
6. Shi Cheng, Hanna Yousef, and Henrik Kratz "79 GHz Slot Antennas Based on SIW in a Flexible Printed Circuit Board" *IEEE Trans. on Antennas and Propa.*, Vol. 57, No. 1 (2009).
7. Soumava Mukherjee, Animesh Biswas, and Kumar Vaibhav Srivastava "Substrate Integrated Waveguide Cavity-Backed Dumbbell-Shaped Slot Antenna for Dual-Frequency Applications" *IEEE Antennas and Wireless Propagation Letters*, vol. 14, pp. 1314–1317 (2015).
8. Dongquan Sun, Jinping Xu and Shu Jiang "SIW horn antenna built on thin substrate with improved impedance matching" *ELECTRONICS Letters*, vol. 51, No. 16 pp. 1233–1235 (2015).
9. Maurizio Bozzi, Luca Perreggini, Ke Wu, Paolo Arcioni "Current and future research trends in substrate integrated waveguide technology" *Radioengineering*, vol. 18, no. 2, pp. 201–207 (2009).

10. Nanda kumar M and T Shanmuganatham “Substrate Integrated Waveguide Cavity Backed Bowtie Slot Antenna for 60 GHz Applications” IEEE International Conference on Emerging Technology Trends (2016).
11. Nanda Kumar M and T shanmuganatham “Substrate Integrated Waveguide Cavity Backed with U and V Shaped Slot Antenna for 60 GHz Applications” International Conference on Smart Engineering Materials (2016).
12. Nanda Kumar M and T Shanmugnantham “Current and Future Challenges in Substrate Integrated Waveguide Antennas –An overview” IEEE International Conference on Advanced Computing (February-2016).
13. Nanda Kumar M and T Shanmugnantham “Substrate Integrated Waveguide π Shaped Slot Antenna for 57–64 GHz Band Applications” ICMEET (Jan-2017).
14. Nanda Kumar M and T Shanmugnantham “Substrate integrated waveguide tapered slot antenna for 57–64 GHz applications” ICCSP (Jan-2017).

A Comparative Analysis of PID Controller Design for AVR Based on Optimization Techniques

Ishita Uniyal and Afzal Sikander

Abstract In this study, an analytic comparison of the design for PID controller based on automatic voltage regulator (AVR) has been presented. The design of proportional-integral-derivative (PID) controller is categorized on the basis of optimization techniques inspired by nature. The objective has been achieved by taking some famous optimization techniques into consideration. These techniques are teaching-learning-based optimization (TLBO), bacterial foraging optimization algorithm (BFO), CAS (chaotic ant swarm), genetic algorithm (GA) and particle swarm optimization (PSO). Each method has been executed ten times with the same data set, and comparative analysis has been done in terms of transient and steady-state characteristics. The present study identifies the best optimization technique among various techniques to design PID controller for AVR.

Keywords PID controller · Automatic voltage regulator · Optimization

1 Introduction

PID controllers are the key elements in industries when it comes to control a particular process. PID controllers are most important and majorly used controllers to control industrial processes. They have been widely used in other areas such as artificial neural network (ANN), fuzzy logic design and adaptive control [1]. PID controllers have three control modes: proportional control, integral control and derivative control, and the composite modes of PID such as P, PI and PD are the most common modes employed for process control in industries. Researchers have found so many techniques for PID tuning from the past decades. The best technique is the one which enhances the dynamic and frequency response of a system. Numerous techniques are available in the literature for PID controller tuning like as

I. Uniyal (✉) · A. Sikander

Department of Electrical Engineering, Graphic Era University, Dehradun 248002, Uttarakhand, India

e-mail: ishitauniyal777@gmail.com

© Springer Nature Singapore Pte Ltd. 2018

R. Singh et al. (eds.), *Intelligent Communication, Control and Devices*,

Advances in Intelligent Systems and Computing 624,

https://doi.org/10.1007/978-981-10-5903-2_138

1315

Ziegler and Nichols methods [2], Tyreus-luyben method [3], Modified Ziegler–Nichols tuning method [3], Damped oscillation [3], Cohen-Coon [4] and advanced techniques, intellectual optimization algorithms like as genetic method [5, 6] and particle swarm algorithm [7] to provide the optimized response of the system. Further; the technique comes with simplified particle swarm optimization [8]. Then after implementing this CAS algorithm [9], at last the TLBO algorithm [10] offers better performance measure values for PID controller.

2 Proportional Integral Derivative (PID) Controller

PID controller is the major widely proposed prevalent controller. It is incorporated in chemical control industry to solve control problems. It is implemented to enhance the transient responses as well as to eliminate the steady-state response. Each term of controller is used with each other. The PID controller's output is written as:

$$u(t) = K_p \zeta(t) + K_i \int_0^t \zeta(\tau) + K_d \frac{d\zeta(t)}{dt} \quad (1)$$

where

- K_p gain for the proportional controller
- K_i integral controller gain
- K_d derivative controller gain
- $\zeta(t)$ error
- t instantaneous time
- τ integration constant

The transfer function of proportional integral derivative controller is written in the following manner:

$$G_{PID}(s) = \frac{U(S)}{E(S)} = K_p \left(1 + \frac{1}{T_I s} + T_D s \right) \quad (2)$$

where $U(S)$ is the signal to be control, $E(S)$ is indicating the error, K_p indicates the proportional constant, T_I is integral time constant, T_D is derivative time constant.

In PID controller design, the tuning of controller parameter is done in a manner to meet the closed loop system objectives as follows:

1. In the frequency domain, stability is measured.
2. In time domain is used to observe transient response, which includes maximum overshoot, settling time and rise time.

3. Truth value for steady state.
4. Interruption in disturbances.
5. Robustness against plant modelling precariousness.

3 Description of AVR System

The automatic voltage regulator is a device which is manipulated for automatically regulating the voltage of a synchronous alternator. It is difficult to find fast and stable response of AVR because of high inductance and load variations of alternator field windings. To maintain the transient stability of power system, synchronous generator is equipped with excitation system.

There are four components in AVR, i.e., sensor, exciter, amplifier and generator. The voltage sensor senses the terminal voltage of the synchronous alternator. Through the comparator, error voltage is generated and from amplifier it is amplified and further it contributes in controlling the alternator field winding.

Figure 1 depicts the block diagram of the AVR system. For analysing dynamic functioning of the AVR, the transfer function of components is given follows [7, 11]:

A. Amplifier Model

It is written in the following form of transfer function:

$$G_A = \frac{K_A}{1 + \tau_A s} \tag{3}$$

where

K_A gain of the amplifier;

τ_A Time constant.

K_A varies from 10 to 40, and τ_A within 0.02 and 0.1 s.

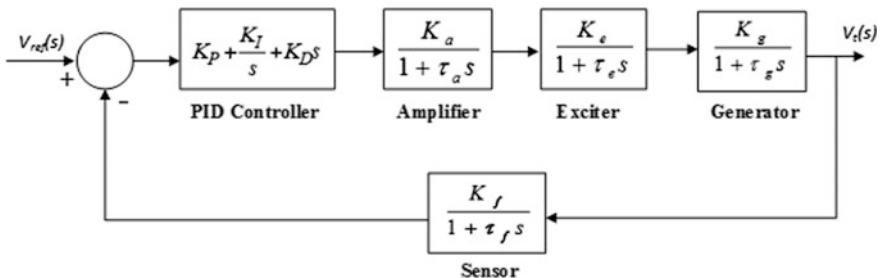


Fig. 1 Automatic voltage regulator with PID controller

B. Exciter Model

The equation for exciter can be given through the constant of gain K_E , and the constant of time τ_E is represented as

$$G_E = \frac{K_E}{1 + \tau_E s} \quad (4)$$

The values of K_E is between 10 and 40, and the time constant τ_E between 0.5 and 1.0 s.

C. Generator Model

The equation for generator is given by:

$$G_G = \frac{K_G}{1 + \tau_G s} \quad (5)$$

where K_G indicates generator gain and τ_G indicates the time constant. K_G ranges from 0.7 to 1.0, and τ_G ranges from 1.0 to 2.0 s.

D. Sensor Model

The equation for sensor circuit is given by

$$G_S = \frac{K_S}{1 + \tau_S s} \quad (6)$$

where τ_S ranges from 0.001 to 0.06 s.

4 Optimization Techniques

The most famous and effective optimization algorithms have been used to establish controller constants for PID controller of AVR system. These techniques are briefly explained below:

4.1 Particle Swarm Optimization (PSO)

Particle swarm optimization is the metaheuristic evolutionary technique proposed in 1995 by Dr. Eberhart and Dr. Kennedy. This algorithm is motivated by the cooperative and societal behaviour of fish schooling and swarming theory [7]. A swarm is an apparently disorganized aggregation of moving individuals may need to flock together. In some cases, individuals want to moves in a random walk.

Swarms are also defined as the certain family of social species. It is a computationally efficient algorithm that gives concept for optimizing nonlinear function.

4.2 Genetic Algorithm

Genetic algorithm is a directed search technique found on a mechanism of biological evolution developed by Prof. John Holland around 1975 and proposed by D. E. Goldberg in 1989 for machine learning [5]. In this, individuals are represented by chromosomes. Basically search algorithm is based on the survival of the fittest concept (Darwinian theory). Genetic algorithm is based on the five component phase: mutation, crossover, population, selection and fitness function.

The population begins with randomly generated states. The next moving on generation of states is given by fitness function. The better state will return with good fitness function. For reproduction, two pairs are selected randomly from the solution. By exchanging between the parents, the offsprings are produced in terms of crossover.

4.3 Teaching–Learning-Based Optimization

It is an evolutionary technique invented by Rao in 2011 [10]. This algorithm is a mimic of teaching–learning process. The algorithm demonstrated two types of learning [10]:

- i. Through interaction with teacher (In teaching mode).
- ii. Through the interaction with scholars (In learning mode).

Teacher plays a vital role in teaching—learning algorithm. Teacher is the one who learns the learners in a perfect way, so they can improve their marks and grades and in other way we say the overall performance. The parameters which are considered in objective function are known as design variables of that particular evolutionary algorithm. The finest resolution in the function is known as the best value of that objective function.

4.4 Chaotic Ant Swarm Optimization

This algorithm was first proposed by Marco Dorigo in 1992. It mimics the behaviour of natural ants. Ant colony optimization is inspired through the activities or behaviour of real ant, and it is also helpful in solving optimization problems in discrete form [9]. Its communication is based on chemicals produced by the ants.

These chemicals are called pheromones. Social behaviour of ants is driven by the trail pheromone. All ants travel at the same speed. All ants deposit an equal amount of pheromone. There are two working modes: forward mode and backward mode, which can be used in dynamic application. Pheromones are only deposited in the backward mode. Ants mark the best solutions and take into account the previous marking to optimize their search.

4.5 *Bacteria Foraging Optimization*

The bacteria foraging is a computational algorithm of biologically inspired computing techniques. BFO is invented by Prof. Revin M. Passino in 2002 based on the social foraging behaviour of bacteria named *E. coli* present in intestine of human being [12]. BFO is a technique inspired through the nature to discover the optimal resolution of the problem. Individual bacteria can communicate with other by sending the signals. Bacteria also guide to cancer as a meta-community of smart social beasts with advanced communication. The bacteria measure the concentration of some chemicals, they make another step and measure it and then they further calculate the difference. BFO is also used as soft filter and social revolutions by chemical tweeting.

5 Results and Discussion

The optimization algorithms discussed in Sect. 4 have been implemented to obtain three parameters: (K_p , K_i and K_d) for PID controller of AVR scheme. The values for these parameters and corresponding time response specifications of AVR along with controller are tabulated in the Table. From this table, it is revealed that the controller designed by CAS optimization exhibits better performance in terms of maximum overshoot, rise time, steady-state error and settling time comparatively among considered five optimization techniques. The time response of AVR along with different controllers when subjected to unit step input is shown in Fig. 3.

Figure 2a depicts the reaction of AVR scheme without controller. In this figure, settling time and rise time achieved the higher values, while we want to reduce these values to obtain the good performance of AVR. Figure 2b depicts the root-locus plot for the AVR scheme without the use of controller. In this, we obtained the gain value as 2; at this value, the system is marginally stable. Above this, the system becomes unstable and goes towards the right-hand side of s-plane. Hence, the system reached the margin of instability. Figure 2c depicts root-locus plot for AVR scheme with different controllers. With the help of this obtained stable system, the roots (poles) are overlapping and lie in the left half of s-plane. So, we obtained the desired response for the system. Figure 2d depicts the frequency

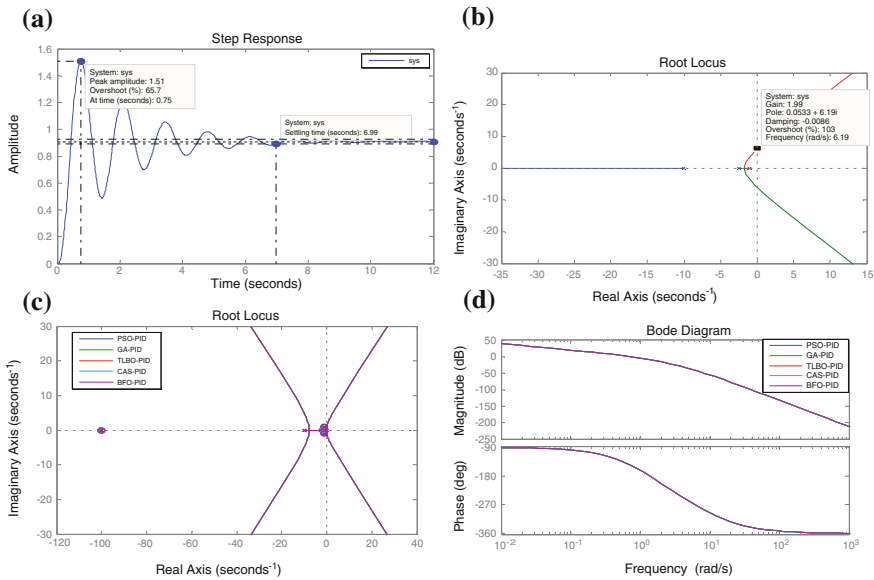


Fig. 2 a Response of AVR without controller; b Root-locus of AVR without controller; c Root-locus of AVR with different controllers; d Bode plot of AVR with different controllers

Table 1 Comparison of time response specifications of AVR

Type of controller	K_p	K_i	K_d	$M_p(\%)$	E_{ss}	T_s	T_r
CAS [9]	0.6202	0.4531	0.2152	0.403	0	0.468	0.304
TLBO [10]	0.5302	0.4001	0.1787	0.61	0	0.618	0.372
PSO [7]	0.6751	0.5980	0.2630	1.68	0	0.495	0.258
GA [5]	0.7722	0.7201	0.3196	4.54	0	0.865	0.214
BFO [12]	0.5462	0.6061	0.2072	4.57	0	2.5	0.328

response providing a good approximation to the PID controller. As it can be verified, the performance meets the specifications.

Table 1 shows the time response specifications of AVR system. The number of generations is considered to be 100. From the table, it is clear that the CAS-PID controller gives the best result as compared with other controllers. So the performance of CAS-PID controller is the best among all the five controllers.

Figure 3 depicts the step response of AVR system with PSO-PID, GA-PID, TLBO-PID, CAS-PID and BFO-PID controllers. From the figure, it is clear that with CAS-PID we obtained the best results. The reason for this is that it is accurate as compared to other controllers in the context of improvement in various transient and steady-state characteristics. So the step response we obtained is most significant in the case of CAS-PID controller.

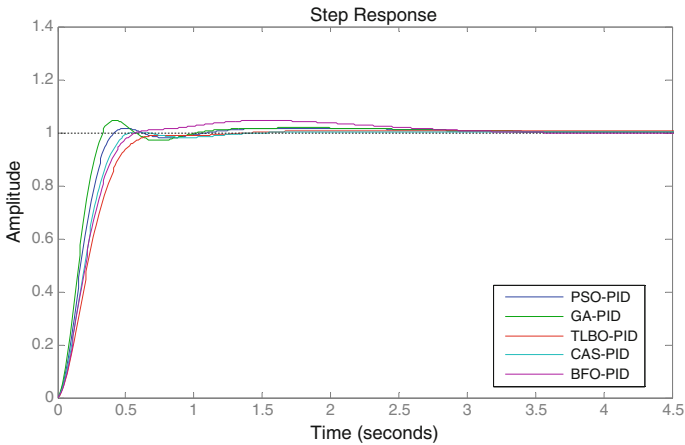


Fig. 3 Step response of AVR with different controllers

6 Conclusion

A comparative analysis of PID controller design methods for AVR is performed in this paper. Five different nature-inspired optimization methods such as PSO, GA, TLBO, CAS and BFO have been considered for this comparative analysis. The comparison has been made in terms of time response specifications and the AVR response with controllers when subjected to unit step input. It is found that among these five optimization methods, CAS optimization method improves the response of AVR better than other optimization methods.

References

1. Hu, H. B., Hu, Q. B., Lu, Z. Y., Xu, D. H.: Optimal PID Controller Design in PMSM Servo System via Particle Swarm Optimization. In: 31st Annual Conference of the IEEE Industrial Electronics Society, IECON 2005, Raleigh, NC. pp. 6–10. USA (2005).
2. Ziegler, J. G., Nichols, N. B.: Optimum Settings for Automatic Controllers. In: *Journal of Dyn Syst Meas Control*, vol. 115, pp. 220–222 (1993).
3. Raut, K. H., Vaishnav, S. R.: Performance Analysis of PID Tuning Techniques based on Time Response Specification. In: *International Journal of Innovative Research in Electrical, Electronics, Instrumentation & Control Engineering*, vol. 2, Issue 1 (2014).
4. Kumar, A., Garg K. K.: Comparison of Ziegler–Nichols, Cohen–Coon & Fuzzy Logic Controllers for Heat Exchanger Model. In: *International Journal of Science, Engineering & Technology Research (IJSETR)*, vol. 4, Issue 6 (2015).
5. Goldberg, D. E.: *Genetic Algorithms in Search, Optimization and Machine Learning*. In: 1st ed. MA: Addison–wesley (1989).
6. Cohen, G. H., Coon, G. A.: Theoretical Consideration of Retarded Control. In: *Trans on ASME*, vol. 75, pp. 827–834 (1953).

7. Gaing, Z. L.: A Particle Swarm Optimization Approach for Optimum Design of PID Controller in AVR System. In: *IEEE Trans on Energy Conversion*, vol. 19, no. 2, pp. 384–391 (2004).
8. Erik, M., Pedersen, H., Chipperfield, A. J.: *Simplifying Particle Swarm Optimization*. (2009).
9. Jiejun, C., Xiaoqian, M. A.: A Multi-Objective Chaotic Ant Swarm Optimization for Environmental/Economic Dispatch. In: *Electrical Power & Energy Systems*, vol. 32, pp. 337–344 (2010).
10. Satapathy, S.: *A Teaching Learning based Optimization based on Orthogonal Design for Solving Global Optimization Problems*. vol. 2, pp. 130–135. Springer Plus (2013).
11. Ula, A., Hasan, A. R.: Design & Implementation of a Personal Computer based Automatic Voltage Regulator for a Synchronous Generator. In: *IEEE Trans Energy Conversion*, vol. 7, no. 1, pp. 125–131 (1992).
12. Sharma, V., Pattnaik, S. S., Garg, T.: A Review of Bacterial Foraging Optimization & its Applications. In: *National Conference on Future Aspects of Artificial Intelligence in Industrial Automation (NCFAAIIA)*, pp. 164–171 (2012).

Aadhaar Card-Based Android Application for Patient Monitoring System

Parth Sharma, Jagriti Raizada, Faraz Siddiqui and Haneet Rana

Abstract Since the past few decades, there has been a rapid increase in the number of diseases which has resulted in enormous increase in the number of patients in hospitals. This increases the workload on doctors and nurses and makes it difficult for them to equally divide their attention among the patients. This might result in unforgivable errors. Therefore, the main focus of this paper is to reduce the workload of hospital workers and to make the process more efficient and organized. This paper proposes a design of a prototype model which implements a well-synchronized patient health monitoring system by utilizing a mobile application that will continuously evaluate the patient's vital parameters, e.g. body temperature, heartbeat and blood pressure, thereby eliminating the constant requirement of an attendant for each patient and also alarming the authorized person whenever any parameter crosses the alarm limits set for it. Additionally, this application will allow the doctor/nurse to access the patient's account which will help the attendant to get a glimpse of the patient's health history making the assessment easy. Diagnosis of the patient can be made without inquiring or any query about patient's health complications. Also, the current health status will accordingly be updated in the database of this application. The paper proposes to use a unique identification Aadhaar card number which will play a key role in providing an access to the patient's data as demonstrated by this prototype model. Since Aadhaar card is a unique number which is owned by every Indian, it possible to access any

P. Sharma (✉) · J. Raizada · F. Siddiqui · H. Rana
Electronics and Communication Engineering, Amity University, Noida, Uttar Pradesh, India
e-mail: parthsharma2708@gmail.com

J. Raizada
e-mail: jagriti95raizada@gmail.com

F. Siddiqui
e-mail: faraz895@gmail.com

H. Rana
e-mail: hrana1@amity.edu

individual's health history which can turn highly beneficial to the treatment of emergency cases.

Keywords Wireless network • IoT technology • Aadhaar card
Patient monitoring system

1 Introduction

Aadhaar number is a twelve digit unique identification number which serves the purpose of a proof of address and identity anywhere in India. It is issued by the unique identity authorization of India on behalf of the Government of India. With the passage of time, the importance of Aadhaar card and Aadhaar number has increased greatly as compared to the time of its inception and has already been incorporated in a number of digital government projects across the country such as marriage, property registration, opening of bank account, applying for PAN card, applying for scholarships.

The recent years have also witnessed the growth of the telemedicine sector in India, and the implementation of Aadhaar card number in this growing sector will introduce a plethora of benefits and ease of diagnosis to the doctors and the medical sector in general. Incorporation of the unique Aadhaar number in the database of the data formed by the collection of wearable sensors will give the doctors the entire past history of the patient and limitations in diagnosis. The database will be stored and accessed by the doctors through an android application, which will also provide the real-time monitoring of the patient's vitals along with displaying a brief history of the patients' medical records and the option of adding a text, that is appropriate diagnosis. The patients can be serialized using their Aadhaar card number, and the creation and accessibility allow the mobility of data and ease of access from anywhere around the world. The sensors used here will be a temperature sensor (LM35).

And a heartbeat sensor is used to give the patient's heart rate.

In this paper, we plan to serialize patients by their unique Aadhaar ID and create a central database which will be accessed through an android application on an Android smartphone which will be interfaced to the patient monitoring system via IoT, reducing time of diagnosis and also increasing the accuracy of diagnosis by giving each patient's medical history.

2 Related Works

In paper [1], the author describes a phone-based system which monitors the vitals such as body temperature, respiratory rate and body posture which further give alerts with the help of intelligent alert system. Additionally, the intelligent data

record system transmits health tips to the patient. The system employs a real-time intelligent content management system (CMS) which is capable of making decisions on the basis of patient's health situation.

In paper [2], the author proposes a real-time patient monitoring system and is based on GSM technology. The model proposes a small portable system which is easy to be carried out by the patient and gives flexibility to the patient to use it. The advantage of this system is that it monitors and records the real-time readings of the various parameters and allows the doctor for accurate diagnosis. However, the system does not allow the doctor to check the patient's condition at any time they want.

In paper [3], the author gives the facility of alerting a doctor whenever a patient crosses a threshold level of the monitoring system. This feature covers a vital role at an emergency situation of the patient. The drawback of the system is that it involves the use of GPS which needs a constant availability of the Internet.

In paper [4], an android application is designed for the diagnosis of the patient. The author employed wireless technology to access patient's information which enables data mobility. Desired signals are extracted by digital filtering. The signals are then processed, and the diagnosis of a disease of the patient is done at the output end.

In paper [5], the author gives Aadhaar-based voting system that comprises of several advantages over the traditional way of voting system. These include cost effectiveness, higher accuracy, fast processing of results, less mechanical and human errors. The system ensures high level of security and privacy with no compromise.

In paper [6], the author proposes an android-based application to monitor parameters such as temperature, ECG, body poster and GPS, and the data is sent to the android application with the help of Bluetooth module. The data is processed, and in the case of emergency, an alert is generated to the concerned doctor or a contact person. The disadvantage of the system is that data sent on the android application is dependent on Bluetooth technology which limits the range of the system.

3 Proposed Methodology

3.1 Objective

The main objective of the proposed system is to provide an access to the patient's data across the country to the concerned doctor:

- at every level of the health sector, i.e. primary level, secondary level and tertiary level;
- at every type of the hospital, i.e. public and private;
- in most of the area across the country, i.e. urban and rural.

For this, this paper proposes a patient monitoring system linked with the Aadhaar card possessed by every Indian citizen. This can be a great asset during emergency cases where every second is crucial. The system will allow the concerned doctor to get a glimpse of the patient's history which helps in saving the time of the doctor for making any kind of diagnosis about the patient and making the treatment process faster. Additionally, in normal times a well-organized personalized app helps the doctor monitor the patient remotely.

3.2 Design

This paper proposes a prototype design of an app which continuously monitors the patient's health vitals by the temperature and heart rate sensors. This data is stored on a Web server via Wi-fi module—ESP8266—and IoT technology. The data is further accessed by the personalized android application authenticated to the concerned doctor. The app mainly performs 3 functions accessed with the help of an Aadhaar card number of the patient:

1. displays the previously diagnosed diseases of the patient.
2. takes the data continuously from sensors embedded on patient and displays real-time information of the patient's health condition on the app.
3. Notifies the concerned doctor or contact person when the patient exceeds risk level.

3.3 Implementation of Design

3.3.1 Software Description

Android Application

Interface basically works on direct manipulation which involves direct touch to produce the outputs. Android, nowadays, is finding wide application in smartphones, gaming controllers, virtual keyboards, etc.

The android application designed by us mainly focuses on four tasks:

- It helps the user to register through an Aadhaar card number. The Aadhaar card number provides a unique identity and removes redundancy which can otherwise create a confusion when two subjects have the same name.
- This application allows the doctor to view the patient's medical history. As it is very difficult to know everything about all the patients in the hospital, this feature will help the doctor to view an updated record about the patient, making the diagnosis more efficient.
- It allows the doctor to enter a diagnosis message after treating the patient, and this is mainly to update the patient's record so that during his/her next visit an updated record is ready.

- Lastly, an alert message appears on the doctor's application whenever the vitals measured through the sensors cross a certain threshold level, indicating immediate attention to be given to the patient.

3.3.2 Hardware Description

Temperature Sensor

Body temperature is the amount of heat that is produced to help us keep healthy. Normally, our body stays at 37 degree Celsius. Our body has a tendency to get back to the normal temperature whenever the temperature outside changes. For example, when too much heat is being produced, then our body tends to sweat trying to cool it down. Similarly, we start shivering when we are cold; here, our body makes the attempt to generate heat to keep us warm.

We have used LM 35 to measure the body temperature, keeping the threshold level as 37.5 °C (99.5 F). LM 35 has an operating range of -55 °C to 150 °C.

Heartbeat Sensor

Heartbeat sensor basically senses the contraction and expansion of heart as it forces the flow of blood from one region to another. This sensor can be manually placed either on the wrist (radial pulse) or on the neck (carotid pulse). This sensor works on the principle of plethysmography. It measures the volume of blood which causes a change in the intensity of the light. Our finger becomes opaque when the heart pumps, and due to which, less light is absorbed. The electrical signal obtained is equivalent to the amount of light absorbed by the blood.

Heart rate in adults ranges between 60 and 100 beats per minute. A lower heart rate implies that the heart functions more efficiently; for example, the heart rate of an athlete ranges from 40 to 45 beats per minute. We have set a threshold of 100 beats per minute.

Arduino Uno

Arduino provides a platform to use both hardware and software. Arduino boards are designed to take the input through a sensor and provide an output which is indicated by a glowing LED, activating a motor or by simply publishing something online. One can easily perform any task by using the Arduino programming language. It is a tool designed for fast prototyping and is used in IOT applications, 3D printing, embedded environments, etc., as it is simple, flexible and easily accessible, and it has thousands of applications.

We are using ATmega 328 to interface the sensors. The data from the sensors is transmitted to the doctor's mobile application through a Bluetooth module, and whenever the incoming values cross the threshold level, an alarm is generated on the mobile application.

Wi-fi Module—ESP8266

This Wi-fi module has an integrated TCP/IP protocol stack which provides Wi-fi access to a microcontroller. Allowing hosting of an application or the functionality to allow offloading all Wi-fi networking functions from some other application

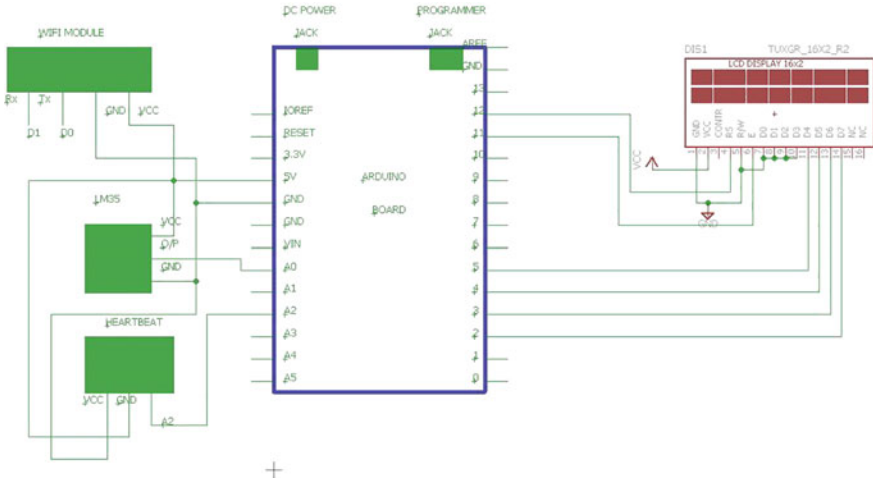


Fig. 1 Schematic diagram of the hardware

processor, the ESP8266 merits its versatility. All ESP8266 modules are pre-programmed which can be simply connected to the Arduino. This module is very cost-effective. The module has a powerful on-board processing and storage compatibility on which the sensors can be easily connected. It has an internally connected RF which allows it to work under all conditions (Fig. 1).

In the figure, Arduino Uno board is connected to the temperature sensor (LM35) and heartbeat sensor which is monitoring patient’s vitals. The Wi-fi module is interfaced with the Arduino board to send the real-time data on to the Web server. The LCD is interfaced with the Arduino board to show real-time data (Fig. 2).

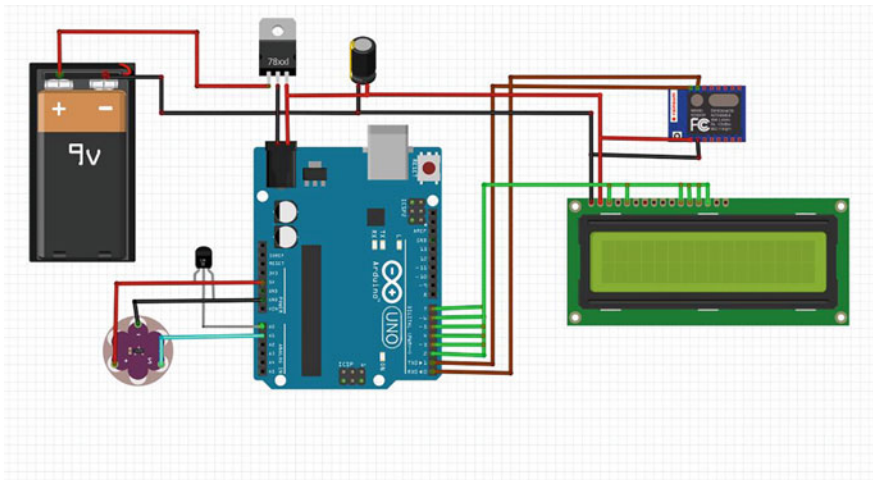
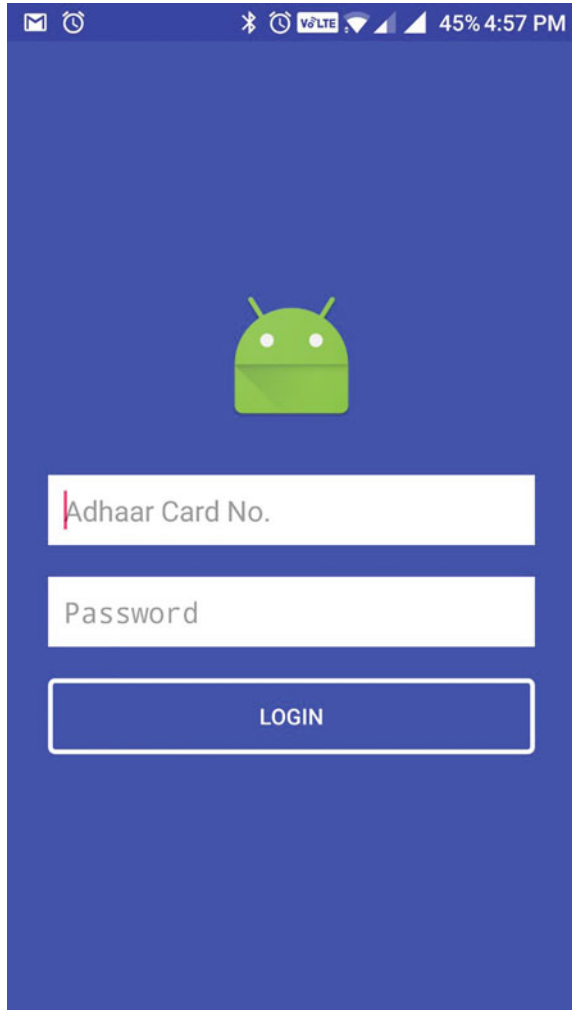


Fig. 2 Picture image of the hardware of the patient monitoring system

4 Results

The results are shown in Figs. 3, 4, 5 and 6.

Fig. 3 Concerned doctor is authorized to access the data of any patient using their Aadhaar card number. The log in process is secured using a password which is known by the doctor or the concerned patient



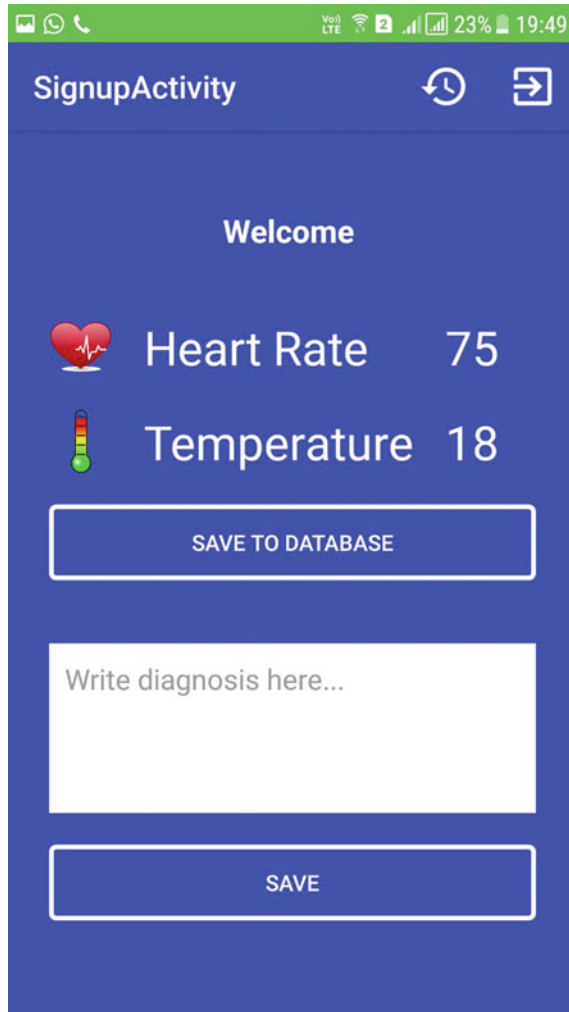


Fig. 4 On logging in, the doctor/patient sees the above page where they can monitor their vitals in real time. On the top right corner, we have the history button and the log out button. The ‘save to database’ button allows the user to save this data. The diagnosis text box allows the doctor to give his/her diagnosis about the patient

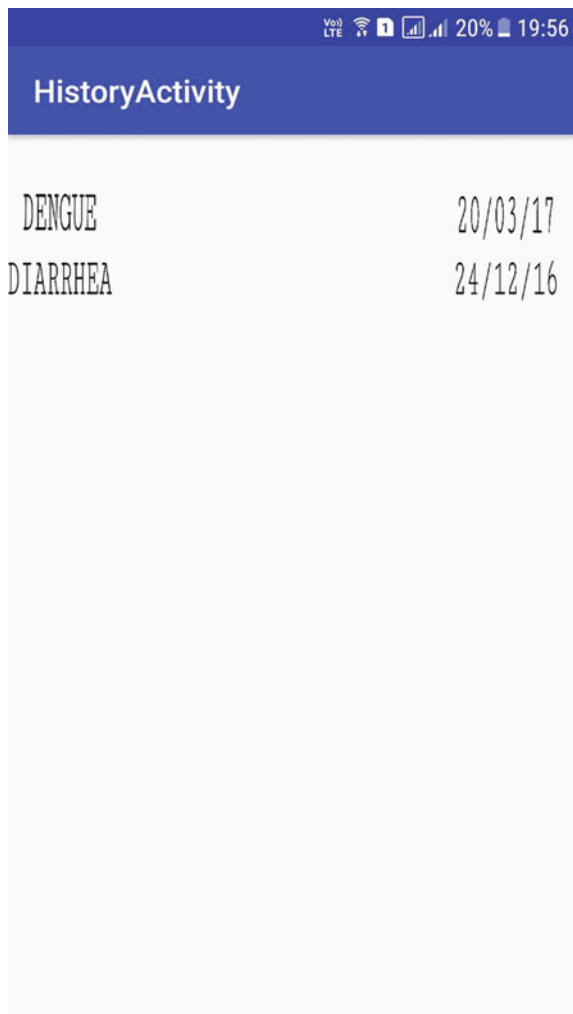


Fig. 5 On tapping the history button, the authorized person can access the past medical records of the patient. This feature helps the doctor to come up with a proper diagnosis as shown in the figure

Analysis of Zernike Moment-Based Features for Sign Language Recognition

Garima Joshi, Renu Vig and Sukhwinder Singh

Abstract This paper discusses a Zernike Moment (ZM) based feature vector that can characterize the alphabets of Indian Sign Language (ISL). Sign Language Recognition (SLR) is a multiclass shape classification problem. Studies of human visual system reveal that while observing any scene, the focus is more on the center part and it decreases toward the edges. This became the basis of calculating the ZMs on a unit circular disk. Continuous orthogonal moments such as magnitude of ZM are well known for their shape representing capabilities. However, for a SLR system the highest order of moments is to be estimated, because with increase in order of moments, the feature vector size increases significantly. In order to find the maximum order that is sufficient to classify the shapes of hand silhouettes, performance of various classifiers is analyzed. Results show that increasing the order of ZM, beyond a certain order does not contribute to the improvement in recognition capability. The results improve when the ZM is combined with some basic geometric features and commonly used shape descriptors such as Hu moments (HMs).

Keywords Sign language recognition · Zernike moments · Shape features

1 Introduction

India has a large population of speech and hearing-impaired people. Indian Sign Language (ISL) is used by the speech and hearing-impaired to communicate. Gesture recognition system can act as an interpreter for Sign Language (SL) [1]. It can eliminate the need of a translator to make conversations with the society at any point of time and can bridge the communication gap. Shape-based features that can be used for shape recognition include Hu Moment (HM), Zernike Moment (ZMs),

G. Joshi (✉) · R. Vig · S. Singh
University Institute of Engineering and Technology, Panjab University,
Chandigarh 160014, India
e-mail: joshi_garima5@yahoo.com

© Springer Nature Singapore Pte Ltd. 2018
R. Singh et al. (eds.), *Intelligent Communication, Control and Devices*,
Advances in Intelligent Systems and Computing 624,
https://doi.org/10.1007/978-981-10-5903-2_140

1335

edge information, and geometric features (GF) [2]. Hand shape is a very important and basic characteristic used to recognize SL [3]. Gesture recognition is the mathematical modeling of hand shapes using appearance-based features. These features can be used to identify different shapes [4]. Moment-based features find applications in shape representation domain. These include non-orthogonal moments, orthogonal moments, continuous and discrete moments [5]. Potocnik assessed the ability of moment-based descriptors to recognize shape [6]. It was found that orthogonal moments such as ZM could also represent minor variations in shape and could represent variation in medical images such as tumor [7]. ZMs are scale invariant, rotation invariant, and translational invariant. Kim et al. compared ZM with various competing descriptors and found ZM as an effective region-based descriptor [8]. Sabhara et al. compared ZM and HM. They reported ZM to be more accurate, flexible, and easier to reconstruct than HM. Increasing the order of the ZM increased the accuracy, and as per the system requirement, an optimal order of ZM could be chosen [9]. Priya and Bora studied the capability of orthogonal moments to address the challenges associated with signer-independent and viewpoint-variant hand gesture recognition system [10].

In pattern recognition domain, moments possess the capability to represent shape. Depending on the order u of the polynomials, moments are divided into lower and higher orders. Primarily, the pattern recognition applications are focused on low-order polynomials. Also, the size of feature vector increases as the order increases. This in turn affects the performance of a classifier. Therefore, there is a need to find the optimal value of order of the moment being derived.

In this work, the performance of a Sign Language (SL) recognition system is analyzed as the order of ZM increases. The order of moments to be included can be estimated by observing the basic characteristic of polynomial order or by using reconstruction process. The polynomial characteristics in 1D are analyzed in Sect. 2. We have created an image dataset for 26 ISL alphabets for 90 subjects. It has total number of 2300 images.

Geometric features are extracted for the binary hand images using region-based parameters (area, moments, and axis) and boundary parameters. The geometrical shape descriptors are listed in Table 1. The details can be found in [11] and in [12].

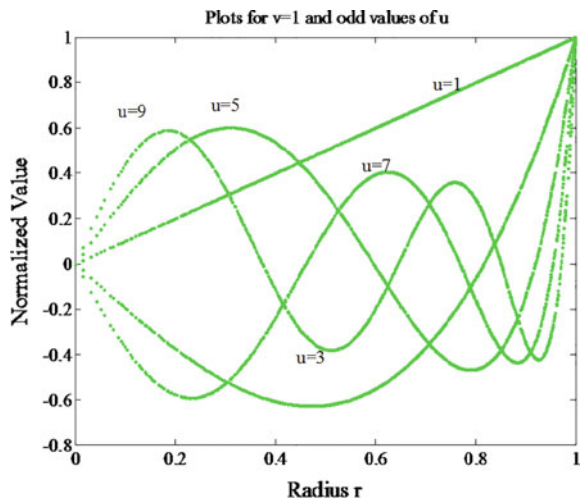
Table 1 Shape-based feature set

Feature type	Feature set
Geometric features (7)	Circularity ratio (CR),
	Spreadness (SS), roundness (RO),
	Solidity (S), average bending energy (BE),
	Eccentricity (E), convexity (CV)
Hu moments (7)	H1, H2, H3, H4, H5, H6, H7
Zernike moments (121)	ZM _{uv} of order $u = 0$ to $u = 20$ and iteration v from ZM _{0 0} to ZM _{20 20}
	Such that $u + v$ is always even with maximum $u = v$

2 Analysis of Zernike Moments

While calculating ZMs, the first step is to convert an image into the unit square image. In the literature, it is revealed that when a person observes an image, center part of the image is more focused. Slowly the attention reduces outward from the center. This study is used in feature extraction and recognition activities. In the calculation of ZMs, this concept is used, so unit disk image is divided into many rings spaced equally outward from the center of the image. Pixels in the different rings carry different weights. This image of unit disk is then projected onto Zernike polynomials, and weights are included in the calculation of Zernike moments [13]. Figure 1 shows the first iteration of odd Zernike polynomial, and it is a sine function. As order increases, the number of zero crossings increases, thus enhancing the ability of ZMs to represent details within an image [14]. Figure 2 shows the behavior of Zernike polynomial for $u = v$. It is observed that for lower values of (u, v) , the plots have distinctive shapes. For higher values of (u, v) , the plots acquire similar shape. Therefore, for the case where u and v are equal, only lower-order ZMs are suitable. ZMs are derived inside a unit disk; in the case of Cartesian coordinates, the drawback of computing ZMs is that the information around the boundary of the disk gets lost, and this leads to geometrical errors. To overcome this problem, the image is resized and ROI is aligned at the center in order to ensure all the pixels lie inside the unit disk.

Fig. 1 Zernike polynomial plots for odd values of u and first repetition



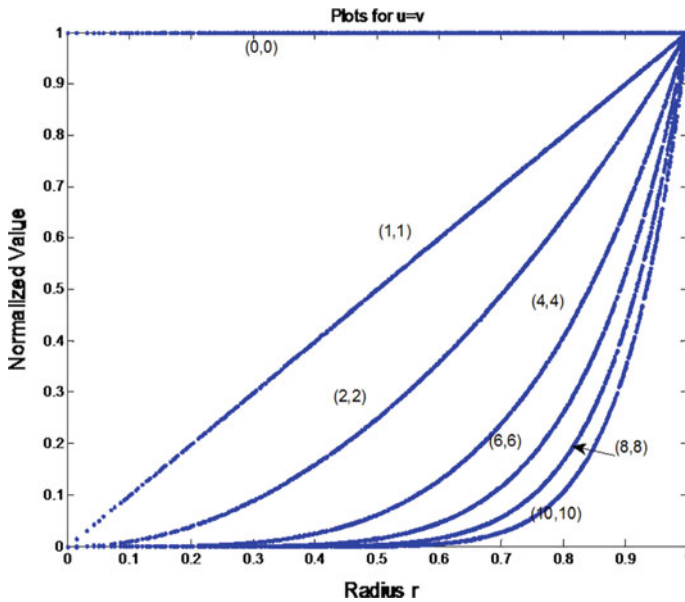
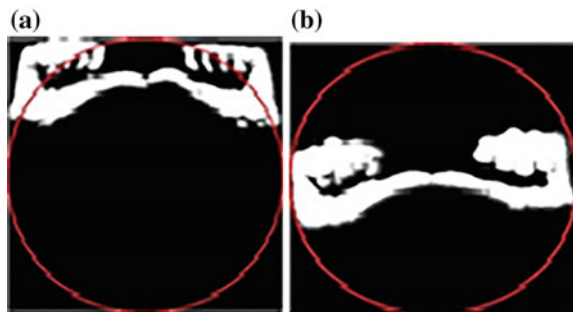


Fig. 2 Zernike polynomial plots $u = [0, 2, 3, 4, 6, 8, 10]$, when $u = v$

Fig. 3 a Improper resizing and b center resizing



2.1 Computational Error in Zernike Moments

Figure 3 shows a unit circle placed on a resized ISL sign of the alphabet A, and the white pixels that come within the circle are included in calculating ZM. In Fig. 3(a), the large white area falls outside the unit circle, whereas in Fig. 3(b) entire hand shape is covered in the circle. Figure 3(b) shows center-aligned resized image; here, the excess number of rows and columns is added in such a way that the center of the image is near to the center of the unit disk of ZM. This helps in the reduction of computational error in ZM. Therefore, the proper center resizing can minimize the computational error in the calculation of ZMs.

3 Results and Discussion

3.1 Preprocessed Image Analysis

In the preprocessing stage, the images without edges, with edges, misaligned, and centrally aligned are classified. Table 2 shows the comparison of results for the ISL database.

For classification, Sequential Vector Machine (SVM), Logistic Model Tree (LMT), Multi-Layer Perceptron (MLP), Bayes Net (BN), Naive Bayes (NB), J48, and k-Nearest Neighbor (k-NN) are compared. The conclusions derived from this experiment are summarized below:

- When edges are not considered, the signs having unique and distinguishable shapes such as alphabets A, C, D, E, G, J, L, U, V, Y, and Z are classified with high accuracy [11]. Considerably, low accuracy is observed for alphabets with similar shape. To distinguish these signs visually, internal edge details are included. Therefore, the performance of all the classifiers improves when edges are included.
- With center resizing, some improvement is observed. SVM gave the highest accuracy. Initially, the highest overall accuracy is 86%. The accuracy improved to 88.4% on the inclusion of edge details, and when images are centrally aligned, 91.1% accuracy is achieved.

3.2 Feature Set Performance Analysis

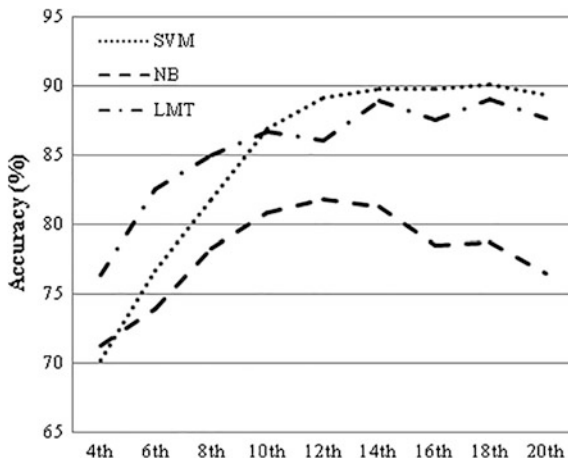
In Fig. 4, the performance of SVM, NB, and LMT is shown for different varying orders of ZMs. For all the classifiers under study and varying feature vectors, the results are summarized in Table 3.

SVM gives good results. Multiclass problems are solved using pair-wise classification. SVM is supposed to be effective in high-dimensional spaces, in cases where a number of feature dimensions are greater than the number of samples. In the case of SVM, the accuracy for ZM_{13} (up to 13th order and all possible values of v) is 89.8%, which saturates for higher orders of ZM. The best result of 93% is obtained for combined feature vector of size 70, which includes ZM_{12} , GF, and HM. In the case of NB, for ZM-based feature vector highest accuracy is 81.8% for ZM_{12} .

Table 2 Performance of the preprocessing stage for ISL database

Edges	Center aligned	SVM	MLP	BN	NB	k-NN	LMT	J48
No	No	86	82.7	74.6	78.9	77.6	80.7	66.2
Yes	No	88.4	88.4	81.3	83.4	82.4	88.4	73.6
Yes	Yes	91.1	88.4	83.8	84.4	83.7	90.6	77.7

Fig. 4 Accuracy of SVM, NB, and LMT for various orders of ZM



It decreases for higher orders. The reason for decrease can be due to the significant increase in feature vector size, which results in a curse of dimensionality called a Hughes effect in probability-based classifiers [15]. Adding GF improves the overall accuracy of NB. Highest accuracy of 84.5% for feature vector of size 63 is achieved. It includes ZM_{12} combined with GF. However, including HM does not contribute to results. For LMT, by including HM to lower-order ZM enhances the performance, whereas further adding GF to this group improves the performance at higher orders of ZM. The performance of LMT is better than all the classifiers at lower feature set. It is 92.1% for combined feature set of size 114. The results for feature vector size variation are summarized in Table 3. Taking the best combination of ZM, GF, and HM into account, a feature vector of size 70 and maximum overall accuracy of 93.7% are obtained with MLP. The next best performer is SVM with 93% at feature vector of size 78 followed by LMT with the feature vector of size 114 and accuracy 92.1%. However, the concern with MLP is the time required to build the model when a feature vector is large. In terms of model building time, it is observed that SVM performs better than MLP and LMT. For other classifiers, accuracy remains less than 85%.

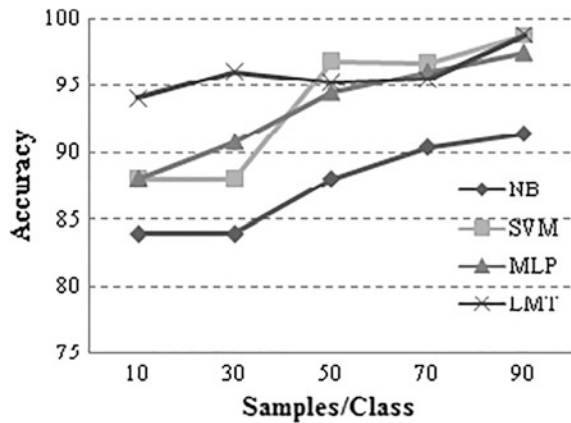
3.3 Analysis of Dataset Size Variation

For the proposed feature set and considering 10 classes only, effect of varying the ISL sample size is analyzed. The percentage split of training/test data is 75/25 percent. The dataset is varied from 10 samples/class (equal to the number of classes) to 90 samples/class (nine times the number of classes). As shown in Fig. 5, even with less number of samples, LMT, SVM, and MLP outperform NB. Performance increases linearly in MLP and NB. It increases considerably for SVM, when size is increased from 30 to 50 samples/class. Therefore, increasing the

Table 3 Comparison of results in terms of accuracy (%)

Classifier	ZM (121)	ZM best result (a)	ZM + GF (b)	ZM + HM (b)	ZM best + HM + GF (c)	All features (135)	Size		
							(a)	(b)	(c)
SVM	89.4	89.8	92.4	90	93	92.7	64	71	70
MLP	89.5	89	89.7	89.8	93.7	92.7	56	63	78
NB	76.5	81.8	84.5	82.2	84.5	80.7	56	63	70
BN	74.7	78.7	82	79.4	82.8	82.8	56	63	70
k-NN	81.1	84.4	83.9	84.2	84	84	56	63	70
LMT	87.7	87.7	90.3	90.1	92.1	91.2	100	117	114
J48	79	73.9	79.1	75.6	79.3	79.3	64	71	78

Fig. 5 Effect of variation of dataset size on classifier performance



dataset size improves the classifier performance. The performance of LMT varies nominally with number of samples per class, it shows better results even for a smaller datasets.

4 Conclusion

From the results presented in the previous section, the following conclusions are drawn:

- Internal edge details improve the results, as the alphabets with similar outside boundary can only be distinguished by including internal details. Also, central alignment of resized images helps in improving the accuracy.
- Combining geometric features and Hu Moments enhances the performance of Zernike Moments.
- For higher orders of ZM, the feature vector size increases considerably, while a significant improvement in accuracy is not achieved. Particularly in the case of Naive Bayes, it decreases due to the considerable increase in feature vector size.
- For combined feature vector, SVM, LMT, and MLP show similar results and are better than BN.
- The performance of LMT is better than all the classifiers even at lower feature set, and it performs at par with MLP and SVM for combined feature set. LMT, MLP, and SVM are capable of handling the larger feature vector.

References

1. Hasan, H. and Kareem, S. A., Static Hand Gesture Recognition using Neural Net-works, *Artificial Intelligence Review*, 37, 1–35 (2012).

2. Zhang, Lu, G., Review of Shape Representation and Description Techniques, *Journal of Pattern Recognition Society*, 37, 1–90 (2004).
3. Kar, P. and Raina, A. M, Semantic Structure of the Indian Sign Language, *International Conference on South Asian Languages*, 1–23 (2008).
4. Ibraheem, P. A. and Khan, R. Z., Survey on Various Gesture Recognition Technologies and Techniques, *International Journal of Computer Applications* 50(7), 38–44 (2012).
5. Shu, H., Luo, L. and Coatrieux, J. L., Moment-based Approaches in Image. Part 1: Basic Features, *IEEE Engineering in Medicine and Biology Magazine*, 25, 70–74 (2007).
6. Potocnik, B., Assessment of Region-based Moment Invariants for Object Recognition., *IEEE International Symposium on Multimedia Signal Processing and Communications*, 27–32 (2006).
7. Nallasivan, G., Janakiraman, S. and Ishwarya, Comparative Analysis of Zernike Moments With Region Grows Algorithm on MRI Scan Images for Brain Tumor Detection, *Australian Journal of Basic and Applied Sciences*, 9, 1–7 (2015).
8. Kim, H. S. and Lee, H. K. Invariant image watermarking using Zernike moments, *IEEE Trans. Image Process*, 13, 766–775, (2003).
9. Sabhara, R. K., Lee, C. P. and Lim, K. M., Comparative Study of Hu Moments and Zernike Moments in Object Recognition, *Smart Computing Review*, 3, 166–173 (2013).
10. Priya, S. P. and Bora, P. K., A Study on Static Hand Gesture Recognition using Moments *IEEE International Conference on Signal Processing and Communication*, 1–5 (2013).
11. Khurana, G., Joshi, G. and Kaur, J., Static Hand Gestures Recognition System using Shape Based Features, *Recent Advances in Engineering and Computational Sciences*, 1–4 (2014).
12. Mingqiang, Y., Kidiyo, K. and Joseph, R., A Survey of Shape Feature Extraction Techniques, *Pattern Recognition Techniques Technology and Applications*, 25, 43–90 (2008).
13. Singh, C., Walia, E. and Upneja, R., Accurate Calculation of Zernike moments, *Information Sciences*, 233, 255–275 (2013).
14. Khalid, M. and Hosny, A Systematic Method for Fast Computation of Accurate Full and Subsets Zernike Moments, *Information Sciences*, 180, 2299–2313 (2010).
15. Kotsiantis, S, Zaharakis, I. and Pintelas, P., Supervised Machine Learning: A Review of Classification and Combining Techniques, *Artificial Intelligence Review*, 26, 159–190 (2006).

Accidents Avoidance Using Smart Traffic Regulation System

Venkata Sai Gokul Gadamssetty, Kiran Kumar Vayalada
and Arpit Jain

Abstract Nowadays, the utilization of sensors is beneficiary in the development of luxury and safety for the automobiles. Smart sensing system has been very effective for the traffic regulation. The autonomous vehicle is automated and equipped with features like environment perception, image sensing, motion planning, proximity alert, and execution features (Ertlmeier and Spannaus in International workshop on intelligent solution in embedded systems, pp 1–9, 2008). Traffic squares and heavy traffic areas are the major accident-prone areas; here, we suggest that in addition to visual display of traffic signal using a transceiver system, the info about the signal status can be gathered by incoming/approaching vehicles and the driver can be alarmed with utilization of a reasonable input (voice caution) appropriately for well-being change. This can be accomplished with the help of an RF module and the unidirectional radio wire for transmitting/accepting the information. Likewise, the security measures at the activity hybrids can be expanded with a period request speed breaker innovation to limit the approach speed of the vehicles amid thin movement hours. And furthermore to reduce the damage brought about to the vehicle because of speed breakers, undesirable braking of the vehicles.

Keywords Smart speed breaker · Micro controller · Wireless transmission
Voice alert · Traffic light detection · Intelligent driver assistance system

V.S.G. Gadamssetty (✉) · K.K. Vayalada · A. Jain
Electronics and Instrumentation Engineering Department,
University of Petroleum and Energy Studies, Dehradun, India
e-mail: gadamssettygokul@gmail.com

K.K. Vayalada
e-mail: kirankumarvayalada@gmail.com

A. Jain
e-mail: ajain@ddn.upes.ac.in

1 Introduction

Among the recent advances in driving, safety, and luxury, Advanced Driver Assistance Systems (ADAS) [1] are one of the promising technologies, utilizing automatic advisory systems. ADAS [1] enhance the passenger safety and driving comfort. Safety features are designed to avoid collisions [2] and to improve the driving experience. Various technologies like taking control over the vehicle and adaptive features like automatic lighting, cruise control [9], [14], assistance in braking, and access to the smartphones for better experiences are also developed to alert the driver to the current situation [3], to guide the driver with crisp information about the vehicle's position or other vehicles approach toward the vehicle [6], and to allow the vehicle to maintain a lane such that traffic will not be unfettered. ADAS [1] are of various forms: Some features are built into cars, and some can be added for extra safety purposes.

ADAS are developing tremendously to meet the requirements of the user and play an important role in automotive electronics segment. Next-generation ADAS will be focusing on wireless connectivity and to provide data car-to-car for improving safety and for communication [4], [6].

Also, there are many types of solutions available. ADAS [1] rely mostly on inputs from multiple data of different sources. Additional inputs are possible from other sources to separate from the primary vehicle platform. The various ADAS features include image sensing, communication, and networking [6], [8], [13].

The main objectives of this project are

- To reduce the rate of accidents by alerting driver about traffic light status.
- To regulate the speed of vehicle indirectly using speed breaker on demand.
- Undesired reduction of speed of the vehicle, the vehicle speed should be unchanged by making the speed breaker disappeared from the road.
- To assist in improving the mileage of vehicles thereby saving a critical and expensive resource.

2 Experimental Studies

Transceiver: Here, an RF module (radio recurrence module) is utilized for correspondence between the autos and the movement lights (central/nearby server). It is utilized to transmit as well as get radio flags between two gadgets. In an inserted framework, it is as often as possible used to speak with another gadget remotely.

Entryway openers, remote caution frameworks, mechanical applications like remote controls, information transmission, shrewd sensor applications [15], and home robotization frameworks are, for the most part, utilized as a part of essential shopper applications. These for the most part infrequently supplant past mode like infrared correspondence plans. These RF gadgets do not require viewable pathway

operation [5]. RF modules may utilize a characterized methodology for RF interchanges, for example, Zig-bee, Bluetooth, and Wi-fi, or they may utilize an elite convention.

IR Sensor: IR sensors use an explicit light sensor to detect a particular wavelength of light in the infrared (IR) spectrum. With the use of LED which emits light at the exact wavelength as what the sensor is in search of, we can measure the intensity of the received light. When the object is in the region of the sensor, the light from the LED bounces off the object to the light sensor. This results in a large variation in the intensity. This can be measured accordingly.

3 Proposed Methodology

The underneath picture demonstrates the schematic of traffic square hardware with handset put on the activity lights, which is utilized to convey and transmit the present status of a traffic light with the assistance of a “unidirectional receiving wire [10], [11],” This radio wire is fixed facing the arriving vehicles and subsequently only these vehicles gets the traffic signal’s flow status (by viewable pathway) hence it helps with giving the fresh data to drivers [12]. At the point when the status is received in the vehicle, an appropriate voice as well as visual alarm is made as needs to be.

What’s more, one of the premier issues at squares is quick moving of the drivers amid late hours (like late night) or when traffic is less. To sidestep high speeds of the vehicle in thin activity, “speed breaker on request” may give a reasonable answer for helping safe driving background. Whenever needed, the speed breakers can work. This time-request speed breaker works just when the speed sensor perceives a vehicle with a speed over than its allowable speed (viz. 60 kmph). In this framework, the speed sensor is sorted out at a predetermined separation from the activity square/hybrid. This speed sensor can be set on the top of a road light which is closer to the activity square (say around 70 m from the square); it detects the vehicle with a speed more noteworthy than the protected bridge speed restrict.

In Fig. 1, we can see a traffic square where the movement of the vehicles is accordingly. In this image, we can see that the traffic signals are shown in their respective directions.

With the help of a microcontroller, data of the traffic lights is stored and the respective data is transmitted to the vehicle in the particular direction with the help of an unidirectional antenna. Here, in Fig. 2, we can see at the transmitter side that, when the signal status is red, the same data is read on the microcontroller, and this data is transmitted with the help of an RF module.

In the receiver’s side, as shown in Fig. 2, we can see that the same data as of the transmitter is read at the receiver’s terminal with the help of an RF module. This data is further processed to get a desired output voice.

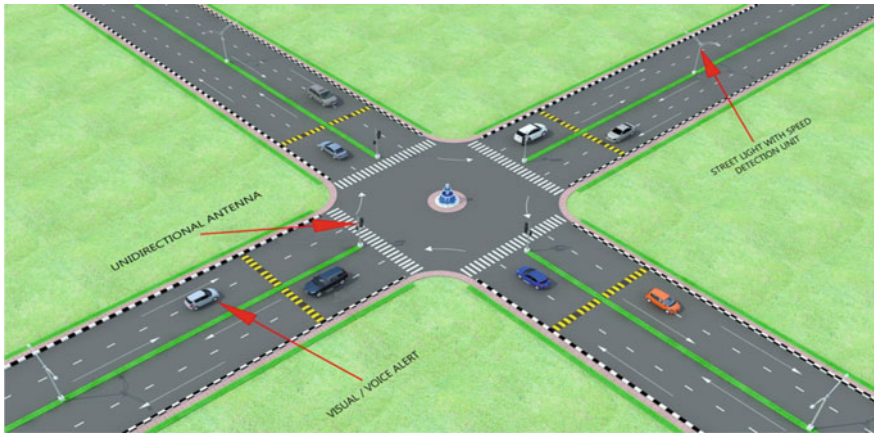


Fig. 1 Schematic of traffic square equipped with unidirectional antenna and speed sensor

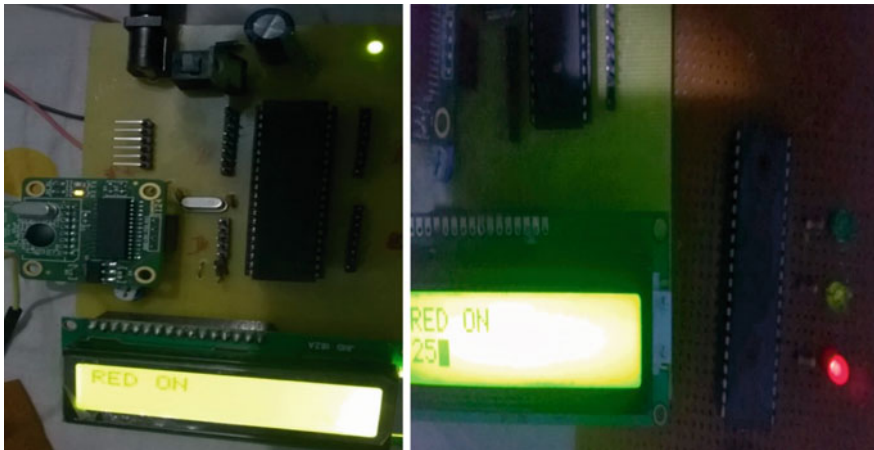


Fig. 2 Transmitter (*left*) side and receiver (*right*) side controllers with their RF modules

The block diagram for traffic signal detection is shown in the Fig. 3. It consists of two sections: One is present at the traffic square and other in the vehicle. The traffic signal with the help of unidirectional antenna transmits the signal, and antenna at the receiver end receives the signal (Fig. 4).

Speed breaker actuation is done with the help of a rack and pinion arrangement. Speed breaker is enabled whenever speed sensor senses a speed more than the predetermined speed (Fig. 5).

We can see two flowcharts: One is for traffic signal detection and other for speed breaker actuation. In flowchart 1, we can see that if traffic signal is either of the

Block Diagram and flowchart:

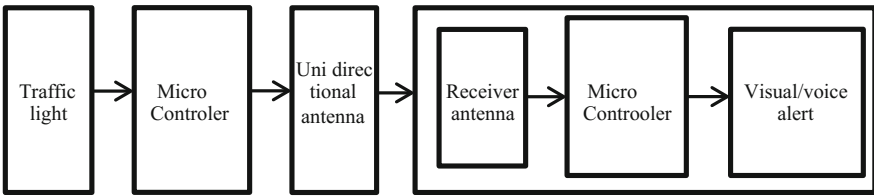


Fig. 3 Block diagram for traffic signal detection

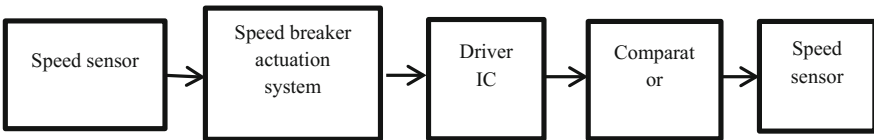


Fig. 4 Block diagram for speed breaker actuation

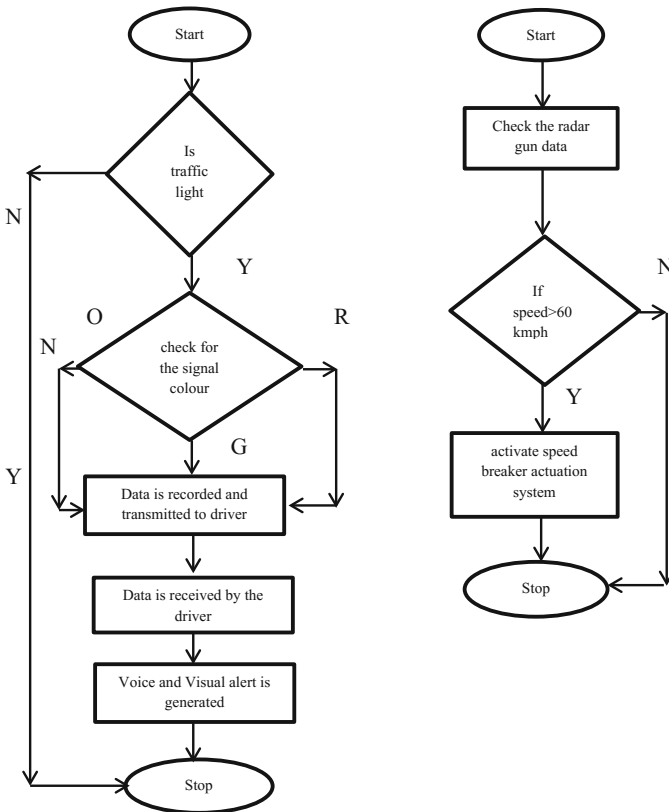


Fig. 5 Flowcharts for traffic signal detection and speed breaker actuation

colors green, red, or orange, it will be detected by the controller and data is recorded and transmitted to the driver. The driver receives the data in the form of voice and visual alert.

In flowchart 2, the process for speed breaker actuation is shown. The speed breaker would actuate if the speed sensor senses the speed of the vehicle more than 60 kmph. If the speed is less than 60 kmph, the speed breaker would not actuate. To sense the speed of the vehicle, radar is used.

4 Results and Discussion

The setup was simulated in PROTEUS software, and various results were acquired. In this project, we controlled the speed of a vehicle in a school zone, work zone, curve zone, highway, and U-turn and prevented accidents by notifying the signal status to the driver and speed using IR sensor. From the setup, we can see that the speed breaker actuation system is very efficient and the data transmission between the vehicle and the traffic light system is quick enough to transmit the status of the current traffic light signal (Table 1).

The method above is the final working model of the project. We enabled only one traffic light and took the observations. A controller has been incorporated at the traffic light which sends the data to the vehicle. The speed breaker would be actuated when the speed sensor senses the vehicle’s speed more than the predetermined speed. The observations for the speed breaker actuation are shown in Table 2 (Fig. 6).

Table 1 Traffic light communication checklist

Signal status	Transmitted signal	Received signal	Time delay (s)
Red	Red	Red	0
Orange	Orange	Orange	0
Green	Green	Green	0

Table 2 Summary of actions taken

S. No.	Speed of the vehicle (kmph)	Smart speed breaker position
1	<60	No change in breaker position
2	=60	Speed breaker actuates
3	>60	Speed breaker actuates

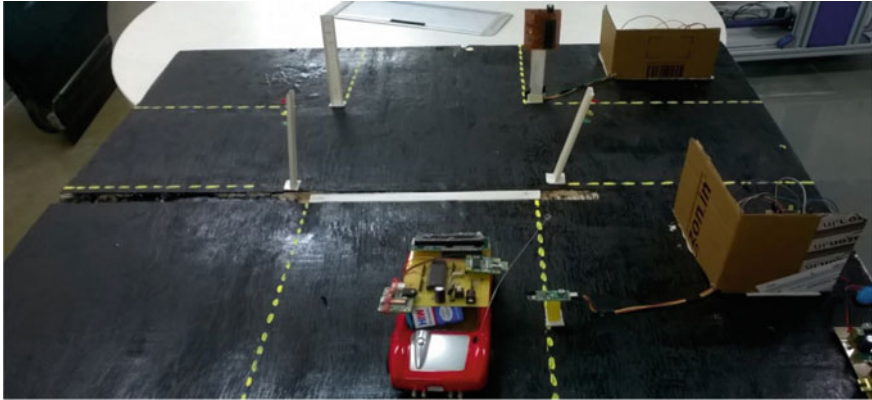


Fig. 6 Working model

5 Conclusion and Future Work

A smart navigation system, which has a direct display of traffic lights, display integrated with vehicles stock satellite navigation system, will be developed and interlinked with the traffic light central control room, which transmits the real-time data accordingly. This system will be very useful such that the driver could change the route during heavy traffic. The speed breaker on demand system can be used as an extension for developing human-free automatic railway crossings. Also, iterations of the system can be implemented near hospitals/educational institutes according to user specifications.

A smart navigation system can be developed where the traffic light loop at the squares would act according to the vehicle density in particular lane, so that the lane with high density, i.e., with heavy traffic, would be given the preference to move forward, while stopping the lane of least density for few minutes through which the traffic can be controlled very easily at the square.

References

1. Ambudkar B., "Sensored car", IEEE 2nd international conference on computer and electrical engg, IEEE computer Society, pp. 335–338, 2009.
2. Bian M, Li K, Jin D, Lian X "A velocity control strategy for vehicular collision avoidance system" Proceedings of the IEEE international conference on mechatronics and automation, Niagars Falls, Canada, pp. 1827–1830, July, 2005.
3. B. Heisele, P. Ho, T. Poggio, "Face Recognition with Support Vector Machines: Global versus Component-based Approach", Proc. of the 8th IEEE International Conference on Computer Vision, ICCV, Vol. 2, pp. 688–694, 2001. International Journal of Distributed and Parallel Systems (IJDPS) Vol. 3, No. 5, September 2012, 157.

4. Brännström, M.; Sjöberg, J.; Coelingh, E. "A situation and threat assessment algorithm for rear-end collision avoidance system", Intelligent Vehicles Symposium, IEEE, pp. 102–107, 2008.
5. Dasgupta C, "Application of GPS and infrared for car navigation in foggy condition to avoid accident", IEEE 2nd international conference on computer Engg and applications, IEEE computer Society, pp. 238–241, 2010.
6. Eidehall A, Pohl J, Gustafsson F and Ekmark J., "Towards autonomous collision avoidance by steering", IEEE transaction on Intelligent transportation system, Vol. 8, No. 1, pp. 84–94, 2007.
7. Ertlmeier R., Spannaus P., "Expanding design process of the airbag control unit ACU-connection of active and passive safety by using vehicle dynamics for rollover and side crash detection", International workshop on intelligent solution in embedded systems, pp. 1–9, 2008.
8. Ferrara A. and Vecchio C., "Cruise control with collision avoidance for cars via sliding models" Proceedings of the IEEE international conference on control applications, Munich, Germany, pp. 2808–2813, 2006.
9. Ferrara A., "Automatic pre-crash collision avoidance in cars", Proceedings of IEEE intelligent vehicles symposium, University of Perma, Italy, pp. 133–138, June, 2004.
10. Hillenbrand Jorg, Kroschel K., " A study on the performance of uncooperative collision migration systems at intersection like traffic situations" IEEE conference on cybernetics and intelligent systems, pp. 1–6, June 2006.
11. Jones W. D., "Black boxes get green light", IEEE Spectrum, pp. 14–15, December, 2004.
12. Nagaraj N.S. "Elements of electronic navigation system", TMH publication, 2008.
13. Nedeveschi Sergiu, Vatavu A., Oniga F. and Meinecke M.M, "Forward collision detection using a stereo vision system", Proceedings of IEEE 4th international conference on intelligent computer and processing, pp. 115–122, 2008.
14. Qingfeng Huang and Ronald Miller and Perry McNeille and David Dimeo and Gruia-Catalin Roman, "Intelligent Vehicle Technologies," Ford Technical Journal, vol. 5, March 2002.
15. www.wikipedia.org.

Prioritization for Regression Testing Using Ant Colony Optimization Based on Test Factors

Sheikh Fahad Ahmad, Deepak Kumar Singh and Preetam Suman

Abstract Regression testing is considered to be one of the most costly, time-taking, and important activity which is performed in an environment with a number of certain restrictions for ensuring the validity of a modified software. Therefore, it becomes necessary to pick the sequence of test cases which is correct as well as it should have the ability to traverse all the faults taking minimum execution time. Prioritizing the test cases helps to achieve performance requirements in which important test cases are executed before than those having lower degree of importance. Studies have shown that prioritization approaches based on test factors like Importance, Volatility, Complexity, Fault Rate, Time, Coverage have good results and also the approaches based on intelligent techniques like Ant Colony, genetic algorithms, have been very promising. Hence, this paper presents a hybrid of these two approaches which first generates the test cases based on the priorities, which are assigned using test factors, and then, the best sequence having least execution time and highest fault rate is calculated by the Ant Colony Optimization algorithm.

Keywords Ant Colony Optimization (ACO) · Regression testing
Prioritizing test cases · Test factors

1 Introduction

There are many testing techniques available but regression testing is one of the most expensive techniques because the whole test suite is executed again and again. It demands execution of huge number of test cases, and also, it consumes lot of time [1]. It becomes very difficult to frequently test the system by running the complete set of software test cases in an environment with resource constraints in limited time. Therefore, the partial test cases at very early stage are selected for fault identification.

S.F. Ahmad (✉) · D.K. Singh · P. Suman
Department of CSE, Integral University, Lucknow, India
e-mail: er.fahad@gmail.com

© Springer Nature Singapore Pte Ltd. 2018
R. Singh et al. (eds.), *Intelligent Communication, Control and Devices*,
Advances in Intelligent Systems and Computing 624,
https://doi.org/10.1007/978-981-10-5903-2_142

1353

Hence, we require applying some type of techniques for prioritizing test cases based on some criterion [2], as it is often not feasible to run exhaustive tests [3]. Thus, if all the test cases are not executed, we can execute the most important ones, and for this, we have to find out the most important test cases.

There are already many test case prioritization techniques [4–11] which have been applied successfully and with good results. But, merging the test case prioritization techniques with the value-based approach, we can get many benefits of test case prioritization, introduced by Barry Boehm. In this type of approach, a higher value or priority is given to those software components that are of utmost importance to the various stakeholders.

Among all these meta-heuristics and search-based techniques, the most extensively applied approach relies on Optimization through Ant Colony. The researchers applied the approach [12] on this problem, as in [9] and [10] which actually succeeded in reducing the overall test case suite execution time.

Hence, in this research, we elect an approach using ACO which is primarily based on test factors for prioritizing test cases.

2 Literature Review

Recent researches have shown that a lot of studies have been done related to the problem of prioritizing test cases using search-based algorithms, and few of them rely on applying ACO for prioritizing test cases. This section will give a brief about only four researches that apply meta-heuristics as a solution to this problem, out of which two are based on ACO.

The technique discussed in [7] for prioritizing test cases relies on genetic algorithm. It rearranges complete regression test suite based on code coverage and time constraints for testing. The objective function of the genetic algorithm is Block Average Percentage Coverage (APBC) metric. The author has shown that, using a case study, this approach performs better than any other approaches.

Authors in [9] compare five search-based techniques which prioritize test cases in regression testing: 2-Optimal, Greedy, Hill-Climbing, Genetic, and Additional Greedy algorithm. The authors have shown that for programs having few lines of code, genetic algorithm performed better than other algorithms and for large or very large programs, Additional Greedy algorithm and 2-Optimal gave better result than others.

The test case prioritization approach discussed in [10] is based on execution time and the fault detection rate. In this approach, a time constraint is used, and hence, it is a test case selection and not the problem of prioritizing test cases. The proposed Ant Colony Optimization technique takes into consideration x number of ants, with x being the count of test cases. Ants chose the graph edges randomly which need to be traversed with the ones having the largest number of pheromones. Results acquired by the proposed approach are found to be better than random ordering of test cases but same as to the technique called Optimal Fault Coverage.

The approach proposed by the author in [11] also uses the execution time and fault-detecting rate of test cases. Authors kept the count of the ants equivalent to the count of test cases, with every ant positioned at a unique vertex which is considered a test case, at the start of the execution. For choosing the next vertex, a heuristic function is used after initialization. This function maximizes the count of faults which are found by the test cases and minimizes pheromones which were previously deposited by the ants as well as execution time. Thus, this process of selecting vertices is continued unless and until each fault is traversed by one of the test cases.

The best and most important solutions are obtained after the pheromones are updated, and then, the technique checks for the runtime constraint. When the solution is invalid, the complete process is expected to be repeated. The author says that the proposed approach reduced the test suite by almost 62% by removing redundancy of faults.

Current trends indicate that the techniques of artificial intelligence techniques nowadays are gaining more popularity in the area of test case prioritization. For test case reordering, Walcott et al. have applied genetic algorithm for the early detection of faults with the help of coverage information [7]. Results disclose that the genetic algorithm is considered one of the most promising techniques under time constraint environment.

The author in [13] has used the concepts of ACO and rough set theory for searching the good quality test cases of unit testing in an object-oriented source code. The natural ants inspired the introduction of a hybrid novel framework. Ant Colony pheromone matrix had been used for Dissemination and finding the best test case value. The authors have also used Bayesian network (BN) technique for the purpose of prioritizing test cases [14]. The authors in [15] used test case coverage along with PSO to evaluate the appropriate position of test cases for the purpose of searching swarm in modified units of software. It was found that PSO was more influential with respect to time and cost than greedy algorithm.

Based upon some common features in ACO-based approaches described above, we conclude that ACO-based approach has best solution and test parameter or value base-testing approach. It also has better test case priority than rest approaches; hence, if we can combine them, then we can come up with an even better approach.

3 Problem Definition

The first phase of the approach prioritizes based upon six factors: (1) importance, (2) volatility, (3) complexity, (4) Fault Rate, (5) Time, and (6) Coverage. The reason why we have chosen these techniques in our approach is discussed below:

- **Importance:** This factor measures how much a requirement is important to the customer. The customer is required to assign appropriate values to every requirement which ranges from 1 to 10 with 10 having the maximum priority.

Relatively, the percentage of software functions which are never used is 45, and 19% of the software functions are hardly used, whereas only 36% are regularly used [16]. Substantial amount of effort must be made to find those faults which are usually encountered during common execution and then eventually leads to repeated failures [17–19].

- **Volatility** is the degree to which a requirement can be changed throughout the entire development period [20].

Out of many faults encountered in a project, roughly 50% are likely to be identified in the requirements phase [21]. The authors in the Standish Group found out that nearly 30% of all the projects are either aborted before ending or failed, and nearly, 70% of the projects degrade the required system performance. The most important reason due to which these projects fail was given to changing requirements. One of the most important reasons for the failed projects is the lack of input from the user, and changing or insufficient requirements [21–23].

- **Complexity** is the degree to which the development team finds the implementation of a requirement difficult. Requirements having very high complexity of implementation are likely to get more number of faults [24]. From the case study of Amland [24], it is quite obvious that the functions having more number of faults have higher McCabe Complexity [24]. Approximately 20% of the modules when executed result in around 80% of the faults [25], whereas the number of fault-free modules was found to be roughly 50% [25].

- **Fault Rate** is the degree of requirements to which the development team identifies and lists those requirements having customer-reported failures. With the advancement of the system, several versions come into existence, and the data collected from previous versions can be used by the developers for the identification of requirements which are fault prone.

Authors of research paper [18] have analyzed and discussed that fault-prone modules are more effective than not fault-prone modules to reduce failures. This paper is focused on refinement of the set of PORT prioritization factors and identification of minimum set of factors for the effective prioritization of system-level test cases.

- **Time** is the subjective measure of total time needed to execute a test case.
- **Coverage** measures the requirements count covered by all the test cases in a test suite. Weight can be assigned on a 10 point scale with 1 being the smallest value and 10 being the largest value.

During the test design analysis phase, each test case is assigned values for all the six factors, and this process is repeated throughout the software development process. The Total Prioritization Value (TPV) for each and every test case can be calculated as follows:

$$TPV_i = \sum_{j=1}^6 (PFV_{ij} * PFW_j)$$

where prioritization factor value for any i th requirement is represented by TPV_i , which is calculated by taking the sum (\sum) of the multiplication of PFV_{ij} (factor value) with PFW_j (factor weight). PFV_{ij} represents the value for every i th requirement for factor j , and PFW_j is used to represent the j th factor weight for a particular product. Let n be the total number of requirements for a product and let's assume that test case j is mapped to i requirements. We can calculate the test case priority by,

$$Priority_j = \left(\frac{\sum_{x=1}^i TPV_x}{\sum_{y=1}^n TPV_y} \right)$$

TPV in a test suite for every test case can be used to calculate these values for the prioritization of test cases based on priority.

4 Proposed Algorithm

In this section, we have proposed our algorithm which primarily relies on ACO, to deal with the issue of optimal sequence of prioritized test cases.

We have done some modeling for the application of the proposed technique to deal with the issue of prioritization of test cases having precedence constraints.

First of all, a directed graph $G = (V, E)$ is generated for the problem, and the vertex of this graph represents each test case of the system, i.e., the set V of this graph contains M elements, with M being the number of test cases. Edges E are generated by connecting vertices with all others. The pheromone information is contained in graph G which is continuously updated.

The Ant Colony Optimization algorithm used in this study is adjusted as follows [9].

```

Set parameters for functions and test cases
Begin initializing the value of pheromone trails
While completion conditions not satisfied
Construct Ant Solutions (Test Case Suites)
Update Pheromones
End while
    
```

The Ant Colony algorithm determines which path each ant will choose when it comes to a fork in the road according to the concentration (high or low) of pheromone. Since the pheromones evaporate slowly over time at a fixed evaporation rate, the long path will take the longer time to walk through. Therefore, the formula of the pheromone update and the pheromone evaporation till test case j from test case i is calculated as follows:

$$T_{ij} \leftarrow (1 - \rho) \cdot T_{ij} + \sum_{k=1}^m \Delta T_{ij}^k$$

$$\Delta T_{ij}^k = \begin{cases} \frac{Q}{L_k} & \text{if ant } k \text{ used edge } (i, j) \text{ in its tour} \\ 0 & \text{otherwise} \end{cases}$$

where

ρ is the pheromone evaporation rate, and this value is set to 10% as a constant;
 ΔT_{ij} stands for the residual pheromone per unit length left by the k th ant;
 L_k stands for the length of a path traveled by the k th ant;
 Q is set as a constant. This term is based on the priority value calculated before in the first phase.

After the pheromone for each path is calculated and assigned to each path in the runtime, this value can be converted to the path probability for the next following ant for path selection. Therefore, the formula of path probability from test case i to test case j is calculated as below.

$$p_{ij}^k = \begin{cases} \frac{T_{ij}^\alpha \cdot n_{ij}^\beta}{\sum_{t \in \text{allowed}_k} T_{ij}^\alpha \cdot n_{ij}^\beta} & \text{if } j \in \text{allowed}_k \\ 0 & \text{otherwise} \end{cases}$$

$$n_{ij} = \frac{1}{d_{ij}}$$

where

Allowed_k is the list of test cases which the K th ant has not traveled through yet;
 α is the variable to control the pheromone concentration;
 β is the variable to control the absolute distance;
 d_{ij} is the distance between i th and j th test cases.

5 Conclusion

ACO-based approach has best solution as shown in related approaches, and factor-based or value-based testing approach also has better test case priority than rest approaches; hence, we have combined the two approaches to come up with an even better approach. Hence, this research emphasizes on prioritization problem of test cases by considering prioritized test cases depending on test factors. This research can also proceed further by implementing the ACO-based algorithm which further can be compared to other search-based algorithms. It can also be applied to other fields [26] of software testing.

References

1. L. Zhang, S. S. Hou, C. Guo, T. Xie and H. Mei "Time Aware Test-Case Prioritization using Integer Linear Programming", ISSTA'09, Chicago, Illinois, USA, Jul 2009.
2. Mathur, A. P.: Foundations of Software Testing, Pearson (2008).
3. Myers, G.: The Art of Software Testing. John Wiley & Sons, Inc, 2nd Edition (2004).
4. B. Boehm and L. Huang, "Value-Based Software Engineering: A Case Study," IEEE Computer, vol. 36, pp. 33–41, Mar 2003.
5. Harman, M., Jones, B. F.: Search-based software engineering. Information and Software Technology, vol. 43, n. 14, pp. 833–839 (2001).
6. Maia, C. L. B., Carmo, R. A. F., Freitas, F. G., Campos, G. A. L., Souza, J. T.: Automated Test Case Prioritization with Reactive GRASP. Advances in Software Engineering (2010).
7. Walcott, K. R., Soffa, M. L., Kapfhammer, G. M., Roos, R. S.: Time-Aware Test Suite Prioritization. In: Proceedings of the International Symposium on Software Testing and Analysis, pp. 1–12 (2006).
8. Mansour, N., Bahsoon, R., Baradhi, G.: Empirical Comparison of Regression Test Selection Algorithms. Journal of Systems and Software, vol. 57, n. 1, pp. 79–90, Elsevier (2001).
9. Li, Z., Harman, M., Hierons, R. M.: Search Algorithms for Regression Test Case Prioritization. IEEE Transactions on Software Engineering, vol. 33, n. 4, pp. 225–237 (2007).
10. Singh, Y., Kaur, A., Suri, B.: Test case prioritization using Ant Colony Optimization. ACM SIGSOFT Software Engineering Notes, vol. 35, n. 4, pp. 1–7 (2010).
11. Suri, B., Singhal, S.: Implementing Ant Colony Optimization for Test Case Selection and Prioritization. International Journal on Computer Science and Engineering, vol. 3, n. 5, pp. 1924–1932 (2011).
12. Dorigo, M., Stutzle, T.: The Ant Colony Optimization metaheuristic: Algorithms, applications, and advances. Handbook of Metaheuristics. Springer, pp. 250–285 (2003).
13. M. Fayoumi, P. Mahanti and S. Banerjee: OptiTest: "Optimizing Test Case Using Hybrid Intelligence" World Congress on Engineering 2007.
14. N S. Mirarab and L.Tahvildari "An Empirical Study on Bayesian Network-based Approach for Test Case Prioritization" Int. Conf. on Software Testing, Verification, and Validation 2008.
15. K. H. S Hla, Y. Choi and J. S. Park "Applying Particle Swarm Optimization to Prioritizing Test Cases for Embedded Real Time Software Retesting", 8th IEEE Int. Conf. on Computer and Information Technology Workshops 2008.
16. F. Moisiadis, "Prioritising Use Cases and Scenarios," 37th International Conference on Technology of OO Languages and Systems, Sydney, NSW, 2000, pp. 108–119.
17. J. Karlsson and K. Ryan, "A Cost-Value Approach for Prioritizing Requirements," IEEE Software, vol. 14, no.5, pp. 67–74, Sep-Oct 1997.
18. J. C. Munson and S. Elbaum, "Software reliability as a function of user execution patterns and practice," 32nd Annual Hawaii International Conference of System Sciences, Maui, HI, 1999, pp. 255–285.
19. J. Musa, Software Reliability Engineering. New York, NY: McGraw-Hill, 1999.
20. Y. K. Malaiya and J. Denton, "Requirements volatility and defect density," 10th Intl' Symposium on Software Reliability Engineering, Boca Ratan, Florida, November 1999, pp. 285–298.
21. G. Mogyorodi, "Requirements-Based Testing: An Overview," 39th International Conference and Exhibition on Technology of Object-Oriented Languages and Systems, Santa Barbara, California, August 2001, pp. 286–295.
22. Computer, vol.29, no. 6 C. Jones, "Software Challenges: Strategies for Managing Requirements Creep," IEEE, pp. 92–94, June 1996.
23. J. O'Neal and D. Carver, "Analyzing the Impact of Changing Requirements," IEEE International Conference on Software Maintenance, Los Alamitos, California, 2001, pp. 190–195.

24. S. Amland, "Risk Based Testing and Metrics," 5th International Conference EuroSTAR'99, Barcelona, Spain, 1999, pp. 1–20.
25. F. Shull, V. Basili, B. Boehm, W. Brown, P. Costa, M. Lindvall, D. Port, I. Rus, R. Tesoriero, and M. Zelkowitz, "What We Learned about Fighting Defects," IEEE Symposium on Software Metrics, Ottawa, Canada, June 2002, pp. 249–258.
26. Sheikh Fahad Ahmad, Mohd. Rizwan Beg, Mohd. Haleem "Test Driven Development with Continuous Integration: A Literature Review", International Journal of Computer Applications Technology and Research (IJCATR).

Optimizing the Available Technology: Tunnel Safety and Energy Conservation System

Sagar Majumdar, Akshansh Jain, Harsh Lawaniya, Kartik Mudgal,
Rajesh Singh and Anita Gehlot

Abstract In order to avoid human life risks due to accidents in a tunnel, safety measures are focused upon along with considering the energy conservation methods. Force on the speed breaker due to vehicle's weight and speed results in power generation, which can be used to light up the whole tunnel. The vehicle counter counts the number of vehicles going inside and coming outside the tunnel, such that traffic inside the tunnel can be controlled using traffic lights, in order to avoid any accident. The proposed system also allows fast evacuation of tunnel when accident occurs, with the help of smoke sensor, hooter as well as manual alarm switch.

Keywords Load cell · Vehicle counter · Smoke sensor · Traffic light
RF modem

S. Majumdar (✉) · R. Singh · A. Gehlot

Electronics Instrumentation and Control, Engineering Department, College of Engineering Studies, University of Petroleum and Energy Studies, Dehradun 248007, Uttarakhand, India
e-mail: sagarnandim@gmail.com

R. Singh

e-mail: rsingh@ddn.upes.ac.in

A. Gehlot

e-mail: anita@ddn.upes.ac.in

A. Jain

Department of Computer Sciences Engineering, University of Petroleum and Energy Studies, Energy Acres, Dehradun, India
e-mail: sherjain98@gmail.com

H. Lawaniya

Department of Automotive Design Engineering, University of Petroleum and Energy Studies, Energy Acres, Dehradun, India
e-mail: harshlawaniya3@gmail.com

K. Mudgal

Department of Power System Engineering, University of Petroleum and Energy Studies, Energy Acres, Dehradun, India
e-mail: kartikmudgal416@gmail.com

© Springer Nature Singapore Pte Ltd. 2018

R. Singh et al. (eds.), *Intelligent Communication, Control and Devices*,
Advances in Intelligent Systems and Computing 624,
https://doi.org/10.1007/978-981-10-5903-2_143

1361

1 Introduction

The fact that *Time flies and never waits for anyone* makes human to search for various methods to utilize time. One such method of minimizing time wastage during traveling is building tunnels in between the mountains. There are a significant number of road tunnels that have been constructed in India and some tunnel projects are still ongoing. With the advent of some system, there come some setbacks too [1]. So, in case of tunnel system, the major concern is regarding the safety of the travelers inside the tunnel, especially in case of long tunnels [2].

Risk analysis depicts that the safety level of long tunnels is quite unsatisfactory, particularly in case of bi-directional traffic and tunnel slopes in the range of 2–3% or higher [3]. Roughly, 25% of the tunnels in India are longer than 3 km (representing roughly 30% of the total tunnel length) [4]. Some obvious reasons of proposing this system are the higher accident rate in the immediate vicinity of the portals, where the environment conditions for the driver change very rapidly, the reduced equipment (e.g., radio, ventilation, water supply, CCTV, etc.), and sometimes reduced availability of escape routes, etc [5]. India consists of several long-distance road tunnels including Rohtang Tunnel (8.8 km), Karbude Tunnel (6.5 km), Jawahar Tunnel (2.85 km), Kamshet Tunnel (1.843 km), Bhatan Tunnel (1.086 km) [6], each of which handles huge traffic. Hence, it is quite important to enhance the safety measures as well as putting forward energy efficient system too.

This write-up suggests a system in which speed breaker in the entrance of a tunnel lights it up using power generated by load sensor. Moreover, traffic control and tackling emergency situations inside a tunnel have also been highlighted in this paper.

2 Theory and Principle Involved

A system is proposed taking in account all the factors affecting humans and environment. This system uses the force exerted by vehicles on the speed breaker equipped with load cell. The power generated by the load cells is sufficient to light up the whole tunnel [7]. This would contribute in conservation of energy as it gets power from running vehicles.

Vehicle counters are also used, keeping in mind the safety aspect of the tunnel. These counters are placed at both the entrance of the tunnel, such that, it informs the microcontroller about the number of vehicles inside the tunnel, which then displays it in the LCD [8]. Use of the vehicle counter is to limit the entry of vehicles inside the tunnel with the help of traffic light, for safety concern. Moreover, if accident occurs, alarm systems are activated automatically using smoke sensor or manually by human, which uses RF modem to communicate with tunnel control room using signal hopping technique [9].

3 Fabrication and Methodology

The system works when the vehicles move through the entrance of a tunnel, passing over the speed breakers, in which load cells are equipped. As soon as the vehicle crosses the speed breaker, load cell generates power due to force exerted by the weight of the vehicle in order to charge up the battery, driving the microcontroller in the tunnel control room [10]. At the same time, vehicle counter counts the number of vehicles passing through the tunnel entrance and acknowledges the microcontroller, which in turn displays the vehicle count in the LCD [11].

Another system works simultaneously, when RF signal is received by the RF modem, connected to the microcontroller. This RF signal is received only when any accident or mishap happens in the tunnel from the sensor nodes, installed inside the tunnel along its wall. As soon as the signal is received by the microcontroller in the tunnel control room, it turns the hooter ON to stop the traffic from going inside the tunnel with the help of traffic light. This is illustrated in Fig. 1.

The sensor nodes, inside the tunnel, consists of microcontroller, smoke sensor, RF modem, street lights, and a switch/button (refer Fig. 2). The street lights are powered up by the energy stored in the battery by load cell [12]. This unit basically works when accident happens inside the tunnel. If a vehicle meets with an accident, smoke sensor will become active and send signal to the input of microcontroller.

Moreover, any person near the accident place can also acknowledge about the same to the microcontroller by pressing the switch/button, connected to it. Now, the RF modem attached to the microcontroller sends signal to the microcontroller of the tunnel control room using signal hopping technology, which then turns ON the hooter to stop the traffic, as discussed earlier.

Figure 3 illustrates the working of complete system. Here, vehicle with green color met with an accident. In this case, smoke sensor of the nearest node, that is, node F (here) acknowledges the microcontroller of that node about it, and this information is passed to the main control room via adjacent nodes using signal

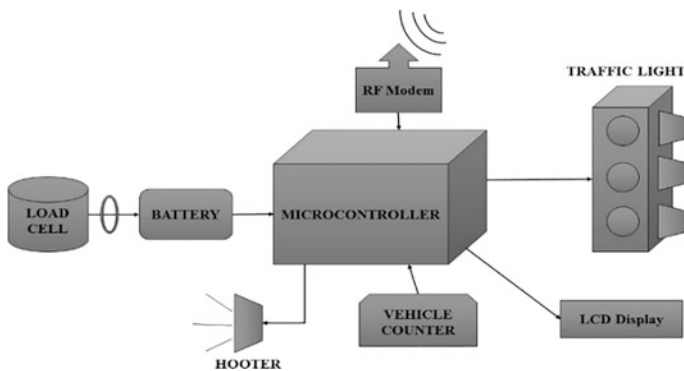


Fig. 1 Tunnel control room unit

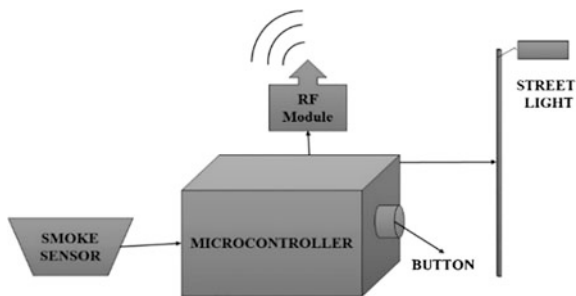


Fig. 2 Sensor node unit

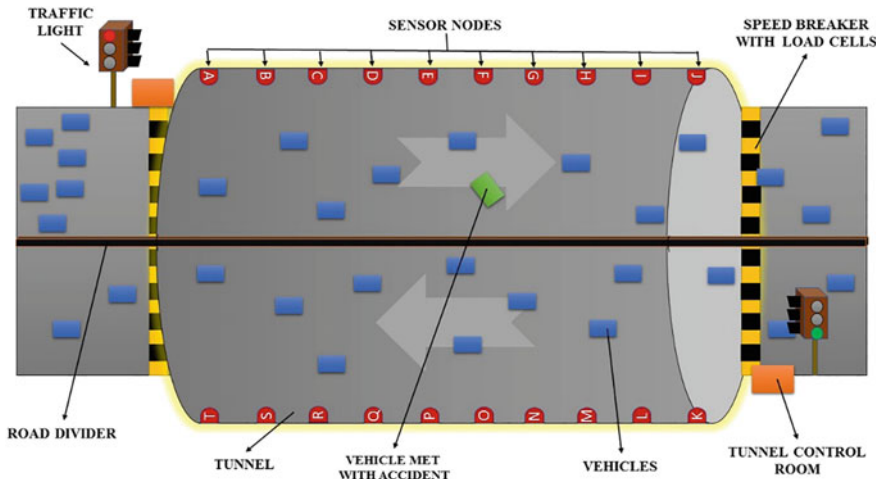


Fig. 3 Top view of the tunnel

hopping technique. The control room then makes the traffic light to signal red for stopping the traffic of that lane [13].

4 Circuit Diagram and Simulation

All the components used in the system can be interfaced with Arduino microcontroller. The proteus simulation of the proposed system has been conducted by burning an appropriate Arduino program into the software and the result obtained is completely appreciable. The Proteus model is illustrated in Figs. 4 and 5.

The circuit used for the Proteus simulation of both the units is illustrated in Figs. 6, 7.

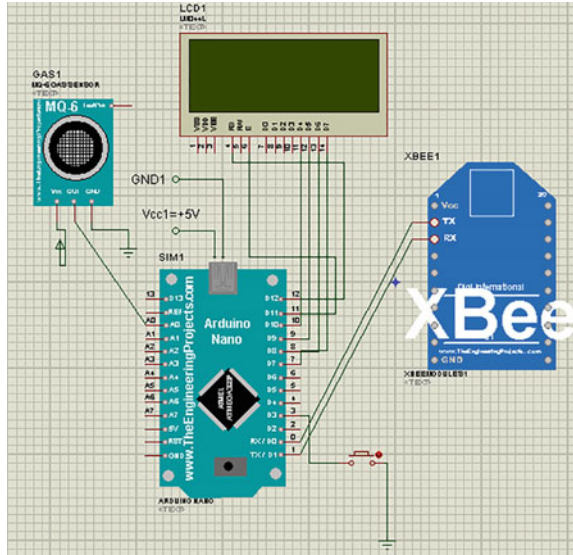


Fig. 4 Sensor node unit

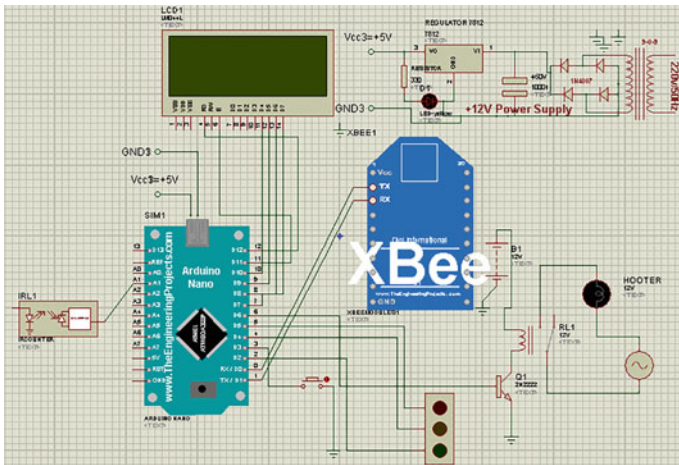


Fig. 5 Tunnel control room unit

From the simulation, it can be seen that all the components used in the system are easily compatible with microcontroller. Moreover, all the processes carried out in the circuit can be easily amalgamated in order to get a fruitful result.

Fig. 6 Sensor node unit

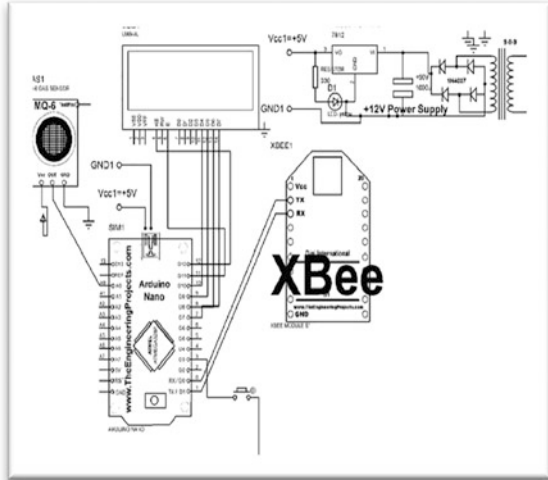
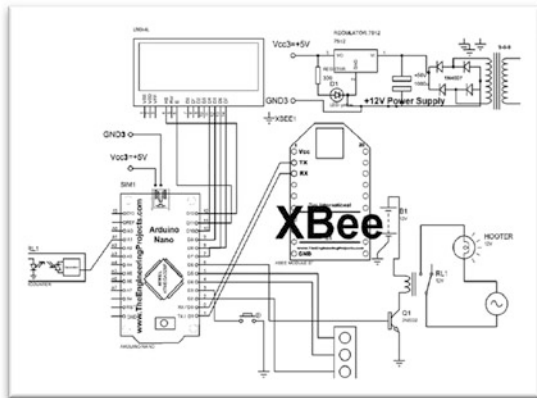


Fig. 7 Tunnel control room unit



5 Mathematical Calculation

5.1 Output Power Generation [14]

Let us consider,

The mass of a vehicle moving over the speed breaker = 10 kg (approximately)

Height of speed brake = 10 cm (approximately)

Work done = Force * Distance.

Here,

- Force = Weight of the Body

$$= 10 * 9.81$$

$$= 98.1 \text{ N}$$

- Distance travelled by the body = Height of the speed brake = 10 cm
- Output power = Work done/s

$$= (89.1 * 0.10)/60$$

$$= 0.1485 \text{ W (For One pushing force)}$$

- Power developed for one vehicle passing over the speed breaker arrangement for 1 min = 0.1485 W

$$\text{For 60 min} = 8.91 \text{ W}$$

$$\text{For 24 h} = 213.84 \text{ W.}$$

This is the power generated by one load cell and considering all the load cell used in the system, the generated power can easily light up the whole tunnel with regular 20–50 W LED-type street lights.

6 Conclusion

The multi-tasking capability of the system for controlling tunnel accidents will certainly help us to switchover to this alternate method. The easy installation of components and benefits to mankind also makes it a reliable system.

Thus, if appreciated it can act very beneficial and ease for controlling traffic inside a tunnel as it involves ‘LIFE SECURITY AND ENERGY CONSERVATION’ with minimum basic requirements.

References

1. Levy, Sidney M. Build, operate, transfer: paving the way for tomorrow’s infrastructure. John Wiley & Sons, 1996.
2. Vashitz, Geva, David Shinar, and Yuval Blum. “In-vehicle information systems to improve traffic safety in road tunnels.” *Transportation Research Part F: Traffic Psychology and Behaviour* 11.1 (2008): 61–74.
3. Beard, Alan N. “Tunnel safety, risk assessment and decision-making.” *Tunnelling and Underground Space Technology* 25.1 (2010): 91–94.
4. Brandt, R., M. Schubert, and N. P. Høj. “On risk analysis of complex road-tunnel systems.” na, 2012.
5. Council, Australasian Fire Authorities. Fire safety guidelines for road tunnels. the Council, 2001.

6. Kulkarni, G. K. "Construction industry: More needs to be done." *Indian journal of occupational and environmental medicine* 11.1 (2007): 1.
7. Dillon, Benny N., Neil C. Griffen, and Mark E. Weihs. "Load cell." U.S. Patent No. 4,815,547. 28 Mar. 1989.
8. Bettelini, Marco, and Nikolaus Seifert. "Automatic fire extinction in road tunnels—State-of-the-art and practical applications." *Proceedings of the Safe Tunneling for the City and Environment-ITA-AITES World Tunnel Congress*. 2009.
9. Durrant, Randolph L., Logan Scott, and John K. Reece. "RF signal repeater, mobile unit position determination system using the RF signal repeater, and method of communication therefor." U.S. Patent No. 6,501,955. 31 Dec. 2002.
10. Liu, Z.G., Kashaf, A., Loughheed, G. D., Crampton, G.P., Ko, Y., Hadjisophocleous, G.V. (2009); Parameters affecting the performance of detection systems in road tunnels; 13th International Symposium on Aerodynamics and Ventilation of Vehicle Tunnels, New Brunswick, New Jersey, 13.05.2009, pp. 389–402.
11. Chou, Pai, Ross Ortega, and Gaetano Borriello. "Synthesis fo the hardware/software interface in microcontroller-based systems." *Proceedings of the 1992 IEEE/ACM international conference on Computer-aided design*. IEEE Computer Society Press, 1992.
12. Dell, Ronald M., and David Anthony James Rand. "Energy storage—a key technology for global energy sustainability." *Journal of Power Sources* 100.1 (2001): 2–17.
13. Zhang, Yuye, and Weisheng Yan. "Research of traffic signal light intelligent control system based on microcontroller." *Education Technology and Computer Science, 2009. ETCS'09. First International Workshop on*. Vol. 2. IEEE, 2009.
14. Das, C. K., S. M. Hossain, and M. S. Hossan. "Introducing speed breaker as a power generation unit for minor needs." *Informatics, Electronics & Vision (ICIEV)*, 2013 International Conference on. IEEE, 2013. <https://www.google.com/patents/US2715912>.

A Navigation Device with Voice for Visually Impaired People

S.K. Nehal, Rajat Kumar Obheroi, Ajay Anand and Haneet Rana

Abstract Mobility of visually impaired people is limited by their inability to recognize their surroundings. So, our goal is to develop a location-aware walking stick for the visually disabled or visually impaired. This self-contained, portable system uses several technologies which include speech recognition, global positioning system (GPS), and embedded systems. The purpose of the system is to provide real-time assistance via global positioning system (GPS). The system will consist of magnetometer, ultrasonic sensors, GPS module, and audio system. It will provide the user with navigation aid, making use of voice to input the destination, using automatic GPS readings, and providing directions using voice outputs.

Keywords GPS · Navigation system · Obstacle sensing

1 Introduction

The ability to see is one of the most important abilities gifted to a human being. About 80% of a human's memory is determined by what they see. A human receives most of the information of the environment through their eyes. According to the statistics of WHO, over 39 million people are blind. Therefore, there is a need for an aid for the visually impaired people [1]. With the advancement of technology

S.K. Nehal (✉) · R.K. Obheroi · A. Anand · H. Rana
Electronics and Communication Engineering, Amity University, Noida, Uttar Pradesh, India
e-mail: nehal.sk.99@gmail.com

R.K. Obheroi
e-mail: ron.rajat@gmail.com

A. Anand
e-mail: anandstark@live.com

H. Rana
e-mail: hrana1@amity.edu

today, there is a need to develop such a device which would not only serve as the eyes of a visually impaired person but also be compact in size in order to be carried around without any difficulty [2]. With the compactness increasing, the cost also increases; hence, the device has to be cheap and affordable. The device we propose consists of a microcontroller, GPS module, microphone, speaker, ultrasonic sensors, and a walking cane. This device solves all the problems by being light in weight, being small in size, and being cheap in cost.

2 System Design

The picture of the layout of our system is shown in Fig. 1.

The system is explained briefly below.

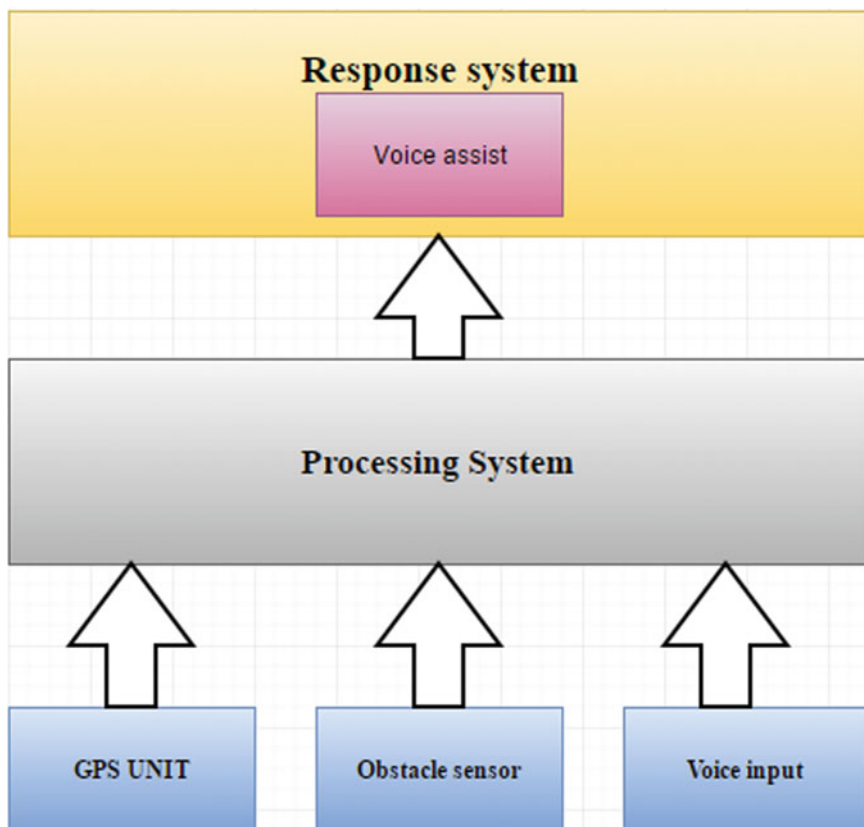


Fig. 1 Block diagram of the system

2.1 Response System

This portion involves the output of the device. It contains a speaker with amplifier which acts as the voice assist and gives the sound output and guides the person concerned to his or her destination by giving instructions in real time.

2.2 Processing System

This portion does all the processing of the device. It contains a microcontroller, Arduino Uno R3. It gathers all the data received from the GPS unit, obstacle sensor and voice input, does the required processing, and provides the appropriate response. It will select the ideal path based on the input (the user's location and desired destination) by applying Dijkstra's algorithm.

2.3 GPS Unit

This consists of Skylab SKM53 GPS module which provides NMEA data to the processing unit which extracts the coordinates of the user.

2.4 Obstacle Sensor

This consists of an ultrasonic sensor which will alert the user of nearby obstacles to avoid collisions.

2.5 Voice Input

This consists of a microphone with preamp. The data collected from the microphone is processed by μ Speech library in the Arduino to identify the destination the user wants to go.

3 Methodology

The methodology we followed divided the process into four major steps. Each step had its own unique approach for the task to be completed successfully. The steps are explained in detail below.

This system is designed to operate in Amity University, Noida. The map used to track the user in this system has been custom made for a few location of Amity University. The map contains coordinates for four landmarks in Amity University; it also contains coordinates defining the paths that connect these landmarks and a reference point (Figs. 2 and 3).

The ellipse represents the area covered by a path or the area between two adjacent nodes which will be used for traveling between them.

3.1 STEP 1: Identifying the User Location

The latitude ($^{\circ}$ N/S) and longitude ($^{\circ}$ E/W) is extracted from the NMEA strings received from the GPS module by the Arduino Uno. The latitude and longitude is converted to Cartesian coordinates $[x(m), y(m)]$ taking the reference point as origin

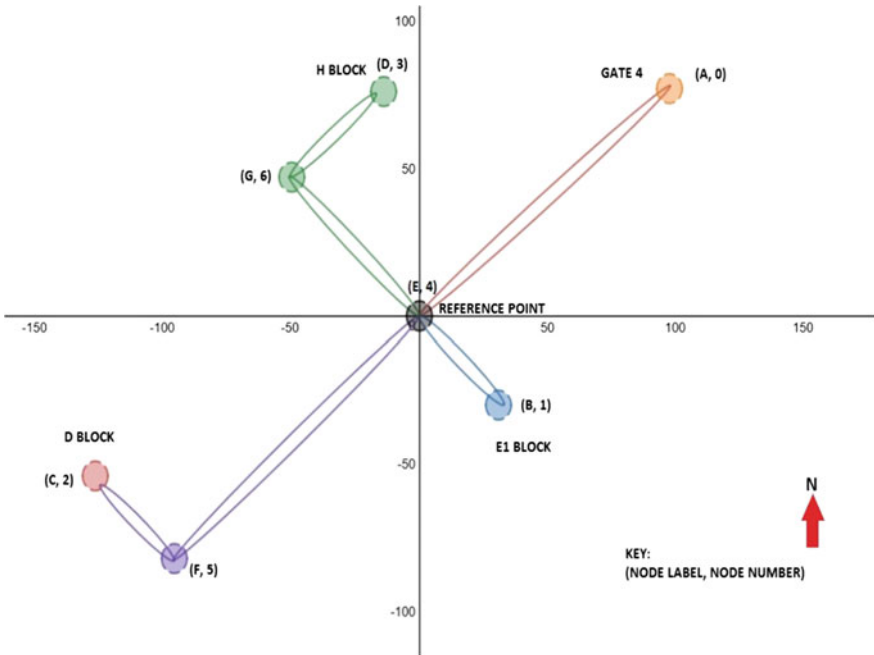


Fig. 2 Coordinate system of the map considered

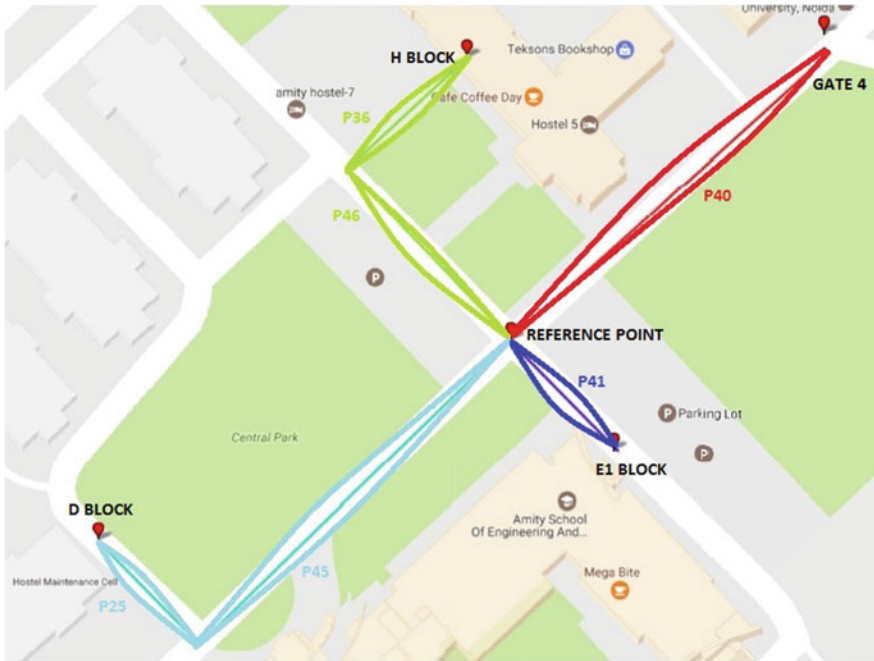


Fig. 3 Map of Amity University Noida which is considered

(0, 0). We put these coordinates (x, y) in the equations of the ellipse of the various path and equations of circles representing the nodes considered. We will get to know which path the user is in by getting to know which equation is satisfied.

For example, if the received coordinates are 28.5454502°N and 77.3344955°E which lies between the nodes *E* and *B*, the coordinates will be converted to Cartesian coordinates using coordinates of reference point which will be *H* (22.05, -18.66). *H* will be the node representing the user’s location. The coordinates of *H* will be applied to various sets of equations representing the path ellipses and circles representing the nodes themselves. In this particular case, the coordinates satisfy the equation:

$$\frac{((x - 19.4) \cos(-0.72) + (y + 17.4) \sin(-0.72))^2}{36.07^2} + \frac{((x - 19.4) \sin(-0.72) - (y + 17.4) \cos(-0.72))^2}{5^2} \leq 1$$

which represents the path between the nodes *E* and *B*. Hence, the location of the user has been identified.

3.2 STEP 2: Identifying the Destination

The user will tell the device the destination he or she wants to go (e.g., if he or she wants to go to *H* Block, he or she will say ‘*D*’). The Arduino will receive this voice command through the microphone, and using the μ Speech library, it will identify the command instructed. The μ Speech library utilizes a special algorithm to enable speech detection. Firstly, the complexity of the signal is calculated by taking the absolute derivative of the signal, multiplying it by a fixed point, and then further dividing by its absolute integral. The consonants other than *R*, *L*, *N*, and *M* have a value above 40, and the vowels have a value below 40. The consonants can be separated into fricatives and plosives. The system determines if the command is a plosive or a fricative by watching the length of the various sections of the speech. Then finally, appropriate character is chosen to that section of the speech. For example, when ‘*D*’ is said, the sound of vowel ‘*e*’ is generated and identified. However, the vowel ‘*e*’ is also generated in the utterance of the letter ‘*B*.’ The two can be separated easily by the number of ‘*e*’ generated as ‘*B*’ generated more number of ‘*e*’ than ‘*D*.’

3.3 Step 3: Identifying the Shortest Path

The shortest path is identified using the Dijkstra’s algorithm. The algorithm uses a cost matrix which stores the distances between the various connected way points.

j ↓ i →	0	1	2	3	4	5	6	7
0	0	999	999	999	116	999	999	999
1	999	0	999	999	22	999	999	999
2	999	999	0	999	999	21	999	999
3	999	999	999	0	999	999	22	999
4	116	22	999	999	0	999	34	999
5	999	999	21	999	63	0	999	999
6	999	999	999	22	34	999	0	999
7	999	999	999	999	999	999	999	0

COST MATRIX

Fig. 4 Cost matrix of the system

Cost matrix is used to identify the shortest path without various way points [3] (Fig. 4).

The symbols ' i ' and ' j ' represent the nodes. Now, the cost matrix represents the distance in meters between two connected nodes. For example, the distance between node 1 and node 4 is 22 m. 999 (any arbitrary distance more than the maximum distance between nodes) represents there is no direct connection between two nodes, and 0 represents it is the same node. The last row and column ($i = 7$ and $j = 7$) represent the distance between the current location of the user and the nodes adjacent to their current location. This row and column are updated after the location of the user has been determined.

For example, if the source node is B (1) and the destination is D (3), the algorithm will determine the shortest path between these nodes as 'BEGD' (Fig. 5).

Applying the Dijkstra's algorithm, we determine the ideal path between the source and destination.

3.4 Step 4: Instruction Using Voice Output

Once the route to be taken is determined, the program will guide the user between nodes. We use the Hmc58931 magnetometer to determine the direction the user is facing ($0^\circ =$ north, $270^\circ =$ west). Then, we use coordinates of the node to be traveled to and the current coordinates of the user to determine the direction user needs to walk in ($0^\circ =$ North, $270^\circ =$ West) to reach the next node. We then subtract these angles to determine the direction the user needs to turn in (left, right, etc.). The instructions are provided to user using a speaker (headphone) using audio files stored on an onboard storage device. The device will provide with corrective directions to the user in case they start moving in the wrong direction. The device will reset when the user reaches their final destination.

4 Result

The GPS system has been simulated using Proteus 7.7 and GPS generator. The GPS generator has been loaded with path file representing our map. It will provide NMEA data to the Arduino Uno in the Proteus through a COMPIM (COM port Physical Interface Model). The COMPIM is connected to GPS generator through a virtual communication port. The GPS generator will simulate a user travelling from an arbitrary point on the map to node D (H-block). The point chosen lies between the nodes B (E-1 block) and E (Reference Point). This point is referred to as node H. The program loaded on Arduino Uno is set to guide the person to node D. The output can be seen on a virtual terminal provided by Proteus (Fig. 6).

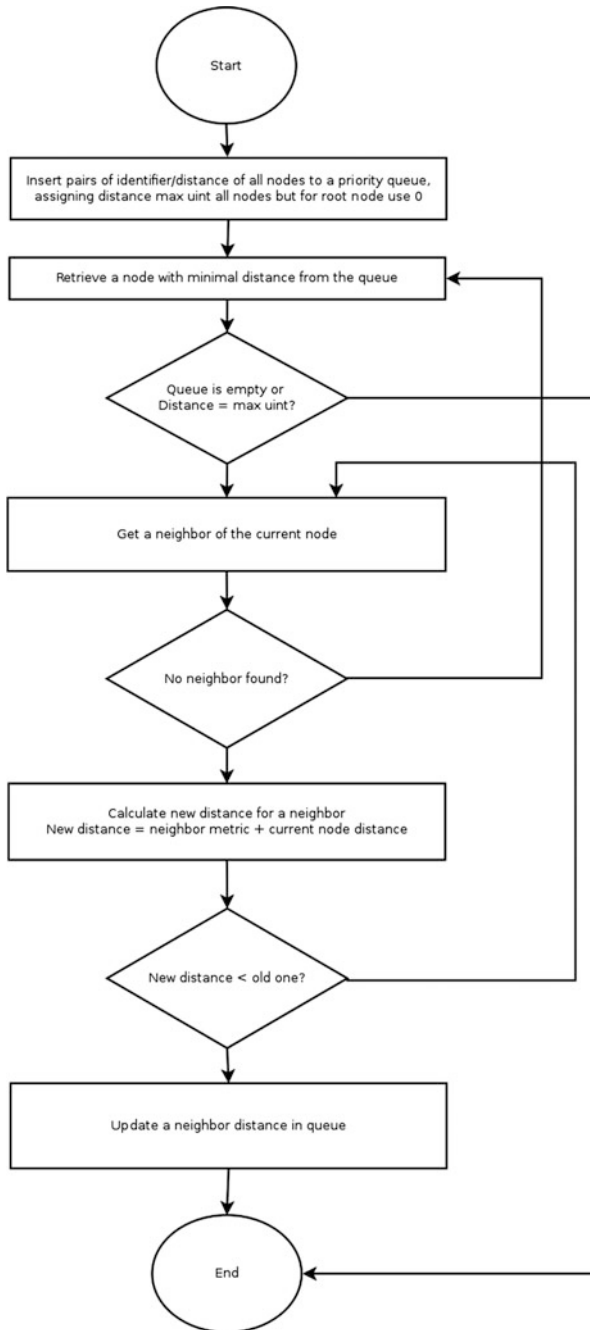


Fig. 5 Flow chart of Dijkstra's algorithm [4]

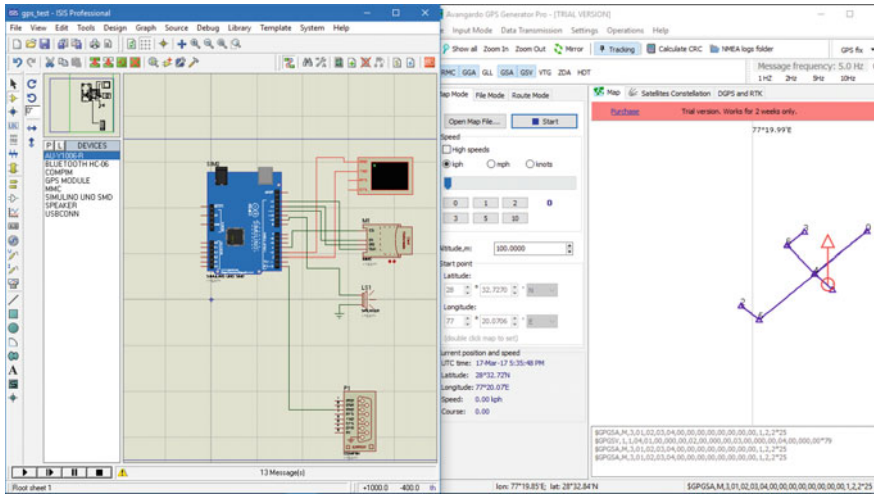


Fig. 6 The simulation uses Proteus and GPS generator

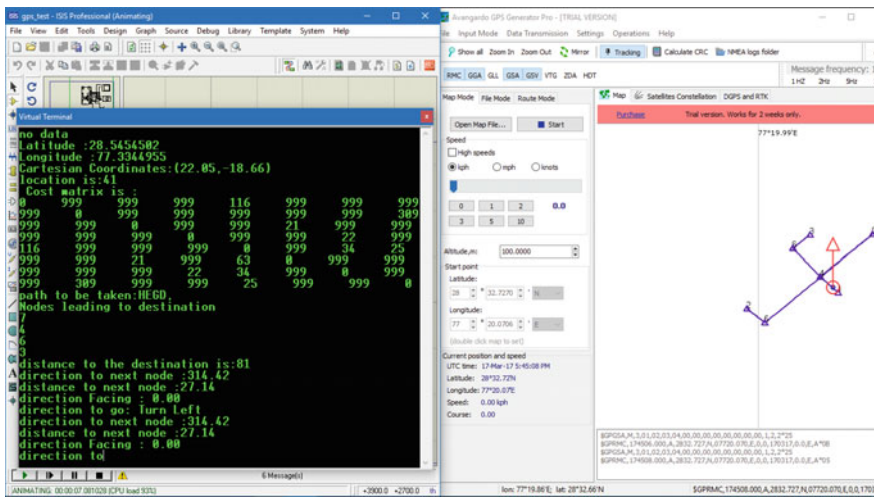


Fig. 7 Instruction generated when user is at a point between *B* and *E*

The initial position is set between nodes *B* and *E*. The red circle represents the user, and arrow represents the direction facing. The initial speed has been set to zero and direction faced to north (Fig. 7).

The simulation is started, and the program prints relevant data to be viewed. The latitude and longitude is printed along with the Cartesian coordinates. The Cartesian coordinates are used to determine the location of the user which is determined as '41' i.e., the user is between nodes 4 and 1. After cost matrix is updated, Dijkstra's

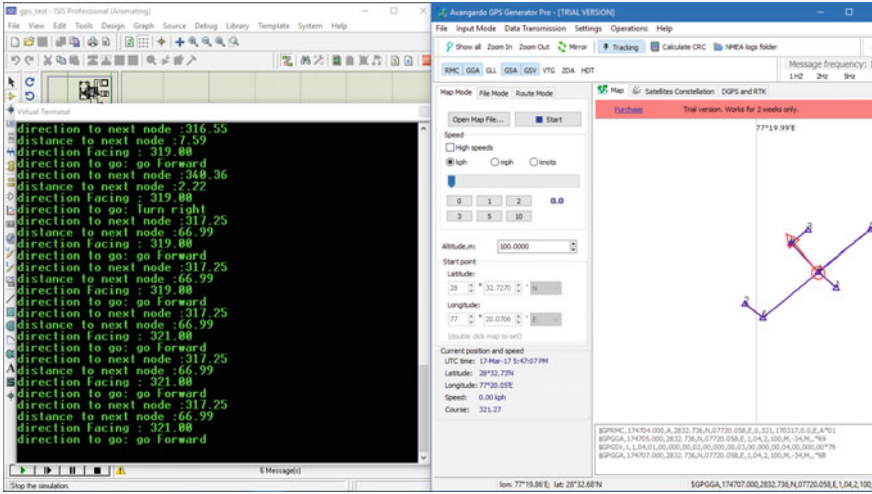


Fig. 8 Instruction generated when user is at node E

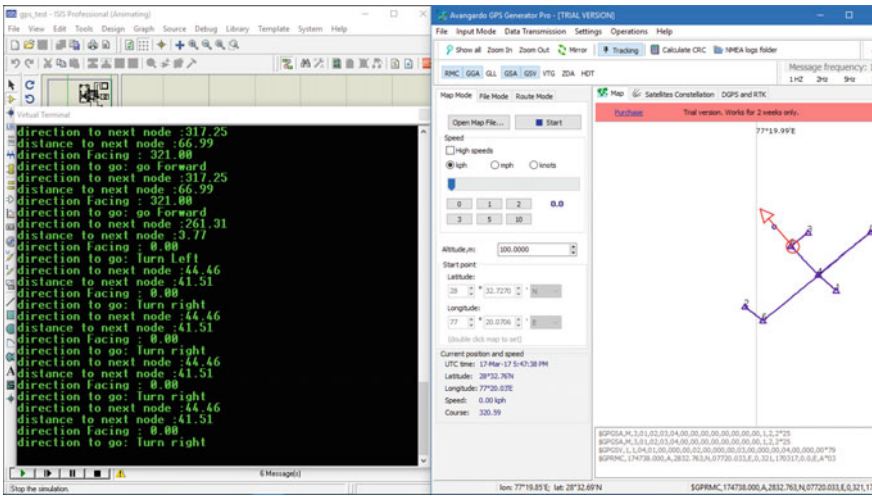


Fig. 9 Instruction generated at node G

algorithm determines the path to be taken is 'HEGD'; the user must walk from H (user's location) to E, then to G, and finally arrive at D (H block). Considering the direction the user is facing, the program then provides the user with instruction to 'turn left' (Fig. 8).

When we place the marker closer to the first node (B), the distance to next node reduces. When it gets close enough, next node is selected, and the distance is updated. The distance to next node changes from 2.22 to 66.99 m, which is the distance to next node (Fig. 9).

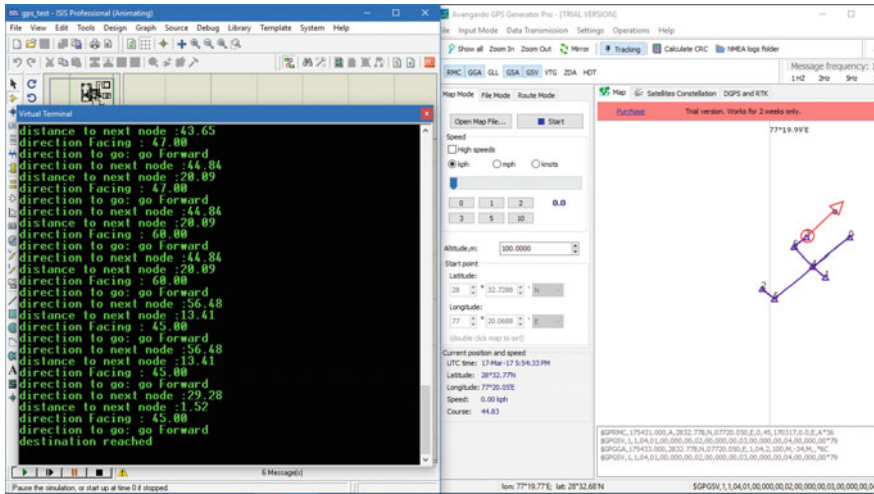


Fig. 10 Instruction on reaching final node

When node G is reached, new instructions are provided to direct the user to the next node (Fig. 10).

When the user reaches the destination, the program informs the user. We have successfully provided navigation instruction to user to reach their destination.

5 Conclusion

The navigation of the visually impaired person was successfully carried out. The navigation from E1 block to H block (node 1 to node 5) of the user was successfully performed. This cost-efficient and compact navigation device could prove to be a very handy tool for visually impaired people. The only drawback of this device is that it does not work accurately inside building or places where a lot of obstructions are present as the GPS does not work properly in these areas. This attempt to navigate visually impaired people was carried out successfully. It helps the users to move without any difficulty over short distances. It also makes the user less dependent on other people for help.

References

1. Review Paper on Navigation System for Visually Impaired People by Chaitali K. Lakde, Dr. Prakash S. Prasad, International Journal of Advanced Research in Computer and Communication Engineering Vol. 4, Issue 1, January 2015.

2. Location Finding for Blind People Using Voice Navigation Stick by Pranjali R Phirke, Jayshree Pande, Prof. Archana Singh, International Journal of Engineering and Technical Research (IJETR) ISSN: 2321-0869, Volume-3, Issue-1, January 2015.
3. https://en.wikipedia.org/wiki/Dijkstra's_algorithm.
4. <https://haryachyy.wordpress.com/tag/dijkstra/>.

Fuzzy Nutrition Recommendation System for Diabetic Patients

Aryaman Gupta and Sanjay Kumar Dubey

Abstract Till 2013, the total number of patients suffering from Diabetes Mellitus reached a total of 382 Million. There is a significant growth from 4.7% in 1980 to 8.5% in 2014 as per the World health organization. Diabetes is not a new word to world now days. It has become a major health problem irrespective of the age group the people belong to. Not just it, most of the times Diabetes is accompanied with other ailments like Hypertension, blood pressure etc. All the researchers, Doctors and Practitioners have a unanimous accord to one fact that Diet plays the most significant role in the cause as well as curb of diabetes. All the fuzzy systems developed so far have given a suitable diet recommendation system or a system for detection and Diagnosis of diabetes. Citing the role of diet to curb the harmful effects of diabetes in the patients, there was a need to come up with a Fuzzy diet recommendation system which is specific to the Diabetes and the diabetic patients and not a diet recommendation system in general. Essentially, the diet of a healthy person should be a lot different from the one suffering from diabetes. The paper uses fuzzy logic to analyze to present a suitable diet recommendation system for the patients suffering from Diabetes.

Keywords Fuzzy logic · Nutrition · Diabetes · System · TSK model

1 Introduction

The number of patients suffering from Diabetes Mellitus was 382 Million in 2013. In the year 2012, an estimated 1.5 Million deaths were directly caused by diabetes and another 2.2 million deaths were attributed to increased blood sugar levels.

A. Gupta (✉) · S.K. Dubey
Department of Computer Science and Engineering, Amity University Uttar Pradesh,
Sec-125, Noida, UP, India
e-mail: aryaman.aryaman.gupta@gmail.com

S.K. Dubey
e-mail: skdubey1@amity.edu

According to the World Health Organization, almost half of the total deaths caused before the age of 70 are attributed to diabetes and increased blood sugar levels. Symptoms of Diabetes include excessive excretion or urination, thirst, constant hunger, weight loss, vision changes and fatigue. There are commonly 3 types of diabetes found in people. Type I diabetes, also known as juvenile diabetes is found in young children. It is a chronic condition in which the pancreas produces little or no insulin. It might be by birth or because of an accident or injury. Only 5% of the people are suffering from this type of diabetes. Type II diabetes is the most common form of Diabetes and happens to adults. This type of diabetes is also known as hyperglycemia. Most of the times, diabetes takes place because of eating habits and unhealthy life style.

There are many other factors which govern what should be your net nutrition intake keeping into account your body type, height weight, physical activities you do in a day, blood sugar levels. The research paper uses all these factors to propose a personalized diet plan for Diabetic Patients [1].

It has been widely acknowledged that fuzzy logic can give excellent outcomes on various real world problems. It can also help to handle uncertain data and knowledge with wide range of applications. Fuzzy logic is one of the ideal methods to map representation of input to outputs. Fuzzy logic is a mathematical model that is applied to a number of fields like control theory, artificial intelligence, Diagnosis of diabetes and the diet recommendation systems [2].

This paper aims to model an intelligent system capable of providing a proper diet recommendation system to patients to support their day to day life and also support medical practitioners in recommending. The proposed system draws and translates knowledge from a diverse array of domains, (including artificial intelligence (AI), biomedical engineering and medicine) into a fuzzy inference mechanism. The fuzzy logic approach is intended to reduce the classification complexities of similar patterns which may exist between individuals requiring different healthcare paths [3].

2 Fuzzy Logic

Whenever we talk of the phrase, Degree of truth in the computing language, Fuzzy logic is the first name that comes to every computer expert's mind. Completely opposite of Boolean logic, which only gives extreme outputs in the form of 0s and 1s Fuzzy logic, is able to give a value between 0 and 1 based upon the degree of truth [4, 5]. We can compare the working of human brain to that of Fuzzy logic. In the modern day developments when the whole world talks about artificially intelligent systems, Fuzzy logic gives the best solutions by developing human like capabilities for it. Fuzzy logic is essential to the development of human-like capabilities for AI [6].

2.1 Membership Functions

Membership function shows a degree of membership in a variable, i.e. to what extent a variable belongs to a given class. Let us consider an example. Let us take the example of temperature. Membership value has to lie between 0 and 1 [7, 8]. There are various curves which could represent the behaviour of membership degrees in fuzzy logic. With increase of functions value, the membership degree might increase, decrease remain constant, first increase then decrease or vice versa. This depends from situation to situation [9].

2.2 Triangular Fuzzy Sets

$$f(x) = \begin{cases} \frac{(x-a)}{(b-a)}, & a < x < b \\ \frac{(c-x)}{(c-b)}, & x \geq 0 \end{cases} \tag{1}$$

3 Fuzzy Inference System (TSK Fuzzy Model)

In case of Fuzzy inference system the chronology starts from crisp input, to fuzzification, to inference system, and finally Defuzzification to get crisp out puts. There are various Fuzzy inference models developed till date. In this research, the inference model used is Takagi-Sugeno-Kang (TSK). TSK model is a fuzzy inference system which uses mathematical equation as a consequent: If x is A and y is B then $z = f(x, y)$ Where A and B are fuzzy sets, and $Z = f(x, y)$ is a crisp function in the consequence [10, 11].

$$\begin{aligned} \alpha &= \min \{ \mu(x_1), \mu(x_2) \} \\ Z &= f(x, y) [\text{mentioned in Table 3}] \end{aligned} \tag{2}$$

To Defuzzyfy the membership degrees method of weighted average is used.

$$Z = \frac{\sum (\alpha_i \times z_i)}{\sum \alpha_i} \tag{3}$$

4 Figures and Parameters

The paper uses to parameters namely

- Blood sugar levels
- The levels of physical activity.

For blood sugar levels the most appropriate range of sugar levels in the body is between 80 and 100 mg/dl below. When the blood sugar levels are below between 50 and 80 mg/dl the person is suffering from a condition called, hypoglycemia. If the blood sugar levels are beyond 100, the person is diabetic (Figs. 1, 2 and 3).

Fig. 2 Triangular fuzzy function showing normal blood sugar levels in the body

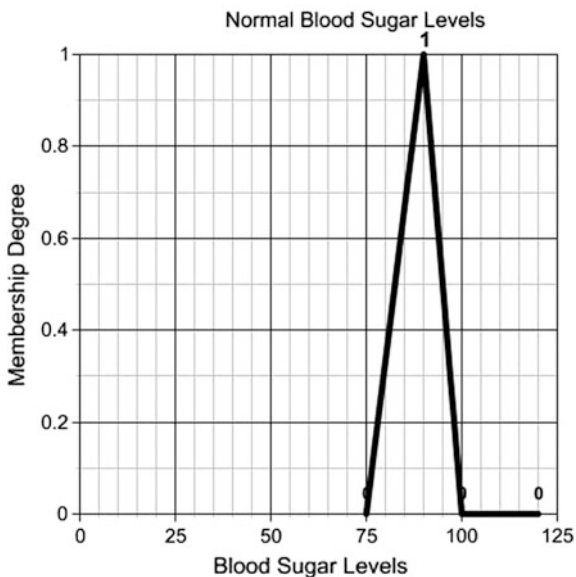


Fig. 1 Triangular fuzzy function showing low blood sugar levels in the body

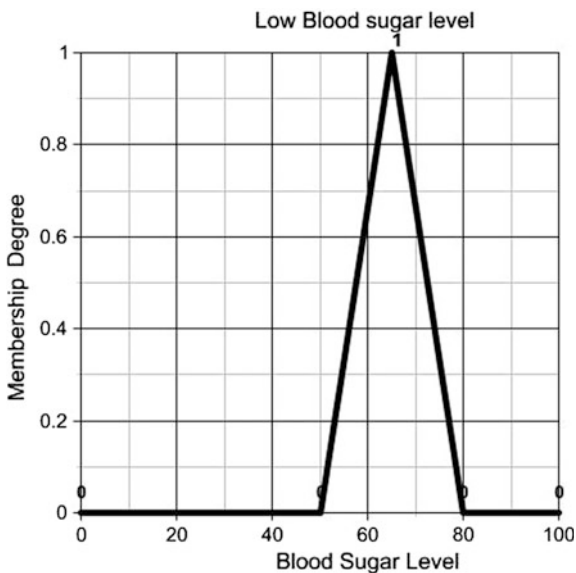
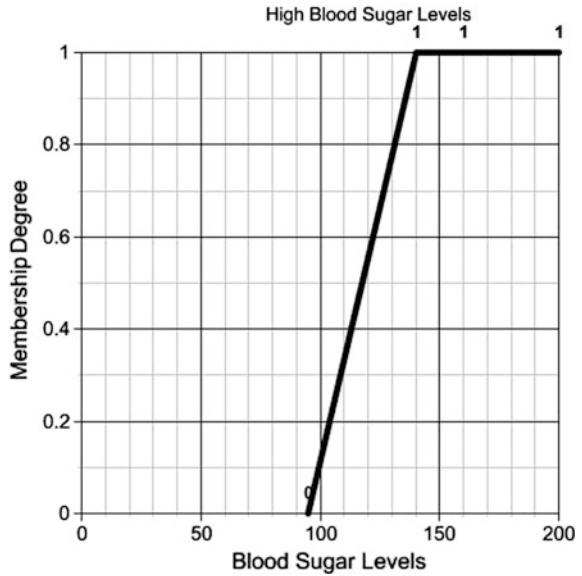


Fig. 3 Triangular fuzzy function showing high blood sugar levels in the body



The most appropriate is 7–10 h of physical activity in form of work, walk, exercise etc. a person working anything between 1 and 7 h, lies in the low category and anything between 10 and 14 h is in high category. Someone working even beyond that lies in the critical level, which is harmful to body (Figs. 4, 5 and 6).

Fig. 4 Triangular fuzzy function showing low physical activity levels in the body

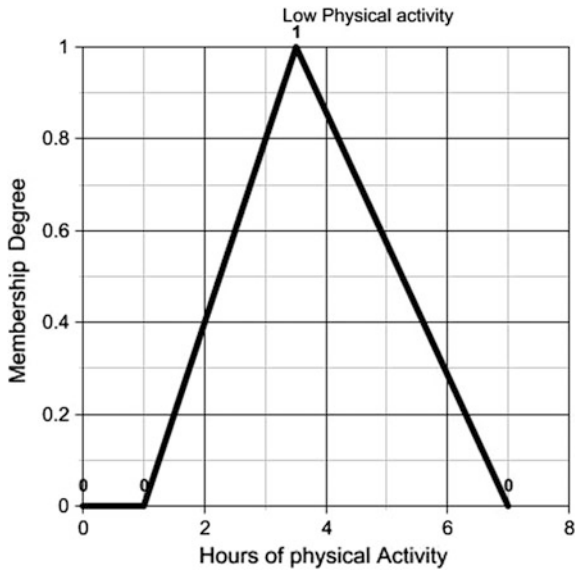


Fig. 5 Triangular fuzzy function showing medium physical activity levels in the body

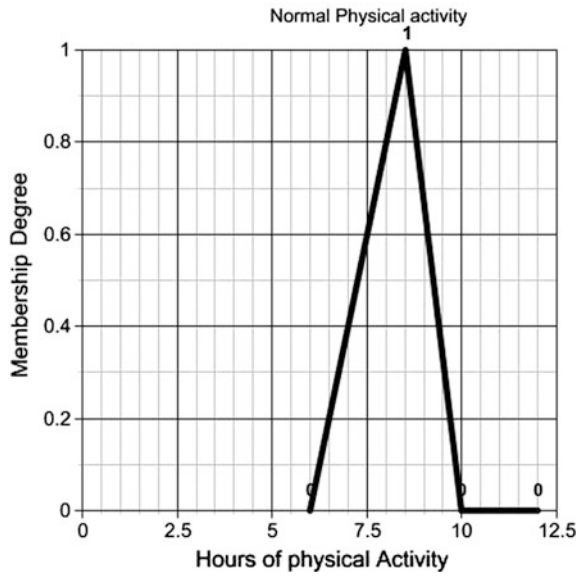
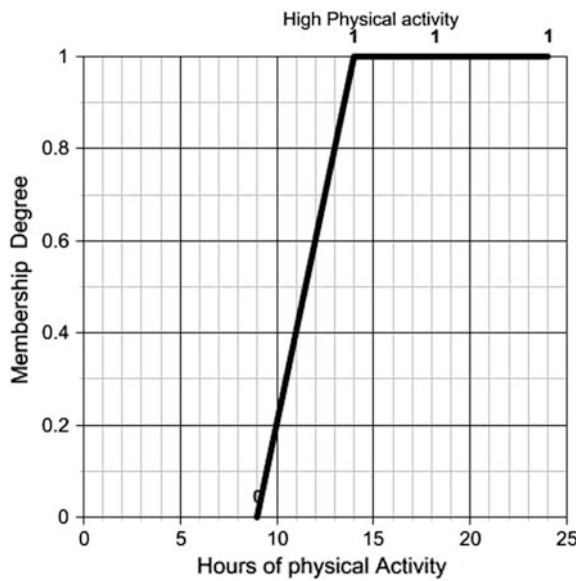


Fig. 6 Triangular fuzzy function showing high physical activity levels in the body



5 Formulas

5.1 Basal Metabolic Rate

Even at rest, there are many functions continuously running in our body. The term BMR or Basal metabolic rate defines the energy needed in calories to carry out all these functions in our body. These processes include circulation of blood, process of respiration, growth of cells, managing body temperature, perspiration, muscular contraction etc. As much as 60–75% of our daily calorie intake is accounted for BMR. Mifflin St Jeor equation used for our work as follows:

$$P = 10 \times m \text{ (kg)} + 6.25 \times h \text{ (cm)} - 5 \times a \text{ (years)} \tag{4}$$

where s is +5 for males and -161 for females, P is the total heat production at complete rest, m is the mass (kg), h is the height (cm) and a is the age (years).

5.2 Weight Adjustment Factor and Daily Energy Requirement

We need energy to carry out voluntary activities like walk, eat, work, exercise etc. We can categorize the levels of physical activities based upon the extent to which a person takes the physical strain. A sports person or a labor might need more calories than someone working on a desk. Also a person with higher blood sugar would want to consume lesser calories than someone with lower blood sugar levels (Table 1).

Here also we can broadly divide the activity level into light, moderate and heavy (Table 2).

Table 1 Activity level [8]

Activity	Male	Female
Very light	1.30	1.30
Light	1.65	1.55
Moderate	1.76	1.70
Heavy	2.10	2.00

Table 2 Weight adjustment

Sugar levels	Calories
High blood sugar	-500
Low blood sugar	+500
Moderate	0

$$\text{Daily Calorie Needs} = \text{BMR} \times \text{Activiy level} \pm \text{weightadjustmen (Reduction in calories)}$$

5.3 Inference Inputs

[R1] IF Blood sugar levels are ‘high’ and Physical activity is ‘high’ then recommendation = $\text{BMR} \times 2.10 - 500$.

[R2] IF Blood sugar levels are ‘High’ and Physical activity level is ‘Medium’ then recommendation = $\text{BMR} \times 1.76 - 500$ (Table 3).

Let us try to understand this with an example Consider a person whose blood sugar is 100, and he is active for almost 12 h a day (we can assume that the person is a sports person or physically very active). We need to suggest a suitable Nutrition recommendation for him. He is a male and his height is 160 cm, and weight is 70 kg and he is 27 years old. Let us use the above algorithm to find the answer.

$$\text{BMR} = 10 \times 70 + 6.25 \times 160 - 27 \times 5 + 5$$

This is equal to 1570 calories.

$$Z1 = 1570 \times 2.10 - 500 = 2797$$

$\alpha_1 = \min \{0.1, 0.3\}$ (from the graph for condition High blood sugar and High Physical activity).

$$Z2 = 1570 \times 1.76 - 500 = 2263$$

$\alpha_2 = \min \{0.1, 0.0\}$ (from the graph for condition High blood sugar and Medium Physical activity).

$$Z3 = 1570 \times 1.76 - 500 = 2763$$

Table 3 Inference condition

Blood sugar	Physical activity (x_2)	Z
H	H	$\text{BMR} \times 2.10 - 500$
H	M	$\text{BMR} \times 1.76 - 500$
H	L	$\text{BMR} \times 1.65 - 500$
M	H	$\text{BMR} \times 2.10$
M	M	$\text{BMR} \times 1.76$
M	L	$\text{BMR} \times 1.65$
L	H	$\text{BMR} \times 2.10 + 500$
L	M	$\text{BMR} \times 1.76 + 500$
L	L	$\text{BMR} \times 1.65 + 500$

Note Above are the Z values for makes, for females refer Table 2

$\alpha_3 = \min \{0.0, 0.0\}$ (from the graph for condition medium blood sugar and medium Physical activity).

Defuzzyfying via weighted average method.

$$Z_0 = (0.1 \times 2797 + 0.0 \times 2263 + 0 \times 2763)/(0.1)$$

$$Z_0 = 2797 \text{ calories}$$

Therefore, the person should consume almost 2800 calories considering that he is working for almost 12 h a day and his blood sugar level is 100.

6 Conclusion

There are three main nutrients that constitute our diet: Fats, Proteins and Carbohydrates. For diabetic patients difference in the approach is that to fulfill the calorie requirement of the body, he should rely on Protein instead of carbohydrates and fats. Now the question is, should he/she stop consuming fat and carbohydrates at all? The answer is NO. This is because for the normal functioning of our body and various organs in it, all types of nutrients are required. Consuming higher amounts of protein can also be harmful to the system because higher is the protein diet in the system, more nitrogen will be released during the digestion of proteins and subsequently more urea will be produced which might be a causative agent for kidney failures. The below table shows the minimum requirement of major nutrients in our body (Table 4).

Also note that each gram of protein contains 4 calories, a gram of carbohydrate contains 4 calories and a gram of fat contains 9 calories. Carbohydrate constitutes 50–55% of our daily calorie requirements, but also suggests that it can be brought down to 40%. Fat doesn't play much role in increasing or decreasing the blood sugar levels. Therefore, the Fat content should be kept 45–50 gm per day for a healthy diet. In general, the protein content of the diet is around 18–20%, and as per world health organization, this can be brought up to 35% of the total diet content. Therefore a Diabetic Patient should essentially consume 30–35% of the daily calorie needs through protein and 20–25% via fat. The Remaining 40–45% should be consumed in form of carbohydrates.

Table 4 Minimum nutrient requirement of the body

Nutrient	Quantity in gm
Carbohydrate	300 gm
Fat	32–35 gm
Protein	0.8 gm per kg

References

1. Y-L. Chi, T.Y. Chen, W.T. Tsai “A Chronic Disease Dietary Consultation System Using OWL-based Ontologies and Semantic Rules” *Journal of Bioinformatics* 53, 2015, pp 208–219.
2. M. Thirugnanam, Dr P. Kumar, S.V. Srivatsan, Narlesh C.R. “Improving the Prediction Rate Of Diabetes Diagnosis Using Fuzzy, Neural Network, Case Based (FNC) approach” *SciVerse Science Direct, Procedia Engineering*, Vol 38, 2012, pp 1709–1718.
3. K. Rajeswari, V.Vaithyanathan, “Fuzzy Based Modelling for Diabetic Diagnostic Decision Support Using Artificial Neural Network” *IJCSNS International Journal of Computer S 126 Science and Network Security*, VOL.11 No.4, April 2011, pp 126–130.
4. R B Lukmanto. Irwansyah. E “The Early Detection of Diabetes Mellitus (DM) Using Fuzzy Hierarchical Model” *ScienceDirect, Procedia Computer Science*, Vol 59, 2012, pp 312–319.
5. C.S. Lee, M.H Wang and H. Hagrais “A Type-2 Fuzzy Ontology and Its Application to Personal Diabetic-Diet Recommendation” *IEEE TRANSACTIONS ON FUZZY SYSTEMS*, VOL. 18, NO. 2, APRIL 2010, pp 374–395.
6. Ahmed Y. Ben Sasi, Mahmud A. Elmalki, “A Fuzzy Controller for Blood Glucose-Insulin System” *Journal of Signal and Information Processing*, 2013, vol-4, pp 111–117.
7. N. Nnamoko, F. Arshad, D. England, J. Vora, “Fuzzy Expert System for Type 2 Diabetes Mellitus (T2DM) Management Using Dual Inference Mechanism” *AAAI Spring Symposium 2013*, pp 67–70.
8. O. Uyar “Preparing Diet List Suggestion with Fuzzy Expert System” *International Journal of Intelligent Systems and Applications in Engineering*, IJISAE, 2016, Vol-4(Special Issue), pp 58–62.
9. Shital V. Chavan “Study of Diet Recommendation System based on Fuzzy Logic and Ontology” *International Journal of Computer Applications (0975–8887) Volume 132—No.12, December 2015* pp 20–24.
10. Joshua M. Krbez, Adnan Shaout “Fuzzy Nutrition System” *International Journal of Innovative Research in Computer and Communication Engineering*, Vol. 1, Issue 7, September 2013, pp 1360–1371.
11. R.A. Priyono, K. Surendro “Nutritional Needs Recommendation Based on Fuzzy Logic” *The 4th International Conference on Electrical Engineering and Informatics (ICEEI 2013)*, *Procedia Technology* 11, 2013, pp 1244–1251.

Physical and Chemical Properties of Mahua and Sal Seed Oils

Deepak Kumar, Vijay Kumar Chibber and Ajay Singh

Abstract Bio-lubricants are the emerging outcomes of the vegetable oils that can be used for several applications in machines and engines. They are very much helpful for providing the frictionless wear and tear operations under certain operating and controlling conditions of machines. Researches have focused in the study and analysis of the tribological characteristics of the vegetable oils. Some vegetable oils are edible, and some are no edible. This chapter focuses on the characteristics of vegetable oils specifically non-edible oils which are great source of bio-lubricants. The petroleum production and final composition in lubricants contain 60–99% base oil and the remaining as additives, based on the desired performance. The main focus of study is carried on mahua and sal seed oils. The oils can be used in electrical machines, mechanical systems and rotary mills. The comparative study is also carried for mahua, coconut, palm, sal, neem, olive, castor, canola, cashew nut and jatropha.

Keywords Bio-lubricants • Oil extraction • Fatty acids

1 Introduction

The vegetable plays [1, 2] a very important role in the production of environment-friendly bio-lubricants. Different types of lubricants have different characteristics in the degradation and produce harmless products. There are many challenges in the utilization of the vegetable oils as biodegradable [3, 4] problems and further convert them into lubricants. The supply and economy factors in the

D. Kumar

Department of Chemistry, Uttarakhand Technical University, Dehradun, India

V.K. Chibber (✉)

Department of Chemistry, Baba Farid Institute of Technology (BFIT), Dehradun, India

e-mail: vijaychibber15@gmail.com

A. Singh

Department of Chemistry, Uttaranchal University, Dehradun, India

© Springer Nature Singapore Pte Ltd. 2018

R. Singh et al. (eds.), *Intelligent Communication, Control and Devices*,

Advances in Intelligent Systems and Computing 624,

https://doi.org/10.1007/978-981-10-5903-2_146

environments are responsible for the human health and safety. In this view point, it is expected that the behaviour of the bio-lubricants should be good in comparison with conventional lubricants, and main focus is taken care of soluble organic fraction (SOF) emissions. Polycyclic aromatic hydrocarbons create the contingency in larger amount for human being, and their health must be less in vegetable oils. Vegetable oils should have the minimum amount of sulphur and its compounds [5] which are great pollutants and mainly responsible for the damage of the catalytic converter and environment. The advantages of the vegetable oils in comparison with the mineral oils in lubricants are biodegradability, non-toxicity, affordable product cost, resources renewability, high viscosity index and base content of the lubricants. The vegetable oils are much cheaper and available in comparison with ester-based oils. Therefore, it is easy to use the vegetable oils as base additive. The presence of polar groups in vegetable and triacylglycerol form structured along with the fatty acid chains creates the oils as amphiphilic in nature. This characteristic of the oils is the perfect solution for the lubricants and its functional fluids. The solid surface is oriented by the triacylglycerol molecules over the polar groups and creates the closed multimolecular and monomolecular layer that results the desired layer of lubricants. Another advantage of this is those triglycerides give the low volatility and have good viscosity properties. The oils available in their natural form cannot be used same as lubricants due to low-temperature conditions, tribochemical process and poor thermo oxidation stability. They have to go several chemical processes.

2 Mahua Oil

Mahua [1, 6] is an Indian tree and majorly found in the north and central regions and its regional forest. The scientific name of mahua is *Madhuca longifolia*. The common name of mahua is mahwa, as mahua or Iluppai. It is one of the fastest and growing trees in India which can vary up to 20 m in height. It belongs to the plant family Sapotaceae. It can grow in arid environments and found in the different states of India such as Madhya Pradesh, Uttar Pradesh, West Bengal, Tamil Nadu, Jharkhand, Maharashtra, Chhattisgarh, Bihar, Telangana, Gujarat, Kerala and Orissa. Other botanical names of mahua oil are *Bassia longifolia* L., *Madhuca indica* J.F. Gmel., *B. latifolia* Roxb., J.F. Macbr., *M. latifolia* (Roxb.) *Illipe latifolia* (Roxb.) and *Illipe malabrorum* (Engl.) F. Muell. The authentic genus *Bassia* is in the Chenopodiaceae. The names *B. latifolia* and *B. longifolia* are illegitimate. In the English language, the name is butter tree, honey tree. In the French language, the name is arbre à beurre, illipe, madhuca bassie. In Sri Lanka, the name is mee. In India also it is called by different names mohua, moha, madhuca, kuligam, madurgam, illuppai, mavagam, tittinam, nattiluppai, mahwa, mowa, mahua, mowrah and moa; in Bengali: mohua, and in oriya: mahula.

The tree is grown in humid and warm regions for its oleaginous seeds. The tree produces 20–200 seeds per annual season. It also depends on the maturity of the tree.

The oil is used for skin-care creams, manufacturing the detergents and soaps also for vegetable butter. The oil is also used for fuel in engines, machines. The outcome after the oil extraction or the seed cakes is used in the fertilization process in fields. The flowers are also used for producing the alcoholic drink in the tropical parts of India. Many tribal communities consider it holy tree, and it is used in many medicines. The drink of the oil also affects the animals and used for animal medicine including the several parts of the tress such as bark. Figure 1 shows the leaves of *M. longifolia*, mahua flowers and mahua seeds.

The tribal community keenly conserves the tree, and it is boon for them. The conservation of this tree is not done by non-tribals, and it is conserved on marginal scale. The leaves of the mahua tree or madhuca indica tree are fed by the moth *Antheraea paphia*, which is used in the production of the tussar silk and used for commercial applications India. Tamil people called it iluppai in Tamil and say “aalai illaa oorukku iluppaip poo charkkarai” that indicates the use of the mahua in unavailability of no cane sugar. The flower of the mahua tree is very sweet and can be used for the same purpose. In some parts of India, people use the madhuca seeds in aquaculture ponds for killing fishes because the availability of alkaloids in the press cake. The contents in mahua flowers are vitamins, 60% sugar, amino acid, organic acid, enzymes, cellulose, aluminous substances, water, yeast and other compounds. The oil is used by many Indian tribal communities in the fermented products, production of alcoholic drink after fermentation, because of high contents of sugar. The rural places in Rajasthan state in India, mahua flowers are used for the treatment in disease such as respiratory disorders in stem powder of mahua flower is used. The fruit of mahua trees is also used as vegetables in coastal and tribal places in India such as Orissa, Chhattisgarh and Maharashtra states. The flow contains 45–50% pale yellow oil. Women use it as one of the nutritive food and massage during breast feeding. The use of mahua flower is also done by many food industries for making jams, jelly, biscuits, alcoholic drinks and milk powder, etc. Mahua flowers are utilized in many medicines for the cough relieving, pain killer,



Fig. 1 a *M. longifolia*. b Mahua flowers. c Mahua seed [8]

skin diseases, pneumonia, vomiting, piles treatment, mouth ulcers, tonsillitis, diabetes, respiratory disorders, lowering the blood pressure and wound healing, etc. Table 1 shows the fatty acid compositions found in mahua oil. Table 2 lists the chemical and physical properties of the mahua oil (Tables 3 and 4).

Table 1 Fatty acid compositions in mahua oil [8]

Fatty acid	Percentage contents
(C16:0) Palmitic acid	24.5
(C17:0) Margaric acid	0.5
(C18:0) Stearic acid	22.7
(C20:0) Arachidic acid	0.1
(C18:1) Oleic acid	37.0
(C18:2) Linoleic	14.5

Table 2 Chemical and physical properties of the mahua oil [8]

Property	Range
Appearance	Yellowish green and pale yellow
Taste	Typical
Odour	Characteristics odour
Specific gravity	0.904
Self-melting point	40–41 °C
Peroxide value	10
Saponification value	187–196
Unsaponifiable matter	1–3
Iodine value	61–71
Refractive index	1.452–1.462
Titer (°C)	220–235

Table 3 Fatty acid compositions in sal oil [7]

Fatty acid	Percentage contents
Palmitic acid (C16:0)	2–8
Margaric acid (C17:0)	0–5.0
Stearic acid (C18:0)	45–60
Arachidic acid (C20:0)	0.5
Oleic acid (C18:1)	35–50
Linoleic (C18:2)	0–8

Table 4 Chemical and physical properties of the sal seed oil [7]

Property	Range
Appearance	Solid white colour
Taste	Typical
Odour	Characteristics odour
Specific gravity	0.8–0.915
Self-melting point	30–35 °C
Peroxide value	4
Saponification value	187–193
Unsaponifiable matter	1.5% max
Iodine value	40–50
Refractive index	1.4500–1.4600
Titer (°C)	46–53

3 Sal Seed Oil

The scientific name of the sal seed oil is *Shorea robusta* [5, 7] seed oil. *Shorea robusta* is called sal in India. This oil is directly extracted from *Shorea robusta* seed, and it is edible. The trees are indigenous to Indian environment and found in two major categories separated by Gangetic Plain based on northern and central part of Indian places. The plant is relating to the Dipterocarpaceae as the family of botanical trees. In different part of India, its nomenclature is different. Its common name is sal. Its hindi name is sal, sakhu, sakher and salwa; Marathi name: sal, rala, guggilu and sajara; Tamil name: attam, kungiliyam and venkungiliyam; Malayalam name: kungiliyam, karimaruthu and maramaram; Kannada name: asina, ashvakarna, bile-bhogimara and asu; Bengali name: sal; Oriya name: sala; Urdu name: safed dammar, ral; Assamese name: hal, sal; and in Sanskrit: ashvakarna, agni-vallabha and ashvakarnika.

The sal tree is a deciduous tree, and its height can reach up to 50 m with a trunk circumference up to 4–5 m. In their normal growth, the average height of the tree is 20–30 m with trunk circumference of 1.5–2 m. The shape of trunk is straight, clean, cylindrical and bearing epicormic branches. The crown is spherical and spreading. The bark colour is dark with brown longitudinal fissures and having thick poles. The variety of tree is found in matured tree also and helpful for fire protection. In their young age, the tree creates a long taproot. The tree is also found in east regions of Himalayas and grows at 200–1000 m altitude. The average temperature bearing for the tree is 25–30 °C and maximum can have 35–45 °C. The rainfall requirement of the tree is 900–3500 mm and maximum of 7000 mm. *S. robusta* flourishes are best in deep, moist, slightly acid, well-drained, sandy to



Fig. 2 a *Shorea robusta* (Sal). b *Shorea robusta* flowers. c *Shorea robusta* seed [7]

clayey soils. The trees are not capable to tolerate the conditions of long-time waterlogging. The presence of soil moisture is essential for the tree, and the great favourable soil is sandy loam with moist and good drainage. Figure 2 shows the leaves of sal tree, sal flowers and sal seeds.

The leaves of the sal are shiny, simple and long (15–25 cm), and the shape is oval with the tapered apex towards a long point. The colour of new leaves is red, and over the time, it becomes green. The colour of flowers is yellow and white. The size of fruits is approximately 1–2 cm length and 1 cm in diameter. The fruit is covered by enlarged calyx segments into 5 unequal wings (5–7 cm) long. The fruit ripen time is May and June, and it contains 66% kernel and pod, 34% calyx and shell. The seed is having wings and calyx with 17–18% fat. There is the existence of de winged seed pod which is brittle and thin. The tree kernel is divided into 5 segments that cover embryo 2 kg of the seeds and give 1 kg of kernel. The major contents of the seeds are 8% protein, 10.8% water, 62.7% carbohydrate, 1.4% fibre 14.8% oil and 2.3% ash contents. The sal is one of the famous trees in different regions of India. The species of sal are found in south and east Himalayan regions such as India, Myanmar and Nepal. The 15% coverage of the forest is covered by the sal tree and covering major states and regions of India such as Assam Valley, Uttarakhand, Himachal Pradesh, Andhra Pradesh, West Bengal, Meghalaya, Himalaya foothills Tripura and Meghalaya, and in central Indian regions such as Chhattisgarh, Madhya Pradesh and Orissa. The larger coverage of the tree is found in Orissa state approximately in 40,000 km², Chhattisgarh 25,000 km² and Madhya Pradesh 28,000 km². The more adoptable process for decortication is the spreading the sal fruits on the ground and set the fire on dry places. Although it is the easiest way by sometime, it may be risky and it can affect the quality production of the sal seed and their oil contents. The collection stores and centres reject the burned seeds. It can contain the stones and sand. To avoid such risk factors, the tradition method can be used in which the wooden stick is used to beat the seed flowers. But it is applicable when the quantity is small. In the larger amount of seed, trading agencies

are helping to get the oil. Storage is an important part and plays a crucial role in the process of collection of sal kernel and their shipment. The sal fat quality is depending on the storage process of their kernels. In the monsoon time, there are the chances of increasing high moist contents and kernel is affected by free fatty acid (FFA) level. It makes unfit for the further use for food and their products. Sometimes the sal seed collection is taken place in monsoon times. So, it is required to use the gunny bags instead of using heavy pesticides because it can reduce the amount of fat. Sometimes, sal is exported to Japan and Europe in which some standards are followed for monitoring pesticides.

The timely collection of the sal seed can enhance the oil quantity. The quantity can be increased if the seed contains minimum value of the moistures. In the dry season, the seed becomes dry 70–80% in fall. The minimum storage and processing at dry place enables the kernel to get the required dryness. In the case of dry kernel collection, the seed should not be burned; otherwise, it increases the free fatty acid (FFA) content and becomes very difficult to export in market. Another important thing for sal oil is that collection time of sal seed and shipment time to factory for crushing should be lesser to keep minimum FFA level. The average time between seed collection and cursing can be 72 h. But the procurement and shipment process is taken place with larger gap and approximately 3–4 months gap is occurring in oil. It can reduce the amount of the oil which should be produced form the sal seeds.

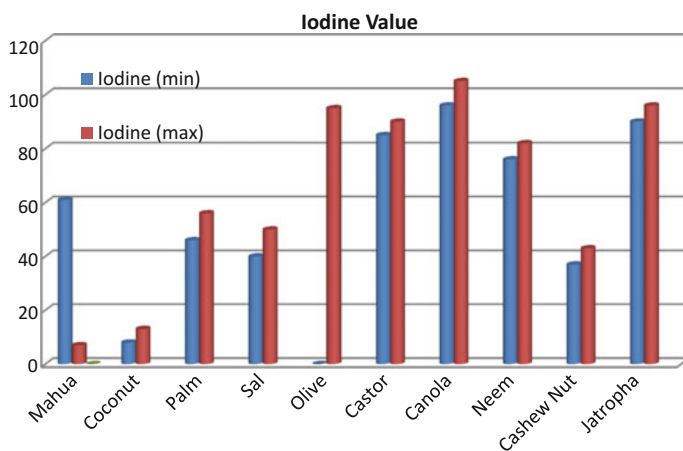
Sal is used as butter in local places in India and also used for soap manufacturing. The modified and refined fats are the substitute of cocoa butter and mostly used by confectionery industries. It is also utilized in vanaspati ghee, which is edible. It is also used in for the production of biodiesel, lubricants, auto oils, paints, cosmetic and pigments. The extraction of the fat in sal oil is done with the help of three methods. One technique is water rendering. The second method is the use of oil expeller and rotary mills with some mechanical system to get the oil; third method is to press the sal seed for a long time and extract the solvents and get the flickers and flakes. The extracted oil has the odour characteristics and greenish brown because of the presence of fatty saturated contents in more amounts. The same oils can be further utilized for cooling and other purpose after refining. Table 2 shows the fatty acid compositions found in sal seed oil. Table 2 lists the chemical and physical properties of the sal seed oil.

4 Comparative Study

The comparative study is also done for comparison table of vegetable oils with melting point, kinematic viscosity, iodine value and flash point. The reviewed oils are mahua, coconut, palm, sal, neem, olive, castor, canola, cashew nut and jatropa. The detailed description of the oils is beyond the scope of this chapter. Table 5 lists the values for these vegetable oils with respect to melting point, kinematic

Table 5 Comparative study of vegetable oils

Oil	Melting point	Iodine value (mg iodine/100 g)	Kinematic viscosity centistokes (cSt)	Flash point (°C)
Mahua	40–41	61–71	26	235
Coconut	22–26	8–13	29	175
Palm	41–42	46–56	43	250
Sal	30–35	40–50	5.9	40
Olive	25–27	82–95	44	205
Castor	4–7	85–90	255	315
Canola	22–24	96–105	115	205
Neem	36–41	76–82	46	257
Cashew nut	19–20	37–43	54	165
Jatropha	30–34	90–96	35.0	226

**Fig. 3** Comparison of vegetable oils with iodine value (mg iodine/100 g) range

viscosity, iodine value and flash point. The comparative graphs are shown in Figs. 3, 4 and 5. The comparison of vegetable oils with iodine value (mg iodine/100 g) range is shown in Fig. 3. The comparison graph of vegetable oils with kinematic viscosity is shown in Fig. 4. The comparison of vegetable oils with melting point is shown in Fig. 5.

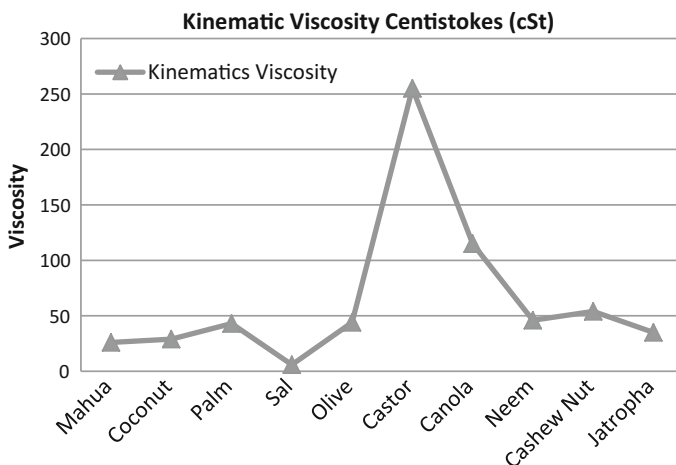


Fig. 4 Comparison graph of vegetable oils with kinematic viscosity centistokes (cSt)

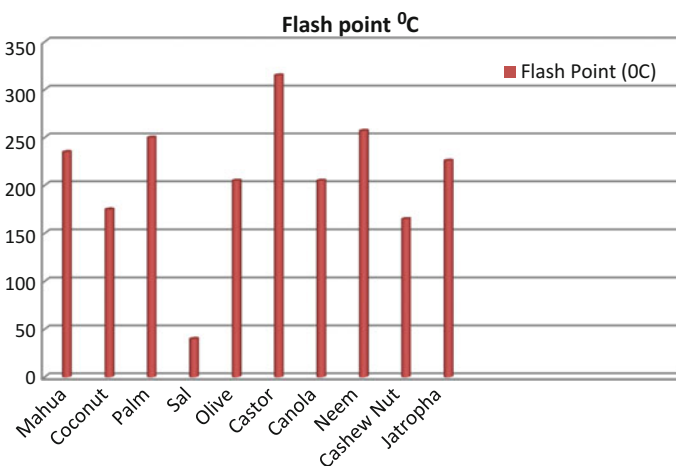


Fig. 5 Comparison of vegetable oils with melting point

5 Conclusions

The minerals oils are ecofriendly and good for health and environment. Vegetable oils are the alternate solution to use additives as the major part of biofuels and engines. Vegetable oils can be utilized as the lubricants especially which are non-edible. We have done the study of fatty acids, chemical and physical

characteristics for mahua and sal seed oils. The comparative study is also done for all oils for kinematic viscosity, flash point and iodine values. This study will be helpful to carry further research in the domain.

References

1. A. Demirbas "Progress and recent trends in biodiesel fuels" "Energy Conversion and Management", Elsevier, Vol. 50, (2009), pp (14–34).
2. A. M. Liaquat, H. H. Masjuki, M. A. Kalam, M. Varman, M. A. Hazrat, M. Shahabuddin, M. Mofijur "Application of blend fuels in a diesel engine" 2nd International Conference on Advances in Energy Engineering (ICAEE), Energy Procedia, Vol. 14, 2012, pp(1124–2233)
3. D. Kumar, G. Kumar, Poonam, C. P. Singh "Fast, easy ethanolsysis of coconut oil for biodiesel production assisted by ultrasonication" Ultrasonics Sonochemistry, Elsevier, Vol. 17 (2010), pp (555–559).
4. D. Lomonaco, F. Jonas N. Maia, C. S. Clemente, J. P. F. Mota, A. E. Costa Junior, S. E. Mazzetto "Thermal studies of new biodiesel antioxidants synthesized from a natural occurring phenolic lipid" Fuel Elsevier, Vol. 97, (2012), pp (552–559).
5. L. F. Chuah, S. Yusup, A. R. A. Aziz, J. J. Klemes, A. Bokhari, M. Z. Abdullah "Influence of fatty acids content in non-edible oil for biodiesel properties" Clean Techn Environ Policy, Springer, Vol. 18, (2016), pp (473–482).
6. C. D. M. Araújo, C. C. Andrade, E. S. Silva, F. A. Dupas "Biodiesel production from used cooking oil: A review" Renewable and Sustainable Energy Reviews Vol. 27, (2013), pp (445–452).
7. https://en.wikipedia.org/wiki/Shorea_robusta_seed_oil
8. https://en.wikipedia.org/wiki/Madhuca_longifolia
9. G. Koçar, N. Civaş "An overview of biofuels from energy crops: Current status and future prospects" Renewable and Sustainable Energy Reviews, Vol. 28, (2013), pp (900–916).
10. L. Simasatitkul, R. Gani, A. Arpornwichanop "20th International Congress of Chemical and Process Engineering CHISA 2012, Prague, Czech Republic" Procedia Engineering, Elsevier, Vol. 42, (2012), pp (1292–1301).
11. K. S. V. Krishna Reddy, Naval Kabra, Umesh Kunchum, and T. Vijayakumar "Experimental Investigation on Usage of Palm Oil as a Lubricant to Substitute Mineral Oil in CI Engines" Chinese Journal of Engineering Volume 2014 (2014), Article ID 643521, 5 pages <http://dx.doi.org/10.1155/2014/643521>.
12. M. H. Ali, M. Mashud, M. R. Rubel, R. H. Ahmad "Biodiesel from Neem oil as an alternative fuel for Diesel engine" 5th BSME International Conference on Thermal Engineering, Procedia Engineering, Elsevier, Vol. 56 (2013), pp (625–630).

Analysis of Sub-threshold Inverter and 6T SRAM Cell for Ultra-Low-Power Applications

D. Sudha, Sreenivasa Rao Ijjada and Ch. Santhirani

Abstract Rapid growth in semiconductor technology extends its applications in the fields of space and communications extensively. VLSI circuits with increased functionality and reduced area is the key factor in the applications. Device scaling yields integration of more functionality, hence increases the portability. Device scaling causes more leakages, and hence wasting more power in the steady state, consequently battery life in those systems reduced very critically. In recent years, the significant use of battery-operated devices leads to the importance of low-power circuit design. This motivates the design of ultra-low power VLSI circuits in the scaled devices. Reduced supply voltage V_{DD} can minimize the energy per operation, active power and leakages, but which are affected by DIBL. And decreased V_{DD} forces the device performance very slow, which causes to increase the power-delay product (PDP). To maintain lowest possible amount point of PDP, it is necessary to operate the devices in its sub-threshold region. In this work, we described the design procedure of sub-threshold inverter and 6T SRAM cell. We used Cadence Virtuoso tools and GPDK 45 nm technology files.

Keywords Inverter • Weak inversion • Strong inversion • SCEs
Power-delay product • SRAM

D. Sudha (✉)

Department of Electronics and Communication Engineering,
Acharya Nagarjuna University, Guntur, Andhra Pradesh, India
e-mail: sudha.dsce2007@gmail.com

S. R. Ijjada

Department of Electronics and Communication Engineering,
GITAM Institute of Technology, GITAM University, Visakhapatnam,
Andhra Pradesh, India
e-mail: isnaidu2003@gmail.com

Ch. Santhirani

Department of Electronics and Communication Engineering,
SVH College of Engineering, Machilipatnam, Andhra Pradesh, India
e-mail: santhirani.ece@gmail.com

© Springer Nature Singapore Pte Ltd. 2018

R. Singh et al. (eds.), *Intelligent Communication, Control and Devices*,
Advances in Intelligent Systems and Computing 624,
https://doi.org/10.1007/978-981-10-5903-2_147

1401

1 Introduction

Extensive use of portable devices in the emerging fields makes rapid changes in the growth of VLSI technology. This gives more impact on the device scaling in order to enhance the chip density. In recent consumer applications, apart from the portability, it leads to include higher functionality, which directly effects the battery life very strongly [1]. Hence, the VLSI people are trying to design the devices with curtail the power in large extent. This interest forces to investigate the causes for higher power consumption in the scaled devices [2]. With all the efforts, it was found that the short-channel effects (SCEs) are the key factors for increasing the power in scaled devices even in the static mode also. Scaling improves the density, hence the portability, consequently, more functionality can be embedded in the chip [3]. The design for low-power in the course of technology down scaling is a big challenging task for the designers. Numerous techniques were proposed to minimize the power in the scaled devices [4]. Even a few gaps are still to fill in this direction of research. Operating the devices in the sub-threshold region produces many advantages, particularly, they are well suited for the portable systems to enhance the battery life. This reduces significant amount of active power ($\sim CV_{DD}^2$) and leakage power. In SRAM cells, energy per operation can be kept low by operating with reduced V_{DD} . But, sharp reduced V_{DD} causes to rise [5]. Typical values of read/write margins of 6T SRAM cell depend on I_{on}/I_{off} ratios set by the transistor length/width ratio. But, process variations make V_{Th} more sensitivity and reduce the I_{on}/I_{off} ratios. The length/width-based ratios contribute wholly the unreliable operation of sub-threshold SRAM devices [6].

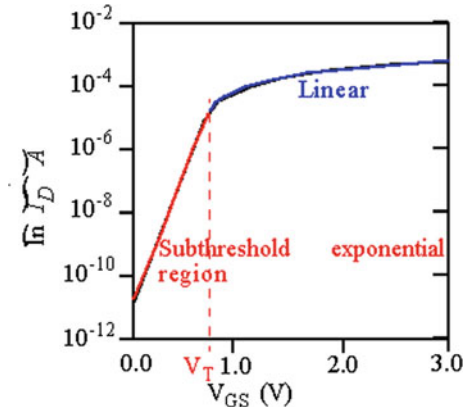
2 Sub-threshold Operation

MOSFETs operation depends on its terminal voltages. The three regions of operations are as given below.

- Weak inversion or cut-off region: When $V_{gs} < V_{Th}$
- Triode mode or linear region: When $V_{gs} > V_{Th}$ and $V_{ds} < (V_{gs} - V_{Th})$
- Active or saturation region: When $V_{gs} > V_{Th}$ and $V_{ds} > (V_{gs} - V_{Th})$

NMOS transistor operates in its sub-threshold region when its gate-to-source voltage (V_{gs}) is under its threshold voltage (V_{Th}) which causes a small current flows from drain to source is usually known as sub-threshold current or minority current [7]. The transfer characteristics of drain current verses gate-to-source voltage is represented as one on the logarithmic scale as shown in Fig. 1. From this, it is observed that the current decreases exponentially when V_{gs} falls below the threshold voltage. But in the case of long channel device, the device V_{Th} does not depend on the channel length and drains voltage. Whereas in the case of

Fig. 1 charecteristic curve of I_D versus V_{GS}



short-channel devices, the depletion regions at source and drain penetrate significantly more into the channel. Hence, the electric field in the channel and potential along the channel are controlled [7].

The current equation for the NMOS transistor when it's biased below V_{Th} is given by

$$I_{ds} = 2n\mu_0c_{ox}\beta^2 \frac{W}{L} \exp(V_{gs} - V_{Th}/n\beta)[1 - \exp(-V_{ds}/\beta)] \tag{1}$$

$$= I_s \exp(V_{gs} - V_{Th}/n\beta)[1 - \exp(-V_{ds}/\beta)]$$

$$S = n\beta \ln(10), \tag{2}$$

where

$$\beta = \frac{KT}{q}$$

- N the slope factor of the MOSFET
- μ_0 zero-bias mobility
- C_{ox} gate oxide capacitance
- W and L the width and length of the MOSFET
- S sub-threshold swing

The prime factor for sub-threshold conduction is in the scaled devices, to supply voltage is also scaling continually with the technology, it lowers dynamic power consumption and makes electric fields inside devices low, consequently achieves good device reliability [8]. Sub-threshold operating voltage depends on the device threshold voltage. Generally, it is in between ground and supply voltage. The gate potential should be kept below the threshold voltage, which makes less swing in

voltage. In sub-threshold region, the current exponentially depends on the gate bias. This becomes more significant in the current technologies.

Triode Mode: In this mode, the transistor works as a variable resistor, and the channel resistance between source and drain is controlled by the amount of gate voltage with respect to the source and drain. When the channel is employed the transistor is switched on, consequently allows flowing current from the drain to source. The current equation in this region is given by

$$I_D = \mu_n c_{ox} \frac{W}{L} (V_{gs} - V_{Th}) V_{ds} - \frac{V_{ds}^2}{2} V \tag{3}$$

Saturation mode: When $V_{gs} > V_{Th}$ and $V_{ds} > (V_{gs} - V_{Th})$, the drain potential is more enough than the gate potential. Hence, the electrons are spread out more. Now the conduction is through boarders instead of narrow channel. This two- or three-dimensional current distribution enhances from the interface and deeper into the substrate. The onset voltage of this state is also known as pinch-off which depicts there is no channel near the drain. At this point, the drain current is weakly influenced by the drain voltage and mostly it is controlled by the gate-to-source voltage, and the current equation in this region is approximated by

$$I_D = \mu_n c_{ox} \frac{W}{2L} (V_{gs} - V_{Th})^2 (1 + \lambda V_{ds}) \tag{4}$$

Sub-threshold NMOS characteristics: The set-up required for operating the NMOS transistor below its threshold voltage is shown in Fig. 2. The transfer characteristics are the set of I_D versus V_{GS} curves for different voltages substrate to source.

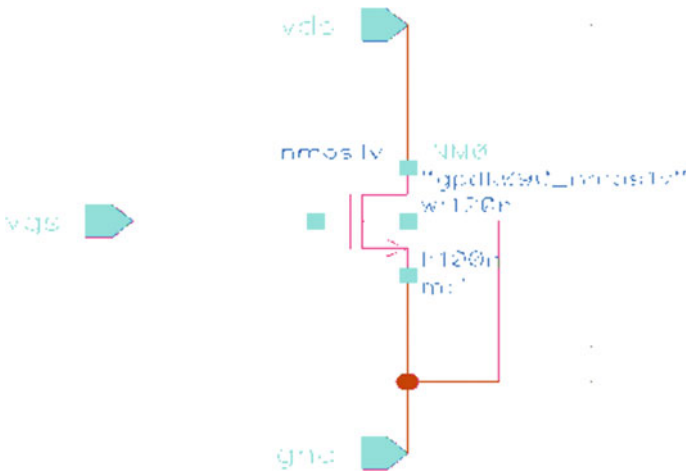


Fig. 2 Sub-threshold NMOS circuit

The characteristics can be drawn by keeping V_{DS} at 0.3 V; vary the V_{GS} from 0.2 to 1.0 V and note the corresponding drain current values finds the current for varying substrate to source voltage as shown in Fig. 3.

Sub-threshold PMOS characteristics: The set-up required for operating the PMOS transistor in sub-threshold region is shown in Fig. 4. The transfer characteristics are the set of I_D versus V_{gs} curves for different substrate to source voltages. The characteristics can be observed with varying the gate-to-source voltage from -0.3 to -1 V with 0.2 V interval [9].

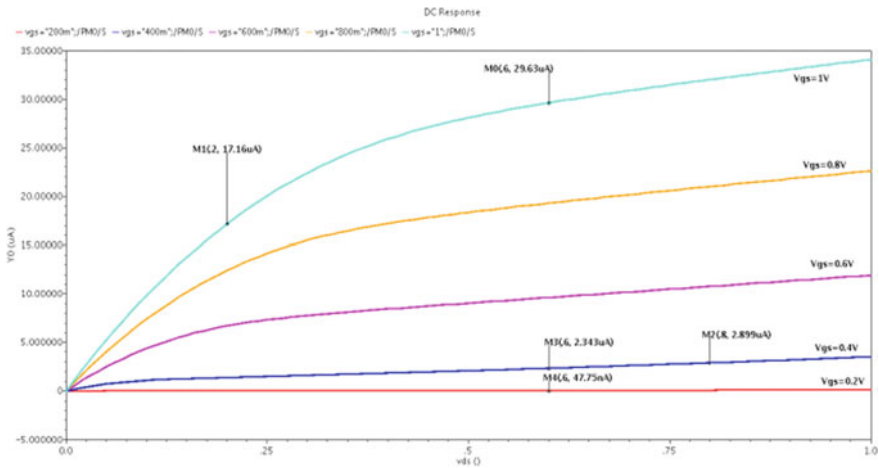


Fig. 3 IV characteristics of NMOS transistor in sub-threshold region

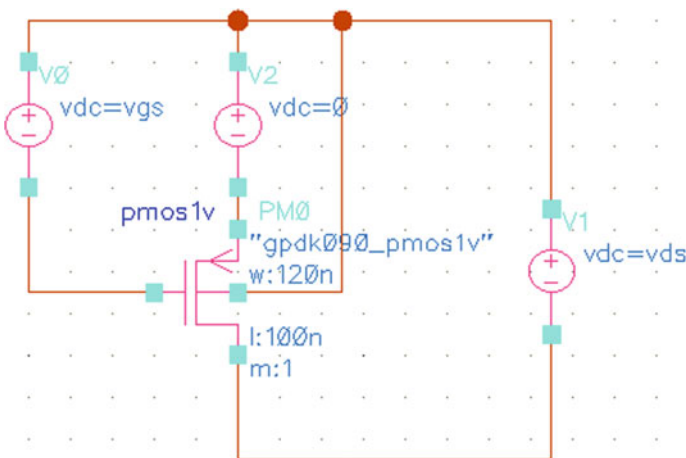


Fig. 4 Sub-threshold PMOS circuit

The transfer characteristics of both NMOS and PMOS transistors are shown in Fig. 5, and the variation of drain currents for different values of V_{gs} and V_{DS} are shown in Table 1.

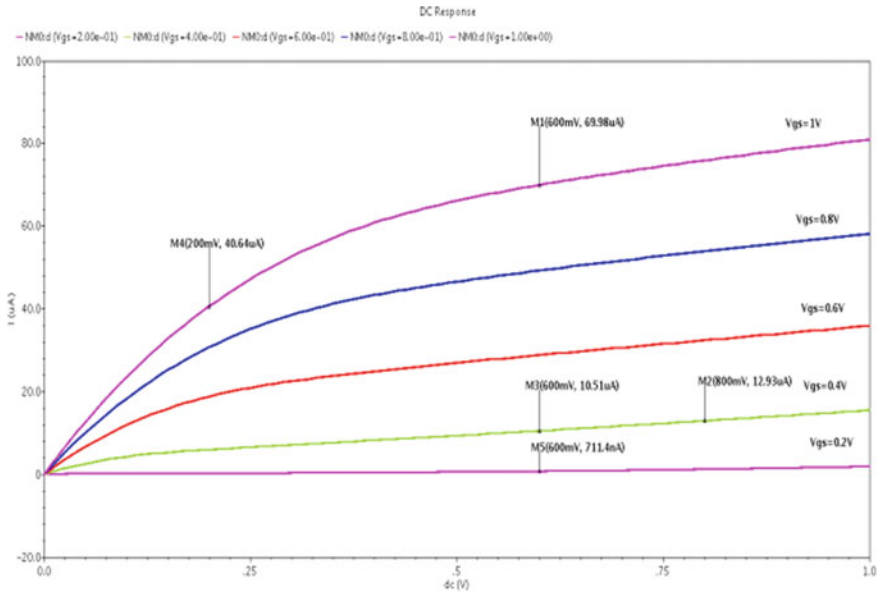


Fig. 5 IV characteristics of PMOS transistor in sub-threshold region

Table 1 Drain currents of NMOS and PMOS devices

		NMOS	PMOS
V_{GS} (V)	V_{DS} (V)	I_D (μA)	I_D (μA)
1.0	0.6	69.98	29.63
1.0	0.2	40.64	17.16
0.8	0.6	31.71	15.28
0.8	0.2	18.22	10.71
0.4	0.6	12.93	4.21
0.4	0.2	10.51	2.34
0.2	0.6	4.02	0.825
0.2	0.2	0.71	0.047

3 Sub-threshold Inverter Design

Inverter is the basic element for all digital circuits. Sub-threshold CMOS inverter logic is similar to the conventional CMOS inverter logic except for the transistors operating in the sub-threshold region [10]. Figure 6 shows the basic CMOS inverter circuit implemented to operate in the sub-threshold region [11].

The voltage transfer characteristics of an inverter as a function of supply voltage is shown in Figs. 7 and 8. Where it is observed that the PMOS width (W_p) is swept

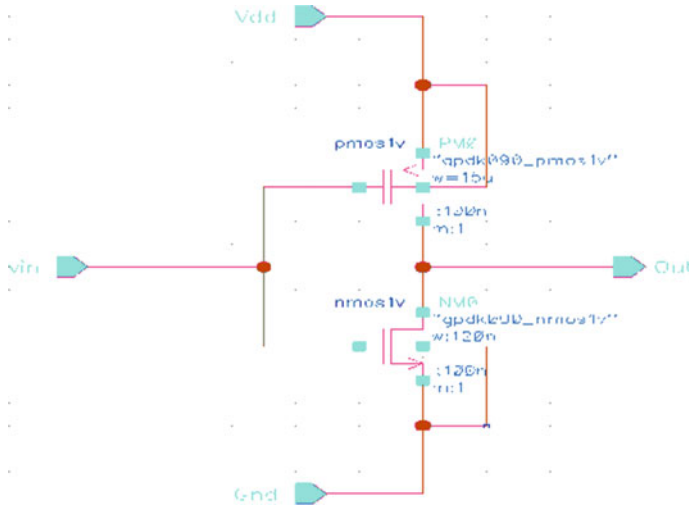


Fig. 6 Sub-threshold CMOS inverter

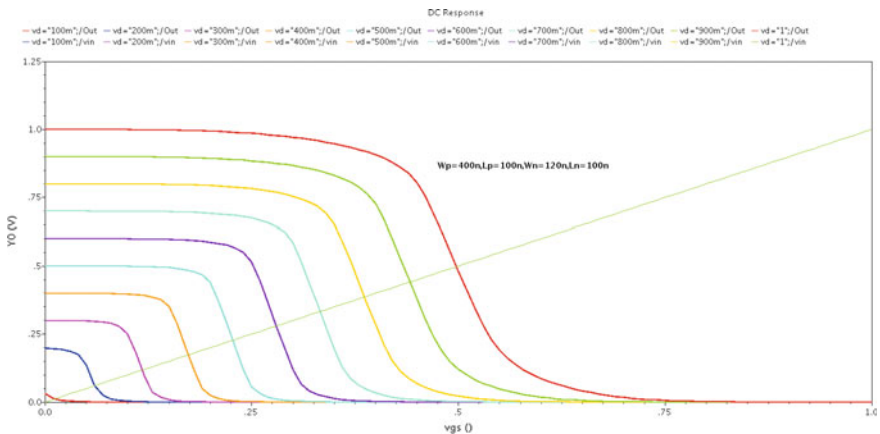


Fig. 7 Voltage transfer characteristics with respect to supply voltage ($W_p = 400$ nm)

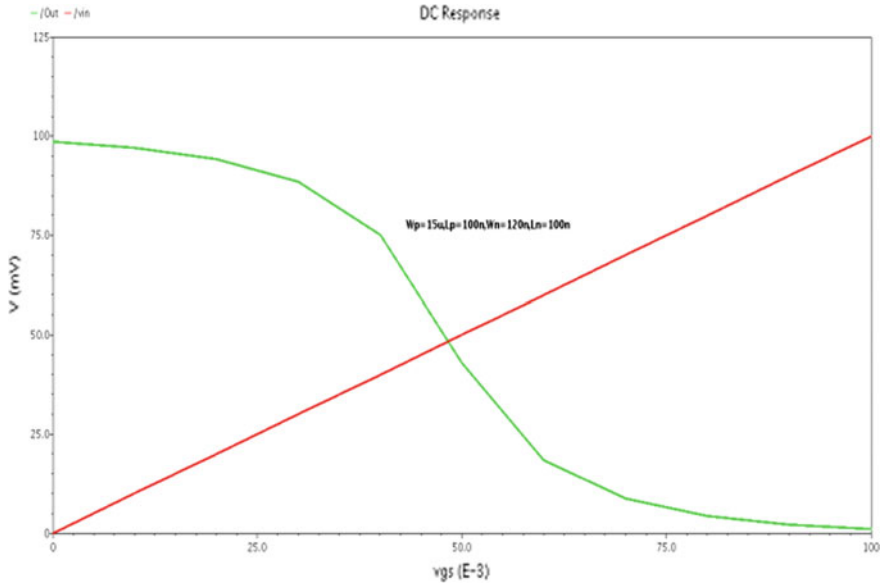
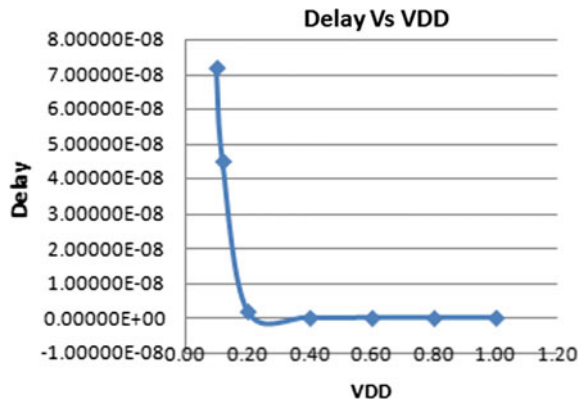


Fig. 8 Voltage transfer characteristics in sub-threshold region ($Wp = 15 \mu\text{m}$)

Fig. 9 Delay versus V_{DD} at 27°C



from 400 nm till 15 μm . Since there is a degradation of logic '1' which occurs in the sub-threshold region, it cannot be deduced below 15 nm.

The major setback of sub-threshold region of operation is the performance degradation. Figure 9 shows that the supply voltage V_{DD} versus delay of the inverter. The sharp decrease in the supply voltage causes the device very slow.

4 Sub-threshold SRAM Design

Basic 6T SRAM cell is shown in Fig. 10 which works in three different states; standby, reading and writing. In read and write cycles, the SRAM cell should have “readability” and “write stability”. **Standby:** When no pulse is applied on the word line, bit lines are disconnected from the cell as the access transistors (M_5 and M_6) are turned off. The two inverters formed by four transistors (M_1 – M_4) are connected in cross-coupled fashion which holds the stored value as long as power supply is switched on. **Reading:** Imagine at the node-1 the stored bit is logic-1. When both the data lines are connected to V_{DD} , the logic-1 stored access transistor starts discharging through M_1 transistor, and hence the corresponding data line voltage starts to decrease, the sense amplifier detects the difference in bit-lines voltages produces logic-1 [12]. **Writing:** To write logic-1 at the node-1 connect BL to V_{DD} , BL bar to GND and apply write pulse of V_{DD} on the word line as shown in Fig. 11. To write logic-0, connect BL to GND and BL bar to V_{DD} . Bit-line drivers are designed strong enough relative to the weak transistors in the cell, and hence it can easily modify the already stored content [13].

6T SRAM Sizing: Readability means, in the read operation the stored content should not be modified. This is achieved when the voltage at the node-1 should not exceed the threshold value of M_2 transistor, otherwise the stored value may flip. Hence, M_2 must be turned off during the read phase.

$$V_{1max} \leq V_{Th2}$$

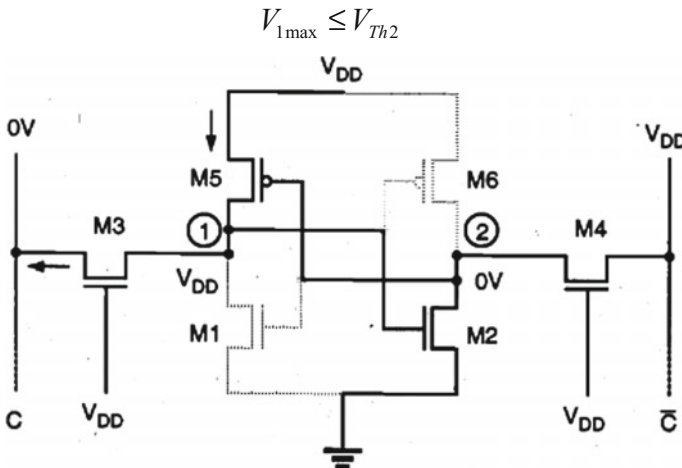


Fig. 10 SRAM cell read operation

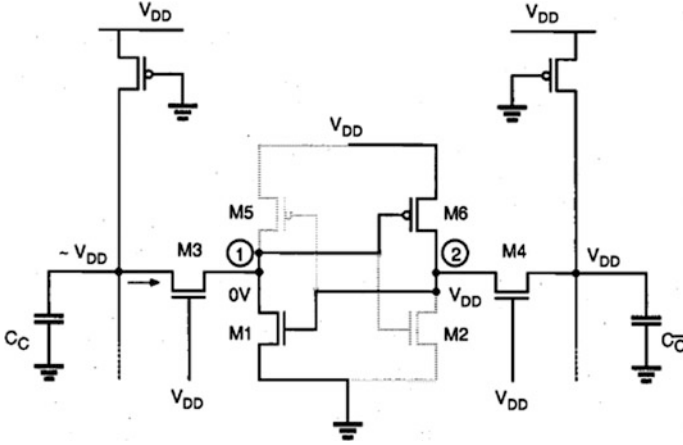


Fig. 11 SRAM cell write operation

Consider a pulse of V_{DD} is on the word line, it makes switch on both the access transistors, and then the bit-line (c) voltage is around V_{DD} . Hence, transistor M_3 works in region of saturation similarly transistor M_1 is the linear region of operation.

$$\frac{k_{p,3}}{2}(V_{DD} - V_1 - V_{Thn})^2 = \frac{k_{n,1}}{2}(2(V_{DD} - V_{Th})V_1 - V_1^2) \quad (5)$$

$$\text{Cell ratio} = \frac{k_{n,3}}{k_{n,1}} = \frac{\left(\frac{W}{L}\right)_3}{\left(\frac{W}{L}\right)_1} < \frac{2(V_{DD} - 1.5V_{Th})V_{Thn}}{(V_{DD} - 2V_{Th})} \quad (6)$$

To modify the stored content, i.e. to store the logic-0 at the node-1 and logic-1 at the node-2, voltage at the node-1 must be reduced below the M_2 threshold voltage. It makes M_2 transistor switched off. Once the node-1 reaches the threshold value of M_3 , it enters into the linear region while M_5 enters into region of saturation [14].

$$\frac{k_{p,5}}{2}(0 - V_{DD} - V_{Th,p})^2 = \frac{k_{n,3}}{2}(2(V_{DD} - V_{Th,n})V_{Th,n} - V_{Th,n}^2) \quad (7)$$

After simplification the pull-up ratio is

$$\frac{k_{p,5}}{k_{n,3}} < \frac{2(V_{DD} - 1.5V_{Th,n})V_{Th,n}}{(V_{DD} + V_{Th,p})^2} \quad (8)$$

5 Simulation Results

The ultra-low-power sub-threshold single-bit 6T SRAM cell implemented in 45 nm technology is shown in Fig. 12.

Figure 13 shows the transient response of the sub-threshold SRAM cell, where it is observed that the stability is severely degraded as the cell more more and more

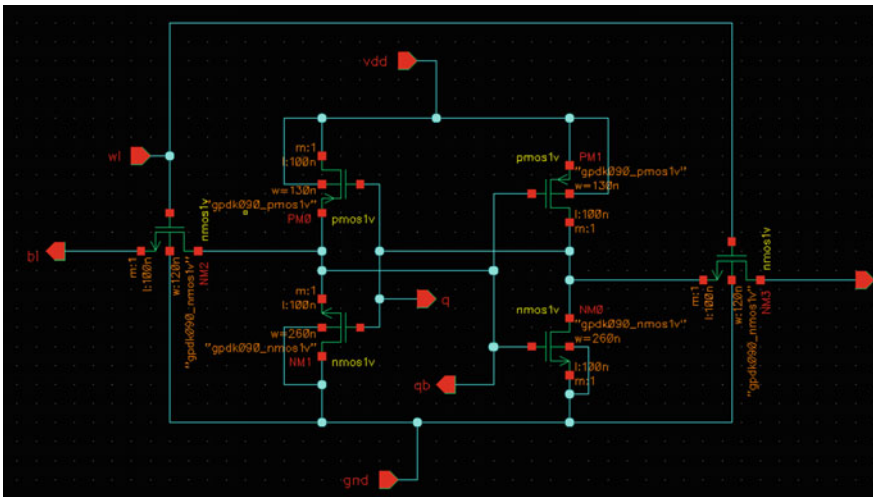


Fig. 12 Schematic implementations of 6T SRAM cell at 45nm technology

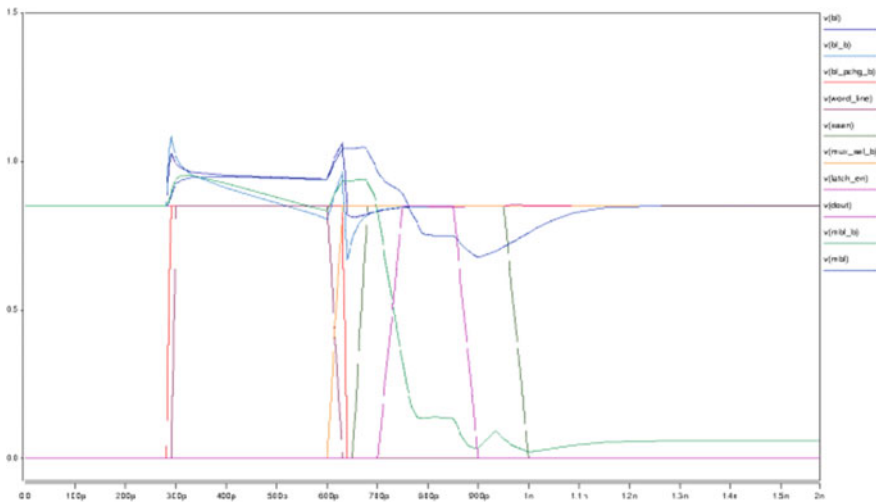
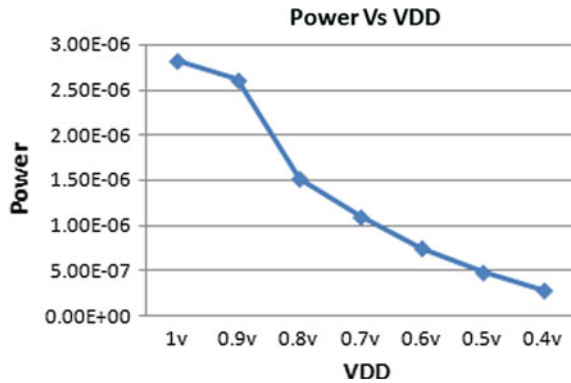


Fig. 13 Simulation results of Sub-threshold 6T SRAM cell

Fig. 14 Variation of SRAM power with respect to the supply voltage



weak. And the Fig. 14 shows the trend of down following of power consumption as the device sub-threshold region of operation improve.

6 Conclusion

Sub-threshold designs reduce the significant amount of power with the supply voltage kept well below the device threshold voltage. Device Scaling reduces the dimensions and hence increases the chip density. Sub-threshold CMOS inverter and 6T SRAM cell is designed in this paper. And observed that the power consumption in these designs reduced from mW to μ W range, but more delay is added when compared with the conventional designs. GPDK 45 nm files and Cadence Virtuoso tools are used for the designs.

References

1. Keejong Kim Mahmoodi, H. Roy, K. Purdue Univ., Lafayette "A Low-Power SRAM Using Bit-Line Charge-Recycling" IEEE J. Solid-State Circuits, vol. 43, pp. 446–459, Feb. 2008
2. Bo Zhai, Sanjay Pant, Leyla Nazhandali, Scott Hanson, Javin Olson, Anna Reeves, Michael Minuth, Ryan Helfand, Todd Austin, "Energy-Efficient Subthreshold Processor Design" IEEE Transactions on VLSI Systems, Vol. 17, NO. 8, 2009
3. A. Pajkanovic, T. Kazmierski and B. Dokic "Adiabatic Digital Circuits Based on Sub-threshold Operation of Pass transistor and Slowly Ramping Signals," *Proceedings of Small Systems Simulation Symposium*, 2012
4. M.R. Bagheri "Ultra Low Power Sub-threshold bridge style adder in nanometer technology" *Canadian Journal on Electrical and Electronics Engineering*, vol. 2, no. 7, pp. 294–299, 2011
5. A. P. Chandrakasan, S. Sheng, and R. W. Brodersen, "Low- power CMOS digital design," IEEE J. Solid-State Circuits, vol. 27, pp. 473–484, Apr. 1992

6. K. Roy, S. Mukhopadhyay, H. Mahmoodi-Meimand, "Leakage Current Mechanisms and Leakage Reduction Techniques in Deep-Submicrometer CMOS Circuits," *Proceedings of the IEEE*, vol. 91, no. 2, Feb. 2003
7. A. Wang, B. H. Calhoun and A. Chandrakasan, *Sub-threshold design for ultra-low-power systems*, Springer publishers, 2005
8. Srinivasa Rao.Ijjada, S.V.Sunil Kumar, M. Dinesh Reddy, Sk.Abdul Rahaman, Dr.V. Malleswara Rao "Design of low power and high speed Inverter" *International Journal of Distributed and Parallel Systems (IIDPS)* Vol. 2, No. 5, September 2011
9. Srinivasa Rao.Ijjada, Raghavendra Sirigiri, B.S.N.S.P. Kumar, V. Malleswara Rao "Design of high efficient & Low Power basic Gates in Sub-threshold region" *International Journal of Advances in Engineering & Technology*, May 2011
10. Priya Gupta, Anu Gupta, Abhijit Asati "A review on ultra low power design technique" *IJCST*, vol-4, issue-2, 2013
11. J. Rabaey, *Low Power Design Essentials*, Springer publications, 2009
12. J. Rabaey, *Digital Integrated Circuit Design* by Jan M. Rabaey, Anantha P. Chandrakasan, Borivoje Nikolić, Borivoje Nikolić, Pearson Education, 2003
13. A. P. Chandrakasan and R.W. Brodersen, "Minimizing power consumption in digital CMOS circuits," *Proc. IEEE*, vol. 83, pp. 498–523, Apr. 1995
14. S. Kang, "Elements of Low Power Design for Integrated Systems," *ISLPED '03*, August, 2003

Temperature- and Color-Based SDSS Stellar Spectral Classification Using Automated Scheme

Amit Goyal, Jayash Kumar Sharma, Darpan Anand
and Manish Gupta

Abstract Automated techniques minimize the complexity, saving time and efforts in the object classification and their analysis. Sloan Digital Sky Survey (SDSS) is one of the spectroscopic surveys releasing large data sets. Astronomers are looking for some automated techniques so that they can analyze these massive data sets which are now publicly available. We use Feed Forward Back Propagation (FFBP) Neural Network for automatic classification. Classification of stars is performed on the basis of two parameters that are temperature and color. 1500 SDSS spectra are classified into 4 spectral types, and around 2359 SDSS spectra are classified into 7 spectral types ranging from A to K and O to M type stars by using color and temperature, respectively.

Keywords Stellar spectra · Spectral type · Sloan digital sky survey (SDSS) Neural network

1 Introduction

Tools of data mining have found applications in various fields like object classification, data compression, etc. They are now being used in star-galaxy classification, stellar classification, etc. In astronomy, databases are getting larger day by

A. Goyal (✉) · J.K. Sharma · D. Anand
Hindustan Institute of Technology and Management, Agra, Uttar Pradesh, India
e-mail: amittech.it@gmail.com

J.K. Sharma
e-mail: jayash.sharma@gmail.com

D. Anand
e-mail: darpan.anand.agra@gmail.com

M. Gupta
Amity University, Gwalior, Madhya Pradesh, India
e-mail: manish_dabra@yahoo.com

day, so there is a need to perform automatic classification of these large data sets. The Sloan Digital Sky Survey is one of such publicly available large source of data that needs to be classified using some automatic technique like ANN.

We use two separate Feed Forward Back Propagation (FFBP) Neural Networks for classification of SDSS stellar spectra on the basis of temperature and color. We have classified 1500 and 2359 SDSS stellar spectra into a set of 4 and 7 spectral types, respectively. SDSS is capturing the details of millions of celestial objects. It provides us a three-dimensional picture of the universe. It consists of images and precise catalogs of all objects discovered including spectra of millions of celestial objects.

The data is available over the Internet in form of data releases from the set of four projects that are SDSS-I/II which include surveys from 2000 to 2008, SDSS-III include surveys from 2008 to 2014, and SDSS-IV consists of current surveys since 2014. Millions of stellar spectra can be accessed from SEGUE and SEGUE-2 surveys.

The paper is structured as follows: Sect. 2 presents the related work. Section 3 describes the methodology used and gives the information about stellar classification using temperature (Sect. 3.1) and color (Sect. 3.2). Section 4 describes the implementation including SDSS spectral data sets used for training and testing (Sect. 4.1) and building the classifier (Sect. 4.2). Section 5 gives the result of simulation using this classifier. Section 6 discusses the conclusion.

2 Related Work

Expert System, K-means, Artificial Neural Networks (ANN), Self-Organizing Map (SOM), and Support Vector Machine (SVM) are the different kinds of techniques that can be used for the classification of astronomical data.

In 2008, Mahdi Bazarghan et al. [1] performed the automated classification of stellar spectra. They used a reference library that consists of 158 spectral types including stars from the range of O to M type classes. 5000 SDSS spectra were then classified by using Probabilistic Neural Network (PNN) into these 158 spectral types. The paper suggested further work of SDSS stellar spectra classification using other parameters like temperature, considering the training data from SDSS itself.

In 2013, Sánchez Almeida et al. [2] used K-means clustering to classify SDSS stellar spectra. In 2016, Kheirdastan et al. [3] used K-means clustering, Support Vector Machine (SVM), and Probabilistic Neural Network (PNN) as automated techniques to explore their applications in the classification of a lot of stellar spectra. SDSS's SEGUE-1 and SEGUE-2 surveys provided the data set of stellar spectra. They found that PNN is a much better technique to classify them as compared to SVM and K-means.

3 Proposed Methodology

Our proposed approach consists of preprocessing the spectral data sets, building the classifier for color and temperature classification, and simulating it with the stellar spectra not seen by classifier before to predict their respective classes.

Preprocessing consists of obtaining the random sample of SDSS stellar spectra separately for color- and temperature-based classification. Samples are divided into two subsets, one for building the classifier and second for its simulation. Building the classifier consists of creating two Feed Forward Back Propagation (FFBP) Neural Networks using the first subset in both cases. Simulation consists of the classification of 1500 SDSS spectra into 4 spectral types and 2359 SDSS spectra into 7 spectral types ranging from A to K and O to M type stars by using color and temperature, respectively.

Back propagation is a part of the general feed-forward model. It is a supervised learning algorithm. It includes two stages that are forward propagation and backward propagation. In training phase, algorithm propagates input data set through the net in a forward way, until we achieve the activation. This phase is named as forward propagation. The difference in between the input and output tells us about the error. This error is used to change the links between layers and propagated backward, so we call this phase as backward propagation.

3.1 Temperature Classification

In the case of stars, the effective temperature is the temperature of a star with the same luminosity per surface area. Our Sun has the effective temperature of around 5780 Kelvin (K). In astronomy, the classification of stars on the basis of their spectral characteristics is called spectral classification. Currently, classification of stars is performed using the sequence of letters O, B, A, F, G, K, and M. Stars fall into the category of O type are hottest, and stars from the category of M type are coolest. Spectral types with their corresponding temperatures are shown in Table 1.

SDSS's SEGUE Stellar Parameter Pipeline (SSPP) measures three primary stellar parameters which are metallicity ($[Fe/H]$), surface gravity ($\log g$), and

Table 1 Temperature of spectral classes

Spectral type	Eff. temperature (K)
O	$\geq 30,000$
B	10,000–30,000
A	7,500–10,000
F	6,000–7,500
G	5,200–6,000
K	3,700–5,200
M	2,400–3,700

effective temperature (Teff), after processing the SDSS stellar spectra. For most of the stars, effective temperature ranges 4000–10,000 K. Due to this limited range, stars with effective temperature lower than 4000 K or greater than 10,000 K i.e., very cool stars and very hot stars, respectively, could not be categorized. Hence, stars are classified into A, F, G, and K spectral type.

3.2 Color Classification

For color, different persons can have a different point of views. If for one individual it is “red,” then for another individual, it can be a different shade of red. If astronomers want to learn something from star color, they require to have a definition of color that is acceptable by everyone; something that everyone can use to perform the comparison between the colors of different stars. For this, they choose color index that is the difference in magnitude between two filters. A number that measures the brightness of a star is called magnitude. In magnitude, lower numbers correspond to brighter objects; higher numbers correspond to fainter objects. Negative magnitude shows that the object is brightest. Index can be measured by observing the magnitude from two different filters say, u and g or g and r, where u is the filter to ultraviolet rays, g and r are filters to visible (green-red) light. By finding the difference in magnitudes, one can find the color index, such as u-g or g-r, respectively. Approximate values of color index of different spectral type shown in Table 2.

SDSS uses five color filters to measure five different colors. A filter only permits a light with specific color and blocks out all other light. The SDSS filters are u, g, r, i, and z. Green and red light filters are termed as g and r. SDSS uses two infrared (i and z) and one ultraviolet filter (u), respectively. Single color index, say, u-g let us know something about a star. By adding more color, we can explore a wider range of the spectrum. But usually, two different colors are enough. Stars can be arranged in a two-dimensional space, referred as Color-color graph where each axis is used for a different color. We have created Color-color graphs of 3150 SDSS spectra from 7 spectral types using MATLAB as shown in Fig. 1. This graph shows locus of stars from lower left to upper right. This shows that we can determine the spectral type of a star using their color index.

Table 2 Color of spectral classes

Spectral type	Color	Color index
O	Blue	-0.4
B	Blue white	-0.3
A	White	0
F	Yellow white	0.3
G	Yellow	0.58
K	Orange	0.81
M	Red	1.4

Fig. 1 Color-color graph of 3150 SDSS spectra where different colors showing different classes

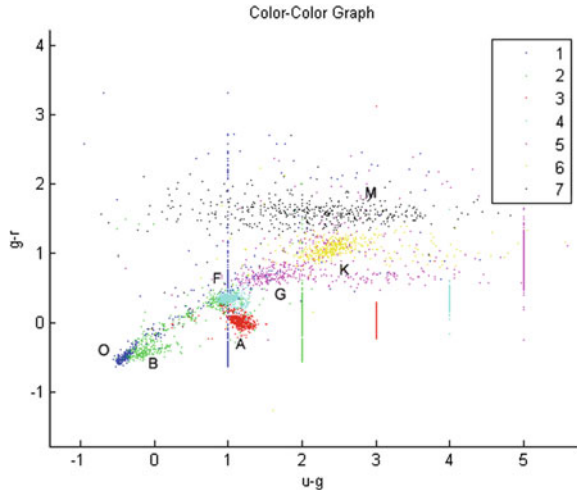


Table 3 SDSS spectra data set for temperature classification

500 spectra	To build the classifier (25% from each spectral type i.e., 125 * 4) includes training, validation and testing data
1500 spectra	To simulate the classifier (75% from each spectral type i.e., 375 * 4) prediction of respective spectral type

4 Implementation

4.1 SDSS Spectral Data Set

The SEGUE and SEGUE-2 surveys from SDSS are used for SDSS spectra. SDSS’s Data Release 7 includes the complete SEGUE data set, and additional spectra are the part of the SDSS 3’s SEGUE-2 extension that is available as part of Data Release 8. We used SDSS Data Release 8 (DR8) Hiroaki et al. [4] to download stellar spectra. Downloaded data is in CSV format acceptable by the neural network.

Temperature Data Set: We used SDSS SkyServer’s SQL interface to select spectra of 2000 stars (500 spectra from four spectral types). This data includes spectra name (plateID-fiberID-MJD), their adopted effective temperature (TEFFADOP), and their respective spectral type. This data is divided into two subsets. The first subset includes 25% data of the entire data set to build the classifier, and the second subset includes 75% data for the simulation of network as shown in Table 3.

Color Data Set: We used SDSS SkyServer’s SQL interface to select spectra of 3150 stars (450 spectra from seven stellar types). This data includes spectra name (plateID-fiberID-MJD); their magnitudes are taken through three color filters (u, g, r) and their respective spectral type. We calculated their color by subtracting the

Table 4 SDSS spectra data set for color classification

791 spectra	To build the classifier (25% from each spectral type i.e., 113 * 7) includes training, validation and testing data
2359 spectra	To simulate the classifier (75% from each spectral type i.e., 337 * 7) prediction of respective spectral type

Table 5 Structure of network

Input matrix of size 1 * 500 (temperature of 500 spectra)
Target matrix of size 1 * 500 (spectral type of 500 spectra)
Number of nodes in hidden layer (12 neurons)
tansig—activation function (hidden layer)
Purelin—activation function (output layer)
traingdx—training function
learnqdm—learning function
mse—performance function

magnitudes: u-g, g-r. This data is divided into two subsets. The first subset includes 25% data of the entire data set to build the classifier, and the second subset includes 75% data for the simulation of the network as shown in Table 4.

4.2 Building the Classifier

Classifier for Temperature Classification: We used neural network toolbox from MATLAB to create a neural network model for classification of stellar spectra. Other tools like SPSS are also data mining tools, but MATLAB gives a large number of functionality supports, so we used NN tool to build our classifier. 500 SDSS stellar spectra were taken to build the classifier. This data set was divided into three subsets:

1. The first subset includes 75% of data that was used to train the model
2. The second subset includes 10% of data that was used for validation
3. The third subset includes 15% of data that was used to test the model.

We have created a two-layer Feed Forward Back Propagation (FFBP) Network using newff command in MATLAB with arguments as shown in Table 5.

Different functions with constant architecture were investigated in the input and output layer for the end results. We found tansig() and purelin() are the best activation functions for hidden and output layers, respectively. The functions are shown in Figs. 2 and 3.

t.trainParam.epochs which tell the algorithm about the maximum number of epochs to train was set to 6 after analyzing the point where mean square error was minimum, and more than that could lead to the overfitting problem. To find the optimum number of hidden nodes, network was trained with 6 up to 16 hidden

Fig. 2 Activation function for hidden layer

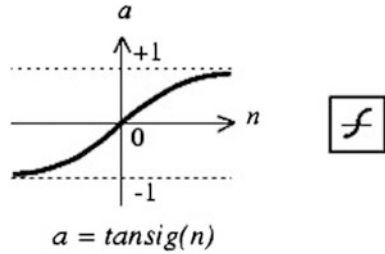


Fig. 3 Activation function for output layer

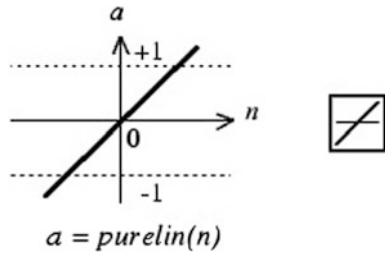


Table 6 Mean performance using different number of hidden nodes

Number of hidden nodes	Mean performance over 10 experiments (%)
6	70.65
7	70.48
8	73.46
9	72.54
10	74.97
11	72.81
12	71.87
13	75.04
14	73.45
15	74.45
16	73.71

nodes using training data, and corresponding performance was measured. For each value, we executed training and evaluation 15 times by changing initial random weight every time.

Table 6 shows the mean performance using a different number of hidden nodes. The network gave us highest mean performance with 13 hidden number of neurons, so we selected it as optimum number of hidden nodes to perform our classification. We got the best performance of 75.04% by using 13 hidden nodes in our network. The performance graph obtained is shown in Fig. 4.

Fig. 4 Performance graph

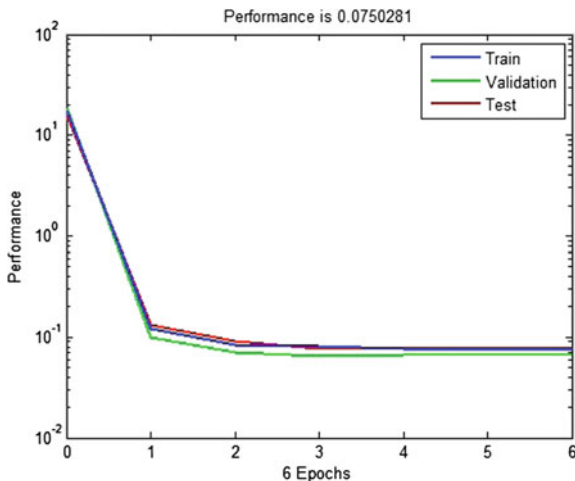
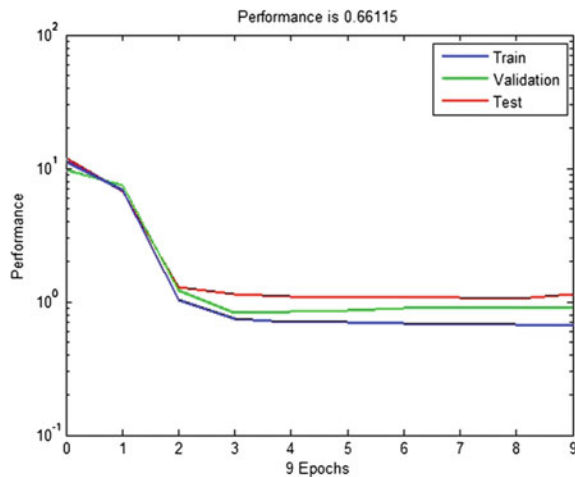


Fig. 5 Performance graph



Classifier for Color Classification: 791 SDSS stellar spectra were taken to build the classifier. This data set was divided into training, validation, and testing data as we have done in temperature classification. The structure of network is also similar, except two arguments i.e., input matrix of size $2 * 791$ (color information of 791 spectra) and target matrix of size $1 * 791$ (spectral type of spectra). Maximum number of epochs was set to 9. The number of hidden neurons was set to 30 to achieve the highest mean performance of 66.182%. The performance graph is shown in Fig. 5.

5 Classification Results (Simulation and Getting Experimental Results)

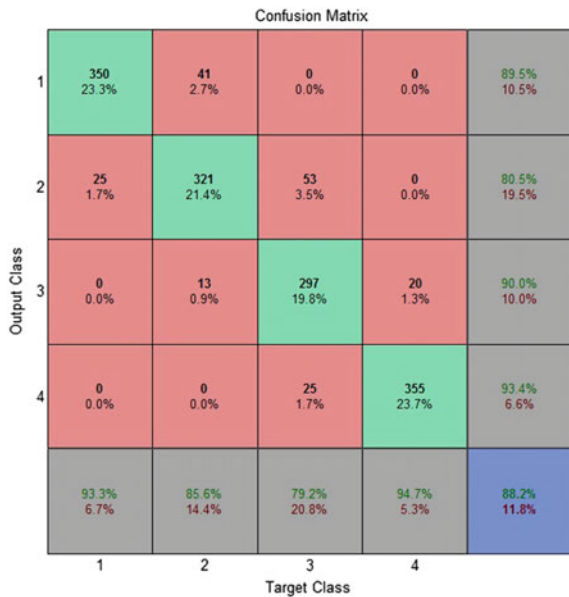
5.1 Results of Temperature Classification

After building the classifier, 1500 SDSS stellar spectra were taken which were not seen by the classifier before and classified them into their respective spectral type. The results of simulation are shown in Table 7. The confusion matrix is shown in Fig. 6. True classes and nearest neighbors classes are listed along the x-axis and the y-axis, respectively. First diagonal shows the correct classifications. The overall accuracy is at the bottom right cell.

Table 7 Temperature classification results

Spectral type	Results (%)
A	93.3333
F	85.6
G	79.2
K	94.6667
Average	88.2

Fig. 6 Confusion matrix obtained after performing temperature classification



5.2 Results of Color Classification

After building the classifier, 2359 SDSS stellar spectra were taken which were not seen by the classifier before and classified them into their respective spectral type. The results of simulation are shown in Table 8. The confusion matrix obtained is shown in Fig. 7.

Table 8 Color classification results

Spectral type	Results (%)
O	55.7864
B	52.819
A	81.8981
F	38.5757
G	51.0386
K	55.4896
M	70.0297
Average	57.9483

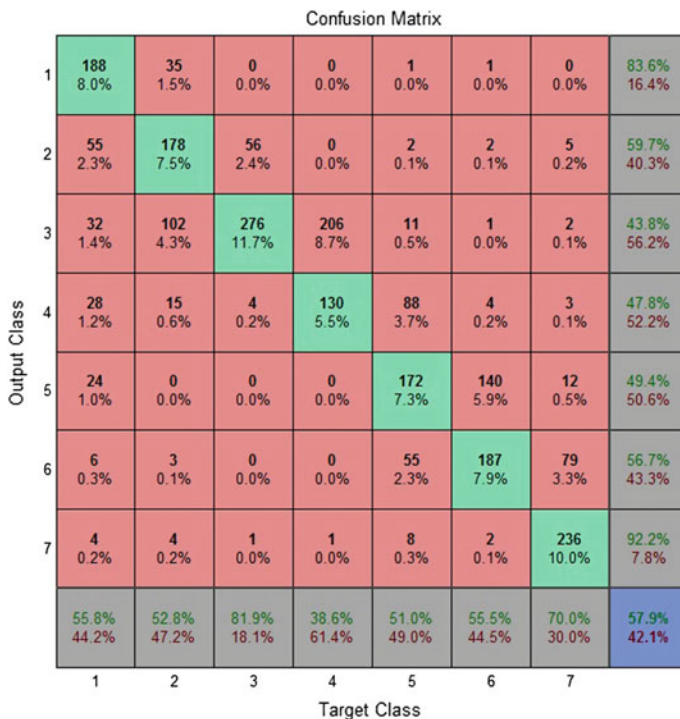


Fig. 7 Confusion matrix obtained after performing color classification

6 Conclusion

In this chapter, we used the Feed Forward Back Propagation (FFBP) Neural Network for classification of bulk of SDSS stellar spectra. The data sets were provided by SEGUE and SEGUE 2 programs of SDSS. Despite the limited samples of stellar population from Milky Way, it provides a large number of stellar types and therefore gives an ideal platform for the classification algorithms.

In our work, we present the results obtained from building a classifier based on Artificial Neural Network (ANN) for classifying stars. We used temperature and color as two different parameters for classification. Temperature-based classification corresponds to a success rate of 88.2%. By color-based classification, we got a success rate of 57.94%. Although classifying stars by color is not a foolproof method, we can learn a lot about stars by looking only at its color. Astronomers use color to classify many objects including stars, galaxies, and quasars.

Future work includes studying the other data from SDSS, such as luminosity that may also prove useful in classifying stars, and this needs to be investigated. In future, we would focus on combining these parameters altogether to get the better results of classification. We would try to apply our method to perform classification to even wider range of data sets.

References

1. Bazarghan, Mahdi and Gupta, Ranjan: Automated classification of sloan digital sky survey (SDSS) stellar spectra using artificial neural networks. In: *Astrophysics and Space Science* (2008)
2. J. Sánchez Almeida, C. Allende Prieto: Automated Unsupervised Classification of the Sloan Digital Sky Survey Stellar Spectra using k-means Clustering. In: *The Astrophysical Journal* (2013)
3. Kheirdastan, S. and Bazarghan, M.: SDSS-DR12 bulk stellar spectral classification: Artificial neural networks approach. In: *Astrophysics and Space Science* (2016)
4. Aihara, Hiroaki, et al.: The eighth data release of the Sloan Digital Sky Survey: first data from SDSS-III. In: *The Astrophysical Journal Supplement* (2011)

Experimental Investigation on SP and TCT PV Array Configurations to Reduce Power Losses During PSC

Aditya Chaudhary and Mamta Chamoli Kala

Abstract In this paper, an analysis of series–parallel and total cross-tied photo-voltaic array (size 3×3) is investigated under irregular irradiation conditions or shading conditions. The artificial shading effect is considered on the PV array with the progression of shadow to investigate the shading effect on PV performance in terms of power and voltage at GMPP and power losses. The performance analysis of system is agreed out in terms of power and voltage at global maximum power point, power and current losses.

Keywords PV array · Series–parallel configuration
Total cross-tied configuration · Power mismatch losses · Shading effect

1 Introduction

Today, maximum energy demand is based upon the fossil fuels in any country. But the fossil fuels have some critical problems such as scarcity, storage capacity, and costliness. It is most urgent to explore more sustainable energy sources. Recently, PV technology is achieving highest popularity due to its advantageous features [1].

The partial shading reduces the PV performance. It is urgently needed to elaborate effective methodologies to reduce the shading effect and/or performance enhancement. In this context, suitable methodology can be adopted to change the electrical connections of PV module in PV array. Moreover, series, series–parallel (SP), total cross-tied (TCT), bridge-link (BL), and honeycomb (HC) interconnections are available to achieve maximum power from PV array.

A. Chaudhary (✉) · M.C. Kala
Department of Electrical Engineering, Faculty of Technology,
Uttarakhand Technical University, Dehradun 248001, India
e-mail: adityachaudhary2017@gmail.com

M.C. Kala
e-mail: nithya12345678@gmail.com

In [2], the authors investigated the partial shading effect on several PV array configurations, e.g., SP, TCT, BL, and HC, and the performance investigation is done in terms of power mismatch losses and FF. In [3], a detailed study is done and analyzes the shading effect on $I-V$ and $P-V$ curves on series and SP configurations with MATLAB/Simulation and experimental analysis. The authors in [4–6] implemented a dynamic switch matrix for adaptive configuration to minimize the shading effect on modules. The experimental work is presented and analyzed the series, SP, and TCT configurations of PV array. The authors of [7] implemented a hardware system, which comprised series and SP configurations to analyze the shading effect under numerous outdoor and laboratory-based irradiation levels. The mathematical modeling is carried out to assess the nature of $I-V$ characteristic of PV array under shading conditions. To validate, the gained results are equated with the bench work analysis [8]. In [9], an investigation and comparative study on obtained results of SP, TCT, and BL PV array configurations are carried out to verify the system performance under the shaded conditions. Moreover, maximum current is achieved in the case of TCT interconnections of PV array. In [10–13], an investigation on the behavior $I-V$ and $P-V$ curves is carried out for the performance analysis, and an experimental setup is implemented to match obtained results.

With the motivation of above literature review, the purpose of this paper is to plan experimental setup for SP and TCT configurations of PV array (size 3×3). Moreover, an investigation is done under the shading conditions in terms of global maximum power point (GMPP) locations, power, current mismatch losses, and FF.

2 Experimental Setup and Specifications

The specifications and utilization of all the supportive components in experimental setup are listed in Table 1. The experimental setup comprises various important components which are shown in Fig. 1.

Table 1 Specifications of components used in experimental setup

Components	Specifications
3×3 PV modules in array	<ul style="list-style-type: none"> • PV array power: 5.087 • O.C.voltage: 10.8 V • S.C.current: 0.59 A • I_{mpp}: 0.55 A, V_{mpp}: 9.25 • No. of PV module: 9 (3×3 array)
Artificial irradiation system	<ul style="list-style-type: none"> • Total number of lamps—16 (4×4) • A potentiometer • Light intensity 50–1650 W/m²
Electromechanical relay circuit board	<ul style="list-style-type: none"> • No. of relay circuits: 4 • Voltage: +5 V, current: 10 A

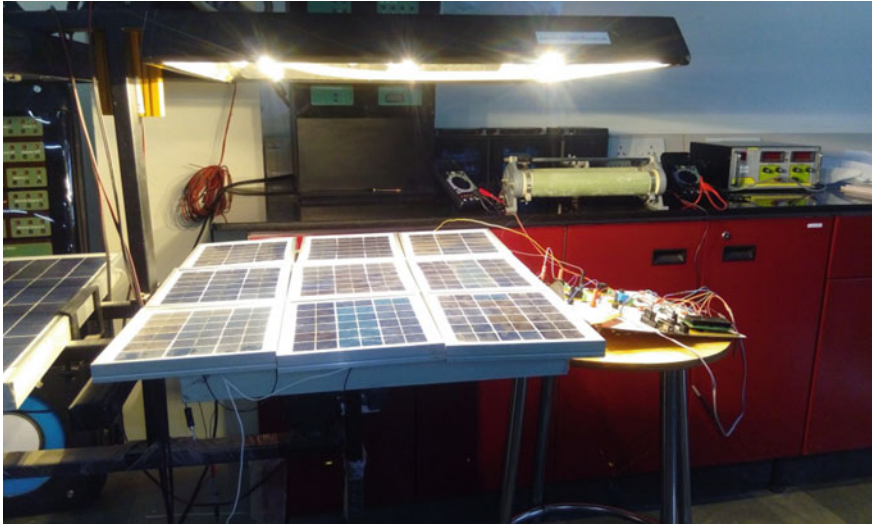


Fig. 1 Experimental setup

3 Modeling of PV System and Array Configurations

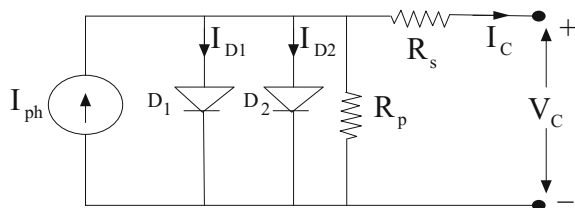
3.1 Mathematical Modeling of PV System

PV array configurations are shaped by interconnecting different PV modules in the combination of series as well as parallel connections to match the demand electrical power to load. This bypass PV module is more accurate and realistic than ideal/single diode especially under the PSC. The electrical circuit of bypass diode PV module is shown in Fig. 2.

The photovoltaic cell voltage (V_C) is given in Eq. (1), and operating temp. of T_C changes with the solar insolation S_C . These types of effects the C_{TV} and C_{TI} (temp. coefficients for voltage and current shown in Eq. (2) [14–16] as,

$$V_C = \frac{AkT_C}{e} \ln\left(\frac{I_{ph} + I_{D1} + I_{D2} - I_C}{I_{D1} + I_{D2}}\right) - I_C \left(\frac{R_s R_p}{R_s + R_p}\right) \tag{1}$$

Fig. 2 Electrical circuit of bypass diode-based PV module



$$C_{TV} = 1 + \beta(T_x - T_x) \quad \text{and} \quad C_{TI} = 1 + \frac{\gamma_T}{S_c}(T_x - T_x). \quad (2)$$

The result of insolation level (S_x) on photocurrent and voltage can be obtained accordingly using correction factors, C_{SV} and C_{SI} , which are used to calculate photocurrent and voltage of cell, and is shown in Eq. (3) as,

$$C_{SV} = 1 + \beta_T \alpha_S (S_x - S_c) \quad \text{and} \quad C_{SI} = 1 + \frac{1}{S_c} (S_x - S_c). \quad (3)$$

The correction factors of temperature and insolation such as C_{TV} , C_{TI} , C_{SV} , and C_{SI} are supportive to express the actual values of voltage (V_{cx}) and photocurrent (I_{phx}) of cell, and are shown in Eq. (4) as

$$V_{cx} = C_{TV} C_{SV} V_c \quad \text{and} \quad I_{phc} = C_{TI} C_{SI} I_{ph}. \quad (4)$$

The power loss on PV array and FFF can be expressed using Eqs. (5)–(6) as

$$\text{Power loss} = \text{MPP without PS} - \text{GMPP with PS} \quad (5)$$

$$FF = \frac{V_{mpp} I_{mpp}}{V_{oc} I_{sc}} \quad (6)$$

The SP and TCT configurations of PV array are given below and shown in Fig. 3a, b.

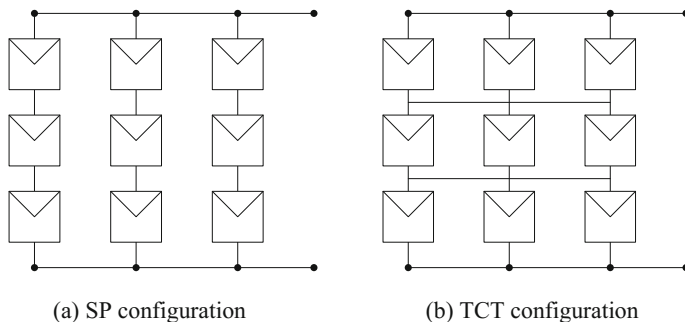


Fig. 3 SP and TCT configurations of size 3×3 PV array

4 Partial Shading Conditions

The shading cases ‘a, b, c’ are categorized under the shading pattern, and each case is considered for experimental investigation for SP and TCT configurations. In present shading pattern, the assumption of the shadow movement is progressive from leftmost PV module (from bottom side to top and right side) of the PV array as shown in Fig. 4.

5 Result Outcomes and Discussion

The performance assessment agreed to analyze the effect of shading under considered shading cases a, b, c of experimental-based SP and TCT configurations of PV array. The salient points of study are carried out as

- Power–voltage ($P-V$) and current–voltage ($I-V$) curves and GMPP of PV array under shading condition
- Power losses and FF assessment of PV array during shading cases

5.1 P–V and I–V Curves and GMPP of PV Array Under Shading Condition

The $P-V$ characteristics of experimental-based PV array interconnections for shading cases ‘a,’ ‘b,’ and ‘c’ of Fig. 4 are depicted in Fig. 5a, c.

In present investigation, the performance assessment is investigated in terms of power and voltage at GMPP, and the obtained result outcomes are summarized in

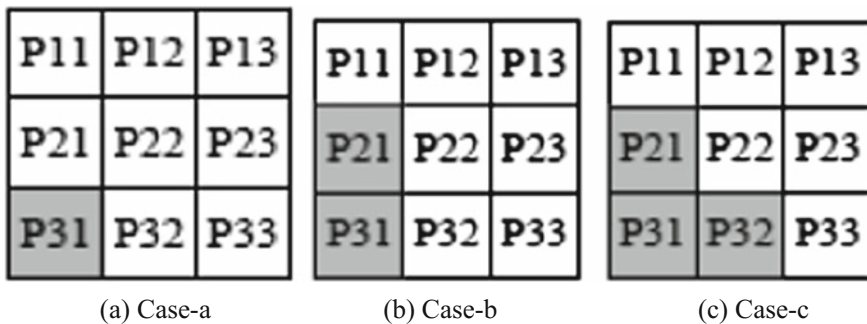


Fig. 4 a–c Partial shading cases ‘a–c’ from bottom side to top and right side

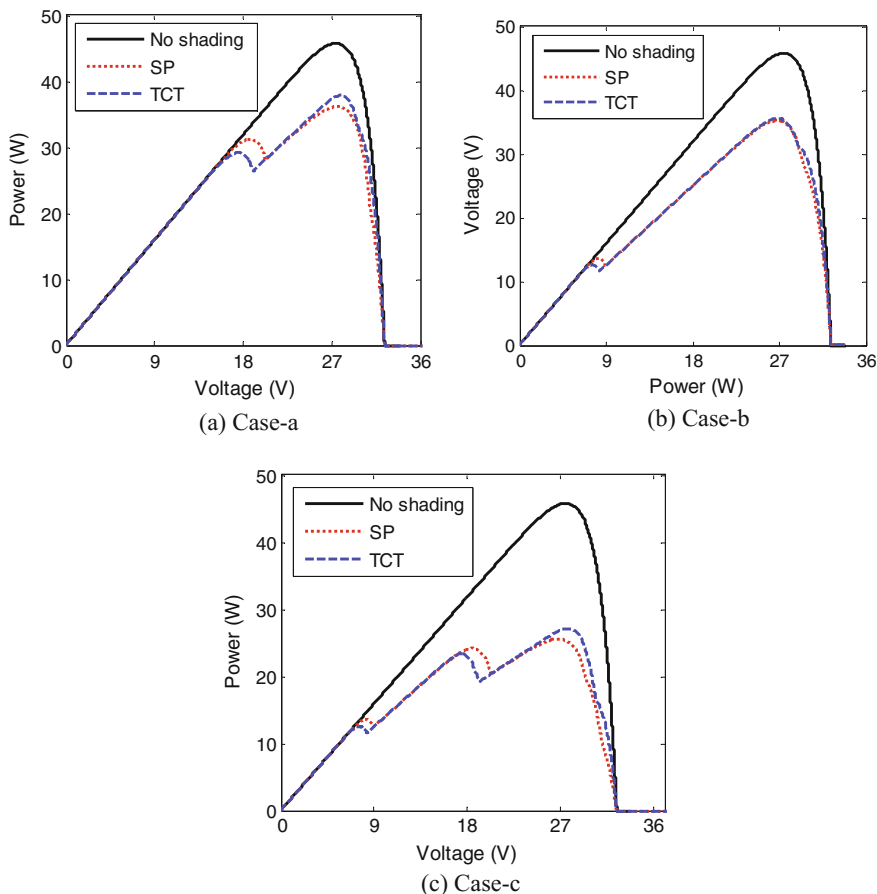


Fig. 5 a–c Effect of shading cases a–c on P–V characteristics

Table 2 Power and voltage at GMPP of SP and TCT PV array configurations

	Power and voltage at GMPP					
	Case a		Case b		Case c	
	P (W)	V (V)	P (W)	V (V)	P (W)	V (V)
SP	36.18	27.59	35.36	26.7	25.27	27.07
TCT	37.88	27.92	35.57	26.7	27.14	27.56

Table 2. The results show that TCT configuration harvests extra power as equated to SP configuration of PV array in experimental analysis. The obtained results are summarized in Fig. 6a, b.

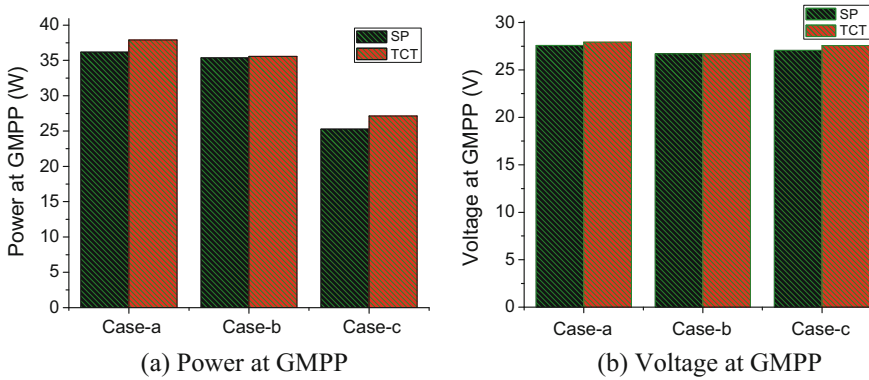


Fig. 6 a, b Effect of shading cases ‘a–c’ on power and voltage at GMPP

5.2 Power Losses and FF Assessment of PV Array During Shading Cases ‘a–c’

During shading pattern/cases ‘a’ to ‘c,’ the performance of TCT configuration is far better than that of SP configuration, and the power mismatch losses are exposed with bar chart in Fig. 7. The power mismatch losses are obtained to be lower in TCT for most of the shading cases. There is increment in shadow on the PV array, which reduces the FF. During shading cases ‘a’ to ‘c,’ the performance of FF is represented graphically. The corresponding values of FF under shading effect are summarized in Table 3. Moreover, it is found that the FF is better for TCT configuration.

Fig. 7 Effect of shading cases ‘a–c’ on power losses

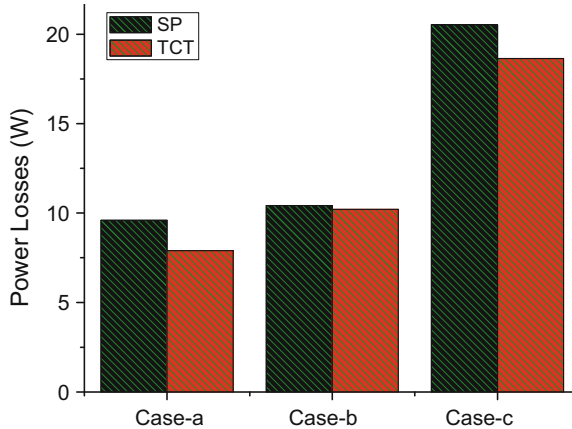


Table 3 Power losses of SP and TCT PV array configurations for shading cases

	Power loss (W)		
	Case a	Case b	Case c
SP	9.6	10.42	20.51
TCT	7.9	10.21	18.64

6 Conclusion

The assessment of functioning of a 3×3 PV array interconnections (configurations) like SP and TCT is studied in detail for experimental system. The parameters such as power and voltage at global MPP (GMPP), power mismatch losses, and evaluation of FF are investigated under such considered shading cases. The results agreed that TCT-based reconfiguration arrangements contain minimum power losses and higher FF of the PV array during considered all the partial shading cases.

References

1. Bishop, J. W., Computer simulation of the effects of electrical mismatches in photovoltaic cell interconnection circuits. *Solar Cells* 25, 73–89, 1988.
2. Karatepe, E., Boztepe, M., Colak, M., Development of a suitable model for characterizing photovoltaic arrays with shaded solar cells. *Solar Energy* 81, 977–992, 2007.
3. Patel, H., Agarwal, V., MATLAB based modeling to study the effects of partial shading on PV array characteristics, *IEEE Transactions on Energy Conversion* 23(1), 302–310, 2008.
4. D. Nguyen, B. Lehman, An adaptive solar photovoltaic array using model-based reconfiguration Algorithm, *IEEE Transactions on Industrial Electronics*, vol. 55, no. 7, pp. 2644–2654, 2008.
5. Chaaban, M. A. et al., Alahmad, M., Neal, J., Shi, J., Berryman, C., Cho, Y., Lau, S., Schwer, A., Shen, Z., Stansbury, J., Zhang, T., 2010. Adaptive Photovoltaic System, In Proc. IEEE conference on Industrial Electronics Safety, pp. 3192–3197, 2010.
6. Quesada, G. V., Gispert, F. G., Lopez, R. P., Lumbreras, M. R., Roca, A. C., Electrical PV array reconfiguration strategy for energy extraction improvement in grid connected PV systems. *IEEE Transactions on Industrial Electronics* 56(11), 4319–4331, 2009.
7. Gao, L., Roger, A., Parallel connected solar PV system to address partial and rapidly fluctuating shadow conditions. *IEEE Transactions on Industrial Electronics* 56(5), 1548–1556, 2009.
8. Moreno, F. M., Munoz, J., Lorenzo, E., Experimental model to estimate shading losses on PV arrays. *Solar Energy Materials and Solar Cells* 94, 2298–2303, 2010.
9. Picalt, D., Raison, B., Bacha, S., Casa, J. D. L., Aguilera, J., Forecasting photovoltaic array power production subject to mismatch losses. *Solar Energy* 84, 1301–1309, 2010.
10. Tsai, H. L., Insolation oriented model of photovoltaic module using MATLAB/Simulink. *Solar Energy* 84, 1318–1326, 2010.
11. Moballegheh, S., Jiang, J., Partial shading modeling of photovoltaic system with experimental validations, in Proc. IEEE conference on Power and Energy Society General Meeting, pp. 1–9, 2011.
12. Santos, P. D., Vicente, E. M., Ribeiro, E. R., Relationship between the shading position and the output power of a photovoltaic panel, in proc. IEEE conference on Power Electronics, pp. 676–681, 2011.

13. Ziar, H., Mansourpour, S., Afjei, E., Kazemi, M., Bypass diode characteristics effect on the behavior of solar array at shadow condition, In proc. IEEE Conference on Power Electronics and Drives Systems Technology, 1–5, 2012.
14. Singh, A., et al., Performance enhancement of partially shaded PV array using novel shade dispersion effect on magic-square puzzle. *Solar Energy*, 144, 780–797, 2017.
15. Gupta, A., Kumar, P., et al., Effect of environmental conditions on single and double diode PV system: a comparative study, *International Journal of Renewable Energy and Research*, 4 (4), 849–858, 2014.
16. Singh, A., et al., comprehensive investigation of PV arrays with puzzle shade dispersion for improved performance, *Solar Energy*, 129, 256–285, 2016.

A Multiband Circular Patch Microstrip Antenna for K and Ka Applications

Ashna Kakkar, Nirdosh and Shalini Sah

Abstract A multiband circular patch microstrip antenna to be used for K and Ka band applications is presented in this manuscript. The designed antenna is composed of circular patch with two inverted U-shaped slots. The antenna presented is designed to function at multiple bands, i.e., 19.14, 23.31, 30.02, 34.91, and 39.05 GHz which improve performance parameters of circular radiating patch antenna like return loss (less than -10 dB), bandwidth, gain, VSWR, and radiation pattern. This patch antenna is useful for satellite and radar communication.

Keywords Circular patch microstrip antenna · Broadband · FR4 substrate K and Ka bands

1 Introduction

In satellite, advanced airship missile moreover other operation where vastness, load, cost, performance and has limitations of streamlined profile. Due to these requirements, microstrip antenna can be used currently [1]. Microstrip antennas are usually called patch antennas in which various components are engraved on dielectric substrate. Radiation part known as patch can be of any random shape [2]. Microstrip antennas designed to operate at a particular frequency, can be used for a single application so it is not preferred, whereas multiband antennas operate at various frequencies can be used for multiple applications and occupy less space. Hence, they are preferred for various required applications. In addition, it is easy to manufacture in large scale which reduces manufacturing cost [1]. Nowadays,

A. Kakkar (✉) · Nirdosh · S. Sah
Department of ECE, ASET, Amity University, Noida, India
e-mail: ashna279@gmail.com

Nirdosh
e-mail: nirdoshtanwar@gmail.com

S. Sah
e-mail: sshah@amity.edu

communication framework such as mobile phones and satellites uses the microstrip patch antenna of little measurements and of best working qualities. Its use is not only limited to communication systems [3]. Today, there is a wide application in many fields [4].

This paper presents a new circular shape antenna, having two inverted U-shaped slots and CPW feed operating in multiband (K and Ka) applications. The proposed antenna can be used in radar and satellite communications, broadcast services, military, and civil applications. As the custom microstrip antennas have low bandwidth and gain which resist and degrade its performance in various applications, the proposed antenna has a high bandwidth percentage of about 32% between frequency 17.9 and 28.4 GHz which is better than earlier proposed antennas in [4, 5]. The given antenna also has a good gain of 5.46, 5.40, 4.41, 6.60, and 1.24 dB at frequencies 19.14, 23.31, 30.02, 34.91, and 39.05 GHz, respectively. Ansoft High Frequency Structural Simulator (HFSS) version 13.0 is used to simulate the proposed antenna. The software works on the finite element method.

2 Antenna Design

A multiband circular-shaped patch antenna having two inverted U-shaped slot and a CPW feed has been proposed as shown in Fig. 1. It is designed on the FR4 substrate with height (h) = 1.6 mm having permittivity of 4.4. The circular patch drawn is of radius 10.1 mm having two inverted U-shaped slot making it suitable for working in the operating frequency of K and Ka band. The formula used to design radius of patch is the following:

$$\text{Radius } (a) = \frac{F}{\left\{ 1 + \frac{2h}{\pi\epsilon_r F} \left[\ln\left(\frac{\pi F}{2h}\right) + 1.7726 \right] \right\}^{1/2}} \quad (1)$$

where $F = \frac{8.791 \times 10^9}{f_r \sqrt{\epsilon_r}}$.

$$\text{Effective Radius } (a_e) = a \left\{ 1 + \frac{2h}{\pi\epsilon_r a} \left[\ln\left(\frac{\pi a}{2h}\right) + 1.7726 \right] \right\}^{1/2}. \quad (2)$$

Resonant frequency for dominant mode TM_{110}^z is given by,

$$(f_r)_{110} = \frac{1.8412 \times v_0}{2\pi a_e \sqrt{\epsilon_r}}. \quad (3)$$

Required measurement of the antenna parameters has been shown in Table 1.

Fig. 1 Front view of proposed antenna

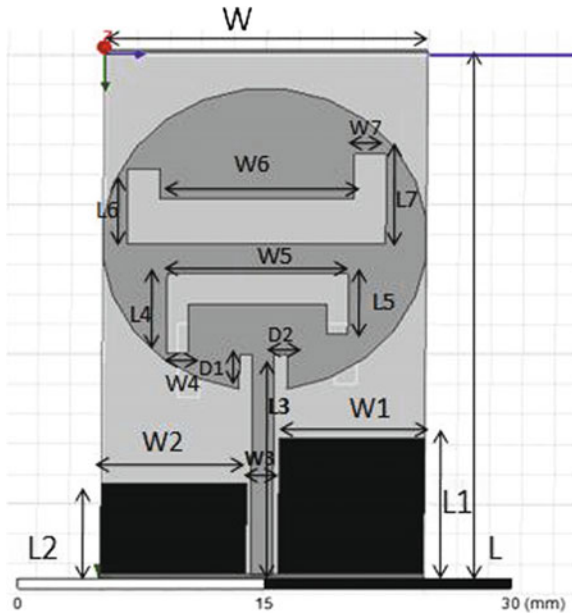


Table 1 Antenna measurement

Length (L) and Width (W)		Dimension (mm)	
L	L1	35	9
W	W1	20	9
L2	W2	6	9
L3	W	12.52	1.35
L4	W4	5.3	1.3
L5	W5	4	11.2
L6	W6	5	12
L7	W7	6	2
D1	D2	2.4	0.8

3 Simulated Result and Discussion

The antenna presented is simulated using software HFSS version 13.0.

Parameters like return loss, VSWR, bandwidth, gain, and radiation pattern are evaluated. Spectrum of designed antenna frequency is from 19 to 40 GHz. In the return loss simulation result which is given in Fig. 2 and Table 2, the observed return loss of the antenna presented is found to be -24.3 dB at 19.14 GHz, -23.3 dB at 23.31 GHz, -18.6 dB at 30.02 GHz, -28.8 dB at 34.91 GHz, and -16.32 dB at 39.05 GHz.

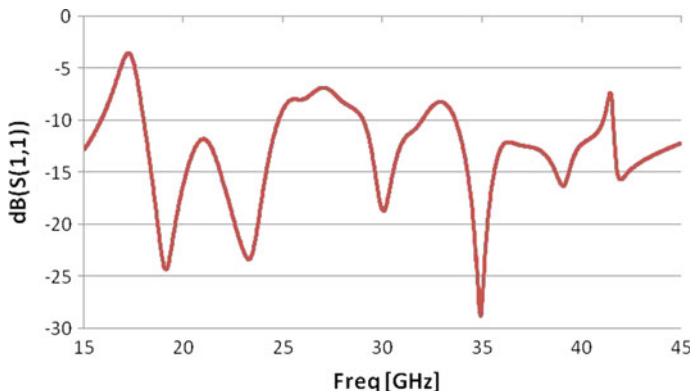


Fig. 2 Return loss of the proposed antenna

Table 2 Characteristics of proposed antenna

Resonant frequency (GHz)	Return loss (dB)	Gain (dB)
19.14	-24.3	5.46
23.31	-3.3	5.40
30.02	-18.6	4.41
34.91	-28.8	6.60
39.05	-16.32	1.24

Proposed antenna gain at resonant frequency of 19.14 GHz is 5.46 dB, and at 23.31 GHz it is 5.40 dB. At third and fourth resonant frequencies that are 30.02 GHz and 34.91 GHz, the gains are 4.41 and 6.60 dB, respectively. In the last resonant frequency that is 39.05 GHz, the gain is 1.24 dB. All the gains which have calculated at five different resonant frequencies are acceptable. According to simulation result, the designed antenna has acceptable impedance matching ($VSWR \leq 2$). The VSWR of the antenna presented is displayed in Fig. 3. The minimum calculated VSWR value of 0.63 dB at 34.91 GHz of resonant frequency. In Table 3, the simulated antenna operates at 17.98 to 24.81 GHz whose bandwidth is 32% which can be used for K band and also better than [4, 5]. Furthermore, the resonant frequencies from 29.01 to 31.97 GHz give bandwidth of 9.69% and from 33.68 to 41.06 GHz offer 20% bandwidth which can be operated for Ka band application (Figs. 4, 5, 6, 7, and 8).

The E and H plane radiation pattern of simulated antenna can be determined at five distinct frequencies which are displayed in Fig. 9a, b.

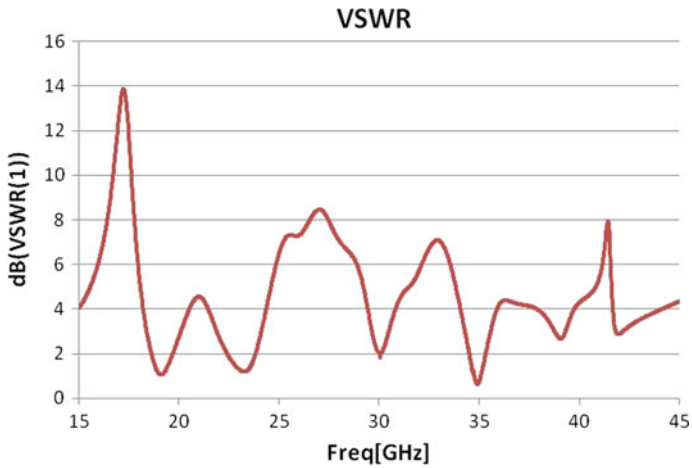


Fig. 3 VSWR of the proposed antenna

Table 3 Simulated frequency bands of designed antenna

Bands	Frequencies (GHz)		Bandwidth (%)
	Lower frequency	Upper frequency	
1	17.986	24.814	32
2	29.017	31.973	9.69
3	33.684	41.068	20

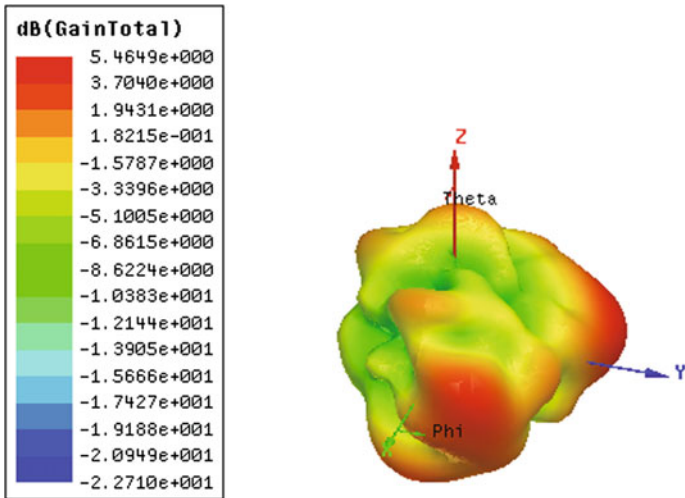


Fig. 4 Gain at resonant frequency of 19.14

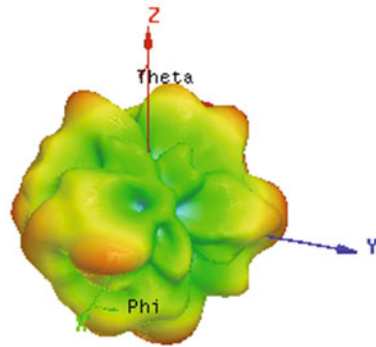
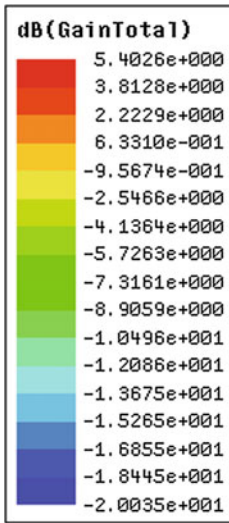


Fig. 5 Gain at resonant frequency of 23.31

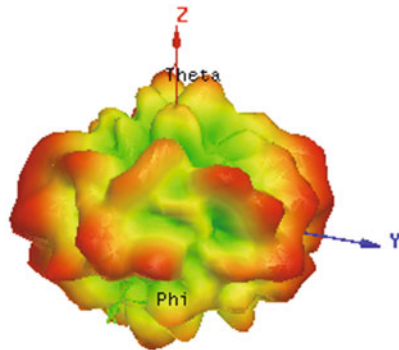
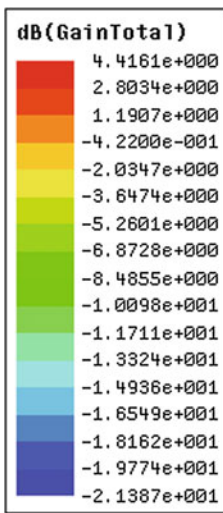


Fig. 6 Gain at resonant frequency of 30.02

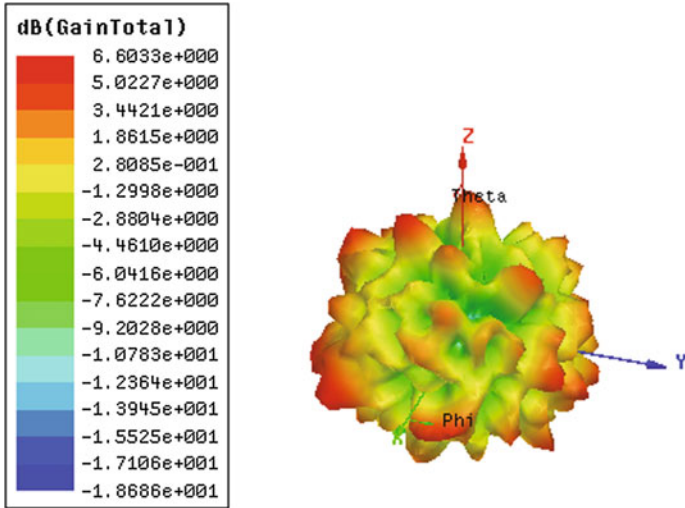


Fig. 7 Gain at resonant frequency of 34.91

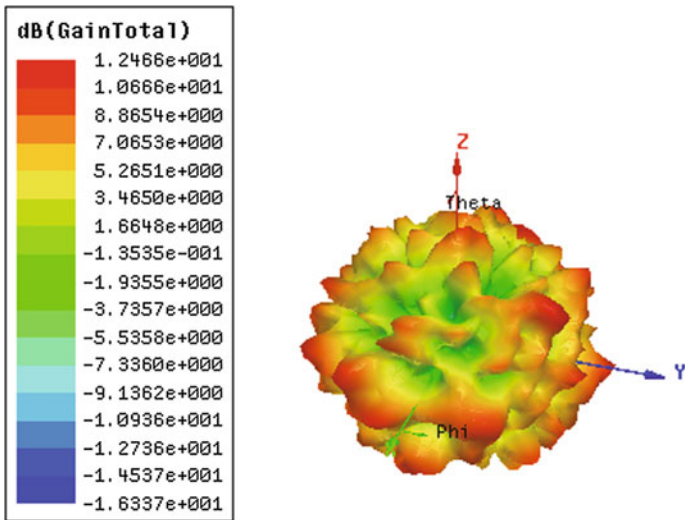


Fig. 8 Gain at resonant frequency of 39.05

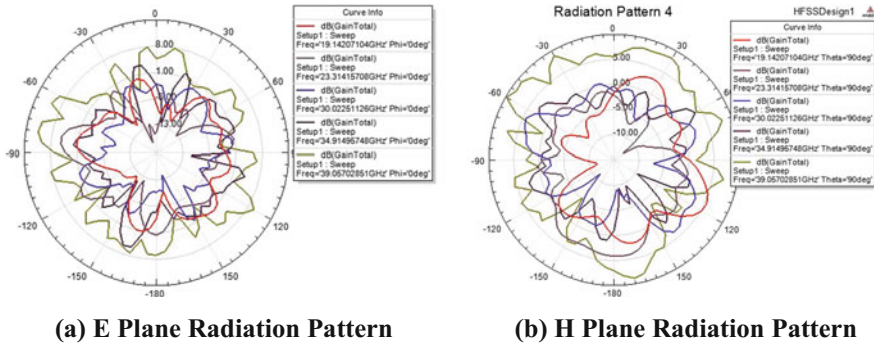


Fig. 9 a E plane radiation pattern. b H plane radiation pattern

4 Conclusion

The multiband circular patch microstrip antenna has been designed. This antenna is operated at five different frequencies that are 19.14, 23.31, 30.02, 34.91, and 39.05 GHz for K and Ka bands applications.

Moreover, the designed antenna demonstrates the better return loss which is less than -10 dB, wide band response (good bandwidth), gain, VSWR which is less than 2, and low cost. Due to these characteristics, it is concluded that this proposed antenna is being well suitable for satellite and radar communications.

References

1. C.A. Balanis, *Antenna Theory*, 2nd Ed., John wily & sons, Inc., NewYork.1982.
2. M. Sekhar, S Nagakishore Bhavanam, P. Siddaiah, "Triple frequency circular patch antenna", IEEE ICCIC, 2014
3. Manik Bhowmik, Brij Bhushan Chowdhury, Ratul De, "Circular patch antenna with modified Swastika shaped slot for multiband applications", IEEE International conference on SPIN, 2016.
4. A. Azman, M. Z. A. Abd Aziz, M. K. Suaidi, A. Salleh, H. Normikman, F. Malek, "CPW-FED Compact Monopole Antenna for Dual-Band WLAN/WiMAX Applications", IEEE International Conference on I4CT (Computer, Communications, and Control Technology), 2015.
5. María Elena de Cos, Mohamad Mantash, Anne-Claude Tarot, Fernando Las-Heras, "Dual-band coplanar waveguide-fed smiling monopole antenna for WiFi and 4G long-term evolution applications", *IET Microw. Antennas Propag.*, 2013, Vol. 7, Iss. 9, pp. 777–782.

RFID Device Based Home Security System to Detect Intruder Trespassing

Sanjana Minocha and Ankur Dumka

Abstract Today in the twenty-first century where digitization and standardization of technology have become prominent, multiple organizations use IoT to streamline cost through collaboration and automation. The applications of automation in home appliances are growing with expansion and innovation in technology. But it can also be considered as the utmost need, for crime is growing at an ever-increasing rate. Thefts, property trespassing, illegal intrusions, etc. are a common story in every neighborhood. The methods previously used in security measurements and risk estimate time, manual power and add to external expense. It is, therefore the purpose of this paper to create a security system using IoT which utilizes RFID technology in which keys will be scanned at door knobs for the purpose of automatic door control system at low cost and reduced manual interruption.

Keywords RFID · Sensor · RFID transponder · RFID interrogator
AIDC

1 Introduction

IoT or Internet of Things is a term which refers to an entwined network of devices, machines, objects or people to connect the unconnected. The transition of web to Internet of things is used for data exchange without human and system interaction

S. Minocha (✉) · A. Dumka
University of Petroleum and Energy Studies, Dehradun, Uttarakhand, India
e-mail: sanjanaminocha17@gmail.com

A. Dumka
e-mail: adumka@ddn.upes.ac.in

© Springer Nature Singapore Pte Ltd. 2018
R. Singh et al. (eds.), *Intelligent Communication, Control and Devices*,
Advances in Intelligent Systems and Computing 624,
https://doi.org/10.1007/978-981-10-5903-2_151

1445

and corporation. The advancement of IoT has resulted from the union of remote infrastructure, micro services, web and frameworks of electromechanical origin. One such remote innovation is Radio Frequency Identification (RFID). It is a nonexclusive term for non-reaching advancements that utilization radio waves to consequently distinguish individuals or articles [1, 2]. Security is ensured by permitting the approved faculty to get to the safe zone. RFID tags are of two types-active and passive depending upon the source of electrical vitality. The active tags have battery as their main source of power and the information from the tags is transmitted on the request of user. In any case, the former tags are extremely costly and rarely utilized. Alternatively, the passive tags depend on external power to control circuit. This power is gained extrinsically from the user. The framework comprises of two segments in particular transponder (label), interrogator (reader). RFID Enable Door Control System imparts between the reader and the transponder. The interrogator peruses the label information and transmits it to the PC for confirmation. The data is handled and upon confirmation, access is granted. This framework will aid in replacing the regular and physical door lock and unlock.

1.1 Background

RFID innovation was initially created as a reconnaissance gadget amid World War II. It took about 30 years of research before it turned into a piece of our regular day to day existence. Initially, RFID tags were invented to work in the long run supplant standardized identifications in various chains. In 1920, Radar was created as a new innovation in the US. RFID which was a blend of radio broadcast innovation and radar, was created long before. In 1930, Britain utilized related software, an IFF transponder, to recognize adversary airplane amid WWII. Radar was refined and RFID was created in 1940. Advancements identified with RFID were investigated in research facilities amid 1950. After this, certain designs were rectified for transponder frameworks for use in flying machinery. Amid the 1960s developers started applying radio recurrence innovation to gadgets for utilization in business sectors past the military [3]. Many organizations invented theft anticipation systems for open utilization that used Electronic Article Surveillance. In 1970, the major references were aimed at electronic toll accumulation, animal and automobile tracking, and production line robotization. The expansion of business was done amid 1980 and till 1990, they became widespread. Their favorable circumstances are that they can be perused remotely with no observable pathway, contain a bigger number of information than standardized tags, and are more grounded. Figure 1 shows the comparability of RFID, GPS and sensor based system in different years. The figure shows that the uses of RFID, GPS and sensor based system is increasing every year.

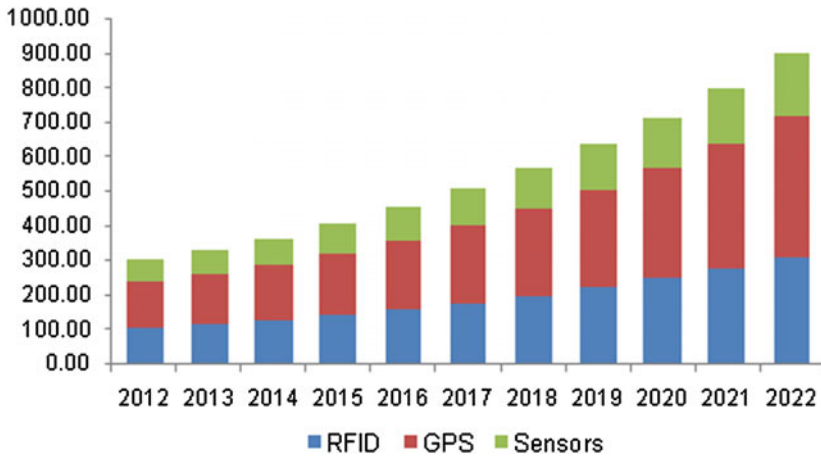


Fig. 1 Use of RFID, GPS, Sensors

1.2 Recent Advancements

With rising technological advancements, RFID has upgraded prompting scaling miniaturization. There is a progressing development in outline and manufacturing of RFID labels. With the rise of Surface Acoustic Wave (SAW) innovation which uses Chipless tags, cost has been conceivably decreased. Other real headways in IC-based label configuration incorporate Smart Active Label (SAL) innovation which gives advantages of upgraded range and precision qualities and without getting irrupted against fluid or metal. Another rising innovation is the ZigBee which is a remote innovation standard that allows interchanges for short and medium range. It is intended for applications which require low-control utilization without any gigantic data throughput.

Hybrid Positioning Systems and Wi-Fi Positioning Systems are the latest arising technologies for regulating path of door systems [4]. Hybrid positioning systems aids in analyzing and locating the position of mobiles of a user with integration of multiple technologies that utilize positioning systems. This provides a new hybrid solution in contrast to the currently available system for positioning and tracking estimation in 4G.

Another arising solution is Wi-Fi-Based Indoor Localization or Wi-Fi Positioning Systems. This system neither requires the installation of software nor requires any modification of hardware. Thus, it aids in determining the location of devices which are compatible with Wi-Fi. These systems have constructed its base extensively in indoor localization due to its advantage of working without line of

Fig. 2 Global RFID Market Revenue, 2014–2020



sight. Figure 2 shows the revenue structure of RFID from 2014 to 2020, which clearly shows that RFID market is trending and increasing in the coming year also.

The above statistic represents to the anticipated size of the market for RFID tags from 2016 to 2020. In 2018, the worldwide market for RFID tags is projected to be estimated at around 17.6 billion U.S. dollars.

RFID increases inventory accuracy, from 65% to more than 95%. Overall, organizations that receive RFID see their inventory count accuracy go from 63 to 95%. In addition, with merchandise labeled with RFID, makers can expand inventory count rates from 200 to 12,000+ things for each hour. Whereas distribution centers and DC's take their inventory perceivability and accessibility from 2 to 20% while implementing RFID technology.

2 Problem Statement

Security and Privacy are the basic concerns of users regarding the use of RFID. Security issues deal with authentic readers accessing data from illegitimate tags, while privacy issues deal with illegitimate readers accessing data from legitimate tags. According to a client's perspective, the security issue is more vital, and therefore media coverage has been significantly higher. Likewise, regulation of RFID security is also gaining utmost importance due to its paradoxical nature [5]. While the utilization of RFID provides security in some territories, the nature of RFID communication represents various protection and security problems [5, 6]. Another issue is related to door access system. The concerns of security mainly deal with fake or illegitimate tags, instead of readers. Tags can be easily duplicated or replicated. The key can be copied and the door can be opened by different techniques. This issue can be resolved by updating the tag key values in the system and replacing the user's previous key with new one each month.

Developers find hard to regulate measures that can provide meaningful metrics for risks in operational security. There are many distinctive reasons in this context namely, problems in validating, updating and estimating risk analysis, the regular transitions in threat landscape [6, 7]. Another reason is the inability in regulating the performance of inclusive calibration of the threat environment, etc. Existing methodologies used for immunity from risks employ measurements of expenditure and time for assessment of steps in which the system is attacked. When the threat or vulnerability landscape changes, the problem becomes more prominent. The change in threat environment occurs due to behavior of agent (e.g., upsurge in the resources possessed by the attacker), while transitions in vulnerability landscape take place due to updates in infrastructure (e.g., decreasing vulnerability of system and inadvertent events by employing patches). In both states, the approximated elucidations will be updated which manifest the properties of agent and the system collectively.

3 Methodology

The planning and development is partitioned into three sections which are research and discovering, equipment usage and programming advancement. The research part will comprise about what is RFID innovation. In hardware part, it will include the utilization of RFID module segment that contains the transmitter and passive tags. This part will likewise incorporate detail of RFID reader and RFID transponder. Last part is software programming which is done with the assistance of embedded C. Figure 3 shows different tags discussed in the previous section of RFID and their utilization weightage.

First, RFID will be utilized to build up the access control system. Second, the system will be installed at the archway of the organization that will allow access only to the approved individual. Clients will have possession of essentially convenient and conveyable RFID tags/keys. These keys will be examined at RFID antenna [8]. The software assimilated hardware will then decide whether the client is certified or not and depending on the output, the system will proceed accordingly. If the card as well as the captured image corresponds to a registered user, access will be permitted, the door will open and the information will be exhibited on LCD; otherwise the system will turn ON the alarm. LEDs will likewise be utilized amid the working of the system. For an approved individual, LED will blink green light and for an unapproved individual, red light will begin flickering. This system works upon Faraday's law of electromagnetic induction. This law states that when current flows through the interrogator coil, magnetic field is produced. This magnetic field associate with the coil of transponder, producing current in the latter's coil. With transitions in load on antenna, the current is fluctuated by the transponder coil.

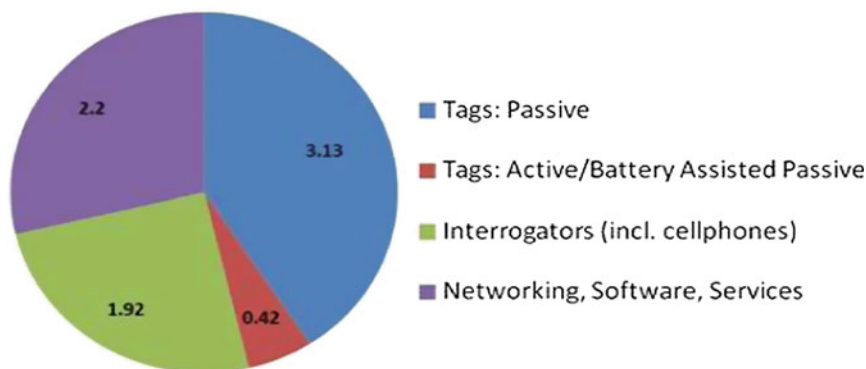


Fig. 3 Utilization of RFID

A cipher form of radio signal is transmitted by the RFID reader for tag interrogation.

After the RFID tag receives this signal or message, it responds with its information and identification. This information may include commodity related data namely, batch number, stock number, date of manufacturing or other related data and exclusive tag serial number.

The RFID system is capable of distinguishing between indefinite tags as it contains eminent serial numbers. These tags might be within the magnitude of the RFID reader. As a result, it can read them simultaneously.

The different scenarios about the working of the system are defined below.

If the person is authorized to open the door, the following steps will take place:

- First, the cards will be scanned at the RFID antenna by the user, where the card's information will be read and stored.
- After proper card scan, the servo motor will turn at 90° (or the direction requisites for practical implementation) and will sustain in that position for time preprogrammed by the developer (5 s). After the timeout period, the server motor will revert back to its last position.
- The door will not remain open for long duration after the success of an authorized attempt. The door will be locked again to prevent any further intrusion entry.

If the person is unauthorized, the following steps will take place:

- If the user scans an unauthorized card, the screen will show an error message e.g. "Entry Not Allowed" after its examination.
- Henceforth servo motor will not depict any further gyration.

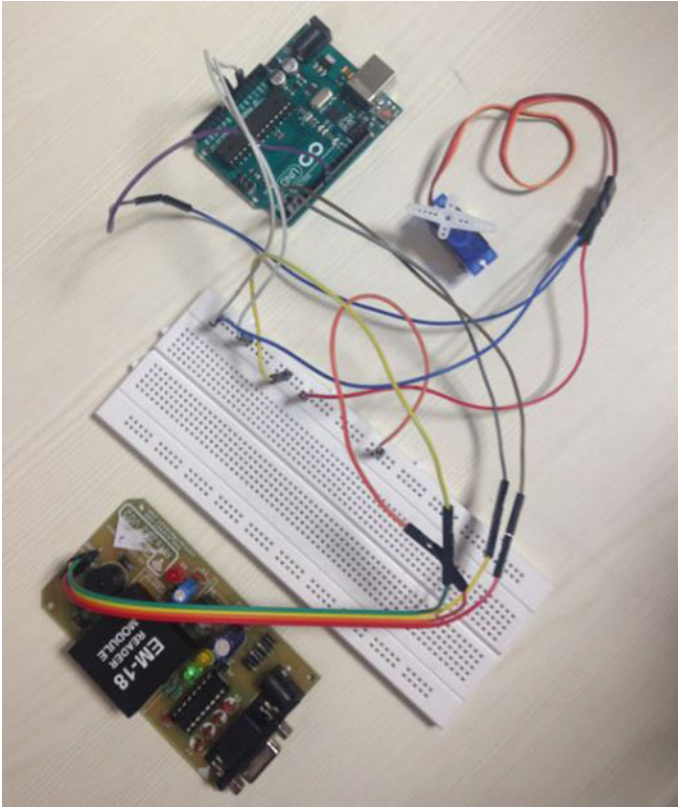


Fig. 4 Designed Model for Home Security System

- If the individual still tries to scan distinct cards to break in the system, a connected alarm alert will begin making boisterous noises to alert the organization about the unauthorized attempt of the intruder.

The Features of proposed system are:

- It is very cheap and affordable.
- It is efficient and portable.
- Reduced manual interruption.
- Maintenance cost is low.
- Less electrical or battery expense.
- Item visibility and status.
- Access control.
- Traceability.

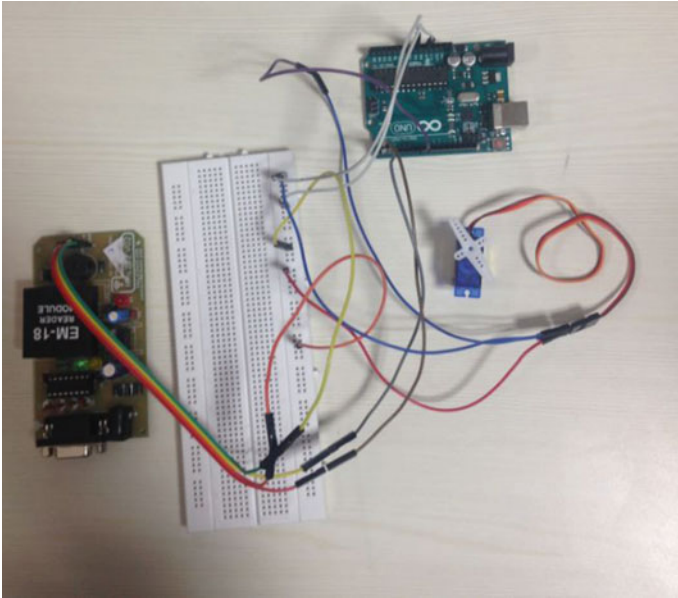


Fig. 5 The Physical Connections of the System

3.1 Algorithm

1. Start.
2. Connect the Piezo buzzer to digital pin 10.
3. Connect the PIR motion sensor to digital pin 7 as an input.
4. LED is connected to digital pin 13.
5. Initially, presume that no motion is detected.
6. Create a variable for reading the pin status.
7. Initialize the library with the numbers of the interface pins.
8. Declare LED as output and sensor as input.
9. Scrutinize values of input from the device.
10. Turn ON the LED, if input is HIGH.
11. Put the buzzer ON.
12. Set LCD cursor position.
13. Print text to LCD as 'Motion Detected'.
14. Stop.

Figures 4, 5 and 6 shows the hardware implementation of RFID based security system established for outcome of the result required.

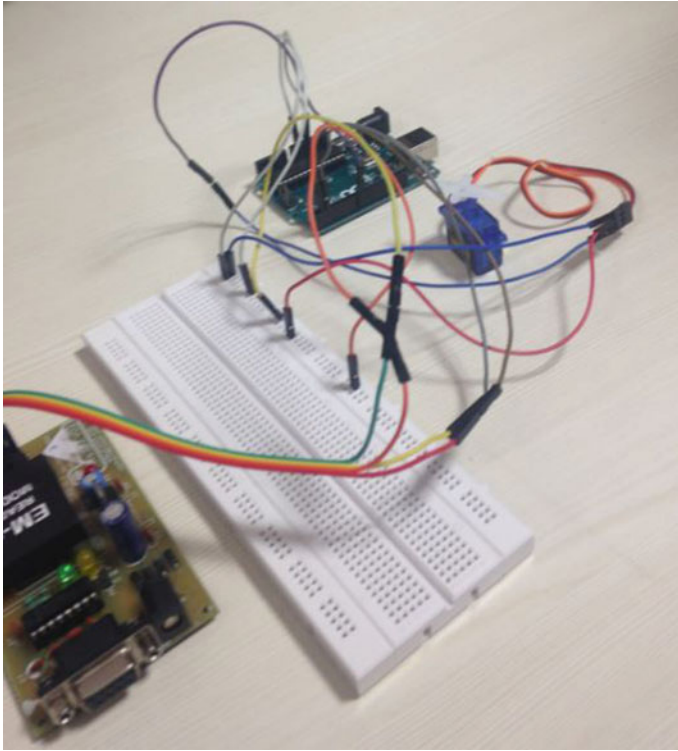


Fig. 6 Use of RFID in the system

4 Result and Conclusion

When the RFID tag that is placed on the RFID reader reads the data, its key value is send to the controller. The controller then matches the received code with the stored code. If both the codes match then the security system gives authorization to user and provides access. Change the tag ID in Access Control into source program with the ID you have noted down earlier and then connect Arduino board with PC, upload the sketch into the board. After access control system the information is displayed on LCD and if the information is not correct, the alarm will start ringing. If uploading is done well, you will see the glowing of LED. It means the system is prepared to read the tag. Now, bring the tag closer to RFID reader, if the tag ID matches with the ID in the code, door lock will open for some time duration. It closes manually after some time. This time can be changed as per the delay in the programming of the software. Glowing of LED indicates that the lock is open. Glowing of caution LED means that you are using the wrong tag. Figure 7 shows

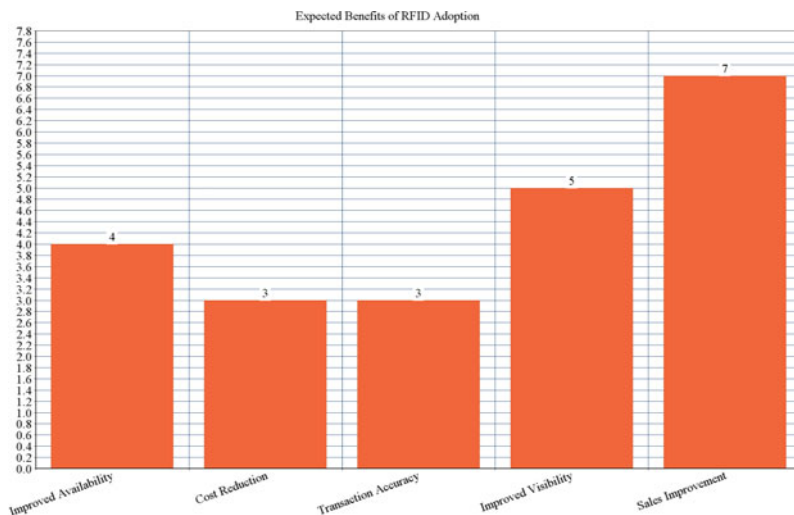


Fig. 7 The advantage of using RFID Home Security System

the benefits of RFID application with respect to non-RFID system and shows the credibility of RFID based system over non-RFID bases system. The figure shows that RFID based system is more vulnerable on factors like availability, cost, transaction accuracy, visibility and sales improvement.

References

1. Bruno Crispo, Melanie R. Rieback, Andrew S. Tanenbaum, A paper on “The Evolution of RFID security.
2. S. Lahiri, RFID sourcebook, IBM Press, Westford, Massachusetts, 2006.
3. R. Weinstein, “RFID: A technical overview and its application to the enterprise,” *IT Professional*, vol. 7, no. 3, May–June 2005, pp. 27–3.
4. D. L. Wu, Wing W. Y. NG, D. S. Yeung, and H. L. Ding, “A brief survey on current RFID applications,” in *Proc. International Conference on Machine Learning and Cybernetics*, Baoding, July 12–15, 2009, pp. 2330–2334.
5. V. Verendel, “Quantified security is a weak hypothesis: A critical survey of results and assumptions,” in *Proceedings of the 2009 New Security Paradigms Workshop*. New York, NY, USA: ACM, 2009, pp. 37–50.
6. G. Kaushal, R. Mishra, N. Chaurasiya, P. Singh, “RFID based security and access control system using Arduino with GSM module”, *Dept. of ECE, Lovely Professional University, IJEEE*, Vol. 2, Issue 2, April, 2015.
7. F. Lourenco and C. Almeida, “RFID based monitoring and access control system,” in *Proc. INFORUM*, 2009.
8. N. Ahmad, S. Butler, and U. Ramachandran, “GuardianAngel: An RFID based indoor guidance and monitoring system,” 2010, pp. 546–551.

Review of Sockets for Transfer of Files Between Systems

Pranav Arora and Ankur Dumka

Abstract The sole purpose in this research is to brief about the (need for, types of) various networking sockets, their various APIs available, and its deployment pertaining to network programming. Sockets are the apex need in client server applications. When there is a need to read or write any message between server and the client, the socket is the apropos choice. The invention of sockets was done during the production of Unix operating system particularly Berkeley Software Distribution OS. And their growth within the Internet is far from invincible now. This paper brings about need and rudimentary factors of socket programming and ideas behind creating sockets for file transfer between the various systems.

Keywords TCP/IP · Sockets · IPv4 · System calls

1 Introduction

According to Merriam-Webster's Dictionary, a socket is "*an opening or hollow that forms a holder for something.*" The "something" in socket programming are computer devices that connect and communicate with each other using these sockets. So without sockets networking is impossible [1]. Two devices that are connected using these sockets are called client and server

"Socket programming involves writing computer programs that enable processes to communicate with each other across a computer network". "A socket is one end-point of a two-way communication link between two programs running on the network."

These sockets do not depend on any particular protocol for building up a network between various threads or executing processes. They can be connectionless or connection-based in nature.

P. Arora · A. Dumka (✉)

University of Petroleum and Energy Studies, Dehradun 248001, India
e-mail: adumka@ddn.upes.ac.in

P. Arora

e-mail: pranav2vis@gmail.com

© Springer Nature Singapore Pte Ltd. 2018

R. Singh et al. (eds.), *Intelligent Communication, Control and Devices*,
Advances in Intelligent Systems and Computing 624,
https://doi.org/10.1007/978-981-10-5903-2_152

1455

Connectionless: It simply means there is no bridge between client and sever. The packets are free from stream and they can be in any order or can be corrupted or lost during transmission.

Connection-oriented: They imply to the fact that is there a connection built for commuting or else the message carries its destination's address with it.

1.1 Request–Response Model for Message Passing

When we wish to write an e-mail or send any message across the Internet or even download any file, we need to build a connection with the local server. This involves the use of a client and a server. The job of the client is to send a request, and server returns a response. A client is the one that asks for a service to be rendered, and server is an amalgam of hardware and software running on hind end machines to render that service. Servers run on pretty advanced machines with high amount of cache for fast processing and core processors to handle network traffic. Clients are applications or desktop apps or laptops which run certain apps. There is a dependency among clients for their applications to be run on servers. The role of sockets comes in here significantly when the apps need to be executed, client and the server create threads or processes that respond to each other by reading from them or writing to them using sockets. The sockets are contract or like an interface given by transport layer protocols for connection-oriented or connectionless protocols, respectively, like TCP and UDP. The client/server application that is covered here is a proprietary client/server application. During the development of socket programs, the programmer needs to implement both client and server side. The programmer is completely aware and has full authority of what goes on in the code on both ends. The problem occurs that these code snippets do not implement protocols that are publically applicable, and all the other developers will not develop codes that sync with this developer's code. So when developing proprietary products, the developer must ensure that all the known port numbers are declared and defined in the remote calls that will be implemented.

1.2 Sockets

We have come across this mediocre term day in and day out. Sometimes, we use it too often to realize in our own homes as well. Sockets can be for electricity or phones or chargers, etc., in non-technical and non-networking terms. In general, sockets act as interfaces which connect a component to its suitable pair. Presenting in network definition, sockets are end points responsible for communication between different processes over a layout of computer networks. Every socket has its address. Consider an analogy of a house. No matter how big or small the house is, every house has the same length address. Similarly, sockets have a unique

address formed by port number (process running) and the layer 3 addressing mechanism, i.e. Internet Protocol address. While using any open source operating system, we come across shell which connects operating system and the user interface through a set of commands. Similarly sockets abstract the ends of networks and represent terminals of a network. Over the various layers of TCP/IP model, the two most concerning layers for sockets are application and TCP layer. They are the key to the door between the transport and app layer. Taking the telephony network as a parameter, we define the major steps in its process. First, the end points (telephone) are created at the two ends. An address (number) is provided at the ends. The call has to be initiated from one end (initiator). The other end waits for the communication to start (receiver). Once they both are set up, the conversation takes place (talking). After the transfer of information or conversation, both the ends hang up. This entire process is the same for any type of network, mobile, satellite, or computer, and the interfaces at the end points of both terminals are called as “sockets.” The telephony analogy will be used in further references too.

2 Types of Sockets

The sockets can be categorized in various perspectives, but broadly they have three subdivisions [2]. The type of sockets to be used generally depends upon the platform and usage of the applications.

- a. Unix-specific sockets.
- b. Internet-specific socket.
 - i. Transmission Control Protocol socket.
 - ii. User datagram protocol socket.
 - iii. Raw Internet Protocol socket.
- c. Ns-specific socket.

Internet-Domain Socket is the celebrity among the range of sockets available and functions on the range of operating systems with different specifications.

- i. **Stream Sockets**—These sockets use Transmission Control Protocol for data transmission. They are connection-oriented sockets with the main aim of carrying packets over a dedicated channel. If the delivery of packets is not possible, the sender receives an error indicator. The special aspect of these sockets is that data has no boundaries over the limit of transfer.
- ii. **Datagram Sockets**—These sockets are meant for situations where connection is not established. There is no need to build a path/bridge between source (client) and server, and they use User Datagram Protocol for its underlying behavior.
- iii. **Raw Sockets**—These sockets are meant to grant permission to users for the underlying communication protocols, which make the encapsulation and

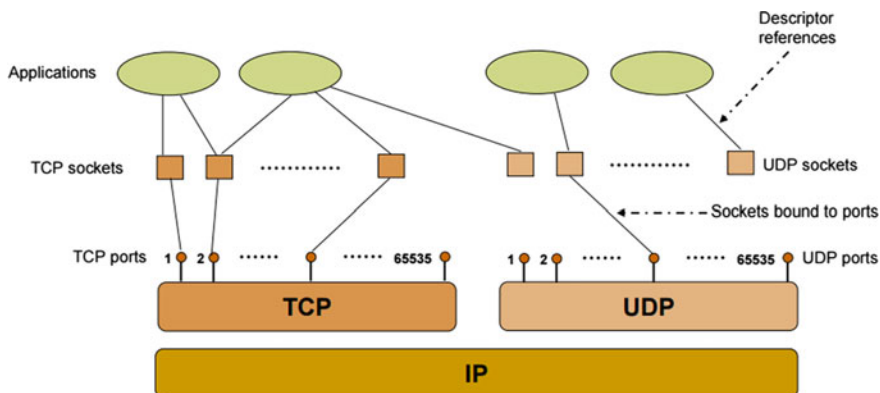


Fig. 1 Basic internet protocol architecture [3]

layering possible for sockets. In computer networking, a **raw socket** is an Internet socket that allows direct transfer of packets and helps in building sockets from ground level up as depicted in (Fig. 1).

2.1 Socket Address and Structure

The essence of socket's address lies within two moieties of it. That is represented by Internet Protocol address and port number.

Port:

A client has an IP address using which it connects to a server. But the client has to identify as to which process it wishes to connect the server on. The problem arises when the network sets up, but there is no logical process known.

Here comes the role of a port. They are prebooked from 0 to 1023 and are defined for various application layer protocols to tell the client as to HTTP, or FTP, or SMTP, or SSH the server for any request. It makes the job of client and server an idyll.

IP Address: The major protocol defined at layer three of Open source Interconnection model has the main focus on providing host-to-host delivery alongside providing a mark to each client on the Web.

Structure of socket varies on address type being used whether IPv4 or IPv6.

The structure of IPv4 uses:

```

#include <sys/types.h>
#include <sys/socket.h>
int getaddrinfo(const char *node, // e.g. "www.xyz.com" or IP
const char *service, // e.g. "http" or port number
const struct addrinfo *hints
struct addrinfo **res);"

```

The below snippet shows if we are sitting on a server and trying to hear to client's IP at port 8080.

This snippet mentioned below is not meant for practical implementation straightforwardly. It might not set up the network and might not perform assigned functions [3].

```

“int status;
Struct addrinfo hints;
Struct addrinfo *servinfo; // will point to the results
memset (&hints, 0, sizeof hints); // make sure the struct is empty
hints.ai_family = AF_UNSPEC; // don't care IPv4 or IPv6
hints.ai_socktype = SOCK_STREAM; // TCP stream sockets
hints.ai_flags = AI_PASSIVE; // fill in my IP for me
if ((status = getaddrinfo(NULL, “3490”, &hints, &servinfo))! = 0) {
fprintf(stderr, “getaddrinfo error: %s”, gai_strerror(status));
} // servinfo now points to a linked list of 1 or more struct addrinfo
//... do everything until you don't need servinfo anymore....
freeaddrinfo(servinfo); // free the linked-list”

```

2.2 *Socket APIs*

Considering the example of telephonic conversation from 1.2.

Socket APIs socket: produces domain-, type-, and protocol-specific sockets (the process of purchasing a telephone).

- bind: portraying a unique telephone number to each assignee.
- Listen: wait for a caller. This is generally the function of server in request-response model.
- accept: when the phone starts to ring you pick up and answer. This is primarily on server/back-end.
- connect: connect is a prequel to accepting. Dialing a number is the analogy of connect.
- Send, sendto: When you talk or connection is written over forms the send function.
- recv, recvfrom: When one talks the other listens in a half-duplex conversation (though being a full duplex communication). This constitutes to reading the connection.
- shutdown: You hang up and complete the conversation by ending the call.

The above APIs are a general overview of what all parameters are involved during client and server conversation.

The following being the similar interfaces but technically sound parameters of what all servers can do over a communication network are mentioned below.

- socket: Server has the sole responsibility of generating a socket which is a logical entity not physical to be precise.
- bind: When the socket's address is thrown at the server is part of bind function.
- listen: It recognizes the epitome of the connections which are now available for the server to hear onto.
- accept: When multiple clients are trying to connect, the accept function selects only one of the client and forms a bond with that particular socket on a singular port.
- send, recv: For Transmission Control Protocol, these are the replicas for read and write functions. These are primarily developed for connection-oriented protocols.
- shutdown: the data structures which bound the kernel are released and the connection is closed.

2.3 Socket/Network Programming Laconic Concept

The Internet as of known today is part of the Web (WWW).

It gained a whole lot of popularity in a very less time than estimated. As the need and the requirement for it is growing exponentially, the demand for the Web/network software has also been on an un-estimated hike. Software development for networks can be done in a variety of pool of languages and frameworks. The major plus point for Java being used to develop Internet is its robust platform which is inhibited in the language. Java being platform independent, robust, reliable, multithreaded gives an excess amount of features and options to develop and choose from [4]. The two main packages of java.net and java.io play a significant role in providing interfaces for uniform resource locators and building sockets through the URL connections. Using java.io package simultaneously eases the work process because independent codes can be written with much exuberance rather than mess creation with pointers and various other data structures. Programming through networks requires multiple processes to run in symphony, and it provides a means to let the processes communicate. The sockets are not individual entities, they are coupled with Transmission Control Protocol layer or various other connection-oriented protocols to maintain sophistication (Fig. 2).

3 Details of Various APIs

3.1 *bind()*—Port is Identified First

The socket creation is a nascent step. Now, the server has done its part, but the client machine needs to establish a port number to link the socket to it. This is

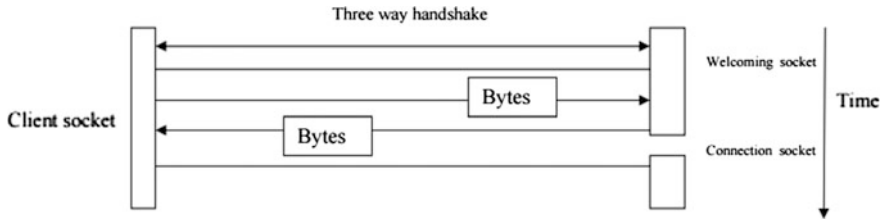


Fig. 2 Various kinds of sockets in three way handshake [5]

preferred during a scenario where a host is listening over multiple connections to join over as in the case of multiplayer gaming. In Unix, everything is in the form of a descriptor so the operating system’s kernel is waiting to match the packet with a process’s socket descriptor. The process for binding is one dimension of connection tree. If connect function is initialized first, then there is no need for it.

3.2 connect()

The binding portion is handled by the server part. Now comes the bridging portion of the connection building process. The TCP client calls the connect () function in order to connect to TCP server. It is a logical connection which is in the form of a fixed path for packets to travel onto. The file descriptor, server’s address, and address length are passed on as parameters to connect function.

3.3 listen()

One of the apogee features of the TCP server is to listen over the network and perform two major functions. First is to change the disconnected socket into a listening socket as in it redirects the message to the kernel to receive and accept any connection request which is meant for that particular socket. The next feature to look at is the most number of connection requests, which the underlying operating system can handle and shoot towards the target sockets. It is a compact function with two arguments, one being the socket descriptor and other being the backlog if the connection crosses the maximum limit for connection.

3.4 accept()—Pickup and Answer

Again, a feature of TCP server is to accept the call made by the client. As mentioned earlier, when someone calls you, we tend to pick up the call if it’s important.

For a server, who is meant to serve the client considers each call as quintessential for it. It is called by the server to tell the next completed connection from the front of queue of completed connections. This function returns a 0 or positive if the acceptance is made. Otherwise, it returns a negative integer, probably -1. The parameters passed into the function are descriptor of the socket, pointer to `sockaddr` structure giving the client IP and port who wants to connect, and finally the length of the address of the socket.

3.5 *send() and recv()*

As read and write are the commands for accessing the server and making amendments onto it, similarly send and receive are the functions which are actually implemented in a language for connected datagram sockets. Taking into consideration the send function, it sends data over a socket stream or in simple words over a logical fixed connection of dgram sockets. It has four arguments in its function as `sockfd`, `msg`, `len` and `flags` which are socket descriptor for the socket, pointer to the message to be transferred, length of the data to be sent and flag is by default 0, respectively. Considering receive function job is moiety to the one of send function. It receives data over stream sockets and has the same number of arguments in its function. One minute detail to focus is that it has buffer as the second argument which maintains a pointer to a data structure which holds the data received.

3.6 *sendto() and recvfrom()*

As discussed about send and receive functions, they are exactly the same in working (not in syntax and function building) but are meant for unconnected datagram sockets or let us just say sockets which do not build any logical connection or a bridge between sender and receiver. Now considering the syntax of `sendto` function, it contains six parameters mainly the socket descriptor, pointer message, length of the message, flags, pointer `*to` pointing to the structure `sockaddr` and `to` length parameter. `Recvfrom()` is used to receive data over unconnected datagram sockets with six parameters in its function and major has two changes. First is the buffer maintained to store the data received and `*from` pointer to the struct `sockaddr` and `*fromlen` to the length of the `sockaddr`.

3.7 *close() and shutdown()*

The client and server have been transferring packets all day. Now, we want to close the communication between them. It is as simple as calling the close file descriptor

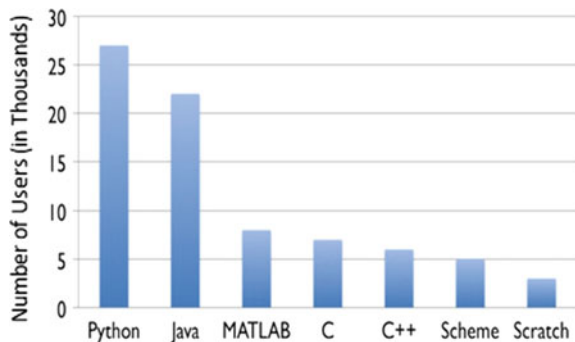
of regular Unix operating system and mentioning `close(sockfd)` which returns 0 in success and `-1` in case of any error. The control over the connection can be gained to a much more certain level and closing can be made elegant by writing the `shutdown()` function which does the same work as `close` but gives megalomaniac feel to the server as well as the client. The function takes input two parameters as `shutdown(int sockfd, int how)` where `how` can be any of the three numbers 0, 1, 2. Here, 0 represents that anymore receiving is not permitted. 1 indicates that send is not permitted, and 2 indicates that both are not allowed. The fun fact is that second parameter passed as “2” would do exact same thing as `close()` function. They both are responsible for handling the socket file descriptor to end its process and leave the system.

4 Result

When it comes to finding the best language to code our sockets in, it is tedious and an unkmpt way to choose one. The need of ours is to go with the one we know the best regardless the ease of syntax it provides. But after our research, we have analyzed the most used languages for socket programming (see Fig. 3). Python being the most human readable and easy to learn language always helps developers to code in a much simpler fashion. The client side and server side sockets can be made in Python or for accessing *Data Object Model characteristics, one could choose JavaScript on front-end. The second to none has to be Java for a few specific reasons.

1. You can literally send and receive objects over sockets.
2. Sending and receiving data belong to basic datatypes such as int, float. Etc., can be done using built-in methods like `writeInt()`, `readInt()`, etc. Thereby reducing the overhead of converting from byte stream to the required datatype.
3. Exception Handling is standardized and hence debugging can be streamlined.

Fig. 3 Inclination of users to respective languages for socket programming [6]



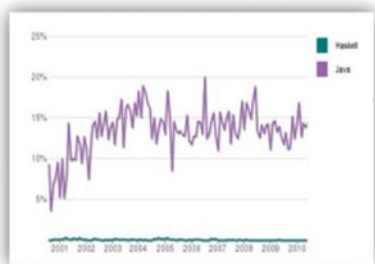


Figure 1: Monthly Lines of Code Changed

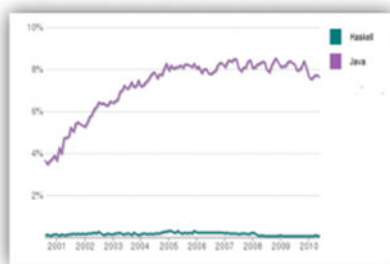


Figure 2: Monthly Project

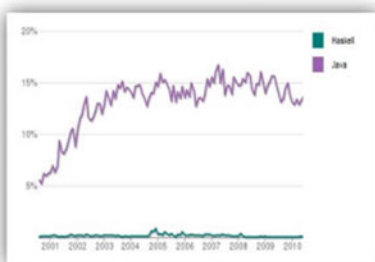


Figure 3: Monthly Commits

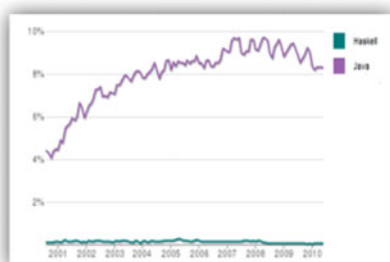


Figure 4: Monthly Contributors

Fig. 4 Java Vs Haskell comparison [6]

The rest languages are used nearly in mediocre fashion and on average have nearly the same number of users e.g. For C, C++, MATLAB have nearly same number of users.

Haskell and Java have a great competition too when it comes to building networks and in terms of easiness of languages. Figure 4 shows that being equally scalable and competent to Java, the number of contributors to Haskell are nearly none (The green being Haskell and magenta being Java).

So these comparison provides us with one lucid reference of the fact that though certain programming languages have their pros and cons and some have a large amount of community support, the best practice is to code the sockets in the language best known, no matter client or server side.

5 Conclusion

This paper deals with cases of sockets, their basic description, their structure and various API's involved in the formation of an established connection. Networks can be mobile, satellite or computer. No matter which type of network is, there is no connection without an interface. That is how the sockets are the crucial point to computer networks. The various API's mentioned are frameworks which can be

embedded in any language (prerequisite is that you know basic data structures and have a clear understanding of any one language) and can be easily coded into. The programming part can be done nearly in any programming language but when it comes to scalability and easiness, there is no comparison to Java or Python. They are much human readable and focus on building connections rather than syntax.

Acknowledgements The research work done during the course of this paper is solely performed under the acute guidance of Dr. Ankur Dumka of University of Petroleum and Energy Studies, Dehradun. I thank my batch mates who gave me strength and provided me with astuteness for pursuing this research. I would like to show my gratitude to the Dean of School of Computer Science, Dr. Manish Prateek, of University of Petroleum and Energy Studies who provided his support and encouragement that gave me a lot of enthusiasm to pursue my work with wholehearted dedication. I am greatly indebted to the Tanenbaum's book on Computer Networks which gave me epiphany on the field of sockets. Any mistake in my work should not put any dark spot on the reputation of these esteemed authors.

References

1. James F. Kurose , Keith W. Ross, Computer Networking: A Top-Down Approach (6th Edition), Pearson, 2012
2. Andrew Tanenbaum, Computer Networks, Prentice Hall Professional Technical Reference, 2002
3. TCP/IP Network Administration by Craig Hunt. Published by O'Reilly & Associates, Inc. ISBN 059600297152
4. TCP/IP Illustrated, volumes 1–3 by W. Richard Stevens and Gary R. Wright. Published by Addison Wesley. ISBNs for volumes 1, 2, and 3 (and a 3-volume set): 020163346948, 020163354X49, 020163495350, (020177631651)
5. Limi Kalita/(IJCSIT) International Journal of Computer Science and Information Technologies, Vol. 5 (3), 2014, 4802
6. Ohloh. 2010. <http://www.ohloh.net> (accessed July 15, 2010)

GSM-Based Prepaid Meter

Shruti Chaudhary, Adesh Kumar and Vivek Kaundal

Abstract Manual reading of meters for electricity measurement has been prevalent for a long time. The drawbacks of having such systems lead to inaccuracies in power consumption data causing problems to both customers and energy providing utility. This has led to large developments in the electronic metering measurements systems which are henceforth more reliable and efficient than the previous systems. This paper presents a design of GSM-based low-cost meter and its associated SMS (short messaging system) interface for remote accessing of data. This system consists of electricity e-billing system at the energy provider side via GSM module and automatic cut off via relay for low balance at the customer side.

Keywords Automatic reading system · GSM module · e-billing
Digital meters · Short messaging system (SMS) service

1 Introduction

Energy scarcity is a major problem in India. So steps need to be initiated on reducing the power consumption in homes. Over past years people have realized the necessity of saving energy which has led to development of many prepaid energy meters. This system helps in guiding people about their usage on daily or monthly basis. The current technology of billing process uses manual process of meter reading by updating the server with data and billing the customer thereafter. It incurs a higher cost on the energy provider side due to involvement of human labor in it. Also becomes difficult to access far flung rural areas. So initially prepaid

S. Chaudhary · A. Kumar (✉) · V. Kaundal
Department of Electronics, Instrumentation and Control Engineering,
University of Petroleum and Energy Studies (UPES), Dehradun 248007,
Uttarakhand, India
e-mail: adeshkumar@ddn.upes.ac.in

V. Kaundal
e-mail: vkaundal@ddn.upes.ac.in

electricity card-based system meters came into market. These card-based systems come under the category of automated meter reading (AMR) systems in which customers are given a prepaid card of particular amount from which they can get their system recharged. The card has to be swiped in front of meter in order to register the amount of recharge. The drawback mainly includes insecurity about this device as if the memory of card will be corrupted or lost then how to recover the recharge amount. Also man power is employed in carrying out the task. Also different cards will be needed for storing different amounts.

So need of automatic reading system is important which saves money on the side of energy provider and enhances knowledge of power consumed on the consumer side, and also which eliminates the defects of card-based system.

2 Related Research Work

Many researches had been done in this field and many are undergone. Like Thien Wan [1] in his paper discusses the need to develop a prepaid wireless meter system using JADE-LEAP (Java agent development environment platform). The system used smart agents for calculating consumed units. Rahman [2] on the other side uses an arduino (Uno) microcontroller, GSM modem, energy meter, and relay circuit. An optocoupler is connected between the load and microcontroller. The microcontroller is responsible for counting number of pulses from the meter. A relay has been connected between energy meter and load which is used for cutting off power supply due to non-payment of dues. Communication of energy consumption is done through GSM modem (SMS service) which has some predefined codes for communicating of data. The major drawback may be the network strength of GSM which may be a hindrance in providing apt communication. Also the cost of project is a detrimental factor in implementing it commercially. Abdollahi et al. [3] and Bashar et al. [4] used ATMEGA microcontroller for counting of pulses and sending it to GSM modem with the help of AT commands. The data is sent to main service center and processing of flow of data from meter side to service center and vice versa is done via SMS. While Noman [5] reads meter energy by using infrared sensor. AT89C51 microcontroller is used for capturing of data from meter and communicating to database through GSM. Database programming is done in MySQL. The whole hardware and software simulation is done in KEIL software. While some researchers like Ahmed [6] use the RFID technology for development of prepaid energy meter. The RFID card can be made to have different credits using software. The data of RFID card reader can be read and write with the help of microcontroller which is the brain of the system. It is this element of the system which sees if the credit is low then sends a message through gem to customer. It also cuts off the power supply through relay connected between microcontroller and load. There is also an LCD which shows the power consumed by the customer. The main drawback is to have different cards having different credits thus complicating the whole process. Nayan Gupta [7] developed a prepaid energy meter using ARM7 as the brain of

microcontroller which collects meter readings from energy meter and forwards to server with the help of GSM and RF technology. The server on the other end sends and receives messages from consumer regarding recharging for prepaid and payment of bills for post-paid meters.

Also theft control has been taken into account to alarm the server. While Ashna [8] developed AMR system comprising of pic microcontroller, GSM modem, LCD, MAX232, MCP3905 ic in order to make an automated online billing system which can readily send SMS about monthly consumption and cost to users or consumers through SMS. The advantage is use of additional components like EEPROM and RTC for storing and reading the data in timely manner. The programming has been done in MICROC IDE using embedded C. Rodney et al. [9] describes how GSM technology can be utilized to build a prepaid metering system. It utilizes the use of e-billing at the energy provider side using database for collection of energy consumed by the respective consumer and Web portal for payment of bills by the customer. It uses the short messaging service (SMS) to communicate the notifications regarding bill payment dues and balance inquiry by the customer.

2.1 Our New Project Addresses the Above Mentioned Problems

The first and foremost is providing a method for energy conservation by instilling the belief in people to know about their energy consumption needs and develops methods in order to reduce their billing, thus solving the problem of energy scarcity. It is capable to access energy data over far flung rural areas. It helps to eliminate or minimize the deficits incurred during manual reading.

It helps to eliminate the deficits incurred during manual reading and provides more accurate billing data. Fewer incidences of tampering and theft of meter. Also customer can have the flexibility to get to know their electricity usage at any time they want. This will help in reducing unwanted power consumption. We are proposing a technology that includes GSM communication to get reading, updating server, and informing consumers about bill units and amount.

This system consists of automatic reading system (AMR) at the energy provider utility, GSM module for recharging and balance notifications via SMS service. Just like we recharge our mobiles we can recharge our electric meter with some amount, and this amount is burned as per the usage in accordance with the current energy tariff. When balance reduces to zero a message will be sent to customer through GSM modem to tell him that the power has been cut off and he has to recharge further in order to reuse the power facility again.

In order to avoid this happen a facility is included in the project which issues a warning message to customer when 10% of balance is left. This gives customer ample time to recharge his system in order to avoid power cutoff. This system will raise the home owner's awareness of how much energy they use and make consumers more energy efficient.

2.2 Main Features of the Project

- (1) Remote recharging to location with GSM.
- (2) Auto cutoff when exiting validity days get over or balance reached to zero.
- (3) Recharge information to customer.
- (4) Customer can check their balance Rupees in the meter.
- (5) Low balance information is automatically sent to the customer.

List of hardware components

Name	Specification
Energy meter	Jaipur 5–20 kWh ac, single phase 2 wire static meter
LCD	16 × 2 LCD display working on 5 V supply
Load	100 W bulb
MCT2E optocoupler	It is a 6 pin ic consisting of gallium arsenide infrared led and a silicon npn phototransistor
PIC16F877A	It has 256 bytes of EEPROM data memory, 2 comparators, 8 channels of 10-bit analog-to-digital converter, 2 capture/compare/PWM functions, serial port facility of SPI, i ² c and USART operating between 2.5 and 5 V
SIM908 GSM modem	It is having both GPRS and GSM facility operating at 12 V DC supply
Relay	Riza relay working for switching on and off the load through driver ic
ULN2003A	Relay driver ic uln2003 is high voltage and high current integrated ic which used Darlington array. It works on 12 V supply

2.3 Working

Figure 1 represents the block diagram of the proposed system. The proposed system has a PIC microcontroller acting as brain of whole prototype. The PIC microcontroller is responsible for counting pulses of the meter through usage of external interrupts in the system. The pulse increments each time an interrupt occurs. To avoid disruption of microcontroller circuit due to high voltage supply in the mains and optocoupler is inserted between the mains supply and microcontroller. This helps to protect circuit for sudden transients of voltage supply. The meter reading in a timely manner is uploaded to server through the GSM modem. The LCD attached to the prototype also shows the balance left when a balance enquiry is sent by the customer. Also the customer has the facility of recharging his meter via short messaging service (SMS) which has particular format of sending the SMS. Also each customer is given a unique id for identification of recharging and balance facilities. To make it more interactive, a warning message will be sent to customer when 10% balance is left. A final message is also sent to indicate that power supply has been cut off and recharge has to be done in order to regain power supply. Coding for this prototype has been done in embedded C.PIC16F877A

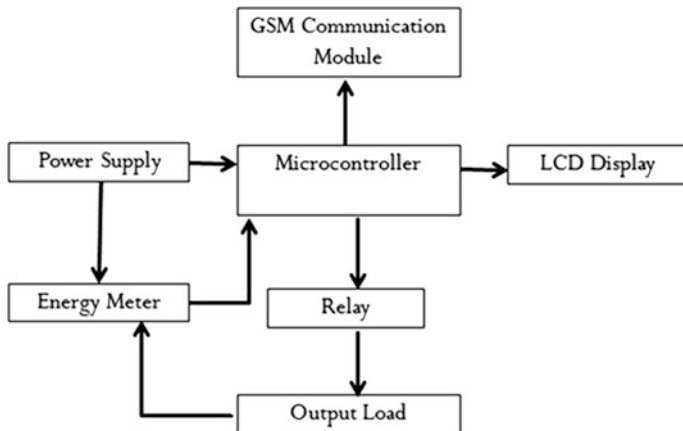


Fig. 1 Block diagram of GSM-based prepaid meter

microcontroller programmed using PICKIT-3 programmer and programming is done in MPLAB X IDE software. Putty software was used for initializing of GSM commands. Logic Analyser is used for verifying of commands of GSM while programming.

2.4 Software Tools Used

MPLAB IDE FEATURES—MPLAB X IDE is a software program for implementation of embedded microcontrollers such as PIC microcontrollers. It works in an integrated development environment (IDE) because it provides a single environment for programming. It supports multiple configurations, many different versions of compiler, and debug Tools. It has inbuilt package of C library which is utilized for programming in this prototype. The compiler used is XC32 (v1.42).

PROTEUS—Proteus is a virtual system modelling (VSM) which utilizes circuit simulation before actually testing your program in real hardware and real environment. It has also different types of libraries consisting of different components, e.g., different microcontrollers, LCDs, switches, buttons, etc., which are utilized in building a hardware prototype. It also has debugging features and single step features in its library.

PUTTY—PUTTY is a free and open-source terminal emulator; serial console, and network file transfer application. It has many features including SCP, SSH, Telnet, rlogin, and raw socket connection. This has been used for testing of AT commands (SMS-based) of GSM.

LOGIC ANALYSER—A logic analyser utilized in this project is an electronic instrument that captures the data from microcontroller and GSM and displays the communication between these systems on its software. It captures data in the form

of timing diagrams consisting of different formats, e.g., hexadecimal or ASCII format. It has the facility of auto detecting the baud rate of connected systems in order to sync captured data properly.

3 Flowchart for the Prepaid Meter

Figure 2 describes the flow of GSM-based meter. It first checks if the balance is low or not. If it is low then the power will be cut off via relay else the counting of pulses will start depending on the energy consumption of the concerned household. Then the pic microcontroller will be continuously monitored for unsolicited message. If a message arrives its mobile number is verified to that of list of customers in database. If it is found it will check whether it is for balance or recharge, else it will be discarded. If it is for recharge then that much amount will be added to customer's meter side balance and an acknowledgement will be sent to the customer. If for balance then the balance left at meter side is grabbed and sent to customer. Also an LCD is there to show balance in case of recharge or balance enquiry.

4 Algorithm for Prepaid Meter

- (1) Set Port D for LCD connections with 0, 1, 2 for rs, r/w, and enable signals and 4, 5, 6, 7 for data pins of lcd. Set Port C.0 pin for relay and Port C.6 and Port C.7 pin for UART transmission and receiving. Set 33 pin of microcontroller for external interrupt.
- (2) Set all pins of Port D and Port C as output pins. Set 7th pin of port c as input pin.
- (3) First initialize LCD with all the following instructions

```
#define LCD_CLEAR      0b00000001    // for clearing all characters written in LCD
#define LCD_HOME      0b00000010    // bringing cursor to initial position
#define LCD_OFF       0b00001000    // turning display off
#define LCD_ON        0b00001100    // turning display on
#define RESET_LCD     0b00110000    // reset the LCD
#define FORMAT_OFF_LCD 0b00101000    // 2line display, 4 bit data
#define SET_CURSOR    0b10000000    // define cursor parameters
```

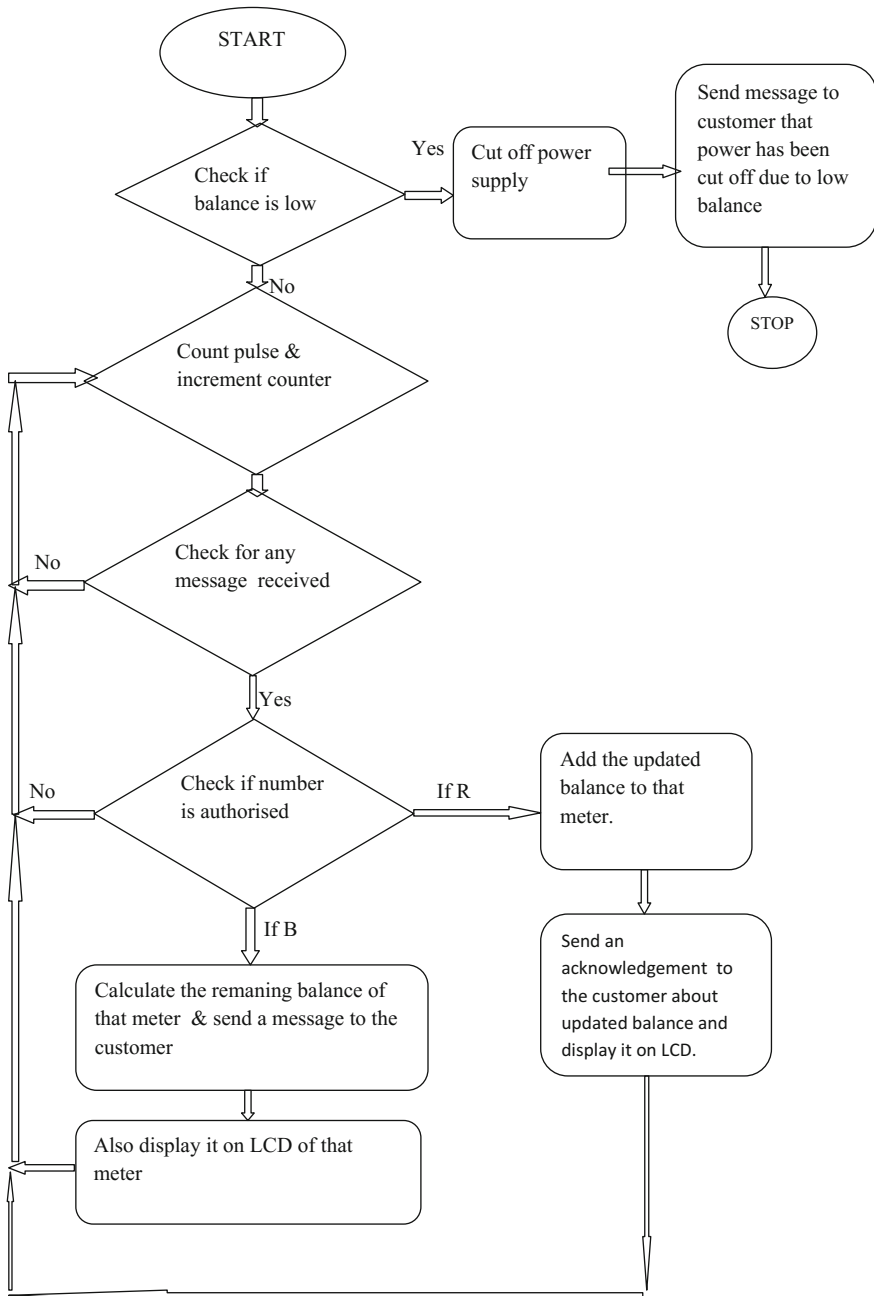


Fig. 2 Flowchart of GSM-based prepaid meter

(4) Initialize GSM

Send AT, ATE0, ATV0, AT + CPIN?, AT + CREG?, AT + CMGF, AT + CNMI for initializing for network checking, registration, setting SMS mode, etc., through UART pins.

- (5) Enable external interrupts and set their respective flags. Set positive edge triggering for the concerned interrupt.
- (6) The energy meter is connected to external interrupt of the pin through the optoisolator. For each increment in pulses counter is incremented in the microcontroller. An ISR routine is made for this.

Check for any response from the GSM modem. The reading of messages will be done by AT + CMGR command.

The response will be of two types—recharge or balance inquiry. They will start with R and B.

The first character will be checked. If it is B then

If any balance enquiry has been done then parse the customer number and find out its meter number and then calculate its pulses and units consumed display it on LCD. Subtract the total balance from the consumed balance and through AT + CMGS command send it to particular number.

If it's R

For recharging from customer number use of *amount# is done, e.g., *32# means recharge of Rupees 32. Through selective parsing numerals will be grasped from this message and converted to integer using a well-defined ASCII to integer function. The amount will be added to that particular meters balance and updated balance will be displayed on to LCD so that customer can see for themselves. Then through GSM modem an acknowledgement message will be sent to customer after recharge with the help of AT + CMGS command.

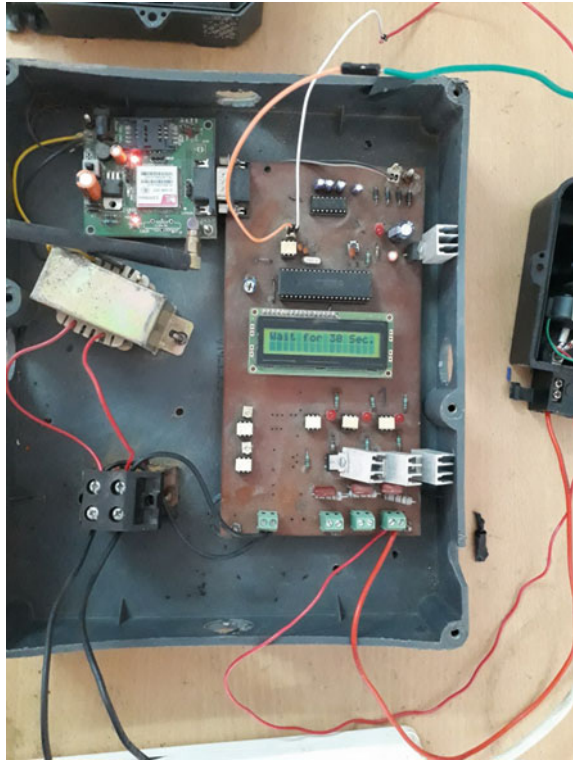
- (7) The last important thing will be the working of relays. The balance of each meter will be checked. If its 90% consumed then a warning message will be sent through AT + CMGS to that particular customer. If the balance is 95% consumed then relay will be switched off through microcontroller Port C pins and power supply will be cut off.

If a customer recharges then again the relay will be switched on and the power supply will be restored.

5 Result and Discussion

Initially on switching on the circuit the LCD will read wait for 30 s which is shown in Fig. 3. After that series of messages will follow as Testing for GSM, Welcome to Naturetech Infra as shown in Figs. 4 and 5.

Fig. 3 LCD displaying delay of 30 s



When no recharge has been done the circuit will show the please recharge message on LCD as reflected in Fig. 6. Then recharge will be done by customer through his mobile number. After the recharge has been done the meter will start working by switching on the power supply and simultaneously the LCD will show the electricity and validity balance of particular customer by as shown in Fig. 7. This will be possible through messages exchanged between customer mobile number and GSM modem of the kit. If 10% of balance will be left a warning message will be sent to customer. Finally if balance is zero then power will be cut off through relay and load will be switched off.

The image of whole working circuit is shown in Fig. 8.

Fig. 4 LCD displaying testing of GSM

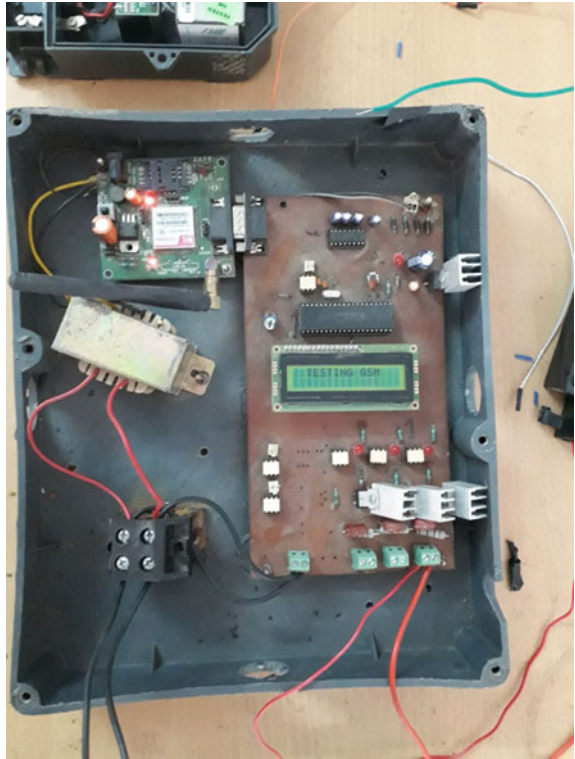


Fig. 5 Displaying welcome to nature tech infra

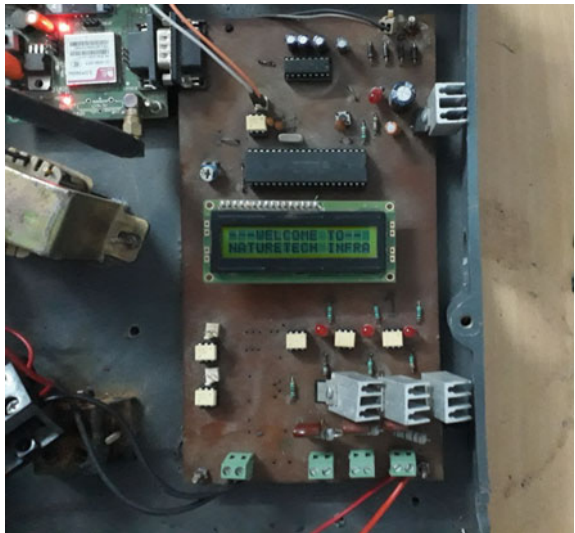


Fig. 6 Displaying please recharge

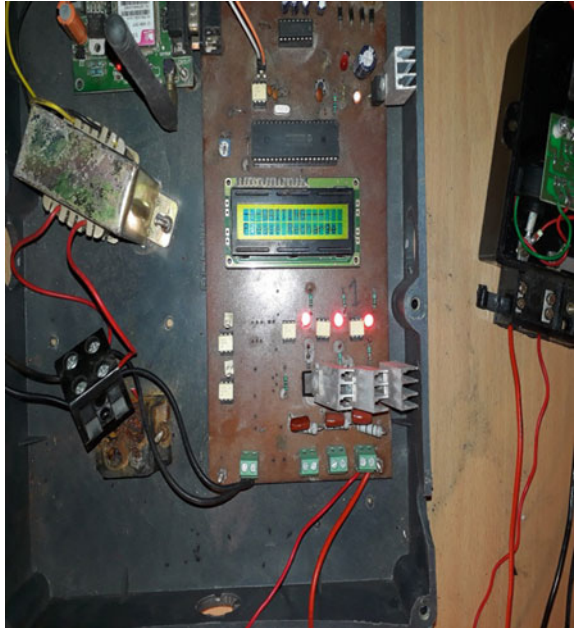


Fig. 7 Displaying balance, validity

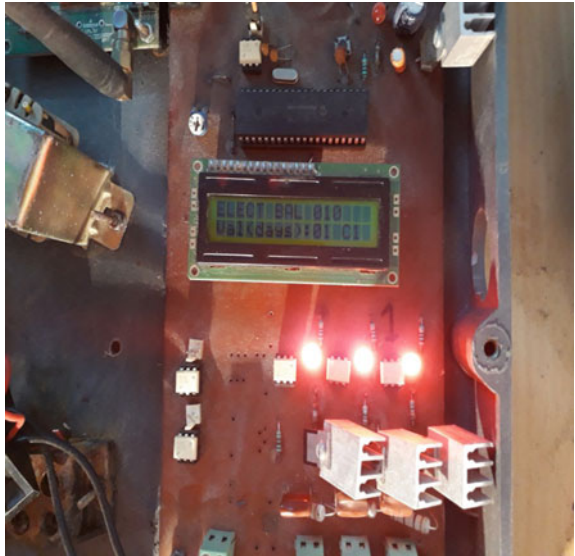


Fig. 8 Displaying the whole working prototype



6 Conclusion

The prepaid meter implemented is a reliable system removing all drawbacks of manual reading. People will also get to know their monthly consumption regarding various seasons of the year and error due to manual calculations will be minimized. Also the facility of recharging and balance inquiry is a much faster process as compared to older technology. The security of the system has been increased with this system as tampering with meters will be lowered. In future, we can further upgrade the system by using RF communication, e.g., use of zigbee as its range is quiet good for transmission of data (units consumed) in our already build project. Use of GSM can be done to upload data to server through GPRS using HTTP protocols.

References

1. Au Thien Wan, Suresh Sankaranarayanan and Siti Nurafifah Binti Sait “Smart Agent Based Prepaid Wireless Energy Meter” International Conference on Cloud Computing and Internet of Things (CCIoT 2014).
2. Md. Masudur Rahman, Noor-E-Jannat, Mohd. Ohidul Islam “Arduino and GSM based smart energy meter for advanced metering and billing system” 2015 International Conference on Electrical Engineering and Information Communication Technology (ICEEICT).
3. Ali Abdollahi, Marjan Dehghani, and Negar Zamanzadeh “SMS-based Reconfigurable Automatic Meter Reading System” 16th IEEE International Conference on Control Applications Part of IEEE Multi-conference on Systems and Control Singapore, 1–3 October 2007.
4. Dr. Md Abul Bashar, Maruf Ahmad, Sobuj Kumar Ray, Fahad Bin Sayed, Asif Ahmed “Economical Way of GPRS Based Fully Automated Energy Metering System”.

5. A.A. Noman, M.F. Rahaman, H. Ullah, R.K. Das “ANDROID BASED SMART ENERGY METER” 4th National Conference on Natural Science and Technology, Asian University for Women, Chittagong, Bangladesh, 2017, pp (1–3)
6. Rozita Teymourzadeh, S. Mahmud Iwan, Ahmed J. A. Abueida “RFID-based prepaid power meter” 2013 IEEE Student Conference on Research and Development (SCOREd), 16–17 December 2013, Putrajaya, Malaysia Vol 13, No 3-E (2013): Global Journal of Computer Science and Technology.
7. Nayan Gupta, Deepali Shukla “DESIGN OF EMBEDDED BASED AUTOMATED METER READING SYSTEM FOR REAL TIME PROCESSING” 2016 IEEE Students’ Conference on Electrical, Electronics and Computer Science.
8. Ashna K, Sudhish N George “GSM Based Automatic Energy Meter Reading System with Instant Billing” 2013 IEEE.
9. H. G. Rodney Tan, C. H. Lee, V. H. Mok “Automatic power meter reading system using GSM network” International Power Engineering Conference, 2007. IPEC 2007.
10. Francesco Benzi, Member, IEEE, Norma Anglani, Member, IEEE, Ezio Bassi, and Lucia Frosini “Electricity Smart Meters Interfacing the Households” IEEE transactions on industrial electronics, vol. 58, no. 10, October 2011.

Design of 2-Bit Vedic Multiplier Using PTL and CMOS Logic

Gaurav Bajaj, Kabir Grover, Anu Mehra and Sachin Kumar Rajput

Abstract The requirement of a high-speed multiplier is expanding. It is one of the most important hardware blocks in a processing system. A multiplier acts as a high delay block, and it also dissipates a lot of power. An ordinary processor requires more time and resources in multiplication operation. The proposed design of the 2-bit Vedic multiplier has been designed using pass transistor logic. The Vedic multiplier is the fastest, reliable, efficient, and low-power multipliers. By reducing the number of partial products, the delay also decreased and the system becomes faster. The design and the properties of this multiplier have been studied and performed using the Pyxis Schematic software (90 nm), and the power dissipation and delay have been compared with 2-bit multiplier using CMOS logic. The analysis is made for voltage range from 0.8 to 1.5 V.

Keywords Vedic multiplier · Pass transistor logic · CMOS logic
Power dissipation · Delay

G. Bajaj (✉) · K. Grover · A. Mehra · S.K. Rajput
ASET, Amity University Uttar Pradesh, Noida, India
e-mail: gaurav_05@hotmail.com

K. Grover
e-mail: kabir1502@gmail.com

A. Mehra
e-mail: amehra@amity.edu

S.K. Rajput
e-mail: skrajput@amity.edu

1 Introduction

Multipliers are widely utilized as a part of microprocessors and digital signal processing (DSP) applications including convolution, filtering, fast Fourier transform (FFT). The requirement of high-speed and low-power multipliers is increasing, and thus, the power dissipation and delay play a crucial role in determining the efficiency of a multiplier [1]. The multiplier can be designed using various algorithms. Algorithms such as Booth multiplier, array multiplier, modified Booth multiplier, carry-save multiplier 2-bit multiplication can also be performed by Wallace multiplier. The fastest multiplier is array multiplier which multiplies all the bits in one go, and it needs a lot of gates which increase the delay and power dissipation and which make array multiplier less efficient. The carry-save adder processes all the bits one by one to add carry in an adder, thereby increasing the execution time as the number of bits increases. The speed of Wallace multiplier is very high because it gives three single bits as an input to one-bit full adder which makes the circuitry complex, and its results show high delay and high power dissipation. Thus, Vedic multipliers are required to remove the disadvantages of the above multipliers.

2 Proposed Algorithm

An ancient mathematician named Sri Bharati Krishna Tirtha Maharaj invented Vedic Mathematics. A total of 16 sutras act as the basis of Vedic Mathematics that deal with algebra, geometry, and operations [2]. The 2-bit Vedic multiplier algorithm is given in Fig. 1. The vertical and crosswise algorithm forms the basis of the architecture used in Vedic multiplier, and this algorithm is called Urdhva Tiryagbhyam (UT) [3]. $A = A_0B_0$ and $B = B_0B_1$ are the two-bit numbers which are used for multiplication. The least significant bit is referred to as LSB. The LSB of the final product is determined by the product of LSB. The LSB of the multiplicand is multiplied with the next higher bit of the multiplier which is then added to the product of the LSB of multiplier and next higher bit of the multiplicand. The resulting sum then gives the second bit of the final product, and then, the carry is added to the partial products that are obtained by the multiplying the most significant bit (MSB) further giving the sum and carry. The third corresponding bit is the sum, and the fourth bit of the final product becomes the carry. The UT algorithm is applicable to both decimals as well as binary numbers [4]. The final result will be $S_3S_2S_1S_0$ where:

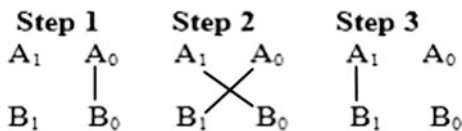


Fig. 1 2-bit UT multiplier

$$\begin{aligned}
 S_0 &= A_0B_0 \\
 S_1 &= (A_0B_1) \text{ XOR } (A_1B_0) \\
 S_2 &= (A_0A_1B_0B_1) \text{ XOR } (A_1B_1) \\
 S_3 &= A_0A_1B_0B_1
 \end{aligned}$$

2.1 Two-Bit Multiplier Using Pass Transistor Logic (PTL)

Several logic families used in the design of integrated circuits can be described by the pass transistor logic (PTL). PTL uses less number of transistors which are used to make different logic gates by eliminating redundant transistors. However, as a lesser number of transistors are used, the output levels are always lower than the input levels. Some basic characteristics of PTL are as follows: (a) Gate is static; i.e., a low rail path exists to both supply rails under all circumstances; (b) N transistors are used instead of 2N; (c) no static power consumption. The implementation of 2-bit multiplier is done in 4 parts. The 4 parts include the simulation of all the 4 multiplier equations separately (S0, S1, S2, S3) and then calculate the delay and the power dissipation of each equation (Figs. 2, 3, 4, and 5).

2.2 Two-Bit Multiplier Using CMOS Logic

The development of digital integrated circuits is done by complementary metal oxide semiconductor technology. It is nowadays being used in all modern digital circuits. The uses of CMOS logic are expanding. Some of the most common uses of CMOS technology are in the field of digital and analog communication (Figs. 6, 7, 8 and 9).

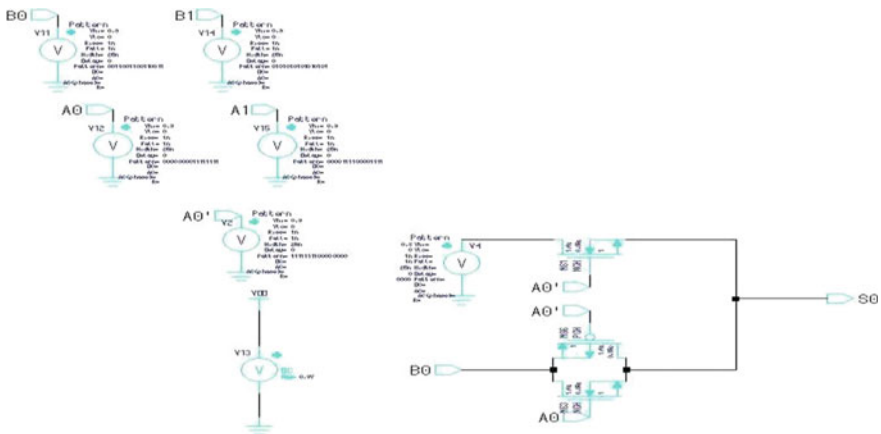


Fig. 2 S0 PTL implementation

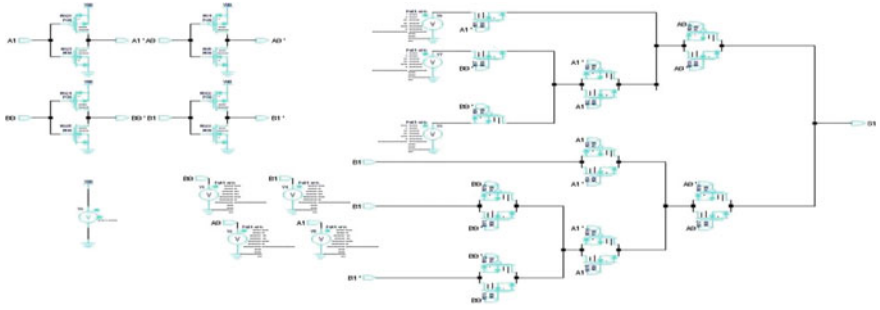


Fig. 3 S1 PTL implementation

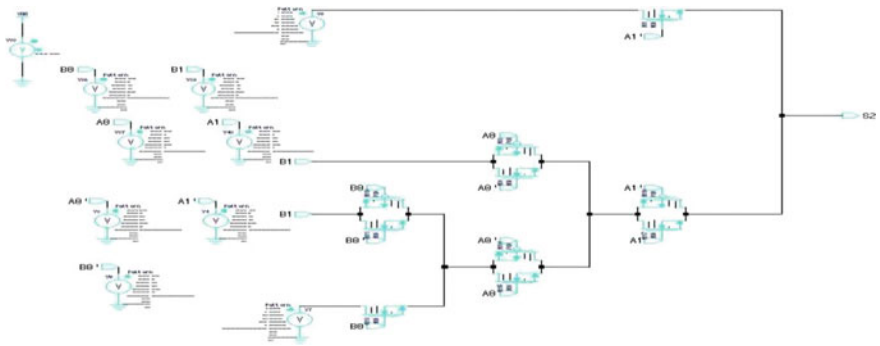


Fig. 4 S2 PTL implementation

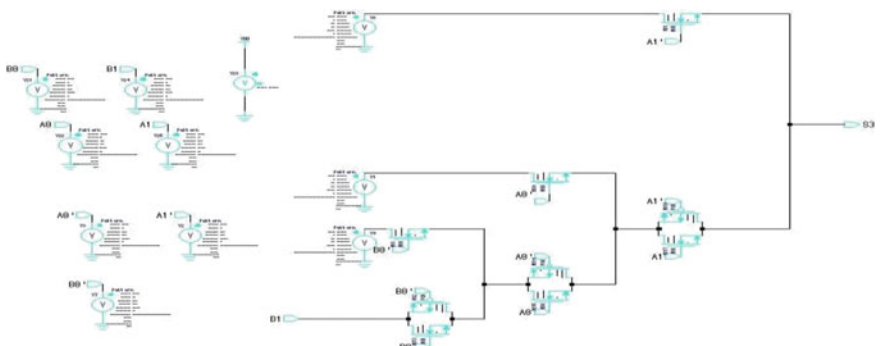


Fig. 5 S3 PTL implementation

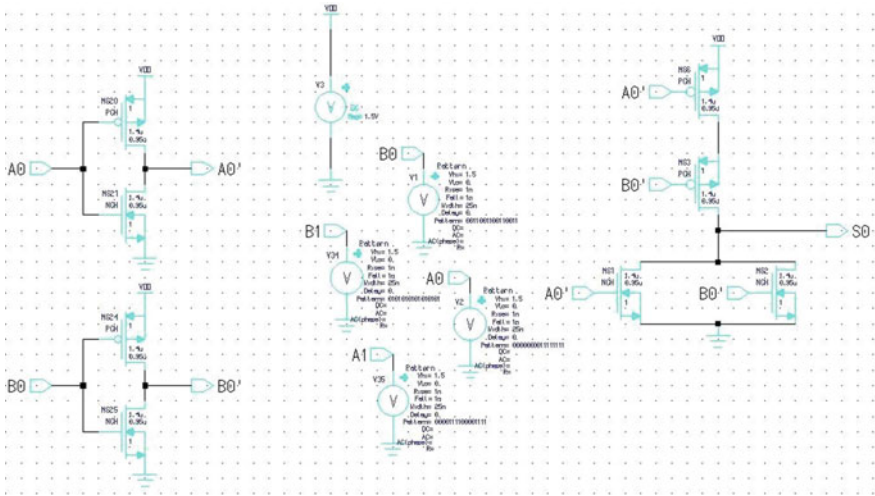


Fig. 6 S0 CMOS implementation

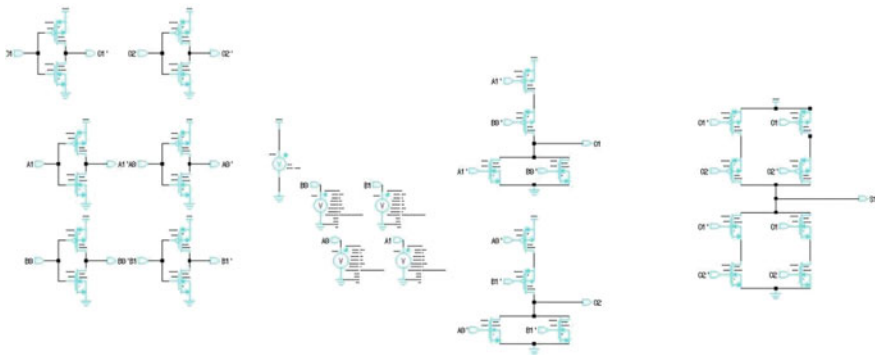


Fig. 7 S1 CMOS implementation

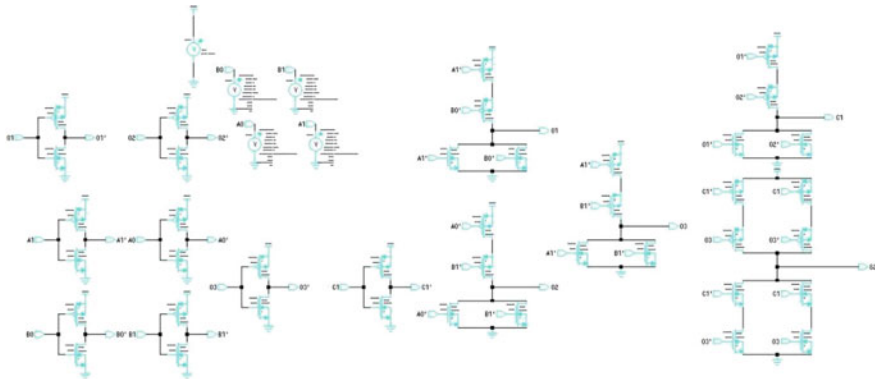


Fig. 8 S2 CMOS implementation

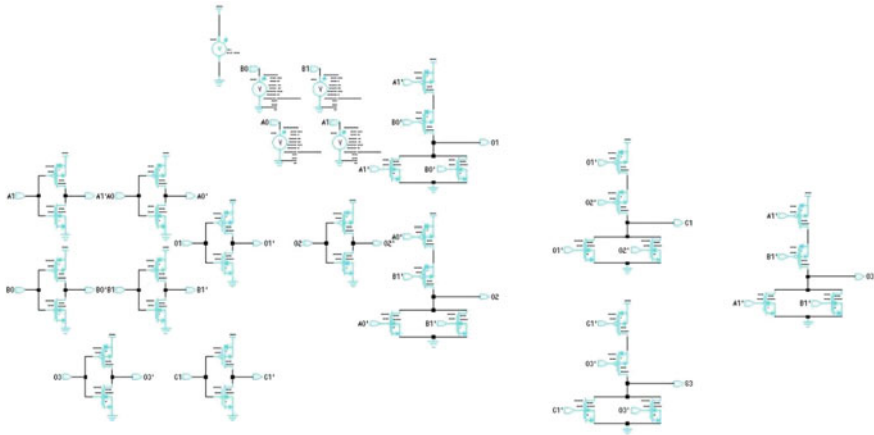


Fig. 9 S3 CMOS implementation

3 Results and Observation

After the simulation of the above PTL and CMOS multiplier circuits, the power dissipation and delay are calculated and compared with each other. In theory, the lower the power dissipation and delay, the higher is the efficiency of the multiplier. The analysis here is made for voltage 1.5 V.

Waveforms of the above equations using the inputs A0, A1, B0, and B1 are shown below.

3.1 *Input and Output Waveforms for 2-Bit Multiplier Using PTL*

See Figs. 10, 11, 12, and 13.

3.2 *Input and Output Waveforms for 2-Bit Multiplier Using CMOS Logic*

The number of transistors, delay, and power dissipation has been calculated for S0, S1, S2, and S3. It has been calculated separately for PTL and CMOS logic (Tables 1, 2, 3, 4 and 5).

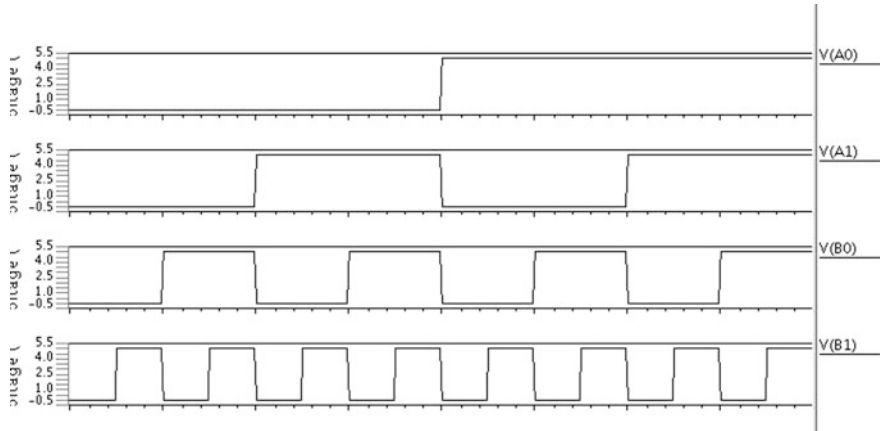


Fig. 10 Input waveforms for PTL multiplier

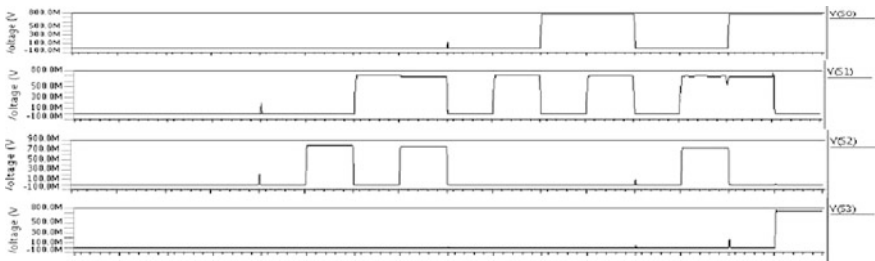


Fig. 11 Output waveforms for PTL multiplier

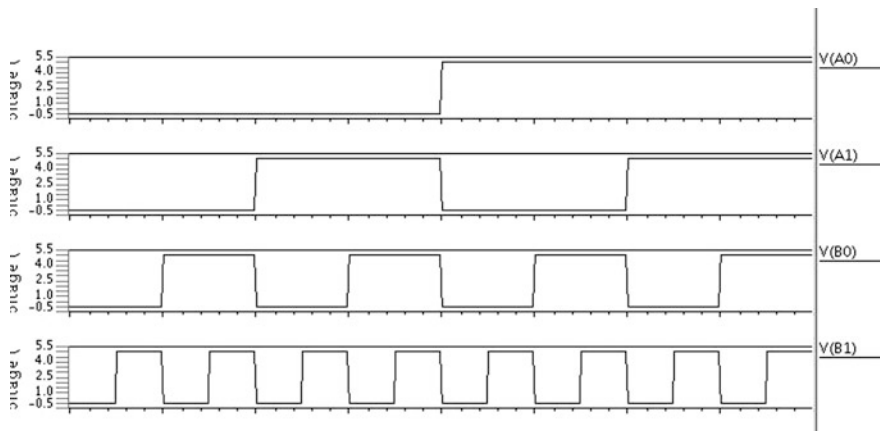


Fig. 12 Input waveforms for CMOS multiplier

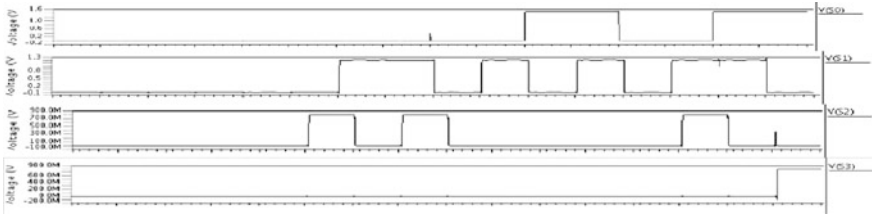


Fig. 13 Output waveforms for CMOS multiplier

Table 1 Number of transistors

Output	Number of transistors used	
	CMOS	PTL
S0	4	3
S1	26	25
S2	16	10
S3	36	9

Table 2 Delay and power dissipation for S0

V _{DD} (V)	Delay (ps)		Power dissipation (nW)	
	CMOS	PTL	CMOS	PTL
0.8	410.84	77.636	0.196	0.0067
0.9	358.19	101.35	0.367	0.011
1.0	317.32	130.65	0.450	0.022
1.1	237.07	157.6	0.553	0.0413
1.2	236.47	182.4	0.687	0.073
1.3	242.79	198.36	0.862	0.127
1.4	241.29	215.84	1.1272	0.217
1.5	224.45	220.83	1.5026	0.363

Table 3 Delay and power dissipation for S1

V _{DD} (V)	Delay (ps)		Power dissipation (nW)	
	CMOS	PTL	CMOS	PTL
0.8	791.066	165.445	1.0815	0.616
0.9	665.84	142.790	1.252	0.885
1.0	566.09	131.825	1.5307	1.2540
1.1	513.43	107.85	1.8736	1.5359
1.2	564.08	86.94	2.314	1.8978
1.3	433.811	83.056	2.9045	2.3833
1.4	416.436	92.86	3.7827	3.061
1.5	398.816	131.586	4.9139	4.0411

Table 4 Delay and power dissipation for S2

VDD (V)	Delay (ps)		Power dissipation (nW)	
	CMOS	PTL	CMOS	PTL
0.8	888.48	262.52	1.3526	0.018
0.9	750.316	205.98	1.6697	0.035
1.0	650.85	169.12	2.0542	0.067
1.1	576.04	162.965	2.5396	0.123
1.2	535.72	112.5016	3.1790	0.219
1.3	497.47	104.13	4.0580	0.380
1.4	470.73	98.77	5.3144	0.647
1.5	447.096	92.29	7.1596	1.804

Table 5 Delay and power dissipation for S3

V _{DD} (V)	Delay (ps)		Power dissipation (nW)	
	CMOS	PTL	CMOS	PTL
0.8	1379.8	150.29	0.816	0.0182
0.9	1126.1	45.100	1.5225	0.0559
1.0	937.44	36.5639	1.8775	0.067
1.1	813.27	88.3398	2.3293	0.123
1.2	709.66	127.5029	2.9377	0.220
1.3	626.71	154.14	3.7684	0.382
1.4	566.90	181.17	4.9829	0.651
1.5	523.31	201.1121	6.7749	1.0918

4 Conclusion

The delay and power dissipation have been calculated for 2×2 multipliers using CMOS logic and PTL. After seeing the results, it has been found that it is much more efficient to design 2×2 multiplier using PTL. The number of transistors has been reduced; the power dissipation and delay are much less when we compare the results with those of CMOS logic. PTL can be further used to design efficient multipliers.

References

1. Jagadguru Swami Sri Bharati Krisna Tirthaji Maharaja, "Vedic Mathematics or Sixteen Simple Mathematical Formulae from the Veda, Delhi (1965)", Motilal Banarsidas, Varanasi, India, 1986.
2. G. Ganesh Kumar, V. Charishma, "Design of High Speed Vedic Multiplier using Vedic Mathematics Techniques", International Journal of Scientific and Research Publications, Volume 2, Issue 3, March 2012 1 ISSN 2250-3153.

3. Sushma R. Huddar, Sudhir Rao Rupanagudi, Kalpana M and Surabhi Mohan, "Novel High Speed Vedic Mathematics Multiplier using Compressors", International Multi conference on Automation, Computing, Communication, Control and Compressed Sensing(iMac4s), 22–23 March 2013, Kottayam, ISBN: 978-1-46735090-7/13, pp.465–469.
4. M.E. Paramasivam, Dr. R.S. Sabeenian, "An Efficient Bit Reduction Binary Multiplication Algorithm using Vedic Methods", IEEE, 2010.

Computer Aided Diagnosis of Cervical Cancer Using HOG Features and Multi Classifiers

Ashmita Bhargava, Pavni Gairola, Garima Vyas and Anupama Bhan

Abstract Cervical cancer is very common in women, and it is the most dreaded disease. Cervical cancer if detected early can be treated successfully. Cervical cancer occurs due to the uncontrolled growth of the cells present in the cervix of the female body, and it also occurs due to the virus human papilloma virus (HPV). Pathologists diagnose cervical cancer by a screening test called Papanicolaou test or Pap smear test. The pap smear test is not always 100% accurate but it helps in early detection of cancerous cells. In this paper, a method is proposed that helps in detection and classification of the cancer using HOG feature extraction and classifying it by the help of support vector machine (SVM), k -nearest neighboring (KNN), artificial neural network (ANN). The database was collected from Air Force Command Hospital, Bengaluru. A total of 66 pap smear images were collected that are 25 normal pap smear images and 41 abnormal pap smear images. Histogram of gradient (HOG) extracts features of the region of interest in the image as it converts pixel-based representation into gradient-based representation. The classification of cervical cells—abnormal cells and normal cells—is done with the help of multi-classifier. The accuracy attained after classification is 62.12, 65.15, and 95.5% for SVM, KNN, and ANN, respectively.

Keywords Cervical cancer · Hog · Artificial neural network
SVM · KNN · Confusion matrix

A. Bhargava (✉) · P. Gairola · G. Vyas · A. Bhan
Amity University, Noida, India
e-mail: ashsnuffle@gmail.com

P. Gairola
e-mail: pawnigai@gmail.com

G. Vyas
e-mail: gvyas@amity.edu

A. Bhan
e-mail: abhan@amity.edu

1 Introduction

Cervix is the narrow part of the lower uterus. That is why it is called the neck of the womb. The cancerous society of the USA gives an estimation for cervical cancer that there is diagnosis of 12,800 new cases of cervix cancer that leads to 4000 deaths which is becoming the most common cause of death amongst women [1]. Most cases reported of cervical cancer lie in the age group below 50 [2]. This cancer is a result of uncontrolled growth of the cervical cells. Every cell has a particular span of life. When they die, new cells replace them. But in the case of cancer, the cells do not die and continue to divide. This continuous division leads to cancer. Some factors alleviate the cancer like the HPV virus which a sexually transmitted virus, smoking, and weak immune system. More than 100 HPV viruses are there out of which 15 causes cancer in the body and other 85 are harmless. The number of reported cases of cervical cancer has been reduced in the last 20 years because of the effective screening test called pap smear test as the cancer if detected at an early stage can be treated successfully [3].

Women now aware of the cancer regularly do the pap smear test as doctors suggest that HPV test and pap smear test should be conducted at the same time. Cervical screening not only detects cancer but also checks for the abnormalities in the cell that is if the nucleus becomes larger in size. If the abnormal cells are not treated, they get converted into malignant cancerous cell. Due to human errors and lack of time of result of pap smear test, the pap smear tests are not always accurate. Therefore, an automated method has to be devised that makes the detection of abnormal cells fast, easy, and accurate. The main contribution of the paper is to diagnose the cervical cancer more correctly and accurately.

2 Related Works

In [4], EDF and EM algorithm for the detection of abnormal cells achieved an accuracy of 70%. In [1], RGVF segmentation classified the normal and abnormal cells using SVM classifier with an accuracy of 93.72. In [5], neural network for pattern recognition and image retrieval is used and accuracy achieved is 80%. In [2], FCM segmentation, features are extracted, and then, classifiers are used for the differentiation of two types of cells. In [6], HEp-2 Cell Image Classification with Deep Convolutional Neural Networks is used. In [3], 22 GLCM features and multiclass SVMs are used, and accuracy of 95% is achieved.

3 Proposed Methodology

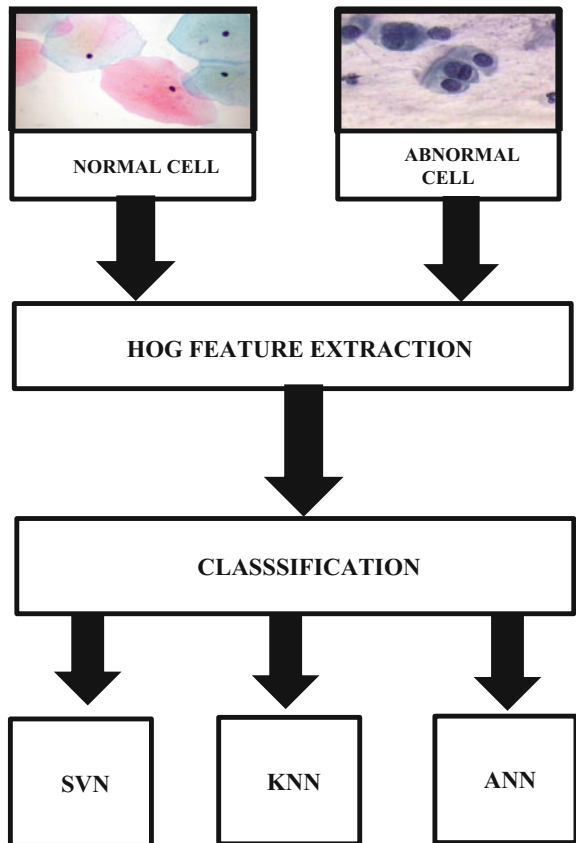
3.1 Flowchart

Normal cell and abnormal cell pap smear images are used. HOG feature extraction is used and 900 features extracted. Multiclassification is done with the help of SVM, KNN, and ANN classifiers. Figure 1 shows the flowchart of proposed methodology.

3.2 HOG Feature Extraction

Feature vector is n dimensions of a vector of an object that depicts numerical features. These features will help in differentiating normal cells to abnormal cancerous cells. HOG is similar to edge-based histograms. Histograms are the

Fig. 1 Flowchart of the methodology



graphical representations of the tone distribution of the image that is the lightness and the intensity of the image. It plots the pixels for each tone of the value. HOG uses global features rather than local features Many algorithms have been used for the feature extraction but in this method, we have used HOG feature extraction. The number of gradient orientation in local portions of the image is counted.

Implementation of the algorithm

1. Gradient computation: Luminous gradient is calculated at each pixel by using Eqs. (1) and (2). Change in lamination is represented by luminous gradient vector where m is the magnitudes, and θ (theta) is the orientation arrangement. L is the lamination value where θ lies between $-\pi/2$ and $\pi/2$. Figure 2 describes the luminous gradient calculation.

$$m(x, y) = \sqrt{L(x + 1, y) - L(x - 1, y) + L(x, y + 1) - L(x, y - 1)} \quad (1)$$

$$\theta(x, y) = \tan^{-1}(L(x, y + 1) - L(x, y - 1)) / (L(x + 1, y) - L(x - 1, y)) \quad (2)$$

2. Orientation binning: This creates the histograms of the cells. The magnitude of luminous gradient plus orientation generates a histogram.
3. Descriptor blocks: Localized normalization of gradient strengths is required to be done for account of localized and contrast changes. By this, the features become robust to changes in the illumination.
4. Block normalization: The features become robust to the changes of the form. Let v be a non-normalized vector that contains all the histograms in the block, and it is the magnitude of each direction.

Fig. 2 Luminous gradient calculation

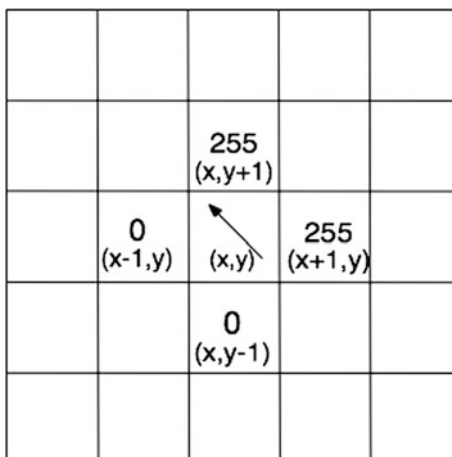


Fig. 3 Basic concept of SVM

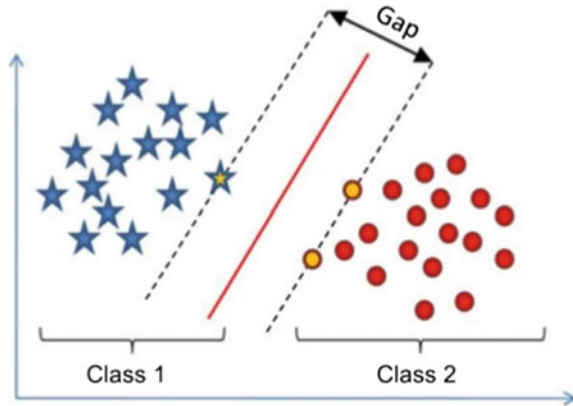
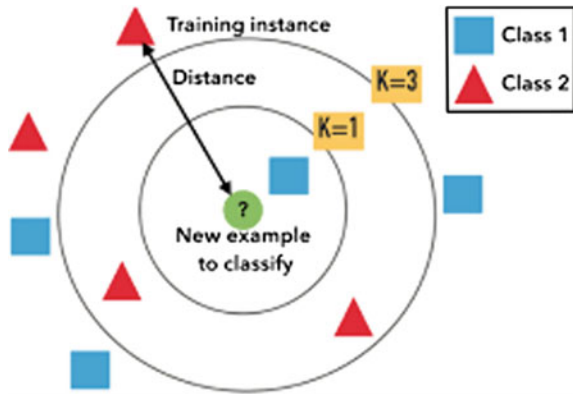


Fig. 4 KNN classifier



3.3 Classification

- i. *Support vector machine classifier*: It is the classifier explained by a separated hyperplane. The training data (supervised-learning) is labeled. Figure 3 shows a basic concept used in SVM classifier.
- ii. *Knearest neighbouring*: KNN is used in classifying objects and does not require parameters. It is the simplest machine learning. Figure 4 shows the KNN classification.
- iii. *Artificial neural network (ANN)*: The artificial neural networks mimic the human body’s nervous system. It consists of three parts—(1) input neuron, (2) hidden neuron, and (3) output neuron. The neural network is used to train the two data and classify them whether they are malignant or not. Figure 3 shows the basic structure of ANN (Fig. 5).

Fig. 5 Structure of ANN

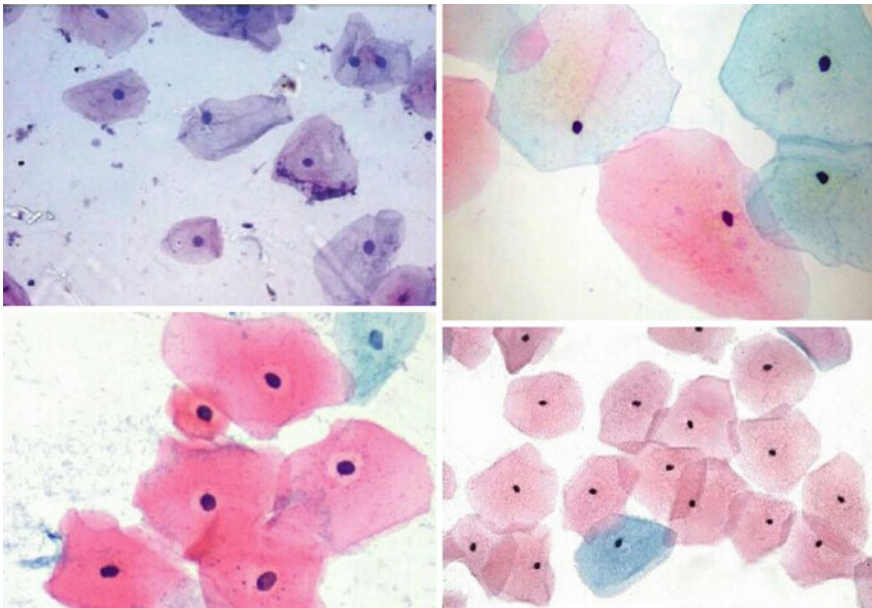
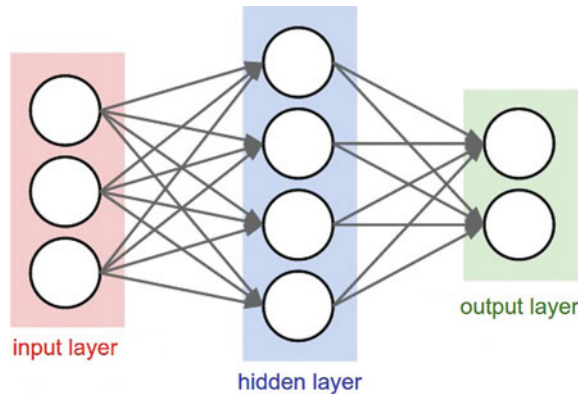


Fig. 6 Normal pap smear

4 Database

The database that is the paps test image of the cancerous and non-cancerous cells was collected from *Air Force Command Hospital, Bengaluru*. Twenty-five normal pap smear cell images and 41 abnormal pap smear images are used. In total, 66 pap smear images of cervical cells are used (Figs. 6 and 7).

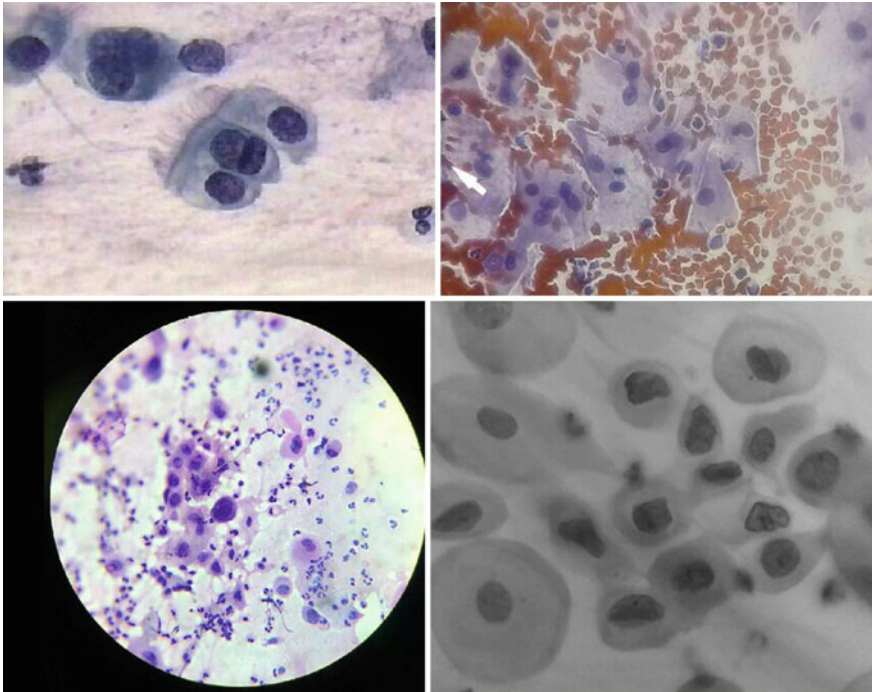


Fig. 7 Abnormal pap smear

Table 1 SVM confusion matrix

$n = 66$	Predicted NO	Predicted YES
Actual NO	TN = 41	FP = 0
Actual YES	FN = 25	TP = 0
Accuracy	TP + TN/total = 41/66	62.12%

Table 2 KNN confusion matrix

$n = 66$	Predicted NO	Predicted YES
Actual NO	TN = 37	FP = 4
Actual YES	FN = 19	TP = 6
Accuracy	TP + TN/total = 43/66	65.15%

5 Experimental Results

Table 1 is the confusion matrix of the SVM classification with accuracy—62.12%.

Table 2 shows the confusion matrix of KNN classifier with an accuracy of 65.15%.

Fig. 8 Npr tool

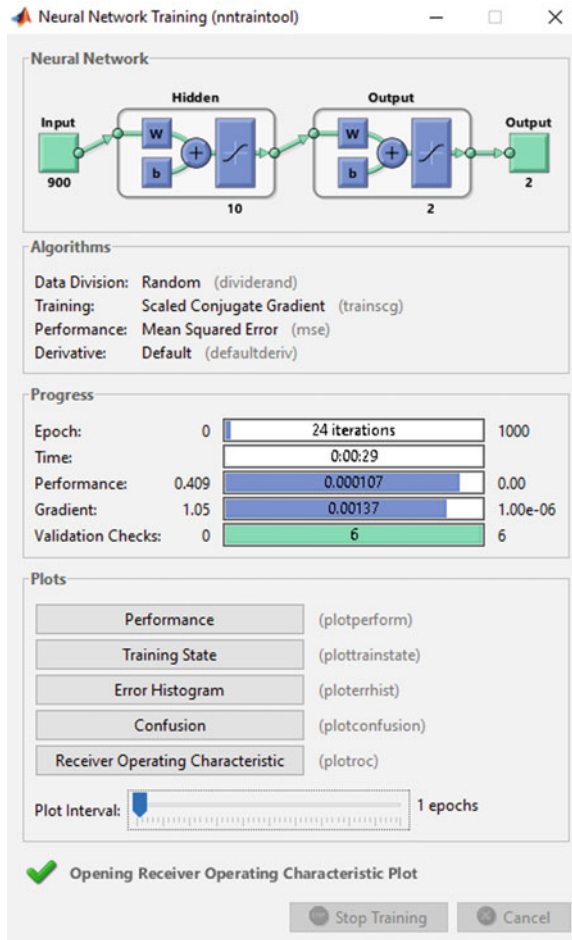


Fig. 9 Performance plot

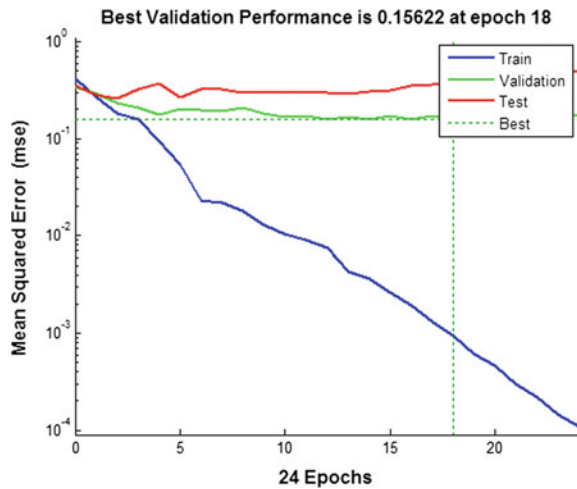


Figure 8 shows the npr tool of the MATLAB. This shows the 900 input layers, ten hidden layers, and two output that is two classes—normal and abnormal.

Figure 9 describes the performance plot of ANN that is the accuracy of train, validation, test, and overall of the dataset that shows the mean square error dynamics (MSE) for all your datasets in logarithmic scale.

Figure 10 describes the training plot. Gradient is a value of back propagation gradient on each iteration in logarithmic scale. Validation fails are iterated when validation MSE increased its value.

Figure 11 shows error histogram plot that visualizes errors between target values and predicted values after training a feed forward neural network.

Fig. 10 Training state plot

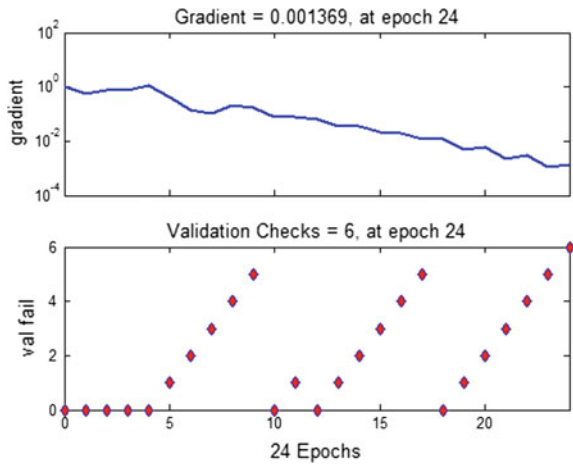
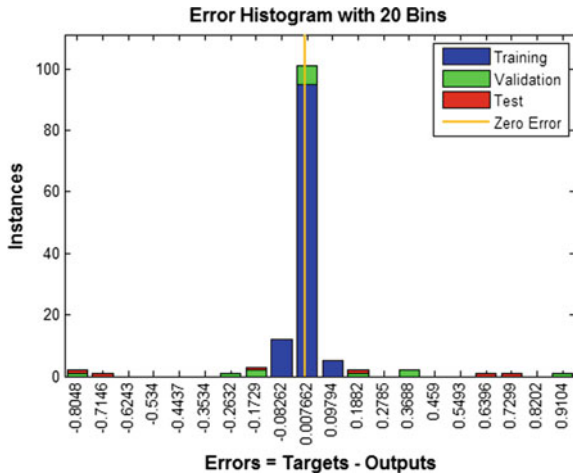


Fig. 11 Error histogram plot



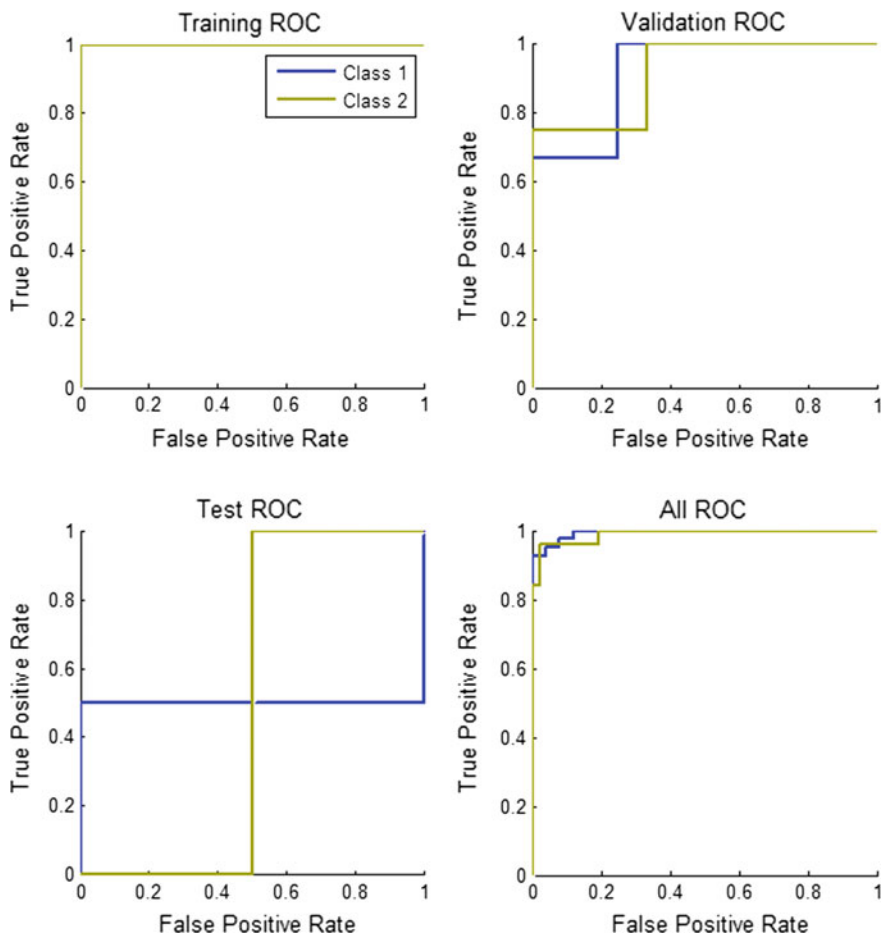


Fig. 12 Receivers operation characteristic (ROC) plot

Figure 12 shows ROC plot that shows the plot of true positive against false positive of classes 1 and 2. In training the accuracy is 100%, in validation the accuracy is decreased, in test it is further decreased but in overall ROC, the accuracy has been increased.

Figure 13 shows the overall confusion matrix with an accuracy of 95.5%.

Table 3 shows the comparison of the accuracy of the classifiers used.

Fig. 13 Overall confusion matrix

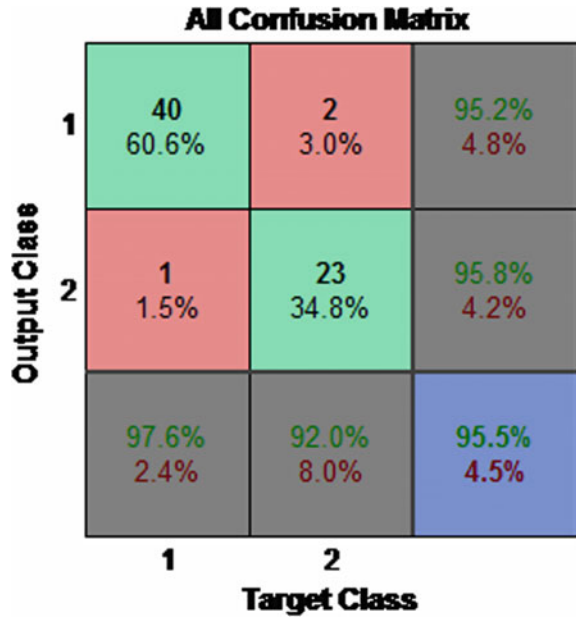


Table 3 Comparison of the accuracy of classifiers

Classifier used	Accuracy (in %)
ANN	95.5
KNN	65.15
SVM	62.12

6 Conclusion

This paper involved the detection and classification of cervical cancer cells. The detection of abnormal and normal cells requires highly qualified pathologists. Detection of cells manually is also a tiresome task. The proposed method is an automated process and improves method for the detection of cervical cancerous cells. The cervical cancer was detected and classified with an accuracy of 95.5%. Table 1 shows the comparison of the three classifiers used. The accuracy of neural network was highest that is 95.5%, second highest was KNN with accuracy of 65.15%, and lastly SVM with an accuracy of 62.12%.

The future work includes the feature extraction of different classes of cancerous cells like ASCUS, ASCH, LSIL, HSIL, and squamous cells and then classifying them using the neural networks. That will be basically grading of the cancerous cells.

References

1. Automated Cervical Cancer Detection through RGVF segmentation and SVM Classification-2015 Intl. Conference on Computing and Network Communications (CoCoNet'15), Dec. 16–19, 2015, Trivandrum, India (2015).
2. Pap smear image analysis for cervical cancer detection-IEEE International Conference on Engineering and Technology (ICETECH), 20th March 2015, Coimbatore, TN, India (2015).
3. Cervical cancer detection and classification using independent level sets and multi SVMs. 2016 39 th International conference on Telecommunications and signal processing (TSP) Debashree Kashyap, Abhishek Somani, Jatin Shekhar, Anupama Bhan, MK Dutaa, Radim Burget and Kamil Riha (2016).
4. A new approach to detect and segment overlapping cells in multi-layer cervical cell volume images Hady Ahmady Phoulady Dmitry B. Goldgof, South Florida, Tampa (2016).
5. International Conference on Communication and Network Technologies (ICCNT) 74 Pattern Recognition: Advanced Development, Techniques and Application for Image Retrieval (2014).
6. HEp-2 Cell Image Classification with Deep Convolutional Neural Networks IEEE International conference of Biomedical and health informatics (2015).

IC Engine-Powered Arial Vehicle for Medical Assistance

Priyal Kumar Sogani, Dushyant Dixit, Rajesh Singh and Anita Gehlot

Abstract The transportation issue is an uncommon kind of direct programming issue where the goal is to limit the cost of distributing a product from various sources or starting points to various goals. In light of its extraordinary structure, the standard simplex technique is not reasonable for taking care of transportation issues. These problems require innovative solution using advanced technology. In case of medical emergencies in remote locations and in hill stations, mobility of medical equipment in shorter time is a challenge. With the existing battery-powered Quadcopters, they have limitations with the payload handling capacity, as well as with their endurance limit. In this work, we will be addressing both mobility problem and the endurance problem using internal combustion engine-powered Quadcopters.

Keywords Alternative fuel (low cost) · Internal combustion engine
Medical assistance · Quadcopter · Transportation

1 Introduction

Heavy consumption of fossil fills and natural debasement has provoked specialists all through the world to look for an appropriate alternative fuel for engine. One such option is to use inexhaustible powers in engine by partial or complete substitution of fossil fuel. In this review, acetylene gas has been considered as an alternative fuel for internal combustion engine, which has grotesque combustion properties [1]. As per a World Bank study, by 2031, somewhere in the range of 600 million individuals are relied upon to live in India's urban areas. Be that as it may, just around

P.K. Sogani (✉) · D. Dixit · R. Singh · A. Gehlot
Department of Electronics Engineering, University of Petroleum
and Energy Studies, Energy Acres, Dehradun, India
e-mail: priyalsogani1996@gmail.com

D. Dixit
e-mail: dixitdushyant.6475@gmail.com

© Springer Nature Singapore Pte Ltd. 2018
R. Singh et al. (eds.), *Intelligent Communication, Control and Devices*,
Advances in Intelligent Systems and Computing 624,
https://doi.org/10.1007/978-981-10-5903-2_156

1503

20 Indian urban communities with populations more than 500,000 have any sort of composed transport frameworks. Since we have seen that because of an absence of current innovations, India is falling behind from different nations. Remembering this, we have composed an idea which is as like as Quadcopter, yet with some real changes. We have seen that it is for the most part utilized as help bot, for military and police divisions for reconnaissance or somewhere in the vicinity, even it is utilized for inquiry and safeguard missions, and so on. Be that as it may, this time we are utilizing Quadcopter idea which can be useful in giving medical assistance. This can make more open doors for Hospitals and Institutions in contacting the concerned individuals. This innovation is as of now being used in some countries, but in India, it is yet to come and we are presenting this innovation at its least expensive way that could be available. So it can without much of a stretch accessible for everybody. For this, we are utilizing acetylene as a fuel in IC engine, and to deliver acetylene, calcium carbide stone and water are utilized.

We are investigating whether the use of unmanned aerial vehicle (UAV) innovation in crisis circumstances would abbreviate reaction time and consequently could enhance patients' result in this covered first stage [2]. Due fundamentally to their mechanical effortlessness, fixed-pitch, battery-fueled multicopters are turning into an undeniably mainstream flying stage for both research and regular citizen exercises. Be that as it may, the flight perseverance of battery-controlled multicopters is for the most part underneath one hour thus of the battery's low vitality thickness, which extraordinarily constrains their useful applications. By introducing a practical and acetylene gas engine, variable-pitch Quadcopter model, this postulation investigates the likelihood to expand multicopter's flight continuance by exploiting petroleum product's high-vitality thickness [3].

2 Use of Acetylene (C_2H_2) [4]

C_2H_2 is the dry gas, having garlic odor introduced from the CaC_2 (calcium carbide), that is gotten from $CaCO_2$ (calcium carbonate). Facilitate the $CaCO_2$ is warmed within the lime heater at around 8250 °C which outlines CaO (lime) liberating CO_2 . CaO is then warmed within the electric-powered radiator with coke (C) to deliver CaC_2 (calcium carbide). Ultimately CaC_2 is hydrolyzed making C_2H_2 . As acetylene is a lackluster gasoline and is tremendously burnable with extra fireplace pace and brief vitality discharge, it may be utilized as choice fuel in ICE. It has a big combustibility variety and minimum start essentialness required for start. in addition differentiating and diverse different gasoline houses, acetylene ended up getting used as a chunk of IC Engine (Table 1).

Table 1 Fuel comparison [5]

Properties of fluid	Acetylene	Hydrogen	Diesel
Chemical representation	C_2H_2	H_2	C_8-C_{20}
Density in kg/m^3 (at STP)	1.092	0.08	840
Autoignition temperature ($^{\circ}C$)	305	572	275
Flammability limits (volume%)	2.5–81	4–74.5	0.06–5.5
LCV (kJ/kg)	48,225	120,000	42,500
Energy of ignition (MJ)	0.019	0.02	–
Lower heating value (kJ/kg)	3396	3399	2930

3 Overview of Project

The procedure we adopt is building a Quadcopter which is powered by ICE which will create more thrust than electric-powered motor for propellers. The fuel which will be used for combustion will be produced by a chemical reaction of calcium carbide stone and water which will produce acetylene gas. This colorless gas is widely used as a welding gas (oxy acetylene). There is a problem which generally comes out while handling C_2H_2 , i.e., when subjected to high temperatures, it changes to benzene to counter that we are going to use ethyl alcohol. For start-up and operation of the motor, two phases are included: First, the motor is begun by auxiliary fuel and after that C_2H_2 can be used as primary fuel. The reaction gives the by-product as calcium hydroxide which can be further used in treating sewage water and thus reusing it. This will generate more thrust. Also we can produce further calcium carbide by reacting calcium hydroxide with carbon in a furnace (Fig. 1).

Using IC Engine will produce torque which can be transmitted to propellers to generate lift. For that, we are adopting chains and shafts mechanism to convert thrust into lift, so that endurance can be enhanced.

A medical kit is kept in a box which prevents it from getting contaminated from foreign particles or pathogens, thus keeping it sterilize. It would be placed over the Quadcopter such that when it reaches to the person in concern, it can be easily accessed. Based on mobile navigation using GPS, medical team can retrieve these vehicles on remote signals (Fig. 2).

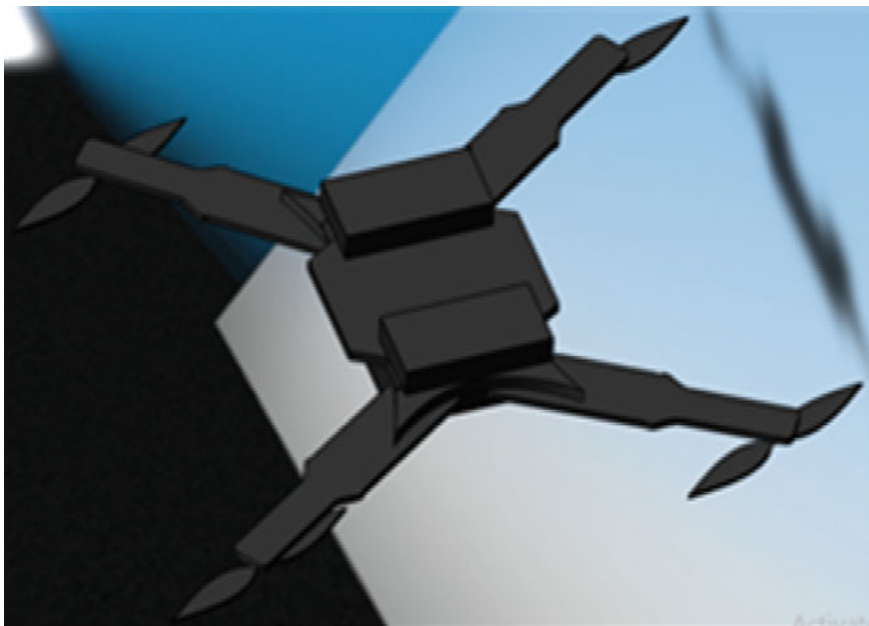


Fig. 1 Quadcopter model

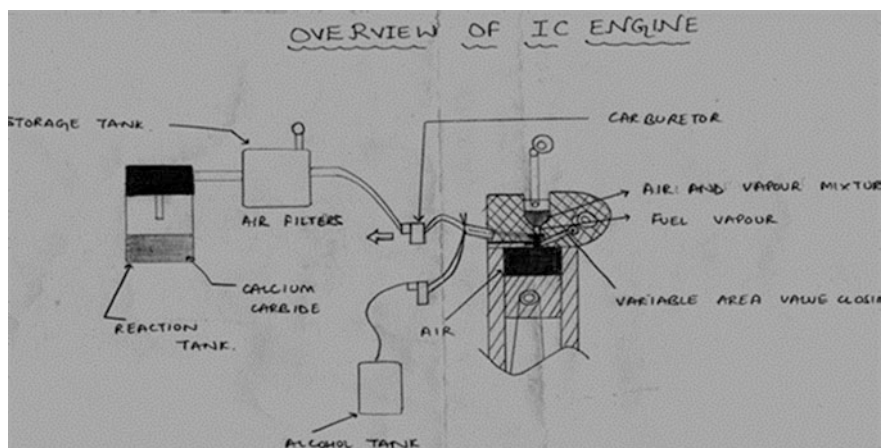
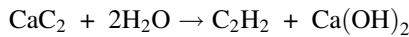


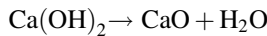
Fig. 2 Engine model [6]

4 Technical Description

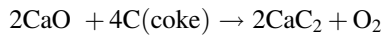
- (1) Design—We are building a Quadcopter and replacing electric motor by a more powerful internal combustion engine (ICE). We are attaching propellers in both sides of it. And also, we are focusing on maintaining the CG (center of gravity) so that our design remains stable while flying. Due to usage of IC engines, we are increasing the overall weight of the Quadcopter. To overcome that we are changing the power-to-weight ratio; thus, it can generate lift.
- (2) Engine—We are using an internal combustion engine (ICE). This works on the concept of combustion of fuel so that we can generate more power. Our engine is attached beneath the front and back sides of our design.
- (3) Fuel—We are using calcium carbide stone as fuel. By reacting it with water, it produces acetylene gas which is colorless gas and is exceptionally flammable with high fire speed and quick vitality discharge [7].



By further reaction of Ca(OH)_2 :



CaO is then warmed in the electric heater with coke (C) to create calcium carbide



We are also using ethyl alcohol as secondary fuel to keep the engine cool. The reaction tank is composed of two chambers:

1. Water is kept in upper chamber in the reaction tank.
2. Calcium carbide is kept in the lower chamber in the reaction tank.

5 Prolog of Auxiliary Fuel

We can demonstrate that presentation of optional fuel is a central bit of this wander as introducing liquor ($\text{C}_2\text{H}_5\text{OH}$ in this venture) decreases the adiabatic fire temperature in the consuming methodology which prompts to keep up a key separation from the auto begin and pounding. The diagram of this wonder is not said here yet rather we can essentially dissect the results from the found out qualities (Table 2).

Table 2 Adiabatic flame temperature comparison [5]

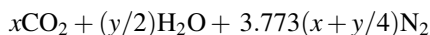
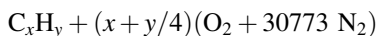
C_2H_2	2908.1	Kelvin
Fossil fuel	2068.9	Kelvin
C_2H_2 with alcohol	2569.5	Kelvin

From consequences we have got, we are able to say that alcohol ought to be acquainted so that to decrease the temperature in ignition chamber. For start-up and operation of the engine, two stages are integrated: First, the engines are started with the aid of assistant fuel (use of ethyl in right here). After a few heat-up period, the second stage carries working the engine with the aid of the usage of fundamental gasoline (acetylene) to make manage yield from the engine.

6 Thermodynamic Evaluation of System

6.1 Stereochemistry Fuel/Calculation for Air Ratio

The combustion equation is given below



$$\begin{aligned} (A/F)C_2H_2 &= (1 + Z/4)(32 + 3.773 * 28.16) / (12.011 + 1.008z) \\ &= 13.28 \quad (z = 1) \end{aligned}$$

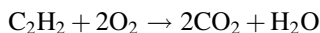
$$\begin{aligned} (A/F)C_8H_{14.96} &= (1 + Z/4)(32 + 3.773 * 28.16) / (12.011 + 1.008z) \\ &= 14.61 \quad (z = 1.87) \end{aligned}$$

6.2 Correlation of Greatest Valuable Work of Acetylene and Gasoline

$$\Delta W_{\text{umax}} \leq -(\Delta H - T\Delta S)$$

$$\Delta W_{\text{umax}} \leq -(H - TS)_{\text{PTA,PA}} - (H - TS)_{\text{RTA,PA}} = (\Delta G)_{\text{TA,PA}}$$

Presently, for the computation of Gibbs free energy of the acetylene for complete combustion, i.e., for identicalness proportion ($\phi \leq 1$), we have the followings.



$$(\Delta G)_{\text{TA,PA}} = (-2 \times 394,360 - 228,590 - 209,170) = 43.326 \text{ MJ/kg}$$

$$((\Delta G)_{\text{TA,PA}})_{\text{gasoline}} = -45.7 \text{ MJ/kg.}$$

7 Environmental Aspects [8]

Depletion of Ozone Layer [Photochemical Ozone Creation Potential (POCP)]

In spite of anticipating a cautious part of the stratosphere, at ground-level ozone is named a hurting take after gas. Photochemical ozone period inside the troposphere, via and large known as summer season cocoa shadowiness, is suspected to underhandedness plant life and material. High centralizations of ozone are risky to humans. Radiation from the Sun and the closeness of nitrogen oxides and hydrocarbons comfy complex substance responses, making severe reaction matters, certainly one of that is ozone. Nitrogen oxides by myself do not apprehend high-ozone fixation tiers. Here is a portion of the examinations of POCP among or three mixes.

The accumulated discharge fluctuates significantly in accordance with the structure of fuel. Mainly this expansive variety has two elements, i.e., reactivity and dissemination.

8 Conclusion and Future Scope

Conclusion This project concludes that engine-powered Quadcopter can be more efficient in terms of stability, endurance and performance when compared to battery-powered Quadcopters, whereas using acetylene can be a good fuel with some safety and control measures that are accounted in gas, precautions involved in gas-phase reaction can cause severe damage.

Future Scope of Proposal

1. This can be used in military operations.
2. In future, it can also be used in accidental relief drone ambulance.
3. It can be used in natural disasters for providing first aid and basic requirements.
4. After a bit of modifications and changes, it can even be used for surveillance.

References

1. Lakshmanan, T., and G. Nagarajan. Experimental investigation on dual fuel operation of acetylene in a DI diesel engine. *Fuel processing technology* 91.5 (2010): 496–503.
2. Young, A., Itzoe, M., Fenton, E., Kucharski, K., Ottoman, P., Clauss, G., Novi, B., Gifford-Hollingsworth, R., Baron, J. and Panchal, C., (2016). Application of Unmanned Aerial Vehicles in Emergency Medical Situations.
3. Tao, P. Design, Prototyping and Autonomous Control of Gasoline-engine Variable-pitch Quadcopter. Diss. 2016.
4. Process of producing carbides and making acetylene therefrom. U.S. Patent 1,996,185, issued April 2, 1935.

5. Sharma, P. K., Kuinkel, H., Shrestha, P., and Poudel, S. (2012). Use of Acetylene as an Alternative Fuel in IC Engine. *Fuel*, 2(H2), C8–C20.
6. Heywood, J. B. *Internal Combustion Engine Fundamentals*, McGraw-Hill, Inc., New York, 1988.
7. Wulff, J., Hulett, W., Sunggyu, L., *Internal combustion system using acetylene fuel*. United States Patent No 6076487.
8. Chigier, N (1981) *Energy, Combustion and Environment*, McGraw Hill.

A Critical Study on Role of Sensor-Based Electronic System for Toxic Gas Identification in the Mining (Coal) Industry

Vishal Sharma, Taksh, Kritarth Srivastav, Priyam and Nihal Anwar Siddiqui

Abstract Mining sector is one of the most vulnerable and hazardous places to work and has constant risks for both human and environment. Due to the presence of various perils, this sector is also prone to various disasters. Every year as the mines are subjected to regular removal of earth resources, the risks for miners, workers, and environment become grave. As there is the presence of toxic gasses such as methane, hydrogen sulfide, sulfur dioxide, therefore, the safety of miners plays an important concern. Therefore, the role of sensors/detectors to detect the concentration of gasses and to make the workplace fit for job becomes the challenging concern for the authorities. This review paper evaluates the present scenario and application of sensors/detectors to detect toxic gases in the mines and to study the dangers and adverse situation which resulted into disasters in past and could be controlled in future by the application of the latest technology in the field of sensors.

Keywords Hazardous place · Toxic gases · Sensors/detectors · Mining · Risk

V. Sharma (✉) · Taksh · K. Srivastav · Priyam · N.A. Siddiqui
University of Petroleum and Energy Studies, Dehradun, India
e-mail: vishalsharma7r@gmail.com

Taksh
e-mail: takshgupta112@gmail.com

K. Srivastav
e-mail: ks5196667@gmail.com

Priyam
e-mail: priyamkaushal46@gmail.com

N.A. Siddiqui
e-mail: nihal@ddn.upes.ac.in

1 Introduction

Country's economy is directly or indirectly linked with its natural resources such as agriculture, forestry, fisheries, and extraction of mineral through mining. Safety is one of the most important aspects, which if ignored can have major impact not only on country's economy but also on workers and the environment [1]. Since safety is one of the most important factors concerning underground coal mine industries so in order to overcome such type of accidents, mining industries should follow basic precautions and rules [2]. To avoid risks and hazards, safety communication is the important tool for an industry today in order to control risk situations and take necessary steps to overcome situations accordingly [3].

The largest coal-producing countries account for over 81% of total world coal production, and nearly about 92% of hard coal is produced by China, India, South Africa, Russia, Ukraine, USA, Australia, Poland, Kazakhstan, Indonesia. The top producers such as China, USA, and India account for over half of global hard coal production [4]. In a queue of toxic or poisonous gases, H₂S and CO are the commonly found gases in underground coal mines. There are different TLVs (Threshold Limit Values) for various mine gases in which a miner can work safely up to a certain duration which has been set by different safety committees of organizations such as OHSAS, DGMS [5]. The distribution of coal production worldwide in 2015 by country is as follows.

2 Some of the World's Worst Record Coal Mining Disasters

2.1 *Benxi Hu Colliery Disaster, China, 1942*

The disaster in the city of Benxi Hu Colliery in China which cost 1,547 lives is considered to be the worst coal mining disaster. The disaster occurred on April 26, 1942, in the Honkeiko mine, located near Benxi in the Liaoning city of China. The day before the explosion, fire was detected around 274 m underground in the Cecil pit. In order to strive the fire pit was closed. A huge explosion emanated from the still-smoldering fire at the pit and caused a blast on the surface which resulted in the killing of disaster [6].

2.2 *Dhanbad Coal Mine Disasters, India, 1965 and 1975*

The coal mine disaster was recorded in the city of Dhanbad on the night between 27 and 28 May. The disaster occurred in Dhori colliery near Dhanbad killing 376 miners according to the government record. On December 27, 1975, disaster took

place in the Chasnala colliery, Dhanbad, after 10 years to the previous one which killed 372 people [7].

2.3 Coal Brook Mine Disaster, South Africa, 1960

The coal brook mine disaster which took away life of 435 people is the worst disaster in South African history. The above examples taken from review paper are concerned regarding the safety aspects related to underground or subsurface mining processes, which is considered to be the most hazardous activity and may cause emission of toxic gasses, fire and might lead to explosion, if proper ventilation is not taken into account. The above scenario relevance is essential for studying the role of sensors and detectors which if used in now-and-then situation could have been beneficial for averting the present and future disaster scenario [8].

3 Causes of Mining Accidents/Disasters

The major causes of accident in mining are mine collapse, emission of toxic gases, and fire in which toxic gas emission is the leading cause in underground mining. There are various disasters reported as mentioned in Table 1, due to toxic gas emission which has adverse effect on miner's health or even death of miners and has environmental impact too. The common gases which are found in the underground coal mines are oxygen (O_2), carbon monoxide (CO), methane (CH_4), carbon dioxide (CO_2), hydrogen sulfide (H_2S), and nitrogen (N_2). Concentration of all of the above-mentioned gases plays an important role [9]. The optimum concentration of these gases decides the extent or degree to which a miner is exposed and up to what duration the worker is exposed.

According to mining laws in India, mine air should contain minimum 19% of O_2 . This minimum limit is 20% in Russia and 19.5% in USA [10]. Similarly, as

Table 1 Distribution of coal production and major accidents worldwide in 2010 [25]

S. No.	Producer country	Hard coal (Mt)	Brown coal (Mt)	Date of accident	Name of coal mine	No. of fatality
1	China	1348	Nil	Feb, 14, 2005	Sunjlawan, haizhou shaft, Fuxin	214
2	USA	909	79	Jan 2, 2006	Sajo, West Virginia	12
3	India	310	23	June 15, 2005	Central Saunda	14
4	Kazakhstan	70	3	Sept 20, 2006	Lenina, Karaganda	43
5	Russia	157	85	March 19, 2007	Ulyanovskaya, kemerovo	108
6	Ukraine	71	5	Nov 19, 2007	Zasyadko, donetzk	80

nitrogen is an inert gas, it has no participation in metabolic functions of human body. When any worker works at pressure higher than atmospheric pressure, the blood and tissues of the body begin to absorb nitrogen. But if the high pressure is abruptly reduced, the nitrogen is given up by the body quickly and thus results in pain and this dangerous condition is referred to as compressed air illness (CAI) which is most commonly observed in workers working in depth. Therefore, role of sensor/detectors and reliable communication systems are essential to overcome the above-stated problem [11].

4 Methane—The Fire Damp

Methane found in underground coal mines are coal mine methane (CMM) or coal-bed methane (CBM). The trapped methane is generally produced during coalification inside the earth strata, and only a fraction of such gases remains bounded under pressure in the coal seam [12]. Coal mine methane (CMM) has always been considered as a dangerous situation for coal miners and engineers as it can create a serious threat to safety and production of mine goods which may cause fire and explosion risk that is why it is commonly known as firedamp in mining areas. Also, methane is about 21 times more potent than carbon dioxide and hence contributes to greenhouse effect and has major environmental impact [13].

4.1 Impact of Methane, H_2S

It is observed that in a coal mine ventilation air contains 0.2–0.9% methane, and also, gas drained before mining contains 61–94% CH_4 depending on the presence of gasses in the coal seam. Gas drained from fractured formations above mined seams (GOBS) may contain 31–96% methane depending on the locations. It is observed that ventilation air methane (VAM) which is the part of shafts in mines results to the emission of 65%. The main reason is found in underground coal explorations. As the mines are mined deeply, the concentration of methane changes [14]. Past records show that there have been many fatalities in coal mine leading to explosions in which CH_4 was one of the factors. Table 1 gives the major mine explosions (USA, 2010) [15].

H_2S is produced when coal containing sulfur is heated with air to a temperature of about 443 °C. H_2S is combustible and does not support combustion, when mixed with air form an explosive mixture. In metal mine, it may be produced by the action of acidic water on sulfide ore. Thus, H_2S gas is very poisonous, and it may cause death in a short time if it is heated in large quantities. The maximum permissible concentration for H_2S (TWA) in room for 8-h exposure is given as 0.02% [16].

Carbon monoxide is very poisonous gas, and its affinity for the hemoglobin of the blood is nearly 300 times that of oxygen. Even if the small quantity of CO is

Table 2 Percentage of CO in surrounding and its health impacts

S. No.	% age of CO in air	Health effect
1	0.02	Headache, discomfort, and possibility of collapse after 45 min at work or 2 h at rest
2	0.12	Palpitation after 10 min at work or 30 min at rest
3	0.2	Unconsciousness after 10 min at work or 30 min at rest
4	0.5–1.0	Death after 10–15 min of work

Table 3 Different mine gases

Name of gas	Common name	Source or cause where found	Effect on life	Explosive	Combustible	Remarks
Carbon dioxide (CO ₂)	Black damp	Respiration of men and animals; fire	May displace O ₂	No	No	TWA(TLV)—0.05% or 500 ppm
Carbon monoxide (CO)	White damp	Incomplete combustion, blasting	Poisonous	Yes	Yes	TWA(TLV)—0.005% or 50 ppm
Nitrogen (N ₂)	Nitrogen	Normal constituent of air	Will not support life	No	No	78% of air
Oxides of Nitrogen (N ₂ O, N ₂ O ₅)	Oxides of nitrogen	Blasting fumes, diesel exhaust	Toxic; causes edema in lungs	No	No	TWA(TLV)—0.0005% or 5 ppm
Methane (CH ₄)	Fire damp	Decaying plants or animals; coal seam	No harmful effect with O ₂ present	Yes	Yes	Expl. Range: 5–15% TWA(TLV)—0.10% or 1000 ppm
Oxygen (O ₂)	Oxygen	Atmosphere	Essential to life	No	No	Supports combustion
Hydrogen sulfide (H ₂ S)	Stink damp	Decomposition of sulfur ores	Paralyze the respiratory system	Yes	Yes	Expl. range: 4.3–4.5%, TWA (TLV)—0.001% or 10 ppm

inhaled which is present in air, then it is difficult to absorb a required quantity of oxygen to survive because carbon monoxide forms a stable compound (i.e., carboxyhemoglobin) when reacts with hemoglobin. In underground coal mine, miner may not know that he/she is inhaling CO unless he/she is equipped with CO detecting devices, and it may result in serious health impacts and even death (Table 2).

The production of CO in a mine may be due to any one or more of the following causes are oxidation of coal and other carbonaceous matter, explosives, spontaneous combustion, methane and coal dust explosion and underground machinery (Table 3).

Factors Responsible for Gas Emission (Commonly Methane) in Underground Coal Mine are

- (1) Pressure change in atmosphere of underground mines.
- (2) During washing and machinery work.
- (3) During ventilating current.
- (4) During roof control (roof bolting).
- (5) Coal rank, coal seam depth.
- (6) Other geological factors such as earthquake and natural disasters.

5 Present Methodologies for Detection of Various Mine Gases

The detection of gases is an integral part of safety system especially when it is linked to an industry such as mine. Detection of these gases is usually governed by the various gas sensors that detect these gases within a particular range of concentration and at a particular area. An electrical response is given by the sensors which are proportional to the concentration of the above-mentioned gases to be detected followed by the alarm when the concentration of these gas levels increases the threshold concentration limit to the close personnel which may activate such preventive actions such as increasing the ventilation, switching off the power supply etc. (Table 4).

Table 4 Different methods for detecting various mine gases (present)

Name	Detectors	Method of detection
Oxygen (O ₂)	O ₂ detector (OXD-2 M), flame safety lamp	Electrochemical, flame lamp
Methane	Methanometer, flame safety lamp	Catalytic oxidation, flame lamp
Carbon dioxide	Multi-gas detector	Optical, infrared
Carbon monoxide	P.S detector, dragger multi-gas detector	Electrochemical, catalytic oxidation, infrared
Sulfur dioxide	Multi-gas detector	Electrochemical, infrared
Oxides of N ₂	Multi-gas detector	Electrochemical
Hydrogen sulfide	Rotten egg odor, Multi-gas detector	Electrochemical, semiconductor

5.1 *Electrochemical Sensors*

These sensors are devices which have cathode, an anode, and electrolyte. The components of the cell are worked upon so that the gas which has to be detected is allowed to diffuse into the cell, causing chemical reactions and generating current. An example of electrochemical gas detector/sensor is the oxygen detector model OXD-2 M which is manufactured by Uptron of Lucknow, is a compact handheld instrument, designed to indicate oxygen deficiency, and incorporates an audible alarm which operates automatically if oxygen level falls below a preset point [17].

Advantage: The electrochemical gas detectors/sensors are used to detect the majority of commonly known toxic gases such as CO, H₂S, Cl₂, SO₂. They can identify particular gas or vapors present in the nearby vicinity. They are typically very accurate and reliable, have fast response and low power, and measure toxic gases in relatively low concentration [18]. **Disadvantage:** The electrochemical gas sensors/detectors have a narrow range of temperature and a short shelf life; they are subjected to various interfering gases, e.g., hydrogen. Sensor lifetime is shortened in very dry and hot areas. It has narrow pressure range and not 'fail-safe' [19].

5.2 *Catalytic Oxidation Sensors*

Mixtures of combustible gases may not burn until they reach an ignition temperature. But in the presence of chemical media, the gas will start to burn or may ignite at lower temperatures and this phenomenon is known as catalytic combustion. In this type of sensor, there is a coil of wire which is coated with ceramic material or glass and with a catalyst. The coated coil is electrically heated to a temperature that will allow it to burn or to catalyze combustible hydro-carbon (CHC) gas being monitored. **Advantage:** It is simple, robust, and inexpensive.

Disadvantage: Sensor Poisoning: Studies conclude that tetraethyl lead, silicon, and sulfur compounds show most poisonous nature in industrial sector which can permanently reduce the quality, performance, and sensitivity of the sensors and are not easily trackable. **Sensor Inhibitors:** The widely noticed inhibitors which are present in mines are H₂S, chlorine, chlorinated hydrocarbons, and halogen compounds [20]. They cause an unnoticed loss of sensitivity to sensor and can recover in the presence of fresh air so that they may perform effectively. **Sensor cracking:** This phenomenon is noticed in the system when sensor is exposed to high level of concentration of gasses, excessive rise in temperature, and other oxidation processes which can take place on the surface of the sensor which then affects the quality and performance of the sensor. **Infrared Gas Sensor:** It is studied that gas molecules are made up of a number of atoms which are clanged together and are of various similar masses. They vibrate with a fixed frequency called natural frequency. The infrared radiations detect and vibrate with the same frequency similar to natural frequency of the molecules. The gas molecules absorb the infrared

radiations, and the molecules gain energy and vigorously vibrate in their positions. Due to the continuous vibrations, there is an increase in temperature which is then detected by the sensor [21]. The basic principle behind infrared detectors is to convert electromagnetic radiation energy and frequent changes in temperature into electrical signals. **Advantage:** The sensor is not affected by contamination and immune to fail-safe operations, and there is no problem with routine calibration and can be operated in the presence of other non-similar gasses. **Disadvantage:** IR sensors are unable to detect some combustible gases like hydrogen. The sensors' performance is affected by humidity and water. The optics of the sensors can be coated by dust and dirt which impairs its performance. **Multi-Gas Detector:** These detectors can be used to detect various types of mine gases using different chemicals in certain different tubes. The change in color of these chemicals indicates a particular type of gas present, and its concentration is determined by the extent of color change. **Advantage:** Various mine gases can be detected. **Disadvantage:** Chemicals in these tubes need to be filled after the use, and life of these tubes is only 2 years. It is time taking; i.e., the whole operation takes about one to two minutes.

6 Need for Modern Technologies

There are various other types of detectors based on different principles which are not so efficient and accurate to detect all the types of mine gasses and are unable to measure the appropriate concentration of the toxic gasses which is the important challenge for the mine industries in terms of safety aspect for the workers working underground or undersurface, and there are various occupational health-related hazards associated with them. Hence, there is a need of latest technologies that could help to reduce human effort and discomfort and can detect these toxic gases before even entering into the tunnels or confined areas where it is quite difficult for the men to enter.

6.1 *About Wireless Controlled Detecting/Sensing System in Mining Industries (The Modern Technology)*

Apart from the present detection technique of various toxic gas releases in mine areas such as explosion of methane, there are several other parameters which must be taken into consideration in order to enhance the safety and productivity in mines. These parameters inside underground coal mines include sudden rise in temperature which may cause fire, increasing humidity which causes uneasiness to the miners working there or sometimes vibration will occur due to landslide or due to some other machinery work in mine areas. Therefore, it is necessary to have a continuous

detecting/sensing system between the workers moving in mines and a fixed station or a control room, which can detect all the necessary parameters in order to create a safe working environment in mine industries.

For successful wireless communication system/detection system and the data transmission, **ZIGBEE** can be properly utilized. It can sense/detect temperature, humidity, fire, gas, as well as vibration inside mines [21]. The modern wireless safety detection/sensing system is divided into two section: One is the transmission section, and other is the receiver section [22]. The transmission section is mounted on a wireless robot which will be in the underground mine and with the help of wireless communication protocol **ZIGBEE**; it will send the necessary data to the receiver section which will be in control room where the analysis of data is done and the necessary action is taken according to it.

The transmitter section consists of a sensor network which senses the respective environmental parameters and gives to microcontroller for further operation. This sensing operation can be made in a specific time intervals according to the need.

Transmitter section (which is mounted on a robot) consists of microcontroller, temperature sensor, humidity sensor, gas sensor, camera, bulb, buzzer IC driver, **ZIGBEE** transceiver [23]. On the wireless robot, wireless camera transmitter is mounted nearby the bulb which will give a live view of underground coal mine [24].

7 Future Scope

The use this modern wireless detection/sensing technology can be utilized to take a initial preventive action against the landslide or damage to miner due to some other reasons such as roof fall and will help to locate the trapped miners in case of rescue operation. This technology is cost-effective and efficient than the present used technologies of detectors/sensors.

With the help of this latest technology, we can identify the toxic as well as inflammable gas emissions using different sensors installed on the wireless robot, as the entire process is automated which requires very less human interactions.

8 Conclusion

There is a growth of fatalities and accidents in mines which are caused due to the release of toxic gasses. As listed, there is a presence of toxic gases in mines, namely carbon dioxide (CO_2), hydrogen (H_2), hydrogen sulfide (H_2S), oxygen (O_2), methane (CH_4), nitrogen (N_2), nitrogen dioxide (NO_2), sulfur dioxide (SO_2), which are not only toxic and problematic to miners but also their release is dangerous. These toxic gases are the major concern for the authorities, and to deal with this problem, innovative techniques such as the use of sensors and detectors can be

helpful to trace, check, and analyze the air quality inside the mines so that working conditions may be improved and safety is ensured. The air quality is the major concern inside the mines and proper ventilation, and uses of PPE (personal protective equipment) are the ways to control the effects of toxic gases. The uses of sensors and detectors therefore are important not only for the detection of toxic gases but also to have data of its release and to map the areas in the mines so that proper preventive and engineering controls shall be implemented. The modern wireless detection/sensing system which is studied and analyzed throughout the review paper will be helpful in safeguarding the inhalation of toxic gasses and will prevent the working of miners in the highly hazardous area as this system is reliable and cost-effective than the presently used sensors which require lots of maintenance. This modern system also reduces the human intervention due to use of wireless robot which is operated from control room. This system is best solution for the complex mine environment as it will consume low power, low cost of ZIGBEE transmission which has the high frequency of data transmission technology with small-size sensors. This system will also provide the proper communication between the control room and underground workers which will further contribute to reduce accidents. Surveillance by these systems will also pave the way for effective safety and protection in mines. In India, we need to implement such systems which could improve present scenario and could laid down foundation for safety not only for engineers and miners but for the contract and indirect labors.

References

1. Paul, P. S., & Maiti, J. (2007). The role of behavioral factors on safety management in underground mines. *Safety Science*, 45(4), 449–471.
2. Laurence, D. (2005). Safety rules and regulations on mine sites—the problem and a solution. *Journal of safety research*, 36(1), 39–50.
3. Pandit, Vaibhav, and U. Rane. Coal mine monitoring using ARM7 and ZigBee. *Int J Emerg Technol Adv Eng* 3.5 (2013): 352–9.
4. Irving, W., & Tailakov, O. (1999). CH₄ Emissions: Coal Mining and Handling. *Good Practice Guidance and Uncertainty Management in National Greenhouse Gas Inventories*.
5. Ruth, J. H. (1986). Odor thresholds and irritation levels of several chemical substances: a review. *American Industrial Hygiene Association Journal*, 47(3), A-142.
6. Dhillon, B. S. (2010). *Mine safety: a modern approach*. Springer Science & Business Media.
7. Choubey, V. D. (1991). Hydrogeological and environmental impact of coal mining, Jharia coalfield, India. *Environmental Geology and Water Sciences*, 17(3), 185–194.
8. Van der Merwe, J. N. (2006). Beyond Coalbrook: what did we really learn? *Journal of the Southern African Institute of Mining and Metallurgy*, 106(12), 857–868.
9. Kuenzer, C., Zhang, J., Tetzlaff, A., Van Dijk, P., Voigt, S., Mehl, H., & Wagner, W. (2007). Uncontrolled coal fires and their environmental impacts: Investigating two arid mining regions in north-central China. *Applied Geography*, 27(1), 42–62.
10. Deshmukh, D. J. (1985). *Elements of mining technology*. Vidyasewa Prakashan.
11. Hendryx, M. (2009). Mortality from heart, respiratory, and kidney disease in coal mining areas of Appalachia. *International archives of occupational and environmental health*, 82(2), 243–249.

12. Irving, W., & Tailakov, O. (1999). CH₄ Emissions: Coal Mining and Handling. Good Practice Guidance and Uncertainty Management in National Greenhouse Gas Inventories.
13. Lawrence, N. S. (2006). Analytical detection methodologies for methane and related hydrocarbons. *Talanta*, 69(2), 385–392.
14. Hartman, H. L., Mutmansky, J. M., Ramani, R. V., & Wang, Y. J. (2012). Mine ventilation and air conditioning. Wiley.
15. Karacan, C. Ö., Ruiz, F. A., Cotè, M., & Phipps, S. (2011). Coal mine methane: a review of capture and utilization practices with benefits to mining safety and to greenhouse gas reduction. *International Journal of Coal Geology*, 86(2), 121–156.
16. Deshmukh, D. J. (1985). Elements of mining technology. Vidyasewa Prakashan.
17. Stevens, B. (1971). U.S. Patent No. 3,612,866. Washington, DC: U.S. Patent and Trademark Office.
18. Becker, W. J., Breuer, W., & Deprez, J. (1977). U.S. Patent No. 4049503. Washington, DC: U.S. Patent and Trademark Office.
19. Takeuchi, T. (1988). Oxygen sensors. *Sensors and Actuators*, 14(2), 109–124.
20. Kumar, A., Kingson, T. M. G., Verma, R. P., Mandal, R., Dutta, S., Chaulya, S. K., & Prasad, G. M. (2013). Application of gas monitoring sensors in underground coal mines and hazardous areas. *International Journal of Computer Technology and Electronics Engineering*, 3(3), 9–23.
21. Yokura, H., Suzuki, Y., & Yoshida, T. (2004). U.S. Patent Application No. 11/019,261.
22. Zhang, Y. P., Ng, T. S., Sheng, J. H., & Zheng, G. X. (2002). A hybrid model for propagation loss prediction in tunnels. *Chinese Journal of Electronics*.
23. Chaamwe, N., Liu, W., & Jiang, H. (2010, August). Seismic monitoring in underground mines: A case of mufulira mine in Zambia: Using wireless sensor networks for seismic monitoring. In *Electronics and Information Engineering (ICEIE), 2010 International Conference On* (Vol. 1, pp. V1–310). IEEE.
24. Kinney, P. (2003, October). Zigbee technology: Wireless control that simply works. In *Communications design conference* (Vol. 2, pp. 1–7).
25. Jinke, L., Hualing, S., & Dianming, G. (2008). Causality relationship between coal consumption and GDP: difference of major OECD and non-OECD countries. *Applied Energy*, 85(6), 421–429.

Companding-Based Technique to Improve Signal to Noise Ratio and Power Dissipation in Analog to Digital Convertor Operating at CTDSP

Anustha, Mahima Gupta, Haneet Rana and Gagan Minocha

Abstract Continuous-time digital signal processing form supports for study and investigation of parameters involved in the analog to digital conversion. The parameters to be improvised are particularly signal to noise ratio and power dissipation. Analog to digital convertors are the backbone of digital world, hence, there is a need to look up on discoveries and researches for the best possible results. With this in consideration, this paper presents a technique to improve the above-mentioned parameters. A 1000 Hz window has been considered for the outcomes of PD. The methodology involves the comparison of SNR and PD in quantization and companding. An in-depth analysis was performed, both forms of uniform quantization were considered which are mid-tread and mid-rise, same is the case with companding as well, A-Law and μ -Law companding techniques were taken into account and best possible results were obtained. Validation was done by accessing and optimizing the outcomes present till date.

Keywords Analog to digital convertor · Quantization · Companding

1 Introduction

Continuous-time digitally processed signals allow for well-ordered outcomes without sampling, thereby producing no aliasing and significant reduction in quantization error. The quality of outputs of analog to digital convertors has a high

Anustha (✉) · M. Gupta · H. Rana · G. Minocha
Electronics & Communication Engineering, Amity University, Noida, Uttar Pradesh, India
e-mail: anushtha212@gmail.com

M. Gupta
e-mail: mahima.gupta07@gmail.com

H. Rana
e-mail: hrana1@amity.edu

G. Minocha
e-mail: genuminocha@gmail.com

correlation with the ability to attain optimized values of signal to error ratio and power dissipation. Recently, continuous-time digital signal processing has gained traction in the quest to find determinants of the mentioned parameters. Yannis Tsvidis [1, 2] has studied that continuous-time operations make possible to evade the aliasing and quantization error altogether because of the association of minimal number of bits for a given signal to noise ratio. C. Vezyrtzis, B. Schell, and Y. Tsvidi [3, 4 5] in their another piece of work have mentioned the techniques for straightforward quantization without the inevitability of intermediate step that is sampling counting level crossing. In achieving this objective, companding-based technique is relevant to optimize the value of power dissipation as well.

2 Quantisation

We have considered as a prototype a transversal analog signal and analyzed its fallout when fed to an uniform quantizer making an allowance for both its forms which are mid-tread and mid-rise. The later does not have zero as a possible value of the signal to error ratio output value as can be seen in Fig. 1. The minimum output for the same has to be half the magnitude of step size, further this quantizer always produce an output breakup of at least 1 bit per sample, if the input data is modeled as a random variable with a probability density function that is proportionate around zero, while, the former quantizer do have a zero output level (Fig. 2) that can reach momentarily low bit rates per sample for input distributions which are proportionate and taper off at higher magnitudes. For few applications, to have a zero output signal representation and to support low output breakup is a necessity. In these cases, using a mid-tread uniform quantizer may be well suited or relevant than using a mid-riser.

Fig. 1 Error in case of mid-tread quantization

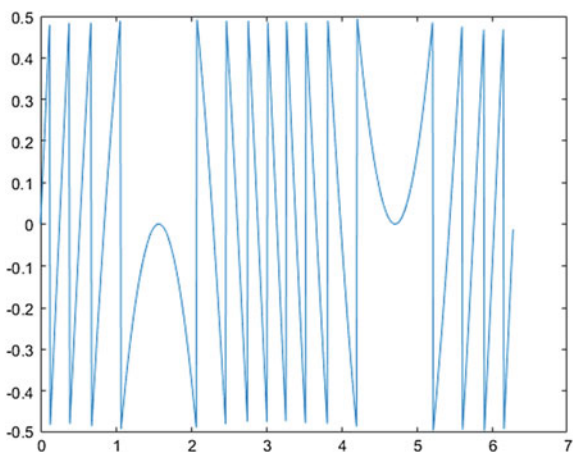
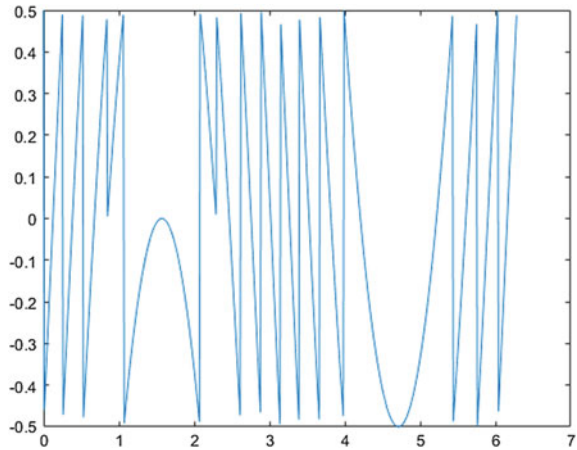


Fig. 2 Error in case of mid-rise quantization



3 Companding

Compressor being a non-linear device contracts the peak amplitudes by surpassing the non-uniform quantized signal through the compressor to acquire uniformity; uniform quantizer employed executes over the signal, and hence non-uniform zones at input correspond to uniform zones at output. The tapered or contracted signal so obtained is passed through expander which is another non-linear device at the receiving end which abolishes the non-linear effect of compressor. Thus, the combination of compression and expansion throughout signal processing is termed as companding. Further seizing into details of the above technique (i.e., compression and expansion) there are two types of it extensively in use worldwide, A-Law and μ -Law companding. This technique also reduces and constricts the bandwidth requirement of the system as companding may decrease the required code word length to 8 bits or less.

3.1 A-Law and μ -Law

A-Law and μ -Law have significantly analogous error introduced in the process, but their results vary in terms of power dissipations. A window of 1000 Hz has been analyzed for deciphering this outcome. In A-Law, the peak to average power ratio (PAPR) experiences a discomfiture which embroider the signal to error ratio, hence the quality of signal. The power intemperate while analog to digital conversion has also been examined using one of the non-parametric approach, i.e., periodogram. This approach has been used for more speculated result as in non-parametric accession no function for spectral density, i.e., spectral density function (SDF) does not abide as initially no pre-assumptions or interpolation of the input signal has

Fig. 3 Power spectral density with A-Law technique

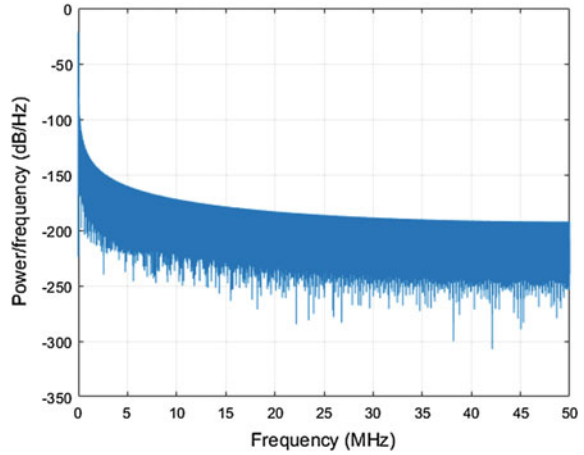
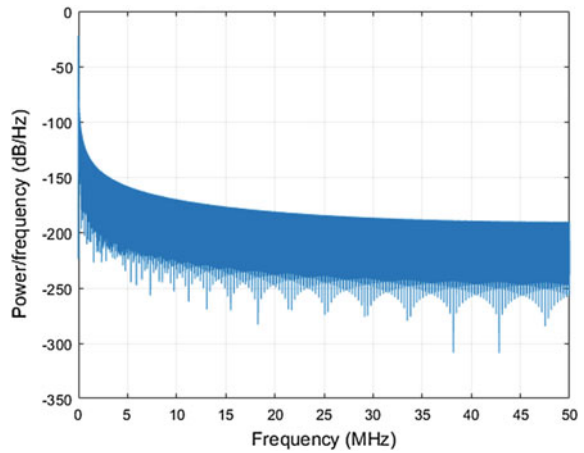


Fig. 4 Power spectral density with μ -Law technique



been done. It is intrinsically the modulus square of digital Fourier transform (DFT) of the signal. The power spectral density acquired with A-Law is far less than that of μ -Law as can be seen in Figs. 3 and 4.

4 Methodology

- Designed a proficient algorithm for companding of an analog signal and compared its results with the quantization in logarithmic domain, aiming at improving the performance parameters of continuous-time-analog to digital converter (CT-ADC).

- Improvement in the power debauched using A-Law companding and maneuvering the results using a non-parametric approach.

5 Results and Discussion

From the adornments of results publicized, it can thereby be implied that, the SER in the event of the logarithmic domain is higher when contemplated with the SER of a conventional quantization technique without compression. A downfall in error power of about 19.97% consequently enhances the signal to error ratio. Thus, it can be deferred that without any deterioration in in-band performance, a commodious decline in error power was detected, thereby further amending the SER, and hence the fulfilment of the objective.

6 Future Scope

Continuous-time domain showed a considerable amount of diminution in quantization error and power dissipation. In addition, an overall augment in signal to error ratio was seen. These improvements and advantages have resulted in this scheme's pervasive applications such as in the field of bio-medical devices, like primarily in bio-medical implantable diagnostic devices which can work on low input power with higher accuracy, hearing aid devices, brain computer interface, bio-potential recording systems, etc.

Acknowledgements The authors express their gratitude to Mr. Gagan Minocha currently working at Mentor Graphics, Noida (U.P.), for his guidance and support.

References

1. Y. Tsividis, "Continuous-time digital signal processing", *El. Letters*, vol. 39, no. 21, pp. 1551–1552, 16 Oct. 2003.
2. Y. Tsividis, "Digital signal processing in continuous time: a possibility for avoiding aliasing and reducing quantization error", *Proc. 2004 IEEE Int. Conf. Acoustics, Speech, and Sig. Proc.*, vol. II, pp. 589–592.
3. Y. Tsividis, "Event-Driven, Continuous-time ADCs and DSPs for Adapting Power Dissipation to Signal Activity", *Proc. 2010 IEEE Int. Symp. Circuits Syst.*, Paris, in press.
4. C. Vezyrtzis and Y. Tsividis, "Processing of signals using level crossing sampling", *Proc. 2009 Int. Symp. Circ. Syst.*, pp. 2293–2296.
5. B. Schell and Y. Tsividis, "A continuous-time ADC/DSP/DAC system with no clock and activity-dependent power dissipation", *IEEE J. Solid-State Circ.*, vol. 43, pp. 2472–2481, Nov. 2008.

Analysis of Parametric Effects on PEMFC Performance and Power Management Schemes

Ekta Joshi and Sandeep Negi

Abstract This paper introduces that the modeling of proton exchange fuel cell has been considered for MATLAB simulation of FC model. Additionally, the possible contrivance of the parametric effects and their interrelationships are deliberated. In this investigation, the significant operating parameters such as reactants (hydrogen and oxygen) flow pressures, membrane resistance, operating temperature are considered. The obtained results as I - V or polarization curves have been carried out for the study of PEMFC behavior. The results show good pacts between the simulated and commercial available PEMFC model. Moreover, the power management schemes are designed and investigated.

Keywords Fuel cell · Parametric effect · Renewable energy
Power management

1 Introduction

FC technology is gaining more popularity for distribution generation (DG) and hybrid power generation with the integration of nonconventional energy sources, e.g., photovoltaic system, wind turbine, micro-turbine system [1, 2]. The FC technology is adopted due to its various advantageous features such as high power density, reliable, portable, fuel availability, and more ecofriendly.

The authors [3] investigated the parametric effects of reactants flow pressure and temperature on FC performance. In [4], the authors analyzed the parametric influence effect and found that the pressure and humidifier temperature were effective parameters to influence the PEMFC performance. The authors [5]

E. Joshi (✉) · S. Negi
Faculty of Technology, Uttarakhand Technical University, Dehradun 248007, India
e-mail: ektajoshi.ddn@gmail.com

S. Negi
e-mail: sandeepnegi80@rediffmail.com

discussed the effect of operating values, e.g., reactants pressure (hydrogen and oxygen) at anode and cathode, temperature and investigated the behavior of $V-I$ curve. In [6], the authors designed a PEMFC model and analyzed the parametric influence by operating parameters, e.g., reactants flow pressure and temperature on the FC system. In [7, 8], the outcome of various parameters effect is calculated for parametric study such as the current density, temperature, pressure, and utilization factors on solid oxide fuel cell performance.

With the help of the given literature review, the planned work additions of the research manuscript are an investigation on the influence effects of significant operating parameters on the performance of PEMFC system. Moreover, proportional-integral-based power management schemes are designed and investigated.

2 Mathematical Modeling of PEMFC System

Generally, PEMFC attains best results at its rated temp. ranges and hydrogen-oxygen reactants pressure. Voltage of FC (V_{fc}) can be stated as Eq. (1) [9, 10] as,

$$V_{fc} = E - V_{act} - V_{conc} - V_{ohm}. \quad (1)$$

The Nernst voltage can be expressed in Eq. (2), and cell potential (E) as,

$$E = E_0 + \frac{RT}{2F} \left[\ln \left\{ \left(\frac{P_{H_2}}{P_{H_2O}} \right) (P_{O_2})^{\frac{1}{2}} \right\} \right]. \quad (2)$$

The activation, concentration, and ohmic drops can be represented in Eqs. (3)–(8) as,

$$V_{act} = -k_1 + k_2 T - \left[\ln \left\{ \frac{(I_{fc})^{k_3}}{(Conc.O_2)^{k_4 T}} \right\} \right] \quad (3)$$

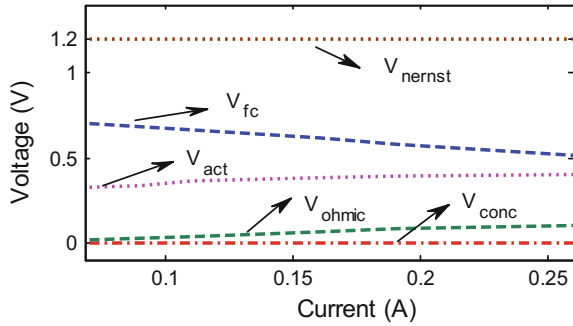
$$Conc.O_2 = \left\{ \frac{PO_2}{5.08 \times 10^6 \times e^{(-498/T)}} \right\} \quad (4)$$

$$V_{ohm} = I_{fc} R_{mem} \quad (5)$$

$$R_{mem} = \frac{t_m}{\sigma} \quad (6)$$

$$V_{conc} = k_1 - k_2 (T - 273) e^{(k_3 T)} \quad (7)$$

Fig. 1 FC polarization $V-I$ curves



Equations (1)–(7) are utilized for cell voltage (V_{fc}) [10]. If all the FC systems are arranged in series, stack voltage (V_{stack}) is the multiplication of FC voltage and N number of cells in the stack, shown in Eq. (8) as,

$$V_{stack} = NV_{fc}. \tag{8}$$

H_2 , O_2 , and H_2O flow pressures can be expressed in Eq. (9) as,

$$P_{H_2} = \left\{ \frac{(m_{H_2} R_{H_2})}{V_{anode}} \right\} T \quad \& \quad P_{O_2} = \left\{ \frac{(m_{O_2} R_{O_2})}{V_{cathode}} \right\} T \quad \& \quad P_{H_2O} = \left\{ \frac{(m_{H_2O})^{\frac{1}{2}}}{k_{cathode}} \right\} q_{H_2O}. \tag{9}$$

The factors that cause voltage drop in FC from ideal voltage such as activation, ohmic, and concentration drops are shown at typical $V-I$ characteristics of a PEMFC in Fig. 1.

3 Results and Discussion

The performance of designed MATLAB/Simulink model of FC system is investigated by significant operating parametric effect for the following test cases as,

- Power management scheme using hydrogen reactant flow pressure control;
- Effect of variation in reactants flow pressures, temperature, and membrane resistance on $I-V$ curve.

3.1 Power Management Scheme Using Hydrogen Reactant Flow Pressure Control

The PI controller is important to increase the speed of the response and also to minimize the steady state error. The proposed strategy for PI controller is shown in Fig. 2.

Mathematically, the PI controller is expressed in Eq. (10) as,

$$u(t) = K_p e(t) + K_i \int e(t) dt. \tag{10}$$

The complete system is of H₂ reactant pressure control schemes as shown in block diagram in Fig. 3.

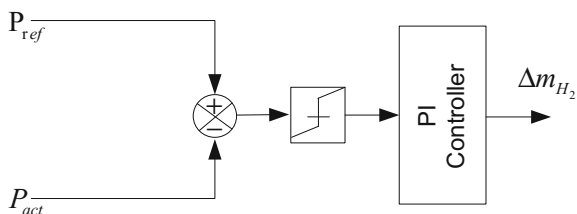


Fig. 2 Schematic diagram of PI-based H₂ flow pressure control scheme

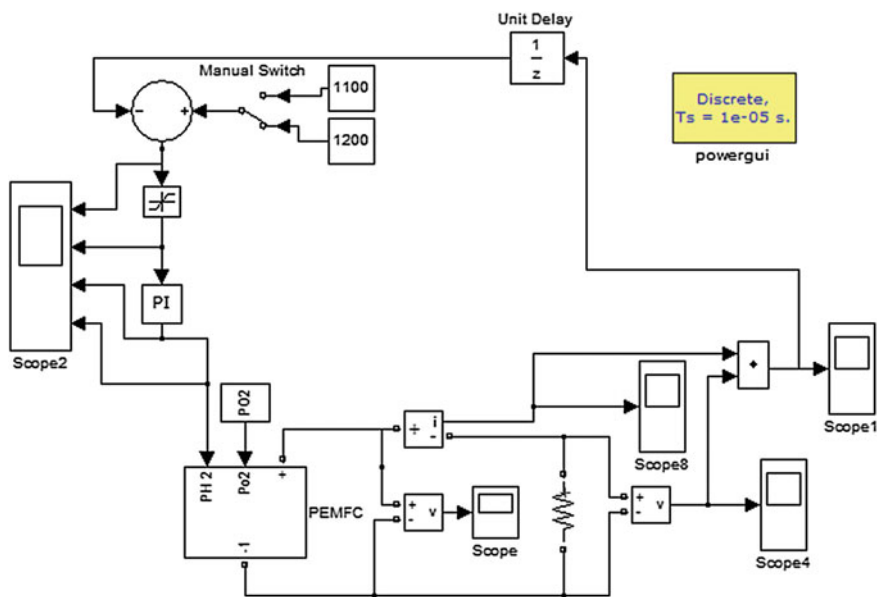


Fig. 3 Simulink model of hydrogen flow pressure-based control scheme

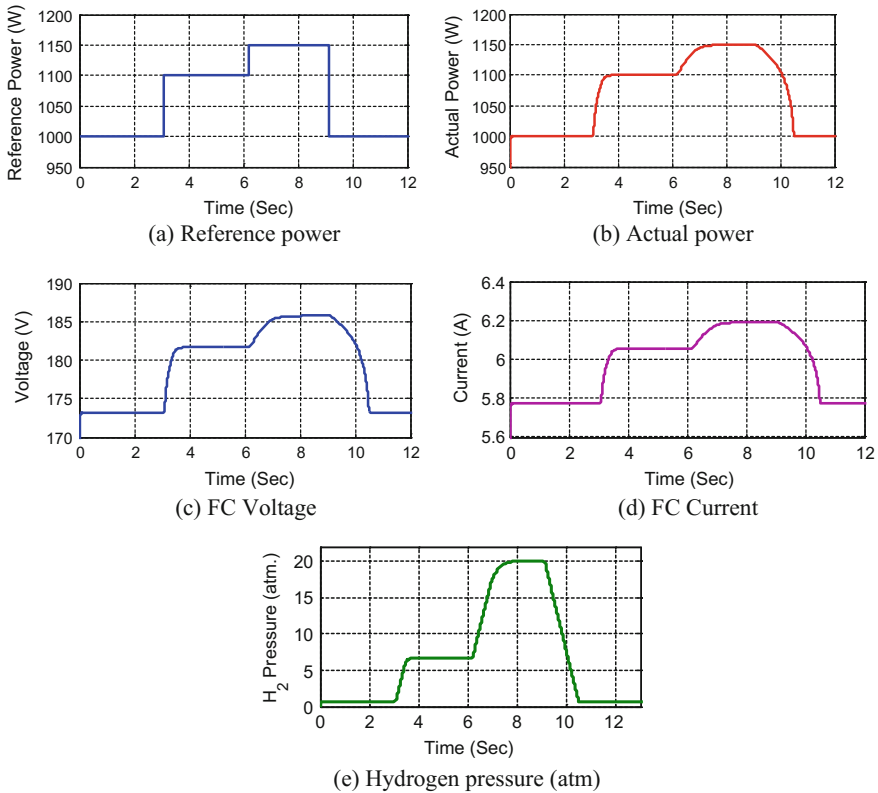


Fig. 4 Performance of PEMFC with hydrogen-based scheme

Under the investigation of hydrogen pressure-based control scheme, the obtained results are given in terms of power reference, actual power, FC voltage, FC current, and H_2 pressure for attaining the reference power as (Fig. 4).

Initially, at $t = 0$ s, the power reference is kept at 1000 W, and the actual power attains the reference power value with 0.8 atm. hydrogen pressure. Furthermore, the power reference is changed up to 1100 W. The actual power attains this power after 0.5 s with transients. At present time, the H_2 pressure is increased up to 7.2 atm. to attain this reference power.

Now, the power reference is changed up to 1150 W. To obtain this reference power by the FC system, the hydrogen pressure consumption is required 20.2 atm. pressure is required with the 0.8 s transients. At $t = 9$ s, the power reference is reduced as 1000 W, and the actual power, voltage, current values are reduced accordingly. The hydrogen pressure consumption is also reduced to achieve this reference power rating. This power management scheme is found satisfactory for the FC performance.

3.2 Effect of Variation in Reactants Flow Pressures, Temperature, and Membrane Resistance on I–V Curve

Figure 5a–d shows V – I characteristics of PEMFC characteristics for different values of operating temperature, H_2 flow pressure, O_2 flow pressure, and membrane resistance (R_{mem}), respectively. In Fig. 5a, the operating temperature ranges increased as $T = 353 + 20\%$ and $353 + 40\%$ °C for the investigation. In this consequence of the obtained results, the decrement of voltage is recorded. Furthermore, the operating temp. range is decreased as $T = 353 - 20\%$ and $353 - 40\%$, and it is found that the voltage is increased, which is shown in Fig. 5a. The H_2 flow pressure is increased as $P_{H_2} = 1 + 20\%$ and $1 + 40\%$, and then the voltage is found to be increased. H_2 pressure is decreased as $P_{H_2} = 1 - 20\%$ and $1 - 40\%$; at this condition, the voltage is decreased, which is shown in Fig. 5b as the output voltage of PEMFC is directly proportional to the H_2 pressure. The O_2 pressure range is increased as $P_{O_2} = 1 + 20\%$ and $1 + 40\%$, and then the voltage is decreased. Furthermore, the O_2 pressure is decreased from its rated value as $P_{O_2} = 1 - 20$ and $1 - 40\%$, and then the voltage is increased, as shown in Fig. 5c. It is evident that at

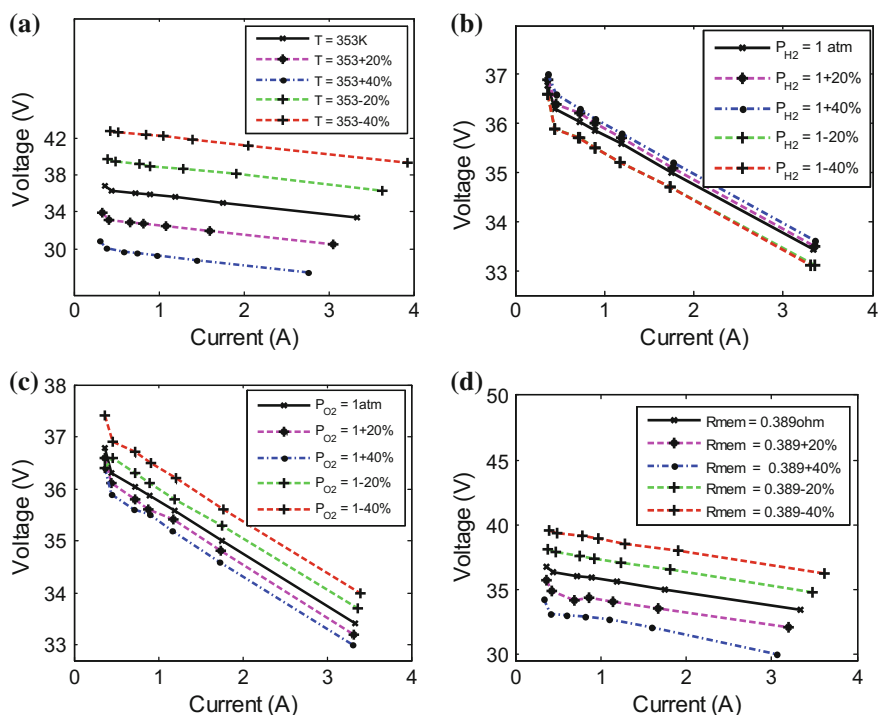


Fig. 5 V – I curves of PEMFC for **a** temp. variation, **b** H_2 pressure, **c** O_2 pressure, **d** membrane resistance (R_{mem})

the lower oxygen flow rate, the reaction rate at cathode is high so the concentration losses are reduced. The R_{mem} is increased as $R_{\text{mem}} = 0.389 + 20\%$ and $0.389 + 40\%$, and then the voltage is reduced and the membrane resistance is decreased as $R_{\text{mem}} = 0.389 - 20\%$ and $0.389 - 40\%$; then the voltage is increased and obtained results are shown in Fig. 5d. It is evident that at the minimum values of R_{mem} , the ohmic losses (V_{ohm}) are reduced, so the concentration losses are reduced.

4 Conclusion

The paper is about the effort that has been completed to join two significant facets of FC. The performance analysis of parametric effects on single FC system, various parameters, e.g., reactants (H_2 and O_2) pressure, rated temp., resistance of membrane, are taken. Furthermore, an extensive simulation of single PEMFC is carried out and found satisfactory results in MATLAB/Simulink environment.

References

1. Peighambaroust, S. J., Rowshanzamir, S., Amjadi, M., Review of the proton exchange membranes for fuel cell applications. *International Journal of Hydrogen Energy*. 35(17), 9349–9384, 2010.
2. Wee, J. H., Applications of proton exchange membrane fuel cell systems. *Renewable and Sustainable Energy Reviews*. 11, 1720–1738, 2007.
3. Benchouia, N., Hadijadeh, A. E., Modeling and validation of fuel cell PEMFC. *Revue des Energies Renouvelables*. 16(2), 365–377, 2013.
4. Kaytakoglu, S., Akyalm, L., Optimization of parametric performance of a PEMFC. *International Journal of Hydrogen Energy*. 32, 4418–4423, 2007.
5. Seyezhai, R., Mathur, B. L., Mathematical modeling of proton exchange membrane fuel cell. *International Journal of Computer Applications*. 20(5), 82–96, 2011.
6. Qingshan, X., Nianchun, W., Ichianagi, K., Yukita, K., PEM fuel cell modeling and parameter influences of performance evaluation. In: *Proceeding International Conference on Electric Utility Deregulation and Restructuring and Power Technologies*, 2827–2832, 2008.
7. Bo, C., Yuan, C., Zhao, X., Parametric analysis of solid oxide fuel cell. *Clean Technology Environmental Policy*. 11, 391–399, 2009.
8. Singh, K., et al., Study of Parametric Effects on Solis Oxide Fuel Cell, in *Proc. Advances in Intelligent Systems and Computing*, 479, 863–869, 2016.
9. Ural, Z., Gencoglu, M. T., Gumus, B., Dynamic simulation of a PEM fuel cell system. In: *Proceeding International Hydrogen Energy Congress and Exhibition*, 1–12, 2007.
10. Chauhan, Y. K., Study and performances analysis of fuel cell assisted vector control variable speed drive system used for electric vehicles. *International Journal of Sustainable Energy*. 35 (1), 1–25, 2015.

Comparative Analysis of MEMS Piezoelectric Materials for the Design of a Piezotube-Type Pressure Sensor

Sachin Kala, Varij Panwar, Lokesh Panwar and Sushant Sharma

Abstract MEMS-based pressure sensors with high voltage sensitivity can be used in many areas of MEMS, biomedical, optical displays, automobile, etc. This paper focuses on the comparison of various types of MEMS piezoelectric materials which sense and convert the mechanical energy into electrical energy using MEMS technology. The model designing and working principle of proposed MEMS Piezotube-type pressure sensor is elucidated here. The modeling and simulation of MEMS Piezotube pressure sensor is done using COMSOL 5.2. The displacement of piezoelectric material and induced electric potential analysis are carried out for various types of MEMS piezoceramic materials. This paper shows the study of voltage generation using direct piezoelectric effect. Here, analysis is done in centimeter range making two sets of boundary conditions where internal fluid pressure of various ranges is applied onto MEMS Piezotube-type pressure sensor using various piezoceramic materials. Furthermore, analyses are done with increased value of pressure, but now the pressure is applied externally. The new result shows that there is a huge increment in induced electric potential on increasing the pressure and dimensions. Indirect piezoelectric effect is also shown in this paper, where on applying the electric field, material becomes strained and strain is directly proportional to electric field.

Keywords Piezoelectric material · Energy harvesting · MEMS

S. Kala (✉) · V. Panwar · L. Panwar · S. Sharma
Graphic Era University, Dehradun, India
e-mail: hiteshhh0007@gmail.com

V. Panwar
e-mail: varijpanwarcertain@gmail.com

© Springer Nature Singapore Pte Ltd. 2018
R. Singh et al. (eds.), *Intelligent Communication, Control and Devices*,
Advances in Intelligent Systems and Computing 624,
https://doi.org/10.1007/978-981-10-5903-2_160

1537

1 Introduction

Today tremendous development has been shown in field of MEMS (microelectromechanical system) in field of energy harvesting. Nowadays various pressure sensor applications have been developed based on MEMS technology which is beneficial to automotive, biomedical, and optical displays, consumer products, fluidics, etc. Conventional pressure sensors were used before, but now these MEMS sensors are mostly used due to their smart function, reliability; they occupy less space, low weight, and low cost [1]. Piezoelectric thin film has been widely used in various MEMS applications such as in pressure sensors, biomedical, and energy harvesting [2, 3]. Many researchers have used piezoceramic sheet elements as sensors in controllable structure systems, health monitoring applications [5], [6] as well as in energy harvesting applications [7]. They are used in sensor and actuators to convert mechanical energy into electrical energy and vice versa. 7S. M. Peelamedu et al. [4] have used lead zirconate titanate (PZT-5H) as a piezoelectric material in their paper where they had illustrated the inverse piezoelectric effect and the direct piezoelectric effect using piezoceramic tube. Here, comparisons are shown for various piezoelectric materials used in this sensor. Section one deals with different results in terms of displacement and induced electric potential when different internal pressure is applied on materials. Finally, comparisons of all piezoceramic materials are made, in which the PZT-7A and barium titanate have highest output voltage of about 2 and 2.8 V, respectively, among all other materials. Section two deals with different results in terms of displacement and induced electric potential when increased external pressure is applied on piezoceramic materials. The results are shown in Table 7, and a huge increment in induced electric potential with increase in pressure and dimensions can be seen there. Hence, this pressure sensor can be widely used in energy harvesting applications. In section three, indirect piezoelectric effect is shown, where on applying the electric field, material becomes strained and strain is directly proportional to electric field. Here, it is found out that PZT-5H shows maximum displacement when potential difference of one volt is applied across it.

1.1 Equation

Piezoceramics are transversely isotropic materials. The piezoelectric constitutive law is defined by two equations shown below. Their combined form in strain-charge form is

$$S = s^E T + dE. \quad (1)$$

$$D = dT + \epsilon^T E. \quad (2)$$

The matrix form of direct piezoelectric effect is shown in Eq. 2, whereas Eq. 1 shows the matrix form of converse piezoelectric effect, where the electric charge displacement components are represented by (D), strain components are represented by (S), field variables are the stress components represented by (T), dielectric constant is denoted by (d), and electric field components are denoted by (E) in Eqs. 1 and 2.

The electric displacement (D) is shown in Eq. 3

$$D = \epsilon_0 \epsilon_r E + dX. \quad (3)$$

$$P = dX. \quad (4)$$

where the electric displacement field is denoted by (D), the electric polarization is denoted by (P), and the electric field is denoted by (E). For more information about piezoelectric sensors refer [9].

2 Sensor Design

The modeling and simulation of pressure sensor is explained in this section. Recently, different transduction methods such as capacitive, thermal transduction, piezoelectric and piezoresistive are explored; each method has their own merits and demerits over each other [10, 11]. The paper shows the static 2D axisymmetric analysis of a piezoelectric actuator utilizing different piezoelectric materials using COSMOL Multiphysics 5.2. A modeling and simulation of radially polarized piezoelectric tube is presented where the direct piezoelectric method is shown. In piezoelectric materials, the negative and positive charges are symmetrically distributed in a crystal. When the pressure is applied on piezoelectric material, it results in formation of the positive charge on the compressed side and the negative charge on the expanded side. On removing the applied pressure, net current flows across the material; this is called as direct piezoelectric method. For case one, the height, inner radius, and outer radius of tube are defined as 3, 4, and 6 cm, respectively, shown in Fig. 1 (radius taken same as of human wrist). In case two, the height, inner radius, and outer radius of piezotube remain same, but the pressure is now applied externally with an increased value of range 80 psi or 551.581 kPa.

3 Simulation of MEMS Piezotube Pressure Sensor

The results of a MEMS Piezotube pressure sensor are presented in this section. The internal fluid pressure is applied to piezoelectric material in the range of 11 to 19 kPa. The normal blood pressure (systolic pressure) of human body is 19 kPa, and lower blood pressure (diastolic) is taken as 11 kPa approximately. The deformation, displacement, and induced voltage sensitivity vary from material to

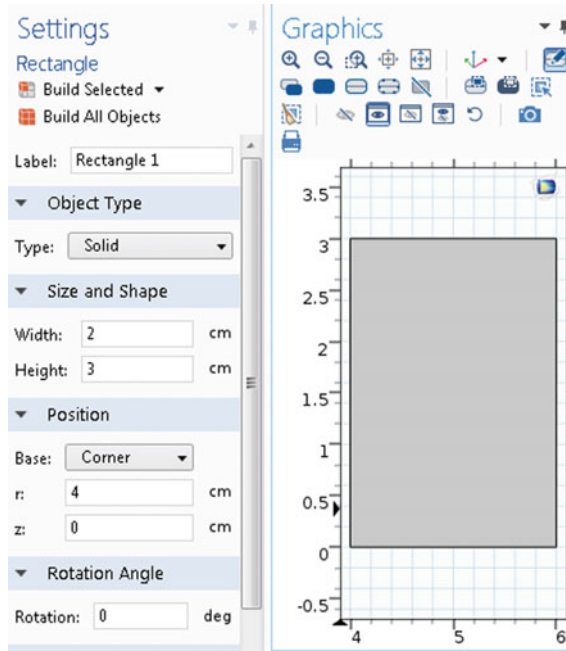


Fig. 1 Geometrical dimensions of MEMS Piezotube-type pressure sensor in centimeter (cm)

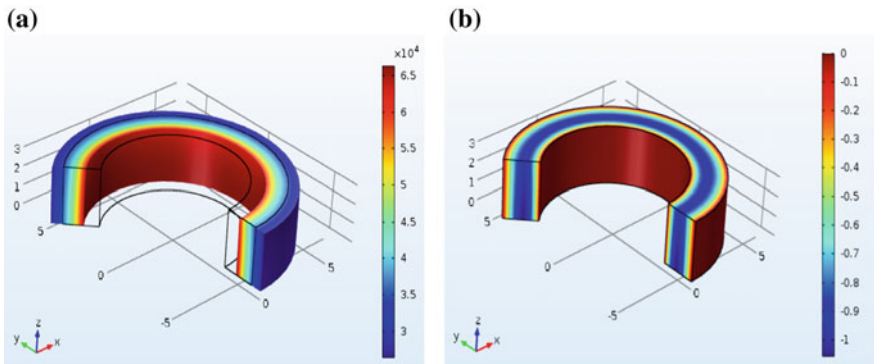


Fig. 2 a 3D displacement view of MEMS Piezotube-type pressure sensor when the pressure is applied internally. b 3D view of induced electric potential when the pressure is applied internally

material depending on their properties. This MEMS pressure sensor is designed using COSMOL Multiphysics 5.1. Figure 2a, b shows the 3D view of displacement and induced electric potential, respectively, when the pressure is applied internally.

The deformation, displacement, and induced voltage sensitivity vary according to the property of material. In second case, the pressure is applied externally and its value is taken as 80 psi or 551.581 kPa which is same as that is applied on normal

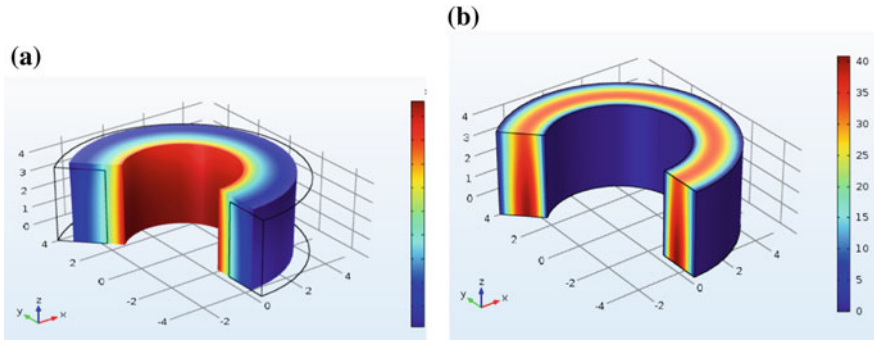


Fig. 3 **a** 3D displacement view when the pressure is applied externally. **b** 3D view of induced electric potential when the pressure is applied externally

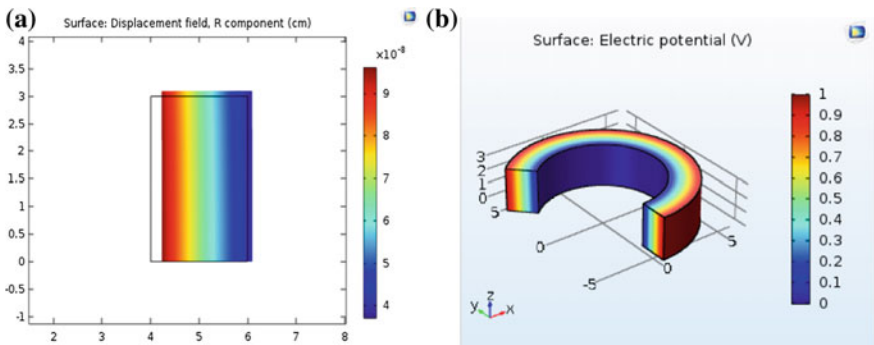


Fig. 4 **a** 2D displacement view of MEMS Piezotube-type pressure sensor when the potential difference of one volt is applied. **b** 3D view of MEMS Piezotube-type pressure sensor when the potential difference of 1 V is applied

cycle tires. Now, every time tire rotates piezomaterial inside it gets deformed. Figure 3a, b shows the 3D view of displacement and induced electric potential, respectively, when the pressure is applied externally.

4 Indirect Piezoelectric Effect

Here, in this section, the height, inner radius, and outer radius of tube are defined as 3, 4, and 6 cm, respectively, shown in Fig. 1. When the potential difference of one volt is applied to various piezoceramic materials, they get strained (deform) and the strain is directly proportional to the electric field shown in Fig. 4b. The piezoelectric material expands or contracts depending upon the applied voltage. When the applied voltage has the same polarity as poling voltage, then material expands

otherwise gets contracts when the applied voltage has opposite polarity that of poling voltage. The 2D and 3D view of displacement and electric potential of pressure sensor are shown in Fig. 4a, b, respectively, when potential difference of one volt is applied across it. The result analyses done in terms of displacement for various piezoelectric materials are shown in Table 8.

5 MEMS Material Analysis for Pressure Sensor

COSMOL Multiphysics 5.1 version provides us various materials. They can be accessed from the material library. But only few MEMS material can be used due to problems that occur during time of microfabrication. Mac Donald [8] has identified that there should be three basic properties of the materials that we are going to use in MEMS technology which are as follows: (a) material must be suitable with semiconductor fabrication technology, (b) material should have good mechanical and electrical properties, (c) intrinsic properties that slow down the rise of high stresses during processing. When the mechanical load, stress, and vibrations are applied on piezomaterials, it results in evolution of piezoelectric, electromagnetic, and electrostatic energies which can be used in harvesting [5]. The study of 5 MEMS piezoceramic materials is shown here one by one. The overall results are explained on the basis of displacement and induced electric potential of each material.

5.1 Lead Zirconate Titanate (PZT-5H)

It belongs to special class of orthotropic materials. We can use it in either zy-plane material orientation or the zx-plane material orientation; the results show that both planes give the same solution; it is because of its transversely isotropic nature. Piezoceramic materials show the same properties or characteristics when lie in one plane, but their properties show sudden changes when they lie in the direction normal to this plane. It has very high coupling coefficient, piezoelectric charge coefficient, and permittivity and hence used for low-power applications where these properties are required. It is the most suitable piezoelectric material for imaging applications, level sensors, field sensors, actuator and accelerometers. Table 1 shows some of its material properties.

Table 1 Material properties of PZT-5H

S. No.	Material property	Value	Units
1	Density	7500	kg/m ³
2	Poisson ratio	0.34	1
3	Dielectric constant	3400	1

Fig. 5 Plot of electric potential for lead zirconate titanate (PZT-5H)

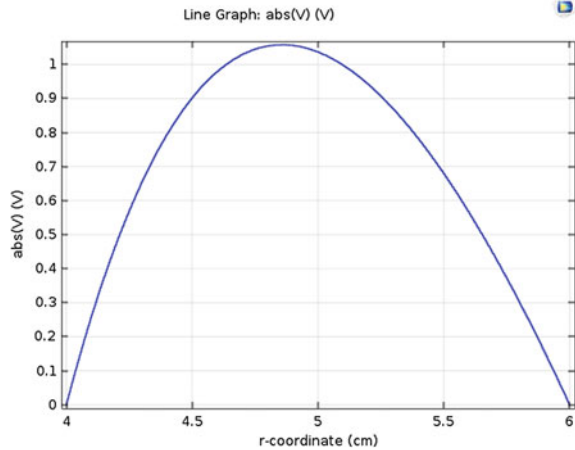


Table 2 Material properties of PZT-5H

S. No.	Material property	Value	Units
1	Density	7750	kg/m ³
2	Poisson ratio	0.35	1
3	Dielectric constant	1800	1

It is used as a piezoelectric material in a piezotube pressure sensor. Figure 5 shows the value of simulated result on induced electric potential, which is about 1 V.

5.2 Lead Zirconate Titanate (PZT-5A)

It is used in low-power applications where high dielectric constant, volume resistivity, high voltage sensitivity, and stability in high temperature ranges are required. It is a piezoceramic material (transversely isotropic) and an excellent source of material for piezo igniters, probes, sensors, and in biomedical areas. Table 2 shows some of its material properties.

It is used as a piezoelectric material in a piezotube pressure sensor. Figure 6 shows the value of simulated result on induced electric potential, which is about 1.3 V.

5.3 Lead Zirconate Titanate (PZT-7A)

It is a piezoceramic material (transversely isotropic). This is used in high-power applications where high coercive field, low dielectric losses, high driving field, and

Fig. 6 Plot of electric potential for lead zirconate titanate (PZT-5A)

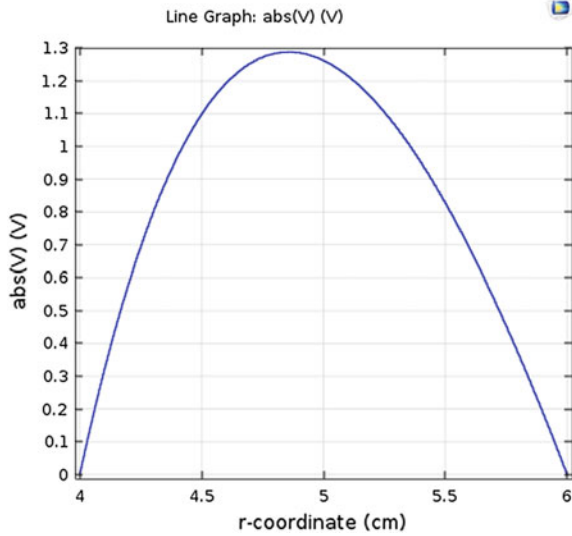


Table 3 Material properties of PZT-7A

S. No.	Material property	Value	Units
1	Density	7700	kg/m ³
2	Poisson ratio	0.35	1

high electromechanical coupling coefficient properties are needed. This is mostly suited for high-power electroacoustic devices, generators, equipments, etc. Table 3 shows some of its material properties.

It is used as a piezoelectric material in a piezotube pressure sensor. Figure 7 shows the value of simulated result on induced electric potential, which is about 2 V.

5.4 Lead Zirconate Titanate (PZT-2)

It is a piezoceramic material (transversely isotropic). We can use it either in the zx -plane material orientation or in the zy -plane material orientation; both give the same solution. It has very high coupling coefficient, piezoelectric charge coefficient, and permittivity and hence used for low-power applications where these properties are required. Table 4 shows some of its material properties.

It is used as a piezoelectric material in a piezotube pressure sensor. Figure 8 shows the value of simulated result on induced electric potential, which is about 1.8 V.

Fig. 7 Plot of electric potential for lead zirconate titanate (PZT-7A)

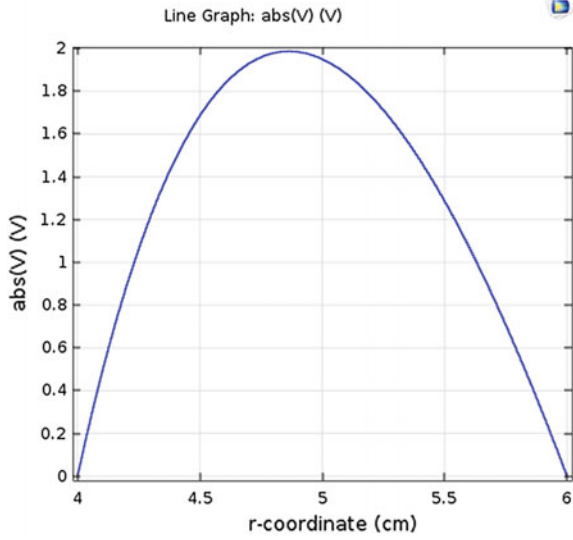
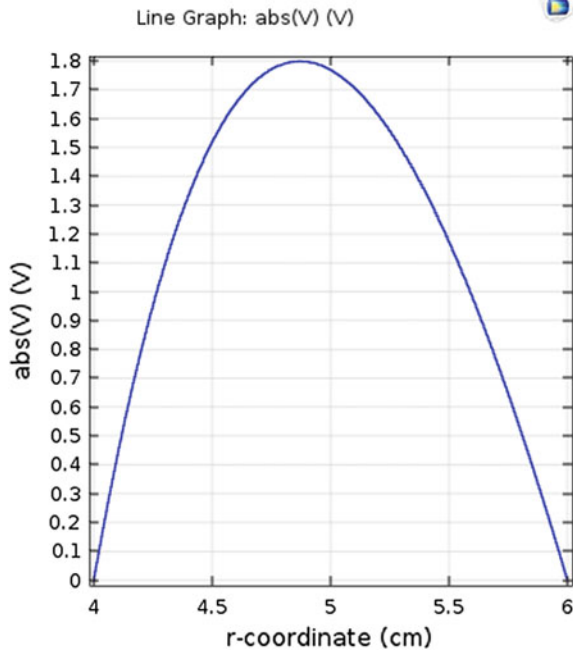


Table 4 Material properties of PZT-2

S. No.	Material property	Value	Units
1	Density	7600	kg/m ³
2	Poisson ratio	560	1
3	Relative permittivity	504.1, 270	1

Fig. 8 Plot of electric potential for lead zirconate titanate (PZT-2)



5.5 Barium Titanate

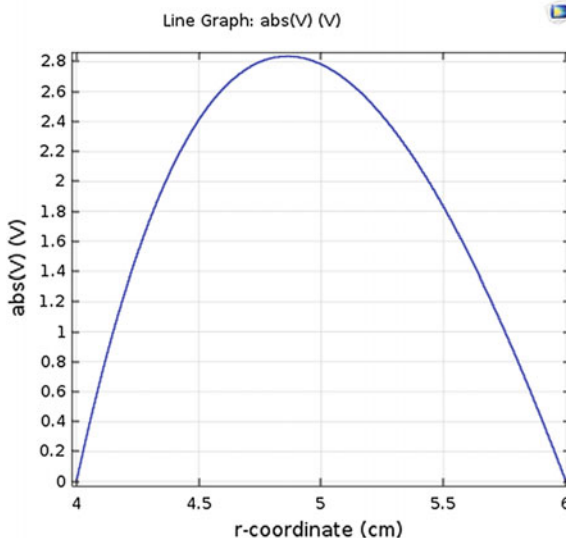
Barium titanate (BaTiO_3) is an inorganic compound. It is a ferroelectric ceramic powder white in color and becomes transparent as grows in larger crystals. This piezoelectric material is used in microphones, sensors, and other transducers. Before it was used as a major source of piezoelectric material, but afterward lead zirconate titanate (PZT) takes its place and replaced it massively. Table 5 shows some of its material properties.

It is used as a piezoelectric material in a piezotube pressure sensor. Figure 9 shows the value of simulated result on induced electric potential, which is about 2.8 V.

Table 5 Material properties of barium titanate

S. No.	Material property	Value	Units
1	Density	7600	kg/m^3
2	Relative permittivity	1976.8, 111.7	1
3	Young modulus	67	GPa

Fig. 9 Plot of electric potential for barium titanate (BaTiO_3)



6 Overall Comparison of Materials

Different piezoelectric materials were used in this sensor. Their design and simulations are done for internal pressure range of about 11–19 kPa in case one and external pressure of about 80 psi or 551.581 kPa in case two. Their analysis was carried out one by one using COSMOL 5.2. The displacement and the induced electric potential vary material to material depending on their properties. In case one, result shows that the PZT-7A and barium titanate as a piezoelectric material have the highest value of induced electric potential of 2 and 2.8 V, respectively, among the all other materials. In case two, analyses are done with increased value of pressure up to 80 psi or 551.581 kPa, which is generally taken same as that of a cycle tire pressure and now the pressure is applied externally. The new result shows that there is a huge increment in induced electric potential on increasing the pressure and dimensions. Case three deals with indirect piezoelectric effect, where on applying the electric field, material becomes strained and strain is directly proportional to electric field. Here, it is found out that PZT-5H shows maximum displacement when potential difference of one volt is applied across it. The results and analysis of different materials and their comparisons are shown in Tables 6, 7, and 8, respectively.

Table 6 Comparative analysis of MEMS piezoelectric materials when the pressure is applied internally

S. No.	Material property	Displacement in nm, when 11 kPa pressure is applied	Electric potential generated in volts, when 11 kPa pressure is applied	Displacement in nm, when 19 kPa pressure is applied	Electric potential generated in volts when 19 kPa pressure is applied
1	pzt-5h	22.5	0.6	39.5	1
2	pzt-5a	22	0.75	38	1.3
3	pzt-7a	14.4	1.1	25	2
4	pzt-2	15.6	1	27	1.8
5	Barium titanate	11.8	1.6	20.2	2.8

Table 7 Comparative analysis of MEMS piezoelectric materials when the pressure is applied externally

S. No.	Material property	Displacement in nm when 80 psi or 551.581 kPa pressure is applied	Electric potential generated in volts when 80 psi or 551.581 kPa pressure is applied
1	Lead zirconate titanate (PZT-5H)	1160	36
2	Lead zirconate titanate (PZT-5A)	1190	45
3	Lead zirconate titanate (PZT-7A)	785	70
4	Lead zirconate titanate (PZT-2)	850	60
5	Barium titanate	550	90

Table 8 Comparative analysis of MEMS piezoelectric materials when potential difference of 1 V is provided across it (indirect piezoelectric effect)

S. No.	Material property	Displacement in nm
1	Lead zirconate titanate (PZT-5H)	0.95
2	Lead zirconate titanate (PZT-5A)	0.6
3	Lead zirconate titanate (PZT-7A)	0.22
4	Lead zirconate titanate (PZT-2)	0.22
5	Barium titanate	0.125

7 Conclusion

The complete study of different MEMS piezoelectric materials used in sensor has been done, and their simulated results are shown in Tables 6, 7, and 8, respectively, where results conclude that for the pressure range of about 11–19 kPa, PZT-7A and barium titanate have the highest electric potential sensitivity among all. For application purpose, this pressure sensor can be used in biomedical, automobile, and many other areas. The radius of piezotube is taken as same as the human wrist so it can be used in blood pressure measurements. The normal blood pressure (systolic pressure) of human body is 19 kPa and lower blood pressure (diastolic) is taken as 11 kPa approximately. Hence, this tube-shaped pressure sensor can be

used as watches to give out blood pressure measurements in terms of voltage whenever the pulses are pressed with the help of piezoelectric material. Using this as an internal fluid pressure, results have been evaluated. In case two, piezoelectric pressure sensors can be used in between tube and tires of cycles, bicycles, automobiles, etc, as an energy harvesting application. Whenever tire rotates, piezoelectric material inside it gets deformed that results in voltage generation; this pressure sensor can be used in many fields such as biomedical, automobile platforms where whenever this pressure sensor gets deformed it results in voltage generation. In case three, the study of indirect piezoelectric effect is done, where it is shown that the lead zirconate titanate (PZT-5H) has maximum displacement of about 0.95 nm among all other piezoceramic materials, when one volt of potential difference is applied across it. These piezoelectric materials are pollution-free, save fossil fuels, and are completely natural sources of energy. So we should use them in our day-to-day life as energy harvesting applications.

References

1. L. Lin and W. Yun, "MEMS Pressure Sensors for Aerospace Applications," Proceeding IEEE Aerospace Conference, vol. 1, Colorado, 21–28, pp. 429–436, March 1998.
2. D. L. DeVoe and A. P. Pisano A P 2001 "Surface micromachined piezoelectric accelerometers (PiXLs)", *J. Microelectromech. Syst* 10, pp. 180–6, 2001.
3. P. Muralt P, "Piezoelectric micromachined ultrasonic transducers based on PZT thin films", *IEEE Trans. Ultrason. Ferroelectr. Freq. Control* 52, 2276–88, 2006.
4. S. M. Peelamedu et al. (Proceedings of the Institution of Mechanical Engineers, Part I: Journal of Systems and Control Engineering March 1, 2000 vol. 214 no. 2 87–97).
5. J. Sirohi and I. Chopra, "Fundamental understanding of piezoelectric strain sensors," *J. Intell. Mater. Syst. Smart Struct.*, vol. 11, pp. 246–257, Apr. 2000.
6. H. A. Tinoco, A. L. Serpa, and A. M. Ramos, "Numerical study of the effects of bonding layer properties on electrical signatures of piezoelectric sensors," *Mecánica Comput.*, vol. 29, no. 86, pp. 8391–8409, Nov. 2010.
7. A. E. Kubba and K. Jiang, "Efficiency enhancement of a cantileverbased vibration energy harvester," *Sensors*, vol. 14, no. 1, pp. 188–211, 2014.
8. MacDonald N C, Chen L Y, Yao J J, Zhang Z L, McMillan J A, Thomas D C & Haselton K R, "Sensors and Actuators", 20, (1989)19.
9. IEEE Standard on Piezoelectricity, ANSI/IEEE Standard 176, 1987.
10. A. Aini, A.N Nordin, H. Salleh, "A comparative study on MEMS piezoelectric microgenerators," *Microsyst Technol*, 2010.
11. S. P. Beeby, M. J. Tudor and N. M. White, "Energy harvesting vibration sources for microsystems applications." *Meas. Sci. Technol.* 2006; 17:R175–R195.

Design and Analysis of SEPIC-Based Single-Stage Three-Phase Inverter

G. Mehta, V.K. Yadav and R. Verma

Abstract This chapter presents a novel design of single-stage three-phase inverter based on SEPIC. The designed inverter has special features that are not seen in the traditional current source inverter (CSI) where DC current at input side is always more than AC current at output side or in the case of traditional voltage source inverter (VSI) where we have voltage at output side smaller than the DC voltage at input side. The presented inverter topology has inherent characteristics of both buck and boost converters. By varying the duty ratio, functioning of the converter can be controlled and thus provide flexibility to the inverter which can be used for both isolated and grid mode cases where desired AC voltage output is either smaller or more than the input voltage. Also, in the proposed inverter, the number of energy storage elements, viz. capacitors and inductors, is substantially reduced so as to improve reliability of the system along with reduction in its overall dimensions and thereby reducing the total cost involved. The proposed inverter is controlled by fuzzy logic by defining various implementation rules along with usage of various membership functions so as to get desired output from the inverter. The converter model along with inverter model, the fuzzy controller and results are presented in the present work in detail.

Keywords SEPIC · fuzzy logic

1 Introduction

Inverter is the power conversion circuit which makes use of source, DC voltage source and/or DC current source, and converting that voltage into AC voltage (or current). It converts energy from DC to AC or an ancillary conversion from AC to AC.

G. Mehta (✉) · R. Verma
School of EE and CE, Galgotias University, Greater Noida, India
e-mail: gitanjali.iitr@gmail.com

V.K. Yadav
Department of Electrical Engineering, Gautam Buddha University, Greater Noida, India

DC to AC conversion is valuable and useful for various fields, which includes power conditioning, compensation of harmonics, motor drives, and grids integrated with renewable energy resources. Input to an inverter is provided with DC source, which can be derived from the AC sources as well, such as a utility AC supply. Therefore, we can take a utility AC voltage supply source as the input power which is converted to DC with the help of an AC to DC converter which then can again be inverted back to AC voltage with an inverter. The final AC voltage obtained as an output can be of different frequency as well as a different magnitude when compared to that of input voltage given out of the utility supply. Value for the input voltages, output voltages, and their corresponding frequencies as well as the overall power-handling capacity depends upon the specific design of the inverter circuit [1–6].

In traditional CSI, the current at input is more than the output. In traditional VSI, the voltage at output side is smaller than the voltage input. Thus, in order to overcome this flipside of traditional inverters, the novel inverter topology has been developed in the present work, which is based on the SEPIC that is having the inbuilt characteristics of buck-boost converters. Also with the usage of this new topology, the value of the inductors and capacitors which are known to be the energy storing elements can be reduced to a great extent so as to improve the reliability along with the reduction in the overall size and thereby reducing the total cost of the inverter [7–9].

The buck-boost inbuilt characteristic of SEPIC varies with the duty ratio which is time dependent, thus providing a large-scale flexibility to be used in isolated and grid-integrated cases where expected voltage at output is either greater or lower than that of voltage at input DC [10–13].

A new model for VSI defined as boost inverter or DC–AC boost converter is given by Caceres and Barbi [1]. The main feature to be focused for the proposed inverter circuit is that it can generate AC voltage at output side which is larger than the DC side input voltage, which is dependent upon the duty ratio. These features are not available in the conventional VSI that give us an output voltage which is always lower than the input side DC voltage. A sliding mode controller is proposed for optimizing out the dynamics of boost inverter, with correct operation in any condition of working.

A single-stage grid-connected inverter topology is designed by Prasad et al. [2], which is matched for applications such as distributed generation area. The inverter is called as universal inverter because of configurable buck, boost, and buck–boost nature using varying PWM control. Jang et al. [3] have designed the boost inverter which is considered as a foundation block for the grid mode FC system employed in single-phase application that offers low cost as well as compactness. Chunkag and Kannan [4] have analyzed and designed a parallel three-phase AC to DC converter based on Cuk converter used for DC DPS. In order to generate three inductor current in compensators, the proposed control scheme is presented as well as to improve dynamic response of rectifier without causing any affect on its steady-state performance.

An advance method for obtaining the maximum available power from the solar array under varying environment situation is given by Chung et al. [5]. This is carried on by connecting a pulse-width-modulated Cuk converter in between the solar PV module and the battery or load. Darwish et al. [6] have presented and designed single-stage three-phase inverter, which is formed using Cuk converter. The designed three-phase inverter is suitable for the use of solar PV applications in which we require input current to be continuous at maximum power point tracking operation.

2 Working and Design of SEPIC

The schematic diagram of single-ended primary-inductor converter (SEPIC) is shown in Fig. 1, whose voltage output is similar to the output of the buck-boost converter but having the same polarity as that of the input voltage. In order to obtain the relation between the input and output voltages, certain assumptions have been made: Inductors are having very large values, and the currents through them are constant. Capacitors are having very large values, and the voltages across them are constant. Circuit operates in the steady state, indicating that the voltage and current waveforms are periodic. Converter with duty ratio of d , the switch is closed for time dT_s and open for $(1 - d)T_s$. Here, ideal switch and diode are considered [10–13].

The SEPIC circuit consists of an input voltage source V_{in} , switch S , and diode D . Capacitor C_1 is used for the transfer of energy between voltage source and the load. Inductors L_1 and L_2 are used for instantaneous storage of energy. The steady-state operation of the circuit can be described easily, considering the switch S off; then, C_1 is charged causing the current I_{L1} to decrease; on the other hand, inductor L_2 is discharged to the load resulting in the increase of current I_{L2} . For the next switching condition, when the switch S is on, L_1 gets charged and the current I_{L1} increases, whereas capacitor C_1 is discharged resulting I_{L2} to increase. We can

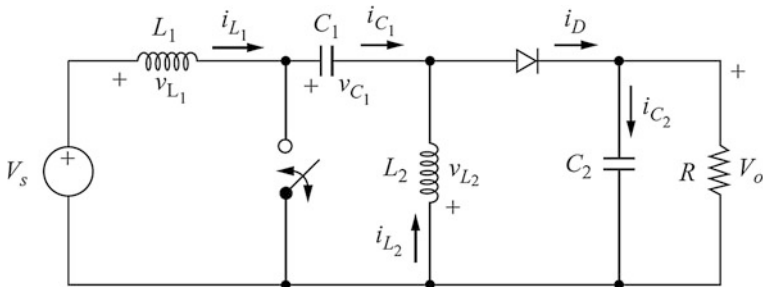


Fig. 1 SEPIC

see that I_{L1} and I_{L2} are correlated by the energy transfer through capacitor C_1 . The SEPIC is modeled using state space model. Assuming the turnoff time for the switch S is T_{off} and turn-on time for the switch S is T_{on} and $T_s = T_{\text{on}} + T_{\text{off}}$, we can write the equations I state space form for the continuous conduction mode as follows:

(1) Switch S is off ($0 < t < T_{\text{off}}$)

$$\begin{aligned}\frac{di_{L1}}{dt} &= \frac{1}{L_1} V_{\text{in}} - \frac{1}{L_1} V_{c1} \\ \frac{dV_{c1}}{dt} &= \frac{1}{C_1} i_{l1} \\ \frac{di_{L2}}{dt} &= -\frac{z}{L_2} i_{l2} \\ \dot{x} &= A_1 x + B_1 V_{\text{in}} \\ V_0 &= Y_1 x \text{ where, } x = [i_{L1}, v_c, i_{L2}]\end{aligned}$$

$$A_1 = \begin{bmatrix} 0 & -\frac{1}{L_1} & 0 \\ \frac{1}{C_1} & 0 & 0 \\ 0 & 0 & \frac{1}{L_2} \end{bmatrix}, \quad B = \begin{bmatrix} \frac{1}{L_1} \\ 0 \\ 0 \end{bmatrix}, \quad \text{and } Y_1 = [0 \quad 0 \quad Z]$$

(2) Switch S is on ($T_{\text{off}} < t < T_s$)

$$\begin{aligned}\frac{di_{L1}}{dt} &= \frac{1}{L_1} V_{\text{in}} \\ \frac{dV_{c1}}{dt} &= -\frac{1}{C_1} i_{l2} \\ \frac{di_{L2}}{dt} &= -\frac{z}{L_2} i_{l2} + \frac{1}{L_2} V_{c1} \\ \dot{x} &= A_2 x + B_2 V_{\text{in}} \\ V_0 &= Y_2 x \text{ where } x = [i_{L1} \quad v_c \quad i_{L2}]\end{aligned}$$

$$A_1 = \begin{bmatrix} 0 & 0 & 0 \\ 0 & 0 & \frac{1}{C_1} \\ 0 & \frac{1}{L_2} & \frac{z}{L_1} \end{bmatrix}, \quad B = \begin{bmatrix} \frac{1}{L_1} \\ 0 \\ 0 \end{bmatrix} \text{ and } Y_2 = [0 \quad 0 \quad Z]$$

Averaged state space expressions over the period $[0 < t < T_s]$ by considering the duty ratio $d = T_{on}/T_s$ we obtain,

$$\begin{aligned}
 A &= A_1(l - d) + A_2d \\
 B &= B_1(l - d) + B_2d \\
 Y &= Y_1(l - d) + Y_2d \\
 \dot{x} &= Ax + BV_{in} \\
 V_0 &= Yx
 \end{aligned}$$

where

$$A = \begin{bmatrix} 0 & -\frac{(1-d)}{L_1} & 0 \\ \frac{(1-d)}{C_1} & 0 & -\frac{d}{L_2} \\ 0 & \frac{d}{L_2} & \frac{Z}{L_1} \end{bmatrix}, \quad B = \begin{bmatrix} \frac{1}{L_1} \\ 0 \\ 0 \end{bmatrix} \quad \text{and} \quad Y_2 = [0 \quad 0 \quad Z]$$

From above equations, we can write the voltage transfer function of the SEPIC $G_v = V_o/V_{in}$ as:

$$G_v = \frac{Zd(1 - d)}{C_1L_1L_2S^3 + C_1L_1ZS^2 + S(L_2 - 2dL_2 + d^2L_2) + (Z - 2dz + d^2z)}$$

3 Inverter Modeling Using SEPIC

The novel three-phase inverter using SEPIC is illustrated in Fig. 2.

All Cuk converter used here provides sinusoidal voltage at output with a DC offset. Assumption of the DC and AC voltage ratio between output and input as H_{dc} and H_{ac} , respectively.

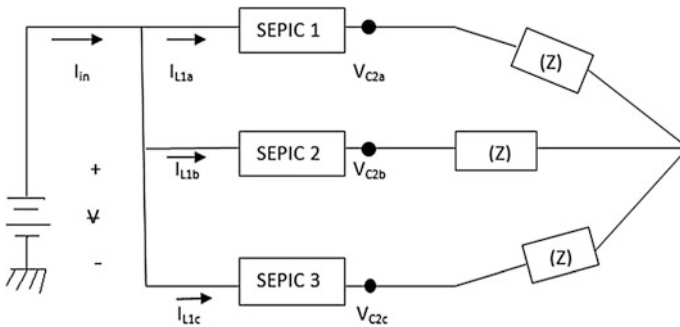


Fig. 2 Three-phase inverter using three SEPICs

$$\begin{aligned}
 V_{c2a} &= H_a V_{in} \\
 H_a &= H_{dc} + H_{ac} \sin(\omega t + \theta) \\
 V_{c2b} &= H_b V_{in} \\
 H_b &= H_{dc} + H_{ac} \sin\left(\omega t - \frac{2\pi}{3} + \theta\right) \\
 V_{c2c} &= H_c V_{in} \\
 H_c &= H_{dc} + H_{ac} \sin\left(\omega t + \frac{2\pi}{3} + \theta\right)
 \end{aligned}$$

As all the three phases operate in the balanced mode, the DC offset of each phase gets cancelled and a pure sinusoidal waveform for the voltage and current is obtained.

A SEPIC is implemented using the SimPowerSystems library blocks as shown in Fig. 3a. A 1-stage 3-phase inverter is formed by integrating three SEPICs in parallel as shown in Fig. 3b. Each of the three phases is displaced to one another by 120° phase shift. The current and voltage outputs obtained from all the three phases are sinusoidal but distorted, so this output cannot be applied to any load as it could produce various side effects on the load such as heating and improper functioning of the device. Thus, we need to improve these output voltage waveforms obtained by the inverter model by using some control strategies so that we could get an output voltage which is purely sinusoidal output waveform. Here, we are using the fuzzy logic control strategy for the same purpose.

4 Fuzzy Logic Controller (FLC) for Inverter

FLC technique has been utilized in the proposed circuit to provide pulses to the inverter switch in order to obtain the desired pure sinusoidal output waveforms.

The fuzzy inference system (FIS) is the tool by which the input values can be mapped to the output values by making use of fuzzy logic. FIS formalizes the process involved in the reasoning capacity by the humans in their language with the means of using fuzzy logic and building the if-then rules for the same. Various rules are formed using the rule viewer in the FIS editor which give rise to a controlling factor on the comparison of the parameter a and center frequency f_b . Based on that controlling factor the pulse generator used in the inverter model, we get the output voltage at various frequencies. These rules are formed under Mamdani's editor

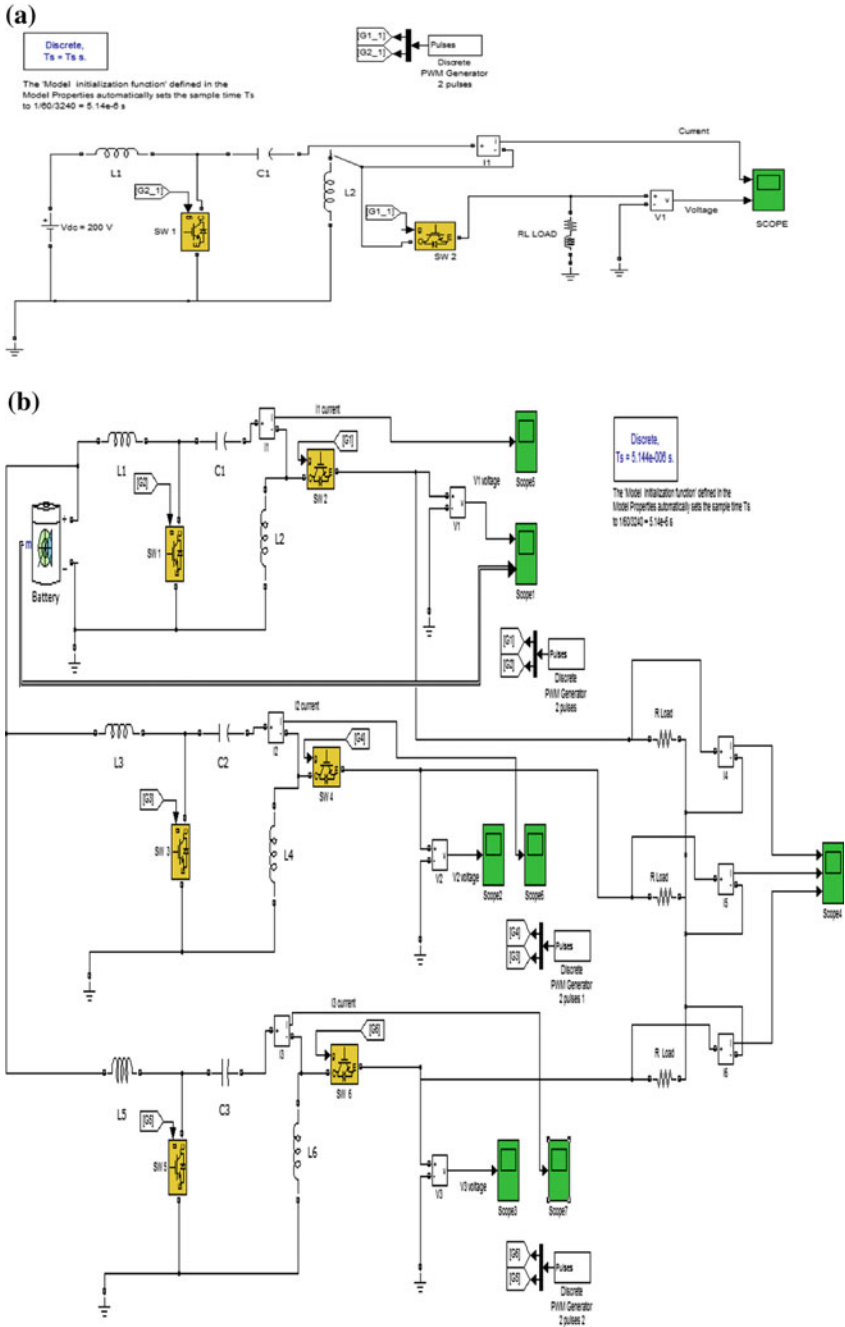


Fig. 3 a SEPIC model in MATLAB, b three-phase inverter model using SEPIC

where we describe the various rules by making use of AND, OR, and NOT operation of the fuzzy logic, and with these rules, we can use any of the membership function, i.e., trapezoidal and triangular [14].

As the inverter designed produces distorted output voltage and current waveform, the fuzzy logic controller is used whose output is given to the switch used in the circuit. As we know by improving the duty ratio of the switches used in the converter, the output which is closer to the sinusoidal waveform can be obtained. With the implementation of the fuzzy controller instead of the PWM pulse generator input to the switch, the duty ratio of the switch has been improved. In this way by including the fuzzy control, we are able to get the sinusoidal waveforms for the output current and voltage.

5 Results and Discussions

The results obtained for both the uncontrolled and fuzzy logic controlled inverters are shown here, and complete analysis is presented. Figure 4 shows the inverter output current waveforms for phase a, b, and c. The output current waveform can be seen to be highly distorted.

Figure 5a shows the phase-a output voltage waveform. An input DC voltage of 100 V is the input to the inverter which is depicted in the second graph of Fig. 5a. In Fig. 5b, c the output voltage waveform is presented for phase-b and phase-c, respectively. These waveforms are not purely sinusoidal as shown in Fig. 4. Thus, in order to get purely sinusoidal current and voltage waveform, fuzzy logic controller is implemented.

After implementing fuzzy logic controller in our inverter model, desirable sinusoidal waveform is obtained as shown in Fig. 6. Figure 6a shows the output current for phase-a, the output voltage for phase-a, and the DC input voltage. It can be observed that the output voltage and current waveform is a pure sine wave having an amplitude of 300 V and 3 A, respectively, which is obtained from 100 V DC supply voltage as an input. Figure 6b, c shows the waveforms for the output current and output voltage for phase-b and phase-c, respectively.

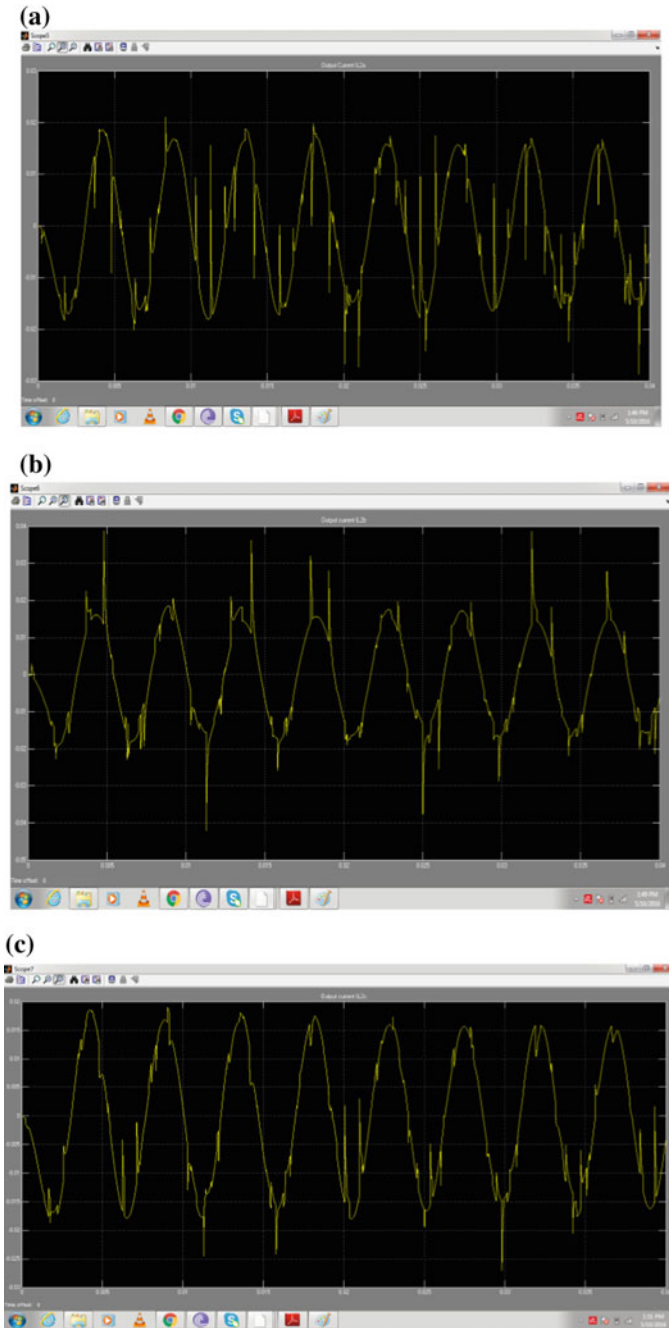


Fig. 4 Waveforms for inverter output current **a** phase-a output current I_{L2a} , **b** phase-b output current I_{L2b} , **c** phase-c output current I_{L2c}

Fig. 5 Waveforms for inverter output voltage
a voltage of phase 'a' V_{C2a} ,
b voltage of phase 'b' V_{C2b} ,
c voltage of phase 'c' V_{C2c}

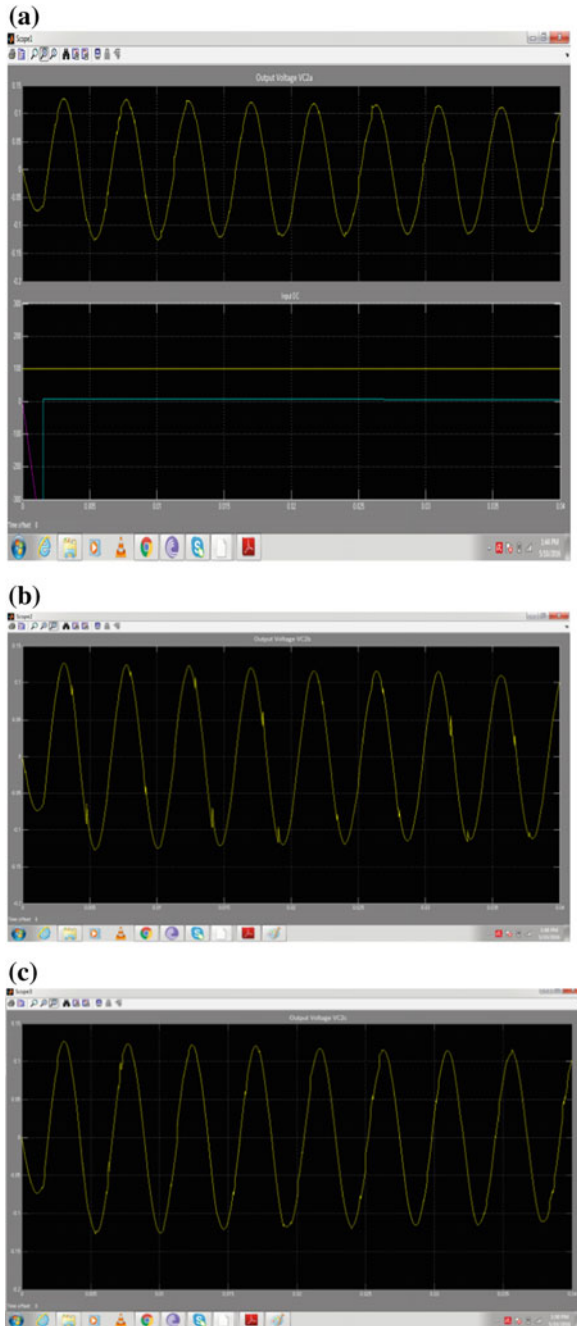
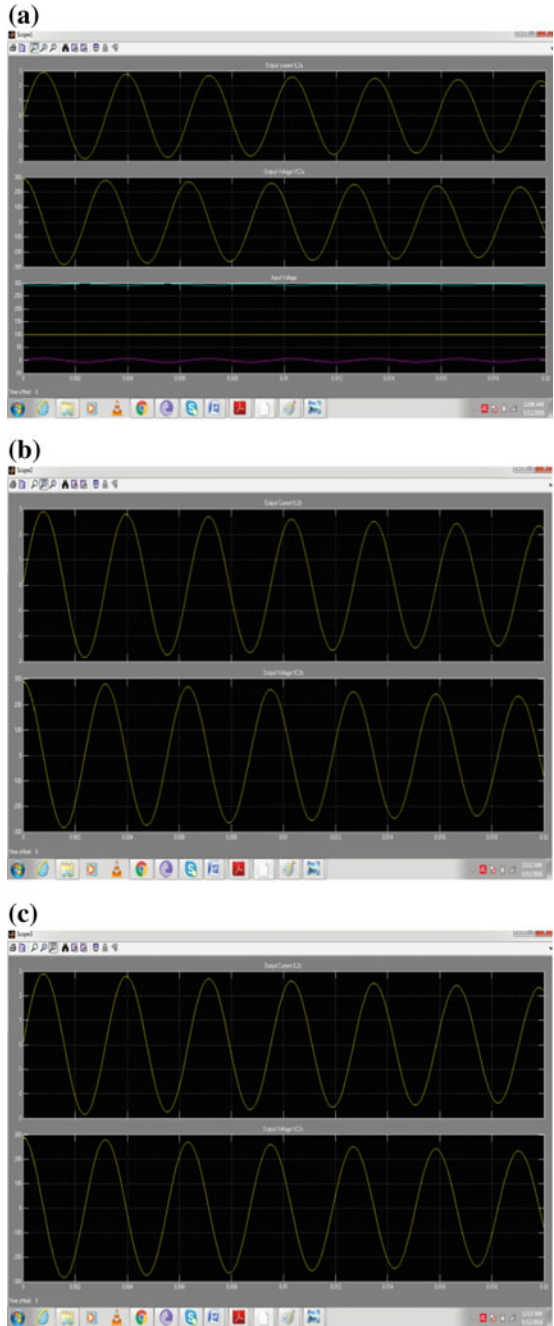


Fig. 6 Inverter output current and voltage **a** current I_{L2a} , voltage V_{C2a} waveform and input DC voltage, **b** output current I_{L2b} and voltage V_{C2b} waveforms, **c** current I_{L2c} and voltage V_{C2c} waveforms



6 Conclusions

A single-stage three-phase inverter using SEPIC operated with fuzzy controller is presented in this chapter. The SEPIC-based inverter has inbuilt characteristics of buck and boost converters, which the traditional inverters lack. With the variation of duty ratio, functioning of the converter can be controlled, and this provides flexibility for the inverter to be used either in case of standalone or grid mode cases where the desired AC voltage at output is either greater or smaller than the DC voltage at input. The number of inductors and capacitors is reduced as well, which increased the reliability of the system along with reduction in the size and total cost of the inverter. The controlling of the designed inverter through fuzzy logics by defining the various implementation rules and membership function so as to get desired output from the inverter also proves to be useful. With usage of fuzzy controller, the complexity of the circuit is reduced as compared to other PI/PID controllers. The results are obtained by MATLAB/Simulink, and satisfactory results in terms of lower second-order harmonic components in the output voltage and current were found.

References

1. R. O. Caceres and I. Barbi, "A boost dc-ac converter: Analysis, design, and experimentation," *IEEE Trans. Power Electronics*, vol. 14, no. 1, pp. 134–141, Jan. 1999.
2. B. S. Prasad, S. Jain, and V. Agarwal, "Universal single-stage grid-connected inverter," *IEEE Trans. Energy Convers.*, vol. 23, no. 1, pp. 128–137, Mar. 2008.
3. M. Jang, M. Ciobotaru, and V. G. Agelidis, "A single-phase grid-connected fuel cell system based on a boost-inverter," *IEEE Trans. Power Electronics*, vol. 28, no. 1, pp. 279–288, Jan. 2013.
4. V. Chunkag and U. Kamnam, "Paralleling three-phase AC to DC converter using Cuk rectifier modules based on power balance control technique," *IET Power Electronics*, vol. 3, no. 4, pp. 511–524, Jul. 2010.
5. H. S.-H. Chung, K. K. Tse, S. Y. R. Hui, C. M. Mok, and M. T. Ho, "A novel maximum power point tracking technique for solar panels using a SEPIC or Cuk converter," *IEEE Trans. Power Electron.*, vol. 18, no. 3, pp. 717–724, May 2003.
6. A. Darwish, D. Holliday, S. Ahmed, A. M. Massoud, and B. W. Williams, "A single-stage three-phase DC/AC inverter based on Cuk converter for PV application," *IEEE Journal of Emerging and Selected Topics in Power Electronics*, vol. 2, no. 4, pp. 797–807, Dec. 2014.
7. W. Zhao, D. D.-C. Lu, and V. G. Agelidis, "Current control of grid-connected boost inverter with zero steady-state error," *IEEE Trans. Power Electron.*, vol. 26, no. 10, pp. 2825–2834, Oct. 2011.
8. J. Knight, S. Shirsavar, and W. Holderbaum, "An improved reliability Cuk based solar inverter with sliding mode control," *IEEE Trans. Power Electron.*, vol. 21, no. 4, pp. 1107–1115, Jul. 2006.
9. Johanna M.A. Myrzlk, "Novel Inverter Topologies for Single-phase Stand-Alone or Grid-Connected Photovoltaic Systems," *IEEE PEDS 2001 Indonesia*, vol. 1, no. 1, pp. 103–108, Oct 2001.
10. J. Hammerbauer and M. Stork, "State space study of the SEPIC converter," *2013 International Conference on Applied Electronics, Pilsen*, 2013, pp. 1–4.

11. H. L. Do, "Soft-Switching SEPIC Converter With Ripple-Free Input Current," in *IEEE Transactions on Power Electronics*, vol. 27, no. 6, pp. 2879–2887, June 2012.
12. S. J. Chiang, S. Hsin-Jang, and C. Ming-Chieh, "Modeling and control of PV charger system with SEPIC converter," *IEEE Trans. Ind. Electron.*, vol. 56, no. 11, pp. 4344–4353, Nov. 2009.
13. El Khateb, A; Abd Rahim, N.; Selvaraj, J.; Uddin, M.N., "Fuzzy-Logic Controller-Based SEPIC Converter for Maximum Power Point Tracking," *Industry Applications, IEEE Transactions on*, vol. 50, no. 4, pp. 2349–2358, July-Aug. 2014.
14. M. N. Uddin, T. S. Radwan, and M. A. Rahman, "Fuzzy-logic controller based cost-effective four-switch three-phase inverter-fed IPM synchronous motor drive system," *IEEE Trans. Ind. Appl.*, vol. 42, no. 1, pp. 21–30, Jan./Feb. 2006.

Inductive Power as Wireless Energy in Electrical Applications

**Shubham Kumar, Adesh Kumar, Vivek Kaundal
and Mukul Kumar Gupta**

Abstract Nowadays, every single person is using mobile phones which became the integral part of their lives. It gives access to internet, movies, videos and books also. Using internet 3G or 4G gives heavy load to the battery which gets discharged soon. If a man using a smartphone and using all of these features then it gives an average of seven hours of battery life. After these seven hours, battery will be discharged. What will a person do when he is travelling and the battery of his smartphone get discharged. As technology improves, we should have a solution to this problem. So a wireless energy transfer car charger can be a solution to this problem. The paper focuses on the wireless charging theoretical aspects and its successful testing environment.

Keywords Self-inductance · Wireless charging

1 Introduction

These days travelling have become an integral part of everyday life. According to a study, on an average a person travels for 50–60 min every day. We can use this time to keep our smartphones operational by charging it. Smartphones which are generally used in India are Samsung, Micromax and Motorola, etc. These phones take about one and half hours to get fully charged. So, a person can charge his

S. Kumar (✉) · A. Kumar · V. Kaundal · M.K. Gupta
Department of Electronics, Instrumentation and Control Engineering, University of
Petroleum and Energy Studies (UPES), Dehradun 248007, Uttarakhand, India
e-mail: sk616391@gmail.com

A. Kumar
e-mail: adeshmanav@gmail.com

V. Kaundal
e-mail: vkaundal@ddn.upes.ac.in

M.K. Gupta
e-mail: mkgupta@ddn.upes.ac.in

phone up to 70%, which is fair enough for use. With wireless energy transfer, it can be possible to charge a phone without connecting it to the charger. Without any effort, a pocketed phone will get charged wirelessly through the transmitter coil fitted under the seat. Nothing is required for the user to charge phone after the initial set-up. The energy to the set-up will be provided by the car battery. The aim of this work is to create wireless energy transfer system [1, 2] which will transfer energy wirelessly to charge mobile phones. Goal is to obtain maximum efficiency at a specific distance as 70% efficiency at a distance of 1–2 ft. In 2010, Android and i-phone users spent an average of 80 min/day to charge their phones. Using mobile apps with video, internet and telecommunication, smartphones need an extended charging period throughout the day to keep them operational. The system that installed in the car constantly charge the phone without any effort and users can use their phones while charging. This will reduce the low battery and switch off condition of phones because every time phone will be in charge. When a user get the notification on his phone that battery is critically low, connect to the charger and then the user rushes to find the charger, in this situation the only solution is to use a car charger, i.e. wireless charger [3, 4]. This wireless system charger will give the solution to the problem of plugging and unplugging of charger. It will remove the need for the charger and will simply start charging on entering the car and stop when exit from the car. This is the time to say goodbye to the wire charger and plugging, unplugging problem.

This system uses common material, such as copper wire and capacitor that cause no danger to human. Yet, there are not any known problems caused by this wireless system. This system is also done with much more powerful magnets but doesn't have produced any harm in human bodies. This system does no harm or any problem when it is housed inside vehicle. To charge a phone, this system requires 5 W from the car battery and 3.5 W to charge a phone. Since, there is wirelessly transmitted energy there will be some power losses, which cause some pollution as compared to solar charger. If the material required for the system comes from outsourced then the manufacturing cost would be around \$20 and manufacture can retail it for \$30 or more. Its cost would decrease if the manufacturer makes their parts. Automotive shopkeeper can charge for installation. There is no additional cost beside the fuel used to charge the car's battery. If there will be any problem in coils then removing or replacement of coils could be done. It's lifelong as it only serves for energy transfer.

One can use this product and its application to make a start-up company. Since, it is the new idea for the product and would rise great opportunity for new company to build business. If a large company would adopt this idea then the investment on this product will be less and there will be a large profit for the company. A wireless energy transfer charger would push a company to a high peak of business.

Now we are going to create a system that will transfer the energy wirelessly and by this energy a mobile phone [6, 7] will charge. Magnetic field [1, 4] plays a main role in transferring energy. This is achieved by connecting a power source to an inductive coupling system that uses magnetic field to transfer energy through air. There will be two coils in coupling system one is transmitting coil component L_1

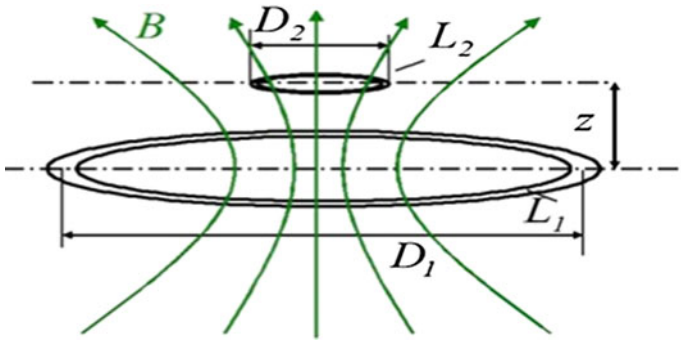


Fig. 1 Inductive coupling system [5, 8]

sending energy to another a receiving coil component L_2 . When L_1 coil is connected to the power source then it creates a magnetic field B . With the help of this magnetic field B created by L_1 coil, L_2 coil creates an energy signal. The inductive coupling system is shown in Fig. 1.

The efficiency is the most important for this system. Higher will be the efficiency, best the product will be. It depends on two factors, the size of both the coils (D_1 and D_2) and the distance between the coils, i.e. Z . As the ratio D_2/D_1 decreases, efficiency will decrease and if the distance between the coils increases efficiency will also decrease. To make the system strong and efficient, we have to add one more coil to transmitting side and one more in receiving side. When the first two transmitting coils are connected to the power source, then the energy will wirelessly transfer to the receiving coils. The energy will then go towards charging the battery of a phone, which would be load.

2 Principle of Operation

The principle is based on the mutual induction, when two inductors are placed in a small and large distance as shown in Fig. 2. The electricity at the source end is converted into magnetic waves and the same magnetic wave is converted into electricity at the load. The diagram is shown in Fig. 3 to support the same function.

The transformer operation is achieved with the help of mutually coupled inductors. The mutually coupled inductors result the application of transformer with the variations in their construction. The coupled inductor is used to store the energy in magnetic field because they are separated by a gap. In a fly back converter, the coupled inductor can be used to store the energy when the switch is in ‘ON’ condition and dump the energy when the switch is in ‘OFF’ condition. The mutual inductance principle is shown in Fig. 4 in which transmitting and receiving coils are arranged and self-induced.

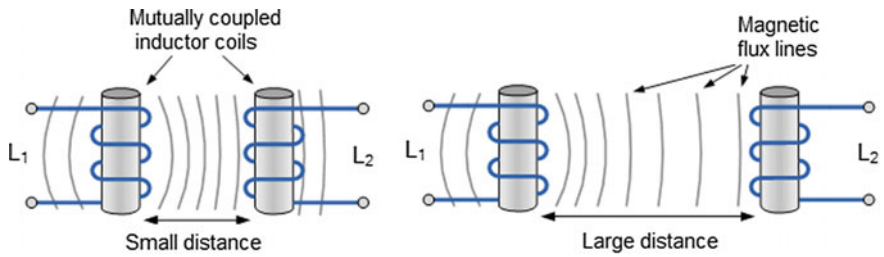


Fig. 2 Mutually connected coils [8]

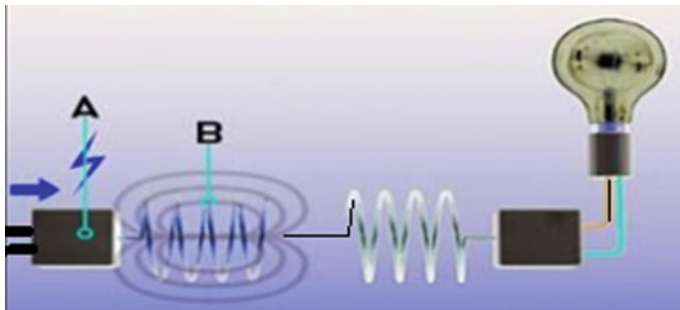


Fig. 3 Energy conversion (electricity—magnetic wave—electricity)

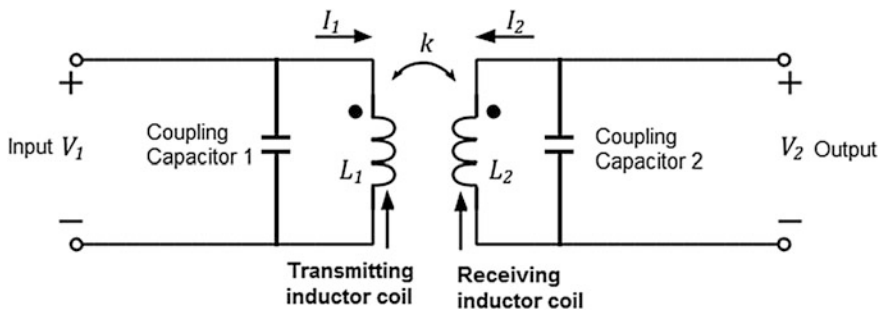


Fig. 4 Mutual inductance in primary and secondary

Let there are N_1 number of turns in primary coil and N_2 number of turns in secondary coil. A current I_1 in the primary coil produces a magnetic field.

$$B = \frac{\mu_0 N_1 I_1}{l}$$

This will give rise in flux

$$\phi_{11} = BN_1A = \frac{\mu_0 N_1^2 AI_1}{l}$$

In the same way, the primary coil gives

$$\phi_{21} = BN_2A = \frac{\mu_0 N_1 N_2 AI_1}{l}$$

In the secondary coil due to current in primary coil, by the definition of self-induction

$$\phi_{11} = L_1 I_1$$

So,

$$L_1 = \frac{\mu_0 N_1^2 A}{l},$$

and by definition of mutual induction

$$\phi_{21} = M_{21} I_1$$

So,

$$M_{21} = \frac{\mu_0 N_1 N_2 A}{l}.$$

Reversing the procedure if we first introduce the current I_2 in secondary coil then we get

$$L_2 = \frac{\mu_0 N_2^2 A}{l}$$

and

$$M_{12} = \frac{\mu_0 N_1 N_2 A}{l}.$$

So L_1 is the self-inductance of primary coil, L_2 is the self-inductance of secondary coil and $M_{21} = M_{12} = M$ is the mutual inductance between two coils. The product of L_1 and L_2 is given as

$$L_1L_2 = \frac{\mu_0^2 N_1^2 N_2^2 A^2}{l^2} = M^2.$$

Hence

$$M = \sqrt{L_1L_2}.$$

In practice, M is always less than equation due to leakage which gives

$$\frac{M}{\sqrt{L_1L_2}} = k,$$

where k is called coefficient of coupling and k is always less than 1.

Equation is written as

$$v_1 = L_1 \frac{di_1}{dt} + M \frac{di_2}{dt},$$

$$v_2 = M \frac{di_1}{dt} + L_2 \frac{di_2}{dt},$$

$$M = k\sqrt{L_1L_2}.$$

3 Block Description of the System

In this design, we take energy from power source and allow transferring it wirelessly. At receiving coil, we receive AC and it can be converted into DC for charging purpose. The block diagram of the wireless charging/energy transfer is shown in Fig. 5. Here, the set-up involves an oscillator which will give frequency to AC supply and rectifier converts AC to pulsating DC, after that an inverter is used to convert DC to AC. Now with the help of impedance matching circuit, the high frequency supply matches the resonance condition so that an efficient transfer of

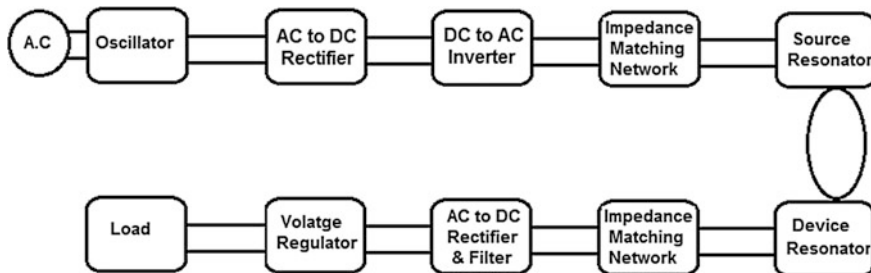


Fig. 5 Block diagram of wireless energy

power takes place. Source resonator is used which produce magnetic lines of force. The energy coupled with the resonator is again rectified to a DC with the use of a rectifier; filtering and voltage regulated output is given to the load requirement such as battery charging.

3.1 Power Transfer

For the wireless transmission of AC power source, we use inductive coupling. For that we measure the inductance of inductor and then couple it with a capacitor to be tuned to a frequency. In order to communicate together much more efficiently, the frequencies are matched in both transmitting and receiving coils. As we receive the AC at the receiving coil it is converted into DC with the help of half wave rectifier and regulator circuit.

3.2 Efficiency

If we want to get maximum efficiency, the ratio of transmitting to receiving coil should be 1:1. In order to get proper efficiency along with larger coil-to-coil ratio, we make transmitting coil larger than receiving coil. If we want to get 70% efficiency, the coil size D_2/D_1 should be 0.3.

3.3 Coil Inductors

Since the size of receiving coil depends on the size of phone, so we have calculated it earlier to be 2.25 in diameter for receiving coil. Size of transmitting coil also depends on size of receiving coil. In order to maintain this ratio $D_2/D_1 = 0.3$. For 70% efficiency, size of transmitting coil will be 7.5 inch in diameter.

3.4 Capacitors

A correct capacitor is needed to be coupled with inductor. We will use this formula,

$$f = \frac{1}{2\pi\sqrt{LC}}.$$

Either we can find frequency with given value of capacitor or we can find capacitor to be coupled for a given value of frequency. Value of the other capacitor which is to be connected to other coil can be found by this formula,

$$C = \frac{1}{4\pi^2 f^2 L}.$$

These capacitors are then connected in parallel with inductors for resonant coupling. Quality factor is ratio of apparent power to the power source. As quality factor increases power factor decreases. The formula for quality factor is,

$$Q = \frac{\omega L}{R}.$$

Quality factor should be around 100 for a useful coil. One way to increase quality factor is to increase frequency. But increasing value of frequency decreases value of capacitor.

4 Results and Discussions

In order to test the efficiency and reliability, a 12 V DC load is tested/used. The distance is set to be 9 times the radius of the coil. The classical Colpitt oscillator has been used to couple inductively which is made up of copper wire of 30 cm in radius. The load consists of DC motors and the current consumed by motors have been monitored using ACS712 module-current sensor based on Hall Effect. The same data is monitored via LCD display and have been logged into SD card module for further assessment. It has been observed that with varying distance the efficiency is decreasing. The efficiency calculated for 100 cm, 175 cm and 225 cm is 0.8, 0.6 and 0.3 respectively. We believe that the efficiency can be further improved with changing the material of coil; for the experiment conducted, the performance characteristics are already up to the mark for designing and implementing the practical application for DC loads (Fig. 6).



Fig. 6 Testing environment

5 Conclusion

The wireless inductive coupling and energy transfer is a forefront technology in the latest development of electronics charging. The applications are involved in solar cells, microwaves, lasers and electromagnetic waves. The main use to this electrical device is to provide continuously charging without the use of power cord. The experiment is successfully tested in variation of distance and the efficiency of the system is also decreased with the large distance. The efficiency calculated for 100 cm, 175 cm and 225 cm is 0.8, 0.6 and 0.3 respectively. In future we are planning to use such charging system for RF applications.

References

1. A. Kurs, A. Karalis, R. Moffatt, J. D. Joannopoulos, P. Fisher, M. Soljacic. "Wireless Power Transfer via Strongly Coupled Magn. Resonances" *Science* Vol. 317, 2007, pp (83–86)
2. B. Choi, J. Nho, H. Cha, T. Ahn, and S. Choi, "Design and implementation of low-profile contactless battery charger using planar printed circuit board windings as energy transfer device," *IEEE Trans. Ind. Electron.*, vol. 51, no. 1, pp. 140–147, Feb. 2004
3. B. Nizam "Inductive Charging Technique" *International Journal of Engineering Trends and Technology (IJETT)* Vol.4, Issue 4–2013, pp (1055-1059)
4. H. Zenkner, W. K. Ngern "Energy Transfer by Resonance Coupling" *International Journal of Electrical and Computer Engineering (IJECE)* Vol. 3, No. 5, 2013, pp. (668–682)
5. R. Sasur Thesis on "Wireless Energy Transfer" Electrical Engineering Department California Polytechnic State University San Luis Obispo 2011, pp (1–40)
6. W. Zhong, C. K. Lee, and S. Y. Ron Hui "General Analysis on the Use of Tesla's Resonators in Domino Forms for Wireless Power Transfer" *IEEE Transactions On Industrial Electronics*, Vol. 60, No. 1, 2013, pp (261–270)
7. Wireless Power Consortium, Transfer efficiency, <http://www.wirelesspowerconsortium.com/technology>
8. <https://www.wirelesspowerconsortium.com/technology/basic-principle-of-inductive-power-transmission.html>

VGA Application in Text Display Using FPGA

Akarsha Mishra, Adesh Kumar and Rakshita Parihar

Abstract This research paper presents the idea of designing and implementing the VGA applications on FPGA. The goal of the first application here is to display a four-bit digit on a VGA screen, and the second application focuses on displaying a 32-bit text on the screen. VGA plays an important role in displaying the data on the screen. VGA cable is connected to the FPGA board easily since a VGA connector is provided on the board. The module is designed by programming of code in VHDL on Xilinx ISE 14.7 software. The synthesis is done with the help of Spartan 3E FPGA which estimate the supporting frame of 50 MHz.

Keywords Field programmable gate array
Very high speed hardware description language · Video graphics array

1 Introduction

Besides of having so many applications of FPGA, one of the applications is to display [1] text or characters on the screen. This application requires the use of VGA [2] controller that reads RGB values from FPGA and accordingly displays these values on the screen. The dimensions of the display which we want to see on the screen can be set in VGA module itself.

FPGA usage is a great improvement for digital designing; it has [3] modular capability, and VHDL programming is concise and clear. The graphics are controlled by the VGA module [4] that controls the screen size of the game and the control of movement of the horizontal and vertical porch of the display. Storage of

A. Mishra (✉) · R. Parihar
University of Petroleum & Energy Studies (UPES), Dehradun, India
e-mail: akarsharr1@gmail.com

A. Kumar
Department of Electronics, Instrumentation and Control Engineering,
University of Petroleum and Energy Studies (UPES), Dehradun 248007, Uttarakhand, India
e-mail: adeshkumar@ddn.upes.ac.in

graphics is done in BRAM, and the graphics are processed by GPU [5, 6]. A graphics processing unit (GPU) is a dedicated circuit that operates on a storage area which is a frame buffer for the purpose of providing display output. Pixel plotting plays a great role in the game control. FPGA Spartan 3E board does the logic processing part to complete the execution. The design has been completely realized on the FPGA chip [7] which communicates with the input and displaying output part through the corresponding interface which is a VGA cable. The horizontal synchronization and vertical synchronization [8, 9] signals are generated by the VGA controller which is responsible to coordinate that the delivery of the data of video is done on each clock of the pixel. The pixel clock [10] is actually a clock that defines the time required to display one pixel of information. The Vsync signal actually is responsible to check the starting and ending line of the screen. As soon as the line ends, all the information is redrawn. The practical refresh frequencies [11] lie in the range of 60–120 Hz. The horizontal retrace frequency is also responsible to check the start and end of the line horizontally, and the information is displayed again at a given refresh frequency. Display part transmits the VGA control [12] signals to the external monitor which shows the game display. No matter how good you could have planned a design, it can always be improved.

2 Related Work

Many researchers have worked on the design and FPGA implementation of games. Bowman et al. [1] have researched about employment of statistical data of the graphics to provide more data to the viewer. Ying and Feng [2] have discussed the design and implementation of VGA controller. The paper has given the design of its top layer module and the simulation of timing function. Detailed information focuses on the system architecture, hardware design, and software programming. Wang et al. [3] have provided graphical programming for different design patterns in FPGA. Yadav and Basha [4] have discussed the design of VGA controller using Verilog HDL language. The development has been developed on FPGA chip of Altera. Zhar et al. [5] have explained an FPGA-based image processing method. Gaikwad [7] has discussed about the top module that he has developed for ps/2 interfacing with monitor. Chu [8] has detailed about the working of ps/2 mouse as a unidirectional as well as bidirectional transmitter and has explained it through the code. Wasu and Wadhankar [9] have also discussed the design of VGA using Verilog to ensure the portability of the user. Radi et al. [13] have discussed the designing and implementing of VGA through FPGA using the test bench to test the accuracy of the system. McMahan et al. [10] have researched on the utilization of commercial video games as a means of enhanced learning, developing skills, etc. Gao et al. [14] address the implementation of multi-pursuit evasion games in which there are multiple agents doing their individual roles and interacting with the real world simultaneously. In such systems, real-time processing is an important issue which cannot be achieved by microcontrollers and therefore, FPGAs are a good

solution for resolving such problems. An efficient learning algorithm is used for each agent to take a required action at each step. Zafar et al. [11] explain how the graphics are processed in FPGA and where they are stored. The paper has explained about the GPU (graphics processing unit) that controls the display of graphics through VGA on screen. Alves et al. [6] have discussed porting as a critical task in mobile game development which is much easier in desktop games. Syed and Shaik [12] have discussed the design of efficient VGA controller hardware architecture which has a compatibility with PLB bus and has a high potential to be used in FPGA-based systems.

3 Block Diagram

Figure 1 shows the structure of VGA module used in the FPGA applications. It has five and eight inputs and outputs, respectively. The input given to the VGA is from the digit module in the first application and from the hex32 module in the second application. These modules have a signal val (4 bit) and hexval (32 bit), respectively, which is an input to the VGA. All the values are stored in a memory unit of FPGA. VGA controller takes these values and displays it on the monitor screen through a VGA cable. There are five signals that play an important role for the display and these are red, green, blue, hsync and vsync. The pin connections for these signals on the Spartan board are given in Table 1.

The Spartan-3E FPGA board contains following signals: Red, Green, Blue, Hsync, and Vsync where are all get connected with the VGA D15 connector. The pins on FPGA that drive the display are shown in Table 1.

Each colour line has a resistor connected in series that provide colours of three bit where each bit is for red, green and blue. To make sure that the colour signals are in the specified range of 0–0.7 V, a series resistor of 75 Ω at the VGA cable termination is used. The Hsync and Vsync signals are TTL-based. We can set the Red, Green and Blue signals ‘0’ or ‘1’ to produce the eight colour combinations shown in Table 2.

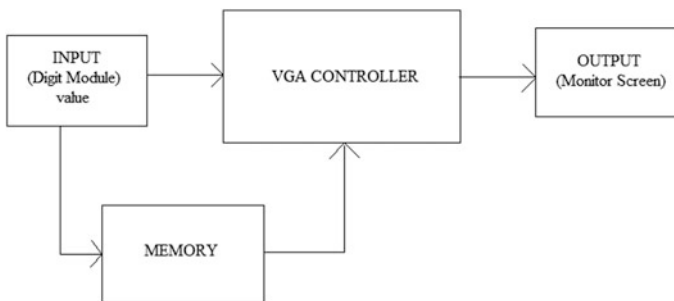


Fig. 1 VGA interface diagram for displaying text

Table 1 VGA port connections for Spartan-3E FPGA

Signal	FPGA pin
Red	H14
Green	H15
Blue	G15
Hsync	F15
Vsync	F14

Table 2 Colour codes for display

Colour formed	Red	Green	Blue
Black is formed	0	0	0
Blue is formed	0	0	1
Green is formed	0	1	0
Cyan is formed	0	1	1
Red is formed	1	0	0
Magenta is formed	1	0	1
Yellow is formed	1	1	0
White is formed	1	1	1

The concept of LCD comes from cathode ray tube displays where they use electron beams that are amplitude-modulated and accelerated. These electron beams when fall on the screen, the information is displayed due to the screen having phosphorous coating while LCD displays use nematic crystals that change their shape when electricity is passed through them. When electricity is passed, the crystals bend allowing the light to fall on the screen. These days LCD's have also started to use the same signal timing like CRT's. Inside a cathode ray tube display, when current passes through the coils they produce magnetic field that deviate the path of electron beams to travel the screen surface in a display pattern. It moves from left to right in horizontal direction, and it moves from top to bottom in vertical direction. The information is displayed when the beam is in between of the starting and ending of the line and not when it is coming back to its original position. Most of the information is therefore lost when the beam is travelling back to its original position. The display resolution is determined by the beam width, the frequency of the beam moving across the display and the frequency at which the modulation of beam takes place. Modern visual graphic array display supports multiple display resolutions, and the resolution is dictated by the VGA controller by producing timing signals which controls the display patterns. In this application, we have the display on LCD having the screen size 640 * 480. The video data comes from the video refresh memory with one or more bytes assigned to every pixel location. The Spartan-3E Starter Kit board which we have used has three bit for each pixel, producing eight possible colours shown in Table 3. The controller moves the buffered data of the video into the memory as the beams traverse across the display. This video data is collected by the controller and then this data is applied to the display at a time when the electron beams moves across a pixel.

Table 3 Signal description of digit module

Signal	Description
Val	Hexadecimal value on 4 bits
posX	X coordinate to display the digit. From 0 to 640
posY	X coordinate to display the digit. From 0 to 480
beamX	Gives current X position of the beam (refreshed pixel) from 0 to 640
beamY	Gives current Y position of the beam (refreshed pixel) from 0 to 480
beamValid	When set ('1'): the beam is in the visible area (640 × 480 area)
Red	Red colour of the digit
Green	Green colour of the digit
Blue	Blue colour of the digit
redOut	Red colour for the beam (refreshed pixel)
greenOut	Green colour for the beam (refreshed pixel)
blueOut	Blue colour for the beam (refreshed pixel)

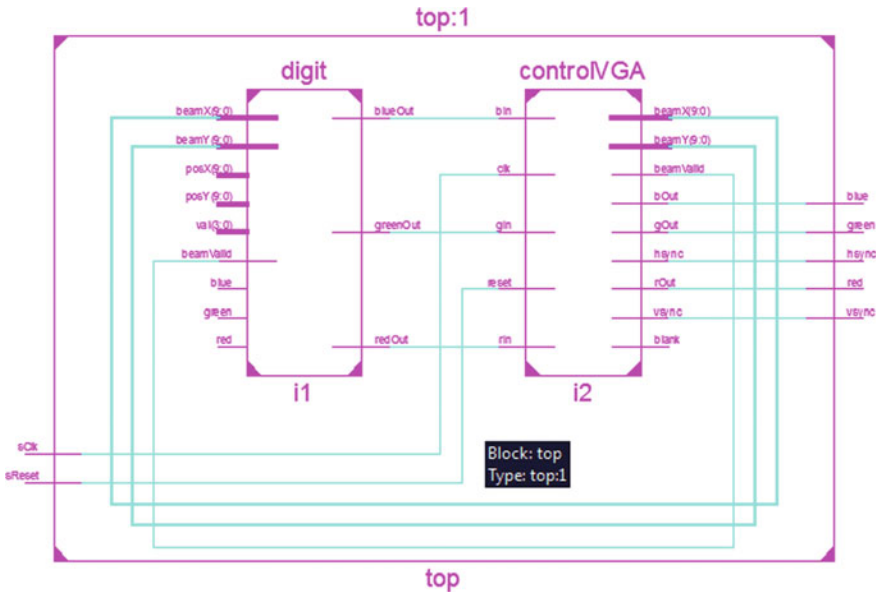


Fig. 2 Data path architecture of top for 4-bit text

4 Screen Display Internal Architecture

Figure 2 shows the data path architecture of the design. There are two modules digit and control VGA. The digit module is responsible for the data control operations like deciding what data needs to be displayed on the screen and at what position.

Table 4 Signal description of VGA module

Signal	Description
Clk50	50 MHz synchronized clock
Reset	Resets the system when high ('1')
rIn	Red In. This signal must be high when you want to turn on the red pixel at coordinate (beamX, beamY)
gIn	Green In. This signal must be high when you want to turn the green pixel on at coordinate (beamX, beamY)
bIn	Blue In. This signal must be high when you want to turn on the blue pixel at coordinate (beamX, beamY)
Red	Red colour of the beam (refreshed pixel)
Green	Green colour of the beam (refreshed pixel)
Blue	Blue colour of the beam (refreshed pixel)
Hsync	Signal for horizontal synchronization
Vsync	Signal for vertical synchronization
blank	The signal shows that the beam is outside the visible area (640 × 480)
beamX	Gives X coordinate of the beam (refreshed pixel) within the visible display (0–640)
beamY	Gives Y coordinate of the beam (refreshed pixel) within the visible display (0–480)
beamValid	When set ('1'): the beam is in the visible area (640 × 480 area)

The other module reads the RGB values and displays it on the screen. The digit module has many inputs and their description is given as follows in Table 3.

The detailed pin description of VGA module is given in Table 4. The main signals that are taken from the board are sclk, sreset, red, green, blue, hsync and vsync. These signals are initialized in top module. Module digit controls all the value-based operations like position value or pixel value, value to be displayed on the screen. Signal val is of four bit since only one digit needs to be displayed. Modules digit and VGA are connected to each other through signals redOut, greenOut and blueOut.

Figure 3 shows the data path architecture for the second application of displaying 32-bit text on the screen. There are also two modules where digit has been named as hex32 in this case since the signal taking the value is of now 32 bit. Rest of the signals have the same function as in the previous application. In this case also, modules hex32 and vga are connected to each other through signals hexblueOut, hexgreenOut and hexredOut.

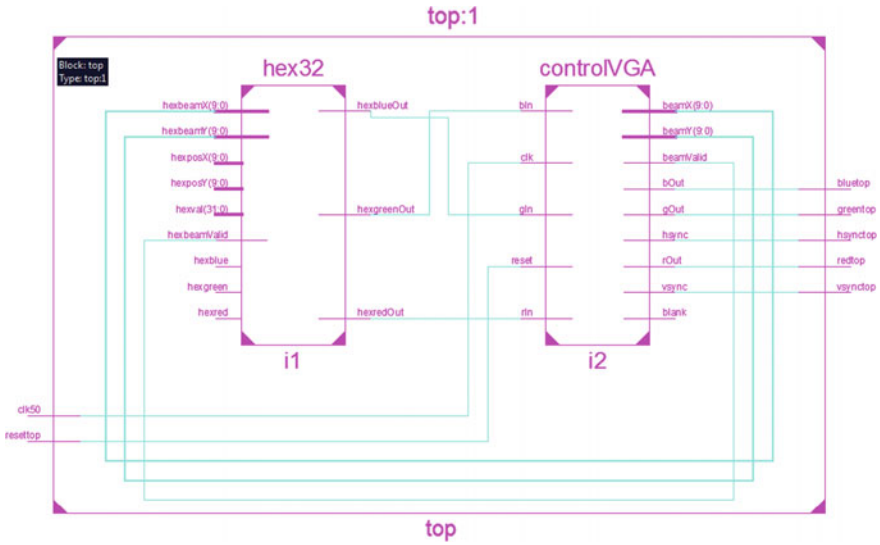


Fig. 3 Data path architecture of top for 32-bit text

5 Results

Figure 4 shows the RTL of top that has two inputs and five outputs. The description of each pin is given in Table 5. Figures 5 and 6 show the simulated waveform of the signals.

The simulation in Fig. 5 shows the resulting values of the signals. Clock operates at 50 MHz with a duty cycle of 50%. Signal reset is zero since it is used

Fig. 4 RTL of top

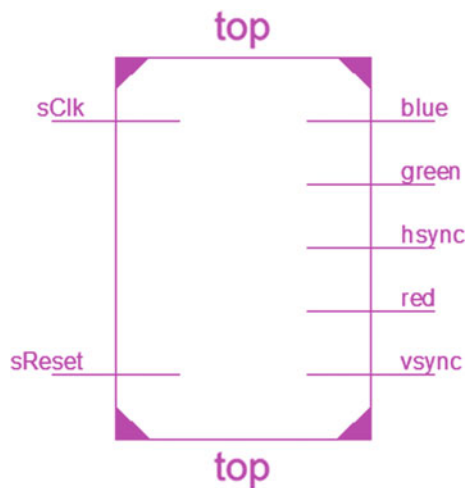


Table 5 Pin description of top

Pin	Description
Sclk	Synchronous clock given from the board
Sreset	Reset is to restart from the beginning
Blue	Blue signal value of vga taken from the board
Green	Green signal value of vga taken from the board
Hsync	Used for horizontal synchronization of the pixels
Red	Red signal value of vga taken from the board
Vsync	Used for vertical synchronization of the pixels

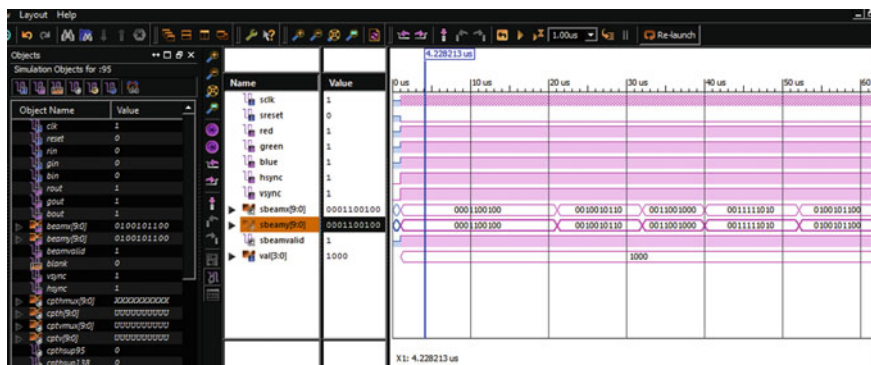


Fig. 5 Simulator waveform for displaying a 4-bit text

only to restart the operation from the beginning. Signals red, blue, green are set to one since the displayed text is white in colour.

Test Case 1: When clock is set, signals hsync, vsync and beamValid becomes high. beamValid will be '1' till it is in the visible are beamX, and beamY has been given a value '100' as a position where the text needs to be displayed. Signal val has a value '8' and '1000' in binary.

Test Case 2: Signal beamX and beamY = '150'. Val = '1000'.

Test Case 3: Signal beamX and beamY = '200'. Val = '1000'.

Test Case 4: Signal beamX and beamY = '250'. Val = '1000'.

Test Case 5: Signal beamX and beamY = '300'. Val = '1000'.

Figure 6 shows the simulated waveform of the signals for the application of displaying a 32-bit text. In this case also the clock is of 50 MHz and signal reset is zero. Signals red, green and blue are '1' since the text displayed is white in colour.

Test Case 1: Signal beamX and beamY = '100'. Val = '88888888'.

Test Case 2: Signal beamX and beamY = '100'. Val = '55555555'.

Test Case 3: Signal beamX and beamY = '100'. Val = '33333333'.

Test Case 4: Signal beamX and beamY = '100'. Val = '11111111'.

Test Case 5: Signal beamX and beamY = '100'. Val = '77777777'.

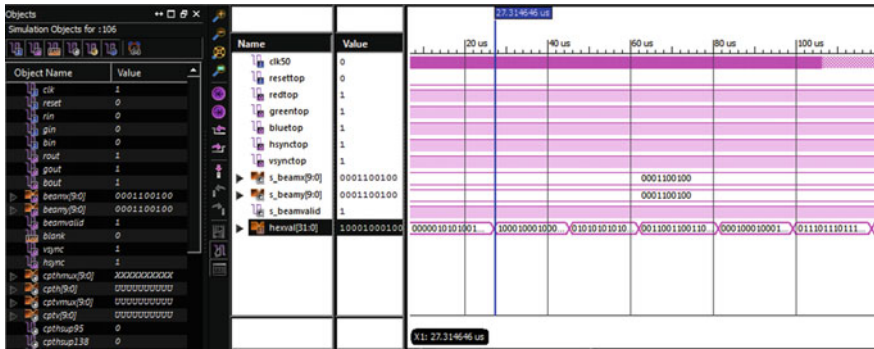


Fig. 6 Simulator waveform for displaying 32-bit text

6 Synthesis

The synthesis work is done on Spartan 3E FPGA. The corresponding design summary and report is given in Table 6. Total CPU time to Xst completion: 0.38 s.

Table 6 Design summary and report

Target device	Xc3s500e-4fg320	Errors	No errors
<i>Device utilization summary</i>			
Utilization of logic	Used	Available	Utilization (%)
Slice flip flop count	121	9312	1
4 input LUT count	955	9312	10
Occupied slices count	558	4656	11
Slices containing only related logic count	558	558	100
Slices containing unrelated logics count	0	558	0
4 input LUTs count	1070	9312	11
Logics used	955		
Route-thru used	115		
Bonded IOBs count	11	232	4
BUFGMUXs count	2	24	8
Average fan out of non-clocked nets	3.30		

7 Conclusion

The project is programmed in ISE Xilinx 14.7 and is simulated in ISim. As FPGA can be used for many applications, it can be used for many display applications also. It can further be used for gaming applications also since the display is possible with FPGA very easily. It was a good choice to implement this application on FPGA which is a suitable board for development that has port for VGA to interface a computer's monitor. To get rid of other dependencies and dependency on operating systems implementing the design on FPGA was a good idea. Also we can also design an ASIC which is a stand-alone chip by simply converting the VHDL code to the Verilog language with the help of Mentor Graphic tools which was one of the reasons to choose this platform, and we can create the final product by creating the layout of the chip. The layout can be made on very big number layers and as in integrated circuits is done, can be done with auto route. This way we can have design implemented on a chip which means that we have a stand-alone device with no speed issues, which would have been there if it would be made on a microcontroller because microcontroller processes small amount of data. And video processing type of processes cannot be handled easily in controllers because of less memory space and timing cycle constraints.

References

1. B. Bowman, N. Elmqvist, T. J. Jankun-Kelly, "Toward Visualization for Games: Theory, Design Space, and Patterns", *IEEE transactions on visualization and computer graphics*, vol. xx, 2012.
2. F. Ying, X. Feng, "Design and Implementation of VGA Controller Using FPGA" *International Journal of Advancements in Computing Technology*, Volume 4, 2012.
3. G. Wang, T. N. Tran, H. A. Andrade, "A Graphical Programming and Design Environment for FPGA-based Hardware" *IEEE*, 2010, pp. 337–340.
4. N. Yadav, Y. Basha, "Algorithm to Design VGA Controller on FPGA Board" *IOSR Journal of VLSI and Signal Processing*, Volume 6, Issue 6, Ver. II, pp. 82–86, 2016.
5. N. Zhar, M. A. Ali, M. Eleuldj, A. Raji, "A Specific-domain Design Tool for FPGA-based Image and Video Processing System" *International Journal of Computer Applications*, Volume 56, 2012, pp. 16–21.
6. V. Alves, I. Cardim, H. Vital, P. Sampaio, A. Damasceno, P. Borba, "Comparative Analysis of Porting Strategies in J2ME Games" *Proceedings of the 21st IEEE International Conference on Software Maintenance (ICSM'05)*, 2005.
7. P. K. Gaikwad, "Development of FPGA based PS/2 Mouse and VGA Monitor Interface Technique" *International Journal of Research in Engineering & Advanced Technology*, Volume 1, 2013.
8. P. P. Chu, "FPGA Prototyping by VHDL Examples" Ch-9, John Wiley & Sons Inc, 2008, pp. 199–214.
9. R. A. Wasu, V. R. Wadhankar, "Design and Implementation of VGA Controller on FPGA" *International Journal of Innovative Research in Computer and Communication Engineering*, Vol. 3, pp 7224– 7231, 2015.

10. R. P. McMahan, E. D. Ragan, A. Leal, R. J. Beaton, D. A. Bowman, "Considerations for the use of commercial video games in controlled experiments" International Federation for Information Processing Published by Elsevier B.V, 2011, pp. 3–9.
11. S. Zafar, S. Kataria, A. Sharma, "Digital design of a dedicated Graphics Processing Unit (GPU) architecture for microcontrollers" International Conference on Electronics and Communication System (ICECS), 2014.
12. Z. Syed, M. Shaik, "Fpga Implementation Of VGA Controller" International Conference on Electronics and Communication Engineering, pp 46–51, 2012.
13. Radi H.R., Caleb W. W. K., M. N. Shah Zainudin, M. Muzafar Ismail, " The Design and Implementation of VGA Controller on FPGA" International Journal of Electrical & Computer Sciences, Vol 12, pp 56–60, 2012.
14. S. Gao, S. N. Givigi, A. JG Beaulieu, "Fpga implementation of multiple pursuit-evasion games with decentralized learning automata" IEEE, 2014.

Survey on Implementation of Security in Cloud

Deepak Garg and Jagpreet Sidhu

Abstract Cloud computing has emerged as one of the next generation computer technologies. It is a model wherein storage, computing facilities, and applications are provided as services on the top of Internet. It permits associations to decrease capital costs, in administration costs, and improve unwavering quality and accessibility by getting administrations and infrastructural assets momentarily in a flexible way utilizing pay-as-you-go demonstrates. These services are provided on resources located at diverse geographical location beneath various service providers. The adjustment of cloud has exchange control of physical assets from potential clients to specialist organizations. This change has offered mount to security dangers and concerns which comes about into absence of certainty of potential clients on distributed computing. The paper displays a short explanatory review on different security issues in distributed computing. It presents a distinct view on classifying various security risks and concerns in cloud computing. A different method of classification varies security frameworks, models, and techniques—selected from latest literature on resources of repute. The paper concludes on realization of some unique cloud security objectives and challenges.

Keywords Cloud · Security · Cloud platforms · Effective citations

1 Introduction

The cloud computing worldview has turned into a standard answer for the arrangement of business procedures and applications, and it is quickly developing. It is giving people in general cloud vision, framework, stage, and programming

D. Garg (✉) · J. Sidhu

Department of Computer Science and Engineering, Chitkara University Institute of Engineering and Technology, Chitkara University, Patiala, Punjab, India
e-mail: deepak.garg@chitkara.edu.in

J. Sidhu

e-mail: jagpreet.sidhu@chitkara.edu.in

© Springer Nature Singapore Pte Ltd. 2018

R. Singh et al. (eds.), *Intelligent Communication, Control and Devices*,
Advances in Intelligent Systems and Computing 624,
https://doi.org/10.1007/978-981-10-5903-2_164

1587

administrations to clients and specialist co-ops on a compensation as-you-go premise. It is also modeled for enabling ever-present, suitable, on-demand network accessibility to a pool of configurable computing resources that are sharable and that can be swiftly provisioned and unrestricted by means of least management effort or service contributor interface. But, security is the major thing where we have to look onto it. Cloud Architecture: Depend on client-server services, we can divide cloud computing into three types: First, Platform-as-a-Service (PaaS): Cloud providers provide a platform where clients can run the applications means cloud providers are delivered the applications to the client that they are able to run the application on their own platform. Platforms are managed by the cloud providers. Second, Software-as-a-Service (SaaS): This service includes computing which is provided by cloud servers, consists of OS, coding language, database management, environment of the platform, etc. Without buying the hardware, customers can run the applications by using the resources. Third, Infrastructure-as-a-Service (IaaS): This is a tune-up of pay-as-you-go same as PaaS and SaaS including resources, storage, etc. (Fig. 1).

Cloud computing can be differentiated into four categories, and in all different categories, there are different security issues. Private cloud: Private cloud is used by a big institutes or societies. But this cloud will be restricted only in that organization means others organization can't share that cloud. Public cloud: This cloud is owned by an organization but other organization also can share that cloud. Hybrid cloud: An organization buys a cloud from another cloud services and uses that cloud. After buying the cloud, only the people of those organizations can only access that cloud. So, hybrid cloud consists of personal cloud and open cloud. The public cloud: This cloud is used by other organization (Fig. 2).

Various security dangers are related with cloud information administrations, such as network eavesdropping, side channel attacks, illegal invasion, virtualization vulnerabilities, abuse of cloud, and denial of service attacks. Security issues in cloud computing: The security issues we face in cloud computing can be categorized into three types:

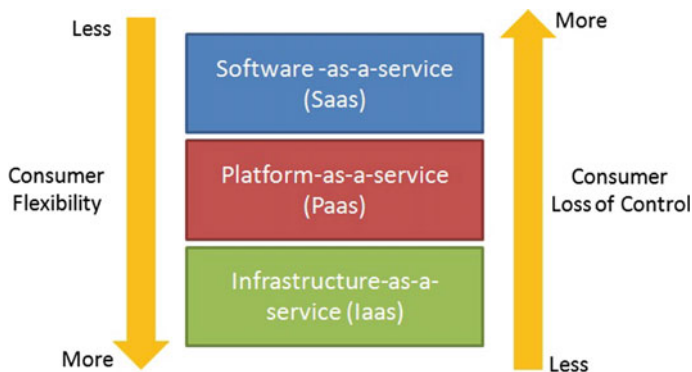
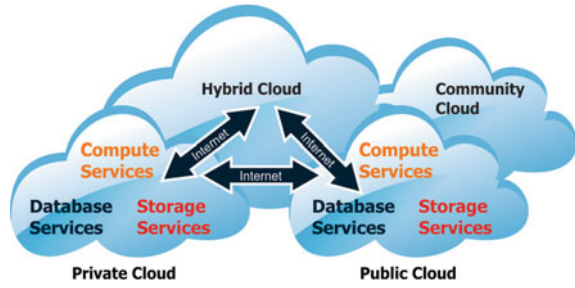


Fig. 1 Cloud deployment model

Fig. 2 Types of cloud deployment model



- Conventional security issues
- Availability issues
- Third-party control-related issues.

2 Literature Review

This paper analyzes the previous works of authors done between 2014 and 2016 in order to critically summarize the current knowledge in the area of security, and new algorithms are developed using some important techniques, and also, various outcomes are discussed. Figure 3 represents the different types of techniques used for evaluating or developing new security models.

However, Table 1 describes what type of dataset, Simulators, Parameters has been used to implement various new applications for security. Dataset is corpus on which the developed algorithm is implemented, and the results are observed. Simulator is software that provides a platform to execute an algorithm developed for various security issues or it is software in which algorithm designed to provide a realistic imitation of operation can be implemented. Constraints are boundaries which define the reach of a particular method or algorithm.

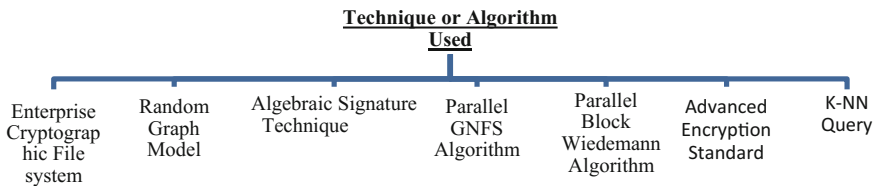


Fig. 3 Techniques or algorithm used

Table 1 Techniques/algorithms used in cloud security

References	Dataset	Simulation	Parameters	Application
[1]	Not discussed	Not discussed	Updated data storage	Created secure record sharing in public storage Outlines a protected and productive stackable framework named Shield
[2]	Not discussed	Actualized utilizing C on a framework with an Intel Core i5-2450 M CPU at 2.5 GHz, and 6 GB RAM	Correspondence cost and computation cost of data auditing and element information refresh	Remote data auditing (RDA) techniques
[3]	MIT reality-mining dataset and Nodobo dataset	Not discussed	Security, cost, and load adjusting in telephone clone provisioning	Developed SWAP a scheme for telephone clones
[4]	Not discussed	Implemented the parallel GNFS algorithm integrated with parallel block Wiedemann algorithm	Not discussed	Not discussed
[5]	Standard HD videos	Not discussed	Not discussed	HEVC encoded video stream
[6]	Not discussed	Not discussed	Improved chaos prediction and suppression methods	CPSS model
[7]	Real datasets (Hong-Kong and SIFT1M) and synthetic datasets (Gaussian64, Gaussian256)	Not discussed	Not discussed	Secure approximate k-nearest neighbor (SANN) query
[8]	Not discussed	There own built simulator	Security and efficiency	Security-aware efficient distributed storage (SA-EDS) model
[9]	TPC-H scale 1.0 dataset	Not discussed	Correctness, security, and theoretical performance	Tree-based order-preserving encryption (OPE) mechanism

(continued)

Table 1 (continued)

References	Dataset	Simulation	Parameters	Application
[10]	Not discussed	Not discussed	Data privacy against CS, key confidentiality against QUs, query privacy against CS and DO, query controllability	Not discussed

3 Findings

In Table 2, we have calculated the effective citations in security domain of cloud computing by using the formula

$$EC_{sdj(y)} = \frac{P_{sdj(y)}}{P_{j(y)}} \times C_{j(y)} \tag{1}$$

where in Eq. (1)

$EC_{sdj(y)}$ signifies effective citations in specific domain (i.e., cloud security) journal of year y . Table 2 represents data.

$P_{sdj(y)}$ signifies total number of publications in specific domain (i.e., cloud security) journal of year y . Table 3 represents data.

Table 2 Effective citations in security domain of cloud computing

	2011	2012	2013	2014	2015
J1	198.47	267.57	511.01	518.18	718.51
J2	0.00	50.66	44.80	253.66	124.27
J3	3.83	48.60	29.74	54.54	35.67
J4	16.95	47.57	121.02	186.35	321.27
J5	38.34	60.86	127.57	154.41	146.69

J1 Future generation computer system

J2 Information sciences

J3 Journal of computer and sciences

J4 Journal of network and computer applications

J5 Journal of parallel and distributed computing

Table 3 Total publications in specific domain journal

	2011	2012	2013	2014	2015
J1	34	40	93	108	76
J2	0	5	5	31	9
J3	1	9	6	12	6
J4	11	14	19	31	33
J5	11	21	32	28	24

Table 4 Total publications in journal of repute

	2011	2012	2013	2014	2015
J1	123	148	188	292	174
J2	360	423	612	871	516
J3	80	65	92	123	109
J4	185	181	157	267	170
J5	136	147	150	136	98

Table 5 Total citations in journal of repute

	2011	2012	2013	2014	2015
J1	718	990	1033	1401	1645
J2	3648	4286	5484	7127	7125
J3	306	351	456	559	648
J4	285	615	1000	1605	1655
J5	474	426	598	750	599

Table 6 Percentage of publications in security domain of cloud computing

	2011	2012	2013	2014	2015
J1	27.64	27.03	49.03	36.99	43.68
J2	0	1.18	0.82	3.56	1.74
J3	1.25	13.85	6.52	9.76	5.5
J4	5.95	7.73	12.1	11.61	19.41
J5	8.09	14.29	21.33	20.59	24.49

$P_{j(y)}$ implies Total Publications in journal of repute. Table 4 represents the data.

$C_{j(y)}$ depicts Total Citations in journal of repute. Table 5 represents data.

In Table 6, we have calculated the percentage of publications in security domain of cloud computing.

Percentage for calculating is

$$\text{Percentage} = \frac{\text{EC}^\#}{\text{TC}^\$} * 100 \quad (2)$$

The term EC means Effective Citations in security field of cloud computing in the journal of repute.

\$ The term TC means Total Number of Effective Citations in security domain of cloud computing in the journal of repute.

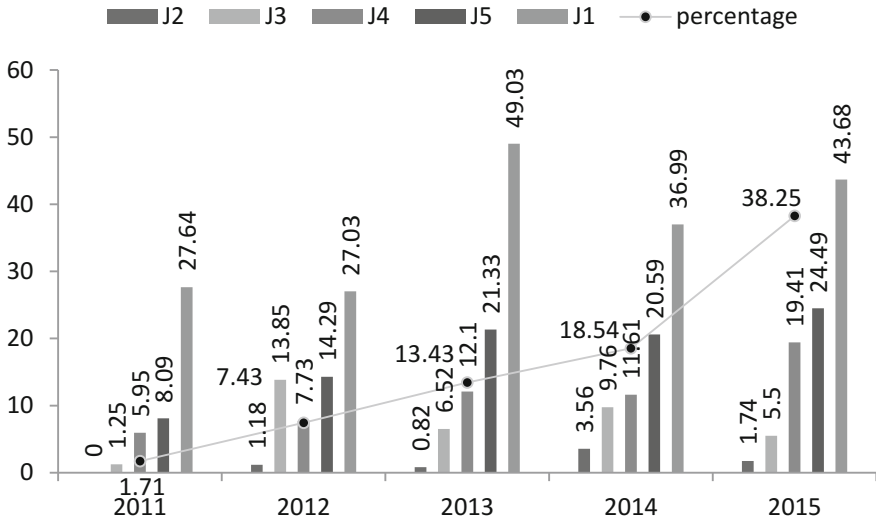


Fig. 4 Journal wise percentage of citations

4 Results

Figure 4 depicts a number of researchers who are citing the works published by Future Generation Computer System journal as it is the prestigious journal in the area of cloud computing.

5 Conclusion

From the above survey, we can conclude that there are various techniques that can be deployed to analyze the results for secured cloud data. Also, to verify results, various datasets are used that are related to user concerns, and security algorithms are proved using that. Before implementing the algorithms onto the data, data cleansing is performed, and this refines the data and makes it ready for analysis. There are also some authors who have not discussed their few parameters. On the basis of this analysis, the above-stated interpretations of result are done. This interpretation of results further provides the outcome of the analysis performed on the gathered data. Graph depicts the number of effective citations to the proportion of total number of citations in relation to a journal of repute.

6 Future Work

We will analyze some more areas where security has to be implemented that are in electronic health records and will be developing some dynamic algorithms that may work at any of the models and also at any of the platform services provided by the cloud providers. Also, we will be using static dataset to prove the results of our developed algorithms.

References

1. Shu, J., Shen, Z., Xue, W.: Shield A stackable secure storage system for file sharing in public storage. *Journal of Parallel and Distributed Computing*, 74(9), 2872–2883 (2014)
2. Sookhak, M., Gani, A., Khan, M. K., Buyya, R.: Dynamic remote data auditing for securing big data storage in cloud computing. *Information Sciences*, 380, 101–116 (2017)
3. Vaezpour, S. Y., Zhang, R., Wu, K., Wang, J., Shoja, G. C.: A new approach to mitigating security risks of phone clone co-location over mobile clouds. *Journal of Network and Computer Applications*, 62, 171–184 (2016)
4. Yang, L. T., Huang, G., Feng, J., Xu, L.: Parallel GNFS algorithm integrated with parallel block Wiedemann algorithm for RSA security in cloud computing. *Information Sciences*, 387, 254–265 (2016)
5. Usman, M., Jan, M. A., He, X.: Cryptography-based Secure Data Storage and Sharing Using HEVC and Public Clouds. *Information Sciences*, 387, 90–102 (2016)
6. Dai, H., Zhao, S., Chen, K.: A chaos-oriented prediction and suppression model to enhance the security for cyber physical power systems. *Journal of Parallel and Distributed Computing*, 103, 87–95 (2016)
7. Peng, Y., Cui, J., Li, H., Ma, J.: A reusable and single-interactive model for secure approximate k-nearest neighbor query in cloud. *Information Sciences*, 387, 147–164 (2016)
8. Li, Y., Gai, K., Qiu, L., Qiu, M., Zhao, H.: Intelligent cryptography approach for secure distributed big data storage in cloud computing. *Information Sciences*, 387, 103–115 (2016)
9. Xiang, T., Li, X., Chen, F., Guo, S., Yang, Y.: Processing secure, verifiable and efficient SQL over outsourced database. *Information Sciences*, 348, 163–178 (2016)
10. Zhu, Y., Huang, Z., Takagi, T.: Secure and controllable k-nn query over encrypted cloud data with key confidentiality. *Journal of Parallel and Distributed Computing*, 89, 1–12 (2016)

Iterative Basic Block Pipelining Implementation as Fast Computation Technique

Parul Shikha, Manish Sharma and Sachin Rajput

Abstract The proposed idea is implementation of a multiplier by using operand decomposition through pipelining so as to do fast computation maximum error reduction (Patricio Bulić et al., A Simple Pipelined Logarithmic Multiplier, IEEE International conference on computer Design, 2010 [1], Mahalingam and Rangantathan, IEEE T Comput, 55(2): 1523–1535, 2006. [2], McLaren, Preceedings of IEEE International SOC Conference 2003, 53–56, 2003 [3]). Implementing the proposed idea with iterative pipelined architecture with less switching activity and this architecture can be opted where speed and accuracy are preferred over complexity.

Keywords Operand decomposition · Mitchel's algorithm · Pipelining

1 Introduction

It has always been a tedious task to multiply numbers manually, for which various multiplication tools were introduced. But these tools have always been time and power consuming [4, 5]. In order to perform fast computation, many different ideas have been proposed, out of which one is operand decomposition method [6]. In the proposed idea, we take operand decomposition method as the method of multiplication and perform this iteratively on hardware through pipelined implementation.

This paper consists of sections which are organized as follows: Sect. 1.1 presents the operand decomposition method. The method in this section is explained with the help of an example. Section 1.2 explains and evaluates the advantages of operand decomposition which is the basis of proposed idea. Section 2 focuses on the approach used for the proposed idea. Sections 3 and 4 explain the method of working of proposed idea through a flowchart. Section 6 shows the simulation result of traditional algorithm as well as the proposed algorithm. Section 7 draws to a conclusion.

P. Shikha (✉) · M. Sharma · S. Rajput
Amity University, Noida, Uttar Pradesh, India
e-mail: Parulshikha94@gmail.com

1.1 Operand Decomposition

In operand decomposition method, we take two numbers that are to be multiplied. These are further decomposed into two more numbers. For instance, consider numbers A and B which are to be multiplied, then by operand decomposition method these numbers are further decomposed into P , Q and R , S , respectively. Then the product is calculated as [6]

$$A * B = [(P * Q) + (R * S)],$$

where

$$P = A \vee B$$

$$Q = A \wedge B$$

$$R = A' \wedge B$$

$$S = A \wedge B'$$

For instance, consider the following example.

Example 1 Consider two numbers 17 and 50 whose multiplication is to be performed.

Then,

$$A = b'\{00010001\} = d'17$$

$$B = b'\{00110010\} = d'50$$

$$P = b'\{00110011\} = d'51$$

$$Q = b'\{00010000\} = d'16$$

$$R = b'\{00100010\} = d'34$$

$$S = b'\{00000001\} = d'01.$$

By formula

$$A * B = ((P * Q) + (R * S))$$

$$A * B = ((51 * 16) + (34 * 1)) \quad A * B = 850.$$

Taking another example,

Example 2 Consider two numbers 18 and 52 whose multiplication is to be performed.

Then,

$$A = b'\{00010010\} = d'18$$

$$B = b'\{00110100\} = d'52$$

$$P = b'\{00110110\} = d'54$$

$$Q = b'\{00010000\} = d'16$$

$$R = b'\{00100100\} = d'36$$

$$S = b'\{00000010\} = d'02.$$

By formula

$$A * B = ((P * Q) + (R * S))$$

$$A * B = ((54 * 16) + (36 * 02)) \quad A * B = 936.$$

1.2 Advantages of Operand Decomposition

1. The number of ones present in data increases the switching activity [6], since in operand decomposition method, the numbers are decomposed into further which reduce the probability of one present in the binary input from '1/2' to '1/4' which automatically reduces the power consumption of the circuit.

In the proposed idea, the first decomposition step is repeated again which results in eight decomposed binary inputs that means the switching activity is further reduced to '1/8,' which is very less than the original which was '1/2'.

2. The main reason for error generation in the output bit is more number of ones present because it contributes to the fractional part [5]; thus, since we are reducing the number of ones in the binary input through operand decomposition, we are reducing the error generation in computation and hence more correct value of output.

2 Approach Used

In the proposed method, the operand decomposed in the previous example is further decomposed such that P is decomposed into $P1$ and $P2$, Q into $Q1$ and $Q2$, and similarly R into $R1$ and $R2$ and S into $S1$ and $S2$, by doing so the number of ones in operand is reduced further so that switching activity is reduced, hence power is reduced. The implementation for product calculation is implemented through

iterative basic block pipelining. The decomposed operands are calculated by the following formulae.

$$\begin{aligned} P1 &= P \vee Q & R1 &= R \vee S \\ P2 &= P \wedge Q & R2 &= R \wedge S \\ Q1 &= P' \wedge Q & S1 &= R' \wedge S \\ Q2 &= P \wedge Q' & S2 &= R \vee S'. \end{aligned}$$

Therefore,

$$A * B = [(P1 * P2) + (Q1 * Q2)] + [(R1 * R2) + (S1 * S2)] \quad (1)$$

Now implementing Example 1 with proposed idea, we have

$$\begin{aligned} P1 &= b'\{00110011\} = d'51 & R1 &= b'\{00100011\} = d'35 \\ P2 &= b'\{00100000\} = d'16 & R2 &= b'\{00000000\} = d'00 \\ Q1 &= b'\{00000000\} = d'00 & S1 &= b'\{00000001\} = d'01 \\ Q2 &= b'\{00100011\} = d'35 & S2 &= b'\{00100010\} = d'34. \end{aligned}$$

From Eq. 1, we have

$$\begin{aligned} A * B &= [(P1 * P2) + (Q1 * Q2)] + [(R1 * R2) + (S1 * S2)] \\ A * B &= [(51 * 16) + (00 * 35)] + [(35 * 00) + (01 * 34)] \\ &= 850. \end{aligned}$$

Similarly, we are proceeding with Example 2

$$\begin{aligned} P1 &= b'\{00110110\} = d'54 & R1 &= b'\{00100110\} = d'38 \\ P2 &= b'\{00010000\} = d'16 & R2 &= b'\{00000000\} = d'00 \\ Q1 &= b'\{00000000\} = d'00 & S1 &= b'\{00000010\} = d'02 \\ Q2 &= b'\{00100110\} = d'38 & S2 &= b'\{00100100\} = 36. \end{aligned}$$

From Eq. 1, we have

$$\begin{aligned} A * B &= [(P1 * P2) + (Q1 * Q2)] + [(R1 * R2) + (S1 * S2)] \\ A * B &= [(54 * 16) + (00 * 38)] + [(38 * 00) + (02 * 36)] \\ &= 936. \end{aligned}$$

As seen in the calculation of proposed idea, the number of zeroes has increased during calculation, due to which, during hardware implementation, there will be less switching activity which will result in comparatively less power consumption with no negative effect on result [7].

3 Flowchart

See Fig. 1.

4 Working

The operand decomposition multiplication algorithm is shown in above flow chart. In the very first step, the two input data A and B are first decomposed into four input data which are P and Q , R and S , respectively. Now according to the proposed idea these four input data are decomposed into $P1$ and $P2$ for P , $Q1$ and $Q2$ for Q , $R1$ and $R2$ for R , and similarly $S1$ and $S2$ for S . These eight input bits are further computed by the proposed idea as mentioned in Eq. 1. Further the log of all these input bits is taken and their product is calculated. At last the antilog is calculated [5] which gives the final product.

5 Hardware Implementation

The above discussed idea of iterative operand decomposition is now implemented on basic block pipelining. The eight decomposed operands are first fed to the leading one detectors (LODs) [4, 6]. This checks the leading one bit, i.e., MSB for the

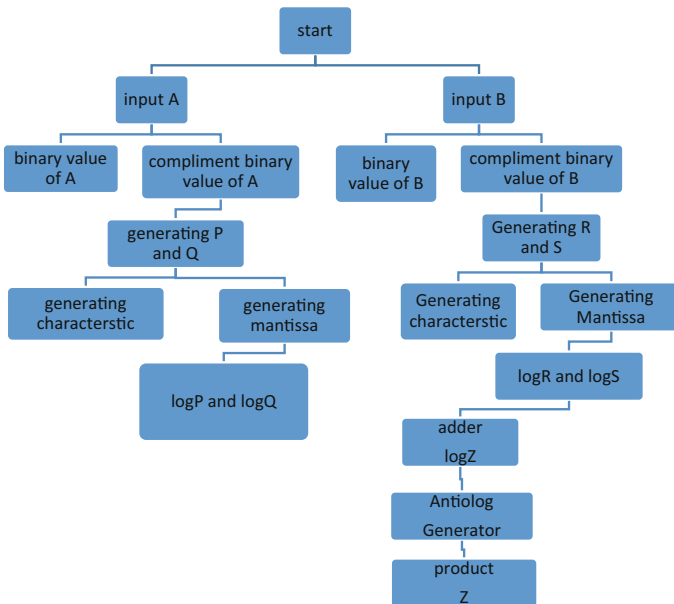


Fig. 1 Design flow of iterative operand decomposition pipelined architecture

mantissa calculation. Now the input bit is further given to priority encoder which detects the MSB. After this the result for mantissa is stored in register. Further from the register, the result is fed to barrel shifter which shifts the ones for obtaining the log value. Again the value is stored in register and then fed to decoder.

For the proposed idea, the same discussed basic block pipelining is implemented iteratively for two more times which generates one approximated product and two correction terms and hence the final result is calculated.

6 Results

After developing the algorithm for proposed idea, simulation is performed on Vivado 2014.14, for both algorithms, i.e., the traditional algorithm as well as the proposed algorithm. Following are the results (Figs. 2 and 3).

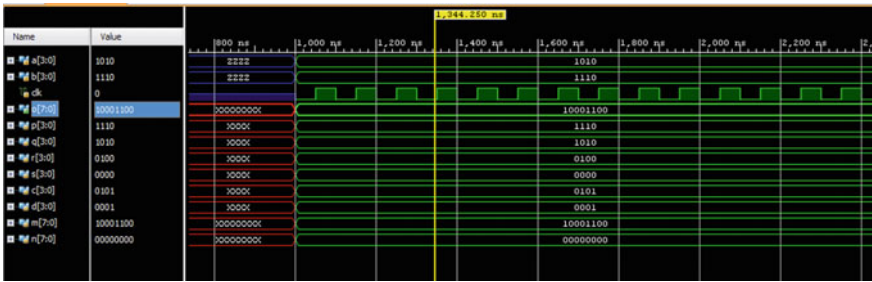


Fig. 2 Simulation result of traditional operand decomposition method

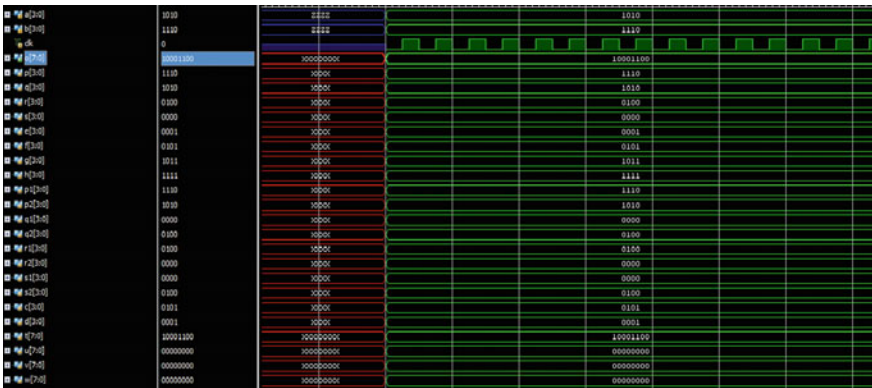


Fig. 3 Simulation result of proposed operand decomposition method

As seen from the simulation result of both algorithms, we see that the number of ones has been decreased [5], which have resulted in less switching activity and eventually power consumption has been decreased. Though this has increased the area of circuit by using more number of registers, but the idea can be used where power is preferred over area.

7 Conclusion

The proposed idea reduces the switching activity which results in less power consumption, and also the operand decomposition method reduces the number of ones and increases zeroes which reduces the fractional value and hence more correct result. The hardware implementation through iterative basic block pipelining [7] also contributes to error reduction. Next, the simulation result for traditional algorithm and proposed algorithm has been shown, which gives a brief comparison of power consumption and area of both circuits.

References

1. Patricio Bulić; Zdenka Babić; Aleksej Avramović, A Simple Pipelined Logarithmic Multiplier, IEEE International conference on computer Design 2010.
2. V Mahalingam, N. Ranganathan, Improving Accuracy in Mitchell's Logarithmic Multiplication Using Operand Decomposition, IEEE Transaction on computers, Vol. 55, No. 2 pp. 1523–1535, December 2006.
3. D.J. McLaren, Improved Mitchell-Based Logarithmic Multiplier for Low-Power DSP applications, Proceedings of IEEE International SOC Conference 2003 pp. 53–56, 17–20 September 2003.
4. K. H. Abed, R. E. Sifred, "CMOS VLSI Implementation of a Low-Power Logarithmic Converter." IEEE Transaction on Computers, Vol 52, No. 11, pp. 1221–1228, September 2003.
5. R. K. Agrawal, and H. M. Kittur, "ASIC Based Logarithmic Multiplier using iterative pipelined architecture," IEEE Conference on information & Communication Technologies (ICT), pp. 362–366 2013.
6. J.N. Mitchell, Computer multiplication and division using binary logarithms IRE Transactions on Electronic Computers, vol. EC-11, pp. 512–517, August 1962.
7. K. Johansson, O. Gustafsson, and L. Wanhammar, "Implementation of Elementary Functions for Logarithmic Number System," IET Computer & Digital Techniques, Vol. 2, No. 4, pp. 295–304, April 2008.

An Approach to Inter-vehicle and Vehicle-to-Roadside Communication for Safety Measures

Rishita Prakash, Himanshu Malviya, Arushi Naudiyal, Rajesh Singh and Anita Gehlot

Abstract This paper represents how the demand for reduction accidents, traffic congestion, transport time, and environmental impact of road transport can be achieved. Nowadays, researchers are keenly interested in developing a system in which vehicles can communicate to vehicles and to roads installed with sensors. There are mainly two types of communication that occur in vehicles that are inter-vehicle and intra-vehicle communication. Vehicles able to communicate provide a fundamental building block for intelligent transport system (ITS) and can provide various applications which will help in traveling. The primary mode of communication is vehicular communication, that is, inter-vehicle communication. The research focuses on the making of intelligent road and intelligent vehicles. The ability of vehicles to exchange information wirelessly is the backbone of Cooperative Intelligent Transport Systems. With such a new technology, fully automatic will provide good driving experience with drivers' comfort and safety. The communication between the vehicles includes information like speed, acceleration, position of vehicle, turn signal status, lane change information, overtaking. [1, 2]. This paper is mainly based on inter-vehicle communication, that is, communication between the vehicles, vehicles to transponders, and vehicle-to-Internet communication. Researchers are trying to implement various ways through which communication may occur between the vehicles. Ways to prevent road accident and

R. Prakash (✉) · H. Malviya · A. Naudiyal · R. Singh · A. Gehlot
Electronics Instrumentation and Control, Engineering Department, College of Engineering Studies, University of Petroleum and Energy Studies, Dehradun 248007, Uttarakhand, India
e-mail: rishitatech0@gmail.com

H. Malviya
e-mail: him14malviya@gmail.com

A. Naudiyal
e-mail: arushi26naudial@gmail.com

R. Singh
e-mail: RSINGH@ddn.upes.ac.in

A. Gehlot
e-mail: anita@ddn.upes.ac.in

traffic congestion are also discussed. The last section of the paper includes vehicle-to-Internet communication in which transmission methods and network model are revised.

1 Introduction

Today's researcher is mainly focusing on how roads can be made safer and smarter. Communication technologies are taken into account for such development and research. Inter-vehicle communication is the communication between the vehicles and vehicles to roadside in which sensors are installed. In this paper, we have discussed the various ways of communication of vehicles which further help in providing safety, comfort, and good driving experience. This paper consists of two areas of research for communication through vehicles, namely mobile ad hoc networking (MANET), the first area of research which will help in vehicle safety, and the concept of 'intelligent road' as the second area of research [1].

The primary modes of communication in inter-vehicle communication are as follows:

2 Vehicle-to-Roadside Communication

This type of communication mode requires sensors which are installed in roads. In this type, both vehicle specific data and locally relevant data broadcast to vehicles can be supported. This type of communication is also known as V2I communication [1].

2.1 Roadside Design

Sensors and equipment are studied in roadside design which will help in establishing communication. For making passing by vehicles to communicate with the road infrastructure, the establishment of broadcast stations and wireless access points is necessary. List of road elements and their V2I applications are as follows [1].

2.1.1 Lane Direction

These are signs to guide the directions to the vehicles and are usually located at a clear view to the drivers. These reduce accidents significantly [1].

2.1.2 Road Junction

The most probable point of accidents is at the road junctions. It can be estimated that in the future, vehicles would possess integrated electronic sensors, which would slow down the speed of the vehicle automatically when it is about to reach a junction on the road [1].

2.1.3 Traffic Lights

Nowadays, the traffic lights integrate various pieces of electronic equipment, which are used for surveying of traffic. Another way that can be implemented and would be effective is to place video cameras at main locations, which would take snaps of the drivers and the number plate of the vehicles that drive breaking the traffic lights [1].

2.2 *Transmission Method*

In this section, we will discuss present standards and ways to establish vehicle-to-infrastructure communication. The USA is keenly interested in the development of V2I communication and is extensively researched the topic in the USA. One most important advantage of V2I communication is the ability to exchange information between the vehicles and in support to the advisories and warning given to the drivers [2].

2.3 *Architecture*

The elements used in V2I communication are usually same. USDOTs' ITS Joint Program Office defines the architecture framework. Minimum components required for V2I communication are as follows:

- Vehicle Onboard Unit or Equipment (OBU or OBE).
- Roadside Unit or Equipment (RSU or RSE).

The vehicles are installed with OBU. OBU is used to perform functions within the vehicle and also perform functions in the transmission of radio element. OBU is made of radio transceiver, a GPS system, an application processor, vehicle human-machine interface (HMI), and interfaces to vehicle systems. The main function OBU provides communication between the vehicles, vehicles to roadside, and also with the passing by vehicle. Messages are transferred to the other OBUs for the protection purpose between the vehicles [2].

Roadside Unit or Equipment can be located at various locations like petrol pumps which within their range provide interface to the vehicles. It consists of radio transceiver, which is an application processor, and also an interface to the V2I communications network. It also has an inbuilt GPS unit. RSU is helpful in V2I communication as it is connected to V2I communication network [5].

2.4 Wireless Technologies

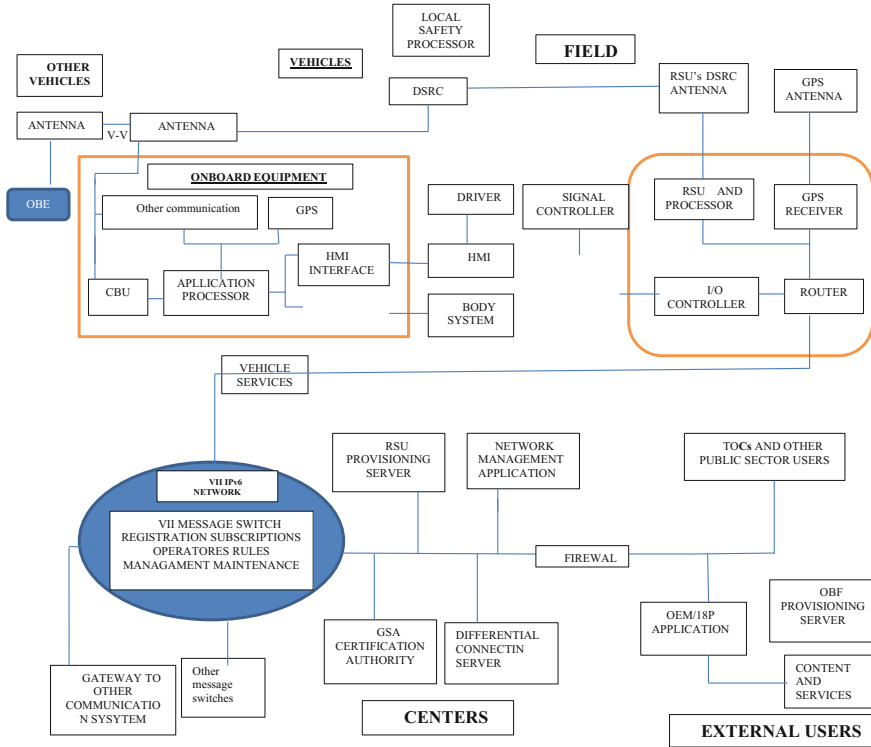
Wireless technology is rapidly evolving in the recent generation. It also plays an important role in people's lives around the entire world. A large percentage of people are dependent on such technology directly or indirectly. The most common example of wireless technology is Wi-Fi, Bluetooth, etc. It has been suggested that wireless is overused in some situations, creating a social nuisance. Some of the wireless technologies which are helpful in communication between the vehicles are given [4].

- DSRC (dedicated short-range communication).
- Bluetooth.

2.4.1 Bluetooth

This wireless technology is the only technology which is easily available to large section of people and is present in most of the devices made for communication, for example, computers, mobile phone, laptops, medical devices. The process of connecting two devices through Bluetooth is called pairing. Once these devices are connected, they can communicate through messages within short range creating an ad hoc network. This network is called piconets. Each device included in piconet is capable to communicate with seven more devices, which makes a larger group of vehicles enable to communicate. The three classes of Bluetooth depending upon their ranges are given [4].

- Class 3 radios (these have the area of 1 m or 3 ft.).
- Class 2 radios (these have upper and lower limits between 10 m or 33 ft and mobile devices generally using this type of radio).
- Class 1 radios (these have upper and lower limits between 100 m or 300 ft. and industries generally using this type of radio).



Construction of V2I systems.

3 Inter-vehicle Communication

Here, we will be discussing various technologies which can be used for communication of two vehicles or group of vehicles (V2V). So it gets essential to form the network. As vehicles are continuously in motion, only one network can support such network, that is, ad hoc network [1].

It is a network which either involves no infrastructure or includes minimum of it that too composed of nodes which combine to become a network. Each node performs a unique role. These include network router, data source/destination. Therefore, if more than two nodes combine into an ad hoc network, they are able to communicate with each other and hence relay information [3].

3.1 *Transmission Methods*

By allowing of very low latencies, it generates advantage of this protocol over point-to-point wireless communications. There are numerous applications which could be enabled by the DSRC protocol [5].

3.1.1 Cooperative Forward Collision Warning

The data which is received from the targetted vehicle along with hosts the information of the host vehicle as to its own position, and also, the roadway information helps to estimate risk of collision. It reduces the chance of collision. Data communicated—Velocity, Heading, Acceleration, vehicle position [5].

3.1.2 Emergency Electronic Brake Light

These provide a message to other vehicles, if the radar sensors are not able to notify due to bad weather conditions and also if the driver's visibility is limited, when a forward vehicle brakes strongly. The following data is communicated—Heading, Velocity, Deceleration, vehicle position [5].

3.1.3 Road Condition Warning

Detection of marginal condition is by using onboard system and sensors, and detection of road warning is communicated to surrounding vehicles using broadcast data communicated—Heading, Road condition, Parameters, vehicle position [5].

4 Vehicle-to-Internet Communication

Internet has become the basic requirement of many technologies without which the implementation is not possible. Day-by-day Internet usage is increasing. Conventionally, vehicle ad hoc network of system was used in the Internet of Vehicles [4].

As the use of IOT in vehicles is increasing rapidly, the vehicle ad hoc networks (VANETs) are switching to Internet of Vehicle (IOV). VANET turns every involved vehicle into a wireless router, which enables the vehicles to connect to with one another. By this, a network is created with a wide range [4].

4.1 Vehicle Networking

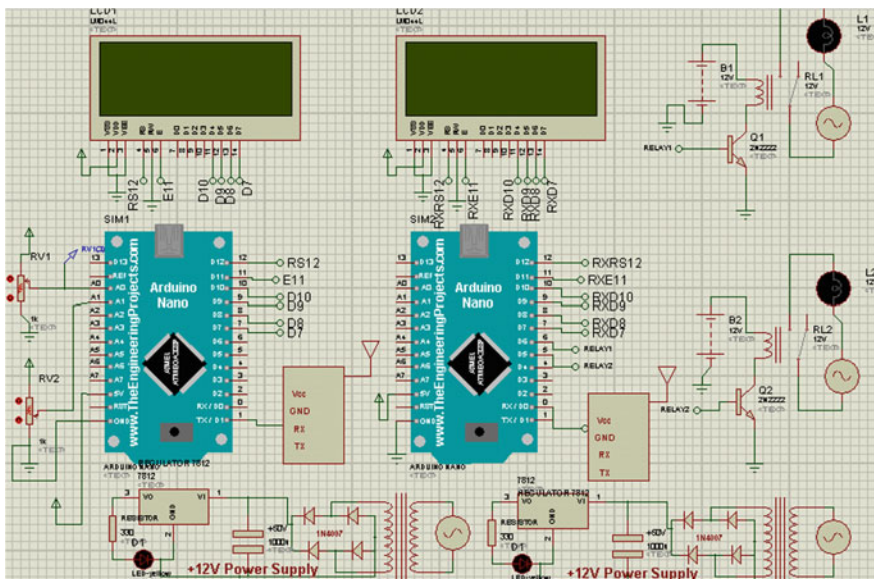
These include VANET (which is also known as vehicles' interconnection), vehicle telematics (which is also called connected vehicles), and mobile Internet (which is also known as the vehicle is as a wheeled mobile terminal) [4].

4.2 Vehicle Intelligence

This is the integration of driver and vehicle as a unit is more intelligent and efficient with making use of network technologies. This refers to deep learning, cognitive computing, swarm computing, uncertainty artificial intelligence, etc. [5].

5 Conclusion

Inter-vehicle communication at present is the vast area of research and development. The implementation of such technology would be helpful in safe driving with good driving experience, comfort, etc. Both V2I and V2V have same applications commonly called intelligent transportation system (ITS). Through communication, number of accidents can be reduced by notifying the driver through the facts obtained through the exchange of information between sensors and vehicles placed on the road. Various other safety applications are such that advance advice for dangerous situations such as traffic, car crash, hinders. Speed management can also be done. Vehicles having emergencies can communicate and can take less time to reach their destination. Traffic jams can be easily operated and can be recognized before [1, 4, 5].



The feasibility of sensor and wireless communication is tested in Proteus simulation. Arduino Nano, LCD, and analog sensor (accelerometer) are used to realize the transmitter and receiver.

References

1. Ana Roxin, "Inter-vehicle communications - research report", October 2014.
2. Adil Mudasir Malla, Ravi Kant Sahu, "Vehicle to Vehicle Communication Protocols in VANETs", Volume 3, Issue 2, February 2013.
3. Andreas Festag, Alban Hessler, Roberto Baldessari, Long Le, Wenhui Zhang, Dirk Westhoff, "Vehicle to vehicle and roadside sensor communication for enhanced road safety".
4. Yang Fangchun, Wang Shangguang, Li Jinglin, Liu Zhihan, Sun Oibo, "An Overview of Internet of Vehicles".
5. Theiry Ernst, Vilmos Nebehaj, Runar Sorasen, "CVIS: Calm Proof of Concept Preliminary Results".
6. Shereen A.M. Ahmed, Sharifah H.S. Ariffin, Norsheila Fisal, "Overview of WAVE Protocols and Standards".

Performance Evaluation of Big Data Frameworks: MapReduce and Spark

Jaspreet Singh, S.N. Panda and Rajesh Kaushal

Abstract Spark and MapReduce are two prominent open-source distributed computing frameworks for big data processing and analytics. These frameworks introduce a simple programming APIs for new users and suppress the complication and fault tolerance of distributed tasks. Most of Internet companies widely deploy these frameworks to process their massive data. Furthermore, all other big communities are adopting these HPC because high-performance data analytics is required to solve big data problems. To provide an efficient framework for processing and analyzing large amount of data, today's researchers correlate both the frameworks. (1) This paper discusses the evaluation of the performance of MapReduce and Spark on page rank, sort and word count. From some existing research, we evaluate page rank and sort algorithms in these frameworks. (2) We provide in-depth analysis of task execution time on word count algorithm in both of these frameworks, through detailed experiment and quantify the performance based on different dataset sizes. Overall experimental results show that Spark is faster than MapReduce. The prime causes of speedups in Spark are the reduced DISK and CPU overheads due to RDD caching.

Keywords Hadoop · Spark · MapReduce · HDFS · Data analytics

J. Singh (✉) · S.N. Panda · R. Kaushal

Department of Computer Science and Engineering, Chitkara University Institute of Engineering and Technology, Chitkara University, Rajpura, Punjab, India
e-mail: jaspreet.cse@chitkara.edu.in

S.N. Panda
e-mail: snpanda@chitkara.edu.in

R. Kaushal
e-mail: rajesh.kaushal@chitkara.edu.in

1 Introduction

Big Data cannot be acknowledged as a precise term with a proper definition. Instead, it is a collection of large amount of various kinds of data, mostly unstructured. This indicates it is very difficult process for relational database managements systems to analyze and process such data, which is of large volume and unstructured nature. To business and big communities should be capable of finding out useful information from this vast amount of data, that helps to grow their existing business and to find out new requirements of their users, so as for better customer experiences in the future. Big Data analytics techniques provide more precise results and solutions [1].

Researchers and Analysts use advanced techniques of analytics such as text and predictive analytics, natural language processing (NLP), data mining and machine learning to figure out more useful insight and information which is very helpful for an enterprise to make right decision. Open-source big data analytics technologies such as Hadoop MapReduce and Spark provide adequate solutions. In this paper, we examine the comparison between Spark and MapReduce frameworks on Hadoop [2].

Section 2 covers Apache Hadoop with MapReduce framework for storage and processing of large dataset. Section 3 discusses about data processing in Apache Spark and Mllib library for iterative machine learning algorithms. Section 4 discusses Hadoop distributed file system (HDFS) to store data in a distributed manner on different nodes. Section 5 shows the comparison of MapReduce and Spark on page rank algorithm and discussion. Section 6 discusses comparison of MapReduce and Spark on sort. Section 7 shows the experimental studies and discussion generated by execution of word count program by using Spark and MapReduce programming framework. Section 8 describes the conclusion.

2 Apache Hadoop

Apache Hadoop is an open-source framework to process and manage Big Data. Big Data is large amount of which can be in any form for example structured, unstructured and semi structured [3]. Hadoop provides a parallel distributed database known as HDFS Hadoop distributed file system, and there are number of tools and frameworks related to Hadoop, which we can use to perform operations on data stored in HDFS. In Hadoop, data is replicate on multiple nodes, if one data node fails, we can recover our data from other nodes [4].

Apache Hadoop includes following modules:

- (a) Hadoop Common: The common utility libraries which help Hadoop components to interact with each other.
- (b) Hadoop distributed file system (HDFS): It is termed as a distributed file system for parallel processing and providing fault tolerant and high throughput which helps to store and process data on multiple nodes in a distributed manner.

- (c) Hadoop YARN: Yarn supervises the cluster resource management and job scheduling during the execution of jobs [5].

3 Hadoop MapReduce

Hadoop MapReduce is a programming framework to process immense data in-parallel distributed manner on large nodes of commodity hardware [6]. It is a fault tolerant and reliable framework. MapReduce programming usually works on map and reduce paradigm [7]. Map phase splits the input dataset into multiple chunks to process in a fully parallel manner, and the output of this stage is input for the next phase which is known as reduce task, and both input and output after the execution of job are stored in HDFS [8]. The MapReduce framework typically works on a <key, value> pair, that is, it splits the input dataset into <key, value> pairs and process output of the job in similar form [9]. Figure 1 represents MapReduce workflow.

4 Apache Spark

Apache Spark is a framework for analyzing Big Data [10] which can process and analyze massive amount of data in distributed manner. Apache Spark uses Resilient Distributed Datasets known as RDDs [11] which is distributed set of instances and an unchallengeable fault tolerant for the execution of parallel operations [12].

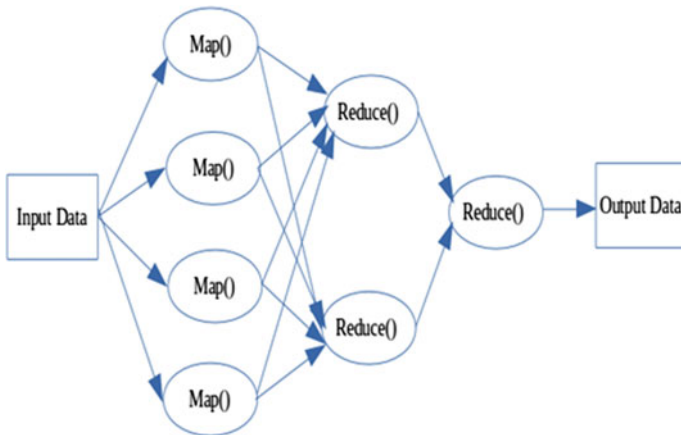


Fig. 1 MapReduce work flow

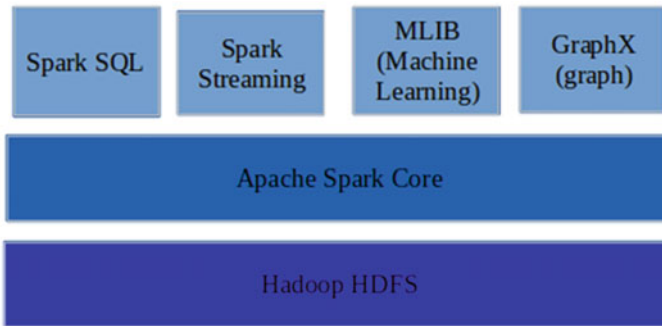


Fig. 2 Apache Spark Stack

As in MapReduce, both Map and Reduce phases use disk read/write operations number of times in the execution of a job, so these read/write operations cause more delay and increase execution time [13].

Apache Spark provides a programming interface where we can write a program, execute it in distributed manner [14], and RDD helps to keep data in RAM and process that data. In this procedure, it utilizes in-memory cache efficiently. During data processing, it puts data on local file system, which reduces read/write disk operations in Spark [15]. Figure 2 describes Apache Spark stack.

5 Page Rank

Page rank is one of the foundational algorithms of Google's indexing process: ranking every web page on the internet by the number and quality of links. It is a procedure to measuring the value and importance of a webpage. PageRank counts the number and quality of links of a webpage to estimate the weight age of webpage [16].

It is assumed that a website which accepts links from another website is very crucial. Different authors performed comparison of page rank algorithm on Hadoop and Spark and according to [2, 17, 18] Spark performs better than Hadoop but according to [19] Hadoop performs better than Spark. Table 1 describes the comparison of page rank algorithm on Hadoop and Spark.

6 Sort

Since data is not reduced through the pipeline, therefore sorting is the most perplexing operation. For moving data on all the machines, shuffle operation is performed at the sorting's core. To sort 1 TB of data, shuffling of this data needs to be

Table 1 Comparison of MapReduce and Spark on PageRank

S. No.	Apache Spark	Apache Hadoop	Results
1	<ol style="list-style-type: none"> IN memory computing (speed processing) (lower latency) Average 40% bandwidth Burst bandwidth is only 47% larger than average 	<ol style="list-style-type: none"> Disk-based processing Average 15% bandwidth 2.198% (larger) which cause traffic and speed slow 	This paper shows Spark is 8x faster than Hadoop in page Rank [17]
2	<ol style="list-style-type: none"> Uses Graphx libraries (better performance and optimization) (reduce network overhead) Page rank is iterative algorithm, caching the input as RDD reduces both CPU and disk i/o so it contributes 90% of speedup 	<ol style="list-style-type: none"> Used Mahout libraries Hadoop uses disk for all operations 	This paper shows Spark is 5x faster than Hadoop in page rank [19]
3	<ol style="list-style-type: none"> There is no memory release phenomenon in Spark Spark outperforms Hadoop When there is enough memory for Spark in the whole iterative process When dataset is large, there is a gradual increment between two consecutive iterations 	<ol style="list-style-type: none"> When map or reduce computation ends it releases memory 	Hadoop performs better if there is insufficient memory to store intermediate results [20]
4	<ol style="list-style-type: none"> OPEN-source MPI library (Message Passing Interface). HPC Load balancing, handles shuffling buffer manager Use 10 iterations so overhead between the iterations is light 	<ol style="list-style-type: none"> Hadoop uses file partitions and store them on disk 	Spark performs better [18]

performed on the network [21]. Different authors performed comparison of sort algorithm on Hadoop and Spark, and according to [22], Spark performs better than Hadoop but according to [19], Hadoop performs better than Spark. Table 1 describes the comparison of sort algorithm on Hadoop and Spark (Table 2).

Table 2 Comparison of MapReduce and Spark on sort

S. No.	Apache Spark	Apache Hadoop	Results
1	Network overhead is caused by and is proportional to the number of files opened simultaneously Low network speed leads to increase cache buffer sparks performance degrades	MapReduce can overlap the shuffle stage with the map stage, which effectively hides the network overhead	MapReduce performs better than Spark on 100 and 500 GB data 1 Gbps ethernet speed MapReduce is 2x faster than Spark [19]
2	Cache buffer decrease	Use disk for read/write operation	100 Tbs and Pbs of data 3x faster 10x fewer machines [22] 200 machines with 10 Gbps link each while 2000 machine

7 Experimental Studies

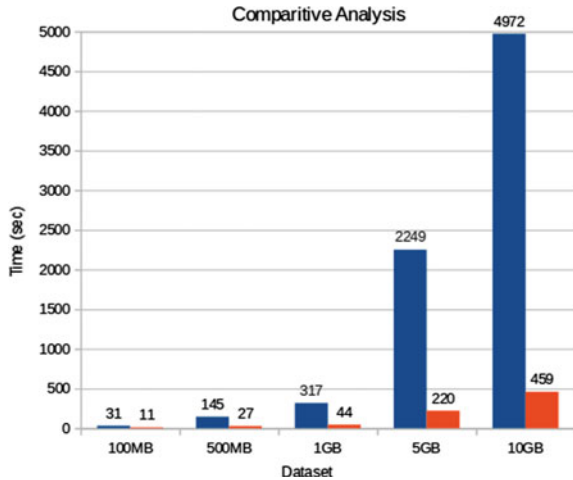
We have evaluated the efficiency of MapReduce and Spark by implementing word count algorithm.

For these experiments, we have used the WC program which we have included in both MapReduce and Spark, and these experiments were performed on five datasets of different sizes on both MapReduce and Spark to calculate the execution time [23]. To perform this experiment, two nodes Hadoop clusters were used. Figure 1 describes the comparison of MapReduce and Spark when word count algorithm was implemented on both the frameworks [15, 24]. Table 3 describes the comparison of MapReduce and Spark on word count on different datasets (Fig. 3).

Table 3 Comparison of MapReduce and Spark on word count

Dataset	MapReduce (s)	Spark (s)
100 MB	31	11
500 MB	145	27
1 GB	317	44
5 GB	2249	220
10 GB	4972	459

Fig. 3 Comparative analysis of Hadoop



8 Conclusion

Both the Spark and MapReduce frameworks are popular distributed computing paradigms for providing an effective solution for handling this large amount of data called Big Data. Today there are many misconceptions about the comparison of Spark and MapReduce framework. Many researchers and bloggers are claiming that Spark is 10–100 times faster than MapReduce framework. In this paper, we are performing the comparative analysis of both the programming frameworks in terms of execution time. We have run word count program on both the programming frameworks with different sized datasets and found that Spark is 10 times faster than Hadoop.

References

1. Landset, S., Khoshgoftaar, T. M., Richter, A. N., & Hasanin, T. (2015). A survey of open source tools for machine learning with big data in the Hadoop ecosystem. *Journal of Big Data*, 2(1). doi:10.1186/s40537-015-0032-1.
2. Elser, B., & Montresor, A. (2013). An evaluation study of Big Data frameworks for graph processing. 2013 IEEE International Conference on Big Data. doi:10.1109/bigdata.2013.6691555.
3. Vavilapalli, V. K., Seth, S., Saha, B., Curino, C., O'malley, O., Radia, S., ... Shah, H. (2013). Apache Hadoop YARN. Proceedings of the 4th annual Symposium on Cloud Computing - SOCC '13. doi:10.1145/2523616.2523633.
4. HDFS Architecture. (n.d.). Retrieved March 2, 2017, from <http://hadoop.apache.org/docs/current/hadoop-project-dist/hadoop-hdfs/HdfsDesign.html>.
5. Cugola G, Margara A (2012) Processing flows of information: from data stream to complex event processing. *ACM Comput Surv* 44(3):15:1–15:62.

6. Dittrich, J., & Quiané-Ruiz, J. (2012). Efficient big data processing in Hadoop MapReduce. *Proceedings of the VLDB Endowment*, 5(12), 2014–2015. doi:10.14778/2367502.2367562.
7. S. G. P., R, N. H., & Prabhu, S. (2017). High Performance Computation of Big Data: Performance Optimization Approach towards a Parallel Frequent Item Set Mining Algorithm for Transaction Data based on Hadoop MapReduce Framework. *International Journal of Intelligent Systems and Applications*, 9(1), 75–84. doi:10.5815/ijisa.2017.01.08.
8. Kabáč, M., Consel, C., & Volanschi, N. (2017). Designing parallel data processing for enabling large-scale sensor applications. *Personal and Ubiquitous Computing*. doi:10.1007/s00779-017-1009-1.
9. Mavridis, I., & Karatza, H. (2017). Performance evaluation of cloud-based log file analysis with Apache Hadoop and Apache Spark. *Journal of Systems and Software*, 125, 133–151. doi:10.1016/j.jss.2016.11.037.
10. Svyatkovskiy, A., Imai, K., Kroeger, M., & Shiraito, Y. (2016). Large-scale text processing pipeline with Apache Spark. 2016 IEEE International Conference on Big Data (Big Data). doi:10.1109/bigdata.2016.7841068.
11. Gopalani, S., & Arora, R. (2015). Comparing Apache Spark and Map Reduce with Performance Analysis using K-Means. *International Journal of Computer Applications*, 113 (1), 8–11. doi:10.5120/19788-0531.
12. Huang, W., Meng, L., Zhang, D., & Zhang, W. (2017). In-Memory Parallel Processing of Massive Remotely Sensed Data Using an Apache Spark on Hadoop YARN Model. *IEEE Journal of Selected Topics in Applied Earth Observations and Remote Sensing*, 10(1), 3–19. doi:10.1109/jstars.2016.2547020.
13. M. Zaharia et al. Resilient Distributed Datasets: A Fault Tolerant Abstraction for In Memory Cluster Computing. NSDI 2012.
14. Liang, F., & Lu, X. (2015). Accelerating Iterative Big Data Computing Through MPI. *Journal of Computer Science and Technology*, 30(2), 283–294. doi:10.1007/s11390-015-1522-5.
15. Wang, K., & Khan, M. M. (2015). Performance Prediction for Apache Spark Platform. 2015 IEEE 17th International Conference on High Performance Computing and Communications, 2015 IEEE 7th International Symposium on Cyberspace Safety and Security, and 2015 IEEE 12th International Conference on Embedded Software and Systems. doi:10.1109/hpcc-css-icess.2015.246.
16. Barrachina, A. D., & O'Driscoll, A. (2014). A big data methodology for categorising technical support requests using Hadoop and Mahout. *Journal Of Big Data*, 1(1), 1. doi:10.1186/2196-1115-1-1.
17. Jiang, T., Zhang, Q., Hou, R., Chai, L., Mckee, S. A., Jia, Z., & Sun, N. (2014). Understanding the behavior of in-memory computing workloads. 2014 IEEE International Symposium on Workload Characterization (IISWC). doi:10.1109/iiswc.2014.698.
18. Liang, F., & Lu, X. (2015). Accelerating Iterative Big Data Computing Through MPI. *Journal of Computer Science and Technology*, 30(2), 283–294. doi:10.1007/s11390-015-1522-5.
19. Shi J., Qiu Y., Minhas U. F., Jiao L., Wang C., Reinwald B., & Ozcan F., “Clash of the titans: MapReduce vs. Spark for large scale data analytics”, In *Proceedings of the VLDB Endowment*, 8(13), pp. 2110–2121, 2015.
20. Apache Spark the fastest open source engine for sorting a petabyte. (2016, October 27). Retrieved March 4, 2017, from <https://databricks.com/blog/2014/10/10/spark-petabyte-sort.html>.
21. Armbrust M., Das T., Davidson A., Ghodsi A., Or A., Rosen J., & Zaharia M., “Scaling spark in the real world: performance and usability”, In *Proceedings of the VLDB Endowment*, 8 (12), pp. 1840–1843, 2015.
22. Awan, A. J., Brorsson, M., Vlassov, V., & Ayguade, E. (2015). Performance Characterization of In-Memory Data Analytics on a Modern Cloud Server. 2015 IEEE Fifth International Conference on Big Data and Cloud Computing. doi:10.1109/bdcloud.2015.37.

23. Liang, F., Feng, C., Lu, X., & Xu, Z. (2014). Performance Benefits of Data MPI: A Case Study with Big Data Bench. *Big Data Benchmarks, Performance Optimization, and Emerging Hardware Lecture Notes in Computer Science*, 111–123. doi:[10.1007/978-3-319-13021-7_9](https://doi.org/10.1007/978-3-319-13021-7_9).
24. Gu L., & Li H., “Memory or time: Performance evaluation for iterative operation on hadoop and spark”, In *High Performance Computing and Communications & 2013 IEEE International Conference on Embedded and Ubiquitous Computing (HPCC_EUC)*, 2013 IEEE 10th International Conference, pp. 721–727, IEEE, November, 2013.

Design and Analysis of PV Analyzer on LabVIEW

Prateek Raj, Ankit Yadav, Farhan Nizam, Vinay Gupta
and Peeyush Garg

Abstract The purpose of this work is to present a data logger to analyze and store the performance record of a PV module using LaAbove mentioned device has given an accurate result under a long time test environment with a specific power rating of PV module and suitably rated devices. However, it has been also tested for various power ratings of module, and it performed well with slight modification in rating of other devices. The data logger consists of a LabVIEW, DAQ card, temperature sensor, voltage sensor, current sensor, and variable rheostat. This data logger can be used to analyze the performance of a solar module and contribute in research to make it more efficient source of energy. The process to install a data logger has been explained below.

Keywords LabVIEW · DAQ card · Data logger · PV analyzer
Voltage measurement · Current measurement · Temperature measurement

P. Raj (✉) · A. Yadav · F. Nizam · V. Gupta · P. Garg
Department of Electrical Engineering, Manipal University Jaipur, Jaipur, India
e-mail: prateeeekraj13@gmail.com

A. Yadav
e-mail: dpkverma786@gmail.com

F. Nizam
e-mail: farhan.nizam@yahoo.co.in

V. Gupta
e-mail: vinra_20@rediff.com

P. Garg
e-mail: peeyush01garg@gmail.com

1 Introduction

In the current world scenario, solar energy is said to be the best source of energy that can fulfill the huge demand of power for the fast-growing technologies. With the rising priorities of environmental issues, clean energy production has become equally important. Solar radiation is a clean energy source resulting in negligible harm to nature. Its resource of energy is sunlight that is abundant and considered to be inexhaustible resource of energy. This is currently fulfilling a huge part of electricity demand in the world but the problem is that it is not used up to best of its efficiency due to some factors. Many research centers and individual ones in the world are currently performing experiments by analyzing its performance under different conditions to enhance its performance. This is already observed that the environmental and eco-friendly solar energy opens the flexible path for research and development with a low cost of economy worldwide [1].

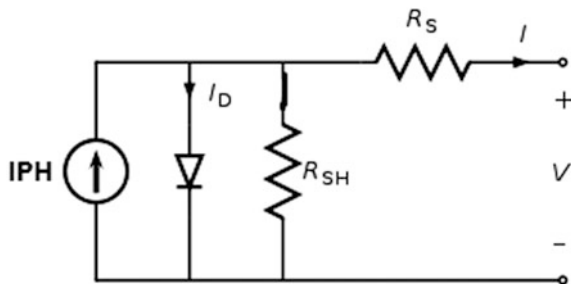
However, the lifetime of solar panels degrades with the years due to the environmental factors, which effect on its characteristics. To evaluate the performance of photovoltaic modules such as fill factor, short-circuit current, open-circuit voltage, and maximum power, the current-voltage (I-V) curve is necessary [2].

By understanding the importance of the above-mentioned research, this data logger design can be used to store and analyze the PV performance data. For the individual experiment performers, it can be very helpful due to its easy installation process and simple design. It can automatically read and store the data at any fixed interval of time which can be used to plot real-time P-V or V-I curves.

2 Electrical Equivalent Circuit of Solar Cell

The solar cell is alike to a single diode model as shown in Fig. 1. The solar cell comprises a current source I_{PH} , diode with internal shunt resistor R_{SH} , and a series resistance R_S , and then the total current is calculated. [3] (Fig. 2).

Fig. 1 Electrical equivalent circuit of single solar cell



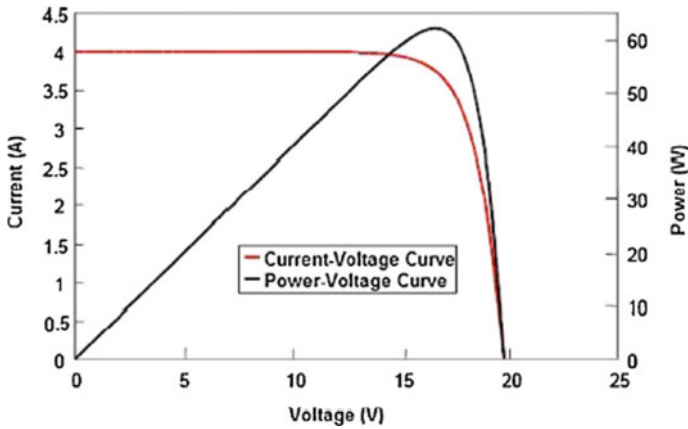


Fig. 2 I-V characteristics of a PV module with the variation of power [5]

$$I = I_{PH} - I_D - \frac{V + IR_S}{R_{SH}} = I_{PH} - I_0 \left[\exp\left(\frac{e(V + IR_S)}{kT_C}\right) - 1 \right] - \frac{V + IR_S}{R_{SH}} \quad (1)$$

It is observed that the value of shunt resistance is more than the value of load resistance, while the value of series resistance is comparatively very low than the value of load resistance. So, the total current I is represented as follows:

$$I = I_{PH} - I_D = I_{PH} - I_0 \left[\exp\left(\frac{eV}{kT_C}\right) - 1 \right] \quad (2)$$

where value of k (Boltzmann’s gas constant) is 1381×10^{-23} J/K, the absolute temperature of the cell is denoted by T_C (in Kelvins), electron charge is denoted by e and is equal to 1602×10^{-19} J/E, voltage across the cell is denoted by V (Volts), dark saturation current is denoted by I_0 , which depends mainly on temperature. Equation for open-circuit voltage V_{oc} is given below:

$$V_{OC} = \frac{kT}{q} \ln\left(\frac{I_{PH}}{I_0} + 1\right) \approx \frac{kT}{q} \ln\left(\frac{I_{PH}}{I_0}\right) \quad (3)$$

3 Design Representation of Data Logger

Design representation of data logger describes the basis of apparatus arrangement and their specifications, as given below:

3.1 Apparatus Description

Designed data logger which is based on LabVIEW using DAQ card will record and save the data in EXCEL file which helps to create the characteristic graphs very easily and accurately with automatic logging and delaying with suitable interval throughout the day. The analysis of generated graph will directly represent the reduction of efficiency percentage due to the environmental factors. This logging system is the best way to analyze the system in real time with very less effort and manpower, resulting in profitable outcome. The detailed connection diagram is shown in Fig. 3.

3.2 Specification of System Components

The logger circuitry is required to have voltage a sensor, a current sensor, a temperature sensor, Data Acquisitioning USB device and a DPDT switch to get the data short circuit current, open circuit voltage to calculate the output power given by the PV Module to get I-V and P-V characteristics with the variation of temperature sensed throughout the day, and Record the data using LabVIEW platform [4].

All the required devices are mentioned below with their ratings:

(a) DAQ card USB6009

- Range of analog output from 0 to 5 V
- Power source—offers +5 V power up to 200 mA
- AI resolution of DAQ 6009: 14 bits differential, 13 bits single-ended

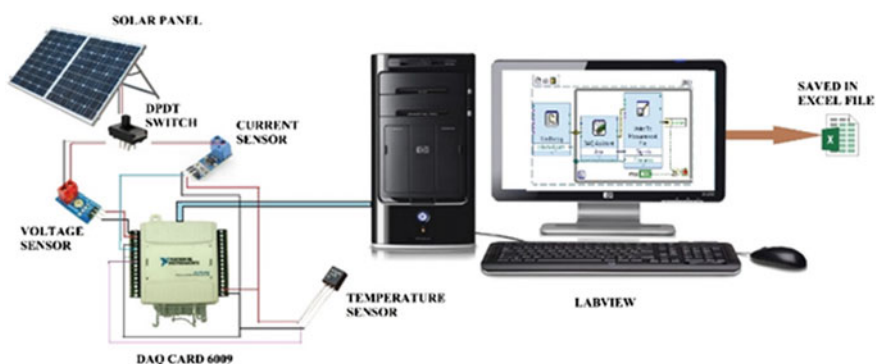


Fig. 3 Schematic diagram of experimental setup

(b) **Current sensor ACS712**

- Pin power supply 5 V
- Onboard indicator
- Current sensing range (-5A) to (+5A), with sensitivity of 66 mV/A

(c) **Voltage sensor**

- Input voltage: direct current type: range—0-25 V
- Voltage measurement range—0.02445-25 V
- Analog voltage resolution—0.00489 V
- Input terminals: positive and negative terminals
- Maximum input voltage: 25 V

d) **Temperature sensor LM 35**

- Operating range -55 °C to 150 °C
- Linearly proportional to the temperature in centigrade
- Accuracy -0.5 °C (at 25 °C)
- Suitable for distance applications
- Low cost, linear output
- Operates voltage range 4-30 V
- Not require any external calibration
- Less output impedance

We connected the designed data logger to the solar panel so that its various parameters were observed and stored in EXCEL sheet. Further, this data has been used to analyze and plot P-V and V-I characteristics (Figs. 4 and 5).

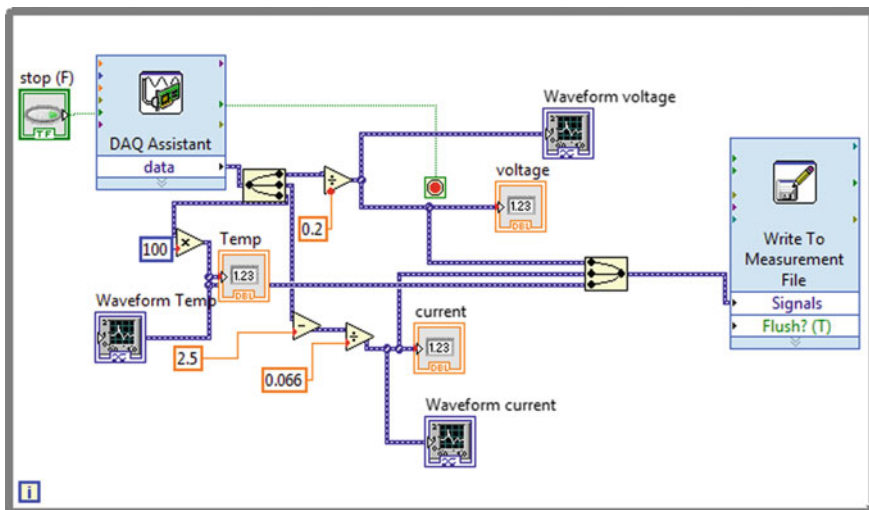


Fig. 4 Block diagram of the acquisition system



Fig. 5 Real-time experimental setup

4 Evaluation and Validation of Designed Data Logger

To determine the accuracy of the designed system, we conducted a small test on 50 W polycrystalline solar panel. The specifications of PV modules are given in Table 1.

The designed system offers the real-time data recording of generated voltage, current, and total power at different temperature environment with the help of data logger. The various characteristic curves are plotted and found near to the ideal, as well described in Fig. 6.

We used a multimeter to note down various readings of solar panel at some specific time. This process helped us to determine the performance accuracy of the system.

By observing the above-mentioned Table 2, it can be determined that the designed data logger is accurate and reliable when compared to traditional method of measurement. It can be used to analyze the data for research purposes.

Table 1 Specification of solar panel

Power max. (P _{mpp})	53.473 W
Voltage at P _{mpp} (V _{mpp})	19.1 V
Current at P _{mpp} (I _{mpp})	2.8 A
Open-circuit voltage	22.905 V
Short-circuit current	2.986 A
Irradiation (watt/m ²)	1000 W/m ²

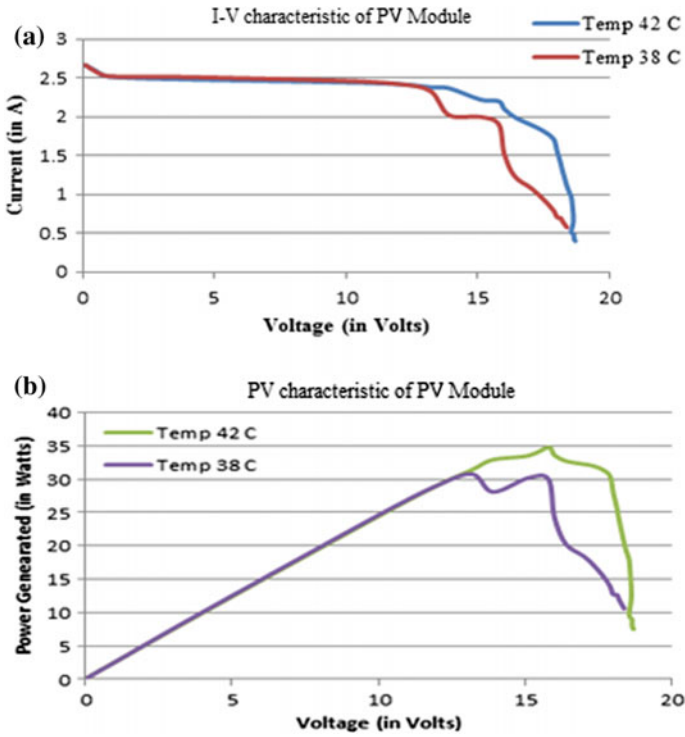


Fig. 6 a, b I-V and PV characteristics at different temperature values

Table 2 Comparison between data logger and standard measuring instrument

Parameters	Using standard measuring instruments	Using data logger
Power (W)	52.98	52.62
Voltage (V)	18.9	18.69
Current (C)	2.78	2.72
Temperature (°C)	42	42

5 Conclusion

The designed system was working properly to measure the various electrical real-time signals' values with environmental parameters like temperature. As per the analysis, the characteristic curve can be tested, and further, the module efficiencies can be predicted with the help of existing data. The available sensors can also be calibrated under suitable range for a PV module. The real-time monitoring and control algorithms for efficiency enhancement of PV panel can also be suggested on the basis of measured data.

References

1. Solanki, C.S.: Solar Photovoltaic- Fundamentals, Technologies and Application, 2nd ed., New Delhi, India, PHI Learning, ch. 1, pp. 04–10 (2011).
2. Batista, V.L.J., Chenlo, F., & Afonso, J.L.: Low-Cost Instrument for Tracing Current-Voltage Characteristics of Photovoltaic Modules. In: International Conference on Renewable Energies and Power Quality (ICREPQ'12) (2012).
3. Mohamed, Z., Yousry, A., Abdullah, A. H., Ihab, E. S.: LabVIEW Based Monitoring system applied for PV power Station, in international conference on Automatic control, modelling & simulation, (ACMOS-10) (2010).
4. National Instruments, <http://www.ni.com>.
5. Pearsall NM, Hill R. Clean electricity from photovoltaics: Imperial College Press; chapter 15, pp. 1–42. (2001).

An Approach to Monitor Construction Site Based on Radio Frequency Identification and Internet of Things

Avi Gaba, Aakanksha Panwar, Rajesh Singh, Anita Gehlot and Vikas Garg

Abstract Monitoring materials and keeping record of the data has always been a problem at the construction sites. Our research is aimed at solving this problem and thus ensuring an increase in assurity of the management of the work at the construction sites. In our study, we have used RFID technology. The materials used at sites will be given a unique tag, and that tool will be recognized by its unique tag only. With the help of these tags, we will be able to recognize the location of each and every tool. Also our study includes a handy device consisting of a screen which will display the distance of the user from a particular tool by taking into account the RSSI of each tag. With the help of RFID technology along with unique tags, it becomes very easy to work at the construction sites without any hustle and bustle. In our study, we have connected a MAX232 after RFID reader to extract the code of each passive RFID tag. As a result with the help of our study, we have proposed the betterment in handling and managing tools at the construction site.

Keywords RFID · Construction tools · Location tracking · IoT

A. Gaba (✉) · A. Panwar · R. Singh · A. Gehlot · V. Garg
College of Engineering Studies, University of Petroleum and Energy Studies, Dehradun,
Uttarakhand, India
e-mail: aaavigaba13@gmail.com

A. Panwar
e-mail: aakankshakpanwar@gmail.com

R. Singh
e-mail: rsingh@ddn.upes.ac.in

A. Gehlot
e-mail: anita@ddn.upes.ac.in

V. Garg
e-mail: vgarg@ddn.upes.ac.in

1 Introduction

According to some researches, it is proved that existing methods for monitoring of tools and equipments on the construction sites still depend wholly on human intervention. Construction materials contributes about 50% of the total project's budget, still their management is not done wisely and most often components got lost at the construction sites. This is so old school and can't cop up with the modern era of technology. Those techniques are old, time consuming, include much labor work, and not reliable. Manager should have a proper record and information about the components and the tools present at the construction site. So by designing an automatic system which can keep the information about the availability and location of construction material, we can have a better management for equipment required. In this research, we are constructing a radio frequency-based identification (RFID)-based construction site monitoring system which will keep an eye-like surveillance on the equipment and tools. It will let us find our needy things which are left somewhere and forgotten. We have divided our construction site into some blocks. For example they are named as, 'Energy house Block 1' and 'Energy house Block 2'. RFID will help us know about the exact location of the tool by which it will be easy to find the object. Received signal strength indicator (RSSI) readings are noted down, and according to the strength of the signal received, the lost object would be found [1].

This research is based on the application of RFID technology to find the lost objects or heavy and important equipment left somewhere at the construction site and forgotten. An automatic system is proposed which includes RFID tags for every tool and object present at the site. We are proposing a research in which every essential tool and components will be tracked and monitored at the construction site. By which no component will ever get lost or the probability of losing an important and costly component falls to almost zero. There are small RFID tags pasted on every component, and each tag has its own identity (assigned by us). According to the RSSI of each RFID tag, a person will get to know about the location of that particular object he/she is looking for. A handy device working as graphical user interface (GUI) is also designed and proposed in this research which will be in the hand of the user and will continuously show the strength of the signal transmitted by particular RFID. User will get a user understandable view of the location of the object. The RSSI of the system is read by the handy device, and it will convert the signal strength into the distance from the object. This work is done by adding some algorithms in the background of that device. As the RFID tags pasted on the objects will transmit a radio signal which is received by a common receiver RFID attached to our computer by using MAX232. As we have assigned a particular identity to each tag (in codes say Z1), the receiver RFID will receive the radio signal and using max232, its code will be extracted and saved in our system. Moreover, all the data regarding to the location and signal strength of the tags will be uploaded to a cloud server time to time. From cloud, we can access our data sitting anywhere using Internet. This research is an example of the futuristic designs

where more application of RFID’s can be added like environment monitoring, human location monitoring, etc. The objective is to dig out more and more methods and ways that will improve this sector technologically, economically, and in many other ways [2].

In this research, we are also checking the capability of passive RFID technology installed at the construction sites. Also we are checking that the received information can help to increase the status and mobility. In addition to this, the main problem at construction sites is wastage of time or lost time that could be utilized in doing the prime task of construction. According to some of the researches, RFID technology is very helpful and efficient in locating tools and equipment along with saving the extra time which is spent while doing some works manually. Manually did work can have human errors in it and is much time consuming when compared to automatically machine handled jobs. This research focuses on the automatic system for collecting data about the availability of the resources and their location at the sites [3].

Each object at the construction site has a RFID tag on it. As every construction site is divided in some areas or blocks say (Block A, Block B, etc.) according to the range of our RFIDs. For Every block, there is assigned a RFID reader. For example in Block 1, the RFID reader assigned have IP address 192.168.0.28 (see Table 1), Likewise the construction site is divided and RFID readers are assigned. Reader RFID will continuously send the radio wave to the RFID tags, and simultaneously all the tags in the range get scanned and data is transferred to a computer connected to it. Code of the particular tag is extracted using MAX232 connected at bray terminal. The nearest reader will read tags, and data is extracted over the connected computer. Using algorithms, all the data is filtered and managed by which it becomes a user understandable layout.

RFID tags have been used which are of very low cost. Each tag is given a known location and is used as a particular reference point. Total of 514 experiments were carried out with the help of 3, 3 m bed. Important thing to note here is that received signal strength indicator (RSSI) has been used for measurement of the signal. Results were like this: number of tags, time duration, tag locations, and interference of metal. Also error occurred when the received signals were not spread within 360° vicinity of the data taking point. Metals objects showed accuracy when it came to

Table 1 Sample data of five tags of different tools

Object ID	Object name	RFID tag value	Time	RFID Reader ID	Description
Z1	Driller1	5000092BE93EF	9:06:15	192.168.0.28	Energy house Block1
Z2	Screw driver1	5000092EA2C04	9:07:35	192.168.0.12	Energy house Block2
Z3	Screw driver2	5000093217F9D	9:08:55	192.168.0.12	Energy house Block 2
Z4	Driller2	5000093228G9X	9:09:12	192.168.0.28	Energy house Block1
Z5	Hammer	5000094217H9A	9:09:44	192.168.0.18	Energy house Block 3

Object ID, object name, RFID tag value, time, RFID reader ID, and reader description

data capturing ability [4]. One of the study showed that an increase of about 32% took place when it was compared to traditional management. The results of this paper showed on how to manage information with the help of RFID taking place at construction environments [5]. This paper tells about the usefulness of supply chain management which is based on RFID. There is also a study tested for a high-tech building of a factory located at Taiwan [6]. This paper includes RFID-based system which showcases itself in areas like managing and filtering. This can also be integrated with PDAs and Web portals for increasing the efficiency of the working of the proposed method. This study mainly focuses on the inspection of the samples and collecting data automatically in test labs. Same kind of study was also tested at Taiwan by some researchers [7].

RFID technology has been considered as an appropriate method for tracking and identifying materials at construction sites. This study depicts a way to do it with the help of RFID technology. Here, sensors in the form of RFID tags are used which do not require human intervention [8]. Our paper showcases the use of tags which are permanently attached to the materials. This study has used a database called building information model (BIM) for resolving the issues of various users to have access to the data. Data is stored on tags in the ifcXML format. This study has been tested and implemented at Concordia University [9]. Another study depicts the use of RFID tags with added security to prevent hackers or unauthorized person to have access to the data. The content on the RFID tags is encrypted to avoid the leak of the information on the system [10]. This study involves usage of RFID technology that works for collecting information and giving it to the decision makers. This system was tested on workers, tools, and materials used [11].

Another study shows a way of material control at sites with the help of RFID. The basic idea behind the study includes RFID checkpoints and types of materials for material control at the sites. This paper has depicted the way to manage construction tools at the sites with the help of RFID [12]. Tracking of the tools and equipment at the construction site and management of all the received data is done with the help of RFID technology. Feasibility of constructing data modeling, traceability, and location services is shown in this paper. By using these information systems, we are decreasing the possibility of human error, or any type of error in the management at the construction site [13].

From last 20 year, RFID technology has been used extensively at the construction sites. From the vast group of applications of RFID, we are proposing one of them here, which is applicable at the construction sites. Conclusion and Future scope are also written at the end of the paper [14]. Effective management of the construction tools and equipment at the active construction site is really a tough task if it is done manually. But with the help of RFID technology, we are introducing an automated tacking system which will make our task much easier. As these construction equipments are made to provide an accurate and precise measurement, all the data is recorded and managed in labs. But, by the time of data reentry if we want to access the information, we require a novel system in which 2D barcode/RFID can be used for data recording and managing. Same is done at a lab in Taiwan [15]. RFID is used in many more areas like in this paper [16], management of waste from

construction sites is done using RFID technology. They made a fuzzy comprehensive evaluation (FCE) method to verify and assure the effectiveness and betterment of this technology over the classical one. Case studies were done in shanghai which clearly show that RFID-based monitoring system is much better and accurate in monitoring transport procedures. Moreover, this technique helped in avoiding the prevailing problems significantly [17].

2 Hardware Development

Figure 1 is the block diagram explaining the extraction of the codes of RFID tags using MAX232 and a USB to serial converter. Whenever any object with the RFID tag comes in the range of RFID reader, the electromagnetic induction will start taking place and this will help in powering the chip which is inside the tag. Further the chip will now send the required code to the RFID reader. As the RFID reader reads the code, it will be transferred to our computer for managing the data more effectively and to make a user understandable layout. Data from the microcontroller will be transferred to computer using MAX232 connected using bray’s terminal via USB to serial converter. Code is extracted, and further data management is done with the help of algorithms running behind in the computer.

The block diagram of the system is shown in Fig. 2. The system consists of a microcontroller Arduino UNO, which is powered by a seperate power supply .Our system consists of +12 V power supply using a 7412 voltage regulator. It is the controlling unit of the system. Each and every tool and equipment is given a unique tag. RFID reader does the work of detecting those tags. It keeps on detecting those tools until they are within a defined range. It stops detecting the material when it goes out of range. We have interfaced a LCD display with ARDUINO UNO through D4, D5, D6, D7 pins. With the help of the programmed code, tag and tool name will be displayed on the LCD. This RFID technique of detecting the tools helps the employees to work very smoothly. This device comes into picture when any tool at the site is not visible, or the person is having difficulty in finding any particular tool. Further, Wi-fi module is connected to the Tx pin of the Arduino UNO from where all the data will be uploaded to a cloud server using IoT

Fig. 1 Block diagram to extract code from RFID

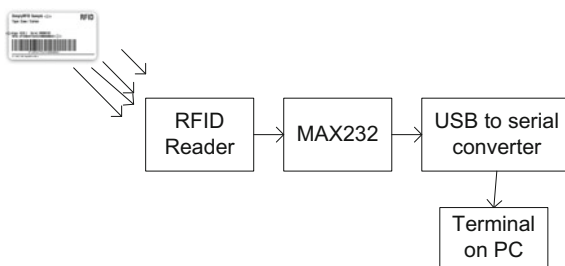


Fig. 2 Block diagram of system

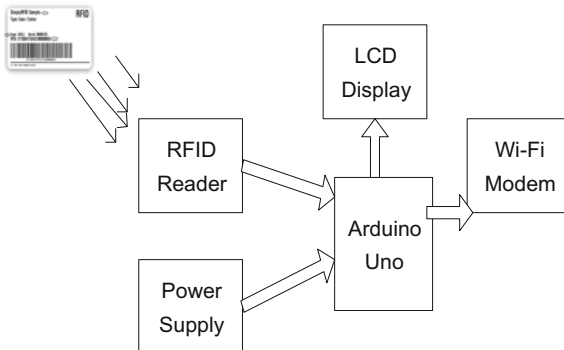
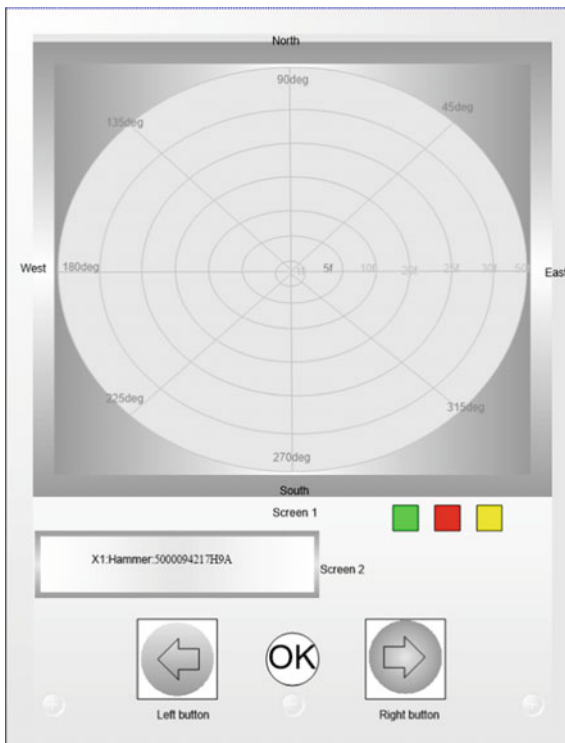


Fig. 3 Remote device for getting the location of the RFID tags



technology. Also all the data will be transferred to a PC connected to the Arduino via MAX232, and all the codes will be extracted and a user understandable layout is created with the help of some algorithms designed for this task.

Figure 3 shows a small portable handy device which is used at construction sites by the manager. This device consists of a RFID reader inside it. An internal replaceable battery is connected to this device for increasing its range up to far

distances. This device contains two screens named as Screen 1 and Screen 2. Screen 2 is a small sized screen on which “code: name: tag” of the tool is displayed. With the help of left and right button, we can scroll to different tools displayed on Screen 2. After choosing the tool by left and right button, we have to press OK button. As soon as we press the Ok button of this device, it will start locating that particular selected device on Screen 1. This device will work by using received signal strength indicator (RSSI). As we select any tool say hammer, the reader will transmit a radio signal and if the hammer is in range, tag over the hammer will receive the signal and in return send its code and with the help of RSSI we’ll get to know about the signal strength of that particular tag. User will have to roam around and have to move the device in different directions and have to follow the direction of maximum signal strength displayed on Screen 1. We have written an algorithm which will convert the signal strength into distance. This device will display the direction, degrees, and distance (in feet) of the tool from this device.

Figure 4 is the circuit diagram of the RFID code extraction circuit. We have interfaced RFID reader with the Arduino. The RFID reader is mainly used to read the RFID tags. We give +5 V power supply to the reader. Now whenever RFID tag comes within the range of the RFID reader, the electromagnetic induction will start taking place and this will help in powering the chip which is inside the tag.

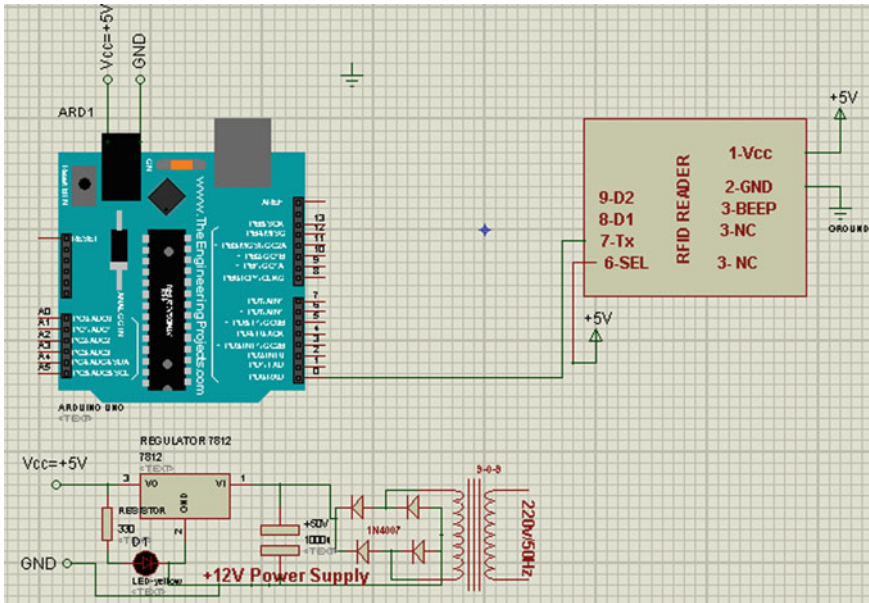


Fig. 4 RFID code extraction circuit

Further the chip will now send the required data to the RFID reader. After receiving the data electromagnetically, the RFID reader outputs the received data serially to the Arduino UNO used in our study. The tx pin of RFID reader is connected to the PD0/RXD pin of the Arduino UNO. RFID reader is connected to +5 V power supply. Further Arduino UNO is given +5 V and ground. A power supply has also been designed with the help of 7812 voltage regulator and four diodes. The output of this power supply is +5 V. Basically, this part is taking input with the help of RFID reader.

Figure 5 is the RFID and Wi-fi modem circuit with Arduino. The details of this circuit are as follows: We have connected a LCD display, Wi-fi modem with the Arduino UNO. ESP8266 Wi-fi module is used which has eight pins. The D4, D5, D6, D7 of the LCD are connected to the D4, D5, D6, D7 pins of the Arduino, respectively. The Wi-fi modem is connected to the Tx pin of the Arduino. Also the Rx pin of the Arduino is taking input from RFID reader through its Tx pin.

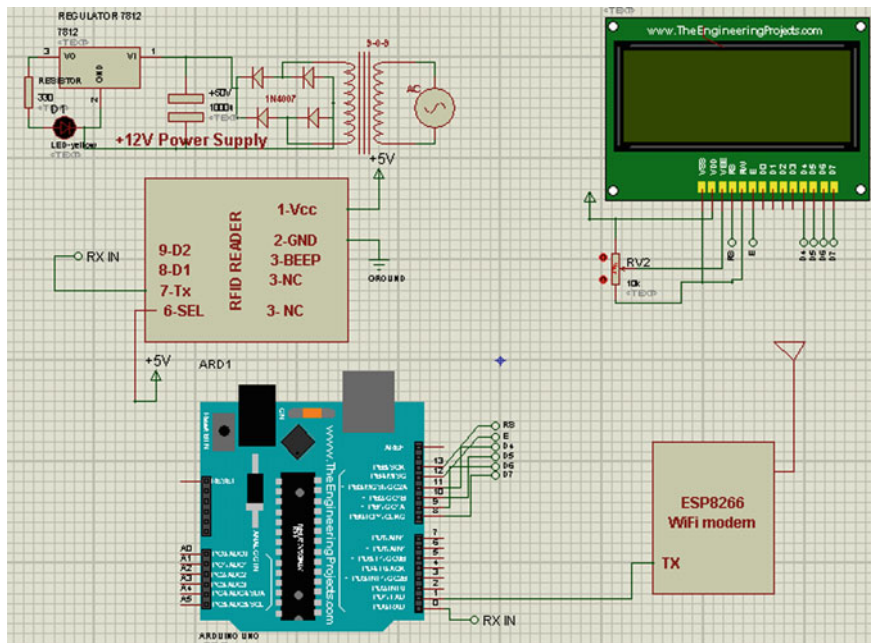


Fig. 5 RFID and Wi-fi modem circuit with Arduino

3 Software Development

See Fig. 6.

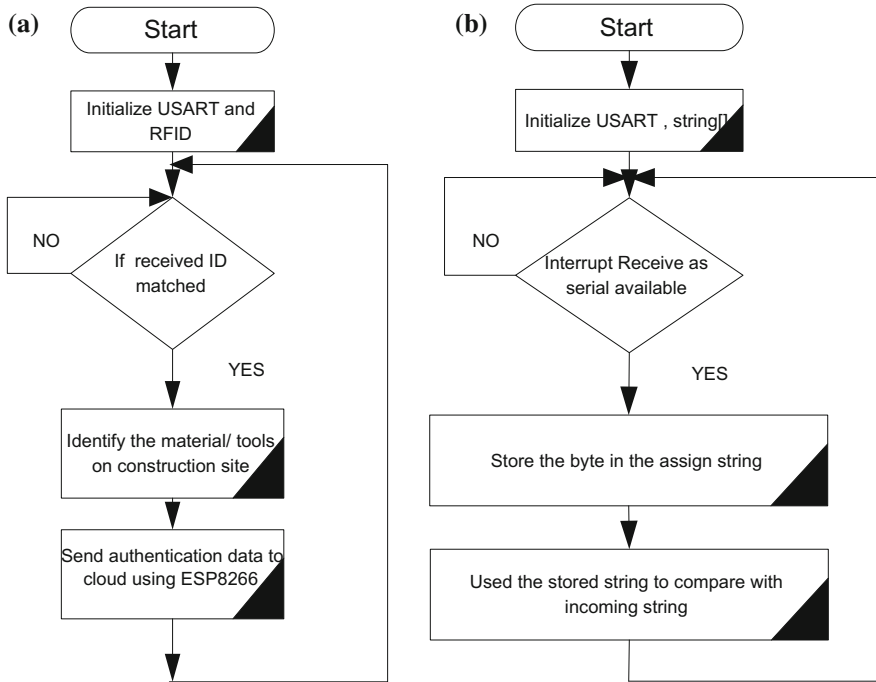


Fig. 6 a Flow chart to identify material/tools using RFID and ESP8266, b RFID card code extraction from RFID

>>>**Function to authenticate/recognize material/Tools using RFID**

```
void Check_RFID_ESP8266()
{
  if(entry_control_RFID_ESP8266==true)
  {
    if(tag_status_RFID_ESP8266==true)
    {
      lcd.setCursor(0,1); set LCD cursor at column0 and Row1
      lcd.print("hammer identified"); // print string on LCD
    }
  }
  else
  {
    lcd.setCursor(0,1); set LCD cursor at colun0 and Row1
    lcd.print("hammer not identified ");// print string on LCD
  }
  entry_control_RFID_ESP8266=false;
  tag_status_RFID_ESP8266=false;
}
```

>>> **function to receive 12 BYTE from RFID**

```
void String_Data_RFID_ESP8266()
{
  if(mySerial.available(>0)
  {
    Char RFID_serial_byte=mySerial.read();//read serial data
    RFID_string_ESP8266[total_count_byte]=RFID_serial_byte;// store data in string
    total_count_byte ++;// increment the counts
  }
}
```

Table 1 gives a glimpse of the result of tracking tools at the construction site. The RFID reader tracks the tools with particular tag. The analysis will be displayed on the computer screen as per the Table 1. Each and every tool at the site will have its own RFID tag value. The particular tool when tracked will be displayed along with its location point and time. The tabular form gives the user an added advantage of carrying out the process very easily thereby increasing the efficiency of the overall system described in our study.

4 Conclusion

This study presents an IoT-based system which works on RFID technology at construction sites. Our study involves a site which consists of various tools having their own RFID tags. The setup is aimed at increasing the efficiency and data collection techniques for the user. With the help of this technology, construction is carried out very smoothly avoiding hustle and bustle at the construction sites. Also with the help

of IoT, the user can easily have a look at the data collection on the system just by using Internet. The employees can easily use these smart electronics systems, thereby eliminating a lot of time during construction work. RFID technology can lead to much advancement if used wisely and can reduce human interference and labor.

References

1. Sardroud, Javad Majrouhi. "Influence of RFID technology on automated management of construction materials and components." *Scientia Iranica* 19.3 (2012): 381–392.
2. Yang, Huanjia, et al. "Design and implementation of an identification system in construction site safety for proactive accident prevention." *Accident Analysis & Prevention* 48 (2012): 193–203.
3. Aaron costin, et al. "RAPIDS Construction Safety and Technology Laboratory" *Automation in Construction* 24 (2012) 1–15.
4. LO, NAN-HAI, and YU-CHENG LIN. "Enhancing Worker Onsite Safety Management Using Rfid Technology In Construction." *Proceedings of the Thirteenth East Asia-Pacific Conference on Structural Engineering and Construction (EASEC-13)*. The Thirteenth East Asia-Pacific Conference on Structural Engineering and Construction (EASEC-13), 2013.
5. Shin, Tae-Hong, et al. "A service-oriented integrated information framework for RFID/WSN-based intelligent construction supply chain management." *Automation in Construction* 20.6 (2011): 706–715.
6. Wang, Lung-Chuang, Yu-Cheng Lin, and Pao H. Lin. "Dynamic mobile RFID-based supply chain control and management system in construction." *Advanced Engineering Informatics* 21.4 (2007): 377–390.
7. Wang, Lung-Chuang. "Enhancing construction quality inspection and management using RFID technology." *Automation in construction* 17.4 (2008): 467–479.
8. Wing, Robert. "RFID applications in construction and facilities management." *Journal of Information Technology in Construction (ITcon)* 11.50 (2006): 711–721.
9. Motamedi, Ali, et al. "Role-based access to facilities lifecycle information on RFID ags. " *Advanced Engineering Informatics* 25.3 (2011): 559–568.
10. Chen, Chun-Te, et al. "Construction of the enterprise-level RFID security and privacy management using role-based key management." *Systems, Man and Cybernetics, 2006. SMC'06. IEEE International Conference on*. Vol. 4. IEEE, 2006.
11. Costin, Aaron, Nipesh Pradhananga, and Jochen Teizer. "Leveraging passive RFID technology for construction resource field mobility and status monitoring in a high-rise renovation project." *Automation in Construction* 24 (2012): 1–15.
12. Lee, Ju Hyun, et al. "Information lifecycle management with RFID for material control on construction sites." *Advanced Engineering Informatics* 27.1 (2013): 108–119.
13. Ikonen, Jouni, et al. "Use of embedded RFID tags in concrete element supply chains." *Journal of Information Technology in Construction (ITcon)* 18.7 (2013): 119–147.
14. Valero, Enrique, Antonio Adán, and Carlos Cerrada. "Evolution of RFID applications in construction: A literature review." *Sensors* 15.7 (2015): 15988–16008.
15. Lin, Yu-Cheng, Weng-Fong Cheung, and Fu-Cih Siao. "Developing mobile 2D barcode/RFID-based maintenance management system." *Automation in Construction* 37 (2014): 110–121.
16. Ruan, Tingting, and Hao Hu. "Application of an RFID-based system for construction waste transport: a case in Shanghai." *International Conference on Computational Logistics*. Springer Berlin Heidelberg, 2011.
17. Montaser, Ali, Roya Azram, and Osama Moselhi. "Experimental Study for Efficient use of RFID in Construction." *FUTURE* (2013).

The Real-Time Hardware of Smart Digital Alarm Clock Integrated with Microcontroller

Ginne Rani, Purnendu Shekhar Pandey, Praful Ranjan, Gaurav Negi and Saurabh Kavi

Abstract This paper is related to new design of a voice-activated smart alarm clock. The device is proposing the new idea to get alert the user time to time as he feeds the schedule of alertness. Proposed system will give the idea to connect this with the Google App of the schedule teller. The time can be flashed using a push button on the development board. At all times, the status of the device can be viewed with the help of the 16×2 alphanumeric LCD display.

Keywords RTC · HM2007

1 Introduction

Nowadays speech processing systems are based on computers which have stretched to composite structure and high accuracy [1, 2], due to refined signal processing algorithms and great computers available. Yet, the performance rise of embedded processors (also called microcontrollers) now permits the implementation of speech recognition in consumer goods, where cost is of supreme importance [3–9]. The aim of this paper is to present a methodology to design a voice-activated smart digital clock. This clock would be capable of taking the time of the reminder and the message from the user and store it in the form of speech [10–16]. The clock also lets the user schedule the time and the date of the reminder.

It will help us to remember our scheduled tasks and appointments in a much efficient way. It is true that the text reminders are presently available on the mobile devices, but scheduling on them is an arduous task [17, 18]. This device aims to make it more convenient and practicable.

G. Rani (✉) · P.S. Pandey · P. Ranjan · G. Negi · S. Kavi
Department of Electronics and Communication Engineering, THDC Institute of Hydropower Engineering and Technology, Bhagirathipuram, Tehri, Uttarakhand, India
e-mail: ginnechaudhary26@gmail.com

2 Hardware Development

The hardware implementation requires the following components: (Fig. 1).

2.1 5 V Power Supply

This module is basically designed to achieve 5 V, 500 mA. This consists of a transformer which is used to step down the AC voltage, IN4007 diodes used to form a bridge rectifier to convert AC to DC, capacitor 1000 μ F which is used as a filter circuit, 7805 regulator to obtain a 5 V at the output of the regulator, 330 ohm resistance, LED as indicator (Fig. 2).

2.2 LM016L

It is a 16×2 alphanumeric LCD. It has been used in 4-bit data mode to preserve the number of pins of the controller for connection with the other peripherals [19–21]. It is used for displaying the time and for assisting the input and the output operations (Fig. 3).

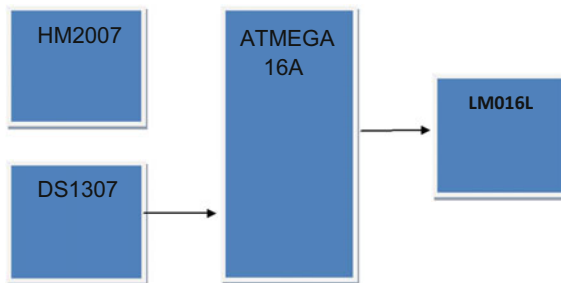


Fig. 1 Block diagram

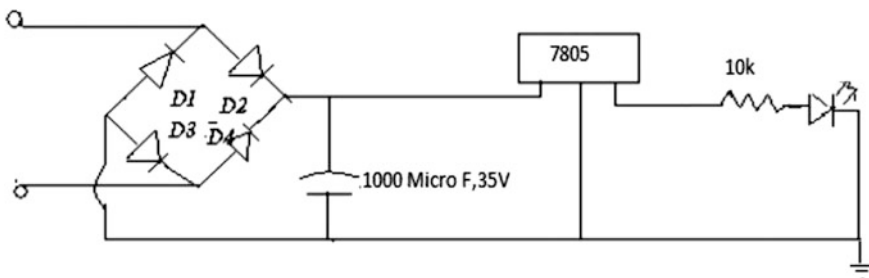


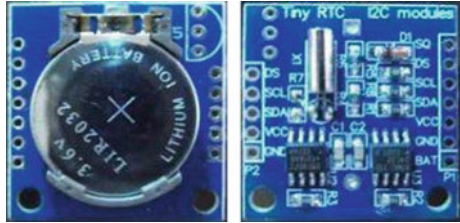
Fig. 2 Power supply circuit



Fig. 3 LCD



Fig. 4 RTC



2.3 DS1307

The DS1307 has been used for time keeping. It is possible to implement the real-time clock using the counters available in the controller also, but it becomes highly ambiguous and all the delays peg up to cause discrepancies in the time-keeping mechanism of the controller (Fig. 4).

The DS1307 has separate registers for time-keeping. It is pre-programmed with correct number of days of every month, and the correction for the leap year is also incorporated in it. Since it works independent of the controller, the time-keeping mechanism is not disturbed [22–25].

It communicates with the controller using the I2C protocol, i.e., by using the SCL, SDA pins.

The module used by us is commonly known as RTC mini.

2.4 HM2007

It is the pre-manufactured module used to provide the input to the controller. Once trained for the voice recognition operation, it has the same utility as the keypad. Firstly, it is trained for the voice recognition, then it is connected to the controller by using the 8-bit data out and is operated as a peripheral (Fig. 5).

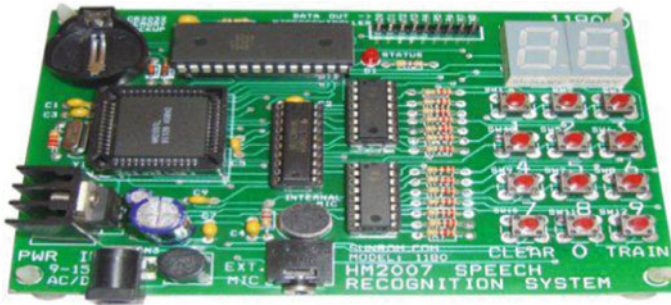


Fig. 5 Voice recognition module

Fig. 6 ATMEGA 16 A



It can be programmed for recognition of 20 words, each of the time duration of 2 s. It has a 3 V battery to retain the programmed commands into its memory even after the power is switched off.

2.5 *ATMEGA 16A Microcontroller*

This microcontroller was chosen because it has all the functionalities required for the implementation of the project, i.e., it has a very efficient implementation of the I2C protocol for interfacing the DS1307 real-time clock (RTC). It has the optimum speed and number of pins. It is also easily available and economically suitable. In the device, it operates at a frequency of 16 MHz. It has a 16 KB flash program memory, 1024-byte SRAM and the 512-byte EEPROM was sufficient for this operation (Fig. 6).

2.6 *Actual Circuit of the Device*

The following figure shows the actual circuit of the fabricated device
It has the peripherals connected on a zero PCB (Fig. 7).

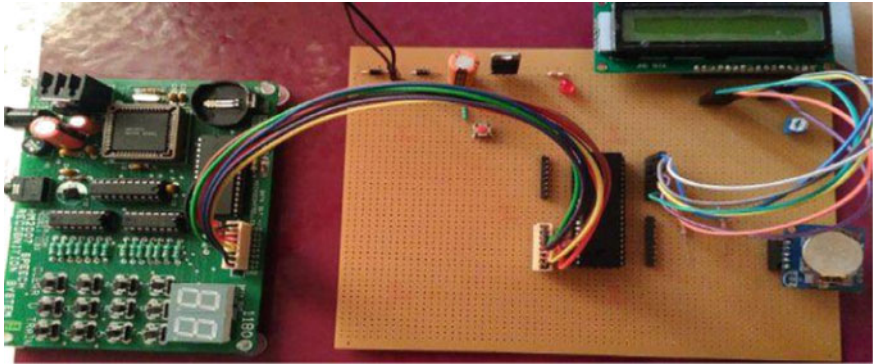


Fig. 7 Actual diagram

3 Software Development

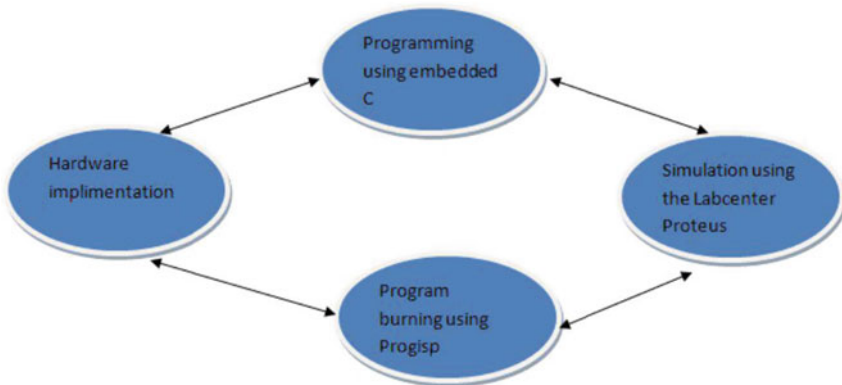
Softwares used and their purposes are as follows:

i. Atmel Studio 7.0—It has been used to program the ATMEGA 16A controller using the embedded C language.

Labcenter Proteus—It has been used for the basic simulation of the circuit before it was implemented on the hardware.

Progisp—It is the software which was used to burn the program in the flash memory of the controller.

3.1 Software Lifecycle of the Project



3.2 Coding and Debugging

The code has been written in the embedded C, which is a high-level, procedure-oriented Language. We used the GCC compiler of the Atmel Studio for writing the code. This series of the IDE is used to program all the RISC-based Atmel AVR's (Advance Virtual RISC) MC.

3.3 Simulation

After writing the code for the controller, it can be simulated on the Labcenter Proteus. In this simulation, the different components are interconnected and their functioning in the real time is observed. With respect to the output simulated, we debug the program of the errors that might have been overlooked by the IDE. It also helps us to define and decide the connections in the circuit, effectively and conveniently.

The following figure is the basic implementation of the device. Here, keypad is used to input the functioning, and it will be replaced by the HM2007 voice recognition module (Fig. 8).

3.4 Burning

It refers to the process of loading the HEX file in the flash memory of the controller. The burner uses open source software called the progisp. It is compatible with all the version of the windows.

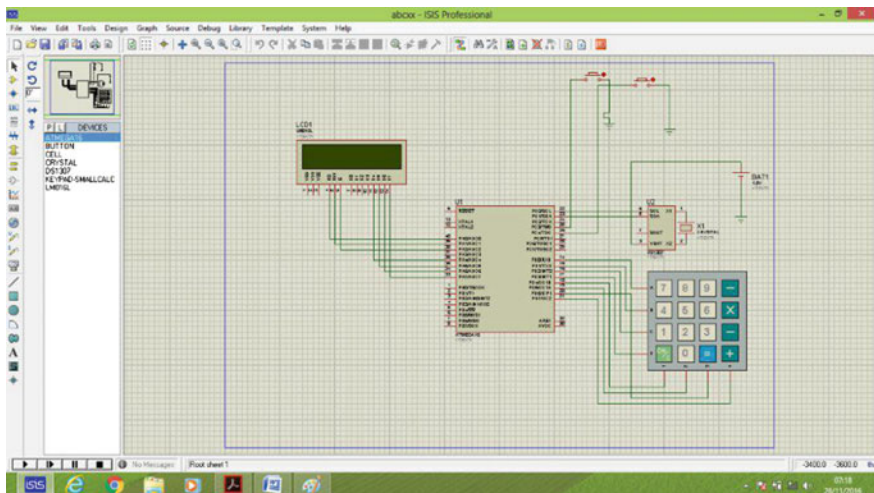


Fig. 8 Simulation

4 Program Specifications

4.1 *The I2C Protocol*

IIC or I2C (Inter-Integrated Circuit)— it is the bus interface connection basically achieves a two-wired interface (TWI) between the controller and the RTC.

In the I2C mode, DS1307 operates as a slave and the controller as a master device. As the name suggests, it requires only two pins for data transfer namely:

SCL—Serial Clock (provided by the master)

SDA—Serial Data

The I2C protocol is ideal for low-speed peripherals to the embedded systems.

4.2 *Voice Recognition System*

The HM2007 IC recognizes the voice commands after it has been trained, by correlating the input against the data stored in the EEPROM. On recognizing, it gives the BCD output on the 8-pin port. This port is connected to the input port of the microcontroller to extract the input.

5 Conclusion and Further Scope

The proposed outcome of this project is a smart device which makes the scheduling easier and completely voice activated.

At the end of this project, we expect a smart clock that performs the following operations:

Reading the time on user's command from the RTC.

Setting the multiple alarms with time set in the form of a structure for easy operation on all its parameter.

It may be further developed to further recording the alarm playback when the time in the set alarm stack matches with the time reading from the RTC.

References

1. N. Mirghafori, "Multi-band speech recognition: A summary of recent work at ICSI", Technical Report TR97-051. ICSI, Berkeley, USA, 1997.
2. H.G. Hirsch and D. Pearce, "The AURORA Experimental Framework for the Performance Evaluations of Speech Recognition Systems under Noisy Conditions", in ISCA, ITRW ASR2000, Paris, France 2000.

3. Sunpreet Kaur Nanda, Akshay P. Dhande, "Microcontroller Implementation of a Voice Command Recognition System for Human Machine Interface in Embedded System", *International Journal of Electronics, Communication & Soft Computing Science and Engineering (IJECSSE)*.
4. Clayder Gonzalez-Cadenillas, Nils Murrugarra-Llerena, "Isolated Words Recognition Using a Low Cost Microcontroller", *Computing Systems Engineering (SBESC) 2013 III Brazilian Symposium on*, pp. 77–82, 2013, ISSN 2324-7894.
5. Mohamed Abd El-Latif Mowad, Ahmed Fathy, Ahmed Hafez, "Smart Home Automated Control System Using Android Application and Microcontroller", *International Journal of Scientific & Engineering Research*, Volume 5, Issue 5, May 2014.
6. A. R. Al-Ali and M. Al-Rousan, "Java-based home automation system", *IEEE Transactions on Consumer Electronics*, vol. 50, no. 2, pp. 498–504, 2004.
7. Alper Gurek, Caner Gur, Cagri Gurakin, Mustafa Akdeniz, Senem Kumova Metin, Ilker Korkmaz, "An Android Based Home Automation System", 2013 10th International Conference on High Capacity Optical Networks and Enabling Technologies (HONET-CNS), December 2013.
8. Thinagaran Perumal, Md Nasir Sulaiman, Khaironi Yatim Sharif, Abd Rahman Ramli, Chui Yew Leong, "Development of an Embedded Smart Home Management Scheme", *International Journal of Smart Home*, Vol. 7, No. 2, March, 2013.
9. D. Naresh, B. Chakradhar, S. Krishnaveni, "Bluetooth Based Home Automation and Security System Using ARM9", *International Journal of Engineering Trends and Technology (IJETT)*, Vol. 4 Issue 9, September 2013.
10. Jieming Zhu, Xucai, Yucang Yang, and Hang Li (2010) "Developing a voice control system for ZigBee based home automation", *Proceedings of IEEE International Conference on network Infrastructure and Digital Content*, September 24–26, Beijing, 2010, pp. 7737–741.
11. Cui Chenguyi, Zhao Guannan, and Jin Mingle (2010) "A ZigBee based embedded remote control System", *Proceedings of the 2nd International Conference on Signal Processing Systems*, 5–7 July, 2010, Dalian, pp. v3–373–376.
12. Simek, M., Fuchs, M, Mraz, L., and Morvek, P. (2011) "Measurement of LowPAN Network coexistence with Home Microwave Appliances in Laboratory and Home Environments", *Proceedings of International Conference on Broadband and Wireless Computing*, October 26–28, 2011, Barcelona, pp. 292–299.
13. Ming Zhi Wu, Wei-Tsang Lee, Ren-JiLino, Chaye, G. (2012) "Development and validation of an integrated dynamic security monitoring platform," *Proceedings of the 6th International Conference on Genetic and Evolutionary Computing*, August 25–28, 2012, pp. 524–517, Kotakushu, 2012.
14. Chunglong Zhang, Min Zhang, Young Sheng Su, and Weillian Wang (2012), "Smart home design based on ZigBee wireless sensor network", *Proceedings of the 7th International ICST Conference on Communications and networking in China*, Kun Ming, pp. 463–466.
15. Nagendra Kumar, Purnendu Shekhar Pandey A paper title "Deregulated AGC scheme using Dynamic Programming Controller "International Journal of Smart Home, Vol. 10, No. 6 (2016), pp. 211–220 <http://dx.doi.org/10.14257/IJSH.2016.10.6.21>, June 2016.
16. Purnendu Shekhar Pandey, Dr. D.S. chauhan, Rajesh Singh, A Paper titled "The Real Time Hardware Design and simulation of moving message Display System Integrated with PLCC Modem" *Innovative Systems Design and Engineering(IISTE) ISSN 2222–1727 (Paper) ISSN 2222-2871 (Online) Vol 3, No 10, 2012*. IC Impact Factor 6.95, Nov 2012.
17. Saurabh Mishra, "Design of Circularly Polarized Rectangular Patch Antenna with Single Cut", *CAC2S 2013*, Atlantis Press pp 174–177, 2013.
18. Praful Ranjan, Purnendu Shekhar Pandey, " Designing of Tracking System and Emergency Vehicle Locator with Ultrasensitive GPS Receiver Antenna", *NCAEM-2016*, ISBN 978-93-82972-12-9.
19. Purnendu Shekhar Pandey, Rajesh Singh, A Paper titled "ECG Monitoring System in Wireless Personal Area Network simulation and design using Zigbee Transceiver Module for Health Care Solution" published in *IJCA (0975–8887) Volume 46 No. 18 on May 2012*.

20. Purnendu Shekhar pandey, Praful Ranjan, A paper title “The Real Time Hardware Design and Simulation of Thermoelectric Refrigerator System Based on Peltier Effect”, ICICCD-2016, Vol 479, pp 581–589, 2016.
21. Y.B. Krishna and S. Nagendram (2012) “ZigBee Based Voice Control System for Smart Home”, International Journal on Computer Technology and Applications, Vol. 3, no. 1 (2012), pp. 163–168.
22. B. Mardiana, H. Hazura, S. Fauziyah, M. Zahariah, A.R. Hanim, and M. K. Noor Shahida (2009) “Home Appliances control Using Speech Recognition in Wireless Network Environment”, Proceedings of the International Conference on Computer Technology and Development, pp. 285–288.
23. N.P. Jawarkar, V. Ahmed, and R.D. Thakare (2007) “Remote Control using mobile through spoken commands”, Proceedings of IEEE International Consortium of Stem Cell Networks”, 2007, pp. 622–625.
24. S.M.A. Haque, S.M. Kamruzzaman, and Md. Islam (2006) “A system for Smart Home Control of Appliances based on timer and Speech Interaction”, Proceedings of the 4th International Conference on Electrical Engineering, January 26–28, pp. 128–13.
25. Ganasekar, A.K., Jayarelu, P., and V. Nagarajan (2012) “Speech recognition based wireless automation of home with fault identification for physically challenged”, Proceedings of International Conference on Communications and Signal Processing, April 4–5 2012, Chennai, pp. 128–132.

Design and Development of Oil Tank Monitoring System Using GSM MODEM in Distribution Transformer

Irfan Ansari, Shubham, Anurag Singh, Puneet Verma, Rajesh Singh and Anita Gehlot

Abstract These features are important for effective power transmission and long life expectancy of industrial transformers. The monitoring and controlling of transformer are done by using microcontroller, GSM transmission is used for wireless communication, and sensors will check the level of oil in oil tank of the transformer. There are various transformer maintenance techniques, but these projects give real-time monitoring and controlling of transformer by using microcontroller. The design is to sense the feature of transformer and send them information regularly to the processor; the processor in turn will make the transmission through GSM MODEM to the client mobile. So, the model makes it possible to do real-time controlling and monitoring of oil in the transformer.

Keywords Oil tank monitoring • Ultrasonic sensor • GSM
Distribution transformer protection • Real-time monitoring system

I. Ansari (✉) · Shubham · A. Singh · P. Verma · R. Singh · A. Gehlot
University of Petroleum and Energy Studies, Dehradun, Uttarakhand, India
e-mail: Irfanansari.ansari76@gmail.com

Shubham
e-mail: rk74817@gmail.com

A. Singh
e-mail: manjraa2022@gmail.com

P. Verma
e-mail: Puneet.verma2796@gmail.com

R. Singh
e-mail: rsingh@ddn.upes.ac.in

A. Gehlot
e-mail: anita@ddn.upes.ac.in

1 Introduction

The various programming and coding systems are developed and now helpful for monitoring the oil level in the oil tank of the transformer. Data logger is very helpful in monitoring the required parameter very effectively and also efficiently. Proteus simulation model is also very helpful in measuring the accuracy of the designed system required for parameter monitoring. The data received is again retransmitted through virtual serial port at a fixed baud rate. The received data is displayed in the graphical user interface. Well, this is very helpful in the designing of the system and further studies are also on for making the system more effective, reliable, efficient, and easier to control [1]. The designed system for monitoring the oil level in the tank collects the data of the level of the oil level in the oil tank and keep transmitting it to the processor. Transmitting the data is done via wireless connection provided in the system using GSM MODEM, and it directly sends the information to the mobile of the operator in charge. In the case, any fault occurs in the oil tank and its oil level affected adversely it immediately transmits an emergency message on the mobile of the operator. Hence, trip signals can be sent by the operator to the relays [2]. The system is designed for measuring the oil level in the oil tank. Different levels of the oil should be measured and recorded while we are filling the oil tank with the oil. During the normal working of the transformer, we should measure and record the different oil levels at different time intervals. We should store this data somewhere in a computerized way. And from the next time, we go for checking the oil level for the same intervals we should match the new data with the previous ones in the computer more accurately and can easily detect that the working condition of the oil tank is normal or not [3]. For continuous monitoring of the oil level in the oil tank, we use ultrasonic sensors in the designed system for monitoring the oil level in the oil tank. Ultrasonic sensor measures the level of the oil and sends this information to Arduino, and from there, it will be sent to the processor and get displayed on LCD via GSM MODEM. These sensors emit radiations toward the oil in the oil tank and these radiations get reflected back after collision with the oil surface; hence, the delay indicates the oil level to the sensors and it further sends by the sensors. This process is on for 24 by 7 [4].

Ultrasonic sensor employed in the system emits radiation or waves which gets reflection from the surface of oil after falling in it. The time delay in the reflection of the sent radiations determines the height of the oil. This determined height is then compared to the data recorded previously if the data matches the previous data; hence, normal, the new data gets stored again and the operator will get update on his/her mobile, and in the case, data does not match the previous data; hence, not normal, an emergency is sent on the operator mobile via GSM MODEM to take the required action immediately [5]. The person in charge for a particular transformer in

a remote area will remain updated with the working and condition of the oil tank of the transformer. The oil requirement, maintenance of the oil tank, and reliability of the oil tank are dependent on the information updating to the person in charge. By this way, better service could be provided to the customers even in the remote areas [6]. For optimization, oil refill, better efficiency, reliability of the oil tank, and the most important customer's satisfaction, the designed system is applicable, reliable, and required very purposely. Very purposeful to minimize the manual maintenance and also in avoiding the excess purchase of the required oil, hence, it is economical to adopt the designed system [7]. The monitoring system is very helpful in detecting any kind of leakage in the oil tank. So that immediate action can be taken by the person in charge [8]. Any kind of leakage detection in the oil tank is reported immediately to the person in charge on his/her mobile via GSM MODEM. So that immediate action can be taken [9]. In this, an analysis has done on oil tank monitoring system during loading test is presented and the result of analysis of actual and practical measurement is compared. And during the experimental test the oil tank was on stiff cohesive soils and on a material used to refill an excavated area can be good with soil cement columns, get with the thoroughly mixing methods. The models used in the technique are good to reproduce the soil nonlinearity and have been calibrated. The measured and analyzed values of pore water pressure are less satisfactory. The capability of the soil improvement program adopted is lastly estimated, comparing the back-analyzed performance with the results of additional analyses, in which no treatment or a different geometry of treatment is hypothesized [10]. The development and uses of an industrial deoiling hydrocyclone equipped with electrical resistance tomographic instrumentation are mentioned. For continuous monitoring of separator operation, electrical sensors are used. A fine distinction of flow among the hydrocyclone can also be sensed by checking its potential for computational fluid dynamics and design prototype [11].

The flow rate of liquid being fed to a point of use is continuously monitored as is the liquid level in the feed tank by detecting the level in a liquid gauge member at two successive locations while feed from the tank is blocked, so that such detected data can be employed in a computer to output the flow rate and tank level [12]. The present invention is an electronic liquid-level monitoring apparatus for an in-ground storage tank. For proper placement of the ultrasonic transducer in a fixed position relative to the fill pipe of the storage tank, transducer is disposed in fill pipe head device and it also provides a combination of a plurality of different fill pipe diameters. The length of time from transmission of ultrasonic pulse to the receipt of the return echo is measured by an electronic control. It then calculates the distance from ultrasonic transducer to the level of liquid in the tank. Using tank parameters stored in a memory as corrected for the speed of sound at the particular temperature measured via a temperature sensor. In this embodiment, a communications device such as a modem can be employed for transmission of the tank data from the

monitoring apparatus to an external device [13]. In the paper, the system is designed for measuring and recording the oil level in the oil tank. In this system, the level of the oil is monitored and recorded continuously. In this system, the oil level is measured and the processor is kept updated with the record in the case if transformer and its oil tank are functioning properly. Also the health of the oil tank is monitored with the oil level in the tank by the system [14]. The sensor deployed in the system is used to monitor the oil level in the oil tank. It is an ultrasonic sensor so it emits ultrasonic waves or radiations toward the oil surface, the waves get reflected back from the oil surface after hitting the surface. The time delay in the reflection of the ultrasonic waves determines the oil level in the oil tank, and this information is sent to the processor and will get displayed on the GUI. The recorded data is also compared with the previously recorded data which was recorded during the normal working conditions of the transformer [15].

Nowadays, power industries require from designers to design and develop a system to monitor the major power equipment mainly transformer located at remote locations or sites. The viscosity of oil changes and it causes losses with the increase in temperature in the industry loading guide. A test program was performed to measure the oil level in the oil tank of the transformer. Some tests were performed for natural and non-directed forced oil calculation. The temperature distribution in the winding was not linear with height as usually assumed. A large number of temperature sensor is required to determine hot spot location. At some areas, the hot spot was found to be different from one another and it is less predictable for natural oil circulation than for non-directed forced oil circulation, during abnormal situation [16]. The viability of applying UHF partial discharge in oil monitoring of all service line is established so that leakage in the line can be detected. Discharge in oil is shown to radiate high-frequency signal which will allow detection. On-site pulse injection is used to test the operation of UHF coupler fitted on the transformer [17]. A vibro-acoustic method is proposed for monitoring the winding pressure clamps and core of the transformer. The basic principle of this method is oscillation frequency spectra on clamping force which allows to differentiate between the core and the winding pressure clamps, for the practical application for the monitoring, a specific software is developed [18]. This paper presents a different type of partial discharge monitoring system is developed which is capable of detecting the possible problems occurred by the partial discharge in the transformer. This is also used in measuring the current pulses and ultrasonic pulses and identifies that the partial discharge is in the transformer or it is any other external noise. So through the different tests in fields and different applications, it is clarified that it can be satisfactorily used [19]. For monitoring the in-service behavior of transformer, the use of dissolved gases is done. Firstly, by portable gas collector the concentration of hydrogen is to be measured at different intervals of few hours. A different model is used which uses fuel cell detector, and a continuous monitoring from the substation

is done. The dissolved gas analysis is used for fault occurring condition [20]. The main component in the transformer which is to be monitored is moisture content in oil. A paper is proposed in which monitoring of moisture is done in oil. The working model estimates the level of moisture in the transformer. Comparing the moisture that had been measured from our model and estimated one, the fault is detected [21]. In this paper, the use of data acquisition system is derived for rehabilitation purpose of the transformer. The aim of standardization is to make the multiple diagnostic models so that different tests can be performed and overall efficiency and maintenance can be done at proper time. The standardization of diagnostic and analytic techniques is improved so that test result can easily be monitored [22].

For continuous monitoring of liquid in underground oil tanks, a different method is proposed. A set of algorithm and hardware make it possible to reduce the losses by continuous monitoring of it. For completion of this task, we require a mechanism in every tank which shows the reading of oil in the oil tank and the temperature condition inside the reservoir. This second system also provides reports to the tank operator and sets an alarm system for a specific time in case there is a loss due to a leak in any part of the tank system so that they can take the further actions [23]. A system is designed for monitoring the conditions inside the oil tank of the transformer. The system includes a sensor communicating data indicative of conditions within the storage tank to a base controller. The graphical display also adds the database of condition inside storage tank of the transformer that may show graphically to track [24]. A different method is designed for monitoring the fluid level in the oil tank of the transformer. The apparatus of the newly invented system includes a rubber which is coated by the magnetic material for holding a pivotally mounted housing to the interior of the storage tank and an ultrasonic sensor is contained within the housing for generating acoustic pulses and for getting reflections of the acoustic pulses through the ultrasonic sensor [25]. In this paper, the theoretical estimations of a derived model for monitoring moisture in the transformer oil are estimated. The moisture model estimates the moisture content inside the transformer oil under the working conditions. Comparing the value of estimated moisture with the measured one, the model can detect failures producing an abnormal water content in the transformer [26].

2 System Description

In Fig. 1, the components are shown which are used to continuously monitor the oil level of the oil tank and the components are oil tank, ultrasonic sensor, Arduino Uno, power supply, GSM MODEM, and mobile phone.

In Fig. 2, a block diagram is there to show how the device will work more efficiently and step-by-step process is also shown that there will be a cutoff level for the tank which will be measured by ultrasonic sensor; then, the microcontroller will

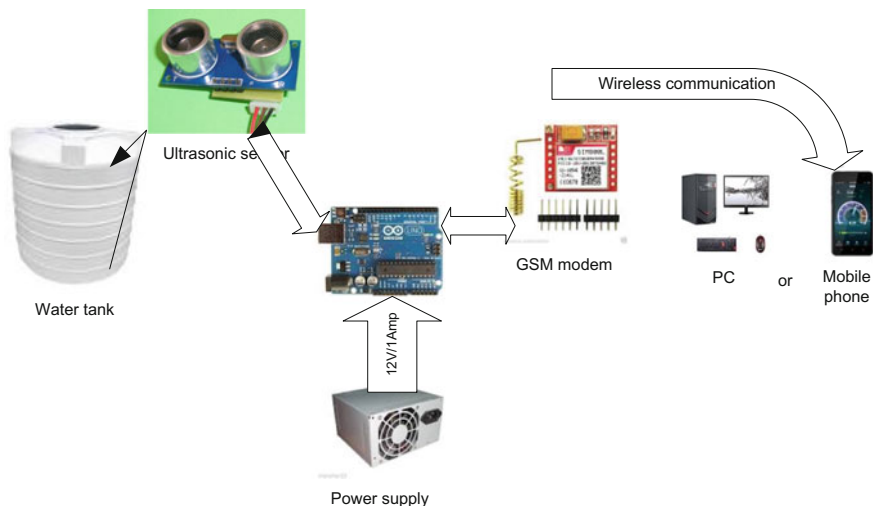


Fig. 1 Generalized block diagram

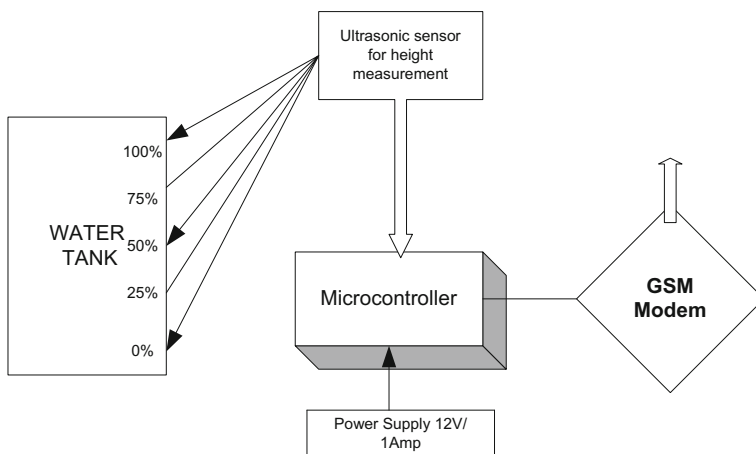


Fig. 2 Block diagram representation of system

analyze the data and it will also show on LCD, if the tank level will fall below the cutoff level, then the message will be sent by GSM MODEM to specific mobile.

In Fig. 3, a complete circuit diagram is shown, and in this paper, Arduino Uno, ultrasonic sensor, GSM MODEM, LCD, and mobile phone are used, and its working is like the following: Initially, sensor will sense the oil in the oil tank of the transformer; then, the sensed information is sent to processor, depending on the sensed information processor that will send respective signals to the peripheral to act. The sensed data will show on LCD, and if the oil in the oil tank of the

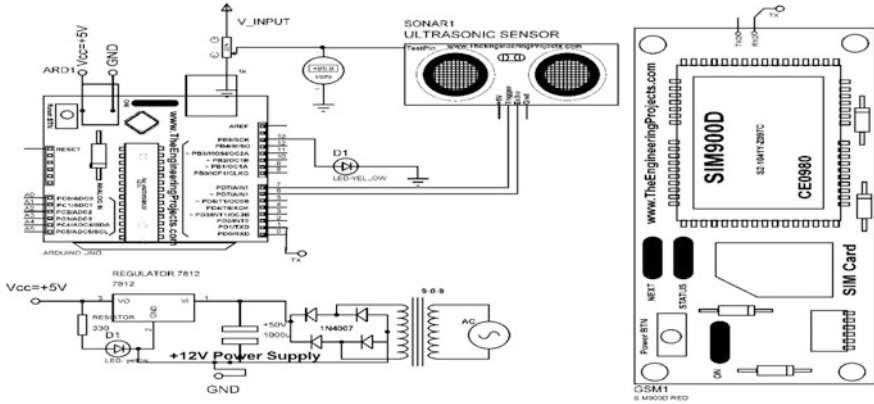


Fig. 3 Circuit diagram of the system

transformer is less than the cutoff level, then the ultrasonic level sensor sent the information to the processor. The sensed data is sent to the operator by the processor using GSM MODEM.

3 Software Development

In Fig. 4, the model of the system is prepared on Proteus and their simulation can also be done. By this, analysis of the device can also be done so that it will work more efficiently and it will be more reliable for the tank.

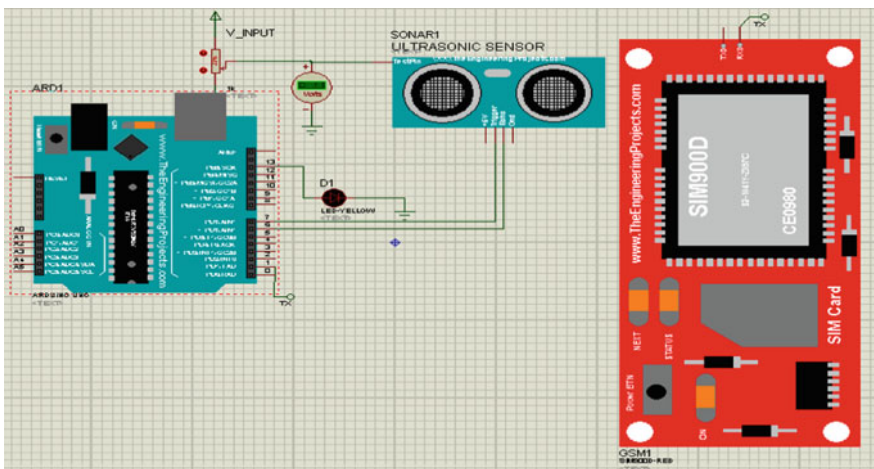


Fig. 4 Proteus model of the system

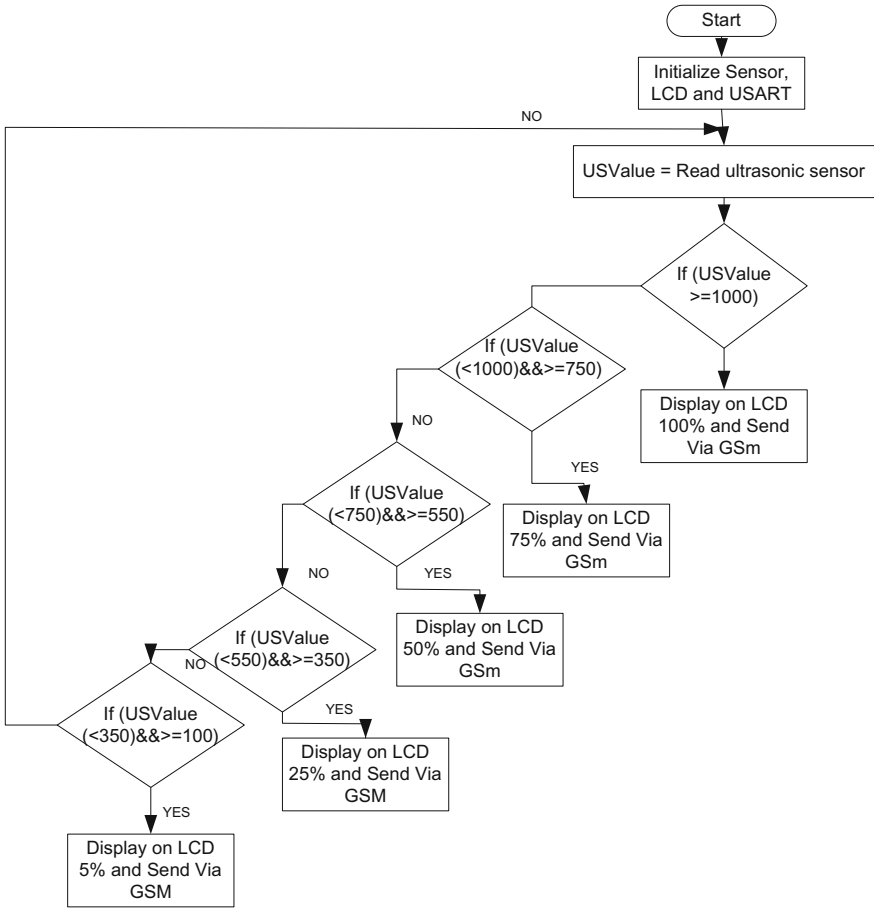


Fig. 5 Flowchart of the system

In Fig. 5, it is shown that before starting the programming part, flowchart is required to follow so that proper algorithm of flowchart is to be followed. By doing this, the device will properly work according to the user requirement. The programming part will be completed on Arduino software by following the above flowchart.

4 Results

The final result of the project is to regular checkup of the oil level in the oil tank of the transformer so that the oil level will continuously be monitored, and at remote sites, regular checkup of oil level will take place. This is also helpful to make the

smart city according to the demand where all the things work on the basis of digitalization. From this project, the labor cost will also be affected so that the manual checking will not be there.

5 Conclusion and Future Scope

Today, the main problem is to take care of the instruments which are at remote location, and because of this, proper maintenance is not done with the equipment. This device is also helpful to make smart city which is totally based on modern technology. By using this device, regular checkup of oil in the oil tank of the transformer will be done so that proper maintenance will be done at proper time, and by this economy, labor cost and time will be saved. This device will remain activated and keep reporting for 24 by 7. Any kind of frequent change in the oil level will be reported immediately by sending SMS on the mobile of the person in charge. This device is also helpful for implementation on monitor scale in the smart cities as it is based on wireless technology.

References

1. Shukla, Abhinav, Rajesh Singh, and Anita Gehlot. "In-campus Generator-Substation Monitoring and Control Using LabVIEW." *Proceeding of International Conference on Intelligent Communication, Control and Devices*. Springer Singapore, 2017.
2. Peters, George W. "Gas/oil well monitoring system." U.S. Patent No. 6,967,589. 22 Nov. 2005.
3. Crawford, Charles D., James A. King Jr., and John H. Randolph. "System for monitoring storage tanks." U.S. Patent No. 5,132,923. 21 Jul. 1992.
4. Sutherland, David B., Fredrick W. Cotton, and Richard M. Zingel. "System for monitoring fills of liquid in a tank container and ongoing liquid condition." U.S. Patent No. 5,351,725. 4 Oct. 1994.
5. Shea, Arthur W. "Residential fuel oil tank level reporting device." U.S. Patent No. 5,619,560. 8 Apr. 1997.
6. Knight, John D., et al. "Residential fuel-oil level reporting and alarm system." U.S. Patent No. 4,845,486. 4 Jul. 1989.
7. Duenas, Roy A. "Method and system for measuring and remotely reporting the liquid level of tanks and the usage thereof." U.S. Patent No. 6,336,362. 8 Jan. 2002.
8. Hendershot, John A., and Leale E. Streebin. "Fluid storage tank system." U.S. Patent No. 4,796,676. 10 Jan. 1989.
9. Butts, Nicholas E. "Subterranean tank leak containment and detection system." U.S. Patent No. 4,672,366. 9 Jun. 1987.
10. Rampell, S., and L. Callisto. "Predicted and observed performance of an oil tank founded on soil-cement columns in clayey soils." *Soils and foundations* 43.4 (2003): 229–241.
11. Bennett, M. A., and R. A. Williams. "Monitoring the operation of an oil/water separator using impedance tomography." *Minerals Engineering* 17.5 (2004): 605–614.
12. Hon, Clarence C. "Monitoring liquid level infed tank and flow rate of liquid therefrom to point of use." U.S. Patent No. 4,856,343. 15 Aug. 1989.

13. Tomecek, Jerry. "Electronic tank level monitoring device." U.S. Patent No. 4,853,694. 1 Aug. 1989.
14. García, Belén, Juan Carlos Burgos, and Ángel Matías Alonso. "Transformer tank vibration modeling as a method of detecting winding deformations-part I: theoretical foundation." *IEEE Transactions on Power Delivery* 21.1 (2006): 157–163.
15. Pahlavanpour, B., and A. Wilson. "Analysis of transformer oil for transformer condition monitoring." *Liquid Insulation (Digest No. 1997/003), IEE Colloquium on An Engineering Review of. IET*, 1997.
16. Pierce, Linden W. "An investigation of the thermal performance of an oil filled transformer winding." *IEEE transactions on power delivery* 7.3 (1992): 1347–1358.
17. Judd, M. D., et al. "Transformer monitoring using the UHF technique." *High Voltage Engineering, 1999. Eleventh International Symposium on (Conf. Publ. No. 467)*. Vol. 5. IET, 1999.
18. Berler, Zalya, et al. "Vibro-acoustic method of transformer clamping pressure monitoring." *Electrical Insulation, 2000. Conference Record of the 2000 IEEE International Symposium on. IEEE*, 2000.
19. Kawada, H., et al. "Partial discharge automatic monitor for oil-filled power transformer." *IEEE transactions on power apparatus and systems* 2 (1984): 422–428.
20. Duval, M. "Dissolved gas analysis: It can save your transformer." *IEEE Electrical Insulation Magazine* 5.6 (1989): 22–27.
21. García, Belén, et al. "A moisture-in-oil model for power transformer monitoring-Part I: Theoretical foundation." *IEEE Transactions on Power Delivery* 20.2 (2005): 1417–1422.
22. Zhang, Xiang, and Ernst Gockenbach. "Asset-management of transformers based on condition monitoring and standard diagnosis [feature article]." *IEEE Electrical Insulation Magazine* 24.4 (2008): 26–40.
23. Williams, Barry N., and Glenn A. Kauffmann. "Method and apparatus for continuous tank monitoring." U.S. Patent No. 5,363,093. 8 Nov. 1994.
24. Duerkop, H. "Tank for fuel oil or other liquids." U.S. Patent No. 3,848,765. 19 Nov. 1974.
25. Conmy, Robyn N., et al. "Submersible optical sensors exposed to chemically dispersed crude oil: wave tank simulations for improved oil spill monitoring." *Environmental science & technology* 48.3 (2014): 1803–1810.
26. Masar, Lubomir, and Gerald T. Boylan. "Method of communicating conditions within a storage tank level." U.S. Patent No. 6,700,503. 2 Mar. 2004.

Trends of Publications and Work Done in Different Areas in Energy Saving in Cloud Computing: A Survey

Nagma, Jagpreet Sidhu and Jaiteg Singh

Abstract Cloud computing is a model that provides a finite pool of virtualized on-demand resources whose mapping on target machines should be done in such a way which prevents their underutilization and overutilization which otherwise lead to high energy consumption. So scheduling of resources should be done in such a way which reduces energy consumption giving rise to energy-aware scheduling. This paper concentrates on integration of scheduling and energy saving in cloud. Also, exploration has been done to find out datasets, tools, applications, and results of work done in the field of energy-aware scheduling in cloud computing and analysis shows the status of numerous publications in this area according to bibliographical citations by taking into consideration diverse global regions involved in research, various journals citing the work, year of publishing, research community involved in exploration, fund provisioning or self-promotion factors. Trends are illustrated in the form of graphs.

Keywords Cloud computing · Green computing · Energy saving
Energy-aware scheduling · Virtual machine migration · Consolidation
Multicore architecture · Power management · Trends · Bibliographical citations

Nagma (✉) · J. Sidhu · J. Singh

Department of Computer Science and Engineering, Chitkara University Institute of Engineering and Technology, Chitkara University, Rajpura, Punjab, India
e-mail: nagma@chitkara.edu.in

J. Sidhu
e-mail: jagpreet.sidhu@chitkara.edu.in

J. Singh
e-mail: jaiteg.singh@chitkara.edu.in

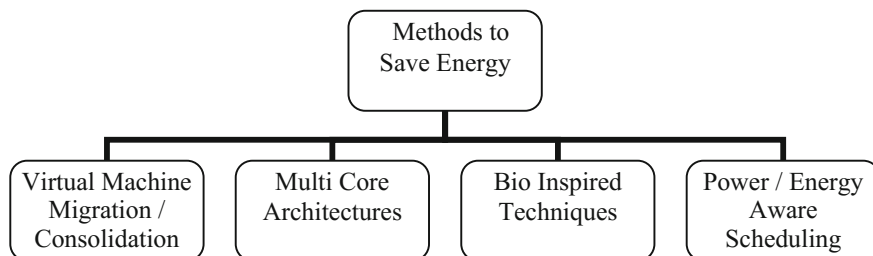


Fig. 1 Classification of work done in energy saving

1 Introduction

Cloud computing is the upcoming phase of evolution of computing systems which facilitate dynamism leading to addition or removal of resources. It provides access to large number of virtualized resources without much managerial involvement [1]. For optimal management of these resources, their mapping on target machines, that is, scheduling should be done in such a way which prevents underutilization and overutilization of resources which otherwise lead to high energy consumption. So mapping of resources should be done in such a way that minimizes energy consumption giving rise to energy-aware scheduling [2]. Thus, integration of scheduling and energy saving can prove really beneficial because energy is the basic necessity for all activities of mankind, so its conservation should be done. As a result, energy-aware scheduling has become an active area of research. There are many ways to save energy in data centers leading to green computing which have been listed in Fig. 1 [2]. After analyzing the literature, it has been found that in all these four methods, scheduling algorithms have been used to save energy. So energy-aware scheduling has largely been explored. This survey provides a clear picture of work done in energy saving in these four different areas, and objectivity/subjectivity of the results has been mentioned.

Also, trends according to bibliographical citations have been shown. Analysis of large number of papers mainly published from 2011 to 2017 has been done. Because of being at a very initial stage of research, this analysis has been done to formulate a problem definition in cloud computing paradigm, so only papers of highly reputed and relevant journals are taken just to know the current scenario and to check the feasibility of pursuing work in future in energy saving. This work may be extended later on by taking papers from various other journals and conferences too.

2 Literature Review

The analysis has been done on the subset of 10 papers that have been selected in each domain in energy saving to find out the techniques, datasets, simulators used by researchers, and also to evaluate objectivity/subjectivity of results. Table 1

Table 1 Techniques/algorithm, dataset, simulation tools used, applications, and results of work done using VM migration/consolidation in energy saving

Ref. No.	Dataset	Simulation environment	Applications/use	Technique/algorithm used	Results
[3]	Used kembench workloads [4]	Xen virtualized platform	Proposed consolidation aware scheduling to improve performance	Yield to head Yield to tail	Subjective Improved VM performance; little overhead
[5]	Used benchmark programs to get power values	Synthetic multiprocessor architecture	Proposed algorithm for solving task migration problem and energy saving	Partitioned scheduling algorithm	Objective Numerical values given for different cases
[6]	Synthetic dataset	Python; Gurobi Used Linux machine and Intel Xeon E5-2440	Derived mathematical formulation for solving server consolidation problem	Best-fit algorithm with consolidation	Objective Truncated runs of the model improve over Best-fit up to 15%
[7]	Data acquisition unit with a digital multimeter was used to collect power consumption values	Implementation in Xen virtualization platform; conducted experiments using profiling software and digital power meters	Proposed and evaluated two power suppressing live migration schemes to resolve the power overshooting issue	Dynamic voltage frequency scaling	Objective The two schemes used reduced power consumption by 3% and 10%
[8]	Generated 100 jobs in the simulation, and VM type is taken randomly from a set of given configurations	Hadoop testbed Sniper; McPAT	Propose a heuristic for consolidation on physical servers to save energy while guaranteeing job service-level agreements (SLA)	Dynamic voltage frequency scaling	Objective Reduced energy consumption, values are given in form of graphs

(continued)

Table 1 (continued)

Ref. No.	Dataset	Simulation environment	Applications/use	Technique/algorithm used	Results
[9]	Measured running time during concurrent execution of pair of 12 benchmarks	Conducted experiments with SPECcpu 2006 benchmark programs	Proposed a performance model that considered interferences in the shared last-level cache and memory bus	Swim VM consolidation method	Objective Different values for cases have been given
[10]	Iteratively generated task requests with a interval time following a pre-specified exponential distribution	Xen virtualization platform	Proposed heuristic algorithm to substantially improve utilization and reduce the physical servers	Splitting-based resource provisioning scheme	Objective 15–22% reduction in the number of physical resources used
[11]	Workload traces from more than 1000 VMs; The statistical data were obtained from the cluster located in Guangdong Key Laboratory of Computer Network	CloudSim	Proposed minimum power and maximum utilization policy and established a SLA violation decision algorithm	Overload decision algorithm VM selection algorithm	Objective It guarantees 21–34% decrease in energy consumption, 84–92% decrease in SLA violation, and 63% decrease in execution time
[12]	10 days data of CoMon project. This data contained CPU utilization in 5-min intervals	CloudSim	Proposed novel proactive online resource management policies to optimize energy, SLA, and number of migrations	Technique for order of preference by similarity to ideal solution (TOPSIS)	Objective 98.11% reduction in the output metric
[13]	Collected a set of processor and disk utilization traces from four different enterprise server types	Matlab	Proposed scheduling algorithm which minimizes the total power consumption in the whole data center	Simulated annealing algorithm	Objective Empirical results showed nearly 24.9% power savings and nearly 1.2% performance degradation

describes the techniques/algorithms, datasets, tools used, applications, and results of the work done in the areas of virtual machine (VM) migration/consolidation in energy saving. Tables 2, 3 and 4 describe the techniques, datasets, tools used, applications, and results of the work done in the areas of using multicore architectures, bio-inspired techniques, and power/energy-aware scheduling, respectively.

Table 2 Techniques/algorithm, dataset, simulation tools used, applications, and results of work done using multicore architectures in energy saving

Ref. No.	Dataset	Simulation environment	Applications/use	Technique/algorithm used	Results
[14]	Used data of Malardalen project [15]	Multi2Sim	Proposed a model to predict distinct task execution times and a scheduler has been evaluated	Earliest deadline first; worst-fit scheduling algorithm	Objective Results turn in important energy savings, by 18% on average
[16]	Synthetic dataset	Not mentioned	Proposed a voltage island largest capacity first (VILCF) algorithm for energy-efficient scheduling of periodic real-time tasks on multicore processors	Dynamic power management technique	Objective The normalized energy of voltage island largest capacity first
[17]	Random variables	Simulation program written in the C++ to run in a Linux environment	Designed and analyzed the performance of heuristic algorithms that employ the equal-speed method	Dynamic voltage scaling Constrained scheduling	Subjective Facts have been mentioned
[18]	Generated random task sets of sizes following certain distributions	Not mentioned	Proposed a technique to find the lowest core speed to schedule individual tasks	Lightest task shifting policy; Rate monotonic algorithm	Objective System utilization and number of tasks executed have been illustrated in the form of graphs
[19]	Not mentioned	Sniper	Proposed a two-tier hierarchical power management methodology	Dynamic voltage frequency scaling	Objective Achieved a performance advantage of 4.2% on average

(continued)

Table 2 (continued)

Ref. No.	Dataset	Simulation environment	Applications/use	Technique/algorithm used	Results
[20]	Got data by running the benchmarks on 48 cores of the Intel SCC	Conducted experiments on 48 cores of the Intel SCC	Proposed a new latency-aware dynamic voltage frequency scaling scheme to adjust the optimal power state accurately	Dynamic voltage frequency scaling	Objective Achieved 24.0% extra energy saving, 31.3% more reduction in the energy-delay product and 15.2% less overhead in execution time
[21]	Test driver generates a set of queries	Maintained a dedicated computing environment to test PostgreSQL	Proposed a toolkit facilitating the evaluation and optimization of energy-efficient multicore-based database systems	Optimization algorithms	Objective Reduces the energy consumption of the 25% CPU utilization by more than 63%
[22]	Poisson stream of tasks generated	Not mentioned	Studied the problem of power and performance management for a multicore server processor in a cloud computing environment	Made models	Subjective Cores should be managed in a centralized way to provide the highest performance
[23]	Poisson stream of tasks	Not mentioned	Formulated and solved problem of multicore server processor partitioning	Speed and power consumption models	Objective Different values have been given in form of tables
[24]	Data are provided by digital elevation models	Experimental setup done using phenom AMD quad and NVIDIA	Presented geographic information systems tool to compute the optimal solar-panel position	Radiation and horizon algorithms	Objective The difference between the expected and the experimental performance is <1%

Table 3 Techniques/algorithm, dataset, simulation tools used, applications, and results of work done using bio-inspired techniques in energy saving

Ref. No.	Dataset	Simulation environment	Applications/use	Technique/algorithm used	Results
[25]	Synthetic dataset	Matlab	Designed and developed a Cloud resource broker for efficiently managing cloud resources	Particle swarm optimization (PSO)	Objective PSO is comparatively 1.23 times better than ant colony optimization, 1.3 times better than genetic algorithms
[26]	Requests accepted from different users	CloudSim	Proposed a novel meta scheduler which consumes minimum power	Self-adaptive particle swarm optimization (SAPSO)	Subjective Significant reduction in the power against the existing strategy and illustrated in the form of graphs
[27]	Scientific workflows such as Montage and Cybershake	JAVA-based simulator	Presented an augmented shuffled frog leaping algorithm (ASFLA) for resource provisioning and scheduling	Meta heuristic optimization techniques	Objective Improved the overall execution cost by approximately 49% on the average with respect to particle swarm optimization
[28]	Real workload traces	Gridsim	Proposed an algorithm which generates an optimal mapping of applications to resources and is fast	Multi-objective genetic algorithm (MOGA)	Objective MOGA obtained median was 10% lower than the First Come First Served heuristic
[29]	Used Cybershake, Montage, Siphit, and inspiral workflows	Not mentioned	Proposed a system to know cost effectiveness	Greedy algorithm	Subjective It gave a promising performance when compared with other state-of-the-art algorithms
[30]	Used Google trace data	Developed a simulator-like CloudSim	Proposed PreAntPolicy that consists of a prediction model	Greedy; Round-robin	Objective 76.17, 75.28, and 60.98% improvement in energy consumption

(continued)

Table 3 (continued)

Ref. No.	Dataset	Simulation environment	Applications/use	Technique/algorithm used	Results
[31]	Data centers for Amazon and Google	Setup a simulation environment	A novel architecture and a key-based scheme were proposed	Genetic algorithms	Objective Proposed algorithm outperforms the baseline and state-of-the-art algorithms by 49 and 40%
[32]	Dataset of genetic algorithm	C programming language LibGa package	Proposed a hybrid algorithm which targets to minimize the total number of running servers	Genetic algorithms	Objective Outperforms permutation pack (PP), first fit (FF) and first fit decreasing (FFD) by 4, 34, and 39%, respectively
[33]	Not mentioned	C++ programming language was used	Proposed a set of service domain-oriented bee colony algorithm	Genetic algorithms	Subjective Extends the theory of swarm intelligence optimization
[34]	Four dataset categories Left skewed Right skewed Uniformdistribution normal	CloudSim	Presented a discrete symbiotic organism search (DSOS) algorithm for optimal scheduling of tasks on cloud resources.	Meta heuristic optimization technique	The average makespan minimization by DSOS was 3.8–25.5% less than that of existing algorithm

Table 4 Techniques/algorithm, dataset, simulation tools used, applications, and results of work done using power/energy-aware scheduling in energy saving

Ref. No.	Dataset	Simulation environment	Applications/use	Technique/algorithm used	Results
[35]	Collected data using real equipment	Green network simulator	Proposed scheme to calculate power of network components	Scheduling techniques	Objective Graphs have been made
[36]	Not mentioned	Wattch simulator	Presented power-aware code scheduling to reduce power	Power gating dynamic voltage scaling	Objective PACS can outperform by more than 33 and 41% in terms of energy-delay product
[37]	All 1000 requests follow the Poisson distribution	A java discrete simulator	Proposed an algorithm for online energy-efficient scheduling of VMs	Round-robin policy; Greedy algorithms	2–10% less energy consumption than Greedy, and 30% less consumption than round-robin
[38]	Used four individual appliance monitors to collect data	OpenStack software	Presented a power-aware scheduling policy for green cloud (GreenC)	Developed algorithms in python script	Objective Energy consumption of GreenC policy was 194.4 which was lesser than others
[39]	Not mentioned	Homogeneous grid environment	Proposed heuristics for scheduling jobs with dependent tasks	Dynamic voltage scaling techniques	Objective Compared techniques; made graphs of power
[40]	Data from CoMon project (a monitoring infrastructure for planet labs)	CloudSim	Proposed a technique for optimum energy consumption and violation reduction	Simulated annealing algorithm in Markov chain model	Objective Violations decreased as compared to the best algorithm by 5% in low load, by 10% in moderate load, and by 12.7% in high load

(continued)

Table 4 (continued)

Ref. No.	Dataset	Simulation environment	Applications/use	Technique/algorithm used	Results
[2]	500 cloudlets whose lengths were randomly generated from 2,400,000 to 3,600,000 MIPS	Matlab	Proposed algorithm for VM scheduling which reduces energy consumption	Dynamic voltage frequency scaling	Objective Reduces energy by 60%, turnaround time by 94%, increases acceptance rate by 96%
[41]	Tested with different DAGs generated at random and real task-based application	Private cloud infrastructure at Barcelona Supercomputing Center	Proposed algorithm minimizes multi-objective function combining energy consumption and execution time	Multi-heuristic scheduling	Objective The scheduling for directed acyclic graph with 500 tasks achieves a reduction of -20.61%.
[42]	Collected solar power traces by installing solar panels on the roof of lab	Matlab	Proposed a scheme re-ups, which shaves data center peak power demand with renewable energy	Power management algorithm	Objective Improved backup energy capacity by 28%, battery lifetime by 42%, green energy utilization by 78%, and reduce degradation by 13%
[43]	Real calculations have been performed on EGI Fed cloud	GAMOS EGI Cloud FLUKA XMM	Schedules resources in multi-cloud environment	Fair sharing algorithms	Objective Values have been given for different cases in tables

3 Findings

Analysis has been done on the subset chosen to evaluate the status of numerous publications in this particular area according to bibliographical citations by taking into consideration diverse global regions involved in research in energy saving in cloud, various journals citing the work, year of publishing, research community involved in exploration, fund provisioning, or self-promotion factors. The interpretations explained below are our way of seeing the things according to the subset chosen. Peer researchers may interpret the trends differently.

Section (a) of Fig. 2 illustrates that Asia is receiving maximum funds in the domain of energy saving in cloud computing while Europe is the second one and other continents have minor contribution in research in this domain. Section (b) of Fig. 2 illustrates that again Asia is publishing maximum number of papers as compared to other continents in this area and after it comes Europe. Section (a) of Fig. 3 shows the combined comparison of published and funded work according to continents making it clear that maximum work done in area of VM consolidation/migration in Asia are funded. While in Europe, all work done in the area of multicore architectures and power/energy-aware scheduling has been funded.

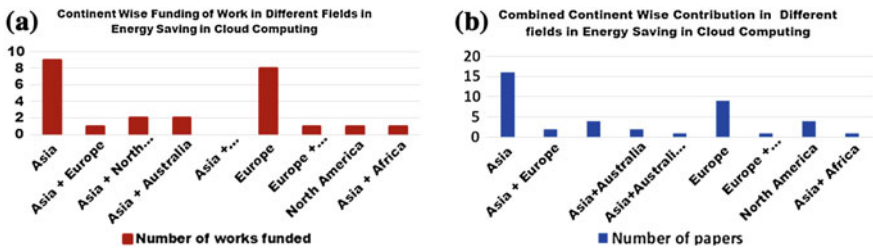


Fig. 2 Trends in publishing and funding of work done in energy saving in all areas in energy saving. **a** Funding of work in energy saving according to continents. **b** Continent-wise publications in energy saving

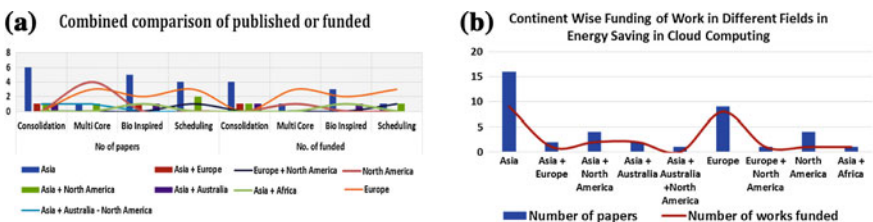


Fig. 3 Trends in publications in all domains in energy saving and comparison of published and funded work. **a** Number of papers published in different areas in energy saving in different continents and number of funds granted. **b** Combined continent-wise publications of all areas in energy saving

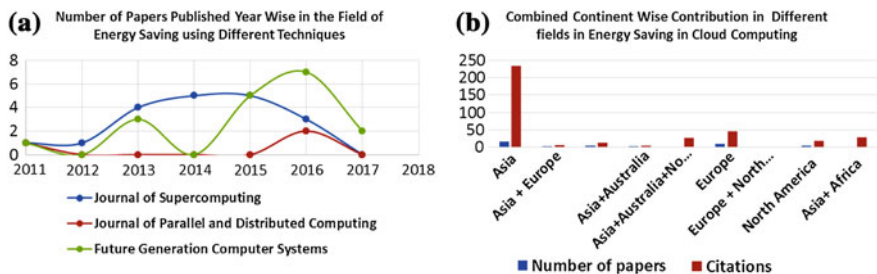
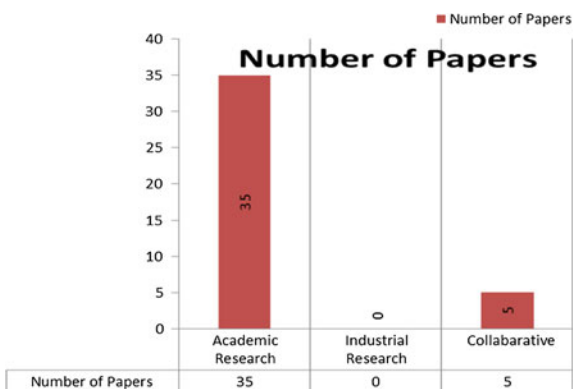


Fig. 4 Trends in citations and year-wise publications of papers by different journals. **a** Articles published year wise in different journals. **b** Continent-wise citations of articles

Fig. 5 Trends in publications according to involved research group



Section (b) of Fig. 3 indicates that more publications are from Asia and Europe, so more funding is provided in these continents only. Thus, it could be interpreted that Asia and Europe are maximum contributors in the field of research in energy saving in cloud in different areas, and hence, they receive maximum number of grants which can be validated from Figs. 2 and 3. Section (a) of Fig. 4 illustrates that highest number of papers are published in year 2015 and 2016 in energy saving and future generation computer systems is publishing maximum papers as compared to other journals. Section (b) of Fig. 4 indicates that Asia and Europe have prominent citations as compared to other continents, thus producing qualitative research articles. So it could be interpreted that 2015 and 2016 are the years in which energy saving in cloud has gained prominent importance, and citations of works done by Asia and Europe are more.

Figure 5 illustrates that there is no research in energy saving in cloud by industry; maximum research is done by academicians, and there is a minor contribution by putting collaborative effort.

4 Conclusion

The integration of scheduling and energy saving in cloud leading to energy-aware scheduling is very significant advancement for future sustainable environment and computing. Scheduling has been used in every area of energy saving, so it has become an active area of research. In this paper, work done in four different areas of energy saving have been analyzed according to five parameters that are datasets, simulation tools, techniques used, applications, and results of the work done to find the objectivity of problem domain, and it has been found that most of work done in this field is objective, so one can pursue research in this field because of the availability of strong literature. To validate the facts objectively, different interpretations have been made which indicate the trends in publications in energy saving according to bibliographical citations and research contribution by different groups across the globe, and it has been concluded that there is ample work done in energy saving from objective point of view, and scheduling is a key parameter that has been used in all areas of energy saving in cloud computing, so integration of energy saving and scheduling giving rise to energy-aware scheduling has gained major attention and different interpretations have been made according to the trends shown in this paper.

References

1. Singh, A., Hemalatha, M.: Cloud computing for academic environment. *International Journal of Information and Communication Technology Research*. 2(2), 97–101 (2012).
2. Hosseinimotlagh, S., Khunjush, F., Samadzadeh, R.: SEATS: smart energy aware task scheduling in real-time cloud computing. *The Journal of Supercomputing*. 71(1), 45–66 (2015).
3. Wang, B., Cheng, Y., Chen, W., He, Q., Xiang, Y., Hassan, M. M., Alelaiwi, A.: Efficient consolidation aware VCPU scheduling on multicore virtualization platform. *Future Generation Computer Systems*. 56, 229–237 (2016).
4. Kernbench, <http://mirror.sit.wisc.edu/pub/linux/Kernel/people/ck/apps/kernbench>.
5. Zeng, G., Matsubara, Y., Tomiyama, H., Takada, H.: Energy-Aware task migration for multiprocessor real-time systems. *Future Generation Computer Systems*. 56, 220–228 (2016).
6. Mazumdar, S., Pranzo, M.: Power efficient server consolidation for Cloud data center. *Future Generation Computer Systems*. (2016) [In Press].
7. Jeong, J., Kim, S. H., Kim, H., Lee, J., Seo, E.: Analysis of virtual machine live-migration as a method for power-capping. *The Journal of Supercomputing*. 66(3), 1629–1655 (2013).
8. Teng, F., Yu, L., Li, T., Deng, D., Magoules, F.: Energy efficiency of VM consolidation in IaaS clouds. *The Journal of Supercomputing*. (2016) [In Press].
9. Kim, S. G., Eom, H., Yeom, H. Y.: Virtual machine consolidation based on interference modeling. *The Journal of Supercomputing*. 66(3), 1489–1506 (2013).
10. Liu, L., Xu, J., Yu, H., Li, L., Qiao, C.: VMSA: a performance preserving online VM splitting and placement algorithm in dynamic cloud environments. *The Journal of Supercomputing*. 72(8), 3169–3193 (2013).
11. Cao, Z., Dong, S.: An energy-aware heuristic framework for virtual machine consolidation in Cloud computing. *The Journal of Supercomputing*. 69(1), 429–451 (2014).

12. Arianyan, E., Taheri, H., Sharifian, S.: Novel heuristics for consolidation of virtual machines in cloud data centers using multi-criteria resource management solutions. *The Journal of Supercomputing*. 72(2), 688–717 (2016).
13. Sharifi, M., Salimi, H., Najafzadeh, M.: Power-efficient distributed scheduling of virtual machines using workload-aware consolidation techniques. *The Journal of Supercomputing*. 61(1), 46–66 (2012).
14. Sahuquillo, J., Hassan, H., Petit, S., March, J. L., Duato, J.: A dynamic execution time estimation model to save energy in heterogeneous multicores running periodic tasks. *Future Generation Computer Systems*. 56, 211–219 (2016).
15. Malardalen Real-Time Research Center, Sweden, WCET Analysis Project, <http://www.mrtc.mdh.se/projects/wcet> (2006).
16. Liu, J., Guo, J.: Energy efficient scheduling of real-time tasks on multi-core processors with voltage islands. *Future Generation Computer Systems*. 56, 202–210 (2016).
17. Li, K.: Scheduling parallel tasks with energy and time constraints on multiple manycore processors in a cloud computing environment. *Future Generation Computer Systems*. (2017) [In Press].
18. Min-Allah, N., Hussain, H., Khan, S. U., Zomaya, A. Y.: Power efficient rate monotonic scheduling for multi-core systems. *Journal of Parallel and Distributed Computing*. 72(1), 48–57 (2012).
19. Jha, S. S., Heirman, W., Falcón, A., Tubella, J., Gonzalez, A., Eeckhout, L.: Shared resource aware scheduling on power-constrained tiled many-core processors. *Journal of Parallel and Distributed Computing*. 100, 30–41 (2017).
20. Lai, Z., Lam, K. T., Wang, C. L., Su, J.: Latency-aware DVFS for efficient power state transitions on many-core architectures. *The Journal of Supercomputing*. 71(7), 2720–2747 (2015).
21. Zhou, Y., Taneja, S., Qin, X., Ku, W. S., Zhang, J.: EDOM: Improving energy efficiency of database operations on multicore servers. *Future Generation Computer Systems*. (2017) [In Press].
22. Li, K.: Optimal configuration of a multicore server processor for managing the power and performance tradeoff. *The Journal of Supercomputing*. 61(1), 189–214 (2012).
23. Li, K.: Optimal partitioning of a multicore server processor. *The Journal of Supercomputing*. 71(10), 3744–3769 (2015).
24. Tabik, S., Villegas, A., Zapata, E. L., Romero, L. F.: Optimal tilt and orientation maps: a multi-algorithm approach for heterogeneous multicore-GPU systems. *The Journal of Supercomputing*. 66(1), 135–147 (2013).
25. Somasundaram, T. S., Govindarajan, K.: CLOUDRB: A framework for scheduling and managing High-Performance Computing (HPC) applications in science cloud. *Future Generation Computer Systems*. 34, 47–65 (2014).
26. Jeyarani, R., Nagaveni, N., Ram, R. V.: Design and implementation of adaptive power-aware virtual machine provisioner (APA-VMP) using swarm intelligence. *Future Generation Computer Systems*. 28(5), 811–821 (2012).
27. Kaur, P., Mehta, S.: Resource provisioning and work flow scheduling in clouds using augmented Shuffled Frog Leaping Algorithm. *Journal of Parallel and Distributed Computing*. 101, 41–50 (2017).
28. Gabaldon, E., Lerida, J. L., Guirado, F., Planes, J.: Blacklist multi-objective genetic algorithm for energy saving in heterogeneous environments. *The Journal of Supercomputing*. 1–16 (2016).
29. Netjinda, N., Sirinaovakul, B., Achalakul, T.: Cost optimal scheduling in IaaS for dependent workload with particle swarm optimization. *The Journal of Supercomputing*. 68(3), 1579–1603 (2014).
30. Duan, H., Chen, C., Min, G., Wu, Y.: Energy-aware scheduling of virtual machines in heterogeneous cloud computing systems. *Future Generation Computer Systems*. (2016) [In Press].

31. Zhang, J., Zhang, L., Huang, H., Jiang, Z. L., Wang, X.: Key based data analytics across data centers considering bi-level resource provision in cloud computing. *Future Generation Computer Systems*. 62, 40–50 (2016).
32. Hallawi, H., Mehnen, J., He, H.: Multi-Capacity Combinatorial Ordering GA in Application to Cloud resources allocation and efficient virtual machines consolidation. *Future Generation Computer Systems*. 69, 1–10 (2017).
33. Xu, X., Liu, Z., Wang, Z., Sheng, Q. Z., Yu, J., Wang, X.: S-ABC: A paradigm of service domain-oriented artificial bee colony algorithms for service selection and composition. *Future Generation Computer Systems*. 68, 304–319 (2017).
34. Abdullahi, M., Ngadi, M. A.: Symbiotic Organism Search optimization based task scheduling in cloud computing environment. *Future Generation Computer Systems*. 56, 640–650 (2016).
35. Niewiadomska-Szynkiewicz, E., Sikora, A., Arabas, P., Kamola, M., Mincer, M., Kolodziej, J.: Dynamic power management in energy-aware computer networks and data intensive computing systems. *Future Generation Computer Systems*. 37, 284–296 (2014).
36. Lee, C. Y., Lin, T. Y., Chang, R. G.: Power-aware code scheduling assisted with power gating and DVS. *Future Generation Computer Systems*. 34, 66–75 (2014).
37. Tian, W., Xiong, Q., Cao, J.: An online parallel scheduling method with application to energy-efficiency in cloud computing. *The Journal of Supercomputing*. 66(3), 1773–1790 (2013).
38. Vilaplana, J., Mateo, J., Teixidó, I., Solsona, F., Giné, F., Roig, C.: An SLA and power-saving scheduling consolidation strategy for shared and heterogeneous clouds. *The Journal of Supercomputing*. 71(5), 1817–1832 (2015).
39. Aziz, A., El-Rewini, H.: Power efficient scheduling heuristics for energy conservation in computational grids. *The Journal of Supercomputing*. 57(1), 65–80 (2011).
40. Rajabzadeh, M., Haghighat, A. T.: Energy-aware framework with Markov chain-based parallel simulated annealing algorithm for dynamic management of virtual machines in cloud data centers. *The Journal of Supercomputing*. 1–17 (2016).
41. Juarez, F., Ejarque, J., Badia, R. M.: Dynamic energy-aware scheduling for parallel task-based application in cloud computing. *Future Generation Computer Systems*. (2016) [In Press].
42. Liu, L., Sun, H., Li, C., Hu, Y., Xin, J., Zheng, N., Li, T.: RE-UPS: an adaptive distributed energy storage system for dynamically managing solar energy in green datacenters. *The Journal of Supercomputing*. 72(1), 295–316 (2016).
43. Rubio-Montero, A. J., Huedo, E., Mayo-García, R.: Scheduling multiple virtual environments in cloud federations for distributed calculations. *Future Generation Computer Systems*. (2016) [In Press].

Arduino- and IoT-Based Tools and Inventory Tracking System in Construction Sites

Aditya Agarwal, Aadrita Tanwar, Rajesh Singh, Vikas Garg and Anita Gehlot

Abstract This paper emphasis on the major drawback in construction sites like diminishing of equipments, shrinkage, wasting of time in searching of equipment and increasing equipments utilization in construction sites. Proficient administration of the supply chain to the materials utilized within development ventures might fundamentally lessen material cost and improve in success meeting project time-scales, exactly where valuable tools and equipment are the key to a successful construction project. Ensuring representatives from conceivably unsafe circumstances will be a critical worry from claiming businesses, the place modern mishaps and harm would at any point introduce peril. So we have designed tool and inventory tracking system with the help of RFID framework which is traceable and will help the manager to track all of his tools on the construction sites. The system consists of RFID tag, RFID reader, sensors, battery, microcontroller, ESP8266, and Node MCU.

Keywords RFID · Equipments · Construction · Sensors

A. Agarwal (✉) · A. Tanwar · R. Singh · V. Garg · A. Gehlot
University of Petroleum and Energy Studies, Dehradun, Uttarakhand, India
e-mail: adityaa235@gmail.com

A. Tanwar
e-mail: adritatanwer21@gmail.com

R. Singh
e-mail: rsingh@ddn.upes.ac.in

V. Garg
e-mail: vgarg@ddn.upes.ac.in

A. Gehlot
e-mail: anita@ddn.upes.ac.in

1 Introduction

This paper introduced an expositive expression audit of remote sensor networks. Also their utilization done BT WSN venture provisions, furthermore distinguished the shortcomings to standalone WSN activities. Similarly as depicted for this thesis, BT Scrutinize need to have a number about noteworthy and forefront sensor system ventures coating an extensive variety about domains. Frequently all these tasks prompted bespoke, stove-piped results that fitted those needs of every project superbly. However, a part of the SNG distinguished this possibility profit from claiming opening these activities out with the goal that information might a chance to be undoubtedly associated with information starting with different WSN tasks, furthermore frameworks to gatherings give rich data. Under BT Research's sensor Virtualization project, a nonexclusive structural engineering to WSNs might have been investigated and the open Geospatial Consortium's (OGC) Sensor Web Enablement (SWE) schema might have been investigated in place with empower the reuse for segments [1]. Apparatus accessibility may be a basic calculation in the gainfulness for development crews. Previously, an expert should enhance the effectiveness of following instruments, what's more in their availability, this research exertion formed an instrument following and stock framework which will be also skilled from claiming storing operation that support (O&M) information utilizing economically accessible dynamic radio recurrence ID number (RFID) tags. With investment about two electrical development firms, those frameworks might have been tried with respect to a number of development jobsites. Those venture exhibited that dynamic RFID could make use of stock little devices that store appropriate O&M information on the devices for development situations in spite of metal obstruction. Economics, absence of standardization, and absence of course what's more range information starting with the tags were identifier concerning illustration the majority noteworthy imperatives restricting animated RFID commercialization to device around following [2]. This paper uses a framework which incorporates Kalman filters (KFs), also a fluffy master framework to track those tip of an affixing device and to identify those attached jolt. This framework utilizes person inertial estimation unit and particular case position sensor which determines the focal point of mass area of the device. Despite a KF may be utilized to those introduction estimations, introduction lapse increments about whether the combination of precise speed lapse [3]. This paper displays a position following framework which estimates the position of tip of an affixing device. The suggested framework utilization a Kalman channel (KF) what's more molecule channel (PF) blending will orchestrate estimations starting with an inertial estimation unit (IMU) furthermore a position sensor. Those KF piece will be used to assess the position of the middle of mass of the tool, and the PF may be used to evaluate the introduction of the device around [4]. A coordinated framework to following stakes is labeled for RFID tags, which would grill during portals, toward portable scanners, or toward work force following units hosting RFID perusing proficiency. The tag book fans and following units would all in correspondence for as a relatable

point “information backbone” and all information may be conveyed to what’s more transformed by a basic summon furthermore control subsystem [5]. RFID has achieved extraordinary profits over the territories through moving forward ongoing data perceivability that’s more traceable [6]. Using economically accessible minimal effort worldwide positioning framework (GPS) gadgets empowers the nonstop information logging of supplies area what’s more to all the recording timestamps [7]. This correctness for a few RSSI-based restriction systems looking into a live jobsite also compares them on outcomes got for an operation fabricating. Four separate restriction calculations (MinMax, most extreme Likelihood, Received Signal Strength Indication RSSI, and k-Nearest Neighbor) were assessed in both areas [8]. Those cost- and time-optimized arranging from claiming earthmoving ventures need been altogether helped, likewise an after effect about deploying recreation systems [9]. US doctor’s facilities use all the millions upon billions of dollars once lost and stolen gear consistently. Radio recurrence ID number (RFID) engineering gives possibility answers for this issue. The nation’s main social insurance suppliers introducing RFID need exhibited the profits of RFID. We need aid utilizing same innovation done on development destinations also [10].

2 Block Diagram and Hardware Implementation

There are two different block diagrams that represent the system using ESP8266 and node MCU. It comprises of microcontroller, RFID tag, RFID reader, battery, ESP8266, and Node MCU. RFID tag will be placed on the tools and instruments. If that tool comes in the range of RFID reader then the system will detect and get the location of that tool. From here, the location of those tools will be stored in the cloud through IoT, i.e., ESP8266 and Node MCU. So it will be available to the workers very easily, this will also be saving some time (Figs. 1 and 2).

The system consists of sensors like inertial measurement unit (IMU), position sensor, accelerometer, and other instruments like calibration filters, microcontroller,

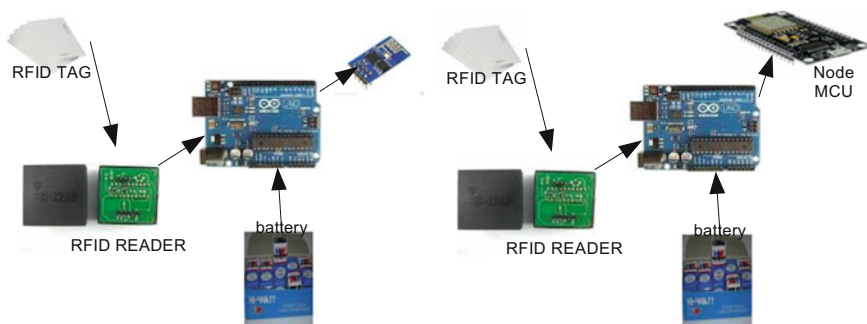
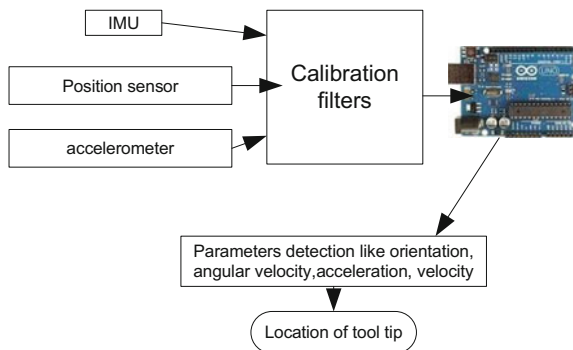


Fig. 1 Generalized block diagram of system using ESP8266 and node MCU

Fig. 2 Block diagram of tool used to tight nut bolt using Arduino



and battery. These sensors are used to define the parameters like orientation of tool tip, angular velocity, and acceleration. By this system, we can select the tool that is needed for a particular nut bolt.

3 Circuit Diagram and Simulation

There are two systems for tracking tools that use RFID technology. One is made with ESP8266 and the other is made with node MCU. Other components are RFID tag, RFID reader, and controller (Arduino). Here, Rx pin of ESP8266 is connected with the 1st pin of Arduino, and 0th pin of Arduino is connected with Tx pin of RFID reader. A battery is connected to give the power to Arduino, ESP8266, node MCU, and RFID reader. In other circuit, only ESP8266 is replaced with node MCU and all other connections are same with controller (Figs. 3 and 4).

Again there are two systems that are made with a basic difference of components node MCU and ESP8266. This circuit can control tools with the help of sensors like inertial measurement unit (IMU), position sensor, and accelerometer. These sensors are used to define the parameters like orientation of tool tip, angular velocity, and acceleration, so the nut bolt can be fitted with a desired tool automatically (Figs. 5 and 6).

4 Software Development

These flowcharts show the functioning of system using ESP8266 and node MCU for monitoring purpose on construction sites. The basic C programming is used to develop the program for both the system. If the RFID reader detects any tool in a particular range with the help of Arduino, then it compares it with the data packet. If it matches then it sends the status of tool via ESP8266 or node MCU (Figs. 7, 8, 9 and 10).

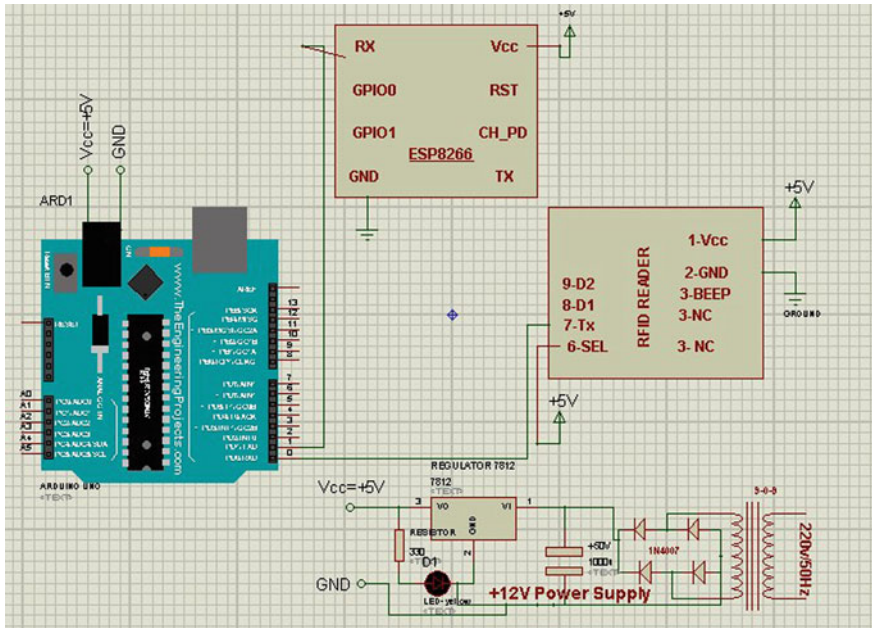


Fig. 3 Circuit diagram of ESP8266 with RFID and Arduino

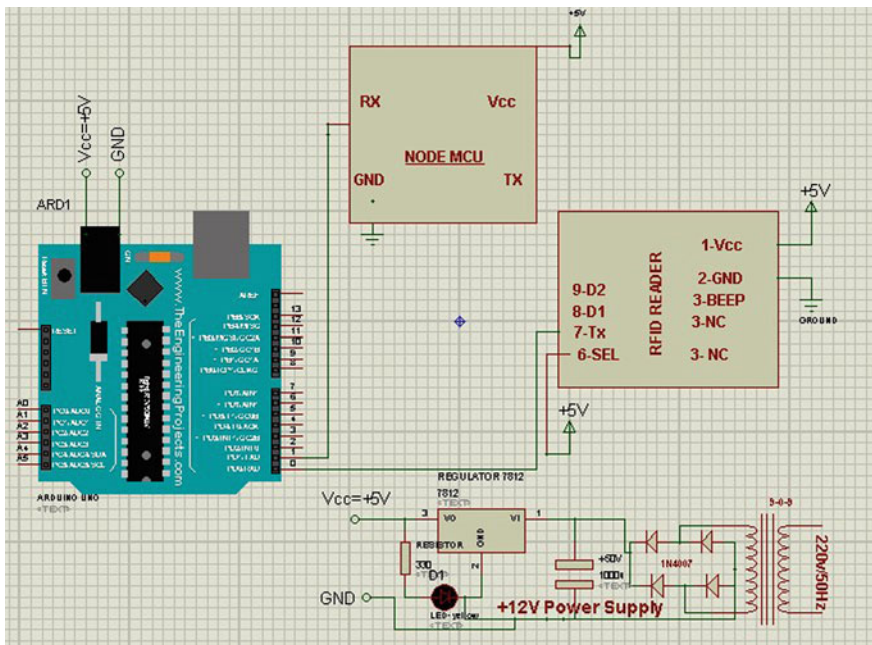


Fig. 4 Circuit diagram of node MCU with RFID and Arduino

Fig. 7 Flowchart of Arduino and ESP8266

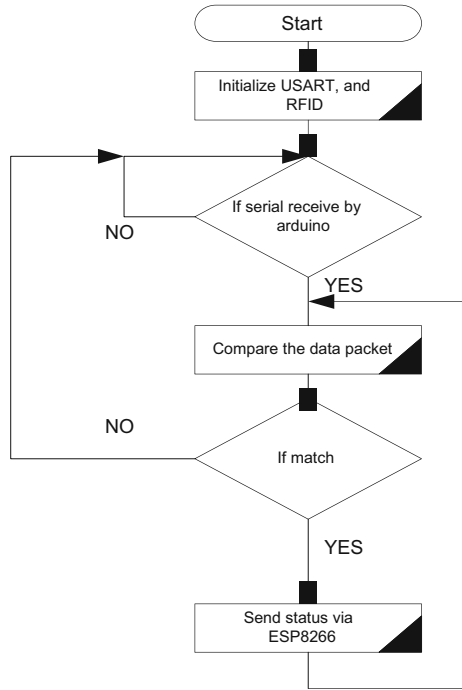


Fig. 8 Flowchart of Arduino and node MCU

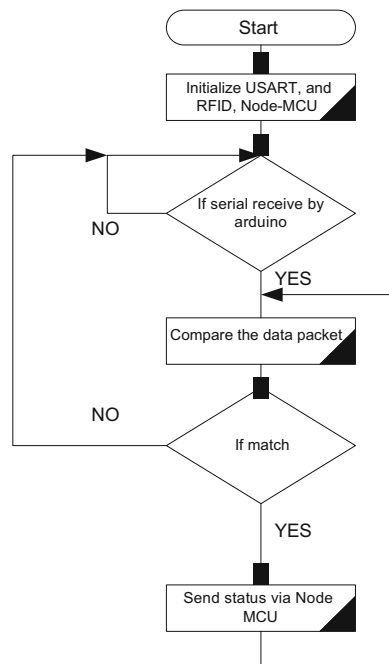


Fig. 9 Flowchart of tools control using ESP8266

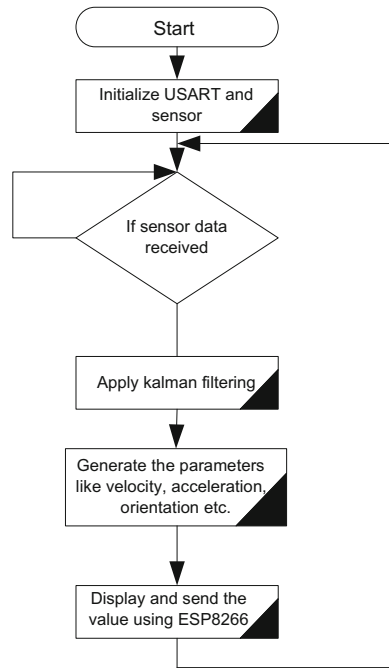
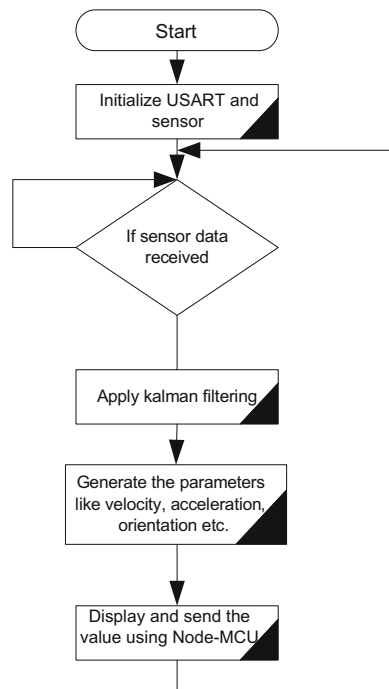


Fig. 10 Flowchart of tools control using node MCU



These flowcharts show the functioning of tool control system using ESP8266 and node MCU on construction sites. The basic C programming is used to develop the program for both the system. When the sensors collect the data and filter it with Kalman filtering, then it generates some parameters like acceleration, velocity, orientation, and it sends the value via ESP8266 or node MCU.

5 Results and Discussion

The RFID monitoring system in nowadays is very important and essential. Nature's domain and attempting states need aid altogether different for every valuable activity. Therefore, a specific RFID framework will be actualized to every connection. Materials need aid different as stated by those sort construction, i.e., climate is separate relying upon those location, and the picked result varies assuming that meets expectations would conveyed crazy indoors, outside alternately covered. The proposed system is efficient, cost effective, and approachable.

6 Conclusion and Future Scope

Radio-frequency ID number (RFID) innovation will be progressively utilized for development activities like increment efficiencies, wrist bindings stakes and diminish robbery. RFID engineering is utilized within a number of provisions that we are likely to be acquainted with such as the E-Z Pass transponder done to our vehicle, alternately those microchip for Fido that serves you find him. The innovation follows its foundations in globe War II. The point when identification, companion or adversary (IFF) frameworks were created utilizing radar. Also, transponders on identify inviting flying machine. It will be supportive over keeping track on tools, moving forward safety, eliminating timecards.

References

1. Foley, Jeffery George. *Sensor Networks and Their Applications: Investigating the Role of Sensor Web Enablement*. Diss. UCL (University College London), 2014.
2. Goodrum, Paul M., Matt A. McLaren, and Adam Durfee. "The application of active radio frequency identification technology for tool tracking on construction job sites." *Automation in Construction* 15.3 (2006): 292–302.
3. Won, Seong-Hoon Peter, Farid Golnaraghi, and Wael William Melek. "A fastening tool tracking system using an IMU and a position sensor with Kalman filters and a fuzzy expert system." *IEEE Transactions on Industrial Electronics* 56.5 (2009): 1782–1792.

4. Won, Seong-hoon Peter, William Melek, and Farid Golnaraghi. "Fastening tool tracking system using a Kalman filter and particle filter combination." *Measurement Science and Technology* 22.12 (2011): 125108.
5. Nowak, Brent M., et al. "Tagging and tracking system for assets and personnel of a commercial enterprise." U.S. Patent No. 7,123,149. 17 Oct. 2006.
6. Lu, Weisheng, George Q. Huang, and Heng Li. "Scenarios for applying RFID technology in construction project management." *Automation in Construction* 20.2 (2011): 101–106.
7. Pradhananga, Nipesh, and Jochen Teizer. "Automatic spatio-temporal analysis of construction site equipment operations using GPS data." *Automation in Construction* 29 (2013): 107–122.
8. Luo, Xiaowei, William J. O'Brien, and Christine L. Julien. "Comparative evaluation of Received Signal-Strength Index (RSSI) based indoor localization techniques for construction jobsites." *Advanced Engineering Informatics* 25.2 (2011): 355–363.
9. Vahdatikhaki, Faridaddin, and Amin Hammad. "Framework for near real-time simulation of earthmoving projects using location tracking technologies." *Automation in Construction* 42 (2014): 50–67.
10. Qu, Xiuli, LaKausha T. Simpson, and Paul Stanfield. "A model for quantifying the value of RFID-enabled equipment tracking in hospitals." *Advanced Engineering Informatics* 25.1 (2011): 23–31.

Circumvention of Friction-Induced Stick-Slip Vibration by Modeling and Simulation

Jitendra Yadav and Geeta Agnihotri

Abstract Present works deal with the insight into the friction-induced stick-slip vibration which takes place by virtue of the difference in the values of static and kinetic friction between the rubbing surfaces, which causes decrease in friction force with velocity. The produced intermittent motion is objectionable as it is the cause of serious nuisance, power loss, quadrant glitch, limit cycle, inaccuracy in control, etc. A comprehensive description of this phenomenon by capturing the effect of influencing parameter has become challenging research task for system dynamics especially for control. In present work, the motion of mass on rough surface, being dragged at constant velocity, is studied by stiction model. In this research work, it has been tried to capture the effect of influencing parameters to define the acceptable and optimum criteria of selecting them to ensure motion without stick slip. The study is performed by varying relevant parameters like coefficient of friction, viscous damping, driving velocity, ratio of static friction to kinetic friction. The outcome of this study is the range of these parameters and their combinations, for which friction-induced disturbances are the minimum. The results obtained in this work may be used as a generalized guide line for reducing and avoiding these disturbances.

Keywords Stick slip · Sticking time · Damping · Friction · Modeling

Notations

c	Damping coefficient
F_c	Coulomb kinetic friction
F_f	Friction force
F_s	Coulomb static friction

J. Yadav (✉)

Mechanical Engineering Department, University of Petroleum and Energy Studies,
Dehradun, Uttarakhand, India
e-mail: jyadav@ddn.upes.ac.in

G. Agnihotri

Mechanical Engineering Department, MANIT, Bhopal, India
e-mail: dr.gagnihotri@gmail.com

k	Spring constant
m	Mass of the moving body
x	Displacement of mass
$\dot{x} = v$	Velocity of mass
y	Displacement of the wall
$\dot{y} = u$	Driving velocity (velocity of wall)
μ	Coulomb friction coefficient
ζ	Damping ratio

1 Introduction

Proper depiction and explanation of friction phenomena are very important to capture the correct system dynamics. Stick slip is one of the phenomena of friction. Stick slip has an adverse effect on system performance and very importantly considered while dealing with the control systems to maintain the control accuracy. Bumpy motion, disquiet, aggravation, and physical damage are some of the effect of stick slip. The proper understanding of stick-slip vibration has indeed become very important for the systems under friction. In past, researchers attempted to capture the facets of these vibrations but quite a well remained untouched for its characterization. Aabdulgalil and Siguerdidjane [1] presented a novel approach to compensate the nonlinear friction of drillstring system by bearing in mind stick-slip behavior at the bit of bottom whole assembly. Di Bernardo et al. [2] ascertained the evidence of stick-slip oscillations in resonant power converters. Huang et al. [3] suggested the control of drive devices with noteworthy stick-slip oscillations. Owen et al. [4] prescribed a solution of friction circumvention. Niemann and Ehrlensp [5] and Rowson [6] analyzed stick-slip motion. Korycki [7] has worked on mathematical modeling of the stick slip. In spite of solving the complex mathematical equation, the effect of sick slip can be obtained directly by simulation [8]. Tool slide ways in machines, extrusion process, and hydraulic cylinder exhibit stick slip at low speeds [9, 10].

There is a research gap found to establish generalized explanation for the effect of influencing parameter and their significance on stick-slip vibrations which is the motive of present work. In the present work, it is tried to observe the effect of parameters on sticking time which is the measure of intensity of stick-slip vibrations.

2 Problem Formulation

The dynamic system for the analysis is modeled in form one degree of freedom system comprises of spring-mass-damper and dragged at constant velocity as shown in Fig. 1. As the spring is pulled by a tension force, it slides with constant velocity. Static friction is for more than kinetic friction. After a unit pulling of distance, when the enough tension is generated in spring, mass starts sliding. Because of the difference of friction in these two phases, the block moves at a faster rate than that of spring, restoring spring to its unscratched length that bring the block to rest thus starting entire process again. In spite of other scenario, this model is selected to make it simplest one for the sake of the feasibility of experimental validation. This model is quite able to capture the stick-slip behavior of many mechanical systems, e.g., piezoelectric actuator and similar machines having sliding motion between parts. The problem is generalized to capture the stick slip by dynamic response of the system as shown in Fig. 1. The governing equations, defining the motion, are Eq. (1).

The governing equation is given as below:

$$m\ddot{x} + c(\dot{y} - \dot{x}) + k(y - x) - F_f = 0 \quad (1)$$

where

- m mass of the block;
- c damping coefficient;
- k stiffness;
- x displacement of mass;
- y displacement of the wall;
- \dot{x} v velocity of mass;
- \dot{y} u velocity of wall.

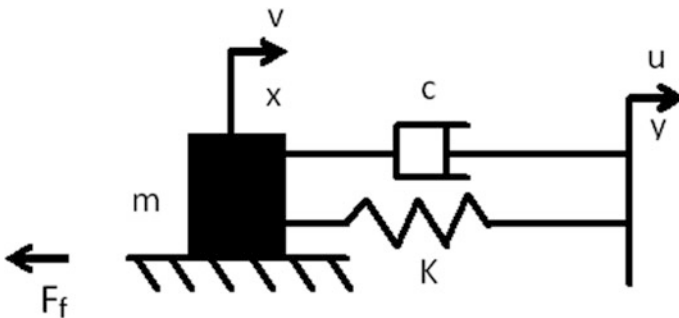
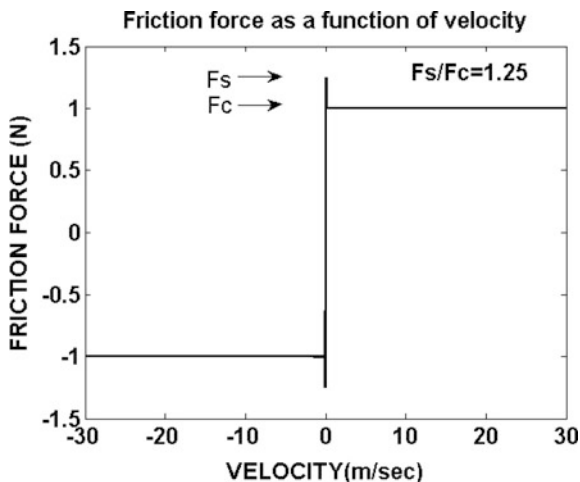


Fig. 1 Spring mass damper system

Fig. 2 Stiction model



3 Modeling of Friction Force

Stiction models deal with the two different regimes of operating friction, i.e., static friction at stagnation and Coulomb friction at motion. The friction imposed by the surfaces at rest is always higher than that of in motion, i.e., kinetic force or Coulomb friction. To initiate the relative motion between the surfaces from rest, an external force more than the force of stiction is needed. During the motion, the friction persisting between the surfaces is the kinetic or Coulomb friction and that causes the motion to be intermittent, known as stick-slip motion. Friction at rest is not only defined by only the velocity but the external force (F_e) too which in deed expressed mathematically by Eq. 2

$$F_f = \begin{cases} F_e & \text{if } v = 0 \text{ and } |F_e| < F_s \\ F_s \text{sgn}(F_e) & \text{if } v = 0 \text{ and } |F_e| \geq F_s. \end{cases} \quad (2)$$

The friction force in Eq. 2 is made as a continuous function of velocity as shown in Fig. 2.

4 System Parameters

System parameters selected for the simulation are shown in table.

Parameter	Value
m	1 kg
K	2 N/m
μ	0.1–0.5@ 0.1
F_c	$\mu^*m^* g$ N
F_s/F_c	1.10, 1.25, 1.40, 1.55 and 1.80
ζ	0, 0.2, 0.3, 0.4, 0.5, 0.6, 0.7, 0.9 and 1.1
u	0.10, 0.20 and 0.30 m/s

5 Results of Simulation

The response of the system is found in terms of displacement versus time and velocity versus time plots for various combinations of influencing parameters.

The sample results for the proposed model are obtained for $F_s/F_c = 1.5$, $\mu = 0.1$, $u = 0.1$ m/s, and $\zeta = 0.141$, as shown in Fig. 3.

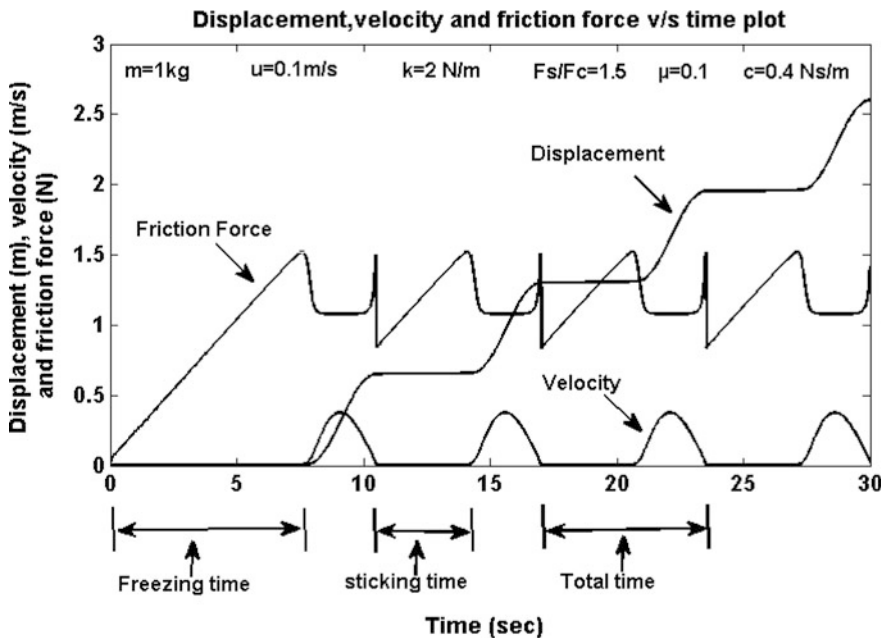


Fig. 3 Sample results

6 Validation of Model

The sample results as shown in Fig. 3 are in perfect compliance with the results of generic paper for LuGre model [10] (refer section D and Table 1). The sample results are obtained with same input parameters as of the LuGre model paper. Viscous damping(c) in the present work has been taken as a lumped parameter of the system, whereas in LuGre model paper it has been considered in the friction force expression itself in the form of the parameter σ_2 ; however, this is not affecting the system dynamics. Thus, the proposed model herein is validated and can be adopted for simulation.

7 Discussion

The results for different values of prevailing parameters, F_s/F_c , driving velocity damping ratio, and coefficient of friction are obtained. The stick slip can be examined by different findings like velocity peak (maximum amplitude of velocity), freezing time (time delayed for the starting of block after the driving force is applied on the wall), sticking time (T_s) (time for which the mass adhere to the surface during the course of motion), and frequency (reciprocal of time period (T_t)) (total time required for complete one cycle of velocity reversal). In the present work, the stick slip is estimated by the sticking time only by the perception that higher the sticking time higher will be the stick slip in the system. Three-dimensional graphs are plotted for variation of two input parameters keeping other constant, to have their effects on the characteristic parameters of stick-slip motion that is the sticking time.

It can be understood from Fig. 4 that the sticking time for constant value of coefficient of friction and driving velocity decreases linearly with the increase of value of damping ratio. The sticking time increases somewhat linearly with the increase of F_s/F_c ratio for all the values of damping ratio. So higher the damping in the system lower will be the sticking time that means the damping has a worst effect on stick slip.

It is clear from Fig. 5 that the sticking time for constant value of coefficient of friction and F_s/F_c ratio decreases linearly with the increase of value of damping ratio for all the values of driving velocity and decreases somewhat linearly with the increase of driving velocity. It is also observed that the sticking time is zero at higher values of damping ratio and driving velocity. So the stick slip diminishes with the higher values of driving velocity and damping ratio.

It is evident from Fig. 6 that the sticking time for constant value of driving velocity and F_s/F_c ratio decreases somewhat exponentially with the increase of value of damping ratio for all the values of coefficient of friction up to the elimination of stick slip and linearly increases with the incremental values of coefficient of friction for all the values of damping ratio.

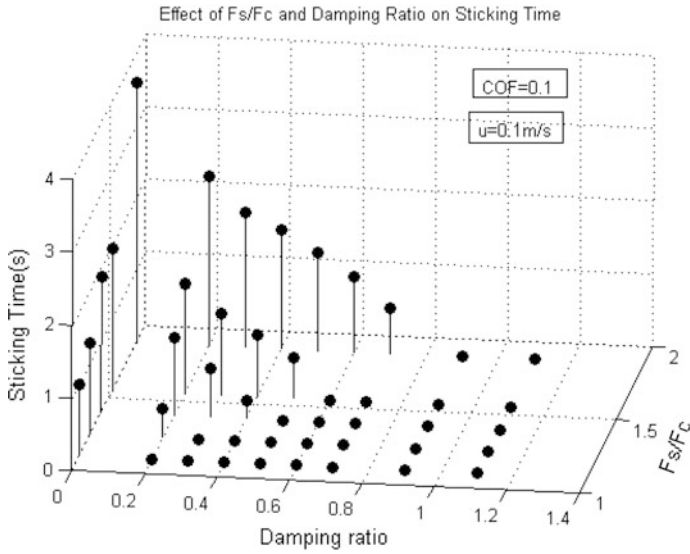


Fig. 4 Effect of F_s/F_c and damping ratio on sticking time for constant value of u and μ , with damping

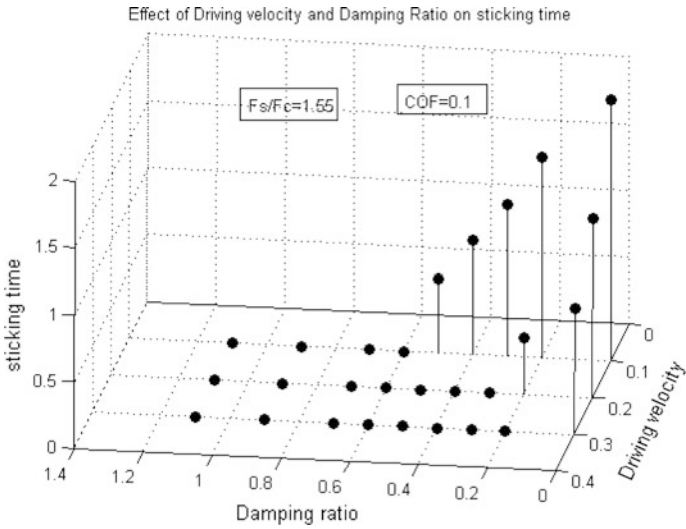


Fig. 5 Effect of driving velocity and damping ratio on sticking time for constant value of F_s/F_c and μ , with damping

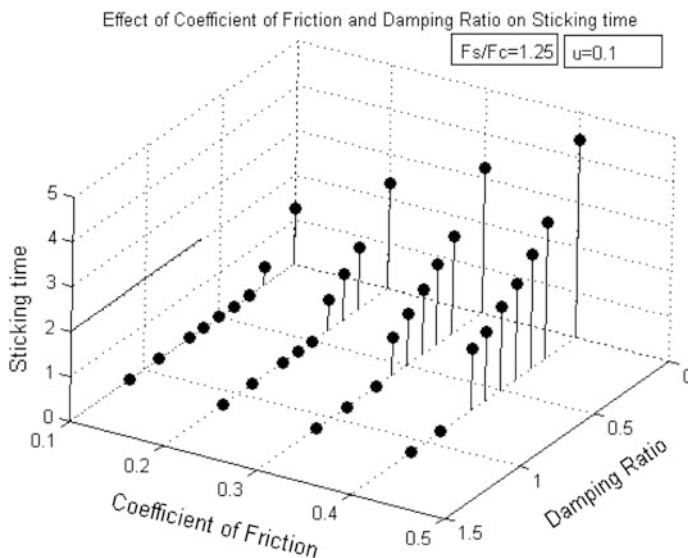


Fig. 6 Effect of μ and damping ratio on sticking time for constant value of F_s/F_c and u , with damping

It can also be observed from Figs. 4, 5, and 6 that there is a combination of the system parameter for which the sticking time is zero. Therefore, by selecting the proper combination of the system parameters the system can be made to be performing without stick slip.

8 Conclusion

It can be concluded that:

1. The sticking time decreases linearly with increase in damping ratio so damping plays a worst role against the stick slip, but the frequency of vibration first increases up to a certain value of damping ratio (that is the point of elimination of stick slip from the system) and then decreases with further increase in the value of damping ratio.
2. The sticking time increases linearly with increase in F_s/F_c ratio, and therefore F_s/F_c is favorable to stick slip and it should be kept minimum as possible as to ensure the system free from stick slip.
3. The sticking time decreases with increase in driving velocity, and therefore the stick slip can be decreased by driving the system at higher velocity.
4. The sticking time increases with the increase in coefficient of friction between the rubbing surfaces so the friction plays a positive role for stick slip. Therefore,

to minimize the stick slip the coefficient of friction between the rubbing surfaces should be kept as minimum as possible.

Sometime, the system might have constraints that do not allow the change in system parameters like coefficient of friction, driving velocity, stiffness, and F_s/F_c though there is an alternative option available to ensure the stick-slip free performance of the system and that is integrating the system with proper viscous damping. Furthermore, it is palpable from the study that by selecting the proper combination of the influencing parameters the system can be kept free from stick slip.

References

1. F. Aabdulgalil and H. Siguerdidjane. "Nonlinear friction compensation for suppressing stick-slip oscillations in oil well drillstring." *Journal of IFAC* 2004.
2. di Bernardo, Mario, and Enric Fossas. "Stick-slip oscillations in resonant power converters." *2005 IEEE International Symposium on Circuits and Systems*. IEEE, 2005.
3. Huang, Chih-Jung, Jia-Yush Yen, and Shu-shung Lu. "Stability of PDF controller with stick-slip friction device." *American Control Conference, Proceedings of the 1995*. Vol. 5. IEEE, 1995.
4. Owen, William Scott. *An investigation into the reduction of stick-slip friction in hydraulic actuators*. Diss. University of British Columbia, 2001.
5. Niemann, G., and EHRENSP. K. "Relative influence of various factors on stick-slip of metals." *Lubrication Engineering* 20.3 (1964): 84.
6. Rowson, D. M. "An analysis of stick-slip motion." *Wear* 31.2 (1975): 213–218.
7. Korycki, Jerzy. "Mathematical model of the stick-slip phenomenon." *Wear* 55.2 (1979): 261–263.
8. Karnopp, Dean. "Computer simulation of stick-slip friction in mechanical dynamic systems." *Journal of dynamic systems, measurement, and control* 107.1 (1985): 100–103.
9. Okamura, K., and MATSUBAR. T. "Frictional vibrations in slide-way." *Journal of Japan Society of Lubrication Engineers* 16.2 (1971): 85.
10. Kato, S., K. Yamaguchi, and T. Matsubayashi. "Stick-slip motion of machine tool slideway." *Journal of Engineering for Industry* 96.2 (1974): 557–566.

Wireless Control System for Enhancing Passenger Safety in the Event of Driver Hostilities for Commercial Vehicles

Aviral Rawat, Gaurav Verma, Navneet Phadke, Yajur Pruthi
and Deepak Kumar

Abstract Majority of passenger mishaps occur in commercial vehicles due to drivers' actions. The control system attempts to protect the passenger in these situations, by integrating modules to measure alcohol levels of the driver, check attempts of passenger abduction, irresponsible driving, and provides an alarming system during perilous circumstances. The module utilizes alcohol sensor and bump sensors, obtains location using GPS module, deactivates ignition using relay, raises alarms by activating the vehicles' preinstalled lights and horn, and wirelessly communicates using fundamental telephony technologies, all incorporated with a microcontroller and drawing power from the standard 12 V vehicle battery. Under those situations, the module would render the vehicle immobile, with lights and horn activated to draw public attention, and location coordinates would be sent to the concerned authorities, thereby providing the passenger means to escape to safety.

Keywords GPS · GSM · DTMF · Alcohol sensor · Bump sensor
AVR ATmega 16 microcontroller · LCD

A. Rawat (✉) · G. Verma · N. Phadke · Y. Pruthi · D. Kumar
University of Petroleum and Energy Studies (UPES), Dehradun 248007, India
e-mail: aviralrawat@outlook.com

G. Verma
e-mail: verma.gaurav1995@gmail.com

N. Phadke
e-mail: navneet.phadke2@gmail.com

Y. Pruthi
e-mail: pruthiyajur@gmail.com

D. Kumar
e-mail: dkumar@ddn.upes.ac.in

1 Introduction

World Bank states that India will have the leading urban population surge by 2050, and thus the pressure on public transportation is increasing at an exponential rate. Safety has taken a hit, and grave criminal incidents have occurred in the recent years with India standing as fourth of the most dangerous places for women to use a commercial transport [1].

Today, commercial vehicles possess either no means of raising alarm in hostile events, or a SOS system, which is relatively easier to bypass, and moreover, time utilizing, for authorities respond after intimation cannot be immediate [2]. We have tried to fill this gap by taking measures to identify the malevolent behaviors in drivers prior to commencement of ride [1]. We not only have installed measures for passenger to seek help in a similar fashion to the existing technologies, but have also empowered her/him to immobilize the vehicle at will and raise alarm on the spot to draw public attention at ground zero [3]. This will emancipate them to take actions before the help arrives and would go a long way in ensuring passenger safety.

In Fig. 1, the control system comprises of two types of sensors: input sensors and the output sensors. DTMF module facilitates communication with mobile phone [4]. GPS module is for the location tracking [3, 5]. Alcohol and bump sensors are for alcohol and impact checks [6, 7]. LCD displays status of the location using GSM for coordinate determination [8]. A 12 V relay is for cutting the

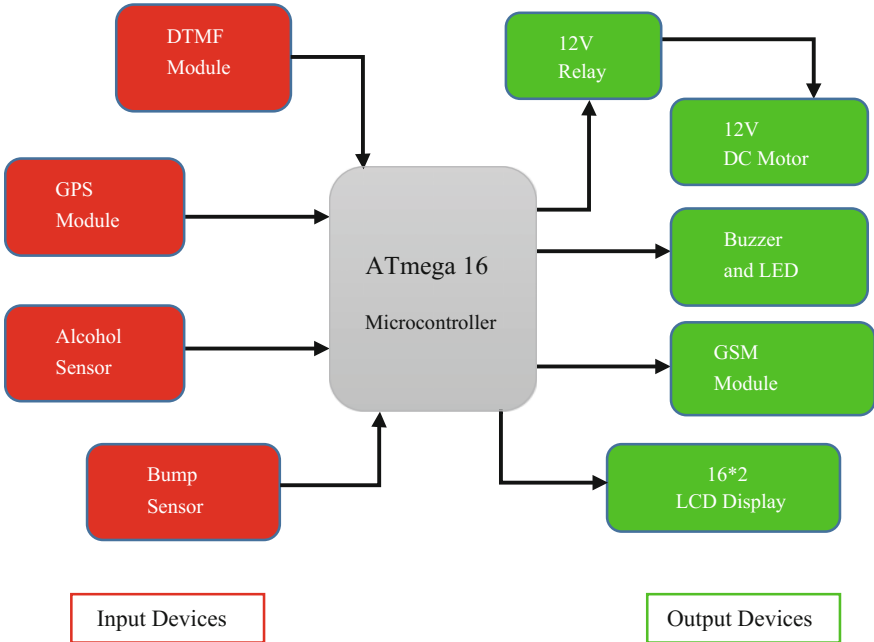


Fig. 1 Functional block diagram of the control system depicting the integrated sensors

electricity to ignition circuitry [9]. The buzzer and LED replicate the horn and lights of the vehicle, and the motor replicates the ignition circuitry [9]. Initially, the motor is on running state, and when the relay is triggered, it is cut off depicting deactivation of the ignition of the vehicle.

All these are integrated with ATmega 16 microcontroller, which has been burned the code in embedded C using AVR Studio. Depending on the logic of the code, appropriate outputs are generated on receiving the inputs by the microcontroller [10].

2 Methodology

2.1 Logic Flow Diagram

From Fig. 2, first step prior to cranking of the engine is the alcohol breath analyzer test. If it is positive, the relay would cut off the ignition circuit and cranking won't happen. Otherwise, the control system checks for accidental impacts while driving and for alarm raised by passenger. For the former case, the GPS module would locate the geo-coordinates of the vehicle and sends it via SMS to the concerned authorities through the GSM module. In the latter case, the relay will cut off the ignition circuit, the GPS would send the coordinates via the GSM module through SMS, as well as the lights and horn of the vehicle would be triggered for capturing attention of the public.

2.2 Circuit Explanation

Figure 3 depicts the circuitry of the control system. It was developed using Proteus software. It provides a fair idea of how the circuit would physically appear in the control system. It depicts all necessary modules required for the control system.

In the testing phase, we sought power through the 240 V household ac stepped down by a 20:1 transformer and converted to dc via a center-tapped bridge rectifier circuit. When installed in vehicles, the power can be directly sought from a standard 12 V battery. The 16 * 2 LCD is connected only for testing purposes and is not a part of standard circuitry to be installed in vehicles. The triggering of the ignition circuitry is done with the help of a relay coil that works on 12 V DC. Alcohol and bump sensors are digital sensors and thus are shown as buttons in Fig. 3. GSM and GPS modules require serial port communication and are interfaced to the microcontroller for universal asynchronous receiver/transmitted. The buzzer and LED are used to indicate the vehicle's lighting and horn system and are powered at 3.5 V using a resistor. The triggering of the ignition coil was tested upon a 12 V DC motor attached to the relay.

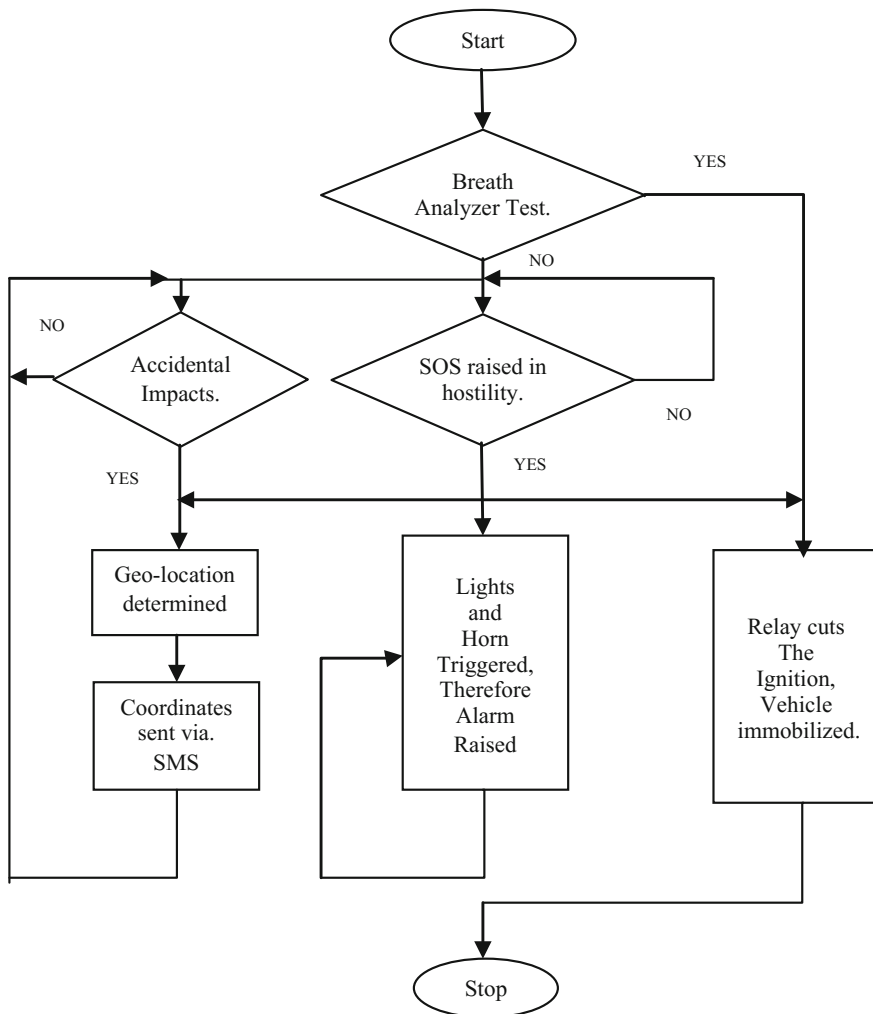


Fig. 2 Logic flow diagram of program burned in the microcontroller

3 Hardware Description

3.1 Alcohol Sensor

In this module, we used MQ3 alcohol gas sensor. The specialty of this sensor is its low cost as well as its ability to detect the alcohol concentration from 0.05 to 10 mg/L. The primary material used in the manufacturing of this sensor is SnO₂. The conductivity of this sensor increases with increase in the concentration of alcohol. This sensor has a very high sensitivity rate toward the alcohol but on the

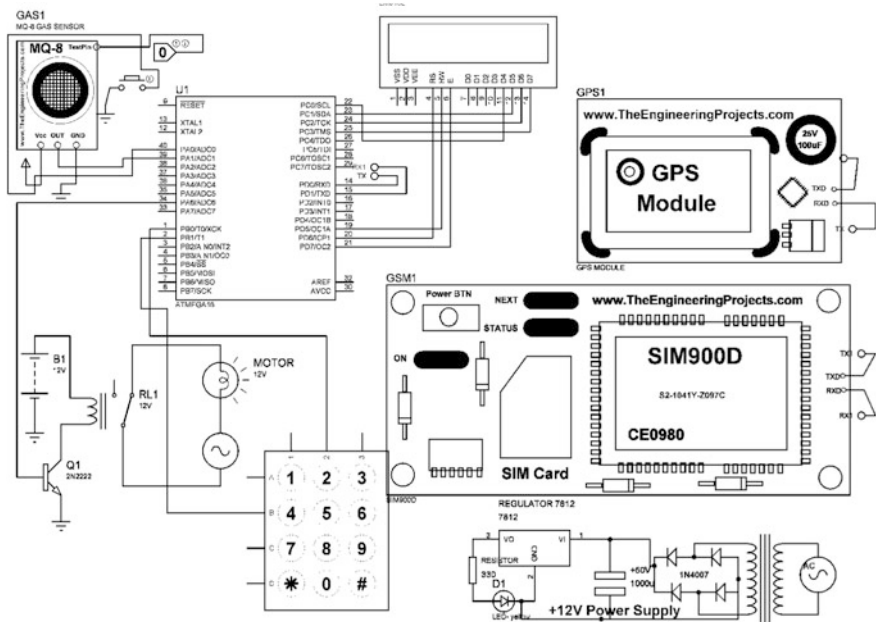


Fig. 3 Sample circuit diagram of the control system

other side, it has good resistance to several disturbances such as vapors, gasoline, and smoke. We have interfaced this MQ3 alcohol sensor with ATmega 16 microcontroller.

Just like common breath analyzer, this sensor can be used to detect the presence of alcohol in our breath. Both its sensitivity and response time are very high. Its operating voltage is 5 V, and current consumption is 150 mA. Both analog and digital output is of 0–5 V. It has four important output pins, i.e., VCC (input power supply), GND (supply ground), DO (digital output), and AO (analog output).

3.2 DTMF Decoder

The DTMF (dual-tone multifrequency) decoder is the best technique which is used to convert analog signal into digital signal. Mostly these decoders are used in the mobile application systems which are used to recognize the sequence of several DTMF tones from the keypad of the mobiles.

This module helps us to decode the audio signal from the phone to 4-bit binary TTL (5 V) output. The IC used in this module is MT8870. This module integrates both the band split filter and digital decoder functions. To decode all the 16 DTMF tone pairs in 4-bit code, the decoder uses digital counting techniques. Its operating voltage is 5 V and operating current is 100 mA. Whenever a new tone is pressed,

an LED is blinked once. It has four output pins on which we get a 4-bit data. This 4-bit data is sent to the microcontroller where it is analyzed, and further steps are taken in order to perform the dedicated operation.

3.3 *LCD Module*

It consists of 16 characters and 2 lines. It can have a 4-bit or an 8-bit MPU interface. The biggest advantage of this module is that it can work with any microcontroller.

3.4 *GSM Module*

GSM (global system for mobile communications) was launched in 1970 developed by Bell Laboratories. GSM architecture comprises of a mobile station, base station subsystem as well as network subsystem. Some of the important features of GSM module are international roaming, FDN (fixed dialing number), SMS (short message service), etc. With the help of GSM, we can communicate with anyone, anywhere and anytime. Required voltage range is 3.4–4.4 V, and it has very low power consumption. Here in this application, the GSM module is used to send a SMS to the concerned person with the current geometrical coordinates of the vehicle.

3.5 *GPS Module*

GPS (global positioning system) is one of the best inventions of US Department of Defense. With this invention, the positioning and navigation has become easier. Here in this module, a GPS receiver is used along with an antenna. These current coordinates are collected by this antenna, having 3 m wire. This data collected is then sent to receiver. An LED light is placed on this receiver circuit whenever the data is collected by the receiver. This collected data is then sent to the microcontroller which then sends this data to the GSM module which sends these coordinates via SMS to the dedicated mobile number. The antenna of the GPS module has a magnetic base. Its working voltage is 3–5 V and 28 dB.

3.6 *AVR ATmega 16*

Here, we are using an 8-bit microcontroller which belongs to the Atmel's Mega AVR family. It has very low power consumption. It is based on reduced instruction set computing (RISC) architecture. Only one machine cycle is used for its most of the instructions. It can work efficiently up to 16 MHz frequency.

Programmable flash memory of 16 kB is provided to this ATmega 16 as well as a static RAM of 1 kB and 512 bytes of EEPROM is also provided. This microcontroller has in total 40 pins. There are 32 input/output lines which are classified into 4 ports. All the operations to be executed and the sequencing and addressing are managed by this AVR ATmega 16 microcontroller. It is the heart of this system. The 4-bit data from the DTMF module is received here and stored, and then the required action is taken whenever necessary.

3.7 Relay

A relay is used for switching applications. Here in our module, we are using a 12 V relay. A relay uses an electromagnet for its switching application. A relay requires one single pulse of coil power, just to move their contacts in one direction and another, pulse to bring it back to its original position. Here, the application of relay is to stop the engine of the car, by stopping the current flow toward the spark plug. Once the electricity is stopped, the vehicle will come to a halt. With the help of DTMF module, by pressing a dedicated number, we can stop the electric supply as well as bring back the relay to its original position and start continuing its electric flow by pressing a separate number.

3.8 LED Indicator and Buzzer

An LED indicator is used in this module which represents the parking lights of the vehicle as well as a buzzer is also used in this module which represents the horn of the car. Whenever any mishap takes place, we are requested to stop the car, then we will do so, as well as start the parking light and start blowing the horn in order to grab the attention of the local people around that car. The LED is red in color and 3 mm in diameter. The buzzer is of 5 V.

4 Results

The module was tested on a sample car ignition circuit model, and its control (a basic phone with number) was given to a person at a remote location at least 50 m away from it (referred to as 'authority' henceforth). The system performed as anticipated. On detection of alcohol or raising of alarm, the ignition was cut, siren was raised and location sent to the authority. Simulated impacts in the sensor caused only the location to be sent to the authority. The sample ignition circuit didn't function until desired by the authority. On forceful removal of the module from the circuit, the sample ignition circuit became permanently disabled (Fig. 4).

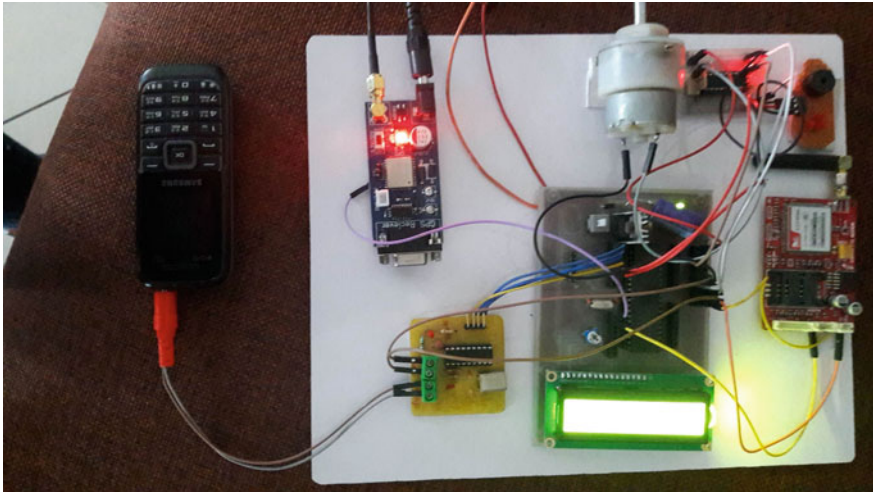


Fig. 4 Sample ignition circuit for of testing the module

5 Discussion

The ideology behind the research was to curb to best extent passenger mishaps in commercial vehicles due to malevolence of the drivers. We took an approach to address the issue in real time on ground zero by providing the passenger means to stop the vehicle at will in case of illegal driving practices or hostile environments.

This control system can be converted into a more reliable tool by using other means for communication than DTMF, which creates a limitation for the module of being operational only in 2G mobile network zones. It can be also reduced significantly in size and made more discreet by adopting lab-on-a-chip approach.

References

1. Thomson Reuters Foundation (31 October 2014). "Most dangerous transport systems for women". <http://news.trust.org>.
2. Transport Department, Government of Andhra Pradesh, India. "Table of Maximum Speed Limit at a Glance". <http://www.aptransport.org>.
3. Alban, Santiago. Design and performance of a robust GPS/INS attitude system for automobile applications. Diss. Stanford University, 2004.
4. Wang, Danping, and Youguo He. "Research and design of the vehicle ranging system based on DTMF." Electrical and Control Engineering (ICECE), 2011 International Conference on. IEEE, 2011.
5. Zhe, X. U., and C. O. N. G. Lin. "The Application of GPS to Automobile Transportation [J]." Shanxi Science & Technology of Communications 2 (2006): 032.
6. Jones, Ian S., and Adrian K. Lund. "Detection of alcohol-impaired drivers using a passive alcohol sensor." Journal of Police Science & Administration (1986).

7. Crandall, Jeffrey R., Kavi S. Bhalla, and N. J. Madeley. "Designing road vehicles for pedestrian protection." *BMJ: British Medical Journal* 324.7346 (2002): 1145.
8. Lili, Wan, and Chen Tiejun. "Automobile anti-theft system design based on GSM." *Advanced Computer Control*, 2009. ICACC'09. International Conference on. IEEE, 2009.
9. Denton, Tom. *Automobile electrical and electronic systems*. Routledge, 2004.
10. Dai, Min, et al. "Design and Implementation of the Control System for Two-Wheeled Self-Balancing Vehicles." *Advanced Materials Research*. Vol. 588. Trans Tech Publications, 2012.

Cybersecurity Issue and Online Information Source

Lalit Mohan Joshi and Rajendra Bharti

Abstract With the occurrence of the advent of social network, this paper illustrates the security issues related to online activity, information source. Here, I discourse on the network information forensic using Python language. As large users connect to the Internet, it magnetizes lots of cybercriminals. Information of gathering footprints and its countermeasures is also explained. Today as the Internet has become more and more widespread, here I discuss the process of discovering e-mail spam and anticipation with protocol analysis and also security issues such as multicast, broadcast, unicast, for communication between receiver and sender. This paper explained how a user can analyze the wireless traffic in an online source and security issues in information theory [1]. The main aim of the system audit by the third-party tools is to secure the online property [2]. This paper ventilates the state of the art for a broad range of cryptographic activity used in networking. This paper also helps to distinguish between hacker, hacking, and penetration techniques.

Keywords Penetration · Impairments · Posterior security · Python

1 Introduction

This paper dissertates the network and cybersecurity issue. The information technology industry has evolved greatly over the last half-century. The original IT industry has increasingly converged with the communication industry into a combined sector commonly called information and communication technology (ICT). In this paper, the definition of hacker, hacktivist, activity of hacker, and types are explained. The next section illustrates how the hacking techniques, such as phishing, vishing, koobface malware attack, are used in the social media via

L.M. Joshi (✉) · R. Bharti
BTKIT, Dwarahat, Uttarakhand, India
e-mail: lalitm.joshi09@gmail.com

R. Bharti
e-mail: rajendramail1980@gmail.com

network. Further, I have discussed the social media app, its advantages and disadvantages [3]. After that come at the main point which is the most concerned issue nowadays is called security. In security section, I have dissertated the multicast, broadcast, unicast security issues with the help of a proper diagram and then stages of security, stages of security provided, measurement of security with time.

I also hold forth about the network information forensic by using Python language with SQL injection. In this paper, researchers also come to know about the gathering footprints of information and its countermeasures. I have also discussed the some morel Web sites those can help to get out the information of any Web sites and domains.

2 Hacker

Hacker may be defined as the person who may alter system or security features to accomplish a goal that differs from the original purpose; hacker is a person which is responsible for the unauthorized intrusion into a computer or network. Hackers are the person those are different from the common person by having knowledge of computer programming deeply. White hat hacker always works for a good thing and save people from online crime [4]. They work like a penetration tester. Black hat hacker always harms people and steals informative data of people from online storage. Grey hat hackers are the mixture of white hat hacker and b hat hacker. Green hat hacker relates to the money or currency. They always debit money from the account and credit/debit card of the people. Scripdeehackers have zero knowledge of computer languages, they are called ethical hacker, and they always use predefined tools. Hacktivists are the cyberarmy of any group of country as they are a politically motivated hacker. “BOTNET is a zombie machine; it is used to perform DDOS Attack” [5, 6, 7].

3 Techniques of Hacking

Phishing is a trap, or we can say a process or attempt to acquire sensitive information such as USERNAME, PASSWORD, CREDIT/DEBIT CARD DETAILS. for a malicious reason, by masquerading as a trustworthy entity in an electronic communication, e.g., receiving e-mail. Vishing is a mixture of phishing and voice, e.g., telephone call.

Koobface malware is created by Facebook to acquire the IP address or some informative data. It is like a vulgar photograph of any ladies, news, or photograph with sympathy attached with a link, as user clicks on it or copies that link to open in a new tab of browser. Due to this activity, authenticated cookies sent to the attacker machine [8]. Hacker can start his/her unauthorized activity and start the same prompt. This is called “power of social engineering.” Vulnerability scanner

technique checks out the weakness of the network or computer. Password cracking is the process of recovering passwords from data stored or transmitted by computer systems [9].

4 Security

Something is hidden from others is called security. There is a key for coding the message, which must be secured. For security reason, we need confidentiality, integrity, and authenticity (CIA). It is raised from the pyramid time in Egypt, 3000 BC before. The original message is sent through sending process, the message is coded, and it is received through receiving process. There are 3 processes in which security may be provided: defense, detection, and decision. There are 3 security stages: The first one is source level, the second one is destination level, and the third one is intermediate network level. There are three types of security: The first one is link to link, the second one is security from one to next node, and the third one is end to end (Fig. 1).

5 Security Issues in Information Theory

5.1 How We Compute Information Source to Destination

The concept of information theory is given by:

American Electrical Engineer: **CLOUD E SHANON** in **1948**.

“**MATHEMATICAL THEORY OF COMMUNICATION**” given by Cloud E Shannon presents the mathematical law of communication when the information is transferred from source to destination. “Numerical Presentation or Quantification/Qualification of Information” is given by Cloud Shannon. Information source is a device that generates random variables:

$$(x_0, x_1, x_2, x_3, x_4, \dots, x_n)$$

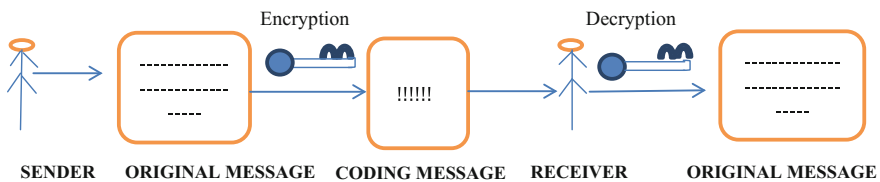


Fig. 1 Message encryption–decryption

Probability of generating variables: $(x_0, x_1, x_2, x_3, \dots, x_n)$

Example of information source:

BINARY INFORMATION SOURCE: It generates (0, 1) random variables.

ENGLISH DICTIONARY ALPHABET: (A, B, a, b)

Types of information source:

ANALOG: human speech, voice of amplifier.

DISCRETE: digital source, computational source, binary Source, English alphabet.

HIGH RANDOMNESS = MORE INFORMATION.

5.2 Information Source Mathematically Presented As

$$\{x_1, A_x, \dots, P_x\}$$

(x) : any random variables.

(A_x) : $(x_0, x_1, x_2, x_3, \dots, x_n)$: set of random variables.

(P_x) : $(p_0, p_1, p_2, p_3, \dots, p_n)$: probability of random variables.

$$P_x(x = x_i) = p_i$$

$$\boxed{E_{x_i} E^{A_x(p_i)} = 1}$$

$$\boxed{\begin{matrix} (0) & \longrightarrow & (x_i) \\ \text{(Information Source)} & & \text{(General Variable)} \end{matrix}}$$

$$\boxed{\begin{matrix} (I) & \propto & \frac{1}{P} \\ \text{(Information Source)} & & \text{(Probability)} \end{matrix}}$$

$$\boxed{\begin{matrix} (0) & \longrightarrow & (x_i) \\ \text{(Information Source)} & & \text{(General Variable)} \end{matrix}}$$

$$I_{(x_i)} \propto 1/P_{(x_i)}$$

$$I_{(x_i)} = \{\log 1/P_{(x_i)}\}$$

$$I_{(x_i)} = \{\log (P_{x_i})^{-1}\}$$

$$I_{(x_i)} = \log P_{(x_i)}$$

$$\boxed{I_{(x_i)} = \log P_{(x_i)}}$$

Here, log is used for RANDOMNESS.

If information source is discrete or binary, then

$$I_{(x_i)} = -\log_2 P_{(x_i)}$$

If information source is ANALOG, then

$$I_{(x_i)} = -\log_e P_{(x_i)}$$

If information source is HARTLY or SHANNON, then

$$I_{(x_i)} = -\log_{10} P_{(x_i)}$$

Range of probability:

1. $0 > P_{(x_i)} < 1$
2. $1 < I_{(x_i)} < 0$

$$I_{(x_i)} = -\log P_{(x_i)}$$

Here, $P_{(x_i)} = 0$

Then, maximum information will get

$$P_{(x_i)} = 1$$

Then, information will be minimum:

$$I_{(x_i)} = -\log P_{(x_i)} = \log 1/P_{(x_i)}$$

Example:

$$I_{(x_i)} = -\log P_{(x_i)} = \log 1/P_{(x_i)}$$

If information source is in a binary form, then

$$X = 0 \text{ or } 1$$

$$A_x = (0, 1)$$

$$P_x = P(0) \text{ or } P(1)$$

$$P(0) = (1/2), \quad P(1) = (1/2)$$

Now for probability

$$I(0) = -\log_2 P_{x_i}$$

$$I(0) = -\log_2^{(-1)} = 1 \text{ bit}$$

If information source as a binary is **M BIT**, then we get

Total output variable = (2^M)

Probability of 1 random variable = $1/2^M = (2^{-M})$

$$I_{(M)} = -\log P(x_i)$$

$$I_{(M)} = -\log_2 2^{(-M)}$$

$$I_{(M)} = M \text{ bit}$$

If binary information source is two digit, then

$$\begin{array}{l}
 A(0/1) \\
 A(0/1)
 \end{array}
 \left. \vphantom{\begin{array}{l} A(0/1) \\ A(0/1) \end{array}} \right] O(C)
 \begin{array}{|c|}
 \hline
 00 \\
 01 \\
 10 \\
 01 \\
 \hline
 \end{array}
 P = 1/4$$

$\{P(00), P(01), P(10), P(11)\}$

$P(C) = P(A) * P(B)$

$P(C) = (0.5) * (0.5)$

$P(C) = 0.25$ or $1/4$

(X) Transmitter \longrightarrow [(Information Source)] CHANNEL (Y) Receiver

Mutual information: When both X and Y provide information mutuality, then

(X) provides information about (Y) .

(Y) provides information about (X) .

Now, information source is:

For $X = (x_1, x_2, x_3, \dots, x_n)$

$$(x_i) = (1, 2, 3, \dots, n)$$

For $Y = (y_1, y_2, y_3, \dots, y_n)$

$$(y_j) = (1, 2, 3, \dots, n)$$

5.3 When Conditional or Transactional Probability Is Used

Conditional probability is:

$$P \left[\frac{X = x_i}{Y = y_j} \right] = \frac{P(x_i/y_j)}{P(x_i)}$$

If probability of $x = 0$, then probability of $y = ?$

If probability of $x = 1$, then probability of $y = ?$

Here, $P(x_i/y_j)$ = posterior probability of (x_i) on (y_j)

$P(X = x_i/Y = y_j)$ = prior probability.

5.3.1 Difference Between Prior and Posterior Probability

1. **Posterior**—Probability obtained after operation (with sampling).
2. **Prior**—Probability obtained before operation (without sampling).

According to Bayes’ theorem, we get

$$P(H/X) = \frac{P(X/H) * P(H)}{P(X)}$$

$$I(X, Y) = \frac{\log P(x_i/y_j)}{P(x_i)}$$

Applying Bayes’ theorem, we get

$$\begin{aligned} I(x, y) &= \frac{\log P(x_j/x_i) * P(x_i)}{P(x_i) P(y_j)} \\ &= \frac{\log P(y_j/x_i)}{P_{y_j}} \end{aligned}$$

$$\boxed{I(x, y) = I(y, x).}$$

5.4 Mutual Information Source

$$I(x_i, y_j) = \log \left[\frac{P(x_i/y_j)}{P(x_i)} \right] \tag{1}$$

Case 1:

$x, y =$ sophisticated independent
then,

$$P(x_i/y_j) = P(x_i)$$

So put the value of $P(x_i/y_j) = P(x_i)$ in formula (1)

$$\begin{aligned} I(x_i, y_j) &= \log P(x_i/x_i) \\ &= \log 1 \end{aligned}$$

$$\boxed{I(x_i y_i) = 0}$$

Case 2:

$$\{P(x_i/y_j) = 1\}$$

Now put the value in formula (1):

$$\begin{aligned} I(x_i/y_i) &= \log P \left[\frac{x_i/y_i}{P(x_i)} \right] \\ I(x_i/y_j) &= \log \{1/P(x_i)\} \\ I(x_i/y_j) &= -\log P(x_i) \\ &= -\log P(x_i) \text{ gives the information of } (x) \end{aligned}$$

5.5 By Using Entropy

$$\text{ENTROPY} = H$$

Behave of Information source is probabilistic is called entropy.

No. of signal: $(S_1, S_2, S_3, S_4, \dots, S_{N-1}, S_K)$

Computing entropy: $H(j)$

Discrete information source: $(S_1, S_2, S_3, S_4, \dots, S_{N-1}, S_K)$

$j = (S_0, S_1, S_2, S_3, S_4, \dots, S_{N-1}, S_K)$

Information of signal: $\{I(S_0), I(S_1), I(S_2), \dots, I(S_{N-1}), I(S_K)\}$

Probability of signals: $\{(P_0), (P_1), (P_2), (P_3), \dots, (P_{N-1}), (P_K)\}$

Collection of average information considering of probability is called entropy.

$$K - 1$$

$$\text{EP}(K - 1) = 1$$

$$K = 0$$

$$I(s_k) = \log(1/P_k)$$

$$I(s_k) = -\log_2(P_k) \tag{1}$$

$$K = 0$$

$$H(J) = EP K^I(SK) \tag{2}$$

$$K = 0$$

Now put the value of (I_{SK}) from Eq. (1) and put this value on Eq. (2):

$$K = 0$$

$$H(J) = +E p_k \log(1/p_k)$$

$$K = 0$$

$$H(J) = +E p_k \log(p_k)$$

$$K = 0$$

For maximum entropy:

Channel is binary source.

This channel transmits signal (0, 1).

Probability P (0, 1).

Probability for (0) = (p_0) ,

Probability for (1) = $(1 - p_0)$.

$$K = 0$$

$$H(J) = -E p_k \log(PK)$$

$$K = 0$$

$$[p_0 \log_2 p_0] \text{ for } (p = 0)$$

$$[p_1 \log_2 p_1] \text{ for } (p = 1)$$

The entropy of binary source/channel is:

$$H(J) = -[p_0 \log_2 p_0 + p_1 \log_2 p_1]$$

Putting value of $[p_1 = (1 - p_0)]$, we get

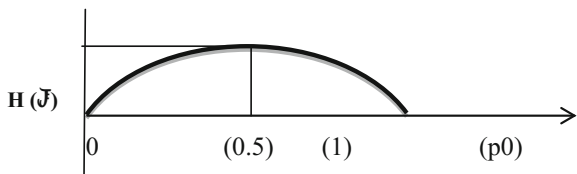
$$[p_0 \log_2 p_0 (1 - p_0) \log_2(1-p_0)]$$

There are 3 cases:

- $p_0 = 0$
- $p_1 = 1$
- $p_0 = 1/2$ or (0.5)

For $p_0 = 0$;
 For $p_0 = 1$;
 For $p_0 = 1/2$ or (0.5)
 Then

$$[H(J) = 1]$$



6 Network Information Forensic Using Python Language

6.1 Sql Injection

Vulnerability starts from the LOGIN pages.

USER NAME.....

PASSWORD

Searching something in GOOGLE.

While logging name if security shows that user name and password are incorrect, then it has back-end security.

USER NAME: (1' OR '1' = 1)

PASSWORD: (1' OR '1' = 1)

Cut the last file name and then confirm login app. You will be accessed.

6.2 *Penetration Testing*

It works for an organization to prevent hacking attempts.

It is different from hacking.

6.3 *Python's Command*

Python.org

Types (3.5, 2.7)

Version (2.7): more powerful

Version (3.5): not stable.

7 **Conclusion**

This paper summarizes that with the occurrence of the advent of social network, security issues across the world produce a huge amount of data daily. Network security issues are now becoming beneficial as society is moving toward cybernetic information era. The process of information gathering footprints and its counter-measures are also explained. Python language is the best procedures to secure online activity either you are a user or a penetration hacker. Here, I have discussed the information in the form of theory as well as mathematical representation. This paper also discoursed on the wireless network, its physical property, its transmission impairments, and the category of mobile transmission by the non-loss condition; also explained a hierarchy of wireless network [10]; and further discussed the information theory, its security issue, and types of information source. The main and beneficial part of my paper ventilates the mathematical presentation of information source with the use of conditional and transactional probability. Here, I applied the Bayes' theorem for information source and then explained how to send information source mutually by two cases. I also used the entropy, a behavior of information source as probabilistic, and have discussed the maximum entropy and binary source entropy.

References

1. K. Summers, W.C. and A. DeJoie. Wireless security techniques: an overview. 2004: ACM.
2. Russell, S. F. Wireless network security for users, 2001. IEEE, p. 172–177.
3. Manley, M., Mcentee, C., Molet, A. & Park, J. Wireless security policy development for sensitive organizations, 2005. IEEE, p. 150–157.

4. Durbin, S. (2011). Tackling converged threats: building a security-positive environment. *Network Security* (6): 5–8.
5. Herath, T. and H. Rao, Encouraging information security behaviors in organizations: Role of penalties, pressures and perceived effectiveness *Decision Support Systems*, 2009. 47(2): p. 154–165.
6. Miller, S.K., Facing the challenge of wireless security. *Computer*, 2001.34(7): p. 16–18.
7. Arbaugh, W.A., Wireless security is different. *Computer*, 2007.36(8): p. 99–101.
8. Dourish, P. et al. Security in the wild: user strategies for managing security as an everyday, practical problem. *Personal and Ubiquitous Computing*, 2004.8(6): p. 391–401.
9. Chenoweth, T., R. Minch, and S. Tabor. User security behavior on wireless networks: An empirical study. 2007: IEEE.
10. Park, J.S. and D. Dicoi, WLAN security: current and future. *IEEE Internet Computing*, 2003. 7(5): p. 60–65.

White Cane Navigation Using Arduino Uno

Mohd. Faizan Khan and Ankita Kumar

Abstract Visually disabled people have always been looked at sympathetically by the society. According to a count around 87% men and 91% women are visually impaired or weak in India alone [1] along with this, globally the estimated count rises as high as 285 million [2]. Our research aims at solving their problem of navigation to a certain extent. This research has been proposed to introduce a device which will help the blind to reach their destination accurately with the help of Google Maps. It proposes a Bluetooth-enabled white cane to help the people reach their destination. The Google Maps API navigation is used and is implemented through an Arduino to navigate the visually disabled via buzzing sensations.

Keywords White cane · Android · Navigation for blind
Visually impaired · Blind aid

1 Introduction

Sight is categorized as one of the most crucial senses and people lacking this sense are always sympathized by others. WHO confirms 39 million people in the world to be visually impaired. 80% people above the age of 50 suffer through any kind of imparity in terms of visual sense [3].

A white cane navigation using Arduino Uno is a research that presents a device that can be used for navigation by the visually impaired where the white cane is Bluetooth enabled and connects with an Arduino Uno device which sends navigating information to the white cane held by the person in the form of mild vibrations to indicate the direction in which the person is supposed to move.

Mohd. F. Khan (✉) · A. Kumar
College of Information Technology, University of Petroleum and Energy Studies,
Dehradun, India
e-mail: mfaizi.k@gmail.com

A. Kumar
e-mail: ankita.kumar76@gmail.com

Earlier work has been done in the area of navigating visually impaired in a close indoor environment, but instead of using RFID in an indoor system, the aim is to present a device to resolve navigation problem for blind people in open environment using Google Map API [4]. First, a connection is established between the stick and Arduino Uno device following which the device acquires the navigation destination. Once this has been done, we start the navigation. Now 4 scenarios are obtained for this (for a white cane held in the right hand):

1. Turn left: Vibration in the thumb,
2. Turn right: Vibration in baby finger,
3. Go straight: Vibration in middle finger,
4. Wrong direction: Vibration in all the fingers.

Once the destination is reached, the Bluetooth navigation stops.

The white cane is held by the person in whichever hand they are comfortable in. A glove is attached to the white cane which fits in the hand of the person and the index finger is pointed along the shaft of the cane which is pointed towards the cane tip resting on the ground [5]. Whenever a navigation signal has to come up, the Arduino Uno will receive this input and accordingly will set up the buzzer. An Arduino Uno has been used as a controller in this research which receives the input from the mobile device over Bluetooth. The Arduino then sends signals accordingly to the indicated buzzer. The buzzer fit here is of very low cost. They have been fit on all five fingers. The vibration is felt accordingly as the signal is received.

The Google Maps navigation API has been taken over in the app and its navigation is used to navigate the person. Google Maps uses a phone's mobile Internet connection to draw out the underlying map, complete with streets and locations. Further, the mobile device's GPS coordinates have been used to integrate its position on top on the map [6].

A triangular button is present on Google Maps which gives the person's current location. This is of great help for the visually impaired person, and once this location is received, the destination has to be entered. Once the destination is entered, the navigation starts with the Google Maps API help. The navigation is commenced and the directions are received by the Arduino Uno. If a left turn has been indicated by the Google Maps navigation, then this is sent to the Arduino Uno over the Bluetooth. The Bluetooth chip HC-05 is fit on the RX/TX pin on the Arduino Uno. It receives from the mobile device and then transmits to the Arduino Uno. The Arduino Uno sends the signals to the buzzer via the digital output pin which is fit on the thumb of the glove and it vibrates (in the given case). This is an indication to the person to turn to the left.

In case the person starts moving in the wrong direction and it is detected by the Google Maps API, then there is a simultaneous vibration on all the five fingers of the person.

Over the last few years, there has been a contribution made to the visually impaired society by the introduction of smart canes or guide canes. These invoke

alertness of through voice messages on the encounter of any obstacle though there was no contribution made for the navigation [3].

This research enhances the mobility of the visually disabled people and removes their dependency of locating the destination through other people’s help.

2 Hardware Development

The block diagram of the system is shown in Fig. 1. The system consists of a microcontroller Arduino Uno. Arduino Uno is given power supply. Our system consists of +12 V power supply using a 7412-V regulator. It is the controlling unit of the system. It receives the navigation as given by the Google Maps API over the Bluetooth to the Arduino Uno. The HC-05 chip attached to the Arduino Uno then transmits these signals to the Arduino which sends it to the buzzer through the digital pins. The HC-05 chip works as RX/TX pin which receives the signals over Bluetooth for effective navigation from the mobile device and then transmits this data to the Arduino Uno for the buzzer activity.

Figure 2 shows Arduino and HC-05 circuit for gloves. Circuit shows the internal wiring of the Arduino Uno as it is connected to the Buzzers (BUZ1, BUZ2, BUZ3, BUZ4, BUZ5) and the HC-05 Bluetooth chip attached to it. The buzzers are connected to the digital pins (D7, D6, D5, D4, D3) which are turned on as per the navigation received from the Google Maps API. The HC-05 chip is connected to RX/TX here. The mobile device sends the navigation details to Bluetooth module which it transmits to the Arduino Uno to process.

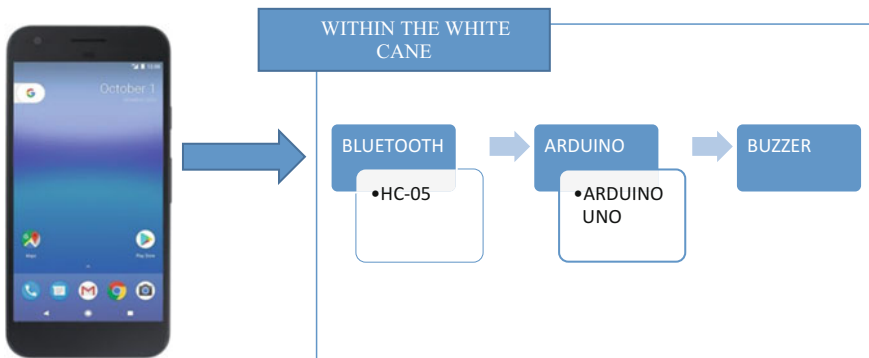


Fig. 1 Block diagram of the system

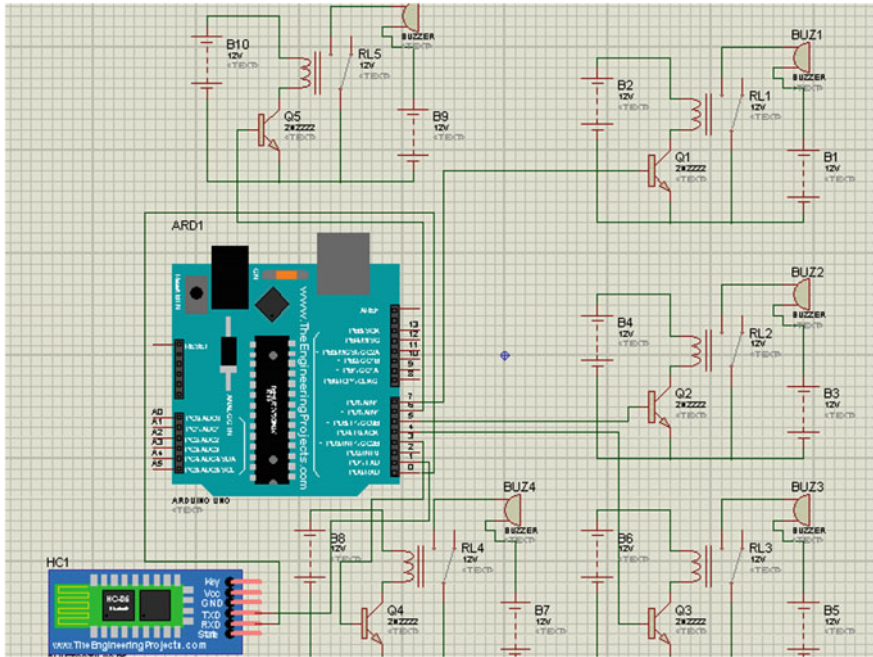


Fig. 2 Arduino and HC-05 circuit for gloves

2.1 HC-05 Bluetooth Module for Receiving Data from Android to Arduino

Bluetooth module HC-05 is a simple Bluetooth SPP (serial port protocol) module which makes wireless serial connection set-up possible. SPP Bluetooth module stack is completely built for Bluetooth V2.0+EDR (enhanced data rate) 3 Mbps modulation along with that; it also supports 2.4 GHz radio transceiver and baseband. CMOS technology is used by the single inbuilt chip and thus holds AFH feature (adaptive frequency hopping). The module is widely used and is easily available over Internet [7].

HC-05 consumes power input of 5 V (Vcc), although TXD and RXD consume 3.3 V for the logical signals. Accordingly, HC-05 module can safely send data to the device as the Arduino digital pins are safely capable to receive up to 5 V, but a voltage divider is required in between to receive a 3.3-V input only [8].

>>>Formula for voltage divider

$$V_{in} = (R2/(R2 + R1))V_{out},$$

where it is known that V_{in} is 5 V and V_{out} has to be 3.3 V. Therefore, voltage could be balanced easily using available resistors [9].

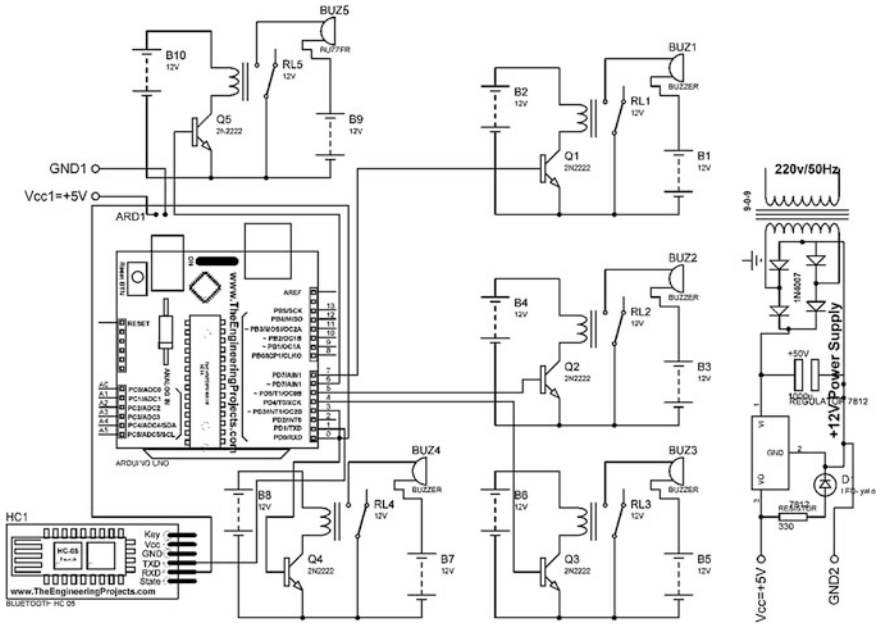


Fig. 3 Proteus simulation of the power supply used in our research

Figure 3 shows the Proteus simulation of 5- and 12-V power supplies. This power supply is used for the entire project to provide VCC and ground to the sensors. This is a simple power supply circuit which is converting 220–240 V into 5- and 12-V output. Here, we are using a step-down transformer “TR1”, for transforming high-voltage AC input to a low voltage. To convert the stepped-down AC voltage into DC, a bridge rectifier is made using diodes. Further, the output of the rectifier is passed through the capacitor for filtering purpose. Capacitor eliminates the fluctuations in the voltage and provides a stable DC voltage, which is then fed to IC 7805 and IC 7812 for getting the desired 5- and 12-V power at the output [10].

3 Software Development

See Figs. 4 and 5.

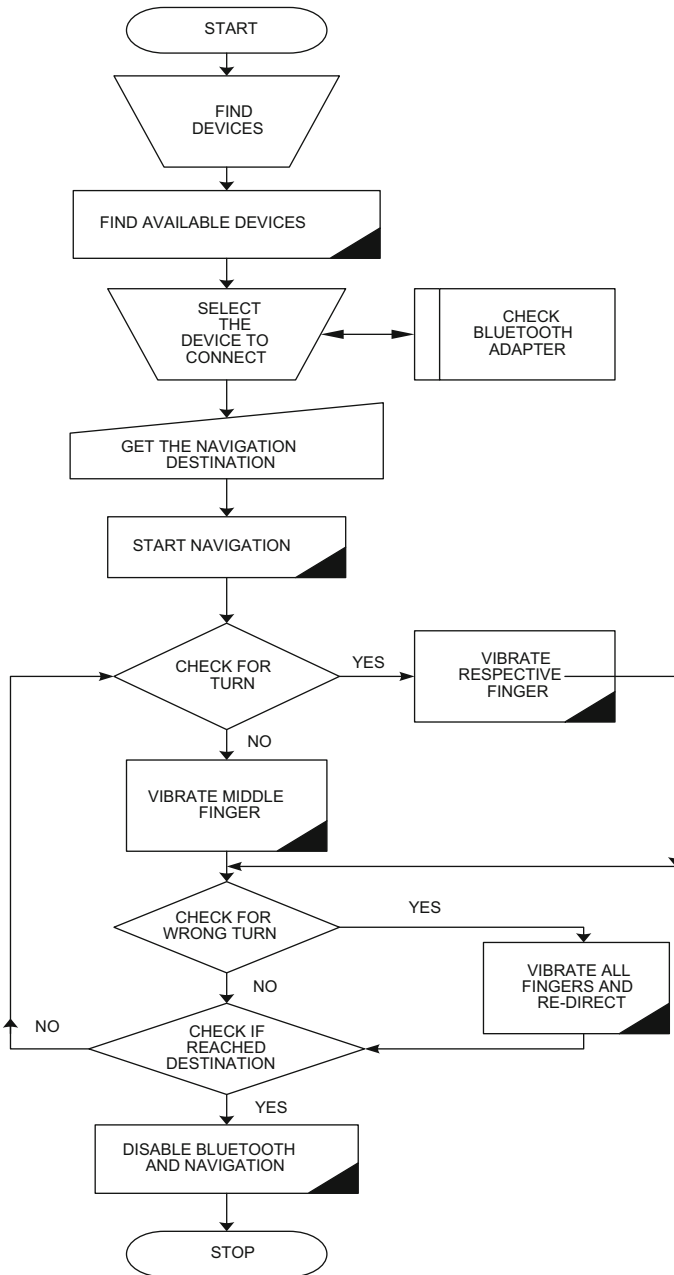


Fig. 4 Flowchart of the white cane android application

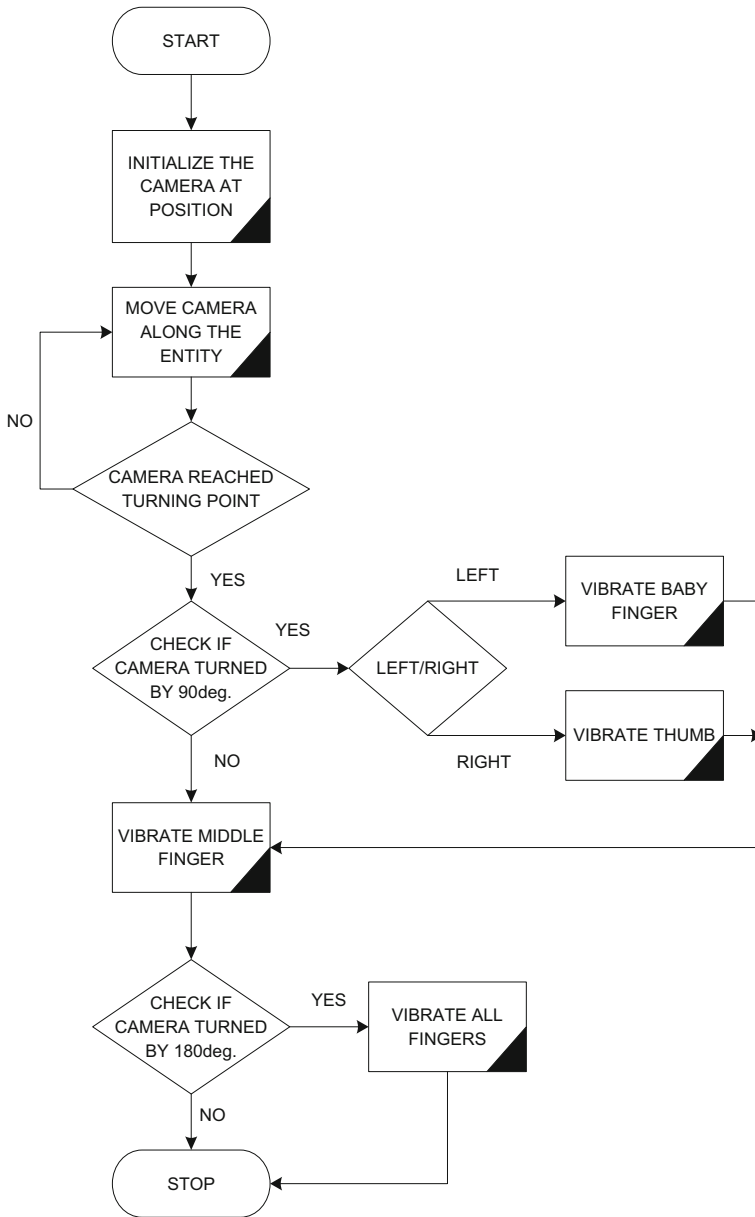


Fig. 5 Flowchart of the navigation using Google Map camera

3.1 *Algorithm for Arduino Uno Device*

- (i) **Initialize HC-05 for communication and establish SPP communication.**

Set the baud rate of HC-05 module to 9600 and read data serially via read function [11].

- (ii) **Receive the data and trigger the buzzer accordingly.**
 (iii) **Continue until data receiving stops.**

3.2 *Algorithm for Android Application*

- (i) **Initialize Bluetooth and make list of visible devices [12].**

Initiate Bluetooth adapter and get pair devices in an array list.
 Get the details of all the visible adapter added to the list.

- (ii) **Connect the selected device to the Bluetooth adapter socket created and begin SSP communication and add permissions to manifest [12].**
 (iii) **Make a Google Map fragment and replace the API key in manifest file.**

>>>**Steps to find Google Map API key [13]**

- Find console API key link in google_maps_api.xml class.
 - Search the link.
 - Accept the condition and build the API key.
 - Copy the API key and use it in the manifest.xml to make a unique connection to Google Maps API.
- (iv) **Make a new intent and pass the navigation details entered by user in a editText field to start navigation service.**
- (v) **Call Google Map API directions and use map camera to tell the direction and send following string through Bluetooth.**
- “l” for left turn.
 - “r” for right turn.
 - “s” for straight.
 - “w” for wrong direction.

Use animateCamera (CameraUpdate update) function for this

- (vi) **Continue till we reach destination.**

4 Conclusion

A life without sight is a very difficult one for an individual. With increase of visual impairment due to cataract and age there is a need of better blind aid products [2]. The thought of being continuously dependent on someone else for any sort of locomotion is a hardship in itself. The research paper proposed here is to tackle this problem to a certain extent. With the help of a navigating tool, a visually disabled person can at least get from one place to another without being dependent on anyone. The person can easily reach his destination with the help of this device, as he receives the navigational direction through vibrations. The Bluetooth connected to white cane serves as a strong support through which it is easy to navigate between two places using an android application. This device can be further enhanced by adding various sensors to detect the obstacles. This may lead to lesser accidents and be a strength to the blind in future. Another improvement can be of detecting the path to be fluid-free and indicating any sort of liquid present on the flood to avoid any sort of slip by the person.

References

1. Murti G.V.S (2005) et al “Current estimates of blindness in India” *Journal of Br J Ophthalmol* Mar; 89(3): 257–260.
2. Mariotti S.P., Pascolini D. (2012) “Global estimates of visual impairment” *Journal of Br J Ophthalmol* May; 96(5):614–8.
3. Masnah, G. (2015). Blind Navigation System using Arduino Uno with 1Sheeld [PDF FILE]. Retrieved from www.eprints.utm.edu.my/.
4. Mau S. (2008) et al “BlindAid: An Electronic Travel Aid for the Blind” *Journal of The Robotics Institute Carnegie Mellon University Pittsburgh, Pennsylvania 15213*.
5. Howell, Jerry. (2000, August). White Cane Basics. Retrieved from www.howellmobility.com/html/basics/.
6. Dube, Ryan. (2010, June 24). Use Google Maps Navigation For Turn-By-Turn GPS [Android]. Retrieved from www.makeuseof.com/.
7. Itead (2017, March 24). *Serial Port Bluetooth Module (Master/Slave)*. Retrieved from <https://www.itead.cc/wiki/>.
8. TechDepot (2008, September 30) *Connecting HC-05 Bluetooth Module to Arduino* Retrieved from <http://www.instructables.com/id/>.
9. Selvam, K.C. (2012) “A novel voltage divider circuit.” *Journal of Engineering, Technology & applied science research*. 2.5: 278–280.
10. Shenoy, M. (2013, May 16) “5 V power supply using 7805 voltage regulator with design”. Retrieved from www.electrosome.com/.
11. “Arduino Bluetooth Basic tutorial” (2016, May 23). Retrieved from www.create.arduino.cc.
12. Google and Open Handset Alliance n.d. Android API guide. <http://developer.android.com/bluetooth>. Accessed March 4, 2017.
13. Google and Open Handset Alliance n.d. Android API guide. <http://developer.android.com/maps/documentation/androiAPI/>. Accessed March 8, 2017.

A Cheiloscopy Approach for Unique Identification Among Indian Subpopulation

Shilpi Jain, V. Poojitha and Madhulika Bhatia

Abstract A biometric is formed on an individual's behavioural or physical features. The main approach is to uniquely identify humans. Identification by biometric factors finishes the complications related with customary approaches used for human identification. The biometric methods that are most commonly being used today are fingerprints, eye retina, iris, etc. This paper shows that just like fingerprints and lip prints are unique in nature and hence can be used as one of the measures to recognize individuals. Also, this paper shows that the nature of lips of an individual varies according to state one belongs to. The lip print samples are taken from different people in different states. After the enhancement of image, existing Sobel edge detection algorithm has been applied to detect the edges of lips. Thereafter, the numValue, i.e. featureValue of the lip print, is extracted and stored which depicts the uniqueness. The graphs have been plotted and examined.

Keywords Cheiloscopy · Lip print · Feature extraction
Biometric identification · Lip prints relation regionwise

1 Introduction

Human identification by making use of their biometric factors has attained great attention recently. Several measures and gestures have been suggested and examined for usage in human identification system. Even though extensive growth has been achieved in the field, it has been witnessed that sometime well-known biometric approaches also could not provide correct outputs in every real-life cir-

S. Jain (✉) · V. Poojitha · M. Bhatia
Computer Science and Engineering, Amity University, Noida, Uttar Pradesh, India
e-mail: jain.shilpi95@gmail.com

V. Poojitha
e-mail: poojithav95@gmail.com

M. Bhatia
e-mail: mbhadauria@amity.edu

cumstance. Human identification methods using biometric features are more reliable and effective as compared to customary validation methods and could be utilized in checking, transaction validation, info recovery, access controller, forensics and many more. Till now, fingerprints, retina, iris and face have been used for identification. Among these characteristics, face recognition has worked at a larger area amid the future users comparing to other kinds of characteristics. One major concern while using the face recognition scheme is that the scheme would not function properly if the object face is not fully exposed. Therefore, taking a minor part of face for advance recognition could be an efficient method to resolve the issue. The usage of lip print characteristics as a factor for biometric identification spans the zone amid the face and other biometric like voice [1].

Lip prints are typical lines and fissures in the forms of wrinkles and grooves existing in the zone of transition of human lip. The grooves on human lips are unique to each individual. Many other features of human are unique and are used for recognizing the identity of a user. But many times, these prints are not available and hence lip prints can be used at such moments. Our project aims to show the unique identification of human beings using lip prints and to determine the predominant lip print patterns in individuals of different states of India. In our study, we have shown the usage of two main algorithms: Sobel edge detection algorithm and fast match algorithm. The former is used to detect the edges of lip from the sample image print. The latter is used to acquire the numValue of the features of the lip print.

2 Literature Review

Shokhan and Khitam in the paper Biometric identification system using lip shape focus on detecting the lip shape. Edge detection method is been used to detect only the lip from the face. The edge detection operator smallest univalue segment assimilating nucleus (SUSAN) had been used. The scheme YCbCr is used next to change into desired colour scheme image. The next part of the algorithm used after changing the image to the colour scheme includes two steps which are locating the lips and defining the lip expression [2].

Lip of individual human being has been detected exclusively by Reshmi M.P. and Arul Karthick in the paper Biometric identification system using lips. At first, the face has been detected using Viola and Jone's algorithm as the algorithm detects the face rapidly. The second major step after face detection was lip extraction. It was done using various calculations using the source and the top right place of the face. After the elimination of the noise and extra lights, the mouth corner was extracted. The final step in the process is to recognize the lip. It is done using support vector machine (SVM) which is a classification technique and prepares a model that calculates the goal values of the data tested.

Bhattacharjee et al. in paper Personal identification from lip print features using a statistical model deals with the recognition of humans from numerical investigation

of the lip prints. Fast match and accurate match algorithms have been used. Feature matrix is been calculated. Feature matrix has been generated for upper and lower lip prints as well. These feature vectors were being compared to the test samples to either reject or accept [3].

Bandyopadhyay et al. describe the identification of human beings using lip prints in their paper. Initially, lip prints are taken on a white background, and it is changed to grey scale. The average grey level is computed using *k*-means clustering algorithm. Fast Fourier transform is used on the grey-scaled image thereafter. Average intensity value or initial threshold value is calculated using transformed matrix of intensity values and the total no. of pixels in the image. Later on, smoothening is done repeatedly using Gaussian filter to reduce noise of the image and to take just the significant grooves on the lip prints. The features of the lips such as vertical and horizontal grooves are detected using Sobel Edge Detector and Canny Edge Detector [4].

2.1 Tabular Representation

The tabular representation of all the literature work has been shown in Table 1.

Table 1 Gaps identified

S. No.	Paper	Methods used	Result	GAPS
1	Biometric identification system by lip shape by Shokhan M.H. and Khitam A.M.	Edge detection method	Identification of lip by extracting lip shape from the face	No study on lip prints was done
2	Biometric identification system using lips by Reshmi M.P. and V. J. Arul Karthick	Face detection: viola and Jone's algorithm lip detection: (ISODA) iterative self-organizing data analysis technique	Extracts lip from the face	Identification of individuals done by lip shape and not by lip prints
3	Personal identification from lip print features using a statistical model by Saptarshi Bhattacharjee	Canny edge detection and feature extraction: fast match and accurate match algorithms	Uniqueness of every individual is shown	Sample space used is very less. The data of only four people has been used
4	Feature extraction using lip prints by Samir Kumar Bandyopadhyay, S. Arunkumar, Saptarshi Bhattacharjee	Sobel and canny edge detections	The method detects the lips' images and recognizes the person based on lip	The lip print must be taken on white background only. It is less effective for forensics and real-time biometric identification of an individual
5	Comparison of lip prints in two different populations of India by Anila Koneru, R. Surekha, Ganesh Shreekanth Nellithady, M. Vanishree, DNSV. Ramesh and Ramesh S. Patil	Lip print patterns and the data are analysed using the z-test for proportions	Predominant features were classified between two populations	

3 Proposed Methodology

3.1 Subjects

The lip prints of four subjects from five states each are taken. A database namely lipPrints_SP_2017 is created as shown in Fig. 1.

3.2 Methodology

We proposed a novel way to show the uniqueness of lip prints and predominant lip print patterns in individuals of different states of India. We have taken four samples from four persons each from every state. This area clarifies the proposed methodology and system. The proposed technique comprises of number of stages, for example, loading of database, grey scaling, image enhancement and edge detection. Later features in the form of numeric values are retrieved. Then evaluation is done by taking the mean of the samples of each individual. The complete procedure is demonstrated in Fig. 2 [5].

		PERSON 1	PERSON 2	PERSON 3	PERSON 4
PUNJAB	Sample 1				
	Sample 2				
	Sample 3				
	Sample 4				
UTTARAKHAND	Sample 1				
	Sample 2				
	Sample 3				
	Sample 4				
BIHAR	Sample 1				
	Sample 2				
	Sample 3				
	Sample 4				
RAJASTHAN	Sample 1				
	Sample 2				
	Sample 3				
	Sample 4				
KARNATAKA	Sample 1				
	Sample 2				
	Sample 3				
	Sample 4				

Fig. 1 Lipprints_SP_2017

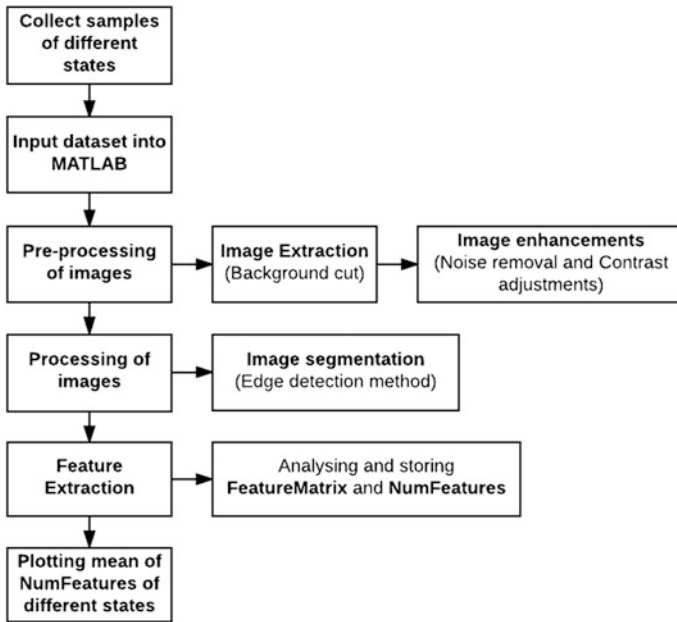


Fig. 2 Complete methodology

3.3 Collection of Lip Print Samples

The total number of samples is 80. A process, very similar to the ones, being applied in forensic laboratories for obtaining relative lip imprints was used.

- Each individual was asked to apply lipstick on their lips.
- Give the lip print on the paper by gently pressing the lips over it.
- After the collection of the lip prints, the photographs of the images have been taken by the camera.

3.4 Load Lip Print Samples

The images of lip print samples are loaded in MATLAB. The data set consists of four samples each of four individuals each from five states, i.e. Punjab, Uttarakhand, Bihar, Rajasthan and Karnataka. The self-created database lipprints_SP_2017 is used.

3.5 Preprocessing of Images

After all the images have been collected, the samples are loaded into MATLAB one at a time, and the data set is obtained for further processing. One of the lip print samples is shown in Fig. 3.

The image is converted into grey scale image [6] in which the hue and saturation information is eliminated, while the luminance is retained as shown in Fig. 4.

The grey-scaled image is further preprocessed by adjusting and enhancing the contrast of the image. The background is then cut from the preprocessed image [7]. The noise is removed by applying predefined function in MATLAB as shown in Fig. 5.

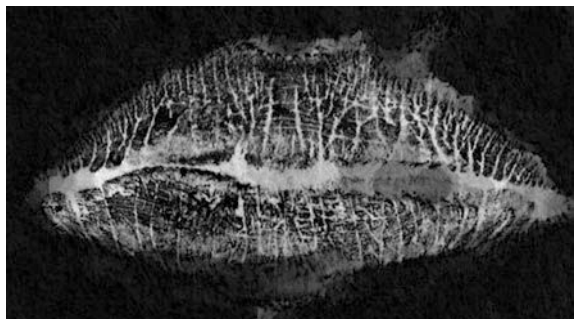
Fig. 3 Sample image



Fig. 4 Grey scaling of lip sample



Fig. 5 Background cut and noise removal of the preprocessed image



3.6 Image Segmentation

Sobel edge detection is applied to affirm each and every groove existing in the image. Sobel edge detection creates an image emphasizing edges [8]. The operator makes use of two 3×3 kernels that are convoluted along the novel image to compute estimates of derivatives—individually for horizontal and vertical changes [9]. Suppose \mathbf{A} is the source image, \mathbf{G}_x and \mathbf{G}_y are two images that at every point comprise the horizontal and vertical derivative estimates, respectively, and the calculations are as follows:

$$\mathbf{G}_x = \begin{bmatrix} +1 & 0 & -1 \\ +2 & 0 & -2 \\ +1 & 0 & -1 \end{bmatrix} * \mathbf{A} \quad \text{and} \quad \mathbf{G}_y = \begin{bmatrix} +1 & +2 & +1 \\ 0 & 0 & 0 \\ -1 & -2 & -1 \end{bmatrix} * \mathbf{A}$$

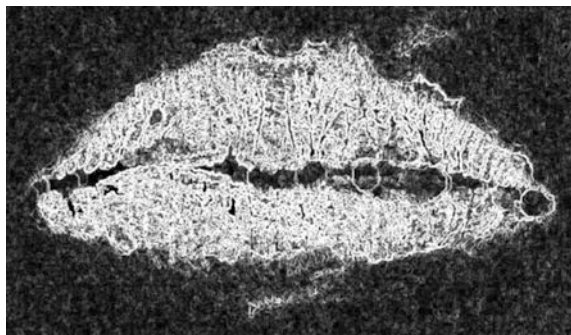
where $*$ symbolizes the 2-D signal processing complexity operation.

Sobel edge detection method basically works like as first-order derivate and computes the change of pixel intensities in edge region. As centre column is of 0, henceforth it does not contain the original values of an image but instead it computes the variance of right and left pixel values around that edge. This contributes extra weightage to the pixel values around the edge region. This upsurge the edge intensity, and consequently, it becomes enhanced when compared to the original image. After applying Sobel edge detection, the image obtained is shown in Fig. 6.

3.7 Feature Extraction

To effectively distinguish each individual, more features are extracted from the lip region. Each image goes under fast match algorithm. This creates a feature matrix. Also a single numValue is obtained which is stored in features. This value is observed for each sample. The mean of the numValue of features of the four samples of same person is taken [10].

Fig. 6 The edge detected image



4 Result

A total of 80 samples from five different states (Punjab, Uttarakhand, Bihar, Rajasthan and Karnataka) were taken. The mean of the numValue obtained is found to be unique for each individual. The unique values show the uniqueness of lip prints among different people. The mean of numValue is shown in Table 2.

A line chart graph is plotted by using the mean of numValue. The graph is shown in Fig. 7.

Also a similar pattern in lines is observed for the people belonging to a same state. The mean value of people from the same state is found to fall in a range which is different from the range of the value of people from another state. This proves that there is common pattern in lip prints of people who are from same place and different from other states (Fig. 8).

Table 2 Mean of numValue

	Person 1	Person 2	Person 3	Person 4
Karnataka	50,160	48,256	54,981	52,787
Uttarakhand	22,857	33,476	20,921	28,407
Bihar	95,354	77,672	86,098	76,821
Punjab	16,389	19,424	11,324	11,214
Rajasthan	126,662	148,728	119,053	108,114

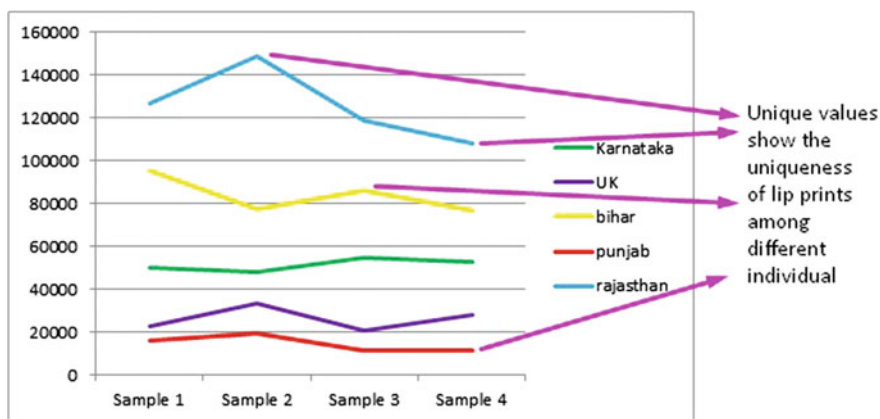


Fig. 7 Line chart graph showing the uniqueness of lip prints

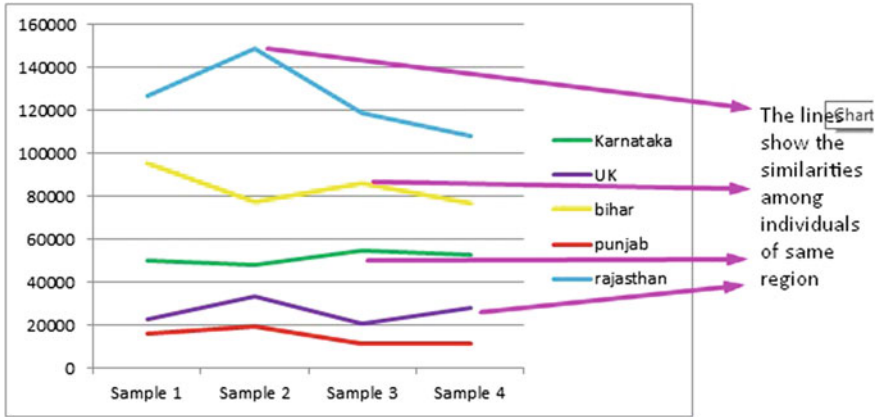


Fig. 8 Line chart graph showing the common pattern within same state and different from different states

5 Conclusion

Cheiloscopy is comparatively a new field among the large number of identification tools available to the forensic expert. Very few literature works have been done on the lip prints for unique identification, but there exist many loopholes. In this paper, feature extraction of lip prints has been used for unique identification of every individual instead of calculating shape and densities for more accurate and better results. Feature extraction provides very descriptive, easy and accurate results than compared to conventional methods. Study of patterns of lip prints of different individuals of different states of India shows significant difference among different regions. Research done on considerably more samples and population leads to the conclusion that every individual lip prints are unique and significantly differs from region to region in India. This result can help us in the future as in forensics a lip print found in crime scene can be matched with the pre-existing database of people to check the involvement or presence of person at the crime scene.

References

1. Kasprzak J, Leczynska B (2001) Chieloscopy. "Human identification on the basis of lip Prints" (in Polish). CLK KGP Press, Warsaw, 2001.
2. Shokhan, M. H., and A. M. Khitam. "Biometric Identification System by Lip Shape." International Journal of Advanced Computer Research 5.18 (2015): 19.
3. Bhattacharjee, Saptarshi, S. Arunkumar, and Samir Kumar Bandyopadhyay. "Personal identification from lip-print features using a statistical model." arXiv preprint [arXiv:1310.0036](https://arxiv.org/abs/1310.0036) (2013).

4. Bandyopadhyay, Samir Kumar, S. Arunkumar, and Saptarshi Bhattacharjee. "Feature Extraction of Human Lip Prints." arXiv preprint [arXiv:1312.0852](https://arxiv.org/abs/1312.0852) (2013).
5. Poojitha, V., et al. "A collocation of IRIS flower using neural network clustering tool in MATLAB." *Cloud System and Big Data Engineering (Confluence), 2016 6th International Conference*. IEEE, 2016.
6. Deepika, C. Lakshmi, and A. Kandaswamy. "An algorithm for improved accuracy in unimodal biometric systems through fusion of multiple feature sets." *ICGST-GVIP Journal, ISSN (2009): 33–40*.
7. Ives, Robert W., et al. "A multidisciplinary approach to biometrics." *IEEE Transactions on Education* 48.3 (2005): 462–471.
8. Sandhu, Parvinder S., et al. "Biometric methods and implementation of algorithms." *International Journal of Electrical and Electronics Engineering* 3.8 (2009): 492–497.
9. Bhatia, Madhulika, et al. "Implementing edge detection for medical diagnosis of a bone in Matlab." *Computational Intelligence and Communication Networks (CICN), 2013 5th International Conference on*. IEEE, 2013.
10. Bhatia, Madhulika, et al. "Proposed algorithm to blotch grey matter from tumored and non tumored brain MRI images." *Indian Journal of science and Technology* 8.17 (2015).

Weighted Transformation and Wavelet Transforms-Based Image Resolution and Contrast Enhancement

N. Prasanthi Kumari, T. V. Hyma Lakshmi, D. Bhavani
and G. Mohana Durga

Abstract Proposed weighted transformation and wavelet transforms-based image resolution and contrast enhancement can be described in two phases. In first phase, input low-resolution image is resolution-enhanced using lifting–stationary wavelet transforms. In this process, input image is decomposed into low-frequency and high-frequency components using lifting and stationary wavelet transforms, and high-frequency components are bi-cubic interpolated to improve the resolution. Finally, inverse lifting wavelet transform is applied to get the high-resolution image. In second phase, resolution-enhanced image is applied to contrast enhancement using weighted transformation function which is obtained from adaptive histograms and mean values from similarities and dissimilarities. Proposed method shows the superiority in experimental results in both quantitatively and visually. Proposed methods are compared with the existing and method with mean square error, Peak signal to noise ratio, noise estimation and entropy and also with visual results.

Keywords Lifting wavelet transform · Stationary wavelet transform
Weighted transformation functions · Peak signal to noise ratio

1 Introduction

Image enhancement is the process of improving the image quality for human perception or to provide a better transformation representation for future automated image processing. Recently, many image enhancement techniques have been

N. Prasanthi Kumari
ECE Department, COES, UPES, Dehradun, Uttarakhand, India
e-mail: prasanti@ddn.upes.ac.in

T. V. Hyma Lakshmi (✉) · D. Bhavani · G. Mohana Durga (✉)
ECE Department, S.R.K.R. Engineering College, Bhimavaram, Andhra Pradesh, India
e-mail: tvhymalakshmi@gmail.com

developed which include both resolution and contrast enhancement using wavelet transforms and different adaptive histogram equalization techniques.

Resolution enhancement can be defined as the improvement of ability to bring out its details of an image. Hasan Demerol and Gholamreza Anbarjafari proposed image resolution enhancement using discrete wavelet transform (DWT) [1]. This methodology decomposes the image into high-frequency pixels sub-band and low-frequency pixels sub-band by applying DWT, and high frequency subbands are interpolated using bi-cubic interpolation. However, during this method, noise enhancement is its significant result. To reduce that noise increment, they introduced SWT as an intermediate stage and proposed image resolution enhancement using DWT and SWT [2]. T.V. Hyma Lakshmi et al. proposed new resolution enhancement technique using DWT and Gaussian mixture model to get sharper edges and smoother details [3]. Later they proposed image resolution enhancement (RE) technique using non-decimated wavelet transform and Gaussian mixture model to overcome the shift variance, time variance, and downsampling in DWT [4].

Contrast enhancement is an improvement of the image quality to finer and more acceptable brightness level for feature extraction or image interpretation. Contrast enhancement techniques have been classified into two principle groups: spatial-domain, transform-domain. Histogram equalization is a method of contrast adjustment [5] which utilizes the image histograms. This method increases the global contrast of images with the help of a gray level transform which tries to flatten the resulting histogram so that processed image looks better. However, HE fails to preserve the mean brightness.

Shashipoddar and SumanTewary introduced [6] contrast enhancement(CE) using adaptive histogram equalization with the help of non-parametric method. Non-parametric method modifies histogram equalization, (NMHE) effectively handles the histogram spikes, and lowers the distortions in smooth regions. without empirical adjustments of parameters. However, this technique provides limited performance for low contrast pictures having finer details. T.V. Hyma Lakshmi et al. proposed image resolution and contrast enhancement using wavelet transforms, and contrast limited adaptive histogram equalization [7] which is CE and RE method and uses the combination of both DWT and SWT for RE along with CLAHE for CE. Drawbacks of CLAHE-DWT are overcome by this CLAHE – DWT and SWT method. Later T.V. Hyma Lakshmi et al. proposed novel Image Resolution and Contrast Enhancement Using SWT and lifting wavelet transform and CLAHE [8] to improve computational efficiency and execution speed.

In this paper, we introduce a new contrast and resolution enhancement technique which combines LWT and SWT for resolution enhancement and weighted transformation functions for contrast improvement.

2 Proposed Methodology

Proposed method uses the combination of LWT–SWT for resolution enhancement which is described by flow chart in Fig. 1. Input image is decomposed using both LWT and SWT with Haar mother wavelet to get the low-frequency sub-bands and high-frequency sub-bands. High-frequency sub-bands consist of edge information. Edge in image can be described as a sudden change in brightness value. All three sub-bands which are called high-frequency sub-bands provide the edge information in horizontal, vertical, and diagonal directions, respectively. Downsampling causes information loss in LWT to produce high-frequency sub-bands. So to overcome this loss, SWT has been used. Bi cubic interpolation has been applied to upsample the high-frequency sub-bands of LWT applied image so that these sub-bands can be added to high-frequency sub-bands of SWT applied image. Finally, by taking the inverse, LWT high resolution image is obtained.

Now, the image is resolution-enhanced, but contrast of image is still poor. Weighted transformation function is used to improve the contrast of image. Let $I(i, j)$ be the original image of size $M \times N$. In the first step, image I is decomposed into different levels with down sampling by 2. Let I^k be the image at k th level. Image decomposed completely at different levels ends up in different mapping functions. To compute the effective transformation function every transform function is allotted some weights. Let h_b^k be the histogram of I^k to increase the dynamic range bins having least contribution are filtered. After this modified histogram is obtained. Final modified histogram is [9] defined as

$$hm_b^k = (1 - \mu)ht_b^k + \mu d_b^k, \tag{1}$$

where μ is the weighting factor and d_b is the uniformly distributed histogram. ht_b^k is obtained by removing bins having less value than threshold. The transformation function is generated as

$$f_b^k = [(B - 1)C_b^k + 0.5]. \tag{2}$$

The average histogram is calculated computed using modified histogram and transformation function as

$$\bar{h}_b^k = \frac{1}{k} \sum_{k=0}^{K-1} hm_b^k. \tag{3}$$

The weights are allocated corresponding to the distance of modified histogram from mean histogram. Higher values of weights are given to the histograms which are nearer to the average histogram. The weighting function is computed as

$$wg_b^k = \frac{\sum_{k=0}^{K-1} \frac{1}{|\bar{h}_b^k - hm_b^k|}}{|\bar{h}_b^k - hm_b^k|} \tag{4}$$

Final transformation function is computed as

$$\bar{T}_b = \sum_{k=0}^{K-1} f_b^k wg_b^k \tag{5}$$

The final smooth transfer function \hat{T}_b is generated as

$$\hat{T}_b = \alpha \bar{T}_b + (1 - \alpha) \bar{T}_{b+1}, \tag{6}$$

where $\alpha = 1/2$ is the weighting factor. The enhanced image is obtained after applying \hat{T}_b on original image

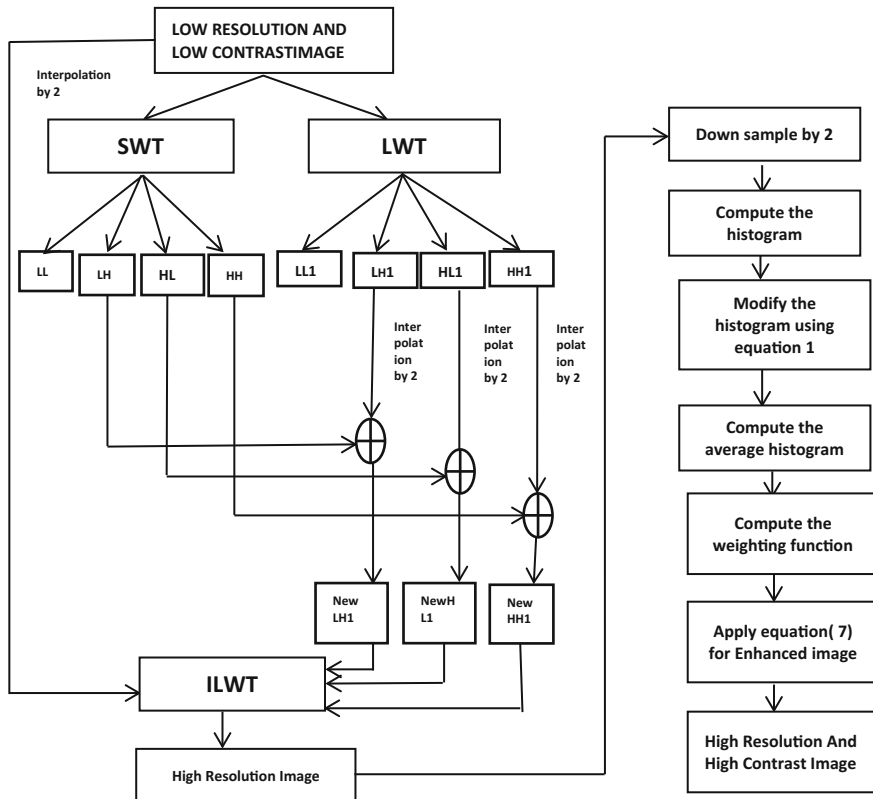


Fig. 1 Flow chart of proposed method results

$$E(i,j) = \widehat{T}_b(I(i,j)). \tag{7}$$

Proposed algorithm is compared with other existing methods on various images for visual results and quantitative results using PSNR, mean square error (MSE) as the performance indexes [10].

PSNR is defined as

$$PSNR = 10 \log_{-10} (255^2/MSE) \tag{8}$$

Where MSE is the mean square error and it is defined as

$$MSE = \frac{1}{MN} \sum_{i=0}^{m-1} \sum_{j=0}^{n-1} [I(i,j) - K(i,j)]^2 \tag{9}$$

Here M, N are the rows and columns of image and I, K are original and enhanced images respectively. Fig. 2 shows proposed method performance with existing methods on test image. From that figure, it can be noticed that NMHE gives better performance on contrast enhancement but at expense of information loss. DWT-SWT gives better enhancement qualitatively but poor performance in

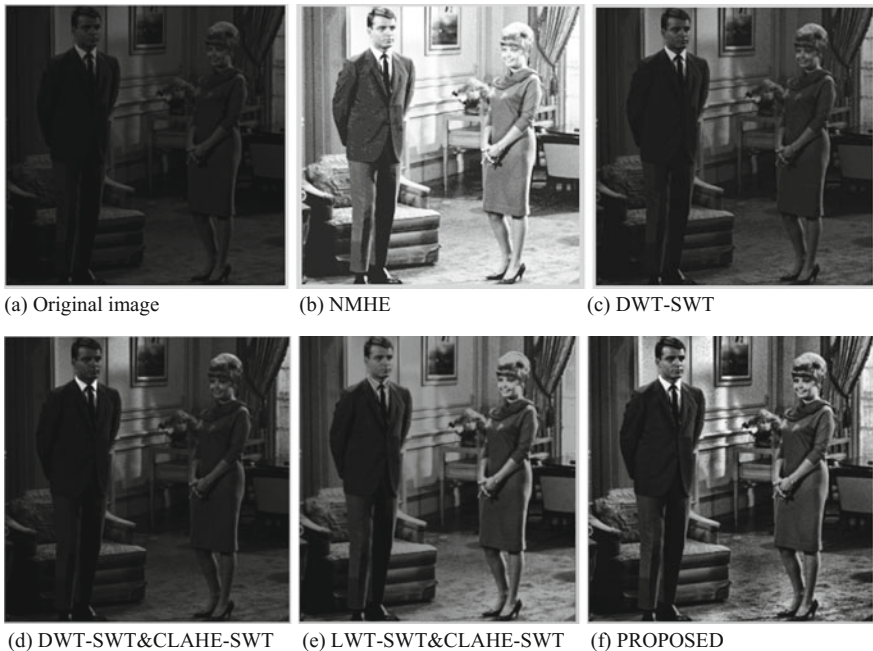


Fig. 2 Test image

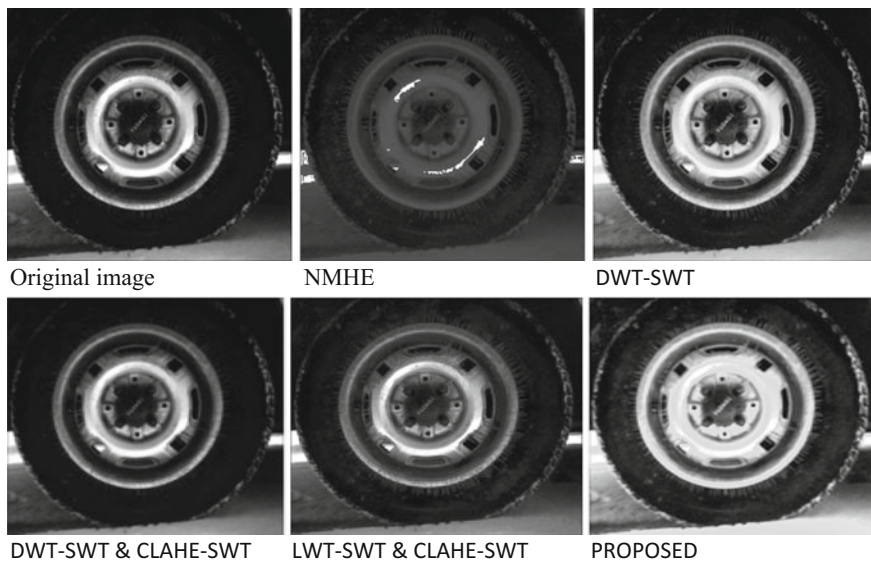


Fig. 3 Test image tire

Table 1 Quantitative analysis

	Techniques	PSNR (dB)	MSE
Bond image	NMHE	43.57	2.8581
	DWT-SWT	53.85	0.2680
	DWT-SWT and CLAHE-SWT	62.79	0.186
	LWT-SWT and CLAHE-SWT	65.79	0.086
	Proposed	68.98	0.0082
Tire image	NMHE	53.25	0.3077
	DWT-SWT	58.92	0.1834
	DWT-SWT and CLAHE-SWT	64.68	0.056
	LWT-SWT and CLAHE-SWT	68.79	0.0086
	Proposed	70.62	0.0021

contrast enhancement. From Figs. 2, 3 and Table 1, it is clear that our proposed method dominates the other existing methods both qualitatively and quantitatively.

Table 1 shows the quantitative comparison of different existing methods over proposed method. Table 1 shows the importance of proposed method. It is to be noted that all the other existing methods suffer the loss of information; especially, NMHE has significant information loss. Higher PSNR values and lower MSE values state the better performance of proposed method.

3 Conclusion

In this paper we proposed image resolution and contrast enhancement methods, which combine LWT with SWT for resolution enhancement and weighted transformation function for contrast enhancement. In this method, the image is decomposed into sub-bands by both LWT and SWT and high frequency sub-bands of LWT are interpolated and combined with high frequency sub-bands of SWT for resolution enhancement, and weighted transformation function improves the contrast of image. Visual results and quantitative results (PSNR, MSE) show the superiority of proposed method than existing methods.

References

1. Hassan Demirel and Gholamreza Anbarjafari. "Discrete Wavelet Transform-Based Satellite Image Resolution Enhancement", IEEE transaction on geosciences and remote sensing, vol. 49, NO. 6, June 2011.
2. Hassan Demirel and Gholamreza Anbarjafari. "Image resolution enhancement by using discrete and stationary wavelet decomposition" IEEE transactions on image processing may 2011.
3. T.V. Hyma Laksmi, T. Madhu, E V Krishna Rao, V. Lakshmi Mounica, "Satellite Image Resolution Enhancement Using Discrete Wavelet Transform and Gaussian Mixture Model", International Research Journal of Engineering and Technology, Volume: 02 Issue: 04, July-2015, Page 95–101.
4. T.V. Hyma Laksmi, T. Madhu, E V Krishna Rao, K.Ch. Sri Kavya, "Satellite Image Resolution Enhancement Using Non-Decimated Wavelet Transform and Gaussian Mixture Model", International Journal of Applied Engineering Research, Volume 10, Issue Number 19 (2015) Pages: 40746–40753.
5. M. Abdullah-Al-Wadud, Md. Hasanul Kabir, M. Ali Akber Dewan, and Oksam Chae, "Dynamic histogram equalization for image contrast enhancement" IEEE Transactions on Consumer Electronics, Vol. 53, No. 2, MAY 2007, pages: 593–600.
6. Shashipoddar and sumanTewary. "Non parametric modified histogram equalization for contrast enhancement". IET image process, 2013, vol. 7, issue. 7, pp. 641–652.
7. T.V. Hyma Laksmi, T. Madhu, K.Ch. Sri Kavya, Shaik. Esub Basha "Novel Image Enhancement Technique Using CLAHE and Wavelet transforms", IJSET, vol. 5, issue no. 6, pp 507–511.
8. T.V. Hyma Lakshmi, T. Madhu, K.Ch. Sri Kavya, A. Geetha Devi "Image Resolution and Contrast Enhancement Using Wavelet Transforms and Contrast Limited Adaptive Histogram Equalization", International Journal of Computer Science and Information Security (IJCSIS), Vol. 14, No. 9, September 2016.
9. S. Poddar, S. Tewary, D. Sharma, V. Karar, A. Ghosh, and S. K. Pal, "Non-parametric modified histogram equalisation for contrast enhancement," IET Image Processing, vol. 7, no. 7, pp. 641–652, 2013.
10. T. V. Hyma Lakshmi, T. Madhu, K.Ch. Sri Kavya, A. Geetha Devi "Image Enhancement using Lifting and Stationary Wavelet Transforms and Contrast limited adaptive Histogram Equalization", International conference on advances in the field of health, safety, fire, environment, allied sciences and Engineering (HSFEA 2016) November 18–19, 2016, UPES, Dehradun.

Author Biographies



N. Prasanthi Kumari mem IEEE., is working as an Associate Professor in the Department of Electronics, Instrumentation and Control Engineering at in UPES Dehradun. She has more than 16 years' experience of teaching under-graduate and post-graduate engineering students. Her areas of research are communication, RF and Antenna Design, VLSI Design, metamaterials. She has published 12 papers in journals and conferences of national and international repute and has reviewed several papers for conferences and journal.



T. V. Hyma Lakshmi obtained her M.Tech.(ECE).. from JNTUCE, Ananthapur and B.E. (ECE) from S.R.K.R, Bhimavaram. Presently working as Assistant Professor in S.R.K.R. Engineering college Bhimavaram and pursuing Ph.D. Program from K L University in the area of Image Processing.



D. Bhavani obtained her M.Tech (ECE) from CMRIT, Hyderabad, and B.E. (ECE) from Adems Engineering College, Khammam. She is presently working as Assistant Professor in SRKR Engineering College, Bhimavaram.



G. Mohana Durga obtained her M.Tech.(ECE)., from S.R.K.R. Engineering College, Bhimavaram and B.E. (ECE) from Vishnu Engineering College, Bhimavaram. Presently working as Assistant Professor in S.R.K.R. Engineering college Bhimavaram.

Fat Tree NoC Design and Synthesis

Arpit Jain, Alok Kumar Gahlot, Rakesh Dwivedi, Adesh Kumar and Sanjeev Kumar Sharma

Abstract Network on chip (NoC) architecture is the promising solution over the limitations of bus-based system. The on-chip communication is addressed by several NoC topological structures and guarantees reliable, fast, and scalable design. The paper addresses the design of fat NoC tree topology that can process the intercommunication from top to root nodes. The tree NoC is indirect topology in which the routers are not dependent on the number of ports. The design is developed in Xilinx ISE 14.2 software with the help of VHDL language, and the design is targeted on Virtex-5 FPGA. The hardware parameters and timing values are estimated to support the functionality of the design.

Keywords Interprocess communication
Field-programmable gate array (FPGA) · Fat tree network on chip (NoC)

1 Introduction

Network on chip (NoC) [1, 2] is the network technology for interconnecting high-performance computers in parallel. The NoC architecture [3, 4] follows the topological structure. The NoC uses the wired link to interconnect and is shared by many signals. The links of the NoC work simultaneously with respect to different data packets' size, and high level of pipelined and parallel processing [5] is required

A. Jain · A.K. Gahlot · R. Dwivedi
Department of Computer Science and Information Technology,
Teerthanker Mahaveer University, Moradabad, India

A. Kumar (✉)
Department of Electronics, Instrumentation and Control Engineering,
University of Petroleum & Energy Studies (UPES), Dehradun, India
e-mail: adeshkumar@ddn.upes.ac.in

S.K. Sharma
Department of Computer Science & Engineering,
JP Institute of Engineering & Technology, Meerut, India

to execute the operations in faster way. The complexity of the integrated electronics systems and ICs is increasing day by day. NoC is the solution over complex integrated system that can provide the better performance and throughput. NoC provides scalable architecture [6, 7] and good performance in comparison with tradition technique used for communication architecture such as shared bus [8], bridges, segmented bus, point to point wires. The routing and addressing of the NOC can be done in such a way that it can support high level of parallelism, and multiprocessor system on chip (MPSoC) interconnections [9] can be configured in scalable design. The methods of networking and on-chip communication techniques are used to configure the specific NoC architecture. The topology of NoC defines the way of connecting the nodes. It can affect the NoC latency and bandwidth requirements. The global interconnection structure helps in reduction of signal latency and wiring of the design. There are many topologies existing for NoC design such as mesh, tree, ring, butterfly, and hybrid topologies. The selection of topology is based on applications and system requirements. The 2D mesh topology [10, 11] is simple and regular in nature and most applicable because of small length of wire among nodes. The NoC communication architecture is following the concept of message transfer among the transmitting and receiving end as response message. The transmitting node transmits the message in the form of packets. The packet data [5, 12] is small and uses small channels. That is why the resource utilization in packet data is small. The data packet is consisting of three main parts: header section, payload section, and tail bit. The information of the destination nodes is addressed by the header and creates the links between source and destination nodes, based on routing mechanism and addressing. The payload section is having actual data required to transmit from sender to receiver node. The tail bit indicates that the packet transmission is ended. The important and fundamental concern in the NoC is fault tolerance [9, 10]. The system failure during runtime and IC defects during the manufacturing and fabrication are inevitable and impossible to remove from the system. The packet data transmission improves the fault tolerance, and NoC follows the fault-tolerant routing mechanism to control the packet transmission and avoids the faulty or defective areas instead of the whole system considered as faulty.

2 Fat Tree NoC

The tree networks [10] are proposed by Charles E. Lesierson 1985. Several nodes are connecting from top to bottom in tree NoC and follow the strategy based on parent child relationship. It can be a layered communication from one parent node to next child node. The number of links connected in the tree network from the top to bottom is equal to the links from bottom to top as siblings are connected in the same way. In the top of the tree network, the links become fatter and the root nodes in the tree are having most of the links in comparison with other topologies. The fat tree structure is shown in Fig. 1. It supports eight root nodes, and its associated

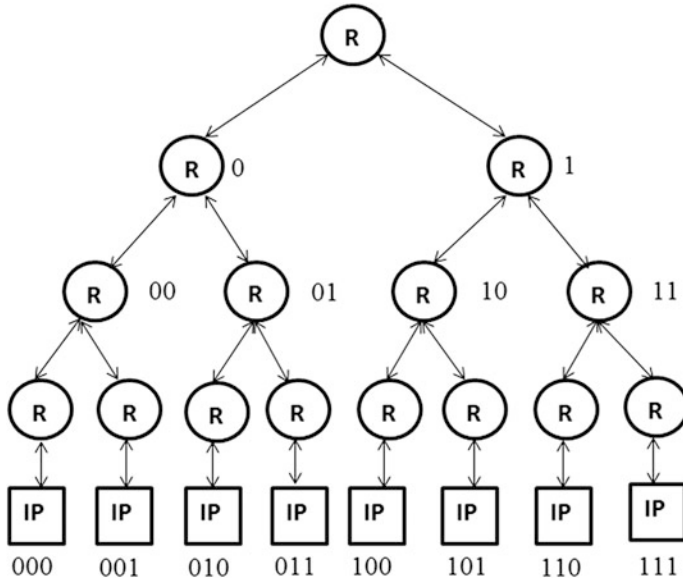


Fig. 1 Fat tree NoC

routers are addressed. The parent router is having its branch “0” and “1” and further distributed in two routers corresponding to each branch. The routers are addressed as “00”, “01” “10”, and “11”. In the last stage, the each router is associated with two roots or child node. The addressing and distribution from the parent to child and again subchild form a tree. The eight cluster nodes in root of the tree NoC are addressed as “000”, “001”, “010”, “011”, “100”, “101”, “110”, and “111”.

3 Results and Discussions

The hardware results are simulated in Xilinx ISE 14.2, and waveform is obtained from Modelsim 10.0 student edition. The Xilinx extracted RTL is presented in Fig. 2. It presents the detailed function of all the pins depicted in the RTL and used in the designed chip. The detail of all these pins is listed in Table 1.

The waveform is obtained from the Modelsim software and verified for different test cases. The simulation waveforms are presented in Fig. 3a–c which correspond to test data 1, test data 2, and test data 3, respectively.

Test data 1: In the simulation waveform, reset = “1”, then forced to run. Clk is applied directly and reset = “0”. The source_node = “001”, target_node = “101”, write = “1” and read = “0”, data_in = 1’hAA00AA00AA00AA00 (hexadecimal) or data_in = “10101010000000001010101000000000101010100000000101010100000000”

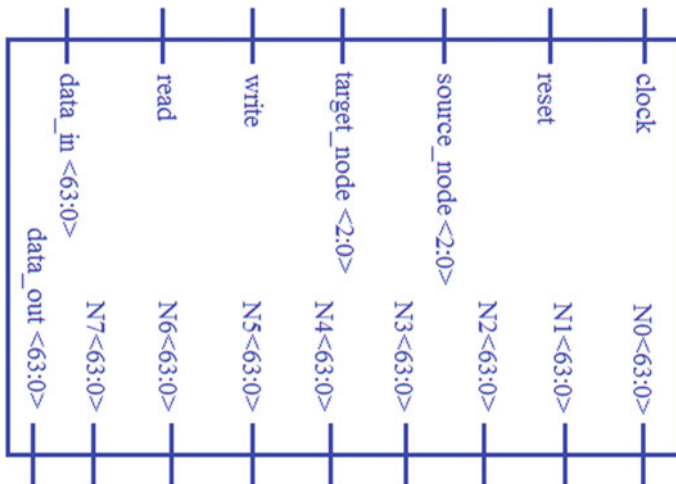


Fig. 2 RTL view of chip

Table 1 Pin explains in the fat tree NoC design

Pins	Description
Reset	It is the input applicable to reset the contents in all the communicating nodes
Clk	It is the default input for the synchronization and associated with all the nodes
source_node (2:0)	It presents the address of the source nodes. In our design, it is of 3 bit
destination_address (2:0)	It presents the address of the targeted communicating nodes. In our design, it is of 3 bits
N ₀ (000)	It is the I/O port corresponds to node 0 with address “000” and 64-bit data transfer
N ₁ (001)	It is the I/O port corresponds to node 1 with address “001” and 64-bit data transfer
N ₂ (010)	It is the I/O port corresponds to node 2 with address “010” and 64-bit data transfer
N ₃ (011)	It is the I/O port corresponds to node 3 with address “011” and 64-bit data transfer
N ₄ (100)	It is the I/O port corresponds to node 4 with address “100” and 64-bit data transfer
N ₅ (101)	It is the I/O port corresponds to node 5 with address “101” and 64-bit data transfer
N ₆ (110)	It is the I/O port corresponds to node 6 with address “110” and 64-bit data transfer
N ₇ (111)	It is the I/O port corresponds to node 7 with address “111” and 64-bit data transfer

(continued)

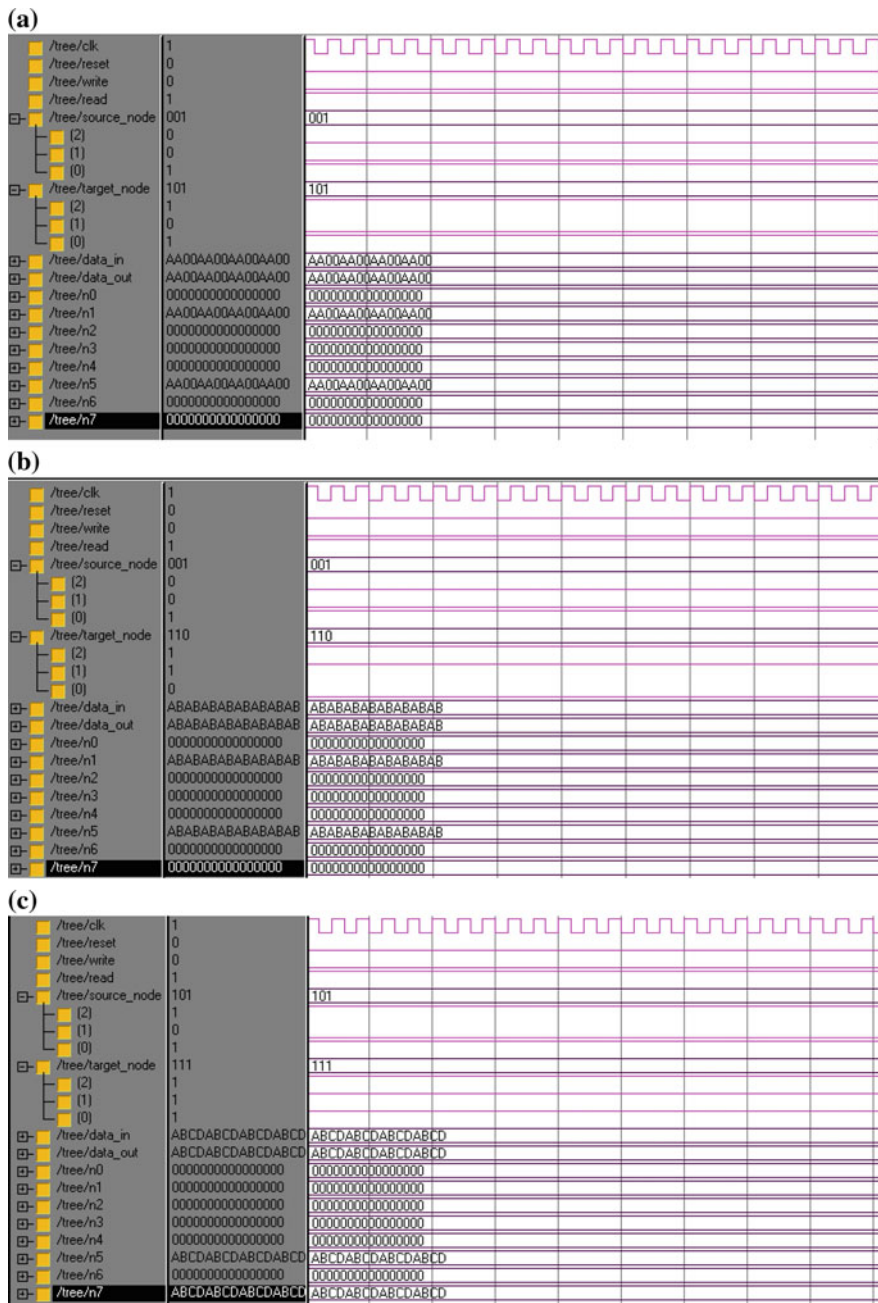


Fig. 3 a Simulation waveform for test data 1. b Simulation waveform for test data 2. c Simulation waveform for test data 3

Table 2 Device utilization summary

Hardware	Description (%)
Slices' usage	105 out of (12,480) 0.84
Slice flip-flops' usage	345 out of (12,480) 2.76
Four-input LUTs' usage	138 out of (403) 34.24
Bonded IOBs' usage	138 out of (172) 80.00
Value of GCLKs	1 out of (32) 3

Table 3 Timing-related parameters' summary

Timing parameters	(2 × 2 × 2)
Period (minimum)	1.270 ns
Frequency (maximum)	400 MHz
Minimum clock duration as input arrival time	1.832 ns
Maximum duration after clock arrival	2.122 ns
Total memory utilization	128,649 kB

5 Conclusions

The paper presented the flat tree NOC design that supports eight nodes in root, and the performance of the design is verified on Virtex-5 FPGA, xc5vlx20t-2-ff323 device. The design is experienced under several test cases. The Modelsim waveform shows the data transfer for the same cluster configuration. The FPGA parameters relating to hardware support and timing are also analyzed. The architecture is modular and scalable in nature. It can be used to form a large scale tree in which multiple nodes can communication in parent to root nodes. The forthcoming research can be in the direction of network security algorithms and integration with large cluster NoC configuration.

References

1. Andreas Hansson, Kees Goossens and Andrei Radulescu “A Unified Approach to Mapping and Routing on a Network-on-Chip for Both Best-Effort and Guaranteed Service Traffic” *Hindawi Publishing Corporation VLSI Design*, pp 1–16, 2007.
2. Adesh Kumar, Piyush Kuchhal, Sonal Singhal “Network on Chip for 3D Mesh Structure with Enhanced Security Algorithm in HDL Environment” *International Journal of Computer Applications (IJCA)* Vol. 59– Number 17, pp 6–13, December 2012.
3. Bergamaschi RA, Cohn J “The A to Z of SoCs. In: *Proceedings of the IEEE/ACM international conference on computer aided design (ICCAD)*”, Yorktown Heights, pp 791–798, 2002.
4. C. Neeb, M.J. Thul, N. When, “Network-on-Chip-Centric Approach to Interleaving in High Throughput Channel Decoders”, *IEEE International Symposium on Circuits and Systems (ISCAS)*, Kobe, Japan, pp 1766–1769, May 2005.
5. D. Wiklund, L. Dake Liu, “SoCBUS: switched network on chip for hard real time embedded systems,” in *Parallel and Distributed Processing Symposium*, pp. 8–9, April 2003.

6. David Atienza, Federico Angiolini, Srinivasan Murali, Antonio Pullinid, Luca Benini, Giovanni De Micheli, "Network-on-Chip design and synthesis outlook", *Integration, the VLSI journal Elsevier* Vol. 41 pp 340–359, 2008.
7. Dally WJ, Towles B "Route packets, not wires: on-chip interconnection networks". In: *Proceedings of the design automation conference (DAC)*, Las Vegas, pp 684–689, 2001.
8. Lu R, Koh C-K "Samba-BUS: high performance BUS architecture for system-on-chips". In: *Proceedings of the IEEE/ACM international conference on computer aided design (ICCAD)*, San Jose, pp 8–12, 2003.
9. Erika Cota, Alexandre de Moraes Amory, Marcelo Soares Lubaszewski Book "Reliability, Availability and Serviceability of Networks on Chip" *Springer New York Dordrecht Heidelberg London*, 2, pp (1–24), 2012.
10. Konstantinos Tatas, Kostas Siozios Dimitrios Soudris, Axel Jantsch Book Ch-1, Ch-2 "Designing 2D and 3D Network-on-Chip Architectures" *Springer New York Heidelberg Dordrecht London*, pp 1–45, 2014.
11. M. Jabbar, D. Houzet, "3D architecture implementation: a survey", in *IP Embedded System Conference (IP-SOC)*, pp. 1–5, 2011.
12. M. Dall'Osso, G. Biccari, L. Giovannini, D. Bertozzi, L. Benini, "Xpipes: a latency insensitive parameterized network-on-chip architecture for multi-processor SoCs," in *International Conference on Computer Design (ICCD)*, pp. 45–48, 2012.

Big Data Issues in Medical Healthcare

Manish Madhava Tripathi and N.K. Joshi

Abstract Due to rapid growth of digitization process, big data size is increasing day by day. In healthcare system, electronic patient data is maintained in hospitals for years of years. As medical data contain patient information, its size and sensitivity increases. These medical data can be accessed after long time as per need of the patient, and therefore the data must be secure for long time as well as can be accessed with ease and speed. In this paper, we have discussed some of the challenges due to rapid growth of digital data and have tried to give solution for it. Further we have given a mechanism to distinguish between useful and waste data.

Keywords Big data · Security · Data mining · Healthcare · Medical data

1 Introduction

Due to the advent of the telecommunication technology, medical data can be transferred from one place to another place all across the countries. In this paper, we first describe some technical implementation of these systems to motivate security and privacy initiatives in medical systems [1].

M.M. Tripathi (✉)
Integral University, Lucknow, India
e-mail: mmt@iul.ac.in

N.K. Joshi
Uttaranchal University, Dehradun, India

1.1 Electronic Health Record (EHR) or Electronic Patient Records (EPR)

With the help of EPR or EHR also known as electronic medical record (EMR), current paper-based medical records or documents are available in digital form so that it can easily accessible online. Physician, nurses, insurance premium providers, and patients all of them can easily access their medical records online. Medical record includes physician notes and prescriptions, MRI, clinical lab results, etc.

Benefits of using EPR or EHR:

1. Minimizes the error rate due to inconsistency and illegibility of terms.
2. Records in the form of EPR can easily backed up then traditional paper-based records which in turn prevent the risk of data loss.

Implementation of EPR requires a local database acquired by hospitals that maintains a record for patients at certain location. Those databases can be connected by Internet for data transmission so that a doctor at one hospital may view a patient's information from another hospital [2]. For example, Vendorbilt and PCASSO patients can be transmitted to a patient portal, a patient's data physician, home-based patient, and other healthcare service providers.

1.2 Remote Patient Monitoring at Home

Every regular patient has been provided some medical equipments to sense his body and report to a system. In this way, body care of the patient can be regularly maintained through this monetary system. This data can be remotely transferred.

1.3 A Hybrid/Integrated System

To provide the benefits of the above two techniques, both hybrid systems are integrated. The sensor data sends the regular update about the patient health to a central monetary system. In this way, a history and track record of the patient health can be recorded in the centralized system [3].

All the technologies described above improve the quality of healthcare delivery. Data quality can be defined as "Data that are fit for use by data consumers." In medical, data consumers may be doctors, nurses, insurance providers, patients, etc. Quality of healthcare data specifies three but most important parameters:

Trustworthiness means to make decisions about treatment regarding the trust of information.

Reliability means on the basis of data, how the system will perform its intended functionality. This valuable data enhances decision making in medical industry in order to proceed the treatment on the basis of reports.

Security: Due to rapid development of technologies for transfer of individual data recorded by sensors over the Internet has increased, the security issues and privacy of the patient health data which must be balanced and analyzed to provide customer satisfaction.

2 Security and Privacy Issues

Adoption of big data in medical industry provides many benefits with the help of various technologies discussed above and also in previous Sect. 2 privacy and security issues must be examined in order to promote electronic healthcare big data industry [4, 5]. Some of them can be pointed out as:

- When and how the data is stored
- Data transfer security and also data at rest
- Real-time security and privacy-preserving analytics
- Access rights to data
- Governing policies
- Future evaluation and current legislations (regulations) and
- Data analysis rights

Many researchers describe two main issues in healthcare big data security and privacy as:

- First, how medical big analytics have to be implemented to prevent the leakage (unauthorized data disclosure or access) of patient's data.
- Second, how medical big data implementation can retain the patient privacy.

To solve above issues, there are five dimensions that can be used as a framework in medical (healthcare) big data:

- Patient privacy risk factors
- Legal and ethical factors
- Preventive practice factors
- Data application factors
- Security threat and data breach factors

2.1 Privacy and Security Issues in Healthcare Information System (HIS)

As per survey, “70–75% of patients are concerned about healthcare sites sharing information without their permission. (Raman 2007).” “Possibly this is because medical data disclosure is the second highest reported break (Hasan and Yurcik).” Some of the researchers also describe security and privacy issues in the form of medical information system are:

1. Threats to Privacy of Information

Threat can be divided into two areas as follows:

(1) Organizational threats and (2) Systematic threats.

Organizational threat arises when some external person get access of the patient data [6]. This external person may be hacker, who do not have right to access any data from the organization. Relatives of organisation employee can easily get access.

Systematic threats arises when some organization member crosses his access limit, and access the data for which he do not have access right (NRC 1997).

2. Web-enabled Healthcare Information Security

Microsoft and Google have opened the Web-based healthcare system and banking access. This also has created security risk to healthcare system and patient’s personal and sensitive information of his health.

Mobile devices have also created a new domain of risks to patient’s data [7]. Nowadays mobile phones come with very high features. By locating the position of the person having mobile phone can harm the patient data. Smart phones also have high resolution camera in it. Intruder can at least take the snapshots of the patient record and can misuse in the future.

3. Information Security for Authorized Data Access (Disclosure)

In medical, it is necessary to share patient data from hospitals to outside industries that specifically involved in health-related cases. When patient data is released, there is chances of its leakage also, so very secret procedure should be adopted at the time of release of the medical data of the patient. This data leakage may affect the socioeconomic condition of the patient. Technological advancement has led too consolidate all the medical data at the single place. Collecting data at the single place can help researchers to use this data for research purposes and improve the algorithm.

4. Information Security and Data Interoperability

Around the world, multiple organizations store medical records in different standard formats. Using such large data formats makes a difficulty in sharing health-related patient data in various organizations as well as to health research [6].

In USA at present, 33 states have developed plan to exchange the medical information and patient data with high security among them [8]. They first try to identify the person who wants to access the medical data, and based on that they provide access or limited access of the data to them.

3 Solutions

In this, we discuss solutions on the basis of the following two classes:

- Some existing solutions
- Open research challenges that further needs to be addressed

3.1 Some Existing Solutions

Some existing solutions discussed by various researchers can be described as follows:

3.2 Encryption

The process of transforming plain text into cipher text will secure the message, so that it can be only readable by sender and receiver. Encryption can be used to secure data and also prevent skimming and eavesdropping. To maintain high level of security, encryption must be done at hardware as well as software levels. Watermarking of the medical data can also be done for encryption at software level [9, 10].

For encryption of medical images [7], several encryption algorithms were used initially but these methods were not secure at both of the ends. So signature methods were adopted before encryption. Nowadays medical image watermarking method for securing medical data has given very promising results. It not only used for authentication and securing the image but it also contains the other information in the form of packets inside the image itself. So separate sending and maintaining of these information is not required.

3.3 Role-Based Access Security and Access Control

In an organization, workers and employees work at different and with different capacity. Everybody cannot be given the authority and privilege and access of medical information of the patient. This authority must be established depending on the nature of the job of the person in the organization [11]. The persons involving in maintenance of the medical data should be authorized by the head of the institution.

3.4 Authentication Mechanism

Authentication means the information sent by the sender and information received by the receiver must be exactly same. Suppose sender sends information I, and receiver receives the information I' then for authentication of the information I

$$I = I'$$

Otherwise message is not an authenticated message, and it should be destroyed and resend. There are a number of algorithms [9] that can be used for authentication; some of them can be pointed out as:

- Digital Signature
- Passwords mechanisms
- Challenge-Response authentication protocol

4 Some Existing Challenges with Their Solutions in Concern to Medical Big Data Security and Privacy Issues

Some existing challenges in medical big data can be described as follows:

4.1 Data Access and Storage

Due to availability of medical records via Internet in the form of EPR or EMR, the record becomes vulnerable to hackers, unauthorized access and malicious attacks. Patient health records require privacy and confidentiality. Confidential data should not be disclosed. Due to distributed nature of sensor networks [12], in-home remote patient monitoring increases the challenges of security, integrity, and privacy compared to traditional paper-based healthcare systems.

There is also a possibility of skimming and eavesdropping when we transmit a sensor data over a wireless network.

There are some key challenges when implementing electronic patient record and also in-home remote patient monitoring using sensor networks:

1. Data Access and Storage
2. Integrity

Some questions need to be answered in order to deal with above-mentioned challenges:

4.2 Who Owns the Data?

The primary question is that who is the actual owner of the patient data. If insurance companies are the owner of the patient of the patient data, they should not refuse to give expenses to patient when needed. If doctors are the owner of the patient data, their recommendation only should be treated as the milestone for getting any kind of medical benefits. But when needed, doctors also tend to refuse to take the responsibility for the ownership of the data.

If these two parties are not the owner of the patient data, whether some third party is the owner of the patient data? If it is so, will they have proper authority and right to handle the patient sensitive data. Whether patient records and data are safe under these custody. These are the questions which have no solution when patient data is accessed and patient tries to get his insurance money.

4.3 Data Types and Its Permissible Storage Limit

Medical record includes data such as physician notes and prescriptions, MRI, clinical lab results, etc. stored in paper-based record. In EMR or EPR, should all this data be stored electronically via the Internet or the subset of such data is sufficient for healthcare EPR users. Similarly in remote patient monitoring (RPM) that makes use of sensor networks, should store the patient information locally like in his personal computer or his personal mobile phone [13, 7]. For village level, it can be stored in the village hospitals under the supervision of the competent authority. For district level, it be maintained in the government medical hospitals and so on. The personal data flow will also be done under this hierarchy. This will serve the patient better as every note will have the personal medical data and information about the patient, and when needed, it can be served without any difficulty and waste of time.

4.4 Who Can Authorize to View Any Patient Record?

EPR users authorize with the following categories:

1. Edit (Read/Write) Privilege—Users have read/write privileges who can view as well as edit the records. For example: physician, nurses.
2. Red only—This kind of access may be limited to read only limit. E.g. insurance companies access can be limited to read only. They can only see the particular portion of the data. They can not edit or modify it any ways.

4.5 *Where Should Medical Big Data Be Stored?*

How can we store medical data and which kind of data is best in order to handle the security and privacy requirements? Here, we describe two storage schemes, centralized versus decentralized storage, for EPR remote patient monitoring (RPM) that can be questioned for providing efficient storage of medical big data and enhance security needs:

1. The first case is that whether data can be stored in a local patient record system where several computer systems are locally connected to each other. If it is so, up to what extent data can be stored.
2. In remote system, data may be send over the Internet for diagnosis purposes, how data can be stored in the local system and what security mechanism have been adopted to send these data while sending over the Internet [13]. Currently watermarking security methods have proved as best for these purposes. For record keeping, fragile watermarking is preferred and for sensitive data some robust procedure may be adopted.

Without consent of patient who can access data:

In certain medical circumstances, patient's medical information needs to be shared without the consent of patient, in the interest of the patient. For example, if patient is very critical. In those cases, the close relative like spouse and parents can have the right of authorization of the data.

4.6 *Health Insurance Portability and Accountability Act of USA (HIPAA)*

To overcome the access difficulty in needy condition for patients, a HIPAA group has been formed in USA, which is controlled and governed by doctors of USA. Any doctor can access the record, can transfer record to other doctor, without the consent of patient. In this way, diagnosis standard has increased. But there are some security concerns also have arisen due to this practice. This can be stated under the following two points:

1. Its primary concern is safety rather than implementation.
2. There are minimum security baseline, and minimum set of patient information protection rules.

At the same time, there are special rules in each state that how health care is controlled, which is well described by the State Health Secrets of the Health Secrets Project. For example, Alabama Code does not have any general law giving patients the right to access their medical records. There are also no general laws restraining the publication of sensitive information, but due to some medical conditions, such as "mental health disorders and sexually transmitted diseases," Alabama has some

methods that control the disclosure of this information along with the patient's information. The Alabama Code also bans the disclosure of medical information by HMO. In contrast, California law provides patients with access to healthcare information from healthcare providers, HMOs, insurance companies, and state agencies.

The Code of California has broad rules on the use of healthcare information and disclosure by these institutions.

References

1. J. Manyika et al., "Big data: The Next Frontier for Innovation, Competition, and Productivity", Zürich, Switzerland: McKinsey Global Inst., Jun. 2011, pp. 1–137.
2. B. Matturdi, X. Zhou, S. Li, and F. Lin, "Big data security and privacy: A review," *China Commun.*, vol. 11, no. 14, pp. 135–145, Apr. 2014.
3. J. Gantz and D. Reinsel, "Extracting value from chaos," in *Proc. IDC IView*, Jun. 2011, pp. 1–12.
4. A. Katal, M. Wazid, and R. H. Goudar, "Big data: Issues, challenges, tools and good practices," in *Proc. IEEE Int. Conf. Contemp. Comput.*, Aug. 2013, pp. 404–409.
5. J. Adler-Milstein, A.K. Jha, Healthcares "Big Data" challenge, *Am. J. Manag. Care* 19 (7) (2013) 537–538.
6. F. Cismondia, A.S. Fialho, S.M. Vieira, S.R. Reti, J.M.C. Sousa, S.N. Finkelstein, Missing data in medical databases: impute, delete or classify?, *Artif. Intell. Med.* 58 (2013) 63–72.
7. Manish Madhava Tripathi, Abhishek Ranjan, "Medical Image watermarking for Mobile Smart phones", *International Journal for Innovations in Engineering, Science and Management*, Volume 2, Issue 11, November 2014.
8. N.O. Skaga, T. Eken, J.M. Jones, P.A. Steen, Different definitions of patient outcome: consequences for performance analysis in trauma, *Injury* 39 (5)(2008) 612–622.
9. Manish Madhava Tripathi, Dr S P Tripathi, "Image Encryption Techniques: A Critical Comparison", *International Journal of Computer Science Engineering and Information Technology Research*, Vol 3, issue 1, March 13.
10. Manish Madhava Tripathi, Md Saif, "HMM Based Offline Signature Forgery Detection", *International Journal of Engineering Technology and Computer Research (IJETCR)*, ISSN: 2348 – 2117, Volume 3; Issue 2; Page No. 41–47.
11. Mohammad Haroon, Mohd Husain, "Interest Attentive Dynamic Load Balancing in distributed systems", Publication date 2015/3/11, Publisher IEEE.
12. Mohd Haroon Ashwani Singh, Mohd Arif, "Routing Misbehaviour In Mobile Ad Hoc Network", *IJEMR*, Volume 4, Issue 5, October 2014.
13. Mohd Haroon, Mohd Husain, Manish Madhav Tripathi, Tameem Ahmad, Vandana Kumari, "Server Controlled Mobile Agent", *International Journal of Computer Applications (0975–8887)*, Volume 11, Issue 4 Pages 13–16.

Android-Based Home Automation Using Bluetooth and ESP8266

Akhil Bhatt, Apurva Saxena, Shubhi Chauhan, Utkarsh Jaiswal and Yashaswi Verma

Abstract This paper exhibits a minimal effort and adaptable home control and checking framework for getting to and controlling gadgets and machines remotely utilizing Android-based smart telephone application. The depiction about the incorporated system architecture and the interconnecting instruments for the solid estimation of parameters by smart sensors and transmission of information by means of web is being exhibited. Home automation or smart home involves the control and computerization of lighting, aerating and cooling, warming, ventilation, and security as well as home appliances. It uses Bluetooth for remote checking and is a component of the Internet of things. The system will be operated on two modes, autonomous and semi-autonomous. To show the plausibility and viability of this framework, gadgets, for example, light switches, control plug, temperature sensor, and humidity sensor, have been coordinated with the proposed home control framework. The framework will consist of an exhaust, water tank, and an LED bulb. The exhaust can be used in kitchen/washroom and work accordingly. Water management is an area of field which needs a thought to work on especially, in India. For this, we will be using a motor which will automatically start when the water level reaches to its bare minimum and stops once the water level reaches to the brim. This will help in conservation of water. The third appliance used is an LED bulb which will start to glow if someone enters a room and stops glowing once the person exits.

Keywords IoT (Internet of Things) · Autonomous · Semi-autonomous Automation · Sensors · Water management

A. Bhatt · A. Saxena · S. Chauhan (✉) · U. Jaiswal · Y. Verma
University of Petroleum and Energy Studies, Dehradun, India
e-mail: shubhi.chauhan22june@gmail.com

U. Jaiswal
e-mail: jaiswalutkarsh15@stu.upes.ac.in

Y. Verma
e-mail: vermayashaswi15@stu.upes.ac.in

1 Introduction

The Internet of things permits elements to be detected or operated remotely crosswise over current system infrastructure, [1] opening the doors for more straightforward reconciliation of the physical world into PC-based frameworks and bringing about enhanced effectiveness, exactness, and financial advantage in addition to decreased human intervention [2–7]. When IoT is expanded with actuators and sensor module or subsystem, the innovation turns into an occurrence of the more broad class of digital physical frameworks, which likewise envelops advances, for example, smart homes, intelligent transportation, and brilliant urban communities. Everything is especially identifiable through its introduced figuring structure, however can function inside the current Internet foundation. Internet of things is about physical things conversing with each other [8, 9]. Specialists estimate that more than 60 billion devices will comprise of IoT by 2022 [10].

One of the most important features of the IoT is information. The achievement of associating gadgets to make them more effective is dependent upon access to and capacity and preparing of information. For this reason, organizations chipping away at IoT gather information and assemble data from various sources and store it in their cloud space for additional handling. This invites protection and security threats and single point vulnerability of different frameworks. IoT is like bringing your dreams to reality; it is not a theoretical concept anymore. IoT is a scenario where machines communicate with each other and with other devices using embedded sensors. Regularly, IoT is required to present propelled network of gadgets, structures, and organizations that goes past machine-to-machine correspondences and spreads a variety of traditions, spaces, and applications [11]. The interlinking of these embedded devices is relied upon to client in computerization in about all fields, while additionally enabling impelled applications like a keen framework, [12] and extending to regions, for example, urban communities. Automation refers to the capacity to program and calendar occasions for the gadgets on the system. The essential point of home automation is to control or screen signals from various apparatuses or fundamental administrations. An advanced cell or web program can be utilized to control or screen the home mechanization framework. The development of indoor regulators empowers computerized control of warming and cooling at a later stage. Present-day frameworks for the most part comprise of switches and sensors associated with a focal center point infrequently called a “network node” from which the framework is operated with a UI that is associated with a divider terminal, mobile phone programming, PC or a web browser, frequently yet not generally by means of web cloud administrations. The other fundamental for front line home automation is remote observing and access. Monitoring applications can give an abundance of data about your home, from the status of the present minute to a point-by-point history of what has occurred up to now. You can check your security framework’s status, regardless of whether the lights are on, whether the entryways are bolted, what the present temperature of your house is and much more. When you begin to comprehend the conceivable

outcomes of home automation, you can think of any number of valuable and creative answers to make your life better. In 2015, the home computerization market was worth US\$6.77 billion (approximately), anticipated to have a market an incentive over US\$10 billion by the year 2025 [13].

A framework is proposed where various sensors are connected with the Arduino board. The Arduino water-level pointer utilizes an ultrasonic sensor to decide the level of water in the tank. The module is first flashed using Arduino and then is programmed to send data to the server. The sensor measures separate utilizing sonar. An ultrasonic heartbeat is transmitted from the ping sensor, and detachment to aimed source is controlled by the time it takes for the echo to return. Output from the sensor is a beat of different length that compares to the separation to the objective. This is then sustained to the microcontroller that decides the water level.

A method for measuring liquid level in a vessel comprises the following steps:

- Attaching an ultrasonic sensor to the wall of a vessel.
- Directing an energy pulse along the sensor waveguide which determines the level of water in the vessel.
- The signal arrival times are then translated into the actual liquid level depth by computation of the pulse travel time.
- The generated data is sent to the application via programmed Arduino whether to trigger the motor if fluid level is below the marked boundary.
- An alert message is sent to the user about the percentage of liquid left in the vessel or how much liquid filled after motor starts pumping the fluid inside the vessel.
- Motor starts pumping the fluid inside the vessel and stops after a specified percentage is programmed inside the Arduino.

Kitchen fans for ventilating oil-loaded air produced combustible vapors from commercial cooking gear, for example, stoves and profound fryers amid cooking are notable. Regularly such fans are physically activated utilizing a toggle switch. Ordinary fans are not reasonable for giving programmed mechanical ventilation, since they are exorbitantly noisy and would have a tendency to stir resting inhabitants of a home when consequently actuated during the evening. In like manner, the need has emerged for a novel range fan electrically connectable to a humidity sensor, which is operable at a diminished sound level in a programmed mode. Humidity sensor fan sense employs unique sensing technology that detects humidity. These fans turn on when they sense a rise in humidity over time and include adjustable sensitivity. This takes into account for faster response to rising humidity levels to clear misted reflects more rapidly than aggressive models which are activated by pre-set humidity levels programmed inside Arduino.

A customary programmed room control circuit has just a single light sensor. So when a man goes into the room, it gets one heartbeat and the lights come. At the point when the individual goes out, it gets another heartbeat and the lights go off. Be that as it may, what happens when two people go into the room, in a steady progression? It gets two heartbeats and the lights stay in off state. The circuit

depicted here beats the previously mentioned issue. It has a little memory which empowers it to naturally switch on/off the lights in a coveted manner. The circuit utilizes PIR sensor which are set in a steady progression (isolated by a separation of say a large portion of a meter) so they may independently detect a man going into the room or leaving the room, the sensor stimulates the bulb/LED to the point that when a man gets into the room it transmits light, and when a man leaves the room it does not radiates. These yields are at the same time connected to two counters. One of the counters will consider +1, +2, +3, and so on when people are getting into the room and the other will consider -1, -2, -3, and so forth when people are escaping the room.

2 Hardware Development

In Figure 1, Arduino mega is used as a microcontroller for the sensors and their outputs. It is the most important unit of the project and links all the sensors with the devices they control as well as control the Bluetooth functioning using an Android device. PIR sensor is based on the detection of heat by sending infrared rays in this project, it will be used to detect motion, and as a prototype an LED/bulb will be lit as a signal of someone entering or leaving the home. LED works according to the PIR sensor attached to transistor and relay. Temperature and humidity sensors identify the relative humidity of the present conditions in which they are put. They measure both the dampness and temperature noticeable all around and express relative humidity as a rate of the proportion of moisture to the most extreme temperature that can be held. The sensor is connected to Arduino mega through a dimmer of 16 levels which will control the speed of the exhaust fan which in this project is depicted by a PC fan.

Ultrasonic sensor is a sensor that senses the time the pulse takes between emitting and detection; it has been connected through a transistor and relay which has a basic functioning to control the power intake of heavy devices like motors and bulbs; all this in turn will control the water pump motor on/off configuration, according to the level detected by the sensor. The whole circuit is finally connected to a Bluetooth module which will be further used to control all functions of equipment by using an Android device in two modes, i.e., autonomous and semi-autonomous.

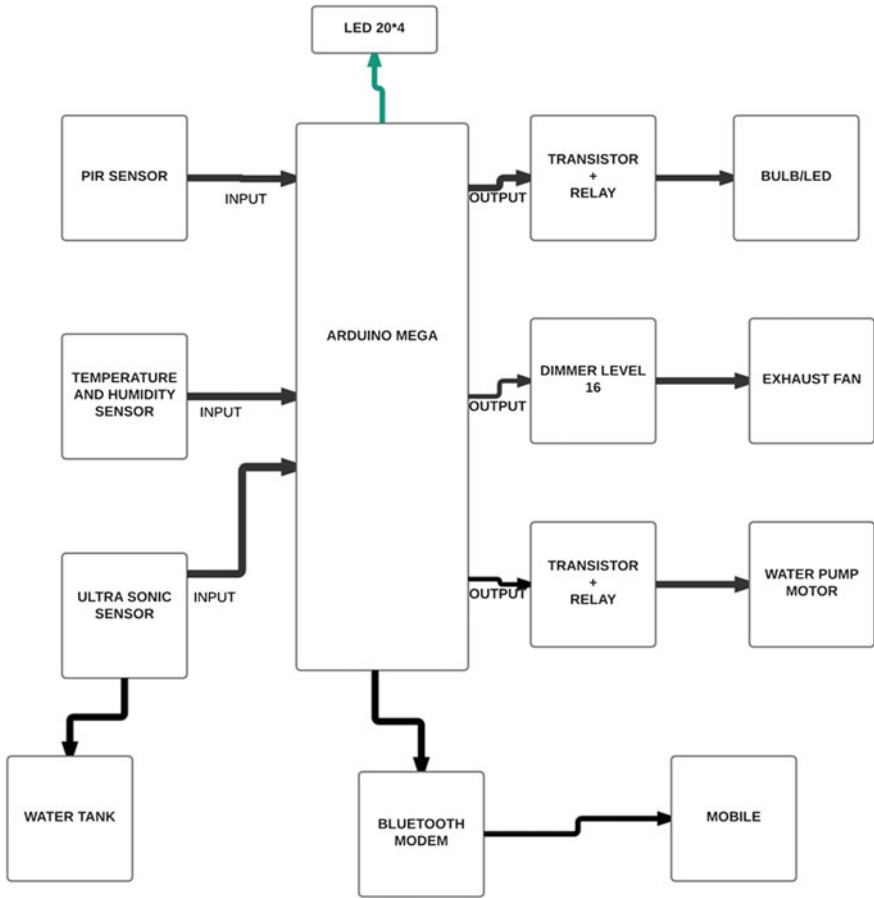


Fig. 1 Flow Diagram of Input Sensors with their respective Outputs

3 Software Development

In Fig. 2, LCD is connected to Arduino on pins 8, 9, 10, 11, 12, and 13. Ultrasonic sensor is connected on pins 5 and 6, and temperature and humidity sensor on pin 0. Bulb is connected to relay (RL1) and on pin 3. Other relay (RL2) is connected to exhaust. Power supply is connected on pin 4 of Arduino. PIR sensor is used to control bulb and is connected to pin 7.

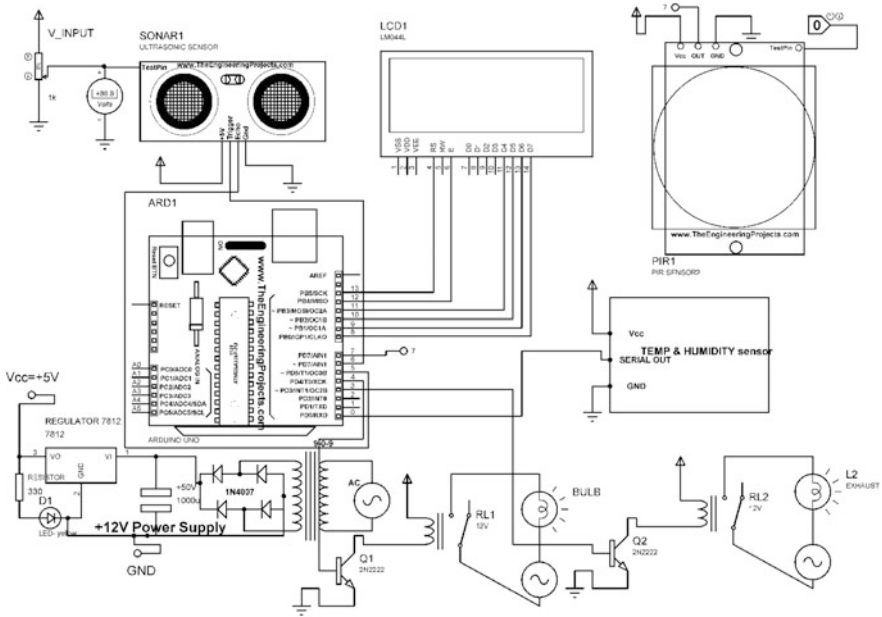


Fig. 2 Model Testing through Proteus Design Suite

3.1 Flow Diagram

Figure 3 explains the working of the model where in data from sensors are fetched in two modes, autonomous and semi-autonomous. If the mode is autonomous, then automatic functioning will be there, otherwise it will take data from app for tank, bulb, and exhaust. For tank, if water level is below certain level then motor will start, and if it is above a certain level then motor will stop. For bulb, if motion is detected, bulb will be switched on. For exhaust, a 16-level dimmer will be used which will regulate the speed of the fan.

In Fig. 4, the first screen of the app shows two modes of selection—autonomous and semi-autonomous. By selecting autonomous, the autonomous mode will be activated. By selecting semi-autonomous, the next screen in the app will be displayed. The second screen is for the LED bulb control, i.e., switching on and off. The third screen displays the control of exhaust fan speed. The slider controls the speed through the app. The fourth screen displays the temperature and humidity control of the exhaust fan. The last screen receives the data, i.e., water level of the tank and displays on the LCD.

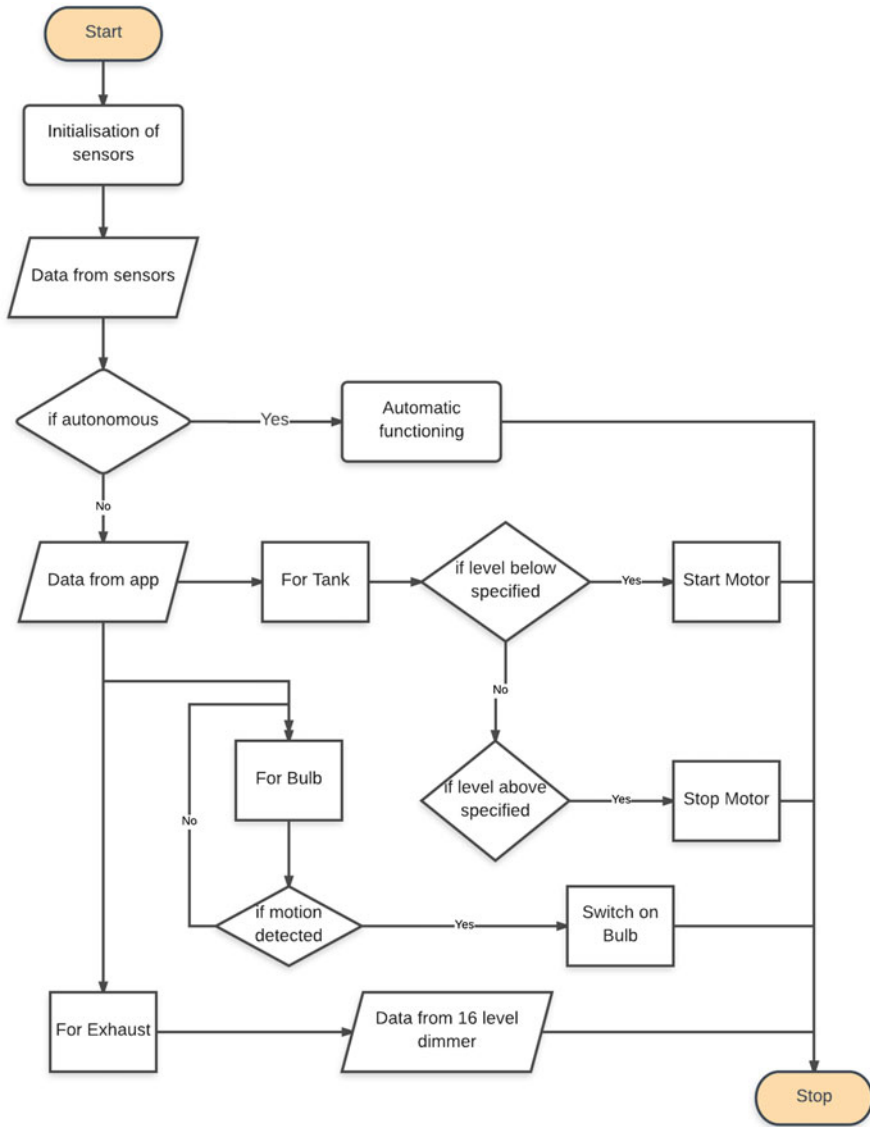


Fig. 3 Flow Chart of proposed Model

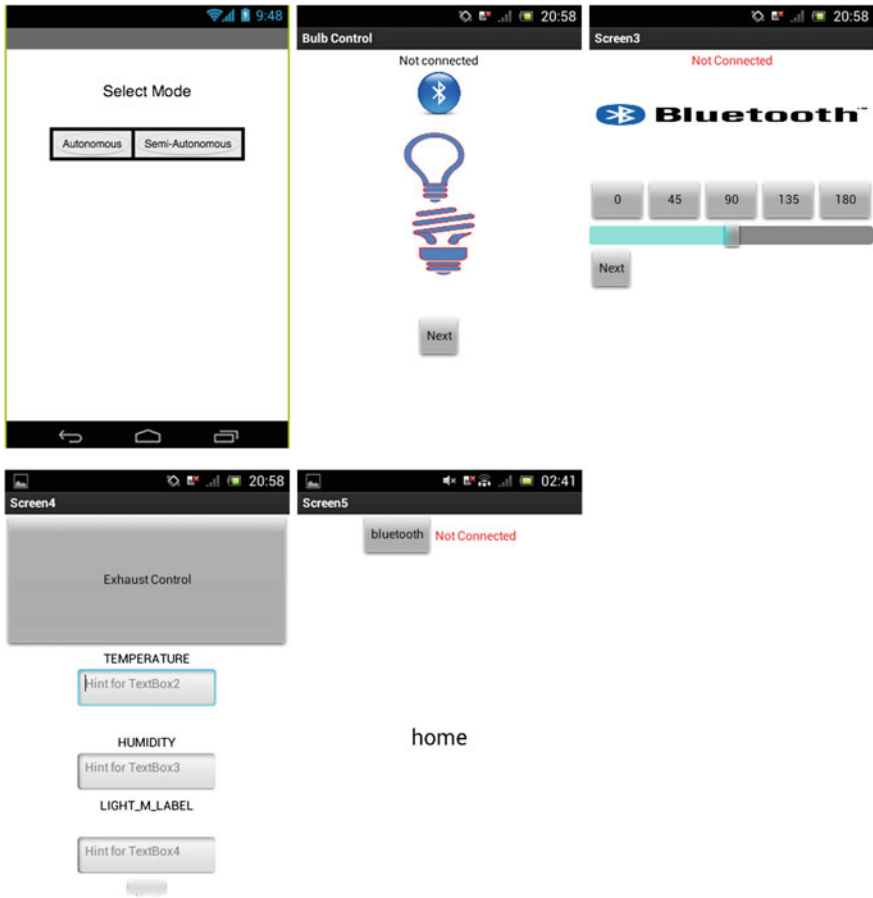


Fig. 4 Screen Layouts of Android App

4 Result and Conclusion

What sorts of things can be a piece of a home automation framework? In a perfect world, anything that can be associated with a system can be mechanized and controlled remotely. In this present reality, home automation most regularly associates straightforward binary devices. This incorporates “on and off” gadgets, for example, lights and electronic locks, additionally gadgets, for example, security sensors which have just two states, open and shut. Usage of home automation facility provides a number of benefits to the users, easy access to diminish or increment the force of lights, control shades, and so on with the touch of a catch on your tablet/cell phone or a dynamic keypad. Automation can introduce conditions for you with no genuine exertion. At the most fundamental level, home automation extends that planned programmability to lighting, with the goal that you can suit

your vitality utilization to your standard day-by-day plan. Using computerization sensors and interchanges advancements, homes can be deliberately and always observed from any place.

The model provides an ultrasonic mechanical assembly and strategy for measuring the fluid level of a vessel subjected to high weights and temperatures without uncovering any sensitive electrical gear to the antagonistic condition. This framework measures the fluid level up through the tank base, “skipping” motions off of the fluid hindrance and afterward registering volume from flag bounce back time, and then via Bluetooth connectivity sends real-time data to the user through the application installed on the smartphone. This can be helpful in managing water management issue and an efficient way of supplying water to households. Keeping in mind the true objective to encourage the diminishment of expenses in the development of residences, without giving up air quality, an existing model must be produced that will provide variety of functions. The kitchen fan with a climatic humidity sensor which naturally turns on the fan at a low speed setting when humidity levels in a residence surpass a pre-set cutoff. This has been proficient in a way that will decrease noise disturbances to dozing inhabitants of the residence. The energy utilizations of private and business structures are developing significantly. One critical commitment to this development originates from the wasteful use of electrical loads, for example, chilling and warming frameworks, lighting framework, and so on. The lighting system is one of the largest single consuming units. A standard customized room control circuit has only a single light sensor—PIR sensor that measures infrared (IR) light transmitting from articles in its field of view. They are regularly utilized as a part of PIR-based motion detectors. The proposed smart LED lightning system normally switches on/off the lights in a pined way when a person enters/leaves the room. This could spare you from wasting energy on overlooked lights and machines once you have left for the day.

References

1. D. Surie O, Laguionie T, Pederson ‘Wireless sensor networking of everyday objects in a smart home environment’ *Proc, Int, Conf, Intell, Sensors Sensor Netw, Inf, Process,* pp. 189–194 2008.
2. Vermesan, Ovidiu; Friess, Peter (2013), *Internet of Things: Converging Technologies for ISBNSmart Environments and Integrated Ecosystems* (PDF), Aalborg, Denmark: River Publishers. ISBN 978-87-92982-96-4.
3. ‘An Introduction to the Internet of Things (IoT)’ (PDF), Cisco.com, San Francisco, California: Lopez Research. November 2013, Retrieved 23 October 2016.
4. Santucci, Gérald, ‘The Internet of Things: Between the Revolution of the Internet and the Metamorphosis of Objects’ (PDF), European Commission Community Research and Development Information Service. Retrieved 23 October 2016.
5. Mattern, Friedemann; Floerkemeier, Christian, ‘From the Internet of Computers to the Internet of Things’ (PDF), ETH,Zurich. Retrieved 23 October 2016.
6. Reddy, Aala Santhosh (May 2014), ‘Reaping the Benefits of the Internet of Things’ (PDF), Cognizant, Retrieved 23 October 2016.

7. Lindner, Tim (13 July 2015), 'The Supply Chain: Changing at the Speed of Technology', Connected World, Retrieved 18 September 2015.
8. H. Sundmaeker P, Guillemin P, Friess S, Woelffle Vision and Challenges for Realizing the Internet of Things Germany Luxembourg: European Union 2010.
9. Internet 3.0: The Internet of Things Singapore Analysis Mason: 2010.
10. Evans, Dave (April 2011), 'The Internet of Things: How the Next Evolution of the Internet Is Changing Everything' (PDF), Cisco, Retrieved 15 February 2016.
11. Höller, J; Tsiatsis, V; Mulligan, C; Karnouskos, S; Avesand, S; Boyle, D, (2014), From Machine-to-Machine to the Internet of Things, Introduction to a New Age of Intelligence, Elsevier. ISBN, 978-0-12-407684-6.
12. Monnier, Olivier (8 May 2014), 'A smarter grid with the Internet of Things', Texas Instruments.
13. 'Research and Markets: Global Home Automation and Control Market 2014–2020 - Lighting Control, Security & Access Control, HVAC Control Analysis of the \$5.77 Billion Industry', Reuters. 2015-01-19, Archived from the original *on* 2016-05-05.

Embedded-Based Smart Solar Grid of 2×2 Monitoring System Using Smart Sensors

Rohit Samkaria, Rajesh Singh, Anita Gehlot, M.S. Yadav, Ashok Kumar, Varchas Choudhary, Sushabhan Choudhury, Rupendra Pachauri and Anvesh Aggarwal

Abstract In this research an embedded-based procedure for automatic fault detection and supervision in 2×2 PV array with possible fault allocation by using voltage and current parameter through embedded. The supervision system is developed with LabView which is acting as real-time data logger. The approach has been validated with experimental setup, and the system is designed with low-cost embedded-based solution to provide reliable and secure monitoring of PV system. The system include the parameter extractions technique to calculate main PV system parameter supervision based method analysis the output of voltage and current sensor present in the solar PV array. In the experimental result, fault detection and supervision system has shown the high accuracy of fault detection and fault classification on the test.

Keywords Solar panel · Current sensor · Arduino control · LabView

1 Introduction

The photovoltaic industry has grown at highly rapid rate due to the solar photovoltaic (PV) generations costs. On the other hand, there are a number of government policies which do the work of promoting the introduction to various grid-connected PV arrays system in different region of the country [1]. There are number of PV systems which are working without any mean of the supervision systems, and this grow in the development of fault detection and supervision system in PV array output level is below than the 25 KWp. Fault detection in PV arrays is a fundamental

R. Samkaria (✉) · R. Singh · A. Gehlot · M.S. Yadav · A. Kumar · V. Choudhary · S. Choudhury · R. Pachauri · A. Aggarwal
Electronics Instrumentation and Control Engineering Department, College of Engineering Studies, University of Petroleum and Energy Studies, Dehradun 248007, Uttarakhand, India
e-mail: rohit.samkaria93@gmail.com

R. Singh
e-mail: rsingh@ddn.upes.ac.in

task in order to increase the efficiency and safety in the PV system [2]. Without the proper fault detection in the PV, the unclear fault not only causes the power loss, but also might lead to safety issue and fire hazards. The wireless-based monitoring technologies nowadays are becoming an important asset in the field of the solar PV array because of their reliable operation and their capabilities to transmit the data to remote location, and from remote location monitoring, the PV system provides high efficient system with reduction to reduce the cost by individually monitoring the whole PV array [3]. By using the Arduino open electronic platform, there are various parameter loggers which store the data that has been developed to solve the current problem of the solar PV array system, and these data loggers meet all the requirements in terms of their reliability and accuracy included in International Electrotechnical Commission IEC Standards [4]. To present the *I-V* characteristics, a circuit-based simulation model for the PV array by PISM software package on 3 kW grid for the SP and TCT has been developed at different surface temperature and isolation under normal operation for PV system, and simulated result shows that the proposed system based on the fault diagnosis and supervision can detect the malfunction very accurately [5]. The developed system which comprises the developed algorithm which has input irradiance level, PV temperature, and proposed system has been successfully validated with experimental setup [6]. Mahmud Dimish et al. presented a system which is automatic fault detection and can detect the possible with the exact location of the fault occurring in Grid-Connected Photovoltaic System (GCPV) of 1.98 kWp plant was installed at University of Huddersfield, UK [7]. To determine the fault location, the values of voltage and current that are received at the receiver section is compared with the theoretical values of the voltage and current, and potting these values live on the graphical user interface developed on virtual instrumentation (VI) LabView software [8]. In summary, this chapter presents the following research contributions:

1. For the first time, embedded-based model is developed to determine the fault and data supervision which has several advantages as fast steps to recognize the fault and having low cost.
2. The proposed embedded-based model is capable to identify faults in the PV system in real time with high rate of accuracy.

2 Proposed System

The system is developed by using Arduino electronic open source platform which acts as the central processing unit of the whole system. As shown in Fig. 1 the generalized block diagram of transmitting unit of the system. The 2×2 matrix of solar panel has rating 9.25 V, 5 W. The parameter of the solar array is monitored by using the following modules:

ACS712 Current Sensor: This module is capable to withstand both DC and AC current up to 20 A.

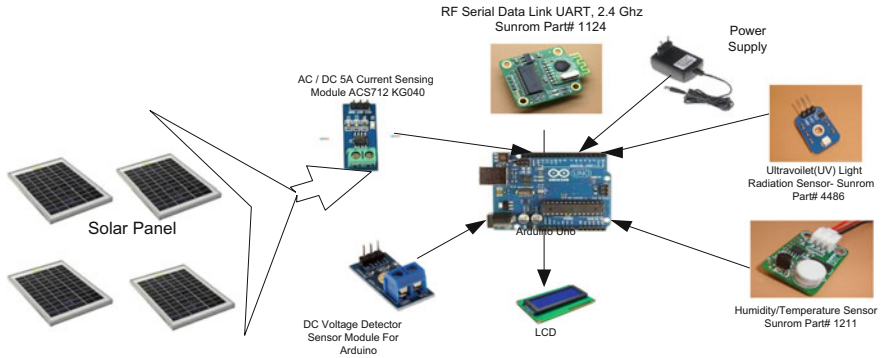


Fig. 1 Generalized block diagram of transmitting unit

DC Voltage Detector: This module is capable to detect up to 35 DC voltage.
RF Modem 2.4 GHz: Wireless data is send using RF modem that works on UART.
Temperature and Humidity Sensor: These both sensors come in a single module which measures the temperature and humidity of the modules.

Figure 2 shows the receiving unit of the system which comprises the Arduino controller unit along with RF modem to receive the data and display unit to display the measured data. This receiving unit is serially interfaced with the system to display data over the GUI developed with LabView.

Figure 3 shows the block diagram of the system where the separate voltage, current, and bump sensors are interfaced with individual solar PV unit. Each solar panel measures its parameters, and individual sensors data is given to multiplexer. This data is given to Arduino unit which took control action over these parameters

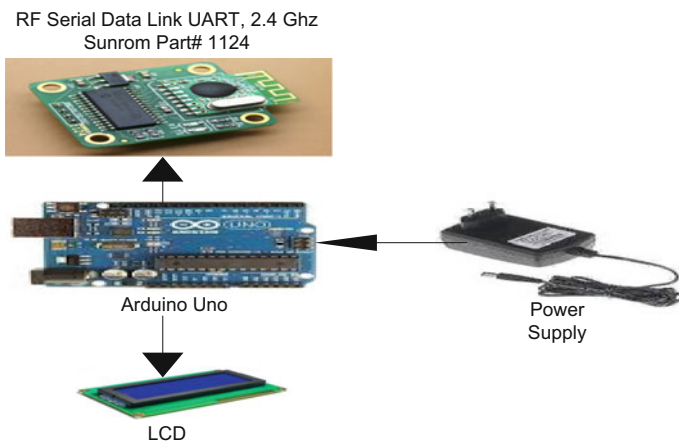


Fig. 2 Generalized block diagram of receiving unit

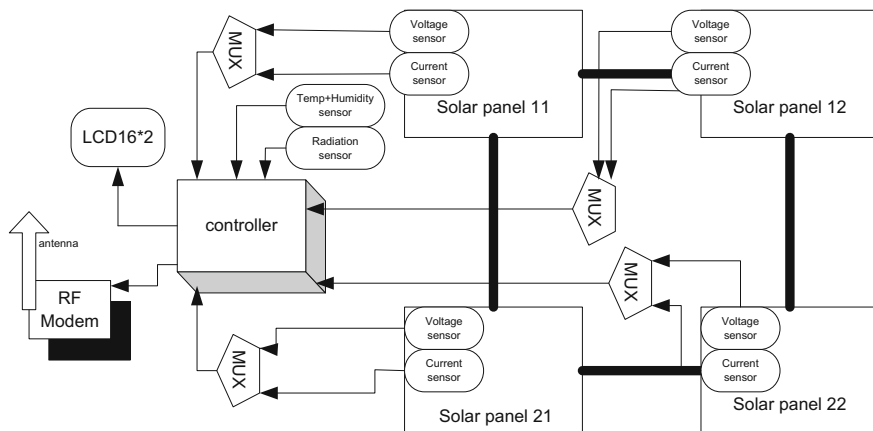


Fig. 3 Block diagram of transmitting unit in SP mode

and displays these parameters over the liquid crystal display (LCD), and at the same time, RF modem receives this data from the Arduino, convert this data into serial format along with start, stop, and parity bit added to data, and send this data to the receiving unit.

Now the system is capable to monitor the data from the PV array, and if there is drop in the current on any of the panel due to shading effect or some other environmental factors, then it auto configures its operating mode from Series Parallel configuration to the TCT configuration to improve the efficiency of the system. Figure 4 shows the block diagram of the system where relay control circuit is connected with the PV array which took action through controller unit as if there are any changes in the current or voltage ration of the PV array system (Fig. 5).

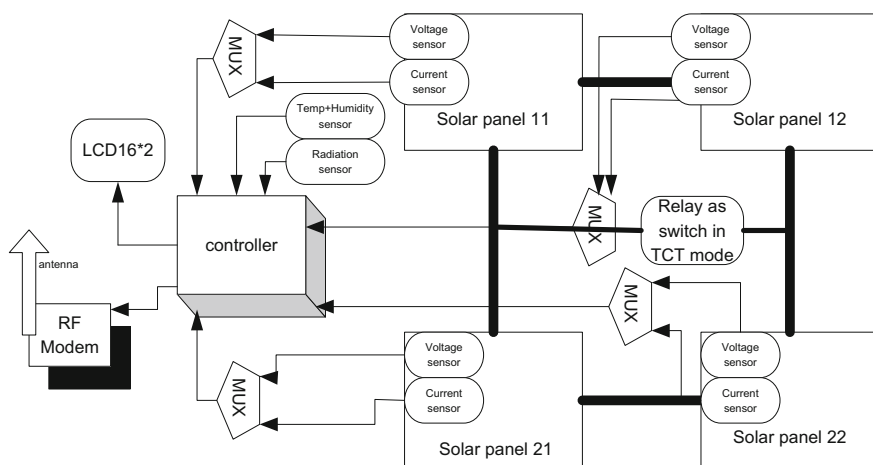
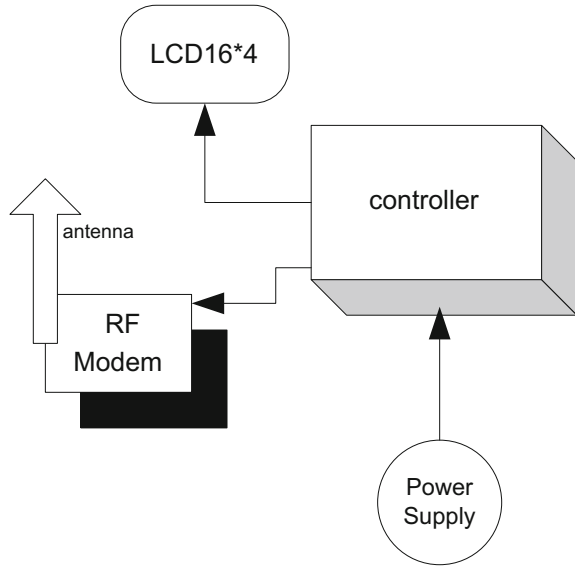


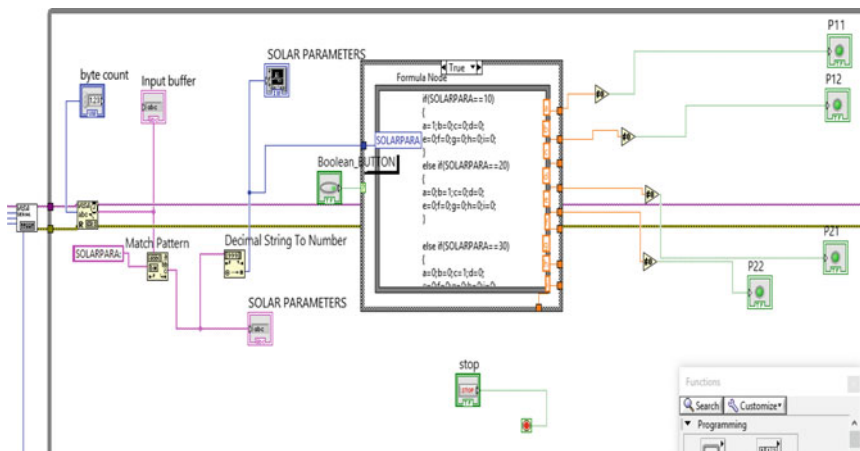
Fig. 4 Block diagram of transmitting unit in TCT mode

Fig. 5 Block diagram of receiving unit in both modes

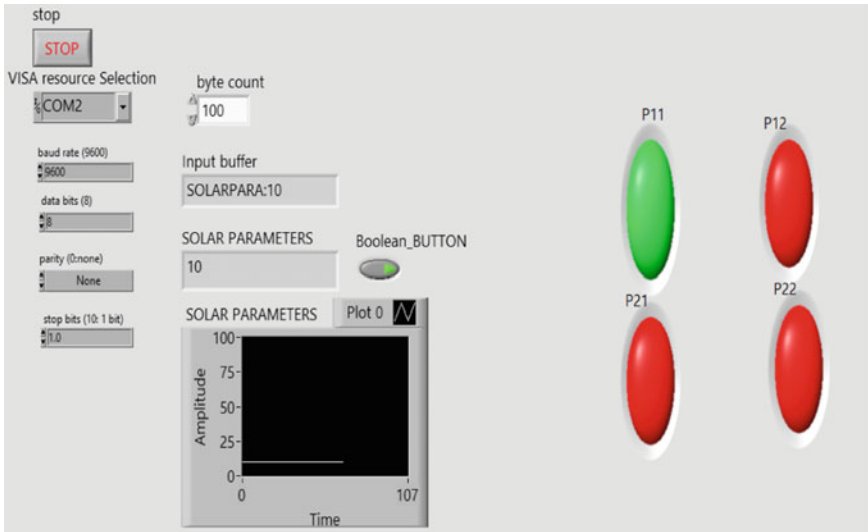


3 Software Development

There is a lot of research has been done over the PV array to diagnose the fault and supervision of the data of PV array, but embedded-based system has high reliability with high rate of accuracy being achieved. The main control action to achieve the high accuracy rate is to develop a software program for the system that is achieved by using open source Arduino fourm (Figs. 6 and 7).



Block diagram representation of LABVIEW GUI



Block diagram representation of LABVIEW GUI

Before actual implementation over the hardware, the system is tested over virtual simulation Proteus software. Figure 8 shows the image of the Proteus simulation of both the transmitter and receiver part of the system (Fig. 9).

Function for transmitting unit to read the sensor and transmit information

```
void loop()
{
  radiationdata=analogRead(radiation);
  set.Cursor(0,2);
  print_lcd("Radiation=");
  set.Cursor(12,2);
  print_lcd(radiationdata);
  if (Transmit_unit_stringComplete)
  {
    Set.Cursor(0,0);
    print_lcd ("HUMD:");
    print_lcd (inputString[3]);
    print_lcd (inputString[4]);
    print_lcd (inputString[5]);
    print_serial (inputString[3]);
    print_serial (inputString[4]);
    print_serial (inputString[5]);
    print_serial (":");
  }
  set.Cursor (10,0);
  print_lcd ("TEMP:");
  print_lcd (inputString[9]);
}
```

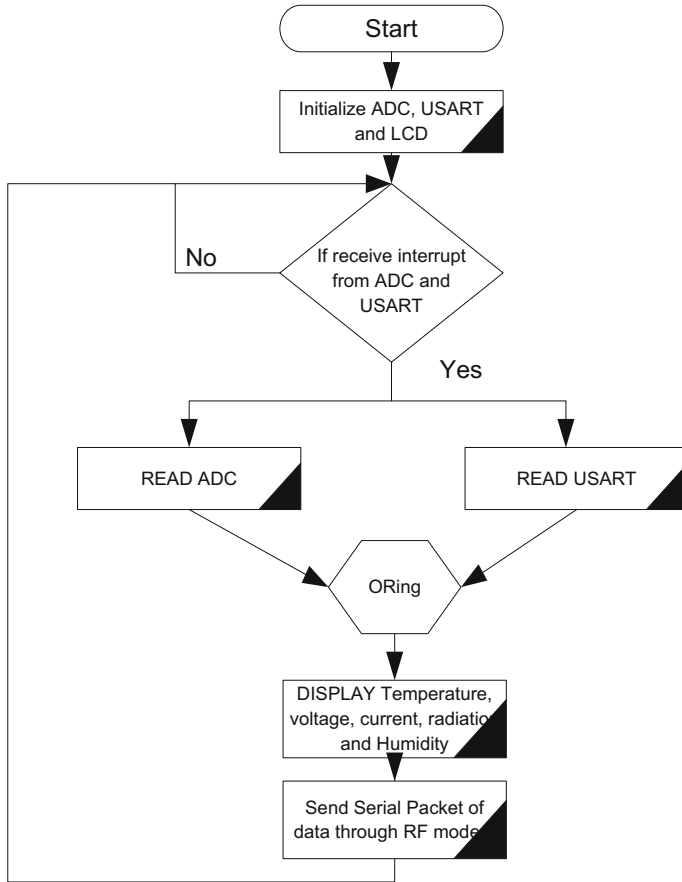


Fig. 6 Flow chart of reading sensors and sending serial data in transmitting unit

```

    print_lcd (inputString[10]);
    print_serial (inputString[10]);
    print_serial (inputString[11]);
    print_serial (":");
}
Transmit_unit_inputString = " ";
Transmit_unit_stringComplete = false;
print_serial (voltage_data);
print_serial (":");
print_serial (current_data);
print_serial (":");
print_serial ln(radiation_data);
}

```

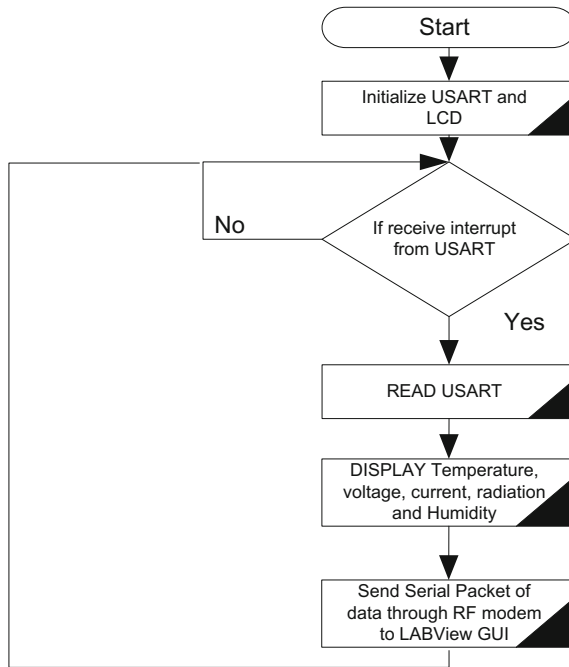


Fig. 7 Flow chart of receiving serial data from transmitting unit in receiver side

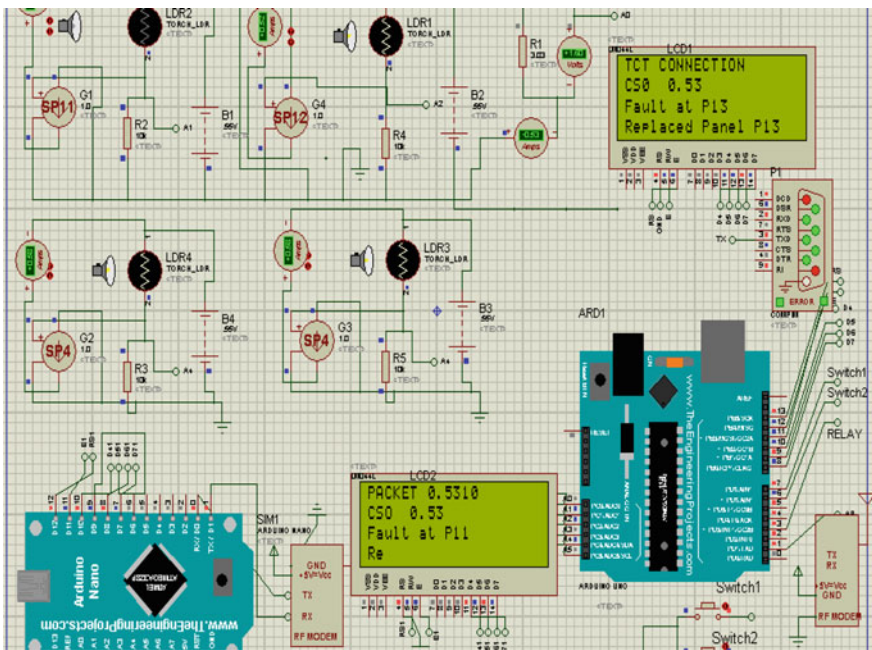


Fig. 8 Proteus model of current sensing-based fault detection

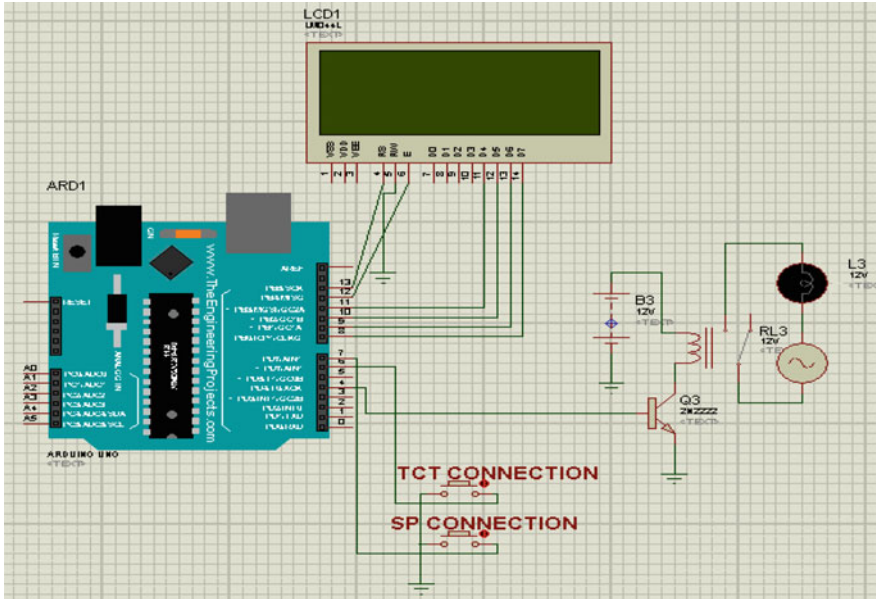


Fig. 9 Proteus model of selection of TCT and SP using switch

Function to read string from Temp and humidity sensor transmitting unit

```
void Transmit_unit_serialEvent ()
{
    while (Serial.available(>0)
    {
        char Transmit_unit_inChar = (char)Serial.read();
        Transmit_unit_inputString += Transmit_unit_inChar;
        if (Transmit_unit_inChar == 0x0A)
        {
            Transmit_unit_stringComplete = true;
        }
    }
}
```

Loop function of data in receiving Unit from transmitting unit

```
void loop()
{
    if (stringComplete)
```

```

{
  lcd.setCursor(0,0);
  print_lcd ("HUMD:");
print_lcd (inputString[0]);
print_lcd (inputString[1]);
  print_lcd (inputString[2]);
set.Cursor (10,0);
  print_lcd ("TEMP:");
print_lcd (inputString[4]);
  print_lcd (inputString[5]);
set.Cursor (0,1);
  print_lcd ("Voltage=");
set.Cursor (8,1);
  print_lcd (inputString[7]);
  set.Cursor (0,2);
  print_lcd ("Radiation=");
  set.Cursor (11,2);
  print_lcd (inputString[9]);
  print_serial ("HUM:");
  print_serial (inputString[0]);
  print_serial (inputString[1]);
  print_serial (inputString[2]);
  print_serial ("TEMP:");
  print_serial (inputString[4]);
  print_serial (inputString[5]);
  print_serial ("VS:");
  print_serial (inputString[7]);
print_serial ("CS:");
  print_serial (inputString[9]);
  print_serial ("RAD:");
  print_serialln(inputString[10]);
}
Receive_inputString = "";
Receive_unit_stringComplete = false;
}

```

Function to receive the data from transmitting unit

```

void Receive_unit_serialEvent ()
{
  while (Serial.available(>0)
  {
    char Receive_inChar = (char)Serial.read();

```

```
Receive_inputString += Receive_inChar;
if (Receive_inChar == 0x0A)
{
    Receive_unit_stringComplete = true;
}
}
}
```

4 Result and Discussion

In this dissertation work, a comprehensive investigation on fault detection and supervision on the self-assembled 2×2 configured PV modules is presented. Extensive analysis has been carried out using two combinations of the PV system, (1) Series Parallel Configuration (2) TCT, and result is analyzed with LabView. The obtained results show that embedded-based fault detection and supervision system has significant effect on the performance of all the considered PV modules. Following are the salient points of this study:

- The investigation on the self-designed 2×2 solar PV array with SP and TCT configurations has been carried out at irradiation level and at different fault condition.
- Performance analysis of the considered PV module configurations has been carried out using embedded-based board to examine the different parameter taking mainly the consideration of $I-V$ characteristics.
- Under both the considered SP and TCT configured, PV module is observed to have better fault detection and supervision performance than the other available systems.

5 Future Scope

In this project, the carried out work for fault detection and supervision has been investigated only on the conventional configurations like series-parallel (SP) and total cross tied (TCT). This can be carried on high PV matrix with other configuration then SP and TCT. In future, this data can be uploaded to server through various techniques available nowadays. There are various other researches have been done over data handling and proposed in some literatures as it may be more effective as compared to proposed system.

References

1. Batista, N. C., et al. "Photovoltaic and wind energy systems monitoring and building/home energy management using ZigBee devices within a smart grid." *Energy* 49 (2013): 306–315.
2. Fuentes, M., et al. "Design of an accurate, low-cost autonomous data logger for PV system monitoring using Arduino™ that complies with IEC standards." *Solar Energy Materials and Solar Cells* 130 (2014): 529–543.
3. Purusothaman, SRR Dhiwaakar, et al. Implementation of Arduino-based multi-agent system for rural Indian microgrids." *Innovative Smart Grid Technologies-Asia (ISGT Asia)*, 2013 IEEE. IEEE, 2013.
4. Papageorgas, P., et al. "Smart Solar Panels: In-situ monitoring of photovoltaic panels based on wired and wireless sensor networks." *Energy Procedia* 36 (2013): 535–545.
5. Hertzog, P., and A. Swart. "A customizable energy monitoring system for renewable energy systems." Presented at the SAUPEC 2015, Resolution Circle Towers in Napier Road in Milpark—Johannesburg (2015).
6. Touati, Farid, et al. "Investigation of solar PV performance under Doha weather using a customized measurement and monitoring system." *Renewable Energy* 89 (2016): 564–577.
7. Peshin, Shwetang, et al. "A photovoltaic (pv) array monitoring simulator." *Modeling, Identification, and control*, int. conf. on, Innsbruck, Austria. 2015.
8. Papageorgas, P., et al. "Wireless sensor networking architecture of polytropon: An open source scalable platform for the smart grid." *Energy Procedia* 50 (2014): 270–276.
9. Dehwah, Ahmad H., Mustafa Mousa, and Christian G. Claudel. "Lessons learned on solar powered wireless sensor network deployments in urban, desert environments." *Ad Hoc Networks* 28 (2015): 52–67.
10. Tushar, Wayes, et al. "Smart grid testbed for demand focused energy management in end user environments." arXiv preprint [arXiv:1603.06756](https://arxiv.org/abs/1603.06756) (2016).
11. Armendariz, Mikel, et al. "A co-simulation platform for medium/low voltage monitoring and control applications." *Innovative Smart Grid Technologies Conference (ISGT)*, 2014 IEEE PES. IEEE, 2014.

Author Index

A

Abhas, 1225
Agarwal, Aditya, 485, 1677
Agarwal, Divya, 1253
Agarwal, S.K., 381
Agarwal, Varima, 197
Aggarwal, Anvesh, 1777
Aggarwal, Ateev, 513
Agnihotri, Geeta, 1687
Agrahari, Ayush, 1171
Agrawal, Krishna Kant, 1267
Ahmad, Jameel, 607
Ahmad, Sheikh Fahad, 1353
Ahmad, Shish, 527, 769, 1079
Ahuja, Neelu J., 855
Alam, Monauwer, 769, 1079
Ali, Sayyed Waize, 889
Anand, Abhineet, 999, 1025
Anand, Ajay, 1369
Anand, Darpan, 1415
Anand, Himanshu Rai, 963
Anil Kumar, Wg. Cdr, 1267
Ansari, Irfan, 1651
Ansari, Mohd. Samar, 23
Anustha, 1523
Arif, Mohammad, 527
Arora, Pranav, 1455
Arora, Sudha, 1145
Asha, Rani, 165, 731
Awasthi, Amit, 493

B

Badgular, Ravindra D., 95
Bajaj, Gaurav, 1481
Bano, Nishat, 769, 1079
Basha, Mudasar, 1243
Bhagwatikar, Govind, 981
Bhan, Anupama, 1491
Bharath Kumar, K., 1127

Bhardwaj, Apoorva, 1275
Bhardwaj, Shubham, 411
Bhargava, Ashmita, 1491
Bhargava, Vani, 687
Bharti, Rajendra, 1707
Bhatia, Madhulika, 1729
Bhattacharya, Subhadip, 289
Bhattacharya, Sudepto, 229
Bhatt, Akhil, 1767
Bhavani, D., 1739
Bhagal, Rosepreet Kaur, 671, 719, 741
Bhuyan, Prashanta, 33
Bijalwan, Anchit, 493
Bishnoi, Shagun, 49
Bisht, Mangal Singh, 277
Bisht, Vijay Singh, 1051
Borah, Abinash, 1191, 1225

C

Chand, Trilok, 335
Chathuranga, G., 65
Chaturvedi, Pranjal, 1225
Chaturvedi, Sudhir Kumar, 49, 83, 799
Chaudhary, Shruti, 1467
Chaudhary, Tanu, 923
Chauhan, Aishwarya, 1137
Chauhan, Shekhar Raj, 553
Chauhan, Shubhi, 1767
Chauhan, Yogesh K., 933, 951, 963, 1033
Chaurasia, R.K., 1019
Chetna, 731
Chhabra, Bharti, 639
Chhabra, Rohit, 805
Chhaya, Lipi, 981
Chibber, Vijay Kumar, 1391
Choudhary, Varchas, 1777
Choudhry, Sushabhan, 1777
Choudhury, Aditya, 1427
Choudhury, S., 513, 933, 963

Chourasia, Vijay S., 129
Chowdary, Vinay, 1111

D

Dar, Ishfaq Gaffar, 811, 819
Dave, M.P., 687
Deepak, Mehta, 731
Deore, Pramod J., 95
Devashrayee, Niranjan M., 209
Dixit, Dushyant, 1503
Dogra, Astha, 139
Dua, Piyush, 633
Dubey, Sanjay Kumar, 239, 839, 847, 1381
Dumka, Ankur, 1445, 1455
Dwivedi, Rakesh, 1749
Dwivedi, R.P., 13

E

Ehtesham, Nazma, 791
Elavarasi, C., 1297

F

Farooq, Sameer, 401

G

Gaba, Avi, 587, 1629
Gadamsetty, Venkata Sai Gokul, 1345
Gahlot, Alok Kumar, 1749
Gairola, Pavni, 1491
Gandhi, Priyesh P., 209
Gangwar, Manjeet Singh, 393
Ganimidi, Mounika, 599
Garg, Deepak, 1587
Garg, Divyanshi, 473
Garg, Lokesh, 381
Garg, Oshin, 455
Garg, Peeyush, 1621
Garg, Vikas, 485, 1629, 1677
Gehlot, Anita, 465, 485, 513, 587, 647, 653, 1191, 1361, 1503, 1603, 1629, 1651, 1677, 1777
Gokhale, S.S., 577
Gopal, Madan, 561
Gowri, R., 1101, 1159
Goyal, Amit, 1415
Grover, Kabir, 1481
Gupta, Abhay Kumar, 1199
Gupta, Apurva, 229
Gupta, Aryaman, 1381
Gupta, Ashutosh, 393
Gupta, Ginni, 943
Gupta, Heena, 839
Gupta, Mahima, 1523
Gupta, Manish, 1415

Gupta, Mukul Kumar, 829, 1111, 1565
Gupta, Neha, 1137
Gupta, Rajeev, 13
Gupta, Shivani, 847
Gupta, Shweta, 1177
Gupta, Vinay, 1621

H

Hak, Sindhu, 1207
Hyma Lakshmi, T.V., 1739

I

Ijjada, Sreenivasa Rao, 1401

J

Jadli, Utkarsh, 1041
Jain, Akansh, 879
Jain, Akshansh, 647, 1361
Jain, Arpit, 829, 1345, 1749
Jain, Prateek, 973
Jain, Sambhav, 1215
Jain, Shilpi, 1729
Jaiswal, Utkarsh, 1767
Jangid, Sandeep, 1191
Jatily, Vibhu, 1145
Jayasinghe, Jeevani, 65
Jha, P.K., 577
Joshi, Ekta, 1529
Joshi, Garima, 1335
Joshi, Lalit Mohan, 1707
Joshi, N.K., 1757
Joshi, R.C., 493
Jyoti, Kiran, 401

K

Kachroo, Beenish, 873
Kakkar, Ashna, 1437
Kala, Mamta Chamoli, 1427
Kala, Sachin, 1537
Kalra, Ashima, 305, 357
Kalra, Nikhil, 465
Kamal, Hutanshu, 799
Kapri, Shivam, 83
Katoch, Rachita, 741
Kaundal, Vivek, 1171, 1467, 1565
Kaur, Iqbaldeep, 1283, 1289
Kaur, Jaspreet, 305
Kaur, Jsvinder, 709
Kaur, Pardeep, 347, 623
Kaur, Prabhjot, 493
Kaur, Rajwanti, 315
Kaur, Ravneet, 537, 991
Kaur, Rupinder, 325
Kaushal, Rajesh, 1611

Kaushiki, 943
 Kavi, Saurabh, 1641
 Khaleelu Rehman, B., 503
 Khan, Azzan, 819
 Khan, Mohd. Faizan, 1719
 Khanum, Akheela, 607
 Khare, P.K., 553
 Khattri, Tanushree, 653
 Khurana, Manpreet Kaur, 805
 Khurana, Sourabh, 1
 Kochhar, Aarti, 347
 Kompella, Surya, 1089
 Kothiyal, Alok Darshan, 277
 Koushal, Anurag, 963
 Kuchhal, Piyush, 633, 829, 907
 Kumar, Abhishek, 419
 Kumar, Adesh, 503, 879, 981, 1177, 1199, 1467, 1565, 1575, 1749
 Kumar, Amit, 33
 Kumar, Anil, 277
 Kumar, Ankita, 1719
 kumar, Arun, 709
 Kumar, Ashok, 513, 1777
 Kumar, Brijesh, 123
 Kumar, Deepak, 33, 943, 973, 1391, 1697
 Kumari, Amisha, 1191
 Kumari, Monisha, 1289
 Kumari, N. Prasanthi, 545
 Kumari, Priyanka, 173, 187
 Kumari, Shraddha, 1009
 Kumar, Kamal, 267
 Kumar, Nitish, 465
 Kumar, Pardeep, 335
 Kumar, Prateek Kumar, 951
 Kumar, Roushan, 855, 879
 Kumar, Sanjeev, 623
 Kumar, Satish, 1051, 1137
 Kumar, Shivam, 473
 Kumar, Shubham, 473, 1565
 Kumar, Sumit, 1199
 Kumar, Sunil, 277
 Kumar, Vivek, 41, 381
 Kumar, Vobulapuram Ramesh, 569
 Kummamuri, Rahul, 799
 Kundu, Sudip, 23
 Kurien, Caneon, 1233
 Kushwaha, Varsha, 779

L

Lal, Kanhaiya, 907
 Lawaniya, Harsh, 1361

M

Madhavi, D., 157

Madhu, Charu, 537, 991
 Madhuri, G.M.G., 545
 Mahreen, S.K., 661
 Maindolia, Ashish, 411
 Majumdar, Sagar, 647, 653, 1361
 Malik, Aditi, 623
 Malik, Ketan, 139
 Mall, Nikhil, 197
 Malviya, Himanshu, 1603
 Manda, Rajarao, 257, 561
 Mathur, Sanjay, 1101, 1159
 Mathur, Vishal, 1019
 Mehra, Anu, 55, 1481
 Mehta, G., 1551
 Mehta, Prateek, 83
 Minocha, Gagan, 1523
 Minocha, Sanjana, 1445
 Mishra, Akarsha, 1575
 Mishra, Raj Gaurav, 65, 633, 1019
 Mishra, Ranjan, 65, 633, 1019
 Mishra, Shubham, 923
 Mittal, Poornima, 107, 115, 123
 Mittal, Arun K., 129
 Mohammad, Salauddin, 561
 Mohana Durga, G., 1739
 Mohit, Jain, 731
 Mohta, Mohit, 913
 Mor, Prashant, 553
 Mudgal, Kartik, 1361
 Mukherjee, Mainak, 197
 Mukherjee, S., 791
 Murthy, K.S.N., 1119

N

Nagma, 1661
 Nagpal, Dimple, 1283
 Nagra, Baljeet Kaur, 639
 Nanda Kumar, M., 1307
 Nath, Ram, 761
 Naudiyal, Arushi, 1603
 Nautiyal, Pranjali, 107, 115
 Nautiyal, Shruti, 107, 115
 Neelam, S.K., 661
 Negi, Gaurav, 1641
 Negi, Sandeep, 1529
 Negi, Shubham, 107, 123
 Nehal, S.K., 1369
 Nikhil, Pachauri, 165
 Nirdosh, 1437
 Nizam, Farhan, 1621

O

Obheroi, Rajat Kumar, 1369
 Olokede, Seyi Stephen, 679, 699

P

Pachauri, Rupendra Kumar, 513, 933, 951,
963, 1033, 1777
Pallavi, G., 1089
Panda, S.N., 1611
Pande, Revant, 1171
Pandey, Alok Kumar, 393, 923
Pandey, Anand, 879
Pandey, Kamlesh, 779, 895
Pandey, Purnendu Shekhar, 41, 1641
Pani, Shuchismita, 865, 1207, 1275
Panwar, Aakanksha, 587, 1629
Panwar, Lokesh, 1537
Panwar, Varij, 1537
Pargain, Vishu, 553
Parihar, Rakshita, 1575
Patel, Dipen, 49
Patel, Hemangi, 907
Patel, Madhukant, 907
Pathak, Diwaker, 1033
Patil, Prashant G., 129
Paul, Babu Sena, 679, 699
Phadke, Navneet, 1697
Poojitha, V., 1729
Prakash, Anshuman, 805
Prakash, Rishita, 1603
Pranav, Vemulapalli Sai, 1243
Prasad, Ajay, 229
Prasad, Dinesh, 429
Prasanthi Kumari, N., 1739
Prashar, Deepak, 401, 419
Praveen Kitti, B., 545
Preeti, 347, 455
Priyam, 1511
Pruthi, Yajur, 1697

R

Rai, Munishwar, 247
Raizada, Jagriti, 1325
Rajale, Sayali, 197
Raja, M., 799
Rajawat, Asmita, 913, 1009
Raj, Prateek, 1621
Rajput, Sachin Kumar, 55, 1481, 1595
Ramesh Kumar, Vobulapuram, 599
Ramesh Patnaik, M., 157
Ramesh, Yenikepalli, 569
Rana, Haneet, 1325, 1369, 1523
Rana, Hukam Singh, 999
Rana, Pradeep, 933
Rana, Sonali, 719
Rani, Ginne, 1641
Rani, Nibha, 779, 895
Ranjan, Praful, 41, 73, 1641

Rathod, Arun Pratap Singh, 115
Rawat, Aviral, 1697
Rehman, Khaleel, 561, 1243
Roy, Ajay, 429
Roy, Arpan, 55

S

Sachan, Shubham, 1009
Sah, Shalini, 1215, 1437
Sai Hemanth, G., 1119
Saini, Devender Kumar, 13
Saini, Parvesh, 1065
Saini, Raj Kumar, 13
Saklani, Rajat, 83
Salaudhin, Mohammad, 257
Samkaria, Rohit, 513, 1777
Sanket, Rohit, 513
Santhirani, Ch., 1401
Saraswat, Jaideep, 197
Satyanarayana, K., 1119
Saxena, Apurva, 1767
Saxena, Mukesh, 855
Sethi, Muneesh, 1
Shaik, Ziaur Rahiman, 147
Shanmuganatham, T., 1127, 1297, 1307
Shanu, Saurabh, 229
Sharawat, Kirti, 239
Sharma, Aashwin, 55
Sharma, Abhay, 173, 187
Sharma, Abhinav, 1101, 1159
Sharma, Abhishek, 465
Sharma, Akshay, 879
Sharma, Devashish, 779
Sharma, Dolly, 305, 315, 325, 335, 639, 1283,
1289
Sharma, Ishan, 999
Sharma, Jayash Kumar, 1415
Sharma, Jyoti, 23
Sharma, Manish, 33, 811, 819, 889, 1595
Sharma, Navodit, 811
Sharma, Neeraj, 753
Sharma, Paawan, 503, 981, 1171
Sharma, Parth, 865, 1207, 1325
Sharma, Prashasti, 473
Sharma, Rohan, 647, 653
Sharma, Sanjeev Kumar, 1749
Sharma, Shilpi, 357
Sharma, Sukesh, 455
Sharma, Sushant, 1537
Sharma, Vishal, 371, 1511
Shikha, Parul, 1595
Shimray, Benjamin A., 289
Shreekant, K., 865, 1207, 1215
Shubham, 1651

Shukla, Anshuman, 393
 Shukla, Vishakha, 485
 Siddiqui, Faraz, 1325
 Siddiqui, Nihal Anwar, 1511
 Sidhu, Jagpreet, 1587, 1661
 Sikander, Afzal, 1315
 Singh, Abhishek, 411
 Singh, Ajay, 1391
 Singh, Anamika, 1225
 Singh, Ankit, 443
 Singh, Anurag, 963, 1651
 Singh, Archana, 895
 Singh, Arpita, 173, 187
 Singh, Atul, 371
 Singh, Deepak Kumar, 1353
 Singh, Deepti, 537, 991
 Singh, Divyansh, 371
 Singh, Dushyant Kumar, 219
 Singh, Gurpreet, 443
 Singh, Jaiteg, 1661
 Singh, Jaspreet, 1611
 Singh, Mandeep, 443
 Singh, Neeraj, 1065
 Singholi, Ajay K.S., 1253
 Singh, Prashant, 83
 Singh, Pratul, 553
 Singh, Preeti, 623
 Singh, Rajesh, 465, 485, 513, 587, 647, 653, 951, 1137, 1191, 1225, 1361, 1503, 1603, 1629, 1651, 1677, 1777
 Singh, Rana Sameer Pratap, 671
 Singh, Satnam, 753
 Singh, Saurabh, 1025
 Singh, Shailendra, 335
 Singh, Sukhwinder, 1335
 Singh, Virendra, 907
 Singh, Vishal Kumar, 411
 Sinha, S.K., 687, 895
 Siva Kumar, M., 1119, 1243
 Sivateja, D., 1119
 Sogani, Priyal Kumar, 1503
 Srivastava, Ajay Kumar, 1233
 Srivastava, Mayank, 429
 Srivastav, Kritarth, 1511
 Sudha, D., 1401
 Sudha, Raga, 1089
 Suhaib, Mohd, 791
 Sukumar, S., 1089
 Suma Bindu, K., 1119
 Suman, Preetam, 1353
 Sumanth Kumar, Ch., 147
 Suri, Karush, 913

T

Taksh, 1511
 Talwar, Meenkshi, 139

Tanwar, Aadrita, 1677
 Tauseef, Sayed Mohammad, 473
 Teja, G.N.L. Ravi, 1089
 Tejaswini, D., 49
 Thakur, Anita, 553
 Thakur, Ritula, 761
 Thakur, Robin, 1
 Thaman, Jyoti, 267
 Thapliyal, Shubhankar, 879
 Thomas, Cris, 799
 Tikku, Revanta, 1199
 Tiwari, Rajeev, 999, 1025
 Tiwari, Rohit, 219
 Tripathi, Manish Madhava, 1757
 Tripathy, M.R., 873, 889

U

Uniyal, Ishita, 1041, 1065, 1315
 Uniyal, Shailesh, 1041

V

Varma, Arun S., 371
 Varshney, Prabhansh, 49
 Vayalada, Kiran Kumar, 1345
 Verma, Aakash, 139
 Verma, Amit, 1289
 Verma, Gaurav, 1199, 1697
 Vermal, Amit, 1283
 Verma, Piush, 13
 Verma, Puneet, 1651
 Verma, R., 1551
 Verma, Shrestha, 923
 Verma, Yashaswi, 1767
 Vig, Renu, 991, 1335
 Vijander, Singh, 165, 731
 Vijayadharshini, S., 1275
 Virk, Kiranpal Singh, 247
 Vivek, Kumar, 731
 Vivek, Pandey, 165
 Vyas, Garima, 1491

W

Warsi, M.R., 661

Y

Yadav, Ankit, 1621
 Yadav, Bharti, 357
 Yadav, Bikarama Prasad, 371, 411
 Yadav, Jitendra, 1687
 Yadav, M.S., 513, 1777
 Yadav, V.K., 1551

Z

Zafar, Aqsa, 1267
 Zilli, A.A., 607